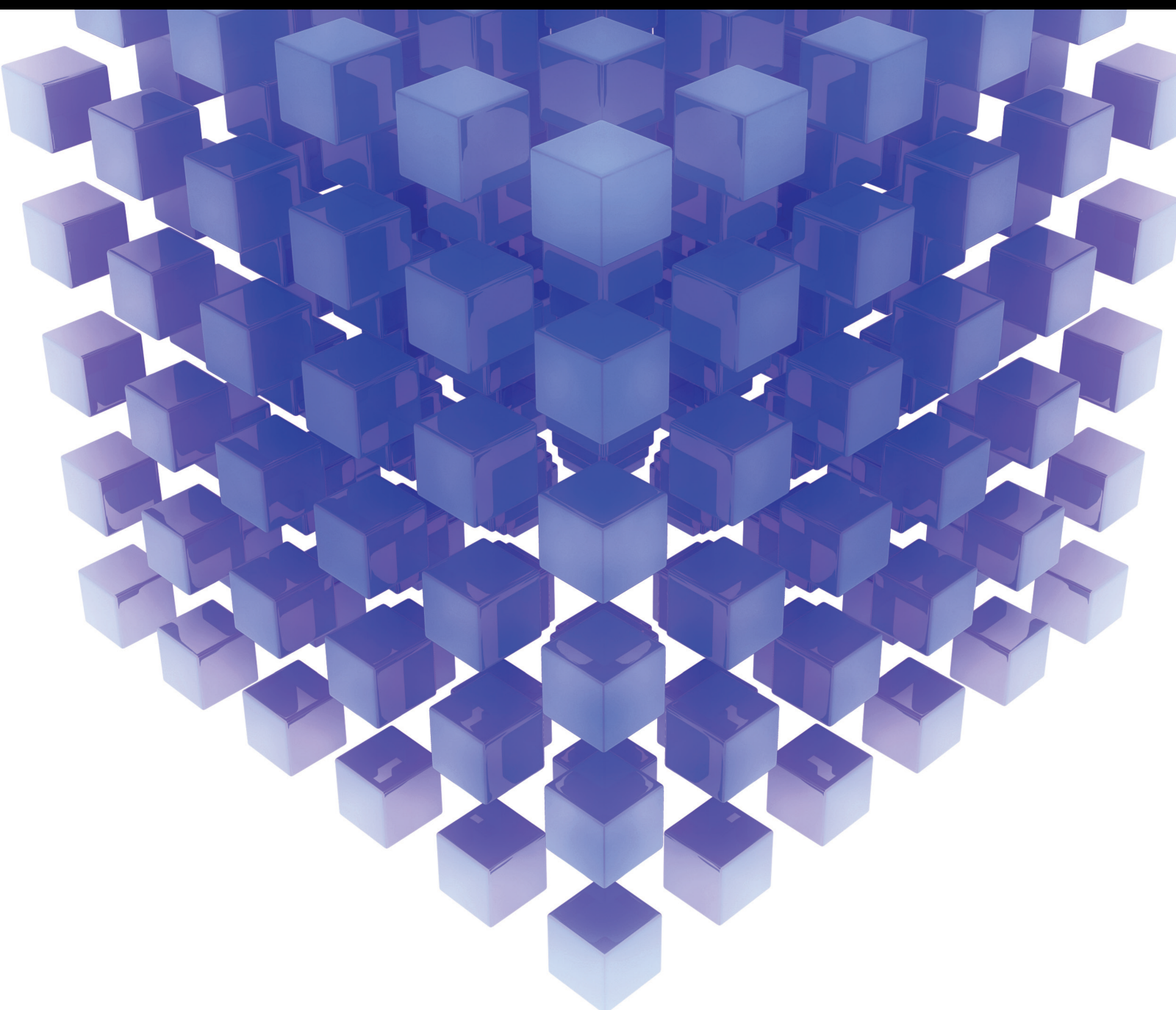


# Bio-Inspired Algorithms and Applications

Lead Guest Editor: Man Fai Leung

Guest Editors: Hangjun Che and Shimin Wang





---

# **Bio-Inspired Algorithms and Applications**

Mathematical Problems in Engineering

---

## **Bio-Inspired Algorithms and Applications**

Lead Guest Editor: Man Fai Leung

Guest Editors: Hangjun Che and Shimin Wang




---

Copyright © 2023 Hindawi Limited. All rights reserved.

This is a special issue published in “Mathematical Problems in Engineering.” All articles are open access articles distributed under the Creative Commons Attribution License, which permits unrestricted use, distribution, and reproduction in any medium, provided the original work is properly cited.

# Chief Editor

Guangming Xie , China

## Academic Editors

Kumaravel A , India  
Waqas Abbasi, Pakistan  
Mohamed Abd El Aziz , Egypt  
Mahmoud Abdel-Aty , Egypt  
Mohammed S. Abdo, Yemen  
Mohammad Yaghoub Abdollahzadeh  
Jamalabadi , Republic of Korea  
Rahib Abiyev , Turkey  
Leonardo Acho , Spain  
Daniela Addessi , Italy  
Arooj Adeel , Pakistan  
Waleed Adel , Egypt  
Ramesh Agarwal , USA  
Francesco Aggogeri , Italy  
Ricardo Aguilar-Lopez , Mexico  
Afaq Ahmad , Pakistan  
Naveed Ahmed , Pakistan  
Elias Aifantis , USA  
Akif Akgul , Turkey  
Tareq Al-shami , Yemen  
Guido Ala, Italy  
Andrea Alaimo , Italy  
Reza Alam, USA  
Osamah Albahri , Malaysia  
Nicholas Alexander , United Kingdom  
Salvatore Alfonzetti, Italy  
Ghous Ali , Pakistan  
Nouman Ali , Pakistan  
Mohammad D. Aliyu , Canada  
Juan A. Almendral , Spain  
A.K. Alomari, Jordan  
José Domingo Álvarez , Spain  
Cláudio Alves , Portugal  
Juan P. Amezcua-Sanchez, Mexico  
Mukherjee Amitava, India  
Lionel Amodeo, France  
Sebastian Anita, Romania  
Costanza Arico , Italy  
Sabri Arik, Turkey  
Fausto Arpino , Italy  
Rashad Asharabi , Saudi Arabia  
Farhad Aslani , Australia  
Mohsen Asle Zaem , USA

Andrea Avanzini , Italy  
Richard I. Avery , USA  
Viktor Avrutin , Germany  
Mohammed A. Awadallah , Malaysia  
Francesco Aymerich , Italy  
Sajad Azizi , Belgium  
Michele Bacciocchi , Italy  
Seungik Baek , USA  
Khaled Bahlali, France  
M.V.A Raju Bahubalendruni, India  
Pedro Balaguer , Spain  
P. Balasubramaniam, India  
Stefan Balint , Romania  
Ines Tejado Balsera , Spain  
Alfonso Banos , Spain  
Jerzy Baranowski , Poland  
Tudor Barbu , Romania  
Andrzej Bartoszewicz , Poland  
Sergio Baselga , Spain  
S. Caglar Baslamisli , Turkey  
David Bassir , France  
Chiara Bedon , Italy  
Azeddine Beghdadi, France  
Andriette Bekker , South Africa  
Francisco Beltran-Carbajal , Mexico  
Abdellatif Ben Makhlof , Saudi Arabia  
Denis Benasciutti , Italy  
Ivano Benedetti , Italy  
Rosa M. Benito , Spain  
Elena Benvenuti , Italy  
Giovanni Berselli, Italy  
Michele Betti , Italy  
Pietro Bia , Italy  
Carlo Bianca , France  
Simone Bianco , Italy  
Vincenzo Bianco, Italy  
Vittorio Bianco, Italy  
David Bigaud , France  
Sardar Muhammad Bilal , Pakistan  
Antonio Bilotta , Italy  
Sylvio R. Bistafa, Brazil  
Chiara Boccaletti , Italy  
Rodolfo Bontempo , Italy  
Alberto Borboni , Italy  
Marco Bortolini, Italy

Paolo Boscariol, Italy  
Daniela Boso , Italy  
Guillermo Botella-Juan, Spain  
Abdesselem Boulkroune , Algeria  
Boulaïd Boulkroune, Belgium  
Fabio Bovenga , Italy  
Francesco Braghin , Italy  
Ricardo Branco, Portugal  
Julien Bruchon , France  
Matteo Bruggi , Italy  
Michele Brun , Italy  
Maria Elena Bruni, Italy  
Maria Angela Butturi , Italy  
Bartłomiej Błachowski , Poland  
Dhanamjayulu C , India  
Raquel Caballero-Águila , Spain  
Filippo Cacace , Italy  
Salvatore Caddemi , Italy  
Zuowei Cai , China  
Roberto Caldelli , Italy  
Francesco Cannizzaro , Italy  
Maosen Cao , China  
Ana Carpio, Spain  
Rodrigo Carvajal , Chile  
Caterina Casavola, Italy  
Sara Casciati, Italy  
Federica Caselli , Italy  
Carmen Castillo , Spain  
Inmaculada T. Castro , Spain  
Miguel Castro , Portugal  
Giuseppe Catalanotti , United Kingdom  
Alberto Cavallo , Italy  
Gabriele Cazzulani , Italy  
Fatih Vehbi Celebi, Turkey  
Miguel Cerrolaza , Venezuela  
Gregory Chagnon , France  
Ching-Ter Chang , Taiwan  
Kuei-Lun Chang , Taiwan  
Qing Chang , USA  
Xiaoheng Chang , China  
Prasenjit Chatterjee , Lithuania  
Kacem Chehdi, France  
Peter N. Cheimets, USA  
Chih-Chiang Chen , Taiwan  
He Chen , China

Kebing Chen , China  
Mengxin Chen , China  
Shyi-Ming Chen , Taiwan  
Xizhong Chen , Ireland  
Xue-Bo Chen , China  
Zhiwen Chen , China  
Qiang Cheng, USA  
Zeyang Cheng, China  
Luca Chiapponi , Italy  
Francisco Chicano , Spain  
Tirivanhu Chinyoka , South Africa  
Adrian Chmielewski , Poland  
Seongim Choi , USA  
Gautam Choubey , India  
Hung-Yuan Chung , Taiwan  
Yusheng Ci, China  
Simone Cinquemani , Italy  
Roberto G. Citarella , Italy  
Joaquim Ciurana , Spain  
John D. Clayton , USA  
Piero Colajanni , Italy  
Giuseppina Colicchio, Italy  
Vassilios Constantoudis , Greece  
Enrico Conte, Italy  
Alessandro Contento , USA  
Mario Cools , Belgium  
Gino Cortellessa, Italy  
Carlo Cosentino , Italy  
Paolo Crippa , Italy  
Erik Cuevas , Mexico  
Guozeng Cui , China  
Mehmet Cunkas , Turkey  
Giuseppe D'Aniello , Italy  
Peter Dabnichki, Australia  
Weizhong Dai , USA  
Zhifeng Dai , China  
Purushothaman Damodaran , USA  
Sergey Dashkovskiy, Germany  
Adiel T. De Almeida-Filho , Brazil  
Fabio De Angelis , Italy  
Samuele De Bartolo , Italy  
Stefano De Miranda , Italy  
Filippo De Monte , Italy



































José António Fonseca De Oliveira  
Correia , Portugal  
Jose Renato De Sousa , Brazil  
Michael Defoort, France  
Alessandro Della Corte, Italy  
Laurent Dewasme , Belgium  
Sanku Dey , India  
Gianpaolo Di Bona , Italy  
Roberta Di Pace , Italy  
Francesca Di Puccio , Italy  
Ramón I. Diego , Spain  
Yannis Dimakopoulos , Greece  
Hasan Dinçer , Turkey  
José M. Domínguez , Spain  
Georgios Dounias, Greece  
Bo Du , China  
Emil Dumic, Croatia  
Madalina Dumitriu , United Kingdom  
Premraj Durairaj , India  
Saeed Eftekhari Azam, USA  
Said El Kafhali , Morocco  
Antonio Elipse , Spain  
R. Emre Erkmen, Canada  
John Escobar , Colombia  
Leandro F. F. Miguel , Brazil  
FRANCESCO FOTI , Italy  
Andrea L. Facci , Italy  
Shahla Faisal , Pakistan  
Giovanni Falsone , Italy  
Hua Fan, China  
Jianguang Fang, Australia  
Nicholas Fantuzzi , Italy  
Muhammad Shahid Farid , Pakistan  
Hamed Faruqi, Iran  
Yann Favennec, France  
Fiorenzo A. Fazzolari , United Kingdom  
Giuseppe Fedele , Italy  
Roberto Fedele , Italy  
Baowei Feng , China  
Mohammad Ferdows , Bangladesh  
Arturo J. Fernández , Spain  
Jesus M. Fernandez Oro, Spain  
Francesco Ferrise, Italy  
Eric Feulvarch , France  
Thierry Floquet, France

Eric Florentin , France  
Gerardo Flores, Mexico  
Antonio Forcina , Italy  
Alessandro Formisano, Italy  
Francesco Franco , Italy  
Elisa Francomano , Italy  
Juan Frausto-Solis, Mexico  
Shujun Fu , China  
Juan C. G. Prada , Spain  
HECTOR GOMEZ , Chile  
Matteo Gaeta , Italy  
Mauro Gaggero , Italy  
Zoran Gajic , USA  
Jaime Gallardo-Alvarado , Mexico  
Mosè Gallo , Italy  
Akemi Gálvez , Spain  
Maria L. Gandarias , Spain  
Hao Gao , Hong Kong  
Xingbao Gao , China  
Yan Gao , China  
Zhiwei Gao , United Kingdom  
Giovanni Garcea , Italy  
José García , Chile  
Harish Garg , India  
Alessandro Gasparetto , Italy  
Stylianios Georgantzinou, Greece  
Fotios Georgiades , India  
Parviz Ghadimi , Iran  
Ştefan Cristian Gherghina , Romania  
Georgios I. Giannopoulos , Greece  
Agathoklis Giaralis , United Kingdom  
Anna M. Gil-Lafuente , Spain  
Ivan Giorgio , Italy  
Gaetano Giunta , Luxembourg  
Jefferson L.M.A. Gomes , United Kingdom  
Emilio Gómez-Déniz , Spain  
Antonio M. Gonçalves de Lima , Brazil  
Qunxi Gong , China  
Chris Goodrich, USA  
Rama S. R. Gorla, USA  
Veena Goswami , India  
Xunjie Gou , Spain  
Jakub Grabski , Poland

Antoine Grall , France  
George A. Gravvanis , Greece  
Fabrizio Greco , Italy  
David Greiner , Spain  
Jason Gu , Canada  
Federico Guarracino , Italy  
Michele Guida , Italy  
Muhammet Gul , Turkey  
Dong-Sheng Guo , China  
Hu Guo , China  
Zhaoxia Guo, China  
Yusuf Gurefe, Turkey  
Salim HEDDAM , Algeria  
ABID HUSSANAN, China  
Quang Phuc Ha, Australia  
Li Haitao , China  
Petr Hájek , Czech Republic  
Mohamed Hamdy , Egypt  
Muhammad Hamid , United Kingdom  
Renke Han , United Kingdom  
Weimin Han , USA  
Xingsi Han, China  
Zhen-Lai Han , China  
Thomas Hanne , Switzerland  
Xinan Hao , China  
Mohammad A. Hariri-Ardebili , USA  
Khalid Hattaf , Morocco  
Defeng He , China  
Xiao-Qiao He, China  
Yanchao He, China  
Yu-Ling He , China  
Ramdane Hedjar , Saudi Arabia  
Jude Hemanth , India  
Reza Hemmati, Iran  
Nicolae Herisanu , Romania  
Alfredo G. Hernández-Díaz , Spain  
M.I. Herreros , Spain  
Eckhard Hitzer , Japan  
Paul Honeine , France  
Jaromir Horacek , Czech Republic  
Lei Hou , China  
Yingkun Hou , China  
Yu-Chen Hu , Taiwan  
Yunfeng Hu, China  
Can Huang , China  
Gordon Huang , Canada  
Linsheng Huo , China  
Sajid Hussain, Canada  
Asier Ibeas , Spain  
Orest V. Iftime , The Netherlands  
Przemyslaw Ignaciuk , Poland  
Giacomo Innocenti , Italy  
Emilio Insfran Pelozo , Spain  
Azeem Irshad, Pakistan  
Alessio Ishizaka, France  
Benjamin Ivorra , Spain  
Breno Jacob , Brazil  
Reema Jain , India  
Tushar Jain , India  
Amin Jajarmi , Iran  
Chiranjibe Jana , India  
Łukasz Jankowski , Poland  
Samuel N. Jator , USA  
Juan Carlos Jáuregui-Correa , Mexico  
Kandasamy Jayakrishna, India  
Reza Jazar, Australia  
Khalide Jbilou, France  
Isabel S. Jesus , Portugal  
Chao Ji , China  
Qing-Chao Jiang , China  
Peng-fei Jiao , China  
Ricardo Fabricio Escobar Jiménez , Mexico  
Emilio Jiménez Macías , Spain  
Maolin Jin, Republic of Korea  
Zhuo Jin, Australia  
Ramash Kumar K , India  
BHABEN KALITA , USA  
MOHAMMAD REZA KHEDMATI , Iran  
Viacheslav Kalashnikov , Mexico  
Mathiyalagan Kalidass , India  
Tamas Kalmar-Nagy , Hungary  
Rajesh Kaluri , India  
Jyotheeswara Reddy Kalvakurthi, India  
Zhao Kang , China  
Ramani Kannan , Malaysia  
Tomasz Kapitaniak , Poland  
Julius Kaplunov, United Kingdom  
Konstantinos Karamanos, Belgium  
Michal Kawulok, Poland



Irfan Kaymaz , Turkey  
Vahid Kayvanfar , Qatar  
Krzysztof Kecik , Poland  
Mohamed Khader , Egypt  
Chaudry M. Khalique , South Africa  
Mukhtaj Khan , Pakistan  
Shahid Khan , Pakistan  
Nam-Il Kim, Republic of Korea  
Philipp V. Kiryukhantsev-Korneev ,  
Russia  
P.V.V Kishore , India  
Jan Koci , Czech Republic  
Ioannis Kostavelis , Greece  
Sotiris B. Kotsiantis , Greece  
Frederic Kratz , France  
Vamsi Krishna , India  
Edyta Kucharska, Poland  
Krzysztof S. Kulpa , Poland  
Kamal Kumar, India  
Prof. Ashwani Kumar , India  
Michal Kunicki , Poland  
Cedrick A. K. Kwuimy , USA  
Kyandoghere Kyamakya, Austria  
Ivan Kyrchei , Ukraine  
Márcio J. Lacerda , Brazil  
Eduardo Lalla , The Netherlands  
Giovanni Lancioni , Italy  
Jaroslaw Latalski , Poland  
Hervé Laurent , France  
Agostino Lauria , Italy  
Aimé Lay-Ekuakille , Italy  
Nicolas J. Leconte , France  
Kun-Chou Lee , Taiwan  
Dimitri Lefebvre , France  
Eric Lefevre , France  
Marek Lefik, Poland  
Yaguo Lei , China  
Kauko Leiviskä , Finland  
Ervin Lenzi , Brazil  
ChenFeng Li , China  
Jian Li , USA  
Jun Li , China  
Yueyang Li , China  
Zhao Li , China































Zhen Li , China  
En-Qiang Lin, USA  
Jian Lin , China  
Qibin Lin, China  
Yao-Jin Lin, China  
Zhiyun Lin , China  
Bin Liu , China  
Bo Liu , China  
Heng Liu , China  
Jianxu Liu , Thailand  
Lei Liu , China  
Sixin Liu , China  
Wanquan Liu , China  
Yu Liu , China  
Yuanchang Liu , United Kingdom  
Bonifacio Llamazares , Spain  
Alessandro Lo Schiavo , Italy  
Jean Jacques Loiseau , France  
Francesco Lolli , Italy  
Paolo Lonetti , Italy  
António M. Lopes , Portugal  
Sebastian López, Spain  
Luis M. López-Ochoa , Spain  
Vassilios C. Loukopoulos, Greece  
Gabriele Maria Lozito , Italy  
Zhiguo Luo , China  
Gabriel Luque , Spain  
Valentin Lychagin, Norway  
YUE MEI, China  
Junwei Ma , China  
Xuanlong Ma , China  
Antonio Madeo , Italy  
Alessandro Magnani , Belgium  
Toqeer Mahmood , Pakistan  
Fazal M. Mahomed , South Africa  
Arunava Majumder , India  
Sarfranz Nawaz Malik, Pakistan  
Paolo Manfredi , Italy  
Adnan Maqsood , Pakistan  
Muazzam Maqsood, Pakistan  
Giuseppe Carlo Marano , Italy  
Damijan Markovic, France  
Filipe J. Marques , Portugal  
Luca Martinelli , Italy  
Denizar Cruz Martins, Brazil

Francisco J. Martos , Spain  
Elio Masciari , Italy  
Paolo Massioni , France  
Alessandro Mauro , Italy  
Jonathan Mayo-Maldonado , Mexico  
Pier Luigi Mazzeo , Italy  
Laura Mazzola, Italy  
Driss Mehdi , France  
Zahid Mehmood , Pakistan  
Roderick Melnik , Canada  
Xiangyu Meng , USA  
Jose Merodio , Spain  
Alessio Merola , Italy  
Mahmoud Mesbah , Iran  
Luciano Mescia , Italy  
Laurent Mevel , France  
Constantine Michailides , Cyprus  
Mariusz Michta , Poland  
Prankul Middha, Norway  
Aki Mikkola , Finland  
Giovanni Minafò , Italy  
Edmondo Minisci , United Kingdom  
Hiroyuki Mino , Japan  
Dimitrios Mitsotakis , New Zealand  
Ardashir Mohammadzadeh , Iran  
Francisco J. Montáns , Spain  
Francesco Montefusco , Italy  
Gisele Mophou , France  
Rafael Morales , Spain  
Marco Morandini , Italy  
Javier Moreno-Valenzuela , Mexico  
Simone Morganti , Italy  
Caroline Mota , Brazil  
Aziz Moukrim , France  
Shen Mouquan , China  
Dimitris Mourtzis , Greece  
Emiliano Mucchi , Italy  
Taseer Muhammad, Saudi Arabia  
Ghulam Muhiuddin, Saudi Arabia  
Amitava Mukherjee , India  
Josefa Mula , Spain  
Jose J. Muñoz , Spain  
Giuseppe Muscolino, Italy  
Marco Mussetta , Italy

Hariharan Muthusamy, India  
Alessandro Naddeo , Italy  
Raj Nandkeolyar, India  
Keivan Navaie , United Kingdom  
Soumya Nayak, India  
Adrian Neagu , USA  
Erivelton Geraldo Nepomuceno , Brazil  
AMA Neves, Portugal  
Ha Quang Thinh Ngo , Vietnam  
Nhon Nguyen-Thanh, Singapore  
Papakostas Nikolaos , Ireland  
Jelena Nikolic , Serbia  
Tatsushi Nishi, Japan  
Shanzhou Niu , China  
Ben T. Nohara , Japan  
Mohammed Nouari , France  
Mustapha Nourelfath, Canada  
Kazem Nouri , Iran  
Ciro Núñez-Gutiérrez , Mexico  
Włodzimierz Ogryczak, Poland  
Roger Ohayon, France  
Krzysztof Okarma , Poland  
Mitsuhiro Okayasu, Japan  
Murat Olgun , Turkey  
Diego Oliva, Mexico  
Alberto Olivares , Spain  
Enrique Onieva , Spain  
Calogero Orlando , Italy  
Susana Ortega-Cisneros , Mexico  
Sergio Ortobelli, Italy  
Naohisa Otsuka , Japan  
Sid Ahmed Ould Ahmed Mahmoud , Saudi Arabia  
Taoreed Owolabi , Nigeria  
EUGENIA PETROPOULOU , Greece  
Arturo Pagano, Italy  
Madhumangal Pal, India  
Pasquale Palumbo , Italy  
Dragan Pamučar, Serbia  
Weifeng Pan , China  
Chandan Pandey, India  
Rui Pang, United Kingdom  
Jürgen Pannek , Germany  
Elena Panteley, France  
Achille Paolone, Italy

George A. Papakostas , Greece  
Xosé M. Pardo , Spain  
You-Jin Park, Taiwan  
Manuel Pastor, Spain  
Pubudu N. Pathirana , Australia  
Surajit Kumar Paul , India  
Luis Payá , Spain  
Igor Pažanin , Croatia  
Libor Pekař , Czech Republic  
Francesco Pellicano , Italy  
Marcello Pellicciari , Italy  
Jian Peng , China  
Mingshu Peng, China  
Xiang Peng , China  
Xindong Peng, China  
Yuexing Peng, China  
Marzio Pennisi , Italy  
Maria Patrizia Pera , Italy  
Matjaz Perc , Slovenia  
A. M. Bastos Pereira , Portugal  
Wesley Peres, Brazil  
F. Javier Pérez-Pinal , Mexico  
Michele Perrella, Italy  
Francesco Pesavento , Italy  
Francesco Petrini , Italy  
Hoang Vu Phan, Republic of Korea  
Lukasz Pieczonka , Poland  
Dario Piga , Switzerland  
Marco Pizzarelli , Italy  
Javier Plaza , Spain  
Goutam Pohit , India  
Dragan Poljak , Croatia  
Jorge Pomares , Spain  
Hiram Ponce , Mexico  
Sébastien Poncet , Canada  
Volodymyr Ponomaryov , Mexico  
Jean-Christophe Ponsart , France  
Mauro Pontani , Italy  
Sivakumar Poruran, India  
Francesc Pozo , Spain  
Aditya Rio Prabowo , Indonesia  
Anchasa Pramuanjaroenkij , Thailand  
Leonardo Primavera , Italy  
B Rajanarayan Prusty, India

Krzysztof Puszynski , Poland  
Chuan Qin , China  
Dongdong Qin, China  
Jianlong Qiu , China  
Giuseppe Quaranta , Italy  
DR. RITU RAJ , India  
Vitomir Racic , Italy  
Carlo Rainieri , Italy  
Kumbakonam Ramamani Rajagopal, USA  
Ali Ramazani , USA  
Angel Manuel Ramos , Spain  
Higinio Ramos , Spain  
Muhammad Afzal Rana , Pakistan  
Muhammad Rashid, Saudi Arabia  
Manoj Rastogi, India  
Alessandro Rasulo , Italy  
S.S. Ravindran , USA  
Abdolrahman Razani , Iran  
Alessandro Reali , Italy  
Jose A. Reinoso , Spain  
Oscar Reinoso , Spain  
Haijun Ren , China  
Carlo Renno , Italy  
Fabrizio Renno , Italy  
Shahram Rezapour , Iran  
Ricardo Rianza , Spain  
Francesco Riganti-Fulginei , Italy  
Gerasimos Rigatos , Greece  
Francesco Ripamonti , Italy  
Jorge Rivera , Mexico  
Eugenio Roanes-Lozano , Spain  
Ana Maria A. C. Rocha , Portugal  
Luigi Rodino , Italy  
Francisco Rodríguez , Spain  
Rosana Rodríguez López, Spain  
Francisco Rossomando , Argentina  
Jose de Jesus Rubio , Mexico  
Weiguo Rui , China  
Rubén Ruiz , Spain  
Ivan D. Rukhlenko , Australia  
Dr. Eswaramoorthi S. , India  
Weichao SHI , United Kingdom  
Chaman Lal Sabharwal , USA  
Andrés Sáez , Spain

Bekir Sahin, Turkey  
Laxminarayan Sahoo , India  
John S. Sakellariou , Greece  
Michael Sakellariou , Greece  
Salvatore Salamone, USA  
Jose Vicente Salcedo , Spain  
Alejandro Salcido , Mexico  
Alejandro Salcido, Mexico  
Nunzio Salerno , Italy  
Rohit Salgotra , India  
Miguel A. Salido , Spain  
Sinan Salih , Iraq  
Alessandro Salvini , Italy  
Abdus Samad , India  
Sovan Samanta, India  
Nikolaos Samaras , Greece  
Ramon Sancibrian , Spain  
Giuseppe Sanfilippo , Italy  
Omar-Jacobo Santos, Mexico  
J Santos-Reyes , Mexico  
José A. Sanz-Herrera , Spain  
Musavarah Sarwar, Pakistan  
Shahzad Sarwar, Saudi Arabia  
Marcelo A. Savi , Brazil  
Andrey V. Savkin, Australia  
Tadeusz Sawik , Poland  
Roberta Sburlati, Italy  
Gustavo Scaglia , Argentina  
Thomas Schuster , Germany  
Hamid M. Sedighi , Iran  
Mijanur Rahaman Seikh, India  
Tapan Senapati , China  
Lotfi Senhadji , France  
Junwon Seo, USA  
Michele Serpilli, Italy  
Silvestar Šesnić , Croatia  
Gerardo Severino, Italy  
Ruben Sevilla , United Kingdom  
Stefano Sfarra , Italy  
Dr. Ismail Shah , Pakistan  
Leonid Shaikhet , Israel  
Vimal Shanmuganathan , India  
Prayas Sharma, India  
Bo Shen , Germany  
Hang Shen, China

Xin Pu Shen, China  
Dimitri O. Shepelsky, Ukraine  
Jian Shi , China  
Amin Shokrollahi, Australia  
Suzanne M. Shontz , USA  
Babak Shotorban , USA  
Zhan Shu , Canada  
Angelo Sifaleras , Greece  
Nuno Simões , Portugal  
Mehakpreet Singh , Ireland  
Piyush Pratap Singh , India  
Rajiv Singh, India  
Seralathan Sivamani , India  
S. Sivasankaran , Malaysia  
Christos H. Skiadas, Greece  
Konstantina Skouri , Greece  
Neale R. Smith , Mexico  
Bogdan Smolka, Poland  
Delfim Soares Jr. , Brazil  
Alba Sofi , Italy  
Francesco Soldovieri , Italy  
Raffaele Solimene , Italy  
Yang Song , Norway  
Jussi Sopanen , Finland  
Marco Spadini , Italy  
Paolo Spagnolo , Italy  
Ruben Specogna , Italy  
Vasilios Spitas , Greece  
Ivanka Stamova , USA  
Rafał Stanisławski , Poland  
Miladin Stefanović , Serbia  
Salvatore Strano , Italy  
Yakov Strelniker, Israel  
Kangkang Sun , China  
Qiuqin Sun , China  
Shuaishuai Sun, Australia  
Yanchao Sun , China  
Zong-Yao Sun , China  
Kumarasamy Suresh , India  
Sergey A. Suslov , Australia  
D.L. Suthar, Ethiopia  
D.L. Suthar , Ethiopia  
Andrzej Swierniak, Poland  
Andras Szekrenyes , Hungary  
Kumar K. Tamma, USA

Yong (Aaron) Tan, United Kingdom  
Marco Antonio Taneco-Hernández , Mexico  
Lu Tang , China  
Tianyou Tao, China  
Hafez Tari , USA  
Alessandro Tasora , Italy  
Sergio Teggi , Italy  
Adriana del Carmen Téllez-Anguiano , Mexico  
Ana C. Teodoro , Portugal  
Efstathios E. Theotokoglou , Greece  
Jing-Feng Tian, China  
Alexander Timokha , Norway  
Stefania Tomasiello , Italy  
Gisella Tomasini , Italy  
Isabella Torcicollo , Italy  
Francesco Tornabene , Italy  
Mariano Torrisi , Italy  
Thang nguyen Trung, Vietnam  
George Tsiatas , Greece  
Le Anh Tuan , Vietnam  
Nerio Tullini , Italy  
Emilio Turco , Italy  
Ilhan Tuzcu , USA  
Efstratios Tzirtzilakis , Greece  
FRANCISCO UREÑA , Spain  
Filippo Ubertini , Italy  
Mohammad Uddin , Australia  
Mohammad Safi Ullah , Bangladesh  
Serdar Ulubeyli , Turkey  
Mati Ur Rahman , Pakistan  
Panayiotis Vafeas , Greece  
Giuseppe Vairo , Italy  
Jesus Valdez-Resendiz , Mexico  
Eusebio Valero, Spain  
Stefano Valvano , Italy  
Carlos-Renato Vázquez , Mexico  
Martin Velasco Villa , Mexico  
Franck J. Vernerey, USA  
Georgios Veronis , USA  
Vincenzo Vespri , Italy  
Renato Vidoni , Italy  
Venkatesh Vijayaraghavan, Australia

Anna Vila, Spain  
Francisco R. Villatoro , Spain  
Francesca Vipiana , Italy  
Stanislav Vitek , Czech Republic  
Jan Vorel , Czech Republic  
Michael Vynnycky , Sweden  
Mohammad W. Alomari, Jordan  
Roman Wan-Wendner , Austria  
Bingchang Wang, China  
C. H. Wang , Taiwan  
Dagang Wang, China  
Guoqiang Wang , China  
Huaiyu Wang, China  
Hui Wang , China  
J.G. Wang, China  
Ji Wang , China  
Kang-Jia Wang , China  
Lei Wang , China  
Qiang Wang, China  
Qingling Wang , China  
Weiwei Wang , China  
Xinyu Wang , China  
Yong Wang , China  
Yung-Chung Wang , Taiwan  
Zhenbo Wang , USA  
Zhibo Wang, China  
Waldemar T. Wójcik, Poland  
Chi Wu , Australia  
Qihong Wu, China  
Yuqiang Wu, China  
Zhibin Wu , China  
Zhizheng Wu , China  
Michalis Xenos , Greece  
Hao Xiao , China  
Xiao Ping Xie , China  
Qingzheng Xu , China  
Binghan Xue , China  
Yi Xue , China  
Joseph J. Yame , France  
Chuanliang Yan , China  
Xinggang Yan , United Kingdom  
Hongtai Yang , China  
Jixiang Yang , China  
Mijia Yang, USA  
Ray-Yeng Yang, Taiwan

Zaoli Yang , China  
Jun Ye , China  
Min Ye , China  
Luis J. Yebra , Spain  
Peng-Yeng Yin , Taiwan  
Muhammad Haroon Yousaf , Pakistan  
Yuan Yuan, United Kingdom  
Qin Yuming, China  
Elena Zaitseva , Slovakia  
Arkadiusz Zak , Poland  
Mohammad Zakwan , India  
Ernesto Zambrano-Serrano , Mexico  
Francesco Zammori , Italy  
Jessica Zangari , Italy  
Rafal Zdunek , Poland  
Ibrahim Zeid, USA  
Nianyin Zeng , China  
Junyong Zhai , China  
Hao Zhang , China  
Haopeng Zhang , USA  
Jian Zhang , China  
Kai Zhang, China  
Lingfan Zhang , China  
Mingjie Zhang , Norway  
Qian Zhang , China  
Tianwei Zhang , China  
Tongqian Zhang , China  
Wenyu Zhang , China  
Xianming Zhang , Australia  
Xuping Zhang , Denmark  
Yinyan Zhang, China  
Yifan Zhao , United Kingdom  
Debao Zhou, USA  
Heng Zhou , China  
Jian G. Zhou , United Kingdom  
Junyong Zhou , China  
Xueqian Zhou , United Kingdom  
Zhe Zhou , China  
Wu-Le Zhu, China  
Gaetano Zizzo , Italy  
Mingcheng Zuo, China

# Contents

---

**Retracted: Study on the Integration of Computer-Assisted Teaching Methods for Teaching Volleyball in College Physical Education**

Mathematical Problems in Engineering

Retraction (1 page), Article ID 9802787, Volume 2023 (2023)

**Retracted: Strategy of Maintainable Renewal of Assembled Residential Buildings Based on PSO-ELM**

Mathematical Problems in Engineering

Retraction (1 page), Article ID 9853265, Volume 2023 (2023)

**Retracted: DARSegNet: A Real-Time Semantic Segmentation Method Based on Dual Attention Fusion Module and Encoder-Decoder Network**

Mathematical Problems in Engineering

Retraction (1 page), Article ID 9762309, Volume 2023 (2023)

**Retracted: Dynamic Simulation Analysis of Carbon-Steel Hybrid Sucker Rod String in Vertical and Directional Wells**

Mathematical Problems in Engineering

Retraction (1 page), Article ID 9829764, Volume 2023 (2023)

**Retracted: The Influence and Prediction of Industry Asset Price Fluctuation Based on the LSTM Model and Investor Sentiment**

Mathematical Problems in Engineering

Retraction (1 page), Article ID 9790419, Volume 2023 (2023)

**Retracted: Question and Answer Techniques for Financial Audits in Universities Based on Deep Learning**

Mathematical Problems in Engineering

Retraction (1 page), Article ID 9876979, Volume 2023 (2023)

**Retracted: Intelligent Deployment and Development Strategy of Agricultural Farmland Based on Improved Architecture of Internet of Things**

Mathematical Problems in Engineering

Retraction (1 page), Article ID 9876547, Volume 2023 (2023)

**Retracted: Intelligent Analysis and Evaluation Method of Athletics Running Data Based on Big Data Statistical Model**

Mathematical Problems in Engineering

Retraction (1 page), Article ID 9873210, Volume 2023 (2023)

**Retracted: Fractal Visual Art Graphic Design Based on Computer-Aided Algorithms**

Mathematical Problems in Engineering

Retraction (1 page), Article ID 9871515, Volume 2023 (2023)

**Retracted: Practice and Research of Blended Learning Model Guided by Deep Learning Model**

Mathematical Problems in Engineering

Retraction (1 page), Article ID 9862714, Volume 2023 (2023)

**Retracted: Development of Interactive Teaching of Physical Dance Based on Dynamic Time Reversion Technique**

Mathematical Problems in Engineering  
Retraction (1 page), Article ID 9843240, Volume 2023 (2023)

**Retracted: Feature Learning-Based Generative Adversarial Network Data Augmentation for Class-Based Few-Shot Learning**

Mathematical Problems in Engineering  
Retraction (1 page), Article ID 9840853, Volume 2023 (2023)

**Retracted: Construction and Knowledge Mining of Traditional Chinese Medicine Ancient Books Bibliographic Abstracts Database Based on Genetic Algorithm and BP Neural Network**

Mathematical Problems in Engineering  
Retraction (1 page), Article ID 9836702, Volume 2023 (2023)

**Retracted: Deep Neural Network-Based Business Data Classification in Intelligent Business Management**

Mathematical Problems in Engineering  
Retraction (1 page), Article ID 9834649, Volume 2023 (2023)

**Retracted: Deep Learning-Based Assessment of Sports-Assisted Teaching and Learning**

Mathematical Problems in Engineering  
Retraction (1 page), Article ID 9831090, Volume 2023 (2023)

**Retracted: Study on Intelligently Designed Business Innovation Service Models Driven by Big Data**

Mathematical Problems in Engineering  
Retraction (1 page), Article ID 9826701, Volume 2023 (2023)

**Retracted: A Deep Learning-Based Framework for Social Data Sensing and Fusion for Enterprise Management**

Mathematical Problems in Engineering  
Retraction (1 page), Article ID 9815707, Volume 2023 (2023)

**Retracted: Construction of an Optimal Scheduling Method for Campus Energy Systems Based on Deep Learning Models**

Mathematical Problems in Engineering  
Retraction (1 page), Article ID 9812456, Volume 2023 (2023)

**Retracted: A Computer-Aided Assessment and Evaluation System for Modern Apprenticeship of Accounting Class On-the-Job Training**

Mathematical Problems in Engineering  
Retraction (1 page), Article ID 9804563, Volume 2023 (2023)

**Retracted: Clustering Merchants and Accurate Marketing of Products Using the Segmentation Tree Vector Space Model**

Mathematical Problems in Engineering  
Retraction (1 page), Article ID 9801626, Volume 2023 (2023)



# Contents

**Retracted: Research on the Efficiency Evaluation of Cross-Organizational Knowledge Synergy in Industry University Cooperation Based on BP Neural Network Algorithm**

Mathematical Problems in Engineering

Retraction (1 page), Article ID 9795454, Volume 2023 (2023)

**Retracted: Teaching Design of Mathematics Application Based on Naive Bayes**

Mathematical Problems in Engineering

Retraction (1 page), Article ID 9787256, Volume 2023 (2023)

**Retracted: A Study on the Usefulness of Stochastic Simulation Algorithms for Teaching and Learning in College Physical Education Classrooms**

Mathematical Problems in Engineering

Retraction (1 page), Article ID 9782972, Volume 2023 (2023)

**Retracted: Effect of Evaluation of Popular Song Creation and Literature Based on RITNN Model**

Mathematical Problems in Engineering

Retraction (1 page), Article ID 9782897, Volume 2023 (2023)

**Retracted: Application and Analysis of Taekwondo Techniques, Tactics, and Movement Trajectories Based on Multi-Intelligent Decision Making**

Mathematical Problems in Engineering



Retraction (1 page), Article ID 9780414, Volume 2023 (2023)

**Retracted: Construction of an Assessment System for Business English Linguistics Based on RNN Multidimensional Models**

Mathematical Problems in Engineering


Retraction (1 page), Article ID 9764598, Volume 2023 (2023)

**Trajectory Planning and Collision Control of a Mobile Robot: A Penalty-Based PSO Approach**

Krishna Kant Pandey , Chandrashekhar Kumbhar, Dayal R. Parhi, Sandeep Kumar Mathivanan, Prabhu Jayagopal, and Aminul Haque 


Research Article (10 pages), Article ID 1040461, Volume 2023 (2023)

**Artificial Intelligence-Based English Self-Learning Effect Evaluation and Adaptive Influencing Factors Analysis**

Xing Shu  and Chengjun Xu

Research Article (9 pages), Article ID 2776823, Volume 2022 (2022)

**Prediction and Industrial Structure Analysis of Local GDP Economy Based on Machine Learning**

Zhiqiang Jiang 

Research Article (9 pages), Article ID 7089914, Volume 2022 (2022)

**[Retracted] A Study on the Usefulness of Stochastic Simulation Algorithms for Teaching and Learning in College Physical Education Classrooms**

Ju Xu 

Research Article (6 pages), Article ID 2779909, Volume 2022 (2022)

### **BP Neural Network-Based Evaluation Method for Enterprise Comprehensive Performance**

Chen Wenjing 

Research Article (11 pages), Article ID 7308235, Volume 2022 (2022)

### **Industrial Land Performance Assessment Based on Fuzzy Analytic Hierarchy Process**

Jing Lv  and Sijia Ge


Research Article (11 pages), Article ID 1384583, Volume 2022 (2022)

### **Evaluation Technology of Students' Learning Status in Chinese Classroom Based on Deep Learning**

Na Li 


Research Article (14 pages), Article ID 9921984, Volume 2022 (2022)

### **Application of PID Control and Improved Ant Colony Algorithm in Path Planning of Substation Inspection Robot**

YeFei Kang, ZhiBin Li, and Tao Wang 

Research Article (10 pages), Article ID 9453219, Volume 2022 (2022)

### **Evaluation and Analysis of Regional Economic Growth Factors in Digital Economy Based on the Deep Neural Network**

Caijun Cheng  and Huazhen Huang


Research Article (10 pages), Article ID 1121886, Volume 2022 (2022)

### **The Path Evaluation of Integrated Development of Leisure Sports and Rural Ecological Environment in Guangxi Based on Fuzzy Comprehensive Evaluation Model**

Qianying Li, Dayao Zhang , Yu Han, and Youchang Xie

Research Article (8 pages), Article ID 5602889, Volume 2022 (2022)

### **Discrete Hyperparameter Optimization Model Based on Skewed Distribution**

Yuqi Li 


Research Article (10 pages), Article ID 2835596, Volume 2022 (2022)

### **Construction of Alumni Information Analysis Model Based on Big Data**

Xue Wang 

Research Article (10 pages), Article ID 1587793, Volume 2022 (2022)

### **The Optimization of Shed-Tunnel Structure in the Confined Environment**

Wu Yi, Huizhao Shao , Zhoutong Cui, Xiaohu Huang, and Ying Zhou

Research Article (9 pages), Article ID 3874783, Volume 2022 (2022)

### **Aerobics Characteristics Analysis and Auxiliary Training Efficiency Improvement Method Based on Deep Learning**

Jiwen Wang, Bingxue Wang, and Shuli Wan 

Research Article (11 pages), Article ID 6073855, Volume 2022 (2022)


# Contents

## **Traffic Flow Prediction and Application of Smart City Based on Industry 4.0 and Big Data Analysis**

Yuqian Gong 

Research Article (11 pages), Article ID 5397861, Volume 2022 (2022)

## **Design of Watercolor Cultural and Creative Products Based on Style Transfer Algorithm**

Qi Wang and Alamusu. H 


Research Article (9 pages), Article ID 2711861, Volume 2022 (2022)

## **[Retracted] A Computer-Aided Assessment and Evaluation System for Modern Apprenticeship of Accounting Class On-the-Job Training**

LinLin Sun, ChunChao Liu , MaoNian Lin, and Ying Zhou



Research Article (11 pages), Article ID 6437885, Volume 2022 (2022)

## **Analysis on the Effect of Intelligitization and Improvement of Tourist Bus Loops Based on Markov Chain Decoupling**

Shousheng Chai, Jun Shan, Chunfeng Long , and Wang Qianyi


Research Article (6 pages), Article ID 9021129, Volume 2022 (2022)

## **[Retracted] Feature Learning-Based Generative Adversarial Network Data Augmentation for Class-Based Few-Shot Learning**

Bharat Subedi, V. E. Sathishkumar , V. Maheshwari, M. Sandeep Kumar, Prabhu Jayagopal, and Shaikh Muhammad Allayear 


Research Article (20 pages), Article ID 9710667, Volume 2022 (2022)

## **Research on Multi-Objective Intelligent Optimization of Financial Resource Management and Allocation Methods in Colleges and Universities**

Shanshan Guo 

Research Article (9 pages), Article ID 1906031, Volume 2022 (2022)

## **Load Balancing of SDN Controller for Migration Optimization Based on Metaheuristics**

Congcong Min 


Research Article (10 pages), Article ID 1169648, Volume 2022 (2022)

## **Innovative Collaborative Design of Ru Porcelain Shape Based on Digital Shape Technology**

Song Bin , Md Ishak Siti Mastura , Shaari Nazlina, Perumal Velu, and Yang Wei


Research Article (9 pages), Article ID 5650673, Volume 2022 (2022)

## **Texture Feature Extraction and Morphological Analysis of Landslide Based on Image Edge Detection**

Feng Wang, E. Wu, Siyan Chen, and Hao Wu 


Research Article (12 pages), Article ID 2302271, Volume 2022 (2022)

## **[Retracted] Development of Interactive Teaching of Physical Dance Based on Dynamic Time Reversion Technique**

Xue Li and Yaqi Yang 


Research Article (8 pages), Article ID 5697041, Volume 2022 (2022)

**Design of Music Teaching System Based on Artificial Intelligence**

Wei Chen 


Research Article (7 pages), Article ID 2627395, Volume 2022 (2022)

**ODL Centralized Control of Power Communication Network Based on Bio-Inspired Algorithms and SDN**

Congcong Min 


Research Article (9 pages), Article ID 9925620, Volume 2022 (2022)

**[Retracted] Dynamic Simulation Analysis of Carbon-Steel Hybrid Sucker Rod String in Vertical and Directional Wells**

Xiurong Sun , Xianbing Ji, Weicheng Li, Lijuan Zhang, and Yang Song


Research Article (14 pages), Article ID 5239355, Volume 2022 (2022)

**[Retracted] Intelligent Deployment and Development Strategy of Agricultural Farmland Based on Improved Architecture of Internet of Things**

Xiaofen Li 


Research Article (8 pages), Article ID 5213535, Volume 2022 (2022)

**Design and Analysis of Intelligent Agricultural Monitoring System Based on Biological Intelligence Optimization Algorithm**

Zhiqin Chen , Zhihao Liao, Deming Qian, and Jie Li

Research Article (8 pages), Article ID 1129419, Volume 2022 (2022)

**[Retracted] Teaching Design of Mathematics Application Based on Naive Bayes**

Huanzhang Ling 




Research Article (6 pages), Article ID 7244001, Volume 2022 (2022)

**Analysis of Big Data Behavior in Sports Track and Field Based on Machine Learning Model**

Qiuping Lin, Xiaoxue Dong, and Minglun Li 



Research Article (10 pages), Article ID 1439993, Volume 2022 (2022)

**Hybrid Genetic Algorithms for the Asymmetric Distance-Constrained Vehicle Routing Problem**

Zakir Hussain Ahmed , Asaad Shakir Hameed , and Modhi Lafta Mutar 



Research Article (20 pages), Article ID 2435002, Volume 2022 (2022)

**Lithium Battery Allocation Decision-Making Scheme Based on K-Means Algorithm**

Dandan Ma  and Xiangge Qin 

Research Article (9 pages), Article ID 7920727, Volume 2022 (2022)


**[Retracted] Study on Intelligently Designed Business Innovation Service Models Driven by Big Data**

Huiying Liu , Jianfeng Shang , and Gang Wan

Research Article (15 pages), Article ID 4468240, Volume 2022 (2022)


# Contents

## **Evaluation and Analysis of High-Quality Development of New Urbanization Based on Intelligent Computing**

Haoran Cheng 

Research Article (8 pages), Article ID 6428970, Volume 2022 (2022)

## **Sports-Assisted Education Based on a Support Vector Machine and Genetic Algorithm**

ChengZhao Li 



Research Article (9 pages), Article ID 5194937, Volume 2022 (2022)

## **Tumor Detection on Microarray Data Using Grey Wolf Optimization with Gain Information**

K. Dhana Sree Devi, P. Karthikeyan, Usha Moorthy , K. Deeba, V. Maheshwari, and Shaikh Muhammad Allayear

Research Article (10 pages), Article ID 4092404, Volume 2022 (2022)

## **[Retracted] Strategy of Maintainable Renewal of Assembled Residential Buildings Based on PSO-ELM**

Yitong Zhang, Yuhang Wu, Jing Sui , and Min Lee 



Research Article (7 pages), Article ID 5813577, Volume 2022 (2022)

## **[Retracted] Research on the Efficiency Evaluation of Cross-Organizational Knowledge Synergy in Industry University Cooperation Based on BP Neural Network Algorithm**

Li Jing 




Research Article (8 pages), Article ID 1873862, Volume 2022 (2022)

## **Comparative Study on the Plastic Zone of Circular Hole Surrounding Rock in Anisotropic In Situ Stress Conditions**

Pei Zhou  and Peng Wu 


Research Article (9 pages), Article ID 2208528, Volume 2022 (2022)

## **[Retracted] DARSegNet: A Real-Time Semantic Segmentation Method Based on Dual Attention Fusion Module and Encoder-Decoder Network**

Yongfeng Xing , Luo Zhong , and Xian Zhong 


Research Article (10 pages), Article ID 6195148, Volume 2022 (2022)

## **Research on Prediction of Physical Fitness Test Results in Colleges and Universities Based on Deep Learning**

Jiwen Wang, Binghui Wu, Yun Jiang, and Yidan Yuan 


Research Article (9 pages), Article ID 6758684, Volume 2022 (2022)

## **Deep Learning for Chinese Language Sentiment Extraction and Analysis**

Zhu Zhu 


Research Article (12 pages), Article ID 8145445, Volume 2022 (2022)

## **[Retracted] Study on the Integration of Computer-Assisted Teaching Methods for Teaching Volleyball in College Physical Education**

Jinfeng Zhang 



Research Article (8 pages), Article ID 5028705, Volume 2022 (2022)

**Performance Prediction and Action Performance Analysis of Sports Competitive Events Based on Deep Learning**

Xiaoying Zhang and Jianqiang Lou 


Research Article (11 pages), Article ID 4170097, Volume 2022 (2022)

**Residential Energy-Saving Lighting Based on Bioinspired Algorithms**

Yuhang Wu, Yitong Zhang, Nah Ilmin , and Jing Sui 

Research Article (9 pages), Article ID 7600021, Volume 2022 (2022)

**[Retracted] Fractal Visual Art Graphic Design Based on Computer-Aided Algorithms**

Qihao Zhou, Teng Liu, Guorong Wu , and Xuhui Chen


Research Article (7 pages), Article ID 3345037, Volume 2022 (2022)

**Research on Optimization and Allocation of English Teaching Resources**

Chongya Liu  and Jue Xia



Research Article (8 pages), Article ID 1342998, Volume 2022 (2022)

**Research on Intelligent Retrieval Method of Teaching Resources on Large-Scale Network Platform**

Xiaofeng Su and Tianjing Zhang 


Research Article (8 pages), Article ID 2745773, Volume 2022 (2022)

**[Retracted] Practice and Research of Blended Learning Model Guided by Deep Learning Model**

Fan Yang  and Yutai Rao 


Research Article (6 pages), Article ID 8915162, Volume 2022 (2022)

**The Database Construction of Intangible Cultural Heritage Based on Artificial Intelligence**

Haixing Zhao 


Research Article (10 pages), Article ID 8576002, Volume 2022 (2022)

**[Retracted] Question and Answer Techniques for Financial Audits in Universities Based on Deep Learning**

Qiang Li 

Research Article (8 pages), Article ID 4875859, Volume 2022 (2022)

**Research and Analysis on the Integration of Artificial Intelligence in College English Teaching**

Dashan Jiang, Yubing Pei , Gongping Yang, and Xue Wang


Research Article (8 pages), Article ID 3997573, Volume 2022 (2022)

**Research on National Costume Design Based on Virtual Reality Technology**

Chunnan Cao  and Yiping Gao 

Research Article (9 pages), Article ID 7503167, Volume 2022 (2022)



**A Research on Library Space Layout and Intelligent Optimization Oriented to Readers' Needs**

Binli Gu  and Kenichi Tanoue

Research Article (12 pages), Article ID 4426091, Volume 2022 (2022)





# Contents

## **3D Reconstruction Method of Virtual and Real Fusion Based on Machine Learning**

Wenyao Zhu  and Shuyue Zhou 



Research Article (11 pages), Article ID 7158504, Volume 2022 (2022)

## **A Multimixed Strategy Improved Sparrow Search Algorithm and Its Application in TSP**

Weizheng Li , Mengjian Zhang , Jing Zhang , Tao Qin, Wei Wei, and Jing Yang 

Research Article (26 pages), Article ID 8171164, Volume 2022 (2022)

## **Study on Strength Theory Effect of Plastic Zone Distribution of Roadway Surrounding Rock**

Pei Zhou  and Peng Wu 


Research Article (9 pages), Article ID 6165652, Volume 2022 (2022)

## **An Improved JADE Hybridizing with Tuna Swarm Optimization for Numerical Optimization Problems**

MuLai Tan , YinTong Li , DaLi Ding , Rui Zhou, and ChangQiang Huang


Research Article (17 pages), Article ID 7726548, Volume 2022 (2022)

## **Green City Landscape Design and Planning Based on GIS and Analytic Hierarchy Process Model**

Daochun Liu, Mingming Tang, and Nan Dong 

Research Article (13 pages), Article ID 7167446, Volume 2022 (2022)

## **Basketball Motion Posture Recognition Based on Recurrent Deep Learning Model**

FeiPeng Liu and Wei Zhang 



Research Article (7 pages), Article ID 8314777, Volume 2022 (2022)

## **[Retracted] Effect of Evaluation of Popular Song Creation and Literature Based on RITNN Model**

Rui Song 


Research Article (9 pages), Article ID 4643674, Volume 2022 (2022)

## **Research on the Change in Public Art Landscape Pattern Based on Deep Learning**

Lei Zhao  and Congcong Tang 





Research Article (10 pages), Article ID 8745174, Volume 2022 (2022)

## **Design and Research of Dynamic Evolution System in Football Tactics Under Computational Intelligence**

Jianming Wang and Jing Chen 


Research Article (12 pages), Article ID 3772236, Volume 2022 (2022)

## **Prediction of Phishing Susceptibility Based on a Combination of Static and Dynamic Features**

Rundong Yang , Kangfeng Zheng , Bin Wu, Chunhua Wu , and Xiujuan Wang 


Research Article (10 pages), Article ID 2884769, Volume 2022 (2022)

## **Market Risk Early Warning Based on Deep Learning and Fruit Fly Optimization**

Liang Chen and Rui Ma 


Research Article (9 pages), Article ID 4844856, Volume 2022 (2022)

**Research on the Evaluation of Industrial Poverty Alleviation under the Background of the Internet**

Ying Tao, Jiazhi Xie, and Jinqiao Yang 


Research Article (11 pages), Article ID 9101772, Volume 2022 (2022)

**[Retracted] A Deep Learning-Based Framework for Social Data Sensing and Fusion for Enterprise Management**

Yu Wang 


Research Article (8 pages), Article ID 3606469, Volume 2022 (2022)

**Research on the Evaluation Model of Dance Movement Recognition and Automatic Generation Based on Long Short-Term Memory**

Xiuming Yuan and Peipei Pan 


Research Article (10 pages), Article ID 6405903, Volume 2022 (2022)

**[Retracted] Deep Learning-Based Assessment of Sports-Assisted Teaching and Learning**

Wei Su and Jian Feng 


Research Article (8 pages), Article ID 7833292, Volume 2022 (2022)

**Research on Dynamic Simulation Technology of Urban 3D Art Landscape Based on VR-Platform**

Yulu Cao  and Zonghan Li


Research Article (9 pages), Article ID 3252040, Volume 2022 (2022)

**Research on Neural Network Machine Translation Model Based on Entity Tagging Improvement**

Xijun Xu 


Research Article (8 pages), Article ID 8407437, Volume 2022 (2022)

**Application Analysis of Emotional Learning Model Based on Improved Text in Campus Review and Student Public Opinion Management**

Zhaofeng Weng 


Research Article (12 pages), Article ID 5135200, Volume 2022 (2022)

**Analysis and Optimization of the Online Vocal Teaching System Based on Intelligent Computing**

Luzhen Jiang 


Research Article (8 pages), Article ID 5320615, Volume 2022 (2022)

**Research on Fault Feature Extraction and Pattern Recognition of Rolling Bearing**

Xiaobin Miao 

Research Article (11 pages), Article ID 9040784, Volume 2022 (2022)

**Interior Space Design and Automatic Layout Method Based on CNN**

WeiPing Wu and Yanshun Feng 

Research Article (14 pages), Article ID 8006069, Volume 2022 (2022)




# Contents

## **Improved Cam Shift Algorithm for Detecting Athletes' Action Targets in Sports Videos**

Yi Yuan 


Research Article (7 pages), Article ID 9401001, Volume 2022 (2022)

## **Effect of Deep Learning on College Students' Career Planning**

Xianhui Gu 


Research Article (12 pages), Article ID 1573635, Volume 2022 (2022)

## **Lute Acoustic Quality Evaluation and Note Recognition Based on the Softmax Regression BP Neural Network**

Lili Liu 


Research Article (7 pages), Article ID 1978746, Volume 2022 (2022)

## **Convolutional Neural Networks for Structural Damage Identification in Assembled Buildings**

Chunhua You , Wenxiang Liu, and Lei Hou


Research Article (11 pages), Article ID 2326903, Volume 2022 (2022)

## **Studying the Coupling and Coordination of Regional Economic and University Development Levels Based on a Deep Learning Model**

Yongfeng Bai , Zaixun Song, and Weimiao Cui

Research Article (7 pages), Article ID 1480173, Volume 2022 (2022)

## **Regional Tourism Economic Forecasting Model Based on GM Grey Forecasting Method**

Bin Li and Jing Gao 


Research Article (9 pages), Article ID 3477246, Volume 2022 (2022)

## **[Retracted] Construction and Knowledge Mining of Traditional Chinese Medicine Ancient Books Bibliographic Abstracts Database Based on Genetic Algorithm and BP Neural Network**

Yongmei Wang , Shujun Ren, Li Song, and Jiang Zhang


Research Article (15 pages), Article ID 6838714, Volume 2022 (2022)

## **[Retracted] Construction of an Optimal Scheduling Method for Campus Energy Systems Based on Deep Learning Models**

Jingyun Li  and Hong Zhao


Research Article (10 pages), Article ID 5350786, Volume 2022 (2022)

## **[Retracted] Application and Analysis of Taekwondo Techniques, Tactics, and Movement Trajectories Based on Multi-Intelligent Decision Making**

Weian Lu and Xiaotao Lin 


Research Article (8 pages), Article ID 8411550, Volume 2022 (2022)

## **[Retracted] Deep Neural Network-Based Business Data Classification in Intelligent Business Management**

Bihong Wang 

Research Article (8 pages), Article ID 7104750, Volume 2022 (2022)

**[Retracted] Clustering Merchants and Accurate Marketing of Products Using the Segmentation Tree Vector Space Model**

Xuwu Ding, Zhong Wu , and Meng Li


Research Article (11 pages), Article ID 7353151, Volume 2022 (2022)

**[Retracted] Intelligent Analysis and Evaluation Method of Athletics Running Data Based on Big Data Statistical Model**

Yushan Ge 





Research Article (8 pages), Article ID 5624482, Volume 2022 (2022)

**[Retracted] Construction of an Assessment System for Business English Linguistics Based on RNN Multidimensional Models**

Yu Shi and Hu Shi 

Research Article (8 pages), Article ID 8446281, Volume 2022 (2022)

**A Comparative State-of-the-Art Constrained Metaheuristics Framework for TRUSS Optimisation on Shape and Sizing**

Bahareh Etaati , Amin Abdollahi Dehkordi, Ali Sadollah , Mohammed El-Abd , and Mehdi Neshat 

Research Article (13 pages), Article ID 6078986, Volume 2022 (2022)

**[Retracted] The Influence and Prediction of Industry Asset Price Fluctuation Based on The LSTM Model and Investor Sentiment**

Wenxiu Hu, Huan Liu , Xiaoqiang Ma, and Xiong Bai

Research Article (8 pages), Article ID 1113023, Volume 2022 (2022)

## *Retraction*

# **Retracted: Study on the Integration of Computer-Assisted Teaching Methods for Teaching Volleyball in College Physical Education**

### **Mathematical Problems in Engineering**

Received 26 September 2023; Accepted 26 September 2023; Published 27 September 2023

Copyright © 2023 Mathematical Problems in Engineering. This is an open access article distributed under the Creative Commons Attribution License, which permits unrestricted use, distribution, and reproduction in any medium, provided the original work is properly cited.

This article has been retracted by Hindawi following an investigation undertaken by the publisher [1]. This investigation has uncovered evidence of one or more of the following indicators of systematic manipulation of the publication process:

- (1) Discrepancies in scope
- (2) Discrepancies in the description of the research reported
- (3) Discrepancies between the availability of data and the research described
- (4) Inappropriate citations
- (5) Incoherent, meaningless and/or irrelevant content included in the article
- (6) Peer-review manipulation

The presence of these indicators undermines our confidence in the integrity of the article's content and we cannot, therefore, vouch for its reliability. Please note that this notice is intended solely to alert readers that the content of this article is unreliable. We have not investigated whether authors were aware of or involved in the systematic manipulation of the publication process.

Wiley and Hindawi regrets that the usual quality checks did not identify these issues before publication and have since put additional measures in place to safeguard research integrity.

We wish to credit our own Research Integrity and Research Publishing teams and anonymous and named external researchers and research integrity experts for contributing to this investigation.

The corresponding author, as the representative of all authors, has been given the opportunity to register their agreement or disagreement to this retraction. We have kept a record of any response received.

### **References**

- [1] J. Zhang, "Study on the Integration of Computer-Assisted Teaching Methods for Teaching Volleyball in College Physical Education," *Mathematical Problems in Engineering*, vol. 2022, Article ID 5028705, 8 pages, 2022.

## *Retraction*

# **Retracted: Strategy of Maintainable Renewal of Assembled Residential Buildings Based on PSO-ELM**

### **Mathematical Problems in Engineering**

Received 19 September 2023; Accepted 19 September 2023; Published 20 September 2023

Copyright © 2023 Mathematical Problems in Engineering. This is an open access article distributed under the Creative Commons Attribution License, which permits unrestricted use, distribution, and reproduction in any medium, provided the original work is properly cited.

This article has been retracted by Hindawi following an investigation undertaken by the publisher [1]. This investigation has uncovered evidence of one or more of the following indicators of systematic manipulation of the publication process:

- (1) Discrepancies in scope
- (2) Discrepancies in the description of the research reported
- (3) Discrepancies between the availability of data and the research described
- (4) Inappropriate citations
- (5) Incoherent, meaningless and/or irrelevant content included in the article
- (6) Peer-review manipulation

The presence of these indicators undermines our confidence in the integrity of the article's content and we cannot, therefore, vouch for its reliability. Please note that this notice is intended solely to alert readers that the content of this article is unreliable. We have not investigated whether authors were aware of or involved in the systematic manipulation of the publication process.

Wiley and Hindawi regrets that the usual quality checks did not identify these issues before publication and have since put additional measures in place to safeguard research integrity.

We wish to credit our own Research Integrity and Research Publishing teams and anonymous and named external researchers and research integrity experts for contributing to this investigation.

The corresponding author, as the representative of all authors, has been given the opportunity to register their agreement or disagreement to this retraction. We have kept a record of any response received.

### **References**

- [1] Y. Zhang, Y. Wu, J. Sui, and M. Lee, "Strategy of Maintainable Renewal of Assembled Residential Buildings Based on PSO-ELM," *Mathematical Problems in Engineering*, vol. 2022, Article ID 5813577, 7 pages, 2022.

## Retraction

# Retracted: DARSegNet: A Real-Time Semantic Segmentation Method Based on Dual Attention Fusion Module and Encoder-Decoder Network

### Mathematical Problems in Engineering

Received 19 September 2023; Accepted 19 September 2023; Published 20 September 2023

Copyright © 2023 Mathematical Problems in Engineering. This is an open access article distributed under the Creative Commons Attribution License, which permits unrestricted use, distribution, and reproduction in any medium, provided the original work is properly cited.

This article has been retracted by Hindawi following an investigation undertaken by the publisher [1]. This investigation has uncovered evidence of one or more of the following indicators of systematic manipulation of the publication process:

- (1) Discrepancies in scope
- (2) Discrepancies in the description of the research reported
- (3) Discrepancies between the availability of data and the research described
- (4) Inappropriate citations
- (5) Incoherent, meaningless and/or irrelevant content included in the article
- (6) Peer-review manipulation

The presence of these indicators undermines our confidence in the integrity of the article's content and we cannot, therefore, vouch for its reliability. Please note that this notice is intended solely to alert readers that the content of this article is unreliable. We have not investigated whether authors were aware of or involved in the systematic manipulation of the publication process.

Wiley and Hindawi regrets that the usual quality checks did not identify these issues before publication and have since put additional measures in place to safeguard research integrity.

We wish to credit our own Research Integrity and Research Publishing teams and anonymous and named external researchers and research integrity experts for contributing to this investigation.

The corresponding author, as the representative of all authors, has been given the opportunity to register their agreement or disagreement to this retraction. We have kept a record of any response received.

### References

- [1] Y. Xing, L. Zhong, and X. Zhong, "DARSegNet: A Real-Time Semantic Segmentation Method Based on Dual Attention Fusion Module and Encoder-Decoder Network," *Mathematical Problems in Engineering*, vol. 2022, Article ID 6195148, 10 pages, 2022.

## *Retraction*

# **Retracted: Dynamic Simulation Analysis of Carbon-Steel Hybrid Sucker Rod String in Vertical and Directional Wells**

### **Mathematical Problems in Engineering**

Received 13 September 2023; Accepted 13 September 2023; Published 14 September 2023

Copyright © 2023 Mathematical Problems in Engineering. This is an open access article distributed under the Creative Commons Attribution License, which permits unrestricted use, distribution, and reproduction in any medium, provided the original work is properly cited.

This article has been retracted by Hindawi following an investigation undertaken by the publisher [1]. This investigation has uncovered evidence of one or more of the following indicators of systematic manipulation of the publication process:

- (1) Discrepancies in scope
- (2) Discrepancies in the description of the research reported
- (3) Discrepancies between the availability of data and the research described
- (4) Inappropriate citations
- (5) Incoherent, meaningless and/or irrelevant content included in the article
- (6) Peer-review manipulation

The presence of these indicators undermines our confidence in the integrity of the article's content and we cannot, therefore, vouch for its reliability. Please note that this notice is intended solely to alert readers that the content of this article is unreliable. We have not investigated whether authors were aware of or involved in the systematic manipulation of the publication process.

Wiley and Hindawi regrets that the usual quality checks did not identify these issues before publication and have since put additional measures in place to safeguard research integrity.

We wish to credit our own Research Integrity and Research Publishing teams and anonymous and named external researchers and research integrity experts for contributing to this investigation.

The corresponding author, as the representative of all authors, has been given the opportunity to register their agreement or disagreement to this retraction. We have kept a record of any response received.

### **References**

- [1] X. Sun, X. Ji, W. Li, L. Zhang, and Y. Song, "Dynamic Simulation Analysis of Carbon-Steel Hybrid Sucker Rod String in Vertical and Directional Wells," *Mathematical Problems in Engineering*, vol. 2022, Article ID 5239355, 14 pages, 2022.

## *Retraction*

# **Retracted: The Influence and Prediction of Industry Asset Price Fluctuation Based on the LSTM Model and Investor Sentiment**

### **Mathematical Problems in Engineering**

Received 13 September 2023; Accepted 13 September 2023; Published 14 September 2023

Copyright © 2023 Mathematical Problems in Engineering. This is an open access article distributed under the Creative Commons Attribution License, which permits unrestricted use, distribution, and reproduction in any medium, provided the original work is properly cited.

This article has been retracted by Hindawi following an investigation undertaken by the publisher [1]. This investigation has uncovered evidence of one or more of the following indicators of systematic manipulation of the publication process:

- (1) Discrepancies in scope
- (2) Discrepancies in the description of the research reported
- (3) Discrepancies between the availability of data and the research described
- (4) Inappropriate citations
- (5) Incoherent, meaningless and/or irrelevant content included in the article
- (6) Peer-review manipulation

The presence of these indicators undermines our confidence in the integrity of the article's content and we cannot, therefore, vouch for its reliability. Please note that this notice is intended solely to alert readers that the content of this article is unreliable. We have not investigated whether authors were aware of or involved in the systematic manipulation of the publication process.

Wiley and Hindawi regrets that the usual quality checks did not identify these issues before publication and have since put additional measures in place to safeguard research integrity.

We wish to credit our own Research Integrity and Research Publishing teams and anonymous and named external researchers and research integrity experts for contributing to this investigation.

The corresponding author, as the representative of all authors, has been given the opportunity to register their agreement or disagreement to this retraction. We have kept a record of any response received.

### **References**

- [1] W. Hu, H. Liu, X. Ma, and X. Bai, "The Influence and Prediction of Industry Asset Price Fluctuation Based on the LSTM Model and Investor Sentiment," *Mathematical Problems in Engineering*, vol. 2022, Article ID 1113023, 8 pages, 2022.

## *Retraction*

# **Retracted: Question and Answer Techniques for Financial Audits in Universities Based on Deep Learning**

### **Mathematical Problems in Engineering**

Received 18 July 2023; Accepted 18 July 2023; Published 19 July 2023

Copyright © 2023 Mathematical Problems in Engineering. This is an open access article distributed under the Creative Commons Attribution License, which permits unrestricted use, distribution, and reproduction in any medium, provided the original work is properly cited.

This article has been retracted by Hindawi following an investigation undertaken by the publisher [1]. This investigation has uncovered evidence of one or more of the following indicators of systematic manipulation of the publication process:

- (1) Discrepancies in scope
- (2) Discrepancies in the description of the research reported
- (3) Discrepancies between the availability of data and the research described
- (4) Inappropriate citations
- (5) Incoherent, meaningless and/or irrelevant content included in the article
- (6) Peer-review manipulation

The presence of these indicators undermines our confidence in the integrity of the article's content and we cannot, therefore, vouch for its reliability. Please note that this notice is intended solely to alert readers that the content of this article is unreliable. We have not investigated whether authors were aware of or involved in the systematic manipulation of the publication process.

Wiley and Hindawi regrets that the usual quality checks did not identify these issues before publication and have since put additional measures in place to safeguard research integrity.

We wish to credit our own Research Integrity and Research Publishing teams and anonymous and named external researchers and research integrity experts for contributing to this investigation.

The corresponding author, as the representative of all authors, has been given the opportunity to register their agreement or disagreement to this retraction. We have kept a record of any response received.

### **References**

- [1] Q. Li, "Question and Answer Techniques for Financial Audits in Universities Based on Deep Learning," *Mathematical Problems in Engineering*, vol. 2022, Article ID 4875859, 8 pages, 2022.



## Retraction

# Retracted: Intelligent Deployment and Development Strategy of Agricultural Farmland Based on Improved Architecture of Internet of Things

### Mathematical Problems in Engineering

Received 18 July 2023; Accepted 18 July 2023; Published 19 July 2023

Copyright © 2023 Mathematical Problems in Engineering. This is an open access article distributed under the Creative Commons Attribution License, which permits unrestricted use, distribution, and reproduction in any medium, provided the original work is properly cited.

This article has been retracted by Hindawi following an investigation undertaken by the publisher [1]. This investigation has uncovered evidence of one or more of the following indicators of systematic manipulation of the publication process:

- (1) Discrepancies in scope
- (2) Discrepancies in the description of the research reported
- (3) Discrepancies between the availability of data and the research described
- (4) Inappropriate citations
- (5) Incoherent, meaningless and/or irrelevant content included in the article
- (6) Peer-review manipulation

The presence of these indicators undermines our confidence in the integrity of the article's content and we cannot, therefore, vouch for its reliability. Please note that this notice is intended solely to alert readers that the content of this article is unreliable. We have not investigated whether authors were aware of or involved in the systematic manipulation of the publication process.

Wiley and Hindawi regrets that the usual quality checks did not identify these issues before publication and have since put additional measures in place to safeguard research integrity.

We wish to credit our own Research Integrity and Research Publishing teams and anonymous and named external researchers and research integrity experts for contributing to this investigation.

The corresponding author, as the representative of all authors, has been given the opportunity to register their

agreement or disagreement to this retraction. We have kept a record of any response received.

### References

- [1] X. Li, "Intelligent Deployment and Development Strategy of Agricultural Farmland Based on Improved Architecture of Internet of Things," *Mathematical Problems in Engineering*, vol. 2022, Article ID 5213535, 8 pages, 2022.

## Retraction

# Retracted: Intelligent Analysis and Evaluation Method of Athletics Running Data Based on Big Data Statistical Model

### Mathematical Problems in Engineering

Received 18 July 2023; Accepted 18 July 2023; Published 19 July 2023

Copyright © 2023 Mathematical Problems in Engineering. This is an open access article distributed under the Creative Commons Attribution License, which permits unrestricted use, distribution, and reproduction in any medium, provided the original work is properly cited.

This article has been retracted by Hindawi following an investigation undertaken by the publisher [1]. This investigation has uncovered evidence of one or more of the following indicators of systematic manipulation of the publication process:

- (1) Discrepancies in scope
- (2) Discrepancies in the description of the research reported
- (3) Discrepancies between the availability of data and the research described
- (4) Inappropriate citations
- (5) Incoherent, meaningless and/or irrelevant content included in the article
- (6) Peer-review manipulation

The presence of these indicators undermines our confidence in the integrity of the article's content and we cannot, therefore, vouch for its reliability. Please note that this notice is intended solely to alert readers that the content of this article is unreliable. We have not investigated whether authors were aware of or involved in the systematic manipulation of the publication process.

Wiley and Hindawi regrets that the usual quality checks did not identify these issues before publication and have since put additional measures in place to safeguard research integrity.

We wish to credit our own Research Integrity and Research Publishing teams and anonymous and named external researchers and research integrity experts for contributing to this investigation.

The corresponding author, as the representative of all authors, has been given the opportunity to register their agreement or disagreement to this retraction. We have kept a record of any response received.

### References

- [1] Y. Ge, "Intelligent Analysis and Evaluation Method of Athletics Running Data Based on Big Data Statistical Model," *Mathematical Problems in Engineering*, vol. 2022, Article ID 5624482, 8 pages, 2022.

## *Retraction*

# **Retracted: Fractal Visual Art Graphic Design Based on Computer-Aided Algorithms**

### **Mathematical Problems in Engineering**

Received 18 July 2023; Accepted 18 July 2023; Published 19 July 2023

Copyright © 2023 Mathematical Problems in Engineering. This is an open access article distributed under the Creative Commons Attribution License, which permits unrestricted use, distribution, and reproduction in any medium, provided the original work is properly cited.

This article has been retracted by Hindawi following an investigation undertaken by the publisher [1]. This investigation has uncovered evidence of one or more of the following indicators of systematic manipulation of the publication process:

- (1) Discrepancies in scope
- (2) Discrepancies in the description of the research reported
- (3) Discrepancies between the availability of data and the research described
- (4) Inappropriate citations
- (5) Incoherent, meaningless and/or irrelevant content included in the article
- (6) Peer-review manipulation

The presence of these indicators undermines our confidence in the integrity of the article's content and we cannot, therefore, vouch for its reliability. Please note that this notice is intended solely to alert readers that the content of this article is unreliable. We have not investigated whether authors were aware of or involved in the systematic manipulation of the publication process.

Wiley and Hindawi regrets that the usual quality checks did not identify these issues before publication and have since put additional measures in place to safeguard research integrity.

We wish to credit our own Research Integrity and Research Publishing teams and anonymous and named external researchers and research integrity experts for contributing to this investigation.

The corresponding author, as the representative of all authors, has been given the opportunity to register their agreement or disagreement to this retraction. We have kept a record of any response received.

### **References**

- [1] Q. Zhou, T. Liu, G. Wu, and X. Chen, "Fractal Visual Art Graphic Design Based on Computer-Aided Algorithms," *Mathematical Problems in Engineering*, vol. 2022, Article ID 3345037, 7 pages, 2022.

## *Retraction*

# **Retracted: Practice and Research of Blended Learning Model Guided by Deep Learning Model**

### **Mathematical Problems in Engineering**

Received 18 July 2023; Accepted 18 July 2023; Published 19 July 2023

Copyright © 2023 Mathematical Problems in Engineering. This is an open access article distributed under the Creative Commons Attribution License, which permits unrestricted use, distribution, and reproduction in any medium, provided the original work is properly cited.

This article has been retracted by Hindawi following an investigation undertaken by the publisher [1]. This investigation has uncovered evidence of one or more of the following indicators of systematic manipulation of the publication process:

- (1) Discrepancies in scope
- (2) Discrepancies in the description of the research reported
- (3) Discrepancies between the availability of data and the research described
- (4) Inappropriate citations
- (5) Incoherent, meaningless and/or irrelevant content included in the article
- (6) Peer-review manipulation

The presence of these indicators undermines our confidence in the integrity of the article's content and we cannot, therefore, vouch for its reliability. Please note that this notice is intended solely to alert readers that the content of this article is unreliable. We have not investigated whether authors were aware of or involved in the systematic manipulation of the publication process.

Wiley and Hindawi regrets that the usual quality checks did not identify these issues before publication and have since put additional measures in place to safeguard research integrity.

We wish to credit our own Research Integrity and Research Publishing teams and anonymous and named external researchers and research integrity experts for contributing to this investigation.

The corresponding author, as the representative of all authors, has been given the opportunity to register their agreement or disagreement to this retraction. We have kept a record of any response received.

### **References**

- [1] F. Yang and Y. Rao, "Practice and Research of Blended Learning Model Guided by Deep Learning Model," *Mathematical Problems in Engineering*, vol. 2022, Article ID 8915162, 6 pages, 2022.

## *Retraction*

# **Retracted: Development of Interactive Teaching of Physical Dance Based on Dynamic Time Reversion Technique**

### **Mathematical Problems in Engineering**

Received 18 July 2023; Accepted 18 July 2023; Published 19 July 2023

Copyright © 2023 Mathematical Problems in Engineering. This is an open access article distributed under the Creative Commons Attribution License, which permits unrestricted use, distribution, and reproduction in any medium, provided the original work is properly cited.

This article has been retracted by Hindawi following an investigation undertaken by the publisher [1]. This investigation has uncovered evidence of one or more of the following indicators of systematic manipulation of the publication process:

- (1) Discrepancies in scope
- (2) Discrepancies in the description of the research reported
- (3) Discrepancies between the availability of data and the research described
- (4) Inappropriate citations
- (5) Incoherent, meaningless and/or irrelevant content included in the article
- (6) Peer-review manipulation

The presence of these indicators undermines our confidence in the integrity of the article's content and we cannot, therefore, vouch for its reliability. Please note that this notice is intended solely to alert readers that the content of this article is unreliable. We have not investigated whether authors were aware of or involved in the systematic manipulation of the publication process.

Wiley and Hindawi regrets that the usual quality checks did not identify these issues before publication and have since put additional measures in place to safeguard research integrity.

We wish to credit our own Research Integrity and Research Publishing teams and anonymous and named external researchers and research integrity experts for contributing to this investigation.

The corresponding author, as the representative of all authors, has been given the opportunity to register their agreement or disagreement to this retraction. We have kept a record of any response received.

### **References**

- [1] X. Li and Y. Yang, "Development of Interactive Teaching of Physical Dance Based on Dynamic Time Reversion Technique," *Mathematical Problems in Engineering*, vol. 2022, Article ID 5697041, 8 pages, 2022.

## *Retraction*

# **Retracted: Feature Learning-Based Generative Adversarial Network Data Augmentation for Class-Based Few-Shot Learning**

### **Mathematical Problems in Engineering**

Received 18 July 2023; Accepted 18 July 2023; Published 19 July 2023

Copyright © 2023 Mathematical Problems in Engineering. This is an open access article distributed under the Creative Commons Attribution License, which permits unrestricted use, distribution, and reproduction in any medium, provided the original work is properly cited.

This article has been retracted by Hindawi following an investigation undertaken by the publisher [1]. This investigation has uncovered evidence of one or more of the following indicators of systematic manipulation of the publication process:

- (1) Discrepancies in scope
- (2) Discrepancies in the description of the research reported
- (3) Discrepancies between the availability of data and the research described
- (4) Inappropriate citations
- (5) Incoherent, meaningless and/or irrelevant content included in the article
- (6) Peer-review manipulation

The presence of these indicators undermines our confidence in the integrity of the article's content and we cannot, therefore, vouch for its reliability. Please note that this notice is intended solely to alert readers that the content of this article is unreliable. We have not investigated whether authors were aware of or involved in the systematic manipulation of the publication process.

Wiley and Hindawi regrets that the usual quality checks did not identify these issues before publication and have since put additional measures in place to safeguard research integrity.

We wish to credit our own Research Integrity and Research Publishing teams and anonymous and named external researchers and research integrity experts for contributing to this investigation.

The corresponding author, as the representative of all authors, has been given the opportunity to register their agreement or disagreement to this retraction. We have kept a record of any response received.

### **References**

- [1] B. Subedi, V. E. Sathishkumar, V. Maheshwari, M. S. Kumar, P. Jayagopal, and S. M. Allayear, "Feature Learning-Based Generative Adversarial Network Data Augmentation for Class-Based Few-Shot Learning," *Mathematical Problems in Engineering*, vol. 2022, Article ID 9710667, 20 pages, 2022.

## *Retraction*

# **Retracted: Construction and Knowledge Mining of Traditional Chinese Medicine Ancient Books Bibliographic Abstracts Database Based on Genetic Algorithm and BP Neural Network**

### **Mathematical Problems in Engineering**

Received 18 July 2023; Accepted 18 July 2023; Published 19 July 2023

Copyright © 2023 Mathematical Problems in Engineering. This is an open access article distributed under the Creative Commons Attribution License, which permits unrestricted use, distribution, and reproduction in any medium, provided the original work is properly cited.

This article has been retracted by Hindawi following an investigation undertaken by the publisher [1]. This investigation has uncovered evidence of one or more of the following indicators of systematic manipulation of the publication process:

- (1) Discrepancies in scope
- (2) Discrepancies in the description of the research reported
- (3) Discrepancies between the availability of data and the research described
- (4) Inappropriate citations
- (5) Incoherent, meaningless and/or irrelevant content included in the article
- (6) Peer-review manipulation

The presence of these indicators undermines our confidence in the integrity of the article's content and we cannot, therefore, vouch for its reliability. Please note that this notice is intended solely to alert readers that the content of this article is unreliable. We have not investigated whether authors were aware of or involved in the systematic manipulation of the publication process.

Wiley and Hindawi regrets that the usual quality checks did not identify these issues before publication and have since put additional measures in place to safeguard research integrity.

We wish to credit our own Research Integrity and Research Publishing teams and anonymous and named external researchers and research integrity experts for contributing to this investigation.

The corresponding author, as the representative of all authors, has been given the opportunity to register their

agreement or disagreement to this retraction. We have kept a record of any response received.

### **References**

- [1] Y. Wang, S. Ren, L. Song, and J. Zhang, "Construction and Knowledge Mining of Traditional Chinese Medicine Ancient Books Bibliographic Abstracts Database Based on Genetic Algorithm and BP Neural Network," *Mathematical Problems in Engineering*, vol. 2022, Article ID 6838714, 15 pages, 2022.

## *Retraction*

# **Retracted: Deep Neural Network-Based Business Data Classification in Intelligent Business Management**

### **Mathematical Problems in Engineering**

Received 18 July 2023; Accepted 18 July 2023; Published 19 July 2023

Copyright © 2023 Mathematical Problems in Engineering. This is an open access article distributed under the Creative Commons Attribution License, which permits unrestricted use, distribution, and reproduction in any medium, provided the original work is properly cited.

This article has been retracted by Hindawi following an investigation undertaken by the publisher [1]. This investigation has uncovered evidence of one or more of the following indicators of systematic manipulation of the publication process:

- (1) Discrepancies in scope
- (2) Discrepancies in the description of the research reported
- (3) Discrepancies between the availability of data and the research described
- (4) Inappropriate citations
- (5) Incoherent, meaningless and/or irrelevant content included in the article
- (6) Peer-review manipulation

The presence of these indicators undermines our confidence in the integrity of the article's content and we cannot, therefore, vouch for its reliability. Please note that this notice is intended solely to alert readers that the content of this article is unreliable. We have not investigated whether authors were aware of or involved in the systematic manipulation of the publication process.

Wiley and Hindawi regrets that the usual quality checks did not identify these issues before publication and have since put additional measures in place to safeguard research integrity.

We wish to credit our own Research Integrity and Research Publishing teams and anonymous and named external researchers and research integrity experts for contributing to this investigation.

The corresponding author, as the representative of all authors, has been given the opportunity to register their agreement or disagreement to this retraction. We have kept a record of any response received.

### **References**

- [1] B. Wang, "Deep Neural Network-Based Business Data Classification in Intelligent Business Management," *Mathematical Problems in Engineering*, vol. 2022, Article ID 7104750, 8 pages, 2022.



## Retraction

# Retracted: Deep Learning-Based Assessment of Sports-Assisted Teaching and Learning

### Mathematical Problems in Engineering

Received 18 July 2023; Accepted 18 July 2023; Published 19 July 2023

Copyright © 2023 Mathematical Problems in Engineering. This is an open access article distributed under the Creative Commons Attribution License, which permits unrestricted use, distribution, and reproduction in any medium, provided the original work is properly cited.

This article has been retracted by Hindawi following an investigation undertaken by the publisher [1]. This investigation has uncovered evidence of one or more of the following indicators of systematic manipulation of the publication process:

- (1) Discrepancies in scope
- (2) Discrepancies in the description of the research reported
- (3) Discrepancies between the availability of data and the research described
- (4) Inappropriate citations
- (5) Incoherent, meaningless and/or irrelevant content included in the article
- (6) Peer-review manipulation

The presence of these indicators undermines our confidence in the integrity of the article's content and we cannot, therefore, vouch for its reliability. Please note that this notice is intended solely to alert readers that the content of this article is unreliable. We have not investigated whether authors were aware of or involved in the systematic manipulation of the publication process.

Wiley and Hindawi regrets that the usual quality checks did not identify these issues before publication and have since put additional measures in place to safeguard research integrity.

We wish to credit our own Research Integrity and Research Publishing teams and anonymous and named external researchers and research integrity experts for contributing to this investigation.

The corresponding author, as the representative of all authors, has been given the opportunity to register their agreement or disagreement to this retraction. We have kept a record of any response received.

### References

- [1] W. Su and J. Feng, "Deep Learning-Based Assessment of Sports-Assisted Teaching and Learning," *Mathematical Problems in Engineering*, vol. 2022, Article ID 7833292, 8 pages, 2022.

## *Retraction*

# **Retracted: Study on Intelligently Designed Business Innovation Service Models Driven by Big Data**

### **Mathematical Problems in Engineering**

Received 18 July 2023; Accepted 18 July 2023; Published 19 July 2023

Copyright © 2023 Mathematical Problems in Engineering. This is an open access article distributed under the Creative Commons Attribution License, which permits unrestricted use, distribution, and reproduction in any medium, provided the original work is properly cited.

This article has been retracted by Hindawi following an investigation undertaken by the publisher [1]. This investigation has uncovered evidence of one or more of the following indicators of systematic manipulation of the publication process:

- (1) Discrepancies in scope
- (2) Discrepancies in the description of the research reported
- (3) Discrepancies between the availability of data and the research described
- (4) Inappropriate citations
- (5) Incoherent, meaningless and/or irrelevant content included in the article
- (6) Peer-review manipulation

The presence of these indicators undermines our confidence in the integrity of the article's content and we cannot, therefore, vouch for its reliability. Please note that this notice is intended solely to alert readers that the content of this article is unreliable. We have not investigated whether authors were aware of or involved in the systematic manipulation of the publication process.

Wiley and Hindawi regrets that the usual quality checks did not identify these issues before publication and have since put additional measures in place to safeguard research integrity.

We wish to credit our own Research Integrity and Research Publishing teams and anonymous and named external researchers and research integrity experts for contributing to this investigation.

The corresponding author, as the representative of all authors, has been given the opportunity to register their agreement or disagreement to this retraction. We have kept a record of any response received.

### **References**

- [1] H. Liu, J. Shang, and G. Wan, "Study on Intelligently Designed Business Innovation Service Models Driven by Big Data," *Mathematical Problems in Engineering*, vol. 2022, Article ID 4468240, 15 pages, 2022.

## *Retraction*

# **Retracted: A Deep Learning-Based Framework for Social Data Sensing and Fusion for Enterprise Management**

### **Mathematical Problems in Engineering**

Received 18 July 2023; Accepted 18 July 2023; Published 19 July 2023

Copyright © 2023 Mathematical Problems in Engineering. This is an open access article distributed under the Creative Commons Attribution License, which permits unrestricted use, distribution, and reproduction in any medium, provided the original work is properly cited.

This article has been retracted by Hindawi following an investigation undertaken by the publisher [1]. This investigation has uncovered evidence of one or more of the following indicators of systematic manipulation of the publication process:

- (1) Discrepancies in scope
- (2) Discrepancies in the description of the research reported
- (3) Discrepancies between the availability of data and the research described
- (4) Inappropriate citations
- (5) Incoherent, meaningless and/or irrelevant content included in the article
- (6) Peer-review manipulation

The presence of these indicators undermines our confidence in the integrity of the article's content and we cannot, therefore, vouch for its reliability. Please note that this notice is intended solely to alert readers that the content of this article is unreliable. We have not investigated whether authors were aware of or involved in the systematic manipulation of the publication process.

Wiley and Hindawi regrets that the usual quality checks did not identify these issues before publication and have since put additional measures in place to safeguard research integrity.

We wish to credit our own Research Integrity and Research Publishing teams and anonymous and named external researchers and research integrity experts for contributing to this investigation.

The corresponding author, as the representative of all authors, has been given the opportunity to register their agreement or disagreement to this retraction. We have kept a record of any response received.

### **References**

- [1] Y. Wang, "A Deep Learning-Based Framework for Social Data Sensing and Fusion for Enterprise Management," *Mathematical Problems in Engineering*, vol. 2022, Article ID 3606469, 8 pages, 2022.

## *Retraction*

# **Retracted: Construction of an Optimal Scheduling Method for Campus Energy Systems Based on Deep Learning Models**

### **Mathematical Problems in Engineering**

Received 18 July 2023; Accepted 18 July 2023; Published 19 July 2023

Copyright © 2023 Mathematical Problems in Engineering. This is an open access article distributed under the Creative Commons Attribution License, which permits unrestricted use, distribution, and reproduction in any medium, provided the original work is properly cited.

This article has been retracted by Hindawi following an investigation undertaken by the publisher [1]. This investigation has uncovered evidence of one or more of the following indicators of systematic manipulation of the publication process:

- (1) Discrepancies in scope
- (2) Discrepancies in the description of the research reported
- (3) Discrepancies between the availability of data and the research described
- (4) Inappropriate citations
- (5) Incoherent, meaningless and/or irrelevant content included in the article
- (6) Peer-review manipulation

The presence of these indicators undermines our confidence in the integrity of the article's content and we cannot, therefore, vouch for its reliability. Please note that this notice is intended solely to alert readers that the content of this article is unreliable. We have not investigated whether authors were aware of or involved in the systematic manipulation of the publication process.

Wiley and Hindawi regrets that the usual quality checks did not identify these issues before publication and have since put additional measures in place to safeguard research integrity.

We wish to credit our own Research Integrity and Research Publishing teams and anonymous and named external researchers and research integrity experts for contributing to this investigation.

The corresponding author, as the representative of all authors, has been given the opportunity to register their agreement or disagreement to this retraction. We have kept a record of any response received.

### **References**

- [1] J. Li and H. Zhao, "Construction of an Optimal Scheduling Method for Campus Energy Systems Based on Deep Learning Models," *Mathematical Problems in Engineering*, vol. 2022, Article ID 5350786, 10 pages, 2022.

## *Retraction*

# **Retracted: A Computer-Aided Assessment and Evaluation System for Modern Apprenticeship of Accounting Class On-the-Job Training**

### **Mathematical Problems in Engineering**

Received 18 July 2023; Accepted 18 July 2023; Published 19 July 2023

Copyright © 2023 Mathematical Problems in Engineering. This is an open access article distributed under the Creative Commons Attribution License, which permits unrestricted use, distribution, and reproduction in any medium, provided the original work is properly cited.

This article has been retracted by Hindawi following an investigation undertaken by the publisher [1]. This investigation has uncovered evidence of one or more of the following indicators of systematic manipulation of the publication process:

- (1) Discrepancies in scope
- (2) Discrepancies in the description of the research reported
- (3) Discrepancies between the availability of data and the research described
- (4) Inappropriate citations
- (5) Incoherent, meaningless and/or irrelevant content included in the article
- (6) Peer-review manipulation

The presence of these indicators undermines our confidence in the integrity of the article's content and we cannot, therefore, vouch for its reliability. Please note that this notice is intended solely to alert readers that the content of this article is unreliable. We have not investigated whether authors were aware of or involved in the systematic manipulation of the publication process.

In addition, our investigation has also shown that one or more of the following human-subject reporting requirements has not been met in this article: ethical approval by an Institutional Review Board (IRB) committee or equivalent, patient/participant consent to participate, and/or agreement to publish patient/participant details (where relevant).

Wiley and Hindawi regrets that the usual quality checks did not identify these issues before publication and have since put additional measures in place to safeguard research integrity.

We wish to credit our own Research Integrity and Research Publishing teams and anonymous and named external researchers and research integrity experts for contributing to this investigation.

The corresponding author, as the representative of all authors, has been given the opportunity to register their agreement or disagreement to this retraction. We have kept a record of any response received.

### **References**

- [1] L. Sun, C. Liu, M. Lin, and Y. Zhou, "A Computer-Aided Assessment and Evaluation System for Modern Apprenticeship of Accounting Class On-the-Job Training," *Mathematical Problems in Engineering*, vol. 2022, Article ID 6437885, 11 pages, 2022.

## *Retraction*

# **Retracted: Clustering Merchants and Accurate Marketing of Products Using the Segmentation Tree Vector Space Model**

### **Mathematical Problems in Engineering**

Received 18 July 2023; Accepted 18 July 2023; Published 19 July 2023

Copyright © 2023 Mathematical Problems in Engineering. This is an open access article distributed under the Creative Commons Attribution License, which permits unrestricted use, distribution, and reproduction in any medium, provided the original work is properly cited.

This article has been retracted by Hindawi following an investigation undertaken by the publisher [1]. This investigation has uncovered evidence of one or more of the following indicators of systematic manipulation of the publication process:

- (1) Discrepancies in scope
- (2) Discrepancies in the description of the research reported
- (3) Discrepancies between the availability of data and the research described
- (4) Inappropriate citations
- (5) Incoherent, meaningless and/or irrelevant content included in the article
- (6) Peer-review manipulation

The presence of these indicators undermines our confidence in the integrity of the article's content and we cannot, therefore, vouch for its reliability. Please note that this notice is intended solely to alert readers that the content of this article is unreliable. We have not investigated whether authors were aware of or involved in the systematic manipulation of the publication process.

Wiley and Hindawi regrets that the usual quality checks did not identify these issues before publication and have since put additional measures in place to safeguard research integrity.

We wish to credit our own Research Integrity and Research Publishing teams and anonymous and named external researchers and research integrity experts for contributing to this investigation.

The corresponding author, as the representative of all authors, has been given the opportunity to register their agreement or disagreement to this retraction. We have kept a record of any response received.

### **References**

- [1] X. Ding, Z. Wu, and M. Li, "Clustering Merchants and Accurate Marketing of Products Using the Segmentation Tree Vector Space Model," *Mathematical Problems in Engineering*, vol. 2022, Article ID 7353151, 11 pages, 2022.

## *Retraction*

# **Retracted: Research on the Efficiency Evaluation of Cross-Organizational Knowledge Synergy in Industry University Cooperation Based on BP Neural Network Algorithm**

### **Mathematical Problems in Engineering**

Received 18 July 2023; Accepted 18 July 2023; Published 19 July 2023

Copyright © 2023 Mathematical Problems in Engineering. This is an open access article distributed under the Creative Commons Attribution License, which permits unrestricted use, distribution, and reproduction in any medium, provided the original work is properly cited.

This article has been retracted by Hindawi following an investigation undertaken by the publisher [1]. This investigation has uncovered evidence of one or more of the following indicators of systematic manipulation of the publication process:

- (1) Discrepancies in scope
- (2) Discrepancies in the description of the research reported
- (3) Discrepancies between the availability of data and the research described
- (4) Inappropriate citations
- (5) Incoherent, meaningless and/or irrelevant content included in the article
- (6) Peer-review manipulation

The presence of these indicators undermines our confidence in the integrity of the article's content and we cannot, therefore, vouch for its reliability. Please note that this notice is intended solely to alert readers that the content of this article is unreliable. We have not investigated whether authors were aware of or involved in the systematic manipulation of the publication process.

Wiley and Hindawi regrets that the usual quality checks did not identify these issues before publication and have since put additional measures in place to safeguard research integrity.

We wish to credit our own Research Integrity and Research Publishing teams and anonymous and named external researchers and research integrity experts for contributing to this investigation.

The corresponding author, as the representative of all authors, has been given the opportunity to register their

agreement or disagreement to this retraction. We have kept a record of any response received.

### **References**

- [1] L. Jing, "Research on the Efficiency Evaluation of Cross-Organizational Knowledge Synergy in Industry University Cooperation Based on BP Neural Network Algorithm," *Mathematical Problems in Engineering*, vol. 2022, Article ID 1873862, 8 pages, 2022.

## Retraction

# Retracted: Teaching Design of Mathematics Application Based on Naive Bayes

### Mathematical Problems in Engineering

Received 18 July 2023; Accepted 18 July 2023; Published 19 July 2023

Copyright © 2023 Mathematical Problems in Engineering. This is an open access article distributed under the Creative Commons Attribution License, which permits unrestricted use, distribution, and reproduction in any medium, provided the original work is properly cited.

This article has been retracted by Hindawi following an investigation undertaken by the publisher [1]. This investigation has uncovered evidence of one or more of the following indicators of systematic manipulation of the publication process:

- (1) Discrepancies in scope
- (2) Discrepancies in the description of the research reported
- (3) Discrepancies between the availability of data and the research described
- (4) Inappropriate citations
- (5) Incoherent, meaningless and/or irrelevant content included in the article
- (6) Peer-review manipulation

The presence of these indicators undermines our confidence in the integrity of the article's content and we cannot, therefore, vouch for its reliability. Please note that this notice is intended solely to alert readers that the content of this article is unreliable. We have not investigated whether authors were aware of or involved in the systematic manipulation of the publication process.

Wiley and Hindawi regrets that the usual quality checks did not identify these issues before publication and have since put additional measures in place to safeguard research integrity.

We wish to credit our own Research Integrity and Research Publishing teams and anonymous and named external researchers and research integrity experts for contributing to this investigation.

The corresponding author, as the representative of all authors, has been given the opportunity to register their agreement or disagreement to this retraction. We have kept a record of any response received.

### References

- [1] H. Ling, "Teaching Design of Mathematics Application Based on Naive Bayes," *Mathematical Problems in Engineering*, vol. 2022, Article ID 7244001, 6 pages, 2022.



## *Retraction*

# **Retracted: A Study on the Usefulness of Stochastic Simulation Algorithms for Teaching and Learning in College Physical Education Classrooms**

### **Mathematical Problems in Engineering**

Received 18 July 2023; Accepted 18 July 2023; Published 19 July 2023

Copyright © 2023 Mathematical Problems in Engineering. This is an open access article distributed under the Creative Commons Attribution License, which permits unrestricted use, distribution, and reproduction in any medium, provided the original work is properly cited.

This article has been retracted by Hindawi following an investigation undertaken by the publisher [1]. This investigation has uncovered evidence of one or more of the following indicators of systematic manipulation of the publication process:

- (1) Discrepancies in scope
- (2) Discrepancies in the description of the research reported
- (3) Discrepancies between the availability of data and the research described
- (4) Inappropriate citations
- (5) Incoherent, meaningless and/or irrelevant content included in the article
- (6) Peer-review manipulation

The presence of these indicators undermines our confidence in the integrity of the article's content and we cannot, therefore, vouch for its reliability. Please note that this notice is intended solely to alert readers that the content of this article is unreliable. We have not investigated whether authors were aware of or involved in the systematic manipulation of the publication process.

Wiley and Hindawi regrets that the usual quality checks did not identify these issues before publication and have since put additional measures in place to safeguard research integrity.

We wish to credit our own Research Integrity and Research Publishing teams and anonymous and named external researchers and research integrity experts for contributing to this investigation.

The corresponding author, as the representative of all authors, has been given the opportunity to register their

agreement or disagreement to this retraction. We have kept a record of any response received.

### **References**

- [1] J. Xu, "A Study on the Usefulness of Stochastic Simulation Algorithms for Teaching and Learning in College Physical Education Classrooms," *Mathematical Problems in Engineering*, vol. 2022, Article ID 2779909, 6 pages, 2022.

## *Retraction*

# **Retracted: Effect of Evaluation of Popular Song Creation and Literature Based on RITNN Model**

### **Mathematical Problems in Engineering**

Received 18 July 2023; Accepted 18 July 2023; Published 19 July 2023

Copyright © 2023 Mathematical Problems in Engineering. This is an open access article distributed under the Creative Commons Attribution License, which permits unrestricted use, distribution, and reproduction in any medium, provided the original work is properly cited.

This article has been retracted by Hindawi following an investigation undertaken by the publisher [1]. This investigation has uncovered evidence of one or more of the following indicators of systematic manipulation of the publication process:

- (1) Discrepancies in scope
- (2) Discrepancies in the description of the research reported
- (3) Discrepancies between the availability of data and the research described
- (4) Inappropriate citations
- (5) Incoherent, meaningless and/or irrelevant content included in the article
- (6) Peer-review manipulation

The presence of these indicators undermines our confidence in the integrity of the article's content and we cannot, therefore, vouch for its reliability. Please note that this notice is intended solely to alert readers that the content of this article is unreliable. We have not investigated whether authors were aware of or involved in the systematic manipulation of the publication process.

Wiley and Hindawi regrets that the usual quality checks did not identify these issues before publication and have since put additional measures in place to safeguard research integrity.

We wish to credit our own Research Integrity and Research Publishing teams and anonymous and named external researchers and research integrity experts for contributing to this investigation.

The corresponding author, as the representative of all authors, has been given the opportunity to register their agreement or disagreement to this retraction. We have kept a record of any response received.

### **References**

- [1] R. Song, "Effect of Evaluation of Popular Song Creation and Literature Based on RITNN Model," *Mathematical Problems in Engineering*, vol. 2022, Article ID 4643674, 9 pages, 2022.

## *Retraction*

# **Retracted: Application and Analysis of Taekwondo Techniques, Tactics, and Movement Trajectories Based on Multi-Intelligent Decision Making**

### **Mathematical Problems in Engineering**

Received 18 July 2023; Accepted 18 July 2023; Published 19 July 2023

Copyright © 2023 Mathematical Problems in Engineering. This is an open access article distributed under the Creative Commons Attribution License, which permits unrestricted use, distribution, and reproduction in any medium, provided the original work is properly cited.

This article has been retracted by Hindawi following an investigation undertaken by the publisher [1]. This investigation has uncovered evidence of one or more of the following indicators of systematic manipulation of the publication process:

- (1) Discrepancies in scope
- (2) Discrepancies in the description of the research reported
- (3) Discrepancies between the availability of data and the research described
- (4) Inappropriate citations
- (5) Incoherent, meaningless and/or irrelevant content included in the article
- (6) Peer-review manipulation

The presence of these indicators undermines our confidence in the integrity of the article's content and we cannot, therefore, vouch for its reliability. Please note that this notice is intended solely to alert readers that the content of this article is unreliable. We have not investigated whether authors were aware of or involved in the systematic manipulation of the publication process.

Wiley and Hindawi regrets that the usual quality checks did not identify these issues before publication and have since put additional measures in place to safeguard research integrity.

We wish to credit our own Research Integrity and Research Publishing teams and anonymous and named external researchers and research integrity experts for contributing to this investigation.

The corresponding author, as the representative of all authors, has been given the opportunity to register their

agreement or disagreement to this retraction. We have kept a record of any response received.

### **References**

- [1] W. Lu and X. Lin, "Application and Analysis of Taekwondo Techniques, Tactics, and Movement Trajectories Based on Multi-Intelligent Decision Making," *Mathematical Problems in Engineering*, vol. 2022, Article ID 8411550, 8 pages, 2022.

## *Retraction*

# **Retracted: Construction of an Assessment System for Business English Linguistics Based on RNN Multidimensional Models**

### **Mathematical Problems in Engineering**

Received 18 July 2023; Accepted 18 July 2023; Published 19 July 2023

Copyright © 2023 Mathematical Problems in Engineering. This is an open access article distributed under the Creative Commons Attribution License, which permits unrestricted use, distribution, and reproduction in any medium, provided the original work is properly cited.

This article has been retracted by Hindawi following an investigation undertaken by the publisher [1]. This investigation has uncovered evidence of one or more of the following indicators of systematic manipulation of the publication process:

- (1) Discrepancies in scope
- (2) Discrepancies in the description of the research reported
- (3) Discrepancies between the availability of data and the research described
- (4) Inappropriate citations
- (5) Incoherent, meaningless and/or irrelevant content included in the article
- (6) Peer-review manipulation

The presence of these indicators undermines our confidence in the integrity of the article's content and we cannot, therefore, vouch for its reliability. Please note that this notice is intended solely to alert readers that the content of this article is unreliable. We have not investigated whether authors were aware of or involved in the systematic manipulation of the publication process.

Wiley and Hindawi regrets that the usual quality checks did not identify these issues before publication and have since put additional measures in place to safeguard research integrity.

We wish to credit our own Research Integrity and Research Publishing teams and anonymous and named external researchers and research integrity experts for contributing to this investigation.

The corresponding author, as the representative of all authors, has been given the opportunity to register their agreement or disagreement to this retraction. We have kept a record of any response received.

### **References**

- [1] Y. Shi and H. Shi, "Construction of an Assessment System for Business English Linguistics Based on RNN Multidimensional Models," *Mathematical Problems in Engineering*, vol. 2022, Article ID 8446281, 8 pages, 2022.

## Research Article

# Trajectory Planning and Collision Control of a Mobile Robot: A Penalty-Based PSO Approach

**Krishna Kant Pandey** <sup>1</sup>, **Chandrashekhar Kumbhar**,<sup>2</sup> **Dayal R. Parhi**,<sup>3</sup>  
**Sandeep Kumar Mathivanan**,<sup>4</sup> **Prabhu Jayagopal**,<sup>4</sup> and **Aminul Haque** <sup>5</sup>

<sup>1</sup>Department of Mechatronics Engineering, Manipal University Jaipur, Jaipur 303007, Rajasthan, India

<sup>2</sup>Learning Facilitator, Educlass Pvt. Ltd., Singapore 408601, Singapore

<sup>3</sup>Mechanical Engineering Department, National Institute of Technology, Rourkela, Odisha 769008, India

<sup>4</sup>School of Information Technology and Engineering, Vellore Institute of Technology, Vellore 632014, Tamil Nadu, India

<sup>5</sup>Department of Computer Science and Engineering, Daffodil International University, Daffodil Smart City, Birulia, Savar, Dhaka 1216, Bangladesh

Correspondence should be addressed to Aminul Haque; aminul.cse@daffodilvarsity.edu.bd

Received 1 July 2022; Revised 5 October 2022; Accepted 24 November 2022; Published 31 January 2023

Academic Editor: Shimin Wang

Copyright © 2023 Krishna Kant Pandey et al. This is an open access article distributed under the Creative Commons Attribution License, which permits unrestricted use, distribution, and reproduction in any medium, provided the original work is properly cited.

In this paper, trajectory planning and navigation control problems have been addressed for a mobile robot. To achieve the objective of the research, an adaptive PSO (Particle Swarm Optimization) motion algorithm is developed using a penalty-based methodology. To deliver the best or collision-free position to the robot, fitness values of the all-random-positioned particles are compared at the same time during the target search action. By comparing the fitness values, the robot occupies the best position in the search space till it reaches the target. The new work integrated with conventional PSO is varying a velocity event that plays a vital role during the position acquisition (continuous change in position during the obstacle negotiation with the communication through random-positioned particles). The obstacle-negotiating angle and positional velocity of the robot are considered as input parameters of the controller whereas the robot's best position according to the target position is considered as the output of the controller. Simulation results are presented through the MATLAB environment. To validate simulation results, real-time experiments have been conducted in a similar workspace. The results of the adaptive PSO technique are also compared with the results of the existing navigational techniques. Improvements in results between the proposed navigation technique and existing navigation techniques are found to be 4.66% and 11.30%, respectively.

## 1. Introduction

In robotics science, navigation and trajectory planning of mobile robots (MRs) using artificial intelligence (AI) approaches are the most common type of research domain. During trajectory planning in the search space, the wheeled mobile robot moves from a source point to the target point by avoiding obstacles present in an arena. Simultaneously, the robot creates a collision-free trajectory in a search space using artificial intelligence (AI) based robot controller. The following control objectives must be followed during the development of any AI-based navigational controller. For the model, the controller should provide good stability (the

signal must be bounded). The controller should have good tracking ability (good understanding) and the controller should be robust (take a self-decision during navigational failures) in nature. In the next section, a detailed review of the literature has been presented addressing strategy, design, and implementation of navigation controllers for wheeled mobile robots in different environments.

Yang et al. [1] developed a layered motion planning scheme for the navigation of a wheeled MR in an unstructured environment using the Fuzzy technique. To produce the intermediate way-point towards the target, the first layer of the planner uses the information about the global end position and the high-range sensory data. Here,

no crucial assumptions have been used regarding the environment. A path-following approach using rule-based fuzzy logic that mimics human behaviour has been proposed by Antonelli et al. [2] for a smart vehicle. Knowledge of the next bend ahead to the vehicle is taken as the fuzzy input data and linear velocity by which the robot can safely move on the path and it is the output of the fuzzy controller. The line following behaviour is executed by the vehicle to validate the proposed algorithm. Gueaieb and Miah [3] developed an intelligent and innovative nonvision-based navigation approach using Radio Frequency Identification (RFID) technology. In their work, only straight path motion has been considered. To mimic human behaviour, they have used single input and single output Mamdani-type fuzzy architecture. Mastrogiovanni et al. [4] developed a new mobile robot navigation approach called “ $\mu$ Nav.” They said, during path planning in a complicated search space, this technique requires a minimum sensory data, less computational power, and memory. Since it gains robustness intrinsically from the  $\mu$ Nav technique, it does not require any self-localization potentiality or inboard geometrical representation. To explore the basic geometrical features of indoor search space and to survive there, a miniaturized triangulation laser scanner-based control architecture has been developed by [5] (using a swarm of the robot). The objectives of the research are to explore the environment using simple, small, low cost, and low power small devices. A fuzzy logic based [6] control algorithm has been trained using an evolutionary-group-based PSO for navigation in an unknown world. The mutation and crossover operation of the fuzzy-based PSO has used group-based framework. The adaptive velocity altered action is presented to enhance the search capability. Takagi–Sugeno–Kang (TSK) type FLC has been used for the navigational analysis. Chou et al. [7] have explored the indoor navigation problems using the dynamic window approach (DWA\*) for navigation in an unfamiliar environment. The local reactive method is used to categorize the environment by which the robot achieves smoothness, speed, and local minima-free navigation. A region study technique has been applied to eliminate inadequate commands. To determine the optimal command, the A\* algorithm is applied with look-ahead verification. Using the tethered coverage (TC) analysis, Shnaps and Rimon [8] emphasized the strategies of MR motion planning in an unknown scenario. They have deployed a mobile robot of size “D” in the fixed pose “S” connected through the cable of length “L.” A novel adaptive localization algorithm [9] performs the estimation of the robot position with great accuracy in an amorphous environment. To estimate the position of the robot, they used image fusion of an omnidirectional visualization system, odometry measurements, and inertial devices (sensors). To decide the robot’s orientation and the robot velocity, odometer and inertial sensors obtained the feature points using the sequence of an image. Using an adaptive fusion (AF) based ACO and PSO (AF-ACPSO) [10], cooperative navigation strategies have been developed for two robots in an unspecified environment. During the navigation, AF-ACPSO-based FLC has been executed the boundary following behaviour and the robot

learn this behaviour. The learning behaviours are completed by a single robot and further applied to the second robot that works as a follower. Ramaithitima et al. [11] proposed the work for navigation control of the MR using a swarm of inexpensive portable sensors. In their work, the robot does not require explicitly metric information during the generation of maps. They have used the Voronoi graph to create an approximate map of the covered environment. The ROS (Robot Operating System) is used to demonstrate the algorithm. Almasri et al. [12] developed a technique for the robotic system, by which the mobile robot follows the line and avoid collision with obstacles. They have used low-cost IR sensors. This methodology includes a satisfactory level of calculation. Hence in real-time applications, it has been efficiently implemented. They have used the e-puck robot on the Webots platform to check the simulation results. Golan et al. [13] proposed an online robot navigation system using artificial temperature gradients techniques. The environment with obstacles is taken as a “hot” junction and the target is taken as a “cold” junction. During the navigation, the temperature gradient is solved using a heat conduction partial differentiation equation. Kanezaki et al. [14] developed a reactive neural network approach to tackle the problem of learning. The author’s key concept is to crop, resize, and rotate an obstacle map which is based on the target location, and to represent the map better, the agent’s current pose is taken rather than the layout of the search space. They have supplied navigation history as input in the robot brain to reduce the rate of failure. Ataka et al. [15] developed an RMF (Reactive Magnetic Field) inspired navigation method in the unspecified 3D convex environment. The robot induced artificial electric current in the obstacle exterior and the MF (magnetic field) guides the robot along with the obstacles surrounding. Hence, the robot does not suffer from the local minima problem in convex obstacles-based 3D environment. Cole and Wickenheiser [16] proposed a path-planning algorithm for multiple mobile robots using a reactive trajectory scheme. The authors stated the route does not disrupt the robot thrust limitation and sensor limitations for the moving obstacles. They used the Sigmoid function for the transition course. Sensor data are updated by matching with sigmoid slopes and curves. Singh et al. [17] developed a vision-based navigational approach for a nonholonomic MR in an unfamiliar known environment. They used switching-based SMC (sliding mode control) methodology for the analysis by which the robot continuously follows the desired route. The robot uses red, green, and blue depth (RGB-D) sensor modules to create angular velocity. In their work, fuzzy logic is used for guidance and the Krasovski method is used to show the asymptotically stable curve. To reference MR applications for the urban search and rescue (USAR), Niroui et al. [18] proposed a deep reinforcement learning strategy for a cluttered environment. The authors combined the Asynchronous Advantage Actor-Critic (A3C) and reinforcement learning to allow the mobile robot to navigate safely. A3C is a technique that accelerates optimization as well as the training process parallelly and maintains the navigational policy.

Due to incomplete information of a mimic and unregular environment, the robot confronts complexity and vagueness during navigation and path planning. It may be that the robot is trapped in the loop due to mimic surrounding inside the environment. Traditional navigational and path-planning approaches such as the Visibility graph [19], Voronoi diagram [20], and Grids [21] are not compatible with navigation and path planning in the mimic and unregular environments. Recently, many researchers have developed various navigation algorithms [22–26] but these methods have still some drawbacks or could not fulfill the desire. These navigational problems are taken as objectives in this analysis. In this research, the mobile robot is using a novel hybrid optimization technique to perform navigation and path-planning tasks. As well as the above problem is expressed as an optimization problem having constraints. The results are compared with other navigational techniques in terms of path length to check the performance of the technique. Using the proposed technique, the robot smartly negotiates obstacles and navigates towards the target. Finally, the mobile robot performs well in the given environment (mimic or unregular environment) and the results are recorded in terms of trajectory length and navigational time.

## 2. The Proposed Work: Adaptive PSO Concept

It is a population-based randomly determined optimization technique and devoted for artificial life phenomenon. The APSO is inspired by the swarm behaviour of insects, birds, and fishes. It is well suited for continuous variable and global search problems. It is effectively applied to a varied series of problems such as network [27], structural optimization [28], and fuzzy control system [29]. In APSO, the system makes it ready to change with the population of a random value and searches for the best by updating the local generation. The APSO technique updates the population of agents according to the values of the fitness function. The fitness function depends upon the swarm behaviour of local particles.

In this analysis, the PSO has been modified using a local search (LS) ability. The constraints are accommodated to obtain better obstacle-negotiation results using the penalty method. Using local search ability, position as well as control

parameters of agents are tuned perfectly. Consequently, the navigational angle performance has been increasing in terms of position accuracy (best fitness).

**2.1. Adaptive Particle Swarm Optimization (APSO) Methodology.** Adaptive PSO algorithm always learns from the situations and utilizes it to optimize the problem state. In APSO, all the agents have some fitness values ( $P_{\text{best}}$ ) but global best ( $G_{\text{best}}$ ) is the solution for all agents, which is surrounded by a flock of agents. The solution to the local search phenomenon is the “footprint between agents moving towards the global best position” in the search space. Furthermore, fitness value has been obtained using fitness calculation criteria. A solution with better fitness value during the local search event is selected as the finest result and appointed as the global best. The agent holds some varying properties like velocity, acceleration, and position when trying to finding out the global best in the environment. As a result, the global best of PSO may be changed as the global best of local search PSO. If agents are moving near to the global best, they sequentially follow the updated optimum position of the agent and it may be based on local search criteria. Figure 1 represents the flowchart of the APSO technique for trajectory planning and navigation control.

In Figure 2, the basic operations of APSO have been presented. The “ $x$ ” is an agent positioned randomly in the search space (“ $x$ ” personal best is  $P_{ij}^n(t)$ ) and searching for global best with time “ $t$ ” to “ $t+1$ ” and so on. In each sequence of iteration, every particle is occupying a new position by following two ‘best’ solutions. The initial best value for all solutions is stored as “ $P_{\text{best}}$ ” (personal best position of an agent). Another value that has been traced by the optimizer is the second-best solution and called a global position ( $g_{\text{best}}$ ). It is stored as a global best ( $g_{\text{best}}$ ) and followed by all agents. “ $P_{\text{best}}$ ” and “ $g_{\text{best}}$ ” are the agent’s personal and global positions, respectively. However, agents are following the global best value and updated their position according to that with varying velocity. By updating velocity ( $v_{ij}^n(t)$ ) and position ( $x_{ij}^n(t)$ ) using equations (1) and (2), the agents update their personal best value ( $P_{\text{best}}$ ) and global best value ( $g_{\text{best}}$ ).

$$x_{ij}^n(t+1) = x_{ij}^n(t) + v_{ij}^n(t+1), \quad (1)$$

$$v_{ij}^n(t+1) = wv_{ij}^n(t) + r_{i_1}C_1[\{P_{ij}^n(t)\} - x_{ij}^n(t)] + r_{i_2}C_2[\{g^n(t)\} - x_{ij}^n(t)]. \quad (2)$$

In equations (1) and (2), “ $w$ ” is inertia weight and  $C_1$  and  $C_2$  are the positive acceleration coefficients [30]. The uniformly distributed random variables (UDRV) are given as ‘ $r_{i_1}$ ’ and ‘ $r_{i_2}$ ’. The costs of UDRV are varied between ‘0’ and ‘1’. The velocity and position of the “ $i^{\text{th}}$ ” particle are denoted as  $x_i = (x_i^1, x_i^2, \dots, x_i^n)$  and  $v_i = (v_i^1, v_i^2, \dots, v_i^n)$ . From equations (3) and (4), the best earlier location ‘ $P_{ij}^n(t)$ ’ and

the global best earlier location ‘ $g^n(t)$ ’ of particles in the swarm are chosen.

$$P_{ij}^n(t) = \{P_{ij}^1(t), P_{ij}^2(t), P_{ij}^3(t), \dots, P_{ij}^n(t)\}, \quad (3)$$

$$g^n(t) = \{g^1(t), g^2(t), g^3(t), \dots, g^n(t)\}, \quad (4)$$

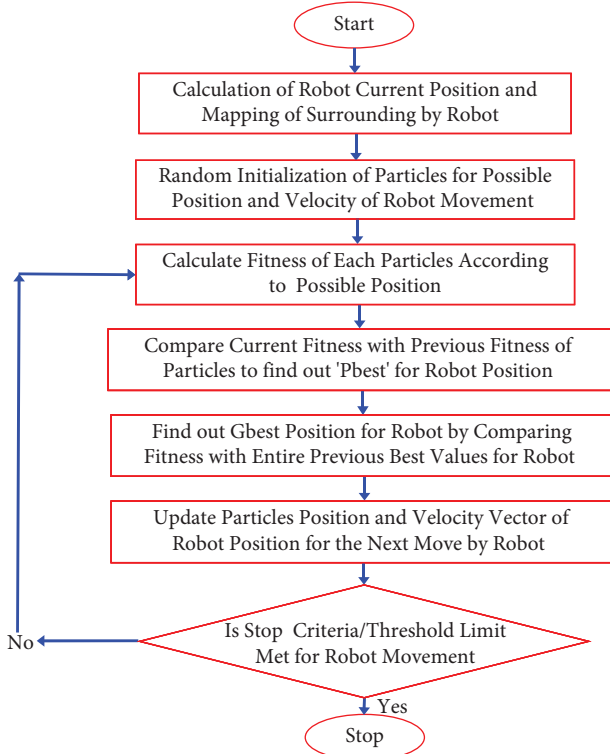


FIGURE 1: Flowchart of the APSO technique.

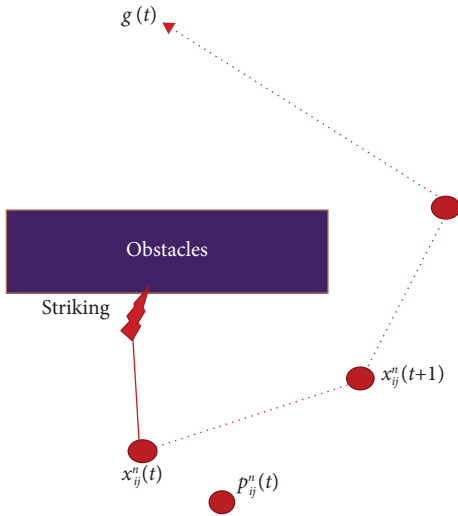


FIGURE 2: Principle diagram of APSO.

$$P_{Ap} = P_{ij}^n(t) + \rho(f). \quad (5)$$

Equations (3) and (4) can be construed in the following way. Let us assume “ $n$ ” searchers act as “ $n$ ” elements stirring in the search environment “ $X$ ,” the locus of the “ $n^{\text{th}}$ ” searcher in the “ $i^{\text{th}}$ ” reiteration is signified as “ $x_{ij}^n \in X_{\text{search-space}} \subset \mathbb{R}^2$ .” The cost function “ $f: \mathbb{R}^2 \rightarrow \mathbb{R}$ ” sustained by each searcher in the adverse of the signal strength established at its existing position [31]. The aim of the searchers is to connect between “ $n$ ” numbers of agents and interchange in a manner to verify and occupy the

TABLE 1: Parameters used in the APSO algorithm architecture.

| Sl. no. | Properties                             | Values |
|---------|--|--------|
| 1       | Population size ( $i$ )                | 100    |
| 2       | “+” acceleration coefficient ( $C_1$ ) | 1.496  |
| 3       | “+” acceleration coefficient ( $C_2$ ) | 1.496  |
| 4       | Alpha                                  | 0.1000 |
| 5       | Iteration                              | 100    |
| 6       | Max iteration                          | 100    |
| 7       | $\eta_{\text{pop}}$                    | 100    |
| 8       | $\eta_{\text{var}}$                    | 3      |
| 9       | Inertia weight ( $w$ )                 | 0.7298 |
| 10      | Penalty                                | 1000   |

universal least of the cost function. Each searcher is expected to know its individual best earlier location and the global best earlier location. Also, each seeker communicates with the agent whose position is overlapped with obstacles but is near to the goal position. If this condition is rising, then the penalty function (using equation (5)) added is with the overlapped agents to separate from the obstacles. The penalty function is taken into account to reduce the navigation time as well as to obtain a smooth path. Table 1 shows the different properties, which are used by the adaptive controller for tuning the navigational path. Furthermore, particles have been accommodated to create a smooth path from the start to the goal position. The adaptive PSO has been analyzed to create optimal and collision-free navigation in an environment using local search methodology.

The negotiation within a threshold range has been performed between obstacles and the robot to obtain the collision-free navigational path. In the next section, the architecture of the controller (APSO) has been demonstrated to tune the navigation path by adding a penalty with colliding agents.

**2.2. The Architecture of APSO Controller.** In Figure 3, a flowchart of the APSO algorithm is shown. By adding a penalty function with the PSO algorithm, the advanced algorithm has been proposed as APSO for trajectory planning, robot navigation, and path optimization. The disorder environments have been taken for the navigation and path-planning analysis in which obstacles shapes are different in size as well as positioned with different orientations. Using APSO “ $G_{\text{best}}$ ” has been calculated and compared with the fitness value of local search “ $G_{\text{best}}$ ” (penalty-based  $G_{\text{best}}$ ). Then, the preferred “ $G_{\text{best}}$ ” from both events (PSO and penalty-based PSO) is appointed as the next possible location and the best location is updated in the robot brain. Hence, the best position vector and velocity vector of the robot have been updated from point to point during the optimized trajectory formation.

Using the adaptive PSO controller, the mobile robot also minimizes decision response time on the operational platform. It is due to local search criteria in APSO. The social and cognitive behaviour of the PSO method has been embedded with the concept of adaptive (local) search to optimize the response time, navigation time, and trajectory length. The robot can perform tasks such as avoiding obstacles, learn



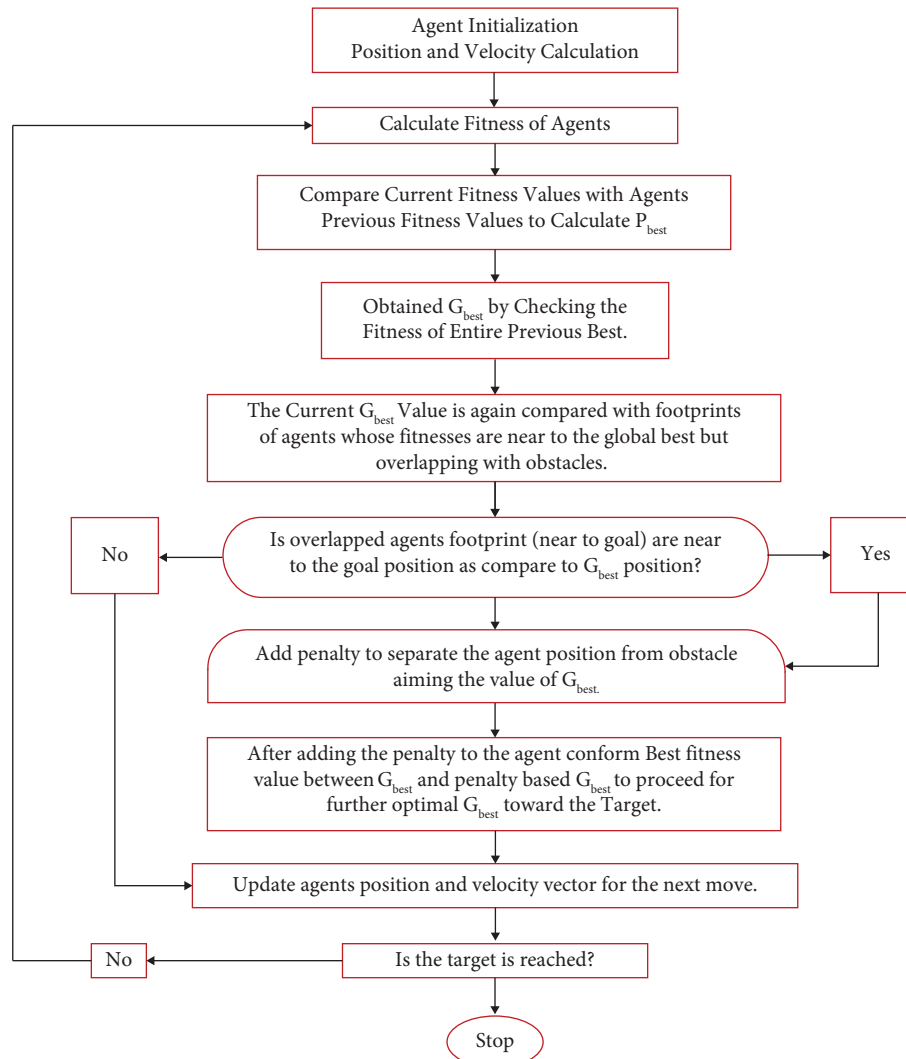


FIGURE 3: Flowchart of the adaptive PSO algorithm.

trajectory, comparing sensors results, and position optimized (aiming the goal) online. The results are analyzed in terms of path cost and path deviation for different environments. The robot reaction time, navigation time, and path length are minimized during the goal search inside the search space. Finally, the robot reaches the goal point smoothly. In the upcoming section, results and discussion using the adaptive PSO algorithm have been presented.

### 2.3. Stability Analysis in the Mimic and Maze Environment.

In this section, results from simulation and real-time experiment have been discussed for the adaptive PSO approach. The results are shown in terms of trajectory length and navigational time. The height and width of the simulation and experimental environments are taken as “10 × 10.” For that, “100 cm” is equal to “10” for simulation and experimental analysis. Two types of simulation environments (Figures 4 and 5) have been created in the MATLAB platform to check the navigational results using the APSO technique. For the real-time experiments, a similar type of

environment (Figures 6 and 7) is taken as compared to the simulation environment. The Khepera II mobile robot has been used in the real-time experiment to validate the simulation results as well as the developed approach. The navigational axis of rotation (obstacle-negotiation angle) has been optimized in a way the robot creates a smooth collision-free trajectory and minimizes navigational time. The robot simultaneously updates its steering angle and positional map using the APSO technique. As a result, the robot has performed an effective exploration work in the given environment.

### 2.4. Experimental Analysis in a Simulation Platform.

In Figures 4 and 5, trajectory planning and navigational results are shown using the APSO technique. The first simulation environment (Figure 4) contains only wall-type obstacles whereas, in the second simulation environment (Figure 5), wall type and irregular obstacles shape are considered.

The robot start position is taken as 0.7 m in the X-direction and 0.05 m in the Y-direction for both of the

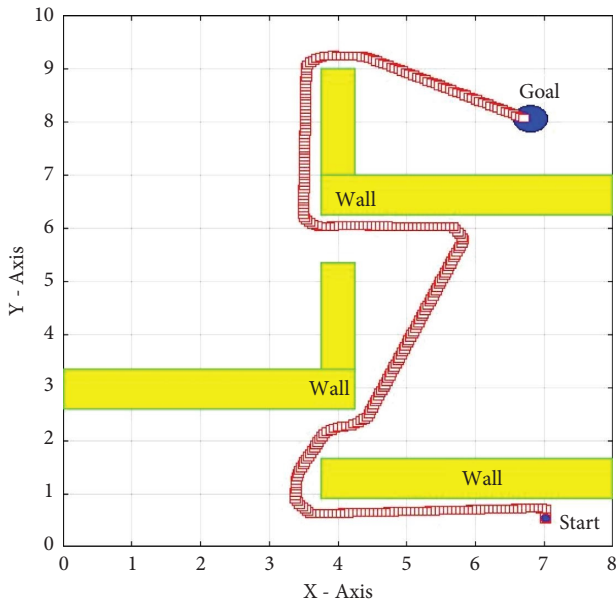


FIGURE 4: The mobile robot control analysis in a mimic environment.

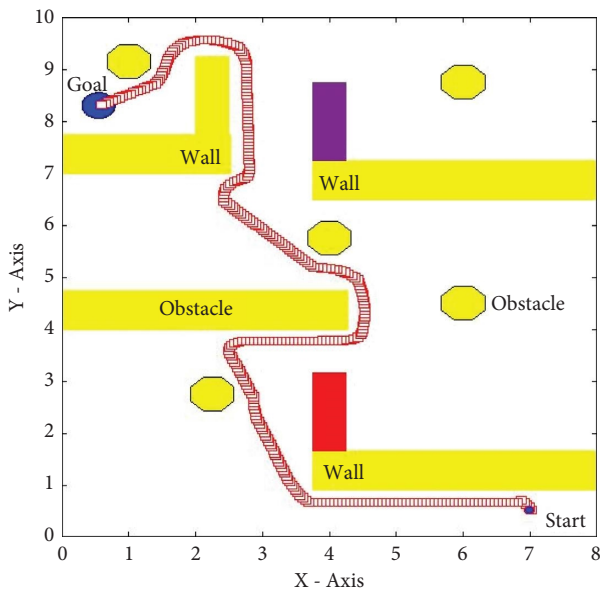


FIGURE 5: The mobile robot control analysis in a maze environment.

environments. The target position is 0.675 m in the  $X$ -direction, and 0.8 m in the  $Y$ -direction has been taken for the first simulation experiment. Similarly, the target position is 0.05 m in the  $X$ -direction, and 0.825 m in the  $Y$ -direction has been taken for the second simulation experiment. In these environments, the robot navigates in the narrow corridor as well as avoids mimic type wall configurations smoothly. Finally, the robot reaches the target efficiently in both of the environments by negotiating the obstacles using APSO. The time taken and path length obtained during the navigation are tabulated in Table 2.

2.5. *Experimental Analysis in a Real-Time Platform Using Khepera-II—A Mobile Robot.* The real-time experiments (Figures 6 and 7) are conducted using a Khepera II mobile robot, and the results are presented in terms of trajectory length (TL) and navigational time (NT) in Table 3. In Figures 6 and 7, the robot starts to point and obstacles position, and the target position are plotted similarly to the simulation environment. The robot successfully reached the target by negotiating the obstacles in the real-time environment.

The deviation in results has been taken in terms of trajectory length and navigational time that are represented in Table 4. Performance and effectiveness of the adaptive PSO algorithm are confirmed by considering the minimum deviation in results between both experiments (Simulation and Real-time). The percentage of deviation in both cases (Time and Trajectory length) is recorded as less than 8.5%.

Due to the use of the best fitness value from the APSO algorithm and the prediction of the next possible position, the PSO algorithm gets smarter. Hence, a smooth and collision-free navigational path has been created from the start to the target position. The robot detects its possible position accurately inside the environment due to penalty-based methodology and local search. The APSO AI technique reduced the trajectory map errors as well as position error (in “ $X$ ,” “ $Y$ ,” and “ $\theta$ ” directions) due to local search and penalty criteria. The wheel slippage is reduced up to 80% in the narrow corridor due to varying velocity events during the obstacle negotiation.

The proposed controller takes minimum reaction time to read the next obstacle-negotiation angle subjecting to the target path. Using the proposed APSO algorithm, the robot does not trap in the loop, or the robot smartly avoids the loop of the search space. Finally, the robot achieved the target without any trouble in an irregular environment. The operational performance and effectiveness of the proposed navigation controller are confirmed by comparing it with other navigational techniques in the next section.

### 3. Simulation Analysis in a Dynamic Environment

3.1. *A Comparative Study between Proposed Algorithm and Existing Algorithm [32] and [33].* APSO navigational results (Table 5) have been compared with ACO with Fuzzy (Garcia [32]) and Fuzzy Logic (Yahmedi and Fatmi [33]) which are already developed. To check the effectiveness of the proposed algorithm, the trajectory length has been considered and compared with other developed techniques. The trajectory length using Simple Ant Colony Optimization distance memory (SACODm) [32] is compared with the trajectory length obtained using the APSO algorithm (Figure 8). It is found that the APSO technique holds good results as compared to SACODm in terms of trajectory length (Table 5). The improvement in trajectory length using the current approach is recorded by 5% as compared to the ‘SACODm’ trajectory length.

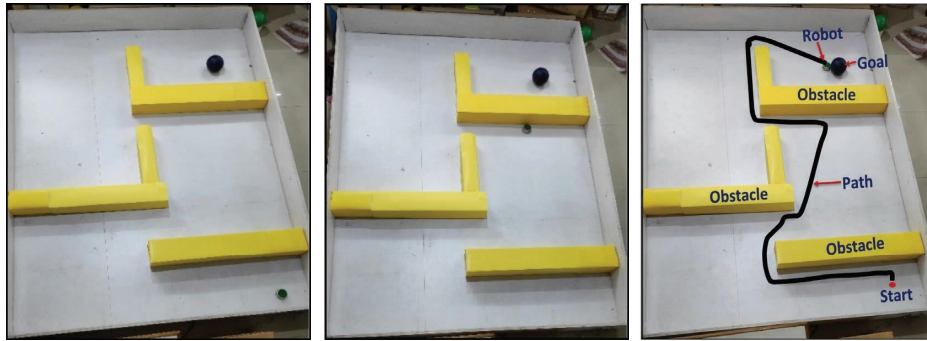


FIGURE 6: Real-time experiment using the APPO algorithm to validate the simulation results (Figure 4).

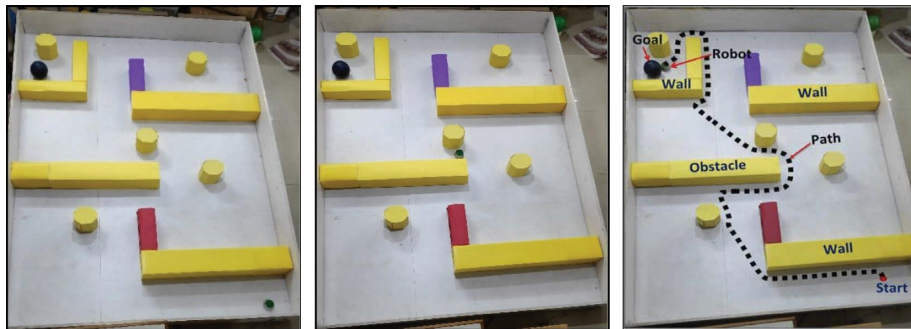


FIGURE 7: Real-time experiment using the APPO algorithm to validate the simulation results (Figure 5).

TABLE 2: Time taken and path length data for the simulation experiment (Figures 4 and 5).

| Sl. no. | Scenario | Time (“s”) | Trajectory length (“m”) |
|---------|----------|------------|-------------------------|
| 1.      | Figure 4 | 21.36      | 1.627                   |
| 2.      | Figure 5 | 27.48      | 1.763                   |

TABLE 3: Time taken and trajectory length data for the real-time experiment (Figures 6 and 7).

| Sl. no. | Scenario | NT (“s”) | TL (“m”) |
|---------|----------|----------|----------|
| 1.      | Figure 6 | 23       | 1.76     |
| 2.      | Figure 7 | 30       | 1.92     |

TABLE 4: Results comparison between simulation and experiment data using APPO (Figures 4–7).

| Sl. no. | Scenario | NT (in second “±0.5”) | “%” deviation | TL (“m” “±0.02”) | “%” deviation |
|---------|----------|-----------------------|---------------|------------------|---------------|
| 1.      | Figure 4 | 21.36                 | 7.13          | 1.627            | 7.55          |
|         | Figure 5 | 23                    |               | 1.76             |               |
| 2.      | Figure 6 | 27.48                 | 8.4           | 1.763            | 8.17          |
|         | Figure 7 | 30                    |               | 1.92             |               |

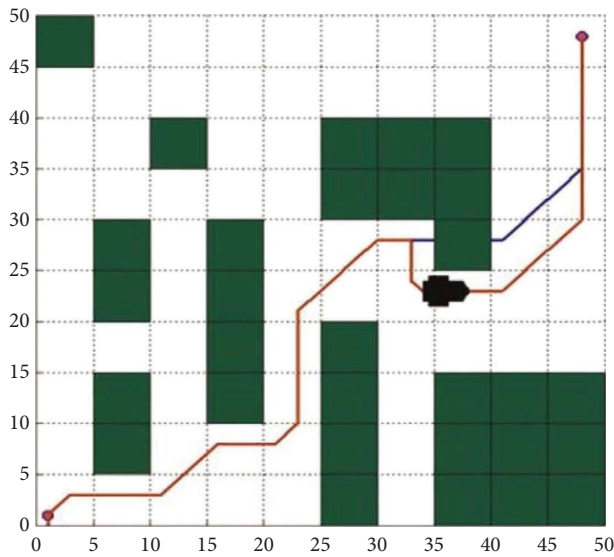
Similarly, the second comparison has been made between ‘Fuzzy logic’ (Yahmedi and Fatmi [33]) and the APPO algorithm in terms of trajectory length (Figure 9). Yahmedi and Fatmi used individual behaviour and action coordination technology with two-layered control. As compared to Yahmedi and Fatmi [33] results in terms of path length, the proposed technique holds improved results by 11% (Table 5).

The simulation and experimental study in various environments are conducted using the proposed methodology (APPO) and results are tabulated in Table 6. To confirm the

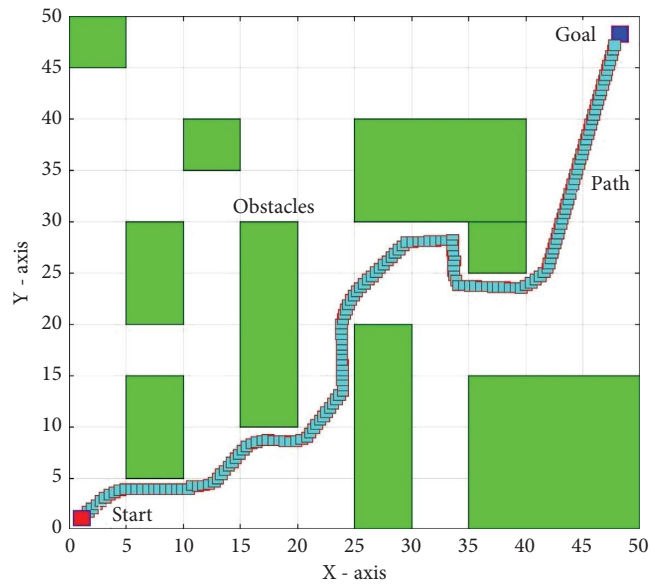
robustness and effectiveness of the proposed methodology during the trajectory planning, the average percentage deviation study between simulation and experimental results are depicted in Table 6. The average deviation in results is confirmed as 5.53 in terms of navigational time (NT) and 5.28 in terms of trajectory length (TL). In this analysis, the average deviation is less than 6% (Table 6) in perspective studies (NT and TL) and improvement in navigational results are greater than 4.5 percent (Table 5) is found. Hence, based upon depicted data in this analysis, the proposed methodology is robust as compared to existing techniques.

TABLE 5: Trajectory length (TL) comparison between APSO and existing techniques [32, 33].

| Sl. no. | Tasks                                | TL      | Improvement (%) |
|---------|--------------------------------------|---------|-----------------|
| 01.     | Figure 8(a), Garcia, [32]            | 03.43 m | 4.66            |
|         | Figure 8(b), proposed technique      | 03.27 m |                 |
| 02.     | Figure 9(a), Yahmedi and Fatmi, [33] | 24.75%  | 10.30           |
|         | Figure 9(b), proposed technique      | 22.20%  |                 |

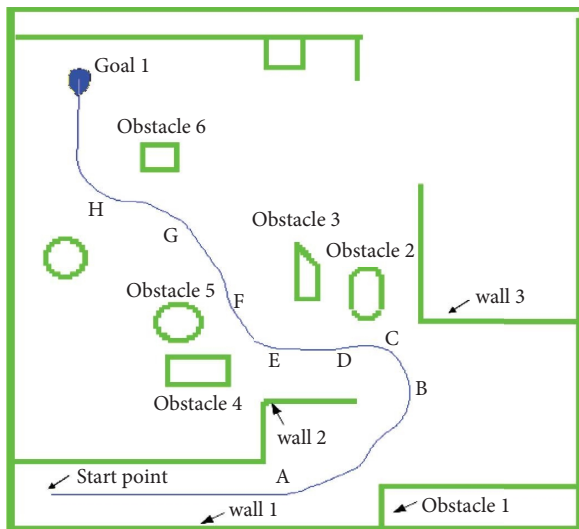


(a)

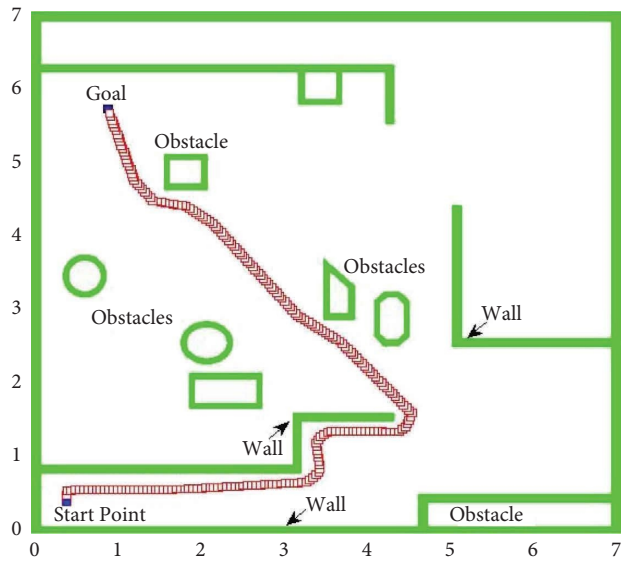


(b)

FIGURE 8: Results comparisons. (a) SACODm [32]. (b) APSO technique (current analysis).



(a)



(b)

FIGURE 9: Results comparisons. (a) Fuzzy Logic [33]. (b) APSO technique (current analysis).

TABLE 6: Study of simulation and experimental data in the various maze environment.

| Sl. No.                      | Scenario      | NT (in second " $\pm 0.5$ ") | "%" deviation | TL (" $m$ " " $\pm 0.02$ ") | "%" deviation |
|------------------------------|---------------|------------------------------|---------------|-----------------------------|---------------|
| 1.                           | Simulation-1  | 22.13                        | 5.43          | 1.78                        | 5.32          |
|                              | Experiment-1  | 23.40                        |               | 1.88                        |               |
| 2.                           | Simulation-2  | 28.18                        | 5.87          | 1.82                        | 5.70          |
|                              | Experiment-2  | 29.94                        |               | 1.93                        |               |
| 3.                           | Simulation-3  | 21.09                        | 5.76          | 1.59                        | 4.40          |
|                              | Experiment-3  | 22.38                        |               | 1.66                        |               |
| 4.                           | Simulation-4  | 26.38                        | 4.70          | 1.71                        | 4.09          |
|                              | Experiment-4  | 27.62                        |               | 1.78                        |               |
| 5.                           | Simulation-5  | 24.56                        | 6.14          | 1.67                        | 5.38          |
|                              | Experiment-5  | 26.07                        |               | 1.76                        |               |
| 6.                           | Simulation-6  | 20.28                        | 6.75          | 1.53                        | 5.22          |
|                              | Experiment-6  | 21.65                        |               | 1.61                        |               |
| 7.                           | Simulation-7  | 20.71                        | 5.98          | 1.57                        | 5.09          |
|                              | Experiment-7  | 21.95                        |               | 1.65                        |               |
| 8.                           | Simulation-8  | 21.13                        | 5.20          | 1.62                        | 4.94          |
|                              | Experiment-8  | 22.23                        |               | 1.70                        |               |
| 9.                           | Simulation-9  | 27.53                        | 4.54          | 1.79                        | 5.58          |
|                              | Experiment-9  | 28.78                        |               | 1.89                        |               |
| 10.                          | Simulation-10 | 28.43                        | 4.92          | 1.81                        | 6.07          |
|                              | Experiment-10 | 29.83                        |               | 1.90                        |               |
| Average deviation in results |               |                              | 5.53          |                             | 5.28          |

#### 4. Conclusions

In this paper, a penalty-based adaptive PSO approach has been developed for the trajectory planning of mobile robot in the wall-type maze environment. The agent overlapped with obstacles is taken under consideration to tune the trajectory path using local search and penalty-based method. To improve the robot position, navigational time, trajectory lengths, and response time penalty-based APSO analysis has been proposed. The agents near to the goal but overlapped with obstacles are added with a penalty to separate from a position of obstacles. Using APSO methodology, the advancement in trajectory planning (10% improvement) has been achieved in this analysis. The performance and effectiveness of the algorithm are validated by comparing the simulation and real-time experimental results. The deviation in results between simulation and real-time experiment has been recorded within 9% in terms of path length and navigational time. To check the authenticity of the proposed technique, its results in terms of the trajectory length are compared with existing techniques. The improvements in the results are recorded by 4% and 10.5%, as compared to existing techniques. The applications of the proposed methodology can be used for AI techniques based on decision-making applications. In future work, we will try to implement in real-time unstructured dynamics environment.

#### Data Availability

The data used to support the findings of this study are included within the article.

#### Conflicts of Interest

The authors declare that there are no conflicts of interest regarding the publication of this article.

#### References

- [1] X. Yang, M. Moallem, and R. V. Patel, "A layered goal-oriented fuzzy motion planning strategy for mobile robot navigation," *IEEE Transactions on Systems, Man, and Cybernetics, Part B (Cybernetics)*, vol. 35, no. 6, pp. 1214–1224, 2005.
- [2] G. Antonelli, S. Chiaverini, and G. Fusco, "A fuzzy-logic-based approach for mobile robot path tracking," *IEEE Transactions on Fuzzy Systems*, vol. 15, no. 2, pp. 211–221, 2007.
- [3] W. Gueaieb and M. S. Miah, "An intelligent mobile robot navigation technique using RFID technology," *IEEE Transactions on Instrumentation and Measurement*, vol. 57, no. 9, pp. 1908–1917, 2008.
- [4] F. Mastrogiovanni, A. Sgorbissa, and R. Zaccaria, "Robust navigation in an unknown environment with minimal sensing and representation," *IEEE Transactions on Systems, Man, and Cybernetics, Part B (Cybernetics)*, vol. 39, no. 1, pp. 212–229, 2009.
- [5] G. Fu, P. Corradi, A. Menciassi, and P. Dario, "An integrated triangulation laser scanner for obstacle detection of miniature mobile robots in indoor environment," *IEEE/ASME Transactions On Mechatronics*, vol. 16, no. 4, pp. 778–783, 2011.
- [6] C. F. Juang and Y. C. Chang, "Evolutionary-group-based particle-swarm-optimized fuzzy controller with application to mobile-robot navigation in unknown environments," *IEEE Transactions on Fuzzy Systems*, vol. 19, no. 2, pp. 379–392, 2011.
- [7] C. C. Chou, F. L. Lian, and C. C. Wang, "Characterizing indoor environment for robot navigation using velocity space

- approach with region analysis and look-ahead verification," *IEEE Transactions on Instrumentation and Measurement*, vol. 60, no. 2, pp. 442–451, 2011.
- [8] I. Shnaps and E. Rimon, "Online coverage by a tethered autonomous mobile robot in planar unknown environments," *IEEE Transactions on Robotics*, vol. 30, no. 4, pp. 966–974, 2014.
- [9] L. Li, Y. H. Liu, K. Wang, and M. Fang, "Estimating position of mobile robots from omnidirectional vision using an adaptive algorithm," *IEEE Transactions on Cybernetics*, vol. 45, no. 8, pp. 1633–1646, 2015.
- [10] C. F. Juang, M. G. Lai, and W. T. Zeng, "Evolutionary fuzzy control and navigation for two wheeled robots cooperatively carrying an object in unknown environments," *IEEE Transactions on Cybernetics*, vol. 45, no. 9, pp. 1731–1743, 2015.
- [11] R. Ramaithitima, M. Whitzer, S. Bhattacharya, and V. Kumar, "Automated creation of topological maps in unknown environments using a swarm of resource-constrained robots," *IEEE Robotics and Automation Letters*, vol. 1, no. 2, pp. 746–753, 2016.
- [12] M. M. Almasri, A. M. Alajlan, and K. M. Elleithy, "Trajectory planning and collision avoidance algorithm for mobile robotics system," *IEEE Sensors Journal*, vol. 16, no. 12, pp. 5021–5028, 2016.
- [13] Y. Golan, S. Edelman, A. Shapiro, and E. Rimon, "Online robot navigation using continuously updated artificial temperature gradients," *IEEE Robotics and Automation Letters*, vol. 2, no. 3, pp. 1280–1287, 2017.
- [14] A. Kanazaki, J. Nitta, and Y. Sasaki, "Goselo: goal-directed obstacle and self-location map for robot navigation using reactive neural networks," *IEEE Robotics and Automation Letters*, vol. 3, no. 2, pp. 696–703, 2018.
- [15] A. Ataka, H. K. Lam, and K. Althoefer, "Reactive magnetic-field-inspired navigation method for robots in unknown convex 3-D environments," *IEEE Robotics and Automation Letters*, vol. 3, no. 4, pp. 3583–3590, 2018.
- [16] K. Cole and A. M. Wickenheiser, "Reactive trajectory generation for multiple vehicles in unknown environments with wind disturbances," *IEEE Transactions on Robotics*, vol. 34, no. 5, pp. 1333–1348, 2018.
- [17] P. Singh, P. Agrawal, H. Karki, A. Shukla, N. K. Verma, and L. Behera, "Vision based guidance and switching based sliding mode controller for a mobile robot in the cyber physical framework," *IEEE Transactions on Industrial Informatics*, vol. 15, no. 4, pp. 1985–1997, 2019.
- [18] F. Niroui, K. Zhang, Z. Kashino, and G. Nejat, "Deep reinforcement learning robot for search and rescue applications: exploration in unknown cluttered environments," *IEEE Robotics and Automation Letters*, vol. 4, no. 2, pp. 610–617, 2019.
- [19] J. S. Mitchell, "An algorithmic approach to some problems in terrain navigation," *Artificial Intelligence*, vol. 37, no. 1–3, pp. 171–201, 1988.
- [20] N. Kalra, D. Ferguson, and A. Stentz, "Incremental reconstruction of generalized Voronoi diagrams on grids," *Robotics and Autonomous Systems*, vol. 57, no. 2, pp. 123–128, 2009.
- [21] M. Weigl, B. Siemiątkowska, K. A. Sikorski, and A. Borkowski, "Grid-based mapping for autonomous mobile robot," *Robotics and Autonomous Systems*, vol. 11, no. 1, pp. 13–21, 1993.
- [22] P. Y. Zhang, T. S. Lü, and L. B. Song, "Soccer robot path planning based on the artificial potential field approach with simulated annealing," *Robotica*, vol. 22, no. 5, pp. 563–566, 2004.
- [23] Y. C. Chang and Y. Yamamoto, "On-line path planning strategy integrated with collision and dead-lock avoidance schemes for wheeled mobile robot in indoor environments," *Industrial Robot: International Journal*, vol. 35, no. 5, pp. 421–434, 2008.
- [24] P. K. Mohanty and D. R. Parhi, "Navigation of autonomous mobile robot using adaptive network based fuzzy inference system," *Journal of Mechanical Science and Technology*, vol. 28, no. 7, pp. 2861–2868, 2014.
- [25] D. R. Parhi, B. B. V. L. Deepak, J. Mohana, R. Ruppa, and M. Nayak, "Immunised navigational controller for mobile robot navigation," in *Soft Computing Techniques in Vision Science*, pp. 171–182, Springer, Heidelberg, Germany, 2012.
- [26] A. Pandey, S. Pandey, and D. R. Parhi, "Mobile robot navigation and obstacle avoidance techniques: a review," *International Robotics & Automation Journal*, vol. 2, no. 3, Article ID 00022, pp. 1–12, 2017.
- [27] S. Goudarzi, W. H. Hassan, M. H. Anisi et al., "ABC-PSO for vertical handover in heterogeneous wireless networks," *Neurocomputing*, vol. 256, pp. 63–81, 2017.
- [28] M. Zawidzki and J. Szklarski, "Transformations of arm-Z modular manipulator with particle swarm optimization," *Advances in Engineering Software*, vol. 126, pp. 147–160, 2018.
- [29] R. Martinez-Soto, O. Castillo, and L. T. Aguilar, "Type-1 and Type-2 fuzzy logic controller design using a Hybrid PSO–GA optimization method," *Information Sciences*, vol. 285, pp. 35–49, 2014.
- [30] B. Song, Z. Wang, and L. Zou, "On global smooth path planning for mobile robots using a novel multimodal delayed PSO algorithm," *Cognitive Computation*, vol. 9, no. 1, pp. 5–17, 2017.
- [31] R. Zou, V. Kalivarapu, E. Winer, J. Oliver, and S. Bhattacharya, "Particle swarm optimization-based source seeking," *IEEE Transactions on Automation Science and Engineering*, vol. 12, no. 3, pp. 865–875, 2015.
- [32] M. P. Garcia, O. Montiel, O. Castillo, R. Sepulveda, and P. Melin, "Path planning for autonomous mobile robot navigation with ant colony optimization and fuzzy cost function evaluation," *Applied Soft Computing*, vol. 9, no. 3, pp. 1102–1110, 2009.
- [33] S. Amur, A. Yahmedi, and M. A. Fatmi, "Fuzzy logic based navigation of mobile robots," *Recent Advances in Mobile Robotics*, pp. 1–12, Intech Open, London, UK, 2011.

## Research Article

# Artificial Intelligence-Based English Self-Learning Effect Evaluation and Adaptive Influencing Factors Analysis

Xing Shu <sup>1</sup> and Chengjun Xu<sup>2</sup>

<sup>1</sup>Foreign Language College, East China Jiaotong University, Nanchang 330013, Jiangxi, China

<sup>2</sup>School of Software Engineering, Jiangxi Normal University, Nanchang 330022, Jiangxi, China

Correspondence should be addressed to Xing Shu; 2820@ecjtu.edu.cn

Received 20 July 2022; Revised 23 August 2022; Accepted 30 August 2022; Published 6 October 2022

Academic Editor: Man Fai Leung

Copyright © 2022 Xing Shu and Chengjun Xu. This is an open access article distributed under the Creative Commons Attribution License, which permits unrestricted use, distribution, and reproduction in any medium, provided the original work is properly cited.

Under the background of continuous development in our country, traditional English education can no longer meet the needs of modern times. Through the evaluation of English autonomous learning effect of artificial intelligence and the analysis of the influencing factors of adaptability, the teaching effect of English class is improved and the students' awareness of autonomous learning is cultivated. In the pilot study, students now have an overall level of adaptation ( $3 < M < 4$ ) supported by English proficiency. That is, the standard deviation is 1. The overall level of self-study in English is higher than that of boys ( $M = 3.40$  for females,  $M = 3.32$  for males, and  $M = 3.32$  for males). Compared with non-English majors, English majors are more suitable for self-study of artificial intelligence in English ( $M = 3.59$  for English majors), ( $M = 3.36$  for non-English majors), and students can improve their adaptive ability to learn AI by creating models. Transfer learning is the key to improving learners' English proficiency, and adaptive learning is the key to achieving this goal. Self-adaptive learning ensures the quality of students' autonomous English homework. Improper English learning not only affects students' learning outcomes but also affects their ability to learn English.

## 1. Introduction

In English learning mode, teachers and students spend a lot of time learning English. Due to the lack of an effective self-learning platform, students' self-learning ability is not strong. English language teaching is changing with the development of artificial intelligence technology. There are some practical steps to use AI tools in the input and output phases of English [1]. Many English lessons are done independently. The model of self-education, however, makes it difficult to increase the effectiveness of the quality of learning English. Poverty that arises at the level of the mind is a self-learning process. In addition, the article describes practical programs based on the characteristics of English-speaking business students, simplifies the maintenance of structured work, and considers the need for independent study to enable students to complete their assignments [2]. Artificial intelligence technology acquires knowledge in lifelong education e-learning through machine

learning to enhance learning effect and application. Introducing artificial intelligence into educational learning can effectively improve learning ability [3]. Learning English requires the use of practical classroom control skills to increase the teacher's level of classroom control as a necessary step in the development of English language learning. By analyzing smart data and analyzing student status, a student's learning status can be understood in a timely and effective manner [4]. The level of teacher control in English classrooms needs to be increased, using the skills of teachers in school management. The use of intelligent data and analysis of student behavior can help students understand how to learn timely and effectively [4]. Teaching English in college is a good way to learn English. However, most of the institute's current English broadcast programs blindly read students' English textbooks on computers [5]. AI is able to communicate better when guided by students' communication strategies. In addition, students were more communicative in the posttest than in the pretest.

According to interviews with students, smart devices with artificial intelligence are used to help them practice outside the classroom [6]. Online teaching methods in English are defined by the area of study and the complexity of online learning. Improve the ability of online English models to monitor and predict student health. Thanks to a combination of brilliant algorithms, a modeling system was developed, and the model performance was tested. The impact of students learning artificial intelligence has been identified in models that accept online learning [7]. The goal of artificial intelligence is to make machines that can understand language, recognize objects in a scene, act as intelligent robots, solve problems, teach students different subjects, and more. Knowledge and strategies may be taught in a content-independent form and then shown how they apply to different content areas. Either approach will help students gain an understanding of a particular knowledge area more easily [8]. Research has seen tremendous growth in AI-based decision-making, with many studies examining the impact of human decision-making using insights from the uncharted field of AI. Human AI decision-making has been shown to work well with textual information, which again constructs systems suitable for teaching human decision-making [9]. AI currently has no significant negative impact on jobs. However, the relationship between vocational training skills and specialized knowledge has a very negative impact on employment inequality [10]. It has become an important task for English educators to improve the initiative of college students in English learning. However, the interaction between vocational learning ability and artificial intelligence has a significant negative impact on job insecurity, and vocational learning ability has a significant moderating effect on job insecurity [11]. Learning motivation is not only a direct reflection of students' learning and living conditions but also an important indicator of the quality of skill development in higher education and teaching. In order to develop effective teaching and assessment methods, the supporting aspects of teaching and assessment in university education need to be considered. Reference [12] explored the application of linear structural equation modeling in analyzing the influencing factors of course learning interest. The main factors affecting students' interest in learning are students' professional foundation and teachers' teaching strategies. Good teaching effects and teaching strategies are very important to stimulate students' interest in learning [13]. The rapid development of modern technologies has promoted the development of smart products based on modern technology. To determine the acceptability of these products, different technology acceptance guidelines were used. The results show that adoption of minimally sophisticated and useful products, such as smart products based on technical expertise, is influenced more by interest in technology than in performance aspects [14].

## 2. The Current Situation and Optimization Strategies of English Autonomous Learning

*2.1. The Status Quo of English Autonomous Learning.* Now, many schools in our country have begun to focus on cultivating students' English language ability, but the effect is not very satisfactory. First, learning activities often do not

have adequate goals and not all learning activities are managed effectively. Although the students actively spoke in some self-directed learning tasks, most of the speeches were not related to the course content, and the students certainly did not participate in the teaching.

*2.2. Problems Existing in the Teaching of English Autonomous Learning.* At present, there are widespread problems in the process of English self-study. First, English teachers do not play the role of teachers because they do not have the right teaching direction. In this traditional teaching method, students do nothing and are based entirely on the teacher's classroom activities. In practical English classes, teachers often use traditional teaching methods to organize self-study classes, which will lead to students' anxiety and boredom in English classes and affect the effectiveness of English physical education teaching. Teachers in English classes do not provide the knowledge they want and neglect to develop students' study skills; students rely on teachers to learn and practice English through research, but they fail to develop their own study skills, as shown in Figure 1.

*2.3. Intervention Strategies in English Autonomous Learning.* All teaching behaviors of teachers should be centered on students' English learning experience, completely subverting the situation that teachers are the main language exporters in the traditional teaching model, and returning the right to speak to students, so as to achieve the return to the origin of the classroom. Let students participate in the classroom, stimulate students' passion for learning, and promote the formation of autonomous learning ability. Teachers should not be immersed in the traditional teaching mode and only study the problem of how to teach. Strengthen the study of learning theory, constantly update the knowledge system, constantly update the learning concept, and incorporate the self-study guide for college students into the learning concept. Teachers should respect and accept the individual differences of students when teaching English and should not use a single standard to evaluate students. The use of learning platforms brings different learning challenges and needs to different students. Recognizing the strengths of each student helps develop students' ability to learn independently, as shown in Figure 2.

- (1) Teachers respect the individual differences of students and make appropriate plans for different students
- (2) Teachers should not immerse themselves in the traditional way of teaching but should update the knowledge system in a timely manner so that the teaching concept can keep up with the times
- (3) Teachers should focus students' attention on learning English, allow students to participate in the classroom, and promote self-reliance in learning English

*2.4. Artificial Intelligence Research on English Autonomous Learning.* In the era of artificial intelligence, English learners should focus on cultivating cognitive driving



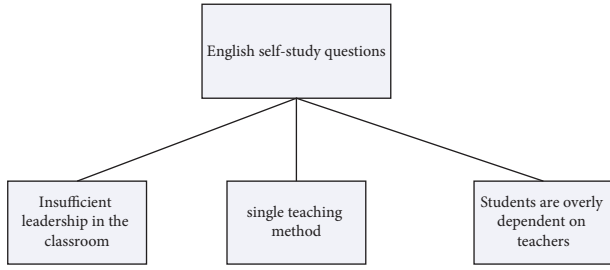


FIGURE 1: Problems existing in English self-study teaching.

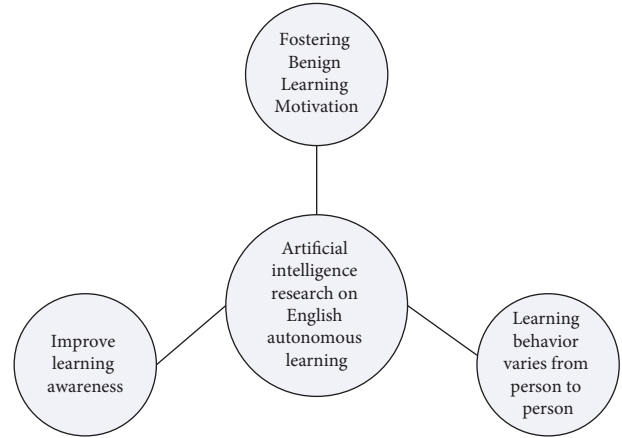


FIGURE 3: Artificial intelligence research on English self-learning.

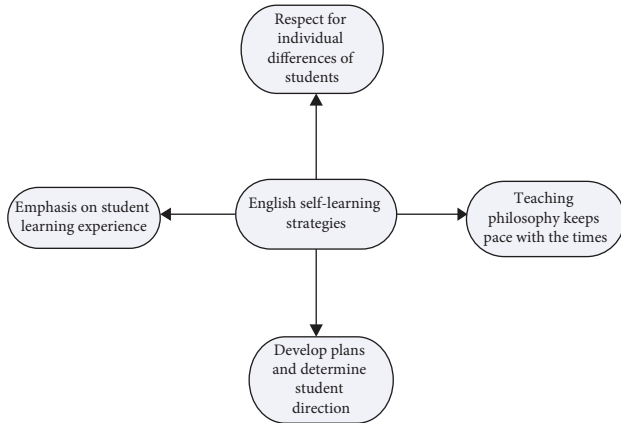


FIGURE 2: English autonomous learning strategies.

force, that is, improving their interest and curiosity in English learning. On this basis, cultivate self-development awareness, work hard for certain goals, and appropriately add some benign auxiliary driving forces, such as family and teacher expectations, to play a supervising role in the learning process. In the process of English learning, to understand the characteristics of one's own English learning, but also to strengthen the cognition of differences between individuals, to see the differences between others and their own English learning, to understand oneself objectively, and to carry out cognitive monitoring, promote strengths and avoid weaknesses, and adjust learning strategies. Online English learning should first have a good learning motivation, and second, improve learning cognition, and then adjust learning strategies according to cognition. The learning behavior can vary from person to person and has no significant impact on the learning effect as shown in Figure 3.

- (1) Artificial intelligence improves students' interest and curiosity in English learning
- (2) Artificial intelligence cultivates continuous and stable benign learning motivation
- (3) You can use artificial intelligence to understand your own English characteristics and strengthen the cognition of differences between individuals

### 3. Research on Artificial Intelligence Algorithms

**3.1. Reactive Power Scheduling Optimization Model.** Due to the ORPD problem, researchers have developed different optimization techniques to better suit different optimization objectives. This article focuses on reducing energy loss. The objective (objective function) is to reduce transmission losses and voltage deviations in the power system to meet energy demand. The problem can be described as a function of  $f(x, u)$ , i.e.,

$$\min[f(x, u)] = \min(g(x, u), h(x, u)),$$

$$\begin{cases} g(x, u) = 0, \\ h(x, u) \leq 0, \end{cases} \quad (1)$$

$g(x, u) = 0$  is an equal form of control;  $f(x, u)$  is a function;  $h(x, u) \leq 0$  is an unequal form of control.

Uneven control includes generator bus voltage, AC ratio, and number of static var compensators. For different control functions,  $x$  and  $u$  are the work-based and control variables, respectively. The purpose of ORPD is to minimize the overall transmission loss of the F-system, i.e.,

$$F_1 = P_{Loss}(x, u) = \sum_{k=1}^{N_L} gk(V_i^2 + v_j^2 - 2V_i V_j \cos(\theta_i - \theta_j)). \quad (2)$$

$N_L$  is the transport line number;  $G_k$  is the  $k$  line;  $V_i$  and  $V_j$  are full voltages. Here,  $j$  is the lines  $i$ ;  $\theta$  is the lines  $i$ ;  $\theta_j$  is the  $j$  end angle label.

Constrained by the equation is the power balance equation, which requires that the power of the power flow be equal; that is, the total energy loss is equal to the total energy production. The problems are

$$P_{Gi} - P_{Di} = V_i \sum_{j \in N_i} V_j (G_{ij} \cos \theta_{ij} + B_{ij} \sin \theta_{ij}),$$

$$Q_{Gi} - Q_{Di} = V_i \sum_{j \in N_i} V_j (B_{ij} \cos \theta_{ij} - G_{ij} \sin \theta_{ij}). \quad (3)$$

$V_i$  is the  $i$  load;  $V_j$  is the  $j$  voltage;  $G_{ij}$  is the conductance between  $i$  and  $j$ ;  $B_{ij}$  is the susceptance between  $i$  and  $j$ ;  $P_{Gi}$  is the  $Q_{Gi}$  active/reactive power;  $Q_{Di}$  is the actual load demand;  $Q_{Di}$  is the reactive load demand.

In ORPD problems, unbalanced basic barriers include barriers that damage generators, transformers, and equipment. As mentioned above, ORPD is a problem related to mobility parameters and loneliness. All unbalanced obstacles are determined by their upper and lower bounds, which leads to a stable solution. The thresholds are generator active power, reactance voltage, and bus voltage, and their upper and lower limits are

$$\begin{aligned} P_{Gi}^{\min} &\leq P_{Gi} \leq P_{Gi}^{\max}, \\ Q_{Gi}^{\min} &\leq Q_{Gi} \leq Q_{Gi}^{\max}, \\ V_{Gi}^{\min} &\leq V_{Gi} \leq V_{Gi}^{\max}, \end{aligned} \quad (4)$$

$i = 1 \dots N_G, N_G$  is the quantity.

The tap distance of the transformer

$$T_i^{\max} \leq T_i \leq T_i^{\min}, \quad (5)$$

$i = 1 \dots N_T, N_T$  is the number of transformers.

The size of the reactive power compensator is limited to

$$Q_{Ci}^{\min} \leq Q_{Ci} \leq Q_{Ci}^{\max}, \quad (6)$$

$i = 1, \dots, N_C, N$  is the number of reactive power compensators.

For obstacle development problems, ORPD handles various parameters such as generator bus voltages, transformer hub connections, and corresponding power compensation pixels, and MATPOWER can handle these changes automatically. Therefore, the bus voltage and reactive power can be limited by taking the PQ voltage amplitude of the bus and the reactive power entering the PV bus as the Penalty rules for objective acts. The above problem can be stated as follows:

$$F = F_X + \sum_{i \in N_V} \lim \lambda_{Vi} (V_i - V_i^{\lim})^2, \quad (7)$$

$F$  is a fitness function;  $F_X$  is the objective function;  $N^{\lim_V}$  is a set of bus numbers that violate the voltage magnitude limit;  $\lambda_{Vi}$  is the penalty function factor.

$V_i^{\lim}$  is calculated according to the following formula:

$$V_i^{\lim} = \begin{cases} V_i^{\max} & V_i > V_i^{\max}, \\ V_i^{\min} & V_i < V_i^{\min}. \end{cases} \quad (8)$$

**3.2. MOTH-FLAME Model.** By updating the BORN-FLAME algorithm, a natural AI update algorithm has several advantages over other incentive algorithms. The MFO algorithm is based on a special night rhythm mechanism. In the MFO model, the location of the problem in the river within the search area is variable. The MFO algorithm is a swarm intelligence algorithm, and an important component is a group of populations displayed in an array. Populations are shown in the array, i.e.,

$$M = \begin{bmatrix} m_{1,1} & m_{1,2} & \cdots & m_{1,d} \\ \vdots & \vdots & \cdots & \vdots \\ \vdots & \vdots & \cdots & \vdots \\ m_{n,1} & m_{n,2} & \cdots & m_{n,d} \end{bmatrix}. \quad (9)$$

$n$  is a numerical value;  $d$  is change researcher. The second most important feature of an MFO is the light matrix.

$$F = \begin{bmatrix} F_{1,1} & F_{1,2} & \cdots & F_{1,d} \\ \vdots & \vdots & \cdots & \vdots \\ \vdots & \vdots & \cdots & \vdots \\ F_{n,1} & F_{n,2} & \cdots & F_{n,d} \end{bmatrix}. \quad (10)$$

During optimization, the taint must update its spatial position according to this matrix. Therefore, in the numerical scheme, the lower edge of the worm is defined based on the fire in the matrix  $F$ . Since the formulas of (9) and (10) are the same, we can assume that there exists a system of conservation of energy values for flight and fire, i.e.,

$$\begin{aligned} O_M &= \begin{bmatrix} O_{M_1} \\ \vdots \\ \vdots \\ O_{M_n} \end{bmatrix}, \\ O_F &= \begin{bmatrix} O_{F_1} \\ \vdots \\ \vdots \\ O_{F_n} \end{bmatrix}. \end{aligned} \quad (11)$$

$O_M$  is the stored value;  $O_M$  is the fitness of the flame. Fitness is the value of the target work or output assigned to each flame.

Moths or flames can be used to solve the problem, but they work and adapt differently. The fire coordinator in the MFO is the ideal site for a kit below the level of current solutions and is the actual inspector of the required area. So, during the discovery process, a fire may appear as a signal for the spider to fall, and each insect turns the flame and adjusts its position to improve the results. This process helps eliminate optimal solutions from the search process. The above process can be illustrated by

$$M_i = S(M_i, F_j). \quad (12)$$

$M_i$  are  $i$  moths,  $F_j$  are  $j$  fires;  $S$  is a function.  $M_i$  are  $i$  moths,  $F_j$  are  $j$  fires;  $S$  is a function.

$$S(M_i, F_j) = D_i \cdot e^{bt} \cdot \cos(2\pi t) + F_j, \quad (13)$$

$b$  is logarithmic spiral shape as always; the interval  $[-1.1]$  contains a random number;  $i$  is followed by the distance between the fly and the flame. Moths can only change

TABLE 1: The way students use artificial intelligence to learn English.

| Educational products               | Frequency | Percentage |
|------------------------------------|-----------|------------|
| Learning to strengthen the country | 111       | 55         |
| Smart work                         | 18        | 8.9        |
| Homework help                      | 22        | 10.9       |
| Speak English fluently             | 31        | 15.3       |
| Tencent translator                 | 131       | 64.9       |
| Little ape search questions        | 55        | 27.2       |
| Learning pass                      | 10        | 5          |
| Xueersi online school              | 5         | 2.5        |
| Xiaodu AI robot                    | 21        | 10.4       |
| Schoolbaglang robot                | 3         | 1.5        |
| Baidu AI platform                  | 32        | 30.7       |
| Tencent cloud platform             | 21        | 10.4       |

TABLE 2: Basic ways of integrating artificial intelligence into education.

|  | Frequency | Percentage |
|--|-----------|------------|
| Conduct artificial intelligence courses                          | 6         | 3          |
| Using artificial intelligence to assist classroom learning       | 63        | 31.2       |
| Using artificial intelligence to assist extracurricular learning | 133       | 65.8       |
| Total  | 202       | 100        |

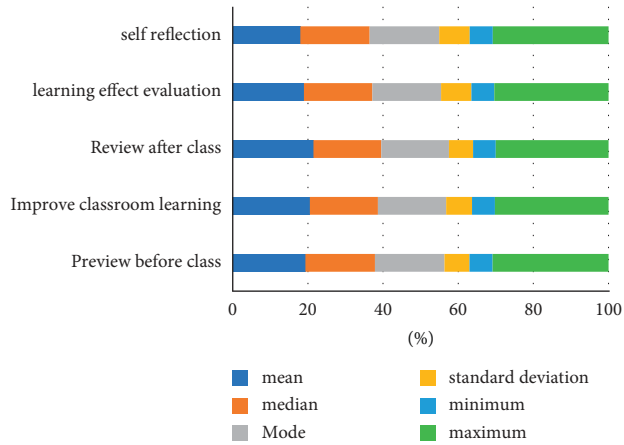


FIGURE 4: The self-learning effect of students using artificial intelligence in English.

position using an equalizer flame to keep the solution out of the atmosphere (13).  $D_i$  represents the distance between the  $j$  th flame and the  $i$  th moth, i.e.,

$$D_i = |F_j - M_i|. \tag{14}$$

$F_j$  is the  $j$  th flame;  $M_i$  is the  $i$  th moth.

Since (13) allows the butterfly to hover around the flame without actually flying between the butterflies, this equation provides an automatic solution process. When the next throttle position is outside the area between the flame and the throttle, the algorithm automatically searches for the throttle position within the space between the fire and the throttle.

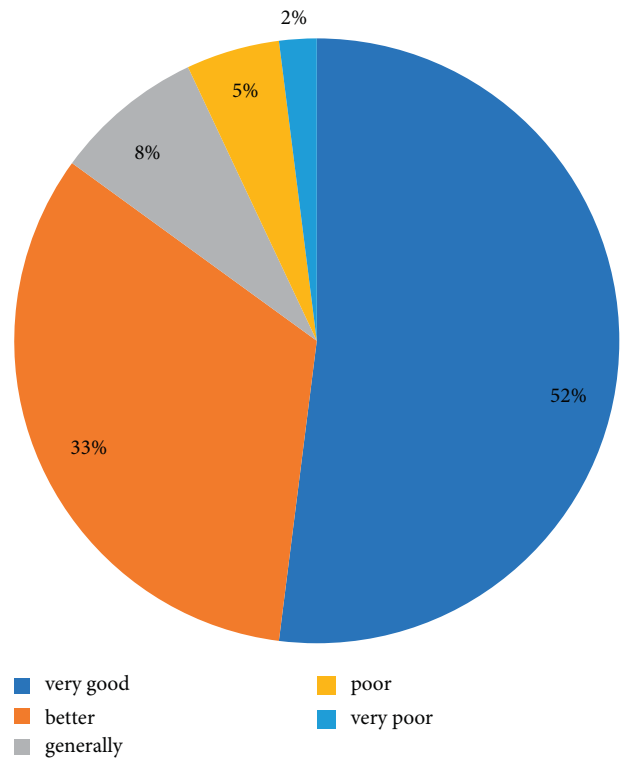


FIGURE 5: Students' evaluation of AI learning and education.

After updating the list, the algorithm ranks the rockets according to their suitability for each iteration. And the butterfly will update its position according to the corresponding flashlight, assuming that there are  $n$  flames in the

TABLE 3: Dimensional division of artificial intelligence English learning adaptability.

| Object                                | Dimension                       | Dimensional division        |
|---------------------------------------|---------------------------------|-----------------------------|
| Learning adaptability                 | Learning attitude adaptation    | Emotional experience        |
|                                       |                                 | Cognitive level             |
|                                       |                                 | Behavioral tendencies       |
|                                       | Self-learning ability           | Learning target             |
|                                       |                                 | Study method                |
|                                       |                                 | Self-assessment             |
|                                       | Learning to interact            | Teacher-student interaction |
|                                       |                                 | Peer interaction            |
|                                       | Learning environment adaptation | Human-computer interaction  |
|                                       |                                 | Resource acquisition        |
| Resource application                  |                                 |                             |
| Physical and mental health adaptation | Environmental choice            |                             |
|                                       | Body function                   |                             |
|                                       | Pressure regulation             |                             |
|                                       |                                 | Attention                   |

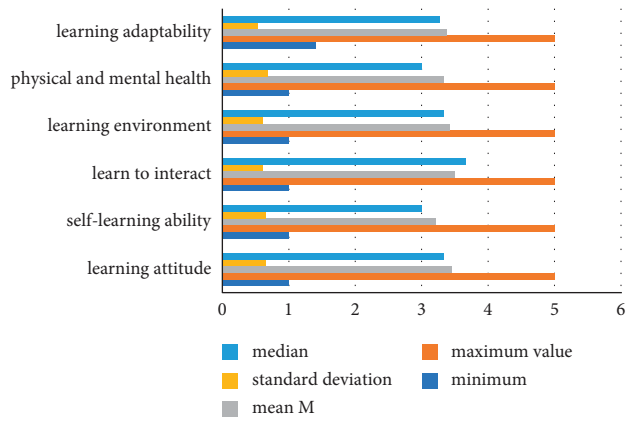


FIGURE 6: The adaptability of college students to English teaching under artificial intelligence.

first stage of the iteration, but the number of flames gradually decreases during the iteration. So, in the last iterative step, the butterfly only updates its position based on its ability to find the optimal position solution. Reducing the number of fires helps to cover the estimated cost of the search area, and the number of fires describing this process can be summed up as

$$N_{flame} = N - l \times \frac{N - 1}{T}, \quad (15)$$

$N$  is the maximum number of flames.  $l$  is the current number of repetitions.  $T$  is the maximum number of repetitions.

#### 4. Artificial Intelligence-Based English Self-Learning Effect Evaluation and Adaptive Impact Analysis

4.1. *Evaluation of English Self-Learning Effect and Adaptive Impact Research Supported by Artificial Intelligence.* The teaching of English has long been flawed, but the method of teaching English is unique. At present, English learning has a complete and mature software and hardware equipment, and human-machine learning is more interactive. The

artificial intelligence learning model improves learner autonomy and teaching performance in English courses, and enhances students' understanding of creativity and independent learning as well as lifelong learning. The ways for AI to learn English are shown in Table 1.

It can be seen from Table 1 that most people choose Tencent translator to learn English, of which 131 people use it, accounting for 64.9%; the use of the schoolbaglang robot is the lowest, and the number of users is 3, which is 1.5%. It shows that in the era of artificial intelligence, students are more inclined to learn independently in learning English, and the channels of seeking help in the learning process have increased, which is more convenient for students to manage time and environment as shown in Table 2.

As shown in Table 2, six students believed their school offered an AI course. It is 3%. 63 students think schools are using artificial intelligence to help them learn in the classroom. Among the 133 students, 31.2% and 65.8%, respectively, think that artificial intelligence has its place for additional training. Better present and understand the latest artificial intelligence and its applications to students, in order to apply them more effectively in the teaching of English courses as shown in Figure 4.

It can be seen from Figure 5 that the learning of artificial intelligence is conducive to after-school English review, preview before English class, improve the effect of English classroom learning, and impact assessment and self-reflection, and the mean size is 3.58, 3.41, 3.39, 3.11, and 2.92 as shown in Figure 5.

52% and 33% of students believe that artificial intelligence has a good effect on self-learning English, 8% believe that the learning effect is average, and 5% and 2% believe that the artificial intelligence is not good for self-learning English.

It can be seen in Figure 5 that students have a high evaluation of teaching AI, which also proves that AI played a good role in students' self-learning English. In the era of artificial intelligence, it is very convenient to repeatedly watch lecture videos or learning materials, and students can also shorten the distance through videos and other forms and adopt peer learning strategies and achieve more communication.

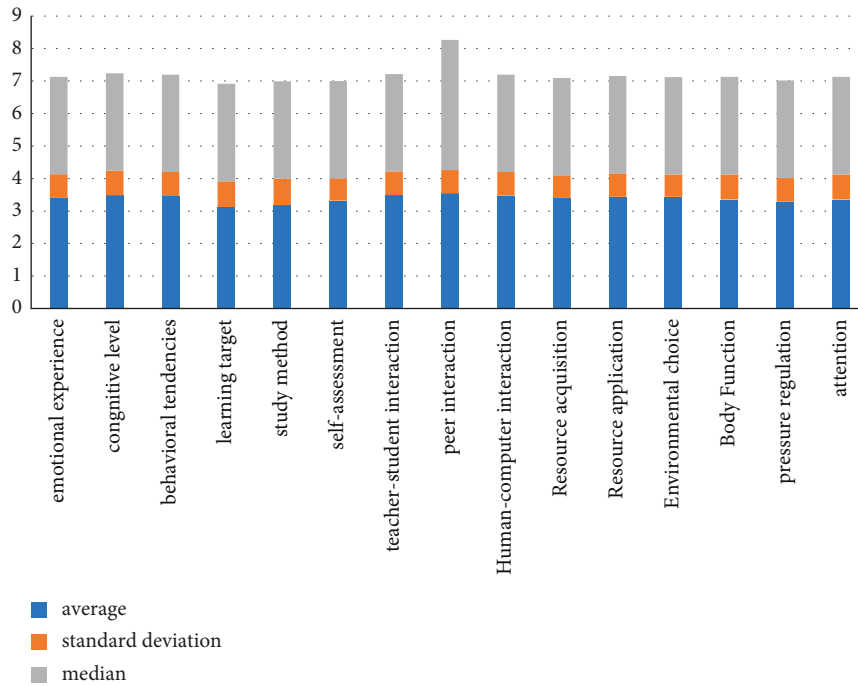


FIGURE 7: The adaptability of each variable in self-learning of artificial intelligence English for college students.

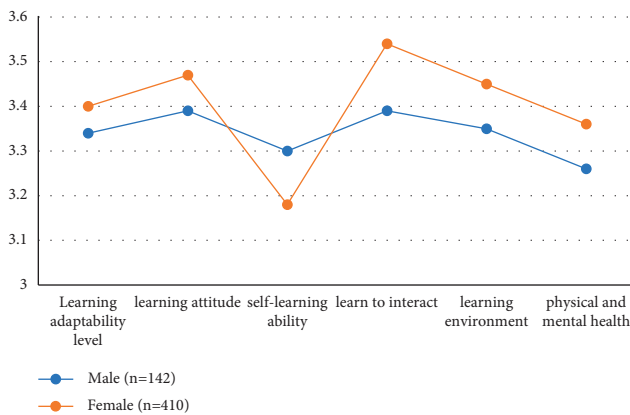


FIGURE 8: The self-learning adaptability of artificial intelligence for students of different genders.

Personalized AI is achieved by creating personalized learning plans based on educational goals, self-monitoring, final evaluation of the learning process, and teaching methods and strategies related to students' learning problems, as shown in Table 3.

Learning by artificial intelligence is collaborative learning between humans and machines, which requires a certain intellectual culture to adapt to student learning and the challenges of the future intelligent society. The experiment uses a score of "5 points." Based on the scores, we were able to distinguish between low fitness levels ( $1 \leq \text{moderate fitness} < 2$ ), normal fitness levels ( $2 \leq \text{moderate fitness} < 3$ ), and moderate levels. According to the score, we can distinguish four levels: low level of adaptability ( $1 \leq \text{fitness value} < 2$ ), normal level of adaptability ( $2 \leq \text{fitness value} < 3$ ), medium level of adaptability level

( $3 \leq \text{fitness value} < 4$ ), and high adaptability level ( $4 \leq \text{fitness value} < 5$ ). Students use artificial intelligence to score the adaptive grade of English autonomous learning. The general level of student adaptation to learning English and the various aspects of adaptation in support of AI are shown in Figure 6.

The results in Figure 6 show that the standard deviation is low and the data that can be analyzed are consistent. At present, the overall learning adaptability level of college students using AI to learn English is 3 to 4, the standard deviation is less than 1, and the sample dispersion is relatively low. The data are relatively small. This suggests that AI supports learning English. The overall level is relatively stable as shown in Figure 7.

The experimental results show that the students' learning goals have the lowest score, indicating that the English goals of AI students are not clear enough, and the learning goals let students know what to do or what to do. If students do not set learning goals before participating in AI learning, it is easy to reduce learning efficiency and even generate learning anxiety.

It can be seen in Figure 7 that the "learning goal" score is the lowest, which indicates that the students' goal of learning English using artificial intelligence is not enough. Setting learning goals can help people get a clear idea of what to do next. Teaching English using artificial intelligence offers students a wealth of English learning resources. If students do not set clear learning goals before they start learning English with AI, they will not have valuable information to learn, and learning will become easier. It can be distracting, reduce learning efficiency, and cause anxiety when learning English as shown in Figure 8.

Figure 8 shows that girls are significantly better at adapting to AI learning English than boys ( $M = 3.54$  for women  $> M = 3.39$  for men). However, on the parameter

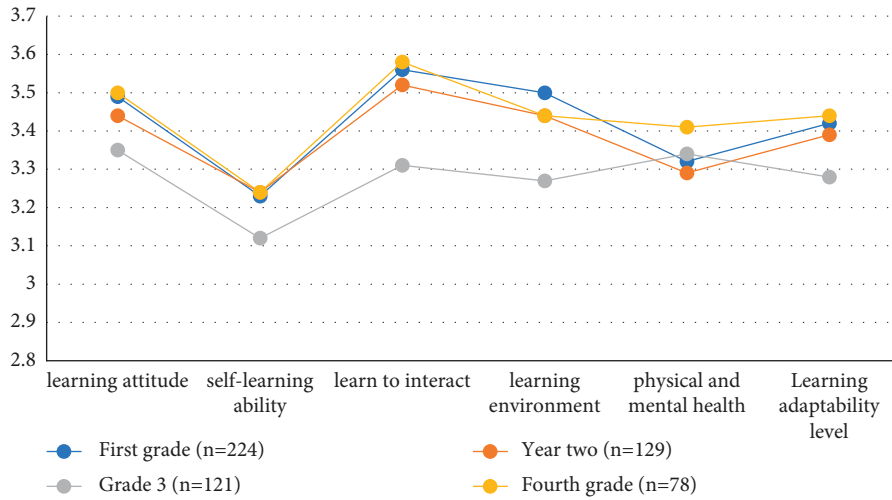


FIGURE 9: The self-learning adaptability of artificial intelligence for students in different grades.

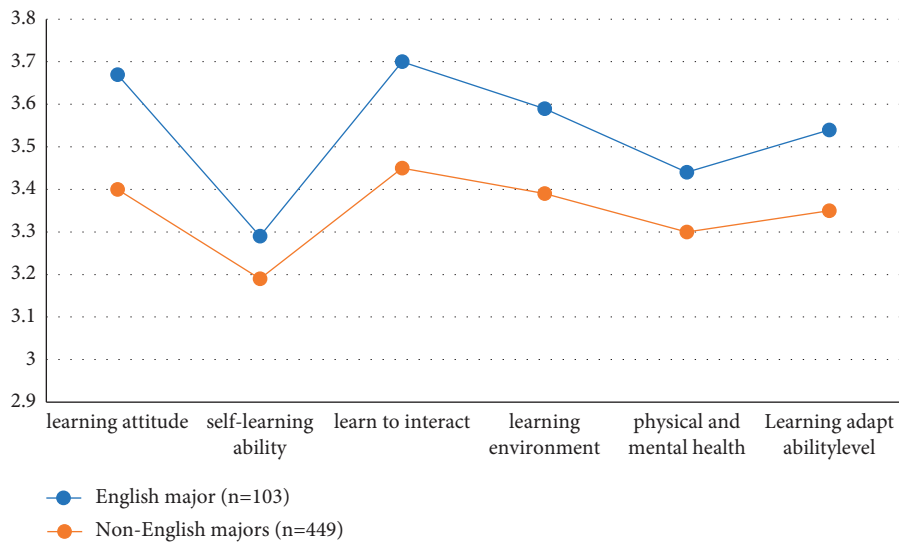


FIGURE 10: English/non-English major students' self-learning adaptability of artificial intelligence in English.

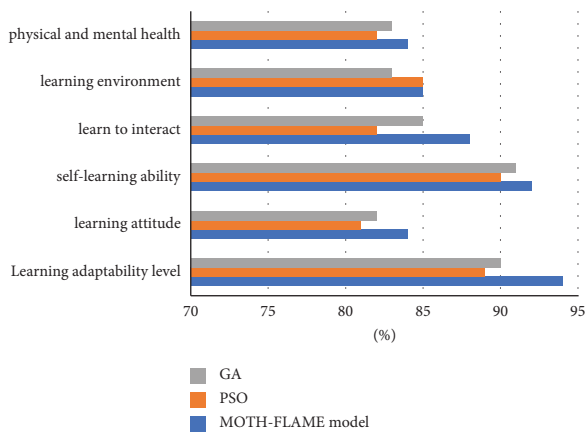


FIGURE 11: Comparison results of the model's adaptability to artificial intelligence English self-learning.

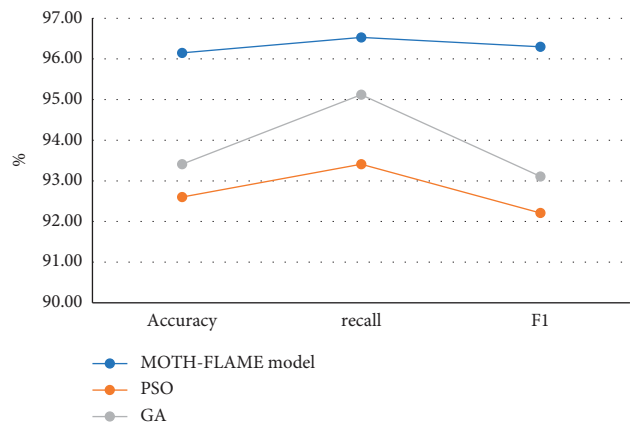


FIGURE 12: The performance of the model on different tests.

“self-learning ability,” men performed better than women as shown in Figure 9.

Figure 9 shows that when using artificial intelligence for teaching English, there is no big difference in the adaptability of learning English in different grades, but there are significant differences in “learning interaction” and “learning environment.” The fitness value of grade four is 3.44, grade one is 3.42, grade two is 3.39, and grade three is 3.28, but the learning adaptability of grade three students is significantly lower than that of other grades (Figure 10).

According to Figure 10, the English/non-English characteristics vary significantly in the level of adaptability to learning English self-taught AI, English majors ( $M = 3.59$ ), and non-English majors ( $M = 3.39$ ). The adaptability of English majors in AI English self-study is significantly higher than that of non-English majors. In order to reflect the practicability and accuracy of this model, we compare the MOTH-FLAME model used in this model with the GA and PSO model, two traditional machine learning algorithms, as shown in Figure 11.

From the comparison in Figure 11, it can be found that the average adaptability to self-learning English of the model established by MOTH-FLAME is 87.83%, while the average adaptability to self-learning of English of the model established by PSO is 84.83%, respectively. The average fitness values were 85.66%. Figure 12.

Comparing the experimental results, it can be known that the accuracy rate of using the MOTH-FLAME model reached 96.15%, while the recall rate and F1 also reached 96.53 and 96.3, while the accuracy rates of using the GA and PSO models were 93.41% and 92.60%, respectively. The recall rate was 95.12% and 93.415, respectively, and F1 was 93.11% and 92.21%, respectively. The prediction effect of the model established using MOTH-FLAME is generally much better than that of the model established using GA and PSO. This evaluation result fully demonstrates the innovation and practicability of the artificial intelligence optimization algorithm selected in this article.

## 5. Conclusion

Many schools in our country emphasize the culture of self-learning English, but this is not enough. I do not think so. First, there are not enough teachers in the schools, and the teachers are not responsible enough. The perfect teaching method is monotonous and retrograde, and students find English lessons interesting. Direct instruction gives poor results; students are too dependent on teachers, which prevent them from cultivating and developing their capacity for independent learning. Artificial intelligence can be used to cultivate students' stable and good mobility and improve the purpose and comprehensiveness of cognitive learning. By integrating AI into English teaching, students can improve and analyze data more effectively to facilitate learning.

## Data Availability

The experimental data used to support the findings of this study are available from the corresponding author upon request.

## Conflicts of Interest

The authors declare that they have no conflicts of interest regarding this work.

## References

- [1] Z. Hou, “Research on adopting artificial intelligence technology to improve effectiveness of vocational college English learning[J],” *Journal of Physics: Conference Series*, no. 4, p. 1744, 2021 (6pp), Article ID 042122.
- [2] Z. Chen, Y. Lian, and Z. Lin, “Research on business English autonomous learning based on artificial intelligence and improved BP network model,” *Journal of Intelligent and Fuzzy Systems*, no. 3, pp. 1–12, 2020.
- [3] C. Rack-In, “Jung-gil. An enhance scheme of effectiveness on lifelong education E-learning through application of artificial intelligence(AI),” *The Journal of Korean Institute of Information Technology*, vol. 10, no. 12, pp. 135–141, 2012.
- [4] Y. Wang, “An improved machine learning and artificial intelligence algorithm for classroom management of English distance education,” *Journal of Intelligent and Fuzzy Systems*, vol. 40, no. 29, pp. 1–12, 2020.
- [5] F. Zhang and M. She, “Design of English reading and learning management system in college education based on artificial intelligence,” *Journal of Intelligent and Fuzzy Systems*, no. 2, pp. 1–10, 2021.
- [6] M. H. Shin, “The effects of communication strategies for EFL students (Applying artificial intelligence) [J],” *Journal of Advanced Research in Dynamical and Control Systems*, vol. 10, no. 3, pp. 126–130, 2018.
- [7] A. Li and H. Wang, “An artificial intelligence recognition model for English online teaching[J],” *Journal of Intelligent and Fuzzy Systems*, vol. 40, no. 1, pp. 1–12, 2020.
- [8] J. S. Brown, A. Collins, G. Harris, I. Artificial, and L. Strategies, “- ScienceDirect,” *Learning strategies*, pp. 107–139, 1978.
- [9] M. Schemmer, P. Hemmer, and M. Nitsche, *A Meta-Analysis on the Utility of Explainable Artificial Intelligence in Human-AI Decision-Making*, vol. 60, no. 1, pp. 47–50, 2020.
- [10] R. Liu and Y. Zhan, “The impact of artificial intelligence on job insecurity: a moderating role based on vocational learning capabilities[J],” *Journal of Physics: Conference Series*, 2020.
- [11] W. J. Huang and M. U. Feng-Ying, “Factors Influencing English Learning Initiative of College Students of Non-English Major[J],” *Journal of Changchun University*, vol. 40, no. 4, pp. 14–20, 2013.
- [12] J. Yan-Ping, “U. Influencing Factors on Learning Motivation of College Students and Group Differences Based on Factor Analysis[J],” *Journal of Taishan University*, vol. 90, no. 1, pp. 102–105, 2019.
- [13] X. Wang and Y. Wu, “A Statistics Model for Influencing Factor Analysis of learning,” in *Proceedings of the 2011 3rd International Conference on Advanced Computer Control (ICACC)*, IEEE, Harbin, January 2011.
- [14] K. Sohn and O. Kwon, “Technology acceptance theories and factors influencing artificial intelligence-based intelligent products - ScienceDirect,” *Telematics and Informatics*, vol. 35, no. 5, pp. 14–20, 2020.

## Research Article

# Prediction and Industrial Structure Analysis of Local GDP Economy Based on Machine Learning

Zhiqiang Jiang 

*School of Business, Huaiyin Institute of Technology, Huaian 223001, China*

Correspondence should be addressed to Zhiqiang Jiang; 11130011@hyit.edu.cn

Received 29 July 2022; Revised 6 September 2022; Accepted 26 September 2022; Published 6 October 2022

Academic Editor: Man Fai Leung

Copyright © 2022 Zhiqiang Jiang. This is an open access article distributed under the Creative Commons Attribution License, which permits unrestricted use, distribution, and reproduction in any medium, provided the original work is properly cited.

The process of regional economic growth is a long-term evolutionary law. During this long evolutionary process, some regions may continue to grow, while others may fall into decline. It takes a long time. For example, from the perspective of our country's regional economic growth since the turn of the century, the east coast has been in a relatively developed state, while the economy of some western regions is relatively backward. Therefore, how to promote the long-term growth of developed regions and revitalize the troubled regional economy by studying the long-term growth mechanism of the regional economy is an important topic of regional economic research. In this context, we can draw the following conclusions. (1) The employment structure of major industries has been declining year by year since 2000, and this trend is relatively obvious and the decline is relatively large. Despite some changes in industrial growth, the overall trend is upward. The employment structure of the service industry has increased year by year, and its proportion in total employment usually exceeds that of major industries, and it is the industry with the largest number of employees. (2) The accuracy under the machine learning model is 79.46%, the reliability is 89.27%, and it is feasible; the accuracy under the data mining model is 68.45%, the reliability is 75.43%, and the feasibility is 86.18%; the accuracy rate under the traditional statistical model is 60.14%, the feasibility is 68.24%, and the reliability is 75.12%. GDP not only is the core indicator of national economic accounting but also can be used to measure the economic status and development level of a country or region. The impact of industrial structure on GDP is huge, and a suitable industrial structure can promote a healthier growth of GDP. In order to analyze the relationship between our country's GDP and industrial structure, the quantitative analysis method of grey correlation analysis is used to study it, and then according to the calculation results, suggestions for adjusting and optimizing the industrial structure will be put forward to the relevant ministries.

## 1. Introduction

In this survey, we review the work of machine learning on methods for dealing with datasets that contain large amounts of irrelevant information. We focus on two key issues: the problem of selecting relevant features and the problem of selecting relevant examples. We describe the progress made on these topics in empirical and theoretical work in machine learning and propose a general framework for comparing different approaches. We conclude with some challenges for future work in this field [1]. Interpretation of brain imaging experiments requires analysis of complex multidimensional data. In recent years, the use of machine learning algorithms has become an increasingly popular diagnostic technique for training classifiers to extract fMRI data of stimuli, mental

states, behaviors, and other variables of interest and to show that the data contain information about them. In reviewing this tutorial, we will understand some of the key options involved in using this technique and how to obtain statistically significant results, illustrating each point with a concrete example [2]. The repeatability and efficiency of the corner detector determines its likelihood of being useful in practical applications. Repeatability is important because the same scene viewed from different locations should yield features corresponding to the same real-world 3D location. Efficiency is important because it determines whether the detector combined with further processing can run at frame rate. The article describes three advances. First, we propose a new feature detection heuristic, and using machine learning, we derive a feature detector from it [3]. We review machine



learning methods using positive definite kernels. These methods formulate learning and estimation problems in reproducing kernel Hilbert spaces (RKHSs) of functions defined over the data domain and are extended in terms of kernels. Working in the linear space of functions facilitates the construction and analysis of learning algorithms, while allowing for large classes of functions. The latter includes non-linear functions as well as functions defined on non-vector data. We cover a wide range of methods, from binary classifiers to complex structured data estimation methods [4]. Feature selection algorithms fall into two broad categories: wrappers that use self-learning algorithms to rank features by their usefulness, and filters that rank features based on heuristics that share features in the data. For applications with large databases, filters have proven to be more practical than wrappers because they are much faster. However, most existing filtering algorithms are only suitable for discrete classification problems. The article describes a fast, correlation-based filter algorithm that can be applied to both continuous and discrete problems [5]. This article discusses factor models that use multiple real-time monthly and quarterly time series to forecast GDP growth in the short term. Factors are estimated using the EM algorithm with basic component estimators, taking into account the different time periods of the data and missing observations at the end of the sample. We discuss some characteristics of real-time estimator samples and provide an alternative approach to forecasting quarterly GDP using monthly ratios [6]. The article compares the performance of a monthly follower model GDP forecast based on time series of the French economy. These models are based on static and dynamic foundations obtained by time and frequency level methods. We question whether it is more appropriate to use aggregated or disaggregated data to derive the factors used in the prediction equations. The accuracy of the forecast for different forecast horizons was evaluated taking into account sliding and recursive patterns [7]. To forecast several epochs into the future, the modeler is faced with a choice: iterative one-step ahead forecasting (IMS technique), or directly model the relationship between observations separated by a periodic interval and use it for forecast (DMS forecast). Structural fractures, unit root non-stationarity, and residual autocorrelation are known to improve DMS accuracy in finite samples, all of which occurred when modeling South African GDP for the period 1965 to 2000 [8]. The impact of monetary policy on the economy has a long and variable lag, so policymakers need reliable forecasts of economic activity. As a result, forecasts of real GDP growth have become increasingly necessary. A new modified ARIMA model is proposed and used to predict China's GDP growth from 1978 to 2004 [9]. Aiming at the development of GDP in the process of urbanization in Zhoushan, establish a GDP measurement model in Zhoushan, open up the measurement relationship between the development of Zhoushan's marine economy and the statistical law of employment growth, and establish a GDP measurement model in Zhoushan. The impact of GDP growth on employment puts forward the predictable stimulating results of Zhoushan's marine economic development on employment, which provides theoretical and practical reference for promoting Zhoushan's

urbanization [10]. The growth of the total economic volume is based on the growth of various industrial sectors. The modern economic growth mode is essentially structure-oriented growth, that is, the core of economic growth is the change of industrial structure. The effectiveness of these factors directly affects economic growth. Therefore, it is very important to examine the impact of industrial scale and efficiency factors on economic growth from the perspective of industrial structure. Scholars at home and abroad have done a lot of research on this topic, using a lot of research methods [11]. Different industries and lifestyles use water in different ways, and different economic development models dramatically change water demand. Therefore, simultaneous (dynamic) analysis of macroeconomic and water resource systems can reveal their intrinsic links. Taking Beijing as an example, this paper analyzes the relationship between industrial structure adjustment and water consumption growth by using relevant theories and analytical methods. Therefore, it is very important to develop the integration of the tertiary industry and the secondary industry to solve the water shortage problem in Beijing [12]. The data from 1978 to 2004 are used as a sample to conduct an empirical analysis on the relationship between urbanization and industrialization. The results show that there is a long-term equilibrium relationship between China's urbanization and industrial structure. Different from their short-term relationship, the one-way Granger causality and their respective variances have inertia [13]. With the help of marine statistical data, the article examines the current situation and development trend of our country's marine industry structure. With the help of econometric methods such as correlation analysis and grey phenomenon theory, the essential factors affecting the growth of the shipping industry are clarified. According to the "Outline of National Marine Economic Development Plan," analyze industrial economy, industrial phenomenon theory, regional economy, and integration of shipping and agriculture, combined with structural problems and measures of our country's marine industry, to provide good technology for the development of marine industry in China [14]. The price structure of forest production in China from 1996 to 2009 was examined using grey relational analysis. Based on the GM(1.1) model, a data model for predicting China's forestry structure in the next 10 years was established. The results show that the grey correlation coefficients between the three forestry industries and forestry output value are 0.8491, 0.7311, and 0.8213, respectively, in the order of secondary industry < tertiary industry < large industry. The prediction results show that our country's forestry is in the middle stage of industrialization, and the secondary and tertiary industries have developed rapidly and become the main industries [15].

## 2. Analysis of Local Economic and Industrial Structure under Machine Learning

### 2.1. Problems Existing in the Economic and Industrial Structure

- (1) Convergence of regional industrial structure: that is, the similarity rate of industrial structure in the eastern, central, and western regions is relatively

high. To adjust our country's current industrial structure, we should follow the basic principles of combining market regulation and government guidance, improving the level of industrial technology through independent innovation, adhering to a new path of industrialization, and promoting the coordinated and healthy development of industries. Continue to promote the construction of energy, transportation, and communication infrastructure, accelerate the adjustment and optimization of industrial product structure, vigorously expand the tertiary industry to absorb labor employment as the main goal, and take practical and feasible adjustment measures.

- (2) According to the actual situation of each region, actively learn from advanced experience, rely on high-quality industries, optimize and adjust the industrial structure, and greatly improve the economic level of the whole region.

With the continuous growth of the economy, capital and labor are transferred to the secondary or tertiary industries, which leads to changes in the industrial structure of the regional economy. The three industries are not coordinated. Development is modernization and industrial transformation. Years of practical experience in adjusting the regional economic and business structure have shown that in the face of these two problems, we must take a holistic approach. For a long time, the primary and secondary industries have been the main body of the market. In order to change the backward situation of our country's "manufacturing industry," actively promote industrial innovation and increase the market share of the tertiary industry. In the process of development and reform, we adhere to the principle of "less but fine" and pay attention to the actual level and standard of the business as well as the structure of the industry. According to the actual situation of each region, actively learn from advanced experience, rely on high-quality industries, optimize and adjust the industrial structure, and greatly improve the economic level of the whole region. It is shown in Figure 1.

**2.2. Adjustment Direction of Regional Economic and Industrial Structure.** Industry is the most important sector supporting the national economy. As the main body of the national economy, the county economy should pay more attention to the development of industrialization. It is also the main direction of today's industrial transformation and meets the needs of our country's economic development. Due to the different economic conditions and industrial development levels in different countries, the actual adaptation process must be realistic and not be successful too quickly but must be gradually improved in industrialized industries. Considering that the current industry is developing in the direction of adapting to the county economy and business structure, we think there are mainly the following reasons. (1) The development of the service industry and service industry is inseparable from industrial support. It is necessary to use the

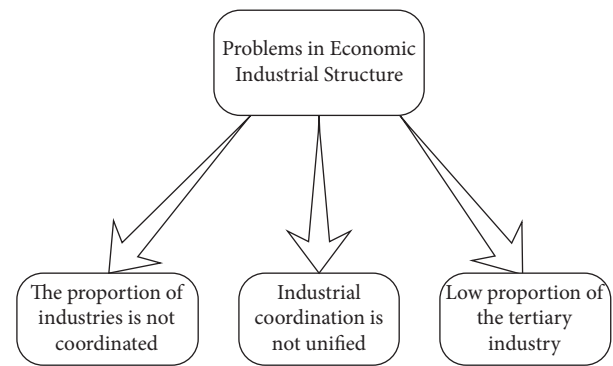


FIGURE 1: Problems existing in the economic and industrial structure.

service industry to drive social concerns and promote economic development and structural adjustment. (2) The demand for service industry in small areas is lower than that in cities. The development of service industry needs to effectively manage the type and scale of service industry in combination with regional characteristics. The over-allocation and waste of resources in the province have created a harsh environment for market competition. (3) According to relevant data, the economic benefits of the manufacturing industry are among the best in many industries, and it has obvious development advantages in terms of national taxation and employment, providing a circular economy for the sustainable development of the industry. Regional industries realize high stability of circular economy. When the state manages the economic restructuring of the whole province, industry not only has an important impact on economic development but also has a good leading role in other industries. The development of high-quality industries can guide many industries, such as the service industry, and is the primary choice for industrial restructuring and development.

**2.3. Breakthroughs in Industrial Structure Adjustment from Key Positions.** Under the new situation, the phenomenon of overcapacity is mainly manifested in the process of regional adaptation of the economic and commercial structure, which exists objectively and is not a random phenomenon. Recovery will come at a huge price. In the process of economic manufacturing, some regional industries do not do temporary work well without new production technology and unique profile products, which brings great challenges to the industry. The following points are investigated and evaluated. (1) From the beginning, comprehensively plan the existing business in the region and implement the upgrading and renewal of the industry based on this. Actively respond to the government's call and adhere to the development policy of "focusing on development, common improvement, and comprehensive coordination." In the early stage before the actual operation, it is necessary to make preparations on the basis of the existing business structure, put forward the basic development policy, and select industries and enterprises for modernization and innovation. Initially, it focused on technological innovation, equipment upgrades, and product improvements to simplify the process, improve

economics, and realize it. Find and deliver the most accurate and personalized guidance to help you succeed. (2) Focus on promoting and developing the industry. Strengthen the improvement of basic equipment and core technologies of relevant enterprises and focus on scientific and technological research and product innovation research. At present, the regionalized production of a large number of imported high-tech equipment and materials in our country not only increases the production cost but also wastes a lot of financial resources. Therefore, it is necessary to actively support the development of science and technology, organize high-tech talents to participate in scientific and technological innovation, participate in major achievements and technologies, and reduce the impact of monopoly technology on enterprise development. Of course, development is inseparable from cooperation and active technological integration. We must focus on promoting the transformation of primary and secondary industries to high-level industries and promote economic and industrial restructuring.

**2.4. Economic and Industrial Forecasting Steps.** Economic forecasts are speculations and estimates of future scenarios for economic phenomena. According to the history and status quo of the economic development process, the scientific forecasting method shows the regularity of the development of economic phenomena and the connection between various economic phenomena and predicts the future development trend and the possible level of the economic phenomenon. The content of economic forecast is very broad: the first is the forecast of domestic economic situation, such as production development, growth rate, economic structure, price development, population employment, tax revenue and expenditure development, supply, production, and sales. At the same time, the international economic situation should also be taken into account, such as the prediction of international economic fluctuations and changes in the international market in region B. Your forecast usually consists of four steps: collecting and analyzing the various data required for the forecast, performing various forecast calculations to outline the preliminary forecast, completing and revising the forecast, and preparing a formal forecast report. The above process is a recurring prognostic process. This cycle typically occurs twice a year, and a forecast report is generated approximately every six months. It is shown in Figure 2.

**2.5. Keep Improving and Become Bigger and Stronger.** As part of the structural adjustment, special jobs should be reserved for regional industries. The Swiss watch industry, for example, is small but has unique high-end brands that have huge growth advantages. We must actively learn from and learn from, focus on developing high-quality industries, make them bigger and stronger, promote industrial transformation, and promote the integration of regional economy and industrial structure. Our country believes that it is very important to adjust the economic and industrial structure of the region, overcome technical difficulties, and vigorously carry out scientific research. At the same time, it is necessary

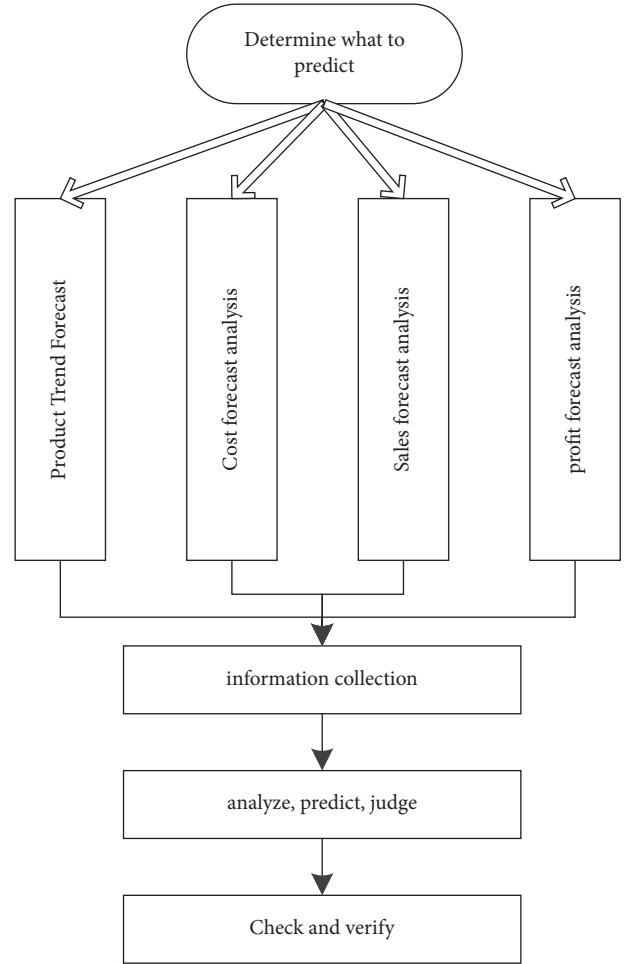


FIGURE 2: Economic and industrial forecasting steps.

to fill the gaps in core industries, closely follow the characteristics of industries, make them bigger and stronger, and actively promote the process of regional economic and trade structure integration.

### 3. Machine Learning Algorithms

**3.1. Classical Machine Learning Algorithms.** KNN algorithm, random forest algorithm, and SVM algorithm are three classic machine learning algorithms in supervised learning. They are commonly used in various intrusion detection scenarios. This section mainly introduces their respective classification ideas. If most of  $K$ 's nearest neighbors belong to a particular class, then the sample also belongs to that class, and that class contains the properties of that sample. The distance formula to calculate the distance between two samples is

$$L_p(x_i, x_j) = \left( \sum_{l=1}^n |x_i - x_j|^p \right)^{1/p}, \quad (1)$$

$$F(x) = \begin{cases} -1, & g(x), \\ +1, & \text{otherwise.} \end{cases} \quad (2)$$

In this attack scenario, the attacker aims to collect proxy records containing malicious samples and normal samples and find out the feature vector space of the target model and the corresponding information parameter vector. If most of  $K$ 's nearest neighbors belong to a particular class, then the sample also belongs to that class, and that class contains the properties of that sample. After the calculation of the result formula (2), the accuracy of the classical machine learning algorithm will be improved even more.

In this case, attackers typically manipulate malicious samples according to conditional probability distributions or feature space distances to get as close as possible to the protected data.

$$\begin{aligned} z^* &= \arg \min g(x) \\ &= \arg \min \omega^T x^j. \end{aligned} \quad (3)$$

Accuracy is the percentage of correctly predicted samples to the total number of samples; response rate is the ratio of the number of positive samples found to the total number of positive samples, reflecting insufficient sample coverage; percentage accuracy means that all predicted positive samples are true. The proportion of positive samples may reflect the problem of false positives. The  $F1$  score is the harmonic mean of recall and precision and is the combined score of recall and precision. The calculation formulas of the four indicators of accuracy, accuracy, recall, and  $F1$  score are as follows:

$$\begin{aligned} \text{accuracy} &= \frac{TP + TN}{TP + FN + FP + TN}, \\ \text{precision} &= \frac{TP}{TP + FP}, \\ \text{recall} &= \frac{TP}{TP + FN}, \\ F1_{\text{score}} &= 2 * \frac{\text{precision} * \text{recall}}{\text{precision} + \text{recall}} \end{aligned} \quad (4)$$

In order to improve the classification accuracy, the corresponding loss function is often developed, and the optimal weight value and paranoia value of the function are obtained by finding the maximum value of the function:

$$\begin{aligned} \min L &= \min \frac{\omega^2}{2} + c \sum_{i=1}^n \max(0, 1 - y_i g(x_i)), \\ \min L &= \min \frac{\omega^2}{2} + c \sum_{i=1}^n \max(0, 1 - y_i (w^T x_i + b)), \\ \text{s.t. } \frac{\sum_{i=1}^d (w_i - w)^2}{k} &\leq w_t. \end{aligned} \quad (5)$$

**3.2. KNN Algorithm Model.** The KNN algorithm continuously finds the best values of  $w$  and  $b$  during the analysis process, so that the loss of the function reaches the lowest

value. The training process randomly assigns final weights. The training process randomly assigns final weights. This training method has no problem in the natural environment, but in a conflict situation, you will be attacked. Attackers can take advantage of this and create malicious samples appropriately to misclassify them. The output can be a combination of several binary decisions, such as whether to evaluate a pixel as the foreground and background of the image, or a more structured output such as a syntax tree or containing box. Multiple binary outputs can simply be represented by multiple independent SVMs.

$$\begin{aligned} \nabla_{\omega} L &\cong \omega + c \sum_{ies} \nabla_l^i x_i, \\ \nabla_{\omega} L &\cong c \sum_{ies} \nabla_l^i. \end{aligned} \quad (6)$$

To visualize the security of classification algorithms, a new concept is introduced here: classifier sensitivity. The higher the sensitivity of the classification, the less secure the algorithm, and vice versa. The security of this algorithm is described as follows:

$$\begin{aligned} \Delta F(x, x') &= \frac{F(x) - F(x')}{||x - x'||} \leq \frac{1}{k} \sum_{K=1}^K |\omega_k|, \\ \frac{dy}{dt} &= ky[y - y_i], \end{aligned} \quad (7)$$

$$C_j = \left( \frac{\sum_{i \in c_j} t_i}{i \sum_{i \in c_j} t_i} \right).$$

When a user selects a service that is interested in interaction, the relevant information of the service can be retrieved, and changes in the community to which the service belongs are highlighted in the adjacent spatiotemporal dimensions.

**3.3. K-Means Machine Learning Model.** The K-means algorithm is an unsupervised learning algorithm that can be applied to unlabeled data. The goal of the algorithm is to find datasets whose number is determined by  $K$ . The algorithm iteratively assigns data to one of  $K$  groups based on the provided features. Group data based on data similarity. In the network model of the query system, the prescribed fusion rules are used to integrate the interactive big data of the educational administration system, so as to realize the interactive query of the big data.

The convergence control function of the interactive big data query in the educational administration system is

$$F(t) = \sum_{j=1} z_j T + (h - f)^2 - \sin(2\pi t), \quad (8)$$

where  $h$  represents the characteristic sampling frequency of the educational administration system and  $f$  is the information transmission rate of the educational administration system data query. The output can be a combination of several binary decisions, such as whether to evaluate a pixel

as the foreground and background of the image, or a more structured output such as a syntax tree or containing box. Multiple binary outputs can simply be represented by multiple independent SVMs.

Based on this, the window width of the interactive big data transmission of the educational administration system is calculated. The calculation formula is

$$u_m = \sum_{j=1} z_j T \sqrt{y+q} - F(t), \quad (9)$$

where  $y$  is the time delay of data transmission and  $q$  is the hidden node of data transmission. Using the adaptive deep learning method, the transmission frequency of interactive big data query data in the educational administration system is obtained as follows:

$$\phi = -\frac{\pi F(t)^2}{\sqrt{y+q}} + \frac{\log_3 \eta + S^2}{c+q}. \quad (10)$$

In the formula,  $\phi$  is the gradient error of data transmission;  $r$  is the iterative step size of deep learning. Through the method of reconstructing the similarity feature of the target sample set, the deep learning of the interactive big data model of the educational administration system is realized, and the global optimal control function of the model is obtained as follows:

$$Y = \sum_{n=1, t=1} \mu_n r + \left[ o - p(t) + \frac{p(y)}{2t\pi} \right]^2, \quad (11)$$

where  $o$  is the step size of adaptive learning. Finally, the optimal model of interactive big data in the educational administration system is obtained as follows:

$$F(k) = F(t) + \sum_{n=1, t=1} \mu_n r - p(t). \quad (12)$$

## 4. Prediction and Industrial Structure Analysis of Machine Learning in Local GDP Economy

*4.1. Local GDP Economic Forecast under Machine Learning.* The process of regional economic growth is a long-term evolutionary law. During this long evolutionary process, some regions may continue to grow, while others may fall into decline. It takes a long time. For example, from the perspective of our country's regional economic growth since the turn of the century, the east coast has been in a relatively developed state, while the economy of some western regions is relatively backward. Therefore, how to promote the long-term growth of developed regions and revitalize the troubled regional economy by studying the long-term growth mechanism of the regional economy is an important topic of regional economic research. Only population, wages, prices, resources, technology, and income distribution affect the long-term growth of regional economies. The flow of these factors, especially the flow of labor and capital, has a greater impact on regional economic growth. The determinants of regional growth can be divided into endogenous and

exogenous factors. The main endogenous factors are the distribution and supply of production factors, such as the distribution and supply of land, labor, and capital. The main external factors are related to the evolution of commodity demand within the region, national investment, and national economy. According to the endogenous and exogenous elements of regional growth and their combinations, from the perspective of integrity and decentralization, distinguish complex models of regional growth, decentralization systems, regional convergence or differentiation growth issues, and social and political factors.

From the data in Figure 3, we can see that from 2017 to 2021, Guangdong Province and Tianjin City have a relatively large number of marine economic structures, indicating that their marine economic structures are more diversified, their marine economic development is relatively stable, and their economic structure is relatively stable. It has not changed much. The marine economy and industrial structure of Liaoning and Shandong have relatively few direct descendants, indicating that the value of marine industry products is relatively concentrated in one or more industries. The industry and business structure dominated by sea fishing will be simplified. The structure is strongly influenced by changes in several major industries, resulting in large fluctuations in overall development and relatively unstable economic development. The number of direct descendants of the industrial structure changed greatly. The impact of Liaoning and Shandong's marine economy and industrial structure is relatively small compared with the previous few years, indicating that the marine economic structure was relatively simple at this time. The industrial structure of different provinces is quite different, which leads to the great fluctuation of the entropy of economic structure in different years. In 2021, the entropy of economic structure in each province is the highest, which indicates that the industrial structure is multidimensional. The large fluctuation in different years indicates that the industrial structure fluctuates greatly in different years, and the structure develops in multiple dimensions. When the change of the entropy of economic structure is small, it shows that the industrial structure depends on less industries.

From the data in Figure 4, we can see that the accuracy under the KNN machine learning model is 79.46%, the feasibility is 89.27%, and the model score is 93.45%; the accuracy under the K-means machine learning model is 68.45%, the feasibility is 75.43%, and the model score is 86.18%; the accuracy under the FM machine learning model is 60.14%, the feasibility is 68.24%, and the model score is 75.12%. The KNN machine learning model has the highest accuracy and feasibility among the three models and is the best performing model among the three models.

From the data in Figure 5 and Table 1, we can see that the actual value of GDP from 2016 to 2021 shows a steady upward trend, and the predicted values under different machine learning models are different. The predicted value of the s-svm model in 2016 was 48188, the predicted value of the K-means model was 47523, and the predicted value of the FM model was 47131; the predicted value of the s-svm model in 2017 was 51469, and the prediction number of the

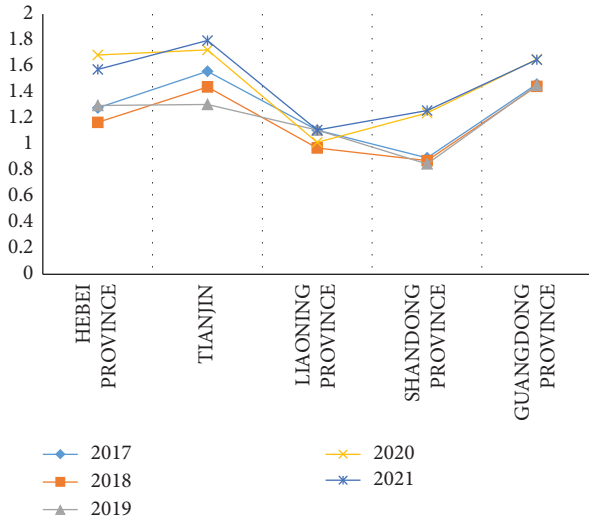


FIGURE 3: Calculation table of the number of direct descendants of the economic and industrial structure in different regions.

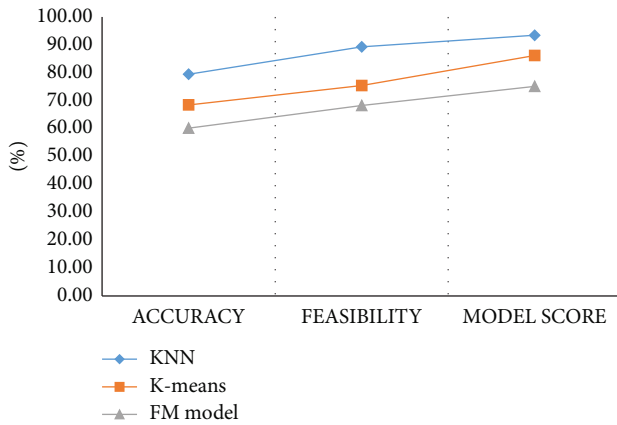


FIGURE 4: Performance tests under different machine learning models.

K-means model is 50279, and that of the FM model is 49946; the prediction number of the s-svm model in 2018 is 56751, that of the K-means model is 55361, and that of the FM model is 54988. In 2019, the number of predictions of the s-svm model is 61516, the number of predictions of the K-means model is 61109, and the number of forecasts of the FM model is 60723. It can be seen that the s-svm model and the predicted values are the closest to the actual values, and the error rate is the smallest. The prediction value of the s-svm model is the closest to the real value in the prediction value of GDP by different algorithms. The prediction accuracy rate can reach more than 96%, and the highest is 99%, which has a high prediction effect. The prediction effect of FM model is poor, and the average prediction accuracy is about 95%. Different models have obvious differences and advantages in predicting GDP growth. Therefore, the S-SVM model has a good application effect in the prediction of GDP.

From the data in Figure 6, we can see that in 2011, the GDP of expenditure was 188.61, consumption expenditure was 136.56, household consumption was 114.13, and

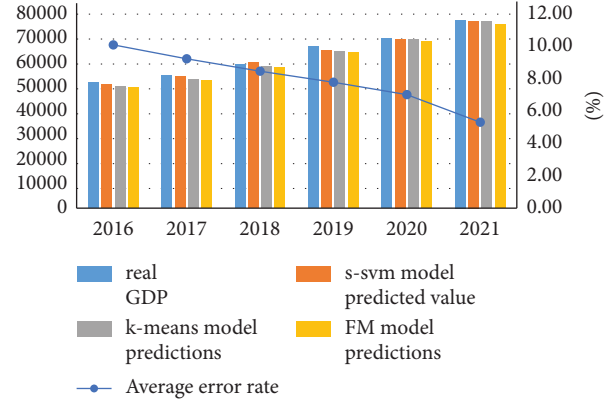


FIGURE 5: GDP forecast and actual GDP under machine learning.

government consumption was 22.43; expenditure GDP was 229.31, consumption expenditure was 164.26, household consumption was 137.32, and government consumption was 26.94. In 2014, expenditure GDP was 242.32, consumption expenditure was 185.47, household consumption was 157.70, and government consumption was 27.77.

**4.2. Forecast and Industrial Structure Analysis in Local GDP Economy.** According to the input-output theory and related mathematical models, most countries in the world began to make input-output tables, and countries began to flexibly use the output model to analyze many important issues of national development. Our country is no exception. The input-output table is used to analyze the relationship between different sectors and end-user sectors in our country to understand the state of economic development. Therefore, many professors and researchers have devoted their efforts to describe the application and analysis of the EC + IO model in our country's economic development. However, since our country does not compile the input-output table every year, we can make statistical improvements to the input-output table for the years that have not been compiled on the original basis. The yearbook data then calculate the overall performance of each department for each year. Compared with previous test results, our test will be more comprehensive, not bound by personal thoughts, and presented to the public more objectively and fairly. From the perspective of the country, it can be viewed more modestly and cautiously, and from the perspective of the troops, it can also be a more objective and fair analysis, which helps to better understand the development of our country. Therefore, the analysis of our country's input-output table is very important for the country and the masses.

From the data in Figure 7 and Table 2, we can see that the employment structure of major industries has been declining year by year since 2000, and this trend is relatively obvious and the decline is relatively large. Despite some changes in industrial growth, the overall trend is upward. The employment structure of the service industry has increased year by year, and its proportion in total employment usually exceeds that of major industries, and it is the industry with the largest number of employees. Judging from the

TABLE 1: 2016–2021 GDP forecast and actual GDP under machine learning.

|      | Real GDP | s-svm model predicted value | K-means model predictions | FM model predictions | Average error rate (%) |
|------|----------|-----------------------------|---------------------------|----------------------|------------------------|
| 2016 | 48946    | 48188                       | 47523                     | 47131                | 9.56                   |
| 2017 | 51751    | 51469                       | 50279                     | 49946                | 8.74                   |
| 2018 | 56197    | 56751                       | 55361                     | 54988                | 8.02                   |
| 2019 | 62966    | 61516                       | 61109                     | 60723                | 7.37                   |
| 2020 | 66309    | 66082                       | 65912                     | 65196                | 6.65                   |
| 2021 | 73438    | 73008                       | 72834                     | 71793                | 5.03                   |

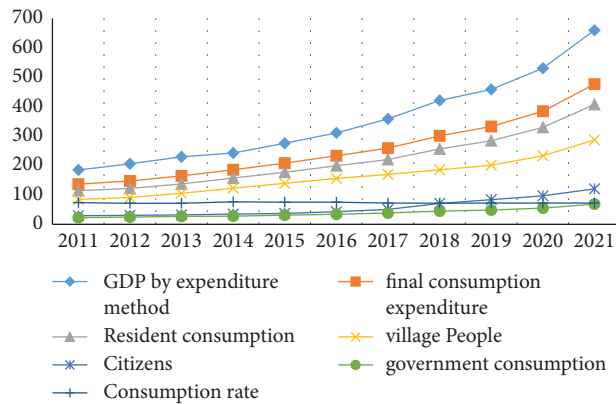


FIGURE 6: 2011–2021 GDP of consumer expenditure in different regions.

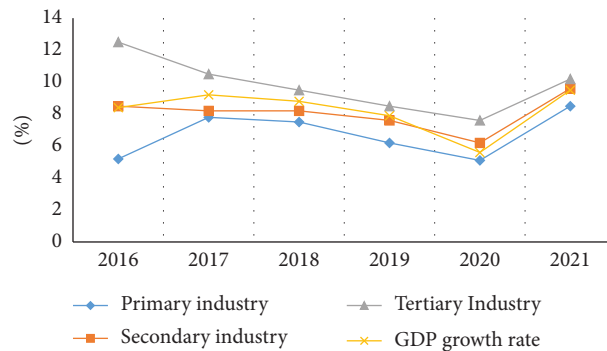


FIGURE 7: Three changes in industrial structure.

TABLE 2: Three changes in industrial structure.

|      | Primary industry (%) | Secondary industry (%) | Tertiary industry (%) | GDP growth rate (%) |
|------|----------------------|------------------------|-----------------------|---------------------|
| 2016 | 5                    | 8.50                   | 12.50                 | 8.40                |
| 2017 | 7.80                 | 8.20                   | 10.50                 | 9                   |
| 2018 | 7.50                 | 8.20                   | 9.50                  | 8.80                |
| 2019 | 6.20                 | 7.60                   | 8.50                  | 7.90                |
| 2020 | 5.10                 | 6.20                   | 7.60                  | 5.60                |
| 2021 | 8.50                 | 9.60                   | 10.20                 | 9.50                |

development situation at home and abroad, the employment structure of our country’s primary industry is still relatively high, the level of agricultural mechanization is insufficient, the employment of the processing industry is obviously sufficient and relatively insufficient, the industrialization still needs to be improved, and the service scope bears the heavy burden of work and needs to be vigorously developed. It needs to continue to grow, and the entire industry structure

also needs to be optimized and improved. From 2016 to 2021, we can see that the GDP growth rate of the region is still relatively high, basically higher than the national growth level. Especially in the past two years, the national growth rate is relatively low, and the GDP growth rate of the region maintains a certain advantage. In the three industrial structures, the proportion of secondary industry is relatively large, and the contribution of growth rate and GDP growth

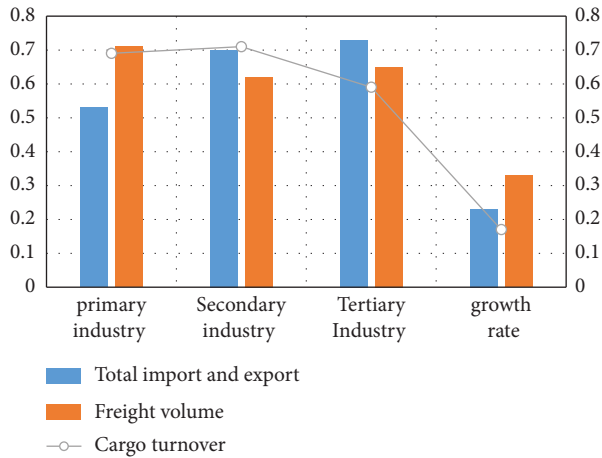


FIGURE 8: The proportion of industrial structure and its predicted value under the machine learning model.

rate is relatively large. In the whole economic structure, different industries have maintained positive growth, so it is necessary to adjust the industrial development strategy for the primary industry and then provide intelligent upgrading services for the primary industry.

From the data in Figure 8, we can see that the actual proportion of the first industry is 23%, the proportion of the second industry is 33%, and the proportion of the third industry is 17%. The proportion of the primary industry predicted by the s-svm model is 26.53%, the proportion of the primary industry predicted by the K-means model is 27.38%, and the proportion of the primary industry predicted by the FM model is 28.91%. It can be seen that the prediction value under the s-svm model is the most accurate among the three models.

## 5. Conclusion

The process of regional economic growth is a long-term evolutionary law. During this long evolutionary process, some regions may continue to grow, while others may fall into decline. It takes a long time. For example, from the perspective of our country's regional economic growth since the turn of the century, the east coast has been in a relatively developed state, while the economy of some western regions is relatively backward. Therefore, how to promote the long-term growth of developed regions and revitalize the troubled regional economy by studying the long-term growth mechanism of the regional economy is an important topic of regional economic research.

## Data Availability

The experimental data used to support the findings of this study are available from the corresponding author upon request.

## Conflicts of Interest

The author declares that there are no conflicts of interest regarding this work.

## References

- [1] C. Andrieu, N. de Freitas, A. Doucet, and M. I. Jordan, "An introduction to MCMC for machine learning," *Machine Learning*, vol. 50, no. 1/2, pp. 5–43, 2003.
- [2] F. Pereira, T. Mitchell, and M. Botvinick, "Machine learning classifiers and fMRI: a tutorial overview," *NeuroImage*, vol. 45, no. 1, pp. 199–S209, 2009.
- [3] I. H. Witten, E. Frank, and M. Hall, "Data mining: practical machine learning tools and techniques, third edition (the morgon kaufmann series in data management systems)," *Acm Sigmod Record*, vol. 31, no. 1, pp. 76–77, 2002.
- [4] E. Rosten, R. Porter, and T. Drummond, "Faster and better: a machine learning approach to corner detection," *IEEE Transactions on Pattern Analysis and Machine Intelligence*, vol. 32, no. 1, pp. 105–119, 2010.
- [5] T. Hofmann, B. Schölkopf, and A. J. Smola, "Kernel methods in machine learning," *Annals of Statistics*, vol. 36, no. 3, 2008.
- [6] C. Schumacher and J. Breitung, "Real-time forecasting of German GDP based on a large factor model with monthly and quarterly data," *International Journal of Forecasting*, vol. 24, no. 3, pp. 386–398, 2008.
- [7] K. Barhoumi, O. Darné, and L. Ferrara, "Are disaggregate data useful for factor analysis in forecasting French GDP," *Journal of Forecasting*, vol. 29, no. 1–2, pp. 132–144, 2010.
- [8] G. Chevillon, "Multi-step forecasting in emerging economies: an investigation of the South African GDP," *International Journal of Forecasting*, vol. 25, no. 3, pp. 602–628, 2009.
- [9] Y. Konchitchki and P. N. Patatoukas, "Taking the pulse of the real economy using financial statement analysis: implications for macro forecasting and stock valuation," *The Accounting Review*, vol. 89, no. 2, pp. 669–694, 2014.
- [10] W. Chihiro, N. Kashif, and T. Yuji, "Measuring GDP in the digital economy: increasing dependence on uncaptured GDP," *Technological Forecasting and Social Change*, vol. 137, Article ID 0040162517313380, 2018.
- [11] H. Zhou, H. E. Guangshun, and X. Wang, "The analysis of ocean industrial structure and the optimized industrial policies in our country," *Marine Science Bulletin*, vol. 24, no. 2, pp. 46–51, 2005.
- [12] G. T. Weng, S. Hu, and Y. L. Wen, "Grey prediction analysis on forestry industrial structure of China," vol. 3, no. 1, pp. 27–29, 2011.
- [13] Y. Guan and M. Li, "Analysis on the degree of the industrial structure's impact on the energy consumption—Based on empirical study of Guangdong Province – ScienceDirect," *Energy Procedia*, vol. 5, no. 1, pp. 1488–1496, 2011.
- [14] L. I. Aimin and A. Wang, "An extension analysis on the urban industrial structure," *Journal of Chongqing Normal University*, vol. 29, no. 6, pp. 105–108, 2012.
- [15] B. Cui, "Analysis on correlation between China's industrial structure and export commodity structure," *Finance & Economics of Xinjiang*, vol. 47, no. 3, pp. 110–129, 2006.



## Retraction

# Retracted: A Study on the Usefulness of Stochastic Simulation Algorithms for Teaching and Learning in College Physical Education Classrooms

### Mathematical Problems in Engineering

Received 18 July 2023; Accepted 18 July 2023; Published 19 July 2023

Copyright © 2023 Mathematical Problems in Engineering. This is an open access article distributed under the Creative Commons Attribution License, which permits unrestricted use, distribution, and reproduction in any medium, provided the original work is properly cited.

This article has been retracted by Hindawi following an investigation undertaken by the publisher [1]. This investigation has uncovered evidence of one or more of the following indicators of systematic manipulation of the publication process:

- (1) Discrepancies in scope
- (2) Discrepancies in the description of the research reported
- (3) Discrepancies between the availability of data and the research described
- (4) Inappropriate citations
- (5) Incoherent, meaningless and/or irrelevant content included in the article
- (6) Peer-review manipulation

The presence of these indicators undermines our confidence in the integrity of the article's content and we cannot, therefore, vouch for its reliability. Please note that this notice is intended solely to alert readers that the content of this article is unreliable. We have not investigated whether authors were aware of or involved in the systematic manipulation of the publication process.

Wiley and Hindawi regrets that the usual quality checks did not identify these issues before publication and have since put additional measures in place to safeguard research integrity.

We wish to credit our own Research Integrity and Research Publishing teams and anonymous and named external researchers and research integrity experts for contributing to this investigation.

The corresponding author, as the representative of all authors, has been given the opportunity to register their

agreement or disagreement to this retraction. We have kept a record of any response received.

### References

- [1] J. Xu, "A Study on the Usefulness of Stochastic Simulation Algorithms for Teaching and Learning in College Physical Education Classrooms," *Mathematical Problems in Engineering*, vol. 2022, Article ID 2779909, 6 pages, 2022.

## Research Article

# A Study on the Usefulness of Stochastic Simulation Algorithms for Teaching and Learning in College Physical Education Classrooms

Ju Xu 

Art and Sports Department, Henan College of Transportation, Zhengzhou 450005, China

Correspondence should be addressed to Ju Xu; [xuju498962466@hncc.edu.cn](mailto:xuju498962466@hncc.edu.cn)

Received 12 April 2022; Accepted 13 May 2022; Published 23 September 2022

Academic Editor: Hangjun Che

Copyright © 2022 Ju Xu. This is an open access article distributed under the Creative Commons Attribution License, which permits unrestricted use, distribution, and reproduction in any medium, provided the original work is properly cited.

In order to address the problem of the absolute nature of the evaluation of superiority and inferiority in the evaluation of physical education classroom in universities and the problem of inconsistency in the conclusion of multiple evaluations, we develop an “autonomous advantage evaluation method to highlight one’s own advantages,” which uses a probabilistic stochastic simulation algorithm to evaluate the advantages of the evaluated objects by calculating the degree of superiority among them. The method is based on an innovative “base to top” approach, with a high degree of independence. The method was validated by means of an algorithm, and the conclusions were obtained with probabilistic information.

## 1. Introduction

University students are the future pillars of our country, and it is only when they have a healthy body that they can be most creative and create more value. Therefore, it is very important for universities to provide physical education to students [1]. The health of students is reflected in all aspects of their lives, and physical education is an integral part of it, as learning more about physical education and acquiring skills through practical application can enhance students' physical fitness [2]. The Ministry of Education is paying more and more attention to the health of students, requiring universities to make reasonable physical education programs to improve the physical fitness of students, and according to the regulations, each school is constantly correcting and improving its teaching methods, and gradually tends to diversify and enrich the teaching content [3–5]. Therefore, it is important to evaluate the quality of physical education in order to judge the quality of teaching and learning [6–8]. Data mining is a popular data analysis technology that has received widespread attention. This technology can use known data resources to discover more potential information and the connection between things, firmly grasp this technology and apply it to the evaluation of the quality of physical education in college students, you can find out the

factors affecting the quality of physical education and effectively enhance the physical fitness of students [9–12].

In China, physical education classroom teaching has been developed for many years, and even though the mechanism of the method varies and the way of solving the problem is different, the conclusion form is mostly determined and consistent, which is expressed as “the absoluteness of superiority and inferiority discrimination” and “the strictness of difference transmission” [13–15]. The use of different evaluation methods for the same evaluation problem usually results in different evaluation conclusions, resulting in the problem of “nonconsistent multievaluation conclusions” [16]. It is now generally accepted that ‘portfolio evaluation’ is an effective solution to this problem, but in reality, this is a compromise approach that does not address the essence of the problem at its root [17].

In this paper, we develop an “autonomous advantage evaluation method to highlight one’s own advantages,” which uses a probabilistic stochastic simulation algorithm to evaluate the advantages of the evaluated objects by calculating the degree of superiority among them [18]. This method produces probabilistic (reliable) evaluation conclusions, which are more interpretable to the actual problem, and proposes an innovative “base to top” comprehensive

evaluation method with a high degree of independence, which is added to the evaluation in the form of “components.” The method is based on an innovative “base to top” approach, with a high degree of independence. The validity of the method is verified by means of an example [19].

## 2. Basic Description of Assessment Issues in Physical Education

There is a multi index evaluation system  $x_{ij} = x_j(x_i)$ , ( $i = 1, 2, \dots, n; j = 1, 2, \dots, m$ ) composed of  $u_1, u_2, \dots, u_n$ ,  $m$  evaluated objects and  $x_1, x_2, \dots, x_m$  indexes, which is about index  $x_j$  for the evaluated object  $u_i$ ; observed value of the evaluation data matrix (decision matrix) can be expressed as

$$A = [x_{ij}]_{n \times m} = \begin{bmatrix} x_{11} & x_{12} & \cdots & x_{1m} \\ x_{21} & x_{22} & \cdots & x_{2m} \\ \cdots & \cdots & \cdots & \cdots \\ x_{n1} & x_{n2} & \cdots & x_{nm} \end{bmatrix}, \quad (1)$$

where  $m, n \geq 3$ , and the data in A is the normalized data after preprocessing the physical education evaluation process we describe as a general transformation:

$$y_i = f(x_{i1}, x_{i2}, \dots, x_{im}), \quad i \in N, \quad (2)$$

where  $f$  is the positive transformation function;  $y_i$  is the comprehensive evaluation value of the object  $u_i$  being evaluated, and  $u_1, u_2, \dots, u_n$  is ranked according to the  $u_1, u_2, \dots, u_n$  value from the largest to the smallest, to complete the  $u_1, u_2, \dots, u_n$  comparison of the advantages and disadvantages.

## 3. Description of the Autonomous Strengths Assessment

*Hypothesis 1.* is that each of the evaluated subjects has the dual objective of “widening the gap between competitors” and “developing their own strengths,” and in doing so, highlights their own strengths in an integrated manner.

A quantitative description of the idea of autonomous strengths evaluation in hypothesis 1:

*Definition.*  $\alpha_{ij}$ ,  $\beta_{ij}$  is the amount of column and row dominance of the evaluated object  $u_i$  ( $i \in N$ ) on indicator  $x_j$  ( $j \in N$ ), respectively, and satisfies

$$\begin{cases} \alpha_{ij} = \frac{1}{n-1} \sum_{k \neq i} (x_{ij} - x_{kj}), & i \in N, \quad j \in M, \quad k \in N, \\ \beta_{ij} = \frac{1}{m-1} \sum_{p \neq j} (x_{ij} - x_{ip}), & i \in N, \quad j \in M, \quad p \in M. \end{cases} \quad (3)$$

If we let  $\lambda_{ij} = \mu\alpha_{ij} + \eta\beta_{ij}$ ,  $i \in N, j \in M$ , then we say that  $\lambda_{ij}$  with is the amount of autonomous advantage of the evaluated object  $u_i$  ( $i \in N$ ) with respect to indicator  $x_j$  ( $j \in N$ ), where  $\mu$  is the competitive target coefficient and  $\eta$  is the developmental target coefficient  $\mu, \eta \in [0, 1], \mu + \eta = 1$ .

Column dominance  $\alpha_{ij}$  ( $i \in N, j \in M$ ) reflects the difference in strength between the  $j$ th indicator of the evaluated object  $\mu_i$  and the  $n-1$  other evaluated objects as a whole, while row dominance  $\beta_{ij}$  reflects the difference in strength between the  $j$ th indicator of the evaluated object  $\mu_i$  and the  $m-1$  other indicators as a whole.

## 4. Stochastic Simulation Algorithm

*4.1. Nonlinear Programming Problems Where the Objective Function Is Linear.* This paper gives a simulated annealing and evolutionary planning algorithm for nonlinear planning problems with linear objective functions, which transforms problems with constraints into unconstrained ones. Numerical results confirm the high computational accuracy of the method and show good convergence, considering the following optimization problem (where  $c$  is a vector):

$$\begin{aligned} \min & c^T x \\ \text{s. t.} & g_i(x) \leq 0 \quad i = 1, \dots, r \\ & Ax \geq b \end{aligned} \quad (4)$$

In order to find a feasible solution that satisfies the constraint, we first solve the subproblem:

$$\begin{aligned} \min, f & = \max\{0, g_i(x) \quad i = 1, \dots, r\}, \\ \text{s. t.} & c^T x \leq c^T x_k^* - \varepsilon, \\ & Ax \leq b, \end{aligned} \quad (5)$$

where  $x_k^*$  is the optimal solution at  $k$  steps and  $\varepsilon$  is a small positive number. Let  $B = \begin{pmatrix} C^T \\ A \end{pmatrix}$ ,  $d = \begin{pmatrix} c^T x_k^* - \varepsilon \\ b \end{pmatrix}$ , the constraint can be reduced to  $Bx \leq d$ .

$Bx \leq d$  can be written as

$$\begin{cases} b_{11}x(1) + b_{12}x(2) + \cdots + b_{1n}x(n) \leq d_1, \\ b_{21}x(1) + b_{22}x(2) + \cdots + b_{2n}x(n) \leq d_2, \\ \cdots \\ b_{m+1,1}x(1) + b_{m+1,2}x(2) + \cdots + b_{m+1,n}x(n) \leq d_{m+1}. \end{cases} \quad (6)$$

*4.2. Simulated Annealing Algorithms for Nonlinear Programming Global Optimization Problems.* Based on the upper and lower bounds of component  $x(L_i)$ , we propose a class of simulated annealing algorithm for solving subproblem (3). The specific steps of the algorithm are as follows: Algorithm 1:

Step 0: initialization: the maximum and minimum temperatures are  $T_{\max}, T_{\min}$ , the number of iterations  $L_{\max}$  and the parameters are given respectively  $\varepsilon > 0$ .

Step 1: use the random process to obtain the initial value of the feasible solution  $x_0 = (x_0(1), \dots, x_0(n))$ , set  $T = T_{\max}$ ,  $t = 0, I = 0$ . If  $f(x_0) \leq 0$ , then  $I = 1, y^* = x_0$ . Otherwise, turn to step 2.

Step 2: While  $(T > T_{\min})$  do

(a) while  $t \leq L_{\max}$  do

(1) randomly select  $l_t \in \{1, 2, \dots, n\}$ , and give a uniformly distributed random number  $\lambda \in [-1, 1]$ . For  $j = 1, \dots, n$ , if  $\lambda > 0$ .

$$z(j) = \begin{cases} x_t(j) + \alpha \times (b_{l_t} - x_t(j)) \times \lambda, & \text{if } j = l_t \text{ and } b_{l_t} \neq \infty, \\ x_t(j) + \alpha \times \lambda, & \text{if } j = l_t, b_{l_t} = \infty, \\ x_t(j), & \text{if } j \neq l_t. \end{cases}$$

$$z(j) = \begin{cases} x_t(j) + \alpha \times (x_t(j) - a_{l_t}) \times \lambda, & \text{if } j = l_t \text{ and } a_{l_t} \neq \infty, \\ x_t(j) + \alpha \times \lambda, & \text{if } j = l_t, a_{l_t} = \infty, \\ x_t(j), & \text{if } j \neq l_t, \end{cases}$$

where  $a_{l_t}$  and  $b_{l_t}$  are lower and upper bounds,  $x_t(l_t)$  comes from Algorithm 1,  $\alpha$  The initial value of is 1, if 444, then  $\alpha = 1$ .

(2) let  $z = (z(1), \dots, z(n))$ , if  $f(z) \leq 0$ , then  $I = 1, y^* = z$ . Algorithm 1 stops. Otherwise, turn (3).

(3) Take  $\eta \in [0, 1]$ , if  $\eta \leq \min\{1, \exp[f(x_t) - f(z)]/T\}$ , set  $x_{t+1} = z$ , otherwise  $x_{t+1} = x_t, t = t + 1$ .

(b)  $L_{\max} = L_{\max} + d, t = 0$ .

(c) by  $T = \delta \times T$  lower the temperature  $T$ . Where parameter  $D, \beta$  And  $\delta$  is a known constant entered in advance.

ALGORITHM 1

Step 1: Given  $\mu$  initial values, let  $k = 1$  and  $I = 0$ . Let the individuals be real-valued vector pairs  $(x_i, \eta_i), \forall i \in \{1, \dots, \mu\}$  [20–22].

Step 2: Calculate the individual adaptation value. If  $\exists i \in \{1, \dots, \mu\}, f(x_i) \leq 0$ , then  $I = 1, y^* = x_i$  otherwise turn Step 3.

Step 3: For each parent  $(x_i, \eta_i), \forall i = 1, \dots, \mu$ , generate a child  $(x'_i, \eta'_i)$  according to the following steps: Randomly select  $l_i$  from the set  $\{1, 2, \dots, n\}$  to generate a uniformly distributed random

parameter  $\lambda$  in the interval  $[-1, 1]$ . For  $j = 1, \dots, n$ , if  $\lambda > 0$

$$x'_i(j) = \begin{cases} x_i(j) + \eta_i(b_j - x_i(j))\lambda, & \text{if } j = l_i \text{ and } b_{l_i} \neq \infty, \\ x_i(j) + \eta_i\lambda, & \text{if } j = l_i, b_{l_i} = \infty, \\ x_i(j), & \text{if } j \neq l_i. \end{cases}$$

$$x'_i(j) = \begin{cases} x_i(j) + \eta_i(x_i(j) - a_{l_i})\lambda & \text{if } j = l_i \text{ and } a_{l_i} \neq \infty, \\ x_i(j) + \eta_i\lambda & \text{if } j = l_i, a_{l_i} = \infty, \\ x_i(j) & \text{if } j \neq l_i, \end{cases}$$

ALGORITHM 2

On the basis of algorithm 1, the initial value of random feasible solution  $x_0$  is given so that  $k = 0$ . If  $I = 1$ , make  $x_{k+1}^* = y^*, T_{\max} = T, L_{\max} = L_{\max}, k = k + 1$ .

If  $I = 0$ , then  $x_k^*$  is the global optimal solution of problem (1).

**4.3. Evolutionary Planning Algorithms for Nonlinear Programming Global Optimization Problems.** This section gives an improved evolutionary planning algorithm for problem (2), where the adaptation value is taken as the objective function value as follows: (Algorithm 2)

The initial value of  $\eta$  is 1 if  $\eta_i < 10^{-4}$ , then  $\eta_i = 1$ .

## 5. Application Examples

This paper uses data from the evaluation of the teaching quality of physical education teachers at a university, with the aim of analysing the factors affecting the quality of physical education. Table 1 shows that the indicators of teaching quality evaluation are divided into

TABLE 1: Teaching quality evaluation form.

| Teacher number | Evaluating indicator |    |    |    | Evaluation results |
|----------------|----------------------|----|----|----|--------------------|
|                | K1                   | K2 | K3 | K4 |                    |
| 1              | B                    | A  | C  | C  | Good               |
| 2              | B                    | B  | C  | B  | Good               |
| 3              | C                    | C  | A  | A  | Secondary          |
| 4              | C                    | B  | B  | C  | Secondary          |
| 5              | A                    | A  | B  | B  | Good               |
| 6              | B                    | C  | B  | C  | Good               |
| 7              | C                    | A  | B  | C  | Secondary          |
| 8              | B                    | B  | A  | C  | Excellent          |
| 9              | B                    | C  | C  | A  | Secondary          |
| 10             | A                    | B  | B  | C  | Good               |

five items based on teaching effectiveness, teaching content, teaching attitudes, and teaching methods [23–25]. It is assumed here that K1: teaching attitude, K2: teaching content, K3: teaching programme, K4: teaching effectiveness, and K5: evaluation result are the data of five training samples, and the evaluation grades

are A: excellent (90–100), B: good (80–90), C: moderate (70–80), D: pass (60–70), and E: fail (<60).

The information entropy of each attribute is calculated first. For K1, there are {1, 2, 6, 8, 9} (3 good, 1 moderate and 1 excellent), {3, 4, 7} (3 moderate), and {5, 10} (2 good) for the evaluation of teaching attitude. Then, the information entropy of K1 is calculated as follows:

$$E(K1) = \frac{1}{5} \times \left[ \frac{3 \cdot (5^3 - 3^3)}{(5+3)^3} + \frac{1 \cdot (5^3 - 1^3)}{(5+1)^3} + \frac{1 \cdot (5^3 - 1^3)}{(5+1)^3} \right] = 0.3445,$$

$$E(K1) = \frac{1}{3} \times \left[ \frac{3 \cdot (3^3 - 3^3)}{(3+3)^3} \right] = 0,$$

$$E(K1) = \frac{1}{2} \times \left[ \frac{2 \cdot (2^3 - 2^3)}{(2+2)^3} \right] \quad (7)$$

The information entropy of the teaching attitude K1 is

$$E(K1) = \frac{5}{10} \cdot 0.3445 + \frac{3}{10} \cdot 0 + \frac{2}{10} \cdot 0 = 0.1772. \quad (8)$$

Similarly, we obtain the information entropy of other attributes:

$$E(K2) = 0.2947, E(K3) = 0.2486, E(K4) = 0.2433. \quad (9)$$

Comparing the entropy of each attribute, the ranking is  $E(K1) < E(K4) < E(K3) < E(K2)$ , so K1 is chosen as the root node and three branches are created, A, B, and C. According to the flow of the algorithm, the test attributes are selected in turn under the branches and nodes are created until the end of the sample division [26].

Based on the decision tree created in Figure 1, we can see that each branch represents the combined set of attributes tested, and the whole decision tree represents the combined destructions.

It is clear from this analysis that teaching attitude is the most important aspect of teaching. When the teaching attitude is excellent, the result of teaching evaluation is good; when the teaching attitude is medium, the result of teaching evaluation is medium; when the teaching attitude is good, the result of teaching evaluation also depends on the teaching programme, but the teaching attitude is still the dominant factor [27, 28].

Evaluation of physical education teaching in universities is ranked. After the calculation of the autonomous evaluation method to obtain the results so that  $b=2$ , we can get the dominant weight vector  $\omega = 0.4546, 0.2908, 0.1637, 0.0726$  to get the ideal order of ranking as

$$u_1 \underset{0.9891}{>} u_2 \underset{0.8971}{>} u_8 \underset{0.5283}{>} u_4 \underset{0.07272}{>} u_5 \underset{0.8306}{>} u_3 \underset{0.5542}{>} u_6 \underset{0.6636}{>} u_7 \underset{0.5464}{>} u_9 \underset{0.7277}{>} u_{10}. \quad (10)$$

The results, e.g.  $u_8 \underset{0.5283}{>} u_4$ , do not mean that  $u_8$  is definitely better than  $u_4$ ,  $u_4$  still has a 04717 probability of being better than  $u_8$ , and this form of conclusion is not

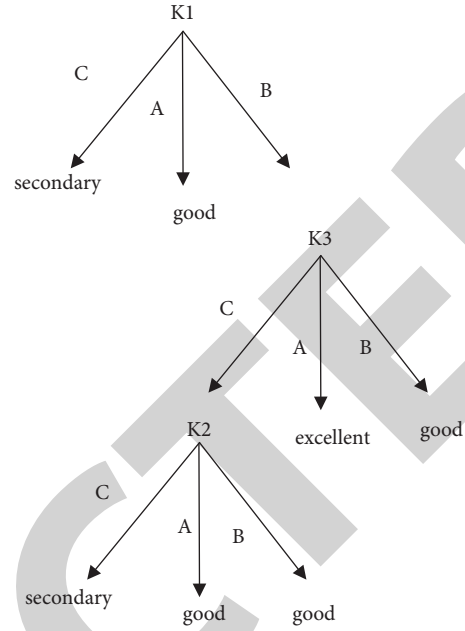


FIGURE 1: Evaluation decision tree.

TABLE 2: Parameter setting values for the simulated annealing algorithm.

| $T_{\max}$ | $T_{\min}$ | $\delta$ | $L_{\max}$ | d | $\alpha$ | $\beta$ |
|------------|------------|----------|------------|---|----------|---------|
| 11         | 0.001      | 0.974    | 3          | 1 | 1        | 1.02    |

TABLE 3: Calculation results based on the simulated annealing algorithm and penalty function method proposed in the paper.

| Functions               | Optimal solution | Worst value | Average best value |
|-------------------------|------------------|-------------|--------------------|
| Paper method            | -10.945          | -10.874     | -10.912            |
| Penalty function method | -10.401          | -10.271     | -10.397            |

suitable for making absolute judgements of superiority between some of the evaluated objects at the intersection of competencies. This form of evaluation gives the most reliable ranking of superiority between objects, but at the same time accommodates a variety of possible rankings (e.g.  $u_8 \underset{0.5283}{>} u_4$  is equivalent to  $u_4 \underset{0.4717}{>} u_8$ ).

This form of evaluation allows multiple absolute evaluation findings to be embedded in a single probabilistic evaluation finding, avoiding the subjective assumptions caused by the “multiple evaluation findings nonconsistency phenomenon” [23–25].

Table 2 shows the parameter settings for the numerical calculations, while Tables 3 and 4 show the results of the numerical calculations.

TABLE 4: Calculation results based on the evolutionary planning algorithm and penalty function method in this paper.

| Functions               | Evolutionary algebra | Population size | Optimal solution | Worst value | Average best value |
|-------------------------|----------------------|-----------------|------------------|-------------|--------------------|
| Paper method            | 1000                 | 10              | -10.967          | -10.875     | -10.926            |
| Penalty function method | 1000                 | 10              | -10.567          | -10.156     | -10.478            |

## 6. Conclusions

In this paper, we address the problem of the absolute nature of the evaluation of the merits of traditional physical education classrooms and the inconsistency of the findings of multiple evaluations, and construct a method to evaluate the merits of the evaluated students by highlighting their own strengths. The validity of the method is verified by calculation, and the evaluation conclusion with probability information is obtained.

## Data Availability

The experimental data used to support the findings of this study are available from the corresponding author upon request.

## Conflicts of Interest

The authors declare that they have no conflicts of interest regarding this work.

## References

- [1] F. J. Hinojo-Lucena, Á. C. Mingorance-Estrada, J. M. Trujillo-Torres, I. Aznar-Díaz, and M. P. Cáceres Reche, "Incidence of the flipped classroom in the physical education students' academic performance in university contexts," *Sustainability*, vol. 10, no. 5, p. 1334, 2018.
- [2] D. J. Barr-Anderson, D. Neumark-Sztainer, K. H. Schmitz et al., "But I like PE: factors associated with enjoyment of physical education class in middle school girls," *Research Quarterly for Exercise & Sport*, vol. 79, no. 1, pp. 18–27, 2008.
- [3] H. Sun and A. Chen, "An examination of sixth graders' self-determined motivation and learning in physical education," *Journal of Teaching in Physical Education*, vol. 29, no. 3, pp. 262–277, 2010.
- [4] C. Lonsdale, R. R. Rosenkranz, L. R. Peralta, A. Bennie, P. Fahey, and D. R. Lubans, "A systematic review and meta-analysis of interventions designed to increase moderate-to-vigorous physical activity in school physical education lessons," *Preventive Medicine*, vol. 56, no. 2, pp. 152–161, 2013.
- [5] J. C. K. Wang, W. C. Liu, N. L. D. Chatzisarantis, and C. B. S. Lim, "Influence of perceived motivational climate on achievement goals in physical education: a structural equation mixture modeling analysis," *Journal of Sport & Exercise Psychology*, vol. 32, no. 3, pp. 324–338, 2010.
- [6] A. Papaioannou, H. W. Marsh, and Y. Theodorakis, "A multilevel approach to motivational climate in physical education and sport settings: an individual or a group level construct?" *Journal of Sport & Exercise Psychology*, vol. 26, no. 1, pp. 90–118, 2004.
- [7] Z. H. A. N. G. Zhengwan, Z. H. A. N. G. Chunjong, L. I. Hongbing, and X. I. E. Tao, "Multipath transmission selection algorithm based on immune connectivity model," *Journal of Computer Applications*, vol. 40, no. 12, p. 3571, 2020.
- [8] Z.-wan Zhang, Di Wu, and C.-J. Zhang, "Study of cellular traffic prediction based on multi-channel sparse LSTM," *Computer Science*, vol. 48, no. 6, pp. 296–300, 2021.
- [9] P. An, Z. Wang, and C. Zhang, "Ensemble unsupervised autoencoders and Gaussian mixture model for cyberattack detection," *Information Processing & Management*, vol. 59, no. 2, Article ID 102844, 2022.
- [10] A. Bekiari and S. Spyropoulou, "Exploration of verbal aggressiveness and interpersonal attraction through social network analysis: using university physical education class as an illustration," *Open Journal of Social Sciences*, vol. 04, no. 06, pp. 145–155, 2016.
- [11] Y. Arslan, "Determination of technopedagogical content knowledge competencies of preservice physical education teachers: a Turkish sample," *Journal of Teaching in Physical Education*, vol. 34, no. 2, pp. 225–241, 2015.
- [12] M. E. Block, Y. Hutzler, S. Barak, and A. Klavina, "Creation and validation of the self-efficacy instrument for physical education teacher education majors toward inclusion," *Adapted Physical Activity Quarterly*, vol. 30, no. 2, pp. 184–205, 2013.
- [13] H. Sun, A. Chen, C. Ennis, R. Martin, and B. Shen, "An examination of the multidimensionality of situational interest in elementary school physical education," *Research Quarterly for Exercise & Sport*, vol. 79, no. 1, pp. 62–70, 2008.
- [14] J. C. Wang, A. J. Morin, R. M. Ryan, and W. C. Liu, "Students' motivational profiles in the physical education context," *Journal of Sport & Exercise Psychology*, vol. 38, no. 6, pp. 612–630, 2016.
- [15] F. Fontana, O. Furtado Jr, O. Mazzardo Jr, D. Hong, and W. de Campos, "Anti-fat bias by professors teaching physical education majors," *European Physical Education Review*, vol. 23, no. 1, pp. 127–138, 2017.
- [16] C. Dai, H. Che, and M. F. Leung, "A neurodynamic optimization approach for L1 minimization with application to compressed image reconstruction," *The International Journal on Artificial Intelligence Tools*, vol. 30, no. 01, Article ID 2140007, 2021.
- [17] Y. Wang, J. Wang, and H. Che, "Two-timescale neurodynamic approaches to supervised feature selection based on alternative problem formulations," *Neural Networks*, vol. 142, pp. 180–191, 2021.
- [18] M. J. Jacobson and U. Wilensky, "Complex systems in education: scientific and educational importance and implications for the learning sciences," *The Journal of the Learning Sciences*, vol. 15, no. 1, pp. 11–34, 2006.
- [19] S. H. Cheon, J. Reeve, and M. Vansteenkiste, "When teachers learn how to provide classroom structure in an autonomy-supportive way: benefits to teachers and their students," *Teaching and Teacher Education*, vol. 90, Article ID 103004, 2020.
- [20] D. A. S. Silva, J. P. Chaput, P. T. Katzmarzyk et al., "Physical education classes, physical activity, and sedentary behavior in children," *Medicine & Science in Sports & Exercise*, vol. 50, no. 5, pp. 995–1004, 2018.
- [21] I. Akour, M. Alshurideh, B. Al Kurdi, A. Al Ali, and S. Salloum, "Using machine learning algorithms to predict

## Research Article

# BP Neural Network-Based Evaluation Method for Enterprise Comprehensive Performance

Chen Wenjing <sup>1,2</sup>

<sup>1</sup>Chaohu University, Hefei 238000, Anhui, China

<sup>2</sup>Philippine Christian University Center for International Education, Manila, Philippines

Correspondence should be addressed to Chen Wenjing; 009009@chu.edu.cn

Received 22 May 2022; Revised 19 June 2022; Accepted 30 June 2022; Published 28 August 2022

Academic Editor: Man Fai Leung

Copyright © 2022 Chen Wenjing. This is an open access article distributed under the Creative Commons Attribution License, which permits unrestricted use, distribution, and reproduction in any medium, provided the original work is properly cited.

Comprehensive performance evaluation is an important basis for improving the training effect of enterprise employees and the effective allocation of enterprise resources. Based on AHP and BP neural network theory, this paper constructs a comprehensive performance evaluation method for enterprises, AHP is used to calculate the weight of the index, and then the importance index is screened. The model proposes a conceptual model of comprehensive performance of manufacturing enterprises from the support layer, core layer, and promotion layer and constructs a manufacturing system from horizontal and vertical. The influencing factors of comprehensive performance solve the quantification problem of enterprise comprehensive performance evaluation and have obvious guiding value for the research on the integration mode and path of industrialization and industrialization of regional manufacturing enterprises. In the simulation process, the weight of each index in the evaluation system is first determined by the analytic hierarchy process; then the evaluation index membership score table is established, and fuzzy mathematics is used to calculate the expert's score, so as to solve the problem caused by the intermediate value. The uncertainty caused by the jump is finally established by the analytic hierarchy process, and the neural network is used to simulate the sample. The experimental results show that by using AHP to collect training samples for neural network evaluation, the comprehensive performance evaluation system has good fitness and achieves the best comprehensive consideration of accuracy and training time when there are 17 hidden layer neurons. The maximum relative error is 1.64%, which is much lower than the general accuracy requirement of 5%, which effectively improves the performance and calculation accuracy of the network.

## 1. Introduction

The comprehensive performance evaluation service has developed rapidly at home and abroad and has received more and more attention [1]. The essence of comprehensive performance evaluation is an innovative product produced by the combination of services, which is a multisubject and multiwin service model [2]. The huge effect of this realistic multiwin model on the participants has made many companies flock to carry out this business. However, when third-party logistics companies carry out comprehensive performance evaluation business, the weak concept of risk management and the low level of risk evaluation also restrict comprehensive performance evaluation [3–5]. R&D's role in enterprise activities has become increasingly obvious. At the same time, R&D activities are also an important part of

scientific research activities and are the foundation of innovation [6, 7].

The comprehensive scientific and technological performance is a special and important resource. Scientific evaluation of them is the premise of recruitment and selection [8], the basis for improving the training effect and the effective allocation of comprehensive performance, and an important factor in formulating employee career planning is given. From the existing research results, it can be seen that most high-tech enterprises do not pay enough attention to the comprehensive performance of science and technology [9], which leads to unreasonable evaluation indicators, single evaluation standards, and unscientific evaluation methods, which brings great influence to the development and management of comprehensive performance. There are big problems [10], such as reduced overall performance

satisfaction, or even resignation. In the long run, the management of the enterprise will fall into chaos, and the goals of the enterprise will be difficult to achieve. Therefore, both internationally and domestically, the quantity and structure of R&D resources are regarded as the core indicators for measuring the comprehensive national strength [11]. R&D has the characteristics of exploratory, creative, uncertain, and risky and is crucial to the productivity that transforms scientific and technological achievements into reality [12–14].

This paper mainly studies the subjective and objective AHP-BP model in the field of comprehensive performance evaluation risk assessment. This paper obtains relevant data through the investigation and analysis of the comprehensive performance of science and technology of a high-tech enterprise and uses the established model to conduct simulation research based on MATLAB software to verify the scientificity of the method. In terms of the risk assessment index system, this paper tries to establish a more comprehensive and practical index system: the first part includes the first three chapters, mainly on the research status, significance, index system construction, and the relevant theoretical basis of model construction. The practicability and accuracy of the paper in the third part is mainly about the shortcomings of this paper and the prospect of future research. Although 26 indicators are selected in this paper, they are all traditional financial indicators. The extent to which visualization should be optimal in both horizontal and vertical directions is not reflected in the text. Too high a degree of visualization will lead to a higher level of complexity in the organization, and too low a degree of visualization may affect the organization's ability to sense. Due to their own limitations, traditional financial indicators pay more attention to the historical information of enterprises. Therefore, it is difficult to fully reveal the potential development capabilities of enterprises.

## 2. Related Work

On the basis of understanding the current research status at home and abroad, combined with the characteristics of high-tech enterprises' comprehensive performance of science and technology, so as to provide scientific and technological comprehensive performance evaluation tools for enterprise managers. To form a more objective and scientific understanding of the current state of enterprise comprehensive performance of science and technology [15], to provide a basis for the development planning and strategy formulation of enterprise comprehensive performance.

Human capital property rights are the rights of its owners to dispose of or utilize their own human capital in order to obtain benefits, including the right to possess, use, dispose of, and benefit from human capital. Some western economists put forward the human capital property right incentive theory from the perspective of human capital participating in income distribution. Profit sharing is a typical contractualization of human capital property rights. Liang and Li [16] believed that compared with the traditional

performance evaluation system, 360-degree evaluation has its advantages and is more comprehensive and accurate. Huang et al. [17] research believes that when the main purpose of the 360-degree evaluation is to serve the development of employees and provide help for employees' careers, the evaluation of evaluators will be more objective and fair. Zhang et al. [18] believe that 360-degree evaluation uses multiple perspectives to evaluate employee performance, especially in providing feedback and guidance, allocating bonuses and opportunities, and avoiding evaluation errors. Cai et al. [19] believe that, according to the characteristics of R&D employees, a four-layer KPI evaluation index system for R&D employees is designed, which combines performance result orientation and workload orientation for evaluation, while realizing the evaluation of the R&D personnel of high-tech enterprises at a single time point, through the multistage information aggregation method of dual incentive control lines, the performance of the R&D personnel of high-tech enterprises can be evaluated in a complete R&D project cycle.

The research group led by Qian [20] is mainly based on the job analysis method of competency characteristics and uses empirical evaluation to construct the structure of the competency characteristics of regional enterprise senior managers, etc. and proposes to first determine a set of general basic competencies, and then these competencies are tailored to specific roles, thereby defining performance levels for each competency. Scholars applied the competency model to the administrative management professional personnel training program and put forward several suggestions for formulating the professional personnel training program. This paper believes that competency is closely related to the job performance of enterprise employees [21]. The use of the competency model can predict the future work performance of enterprise employees and can distinguish the outstanding performers and the average ones in the enterprise. It is multilevel, multidimensional, cross-organizational, linked to task scenarios, and dynamic [22]. Through the performance-oriented comprehensive performance management system, the R&D personnel are implemented performance management, and targeted and personalized incentive measures are taken [23–25].

## 3. Construction of an Enterprise Comprehensive Performance Evaluation Method Based on AHP and BP Neural Network

*3.1. Analytic Hierarchy Architecture.* The factor analysis hierarchy process can be divided into R-type factor analysis and Q-type factor analysis according to the different research objects to find several common factors that control all variables through the study of the correlation matrix or the internal dependence of the covariance matrix of the variables through the study of the internal structure of the similar matrix of the samples, to find out the main analytic hierarchy process factors that control all the samples.



$$\begin{aligned}
 X(i, j) &= \begin{cases} \sum_{i,j=1} \overline{x(i)/x(j)}, i > j, \\ \text{miu}(\sum x(i+j) - \sum x(i-j)), i < j, \end{cases} \\
 G_i(i, j) &= \begin{cases} [F_i(x=1, 2, \dots, i) + F_i(y=1, 2, \dots, j)], (i > 0), \\ [F_i(x=1, 2, \dots, i) - F_i(y=1, 2, \dots, j)], (i \leq 0). \end{cases}
 \end{aligned} \tag{1}$$

There are many calculation methods for calculating the single-level sorting of each layer to the previous layer, such as the sum method, root method, characteristic root method, and least square method. The existing research and application show that the root method is accurate and the evaluation effect is better. Therefore, this paper intends to use the root method to calculate the relative weight. It can be seen that the coefficient of variation of the inventory comprehensive performance evaluation rate is 1.74, and the variation coefficient of the business cycle is 1.37, indicating that the inventory comprehensive performance evaluation rate has a greater degree of variation and reflects a relatively large amount of information. Therefore, this paper chooses the comprehensive performance evaluation rate of inventory as one of the representative indicators.

$$\begin{aligned}
 &\begin{cases} f(\text{net}, i, j) \longrightarrow \text{net}(i, j), \\ \sum_{i,j=1} \frac{\text{net}(i) - 1/\text{net}(j)}{1-i} \longrightarrow \frac{\text{net}(i) - 1/\text{net}(j)}{1-i}, \end{cases} \\
 f(\text{omiga}, i, j) &= \begin{cases} \sum_{i,j=1} (\text{omiga}^{t-i} (i-x)) / (1-j-\text{alpha}), \\ \sum_{i,j=1} (\text{omiga}^{t-i} (i)) / f^{t-j} (j-\text{alpha}). \end{cases}
 \end{aligned} \tag{2}$$

Here, *K* represents knowledge of comprehensive performance; *S* represents skills of comprehensive performance; *A* represents the ability of comprehensive performance; *I* represents the mediating variable, including motivation and attitude; *B* represents the behavior of comprehensive performance. The theory holds that behavioral change is the result of a series of jobs and is the primary concern of comprehensive performance development like changes in knowledge, skills, and abilities enable changes in behavior, and the translation of this possibility into reality requires the role of mediating variables such as motivation and attitude. DEA deals with the same type of DMU and indicators with the same input and output, so the DEA method can perform a time series analysis; that is, each time point is a decision-making unit; it can also perform a cross-sectional analysis; that is, each individual are decision-making units.

Figure 1 further judges the influence of indicators by using multiple indicators, if the unit of measurement is the same as the mean, the standard deviation can be directly used for comparison. Among the other five indicators of their own kind, the multiple correlation coefficients of nonperforming assets ratio, long-term asset suitability ratio,

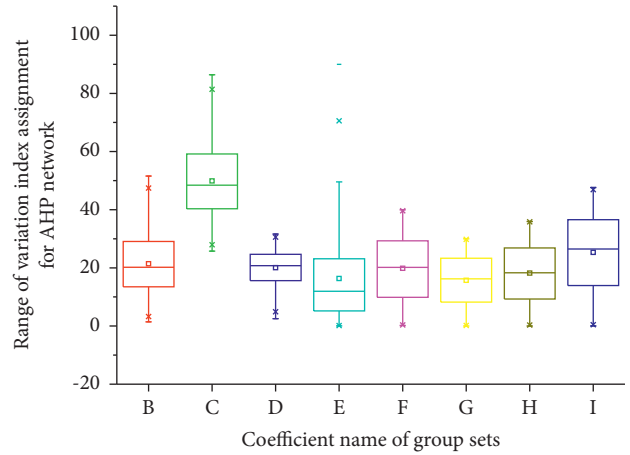


FIGURE 1: Coefficient of variation index assignment of AHP.

accounts payable turnover ratio, comprehensive performance evaluation rate of fixed assets, and comprehensive performance evaluation rate of accounts receivable are 0.266, respectively. Sometimes a single neural network works better than a modular neural network for some data. The reasons are analyzed as follows: the insufficient number of samples after the modules are divided makes the neural network inferior to a single neural network, so such a problem can only be solved by ensuring a number of standard samples. Therefore, this paper selects the comprehensive performance evaluation rate of fixed assets and the comprehensive performance evaluation rate of accounts receivable as reflecting the enterprise for the representative indicator of comprehensive performance evaluation capabilities.

**3.2. BP Neural Network Topology.** Before using large size kernels, GoogLeNet scales the computation by adding a bottleneck layer with 11 convolution kernels. It uses sparse connections to overcome the problems of information redundancy and high computational cost by omitting irrelevant feature maps. In addition, GoogLeNet innovatively uses global average pooling in the last layer to reduce the density of connections. These parameters are adjusted which resulted in a significant reduction in the number of parameters from 40 million to 5 million. If it is the Inception module of GoogLeNet without dimension reduction, it is the Inception module after adding dimension reduction in Figure 2, subcriteria layers should be further decomposed.

The judgment matrix and scale meaning are as shown, where the middle value of the two values indicates the importance between the two. The neural network will inevitably lose some image feature information due to the deepening of the number of network layers. At the same time, the low-level feature information cannot be directly transmitted to the high-level, and the network cannot learn more robust features. The higher the number of network layers, the better the fitting ability will be, but it may cause the gradient to disappear or the gradient to explode, and the network cannot continue to learn effective features and the network training stops.

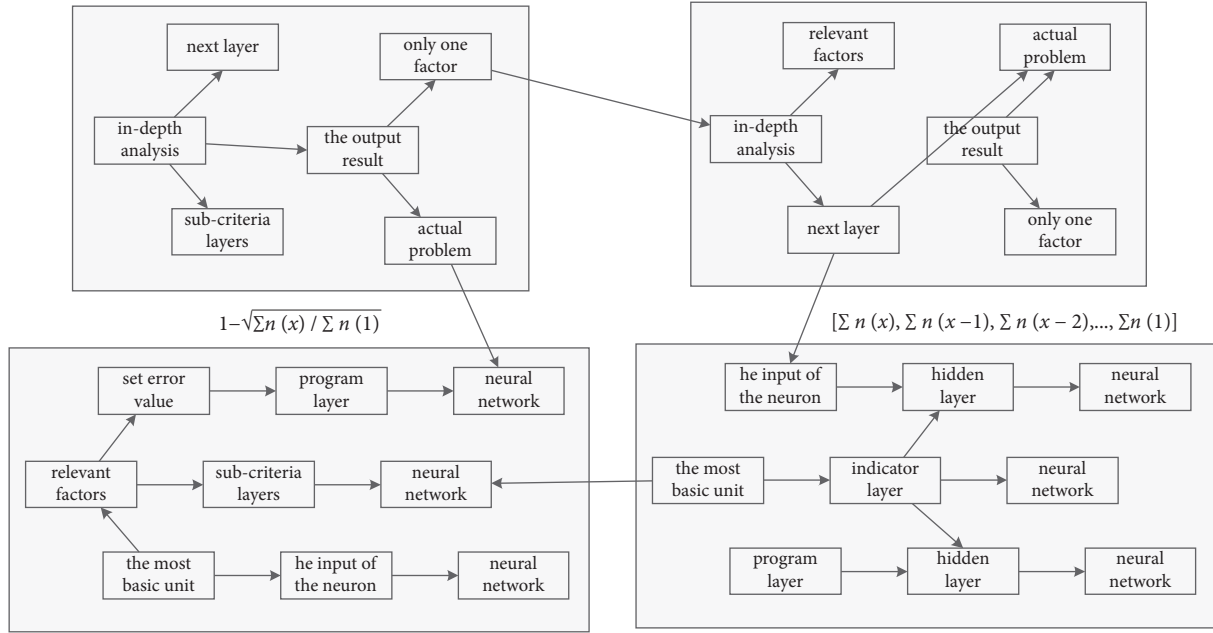


FIGURE 2: Topological unit of BP neural network.

$$\text{far}(x, y, t) = \begin{cases} \sum_{i+j=1} \frac{m(x) + m(y)}{m(x) - m(y)}, \\ \sum u^{t-i} (i-j) / u^{t-j} (j), \\ \sum u^{t-i} (i) / u^{t-j} (j-i), \end{cases}$$

$$\sum_{m,n=1} \frac{1}{\text{lameda} - 1} - m \sum_{m,n=1} 1 - \left| \frac{1 - \text{lameda}}{f(m)} \right|$$

$$- \left| \frac{\text{lameda}}{f(n)} \right| \in CI. \quad (3)$$

The six regions are convolved to extract feature information and then cascaded to extract higher-level feature information so that each pixel can jointly represent and exchange information to ensure richer and more robust feature information. The model in this chapter not only has fewer network layers and fewer parameters but also has a higher accuracy of image classification.

$$\sum_{m,n=1} 1 - \frac{1 - w(a) - w(b)}{w(a) - w(b)} = \sum \text{tra}(w(a), w(b)) - w(a)v(b),$$

$$\cdot \sum_{i,j=1} \frac{\text{lameda}(i) - \exp(i, j)}{1 - \exp(i, j)}$$

$$- \sum f(i, j) \left( \frac{1 + \text{lameda}(i, j)}{1 - \text{lameda}(i, j)} \right) = 0. \quad (4)$$

In the task of neural network processing image classification, the conventional operation is to preprocess the image first, then input the whole image to the

convolutional neural network model and then output the classification. However, since the category targets of different images may have regional differences, different categories may have highly similar feature information, so the accuracy of image classification only by global features is not high.

$$\begin{cases} \sum_{i,j=1} \frac{e(i) - p(i, j)}{1 - p(i, j)} \leq \sum f(d(i) - d(j)), \\ \sum f(d(i) - d(j)) \leq \sum \left( \frac{1 + p(i, j)}{1 - p(i, j)} \right) - 1. \end{cases} \quad (5)$$

The indicators of each enterprise in the neural network sample use standardized data, and the target data use the data evaluated by AHP. The specific evaluation steps are as follows: determine the evaluation index set and output set and determine the number of nodes in the input layer, output layer, and hidden layer. Initialize the weights and thresholds of the neural network nodes. The commonly used method is to assign a random number between 0 and 1. Input neural network learning step size, error target, momentum coefficient, maximum number of iterations, etc. Input sample data, the indicators of the data are standardized data, and the target output is the AHP evaluation value. The neural network propagates forward and calculates the node output values of the input layer, output layer, and hidden layer, respectively.

$$\sum_x^{x-i} \frac{a(x-1) \sqrt{p(x-m)(x+m)}}{a(x) \sqrt{w(x-n)(x+n)}} + \sum_x^{x-n} = 1, \quad (6)$$

$$\cdot t(ma, i, j) = \left\{ \prod w(c(i)di), \prod m(c(i)di), \prod n(c(i)di) \right\}.$$

The network often uses sigmoid log or tangent activation functions and linear functions. When it is desired to limit the output of the network, such as limiting the output between 0

and 1, the logarithmic s-type activation function should be used in the output layer. In general, the s-type activation

function is used in the hidden layer, while the output layer uses a linear activation function.

$$\sum_{i+j=1} \sqrt{n(x, y)m(x, y)} \cup \sqrt{\sum n(x)/\sum n(y)} = \sqrt{\sum n(i, j) - \sum m(i, j)},$$

$$\frac{1 - \sqrt{\sum n(x)/\sum n(y)}}{\sqrt{\sum n(x)/\sum n(y)}} = \lim(n, m) \begin{bmatrix} \sum n(x) & i \\ i & 1 - \sum n(x) \end{bmatrix}, \quad (7)$$

$$\begin{bmatrix} [\sum n(x), \sum n(x-1)] \\ [\sum n(x-2), \dots, \sum n(1)] \end{bmatrix} \xrightarrow{n, m} \begin{cases} 1 - \sqrt{x/\sum n(1)}, \\ 1 - \sqrt{\sum n(x)/\sum n(1)}. \end{cases}$$

When analyzing the dendrogram in the cluster analysis results obtained by using the systematic clustering method, a threshold value needs to be set manually because the category number system will not be given. Therefore, the threshold value can be determined according to the needs of the research setting, which in turn determines the number of subcategories. According to the cluster analysis results in the above figure, the threshold value selected in this paper is about 22. This paper divides the above 10 indicators into 6 subcategories. Period, current assets, comprehensive performance evaluation rate of total assets, and cash comprehensive performance evaluation period are classified into one category, and the other five indicators are each classified into one category.

**3.3. Analysis of Performance Evaluation Indicators.** For performance evaluation indicators, quantitative indicator evaluation does not require the participation of multiple evaluators but is obtained by a special responsible person such as an HR assessment specialist based on the real performance of the R&D personnel and comparing it with the performance plan. The performance indicators in this paper are quantitative indicators of R&D personnel, and their scores are related to the corporate objectives of the indicators. The expected objectives of R&D personnel include the target threshold value and the target challenge value. If the target threshold value cannot be reached, the assessment is 0. The basic requirements are for employees, and the target challenge value is the cut-off point of the performance full score of 1, which requires employees to make more efforts to achieve. The samples of 8 belong to ordinary modules and are divided into STU2, and these data are put into Matlab and then simulated, and STU1, STU2, and a single neural network are compared, respectively. In most scenarios, the larger the coefficient, the faster the collection, the smaller the risk of bad debts, and the stronger the ability to repay short-term debts. SSE represents the sum of squares of errors, SSW refers to the sum of squares of network weights, ENP represents effective weights and thresholds, and TPR refers to the number of training steps.

The application value of research results can be divided into parts in Figure 3 for statistics: one is the patent score, that

is, regardless of the field and type of the patent, each patent is awarded 5 points; the second is the achievement score; that is, the patent application and the economic value generated in real life is recorded as 1 point for every 20,000 yuan of benefits. The calculation method of multi-person cooperation refers to the calculation of the paper or monograph. The evaluation of qualitative indicators is generally completed by an expert group composed of multiple evaluators. The members of the expert group get the corresponding weights according to their roles with the R&D personnel and calculate the fuzzy membership degree according to the different evaluation levels. Firstly, the actual situation of model initialization is analyzed, then the assessment span is determined, and the weights of assessment personnel are allocated. The members of the assessment team divide the level of the  $k$ -th R&D personnel. For example, the indicators can be divided into A, B, C, D, and E grades.

It can be seen that the multiple correlation coefficients of the comprehensive performance evaluation rate of inventory and the operating cycle in the indicators in Figure 4 are 0.963 and 0.966, respectively. After calculating with AHP, the adaptive force evaluation of each manufacturing enterprise can be obtained, which can be expressed as it, the neural network provides training samples. After data processing and normalization or fuzzification, the data is input, and simulation experiments are carried out. After calculation, 8 groups were selected as training data. As long as the index information of the R&D personnel to be evaluated is input into the system, accurate evaluation results can be obtained. We can also multiply the result by 10 or 100 according to the individual needs of the enterprise and restore it to the competency evaluation score suitable for the enterprise. And, with the increase of learning samples, the accuracy of evaluation can be further improved, so it has wide applicability. The results of the multi-index comprehensive evaluation realized by the BP neural network are convincing. It overcomes the influence of human factors, ambiguity, and randomness on evaluation and is an intelligent comprehensive evaluation method.

**3.4. Comparison of Network Data Fitness.** After investigation, we obtained the values of network data fitness among

Analysis of the weight and share level of performance evaluation

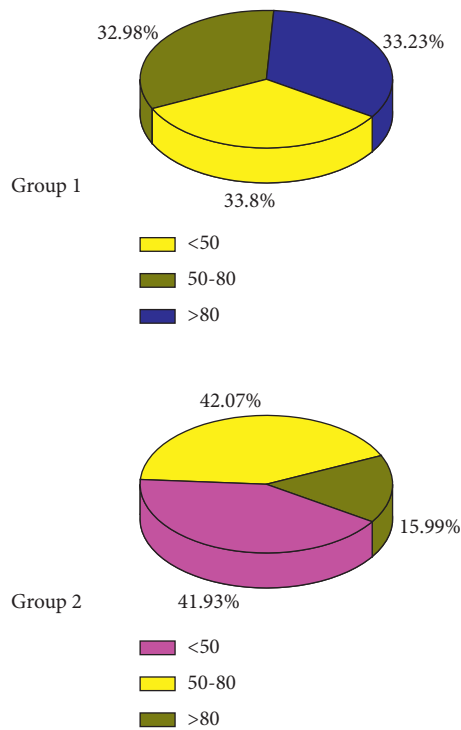


FIGURE 3: Analysis of the weight share level of performance evaluation.

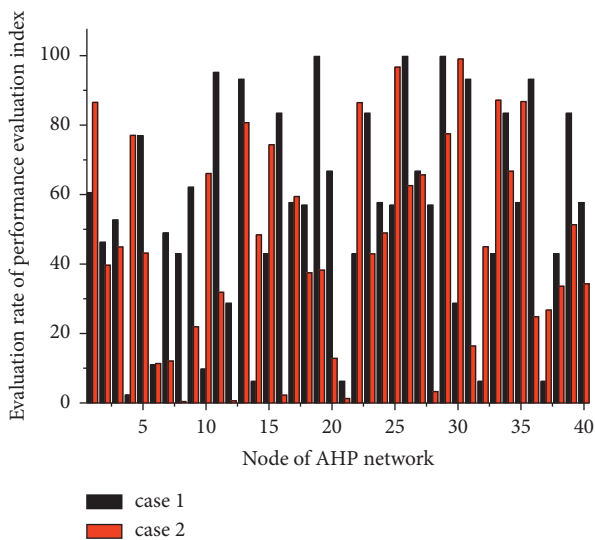


FIGURE 4: Analysis of the evaluation rate of performance evaluation indicators.

12 evaluation indicators. Among them, the economic benefit index generated by patent and achievement application has not obtained comprehensive information due to the difficulty of investigation, so this paper will not calculate it for the time being. See below for the survey data. Since the index  $c$  itself is a value between 0 and 1, no normalization is required, and the other index values are between 0 and 100, it

is divided by 100 to obtain the normalized data. In this paper, the first 12 samples of the samples are selected as training samples to test the BP neural network. After comparative analysis, it is determined that the number of nodes in the hidden layer is 8, the convergence speed is fast, and the error can meet the requirements. The output value of the network after training is: 0.9701, 0.7801, 0.6294, 0.78012, 0.6084, 0.6620, 0.58971, 0.8380, 0.6193, 0.6281, 0.7185, and 0.58900.

Figure 5 selects 91 indicators that can basically cover all the information of listed companies. According to the principle of maximum membership, we can see from the judgment matrix month that the evaluation of enterprise B's manufacturing system self-adaptation is medium. Among its first-level indicators, flexibility is good, visualization is medium, and self-knowledge is medium. Among them, in the evaluation of flexibility, it can be seen from the data that the evaluation is not consistent in this indicator (between good and medium, slightly biased and good). Scoring rules: for quantitative competency indicators, the comprehensive performance management personnel will compare the employee's performance data with the performance target schedule, analyze, and finally obtain the precise score. Qualitative competency indicators are divided into 5 grades: A, B, C, D, and E. The corresponding grades are evaluated by a 360-degree assessment of the competency of R&D personnel, including experts from the company's R&D personnel competency evaluation team. For the index rating, the corresponding scores are 10, 8, 6, 4, and 2, respectively. After the rating, fuzzy membership processing is performed, and the scores of the quantitative and qualitative indicators in Table 1 are standardized to [0, 1].

This paper analyzes the application data of R&D personnel in a high-tech enterprise. Quantitative indicators are mainly derived from statistics on the R&D statistical records of the high-tech enterprise, and qualitative indicators are mainly derived from the evaluation records and interviews of employees of the enterprise. The original data of the enterprise are shown in Figure 6. Before training the network, it is necessary to initialize the thresholds and weights of the network. The command newff to establish the network will directly initialize the thresholds and weights of the network when the network is established. Since the input data and output data are both between 0 and 1, the Logsig transformation function is applied to both the hidden layer.

Divide the value data of the 13 groups of R&D personnel competency indicators in Part 01 into the parts in Figure 6, select the first 7 groups of data in Part 01 and the 13 groups of data in Part 02 as learning samples, train neurons to connect weights and thresholds, select after the 01 part, 6 groups of data are checked and tested. When the number of training reaches 1 to 150, the training meets the required accuracy. It can be seen that the maximum relative error between the expected output and the training result is 0.15%, which meets the required accuracy. It can clearly reflect the importance of various indicators, including the application of information technology, the degree of perfection of information communication mechanism, the degree of information sharing, the real-time monitoring of WIP, RM, and

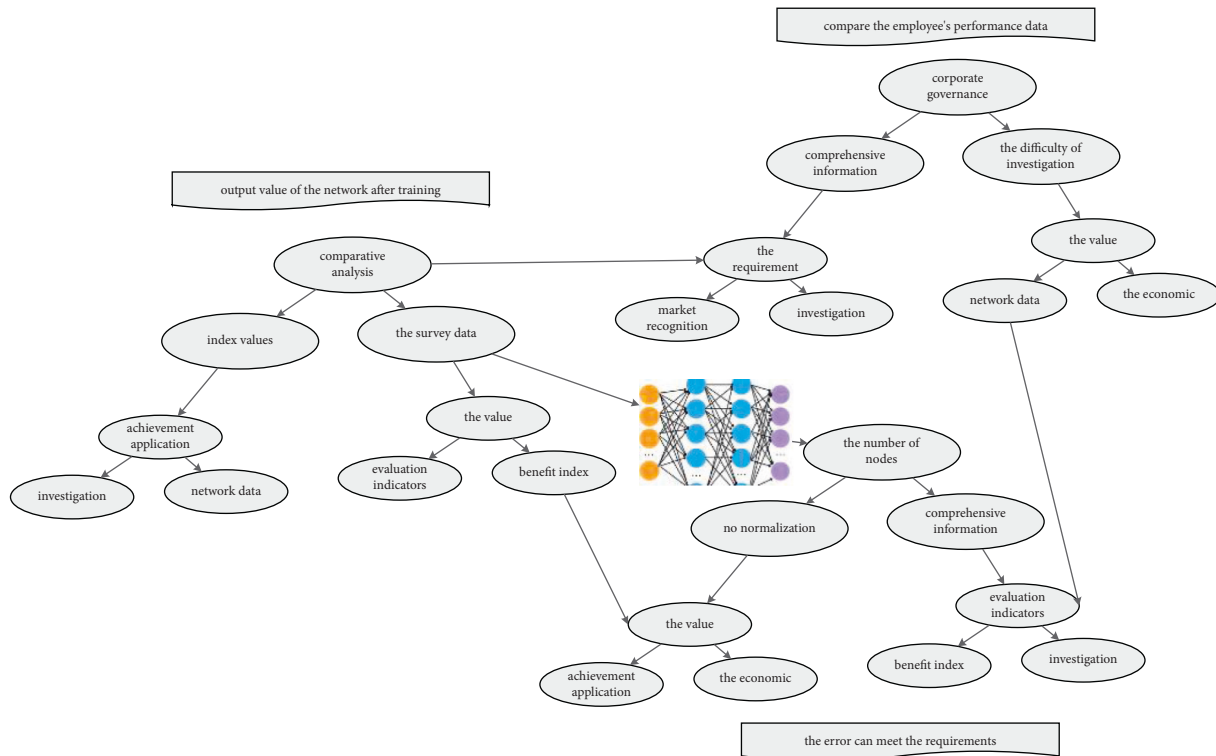


FIGURE 5: AHP and BP neural network data nodes.

TABLE 1: Description of network data fitness.

| Network | Mode 1 | Mode 2 | Mode 3 | Mode 4 | Mode 5 | Mode 6 | Mode 7 |
|---------|--------|--------|--------|--------|--------|--------|--------|
| Layer 1 | 0.45   | 0.76   | 0.95   | 0.16   | 0.49   | 0.56   | 0.27   |
| Layer 2 | 0.87   | 0.91   | 0.21   | 0.45   | 0.76   | 0.95   | 0.59   |
| Layer 3 | 0.67   | 0.45   | 0.33   | 0.87   | 0.91   | 0.21   | 0.80   |
| Layer 4 | 0.71   | 0.73   | 0.75   | 0.77   | 0.79   | 0.81   | 0.83   |
| Layer 5 | 0.18   | 0.16   | 0.14   | 0.12   | 0.1    | 0.08   | 0.06   |

FM, and the weights of the utilization rate of production forms and electronic case indicating that the lower-level indicators in the visualization have an impact on the adaptive force of the manufacturing system. This method is very convenient to apply, and the evaluation result can be obtained by inputting the information of the object to be evaluated.

#### 4. Application and Analysis of an Enterprise Comprehensive Performance Evaluation Method Based on AHP and BP Neural Network

4.1. AHP and BP Neural Network Data Pooling. DDU (Decomposition Decision Unit) is a decision subunit that decomposes AHP and BP neural network data. AHP is mainly used to normalize data, make evaluations, generate training samples and weights of various indicators, and input them into different data processing in STU. Among them, STU is a subtask processing unit (Subtask Processing

Unit), and the number of STUs is determined by DDU. The selected neural network implements the function of STU, and the neural network is trained according to the data sent by DDU. The data sent in different ranges are trained at the same time using different neural networks. In this paper, MATLAB software is used to program, the financial data of 20 three-level indicators of the previous 15 listed companies are used as the input of the network, the comprehensive score value is used as the output, and the dimensionless data is used to calculate the model. The comprehensive evaluation results and network fitting errors are shown in Figure 7.

The judgment matrix is obtained by sending out questionnaires to experts to collect the data. In this paper, the calculation process and numerical model of AHP are introduced. Combined with the obtained judgment matrix, the relative weights and total weights of each layer of indicators are calculated, and the RI and CI of the weights are tested to judge their validity. By distributing the judgment matrix questionnaire to 8 experts, the judgment matrix is constructed, the weight value obtained by each expert's judgment matrix is calculated, and then the average value of all

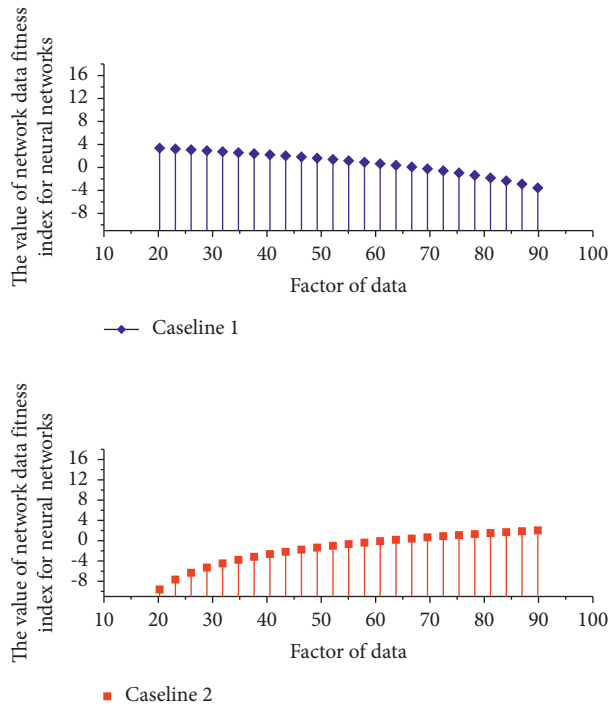


FIGURE 6: Values of network data fitness indicators.

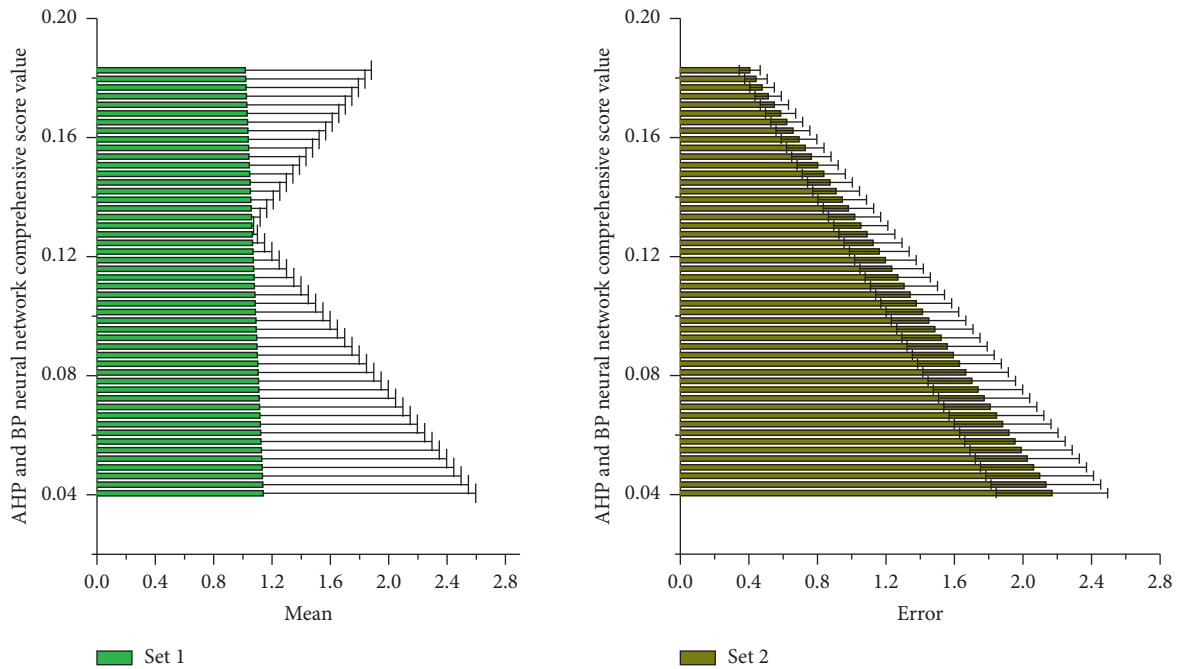


FIGURE 7: AHP and BP neural network comprehensive score value output.

weights is calculated by the average method to determine the indicators at all levels. In production flexibility, the application of information technology, the perfection of information communication mechanism, and judgment matrix for the degree of information sharing. From the table, it can be seen that the application of information technology has the largest weight, followed by the perfection of the information communication mechanism and the degree of

information sharing. Among them, in the evaluation of comprehensive performance, it can be seen from the data that the evaluation is not consistent in this indicator (between good and medium, slightly biased and good).

By analogy, the weights and consistency tests of the judgment matrices of the remaining experts are calculated. Figure 8 uses the average algorithm to take into account the opinions of each expert, weakening the bias caused by

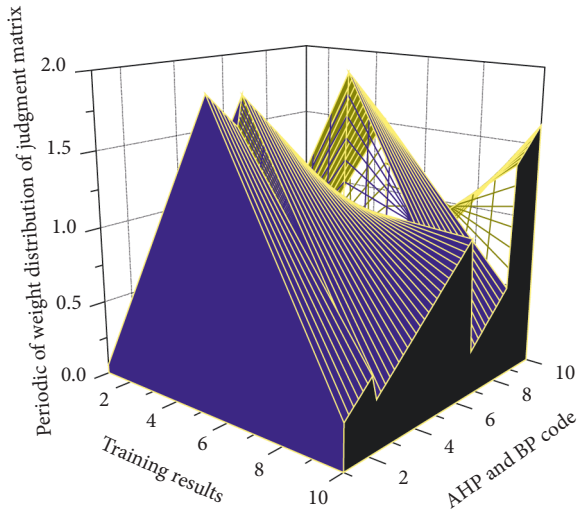


FIGURE 8: Weight distribution of judgment matrix of AHP and BP neural network.

personal subjectivity, and finally obtains the ranking of the weights of each single layer. Assuming that external factors (such as social environment, economic environment, and market environment) remain unchanged, according to the principle of index system construction, five categories of second-level indicators and corresponding 20 third-level indicators are selected, and AHP is used to construct the level of financing ability evaluation. structural model. The weight of each indicator is calculated based on the expert scores. The weights of the usage rate account for 0.1291, 0.0645, 0.0645, 0.0644, and 0.0645, respectively, and these weights are the largest values in the total ranking of the hierarchy, indicating that the lower-level indicators in the visualization have an impact on manufacturing. The overall performance of the system has a greater impact.

**4.2. Simulation Realization of Enterprise Comprehensive Performance Evaluation.** Based on 20 business sample data that have occurred in company A as the original data, this paper evaluates the accuracy and usability of the model through the evaluation of the AHP-BP model. According to the risk management rules of company A, the risk level of loan companies is generally divided into five grades: excellent, good, medium, poor, and extremely poor. The data involved in this paper are both quantitative and qualitative. Quantitative data can be obtained directly, while qualitative data are scored by experts to quantify qualitative data. Experts' scoring of quantitative data is based on the actual performance of related companies and the risk classification standards of company A. The expert scores are [0–10], “extremely poor” is [0–2), “poor” is [2–4), “moderate” is [4–6), and “good” is [6–8), “excellent” is [8–10]. According to the original data of company A and expert scores, the risk assessment samples are shown in Table 2.

In the Matlab programming of this article, the error precision is set to 0.15, the maximum number of iterations is

TABLE 2: Enterprise comprehensive performance evaluation score.

| Evaluation set | Poor  | Moderate | Good  | Excellent |
|----------------|-------|----------|-------|-----------|
| Data 1         | 39.65 | 71.90    | 87.17 | 90.88     |
| Data 2         | 44.90 | 43.33    | 66.71 | 44.61     |
| Data 3         | 77.04 | 76.38    | 86.77 | 98.35     |
| Data 4         | 43.14 | 42.62    | 24.80 | 26.52     |
| Data 5         | 11.34 | 88.06    | 26.74 | 97.92     |
| Data 6         | 12.06 | 99.31    | 33.62 | 20.12     |
| Data 7         | 0.39  | 55.34    | 51.31 | 61.42     |

5000 times, the step size is 0.05, the momentum coefficient is 0.25, and the initial weight and threshold are all assigned gradients with random numbers between [0, 1], and validation check are all system defaults. Too few neurons in the hidden layer will make the trained neural network not “robust” enough, and at the same time, the fault tolerance is poor, and there are too many neurons. It will make the network training time too long, and the error may not be the best. The most commonly used membership functions in current research are trapezoidal distribution, triangular distribution, rectangular distribution, and normal distribution. In the specific application process, the appropriate function can be selected as the membership function according to the actual situation of the research object, and the undetermined parameters in the membership function can be determined. After calculation, 8 groups are selected from Figure 9 as training data.

The model in this paper has tested the network training situation from 14 to 20 hidden layer neurons, and the accuracy is all up to the requirements, but although increasing the number of neurons will improve the accuracy, it will also change the training time and error. The best combination of accuracy and training time is achieved when there are layers of neurons. The maximum relative error of the neural network simulation is 1.64%, which is far below the general accuracy requirement of 5%, and the neural network evaluation performs well. According to the simulation diagram, the risk level of each assessed enterprise can be clearly displayed: No. 17 enterprise is “good”, No. 18 and 19 enterprises are “medium”, and No. 20 enterprise is “excellent”. In DDU, the agility value is 0. The membership value of each index is calculated by the method of a trigonometric linear function, and finally, the evaluation result is obtained. Then, the obtained data is used as a sample for neural network training to be simulated and tested. From the analyzed data, the effect of the modular neural network is better.

According to the steps of the analytic hierarchy process, first determine the index weight and obtain the index weight from the formula:  $W = [0.0292, 0.0118, 0.0719, 0.0252, 0.0444]$ . Experts scored each sample in Figure 10 according to the original data and enterprise risk assessment standards and obtained the AHP evaluation score of each sample according to the above weights. The scores in the original table will no longer be included in the evaluation, and only some raw data will be scored. From the image before improvement, we can see that the fitness rises relatively slowly, and even the maximum fitness is still declining at the beginning, and it falls into a local optimal solution later. This

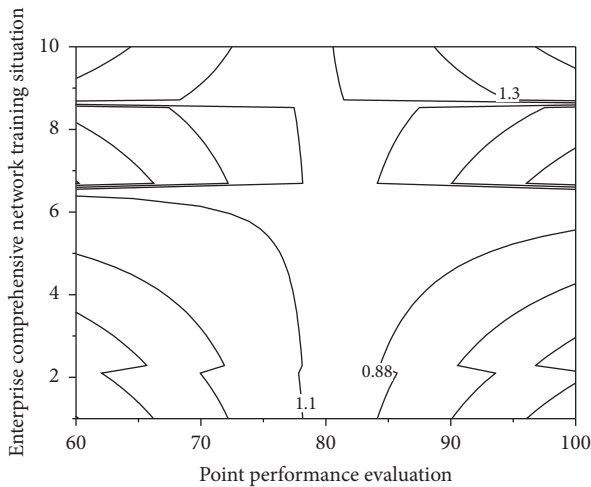


FIGURE 9: Network training situation of enterprise comprehensive performance evaluation.

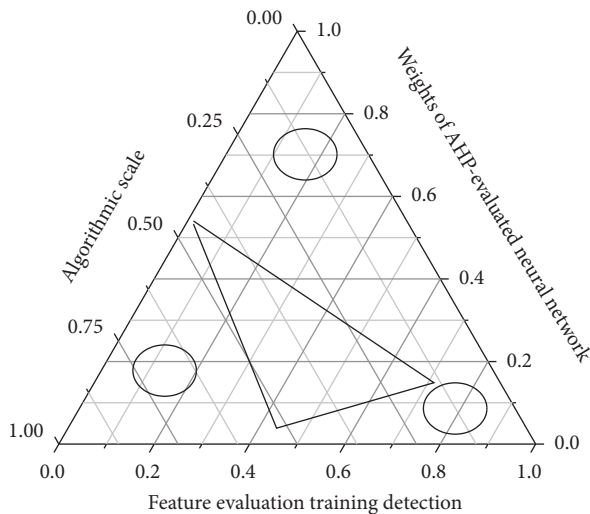


FIGURE 10: Neural network evaluation training situation for AHP evaluation.

coefficient is the actual embodiment of the main content of operating profit and is very important to the current assets of the sample. If it is measured by time, it means the time from the establishment of the account receivable to the account. It can be seen from the table that the improved BP algorithm can obtain a high-quality solution in a short time, greatly improve the convergence speed of the search, and significantly improve the global optimization performance.

## 5. Conclusion

Based on the research on modern comprehensive performance evaluation methods, this paper determines the evaluation method combining AHP and BP neural network. Firstly, the AHP and BP neural networks are summarized, respectively, and their basic principles and application processes are introduced; secondly, the process of calculating index weights and screening important indicators is

proposed; finally, based on the screening results, BP neural network is used to carry out scientific case. In the comprehensive performance evaluation, the BP neural network is trained first with the learning samples, and then the performance of the network is verified with the test samples; the simulation research proves that the method is effective. In the comprehensive performance indicators, the relevant research on agility indicators is referenced, which shows that comprehensive performance and agility have something in common, and the research on comprehensive performance is the inheritance and development of agility. The advantage of the neural network is that according to the operation performance of the manufacturing system in the actual process, through self-learning and self-correction, the evaluation results are more in line with the actual situation. In future research, attention should be paid to finding more reasonable and feasible methods to process the data more reasonably. The research method in this paper can effectively absorb the advantages of the two methods, simplify the difficulty of system decision-making, and improve the efficiency and accuracy of evaluation.

## Data Availability

The data used to support the findings of this study are available from the author upon request.

## Conflicts of Interest

The author declares that there are no conflicts of interest.

## Acknowledgments

This work was supported by the 2019 School Level Teaching and Research Project: Audit virtual simulation experiment teaching center (Project no: ch19xfn02).

## References

- [1] W. Li, G. Xu, D. Zuo, and J. Zhu, "Corporate social responsibility performance-evaluation based on analytic hierarchy process-fuzzy comprehensive evaluation model," *Wireless Personal Communications*, vol. 118, no. 4, pp. 2897–2919, 2021.
- [2] Y. Shu and G. h Xu, "Multi-level dynamic fuzzy evaluation and BP neural network method for performance evaluation of Chinese private enterprises," *Wireless Personal Communications*, vol. 102, no. 4, pp. 2715–2726, 2018.
- [3] W. Li, G. Xu, Q. Xing, and M. Lyu, "Application of improved AHP-BP neural network in CSR performance evaluation model," *Wireless Personal Communications*, vol. 111, no. 4, pp. 2215–2230, 2020.
- [4] G. Candan and M. Cengiz Toklu, "Sustainable industrialization performance evaluation of European Union countries: an integrated spherical fuzzy analytic hierarchy process and grey relational analysis approach," *The International Journal of Sustainable Development and World Ecology*, vol. 24, pp. 12–14, 2022.
- [5] J. Gao, "Performance evaluation of manufacturing collaborative logistics based on BP neural network and rough set," *Neural Computing & Applications*, vol. 33, no. 2, pp. 739–754, 2021.



- [6] Z. Geng, D. Shang, Y. Han, and Y. Zhong, "Early warning modeling and analysis based on a deep radial basis function neural network integrating an analytic hierarchy process: a case study for food safety," *Food Control*, vol. 96, pp. 329–342, 2019.
- [7] C. Yujie, G. Weimin, K. Chelli, and K. M. Ahmed, "Performance evaluation of college laboratories based on fusion of decision tree and BP neural network," *Applied Mathematics and Nonlinear Sciences*, vol. 2022, 2022.
- [8] Y. Wan, "Research on performance evaluation index system and empiricism of network marketing," *International Symposium on Social Science*, vol. 5, pp. 579–583, 2018.
- [9] Y. Xiong, J. Zhao, and J. Lan, "Performance evaluation of food cold chain logistics enterprise based on the AHP and entropy," *Research Anthology on Food Waste Reduction and Alternative Diets for Food and Nutrition Security*, vol. 2, pp. 395–405, 2021.
- [10] Y. Luo and D. Ren, "Influence of the enterprise's intelligent performance evaluation model using neural network and genetic algorithm on the performance compensation of the merger and acquisition parties in the commitment period," *PLoS One*, vol. 16, no. 3, Article ID e0248727, 2021.
- [11] Z. Geng, L. Liang, Y. Han, and T. Guangcan, "Risk early warning of food safety using novel long short-term memory neural network integrating sum product based analytic hierarchy process," *British Food Journal*, vol. 2, 2021.
- [12] Y. Li, S. Huang, C. Yin, G. Sun, and C. Ge, "Construction and countermeasure discussion on government performance evaluation model of air pollution control: a case study from Beijing-Tianjin-Hebei region," *Journal of Cleaner Production*, vol. 254, Article ID 120072, 2020.
- [13] Q. Y. Zhang, "Research on hybrid intelligent algorithm for comprehensive evaluation of aviation logistics performance," in *Proceedings of the Intelligent transportation, big data & smart city (ICITBS)*, pp. 477–480, Xi'an, China, March 2021.
- [14] H. Wu and Y. Qi, "Computer performance appraisal system based on balanced scorecard under the internet background," *Journal of Physics: Conference Series*, vol. 1881, no. 3, Article ID 032012, 2021.
- [15] Y. Zhao, "Influence of deep learning neural network on performance evaluation of sustainable development of international trade," *Academic Journal of Business & Management*, vol. 2, no. 2, 2020.
- [16] W. Liang and T. Li, "Research on human performance evaluation model based on neural network and data mining algorithm," *EURASIP Journal on Wireless Communications and Networking*, vol. 4, no. 1, pp. 11–14, 2020.
- [17] Z. Huang, J. He, and X. Ren, "Application of artificial intelligence in enterprise knowledge management performance evaluation," *Knowledge Management Research and Practice*, vol. 7, pp. 7–9, 2021.
- [18] Y. Zhang, Q. Ding, and J. B. Liu, "Performance evaluation of emergency logistics capability for public health emergencies: perspective of COVID-19," *International Journal of Logistics Research and Applications*, vol. 11, pp. 1–14, 2021.
- [19] X. Cai, Y. Qian, Q. Bai, and W. Liu, "Exploration on the financing risks of enterprise supply chain using Back Propagation neural network," *Journal of Computational and Applied Mathematics*, vol. 367, Article ID 112457, 2020.
- [20] S. Qian, "Construction of financial credit risk evaluation system model based on analytic hierarchy process," *Cyber Security Intelligence and Analytics*, vol. 9, pp. 488–496, 2022.
- [21] G. Wang, "Research on network security risk assessment method based on improved analytic hierarchy process[[]]," *International Journal on Network Security*, vol. 23, no. 3, pp. 515–521, 2021.
- [22] I. Yazici, O. F. Beyca, and O. F. Gurcan, "A comparative analysis of machine learning techniques and fuzzy analytic hierarchy process to determine the tacit knowledge criteria," *Annals of Operations Research*, vol. 308, pp. 21–24, 2020.
- [23] A. Yu, Z. Jia, W. Zhang, K. Deng, and F. Herrera, "A dynamic credit index system for TSMEs in China using the delphi and analytic hierarchy process (AHP) methods," *Sustainability*, vol. 12, no. 5, p. 1715, 2020.
- [24] Y. Wang and P. Fu, "Integration performance statistics of green suppliers based on fuzzy mathematics and BP neural network," *Journal of Intelligent and Fuzzy Systems*, vol. 40, no. 2, pp. 2083–2094, 2021.
- [25] H. Li, Q. Zhang, and Z. Zheng, "Research on enterprise radical innovation based on machine learning in big data background," *The Journal of Supercomputing*, vol. 76, no. 5, pp. 3283–3297, 2020.

## Research Article

# Industrial Land Performance Assessment Based on Fuzzy Analytic Hierarchy Process

Jing Lv  and Sijia Ge

Jilin Jianzhu University, ChangChun 130118, JiLin, China

Correspondence should be addressed to Jing Lv; lvjing@jlju.edu.cn

Received 24 June 2022; Revised 15 July 2022; Accepted 22 July 2022; Published 25 August 2022

Academic Editor: Man Fai Leung

Copyright © 2022 Jing Lv and Sijia Ge. This is an open access article distributed under the Creative Commons Attribution License, which permits unrestricted use, distribution, and reproduction in any medium, provided the original work is properly cited.

The use of industrial land tends to be standardized and rational, but the total amount of developed industrial land has reached its limit in many places. Under such circumstances, industrial transformation and upgrading are difficult, and how to improve the quality and efficiency of the stock space must become the key to the problem. Therefore, this paper proposes to take X city industrial land as the research object, with the help of multidimensional feature analysis of spatial performance evaluation, and apply the method of Fuzzy analytic hierarchy process to explore the refined utilization of industrial land promoted by spatial calculation. Through example analysis, the results of site-specific spatial performance evaluation are derived by using various weighted evaluation factors.

## 1. Introduction

With the acceleration of global industrial reform and urbanization, the “bottom-up” process of rural industrialization has led to a low threshold for industrial land access, which is reflected in a high degree of spatial fragmentation and wasteful allocation of resources. Although the intensive industrial land development model of “farmers in the city, industry in the park” has been the mainstream of planning since the 1990s, the complex entanglement of property rights and the redistribution of differential land rent have made this model unsustainable. With the advent of the new economic norm, land is bound to undergo a functional transformation. How to find a balance in the reform and how to scientifically judge the reorganization function of urban and rural land is an urgent issue for local governments in the Pearl River Delta. The spatial performance of land use is a reflection of the comprehensive effectiveness of urban land use function. The systematic study of “urban spatial performance” according to the law of urban space operation is conducive to improving the effectiveness and relevance of planning disciplines and planning practices. Only by meeting the development needs of various urban functions to the maximum extent and allocating various spatial

resources reasonably can we effectively improve the comprehensive benefits of cities. Therefore, the establishment of a spatial performance assessment system for industrial land can help the government scientifically formulate public policy tools, including urban planning, and facilitate the effective operation of the land market. Currently, China’s industrial economy is moving toward a new normal of slow speed and good structure, facing problems such as industrial structure adjustment and stable growth rate, development of high-tech industries, and the tightening of resource and environmental constraints [1].

Development zone construction includes regional development such as economic and technological development zones, high-tech development zones, bonded zones, border economic cooperation zones, tourist resorts, and similar regional development projects such as industrial parks. With the rapid development of various development activities, the demand for land in China is increasing at this stage and land development has to be expanded to land that was previously considered unsuitable for development. The construction of development zones is bound to occupy a certain amount of agricultural land, thus making the conflict between industrial land and agricultural land increasingly acute. According to statistics, in 2000, China had 128 million  $\text{hm}^2$  of

agricultural land with  $0.101 \text{ hm}^2$  of agricultural land per capita, less than half of the world's per capita agricultural land. In 2000, various kinds of construction occupied  $163,000 \text{ hm}^2$  of agricultural land, according to which, the situation of land resources in China is very serious. Moreover, from the total natural productivity of land in 2000, the annual biological production is about  $32 \times 10^8$  tons of dry matter, and the reasonable carrying capacity of the population is 950 million. Land resource conservation and rational development and utilization of land resources are the urgent problems facing the sustainable use of land in China.

As an important carrier of industrial undertaking, China's industrial land has maintained rapid growth and has undergone changes from scattered layout to park agglomeration. At the same time, due to the dual effects of urbanization and post-industrialization, the overlap between industrial land and urban land, lack of planning, duplication of structure, and confusion about the layout of industrial land have become increasingly acute. Ensuring the rational layout and effective supply of industrial land and promoting the safe integration of production cities have become bottlenecks in the development of many cities. Space security for industrial land will be directly related to the socio-economic and ecological security of the region and the scientific assessment of the space security of industrial land will be conducive to optimizing the allocation of land resources. Realizing the "win-win" between industrial development and land space security finally realized the integration development of town, people, and industry in function and space, that is, the integration of production city [2].

In regional natural resources, land resources are non-renewable resources on which the regional economy depends. It has become an important part of urban ecosystems through various construction activities, such as regional infrastructure land, corresponding supporting facilities in parks, etc. However, if the land to be exploited and the whole natural environment are not clearly understood, the capacity of natural environment and the appropriateness of land use are ignored, the overexploitation will lead to the occurrence of natural disasters, ecosystem damage, and other serious ecological negative effects.

Economic development will lead to the destruction of the ecological environment. But as the population grows and the demand for consumption increases, there is also an urgent need to develop the economy to improve people's lives [3]. To coordinate the relationship between the two in the face of the contradiction between economic development and ecological protection, a win-win situation is an important task [4]. History has told us that the path to pollution and then management is not feasible. Therefore, according to the principle of ecological priority, the quality of the ecological environment can be reasonably evaluated to determine whether it is suitable for industrial development. To put forward, reasonable environmental protection measures for existing problems will play a fundamental role in regional sustainable development and ecological environment management. Therefore, for urban land resources, cherish

every inch of urban land, we should develop and utilize land resources scientifically and rationally.

Theoretical studies on the ecological safety of industrial land have always accompanied the stages of industrial development. At the early stage of industrialization, the ecological safety of industrial land mainly focused on suitability evaluation [5], and the scope of research ranged from individual industrial parks to cities [6] and larger regions [7]. With the explosive growth of industrial parks, intensive and economical utilization within the industrial land has gradually become the focus of research [8], and scholars have combined different scales to propose various evaluation indexes [9], mainly involving the degree of land development, the degree of land input, land use intensity, land use efficiency, and land structure. With the advent of post-industrialization and comprehensive urbanization era, scholars mostly start from the urban construction land as a whole and conduct research on the evolution of urban spatial structure [10], urban land scale boundary [11], and optimization of land use pattern [12] to provide technical support for the safe and efficient use of urban land [13]. In contrast, there are few studies on the relationship between the layout of industrial land and other land and the performance evaluation of industrial land layout.

After reform and opening up, the development of both local and foreign industries is based on cheap resources, including land, labor, environmental costs, etc., and with the process of the localized economy, many small industrialized towns are formed, becoming the main areas carrying primary processing industries. However, after the rapid development of these small towns in the early stages, the characteristics of inadequate land use and inefficient land use gradually emerged. On the one hand, the proportion of industrial land has long exceeded reasonable limits. For example, in some small towns in the Yangtze River Delta and the Pearl River Delta, the built-up area covers not only the entire town area but also the proportion of industrial land far exceeds the standard. On the other hand, the industrial structure is unreasonable, used inefficiently, and occupies a large amount of land. Related research reveals the fragmentation and inefficient utilization of industrial land at different levels and gives the countermeasures in combination with the forming reasons, but it is limited to qualitative research whether it is an integrated layout or optimized configuration. The land use performance evaluation can be traced to the land rent theory of classical political economy at the earliest. However, in China, due to the restriction of industrial land data acquisition, the performance evaluation can be carried out gradually after 2000. The content of the evaluation usually focuses on the intensity of industrial land development, input and output, and economic benefits, and different methods are used for industrial land performance evaluation (1) to strengthen the intensive use of industrial land by evaluating the intensity of land use, the degree of input, the efficiency of use, and other core elements [14], and to propose ways and measures for intensive use of industrial land; (2) to explore ways and systems for the supply of industrial land, to study the performance of industrial land use using an industrial land

renewal benefit reduction mechanism or an industrial land use based on liability positioning method [15]. A quantitative evaluation study on the performance of industrial land supply, and according to the development process and characteristics of industrial land in China, explore the path of innovation evaluation [16]; (3) to update the stock of industrial land, quantify it with indicators such as location, plot ratio, production efficiency, property rights, etc., performance evaluation of inefficient industrial land through hierarchical analysis and to explore the application in planning control [17]. These studies are gradually establishing methods for evaluating the performance of industrial land in different dimensions. The evaluation, however, ignores businesses that are land users. This is the core element of the current industrial development and transformation period.

The regional land ecological environment is a complex giant system containing many factors. Only by reasonably selecting the evaluation factors, establishing a hierarchical index system, and assigning reasonable weight values to each index can, we ensure the reasonableness of the evaluation results. Since the evaluation of regional ecological environment quality involves not only a large number of complex phenomena and the interaction of many factors, there are a lot of fuzzy phenomena and fuzzy concepts in the evaluation, which requires a clear quantitative concept to reflect the severity of ecological damage, but also requires that the quantitative index can appropriately reflect the inherent criteria of environmental quality classification and the continuity of environmental quality changes. The fuzzy theory is an effective tool to deal with the problem of ambiguity. Therefore, in this study, the Fuzzy analytic hierarchy process (FAHP) was considered for the evaluation of industrial land performance indicators. The specific technical route is described in Figure 1.

## 2. Fuzzy Analytic Hierarchy Process

**2.1. Fuzzy Set Theory.** Fuzzy mathematics is based on the theory of fuzzy sets. The concept of fuzzy sets corresponds to the classical notion of either/or sets, describing sets without clear and well-defined boundaries. It emerged in the 1960s as a mathematical approach to the study and treatment of “fuzzy” phenomena. The so-called fuzziness refers to the indistinctness and uncertainty of objective things, which is rooted in the existence of a mid-valve transition between objective differences, such as “good and bad” in the evaluation of environmental quality. In daily life “Early and late,” “more and less,” etc., are difficult to draw a clear line. Auxiliary mathematics is based on set theory. According to the requirements of set theory, an object either belongs to a set or not. There are no ambiguous cases of belonging and not belonging at the same time. This precision of set theory greatly limits its scope of application. It makes it unable to deal with the ambiguities of everyday life. Faced with this situation, in 1965, the American cybernetics expert Zadeh [18] published his famous paper marking the birth of the new discipline of fuzzy mathematics. Although only 40 years

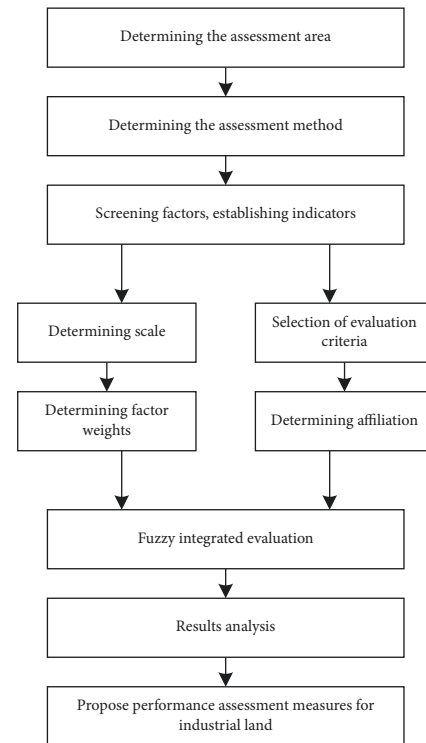


FIGURE 1: Schematic diagram of the basic research route.

have passed, the development of fuzzy mathematics has been exceptionally rapid, and its application has involved almost all fields and sectors of the national economy. Fuzzy mathematics has been widely and successfully used in agriculture, forestry, meteorology, environment, geological survey, military, and other fields.

The theory and method of fuzzy mathematics show its superiority when the object cannot be accurately described by classical mathematics. The appropriateness of industrial supervisory land is determined by various factors. When evaluating the suitability of industrial land at the location of the development zone, it is impossible to get a very precise result. The main problems that need to be determined by the evaluation of fuzzy mathematical theory are the determination of factor weight, the establishment of affiliation dispersion, and the selection of the evaluation model.

The main difference between fuzzy sets and ordinary sets is that there are only two relations between elements in the domain and ordinary sets. There are many relationships between fuzzy sets and elements, which can be represented by any value on  $[0, 1]$ . Taking “0” means that the element does not belong to the fuzzy set, taking “1” means that the element belongs entirely to the fuzzy set, taking “0.3” means that the element belongs to the fuzzy set to a degree of 0.3, and so on. The number taken is called the affiliation of the element to the fuzzy set. Affiliation is an indicator of the fuzziness of characterization factors. It can be said to be the cornerstone of fuzzy sets is applied to practical problems. If this affiliation varies with a variable, the affiliation function needs to be established. The membership function is generally denoted by  $A(x)$ .

To solve a practical problem, generally, is to determine the degree of affiliation function scatter. However, the affiliation function is often not declared and given, and its determination is generally approximated by using the method of inference. Its determination process is objective in nature. However, a certain amount of artificial skill is allowed, and sometimes the artificial skill plays a decisive role in the solution of the problem. It is worth noting that the artificial skill should be reasonable and not contrary to the objective reality. It can be given by fuzzy statistical tests or by the typical function method summarized by practical experience.

The weight coefficient is a quantitative description of the importance of each factor in the evaluation domain, which can be regarded as the affiliation of each factor in the evaluation domain with respect to the "importance." The assigned weights in common evaluation problems are generally subjective based on experience and are highly subjective. In some cases, the subjective determination of weights has an objective aspect and reflects the actual situation to a certain extent. However, in most cases, the evaluation results of the subjective determination method are usually seriously distorted and may lead to misjudgment of decision makers. As a rule, mathematical methods should be used more often to determine weights, although they are also subjective in nature. However, due to the strict logic of mathematical methods, the determined weights can be processed, thus eliminating as much subjective components as possible and conforming to objective facts.

There are various methods for determining the weights, such as expert empirical estimation, survey statistics, hierarchical analysis, fuzzy inverse equation method, and sequential synthesis method. The literature points out that the accuracy of the hierarchical analysis method in weight calculation is relatively better [19]. Moreover, the hierarchical analysis method requires less data, takes less time to score, has less computational effort, and is easy to understand and master. In view of the advantages of the hierarchical analysis method, and considering the popularity and relative objectivity of the expert empirical estimation method in practice, this study uses the combination of the hierarchical analysis method and the expert scoring method to determine the weights of each index affecting the suitability of the industrial land.

The analytic hierarchy process (AHP) is essentially a way of thinking about decision-making, that is, decomposing a complex problem into component factors, grouping these factors into an orderly hierarchical structure according to the dominant relationship, determining the relative importance of each factor in the hierarchy through a two-by-two comparison, and then integrating human judgment to determine the total relative importance of each factor. This is a reasonable way to solve the process of quantifying qualitative problems. The basic steps of using hierarchical analysis to solve the intrusion problem are as follows: (1) clarify the problem and establish the hierarchical structure; (2) construct a two-by-two judgment matrix; (3) calculate the relative weights of the elements being compared; (4) calculate the combined weights of the elements in each hierarchy.

Defining the problem and establishing the hierarchy is the most important step of AHP. First, the complex problem is decomposed into component elements, and these elements are divided into groups according to different attributes to form different levels. The elements of the same level act as a criterion to dominate some elements of the next level, and at the same time, it is dominated by the elements of the previous level. This top-down dominance relationship forms a hierarchy. A typical hierarchy can be represented in Figure 2. In a recursive hierarchy, the number of levels generally depends on the complexity of the intrusion and the level of detail required for the analysis. The number of elements contained in the same hierarchy is usually no more than 9. The number of elements included is too large, which can make it difficult to compare two comparisons. The index system established in this study is a recursive hierarchy, including three levels, target level, criterion level, and sub-criterion level, in which the regional industrial land suitability level is the target of evaluation.

The hierarchical analysis method is also based on expert survey scoring, but the method of comparing grading and calculating weight coefficient is different. The experiments show that when people compare the different important degrees of multiple factors, they cannot compare and judge too much. Usually, the number of factors a person can compare simultaneously cannot exceed 9. However, a comparison of the degree of importance difference between the two factors. Man is perfectly competent. Therefore, the "two-two comparison method" can be used for multi-factor weight analysis, and only two factors are of relative importance to each other in  $n$  factors. A measure of relative importance between factors is called a judgment scale.

*2.2. Fuzzy Integrated Evaluation.* Here, it is assumed that the upper-level element  $C$  is the criterion or sub-criterion, and the elements governing the next level are  $u_1, u_2, \dots, u_n$ . The judgment matrix is the basic information of the hierarchical analysis method, and it is also an important basis for the relative importance calculation of each factor in this study. The judgment matrix is a two-by-two comparison of the elements of this level to determine the elements in the matrix with the upper-level element  $C$  as the evaluation criterion, and the judgment matrix with  $n$  factors with  $C$  as the evaluation criterion is as follows in Table 1.

So the judgment matrix  $A$  could be expressed as equation (1):

$$A = [a_{ij}]_{n \times n} \quad (1)$$

In the general evaluation problem, the evaluator cannot judge the value of the weight indicator  $w_i / w_j$  very precisely, but can only estimate it. If there is an error in the estimation, it will inevitably lead to deviations in the eigenvalues of the judgment matrix as well. This means that the judgment matrix obtained by the two-by-two comparison method may have inconsistent judgments, so a consistency test is required. By consistency, it means that when  $X_1$  is more important than  $X_2$  and  $X_2$  is more important than  $X_3$ , then  $X_1$  must be considered more important than  $X_3$ . When the

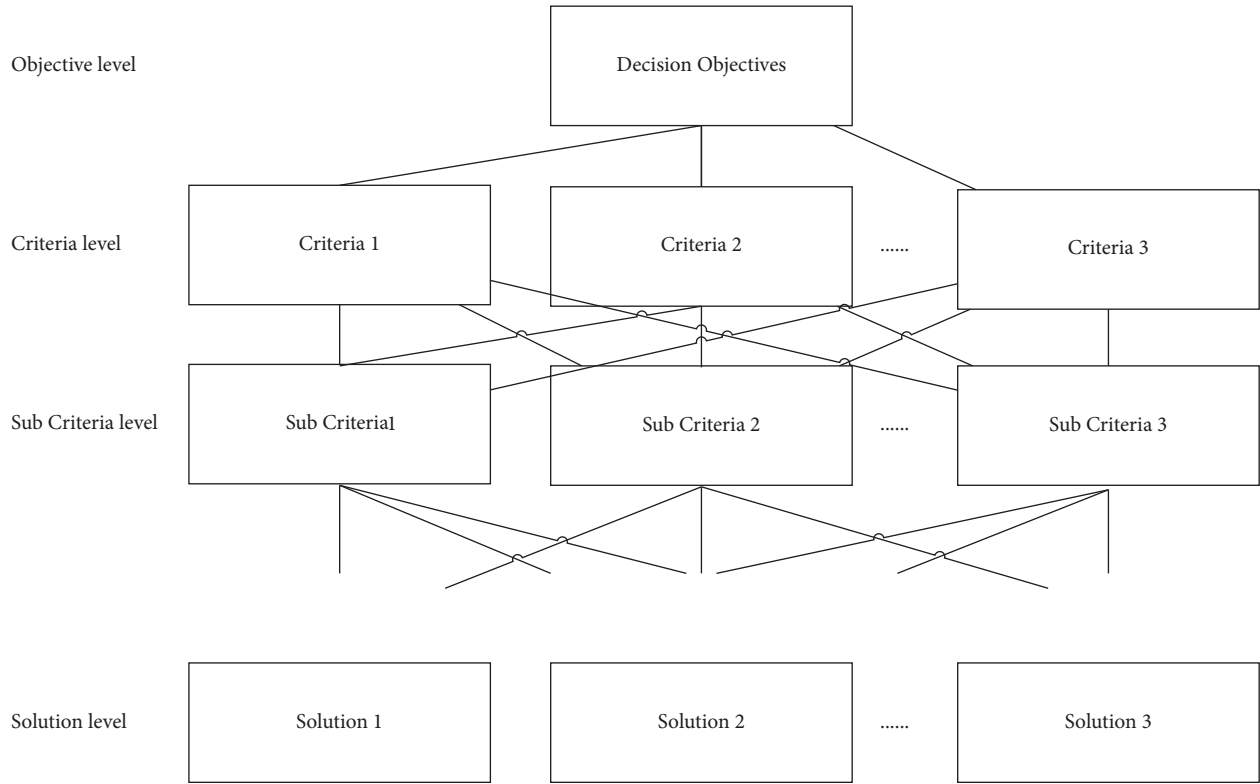


FIGURE 2: Schematic diagram of the recursive hierarchy.

TABLE 1: Form judgment matrix.

| $C$   | $u_1$    | $u_2$    | ... | $u_j$    | ... | $u_n$    |
|-------|----------|----------|-----|----------|-----|----------|
| $u_1$ | $a_{11}$ | $a_{12}$ | ... | $a_{1j}$ | ... | $a_{1n}$ |
| $u_2$ | $a_{21}$ | $a_{22}$ | ... | $a_{2j}$ | ... | $a_{2n}$ |
| ...   | ...      | ...      | ... | ...      | ... | ...      |
| $u_i$ | $a_{i1}$ | $a_{i2}$ | ... | $a_{ij}$ | ... | $a_{in}$ |
| ...   | ...      | ...      | ... | ...      | ... | ...      |
| $u_n$ | $a_{n1}$ | $a_{n2}$ | ... | $a_{nj}$ | ... | $a_{nn}$ |

judgments are in complete agreement, there should be  $\lambda_{\max} = n$ . Consistency indicators, CI, can be written as equation (2):

$$CI = \frac{\lambda_{\max} - n}{n - 1}. \tag{2}$$

When consistent,  $CI = 0$ , and  $CI > 0$  when non-consistent. Regarding how to measure the acceptability of CI values, Saaty [20, 21] constructed the most inconsistent case by taking  $1/9, 1/7, 1/5, \dots, 5, 7, 9$  randomly taken values of elements in the judgment matrix for different  $n$ , and used 100 to 500 subsamples for different  $n$  to calculate their consistency indexes, and then found the average value, noted as RI.

Fuzzy synthesis evaluation is a proven decision-making method to solve multi-factor and multi-indicator synthesis problems. It applies the characteristics of fuzzy relationship synthesis and makes a comprehensive evaluation of the affiliation level of the evaluated thing from multiple indicators according to the given evaluation criteria and the

measured values. It divides the change interval of the evaluated thing and analyzes the degree of the thing belonging to each level, which makes the description of the thing more in-depth and objective, and the analysis result more accurate. The operation process of fuzzy comprehensive evaluation is shown in Figure 3.

One-level evaluation is the basis of multi-level evaluation. Generally speaking, the first-level fuzzy comprehensive evaluation is carried out mainly in the following steps.

- (1) Determine the set of factors and the set of comments to establish the set of factors and the set of comments is the first step of evaluation. A fuzzy comprehensive evaluation is a comprehensive evaluation that considers all factors related to the evaluated thing, and its focus is on all relevant factors to be considered. Therefore, a factor set is created. To clearly describe the evaluation results, it is necessary to classify the evaluation results into certain levels, so it is necessary to establish a set of comments at the same time.
- (2) Determining the affiliation function based on the evaluation criteria. The affiliation function is based on the established evaluation criteria, and the purpose is to evaluate the affiliation level by dividing the evaluation factors through certain function operations to make the original ambiguous mathematical concept intuitive. At present, the affiliation function is widely used in a variety of affiliation functions, and I used the actual frequency of the current ascending

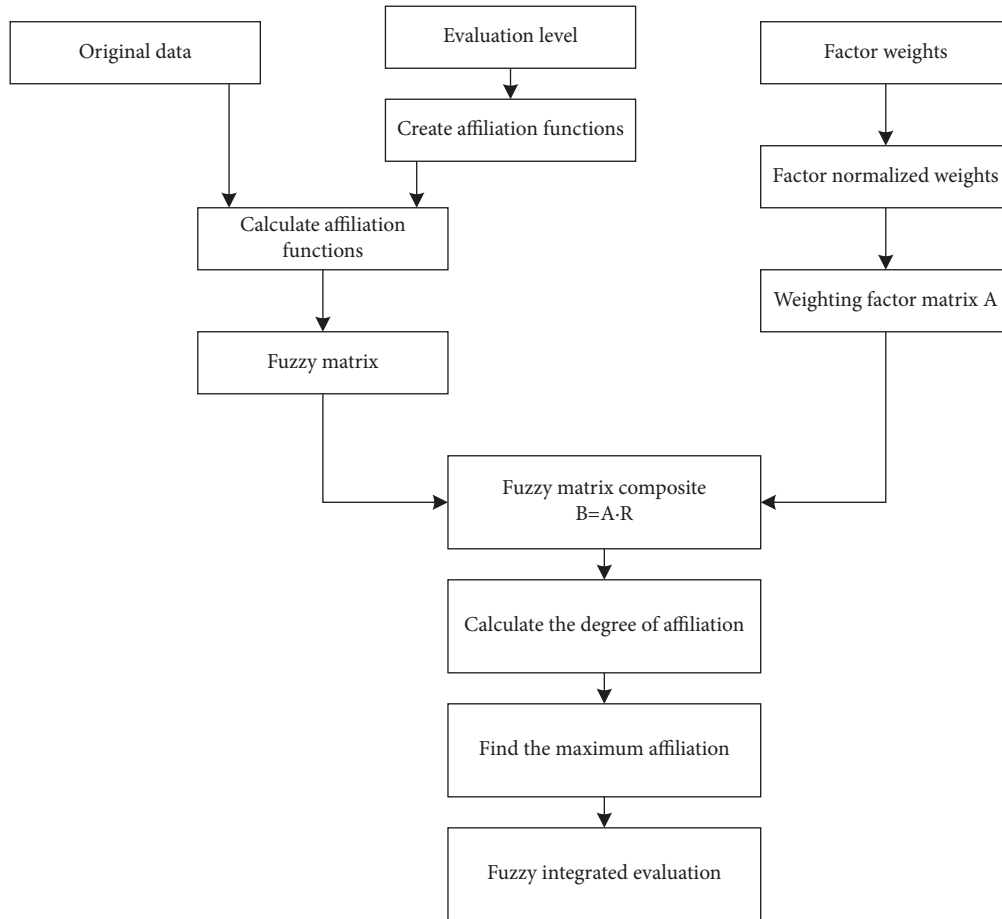


FIGURE 3: Fuzzy comprehensive evaluation flow diagram.

semi-trapezoidal affiliation function and descending semi-trapezoidal affiliation function. The ascending semi-trapezoidal affiliation function is applied to those negative effect indicators that are less applicable to industrial sites with higher values. The descending semi-trapezoidal affiliation function is applied to those positive indicators whose larger values indicate better suitability of industrial land. In practical application, the affiliation function should be selected scientifically according to the focus of evaluation work and the change rule of factors.

- (3) Determine the affiliation degree of each indicator. Based on the affiliation function constructed in step 2, the affiliation degree of  $u_i$  on the rubric  $v_j$  level can be solved - denoted by  $\gamma_{ij}$ . The affiliation degree of each factor for each evaluation level constitutes a vector  $R_i = (\gamma_{i1}, \gamma_{i2}, \gamma_{i3}, \dots, \gamma_{in})$ . It is a fuzzy subset on the decision rubric  $V$ .
- (4) Determine the weights of the factors. In the comprehensive evaluation, it is necessary to know the relative importance of each factor with respect to  $C$ , i.e., the weight of each factor. To do this, we can find the eigenvector  $W$  of the judgment matrix  $A$  and then normalize it to find the relative importance (weight) of each factor with respect to  $C$ .

- (5) The fuzzy matrix composite operation is to synthesize the weight set  $A$  and the affiliation set  $R$  rows according to a certain algorithm, such as equation (3).

$$B = A \cdot R = (b_1, b_2, \dots, b_n)$$

$$= (a_1, a_2, \dots, a_n) \cdot \begin{pmatrix} \gamma_{11} & \gamma_{21} & \dots & \gamma_{1n} \\ \gamma_{21} & \gamma_{22} & \dots & \gamma_{2n} \\ \dots & \dots & \dots & \dots \\ \gamma_{m1} & \gamma_{m2} & \dots & \gamma_{mn} \end{pmatrix}. \quad (3)$$

$B$  is the rank fuzzy subset on the set of decision rubrics  $V$ , and  $b_j$  ( $j = 1, 2, 3, \dots, n$ ) is the affiliation of rank  $V_j$  to the set of rank fuzzy subsets obtained from the composite rubric.

- (6) Draw the conclusion.

If  $b_j = \max(b_1, b_2, \dots, b_n)$ , then make a comment on the judged object  $v_j$ .

In the more complex system, when many factors need to be considered and the evaluation elements have a mutual influence on each other, it is inevitable that each factor is assigned a small weight, and it is not easy to determine. At this time, the first level of comprehensive evaluation may be that too small weights do not work and lose a lot of useful

information, so the results should not be obtained. However, we can divide all the factors into several categories to determine the relative importance of the factors in a smaller range more accurately, set the weight vector, and then perform the comprehensive evaluation.

**2.3. One-Level Comprehensive Evaluation for Spatial Performance.** The purpose of spatial performance evaluation is to grasp the status of industrial land use and provide a basis for formulating land use and industrial development strategies. In addition to the selection of indicators for the industrial land itself, the indicator system also needs to consider the spatial characteristics of the hosted industrial enterprises. Moreover, the use of industrial land in small towns not only affects the development of towns but also directly affects the interests of grassroots communities in the case of collective industrial land in villages. Therefore, the evaluation indicators need to consider the multidimensional characteristics of spatial attributes in the hierarchical framework, including four aspects of social benefits, economic benefits, environmental benefits, and development potential, specifically divided into six positive indicators of average number of employees, average rent, average production value, innovation capacity, industrial relevance [22] and industrial aggregation [23], and two negative indicators of energy consumption and pollution intensity (see Table 2).

Considering the availability and authenticity of data and the sustainability of evaluation, the basic data in this paper are obtained through the mutual support of enterprise census data and geographic information data. Among them, industrial land use status is based on town planning and is combined with on-site research to obtain relevant data; industrial enterprises' spatial distribution, output value scale, pollution and energy consumption, innovation input, and industry type data are based on enterprise surveys [24], including enterprises' spatial positioning, statistical yearbooks, and communication interviews [25]. These processing methods can clearly and effectively reflect the use status of industrial land and help to more clearly understand the characteristics of each index of spatial performance.

According to the weight of each indicator, the weighted superposition is carried out to obtain a comprehensive evaluation score. Comprehensive evaluation score calculation adopts the weighted summation method of factor scores, and its calculation formula is shown in equation (4).

$$S = \sum_{i=1, j=1}^n v_i u_{ij} w_j = \{S_1, S_2, S_3, S_4\} \quad (4)$$

$$= \{\text{NSPL}, \text{LSPL}, \text{MSPL}, \text{HSPL}\},$$

where  $S$  is the comprehensive evaluation score;  $v_i$  is the weight of the  $i$ th evaluation index, which is determined by the 6th process in the last section;  $n$  is the total number of impact factors. Here,  $u_{ij}$  is the present value of the characteristic evaluation index, which is the data acquired from geographic information, and  $w_j$  is the corresponding weight. The NSPL, LSPL, MSPL, HSPL stand for No Space

Performance Land, Low Space Performance Land, Mid Space Performance Land, and High Space Performance Land.

### 3. Case Study Based on X City

The case chosen for this paper is X city in Guangdong Province, which, as a national economic powerhouse and a central town in Guangdong Province, has a tradition of doing business, and is a typical representative of small-town development in the Pearl River Delta region. Since the reform and opening up, the modern industry in X city developed rapidly and the industrial output value increased more than ten times in just a few years in the 1990s, and the corresponding industrial land also expanded rapidly. By 1996, the industrial land area reached 603.9 hm<sup>2</sup>, accounting for 18% of the total urban and rural construction land area, including 244.0 hm<sup>2</sup> of rural industrial land. By the beginning of this century, only the rural industrial land had increased by 446.5 hm<sup>2</sup>, and the total industrial land reached 1318.9 hm<sup>2</sup> in 2002, accounting for 36.5% of the rural construction land. Although the total industrial output value in the same period was as high as 14.3 billion yuan, the layout of industrial land was confusing and the efficiency of the land was not high.

For this reason, X city focused on industrial restructuring and industrial zone construction in the recent plan (2001–2005). Since then, the total industrial output value is continuously increasing, but the industrial land development is well controlled, and by 2015, the industrial land area only rose to 1,320 hm<sup>2</sup>. During this period, due to a series of regulatory policies, the industrial land layout tends to be rationalized, and different industrial zones are intentionally specialized and networked to create industrial clusters. However, in general, the inefficiency of land use still exists, and the more problematic issue is that there is no more incremental industrial land, and these have become obstacles to industrial transformation and upgrading.

Since this study focuses on industrial land and the bearing industrial enterprises, it is necessary to analyze the spatial association of the enterprises in a certain range, so the industrial land is divided into eight zones according to the existing division of industrial land and its proximity in space, combined with the administrative boundary of the town community. For simplicity, they are referred to as 1–8 in this study.

At present, X city has nearly 10,000 industrial enterprises, mostly small, medium, and micro enterprises, and this paper selects 337 of the state-listed enterprises for statistical analysis [26], shown in Figure 4. In general, X city has formed an industrial spatial pattern with technology-intensive industries in the southern industrial zone, technology- and capital-intensive industries in the east, and labor- and technology-intensive industries in the rest of the industrial zone. The statistical results show that the manufacturing sector of X city is complete, but the layout of different manufacturing sectors is more arbitrary. Among them, the total industrial output value of the southern district 3 is the largest and the industrial categories are the most numerous, and the technology-intensive electronic



TABLE 2: Spatial performance evaluation index system for industrial land.

| Objective                        | Classification               | Indicator                             | Relevancy  | Remark  |
|----------------------------------|------------------------------|---------------------------------------|------------|---|
| Effective use of industrial land | Social benefits $U_1$        | Number of employees per land $u_{11}$ | Positively |   |
|                                  | Economic benefits $U_2$      | Average land rent $u_{21}$            | Positively |   |
|                                  |                              | Average land value $u_{22}$           | Positively |   |
|                                  | Environmental benefits $U_3$ | Energy consumption $u_{31}$           | Negatively | Per unit industrial land                            |
|                                  |                              | Pollution intensity $u_{32}$          | Negatively | Per unit industrial land                            |
|                                  | Potential benefits $U_4$     | Industrial correlation $u_{41}$       | Positively | The degree of correlation between industries        |
|                                  |                              | Industrial aggregation $u_{42}$       | Positively | Location entropy of leading industries              |
|                                  |                              | Innovation capacity $u_{43}$          | Positively | R&D (research and development) investment intensity |

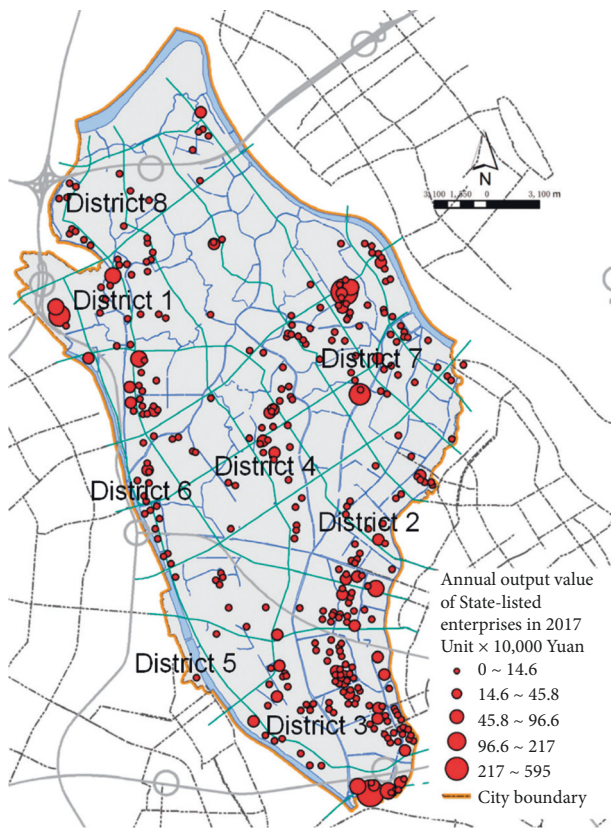


FIGURE 4: X city Industrial land and industrial enterprises spatial distribution map.

equipment manufacturing is the pillar industry of this district; the eastern district 7 is mainly dominated by capital-intensive daily chemical and beverage enterprises, while the labor-intensive plastic products and paper products, in addition to the technology-intensive electronic equipment manufacturing, also occupy the majority in district 1, but lack the core industry; similar to the situation in district 1, there are also several other districts. This is different from the industrial layout plan of X city and may cause internal competition among industrial zones to attract advantageous industries to move in.

X city is guiding the construction of “big project - industrial chain - industrial cluster - industrial base”

development model to strengthen the industrial clustering effect of different industrial zones, but due to differences in economic base, land conditions, and traffic factors, the development of each industrial zone is increasingly uneven. However, due to the differences in economic base, land conditions and transportation factors, the development imbalance among industrial zones has become increasingly prominent. To analyze the characteristics of industrial land use in X city, this study calculates the index values of eight industrial zones based on the basic data of industrial land, and by comparing the advantages and disadvantages of the indexes and combining the essential characteristics of the clustering economy of the zones, the eight zones are shown in Figure 5.

Based on the original data, we analyzed the elements of external scale development, internal scale development, area homogeneous development, and lagging loose development of each district from the radar chart. The above preliminary analysis shows that District 3 has obvious advantages in terms of industrial spatial correlation, innovation capacity, and the number of employees per place; in terms of the output value per place and industrial aggregation, District 7 has obvious advantages, but pollution and energy consumption are also the most prominent. The rest of the industrial zones have their own characteristics, except for District 8, which has obvious disadvantages. It is difficult to judge their spatial performance from a single level, and further comprehensive evaluation will be conducted on this basis.

The sub-study of comprehensive evaluation indexes of spatial performance helps to objectively understand the real characteristics of industrial land use so that effective development strategies can be formulated. However, if the spatial performance of industrial zones is evaluated by the virtue of a single indicator only, it is one-sided to a certain extent. Therefore, the study further calculates the evaluation indicators and weights of each indicator according to formulae (1) and (2), and then calculates the indicator values and ranks the scores of eight industrial zones in X city according to formulae (3) and (4), and then carries out a comprehensive evaluation. Details are shown in Tables 3 and 4.

Among the index weights, the industrial agglomeration ( $u_{42}$ ) has the largest weight, while the weights of industrial association ( $u_{41}$ ), average land value ( $u_{22}$ ), and innovation capacity ( $u_{43}$ ) are at the second level. From the magnitude of

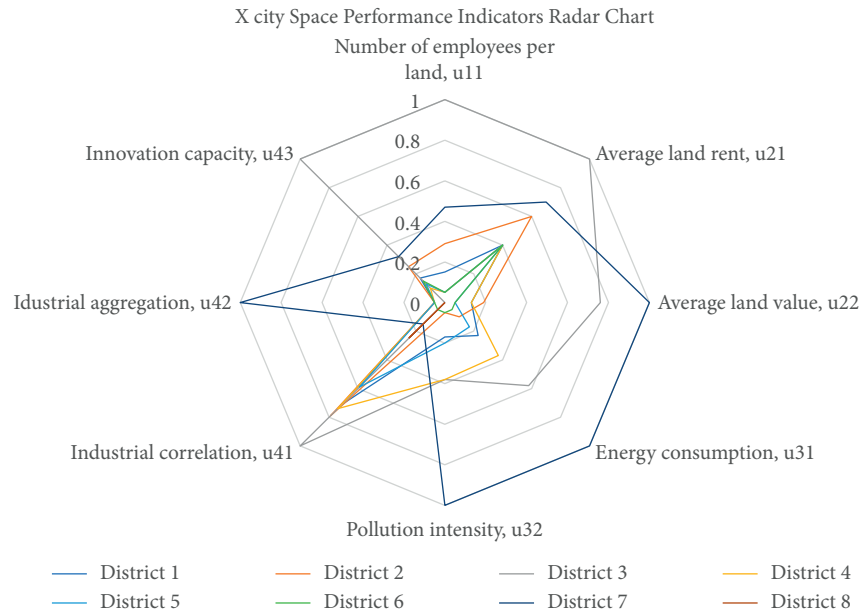


FIGURE 5: X city space performance indicators radar chart.

TABLE 3: Weighting of each indicator.

| indicator        | $u_{11}$ | $u_{21}$ | $u_{22}$ | $u_{31}$ | $u_{32}$ | $u_{41}$ | $u_{42}$ | $u_{43}$ |
|------------------|----------|----------|----------|----------|----------|----------|----------|----------|
| Weight ( $w_j$ ) | 0.0978   | 0.0521   | 0.1696   | 0.0416   | 0.0379   | 0.1914   | 0.3526   | 0.1270   |

TABLE 4: Comprehensive evaluation score of industry zoning space performance.

| District | Comprehensive evaluation score (S) | Ranking |
|----------|------------------------------------|---------|
| 1        | 44.05                              | 4       |
| 2        | 51.90                              | 2       |
| 3        | 66.01                              | 1       |
| 4        | 39.00                              | 7       |
| 5        | 41.32                              | 5       |
| 6        | 40.51                              | 6       |
| 7        | 49.24                              | 3       |
| 8        | 38.58                              | 8       |

the weights, it can be seen that the spatial aggregation of industries in the area has the largest weight in spatial performance, followed by spatial correlation and industrial scale, reflecting that the selection and leading of leading industries is the basis of spatial performance of industrial land, and industrial chain, industrial scale, and innovation capacity are the driving factors and potential factors of industrial land development. Special attention is paid to the fact that the high or low innovation capacity is not only a potential factor for the development of industrial enterprises, but also a side reflection of the number of regional investments.

Since the infrastructure of industrial land is relatively homogeneous and the layout of industrial zones is relatively close, the weights of the average number of employees ( $u_{11}$ ) and the average rent ( $u_{21}$ ) are smaller. However, for industrial zones with poor spatial performance, the lack of industrial land development planning and weak human resources are also important reasons for their difficulties in further development.

#### 4. Discussion and Conclusion

This paper adopts a spatial performance evaluation method to conduct a more comprehensive analysis of the situation of industrial land in X city. The selection of spatial performance indicators in this study is based on the traditional performance evaluation index system, with more emphasis on the extraction of spatial element characteristics. Through spatial performance analysis, this study systematically understands the use status of industrial land in X city and calculates that the main factors affecting the performance of industrial land in X city are industrial spatial agglomeration, industrial spatial correlation, and industrial scale through the Fuzzy comprehensive evaluation method, which also reflects to a certain extent the future development direction of industrial land in X city. This also reflects to a certain extent the future development direction of industrial land in X city.

Based on the evaluation results of spatial performance, we will fully consider the possible potential factors, promote the intensive development of industrial land in an orderly manner with enterprises as the core, and establish a long-term regulation and control mechanism, thus realizing the optimization and upgrading of industries under the dynamic adjustment of industrial land spatial structure. Specific recommendations include.

- (1) In the industrial land, which is dominated by internal economies of scale, we should pay attention to industrial linkage development, increase industrial spatial correlation, and mobilize ecological restoration and improvement of the industrial system. We

should consciously cultivate the leading role of core industries in surrounding industries, emphasize the relatively concentrated “clusters” and “nets” industrial spatial models, and then form a good industrial upgrading environment [27];

- (2) Industrial land for the development of industry homogenization needs to promote the development of advantageous industries through the centralized space platform and increase the concentration of the industrial space and the scale of the industry. This requires industrial land to attach importance to the selection of industrial enterprises in development, to plan the industrial structure scientifically and rationally, and increase the scientific and technological support to the industry in a targeted manner, cultivate its independent innovation ability, and on this basis, to control the intensity of industrial land use and avoid uneconomical phenomena that are too scattered or concentrated.
- (3) For the lagging development of industrial land, there are obvious defects in its industrial dynamics. In its own development, we should cultivate the “shared concept” and consolidate resources so as to proceed step by step. With the help of the transformation and upgrading of urban industries, full consideration is given to multifunctional embedding in production, circulation, and innovation. Promoting the renewal of industrial land and the improvement of the soft and hard environment [28]. Promote the full utilization of stock space and the concentration of higher efficiency.

Urban space performance refers to the combined effect or effect of urban space. Only to maximize the development needs of the city’s functions and rationally allocate all kinds of space resources to promote balanced development of all elements, “Performance is a multidimensional structure. Different angles are observed and measured, and the results are different” [29]. The performance of urban spatial structure development refers to the internal effect and external effect of the change of spatial structure in the development process, namely, the shaping and tear change of urban spatial structure to the society of the city ontology and its radiation, economic, ecological, and other effects. These effects are manifested specifically in urban economic gains, social differentiation ecological control, urban form, and transportation network [30]. The evaluation of the performance of urban spatial development is the qualitative and attributive analysis of these changes.

The hierarchical analysis–fuzzy evaluation method combines hierarchical analysis and fuzzy comprehensive evaluation method, which can not only establish a hierarchical index relationship tree, avoid information overlap and information loss among the indicators but also use fuzzy set and fuzzy logic to delineate the affiliation of each indicator to the evaluation level according to certain rules so that the evaluation result level value has continuity. In this paper, the factors affecting the spatial performance of industrial land in development zones are screened. The index system of spatial performance analysis of industrial land in the development zone is established by

using the hierarchical analysis method. By using the combination of fuzzy evaluation model calculation and hierarchical analysis method, the spatial performance of industrial land in the development zone is analyzed. Thus, a complete analysis of whether the development zone is suitable for industrial construction is carried out. This paper is a new attempt to apply the hierarchical analysis-fuzzy evaluation method to the practical work of specific development zones, which makes the method more complete in practice and develops a practical method for spatial performance assessment of industrial parks.

In this paper, the spatial performance study of X city is comprehensively analyzed by FAHP method, which can evaluate and grade the determination of individual impact factors as well as realize the overall spatial positioning and grade classification. The study shows that the hierarchical fuzzy object metamodel can also realize a comparative analysis of multiple evaluation objects, and should continue to innovate in terms of multi-regional comparison and evaluation index selection and rank classification in subsequent studies to make the evaluation results more valuable in practice.

Overall, this study tries to explore the evaluation method of industrial land spatial performance at multiple levels, but the extension in vertical and horizontal directions is not yet very deep. Therefore, future research should include a longitudinal comparison of the time dimension while appropriately adding a horizontal comparative analysis of relevant indicators of neighboring towns, so as to reflect the use status of industrial land in more dimensions. The evaluation of the spatial performance of industrial land is an extremely complex task that involves a wide range of knowledge. This study has only developed and improved the evaluation method to a certain extent, but it is far from perfect. It needs to be further researched and improved continuously. On the other hand, in future development, we can try to use the method to conduct evaluation studies on regions of different sizes and different degrees of economic development and industrial structure.

## Data Availability

The experimental data used to support the findings of this study are available from the corresponding author upon request.

## Conflicts of Interest

The authors declare that they have no conflicts of interest to report regarding the present study.

## References

- [1] P. Li, “China’s industry in ‘new normal’ of Chinese economy—survey of ‘the 3rd China’s industrial development forum,’” *China Ind. Econ.*, vol. 1, pp. 45–51, 2015.
- [2] W. Li and H. Chen, “Analysis of city industry integration and planning strategies,” *Urban Plan. Forum*, vol. 7, pp. 99–103, 2012.
- [3] L. Yan, X. Jin, and Y. Zhang, “Effects of virtual reality technology in disaster news coverage based on MAIN model,”

- in *Proceedings of the HCI International 2022 Posters*, pp. 122–129, Springer Cham, New York, NY, USA, June 2022.
- [4] Y. Jiang, X. Jin, and Q. Deng, “Short Video Uprising: How #BlackLivesMatter Content on TikTok Challenges the Protest Paradigm,” 2022, <https://arxiv.org/abs/2206.09946>.
  - [5] Q. Wang, Y. Jiang, and G. Zhao, “Method and application of land use suitability evaluation based on GIS: Singapore-Huaihua industrial park example,” *The Planner*, vol. 27, no. 4, pp. 52–56, 2011.
  - [6] Q. Ding, Y. Zhang, and Y. Liu, “Ecological suitability evaluation on industrial land based on RS and GIS in Wuhan City,” *Territ. Nat. Resour. Study*, vol. 5, pp. 56–58, 2011.
  - [7] L. Zhang, X. Long, and J. Su, “Geo-environmental suitability assessment of industrial land in the Yangtze River Delta economic zone,” *Hydrogeology & Engineering Geology*, vol. 38, no. 3, pp. 124–128, 2011.
  - [8] X. Gu, H. Jiang, and T. Wang, “Evaluation of intensive use of industrial land and industrial structure adjustment: a case study of Jiangsu Province,” *Resources Science*, vol. 31, no. 4, pp. 612–618, 2009.
  - [9] Y. Chen, Y. Chen, and W. Ma, “Evaluation of industrial land’s intensive use and analysis of potential mining with Bayes discrimination: a case study of typical enterprises in Hubei Province,” *Resources Science*, vol. 34, no. 3, pp. 433–441, 2012.
  - [10] Y. Hu and J. Zhang, “Economic space evolution of Yangtze River Delta City group based on county scale,” *Economic Geography*, vol. 30, no. 7, pp. 1112–1117, 2010.
  - [11] Q. Ye, “The transfer trend and undertaking competitive situation of China’s regional industry,” *Economic Geography*, vol. 34, no. 6, pp. 38–45, 2013.
  - [12] H. Xie, “Review and the outlook of land use ecological security pattern,” *Acta Col. Sin.*, vol. 28, no. 12, pp. 6305–6311, 2008.
  - [13] Q. Liu and L. Chen, “Comprehensive evaluation and spatial partition of sustainable utilization of land in Chang-Zhu-Tan region,” *Transactions of the Chinese Society of Agricultural Engineering*, vol. 29, no. 6, pp. 245–253, 2013.
  - [14] J. Zhen, S. Cheng, Y. Guo, and M. Zhang, “Preliminary study on the evaluation of land intensive use potential of industrial land in baotou city,” *Economic Geography*, vol. 24, no. 2, pp. 250–253, 2004.
  - [15] W. Li, X. Wu, and X. Yang, “Study on the conservation and intensive use of industrial land in Ningbo,” *China L. Sci.*, vol. 22, no. 5, pp. 23–27, 2008.
  - [16] G. Guo and qiang Xiong, “A study of regional differences in urban industrial land efficiency and influencing factors,” *China L. Sci.*, vol. 28, no. 4, pp. 45–53, 2014.
  - [17] Q. Zhang and C. Qin, “Analysis of the theory and practice of small town construction at home and abroad,” *Dev. Manag.*, pp. 100–104, 2008.
  - [18] L. A. Zadeh, “Fuzzy sets,” *Information and Control*, vol. 8, no. 3, pp. 338–353, 1965.
  - [19] W. Liu, *Research and Implementation of Fuzzy Comprehensive Evaluation System*, Chongqing University, Chongqing, China, 2003.
  - [20] T. L. Saaty, *The Analytic Hierarchy Process*, McGraw-Hill, New York City, NY, USA, 1980.
  - [21] R. W. Saaty, “The analytic hierarchy process—what it is and how it is used,” *Mathematical Modelling*, vol. 9, no. 3–5, pp. 161–176, 1987.
  - [22] X. Chen, “Deepening the understanding regarding the overall economic and socialist development of urban and rural areas; taking a solid step to push on the development of new socialist countryside,” *Dev. Small Cities Towns*, vol. 11, pp. 17–20, 2005.
  - [23] Y. Tang and M. Gao, “Review about the industrial land supply system and its performance evaluation,” *Areal Res. Dev.*, vol. 31, no. 4, pp. 113–117, 2012.
  - [24] C. Xi, X. Qiangmin, and L. Guoping, “Industrial linkage and spatial distribution of manufacturing industry,” *Geographical Research*, vol. 34, no. 10, pp. 1943–1956, 2015.
  - [25] G. Dang, “Problems and the way out of the reform of township institutions,” *Dev. Small Cities Towns*, 2006.
  - [26] T. Jing, Y. Liu, and J. Cheng, “The spatial performance of industrial land in small towns: a case study of xl town in zhongshan city,” *Dev. Small Cities Towns*, vol. 37, no. 8, pp. 27–35, 2019.
  - [27] A. Wu, L. Sun, G. Li, and H. Yang, “A theoretical construction and empirical study on the determinants of manufacturing aggregation in China,” *Inq. into Econ. Issues*, vol. 2, pp. 6–13, 2012.
  - [28] G. Li, G. Chi, and Y. Cheng, “Evaluation model and empirical study of human all-round development based on entropy weight and TOPSIS,” *Journal of Systems Engineering*, vol. 3, pp. 400–407, 2011.
  - [29] M. Armstrong and A. Baron, *Performance Management*, The Cromwell Press, London, UK, 1998.
  - [30] J. Sohn, T. John Kim, and G. J. D. Hewings, “Information technology and urban spatial structure: a comparative analysis of the Chicago and Seoul regions,” *The Annals of Regional Science*, vol. 37, no. 3, pp. 447–462, Sep. 2003.

## Research Article

# Evaluation Technology of Students' Learning Status in Chinese Classroom Based on Deep Learning

Na Li 

*Department of Education and Modern Art, Shangqiu Institute of Technology, Shangqiu 476000, China*

Correspondence should be addressed to Na Li; 1350008004@sqgxy.edu.cn

Received 19 May 2022; Revised 15 July 2022; Accepted 22 July 2022; Published 23 August 2022

Academic Editor: Man Fai Leung

Copyright © 2022 Na Li. This is an open access article distributed under the Creative Commons Attribution License, which permits unrestricted use, distribution, and reproduction in any medium, provided the original work is properly cited.

The evaluation of students' learning status has a strong guiding role. What is taken as the evaluation standard will determine what education teaches and what students learn. As a basic subject and a lifelong art, Chinese in senior high school plays an important role in the college entrance examination; its importance can be imagined; and it has also attracted more and more attention. The assessment of students' learning status can greatly promote students' learning quality and values. However, the current evaluation of students' learning status still has the score-oriented problem, and lacks enough attention to students' interests, skills, potential, thinking, values, and other aspects, which is worrying. The function of Chinese evaluation has been narrowed to evaluate students' knowledge and skills, and it has been euphemistically called the focus of classroom teaching. In Chinese class, the role of students' learning status assessment has received a lot of attention, and it should play more roles in promoting students' deep learning, so as to improve the thinking quality of learning and find appropriate learning methods. Deep learning requires students to have strong autonomous learning ability and problem-solving ability, etc. Students will benefit from developing these good habits in their future work and life.

## 1. Introduction

Computer vision measures people's perception of urban environment and is increasingly used to study the relationship between urban appearance and residents' behavior and health. We train Siamese convolution neural structure, which learns the loss of common classification and arrangement to predict people's judgment on pair image comparison. The results show that clustering combined with the neural network can generate global urban observation data [1]. At present, the popular digital image steganography communication recognition method mainly includes three steps: residual calculation, feature extraction, and binary classification. In this paper, a digital image steganalysis method based on a convolutional neural network (CNN) is proposed, which can correctly reproduce and optimize these key steps in a unified framework, thus learning hierarchical representation directly from the original image. Compared with SRM (switched reluctance motor) and its selective channel-aware variant maxSRMd2, our model surpasses all

test algorithms with different loads [2]. For categorization tasks, we always want to choose the attributes that keep the categories separate in the most efficient way. In this paper, a new feature separation method is proposed, which uses the deep neural network to learn the explicit mapping from sample space to feature space, and improves the feature separability according to Fisher's criterion. For highly flexible models, the optimal Fisher function can find a balance between uniqueness and descriptivity [3]. Because the reliability of each pixel attribute determines the classification accuracy, it is very important to design the feature extraction algorithm for hyperspectral image classification. We propose a very effective hyperspectral image classification learning algorithm-context deep learning. A large number of experiments show that the context deep learning algorithm proposed in this paper is an excellent function learning algorithm, which can achieve good performance only by simple classification [4]. The deep neural networks are usually optimized by the stochastic gradient descent (SGD) method. In this paper, a new second-order stochastic

optimization algorithm is proposed. We find this structure very useful, not only because it speeds up training and decoding, but also because it is a very effective method against overfitting. The convergence speed of our algorithm is faster than that of SGD [5]. A new probabilistic model for the analysis of time-varying patterns in rs-fMRI intrinsic functional networks, combined with a methodological architecture of deep learning and spatial modeling, examines the functional relationships assessed between mild cognitive impairment and normal healthy controls [6]. The convolutional neural network is the core of deep learning application. They did not consider weight updates and complex data dependencies during exercise. In the training process, batch processing limits the number of images that can be processed continuously, because the next batch of images must be processed according to the updated weight [7]. The focus of local space design research has gradually changed from the manual design method to the learning method. In this paper, a convolutional neural network (CNN) is proposed for learning efficient graphs in Euclidean space. Experimental results show that L2-Net has good generalization ability and can directly replace the existing artificial graphs. The second language network is trained [8]. More and more unstructured text data appear on social media among enterprises, forming a social environment with many production relations, which can be used as decision support information to match the production capacity needs among enterprises. The ultimate goal of this study is to promote knowledge transfer and sharing in the context of business and social interaction, so as to support the integration of resources and capabilities among different companies. Experimental results show that this method can achieve the same performance as the existing learning models and is well suitable for the network-based social production interaction environment [9]. According to research, the growth of online education is more driven by economic forces than its long-term effectiveness [10]. This paper discusses the role of classroom feedback in the assessment of students' learning status. Using the proportional sampling method, this paper studies the influence of teacher-student interaction and classroom environment on students' classroom learning process [11]. The assessment of students' learning status can improve the quality of education. Learning evaluation pays more attention to students' learning process and lets teachers know how to improve their own development, so it is a change of classroom evaluation form [12]. In this paper, teachers and students can establish a more successful relationship. In order to overcome students' prejudice, teachers should always be fair and sincere in their affairs and evaluation process [13]. Research shows that most students think that classroom evaluation plays an important role in teaching quality monitoring [14]. Educational evaluation is a very important part of the education system. This paper analyzes the problems encountered in classroom teaching evaluation and puts forward various improvement measures to improve the level of classroom teaching evaluation [15]. In the abovementioned related literature research, some technical problems are discussed and applied, but there are many problems in the classroom teaching process, for

example, the adopted technology does not improve the corresponding accuracy and it is difficult to identify. However, using a single technology to solve teaching problems is not effective in the implementation of teaching details. Therefore, using deep learning to solve students' learning situation and application can improve the autonomous learning mode, and effectively improve the classroom teaching quality and the recognition effect of teaching behavior.

## 2. Characteristics of Deep Learning

*2.1. In-Depth Study and Participation.* First is the deep emotional input. We encourage students to put in positive emotions and stimulate students' correct learning attitude. At this time, the input is a kind of active learning, and the students' emotional state is positive. They pour their emotions into the learning process and pay attention to and focus on the learning tasks in class for a long time. Second, the integration of learning methods is deep. Different learning methods are needed. For example, when previewing before class, we mainly focus on self-study, and when listening to teachers in class, we mainly focus on listening with energy. Third is high investment in the learning process, positive emotional state, and deep participation. For different learning tasks, we use different thinking to solve them. We can transform knowledge into their own information and get through the key points; link the learned knowledge with the old knowledge and connect at multiple points; and use knowledge structure to solve different types of tasks and problems. In the whole learning process, students' thinking is very active and their operation is relatively fast.

*2.2. High Level of Thinking Development.* Deep learning requires students to have certain innovative thinking. The thinking structure includes five levels: pre-, single, pluralistic, related, and abstract expansion. Association structure can integrate the existing information into a whole connection framework and become a logical and orderly internal structure. The abstract extended structure can not only use all available data and connect them, but also test the reasonable abstract structure obtained from data, which can surpass the given information and infer the structure, and can carry out logical reasoning from concrete to general; able to induce and make assumptions; can use many methods to use reasoning results in conclusions; can use more abstract functions to expand the knowledge structure; and be able to understand the role of change in the change method. It can be noted that some structures come from different ideas and migrate these ideas to new fields.

*2.3. Strong Application Migration Ability.* After a deep study, students can find the key to the problem and then combine the known knowledge to solve the problem. After firmly mastering the knowledge in class, even if you encounter new problems or situations, you can still successfully complete various learning tasks, identify the core elements in the situations, relate and utilize them, and even better migrate to

the actual life. If the learned knowledge and skills cannot be used to solve problems in various situations, then this simple copying and mechanical memory are still in the shallow learning stage. In the process of Chinese learning, learners must actively learn, creatively use their knowledge and skills to solve problems when encountering complex situations, and realize the flexible transfer and application of knowledge and skills, so as to achieve the effect of “drawing inferences from others” and “learning by analogy.”

In this paper, the practical application of classroom teaching has a good application. The second part of this paper explains the relevant theories, especially the characteristics of deep learning in teaching practice. The third part explains the application model of the DDS algorithm and the data processing flow. In the fourth part, the application of different algorithms in teaching scenes is compared, and the effect of the deep learning mode is obvious.

### 3. Improvement Strategy of SSD Algorithm

*3.1. Infrastructure Network Improvement.* The goal of the basic grid upgrade is to replace the original backbone VGG16 with the lightweight grid. By studying the data and analyzing different models, we know that the MobileNet network meets the requirements. It replaces standard convolution with deep separation convolution to reduce the number of parameters. MobileNet has only 4.2 million parameters, compared with 133 million in VGG16. The test results of the ImageNet dataset show that MobileNet is obviously faster, but the accuracy rate is only 0.9 percentage points lower than VGG16. Therefore, this paper is based on the original MobileNet, after some modification, as the core network of SSD.

*3.1.1. Improvement of MobileNet.* The reason MobileNet is faster and less computational than VGG16 is because there are two differences between MobileNets. First, depth analysis rounds are used in network synthesis, and width coefficient and resolution coefficient are also used. Deep convolution is the main part, and two parts are used to supplement convolution operation, namely, deep convolution and point convolution. MobileNet’s network structure has 28 layers if both are considered two and 14 layers if both are considered one.

Formula (1) can be used to judge its parameter ratio.

$$\frac{F_k * F_k * F_f * F_f * R + 1 * 1 * F_f * F_f * R * P}{F_k * F_k * R * P * F_f * F_f} = \frac{P + F_k^2}{PF_k^2}, \quad (1)$$

where  $P$  represents the size of the output channel;  $R$  represents the size of the input channel;  $F_k$  represents the size of the output feature map; and  $F_f$  represents the size of the feature map.

In order to reduce network parameters, in addition to depth separation convolution, width factor  $\alpha$  and resolution factor  $\rho$  with values between 0 and 1 are used. The impact of  $\alpha$  is declining. For example, for an input channel with a value of  $R$ , it becomes  $\alpha R$ , which greatly reduces the computation.

Another factor greater than  $\alpha^2$  that affects the amount of computation is the resolution, so  $\rho$  is used to reduce the resolution of the image. After using this coefficient and reducing the value of  $\alpha$ , the calculation times of the pixel value of  $\rho^2$  are reduced.

On the basis of the above introduction, this paper improves MobileNet in two aspects.

Based on the above analysis, in order to further reduce the calculation of the BN layer, this paper combines it with the previous convolution, so that the speed will be improved on the previous basis.

The input size of MobileNet is changed from  $224 \times 224$  to  $300 \times 300$ . There are two reasons for this modification: first, increasing the input size can improve the information capacity of the feature map and then improve the detection accuracy, but the input size should not be too large, which greatly increases the network parameters, thus making MobileNet lose the advantages of the lightweight model; on the other hand, the input size of SSD network structure used in this paper is  $300 \times 300$ , which makes basic preparation for the combination of the following two networks after modification.

*3.1.2. Replacement of SSD Basic Network.* In order to improve the feature extraction ability of the model, this paper combines eight standard smaller convolutional layers behind the replaced core network to further obtain the depth information of the image. At the end of the network, a classification layer for judging categories and a nonmaximum suppression layer for screening regression boxes are connected, thus completing the replacement of the basic network. In this paper, the deep convolution and the subsequent  $1 \times 1$  point convolution are regarded as one layer, and there are 14 layers, which are denoted from Conv0 to Conv13, respectively. Where s1 represents a step size of 1, s2 represents a step size of 2, and Convdw means that deep convolution will be followed by a  $1 \times 1$  point convolution to process the channel.

Finally, like SSD, six feature layers are selected to complete the following work, and the depth of this layer should be considered when selecting. If it is too shallow, enough image information cannot be extracted. Therefore, this paper selects six feature layers to reduce the size from front to back and realize multiscale prediction. The SSD algorithm is an application form of deep learning. SSD belongs to the one-stage detection method, which mainly regresses the target category and location directly. In the process of prediction, it is precisely because of the prediction on the feature layer of different scales that the target can be detected well when the image is of low resolution, and its accuracy can be guaranteed. In the process of training, end-to-end training is adopted.

In this paper, using the SSD algorithm in the application class students’ learning picture processing and application has a good effect, especially some learning behaviors can use action behavior to identify the corresponding state.

*3.2. Feature Fusion of Network Model.* In the previous step, the replacement of the basic network improves the detection speed but does not improve the accuracy of small target

detection. It is a common improvement strategy to improve the model performance by fusing different scale features. Therefore, this section introduces the method of feature fusion and, on this basis, puts forward the model fusion strategy in this paper.

**3.2.1. Feature Fusion Method.** When an image is put into a convolution network, different levels of the network get different image information. The shallow layer, also known as the low layer, is at the initial stage of convolution, so only limited information can be obtained. However, due to its good resolution, its main function is to obtain some visible features, such as the position information and edge information of the target object in the image. The deep layer is also called the high layer, that is, when the network depth is very large and convolved many times, what we get at this time is some abstract information invisible to the naked eye, which has strong semantic characteristics. Through the above analysis, we can see that the advantages between shallow layer and deep layer can complement the shortcomings of both, so there is a method to merge the two, which is uniformly named as feature fusion. However, according to the order of feature fusion and target prediction.

Early fusion refers to feature fusion first; then, predictor training is carried out on the basis of fused features; and predictor training will not be carried out before complete fusion. There are two common fusion methods: concat and add.

The concat method directly adds attributes and can also be understood as a combination of channels, each of which is associated with a convolution sum. This method adds information to the image itself but does not add information about the attributes of each layer. The add method is to combine feature vectors into a combined vector and simply add a value, but the number of channels remains unchanged, which is a convolution operation after adding feature graphs. This method increases the amount of information to describe image features, but the dimension of description graphics remains unchanged. Usually, the parameter quantity of the add method is less than concat. Assuming that there are only two channels and the number of channels is the same, the concat method and the add method can be expressed by formulas (2) and (3), respectively, where  $X$  and  $Y$  represent two channels to be fused, and the number of channels is  $N$ , and the fusion results of the two methods are  $R_{\text{concat}}$  and  $R_{\text{add}}$ , respectively.

$$R_{\text{concat}} = \sum_{i=1}^N X_i * K_i + \sum_{i=1}^N Y_i * K_{i+N}, \quad (2)$$

where  $X$  and  $Y$  are the channels to be fused;  $K_i$  is the weight of the  $i$ -th channel;  $R_{\text{concat}}$  is the fusion results.

$$R_{\text{add}} = \sum_{i=1}^N (X_i + Y_i) K_i = \sum_{i=1}^N X_i * K_i + \sum_{i=1}^N Y_i * K_i, \quad (3)$$

where  $X$  and  $Y$  are the channels to be fused;  $K_i$  is the weight of the  $i$ -th channel;  $R_{\text{add}}$  is the fusion results.

Late fusion refers to the fusion of the detection results of each layer, so as to get a better model and meet the requirements, that is, each layer will have detection results and then fuse them to get the final result. By dividing the late fusion once again, we can get two late fusion modes in different directions. The first direction is to adopt multiscale features. Different scales contain different information, so different results will be obtained. Integrating these different results into one piece will get the final results with rich information. In the second direction, a pyramid feature set will be obtained by arranging different features from small to large; then, the feature information of each layer will be fused step by step from shallow to deep; and each layer will be detected at the same time of fusion, without getting all the fusion to complete redetection. Common late fusion methods include SSD, MS-CNN, FPN, and so on.

**3.2.2. Model Fusion Process in This Paper.** Combined with the nature of the network model structure and the combination of various functions, this paper chooses to add a combination of functions to connect the network. It can be seen from the model structure that the size of the extracted six feature layers gradually decreases from shallow to deep, and the more the first one contains, the less the abstract information, so the purpose of feature fusion is to transmit abstract information from deep functional floor to lower floor. Considering that Conv17\_2 and Conv16\_2 are too small to have much information, only Conv11, Conv13, Conv14\_2, and Conv15\_2 are selected for fusion operation.

**3.3. Model Optimization Algorithm.** When training the model, we pay attention to the change of loss function. As the value of the loss function decreases, it shows that the result of model training is approaching the actual result, so the loss function must be pointed downward to find the minimum value of the loss function. However, in the process of gradient calculation, the value ferry amplitude may be too large or unchanged, which leads to slow gradient descent. Therefore, in order to speed up the descent, we usually need to use optimization algorithms, such as momentum, RMSProp, and Adam.

In this paper, the RMSProp algorithm proposed by Geoffrey E. Hinton is adopted. The algorithm calculates the historical gradient of each dimension, superimposes the sum of its squares, and obtains the sum of historical gradients by applying the attenuation rate. When updating parameters, the learning rate is divided by the above result. After using the optimization algorithm, the gradient direction still changes in a small range, which accelerates the convergence of the network. The specific calculation formulas are shown in formulas (4) and (5).



$$S_{dR} = \beta S_{dR} + (1 - \beta) (dR)^2, \quad (4)$$

$$R = R - \rho \frac{dR}{\sqrt{S_{dR} + a}}, \quad (5)$$

where  $R$  is the parameter.

**3.4. Principles of Model Training and Prediction.** After completing the network building, the model needs to be trained to complete the recognition task. The training process is mainly to find a prior frame matching with the target frame marked in advance in the picture. Unlike YOLO, SSD uses multiscale feature layers to detect images, so the prior frames will be different with the change of feature layer scale. The prior frame includes two aspects, namely, scale and aspect ratio, in which there is a linear relationship between scale and feature map size as in formula (6).

$$X_k = X_{\min} + \frac{X_{\max} - X_{\min}}{m - 1} (k - 1), k \in [1, m], \quad (6)$$

where  $X_{\min}$  is the minimum value of the ratio of frame size to feature diagram;  $X_{\max}$  is the maximum ratio of frame size to feature map;  $M$  is the eigenvalue number;  $K$  is a certain feature layer; and  $X_k$  is the ratio of a priori frame to the  $k$ -th feature graph.

In this paper,  $X_{\min}$  is 0.2 and  $X_{\max}$  is equal to 0.9. The scales of the smallest and largest prior boxes in the six feature graphs are {30.0, 60.0, 111.0, 162.0, 213.0, 264.0} and {60.0, 110.0, 162.0, 213.0, 264.0, 315.0}, respectively. At the same time, in order to predict the targets of different shapes, different aspect ratios  $\alpha_r$  are set according to the minimum size prior frame of each layer, and the values are {2 : 2, 2 : 1, 3 : 1, 1 : 2, 1 : 3}, so the calculation method of width and height is as shown in formula (7).

$$M_k^a = X_k \sqrt{\alpha_r}, N_k^a = \frac{X_k}{\sqrt{\alpha_r}}, \quad (7)$$

where  $M_k^a$  is the prior box width value;  $N_k^a$  is a priori box height value; and  $X_k$  is the ratio of prior frame to the characteristic graph.

The matching of prior boxes in this paper follows two principles.

The first principle is as follows: we find the prior frame with the largest IOU (intersection over union) (referring to the coincidence rate between the two) for each real frame in the image so that each real frame has a matching prior frame. Some prior frames may not find matching target frames, that is, there are no targets to be identified in their range. These kinds of prior frames are located as negative samples, and if there are any, they are positive samples. Negative samples are classified as background, while positive samples are the targets to be found.

The second principle is as follows: after the implementation of the first principle, a large number of negative samples will be produced, resulting in extremely unbalanced positive and negative samples, so the second principle is put

forward. For a matching prior box, if its IOU in a real box is greater than a certain threshold, it is also considered to be matched. That is to say, a real box has multiple matching prior boxes, and vice versa. The second principle must be based on the premise of the first principle before it can be established.

Even if there is the second principle, the gap between the number of positive and negative samples is very large, and too large a number difference will cause a very large loss function value. Therefore, this paper artificially reduces the number of negative samples, that is, removes some negative samples in training, so that the ratio of positive to negative is about 1 : 3. Every time the training is completed, the parameters need to be updated until the expected effect is achieved, so the loss function and nonmaximum suppression are needed to assist the training process.

**3.4.1. Loss Function.** In this paper, the loss function consists of two parts, namely, location loss and confidence loss, which are obtained by the weighted sum of the two parts. The loss function formula is shown in formula (8) as follows:

$$L(x, c, l, g) = \frac{1}{S} (L_{\text{conf}}(x, c) + \alpha L_{\text{loc}}(x, l, g)), \quad (8)$$

where  $c$  is the confidence value;  $L$  represents the prediction box;  $g$  denotes the true box;  $S$  is the default number of boxes;  $\alpha$  is the weight value of the two;  $L_{\text{conf}}$  is the value of confidence loss;  $L_{\text{loc}}$  is the location loss value.

The formulas of location loss and confidence loss are as follows, where  $P$  represents the category serial number, and when  $P$  is 0, it represents the background;  $x_{ij}^p = \{0, 1\}$ . When 1 is taken, it means that the predicted box and the real box match, and the matching category is  $p$ .

The confidence loss function formula is shown in formula (9) as follows:

$$L_{\text{conf}}(x, c) = \sum_{i \in \text{Pos}} x_{ij}^p \log(\hat{c}_i^p) - \sum_{i \in \text{Neg}} \log(\hat{c}_i^0), \quad (9)$$

where  $\hat{c}_i^p$  is the probability value predicted as category  $p$ ;  $P$  denotes the category;  $x_{ij}^p$  is whether the discriminant value is matched.

The positioning loss function formula is shown in formula (10) as follows:

$$L_{\text{loc}}(x, l, g) = \sum_{i \in \text{Pos}} \sum_{m \in \{cx, xy, w, h\}} x_{ij}^p \text{smooth}_{L1}(l_i^m - \hat{g}_j^m), \quad (10)$$

where  $g_j^m$  is the real box;  $l_i^m$  is the prediction box.

**3.4.2. Nonmaximum Suppression.** When the image passes through the prediction network, there will be a large number of regression boxes to be selected for each category, many of which are wrong and there are a large number of repetitions. Selecting an accurate regression box from these results cannot be accomplished only by IOU, so a nonmaximum suppression method is proposed to remove useless information and keep the waiting box with the most targets.

**3.5. Behavior Database Construction Method.** The good classification effect of the deep learning network model needs to be based on a large amount of data, which constitutes an image database. Different application fields have their own image databases, such as medical image database in the medical and health field, fundus disease image database, disease pattern image database, etc.; vehicle image database and road sign image database in the field of transportation; and MNIST handwritten digital database, ImageNet database, COCO (collation of cortical) database, PASCAL VOC database, CIFAR-10 database, etc., which are commonly used in image recognition theory research. The experiment in this chapter needs a large amount of classroom behavior image data, but there is no special database for students' classroom behavior recognition at present, so it needs to be built by individuals. This section will detail the process of creating the classroom behavior database.

### 3.5.1. Dataset Acquisition

(1) *Image Acquisition.* The datasets used in this paper are source classroom surveillance video and network pictures. In order to ensure the recognition effect, we try to make the collected image a background classroom. Video images need to be processed before they can be used as datasets, which contain many video segments including raising hands, sitting up, sleeping, and writing appear. Then, we use OpenCV to sample the selected video frames and select the pictures containing the above five actions to save. In order to ensure the speed of training, we try to ensure that the size of the picture is 200 k left. If the picture is too large, the training will be slow.

(2) *Data Enhancement.* Because there are not much image data collected in this paper, and the accuracy of model training needs a large amount of data as support, this paper uses the method of data enhancement to increase the amount of data. It mainly includes flipping the image horizontally, left and right and randomly, translating the image horizontally and vertically, and randomly changing the color of the image. After data enhancement, there are 2000 pictures in this dataset.

### 3.5.2. Dataset Preprocessing

(1) *Grayscale Processing.* By comparing the mean value method adopted in this paper, the mean value of each pixel value point is calculated to realize gray processing, and the calculation is as shown in formula (11) as follows:

$$R = G = B = \frac{(R + G + B)}{3}, \quad (11)$$

where  $R$ ,  $G$ , and  $B$  are three color channels.

(2) *Bilateral Filtering.* The change of color image into a gray image only reduces the parameter quantity of color, and cannot eliminate the noise of the original image, but the data needed in this paper cannot have too much noise, so the

related methods are explained in the second chapter. Combined with the actual needs and comparing the differences of various methods, this paper chooses bilateral filtering denoising technology. When the selected method is used to filter the noise, it not only reduces the image noise but also preserves the edge information. In an operation similar to Gaussian filtering, every pixel of the picture is scanned once, and then, the weighted sum of pixel value weights is added on the basis of the operation of finding the weighted sum of each pixel value and the corresponding position weights in the field. When calculating, the closer to the center, the greater the weight, the closer the pixel value, and the greater the weight, as shown in formulas (12) and (13).

$$G_s = \exp\left(-\frac{\|p - q\|^2}{2\sigma_s^2}\right), \quad (12)$$

$$G_r = \exp\left(-\frac{\|I_p - I_q\|^2}{2\sigma_s^2}\right), \quad (13)$$

where  $G_s$  is the weight of spatial distance;  $G_r$  is the pixel value weight;  $Q$  is the center point of a window;  $P$  is a certain point;  $I_q$  is the input image; and  $I_p$  is the filtered image.

The entire filter is represented by  $BF$ , as shown in formula (14) as follows:

$$\begin{aligned} BF &= \frac{1}{W_q} \sum_{p \in \epsilon_s} G_s(p) G_r * I_p \\ &= \frac{1}{W_q} \sum_{p \in \epsilon_s} \exp\left(-\frac{\|p - q\|^2}{2\sigma_s^2}\right) \exp\left(-\frac{\|I_p - I_q\|^2}{2\sigma_s^2}\right) * I_p, \end{aligned} \quad (14)$$

where  $W_q$  is shown by formula (15) as follows:

$$W_q = \sum_{p \in \epsilon_s} G_s(p) G_r(p) = \sum_{p \in \epsilon_s} \exp\left(-\frac{\|p - q\|^2}{2\sigma_s^2}\right) \exp\left(-\frac{\|I_p - I_q\|^2}{2\sigma_s^2}\right), \quad (15)$$

where  $G_s$  is the space distance weight;  $G_r$  is the pixel value weight; and  $W_q$  is the sum of the weights of each pixel value.

(3) *Target Enhancement.* The working principle of the USM algorithm is as follows: we use a low-pass filter to process the input image to get a low-pass component, calculate the difference between the original image and this component to get a high-pass component, and superimpose the high-pass component on the original image to get a sharpened image. Usually, Gaussian ambiguity is used to obtain low-pass components. The calculation formula is shown in formula (16), where the value of  $W$  is 0.1 to 0.9 and is usually 0.6.

$$y = \frac{(x - w * z)}{(1 - w)}, \quad (16)$$

where  $y$  is the output image;  $X$  is the input image;  $W$  is the Gaussian ambiguity; and  $Z$  is the weight value.

**3.6. Model Evaluation Criteria.** In this paper, the model is evaluated from the detection time of a single-frame image and the average accuracy of image detection. The MAP (mean average precision) is the average value of all AP-like values. AP is the area below the line of the curve of accuracy and recall.

The accuracy rate formula is shown in formula (17) as follows:

$$\text{Precision} = \frac{TP}{TP + FP} \quad (17)$$

In the formula, TP refers to the number of positive samples of the classifier; FP refers to the number of negative samples of the classifier. The whole model reflects the accuracy function.

The recall rate formula is shown in formula (18) as follows:

$$\text{Recall} = \frac{TP}{TP + FN} \quad (18)$$

where  $T_n$  refers to the number of positive samples of the classifier.

The whole formula reflects the checking function of the whole class of the model.

## 4. Experimental Analysis

**4.1. Performance Comparison.** In order to achieve the expected accuracy of our experiment, we compared the performance ability of fuzzy learning, shallow learning, and deep learning in complexity, learning ability, and number of parameters six times. The results are shown in Figures 1–3. The comparison in Figures 1–3 was performed with six independent experiments at random, which does not mean that performance increases as the number of experiments increases. The performance is different in different stages, and the performance degradation in the following experiments is also random.

By observing Figures 1–3, we can see that deep learning has the best performance ability in all aspects, so this paper adopts the deep learning method to carry out the following experiments. Performance is the coefficient of performance of different algorithms, with the highest being 10 and the lowest being 0.

**4.2. Present Situation and Problems of Chinese Classroom Evaluation in Senior High Schools.** Questionnaire from the understanding of classroom evaluation, classroom evaluation participation, classroom evaluation content, and evaluation feedback are four aspects to investigate and grasp the current students in all aspects of the basic situation of classroom evaluation. It is shown in Figure 4.

### 4.2.1. Student Questionnaire

**(1) Students' Understanding of Evaluation Function.** In Table 1, 69.5% of the students think that Chinese classroom evaluation can help them find the advantages and

disadvantages of learning, 20.9% of the students say “uncertain,” and 9.6% of the students think they cannot. Most students can realize the role of classroom evaluation and hope to get feedback from it, so as to use this feedback to better understand themselves.

In Table 2, 65.9% of the students think that Chinese classroom evaluation can make them reflect on their learning strategies, these students can have a deep understanding of their own learning situation, and 26.1% of the students are not clear whether classroom evaluation is helpful to their learning strategies. These students lack serious attention to learning strategies, and 8% of the students think that classroom evaluation will not have any effect on learning strategies.

In Table 3, it can be seen that 65.9% of the students think that Chinese classroom evaluation can stimulate their strong learning motivation, 26.1% of the students say “uncertainty,” and only 8% of the students think that “Chinese classroom evaluation can promote learning motivation” does not conform to their actual situation. Most students are aware of the stimulating effect of Chinese classroom evaluation on learning motivation, which is a good phenomenon, which shows that students have a great demand for classroom evaluation and have a correct understanding. If teachers can make more evaluations, it must be in line with students' inner learning wishes.

**(2) Content of Chinese Classroom Evaluation.** In Table 4, 71.6% of students think that students who can draw inferences from others are often praised, which shows that teachers attach great importance to students' ability to draw inferences from others and integrate them, which are all manifestations of deep learning. About 18.0% of the students chose “uncertainty,” while 10.4% of the students thought that this situation was not in line with reality. It can be seen that Chinese teachers in senior high schools pay more attention to the development of students' transfer ability, but it may be due to some improper handling in the implementation of evaluation, which leads some students to fail to recognize the statement that “students who can draw inferences from others are often praised.”

In Table 5, it can be seen that 20.8% of the students choose “completely consistent” on the issue of “Chinese teachers often evaluate students' learning attitude in class,” which shows that the situation is not ideal, and teachers may not pay enough attention to students' learning attitude in class. About 50.0% of the students chose “basic compliance,” accounting for the largest proportion. Students who chose “uncertain” accounted for 19.6%, students who chose “somewhat inconsistent” accounted for 6.8%, and students who chose “completely inconsistent” accounted for 2.8%.

In Table 6, 67.5% of the students think that Chinese teachers often evaluate students' learning methods in class, 14.9% of the students say “uncertainty,” and 17.7% of the students think that teachers do not often pay attention to students' learning methods.

In Table 7, on the issue of “Chinese teachers often evaluate students' thinking logic ability in class,” 20.5% of the students chose “complete conformity,” which shows that

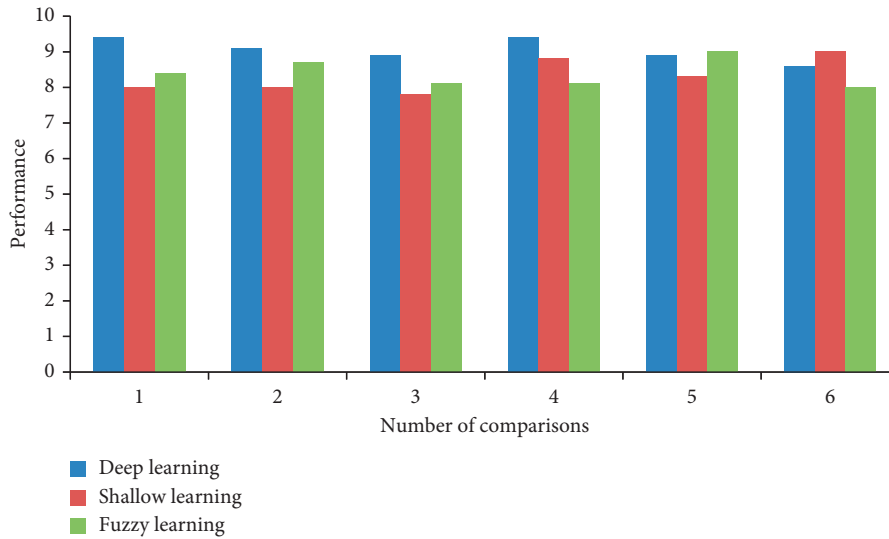


FIGURE 1: Complexity comparison of different algorithms.

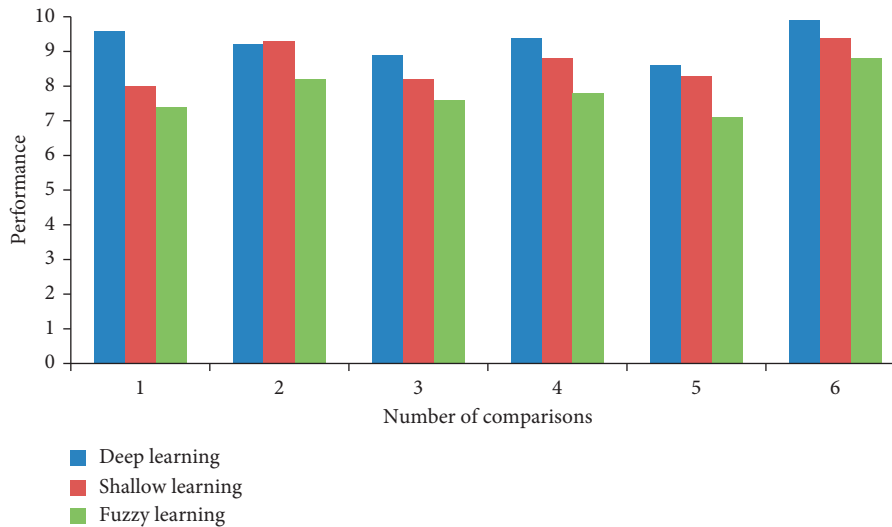


FIGURE 2: Learning ability comparison of different algorithms.

one fifth of the students think that teachers pay attention to students' thinking logic, and 39.4% of the students choose "basic conformity," which shows that more than one third of the students think that teachers pay average attention to students' thinking logic. About 23.7% of the students chose "uncertain," 12.4% chose "somewhat inconsistent" and 4.0% chose "completely inconsistent." There are still nearly 40% of students who do not explicitly recognize that Chinese teachers have evaluated students' logical thinking ability in class, which shows that in the process of classroom evaluation, attention to logical thinking ability still needs continuous investment.

(3) *Students' Participation in Evaluation in Chinese Class.* In Table 8, the average value of this question is 2.89, which is lower than the median value. It shows that students' evaluation of others is not ideal. About 36.6% of the students think that they often have the opportunity to

evaluate others' learning, 24.8% say "uncertain," and 38.6% think that "they often have the opportunity to evaluate others' learning in Chinese class" is inconsistent with their actual situation. It can be seen that in the practice of Chinese classroom evaluation in senior high schools, students' participation is insufficient, so teachers need to find ways to organize students to go to the classroom and encourage more students to participate in it to express their ideas.

In Table 9, the average value of this question is lower than the median value. Among them, 37.9% of the students expressed their willingness to evaluate other students' learning in class, 23.4% of the students held an "uncertain" attitude, and 38.7% of the students were unwilling to evaluate others in class. It shows that students are unwilling to participate in the evaluation of Chinese classroom in senior high schools, and most people do not want to make an evaluation.

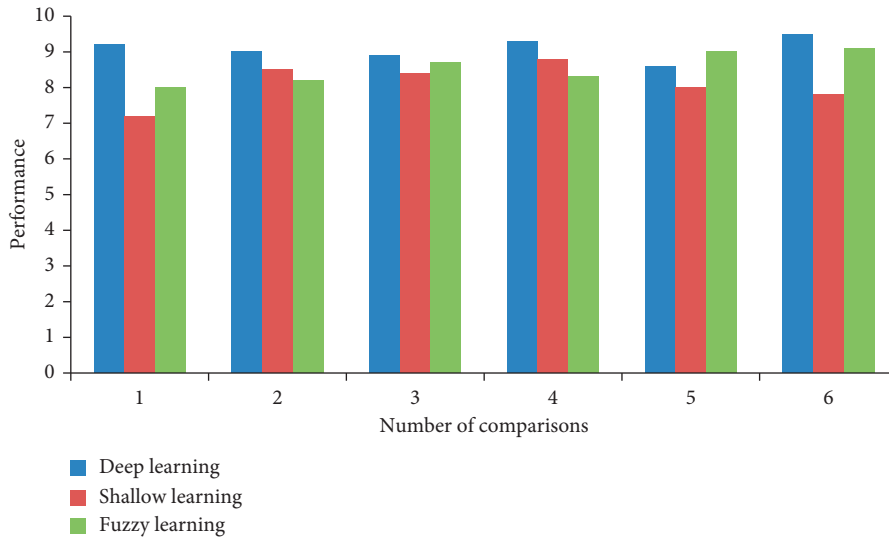


FIGURE 3: Parameters' comparison of different algorithms.

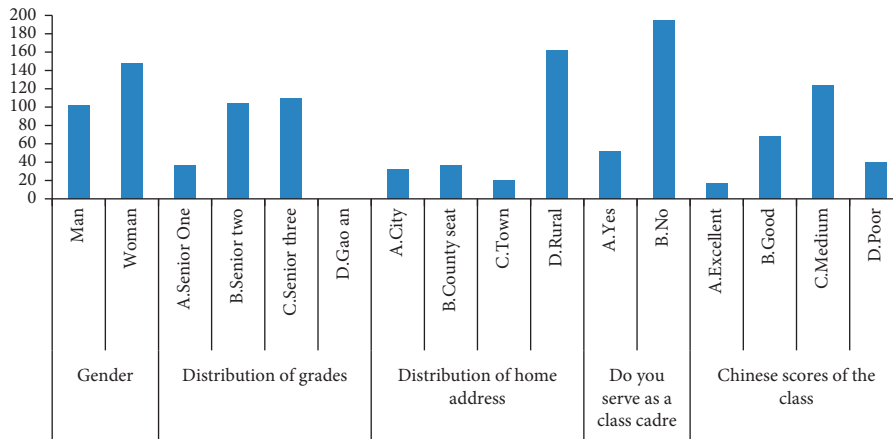


FIGURE 4: Sample distribution diagram of questionnaire survey.

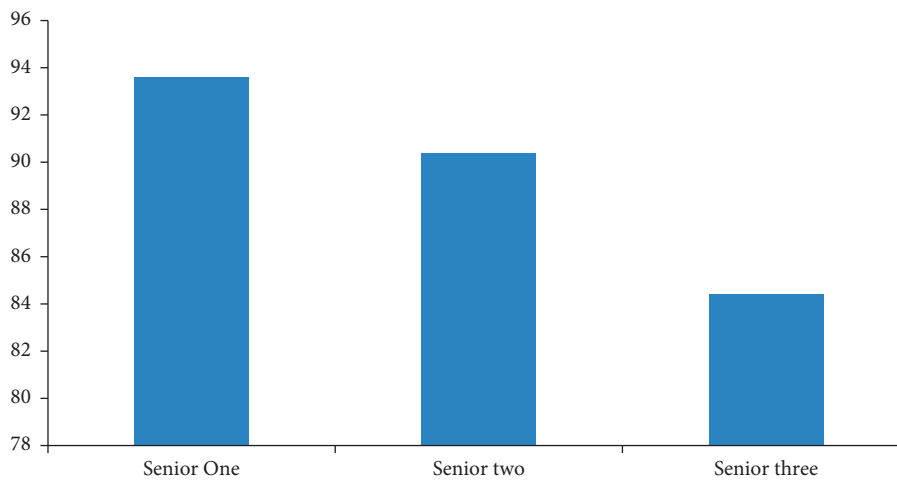


FIGURE 5: Analysis of the differences in the total scores of senior high school students' classroom evaluation in grades.

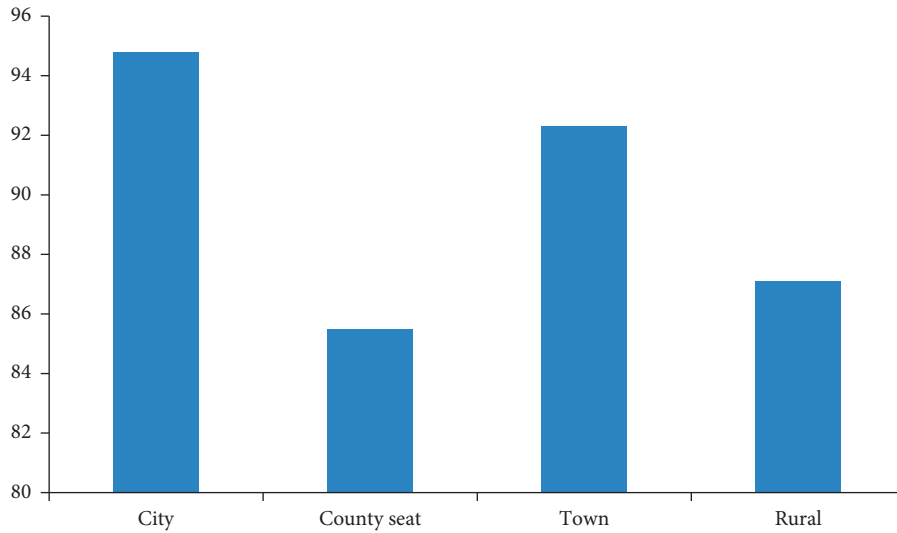


FIGURE 6: Difference analysis of total scores of classroom evaluation of senior high school students in family residence.

TABLE 1: Chinese teacher's evaluation in class can help me find the advantages and disadvantages of learning.

| Title   | Options                     | Frequency | Percentage (%) |
|---|-----------------------------|-----------|----------------|
| The Chinese teacher's evaluation in class can help me find the advantages and disadvantages of learning | (1) Completely inconsistent | 5         | 2.0            |
|   | (2) Some do not match       | 19        | 7.6            |
|   | (3) Uncertainty             | 52        | 20.9           |
|   | (4) Basically accord        | 136       | 54.6           |
|   | (5) Completely accord with  | 37        | 14.9           |

TABLE 2: Chinese classroom evaluation can make me reflect on learning strategies.

| Title  | Options                     | Frequency | Percentage (%) |
|--|-----------------------------|-----------|----------------|
| Chinese classroom evaluation can make me reflect on my learning strategies | (1) Completely inconsistent | 5         | 2.0            |
|  | (2) Some do not match       | 15        | 6.0            |
|  | (3) Uncertainty             | 65        | 26.1           |
|  | (4) Basically accord        | 123       | 49.4           |
|  | (5) Completely accord with  | 41        | 16.5           |

TABLE 3: Chinese evaluation can stimulate my strong learning motivation.

| Title   | Options                     | Frequency | Percentage (%) |
|---|-----------------------------|-----------|----------------|
| Chinese class can stimulate my strong learning motivation | (1) Completely inconsistent | 5         | 2.0            |
|   | (2) Some do not match       | 15        | 6.0            |
|   | (3) Uncertainty             | 65        | 26.1           |
|   | (4) Basically accord        | 123       | 49.4           |
|   | (5) Completely accord with  | 41        | 16.5           |

In Table 10, the average value of this question is 3.17, slightly higher than the median value. About 43.4% of the students will participate in the classroom evaluation of Chinese class in various ways, 25.7% of the students say they are "uncertain," and 30.9% of the students think they cannot participate in the classroom evaluation in various ways.

In Table 11, the average value of this question is 3.41, slightly higher than the median value. On the question of "Chinese teachers often encourage us to evaluate others in class," 18.5% of students chose "complete conformity," 37.1%

chose "basic conformity," 21.8% expressed "uncertainty," 12.9% chose "some inconformity," and 9.7% chose "complete inconformity." About 45% of the people did not explicitly indicate that Chinese teachers encourage students to make other evaluations. It can be seen that in order to improve students' participation in Chinese classroom evaluation in senior high schools, teachers must first constantly encourage students to join, create an environment that can attract students to join, and let students make evaluations in a comfortable and stable classroom environment.

TABLE 4: Students who can draw inferences from others are often praised.

| Title  | Options                     | Frequency | Percentage (%) |
|--|-----------------------------|-----------|----------------|
| Students who can draw inferences from others are often praised | (1) Completely inconsistent | 4         | 1.6            |
|  | (2) Some do not match       | 22        | 8.8            |
|  | (3) Uncertainty             | 45        | 18.0           |
|  | (4) Basically accord        | 118       | 47.2           |
|  | (5) Completely accord with  | 61        | 24.4           |

TABLE 5: Do teachers often evaluate students' learning attitude in class.

| Title  | Options                     | Frequency | Percentage (%) |
|--|-----------------------------|-----------|----------------|
| Chinese teachers often evaluate students' learning attitude in class | (1) Completely inconsistent | 7         | 2.8            |
|  | (2) Some do not match       | 17        | 6.8            |
|  | (3) Uncertainty             | 49        | 19.6           |
|  | (4) Basically accord        | 125       | 50.0           |
|  | (5) Completely accord with  | 52        | 20.8           |

TABLE 6: Teachers often evaluate students' learning methods.

| Title   | Options                     | Frequency | Percentage (%) |
|---|-----------------------------|-----------|----------------|
| Chinese teachers often evaluate students' learning methods in class | (1) Completely inconsistent | 10        | 4.0            |
|   | (2) Some do not match       | 34        | 13.7           |
|   | (3) Uncertainty             | 37        | 14.9           |
|   | (4) Basically accord        | 125       | 50.2           |
|   | (5) Completely accord with  | 43        | 17.3           |

TABLE 7: Teachers often evaluate students' thinking ability in class.

| Title   | Options                     | Frequency | Percentage (%) |
|---|-----------------------------|-----------|----------------|
| Chinese teachers often evaluate students' thinking logic ability in class | (1) Completely inconsistent | 10        | 4.0            |
|   | (2) Some do not match       | 31        | 12.4           |
|   | (3) Uncertainty             | 59        | 23.7           |
|   | (4) Basically accord        | 98        | 39.4           |
|   | (5) Completely accord with  | 51        | 20.5           |

TABLE 8: Do students often have the opportunity to evaluate others' learning in class.

| Title   | Options                     | Frequency | Percentage (%) |
|---|-----------------------------|-----------|----------------|
| I often have the opportunity to evaluate other people's learning in Chinese class | (1) Completely inconsistent | 49        | 19.9           |
|   | (2) Some do not match       | 46        | 18.7           |
|   | (3) Uncertainty             | 61        | 24.8           |
|   | (4) Basically accord        | 63        | 25.6           |
|   | (5) Completely accord with  | 27        | 11.0           |

(4) *Students' Feedback on Classroom Evaluation.* In Table 12, 64.8% of the students think that the Chinese teacher's evaluation can truly reflect the students' learning situation, 23.6% of the students hold an "uncertain" attitude, and 11.6% of the students think that the teacher's evaluation cannot truly reflect the students' situation. It shows that from the perspective of students, students' learning situation is not completely reflected by the evaluation of Chinese teachers.

In Table 13, 75.2% of the students said that Chinese teachers often communicate the results of learning evaluation with their classmates, 15.2% said they were

"uncertain," and only 9.6% thought it was not the case. It shows that Chinese teachers in senior high schools will evaluate and communicate with their classmates at present, but about a quarter of the students still have no clear supporters of this view.

In Table 14, 76% of the students think that Chinese teachers can use the evaluation results to guide people to study deeply, 17.6% think it is "uncertain," and only 6.4% of the students hold the opposite view.

In Table 15, on the question of "whether Chinese teachers will guide students to reflect on learning according to the evaluation results," 32.4% of students choose "complete

TABLE 9: Students are willing to evaluate other students' learning in class.

| Title  | Options                     | Frequency | Percentage (%) |
|--|-----------------------------|-----------|----------------|
| I am happy to evaluate other students' learning in Chinese class | (1) Completely inconsistent | 43        | 17.3           |
|  | (2) Some do not match       | 53        | 21.4           |
|  | (3) Uncertainty             | 58        | 23.4           |
|  | (4) Basically accord        | 64        | 25.8           |
|  | (5) Completely accord with  | 30        | 12.1           |

TABLE 10: Participate in classroom evaluation of Chinese class in various ways.

| Title   | Options                     | Frequency | Percentage (%) |
|---|-----------------------------|-----------|----------------|
| I participate in the classroom evaluation of Chinese class in many ways | (1) Completely inconsistent | 22        | 8.8            |
|   | (2) Some do not match       | 55        | 22.1           |
|   | (3) Uncertainty             | 64        | 25.7           |
|   | (4) Basically accord        | 73        | 29.3           |
|   | (5) Completely accord with  | 35        | 14.1           |

TABLE 11: Encourage students to evaluate each other in class.

| Title   | Options                     | Frequency | Percentage (%) |
|---|-----------------------------|-----------|----------------|
| Chinese teachers often encourage us to make comments on others in class | (1) Completely inconsistent | 24        | 9.7            |
|   | (2) Some do not match       | 32        | 12.9           |
|   | (3) Uncertainty             | 54        | 21.8           |
|   | (4) Basically accord        | 92        | 37.1           |
|   | (5) Completely accord with  | 46        | 18.5           |

TABLE 12: Chinese teachers' evaluation can truly reflect students' learning situation.

| Title   | Options                     | Frequency | Percentage (%) |
|---|-----------------------------|-----------|----------------|
| The evaluation of Chinese teachers can truly reflect students' learning situation | (1) Completely inconsistent | 4         | 1.6            |
|   | (2) Some do not match       | 25        | 10.0           |
|   | (3) Uncertainty             | 59        | 23.6           |
|   | (4) Basically accord        | 114       | 45.6           |
|   | (5) Completely accord with  | 48        | 19.2           |

TABLE 13: Results of teacher-student exchange evaluation.

| Title   | Options                     | Frequency | Percentage (%) |
|---|-----------------------------|-----------|----------------|
| Chinese teachers often communicate the results of learning evaluation with students | (1) Completely inconsistent | 9         | 3.6            |
|   | (2) Some do not match       | 15        | 6.0            |
|   | (3) Uncertainty             | 38        | 15.2           |
|   | (4) Basically accord        | 124       | 49.6           |
|   | (5) Completely accord with  | 64        | 25.6           |

compliance,” and about one third of students think that teachers can inspire students to think and examine their learning behavior and state through the evaluation results. About 46.8% of the students chose “basic conformity,” which accounts for nearly half, indicating that teachers' performance in handling the evaluation results is satisfactory.

*4.2.2. Difference Analysis of Total Scores of Classroom Evaluation of Senior High School Students.* This study will analyze the differences in the total scores of classroom evaluation of Chinese teachers in senior high schools in various demographic variables. These variables involve five

factors, namely, teachers' gender, grade, family residence, whether they serve as class managers or not, and Chinese scores in classes. An independent sample  $t$ -test was used to analyze the variance between gender and class cadre, and single-factor variance was used to analyze the variance between class, grade, and family residence. The overall analysis ideas and results are roughly consistent with the teachers' questionnaires, so they will not be repeated here.

(1) *Grade Difference.* From the grade difference of students in Figure 5, the  $F$  value of one-way ANOVA is 7.124,  $P < 0.05$ , which shows that the difference between groups has reached a very significant level; different grades have different evaluation



TABLE 14: Guiding students to conduct in-depth learning.

| Title   | Options                     | Frequency | Percentage (%) |
|---|-----------------------------|-----------|----------------|
| Chinese teachers use evaluation results to guide students to study deeply | (1) Completely inconsistent | 4         | 1.6            |
|   | (2) Some do not match       | 12        | 4.8            |
|   | (3) Uncertainty             | 44        | 17.6           |
|   | (4) Basically accord        | 135       | 54.0           |
|   | (5) Completely accord with  | 55        | 22.0           |

TABLE 15: Guide students to reflect on their own learning.

| Title   | Options                     | Frequency | Percentage (%) |
|---|-----------------------------|-----------|----------------|
| Chinese teachers will guide students to reflect on their own learning according to the evaluation results | (1) Completely inconsistent | 6         | 2.4            |
|   | (2) Some do not match       | 10        | 4.0            |
|   | (3) Uncertainty             | 36        | 14.4           |
|   | (4) Basically accord        | 117       | 46.8           |
|   | (5) Completely accord with  | 81        | 32.4           |

scores; and at least one group has significant differences. After the multiple comparative tests, we can see that there are significant differences between senior three students and senior one students ( $P < 0.05$ ) and senior two students ( $P < 0.05$ ). By observing the average value, it can see that in the survey of Chinese classroom evaluation in senior high schools that promotes deep learning, the scores of students in Grade One and Grade Two are higher than those in Grade Three.

Looking at the above table, we can see that the average evaluation scores of senior one students are 93.5556, the average evaluation scores of senior two students are 90.4423, and the average evaluation scores of senior three students are only 84.4312, which is obviously different from the other two groups. Generally speaking, the higher the grade, the lower the score in the classroom evaluation of promoting deep learning. In the third year of senior high school, the new teaching has been greatly reduced, and students have gradually turned to comprehensive review, paying more attention to the consolidation of knowledge points. Teachers' evaluation focus in class will also turn to the detection of knowledge points and the investigation of test-taking skills, thus ignoring the cultivation of deep learning ability of senior high school students.

(2) *Difference in Family Residence.* From Figure 6, it can be seen that the F value of one-way ANOVA is 3.296, and the  $P < 0.05$ , which shows that the difference between groups has reached a very significant level. Different families live in different places in terms of evaluation scores, and at least one group has significant differences, but it is unclear which group is at present. Further looking at the data, we can see that there are significant differences between the students who live in cities and the students who live in county towns ( $P < 0.05$ ) and the students who live in rural areas ( $P < 0.05$ ). Because of the differences in educational level and other factors, the average score of students in cities is higher than that of students in other places.

Teachers' classroom evaluation is still knowledge oriented. Although they sometimes know how to encourage students, they still tend to test students' mastery of knowledge

in the actual classroom, lacking attention to students' learning interest, learning methods, and thinking structure. In the questionnaire survey, teachers generally know more about the evaluation of promoting deep learning. However, when asked about the relevant contents of deep learning, teachers are somewhat vague, unable to really understand the meaning and characteristics of deep learning, and unable to make in-depth connection between evaluation and deep learning. During the interview, some teachers asked what deep learning is like, which can also reflect that some teachers have less awareness of promoting the evaluation of deep learning, let alone how to make in-depth management of classroom evaluation and deep learning. In the Chinese classroom of real frontline teachers, deep learning-oriented evaluation is still difficult to implement, due to external evaluation reasons, and factors such as poor self-grasp, difficult implementation, and unwillingness to try.

## 5. Conclusions

Learning to evaluate students' learning status in different ways is a necessary process to guide students to study deeply. The original starting point of evaluating students includes thinking level, knowledge reserve, learning skills, psychological characteristics, interest tendency, self-cognition, learning attitude, and so on. We can use the question-and-answer style of direct inquiry in class; we can also use the description of other teachers to evaluate others; and we can also infer other information about students' learning by looking at previous learning works. Calling student status files is the most convenient way to have an overall understanding of students. If you need to examine students' knowledge and ability, the best way is to use a thorough test paper and intuitively understand it through test scores. However, for the information of interest and self-cognition, we take the interest scale and self-evaluation scale to fill in for students, so that they can scientifically predict their emotional content. After measuring and evaluating in many aspects, teachers can deeply understand the starting point of students' learning and lay a solid data foundation for the analysis of learning situation.

## Data Availability

The experimental data used to support the findings of this study are available from the author upon request.

## Conflicts of Interest

The author declare that they have no conflicts of interest regarding this work.

## Acknowledgments

This work was sponsored in part by the Research on Critical Thinking Cultivation in Chinese Reading Teaching Based on Core Literacy (SKG-2019-102).

## References

- [1] B. Leibe, J. Matas, N. Sebe, and M. Welling, "Deep learning the city: quantifying urban perception at a global scale," in *Proceedings of the European Conference on Computer Vision*, Springer, Cham, The Netherlands, Amsterdam, 2016.
- [2] Y. Jian, J. Ni, and Y. Yang, "Deep learning hierarchical representations for image steganalysis," *IEEE Transactions on Information Forensics and Security*, vol. 12, no. 11, pp. 2545–2557, 2017.
- [3] W. K. Wong and M. Mingming Sun, "Deep learning regularized Fisher mappings," *IEEE Transactions on Neural Networks*, vol. 22, no. 10, pp. 1668–1675, 2011.
- [4] X. Ma, J. Geng, and H. Wang, "Hyperspectral image classification via contextual deep learning," *EURASIP Journal on Image and Video Processing*, vol. 2015, no. 1, p. 20, 2015.
- [5] S. Wiesler, A. Richard, R. Schlüter, and H. Ney, "Mean-normalized stochastic gradient for large-scale deep learning," in *Proceedings of the IEEE International Conference on Acoustics*, Florence, Italy, 2014.
- [6] H.-Il Suk, C. Y. Wee, S. W. Lee, and D. Shen, "State-space model with deep learning for functional dynamics estimation in resting-state fMRI," *NeuroImage*, vol. 129, pp. 292–307, 2016.
- [7] L. Song, X. Qian, L. Hai, and Y. Chen, "PipeLayer: a pipelined ReRAM-based accelerator for deep learning," in *Proceedings of the 2017 IEEE International Symposium on High Performance Computer Architecture (HPCA)*, IEEE, Austin, TX, USA, 2017.
- [8] Y. Tian, B. Fan, and F. Wu, "L2-Net: deep learning of discriminative patch descriptor in euclidean space," in *Proceedings of the 2017 IEEE Conference on Computer Vision and Pattern Recognition (CVPR)*, IEEE, Honolulu, HI, USA, 2017.
- [9] J. Leng and P. Jiang, "A deep learning approach for relationship extraction from interaction context in social manufacturing paradigm," *Knowledge-Based Systems*, vol. 100, no. 15, pp. 188–199, 2016.
- [10] J. A. O'Flaherty and T. A. Laws, "Nursing student's evaluation of a virtual classroom experience in support of their learning Bioscience," *Nurse Education in Practice*, vol. 15, no. 5, pp. 232–267, 2014.
- [11] A. Saeed, M. Fauzia, S. Malik Muhammad, and M. Sidra, "Sociology of classroom: role of perceived pedagogical skills, andragogy and social capital in evaluation of students' learning," *The Pakistan Journal of Social Issues*, vol. 6, no. 3, pp. 128–162, 2017.
- [12] M. Shi, "Learning classroom Assessment is missing in the evaluation of education in China," *The Guide of Science & Education*, vol. 8, no. 11, pp. 423–469, 2015.
- [13] K. Tomul, "Çelik ali taş. Justice in the classroom: evaluation of teacher behaviors according to students' perceptions," *European Journal of Educational Research*, vol. 12, no. 48, pp. 59–72, 2009.
- [14] X. Huang and L. Han, "Empirical analysis of students' participation in the online evaluation of classroom teaching quality," *Higher Education Development and Evaluation*, vol. 13, no. 24, pp. 326–389, 2010.
- [15] H. Zhu and S. Lan, "Classroom teaching evaluation of Chinese painting as a form of fine arts in rural junior high schools," *Asian Agricultural Research*, vol. 12, no. 12, pp. 4–14, 2020.

## Research Article

# Application of PID Control and Improved Ant Colony Algorithm in Path Planning of Substation Inspection Robot

YeFei Kang, ZhiBin Li, and Tao Wang 

*School of Automation Engineering, Shanghai University of Electric Power, Shanghai 200090, China*

Correspondence should be addressed to Tao Wang; wangtao@mail.shiep.edu.cn

Received 30 June 2022; Revised 1 August 2022; Accepted 3 August 2022; Published 23 August 2022

Academic Editor: ManFai Leung

Copyright © 2022 YeFei Kang et al. This is an open access article distributed under the Creative Commons Attribution License, which permits unrestricted use, distribution, and reproduction in any medium, provided the original work is properly cited.

The purpose is to improve the effect of substation inspection and ensure the safety of power consumption in human society. First, this work discusses the current substation inspection-oriented robot path planning situation. Then, the proportional integration differentiation (PID) control algorithm is introduced and optimized. Ant colony algorithm (ACA) is improved. The substation inspection-oriented RPP model is designed based on the PID algorithm and optimized ACA (the proposed model is denoted as the Ant-PID algorithm). Afterward, the Ant-PID algorithm is compared with the PID control algorithm and ACA. The results show that the longest robot path of the proposed Ant-PID algorithm in different data sets is about 28 m. The shortest is about 26 m, and the number of optimal solutions is maintained at about 45–49. By comparison, the average response time of the PID algorithm is about 25 s to 28 s. The shortest response time of ACA is about 24 s, the shortest average response time is about 27 s, and the longest is about 30 s. The average response time of the proposed ant PID model is about 17 s to 20 s. Therefore, the Ant-PID algorithm can improve the substation inspection robots' path planning effect. The research results provide technical support for improving the effect of substation inspection and contribute to social power transmission.

## 1. Introduction

With science and technological progress, power transmission engineering is expanding. As the intermediate medium of power transmission, substation plays an important role. The substation has a tricky structure, with heavy maintenance costs and complex detection flow. Therefore, real-time substation monitoring in power transmission is critical and challenging [1]. As a technological product to mimic and replace human intelligence, robot technologies have found applications in substation inspection, only far from mature. In particular, the inspection task-oriented robot path planning (RPP) is worthy of in-depth exploration, and the robot response time cannot meet the needs of current substation inspection to improve the working efficiency of the robot in substation inspection [2].

Although the current research on applying robots in substation inspection is not perfect, many studies have provided technical support. Tao et al. proposed a based robot to replace real-time manual inspection of substations. The

optimal RPP and two-way walking were realized following the magnetic trajectory to inspect the primary equipment in the station. The designed robot could make an autonomous decision or be remotely controlled to find the thermal defects and equipment abnormalities in time. Image processing and pattern recognition distinguished the opening and closing states of switches and knife switches. When under remote control or sequential control of the intelligent substation, the robot could replace manual inspection in positioning and controlling the equipment [3]. Li et al. observed that the power grid security maintenance was becoming more intelligent with the development of information and intelligence. Major power grid companies and enterprises loved the substation inspection robot, upgrading every day as a key component in intelligent power grid development. Therefore, the research on substation inspection-oriented RPP was a hot research spot. However, the current research was challenged by real-time RPP [4]. Melo et al. implemented the substation maintenance-oriented RPP through an ant colony algorithm (ACA) and achieved an effective outcome by

continuously optimizing the robot paths. ACA provided a more comprehensive and effective RPP reference through the distributed node calculation. Besides, ACA analyzed the system error through positive feedback to encourage the system's self-optimization through iterative training. However, ACA was still in its infancy and must be further explored to provide better technical support for RPP [5]. Ekinci et al. divided the mobile robot's path tracking, control, and planning into two modules according to the kinematic model and using the hierarchical control theory: trajectory tracking controller and proportion integration differentiation (PID)-based robot speed controller. Based on the backstepping time-varying state feedback method and Lyapunov theory, a mobile robot-oriented global trajectory tracking algorithm was designed by introducing a virtual feedback quantity with hyperbolic tangent characteristics. PID controller was adopted to meet the real-time speed regulation requirements of the robot drive motor. Regarding the dynamic constraints of the robot, a strategy was introduced to ensure its smooth motion. The real-time trajectory tracking experiment of the algorithm was carried out on a two-wheel drive mobile robot, obtaining satisfactory results. It was found that the PID algorithm must integrate other algorithms in RPP, and more research was needed to support its development [6]. To sum up, the current research has provided a theoretical reference for applying robot technologies in substation inspection. Nevertheless, the current technical means are not perfect. For example, the system response time is long, and the intelligent RPP is not reasonable. To this end, more research is needed to support RPP's technical improvement.

Based on the above problems of substation inspection robots and the specific research directions, this work summarizes the substation inspection-oriented RPP and the inspection robot's specific design concept. Then, the PID algorithm is optimized. Finally, the ACA is improved, and the substation inspection-oriented RPP model is designed by integrating PID and ACA. The finding provides an essential guarantee for the regular operation of the substation and contributes to the normal power consumption of human society.

## 2. Research Theories and Methods

*2.1. Comprehensive Design Concept of Substation Inspection Robot.* Artificial intelligence (AI) equipment has become the first choice to replace humans. For example, intelligent robots have been widely used in various fields and have become the main productivity of human society [7]. As the main supporting point of human use of electricity, substation inspection plays a vital role in ensuring its normal work and the normal operation of human life. The substation inspection is a critical but boring task. Traditionally, the manual inspection often overlooks many faults and failures because the result is subjective, and individual experience and human vision are unsuitable for such missions. Therefore, the AI robot has become an essential technology for substation inspection [8]. The main task of the substation inspection robot is to reduce the labor intensity of inspection

workers. During the daily inspection, the inspection robot mainly obtains the power equipment video through the camera. It transmits the data to the background for processing to repair the power equipment with potential safety hazards in time [9]. In order to complete the daily inspection work, the robot needs to integrate vision technology and path planning technology, additionally, to process the inspection results, and to transmit the information obtained by the robot to the background processing end in real time. The inspection robot should also combine multisensor information fusion technology, wireless communication, and wireless transmission technology. Last but not least, the substation inspection robot has special requirements in the overall structural design and functional hardware selection [10].

The substation has many characteristics as the main supporting point of electric power transmission (EPT). First, the overall environment is static. Substation equipment is divided into outdoor open type and indoor integrated type. Currently, the conventional outdoor open type is more used in the substation. Different equipment is assembled according to the functional objectives of the substation. The equipment is arranged in turn according to the functions, and the wiring between the equipment is safe and beautiful [11]. The building structure of the substation is reasonable, and the appearance is neat. After using robots to replace manual inspection, few people are active in the substation, so the overall environment of the substation is an overall static environment for the substation inspection robot. Thus, the substation topology can be stored in the database for the convenience of robots [12]. Second, the environment is full of high electromagnetic interference (EMI). There are transformers, high-voltage, or ultrahigh voltage (UHV) equipment in the substation, producing all kinds of corona phenomena. The high-voltage line of the substation will produce a strong electromagnetic field. Transient UHV occurs during operation [13]. Thus, complex EMI makes the electromagnetic environment of substations particularly complex. There is a clear distinction between environmentally feasible areas and obstacle areas. The overall design of the substation is relatively clean, with clear obstacle areas and feasible areas. The robot must keep a safe distance from the obstacle areas during the inspection process. Some feasible areas of the substation are relatively narrow, so the robot foothold should be minimum [14]. Finally, the feasible area is generally flat, but some potholes, slopes, and steps will be. In the substation design, the roads in feasible areas are mostly flat. However, the substation roads in mountainous areas might have potholes, and there will be slopes or steps in places with large drops [15].

The inspection robot needs to regularly conduct comprehensive and detailed inspections on the power equipment in the substation, greatly improving the efficiency and accuracy of inspection. In order to realize all-weather and no dead corner inspection, the inspection robot needs to have some functions [16]. First, the substation inspection robot can perceive the information of the environment and determine when to stop or bypass [17]. At the same time, the substation inspection robot must be timely aware of its self-

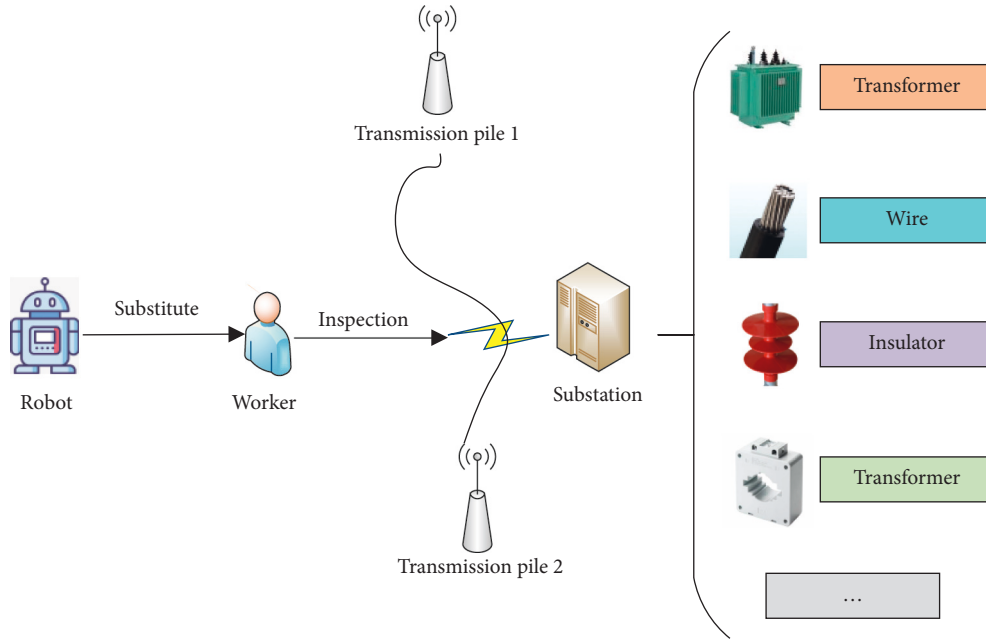


FIGURE 1: Basic characteristics of substation and main working conditions of inspection robot.

position through relevant technologies. Second, the substation inspection robot can carry out path planning. It can plan a path that traverses all stops and has the shortest distance suitable for the substation inspection [18]. Then, the substation inspection robot can feedback a clear image of the detected power equipment in real time through the communication module for expert observation and analysis [19]. Finally, the substation inspection robot can be remotely controlled. During the inspection process, the robot can receive the command from the background, change to the manual remote-control state, and monitor the abnormal power equipment at a specific position in the substation [20]. Figure 1 shows the substation's basic characteristics and the inspection robot's main working conditions.

As shown in Figure 1, as a substitute for substation patrol workers, the robot undertakes the main responsibility of substation inspection. Doing so prevents human injury to substation equipment and improves inspection efficiency. However, the robot inspection path needs to be designed to provide better technical support for improving the efficiency of substation inspection.

**2.2. PID Control Algorithm.** PID control algorithm plays a vital role in the industrial control process. With the support of the PID control algorithm, various industrial production processes have been refined. PID algorithm refers to proportional, integral, and differential linear control algorithms [21]. Figure 2 draws the main flow of the PID control algorithm.

As shown in Figure 2, in the PID control algorithm, the proportional, integral, and differential linear calculations shall be carried out, respectively. Then, the calculation results of the three shall be integrated to strengthen the control

effect of the system [22]. The calculation of differential equation and transfer function of PID controller read

$$u(t) = K_p \left[ e(t) + \frac{1}{T_I} \int_0^t e(t)dt + T_D \frac{de(t)}{dt} \right], \quad (1)$$

$$D(S) = \frac{U(S)}{E(S)} = K_p \left[ 1 + \frac{1}{T_I S} + T_D S \right], \quad (2)$$

$$e(t) = r(t) - c(t). \quad (3)$$

In (1)–(3),  $K_p$  is the scale factor.  $T_I$  denotes the integral time constant.  $T_D$  represents the differential time constant.  $d$  stands for the calculated bias, and  $t$  signifies the time [23]. The functions of the three modes are different. The proportional function is to map the deviation signal in the control process through a certain proportion. In other words, the proportional function will react when the system has a control deviation to reduce the control deviation of the system [24]. The integration function mainly removes the static error so that the control result of the system is the same as the final setting result. The relationship between the action effect of the integration link and the integration time constant is inversely proportional. The integration time constant is the main factor determining the action of the integration link [25]. The function of the differential link is mainly to map the changing state of the deviation signal of the slice. Suppose the changing state of the deviation signal is stronger. In that case, the system will modify the control quantity faster to effectively reduce the delay of system error

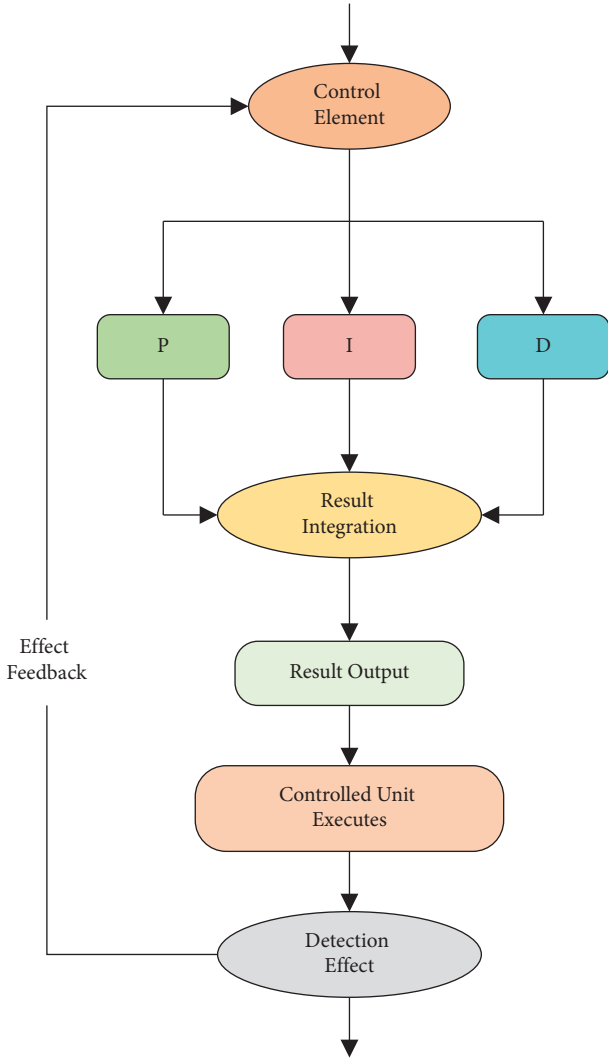


FIGURE 2: Calculation flow of PID control algorithm.

modification [26]. The main control mode of the PID control algorithm is the digital calculation, so it is necessary to discretize the PID algorithm. That is, each element in the PID algorithm is approximately discretized [27]. The discretization reads

$$t \approx kT (k = 0, 1, 2, \dots), \quad (4)$$

$$e(t) \approx e(kT), \quad (5)$$

$$\int e(t)dt \approx \sum_{j=0}^k e(jT)T = T \sum_{j=0}^k e(jT), \quad (6)$$

$$\frac{de(t)}{dt} \approx \frac{e(kT) - e[(k-1)T]}{T}. \quad (7)$$

In (4)–(7), each element shares the same meaning as the above equations. If  $kT$  is represented by  $k$ , the specific calculation reads

$$K_I = K_P \frac{T}{T_I}, K_D = K_P \frac{T_D}{T}, \quad (8)$$

$$u(k) = K_P e(k) + K_I T \sum_{j=0}^k e(j) + K_D [e(k) - e(k-1)].$$

This work optimizes the PID algorithm through position and increment. The first is the position PID control algorithm. In this algorithm, the system controls the control unit through  $u(k)$ , and the calculated value of  $u(k)$  is the position output of the controlled unit. The second is the incremental control algorithm [28]. In this algorithm,  $u(k)$  represents the change in the position of the control unit. This algorithm is widely used because it is safer and does not need cumulative calculation. Thereby, it shortens the system calculation time and improves work efficiency [29]. Fusing position control algorithms (8) and (9) can obtain the calculation of the incremental control algorithm:

$$u(k-1) = K_P e(k-1) + K_I \sum_{j=0}^{k-1} e(j) + K_D [e(k-1) - e(k-2)], \quad (9)$$

$$\Delta u(k) = K_P [e(k) - e(k-1)] + K_I e(k) + K_D [e(k) - 2e(k-1) + e(k-2)]. \quad (10)$$

In (10) and (11), the result of  $\Delta u(k)$  represents the position change of the controlled unit in the control process of the PID algorithm. Only the recent errors are sampled [30]. Figure 3 presents the design concept of optimizing the PID control algorithm through position and incremental algorithms.

As shown in Figure 3, an incremental algorithm is extended based on the positional algorithm. In simple terms, the positional algorithm provides a basic concept for the incremental algorithm, and the incremental algorithm is the optimization result of the positional algorithm [31]. Therefore, in the PID optimization algorithm, the control accuracy of the incremental control algorithm is higher, and the calculation result of the algorithm is more reliable.

**2.3. Optimizing ACA.** ACA is designed according to the ant colony foraging process. Its main connotation is to seek simpler results in the calculation process. The robot path control calculation selects a shorter route with a high algorithm accuracy to make a more efficient substation inspection. ACA features distributed computing, self-organization, and positive feedback [32]. Distributed computing means the ant colony algorithm distributes the global computing tasks to each node in the computing process. That is, the ant individuals in the ant colony calculate independently. When the node-independent computing task is completed, the system integrates all the calculation results. Then, it compares and analyzes the integration results

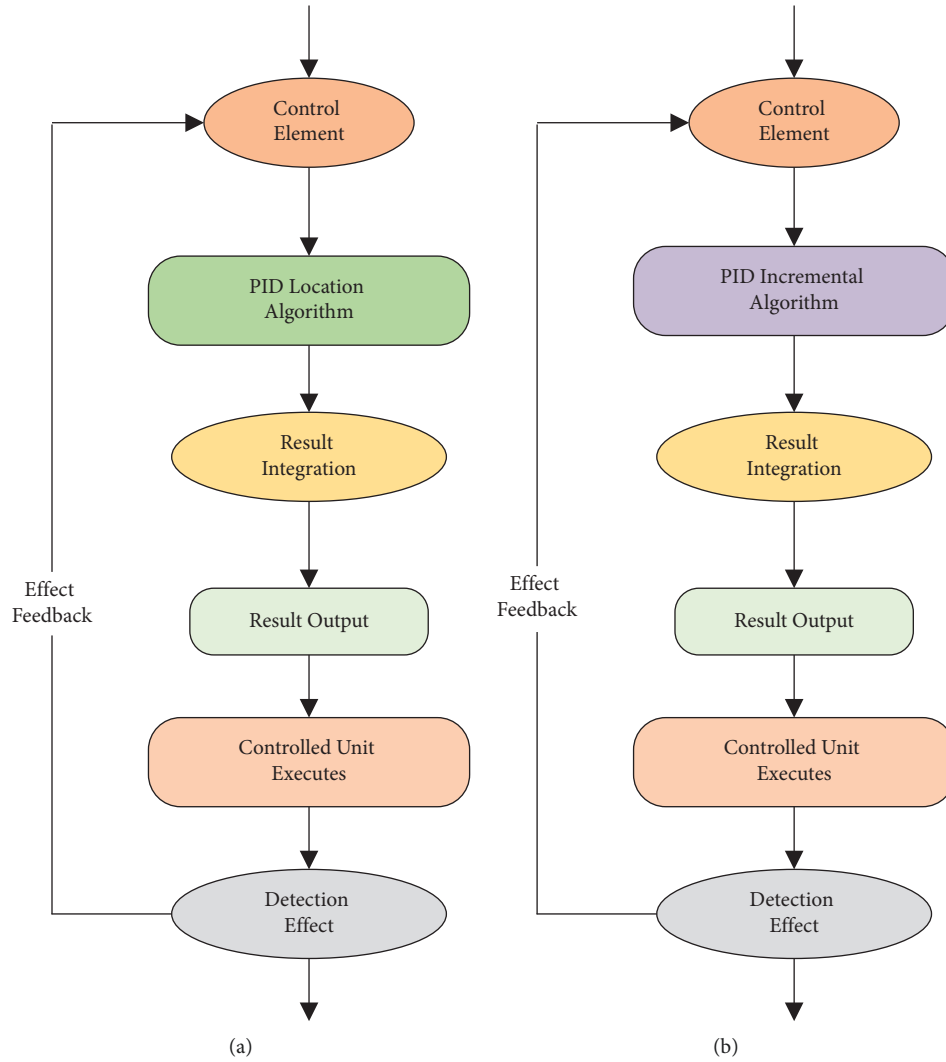


FIGURE 3: The design concept of optimizing PID control algorithm through position algorithm and incremental algorithm ((a) is position algorithm, and (b) is incremental algorithm).

and finally outputs the optimal solution of the system calculation. Therefore, in ACA, the feasibility of the system results will not be affected by the individual calculation error. The self-organization characteristic means that the ant colony is not affected by external factors in the calculation process. The ant colony individuals independently seek the optimal solution in the calculation process. The system selects the path with the most individuals after specific iterations, namely, the result with the most individual calculation frequency [33]. The positive feedback characteristic means that when the ant colony selects a path, the individual ants generate pheromones on the shortest path. Then, the ant colony will feedback the shortest path selected most according to the pheromone concentration (PC). Thereby, it helps the ant colony chooses more shortest paths [34]. The calculation of the transition probability of ant colony selection reads

$$p_{ij}^k = \frac{(\tau_{ij}^\alpha)(\eta_{ij}^\beta)}{\sum_{z \in \text{allowed}_x} (\tau_{ij}^\alpha)(\eta_{ij}^\beta)}. \quad (11)$$

In (11),  $i$  and  $j$  are the selected location nodes of the ant colony.  $z$  is the specific location.  $\text{allowed}$  represents the location set, and  $dx$  denotes the location deviation.  $\tau$  refers to the PC. The specific calculation reads

$$\tau_{ij}(t+1) = \rho * \tau_{ij}(t) + \Delta\tau, \quad (12)$$

$$\Delta\tau_{ij} = \sum_{k=1}^m \Delta\tau_{ij}^k. \quad (13)$$

In (12) and (13),  $\rho$  is the volatilization coefficient.  $k$  denotes the calculation position point. The PC calculation of the heuristic function reads

$$\eta_{ij} = \frac{1}{d_{ij}}. \quad (14)$$

In (14),  $d$  is the Euclidean distance (ED) between location nodes. In this work, the pheromone updating mechanism is used to improve ACA. That is, in the

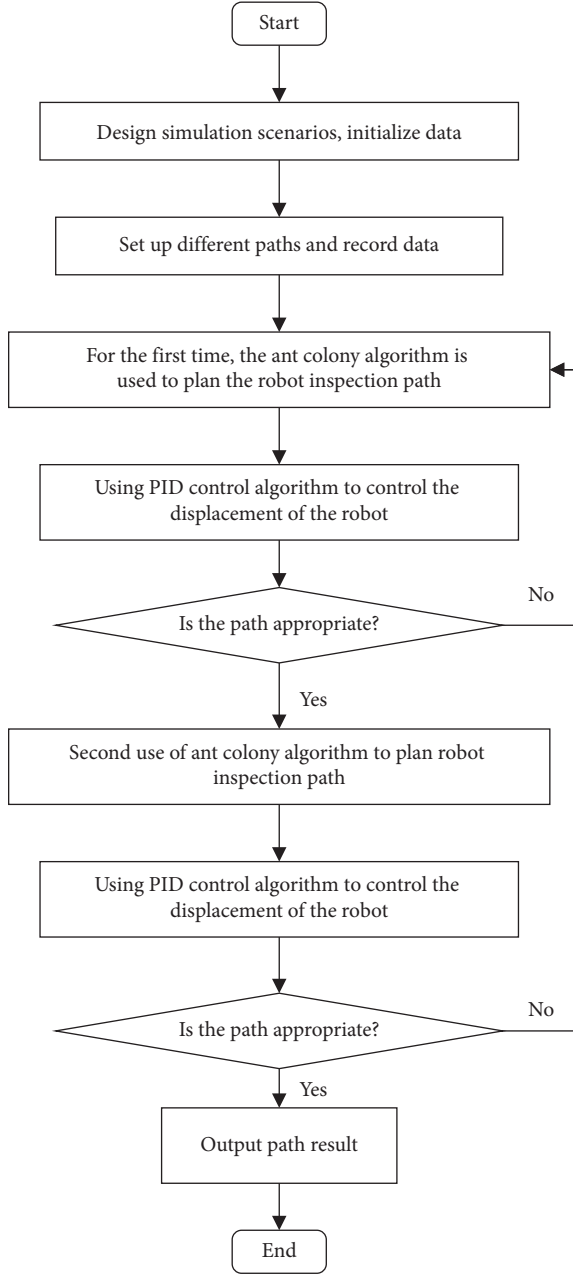


FIGURE 4: Calculation flow of PID control algorithm and twice path planning ACA.

calculation process, only individuals who can reach the target point are selected. In each iteration process, individuals who can reach the target point and have the shortest path are selected to improve the calculation results of ACA [35] gradually. The pheromone update calculation reads

$$\tau_{ij}(t+1) = (1 - \rho)\tau_{ij}(t) + \rho\Delta\tau_{ij}(t, t+1), \quad (15)$$

$$\tau_{ij}(t+1) = (1 - \rho)\tau_{ij}(t) + \eta\rho\Delta\tau_{ij}(t, t+1), \quad (16)$$

$$\tau_{ij}(t+1) = (1 - \rho)\tau_{ij}(t) - \eta\rho\Delta\tau_{ij}(t, t+1). \quad (17)$$

In (16) and (17),  $\eta$  is the increased range coefficient of pheromone.  $\rho$  is of utmost importance. The volatilization coefficient can adjust the pheromone distribution to find the optimal solution. Therefore, the selection of the volatilization coefficient is crucial. The adjustment of the volatilization coefficient reads

$$\rho(t+1) = \begin{cases} \gamma \cdot \rho(t), & \gamma \cdot \rho(t) \geq \rho_{\min}, \\ \rho_{\min}, & \text{others.} \end{cases} \quad (18)$$

In (18),  $\rho_{\min}$  is the minimum volatilization coefficient.  $\gamma$  represents the attenuation coefficient, which is less than 1. This work designs the twice-path planning method to improve the calculation results of the ACA. Then, Figure 4 demonstrates the calculation process of the PID control algorithm combined with the proposed twice-path planning ACA.

As shown in Figure 4, based on the calculation of ACA, the twice path planning mechanism is added to increase the calculation frequency of ACA. This can effectively improve the accumulation effect of pheromone to help the substation inspection robot find a better inspection route. Integrating the PID control algorithm can effectively provide a better inspection path for the substation inspection robot. Therefore, the proposed Ant-PID control algorithm fusing the PID algorithm and ACA can improve the efficiency of the substation inspection robot.

**2.4. Research Data Settings.** The data set is mainly used to evaluate the comprehensive performance of the model. The data sets include (1) supersizing self-supervision (SS) dataset, containing 50 K data points and 700 hours of robot experiment and error experiment. At the same time, the data set collects more than 150 objects with different graspability. (2) Learning hand-eye coordination (LH) dataset describes two large-scale experiments on two independent robot platforms. The first experiment collects about 800,000 grab attempts over two months. In the second experiment, different robot platforms and eight robots collect data sets containing more than 900,000 grab attempts. (3) Scene understanding (SUN) dataset contains 10,335 robot detection results of different scenes, 146,617 2D polygon annotations (which should refer to 2D segmentation), and 58,657 3D frames. (4) The RoboTurk Real Robot (RTRR) dataset contains 2,144 different presentations from 54 users. This includes 111 hours of robot operation data for three challenging operation tasks. This work comprehensively evaluates the performance optimization of substation robots through robot path selection simulation. The comparison algorithms used in the evaluation process include the PID algorithm and ACA.

### 3. Performance Optimization Evaluation of Substation Inspection Robot

**3.1. Path Selection Performance Evaluation.** This section uses the proposed Ant-PID control algorithm to design the substation inspection-oriented RPP model. Then, it evaluates the displacement of the robot through the PID control algorithm and carries out twice path planning through ACA to



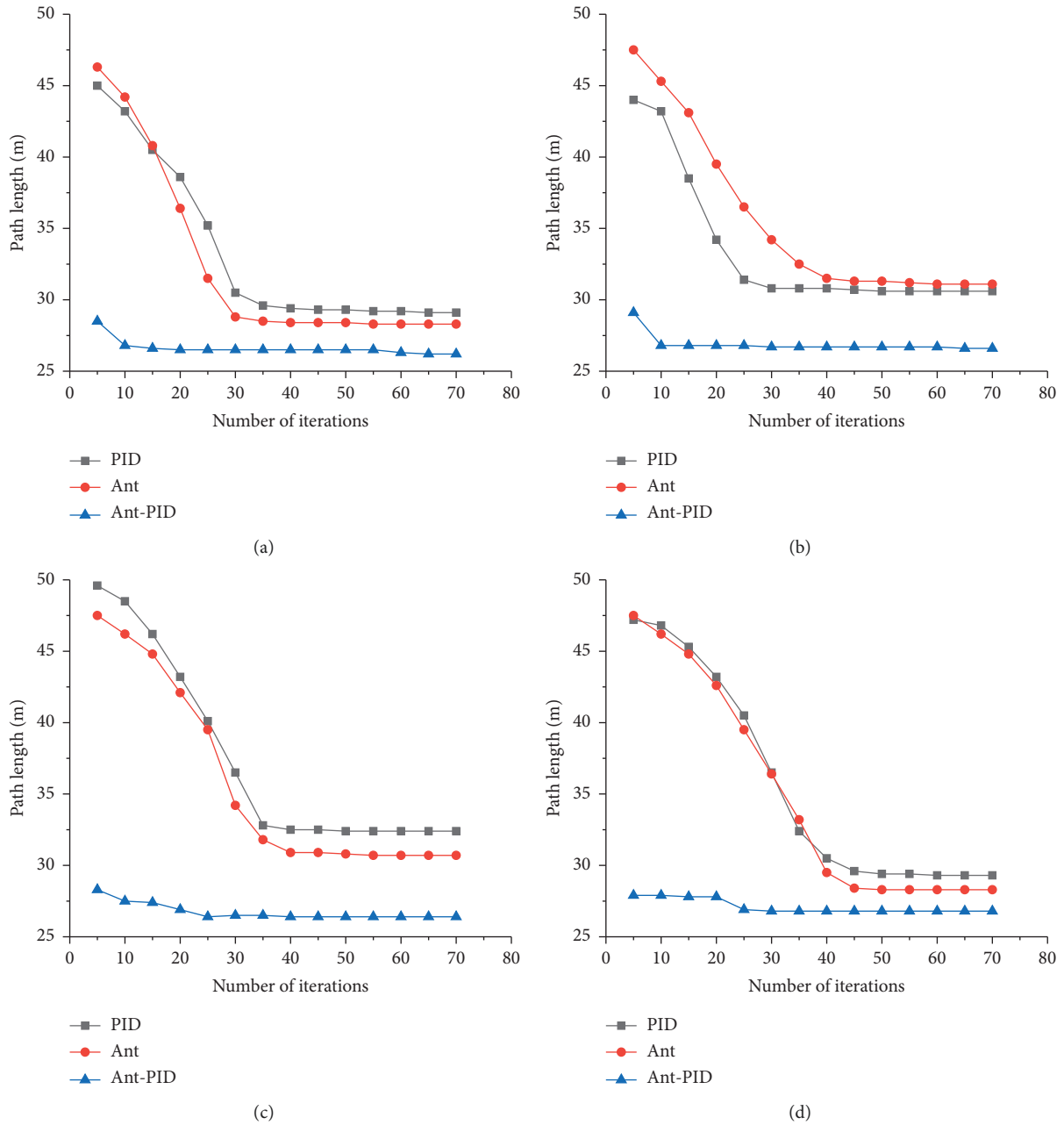


FIGURE 5: Optimization performance evaluation of robot path selection ((a) is SS data set, (b) is LH data set, (c) is SUN data set, and (d) is RTRR dataset).

strengthen the path planning performance of the model. Specifically, a simulation scenario with the shortest length of 25 m is designed to evaluate the model. Figure 5 demonstrates robot path selection’s optimization performance evaluation results under the proposed Ant-PID algorithm.

As shown in Figure 5, the proposed Ant-PID algorithm integrates the performance of the PID algorithm for robot displacement optimization control and the comprehensive optimization performance of ACA for robot path selection. Therefore, the path selection of the proposed Ant-PID algorithm is optimal. According to Figure 5, the longest robot path taken by the proposed Ant-PID algorithm in different data sets

is about 28 m, and the shortest is about 26 m. The longest path selection of the PID control algorithm is about 50 m, and the shortest is about 28 m. The longest path selection of ACA is about 47 m, and the shortest is about 27 m. Thus, the evaluation curve convergence effect of the proposed Ant-PID algorithm is better, and the path design result is better.

3.2. *Effect Evaluation of RPP.* In evaluating the RPP effect of the proposed Ant-PID algorithm, this work uses the simulation scene with the shortest length of 25 m. It evaluates the path planning results of the model on different data sets

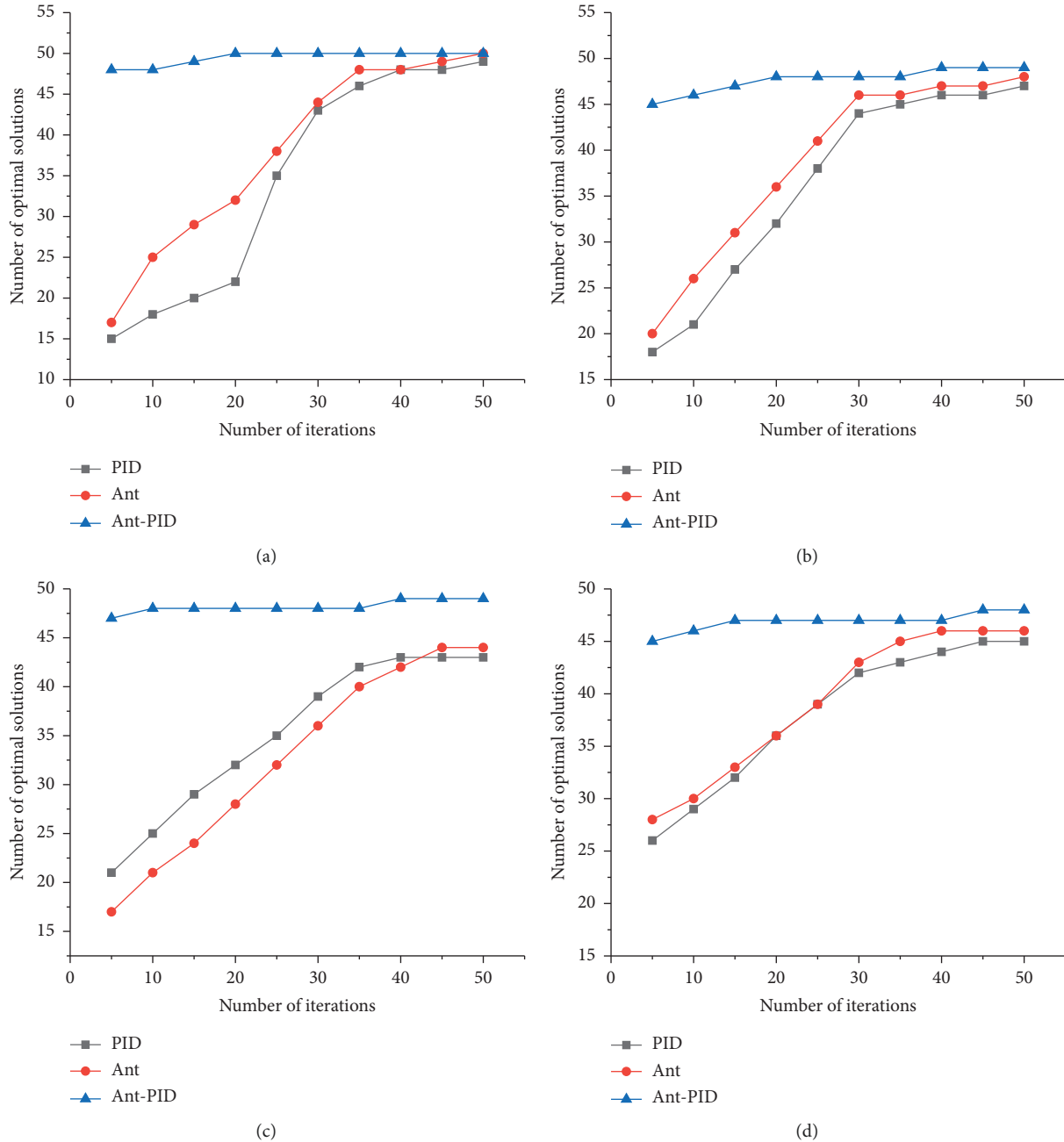


FIGURE 6: Evaluation results of RPP effect ((a) is SS data set, (b) denotes LH data set, (c) represents SUN data set, and (d) indicates RTRR data set).

50 times under different iterations. Figure 6 portrays the RPP evaluation results of the proposed Ant-PID algorithm.

As shown in Figure 6, the proposed Ant-PID algorithm still performs well in the RPP effect. On various data sets, the optimal solution times of the proposed Ant-PID algorithm are maintained at about 45–49 times. By comparison, the performance of the other two models is poor. For example, the optimal solution times of the PID algorithm are about 15–48 times. The minimum number of optimal solutions of ACA is about 17, and the maximum number is about 49. Therefore, the proposed Ant-PID algorithm has a good RPP effect. The comprehensive RPP effect of the model also needs

to evaluate the path planning efficiency of the model by factoring in the response time. Figure 7 compares the response time of the proposed Ant-PID algorithm and the other two algorithms.

Obviously, the average response time of the PID algorithm is about 25 s at the shortest and about 28 s at the longest. The shortest response time of ACA is about 24 s. The shortest average response time of ACA is about 27 s, and the longest is about 30 s. The average response time of the proposed Ant-PID algorithm is about 17 s to 20 s. Hence, the proposed Ant-PID algorithm has a quicker response in robot inspection path planning.

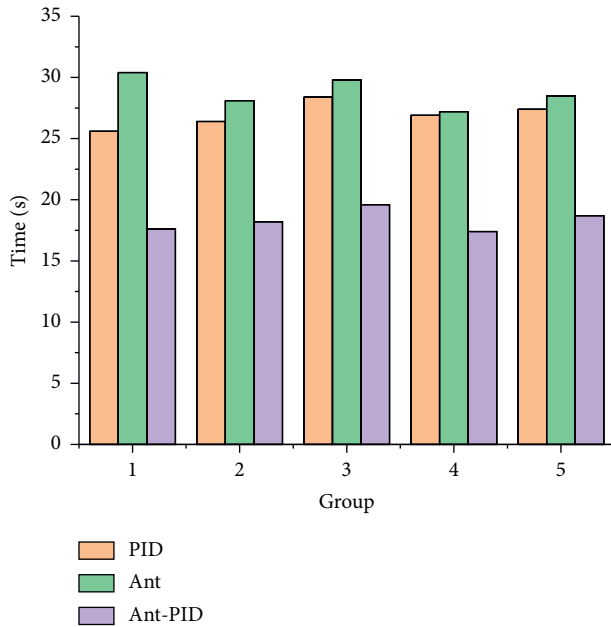


FIGURE 7: Evaluation results of model response time.

#### 4. Conclusion

With science and technological development, human beings use electricity more and more. The substation plays a vital part in transmitting power and power grids. Based on this, to improve the comprehensive efficiency of substation inspection, this work first discusses the status of substation inspection. Then, the PID control algorithm is introduced and optimized. Finally, the ACA is comprehensively improved. The Ant-PID algorithm is designed by fusing the PID algorithm and ACA, and the effect of the model in the substation inspection RPP is comprehensively evaluated. The results show that the longest robot path taken by the proposed Ant-PID algorithm in different data sets is about 28 m, and the shortest is about 26 m. The longest path selection of the PID control algorithm is about 50 m, and the shortest is about 28 m. The longest path selection of ACA is about 47 m, and the shortest is about 27 m. Second, the optimal solution times of the proposed Ant-PID algorithm are maintained at about 45–49 times, while the performance of the other two models is poor. Specifically, the optimal solution times of the PID algorithm are at least about 15 times and at most about 48 times. The minimum number of optimal solutions of ACA is about 17, and the maximum number is about 49. Finally, the average response time of the PID algorithm is about 25 s and 28 s; the shortest average response time of ACA is about 27 s, and the longest is about 30 s. The average response time of the proposed Ant-PID algorithm is about 17 s to 20 s. Although this work optimizes and designs a relatively perfect RPP model, there is less research on its practical application. Therefore, the research finding will be strengthened and generalized in future work.

#### Data Availability

The data used to support the findings of this study have been deposited in the Baidu Netdisk repository (<https://pan.baidu.com/s/1hqstBmcaX7rfRWAYnzMxNA>; password: suep).

#### Conflicts of Interest

The authors declare that they have no conflicts of interest.

#### Acknowledgments

This research was funded by the Shanghai Key Laboratory of Power Station Automation Technology (13DZ2273800) Project Funding.

#### References

- [1] X. Lai, J. Li, and J. Chambers, “Enhanced center constraint weighted A\* algorithm for path planning of petrochemical inspection robot,” *Journal of Intelligent and Robotic Systems*, vol. 102, no. 4, pp. 78–15, 2021.
- [2] M. V. J. Muthugala, S. B. P. Samarakoon, and M. R. Elara, “Toward energy-efficient online complete coverage path planning of a ship hull maintenance robot based on gladius bio-inspired neural network,” *Expert Systems with Applications*, vol. 187, no. 4, Article ID 115940, 2022.
- [3] Y. Tao, Y. Wen, H. Gao, T. Wang, J. Wan, and J. Lan, “A path-planning method for wall surface inspection robot based on improved genetic algorithm,” *Electronics*, vol. 11, no. 8, p. 1192, 2022.
- [4] J. Li, S. Jin, C. Wang, J. Xue, and X. Wang, “Weld line recognition and path planning with spherical tank inspection robots,” *Journal of Field Robotics*, vol. 39, no. 2, pp. 131–152, 2022.
- [5] A. G. Melo, M. F. Pinto, A. L. M. Marcato, L. M. Honório, and F. O. Coelho, “Dynamic optimization and heuristics based online coverage path planning in 3D environment for UAVs,” *Sensors*, vol. 21, no. 4, p. 1108, 2021.
- [6] S. Ekinçi, B. Hekimoğlu, and D. Izci, “Opposition based Henry gas solubility optimization as a novel algorithm for PID control of DC motor,” *Engineering Science and Technology, an International Journal*, vol. 24, no. 2, pp. 331–342, 2021.
- [7] I. Z. Biundini, M. F. Pinto, A. G. Melo, A. L. M. Marcato, L. M. Honório, and M. J. R. Aguiar, “A framework for coverage path planning optimization based on point cloud for structural inspection,” *Sensors*, vol. 21, no. 2, p. 570, 2021.
- [8] H. Lu, Y. Chen, H. Wu, and L. Cheng, “Path planning of substation inspection robot under road network and measurement constraints,” *China Mechanical Engineering*, vol. 32, no. 16, 2021.
- [9] J. O. Adibeli, Y. K. Liu, A. Ayodeji, and N. J. Awodi, “Path planning in nuclear facility decommissioning: research status, challenges, and opportunities,” *Nuclear Engineering and Technology*, vol. 53, no. 11, pp. 3505–3516, 2021.
- [10] A. Majumder, A. Majumder, and R. Bhaumik, “Teaching-Learning-based optimization algorithm for path planning and task allocation in multi-robot plant inspection system,” *Arabian Journal for Science and Engineering*, vol. 46, no. 9, pp. 8999–9021, 2021.

- [11] R. Bausys, E. K. Zavadskas, and R. Semenas, "Path selection for the inspection robot by m-generalized q-neutrosophic PROMETHEE approach," *Energies*, vol. 15, no. 1, 2021.
- [12] A. Pérez-González, N. Benítez-Montoya, Á. Jaramillo-Duque, and J. B. Cano-Quintero, "Coverage path planning with semantic segmentation for UAV in PV plants," *Applied Sciences*, vol. 11, no. 24, Article ID 12093, 2021.
- [13] L. M. González de Santos, E. Frías Nores, J. Martínez Sánchez, and H. González Jorge, "Indoor path-planning algorithm for UAV-based contact inspection," *Sensors*, vol. 21, no. 2, p. 642, 2021.
- [14] R. Almadhoun, T. Taha, L. Seneviratne, and Y. Zweiri, "Multi-robot hybrid coverage path planning for 3D Reconstruction of large structures," *IEEE Access*, vol. 10, no. 3, pp. 2037–2050, 2022.
- [15] K. G. S. Apuroop, A. V. Le, M. R. Elara, and B. J. Sheu, "Reinforcement learning-based complete area coverage path planning for a modified hTrihex robot," *Sensors*, vol. 21, no. 4, p. 1067, 2021.
- [16] B. Hadi, A. Khosravi, and P. Sarhadi, "A review of the path planning and formation control for multiple autonomous underwater vehicles," *Journal of Intelligent and Robotic Systems*, vol. 101, no. 4, pp. 67–26, 2021.
- [17] A. S. Afroz, F. Inglese, C. Stefanini, and M. Milazzo, "STL\_Process: A STL-based preprocessor for robot path planning in manufacturing and quality control processes," *SoftwareX*, vol. 15, no. 5, Article ID 100725, 2021.
- [18] H. Azpúrua, A. Rezende, G. Potje et al., "Towards semi-autonomous robotic inspection and mapping in confined spaces with the espeleorobô," *Journal of Intelligent and Robotic Systems*, vol. 101, no. 4, pp. 69–27, 2021.
- [19] F. Kiani, A. Seyyedabbasi, S. Nematzadeh et al., "Adaptive metaheuristic-based methods for autonomous robot path planning: Sustainable agricultural applications," *Applied Sciences*, vol. 12, no. 3, p. 943, 2022.
- [20] A. Khan, C. Mineo, G. Dobbie, C. Macleod, and G. Pierce, "Vision guided robotic inspection for parts in manufacturing and remanufacturing industry," *Journal of Remanufacturing*, vol. 11, no. 1, pp. 49–70, 2021.
- [21] R. P. Borase, D. K. Maghade, S. Y. Sondkar, and S. N. Pawar, "A review of PID control, tuning methods and applications," *International Journal of Dynamics and Control*, vol. 9, no. 2, pp. 818–827, 2021.
- [22] G. Dei, D. K. Gupta, B. K. Sahu et al., "Improved squirrel search algorithm driven cascaded 2DOF-PID-FOI controller for load frequency control of renewable energy based hybrid power system," *IEEE Access*, vol. 10, no. 2, pp. 46372–46391, 2022.
- [23] A. A. Jamil, W. F. Tu, S. W. Ali, Y. Terriche, and J. M. Guerrero, "Fractional-order PID controllers for temperature control: a review," *Energies*, vol. 15, no. 10, p. 3800, 2022.
- [24] B. Ozgenc, M. S. Ayas, and I. H. Altas, "Performance improvement of an AVR system by symbiotic organism search algorithm-based PID-F controller," *Neural Computing & Applications*, vol. 34, no. 10, pp. 7899–7908, 2022.
- [25] E. S. Ghith and F. A. A. Tolba, "Design and optimization of PID controller using various algorithms for micro-robotics system," *Journal of Robotics and Control (JRC)*, vol. 3, no. 3, pp. 244–256, 2022.
- [26] W. Zeng, Q. Jiang, Y. Liu et al., "Core power control of a space nuclear reactor based on a nonlinear model and fuzzy-PID controller," *Progress in Nuclear Energy*, vol. 132, no. 8, Article ID 103564, 2021.
- [27] H. Feng, W. Ma, C. Yin, and D. Cao, "Trajectory control of electro-hydraulic position servo system using improved PSO-PID controller," *Automation in Construction*, vol. 127, no. 5, Article ID 103722, 2021.
- [28] Q. Bu, J. Cai, Y. Liu et al., "The effect of fuzzy PID temperature control on thermal behavior analysis and kinetics study of biomass microwave pyrolysis," *Journal of Analytical and Applied Pyrolysis*, vol. 158, no. 5, Article ID 105176, 2021.
- [29] A. K. Kashyap and D. R. Parhi, "Particle swarm optimization aided pid gait controller design for a humanoid robot," *ISA Transactions*, vol. 114, no. 9, pp. 306–330, 2021.
- [30] B. Guo, Z. Zhuang, J. S. Pan, and S. C. Chu, "Optimal design and simulation for PID controller using fractional-order fish migration optimization algorithm," *IEEE Access*, vol. 9, no. 4, pp. 8808–8819, 2021.
- [31] A. Boudia, S. Messalti, A. Harrag, and M. Boukhnifer, "New hybrid photovoltaic system connected to superconducting magnetic energy storage controlled by PID-fuzzy controller," *Energy Conversion and Management*, vol. 244, no. 4, Article ID 114435, 2021.
- [32] D. Di Caprio, A. Ebrahimnejad, H. Alrezaamiri, and F. J. Santos-Arteaga, "A novel ant colony algorithm for solving shortest path problems with fuzzy arc weights," *Alexandria Engineering Journal*, vol. 61, no. 5, pp. 3403–3415, 2022.
- [33] N. Rokbani, R. Kumar, A. Abraham et al., "Bi-heuristic ant colony optimization-based approaches for traveling salesman problem," *Soft Computing*, vol. 25, no. 5, pp. 3775–3794, 2021.
- [34] S. Sefati, M. Abdi, and A. Ghaffari, "Cluster-based data transmission scheme in wireless sensor networks using black hole and ant colony algorithms," *International Journal of Communication Systems*, vol. 34, no. 9, Article ID e4768, 2021.
- [35] G. Rivera, C. A. Coello Coello, L. Cruz-Reyes, E. R. Fernandez, C. Gomez-Santillan, and N. Rangel-Valdez, "Preference incorporation into many-objective optimization: an Ant colony algorithm based on interval outranking," *Swarm and Evolutionary Computation*, vol. 69, no. 8, Article ID 101024, 2022.

## Research Article

# Evaluation and Analysis of Regional Economic Growth Factors in Digital Economy Based on the Deep Neural Network

Caijun Cheng <sup>1,2</sup> and Huazhen Huang<sup>3</sup>

<sup>1</sup>Center for Social Security Studies of Wuhan University, Wuhan 430072, China

<sup>2</sup>College of Computer Information and Engineering, Nanchang Institute of Technology, Nanchang 330044, China

<sup>3</sup>College of Finance and Economics, Nanchang Institute of Technology, Nanchang 330044, China

Correspondence should be addressed to Caijun Cheng; [chengcaijun58959703@nut.edu.cn](mailto:chengcaijun58959703@nut.edu.cn)

Received 31 March 2022; Revised 5 May 2022; Accepted 14 June 2022; Published 22 August 2022

Academic Editor: Man Fai Leung

Copyright © 2022 Caijun Cheng and Huazhen Huang. This is an open access article distributed under the Creative Commons Attribution License, which permits unrestricted use, distribution, and reproduction in any medium, provided the original work is properly cited.

With the rise of deep learning technology, due to the superior performance of the deep neural network, its application in the digital economy has attracted extensive attention of scholars. Since the beginning of the 21st century, my country's digital economy has developed rapidly, and its universalization and other characteristics have created favorable conditions for the optimal allocation of resources in underdeveloped regions and the exertion of comparative advantages. The digital economy will play a key role in poverty alleviation, promoting coordinated regional development, narrowing regional gaps, and improving the spatial layout of my country's reform and opening up. This paper studies the factors that the digital economy based on deep neural networks has on regional economic growth. Simulation experiment conclusions are as follows: (1) the digital economy of Guizhou, Beijing, Chongqing, Anhui, and Tibet is growing rapidly. The central and western regions are in a period of rapid growth. For the gap between major industrial provinces, the coefficient of variation reached about 1 before 2013, then it declined rapidly, and slowed down, and steadily declined after 2019, indicating that the gap in the digital economy in various regions is narrowing in general. (2) From the national level, the digital economy index coefficient is 1.24, that is, for every 1% increase in digital economy investment, GDP will increase by about 0.24%. The labor force increased by 1% and the GDP increased by about 0.22%. This promotion effect is also very obvious. (3) Judging from the above data, the western region urgently needs to promote the construction of the digital economy and introduce high-tech digital economy talents. The talent effect in the Midwest has a significant effect on GDP. (4) From the perspective of the whole country and other regions, the parameter coefficients and signs have not changed significantly, so the original model is robust, and so the conclusion is desirable.

## 1. Introduction

At present, there is no clear definition of the deep neural network in the field of computer vision. Broadly speaking, it is considered to include specific variants such as convolutional neural networks and recurrent neural networks. In practical applications, deep neural networks often incorporate a variety of known structures [1, 2], for example, restricted Boltzmann machines and long and short-term memory units.

The current level of digital technology development is changing with each passing day in the context of economic globalization. Information technology in various countries is

infiltrating and integrating with all walks of life and is constantly injecting new vitality into the global economy. It has become a powerful driving force to promote economic growth [3, 4]. The fields involved are not only in manufacturing and business management but also in the fields of population employment, education, and people's livelihood. It is to promote national economic development and also to promote the smooth advancement of digital transformation in various regions [5, 6].

On the one hand, it encounters challenges such as complex international environment, great downward pressure on the economy, and slow industrial transformation. On the other hand, the country is also in an

environment of major opportunities such as the vigorous rise of new technology revolution and the integration and interconnection of data resources [7–10]. Since the outbreak of the new crown pneumonia epidemic, the traditional manufacturing industry has been greatly impacted, which has brought great challenges to economic development around the world, and has also triggered many people's thinking about economic growth. The global economy will enter a new cycle of economic growth led by innovation [11, 12].

Economic growth is the basis and premise of regional economic and social development and progress, but there are always differences between and within countries or regions. Developing countries consider how to increase their economic growth rate to approach developed countries; within countries or regions, they consider how to adjust the economic structure, narrow the internal gap, and improve the overall social welfare level [13].

China has continuously created miracles in the history of human development, but the gap in economic strength between regions has always existed. How to gradually reduce the economic gap between regions while maintaining stable economic development is a problem that our government has always attached great importance to. The digital economy is an emerging economic form [14–17]. The digital economy has penetrated into all fields of society and has changed the way of social organization to a large extent. Similarly, the digital economy has also had a certain impact on economic growth in terms of economic theory and policy systems.

The specific aspects are shown in Figure 1.

For the empirical research on the promotion of economic growth by the digital economy, many research results have achieved the world's advanced level in new development fields. The impact of the digital economy on the economy is mainly manifested in the following aspects: the digital economy puts forward new requirements for energy distribution and environmental protection, the digital economy also presents new challenges for taxation as it affects economic growth, and the digital economy changes business and social behavior. Due to the various characteristics and advantages of deep neural networks, we propose to study the evaluation and analysis of regional economic growth factors in the digital economy based on deep neural networks [18, 19].

## 2. Basic Theory Related to the Deep Neural Network and the Digital Economy

*2.1. Deep Neural Network Model.* A deep neural network and its idea come from the human brain's hierarchical processing mechanism for visual information. Starting from the original data, it automatically learns effective feature expressions through a multilayer structure and realizes classification and recognition at the output layer. Its advantages are that it overcomes the time-consuming and laborious shortcomings of the manual feature design; the primary features of each layer are obtained through layer-by-layer data pretraining; distributed data learning is more effective

(exponential); and compared with shallow modeling methods, deep modeling can be more detailed and efficient representation of actual complex nonlinear problems. At present, both the theoretical research on the deep neural network algorithm and its application research have reached a peak. As the core model of deep learning, the deep neural network is often designed for image classification, speech recognition, and other fields, and has achieved good results. The different models differ mainly in their different model structures and have little to do with other parameters.

If the deep structure is regarded as a neuron network, the idea of the deep neural network can be described as follows: the pretraining of each layer of the network adopts unsupervised learning; input to one layer; supervised learning to fine-tune all layers (plus a classifier for classification). The main difference between deep neural networks and traditional neural networks is the training mechanism. The deep neural network adopts the training mechanism of layer-by-layer pretraining as a whole rather than the back-propagation training mechanism of the traditional neural network. The related theory is shown in Figure 2.

The encoder is one of the building blocks of the deep neural network. It is an unsupervised learning algorithm and a nonlinear neural network structure that reproduces the input signal as much as possible. The training difficulty of the convolutional neural network is more difficult, and the design of its network structure is also more complicated. Therefore, when designing a convolutional neural network, it is necessary to optimize its structural design.

*2.2. Theories Related to Digital Economy.* The digital economy takes digital knowledge and information as the key production factors [20], takes digital technology innovation as the core driving force, takes the modern information network as an important carrier, and deeply integrates Internet technology with the real economy to enhance industrial intelligence, digitization, and speed up the new economic form formed by reconstruction. Among them, industries such as computer manufacturing, electronic equipment manufacturing, radio and television and satellite transmission services, and information technology services are the basic industries of the digital economy. Internet retail, e-commerce, financial service platforms, and logistics services are based on digitalization and can be regarded as the category of digital economy [21].

The digital economy can be divided into digital industrialization and industrial digitization. Digital industrialization transforms scientific and technological innovation achievements into the driving force of economic and social progress through the market-oriented application of modern digital technology. Industrial digitalization means that traditional industries can improve themselves in an all-round and full-chain manner by introducing digital technology and in-depth integration, such as industrial Internet, intelligent manufacturing, and digital agriculture. From the 1990's to the first decade of the 21st century, the electronic information manufacturing and software industries were booming. The main feature of the digital economy in this

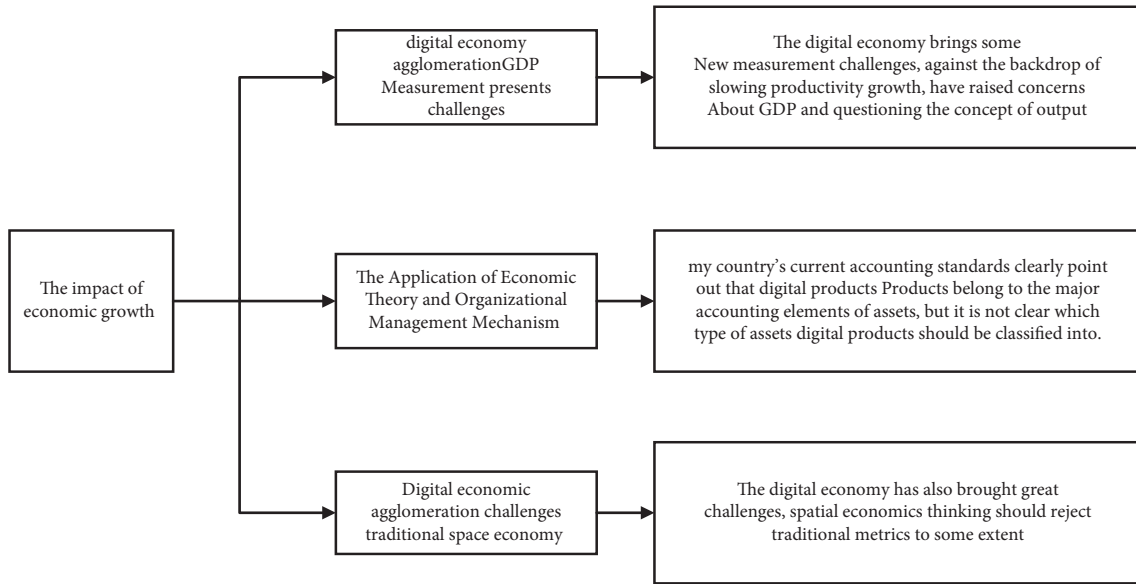


FIGURE 1: The impact of economic growth.

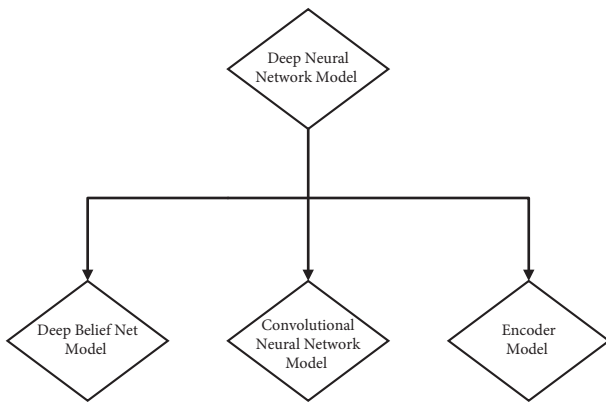


FIGURE 2: Common models of deep neural networks.

period was informatization, and information technology began to be widely embedded in the traditional neural network. In the industry, new business models have been conceived, but they are not yet mature. The accumulation of sufficient quantitative changes in the application of information technology began to produce a qualitative leap. After 2010, the main feature of the digital economy changed to digitization. In addition, the digital economy has three major characteristics [22].

First is platformization. The Internet platform makes information flow no longer monopolized by giants in the industry chain, promotes direct communication between suppliers and consumers, and realizes a large-scale division of labor and cooperation systems. Second is data. Data has become a key production factor for the development of the digital economy. Third is universalization. Inclusiveness embodies the concept of “everyone participates and everyone shares,” and representative fields include inclusive technology, inclusive finance, and inclusive trade. Figure 3 shows the three laws of the digital economy [23].

*2.3. The Impact of the Digital Economy on Regional Economic Development.* The digital economy has become a driving force, one is to promote production innovation. Digital, networked, and intelligently guided production methods are in line with the trends of precise resource allocation, automated production organization, and enterprise interconnection. The second is to promote consumption upgrading. The wide application of information products and information services makes the Internet penetrate into almost every detail of people’s consumption life. Mobile payment, with its convenience and efficiency, lowers the payment threshold and fully releases the consumption potential of urban and rural residents. The third is to change the trade pattern, such as books, audio and video, software, and services, such as R&D, finance, and advertising, can easily and quickly realize cross-border transactions through Internet transmission. Such digital trade products are growing rapidly. Digital trade will lead a world trade into a new stage and become a new economic growth pole.

Secondly, the digital economy has spillover effects on the economic development of other regions [24]. The digital economy not only empowers the economic development of the region but also promotes the economic development of other regions due to the spillover effect of digital technologies such as the Internet. The real-time, shared, and open nature of the Internet, as a core digital technology, connects multiple regions into a whole, breaks geographic barriers, and provides great convenience for the development of economic activities. Zhejiang regards the digital economy as “Project No. 1.” The difference in Shandong’s digital economy policy lies in the inclination towards the primary industry, which proposes to speed up the development of smart agriculture. Guangxi proposes to improve the foundation and governance of the digital economy and create a highland for ASEAN-oriented digital economic cooperation. The Yangtze River Delta region will focus on building key industries and promoting digital economy industrial clusters [25].

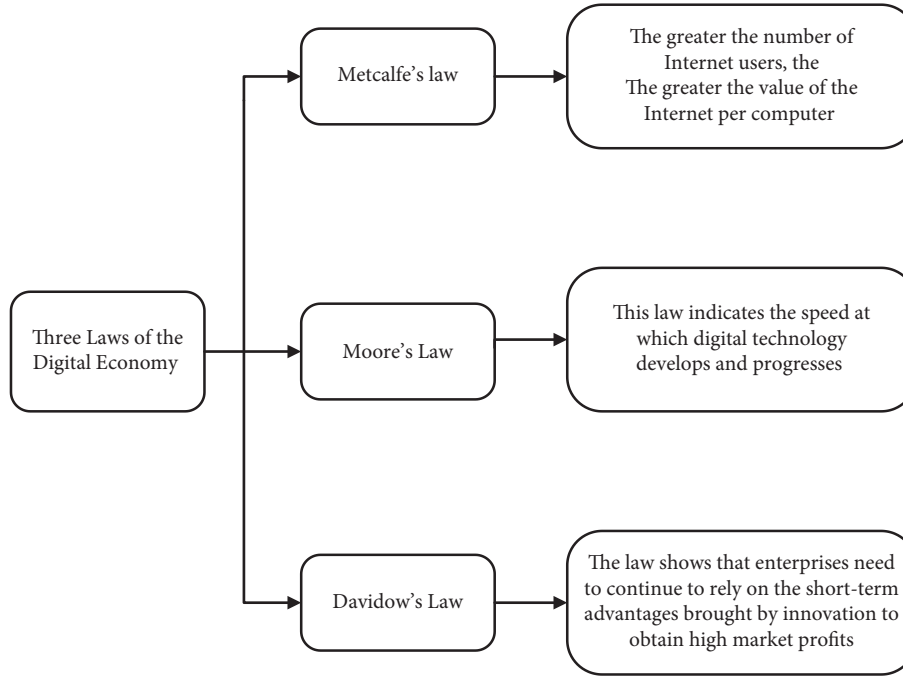


FIGURE 3: Three laws of the digital economy.

The role of the digital economy on the regional economy can be represented in Figure 4.

### 3. Basic Theory Related to the Deep Neural Network and the Digital Economy

**3.1. Multihidden Layer Multilayer Perceptron.** Multilayer perceptron: usually, this model is also called multihidden layer multilayer perceptron. Figure 5 shows the general structure of the multilayer perceptron model.

We deduce the learning process of the network through mathematical formulas. Suppose the input variable is  $net_i$ , then we get

$$net_i = \sum_{i=1}^M x_i + \theta_i. \quad (1)$$

The corresponding output is

$$a_i = f(net_i). \quad (2)$$

Sigmoid function is

$$f(x) = \frac{1}{1 + \exp(-x)}. \quad (3)$$

When the value of the mapping function is in the positive and negative range, the symmetrical function is used as the excitation function:

$$f(x) = \tanh(x) = \frac{1 - \exp(-x)}{1 + \exp(-x)}. \quad (4)$$

General order is

$$a_i = x_i. \quad (5)$$

Then the input of the  $j$ th neuron in the hidden layer  $net_j$  is

$$net_j = \sum_{j=1}^N w_{ij}a_i + \theta_j. \quad (6)$$

The corresponding output is  $a_j$ :

$$a_j = f(net_j). \quad (7)$$

Then the input of the  $k$ th neuron in the output layer  $net_k$  is

$$net_k = \sum_{k=1}^L w_{jk}a_j + \theta_k, \quad (8)$$

where  $w_{jk}$  and  $\theta_k$  are the weight and threshold, respectively. The corresponding output is  $y_k$ :

$$y_k = f(net_k). \quad (9)$$

**3.2. Long Short-Term Memory Network.** Long short-term memory network is a special kind of a neural network. This kind of a neural network is different from the general feedforward neural network, LSTM can use time series to analyze the input. Recurrent neural networks learn sequential information through inner loops. The slope obtained by the chain rule is propagated to the activation function, and then the slope becomes very small or very large, which is the problem of vanishing or exploding gradients.

The long-short-term memory network forgetting gate is



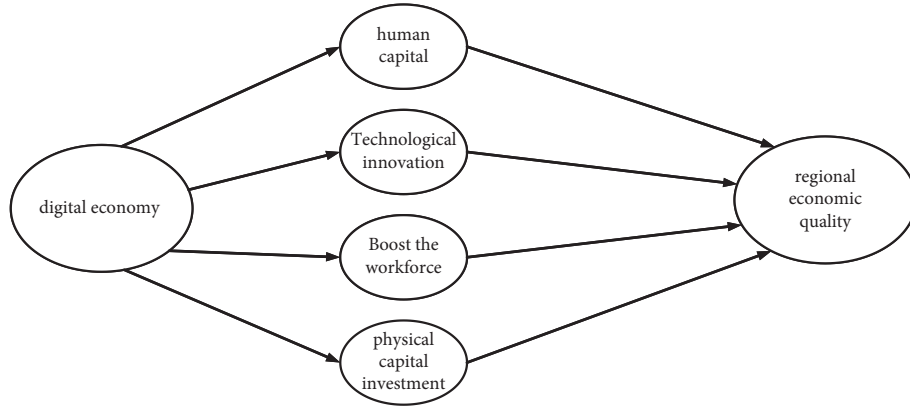


FIGURE 4: Action diagram.

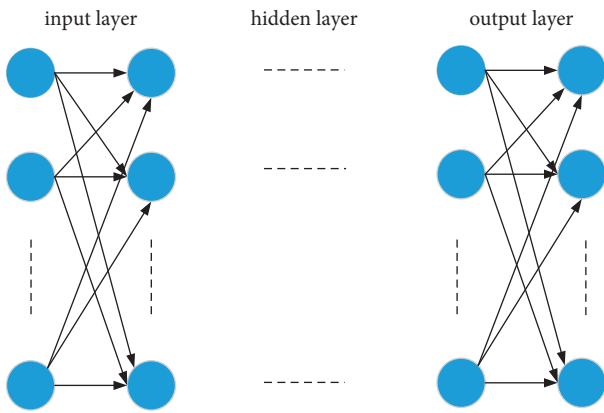


FIGURE 5: Multihidden layer multilayer perceptron network.

$$f_t = \sigma(U_g x_t + W_g h_{t-1} + b_f). \quad (10)$$

The input gate of the long short-term memory network is

$$\begin{aligned} i_t &= \sigma(U_i x_t + W_i h_{t-1} + b_i), \\ \bar{c}_t &= \tanh(U_c x_t + W_c h_{t-1} + b_c). \end{aligned} \quad (11)$$

The current memory cell state is

$$c_t = f_t c_{t-1} + i_t \cdot \bar{c}_t. \quad (12)$$

Then the output gate of the long-short-term memory network is

$$o_t = \sigma(U_o x_t + W_o h_{t-1} + b_o). \quad (13)$$

Then the state of the current hidden layer is

$$h_t = o_t \cdot \tanh(c_t). \quad (14)$$

**3.3. Entropy Method.** Indicator selection: if there are  $m$  indicators,  $n$  regions, and  $r$  years, then  $x_{ijt}$  is the observed value of the  $j$ th indicator in region  $i$  in year  $t$ . Then, standardize the indicators as follows:

Positive indicators are

$$x_{ijt}^* = \frac{(x_{ijt} - m_j)}{(M_j - m_j)}. \quad (15)$$

Negative indicators are

$$x_{ijt}^* = \frac{(M_j - x_{ijt})}{(M_j - m_j)}, \quad (16)$$

$$M_j = \max\{x_{ijt}\}, m_j = \min\{x_{ijt}\}.$$

We determine the proportion of observations of the  $j$ th indicator for region  $i$  in year  $t$ :

$$p_{ijt} = \frac{x_{ijt}^*}{\sum_t x_{ijt}^*}, p_{ijt} \in [0, 1]. \quad (17)$$

We determine the entropy value of the  $j$ th index as

$$e_j = \left[ -\frac{1}{\ln(rn)} \right] \times \sum_t \sum_i p_{ijt} \ln(p_{ijt}), e_j \in [0, 1]. \quad (18)$$

We determine the information utility value of the  $j$ th indicator as

$$g_j = 1 - e_j. \quad (19)$$

We determine the weight of the  $j$ th indicator as

$$w_j = \frac{g_j}{\sum_j g_j}. \quad (20)$$

We determine the index for year  $t$  of region  $i$  as

$$H_{it} = \sum_j w_j x_{ijt}^*. \quad (21)$$

This defines a set of data information entropy as

$$E_j = -\ln(n)^{-1} \sum_{i=1}^n p_{ij} \ln p_{ij}, \quad (22)$$

where  $p_{ij}$  is

$$p_{ij} = \frac{Y_{ij}}{\sum_{i=1}^n Y_{ij}}. \quad (23)$$

TABLE 1: Digital economy indicator system.

| First-level indicator |     | Secondary indicators  | Weights |
|-----------------------|-----|---|---------|
| Infrastructure        | x1  | Mobile telephone exchange capacity per capita                             | 0.0501  |
|                       | x2  | Length of long-distance optical cable per square kilometer                | 0.0507  |
| Digital industry      | x3  | Telecommunication traffic per capita                                      | 0.0701  |
|                       | x4  | Computer main business income as a percentage of GDP                      | 0.1735  |
|                       | x5  | Software main business income as a percentage of GDP                      | 0.1702  |
|                       | x6  | The proportion of electronic information product exports in total exports | 0.1036  |
| Creativity            | x7  | Number of domestic patent authorizations per 10,000 people                | 0.1743  |
|                       | x8  | Internal expenditure of R&D funds as a percentage of GDP                  | 0.0641  |
|                       | x9  | Education spending as a share of GDP                                      | 0.0456  |
| Digital livelihood    | x10 | Internet penetration  | 0.0533  |
|                       | x11 | The household rate of cable broadcasting and TV                           | 0.0336  |

## 4. Simulation Experiment

**4.1. Experimental Data and the Digital Economy Indicator System.** This article selects the national provincial unit data from 2011 to 2021. The constructed digital economy indicator system includes first-level indicators: infrastructure, digital industry, innovation capability, and digital livelihood, and second-level indicators, as shown in Table 1.

According to the formula in Figure 6, this paper calculates the digital economy index of each province, municipality, and autonomous region. The highest ranking province and city in the digital economy index in 2021 is Beijing, which is 0.49. In Beijing, Tianjin, Hebei, and Sichuan, the digital economy index is relatively high. The digital economy indicator system constructed in this paper is relatively robust and suitable for empirical research. The coefficient of variation reached around 1 before 2013, then decreased rapidly, and then slowed down, and decreased steadily after 2019, indicating that the overall digital economy gap between regions is narrowing, and the gap before 2019 is significantly larger than after 2019. The Moran index was stable at 0.2–0.3, and passed the 5% significance test except in 2016 and 2017, as shown in Figure 7 and Table 2.

**4.2. Construction of the Digital Economy and Economic Growth Model Based on the Deep Neural Network.** Among them,  $\ln Y$  represents the total economic volume,  $\ln L$  represents the labor force,  $\ln K$  represents the capital stock, and  $\ln T$  represents the digital economy index. This paper uses regional per capita GDP data to measure, labor is one of the main endogenous variables in the economic growth model, and the digital economy index uses the above measurement data results. According to the above-mentioned selected variables and methods for calculation, the following data results are obtained. As shown in Table 3 and Figure 8, the following are the statistical description values of the data.

**4.3. An Empirical Analysis of the Impact of the Digital Economy on Economic Growth.** In this paper, the LSTM regression model is used for regression analysis and operation. The analysis will be carried out from four perspectives.

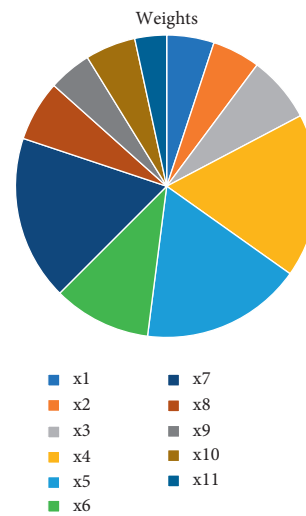


FIGURE 6: Weight of each indicator.

From the results of the regression test values in the above table, the model fitting effect is good. Previous empirical studies have consistently shown that the digital economy index has a positive relationship with GDP, which is confirmed in this paper. At the national level, the digital economy index coefficient is 1.24, which shows that the digital economy has a good role in promoting economic growth, that is, for every 1% increase in the digital economy input, GDP will increase by about 0.24%, the labor force increased by 1%, and the GDP increased by about 0.22%. This promotion effect is also very obvious and are shown in Table 4 and Figure 9.

In the current digital economy era, innovation is the main driving force for development, and talents are the main body of innovation. Among them, including Beijing, Guangdong, and other regions are regions with relatively good digital economy development. The digital economy foundation, digital economy development resources, and digital economy innovation in this region are with the best ability in the country. From the point of view of the digital economy index coefficient, the digital economy grows by 1%, the GDP increases by about 0.30%, the labor input increases by 1%, the regional economy increases by about 0.24%, the capital investment increases by 1%, and the GDP increases

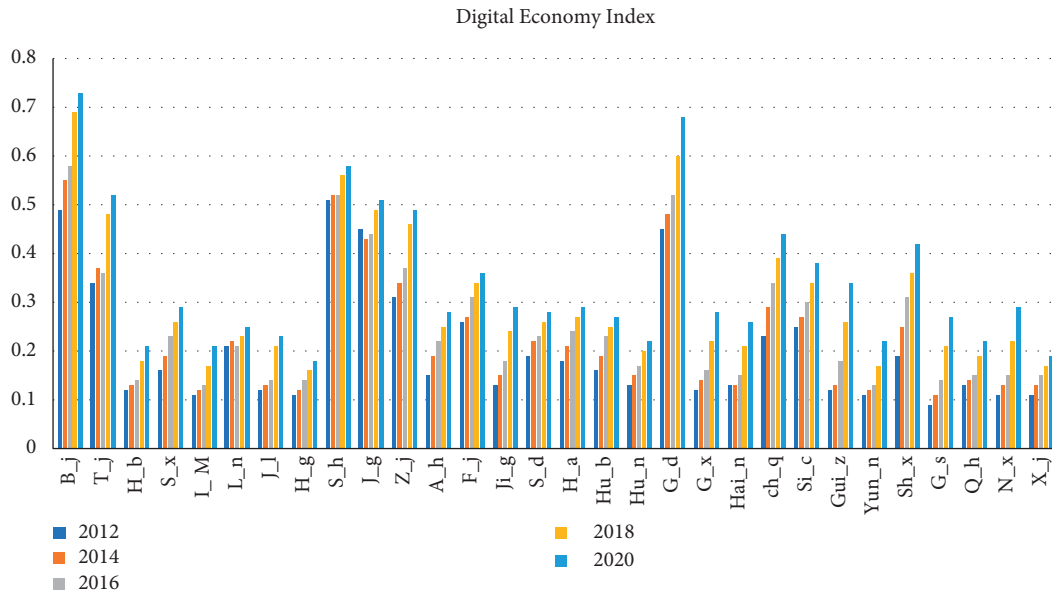


FIGURE 7: Differences in digital economy indices.

TABLE 2: Digital economy index.

| Area  | 2012 | 2014 | 2016 | 2018 | 2020 |
|-------|------|------|------|------|------|
| B_j   | 0.49 | 0.55 | 0.58 | 0.69 | 0.73 |
| T_j   | 0.34 | 0.37 | 0.36 | 0.48 | 0.52 |
| H_b   | 0.12 | 0.13 | 0.14 | 0.18 | 0.21 |
| S_x   | 0.16 | 0.19 | 0.23 | 0.26 | 0.29 |
| L_M   | 0.11 | 0.12 | 0.13 | 0.17 | 0.21 |
| L_n   | 0.21 | 0.22 | 0.21 | 0.23 | 0.25 |
| J_l   | 0.12 | 0.13 | 0.14 | 0.21 | 0.23 |
| H_g   | 0.11 | 0.12 | 0.14 | 0.16 | 0.18 |
| S_h   | 0.51 | 0.52 | 0.52 | 0.56 | 0.58 |
| J_g   | 0.45 | 0.43 | 0.44 | 0.49 | 0.51 |
| Z_j   | 0.31 | 0.34 | 0.37 | 0.46 | 0.49 |
| A_h   | 0.15 | 0.19 | 0.22 | 0.25 | 0.28 |
| F_j   | 0.26 | 0.27 | 0.31 | 0.34 | 0.36 |
| Ji_g  | 0.13 | 0.15 | 0.18 | 0.24 | 0.29 |
| S_d   | 0.19 | 0.22 | 0.23 | 0.26 | 0.28 |
| H_a   | 0.18 | 0.21 | 0.24 | 0.27 | 0.29 |
| Hu_b  | 0.16 | 0.19 | 0.23 | 0.25 | 0.27 |
| Hu_n  | 0.13 | 0.15 | 0.17 | 0.2  | 0.22 |
| G_d   | 0.45 | 0.48 | 0.52 | 0.6  | 0.68 |
| G_x   | 0.12 | 0.14 | 0.16 | 0.22 | 0.28 |
| Hai_n | 0.13 | 0.13 | 0.15 | 0.21 | 0.26 |
| ch_q  | 0.23 | 0.29 | 0.34 | 0.39 | 0.44 |
| Si_c  | 0.25 | 0.27 | 0.3  | 0.34 | 0.38 |
| Gui_z | 0.12 | 0.13 | 0.18 | 0.26 | 0.34 |
| Yun_n | 0.11 | 0.12 | 0.13 | 0.17 | 0.22 |
| Sh_x  | 0.19 | 0.25 | 0.31 | 0.36 | 0.42 |
| G_s   | 0.09 | 0.11 | 0.14 | 0.21 | 0.27 |
| Q_h   | 0.13 | 0.14 | 0.15 | 0.19 | 0.22 |
| N_x   | 0.11 | 0.13 | 0.15 | 0.22 | 0.29 |
| X_j   | 0.11 | 0.13 | 0.15 | 0.17 | 0.19 |

by about 0.16%. From the perspective of the provinces in the central region represented by Shanxi and Hunan, the basic digital economy has developed well, and the fiber optic laying range basically covers the whole province. The

electronic information industry and the software service industry play a significant role in the economic contribution of this region. The digital economy index coefficient of the western region is 1.35, indicating that the digital economy

TABLE 3: Statistical description of the data.

| Variable | Mean | Standard | Minimum | Maximum |
|----------|------|----------|---------|---------|
| lnY      | 9.5  | 1.1      | 5.9     | 11.5    |
| lnL      | 5.9  | 0.9      | 3.1     | 7.6     |
| lnK      | 10.5 | 1.2      | 6.7     | 12.6    |
| lnE      | 8.1  | 1.1      | 4.6     | 10.6    |

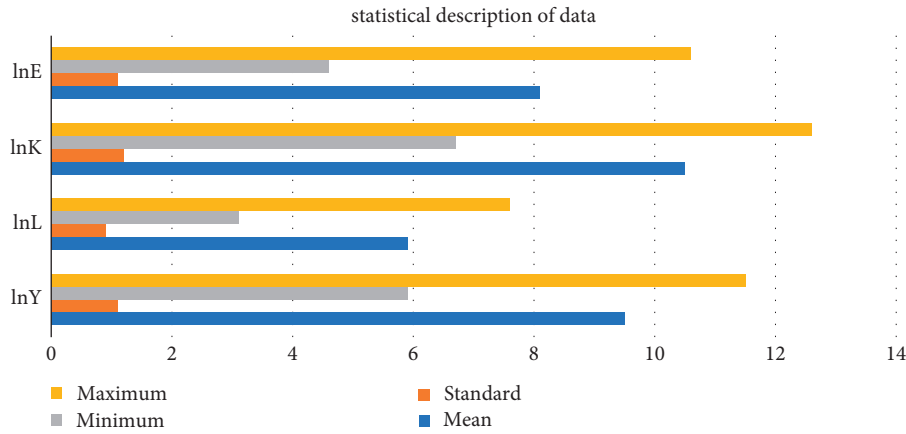


FIGURE 8: Data statistical descriptive value analysis.

TABLE 4: National-level panel regression.

|          | National | East area | Central | Western |
|----------|----------|-----------|---------|---------|
| lnE      | 1.24     | 1.19      | 1.34    | 1.35    |
| lnk      | 1.22     | 1.15      | 1.22    | 1.39    |
| lnL      | 1.26     | 1.32      | 1.15    | 1.14    |
| Cons     | 1.45     | 1.68      | 1.86    | 1.72    |
| R square | 1.95     | 1.93      | 1.84    | 1.92    |

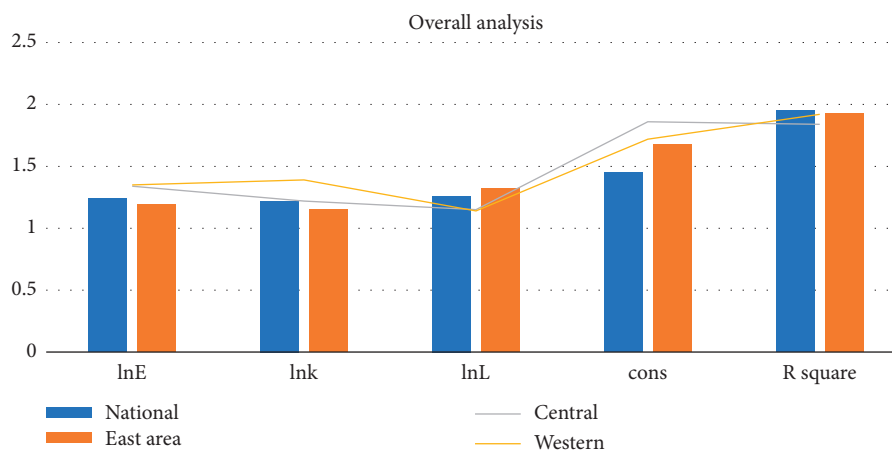


FIGURE 9: Analysis from the overall perspective of the country.

investment increases by 1%, and the GDP increases by about 0.35%. The labor coefficient is 1.39, indicating that labor input increases by 1%, GDP increases by about 0.39%, and the capital coefficient is 1.14, indicating that capital investment increases by 1%, GDP increases by about 0.14%.

Judging from the above data, and the construction of digital talents and the introduction of digital talents are a solid foundation for further sustainable innovation and development in various regions. Table 5 and Figure 10 shows the F test value and the Hausman test value.

TABLE 5: F test value and Hausman test value.

|              | National | East area | Central region | Western region |
|--------------|----------|-----------|----------------|----------------|
| F test value | 67.6     | 82.9      | 36.53          | 58.96          |
| Hausman test | 124.9    | 43.5      | 8.96           | 66.75          |

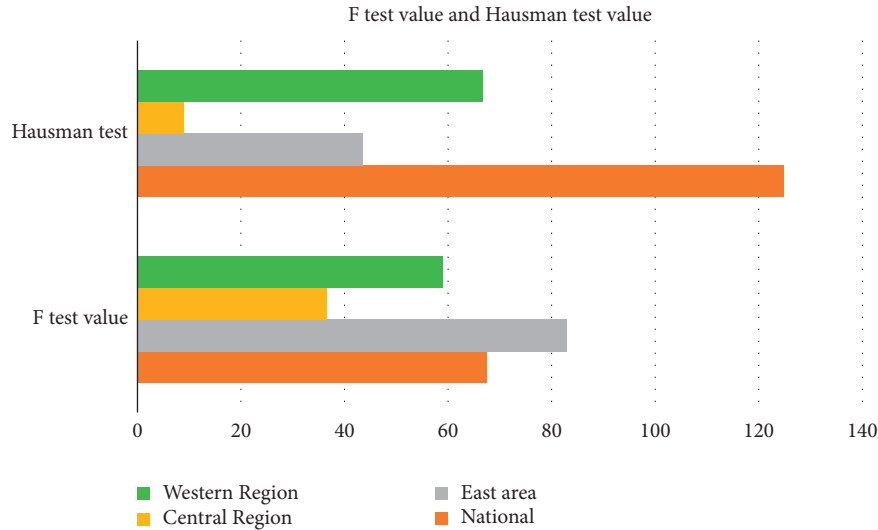


FIGURE 10: F test value and Hausman test value of each region.

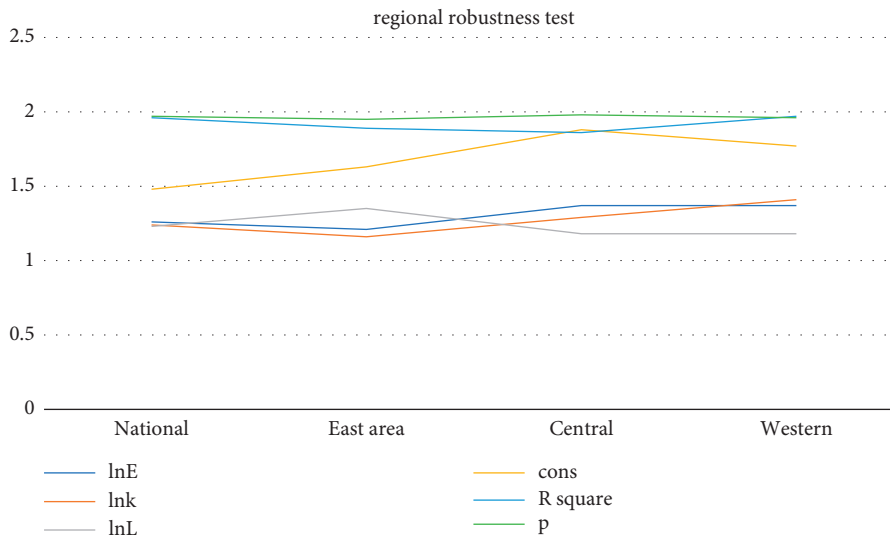


FIGURE 11: Robustness analysis.

4.4. *Robustness Check.* In order to ensure the reliability of the research conclusions, this paper does a robustness test on the national, eastern, central, and western data, and removes the explanatory variables one by one. The reason is that when calculating the digital economy index in this paper, these variables may be superimposed with labor and capital stock data. Sex test: Judging from the three models of the national, eastern, central, and western models, the parameter coefficients and signs have not changed significantly, so the original model is robust, and so the conclusion is desirable, as shown in Figure 11.

## 5. Conclusion

According to the calculation results of the digital economy index, it is concluded through this topic: (1) the digital economy of Guizhou, Beijing, Chongqing, Anhui, and Tibet is growing rapidly, and the central and western regions are in a period of rapid growth. For the gap between major industrial provinces, the coefficient of variation reached about 1 before 2013, and then declined rapidly, and slowed down, and steadily declined after 2019, indicating that the gap in the digital economy in various regions is narrowing in general. (2) From

the national level, the digital economy index coefficient is 1.24, that is, for every 1% increase in digital economy investment, GDP will increase by about 0.24%. The labor force increased by 1% and the GDP increased by about 0.22%. This promotion effect is also very obvious. (3) Judging from the above data, the western region urgently needs to promote the construction of the digital economy and introduce high-tech digital economy talents. The talent effect in the Midwest has a significant effect on GDP. (4) From the perspective of the whole country and other regions, the parameter coefficients and signs have not changed significantly, so the original model is robust, so the conclusion is desirable.

## Data Availability

The data used to support the findings of this study are available from the corresponding author upon request.

## Conflicts of Interest

The authors declare that they have no conflicts of interest regarding this work.

## Acknowledgments

This study was supported by the Humanities and Social Science Project of Universities in Jiangxi Province: "Research on the Development Status and Countermeasures of Digital Economy in Jiangxi Province" (Project number: JJ20116).

## References

- [1] J. Xiuliang, "Zhenhai. Deep neural network algorithm for estimating maize biomass based on simulated Sentinel 2A vegetation indices and leaf area index," *The Crop Journal*, vol. 8, no. 01, pp. 91–101, 2020.
- [2] Y. Sun, B. Pan, and Y. Fu, "Lightweight deep neural network for real-time instrument semantic segmentation in robot assisted minimally invasive surgery," *IEEE Robotics and Automation Letters*, vol. 6, no. 99, p. 1, 2021.
- [3] W. Xing, T. Lyu, X. Chu et al., "Recognition and classification of single melt tracks using deep neural network: a fast and effective method to determine process windows in selective laser melting," *Journal of Manufacturing Processes*, vol. 68, pp. 1746–1757, 2021.
- [4] M. J. Shafiee, A. Jeddi, A. Nazemi, P. Fieguth, and A Wong, "Deep neural network perception models and robust autonomous driving systems: practical solutions for mitigation and improvement," *IEEE Signal Processing Magazine*, vol. 38, no. 1, pp. 22–30, 2021.
- [5] P. Surendar and B. M. Ponni, "Diagnosis of lung cancer using hybrid deep neural network with adaptive sine cosine crow search algorithm," *Journal of Computational Science*, vol. 53, no. 2, Article ID 101374, 2021.
- [6] A. Bose, C. H. Hsu, S. S. Roy, K. C. Lee, B. Mohammadi-ivatloo, and S Abimannan, "Forecasting stock price by hybrid model of cascading multivariate adaptive regression splines and deep neural network," *Computers & Electrical Engineering*, vol. 95, no. 15-16, Article ID 107405, 2021.
- [7] M. Salahuddin and J. Gow, "The effects of Internet usage, financial development and trade openness on economic growth in South Africa: a time series analysis," *Telematics and Informatics*, vol. 33, no. 4, pp. 1141–1154, 2016.
- [8] A. Marshall, M. Dezuanni, J. Burgess, J. Thomas, and C. K Wilson, "Australian farmers left behind in the digital economy – i," *Journal of Rural Studies*, vol. 80, no. 2, pp. 195–210, 2020.
- [9] E. G. Popkova and B. S. Sergi, "A digital economy to develop policy related to transport and logistics. Predictive lessons from Russia," *Land Use Policy*, vol. 99, no. 6, Article ID 105083, 2020.
- [10] J. . Morris, "Invisibility by design: women and labor in Japan's digital economy, by GabriellaLukacs," *British Journal of Industrial Relations*, vol. 59, no. 1, pp. 246-247, 2021.
- [11] A. Androutsos, "Access link bandwidth externalities and endogenous Internet growth: a long-run economic approach," *International Journal of Network Management*, vol. 21, no. 1, pp. 21–44, 2011.
- [12] N. C. Jackson and L. M. Dunn-Jensen, "Leadership succession planning for today's digital transformation economy: key factors to build for competency and innovation," *Business Horizons*, vol. 64, no. 3, 2021.
- [13] A. Datta and S. Agarwal, "Telecommunications and economic growth: a panel data approach," *Applied Economics*, vol. 36, no. 15, pp. 1649–1654, 2014.
- [14] Y. Zou and Y. Zhang, "Analysis on the coupling coordination degree between regional economy and old-age service—a case study of Sichuan province," *Journal of Physics: Conference Series*, vol. 1774, no. 1, Article ID 012022, 2021.
- [15] S. K. Chowdhury and M. L. Endres, "The influence of regional economy- and industry-level environmental munificence on young firm growth," *Journal of Business Research*, vol. 134, no. 3, pp. 29–36, 2021.
- [16] A. Bayraktar, "OECD (organisation for economic cooperation and development) and environment," *Journal of European Economy*, vol. 138, no. 10, pp. 200–207, 2010.
- [17] L. Zhu, Z. Yu, and H. Zhan, "Impact of industrial agglomeration on regional economy in a simulated intelligent environment based on machine learning," *IEEE Access*, vol. 9, no. 99, p. 1, 2020.
- [18] B. R. Moulton, "Getting the 21st-century GDP right: what's underway?" *The American Economic Review*, vol. 90, no. 2, pp. 253–258, 2000.
- [19] A. Crabtree, T. Lodge, J. Colley, C. Greenhalgh, R. Mortier, and H Haddadi, "Enabling the new economic actor: data protection, the digital economy, and the Databox," *Personal and Ubiquitous Computing*, vol. 20, no. 6, pp. 947–957, 2016.
- [20] C. I. Fu-yi, "Regional green innovation system mode and its implication:Acase study in eastern China coastal areas," *Ecological Economy*, vol. 16, no. 01, pp. 37–59, 2020.
- [21] M. Cheng, "Sharing economy: a review and agenda for future research," *International Journal of Hospitality Management*, vol. 57, pp. 60–70, 2016.
- [22] B. Carlsson, "The Digital Economy: what is new and what is not?" *Structural Change and Economic Dynamics*, vol. 15, no. 3, pp. 245–264, 2004.
- [23] R. Ghosh, "CODE: collaborative ownership and the digital economy," *Technology and Culture*, vol. 47, no. 3, pp. 1854-1855, 2006.
- [24] E. Turban, *Information Technology for Management: Transforming Organizations in the Digital Economy Wiley Plus Stand-alone*, John Wiley, New Jersey, NJ, USA, 1997.
- [25] A. D. Borremans, I. M. Zaychenko, and O. Y. Iliashenko, "Digital economy:IT strategy of the company development," *EDP Sciences*, vol. 170, Article ID 01034, 2018.

## Research Article

# The Path Evaluation of Integrated Development of Leisure Sports and Rural Ecological Environment in Guangxi Based on Fuzzy Comprehensive Evaluation Model

Qianying Li,<sup>1</sup> Dayao Zhang ,<sup>2</sup> Yu Han,<sup>1</sup> and Youchang Xie<sup>1</sup>

<sup>1</sup>Guangxi Sports College, Nanning 530000, Guangxi, China

<sup>2</sup>Guangdong Ocean University, College of Sports and Leisure, Zhanjiang 524088, Guangdong, China

Correspondence should be addressed to Dayao Zhang; zhangdayao2022@gdou.edu.cn

Received 18 May 2022; Revised 2 July 2022; Accepted 13 July 2022; Published 10 August 2022

Academic Editor: Man Fai Leung

Copyright © 2022 Qianying Li et al. This is an open access article distributed under the Creative Commons Attribution License, which permits unrestricted use, distribution, and reproduction in any medium, provided the original work is properly cited.

Sports tourism is a new form of tourism based on sports resources, which attracts people to participate and feel the interest of sports activities and nature, and is an important part of sports industry. Through the field survey method and logical analysis method, we make a comparative analysis of the five existing rural sports tourism integration development models in Guangxi, analyze the problems of the existing rural sports tourism integration development models in Guangxi from macro-, meso-, and microdimensions, propose corresponding development countermeasures, provide reference for promoting the national strategy of building important tourism bases in Guangxi and theoretical system construction, use the method of fuzzy mathematics to construct a fuzzy comprehensive evaluation model, and apply this model to objectively evaluate the sports tourism resources in Guangxi Province. Finally, in response to the evaluation results, it is proposed to deeply develop characteristic advantageous sports tourism resources, focus on breakthroughs, develop fitness and leisure participation sports tourism industry, and reasonably lay out and cultivate some attractive sports tourism products.

## 1. Introduction

The tourism + folk sports culture development model is a special cultural development model based on folk customs, folk culture, and folk way of life to meet people's multiple travel needs [1–3]. This development model has greatly increased the popularity of the tourist area, broadened the market of sports tourism sources, and driven the sustainable development of the local economy [4].

Tourism + sports town development model's basic features are as follows: the market as the goal to create a set of traditional culture, ecological tourism, health and leisure sports, parent-child leisure play, and pension to enjoy the old in one of the cultural and health tourism areas [5, 6]. At present, many sports and leisure characteristic towns have been built in Guangxi (Nanning City Beautiful South Sports and Leisure Base, Liuzhou City Luzhai County Zhongdu Shilujiang Sports and Leisure Characteristic Town, Hechi City Desheng Lalang Ecological Sports and Leisure

Characteristic Town, etc.). This model takes sports as the core of development and cross-border integration with culture, education, health, and other industries, forming an intelligent and comprehensive public sports service platform, which is essential for enhancing tourists' experience and coordinating regional economic development [7, 8]. It has a nonnegligible role in enhancing tourists' experience and coordinating regional economic development [9, 10]. This development mode can effectively promote the mutual integration of Guangxi sports industry and red tourism area on the one hand and drive the good development of old revolutionary areas and economy and society in Guangxi on the other hand. In addition, it can effectively strengthen the education of traditional culture in old revolutionary areas, enhance the patriotism sentiment, and promote the national spirit of people all over the country [11, 12].

The construction of rural sports tourism circle development mode refers to the core of sports tourism resources to form a collaboration area with certain geographical scope

in order to obtain the best economic, social, and environmental benefits, and its basic features are taking sports industry as the core, referring to the actual situation of the development of major domestic sports tourism circles, integrating various types of tourism resources in Guangxi area, and creating a new brand about sports tourism products [13, 14]. This development mode promotes and strengthens the tourism economic cooperation between regions to a certain extent, promotes the construction of cross-regional tourism bases, improves the development environment of regional tourism economy, and promotes the overall characteristic and sustainable development of regional economy [15].

The rural sports tourism theme-based integration development model is a new model of integrated development of rural sports tourism [16]. Its main feature is to create theme lines, theme festivals, theme events, theme parks, featured villages, featured hotels, featured shopping, and other sports tourism products with different functions to meet the tourism needs of tourists, optimize the regional industrial structure, and promote the sustainable and healthy development of regional sports tourism and economy [17, 18]. On the one hand, this model can effectively avoid or reduce repetitive sports tourism market competition to guarantee the innovation and diversity of products; on the other hand, it can effectively allocate the specific resources of sports tourism so that they can be utilized in different time periods, geographical spaces, and functional uses. However, it will encounter obvious limitations in the implementation process, such as the theme tourism developed under this model can be easily imitated or copied [19, 20].

In this paper, we make a comparative analysis of the five existing rural sports tourism integration development models in Guangxi, analyze the problems of the existing rural sports tourism integration development models in Guangxi from macro-, meso-, and microdimensions, propose corresponding development countermeasures, provide reference for promoting the national strategy of building important tourism bases in Guangxi and theoretical system construction, use the method of fuzzy mathematics to construct a fuzzy comprehensive evaluation model, and apply this model to objectively evaluate the sports tourism resources in Guangxi Province. Finally, in response to the evaluation results, it is proposed to deeply develop characteristic advantageous sports tourism resources, focus on breakthroughs, develop fitness and leisure participation sports tourism industry, and reasonably lay out and cultivate some attractive sports tourism products.

## 2. Integration Path

Industrial integration needs to go through a very complicated process, generally needs to go through the implicit to explicit process, industry through cross-penetration and complementarity, as far as possible to reduce costs, in order to achieve a win-win situation in the competition. Guangxi sports tourism and rural tourism integration is the result of multilevel, multipath, and all-round integration of industries

(see Figure 1). Through the policy support of Guangxi municipal government, the pull of market demand, the internal promotion of enterprises, and the drive of scientific and technological development, the two sides achieve the integration in resources, market, products, and technology and form the new business mode of integration, thus producing corresponding economic and social benefits. The whole process has the characteristics of low consumption and high enjoyment; it is both the process of tourism and sports and leisure. Visitors not only directly participate in various sports but also make full use of various rural resources to carry out sports activities, thus realizing the integration of sports tourism resources and rural tourism resources and ultimately achieving the purpose of increasing income and promoting the construction of beautiful countryside.

## 3. Integration Model

This study adopts the cross-combination method of tourism activity attributes and resource attributes to determine the type of fusion formation. According to the activity attributes of Guangxi sports tourism, it is divided into three main types: recreation and health type, ornamental experience type, and competition participation type; according to the resource attributes of Guangxi tourism, it can be divided into natural resources type, human resources type, and artificial resources type. The 9 theoretical types of composite classification method are natural recreation and health type rural tourism, natural ornamental experience type rural tourism, natural competition participation type rural tourism, humanistic recreation type rural tourism, humanistic experience type rural tourism, humanistic participation type rural tourism, artificial recreation type rural tourism, artificial ornamental experience type rural tourism, and artificial participation type rural tourism (see Figure 2). In the process of promoting school aesthetic education, some schools have some problems, such as insufficient construction of campus aesthetic education environment and lack of aesthetic thinking in various disciplines. In view of these problems, combined with the concept of flipped classroom and the characteristics of artificial intelligence task-driven teaching, taking PHP, HTML + CSS + JS, and other development technologies as the main development technologies, and relying on the flipped classroom teaching mode of network learning space, this paper constructs an artificial intelligence core course website as a teaching platform for graduate teaching and undergraduate extended learning. The platform seeks the optimal solution of multiple combination optimization based on genetic algorithm and effectively improves the teaching quality of artificial intelligence course and students' learning efficiency.

Comparing and analyzing the 118 rural tourism areas in Guangxi city with the 9 major types formed by composite, it is determined that the fusion of sports tourism and rural tourism in Guangxi can form 4 major types, such as ornamental and playful rural tourism, recreation and health rural tourism, sports and leisure rural tourism, and folklore experience rural tourism. The characteristic resources of the



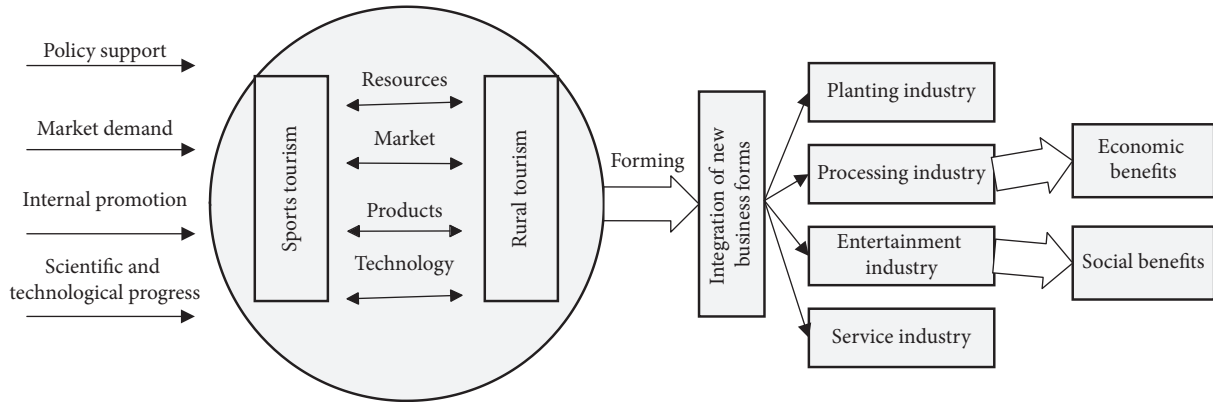


FIGURE 1: Development path of convergence.

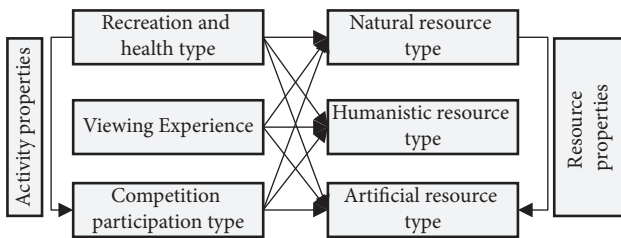


FIGURE 2: Types of integration.

4 fusion tourism types and the main representative tourist places are shown in Table 1. Through the multilevel fuzzy comprehensive evaluation of sports tourism resources, we can judge the value of sports tourism resources and provide a scientific basis for the development and protection of sports tourism resources. The evaluation model of sports tourism resources constructed in the evaluation process can adjust the index system appropriately according to the specific situation, which is also applicable to the evaluation of sports tourism resources in other regions. In this study, only representative sports tourism scenic spots as shown in Table 1 are selected for resource evaluation, which does not involve all scenic spots. In the future, more in-depth statistical analysis and evaluation of resources can be carried out from a more comprehensive perspective and the research conclusions will be more practical and targeted.

#### 4. Diversified Demand

It is found that the influencing factor of tourism motivation of tourists over 56 years old in Guangxi is mainly health factor, and the selected tourism type is mainly recreation and health type; the influencing factor of tourism motivation of tourists between 35 and 56 years old is mainly experience factor, and the selected tourism type is mainly viewing and playing type and folklore experience type; the influencing factor of tourism motivation of tourists under 35 years old is mainly breakthrough factor, and the selected tourism type is mainly sports leisure type (see Table 2).

As mentioned in Table 2, the tourism needs and motives of tourists of different ages are different; middle-aged and elderly people prefer the types of projects with relatively

small sports intensity and volume, such as hiking, traditional ethnic sports, fishing, ornamental and amusement, while young people prefer the types of projects with larger sports intensity and volume and stronger excitement, such as rafting, mountaineering, rock climbing, mountain biking, and orienteering. At present, Guangxi's sports tourism and rural tourism resources are not fully utilized and tourism-related industrial resources such as business, learning, and leisure are not fully integrated, not to mention the formation of a complete set of industrial system, which has caused the contradiction between a single tourism product and diversified and diverse tourism needs. For example, in Xitou Village of Conghua District, although there are a series of tourism projects under the government planning, such as riding, camping, and viewing, the business model is relatively single and the consumption characteristics are mainly "one-day trip," "overnight mode" has not been formed. Therefore, we should make use of the radiation advantage of urban areas in Guangxi city, continuously enrich and develop tourism resources in rural areas, meet the diversified tourism demand of tourists, create diversified and upgraded sports and rural tourism products to promote the horizontal development of rural leisure in Guangxi city, and break the dual economic structure of urban and rural areas in Guangxi [21–23].

#### 5. Evaluation of Sports Tourism Resources in Guangxi Province

5.1. Construction of Sports Tourism Resources Evaluation System. According to the principles of concise scientificity, systematic wholeness, operability, and comparability, the evaluation indexes are selected by the theoretical analysis method and expert consultation method. The theoretical analysis method is to analyze, compare and synthesize the issues related to sports tourism, and select the important and targeted indicators; the expert consultation method is to further consult the relevant experts and adjust the indicators on the basis of the preliminary proposed evaluation indicators. By combining these two methods, the evaluation index system will be finally obtained and the indexes will be divided into target layer A, criterion layer B, and indicator

TABLE 1: Characteristic resources and main representative villages (towns) of the integration type.

| Type                       | Characteristics  | Rural (town)  |
|----------------------------|--|---|
| Spectator type             | Nature, ecological parks, hiking, kite flying, cycling, sports towns, iconic venues, etc.  | Xiaozhou Village (Haizhu district), Wanha Sha Town (Nansha district), and Xigeng Village (Zengcheng district) |
| Recreation and health type | Resorts, farms, fruit picking, island tours, hiking, hot springs, etc.   | Changzhou Island (Huangpu district), Taitian Town (Huadu district), and Hot Spring Town (Conghua district)    |
| Sports and leisure type    | Farming, rafting, climbing, kayaking, marathon orienteering, rock climbing, etc.   | Asian Games Village (Panyu), Xitou Village (Conghua district), and Paitan Village (Zengwei district)          |
| Folklore experience type   | Cultural sites characteristic villages, educational and cultural science and technology museums, traditional ethnic sports, etc. | Shawan Town, Daling Village, Zhong Village (Panyu district), and Taiping Town (Nansha district)               |

TABLE 2: Analysis of tourism motivation of tourists of each age group in Guangxi city.

| Age stage          | Impact factor       | Selection type                             |
|--------------------|---------------------|--|
| Over 56 years old  | Health factor       | Recreation and health type                 |
| 35–56 years old    | Experience factor   | Entertainment and folklore experience type |
| Under 35 years old | Breakthrough factor | Sports and leisure type                    |

layer C according to their attributes and hierarchical relationships (see Figure 3).

**5.2. Determination of Evaluation Index Weights.** The weight of evaluation indexes is determined by using the hierarchical analysis method (AHP), and relevant experts are invited to make a two-by-two comparison of the importance of each factor in each level of evaluation by issuing questionnaires, and the results of the comparison are used to establish the distribution weights of the AHP judgment matrix. Taking the evaluation of comprehensive level B as an example, judgment matrix A is constructed.

$$A = \begin{Bmatrix} 1 & \frac{7}{5} & 3 \\ \frac{5}{7} & 1 & \frac{7}{4} \\ \frac{1}{3} & \frac{4}{7} & 1 \end{Bmatrix}. \quad (1)$$

Take the calculation of the weights of layer B relative to layer A as an example, and use the sum-product method to solve it as follows:

- (1) Normalize each column of the judgment matrix A, i.e., with  $\bar{a}_{11} = a_{11} / \sum_{i=1}^3 a_{i1} = 1/1 + 5/7 + 1/3 = 0.4883$ , and calculate the other terms in turn to obtain the following matrix:

$$\bar{A} = \begin{Bmatrix} 0.4884, 0.4712, 0.5217 \\ 0.3848, 0.3365, 0.3043 \\ 0.1628, 0.1923, 0.1740 \end{Bmatrix}.$$

- (2) Adding the elements in  $\bar{A}$  by rows gives the vector  $\bar{w}$  whose components  $\bar{w} = (1.4813 \ 0.9896 \ 0.5291)$ .

- (3) Normalize  $\bar{w}$  to obtain the weight  $w = (0.4938 \ 0.3298 \ 0.1764)$  of the relevant elements in layer B with respect to layer A.

- (4) Input the judgment matrix A into MATLAB 6.5 software, and calculate the maximum characteristic root  $\lambda_{\max} = 3.0046$  of the judgment matrix A [12].

$$CI = \frac{\lambda_{\max} - n}{n - 1} = \frac{3.0046 - 3}{2} = 0.0023. \quad (2)$$

Since the number of dimensions is  $n = 3$ , checking the table shows that  $RI = 0.58$ ; then, we have

$$CR = \frac{CI}{RI} = \frac{0.0023}{0.58} = 0.0039 < 0.1. \quad (3)$$

Therefore, the above weights of the relevant elements in layer B were confirmed relative to layer A by consistency tests. Using the same approach, the weights of the indicators in layer C were determined to be equivalent to the weights in layer B (see Table 3).

## 6. Evaluation Effects

### 6.1. Factor Set and Evaluation Set of the Evaluation Object.

Factor set is a general collection of factors affecting the evaluation object; the first top evaluation set  $A = \{B_1, B_2, B_3\} = \{\text{resource elements value, scenic environment conditions, development conditions}\}$ , index evaluation set  $B_1 = \{C_{11}, C_{12}, C_{13}, C_{14}\} = \{\text{sports culture value, spectacle value, recreation value, sports education value}\}$ ,  $B_2 = \{C_{21}, C_{22}, C_{23}, C_{24}\} = \{\text{scenic attractions portfolio, environmental quality and capacity, touring period, safety}\}$ , and  $B_3 = \{C_{31}, C_{32}, C_{33}, C_{34}\} = \{\text{regional economic conditions, tourism service system, infrastructure conditions, visitor market conditions}\}$ .

The evaluation factor indexes are quantified in a hierarchical manner (see Table 4).

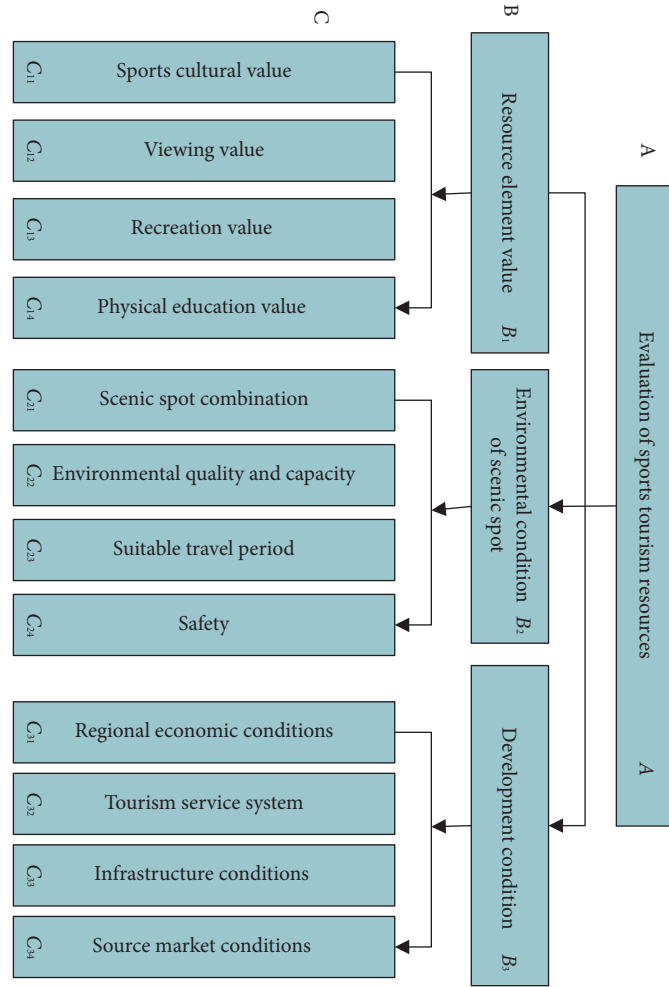


FIGURE 3: The sports tourism resource evaluation hierarchy diagram of Henan Province.

TABLE 3: Weights for each evaluation.

| Target layer A   | Criterion layer B                            | Index weight | Index layer C   | Index weight | Total weight of indicators |
|--|--|--------------|---|--------------|----------------------------|
| Evaluation of sports tourism resources in Henan Province A | Resource element value $B_1$                 | 0.485<br>8   | Sports cultural value $C_{11}$<br>(0.322 3)           | 0.317 4      | 0.157 3                    |
|  |  |              | Viewing value $C_{12}$ (0.202 7)                      | 0.202 8      | 0.101 7                    |
|  |  |              | Recreation value $C_{13}$ (0.344 2)                   | 0.344 2      | 0.171 5                    |
|  |  |              | Physical education value $C_{14}$<br>(0.137 8)        | 0.141 9      | 0.069 5                    |
|  | Environmental condition of scenic spot $B_2$ | 0.332<br>8   | Scenic spot combination $C_{21}$<br>(0.267 7)         | 0.271 7      | 0.089 6                    |
|  |  |              | Environmental quality and capacity $C_{22}$ (0.208 5) | 0.207 6      | 0.068 2                    |
|  |  |              | Suitable travel period $C_{23}$ (0.303 5)             | 0.302 5      | 0.099 5                    |
|  |  |              | Safety $C_{24}$ (0.225 3)                             | 0.232 3      | 0.074 7                    |
|  | Development condition $B_3$                  | 0.177 4      | Regional economic conditions $C_{31}$ (0.387 6)       | 0.387 6      | 0.069 2                    |
|  |  |              | Tourism service system $C_{32}$<br>(0.135 7)          | 0.135 7      | 0.024 8                    |
|  |  |              | Infrastructure conditions $C_{33}$<br>(0.236 5)       | 0.232 6      | 0.042 5                    |
|  |  |              | Source market conditions $C_{34}$<br>(0.246 2)        | 0.255 2      | 0.044 1                    |

TABLE 4: Quantitative evaluation index fuzzy evaluation form of sports tourism resources.

| Evaluation factor                  | Weight  | Evaluation grade |        |        |        |       |
|------------------------------------|---------|------------------|--------|--------|--------|-------|
| Sports cultural value              | 0.155 2 | Very high        | Higher | High   | Fair   | Low   |
| Viewing value                      | 0.089 7 | Very high        | Higher | High   | Fair   | Low   |
| Recreation value                   | 0.171 6 | Very high        | Higher | High   | Fair   | Low   |
| Physical education value           | 0.069 5 | Very high        | Higher | High   | Fair   | Low   |
| Scenic spot combination            | 0.089 6 | Excellent        | Good   | Medium | Poor   | Bad   |
| Environmental quality and capacity | 0.069 2 | Excellent        | Good   | Better | Fair   | Poor  |
| Suitable travel period             | 0.098 4 | Very long        | Longer | Long   | Normal | Short |
| Safety                             | 0.075 6 | Very high        | Higher | High   | Fair   | Low   |
| Regional economic conditions       | 0.069 2 | Excellent        | Good   | Medium | Poor   | Bad   |
| Tourism service system             | 0.024 8 | Excellent        | Good   | Medium | Poor   | Bad   |
| Infrastructure conditions          | 0.042 4 | Excellent        | Good   | Medium | Poor   | Bad   |
| Source market conditions           | 0.043 2 | Excellent        | Good   | Medium | Poor   | Bad   |

TABLE 5: The fuzzy evaluation form of sports tourism resources in the Songshan Shaolin Temple.

| Criterion layer B   | Index layer C  | Average value degree |      |        |      |      |
|---|--|----------------------|------|--------|------|------|
|   |  | Very good            | Good | Better | Fair | Poor |
| <i>Resource element value B<sub>1</sub></i> (0.485 8)                 | Sports cultural value $C_{11}$ (0.3223)              | 0.31                 | 0.33 | 0.27   | 0.09 | 0.01 |
|   | Viewing value $C_{12}$ (0.2027)                      | 0.22                 | 0.33 | 0.37   | 0.10 | 0.02 |
|   | Recreation value $C_{13}$ (0.3442)                   | 0.27                 | 0.43 | 0.19   | 0.11 | 0    |
|   | Physical education value $C_{14}$ (0.1378)           | 0.32                 | 0.30 | 0.23   | 0.18 | 0.01 |
| <i>Environmental condition B<sub>2</sub> of scenic spot</i> (0.332 8) | Scenic spot combination $C_{21}$ (0.2677)            | 0.19                 | 0.37 | 0.33   | 0.12 | 0.02 |
|   | Environmental quality and capacity $C_{22}$ (0.2085) | 0.25                 | 0.39 | 0.36   | 0.13 | 0    |
|   | Suitable travel period $C_{23}$ (0.303 5)            | 0.33                 | 0.35 | 0.29   | 0.02 | 0.01 |
|   | Safety $C_{24}$ (0.2253)                             | 0.26                 | 0.37 | 0.40   | 0.09 | 0    |
| <i>Development condition B<sub>3</sub></i> (0.177 4)                  | Regional economic conditions $C_{31}$ (0.3876)       | 0.19                 | 0.49 | 0.28   | 0.07 | 0.01 |
|   | Tourism service system $C_{32}$ (0.1357)             | 0.22                 | 0.44 | 0.33   | 0.05 | 0.02 |
|   | Infrastructure conditions $C_{33}$ (0.2365)          | 0.27                 | 0.39 | 0.27   | 0.05 | 0.03 |
|   | Source market conditions $C_{34}$ (0.2462)           | 0.31                 | 0.35 | 0.26   | 0.10 | 0.01 |

The data in parentheses are the weight values of each indicator.

6.2. *Comprehensive Evaluation of Sports Tourism Resources in Guangxi Province.* According to the evaluation index, design the relevant questionnaire and finally get the set of comments of qualitative index. Each member of the rubric evaluates each evaluation factor of each scenic spot according to the identified evaluation level criteria, and the arithmetic mean is used to calculate the affiliation value of each attraction index. For example, 30% of the people thought that the sports and cultural value of Songshan Shaolin Temple was very high, and the affiliation degree of “very high” was 0.30; 32% thought that the sports and cultural value of Songshan Shaolin Temple was high, and the affiliation degree of “high” was 0.32; and 26% thought that the sports and cultural value of Songshan Shaolin Temple was average, and the affiliation degree of “average” is 0.10; 2% of people think that the sports and cultural value of Songshan Shaolin Temple is high, and the affiliation degree of “average” is 0.10; and 2% of people think that the sports and cultural value of Songshan Shaolin Temple is high. Thus, the fuzzy evaluation matrix of  $C_{11}$  is [0.30, 0.32, 0.26, 0.10, 0.02].

For simplicity, in the fuzzy evaluation table, each single-factor evaluation level is recorded as “very good, good, better, average, and poor.” The fuzzy comprehensive evaluation of sports tourism resources of Songshan Shaolin Temple is still taken as an example (see Table 5). After calculation, the first-level fuzzy comprehensive evaluation result  $B_1$  has 3 single-factor fuzzy comprehensive evaluation:  $B_{11}, B_{12}, B_{13}$ ; then, the second-level comprehensive evaluation and the above 3 single-factor first-level comprehensive evaluation result together form the second-level fuzzy comprehensive evaluation judgment matrix  $R_2$ . Then, the second-level fuzzy comprehensive evaluation result is

$$\begin{aligned}
 A &= A_w \times R_1 = (0.4938, 0.3298, 0.1764) \times \\
 &\left\{ \begin{array}{l} 0.2427, 0.3804, 0.2472, 0.1159, 0.0138 \\ 0.2509, 0.3635, 0.3358, 0.0816, 0.0072 \\ 0.2354, 0.4181, 0.2656, 0.0622, 0.0187 \end{array} \right\} \quad (4) \\
 &= (0.2429, 0.3815, 0.2671, 0.0951, 0.0124),
 \end{aligned}$$

where  $A$  is the comprehensive evaluation result of the sports tourism resources of Songshan Shaolin Temple. According to the principle of maximum affiliation, the sports tourism resources of Songshan Shaolin Temple are of “good” level.

TABLE 6: The fuzzy evaluation form of typical sports tourism scenic resources in Henan Province.

| Sports tourism scenic spot              | Fuzzy evaluation matrix                      | Individual evaluation results |   |                        | Overall evaluation results |
|---|--|-------------------------------|---|------------------------|----------------------------|
|   |  | Resource element value        | Environmental conditions of scenic spot | Development conditions |                            |
| Songshan Shaolin Temple                 | (0.244 9 0.382 5 0.268 1<br>0.094 1 0.013 5) | Good                          | Good                                    | Good                   | Good                       |
| Chenjiagou Taijiquan                    | (0.246 7 0.362 8 0.288 1<br>0.087 7 0.029 9) | Good                          | Good                                    | Preferably             | Good                       |
| Funiu Mountain Ski Resort               | (0.189 2 0.311 6 0.385 5<br>0.075 4 0.052 3) | Good                          | Preferably                              | Preferably             | Preferably                 |
| Songshan Ski Resort                     | (0.134 5 0.307 7 0.344 3<br>0.087 6 0.158 9) | Preferably                    | Preferably                              | Commonly               | Preferably                 |
| Xinxiang Wanxianshan Rock Climbing Park | (0.185 6 0.326 6 0.368 7<br>0.103 3 0.030 0) | Good                          | Commonly                                | Commonly               | Preferably                 |
| Luoyang Chongdugou scenic spot          | (0.204 7 0.333 3 0.296 6<br>0.092 1 0.075 5) | Good                          | Good                                    | Preferably             | Good                       |
| Qingming Shanghe Garden (Kaifeng Cuju)  | (0.114 1 0.165 3 0.431 6<br>0.365 6 0.022 6) | Preferably                    | Commonly                                | Commonly               | Commonly                   |

Using the same method, the fuzzy evaluation results of several other sports tourism scenic spots were obtained (see Tables 5 and 6).

6.3. *Analysis of Evaluation Results and Suggestions for Countermeasures.* Guangxi Province is rich in types of sports tourism resources, which can well satisfy tourists with different needs. There are both traditional national sports tourism resources and new sports tourism resources, which provide a rich resource base for the development of sports tourism.

Establish the overall development strategy in the province, based on the comprehensive evaluation of the quantity, quality, and scale of sports tourism resources in the province, determine the areas more suitable for the development of sports tourism, form the core area of sports tourism, and achieve the coordinated development of resources, benefits, and brands. Taking the “national fitness project” as the strategy and taking the development mode of domestic major sports tourism circle as the reference, construct a sports tourism area in Central Plains, which is highly integrated with tourism development and scenic spot construction in Guangxi Province, and tourists demand for sports and leisure vacation, making Guangxi sports tourism become a unique charming tourist destination in China.

## 7. Conclusion

Through multilevel fuzzy comprehensive evaluation of sports tourism resources, the high and low merits of sports tourism resources value can be discerned, providing a scientific basis for the development and protection of sports tourism resources. The sports tourism resources evaluation model constructed in the evaluation process can be appropriately adjusted according to the specific situation, and it is also applicable to the evaluation of sports tourism resources in other regions. In this study, only seven representative sports tourism scenic spots in Guangxi Province

were selected for resource evaluation, and not all the spots were involved. In the future, more in-depth statistical analysis and evaluation of resources can be carried out from a more comprehensive perspective and the research conclusions will have more practical guidance and relevance.

## Data Availability

The dataset used in this study is available from the corresponding author upon request.

## Conflicts of Interest

The authors declare that they have no conflicts of interest regarding this work.

## Acknowledgments

This study was supported by the Guangxi Sports Distinctive Town Constructive Route and Development Model (Grant no. 2019KY1169).

## References

- [1] S. Feng and L. D. Xu, “Decision support for fuzzy comprehensive evaluation of urban development,” *Fuzzy Sets and Systems*, vol. 105, no. 1, pp. 1–12, 1999.
- [2] C. Lai, X. Chen, X. Chen, Z. Wang, X. Wu, and S. Zhao, “A fuzzy comprehensive evaluation model for flood risk based on the combination weight of game theory,” *Natural Hazards*, vol. 77, no. 2, pp. 1243–1259, 2015.
- [3] Z. Liang, K. Yang, Y. Sun, J. Yuan, H. Zhang, and Z. Zhang, “Decision support for choice optimal power generation projects: fuzzy comprehensive evaluation model based on the electricity market,” *Energy Policy*, vol. 34, no. 17, pp. 3359–3364, 2006.
- [4] L. Meng, Y. Chen, W. Li, and R. Zhao, “Fuzzy comprehensive evaluation model for water resources carrying capacity in Tarim River Basin, Xinjiang, China,” *Chinese Geographical Science*, vol. 19, no. 1, pp. 89–95, 2009.

- [5] Z. Zhou, X. Zhang, and W. Dong, "Fuzzy comprehensive evaluation for safety guarantee system of reclaimed water quality," *Procedia Environmental Sciences*, vol. 18, pp. 227–235, 2013.
- [6] M. Wang and D. Niu, "Research on project post-evaluation of wind power based on improved ANP and fuzzy comprehensive evaluation model of trapezoid subordinate function improved by interval number," *Renewable Energy*, vol. 132, pp. 255–265, 2019.
- [7] X. Lin, J. Wu, S. Mumtaz, S. Garg, J. Guizani, and M. Guizani, "Blockchain-based on-demand computing resource trading in IoV-assisted smart city," *IEEE Transactions on Emerging Topics in Computing*, vol. 9, no. 3, pp. 1373–1385, 2021.
- [8] A. Ramesh Khaparde, F. Alassery, A. Kumar et al., "Differential evolution algorithm with hierarchical fair competition model," *Intelligent Automation & Soft Computing*, vol. 33, no. 2, pp. 1045–1062, 2022.
- [9] J. Liang, S. Xu, Y. Li, and Y. Xie, "Inheritance and protection of Guangxi national sports culture under the background of new urbanization," *Nanotechnology for Environmental Engineering*, vol. 6, no. 3, p. 51, 2021.
- [10] D. Xingme, "Integrated Development of Health Tourism under the Background of Rural Revitalization Strategy," *Forest Chemicals Review*, vol. 12, pp. 247–254, 2021.
- [11] X. Su, D. Lu, H. Yu, and W. Qin, "Evaluation of forest tourist resources and analysis on environmental capacity of Damingshan in Guangxi," *Guangxi Agricultural Sciences*, vol. 40, no. 6, pp. 777–781, 2009.
- [12] K. Day, "Built environmental correlates of physical activity in China: a review," *Preventive medicine reports*, vol. 3, pp. 303–316, 2016.
- [13] T. Wang, G. Han, S. Liang et al., "The path of increasing income for new agricultural enterprises in Guangxi," *Journal of Southern Agriculture*, vol. 50, no. 7, pp. 1640–1646, 2019.
- [14] S. L. Wang, Y. C. Li, and C. P. Zhang, "Analysis of the effect of social support on sustainable competitive advantage in tourism industry - based on the perspective of living-ecology-production integrated space," *Revista de Cercetare și Intervenție Socială*, vol. 71, pp. 250–263, 2020.
- [15] Y. Z. Huang and C. J. Chen, "Ecological integration of new ideas for urban tourism space resources—nanning watertown tourism space resources integration," *Advanced Materials Research*, vol. 368, pp. 1889–1894, 2012.
- [16] Z. Yongxun and H. Lulu, "Protecting important agricultural heritage systems (IAHS) by industrial integration development (IID): practices from China," *Journal of Resources and Ecology*, vol. 12, no. 4, pp. 555–566, 2021.
- [17] Y. Wu, "Theoretical definition and evaluation of marine cultural resources from the perspective of rural revitalization: a literature review," *Environment, Resource and Ecology Journal*, vol. 5, no. 2, pp. 49–52, 2021.
- [18] W. Huizhen, "Integration development and protection of sports intangible cultural heritage and cultural tourism in the yellow river basin based on GIS," *Tobacco Regulatory Science*, vol. 7, no. 6, pp. 5514–5522, 2021.
- [19] L. Zhang, J. Zhang, L. Zhang, C. Wu, and Y. Zhang, "Study on the classification of forestry infrastructure from the perspective of supply based on the classical quartering method," *Applied Mathematics and Nonlinear Sciences*, vol. 6, no. 2, pp. 447–458, 2021.
- [20] P. Li, C. Ryan, and J. Cave, "Chinese rural tourism development: t," *Anhui.-2008-2015. Tourism Management*, vol. 55, pp. 240–260, 2016.
- [21] J. J. Chang, R. F. Chen, and C. L. Lin, "Exploring the driving factors of urban music festival tourism and service development strategies using the modified SIA-NRM approach," *Sustainability*, vol. 14, no. 12, p. 7498, 2022.
- [22] C. Yu, L. Zhang, R. Miao, and M. Wang, "Changes and prospects of rural teacher compensation policy from the perspective of positive psychology," *Psychiatria Danubina*, vol. 33, no. suppl 6, pp. 265–270, 2021.
- [23] R. L. Daft and R. H. Lengel, "Organizational information requirements, media richness and structural design," *Management Science*, vol. 32, no. 5, pp. 554–571, 1986.

## Research Article

# Discrete Hyperparameter Optimization Model Based on Skewed Distribution

Yuqi Li 

*School of Economics and Management, Beijing University of Posts and Telecommunications, Beijing 100876, China*

Correspondence should be addressed to Yuqi Li; [liyuyi@bupt.edu.cn](mailto:liyuyi@bupt.edu.cn)

Received 21 March 2022; Revised 15 June 2022; Accepted 21 June 2022; Published 9 August 2022

Academic Editor: Man Fai Leung

Copyright © 2022 Yuqi Li. This is an open access article distributed under the Creative Commons Attribution License, which permits unrestricted use, distribution, and reproduction in any medium, provided the original work is properly cited.

As for the machine learning algorithm, one of the main factors restricting its further large-scale application is the value of hyperparameter. Therefore, researchers have done a lot of original numerical optimization algorithms to ensure the validity of hyperparameter selection. Based on previous studies, this study innovatively puts forward a model generated using skewed distribution (gamma distribution) as hyperparameter fitting and combines the Bayesian estimation method and Gauss hypergeometric function to propose a mathematically optimal solution for discrete hyperparameter selection. The results show that under strict mathematical conditions, the value of discrete hyperparameters can be given a reasonable expected value. This heuristic parameter adjustment method based on prior conditions can improve the accuracy of some traditional models in experiments and then improve the application value of models. At the same time, through the empirical study of relevant datasets, the effectiveness of the parameter adjustment strategy proposed in this study is further proved.

## 1. Introduction

The whole Pareto/NBD model was created by Abramowitz and Stegun. The practical problem corresponding to the initial modeling is to analyze the behavior of consumers, especially the repeated purchase of related products, so that managers can evaluate the purchasing intention of future consumers and better arrange production and marketing activities. For the whole model itself, the description of consumer behavior is reflected in the following two important parts [1]. First, it is about the probability distribution or the probability distribution density of the consumer's survival over the entire product purchasing cycle; second, it is about the description of the mathematical expectation of consumers' purchasing behavior randomly selected in a certain consumption period in the future.

For the construction of the whole Pareto/NBD model, the most critical part is to get the exact mathematical analytical expression of conditional mathematical expectation through appropriate mathematical assumptions and strict mathematical reasoning [2–4]. This work is very difficult for many researchers who are familiar with the SMC model. An

important objective of this study was to prove the accuracy of some key conclusions about the Pareto/NBD model through mathematically deriving relevant important intermediate results (especially probability distribution function and probability distribution density function) within the framework of Pareto/NBD model. At the same time, the analytical framework of this model is combined with the hyperparameter optimization problem of discrete SMBO type to achieve the accuracy of mathematical description of the whole model.

First of all, we need to introduce a special function, Gauss hypergeometric function, and the mathematical expression of this function in the form of power series [5] is as follows:

$${}_2F_1(a, b; c; z) = \sum_{j=0}^{\infty} \frac{(a)_j (b)_j}{(c)_j} \frac{z^j}{j!}, \quad (1)$$

where  $c \neq 0, -1, -2, \dots$ ,  $(a)_j$  is the factorial power (Pochhammer's symbol) operation, and specific mathematical calculation formula is  $a(a+1) \cdots (a+j-1)$ . In contrast to the forming operation, it is about the parameter  $a$  of the

ascending factorial power operation, and according to the assessment method of Abel, the convergence of the factorial power operation depends on the parameter  $z$ , in the case of  $|z| < 1$  throughout the series converges to 1, in the case of  $|z| > 1$  tends to spread the whole series,  $|z| = 1$ , the series converges to the  $c - a - b > 0$ .

The ascending joint operation  $(a)_j$  can be expressed by two gamma functions with related parameters, which can be expressed by mathematical formula as follows:

$$(a)_j = \frac{\Gamma(a+j)}{\Gamma(a)}. \quad (2)$$

With the help of this nature, the mathematical expression of the whole Gauss hypergeometric function can be further expressed as follows:

$${}_2F_1(a, b; c; z) = \frac{\Gamma(c)}{\Gamma(a)\Gamma(b)} \sum_{j=0}^{\infty} \frac{\Gamma(a+j)\Gamma(b+j)}{\Gamma(c+j)} \frac{z^j}{j!}. \quad (3)$$

According to the above mathematical expression form of Gauss hypergeometric function, combined with the nature of gamma function, the whole function is still expressed in discrete form, and the whole Gauss hypergeometric function is mutually symmetric for two parameters  $a$  and  $b$  [6], which is expressed in mathematical form as follows:

$${}_2F_1(a, b; c; z) = {}_2F_1(b, a; c; z). \quad (4)$$

Furthermore, to further deepen the understanding of Gauss hypergeometric functions and facilitate the next model derivation, we must introduce the representation of Gauss hypergeometric functions in the form of Euler integral:

$${}_2F_1(a, b; c; z) = \frac{1}{B(b, c-b)} \int_0^1 t^{b-1} (1-t)^{c-b-1} (1-zt)^{-a} dt, \quad c > b. \quad (5)$$

Through the above mathematical expressions, we get the continuous expression of the Gauss hypergeometric function, where  $B(\cdot, \cdot)$  is the beta function.

## 2. Model Assumptions

Many aspects of BG/NBD model are similar to the Pareto/NBD model, but there are still many differences between models. The most important part is whether the hyperparameters change with each experiment/test. In the Pareto model, the hyperparameters change in any interval of each experiment/test interval, which is further independent of the selection and change in datasets. In the BG/NBD model, we assume that the timing of determining whether the hyperparameters change is controlled after each new dataset test; that is, the continuous discrimination interval in Pareto/NBD is changed into discrete decision interval, and then, the beta-geometric (BG) model can be established [7]. On the whole, the following five basic assumptions are needed for the new model.

- (1) When dataset testing further influences the change in hyperparameters, the change in hyperparameters is subject to the Poisson process with parameter  $\lambda$  as a whole; that is to say,

$$P(\Theta(d_t) = x|\lambda) = \frac{(\lambda d_t)^x \exp(-\lambda d_t)}{x!}, \quad (6)$$

$$x = 0, 1, 2, \dots,$$

where  $d_t = \|D_t - \emptyset\|$  represents the difference between different datasets and empty sets, which can be the complexity change between datasets or the size change in datasets. For Poisson process distribution, the exponential distribution with parameter  $\lambda$  is followed between every two dataset experiments, and the mathematical expression is as follows:

$$g(d_j - d_{j-1}|\lambda) = \lambda \exp[-\lambda(d_j - d_{j-1})], \quad d_j > d_{j-1} \geq 0, \quad (7)$$

where  $g$  stands for probability density function.

- (2) For parameter  $\lambda$ , we assume that it is subject to the gamma distribution of parameters  $r$  and  $\alpha$ , and the mathematical expression is as follows:

$$g(\lambda|r, \alpha) = \frac{\alpha^r \lambda^{r-1} \exp(-\lambda\alpha)}{\Gamma(r)}, \quad \lambda > 0, \quad (8)$$

where  $r$  and  $\alpha$  are the known and determined constants, which are determined by exogenous factors and not affected by the model itself.

- (3) After each experiment/test, the probability  $p$  of the hyperparameter  $\theta$  will remain unchanged. In other words, after any experiment/test, a judgment should be made on whether the next hyperparameter  $\theta$  will change further. Then, the probability of the hyperparameter  $\theta$  remaining unchanged should follow the geometric distribution of the parameter  $p$ :

$$P(\text{unchange}) = p(1-p)^{j-1}, \quad (9)$$

$$j = 1, 2, 3, \dots,$$

where  $j$  is the number of experiments/tests.

- (4) To ensure that there is an analytic solution to the posterior distribution involving hyperparameters when solving the Bayesian estimation, it is necessary to assume that the parameter  $p$  is also determined by the exogenously given probability distribution, namely,

$$g(p|a, b) = \frac{p^{a-1} (1-p)^{b-1}}{B(a, b)}, \quad 0 \leq p \leq 1, \quad (10)$$

where  $a$  and  $b$  are the known and determined constants, which are determined by exogenous factors and not affected by the model itself.

- (5) To eliminate the interaction between parameters and simplify the complexity of the overall model analysis, we need to assume the independence of parameters  $\lambda$



and  $p$  of the two models; that is, with the progress of the experiment/test,  $\lambda$  and  $p$  are independent of each other and not affected by each other.

### 3. Model Evolution

*3.1. Derivation of Likelihood Function.* We may consider that for the hyperparameter  $\theta$ , it has experienced  $x$  changes in the known experimental/test interval  $(0, d_T]$ . These changes may occur in  $x$  interval  $d_1, d_2, \dots, d_x$  in the whole test interval, which can be represented by the number line graph as follows.

To ensure that a relatively complete likelihood function of relevant parameters can be derived [8], we carry out the following technical operation and further assumption:

- (1) The probability of hyperparameter  $\theta$  changing between  $d_1$  in the first experiment/test area is a standard exponential distribution model, and the probability of event occurrence should be  $\lambda \exp(-\lambda d_1)$ .
- (2) The probability that the second change in hyperparameter  $\theta$  happens to be in the second experiment/test interval  $d_2$  is in the first experiment/test interval  $d_1$ . The probability of hyperparameter  $\theta$  still continues to change with the product of the probability of  $d_1$  and  $d_2$  changes within the range of test; that is to say, in the whole experiment/test interval, the probability of  $\theta$  hyperparameter change still obeys the standard of exponential distribution, but needs to multiply by the probability that the hyperparameter  $\theta$  will still change in the first test interval. The specific expression is as follows:

$$(1-p)\lambda \exp[-\lambda(d_2 - d_1)]. \quad (11)$$

- (3) Further extend to the probability that the hyperparameter  $\theta$  changes at the  $x$ th experiment/test interval  $d_x$  should be equal to the standard exponential distribution times the probability that the change will occur after the previous experiment/test interval  $d_{x-1}$ , and the mathematical expression is as follows:

$$(1-p)\lambda \exp[-\lambda(d_x - d_{x-1})]. \quad (12)$$

- (4) Finally, to ensure the likelihood function expression of completeness, we must make mandatory assumptions about the predicted change probability after the first experiment/test  $d_1$ , assuming that the first test/test must be changed, but the changes can take 0 concrete or other step length, so overall hyperparameter  $\theta$  in  $(d_x, d_T]$  interval constant probability is composed of two parts. The first part is the first time the experiment/test has changed, both of which do not change afterwards, and the second part is just the possibility just there is no change in  $(d_x, d_T]$  interval, where the specific expression is as follows:

$$p + (1-p)\exp[-\lambda(d_T - d_x)]. \quad (13)$$

Further, we can obtain the likelihood function of the parameter  $d_1, d_2, \dots, d_x, d_T$  when  $\lambda$  and  $p$  are known:

$$\begin{aligned} L(\lambda, p|d_1, d_2, \dots, d_x, d_T) &= \lambda \exp(-\lambda d_1)(1-p) \\ &\quad \cdot \lambda \exp[-\lambda(d_2 - d_1)] \dots (1-p) \\ &\quad \cdot \lambda \exp[-\lambda(d_x - d_{x-1})] \\ &\quad \cdot \{p + (1-p)\exp[-\lambda(d_T - d_x)]\} \\ &= p(1-p)^{x-1} \lambda^x \exp(-\lambda d_x) \\ &\quad + (1-p)^x \lambda^x \exp(-\lambda d_T). \end{aligned} \quad (14)$$

Just like our Pareto/NBD model above, the change in hyperparameter  $\theta$  is still uncertain and random, and the prediction of the overall hyperparameter change depends on the historical information of the whole experiment/test:  $(\Theta = x, d_x, d_T)$ .

At the zero point of the initial experiment/test preparation stage, we must ensure that the hyperparameter  $\theta$  will change, but there is a difference in the change step size, and then, we can get the probability likelihood function of the hyperparameter  $\theta$  remaining at 0 in the whole historical information range of  $(0, d_T]$ , which can be further obtained using the exponential distribution:

$$L(\lambda|\Theta = 0, d_T) = \exp(-\lambda d_T). \quad (15)$$

Further, for a single hyperparameter  $\theta$ , we can obtain a probability likelihood function, and the mathematical expression is as follows:

$$\begin{aligned} L(\lambda, p|\Theta = x, d_T) &= (1-p)^x \lambda^x \exp(-\lambda d_T) \\ &\quad + I_{x>0} p(1-p)^{x-1} \lambda^x \exp(-\lambda d_x), \end{aligned} \quad (16)$$

where  $I_{x>0} = 1$ , when  $x > 0$ , and  $x \leq 0$  is less than minus, and the value of the whole is 0.

*3.2. Derivation of the Probability Distribution of the Hyperparameter  $\theta$ .* For  $\theta$  hyperparameter probability distribution, the application of mathematical formula is expressed as  $P(\Theta(d_t) = x)$ , where the  $\Theta(d_t)$  represents the specific value of hyperparameter  $\theta$  in the whole experiment/test interval  $d_t$ , so  $\Theta(d_t)$  becomes a random variable, so that you can establish the basic relationships between experiment/test interval and hyperparameter  $\theta$ :  $\Theta(d_t) \geq x \Leftrightarrow T_x \leq d_t$ . Among them,  $T_x$  shows experiment/test range when  $\theta$  hyperparameter is  $x$  changed. According to the corresponding relationship, we can get approximate mathematical expressions about  $P(\Theta(d_t) = x)$ :

$$\begin{aligned} P(\Theta(d_t) = x) &= P(\text{change}) \cdot P(T_x \leq d_t, T_{x+1} > d_t) \\ &\quad + I_{x>0} \cdot P(\text{unchange}) \cdot P(T_x \leq d_t). \end{aligned} \quad (17)$$

Considering that the experimental/test interval in which the hyperparameter  $\theta$  changes follows an exponential distribution (for specific content, see model hypothesis part), according to random variable for the hyperparameter itself, an important part of the probability distribution function is

$P(T_x \leq d_t, T_{x+1} > d_t)$ , a Poisson probability problem; among them,  $\Theta(d_t) = x$  and  $P(T_x \leq d_t)$  (Erlang— $x$ ) are the arrival time distribution. Furthermore, we can derive the conditional distribution function of hyperparameter with  $\theta$  machine variable under the known condition of RP [9]:

$$P(\Theta(d_t) = x | \lambda, p) = (1-p)^x \frac{(\lambda d_t)^x \exp(-\lambda d_t)}{x!} + I_{x>0} p (1-p)^{x-1} \cdot \left[ 1 - \exp(-\lambda d_t) \sum_{j=0}^{x-1} \frac{(\lambda d_t)^j}{j!} \right]. \quad (18)$$

**3.3. Derivation of Mathematical Expectations for the Hyperparameter  $\theta$ .** Since the change in the hyperparameter  $\theta$  follows the Poisson process with the parameter  $\lambda d_t$ , the mathematical expectation of the value change in the hyperparameter  $\theta$ , i.e.,  $E[\Theta(d_t)]$ , should be  $\lambda d_t$ , within the given experimental/test interval. Then, for the hyperparameter  $\theta$ , there are no longer changes in the experimental/test interval  $d_\tau \leq d_t$ ; then, the mathematical expectation of  $E[\Theta(d_t)]$  in  $(0, d_\tau)$  with respect to the hyperparameter  $\theta$  should be equal to  $\lambda d_\tau$ .

Then, for the change occurring outside the experimental/test interval  $d_\tau$ , the probability distribution of the change in the value of the hyperparameter  $\theta$  should follow the conditional probability model about  $\lambda$  and  $p$ , that is,

$$P(d_\tau > d_t) = P(\text{change} | \lambda, p) = \sum_{j=0}^{\infty} (1-p)^{j-1} \frac{\exp(-\lambda d_t) (\lambda d_t)^j}{j!} = \exp(-\lambda p d_t). \quad (19)$$

This expression further indicates the probability density function for no-answer experiment/test interval  $d_\tau$ ; that is to say,  $g(d_\tau | \lambda, p) = \lambda p \exp(-\lambda p d_\tau)$ . It shall be highlighted that no-answer experiment/test interval  $d_\tau$  is an exponential form, but the relevant parameter arrangement depends on the probability for the recognition of each experiment/test  $p$ . However, in a Pareto/NBD model, the overall model assumes that no-answer experiment/test interval  $d_\tau$  is specified by the probability density function, and there is no relevant information for the discrimination of probability  $p$ . Then, we can further work out the conditional expectation expression about  $\Theta(d_t)$  in the case that  $\lambda$  and  $p$  know, and the specific mathematical expression is as follows:

$$E[\Theta(d_t) | \lambda, p] = \lambda d_t \cdot P(d_\tau > d_t) + \int_0^{d_t} \lambda d_\tau g(d_\tau | \lambda, p) d(d_\tau). \quad (20)$$

By substituting relevant intermediate variables into the above formula and further simplifying, we can get a very concise formula:

$$= \frac{1}{p} - \frac{1}{p} \exp(-\lambda p d_t). \quad (21)$$

**3.4. Derivation of the Transcendental Posterior Expectation.** By the content of the previous section, we discuss the core of the problem is to deduce the mathematical expectation of  $E[\Theta(d_t) | \lambda, p]$  involving  $\theta$  hyperparameter under the condition of known parameters  $\lambda$  and  $p$ , that is, under the premise of arrival rate  $\lambda$  of the test data and the know  $p$ , the conditional expectation expression of the hyperparameter  $\theta$  is obtained, but in fact, according to the previous hypothesis, according to  $\lambda$  and  $p$ , we set and select the two parameters that obey the distribution types and determined parameters. This part mainly focuses on the content of the derivation in  $\lambda$  to gamma distribution and  $p$  to beta distribution of cases, that is, to derive the posterior conditional expectation of  $\Theta(d_t) = x$  involving the parameters  $r, \alpha, a, b$  when we assume that the conditions (1) and (2) meet. The whole derivation process is relatively complex, and we will treat the proof content as an appendix. This summary mainly lists the main results in the derivation process.

- (1) According to the content of Section 3.1, we have derived the probability likelihood function of the related parameters  $\lambda$  and  $p$  when the hyperparameter and the whole experimental/test interval are known, in the form of formula (3). Furthermore, we will make parameters  $r, \alpha$  obey the parameters for the gamma distribution and  $a, b$ , respectively, the assumptions for the beta distribution into the middle of the derived formula; note that we need to emphasize that the entire  $(r, \alpha, a, b)$  parameter set is given and then get in the whole experiment/test cycle ( $\Theta = x, d_x, d_T$ ) known cases, and related parameter ( $\Theta = x, d_x, d_T$ ) probabilistic likelihood function is expressed as follows:

$$L(r, \alpha, a, b | \Theta = x, d_x, d_T) = \frac{B(a, b + x)}{B(a, b)} \frac{\Gamma(r + x) \alpha^r}{\Gamma(r) (\alpha + d_T)^{r+x}} + I_{x>0} \frac{B(a + 1, b + x - 1)}{B(a, b)} \cdot \frac{\Gamma(r + x) \alpha^r}{\Gamma(r) (\alpha + d_x)^{r+x}} \quad (22)$$

All the four variables  $(r, \alpha, a, b)$  in the above formula can be estimated by means of maximum-likelihood estimation. That is to say, in the whole known experiment/test cycle  $(0, d_T)$ , for  $\Theta = x$ , the probability likelihood function after the log operation occurred in the  $d_x$  experiment/test interval can be expressed as follows:

$$LL(r, \alpha, a, b) = \ln[L(r, \alpha, a, b | \Theta = x, d_x, d_T)]. \quad (23)$$

The estimation of this formula can follow the general numerical optimization method and determine the optimal solution by finding the stagnation point of the first derivative and solving the extreme value, because the nature of the likelihood function must be convex.

- (2) According to the conditional probability distribution of hyperparameter  $\theta$ , the form is shown in formula (4). Considering that the specific distribution of  $\lambda, p$  has been given and the parameters have been determined, we can further express formula (4) as the conditional probability distribution under the condition that parameter set  $(r, \alpha, a, b)$  is known:

$$\begin{aligned}
 P(\Theta(d_t) = x | r, \alpha, a, b) &= \frac{B(a, b + x) \Gamma(r + x)}{B(a, b) \Gamma(r)x!} \left(\frac{\alpha}{\alpha + d_t}\right)^r \left(\frac{d_t}{\alpha + d_t}\right)^x \\
 &+ I_{x>0} \frac{B(a + 1, b + x - 1)}{B(a, b)} \\
 &\cdot \left[ 1 - \left(\frac{\alpha}{\alpha + d_t}\right)^r \left\{ \sum_{j=0}^{x-1} \frac{\Gamma(r + j)}{\Gamma(r)j!} \right\} \left(\frac{d_t}{\alpha + d_t}\right)^j \right].
 \end{aligned} \tag{24}$$

- (3) Finally, according to the condition of known parameters of  $\lambda, p$ , the hyperparameter  $\theta$  conditional expectation, the concrete mathematical expression such as formula (5), combined with the  $\lambda, p$  two parameters, follows gamma distribution and beta distribution in concrete form, and we can get in any experiment/test interval length  $d_t$ , under the condition of the parameters in the parameter set  $(r, \alpha, a, b)$  known, hyperparameter  $\theta$  conditional expectation, which can also be called the posterior conditional expectation; the mathematic expression of the specific is as follows:

$$\begin{aligned}
 E[\Theta(d_t) | r, \alpha, a, b] &= \frac{a + b - 1}{a - 1} \\
 &\cdot \left[ 1 - \left(\frac{\alpha}{\alpha + d_t}\right)^r F_1\left(r, b; a + b - 1; \frac{d_t}{\alpha + d_t}\right) \right],
 \end{aligned} \tag{25}$$

where  $F_1(\cdot)$  is Gauss hypergeometric function; refer to the explanation in the proof for the simple derivation, and refer to the relevant introduction in the model introduction for the specific content.

---


$$\begin{aligned}
 E[Y(d_t) | \Theta = x, d_x, d_T, r, \alpha, a, b] &= \frac{a + b + x - 1/a - 1 \left[ 1 - (\alpha + d_T/\alpha + d_T + d_t)^r F_1(r + x, b + x; a + b + x - 1; d_t/\alpha + d_T + d_t) \right]}{1 + I_{x>0} a/b + x - 1 (\alpha + d_T/\alpha + d_x)^{r+x}},
 \end{aligned} \tag{26}$$

where  $\Theta = x, d_x, d_T$  stands for the known experimental/test information,  $(r, \alpha, a, b)$  stands for the known parameter set by calculation, and  $F_1(\cdot)$  stands for the Gauss hypergeometric function.

Once again, the whole formula uses the Gauss hypergeometric function, and a mathematical expression formula is the same, of course, where the Gauss hypergeometric function parameters are known, and the calculation of the precise value is guaranteed. To reduce the computation

It is important to note that the final expression of posterior conditional expectation about hyperparameter  $\theta$  needs a value about Gauss hypergeometric function; of course, this value has nothing to do with hyperparameter  $\theta$ . On the contrary, due to the parameter set  $(r, \alpha, a, b)$  can be obtained by maximum-likelihood estimate of the traditional method, and the experiment/test interval length is also a known quantity, so the overall Gauss hypergeometric function value is also determined. Compared with other estimated results, using the Gauss hypergeometric function to express the hyperparameter  $\theta$  of the posterior conditional expectation is more direct and simple, and polynomial sequence can be used for approximate calculation, so the convenience for the late of simulation is very good, which can greatly simplify the computing complexity and try to solve the corresponding parameter selection in a timely manner.

Of course, the above content is just based on known sequence information  $(\Theta = x, d_x, d_T)$  cases and makes the probability model for how hyperparameter  $\theta$  values. In addition to accommodating more known conditions and historical information as much as possible to make accurate simulation of the structure of past data, the final purpose of establishing BP/NBD model shall also focus on a given new experiment/test dataset case and how to utilize the known datasets and the relationship between the parameter  $\theta$ , given the new dataset the parameters of an approximate estimate [10], and the key of the whole model application on the new dataset corresponds to the hyperparameter of the prediction is that we more concern.

$(\Theta = x, d_x, d_T)$  in the history of the experiment/test information has been confirmed, we can have  $\theta$  hyperparameter values on the new experiment/test interval  $d_t$ , we give an approximate posterior conditional expectation, the specific detailed process can see behind a certificate, and here we give the concrete mathematical expression of this posterior conditional expectation:

burden on the computer simulation process, the actual operation often uses polynomial equations to approximate its numerical calculation and will not cause enormous computation burden. The rest of the whole formulas are simple numerical calculations and would not form the computing burden.

The overall content of the appendix mainly focuses on the mathematical description of the key process in the model derivation process. On the one hand, through mathematical

rigour, it indicates the credibility of model content; on the other hand, it also provides mathematical support for transforming the mathematical model into computer model. The main purpose is the mathematical expectation for hyperparameter  $\theta$ ,  $E[\Theta(d_t)]$ , and ultimately predictable  $\theta$  hyperparameter posterior mathematical expectation of mathematical deduction, and the derivation process of the intermediate links is the Euler integral for Gauss hypergeometric function:

$${}_2F_1(a, b; c; z) = \frac{1}{B(b, c-b)} \int_0^1 t^{b-1} (1-t)^{c-b-1} (1-zt)^{-a} dt, c > b. \quad (27)$$

**3.5. Derivation of Mathematical Expectation  $E[\Theta(d_t)]$  for the Hyperparameter  $\theta$ .** To get the mathematical expectation  $E[\Theta(d_t)]$  about hyperparameter  $\theta$ , according to the condition of known parameter set  $\lambda, p$ , we must use formula about the conditional expectation of hyperparameter  $\theta$  and assumptions about the distribution of  $\lambda$  and  $p$ ,  $\lambda$ , parameters of  $r, \alpha$  gamma distribution on  $p$  obedience of  $a, b$  beta distribution parameters; first of all, we will bring the probability distribution density of  $g(\lambda|r, \alpha) = (\alpha^r \lambda^{r-1} \exp(-\lambda\alpha)/\Gamma(r))$ ,  $\lambda > 0$ , related to  $\lambda$  into formula (4) and get preliminary mathematical expressions:

$$E[\Theta(d_t)|r, \alpha, p] = \frac{1}{p} - \frac{\alpha^r}{p(\alpha + pd_t)^r}. \quad (28)$$

Further, we substitute the beta probability distribution density  $g(p|a, b) = (p^{a-1}(1-p)^{b-1}/B(a, b))$ ,  $0 \leq p \leq 1$ , of  $p$  subject to the overall conditional expectation formula of hyperparameter  $\theta$ , and we first calculate a definite integral as follows:

$$\int_0^1 \frac{1}{p} \frac{p^{a-1}(1-p)^{b-1}}{B(a, b)} dp = \frac{a+b-1}{a-1}. \quad (29)$$

Further, a more complex definite integral needs to be calculated:

$$\begin{aligned} & \int_0^1 \frac{\alpha^r}{p(\alpha + pd_t)^r} \frac{p^{a-1}(1-p)^{b-1}}{B(a, b)} dp \\ &= \alpha^r \frac{1}{B(a, b)} \int_0^1 p^{a-2} (1-p)^{b-1} (\alpha + pd_t)^{-r} dp. \end{aligned} \quad (30)$$

To ensure that the definite integral form at the end is consistent with the form of Gauss hypergeometric function, we need to make a variable substitution, so  $q = 1 - p$ ; of course, in the process of variable substitution, the form of the differential will also change  $dp = -dq$ . The integral form above further becomes the following:

$$= \left( \frac{\alpha}{\alpha + d_t} \right)^r \frac{1}{B(a, b)} \int_0^1 q^{b-1} (1-q)^{a-2} \left( 1 - q \cdot \frac{d_t}{\alpha + d_t} \right)^{-r} dq. \quad (31)$$

The Euler integral form and parameter  $r, b; a + b - 1; (d_t/\alpha + d_t)$  of the Gauss hypergeometric function mentioned above are further applied, and the

corresponding parameters in the integral form are expressed, respectively; then, the definite integral can be further formalized as follows:

$$= \left( \frac{\alpha}{\alpha + d_t} \right)^r \frac{B(a-1, b)}{B(a, b)} {}_2F_1 \left( r, b; a + b - 1; \frac{d_t}{\alpha + d_t} \right), \quad (32)$$

where  $F_1(\cdot)$  is a Gauss hypergeometric function.

Finally, the conditional expectation formula of the hyperparameter  $\theta$  can be obtained, and its mathematical expression is as follows:

$$\begin{aligned} & E[\Theta(d_t)|r, \alpha, a, b] \\ &= \frac{a+b-1}{a-1} \left[ 1 - \left( \frac{\alpha}{\alpha + d_t} \right)^r {}_2F_1 \left( r, b; a + b - 1; \frac{d_t}{\alpha + d_t} \right) \right]. \end{aligned} \quad (33)$$

**3.6. Derivation of the Conditional Expectation  $E[Y(d_t)|\Theta = x, d_x, d_T]$  for the Hyperparameter  $\theta$  with Known Historical Information.** We further define the variation of  $(d_T, d_{T+t})$  hyperparameter  $\theta$  in the new experimental/test interval of  $Y(d_t)$ . As a prediction of hyperparameter  $\theta$  in the new dataset, we focus on the conditional expectation of the value of hyperparameter  $B$  under the premise that the historical information is known; i.e.,  $\Theta = x, d_x, d_T$  is determined, which is expressed as  $E[Y(d_t)|\Theta = x, d_x, d_T]$  by mathematical formula.

If the hyperparameter  $\theta$  still changes further in  $d_T$  experiments/tests, then the conditional mathematical expectation of  $Y(d_t)$ , the corresponding random variable, can be expressed as follows:

$$E[Y(d_t)|\lambda, p] = \frac{1}{p} - \frac{1}{p} \exp(-\lambda pd_t). \quad (34)$$

Then, further, we need to make sure that in the new experiment/test sequence, how much probability that hyperparameter  $\theta$  will change. According to our hypothesis in the second section, all the experiment/test sequence for each group in the initial state can keep a change state, the purpose of which is to ensure the overall model can be used to measure is in complete probability space, that is to say, in  $d_T$ /tests, hyperparameter  $\theta$  keeps changing the state of the conditional probability, which can be expressed as follows:

$$P(\text{change}|\Theta = 0, d_T, \lambda, p) = 1. \quad (35)$$

As for  $(0, d_T)$  experiment/test interval, the conditional probability of the hyperparameter  $\theta$  remaining changing state can be approximately expressed, in the case that historical

information  $\Theta = x, d_x, d_T$  and parameters  $\lambda$  and  $p$  have been determined:

$$P(\text{change}|\Theta = x, d_x, d_T, \lambda, p) = \frac{(1-p)\exp[-\lambda(d_T - d_x)]}{p + (1-p)\exp[-\lambda(d_T - d_x)]} \quad (36)$$

Among them, the molecules represented in  $d_x$ /tests still keep change state, but that in the experiment/test interval of  $(d_x, d_T]$  keep zero step change probability, and the denominator is the probability that nothing has changed from the beginning of the experiment/test to the end of the historical information, as the case is in assumption (4) in Section 3.1.

Here, we apply a small trick of conditional probability. For the clever treatment of “1,”  $[(1-p)\exp[-\lambda(d_T - d_x)]]/$

$[(1-p)\exp[-\lambda(d_T - d_x)]] = 1$ ; multiplied by the above equation, we can get an important intermediate result:

$$P(\text{change}|\Theta = x, d_x, d_T, \lambda, p) = \frac{(1-p)^x \lambda^x \exp(-\lambda d_T)}{L(\lambda, p|\Theta = x, d_x, d_T)}, \quad (37)$$

where  $L(\lambda, p|\Theta = x, d_T) = (1-p)^x \lambda^x \exp(-\lambda d_T) + I_{x>0} p(1-p)^{x-1} \lambda^x \exp(-\lambda d_x)$ , as previously concluded in formula (3); note that we need to assume that, at  $x = 0$ , the whole A2 formula should be equal to 1.

We multiply the two important intermediate variables A1 and A2 to obtain the following further results:

$$\begin{aligned} E[Y(d_t)|\Theta = x, d_x, d_T, \lambda, p] &= \frac{(1-p)^x \lambda^x \exp(-\lambda d_T) (1/p - 1/p \exp(-\lambda d_t)/p)}{L(\lambda, p|\Theta = x, d_x, d_T)} \\ &= \frac{p^{-1} (1-p)^x \lambda^x \exp(-\lambda d_T) - p^{-1} (1-p)^x \lambda^x \exp[-\lambda(d_T + p d_t)]}{L(\lambda, p|\Theta = x, d_x, d_T)}. \end{aligned} \quad (38)$$

It should be noted that the case of A1 when  $x = 0$  is eliminated, because the premise for the existence of the entire posterior probability and the posterior mathematical expectation is that the entire historical information should remain in the new interval  $(d_T, d_{T+t}]$  state at  $d_T$ , and the hyperparameter  $\theta$  must be able to connect with each other.

Because the above results are involved parameters  $\lambda$  and  $p$ , they are still incomplete expressions of random variable  $Y(d_t)$  on posterior mathematical expectation. Therefore, according to Section 2 of model assumptions,  $g(\lambda|r, \alpha) = (\alpha^r \lambda^{r-1} \exp(-\lambda \alpha))/\Gamma(r)$ ,  $\lambda > 0$ , and  $g(p|a, b) = (p^{a-1} (1-p)^{b-1})/B(a, b)$ ,  $0 \leq p \leq 1$ ; further processing, since the probability distribution density of these two parameters is continuous, we can adopt the method of integral and further improve A3 posterior mathematical expectation and add more uncertainty information, especially the hidden information about parameters  $\lambda, p$  that express explicit use of parameter set  $(r, \alpha, a, b)$ :

$$\begin{aligned} E[Y(d_t)|\Theta = x, d_x, d_T, r, \alpha, a, b] &= \int_0^1 \int_0^\infty E[Y(d_t)|\Theta \\ &= x, d_x, d_T, \lambda, p] \cdot g(\lambda, p|\Theta = x, d_x, d_T, r, \alpha, a, b) d\lambda dp, \end{aligned} \quad (39)$$

where  $g(\lambda, p|\Theta = x, d_x, d_T, r, \alpha, a, b)$  is the joint posterior probability distribution density of the parameters  $\lambda, p$ .

According to the basic theory of Bayesian estimation and Bayesian optimization, under the condition that the parameters  $\lambda, p$  is independent, their joint posterior probability distribution density can be expressed in the following complex form:

$$\begin{aligned} g(\lambda, p|\Theta = x, d_x, d_T, r, \alpha, a, b) &= \frac{L(\lambda, p|\Theta = x, d_x, d_T) g(\lambda|r, \alpha) g(p|a, b)}{L(r, \alpha, a, b|\Theta = x, d_x, d_T)}. \end{aligned} \quad (40)$$

By combining the key intermediate variables A5 and A3 in formula A4, the posterior mathematical expectation related to the hyperparameter  $\theta$  can be further deduced:

$$\begin{aligned} E[Y(d_t)|\Theta = x, d_x, d_T, r, \alpha, a, b] &= \frac{A - B}{L(r, \alpha, a, b|\Theta = x, d_x, d_T)}, \end{aligned} \quad (41)$$

where two parameters  $A$  and  $B$ , respectively, represent the following two operation results:

For A,

$$A = \int_0^1 \int_0^\infty p^{-1} (1-p)^x \lambda^x \exp(-\lambda d_T) g(\lambda|r, \alpha) g(p|a, b) d\lambda dp$$

$$= \frac{B(a-1, b+x)}{B(a, b)} \frac{\Gamma(r+x)\alpha^r}{\Gamma(r)(\alpha+d_T)^{r+x}} \quad (42)$$

For B,

$$B = \int_0^1 \int_0^\infty p^{-1} (1-p)^x \lambda^x \exp[-\lambda(d_T + pd_t)]$$

$$g(\lambda|r, \alpha) g(p|a, b) d\lambda dp$$

$$= \int_0^1 \frac{p^{a-2} (1-p)^{b+x-1}}{B(a, b)}$$

$$\left\{ \int_0^\infty \frac{\alpha^r \lambda^{r+x-1} \exp[-\lambda(d_T + pd_t + \alpha)]}{\Gamma(r)} d\lambda \right\} dp$$

$$= \frac{\Gamma(r+x)\alpha^r}{\Gamma(r)B(a, b)} \int_0^1 p^{a-2} (1-p)^{b+x-1} (\alpha + d_T + pd_t)^{-(r+x)} dp. \quad (43)$$

To achieve formal matching with the Gauss hypergeometric function in the form of Euler integral, we need to further realize variable substitution, and let  $q = 1 - p$  and

also make corresponding change  $dp = -dq$  for the differential variable. Further calculation results are as follows:

$$= \frac{\Gamma(r+x)\alpha^r}{\Gamma(r)B(a, b)(\alpha + d_T + d_t)^{r+x}} \cdot \int_0^1 (1-q)^{a-2} (q)^{b+x-1} \left(1 - \frac{d_t q}{\alpha + d_T + d_t}\right)^{-(r+x)} dq. \quad (44)$$

By combining the Gauss hypergeometric function in the form of Euler integral, we get the parameter  $r, b; a + b - 1; (d_t/\alpha + d_t)$ , which corresponds to the corresponding parameter expression in the form of integral function respectively, and we get:

$$= \frac{B(a-1, b+x)}{B(a, b)} \frac{\Gamma(r+x)\alpha^r}{\Gamma(r)(\alpha + d_T + d_t)^{r+x} \cdot 2}$$

$$F_1\left(r+x, b+x; a+b+x-1; \frac{d_t}{\alpha + d_T + d_t}\right). \quad (45)$$

Under the condition of formula A6, according to the mathematical expression formula of  $L(r, \alpha, a, b|\Theta = x, d_x, d_T)$  (6), the middle of the two key variables A7 and A8, after reduction, we can get the ideal result, under the BP/NBD model; the mathematical expectation of overall  $\theta$  hyperparameters under the posteriori probability has analytical solution, and the mathematic expression of the specific is as follows:

$$E[Y(d_t)|\Theta = x, d_x, d_T, r, \alpha, a, b]$$

$$= \frac{(a+b+x-1/a-1)[1 - ((\alpha + d_T)/(\alpha + d_T + d_t))^r {}_2F_1(r+x, b+x; a+b+x-1; (d_t/\alpha + d_T + d_t))]}{1 + I_{x>0}(a/(b+x-1))(\alpha + d_T/\alpha + d_x)^{r+x}} \quad (46)$$

## 4. Experimental Analysis

**4.1. Dataset of an Industry Competition.** The premise of text mining of the entries requires complete project information:

- (1) Most of the projects in the prototype design stage are in the initial stage, and there are some problems such as incomplete application materials. In this mining modeling process, the projects in the prototype design stage are eliminated.
- (2) Projects without declaration materials (project documents) cannot pass the preliminary examination. In this mining modeling process, enterprises without declaration materials will be eliminated.

Finally, 143 project contents are reserved for topic mining, and the case content and project output value are mined separately to extract important information and

explore the application field, current situation, and key points of value promotion of industrial Internet.

The main purpose of using this dataset is to adjust the discrete hyperparameters of the relevant prediction or classification model and compare the differences between the results before and after the adjustment, to form the experimental conclusion.

**4.2. Participle.** Jieba Chinese word segmentation component [10–12] is called, industrial Internet-related special words such as VR, AR, and smart Park are added into Jieba library, and precise mode is used to segment each document by default. In the process of word segmentation, function words and meaningless symbols are removed. To unify the expression of professional vocabulary, a thesaurus is set to merge synonyms to improve the effect of later topic extraction. For example, “artificial intelligence” and “Ai” are synonyms and merged into “Ai.” The unimportant words are

TABLE 1: Confusion matrix.

| Classification        | Forecast positive class | Forecast negative class |
|-----------------------|-------------------------|-------------------------|
| Actual positive class | TP—true positive        | FN—false negative       |
| Actual negative class | FP—false positive       | TN—true negative        |

(1) Accuracy (ACC):  $accuracy = (TP + TN) / (TP + FN + FP + TN)$ , the percentage of the correct results. (2) Precision:  $precision = TP / (TP + FP)$ . In the records with positive prediction, how many are actually positive. (3) Recall rate (recall):  $recall = TP / (TP + FN)$ ; in the actual positive records, how many predictions are positive. (4) F1 score:  $2 / F1 = 1 / precision + 1 / recall$ .

filtered according to the part of speech, and the related words are finally reserved.

**4.3. LDA Topic Extraction.** The generated dictionary and corpus are in accordance with the input format of the model, and the open-source Gensim package [13] is used to construct the topic model and estimate the parameters. The default value of parameter selection is  $a = 0.37$  and  $B = 0.02$ . The optimal topic number  $k$  is determined according to the perplexity of the model. In theory, the  $k$ -nearest neighbor with low confusion degree should be selected, but under the premise of small corpus database capacity, more topics may lead to overfitting phenomenon. Therefore, this time, the number of topics is adjusted by combining the coincidence degree of the visualization results. Finally, the optimal number of topics is 4, the optimal number of output value topics is 2, and there is no coincidence between topics.

**4.4. Basic Model.** According to the results of index analysis and LDA theme mining [14–16], the projects that are in the prototype design stage and lack of application materials are selected to be eliminated. Finally, 143 projects are retained to enter the modeling stage, of which 67.83% can enter the second round. Considering that there are many projects in the preliminary evaluation stage, which are not easily affected by external factors and can better reflect the development trend of current related industries, the paper uses XGBoost and multinomial NB to predict and model the preliminary evaluation results of 2020 related industry competition. The discrete hyperparameter indexes of the correlation model are the highest polynomial degree (multinomial NB) and the number of root nodes (XGBoost).

**4.5. Evaluation Index.** Because of the classification model prediction, the confusion matrix is selected as the basic evaluation index, and the evaluation index is derived from confusion matrix, as given in Table 1.

**4.6. Comparison of Experimental Results.** In this modeling process, the polynomial naive Bayesian model (multinomial NB) and integrated model (XGBoost) are selected as training models (lack of specific mathematical description of the two methods). 70% of the samples are used for model training

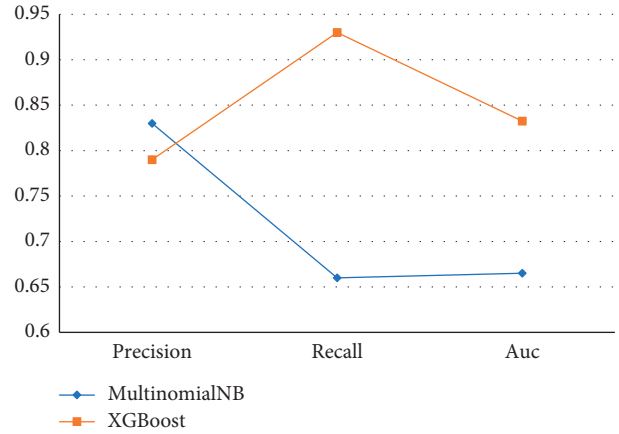


FIGURE 1: Results using original discrete hyperparameters.

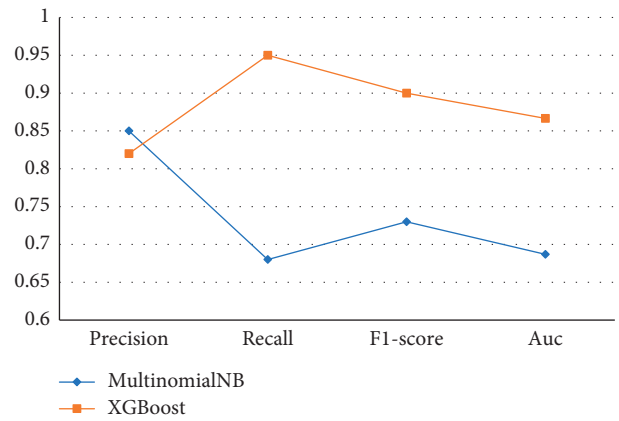


FIGURE 2: Results after adjusting the discrete hyperparameters using the expected results of skew distribution.

and 30% for testing. The parameters are adjusted in the training set dataset combined with threefold cross-validation, and “AUC” is used for training in the parameter adjustment process Figures 1 and 2 show the effect of the model after adjusting the parameters, which has a certain reference value for the actual prediction performance of the model. On the test set, the effect of the model is as follows.

Through the comparison of experiments, we can find that

- (1) From the classification prediction results of the whole model, the final result of XGBoost method is obviously better than the traditional Bayesian model in both the original configuration and the adjusted configuration
- (2) The method of adjusting discrete hyperparameters based on skew distribution is effective. Through the empirical results of data experiments, the overall model, whether XGBoost or Bayesian model, achieves the improvement of relevant evaluation indicators under the new hyperparameter adjustment strategy.

## 5. Conclusion

Through the combination of mathematical analysis and empirical research, this study focuses on the optimization method of the hyperparameters of the relevant machine learning model under the condition of skew distribution, especially the discrete hyperparameters. Through strict mathematical assumptions and mathematical derivation, the expected value of the discrete hyperparameters is obtained, and then, the actual data test is carried out through the empirical dataset. The experimental results show that this heuristic parameter adjustment method is feasible and effective for XGBoost and Bayesian models.

## Data Availability

The data used to support the findings of this study are available from the corresponding author upon request.

## Conflicts of Interest

The author declares that there are no conflicts of interest.

## References

- [1] M. Abramowitz and I. A. Stegun, *Handbook of Mathematical Functions*, Dover Publications, Mineola, NY, USA, 1972.
- [2] D. Bell, J. Deighton, W. J. Reinartz, R. T. Rust, and G. Swartz, "Seven barriers to customer equity management," *Journal of Service Research*, vol. 5, no. 1, pp. 77–85, 2002.
- [3] P. D. Berger and N. I. Nasr, "Customer lifetime value: marketing models and applications," *Journal of Interactive Marketing*, vol. 12, no. 1, pp. 17–30, 1998.
- [4] G. Casella and R. L. Berger, *Statistical Inference*, Duxbury, Pacific Grove, CA, 2nd edition, 2002.
- [5] P. S. Fader, B. G. S. Hardie, and K. L. Lee, "A note on implementing the Pareto/NBD model in MATLAB," 2005, <http://brucehardie.com/notes/008/>.
- [6] P. S. Fader, B. G. S. Hardie, and Ka L. Lee, "RFM and CLV: using iso-value curves for customer base analysis," *Journal of Marketing Research*, vol. 42, no. 4, pp. 415–430, 2005.
- [7] D. Jain and S. S. Singh, "Customer lifetime value research in marketing: a review and future directions," *Journal of Interactive Marketing*, vol. 16, no. 2, pp. 34–46, 2002.
- [8] F. J. Mulhern, "Customer profitability analysis: measurement, concentration, and research directions," *Journal of Interactive Marketing*, vol. 13, no. 1, pp. 25–40, 1999.
- [9] A. M. Mood, F. A. Graybill, and D. C. Boes, *Introduction to the Theory of Statistics*, McGraw-Hill Publishing Company, New York, NY, USA, 1974.
- [10] D. C. Schmittlein, D. G. Morrison, and R. Colombo, "Counting your customers: who-are they and what will they do next?" *Management Science*, vol. 33, no. 1, pp. 1–24, 1987.
- [11] I. Guyon, K. Bennett, G. Cawley et al., "Design of the 2015 ChaLearn AutoML challenge," in *Proceedings of the 2015 International Joint Conference on Neural Networks (IJCNN)*, Killarney, Ireland, July 2015.
- [12] C. Wang, X. Wang, J. Zhang et al., "Uncertainty estimation for stereo matching based on evidential deep learning," *Pattern Recognition*, vol. 124, Article ID 108498, 2021.
- [13] E. Mulholland, P. M. Kevitt, T. Lunney, J. Farren, and J. Wilson, "360-MAM-Affect: sentiment analysis with the google prediction API and EmoSenticNet," in *Proceedings of the International Conference on Intelligent Technologies for Interactive Entertainment*, IEEE Computer Society, Turin, Italy, June 2015.
- [14] G. Luo, B. L. Stone, M. D. Johnson, and F. L. Nkoy, "Predicting appropriate admission of bronchiolitis patients in the emergency department: rationale and methods," *JMIR Research Protocols*, vol. 5, no. 1, p. e41, 2016.
- [15] X. Ning, K. Gong, W. Li, and L. Zhang, "JWSAA: joint weak saliency and attention aware for person re-identification," *Neurocomputing*, vol. 453, pp. 801–811, 2021.
- [16] G. Luo, "Automatically explaining machine learning prediction results: a demonstration on type 2 diabetes risk prediction," *Health Information Science and Systems*, vol. 4, no. 1, p. 2, 2016.



## Research Article

# Construction of Alumni Information Analysis Model Based on Big Data

**Xue Wang** 

*Foreign Language Department, Shanghai Xingjian College, Shanghai 200072, China*

Correspondence should be addressed to Xue Wang; wangxue6636@163.com

Received 25 May 2022; Revised 27 June 2022; Accepted 2 July 2022; Published 9 August 2022

Academic Editor: Man Fai Leung

Copyright © 2022 Xue Wang. This is an open access article distributed under the Creative Commons Attribution License, which permits unrestricted use, distribution, and reproduction in any medium, provided the original work is properly cited.

In order to integrate and utilize alumni resources in a better way, big data is utilized to construct alumni information analysis model based on improved hierarchical clustering algorithm, so as to realize mining and retrieval of alumni information. First, the basic principle of hierarchical clustering algorithm is analyzed concretely. Moreover, the improvement is performed on this basis, and a method of calculating the distance between class clusters based on the ant colony optimization is proposed, which uses the shortest distance of the ant colony algorithm to optimally solve the distance between hierarchical class clusters, so as to improve the clustering accuracy. Then, the alumni information analysis model based on improved hierarchical clustering algorithm is constructed, and the model is divided into text preprocessing, keyword extraction, text feature vector generation, name disambiguation, and alumni recognition modules. Finally, the improved hierarchical clustering algorithm and construction of model are verified by experiments. The results show that the accuracy of the improved agglomerative hierarchical clustering algorithm is as high as 86.4% on average and 3.8% and 4.8% more than the two traditional algorithms. Thus, the clustering effect of the algorithm is better, and the proposed alumni analysis model can effectively process text disambiguation of web pages and identification of alumni information, which has certain effectiveness.

## 1. Related Work

For school, alumni resources are the favorable support and key to school development and construction. The effective integration and tracking of alumni information plays a crucial role for schools. For example, schools can evaluate teaching quality according to the alumni information, so as to continuously improve and perfect their teaching methods and concepts. Furthermore, the latest trends of alumni may be able to provide support and help for the development and construction of school. Therefore, it is necessary for school to manage alumni resources and information effectively. However, there are so many graduates, that it seems impractical to keep track of every alumni.

In recent years, with the development and application of big data and Internet, it has become possible to obtain alumni information and update it in real time. At the same time, the Internet information is very large, so how to accurately identify alumni-related information is the

current challenge. In addition, how to quickly and accurately identify alumni information from many pieces of information and exclude the people with the same name to obtain the final target is the current urgent problem to be solved. Barnea Avner et al. constructed an emergency intelligence analysis model based on big data and utilized big data analysis technology to analyze and predict various emergencies in advance, which has certain effectiveness [1–3]. Li Hong et al. studied the information analysis model based on complex network deeply and then used Internet technology to classify and identify complex information on the network. Thus, the accuracy of information analysis is improved [4–6]. Jiho Lee et al. proposed a hierarchical clustering analysis algorithm to construct a learner emotion analysis model for learning experience text and classified learners through hierarchies. Thus, the emotion analysis of each learner is realized [7, 8]. Agnivesh et al. applied clustering algorithm to data classification, which showed good performance and effect

[9]. Ko applied big data to the parallel improvement of clustering and concluded that clustering can be used in massive data classification [10]. On this basis, taking the alumni information in the school campus network as the basic data, and combined with the above research results, the current widely used hierarchical clustering method is improved and applied to analyze the alumni resources information; thus, the corresponding analysis model is constructed, which realizes the accurate identification and classification of alumni resources, so as to provide technical reference and research direction for the analysis of alumni information.

## 2. Basic Methods

**2.1. Hierarchical Clustering Algorithm.** Hierarchical clustering algorithm is one of the common algorithms in clustering algorithm, and its basic principle is clustering through the distance between objects [11]. This algorithm can also be called tree clustering, which is mainly divided into two forms of agglomeration and split.

Among them, agglomerative clustering means to calculate the distance between class clusters and merge its various categories. The clustering form is bottom-up. Multiple iterations and merges are carried out on a cluster. When all the data are concentrated in one cluster and the set standard is reached, the calculation can be completed [12]. The basic principle is shown in Figure 1.

The clustering form of split cluster is opposite to that of agglomerative clustering, and its split form is top-down. New clusters are obtained by repeatedly decomposing a data set.

In hierarchical clustering, each cluster is classified by evaluation criteria and usually by means of distance between points and distance between class clusters [13]. The calculation formulas of the two methods are as follows.

**2.1.1. Calculation Method of the Distance between Points.** If there are two  $n$ -dimensional vector data points  $A, B$ ,  $A = \{A_1, A_2, \dots, A_n\}$  and  $B = \{B_1, B_2, \dots, B_n\}$ , then the distance between the two points can be calculated by cosine similarity, that is, to figure out the cosine value of the included angle [14]. The calculation formula is as follows:

$$\cos\theta = \frac{\sum_{i=1}^n A_i \cdot B_i}{\sqrt{\sum_{i=1}^n A_i^2} \sqrt{\sum_{i=1}^n B_i^2}} \quad (1)$$

Euclidean distance can measure the absolute distance between two vectors. The solution formula is as follows:

$$d(A, B) = \sqrt{\sum_{i=1}^n (A_i - B_i)^2} \quad (2)$$

**2.1.2. Measuring the Distance between Class Clusters.** At present, clustering is mainly achieved by calculating the distance between class clusters. The common method for

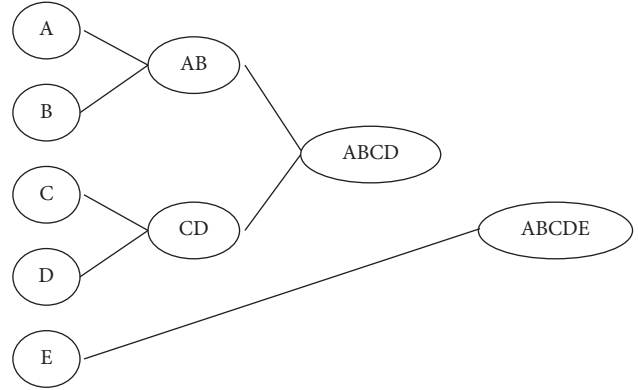


FIGURE 1: Clustering principle of agglomerative hierarchical clustering algorithm.

measuring the distance is to solve the minimum, maximum, average value, and average distance of class clusters, which are shown in formulas (3–6):

$$d_{\min}(c_i, c_j) = \min\|p_i - p_j\|, \quad (3)$$

$$d_{\max}(c_i, c_j) = \max\|p_i - p_j\|. \quad (4)$$

Here,  $(p_i \in c_i, p_j \in c_j)$ .

$$d_{\text{mean}}(c_i, c_j) = \max\|m_i - n_j\|, \quad (5)$$

where  $m_i, n_j$  and  $m_i, n_j$  are the centroids of  $c_i, c_j$  and  $c_i, c_j$ , respectively.

$$d_{\text{avg}}(c_i, c_j) = \frac{1}{n_i n_j} \sum \sum \|p_i - p_j\|, \quad (6)$$

where  $(p_i \in c_i, p_j \in c_j)$ ,  $n_i, n_j$ , and  $n_i, n_j$  are the sample numbers of class  $c_i, c_j$  and  $c_i, c_j$ , respectively.

**2.2. Algorithm Improvement.** The traditional hierarchical clustering algorithm is simple, and the accuracy of distance calculation is not high, which is easy to be interfered by outliers in the class cluster. Therefore, to better represent the distance between clusters, avoid interference, and improve the clustering effect, the ant colony optimization algorithm is added to the agglomerative hierarchical algorithm. Based on the pheromone characteristics of the ant colony optimization algorithm, the optimal path is solved, so as to improve the clustering accuracy and achieve global optimization [15].

**2.2.1. Ant Colony Optimization Algorithm.** The basic principle of the ant colony optimization is global search, and it is an intelligent optimization algorithm. Simulating real ant behavior, the algorithm is constantly improved and optimized to identify the direction through pheromone concentration, so as to find the optimal path and achieve global optimization [16].

The ant colony optimization algorithm can also be called traveling salesman problem (TSP). If there are  $n$  cities, TSP will implement the algorithm.

- (1) When the ant colony reaches  $n$  cities, ants will update pheromones in the path, and the update formulas are as follows:

$$\begin{aligned} \tau_{ij}(t+n) &= \rho^* \tau_{ij}(t) + \Delta\tau_{ij} \\ &= \sum_{k=1}^m \Delta\tau_{ij}^k, \\ \Delta\tau_{ij}^k &= \frac{Q}{L_k}, \end{aligned} \quad (7)$$

where  $m$  represents the total number of ants and  $Q$  represents the constant.  $\rho < 1$ ,  $L_k$  is the distance between two points;  $\tau_{ij}(t)$  represents the pheromone on edge  $(i, j)$  at time  $t$ ;  $\Delta\tau_{ij}^k$  is the pheromone quantity generated by ant  $k$  on edge  $(i, j)$  between time  $t$  and  $t+n$  [17].

- (2) The ant colony cannot return to the previous city until it reaches  $n$  cities.
- (3) The ant colony starts from a certain point, and the probability of selecting the next target is

$$p_{ij}^k(t) = \frac{[\tau_{ij}(t)]^{\alpha} [\eta_{ij}(t)]^{\beta}}{\sum [\tau_{ij}(t)]^{\alpha} [\eta_{ij}(t)]^{\beta}} j \in T_k, \quad (8)$$

where  $T_k$  is the city that ants can choose;  $\eta_{ij}$  is the heuristic information;  $\alpha$  is the relative importance of pheromone heuristic factor; and  $\beta$  is the relative importance of heuristic information.

### 2.2.2. Agglomerative Hierarchical Clustering Algorithm Based on the Ant Colony Optimization

- (1) *Standard Distance.* Euclidean distance is used to figure out the distance between two data points, and the solution formula is as follows:

$$\begin{aligned} d_{ij} &= \sqrt{(x_{i1} - x_{j1})^2 + \dots + (x_{im} - x_{jm})^2}, \\ x_i &= (x_{i1}, \dots, x_{im}), \\ x_j &= (x_{j1}, \dots, x_{jm}), \end{aligned} \quad (9)$$

where  $x_i$  and  $x_j$  represent two  $m$ -dimensional data points.

The similarity can be measured by calculating the distance between two clusters, and the distance between clusters can be calculated by the minimum distance formula (3) in agglomerative hierarchical clustering.

- (2) *Objective Function.* Objective function is set as the clustering error square sum (suppose there are  $c$  clustering centers after clustering is completed):

$$E = \sum_{l=1}^c \sum_{x_i \in c_j} x_i - c_l^2, c_j = \frac{1}{m_j} \sum_{i=1}^{m_j} x_i, \quad (10)$$

where  $C_j$  represents the centroid, which is calculated by a specific cluster  $j$  and  $m_j$  represents the amount of data in the cluster.

- (3) *Agglomerative Hierarchical Clustering Based on the Ant Colony Optimization.* The objective of this algorithm is to find a shortest path in all the data to improve the clustering efficiency and accuracy. Utilizing the ant optimization, ants are taken as the research object, and food is taken as the clustering center. The probability of ants searching food is put into the clustering algorithm, and data are classified by probability [18].

There are six steps improving algorithm, and the specific steps are as follows.

It can be seen from Figure 2 that the process of improving algorithm is mainly divided into six steps, which are as follows:

- (1) Initialize parameters, such as the number of ants  $m$ , weight parameter  $\alpha$ , and volatile factor  $\rho$ .
- (2) Set an ant as  $m$ , calculate the distance and pheromone between data points, evaluate the transition probability, and determine the merger probability between data points and alternative points. The merger probability formula is as follows:

$$p_{ij}^m = \frac{(\tau_{ij})^{\alpha} (\eta_{ij})^{\beta}}{\sum_i \bullet N_i^m (\tau_{il})^{\alpha} (\eta_{il})^{\beta}} J \in N_j^m \eta_{ij} = \frac{\pm}{d_{il}}, \quad (11)$$

where  $d_{ij}$  is the distance between two data points;  $\eta_{ij}$  is the distance-based heuristic information; and  $\alpha$  and  $\beta$  are weight parameters, which have a great influence on pheromones [19].

If  $p_{ij}^m \geq p_0$ ,  $x_j$  merges with  $x_i$ ; otherwise, there is no merger.

- (3) Judge whether the number of ants  $k$  reaches the total number of ants; if not, set  $k = k + 1$ , and go back to Step (2) for calculation.
- (4) After ants complete clustering, the clustering center and pheromone will be updated, where the expression of clustering center is

$$c_j = \frac{1}{m_j} \sum_{i=1}^{m_j} x_i, \quad (12)$$

where  $m_j$  is the total amount of data points classified in  $c_j$ .

In the process of optimization, the pheromone concentrations in the paths passed by ant are different [20]. After clustering, ants' pheromones will constantly evaporate, and the evaporation formula can be expressed as follows:

$$\tau_{ij} = (1 - \rho)\tau_{ij}, \quad (13)$$

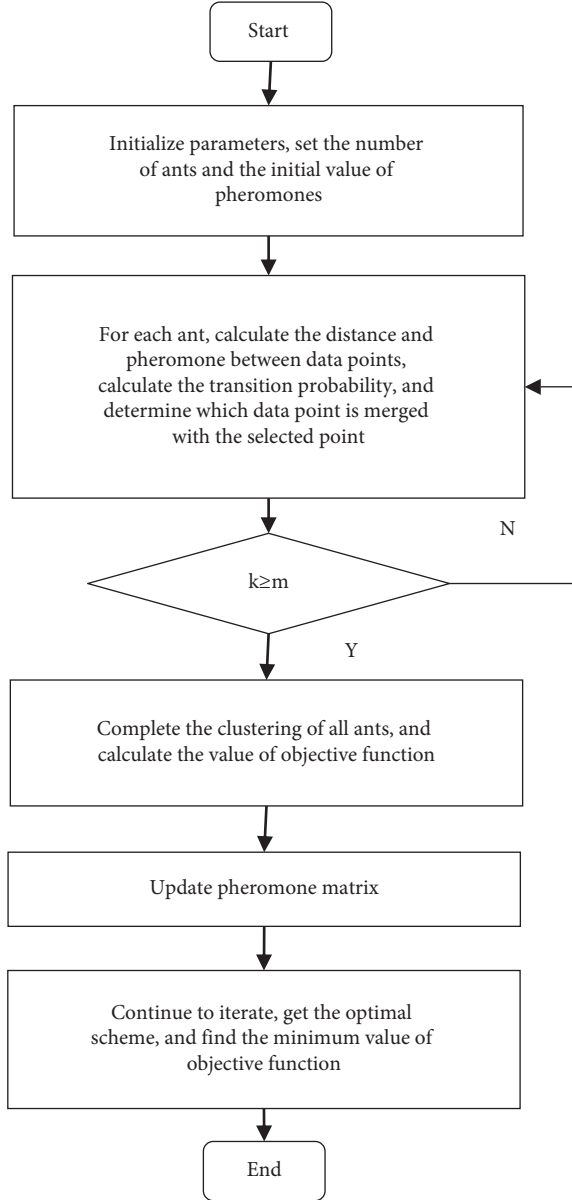


FIGURE 2: Flow chart of improving algorithm.

where  $\rho$  represents pheromone evaporation rate. When  $0 < \rho \leq 1$ , it can enable the algorithm to delete long paths and avoid pheromone accumulation.

After completing evaporation, all ants will leave pheromones again:

$$\tau_{ij} = \tau_{ij} + \sum_{k=1}^m \Delta\tau_{ij}^k, \quad (14)$$

where  $\Delta\tau_{ij}^k$  represents the amount of information from data  $x_i$  to class cluster  $c_j$  of the  $k$ th ant.

$$\Delta\tau_{ij}^k = \frac{1}{d(x_i, c_j)}. \quad (15)$$

- (5) Figure out the solution of objective function.
- (6) Return to steps (2)–(4) until the minimum target is calculated, and then the calculation can be completed.

### 3. Model Construction

**3.1. Design of the Alumni Recognition Model Based on Improved Algorithm.** There are too much alumni information on the Internet. The structure of the web page is complex, and the data format is not standard, which means that it is difficult to extract features of alumni information and fail to accurately identify alumni information. Therefore, an alumni recognition model based on the improved agglomerative hierarchical clustering algorithm is proposed, which is shown in Figure 3. Firstly, alumni information is collected and preprocessed. Secondly, text features are extracted by embedding technology. Moreover, text representation model and feature vector are constructed. Finally, name disambiguation and alumni identification are carried out. Thus alumni information analysis is realized.

As can be seen, alumni information identification process is mainly divided into six steps, as follows:

- (1) Classify the text data and name entity recognition
- (2) Filter stop words and delete useless interjections, modal particle, personal pronouns, and so on [21]
- (3) Extract keywords and use TF-IDF algorithm to select key information
- (4) For text representation, use the word embedding tool to complete the word embedding of keywords and obtain the vectorization expression of keywords
- (5) For text clustering, adopt cosine similarity calculation method to cluster document vector
- (6) Analyze clustering results

**3.2. Data Collection and Preprocessing.** To perform the data collection and preprocessing, the first step is to collect the web page documents, and the original alumni data are collected by using the Python programming of Baidu's search engine API. The second step is to specify a person's name as a search term for the web page retrieval; thus, the web document is obtained and it is stored in a local folder. Then, the web page file is processed by the Python programming, and the web page information is extracted. Furthermore, the text content is extracted by regular expression. The specific work includes tag attribute extraction, tag filtering, and character filtering [22].

**3.3. Text Feature Extraction.** The python package pynlpir based on mlpir natural language processing system of Chinese Academy of Sciences is utilized to annotate text sequences and complete text classification.

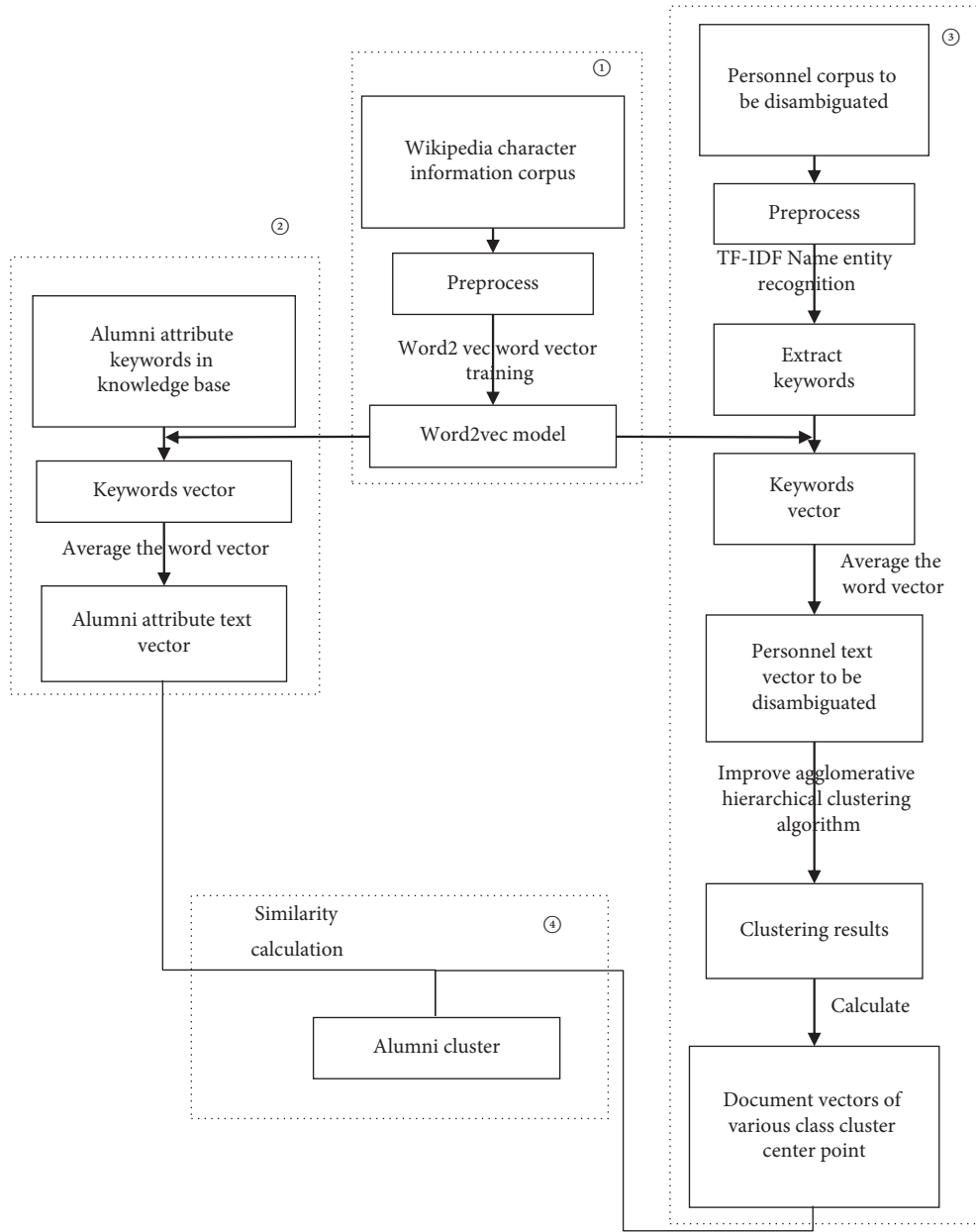


FIGURE 3: Alumni recognition model based on improved agglomerative hierarchical clustering algorithm.

The TF-IDF algorithm is used to extract keywords, each information is named, and its entity is taken as the final text keyword. The algorithm flow is in Figure 4.

The TF-IDF algorithm is used to calculate word frequency of text and inverse document frequency; thus, TF-IDF value is obtained to measure the importance of words. The solution formula is as follows:

$$tf - idf = tf * idf, \tag{16}$$

where  $tf$  (text frequency) represents the occurrence frequency of words in the document, and the solution formula is as follows:

$$tf_{i,j} = \frac{n_{ij}}{\sum_k n_{k,j}}, \tag{17}$$

where  $n_{ij}$  is the number of occurrences of word  $i$  in document  $j$ ;  $\sum_k n_{k,j}$  is the sum of occurrences of all words in document  $j$ ; and IDF (inverse document frequency) indicates the rarity of the word in the document, namely, the importance of the word. The expression is as follows:

$$idf_i = \lg \frac{|D|}{|\{j: c_i \in d_j\}|}. \tag{18}$$

Here,  $|D|$  is the number of all documents in the corpus and  $|\{j: c_i \in d_j\}|$  is the number of documents containing word  $c_i$ .

### 3.4. Construction of Text Representation Model and Feature Vector

**3.4.1. Construction of Word2Vec Text Representation Model.** Before classifying text, it is necessary to select an appropriate model to represent text. The quality of text representation has a great influence on the text clustering result. However, many text models are deficient in information and incomplete, which leads to poor clustering effect in the later stage. Therefore, word embedding model is used to represent text content, so as to improve the effect of text clustering.

Word embedding model improves text quality by transforming text dimensions and filling in missing information. On this basis, Skip-gram, which has a good application effect at present, is used to train model and generate word vector.

**3.4.2. Construction of Text Feature Vector.** The construction process of text feature vector is shown in Figure 5. The first step is to use trained Word2Vec model to generate word vector. The second step is to find the average value of keywords; thus, the text feature vector is obtained.

If there are  $n$  keywords in the text, the text representation model  $d = \{c_1, c_2, \dots, c_n\}$ , and the word vector  $v(c_i)$  can be obtained by training. Thus, the feature vector expression of document is

$$v(d) = \frac{1}{n} \sum_{i=1}^n v(c_i), \quad (19)$$

where  $v(d)$  is the feature vector representation of a document and  $v(c_i)$  is the word vector of the  $i$ th feature word  $c_i$ , namely, the average value of sum of the document vector and all the keyword vectors.

The personnel text feature vector to be disambiguated and the text vector of alumni attribute in the knowledge base can be obtained by the above model.

**3.5. Name Disambiguation and Alumni Identification.** Using text feature vector, text is clustered based on the improved agglomerative hierarchical clustering algorithm. Through clustering, people with the same name is distinguished, and the texts related to the same person are divided into the same category, which achieves name disambiguation. Then, the knowledge base information is used to assist identification to find the class cluster to which a specific person belongs, so as to realize the information identification of specific person. The disambiguation process is shown in Figure 6.

The improved condensed hierarchical clustering algorithm proposed in this paper is utilized to cluster text information, and the central point of each cluster is figured out. The calculation formula is shown in formula (22) [23–27]:

$$v(C_i) = \frac{1}{m} \sum_{j=1}^m v(d)_j, \quad (20)$$

where  $v(C_i)$  represents the feature vector of the center point of the  $C_i$ th class cluster;  $m$  represents the number of data points in class cluster  $C_i$ ; and  $v(d)_j$  represents the feature vector of the  $j$ th data point.

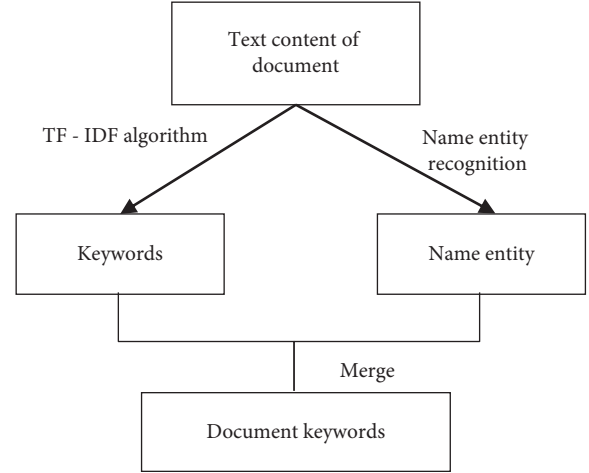


FIGURE 4: Keyword extraction process.

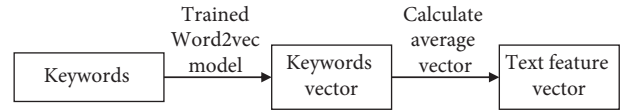


FIGURE 5: Construction process of text feature vector.

Comparing the similarity between the feature vector of center point of the class cluster and the feature vector of target personnel information constructed based on the knowledge base and if the similarity is greater than threshold value, the target personnel class cluster can be obtained, namely, relevant web page text information of the target person.

## 4. Experimental Results and Analysis

**4.1. Experimental Data.** To verify the effectiveness of the improved method, there are 8000 text corpus about sports, government, commerce, culture and scientific research obtained from the Python web crawler as experimental data, and the data set D1 and D2 of alumni with the same name are divided into 5000 training sets and 3000 testing sets.

**4.2. Experimental Environment and Parameter Setting.** To obtain better experimental results, the experimental processor is the 9th generation of Intel core i5, and the operating system is windows 64-bit. In addition, cas NLPiR word segmentation system and python language are adopted in the experiment.

The parameter value setting of the algorithm is shown in Table 1.

**4.3. Evaluation Indicators.** To evaluate the experiment more objectively, accuracy, recall rate, and F1 value are adopted as evaluation indicators. The accuracy is the ratio of correct number to total number, and the recall rate is the ratio of correct number to real number of texts. The expression of accuracy and recall rate is as follows:

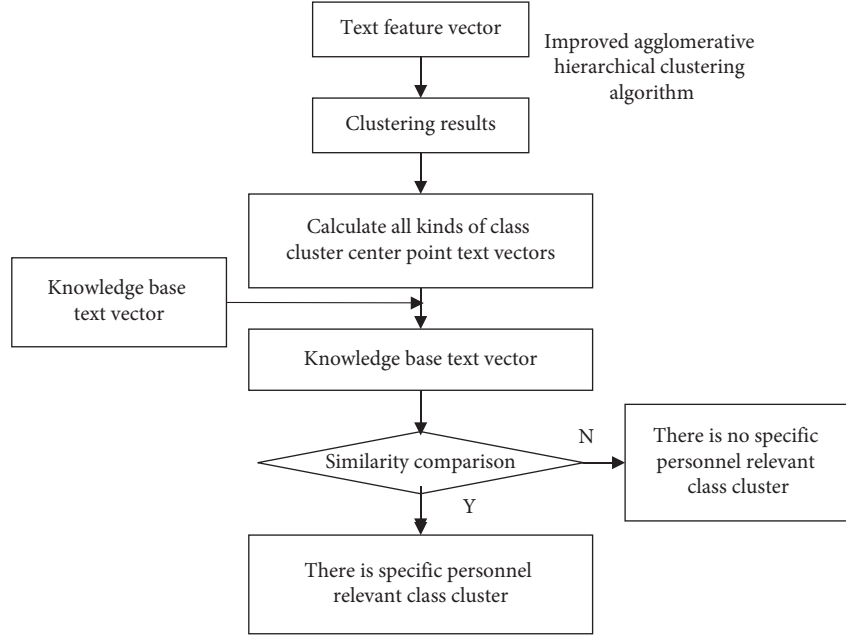


FIGURE 6: Name disambiguation process.

TABLE 1: Experimental parameter setting.

| Parameter                 | Parameter value        |
|---------------------------|------------------------|
| Number of ants            | $m = 7$                |
| Pheromone volatile factor | $p = 0.8$              |
| Weight parameters         | $\alpha = \beta = 0.5$ |
| Merger probability        | $P_0 = 0.6$            |

$$\text{precision} = \frac{a}{a + b}, \quad (21)$$

$$\text{recall} = \frac{a}{a + c}, \quad (22)$$

where precision represents accuracy; recall stands for recall rate;  $a$  is the number of text correctly identified by algorithm;  $b$  is the number of text incorrectly identified by algorithm; and  $c$  is the number of text belonging to a certain category that algorithm does not recognize.

$F_1$  value is the comprehensive analysis standard of the clustering algorithm. The higher the value of  $F_1$  is, the better the clustering effect of algorithm is. Formula of  $F_1$  value is as follows:

$$F_1 = 2 \times \frac{\text{precision} \times \text{recall}}{(\text{precision} + \text{recall})}. \quad (23)$$

**4.4. Improved Algorithm.** To test the effectiveness of the proposed improved algorithm, the experiment compares the algorithm before and after improvement with the K-means algorithm. The experimental results are shown in Table 2.

It can be seen from Table 2 that the accuracy of the improved algorithm is 84.2% and 85.6% in D1 and D2 data sets, respectively, which is higher compared to the accuracy of the algorithm before improved and the traditional

clustering algorithm, which indicates that the improved algorithm proposed in the paper is effective.

To test the performance of the improved algorithm, the comparison curves of accuracy, recall rate, and  $F_1$  value of the three algorithms are as follows.

As can be seen from Figure 7, the highest accuracy of the improved algorithm is 89% and the average rate is 86.4%, which are higher compared to those of the other two algorithms by 3.8% and 4.5% respectively, which means that adding the ant colony optimization algorithm can improve the clustering accuracy.

As can be seen from Figures 8 and 9, the highest recall rate of the improved algorithm is 89% and the average rate is 86.5%, which are 3% and 3.5% higher compared to those of the other two algorithms. The  $F_1$  value of the improved algorithm is as high as 88% and as low as 86%, which is obviously higher compared to that of the other two algorithms. Thus, the improved algorithm has better effect on text classification and better algorithm performance.

**4.5. Alumni Recognition Model Based on the Improved Algorithm.** To verify the validity of the constructed alumni information recognition and analysis model, there are 5 alumni information selected from the above data set for experimental verification. The Word2Vec tool is adopted to train word vector, and the hyperparameter settings of the model during training are in Table 3.

After name disambiguation and recognition are performed by the alumni information recognition model, the statistical results obtained are shown in Table 4.

As can be seen from Table 4, using this model to identify and classify 5 alumni, alumni with the same name is accurately distinguished, name disambiguation is realized, and the class cluster of 5 alumni is also accurately

TABLE 2: Comparison results of the accuracy of the three algorithms.

| Data set | Number of samples | Agglomerative hierarchical clustering [28] (%) | K-means (%) | The proposed algorithm (%) |
|----------|-------------------|--|-------------|----------------------------|
| D1       | 4000              | 76.3   | 79.4        | 84.2                       |
| D2       | 4000              | 78.7   | 80.1        | 85.6                       |

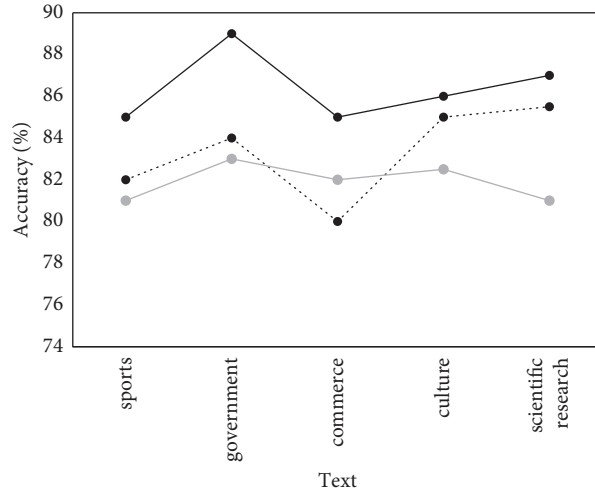


FIGURE 7: Algorithm accuracy.

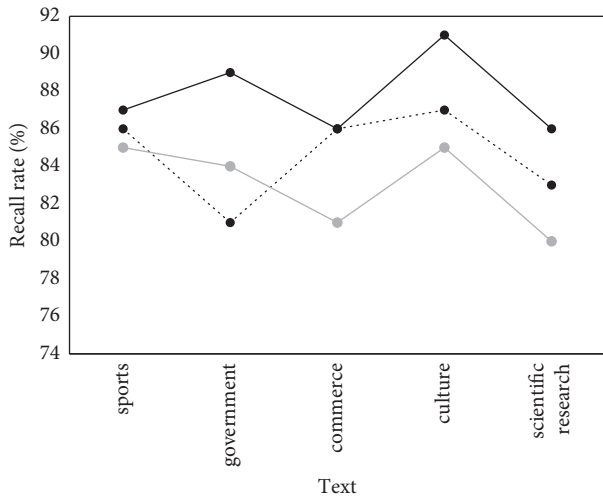


FIGURE 8: Recall rate of algorithm.

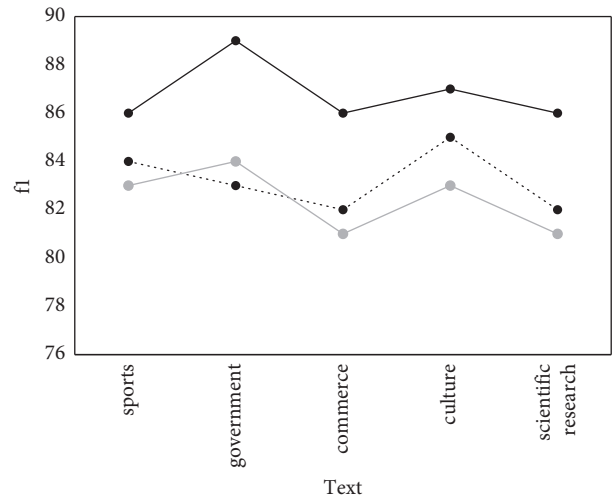


FIGURE 9: F1 value of algorithm.



TABLE 3: Hyperparameter settings.

| Hyperparameter nam | Hyperparameter description                 | Hyperparameter values |
|--------------------|--|-----------------------|
| Size               | Adjust the dimension of word vector        | 100                   |
| Min-count          | Adjust the minimum frequency value of word | 2                     |
| cbow_mean          | Select the training model                  | 1                     |
| Window             | Adjust the size of context window          | 5                     |
| Worker             | Adjust the number of computing cores       | 10                    |

TABLE 4: Statistical table of clustering results.

| Personnel | Number of class clusters | Class clusters of alumni |
|-----------|--------------------------|--------------------------|
| Alumni 1  | 22                       | 3                        |
| Alumni 2  | 6                        | 5                        |
| Alumni 3  | 13                       | 7                        |
| Alumni 4  | 34                       | 26                       |
| Alumni 5  | 11                       | 11                       |

located. Thus, alumni information identification is realized, which shows that the constructed recognition model is feasible.

## 5. Conclusion

The proposed ant colony optimization clustering algorithm can achieve accurate clustering of alumni information, and the clustering effect is good. Moreover, the constructed model can disambiguate alumni name information and improve the accuracy of alumni information identification. The results show that the improved agglomerative hierarchical clustering algorithm has higher recognition accuracy, recall rate, and F1 value compared to traditional agglomerative hierarchical clustering algorithm and K-means algorithm. The corresponding average rates are 86.4%, 86.5%, and 87%, which shows that adding the ant colony algorithm into traditional agglomerative hierarchical clustering algorithm can figure out the optimal solution. Applying the modified algorithm to the alumni analysis model can further improve the recognition accuracy and clustering effect, which makes the model be extended and applied in the field of alumni analysis. The contribution of this study is to improve hierarchical clustering by using the ant colony algorithm; thus, the accuracy of massive data classification is improved. This method is applied to the analysis of alumni information, which provides a reference for the extension of informatization in various fields.

However, due to the lack of experimental conditions and research experience, there are still certain limitations. The future research is to improve the execution efficiency of the improved hierarchical clustering algorithm, so as to complete text data clustering and analysis in a shorter time.

## Data Availability

The experimental data used to support the findings of this study are available from the corresponding author upon request.

## Conflicts of Interest

The author declares that there are no conflicts of interest regarding this work.

## Acknowledgments

This study was supported by Research Project on the Work of the Communist Youth League in Shanghai Schools in 2020, the Research on Tracking Service Mechanism of the Student Leaders after Graduate by Searching the Past Ones, taking Shanghai Xingjian College as an example, Project Approval No. 2020YB116.

## References

- [1] B. Meshulach and M. Avi, "Forecasting for intelligence analysis: scenarios to abort strategic surprise," *International Journal of Intelligence & Counter Intelligence*, vol. 34, no. 1, pp. 106–133, 2021.
- [2] S. José Ramón and R. Dag, "A three-stage method for data text mining: using UGC in business intelligence analysis," *Symmetry*, vol. 11, no. 4, p. 519, 2019.
- [3] C. Zhang, "User multi-modal emotional intelligence analysis method based on deep learning in social network big data environment," *IEEE Access*, vol. 7, pp. 181758–181766, 2019.
- [4] Li Hong, Z. Chen, and Q. Guo, "The evolution and approaches of information analysis service of university libraries in China," *Science & Technology Libraries*, vol. 40, no. 1, pp. 52–64, 2021.
- [5] B. Azeddine, M. A. Qureshi, S. A. Amirshahi, A. Chetouani, and M. Pedersen, "A critical analysis on perceptual contrast and its use in visual information analysis and processing," *IEEE Access*, vol. 8, pp. 156929–156953, 2020.
- [6] W. Zhang, K. Yang, and X. Guo, "Design and implementation of the pedestrian information analysis system," *IOP Conference Series: Materials Science and Engineering*, vol. 439, no. 3, 2018.
- [7] J. Lee, H. S. Yang, H. Jeong, J. H. Kim, and H. Yang, "Targeted isolation of lignans from *Trachelospermum asiaticum* using molecular networking and hierarchical clustering analysis," *Biomolecules*, vol. 10, no. 3, p. 378, 2020.
- [8] H. A. H. Naji, Q. Xue, K. Zheng, and N. Lyu, "Investigating the significant individual historical factors of driving risk using hierarchical clustering analysis and quasi-Poisson regression model," *Sensors*, vol. 20, no. 8, p. 2331, 2020.
- [9] A. Agnivesh, R. Pandey, and A. Singh, "Improved K-means map reduce algorithm for big data cluster Analysis[J]," *International Journal of Innovative Technology and Exploring Engineering*, vol. 8, no. 8, pp. 1796–1802, 2019.

- [10] S. Ko, "Predicting learning achievement using big data cluster Analysis: focusing on longitudinal study," *Journal of Digital Contents Society*, vol. 19, no. 9, pp. 1769–1778, 2018.
- [11] S. Balakrishna, M. Thirumaran, R. Padmanaban, and V. K. Solanki, "An efficient incremental clustering based improved K-Medoids for IoT multivariate data cluster analysis," *Peer-to-Peer Networking and Applications*, vol. 13, no. prepublsh, pp. 1–24, 2019.
- [12] F. Nan, Y. Li, X. Jia, L. Dong, and Y. Chen, "Application of improved SOM network in gene data cluster analysis," *Measurement*, vol. 145, pp. 370–378, 2019.
- [13] Y. Wang, "Application of ant colony algorithm and artificial intelligence in training simulation of athletes in sports arena," *Journal of Ambient Intelligence and Humanized Computing*, pp. 1–10, 2021.
- [14] L. Niu and L. Xiong, "Optimisation and application research of ant colony algorithm in vehicle routing problem," *International Journal of Computing Science and Mathematics*, vol. 13, no. 2, 2021.
- [15] Y. Lin and Lu Han, "Diagnosis strategy design method based on ant colony algorithm," *Journal of Physics: Conference Series*, vol. 1894, no. 1, 2021.
- [16] J. Ge, D. Yu, and Y. Fang, "Multi-dimensional QoS cloud computing task scheduling strategy based on improved ant colony algorithm," *Journal of Physics: Conference Series*, vol. 1848, no. 1, 2021.
- [17] X. Tian, L. Li, L. Shuang, D. Zhiping, and P. Ming, "Path planning of mobile robot based on improved ant colony algorithm for logistics," *Mathematical biosciences and engineering: MBE*, vol. 18, no. 4, pp. 3034–3045, 2021.
- [18] K. Bilal, K. Ali, and A. Yassine, "Open capacitated ARC routing problem by hybridized ant colony algorithm," *RAIRO - Operations Research*, vol. 55, no. 2, pp. 639–652, 2021.
- [19] M. Khodabandeh, M. Ghassabzadeh Saryazdi, and A. Ohadi, "Multi-objective optimization of auto-body fixture layout based on an ant colony algorithm," *Proceedings of the Institution of Mechanical Engineers - Part C: Journal of Mechanical Engineering Science*, vol. 234, no. 6, pp. 1137–1145, 2020.
- [20] X. Wang, H. Li, J. Yang, C. Yang, and H. Gui, "Optimal path selection for logistics transportation based on an improved ant colony algorithm," *International Journal of Embedded Systems*, vol. 13, no. 2, 2020.
- [21] J. X. Liu, T. Z. Huang, and X. i. Duan, "Application of improved ant colony algorithm in optimal planning of dynamic distribution network," *Journal of Physics: Conference Series*, vol. 1533, no. 3, 2020.
- [22] L. i. Xiao, J. Wei Yang, and L. i. Nai Qian, "Multi-feature fusion energy-saving routing in internet of things based on hybrid ant colony algorithm," *International Journal of Innovative Computing and Applications*, vol. 11, no. 2-3, pp. 103–108, 2020.
- [23] P. Praveen, M. R. Kumar, M. A. Shaik, R. Ravikumar, and R. Kiran, "The comparative study on agglomerative hierarchical clustering using numerical data," *IOP Conference Series: Materials Science and Engineering*, vol. 981, no. 2, Article ID 022071, 2020.
- [24] P. Shi and Z. Zhao, H. Zhong, H. Shen, and L. Ding, "An improved agglomerative hierarchical clustering anomaly detection method for scientific data," *Concurrency and Computation: Practice and Experience*, vol. 33, no. 6, 2020.
- [25] S. Lim, "Sequential batching with minimum quantity commitment in N-level non-exclusive agglomerative hierarchical clustering structures," *International Journal of Industrial Engineering Computations*, vol. 11, no. 3, pp. 317–340, 2020.
- [26] X. Cai and Q. Wang, "Educational tool and active-learning class Activity for teaching agglomerative hierarchical clustering," *Journal of Statistics Education*, vol. 28, no. 3, pp. 1–15, 2020.
- [27] S. Saurabh and S. Gautam, "Modelling and statistical analysis of YouTube's educational videos: a channel Owner's perspective," *Computers & Education*, vol. 128, pp. 145–158, 2019.
- [28] P. Garikapati, K. Balamurugan, T. P. Latchoumi, and R. Malkapuram, "A cluster-profile comparative study on machining AlSi 7/63% of SiC hybrid composite using agglomerative hierarchical clustering and K-means," *Silicon*, vol. 13, pp. 1–12, 2020.

## Research Article

# The Optimization of Shed-Tunnel Structure in the Confined Environment

Wu Yi,<sup>1,2,3</sup> Huizhao Shao ,<sup>1,2,3</sup> Zhoutong Cui,<sup>4</sup> Xiaohu Huang,<sup>1,2,3</sup> and Ying Zhou<sup>5</sup>

<sup>1</sup>National Field Observation and Research Station of Landslides in Three Gorges Reservoir Area of Yangtze River, Three Gorges University, Yichang 443002, Hubei, China

<sup>2</sup>Collaborative Innovation Center for Geo-Hazards and Eco-Environment in Three Gorges Area, Three Gorges University, Yichang 443002, Hubei, China

<sup>3</sup>Hubei Key Laboratory of Disaster Prevention and Mitigation, Three Gorges University, Yichang, Hubei 443002, China

<sup>4</sup>China Metallurgical Group Wuhan Survey and Research Institute Co, Wuhan 430080, Hubei, China

<sup>5</sup>Fifth Geological Brigade of Hubei Geological Bureau, Ezhou 436000, Hubei, China

Correspondence should be addressed to Huizhao Shao; 201908180021008@ctgu.edu.cn

Received 23 May 2022; Revised 24 June 2022; Accepted 29 June 2022; Published 5 August 2022

Academic Editor: Man Fai Leung

Copyright © 2022 Wu Yi et al. This is an open access article distributed under the Creative Commons Attribution License, which permits unrestricted use, distribution, and reproduction in any medium, provided the original work is properly cited.

The design of shed-tunnel structure in the confined environment can help to avoid the safety of passing vehicles and pedestrians from being threatened by the impact of upper rockfall in highway, railway, and other rockfall disaster protection engineering. Due to the limitation of the space environment, it is necessary to optimize the shed-tunnel structure to provide enough space for passing vehicles and pedestrians. In this study, a case study was made on the passing shed tunnel of Badong Juebitianhe Revolutionary Education Base. First, the theoretical calculation of rockfall impact force was compared and optimized. Then, the optimization scheme of “column + anchor bolt + buffer layer” was proposed based on the commonly used shed-tunnel form and was verified by ABAQUS numerical simulation. The performance of the optimized shed-tunnel structure is greatly improved in terms of the space utilization rate of shed tunnel and the impact resistance of rockfall.

## 1. Introduction

Confined environment refers to the environment with limited space. In the theory system of geological disaster prevention and control, confined environment is mainly manifested by high and steep slope in the inner side and gully cliff in the outer side of the mountain road with limited passage width. Under the impact of natural factors, the inner slope is prone to collapse and rockfall disaster, especially the high and steep rock slopes with sparse vegetation and developed rock fissures. Affected by rainfall and dead weight, such slopes tend to form negative terrain such as local inverted ridge and cause rockfall disaster, which seriously affect road passage and vehicle and pedestrian safety.

Shed-tunnel structure protection is commonly used for preventing dangerous rock collapse in such geological environments. New structural forms such as frame shed

tunnel, skew joist shed tunnel, and all-steel shed tunnel are often adopted at tunnel entrances [1]. To a certain extent, the shed-tunnel structure solves the difficulties brought by bad geological problems to railway construction. Yang et al. [2] proposed a new type of flexible shed tunnel, which achieved buffer energy dissipation by flexible using the energy-dissipating structure formed by flexible metal mesh and spring struts to replace the sand-gravel cushion laid at the top of the traditional reinforced concrete shed tunnel. Jiang et al. [3] conducted a related study by establishing two simulation models of frame portal shed tunnel through the ANSYS/LS-DYNA finite element software. The research results show that the impact resistance of the shed tunnel can be improved to some extent by changing the structure roof angle. Based on the numerical simulation on the impact process of rockfall using a dynamic finite element, Wu et al. [4] obtained the dynamic and mechanical responses of the

structure under different impact angles of rockfall and concluded that the deflection deformation of the roof plate and the roof beam of the shed tunnel presented a quadratic parabolic shape. According to the comparative analysis of experiments of ordinary support shed tunnel and energy dissipation support shed tunnel, Bertrand et al. [5] concluded that the energy dissipation support made of mild steel could improve the bearing performance of the shed tunnel. In addition, Delhomme et al. [6] replaced the sand-gravel cushion by adding structurally dissipating rock-sheds (SDR) at the support of concrete shed tunnel to absorb rockfall impact energy and studied its dynamic behavior by scale test. In addition, many scholars have conducted a lot of theoretical analyses on the numerical simulation of shed tunnel. For example, Labiouse et al. [7] summarized the empirical algorithm of rockfall impact force by combining it with the field rockfall impact test. Yang and Guan [8] studied the factors affecting the impact force by using a hammer impact buffer layer through an indoor model test and proposed relevant formulas for rockfall impact calculation. Pichler et al. [9] studied the impact characteristics of rockfall by using a numerical simulation method and combining it with the pipeline protection structure in sandy cobble stratum.

The traditional shed tunnel can ensure the safety of management engineering in a confined environment, but it can not meet the requirements in terms of economic cost and impact resistance. Therefore, it is necessary to optimize the shed-tunnel structure. With the shed tunnel of Badong Juebitianhe Revolutionary Education Base, as an example, first of all, the rockfall impact theory calculation methods of confined environment were compared, and the traditional methods were optimized. Second, based on the optimal impact theory, the optimized shed-tunnel structure was put forward. Next, numerical simulation was conducted on the stress and displacement in the different parts (beams and columns) of the optimized shed tunnel through the ABAQUS software.

## 2. Comparison and Optimization of Theoretical Calculation of Rockfall Impact Force in a Confined Environment

Few people pass through a confined environment. Besides, there are mostly steep cliffs in the mountain area, resulting in a low safety index. The shed-tunnel structure mainly needs to bear the external load of the impact load of rockfall. Thus, the calculation of the impact force of rockfall can provide a basis for the practical engineering prevention and control.

The existing impact force algorithms include the sub-grade code method, tunnel manual method, Yang Qixin method, Japanese road authority method, Swiss method, Ye Qiqiao method, and Xiang Xin method. The following assumptions were made before comparing these methods:

- (1) Rockfall was assumed to be a homogeneous sphere. Besides, both the fragmentation of rockfall and the splashing of buffer soil were ignored in the impact process.

- (2) The rockfall height group setting is as follows: 15 m, 30 m, 45 m, 60 m, and 75 m.

*2.1. Introduction to Existing Calculation Methods.* The different calculation methods and formulas are summarized in Table 1.

The following results were obtained according to the comparison of different calculation methods of impact force: with the increase of rockfall radius, the impact force calculated by all methods kept increasing trend. To be specific, the impact force calculated by the Xiang Xin method had the fastest increase and the largest calculated impact force, followed by the Japanese road authority method and the Swiss method; the impact force calculated by the tunnel manual method had the slowest increase and the least calculated impact force. With the increase of the height of free fall, however, the difference between the methods became larger and larger.

*2.2. Comparison of Each Method with Simulation Results.* According to the comparison and analysis of the impact force of rockfall with an equivalent radius of 0.2–0.5 m falling from a height of 20–100 m, it was concluded that the simulated values were close to those calculated by the Xiang Xin method and Japanese road authority method. The deviations between the simulated values and the values calculated by the above two methods were 1.9% and 20.62%, respectively, when the equivalent radius of rockfall was 0.2 m and the height of rockfall was 100 m. With the increase of rockfall mass and falling height, however, the simulated values gradually approached the values calculated by the Xiangxin method. The deviation between the simulated values and the values calculated by above two methods was –1.85% and 40.67%, respectively when the equivalent radius of rockfall was 0.5 m and the falling height was 100 m. The impact force calculated by the Xiangxin method was the closest to the simulated value, and the deviations were all within 10%. However, the amplification coefficient of the impact force in this method needed to be improved because of the large mass and height of rockfall in a confined environment.

*2.3. Advantages and Disadvantages of Each Method.* Among the above methods, the value obtained by the tunnel manual method was the minimum. The effect of gravity in the process of rockfall was not considered; the rockfall did not rebound after the regulated impact; the impact duration obtained by this method was too long. Hence, the values obtained were smaller. Some experiments proved that the impact duration of rockfall generally did not exceed 0.14 s. In fact, the value obtained by this method was the average value of the impact process, rather than the maximum impact force.

Similarly, the value obtained by Yang Qixin was also the average value in the process of rockfall impact, rather than the maximum impact force. In addition, the effect of gravity in the process of rockfall was not considered, so the impact

TABLE 1: Different calculation methods and formulas.

| Calculation method    | Calculation formula   |
|-----------------------|---|
| Subgrade code method  | $P = P(Z)F = 2\gamma Z[2 \tan^4(45^\circ + (\phi/2)) - 1]F$ , where $Z = V_R \sqrt{(Q/2g\gamma F)} \times \sqrt{(1/2 \tan^4(45^\circ + (\phi/2)) - 1)}$   |
| Tunnel manual method  | $\begin{cases} p = (Qv_0/gt) \\ t = (2h/c) \\ c = \sqrt{1 - \mu/(1 + \mu)(1 - 2\mu)} \times (E/\rho) \end{cases}$   |
| Yang Qixin method     | $\begin{cases} p = \zeta m a_{\max} \\ a = \sqrt{(2gh/t)} \\ t = ((1/100)(0.097mg + 2.2h + 0.045/H + 1.2)) \end{cases}$   |
| Xiang Xin method [10] | $F = 3.2377(l \times \gamma \times N_\gamma)^{(1/3)} (mgH)^{(2/3)}, N_\gamma = 1.8(N_q - 1)\tan\phi, N_q = \tan^2(45^\circ + (\phi/2))e^{\gamma \tan\phi},$ $F_{\max} = 7.412(l \times \gamma \times N_\gamma)^{(1/3)} (mgH)^{(2/3)}$ |

Note. In the formula of the existing calculation method,  $P$  denotes the impact force of falling rock, (kN);  $P(Z)$  denotes the unit resistance of rockfall impact on the buffer layer (kPa);  $V_R$  denotes the impact velocity (m/s) when rockfall contacts the buffer soil layer;  $\Phi$  denotes the density of the layer (kN/m<sup>3</sup>);  $g$  denotes the acceleration of gravity (m/s<sup>2</sup>); and  $F$  denotes the cross-sectional area of the equivalent sphere of rockfall (m<sup>2</sup>).

force calculated by this method was still smaller, being similar to the value obtained by the tunnel manual method.

According to the functional principle, the value obtained by the subgrade code method was actually also the average impact force and was smaller. Its calculation result was close to that of Yang Qixin and could not reflect the changing relationship between rockfall and the thickness of buffer layer.

As for the Japan Road community method and Switzerland method, the empirical formula was established based on a field test. The calculation result was the maximum impact, and it was more in line with the engineering practice. The value obtained by the Japan Road community method was larger. The two methods were different in terms of the selection of lame constant and deformation modulus, but they did not consider the effect of buffer layer thickness of rockfall impact.

Based on the theory of energy conservation and foundation bearing capacity, the Xiang Xin method calculated the reaction force of buffer layer, so the impact force obtained was the maximum, being the calculated maximum value among the above methods. It was more consistent with the actual rockfall engineering of free-falling body, but it was highly sensitive to rockfall.

Therefore, the Xiang Xin method was the most suitable for the calculation of rockfall impact force in a confined environment, and it is reasonable and feasible to optimize the shed-tunnel structure by using the Xiang Xin method as the calculation method of rockfall impact force in a confined environment.

### 3. The Design Optimization of Shed-Tunnel Structure Based on Optimization Impact Force Theory

3.1. *Shed-Tunnel Structure Type.* The design of shed tunnel needs to be considered for mountainous areas where most

geological disasters occur, so the classification of shed tunnel in mountainous areas is of great significance [11]. Shed tunnel has various structure forms, which is mainly composed of five parts, namely, outer support structure, inner wall, roof, transverse connection at the bottom, and the outer foundation [12]. To be specific, the outer supporting structure is in the form of straight column, inclined column, cantilever, wall type, and arch beam; the inner wall is in the form of retaining wall and curved arch; the roof is in the form of flat plate and curved arch; the outer foundation structure is in the form of independent foundation, strip foundation, pile foundation, and underground continuous wall.

3.2. *Optimization of Shed-Tunnel Structure.* Shed tunnel can help to avoid endangering the lives of passing vehicles and pedestrians. Due to the limitation of the space environment, however, it is necessary to optimize the structure form of the shed tunnel. In the study, by comparing with the traditional shed-tunnel structure, the shed tunnel was optimized from the aspects of structure shape, connection mode of the shed tunnel and the rock mass, and the buffer layer material of the roof board to improve the utilization rate of space while satisfying the structural performance.

Therefore, based on the comparison with the ordinary shed-tunnel structure described in Section 3.1, the following optimization measures were proposed for shed-tunnel structure:

- (1) Shed tunnel has more strict requirements for concrete material. Thus, the rock mass was replaced by shed-tunnel stress components; the original internal and external pillars as the main stress components were replaced by only lateral pillars. Besides, the inner pillars were removed and replaced by the slope rock mass and anchor bolt.
- (2) According to the study of Luo Wenjun and Cao [13], the vibration isolation effect of the barrier filled with tire debris was optimal within the frequency band of

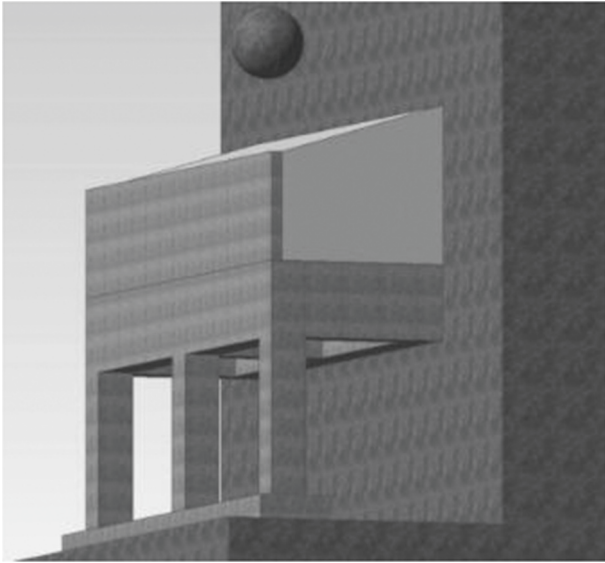


FIGURE 1: Three-dimensional schematic diagram of portal anchoring shed tunnel.

1–10 Hz and 15–25 Hz. Therefore, abandoned tires were used to provide the buffer energy dissipation effect of rockfall for the buffer soil layer of the shed tunnel.

The optimized shed-tunnel structure model is shown in Figure 1.

Figure 1 shows a three-dimensional schematic diagram of an optimized shed-tunnel structure. In the figure, the main stressed components of the shed tunnel are the roof plate and column. The overall enhancement inside is achieved by embedding the shed-tunnel with the rock slope body by anchor rods.

The section drawings of shed-tunnel structure before and after optimization are shown in Figures 2 and 3:

The comparison of shed tunnel before and after optimization is listed in Table 2.

#### 4. Engineering Cases

In this study, the optimization scheme of the traditional shed tunnel was explained by taking the shed-tunnel design of the geological disaster spot of Juebitianhe in Juebitianhe as an example. Juebitianhe Revolutionary Education Base is located in Qingtaiping Town and Shuibuya Town, Badong County. There are a certain number of disaster spots along the base. Any instability will affect the normal operation of irrigation canals, drinking water, and irrigation for tens of thousands of people in Badong and Changyang counties. Besides, it will affect the lives and property safety of more than 200 households below the canal. In addition, it will pose a serious threat to the life safety of students, party cadres, and tourists who come here to carry out party day activities.

The destroying modes of the dangerous rock mass in the rocky slope were dominated by falling type and dumping type. Moreover, lithologic was hard limestone rock mass.

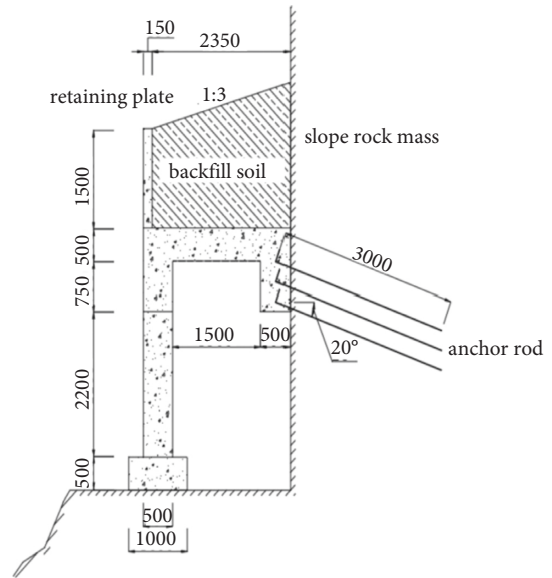


FIGURE 2: Section of portal anchoring shed tunnel.

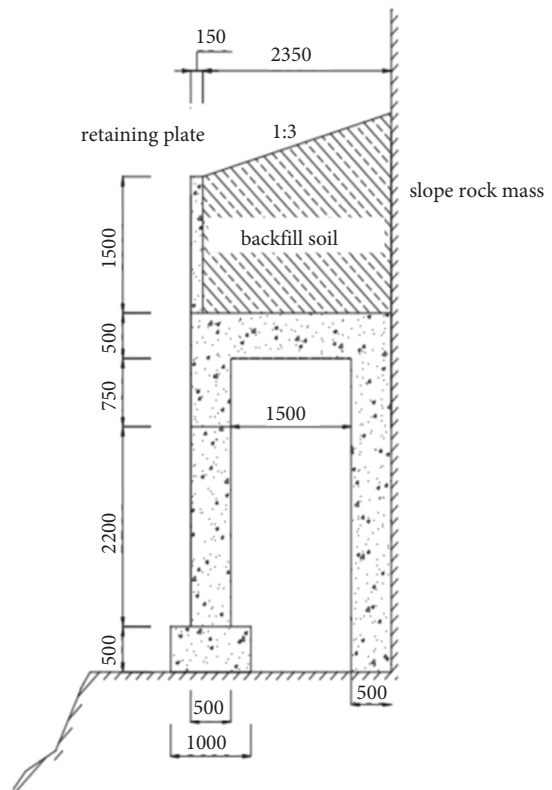


FIGURE 3: Section of portal wall shed tunnel.

Therefore, the ordinary shed-tunnel structure was optimized as follows: the inter side and rock mass were built-in into an organic whole through an anchoring bolt; as the contact of the shed-tunnel structure, the outer side held the stress passed to the pillar from the top of the shed tunnel through the pile foundation. The engineering geology section is shown in Figure 4, and the elevation layout of the engineering is shown in Figure 5.

TABLE 2: Comparison of shed tunnel before and after optimization.

| Contrast factor                        | Before optimization   | After optimization    | Optimization results                     |
|--|-----------------------|-----------------------|--|
| Available volume of space              | 5.05 m <sup>3</sup>   | 6.313 m <sup>3</sup>  | Being improved by 25%                    |
| Useable volume of concrete             | 6.375 m <sup>3</sup>  | 5.025 m <sup>3</sup>  | Economic returns increased significantly |
| Peak value of impact force on the roof | 5.7 N/mm <sup>2</sup> | 2.8 N/mm <sup>2</sup> | Being improved by 50%                    |

Note. The extension length of the shed tunnel is 1 m.

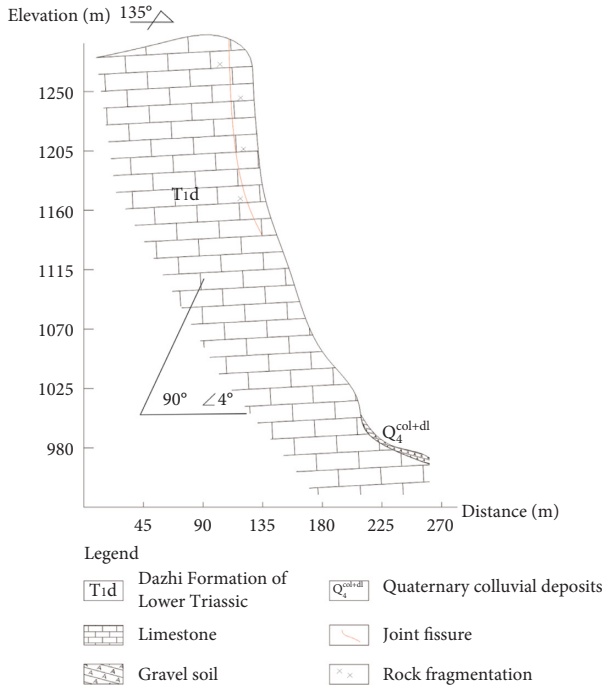


FIGURE 4: Section of engineering geology.

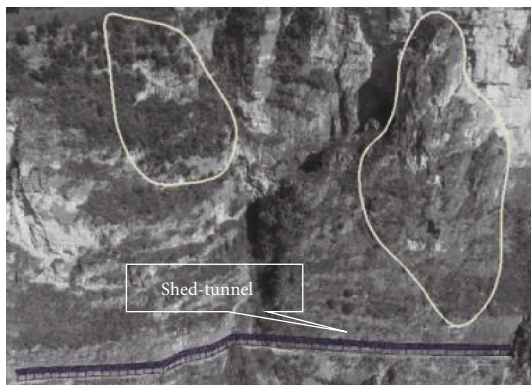


FIGURE 5: Elevation layout of the engineering.

Stratigraphic lithology of Badong Juebitianhe Revolutionary Education Base is listed in Table 3.

The mountain terrain in the Juebitianhe area has a large slope, generally reaching 60°–80°, and most of them are steep cliffs, which provide good space conditions for the formation of dangerous rock masses. The dangerous rock mass is composed of thin layer and middle layer of limestone with hard brittle lithology, which provides a material source for the formation of dangerous rock mass. The rock mass

fractures are complexly developed and are dominated by steeply inclined fractures, and they can deform and expand under gravity unloading. Besides, the weathering of rock mass, the infiltration of fissure water, and the wedging of plant roots can quicken the collapse and deformation of dangerous rock mass. The space is limited in the construction process. The traditional shed tunnel was optimized by the optimization scheme proposed in this study. The optimized shed tunnel not only facilitated the construction but also took into account the requirements of the confined construction site under the actual environmental conditions.

4.1. *Contrastive Analysis of Stress.* The portal wall shed-tunnel structure was taken as an example before the optimization. The optimization model in this study used ABAQUS as simulation software, and the material constitutive model was mainly based on the actual optimization project in Enshi, Hubei province, are calculated and simulated, as listed in Table 4. The stress nephogram is shown in Figure 6.

The portal anchoring shed-tunnel structure is taken as an example after the optimization, with the stress nephogram, as shown in Figure 7.

Based on the comparison and analysis of Figures 6 and 7, it was found that the external force on the joints between columns and beams of the portal wall shed tunnel was much greater than that of the portal anchoring shed tunnel.

According to the equivalent stress nephogram, the unit stress curves of the key parts of the jack stringer of the shed tunnels could be obtained, as shown in Figures 8 and 9.

Based on the comparison and analysis of Figures 8 and 9, it was found that the peak value of unit stress in the key position of the jack stringer of the anchoring shed tunnel and the unit stress value after the structure was stabilized were lower than the corresponding position of the wall shed tunnel.

According to the equivalent stress nephogram, the unit stress curves of the key parts of the center pillars of the shed tunnels could be obtained, as shown in Figures 10 and 11.

As seen from the comparison and analysis of Figures 10 and 11, the peak value of unit stress in the key position of the center pillars of the anchoring shed-tunnel and the unit stress value after the structure was stabilized were lower than those at the corresponding positions of wall shed-tunnel.

In conclusion, the stress values of the key parts of the jack stringer and center pillars of the anchoring shed tunnel were smaller than those of the corresponding positions of the wall

TABLE 3: The stratigraphic lithology of Badong Juebitianhe revolutionary education base.

| Formation      |  | Distribution location and material composition   |
|----------------|--|--|
| Q <sub>4</sub> | Quaternary colluvial deposits (Q <sub>4</sub> <sup>col+dl</sup> )        | It is distributed below the cliff Tianhe channel of the exploration route of Shuibuya Section of the exploration line, with an uneven thickness of generally 3–5 m. It is mainly composed of collapsed stones with diameters of generally 0.5–1 m and 1.8 m at most.   |
|                | Quaternary artificial accumulation layer (Q <sub>4</sub> <sup>ml</sup> ) | It is distributed below the precipitous Tianhe channel of the exploration route from Sanlicheng to Baishuoping Section. The main material composition is gravel soil, with the soil-rock ratio of 7 : 3, presenting a loose to slightly dense state, with a distribution thickness of 1–3 m.   |
|                | Quaternary landslide deposits (Q <sub>4</sub> <sup>del</sup> )           | It is distributed in the exploration route from Shuiliuping Section to Baishuoping Section, that is, the large landslide, which is composed of gravel soil, with the content of about 40%–50%; gravel components are limestone, with the diameter of generally 5 cm–30 cm and about 1 m at most; the soil has a high content of yellowish-brown clay particles. The accumulation layer has an average thickness of 4 m, and a total volume of about 3.2 × 10 <sup>4</sup> m <sup>3</sup> . |
| Bed rock       | Lower triassic daye formation (T <sub>1</sub> D)                         | The lithology of the stratum is a thin layer and medium-thick layer limestone, with the stratum occurrence of 135–240°∠4–15°, serious surface weathering, and local small-scale falling. Rock mass and slope form tangential slope and reverse slope structure.  |

TABLE 4: Physical parameter values of materials.

| Density ρ (kg/m <sup>3</sup> ) | Elasticity modulus E (Mpa) | Poisson's ratio μ | Cohesion c (kPa) | Friction angle φ (°) |
|--------------------------------|----------------------------|-------------------|------------------|----------------------|
| 7850                           | 200000                     | 0.3               |                  |                      |
| 2500                           | 5000                       | 0.24              |                  |                      |
| 1850                           | 35                         | 0.35              | 20               | 25                   |
| 2500                           | 30000                      | 0.2               |                  |                      |

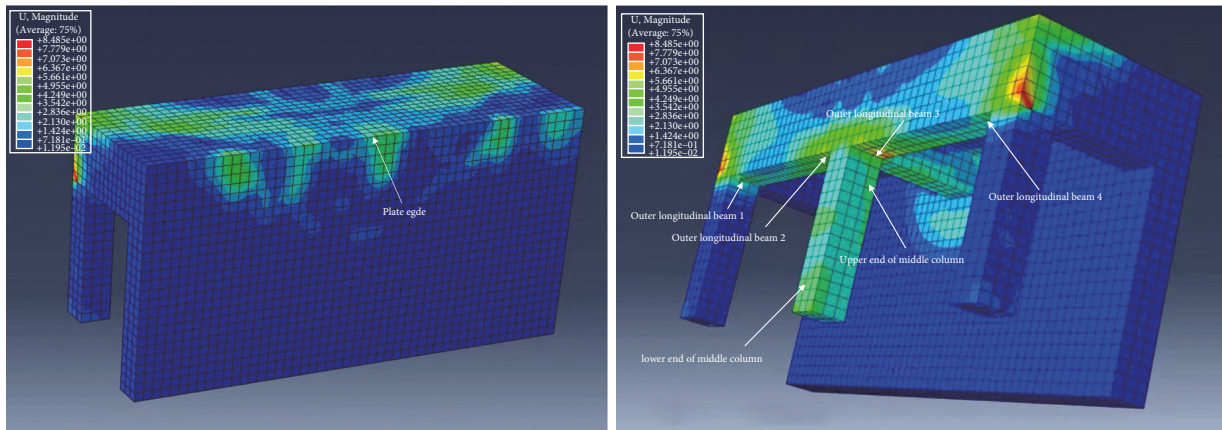


FIGURE 6: Equivalent stress nephogram of portal wall shed-tunnel structure.

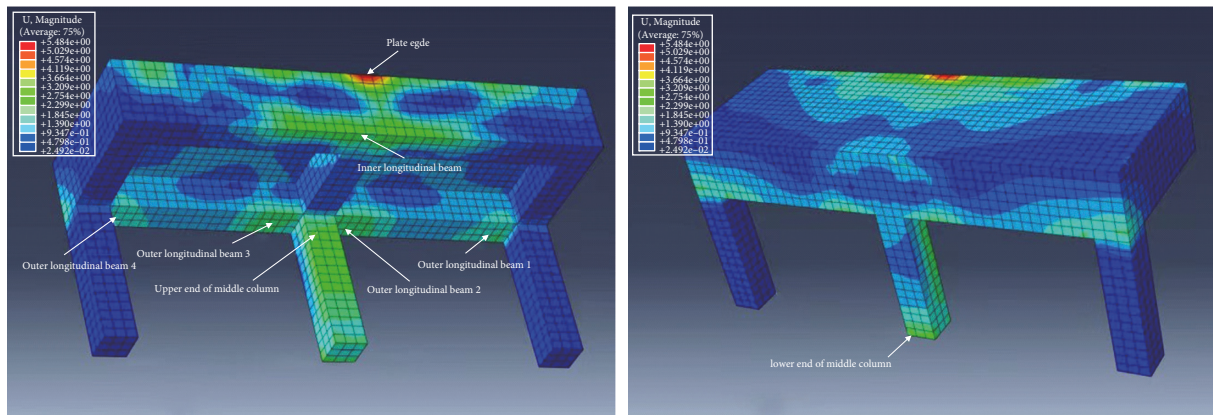


FIGURE 7: Equivalent stress nephogram of portal anchoring shed-tunnel structure.



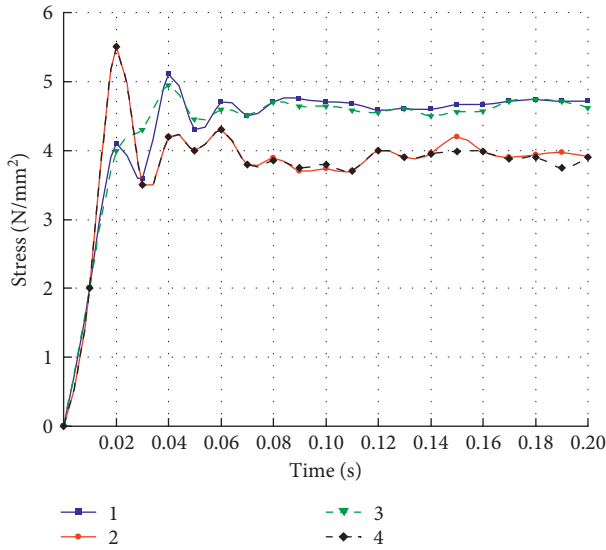


FIGURE 8: The unit stress curves of the key parts of the jack stringer of the portal wall shed tunnel.

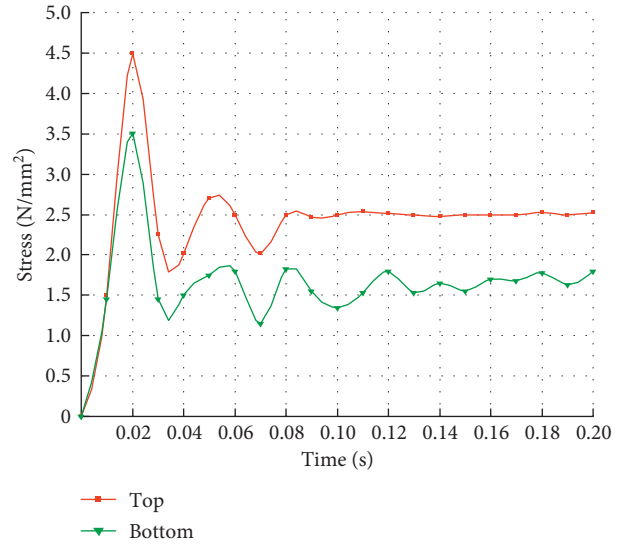


FIGURE 10: The unit stress curves of the key parts of the center pillars of the portal wall shed tunnel.

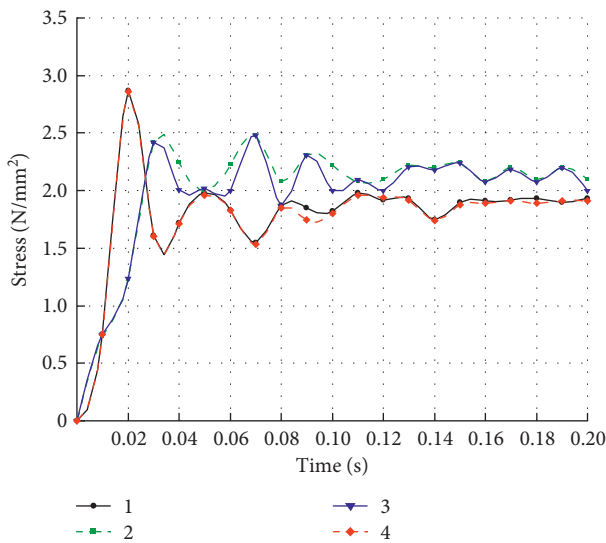


FIGURE 9: The unit stress curves of the key parts of the jack stringer of the portal anchoring shed tunnel.

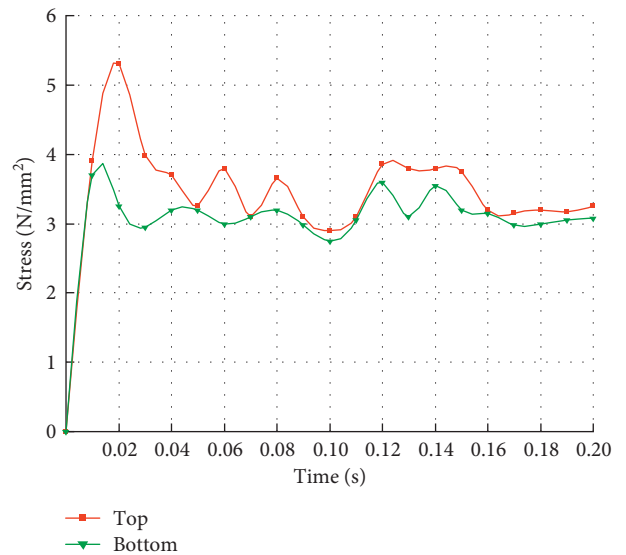


FIGURE 11: The unit stress curves of the key parts of the center pillars of the portal anchoring shed tunnel.

shed tunnel. Thus, the anchoring shed tunnel was more suitable in confined environment.

4.2. Comparative Analysis of Displacement. The displacement of portal shed tunnel was analyzed. The displacement nephograms of portal wall shed tunnel and portal anchoring shed tunnel were obtained, as shown in Figures 12 and 13.

The portal wall shed-tunnel structure was the shed-tunnel structure before optimization. Based on the analysis of the displacement variation of the maximum displacement nephograms of the portal wall shed-tunnel structure, it was found that the beam-column joints of the portal wall shed tunnel had obvious displacement variation under the action of the great external force. Based on the analysis of the

maximum displacement nephograms of the portal anchoring shed-tunnel structure in Figure 13, it was found that the beam-column joints of the optimized shed tunnel received relatively small external forces under the same position.

The structure displacement first occurred at the center of the roof plate of the shed-tunnel just below the rockfall and the middle position of the jack stringer when the rockfall initially contacted with the cushion. With the gradual contact between rockfall and cushion, the displacement range gradually expanded to the jack stringer and the center pillar, and the maximum displacement of the roof extended to the inside. When the rockfall movement stopped and the structure tended to be stable, the maximum displacement occurred in the center pillar and the jack stringer. The

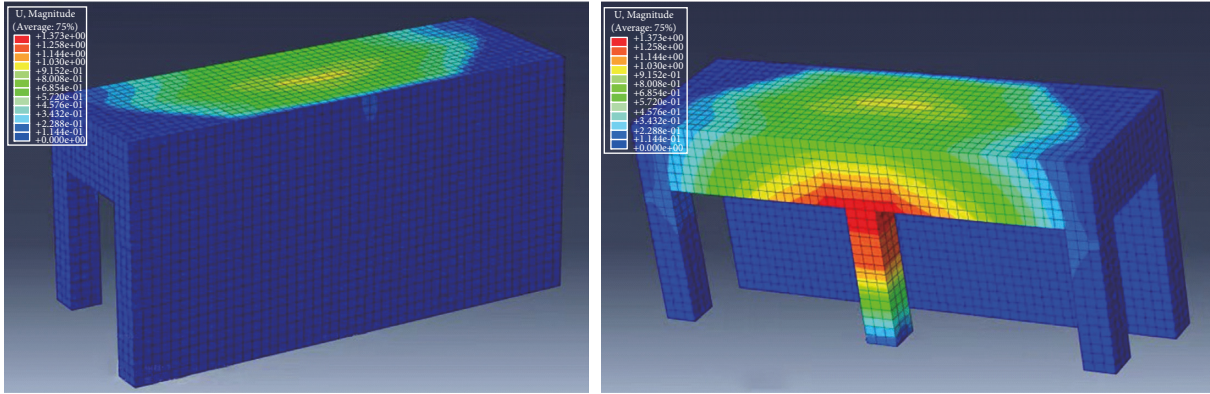


FIGURE 12: The maximum displacement nephograms of portal wall shed-tunnel structure.

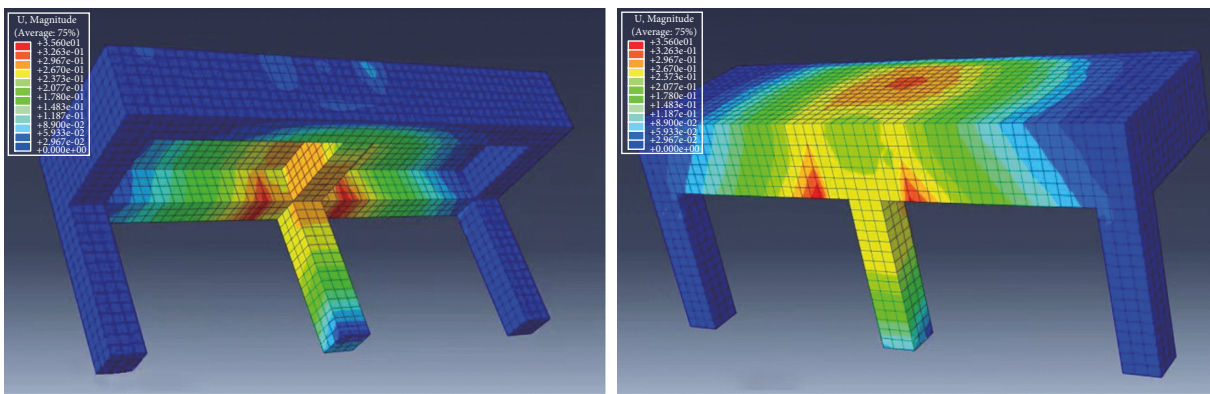


FIGURE 13: The maximum displacement nephograms of portal anchoring shed-tunnel structure.

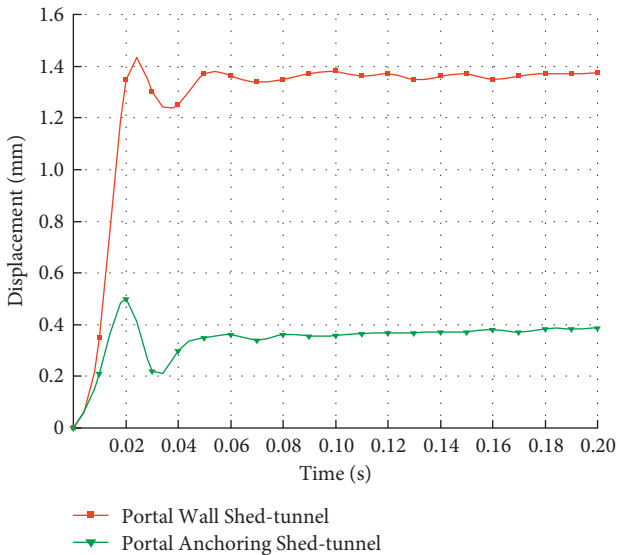


FIGURE 14: Diachronic curves of the maximum displacement of the jack stringer of the anchoring shed tunnel and wall shed tunnel.

displacement boundary was relatively clear, and the maximum displacement also occurred at the structure stress concentration.

The diachronic curves of the maximum displacement of the jack stringer of the portal anchoring shed tunnel and portal wall shed tunnel are shown in Figure 14.

As shown in Figure 14, the maximum displacement of the jack stringer of the wall shed tunnel was significantly greater than that of the anchoring shed tunnel. Based on the comparison of the maximum displacement values of representative units in the key parts of the structure, such as the jack stringer, roof plate, and interior stringer, it could be concluded that the anchoring shed tunnel was more suitable for a confined environment than the wall shed tunnel under the same conditions.

### 5. Conclusion

In this study, the optimization of shed-tunnel structure in a confined environment is studied, and the following conclusions are drawn:

- (1) Through comparative analysis of traditional impact force calculation methods, the Xiang Xin method is most suitable for the calculation of rockfall impact force in a confined environment.
- (2) The optimization of the shed tunnel increases the space utilization rate, reduces the cost, and greatly

improves the impact resistance of rockfall. The results provide a reference for similar shed-tunnel management.

- (3) The shed-tunnel design still can be further optimized for Juebitianhe geological disaster site in Enshi. If there are difficulties in the actual construction process, then the potential safety threats in the construction process still exist. Because the main force falls on the column, high requirements are proposed for the concrete used by the column. In the later stage, the model can also optimize the shed-tunnel structure by changing the bending moment, shear force, and energy.

### Data Availability

The experimental data used to support the findings of this study are available from the corresponding author upon request.

### Conflicts of Interest

The authors declare that they have no conflicts of interest.

### Acknowledgments

The study was supported by the National Natural Science Foundation of China (no. 42007237), Hubei Provincial Key Laboratory of Intelligent Vision Monitoring for Hydro-power Engineering (no. 2020SDSJ02), and Natural Science Foundation of Hubei Province (no. 2017CFB436).

### References

- [1] L. Ran and C. Chen, "Design of railway shed-tunnel," *Journal of Railway Engineering*, vol. 25, no. 6, pp. 61–66, 2008.
- [2] J. Yang, Y. Bai, and X. Yang, "Numerical simulation and experimental study on rockfall impact of flexible shed-tunnel structure," *Journal of Vibration and Shock*, vol. 36, no. 9, pp. 172–178, 2017.
- [3] J. Guo, Q. Wang, and Q. Zhang, "Optimization of frame portal shed-tunnel structure under rockfall impact load," *Hydrogeology & Engineering Geology*, vol. 41, no. 6, pp. 92–97, 2014.
- [4] Y. Wu, S. He, and J. Shen, "Dynamic response of shed-tunnel structure under rockfall impact load," *Rock and Soil Mechanics*, vol. 32, no. 3, pp. 781–788, 2011.
- [5] D. Bertrand, F. Kassem, F. Delhomme, and A. Limam, "Reliability analysis of an RC member impacted by a rockfall using a nonlinear SDOF model," *Engineering Structures*, vol. 89, pp. 93–102, 2015.
- [6] F. Delhomme, M. Mommessin, J. P. Mougou, and P. Perrotin, "Behavior of a structurally dissipating rock-shed: experimental analysis and study of punching effects," *International Journal of Solids and Structures*, vol. 42, no. 14, pp. 4204–4219, 2005.
- [7] V. Labiouse, F. Descoedres, and S. Montani, "Experimental study of rock sheds impacted by rock blocks," *Structural Engineering International*, vol. 6, no. 3, pp. 171–176, 1996.
- [8] Q. Yang and B. Guan, "Experimental study on calculation method of rockfall impact force," *Journal of the China Railway Society*, vol. 18, no. 1, pp. 101–106, 1996.
- [9] B. Pichler, Ch. Hellmich, and H. A. Mang, "Impact of rocks onto gravel Design and evaluation of experiments," *International Journal of Impact Engineering*, vol. 31, no. 5, pp. 559–578, 2005.
- [10] X. Xiang, *The Rockfall Movement Characteristics and Collision Impact Effect along the Slope*, pp. 68–79, China University of Geosciences, Wuhan, 2010.
- [11] Y. Zheng, *The Adaptability of Greenhouse-Cave Structure, Backfill Buffer and Mountain*, pp. 15–27, Chongqing Jiaotong University, Chongqing, 2015.
- [12] F. Wang, "Application and development of new type shed-tunnel in control of vertical slope diseases of existing cable bridge and tunnel," *Building Materials and Decoration*, vol. 16, no. 5, pp. 256–257, 2020.
- [13] W. Luo and H. Cao, "Finite element analysis of vibration isolation effect by filling ditches with ditches and waste tire," *Building Structure*, vol. 50, no. S2, pp. 360–365, 2020.

## Research Article

# Aerobics Characteristics Analysis and Auxiliary Training Efficiency Improvement Method Based on Deep Learning

Jiwen Wang,<sup>1</sup> Bingxue Wang,<sup>2</sup> and Shuli Wan <sup>3</sup>

<sup>1</sup>Shijiazhuang Information Engineering Vocational College, Hebei, Shijiazhuang 050000, China

<sup>2</sup>Hebei Institute of Communications, Hebei, Shijiazhuang 050000, China

<sup>3</sup>The Department of Basic Education, Shanghai Urban Construction Vocational College, Shanghai 201415, China

Correspondence should be addressed to Shuli Wan; [wanshuli@succ.edu.cn](mailto:wanshuli@succ.edu.cn)

Received 24 February 2022; Revised 18 April 2022; Accepted 3 June 2022; Published 2 August 2022

Academic Editor: Man Fai Leung

Copyright © 2022 Jiwen Wang et al. This is an open access article distributed under the Creative Commons Attribution License, which permits unrestricted use, distribution, and reproduction in any medium, provided the original work is properly cited.

Aerobic exercise is the predecessor of aerobics. Aerobics is a kind of young and energetic sports, although it is only popular in recent years, but because of its strong ornamental, very beautiful, so many people like it. Now, the characteristic of sports development is to integrate competitive sports into schools, and the establishment of high-level sports teams in Chinese colleges and universities is the need of the current development trend and adapts to the trend of the times. Many colleges and universities have invested a lot of time, money, and energy. It is to set up a high-level sports team. It has provided great help to physical education and athletes. Therefore, it is very beneficial to the sustainable development of aerobics of high-level sports teams in colleges and universities to compare, analyze, and study the aerobic training methods of high-level sports teams in colleges and universities, and find out the existing problems in current training, correct them in time, and find out more suitable training methods.

## 1. Introduction

An opponent is established for the deep learning system applied to image object recognition, and the system parameters are used to find the minimum disturbance of the input image so that the system can misclassify with high confidence. We use this method to construct and deploy an opponent of a deep learning system applied to music content analysis. We find that the convolution architecture is more robust than the majority vote system based on a single classified audio frame [1]. Large-scale gene expression profiles have been widely used to describe the response of cells to various disease conditions, genetic interference, and so on. Although the cost of genome-wide expression profiles has been steadily decreasing, it is still very expensive to generate a compilation of expression profiles on thousands of samples. Deep learning is still better than linear regression with a relative improvement of 6.57% and achieves lower error on 81.31% of target genes [2]. The emergence of electronic medical records with large electronic image databases and the progress of deep neural networks with machine learning provide unique opportunities to achieve milestones in

automated image analysis. As a new image classification technology, deep learning technology has high classification accuracy and effectiveness [3]. A long-term memory network is the most advanced technology for sequence learning. They are not often applied to financial time-series forecasting, but they are essentially suitable for this field. We find that the daily return rate of the LSTM network is 0.46%, and the Sharpe ratio before transaction cost is 5.8, which is superior to memoryless classification methods, namely, random forest, deep neural network, and logistic regression classifier [4]. We propose a consistency-aware depth learning (CADL) framework for personnel rerecognition in camera networks. Under the framework of deep learning, we use this consistency perception information to automatically learn feature representation and image matching under certain consistency constraints. Experimental results show that the performance of this method is greatly improved, which is much better than the existing methods [5]. A new scalable training method for deep learning machines is proposed, which utilizes data parallelism through incremental block training and intrablock parallel optimization, and stabilizes the learning process through block model update filtering.

Compared with the traditional random gradient descent training based on a small batch on a single GPU, we have achieved linear acceleration of 16 GPUs on the LSTM task and 64 GPUs on the DNN task, and the recognition accuracy has not decreased or improved [6]. Defect prediction is a very interesting topic, especially at the change level. Deep learning is a research hotspot in the field of machine learning. Whether deep learning can be used to improve the performance of just-in-time defect prediction has not been studied. The experimental results show that in 4 of the 6 items, this is statistically significantly higher than Yang et al.'s method [7]. The practical success of deep neural networks has not matched the theoretical progress of satisfactorily explaining their behavior. In this study, the information bottleneck theory of deep learning is studied. By combining the analysis results with the simulation results, we prove that the information plane trajectory is mainly a function of neural nonlinearity [8]. Finding the parameters that minimize the loss function is the core of many machine learning methods. The random gradient descent algorithm is widely used and provides the most advanced results for many problems [8]. Nowadays, many diseases are gradually becoming younger, and stroke is one of them. This study found that aerobics can assist in the treatment of stroke [9]. Aerobics can make people's joints and muscles get good exercise, thus reducing symptoms such as joint sprain and muscle strain. This study found that aerobics is a means to improve the important system of the body and improve the efficiency of the body system through physical exercise [10]. This study found that aerobics can reduce overweight and adipose tissue, coordinate human limbs, and strengthen explosive force and flexibility [11]. Because aerobics has many benefits to people's health, people like this sport more and more. It can cultivate students' innovative abilities, so it is necessary to improve teachers' professional skills in the teaching process [12]. This study uses imagery training to improve the teaching method of aerobics. The research shows that this method can improve our understanding of aerobics and adjust our emotions [13]. In this study, yoga, aerobics, and aerobics combined with yoga training are divided into groups. The analysis results show that the fitness effect of yoga and aerobics on women is better than that of single training [14].

## 2. An Analysis of the Problems Existing in the Traditional Aerobics Teaching Mode

*2.1. Action Name Confusion.* Under the traditional aerobics teaching, students learn to cope with examinations, which is very common. At the end of the assessment, the actions are forgotten. After the course, 90% of the students cannot answer the terms, basic action names, and action methods of aerobics. Even in the process of learning, it will be found that the focus of contact with this subject is on the imitation learning and memory of complete sets of movements, ignoring the repeated practice and memory of basic movements, resulting in poor standardization of the final complete sets of movements. For example, kicking and bouncing are indistinguishable, word step and man step are indistinguishable, and the transition from low-impact step

to high-impact step-bouncing kick and bouncing kick jump, leg sucking, and leg sucking jump are indistinguishable, which are caused by unclear basic action concepts, unclear action names, or confusion, which will not be conducive to subsequent learning and memory.

*2.2. Poor Standardization of Movements.* One of the most basic elements of aerobics is that the movements should be elastic, due to lack of practice and poor coordination of limbs. For example, when sucking legs in the last step, the thighs are uneven, the toes are hooked, and the crotch is swung forward. In the "V" step, the center of gravity fluctuates too much, wraps the legs outward, and swings the hip joints in turn. These are the problems caused by unclear action essentials. Therefore, the essentials and norms of basic movements should be the focus of learning at the beginning, instead of rushing to remember the sequence of complete sets of movements.

*2.3. Insufficient Movement Practice.* In the process of students' learning, you will find that some students' poor movement quality is due to the lack of exercise, which leads to poor physical coordination. After a month's class with the same teacher and the same basic movement training methods, it is finally found that the coordination and standardization of students' movements improved by the main items are better than those of students in general classes, no matter which set of exercises. Therefore, the number of exercises is the decisive factor to change the coordination of movements, that is, the so-called quantitative change causes qualitative change. In addition, the quality of flexibility is congenital, but there is a lot of room for change the day after tomorrow. In the learning process of basic movements, continuous and special training for the completion of movements will greatly improve and enhance the standardization of movements. For example, lifting and side lifting are the worst standardized movements for beginners, and it is difficult to get in place at once. However, after repeated targeted positioning control exercises, increasing muscle memory, and shoulder joint flexibility exercises, these movements, especially lifting movements, have been greatly improved.

## 3. Collaborative Filtering Algorithm

The collaborative filtering algorithm, as the most practical and popular recommendation algorithm at present, makes use of the collaborative wisdom among users to make recommendation judgments. Generally speaking, collaborative filtering algorithms are divided into two ways: nearest neighbor-based collaborative filtering and model-based collaborative filtering.

*3.1. Collaborative Filtering Algorithm Based on Nearest Neighbor.* The basic idea of the nearest neighbor-based collaborative filtering algorithm is as follows: in order to recommend the potentially interesting content to a specific user, first, other users with some similar characteristics are

found, and based on the content objects that similar users are interested in, the content objects are pushed to specific users. Therefore, the nearest neighbor-based collaborative filtering algorithm mainly includes two main steps: (1) to find the user set similar to the target user, and (2) find the objects that users like in this collection and the target users have not made a relevant evaluation and recommend them to the target users. First, the user-object rating matrix is used to represent the user's historical behavior. For user  $I$ , the vector ruler  $R_{i*}$  (representing the matrix  $R$  and the  $i$ -th row) is used to represent the user's historical behavior. Next, we need to find out the user set similar to user  $I$ . In order to find out the similar users, researchers put forward two commonly used similarity measurement methods: Jaccard similarity and cosine similarity.

Jaccard similarity can be expressed as formula (1) as follows:

$$\text{JaccardSimilarity} = \frac{|W_i \cap W_j|}{|W_i \cup W_j|}. \quad (1)$$

Cosine similarity can be expressed as formula (2) as follows:

$$\text{CosineSimilarity} = \frac{R_{i*} \cdot R_{j*}}{\|R_{i*}\| \times \|R_{j*}\|}, \quad (2)$$

where  $R_{i*}$  and  $R_{j*}$  represent the historical behavior of users  $I$  and  $J$  in the user-object scoring matrix,  $\cdot$  represents the inner product of vectors, and  $\|\cdot\|$  represents the modulus of vectors.

After determining the similarity measurement method,  $K$  users with the highest similarity with the target user  $I$  are formed into a similar user set  $U(i, k)$ . Finally, formula (3) is used to calculate the score prediction of the object whose evaluation is not made by the target user  $I$ .

$$\hat{R}_{is} = \sum_{j \in U(i,k) \cap N(s)} w_{ij} R_{js}, \quad (3)$$

$\hat{R}_{is}$  represents the evaluation prediction of user  $I$  on object  $S$ ,  $w_{ij}$  represents the similarity between user  $I$  and user  $J$ ,  $R_{js}$  represents the score of user  $J$  on object  $S$ ,  $U(i, k)$  represents the collection of  $K$  users most similar to user  $I$ , and  $N(s)$  represents the collection of users who have evaluated article  $S$ .

After predicting the ratings of the target user  $I$  for all potential recommendation targets (objects that make evaluations),  $K$  objects with the highest predicted ratings are recommended to user  $I$ .

The nearest neighbor-based collaborative filtering algorithm is also called the user-based collaborative filtering algorithm, because the overall idea of its algorithm is to calculate the user set most similar to the target user from the user's point of view, then calculate the score prediction of the target user to the potential recommendation target, and finally recommend it. In addition to the user-based collaborative filtering algorithm, there is also an object-based collaborative filtering algorithm, whose ideas and steps are almost the same as those of the user-based collaborative filtering algorithm. The object-based collaborative filtering

algorithm is to find the object that is most similar to the target object from the perspective of the object, then predict the prediction score between the object and the user, and finally recommend it.

The user-based collaborative filtering algorithm needs to maintain a user similarity matrix whose size is  $m \times m$ , and the object-based collaborative filtering algorithm needs to maintain an object similarity matrix whose size is  $n \times n$ . From the storage point of view, if the number of users is huge, it needs a lot of storage space to use user CF. Similarly, if the number of items is large, using item CF also requires a large maintenance cost.

**3.2. Model-Based Collaborative Filtering Algorithm.** In October 2006, Netflix, a DVD retailer, announced a competition in which anyone who invented a new method 10% better than its existing movie recommendation algorithm, CineMatch, won a seven-figure prize. The algorithm that shines brilliantly in the competition is the model-based collaborative filtering algorithm, which is also called the LFM hidden factor model or probability matrix decomposition model. The gradual implicit factor model has become the most common algorithm in recommendation algorithm and also become the most important model in recommendation algorithm research.

The PMF model directly models the user-object evaluation matrix  $R$ , making  $R \approx U^T V$ . The algorithm uses two parameter matrices  $U$  and  $V$  to describe the features of users and objects, where  $K$  is used to describe the dimension of feature vectors of users and goods. The parameters in  $U$  and  $V$  are trained by using the score data made by users in  $R$ , then, the vacant score in  $R$  is predicted by using  $R \approx U^T V$ , and finally, the object with the highest predicted score is selected as the recommendation object for the target users. The whole algorithm can be regarded as a process of matrix factorization, so the LFM model is often called matrix factorization model.

The mathematical expression of score prediction in PMF is the following formula:

$$r_{ij} = U_{i*} \cdot V_{*j}, \quad (4)$$

where  $r_{ij}$  represents the score of user  $I$  on object  $J$ ,  $U_{i*}$  represents the  $i$ -th row of  $U$  matrix, that is, the eigenvector of user  $I$ , and  $V_{*j}$  represents the  $j$ -th column of  $V$  matrix, that is, the eigenvector of object  $J$ . Formula (4) represents the construction method of the scoring model in PMF. In order to solve the parameter matrices  $U$  and  $V$ , the PMF model constructs a loss function  $J(U, V)$  as follows:

$$J(U, V) = \sum_{R_{ij} \in S} (U_{i*} \cdot V_{*j} - r_{ij})^2 + \lambda_1 \|U\|_F^2 + \lambda_2 \|V\|_F^2. \quad (5)$$

The first term in formula (5) is a fidelity term, which ensures that the parameter matrices  $U$  and  $V$  are consistent with the training data, while the last two terms are regular terms or constraint terms, and the matrix Frobenius norm is generally used as the regular term, where  $S$  represents the set of non-null scoring items in the user-object scoring matrix,

indicating that the loss function  $J(U, V)$  only fits the non-null items in the user-object scoring matrix;  $\lambda_1$  and  $\lambda_2$  are regularity parameters, which are used to adjust the degree of strong-weak relationship between fidelity term and regularity term. The solution problem of LFM is transformed into the following optimization problem, as shown in formula (6).

$$U, V = \arg \min_{u, v} J(U, V). \quad (6)$$

In order to solve formula (6), the most common optimization algorithm, batch gradient descent method, is introduced. The BGD is an iterative optimization algorithm by constantly updating each element  $U_{im}$  and  $V_{mj}$  in the  $U$  and  $V$  matrices, so that each update can approach the minimum value of the objective function  $J(U, V)$ . The updating rules are formulas (7) and (8).

$$U_{im}^{n+1} := U_{im}^n - \frac{\partial}{\partial U_{im}} J(U, V) * \alpha, \quad (7)$$

$$V_{mj}^{n+1} = V_{mj}^n - \frac{\partial}{\partial V_{mj}} J(U, V) * \alpha, \quad (8)$$

$N$  in the above formulas (7) and (8) denotes the current number of iterations, and  $\alpha$  is the learning rate or iteration step. Then, the partial derivatives of the objective function  $J(U, V)$  with respect to  $U_{im}$  and  $V_{mj}$  are solved, as shown in formulas (9) and (10).

$$\frac{\partial}{\partial U_{im}} J(U, V) = \sum_j 2V_{mj}(U_{i*} \cdot V_{*j} - r_{ij}) + 2\lambda_1 U_{im}, \quad (9)$$

$$\frac{\partial}{\partial V_{mj}} J(U, V) = \sum_i 2U_{im}(U_{i*} \cdot V_{*j} - r_{ij}) + 2\lambda_1 V_{mj}. \quad (10)$$

The complete iterative formula of BGD can be obtained by bringing formulas (9) and (10) into (7) and (8).

There are four hyperparameters in the PMF model, including the number of hidden factors  $k$ , regularization parameters  $\lambda_1$  and  $\lambda_2$ , and learning rate  $\alpha$ , where  $k$  describes the size of the model, which is generally related to the density of data,  $\lambda_1$  and  $\lambda_2$  describe the strength of regularization terms, which are generally used to overcome the overfitting problem of the model, and  $\alpha$  represents the adjustment degree and convergence rate of each update. Usually, the selection of super-parameters needs to be decided by experiments, and there are also cross-validations or Bayesian methods to help select super-parameters.

Subsequently, the probability model of PMF and its derivation process are explained. Because the essence of the

PMF model is to fit the  $R$  of score data, the PMF is a regression model on the whole. Based on the basic modeling idea of the regression model, it is assumed that the prediction error obeys the normal distribution with an expectation of 0, as shown in formulas (11) and (12).

$$\varepsilon \sim N(0, \sigma^2), \quad (11)$$

$$\varepsilon = r_{ij} - U_{i*} \cdot V_{*j}. \quad (12)$$

As shown in formula (12), the error is equal to the difference between the predicted value and the true value, from which the probability of the occurrence of the true value can be deduced as shown in formula (13).

$$p(r_{ij} | U_{i*}, V_{*j}, \sigma) = \frac{1}{\sqrt{2\pi}\delta} \exp\left(-\frac{(r_{ij} - U_{i*} \cdot V_{*j})^2}{2\delta^2}\right). \quad (13)$$

Formula (13) is arranged into a matrix expression as shown in formula (14).

$$p(R | U, V, \sigma) = \prod_{i=1}^m \prod_{j=1}^m \left[ \frac{1}{\sqrt{2\pi}\delta} \exp\left(-\frac{(r_{ij} - U_{i*} \cdot V_{*j})^2}{2\delta^2}\right) \right]^{I_{ij}}. \quad (14)$$

The goal of the model is to solve  $U$  and  $V$ , so the Bayesian formula is used to find the conditional probability expression of  $U$  and  $V$  and  $R$ , where  $I_{ij}$  is the indicator function, indicating whether  $r_{ij}$  is empty, as shown in formula (15).

$$p(U, V | R) = \frac{p(R | U, V)p(U)p(V)}{p(R)} \propto p(R | U, V)p(U)p(V). \quad (15)$$

Then, it is assumed that the parameters in  $U$  and  $V$  also obey a normal distribution with an expectation of 0 as shown in formula (16).

$$p(U | \sigma_U^2) = \prod_{i=1}^m N(U_i | 0, \sigma_U^2 I), p(V | \sigma_V^2) = \prod_{i=1}^m N(V | 0, \sigma_V^2 I). \quad (16)$$

According to formulas (14)–(16), conditional probability expressions for  $U$  and  $V$  and  $R$  can be obtained from the maximum a posteriori estimation framework. In order to simplify the calculation, the logarithmic form of the conditional probability will be obtained here, as shown in formula (17).

$$\begin{aligned} \ln p(U, V | R, \sigma, \sigma_U, \sigma_V) = & -\frac{1}{2\sigma^2} \sum_{i=1}^m \sum_{j=1}^m I_{ij} (r_{ij} - U_{i*} \cdot V_{*j})^2 - \frac{1}{2\sigma_U^2} \sum_{i=1}^m U_{i*}^T U_{i*} - \frac{1}{2\sigma_V^2} \sum_{j=1}^m V_{i*}^T V_{i*} \\ & - \frac{1}{2} \left( \left( \sum_{i=1}^m \sum_{j=1}^m I_{ij} \right) In\sigma^2 + nkIn\sigma_U^2 + mkIn\sigma_V^2 \right) + C. \end{aligned} \quad (17)$$

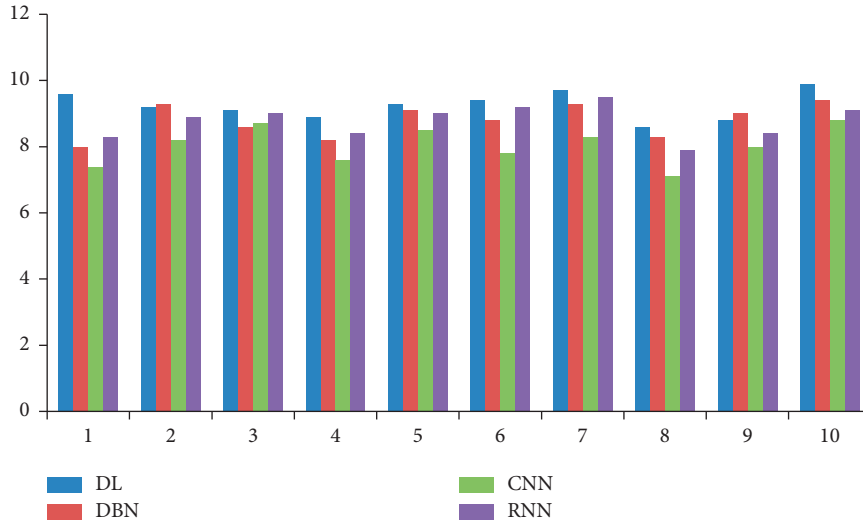


FIGURE 1: Comparison of the number of parameters.

$N$  denotes the number of users in the system,  $M$  denotes the number of objects in the system,  $K$  denotes the number of implicit factors, and formula (18) can be obtained by sorting out formula (17).

$$E = \frac{1}{2} \sum_{i=1}^m \sum_{j=1}^m I_{ij} (r_{ij} - U_{i*} \cdot V_{*j})^2 + \frac{\lambda_U}{2} \sum_{i=1}^m \|U_{i*}\|_F^2 + \frac{\lambda_V}{2} \sum_{j=1}^m \|V_{*j}\|_F^2 \quad (18)$$

According to the definition of the MAP framework, the solution goal is to find the parameters  $U$  and  $V$  so that the value in formula (7) is as large as possible, and the value of  $E$  in formula (18) is as small as possible. It can be found that the objective function and solution objective in formula (18) are consistent with those in the previous formula (5).

## 4. Experimental Analysis

**4.1. Performance Comparison.** In order to improve the accuracy of our later experiments, we have performed 10 experiments on the number of parameters, learning ability, and complexity of DL, DBN, CNN, and RNN, and compared the performance of the four algorithms, as shown in Figures 1–3.

Looking at Figures 1–3, we can clearly see that the DL algorithm has the strongest performance ability in terms of parameter number, learning ability, and complexity, so we choose the DL algorithm for the next experiment.

### 4.2. Analysis of the Proportion of Completed Points and Reduced Point Units in the Complete Set of Competitive Events

**4.2.1. Complete the Proportion Analysis of Subunit and Subunit.** In the evaluation part of the completion of the rules, the units of each action content reduction unit are

different. The difficulty/skill is to reduce the points once for each complete action, the operation action is to reduce the points once for each eight-beat action, and the main content (transition connection, cooperation, and lifting action) is to reduce the points once for each action. According to expert interviews, the principle of completing score reduction is to take the first grade of score reduction when multiple errors of the same grade (deviating from the degree of perfect completion) occur at the same time, and when errors of different grades occur, the light is avoided and more attention is paid.

Table 1 is obtained by video analysis and writing of the men's singles final set of the 15th World Championships. It can be seen from the following table that the number of difficulty reduction units in each group of men's singles is 80, and the proportion (40.00%) is the highest among all action contents. Followed by exercises, the total number is 65 (33.50%). Finally, there are transition connections, with a total number of 53 (26.50%).

Table 2 is obtained by video analysis and writing of the women's singles final set in the 15th World Championships. As can be seen from the following table, the number of difficulty reduction units in each group of women's singles is 80, accounting for 39.60%, which is the highest among all movements, followed by exercises, with a total number of 67 (33.17%).

Table 3 is obtained by video analysis and writing of the mixed doubles final set of the 15th World Championships. It can be seen from the following table that the number of difficulty reduction units in each group of mixed doubles is 72, accounting for 33.80%, which is the highest among all action contents. Then, there are transition connections, with a total number of 36 (16.90%) and, finally, cooperation, with a total number of 33 (15.49%). Lifting is the fixed content of collective projects, so each set has a reduction unit.

Table 4 is obtained by video analysis and writing of the 15th World Championships three-person final set. As can be seen from the following table, the number of difficulty



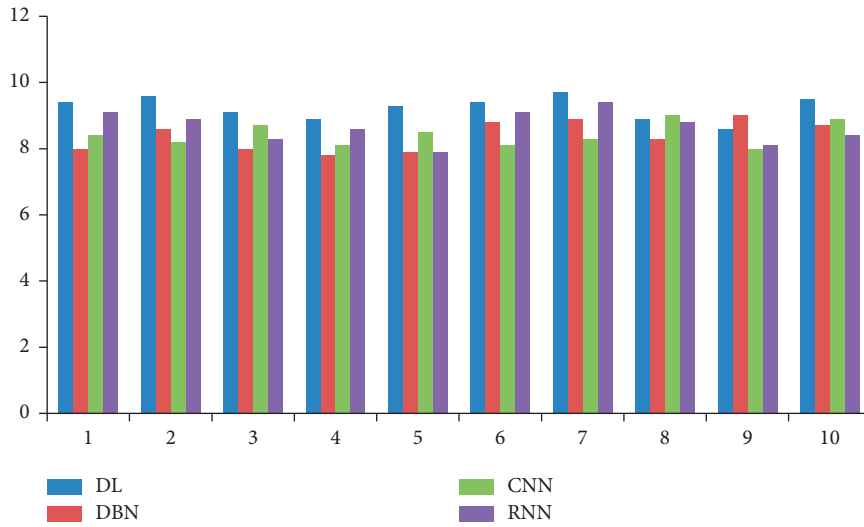


FIGURE 2: Comparison of learning ability.

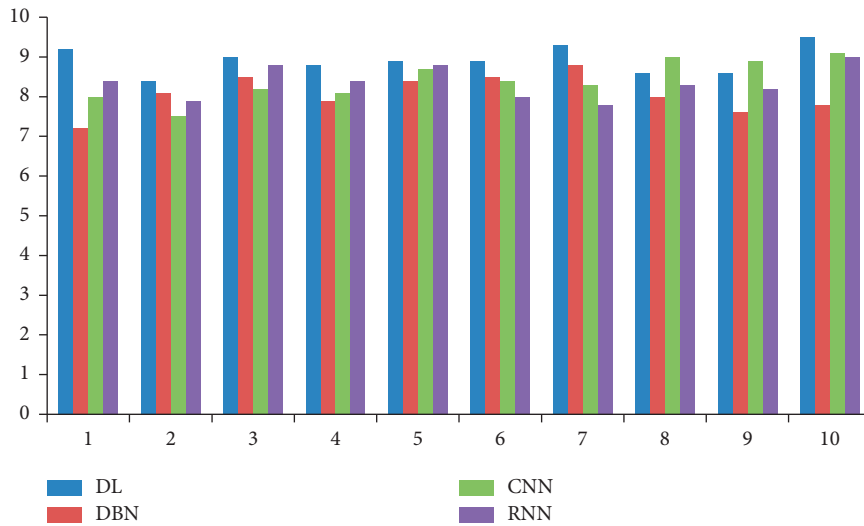


FIGURE 3: Comparison of complex capabilities.

TABLE 1: Statistics on the number of reduced units in men’s singles.

| Ranking    | Difficult movement | Exercise action | Transition connection | Total |
|------------|--------------------|-----------------|-----------------------|-------|
| 1          | 10                 | 8               | 7                     | 25    |
| 2          | 10                 | 8               | 5                     | 23    |
| 3          | 10                 | 9               | 6                     | 25    |
| 4          | 10                 | 9               | 8                     | 27    |
| 5          | 10                 | 8               | 7                     | 25    |
| 6          | 10                 | 9               | 7                     | 26    |
| 7          | 10                 | 8               | 6                     | 24    |
| 8          | 10                 | 8               | 7                     | 25    |
| Total      | 80                 | 65              | 53                    | 198   |
| Percentage | 40.00%             | 33.50%          | 26.50%                |       |

TABLE 2: Statistics of the number of women’s singles reduced units.

| Ranking    | Difficult movement | Exercise action | Transition connection | Total |
|------------|--------------------|-----------------|-----------------------|-------|
| 1          | 10                 | 8               | 6                     | 24    |
| 2          | 10                 | 9               | 8                     | 27    |
| 3          | 10                 | 8               | 8                     | 26    |
| 4          | 10                 | 8               | 6                     | 24    |
| 5          | 10                 | 8               | 7                     | 25    |
| 6          | 10                 | 9               | 8                     | 27    |
| 7          | 10                 | 9               | 7                     | 26    |
| 8          | 10                 | 8               | 5                     | 23    |
| Total      | 80                 | 67              | 55                    | 202   |
| Percentage | 39.60%             | 33.17%          | 27.23%                |       |

reduction units in each group of the three people is 72, accounting for 33.49%, which is the highest among all action contents. Followed by exercises, the total number is 66 (30.70%). Then, there are transition connections, with a total

number of 48 (16.90%) and, finally, cooperation, with a total number of 21 (9.77%).

Table 5 is obtained by video analysis and writing of the five-person final set of the 15th World Championships. As can be

TABLE 3: Statistics on the number of reduced units in mixed doubles in the 15th World Championships.

| Ranking    | Difficult movement | Exercise action | Transition connection | Collaboration | Lifting action | Total |
|------------|--------------------|-----------------|-----------------------|---------------|----------------|-------|
| 1          | 9                  | 8               | 4                     | 4             | 1              | 26    |
| 2          | 9                  | 8               | 4                     | 4             | 1              | 26    |
| 3          | 9                  | 9               | 5                     | 4             | 1              | 28    |
| 4          | 9                  | 8               | 6                     | 5             | 1              | 29    |
| 5          | 9                  | 8               | 5                     | 3             | 1              | 26    |
| 6          | 9                  | 6               | 5                     | 5             | 1              | 26    |
| 7          | 9                  | 8               | 5                     | 4             | 1              | 27    |
| 8          | 9                  | 9               | 2                     | 4             | 1              | 25    |
| Total      | 72                 | 64              | 36                    | 33            | 8              | 213   |
| Percentage | 33.80%             | 30.05%          | 27.23%                | 15.49%        | 3.76%          |       |

TABLE 4: Statistics on the number of reduction units completed by three people in the 15th World Championships.

| Ranking    | Difficult movement | Exercise action | Transition connection | Collaboration | Lifting action | Total |
|------------|--------------------|-----------------|-----------------------|---------------|----------------|-------|
| 1          | 9                  | 9               | 8                     | 2             | 1              | 29    |
| 2          | 9                  | 8               | 4                     | 3             | 1              | 25    |
| 3          | 9                  | 9               | 7                     | 2             | 1              | 28    |
| 4          | 9                  | 8               | 8                     | 3             | 1              | 29    |
| 5          | 9                  | 8               | 5                     | 2             | 1              | 25    |
| 6          | 9                  | 8               | 6                     | 2             | 1              | 26    |
| 7          | 9                  | 8               | 5                     | 3             | 1              | 26    |
| 8          | 9                  | 8               | 5                     | 4             | 1              | 27    |
| Total      | 72                 | 66              | 48                    | 21            | 8              | 215   |
| Percentage | 33.49%             | 30.70%          | 22.33%                | 9.77%         | 3.72%          |       |

TABLE 5: Statistics of the number of reduced units completed.

| Ranking    | Difficult movement | Exercise action | Transition connection | Collaboration | Lifting action | Total |
|------------|--------------------|-----------------|-----------------------|---------------|----------------|-------|
| 1          | 8                  | 9               | 4                     | 5             | 1              | 27    |
| 2          | 9                  | 8               | 5                     | 4             | 1              | 27    |
| 3          | 9                  | 8               | 6                     | 4             | 1              | 28    |
| 4          | 9                  | 8               | 4                     | 4             | 1              | 26    |
| 5          | 8                  | 10              | 5                     | 3             | 1              | 27    |
| 6          | 9                  | 9               | 7                     | 3             | 1              | 29    |
| 7          | 8                  | 8               | 5                     | 4             | 1              | 26    |
| 8          | 9                  | 9               | 6                     | 2             | 1              | 27    |
| Total      | 69                 | 69              | 42                    | 29            | 8              | 217   |
| Percentage | 32.73%             | 31.36%          | 22.33%                | 9.77%         | 3.64%          |       |

TABLE 6: Statistics on the number of reduced point units completed in the finals of the 15th World Championships.

|                 | Difficult movement | Exercise action | Transition connection | Collaboration | Lifting action |
|-----------------|--------------------|-----------------|-----------------------|---------------|----------------|
| Men's singles   | 10                 | 8.38            | 6.63                  |               |                |
| Women's singles | 10                 | 8.38            | 6.88                  |               |                |
| Mixed doubles   | 9                  | 8               | 4.5                   | 4.13          | 1              |
| Three persons   | 9                  | 8.25            | 6                     | 2.63          | 1              |
| Five people     | 9                  | 8.63            | 5.25                  | 3.63          | 1              |

seen from the following table, the number of difficulty reduction units in each group of five people is 72, accounting for 32.73%, which is the highest among all action contents, followed by exercises, with a total number of 69 (31.36%); then, there are transition connections, with a total number of 42 (19.09%) and, finally, cooperation, with a total number of 29 (13.18%).

4.2.2. Overall Analysis of Point Reduction Units in Complete Sets of Competitive Events. By writing 40 sets of videos, the number of units for completing points and reducing

points of different action contents in each competition routine is obtained, and Table 5 is calculated according to the average of the total number of individual items. As can be seen from Table 6, the average number of difficulty units in single events is 10 and that in collective events is 9. There are more than 8 units in each routine on average; because, in this cycle rule, it is required that there must be 8 complete operation units in each set, among which the average value of five people is the highest (8.63) and the average value of mixed doubles is the lowest (8). In the

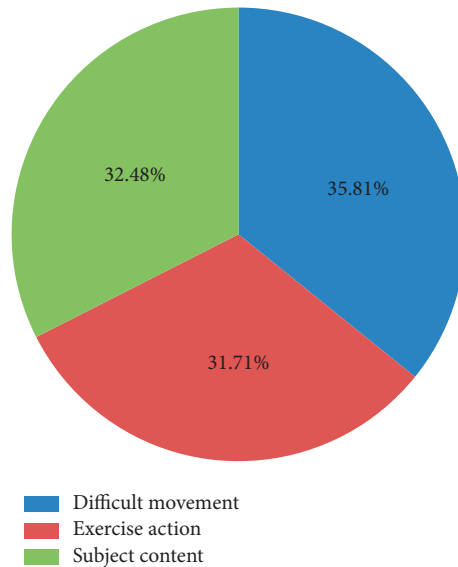


FIGURE 4: Percentage statistics of completed point reduction units.

TABLE 7: Statistics on the reduction of points in the contents of men’s singles in the 15th World Championships.

| Ranking    | Difficult movement | Exercise action | Transition connection |
|------------|--------------------|-----------------|-----------------------|
| 1          | 0.5                | 0.2             | 0.1                   |
| 2          | 0.9                | 0.1             | 0                     |
| 3          | 0.9                | 0.2             | 0                     |
| 4          | 0.5                | 0.7             | 0.2                   |
| 5          | 1                  | 0.2             | 0.1                   |
| 6          | 0.8                | 0.2             | 0.3                   |
| 7          | 1.2                | 0.2             | 0                     |
| 8          | 1.4                | 0.1             | 0                     |
| Total      | 7.2                | 1.9             | 0.7                   |
| Percentage | 73.47%             | 19.39%          | 7.14%                 |

TABLE 8: Statistics on the reduction of points in the completion of each movement content of women’s singles.

| Ranking    | Difficult movement | Exercise action | Transition connection |
|------------|--------------------|-----------------|-----------------------|
| 1          | 1                  | 0               | 0.2                   |
| 2          | 0.9                | 0.2             | 0.1                   |
| 3          | 0.9                | 0.4             | 0.3                   |
| 4          | 1.2                | 0.1             | 0.1                   |
| 5          | 1                  | 0.2             | 0.1                   |
| 6          | 1.1                | 0.3             | 0.2                   |
| 7          | 1.1                | 0.3             | 0.2                   |
| 8          | 1.8                | 0.3             | 0.2                   |
| Total      | 9                  | 1.8             | 1.4                   |
| Percentage | 73.77%             | 14.75%          | 11.48%                |

rules of this cycle, it is required that there must be no less than 4G+ actions in each set, and only G+ can be expressed by transitional connections in single events. Therefore, the average value of transitional connections in single events is significantly higher than that in collective events. In collective events, the average value of three-person exercises (6) is the highest and closest to single events, while mixed doubles events are the lowest (4.5). In cooperation, the average number of units in mixed doubles is the highest (4.13), while that in triple doubles is the lowest (2.63).

Figure 4 is obtained by adding the total data of each item and calculating the percentage. It can be seen that the number of units with difficulty to complete the reduction is the largest, accounting for 35.81%.

4.3. Complete the Statistics and Analysis of Points and Reductions. The reduction statistics studied in this section are based on the rules, and the error between the final reduction scores and the actual reduction scores of the complete set is within the allowable range of the rules.

It can be seen from Table 7 that the action content with the most point reduction in men’s singles is the difficulty action, and the total difficulty reduction is 7.2, accounting for 73.47% and, finally, the transition connection, with a total reduction of 0.7, accounting for 7.14%.

It can be seen from Table 8 that the action content with the most point reduction in men’s singles is the difficulty action, and the total difficulty reduction is 9.0, accounting for 73.77% and, finally, the transition connection, with a total reduction of 1.4, accounting for 11.48%.

From Table 9, it can be seen that the highest ranking of mixed doubles is the difficulty movement, and the lowest ranking is the transition connection. The total difficulty reduction is 6.3, accounting for 57.27%. The total reduction score of consistency is 2.1, accounting for 19.09%. The total reduction score of maneuvering movements is 1.3, accounting for 11.82%. The total reduction of cooperation is 0.3, accounting for 2.73%. The total deduction of overlink is 0.1, accounting for 0.91.

It can be seen from Table 10 that the contents of the three-person project from high to low are difficulty action, consistency, operation action, lifting action, cooperation,

TABLE 9: Statistics on the reduction of points for each action content of mixed doubles.

| Ranking    | Difficult movement | Exercise action | Transition connection | Collaboration | Lifting action | Consistency |
|------------|--------------------|-----------------|-----------------------|---------------|----------------|-------------|
| 1          | 0.8                | 0               | 0                     | 0.1           | 0.1            | 0.1         |
| 2          | 0.9                | 0.1             | 0                     | 0             | 0.1            | 0.3         |
| 3          | 0.5                | 0.1             | 0                     | 0.1           | 0.3            | 0.3         |
| 4          | 0.8                | 0.1             | 0                     | 0.1           | 0.1            | 0.3         |
| 5          | 0.9                | 0.1             | 0.1                   | 0             | 0              | 0.2         |
| 6          | 1                  | 0.3             | 0                     | 0             | 0.1            | 0.1         |
| 7          | 0.4                | 0.5             | 0                     | 0             | 0.1            | 0.5         |
| 8          | 1                  | 0.1             | 0                     | 0             | 0.1            | 0.3         |
| Total      | 6.3                | 1.3             | 0.1                   | 0.3           | 0.9            | 2.1         |
| Percentage | 57.27%             | 11.82%          | 0.91%                 | 2.73%         | 8.18%          | 19.09%      |

TABLE 10: Statistics on the reduction of points in each action content of the three people in the 15th World Championships.

| Ranking    | Difficult movement | Exercise action | Transition connection | Collaboration | Lifting action | Consistency |
|------------|--------------------|-----------------|-----------------------|---------------|----------------|-------------|
| 1          | 0.6                | 0.2             | 0                     | 0             | 0              | 0.4         |
| 2          | 0.7                | 0.2             | 0.2                   | 0             | 0.1            | 0.2         |
| 3          | 0.5                | 0.3             | 0.1                   | 0.1           | 0.1            | 0.3         |
| 4          | 0.6                | 0.2             | 0.2                   | 0.1           | 0.1            | 0.2         |
| 5          | 0.9                | 0.2             | 0                     | 0.1           | 0.1            | 0.2         |
| 6          | 0.7                | 0.1             | 0                     | 0.2           | 0.1            | 0.4         |
| 7          | 0.6                | 0.3             | 0                     | 0.2           | 0.3            | 0.2         |
| 8          | 1.5                | 0               | 0                     | 0             | 0              | 0.3         |
| Total      | 6.1                | 1.5             | 0.5                   | 0.7           | 0.8            | 2.2         |
| Percentage | 51.69%             | 12.71%          | 4.24%                 | 5.93%         | 6.78%          | 18.64%      |

TABLE 11: Statistics of score reduction of action content completion.

| Ranking    | Difficult movement | Exercise action | Transition connection | Collaboration | Lifting action | Consistency |
|------------|--------------------|-----------------|-----------------------|---------------|----------------|-------------|
| 1          | 0.8                | 0.2             | 0                     | 0.1           | 0              | 0.4         |
| 2          | 0.9                | 0.2             | 0                     | 0             | 0.1            | 0.2         |
| 3          | 0.7                | 0.2             | 0                     | 0.1           | 0.1            | 0.3         |
| 4          | 0.7                | 0.1             | 0                     | 0.1           | 0              | 0.5         |
| 5          | 0.6                | 0.2             | 0                     | 0.1           | 0.1            | 0.4         |
| 6          | 1                  | 0               | 0.2                   | 0             | 0              | 0.3         |
| 7          | 1.1                | 0.1             | 0.1                   | 0.1           | 0.1            | 0.2         |
| 8          | 1                  | 0.2             | 0                     | 0.2           | 0.1            | 0.3         |
| Total      | 6.8                | 1.2             | 0.3                   | 0.7           | 0.5            | 2.6         |
| Percentage | 56.20%             | 9.92%           | 2.48%                 | 5.79%         | 4.13%          | 21.49%      |

and transition connection, and the total difficulty reduction is 6.1, accounting for 51.69%. The total consistency reduction is 2.2, accounting for 18.64%. The total reduction of maneuvering movements is 1.5, accounting for 12.71%. The total reduction of cooperation is 0.7, accounting for 5.93%. The total reduction of transition connection is 0.5, accounting for 4.24%.

From Table 11, it can be seen that the contents of the five-person project from high to low are difficulty action, consistency, operation action, cooperation, lifting action, and transition connection. The total reduction score of difficulty action is 6.8, accounting for 56.20%. The total reduction score of sex is 2.6, accounting for 21.49%. The total reduction of cooperation is 0.7, accounting for 5.79%. The total reduction of lifting action is 0.5, accounting for 4.13%. The total reduction score of transition connection is 0.3, accounting for 2.48%.

Figure 5 is the statistics of the percentage of points reduced in the final of a single event. As can be seen from the following figure, the difficulty is to complete the action

content with the largest proportion of point reduction, accounting for 74% of the total point reduction, followed by exercises, accounting for 17% and, finally, transition connection, accounting for 9%.

Figure 6 is the statistics of point reduction in the final completion of collective events. As can be seen from the following figure, the highest ranking for reducing points is the difficult action, and the lowest ranking is the transition connection. Among them, the proportion of difficult movements is 55%.

This study found that in collective events, the proportion of consistency reduction is second only to the proportion of difficulty reduction, and collective events should be paid attention to in training. Exercise movement is a complete set of movement content second only to difficulty reduction, and the reduction of exercise movement is mainly posture reduction. Athletes should also pay attention to the training of basic skills while improving the complete set of difficulties.

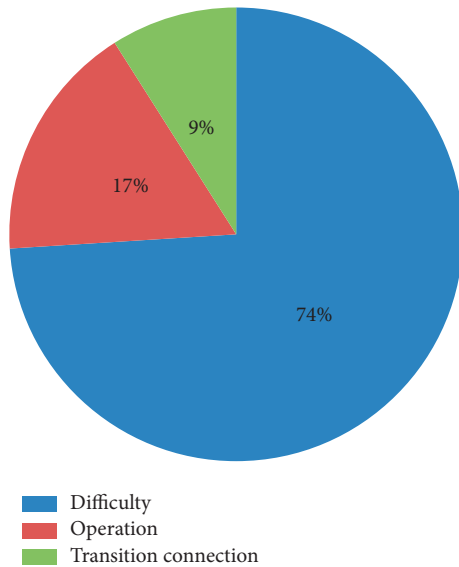


FIGURE 5: Statistics on the proportion of point reduction completed by a single project.

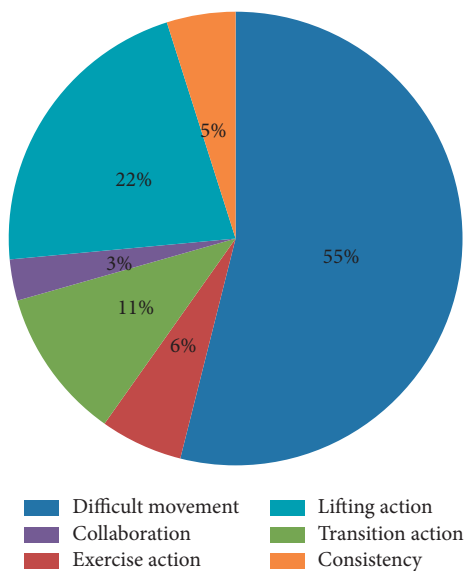


FIGURE 6: Statistics on the proportion of point reduction completed by collective projects.

## 5. Conclusions

The society attaches great importance to physical education and sports training. There are many kinds of modern sports, and aerobics is one of the sports. It plays an important role in losing weight, strengthening the body, and exercising cardiopulmonary function. Therefore, it is necessary to strengthen aerobics teaching and training, realize the integrated development of theoretical teaching and skill training, analyze the problems existing in the concrete practice of aerobics teaching and training mode in time, actively explore and study the construction methods of aerobics teaching and training mode, and continuously improve the overall level and quality of aerobics teaching and training. In the

dimension of completing point reduction, through the statistics and analysis of 40 sets of final videos of competitive events in the 15th World Championships, it is found that difficult movements account for the largest proportion of the number of units completing point reduction and completing point reduction. The highest score for a single-player project is the difficulty action, and the lowest is the transition connection. Difficult movements rank highest in the scores of collective events.

## Data Availability

The experimental data used to support the findings of this study are available from the corresponding author upon request.

## Conflicts of Interest

The authors declared that they have no conflicts of interest regarding this work.

## References

- [1] C. Kereliuk, B. L. Sturm, and J. Larsen, "Deep learning and music adversaries," *IEEE Transactions on Multimedia*, vol. 17, no. 11, pp. 2059–2071, 2015.
- [2] Y. Chen, Y. Li, N. Rajiv, A. Subramanian, and X. Xie, "Gene expression inference with deep learning," *Bioinformatics*, vol. 32, Article ID 1832, 2016.
- [3] C. S. Lee, D. M. Baughman, and A. Y. Lee, "Deep learning is effective for classifying normal versus age-related macular degeneration OCT images," *Ophthalmology Retina*, vol. 1, no. 4, pp. 322–327, 2017.
- [4] T. Fischer and C. Krauss, "Deep learning with long short-term memory networks for financial market predictions," *European Journal of Operational Research*, vol. 270, no. 2, 2017.
- [5] L. Ji, L. Ren, J. Lu, J. Feng, and J. Zhou, "Consistent-aware deep learning for person Re-identification in a camera network," in *Proceedings of the 2017 IEEE Conference on Computer Vision and Pattern Recognition (CVPR)*, IEEE, Honolulu, HI, USA, July 2017.
- [6] C. Kai and H. Qiang, "Scalable training of deep learning machines by incremental block training with intra-block parallel optimization and blockwise model-update filtering," in *Proceedings of the 2016 IEEE International Conference on Acoustics, Speech and Signal Processing (ICASSP)*, IEEE, Shanghai, China, March 2016.
- [7] X. Yang, D. Lo, X. Xia, Y. Zhang, and J. Sun, "Deep learning for just-in-time defect prediction," in *Proceedings of the IEEE International Conference on Software Quality*, IEEE, Vancouver, BC, Canada, August 2015.
- [8] A. M. Saxe, Y. Bansal, J. Dapello et al., "On the information bottleneck theory of deep learning," in *Proceedings of the ICLR 2018*, Vancouver, Canada, 2018.
- [9] P. Yan, "Aerobics factors for youth stroke auxiliary therapeutic effect," *Bulletin of Science and Technology*, vol. 3, no. 2, pp. 37–86, 2014.
- [10] A. A. Behery, "Effects of a training program using aqua aerobics on improving the functional status of individuals with Diabetes," *Journal of American Science*, vol. 7, no. 13, pp. 361–419, 2004.
- [11] N. Viski-Stalec, J. Stalec, R. Kati, Đ. Podvorac, and D. Katović, "The impact of dance-aerobics training on the morpho-motor

- status in female high-schoolers," *Collegium Antropologicum*, vol. 31, no. 1, 259 pages, 2007.
- [12] Z. Ping, "Research on using modern educational technology to training students ability of producing aerobics," *Information Technology Journal*, vol. 13, no. 5, pp. 954–959, 2014.
- [13] S. Hong and M. Guo, "Survey of the course and characters during the image training of aerobics," *Journal of Shaoguan University*, vol. 21, no. 9, pp. 832–896, 2006.
- [14] C. Lu and J. S. Armstrong, "Role of calcium and cyclophilin D in the regulation of mitochondrial permeabilization induced by glutathione depletion," *Biochemical and Biophysical Research Communications*, vol. 363, no. 3, pp. 572–577, 2007.

## Research Article

# Traffic Flow Prediction and Application of Smart City Based on Industry 4.0 and Big Data Analysis

**Yuqian Gong**

*Beijing Huak Technology Development Co Ltd., Beijing 10002865292, China*

Correspondence should be addressed to Yuqian Gong; kevin\_space@163.com

Received 6 April 2022; Revised 6 June 2022; Accepted 13 June 2022; Published 1 August 2022

Academic Editor: Man Fai Leung

Copyright © 2022 Yuqian Gong. This is an open access article distributed under the Creative Commons Attribution License, which permits unrestricted use, distribution, and reproduction in any medium, provided the original work is properly cited.

For smart city traffic flow prediction in the period of big data and industry 4.0, the prediction accuracy is low, the prediction is difficult, and the prediction effect is different in different geographical locations. This paper proposes a smart city traffic communication forecast based on Industry 4.0 and big data analysis application. Firstly, this paper theoretically explains the application scenario of urban traffic fault text big data and analyzes the characteristics of related problems, especially the fault problems. Secondly, the AC traffic prediction algorithm is studied, and the application analysis of PVHH, IDT, and Ford-Fulkerson algorithms is applied, respectively. Finally, the above three algorithms are used to predict and analyze traffic flow.

## 1. Introduction

With the advent of the industry 4.0 era, artificial intelligence and big data analysis play an important role in China's information construction. In order to understand the occurrence, development, diagnosis, and treatment of diseases more accurately, it is necessary to analyze the whole molecular measurement in multiple groups and obtain more abundant information resources from the analysis, so it is necessary to evaluate more data. At this time, the above problems can be effectively solved by using artificial intelligence [1]. Depression is a common psychological disease in today's society. There are many people suffering from this disease, which seriously affects everyone's health and social function [2]. Depression alone affects 11% of the world's population, where mental health has caused great pain and damage. In order to effectively treat this disease, artificial intelligence and big data technology are increasingly used in depression, providing new methods for clinical diagnosis and treatment. Of course, there are not many markers to prove mental health, so that it depends on the questionnaire data of patients and doctors for explanation [3]. Nowadays, microbiology is one of the important disciplines in biology, which includes a wide range of bacteria, viruses, and fungi, and all belong to microorganisms, and it is closely related to

human beings [4–6]. It has been identified as one of the causes of many cancers, such as *Helicobacter pylori*. Man is its only host, and it is almost impossible to heal after being infected. *Helicobacter pylori* plays a very important role in the treatment of gastric cancer. With the development of sequencing technology, a large number of complex data has been generated. However, there are still obstacles in the analysis of these data, which is not conducive to making correct decisions. However, the emergence of artificial intelligence helps and properly solves the doctors' processing of these data [7].

The rapid development of artificial intelligence (AI) and big data has stimulated the tide of various social networks and produced a lot of social data worth analyzing [8]. Mining the relationship among social organizations, networks, and media is a key point of social computing. The large increase of these data makes it more difficult to mine large-scale social data. Now, the combination of human intelligence and artificial intelligence is applied to social computing, which provides more methods for the analysis and detection of social data, and is a new direction of artificial intelligence and big data research [9]. Today's electromagnetic environment is still not optimistic, and spectrum resources are relatively few. In actual division, there will be uneven distribution, and the existing

monitoring level is not enough, so there is no way to fully grasp the frequency usage. In order to solve this problem, an electromagnetic spectrum monitoring scheme combining big data and artificial intelligence is proposed, which mainly aims at various applications and related businesses and strengthens the construction of handheld monitoring systems, big data analysis systems, and electromagnetic spectrum monitoring system [10].

In teaching, the effect of online education is far less than that of actual classroom teaching. In order to improve the learning effect of online teaching combined with the actual needs of online education, the evaluation technology based on artificial intelligence big data technology is established with evaluation as the center of teaching, Model analysis is carried out through actual teaching, and various functional modules are established based on learning objectives, all of which are aimed at developmental evaluation. The results show that some models have good performance [11].

The safety of urban traffic is a permanent theme. Bus, as an important national facility and a means of transportation with high frequency, has a great responsibility for ensuring the safety of people's lives and property. In recent years, with the rapid development of expressways in China, expressway undertakes more important transportation tasks. However, the occurrence of various disasters and other unexpected events also bring great hidden dangers to highway transportation safety. This paper focuses on the research and application of big data analysis technology for urban traffic accidents, as well as the establishment of cloud service network for urban traffic emergency management and the proposal of highway cloud resource scheduling based on cloud computer and double-layer particle swarm optimization. The integrated management of high-speed emergency big data and the optimization of the emergency scheme were studied, and good results were achieved [12–15].

## 2. Theoretical Basis

**2.1. Analysis and Application of Urban Traffic Fault Text Big Data.** Urban transportation has entered the era of big data. The analysis of urban traffic faults should be composed of safety supervision report, accident database, and other parts. Big data analysis is used to realize the functions of retrieval, extraction, intelligent classification, and related analysis of urban traffic faults [16, 17].

China's urban traffic safety monitoring system is composed of monitoring object layer, monitoring layer, and management layer. Because of the different monitoring objects, it can be divided into three types: people, equipment, and environment. Its dataset has four characteristics, namely, scale, diversity, rapidity, and value.

- (1) Scale generally refers to the amount of data.
- (2) Diversity: It means that its data comes from many kinds of sources, which is beyond the data range previously included, including semistructured data and unstructured data. In addition, it also analyzes various data such as weather, earthquake, and

ministry of public security, shown as follows: Figure 1 describes the classification of traffic big data and whether the internal data and external data mainly come from the transportation department are being judged. In internal data, structured data can be stored directly while Figure 1 unstructured data cannot be stored directly, so it needs to be converted into structured data for storage by technical means.

- (3) Fast speed: big data mining lies in the fast processing speed, that is to say, data streams are mostly high-speed and need fast and continuous real-time processing by processing all kinds of data in time to ensure the safety of urban road driving.
- (4) Value: the value of road safety lies in the use of data, statistical analysis, and classification algorithm to analyze big data, so as to find correlation and knowledge, predict accident failure safety problems, and provide basis for ensuring driving safety.

Urban traffic is a complex transportation system. Many experts analyze accidents and faults around safety evaluation, which provides favorable decisions for the prevention of safety accidents and faults. Experts use the accident fault data accumulated over the years to analyze the development rules of accident fault from the perspective of data analysis. This paper uses text big data analysis technology for statistical analysis to promote the application of urban traffic safety big data.

The application of fault analysis to accidents includes the following functions: feature extraction, accident-prone areas, fault analysis, full-text search, association analysis, and system management (Figure 2).

**2.2. Full-Text Retrieval of Urban Traffic Faults.** In the era of big data, it is of great significance to realize full-text retrieval through urban traffic big data technology. In this paper, through the establishment of full-text retrieval, combined with the actual traffic situation, the storage of traffic unstructured accident fault text, index building, Chinese word segmentation, and full-text retrieval is realized to find important messages in accident fault text.

Failure text retrieval is about indexing documents, queries, and the relationship between the users by using TF-IDF to retrieve and text analysis.

TF denotes word frequency, and the formula is as follows:

$$TF_{i,j} = \frac{n_{i,j}}{\sum_k n_{k,j} + 1}. \quad (1)$$

In the above formula,  $n_{i,j}$  represents the number of occurrences,  $\sum_k n_{k,j}$  represents the second sum of occurrences, and the denominator is added with 1 to prevent the denominator from being 0.

IDF denotes the reverse document frequency as follows:

$$IDF_i = \log \frac{N}{k_i + 1}, \quad (2)$$



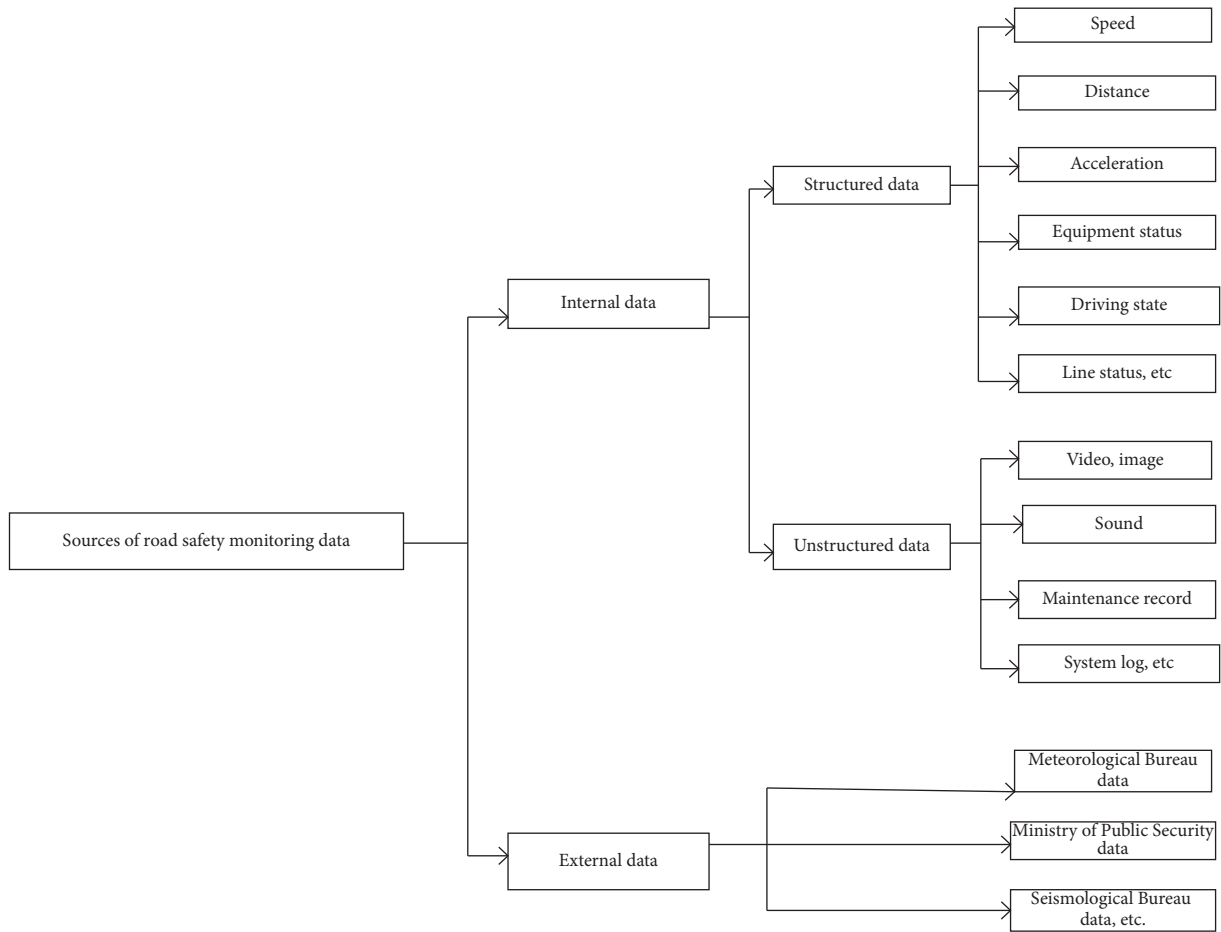


FIGURE 1: Sources of road safety data.

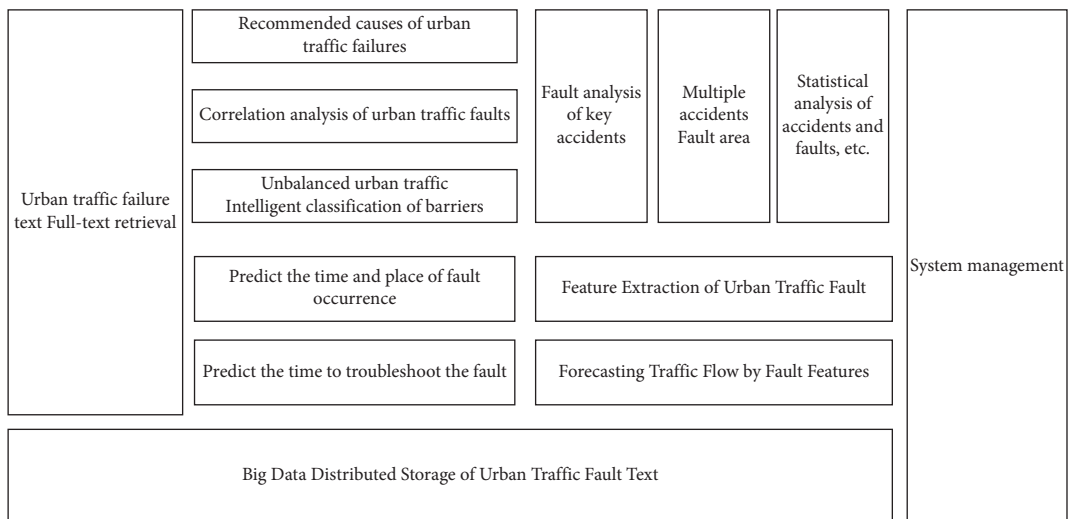


FIGURE 2: Functional architecture.

where  $k_i$  represents the number of documents and  $N$  represents the size of  $D$ . The denominator is added by 1 to prevent the denominator from being 0.

Combine TF with IDF to get the weight:

$$W_{i,j} = TF_i \times IDF_i. \tag{3}$$

Document  $D_j$  is reorganized into vectors with word weights:

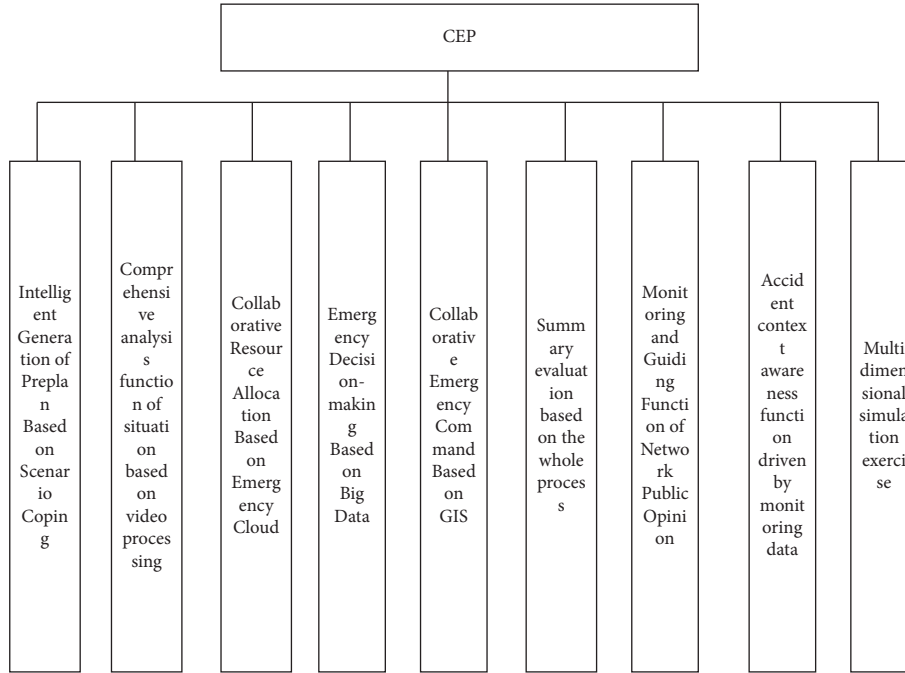


FIGURE 3: Functional diagram of urban traffic emergency platform.

$$d_j = \langle W_{1,j}, W_{2,j}, W_{3,j}, \dots, W_{n,j} \rangle. \quad (4)$$

The cosine distance is calculated as follows:

$$\text{sim}(q, d) = \frac{\sum W_{i,j}^q \times W_{i,j}}{|q_j| \times |d_j|}. \quad (5)$$

Finally, according to the results, the documents can be arranged to select the most suitable document for the user.

**2.3. Technical Research and Analysis of Urban Traffic Emergency Management.** The achievements of China's urban transportation can be said to attract worldwide attention, and it has won worldwide recognition for its characteristics of "high efficiency, high safety, and high quality service." It is very important to establish a perfect safety early warning and emergency management model. Because emergencies are unpredictable, an emergency management mode derived from cloud computing can be formed, a cloud service network can be established, and technologies such as Internet of Things and big data can be used to improve the efficiency of dealing with emergencies.

**2.3.1. The Main Functions of the Urban Traffic Emergency Platform (CEP).** Figure 3 illustrates the main functions of the urban traffic emergency platform (CEP), which is mainly divided into 9 functions, each of which can achieve different target requirements. It has certain intelligent control value for traffic control and realizes the goal of intelligent transportation in Industry 4.0 (Figure 3).

By establishing an "emergency cloud" to realize the application and deployment of network resources, the utilization rate of resources is greatly improved.

**2.3.2. Emergency Cloud Service Virtualization Modeling.** In the field of cloud computing, virtualization technology is a very important key technology.

For virtualized storage resources, the formula is as follows:

$$D_i = \{D_{i1}, D_{i2}, D_{i3}, \dots, D_{ij}, \dots, D_{is_i}\}, \quad (6)$$

where  $D_{ij}$  is the  $J$ th virtual machine virtualized from the  $I$ -th storage server and  $s_i$  is the number of virtual machines in the storage.

For computational virtualization, the formula is as follows:

$$C_i = \{C_{i1}, C_{i2}, C_{i3}, \dots, C_{ij}, \dots, C_{is_i}\}, \quad (7)$$

where  $C_{ij}$  has similar functionality to  $D_{ij}$ .

For virtualized rescue services, the formula is as follows:

$$T_i = \{T_{i1}, T_{i2}, T_{i3}, \dots, T_{ij}, \dots, T_{is_i}\}, \quad (8)$$

where  $T_{ij}$  is the virtual rescue vehicle service from the  $i$ -th rescue vehicle server and 4S is the virtual service number in the rescue vehicle service.

**2.3.3. Cloud Service.** The virtualized storage resources of the emergency cloud are gathered together to form a storage pool, and the formula is as follows:

$$\begin{aligned} DP &= \{D_1 \cup D_2 \cup D_3 \cup \dots \cup D_{n_1-1} \cup D_{n_1}\} \\ &= \{D_{1,1}, D_{1,2}, D_{1,3}, \dots, D_{1,s_1}\} \cup \{D_{2,1}, D_{2,2}, D_{2,3}, \dots, D_{2,s_1}\} \cup \\ &\quad \{D_{3,1}, D_{3,2}, D_{3,3}, \dots, D_{3,s_1}\} \cup \dots \cup \{D_{n_1,1}, D_{n_1,2}, D_{n_1,3}, \dots, D_{n_1,s_1}\}, \end{aligned} \quad (9)$$

where  $n_1$  refers to the number of storage servers.

The virtual network energy gathered together is the network pool, and the formula is

$$\begin{aligned}
 NP &= \{N_1 \cup N_2 \cup N_3 \cup \dots \cup N_{n_3-1} \cup N_{n_3}\} \\
 &= \{N_{1,1}, N_{1,2}, N_{1,3}, \dots, N_{1,s_3}\} \\
 &\cup \{N_{2,1}, N_{2,2}, N_{2,3}, \dots, N_{2,s_3}\} \\
 &\cup \{N_{3,1}, N_{3,2}, N_{3,3}, \dots, N_{3,s_3}\} \\
 &\cup \dots \cup \{N_{n_3,1}, N_{n_3,2}, N_{n_3,3}, \dots, N_{n_3,s_3}\},
 \end{aligned} \tag{10}$$

where  $n_3$  is the number of network servers.

**2.3.4. Cloud Computing Model.** The resources used by the emergency platform are virtual cloud services and they are shared, but there are also constraints as follows.

All rescue system resources should be less than the total storage pool resources, and the formula is

$$\sum_{i=1}^{y_n} k'_1(i) \langle DG_{\max} \rangle \tag{11}$$

In the above formula,  $y_n$  is the number of emergency rescue systems and  $DG_{\max}$  is the total number of virtual resources in the storage pool.

$$\sum_{i=1}^{y_n} k'_2(i) \langle CG_{\max} \rangle \tag{12}$$

In the above formula,  $CG_{\max}$  is the total number of virtual resources in the calculation pool.

$$\sum_{i=1}^{y_n} k'_3(i) \langle NG_{\max} \rangle \tag{13}$$

In the above formula,  $NG_{\max}$  is the total number of virtual resources in the network pool.

$$\sum_{i=1}^{y_n} k'_4(i) \langle TG_{\max} \rangle \tag{14}$$

In the above formula,  $TG_{\max}$  is the total number of virtual resources in the rescue vehicle service pool.

$$\sum_{i=1}^{y_n} k'_5(i) \langle PG_{\max} \rangle \tag{15}$$

In the above formula,  $PG_{\max}$  is the total number of virtual resources in the rescue team service pool.

$$\sum_{i=1}^{y_n} k'_7(i) \langle RG_{\max} \rangle \tag{16}$$

In the above formula,  $RG_{\max}$  is the total number of virtual resources in the emergency materials service pool.

Through the above establishment and application research of emergency cloud, cloud computing, and big data technologies, the application and deployment of emergency platform network resources are completed, and a double-layer particle swarm optimization algorithm is proposed to establish constraints and effectively determine the number of emergency cloud resource scheduling.

**2.3.5. Urban Traffic Operation Model.** With the rapid development of urban transportation in China, the demand for passenger transport is also growing day by day, and various capacity scheduling problems in passenger transport are obvious. In order to solve the capacity problems, the adjustment of operation scheme and operation diagram has become very frequent. Passenger flow is the basic basis for determining the operation plan. Short-term passenger flow forecasting method and gradient lifting decision tree method are used for comparative analysis.

- (1) The classification of short-term passenger flow forecasting methods is as follows (Figure 4): Passenger flow forecasting is based on the time characteristics of historical passenger flow and predicts the total amount and distribution of future passenger flow. Measurement, such as the prediction of future lines and related traffic at each station.
- (2) CART decision tree and gradient lifting algorithm.

Decision tree model is a nonparametric classifier, which is composed of regression tree and classification tree, and the two tree types are different in essence.

The CART decision tree formula is as follows:

$$F(j, s) = \arg \min \left[ \min_{x_i \in R_1(j, s)} \sum (y_i - C_1)^2 + \min_{x_i \in R_2(j, s)} \sum (y_i - C_2)^2 \right] \tag{17}$$

In the above formula,  $C_m$  is the mean value generated after division.

J.H. Friedman, a professor at Stanford, invented gradient lifting method, which is one of the ensemble algorithms. As an iterative decision tree algorithm, it has fast training speed and can reduce prediction deviation, so it is one of the most effective methods in machine learning algorithms. Its basic origin is as follows:

$$F(x) = \sum_{m=0}^M \beta_m h(x; a_m) \tag{18}$$

In the above formula,  $h(x; a_m)$  is the subtree,  $a_m$  is the parameter, and  $\beta_m$  is the weight in the prediction function.

The first regression tree:

$$F_0 = \arg \min \sum_{i=1}^N L(y_i, h_0(x_i, a)) \tag{19}$$

Negative gradient of loss function:

$$\tilde{y}_{mi} = - \left[ \frac{\partial L(y_i, F(X_i))}{\partial F(X_i)} \right]_{F(x)=F_{m-1}(x)},$$

$$a_m = \arg \min \sum_{i=1}^N [\tilde{y}_{mi} - h(X_i; a)]^2 \tag{20}$$

$$\beta_m = \arg \min \sum_{i=1}^N L(y_i, F_{m-1}(X_i) + \beta h(X_i; a_m))$$

Update prediction function:

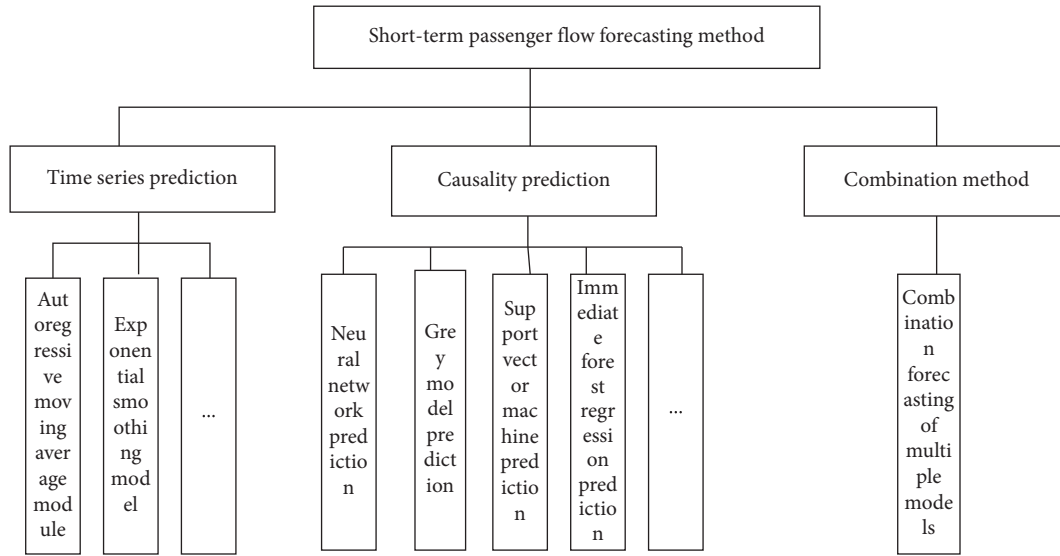


FIGURE 4: Short-term passenger flow forecasting method.

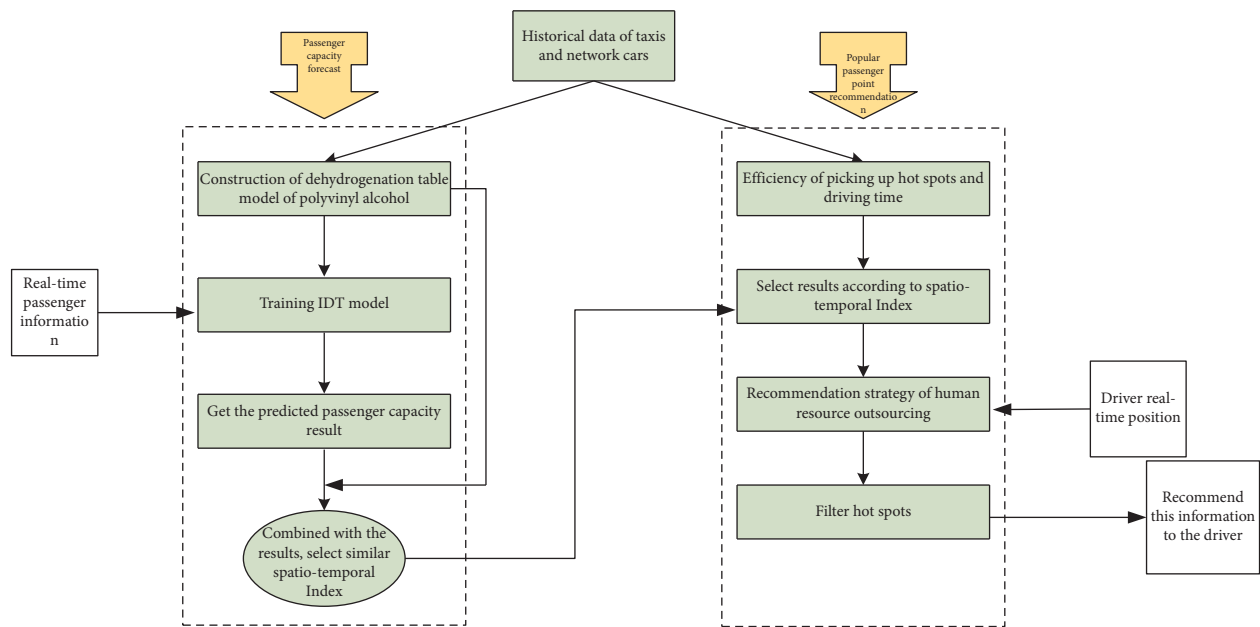


FIGURE 5: Popular passenger frame model of taxis and network cars.

$$F_m(X) = F_{m-1}(X) + v\beta_m h(X; a_m). \quad (21)$$

### 3. Model Application

3.1. PVHH Prediction Model and IDT Prediction Algorithm. Combining the model analysis of urban traffic in the previous chapter with the passenger data of Tianjin network car and taxi, this paper puts forward the PVHH prediction model and IDT prediction algorithm of passenger capacity. The general framework of its passenger hotspots is shown in Figure 5.

The PVHH prediction model is based on the collected data of taxis and network cars and then analyzes the popular passenger points in the past, extracts the flow and distribution of passengers, and understands the trend of mobile personnel in the whole city.

The IDT algorithm mainly uses the information gain theory in decision tree to analyze the influence of different data at each moment on the predicted value. The labels of prediction models are original features (hotspots<sub>i</sub>, m) and original labels (hotspots<sub>i</sub>, m), respectively. In order to be suitable for machine learning classification algorithms, it is especially necessary to quantify data and weigh them. The

```

Input: import trainset (hotspotsi,  $m$ ,  $w$ )--dataset R;
Number of times—K;
Scheme—single-level decision tree;
Output: composite model.
(1) Start;
(2) weight setting— $1/[R]$ ;
(3) for( $i = 1; i < K; i++$ );
(4) Sampling put back— $R_i$  and forecasting model— $M_i$ ;
(5) Error rate  $\Theta$  of model  $M_i$ ;
(6) if  $\Theta > 0.5$  return to step 6;
(7) for (all data  $R_{ij}$  in  $R_i$ );
(8) Update the weight of data  $R_{ij}$ ;
(9) end for;
(10) return to K group training model;
(11) End.

```

ALGORITHM 1: IDT algorithm code.

specific characteristics of prediction model labels are as follows:

$$\begin{aligned}
 \text{features}(\text{hotspots}_i, m, w) &= \begin{bmatrix} \hat{P}_{i1}^{m-k} * w_{m-k}, \hat{P}_{i1}^{m-k+1} * w_{m-k+1}, \dots, \hat{P}_{i1}^{m-1} * w_{m-1} \\ \hat{P}_{i2}^{m-k} * w_{m-k}, \hat{P}_{i2}^{m-k+1} * w_{m-k+1}, \dots, \hat{P}_{i2}^{m-1} * w_{m-1} \\ \dots \\ \hat{P}_{in}^{m-k} * w_{m-k}, \hat{P}_{in}^{m-k+1} * w_{m-k+1}, \dots, \hat{P}_{in}^{m-1} * w_{m-1} \end{bmatrix}, \\
 \text{labels}(\text{hotspots}_i, m) &= [q_{i1}, q_{i2}, \dots, q_{in}].
 \end{aligned} \tag{22}$$

Adaboost algorithm constantly updates the sample weight value to achieve the correct sample weight value reduction. The wrong sample weight value increases this classification purpose. Because taxis and network cars need to update the data of popular passenger points in real time, the Adaboost algorithm can update the prediction model. The IDT algorithm is shown in Algorithm 1.

**3.2. Ford–Fulkerson Algorithm.** Nowadays, urban traffic congestion is becoming more and more serious, so it is very important to analyze and evaluate traffic bottlenecks. Aiming at the three problems of node bottleneck, road bottleneck, and regional bottleneck, taking Chaoyang road for 4 days as an example, the congestion situation of this road section is studied, as shown in Figure 6.

It is of new reference significance to analyze traffic flow through data statistics in different time periods, and the traffic state in different time periods is different. Therefore, it is necessary to adopt the most reasonable and scientific forecasting methods for traffic conditions in different time periods. Generally, the traffic pressure is large in the morning and evening, and there are many geographical locations for analysis, so the global analysis scope is large. It can effectively reflect the advantages of the algorithm, can be analyzed for different time periods, and has the advantage of fast convergence speed.

Algorithm is the core model to solve the bottleneck of traffic flow. It uses labeling method to search the augmented path continuously until there is no path to search, and then get the maximum feasible flow. In order to identify the bottlenecks that lead to traffic obstruction and minimize the traffic flow, a bottleneck identification model of urban traffic network can be established by combining the road network framework, as shown in Figure 7.

The bottleneck identification model of urban traffic network is shown as follows:

$$\begin{cases} C_p(i, j) \forall P \in P_{D_k}, \\ P \in P_{O_k}, \\ \forall_{i,j} \in M_p, \end{cases} \tag{23}$$

#### 4. Experimental Simulation Comparison

To establish the Ford–Fulkerson traffic flow prediction and analysis model, it is necessary to analyze and apply the whole traffic flow effectively. This paper analyzes the traffic flow data of taxis to analyze the prediction effect and application of traffic flow in different places and different time periods. The four intelligent algorithms used in this paper have the effect of traffic prediction. They have a good application prospect in the field of transportation, especially when there is an optimal problem between global and local. Therefore,

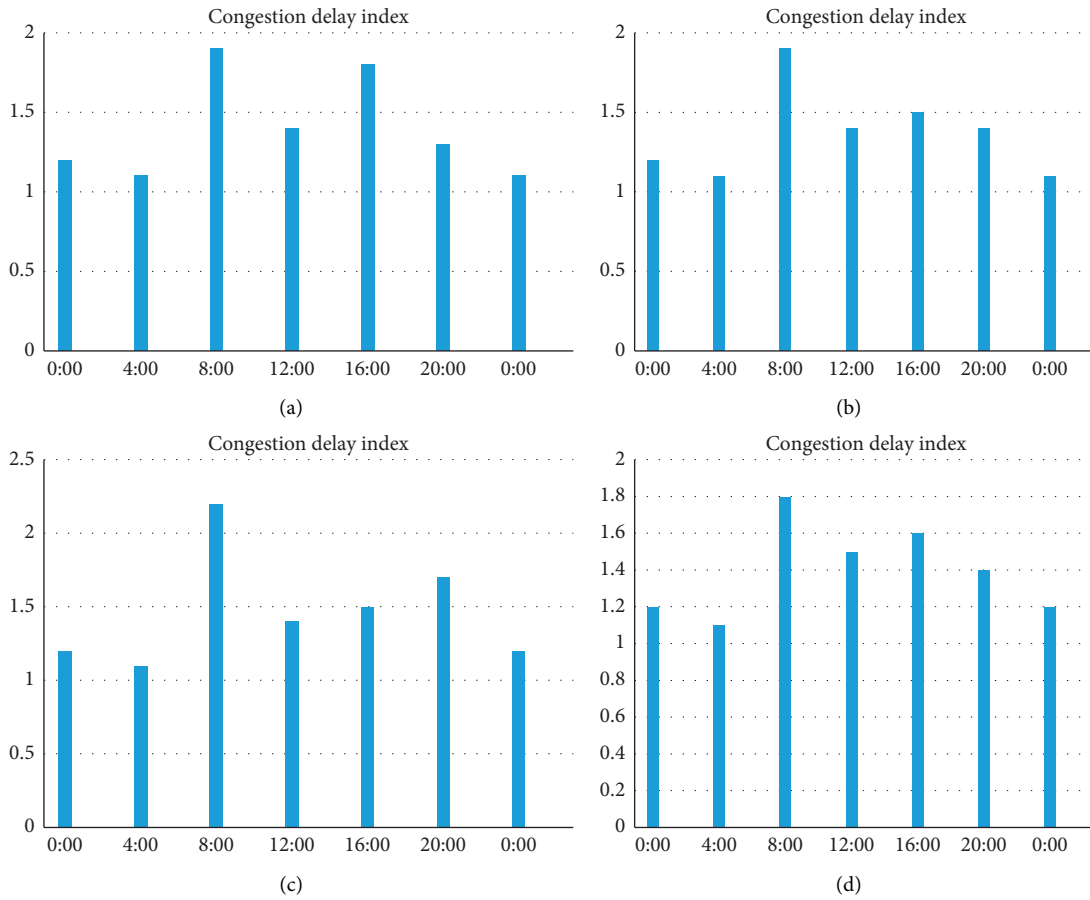


FIGURE 6: Traffic congestion on Chaoyang road in different time periods Ford–Fulkerson: (a) traffic congestion on 5 May; (b) traffic congestion on 12 May; (c) traffic congestion on 24 May; (d) traffic congestion on 28 May.

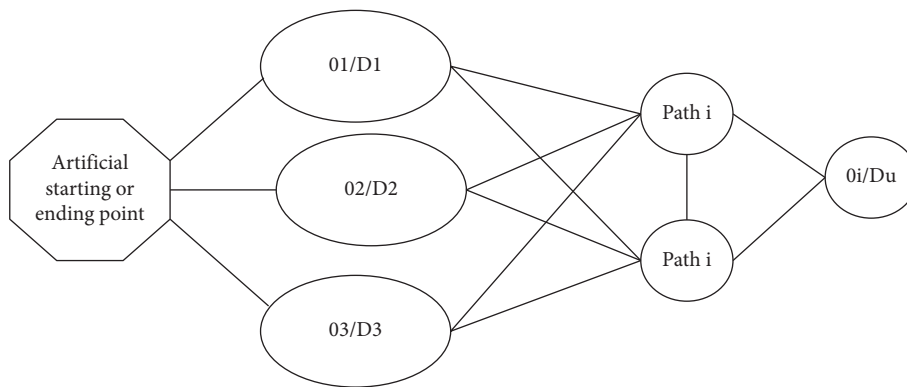


FIGURE 7: Network flow framework.

traffic flow forecasting is a global optimal problem, and intelligent algorithms can quickly realize the global minimum cost to achieve traffic forecasting and guide traffic planning.

Among the traffic flow forecasting methods under different algorithms in Figure 8, Ford–Fulkerson has certain advantages, with an average error of 0.31. Other algorithms have large errors and are unstable in prediction accuracy.

In order to forecast the traffic flow at different locations, the paper selects 10 traffic centers to forecast the traffic flow. The prediction effect is shown in Figure 9.

Then, analyze the error comparison of experiments under different algorithms, as shown in Figure 10.

In Figure 10, the prediction error comparison of different algorithms in different time periods every day is based on the deviation of relevant positions after 10 positions are

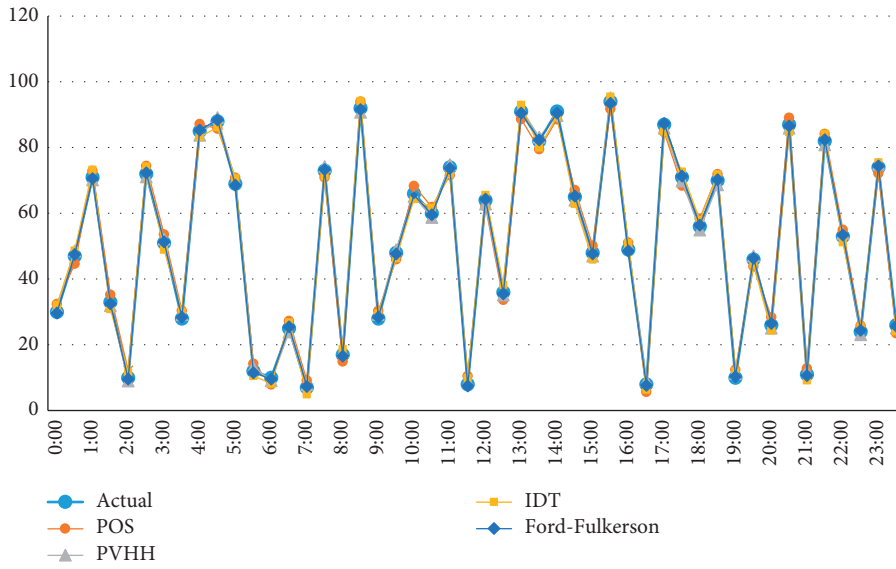


FIGURE 8: Traffic flow forecast in different time periods.

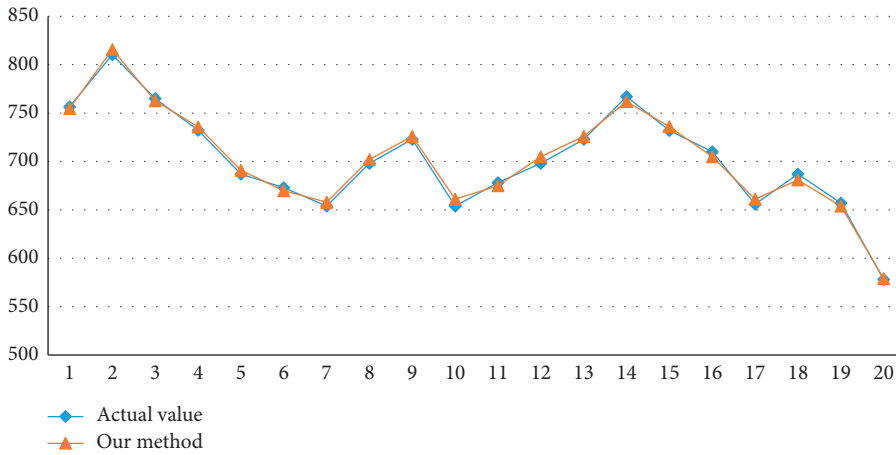


FIGURE 9: Comparison of average time period traffic prediction at different address locations.

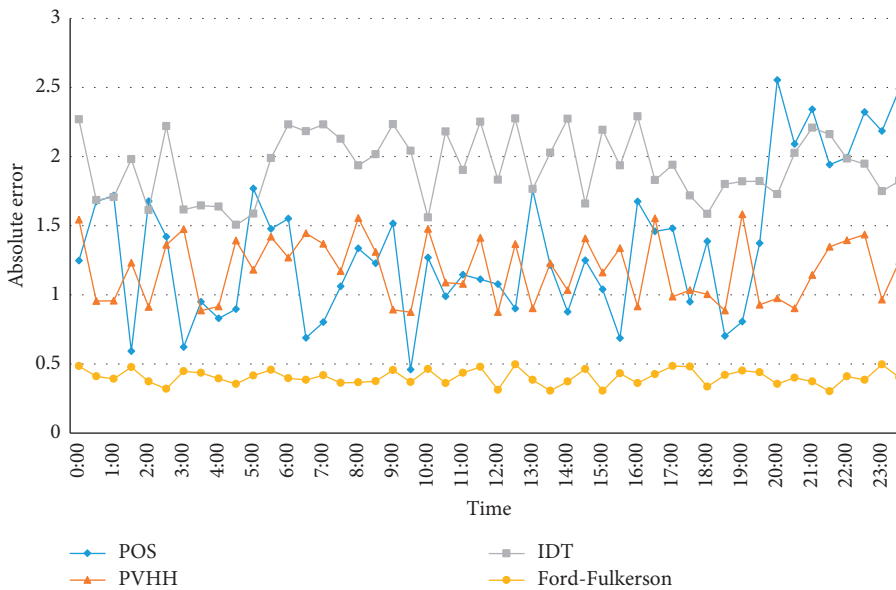


FIGURE 10: Error comparison of different algorithms.

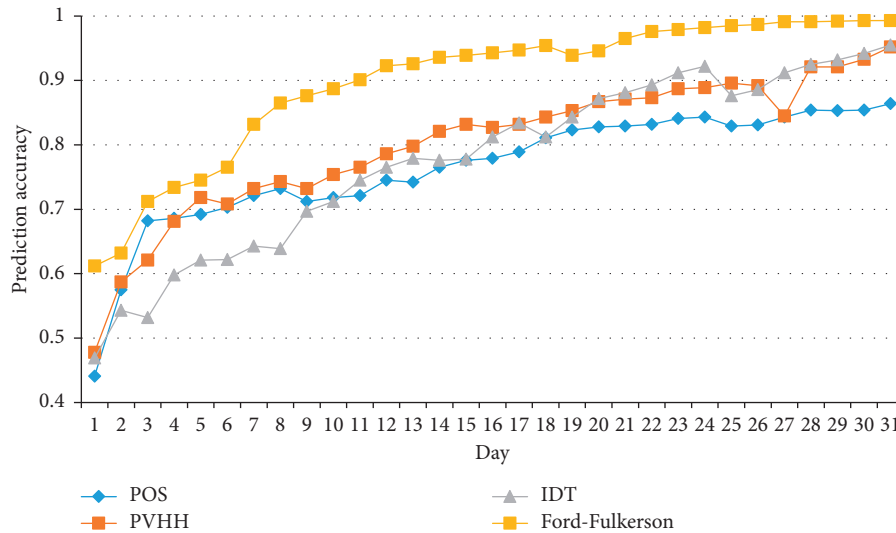


FIGURE 11: Comparison of prediction accuracy in different time periods.

predicted as the position error comparison. Ford–Fulkerson has lower error and better stability (Figure 10).

Next, the prediction effect is analyzed from the prediction accuracy, as shown in Figure 11.

In Figure 11, the prediction accuracy of the above four algorithms is compared for different days in one month. The prediction results of the four algorithms are not ideal in the early stage, and the highest prediction results of Ford–Fulkerson are 0.62. With the increase of days, the accuracy of the four algorithms is also improving. Because there are many early learning data, it can provide some reference for later prediction, and the accuracy is constantly improving. Finally, the Ford–Fulkerson accuracy rate is above 0.96, and the prediction effect is good.

## 5. Conclusion

With the in-depth development and technology application of smart cities, intelligent transportation technology has become a new technical means of urban development. This paper puts forward the prediction and analysis of traffic flow supported by Industry 4.0 and big data technology, which can play a key role in traffic development in smart cities. There are still some problems in the proposed algorithms, such as prediction accuracy, time, and other factors. Future work focuses on time delay and unpredictable factors in traffic forecasting and then puts forward corresponding models and solutions.

## Data Availability

The experimental data used to support the findings of this study are available from the corresponding author upon request.

## Conflicts of Interest

The author declares that there are no conflicts of interest regarding this work.

## References

- [1] M. T. Odenkirk, D. M. Reif, and E. S. Baker, “Multiomic big data analysis challenges: increasing confidence in the interpretation of artificial intelligence assessments,” *Analytical Chemistry*, vol. 93, no. 11, 2021.
- [2] W. W. K. Zung, “A self-rating depression scale,” *Archives of General Psychiatry*, vol. 12, no. 1, p. 63, 1965.
- [3] A. Rosenfeld, D. Benrimoh, and C. Armstrong, “Big Data analytics and artificial intelligence in mental healthcare,” *Applications of Big Data in Healthcare*, pp. 137–171, 2021.
- [4] R. Simon, U. Priefer, and A. Puhler, “A broad host mobilization system for in vivo genetic engineering: transposon mutagenesis in Gram-negative bacteria,” *Bio/Technology*, vol. 1, no. 9, pp. 37–45, 1983.
- [5] Y. Zhen, Z. Lan, and Z. Jin-Fa, “New geographic distribution and molecular diversity of Citrus chlorotic dwarf-associated virus in China,” *Journal of European Economy*, vol. 21, no. 1, p. 6, 2022.
- [6] L. Schütz, K. Saharan, and P. Mder, “Rate of hyphal spread of arbuscular mycorrhizal fungi from pigeon pea to finger millet and their contribution to plant growth and nutrient uptake in experimental microcosms,” *Applied Soil Ecology*, vol. 169, no. 248, Article ID 104156, 2022.
- [7] Z. M. Li and X. Zhuang, “Application of artificial intelligence in microbiome study promotes precision medicine for gastric cancer,” *Journal of European Economy*, vol. 2, no. 4, p. 6, 2021.
- [8] G. He and Z. Luo, “Artificial intelligence in second language learning,” *Raising Error Awareness*, no. 3, pp. 74–80, 2008.
- [9] W. Zhang, H. Ning, and L. Liu, “Guest editorial: special issue on hybrid human–artificial intelligence for social computing,” *IEEE Transactions on Computational Social Systems*, vol. 8, no. 1, pp. 118–121, 2021.
- [10] L. Qiao and X. Zhang, “Frequency management method based on cloud computing, big data and artificial intelligence,” *Journal of Physics: Conference Series*, vol. 1757, no. 1, (8pp), Article ID 012106, 2021.
- [11] X. Bai and J. Li, “Personalized dynamic evaluation technology of online education quality management based on artificial intelligence big data [J],” *Journal of Intelligent and Fuzzy Systems*, no. 3, pp. 1–10, 2021.



- [12] J. Rasmussen, "Human errors - a taxonomy for describing human malfunction in industrial installations," *Journal of Occupational Accidents*, vol. 4, no. 2-4, pp. 311-333, 1982.
- [13] F. Zegrari and A. Idrissi, "Modeling of a dynamic and intelligent simulator at the infrastructure level of cloud services," *Journal of Automation Mobile Robotics & Intelligent Systems*, vol. 14, no. 3, pp. 65-70, 2021.
- [14] C. Qiu and N. Liu, "A novel three layer particle swarm optimization for feature selection," *Journal of Intelligent and Fuzzy Systems*, no. 3, pp. 1-15, 2021.
- [15] Y. Wang, "'Co-Construction' to 'symbiosis'," *Research on the Integrated Governance Mechanism of Industrial Colleges in Higher Vocational Colleges*, no. 9, pp. 142-146, 2021.
- [16] Y. Li, S. Wang, and Y. Yang, "Multiscale symbolic fuzzy entropy: an entropy denoising method for weak feature extraction of rotating machinery [J]," *Mechanical Systems and Signal Processing*, vol. 162, no. 7, Article ID 108052, 2022.
- [17] S. Zhang and E. Forssberg, "Intelligent Liberation and classification of electronic scrap," *Powder Technology*, vol. 105, no. 1-3, pp. 295-301, 1999.
- [18] L. Ping, W. Pu, and Z. Jinzi, "Research on global optimization scheduling method of high-speed railway emergency resource based on service pool," in *Proceedings of the IEEE International Conference on Advances in Electrical Engineering and Computer Applications (AEECA)*, pp. 100-108, DalianChina, August 2020.

## Research Article

# Design of Watercolor Cultural and Creative Products Based on Style Transfer Algorithm

Qi Wang<sup>1</sup> and Alamusi. H <sup>2</sup>

<sup>1</sup>Hebei Academy of Fine Arts, Shijiazhuang 050700, Hebei, China

<sup>2</sup>Hebei Academy of Fine Arts, School of Architecture and Artistic Design, Shijiazhuang 050700, Hebei, China

Correspondence should be addressed to Alamusi. H; [alamusi@hbafa.edu.cn](mailto:alamusi@hbafa.edu.cn)

Received 4 March 2022; Revised 6 May 2022; Accepted 23 May 2022; Published 31 July 2022

Academic Editor: Man Fai Leung

Copyright © 2022 Qi Wang and Alamusi. H. This is an open access article distributed under the Creative Commons Attribution License, which permits unrestricted use, distribution, and reproduction in any medium, provided the original work is properly cited.

Due to the long design cycle of watercolor cultural and creative products, a design method based on style transfer algorithm is proposed. Here, the design of Shanghai style watercolor painting cultural and creative products is taken as the research object, VGG-19 network is used as the style transfer model, and the loss function of style transfer algorithm is designed. The simulation results show that the proposed method can effectively extract and reconstruct the color, texture, brushstroke, and other styles of Shanghai style watercolor painting. The generated new images are added as design elements, which makes the cultural and creative products have both appearance and personalization. In addition, the newly generated cultural and creative products have also obtained high satisfaction from experts and users, which meet the aesthetic changes. It can be seen that proposed method provides a new idea for the design of watercolor cultural and creative products, which shortens the product design cycle, reduces the design cost, and has a certain practicality.

## 1. Related Work

Cultural and creative product design integrates cultural elements and creative thinking into products in a modern way. In recent years, the rich and colorful forms are more and more in line with modern people's aesthetics and are gradually accepted, sought after and loved by the public. However, the design is a creative work, with the characteristics of a long design cycle, and the time cost is high for designers and users. Thus, relevant practitioners have carried out in-depth research. Liu Yuan proposed an improved generative adversarial network based on gradient penalty. The migration and reconstruction of image oil painting style are studied by constructing a total variance loss function, which could provide good edge and texture details for the migration process of image oil painting style. In addition, the generation rate and image quality of oil painting style images are improved [1]. Cai et al. proposed a method of image color style transfer. Dichotomy is utilized to extract color features of template images. The color style of the source image can be transferred to a new image, which can be used

as a design element in product design to improve the speed of product design [2]. Bai et al. proposed a multiscale and multilayer feature fusion network, which uses a local binary pattern to generate three LBP-RGB feature maps. Furthermore, a neural network model is constructed to better express the rotation features of images, which can realize automatic directional detection and feature extraction of abstract paintings. By applying the extracted features to product design, the design speed is improved to a certain extent [3]. Wei proposed a painting image style feature extraction algorithm based on intelligent vision [4]. Here, similarity analysis, pixel smooth transfer, and semi-supervised learning methods are adopted. On this basis, the similarity rule of painting image style is established, and all style features are quantified. Using intelligent vision technology to extract the style features of painting images can effectively reduce the average running time and improve the success rate of feature extraction. Thus, the design speed is improved. de Manincor et al. proposed to use the principal component analysis method to analyze the image sample data, and the data to be analyzed are made as a separate

contribution, and thus, the analysis of carpaccio large-scale canvas paintings is realized, which lays a theoretical foundation for the product's design [5]. Based on the style transfer algorithm, Guo et al. determined three main factors affecting human visual complexity perception, by collecting subjective complexity labels of painting images [6]. On the basis of psychology and art theory, there are 29 regional feature painting images representing the above three factors designed. The experimental results show that the proposed method can predict the visual complexity perception of paintings, and the prediction accuracy is 86.78%. It has a high correlation coefficient between subjective complexity and objective complexity, which is superior to other image complexity measurement methods. Wang et al. used the style transfer algorithm to propose a subgraph exchange method [7, 8]. The wall painting works selected by users are fused with the simulated environment image, and thus, the wall painting simulation renderings are generated. As can be seen, the design is highly innovative. Jeremiah and others put forward the use of the neural network to detect artistic style, which provides a reference for the neural network in the extraction of artistic style [9]. Kang and others proposed to improve the quality of artistic style pictures through texture transmission, which provides a set of image processing technology for the improvement of artistic style [10]. Gardini et al. applied a convolutional neural network to high-dimensional art image processing, thus realizing the transformation of music and visual art [11]. Yang and others applied deep learning to the classification of art images [12].

Based on the above research results, the style transfer algorithm has certain advantages in product design. Therefore, based on the style transfer algorithm and taking the Shanghai-style watercolor paintings transfer as the research object, a new design method is proposed.

## 2. Introduction to Style Transfer Algorithm

Style transfer algorithm means that the computer will specify content samples and style samples through operation to generate new samples with both content characteristics and artistic style characteristics [13]. The new sample has both the shape and outline of the content sample and the texture and color of the style sample. Gatys' transfer algorithm is the most widely used style transfer algorithm at present. Moreover, it is divided into three parts: content reconstruction, style reconstruction, and style transfer.

**2.1. Content Reconstruction.** Assuming that there are content image  $\vec{p}$  and a trained convolutional neural network, the number of filters at each layer is  $N^l$ , and thus, multiple feature maps can be obtained at each layer. Vectorizing feature map can obtain  $M^l$ . Save  $N^l$  to  $F^l \in R^{N^l \times M^l}$ , specify a layer of feature representation, and generate a new image  $\vec{x}$  such that the layer of feature representation  $P^l$  is equal to the original feature representation  $F^l$ . The loss function is defined as [14] follows:

$$L_{\text{content}}(\vec{p}, \vec{x}, l) = \frac{1}{2} \sum_{i,j} (F_{ij}^l - P_{ij}^l)^2. \quad (1)$$

Element  $F_{ij}^l$  is the corresponding activation of  $i$ th filter at position  $j$  at layer  $l$ .

**2.2. Style Reconstruction.** Gram matrix is adopted as the style image style, which is defined as follows [15]:

$$G_{ij}^l = \frac{1}{2} \sum_k F_{ik} F_{jk}, \quad (2)$$

$G^l \in R^{N^l \times M^l}$  is the style representation. In order to make the style feature consistent with the original style feature, back propagation algorithm is used to optimize the white noise image. Assuming that the style image is  $\vec{a}$ , the image expected to be generated is  $\vec{x}$ , and the corresponding gram matrices of  $l$  layer are  $A^l$  and  $G^l$ , and then, the loss function of this layer is [16]

$$E_l = \frac{1}{4N_l^2 M_l^2} \sum_{i,j} (G_{ij}^l - A_{ij}^l)^2. \quad (3)$$

The total loss function is

$$L_{\text{style}} = \sum_{l=0}^L \omega_l E_l, \quad (4)$$

where  $\omega_l$  is the weight of each layer.

**2.3. Style Transfer.** To generate a new image  $\vec{x}$  integrating the style of image  $\vec{a}$  and the content of image  $\vec{p}$ , the gap between a layer content representation of  $\vec{x}$  and  $\vec{p}$  and the gap between the multiple layers style representation of  $\vec{x}$  and  $\vec{a}$  are minimized at the same time. The loss function is [17]

$$L_{\text{total}}(\vec{p}, \vec{a}, \vec{x}) = \alpha L_{\text{content}}(\vec{p}, \vec{a}) + \beta L_{\text{style}}(\vec{a}, \vec{x}). \quad (5)$$

## 3. Design of Watercolor Cultural and Creative Products Based on Style Transfer Algorithm

**3.1. Selection of Style Transfer Model.** VGG network is a deep convolutional neural network with convolution operation, which is composed of a convolutional layer, pooling layer, full connection layer, and Softmax layer. It has various variations and is often used in object classification and other fields [18]. At present, the commonly used VGG model is VGG-19 (VGG-E) model. The structure of this model is shown in Figure 1. There is a  $3 \times 3$  convolution kernel used for convolution operation to extract more significant features of input images, and classification is achieved through activation function and Softmax layer [19].

The convolution operation formula of the VGG-19 model is as follows [20]:

$$y_{\text{conv}} = \delta(\text{Mat} \bullet W + b), \quad (6)$$

where  $y_{\text{conv}}$  is output result;  $\delta$  is activation function; Mat is grayscale matrix;  $W$  is convolution kernel;  $\bullet$  is convolution operation; and  $b$  is bias value.

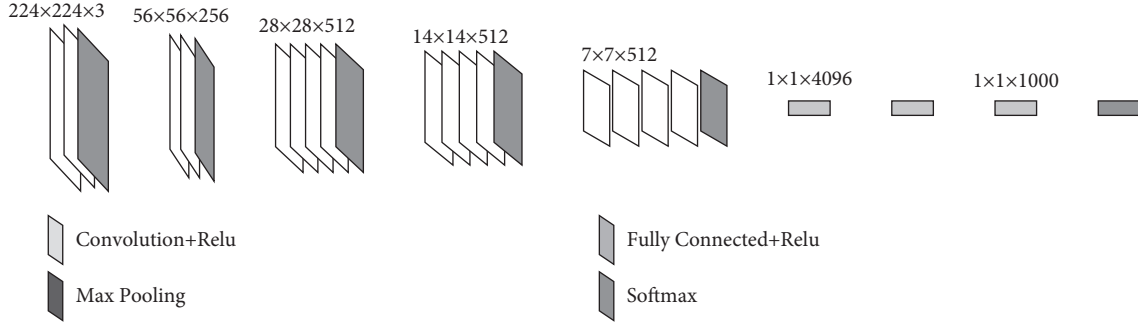


FIGURE 1: VGG-19 network structure.

The convolution operation is included in the activation function, as shown in formula (7) [21], to reduce the amount of computation of the network and avoid the over-fitting phenomenon.

$$f_{\text{relu}}(x) = \begin{cases} x, & x \geq 0, \\ 0, & x < 0, \end{cases} \quad (7)$$

where  $x$  is output value of the convolution operation.

After entering the pooling layer, in order to reduce parameters, the maximum pooling with step size of 2 and box size of  $2 \times 2$  is adopted for pooling operation.

$$f_{\text{pool}} = \text{Max}(x_{m,n}, x_{m+1,n}, x_{m,n+1}, x_{m+1,n+1}), \quad (8)$$

$$0 \leq m \leq M,$$

$$0 \leq n \leq N,$$

where  $M$  and  $N$  are the length and width of two-dimensional vector of image, respectively.

The regression multiclassification data label of Softmax layer  $y \geq 2$ , and the training set is  $k$ -labeled samples.

$$T = [(x_{(1)}, y_{(1)}), (x_{(2)}, y_{(2)}), \dots, (x_{(k)}, y_{(k)})], \quad (9)$$

$$y(i) \in \{1, 2, \dots, k\},$$

where  $y(i)$  is classification label, and  $x_{(i)}$  is sample set. Assume that  $j$  is a different category and the probability value of  $j$  is estimated. For each sample, the probability of the  $k$ th label is [22]

$$P(y = j|x) j = 1, 2, \dots, k. \quad (10)$$

Transform the regression sample into a  $k$ -dimensional probability vector, and then, there is

$$h(x_{(i)}|\theta) = \begin{bmatrix} p(y_{(i)} = 1|x_{(i)}, \theta) \\ p(y_{(i)} = 2|x_{(i)}, \theta) \\ \dots \\ p(y_{(i)} = k|x_{(i)}, \theta) \end{bmatrix}. \quad (11)$$

The learning parameters of model are

$$\theta = [\theta_1^T, \theta_2^T, \dots, \theta_k^T],$$

$$\theta_1^T, \theta_2^T, \dots, \theta_k^T \in R^{n+1},$$

$$y = \frac{1}{\sum_{j=1}^k e^{x^{(i)} \theta_j^T}} = \frac{1}{\sum_{j=1}^k e^{x^{(i)} \theta_j^T}} \begin{bmatrix} e^{\theta_1^T x^{(i)}} \\ e^{\theta_2^T x^{(i)}} \\ \dots \\ e^{\theta_k^T x^{(i)}} \end{bmatrix}. \quad (12)$$

The sum of all probabilities in formula (11) is 1. For sample training, the loss function can be expressed in the following formula [23]:

$$J(\theta) = -\frac{1}{m} \left[ \sum_{i=1}^m \sum_{j=1}^k 1\{y(i) = j\} \log \frac{e^{x^{(i)} \theta_j^T}}{\sum_{j=1}^k e^{x^{(i)} \theta_j^T}} \right]. \quad (13)$$

In the back propagation of the VGG-19 network, the error function cannot be used in the hidden layer of the network, so the residual is adopted for propagation. The back propagation expressions are

$$\frac{\partial J(W, b; x_{(i)}, y_{(i)})}{\partial w_{ij}^{(l)}} = a_j^{(l)} \delta_i^{(l+1)}, \quad (14)$$

$$\frac{\partial J(W, b; x_{(i)}, y_{(i)})}{\partial w_{ij}^{(l)}} = \delta_i^{(l+1)}, \quad (15)$$

where  $a_j^{(l)}$  is the output value of the node  $j$  at the output layer  $l$ , and  $\delta_i^{(l+1)}$  is the residual of the node  $i$  whose output is  $l+1$ .

According to formulas (13)~(15), the updated amount of weight  $w_{ij}^l$  and bias  $\partial b_i^{(l)}$  can be obtained as follows:

$$\frac{\partial J(W, b)}{\partial w_{ij}^{(l)}} = \left[ \frac{1}{m} \sum_{i=1}^m a_j^{(l)} \delta_i^{(l+1)} \right] + \lambda w_{ij}^l, \quad (16)$$

$$\frac{\partial J(W, b)}{\partial b_i^{(l)}} = \frac{1}{m} \sum_{i=1}^m \delta_i^{(l+1)}, \quad (17)$$

where  $1\{y(i) = j\}$  indicates that when  $y(i) = j$ , its value is 1. When  $y(i) \neq j$ , its value is 0. As can be seen from the formula, adjusting parameters can be realized by adjusting parameter  $\theta$ .

VGG-19 network has a strong ability for feature presentation and detail description and can extract more features and details [24, 25]. Therefore, based on the VGG-19 network model, the Shanghai-style watercolor painting style is transferred.

**3.2. Design of Style Transfer Loss Function.** Gatys' migration algorithm is adopted to minimize the objective function through iteration and transfer the style of content image  $S$  to style image  $I$  [26].

$$\text{Loss}_{\text{total}} = \sum_{l=1}^L \alpha_l \text{Loss}_c^l + \Gamma \sum_{l=1}^L \beta_l \text{Loss}_s^l,$$

$$\text{Loss}_c^l = \frac{1}{2N_l D_l} \sum_{ij} (F_l[O] - F_l[I])_{ij}^2, \quad (18)$$

$$\text{Loss}_s^l = \frac{1}{2N_l^2} \sum_{ij} ((G_l[O] - G_l[S]))_{ij}^2,$$

where  $\text{Loss}_{\text{total}}$  is the total loss function,  $\text{Loss}_c^l$  is the content image loss function, and  $\text{Loss}_s^l$  is the style image loss function.  $I$  is the  $l$ -layer model of depth model, and  $\Gamma$  is the weight distinguishing influence of formulas (15) and (16) on the total loss function.  $F$  is the feature matrix, and  $G$  is the Gram matrix.

**3.3. Scheme Design of Style Transfer.** Based on the above analysis, the Shanghai-style watercolor painting style is adopted as a transfer style to design cultural and creative products. The specific scheme is as follows.

Firstly, the style transfer algorithm is used to extract and reconstruct style characteristics of Shanghai-style watercolor paintings, including brushstroke, color, and texture, to generate a new image example. In the design process, besides the decoration of the product, the practicality of products should meet the needs of users. Furthermore, the design should not be limited to a two-dimensional plane, so as to enrich the product style. The color collocation can choose the color close to the original Shanghai-style watercolor style or boldly choose a contrasting color. The materials can choose high-quality and inexpensive acrylic, paper, and other materials to reduce the selling price of products and improve the cost performance of products.

According to the above design scheme, the watercolor cultural and creative products are designed, and Figures 2 and 3 are the sketches of the product design.

## 4. Simulation Experiment

**4.1. Construction of Experimental Environment.** This experiment is conducted on tensorflow-gpu1.9.0, deep learning framework, and torch7 environment. It is run in Linux operating system. The GPU is GTX P102-100, which is

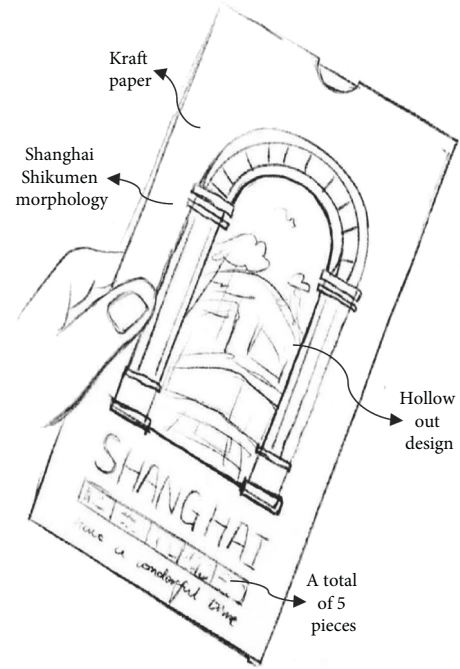


FIGURE 2: Design sketch of postcard.

a 4-core 24G E5-2660 V2, and the hard disk is 500 GB SSD. And Python, OpenCV, and other support libraries are installed.

**4.2. Data Sources and Processing.** The sample data of this experiment include style sample data and content sample data. Among them, style sample data are divided into realistic style data, freehand style data, and abstract style data, and the three kinds of data are, respectively, selected from the works of Shanghai-style watercolor painters Pan Sitong, Ran Xi, and Ping Long [27]. The content samples are selected from Shanghai landmark Hudecs buildings, including Wu Tongwen Residence, Hudecs Private Residence, Joint Saving Society Bank, Park Hotel, and Wukang Building.

There are certain errors in the iterative process of the model resulting in problems such as noise or blurry images in the final style transfer image [28]. To solve this problem, Gaussian filtering, median filtering, and other methods are adopted for processing, and it finds that the image processed by Gaussian filtering is closer to the reality, and the details are richer. Therefore, Gauss filtering is used to process style transfer watercolor paintings. Figure 3 shows the calculation process of style migration.

Considering that the model has some errors during iteration, and the images obtained through style transfer contain noise or blurred image [24], this paper tries to optimize the number of iterations, content weight, and style weight, and filtering smoothing to solve these problems. The specific operations are as follows.

**4.2.1. Number of Iterations.** Due to the different difficulties of learning different styles of watercolor painting, adjusting

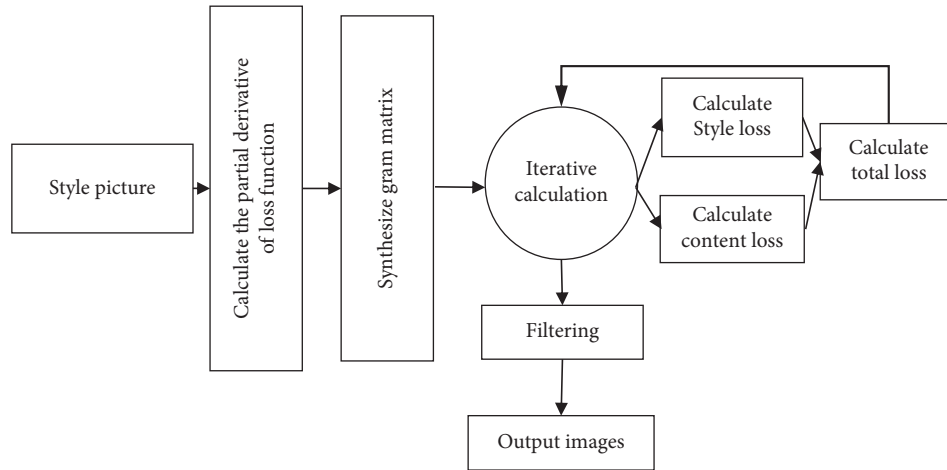


FIGURE 3: Calculation process of style transfer.

the number of iterations properly to learn different levels of watercolor paintings to a varying degree, which is conducive to improving the transfer effect of watercolor painting styles. Table 1 shows the change process of the watercolor style transfer effect under different iterations. According to the figure, when the number of iterations is 1000, the watercolor style transfer effect is the best.

**4.2.2. Content Weight and Style Weight.** The content weight and style weight of watercolor have a great influence on the transfer effect, too high content weight will lead to full style transfer, and too high style weight will lead to the loss of details. Therefore, in order to achieve the ideal transfer effect, different content weights and style weights are tested, and the results are shown in Table 2. According to the figure, when the content weight is 5 and the style weight is 200, the migration effect is the best.

**4.2.3. Filtering Smoothing.** Filtering smoothing usually includes Gaussian filtering, median filtering, and other processing methods. In order to select the best filtering smoothing method, different filtering smoothing methods are used in this paper to process watercolor paintings, and the results are shown in Table 3. As can be seen from the figure, compared with mean filtering, median filtering, and bilateral filtering, the image processed by Gaussian filtering is closer to reality and has richer details. Therefore, a Gaussian filter is used to process the style transfer of watercolor paintings.

Figure 4 shows the comparison of results of the Wukang Building before and after Gaussian filtering after style transfer. In the picture, the style pictures from top to bottom are Pan Sitong style, Ran Xi style, and Ping Long style. As can be seen, compared with the image before processing, the image processed by Gaussian filtering has more clear stylized features, stronger color features, more natural brushstroke edges, and more realistic light and shade of the overall composition, which indicates that Gaussian filtering has obvious treatment effect and certain effectiveness. In addition, by comparing the

transferred images of Pan Sitong, Ran Xi, and Ping Long, it can be seen that Pan Sitong's works are more realistic in color and composition, and the overall treatment of light and shade and details of virtual and real are more balanced and unified than those of Ran Xi and Ping Long. Therefore, the Pan Sitong style is finally transferred to the cultural and creative products.

**4.3. Parameter Settings.** Initial model training parameters are set as follows: epoch = 500, batch\_size = 1, learning rate  $\eta = 1e0$ , style image weight  $\alpha = 1e5$ , and content loss weight  $\beta = 1e2$ . Through repeated experiments, the optimal training parameters of the model are determined as epoch = 1000, batch\_size = 1,  $\eta = 1e0$ ,  $\alpha = 1e200$ , and  $\beta = 1e5$ .

#### 4.4. Experimental Results

##### 4.4.1. Experimental Results of Style Transfer

**(1) Style Transfer Results.** To verify the transfer effect of the proposed method, Pan Sitong style transfer is applied to Residence, Building successively. The results are shown in Figure 5. As can be seen, the proposed method realizes the transfer and lays a foundation for the secondary creation of Shanghai-style watercolor paintings.

**(2) Evaluation of Style Transfer Effect.** In this experiment, user satisfaction is selected to evaluate the effect of the proposed style transfer method. Three art-related practitioners, three design professionals, and four ordinary people are selected to score the generated style transfer effect images on an integer scale of 1~5 and calculate the average of final evaluation scores. The evaluation results are shown in Table 4. The proposed style migration algorithm based on VGG-19 can generate relatively satisfactory transfer images for users, and there are 4 samples with satisfaction scores higher than 3, accounting for 80%. This shows that the proposed style transfer algorithm can extract and reconstruct the color, texture, brushstroke, and other styles of Shanghai-style watercolor paintings and generate new images with high user satisfaction.

TABLE 1: Changes of style transfer effect with the number of iterations.






| Content image   | Style image   | Iterations 100  | Iterations 800   | Iterations 1500   |
|---|---|---|--|---|
|  |  |  |  |  |

TABLE 2: Changes of style transfer effect with content weight and style weight.






| Content image   | Style image   | Style weight 100  | Style weight 500   | Style weight 1000   |
|---|---|---|--|---|
|  |  |  |  |  |

TABLE 3: Processing results of different filtering smoothing methods.

| Original image  | Mean filtering  | Median filtering  | Bilateral filtering  | Gaussian filtering  |
|---|---|---|--|---|
|  |  |  |  |  |


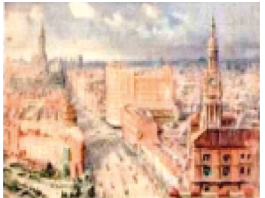
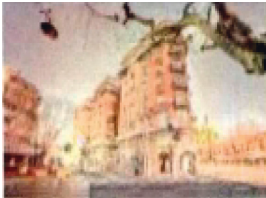





| Content images  | Style images  | Before Gaussian filtering  | After Gaussian filtering  |
|---|---|--|---|
|  |  |  |  |
|  |  |  |  |

FIGURE 4: Comparison of results before and after Gaussian filtering after image style transfer.







| Content sample  | Style sample  | Generated results sample  |
|---|---|---|
|  |  |  |
|  |  |  |

FIGURE 5: Style transfer results.

TABLE 4: Evaluation results.

User satisfaction evaluation table of Shanghai-style watercolor painting style transfer generated effect (a scale of 1 to 5, 1 point means that very dissatisfied. Note: the score can be comprehensively considered from the dimensions of color, brushstroke, and composition)





| Content samples   | Style samples   | Results of experiment 2  | Satisfaction scoring |
|---|---|--|----------------------|
|  |  |  | 4.6                  |

TABLE 5: Expert satisfaction score.

| Evaluation dimensions/cultural and creative products                              |     |
|---|-----|
|  |     |
| Cultural connotation  | 4.2 |
| Appearance  | 3.8 |
| Personalization   | 4.4 |
| Practicality  | 4   |

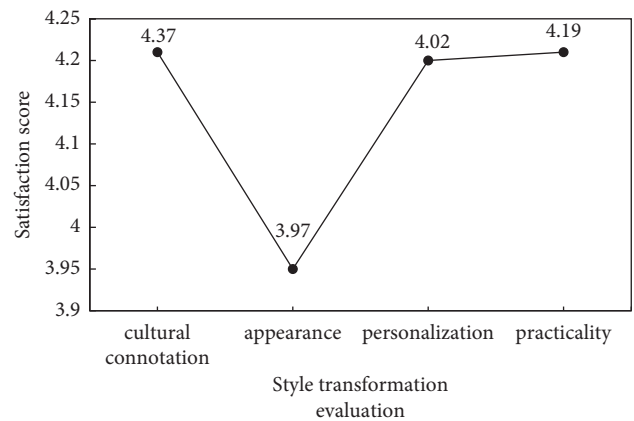


FIGURE 7: User satisfaction with postcards.



FIGURE 6: Effect diagram of postcard.

#### 4.4.2. Design Results of Cultural and Creative Products

(1) *Design Effect Display.* Figure 6 shows the design effect diagram of products. The style transfer algorithm can quickly generate design materials, reduce design time, improve design efficiency, and reduce the design cost. At the same time, cultural and creative products can be customized for different users, which meets the aesthetic trend of the era.

(2) *Design Evaluation.* There are 10 professionals, including art museum experts, students majoring in design, and painters, invited to use a scale of 1 to 5 to score the products

from appearance [29], cultural connotation, practicality, and personalization, so as to realize the evaluation of designed watercolor cultural and creative products. The results are as shown in Table 5. Here, content images can reflect the characteristics of Shanghai. Moreover, the newly generated images are added to cultural and creative products as design elements, which can make products have both cultural connotation and personalization. Therefore, the products have obtained a high expert satisfaction score, and the overall satisfaction is more than 3.4 points.

To evaluate the market demand for designed watercolor cultural and creative products, a questionnaire survey is conducted on random passers-by, and 100 questionnaires are sent and collected, among which 61 questionnaires are valid. In the valid questionnaire, there are 31 male and 30 female users. Among them, 37 users are aged between 18 and 25, and 24 users are aged between 26 and 55. The scores of users on the designed cultural and creative products are counted, and the average scores are calculated, which are shown in Figure 7. Here, users have high overall satisfaction with the designed postcards, with an average score close to 4, indicating that the designed watercolor cultural products are popular with the public and can simultaneously meet users' needs for cultural connotation, appearance, personalization, and practicality.

## 5. Conclusion

To sum up, the proposed watercolor product design method based on the style transfer algorithm adopts the VGG-19 network as the basic model to migrate the Shanghai-style



watercolor painting style. In addition, the loss function of the style transfer algorithm is designed. Thus, the rapid extraction and reconstruction of the color, texture, brush-stroke, and other styles are achieved. Moreover, the design cost is reduced, and the design process is shortened. Adding newly generated images as design elements to cultural and creative products can make products meet the needs of appearance, personalization, cultural connotation, and practicality. There is no doubt that these products can obtain high expert and user satisfaction and meet the aesthetic changes in the market, which is conducive to the spread of watercolor painting. The innovation of this study is to apply the deep learning algorithm to the specific artistic style extraction and apply the extracted style to the actual design, so as to provide a more practical case for the information design of artistic style.

Although certain results have been achieved, due to the limitations of conditions, there are still some deficiencies to be improved and perfected. On the one hand, the proposed style transfer algorithm has a good style transfer effect on Pan Sitong's realistic style watercolor paintings, but the transfer effect of freehand style and abstract style still needs to be improved. On the other hand, the proposed method has been verified using Hudec architecture as an example, but the themes such as landscapes and people have not been selected in the content sample. Therefore, in future research, improvements should be considered from the above deficiencies to optimize the algorithm and improve the generalization of the algorithm.

## Data Availability

The experimental data used to support the findings of this study are available from the corresponding author upon request.

## Conflicts of Interest

The authors declare that they have no conflicts of interest regarding this work.

## References

- [1] Y. Liu, "Improved generative adversarial network and its application in image oil painting style transfer," *Image and Vision Computing*, vol. 105, Article ID 104087, 2021.
- [2] X. Cai, Y. Ge, R. Cai, and T. Guo, "Image color style migration method for mobile applications based color feature extraction," *Journal of Computational Methods in Science and Engineering*, vol. 19, no. 4, pp. 879–890, 2019.
- [3] R. Bai and X. Guo, "Automatic orientation detection of abstract painting," *Knowledge-Based Systems*, vol. 227, Article ID 107240, 2021.
- [4] N. Wei, "Research on the Algorithm of Painting Image Style Feature Extraction Based on Intelligent vision[J]," *Future Generation Computer Systems*, vol. 1, 2021.
- [5] N. de Manincor, G. Marchioro, E. Fiorin, M. Raffaelli, O. Salvadori, and C. Daffara, "Integration of multispectral visible-infrared imaging and pointwise X-ray fluorescence data for the analysis of a large canvas painting by Carpaccio," *Microchemical Journal*, vol. 153, no. C, Article ID 104469, 2020.
- [6] X. Guo, Y. Qian, L. Li, and A. Asano, "Assessment model for perceived visual complexity of painting images," *Knowledge-Based Systems*, vol. 159, pp. 110–119, 2018.
- [7] H. Wang, H. Zhang, and A. Syed Hassan, "Visual mechanism characteristics of static painting based on PSO-BP neural network," *Computational Intelligence and Neuroscience*, vol. 2021, pp. 1–10, Article ID 3835083, 2021.
- [8] F. Xue, "Innovative design of wall painting pattern based on microprocessor system and evolutionary computer technology," *EURASIP Journal on Applied Signal Processing*, vol. 1, p. 100, 2021.
- [9] W. Jeremiah, "Johnson. Towards the algorithmic detection of artistic style[J]," *International Journal of Advanced Computer Science and Applications*, vol. 10, no. 1, 2019.
- [10] D. Tian, F. Seo, and S. Seo, "Perceptually inspired real-time artistic style transfer for video stream," *Journal of Real-Time Image Processing*, vol. 13, no. 3, pp. 581–589, 2017.
- [11] E. Gardini, M. J. Ferrarotti, A. Cavalli, and S. Decherchi, "Using Principal Paths to Walk through Music and Visual Art Style Spaces Induced by Convolutional Neural Networks[J]," *Cognitive Computation*, vol. 13, pp. 1–13, 2021.
- [12] Z. Yang, "Classification of picture art style based on VGGNET," *Journal of Physics: Conference Series*, vol. 1774, no. 1, Article ID 012043, 2021.
- [13] H. Liu, "Pixel domain multi-resolution minimum variance inpainting of CMB maps," *Journal of Cosmology and Astroparticle Physics*, vol. 2021, no. 01, p. 026, 2021.
- [14] P. M. Hall, "Video Paintbox: the fine art of video painting," *Computers & Graphics*, vol. 29, no. 6, pp. 862–870, 2005.
- [15] R. N. Abiram and P. M. D. R. Vincent, "Identity preserving multi-pose facial expression recognition using fine tuned VGG on the latent space vector of generative adversarial network," *Mathematical Biosciences and Engineering*, vol. 18, no. 4, pp. 3699–3717, 2021.
- [16] W. Tan, P. Liu, X. Li et al., "Classification of COVID-19 pneumonia from chest CT images based on reconstructed super-resolution images and VGG neural network," *Health Information Science and Systems*, vol. 9, no. 1, p. 10, 2021.
- [17] K. H. Cheah, H. Nisar, V. V. Yap, C.-Y. Lee, and G. R. Sinha, "Optimizing residual networks and VGG for classification of EEG signals: identifying ideal channels for emotion recognition," *Journal of Healthcare Engineering*, vol. 2021, pp. 1–14, Article ID 5599615, 2021.
- [18] R. Dhiraj and N. Ghattamaraju, "An effective analysis of deep learning based approaches for audio based feature extraction and its visualization," *Multimedia Tools and Applications*, vol. 78, no. 17, pp. 23949–23972, 2019.
- [19] K. Wang, Z. Chen, Q. M. Jonathan Wu, and C. Liu, "Face recognition using AMVP and WSRC under variable illumination and pose," *Neural Computing & Applications*, vol. 31, no. 8, pp. 3805–3818, 2019.
- [20] R. Lakshmi, "Mixed data through multiple input for price prediction with multilayer perception and mini VGG net[J]," *International Journal of Recent Technology and Engineering*, vol. 8, no. 2, pp. 6317–6320, 2019.
- [21] F. Wang, S. Zhao, X. Zhou, C. Li, M. Li, and Z. Zeng, "An recognition-verification mechanism for real-time Chinese sign language recognition based on multi-information fusion," *Sensors*, vol. 19, no. 11, p. 2495, 2019.
- [22] A. R. Saikia, K. Bora, L. B. Mahanta, and A. K. Das, "Comparative assessment of CNN architectures for classification of breast FNAC images," *Tissue and Cell*, vol. 57, pp. 8–14, 2019.

- [23] B. Hao and D. S. Kang, "Research on image semantic segmentation based on FCN-VGG and pyramid pooling module [J]," *Journal of Korean Institute of Information Technology*, vol. 16, no. 7, pp. 1–8, 2018.
- [24] Z. Yang, J. Yue, Z. Li, and L. Zhu, "Vegetable image retrieval with fine-tuning VGG model and image hash," *IFAC-PapersOnLine*, vol. 51, no. 17, pp. 280–285, 2018.
- [25] S.-L. Hsueh, B. Zhou, Y. L. Chen, and M. R. Yan, "Supporting technology-enabled design education and practices by DFuzzy decision model: applications of cultural and creative product design[J]," *International Journal of Technology and Design Education*, vol. 12, pp. 1–18, 2021.
- [26] Y. Wu, "Design of tourism cultural and creative products based on regional historical and cultural elements," in *Proceedings of the 2021 International Conference on Tourism, Economy and Environmental Sustainability (TEES 2021)*, vol. 251, p. 03004, Kiamen China, 5-7 March 2021.
- [27] C. Zhao, "Strategies for promoting the value of tourist cultural and creative brands based on cultural elements," in *Proceedings of the E3S Web of Conferences*, vol. 251, p. 03028, Kiamen, China, June 2021.
- [28] C. Pei, "Tourism cultural and creative product design for guye shell mound archaeological site based on SIPS model," in *Proceedings of the E3S Web of Conferences*, vol. 251, p. 03002, Kiamen, China, July 2021.
- [29] H. Hui, "Research of user-centered intelligent technology in China's cultural and creative product design," in *Proceedings of the E3S Web of Conferences*, vol. 236, pp. 04050–04059, Kiamen, China, October 2021.

## *Retraction*

# **Retracted: A Computer-Aided Assessment and Evaluation System for Modern Apprenticeship of Accounting Class On-the-Job Training**

### **Mathematical Problems in Engineering**

Received 18 July 2023; Accepted 18 July 2023; Published 19 July 2023

Copyright © 2023 Mathematical Problems in Engineering. This is an open access article distributed under the Creative Commons Attribution License, which permits unrestricted use, distribution, and reproduction in any medium, provided the original work is properly cited.

This article has been retracted by Hindawi following an investigation undertaken by the publisher [1]. This investigation has uncovered evidence of one or more of the following indicators of systematic manipulation of the publication process:

- (1) Discrepancies in scope
- (2) Discrepancies in the description of the research reported
- (3) Discrepancies between the availability of data and the research described
- (4) Inappropriate citations
- (5) Incoherent, meaningless and/or irrelevant content included in the article
- (6) Peer-review manipulation

The presence of these indicators undermines our confidence in the integrity of the article's content and we cannot, therefore, vouch for its reliability. Please note that this notice is intended solely to alert readers that the content of this article is unreliable. We have not investigated whether authors were aware of or involved in the systematic manipulation of the publication process.

In addition, our investigation has also shown that one or more of the following human-subject reporting requirements has not been met in this article: ethical approval by an Institutional Review Board (IRB) committee or equivalent, patient/participant consent to participate, and/or agreement to publish patient/participant details (where relevant).

Wiley and Hindawi regrets that the usual quality checks did not identify these issues before publication and have since put additional measures in place to safeguard research integrity.

We wish to credit our own Research Integrity and Research Publishing teams and anonymous and named external researchers and research integrity experts for contributing to this investigation.

The corresponding author, as the representative of all authors, has been given the opportunity to register their agreement or disagreement to this retraction. We have kept a record of any response received.

### **References**

- [1] L. Sun, C. Liu, M. Lin, and Y. Zhou, "A Computer-Aided Assessment and Evaluation System for Modern Apprenticeship of Accounting Class On-the-Job Training," *Mathematical Problems in Engineering*, vol. 2022, Article ID 6437885, 11 pages, 2022.

## Research Article

# A Computer-Aided Assessment and Evaluation System for Modern Apprenticeship of Accounting Class On-the-Job Training

LinLin Sun, ChunChao Liu , MaoNian Lin, and Ying Zhou

*School of Economics and Management, Hainan College of Vocation and Technique, Haikou 570216, Hainan, China*

Correspondence should be addressed to ChunChao Liu; 100090@hainnu.edu.cn

Received 17 May 2022; Revised 21 June 2022; Accepted 1 July 2022; Published 30 July 2022

Academic Editor: Man Fai Leung

Copyright © 2022 LinLin Sun et al. This is an open access article distributed under the Creative Commons Attribution License, which permits unrestricted use, distribution, and reproduction in any medium, provided the original work is properly cited.

With China's economy and the accelerated pace of globalization, the accounting environment is constantly changing, some accounting laws and regulations are constantly being revised or promulgated, and the accounting system and system are gradually being improved. At the same time, breach of trust in economic activities and violation of financial laws and regulations are common, making the accounting environment more complex. All these have put forward higher requirements for accounting practitioners, which require accounting personnel to receive systematic and professional accounting professional training. Therefore, it is very important for the construction of the assessment and evaluation system for accounting internship. Based on this paper, we study the construction of the computer-aided implementation of the assessment and evaluation system of accounting internship for modern apprenticeship in order to improve the practical and effective help for the employment of accounting students.

## 1. Introduction

College accounting majors will teach students the theoretical knowledge of accounting, but with the practical accounting operation, there is still a big gap with the actual operation in enterprises. Therefore, the expectation of college accounting graduates is that accounting students can enter the accounting position as soon as possible to do accounting work [1–3]. Especially in small and medium-sized enterprises, the recruited accounting personnel need to be able to immediately adapt and be competent in their accounting work, so the accounting students to carry out on-the-job internship so that the accounting theory learned in school and practical operation combined to enhance their professional accounting skills have become a realistic demand and urgent task [4]. This requires institutions to make efforts to train professional financial personnel who can quickly adapt to and be competent for their jobs according to the needs of society and enterprises. In order to let their students have zero contact with the job as much as possible, the institutions have reformed the teaching system of accounting

profession one after another, combining theoretical teaching with practice and requiring students to have at least half a year of on-the-job internship [5]. Although it is said that the internship is very important in the teaching system, the accounting talents who can really adapt to the development needs of society and enterprises are not produced in large quantities [6]. All these problems exist which affect the effect and quality of on-the-job internship of accounting students in colleges and universities and many students of accounting majors. It is difficult for many accounting students to enter into the role of accounting work as soon as possible after they leave school, and it is urgent to conduct systematic research on the top-up internship for accounting students from the aspects of theory and practice.

Accounting professional internship generally adopts “2.5 + 0.5” model or “2 + 1” model, that is, out of 3 years of study, 2 or 2.5 years are for professional study and 0.5 or 1 year is for internship [7]. These two models have problems; on the one hand, students do not have contact with the real business of enterprises during their school years, and on the other hand, in the final 0.5 or 1 year of internship, almost all

students find enterprises and positions on their own so that the professional match is difficult to ensure resulting in accounting students going to work in sales, clerical work, e-commerce work so that the professional internship has lost its meaning [8, 9].

Schools that offer accounting majors generally have higher enrollment scores and more students, but with the national policy of “decentralization,” industrial transformation and upgrading, and the continuous updating of information technology, the current accounting industry has undergone tremendous changes, and with the rapid development trend of management accounting, large enterprises tend to financial sharing and small enterprises choose to bookkeeping [10]. This has led to a gradual decrease in the demand for accounting personnel in the accounting industry while most of the accounting graduates can only go to small enterprises for internship and while the market has seen a relatively small increase in the income of accounting personnel in the past decade, and some students cannot get basic pay during their internship, resulting in some students not wanting to engage in accounting work [11]. Therefore, if students look for their own units for the internship, it is inevitable that some students cannot work in accounting-related positions. In addition, some students are unable to find internship units within the time limit set by the school, some students choose to prepare for the college entrance examination, and some choose to start their own business. A variety of situations have led to the emergence of multiple forms of top-up internship for accounting students.

Due to the large number of accounting students, there are many schools with hundreds or even thousands of accounting students while the number of teachers is relatively small; according to the regulations of the Ministry of Education, the student-teacher ratio should reach 20 : 1; however, the reality is that many schools have 30 : 1, and private schools even reach 40 : 1, which is far from being able to meet the various needs of students, resulting in teachers basically working beyond their workload [12]. In addition to the teaching workload, they also need to undertake scientific research and social service work, which inevitably leads to the lack of energy and cannot guarantee the quality of teaching, and the assessment of students’ on-the-job practice cannot be refined.

Whether it is the diversification of the types of student internships or the overload of teachers, the assessment and evaluation of liberal arts majors in most schools is basically standardized, mainly including process assessment and result assessment. However, due to the small number of teachers and large number of students, each instructor instructs more students, less than a dozen, and more than a few dozen, which makes teachers unable to grasp the internship status of each student, unable to follow the guidance, and unable to do a good process. In addition, the school also incorporates the evaluation of students by enterprise instructors into the assessment and evaluation content, but many of the enterprise evaluations are also formal. The result evaluation is based on the students’ weekly diary and internship summary, thesis or graduation survey report, and

other written materials, and the evaluation results may not be very accurate. Therefore, the standardized assessment and evaluation do not match the diversity of students’ internship and the overload of teachers’ workload.

## 2. Related Work

The apprenticeship system has a long history in factories, i.e., the master leads the apprentice to carry out practical operations in a one-to-one manner so that he or she has the ability to operate the equipment independently on the basis of comprehending and learning the master’s professional skills; therefore, the traditional apprenticeship system is less efficient. Students have double mentors, with enterprises (industry) as the main body, colleges and universities as the basis, school-enterprise division of labor, “school classroom education + job teacher-apprentice skills training” as the main way, combining theory and practice and realizing the complete docking and integration of occupation and profession, job and curriculum, and the professional skills and professional spirit throughout the education process [13].

At present, many teachers in institutions lack practical experience in the industry, not to mention being successful in the industry. To become a true “master,” teachers need to combine professional skills with industry practice and have a high level of practical experience to be able to train qualified students. Modern apprenticeship is a combination of production and teaching, the core of which lies in the production activities of students rather than the teaching activities of teachers. The teaching method is theory-practice, and practical activities are carried out on the basis of theoretical learning; therefore, students will have a sense of achievement in the practical activities. At the same time, in response to the lack of teachers for professional skills, schools can recruit some part-time educators in the society. Among them, the school is only responsible for providing the venue and related teaching equipment, the part-time staff is responsible for teaching professional skills, and the teachers are responsible for teaching professional theoretical knowledge, thus maximizing the use of existing teaching resources and also focusing on training the backbone teachers of the school so that they can become strategic reserve talents of the school after the completion of their studies [14].

The purpose of vocational education is to cultivate students with strong professional skills, requiring them to have strong practical skills, but everyone’s learning and understanding abilities are different. Therefore, students in large classes cannot fully understand what the teacher is teaching, let alone thoroughly master the operational skills. However, teaching in the modern apprenticeship system allows a master to provide skills instruction, which greatly improves their hands-on skills. For example, when conducting an internship in an electronics factory, students need to know enough about soldering and electronic equipment that the author cannot instruct the students one by one. The factory is equipped with a corresponding master for each student to lead them in production practice, and the author will also give them corrective advice for some

common problems that arise among students, which is also more conducive to their smooth growth.

Since the proportion of institutions in the whole education system in China is not high, there are few articles about research institutions accounting students on top of the internship, usually with higher vocational institutions as the research object, while foreign countries focus on the combination of teaching and practical operation in the educational approach, in terms of professional career development and close cooperation with enterprises, so the research starts earlier than domestic and the number of research literature is more than domestic. Foreign research focuses on vocational education with the guidance of government departments, which has a strong theoretical guidance and grasps the talent training mode of combining theory and practice from the macro level, while domestic research mainly focuses on the current situation of students' on-the-job internship from the microlevel and makes corresponding research on the specific problems and improvement methods of on-the-job internship.

In recent years, with the development of China's economy, enterprises pay more attention to financial management and also to the comprehensive quality and ability of accounting talents in all aspects, and the role of internship in improving the ability of accounting students has received the attention and recognition of education and accounting experts and scholars, and many research results with certain theoretical depth have emerged. The Dictionary of Education, edited by the famous scholar Gu Mingyuan, has a clear definition of "internship." The so-called internship is generally a kind of internship in which students complete their work tasks alone in production, management, service, and other production positions. For example, in vocational schools, before graduation, students usually have a half-year internship, which is arranged in factories or other departments to perform their duties and complete production tasks independently according to the job specifications of production workers with the aim of making them proficient in operating procedures and being able to adapt to their work needs quickly, both psychologically and physically, after joining the workforce.

In our country, the education of university-industry cooperation has experienced five periods of development and changes. In the first stage, under the guidance of the party's education policy and science and technology policy, in the 1950s and 1960s, the scientific and educational personnel of colleges and universities actively participated in production practice and began to take steps to cooperate with enterprises, and the cooperation at this stage was mainly government-driven [15]. In the second stage, the reform and opening up started in the late 1970s injected new connotation to the cooperation between industry, university, and research, and the resource allocation system was reformed to increase the vitality of enterprises, and the government-driven cooperation between industry, university, and research gradually changed to the interest-driven type of both parties [16]. The third stage, in 1985, began to cooperate with foreign countries and established its own joint development institutions of industry-

university research. In 1991, Shanghai took the first step to establish the National Association of Research, Education, and Research [17]. In the fourth stage, in 1997, our universities responded positively to the relevant circulars and regulations of the Ministry of Education to vigorously promote the development and in-depth promotion of university-industry research [18]. In the fifth stage, in 2008, the Ministry of Education once again emphasized the importance of university-industry research, which further pointed out the direction for the philosophy of running universities [19, 20]. At present, there is no unified standard in terms of awareness and execution when institutions carry out accounting capstone internship. This thesis takes the research object from three aspects: enterprises, teachers, and students, and based on the research of combining theory and practice in talent training mode, through some discussions on the significance of top-up internship for accounting students in institutions, possible problems, as well as difficulties encountered in the process of internship and policy measures, it is believed that carrying out top-up internship for students requires close cooperation among enterprises, schools, and students; the theory of top-up internship in institutions is improved and supplemented; and the theoretical research in this field is enriched and developed.

### 3. Methods

This paper explores the design of a computer-assisted accounting internship evaluation from the perspective of modern apprenticeship system, aiming to realize the mutual integration and penetration of teachers and apprentices and the effective use of internship resources. The purpose of this paper is to develop a computer-assisted accounting internship evaluation in the perspective of modern apprenticeship system, which is divided into a mobile client and a web server. The mobile client is mainly for course information browsing and online communication. The web server side mainly manages and maintains various modules in the background, such as internship data management and statistical analysis of results.

The main users of the system are students and teachers. The student use cases include login and registration, viewing internship resources, teacher-apprentice communication, and other options; the teacher use cases include publishing microvideo content and assignment management. The system administrator maintains the users and the system, etc. The use case diagrams of students and teachers are shown in Figures 1 and 2.

The system is divided into an Android client and a web server. Students learn through the Android client. The administrator manages users and internship materials through the server side. The system is divided into functional modules as shown in Figure 3.

The Android client mainly contains the following functional modules: internship materials, microlesson videos, teacher-apprentice exchange, knowledge vault, bulletin board, query, etc. The web server completes all the information and data related to the system, such as adding,

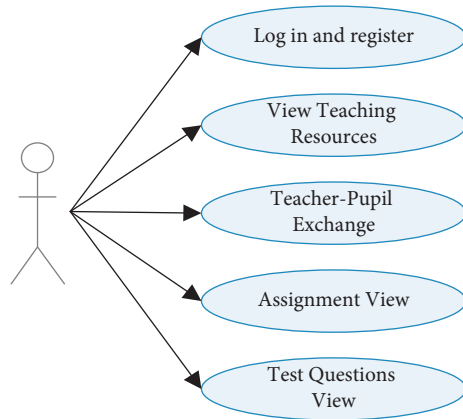


FIGURE 1: Student use case.

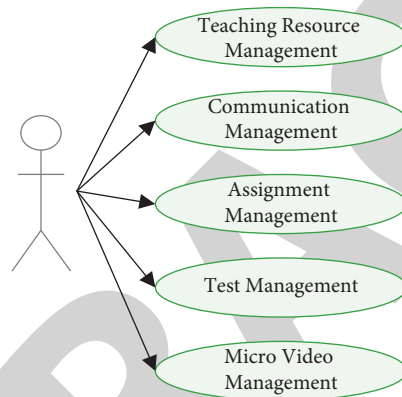


FIGURE 2: Teacher use case.

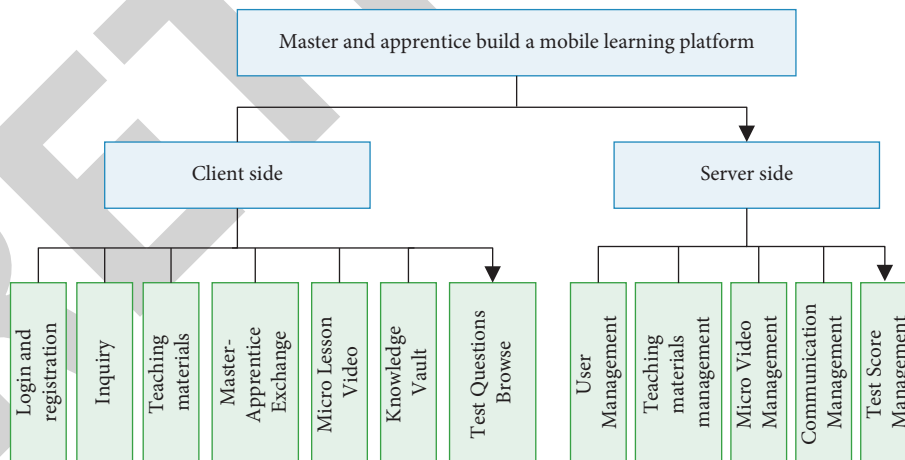


FIGURE 3: Functional modules of the system.

deleting, modifying, importing data, and other information maintenance functions; listens to the database server; and pushes the newly added information to the server in real time.

The system contains information such as user, student, and teacher entities; course and courseware entities; question and answer entities; assignment and learning resource table entities; and test question entities. The teacher and

student entities are designed as shown in Figure 4. The administrator and course information entity diagram is shown in Figure 5.

The server side interacts with the Android side through the Web Service interface, and the Android side interacts with the server side through two interfaces. The server side and the client side interact with each other through the JSON data format, where the data obtained from the database is

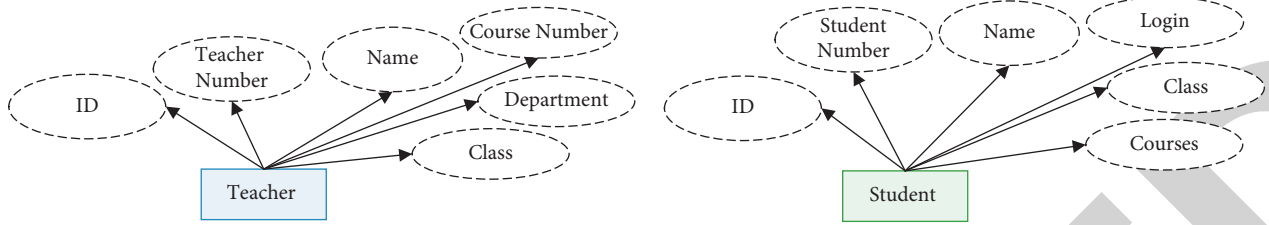


FIGURE 4: Teacher and student entity diagram.

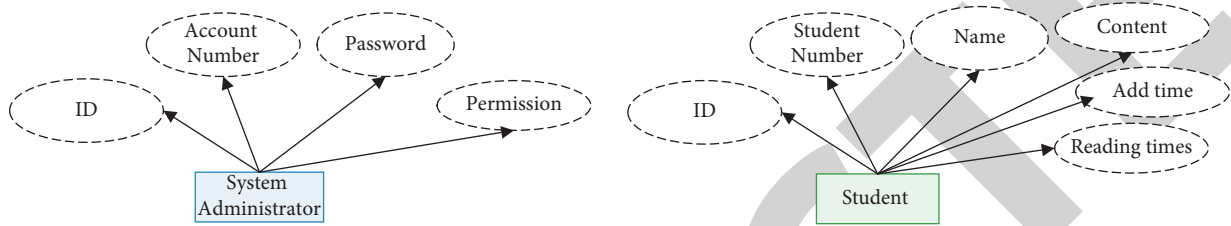


FIGURE 5: Entity diagram of administrator and course information.

converted into JSON data format and the generic type is converted into JSON.

The module implementation takes the microvideo list implementation as an example. When the user clicks on the microvideo courseware in the Android client, the corresponding function of Web Service reads out the content and passes it to the Android client for playback.

The server-side function modules of the mobile internship system are as follows: teacher module, student module, and administrator module. Through the server side, teachers and students can carry out classroom learning, testing, and review and realize the sharing of teachers and students to build a vault of resources. In addition, teachers can assign homework and tasks for students in the online classroom, and students can conduct independent learning and realize online discussion and research, constituting an online and offline interaction mechanism, thus stimulating students' learning enthusiasm. The specific grading index system of the top-up internship is shown in Figure 6.

In view of the characteristics of the accounting professional on-the-job internship, an assessment and evaluation system combining the school-enterprise double main body, process assessment, and result assessment is established. The appraisal and evaluation system should consider five aspects such as school instructor evaluation, enterprise instructor evaluation, student self-evaluation, enterprise evaluation, and parent evaluation. The proportion of the five aspects is positioned 30%, 40%, 10%, 10%, and 10%, respectively. The specific contents are as follows:

- (1) On-campus instructor evaluation should be assessed and evaluated in terms of learning ability, vocational job adaptation ability, teamwork ability, social practice ability, internship reality performance, and internship effect as shown in Table 1.
- (2) The evaluation of external instructors should be assessed and evaluated in terms of students' professionalism, ability to apply professional skills and

public knowledge, ability to solve practical problems at work, work efficiency, and teamwork ability as shown in Table 2.

- (3) Students' self-assessment should be assessed and evaluated in terms of the realistic performance of the on-the-job internship, teamwork ability, work practice ability, and the effectiveness of the internship as shown in Table 3.
- (4) Enterprise assessment and evaluation should be conducted in terms of job adaptability, work attitude, teamwork spirit, and internship performance as shown in Table 4.
- (5) Parental assessment and evaluation should be conducted in terms of job matching, employability, social practice ability, and internship effectiveness as shown in Table 5.

#### 4. Case Study

Taking a higher vocational institution as an example, we analyze the overall situation of students' top job placement, specifically.

On-job internship means that students have to leave school and step into society to participate in work, during which many students avoid and are unwilling to participate in the on-the-job internship due to various reasons such as poor adaptability and inability to bear hardship, and even have a negative psychology. As shown in Figure 7, more than half of the students only passively insist on their internship as a task, only about 37% of the students actively participate in the internship, nearly 7% of the students leave the internship midway and do not want to continue to participate in the internship, and even a small number of students avoid the internship for various reasons at the beginning and do not participate in the internship. There are even a few students who avoid



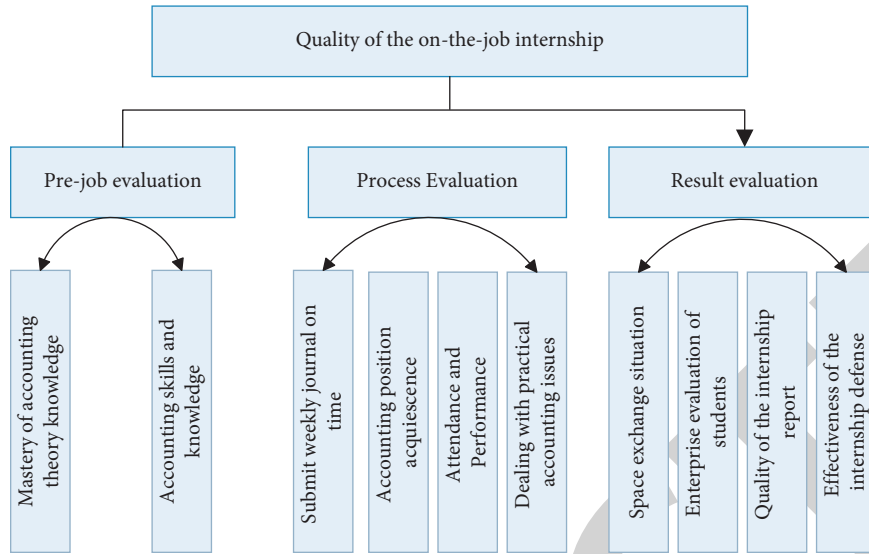


FIGURE 6: Top-up internship rating index system.

TABLE 1: Assessment and evaluation of in-school instructors of accounting students' on-the-job internship.

| Student name : Major: Class: School instructor: |  |  |       |       |
|---|--|--|-------|-------|
| Serial number                                   | Evaluation items                           | Evaluation content   | Score | Score |
| 1   | Self-learning ability                      | The ability of self-learning and transferring new things and knowledge in the context of transformation and upgrading of accounting industry and the ability to collect and organize information by using the internet and other media | 20    |       |
| 2   | Ability to adapt to professional positions | The degree of understanding and acceptance of the professional competence of the internship and the degree of adaptation to changes in the accounting profession in the new situation  | 20    |       |
| 3   | Teamwork ability                           | The ability to communicate and coordinate with colleagues, school instructors, and classmates in the workplace and to deal with problems   | 20    |       |
| 4   | Social practice ability                    | To be able to collect information about job recruitment and find suitable jobs on their own  | 20    |       |
| 5   | Realistic performance of internship        | Correct understanding of the relationship between the internship and the job, the actual work attitude, the writing of the internship data, and the timeliness and comprehensiveness of the data submitted                             | 10    |       |
| 6   | Effect of internship                       | The results obtained in the internship and the help to the graduation design   | 10    |       |
| Total   | 100  |  |       |       |

TABLE 2: Assessment and evaluation table of instructors of accounting students' on-the-job internship enterprises.

| Student name : Major: Class: School instructor: |  |  |       |       |
|---|--|--|-------|-------|
| Serial number                                   | Evaluation items   | Evaluation content   | Score | Score |
| 1   | Professionalism  | The degree of identification with the internship company, love of work and dedication to observe labor discipline, and work carefully and meticulously                                   | 30    |       |
| 2   | Professional skills and ability to apply comprehensive knowledge | The ability to read and write documents such as financial analysis reports and the ability to apply financial professional skills and comprehensive knowledge in the internship position | 20    |       |
| 3   | Practical problem-solving ability                                | Attitude and ability to deal with the actual production and operation process events   | 30    |       |
| 4   | Work efficiency  | Ability to complete the required work tasks on time and with quality   | 10    |       |
| 5   | Collaboration ability  | Able to pay attention to teamwork, work with colleagues to complete work tasks, timely communicate to the leadership of the instructor, and communication                                | 10    |       |
| Total   | 100  |  |       |       |

TABLE 3: Self-evaluation table of accounting students' on-the-job internship.

| Student name : Major: Class: School instructor: |                       |  |       |       |
|---|-----------------------|--|-------|-------|
| Serial number                                   | Evaluation items      | Evaluation content   | Score | Score |
| 1   | Realistic performance | 0.5 points for each day of diligence and 1 point for violation of discipline   | 30    |       |
| 2   | Teamwork ability      | Work can pay attention to the sense of teamwork, can use existing relationships to solve problems, work with colleagues to complete the task, timely communicate to the leadership instructor, and communication | 20    |       |
| 3   | Work practice ability | Skilled in Min bit technology and can complete independently or collaboratively  | 20    |       |
| 4   | Effect of internship  | The work tasks of the vocational position of the vocational subministry counterpart and the internship process have been praised by the unit and colleagues  | 30    |       |
| Total   | 100                   |  |       |       |

TABLE 4: Accounting students' on-the-job internship enterprise assessment and evaluation table.

| Student name : Major: Class: School instructor: |                      |  |       |       |
|---|----------------------|--|-------|-------|
| Serial number                                   | Evaluation items     | Evaluation content   | Score | Score |
| 1   | Job adaptability     | The understanding and acceptance of the internship job vocational subcapacity of the job slot frequency  | 20    |       |
| 2   | Work attitude        | The degree of recognition of the internship enterprise, love and dedication to the job, abide by labor discipline, and work carefully and meticulously   | 30    |       |
| 3   | Teamwork ability     | The work can pay attention to the group knowledge and can use the existing department to solve problems  | 20    |       |
| 4   | Effect of internship | The ability to apply professional financial skills and comprehensive knowledge in the internship, as well as the ability to read and write documents such as financial analysis reports, and the ability to complete the work of professional positions independently or collaboratively | 30    |       |
| Total   | 100                  |  |       |       |

TABLE 5: Parents' assessment and evaluation of accounting students' on-the-job internship.

| Student name : Major: Class: School instructor: |                         |   |       |       |
|---|-------------------------|---|-------|-------|
| Serial number                                   | Evaluation items        | Evaluation content  | Score | Score |
| 1   | Job matching            | The internship position and the professional counterpart count as full points, not the counterpart count as 0 points  | 20    |       |
| 2   | Employability           | Able to work independently or collaboratively to complete practical tasks, collect relevant information, and independently find a suitable job position   | 30    |       |
| 3   | Social practice ability | Able to deal with various unexpected problems in daily life and work  | 20    |       |
| 4   | Effect of internship    | The ability to apply professional financial skills and knowledge in the internship ability to read and write documents such as financial analysis reports and to complete the work tasks of professional positions independently or collaboratively | 30    |       |
| Total   | 100                     |   |       |       |

participating in the internship for various reasons at the beginning and have aversion to the internship.

Whether or not to get a job position corresponding to their majors determines the improvement of students' practical ability and lays the foundation for their future employment, which is an important index to determine the effect of top-up internship. In the survey, it is found that the rate of students' job matching with their majors is low, and most of the students are engaged in basic text entry and checking work or jobs not

related to their majors after arriving at the enterprises, and they can rarely come into contact with the core work content of accounting majors, such as bookkeeping, accounting, and reporting. As can be seen from Figure 8, the proportion of professional mismatch is 46.8%, in which the proportion of complete mismatch is only 22.5% and the proportion of incomplete mismatch is 24.3%; the proportion of mismatch between professional and internship positions is more than 50%, in which the proportion of complete mismatch is 39.5%.

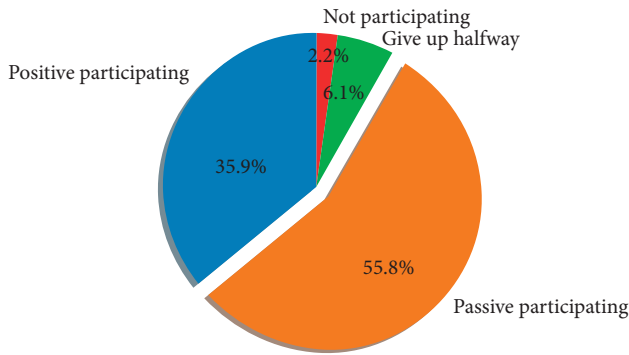


FIGURE 7: The enthusiasm of participation in the internship.

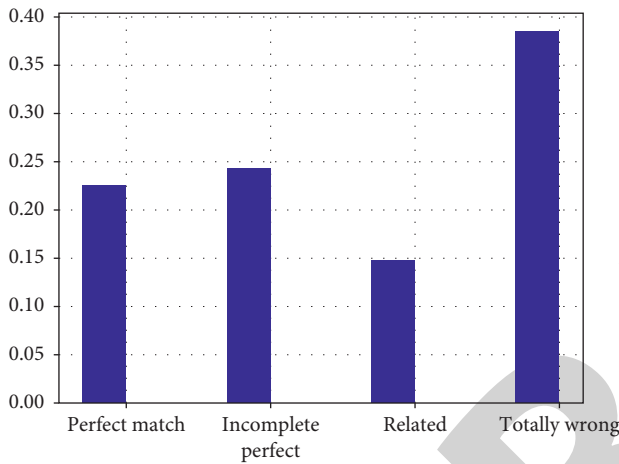


FIGURE 8: Professional counterparts in the internship.

Through interviews, it is found that state-owned enterprises generally attach more importance to the academic qualifications of interns and have a higher threshold, while private enterprises accept students' internships with a stronger acceptance. From the data of this survey (see Figure 9), the nature of the internship unit is state-owned or collective enterprises accounted for only 3.1% and private enterprises up to 93.4%, and a few students' internship unit is the family business founded by their own families, which makes the internship as "formal."

What kind of mentality students put into the internship has a decisive influence on the purpose of the internship. The differences in learning ability and family background make students' understanding of the purpose of the internship vary greatly. It can be roughly divided into four aspects: equivalence to employment, skill enhancement, completion of studies, and preparation for employment. In Figure 10, more than 40% of students think that the main purpose of participating in the internship is to graduate while more than 10% think that the internship is to join the workforce. The proportion of those who think the main purpose of the internship is to learn skills and prepare for future employment also exceeds 40%. It can be seen that students do not have a strong purpose to improve their skills through the internship.

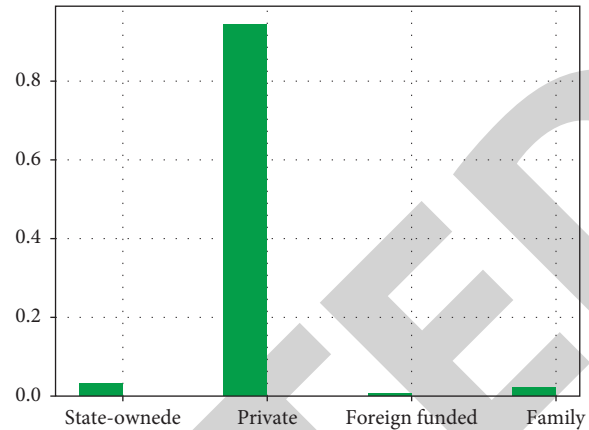


FIGURE 9: Investigation of the nature of top position internships.

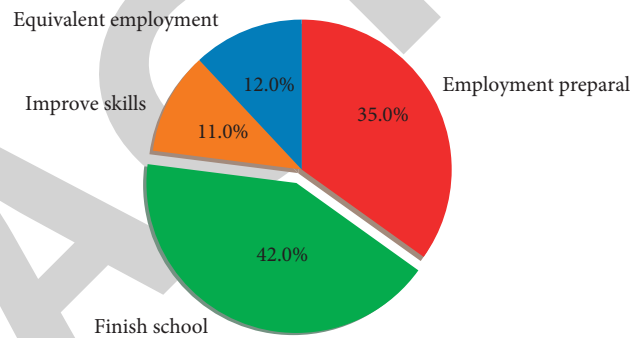


FIGURE 10: Understanding the objective of the internship.

Prejob mobilization education is the preparation link to help students get familiar with the enterprise where they are doing their own internship, and it has an important basic role in the smooth development of future internship management. The survey found that, as shown in Figure 11, more than 60% of the students said it was necessary to receive pre-post training, and 30% of the students thought the pre-post training received was only a simple introduction by the class teacher, and the pre-post training was generally accepted. Another 7.92% of students said they were not willing to receive any kind of preservice training.

Since the students' internship is off-campus, the management of the school in the internship is an important support to ensure the effective functioning of this form of practical teaching, so the management form may also be different from that of school teaching. As shown in Figure 12, 68.5% of the students are managed by teachers through the Internet and telephone, 5.4% are managed by teachers on-site, 11.6% are managed by teachers on rounds, 7.1% are managed by teachers returning to school regularly, and 7.4% are not managed at all.

As can be seen from Figure 12, the current management mode of students' on-the-job internship is basically based on information technology communication such as network and telephone, and some schools even stay in the guidance and management mode of having the former class teacher as the internship instructor, which is relatively insufficient for technical guidance and education work with practical effect

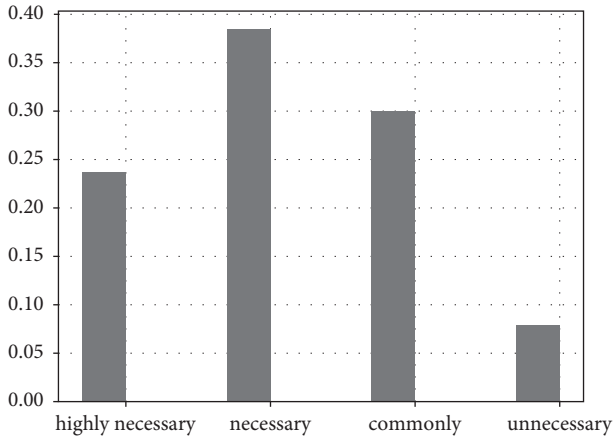


FIGURE 11: Whether pre-post training is necessary.

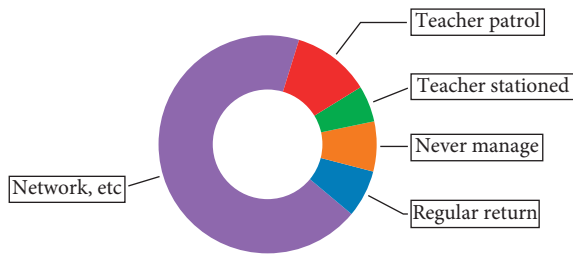


FIGURE 12: Modes of management practice for schools.

and is only responsible for conveying some routine school notices to students.

The implementation of the management of the students by the internship unit directly restricts the achievement of the purpose of the internship. As shown in Figure 13, almost all students said that they had a special master to guide them in the internship process, and 35.8% felt that the effect was good, 42.7% had an average effect, 21.1% had a poor effect, and only 0.4% of students said that they did not have a special master to guide them, which shows that as finance workers, master guidance is essential. However, as far as the effect of guidance is concerned, the reasons are many. Meanwhile, during the survey, it was found that only 16% of the enterprises receiving students for top-up internship really have a system charter specifically for internship management.

Although many colleges and universities ask internship companies to provide rotation opportunities for students participating in internships, which can expose students to more positions and effectively solve students' boredom with internships, master more skills, and create strong conditions for future career selection and employment. In the accounting profession, the proportion of enterprises that really provide students with job rotation during the survey is only 23%, and the majority of internship enterprises arrange students in the finance and taxation departments to carry out daily information reconciliation, sorting and binding of accounting vouchers, reconciliation with bank current account information, simple information aggregation, report production, etc. The one-year

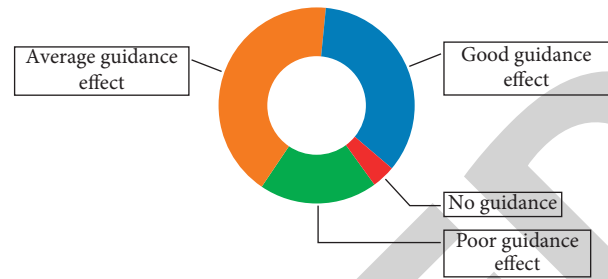


FIGURE 13: The effect of teachers' guidance.

internship period rarely carries out job rotation, which is also due to the small scale of the enterprise itself and the small number of positions in the finance department. The one-year internship period is rarely rotated, which is also due to the small size of the company itself and the few positions in the finance department.

The essence of the internship is the relearning process in the social context. During this period, the guidance contents of enterprises and schools mainly include vocational skills, career planning, professional ethics, and interpersonal relationship. The detailed data of the necessity of the above guidance contents for the students participating in the internship can be seen in Table 6.

From the table below, it can be seen that students participating in the internship have more balanced requirements for each guidance content, and they can realize that comprehensive practice will largely affect their future career choice, so they are more eager to receive career guidance from all aspects. In the actual survey, it is found that the internship students are eager to receive timely and effective guidance when they encounter problems in the practice process, such as the problems they should pay attention to in the actual operation of accounting computerization and red-letter flushing when filling out vouchers and bills with errors.

In the survey, it is found that the assessment of school's top-up internship mainly focuses on students' internship handbook, internship log, and summary report, and the internship grades are given through the scoring by internship instructors and scoring by enterprise masters. In terms of the assessment process, only 17.3% of the students said that the school's assessment ran through the whole process of the top-up internship, and 82.7% of the students said that they only did the two mid-term summary and final assessment. The school still adopts the traditional evaluation by paper summary, internship report, and internship appraisal signed and stamped by the enterprise, which is neither comprehensive nor objective. In the main body of the evaluation, the teachers of the school are still mainly involved, the supervisors of the enterprises are less involved, and the content of the evaluation only lies in whether they have complied with the rules and regulations of the enterprises and made a simple assessment of the attendance. In the final survey, only 40% of the students think that the way of internship assessment is reasonable, and more than half of them think that the way of internship assessment is unreasonable. This shows that there is not yet

TABLE 6: Comparison table of hoped and actually obtained guidance contents in internship practice.

| Serial number | Option content             | Demand proportion (%) |           |         | Actual percentage of receiving guidance |
|---------------|----------------------------|-----------------------|-----------|---------|---|
|               |                            | Very Necessary        | Necessary | General |   |
| 1             | Career skills              | 44.55                 | 61.64     | 23.85   | 52.38                                   |
| 2             | Career planning            | 23.97                 | 35.63     | 40.3    | 5.99                                    |
| 3             | Interpersonal relationship | 13.70                 | 5.26      | 31.03   | 8.65                                    |
| 4             | Professional ethics        | 35.70                 | 55.62     | 6.67    | 29.69                                   |
| 5             | Psychological counseling   | 19.87                 | 35.20     | 44.92   | 3.32                                    |

a special system to stipulate how to evaluate students systematically at the end of the top-up internship.

Students' own feelings are one of the criteria to measure the effectiveness of guidance and management. Satisfaction analysis is carried out through five aspects: salary and remuneration, interpersonal communication, skill enhancement, job matching, and guidance effect. The results show that students are more satisfied with the place focused on career skill enhancement, which shows that students attach more importance to the improvement of self-worth and hope to learn real knowledge through their own efforts and also reflects the importance of top-up internship for accounting students. Dissatisfaction is concentrated mainly in the aspect of salary and wages. Internship students generally think that their efforts are not proportional to their rewards. Those with general attitudes are mainly in interpersonal interaction, job matching, and guidance effect as shown in Figure 14. In addition, schools and enterprises do not pay enough attention to students' psychological counseling, which causes students' self-identity and poor stress resistance, and is also one of the reasons for students' dissatisfaction.

In the conversation with class teachers, internship teachers, and school officials, we learned that the school is generally satisfied with the students' internship, mainly because the school believes that the students' skills have been improved and their interpersonal skills have been strengthened during the internship, and some students have signed labor contracts with the enterprises directly during the internship and participated in the work directly after graduation. The employment rate of the school is improved, and the task of the internship can be completed well. The dissatisfaction is concentrated in the fact that the employer pays too much attention to the economic interests and only asks the students to work seriously without paying attention to the process management of the students, and the students do not communicate well with the school when there are problems in the enterprise, and the school often knows about it only afterwards.

In a survey of 14 people, including finance team leaders, cashiers, and department heads of enterprises, it was found that the satisfaction of enterprises with the top job placement is still relatively low. In the interview, a finance section chief said: "The basic ability of the interns sent here is so poor that they are completely unable to complete the registration of bills independently, and even the simplest journal entries are often wrong." The reason for this is that the intern's own lack of ability greatly affects the effectiveness of the internship.

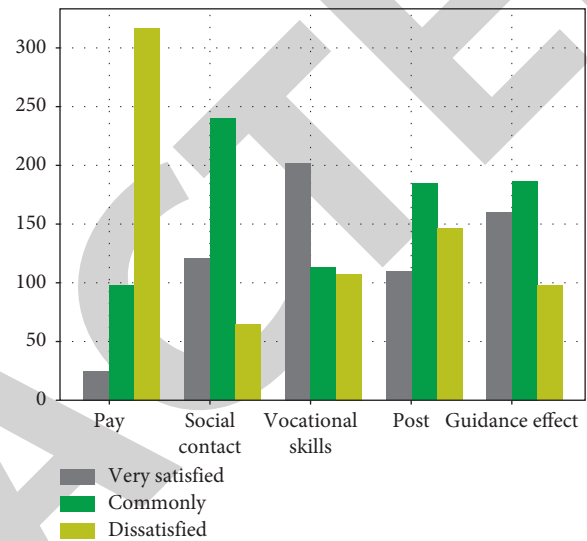


FIGURE 14: The satisfaction of secondary vocational students in the internship.

This is one of the reasons why enterprises are not satisfied with the internship [21, 22].

## 5. Conclusion

Through the multifaceted survey visits to the students involved in the top-up internship in the institution, the school, and the enterprises receiving the top-up students, we have gained an in-depth understanding of the current situation of the top-up internship of students in a school. From the results of the survey, most of the institutions have formulated relevant management systems, prepared the teaching syllabus of the top-up internship, and appointed special internship instructors. In general, the internship in China is at the exploration stage, and many processes and links are still in the early stage of encountering problems and then trying to solve them, and there are still many places that can be further improved.

## Data Availability

The data set used in this paper is available from the corresponding author upon request.

## Conflicts of Interest

The authors declare that they have no conflicts of interest regarding this work.

## Research Article

# Analysis on the Effect of Intelligentization and Improvement of Tourist Bus Loops Based on Markov Chain Decoupling

Shousheng Chai,<sup>1</sup> Jun Shan,<sup>1</sup> Chunfeng Long ,<sup>2</sup> and Wang Qianyi<sup>3</sup>

<sup>1</sup>School of Management, Ocean University of China, Qingdao 266100, China

<sup>2</sup>School of Business Administration, Chongqing Technology and Business University, Chongqing 400061, China

<sup>3</sup>Economic School of Shandong Technology and Business University, Yantai, Shandong 264500, China

Correspondence should be addressed to Chunfeng Long; [long\\_cf@ctbu.edu.cn](mailto:long_cf@ctbu.edu.cn)

Received 26 May 2022; Revised 22 June 2022; Accepted 1 July 2022; Published 21 July 2022

Academic Editor: Hangjun Che

Copyright © 2022 Shousheng Chai et al. This is an open access article distributed under the Creative Commons Attribution License, which permits unrestricted use, distribution, and reproduction in any medium, provided the original work is properly cited.

Based on vehicle positioning and remote data transmission technology, a quantitative analysis method for the impact of intelligent tour bus loops on the choice of transportation means between tourist attractions is developed. Aiming at the problem of undirected graph path planning where the influence of time series is known and the edge weights are known, Markov chains are introduced on the basis of the “0-1-like planning under time series” model, and a Markov chain-based algorithm is established. In this article, we proposed a model for route planning of a tourist bus. When solving, it is assumed that the weight of the edge changes with time, and random variables are introduced, but the past state will not affect the current state, and other conditions remain unchanged. After the constraint model is established, it is simulated by computer and solved using the stochastic gradient descent algorithm. The model makes the tour bus loop intelligent and has good interpretability and robustness.

## 1. Introduction

With the development of economy, holiday tourism is more and more popular among people. Every city regards tourism as an emerging industry and increases efforts to build and improve tourist attractions [1–3]. However, holiday tourism also greatly increases traffic. Especially during the long holiday, the traffic demand of various tourist cities has caused great pressure on the city’s transportation network. Drawing on the advanced experience of developed countries, it is necessary to improve the supply of tourism transportation in tourist cities, especially the accessibility of scattered tourist attractions. This paper proposes a scheme and method for building an intelligent tourism bus loop based on Markov chain decoupling and develops a quantitative analysis model to evaluate the system’s choice of transportation means between scenic spots.

The main purpose of the tourist bus loop is to provide services for tourists who move between scenic spots. It should connect the main scenic spots in the city, and at the

same time, it can enable tourists to reach any major scenic spot by one bus. At present, China’s urban tourist attractions are relatively scattered, especially a considerable number of tourist attractions are located on the edge of relatively remote cities, so the accessibility of urban attractions on the bus network is very poor [4–7]. In order to improve urban tourism traffic conditions and provide tourists with comprehensive bus services, it is necessary to set up circular bus routes so that tourists can enjoy one-stop bus services when moving between scenic spots. The intelligent public transportation system refers to the real-time information exchange between the vehicle station, the scenic spot, and the control center, so as to realize the flexible operation and management of the vehicle, the adjustment of the number of people in the park, and the reasonable arrangement of tourism for tourists. The construction of an intelligent tourist bus system in a developed tourist city can provide experience and methods for the construction of the whole city’s intelligent transportation system IST [8–10]. In order to reasonably grasp the tourists’ understanding and needs of

the intelligent tourism bus loop, a questionnaire survey was conducted among tourists in Dalian, and a total of 104 valid answers were obtained, which were composed of 7% by car, 12% by taxi, 70% by bus; tourists' satisfaction with public transportation between scenic spots is 20%, very satisfied or %, dissatisfied or %, slightly Satisfied 60%.

After clarifying the necessity of building an intelligent tourism bus line, its spatial orientation has become a prerequisite for meeting the requirements of tourists. The spatial layout must first be able to connect with the main scenic spots in the city; it should try not to overlap with conventional buses; the scenery on both sides of the line should be beautiful. The purpose of introducing an intelligent system is to achieve interaction between traffic suppliers, traffic demanders, and scenic spot operators. The core technology of intelligent tourism loops is automatic vehicle positioning system (AVL) [11, 12]. Many cities are equipped with bus vehicles. With AVL equipment, the system has the following functions: (1) real-time monitoring of the dynamics of running vehicles in order to improve fleet management and improve running schedules; (2) providing passengers with real-time vehicle arrival forecast information at stations; and (3) implementing the bus signal priority to locate each vehicle. This paper designs a travel bus loop intelligence based on Markov chain decoupling. Aiming at the problem of undirected graph path planning where the influence of time series is known and the edge weights are known, in order to simulate the situation that the degree of traffic congestion changes with weather changes in reality, based on the model of "class 0-1 planning under time series," the Markov chain is introduced, and a multi-objective path planning model based on the Markov chain is established.

## 2. Theoretical Background

**2.1. Intelligent Tourism Bus Routes.** To determine which improvements would increase the attractiveness of public transport, we designed a questionnaire. Three questions are designed. Is it necessary to display the running status of vehicles on the route on the bus stop sign? Is it necessary to display the admission status of each main scenic spot in the bus? Is it necessary to open the intelligent communication between the main tourist attractions? In terms of the necessity of displaying vehicle operation information at bus stops, 8% think it is not necessary, 2% think it is unnecessary, 24% think it is basically necessary, and 6% think it is necessary. In terms of the necessity of garden information, 14% thought it was not very necessary, 2% thought it was unnecessary, 16% thought it was basically necessary, and 68% thought it was necessary.

Using differential global positioning system (DGSP) and wireless communication technology to realize intelligent tour bus loop, information exchange between vehicles and control center and information release between stations and vehicles are realized. The vehicle equipped with the GSP receiver transmits its coordinates to the control center through wireless transmission, and the control center processes these coordinates to obtain the arrival time of the next vehicle at each station and then displays the time on the

display screen of the station through data transmission. At the same time, each scenic spot transmits its congestion level to the control center by playing at a certain time interval, and the center then publishes the information on the station and vehicles in a zero-delay manner. The technology required for the entire system is formed. The technology and the price of its products are not high, which is suitable for tourist cities with certain financial resources.

**2.2. Markov Chain.** A Markov chain is a stochastic process with Markov properties in probability theory and mathematical statistics that exists in discrete exponential sets and state spaces [13]. Markov chains that apply to sets of continuous exponentials are called Markov processes but are also sometimes regarded as a subset of Markov chains, i.e., continuous-time Markov chains, which correspond to discrete-time Markov chains. Therefore, Markov chain is a relatively broad concept.

Markov chains can be defined by transition matrices and transition graphs. In addition to Markov properties, Markov chains may be irreducible, recursive, periodic, and ergodic. An irreducible and normally recursive Markov chain is a strictly stationary Markov chain with a unique stationary distribution. A limiting distribution that traverses a Markov chain converges to its stationary distribution.

A Markov chain is a set of discrete random variables with Markov properties. Specifically, for the set of random variables in the probability space with a one-dimensional countable set as the exponential set, if the values  $X = s_i, s_i \in S$  of the random variables are all in the countable set and the conditional probability of the random variable satisfies the following relationship [14]:

$$P(X_{t+1}|X_t, \dots, X_1) = P(X_{t+1}|X_t), \quad (1)$$

then  $X$  is called the Markov chain, the countable set  $S$  is called the state space, and the value of the Markov chain in the state space is called the state. The Markov chain defined here is a discrete-time Markov chain, and although it has a continuous exponential set, it is called a continuous-time Markov chain, but it is essentially a Markov process. Commonly, exponential sets of Markov chains are called "steps" or "time steps."

The above formula defines the Markov property while defining the Markov chain, which is also called "memoryless," that is, the random variable at step  $t+1$  is given the random variable at step  $t$  and the rest of the random variables. The variables are conditionally independent. On this basis, Markov chains have strong Markov properties. That is, for any stopping time, the states of the Markov chain before and after the stopping time are independent of each other.

## 3. Intelligent Model of Tourist Bus Loop Based on Markov Chain Decoupling

The path planning problem is to plan an optimal path after a given goal and cost. Different combinations of conditions and goals will produce different planning problems. For example, the planning of multiple goals is multi-objective

planning [15], and the loss can be abstracted into yes or no, which is a 0-1 plan. According to the basic Markov chain model in Section 2.2 and the conversion rules between random Petri nets and Markov chains [16], an intelligent model of tourist bus loops based on Markov chain decoupling can be constructed. The algorithm flowchart is shown in Figure 1. After the Markov chain is constructed, the time factor needs to be introduced.

Markov chain is widely used in the analysis and modeling of systems with random processes. It regards time series as a random process and then determines the changing trend of things by calculating the initial probability and state transition probability of the same state. The bus departure and arrival time series is regarded as a random process, and the Markov chain is used to predict the state change of single-line intelligent bus and estimate the delay propagation probability. The evolution process of delays with time and space is regarded as a non-stationary Markov chain, and the arrival/departure delays of smart buses in consecutive stations are defined as random variables and classified into early, small, and large states, and the probability distribution of delays is predicted, and the prediction accuracy is 71% increase. All the above studies have achieved good results, but the influence of joint delay on the transmission process cannot be considered alone. In this paper, the Markov chain is used to intelligentize the tourist bus loop. The research assumptions in this paper are as follows. (1) The bus operation is based on the map. If the delay propagation process between trains is determined, then the train's on-time delay status remains unchanged, and the propagation probability remains 1. However, there are still random disturbances in the actual operation process, such as the influence of bad and abnormal weather, equipment failures and human operation errors, and so on, and there are differences in the driver's operation. The influence of the difference of traction and braking performance of EMU, as well as the situation that the passenger car uses the redundant time to rush to the point, are random events based on the graph driving. So, these events can be described by probability model. (2) Redundancy time, including station interval operation, tracking operation, redundant time, and so on, is mainly used to control the delay propagation intensity and improve the delay recovery ability. This paper studies the intelligentization of tourist bus routes because the speed scale of tourist buses in the interval is basically the same, that is, the front and rear buses can be used.

When the initial state vector of the train is  $T = \{1, 0, 0\}$ , with the increase of the interval between arrivals, the probability of joint delay gradually increases, but the probability of joint delay is always smaller than the other two delay probabilities. When  $T = \{0, 1, 0\}$ , with the increase of arrival interval, the probability of non-delay and joint delay state gradually decreases, and the probability of initial delay gradually increases. In addition, the first train following the initial delayed train is most likely to have joint delays. When  $T = \{0, 0, 1\}$ , with the increase of arrival interval, the probability of non-delay and joint delay state gradually increases, and the probability of initial delay gradually increases. In addition, the probability of joint delay of the first

train after the joint delayed train is also high. If the homogeneous Markov chain starts from three different initial states, after 6 arrival intervals, the probability of each train arrival state is basically stable. It can be shown that regardless of the distribution of the initial arrival state, after 6 probability transitions, a stable state will always be reached. It can also be shown that when the joint delay propagation range of the intelligent bus is 6 buses, the following bus is no longer affected by the current delay state. Combined with the above analysis, since the state transition probability of each station is different, in the scheduling adjustment, it is necessary to pay more attention to the high probability of delay propagation, especially the stations that are likely to cause long delays, and organize trains to catch up in the forward interval.

#### 4. The Impact of Intelligent Tourism Loop on Traffic between Scenic Spots

Since the annual total number of tourists in a city and the traffic demand between scenic spots can be regressed through statistical data, the key to quantitative analysis is to accurately predict the impact of the system on the choice of transportation means between scenic spots after the system guides people. The maximum likelihood utility theory is considered to be the most effective and conventional method when selecting means, and the analysis method is structured as follows:

$$P_i = \frac{U_i^a}{\sum_j U_j^a}, \quad (2)$$

where  $U$  is the utilization utility of transportation means  $i$ . It varies according to personal preferences, and the reason for this contingent variable is that some passengers do not always use the most efficient means of transportation.  $P_i$  represents the probability that the passenger chooses the means of transportation  $i$ .

Equation (2) is a very typical mode of transportation means selection. The form of the function  $f(x)$  is usually linear, exponential, or logarithmic, and the unknown coefficients need to be calibrated by regression using the existing data. The advantage of this method is that it has sufficient theoretical basis and is easy to understand. The disadvantage is that it requires a large amount of existing data to calibrate the unknown coefficients, and the calibrated coefficients reflect the behavioral awareness of people in the past, and there may be large errors in the prediction of the future. The intelligent tourism bus loop is a brand-new means of transportation, there is no existing data to use, and there are some unquantifiable elements in the subjective evaluation of the means of transportation between scenic spots by tourists, so it is difficult to obtain the open intelligent transportation by using the conventional utility function. This paper proposes to use the analytic hierarchy process to calculate the utility of various means of transportation between scenic spots. The analytic hierarchy process (AHP) was proposed by an American operations researcher. The advantage of AHP is to determine the



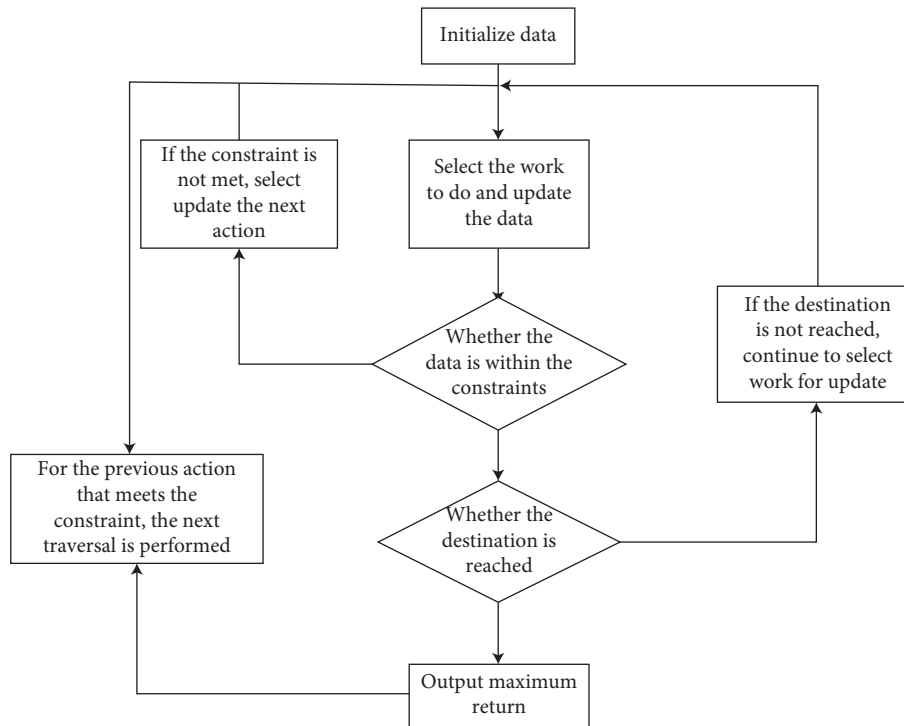


FIGURE 1: The algorithm flowchart.

importance of various factors in people's subjective consciousness when making decisions through questionnaires, so as to quantify people's subjective consciousness  $I$  in the decision-making process. The choice of transportation means for tourists to move between scenic spots is also a decision-making process. According to a large number of previous studies, it is reasonable to believe that the factors ( $X_i$ ) that affect tourists' decision making include cost ( $x_1$ ), time ( $x_2$ ), comfort level ( $x_3$ ), and information provision ( $x_4$ ).

In order to use AHP to calculate the utility of various means of transportation, a hierarchical structure is designed. Generally speaking, the top layer obtains the priority of tourists' subjective awareness of each means of transportation. Since tourists do not always choose the most transportation, some contingent factors can also influence their final choice. So, the chance factor is entered into the equation (1) as the utility of the various vehicles. So, the probability of each vehicle being selected is calculated. The second layer refers to the factors that affect the choice of transportation means for tourists, in which cost and time are continuous numerical indicators, while comfort and information provision are qualitative indicators, which are quantified here using discrete indicators.

When using AHP to make decision-making judgments, weight data must be obtained through surveys. The weight is determined by integrating the subjective consciousness of experts in the corresponding field, but most studies calculate the weight by conducting a sample survey of all relevant personnel. Here, the weight of each factor is determined by conducting a questionnaire survey of tourists at the scenic spot. In order to determine the effect of tourists on the four

elements of the second layer in the means of transportation and to avoid contradictions in the pairwise comparisons, here, according to the order of the elements arranged by the experts, the respondents are asked to make a stepwise comparison. According to the traditional practice of the AHP method, the importance is assigned to the corresponding value, where very important = 5, important = 3, not very important = 1, not important = 0, and then 104 answers are counted.

In order to determine tourists' awareness of the four aspects of various means of transportation in the second layer, the purpose is to find the critical value that tourists care about each element. Through statistical analysis of the survey results, the proportion of tourists who care about each element and various states is obtained. The marginal value of cost difference that tourists care about: 2-6 yuan accounts for 29%, 6-10 yuan accounts for 43%, 10-12 yuan accounts for 20%, and 12 yuan accounts for 8%. The time boundary value that tourists care about: 31% below 10min, 33% 10-20min, 20% 20-30min, 2% 30-40min, and 14% above 40 yuan. Boundary values for comfort differences: 14% accept no-seat crowding, 18% may have a seat, 24% are seated but not crowded, and 4% have a seat. Smart supply boundary value difference: 8% is slightly needed, 2% is not needed, 24% is needed very much, and 66% is needed%. Combining the above survey results, we can get the priority matrix of various means of transportation relative to each element.

According to the above route layout and survey results, AHP can be used to quantitatively analyze the effectiveness of various means of transportation between tourist attractions. However, due to the large OD matrix of tourist

attractions, it is impossible to calculate the utility of various means of transportation for each OD. In this paper, the average value of OD is used to quantitatively analyze the utility of various means of transportation between scenic spots. According to the model results, we give the priority matrix of tourism bus intelligence in 4 aspects (Table 1). It can be seen that information provision is the most important demand in the loop line performance bus. Then, there is comfort, time, and expense. This is because the price of bus loop travel is relatively low and does not fluctuate much.

## 5. Improvement of the Tourist Loop

Since the 21st century, country's social economy has continued to develop and various systems have been continuously improved and perfected. The improvement of people's living standards has led to the vigorous development of leisure tourism. Faced with the current development background and strong development impetus, the state has formally incorporated leisure tourism into the major strategic plan of national development, and tourism development is regarded as an important strategic plan for implementation and national layout. The new pillar industry of our country's national economy promotes the development of our country's economy. The scenic tourist road itself is also a part of the scenery. It is different from ordinary highways in that it has few freight services and has higher requirements for aesthetics. The characteristics of tourist highways around scenic spots are studied and analyzed, and targeted landscape construction can realize highways. The organic unity with tourism provides a pleasant driving environment for tourists.

In the long-term development process of highway construction and governance, the state usually only focuses on the corresponding construction and maintenance of the use function of the highway but does not pay much attention to the landscape and characteristics of the highway itself, including the surrounding environment, even if there are some highways. In the process of construction or governance, the factors of the environment or landscape are considered, and it is also a relatively superficial governance, or it just stays on the repetition of some simple content, or the decoration and creation of the surface of the road, which leads to the development of the road. The disharmony between the overall structure and the landscape environment will even cause damage to many natural landscapes around the highway and along the route, resulting in environmental deterioration. At the same time, many highways in our country are beautifying the landscape along the route or the surrounding environment. In the process of construction, it only stays on the general greening tree design, and the patterns and methods used are relatively simple, resulting in too monotonous road landscape. No systematic design research has been carried out, so the corresponding road landscape is very scattered, which not only affects the road landscape but also affects the use of highways as a transportation channel to a certain extent. For tourist highways, in addition to satisfying the most basic driving and use functions, the landscape organization along the tourist

TABLE 1: Relative importance of four factors in traffic mode choice.

|                      | Cost | Time | Comfort | Information provided |
|----------------------|------|------|---------|----------------------|
| Cost                 | 1    | 2.05 | 4.63    | 11.58                |
| Time                 | 0.49 | 1    | 2.26    | 5.65                 |
| Comfort              | 0.21 | 0.44 | 1       | 2.50                 |
| Information provided | 0.09 | 0.18 | 0.4     | 1                    |
| The eigenvalue       | 0.64 | 0.25 | 0.08    | 0.03                 |

highways should also be given full attention. Whether the tourism highway landscape organization is reasonable or not plays a pivotal role in the overall planning of the highway landscape.

Tourism highway landscape is a complex landscape, including the landscape formed by the highway itself, as well as the natural landscape and human landscape along its route. The interpretation of tourist highway landscape should pay attention to the following. (1) From the perspective of internal and external scope, the tourist highway landscape not only includes the landscape within the scope of the highway but also includes the sight-seeing landscape outside the scope of the highway. Tourism highway landscape is a combination of various natural and cultural landscapes and highway traffic elements visually seen by highway users. As a highway construction mode integrating tourism traffic and economic development, the landscape construction of tourist highway goes beyond the content and scope of the usual highway landscape. (2) From the perspective of landscape components, the tourist road landscape covers natural landscapes and human landscapes. Natural landscapes include topography and landforms in the natural environment (such as plains and hills, snow-capped mountains, forests, seas, wetlands, deserts, and gobi), animals, plants, celestial phenomena, and so on. Human landscape refers to various artificial structures or settlement landscapes created by human beings in the long social production activities, including various types of towns, suburbs, rural landscapes, and social and cultural landscapes such as transportation facilities, historical sites, and religious buildings. (3) According to the different viewing methods of the tourist road landscape, the tourist road landscape includes dynamic and static landscapes. The dynamic landscape and the static landscape correspond to the dynamic viewing mode and the static viewing mode, respectively, and are suitable for studying the physiological and psychological feelings of the dynamic landscape and the static landscape due to the high-speed driving, slow driving, or stillness of the landscape subjects. Visual view, corresponding space design, and dynamic landscape sequence space design are important techniques and means of landscape composition.

## 6. Conclusion

The establishment of tourist loops in large cities with insufficient urban rail networks will play a significant role in improving the supply level of tourist traffic, improving

tourist traffic services, and improving the soft and hard environment of tourism. The intelligent system of tourist bus loops is based on Markov chain decoupling. The introduction will not only improve the efficiency of a single tourist bus route but also provide experience and methods for the construction of the city's overall intelligent transportation system. It is entirely possible for the construction of intelligent tourism bus lines to take the line to the surface to accelerate the intelligent process of the urban transportation system.

### Data Availability

The raw data supporting the conclusions of this article will be made available by the authors, without undue reservation.

### Conflicts of Interest

The authors declare that they have no conflicts of interest regarding this work.

### References

- [1] J. Yuan and I. A. Hansen, "Optimizing capacity utilization of stations by estimating knock-on train delays," *Transportation Research Part B: Methodological*, vol. 41, no. 2, pp. 202–217, 2007.
- [2] M. Carey and S. Carville, "Testing schedule performance and reliability for train stations," *Journal of the Operational Research Society*, vol. 51, no. 6, pp. 666–682, 2000.
- [3] W. Daamen, T. Houben, and R. Goverde, "Monitoring system for reliability of rail transport chains Winnie Daamen1, Toine Houben2, Rob Goverde1, Ingo Hansen1, Adeodat Weeda1 [J]," *Technology*, vol. 2003, p. 129, 2004.
- [4] W. Daamen, R. M. P. Goverde, and I. A. Hansen, "Non-discriminatory automatic registration of knock-on train delays," *Networks and Spatial Economics*, vol. 9, no. 1, pp. 47–61, 2009.
- [5] R. M. P. Goverde, "A delay propagation algorithm for large-scale railway traffic networks," *Transportation Research Part C: Emerging Technologies*, vol. 18, no. 3, pp. 269–287, 2010.
- [6] T. Büker and B. Seybold, "Stochastic modelling of delay propagation in large networks," *Journal of Rail Transport Planning & Management*, vol. 2, no. 1-2, pp. 34–50, 2012.
- [7] T. Huisman, R. J. Boucherie, and N. M. van Dijk, "A solvable queueing network model for railway networks and its validation and applications for The Netherlands," *European Journal of Operational Research*, vol. 142, no. 1, pp. 30–51, 2002.
- [8] X. Wang, N. I. E. Lei, and W. Li, "Study on robustness of high-speed train working diagram based on EMU utilization[J]," *Railway Transport and Economy*, vol. 36, no. 11, pp. 50–55, 2014.
- [9] L. Meng and R. M. P. Goverde, "A method for constructing train delay propagation process by mining train record data [J]," *Journal of Beijing Jiaotong University*, vol. 36, no. 6, pp. 15–20, 2012.
- [10] Y. Yin, J. Liu, and Q. Liu, "Simulation research of station delay propagation based on SIR model[J]," *China Transportation Review*, vol. 39, no. 7, pp. 60–65, 2017.
- [11] P. Huang, Q. Peng, and C. Wen, "Random forest prediction model for Wuhan-Guangzhou HSR primary train delays recovery[J]," *Journal of the China Railway Society*, vol. 40, no. 7, pp. 1–9, 2018.
- [12] P. Huang, C. Wen, and Z. Li, "A neural network model for real-time prediction of high-speed railway delays[J]," *China Safety Science Journal*, vol. 29, no. S1, pp. 20–26, 2019.
- [13] Qi Zhang, F. Chen, and T. Zhang, "Intelligent prediction and characteristic recognition for joint delay of high speed railway trains[J]," *Acta Automatica Sinica*, vol. 45, no. 12, pp. 2251–2259, 2019.
- [14] H. Wu, *Research on Game Theory of Contract Water-Saving Projects in Colleges and universities[D]*, Xi'an University of Technology, vol. 19, no. 5, China, Shaanxi, Xi'an, Beilin, 2020.
- [15] İ Şahin, "Markov chain model for delay distribution in train schedules: assessing the effectiveness of time allowances," *Journal of Rail Transport Planning & Management*, vol. 7, no. 3, pp. 101–113, 2017.
- [16] P. Kecman, F. Corman, and L. Meng, "Train delay evolution as a stochastic process[C]," in *Proceedings of the 6th International Conference on Railway Operations Modelling and Analysis*, Narashino, Japan, Tokyo, March, 2015.

## *Retraction*

# **Retracted: Feature Learning-Based Generative Adversarial Network Data Augmentation for Class-Based Few-Shot Learning**

### **Mathematical Problems in Engineering**

Received 18 July 2023; Accepted 18 July 2023; Published 19 July 2023

Copyright © 2023 Mathematical Problems in Engineering. This is an open access article distributed under the Creative Commons Attribution License, which permits unrestricted use, distribution, and reproduction in any medium, provided the original work is properly cited.

This article has been retracted by Hindawi following an investigation undertaken by the publisher [1]. This investigation has uncovered evidence of one or more of the following indicators of systematic manipulation of the publication process:

- (1) Discrepancies in scope
- (2) Discrepancies in the description of the research reported
- (3) Discrepancies between the availability of data and the research described
- (4) Inappropriate citations
- (5) Incoherent, meaningless and/or irrelevant content included in the article
- (6) Peer-review manipulation

The presence of these indicators undermines our confidence in the integrity of the article's content and we cannot, therefore, vouch for its reliability. Please note that this notice is intended solely to alert readers that the content of this article is unreliable. We have not investigated whether authors were aware of or involved in the systematic manipulation of the publication process.

Wiley and Hindawi regrets that the usual quality checks did not identify these issues before publication and have since put additional measures in place to safeguard research integrity.

We wish to credit our own Research Integrity and Research Publishing teams and anonymous and named external researchers and research integrity experts for contributing to this investigation.

The corresponding author, as the representative of all authors, has been given the opportunity to register their agreement or disagreement to this retraction. We have kept a record of any response received.

### **References**

- [1] B. Subedi, V. E. Sathishkumar, V. Maheshwari, M. S. Kumar, P. Jayagopal, and S. M. Allayear, "Feature Learning-Based Generative Adversarial Network Data Augmentation for Class-Based Few-Shot Learning," *Mathematical Problems in Engineering*, vol. 2022, Article ID 9710667, 20 pages, 2022.

## Research Article

# Feature Learning-Based Generative Adversarial Network Data Augmentation for Class-Based Few-Shot Learning

**Bharat Subedi,<sup>1</sup> V. E. Sathishkumar<sup>2</sup>, V. Maheshwari,<sup>3</sup> M. Sandeep Kumar,<sup>3</sup> Prabhju Jayagopal,<sup>3</sup> and Shaikh Muhammad Allayear<sup>4</sup>**

<sup>1</sup>AgileSoDa, Seoul, Republic of Korea

<sup>2</sup>Department of Industrial Engineering, Hanyang University, 222 Wangsimni-ro, Seongdong-gu, Seoul, Republic of Korea

<sup>3</sup>School of Information Technology and Engineering, Vellore Institute of Technology, Vellore, Tamil Nadu, India

<sup>4</sup>Department of Multimedia and Creative Technology, Daffodil International University, Daffodil Smart City, Khagan, Ashulia, Dhaka, Bangladesh

Correspondence should be addressed to V. E. Sathishkumar; [sathishkumar@kakao.com](mailto:sathishkumar@kakao.com)

Received 10 May 2022; Revised 21 June 2022; Accepted 23 June 2022; Published 21 July 2022

Academic Editor: Shimin Wang

Copyright © 2022 Bharat Subedi et al. This is an open access article distributed under the Creative Commons Attribution License, which permits unrestricted use, distribution, and reproduction in any medium, provided the original work is properly cited.

As training deep neural networks enough requires a large amount of data, there have been a lot of studies to deal with this problem. Data augmentation techniques are basic solutions to increase training data using existing data. Geometric transformations and color space augmentations are well-known augmentation techniques, but they still require some manual work and can generate limited types of data only. Therefore, there are many interests in generative-model-based augmentation lately, which can learn the distribution of data. This study proposes a set of GAN-based data augmentation methods that can generate good quality training data. The proposed networks, f-DAGAN (data augmentation generative adversarial networks), have been motivated by the DAGAN that learns data distribution from two real data. The basic f-DAGAN uses dual discriminators handling both generated data and generated feature spaces for better learning the given data. The other versions of f-DAGANs have been proposed for generating hard or easy data that have additional dual classifiers for both generated data and feature spaces to control the generator. Hard data is useful for optimized training to increase the target performance such as classification accuracy. Easy data generation can be used especially in few-shot learning. The quality of generated data has been validated in two ways: using t-SNE visualization of generated data and classification accuracy by training with generated data using the MNIST data set. The t-SNE representations show that data generated by f-DAGAN are evenly distributed for every class better than the exiting generative model-based augmentation methods. The f-DAGAN also shows the best classification accuracy by training with generated data. The f-DAGAN version for easy and hard data generation generates data well from five-shot learning and performs well in sample data generation experiments.

## 1. Introduction

Machine learning (ML) is a subset of artificial intelligence (AI), which imparts the framework and the advantages to naturally gain from the ideas and information without being unequivocally customized. Deep learning depends on the assortment of ML techniques that models significant level deliberations in the data with numerous nonlinear changes. Deep learning is otherwise called deep structure learning and various leveled discoveries that comprise different layers that incorporate nonlinear preparing units with the end goal of change and

highlight extraction. A deep learning innovation takes a shot at the artificial neural system (ANNs). These ANNs continually take learning techniques, and by constantly expanding the measure of data, the proficiency in preparing procedures can be improved. The learning procedure can be the supervised or semisupervised path by utilizing unmistakable phases of reflection and complex degrees of portrayals [1].

The general focal point of deep learning is the portrayal of the independent data and speculation of the educated examples for use on data unseen. The decency of the data portrayal largely affects the presentation of data by machine

learners; an unfortunate data portrayal is probably going to decrease the exhibition of even a propelled machine learner, while a decent data portrayal can prompt superior for a moderately easier machine learner. These features include designing, which centers on building highlights and data portrayals from actual data [2], which is a significant component of deep learning. Key idea basic deep learning (DL) strategies are dispersed portrayals of the data, in which countless potential arrangements of the theoretical highlights of the information are achievable, taking into consideration a conservative portrayal for each example and prompting a more extravagant generalization. The quantity of potential designs is exponentially identified with the quantity of removed conceptual highlights. Taking note of that they watched information was created through connections of a few known/obscure variables, and along these lines, when an information design is gotten through certain setups of educated components, inconspicuous information examples can probably be depicted through new arrangements of the scholarly factors and examples [3, 4]. Compared to learning dependent on nearby generalizations, the number of examples that can be obtained utilizing an appropriated portrayal scales rapidly with the number of learned elements.

In the following sections, a brief introduction of the few-shot learning approach, data augmentation approach, and the importance of the data augmentation approach will be presented.

Current DL methods cannot quickly sum up from a couple of models. The previously mentioned effective DL applications depend on gaining from huge scope of information. Conversely, people are fit for learning new assignments quickly by using what they realized previously. Overcoming this issue among DL and people is a significant heading. It very well may be handled by DL, which is worried about the subject of how to build PC programs that naturally improve with experience [5, 6]. To gain from a pre-determined number of models with directed data, another AI worldview called few-shot learning (FSL) [7, 8] is proposed. FSL can help calm the weight of gathering huge scope-directed information. Driven by the scholastic objective for DL to move toward people and the modern interest for inexpensive learning, FSL has drawn a lot of ongoing consideration and is currently a hot research territory.

Existing information growth strategies can be separated into two general classes: conventional, white box strategy, or discovery techniques dependent on deep neural networks. The most well-known customary methodology is to perform a mix of relative picture transformation and shading alteration. Geometric mutilations are generally used to expand the number of tests for preparing the deep neural networks, to adjust the size of data sets also for their productivity improvement. The most mainstream strategies are histogram evening out, upgrading complexity or splendor, white-adjust, sharpen, and blur.

Generative adversarial network (GAN) is a generally amazing asset to perform unsupervised actual data utilizing the min-max technique [9]. GANs are seen as very helpful in a wide range of information age and control issues such as text-to-image translation, the image in a painting, and so on.

One of the significant tests to utilize DL models is any way to accumulate and clarify enough data training. Fluctuates heuristics are normally used to prevent overfitting, for example, dropout, penalizing the standard of the system parameters, or early halting of the improvement technique. Aside from the regularization strategies identified with the optimized strategy, diminishing overfitting can be accomplished with data argumentation. Another significant purpose of data argumentation is to build the size of data and sum up a model for better forecast outcomes for unseen data.

The main contributions of this work include

- (1) We examine and compare several data augmentation techniques for a few-shot image classifications using metric learning, in order to compare with different generative-based data augmentation techniques.
- (2) We designed two different types of feature learning generative models for data augmentation.
- (3) We successfully build a model that can generate realistic images even a few samples available in the training set.
- (4) This work shows the feasibility of generating synthesized training data generation using adversarial training with few training data required to achieve the performance of the analysis.

The remainder of the paper is organized as follows. Section 2 describes the related works published in the field of data augmentation and few-shot learning. Section 3 gives an overview of data augmentation. Hallucination-based few-shot learning is explained in Section 4. Proposed work is elaborated in Section 5, and augmentation considering a class is described in Section 6. The evaluation process design and the result of the one-class-based augmentation are described in Sections 7 and 8, respectively. Section 9 concludes the paper.

## 2. Related Works

Few-shot learning (FSL) is the method of taking care of a learning model with a limited quantity of preparing information, rather than utilizing an enormous measure of preparing information to the generalized model for inconspicuous information. This strategy is for the most part used in the field of computer vision, where utilizing an item arrangement model despite everything gives proper outcomes even without having a few preparing tests. The basic FSL situation is the place models with supervised data are hard or difficult to obtain because of security, well-being, or ethical issue. A run of the model is drug revelation, which attempts to find properties of new atoms to distinguish valuable ones as new medications [10]. FSL can lessen the information gathering exertion for information serious applications, for example, picture arrangement, picture recovery, object following, video occasion discovery, language demonstrating, and neural engineering search.

FSL is called one-shot learning. One set of one-shot learning algorithms achieves an information transfer focused on the similarities between previous and recent classes

by reuse model parameters. Classes of objects are learned first by numerous training examples, and then new classes of objects were also learned by transforming model parameters from previously learned classes or selecting appropriate classifier parameters. A further class of algorithms ensures the transfer of knowledge through the sharing of object categories or functions. In patches of already-learned classes, the machine-learning algorithm extracts “diagnostic knowledge” from shared information patches and then applies it to new class learning. One shot of prior experience in horse and cow classes, for example, may be acquired in a dog class, as dog items can have identical distinctive patches. The one-shot research focused on the similarities of new classes of objects and their previously studied ones passes qualitative awareness to a worldwide experience of the object’s environment.

Zero-shot learning expects to perceive objects whose occasions might not have been seen during preparation [11, 12]. It involves the grouping of pictures where there is no named preparing information, and a few methodologies have been proposed; each year has been expanding quickly with no specific benchmark. For a solid model, envision recognizing a class of items in photographs without ever having seen a photograph of that sort of article previously. Most zero-shot learning techniques utilize some association between accessible data and inconspicuous classes. Early works of zero-shot learning [13, 14] utilize the traits inside a two-phase way to deal with construing the name of a picture that has a place with one of the concealed classes. In the broadest sense, the features of an information picture are anticipated in the principal stage; at that point, its class mark is surmised via looking through the class that accomplishes the most comparative arrangement of features.

While a large portion of zero-shot learning strategies gets familiar with the cross-model mapping between the picture and class installing space with discriminative misfortunes, there are a couple of generative models [15, 16], which address each class as a likelihood appropriation [17].

Few-shot learning (FSL) techniques can be generally sorted into three classes: hallucination-based data argumentation, meta-learning, and metric-learning. Data augmentation is a great method to expand the measure of accessible information and accordingly valuable for few-shot learning [18–20]. A few strategies propose to gain proficiency with an information generator for example adopted on Gaussian noisy [21, 22]. Be that as it may, the age models regularly fail to meet expectations when trained on not many shot information. An option is to combine information from numerous tasks that, be that as it may, is not successful because of fluctuations of the information across undertakings [23].

Meta-Learning few-shot is based on aggregate understanding from learning numerous assignments [24, 25], while base-learning centers display the information appropriation of a solitary understanding. A best-in-class illustrative of this, in particular model-agnostic meta-learning (MAML), figures out how to scan for the ideal introduction state to quick-adjust a base-student to another assignment. Its task-agnostic property makes it conceivable to sum up the

few-shot supervised learning just as unsupervised reinforcement learning [26, 27]. In any case, in our view, there are two primary constraints of this sort of approach restricting their adequacy: (i) these techniques, as a rule, require countless comparable errands for meta-training, which is costly, and (ii) each assignment is commonly displayed by a low-complexity base learner (for example, a shallow neural system) to keep away from model overfitting, hence being not able to utilize further and all the more impressive structures [28].

The objective of metric learning is to limit intra-class varieties and maximize between-class varieties. Early works utilized Siamese engineering [29, 30] to catch the likeness between pictures. The ongoing works [31] received the deep systems as feature embedded method and utilized triplet misfortunes rather than pairwise limitations to get familiar with the measurement. These measurement-learning techniques have been generally utilized in picture recovery [32], face acknowledgment, and individual redistinguishing proof [33]. Duan et al. [34] introduced a deep adversarial metric learning (DAML) to create manufactured hard negatives from the watched negative examples, where the potential hard negatives are produced for scholarly measurement as supplements. All the more as of late, Wu et al. [35] introduced a feature embedding method dependent on the neighborhood part examination. These works show that joining a deep model with appropriate targets is successful in learning the likenesses. In contrast to these techniques, we consider utilizing triplet-like systems to improve the component separation on the concealed class pictures for few-shot learning issues [36].

Metric learning-based strategies gain proficiency with a lot of project functions (embedding functions) and measurements to quantify the similitude between the question and test pictures and group them in a feed-forward way. Snell et al. [36] broadened the coordinating system by utilizing the Euclidean separation rather than the cosine separation and building a model portrayal of each class for a couple of shot learning situations, to be a specific prototypical system. Sung et al. [37] contended that the inserting space ought to be characterized by a nonlinear classifier and planned the connection module to get familiar with the separation between the feature embedding of support images and query images shown in Figure 1. The key distinction among metric-learning-based techniques lies in the way they get familiar with the measurement. Vinyals et al. [19] planned to start to finish trainable k-nearest neighbors utilizing the cosine separation on the picked-up inserting highlight, to be a specific coordinating system. Of late, Mehrotra and Dukkipati [21] prepared a deep leftover system along with a generative model to rough the expressive pairwise closeness between tests. This network is trained to learn relations between features of support and query images. The connection categories broadens the coordinating system and prototypical system by including a learnable nonlinear comparator. Jin et al. utilized several deep learning models for predicting the crack width of Longyangxia Dam, and the importance of influencing factors in cracks is analyzed [38]. Cen et al. [39] utilized recent

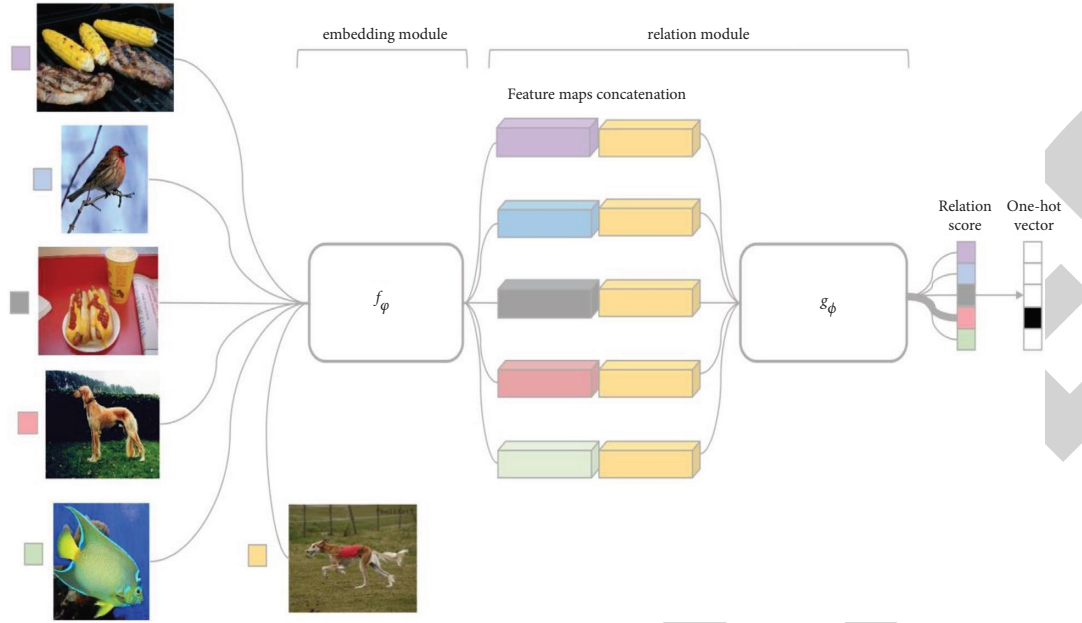


FIGURE 1: Learn to compare relation networks for few-shot learning.

graph neural networks for few-shot learning to represent fully connected graph samples of interest. Cao et al. proposed a BERT-based deep spatial-temporal network for taxi demand prediction by modeling complex spatial-temporal relations using global and local features that are heterogeneous [40]. Pu et al. used a convolutional neural network and recurrent neural network to fit the motion representation and spatial sequence in a video stream to improve the accuracy of fetal ultrasound standard plane recognition [41]. Several big data service architectures were discussed by Wang et al. [42]. Li et al. proposed a data-driven adversarial capsule network for regional traffic flow prediction with highly challenging data sets [43]. Blockchain-based technologies also play a vital role in several applications [44].

### 3. Data Augmentation

Argumentation of data involves a number of techniques that increase the size and consistency of training data sets in order to create stronger deep learning models. The augmentation algorithms addressed in this research includes mathematical augmentation technique and generative adversarial networks (GAN) based technique.

**3.1. Mathematical Augmentation.** An exceptionally conventional and acknowledged current practice for augmenting picture data is to perform geometric and color augmentations, for example, mirroring the picture, flipping, revolution, translation, noise injection, cropping, translating the picture, and changing the color palette of the picture [45]. The entirety of the transformation is the relative transformation of the first picture that takes the structure as follows:

$$y = wx + b. \quad (1)$$

The well-being of rotate argumentation is vigorously dictated by the rotate degree parameter. Moving pictures left, right, up, or down can be an extremely valuable chance to keep away from positional predisposition in the data. Another significant numerical argumentation technique is a noisy infusion, which comprises infusing a network of irregular qualities normally drawn from Gaussian dissemination. A noisy infusion of pictures can help CNNs learn progressively strong highlights. Picture data is encoded into pixel esteems for individual RGB color esteem. Lighting bias is among most of the time happening difficulties to picture recognition issues. A handy solution to excessively splendid or dim pictures is to circle through the pictures and decrease or increment the pixel esteems by a constant value can assist with learning the high dimensional feature of pictures. The mathematical augmentation technique is not suitable for all types of data set illustrated in Figure 2 in numeric data if rotation degree increases the label of data that is no longer preserved.

**3.2. Generative Model-Based Augmentation.** Later and additionally, an exciting technique for data augmentation is generative demonstrating. In Figure 3, two neural networks are trained opposite one another in a generative adversarial network (GAN). The generator  $G$  takes as input a noise vector  $z$  and outputs an image  $X_{fake} = G(z)$ . The discriminator  $D$  receives a training image or synthesized image as an input from the generator and outputs a distribution of probabilities  $P(S|X) = D(X)$  over potential sources of image data. The discriminator is trained to optimize the log-likelihood of the source as follows:

$$L = E[\log P(S = real|X_{real})] + E[\log P(S = fake|X_{fake})]. \quad (2)$$





FIGURE 2: Rotation and flipping.

The generator has the task of generating convincing fake data from random noise. The discriminator gets as input either fake or real data and has to determine whether its input is real or fake.

Generative displaying refers to the act of making artificial cases from a data set with the end goal that they hold comparative qualities to the first set. The standards of adversarial training prompted an extremely intriguing and hugely famous generative system known as GANs. GAN is an approach to open extra data from a data set. GANs are by all accounts not the only generative displaying procedure that exists; anyway, they are drastically driving the path in calculation speed and nature of results. The impressive presentation of GANs has brought about expanded consideration on how they can be applied to the undertaking of data argumentation. These systems can create new training data for those outcomes in better performing order models.

Another valuable system for generative displaying worth referencing is variational autoencoder (VAE), which is described in Figure 4. The GAN system can be stretched out to improve the nature of tests delivered with variational autoencoders. Variational autoencoder gains proficiency with a low-dimensional portrayal of data focuses. An autoencoder organized is a couple of two associated systems, an encoder and a decoder. An encoder arranged takes in an independent variable and changes over it into a littler, thick portrayal, which the decoder system can use to change over it back to the actual independent variable. Variational autoencoders (VAEs) have a very simple property that isolates them from vanilla autoencoders, and that property makes them so useful for generative demos.

The model contains an encoder function  $g(\cdot)$  parameterized by  $\Phi$  and a decoder function  $f(\cdot)$  parameterized by  $\theta$ . The encoding for input  $x$  on the bottleneck layer is  $z$ , and the data restored is given in

$$x' = f_{\theta}(g_{\Phi}(x)). \quad (3)$$

#### 4. Hallucination-Based Few-Shot Learning

Hallucination-based learning is to straightforwardly manage data inadequacy by figuring out how to enlarge like humans imagination illustrated in Figure 5. This class of technique takes in a generator from data in the base classes and utilizes the educated generator to hallucinate new novel class data for data argumentation. These generators either move fluctuation in base class data to novel classes since hallucination-based techniques frequently work with other few-shot strategies together (e.g., use hallucination-based and metric learning-based techniques together) and lead to entangled

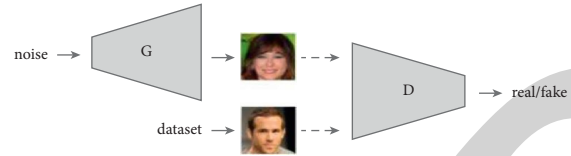


FIGURE 3: A simple graphical representation of the GAN setting.

correlation. Numerous conventional meta-learning strategies treat pictures as black boxes, disregarding the structure of the visual world. As humans, our insight into the class's diverse variety of articles may permit us to imagine what a novel item may resemble in other posture or environmental factors. On the off chance that machine vision could do such hallucinated samples, at that point, the fantasized models could be utilized as extra training data to manufacture better classifiers. Building models that can perform hallucination is hard. For general pictures, while extensive advancement has been made as of late in creating sensible examples, most current generative demonstrating approaches experience the ill effects of the issue of mode breakdown; they are just ready to catch a few methods of the data.

The key insight hallucination technique is the hallucination model that is valuable for learning classifiers. For expanding the classification, the accuracy utilizing daydream models a model that needs to map genuine guides to hallucination models. In the hallucination approach, training is first taken care of by the hallucinator; it delivers an extended preparation set, which is then utilized by the student. Utilizing meta-learning out how to train the hallucinator and the classification has two advantages. To start with, the hallucinator is legitimately prepared to deliver the sorts of fantasies that are valuable for class differentiation, evacuating the need to accurately tune authenticity or assorted variety or the correct methods of variety to hallucinate. Second, the classification technique is trained mutually with the hallucinator, which empowers it to consider any mistakes in the hallucination. On the other hand, the hallucinator can spend its ability to smother the blunders, which perplex the classification technique.

The contingent generative model incorporates highlights of unseen classes F-CLSWGAN by optimizing the Wasserstein separation regularized by a classification misfortune demonstration in Figures 6 and 7. F-CLSWGAN that produces features includes rather than pictures and is trained with a novel misfortune improving over option GAN-models. The principle key of feature-based classification is the capacity to create semantically rich CNN feature disseminations molded on class explicit semantic vector, for example, properties, without access to any pictures of that class. This reduces the irregularity among seen and unseen classes, as there is no restriction on the quantity of engineered CNN features that the model can produce.

#### 5. Proposed Method

We proposed a new generative adversarial network for image data augmentation by conducting various feature vectors-based approaches. Furthermore, we interpreted data augmentation for class-based few-shot learning. Finally, we inform the application areas of the data augmentation.

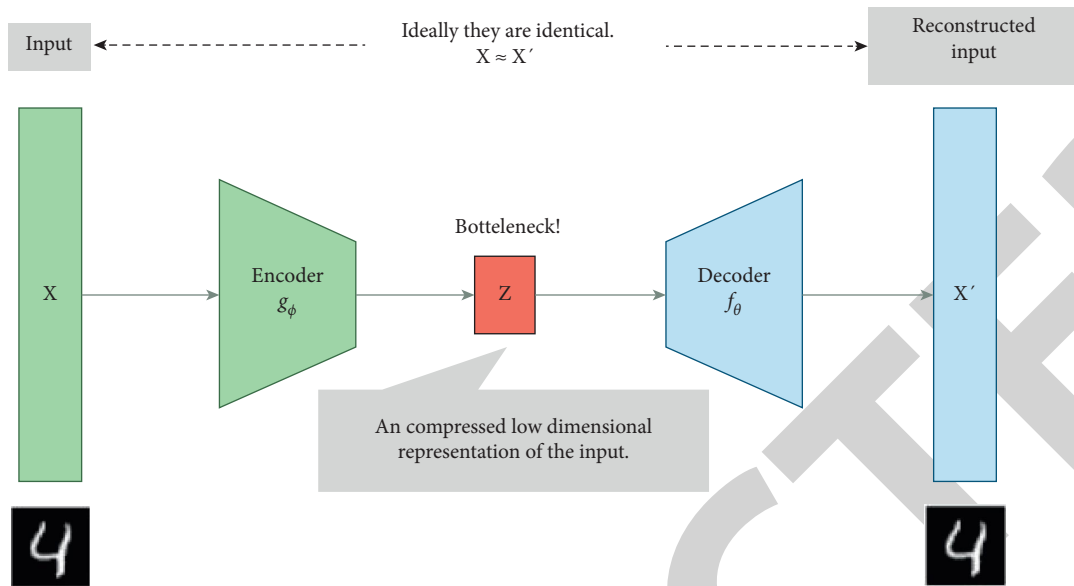


FIGURE 4: Illustration of autoencoder model architecture.



FIGURE 5: Humans are good at imagination.

*5.1. The Proposed Approach.* The proposed feature learning-based data augmentation generative adversarial network is given in Figures 8 and 9. In two different ways, we tried to design networks and present the output result of networks [1]. The overall flow of the proposed system is shown in Figure 10.

## 6. Data Augmentation for Class-Based Few-Shot Learning

The general idea of class-based data augmentation is to increase the number of data by changing data slightly to be different from the original data in a few-shot approach, but the data still can be recognized by humans. The generated

data involved the same training classes are identical to the original class. Class-based data augmentation randomly interchanged regions between various images of the same class for improving the generalization of feature distribution. To use GAN for class-based data augmentation, we design our generative network that can extract features from random Gaussian noise, which is an input of the generator network and concatenation of those features with real image features generated by CNN, which is the input for the discriminator.

*6.1. Augmentation considering a Class.* To achieve our goal, we purposed the f-DAGAN network for a single class

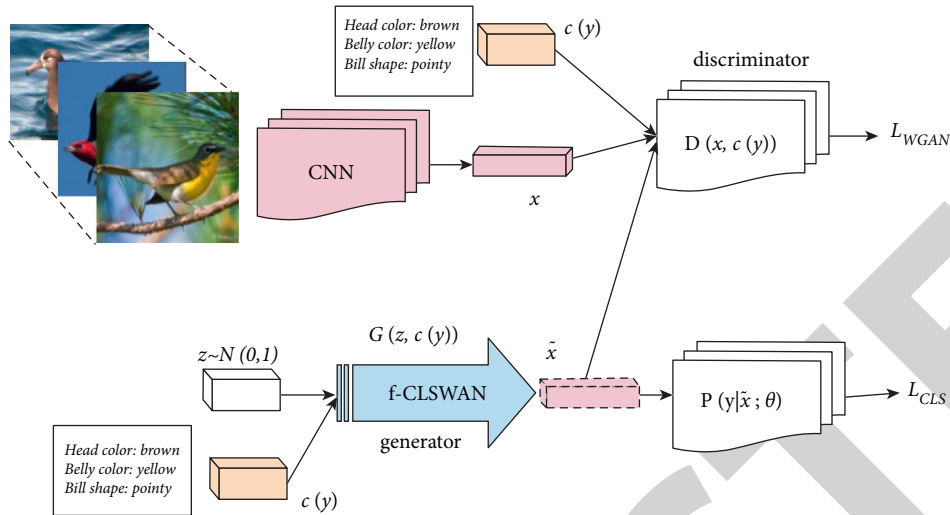


FIGURE 6: F-CLSWGAN.

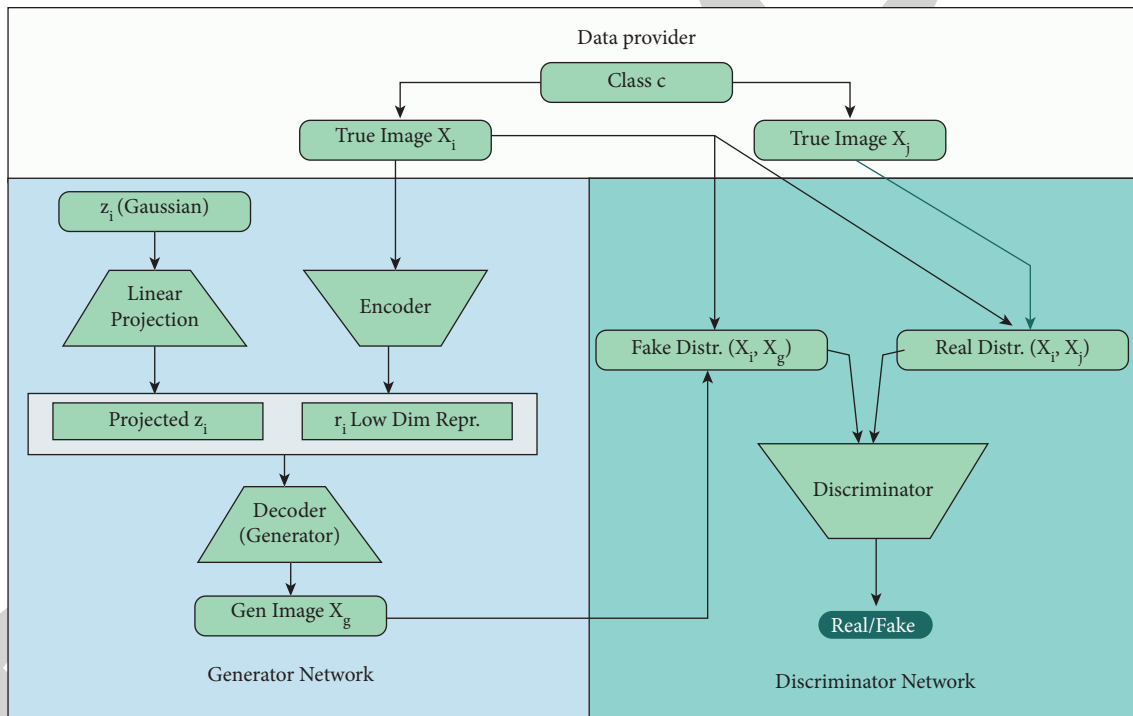


FIGURE 7: AGAN architecture [46].

augmentation and the h-DAGAN network for hard example generation. The data augmentation for both networks can be learned using an adversarial approach. Consider a source image class consisting of data  $D = \{x_1, x_2, \dots, x_n\}$ . Our networks take some input data point  $x_i$  and a second data point from the same class  $x_j$ .

The main idea of our first purposed architecture f-DAGAN for a single class is that we combined the generator feature and CNN feature of a real image to create realistic images. This can be done by concatenating both image features and random noise features along the channel axis. For example, a given image of dimensions  $[W \times H \times$

$C]$  with its corresponding generator feature of dimensions  $[W \times H \times C]$  results in a feature with dimensions of  $[W \times H \times 2C]$ . When training the GAN, the generator is now modified to generate a feature vector, instead of just an image. This change, in its most trivial form, can be achieved by simply modifying the convolutional layer in the generator, such that the number of channel outputs is equal to the number of channels of the required CNN feature of an input image.

For the discriminator network, we used two discriminators. One discriminator is used to discriminate between real and fake features and another discriminator to

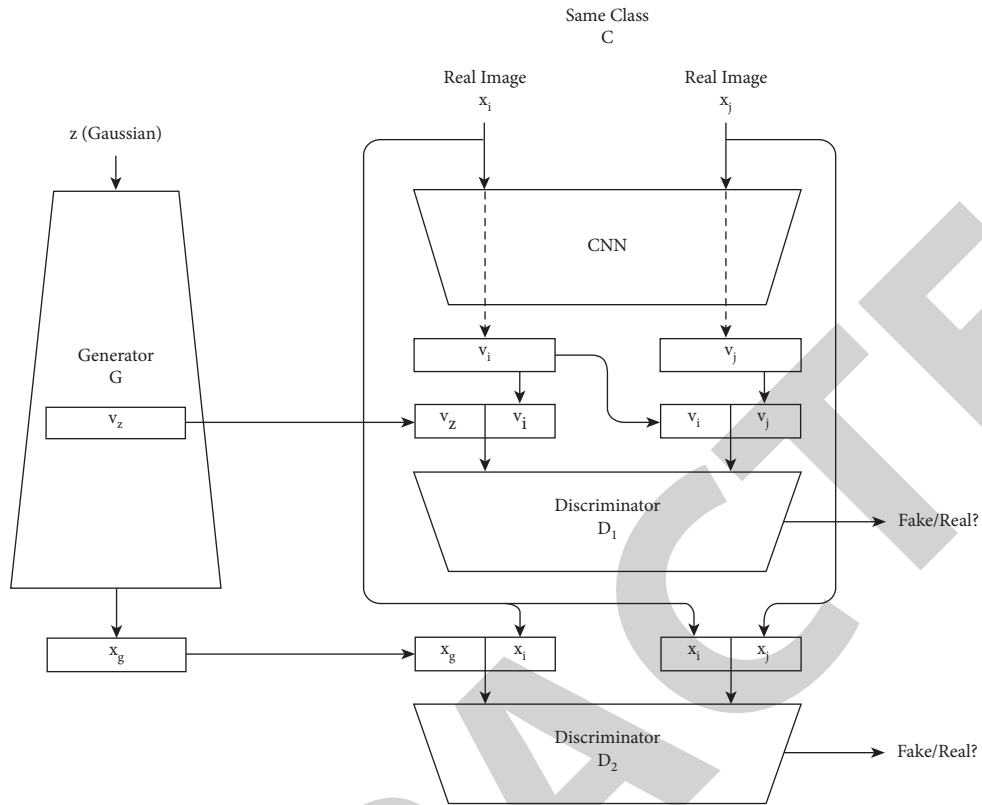


FIGURE 8: f-DAGAN structure.

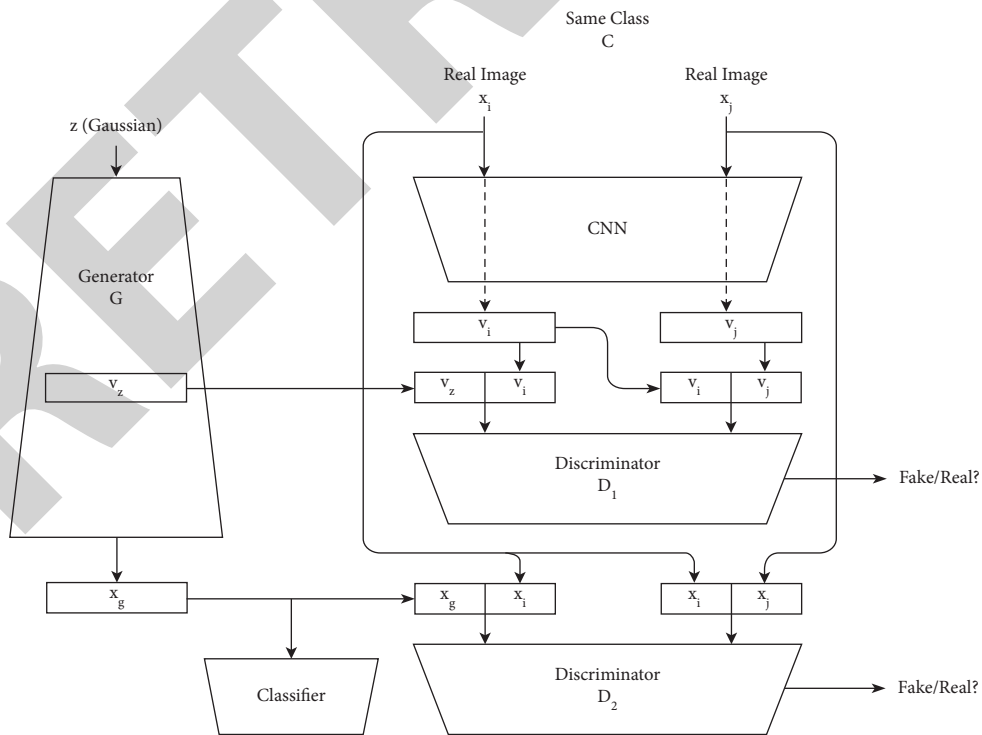


FIGURE 9: DAGAN few samples training.

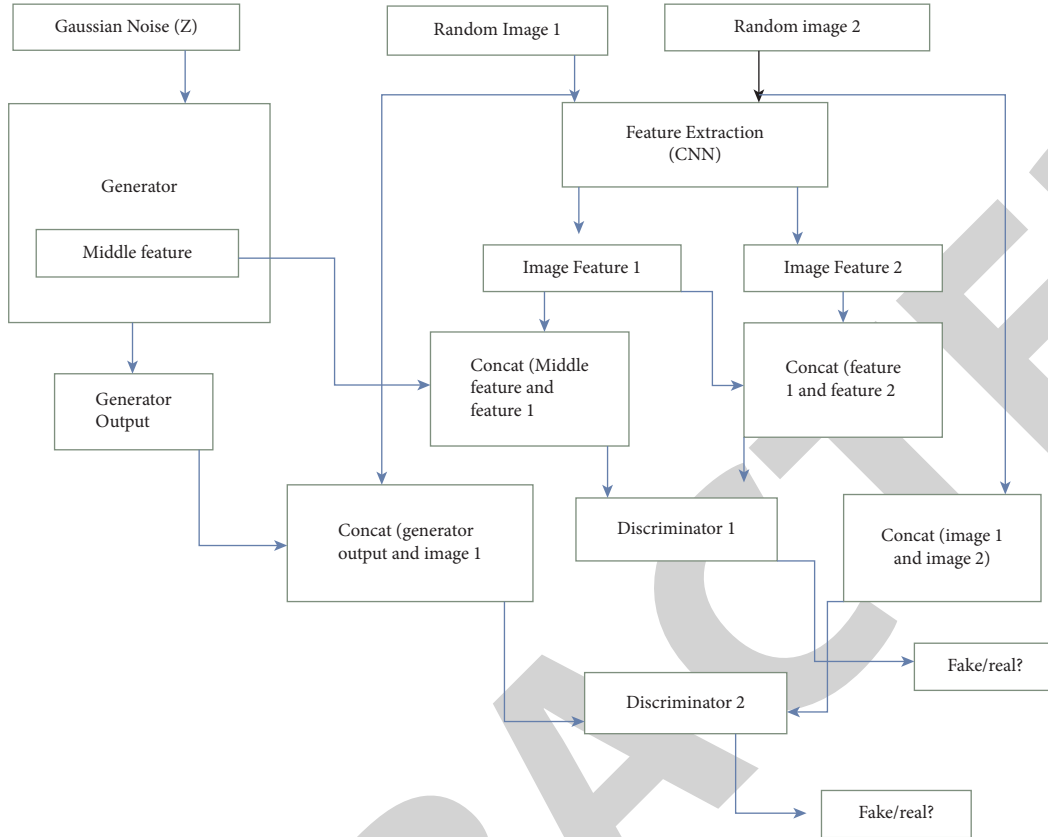


FIGURE 10: System workflow.

discriminate between real and generator images. At first, the feature discriminator network now takes a concatenated feature of the generator network and real image  $x_i$  feature as input, and its goal is to correctly decide if any given feature is real or synthetic. Second, the input of the feature discriminator network is the concatenated feature of pairs of real images  $x_i$  and  $x_j$ . At first, the image discriminator takes concatenated fake image generated by the generator and real image  $x_i$  as input, and its main goal is to correctly decide if any given image is real or synthetic. Second, the input of the discriminator network is the concatenation of pairs of real images  $x_i$  and  $x_j$ . To calculate the final loss of the discriminator, we used the sum of feature discriminator network loss and image discriminator loss.

Our second purposed architecture h-DAGAN is an example for augmentation. Classifiers are used for calculating feature and image-based easiness (hardness) of generating samples. This can be done by implementing classifiers for both fake image  $x_g$  generated by the generator and latent vector features generated by the generator network. We calculate classification loss in two ways, one for feature classification and another for fake image classification using binary cross-entropy loss. The final classification loss is the combination of feature and fake image loss. In the second step, we concatenate the concatenated feature from the generator network with a real image  $x_i$  feature from CNN, which is one of the inputs of the feature discriminator network. Another input of the feature

discriminator network is the concatenated pairs of real images  $x_i$  and  $x_j$  features from CNN. To calculate feature discriminator network loss, we utilized fake feature logits and real feature logits.

For image discriminator networks, we utilized pairs of real images  $x_i$  and  $x_j$  and images generated by the generator network. The first input of the image discriminator network is the concatenation of randomly selected one real image  $x_i$  and a fake image from the generator network. The second input of the image discriminator network is the concatenation of randomly selected real image pairs  $x_i$  and  $x_j$ . We calculate image discriminator loss by using combined fake and real image logits. The total discriminator loss is the addition of feature discriminator loss and image discriminator loss with the subtraction of total classification loss. Classifier  $C_1$  is used for classifying fake image feature vectors, and classifier  $C_2$  is used for classifying fake images. Probabilities of the target class in  $C_1$  and  $C_2$  are used for class loss  $CL_1$  and  $CL_2$  using binary cross-entropy loss. Total classifier loss  $Cl$  is calculated as follows:

$$CL = \alpha CL_1 + \beta CL_2. \quad (4)$$

The final generator loss is the sum of fake feature logits loss and fake image logits loss. Our second GAN architecture that we use to generate the image is illustrated in Figure 10. In both networks, every generated sample has a corresponding class pair of two images,  $x_i \sim p_{x_j}$  in addition to the noise  $z$ .  $G$  uses both to generate images  $X_{fake} =$

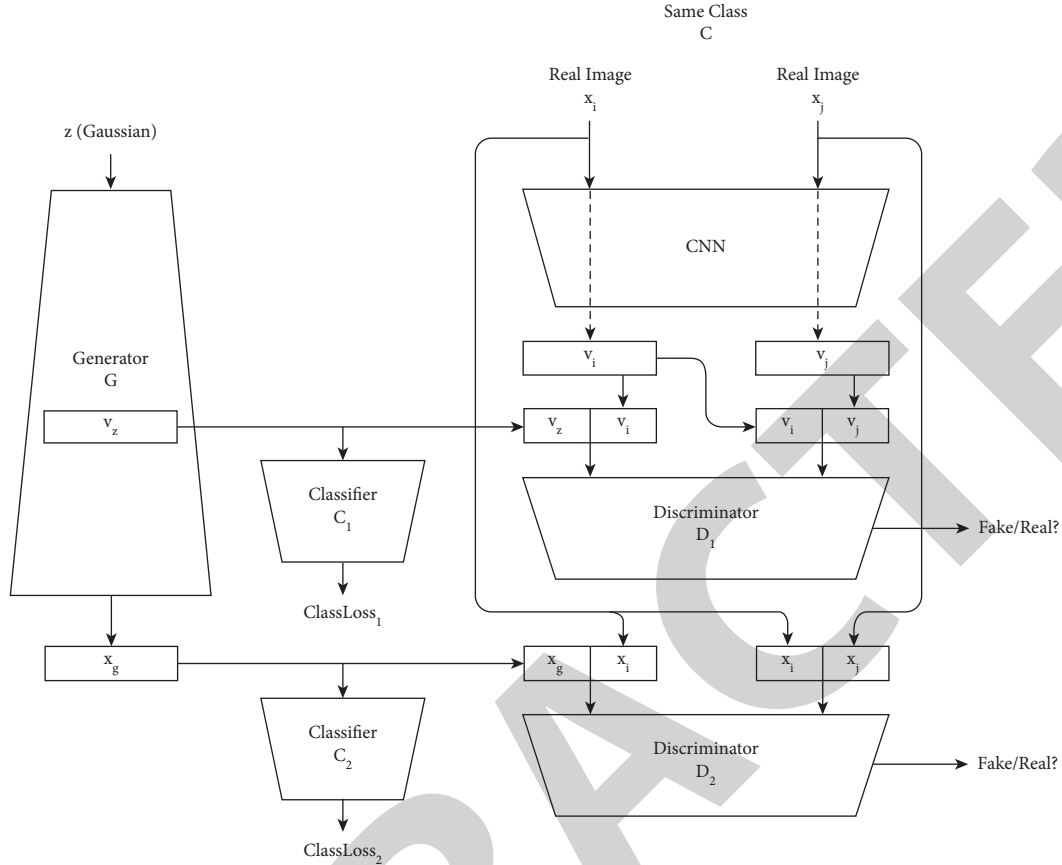


FIGURE 11: h-DAGAN hard example generation network.

$G((x_i, x_j), z)$ . The discriminator gives both a probability distribution over sources  $x_i$  and  $x_j$  as follows:

$$P(x_i|X), P(x_j|X) = D(X). \quad (5)$$

GAN is studied as a minimax game and uses the alternating gradient descent on the cost function  $J$  to optimize the discriminator  $D$  and generator  $G$ . The objective function is defined as follows:

$$J^{(D)}(\Phi, \theta) = -E_{x \sim p_{real}} \log D_\theta(x) - E_z \log(1 - D_\theta(G_\Phi(z))), \quad (6)$$

$$J^{(G)}(\Phi, \theta) := -J^{(D)}(\Phi, \theta). \quad (7)$$

The complete game can be specified as follows:

$$\min_{\Phi} \max_{\theta} \{J(\Phi, \theta) = E_{x \sim p_{real}} \log D_\theta(x) + E_z \log(1 - D_\theta(G_\Phi(z)))\}. \quad (8)$$

In f-DAGAN, we want to find the equilibrium where the discriminator  $\theta$  maximizes  $J$  and the generator  $\Phi$  minimizes it. f-DAGAN learns a representation for  $z$  that is independent of different source images. Structurally, this model is not tremendously different from many existing few-shot models. The final discriminator loss of h-DAGAN is the difference between total discriminator loss and classifier loss.

**6.2. Network Structure.** During this research work, we designed and implemented feature generative networks. Our feature vector-based data augmentation generative adversarial network (f-DAGAN) as shown in Figure 11 and feature vector-based hard data augmentation generative adversarial network (h-DAGAN) are implemented based on feature space learning. We designed f-DAGAN for feature vector-based data augmentation and h-DAGAN for hard example generation. We already discussed our f-DAGAN network. The main objective of our h-DAGAN network is to create hard sample data that can help generalize the classifier and increase the accuracy of the network. Furthermore, the classifier becomes more robust when we trained on hard example data. For a training network with a few examples, we design another network. The main objective to add a classifier is to control the generator during the training network with a few examples.

**6.3. Training Process and Implementation Details.** Our single-class GAN was trained on the MNIST data set using ResNet50 architecture. During the training phase, there are three parts to the network. The CNN network takes in two images from the same class as the input image and returns a feature of input images. The concatenate CNN features of two images are then passed into the feature discriminator network. The generator network takes a random noise vector and generates a feature of a random vector and a fake image.

The  $x_i$  image feature concatenates with the generator generate feature also passed into the feature discriminator network. On the other side, the concatenated image of the generator image and real image  $x_i$  is passed into the image discriminator network, and concatenated image of real  $x_i$  and  $x_j$  images is passed into the image discriminator network. In each training cycle, a randomly selected sample from the source was provided for each real example.

For few-shot training, we divided the MNIST data set into small sets of data. To create 5 images sample set of the data set, we randomly selected 50 images from each class; for 10 images sample set of the data set, we randomly selected 100 images from each class, and similarly for 100 and 1,000 images sample set. We trained our f-DAGAN and h-DAGAN networks using a generator learning rate of 0.0005, and the discriminator learning rate is 0.002 with Adam optimizer parameters of  $\beta_1 = 0.2$  and  $\beta_2 = 0.9$ . The generator has a total of 3 ResNet blocks, each block having 4 convolutional layers (ReLU activations and batch normalization) followed by one downscaling or upscaling layer. Downscaling layers were convolutions with stride 2, followed by ReLU and batch normalization. Upscaling layers were stride 1/2 replicators, followed by a convolution, ReLU, and batch normalization. Feature generated by the first ResNet block is followed by the attention block. During h-DAGAN, we used  $\alpha = 0.1$   $\beta = 0.5$  for controlling loss of classifiers.

The feature generative network has a total of 2 ResNet blocks; each block consists of 4 convolutional layers with the ReLU activation and batch normalization that is followed by one downscaling layer. Feature discriminator network has a total of 3 ResNet blocks, having 4 convolution layers with ReLU activation function and batch normalization layers followed by 1 downscaling layer and dense layer. Downscaling layers were convolutions with stride 2. The image discriminator network consists of 4 ResNet blocks followed by a downscaling layer. Also, each block of ResNet had skip connections. For training and validation, we used an AMD server with 1920X CPU and NVIDIA RTX 1080ti GPU. As the deep learning framework, Python 3.7 and the GPU version of TensorFlow 2.3 were used. The configuration of the h-DAGAN network is the same as f-DAGAN; only the difference is the addition of feature and fake image classifier shown in Figure 10. Feature and image classifier network consist of two convolution blocks; each convolution block contains a 64-filter  $3 \times 3$  convolution, a batch normalization,  $2 \times 2$  max polling, ReLU nonlinearity layer, and fully connected layer with Sigmoid layer.

## 7. Evaluation

In this section, we report a series of experiments conducted on a different set of MNIST data sets, and the results of these experiments are followed by a discussion of the findings in this research work. A performance comparison of the different network architectures introduced in the previous sections (DAGAN, VAE, f-DAGAN, and C-GAN) is also presented. As a performance evaluation metric, classification accuracy is primarily used. For a detailed investigation of the



FIGURE 12: MNIST data set samples visualization.

classification accuracy of different network-generated data sets, we used the ResNet50 network.

**7.1. Evaluation Process Design.** It is difficult to assess the quality of data generated by GANs. This also causes it to be challenging to accurately compare the quality of data produced by different GAN architectures, algorithms, and hyperparameter settings. One way to measure the performance of generative models is an evaluation by humans. However, next to being time-consuming and expensive, this method also varies under evaluation conditions. Specifically, the evaluation setup and motivation of the annotators affect the scoring. Furthermore, when annotators are given feedback, they learn from their mistakes and make fewer errors. The (part of the) output of the discriminator that indicates whether the generated data is regarded as real could be used to monitor the convergence of GANs. However, for any specific discriminator, this output heavily depends on the generator that it is trained with. Therefore, the discriminator output cannot be used trivially to quantitatively evaluate the quality of the generated data. To overcome the problem of generated data evaluation, we used two ways that were employed to measure visual quality and data generation diversity. The classification accuracy measured how generated data performed classification on the original MNIST data set. The t-SNE visualization creates a probability distribution using the Gaussian distribution that defines the relationships between the data points in high-dimensional space [47].

**7.1.1. Purposes and Performance Metrics.** The use of these as feature extractors on labeled data sets is one common learning technique for evaluating the quality of unsupervised representative learning algorithms and for assessing the performance of linear model models on generated images. To evaluate for instance the consistency of the GAN model representations trained the GAN model on the MNIST data set and generate synthesized images, then CNN is used to classify them. If the CNN classifier performs well on the original data set, this indicates that the GAN synthesized images are accurate and sufficient to be informative about object class.

In order to test GANs, Ye et al. [48] suggested an analytical metric known as the GAN Consistency Index. Firstly, a generator  $G$  is trained on a labeled real data set with  $N$  classes. Secondly, a classifier  $C_{real}$  is trained on the real data set. A second classifier, called the GAN-induced

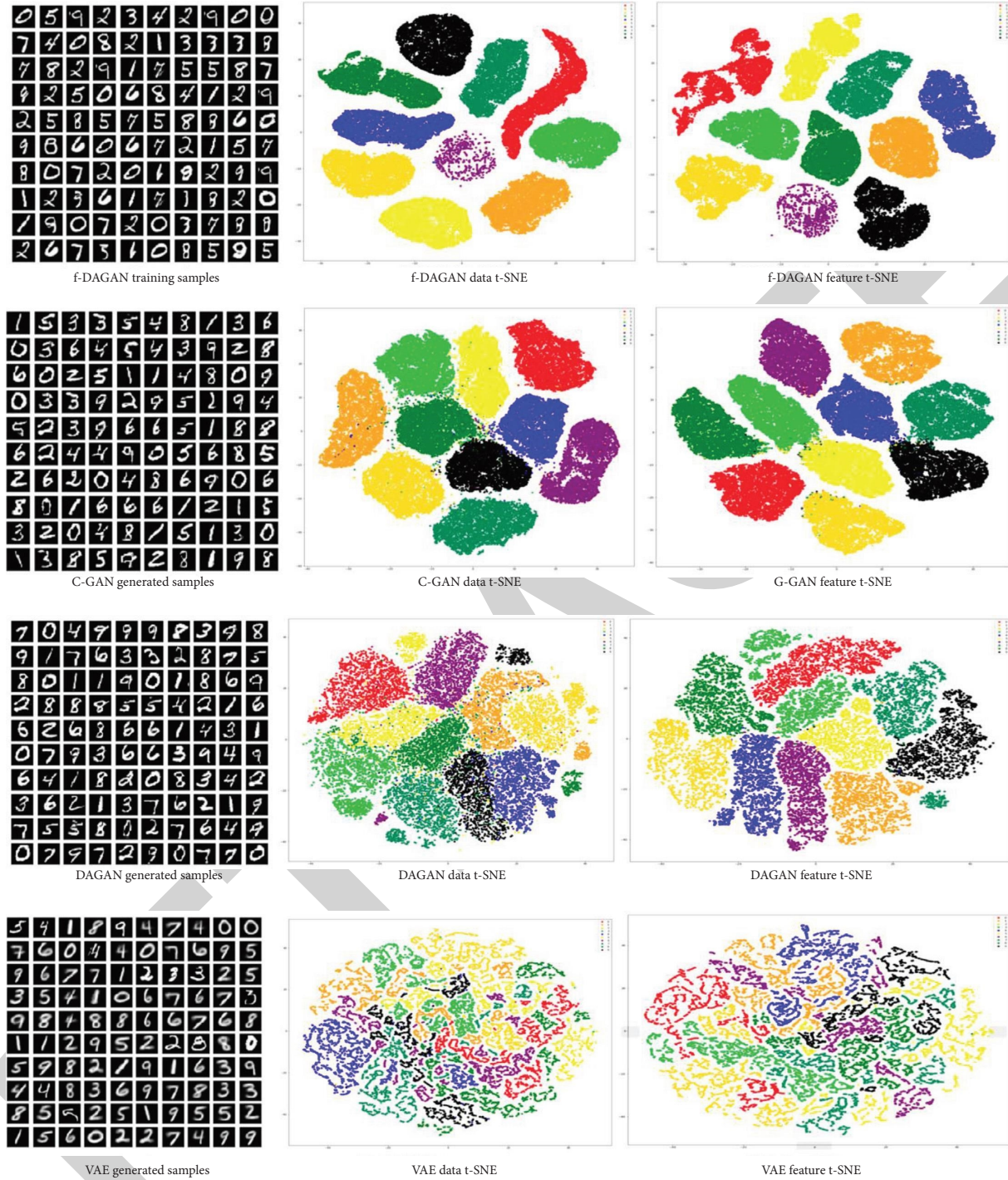


FIGURE 13: t-SNE for 5 samples data and feature spaces distribution.

classifier  $C_{GAN}$ , is trained on the generated data [49]. Finally, the GQI is defined as the ratio of the accuracies of the two classifiers. The formula for calculating GQI is as follows:

$$GQI = \frac{ACC(C_{GAN})}{ACC(C_{real})} \times 100. \quad (9)$$

GQI is an integer between 0 and 100. In higher GQI, the GAN distribution correlates best with the actual data distribution.

**7.1.2. Data Sets.** The MNIST data set is the application used for the analysis studies. A sample of the MNIST data set is shown in Figure 12. This data set consists of black and white images of handwritten instances of the digits 0–9 having class labels of the corresponding integers. The data set comprises a training set of 60,000 images and a test set of 10,000 images. The digits in the training and test sets were written by disjoint sets of writers. The size of the MNIST images is  $28 \times 28$  pixels. Figure 11 shows a sample of the



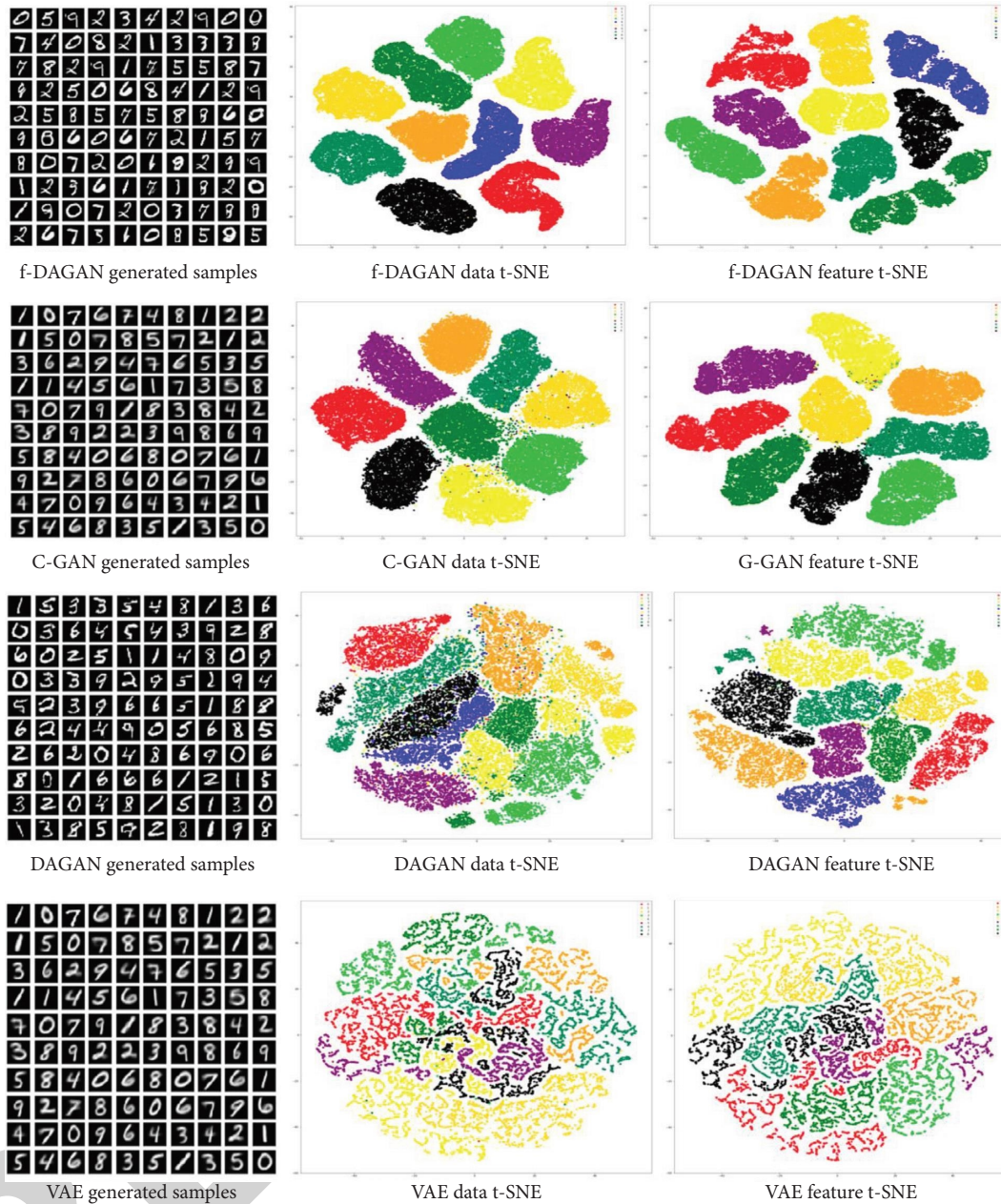


FIGURE 14: t-SNE for 10 samples data and feature spaces distribution.

MNIST data set. For the few-shot approach of training and generating synthesized images, we used a different version of the MNIST data set by splitting the training set of the MNIST data set. We split the MNIST data set into two categories:

- (a) Randomly selected 5 images from each class
- (b) Randomly selected 10 images from each class
- (c) Randomly selected 100 images from each class
- (d) Randomly selected 1,000 images from each class

The main purpose of splitting the original data set into a subset of a data set is to identify how our GAN can generalize data consisting of unseen classes.

*7.1.3. References Network for Comparisons.* We wanted to demonstrate that f-DAGAN could be used for data augmentation for few-shot learning, and hard example can help increase the performance of the network, as comparison of our network with other popular data augmentation architectures like DAGAN, C-CAN, and VAE. We trained each architecture until convergence as deemed their respective implementation on the MNIST data set. Then we sample 6,000 images each class uniformly at random from each generator to use as our generated set.

Here, we demonstrate that our GAN best approximates the true distribution, while DAGAN performs slightly worse. The worst performing model is the VAE, as expected.

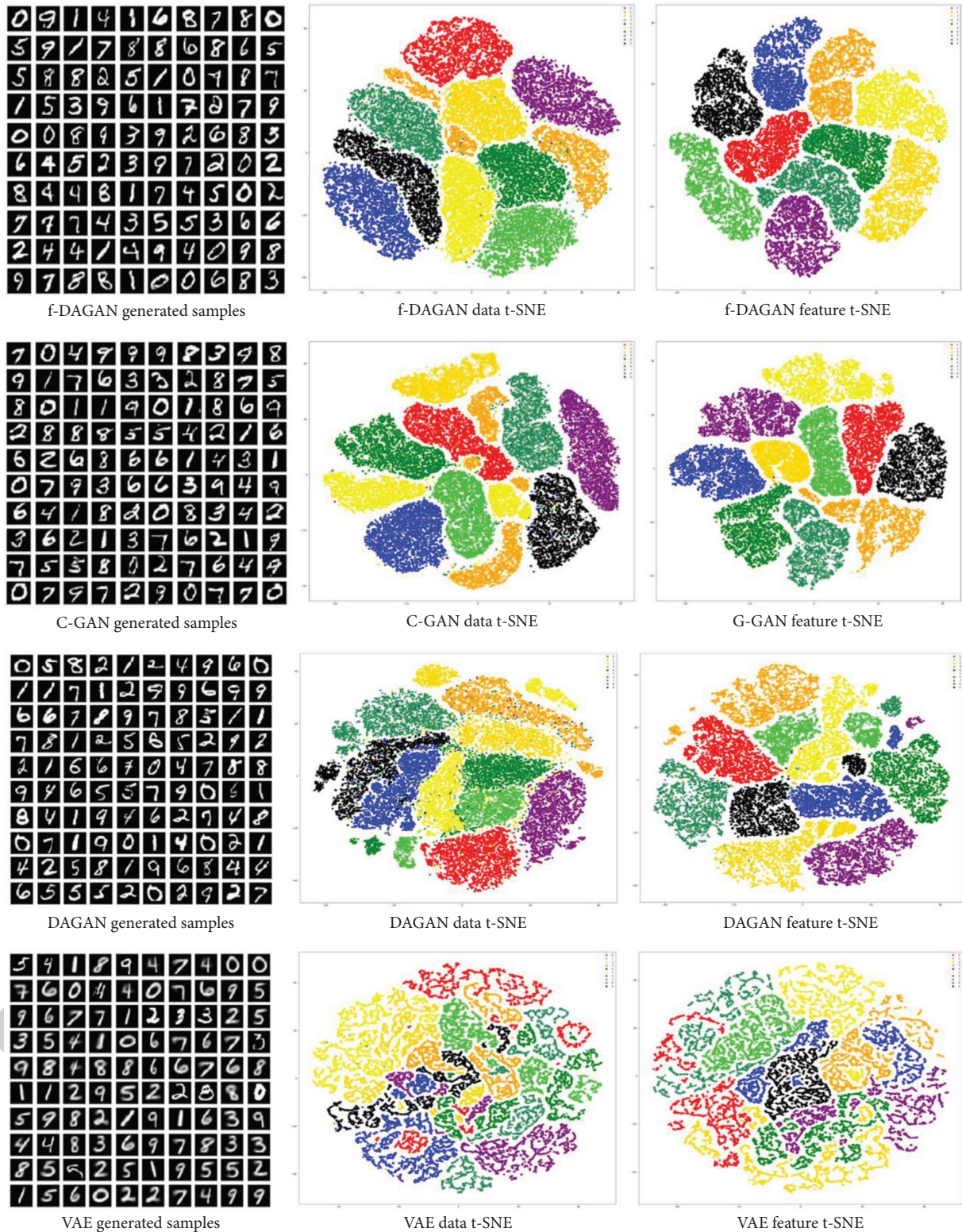


FIGURE 15: t-SNE for 100 samples data and feature space distribution.

### 8. Result of the One-Class-Based Augmentation

In this section, we compute the classification accuracy, our GAN, on different subsets of MNIST data sets and compare

the results of the architectures described. We demonstrate that our GAN achieves the correct ordinal rankings for each subset of the data set. Due to the architectures having a great dissimilarity in their outputs, we want to start with a baseline

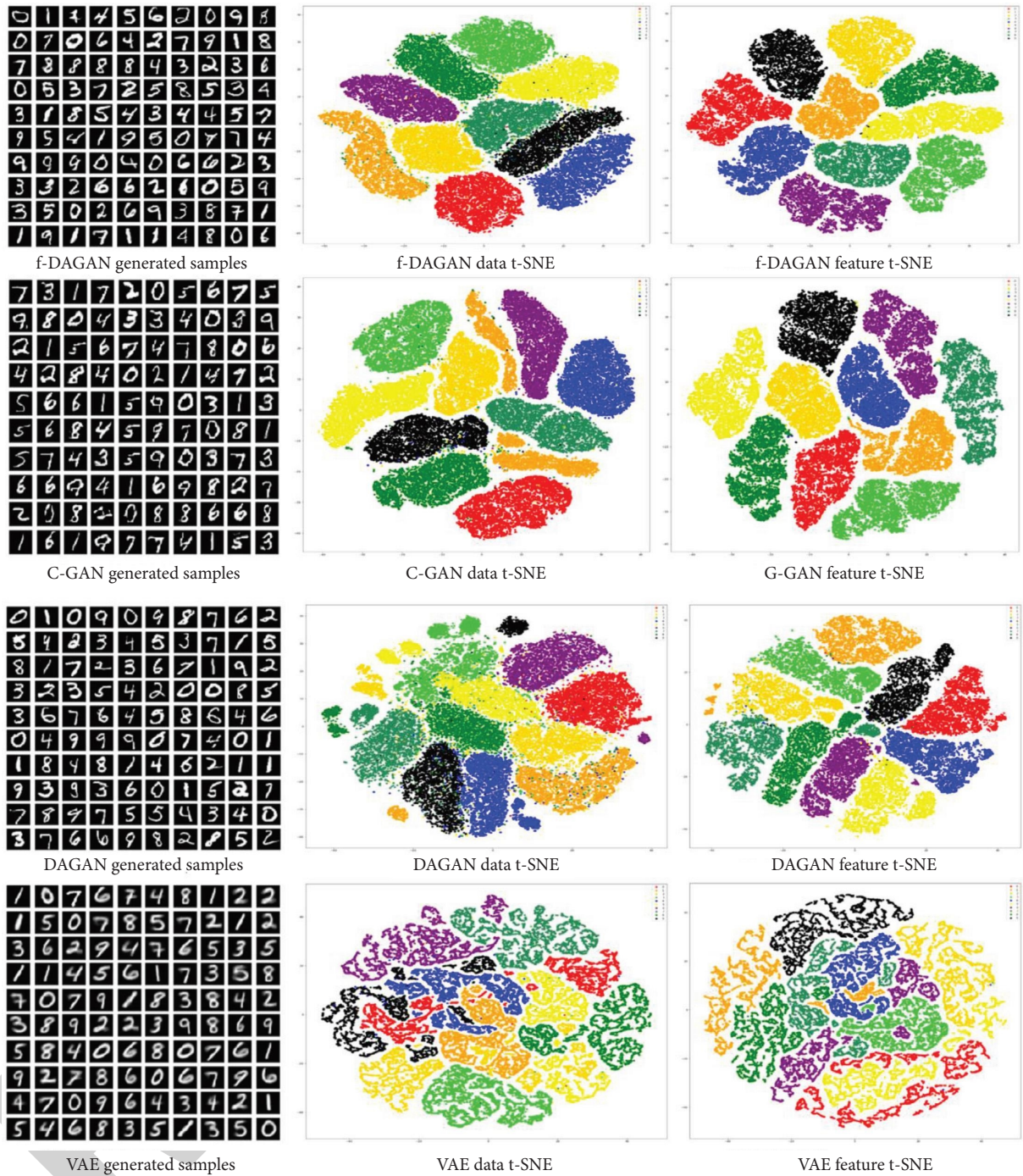


FIGURE 16: t-SNE for 1,000 samples data and feature spaces distribution.

task to ensure the model works under supervision before proceeding to more complicated comparisons that may look equivalent to human observers and vary subtly. For our MNIST experiment, we tested DAGAN, VAE, C-GAN, and f-DAGAN. We can observe that the correct ordinal ranking is achieved by the measure, highlighting that the measure detects the missing modes of the distribution. By ranking the small DCGAN better than weakened GAN, it highlights that it is not fooled by noise and by ranking C-GAN better than small GAN; it further highlights the importance of the full distribution for a better score.

8.1. *Quality of Augmented Data.* We demonstrate visualization maps of the generated feature and data from different models (Figures 13–17). Figure 12 shows the MNIST data set and their corresponding data and feature visualization, and Figure 18 shows the hard example generated (Figure 19) from h-DAGAN and their respective data and feature distribution.

### 9. Classification Performance

We evaluated the classification accuracy of the output obtained by different network ResNet50 classifiers. The

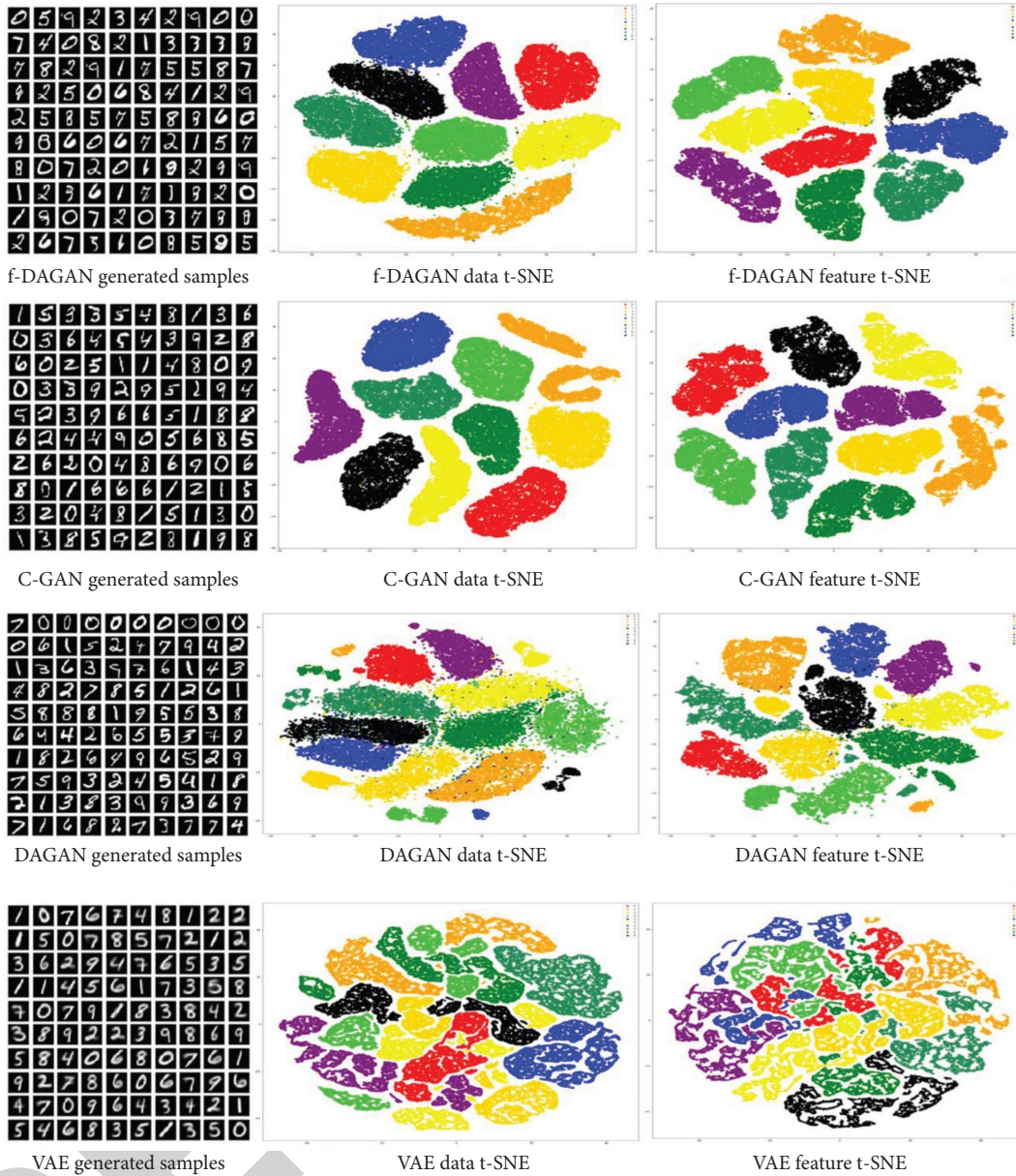


FIGURE 17: t-SNE for all MNIST data and feature spaces distribution.

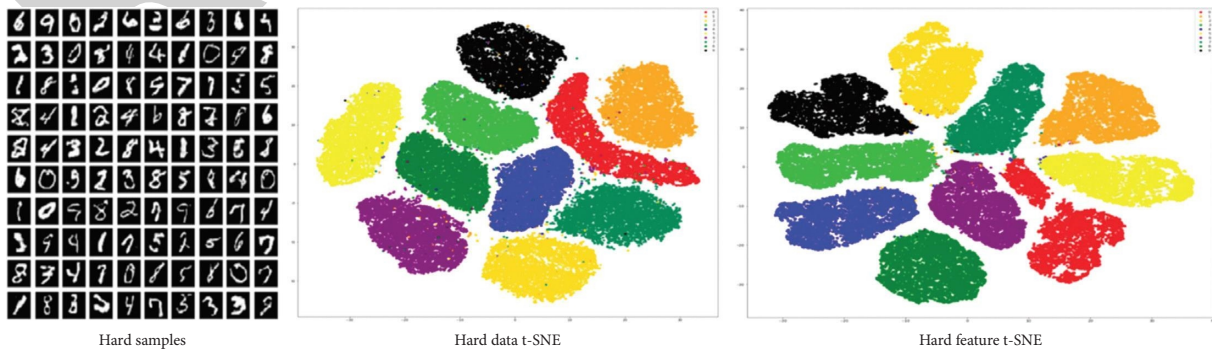


FIGURE 18: t-SNE for h-DAGAN data and feature distribution.

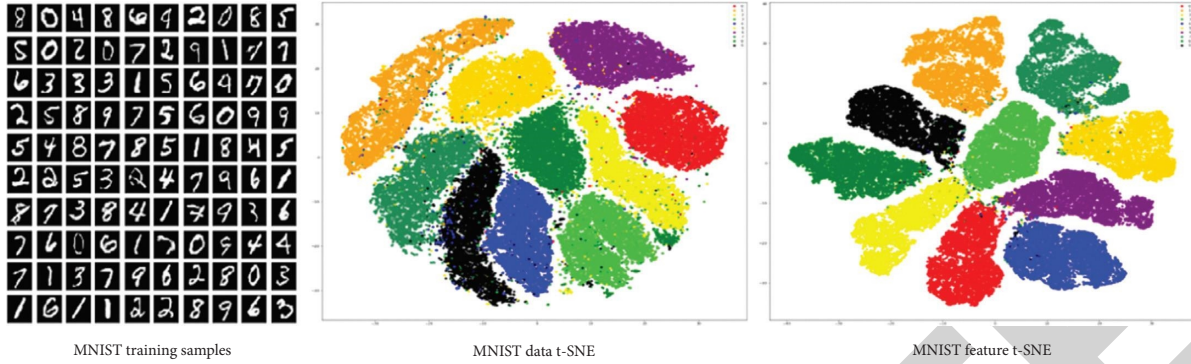


FIGURE 19: t-SNE for MNIST data and feature distribution.

evaluation metric we employ to measure the accuracy of the ResNet50 classifier is defined as the total number of correctly classified samples divided by the total number of test samples. To compute various networks, we train an image classification network created by different networks and then evaluate its output in a real-world image test set. To evaluate the creation of synthetic data the experiments were done using the following steps:

- (1) Trained the different networks using the randomly selected 50 samples (each class 5 samples), 100 samples (each class 10 samples), 1,000 (each class 100 samples), 10,000 (each class 1,000 samples), and a full training set of original data sets.
- (2) Used the trained different networks to generate a new synthetic data set with the exact size of the original.
- (3) The new data set is used to train classification accuracy using ResNet50. For training ResNet50, we used a total of 60,000 data sets with different combinations such as:
  - (a) 50 selected samples (5 from each class) and generated samples of 59,050
  - (b) 100 selected samples (10 from each class) and generated samples of 59,900
  - (c) 1,000 selected samples (100 from each class) and generated samples of 59,000
  - (d) 10,000 selected samples (1,000 from each class) and generated samples of 50,000
- (4) The ResNet50 network is tested using the test set of the original data set.

Intuitively, this measures the difference between the learned (i.e., generated image) and the target (i.e., real image) distributions. We can conclude that the image generated is similar to real images if the classification network can correctly classify real images, which learns features for discriminatory images generated for different classes. In other words, network training is akin to a recall measure, as a good network training performance shows that the generated samples are diverse enough. Network testing often needs adequate precision because the consistency of the sample may influence the classifier.

TABLE 1: Random five samples classification accuracy and GQI.

| Data sets    | Accuracy (%) | GQI    | LS    |
|--------------|--------------|--------|-------|
| MNIST (full) | 99.13        | 1      | 0.873 |
| VAE          | 91.18        | 0.9199 | 0.471 |
| CGAN         | 92.43        | 0.9325 | 0.637 |
| DAGAN        | 92.57        | 0.9339 | 0.732 |
| f-DAGAN      | 93.14        | 0.9396 | 0.739 |

TABLE 2: Random 10 samples classification accuracy and GQI.

| Data sets    | Accuracy (%) | GQI    | LS    |
|--------------|--------------|--------|-------|
| MNIST (full) | 99.13        | 1      | 0.861 |
| VAE          | 92.07        | 0.9287 | 0.433 |
| CGAN         | 92.93        | 0.9375 | 0.615 |
| DAGAN        | 92.97        | 0.9379 | 0.717 |
| f-DAGAN      | 94.42        | 0.9526 | 0.702 |

We reported the quantitative results of classification accuracy and GQI in Tables 1 and 2. Tables 3 and 4 is for experiments using the ResNet50 classifier. ResNet50 classifier provides the lower result in less number of training images. Because the ResNet50 network structure requires a large amount of data to train. We can test sample images that are collected from the MNIST test set. MNIST 50 consists of 5 samples from each class; MNIST 100 consists of 10 samples from each class; MNIST 1,000 consists of 100 samples from each class; MNIST 10,000 consists of 1,000 samples from each class; and MNIST 60,000 unlabeled data are used for adversarial training. In Table 1, our f-DAGAN performs better results than other networks. However, C-GAN classification accuracy is quite similar to DAGAN and higher than VAE. Then, for each trained GAN generated, we make random synthetic images samples, and we applied the LS and other GQI measures to the generated image sets and the original image subset. Results are shown in Tables 1–4. LS agrees with FID; F-DAGAN is the best; GAN is the worst model.

We choose different samples from a single class for a few-shot purpose to visualize in supporting and classify the pattern of data generate with various scenerios such as number of training samples is selected. Further, distribution of generated data with different class. It shows that our

TABLE 3: Random 100 samples classification accuracy and GQI.

| Data sets    | Accuracy (%) | GQI    | LS    |
|--------------|--------------|--------|-------|
| MNIST (full) | 99.13        | 1      | 0.851 |
| VAE          | 93.76        | 0.9459 | 0.418 |
| CGAN         | 94.31        | 0.9514 | 0.652 |
| DAGAN        | 95.12        | 0.9597 | 0.783 |
| f-DAGAN      | 96.51        | 0.9736 | 0.710 |

TABLE 4: Random 1,000 samples classification accuracy and GQI.

| Data sets    | Accuracy (%) | GQI    | LS    |
|--------------|--------------|--------|-------|
| MNIST (full) | 99.13        | 1      | 0.886 |
| VAE          | 95.92        | 0.9677 | 0.497 |
| CGAN         | 96.63        | 0.9748 | 0.698 |
| DAGAN        | 96.72        | 0.9756 | 0.738 |
| f-DAGAN      | 98.93        | 0.9979 | 0.746 |

approach have capable to distribute with other methods. We used other GAN measures also for comparison with different methods even in every method our approach performed well.

## 10. Conclusion and Future Work

In the few shot context, lack of training data, classifying images, and labeling training data remain still a challenging problem. In this project, we concentrate on f-DAGAN design architecture by combining different feature vectors; we successfully build a model that can generate realistic images even a few samples available in the training set. In conclusion, this work shows the feasibility of generating synthesized training data generation using adversarial training with few training data required to achieve the performance of the analysis. We trust that our method provides valuable insights into the fine-grained data augmentation problem and opens a new horizon for deep learning with fewer amounts of data.

In the future, our f-DAGAN framework can be extended in various directions. For example, it is possible to utilize other different layers features or more proper architectures or training schemes that could further improve f-DAGAN performance. Specifically, the concatenation of the generator feature and image feature improves the visual quality and image diversity. The current study provides a basis for work employing various features or prior information to better design GAN generators and discriminators. In addition, we have planned to implement a hard example generation network to improve classification accuracy.

## Abbreviations

|              |                          |
|--------------|--------------------------|
| $D$ :        | Discriminator            |
| $G$ :        | Generator                |
| $X_{fake}$ : | Outputs on image         |
| $L$ :        | Log-likelihood of source |
| $X_{real}$ : | Original image           |
| $g(\cdot)$ : | Encoder function         |
| $f(\cdot)$ : | Decoder function         |

|                           |                    |
|---------------------------|--------------------|
| $z$ :                     | Bottleneck layer   |
| $D$ :                     | Dimensions         |
| $[W \times H \times C]$ : | Feature dimensions |
| CL:                       | Classifier loss    |
| $x_i$ and $x_j$ :         | Sources            |
| $x_i$ and $p_{x_j}$ :     | Images.            |

## Data Availability

The data used to support the findings of this study are included within the article.

## Conflicts of Interest

The authors declare that there are no conflicts of interest regarding the publication of this article.

## References

- [1] G. Yang, S. Yu, H. Dong et al., "DAGAN: deep de-aliasing generative adversarial networks for fast compressed sensing MRI reconstruction," *IEEE Transactions on Medical Imaging*, vol. 37, no. 6, pp. 1310–1321, 2017.
- [2] S. Rajendran, S. K. Mathivanan, P. Jayagopal et al., "Emphasizing privacy and security of edge intelligence with machine learning for healthcare," *International Journal of Intelligent Computing and Cybernetics*, vol. 15, no. 1, pp. 92–109, 2021.
- [3] S. Rajendran, S. K. Mathivanan, P. Jayagopal et al., "Language dialect based speech emotion recognition through deep learning techniques," *International Journal of Speech Technology*, vol. 24, no. 3, pp. 625–635, 2021.
- [4] K. Gao, F. Han, P. Dong, N. Xiong, and R. Du, "Connected vehicle as a mobile sensor for real time queue length at signalized intersections," *Sensors*, vol. 19, no. 9, p. 2059, 2019.
- [5] W. Guo, N. Xiong, H. C. Chao, S. Hussain, and G. Chen, "Design and analysis of self-adapted task scheduling strategies in wireless sensor networks," *Sensors*, vol. 11, no. 7, pp. 6533–6554, 2011.
- [6] X. Wang, Q. Li, N. Xiong, and Y. Pan, "Ant colony optimization-based location-aware routing for wireless sensor networks," in *Proceedings of the International Conference on Wireless Algorithms, Systems, and Applications*, pp. 109–120, Dallas, TX, USA, October 2008.
- [7] Y. Jiang, G. Tong, H. Yin, and N. Xiong, "A pedestrian detection method based on genetic algorithm for optimize XGBoost training parameters," *IEEE Access*, vol. 7, pp. 118310–118321, 2019.
- [8] R. Wan and N. Xiong, "An energy-efficient sleep scheduling mechanism with similarity measure for wireless sensor networks," *Human-centric Computing and Information Sciences*, vol. 8, no. 1, pp. 1–22, 2018.
- [9] E. Gayakwad, J. Prabhu, R. V. Anand, and M. S. Kumar, *Training time reduction in transfer learning for a similar dataset using deep learning. Intelligent Data Engineering and Analytics*, pp. 359–367, Springer, Singapore, 2021.
- [10] H. Altae-Tran, B. Ramsundar, A. S. Pappu, and V. Pande, "Low data drug discovery with one-shot learning," *ACS Central Science*, vol. 3, no. 4, pp. 283–293, 2017.
- [11] C. H. Lampert, H. Nickisch, and S. Harmeling, "Attribute-based classification for zero-shot visual object categorization," *IEEE Transactions on Pattern Analysis and Machine Intelligence*, vol. 36, no. 3, pp. 453–465, 2013.

- [12] H. Larochelle, D. Erhan, and Y. Bengio, "Zero-data learning of new tasks," in *Proceedings of the 23rd national conference on Artificial intelligence/AAAI*, vol. 1, Chicago, Illinois, July 2008.
- [13] Z. Al-Halah, M. Tapaswi, and R. Stiefelhagen, "Recovering the missing link: predicting class-attribute associations for unsupervised zero-shot learning," in *Proceedings of the IEEE Conference on Computer Vision and Pattern Recognition*, pp. 5975–5984, Las Vegas, NV, USA, June 2016.
- [14] M. Norouzi, T. Mikolov, S. Bengio et al., "Zero-shot Learning by Convex Combination of Semantic Embeddings," 2013, <http://arxiv.org/abs/1312.5650>.
- [15] V. K. Verma and P. Rai, "A simple exponential family framework for zero-shot learning," in *Proceedings of the Joint European Conference on Machine Learning and Knowledge Discovery in Databases*, pp. 792–808, September 2017.
- [16] Y. Li and D. Wang, "Zero-shot Learning with Generative Latent Prototype Model," 2017, <http://arxiv.org/pdf/1705.09474>.
- [17] W. J. Scheirer, A. Rocha, A. Sapkota, and T. E. Boult, "Towards open set recognition," *TPAMI*, vol. 36, 2013.
- [18] G. Koch, R. Zemel, and R. Salakhutdinov, "Siamese neural networks for one-shot image recognition," *ICML deep learning workshop*, vol. 2, no. 0, 2015, July.
- [19] O. Vinyals, C. Blundell, T. Lillicrap, and D. Wierstra, "Matching networks for one shot learning," *Advances in Neural Information Processing Systems*, vol. 29, 2016.
- [20] A. Khoreva, R. Benenson, E. Ilg, T. Brox, and B. Schiele, "Lucid data dreaming for video object segmentation," *International Journal of Computer Vision*, vol. 127, no. 9, pp. 1175–1197, 2019.
- [21] A. Mehrotra and A. Dukkipati, "Generative Adversarial Residual Pairwise Networks for One Shot Learning," 2017, <http://arxiv.org/abs/1703.08033>.
- [22] E. Schwartz, L. Karlinsky, J. Shtok et al., "Delta-encoder: an effective sample synthesis method for few-shot object recognition," *Advances in Neural Information Processing Systems*, vol. 31, 2018.
- [23] Y. X. Wang, R. Girshick, M. Hebert, and B. Hariharan, "Low-shot learning from imaginary data," in *Proceedings of the IEEE Conference on Computer Vision and Pattern Recognition*, pp. 7278–7286, Salt Lake City, UT, USA, June 2018.
- [24] C. Finn, P. Abbeel, and S. Levine, "Model-agnostic meta-learning for fast adaptation of deep networks," in *Proceedings of the International Conference on Machine Learning*, pp. 1126–1135, PMLR, July 2017.
- [25] S. Ravi and H. Larochelle, "Optimization as a Model for Few-Shot Learning," 2016.
- [26] E. Grant, C. Finn, S. Levine, T. Darrell, and T. Griffiths, "Recasting Gradient-Based Meta-Learning as Hierarchical Bayes," 2018, <http://arxiv.org/abs/1801.08930>.
- [27] C. Finn, K. Xu, and S. Levine, "Probabilistic model-agnostic meta-learning," *Advances in Neural Information Processing Systems*, vol. 31, 2018.
- [28] M. S. Kumar, M. Z. Khan, S. Rajendran, A. Noor, A. S. Dass, and J. Prabhu, "Imbalanced Classification in Diabetics Using Ensemble Machine Learning," *Computers, Materials and Continua*, vol. 72.
- [29] R. Hadsell, S. Chopra, and Y. LeCun, "Dimensionality reduction by learning an invariant mapping," vol. Vol. 2, pp. 1735–1742, in *In Proceedings of the 2006 IEEE Computer Society Conference on Computer Vision and Pattern Recognition (CVPR'06)*, vol. Vol. 2, pp. 1735–1742, IEEE, New York, NY, June 2006.
- [30] S. Chopra, R. Hadsell, and Y. LeCun, "Learning a similarity metric discriminatively, with application to face verification," vol. 1, pp. 539–546, in *In Proceedings of the 2005 IEEE Computer Society Conference on Computer Vision and Pattern Recognition (CVPR'05)*, vol. 1, pp. 539–546, IEEE, San Diego, CA, USA, June 2005.
- [31] F. Schroff, D. Kalenichenko, and J. Philbin, "Facenet: a unified embedding for face recognition and clustering," in *Proceedings of the IEEE Conference on Computer Vision and Pattern Recognition*, pp. 815–823, Boston, MA, USA, June 2015.
- [32] J. Wang, Y. Song, T. Leung et al., "Learning fine-grained image similarity with deep ranking," in *Proceedings of the IEEE Conference on Computer Vision and Pattern Recognition*, pp. 1386–1393, San Juan, PR, USA, June 2014.
- [33] T. Xiao, S. Li, B. Wang, L. Lin, and X. Wang, "Joint detection and identification feature learning for person search," in *Proceedings of the IEEE Conference on Computer Vision and Pattern Recognition*, pp. 3415–3424, Honolulu, HI, USA, July 2017.
- [34] S. Bai, Y. Li, Y. Zhou, Q. Li, and P. H. Torr, "Adversarial metric attack and defense for person re-identification," *IEEE Transactions on Pattern Analysis and Machine Intelligence*, vol. 43, no. 6, pp. 2119–2126, 2020.
- [35] Z. Wu, A. A. Efros, and S. X. Yu, "Improving generalization via scalable neighborhood component analysis," in *Proceedings of the European Conference on Computer Vision (ECCV)*, pp. 685–701, September 2018.
- [36] J. Snell, K. Swersky, and R. Zemel, "Prototypical networks for few-shot learning," *Advances in Neural Information Processing Systems*, vol. 30, 2017.
- [37] F. Sung, Y. Yang, L. Zhang, T. Xiang, P. H. Torr, and T. M. Hospedales, "Learning to compare: Relation network for few-shot learning," in *Proceedings of the IEEE Conference on Computer Vision and Pattern Recognition*, pp. 1199–1208, Salt Lake City, UT, USA, June 2018.
- [38] J. Wang, Y. Zou, P. Lei, R. S. Sherratt, and L. Wang, "Research on recurrent neural network based crack opening prediction of concrete dam," *Journal of Internet Technology*, vol. 21, no. 4, pp. 1161–1169, 2020.
- [39] C. Chen, K. Li, W. Wei, J. T. Zhou, and Z. Zeng, "Hierarchical graph neural networks for few-shot learning," *IEEE Transactions on Circuits and Systems for Video Technology*, vol. 32, no. 1, pp. 240–252, 2021.
- [40] D. Cao, K. Zeng, J. Wang et al., "Bert-based deep spatial-temporal network for taxi demand prediction," *IEEE Transactions on Intelligent Transportation Systems*, 2021.
- [41] B. Pu, K. Li, S. Li, and N. Zhu, "Automatic fetal ultrasound standard plane recognition based on deep learning and IIoT," *IEEE Transactions on Industrial Informatics*, vol. 17, no. 11, pp. 7771–7780, 2021.
- [42] J. Wang, Y. Yang, T. Wang, R. S. Sherratt, and J. Zhang, "Big data service architecture: a survey," *Journal of Internet Technology*, vol. 21, no. 2, pp. 393–405, 2020.
- [43] J. Li, H. Li, G. Cul, Y. Kang, Y. Hu, and Y. Zhou, "Gacnet: a generative adversarial capsule network for regional epitaxial traffic flow prediction," *CMC-COMPUTERS MATERIALS & CONTINUA*, vol. 64, no. 2, pp. 925–940, 2020.
- [44] R. Jothikumar, *Applying blockchain in agriculture: a study on blockchain technology, benefits, and challenges*. *Deep Learning and Edge Computing Solutions for High Performance Computing*, pp. 167–181, Springer, Heidelberg, Germany, 2021.
- [45] F. Zhang, H. Zhao, W. Ying, Q. Liu, A. N. J. Raj, and B. Fu, "Human face sketch to RGB image with edge optimization

## Research Article

# Research on Multi-Objective Intelligent Optimization of Financial Resource Management and Allocation Methods in Colleges and Universities

Shanshan Guo 

Hebei University of Chinese Medicine, Shijiazhuang 050200, Hebei, China

Correspondence should be addressed to Shanshan Guo; [guoshanshan@hebcm.edu.cn](mailto:guoshanshan@hebcm.edu.cn)

Received 14 April 2022; Revised 23 May 2022; Accepted 1 June 2022; Published 20 July 2022

Academic Editor: Man Fai Leung

Copyright © 2022 Shanshan Guo. This is an open access article distributed under the Creative Commons Attribution License, which permits unrestricted use, distribution, and reproduction in any medium, provided the original work is properly cited.

Higher education is the cornerstone of national development. With the rapid development of higher education, it puts forward requirements for the management and allocation of financial resources in colleges and universities. In order for sustainable development of colleges and universities, how to optimize the management and allocation of financial resources has become an important condition. To ensure the smooth implementation and development of various works in colleges and universities and to improve the scientific rationality of college financial budgets, this paper starts with the challenges faced by the college financial work in the new era, analyzes the problems of the college financial resource management, and proposes relevant solutions. Method: combined with the intelligent optimization algorithm, the method used in different situations of financial configuration is introduced, and compared with different algorithms, according to the comparison results, we can get the better intelligent optimization algorithm we want and find the optimal solution among global instances.

## 1. Introduction

The financial resource allocation system of some colleges and universities is gradually reformed, but there are problems and difficulties in its operation efficiency and work quality. These problems indicate that we need to further optimize the management system and allocation methods [1]. In some universities, seeking to maximize the quality of the educational experience provided to students, there is a hierarchical structure in the quality of schools between different schools, with significant stratification of income and ability, and the pricing policies adopted by schools also vary [2] and adopt corresponding management of school financial resources. In the early days, UMMS responded to the changing trend of traditional funding and changed the financial structure and financial culture of the school. The school began to offer a course to change the traditional budget thinking and develop related indicators to show how resources are affected by related activities [3]. From today's point of view, the school's budget declaration concept should establish authority and

expenditure responsibility, form authority departments, disclose budget declaration information, and participate in the declaration and supervision of all staff [4]. Under the current background, colleges and universities should establish a comprehensive budget system, guide scientific budget preparation activities, improve relevant systems and organizational structures, and reconstruct the implementation process [5]. In the background of the domestic college education system, financial management is an important part of college management. Colleges and universities should improve financial management and other related management to promote school development [6]. Similarly, literature [7] analyzed that with the increase of national financial and social capital investment in higher education, colleges and universities should optimize the allocation of resources, improve the financial management work and level of colleges and universities, and promote the high-quality development of schools. Under multi-objective conditions, choosing intelligent optimization is required for our financial management and allocation methods, so we



need optimized algorithms. Reference [8] describes the related algorithms and their practical application cases. Swarm intelligence optimization algorithms use the advantages of groups to find solutions to difficult problems [9]. For example, the optimization algorithm case [10] uses this algorithm to solve the relevant algorithm requirements, which shows that it is promising to find the optimal solution and proves that the algorithm in the literature has the property of value convergence. Today, there are many intelligent optimization algorithms for our reference. In the above literature, more or less the improvement methods of financial management in colleges and universities are given, but they are only limited to a part of financial management and configuration in colleges and universities and have not been fully implemented. They run through the entire organizational framework and only improve within the framework. The given intelligent optimization algorithm is listed at one time but not expressed by situation, or the algorithm itself is no longer suitable for the requirements of current university financial resource management and allocation. This paper will restructure the university financial resource management system from the perspective of intelligence, based on the fact that this provides intelligent optimization algorithms that seek optimal solutions for financial allocation.

## 2. University Financial Organization System and Intelligent Optimization Algorithm

*2.1. University Financial Organization System.* Pyramid organizational structure causes items to be approved layer by layer [11], lack of horizontal communication, which is not conducive to financial management activities, and the efficiency of layer approval is low. It is easy to cause lag in information transmission and information asymmetry. In the actual functional division of labor, some functional personnel do not understand the relevant project budget, which is prone to misunderstanding and affects execution. Let us take Sunshine University as an example as shown in Figure 1.

*2.1.1. Optimization of University Financial Organization System.* The school's business volume and financial income have increased year by year. In the existing organizational structure, the finance department needs to invest a considerable amount of personnel to maintain a normal operation. Too many departments and levels have resulted in overlapping functions and redundant personnel resulting in wasted manpower and low efficiency. Here, we can take advantage of the decentralized features of the blockchain to promote the flattening of the organizational structure [12], streamlining departments, and compressing management. Therefore, we can set three levels: financial management level, financial service level, and financial business level, to optimize the organizational structure as shown in Figure 2.

In order to better highlight the flattening, the three major levels should be under the same framework and restrict each other.

After the departmental organization is optimized, it is the sorting and adjustment of the relevant financial personnel levels. The relationship between the superiors and employees of the college is not the relationship between the leader and the led. The superiors and employees receive tasks according to relevant task instructions and individual talents and arrange personnel at other levels. Complete tasks together, strengthen horizontal communication, and promote the enthusiasm of employees in the department. The superior is responsible for answering, guiding, and supervising.

*2.2. Multiple Objective Intelligent Optimization Algorithm.* After the above effective optimization of the financial organizational structure of colleges and universities, the efficiency of the financial department in managing financial-related resources has increased, the speed of multi-directional information transmission has been accelerated, the transparency of data has increased, and the problems that various functional departments have discovered and need to deal with have increased. We need to introduce multi-objective intelligent optimization algorithms to help us find the optimal solution to financial-related problems.

*2.2.1. Quantum Algorithms.* Different from simulated annealing, quantum annealing [13] can jump out of the local optimum by virtue of its quantum-specific effects.

Many optimization problems require a mapping before they can be solved by quantum algorithms:

$$H_p = \sum_{i=1}^n h_i \sigma_i^2 + \sum_{i,j=1}^n J_{ij} \sigma_i^z \sigma_j^z. \quad (1)$$

Among them,  $h_i$  is the degree of offset and  $J_{ij}$  represents the degree of fit between  $i$  and  $j$ .

Then, the function of quantum annealing is

$$H(t) = H_p + \Gamma(t) \sum_{i=1}^n \Delta \sigma_i^x. \quad (2)$$

$\Gamma$  is the field strength, similar to the temperature  $T$  in the simulated annealing function.

It can be seen that the quantum algorithm converges faster, can obtain the desired data more accurately, and is expected to reach the global optimal solution in the search target.

*2.2.2. Firefly Algorithm.* The above quantum algorithm is suitable for finding the solution of the problem when the problem is relatively clear, but usually in our actual financial resource management and allocation, the multi-objective problem algorithm encountered is large in scale and when the complexity is more complex it needs a group. Action to find the global ideal solution. Here, we need the firefly algorithm [14].

We assume that there are  $N$  fireflies and the search space is  $H$  dimension, then the initial space of fireflies in  $H$  space can be expressed as  $X_i = [x_i, 1x_i, 2, \dots, x_i, n]$

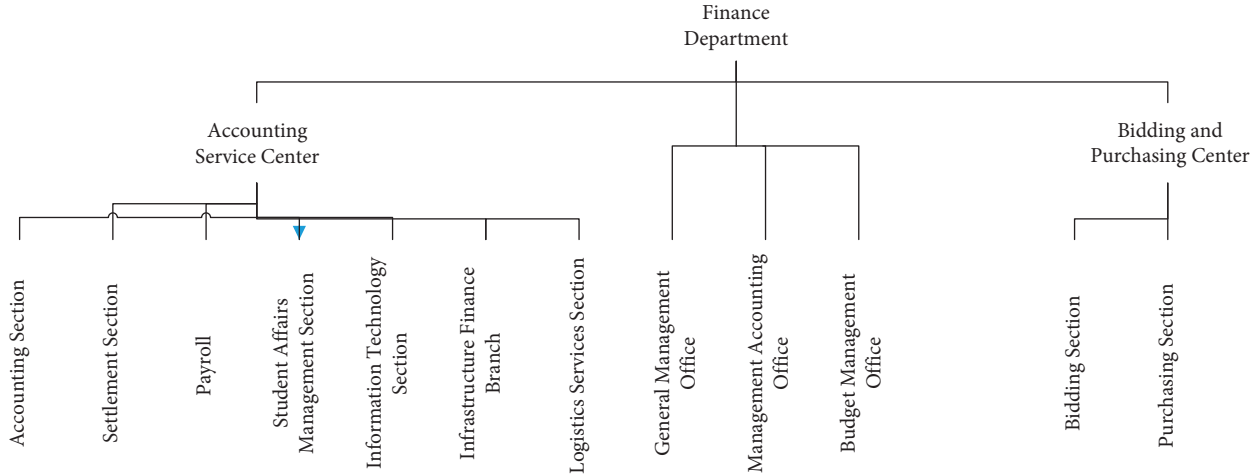


FIGURE 1: Organizational structure of the finance department of Sunshine University.

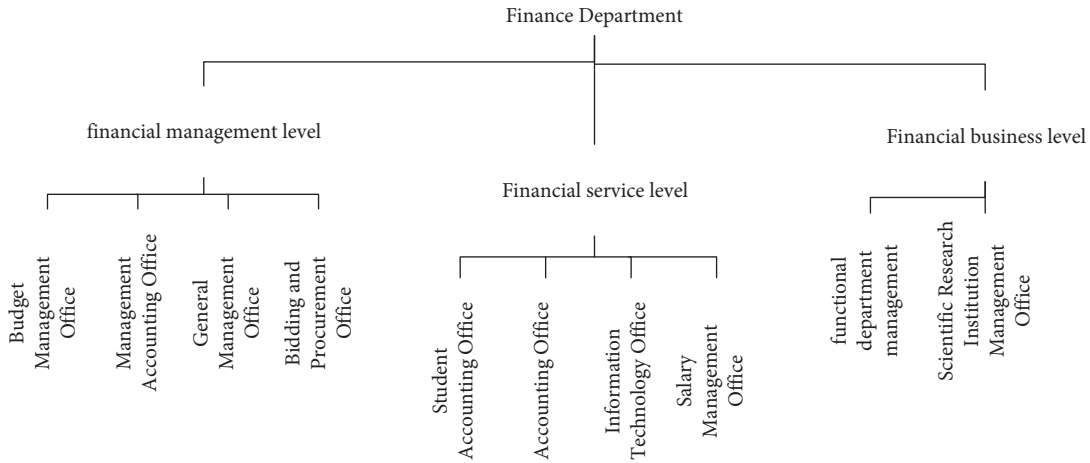


FIGURE 2: Optimization of the organizational structure of the financial department of C major.

Brightness of the 1-th firefly

$$I_{oi} = f(x_i). \quad (3)$$

Relative brightness of the 1-th firefly:

$$I_i = I_{oi} \cdot e^{-\lambda \cdot r_{ij}}. \quad (4)$$

The parameter is related to the area, and represents the distance between the target and another target firefly.

Attractiveness:

$$\beta = \beta_o \cdot e^{-\lambda \cdot r_{ij}^2}. \quad (5)$$

$\beta_o$  represents the maximum attraction between fireflies.

We need to increase the range of search objects to prevent the algorithm from converging prematurely. So join  $\alpha(\text{rand} - 1/2)$ :

$$X_i^{t+1} = X_i^t + \beta \cdot (X_j^t + X_i^t) + \alpha \left( \text{rand} - \frac{1}{2} \right). \quad (6)$$

Here, we get the firefly algorithm, which converges to obtain the best quality by moving the firefly to the brighter

part. When dealing with how to optimize the management and allocation of financial resources, you can select the relevant financial resources to be processed according to different situations and conditions, substitute the algorithm, and conduct simulations to find the ideal solution for resource allocation.

### 3. Multiple Objective Intelligent Optimization Algorithm Improvement

3.1. Quantum Model of Intelligent Optimization Algorithm. On the basis of the above, we can establish the intelligent optimization algorithm equation:

$$i\hbar \frac{\partial \psi(x, t)}{\partial t} = \left[ -\frac{\hbar^2}{2m} \frac{\partial^2}{\partial x^2} + f(x) \right] \psi(x, t). \quad (7)$$

This idea has also been adopted in other algorithms of the same type [15]. But it does not realize the relationship between target and potential energy.  $\tau = it/\hbar$ ,  $D = \hbar/2m$ :

$$\frac{\partial \psi(x, \tau)}{\partial \tau} = \left[ D \frac{\partial^2}{\partial x^2} - f(x) \right] \psi(x, \tau). \quad (8)$$

But because the introduction of the constraints of our optimization problem destroys the unity of Green's conditions, we introduce a convergence factor, and after adjustment we finally get

$$\frac{\partial \psi(x, \tau)}{\partial \tau} = \left\{ D \frac{\partial^2}{\partial x^2} - [f(x) - E_r] \right\} \psi(x, \tau). \quad (9)$$

For the application of financial resource management and configuration in colleges and universities, iterative operations can be designed according to the reference data to be obtained, and the specific data to be obtained in the application scenario can be calculated through the iterative function.

We want to describe the path of the target resource from  $m$  to  $n$ , which is obtained by deforming the optimization algorithm equation :

$$\psi(x, \tau) = \lim_{n \rightarrow \infty} \int_{-\infty}^{\infty} \left( \prod_{j=0}^{n-1} dx_j \right) \prod_{n=1}^n W(x_n) P(x_n, x_{n-1}). \quad (10)$$

In the above formula, we have to find out the motion behavior of the target resource, and the formula related to its location and size is

$$P(x_n, x_{n-1}) = \left( \frac{m}{2\pi\hbar\Delta\tau} \right)^{1/2} \exp \left[ \frac{m(x_n - x_{n-1})^2}{2\hbar\Delta\tau} \right]. \quad (11)$$

$$X_i^{t+1} = \begin{pmatrix} X_i^t; & \text{if } f(X_i^{t+1}) > f(X_i^t), \\ X_i^t + \beta \cdot (X_j^t - X_i^t) + \alpha \left( \text{rand} - \frac{1}{2} \right); & \text{else.} \end{pmatrix}. \quad (16)$$

In order to optimize the firefly algorithm, we introduce a random flight distribution:

$$s_i = \frac{\mu}{|v|^{1/\beta}}. \quad (17)$$

Among them,

$$\begin{pmatrix} \mu \sim n(0, \sigma_\mu^2) \\ \mu \sim n(0, \sigma_v^2) \end{pmatrix}. \quad (18)$$

Also,

$$\begin{pmatrix} \sigma_\mu = \left\{ \frac{\Gamma(1+\beta)\sin(\pi\beta/2)}{\Gamma[(1+|\beta/2])2^{(\beta-1)/2}} \right\}^{1/\beta} \\ \sigma_v = 1. \end{pmatrix}. \quad (19)$$

Then, the optimized firefly algorithm gets

To get the probability that the target resource appears in the position of the specified scheme, we need

$$W(x_n) = \exp \left\{ -\frac{[f(x_n) - e_r]\Delta\tau}{n} \right\}. \quad (12)$$

Similarly, we can use a Monte Carlo method to find the expectation under

$$\int_a^b h(x)dx = \int_a^b f(x)p(x)dx = E_{p(x)}[f(x)]. \quad (13)$$

Then, the density function of the target is

$$p(x_1 \dots x_n) = \prod_{n=1}^n P(x_n, x_{n-1}). \quad (14)$$

The function is

$$f(x_1 \dots x_n) = \prod_{n=1}^n W(x_n),$$

$$\psi(x, \tau) = E_{p(x)}[f(x)] \cong \frac{1}{n} \sum_{i=1}^n \psi(x_0, 0) \prod_{n=1}^n W(x_n). \quad (15)$$

The process of changing the target can be obtained intuitively.

**3.2. Improved Firefly Algorithm.** The traditional firefly algorithm may have problems such as weak local discovery ability. We improved the individual and the direction of its distribution:

$$X_i^{t+1} = X_i^t + \beta \cdot (X_j^t - X_i^t) + \alpha \cdot \text{sign} \left( \text{rand} - \frac{1}{2} \right) \oplus \text{Levy} \sim \frac{\mu}{|v|^{1/\beta}}. \quad (20)$$

After we introduce the random flight distribution, the ability of the firefly algorithm to search for an ideal solution globally is improved, but the accuracy may be reduced when the target acquisition solution is carried out in a specific range. To solve this problem, we obtain a good resource factor which is

$$X_{best}^t = X_j^t, \quad \text{if } f(X_j^t) \leq f(X_i^t), \forall i \in \{1, 2, \dots, n\}. \quad (21)$$

Then, we overlap the positions of good individuals and nongood individuals and then compare the values before and after the overlap to select better individuals:

$$X_n^t \begin{pmatrix} c_1; & \text{if } f(c_1) \leq \min(f(c_2), f(X_n^t)), \\ c_2; & \text{if } f(c_2) \leq \min(f(c_1), f(X_n^t)), \\ X_n^t. \end{pmatrix} \quad (22)$$

Finally, combined with the above formula, we consider the time situation  $x(1)$  in the best case of the time situation considered by financial resources:

$$T_{\text{iteration}} \times (o((D + f(D) + 1)n + x_1) + o(n^2) + o(I(D) \times n) + o(1) + o(1)). \quad (23)$$

The worst situation:

$$T_{\text{iteration}} \times (o((D + f(D) + 1)n + x_1) + o(n^2) + o(I(D + x_2) \times n) + o(1 + g(n)) + o(1)). \quad (24)$$

Although we optimize the firefly algorithm to the end, the complexity of its equations increases, but it can quickly and effectively find the optimal configuration scheme we want in dealing with the complex and huge financial management configuration applications in colleges and universities.

## 4. Experiment

**4.1. Comparison of the Actual Ability of Various Algorithms to Seek the Optimal Financial Solution.** Considering that most of the algorithms we face in the processing of financial resources are relatively large and difficult, we set up 20 schemes related to the management and allocation of financial resources in colleges and universities, give the target financial resources, and then set the resource parameters into the improved firefly algorithm and other swarm intelligence optimization algorithms, and then compare the optimal choices of the six algorithms in the experiment for these 20 schemes.

We can make initial settings for a variety of algorithms as shown in Table 1.

**4.2. Optimal Solutions of Different Algorithms to the Scheme.** The choices of algorithms are as shown in Figures 3–8.

Figure 9 shows a bar graph that can more intuitively show the superiority of the optimized firefly algorithm.

It can be seen that after incorporating the random flight mechanism and good individuals, the optimized algorithm (LEEFA) converges significantly faster than other algorithms in more than 2,000 uninterrupted iterations and can avoid falling into the local solution like other algorithms. Youzhong found the global best financial solution. Therefore, in the face of complex and huge plan decisions in the future, choosing the optimized firefly algorithm is more conducive to us than choosing the optimal one among many financial resource decision-making plans in the future.

Comparison of different search targets, convergence accuracy under different parameters, etc. However, it is sufficient to select a suitable intelligent algorithm under this experiment.

TABLE 1: Algorithm parameters.

| Model | Parameter setting  |
|-------|--|
| LEEFA | $\alpha = 0.1, \beta_0 = 1, \gamma = 0.002, l_{\text{threshold}} = 0.1$  |
| PSO   | $C_1 = 1.8, C_2 = 1.8, w = 0.8, v_{\text{max}} = 1, v_{\text{min}} = -1$ |
| GA    | $p_m = 0.01, p_c = 0.8$  |
| ABC   | $l_{\text{limit}} = N \cdot D$   |
| FA    | $\alpha = 0.1, \beta_0 = 1, \gamma = 1$                                  |
| LFFA  | $\alpha = 0.1, \beta_0 = 1, \gamma = 1$                                  |

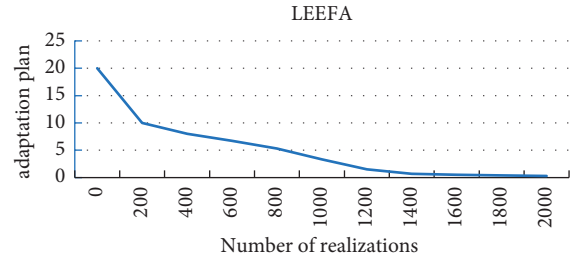


FIGURE 3: The choice of LEEFA algorithm.

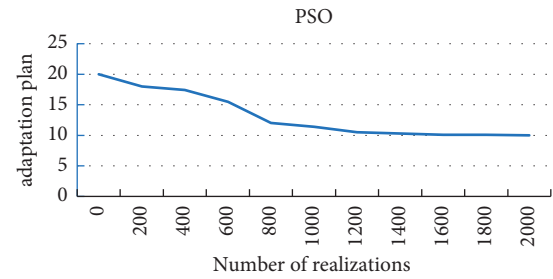


FIGURE 4: The choice of PSO algorithm.

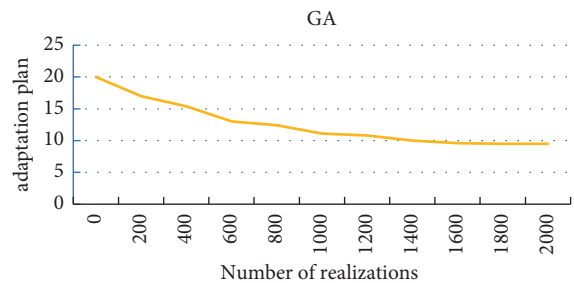


FIGURE 5: The choice of GA algorithm.

### 4.3. Performance Comparison after Optimization of Resource Allocation in Colleges and Universities

**4.3.1. Optimization Scheme.** We apply the selected firefly intelligent optimization algorithm. Taking Sunshine University as an example, on the basis of the optimization of the financial organization structure of Sunshine University, we use the algorithm to select an optimal financial reimbursement method to prove that the optimization algorithm is effective for multi-objective financial management, and

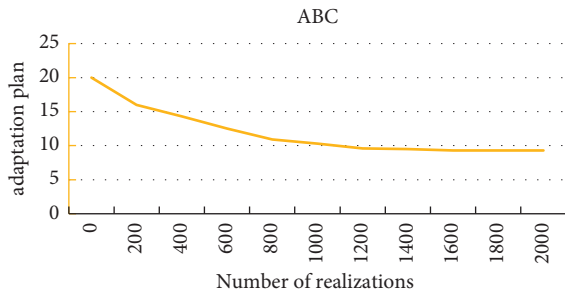


FIGURE 6: The choice of ABC algorithm.

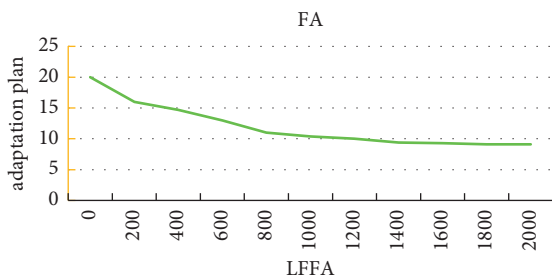


FIGURE 7: The choice of FA algorithm.

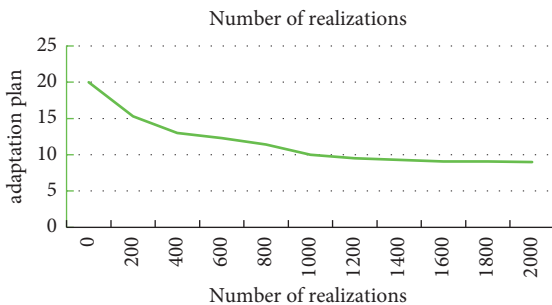


FIGURE 8: The choice of LFFA algorithm.

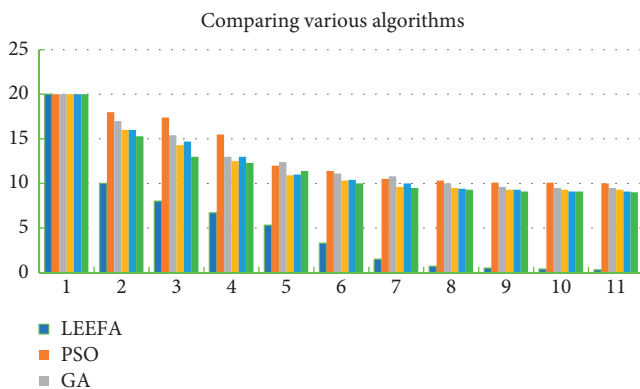


FIGURE 9: Comprehensive comparison chart of six algorithms.

the solution of the ideal scheme of the configuration method is shown in Figures 10 and 11.

The “Network Image Comparison” logo from the “Generate Order Number” link to the “Project Leader’s Online Approval” link, and add the “Enter Online Banking Payment” logo from the “Review” link to the “Settlement and Payment” link.

Simplify the application process. The applicant only needs to upload the bill through the network, and then automatically generate the order number. The approval and accounting are integrated, and the automatic review is carried out through the comparison of network electronic images, which reduces the possibility of forgery and alteration of bills and reduces the malicious use of financial resources. Probability upon entering the payment state, each payment of funds will be recorded in the entire link chain. If relevant departments want to obtain payment vouchers, they can also download relevant voucher records from the internet and print them. Prevent the movement of non-compliant funds. In the final filing process, the relevant vouchers will be stored in the school’s intranet, and relevant personnel can refer to them at any time when necessary, but the access records will be recorded.

4.3.2. *Performance Comparison.* We compare the processing performance of the two schemes with 50 people participating in financial reimbursement as a reference as shown in Figure 12.

It can be clearly seen from the picture that the number of participants in the process is also increasing rapidly in the traditional financial reimbursement process as the number of reimbursements increases. Because in the traditional reimbursement process, reimbursement personnel need to deliver the sorted bills to the reimbursement center. The staff of the reimbursement center will effectively distribute the documents due to the increase of reimbursement documents. Each type of bills and documents needs to be sorted by corresponding staff, thereby increasing the number of personnel involved in the process. The same is true for the increase in the number of trial and induction personnel in the process. In the algorithm-optimized process, the corresponding trial sections have been electronically integrated, and the progressive reimbursement process structure has been compressed to increase efficiency and reduce the number of personnel required.

The above histogram can clearly reflect the change in response time between the traditional reimbursement process and the optimized reimbursement process. The traditional reimbursement process adopts the classic layer by layer transmission of information. After the reimbursement personnel hand in the corresponding bills, the reviewer manually scans and uploads them with an electronic scanner and then confirms them layer by layer. The existence of information difference between them leads to the need to look for integration and confirm with the information in the process of information transmission in the network. Therefore, in the traditional reimbursement process, the network response time is longer and the number of

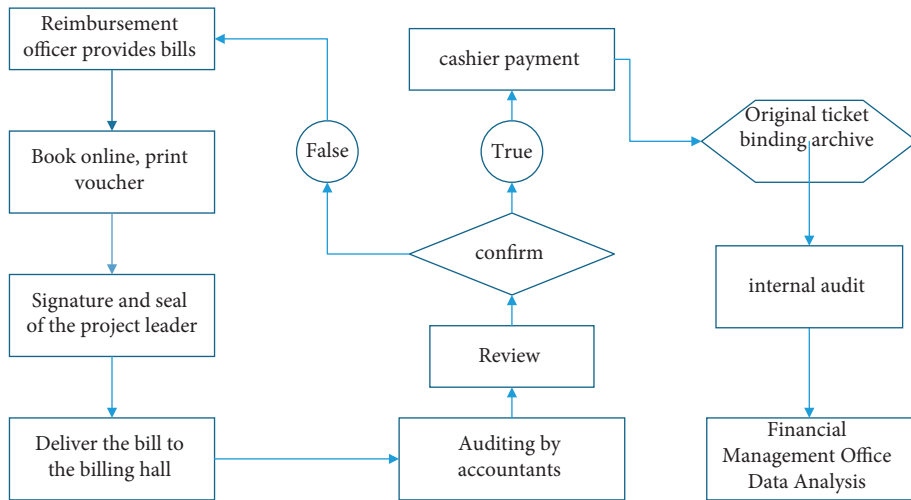


FIGURE 10: Sunshine University reimbursement financial process.

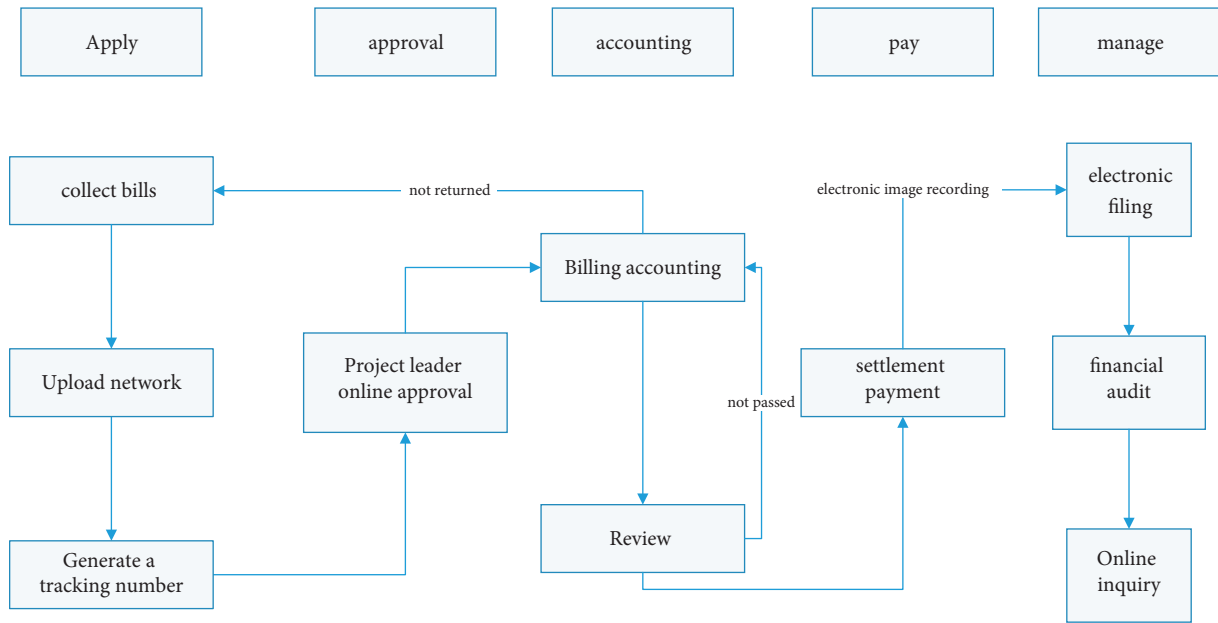


FIGURE 11: The optimized financial reimbursement process of Sunshine University. The payment optimization flow chart, the budget management optimization flow chart, etc.

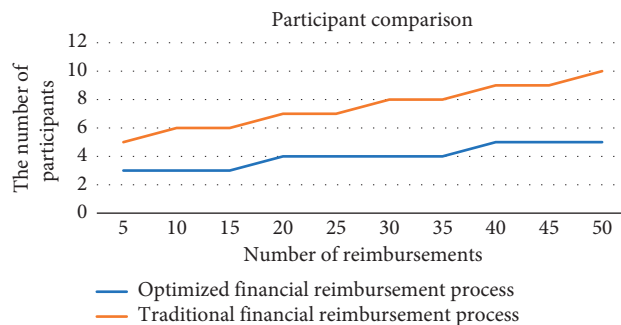


FIGURE 12: Participant comparison chart.

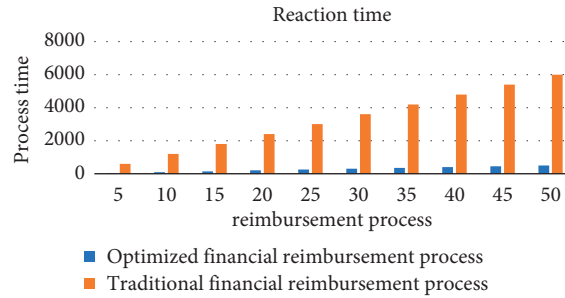


FIGURE 13: Response time comparison chart.

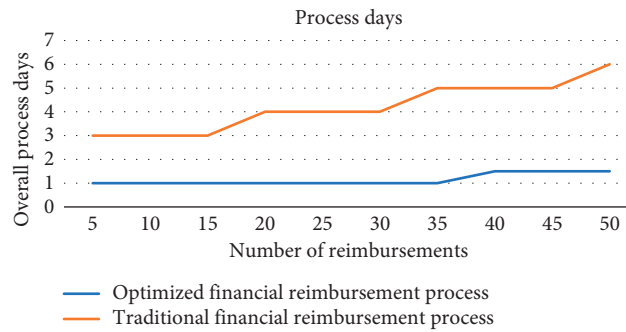


FIGURE 14: Process days comparison chart.

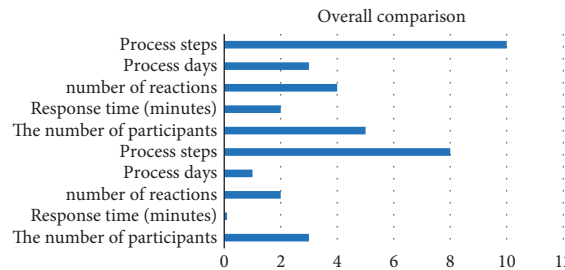


FIGURE 15: Performance comparison of a single reimbursement process.

responses is higher. After the optimization of the intelligent algorithm, our process has been simplified a lot, and the electronic integrated scanning and auditing is adopted as shown in Figure 13.

In the traditional financial reimbursement process, the time required at the end of the reimbursement process, that is, the final filing increases as the number of reimbursed persons increases. The reimbursement process without optimization adopts the form of data submission layer by layer. The core element is the time arrangement of the management personnel, which has too many subjective elements. Therefore, the actual time to finally obtain the bill voucher file will increase due to the increase of reimbursement materials. The most likely consequence is to delay the timeliness of financial data analysis. In the optimized process plan, most of the processes adopt flat integrated design and network intelligent processing. Therefore, it only takes a short time from the submission of data by reimbursement personnel to the final data entry into the file,

which ensures the timeliness of financial analysis to the greatest extent as shown in Figure 14.

There is a lack of combining actual cases, and you can also increase your own practice after selecting a plan to reflect whether the plan is optimal.

When the above is a single reimbursement process, it can be clearly seen that the financial reimbursement process method selected by our intelligent algorithm has obvious optimization in terms of time, number of participants, and process steps compared with the previous process. From the above process, the overall network response processing time has changed from 120 seconds to 10 seconds after optimization, not only because of the advantages brought by blockchain but also because of the simplified process and optimized overall network response time. The overall process days have also changed from the original three days to only one day. The optimized process integrates the document approval, review, and other processes, and the entire process of electronic inspection and verification in addition

to approval greatly reduces the number of process days and the overall process. The number of people needed is the number of responses for the network to process the agent, and the reduction of the number of responses is beneficial to the processing of other situations and reduces the waste of financial resources as shown in Figure 15.

It should also be compared with the optimization process selected by other algorithms, such as the particle swarm algorithm and the financial reimbursement process plan selected by the gray wolf algorithm.

## 5. Conclusion

In order to explore the method of optimizing the management and allocation of financial resources in colleges and universities oriented to multi-objective intelligence, this paper analyzes that the current financial organization system of Sunshine University is a classic pyramid model, which is not conducive to the exchange of information within the financial organization and the motivation of employees. Therefore, an improvement plan is proposed, using the blockchain technology as the prototype, using its core idea of decentralization, the design flattens the financial organization, changes the original hierarchical relationship, strengthens horizontal communication, and increases employee satisfaction. On this basis, we have the conditions to efficiently select a good optimization algorithm for scheme selection. When choosing an intelligent optimization algorithm, we consider the number of algorithms faced by multi-objective method selection and the complexity of the problem. In general, we choose an intelligently optimized quantum algorithm to help us choose the optimal solution. When the algorithm is complex and the algorithm is huge, we choose the optimized firefly algorithm. In the experiment, after comparing with other algorithms, the performance of this algorithm is significantly better than other algorithms, which is the ideal algorithm we want. Then we use this algorithm to optimize the financial resource management and allocation methods. For example, in the experimental example, we intelligently optimize the reimbursement financial process, and the optimized process method has made great progress compared with the previous one.

## Data Availability

The experimental data used to support the findings of this study are available from the corresponding author upon request.

## Conflicts of Interest

The authors declare that they have no conflicts of interest.

## References

- [1] H. Liu, Y. Tang, T. Liu, D. Qiu, and H. K. Hu, "On the diversified structure of financial allocation system for local universities and colleges," *Educational Research*, vol. 38, no. 1, pp. 93–98, 2003.
- [2] T. M. Breyer and R. L. Raab, "Efficiency and perceived quality of the nation's "top 25" National Universities and National Liberal Arts Colleges: an application of data envelopment analysis to higher education," *Socio-Economic Planning Sciences*, vol. 28, no. 1, pp. 33–45, 1994.
- [3] W. R. Elger, "Managing resources in a better way: a new financial management approach for the university of Michigan medical school approach for the university of Michigan medical school," *Academic Medicine*, vol. 81, no. 4, pp. 301–305, 2006.
- [4] W. Meng and Bo Huang, "Research on the design of optimal allocation mechanism of university resources based on comprehensive budget management," *Journal of Chongqing University: Social Science Edition*, vol. 15, no. 4, p. 6, 2009.
- [5] Y. Zhao, "Research on the construction of comprehensive budget management system in private colleges and universities—taking xi'an institute of translation and interpretation as an example," *Value Engineering*, vol. 031, no. 033, pp. 225–227, 2012.
- [6] R. Lin, "An empirical study on several issues of financial management in colleges and universities in my country," *Open Education Research*, vol. 17, no. 1, p. 7, 2011.
- [7] X. Yu, "How does finance optimize resource allocation to promote high-quality development of colleges and universities," *Accountant*, vol. 21, p. 2, 2019.
- [8] Y. Gao and S. Xie, "Particle swarm optimization algorithm based on simulated annealing," *Computer Engineering and Applications*, vol. 40, no. 1, p. 4, 2004.
- [9] Y. Wang, L. Li, and Z. Hu, "Swarm intelligence optimization algorithm," *Computer Technology and Development*, vol. 18, no. 8, p. 4, 2008.
- [10] H. H. Shah, "Intelligent water drops algorithm A new optimization method for solving the multiple knapsack problem," *International Journal of Intelligent Computing & Cybernetics*, vol. 1, no. 2, pp. 193–212, 2008.
- [11] Li Wang, "Thinking on the innovation of internal administrative management in higher vocational colleges based on flat organization theory," *Journal of Xiangfan Vocational and Technical College*, vol. 5, no. 6, p. 3, 2006.
- [12] X. Li, "The challenge of organizational structure flattening to human resource management—taking zhejiang R bank as an example," *Journal of Shaoxing University of Arts and Sciences*, vol. 34, no. 2, p. 6, 2014.
- [13] W. Du, B. Li, and Yu Tian, "Research progress of quantum annealing algorithm," *Computer Research and Development*, vol. 45, no. 9, p. 8, 2008.
- [14] C. Liu and C. Ye, "A novel bionic swarm intelligence optimization algorithm: firefly algorithm," *Computer Application Research*, vol. 28, no. 9, p. 3, 2011.
- [15] H. Zhang, H. Xiong, and L. Tu, "An improved quantum annealing algorithm," *Journal of Jiangxi Normal University: Natural Science Edition*, vol. 40, no. 5, p. 3, 2016.



## Research Article

# Load Balancing of SDN Controller for Migration Optimization Based on Metaheuristics

Congcong Min 

*Guangdong Communications & Networks Institute, Guangzhou 510671, China*

Correspondence should be addressed to Congcong Min; [epcheesefitness@mail.scut.edu.cn](mailto:epcheesefitness@mail.scut.edu.cn)

Received 23 March 2022; Revised 20 May 2022; Accepted 28 May 2022; Published 13 July 2022

Academic Editor: Man Fai Leung

Copyright © 2022 Congcong Min. This is an open access article distributed under the Creative Commons Attribution License, which permits unrestricted use, distribution, and reproduction in any medium, provided the original work is properly cited.

With the existing power SDN network architecture, the improved switches migration algorithm is put forward. Through the advantages of the ant colony algorithm and genetic algorithm fusion, the migration process is optimized, and the fusion algorithm in switches uses the operation, such as restrictions in advance and pruning algorithm efficiency to eventually apply migration under multiple controllers to the switch. The efficiency and stability of switch migration under multicontroller are improved, and the performance of the RYU controller is compared with other algorithms. The results of the algorithm and performance comparison test show that the improved ant colony algorithm is reduced by 12.5% and 1.5%, which is a comparison of response delay; the accuracy of the migration operation of the algorithm can make full use of the resources of the controller and achieve the purpose of improving the migration efficiency and load balancing among multiple controllers.

## 1. Related Work

In the new network architecture of SDN, load balancing between multiple controllers is realized by switch migration. During switch migration, the first problem to be solved is how to migrate the switch the fastest without losing data. To solve this problem, Haller et al. mentioned the seamless migration mode, that is, the switch is connected to two controllers at the same time, and the roles of the two controllers are changed at the same time, so as to achieve rapid data migration. However, for the existing SDN network, and due to the instantaneous network traffic, controllers in the same cluster may not only be overloaded with one controller but may be overloaded with two or more controllers at the same time [1, 2]. In this case, no matter how efficiently the switch migration is performed, the stability of the network cannot be restored quickly. Therefore, a switch migration optimization algorithm is proposed. Classical optimization algorithms include nearby selection algorithms [3], genetic algorithms [4–6], immune particle swarm optimization algorithms, and so on [5–8].

Among them, the nearby migration algorithm is to select the controller with the lowest migration cost as the target

controller for migration by calculating the path between the global controller and the overload controller when the controller overload is detected. This method is fast, but when multiple controllers are overloaded at the same time, two or more controllers may migrate to one controller, resulting in a secondary overload of the target controller. In this case, one switch migration cannot complete load balancing, and multiple switches are required to achieve load balancing. To solve this problem, both genetic algorithm and improved particle swarm optimization (PSO) have been improved [9–11]. However, due to the complexity of particle swarm optimization and genetic algorithm and the problem of long calculation time under single controller overload, there is still a lot of research direction in the optimization of switch migration algorithm. The classical optimization algorithm tries to solve the load balancing of multicontrol architecture by unified scheduling in the control plane, which has achieved good results. In view of the actual situation of existing algorithms and switch migration process, heuristic algorithms, such as ant colony algorithm and genetic algorithm, have very good advantages in computing speed and resource consumption [12, 13]. However, both ant colony algorithm and genetic algorithm have exposed many

shortcomings in the course of many years of practice. Ant colony algorithm has fast global search ability, but poor local search ability, while genetic algorithm has good local search ability but poor global search ability. In this regard, the research focus of this paper is to integrate the ant colony algorithm and genetic algorithm and improve the actual application scenarios under the SDN architecture, so as to improve the performance of SDN and maintain the load balancing of SDN.

## 2. Traditional Ant Colony Algorithm

At present, the ant colony algorithm has been used in the path planning of AGV vehicles. In application, it can be divided into three parts: foraging, movement, and pheromone rules. Foraging rules are used to determine the impassable locations, which depends on the set tabu list, and then the ant's current location is added to it [14–16].

Movement rules are used to determine the ant's transition probability in different nodes, which needs to use heuristic functions and pheromone concentrations. If there are no movable nodes obtained, the current search process ends. In addition, in order to improve the search ability of the algorithm, the roulette method is introduced to ensure that all nodes can be selected. The formulas of transition probability are as follows [17]:

$$p_{ij}^k(t) = \begin{cases} \frac{[\tau_{ij}(t)]^a \times [\eta_j(t)]^\beta}{\sum_{s \in \text{allowed}_k} [\tau_{is}(t)]^a \times [\eta_j(t)]^\beta, j \in \text{allowed}_k, 0, j \notin \text{allowed}_k}, \\ \eta_j = \frac{1}{d_j}, \\ d_j = \sqrt{(J_x - E_x)^2 + (J_y - E_y)^2}, \end{cases} \quad (1)$$

where  $a$  and  $\beta$  are the important factors of pheromone and heuristic function, respectively.  $k$  represents an ant. Moreover,  $p_{ij}^k(t)$  and  $\text{allowed}_k$  represent the transition probability and corresponding set of  $k$  at the lower node respectively.  $\eta_j(t)$  represents the heuristic function, which is related to the distance  $d_j$  between endpoint  $E$  and node  $j$ , and  $\tau_{ij}(t)$  represents the pheromone concentration transferred at nodes  $i$  and  $j$ .

For the pheromone rule, pheromones in the path do not increase with the ant's release, but some of them volatilize. After multiple loops, the updated formula of pheromone in the path is as follows [18]:

$$\tau_{ij}(t+1) = (1-\rho)\tau_{ij} + \sum_{k=1}^m \Delta\tau_{ij}^k, \quad (2)$$

where  $m$  represents the number of ants and  $\rho$  represents the volatilization factor of pheromone, which takes values between 0 and 1. Furthermore,  $\Delta\tau_{ij}^k$  represents the pheromone left by ant  $k$  in the iteration, whose form is as follows [19]:

$$\Delta\tau_{ij}^k = \begin{cases} \frac{Q}{L_k}, & \text{kth ant goes from node } i \text{ to node } j, \\ Q, & \text{Others,} \end{cases} \quad (3)$$

where  $L_k$  represents the total length of the ant's path and  $Q$  means a constant.

## 3. Switch Migration Algorithm Based on Improved Ant Colony

Combined with the previous analysis, the basic principle of the ant colony algorithm has been defined. This algorithm has some advantages in convergence and local search, but there are also some obvious shortages, which embodies that the global search ability is poor. And, for large network architecture, the generation of initial pheromone takes a long time occupying the algorithm more than 60% of the total execution time, which reduces the efficiency significantly. On the other hand, genetic algorithm is also widely used to solve optimization problems. The algorithm has good global search ability, but it is difficult to maintain high convergence when the network scale is large. Considering the above problems comprehensively, the two algorithms mentioned above can be combined in the new SDN network architecture, which makes up for the shortcomings of the single algorithm. The advantages of the two algorithms can be given full play; thus, the effect of load balancing is improved. In addition, SDN is a cloud computing method that can realize network configuration by programming controller, so as to fundamentally solve the problem of decentralized and complex static architecture in traditional networks, which improves the performance and processing efficiency of the network. However, the current network requires greater flexibility and simple troubleshooting. SDN realizes centralized and unified control of the network through the control plane, thus greatly improving the performance of the network. Therefore, this study attempts to optimize the load balancing problem of SDN under the control plane through the ant colony algorithm.

As can be seen, the ant colony algorithm and genetic algorithm are integrated to design an improved ant colony switch migration algorithm. The parameters of the algorithm are optimized to improve the effect of load balancing.

**3.1. Load Balancing Strategy of Migration Algorithm.** Analyzing the problems in the fusion algorithm, the optimization strategy is proposed, which is embodied in the selection of switch and target controller. Given that  $C = \{c_1, c_2, \dots, c_M\}$  represents all controller nodes in  $G$  of the SDN area and  $S = \{s_1, s_2, \dots, s_N\}$  represents the set of switches. The control relation between the two is expressed as  $F = (f_{ij})_{M \times N}$ , where when  $c_i$  controls  $s_j$ , there is  $f_{ij} = 1$ , and when other cases occur, there is  $f_{ij} = 0$ .  $c_i$  can be used as the source node or the target node. If  $\forall c_i \in c$  and it is overloaded,  $c_i$  needs to be migrated, and the controller is the source node. When  $c_i$  receives the migrated computer, the corresponding controller is the target node. If the number of

migration switches and overloaded controllers is  $N$  and  $M$ , respectively,  $c_i$  can obtain the number of current requests  $r_{ij}$  of switch  $s_j$ . Meanwhile, the controller is used to load, and the load comes from multiple sources, including memory, CPU utilization  $U_{\text{mem}}$ ,  $U_{\text{cpu}}$ , and number of switches  $N$ . The specific formula is shown as follows.

**3.1.1. Migration Time.** The controller's resource utilization  $U_c$ , the current CPU utilization  $U_{\text{cpu}}$ , the current memory utilization  $U_{\text{mem}}$ , and the network bandwidth utilization  $U_{\text{net}}$  are taken as main performance parameters, wherein the controller's resource utilization is expressed by the percentage of all switch requests under the current controller and the maximum request volume accepted by the controller.

Set Threshold ( $U_c$ ,  $U_{\text{cpu}}$ ,  $U_{\text{mem}}$ , and  $U_{\text{net}}$ ) as the triggering policy. Within a period  $T$ ,  $c_i$  collects parameters once and compares them with matched load characteristic thresholds ( $u_{\text{cth}}$ ,  $u_{\text{cpth}}$ ,  $u_{\text{mth}}$ , and  $u_{\text{nth}}$ ). If a parameter is greater than the maximum threshold for several consecutive times, the controller  $c_i$  is considered to be overloaded, and the switch must be migrated. If none of the parameters is higher than the threshold, the controller is considered to be idle, and the switch can be migrated in.

**3.1.2. Switch Selection.** In this paper, the probability formula is used to select switches, and the switch selection probability  $p_{ij}$  is shown in the following formula:

$$p_{ij} = \frac{\exp(-r_{ij}/\mu_{ij})}{\sum_{j \in S_i} \exp(-r_{ij}/\mu_{ij})}, \quad (4)$$

where  $r_{ij}$  is the number of flow requests from  $s_j$  to  $c_i$ ,  $\mu_{ij}$  is the hop number between  $s_j$  and  $c_i$ , and  $S_i$  is the set of  $s_j$  controlled by  $c_i$ .

Assume that  $X$  is the load volume that exceeds the overload controller  $c_i$  and  $a$  is the load of the switch in set  $S$ . Only when  $n$ , the number of switches migrated by the overload controller, meets the condition  $\sum_{i=1}^n a_j > X$  can flow requests be processed in time in this area.

**3.1.3. Selection of Target Controller.** After the migration controller and migration switch are determined, this paper mainly uses the improved ant colony algorithm to select the appropriate immigration controller. Firstly, for the immigration controller, the more the idle resources, the higher the probability of occurrence in the process of crossover and mutation, and the higher the probability of eventually appearing in the initial pheromone set of the ant colony algorithm. Secondly, the larger the hop number between the migration controller and the immigration controller, the longer the communication time between the two controllers, and the smaller the number of ants appearing on the path. Therefore, the function  $v_{ij}$  for searching the target controller in the improved ant colony algorithm is defined as follows:

$$v_{ij} = r_{ij} \frac{\mu_i^s}{d_{ij} (1 - \mu_i^s)}, \quad (5)$$

where  $r_{ij}$  is the number of flow requests from  $s_j$  to  $c_i$ ,  $\mu_{ij}$  is the hop number between  $s_j$  and  $c_i$ , and  $S_i$  is the set of  $s_j$  controlled by  $c_i$ .

Thus, to solve the switch migration problem is to solve a typical traveling salesman problem of the ant colony algorithm.

**3.2. Solving Migration Problem.** At present, the ant colony algorithm has been widely used to solve optimization problems. The characteristics of the algorithm are high convergence, strong concurrency, good local search performance, and so on. In principle, the method is designed mainly according to the ants foraging rule in nature, and the optimal path is obtained through positive feedback, namely the optimal solution to the problem. In addition to this algorithm, genetic algorithm is also widely used to solve optimization problems. Genetic algorithm has strong global search ability, randomness, and rapidity. The algorithm is designed according to the law of evolution in nature, and high-quality offspring can be generated through crossover, mutation, and other ways. On this basis, the optimal solution can be obtained by coding.

However, there are some problems in the application of the above two algorithms. On the one hand, the efficiency of the ant colony algorithm is low in the initial search, although it will be improved in the process of pheromone accumulation. On the other hand, the convergence of the genetic algorithm is fast in the initial search, but it will decrease significantly in the later stage. Thus, after fusing the two algorithms, the advantages of the two algorithms can be given full play, which can keep high efficiency while obtaining the optimization results. At present, there are many researches in this field, and different methods have been formed. The common fusion strategies are divided into two categories: firstly, a genetic algorithm is used to get the initial pheromone solution, and then it is applied to the ant colony algorithm to get the optimal solution. Secondly, the genetic operation is added to the ant colony algorithm to diversify the solutions. After analysis, the second strategy is finally adopted in this paper.

**3.2.1. Algorithm Design and Implementation.** Adopting coded parameters is the significant difference between the genetic algorithm and other algorithms. Therefore, when using a genetic algorithm, the first is to determine the appropriate coding  $G$ , which generally is binary coding. Besides this method, tree code or volume number code can also be adopted. In addition, when using the ant colony algorithm, it often needs to transform the problem to be solved. Only after it is transformed into the traveling merchant problem can it be solved.

The above factors are considered in the design of the fusion algorithm. For example, for the ant colony algorithm, there are only two selection paths for each node except the

last node. And ant pheromone distribution is used to solve the continuous calculation problem. After analysis, for the genetic algorithm, the binary coding method is adopted. On this basis, the fusion of two algorithms is carried out.

At present, some scholars have studied the fusion of two algorithms and put forward different fusion strategies, which can be generally divided into two categories. The first one is that the ant colony algorithm takes a higher proportion of the whole algorithm, and the genetic algorithm serves as an auxiliary part. The second is the opposite, with a higher proportion of genetic algorithms and ant colony algorithms as auxiliary.

A genetic algorithm (binary coding) and ant colony algorithm (double subsequent nodes) can be used to design a fusion algorithm. The first algorithm needs to adopt the genetic algorithm firstly and then uses the ant colony algorithm. Specifically, the initial solution set is firstly obtained by the genetic algorithm, and then it is input into the ant colony algorithm as the initial pheromone path; thus, the optimal solution is further calculated. The second algorithm mainly uses the ant colony algorithm. Adding genetic and mutation operations to the ant colony algorithm is helpful for the improvement of global optimization ability. Considering various factors, the second algorithm is finally selected in this paper.

In the research, the fusion algorithm is used to solve the load balancing problem of multiple controllers, which needs to transform the problem first. And using a cross way to combine the original paths can make the algorithm achieve higher global search ability. Finally, the pheromone concentration of a new path needs to be updated. In the fusion algorithm, the selection and mutation of a genetic algorithm are introduced. In the crossover process, the intersection position between the ant colony algorithm path and genetic algorithm should be selected randomly, and then the corresponding new path can be obtained by selecting the crossover.

The basic principle of path crossing is shown in Figure 1.

When ants pass by, a pheromone is left over in each path, which is updated by pheromone concentration in the algorithm.

Here, Knot -  $j$  ( $j = 1, \dots, r, i = 0, 1$ ) represents the migration path of  $(j, i)$ , and each node has two migration nodes, which are Next - knot - 0 and Next - knot - 1, respectively. The connected edge is represented as edge  $(j, i, 1)$ . Thus, the formulas of a pheromone update are as follows:

$$\tau_{j,i,1}(t+1) = \rho\tau_{j,i,1}(t) + \Delta\tau_{j,i,1},$$

$$\Delta\tau_{j,i,1} = \sum_{k=1}^m \tau_{j,i,1}^k,$$

$$\Delta\tau_{j,i,1}^k = \begin{cases} \frac{Q}{F^k(x_1, x_2, \dots, x_n)}, & \text{When the } k\text{th ant passes by the edge,} \\ 0, & \text{Otherwise,} \end{cases} \quad (6)$$

where  $m$  represents the number of ants,  $F^k(x_1, x_2, \dots, x_n)$  represents the final obtained optimal solution, and  $\Delta\tau_{j,i,1}^k$

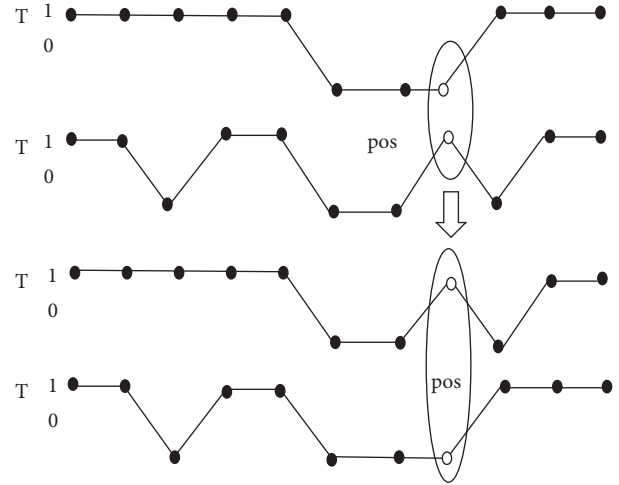


FIGURE 1: Operation principle of path crossing.

represents the pheromone concentration increased in edge  $(j, i, ij)$  during the movement of ants. The probability formula of ant selecting subsequent nodes is as follows:

$$P_{j,i,i_j}^k = \frac{[\tau_{j,i,i_j}]^\alpha [\eta_{j,i,i_j}^k]^\beta}{[\tau_{j,i,0}]^\alpha [\eta_{j,i,0}^k]^\beta + [\tau_{j,i,1}]^\alpha [\eta_{j,i,1}^k]^\beta} \quad (7)$$

where  $\tau_{j,i,0}$  and  $\tau_{j,i,1}$  represent the pheromone concentration of Edge  $(j, i, 0)$  and Edge  $(j, i, 1)$ , respectively.  $\eta_{j,i,0}, \eta_{j,i,1}$  represent the visibility function of the two edges.  $\alpha$  and  $\beta$  are the coefficients associated with node selection.

3.2.2. *Specific Solution Steps.* The improved algorithm is described as follows:

- (1) Initialize related parameters  $\alpha, \beta, \rho$ , and so on of ant colony algorithm
- (2) Calculate iteratively
- (3) While  $t < \text{iteration period } c$ , output the final optimal solution

The improved ant colony algorithm is applied to the load balancing problem of SDN, which can ensure the dynamic selection of migration objects. However, if the scale of network topology is large, it cannot maintain a high convergence rate. Therefore, the genetic algorithm can be introduced to solve the above problems effectively, so as to further improve the global search ability and convergence performance of the algorithm.

For the problem of load balancing, it is difficult to migrate each switch to other switches randomly due to the influence of the subdomain division of the controller. Therefore, pruning is carried out for the genetic algorithm to ensure that ant paths are all in the subdomain. The specific process is as follows: firstly, the pruning is carried out by the genetic algorithm to obtain the initial pheromone. Then the ant colony algorithm is used for processing, and the global optimal solution is obtained by an iterative method. In this way, the optimal migration path can be obtained. The fusion

algorithm designed in this paper, namely, the GA-ACO algorithm, is as follows:

- (1) Related parameters of the improved ant colony algorithm
- (2) Path crossover probability  $P_c$
- (3) Perform improved ant colony algorithm
- (4) While  $t <$  iteration period  $c$ , output the results

## 4. Simulation Experiment and Performance Analysis

**4.1. Construction of Simulation Environment.** In the simulation process, Open vSwitch 1.4.6, Zookeeper 3.4.5, and so on are used. The hardware should ensure that the processor is Intel I7, and hard disk and memory are not less than 500 G and 12 G, respectively. Software configuration is Windows 10 system, and the virtual machine is VMware.

In addition, the number of OVS switches and controllers used in the simulation is 12 and 4, respectively, and the processing performance of each controller is different. The load threshold of the controller is  $\max(u_{cth}, u_{cpth}, u_{mth}, u_{nth}) = (0.9, 0.9, 0.85, 0.95)$ , and the sampling period is 10 s. In the

simulation, the data flow speed of the switch is improved step by step, and the response delay of the controller, the resource utilization ratio, and other indicators are recorded and analyzed.

Analyzing the application effect of improved ant colony algorithm to compare with proximity migration algorithm, its influence on load balancing is discussed.

### 4.2. Parameter Setting of Improved Ant Colony Algorithm.

The application effect of the ant colony algorithm will be affected by the parameter setting. If the parameter setting is not reasonable, the effectiveness of the algorithm will be inevitably reduced. In this paper, the effects of various parameters are analyzed, including hormone volatility coefficient  $\rho$ , heuristic factor  $\alpha$  and  $\beta$ , ant number  $m$ , and so on. The influence of each parameter is discussed, and the relevant parameters are reasonably set, which makes the improved algorithm can play a better role in the load balancing.

**4.2.1. Setting of Hormone Volatility Coefficient.** The global update method is adopted, and the form of  $\Delta\tau_{ij}^k(t)$  is as follows:

$$\Delta\tau_{ij}^k(t) = \begin{cases} \frac{Q}{\cos t_{ij}}, & \text{The path that ant } K \text{ passing through node } i \text{ and node } j \text{ in a loop,} \\ 0, & \text{Otherwise,} \end{cases} \quad (8)$$

where there are two nodes  $i$  and  $j$ .  $\cos t_{ij}$  represents the overhead of  $i$  and  $j$ .  $\rho$  and  $1 - \rho$  represent the volatility coefficient and retention coefficient of hormones, respectively. The improved algorithm still has problems of falling into local optimum and low convergence speed, which is directly related to the rationality of setting  $\rho$ .

Hormone volatility coefficient  $\rho$  is an important parameter that if it is not set or set unreasonable, the application effect of the fusion algorithm will be adversely affected. Specifically, if the parameter is not set, the subsequent nodes may still have paths that do not belong to alternative paths due to the influence of crossover operations, thus affecting the convergence of the algorithm. If this parameter is too small, the volatility speed of the hormone is significantly reduced. At this time, it is difficult for the pheromones in the path to forming a large difference so the global optimal solution cannot be achieved. However, if this parameter is too large, the pheromone in the path volatilizes quickly, which increases the randomness of the ant's selection of subsequent nodes and reduces the convergence of the algorithm. Therefore, it is necessary to determine the hormone volatility coefficient in an appropriate way, and the specific process is shown as follows.

To research the setting of hormone volatility coefficient  $\rho$ , the first is to set relevant parameters. The expected factors are set as  $\alpha = 1$  and  $\beta = 2$ . The number of ants is set as  $M = 5$ .

Given that  $p = 1$ ,  $\rho$  is 0.1, 0.3, 0.5, 0.7, or 0.9, and the influence of  $\rho$  on the performance of the improved ant colony algorithm is changed. After each parameter is set, iteration begins. If the difference between the maximum  $v_{\max}$  of hormone concentration and the minimum  $v_{\min}$  in each path exceeds 10%, the iteration process can be ended. The final results are shown in Figure 2.

The relationship between the iteration number and the hormone volatility coefficient is shown in Figure 3.

As can be seen, there is a positive correlation between the number of iterations and the hormone volatility coefficient on the whole. If the hormone volatility coefficient is higher, it means the number of iterations also is higher. In this case, the influence of hormones on path selection is small, but it affects the convergence of the algorithm. When the value of the volatility coefficient is small, although the number of iterations is small, the convergence speed is improved. The algorithm is prone to local convergence; thus, the global optimal solution ultimately cannot be obtained.

Combined with the above analysis, when determining the hormone volatility coefficient, the convergence of the algorithm and the global search ability should be taken into consideration. Here, the hormone volatility coefficient is appropriately set between 0.3 and 0.5 to ensure the stability and convergence of the algorithm. At the same time, the global optimization result can be obtained. After the above

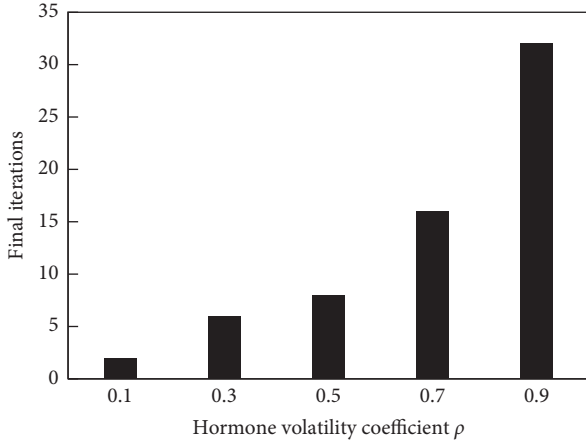


FIGURE 2: Influence of hormone volatility coefficient on the improved ant colony algorithm.

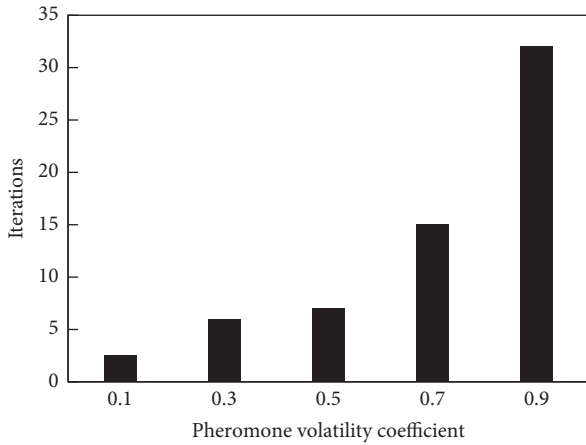


FIGURE 3: Relationship between pheromone volatility coefficient  $p$  and iterations.

analysis, the hormone volatility coefficient is finally set as 0.3.

**4.2.2. Setting of Heuristic Factors  $\alpha$  and  $\beta$ .** Pheromone heuristic factors  $\alpha$  and  $\beta$  mainly express the role of the improved algorithm in ants' path search, which represent the hormone-dependent size and preference coefficient of path selection, respectively. When the former is larger, it means that the randomness of the ant's path selection is small, and the ant is more inclined to choose the path previously traveled. In this case, it is easy to lead to local convergence, and it is difficult to obtain the global optimal solution. When the latter is large, it indicates that the ant has a higher probability to choose the local shortest path at a node. Although the convergence speed can be improved, the problem of local optimization also exists. Therefore, it is necessary to set the two reasons, so as to meet the requirements of convergence and optimization.

To solve the load balancing problem of SDN architecture, the network scale is usually high. It is necessary to ensure that ants can achieve a certain random search ability

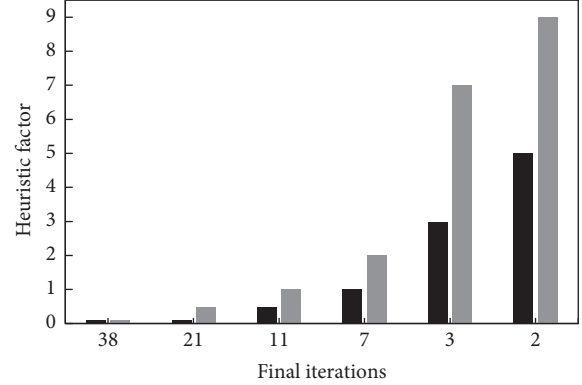


FIGURE 4: Iterations of heuristic factors  $\alpha$  and  $\beta$  under different combinations.

in the path search process and meet the requirements of convergence, which will have a great impact on the application effect of the whole algorithm. Therefore, it is necessary to keep a balance between the certainty and randomness of the search, so as to improve the performance of the algorithm.

According to the above analysis, the heuristic factor can be set reasonably in combination with the previous simulation. During the simulation process, the hormone volatility coefficient is set as 0.3, and then several groups of heuristic factors are set. The relationship between the algorithm performance and the combination of heuristic factors is verified by simulation. Moreover, the influence of the combination of heuristic factors is discussed; thus, the optimal value of the heuristic factor is determined. The iteration number of different combinations of heuristic factors obtained in the simulation is shown in Figure 4.

It can be seen from Figure 4 that when the combination of heuristic factors is different, the corresponding number of iterations changes significantly. When both pheromone heuristic factors  $\alpha$  and  $\beta$  are high, the roles of the two are different. The former makes the ant excessively depend on the pheromone concentration to determine the moving path. The latter makes the ant more dependent on the positive feedback and is easy to obtain the local optimal solution. When both are small, the former significantly reduces the dependence of ant on hormone concentration and basically did not use hormone concentration information when determining the path. The latter increases the randomness of path search, which leads to more redundant paths and lower convergence speed, making it difficult to obtain the optimal path. Taking into account the above factors, it is appropriate to set the two to 1 and 2, respectively.

**4.2.3. Setting of the Number of Ants.** The improved ant colony algorithm needs to obtain the optimal solution from the solution set, which requires the participation of all ants. And the optimal solution can be obtained by iteration. Since each ant will search for an optimal solution, the solution obtained by all ants can form a solution set, so the number of ants will inevitably affect the algorithm performance. If the

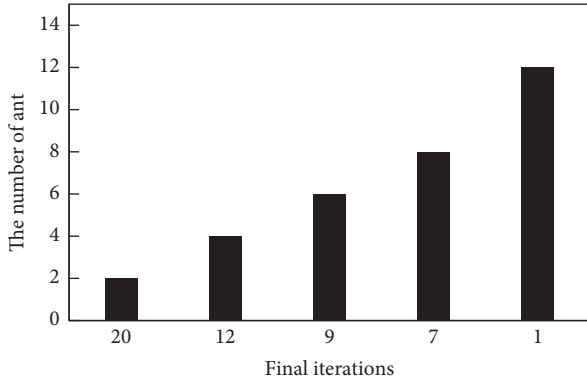


FIGURE 5: Iterations under different ant numbers.

number is large, the global search ability of the algorithm is stronger, which improves the reliability of the algorithm significantly. However, there may be many invalid paths in the solution set, which reduces the convergence speed and affects the algorithm performance to a certain extent. If the number is too small, it is difficult to maintain a high global search capability, and only a local optimal solution can be obtained.

To solve the above problems, it is necessary to set the number of ants reasonably. Here, the previous simulation method is adopted to determine the number of ants. The first is to set the hormone volatility coefficient and two heuristic factors, which are 0.3, 1, and 2, respectively. The second is to set multiple ant numbers for comparison, and the number of ants is 2, 4, 6, 8, and 12. The optimal number is determined according to its influence on algorithm performance. The final results are shown in Figure 5.

According to the information in the table, there is a negative correlation between the number of ants and the corresponding number of iterations. When the number of ants is small, the corresponding solution set is relatively small, while the number of iterations is large. If the network scale is large, the global optimal solution cannot be obtained. When the number of ants is large, the search performance is improved. However, when the network is complex, some invalid paths are easily introduced, which affects the convergence. After comprehensive consideration, the number of ants is finally set to 8.

To sum up, the number of ants  $M=8$ , pheromone heuristic factor  $\alpha=1$ , expected value heuristic factor  $\beta=2$ , and hormone volatilization coefficient  $\rho=0.3$ .

### 4.3. Optimization Results

#### 4.3.1. Comparison of Resource Utilization Rate of Controller.

The migration efficiency of the switch is directly affected by the utilization rate of the controller and can represent the load balancing degree of the controller to a certain extent. Set different load states for each controller, where 1 and 2 are overload and 3 and 4 are light load. Then send data packets to each controller to analyze the changes in resource utilization rate. It is necessary to ensure that controller resources are properly used so that the overload controller can recover.

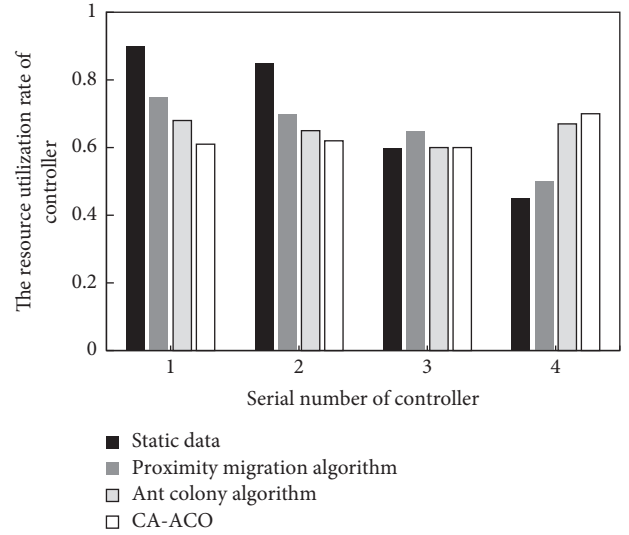


FIGURE 6: Comparison diagram of resource utilization rate.

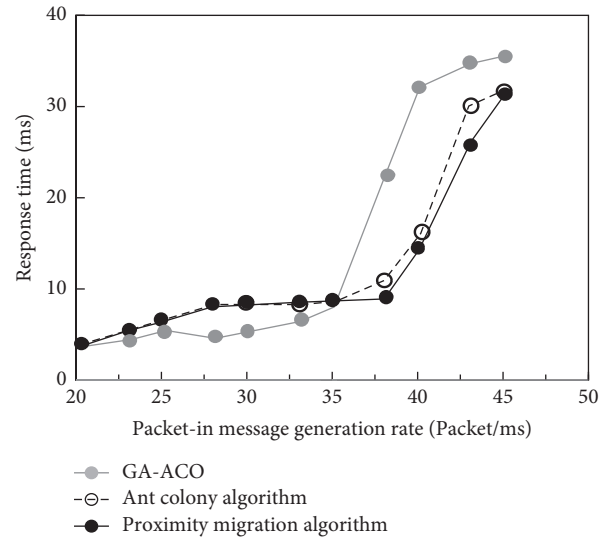


FIGURE 7: Comparison of response delay.

The calculation formula of the resource utilization rate of controller is as follows:

$$U_c = \frac{U_i}{U_{max}}, \quad (9)$$

where  $U_i$  and  $U_{max}$  need to be obtained in certain ways, among which the former is queried by the Zookeeper module and the latter is obtained based on experimental data. According to existing studies, memory resource utilization is related to many factors. Under the condition that the number of switches and network structure remain unchanged, resource loss in packet-in message processing is an important influencing factor, which is involved in the controller overload. That is, the controller occupies too many resources, affecting functions and performance and making it difficult to process requests in a timely manner. In this paper, experiments are carried out to solve this problem.

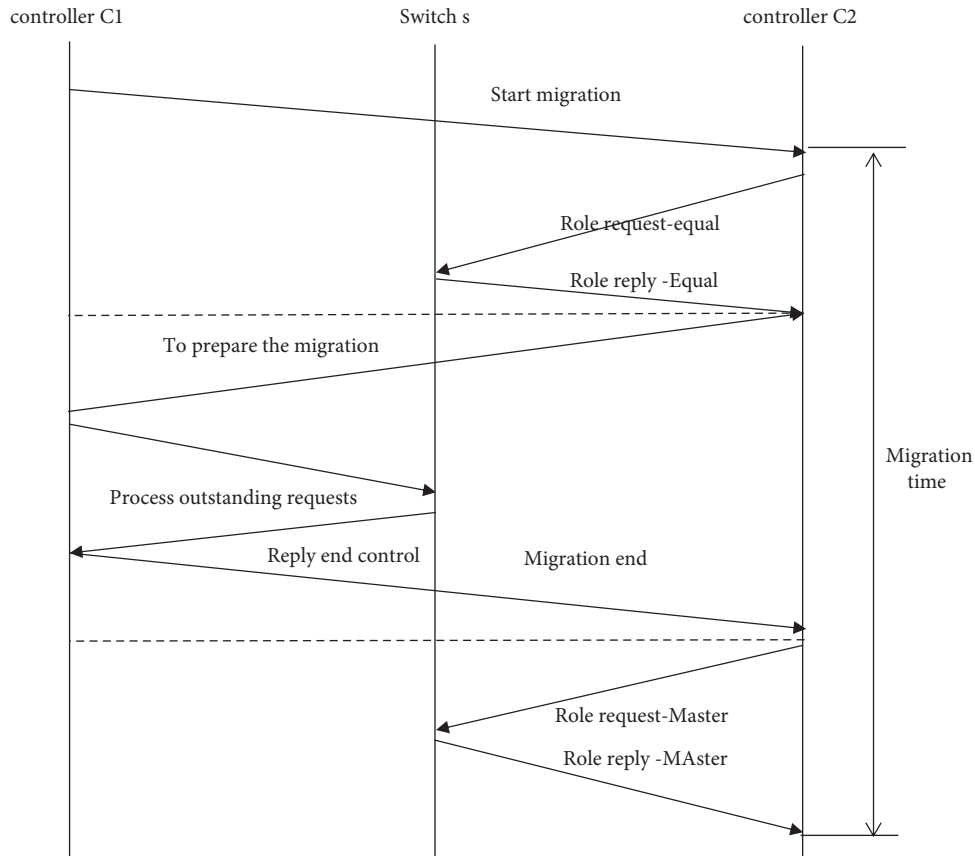


FIGURE 8: Switch migration process.

Furthermore, on the basis of improving packet-in transmission rate to simulate overload, the application effects of different migration algorithms can be analyzed. The final experimental results are shown in the following Figure 6.

It can be seen that controllers are always overloaded before the migration. There are three control strategies used to implement the migration [20–22]. And resource utilization is at a normal level to avoid overload problems. The variance of the proximity migration algorithm, ant colony algorithm, and GA-ACO algorithm are 0.0196, 0.0054, and 0.0041, respectively.

The results show that compared with the other two strategies, the proximity migration strategy has obvious disadvantages in achieving load balancing. And, after analysis, it is found that the strategy adopts the principle of proximity during migration. Although it is relatively simple and reduces the delay, it is easy to cause secondary overload. The other two algorithms can effectively avoid the above problems, and both can select the controller for migration according to the load conditions, so as to meet the requirements of load balancing.

**4.3.2. Comparison of Response Delay.** In load algorithm evaluation, the response delay index is generally used to evaluate controller performance. If the index is small, it means that high performance can be achieved. In this part, detection and analysis are carried out for this indicator, and

specifically, the Cbench tool is used to obtain the response delay according to the time difference between the sent packet-in and the received Flow-MODs.

To measure and compare the response delays of the three algorithms, set controllers 1 and 2 to be overloaded, and the rest to be a light load. A total of 50 tests are carried out, and the mean value is calculated as the final response delay to ensure the reliability of the test results. The final results are shown in Figure 7.

According to the information in the above figure, there are certain differences in the response delay of the three algorithms, among which compared with the proximity migration and ant colony algorithms, the improved ant colony algorithm is reduced by 12.5% and 1.5%, respectively. If the migration strategy is not adopted when the controller is overloaded, it is difficult for the controller to process subsequent package-in requests in a timely manner, which ultimately reduces the performance of the controller.

If the load is not large, compared with the other two algorithms, the proximity migration algorithm has the smallest response delay. After analysis, the response delay is related to the processing speed of the controller and the distance of switches. And, compared with the other two algorithms, the complexity of the proximity migration algorithm is relatively low; thus, the response delay is small.

If the load is heavy, there may be an overloading problem of multiple controllers in the network. At this time, the use of proximity is difficult to meet the requirements, which easily



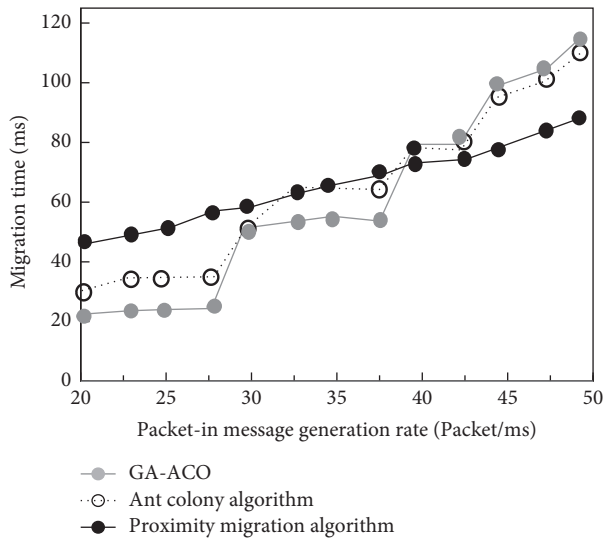


FIGURE 9: Comparison of controller migration time.

lead to an increase in a response delay. The use of the ant colony algorithm can easily lead to misjudgment of the number of overload controllers, resulting in migration redundancy problems, which will also prolong the response delay. The use of the improved ant colony algorithm has obvious advantages, which not only controls the response delay at a reasonable level but also reduces the network load and improves the rationality of controller resource utilization.

When the message generation rate exceeds 45 packet/ms, all controllers are basically in an overload state. In this case, to meet the requirements of load balancing, other controllers must be added.

**4.3.3. Comparison of Migration Time.** Migration time is an important index, which reflects the migration efficiency of the controller. In the process of migration, the controller is divided into two parts, namely the master controller and the slave controller. The former has only one controller, and the latter can have multiple controllers. The requirements of migration can be met by adjusting the master and slave controllers.

Figure 8 is the specific process of switch migration, in which the role needs to be changed to a peer role through controller C2. After the target controller C2 becomes a peer controller, it begins to receive the information sent by C1 and begins the migration process. Then C2 receives the information from S, and after C1 sends the flow table, C2 issues a request to change to the master controller and updates the distributed data. After the above operations are complete, the migration process is completed.

The time of a migration can be expressed as the time interval between two role requests: role request-Equal and role response-Master. If multiple controllers are loaded during this period, migrate multiple switches to meet load balancing requirements. In this paper, the average time in multiple migrations is calculated, and the final results are shown in Figure 9.

As can be seen from the figure, significant segmentation points appear around 35 packets/ms, which are mainly related to the load flow limitation of delay and migration time. If the load flow is small, the improved ant colony algorithm has a longer migration time than the other two algorithms. To analyze this phenomenon, the main reason is that the number of migration switches and controllers is relatively small. In addition, load balancing can be realized through simple methods such as proximity migration and so on, and the efficiency is high.

When the load is too heavy, the controller overload is more significant, resulting in more switch migrations. If only one switch is migrated each time, the migration time and communication cost will be increased. The improved ant colony algorithm can solve the above problems; thus, more switches can be migrated each time, and the convergence speed is high, which can efficiently achieve the goal of load balancing.

## 5. Conclusion

As can be seen from the above studies, the advantages of the genetic algorithm and ant colony algorithm are integrated, which improves the performance of SDN to a certain extent. It is concluded that when solving the problem that multiple controllers are overloaded simultaneously, there are obvious advantages in processing time effect and complexity. The reason for the above results is that the advantages of the ant colony algorithm and genetic algorithm in global and local optimization are fully utilized to greatly improve the efficiency of SDN load optimization so that the overall network can better handle the load, and the dual purposes of migration and load balancing between multiple controllers are finally achieved. The innovation of this research is to regard the SDN load balancing problem as a traveling salesman problem and solve it with an improved ant colony algorithm, so as to greatly optimize the SDN network load and improve the operation efficiency of the network.

## Data Availability

The experimental data used to support the findings of this study are available from the author upon request.

## Conflicts of Interest

The author declares that there are no conflicts of interest.

## References

- [1] M. Yelmo, Y. Isaias, and Alvarez-Horcajo, "EHDDP: enhanced Hybrid Domain Discovery Protocol for network topologies with both wired/wireless and SDN/non-SDN devices," *Computer Networks*, vol. 191, Article ID 107983, 2021.
- [2] N. V. N. V., "Application of SDN for secure communication in IoT environment," *Computer Communications*, vol. 151, no. C, pp. 60–65, 2020.
- [3] Z. Ma and B. Li, "A DDoS attack detection method based on SVM and K-nearest neighbour in SDN environment,"

- International Journal of Computational Science and Engineering*, vol. 23, no. 3, 2020.
- [4] X. P. Zhou, X. C. Huang, and X. F. Zhao, "Optimization of the critical slip surface of three-dimensional slope by using an improved genetic algorithm," *International Journal of Geomechanics*, vol. 20, no. 8, 04020120 pages, 2020.
  - [5] A. Hossein, H. Zaji Bonakdari, H. Z. Khameneh, and S. R. Khodashenas, "Application of optimized Artificial and Radial Basis neural networks by using modified Genetic Algorithm on discharge coefficient prediction of modified labyrinth side weir with two and four cycles," *Measurement*, vol. 152, no. C, 107291 pages, 2019.
  - [6] F. Mordecai, "Raji and Huapeng Zhao and Happy N. Monday. Fast optimization of sparse antenna array using numerical Green's function and genetic algorithm," *International Journal of Numerical Modelling: Electronic Networks, Devices and Fields*, vol. 33, no. 4, 2020.
  - [7] Y. Wang, L. Wang, X. Yan, and P. Shen, "Fuzzy immune particle swarm optimization algorithm and its application in scheduling of MVB periodic information 1," *Journal of Intelligent and Fuzzy Systems*, vol. 32, no. 6, pp. 3797–3807, 2016.
  - [8] Y. Yan, L. Zhang, and J. Gao, "Tool path planning for flank milling of non-developable ruled surface based on immune particle swarm optimization algorithm," *International Journal of Advanced Manufacturing Technology*, vol. 115, pp. 1–12, 2021.
  - [9] S. Li and X. Pan, "Adaptive management and multi-objective optimization of virtual machine in cloud computing based on particle swarm optimization," *EURASIP Journal on Wireless Communications and Networking*, vol. 2020, no. 1, pp. 3207–3211, 2020.
  - [10] Q. Feng, J. Zheng, and S. Zheng, "Optimization design of the key parameters of McPherson suspension systems using generalized multi-dimension adaptive learning particle swarm optimization," *Proceedings of the Institution of Mechanical Engineers-Part D: Journal of Automobile Engineering*, vol. 233, no. 13, pp. 3403–3423, 2019.
  - [11] M. Cheng and M. Xiang, "Application of a modified CES production function model based on improved firefly algorithm," *Journal of Industrial and Management Optimization*, vol. 16, no. 4, pp. 1571–1584, 2020.
  - [12] B. S. Oh, J. Cho, B. Choi, H. W. Choi, M. S. Kim, and G. Lee, "Application of heuristic algorithms for design optimization of industrial heat pump," *International Journal of Refrigeration*, vol. 134, pp. 1–15, 2022.
  - [13] A. Kramer, "Exact and heuristic algorithms for scheduling problems," *4Or*, vol. 18, no. 1, pp. 123–124, 2020.
  - [14] M. Saryazdi, M. Ohadi, and A. Ohadi, "Multi-objective optimization of auto-body fixture layout based on an ant colony algorithm," *Proceedings of the Institution of Mechanical Engineers - Part C: Journal of Mechanical Engineering Science*, vol. 234, no. 6, pp. 1137–1145, 2020.
  - [15] Yu Jin, X. You, and S. Liu, "Ant colony algorithm based on magnetic neighborhood and filtering recommendation," *Soft Computing*, vol. 25, pp. 1–16, 2021.
  - [16] Y. Zhou and X. Fu, "Research on the combination of improved Sobel operator and ant colony algorithm for defect detection," *MATEC Web of Conferences*, vol. 336, Article ID 01009, 2021.
  - [17] L. Zhang and Cai, "Multi-Objective optimal management of building engineering based on ant colony algorithm," *IOP Conference Series: Earth and Environmental Science*, vol. 598, no. 1, Article ID 012031, 2020.
  - [18] G. Yuan, J. Li, and H. Hua, "Image matting trimap optimization by ant colony algorithm," *Multimedia Tools and Applications*, vol. 80, no. 4, pp. 6143–6169, 2020.
  - [19] C. Gao, J. Chen, L. Zhou, Z. Lu, and Q. Qu, "Guide circle-based improved ant colony algorithm," *Journal of Physics: Conference Series*, vol. 1634, no. 1, Article ID 012057, 2020.
  - [20] M. Bai, M. Tian, and J. Bai, "Resource allocation based on chaotic ant colony algorithm in self-organizing wireless sensor network," *Journal of Physics: Conference Series*, vol. 1673, no. 1, Article ID 012027, 2020.
  - [21] L. Li, Z. Zhou, Q. Han, J. Yu, X. Lv, and S. Bi, "Application of ant colony algorithm to air route planning in helicopter submarine searching," *Journal of Physics: Conference Series*, vol. 1650, no. 3, Article ID 032004, 2020.
  - [22] L. Chen, W. Liu, and J. Zhong, "An efficient multi-objective ant colony optimization for task allocation of heterogeneous unmanned aerial vehicles," *Journal of Computational Science*, vol. 58, Article ID 101545, 2021.

## Research Article

# Innovative Collaborative Design of Ru Porcelain Shape Based on Digital Shape Technology

**Song Bin** <sup>1,2</sup>, **Md Ishak Siti Mastura** <sup>1</sup>, **Shaari Nazlina**,<sup>1</sup> **Perumal Velu**,<sup>1</sup> and **Yang Wei**<sup>2</sup>

<sup>1</sup>Universiti Putra Malaysia, Kuala Lumpur 43400, Malaysia

<sup>2</sup>Pingdingshan University, Pingdingshan 467000, Henan, China

Correspondence should be addressed to Md Ishak Siti Mastura; [ct\\_mastura@upm.edu.my](mailto:ct_mastura@upm.edu.my)

Received 24 March 2022; Revised 18 April 2022; Accepted 26 May 2022; Published 9 July 2022

Academic Editor: Man Fai Leung

Copyright © 2022 Song Bin et al. This is an open access article distributed under the Creative Commons Attribution License, which permits unrestricted use, distribution, and reproduction in any medium, provided the original work is properly cited.

Under the background of digital technology, computer-aided design is still in the initial stage of application in the field of design and manufacture of ceramic products. In order to improve the informatization degree of ceramic industry, advance the efficiency of product design, and satisfy the demand of personalized customization, in this paper, Ru porcelain is selected as the research object, and according to its shape characteristics, based on the 3D evolution of data combined with the image shape method and entity design, the design process of Ru porcelain shape was put forward, and the collaborative design of Ru porcelain was implemented with Yuhu spring bottle as the representative. The simulation results show that the model is highly practical and helpful to realize the convenient design of ceramic products.

## 1. Introduction

Innovative design of daily-use ceramics is a process of creative labor and a systematic project. Faced with the existing achievements and the ever-changing consumer demand and aesthetic demand of the public, numerous ground work has been completed by designers, including early market research, design positioning, and new product testing. As an important component of products, sculpt plays the role of transmitting information between products and consumers, designers and consumers, which can show certain personality characteristics in combination with consumers' cognition [1, 2]. Function is the decisive factor of daily ceramic shape, and it is the purpose of daily ceramic shape. The function of daily-use ceramic is realized through shape, so its shape design occupies a dominant position in the whole design process. With the increasing demands of consumers on the function and aesthetics of daily-use ceramics, designers pay more attention to its design.

Due to the lack of innovation in ceramic design, it is losing its attraction, and because of the complexity of ceramic technology's own manufacturing process and the combination of various techniques, in pattern design,

colorful patterns require craftsmen to have enough patience and aesthetic capability. In addition, the ceramic industry is fragmented without satisfactory ecology and system model. It is mainly based on traditional small workshops, which leads to the stereotyped shapes and patterns in the ceramic market. At the same time, because of its small scale, they are unable to introduce more advanced technologies and feed them back into ceramic production, which leads to a further decline in the competitiveness and attraction of ceramics [3–5].

In recent years, the application of computer-aided technology in product design has stimulated the collision of diversified design thinking, touched new design pain points and design ideas, and became a new pattern, which breaks the limitations of traditional design patterns and effectively discovers new design opportunities. However, in the field of ceramic product design, it still relies on traditional manual work, which is cumbersome and inefficient, and it has been difficult to meet customers' aesthetic demand for ceramic ware shape and the development demand of large-scale personalized customization [6, 7]. Therefore, it is imperative to combine computer aesthetics with product design by applying 3D parametric technology in design and creation of



FIGURE 1: Shape of Ru porcelain: (a) plum bottle; (b) Yuhu spring bottle.

ceramic product. In this paper, Ru porcelain, an excellent porcelain in celadon series, is selected as the research object, and its shape design under the background of digital technology is studied.

## 2. Basis of Product Design of Ru Porcelain

Ru porcelain was attractive with its unique glaze color and flourished in the Song Dynasty. “Ru” refers to the geographical location of the Tang and Song dynasties as the “Ruzhou.” Ru porcelain is an excellent porcelain in celadon series, and its glaze color is just like “after a storm, the sky is clear and the clouds are broken,” where the glaze shows small pieces of cicada pattern [8, 9].

### 2.1. Artistic Features of Ru Porcelain

**2.1.1. Shape Characteristics.** The shape design of ceramics needs to meet its practical use needs. On this basis, the artistic elements of shape beauty and style are integrated into it, so that the function, form, and style form a unified whole. Seeking beauty from nature, an elegant and quiet aesthetic concept is shown through linear and three-dimensional structure. The shape of Ru kiln in Northern Song Dynasty has the regularity of formal beauty to a certain extent [10, 11]. Through various geometric structures, people in Song Dynasty advocated roundness at that time. This was because many objects that people saw in nature at that time were round, and they showed this emotion through ceramic shape, which is also the most practical in terms of firing process and use function. The most typical ceramic shape of Ru kiln is bottles, which is related to the culture and times at that time [12]. As shown in Figure 1, plum bottles and Yuhu spring bottles are porcelain used to hold wine. Because of different uses, there are great differences in design. The

mouth of Yuhu spring bottle is curled outside, the neck is easy to grasp, and the center of gravity is below the abdomen after drinking, which is a kind of bottle that is convenient for scalding and drinking, while plum bottles have short mouth, abundant shoulders, and astringent abdomen.

Before the Tang and Song Dynasties, the overall design of shape was mainly based on demand of usage, followed by aesthetics. Since the Song Dynasty, aesthetic needs have been brought to the forefront of design. The literati sentiment and simple aesthetic style of the Song Dynasty led to the trend of the overall design, which pursues the flowing texture of lines.

**2.1.2. Cultural Heritage.** The celadon produced by Ru kiln not only meets the requirements of people’s life but also pursues aesthetics, which integrates the culture and customs of the Song Dynasty into creation of Ru porcelain. Different from the rough and majestic style of the Han Dynasty, the ornate and complicated decoration of the Tang Dynasty, the aesthetic style of the Song Dynasty pursued a simple and tranquil artistic style, whose aesthetic of purity and inaction had a profound influence on the aesthetic thought at that time [13, 14]. Song Huizong liked to drink tea and believe in Taoism, which also had a great influence on the aesthetic development of that time. Ru porcelain modeling is simple, in the process of high-temperature firing, the use of the different shrinkage coefficient between the glaze, the formation of cracks of different sizes on the glaze for natural decoration, as ice cracks in general, usually known as “ice cracks.” This kind of crack is naturally produced, and it is not intentional or intentional by craftsmen. This natural decoration perfectly fits the aesthetic concept of ancient China.

**2.2. 3D Evolution Algorithm.** One of the main forms of digital technology is image 3D reconstruction. Stereo vision performance by 3D evolution algorithm, the realization of

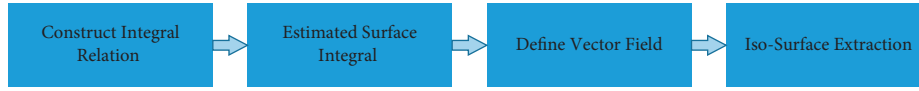


FIGURE 2: The flow of the 3D evolution algorithm for Ru porcelain.

the stereo vision three-dimensional evolution process is stereo image matching and the label calibration process, each label corresponding to pixels of parallax in Markov random field is including three collections: network node set  $L$ , neighboring relations system set (N), and collection of random variables (F). Among them, the set of sampling points is the set of network nodes, the set of connection relation between nodes is the set of adjacent relation system, and the set of possible values of a node element is the set of random variables.

Defining energy function is to transform matching problem into energy function problem. Therefore, stereo matching can be described as the energy function minimization problem. The matching algorithm can specify a label value for each pixel point. The operation is to find the appropriate label among all possible labels and quantify the label as an energy function. In the case of stereo matching, the label is parallax, reaching a set of parallax function values that minimize the energy function. The essence of stereo matching is to obtain the parallax value and parallax relation between pixels of different images. Therefore, the image segmentation stereo matching algorithm is divided into the following steps: composition  $\rightarrow$  edge sorting  $\rightarrow$  initialization  $\rightarrow$  merging image regions  $\rightarrow$  iterative output. Image segmentation through the above steps basically reflects the structure of the real scene, where the connection between images is a deep discontinuous area.

It is pointed out in the literature [15] that the integration of digital interactive technology into ceramic product design conforms to the requirements of The Times. Therefore, this paper proposes the modeling design of ceramic products based on 3D evolution algorithm of digital interactive image. The image based on this algorithm uses the implicit fitting Poisson 3D reconstruction algorithm, uses the indicator function to extract the isosurface and generate the triangulated surface prediction function, and uses the relationship between the constructed vector domain and the indicator function to realize the Poisson reconstruction, and completes the 3D modeling design of ceramic products through the above steps [16, 17].

According to the characteristics of ceramic products, the image modeling method is combined with solid design, and the design process is realized by data interaction and 3D evolution. Therefore, the Poisson reconstruction algorithm is proposed, which is a global solution. It adopts the sample points after the image segmentation in the previous section and does not need to be resegmented or fused. The reconstruction method limits the implicit function gradient at all spatial points with few errors [18]. The flow of the 3D evolution algorithm for Ru porcelain is shown in Figure 2.

Set the input data  $S$  as the set of sampling points  $s$ . Any sampling point includes two properties: position  $s$ .  $p$  and

normal  $s.\bar{N}$ . The sampling point is the point or approach point of the surface  $\partial M$  of the mold  $M$ . The Poisson reconstruction is to extract the isosurface from the estimation model and present a closed triangulated surface prediction function by using the indicator function of the estimation model.

**2.2.1. Construct the Integral Relation.** Firstly, the integral relationship between the indicator function gradient and the construction vector domain is expressed, and the surface integral, that is, the gradient domain is summed and estimated by the point set. Then, the gradient domain is used to calculate the exponential function.

Set a ceramic with a surface estimated as  $\partial M$  surface, set  $\chi_M$  to represent the indicator function of  $M$ , the inner surface normal is represented by  $\bar{N}_{\partial M}(p)$ , and the point  $p \in \partial M$ ,  $\bar{F}(q)$  represents the smooth filter.  $\bar{F}_p(q) = \bar{F}(p - q)$  represents the transformation of point  $p$ , and the normal vector domain of the surface after the smoothing is equal to the surface after the slide; therefore,

$$\nabla(\chi_M * \bar{F})(q_0) = \int_{\partial M} \bar{F}_p(q_0) \bar{N}_{\partial M}(p) dp. \quad (1)$$

Among them,  $\bar{F}$  represents a universal smoothing filter;  $q_0$  represents the smoothed sampling point; and  $\bar{F}_p(q_0)$  is the transformation of smooth filter at the sampling point  $p$ .

**2.2.2. Estimate Surface Integral.** According to the surface geometry information, the surface integrals are estimated by using point sets in the model.  $\partial M$  is segmented into the independent plane set  $\{p_s \subset \partial M\}$  by point set  $S$ , and the integral on the independent plane  $p_s$  is predicted by the position  $s$ .  $p$  of the sampling point set, and  $p_s$  region determines the sampling point set region; therefore,

$$\begin{aligned} \nabla(\chi_M * \bar{F})(q) &= \sum_{s \in S} \int_{p_s} \bar{F}_p(q) \bar{N}_{\partial M}(p) dp = \\ & \sum_{s \in S} |p_s| \bar{F}_{s,p}(q) s.\bar{N} = \bar{V}(q). \end{aligned} \quad (2)$$

In formula (2),  $\bar{F}_{s,p}(q)$  express  $\bar{F}(q)$  transform of sampling point position  $s$ .  $p$  by smoothing filter;  $\bar{V}(\cdot)$  represents the vector field.

$\bar{F}_{s,p}(q)$  is the transform of  $\bar{F}(q)$  smooth filter at the sampling point  $s$ .  $p$ , and  $\bar{V}(\cdot)$  represents the vector domain of construction.

**2.2.3. Define Vector Field.** In order to solve the indicator function accurately, it is necessary to define the vector field, which can transform the sampling point into its

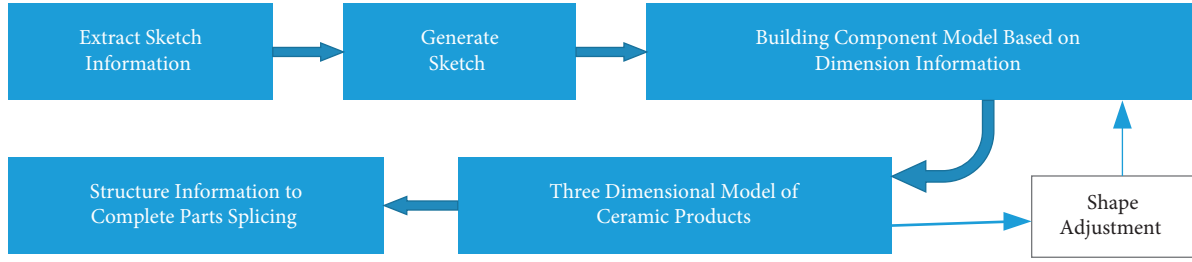


FIGURE 3: Product design of Ru porcelain.

corresponding node center, and classify the sampling points on eight nearest neighboring nodes by using three-line interpolation, and then the indicator function gradient field can be described as

$$\bar{V}(q) = \sum_{s \in S} \sum_{N_{o,ggB}(s)} \alpha_{o,s} F_o(q) s \cdot \bar{N}, \quad (3)$$

where  $o$  represents the node corresponding to the sampling point; the node with the nearest depth  $D$  from the sampling point  $s$ .  $P$  is represented by  $N_{gbrD}(s)$ , and  $\alpha_{o,s}$  represents the trilinear interpolation weights. The underlying function of node  $o$  is expressed by  $F_o$ .

**2.2.4. Extract Isosurface.** To obtain the reconstructed surface  $\partial M$ , the isosurface is extracted by selecting the appropriate exponential function value, which should meet the requirement that the sampling point set is distributed near the isosurface as much as possible. The indicator function  $\chi_M$  was estimated according to the sampling point set, and the mean value was used for isosurface extraction; therefore,

$$\begin{aligned} \partial M &\equiv [q \in R^3 | \chi(q) = \gamma], \\ \gamma &= \frac{1}{|S|} \sum_{s \in S} \chi(s, q), \end{aligned} \quad (4)$$

where  $R$  represents the set of functions of sampling point set acquired by scaling or transformation;  $\chi(q)$  is the indicator function of sample point  $q$ .  $\gamma$  represents constant;  $\chi(s, q)$  indicates the location of sampling points.

Assuming that the sampling point set is distributed on the surface of the model, the vector domain is constructed, expressed by the function in space, and then the surface estimation of the isosurface is obtained from the generated indicator function, and the 3D modeling design of ceramic products is realized by the above digital interactive 3D evolution algorithm.

### 3. Collaborative Product Design of Ru Porcelain

In this paper, the Yuhu spring bottle is designed as the representative, which is a shape with curled mouth, thin neck, drooping belly and round feet, and a soft curve as the contour line. Its basic shape is composed of two symmetrical S-shaped curves on the left and right, with graceful and soft lines with a kind of oriental feminine softness, reflecting the

oriental aesthetic of porcelain [19]. In this paper, the generation of 3D Yuhu spring bottle model is shown in Figure 3. The feature information of product sketch pixel was extracted, the model components were constructed by parametric pixel method, and the model was constructed by geometric rotation stitching. To generate the model, global shape and local shape of products are converted into parameter requirements, and graphic element shape changes accordingly. At the same time, the linear model of 3D model is manually adjusted to realize rapid shape and collaborative change of the 3D ceramic model.

**3.1. Simulation of 2D Image.** Parameterized design means that when the dimension parameters of a certain part of the graphic element are changed or the defined part parameters are modified, the system automatically completes the change of the graphic related parts to realize the graphic driving [20]. It connects the shapes, features, and functions of products through constraints, which constrains the size and geometric structure of graphic elements, and combines them into design drawings. The parameterized design methods include parameterized pel and parameterized modification engine [21]. Parameterized pel controls the geometry and features of the underlying controls of the model through input data, and parameterized modification engine controls the correlation between each module. With the help of parameterization, the sketch is divided into  $n$  components, which are defined as  $\{Pi\}$ , and the parameter information of basic geometric primitives is extracted and given different descriptions, which is shown in Figure 4.

Pels are the basic elements of 3D entities. All pels can be decomposed into four basic elements: point, line, arc, and circle [22], as shown in Figure 5.

The parametric curve  $SpL = \{Sp, L\}$  consists of a series of three-dimensional curve control points  $Sp = \{Sp_i\}$  and discrete line segment control points  $L = \{Lp_i\}$ . A set of spatial closed plane domains  $G = \{A_r, C, P_o, R_p\}$  is defined. The closed plane domain includes a circle  $C = (Cp_0, Cp_1)$  controlled by the center and a point on the circumference, and an ellipse  $A_r = (Ap_0, Ap_1)$  controlled by the corner points on the center and the surrounding rectangle.

$D$  is defined as position stitching constraint,  $D = \{D_i | i = 0, 1, \dots, 3(n-1)\}$ ,  $n$  is the number of parts in the sketch, and  $D_i$  realizes position stitching between parts.  $H$  is the hollow-out constraint,  $\alpha$  is the hollow-out rate,  $M$  is the collision stitching constraint,  $M = \{(p, M_c) | p = 1, 2$

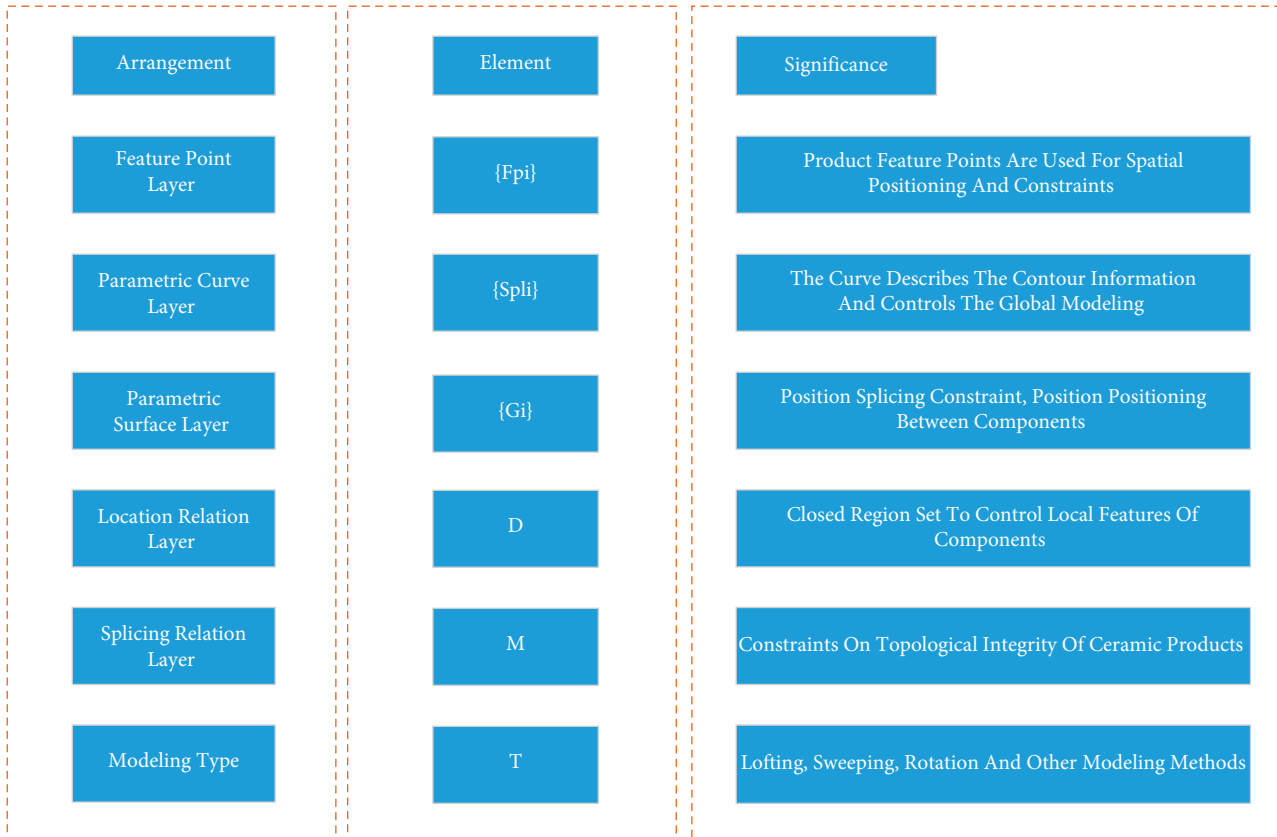


FIGURE 4: Parametric simulation of 2D image.

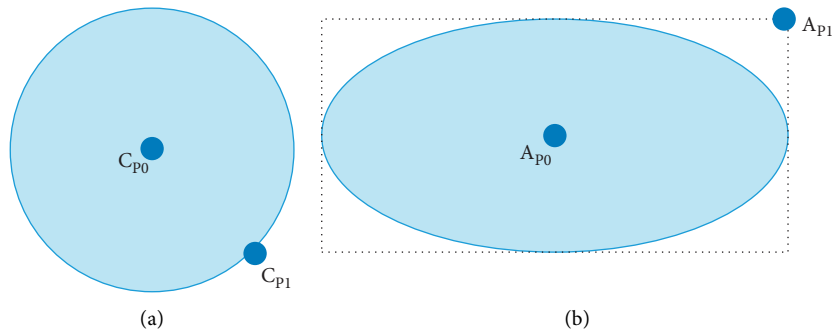


FIGURE 5: Definition of primitive parameters: (a) parametric circle C; (b) parametric ellipse A<sub>r</sub>.

$\dots, n\}$ ,  $p$  is the component identification, and  $(p, M_c)$  defines the type of stitching between component  $p$  and the stitching body as  $M_c$ . According to the above description, the parameterized expression of ceramic products is

$$Z = (\{P_i \mid i = 0, 1, \dots, n\}, D, M, \alpha) P_i = (G, Sp, T, H). \quad (5)$$

**3.2. Assembly Simulation of Each Component.** The construction of 3D model makes the effect of product design closer to reality and displays it in the most intuitive way. The complete 3D entity has a complex structure, which can

be divided into several components, modeled separately and then spliced and merged. As shown in Figure 6, ceramic products are divided into multiple components, and each product component is generated in three dimensions, and a complete 3D model is generated by geometric splicing and merging of components and modeling adjustment.

The splicing of product shall be carried out within the same size to show that they are the main body, and the splicing display parts shall perform uniform size operation. The distance formula  $\text{dis}(p_1, p_2)$  and the scale factor  $d$  are defined as follows:

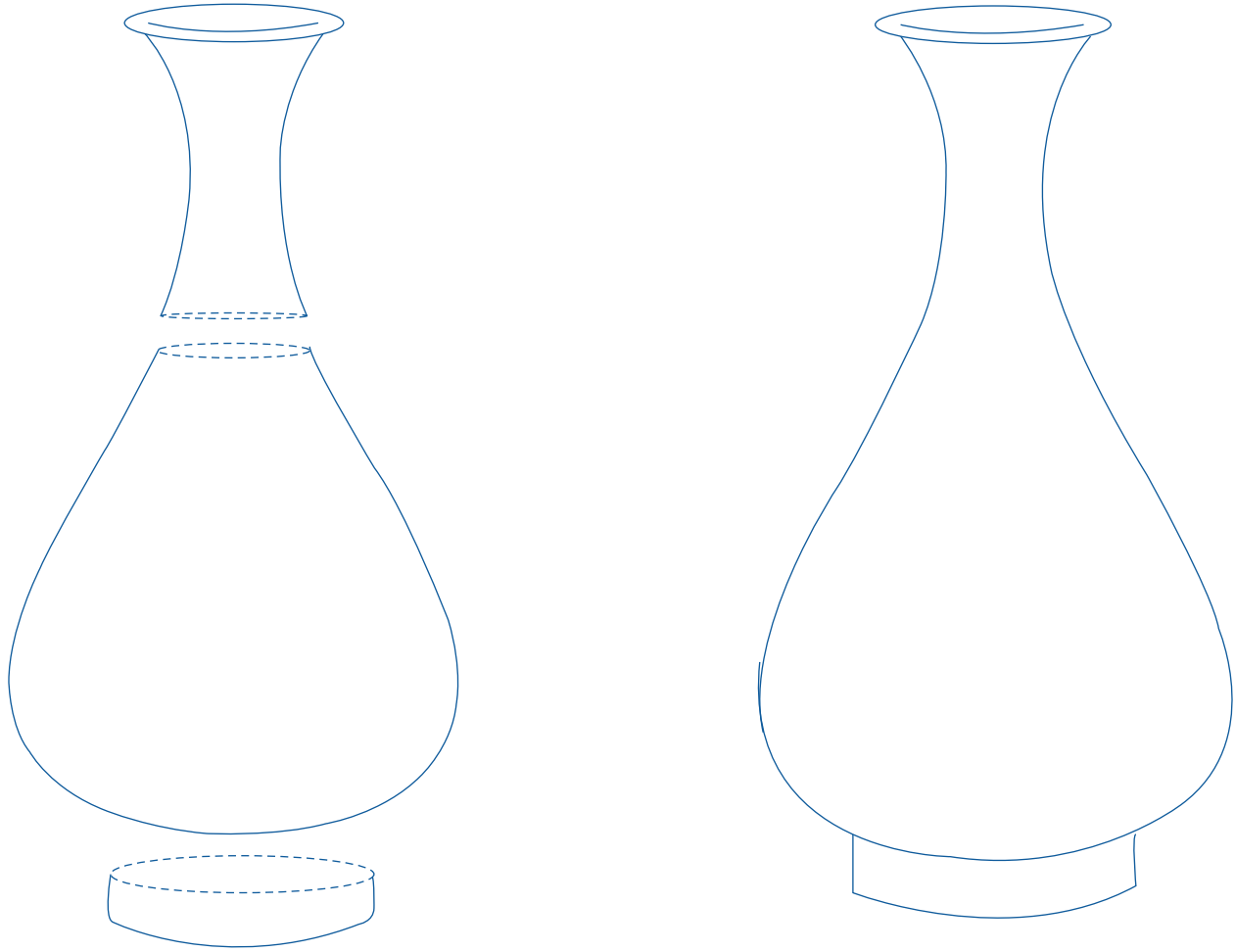


FIGURE 6: Combination of components of Yuhu spring bottle.

$$\text{dis}(p_1, p_2) = \sqrt{(p_1 \cdot x - p_2 \cdot x)^2 + (p_1 \cdot y - p_2 \cdot y)^2 + (p_1 \cdot z - p_2 \cdot z)^2}, \quad (6)$$

$$d = \frac{h_2}{h_1} = \frac{\text{dis}(D_{11}, D_{12})}{\text{dis}(D_{21}, D_{22})}. \quad (7)$$

As shown in Figure 6, the identification of feature points is transformed in the 2D image, where  $D_0$  is the coordinate of the center point of the nozzle section in the sketch, and  $D_1$ ,  $D_2$  are the coordinate of the characteristic point at the joint of two parts in the sketch; in the entity to be spliced,  $D_{01}$ ,  $D_{11}$ , and  $D_{21}$  are the feature points corresponding to the sketch in the entity part; in the entity of body part,  $D_{02}$  is the corresponding position of the center to be splice, and  $D_{12}$ ,  $D_{22}$  are the corresponding feature point in the body entity of bottle.

By defining the connection and inclusion relationship between components, the components are spliced and merged to generate the 3D entity. The stitching of ceramic

parts contains the constraints of position stitching, when the modeling of different parts is merged into the same entity, it needs to be transformed into the same modeling space in position, and the transformation process involves the size change, position conversion, and rotation operation of parts. The stitch of pot is taken as an example to give the operation process, as shown in Figure 7.

In order to realize the stitch of entity, coordinate  $D_{02}$  needs to be solved according to two-position image information, and the solving process is as follows:

$$g_1 = \frac{\text{dis}(D_{12}, D_{22})}{\text{dis}(D_1, D_2)}. \quad (8)$$

$$D_{02} = D_{12} - g_1 \times (D_1 - D_0). \quad (9)$$

Given three points  $D_{01}$ ,  $D_{11}$ ,  $D_{21}$  and corresponding coordinate points  $D_{02}$ ,  $D_{12}$ ,  $D_{22}$  after transformation,  $R$ ,  $T$



can be solved, and then the transformation matrix of pot is

$$R_\varphi = \begin{bmatrix} R & T \\ 0 & 1 \end{bmatrix}.$$

Assuming that the corresponding three points after the transformation of  $R$  are  $3 \times 3$  matrix  $T$  are  $3 \times 1$  matrix sequence,  $B = R \times A + T$ . The transformation matrix can be obtained by solving

$$\begin{cases} \mu_A = \frac{1}{N} \sum_{i=1}^N D_{A_i} \\ \mu_B = \frac{1}{N} \sum_{i=1}^N D_{B_i} \\ \begin{cases} A'_i = \{D_{A_i} - \mu_A\} \\ B'_i = \{D_{B_i} - \mu_B\} \end{cases} \end{cases} \quad (10)$$

$$H = \sum_{i=1}^N A'_i B_i'^T = \sum_{i=1}^N (D_{A_i} - \mu_A)(D_{B_i} - \mu_B)^T$$

$$[U, S, V] = \text{SVD}(H)$$

$$R = VU^T$$

$$T = -R \times \mu_A + \mu_B.$$

According to equation (10), the transformation matrix

$$\begin{bmatrix} R & T \\ 0 & 1 \end{bmatrix}$$

is obtained to realize position stitching.

**3.3. Assembly Optimization of Ceramic Parts.** The position constraint realizes the seamless stitching between ceramic parts, and the Boolean operation between parts completes the processing of the overlap area between parts in the stitching process. To perform Boolean operations on product parts, two parts need to intersect, and there is a common area.  $M \in \{M_0, M_1\}$ , where  $M_0$  represents adjacency and merge and  $M_0$  removes the intersection and merge. Using Boolean operation, adjacency merges two parts of geometry space, removing the intersection and merge means remove two common parts and then execute operation of merge. Meanwhile, for a single component,  $H \in \{0,1\}$  can be defined to perform the hollow operation of the component entity, where  $\alpha$  is the hollow coefficient. The optimization process is calculated by the following formulas:

$$S = \begin{cases} S & H = 0 \\ S \times (1 - \alpha) & H = 1 \end{cases} \quad (11)$$

$$S_i = \begin{cases} S_i \cup S_{i+1} & M = M_0 \\ S_{i+1} \cup (S_i - S_i \cap S_{i+1}) & M = M_1 \end{cases} \quad (12)$$

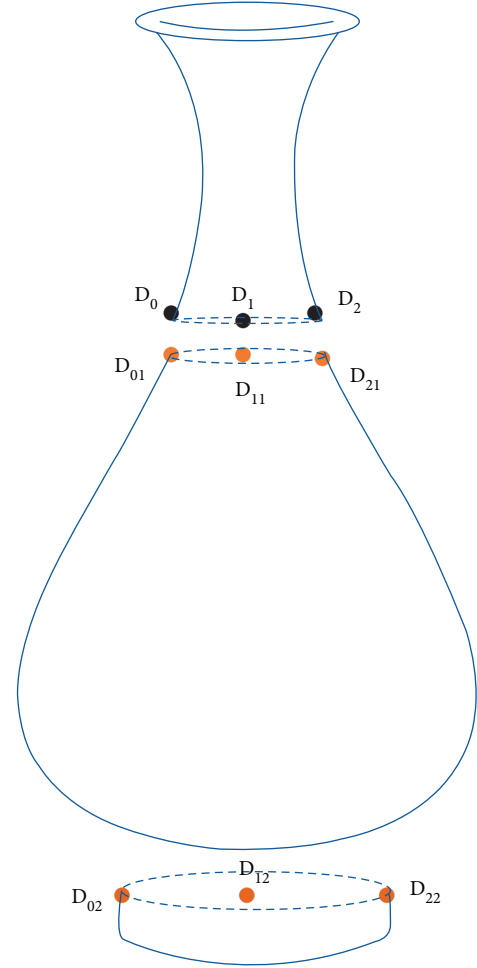


FIGURE 7: The stitch of pot.

$$S_i(m) = \begin{bmatrix} m_x & 0 & 0 \\ 0 & m_y & 0 \\ 0 & 0 & m_z \end{bmatrix}, \quad (13)$$

where  $S_i$  controls position adjustment, allowing the model components to rotate as required. The scale adjustment is shown in formula (13), and the global variable  $m = (m_x, m_y, m_z)$  is defined as the size variable constraint, and  $m_x, m_y, m_z$  are the scaling proportion of components in X, Y, and Z axes. Users perform global adjustments to each component or entity, including scaling and positioning. Proportional adjustment supports horizontal, vertical, and all-round size of the product proportional transformation, only changes the size of the shape without changing the shape of the shape.

**3.4. Process of Collaborative Design.** Based on the user experience, collaborative design aims to design products that meet the user's needs, which are convenient and efficient to use. It allows users to learn better, complete tasks faster, and satisfy the unique experience of them in the process of experience. In addition, users are no longer inclined to the invariable design of ceramic products aesthetic, but more



FIGURE 8: Simulation of Ru porcelain characteristic.

inclined to diversified, special-shaped product design. Parametric 3D model generation, which can quickly generate 3D model with input of feature point, is suitable for mass production but not for personalized customization by users. Therefore, the shape design method of collaborative ceramic product is introduced to personalize the products in fixed mode, so as to realize the interaction between people and products with convenient operation and excellent real-time effect [23]. The collaborative design in Ru porcelain makes it difficult to adjust the shape of the generated 3D models. Therefore, this paper draws a 3D linear model to describe the outline information and cross section feature information of the model. According to the user's own requirements, manually stretch and drag the position of each feature point on each line and section of the linear model to realize the change of sketch outline and section shape, and constrain the corresponding primitives in the 3D model entity to realize the 3D model reconstruction. According to the change effect, users can further adjust to realize real-time collaborative design of products. The shape of the generated 3D model can be further adjusted, where online space mouse manually changes the position of contour curve and the size of primitive, and realizes the shape change of Ru porcelain.

#### 4. Analysis of Simulation Results

The effective application of digital technology improves the level of product design. In order to verify the feasibility of the algorithm in this paper, the following simulation experiments are carried out. Based on the image feature of Ru porcelain as the basis of 3D product design, the shape design of ceramic products is carried out by using the Poisson reconstruction algorithm and subdivision surface reconstruction algorithm. Four groups of image feature data of Ru porcelain are shown in Figure 8.

Compare the design time and effect differences of each group among Ru porcelain products. The specific data are shown in Tables 1 and 2.

Table 1 shows the statistical data of shape design of ceramic products using the Poisson reconstruction algorithm, and Table 2 adopts the subdivision surface reconstruction algorithm. From the perspective of shape design time in Table 1, the subdivision surface reconstruction algorithm takes more than 60 minutes for shape design of Ru porcelain, and the maximum time has reached 80 minutes, which shows that the design efficiency by this algorithm is low. However, the algorithm in this paper takes less time for shape design of Ru porcelain, which is basically around

TABLE 1: 3D design effect of Ru porcelain products.

| Group | Design time/min | Output clarity/% |
|-------|-----------------|------------------|
| 1     | 20.5            | 99.34            |
| 2     | 19.5            | 98.23            |
| 3     | 20.0            | 97.98            |
| 4     | 22.5            | 93.82            |

TABLE 2: Subdivision surface effect of Ru porcelain products.

| Group | Design time/min | Output clarity/% |
|-------|-----------------|------------------|
| 1     | 70.5            | 47.34            |
| 2     | 79.5            | 54.26            |
| 3     | 80.0            | 48.89            |
| 4     | 72.5            | 43.28            |

16 min, indicating that the algorithm in this paper is efficient. Moreover, from the output effect of Ru porcelain, the clarity of shape output in this paper is over 95%, while that of subdivision surface reconstruction algorithm is less than 50%. Therefore, comparing the two algorithms, the performance of the algorithm in this paper is better.

The method has real-time interactivity and adjustability of the model, which meets the personalized design requirements, allows users to quickly complete the 3D model construction of ceramic products under a fixed model, simultaneously meets the user's requirements for the change of the width-height ratio and the shape of each component, and greatly improves the efficiency and convenience of design. In addition, it has practical significance for professional and nonprofessional people to design the appearance of Ru porcelain, which provides great convenience and portability for ceramic product design.

#### 5. Conclusion

By applying 3D parametric technology to the design and creation of ceramic, the combination of computer aesthetics and product design is helpful to stimulate the collision of diversified design ideas and trigger a brand-new design mode of ceramic. In this paper, Ru porcelain, an excellent porcelain in celadon series, is selected as the research object. According to its artistic characteristics and cultural heritage, innovative collaborative design based on 3D evolution was carried out for its shape. The simulation results show that the clarity of Ru porcelain designed by the algorithm in this paper is more than 95%, and the design time is less than 20 min, which greatly improves the efficiency and

convenience of design, and is of practical significance to professional and nonprofessional shape design, thus providing great convenience and portability for design of Ru porcelain.

### Data Availability

The data used to support the findings of this study are available from the corresponding author upon request.

### Conflicts of Interest

The authors declare that there are no conflicts of interest.

### Acknowledgments

This work was supported by (1) Horizontal Fund Project of Pingdingshan University, “Development of Ru porcelain new technology,” the project number is PHY-HX-202185; (2) supported by Henan Lushan Flower Porcelain Engineering Technology Research Center, the project number is ZYGTCXW2018-01, and (3) supported by Development of new ceramic technology for daily use, the project number is PXY-HX-2022013.

### References

- [1] J. Su, P. Wang, S. Zhang, A. S. Zhao, and A. M. Zhou, “Research progress of key technologies of product image shape design,” *Mechanical Design*, vol. 30, no. 01, pp. 97–100, 2013.
- [2] J. Sun, “Daily ceramic design based on emotional appeal,” *China Ceramic Industry*, vol. 19, no. 05, pp. 39–41, 2012.
- [3] aihong Wang and H. Chen, “Development trend of daily ceramic products design in information time,” *Packaging Engineering*, vol. 34, no. 22, p. 89–92, 2013.
- [4] C. Peng, “Humanized design process and analysis of household ceramics,” *China Ceramics*, vol. 47, no. 11, pp. 46-47+56, 2011.
- [5] Y. Li and L. Zhu, “Research on product design method based on Kansei Engineering,” *Packaging Engineering*, vol. 29, no. 11, pp. 112–114, 2008.
- [6] W. Lin, “Design of daily-use ceramics based on Perceptual Engineering,” *China Ceramics*, vol. 47, no. 08, pp. 39-40+49, 2011, (in Chinese ).
- [7] L. Huang and Z. Wang, “Research on the method of product experience design,” *Packaging Engineering*, vol. 34, no. 6, p. 64–67, 2013.
- [8] J. Cheng, *Chinese Ceramic Aesthetics*, Gansu People’s Fine Arts Publishing House, 2007.
- [9] G. Wang, “Viewing Ru kiln from the official handicraft system,” *Journal of Palace Museum*, 2002.
- [10] J. Huang, “Research on the development of cultural industry in Ru porcelain,” *Ruzhou [J]. Art Guide*, no. 09, pp. 12-13, 2018.
- [11] J. Zhu, “Ru porcelain: past lives of millennium brand — design culture of Ru porcelain in northern Song dynasty and development characteristics of contemporary Ru porcelain industry,” *Corporate Culture*, no. 10, pp. 78-79, 2019.
- [12] P. Zhu, “Research on the inheritance and innovation of traditional cultural industry in the Internet age — taking Ru Porcelain as an example,” *Journal of Hebei Youth Management Cadre College*, vol. 31, no. 03, pp. 102–109, 2019.
- [13] Z. Wu, *Research on the Design Culture of Ru Porcelain in Northern Song Dynasty and the Development of Contemporary Ru Porcelain Industry*. Xi’an, Shaanxi University of Science and Technology, 2017.
- [14] Z. Wu and Z. Liu, “Research on the design culture of Ru porcelain in northern Song dynasty and the development of contemporary Ru porcelain [J],” *Tomorrow Fashion*, no. 04, p. 49+94, 2017.
- [15] J. Zych, J. Kolczyk, and Ł. Jamrozowicz, “The influence of the shape of wax pattern on the kinetics of drying of ceramic moulds,” *Metalurgija*, vol. 54, no. 1, pp. 15–18, 2015.
- [16] X. Dandan, G. Shengguo, and Y. Zhixiao, “Three dimensional modeling and simulation analysis for multi-angle image of huge buildings,” *Computer Simulation*, vol. 32, no. 11, p. 255, 2015.
- [17] yongqiang Wang and qingli Li, “Defect image recognition of sanitary ceramics based on color features,” *Computer Systems & Applications*, vol. 24, no. 6, pp. 258–261, 2015.
- [18] Y. Wu, Yu Cheng, Y. Bai et al., “Structure and parameters research for the machine of molding heterotype ceramic products,” *Machine Design And Manufacturing Engineering*, vol. 45, no. 5, pp. 81–84, 2016.
- [19] Hailin, *Ru Porcelain Research Based on Redesign Concept*, South China University of Technology, Guangzhou, 2015.
- [20] A. Coates, H. Lee, and A. Y. Ng, “An analysis of single-layer networks in unsupervised feature learning[C]//Proceedings of the 14th International Conference on Artificial Intelligence and Statistics,” *JMLR*, pp. 215–223, 2011.
- [21] K. He, X. Zhang, S. Q. Ren, and J. Sun, “Deep Residual Learning for Image recognition,” in *Proceedings of the IEEE Conference on Computer Vision and Pattern Recognition*, pp. 770–778, Las Vegas, NV, USA, October 2016.
- [22] J. Mairal, P. Koniusz, Z. Harchaoui, and C. Schmid, “Convolutional Kernel networks,” 2014, <https://arxiv.org/abs/1406.3332>.
- [23] L. Yang, “Research on application of AutoCAD in three-view drawings for ceramic product design,” *Modern Electronics Technique*, vol. 38, no. 17, p. 135–138, 2015.

## Research Article

# Texture Feature Extraction and Morphological Analysis of Landslide Based on Image Edge Detection

Feng Wang,<sup>1,2</sup> E. Wu,<sup>1</sup> Siyan Chen,<sup>1,3</sup> and Hao Wu <sup>1,2,4</sup>

<sup>1</sup>Sichuan Huadi Building Engineering Co. Ltd., Chengdu 610081, China

<sup>2</sup>Chengdu University of Technology, Chengdu 610059, China

<sup>3</sup>The Engineering & Technical College of Chengdu University of Technology, Leshan 614000, China

<sup>4</sup>School of Geographic Science and Remote Sensing, Guangzhou University, Guangzhou 510006, China

Correspondence should be addressed to Hao Wu; 1819400072@e.gzhu.edu.cn

Received 30 March 2022; Revised 30 May 2022; Accepted 7 June 2022; Published 7 July 2022

Academic Editor: Man Fai Leung

Copyright © 2022 Feng Wang et al. This is an open access article distributed under the Creative Commons Attribution License, which permits unrestricted use, distribution, and reproduction in any medium, provided the original work is properly cited.

Landslides in nature are harmful to economic development and people's lives and cause irreparable losses to the environment. With the application of image detection technology and intelligent algorithm, a new way for landslide detection is proposed to achieve effective detection and identification of hazards. This paper takes the landslide as the data set, carries on the noise reduction, the image expansion, and the image segmentation processing to the image, and extracts the object region information. The quantitative description of the azimuth displacement and displacement change of the crack curve is completed in this paper. This method is suitable for 3D simulation model, sand and stone model, soil model, and the sliding test results of Panzhihua Flight Field, which proves that the design method is effective. Experiments show that when sliding occurs, the texture and color become chaotic, the usual mountain becomes more in the regular state, and the extraction of features is very different. The method has better recognition effect for the hillside covered with vegetation, the recognition time is short, and the recognition rate can reach 90%.

## 1. Introduction

As a common kind of geological disasters [1], the frequency of landslides is increasing year by year. According to the National Geological Disaster Bulletin, 9710 geological disasters occurred in China in 2020, of which 7403 accounted for 76.2% of the total geological disasters. Therefore, it is very important to implement sliding monitoring alarm for disaster prevention and mitigation [2, 3].

Intermittent cracks occur at the trailing edge. If the length of cracks remains unchanged, it indicates the slope shape that begins to slide. The cracks at the trailing edge occur continuously, and if the crack length tends to expand, it means that the sliding becomes fierce slowly [4]. Therefore, it is of great significance for monitoring and alarming sliding slope to monitor the crack change trend at the sliding edge and reflect the sliding displacement trajectory in time. Independent component analysis is used for feature extraction,

and basis function is used as pattern template for natural image feature detection [5]. The successful application of this method in edge detection and texture segmentation is given. Remote sensing technology is used to monitor disasters, thus improving the efficiency. In this paper, CNN and texture change are proposed to detect landslides intelligently [6].

At present, landslide monitoring methods are mainly divided into displacement monitoring, physical field monitoring, groundwater monitoring, and external trigger factor monitoring, in which the surface displacement is an important basis for judging the stability of the slope, and also an important indicator for studying the evolution process of the landslide and the management of hidden danger areas, so the accuracy and effectiveness of displacement data in monitoring is particularly important. The technical scheme of landslide disaster monitoring is gradually developing towards more accurate, intelligent, and real-time research. There are some difficulties in landslide monitoring, and

there are signal errors and non-real-time characteristics in the use of sensors. Therefore, using image processing technology to deal with the hillside covered with vegetation has better recognition effect, shorter recognition time, and higher recognition rate. Landslide movement is highly complex and affected by many factors, so it is difficult to understand the internal characteristics of each landslide thoroughly at present, but landslide monitoring is helpful to master and analyze the evolution and characteristics of the landslide body. With the continuous progress of landslide monitoring technology, in order to obtain more detailed landslide data and understand the landslide more deeply, it is necessary to design a universal landslide early warning system which is easy to install.

## 2. Identification of Crack Curve at the Trailing Edge of Landslide

**2.1. Characteristics of Cracks at the Trailing Edge of Landslide.** After the landslide disaster [7], the soil and rock mass, which were originally a part of the mountain, leave the main body of the mountain due to gravity, and the cracks formed between the trailing edge of the landslide and the immobile mountain are mainly characterized as shown in Table 1.

**2.2. Image Recognition.** The image processing technology is a technology for processing an image such as noise removal [8], enhancement, restoration, segmentation, and feature extraction. The main contents included in the image processing are shown in Table 2.

Image processing technology is more mature, widely used in various industries, and the work efficiency is greatly improved [9]:

- (1) In road detection, image processing technology is used to quickly detect the crack position and crack width of road [10]

- (2) In residential buildings, image processing technology is used to detect the crack information of concrete [11]
- (3) In bridge monitoring, image processing technology is used to monitor whether there are cracks at the bottom of the bridge [12]
- (4) In the tunnel, image processing technology is used to collide with the tunnel
- (5) In edge monitoring, image processing technology is used to monitor the changes of mountain and obtain real-time changes, but it is difficult to record and compare the changes of the whole mountain, for example, it is difficult to analyze the more detailed changes of mountain by using methods such as dividing and strengthening, so as to obtain accurate and comprehensive monitoring data [13]
- (6) Image processing technology can also be used for small displacement motion

### 2.3. Color Model

**2.3.1. RGB Model.** Because RGB model quantitatively represents the brightness of three basic colors: red, green, and blue, it is also called additive color mixing model [14]. However, when the brightness values of the three basic colors are the lowest (0), it is set to black. When the brightness values of the three primary colors reach the highest value (255), they are white [15].

This is a basic method of mixing colors by adding colors and mixing colors.  $red + green = yellow$ ,  $green + blue = cyan$ ,  $red + green + blue = white$ .

The color matching equation of the color mixing model is

$$F(\text{objectcolor}) = R(\text{redpercentage}) + G(\text{green percentage}) + B(\text{blue percentage}). \quad (1)$$

**2.3.2. HSV Model.** HSV is created based on the visual property parameters of three colors. Hue (H), chromaticity (S), and brightness (V) are different [16]:

**Hue H:** hue  $H$  stipulates that the color should be measured with a 360 disc and driven counterclockwise from 0. Common colors are red at 0, green at 120, and blue at 240.

**Saturation S:** chroma  $S$  is based on spectral color. The closer the color is to spectral color, the higher the saturation of its color. On the contrary, the lower the chroma.

**Brightness V:** brightness  $V$  is used to indicate the brightness of color, and the brightness depends on the brightness of light source.

In the landslide monitoring system, images with different RGB color ratios show different image effects. The analysis of landslide monitoring images can improve the image processing quality and analysis accuracy. Usually, hue and saturation are commonly called chromaticity, which is used to express the category and depth of the color. Because people's vision is more sensitive to brightness than to shade of color, HIS color space is often used to facilitate color processing and recognition, which is more in line with people's visual characteristics than RGB color space. In image processing and computer vision, a large number of algorithms can be used in HIS color space, and they can be processed separately and independently of each other. Therefore, the workload of image analysis and processing can be greatly simplified in HIS color space.

TABLE 1: Characteristics of cracks at the trailing edge of landslide.

| Characteristic   | Elaborate   |
|--|---|
| The color contrast on both sides of the curve is large | The occurrence of landslide disaster is generally accompanied by the collapse of rock and soil. In the stable state of landslide, there is a great color difference between the immovable mountain (green vegetation, etc.) and the trailing edge of landslide (like rock). This provides a theoretical basis for the design method of this system. |
| The curve shape is tortuous                            | The crack curve of inclined back edge is mostly curved and folded.  |
| The curve develops gradually                           | The movement of landslide disaster body is generally a very slow process.   |

TABLE 2: Main internal customers of image processing.

| Classification | Features  |
|----------------|---|
| 1              | By thinning the smallest display unit of the image, the pixels of the image are usually suppressed and strengthened, or geometric transformation is performed. Reduce or remove the noise that may exist in the image, and emphasize the information sensitive to the image.  |
| 2              | Look for important features and features of images. For example, the change of color, the positioning of boundaries, the division of regions, and so on. General methods include image segmentation and image recognition. In addition, the segmentation criteria for image segmentation need to be set based on different image features to find a commonly used segmentation method. Image recognition has been widely used in recent years. The rapid development of machine learning provides powerful technical support for image recognition. |
| 3              | Compared with the expressive impression, there is also a lot of resource space. Therefore, the mature image protocol is used for coding and compression, and the memory capacity is reduced. Then, accelerate the transmission speed.   |

## 2.4. Image Preprocessing

**2.4.1. Image Preprocessing.** The purpose of image digitization is to convert continuous analog images into discrete digital images [17]. Sampling quantization or coding is usually used to convert the original continuous space and brightness into discrete space and brightness.

As shown in Figure 1(a) of a digital image sample diagram, the original image is divided into an array of  $M * N$  in a fixed unit size in a two-dimensional space to generate a "dot" image (Figure 1(b)) in which the number of dots that are finally available is explained. The output efficiency is high, and the images are easily connected among various system platforms.

$$f(x, y) = \begin{pmatrix} f(0, 0) & \cdots & f(0, N-1) \\ \vdots & \ddots & \vdots \\ f(M-1, 0) & \cdots & f(M-1, N-1) \end{pmatrix}. \quad (2)$$

**2.4.2. Domains and Connected Domains.** Since the pixel points of the digital image are arranged in a 2-bit array, these remaining pixel points are close to 4 (upper, lower, left, and right) and D (diagonal) in common with the pixel points in the vicinity of the pixel point of interest, and as shown in Figure 2, the nearest eight pixel points of interest are P, and the coordinate points are  $(Z, Y)$ .

Two pixels on the image are adjacent, and the pixel gray values satisfy specific similarity. If they are further equal, the two pixels are called connection area relationship. As shown in Figure 3,  $p$  and  $q$  constitute a connected region.

**2.4.3. Grayscale.** Because the CCD image is a color image, it takes a lot of time to calculate and process, so the CCD image is usually converted into a corresponding gray image.

(1) *Component Method.* Three color fluxes of the three channels of the color image are used as the gray value of the corresponding image:

$$\text{Gray}_g(x, y) = R(x, y), \quad (3)$$

$$\text{Gray}_G(x, y) = R(x, y), \quad (4)$$

$$\text{Gray}_B(x, y) = R(x, y). \quad (5)$$

We choose the best conversion method according to the conversion effect.

(2) *Maximum Value Method.* The maximum value of the channel component of the color image 3 is used as the grayscale value of the corresponding grayscale image:

$$\text{Gray}(x, y) = \max\{R(x, y), G(x, y), B(x, y)\}. \quad (6)$$

(3) *Average Method.* The average value of the channel components of the color image 3 is used as the grayscale value of the corresponding grayscale image:

$$\text{Gray}(x, y) = \frac{\{R(x, y), G(x, y), B(x, y)\}}{3}. \quad (7)$$

(4) *Weighted Average Method.* The weighted average value of the 3-channel components of the color image is used as the grayscale value of the corresponding grayscale image:

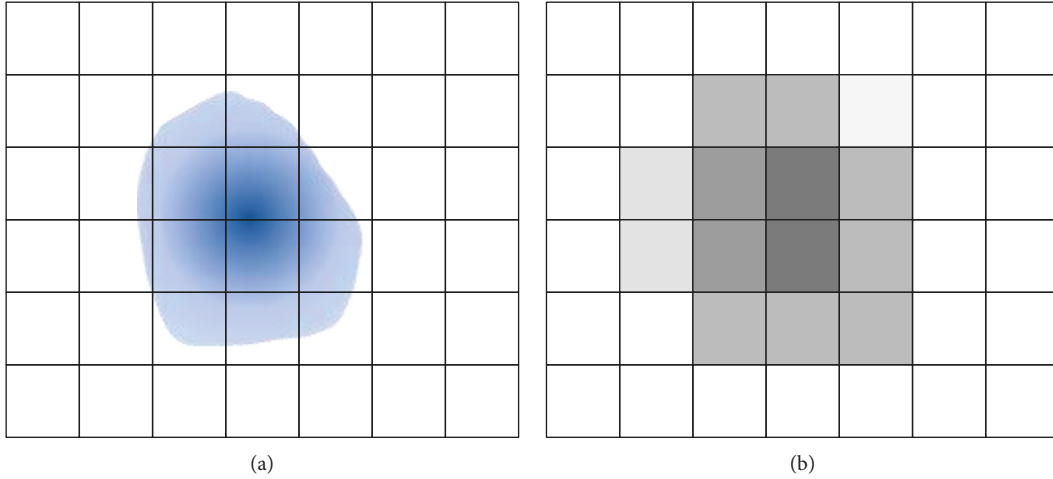


FIGURE 1: Image sampling schematic. (a) Original drawings. (b) Sampled images.

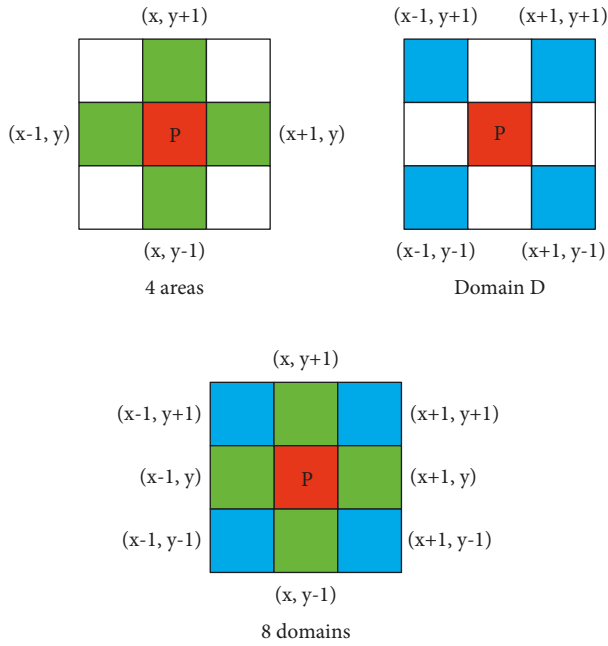


FIGURE 2: Neighborhood diagram.

$$Gray(x, y) = 0.299R(x, y) + 0.587G(x, y) + 0.114B(x, y). \quad (8)$$

**2.4.4. Histogram Correction.** Histogram correction belongs to the category of image enhancement, and its essence is to open gray interval or uniform gray distribution. Balance of histogram and specification of histogram are two commonly used correction methods.

(1) *Histogram Balance.* Histogram equalization refers to the use of one-time gray mapping function to process the

original image pixels, and the uniform distribution of the image after the gray probability distribution:

(1) Set the gray level of the original image and the gray level of the object image as  $r$  and  $s$ , respectively. If  $0 \leq r, s \leq 1$ ,  $s = T(r)$ , then  $T$  is a unified gray level mapping function.

(2) When the distribution function of gray level  $s$  of the target image is expressed in  $f(s)$ , then

$$f_s(s) = \int_{-\infty}^s P_r(r) dr \Rightarrow P_s(s) = P_r \frac{dr}{ds} \Big|_{r=T^{-1}(s)}. \quad (9)$$

(3) Unified gray mapping function is

$$s = T(r) = \int_0^r P_r(\omega) d\omega. \quad (10)$$

(4) Derivative of  $s$  in the mapping function is

$$\frac{ds}{dr} = \frac{dT(r)}{dr} = P_r(r). \quad (11)$$

(5) Substituting equations (11) into (9) results in

$$P_s(s) = P_r \frac{1}{P_r} \Big|_{r=T^{-1}(s)} = 1. \quad (12)$$

(2) *Specification of Histograms.* Histogram specification refers to the step of transforming the gray histogram within a specific gray range into a target histogram by using a gray image function:

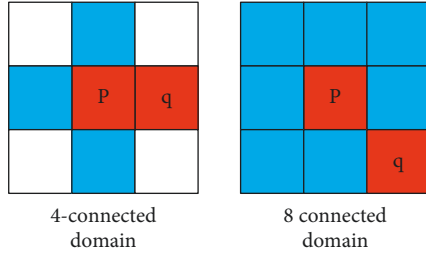


FIGURE 3: Schematic diagram of the connected domain.

- (1) Integrate the gray probability density function  $P_r(R)$  of the original image and the gray probability density function  $P_z(Z)$  of the object image:

$$v = G(z) = \int_0^z P_z(z) dz, \quad (13)$$

$$s = T(r) = \int_0^r P_r(r) dr. \quad (14)$$

- (2) The gray probability density function of inverse transformation target image is

$$z = G^{-1}(v). \quad (15)$$

- (3) Replace  $V$  in the inverse transformation of the above formula with the gray level of the original image:

$$z = G^{-1}(s). \quad (16)$$

**2.4.5. Image Noise Reduction Processing.** Due to the limitation of photography conditions, outdoor slider images usually contain various noises. Identifying these images directly may not achieve the desired effect.

Image noise reduction processing can improve image recognition and image quality. General noise reduction schemes are average filtering and median filtering in Figure 4.

Generally, the discrete subsequence input into the database is assumed to be  $\{X_0, X_1, \dots, X_8\}$ , and the corresponding non-negative integer weights are  $\{W_0, W_1, \dots, W_8\}$ . Weighted median filtering is defined as  $Y = M_{ed} \times (X_0 W_0, X_1 W_1, \dots, X_8 W_8)$ , where  $Y$  represents the filtered output of the database and  $M_{ed}$  represents the copy of image data.

**2.4.6. Image Binarization Processing.** In the image binarization process, if the preset threshold value is small, the gray value is set to 0, otherwise it is set to 255, which indicates the effect of whether the image is black or white, and a foreground region and a background region can be distinguished.

The total number of pixels in the image is

$$M = \sum_{i=0}^{n-1} m_i. \quad (17)$$

The frequencies of pixels with different gray values are also different. The calculation formula of frequency is

$$P_i = \frac{m_i}{M}. \quad (18)$$

Set the threshold  $T$  to divide the image into foreground and background, and the frequency of foreground and background is as follows:

$$P_a = \sum_{i=0}^r P_i, \quad (19)$$

$$P_b = \sum_{i=T+1}^{n-1} P_i = 1 - P_a. \quad (20)$$

The average of foreground and background gray values is

$$W_a = \sum_{i=0}^r \frac{iP_i}{P_a}, \quad (21)$$

$$W_b = \sum_{i=T+1}^{n-1} \frac{iP_i}{P_b}. \quad (22)$$

The average value of the overall gray value of the image pixels is

$$W_0 = P_a W_a + P_b = \sum_{i=0}^{n-1} iP_i. \quad (23)$$

Maximum variance between foreground and background is

$$\delta^2 = P_a (W_a - W_0)^2 + P_b (W_b - W_0)^2. \quad (24)$$

$T^*$  is the optimal threshold. Namely,

$$T^* = \text{ArgMax} [P_a (W_a - W_0)^2 + P_b (W_b - W_0)^2], \quad (25)$$

where  $\delta$ ,  $P_a$ ,  $P_b$ ,  $W_a$ ,  $W_b$ , and  $W_0$  are all functions of the threshold value  $T$ ,  $\delta^2$  is the maximum, and  $T^*$  is the optimal threshold value.

**2.5. Image Morphological Processing.** Non-morphological algorithm can obtain processing effect through function modeling, convolution transformation and other methods, and play an active role in correcting the pixels of multiple images, but there are few inactive pixels of some images, such as correcting abnormal points through the consistency of functions. Pixel units are also referred to as structural elements and the structural elements typically select a relatively small set of pixel points.

The two basic processing methods of mathematical form processing are corrosion and expansion, and the resulting morphological algorithms include open operation and closed operation.



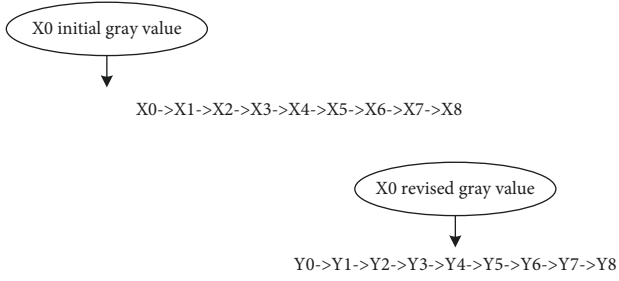


FIGURE 4: Schematic diagram of median filtering.

**2.5.1. Expansion.** If the original image is  $Z^2$ , in the mathematical form dilation processing, when the pixel group  $X$  is scanned using the dilation structure element  $D$  and crosses the pixel group after the dilation structure element  $D$  moves parallel to  $Z$ , the dilation result group can be considered:

$$X \oplus D = \{Z | (D)_z \cap X \neq \emptyset\}. \quad (26)$$

The bright part (white area) of the image can be enlarged and all background points in contact with the foreground area can be integrated with the object to fill the cavity and narrow gap of the foreground area, and intermittent parts of the image can be connected.

**2.5.2. Corrosion.** If the original image is  $Z^2$ , in the mathematical form of etching treatment, if the etching structural element  $E$  scans the pixel group  $X$  and the etching structural element  $E$  belongs to the pixel group  $X$  after moving  $Z$  in parallel, the group is considered as the etching result group:

$$X \ominus E = \{Z | (E)_z \in X\}. \quad (27)$$

The cross-difference approximate gradient width of  $f(x, y)$  in the image is

$$f(x, y) = |G_x| + |G_y| = |f(x+1, y) - f(x, y)| + |f(x, y+1) - f(x, y)|. \quad (29)$$

$$f(x, y) = |G_x| + |G_y| = |f(x, y) - f(x+1, y+1)| + |f(x+1, y) - f(x, y+1)|. \quad (30)$$

When  $G(X, Y)$  is greater than a preset threshold, points  $(Z, Y)$  are regarded as edge points.

**2.6.2. Sobel Edge Detection Algorithm.** Sobel operator was proposed by Irwin Sobel in 1973. As a weighted average edge

**2.5.3. Open Operation.** Open operation will corrode the image and expand. The arithmetic expression is

$$X \diamond B = (X \ominus B) \oplus B. \quad (28)$$

The calculation may filter the details of the protrusions smaller than the structural element  $B$  to segment the edges of the slender connection destination and the smooth object region. This method is inconvenient to preserve the cracks in the sliding trailing edge on the fine edge.

**2.6. Boundary Detection.** In order to obtain the crack curve of sliding trailing edge, it is necessary to extract cracks in the connection between sliding trailing edge (rock and soil) and immovable mountain (green vegetation). Because of the difference in color gray between sliding trailing edge and immovable mountain, the pixel gray ladder of edge pixels and nearby pixels in the image is large, so edge detection algorithm can be used to extract sliding trailing edge crack curve.

The global search class focuses on the calculation of edge strength, using the main function to represent the pixel gradient pattern value, and replacing the local direction of edge motion with the gradient direction. There are Roberts operator and Sobel operator for global search once edge detection.

**2.6.1. Roberts Edge Detection Algorithm.** The Roberts operator is proposed by Lawrence Roberts in 1963. The local difference operator is used to find the edge operator. It is shown in Figure 5.

The magnitude of the vertical and horizontal difference approximate gradient in the image is

detection operator, Sobel operator thinks that the influence of nearby pixels on the current pixel is not equal, so different weight operators have different influences on the results of pixels with different distances.

Sobel's nuclear accumulation factor is

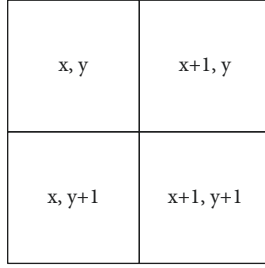


FIGURE 5: Schematic diagram of coordinate points of digital image pixels.

$$G_x = \begin{vmatrix} -1 & 0 & 1 \\ -2 & 0 & 2 \\ -1 & 0 & 1 \end{vmatrix} \quad G_y = \begin{vmatrix} -1 & -2 & -1 \\ 0 & 0 & 0 \\ 1 & 2 & 1 \end{vmatrix}. \quad (31)$$

The factor consists of two sets of  $3 \times 3$  matrices, which represent transverse and longitudinal directions, respectively. Convolution operations are performed near  $3 \times 3$  centered on  $F(X, Y)$  to calculate the deviation in  $Z$  and  $Y$  directions.

Set the image to  $I$  and the threshold to  $T$ :

$$T = (I \otimes G_x)^2 + (I \otimes G_y)^2. \quad (32)$$

$F(X, Y)$  is regarded as an edge point when the gray degree is greater than the threshold  $T$ .

**2.6.3. Gauss-Laplacian Edge Detection Algorithm.** If only one differential is performed, the gradient change can be a local extreme value, so it is impossible to judge the position of the edge point, so we continue to find the first differential from the second differential. After the zero point is obtained from the meta-pole, there is a peak and a trough before and after the zero point.

And finally, we have

$$L(x, y) = \Delta G(x, y, \sigma) = \frac{x^2 + y^2 - 2\sigma^2}{\sigma^4} e^{x^2 + y^2 / 2\sigma^2}. \quad (33)$$

**2.6.4. Canny Edge Detection Algorithm.** The Canny operator was proposed by John-F. Conny in 1986. As the most common edge detection method, the steps are as follows.

(1) *Noise Removal.* Like the Gaussian Laplace transform, in order to reduce the interference to the processing result caused by noise or the like, noise removal processing of the object image is required.

The coordinate point  $(x, y)$  means close to  $3 \times 3$ , and the coordinate of the center point is  $(0, 0)$ .  $X, Y$  are integrals, and  $I$  take the value of  $0-8$ . Because of standard deviation, the smaller the value, the better the smoothing effect. The formula of quadratic Gaussian function is

$$G_i(x, y) = \frac{1}{2\pi\sigma^2} e^{x^2 + y^2 / 2\sigma^2}. \quad (34)$$

The gray values of the  $3 \times 3$  region are assumed to be  $Z_0-Z_8$ :

$$G_i = Z_i \times Y_i. \quad (35)$$

Plus these nine values. This is the Gaussian ambiguity value of the center point  $X_0$ :

$$M_0 = \sum_{i=0}^8 G_i. \quad (36)$$

(2) *The Amplitude and Direction of Gradient Are Calculated by Finite Difference of Principal Deviation.* Image edge detection is divided into two parameter attributes: direction and amplitude, and the gray value is displayed along the moving direction of the edge.

The change is slow, but perpendicular to the moving direction of the edge, the gray value changes strongly.

The Gaussian filtered image is a  $2 \times 2$  region, and two gradients in the  $x$ -direction and  $y$ -direction are calculated by the principal finite difference approximation, and as shown in Figure 6.

The gradients in the  $X$  and  $Y$  gate directions are

$$g_x = \frac{(h_1 - h_0 + h_3 - h_2)}{2}, \quad (37)$$

$$g_y = \frac{(h_2 - h_0 + h_3 - h_1)}{2}. \quad (38)$$

Thus, the distribution value and direction of the point gradient are obtained:

$$M(x, y) = \sqrt{(g_x^2 + g_y^2)}, \quad (39)$$

$$\alpha(x, y) = \arctan\left[\frac{g_x}{g_y}\right]. \quad (40)$$

(3) *Suppressing the Nonmaximum Value of Gradient Amplitude.* For the 8 adjacent spaces of the  $3 \times 3$  region, as shown in Figure 7, the gradient direction can be four directions of  $0, 45, 90,$  and  $135$ .

(4) *Edge Connections Are Detected by Two Threshold Algorithms.* By setting two default values  $T_1$  and  $T_2$  to obtain  $2T_1 = T_2$  the two threshold edge images  $N_1$  and  $N_2$  have values using low thresholds and include a number of false edges.  $N_2$  is intermittent (not off) by using a high threshold. Therefore, with respect to edge connection, if a cut-off point  $N_2[X, Y]$  of the edge appears in the  $N_2$  image, the algorithm is looking for eight locations that can connect the cut-off points before the  $N_1[X, Y]$  image is disconnected. As shown in Figure 8, the flowchart turns off the  $n_2$  image.

**2.6.5. Comparison of Edge Detection Operators Tab.** Table 3 shows a comparison of the advantages and disadvantages of each edge detection operator.

Here, the image used in the edge detection step is a binary image, and the position of edge points needs to be correctly determined. In order to integrate the advantages

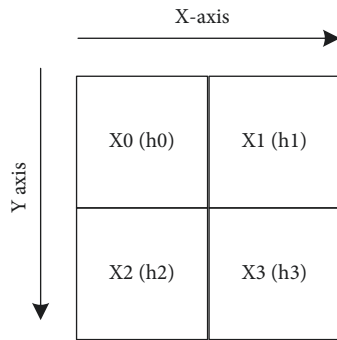


FIGURE 6: Gradient bat value and direction.

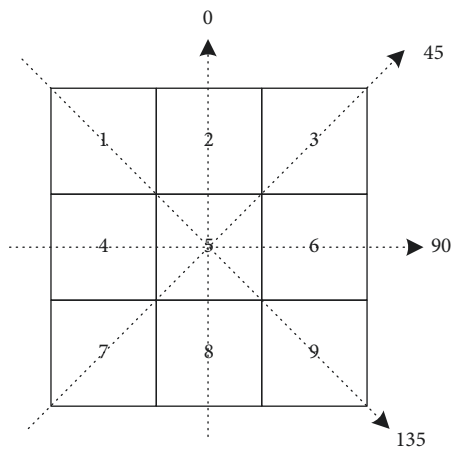


FIGURE 7: Gradient direction value.

and disadvantages of these operators, canny operator is used for edge detection.

**2.7. Feature Parameter Setting.** Image feature is a response feature or feature that distinguishes a certain object from the other types of objects, and it is the proportion of features or features of objects different from feature parameters to the whole image source, with numbers ranging from 0 to 1.

Because the interference region and crack curve in the graph are included in the connection region depicted by Carney edge detection operator, it is necessary to set the characteristic parameters to remove the gold crystals in the connection region formed between branches and boulders.

The length of the foreground region projected onto the width of the image length is a projection coefficient occupying the entire width of the image source. In the case that the ratio coefficient is larger than a preset characteristic parameter, the connecting region is considered to contain a sliding trailing edge crack curve.

As shown in Figure 9, the width of the image length is  $X$  and  $Y$ , respectively, and there are rectangular boxes cutting off the two connecting areas  $A$  and  $B$  and their edges.

### 3. Experimental Process and Analysis

This experiment uses MATLAB development platform. The hardware composition of this experiment is a computer with "Pentium 2 CPU 3.00 GHz and 2.0 GHz memory." Randomly select 173 mountain muscle images without skiers, and generate 110 skier images. Image sources mainly come from network search. When the system detects the position of the image moving mark, the digital image processing module is executed. According to the algorithm design, the digital image processing module uses Wang subroutine to complete RGB color feature extraction, HSI color feature extraction, and gray level co-occurrence matrix texture feature extraction, and finally uses a subroutine to complete the recognition of landslide state.

Taking the typical images of four mountains and the normal images of four mountains as examples, the experimental analysis is carried out. This experiment consists of three stages: image preprocessing, feature extraction, and classifier design as shown in Figures 10 and 11.

The purpose of the standardized size is to reduce the image to the same size, so as to extract the features easily.

**3.1. Texture Feature Extraction Experiment.** Tables 4 and 5 show that the texture features of each subregion do not change greatly, and the feature values are relatively stable. If the mountain slides, the texture characteristics of the slope will change greatly.

**3.2. HIS Color Feature Extraction Experiment.** Tables 6 and 7 show the color characteristics obtained after obtaining the dominant color of each subregion according to the histogram.

Analysis of Tables 6 and 7 shows that there is no significant change in the color characteristics of each subregion of a typical mountain image. If a landslide occurs, the color characteristics of the subarea of the slope will change greatly, and the dispersion will increase significantly.

**3.3. Design of the BP Neural Network Classifier.** In the identification of landslide disaster of railway line, there are only two outputs, and the nodes of output layer are  $p = 1$  and  $h = 5 \sim 14$ . The selected parameters are displayed in Table 8, and the network structure and the selection of training parameters are displayed in Table 8.

**3.4. Landslide Identification Experiment Results.** From the collected 173 images of mountain muscle without landslide and 110 images of mountain muscle with landslide, 40 images and 80 images were randomly selected for testing, and the rest were reserved as training images. Among them, 133 common mountain muscle images constitute the training sample group, and 70 slippery mountain images constitute the training negative sample group to train the classifier. Tables 9 and 10 show the recognition results of 80 test images, respectively.

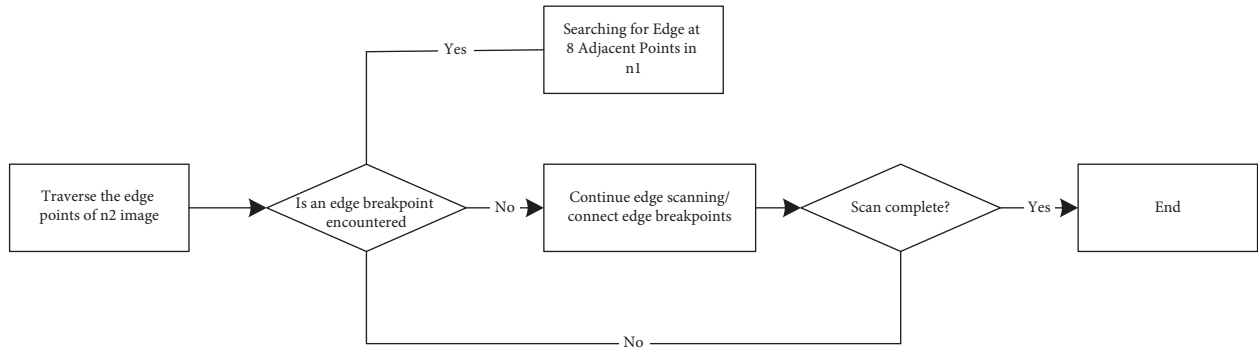


FIGURE 8: Flowchart of double threshold algorithm.

TABLE 3: Comparison of edge detection operators.

| Operator name         | Comparison of advantages and disadvantages   |
|-----------------------|--|
| Roberts operator [18] | It is effective for steep and low-noise image processing, but the edges extracted by the operator are rough. Therefore, it is not advantageous to position the edge correctly.   |
| Sobel operator [19]   | It performs more efficient processing of grayscale gradation and noisy images.   |
| LOG operator [20]     | The ability to identify edge points is strong, and only pay attention to the position with strong gray level change, but the second German action enhances the influence of noise, and the edge direction information is not discussed.  |
| Canny operator [21]   | Noise interference can be effectively avoided, and the inconspicuous position of edge information can be correctly extracted. Its advantage is that different thresholds are used to detect all strong edges and weak edges, respectively. Filter “pseudo weak edges,” which can include weak edges in the output image. |

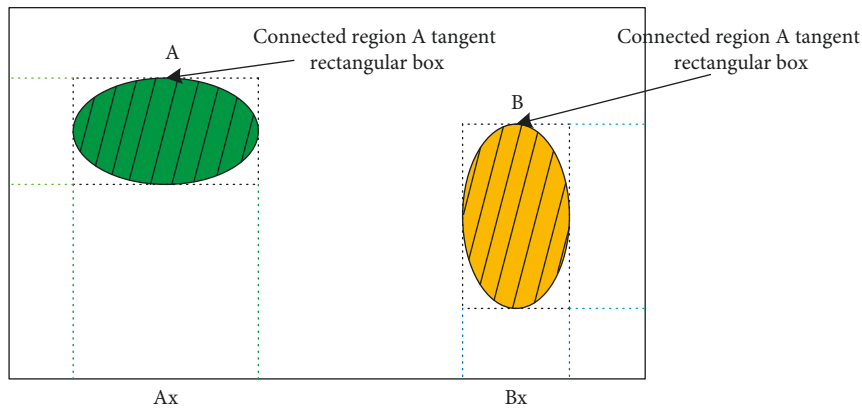


FIGURE 9: Schematic diagram of image feature recognition.

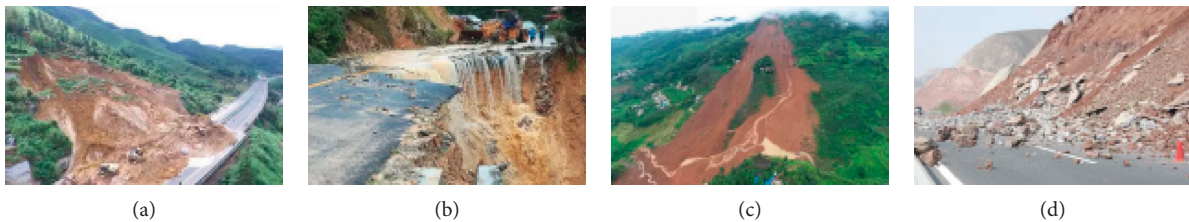


FIGURE 10: Example of typical landslide mountain.

The analysis and experimental results show that the recognition rate of SVM method is 90%, while that of BP neural network is only 77.5%. Then, after training the classifier in recognition time, SVM algorithm is better than BP neural network for a single  $200 \times 150$  (or  $150 \times 200$ ) image, but the

recognition time is within the allowable range. Images of mountains without slopes are more accurate than those of Sakamoto, and vary according to the condition of the mountains, the shape of the slopes, and the quality of photography. The scope and area are also very different.



FIGURE 11: Typical normal mountain image.

TABLE 4: Comparison of texture features of typical landslide images.

| Texture feature       | Figure 10(a) | Figure 10(b) | Figure 10(c) | Figure 10(d) |
|-----------------------|--------------|--------------|--------------|--------------|
| Contrast              | 11.2260      | 5.3456       | 9.2341       | 2.4351       |
| Correlation           | 2.3245       | 1.3245       | 1.2345       | 1.5674       |
| Angular binary matrix | 2.8908       | 47.7892      | 4.4567       | 4.2314       |
| Entropy               | 385.6444     | 60.0974      | 24.3456      | 32.4355      |
| Locally stationary    | 2.5645       | 1.3566       | 1.7456       | 1.3467       |

TABLE 5: Comparison of texture features of typical normal mountain images.

| Texture feature       | Figure 11(a) | Figure 11(b) | Figure 11(c) | Figure 11(d) |
|-----------------------|--------------|--------------|--------------|--------------|
| Contrast              | 1.3435       | 1.5675       | 1.2346       | 1.5736       |
| Correlation           | 1.1234       | 1.1234       | 1.0453       | 1.9098       |
| Angular binary matrix | 1.0753       | 1.5432       | 1.8546       | 1.4326       |
| Entropy               | 1.0435       | 0.6543       | 2.3256       | 2.5231       |
| Locally stationary    | 1.3432       | 1.3245       | 1.1234       | 1.1234       |

TABLE 6: Comparison of color characteristics of typical landslide images.

| Color feature | Figure 10(a) | Figure 10(b) | Figure 10(c) | Figure 10(d) |
|---------------|--------------|--------------|--------------|--------------|
| Subregion 1   | 0.2349       | 0.2189       | 2.2345       | 0.0324       |
| Subregion 2   | 0.2134       | 1.2234       | 0.5234       | 0.3213       |
| Subregion 3   | 0.9213       | 0.1245       | 0.8252       | 0.3142       |
| Subregion 4   | 3.1412       | 4.2134       | 3.4363       | 1.2134       |
| Subregion 5   | 11.2314      | 16.2345      | 16.3245      | 4.2134       |
| Mean value    | 3.3255       | 4.3145       | 4.2132       | 1.2134       |
| Variance      | 24.2322      | 43.1234      | 47.3242      | 2.2355       |

TABLE 7: Comparison of color characteristics of typical normal mountain images.

| Color feature | Figure 11(a) | Figure 11(b) | Figure 11(c) | Figure 11(d) |
|---------------|--------------|--------------|--------------|--------------|
| Subregion 1   | 0.0123       | 0.0213       | 0.0213       | 0.0213       |
| Subregion 2   | 0.2312       | 0.3123       | 0.2325       | 0.1234       |
| Subregion 3   | 0.0213       | 0.1234       | 0.2314       | 0.2131       |
| Subregion 4   | 0.3214       | 0.3214       | 0.5123       | 0.3451       |
| Subregion 5   | 0.9435       | 1.5453       | 2.3246       | 1.3526       |
| Mean value    | 0.3214       | 0.43623      | 0.6234       | 0.2344       |
| Variance      | 0.1324       | 0.4325       | 0.7345       | 0.2336       |

TABLE 8: Neural network structure and training parameters.

| Input layer node | Hidden layer node | Output layer node | Initial weight | Expected error | Momentum term | Training coefficient | Learning rate |
|------------------|-------------------|-------------------|----------------|----------------|---------------|----------------------|---------------|
| 15               | 8                 | 1                 | (-1, 1)        | 0.02           | 0.9           | 2000                 | 0.05          |

TABLE 9: Landslide identification results based on SVM algorithm.

|           | Number of images | Number of correct detections | Number of false detections | Detection rate (100%) |
|-----------|------------------|------------------------------|----------------------------|-----------------------|
| Normal    | 40               | 37                           | 3                          | 92.5%                 |
| Landslide | 40               | 35                           | 5                          | 87.5%                 |
| All       | 80               | 72                           | 8                          | 90.0%                 |

TABLE 10: Landslide identification results based on BP neural network algorithm.

|           | Number of images | Number of correct detections | Number of false detections | Detection rate (100%) |
|-----------|------------------|------------------------------|----------------------------|-----------------------|
| Normal    | 40               | 32                           | 8                          | 80.0                  |
| Landslide | 40               | 30                           | 10                         | 75.0                  |
| All       | 80               | 62                           | 18                         | 77.5                  |

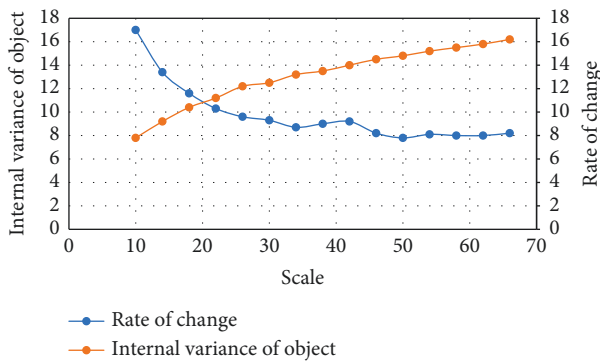


FIGURE 12: LV-ROC trend chart of image in the study area.

Based on high-resolution images, 30m resolution SRTM highway data, and its derived gradient data, landslides are extracted by object-oriented method. First, a sliding optimum segmentation ratio of the image is determined using the station partial divergence method, and the LV-ROM curve of the image is shown in Figure 12. The image is segmented in this ratio, and the weight of each frequency band is set to 1, the shape index is set to 0.3, and the contraction index is set to 0.3.

#### 4. Conclusion

In this paper, the image processing technology is used to deal with the hillside covered by vegetation, and the recognition effect is good, the recognition time is short, and the recognition rate is high. Using image processing and SVM algorithm, the recognition rate of sliding mountain is higher than that of BP neural network. After training the classifier with recognition time, for a single 200 × 150 image, the proposed method is superior to BP neural network, but the recognition time is within the allowable range. The results of the article have a high recognition rate, and further research needs to analyze the terrain, through the analysis of different mountain characteristics and soil and other factors. Through the comprehensive analysis of different advancing locations and different characteristics of the mountain, the corresponding identification methods are obtained, respectively.

#### Data Availability

The experimental data used to support the findings of this study are available from the corresponding author upon request.

#### Conflicts of Interest

The authors declare that they have no conflicts of interest regarding this work.

#### References

- [1] C. Zhang, "Retracted article: warning of regional landslide disaster based on sensors and the effect of aerobic exercise of obese students," *Arabian Journal of Geosciences*, vol. 14, no. 16, p. 1633, 2021.
- [2] X. Wu, Z. Wang, G. Gao, J. Guo, and P. Xue, "Disaster probability, optimal government expenditure for disaster prevention and mitigation, and expected economic growth," *The Science of the Total Environment*, vol. 709, no. Mar.20, Article ID 135888.1, 2020.
- [3] C. C. Chou, Y. T. Wang, J. J. Hu, S. Liao, and C. Hsu, "Materials science introduces disaster prevention and mitigation education experiment," *Applied Mechanics and Materials*, vol. 897, pp. 221–225, 2020.
- [4] H. Wang, D. Nie, X. Tuo, and Y. Zhong, "Research on crack monitoring at the trailing edge of landslides based on image processing," *Landslides*, vol. 17, no. 4, pp. 985–1007, 2020.
- [5] C. Yenwei and Z. Xianyan, "Edge Detection and Texture Segmentation Based on Independent Component analysis," in *Proceedings of the 16 Th International Conference on Pattern Recognition*, Quebec City, QC, Canada, August2002.
- [6] A. Ding, Q. Zhang, X. Zhou, and B. Da, "Automatic Recognition of Landslide Based on CNN and Texture Change detection," in *Proceedings of the Chinese Association of Automation*, IEEE, 2017.
- [7] W. Lin, K. Yin, and N. Wang, "Landslide hazard assessment of rainfall-induced landslide based on the CF-SINMAP model: a case study from Wuling Mountain in Hunan Province, China," *Natural Hazards*, no. 11, pp. 1–22, 2021.
- [8] Y. Wang, Y. Yu, X. Zhu, and Z. Zhang, "Pattern recognition for measuring the flame stability of gas-fired combustion based on the image processing technology," *Fuel*, vol. 270, Article ID 117486, 2020.
- [9] N. Fan, "Application of CAD combined with computer image processing technology in mechanical drawing," *Application of*

- Intelligent Systems in Multi-modal Information Analytics*, vol. 1234, pp. 319–324, 2020.
- [10] G. Yang, J. Wu, and Q. Hu, “Rapid detection of building cracks based on image processing technology with double square artificial marks,” *Advances in Structural Engineering*, vol. 22, no. 5, pp. 1186–1193, 2019.
- [11] Y. Wang, J. Y. Zhang, J. X. Liu et al., “Research on crack detection algorithm of the concrete bridge based on image processing,” *Procedia Computer Science*, vol. 154, pp. 610–616, 2019.
- [12] D. H. Kim, Y. G. Hong, D. W. Seo, and K. T. Park, “Development of structural health monitoring technology for internal tendon of PSC bridge using acoustic emission technology,” *Journal of Acoustic Emission*, vol. 36, pp. S142–S147, 2019.
- [13] V. Sood, H. S. Gusain, S. Gupta, and S. Singh, “Topographically derived subpixel-based change detection for monitoring changes over rugged terrain Himalayas using AWiFS data,” *Journal of Mountain Science*, vol. 18, no. 1, pp. 126–140, 2021.
- [14] P. M. Nowak and P. Kościelniak, “What color is your method? Adaptation of the RGB additive color model to analytical method evaluation,” *Analytical Chemistry*, vol. 91, no. 16, pp. 10343–10352, 2019.
- [15] C. U. Hail, G. Schnoering, M. Damak, D. Poulidakos, and H. Eghlidi, “A plasmonic painter’s method of color mixing for a continuous red-green-blue palette,” *ACS Nano*, vol. 14, no. 2, pp. 1783–1791, 2020.
- [16] R. Kondel, N. Shafiq, I. P. Kaur et al., “Effect of acyclovir solid lipid nanoparticles for the treatment of herpes simplex virus (HSV) infection in an animal model of HSV-1 infection,” *Pharmaceutical Nanotechnology*, vol. 7, no. 5, pp. 389–403, 2019.
- [17] C. L. Deufel, S. Tian, B. B. Yan, B. D. Vaishnav, M. G. Haddock, and I. A. Petersen, “Automated applicator digitization for high-dose-rate cervix brachytherapy using image thresholding and density-based clustering,” *Brachytherapy*, vol. 19, no. 1, pp. 111–118, 2020.
- [18] S. Tian, J. Kong, X. Wang, L. Zhao, and X. Jianliang, “Improved Roberts Operator for Detecting Surface Defects of Heavy Rails with superior Precision and Efficiency,” *High-tech communication*, no. 2, p. 8, 2016.
- [19] Z. Hui, Q. Zhu, and X. F. Guan, “Probe into Image Segmentation Based on Sobel Operator and Maximum Entropy Algorithm,” in *Proceedings of the International Conference on Computer Science & Service System*, Nanjing, China, August 2012.
- [20] Y. Li and J. X. Pang, “Sub-pixel edge detection based on spline interpolation of D<sub>2</sub> and LOG operator[J],” *Journal of Huazhong University Ofence & Technology*, vol. 28, no. 3, pp. 77–79, 2000.
- [21] D. D. Zhang and S. Zhao, “An improved edge detection algorithm based on canny operator,” *Applied Mechanics and Materials*, vol. 347–350, no. 4, pp. 3541–3545, 2013.

## *Retraction*

# **Retracted: Development of Interactive Teaching of Physical Dance Based on Dynamic Time Reversion Technique**

### **Mathematical Problems in Engineering**

Received 18 July 2023; Accepted 18 July 2023; Published 19 July 2023

Copyright © 2023 Mathematical Problems in Engineering. This is an open access article distributed under the Creative Commons Attribution License, which permits unrestricted use, distribution, and reproduction in any medium, provided the original work is properly cited.

This article has been retracted by Hindawi following an investigation undertaken by the publisher [1]. This investigation has uncovered evidence of one or more of the following indicators of systematic manipulation of the publication process:

- (1) Discrepancies in scope
- (2) Discrepancies in the description of the research reported
- (3) Discrepancies between the availability of data and the research described
- (4) Inappropriate citations
- (5) Incoherent, meaningless and/or irrelevant content included in the article
- (6) Peer-review manipulation

The presence of these indicators undermines our confidence in the integrity of the article's content and we cannot, therefore, vouch for its reliability. Please note that this notice is intended solely to alert readers that the content of this article is unreliable. We have not investigated whether authors were aware of or involved in the systematic manipulation of the publication process.

Wiley and Hindawi regrets that the usual quality checks did not identify these issues before publication and have since put additional measures in place to safeguard research integrity.

We wish to credit our own Research Integrity and Research Publishing teams and anonymous and named external researchers and research integrity experts for contributing to this investigation.

The corresponding author, as the representative of all authors, has been given the opportunity to register their agreement or disagreement to this retraction. We have kept a record of any response received.

### **References**

- [1] X. Li and Y. Yang, "Development of Interactive Teaching of Physical Dance Based on Dynamic Time Reversion Technique," *Mathematical Problems in Engineering*, vol. 2022, Article ID 5697041, 8 pages, 2022.



## Research Article

# Development of Interactive Teaching of Physical Dance Based on Dynamic Time Reversion Technique

**Xue Li and Yaqi Yang** 

*College of Sports and Art, Shandong Sports University, JiNan 25000, ShanDong, China*

Correspondence should be addressed to Yaqi Yang; yangyaqi@sdpei.edu.cn

Received 7 April 2022; Revised 25 May 2022; Accepted 8 June 2022; Published 6 July 2022

Academic Editor: Hangjun Che

Copyright © 2022 Xue Li and Yaqi Yang. This is an open access article distributed under the Creative Commons Attribution License, which permits unrestricted use, distribution, and reproduction in any medium, provided the original work is properly cited.

In order to cultivate students' dance expression, in physical dance teaching, emphasis should be placed on cultivating students' interest in physical dance, strengthening the training of movement skills and musical rhythm, training of cultural cultivation, and training of coordination and cooperation between male and female partners. In this paper, we design a dance teaching aid based on DTW (Dynamic Time Warping) movement similarity evaluation algorithm. The evaluation of movement similarity is difficult because each movement is multidimensional, there is a lot of noise when the movement data are collected, and there is high variability in the performance of different individuals, and the real-time requirement of movement similarity evaluation. In the teaching practice, we should pay attention to the cultivation of students' dance expression, so that students can match the music and make coordinated sports dance movements, realize the integration of music and dance, and improve the professional standard.

## 1. Introduction

Sports dance is a kind of walking duo dance with male and female partners, which is one of the sports competition items and was introduced to China in the 1990s [1]. In the item group training theory of sports training, sports dance is categorized in the skill-driven category of performance difficulty and aesthetic item group, which indicates that sports dance participants should not only have a high technical level but also need rich artistic expression [2]. Expression in sports dance refers to the ability of dancers to show their thoughts and emotions with body language and facial expressions within the competition rules [3].

Sports dance takes human body movements as the main means of expression, while music is the soul of sports dance and is the specific object of expression of dance movements [4]. In the competition, sports dancers must deeply understand the connotation and meaning of the music and then use the special skills learned to express it, in order to show a qualified performance [5]. While teaching, teachers

should let students listen and practice more, immerse themselves in the world of music, comprehend the thought and emotion expressed by music or lyrics, and then follow the melody and rhythm of the music to complete sports dance movements, which can effectively improve students' appreciation of music and expression ability [2].

Sports dance is a kind of competitive sport, and the strength of psychological quality will directly affect the performance of the participating athletes on the field [6]. Athletes with poor psychological quality will easily become nervous and anxious during the competition, leading to some movement mistakes or even forgetting the movements during the competition and also affecting their ability to play on the field [7, 8].

Sports dance requires two people to work together to complete the highest level of performance, and to become one, the two people should be in tune with each other and cooperate seamlessly as if a person performing [9]. To achieve this state, both men and women in sports dance performances must maintain the same technical level of movement and have a high degree of compatibility in body

language, facial expressions, and emotional expressions [2]. There are many sports dance events, and different dances have different requirements for emotional expression. For example, the tango needs to show a high degree of defensiveness and vigilance, the rumba needs to show the lingering love between lovers, and the cowboy dance needs to show a sense of cheerfulness [10].

Sports competition is extremely physically demanding for the participants, and the higher the level of competition in sports dance, the higher the physical demands on the participants [11]. Sports dance is categorized as a skill-led performance of difficult aesthetic items, without sufficient physical strength, their speed, strength, endurance, flexibility, and coordination will certainly be affected, the artistic expression will be greatly reduced, and it is difficult to perfectly show the musical content [12].

In the process of competition or performance, players need to cooperate with the music, with flexible steps, beautiful dance, and rhythmic movements, to express the connotation and emotion of the music [13]. Back to the dance itself, in addition to a deep understanding of the connotation of the music, players must also have a strong sense of dance, to be able to expressions, eyes, gestures, steps, rotations, and other technical movements, the perfect presentation of the content of the music, to provide the audience with a visual feast [14].

## 2. Key Technology Research

**2.1. Beat Control.** Music is a very important part of the dance game, which plays a very important role in defining the overall style of the game, controlling the rhythm, and dividing the system structure in the game development process [15]. For example, in the menu control part of the game, the players need to switch the current background music in real time so that the player can have a preview of the song. At the beginning of the game, the playback of standard dance moves and the real-time recording and evaluation of the player's moves, the playback of game effects, and the rhythm control of UI all rely on beat control [16].

Since there are several game objects that depend on the music beat for updates, a separate music beat component is needed to send events for other modules at the right time. The module has a "one-to-many" feature, and the "many" end is easy to change, so the "observer pattern" is used for the design, as shown in Figure 1. The observer pattern is to separate the observer from the observed object, with the action evaluation module, UI module, cue module, and background control module as the observers, and the music beat as the observed object, and the observer will do the corresponding processing itself according to the data changes of the observed object [17]. In this way, each module can be clearly divided out and the overall reusability and maintainability of the system can be improved. In the design and development process of the game, we set up a special beat control module, using the observer mode, to control the rhythm of the game as a whole [18].

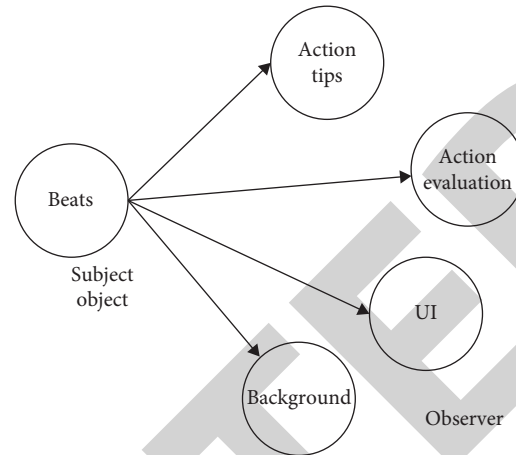


FIGURE 1: Observer model of music beat control.

**2.2. Movement Evaluation Algorithm.** Traditional dance learning methods include video teaching methods and live demonstration teaching. For people with no or only a small amount of dancing experience, the video teaching method has low learning effect and large deviation of movements because of the lack of control object and no evaluation of whether the movements are standard or not. On the other hand, the real-person teaching can achieve a better learning effect, but it consumes a lot of manpower and cannot be studied at any time. Therefore, this paper considers an action evaluation algorithm in designing a square dance game to provide real-time feedback to players' actions and achieve a good learning effect.

The main task of action similarity evaluation is to enable the computer to automatically sense "where" a person is in a scene and determine "what" a person is doing. The first step of action similarity evaluation is to perform pose estimation. Pose evaluation is the process of identifying the pose parameters of each human body part in each frame based on a specific input image sequence. For example, the position and orientation of each body part in the whole 3D space is a set of pose parameters, which is usually done by the motion capture devices. The motion similarity evaluation is based on pose estimation, extracting features from motion frames and obtaining the similarity between 2 motion sequences by calculating the distance between the feature vectors of the reference motion sequence and the comparison motion sequence. Since the motion similarity evaluation algorithm relies heavily on the results of pose estimation, the accuracy of pose estimation will have some influence on the accuracy of motion similarity evaluation, so some preprocessing work, such as data noise reduction, needs to be performed on the motion data before the motion similarity evaluation.

The specific implementation process of the action evaluation algorithm with adaptive joint weights and interpolation wavelets is expressed as follows:

### (1) Data noise reduction

Firstly, a combination of Faber-Schauder interpolation wavelet and mean filtering is used to reduce the noise of the acquired motion data. In the

background with little noise, some motion details in the strenuous movements are easily treated as noise, which is suitable for using interpolation wavelet; in the background with more noise, the combination of mean filtering can obtain better noise reduction effect.

(2) The evaluation method of adaptive joint weights

Starting from the motion characteristics, the action sequence is divided into multiple subsegments, and the cascaded joint direction data are used as features to calculate and compare the joint weights of the action, which can be calculated to get the distance between any 2 frames.

To accommodate users of different body sizes, time-series data of joint directions are used to describe the human skeleton posture and the action sequence can be expressed as  $P = [P^1, P^2, \dots, P^i, \dots, P^T]$ , where  $P^i$  is the time series data of the  $i$ -th joint direction and  $T$  is the number of joints. Using the action fragment division method with fixed time length, normalization can be achieved for different length action sequences when using the dynamic time regularization method for action sequence matching.

The adaptive joint weights are calculated as follows. Cascaded joint orientation data are used as features.

The action sequence  $P$  consists of several frames of skeleton data, and each frame can be regarded as static human skeleton structure data. The similarity of the cascaded quaternion of joint direction data, i.e., the static human skeleton structure, is measured by using a measure of 2 quaternion distances as defined in the literature.

Adaptive joint weights are calculated.

The adaptive joint weights are calculated as follows:

- (1) The length of the time segment is selected, and the action sequence  $P$  is divided into  $N$  segments.
- (2) Calculate the relative motion energy size  $f(P_n^i)$  of the action segments  $P_n^i$ . All joints of  $P_n^i$  are arranged in descending order of motion energy to obtain  $T_n$ . Take the first  $H$  joints with large energy of  $T_n$  to obtain  $T_n^H$ . Repeat this step for  $N$  segments of  $P$  to obtain  $TH = [T_1^H, T_2^H, \dots, T_n^H, \dots, T_N^H]$ . The relative motion energy in this step is measured by the definition of entropy in information theory. Assuming that each joint motion  $P_n^i$  of each action segment obeys Gaussian distribution, the information entropy of  $P_n^i$  can be calculated and used to represent the relative value of motion energy. The variance of joint motion is used to represent the function  $f(P_n^i)$ .
- (3) Counting the number of occurrences of each joint  $ID (i = 1, \dots, T)$  in vector  $TH$ , the proportion of segments with higher energy of joint  $i$  to all segments can be found  $S_i$ .
- (4) Calculate the joint weights. The  $m$  largest elements in  $S'$  are taken until the sum of these elements is greater than  $\alpha$ . The proportion  $\alpha$  can be regarded as the overall weight of the more vigorous joints, and the evaluation result of movement similarity will be

affected by the value of  $\alpha$ . The weights  $\omega_i$  of these joints are calculated as shown in

$$\omega_i = \begin{cases} \frac{S_i \cdot \alpha}{\sum_{j=1}^m S_j}, & i \in C, \\ \frac{(T-m)}{(1-\alpha)}, & i \notin C. \end{cases} \quad (1)$$

The remaining joints share the remaining weights equally, and equation (2) is the formula for calculating the weights.

$$\omega_i = \begin{cases} \frac{S_i \cdot \alpha}{\sum_{j=1}^m S_j}, & i \in C, \\ (T-m)/(1-\alpha), & i \notin C, \end{cases} \quad (2)$$

where  $i = 1, \dots, T$ . Let  $p_r^i, q_r^i$  be the quaternion representation of the  $i$ -th joint direction data of  $P$  and  $Q$ , respectively. The joint weights  $\omega_i'$  of  $Q$  are calculated according to equation (2), and the distance of any 2 frames  $p_r, q_r$  can be obtained with the metric equation.

$$\text{dist}(p_r, q_r) = \sum_{i=1}^T \frac{\omega_i + \omega_i'}{2} \cdot |d(p_r^i, q_r^i)|. \quad (3)$$

After the experiments on the test set,  $H = 6$  and  $\alpha = 0.7$ , and the segmentation time fragment is 0.8 s. The optimal solution can be obtained at this time.

Next, we determine the action sequence mapping relationship.

The DTW action sequence matching algorithm is used to determine the unique mapping relationship between the reference action sequence  $P$  and the comparison action sequence  $Q$ . Record the set of matching relations between them.

The DTW-based action sequence matching algorithm is described as follows:

- (1) Starting from the first node, the path distance is calculated cyclically. Based on the interframe distance measure and the three conditions of DTW, the smallest one is selected and the current distance is added to obtain the minimum distance of the path.
- (2) Repeat the previous step until the complete regularized path is obtained.
- (3) Create an array MapFrame to record the unique mapping relationship of all frames in the reference action sequence  $P$  to the comparison action sequence  $Q$ . Iterate through the regularized paths and store their mapping relationships in MapFrame.

Finally, we extract multidimensional action sequence keyframes.

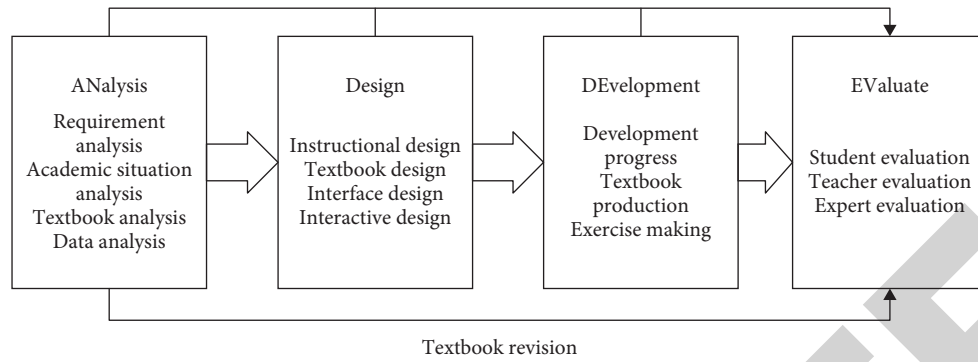


FIGURE 2: Instructional design model for this study.

The key frame extraction method based on multiscale Faber–Schauder interpolation wavelet and interval interpolation wavelet based on central affine transform performs wavelet decomposition on the joint with the largest motion energy of each segment, calculates the wavelet coefficients, extracts the key frames of  $P$ , and obtains the set of key frames  $K_{p_r} = (r = 1, \dots, R)$ , where  $R$  is the number of key frames of the action sequence, and then, combined with the set of matching relations obtained in step 3, the keyframes of  $Q$  are obtained  $K_{q_r} = (r = 1, \dots, R)$ , where  $r$  is the number of keyframes of the action sequence.

### 3. Instructional Design

The instructional design process consists of analysis, design, development, and evaluation. The analysis step analyzes the instructional needs, students, content, and data. The design step follows the results of the first phase of analysis in terms of instructional strategy, curriculum, user interface, and interaction. The development step focuses on the development and production of instruction, and the evaluation part invites experts and users to evaluate instruction. The development step focuses on the development and production of the instruction; the evaluation part invites experts and users to evaluate the instruction. In summary, the instructional design model of this study is shown in Figure 2.

**3.1. Analysis Phase.** The purpose of the demand analysis is to understand the demand of the relevant courses according to the literature, domestic and international online physical dance courses, and the discussion of the research subjects of this study before the design and development of this study. According to the results of the questionnaire and analysis, most of the students have some knowledge about the content of physical dance. The main purpose of the pedagogical analysis was to review the focus of the course content and to determine the course objectives and content of this study. Based on the demand analysis, student analysis, and pedagogical analysis, an appropriate media presentation was selected [19–23].

**3.2. Design Phase.** The instructional design and materials design, according to the themes and course content

summarized by the pedagogical analysis, was designed using task problem-solving teaching strategies, allowing students to apply the problem-solving model with the physical interaction of physical dance and Kinect somatic technology to enhance students' interest in learning, allowing students to learn and apply mathematical concepts that were not easily understood in the process of designing and verifying physical dance. The course content topics are organized by literature exploration and references to relevant books and web-related resources.

**3.3. Development Stage.** The development phase is mainly divided into three parts: development progress, teaching production, and exercise production. After studying the relevant teaching platforms at home and abroad, web design software, image processing software, and audio-visual editing software are chosen as the tools for teaching development.

**3.4. Evaluation Stage.** In the process of teaching, production, and development, relevant data must be collected continuously to evaluate whether the teaching content and structure meet the teaching needs. In this study, the evaluation was conducted according to three aspects: teaching content, teaching design, and user interface design. The survey was conducted in two phases: in the first phase, expert evaluations were conducted to modify inappropriate content and instructional planning, and in the second phase, evaluation work was conducted with students and teachers to understand the strengths and weaknesses of instructional design and development as a basis for instructional improvement.

### 4. Testing Effectiveness

The development of intelligent Agent applications can use a variety of distributed object building block technologies such as CORBA, DCOM, and Java RMI. The interface definition language IDL in CORBA also provides mapping to Java, C++, Smalltalk, and other languages, allowing easy interaction between objects from different platforms on the web. Therefore, the best solution for implementing an Agent-based web-based teaching system is to use a

TABLE 1: Comparison of 2007 computer class results.

|                      | Fundamentals of computer (average) | Software engineering (average) | Assembly language (average) | Java language (average) | Visual basic language (average) | Network technology (average) |
|----------------------|------------------------------------|--------------------------------|-----------------------------|-------------------------|---------------------------------|------------------------------|
| Network technique    | 82.3                               | 71.2                           | 77.4                        | 77.5                    | 75.2                            | 78.2                         |
| Software technology  | 79.1                               | 73.9                           | 79.4                        | 78.1                    | 76.2                            | 79.4                         |
| Computer application | 79.2                               | 72.4                           | 79.9                        | 78.4                    | 75.2                            | 78.4                         |
| Animation technology | 79.572.8                           | 77.4                           | 77.5                        | 74.3                    | 75.2                            | 77.1                         |

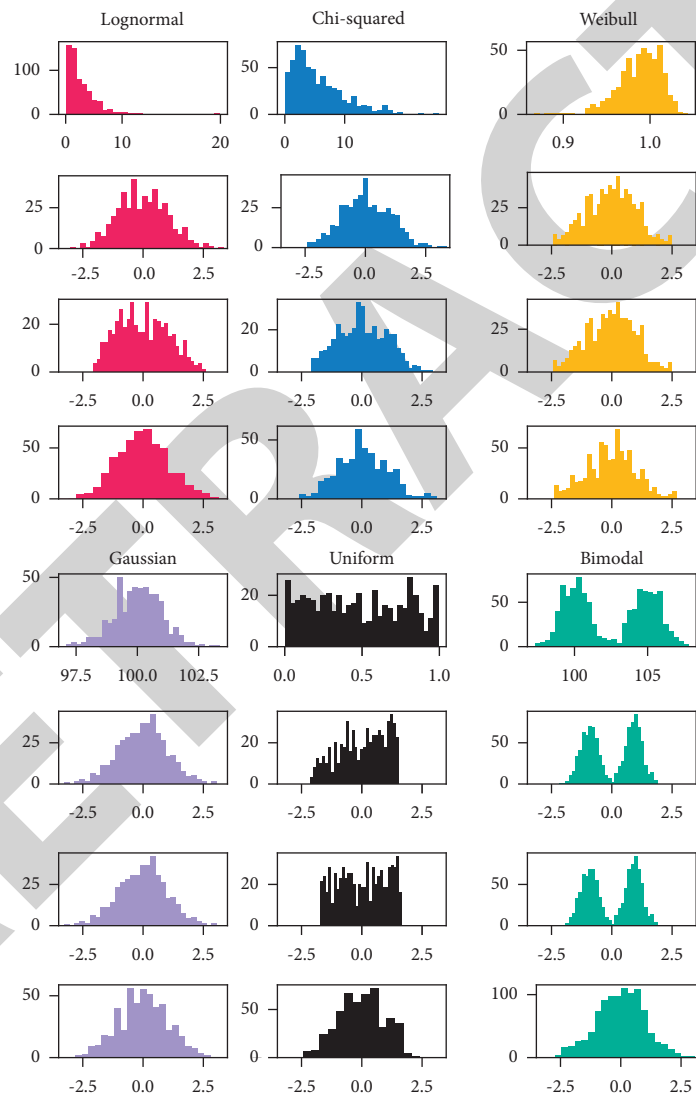


FIGURE 3: Distribution of online learning outcomes for vocal students by year.

combination of CORBA and Java technology. The B/A/S model is used, i.e., Browser/Agent/Central Server. Windows XP is used, and NT is used as the server.

In 2020, we used traditional computer-based teaching methods, and in 2021, we piloted the implementation of networked teaching for vocal courses using intelligent Agent

technology and are now conducting a comparison experiment between the two years of the vocal course (see Table 1).

The results of the comparison and interviews with some students show that students' motivation to learn is significantly improved, their hands-on skills are significantly enhanced, and the difficulty of the course is intelligently adjusted according to

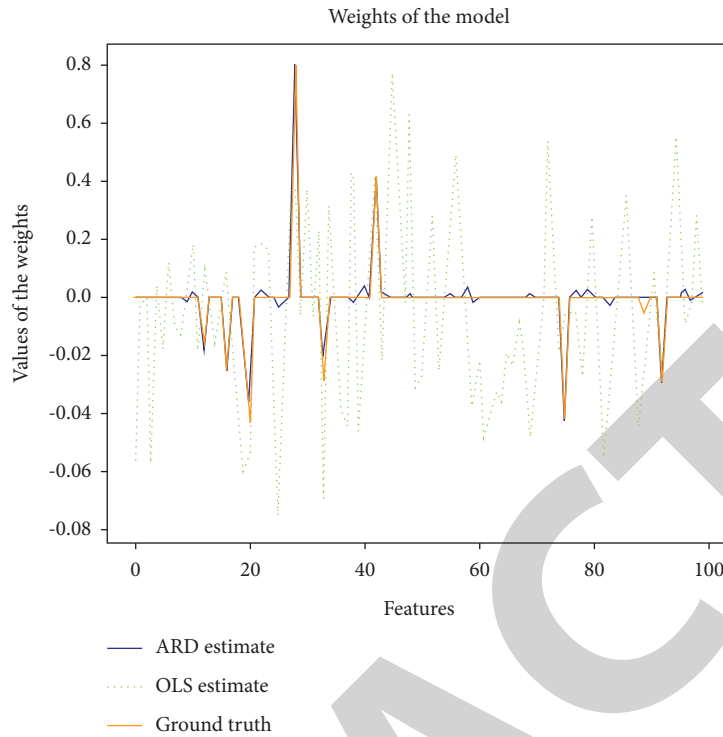


FIGURE 4: Assessment of vocal effects.

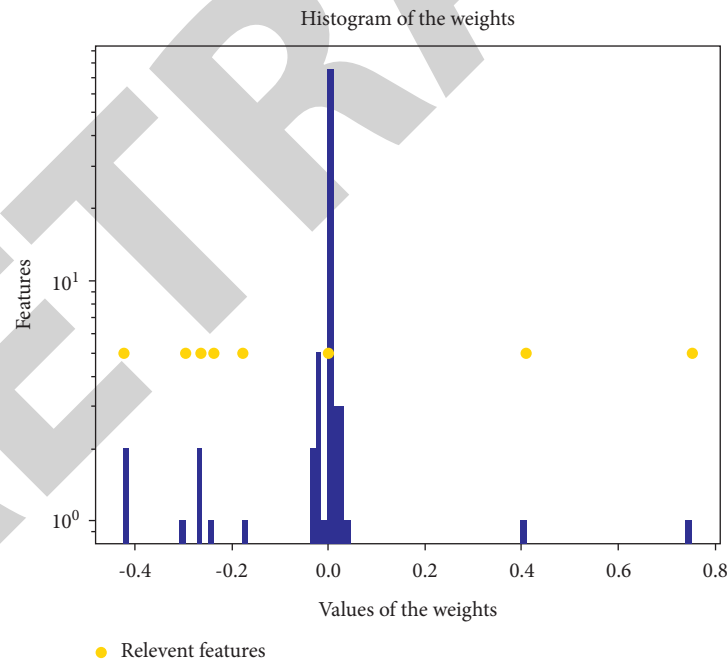


FIGURE 5: Correlation of vocal characteristics.

the level of the students, so that the potential of each individual can be maximized and students can be effectively guided to learn better. It provides an effective platform for teachers to innovate in the curriculum, reduces duplication of effort, accurately grasps students' mastery of knowledge, provides targeted instruction and improves teaching efficiency, and is welcomed by teachers [24].

As shown in Figure 3, digital technology full media bring certain facilities for vocal teaching and provide modern resources for the improvement of vocal teaching techniques. There are two sides to everything, and the same is true for modern media technology. If used accurately, it can quickly improve singing skills and enhance the knowledge and techniques we learn. The Gaussian distribution of vocal

learning results across students shows that the use of full media technology in vocal performance teaching methods and the promotion and dissemination of vocal performance teaching methods through digital technology makes it easier to improve teaching efficiency and enable students to acquire the latest knowledge [25].

As shown in Figure 4 for the vocal effect application, our students' video and audio were recorded at the beginning of their enrolment to create a record of their initial learning status. Through the intervention of digital teaching methods, students can realize their shortcomings and identify ways and means to solve their problems. At special times when parents cannot be present to watch their students' examinations, the digital network technology allows parents to see their students' learning status at school without having to leave home, greatly facilitating communication between school and parents.

In the process of learning vocal lessons in colleges and universities, vocal practice and singing songs remain an unavoidable process in vocal lessons and vocal skills are basically addressed in vocal practice pieces and songs. Due to the instability of the signal transmission or the sensitivity of the receiving equipment, the transmission of information in online courses is more or less delayed. As shown in Figure 5 for the correlation of vocal characteristics in this paper program, the network reception delay can be as much as five or six seconds in some cases if the student is in a different area. Vocal lessons require student singing and teacher accompaniment at the same time, in order to reduce the delay caused by teacher accompaniment of student singing.

## 5. Conclusion

The goal of information technology-assisted education should be to enable students to learn knowledge and skills within the limited content of the instructional curriculum, which in turn will enable students to actively use information technology to improve learning. Based on the results of the user satisfaction assessment, it was found that 89% of the students indicated that the system was helpful in mastering the details of physical dance and comprehending the connotations of the dance and thus enjoyed the physical dance, course, and more. The visual operation of the system can reduce the difficulty of learning, and the combination of DTW interactive physical and problem-oriented teaching can increase students' interest in learning and help them in learning physical dance with a more rigorous attitude. In the future, the system will also try to combine with other disciplines to implement integrated learning and enhance the learning effect. This will not only achieve the learning goals of each learning area but also develop creative thinking and problem-solving skills, achieving a win-win effect, which is also the future trend of information education.

## Data Availability

The raw data supporting the conclusions of this article will be made available by the authors, without undue reservation.

## Conflicts of Interest

The authors declare that they have no conflicts of interest regarding this work.

## References

- [1] C. J. Su, C. Y. Chiang, and J. Y. Huang, "Kinect-enabled home-based rehabilitation system using Dynamic Time Warping and fuzzy logic," *Applied Soft Computing*, vol. 22, pp. 652–666, 2014.
- [2] K. E. Raheb, M. Stergiou, A. Katifori, and Y. Ioannidis, "Dance interactive learning systems: a study on interaction workflow and teaching approaches," *ACM Computing Surveys*, vol. 52, no. 3, pp. 1–37, 2020.
- [3] D. J. Dürrenmatt, D. Del Giudice, and J. Rieckermann, "Dynamic time warping improves sewer flow monitoring," *Water Research*, vol. 47, no. 11, pp. 3803–3816, 2013.
- [4] C. Tapia Cortez, S. Saydam, J. Coulton, and C. Sammut, "Alternative techniques for forecasting mineral commodity prices," *International Journal of Mining Science and Technology*, vol. 28, no. 2, pp. 309–322, 2018.
- [5] Z. Gao, P. Zhang, and L. W. Podlog, "Examining elementary school children's level of enjoyment of traditional tag games vs. interactive dance games," *Psychology Health & Medicine*, vol. 19, no. 5, pp. 605–613, 2014.
- [6] C. Huang and Z. Gao, "Associations between students' situational interest, mastery experiences, and physical activity levels in an interactive dance game," *Psychology Health & Medicine*, vol. 18, no. 2, pp. 233–241, 2013.
- [7] P. A. Hastie, A. MacPhail, A. Calderón, and O. A. Sinelnikov, "Promoting professional learning through ongoing and interactive support: three cases within physical education," *Professional Development in Education*, vol. 41, no. 3, pp. 452–466, 2015.
- [8] K. Chandra, A. S. Marcano, S. Mumtaz, R. V. Prasad, and H. L. Christiansen, "Unveiling capacity gains in ultradense networks: using mm-wave NOMA," *IEEE Vehicular Technology Magazine*, vol. 13, no. 2, pp. 75–83, 2018.
- [9] J. Du, C. Jiang, Z. Han, H. Zhang, S. Mumtaz, and Y. Ren, "Contract mechanism and performance analysis for data transaction in mobile social networks," *IEEE Transactions on Network Science and Engineering*, vol. 6, no. 2, pp. 103–115, 2019.
- [10] A. Dania, D. Hatziharistos, M. Koutsouba, and V. Tyrovolas, "The use of technology in movement and dance education: recent practices and future perspectives," *Procedia-Social and Behavioral Sciences*, vol. 15, pp. 3355–3361, 2011.
- [11] N. Subramani, P. Mohan, Y. Alotaibi, S. Alghamdi, and O. I. Khalaf, "An efficient metaheuristic-based clustering with routing protocol for underwater wireless sensor networks," *Sensors*, vol. 22, no. 2, p. 415, 2022.
- [12] H. Singh Gill, O. Ibrahim Khalaf, Y. Alotaibi, S. Alghamdi, and F. Alassery, "Multi-model CNN-RNN-LSTM based fruit recognition and classification," *Intelligent Automation & Soft Computing*, vol. 33, no. 1, pp. 637–650, 2022.
- [13] C. Steinberg and F. Steinberg, "Importance of students' views and the role of self-esteem in lessons of creative dance in physical education," *Research in Dance Education*, vol. 17, no. 3, pp. 189–203, 2016.
- [14] O. A. Sinelnikov, "Using the iPad in a sport education season," *Journal of Physical Education, Recreation and Dance*, vol. 83, no. 1, pp. 39–45, 2012.

## Research Article

# Design of Music Teaching System Based on Artificial Intelligence

Wei Chen 

Music and Dance Department, Zhengzhou Normal University, Zhengzhou 450000, Henan, China

Correspondence should be addressed to Wei Chen; [chenwei@zznu.edu.cn](mailto:chenwei@zznu.edu.cn)

Received 6 May 2022; Revised 17 June 2022; Accepted 20 June 2022; Published 6 July 2022

Academic Editor: Hangjun Che

Copyright © 2022 Wei Chen. This is an open access article distributed under the Creative Commons Attribution License, which permits unrestricted use, distribution, and reproduction in any medium, provided the original work is properly cited.

This paper analyzes the application basis of AI technology in music teaching and realizes the extraction of music features. In addition, an intelligent music teaching model based on the RBF algorithm is constructed, which determines the way of music learning, and thus, an intelligent music teaching system is designed. The system constructed can realize the effective interaction between teachers and students, improve learners' singing style to the maximum extent, and play a good auxiliary role in students' music knowledge learning.

## 1. Introduction

Learning music is very important for students' long-term development, and music is also a compulsory course in basic education. Besides imparting theoretical knowledge, music teaching should pay more attention to the cultivation of students' music skills. However, the present situation of music teaching cannot meet people's expectations. Traditional music teaching belongs to the class teaching system where there are not many music lessons per week, and students must learn theoretical knowledge and singing practice at the same time [1,2]. With the rapid development of the economy, in the Internet era, intelligent electronic musical instruments are constantly being introduced [3]. These intelligent electronic musical instruments can not only store a wide variety of musical instrument timbres but also realize the effective arrangement of them, so that they can perform orderly music according to the corresponding behavior instructions. Obviously, the function of this musical instrument is difficult for traditional musical instruments to realize. Therefore, AI has a unique advantage in music education. Digitizing sound signals through AI technology is not only convenient for preservation and reproduction but also characterized [4,5]. Digital audio is easy to record, easy to store, and spread, so it can be combined with traditional music teaching to help teachers give feedback and guidance to students' singing and make up

for the current situation of traditional music teaching with few class hours and lack of teachers.

In addition, the AI music software makes music tasks that used to be edited by music synthesizers or music practitioners only need to be handed over to the computer, thus greatly improving the processing capacity of music data and broadening the storage space of music information. Users can freely edit, adjust, record, and carry out AI processing on a variety of different musical elements [6–8]. The application of artificial music software in music teaching provides an interactive platform for teachers and students to teach and learn, which greatly changes traditional music teaching methods.

In view of the present situation of traditional music teaching in the basic education stage, such as students' weak music foundation, large differences in individual learning progress, lack of music equipment, shortage of teachers, and limitation of music hours, this study integrates AI technology into music teaching, aiming at developing a set of music teaching system based on a feature comparison.

## 2. Theoretical Basis of AI in Music Education

*2.1. Emotional Interaction Theory.* Emotion is a special way of thinking of human beings, which contains a complex operating mechanism. The emotion obtained by molding machines to develop technical problems of AI is mainly



applied to music teaching by creating six dimensions of emotional machines, namely consciousness, mental activity, common sense, thinking, intelligence, and self [9]. This explains the complex mechanism of the human brain and confirms the possibility of applying emotional machine to music teaching. Emotion interaction is emotion calculation based on AI, which endows computers or machines with the ability of human beings to communicate similar or identical observations, understanding, and various emotions. In the process of communicating with machines or computers, it is more natural and convenient that for personalized music education, AI teachers are used to solve problems that students encounter, and when there is an error in music practice, the intelligent system talks about the error, as shown in Figure 1.

Music learners access the learning combination, generally a learning platform, by logging in to the client, and then presenting the learning results to the teachers through the man-machine interaction mode. However, the teachers improve the new teaching model through their achievements and improve the learners' learning awareness and learning ability based on negative feedback, thus forming an interactive closed loop. Compared with the traditional evaluation methods, the teaching system based on AI adopts developmental feedback and reasonably applies emotional evaluation to improve the teaching efficiency of music learners.

**2.2. Evaluation Criteria.** Although it is difficult for computers to perceive people's emotions, there are ways to detect intonation, rhythm, and breath smoothness. In terms of intonation, this study decided to use a pitch feature sequence to represent it. Taking time as a unit, the sound signal is divided into small enough frames, and the pitch of them is extracted to generate a sequence of sound features. In addition, by calculating the number of consecutive pitches with the same pitch value, the sound length of a note can be calculated.

In the aspect of rhythm, it is particularly important to judge the rhythm after extracting the pitch characteristic sequences of singing signals and template music, respectively. The judgment of rhythm is realized by comparing the values of template music pitch and singing voice pitch at the same time. If the pitch value of the template music is 0 but the singing voice pitch value is not negative, or if the pitch value of the template music is not only the pitch value of the singing voice but also the pitch values of more than a dozen or even dozens of tones in succession appear in this situation, it can be judged that the singing rhythm does not correspond.

### 2.3. Extraction of Music Feature

**2.3.1. Pitch Characteristics.** As a whole, the sound is constantly changing with time, so it cannot be analyzed and processed by ordinary methods. However, in a short time range, its characteristics basically remain unchanged, so it is considered that the speech signal has short-term stationarity.

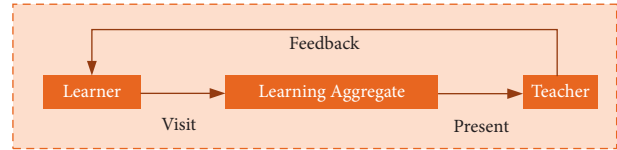


FIGURE 1: Emotional interaction in music teaching.

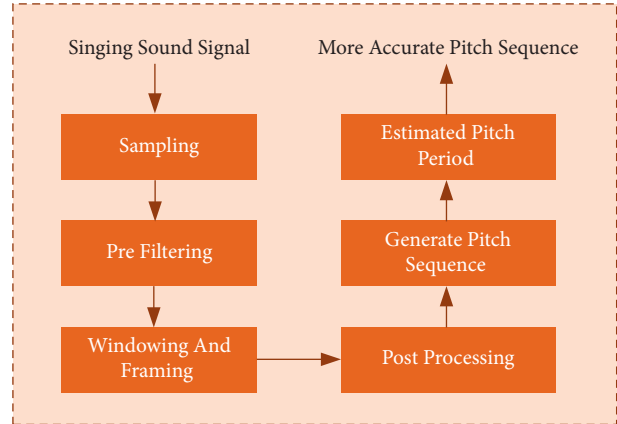


FIGURE 2: Process of pitch extraction.

According to the characteristics of short-term stationarity of speech signals, by adding a rectangular window or Hamming window to it, the speech signal is split into a series of small speech signals, each of which is a pause, and then, the pitch period of each signal is calculated, as shown in Figure 2.

**2.3.2. Melody Features.** Compare the students' singing voice with the standard music to judge. As MIDI files are instruction music files, similar to music scores, from which more accurate music information can be directly extracted, therefore, taking MIDI files as a template for singing comparison can make the judgment result more accurate and more reliable. The results are taken as music templates for students to sing for comparative assessment. MIDI files are composed of a header block and one or more audio track blocks. One of the tracks contains the singing score information of the song, which is the main track. If it has only one track, this track is the main track, and while there are multiple tracks, it is necessary to judge the main track by extracting the main track in the song file and then extracting melody features.

**2.4. Application of FMS.** Flash Media Server (FMS) is mainly used as a platform for users to communicate with each other, which has the characteristics of multimedia interaction, real-time audio, real-time video, and real-time data stream. By installing FMS3 on the Windows platform, there will be an applications folder under the installation directory, and all the server applications will be placed in it. The folder name of the application must be consistent with the name of the application; that is, if the application name is "micRecord," it must be placed under a folder called "micRecord." Then, FlashDevelop software is adopted to program, which realizes

the connection between microphone and FMS. The flow chart is shown in Figure 3.

The program is written in AS3 language, and its function is to complete the generation operation of WAV format music files according to the WAV format standard. Afterwards, the sound signal is saved as an audio file in WAV format, which is convenient for students to call out the original singing and self-singing for voice comparative analysis. Before using THE AS3WavSound program to generate WAV files, you can freely make some presets to determine the generation of a WAV file, such as mono or stereo, the sampling frequency can choose 11025 Hz, 22050 Hz, or 44100 Hz sample bit rate can choose 8 bit or 16 bit.

### 3. Intelligent Music Teaching Model

The intelligent music teaching system proposed in this paper adopts the RBF algorithm, which is a neural network composed of locally adjusted neurons [10,11]. It generally has a five-layer network, as shown in Figure 4.

The first layer is the information factors related to the case, and these inputs can be summarized into different music item indicators, which are input into the neural network structure.

The second layer is the membership function, and its mathematical expression is as follows:

$$\mu_{ij}(x_i) = \exp\left[-\frac{(x_i - c_{ij})^2}{\sigma_j^2}\right], \quad (1)$$

$$i = 1, 2, \dots, r; j = 1, 2, \dots, u.$$

The third layer describes the number of fuzzy rules. By learning the samples, the number of learned rules is trained the least and the most important. Among them, the output calculation of the  $j$ -th rule is shown in the following formula:

$$\phi_j = \exp\left[-\frac{\sum_{i=1}^r (x_i - c_{ij})^2}{\sigma_j^2}\right] = \exp\left[-\frac{\|X - C_j\|^2}{\sigma_j^2}\right], \quad j = 1, 2, \dots, u, \quad (2)$$

where  $c_j = (c_{1j}, \dots, c_{rj})$  represents the center of the  $j$ -th RBF unit. The characteristic of the RBF neural network is that the closer the neuron is to the center, the higher its activation degree, which is very consistent with the teaching mode of influencing factors of interactive music learning.

The fourth layer is the normalization layer. The nodes of this layer should be consistent with the fuzzy rule nodes, and the output  $N_j$  of the  $j$ -th node is shown in the following formula:

$$\Psi_j = \frac{\phi_j}{\sum_{k=1}^N \phi_k}, \quad j = 1, 2, \dots, u. \quad (3)$$

The fifth layer is the output layer, which outputs the evaluation of each skill in music performance. It is mainly based on TS fuzzy model in the RBF algorithm, and its output is shown in the following formula:

$$y(x) = \frac{\sum_{i=1}^u \left[ (a_{i0} + a_{i1}x_1 + \dots + a_{ir}x_r) \exp\left(-\left(\|x - c_i\|^2/\sigma_i^2\right)\right) \right]}{\sum_{i=1}^u \exp\left(-\left(\|x - c_i\|^2/\sigma_i^2\right)\right)}, \quad (4)$$

where  $w_k$  is the connection mode representing the  $k$ -th rule, that is, the sum of the weight products of the output variables, as shown in the following formula:

$$y(x) = \sum_{k=1}^u w_k \cdot \Psi_k. \quad (5)$$

The music learning mode based on the RBF algorithm is to integrate the algorithm idea into the design of the platform and fully show the algorithm when writing the code, which realizes the function of the platform interface, so that it can effectively match with the interactive learning mode. Among them,  $X$  is the proportion of learning time consumed by 100 students in the music system;  $c_j$  and  $\sigma_j$  refer to the distribution of hidden layer in each music learning courseware for excellent students in  $X$ . The hidden layer category of these learning samples is relatively parallel; in addition,  $Y$  is the best music score corresponding to each input layer.

In order to simplify the RBF algorithm, the second, third, and fourth layers can be classified as hidden layers, and the first and fifth layers are input layers and output layers, respectively, which are used as input layers for different aspects of music teaching. When aiming at a series of large-scale data, the first  $m$  data of music data are taken as initial training, and then, an RBF model for students to learn music knowledge can be constructed, as shown in Figure 5.

### 4. Design of Intelligent Music Teaching System

**4.1. Demand Analysis.** There are two main target users of this system. The first target is students, especially those in basic education. Because their knowledge construction ability is not perfect, they need to understand abstract music knowledge such as pitch, melody, whole tone, and semitone in the study of music. In the process of music learning, it is necessary to train pronunciation and correct intonation. Because there are also remote areas where music teachers are scarce, it is urgent to find a channel that can provide professional guidance for one's own theoretical study and singing.

The next target is music teacher. They should have rich professional knowledge of music and be able to guide students in singing training to practice pitch and intonation and improve their singing level.

Based on the characteristics and needs of target users, this system emphasizes more on education. Therefore, in the design and development of the system, more emphasis should be placed on the standardization of reference audio, the accuracy of data processing, and the professionalism of feedback guidance. Therefore, it should have the following functions: selecting songs, listening to songs, recording singing, grading, correcting errors, saving recording and

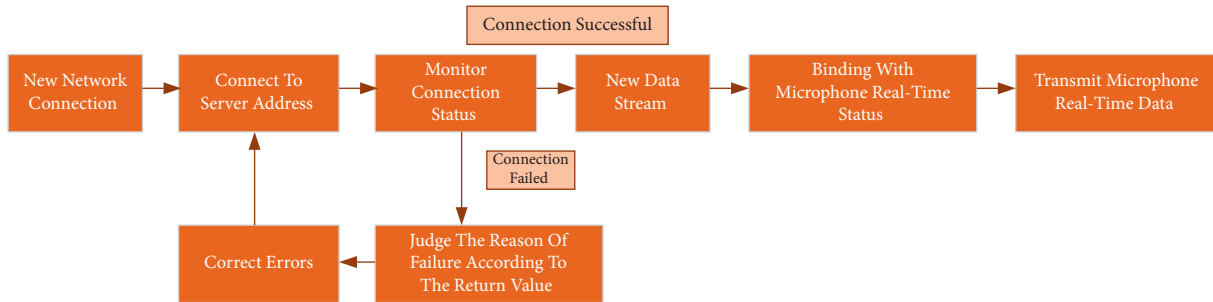


FIGURE 3: Transmission of FMS data.

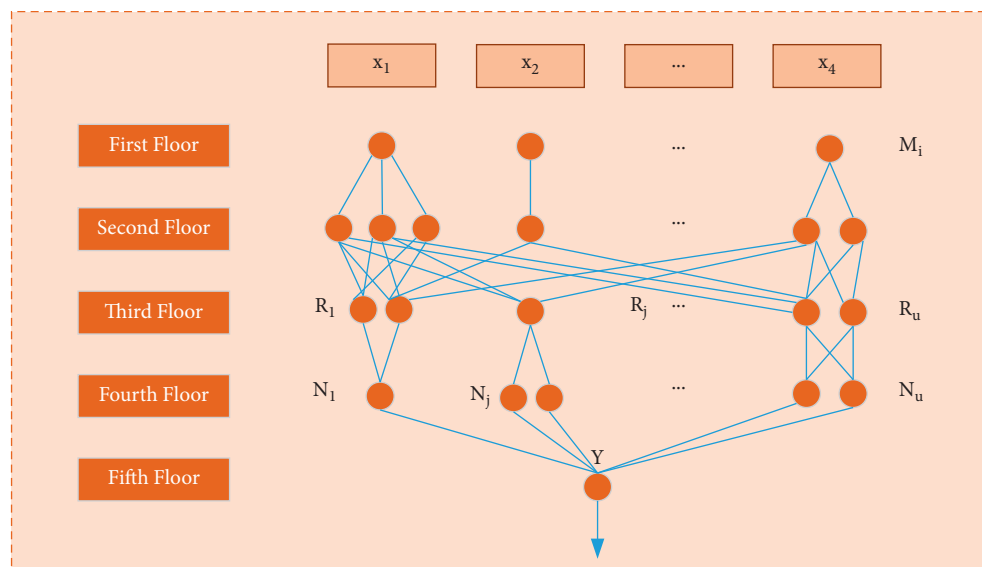


FIGURE 4: Structure of RBF neural network.

evaluation results, and comparing original and self-singing and uploading music templates.

**4.2. Frame Design.** According to the demand analysis of the music teaching system, the design of the systematic framework is shown in Figure 6.

The user module converts the analog signal of students' singing voice into a digital signal and then transmits it to the audio feature extraction module. The module extracts the pitch characteristics of the audio input by the user to obtain the singing pitch sequence to be compared. On the other hand, after the students select the track, the system will call out the template audio sequence of the corresponding track from the music feature library. The music feature library contains the audio files of all songs in the template music library, which is generated by the feature extraction module.

After singing, the similarity comparison module compares the singing pitch sequence with the template pitch sequence and finally obtains the short-term score and the total score. Afterwards, the feedback module lists the five items with the lowest short-term scores, determines the causes of errors according to the pitch data, and gives improvement strategies to learners, so that students can practice singing next time.

The operation process of users is as follows:

- (1) Select songs through the user input interface, then enter the singing stage, and grasp the overall rhythm according to the information such as song mode, beat, and speed displayed on the interface
- (2) Sing it through the microphone at the right time when listening to the accompaniment of the song
- (3) After singing, the system will give the singing score, the reasons for mistakes, and suggestions for improvement

In addition, students can select a section of audio according to the visual pitch curve, freely switch between self-singing and original singing, visually and audibly compare the difference between self-singing and original singing, and correct mistakes.

#### 4.3. Design of Functional Modules

**4.3.1. Template Music Library Module.** At present, the accuracy rate of extracting the main melody of multimusic is low, and only with accurate template data can the scoring results and feedback information be calculated with high credibility. Because this system is designed for music

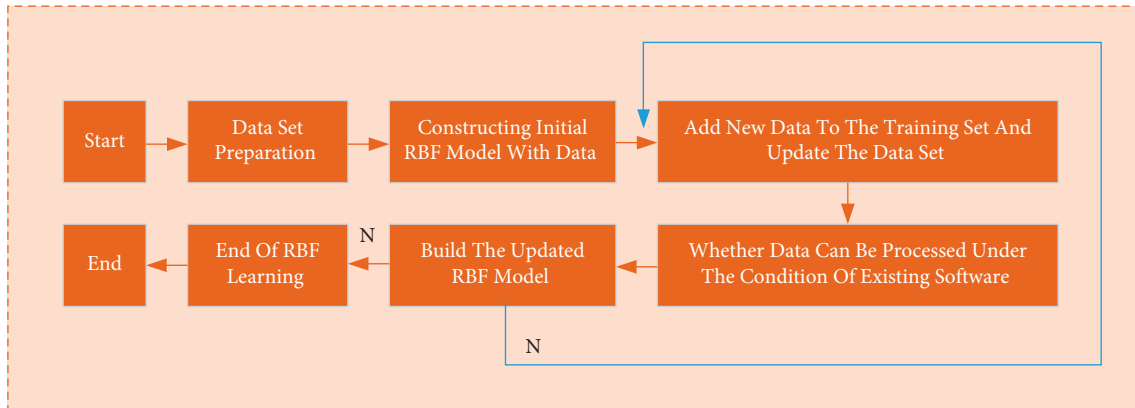


FIGURE 5: Implementation process of RBF model.

education, it requires high accuracy of music data, and it is necessary to avoid using polyphonic music to build a database. The construction of a common music feature database is mainly divided into three types: WAV files, music score information, and MIDI analysis.

This system uses MIDI to build a database. In addition to the large amount of music data that comes with the system, it also supports music teachers to upload MIDI files to expand the music library. Ways for teachers to obtain MIDI files are included as follows:

- (1) *Download MIDI files through the network.* MIDI files are small in size, easy to store, spread, and make, which makes many MIDI files available for downloading on the network.
- (2) *Creating MIDI music.* MIDI music can be made by software such as Sonar or connected to the computer by devices with MIDI interface, such as the electronic keyboard. By playing music, MIDI data can be directly input into the computer through a sound card to synthesize MIDI files.

In addition, in the music template library, the extracted MIDI main melody pitch feature sequence of a song is associated with the song name, accompaniment, and lyrics and stored in the database together. When the user selects the song, the system can directly call up the template pitch data for comparison.

**4.3.2. User Input Module.** The most important function of the module is real-time recording, which converts the analog signals of students' singing practice into digital signals and stores them for later processing. Besides, it also includes some interactive functions, such as selecting practice tracks, playing accompaniment, starting, pausing, ending, and other control functions, and some display functions, such as displaying the name and duration of the selected song, as well as melody information such as mode, beat, and speed.

**4.3.3. Music Feature Extraction Module.** The function of the feature extraction module is to extract the feature information of music, which is convenient for similarity

comparison and as the basis for error correction. The difference between music lies mainly in the difference in the melody that is related to pitch, length, and rhythm. As the sound length involves cutting notes, accurate cutting of notes is always a difficult point in the field of audio processing. Especially, for the audio input by the user, it will reduce the credibility of the later comparison results. Therefore, this system uses pitch as a feature vector to represent music. Since time has absolute correspondence with audio signals, the sound length can be understood as the number of frames with the same pitch.

**4.3.4. Similarity Comparison Module.** The function of the similarity comparison module is to compare the extracted singing pitch feature sequence with the template pitch feature sequence and get the scoring result. The purpose is to compare the students' singing situation with the template and evaluate whether the students' singing is accurate. In the course of students' singing, the pitch sequence of singing and template audio is compared in sections with a fixed duration as a unit, and the short-term singing score is obtained. The system sets this fixed duration to seconds. After the singing is finished, the system will normalize the vocal data and calculate its total score, which can give feedback to students in time during the singing process and facilitates the system to locate the wrong position according to the score.

**4.3.5. Feedback Module.** The feedback module is the most important module in this system. Only by accurately analyzing students' problems in singing and reminding them to make targeted corrections can we really improve students' singing levels. The study of singing or performance belongs to the study of motor skills which refers to the process of relatively lasting changes in athletic ability caused by practice or experience.

In this paper, the content of feedback includes not only the overall evaluation of the singing situation but also the short-term scoring of the lowest scores, analysis of the causes of errors, and suggestions for correction. In addition, the demonstration of the original singing in the wrong position is also provided for students to compare and then carry out

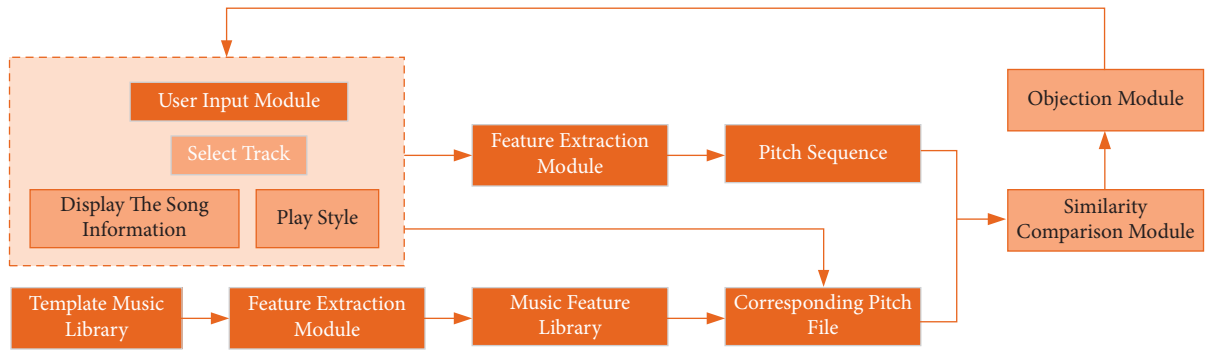


FIGURE 6: Systematic framework.

| Feedback Category  | Feedback Mode   | Presentation Mode | Sensory Experience |
|--------------------|---|-------------------|--------------------|
| Immediate Feedback | Real Time Display Of Pitch Curve Of Original Singing And Self Singing | Image             | Vision             |
| Delayed Feedback   | Total Score   | Written Words     | Vision             |
| Delayed Feedback   | Error Location And Correction Suggestions                             | Text, Image       | Vision             |
| Delayed Feedback   | Comparison Of Original Singing, Self Singing Audio And Pitch Curve    | Audio, Image      | Hearing And Vision |

FIGURE 7: Characteristics of different feedback methods.

the targeted practice. Finally, guidance, demonstration, practice, and feedback are carried out circularly.

The feedback mode adopted by this system is shown in Figure 7.

When designing feedback methods, the advantages and disadvantages of immediate feedback and delayed feedback are considered. Immediate feedback is to give feedback information in real time during students’ singing or playing; delayed feedback refers to giving feedback information after singing or playing. In this study, the system uses a combination of immediate feedback and delayed feedback. The advantages of storage and analysis of delayed feedback are used to make up for the shortness of immediate feedback. The immediate feedback is used, because the delayed feedback cannot remind students to correct pitch immediately.

### 5. Conclusion

Through the extraction of music features, this paper puts forward an intelligent music teaching model based on the RBF algorithm, determines the way of music learning, and designs an intelligent music teaching system. According to

the result of the requirement analysis, the design of the systematic flow is completed, and the function design of each module of the system is carried out. Among them, the template music library module is constructed by MIDI music files to obtain more accurate comparison templates; the user input module uses FMS to record and save students’ singing voice in real time; the feature extraction module realizes the feature extraction of singing audio and template music, so that the similarity comparison module can get accurate comparison results; feedback module can improve learners’ singing style to the maximum extent.

### Data Availability

The dataset can be accessed upon request.

### Conflicts of Interest

The authors declare that they have no conflicts of interest.

### References

[1] M. Zou, “AI and its application in music education,” *Northern Music*, vol. 38, no. 15, p. 162, 2018, in Chinese.

- [2] J. Zhang and P. Han, "Research on the application of AI in network education," *Computer Simulation*, vol. 31, no. 2, pp. 259–263, 2014, in Chinese.
- [3] J. Liu, "Application of AI in network education," *Computer CD-ROM Software and Application*, vol. 9, no. 6, p. 244, 2014, in Chinese.
- [4] D. Williams, A. Kirke, E. Miranda et al., "Affective calibration of musical feature sets in an emotionally intelligent music composition system," *ACM Transactions on Applied Perception*, vol. 14, no. 3, 2017.
- [5] D. Liu, N. Zhang, and H. Zhu, "Review of music feature recognition," *Computer Engineering and Application*, no. 24, pp. 74–77, 2002, in Chinese.
- [6] Y. Gu, "Modern music education and modern AI/IT technology," *Music Exploration*, no. 2, pp. 104–107, 2007, in Chinese.
- [7] X. Hang, "Present situation and future development of music education software in teaching," *Contemporary music*, no. 1, pp. 154–157, 2021, in Chinese.
- [8] J. Zhang and Y. Zhao, "Research and application of intelligent system of interactive teaching music based on AI," *Micro-computer Applications*, vol. 37, no. 4, pp. 45–48, 2021, in Chinese.
- [9] X. Liu and F. Yin, "Research on automatic piano accompaniment system with human-computer interaction," *Computer Knowledge and Technology*, vol. 7, no. 12, pp. 2748–2750, 2011, in Chinese.
- [10] H. Zhang and W. Luo, "Analysis of the application of AI in computer network technology in the era of big data," *Communication and Information Technology*, vol. 392, no. 3, pp. 52–53, 2019, in Chinese.
- [11] Y. Chao and W. Guo, "Application of AI system in music education and teaching in primary and secondary schools," *Art Review*, vol. 2019, no. 15, pp. 107–108, 2019, in Chinese.

## Research Article

# ODL Centralized Control of Power Communication Network Based on Bio-Inspired Algorithms and SDN

Congcong Min 

*Guangdong Communications & Networks Institute, Guangzhou 510671, Guangdong, China*

Correspondence should be addressed to Congcong Min; [epcheesefitness@mail.scut.edu.cn](mailto:epcheesefitness@mail.scut.edu.cn)

Received 23 March 2022; Revised 20 May 2022; Accepted 1 June 2022; Published 30 June 2022

Academic Editor: Man Fai Leung

Copyright © 2022 Congcong Min. This is an open access article distributed under the Creative Commons Attribution License, which permits unrestricted use, distribution, and reproduction in any medium, provided the original work is properly cited.

An ODL centralized control strategy is designed to study the problem of heavy load in the power communication network, in which the machine learning method is introduced. SDN technology is used to establish SDN cluster control structure, and different algorithms, such as genetic algorithm, are utilized to optimize resource scheduling. The results show that the improved algorithm obtains the shortest link path through 28 iterations. At the same time, AHP is used to switch the network spectrum. Moreover, the application effect of the control strategy is simulated and analyzed, and its effect on network communication application is verified.

## 1. Related Work

Technologies such as cloud computing and big data continue to develop but, at the same time, begin to penetrate into traditional industries. Among them, the construction and management of power grid began to adopt intelligent new technology, and the construction of smart power grid has become an inevitable trend. However, with the growth of the power communication network business, the network load increases gradually. In addition, the problems of resource waste and low compatibility in the traditional electric power communication system affect the quality of electric power service. Therefore, people propose to introduce SDN into network deployment. Software-defined networking (SDN) is also gaining popularity in power systems [1]. It is a new software-defined network model, which separates control and data forwarding functions, so as to realize centralized operation and maintenance control of power communication network resources. At the same time, its programmable advantage can achieve a wide range of power communication business expansion. Standard southbound interface and virtual network layer can promote the close integration of new power equipment and control network. In a word, it liberates a lot of manpower, avoids many configuration failures, and is easy to deploy uniformly and quickly, so as to

make up for the defects of traditional communication network single decentralized control, which has been successfully applied in some data centers and cloud computing networks [2, 3]. Therefore, the centralized management and control architecture of distribution communication network based on SDN is designed, and the realization scheme of various control functions is studied, so as to provide a theoretical basis and demonstration reference for the construction of a new generation of power communication network, in which resources are uniformly controlled, network and data are coscheduled, and business needs are rapidly answered. At present, there are many researches on SDN deployment. For example, in April 2014, Beijing Telecom completed the commercial deployment of SDN in cooperation with Huawei, successfully applied SDN technology to IDC (Internet data center) network, and released a series of new IDC businesses based on SDN [4, 5]. In 2017, the ZENIC SDON innovation scheme of ZTE applied SDN technology to the WDM/OTN network, which can provide BoD, PoD, and OoD services on demand and support rapid deployment of multilevel services including L3/L2/L1/L0.

At the same time, aiming at the optimization problem of the power network, some scholars have proposed a large number of artificial intelligence algorithms. For example, Liu applied the genetic algorithm to network QoS optimization

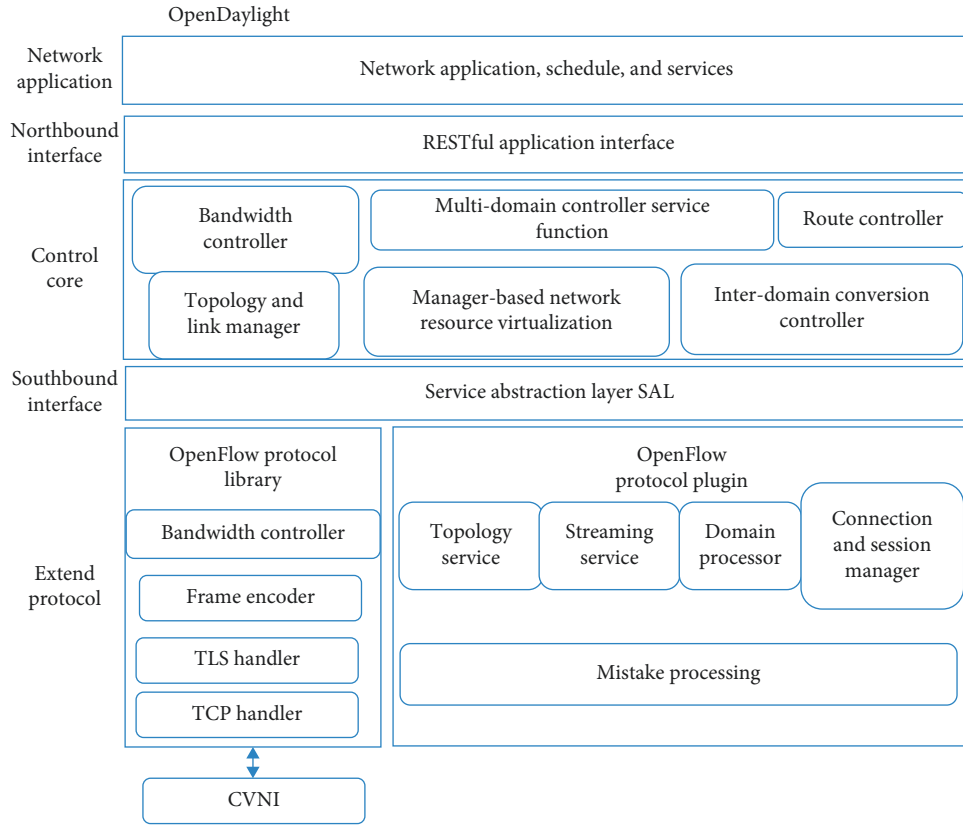


FIGURE 1: Overall architecture of ODL.

and obtained the scheduling sequence with the shortest task span and average task calculation time, which greatly improved the performance of the network [6]; Wang et al. put forward the bandwidth and capacity optimization method of elastic optical networks (eon) based on mixed-integer linear programming model [7]. The results show that this method can not only improve the overall network capacity but also minimize the number of allocated time slots and service request blocking rate; Rongheng Lin and others proposed a bat SDN network scheduling method, which transforms the resource reservation problem into a multiknapsack problem [8]; Liang et al. used ant colony algorithm to schedule network resources. Experiments show that this method can effectively reduce the time of network resource scheduling [9]; Lalitha Devi et al. and Yi et al. proposed a joint beam and power scheduling scheme and solved the scheduling scheme by Bayesian algorithm [10, 11]; Praveena and Vijayarajan proposed that the energy consumption of mobile cloud network through the neural network is the lowest [12]. The results show that through optimization, the power consumption is reduced by 53.68%; Faroqal Tam and others introduced the deep reinforcement learning method to schedule the resources of a 5g MAC layer wireless network [13]. The results show that this method has a positive impact on network resource scheduling. Aiming at the resource control problem in the SDN network, this study proposes a centralized control scheme based on ODL, so as to better promote the scheduling and effective utilization of SDN network resources. The innovation of this research is that

combined with the ODL centralized control method, two methods are proposed for optimization, and a variety of machine learning algorithms are introduced for optimization, so as to greatly improve the efficiency of ODL centralized control and provide a reference for the multialgorithm application of ODL control.

## 2. The ODL Centralized Control Framework in This Paper

ODL is generally divided into the controller, network application layer, and north-south interface, and each part has different functions. The southbound protocol layer is a module that provides support for different protocols of the device, such as LISP. The northbound interface layer provides a standard set of Rest interfaces to external applications while supporting the cluster working mode. The ODL is the core of SDN control. Among them, the controller supports link management, bandwidth control, application development, and other functions, which is essentially a platform with a high open degree. The network application layer can be used to obtain network information, so as to achieve effective control of network behavior, which has high flexibility. For the north-south interface, the southbound interface is related to format conversion and data transmission, which supports different types of protocols. And northbound interface adopts RESTful protocol to expand interactive interfaces [14–17]. The specific structure is shown in Figure 1.



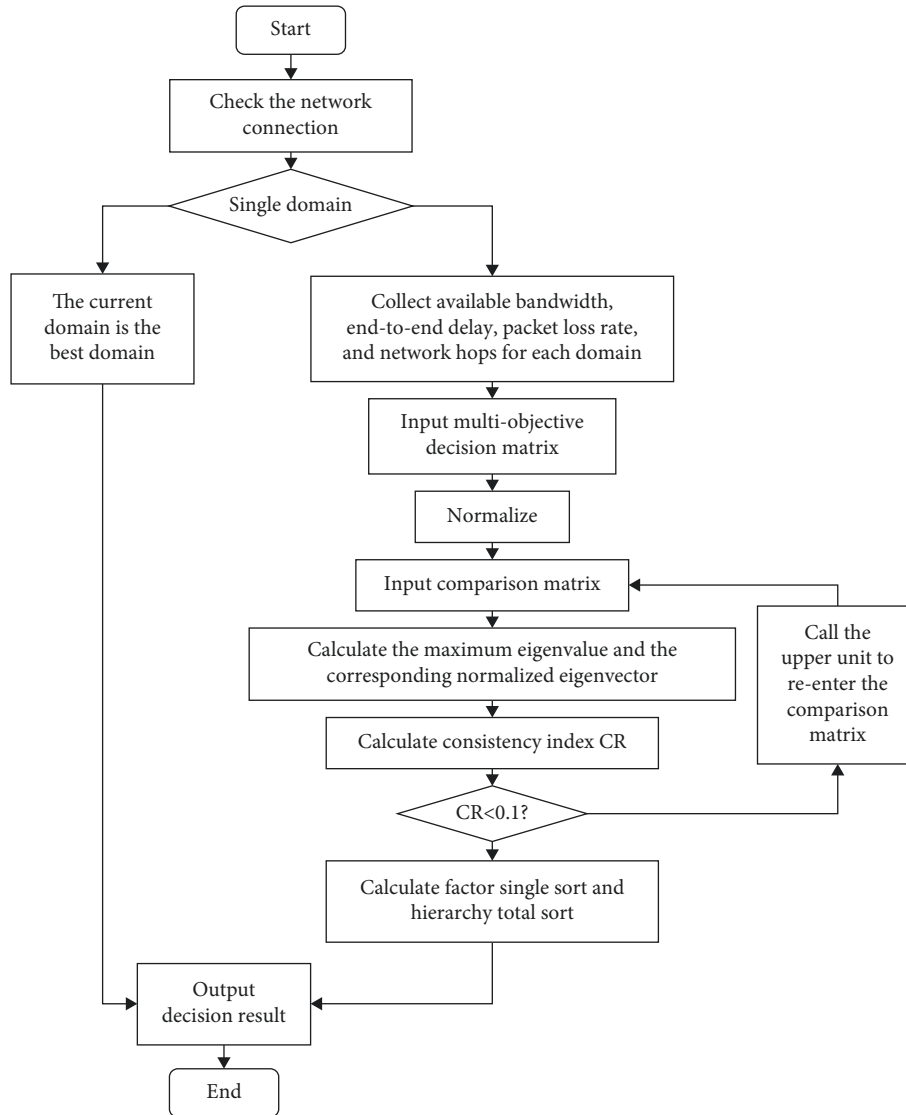


FIGURE 2: Basic process of the algorithm.

In order to realize the virtualization expansion of the network, the open switch software is introduced in this design, which is convenient to control virtual machines and traffic effectively.

### 3. Research on Bandwidth Resource Allocation Combining Genetic and Ant Colony Algorithm

Combined with the background of the ODL overall control framework in Figure 1, this study mainly studies and analyzes from the perspective of spectrum resource allocation and spectrum switching [18–20].

*3.1. Power Distribution Communication Service Spectrum Arrangement Based on Genetic Algorithm.* With the continuous development of the power distribution business, various types of services have also begun to appear, showing

a general trend of diversified development, which further optimizes the network of Figure 2 and strengthens the scheduling of spectrum resources of SDN networks. There are also certain differences in communication nodes for the management of various business facilities, which put forward different requirements for the communication link spectrum. In this kind of business, communication spectrum needs to be allocated, which is studied deeply. Comparing different algorithms, and after analysis, a genetic algorithm is used in this study. The user ids are 1, 2, 3, ..., N, and the L matrix is utilized to select the user’s free spectrum, and then, all are matched one by one with users. It is known that users 1 and 2 are matched with spectrum B and C, respectively, which are represented as  $1^B$  and  $2^C$  in turn. According to this matching method, chromosome  $1^B, 2^C, \dots, N^A$  can be obtained. If the evolution rate needs to be compared,  $1^{0010}, 2^{0011}, \dots, N^{0001}$  can be obtained in binary form.

Chromosomes that meet the requirements can be obtained by random matching of spectrum resources. Then, the

corresponding chromosomes are obtained on the basis of the reasonable grouping of genes. For reasonable settings of algorithm parameters, the population size is set to 50.

The basic process of crossing is as follows: the first is to set the crossing probability  $P_c=0.6$ . If the probability is lower than this value, the crossing operation is performed. The crossover points need to be set arbitrarily at first, and the value range is  $[1, n]$ , and then, the chromosome segments are crossed. Moreover, the remaining fragments are stored in arrays  $x []$  and  $y []$ . Comparing the fragments after crossing, if there are different elements, replacement is performed. The specific mutation is as follows: the value of any generated integer rand key is 1, 2, and 3, which corresponds to the insertion, inversion, and swap operations, respectively.

When using a genetic algorithm, appropriate parameters need to be set. Here, the minimum value of evolution rate and the corresponding continuous algebra are represented as  $Gene_{min-imprion-rane}$  and  $Gene_{die}$ , respectively, and the maximum and minimum values of iteration are  $Gene_{max}$  and  $Gene_{min}$ , respectively. In the iteration process, if the conditions are met, the iteration ends, which includes the continuous  $Gene_{die}$  generation of iteration or the number of iterations reaching  $Gene_{max}$ . The resolution improvement rate is lower than  $Gene_{min-imprion-rane}$ .

### 3.2. Power Distribution Communication Service Spectrum Selection Based on Ant Colony Algorithm.

$$\begin{cases} \Delta r'_{ij} = Q * b_{ij}, \text{ there is an edge between cognitive user } i \text{ and authorized user } j \\ \Delta r'_{ij} = 0, \text{ there is no edge between cognitive user } i \text{ and authorized user } j, \end{cases} \quad (2)$$

where  $b_{ij}$  and  $Q$  represent the benefit and adjustment coefficient, respectively.

(2) Use authorize user nodes to select policies. The formula for selecting node  $j$  is as follows:

$$\begin{cases} j = RW(p_j^x), q \leq q_0 \\ j = \arg \max(p_j^x), \text{ other,} \end{cases} \quad (3)$$

where  $P_j^x$  and  $q_0$  represent transition probability and threshold parameters, respectively, and the latter is set to 0.9.  $Q$  stands for a random number, and its value ranges from 0 to 1.

$$P_j^k = \frac{(r_{ij}(t))^\alpha (b_{ij})^\beta}{\sum_{w \in j} [(r_{ij}(t))^\alpha (b_{ij})^\beta]}, \quad (4)$$

where  $i$  represents the nodes that ants can access and and is not a node in the tabu table.

(3) Set algorithm parameters, where  $Q=10$ ,  $\rho=0.2$  and  $\alpha=\beta=1$ , respectively.

(4) Set the number of ants, namely the number of user nodes  $n$ .

(1) Ant colony algorithm (ACO) is introduced in spectrum allocation of power communication network, which is helpful to improve the reliability and efficiency of spectrum allocation [21–23]. In the study of spectrum allocation, a bipartite graph  $G = V, U, E$  is adopted, where  $V$ ,  $U$ , and  $E$  represent the user, the authorized user, and the connection edge, respectively. Furthermore, there is  $E = \{e_{ij} | i = 1, 2, \dots, n; j = 1, 2, \dots, l\}$ , and edge  $e_{ij}$  connected represents that  $i$  is matched to the authorized user  $i$ .  $T_{ij}$  represents the trace of this edge. If  $i$  and  $j$  are not connected,  $T_{ij} = 0$  can be obtained.

(i) *Update pheromone.* The specific update formula is as follows:

$$\begin{cases} \tau_{ij}(t) = (1 - \rho) \tau_{ij}(t) + \Delta'_{ij} \\ \tau_{ij}(t) = \tau_{ij}(t)_{\max}, \tau_{ij}(t) > \tau_{ij}(t)_{\max}, \\ \tau_{ij}(t) = \tau_{ij}(t)_{\min}, \tau_{ij}(t) < \tau_{ij}(t)_{\min} \end{cases} \quad (1)$$

where  $T_{ij}(t)_{\max}$  and  $T_{ij}(t)_{\min}$  represent the maximum and minimum pheromone values of  $e_{ij}$  in turn. The former value is infinite, and the latter is set to 60.  $\rho$  represents the volatilizing rate of pheromone.  $\Delta'_{ij}$  refers to the increased value in trace on  $e_{ij}$ , and its formula is as follows:

(5) The ending condition of the ant colony algorithm is as follows: the first iteration number reaches  $Ant_{\max}$ ;  $b$  iterates continuous  $Ant_{dot}$ , and the improvement rate of the child optimization solution is always less than  $Ant_{max-imprion-rane}$ .

3.3. *Bandwidth Resource Optimization Strategy Based on Ant Colony Algorithm and Genetic Algorithm.* A genetic algorithm is mainly used to get the best spectrum allocation combination, which is used as the initial pheromone matrix  $T(i, j)$  and applied to the ant colony algorithm. In this way, the problem of insufficient initial pheromone is solved, and the efficiency of bandwidth allocation is improved. The specific algorithm is shown in Figure 3.

The optimization process based on a genetic algorithm (GA) is as follows:

- (1) Determine the end conditions of GA first
- (2) Then, set the initial value of the ant colony algorithm trace, which is shown as follows:

$$T_{ij}(t_0) = T_0 + \Delta T_{ij}, \quad (5)$$

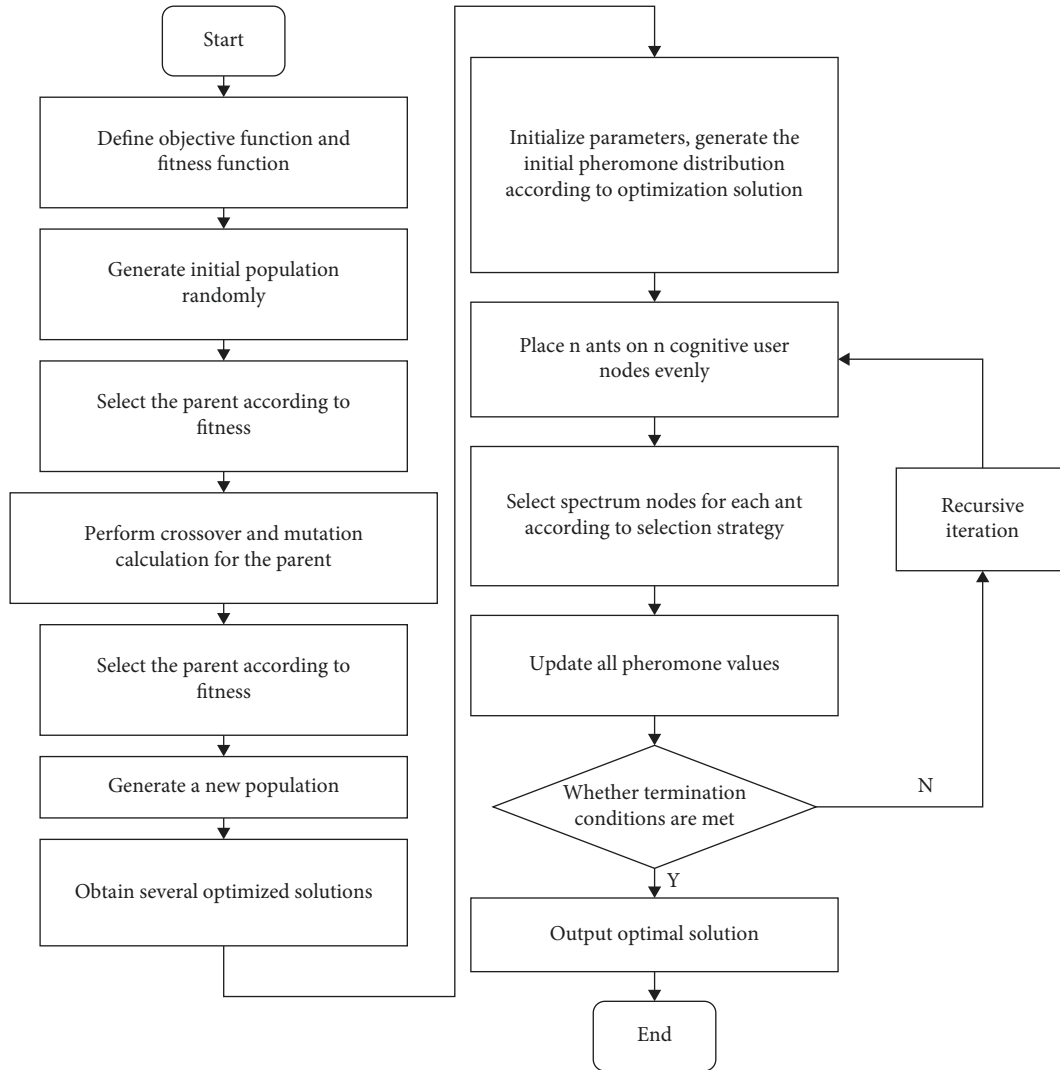


FIGURE 3: Node allocation algorithm combining genetic and ant colony algorithm.

where  $T_0$  represents the pheromone, which is set to 60;  $\Delta T_{ij}$  represents the obtained pheromone increment.

- (3) Obtain pheromone increment: sort the results of the solution and get the results according to the fitness where the first 10% is represented as  $S_{10\%}$ ;  $\Delta T_{ij}$  starts at 0, and if some solution in  $S_{10\%}$  passes through  $e_{ij}$ , then  $\Delta T_{ij}$  plus 20.

The maximum point of the function can be obtained by a genetic algorithm, which is helpful to improve the network performance.

The objective function satisfies the principle of optimal network average benefit, and the specific form is as follows:

$$U_{msrm} = \frac{1}{N} \sum_{i=1}^N r_n = \frac{1}{N} \sum_{i=1}^N \sum_{m=1}^N a_{n,m} \bullet b_{n,m}, \quad (6)$$

where  $a$  and  $b$  represent allocation matrix and benefit matrix, respectively;  $a_{n,m}$  represents whether  $m$  frequency band is allocated to  $n$  users;  $b_{mm}$  represents the distributed network benefit.  $X$  represents spectrum allocation, and each

$x$  keeps corresponding to a set of matrix  $a$  and  $b$ . Spectrum and the number of users are set to 64 and 16, respectively.

## 4. Power Service Switching of SDN Multidomain Network

*4.1. Switching Strategy of Multidomain Network.* Multidomain network switching can rearrange different services. In practice, multiple types of distribution communication network services are involved, in which service quality must be guaranteed based on appropriate policies. When switching target domains, it is necessary to reallocate network resources. In this case, a resource allocation strategy is designed to allocate resources based on service quality requirements, which is shown as follows:

- (1) If the business does not put forward high requirements for service quality, it only needs to allocate certain free resources in the target domain.
- (2) If the service quality requirements are high, the service can be divided into two types of switching,

namely low-to-high-capacity domain and high-to-low-capacity domain. For the former, a high-capacity network has more resources, which can improve the service quality. Therefore, the service requirements can be met as long as appropriate resources are configured. For the latter, more emphasis should be given to quality requirements, and appropriate resources should be allocated.

The switching problem of the multidomain network is studied to improve the rationality of resource allocation and meet the basic requirements of service quality. The controller needs to be used in network topology management. The basic control process is as follows:

- (1) Determine the original domain and target domain reasonably first, and obtain the control command
- (2) Then, locate the services involved, and obtain information such as the status of subdomains
- (3) Reallocate business resources in combination with resource usage information
- (4) After the completion of the allocation, build the switched link, then migrate the switched services, and record the relevant information in the database

*4.2. Switching Algorithm between Domains Based on Analytic Hierarchy Process.* At present, there are many scholars have studied the switching algorithm between domains, and a variety of algorithms are proposed. Algorithms have different characteristics and can achieve different effects. In this paper, the switching algorithm of a multidomain network is studied, and the analytic hierarchy process (AHP) is introduced. This method analyzes many factors that affect things at multiple levels, and the relative importance of things is determined based on the comparison between the two. According to the process of AHP hierarchy analysis, a multiobjective decision algorithm is constructed, and the adopted decision indicators include packet loss rate, delay, and bandwidth. The basic process of the algorithm is shown in Figure 2 [24–28].

## 5. Analysis of Simulation Results

*5.1. Simulation Results of Bandwidth Resource Optimization.* It is necessary to set the parameters of the genetic algorithm reasonably, in which the probability of mutation and crossover is 0.03 and 0.70, respectively; the number of iterations and population size are 40 and 50, respectively. After the parameter setting is completed, the MATLAB tool is used to simulate the designed algorithm, and the data and models refer to Li Ling. The results obtained after several iterations are shown in Figure 4.

It can be seen from Figure 7 that the average network benefit shows an upward trend with the increase of the number of evolution.

In the above process, matrix  $a$  actually belongs to a distribution mode, that is,  $m$  spectrum fragments can be allocated to  $n$  users. The ant colony algorithm can solve two problems: the first is to arrange the spectrum, especially

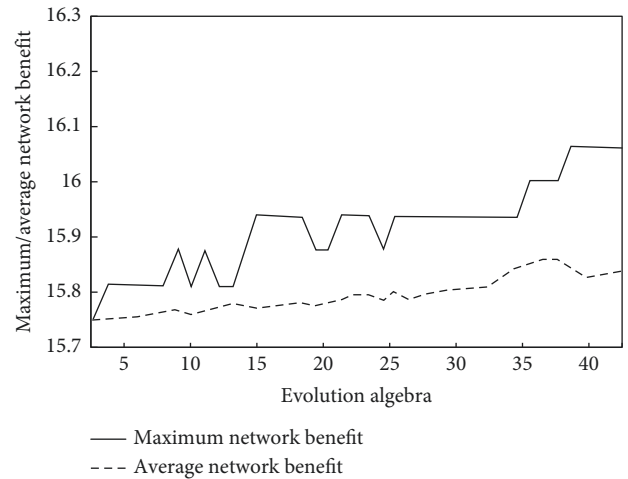


FIGURE 4: Relationship between iterations and frequency spectrum benefit of power distribution network.

when new fragments are obtained; the second is to arrange the continuous spectrum.

Given that  $T(i, j)$  represents the pheromone distribution matrix, and its initial value is the connection relation of  $a$  and  $b$ . The new spectrum number is  $K$ , which is extended to  $m + k$  dimensions, and then, the bandwidths are divided into multiple subsets. Here, the new set is expressed as  $S$ , and based on the ant colony algorithm, each subset is processed, and thus, the corresponding spectrum connection mode can be obtained. The ant colony algorithm is used for simulation, and the specific parameter settings are shown in the following Table 1.

After setting each parameter, the simulation can be carried out, and the final results are shown in Figure 5.

According to the information in above Figure 5, the optimal path obtained by simulation is expressed. The optimal convergence results in the power distribution network are shown in Figure 6.

Based on the above results, it can be seen that the ant colony algorithm can not only obtain the optimal loop route but also has fewer iterations and higher convergence. When the number of iterations reaches 28 times, the minimum value is obtained. Therefore, the application of this method can meet the requirements of node allocation and is suitable for power grid communication resource allocation.

*5.2. Simulation Results of Interdomain Handoff.* MATLAB tool is used to simulate the designed algorithm to realize the selection of multidomain network. In addition, bandwidth, packet loss rate, delay, and network hop are utilized to evaluate the performance of network.

*5.2.1. Power Distribution Video Surveillance Service.* In the operation process of a power communication system, there are many kinds of monitoring services, which generally have relatively low requirements for packet loss rate and pay more attention to delay and bandwidth.

TABLE 1: Ant colony algorithm model parameters.

| Number of ant | Constant coefficient | Maximum iterations | Pheromone importance factor $\alpha$ | Heuristic function importance factor $\beta$ | Pheromone volatile factor $\rho$ |
|---------------|----------------------|--------------------|--------------------------------------|--|----------------------------------|
| 30            | 17                   | 50                 | 1                                    | 4  | 0.1                              |

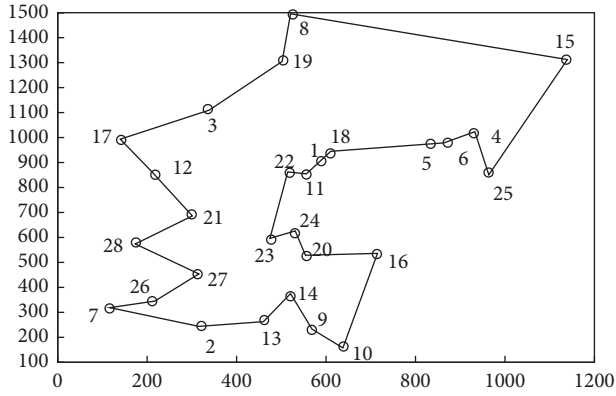


FIGURE 5: Optimal loop diagram in the power distribution network.

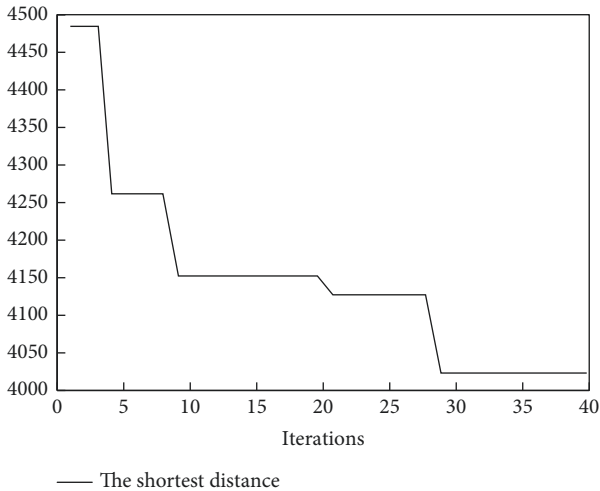


FIGURE 6: Convergence curve of the optimal solution in the power distribution network.

TABLE 2: Comparison matrix of power distribution video surveillance service.

| Comparative indicators | Delay | Bandwidth | Packet loss rate | Hop |
|------------------------|-------|-----------|------------------|-----|
| Delay                  | 1     | 1/3       | 5                | 5   |
| Bandwidth              | 3     | 1         | 9                | 8   |
| Packet loss rate       | 1/5   | 1/9       | 1                | 3   |
| Hop                    | 1/5   | 1/8       | 1/3              | 1   |

In this process, the eig function is mainly used to calculate the eigenvalue  $\lambda_{\max}(C)$  and eigenvector  $1^r$  of  $C$ . The calculated CR is lower than 0.1, and thus, the consistency test is passed. On this basis, the combination of the single factor and weight coefficient of business 1 is further obtained. The comparison matrix is shown in Table 2.

$$W^r = \{w_1, w_2, w_3, w_4\} = \{0.0483, 0.0935, 0.3775, 0.4807\}$$

$$W^p = \begin{pmatrix} w_1, w_2, w_3, w_4 \\ w_1, w_2, w_3, w_4 \end{pmatrix} = \begin{pmatrix} 0.2500, 0.7500, 0.2500, 0.2000 \\ 0.7500, 0.2500, 0.7500, 0.8000 \end{pmatrix}. \quad (7)$$

The total hierarchical distribution coefficient is obtained based on the decision coefficient, and the utility comparison diagram of business 1 is  $ts = (0.2823, 0.7177)$ ;  $f_{\text{Business1}} = \max(ts) = 0.7177$ .

According to the above information, 0.2823 and 0.7177, respectively, represent the utility values of service 1 in access domains 1 and 2. Therefore, domain 2 is the optimal switching network for this service.

5.2.2. *Electricity Information Collection Service.* This service has high requirements for bandwidth and delay, and the corresponding comparison matrix is shown in Table 3:

The combinations of single factor and weight coefficient for business 1 are as follows:

$$W^r = \{w_1, w_2, w_3, w_4\} = \{0.2736, 0.3359, 0.2986, 0.0919\}$$

$$W^p = \begin{pmatrix} w_1, w_2, w_3, w_4 \\ w_1, w_2, w_3, w_4 \end{pmatrix} = \begin{pmatrix} 0.8333, 0.8000, 0.3333, 0.2500 \\ 0.1667, 0.2000, 0.6667, 0.7500 \end{pmatrix}. \quad (8)$$

The total hierarchical distribution coefficient is obtained based on the decision coefficient, and the utility comparison diagram of business 2 is  $ts = (0.6068, 0.3932)$ ;  $f_{\text{Business2}} = \max(ts) = 0.6068$ .

According to the above information, 0.6068 and 0.3932, respectively, represent the utility values of business 2 in the optimal access domain 1 and 2. It can be clearly seen that the optimal switching network for this business is domain 1.

5.2.3. *Distributed Generation Access Service.* The comparison matrix for this service is shown in Table 4.

The combinations of single factor and vector weight coefficient are further obtained as follows:

$$W^r = \{w_1, w_2, w_3, w_4\} = \{0.2573, 0.5458, 0.1305, 0.0664\}$$

$$W^p = \begin{pmatrix} w_1, w_2, w_3, w_4 \\ w_1, w_2, w_3, w_4 \end{pmatrix} = \begin{pmatrix} 0.8633, 0.8000, 0.2500, 0.3333 \\ 0.1367, 0.2000, 0.7500, 0.6667 \end{pmatrix}. \quad (9)$$

The total hierarchical distribution coefficient is obtained based on the decision coefficient, and the utility comparison diagram of business 3 is  $ts = (0.7167, 0.2833)$ ;  $f_{\text{Business3}} = \max(ts) = 0.7167$ .

TABLE 3: Comparison matrix of electricity information collection service.

| Comparative indicators | Delay | Bandwidth | Packet loss rate | Hop |
|------------------------|-------|-----------|------------------|-----|
| Delay                  | 1     | 2         | 1/2              | 5   |
| Bandwidth              | 1/2   | 1         | 2                | 2   |
| Packet loss rate       | 3     | 1/2       | 1                | 2   |
| Hop                    | 1/5   | 1/3       | 1/2              | 1   |

TABLE 4: Comparison matrix of distributed generation access service.

| Comparative indicators | Delay | Bandwidth | Packet loss rate | Hop |
|------------------------|-------|-----------|------------------|-----|
| Delay                  | 1     | 1/5       | 2                | 3   |
| Bandwidth              | 5     | 1         | 2                | 4   |
| Packet loss rate       | 1/2   | 1/2       | 1                | 2   |
| Hop                    | 1/3   | 1/4       | 1/2              | 1   |

TABLE 5: Comparison matrix of power distribution automation service.

| Comparative indicators | Delay | Bandwidth | Packet loss rate | Hop |
|------------------------|-------|-----------|------------------|-----|
| Delay                  | 1     | 1/3       | 1/3              | 1/2 |
| Bandwidth              | 3     | 1         | 1/2              | 2   |
| Packet loss rate       | 3     | 2         | 1                | 4   |
| Hop                    | 2     | 1/2       | 1/4              | 1   |

According to the above information, 0.7167 and 0.2833, respectively, represent the utility values of business 3 in the best access domain 1 and 2. It is obvious that domain 1 should be selected for this business.

**5.2.4. Power Distribution Automation Service.** The comparison matrix for this service is shown in Table 5.

The combinations of single factor and weight coefficient are shown as follows:

$$W^r = \{w_1, w_2, w_3, w_4\} = \{0.1038, 0.1765, 0.4642, 0.2555\}$$

$$W^p = \begin{pmatrix} w_1, w_2, w_3, w_4 \\ w_1, w_2, w_3, w_4 \end{pmatrix} = \begin{pmatrix} 0.1377, 0.7500, 0.5000, 0.3333 \\ 0.8623, 0.2500, 0.5000, 0.6667 \end{pmatrix}. \quad (10)$$

The total hierarchical distribution coefficient is obtained based on the decision coefficient, and the utility comparison diagram of business 4 is  $ts = (0.4756, 0.5244)$ ;  $f_{\text{Business4}} = \max(ts) = 0.5244$ .

According to the above information, 0.4756 and 0.5244, respectively, represent the utility values of business 4 in the best access domain 1 and 2. It is obvious that domain 2 should be selected for this business.

## 6. Conclusion

To sum up, it can be seen that the performance of the SDN network is improved to a certain extent by introducing the

spectrum scheduling of the improved genetic algorithm and switching method of AHP. After parameters are optimized, the optimal spectrum resource optimization path of the SDN network can be obtained. Moreover, the switching of AHP shows that domain 2 is the best access domain, so as to better improve the performance of the whole network.

## Data Availability

The experimental data used to support the findings of this study are available from the corresponding author upon request.

## Conflicts of Interest

The authors declare that they have no conflicts of interest regarding this work.

## References

- [1] L.-H. Chang, "Application-based online traffic classification with deep learning models on SDN networks," *Advances in Technology Innovation*, vol. 5, no. 4, pp. 216–229, 2020.
- [2] S. Rui, "A hybrid SDN solution for mobile networks," *Computer Networks*, vol. 190, 2021.
- [3] Ma Zheng, "Research on the on-demand scheduling algorithm of intelligent routing load based on SDN," *International Journal of Internet Protocol Technology*, vol. 14, no. 1, 2021.
- [4] K. Qin, B. Fu, P. Chen, and J. Huang, "MCRA: multicost rerouting algorithm in SDN," *Journal of Advanced Computational Intelligence and Intelligent Informatics*, vol. 24, no. 6, pp. 728–737, 2020.
- [5] D. Li, H. Liu, and Y. Jin, "MPF-MLBS: a multi-path load balancing strategy for SDN networks based on multiple performance factors," *Mathematics and Computer Science*, vol. 5, no. 3, p. 64, 2020.
- [6] Z. Liu, "QoS oriented task scheduling based on genetic algorithm in cloud computing," *Computer Systems Science and Engineering*, vol. 30, no. 6, pp. 481–487, 2015.
- [7] R. Wang, S. Bidkar, F. Meng, R. Nejabati, and D. Simeonidou, "Load-aware nonlinearity estimation for elastic optical network resource optimization and management," *Journal of Optical Communications and Networking*, vol. 11, no. 5, p. 164, 2019.
- [8] R. Lin and Z. Ye, "A bat algorithm for SDN network scheduling," *EURASIP Journal on Wireless Communications and Networking*, vol. 2018, no. 1, p. 120, 2018.
- [9] P. Liang, H. Zhao, and G. Caner, "Network resource information scheduling based on non-convex function optimization algorithm," *Journal of Intelligent and Fuzzy Systems*, vol. 35, no. 4, pp. 4215–4224, 2018.
- [10] K. Lalitha Devi and S. Valli, "Multi-objective heuristics algorithm for dynamic resource scheduling in the cloud computing environment," *The Journal of Supercomputing*, pp. 1–29, 2021.
- [11] W. Yi, Y. Yuan, R. Hoseinnezhad, and L. Kong, "Resource scheduling for distributed multi-target tracking in netted colocated MIMO radar systems," *IEEE Transactions on Signal Processing*, vol. 68, pp. 1602–1617, 2020.
- [12] A. Praveena and V. Vijayarajan, "ENergy efficient resource scheduling using optimization based neural network in mobile cloud computing," *Wireless Personal Communications*, vol. 114, pp. 1–20, 2020.

- [13] F. Al-Tam, J. Correia, and J. Rodriguez, "Learn to schedule (leasch): a deep reinforcement learning approach for radio resource scheduling in the 5G MAC layer," *IEEE Access*, vol. 8, Article ID 108088, 2020.
- [14] Y. Wu, "Editorial: special issue on SDN-based wireless network virtualization," *Concurrency and Computation: Practice and Experience*, vol. 32, no. 16, p. n/a, 2020.
- [15] Z. Wang, Z. Lu, and C. Li, "Research on deep reinforcement learning multi-path routing planning in SDN," *Journal of Physics: Conference Series*, vol. 1617, no. 1, Article ID 012043, 2020.
- [16] M. Sharma, "To eliminate the threat of a single point of failure in the SDN by using the multiple controllers," *International Journal of Recent Technology and Engineering*, vol. 9, no. 2, pp. 234–241, 2020.
- [17] D. Eddine Henni, A. Ghomari, and Y. Hadjadj-Aoul, "A consistent QoS routing strategy for video streaming services in SDN networks," *International Journal of Communication Systems*, vol. 33, no. 10, p. n/a, 2020.
- [18] L. Liao, V. C. M. Leung, Z. Li, and H.-C. Chao, "Genetic algorithms with variant particle swarm optimization based mutation for generic controller placement in software-defined networks," *Symmetry*, vol. 13, no. 7, p. 1133, 2021.
- [19] A. Shahid, "Securing genetic algorithm enabled SDN routing for blockchain based internet of things," *IEEE Access*, vol. 9, Article ID 139739, 2021.
- [20] H. Xue, K. Kim, and H. Youn, "Dynamic load balancing of software-defined networking based on genetic-ant colony optimization," *Sensors*, vol. 19, no. 2, p. 311, 2019.
- [21] M. S. Han, "Optimal routing path calculation for SDN using genetic algorithm," *International Journal of Hospitality Information Technology*, vol. 11, no. 3, pp. 7–12, 2018.
- [22] M. V. O. De Assis, A. H. Hamamoto, T. Abrao, and M. L. Proenca, "A game theoretical based system using holt-winters and genetic algorithm with fuzzy logic for DoS/DDoS mitigation on SDN networks," *IEEE Access*, vol. 5, pp. 9485–9496, 2017.
- [23] Z. Stanislav Igorovych, "Genetic algorithm for SDN protection against network attacks[J]," *System research and information technologies*, vol. 0, no. 2, p. 14, 2016.
- [24] A. M. Tobie, R. A. Etoundi, and J. Zoa, "A literature review of ERP implementation in african countries," *The Electronic Journal on Information Systems in Developing Countries*, vol. 76, no. 1, pp. 1–20, 2017.
- [25] L. Yan, "Voltage sag severity analysis based on improved FP-Growth algorithm and AHP algorithm," *Journal of Physics: Conference Series*, vol. 1732, no. 1, Article ID 012088, 2021.
- [26] Ba D. Nguyen, "The role of factors affecting flood hazard zoning using analytical hierarchy process: a review," *Earth Systems and Environment*, pp. 1–17, 2021.
- [27] M. Mishra and S. Chatterjee, "Application of Analytical Hierarchy Process (AHP) algorithm to income insecurity susceptibility mapping - a study in the district of Purulia, India," *Socio-Economic Planning Sciences*, vol. 62, pp. 56–74, 2018.
- [28] L. Li, T.-S. Pan, X.-X. Sun, S.-C. Chu, and J.-S. Pan, "A novel binary slime mould algorithm with AU strategy for cognitive radio spectrum allocation," *International Journal of Computational Intelligence Systems*, vol. 14, no. 1, p. 161, 2021.

## Retraction

# Retracted: Dynamic Simulation Analysis of Carbon-Steel Hybrid Sucker Rod String in Vertical and Directional Wells

### Mathematical Problems in Engineering

Received 13 September 2023; Accepted 13 September 2023; Published 14 September 2023

Copyright © 2023 Mathematical Problems in Engineering. This is an open access article distributed under the Creative Commons Attribution License, which permits unrestricted use, distribution, and reproduction in any medium, provided the original work is properly cited.

This article has been retracted by Hindawi following an investigation undertaken by the publisher [1]. This investigation has uncovered evidence of one or more of the following indicators of systematic manipulation of the publication process:

- (1) Discrepancies in scope
- (2) Discrepancies in the description of the research reported
- (3) Discrepancies between the availability of data and the research described
- (4) Inappropriate citations
- (5) Incoherent, meaningless and/or irrelevant content included in the article
- (6) Peer-review manipulation

The presence of these indicators undermines our confidence in the integrity of the article's content and we cannot, therefore, vouch for its reliability. Please note that this notice is intended solely to alert readers that the content of this article is unreliable. We have not investigated whether authors were aware of or involved in the systematic manipulation of the publication process.

Wiley and Hindawi regrets that the usual quality checks did not identify these issues before publication and have since put additional measures in place to safeguard research integrity.

We wish to credit our own Research Integrity and Research Publishing teams and anonymous and named external researchers and research integrity experts for contributing to this investigation.

The corresponding author, as the representative of all authors, has been given the opportunity to register their agreement or disagreement to this retraction. We have kept a record of any response received.

### References

- [1] X. Sun, X. Ji, W. Li, L. Zhang, and Y. Song, "Dynamic Simulation Analysis of Carbon-Steel Hybrid Sucker Rod String in Vertical and Directional Wells," *Mathematical Problems in Engineering*, vol. 2022, Article ID 5239355, 14 pages, 2022.



## Research Article

# Dynamic Simulation Analysis of Carbon-Steel Hybrid Sucker Rod String in Vertical and Directional Wells

Xiurong Sun <sup>1</sup>, Xianbing Ji,<sup>1</sup> Weicheng Li,<sup>2</sup> Lijuan Zhang,<sup>1</sup> and Yang Song<sup>1</sup>

<sup>1</sup>Department of Environmental Engineering, Hebei University of Environmental Engineering, Qinhuangdao 066102, China

<sup>2</sup>School of Mechanical Engineering, Yanshan University, Qinhuangdao 066004, China

Correspondence should be addressed to Xiurong Sun; [sunxiurong@hebeuee.edu.cn](mailto:sunxiurong@hebeuee.edu.cn)

Received 28 April 2022; Revised 24 May 2022; Accepted 2 June 2022; Published 29 June 2022

Academic Editor: Man Fai Leung

Copyright © 2022 Xiurong Sun et al. This is an open access article distributed under the Creative Commons Attribution License, which permits unrestricted use, distribution, and reproduction in any medium, provided the original work is properly cited.

Carbon fiber composite continuous sucker rod string is more and more widely used in deep and ultradeep wells because of its light weight, high strength, and corrosion resistance. In order to analyze the dynamic problems of carbon fiber sucker rod string in actual oil wells, a transverse vibration simulation model of carbon fiber and steel (carbon-steel) hybrid rod string excited by buckling deformation in vertical wells is established with the compression buckling deformation of weighting rod. Considering the influence of wellbore trajectory and the constraint of tubing, the transverse vibration simulation model of carbon-steel hybrid rod string in directional wells under borehole trajectory excitation is also established in this paper. The finite difference method is used to discretize the well depth node, the numerical integration method (Newmark- $\beta$ ) is used to discretize the reciprocating periodic time node, and simulation methods for the contact and collision dynamics of rod-tubing in vertical wells and directional wells are formed. Through programming calculation, the distribution laws of transverse displacement, contact force, collision force, and bending stress of carbon-steel hybrid sucker rod string in vertical wells and directional wells along well depth are obtained. The simulation results in vertical wells show that the strong collision between the rod and tubing occurs near the bottom steel rod, while the upper load is small and the rod-tubing collision load of the upper rod of the carbon-steel hybrid rod string is much lower than that of the traditional steel rod string at the same position. Furthermore, the bending stress of the upper carbon fiber is also much less than that of the bottom steel rod. The simulation results in directional wells show that the collision phenomenon of the deflecting section and the bottom weighting rod compression section are the strongest and the rod-tubing contact pressure is also the largest. Second, the impact force of the upper carbon fiber rod is also much lower than that of the steel rod. Again, the maximum bending stress of the whole well occurs near the deviation section where the deviation angle changes suddenly. The transverse vibration mechanical model in directional wells in this paper lays a theoretical foundation and provides theoretical support for the optimal design of fracture and splitting prevention measures of carbon fiber sucker rod.

## 1. Introduction

Compared with the traditional steel sucker rod, carbon fiber sucker rods have obvious advantages such as light weight, high strength, corrosion resistance, reducing suspension point load, and increasing pump depth [1] and are more and more widely used in oil fields [2, 3]. Carbon fiber sucker rod string is not used alone, but mixed with steel rod. The mixing system consists of the upper carbon fiber rod and the bottom steel rod or weighting rod [4].

At present, the research on the mechanical properties of carbon-steel hybrid rod string system is still based on the theory of traditional steel rod string: that is, the buckling analysis of sucker rod in quasistatic state and the mechanical analysis of longitudinal and transverse vibration in dynamic state.

The static buckling deformation of traditional steel sucker rod string has laid a good research foundation for the study of carbon fiber rod string mechanics [5, 6]. Sun et al. have established the simulation model of the buckling configuration of the traditional steel sucker rod string in the tubing and concluded that the buckling configuration below

the neutral point has an important impact on the entire rod string deformation and rod-tubing collision [7, 8].

Wu et al. and Xing et al. have systematically studied the longitudinal vibration and rod-tubing-liquid coupling vibration of sucker rod string in vertical wells and got the numerical simulation result of top suspension point load, bottom pump axial load, natural frequency of rod string, and so on [9, 10]. Sun et al. established the simulation model of the axial distributed load of the sucker rod string based on the wave equation and further pointed out that the axial distributed load changes along the axial position of the sucker rod string, which has significant nonuniform distribution characteristics [7].

Based on the understanding of the alternating shape of sucker rod string in vertical wells in tubing, Sun proposed the rod-tubing lateral collision theory of the traditional sucker rod string under the excitation of buckling deformation in vertical wells [11], but it cannot be applied to the carbon fiber rod string system.

The mechanical research of directional well is also based on the traditional steel rod string. Dong and Di established the static finite element model of the traditional steel rod string in the tubing in the directional well: the bending deformation, the eccentric wear position, and the contact pressure between the rod and tubing [12, 13]. Wang et al. and Yang et al. studied the longitudinal vibration of sucker rod string, realizes the simulation of axial distributed load and bottom axial load of sucker rod string [14, 15]. Through the quasistatic method, the bending deformation of sucker rod string in tubing, the eccentric wear position, and the contact pressure of rod-tubing in any instantaneous directional well are also simulated by the finite element method. Yang et al. and Zhu et al. established the simulation model of vertical-horizontal-torsional coupling vibration of sucker rod string in directional wells, which is mainly used to analyze the motion law and force of sucker rod string [16, 17]. The above mechanical model is not based on carbon-steel hybrid rod string.

With the strengthening of the application of carbon fiber sucker rod in oil wells, the research on its mechanical properties has gradually attracted much attention. Wang et al. and Zhang et al. theoretically analyzed the over stroke behavior of carbon fiber sucker rod string [18, 19]. Lv et al. obtained the variation laws of longitudinal vibration and natural frequency of carbon fiber sucker rod string [20–22]. The above studies are carried out for the axial movement of carbon fiber sucker rod, which lays a good foundation for the study of the mechanical properties of carbon fiber sucker rod string. The transverse bending deformation of carbon fiber sucker rod is not only constrained by the well wall, but also affected by the wellbore trajectory, which is reflected in

the influence of the compression buckling deformation of the bottom steel rod string on the transverse vibration of the integral hybrid rod string in vertical wells and the influence of the wellbore trajectory in the directional well on the transverse vibration of the integral hybrid rod string.

At present, the mechanical analysis of carbon fiber rod string does not consider the above effects. Although carbon fiber sucker rods have been applied in actual oil wells in batches, the mechanical mechanism of fracture and splitting of sucker rod body is not well understood, and the mechanical model needs to be further improved. It is urgent to carry out the theoretical research of transverse vibration mechanics based on carbon-steel hybrid rod string.

In this paper, the transverse vibration simulation models of carbon-steel hybrid rod string in vertical wells and directional wells are established, respectively. In the vertical well, the excitation of the transverse vibration caused by the buckling deformation of the bottom steel rod is considered. In the directional well, the excitation of the transverse vibration of the integral rod string caused by the wellbore trajectory is considered. The rod string length is discretized into spatial nodes  $J$  along the well depth, and the time of periodic change is discretized into time nodes  $I$ . Through simulation analysis, the variation laws of transverse vibration, rod-tubing collision, and bending of hybrid rod string in vertical and directional wells are obtained with well depth and period time, which lays a theoretical foundation for the phenomenon of rod string breaking and splitting failure of carbon fiber sucker rod in oil well.

## 2. Simulation Analysis in Vertical Wells

*2.1. Mechanical Model.* Regardless of the torsional deformation of rod string, assuming that the oil tubing is completely vertical, and the axis of rod string coincides with the center of oil tubing.

The coordinate system origin is established at the top of the carbon fiber rod string. The rod string in the oil liquid is not only subjected to the reciprocating end load  $P(t)$  at the bottom end, but also subjected to the node load  $q(x)$  distributed at different depths of the oil tubing.

Based on the above assumptions, the mechanical model of transverse bending deformation of hybrid rod string in vertical wells is established as shown in Figure 1.

*2.2. Mathematical Model.* Based on the theory of elastic body dynamics, the differential equation of transverse vibration of sucker rod string in vertical wells is established as follows:

$$\left\{ \begin{array}{l} \rho_i A_i \frac{d^2 u}{dt^2} = \frac{\partial Q}{\partial s} - \varepsilon \frac{du}{dt}, \\ Q = N \frac{\partial u}{\partial s} - \frac{\partial M}{\partial s}, \\ M = E_i I_i \left( \frac{\partial^2 u}{\partial s^2} + \frac{\partial u}{\partial s} \right), \\ N = P(t) + \int_s^l q(s, t) ds. \end{array} \right. \quad (1)$$

$$\left\{ \begin{array}{l} x = s - (S - u_A(t)), \\ \int_s^l q(s, t) ds = \int_s^{L_1} q_1(s, t) ds + \int_{L_1}^L q_2(s, t) ds \quad (0 < x < L_1), \\ \int_s^l q(s, t) ds = \int_s^L q_2(s, t) ds \quad (L_1 < x < L), \\ \frac{d^2 u}{dt^2} = a \frac{\partial u}{\partial s} + v^2 \frac{\partial^2 u}{\partial s^2} + 2v \frac{\partial^2 u}{\partial s \partial t} + \frac{\partial^2 u}{\partial t^2}. \end{array} \right. \quad (2)$$

In which,  $i$  is the number of rod ( $i = 1, 2$ ). When  $i = 1$ , it represents the carbon fiber material (rod length  $L_1/m$ ). When  $i = 2$ , it represents the steel material (rod length  $L_2/m$ ). Total length of sucker rod string is  $L = L_1 + L_2$ .  $N(s, t)$  is the axial load at instantaneous  $t$  at any section  $s$  of the rod string,  $N$ .

$u(s, t)$  is the transverse displacement;  $Q(s, t)$  is the shear force at any moving coordinate position  $s$ ;  $M(s, t)$  is the bending moment at any moving coordinate position  $s$ ;  $P(t)$  is the axial load at the bottom of the sucker rod string at any instantaneous  $t$ ;  $N$ ;  $S$  is stroke,  $m$ ;  $u_A(t)$  is the suspension point displacement with time;  $\varepsilon$  is the lateral damping coefficient.

The junction of carbon-steel material rod string meets the continuity of displacement, rotation angle, and bending moment, namely, the continuity condition is

$$\left\{ \begin{array}{l} u_{s=L_1^-} = u_{s=L_1^+}, \\ = \frac{du}{ds} \Big|_{s=L_1^+} E_1 I_1 \frac{d^2 u}{ds^2} \Big|_{s=L_1^-}, \\ = E_2 I_2 \frac{d^2 u}{ds^2} \Big|_{s=L_1^+} E_1 I_1 \frac{d^3 u}{ds^3} \Big|_{s=L_1^-}, \\ = E_2 I_2 \frac{d^3 u}{ds^3} \Big|_{s=L_1^+}. \end{array} \right. \quad (3)$$

Initial conditions: the rod string is initially in a static state; that is, the rod string lies in the wellbore, the initial state of the rod string central axis coincides with the trajectory line of the wellbore, and the suspension point is at the

top dead center at this time. The initial condition can be further expressed as

$$\left\{ \begin{array}{l} u(s, 0) = \varphi(s) = 0, \\ u_A(0) = 0, \\ \frac{\partial u}{\partial t}(s, 0) = g(s) = 0. \end{array} \right. \quad (4)$$

Boundary conditions: the boundary position both top and bottom end of rod string are constrained by transverse displacement and angular displacement. The boundary condition at the top of the carbon fiber rod string can be simplified as a sliding fixed end. The bottom of the steel rod string is also constrained by transverse displacement and angular displacement, whose boundary condition can be simplified as a sliding fixed end. Therefore, the boundary condition of the rod string can be expressed as

$$\left\{ \begin{array}{l} u(s, t) = 0 \frac{\partial u}{\partial s}(s, t) = 0, \\ u(L, t) = 0 \frac{\partial u}{\partial s}(L, t) = 0. \end{array} \right. \quad (5)$$

The reason of hybrid rod string producing bending deformation and contacting with the inner wall of the tubing, on the one hand, is the transverse load generated by the viscous resistance of the oil fluid. On the other hand, it is the collision between the bent rod string and the inner wall of the oil tubing, and the motion of nodes rebound after the collision. This process is equivalent to the collision of the impulse theorem, and the contact force is the resultant force of collision force and lateral force generated in the collision process.

**2.3. Numerical Simulation Method.** This (1) is a high-order linear differential equation with variable coefficients, including time variable  $t$  and space variable  $x$ . When the bending deformation of the rod string contacts with the inner wall of the tubing, it will rebound after collision. The collision process is a nonlinear contact problem. Therefore, the whole analysis process needs to be divided into two parts: solving high-order linear coupled differential equations with variable coefficients and simplifying the collision problem.

For the problem of collision here, the commonly used recovery coefficient method is introduced here, that is, when the rod string node collides with the oil tubing wall, the speed along the circumferential radial direction is reversed, while the speed direction and size of the tangential direction remain unchanged, and the motion node falls on the inner wall of the oil pipe after the collision; see the literature [23, 24].

It is difficult to solve the higher-order linear coupled differential equations with variable coefficients by the analytical method, and the better way is to use numerical integration. So, this paper adopts the method of combining finite difference and Newmark- $\beta$ . The finite difference

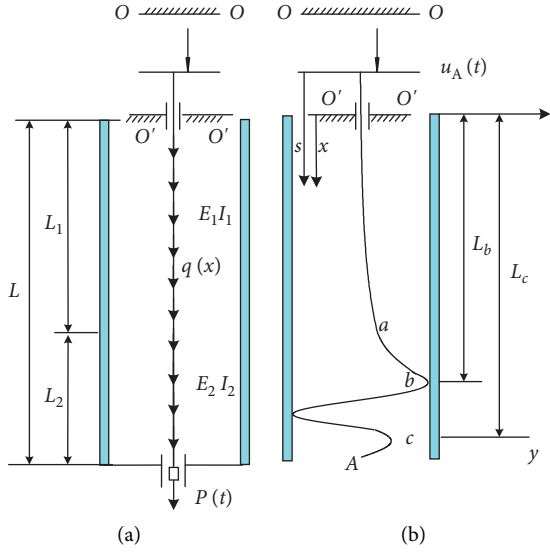


FIGURE 1: Load model and transverse bending deformation of hybrid rod string. (a) Load model. (b) Transverse bending.

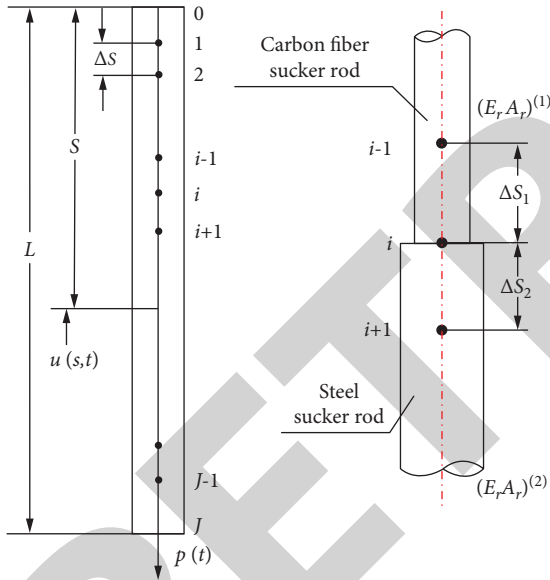


FIGURE 2: Discrete nodes of carbon-steel hybrid rod string length in vertical wells.

method is used to discrete space variables quantity  $x$ , and the Newmark- $\beta$  method is used for discrete time variable quantity  $t$ . The space discrete model is shown in Figure 2. The whole slender rod string is discretized into  $n$  elements and  $N+1$  nodes. Taking the joint position between carbon fiber rod string and steel rod string as the dividing point, steps lengths are  $\Delta x_1$  and  $\Delta x_2$ , respectively, and the time steps are  $\Delta t$ :

$$\begin{cases}
 u_1^{(4)} = \frac{7u_1 - 4u_2 + u_3}{\Delta s^4}, \\
 u_2^{(4)} = \frac{6u_2 - 4(u_1 + u_3) + u_4}{\Delta s^4}, \\
 u_j^{(4)} = \frac{6u_j - 4(u_{j-1} + u_{j+1}) + u_{j-2} + u_{j+2}}{\Delta s^4} \quad (3 \leq j \leq J-3), \\
 u_{J-2}^{(4)} = \frac{6u_{J-2} - 4(u_{J-1} + u_{J-3}) + u_{J-4}}{\Delta s^4}, \\
 u_{J-1}^{(4)} = \frac{7u_{J-1} - 4u_{J-2} + u_{J-3}}{\Delta s^4}, \\
 u_1'' = \frac{u_2 - 2u_1}{\Delta s^2}, \\
 u_j'' = \frac{u_{j+1} - 2u_j + u_{j-1}}{\Delta s^2} \quad (2 \leq j \leq J-2), \\
 u_{J-1}'' = \frac{u_{J-2} - 2u_{J-1}}{\Delta s^2}, \\
 u_1' = \frac{u_2}{2\Delta s} \\
 u_j' = \frac{u_{i+1} - u_{i-1}}{2\Delta s} \quad (2 \leq j \leq J-2), \\
 u_{J-1}' = \frac{-u_{J-2}}{2\Delta s}.
 \end{cases} \quad (6)$$

Next, the Newmark- $\beta$  method is used to discretize the time variable  $t$ , i.e.,

$$\begin{cases}
 \dot{u}_{t+\Delta t} = \dot{u}_t + [(1-\gamma)\ddot{u}_t + \gamma\ddot{u}_{t+\Delta t}]\Delta t, \\
 u_{t+\Delta t} = u_t + \dot{u}_t\Delta t + \left[\left(\frac{1}{2} - \beta\right)\ddot{u}_t + \beta\ddot{u}_{t+\Delta t}\right]\Delta t^2.
 \end{cases} \quad (7)$$

In which,  $\beta$  and  $\gamma$  are the integration accuracy parameters. When  $\beta \geq 0.5$ ,  $\gamma \geq 0.25(0.5 + \beta)^2$ , the numerical method is unconditionally convergent. This paper takes  $\beta = 0.5$ ,  $\gamma = 0.25$ , and at this time, the stability and accuracy are both high. The recursive expression is further obtained from (7), i.e.,

$$\begin{cases} \ddot{u}_{t+\Delta t} = \alpha_0 (u_{t+\Delta t} - u_t) - \alpha_2 \dot{u}_t - \alpha_3 \ddot{u}_t, \dot{u}_{t+\Delta t} = \alpha_1 (u_{t+\Delta t} - u_t) - \alpha_4 \dot{u}_t - \alpha_5 \ddot{u}_t, \alpha_0 = \frac{1}{\beta \Delta t^2} \alpha_1 = \frac{\gamma}{\beta \Delta t} \alpha_2 = \frac{1}{\beta \Delta t}, \\ \alpha_3 = \frac{1}{2\beta} - 1\alpha_4 = \frac{\gamma}{\beta} - 1\alpha_5 = \frac{\Delta t}{2} \left( \frac{\gamma}{\beta} - 2 \right). \end{cases} \quad (8)$$

The equilibrium differential equation at time  $t+\Delta t$  satisfies as follows:

$$[\mathbf{M}]\ddot{u}_{t+\Delta t} + [\mathbf{C}]\dot{u}_{t+\Delta t} + [\mathbf{K}]u_{t+\Delta t} = \mathbf{R}_{t+\Delta t}. \quad (9)$$

Substituting (7) and (8) into (9), the equation about  $\{u\}_{t+\Delta t}$  is obtained:

$$[\bar{\mathbf{K}}]\{y\}_{t+\Delta t} = \{\bar{\mathbf{R}}\}_{t+\Delta t}, \quad (10)$$

in which

$$\begin{cases} [\bar{\mathbf{K}}] = [\mathbf{K}] + \alpha_0 [\mathbf{M}] + \alpha_1 [\mathbf{C}], \\ \{\bar{\mathbf{R}}\}_{t+\Delta t} = \{\mathbf{R}\}_{t+\Delta t} + [\mathbf{M}] (\alpha_0 \{y\}_t + \alpha_2 \{\dot{y}\}_t + \alpha_3 \{\ddot{y}\}_t) + [\mathbf{C}] (\alpha_1 \{y\}_t + \alpha_4 \{\dot{y}\}_t + \alpha_5 \Delta t \{\ddot{y}\}_t), \end{cases} \quad (11)$$

in which  $[\mathbf{K}]$ ,  $[\mathbf{M}]$ , and  $[\mathbf{C}]$  represent stiffness matrix, mass matrix, and damping matrix, respectively.

After sorting, the discrete form of (10) is expressed by

$$\begin{cases} G_{i,j}^k = A_i y_{j-2}^k + B_{i,j-1}^k y_{j-1}^k + C_{i,j}^k y_j^k + D_{i,j+1}^k y_{j+1}^k + F_i y_{j+2}^k \quad (3 \leq i \leq N-3), \\ A_i = F_i = \frac{E_i I_i}{\Delta s^4}, \\ B_{i,j-1}^k = \rho_i A_i \left( \frac{a}{2\Delta s} + \frac{v^2}{\Delta s^2} - \frac{v\alpha_1}{\Delta s} \right) - \frac{4E_i I_i}{\Delta s^4} - \frac{N}{\Delta s^2} + \frac{\partial N}{\partial s} \frac{1}{2\Delta s} - \frac{\varepsilon v}{2\Delta s}, \\ C_i^k = \frac{6E_i I_i}{h^4} + \rho_i A_i \left( \alpha_0 - \frac{2v^2}{\Delta s^2} \right) + 2N \frac{1}{\Delta s^2} + \varepsilon \alpha_1, \\ D_{i,j+1}^k = \rho_i A_i \left( \frac{a}{2\Delta s} + \frac{v^2}{\Delta s^2} + \frac{v\alpha_1}{\Delta s} \right) - \frac{4E_i I_i}{\Delta s^4} - \frac{N}{\Delta s^2} - \frac{\partial N}{\partial s} \frac{1}{2\Delta s} + \frac{\varepsilon v}{2\Delta s}, \\ G_{i,j}^k = \rho_i A_i (\alpha_0 u_j^{k-1} + \alpha_2 \dot{u}_j^{k-1} + \alpha_3 \ddot{u}_j^{k-1}) + \rho_i A_i v \frac{(\alpha_1 u_{j+1}^{k-1} + \alpha_4 \dot{u}_{j+1}^{k-1} + \alpha_5 \ddot{u}_{j+1}^{k-1})}{\Delta s} + \rho_i A_i v \frac{(\alpha_1 u_{j-1}^{k-1} + \alpha_4 \dot{u}_{j-1}^{k-1} + \alpha_5 \ddot{u}_{j-1}^{k-1})}{\Delta s} + \varepsilon (\alpha_1 u_j^{k-1} + \alpha_4 \dot{u}_j^{k-1} + \alpha_5 \ddot{u}_j^{k-1}), \end{cases} \quad (12)$$

in which  $i$  is the same as the meaning of (1),  $j$  is the rod string length node, and  $k$  is the time node.

When the rod string length node collides with the tubing wall, it is considered that the transverse displacement of rod string exceeds the boundary of the tubing wall. After the collision, the displacement and velocity of the node meet the following relationship:

$$\begin{cases} u(s, t)|_{t^+} = \text{sgn}(u(s, t)|_{t^-}) (R - r), \\ \frac{du(s, t)}{dt}|_{t^+} = -\gamma_e \frac{du(s, t)}{dt}|_{t^-}. \end{cases} \quad (13)$$

$\gamma_e$  is the collision recovery coefficient, and its value is determined by the collision material. For further analysis, see reference [23].

Furthermore, the calculation formulas of collision force and transverse pressure are

$$\begin{cases} F_{i,n} = -\rho_i A_i \frac{(1+\gamma)}{\Delta\tau} \frac{du(s,t)}{dt} \Big|_{t-}, \\ F_{i,s} = E_i I_i \frac{\partial^2 u}{\partial s^2} - \frac{\partial}{\partial s} \left( T \frac{\partial u}{\partial s} \right). \end{cases} \quad (14)$$

The total contact force of rod-tubing is composed of the resultant force of collision force and transverse pressure.

$\Delta\tau$  is the time step of collision, and its value can be found in reference [24].

### 3. Simulation Analysis in Directional Wells

**3.1. Mechanical Model.** In directional wells, the upper carbon fiber sucker rod is regarded as a continuous rod string without coupling, and the bottom influence of the coupling and centralizer of the weighted steel rod is ignored. The overall rod string structure and load diagram in directional wells are shown in Figures 3(a) and 3(b), respectively. In order to facilitate modeling, two coordinate systems are established to express the rod string position in the well depth: the first one is the static coordinate system fixed at the top, with the position of well depth being represented by  $x$ . The second one is the dynamic coordinate system, with the position of well depth by  $s$ .

In Figure 3,  $q(s,t)$  or  $q(x,t)$  is the axial distributed force at the axis position  $s$  or  $x$ .  $P(t)$  is the concentrated axial force at the bottom of the sucker rod.  $q_u(s,t)$  or  $q_u(x,t)$  is the transverse distributed load.  $L_1$  and  $L_2$  are the lengths of carbon fiber rod and steel rod, respectively.  $u_A(t)$  is the suspension point position.

According to Figure 3, further assumptions are made as follows. First the well trajectory appears only in the 2D plane. Second, ignore the effect of torsional deformation of rod string. Third, the axis line of the overall rod string and the center of the tubing coincides with the well trajectory line. Fourth, in addition to the concentrated axial load  $P(t)$ , the bottom of the weighting rod is also subjected to the distributed load  $q(s,t)$  or  $q(s,t)$  at different well depth positions.

**3.2. Mathematical Model.** Based on the theory of elastomer dynamics, the differential equation of transverse vibration of sucker rod string in directional wells is established as follows:

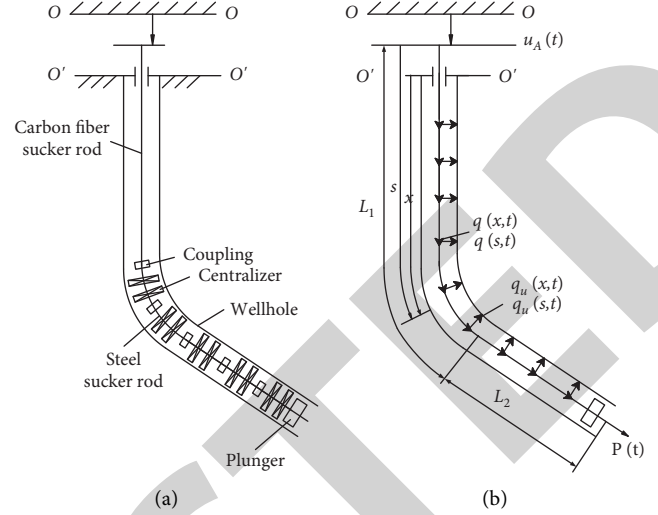


FIGURE 3: Rod string structure and load model of carbon-steel hybrid rod string in directional wells. (a) Schematic diagram of hybrid rod string. (b) Load model.

$$\begin{cases} \rho_i A_i \frac{d^2 u}{dt^2} = \frac{\partial Q}{\partial s} + N \frac{\partial \alpha(x)}{\partial s} + q_{ub}(x,t), \\ Q = N \frac{\partial u}{\partial s} - \frac{\partial M}{\partial s}, \\ M = E_i I_i \left( \frac{\partial^2 u}{\partial s^2} + \frac{\partial u}{\partial s} \right), \\ x = s - (S - u_A(t)), \\ N = P(t) + \int_s^l q(s,t) ds, \\ q_{ub}(x,t) = -(\rho_i - \rho_l) A_i g \sin \alpha(x) - \varepsilon \frac{du}{dt}, \\ \int_s^l q(s,t) ds = \int_s^{L_1} q_1(s,t) ds + \int_{L_1}^L q_2(s,t) ds \quad (0 < s < L_1), \\ \int_s^l q(s,t) ds = \int_s^L q_2(s,t) ds \quad (L_1 < s < L). \end{cases}$$

$$\frac{d^2 u}{dt^2} = a \frac{\partial u}{\partial s} + v^2 \frac{\partial^2 u}{\partial s^2} + 2v \frac{\partial^2 u}{\partial s \partial t} + \frac{\partial^2 u}{\partial t^2}. \quad (15)$$

In which,  $\rho_i$  is the material density of corresponding rod number,  $\text{kg/m}^3$ .  $A_i$  is the cross-sectional area of rod string.  $\rho_l$  is the oil liquid density,  $\text{kg/m}^3$ .  $q(s,t)$  is the axial distributed load at any section position  $s$ ,  $\text{N/m}$ .  $q_{ub}(x,t)$  is the transverse distributed load at any section position  $s$ , and  $\text{N/m}$ .  $\alpha(x)$  is the well deviation angle at any static coordinate position  $x$ .

The continuity conditions are the same as those in Section 2.2, the junction of carbon fiber material rod string and steel material rod string both meet the continuity of displacement, and rotation angle and bending moment, namely, the continuity condition are

$$\left\{ \begin{aligned} u_{s=L_1^-} &= u_{s=L_1^+} \frac{du}{ds} \Big|_{s=L_1^-} \\ &= \frac{du}{ds} \Big|_{s=L_1^+} E_1 I_1 \frac{d^2 u}{ds^2} \Big|_{s=L_1^-} \\ &= E_2 I_2 \frac{d^2 u}{ds^2} \Big|_{s=L_1^+} E_1 I_1 \frac{d^3 u}{ds^3} \Big|_{s=L_1^-} \\ &= E_2 I_2 \frac{d^3 u}{ds^3} \Big|_{s=L_1^+} \end{aligned} \right. \quad (16)$$

Initial conditions: the rod string is initially in a static state, also the same as section 2.2. That is, the initial condition can be expressed as

$$\left\{ \begin{aligned} u(s, 0) &= \varphi(s) = 0, \\ u_A(0) &= 0, \\ \frac{\partial u}{\partial t}(s, 0) &= g(s) = 0. \end{aligned} \right. \quad (17)$$

Boundary conditions: the boundary position between the top of the carbon fiber rod string and the wellhead is also the same as Section 2.2. Therefore, the boundary condition of the rod string can be expressed as

$$\left\{ \begin{aligned} u(s, t) &= 0, \quad \frac{\partial u}{\partial s}(s, t) = 0, \\ u(L, t) &= 0, \quad \frac{\partial u}{\partial s}(L, t) = 0. \end{aligned} \right. \quad (18)$$

**3.3. Numerical Simulation Method.** The transverse vibration equation of carbon-steel hybrid rod string is a high-order partial differential equation. The time variable  $t$  and the curvilinear coordinate variable  $s$  are coupled together, so it is almost impossible to separate the variables to obtain the analytical solution. As Section 2.3, the finite difference method and the Newmark method are combined for numerical analysis to obtain the numerical solution. It should be noted that the finite difference method can solve the linear problem, but this paper presents a special, the curved wellbore of directional well can be regarded as a straight line and then can be simulated according to the finite difference method.

The discrete model of carbon-steel hybrid rod string along the coordinate variable  $s$  is shown in Figure 4 ( $\Delta s$  is the differential step size). The junction of the two-stage rod meets the continuity condition of (16). The central finite difference method is used to discretize the variables  $u'$ ,  $u''$ ,  $u'''$ ,  $u^{(4)}$  about  $s$ .

The simulation method of transverse vibration of hybrid rod string in directional wells is similar to Section 2.3. So, the discrete form of equation (11) in directional wells is

$$\left\{ \begin{aligned} G_{i,j}^k &= A_i y_{j-2}^k + B_{i,j-1}^k y_{j-1}^k + C_{i,j}^k y_j^k + D_{i,j+1}^k y_{j+1}^k + F_i y_{j+2}^k \quad (3 \leq i \leq N-3), \\ A_i &= F_i = \frac{E_i I_i}{\Delta s^4}, \\ B_{i,j-1}^k &= \rho_i A_i \left( \frac{a}{2\Delta s} + \frac{v^2}{\Delta s^2} - \frac{v\alpha_1}{\Delta s} \right) - \frac{4E_i I_i}{\Delta s^4} - \frac{N}{\Delta s^2} + \frac{\partial N}{\partial s} \frac{1}{2\Delta s} - \frac{\varepsilon v}{2\Delta s}, \\ C_i^k &= \frac{6E_i I_i}{h^4} + \rho_i A_i \left( \alpha_0 - \frac{2v^2}{\Delta s^2} \right) + 2N \frac{1}{\Delta s^2} + \varepsilon \alpha_1, \\ D_{i,j+1}^k &= \rho_i A_i \left( \frac{a}{2\Delta s} + \frac{v^2}{\Delta s^2} + \frac{v\alpha_1}{\Delta s} \right) - \frac{4E_i I_i}{\Delta s^4} - \frac{N}{\Delta s^2} - \frac{\partial N}{\partial s} \frac{1}{2\Delta s} + \frac{\varepsilon v}{2\Delta s}, \\ G_{i,j}^k &= \rho_i A_i (\alpha_0 u_j^{k-1} + \alpha_2 u_j^{k-1} + \alpha_3 u_j^{k-1}) + \rho_i A_i v \frac{(\alpha_1 u_{j+1}^{k-1} + \alpha_4 u_{j+1}^{k-1} + \alpha_5 u_{j+1}^{k-1})}{\Delta s} + \rho_i A_i v \frac{(\alpha_1 u_{j-1}^{k-1} + \alpha_4 u_{j-1}^{k-1} + \alpha_5 u_{j-1}^{k-1})}{\Delta s} - E_i I_i \frac{\partial^3 \alpha(x)}{\partial s^3} + N \frac{\partial \alpha(x)}{\partial s} - (\rho_i - \rho_l) A_i g \sin \alpha(x) + \varepsilon (\alpha_1 u_j^{k-1} + \alpha_4 u_j^{k-1} + \alpha_5 u_j^{k-1}). \end{aligned} \right. \quad (19)$$

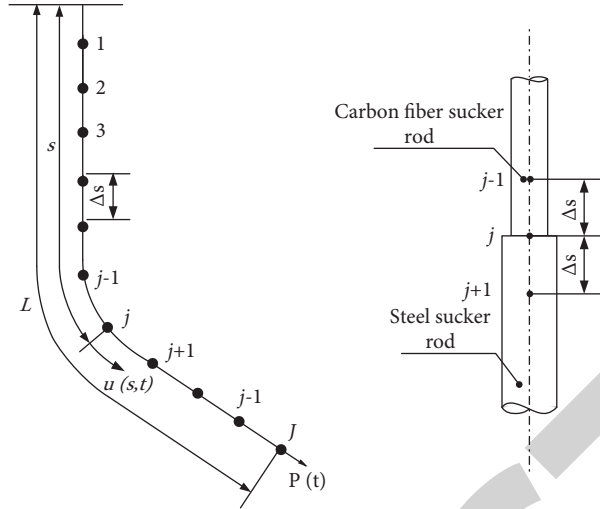


FIGURE 4: Discrete nodes of hybrid rod string length of directional well.

After collision, the node displacement and velocity meet the following relationship:

$$\begin{cases} u(s, t)|_{t^+} = \text{sgn}(u(s, t)|_{t^-})|(R - r), \\ \frac{du(s, t)}{dt}|_{t^+} = -\gamma_e \frac{du(s, t)}{dt}|_{t^-}. \end{cases} \quad (20)$$

Accordingly, the calculation formulas of impact force and transverse pressure of directional well rod-tubing are expressed as follows:

$$\begin{cases} F_{i,n} = -\rho_i A_i \frac{(1 + \gamma)}{\Delta \tau} \frac{du(s, t)}{dt}|_{t^-}, \\ F_{i,s} = E_i I_i \left( \frac{\partial^2 u}{\partial s^2} + \frac{\partial^3 \alpha(x)}{\partial s^3} \right) - T \frac{\partial \alpha(x)}{\partial s} + (\rho_i - \rho_l) A_i g \sin \alpha(x) - \frac{\partial}{\partial s} \left( T \frac{\partial u}{\partial s} \right). \end{cases} \quad (21)$$

The total contact force of rod-tubing is composed of the resultant force of collision force and transverse pressure.

$\Delta \tau$  is the time step of collision, and its value can be found in reference [24].

## 4. Simulation Result

**4.1. Basic Parameters.** Both vertical and directional wells are 2200 m deep. The wellbore trajectory of vertical well is an idealized vertical wellbore, and the curved trajectory of directional well is shown in Figure 5. Combination form of carbon-steel hybrid rod string is as follows: 19 mm × 1650 m + 25 mm × 550 m. The upper part is continuous carbon fiber sucker rod, and the lower part is steel weighting rod. The respective elastic modulus is  $E_1 = 103$  GPa and  $E_2 = 206$  GPa, respectively. Other corresponding parameters in both well types are shown in Figure 6.

## 4.2. Simulation Results of Impact Force and Contact Pressure

**4.2.1. The Impact Force and Contact Pressure in Vertical Wells.** Through numerical simulation of vertical well, the variation laws of rod string with well depth and time are obtained as shown in Figure 7, which shows two different results between the traditional steel rod and new carbon-steel hybrid rod string in this paper. It can be seen that the similarities between Figures 7(a) and 7(b) are the largest impact force with the same level value distributed on the steel rod at bottom. However, the impact contact force of the upper part in new carbon-steel hybrid rod string in Figure 7(a) is greatly reduced compared with the traditional steel rod string in the same position in Figure 7(b). This means that the carbon fiber rod string can effectively reduce the contact and collision of rod-tubing, especially in the upper part of the wellbore and prolong the service life of the rod accordingly.



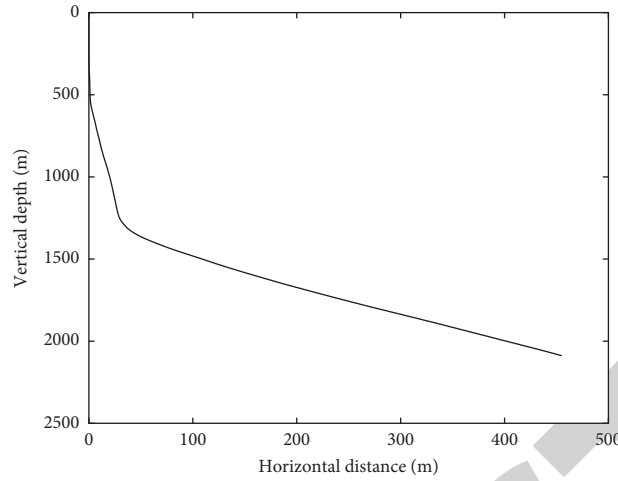


FIGURE 5: Wellbore trajectory of directional well.

| Oil well parameters   |               |  |   |
|---|---------------|--|---|
| Dynamic viscosity of oil (pa/s):  | 0.6           | Oil pressure (mpa):                    | 0.3                                     |
| Oil density (kg/m <sup>3</sup> ):   | 880           | Casing pressure (mpa):                 | 0.6                                     |
| Moisture content:   | 0.85          | Oil temperature at pump (°C):          | 60                                      |
|   |               | Gas density (kg/m <sup>3</sup> ):      | 0.7174                                  |
|   |               | Dynamic liquid level(m):               | 1310                                    |
|   |               | GOR:                                   | 20                                      |
|   |               | Pump depth (m):                        | 1700                                    |
|   |               | Pump diameter (m):                     | 0.056                                   |
| Parameters of beam pumping unit   |               |  |   |
| Crank Length (m):   | 1.32          | Connecting rod length (m):             | 3.8                                     |
| Length of rear arm of walking beam (m):   | 2.85          | Crank angular velocity (rad/s):        | 0.6283                                  |
| Height difference between beam rotation center and crank rotation center H-G (m): | 3.8           | Horizontal projection of base rod (m): | 2.525                                   |
|   |               | Length of walking beam forearm (m):    | 4.36                                    |
| Sucker rod parameters   |               |  |   |
|   | Diameter (m): | Density (kg/m <sup>3</sup> ):          | Elastic modulus (pa)*10 <sup>11</sup> : |
| First stage   | 0.019         | 1620                                   | 1.03                                    |
| Second stage  | 0.025         | 7850                                   | 2.06                                    |
| Third stage   | 0             | 0                                      | 0                                       |
| Fourth stage  | 0             | 0                                      | 0                                       |
| Fifth stage   | 0             | 0                                      | 0                                       |
|   |               | Length (m):                            | Inner diameter of tubing                |
|   |               | 1650                                   | 0.0635                                  |
|   |               | 550                                    |   |
|   |               | 0                                      |   |
|   |               | 0                                      |   |
|   |               | 0                                      |   |

Calculate

FIGURE 6: Basic parameters of simulation interface.

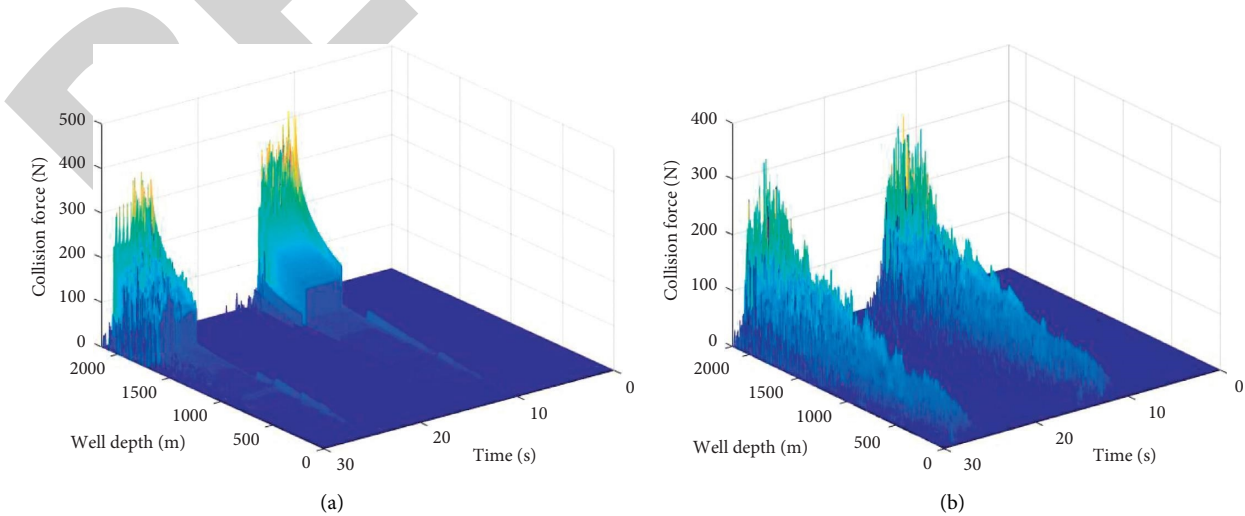


FIGURE 7: Variation of collision contact force with well depth. (a) Carbon-steel hybrid rod string. (b) Traditional steel rod string.

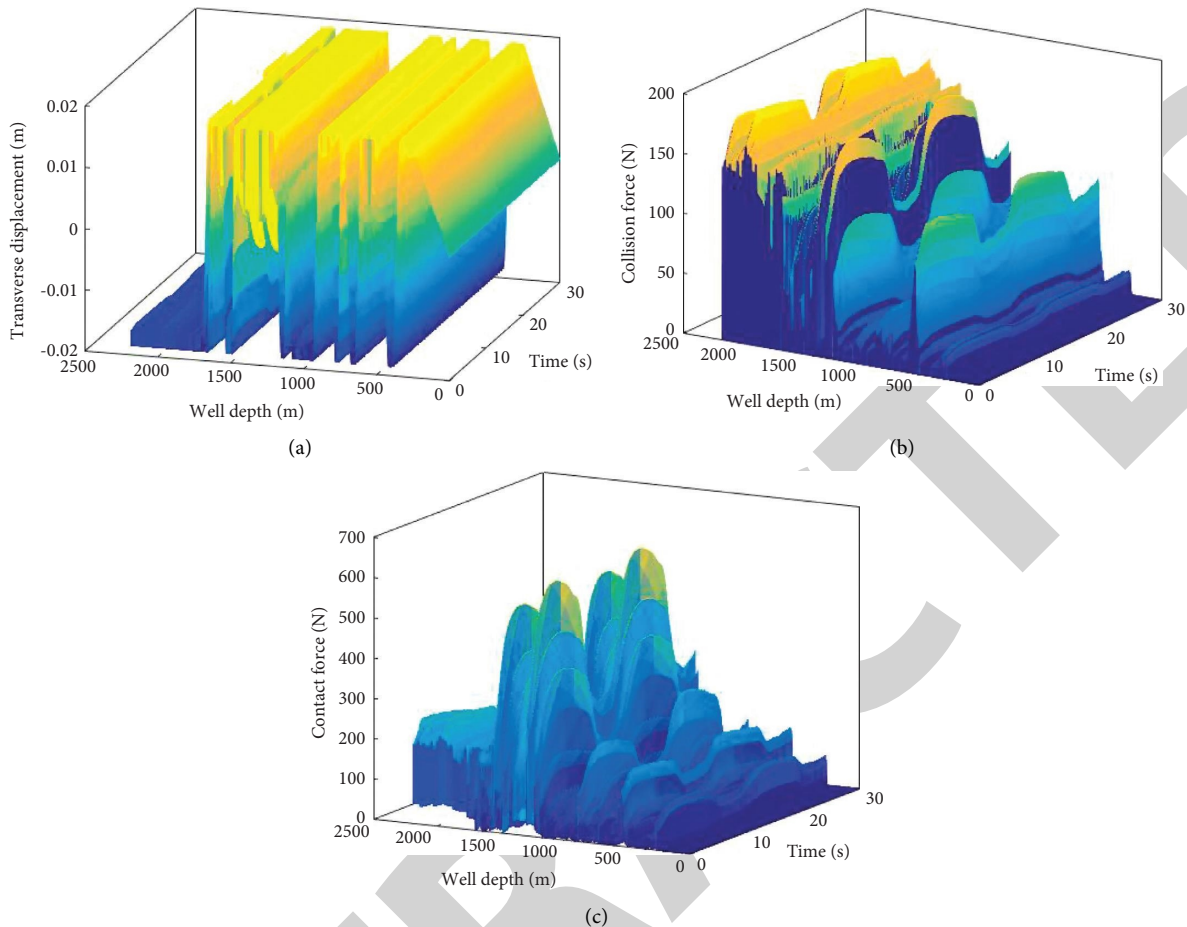


FIGURE 8: Simulation results of carbon-steel hybrid rod string. (a) Transverse displacement varies with well depth and time. (b) The impact force varies with well depth and time. (c) Rod-tubing contact force varies with well depth and time.

**4.2.2. The Impact Force and Contact Pressure in Directional Wells.** Through the simulation analysis of the transverse vibration of carbon-steel hybrid rod string in directional wells, the variation laws of rod string transverse displacement, collision force, and contact force of rod-tubing with well depth and time are obtained, as shown in Figure 8.

It can be seen from Figure 8 that the largest transverse displacement is at the bottom steel rod with almost all the rod string nodes attached to the oil well wall. Second, except for the deflecting section of wellbore, the collision force of the upper carbon fiber sucker rod is significantly lower than that of the bottom steel rod. At the inclined section and the bottom steel rod part, the collision force increases significantly. Again, the area with the maximum contact force occurs in the deviation section with large deviation angle, which indicates that the eccentric wear of rod-tubing in the deviation section will be the most serious.

Figures 9(a)–9(c) show the simulation results of traditional steel rod string in directional wells under the same condition as carbon fiber rod string. It can be seen from the comparison between Figures 8 and 9 that the maximum transverse displacement of the new and old rod string system occurs all in the compression section of the bottom rod. Again, the collision force and contact force of the rod-tubing

at the inclined section are almost the largest, indicating that the inclined section has a significant impact on the collision and extrusion of rod-tubing.

### 4.3. Bending Stress Simulation Results

**4.3.1. Bending Stress in Vertical Wells.** After further processing of the vertical well numerical simulation results, the bending stress distribution of the rod string after dynamic deformation in the tubing is obtained, as shown in Figure 10. We can get the bending stress of new carbon-steel hybrid rod string (1650–2200 m) from Figure 10(a) and the bending stress of new carbon-steel hybrid rod string (0–1650 m) from Figure 10(b), and also bending stress of traditional steel rod string (0–2200 m) from Figure 10(c).

It can be seen from the figure that the maximum bending stress of carbon-steel rod increases with the increase of well depth in a stroke. The maximum bending stress of the upper carbon fiber rod (0–1650 m) can reach 30 MPa compared with the bottom steel rod (1650–2200 m) 150 MPa. The bending stress of the traditional steel rod (0–1650 m) reaches 80 MPa. Although the bending stress does not exceed their yield limit, the stress of the traditional steel rod in the wellbore is mostly reciprocating wear and fatigue failure. On

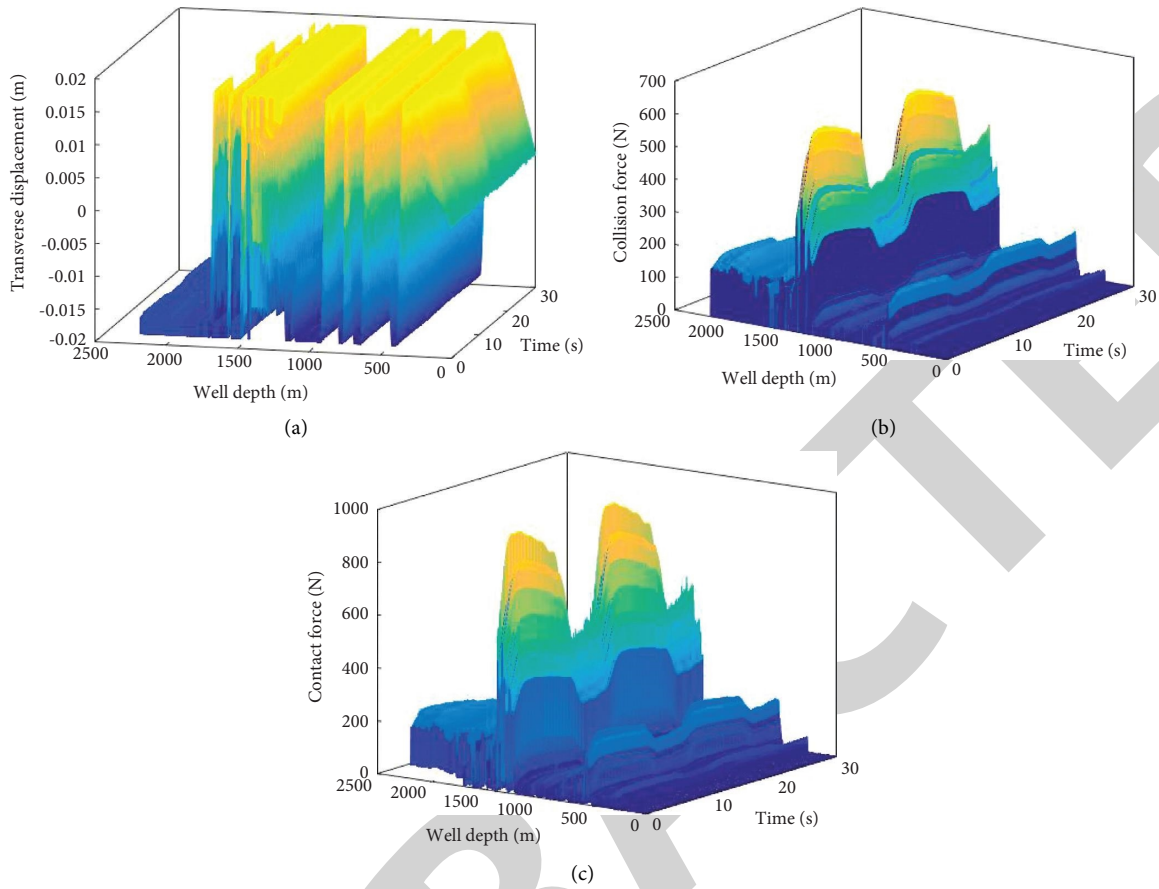


FIGURE 9: Simulation results of traditional steel rod. (a) Transverse displacement varies with well depth and time. (b) The impact force varies with well depth and time. (c) Rod-tubing contact force varies with well depth and time.

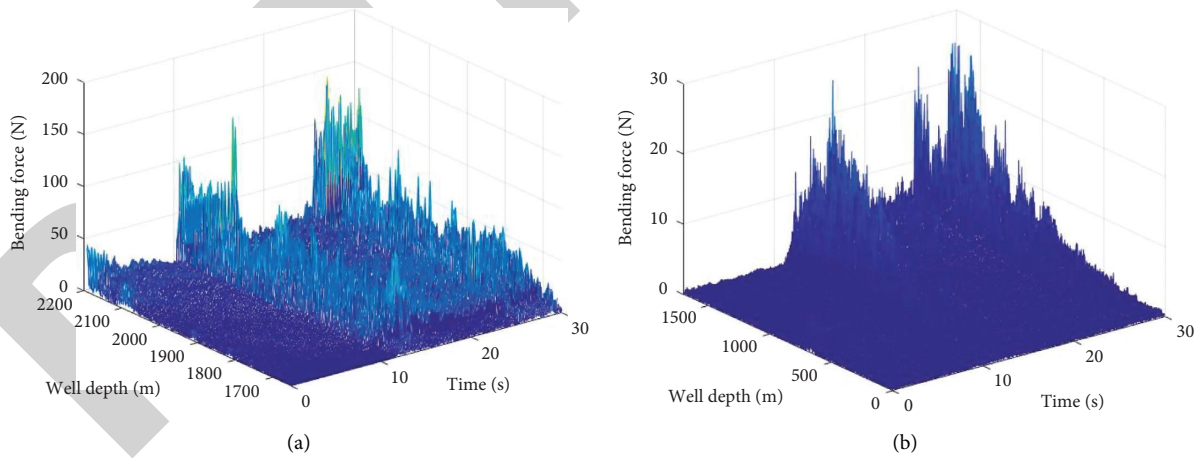


FIGURE 10: Continued.

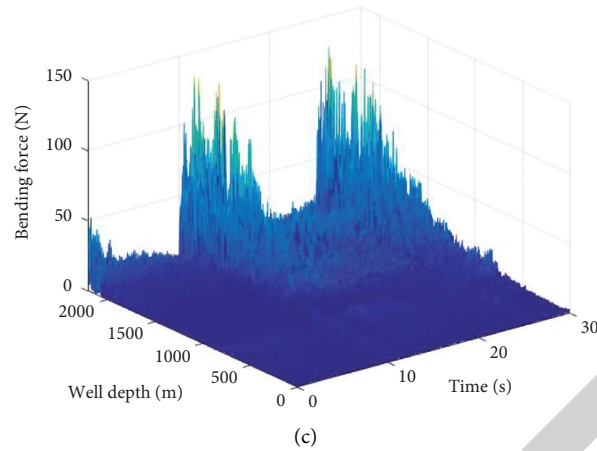


FIGURE 10: Variation of bending stress of new and traditional rod string in vertical wells. (a) Bending stress of new carbon-steel hybrid rod string (1650–2200 m). (b) Bending stress of new carbon-steel hybrid rod string (0–1650 m). (c) Bending stress of traditional steel rod string (0–2200 m).

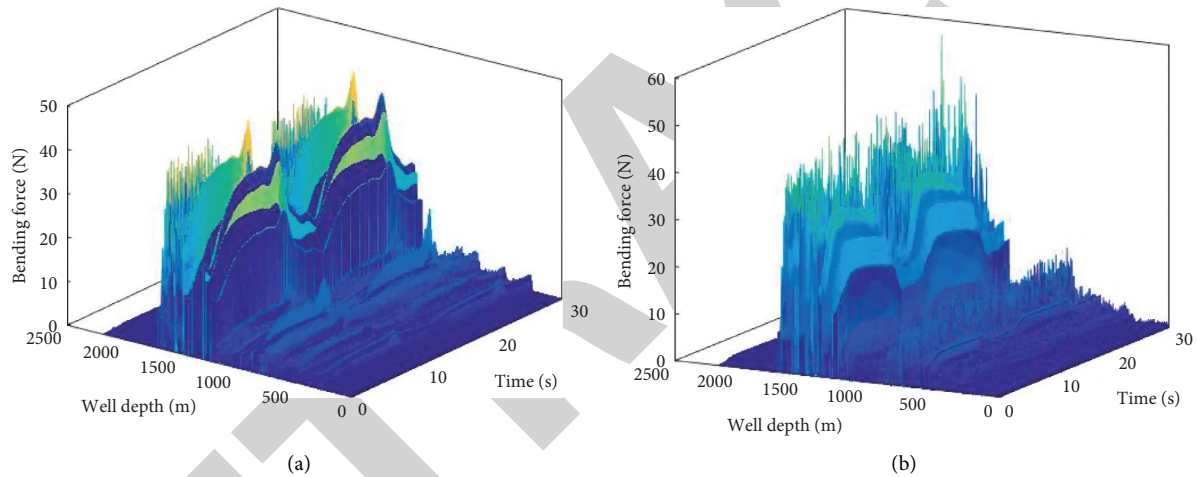


FIGURE 11: Change of bending stress of carbon fiber hybrid rod string and traditional steel rod string in directional well. (a) Change of bending stress of carbon fiber hybrid rod string. (b) Variation of bending stress of traditional steel rod string.

the contrary, the bending stress of carbon fiber rod is greatly reduced, and the service life of carbon fiber rod is greatly prolonged.

**4.3.2. Bending Stress in Directional Wells.** Based on the above simulation model of carbon-steel hybrid rod string in directional wells, the bending stress of hybrid rod string after transverse vibration deformation in tubing is obtained, as shown in Figure 11(a). The second model replaces the upper carbon fiber rod string with steel rod with the same size to obtain the bending stress, as shown in Figure 8(b). It can be seen from Figures 11(a) and 11(b) that, whether it is an integral steel rod or a carbon and steel hybrid rod string, when the sucker rod string reciprocates in the directional well, the bending stress at the inclined section is almost the largest in the whole well.

In the above two comparative models, the maximum bending stress of the above two kinds of rod forms appears

near the inclined section. The simulation results are consistent with the fact that the actual rod string is the easiest to be damaged at the inclined section.

## 5. Conclusions

In this paper, the dynamic simulation models of carbon-steel hybrid rod string in vertical wells and in directional wells are established, and the dynamic behavior of hybrid rod string above in tubing is simulated and analyzed with the following conclusions.

In vertical wells, the severe collision between the carbon-steel hybrid rod string and the oil tubing is near the bottom, which is consistent with the actual situation of the oilfield. Second, the collision of the upper carbon fiber rod is obviously weak and low, which indicates that the eccentric wear of the carbon-steel hybrid rod string mainly occurs at the bottom of the steel rod. However, the eccentric wear of

the traditional pure steel rod string almost occurs in the whole well. Therefore, the eccentric wear of carbon-steel hybrid rod is greatly reduced and also more and more widely used. Again, the stress of bending deformation of rod string in tubing does not exceed the allowable stress of the material itself in vertical wells, which is still deformed within the elastic range. This proves that the failure of the rod string is mainly fatigue wear.

In directional wells, the contact force at inclined section is almost at the maximum in the whole well, where the transverse vibrating collision phenomenon is almost the most intense. Second, whether it is a new type of carbon-steel rod string or a traditional pure steel rod string, the bending stress at the inclined section is nearly the largest. Again, carbon fiber sucker rod instead of pure steel rod string can significantly reduce the impact force and prolong the service life of rod string.

The transverse vibration simulation analysis in this paper provides the result that the carbon fiber sucker rod itself has low collision contact force, which means that the carbon fiber sucker rod can prolong the pump inspection cycle and improve the service life of oil wells. The research results lay a theoretical foundation for the practical application of carbon fiber sucker rod string in oil field.

## Data Availability

The simulation experiment data used to support the findings of this study are available from the corresponding author upon request.

## Conflicts of Interest

The authors declare that there are no conflicts of interest regarding the publication of this paper.

## Acknowledgments

This work was supported in part by the Hebei Province Natural Science Foundation of China (Grant no. E2021203095), the Science and Technology Key Project of Hebei University of Environmental Engineering (Grant no. 2020ZRZD01), the basic innovation and scientific research cultivation project of Yanshan University (Grant no. 2021LGQN009).

## References

- [1] J. Gao, "Failure analysis and countermeasures of carbon fiber continuous sucker rod," *Inner Mongolia Petrochemical Industry*, vol. 35, no. 03, pp. 45–47, 2009.
- [2] J. Li, L. Xu, and L. Li, "Application of carbon fiber continuous sucker rod in different types of pumping units," *Energy Conservation in Petroleum & Petrochemical Industry*, vol. 11, no. 12, pp. 20–22, 2021.
- [3] L. Zhang, Z. Zhang, and Q. Zheng, "Simulation study on energy saving performance and mechanism of carbon fiber rod pumping system," *China Petroleum Machinery*, vol. 49, no. 04, pp. 109–116, 2021.
- [4] Y. Zhu, "Application of continuous sucker rod of carbon fiber in oilfield production," *Energy Conservation in Petroleum & Petrochemical Industry*, vol. 7, no. 11, pp. 26–28, 2017.
- [5] W. Huang, D. Gao, and Y. Liu, "A study of tubular string buckling in vertical wells," *International Journal of Mechanical Sciences*, vol. 118, pp. 231–253, 2016.
- [6] A. A. Almet, H. M. Byrne, P. K. Maini, and D. E. Moulton, "Post-buckling behaviour of a growing elastic rod," *Journal of Mathematical Biology*, vol. 78, no. 3, pp. 777–814, 2019.
- [7] X. Sun, S. Dong, H. Wang, W. C. Li, and L. Sun, "Comparison of multistage simulation models of entire sucker rod with spatial buckling in tubing," *Journal of Jilin University (Engineering and Technology Edition)*, vol. 48, no. 04, pp. 1124–1132, 2018.
- [8] X. Sun, S. Dong, W. Li, and W. Zhang, "The numerical simulation of entire sucker rod string buckling with couplings in vertical wells," *Cluster Computing*, vol. 22, no. S5, Article ID 12295, 2019.
- [9] X. Wu, Z. Li, and Y. Hao, "A mathematical simulation Technology for beam pumping well," *Acta Petrolei Sinica*, vol. 21, no. 5, pp. 75–81, 2009.
- [10] M. Xing and S. Dong, "An improved longitudinal vibration model and dynamic characteristic of sucker rod string," *Journal of Vibroengineering*, vol. 16, no. 7, pp. 3432–3448, 2014.
- [11] S. Dong, X. Sun, M. Liu, and J. Zhang, "The simulation model of sucker rod string transverse vibration under the space buckling deformation excitation and rod-tubing eccentric wear in vertical wells," *Journal of Vibroengineering*, vol. 20, no. 1, pp. 283–299, 2018.
- [12] S. Dong, W. Zhang, Z. Hong, and C. F. Wang, "Research on the distribution contact pressure between sucker rod and tubing string of rod pumping system in directional wells," *Engineering Mechanics*, vol. 10, no. 28, pp. 179–184, 2011.
- [13] Q. Di, W. Wang, Y. Hu, and S. Dou, "Calculation method of sucker rod strings space configuration in directional well," *Journal of China University of Petroleum*, vol. 35, no. 3, pp. 72–75, 2011.
- [14] Y. Wang, M. Li, Y. Zhang, and S. M. Dong, "3D mechanical model of directional well sucker rod and its application in eccentric wear," *Drilling and Production Technology*, vol. 34, no. 1, pp. 65–68, 2011.
- [15] H. Yang, Q. Di, and W. Wang, "Prediction of serious abrasion position and mechanism of uneven abrasion between sucker rod string and tubing," *Acta Petrolei Sinica*, vol. 26, no. 2, pp. 100–103, 2005.
- [16] H. Yang, Q. Di, and X. Bu, "Establishment of dynamic model of suck rod string of 3D bending well bores and its simulation," *Journal of the Daqing Petroleum Institute*, vol. 28, no. 5, pp. 39–42, 2004.
- [17] X. H. Zhu, B. Li, Q. Y. Liu et al., "New Analysis Theory and Method for Drag and Torque Based on Full-Hole System Dynamics in Highly Deviated Well," *Mathematical Problems in Engineering*, vol. 2015, Article ID 535830, 1–13 pages, 2015.
- [18] H. Wang, X. Lu, Y. Liu, C. Yanxin, and L. Shengshan, "Mechanism of plunger over stroke in oil production system using carbon fiber sucker rod," *Acta Petrolei Sinica*, vol. 40, no. 12, pp. 1531–1541, 2019.
- [19] L. Zhang, X. Lv, and D. Jiang, "Over stroke of carbon fiber continuous sucker rod," *China Petroleum Machinery*, vol. 47, no. 7, pp. 87–92, 2019.
- [20] L. Xiaoxiao, W. Hanxiang, Z. Xin, L. Yanxin, and C. Shengshan, "An equivalent vibration model for optimization design of carbon/glass hybrid fiber sucker rod pumping

## Retraction

# Retracted: Intelligent Deployment and Development Strategy of Agricultural Farmland Based on Improved Architecture of Internet of Things

### Mathematical Problems in Engineering

Received 18 July 2023; Accepted 18 July 2023; Published 19 July 2023

Copyright © 2023 Mathematical Problems in Engineering. This is an open access article distributed under the Creative Commons Attribution License, which permits unrestricted use, distribution, and reproduction in any medium, provided the original work is properly cited.

This article has been retracted by Hindawi following an investigation undertaken by the publisher [1]. This investigation has uncovered evidence of one or more of the following indicators of systematic manipulation of the publication process:

- (1) Discrepancies in scope
- (2) Discrepancies in the description of the research reported
- (3) Discrepancies between the availability of data and the research described
- (4) Inappropriate citations
- (5) Incoherent, meaningless and/or irrelevant content included in the article
- (6) Peer-review manipulation

The presence of these indicators undermines our confidence in the integrity of the article's content and we cannot, therefore, vouch for its reliability. Please note that this notice is intended solely to alert readers that the content of this article is unreliable. We have not investigated whether authors were aware of or involved in the systematic manipulation of the publication process.

Wiley and Hindawi regrets that the usual quality checks did not identify these issues before publication and have since put additional measures in place to safeguard research integrity.

We wish to credit our own Research Integrity and Research Publishing teams and anonymous and named external researchers and research integrity experts for contributing to this investigation.

The corresponding author, as the representative of all authors, has been given the opportunity to register their

agreement or disagreement to this retraction. We have kept a record of any response received.

### References

- [1] X. Li, "Intelligent Deployment and Development Strategy of Agricultural Farmland Based on Improved Architecture of Internet of Things," *Mathematical Problems in Engineering*, vol. 2022, Article ID 5213535, 8 pages, 2022.

## Research Article

# Intelligent Deployment and Development Strategy of Agricultural Farmland Based on Improved Architecture of Internet of Things

**Xiaofen Li** 

*Jiangxi University of Technology, Nanchang 330098, China*

Correspondence should be addressed to Xiaofen Li; [lixiaofen@jxut.edu.cn](mailto:lixiaofen@jxut.edu.cn)

Received 20 April 2022; Revised 10 June 2022; Accepted 17 June 2022; Published 28 June 2022

Academic Editor: Hangjun Che

Copyright © 2022 Xiaofen Li. This is an open access article distributed under the Creative Commons Attribution License, which permits unrestricted use, distribution, and reproduction in any medium, provided the original work is properly cited.

Agricultural modernization has gradually become the direction of future agricultural development. With the improvement of the technical capacity of the Internet of things, a new agricultural development model, namely, intelligent agriculture, has gradually emerged. It can not only improve the production efficiency of agriculture but also improve the efficiency of resource utilization. The main work of the software design of the terminal node is the IoT network connection, the sensor work acquisition, and the packaging of the collected data for transmission and acceptance control to fundamentally alleviate the pressure on food security and ensure the sustainable development of China's agriculture. The experiment demonstrates that the curve temperature cycle of the agricultural greenhouse monitored by the system in this paper is normal, and the maximum temperature has been constant under different time cycles. For example, the maximum values of 5, 15, and 20 are all 0.67.

## 1. Introduction

With the change of lifestyle and consumption concept, urban and rural residents' demand for high-quality, green, safe, and healthy agricultural products has further increased. As food manufacturing involves multiple links/subjects such as production, processing, circulation, and sales, it is restricted by many factors such as inputs, environment, technology, opportunistic behavior of business subjects, and the information asymmetry among producers, consumers, and regulatory authorities, resulting in great difficulty in monitoring the quality of agricultural products, repeated prohibition of food safety incidents, and lack of public confidence in agricultural products. In the context of building a new development pattern of domestic and international double circulation, the development of smart agriculture is conducive to enhancing the market competitiveness of agricultural products in various countries, which is an important aspect of China's high-quality agricultural development. It is urgent to enhance the value chain of agricultural industry through smart agricultural technology and promote the core competitiveness of China's agricultural

industry to approach the level of agricultural developed countries as soon as possible [1].

Since 1982, the central government has issued many No. 1 documents on the subject of the three agricultural issues, and the National Medium and Long-term Development Plan for Agriculture clearly proposes the development of special agriculture, intelligent agriculture, ecological agriculture, tourism agriculture, and water-saving agriculture [2]. At this stage, as society continues to develop and as technology progresses, the creation of IoT provides strong technical support for the development of smart agriculture, which promotes the smart agriculture to become an important part of modern agriculture [3], to implement the national policy on agricultural development, in order to fundamentally solve the "three rural" problem.

IoT is a network model that uses sensors, global positioning systems, global geographic information systems, gas sensors, and laser scanners to monitor, interact with, and connect processes or objects in real time, in particular by collecting a wide range of information such as light, heat, electricity, chemistry, sound, physics, location, and mechanics, and then integrating them with the Internet [4]. The biggest advantage of the IoT is that it allows all objects to be

connected to the network, thus making them easier to detect and manage. At this stage, the IoT can be divided into 3 levels [5]. First, there is the sensing layer, which is formed mainly based on various sensors that can use information to sensing devices, thus collecting the required information and then carrying out intelligent analysis, and finally enabling the connection between the device and the network. In fact, it is the network layer, which mainly includes the network management system, the cloud computing system, and the Internet system, whose main function is to sense the processing and transmission of the data obtained. Finally, there is the application layer, which can fully realize the sensing and identification between people and things, things and things, so as to complete the research and analysis of the data and play the intelligent function of the IoT itself [6, 7].

Smart agriculture integrates the emerging mobile communication network system, Internet system, and cloud computing system, and uses various sensors and wireless sensors to achieve intelligent warning, intelligent identification, intelligent sensing, and intelligent decision making, thus providing strong technical support for agricultural development and forming visual and refined decisions [8]. The smart agriculture model mainly consists of several systems such as remote monitoring system, expert system, data analysis and collection system, wireless sensor system, and data analysis and processing system, thus being able to solve different kinds of problems existing in agricultural production.

## 2. Related Work

In the context of the development of the new era, agricultural development urgently needs to face transformation, from the once semimechanized to a modern informatization and mechanization stage of development [9]. The vigorous development of modern agriculture requires the support of modern information technology such as the IoT and cloud computing. The new IoT technology NB-IoT, known as NarrowBand-Internet of Things, is a LPWA technology led by Huawei and has become a 3GPP standard [10]. At present, China's NB-IoT industrial development is also in a leading position in the world. Reference [11] clearly proposed that the infrastructure of narrowband IoT should be built and perfected to achieve its large-scale application in urban ones. In the five-year plan for the development of the information and communications industry (2016–2020), the Ministry of Information and Communications has clearly proposed to build and improve the infrastructure of narrowband IoT and realize its large-scale application in urban management and key industries, and issued a notice on comprehensively promoting the construction and development of mobile IoT [12].

Previously, Deutsche Telekom announced that its NB-IoT network has been commercially available in eight European markets, and its US company T-MobileUS will also build a NB-IoT network covering the entire US in 2018 [13–15]. To promote the development of NB-IoT, Deutsche Telekom has established a special R&D lab, WARP NB-IoT, to provide technical support to the relevant terminal and

product manufacturing companies [16]. As of June 2017, a total of 26 operators worldwide are deploying cellular LPWAN networks, mainly concentrated in Asia, Europe, and North America. It can be seen that NB-IoT technology is currently focused on development and promotion both at home and abroad, and there is still much room for future development, gradually coming into our lives and serving the public [17, 18].

*2.1. System Solutions.* Today's agriculture is gradually moving towards an era of unmanned, regionalized, professional, and efficient agriculture, relying on modern technology to develop agriculture so that fields are not manned, digital irrigation is achieved, and computerized automatic control and software data systems are used across the board to ensure production reliability and increase efficiency while steadily increasing returns [19].

The NB-IOT-based agricultural environment monitoring system can remotely acquire the air temperature and humidity, soil moisture temperature, carbon dioxide concentration, light intensity, and video images in the field or greenhouse in real time. Through model analysis, it can automatically control the greenhouse wet curtain fan, sprinkler drip irrigation, internal and external shading, top window side window, heating and lighting, and other equipment. At the same time, the system can also push real-time monitoring information and alarm information to managers through mobile phones, PDAs, computers, and other information terminals so as to realize greenhouse informatization and intelligent remote management, which give full play to the role of Internet of things technology in facility agricultural production, ensure that the environment in greenhouse is suitable for crop growth, realize fine management, and create conditions for high yield, high quality, high efficiency, ecology, and safety of crops, help customers improve efficiency, reduce costs, and increase revenue.

The information collected by sensors in the sensing layer by means of wired or wireless is transmitted to local area networks and wide area networks using a variety of communication protocols [20]. The platform layer is to transmit the collected data to the central server side of the platform and to carry out analysis and aggregation processing of the data, displaying real-time data in a database in the form of graphs and other forms [21]. In the application layer, the manager understands the real-time crop growth condition and makes scientific decisions to achieve remote control of the agricultural production process. The specific system structure is shown in Figure 1.

In-depth understanding of the crop growth environment, and making full use of the advantages of modern wireless sensor network technology, combined with this design specific implementation project functional requirements of the background, the overall scheme of the NB-IOT-based agricultural environment monitoring system is proposed [22].

The hardware sensor collection and transmission terminal are designed, and the software monitoring platform is



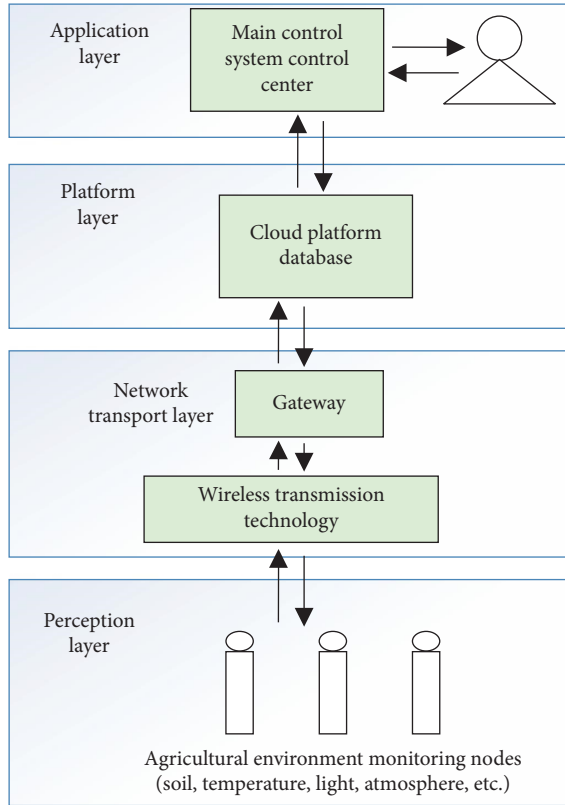


FIGURE 1: Overall architecture of the agricultural IoT system.

designed to make it a complete agricultural environment monitoring system. The design takes into account the actual use of environmental conditions, transmission distance, maintenance difficulties, and power consumption to ensure stable monitoring data collection and transmission, and to achieve synchronous storage and real-time query of the server side, issuing instructions to control and other functions [23].

On comprehensive analysis of the above considerations, the overall system design is ultimately to achieve data collection. The overall system hardware scheme structure is shown in Figure 2.

The whole design consists of three main parts: control part, communication part, and collection part. The IoT platform required plug-ins, profile file writing and IOT terminal device registration and installation, etc [24].

**2.2. Node Hardware Architecture.** The hardware part of the node is designed mainly around the control circuit, connection SIM module, the step-down circuit, and some peripheral circuits, etc. Figure 3 shows the hardware block diagram of the node.

**2.3. Main Software Processes.** The main work of the software design of the terminal node is the IoT network connection, the sensor work acquisition, and the packaging of the collected data for transmission and acceptance control. The software works in the following steps: first, the initialization

of the configuration microcontroller, closing the watchdog, and configuring SMLK as the clock source to ensure that it can be woken up in the LPM3 mode via the UART serial port [25]. And then initialize each other interface, and initialize variables such as clearing the serial buffer, then it enters the sleep power saving mode and enables interruptions, waiting for the next attempt to turn on the network and carry out data collection and transmission. Software workflow of the specific end node is shown in Figure 4.

### 3. Nodal Energy Model Analysis

**3.1. Cause Analysis.** The current IoT technology mainly uses sensors to collect parameters, a wide range of sensors and some of the power is large, but the actual use of IoT nodes mostly use battery power supply such as solar energy combined with battery storage power supply, light and high energy density lithium battery power supply, etc., without the need for cumbersome external utility not only to meet the field production environment requirements but also to reduce development costs to promote the rapid implementation of the project [26].

Most of the nodes in the IoT application are powered by batteries, which also bring its limitations. The key to the research is to balance the energy consumption of the nodes with the energy efficiency of the batteries so that the nodes can work for as long as possible and the batteries can ensure the stability of the monitoring network for a controlled period of time. This requires the selection of the battery energy size according to the energy consumption of the node and the comprehensive calculation of the node's stable working cycle to ensure the normal operation of the whole monitoring network. The loss of energy in the communication of the end nodes is difficult to measure through the instrumentation and needs to be modeled for analysis [27].

**3.2. Communication Energy Consumption Model.** The node energy consumption is analyzed here using the commonly used first-order energy loss model, which is also used in the study of clustered routing algorithms. In this design, the node contains both transmit and receive energy losses. The energy consumption of sending a  $k$ -bit packet through the transmitter circuit is  $E_{TX}(k)$ , the wireless transmission distance is  $L$ , and the energy consumption of receiving data in the receiver circuit is  $E_{RX}(k)$ . Figure 5 illustrates the energy consumption model of the node [28].

The energy consumption of node communication can be simply represented by the above diagram

$$P_E = P_{TX} + P_{RX}, \quad (1)$$

where  $P_{TX}$  is the transmitter energy consumption and  $P_{RX}$  is the receiver energy consumption, both of which are related to the distance of the wireless signal and the size of the transmitted packet  $k$  which can be expressed as

$$E = E_{TX}(k, l) + E_{RX}(k). \quad (2)$$

The energy consumed by the sensor node to transmit  $K_{bit}$  of data over a distance of  $L$  is

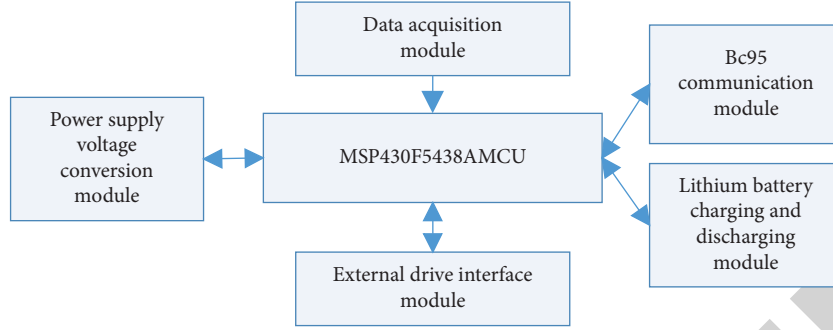


FIGURE 2: Overall system hardware scheme structure.

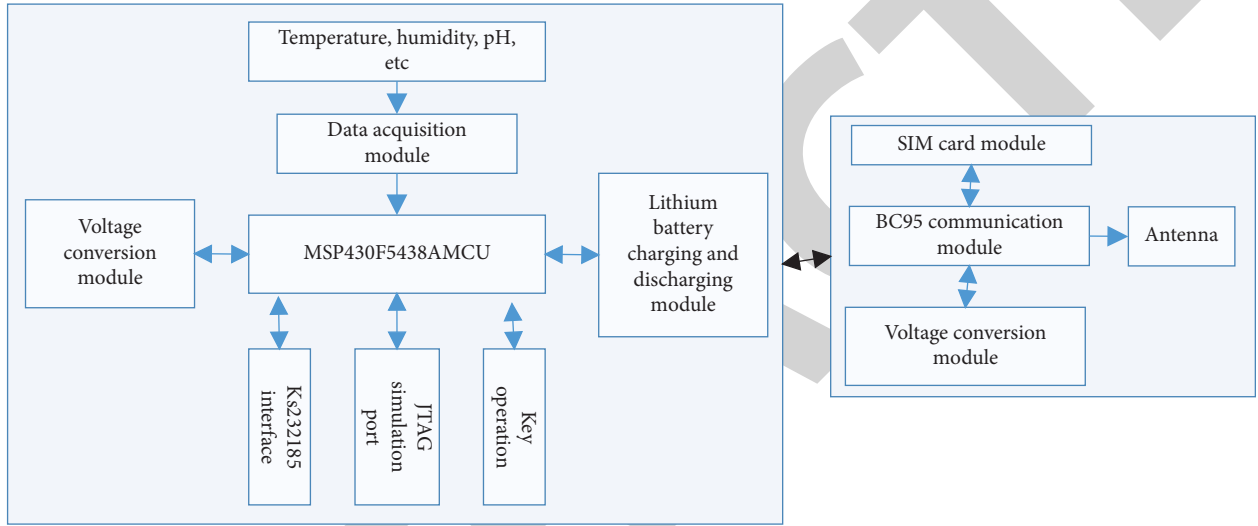


FIGURE 3: Node hardware block diagram.

$$E_{rx}(k, l) = E_{rx\_elec} \cdot k + \varepsilon_{amp} \cdot l \cdot k, \quad (3)$$

where  $E_{rx\_elec}$  is the energy consumption per bit in the transmitter circuit and  $\varepsilon_{amp}$  is the energy consumption of the amplifier in the discharge circuit. The energy consumption can be divided into two cases depending on the threshold value; when the distance is greater than  $l_0$ , the multipath fading channel model is used, while when the distance is less than  $l_0$ , the self-using spatial channel model is used to calculate the energy consumption.

Therefore, based on the relationship between the transmission distances  $l$  and  $l_0$ , the energy required to send  $K_{bit}$  data is

$$\begin{aligned} E_{rx}(k, l) &= E_{rx\_elec} \cdot k + \varepsilon_s \cdot l^2 \cdot k \quad l < l_0, \\ E_{rx}(k, l) &= E_{rx\_elec} \cdot k + \varepsilon_{mf} \cdot l^4 \cdot k \quad l \geq l_0. \end{aligned} \quad (4)$$

The formula for the critical distance threshold  $l_0$  is

$$\sqrt{\frac{\varepsilon_s}{\varepsilon_{mf}}}, \quad (5)$$

where  $\varepsilon_{fs}$  represents the fading coefficient in the self-use spatial channel model,  $E_{TX}$  represents the fading coefficient

in the multipath fading channel model, and  $E_{RX}$  is the energy loss in the circuit [29].

The energy consumption of the received data is

$$E_{RX} = E_{RX\_elec} \cdot k. \quad (6)$$

From equation (6) above, whether in the free space model or in the fading space model, the received data energy consumption is only related to the amount of data received. The energy loss from channel transmission in the node is much greater than the energy loss from the sensor acquisition and data integration, and the internal energy consumption is relatively small. Therefore, it is necessary to consider reducing the transmission distance and keeping the node location and the base station within a reasonable range. The energy consumption algorithm can be used to calculate the node placement and a number of nodes in the communication grid in relation to the base station to obtain the best area with low energy consumption for node communication. According to the common selection criteria for wireless sensor networks, the energy consumption of the transmitting circuit is determined, the initialized node energy is 0.3 J, the fading factor  $\alpha$  in the spatial channel model is 10 pJ/(bit<sup>2</sup>), the fading factor  $\alpha_m$  in the multipath fading channel model is 0.0013 pJ/(bit<sup>4</sup>), the packet size  $k$  is 2000it,

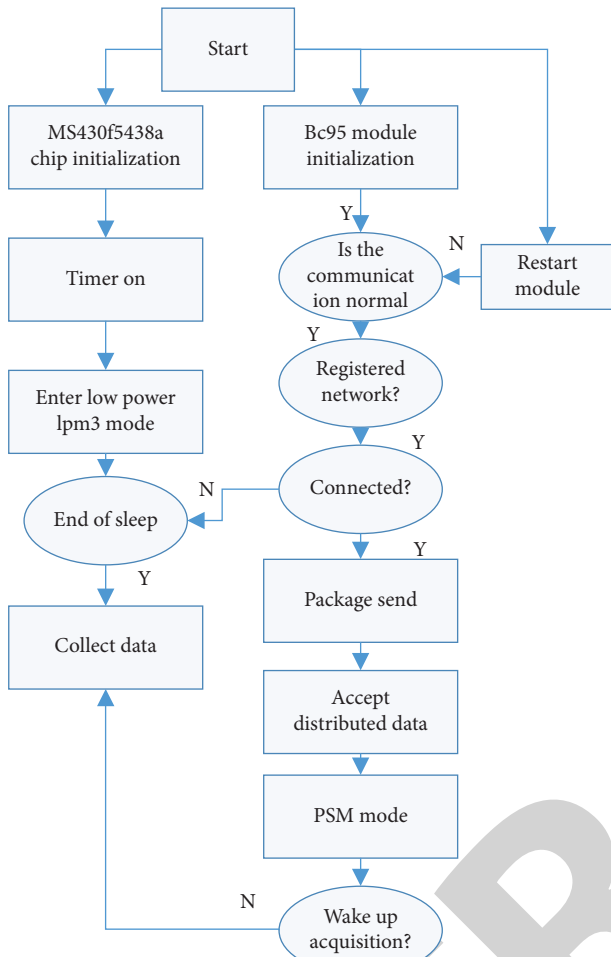


FIGURE 4: Workflow diagram of the end node.

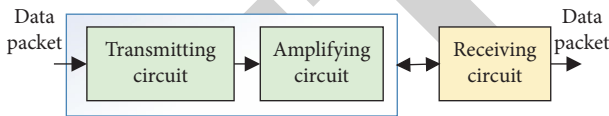


FIGURE 5: Energy consumption model diagram.

the transmission radius of the wireless network is 100m, and the threshold value  $l_{Ex}$  is  $1.026 \times 10^7$ J according to the energy consumption formula, and the capacity of the battery is 169mAh at 3.7V according to the transmission time of 5s per transmission, 12 times per day, and the working life is of at least 1 year [30, 31].

#### 4. Case Applications

This study takes a modern agricultural intelligent park project as the background and uses IoT technology and wireless networking technology to build an intelligent sensor monitoring network in the demonstration area and construct a real-time monitoring system for the rice crop growth environment in the demonstration area. The monitoring parameters of the system mainly include regional meteorological parameters monitoring (temperature, humidity,

rainfall, etc.), rice growth soil and fertilizer environment monitoring (groundwater level, pH value,  $CO_2$ , light level, etc.), and finally build a demonstration area pump station remote computer automation control system integrating data acquisition, image transmission, and automatic control. The field application of this R and D is mainly the field commissioning and application of the nodes based on NB-IoT technology. Figure 6 below is a schematic diagram of the system structure of an intelligent modern agricultural park [12].

After the hardware design is completed, on-site commissioning will be carried out and the collected environmental data and information such as pumping stations of the intelligent modern agricultural park will be gathered in the application platform of the project. The environmental data collected by the nodes will be subscribed to the application data through the IoT platform. The URL of the local system server will be filled in the subscription address field and the subscription will be successful when the platform is automatically detected, and the data will be sent to the local management system server simultaneously. Figure 7 shows the field system platform transfer attempt.

In recent years, after years of development, China's IoT technology has made certain achievements, taking shape specifically, and Internet of Things technology can detect and control the production environment of intelligent agriculture. This requires farmers to go out to the fields regularly to observe the growth of their crops, which consume a lot of resources, human, financial, and material resources. Use of IoT technology allows for timely and effective irrigation, spreading, sowing, and fertilization of crops, thus eliminating the drawbacks of traditional agriculture, improving the quality and yield of crops, and saving resources.

It can be seen from Figure 8 that the curve temperature cycle of the agricultural greenhouse monitored by the system in this paper is normal, and the maximum temperature has been constant under different time cycles. For example, the maximum values of 5, 15, and 20 are all 0.67. An IoT technology can provide protection for the food safety of agricultural products. The proverb "disease enters through the mouth" shows that food safety is directly related to human health, so the safety and quality of agricultural products need to be strictly controlled so as to provide a safe dining environment for the general public. The use of the IoT technology can be used to measure and control the quality and safety of agricultural products throughout the whole process, from the field to the table management will be transparent, so as to ensure the safety of agricultural products. This technology can be used in greenhouses, highways, irrigated areas, and gardens. This technology can also be used in greenhouses, highway barriers, agricultural irrigation areas, and garden green areas. In addition, IoT technology has been significantly developed in the network management, intelligent computing, and communication protocols of smart agriculture and has received good results in the agricultural fields of electricity, environmental protection, food, transportation, logistics, and medical care, with temperature monitoring as shown in Figure 9.

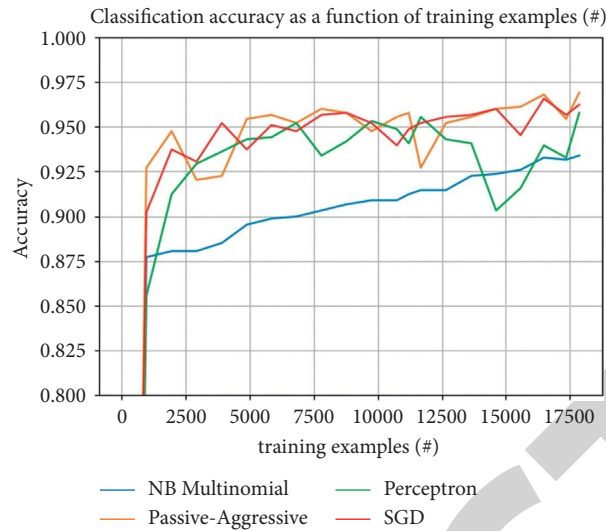


FIGURE 6: Schematic diagram of the system structure of the intelligent park.

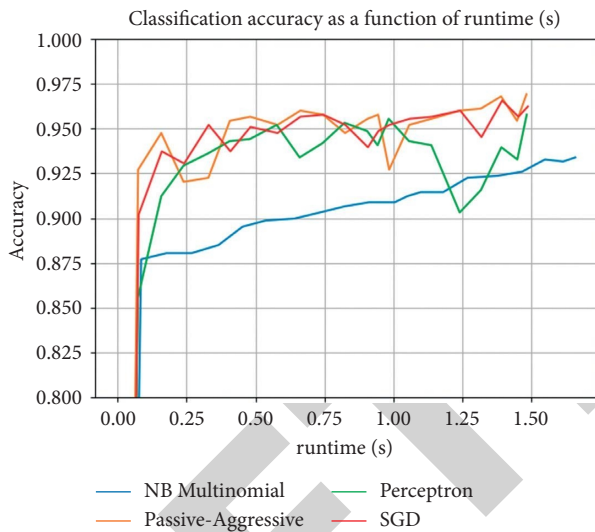


FIGURE 7: Temperature control effect.

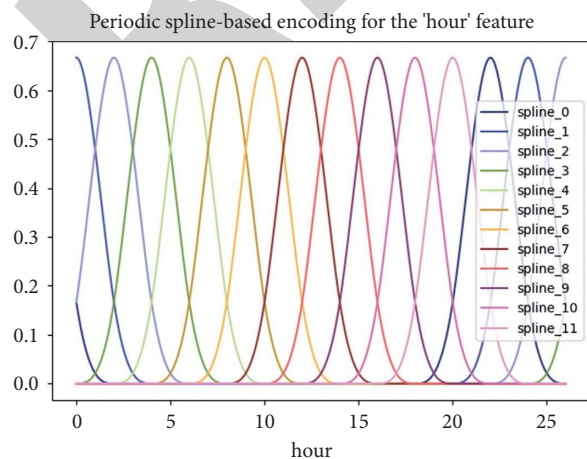


FIGURE 8: Different monitoring data.

Logistics network technology in the development of smart agriculture also has certain shortcomings, such as the slow degree of construction of basic information in agriculture, the lack of relevant norms and standards for agricultural development, the lack of professional and technical personnel, the lack of unified technical means in agriculture, the lack of maturity in the development of IoT, the lack of strength in agricultural production, and the inability to enable farmers to receive appropriate technical training, specifically for the application of IoT in smart agriculture technology. There are problems between the standard and cost of the IoT technology; compared with foreign technology, China's technology still has more drawbacks and needs to be further improved, and the maturity of the IoT technology directly restricts the scale of the development of smart agriculture, the lack of unified technical standards in the reading of information, the transmission of information, and the analysis of data and human-computer interaction, as shown in Figure 10.

This directly leads to the fact that manufacturers cannot organize their production according to uniform regulations and, therefore, costs are increased and can only be applied to some high value agricultural products. At this stage, there is a lack of professional and technical personnel to apply IoT technology. There are not many experts in Chinese agriculture, and there are many computer professionals and technical personnel who do not understand the science of smart agriculture, which is an inherent deficiency. The commercial form of smart agriculture is backward. At this stage, the commercial form of Chinese agricultural IoT is by and large the production units of agriculture themselves which pay for the needed projects, and even some large farms need to pay for their own application of IoT projects, which all lead to high cost and low motivation and insufficient multisectoral coordination of IoT technology. The development of smart agriculture using IoT technology requires the collection of a wide range of information, requiring a lot of information analysis and transfer from the environment, government, meteorological offices, farmers and business, etc.

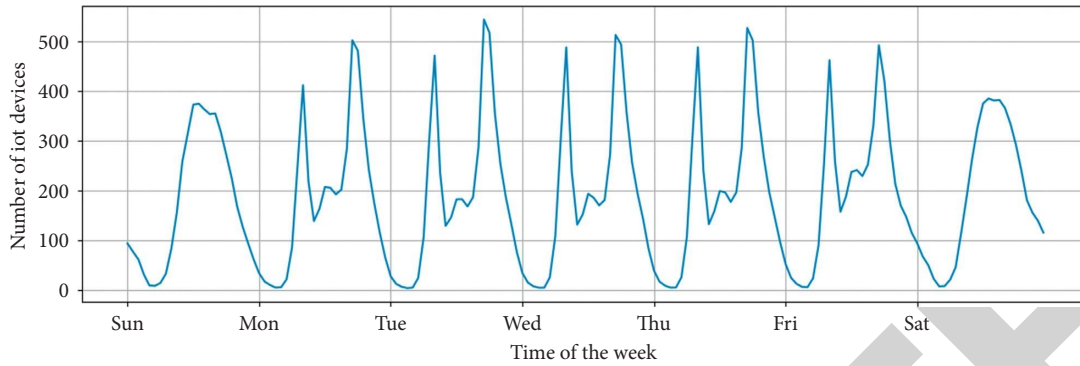


FIGURE 9: Monitoring of different IoT devices.

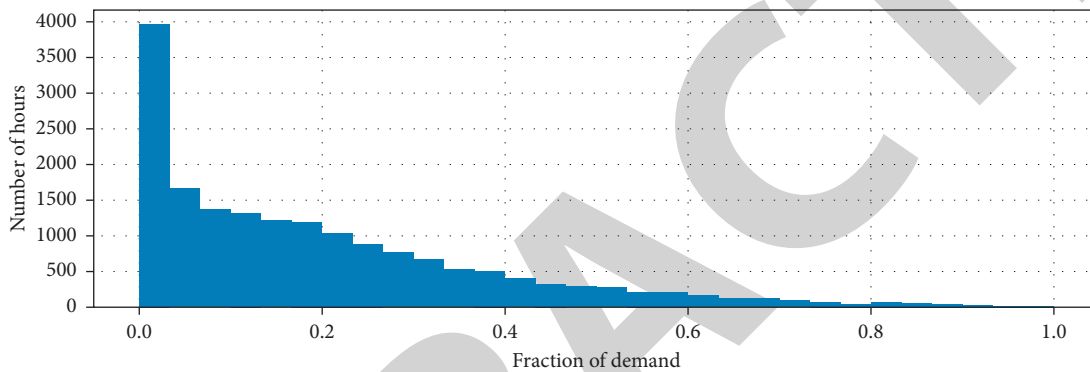


FIGURE 10: Different need ratios.

## 5. Conclusions

IoT, with its ubiquitous information data perception, intelligent information analysis and processing, massive information data storage and analysis, and ubiquitous network connectivity, can not only combine the real world and the virtual network but also promote the transformation of agricultural production methods and improve the efficiency of resource utilization.

Although there are many problems in applying IoT technology to smart agriculture, with the continuous development of science and technology, smart agriculture has become the inevitable trend of the times, and we believe that combining IoT and smart agriculture is an effective strategy to achieve sustainable agriculture. In short, the application of IoT technology in smart agriculture is a long way to go and requires the joint efforts of the party and the state, the agricultural sector, and all sectors of society. [32].

## Data Availability

The raw data supporting the conclusions of this article will be made available by the authors, without undue reservation.

## Conflicts of Interest

The authors declared that they have no conflicts of interest regarding this work.

## Acknowledgments

The research was supported by the Science and Technology Research Project of Jiangxi Provincial Education Department, Research on the Relationship between Financial Market Development and Enterprise Technological Innovation in Six Central Provinces, No. GJJ171023.

## References

- [1] S.-H. Han, "A review of research on restaurant brand personality: a focus on the hospitality and tourism journals listed at korea research foundation," *Journal of Tourism Sciences*, vol. 35, no. 2, pp. 337–353, 2011.
- [2] R. S. Sinha, Y. Wei, and S.-H. Hwang, "A survey on LPWA technology: LoRa and NB-IoT," *Ict Express*, vol. 3, no. 1, pp. 14–21, 2017.
- [3] T. Xie, C. Zhang, Z. Zhang, and K. Yang, "Utilizing active sensor nodes in smart environments for optimal communication coverage," *IEEE Access*, vol. 7, pp. 11338–11348, 2019.
- [4] J. Shi, L. Jin, J. Li, and Z. Fang, "A smart parking system based on NB-IoT and third-party payment platform," in *Proceedings of the 2017 17th International Symposium on Communications and Information Technologies (ISCIT)*, pp. 1–5, IEEE, Cairns, QLD, Australia, 2017, September.
- [5] J. Zhang, P. Liu, W. Xue, and Z. Rui, "Farmland intelligent information collection system based on NB-IoT," in *Proceedings of the International Conference on Cloud Computing and Security*, pp. 331–343, Springer, Haikou, China, 2018, June.

## Research Article

# Design and Analysis of Intelligent Agricultural Monitoring System Based on Biological Intelligence Optimization Algorithm

Zhiqin Chen <sup>1</sup>, Zhihao Liao,<sup>1</sup> Deming Qian,<sup>1</sup> and Jie Li<sup>2</sup>

<sup>1</sup>School of Electronic Commerce, Jieyang Polytechnic, Jieyang, Guangdong 522000, China

<sup>2</sup>Jieyang Administration for Market Regulation, Jieyang, Guangdong 522000, China

Correspondence should be addressed to Zhiqin Chen; [chenzq@jyc.edu.cn](mailto:chenzq@jyc.edu.cn)

Received 31 March 2022; Revised 9 May 2022; Accepted 17 May 2022; Published 24 June 2022

Academic Editor: Man Fai Leung

Copyright © 2022 Zhiqin Chen et al. This is an open access article distributed under the Creative Commons Attribution License, which permits unrestricted use, distribution, and reproduction in any medium, provided the original work is properly cited.

The traditional optimization method has insufficient intelligence, slow operation speed, and some problems in the calculation of optimal parameters when facing the relationship between too large sample size and complex thread. The biological intelligence optimization algorithm is based on the genetic and evolutionary mechanism of the genetic system. The smart agricultural system is the application of new IOT technology in the field of smart agriculture, mainly including real-time monitoring, wireless monitoring, and remote image and analysis functions. Through this topic, it is concluded that (1) when the parameter is set to  $\mu = 0.02$ ,  $\beta = 0.99$ , the deviation of the optimal value = 1.74, the deviation of the average value = 3.86, the standard deviation of the experimental value = 3.81, the performance evaluation = 2.68, and the maximum number of peaks = 4. It can give full play to the advantages of various algorithms and learn from each other's strengths. (2) The sNIOA algorithm is the best. Compared with the NIOA algorithm, the accuracy of N is increased by 50% and the accuracy of  $L = 8$  is increased by 20%. Compared with the NGA algorithm, the error of I is reduced by 23.5% and the offset of M is reduced. NPSO algorithm pm performance is improved by 20%, and pmk peak value is reduced by 20%. The domestic research on smart agriculture has experienced explosive growth, and the research has been carried out from the concept of smart agriculture, related technologies, constraints, industrial chain, etc., to provide theoretical guidance for the development of smart agriculture. The worst algorithm parameter is the NIOA model whose offset increases little, the performance decreases by 20%, and the peak value becomes worse. (3) The smart agriculture project uses the latest Internet of Things and cloud computing technology, and based on the analysis of big data and artificial intelligence technology, a new service form is proposed, that is, a cloud, network, and platform composite service system to establish a regional closed-loop ecological chain integrating agricultural production, processing, and marketing. (4) In the biological genetic algorithm model, the recall rate of Cp is low, the ROC curve fluctuates greatly, the specificity AEa is poor, and the sensitivity is not high. Using the integrated technology integrating GIS technology, RS technology, spatial statistics, mathematical models, and other methods, based on the differences of various temporal and spatial scales and their monitoring methods, combined with regression model and spatial sampling method, quantitative analysis was performed, and its influencing factors were analyzed. The comparison shows that the optimal F1 score of biological intelligence optimization parameters is up to 23% higher, the accuracy rate Ao is increased by 20%, and the accuracy rate is high.

## 1. Introduction

Artificial intelligence control is used to express human reasoning and decision-making behavior in the form of computer language and apply it to the control process. An immune feedback controller is proposed based on the feedback mechanism of the immune system [1–3]. On this basis, combined with fuzzy theory, a novel fuzzy self-

adjusting immune feedback control system is proposed. Based on the interconnection between the three major systems in the organism, a biological network structure is constructed, which is the solution to the overall intelligence of complex systems. Behavior provides ideas. The neuro-endocrine immune network is a complex large system with deep negative feedback and high stability, with unique adaptability and stability. Intelligent control is used to

intelligentize the control process. The intelligence here is inseparable from the study of biological intelligent behavior, especially the study of human intelligent behavior. These algorithms are widely used in practical optimization problems due to their excellent performance and simplicity. The immune system is a delicate, complex, and complete physiological defense system with the characteristics of diversity, adaptability, robustness, memory, immune self-regulation, and evolution. Fuzzy control imitates human's fuzzy reasoning and decision-making process. Expert control imitates the process of human experts making decisions based on experience and knowledge. Neural network simulates the information transmission of the human brain in many aspects. Besides, genetic algorithms are produced by simulating biological genetic and evolutionary mechanisms. The search range of genetic algorithm docking is much larger than that of ordinary docking. The search algorithm has to face the more complex energy landscape of the entire genetic surface, and for search algorithms of different sizes, the search range of blind docking is regarded as rigid and small molecules. For a problem to be solved by AIS algorithm, it should firstly be clear whether the field corresponding to the problem belongs to optimization problem or classification problem. Fuzzy control, as the earliest intelligent control, and its entire development process are of great significance to the development of intelligent control. Heuristic search algorithms (such as particle swarm algorithm) are used to make targeted adjustments to the pose of the ligands to try to find the ideal pose for small molecules and proteins to bind. Since the fuzzy set theory and the basic principles of fuzzy control were proposed [4–6], people continue to research and innovate on the basis of its theory. The aforementioned basic fuzzy models have been improved in many ways [7–10]. Blind docking experiments are very different from ordinary docking experiments. On one hand, the search range of blind docking experiments is much larger than that of ordinary docking experiments, so the search algorithm will face more energy "trap" (i.e., local optima regions) on larger protein surfaces, which gives a greater challenge to the algorithm. On the other hand, since the blind docking box needs to contain the whole protein, the search range size of the blind docking is different for different docking cases, which tests the adaptability of the algorithm to the search range of different sizes. For results related to the mean lowest binding energy, LGA performed much better, second only to GDCGL-RDPSO and MSPL-RDPSO-S6, but LPSO was still the worst, suggesting that LPSO may not be suitable for the search range much bigger blind docking problem. The number of best scoring conformations and the best-sampled RMSD for successful docking are somewhat more important results for blind docking. Because for the blind docking problem, the user is likely to examine all the conformations found one by one according to the binding energy ranking given by the docking software. Therefore, if the algorithm can find the best scoring conformation for successful docking, it can save a lot of research time. The best sampled RMSD correlation results (including the number of best sampled conformations successfully docked and the mean of the best sampled RMSDs) refer to the user evaluating all

conformations found by the algorithm one by one. The user is able to successfully reproduce the crystal conformation, and that crystal conformation are sufficiently similar.

The smart agricultural system is the application of new IOT technology in the field of smart agriculture, mainly including real-time monitoring, wireless monitoring, and remote image and analysis functions. Real-time monitoring: according to the information of animal and plant growth environment obtained by wireless network. The system is responsible for receiving the data sent by the wireless sensors, realizing the acquisition, management, dynamic display, and analysis processing of all information, and displaying it to the user in the form of intuitive charts and curves. Control: these are crucial for China in a transitional period. SMS alarm information is provided according to different needs. Empirical models are used with very little ground data [11–14]. Compared with traditional data, the error of simulation results is smaller. RS technology has multiple functions, among which information is based on the growth characteristics of crops, and is used to evaluate the damage degree and area of crops. The intelligent agricultural problem has high requirements on the quality of the search algorithm, but it is difficult to find a solution of sufficient quality in a short time only by relying on the partial global intelligent search algorithm. The search algorithm developed based on intelligent optimization usually makes the search behavior more global. The algorithm is used in conjunction with the PSW local search algorithm. Using a hybrid algorithm framework can calculate the optimal solution more sensitively [15].

## 2. Biosmart Agriculture

*2.1. Biological Information Processing System.* People have proposed the genetic and evolutionary mechanism of artificial neural network based on the genetic system. People have proposed the mechanism of immune recognition and immune regulation based on the immune system of genetic algorithm. Introductory books include artificial neural networks, genetic algorithms, particle swarm optimization, simulated annealing, immune algorithms, and combinatorial optimization algorithms. Then, the basic AIS model is selected according to the nature of the problem. Finally, choose the corresponding AIS algorithm [16–19]. The combination of fuzzy control and neural network makes full use of the adaptive learning ability of neural network and the ability of fuzzy control to express qualitative knowledge. The original data stream is denoised, as shown in Figure 1. Population Parallelism (MSP) strategy is combined with the RDPSO algorithm to form the MSP-RDPSO algorithm. The MSP strategy draws on the idea of part of the island model and part of the CPSO algorithm architecture, divides the entire population into multiple subpopulations evenly, and assigns characteristic components to each subpopulation. The algorithm uses the feature exchange method to realize the information exchange between the subpopulations and every certain number of iterations. Since the iterative process of RDPSO and the exchange of feature components in each subpopulation can be executed evenly in the unit of

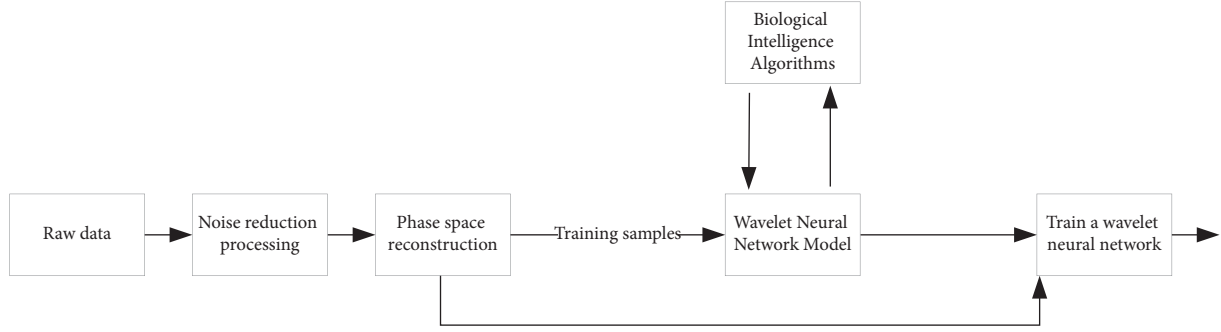


FIGURE 1: Modeling process of biological intelligence algorithms.

subpopulation, the MSP-RDPSO algorithm can be fully parallelized. The interval between the two feature exchange methods and the value range of the number of subpopulations are determined. The value has an important impact on the performance of the algorithm. Multiple MSP-RDPSO versions are compared with the classic version of the RDPSO algorithm and the RDPSO algorithm based on the classic island model. The performance comparison is carried out to prove the effectiveness of the MSP strategy in improving the performance of the algorithm. After wavelet noise reduction, it enters the phase space reconstruction and uses the training wavelet model to perform biological intelligence algorithms on the training samples to obtain the optimal parameter model.

**2.2. Grey Linear Programming.** It takes a long time for each subpopulation to continuously perform the RDPSO search behavior, and each subpopulation has converted to a relatively small area before the FE operation. At this time, even if the FE operation is performed again, it is difficult to expand the search range of the particle swarm to a very small area. Large range, which is obviously disadvantageous for multimodal problems, but more local searches are more beneficial for unimodal problems. When it is larger, the number of iterations between two FE operations is relatively small, so that the entire search process is interrupted by the FE operation before the subpopulation converges to a smaller area for a more local search. In this case, the algorithm cannot achieve better results on the unimodal function, but more FE operations mean more frequent information exchange between subpopulations, which is conducive to maintaining the diversity of the entire population, which can help the algorithm to better solve the problem. As a veritable agricultural country, there are significant differences in agricultural resources and conditions in various regions of our country. It is precisely because of this that it is very necessary to further develop smart agriculture. Smart agriculture simulates the information transmission of the human brain in many aspects and is becoming mature in the continuous research and development, which can effectively achieve the goal of increasing food production and provide reliable food security for human beings. Simulation of biological genetics and evolutionary

mechanism produces genetic algorithm, which is mainly based on professional technology and operation platform research. From the perspective of policy supply and demand, macro research on the development of smart agriculture and its application in each link of the industrial chain is less involved, as shown in Figure 2.

### 3. Biological Intelligence Optimization Algorithm

**3.1. sNIOA Algorithm.** Biological intelligence [20–23]:

$$I_{e_i} = I_{p_e} \frac{I_{f_i}}{\sum_{i=1}^n I_{f_i}} + (1 - I_{p_e}) \frac{I_{c_i}}{\sum_{i=1}^n I_{c_i}}. \quad (1)$$

Blur self-adjustment:

$$\{(x^{(1)}, y^{(1)}), \dots, (x^{(k)}, y^{(k)})\}, \dots, y^{(i)} \in \{1, 2, \dots, k\}, \quad (2)$$

$$h_{\theta}(x^{(i)}) = p(y^{(i)} + x^{(i)}).$$

Artificial intelligence control:

$$\Gamma_i = \frac{1}{\sum_{j=1}^k e^{\theta x^{(i)}}}, \quad (3)$$

$$p(y^{(i)} = jx^{(i)}).$$

**3.2. NIOA Algorithm [24, 25].** Reasoning and decision-making:

$$J(\theta) = -\frac{1}{m} \left[ \sum_{i=1}^m \sum_{j=1}^k \{y^{(i)} = j\} \log e^{\theta_j x^{(i)}} \right]. \quad (4)$$

Immune intelligent controller:

$$f(x, y) = 0.5 + \frac{\sin^2(\sqrt{x^2 + y^2}) - 0.5}{1 + 0.001(x^2 + y^2)}, \quad (5)$$

$$R = \{r_1, r_2, \dots, r_q\},$$

$$T = \{t_1, t_2, \dots, t_s\}.$$

Intelligent control:



$$\begin{aligned} \min f &= \sum_{j=1}^s c_{ij} k_{ij} p_j, \\ \text{s.t. } \sum_{j=1}^s k_{ij} &= 1, \forall i = 1, 2, \dots, q, \\ \sum_{i=1}^q \sum_{j=1}^s k_{ij} &= s. \end{aligned} \quad (6)$$

Evolutionary computation:

$$i = 1, 2, \dots, q. \quad (7)$$

Remote sensing data:

$$\begin{aligned} j &= 1, 2, \dots, s, \\ s &\leq q, \\ k_{ij} &\in \{0.1\}, \quad \forall i, j. \end{aligned} \quad (8)$$

### 3.3. NGA Algorithm [26]

$$\begin{aligned} T_i &= \{t_i^1, t_i^2, \dots, t_i^j\}, \\ D_i &= \{A_\varphi, T_i, A_\varphi\}. \end{aligned} \quad (9)$$

Smart agriculture:

$$\min f = \sum_{i=1}^q \sum_{u=1}^{D_i} \sum_{v=1}^D \delta_{uv} \zeta_{uv}, \psi(i) = \{j, k_{ij} = 1, \forall j \in R\}. \quad (10)$$

Real-time monitoring:

$$\psi^{-1}(i) = \{i, k_{ij} = 1, \forall i \in V\}. \quad (11)$$

Empirical model:

$$\begin{aligned} N(i) &\in \{1, 2, \dots, n\}, \\ \alpha_i &= \frac{r_c - d_{iC}}{r_C}. \end{aligned} \quad (12)$$

Wireless monitoring:

$$d_{AB} \sqrt{(x_A - x_B)^2 + (y_A - y_B)^2}. \quad (13)$$

Image and analysis:

$$\begin{aligned} \min f &= \sum_{i=1}^m \alpha_i \Phi(i), \\ \rho_i &= r_i \frac{\sum_{\mu=0}^{e_p-1} 2^\mu b \mu}{2^{e\mu}}. \end{aligned} \quad (14)$$

## 4. Simulation Experiment

**4.1. Smart Agriculture.** Smart agriculture is mainly based on professional technology and operation platform research, and there is less macro research on the development of smart agriculture and its application in various

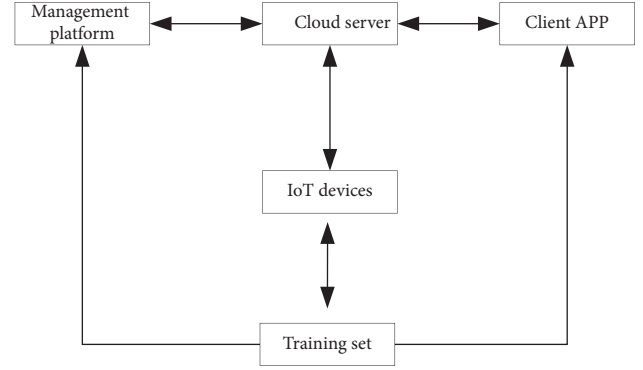


FIGURE 2: Grey linear programming model.

links of the industrial chain from the perspective of policy supply and demand. Under the guarantee of policy, science and technology, and the popularization of education, smart agriculture in developed countries has developed better. Each country develops suitable smart agriculture models according to their specific national conditions, and each country has its own characteristics of smart agriculture. The experimental results of parameter analysis are shown in Table 1 and Figures 3 and 4. When  $\mu=0.02$ ,  $\beta=0.99$ , deviation from optimal value = 1.74, deviation from mean value = 3.86, standard deviation of experimental value = 3.81, performance evaluation = 2.68, and the maximum number of peaks = 4. In the academic field of biological sciences, the interaction between them, that is, the “neuroendocrine immune network”, has attracted the attention of scholars and carried out systematic research since the 1990s. In the parameter setting, when  $\mu=0.05$ ,  $\beta=0.67$  is the optimal value in the prediction result of smart agriculture, the optimal value deviation = 2.05, the average deviation = 3.22, the experimental value standard deviation = 3.24, the performance evaluation = 1.47, and maximum number of peaks = 4. When  $\mu=0.1$ , the predicted result  $\beta=0.88$  is the optimal value, the optimal value deviation = 1.47, the average deviation = 3.35, the experimental value standard deviation = 3.07, the performance evaluation = 1.61, and the maximum number of peaks = 5.

**4.2. Grey Linear Programming Model.** GLP refers to the gray linear programming model and finally configures the results of the two optimization schemes and applies them to the space unit. As a veritable agricultural country, there are significant differences in agricultural resources and conditions in various regions of our country. It is precisely because of this that it is very necessary to further develop smart agriculture. The construction of smart agriculture will help to increase farmers’ income, agricultural growth, and balance the total area of arable land. Realized by neural networks, biological intelligent controllers inspired by biological physiological structures and regulatory mechanisms have emerged. The parameter settings are shown in Table 2 and Figure 5. The sNIOA algorithm is optimal,  $N=5$ ,  $L=8$ ,  $I=6$ ,  $M=8$ ,  $Pc=6$ ,  $pm=5$ ,  $pmk=6$ ,  $Ip=9$ ,  $\mu n=6$ , and

TABLE 1: Parameter analysis experimental results.

| Parameter | Experimental results |         |                         |                |  |                           |                      |
|-----------|----------------------|---------|-------------------------|----------------|--|---------------------------|----------------------|
|           | $\mu_n$              | $\beta$ | Optimal value deviation | Mean deviation | Standard deviation of experimental value | Function evaluation times | The most peak number |
| 0.02      |                      | 0.99    | 1.74                    | 3.86           | 3.81                                     | 2.68                      | 4                    |
|           |                      | 0.19    | 2.63                    | 3.89           | 3.36                                     | 2.16                      | 3                    |
|           |                      | 0.86    | 2.75                    | 2.10           | 3.71                                     | 2.12                      | 5                    |
|           |                      | 0.26    | 2.34                    | 3.79           | 3.12                                     | 2.93                      | 3                    |
| 0.05      |                      | 0.90    | 2.54                    | 2.73           | 3.20                                     | 1.13                      | 5                    |
|           |                      | 0.67    | 2.05                    | 3.22           | 3.24                                     | 1.47                      | 4                    |
|           |                      | 0.95    | 2.77                    | 3.92           | 3.63                                     | 2.59                      | 4                    |
|           |                      | 0.40    | 1.33                    | 3.21           | 3.91                                     | 1.41                      | 5                    |
| 0.1       |                      | 0.76    | 2.77                    | 3.57           | 3.45                                     | 1.70                      | 5                    |
|           |                      | 0.88    | 1.47                    | 3.35           | 3.07                                     | 1.61                      | 5                    |
|           |                      | 0.61    | 2.83                    | 2.07           | 3.36                                     | 2.66                      | 2                    |
|           |                      | 0.11    | 1.71                    | 3.37           | 3.74                                     | 1.30                      | 4                    |
| 0.2       |                      | 0.23    | 1.94                    | 3.67           | 3.87                                     | 2.52                      | 2                    |
|           |                      | 0.06    | 2.16                    | 3.63           | 3.90                                     | 2.92                      | 2                    |
|           |                      | 0.70    | 1.98                    | 2.28           | 3.45                                     | 1.39                      | 2                    |
|           |                      | 0.55    | 1.28                    | 3.30           | 3.23                                     | 2.47                      | 2                    |

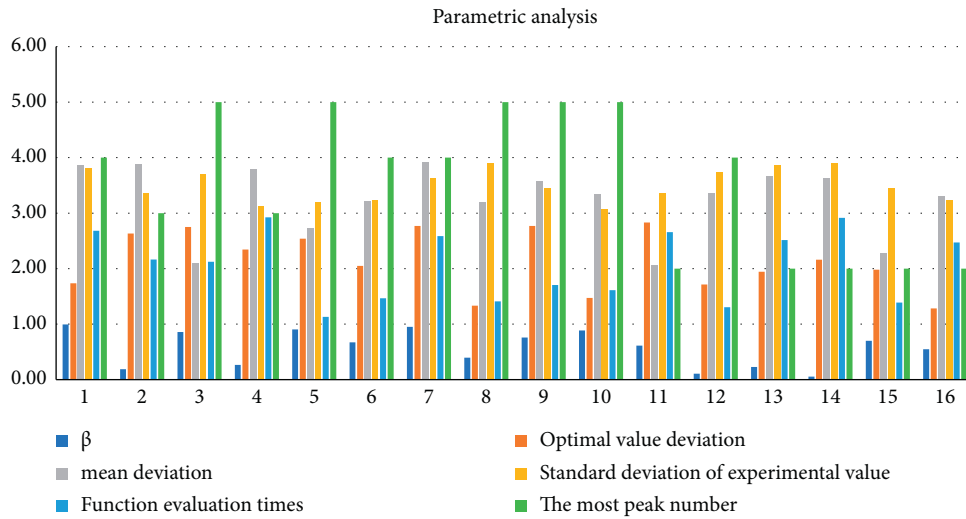


FIGURE 3: Parameter analysis.

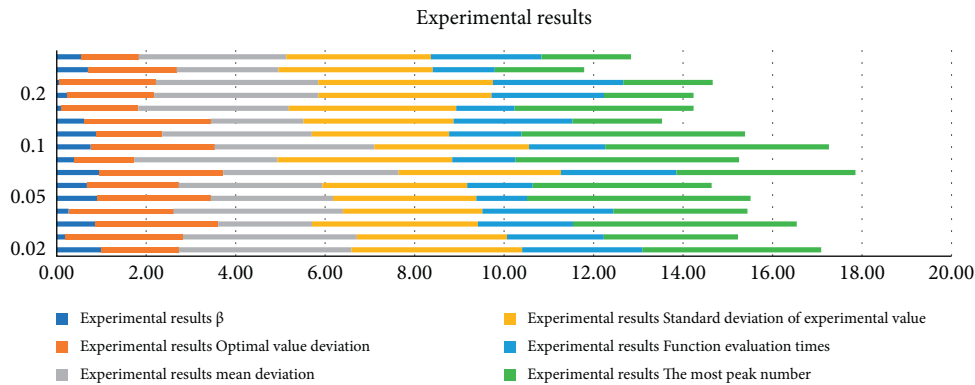


FIGURE 4: Experimental results.

$\beta=8$ . The domestic research on smart agriculture has experienced explosive growth, and the research has been carried out from the concept of smart agriculture, related

technologies, constraints, industrial chain, etc., to provide theoretical guidance for the development of smart agriculture. The worst algorithm parameters are NIOA model,

TABLE 2: Comparison algorithm parameter settings.

|          | sNIOA | NIOA | NGA | NPSO |
|----------|-------|------|-----|------|
| N        | 5     | 10   | 5   | 8    |
| L        | 8     | 10   | 8   | 8    |
| I        | 6     | 7    | 8   | 9    |
| M        | 8     | 9    | 5   | 6    |
| $P_c$    | 6     | 8    | 10  | 9    |
| $p_m$    | 5     | 5    | 6   | 7    |
| $p_{mk}$ | 6     | 5    | 7   | 9    |
| $I_p$    | 9     | 8    | 9   | 6    |
| $\mu_n$  | 6     | 9    | 9   | 10   |
| $\beta$  | 8     | 10   | 8   | 7    |

TABLE 3: Model comparison.

|                                    | KA | NOI | Cp | Mina | Maxa | AEa | Ao |
|------------------------------------|----|-----|----|------|------|-----|----|
| Genetic algorithm                  | 2  | 3   | 2  | 4    | 1    | 3   | 5  |
| Biological intelligence algorithms | 2  | 4   | 1  | 4    | 4    | 4   | 2  |

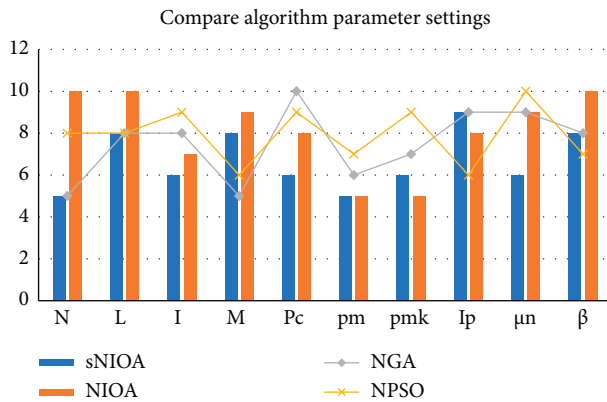


FIGURE 5: Comparison algorithm parameter settings.

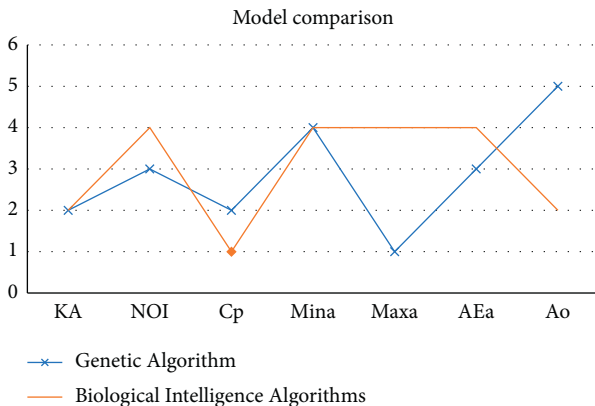


FIGURE 6: Algorithm comparison.

$N = 10, L = 10, I = 7, M = 9, P_c = 8, p_m = 5, p_{mk} = 5, I_p = 8, \mu_n = 9,$  and  $\beta = 10$ . The gray linear programming model was performed at NGA parameters set to  $N = 5, L = 8, I = 8, M = 5, P_c = 10, p_m = 6, p_{mk} = 7, I_p = 9, \mu_n = 9,$  and  $\beta = 8$  around the average. The results of NPSO parameter setting and NGA parameter setting are similar to  $N = 8, L = 8, I = 9, M = 6, P_c = 9, p_m = 7, p_{mk} = 9, I_p = 6, \mu_n = 10,$  and  $\beta = 7$ .

4.3. *New Management Model of Smart Agriculture.* The smart agriculture project uses the data of the original system of an agricultural company and adds modern information technology means on this basis, as shown in Figure 6. The basic

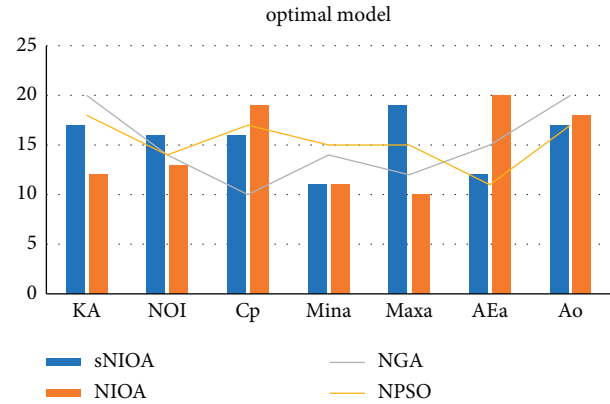


FIGURE 7: Optimal model.

agricultural information was replaced by KA, NOI, Cp, Mina, Maxa, AEa, and Ao, and the two models were optimized and compared.

4.4. *Model Comparison.* The biological intelligence algorithm consists of two parts: the global directional optimization unit and the local fine optimization unit. The biological intelligence optimization model consists of KA = 2, NOI = 4, Cp = 1, Mina = 4, Maxa = 4, AEa = 4, and Ao = 2, and in the global directional optimization unit, a large-scale global optimization and a local fine optimization are performed. As shown in Table 3 and Figure 7, in the biological genetic algorithm model: KA = 2, NOI = 3, Cp = 2, Mina = 4, Maxa = 1, AEa = 3, and Ao = 5. Using the integrated technology integrating GIS technology, RS technology, spatial statistics, mathematical models, and other methods, based on the differences of various temporal and spatial scales and their monitoring methods, combined with regression model and spatial sampling method, quantitative analysis was performed and its influencing factors were analyzed.

### 5. Conclusion

The smart agricultural system is the application of new IOT technology in the field of smart agriculture, mainly including real-time monitoring, wireless monitoring, remote image, and analysis functions. Through this topic, it is concluded that (1) when the parameter is set to  $\mu = 0.02, \beta = 0.99,$  the deviation of the optimal value = 1.74, the deviation of the average value = 3.86, the standard deviation of the experimental value = 3.81, the performance evaluation = 2.68, and the maximum number of peaks = 4. It can give full play to the advantages of various algorithms and learn from each other's strengths. (2) The sNIOA algorithm is the best. Compared with the NIOA algorithm, the accuracy of N is increased by

50% and the accuracy of  $L=8$  is increased by 20%. Compared with the NGA algorithm, the error of I is reduced by 23.5% and the offset of  $M$  is reduced. NPSO algorithm pm performance is improved by 20%, and pmk peak value is reduced by 20%. The domestic research on smart agriculture has experienced explosive growth, and the research has been carried out from the concept of smart agriculture, related technologies, constraints, industrial chain, etc., to provide theoretical guidance for the development of smart agriculture. The worst algorithm parameter is the NIOA model whose offset increases little, the performance decreases by 20%, and the peak value becomes worse. (3) The smart agriculture project uses the latest Internet of Things and cloud computing technology, and based on the analysis of big data and artificial intelligence technology, a new service form is proposed, that is, a cloud, network, and platform composite service system to establish regional closed-loop ecological chain integrating agricultural production, processing and marketing. (4) In the biological genetic algorithm model, the recall rate of  $C_p$  is low, the ROC curve fluctuates greatly, the specificity  $AEa$  is poor, and the sensitivity is not high. Using the integrated technology integrating GIS technology, RS technology, spatial statistics, mathematical models, and other methods, based on the differences of various temporal and spatial scales and their monitoring methods, combined with regression model and spatial sampling method, quantitative analysis was performed and its influencing factors were analyzed. The comparison shows that the optimal  $F1$  score of biological intelligence optimization parameters is up to 23% higher, the accuracy rate  $Ao$  is increased by 20%, and the accuracy rate is high.

### Data Availability

The experimental data used to support the findings of this study are available from the corresponding author upon request.

### Conflicts of Interest

The authors declare that they have no conflicts of interest regarding this work.

### Acknowledgments

This work was sponsored in part by Science and Technology Program of Jieyang, China, Research and Development of Internet of Things Monitoring System for Planting Smart Agriculture in Chinese Yam (Grant no. skjcx001), and Jieyang Polytechnic Science Foundation, China (Research on Intelligent Agricultural Monitoring System Based on High Performance Fusion Algorithm, Grant no. 2021JYCKY24).

### References

- [1] S. Barman, P. K. Neog, and P. K. Pathak, "Adoption consistency of climate smart agriculture practices among farmers of vulnerable areas to flood in Assam," *Indian Research Journal of Extension Education*, vol. 19, no. 4, p. 1, 2021.
- [2] G. Asefa and T. F. Negewo, "The potential contribution of carbon sequestration in soil and forest to enhanced climate smart agriculture in Ethiopia," *Journal of Earth Science and Climatic Change*, vol. 12, no. 6, p. 7, 2021.
- [3] M. W. Thongoh, H. M. Mutembei, J. Mburu, and B. E. Kathambi, "Evaluating knowledge, attitudes and practices of livestock value chain actors on climate smart agriculture/livestock (CSA/L) in kajiado county, Kenya," *Asian Journal of Agricultural Extension, Economics & Sociology*, vol. 12, pp. 134–148, 2021.
- [4] R. Hou, S. Li, and H. Chen, "Coupling mechanism and development prospect of innovative ecosystem of clean energy in smart agriculture based on blockchain," *Journal of Cleaner Production*, vol. 319, 128466 pages, 2021.
- [5] M. Scimeca, N Urbano, N. Toschi, E Bonanno, and O Schillaci, "Precision medicine in breast cancer: from biological imaging to artificial intelligence," *Seminars in Cancer Biology*, vol. 72, pp. 1–3, 2021.
- [6] T. Sovhyra, "Methods OF decoding data using biological research and artificial intelligence IN culture practice," *Interdisciplinary Research of Complex Systems*, vol. 67, no. 18, pp. 5–14, 2021.
- [7] S. S. Mailumo, G. C. Onuwa, and S. Oyewole, "Adoption OF climate smart agriculture among food crop farmers IN birnin-kudu local government area, jigawa state, Nigeria," *Russian Journal of Agricultural and Socio-Economic Sciences*, vol. 110, no. 2, pp. 169–176, 2021.
- [8] J. R. Liao, H. C. Lee, M. C. Chiu, and C. C Ko, "Semi-automated identification of biological control agent using artificial intelligence," *Scientific Reports*, vol. 10, no. 1, 14632 pages, 2020.
- [9] T. Yang, Y. Luo, and W. Ji, "Advancing biological super-resolution microscopy through deep learning: a brief review," vol. 7, no. 4, p. 14, 2021.
- [10] E. L. Mellor, M. D. Kinkaid, and M. T. Mendl, "Nature calls: intelligence and natural foraging style predict poor welfare in captive parrots," *Proceedings of the Royal Society B: Biological Sciences*, vol. 2021, p. 288, 1960.
- [11] J. X. Wang, "Meta-learning in natural and artificial intelligence," *Current Opinion in Behavioral Sciences*, vol. 38, pp. 90–95, 2021.
- [12] J. Bensemann, Q. Bao, and G. Gendron, "Relating blindsight and ai: a review," *Journal of Artificial Intelligence and Consciousness*, pp. 1–15, 2021.
- [13] C. Gonthier, J. Grégoire, and M. Besanon, "No negative Flynn effect in France: why variations of intelligence should not be assessed using tests based on cultural knowledge," *Intelligence*, vol. 84, 2021.
- [14] A. Rivas-Ubach, B. Stanfill, and S. China, "Deciphering the source of primary biological aerosol particles: a pollen case study," *ACS Earth and Space Chemistry*, vol. 34, no. 3, 2021.
- [15] A. D. Malik, A. Jamil, K. A. Omar, and M. H. A. Wahab, "Implementation of faulty sensor detection mechanism using data correlation of multivariate sensor readings in smart agriculture," *Annals of Emerging Technologies in Computing*, vol. 5, no. 5, pp. 1–9, 2021.
- [16] C. H. Nguyen, "Structured learning in biological domain," *Journal of Systems Science and Systems Engineering*, vol. 29, no. 4, p. 14, 2020.
- [17] B. L. M. E. Staub, "The mismeasure of minds: debating race and intelligence between Brown and the bell curve," *Chapel Hill: The University of North Carolina Press, Social History of Medicine*, vol. 95, p. 232, 2020.

- [18] E. Kapetanios, "Humans and machines at work: monitoring, surveillance and automation in contemporary capitalism," *Computing Reviews*, vol. 61, no. 5, pp. 173-174, 2020.
- [19] A. D. Visscher, "Artificial versus biological intelligence in the cosmos: clues from a stochastic analysis of the drake equation," *International Journal of Astrobiology*, vol. 19, no. 5, pp. 1-7, 2020.
- [20] R. P. Badman, T. T. Hills, and R. Akaishi, "Multiscale computation and dynamic attention in biological and artificial intelligence," *Brain Sciences*, vol. 10, no. 6, p. 396, 2020.
- [21] D. Yadav, R. K. Garg, D. Chhabra, R. Yadav, A. Kumar, and P. Shukla, "Smart diagnostics devices through artificial intelligence and mechanobiological approaches," *3 Biotech*, vol. 10, no. 8, p. 351, 2020.
- [22] J. Beyerer, G. Bretthauer, and T. Längle, "Smart agriculture," *AT - Automatisierungstechnik*, vol. 69, no. 4, pp. 275-277, 2021.
- [23] E. Zossou, A. R. Agboh-Noameshie, and A. Assouma-Imorou, "Closing gender gaps in climate-smart agriculture through strengthening women rice seed farmer's capacities and access to quality stress-tolerant seed in Benin," *Sustainable Agriculture Research*, vol. 10, 2021.
- [24] H. S. Jat, A. M. Datta, and H. Choud, "Soil enzymes activity: effect of climate smart agriculture on rhizosphere and bulk soil under cereal based systems of north-west India," *European Journal of Soil Biology*, vol. 103, no. 3, 103292 pages, 2021.
- [25] L. Molieleng, P. Fourie, and I. Nwafor, "Adoption of climate smart agriculture by communal livestock farmers in South Africa," *Sustainability*, vol. 13, no. 12, 126940 pages, 2021.
- [26] S. U. Haq, I. Boz, and P. Shahbaz, "Adoption of climate-smart agriculture practices and differentiated nutritional outcome among rural households: a case of Punjab province, Pakistan," *Food Security*, vol. 13, pp. 1-19, 2021.

## Retraction

# Retracted: Teaching Design of Mathematics Application Based on Naive Bayes

### Mathematical Problems in Engineering

Received 18 July 2023; Accepted 18 July 2023; Published 19 July 2023

Copyright © 2023 Mathematical Problems in Engineering. This is an open access article distributed under the Creative Commons Attribution License, which permits unrestricted use, distribution, and reproduction in any medium, provided the original work is properly cited.

This article has been retracted by Hindawi following an investigation undertaken by the publisher [1]. This investigation has uncovered evidence of one or more of the following indicators of systematic manipulation of the publication process:

- (1) Discrepancies in scope
- (2) Discrepancies in the description of the research reported
- (3) Discrepancies between the availability of data and the research described
- (4) Inappropriate citations
- (5) Incoherent, meaningless and/or irrelevant content included in the article
- (6) Peer-review manipulation

The presence of these indicators undermines our confidence in the integrity of the article's content and we cannot, therefore, vouch for its reliability. Please note that this notice is intended solely to alert readers that the content of this article is unreliable. We have not investigated whether authors were aware of or involved in the systematic manipulation of the publication process.

Wiley and Hindawi regrets that the usual quality checks did not identify these issues before publication and have since put additional measures in place to safeguard research integrity.

We wish to credit our own Research Integrity and Research Publishing teams and anonymous and named external researchers and research integrity experts for contributing to this investigation.

The corresponding author, as the representative of all authors, has been given the opportunity to register their agreement or disagreement to this retraction. We have kept a record of any response received.

### References

- [1] H. Ling, "Teaching Design of Mathematics Application Based on Naive Bayes," *Mathematical Problems in Engineering*, vol. 2022, Article ID 7244001, 6 pages, 2022.

## Research Article

# Teaching Design of Mathematics Application Based on Naive Bayes

Huanzhang Ling 

Harbin Engineering University, Harbin 150001, Heilongjiang, China

Correspondence should be addressed to Huanzhang Ling; lghan@hrbeu.edu.cn

Received 13 April 2022; Revised 23 May 2022; Accepted 8 June 2022; Published 24 June 2022

Academic Editor: Hangjun Che

Copyright © 2022 Huanzhang Ling. This is an open access article distributed under the Creative Commons Attribution License, which permits unrestricted use, distribution, and reproduction in any medium, provided the original work is properly cited.

There is a huge amount of mathematical information in the world, and mathematics is everywhere and nowhere. Bayesian theory is based on a process of statistical inference that requires the calculation of general and prior information to obtain a posteriori information. Its main features are the use of probabilities to represent all forms of uncertainty and the use of probabilistic rules to enable learning and inference, estimating the probability of future occurrences by calculating the probability of a past time. In order to bring mathematics closer to life, this paper explores the teaching of mathematical applications in terms of material selection, teaching arrangement, and professional integration. At the same time, in order to better realize mathematics application teaching, effectively improve the classroom effect of mathematics application teaching, and make students better accept mathematical knowledge and apply it to practical applications, the design of mathematics application teaching in this paper is also based on Naive Bayes.

## 1. Introduction

The focus on the development of students' abilities and application awareness, and the internalization of the teaching process from teacher instruction to the development of students' abilities, is an issue of concern in applied mathematics teaching [1]. Owhadi [2] said the following: "Education can only be effective and truly educational through life." Therefore, mathematics itself is not just "number symbols," and mathematics teaching is not only about making students do mathematical problems but also about making students learn mathematics with certain logical thinking skills and using mathematical methods to solve problems they encounter. Mathematics has its rich connotation; it originates from life and serves life.

What role does mathematics play in human life? Dogan and Aydin [3] divide the role of mathematics into three levels. The first level provides language, concepts, ideas, theories, and methods for other disciplines. The natural sciences and social sciences such as economics and management cannot be developed without mathematics. The second level is the direct application to engineering and

production activities, of which there are many examples [4]. The third level is as a culture that plays a subtle role for all members of society. The level of mathematical training of a nation has a great influence on the civilization of this nation [5].

Mathematics is an important basic course for many majors in colleges and universities and plays an important role in the education of higher technical and application-oriented specialists for the first line of production [6, 7]. Therefore, the traditional mathematics education can no longer adapt to and meet the needs of talent training mode, and the application of mathematics teaching has become an important issue that many institutions urgently need to solve [8].

## 2. Mathematics Application Teaching Exploration

Mathematical problems in life often involve different fields; although not as systematic as mathematical theories, they are logically connected, and when solving mathematical problems, you can properly organize the relevant content,

according to the order of the shallow to the deep rational arrangement of teaching. Let us look at three examples; they seem unrelated, but they are logically linked [9–13].

A mathematical problem is fragmented if it is not supported by theory. When solving practical problems, we link the teaching of problem solving and theory to emphasize the mathematical ideas and theories used in the process of problem solving, so that we can achieve the effect of learning from one to three [14, 15]. This not only cultivates students' ability to solve practical problems but also deepens their understanding of mathematical theories.

For example, consider the population increment problem. It is known that the population in  $t_0$  years is  $N_0$ , the growth rate of the population is proportional to the total number of people, and other factors are ignored for the time being, so how does the number of people change? Before solving this problem, we can ask students to go back to the theory of differential equations, such as the initial conditions of differential equations, general solutions, special solutions, and other concepts, for students to review the solution of differential equations, and then we can suggest that the rate of change in mathematics is expressed by the derivative. If the symbol  $N(t)$  is used to represent the number of people as a function of time  $t$  and  $k$  represents the ratio of the population growth rate to the total population, an equation is obtained as follows:  $d(N(t))/dt = kN(t)$ . The initial condition is  $N(t_0) = N_0$ , and then the solution by separating the variables gives  $N(t_0)e^{t-t_0}$  ( $t \geq t_0$ ).

For the school, mathematics is a basic course and is the basis for learning other professional courses. With the emphasis on the requirement of "moderate enough" and the reduction of the number of mathematics hours, some problems related to the profession should be selected in a targeted way [16]. For example, for marketing majors, they can be introduced to the problem of optimizing the purchase of goods; when the demand is random, what ordering scheme can maximize the total profit. In addition, for logistics students, you can introduce them to some examples of graph theory, such as the seven bridges problem, the merchant crossing the river problem, and so on, so that students can understand the basic ideas of graph theory and lay the foundation for their future professional knowledge [17]. For example, when introducing the concept of derivative, different examples can be introduced according to different majors, such as the concept of margin for economics and management majors and rate and linear density for electromechanics majors.

On the one hand, be good at finding out some problems that enhance students' thinking. Use these problems to liven up the classroom atmosphere. Here are a few interesting mathematical problems. "What is the probability that a couple will sit together when 15 couples attend a party, but the person who arranges the seats does not know the 30 people?" Someone says something like "I'm wrong about this," so is what he said right or wrong? "If  $n$  people attend a party and no one is known to know all of them, ask if there are two people who know as many people?"

On the other hand, step-by-step questions provoke students' thinking. When using mathematical methods to

solve real-world problems, students do not think in one step, so you can use questions to prompt students, stimulate their thinking, and develop their ability to think independently [18].

When teaching, introduce students to the content of the history of mathematics. For example, when we talk about infinitesimals in advanced mathematics, we can add the arguments about infinitesimals to students; when we talk about some paradoxes in mathematics, we can introduce the mathematical crisis caused by mathematical paradoxes [19, 20].

### 3. Method

Bayesian theory is based on a statistical inference process that requires the calculation of general and prior information to obtain a posteriori information. Its main features are the use of probabilities to represent all forms of uncertainty and the use of probabilistic rules to enable learning and inference by calculating the probability of occurrence at a past time to estimate the probability of future occurrence.

Bayesian classifier is a simple probabilistic classifier based on the application of Bayesian independence assumption theory. The relationship between conditional and inverse conditional probabilities in Bayes' theorem can be expressed as

$$P(Y | X) = \frac{P(Y | X)}{P(X)}, \quad (1)$$

where  $P(Y)$  is the prior or marginal probability of  $Y$ , i.e., the probability that does not take into account any information about  $X$ .  $P(Y|X)$  is the conditional probability of  $Y$  given  $X$ , whose value is derived from or depends on the value of  $X$ . When constructing posterior probabilities, in many cases, it is necessary to find the conditional probability  $P(E|D)$  in the dataset  $E$ , given data  $D$ . Assuming that the maximum value  $e$  is contained in  $E$ , any hypothesis of maximum probability is called the maximum a posteriori hypothesis and is labeled as  $E_{MAP}$ , i.e.,

$$P(E | D)E_{MAP} = \arg \max_{e \in E}, \quad (2)$$

$$P(E | D) = \arg \max_{e \in E} \frac{P(D | E)P(E)}{P(D)}.$$

**3.1. Naive Bayesian Principle.** Let  $U = \{X, C\}$  be a finite set of random variables, where  $X = \{X_1, \dots, X_n\}$  is the set of attribute variables and  $C$  is a class variable taking values in the range  $\{c_1, \dots, c_j\}$ , and  $x_i$  is the value of attribute  $X_i$ . The probability that sample  $x_i = (x_1, \dots, x_n)$  belongs to  $c_i$  can be expressed by Bayes' theorem as

$$P\left(\frac{C = c_j}{X = x_i}\right) = \frac{P(c_j) \cdot P(x_1, \dots, x_n/c_j)}{P(x_1, \dots, x_n)} \quad (3)$$

$$= \alpha \cdot P(c_j) \cdot P\left(\frac{x_1, \dots, x_n}{c_j}\right),$$



where  $\alpha$  is the regularization factor,  $P(c_j)$  is the prior probability of class  $c_j$ , and  $P(x_1, \dots, x_n/c_j)$  is the likelihood of class  $c_j$  with respect to  $X_i$ .

By the chain rule of probability, equation (3) can be expressed as

$$p(c_j)c_jP(c_j|x_1, \dots, x_n) = \alpha \cdot P(c_j) \cdot \prod_{i=1}^n P(x_i|x_1, \dots, x_{i-1}, c_j). \quad (4)$$

Given a training sample set  $D = \{u_1, \dots, u_N\}$ , the goal of the classification task is to analyze the training sample set  $D$  and determine a mapping function  $f: (x_1, \dots, x_n) \rightarrow C$ , such that the class label can be labeled for any instance  $x_i = (x_1, \dots, x_n)$  of an unknown class. According to the Bayesian maximum posterior criterion, given a certain instance and  $x_i = (x_1, \dots, x_n)$ , the Bayesian classification model selects the class with the largest posterior probability  $P(c_j|x_1, \dots, x_n)$  as the class label for that instance.

Using Bayesian networks as a classification tool is actually solving equation (4) with Bayesian networks, and it is possible to find  $P(x_i|x_1, \dots, x_{i-1}, c_j)$  and determine the category from equation (4) according to the Bayesian maximum posterior criterion.

**3.2. Bayesian Networks.** A Bayesian network is a joint  $U = \{X_1, \dots, X_n\}$ , coding of probability distributions consisting of a collection of random variables. Formally a pair of binary groups  $B = \langle G, \Theta \rangle \cdot G$  is a directed acyclic graph (DAG) whose nodes correspond to random variables  $X_1, \dots, X_n$  and whose directed edges represent the dependencies between variables, and the structure  $G$  of the graph encodes the independence assumption that given the parent of each node, the node is independent of its non-self-derived children; the second part of the binary, i.e.,  $\Theta$ , represents the set of conditional probability distributions for each variable of this network, and each element of the set represents the probability corresponding to  $X_i$  taking the value  $x_i$  under the  $pa(x_i) \in Pa(X_i)$  condition, where  $Pa(X_i)$  is the set of  $X_j$ , the parent variables in  $G$ , and  $Pa(X_i)$  is a composition of  $Pa(X_i)$ .  $B$  defines on  $U$  the unique joint probability distribution:

$$P_B(X_1, \dots, X_n) = \prod_{i=1}^n P_B((X_i|P_a(X_i))). \quad (5)$$

Learning Bayesian networks from data can be formulated as follows: given a training sample set  $D = \{u_1, \dots, u_N\}$  defined on  $U$ , find the network  $B$  that best matches  $D$ . The usual approach is to introduce a scoring function to compute every possible network on this training set and find the optimal one. General Bayesian network classifier (GBN) treats class nodes and attribute nodes as network nodes of equal status and trains Bayesian networks based on the selected scoring function and sample data, which are directly used as classification models. Since the structure learning of Bayesian networks is itself an NP-complete problem, it is impossible to search the entire network structure space under the current

conditions, so this paper is limited to studying a special Bayesian classification model, i.e., the tree-enhanced Naive Bayesian classification model.

### 3.3. Tree Augmented Naive Bayesian Classification Model.

The tree augmented Naive Bayesian classifier (TAN) is a constrained Bayesian net defined on  $U^* = \{A_1, \dots, A_n, C\}$ , where  $A$  is a discrete attribute variable and  $C$  is a class variable. The attributes  $Pa(C) = \emptyset$  and  $Pa(A_i)$  of Bayesian network are shown in Figure 1. This type of model has been proved by Geiger and learned by Bayesian net algorithm with Chow and Liu learning tree structure. The TAN classification model constructed in this way has been widely used because it has been shown experimentally that it usually has good classification accuracy at a small cost. However, TAN requires variables to be discrete, and credit assessment problems often involve mixed variables (attribute variables that contain both discrete and continuous variables), so if TAN is used directly in credit assessment, the attributes containing continuous variables need to be pre-dissociated, which loses the information contained in continuous variables and increases the computational effort itself (the size of the cardinality is also difficult to determine in advance). Moreover, too many discrete values will increase the computational complexity by increasing the storage space required by the algorithm, so it is necessary to consider the case of continuous attributes.

### 3.4. Constructing a Naive Bayesian Network Mathematics Application Teaching Model.

Regarding the construction method of the model conditional probability distribution, it is as follows. The establishment of a Bayesian network classification model for teaching mathematics applications mainly requires consideration of two aspects: first, determining the structure of the network; second, learning the conditional probability distributions of the attribute variables and determining the class prior probabilities. For the case where the attribute variables are all discrete, the learning can be done according to the conditional probability distribution table, and the learning method also adopts the method of great likelihood estimation, which is estimated by the empirical frequency of the training samples [21, 22].

There are many parametric probability models to express the distribution of continuous variables, and in this paper, we assume Gaussian distribution. There are three cases in ETAN.

- (1) Only class variables are parents of continuous variables  $X_i$ : for each value of  $C$ ,  $C = k$  corresponds to a one-dimensional Gaussian distribution with mean  $\mu_k = E(X_i|C = k)$  and variance  $\sigma_k^2 = E(X_i^2|C = k) - E^2(X_i|C = k)$ .
- (2) The class variable  $C$  and a discrete variable  $A_j$ , which is the parent of the continuous variable  $X_i$ : for each value of  $c$  and  $A_j$ ,  $C = k$ ,  $A_j = l$  corresponds to a one-dimensional Gaussian distribution with a mean of

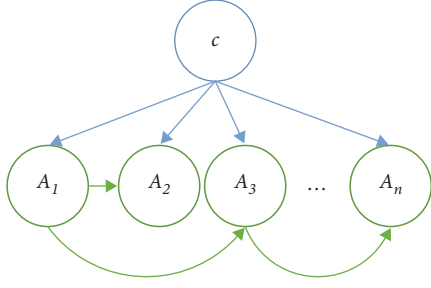


FIGURE 1: Structure of tree-enhanced Naive Bayesian network.

$\mu_{k,l} = E(X_i|C = k, A_j = l)$  and a variance of  $\sigma_{k,l}^2 = E(X_i^2|C = k, A_j = l) - E^2(X_i|C = k, A_j = l)$ .

- (3) With class attribute  $c$  and continuous variables  $X_i, X_j$  as parents: for each  $C = k$  after setting  $X_i, X_j$  the joint distribution function to be a binary Gaussian distribution, the conditional distribution of  $X_i$  given  $C = k, X_j = x_j$  is a normal distribution with mean  $\alpha_{ijk} + x_j\beta_{ijk}$  and variance  $\sigma_{ijk}^2$ , where

$$\beta_{ijk} = \frac{E[(X_i X_j|C = k)] - E[(X_i|C = k)]E[(X_j|C = k)]}{E[(X_j^2|C = k)] - E^2[(X_j|C = k)]}$$

$$\alpha_{ijk} = E[(X_i|C = k)] - \beta_{ij} \times E[(X_j|C = k)]$$

$$\sigma_{ijk}^2 = E[(X_i^2|C = k)] - E^2[(X_i|C = k)] - \frac{([E[(X_i X_j|C = k)] - E[(X_i|C = k)]E[(X_j|C = k)]]^2}{E[(X_j^2|C = k)] - E^2[(X_j|C = k)]}$$

(6)

- (4) For a conditional probability distribution where the other parent variable is continuous and the child variables are discrete, in addition to the class variables, the following variant is used. Let  $A_i$  be the discrete variable,  $X_j$  be the continuous variable,  $f(x_j; C = k, A_i = l)$  be the distribution density function of  $X_j$  under  $C = k, A_i = l$  conditions, and  $g(x_j; C = k)$  be the distribution density function of  $x_j$  under  $C = k$  conditions. For any fixed  $\varepsilon > 0$  and for any  $x_j$ , considering the following conditional probabilities, we have

$$P(A_i = l | x_j < X_j \leq x_j + \varepsilon, C = k)$$

$$= \frac{P(A_i = l, x_j < X_j \leq x_j + \varepsilon | C = k)}{P(x_j < X_j \leq x_j + \varepsilon | C = k)}$$

$$= \frac{P(x_j < X_j \leq x_j + \varepsilon | A_i = l, C = k)P(A_i = l | C = k)}{P(x_j < X_j \leq x_j + \varepsilon | C = k)} \quad (7)$$

$$= \frac{\int_{x_j}^{x_j+\varepsilon} f(x_j; C = k, A_i = l) dx_j P(A_i = l | C = k)}{\int_{x_j}^{x_j+\varepsilon} g(x_j; C = k) dx_j}$$

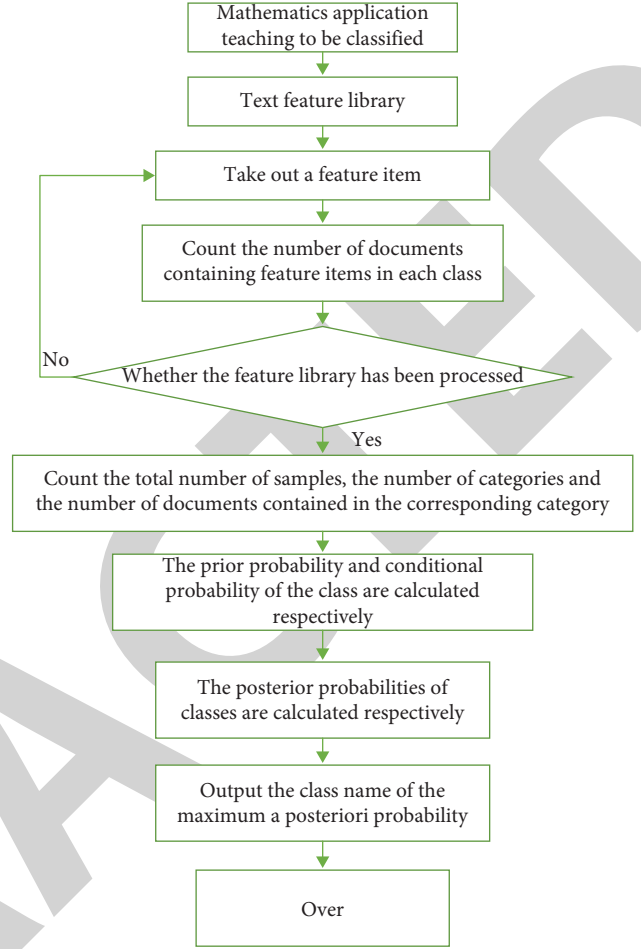


FIGURE 2: Teaching design process of mathematical application based on Naive Bayes.

**Theorem 1.** If  $f(x), g(x)$  is continuous on  $[a, b]$ ,  $g(x) \neq 0$ , and  $x \in [a, b]$ , then there exists at least one point  $\xi$  in  $(a, b)$  such that

$$\frac{\int_a^b f(x) dx}{\int_a^b g(x) dx} = \left( \frac{f(\xi)}{g(\xi)} \right) \quad (a < \xi < b). \quad (8)$$

From Theorem 1 and  $g(x_j; C = k) > 0$  ( $g(x_j; C = k)$ ), which are normal density functions, we have

$$P(A_i = l | x_j < X_j \leq x_j + \varepsilon, C = k)$$

$$= \frac{f(\xi; C = k, A_i = l)P(A_i = l | C = k)}{g(\xi; C = k)} (x_j < \xi < x_j + \varepsilon). \quad (9)$$

When  $\varepsilon \rightarrow 0$ , then

$$\lim_{\varepsilon \rightarrow 0} P(A_i = l | x_j < X_j \leq x_j + \varepsilon, C = k)$$

$$= \frac{f(x_j; C = k, A_i = l)P(A_i = l | C = k)}{g(x_j; C = k)}. \quad (10)$$

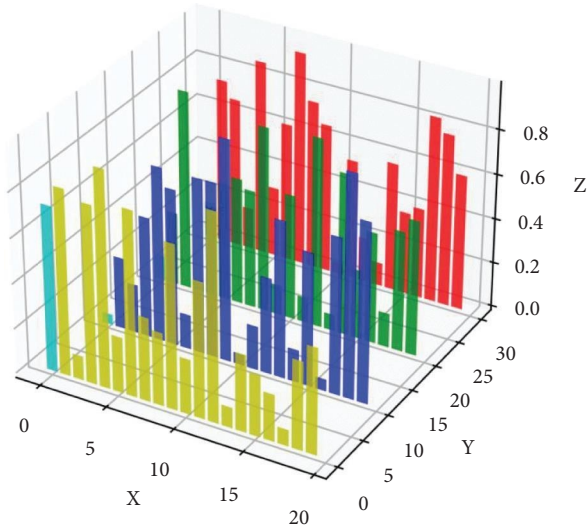


FIGURE 3: The results of students' adaptation to mathematics application teaching.

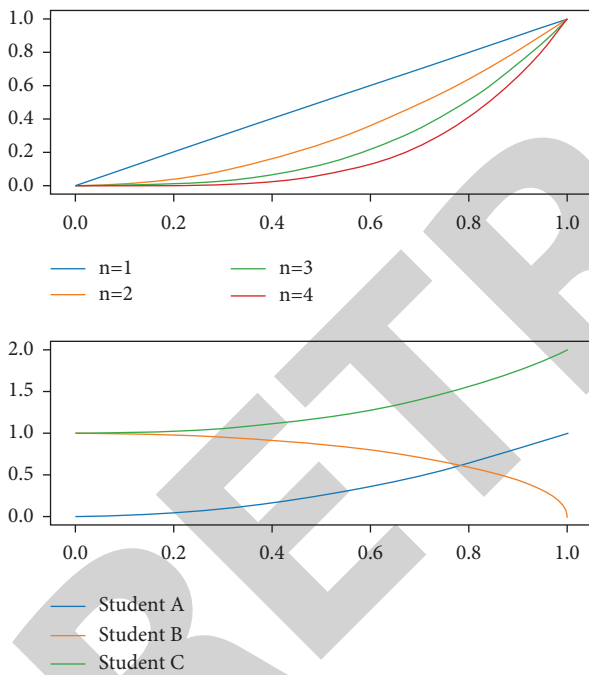


FIGURE 4: The comparison of different students.

The prior probability of each category, which can be specified based on expert knowledge, must be guaranteed ( $\sum P(C = c_j) = 1$ ) and can be estimated as the proportion of each category in the training sample if there is no reliable experience [23–25].

The complete design process for teaching mathematical applications based on Naive Bayes is shown in Figure 2.

#### 4. Case Study

Based on the mathematics application teaching course of a middle school, we evaluate the teaching design based on

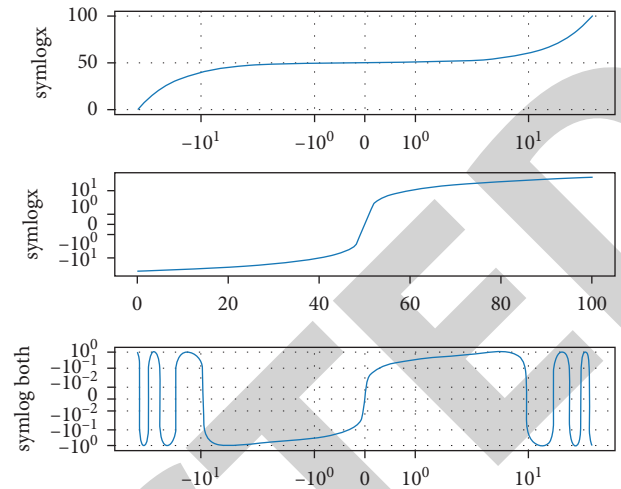


FIGURE 5: The efficiency of different students in this method is different.

Naive Bayes. The specific experimental results are shown in Figure 3.

The assessment indexes commonly used in teaching mathematical applications are generally selected from three aspects: selection of materials, teaching arrangement, and professional integration. The results are shown in Figure 4.

The relationship between mathematics and various fields has become increasingly close, which has put forward newer and higher requirements for mathematics education, as shown in Figure 5.

#### 5. Conclusion

By guiding students to discover mathematical problems in their lives and cultivating their sense of application, we have changed the passive state of students in the learning process and encouraged them to explore more actively and proactively. When teaching, introduce students to the content of the history of mathematics. For example, when we talk about infinitesimals in advanced mathematics, we can add the arguments about infinitesimals to students; when we talk about some paradoxes in mathematics, we can introduce the mathematical crisis caused by mathematical paradoxes. It also enhances students' interest in learning and confidence in learning mathematics; develops students' ability to collect and process information; develops students' sense of cooperation and ability to work together; and develops students' ability to apply their knowledge to solve problems.

#### Data Availability

The raw data supporting the conclusions of this article will be made available by the author, without undue reservation.

#### Conflicts of Interest

The author declares that there are no conflicts of interest.

## Research Article

# Analysis of Big Data Behavior in Sports Track and Field Based on Machine Learning Model

Qiuping Lin,<sup>1</sup> Xiaoxue Dong,<sup>2</sup> and Minglun Li <sup>3</sup>

<sup>1</sup>Department of Physical Education, Weifang Medical University, Weifang 261053, China

<sup>2</sup>Physical Education Center, Weifang University of Science and Technology, Shouguang 262700, China

<sup>3</sup>Department of Science and Humanities, Shandong College of Economics and Business, Weifang 261011, China

Correspondence should be addressed to Minglun Li; [liminglunplus@sdecu.edu.cn](mailto:liminglunplus@sdecu.edu.cn)

Received 31 March 2022; Revised 9 May 2022; Accepted 17 May 2022; Published 23 June 2022

Academic Editor: Man Fai Leung

Copyright © 2022 Qiuping Lin et al. This is an open access article distributed under the Creative Commons Attribution License, which permits unrestricted use, distribution, and reproduction in any medium, provided the original work is properly cited.

At present, machine learning is more efficient and accurate for the efficiency of operation logic after four stages of reform. In order to improve the participation rate of the whole people in track and field sports and get a better level and ranking in track and field competitions, the ATI model under the machine model is used to deeply analyze the behavior of track and field sports in order to get more accurate data. There are a series of problems in the process of correlation analysis, such as the loss caused by the analysis process, the error in the analysis process, and the lack of understanding of track- and field-related data. In order to solve this series of problems, this study optimizes the behavior analysis through related experiments. The experiment proves the correlation between learning rate and loss. When the learning rate is 0.1, the loss caused by behavior analysis is lower. For the 23rd–28th session, the number of gold medals and the number of medals won in track and field were analyzed. By comparing the ATI model with the ATT model, ATT-Net model, and WAT model, it is concluded that the ATI model has a lower error rate for behavior analysis under big data. The coverage rate of behavior analysis data is wider. Therefore, in order to make track and field behavior analysis more accurate and stable under big data, the ATI model under machine learning should be preferred for data collection, collation, analysis, and summary. Through the ATI model to analyze the related behavior of track and field under big data, there are the following advantages: when the learning speed is 0.1, the loss value in the analysis process is reduced; the number of neurons is increased, and the dropout rate is reduced to reduce NPMSE value; and the error loss rate of behavior analysis is reduced, and the analysis coverage rate is increased.

## 1. Introduction

Through correlation analysis, we can get safer training methods and more accurate track and field data, so as to obtain better track and field results. In this study, the ATI model is proposed to analyze track and field data, and the error rate and coverage rate of the model are compared and analyzed. It is concluded that the ATI model under the machine learning model can be combined with big data to more accurately and stably analyze track and field behavior. By combining the behavior analysis model ATI with track and field sports, we can analyze more accurate and stable data, so as to increase the participation rate of track and field sports and analyze athletes' behaviors, reduce unnecessary sports injuries of athletes in the process of sports, and get better competition results.

In this study, various technical ports are used to solve technical problems. It qualitatively criticizes the extent to which the work under review meets these requirements, discussing the outstanding issues, and challenges in this area [1]. By studying the convenient technology brought by the related technical level, an online recursive algorithm for training support-vector machines is proposed, one vector at a time [2]. Data integration systems provide access to a large number of data sources through a single mediation pattern [3]. Machine learning tasks have become common in a wide range of fields and systems (from embedded systems to data centers) [4]. This study summarizes the current situation of deep machine learning and puts forward some views on how it may develop [5]. This study focuses on the statistical analysis of the results in the field of machine learning based on genetics [6]. They collect content from the web and

organize it for easy access, retrieval, and search [7]. This study studies and analyzes the related track and field athletes, so as to reduce the accidental injuries of athletes. Microfracture is an effective first-line treatment, which can make young athletes with short symptom interval and less knee cartilage injury return to high-intensity track and field sports [8]. Preventive intervention should mainly focus on the overuse of injuries and full rehabilitation of previous injuries [9]. We report the incidence, risk, and severity of knee joint injuries across exercise, sex, and exposure type in high school [10]. Consistent use of definitions and methodological guidance will lead to more reliable and comparable evidence [11]. Future research needs to determine whether proving normal lower limb function before resuming exercise can effectively reduce the rate of reinjury [12]. Genes and environment are the basic and interdependent determinants of behavioral response [13]. These devices are inexpensive, easy to manufacture, reusable, and suitable for providing any liquid stimulation [14]. This study analyzes behavior through physical cognition, stress, and characteristics. The main goal is to overcome some of the main disadvantages of online communication, namely, the lack of contextual information such as body language or gestures [15].

## 2. Machine Learning Model and Track and Field Behavior Analysis

*2.1. Machine Learning Model.* There are four stages in the development of machine learning [16], as shown in Table 1.

Machine learning is based on physiology, cognitive science, and other studies on human learning mechanism [17]. Through GA, learning theory, analogy, induction, clustering, and other methods, machine learning is deeply studied and understood [18], as shown in Figure 1.

From Figure 1, it can be analyzed that the calculation methods related to machine learning are related to the computable determinacy of mathematics, the inductive analysis of philosophy, the study of the central nervous system in biology, the Bayesian judgment rules related to statistics, and the behaviorism of psychology.

*2.2. Correlation Behavior Analysis.* Big data-related behavior analysis of sports track and field includes ideological education analysis, daily management analysis, and training and competition guidance behavior [19]. Among them, the analysis of ideological education includes the following: the analysis of will, morality, values, and other behaviors; daily management analysis includes the following: life, spirit, interpersonal analysis, etc.; the analysis of competition guidance includes the following: training, training plan, feedback, sports behavior, and other analysis contents [20], as shown in Figure 2.

The analysis of track and field behavior can analyze athletes' sports behavior, athletes' training methods, and athletes' psychological literacy. Through more accurate analysis of the statistics of the data and the analysis of the

TABLE 1: Development history table.

| Stage   | History of development   |
|---|--|
| The first stage is the mid-1950s              | Inspired by neurophysiology and biology, he mainly studies neural network system   |
| The second stage is the early 1960s           | Enlightened by psychology and human learning, it mainly obtains conceptual learning and language   |
| The third stage is the middle and late 1970s  | On the one hand, a large number of domain knowledge is introduced into the learning program; on the other hand, knowledge is acquired automatically          |
| The fourth stage is the middle and late 1980s | Neural networks are emerging again, and multilayer neural networks and backpropagation algorithms are proposed to overcome the limitations of the early days |

athletes' data, we can improve the athletes' behavior, psychology, and training methods, and get better results.

## 3. Correlation Formula

### 3.1. Machine Learning Model

*3.1.1. Learning Theory.* Output variable  $X$  and output variable  $Y$  form a joint distribution  $F(X, Y)$ , with  $L$  independent observation samples [21].

$$z = \{(x_1, y_1), (x_2, y_2), \dots, (x_l, y_l)\}. \quad (1)$$

The probability measure  $F(z) = F(x, y)$ .

$$R(\alpha) = \int Q(z, \alpha) dF(z). \quad (2)$$

Loss function variable  $z, \alpha$  is as follows [22]:

$$Q(z, \alpha) = L(z, f(z, \alpha)). \quad (3)$$

The loss function is defined as follows:

$$L(y, f(x, \alpha)) = \begin{cases} 0, & y = f(x, \alpha), \\ 1, & y \neq f(x, \alpha). \end{cases} \quad (4)$$

If the output variable  $y$  is a real value,  $f(x, \alpha), \alpha \in \Lambda$  is a real function set.

$$L(y, f(x, \alpha)) = (y - f(x, \alpha))^2, \quad (5)$$

$$L(y, f(x, \alpha)) = |y - f(x, \alpha)|.$$

Density estimation probability loss function is as follows:

$$L(p(x, \alpha)) = - \sum_{i=1}^l \log p(x_i, \alpha). \quad (6)$$

*3.1.2. Learning the Concept of Consistency.*  $R(\alpha)$  is the universal function of minimizing risk [23].

For the same limit of function set and probability distribution function,

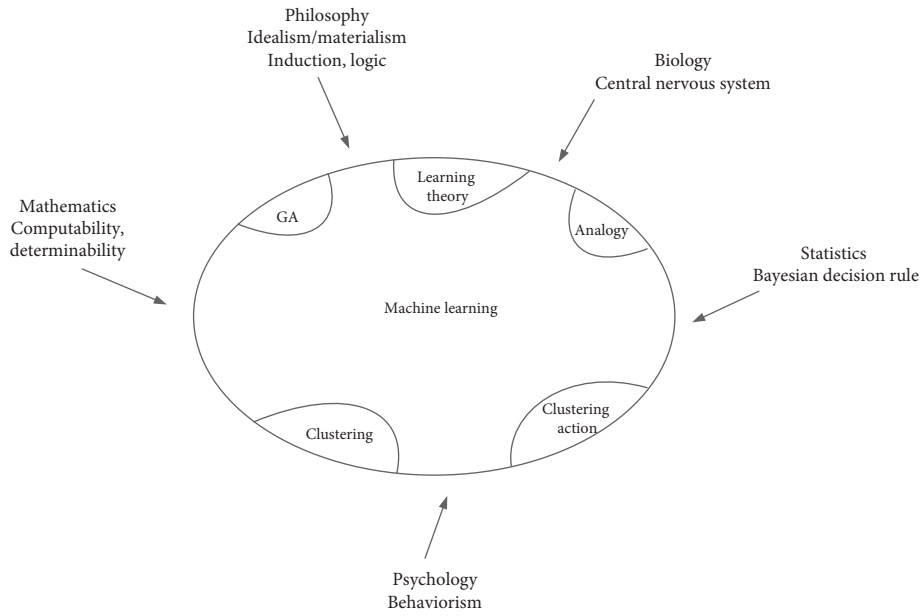


FIGURE 1: Machine learning model.

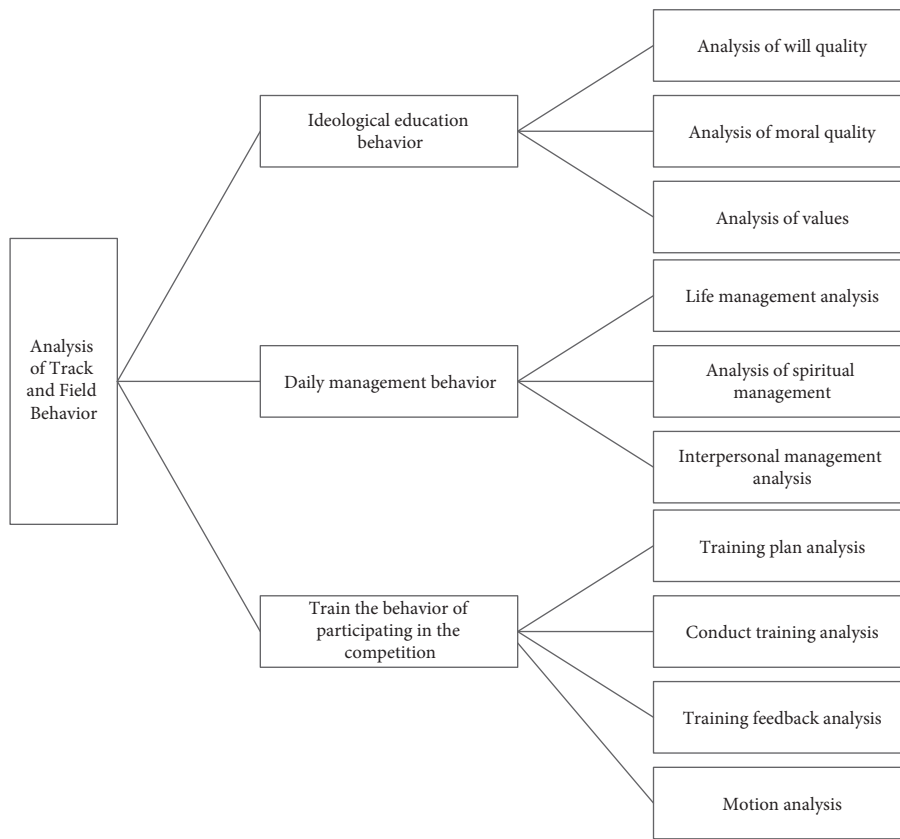


FIGURE 2: Track and field behavior analysis.

$$R_{\text{emp}} = \frac{1}{l} \sum_{i=1}^l Q(z_i, \alpha), \quad \alpha \in \Lambda,$$

$$R(\alpha_l) \xrightarrow{l \rightarrow \infty} \inf_{\alpha \in \Lambda} R(\alpha_l), \quad (8)$$

$$R_{\text{emp}}(\alpha) \xrightarrow{l \rightarrow \infty} \inf_{\alpha \in \Lambda} R(\alpha).$$

Function  $N^\wedge(Z_m)$  is defined as follows:

$$N^\wedge(Z_m) = \max\{N(F, Z_m): Z_m = \{z_1, \dots, z_m\} \subset Z\},$$

$$\text{VCdim}(Q) = \max\{m: N^\wedge(Z_m) = 2^m\}. \quad (9)$$

**3.1.3. Milestones in Learning Theory.** Sufficient conditions for consistency are as follows:

$$\lim_{l \rightarrow \infty} \frac{H^\wedge(l)}{l} = 0. \quad (10)$$

Sufficient conditions are as follows:

$$\lim_{l \rightarrow \infty} \frac{H_{\text{ann}}^\wedge(l)}{l} = 0. \quad (11)$$

Sufficient and necessary conditions are as follows:

$$\lim_{l \rightarrow \infty} \frac{G^\wedge(l)}{l} = 0. \quad (12)$$

Minimization principle is as follows.

$H$  is the VC dimension of the exponential function set, and  $L$  is the number of samples.

$$R(\alpha) \leq R_{\text{emp}}(\alpha) + \sqrt{\frac{h(\ln(2l/h) + 1) - \ln(\eta/4)}{l}}. \quad (13)$$

The relationship between empirical risk and actual risk is as follows:

$$R(\alpha) \leq R_{\text{emp}}(\alpha) + \Phi(h/l), \quad (14)$$

where  $\Phi \propto h$ ,  $\Phi \propto (1/l)$ .

### 3.2. Big Data Analysis of Sports Track and Field

#### 3.2.1. Gray Prediction of Track and Field Results.

$$X^{(0)} = [X^{(0)}(1), X^{(0)}(2), X^{(0)}(3), \dots, X^{(0)}(n)]. \quad (15)$$

We calculate the stage ratio as follows:

$$Q(m) = \frac{X(m-1)}{X(m)}. \quad (16)$$

We calculate to obtain the following:

$$Q = (Q(1), Q(2), \dots, Q(n)),$$

$$Q(m) \in (e^{-2/m+1}, e^{2/m+1}). \quad (17)$$

We solve coefficients by the least squares method.

$$u = \begin{pmatrix} a \\ b \end{pmatrix} = (B^T B)^{-1} B Y^T. \quad (18)$$

We get the response function as follows:

$$\hat{X}^{(1)}(m+1) = \left( X^{(0)}(1) - \frac{b}{a} \right) e^{-am} + \frac{b}{a}. \quad (19)$$

Data restoration through first-order cumulative reduction is as follows:

$$\hat{X}^{(0)}(m+1) = \hat{X}^{(1)}(m+1) - \hat{X}^{(1)}(m), \quad m = 1, 2, 3, \dots \quad (20)$$

**3.2.2. Relative Error Test Steps.** We find relative residuals as follows:

$$e^{(0)}(m) = X^{(0)}(m) - \hat{X}^{(0)}(m). \quad (21)$$

We calculate the relative residual rate as follows:

$$P(e^{(0)}(m)) = \frac{e^{(0)}(m)}{X^{(0)}(m)} * 100\%. \quad (22)$$

We calculate the average residual rate as follows:

$$P(e^{(0)}(\text{avg})) = \frac{1}{n-1} \sum_{m=2}^n |e^{(0)}(m)|. \quad (23)$$

## 4. Machine Learning and Behavior Analysis

### 4.1. ATI Machine Learning Model

**4.1.1. Loss Curve Analysis of ATI Model.** In order to analyze the related data of sports track and field, this study proposes the ATI model under machine learning (ML) to analyze the behavior of big data [24]. The loss curve of the ATI model is analyzed by designing experiments. In the iterative epoch of 0–500 learning rates, loss experiments are carried out on learning rates of 0.0001, 0.001, 0.01, and 0.1, respectively, to obtain correlation loss values. From the images, when learning rates are 0.001, 0.01, and 0.1, respectively, the loss value of the correlation curve greatly decreases, shows a gradual downward trend, and gradually tends to be stable. Experiments and data show that when the learning rate is 0.1, the loss gradually decreases from 0.00025 when the iteration era is 0, 0.0002 when the iteration era is 100, 0.0001 when the iteration era is 200, and the loss of the ATI model decreases to zero when the iteration era is 300, and the loss is zero when the iteration era is 400 and 500, indicating that the loss rate of the ATI model decreases to zero when the iteration era is 300 [25]. When the learning rate is 0.01, the loss rate in 0–200 iteration era is similar to that in 0–200 iteration era, the loss is 0.00015 when the iteration era is 300, 0.0001 when the learning rate is 400, and the loss drops to zero when the iteration era is 500. When the learning rate is 0.0001, the loss is higher, which is 0.0014 at 300 era, 0.0005 at 400 era, and 0.0003 at 500 era. Therefore, in order to

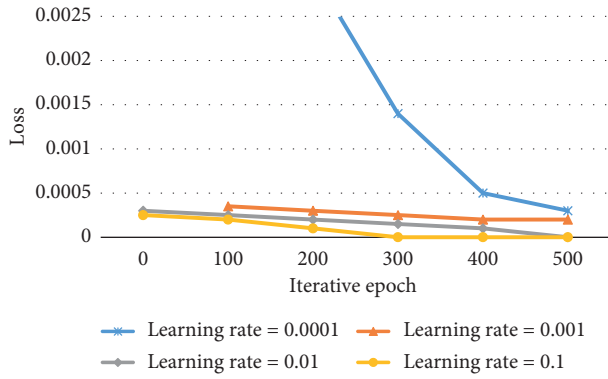


FIGURE 3: Loss analysis table.

minimize the loss, the ATI model proposed in this study should be used. When the learning rate is 0.1, the corresponding loss is lower than other learning rates. When the learning rate is 0.0001, the loss is too serious, which will easily lead to an inaccurate analysis of related behaviors, as shown in Figure 3.

4.1.2. ATI Machine Learning and Hidden Neurons.

Through relevant experiments and data, it can be seen that when the number of hidden neurons is fixed, the analysis of the dropout rate and NRMSE data shows that when the dropout rate is from 0 to 0.9, the NRMSE value approximately gradually increases, and when the dropout rate is 0.9, the NRMSE value reaches the highest value of 0.8. When the number of neurons increased from 8 to 16, 24, and 32, the NRMSE value gradually increased with the increase in the dropout rate. When the number of neurons was 16, the highest NRMSE value was 0.75 when the dropout rate was 0.9. When the number of neurons is 24 hours, with the increase in the dropout rate, the NRMSE value also gradually increases, reaching the highest value of 0.4 at 0.9. As shown above, when the number of neurons is 32 and the dropout rate is 0.9, the highest NRMSE value is 0.3. On the other hand, when the dropout rate is fixed and the neural network gradually increases, the NRMSE value gradually decreases. According to the experiment and related data, the following conclusions are drawn: when the dropout rate is constant, with the increase in hidden neurons, the NRMSE value gradually decreases. When the number of hidden neurons is constant, the NRMSE value gradually increases with the increase in dropout rate. This shows that the relationship between the ATI machine learning model and NRMSE value is related to the number of hidden neurons and dropout rate. When the number of neurons increases to 32, the lower the dropout rate, the lower the NRMSE value, and vice versa, as shown in Figure 4.

4.2. Analysis of Sports Track and Field

4.2.1. Big Data Analysis of Track and Field Performance.

The number of medals, gold medals, silver medals, and bronze medals is statistically analyzed through the number of track and field competitions. In the 24th competition, the

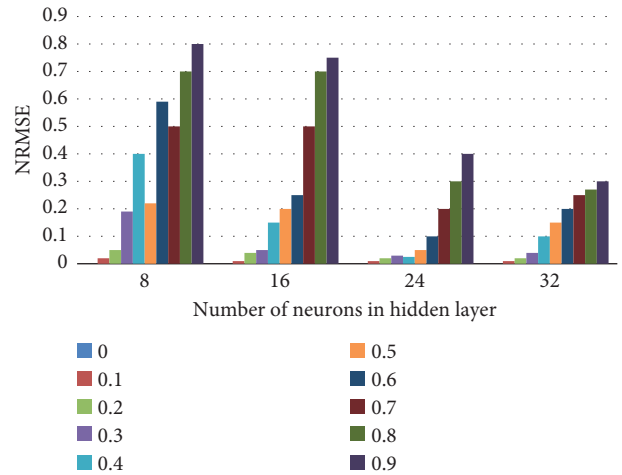


FIGURE 4: NRMSE data analysis.

total number of medals won was 1, which was the bronze medal won by the shot put competition. In the 25th competition, the total number of medals won was 4, including 1 gold medal, a silver medal in walking race and shot put competition, and a bronze medal in walking race and middle and long-distance running, respectively, totaling 4 medals. In the 26th competition, he won a gold medal in middle and long-distance running, a bronze medal in middle and long-distance running and shot put, respectively, and a bronze medal in walking race, totaling 4 medals; Won a gold medal in walking race in the 27th competition. In the 28th competition, he won two gold medals in hurdle and middle and long-distance running, respectively. In the 23rd to 28th competitions investigated, a total of 13 medals were won. As shown in Table 2.

Through relevant investigation and data drawn into the icon, the number of participants, the number of top eight, and the number of gold medals in the 23rd to 28th track and field competitions were statistically analyzed. According to the chart, the number of participants will be 22 in the 23rd session, which is the least in the survey session. By the 28th session, the number of participants will be 52, which has been greatly improved. It shows that with the development of the times, track and field are known and liked by more people, and the promotion of track and field events has played a role in promoting national fitness. Through the analysis of the overall data, it can be seen that from the 23rd to the 28th, track and field sports have been better popularized, and more people have participated in them, as shown in Figure 5.

According to the analysis of the number of people who entered the top eight in the competition, in the 24th to 25th sessions, from 27th to 28th, it showed an upward trend. At the 25th time, the number of people entering the top eight competitions reached the highest of 12 in the survey session, the lowest is the 27th session, and only three people enter the top eight of the competition. According to the relevant data, there is no obvious rule in the number of people entering the top eight, which shows that in the track and field competition, the participants are unstable. It is necessary to



TABLE 2: Analysis of the number of medals.

| Number of sessions | Gold medal (pieces)                           | Silver medal (pieces)                              | Bronze medal (pieces)                                  | Total medals (medals) |
|--------------------|---|--|--|-----------------------|
| 23rd session       | 0   | 0  | 1 (high jump)  | 1                     |
| 24th session       | 0   | 0  | 1 (shot put)   | 1                     |
| 25th session       | 1 (race walking)                              | 1 (shot put)                                       | 2 (race walking, and middle and long-distance running) | 4                     |
| 26th session       | 1 (middle and long-distance running)          | 2 (middle and long-distance running, and shot put) | 1 (race walking)                                       | 4                     |
| 27th session       | 1 (race walking)                              | 0  | 0  | 1                     |
| 28th session       | 2 (hurdle, middle, and long-distance running) | 0  | 0  | 2                     |
| Total              | 5   | 3  | 5  | 13                    |

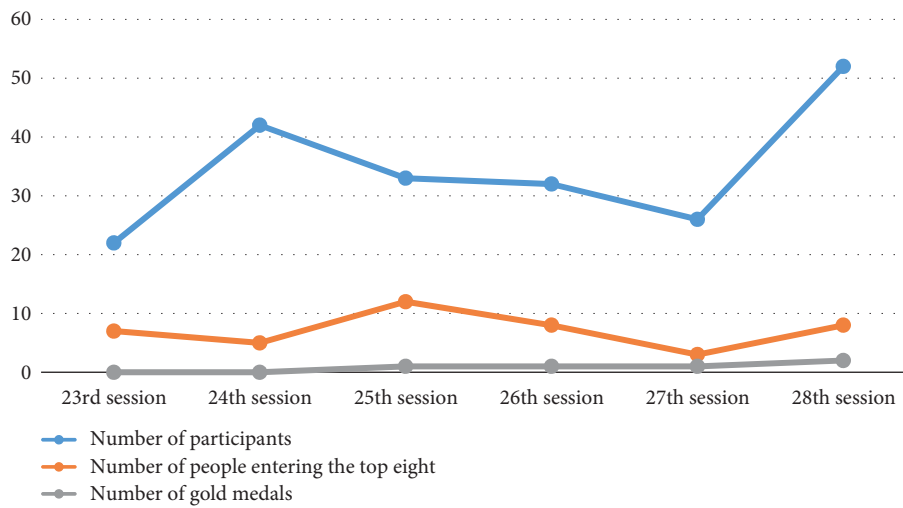


FIGURE 5: Track and field data statistics.

strengthen the behavior analysis of sports track and field big data in order to carry out training reform in track and field training. Through the data analysis of the number of gold medal winners, it can be seen that the number of gold medal winners in the 23rd to 28th track and field competitions is on the rise, the number of gold medals in the 23rd and 24th track and field competitions is 0, the number of gold medals in the 25th to 27th track and field competitions is 1, and the number of gold medals in the 28th track and field competition is 2.

4.2.2. *Data Analysis of Men’s Track and Field.* In order to accurately analyze the related behaviors of sports track and field big data, this experiment makes a more accurate behavior analysis through statistical analysis and comparative analysis of men’s track and field-related data, so as to make more right people join the track and field competition. Linear 100 m, linear 200 m, and linear 400 m curve data are obtained by calculating relevant data. Compared with linear data, the absolute data of linear 100 m, linear 200 m, and linear 400 m are 2.1, 2.25, and 1.1, respectively, while the average progressive coefficient of 100 m, 200 m, and 400 m is  $2.25 > 2.1 > 1.1$ , indicating that the stability of 200 m performance is greater than 100 m and 400 m. Through

experiments, the behavior analysis of 200-meter training mode under big data is carried out, and the training mode of 100-meter and 400-meter men’s track and field competition is improved according to the results of relevant behavior analysis, so as to improve the performance and stability of 100-meter and 200-meter running, as shown in Figure 6.

Through the analysis of the relevant data in Figures 6 and 7, it can be known that the women’s 100-meter, 200-meter, and 400-meter track and field sprint results are more stable than those of men. Therefore, from the results of correlation analysis to find out the differences between men’s and women’s training methods, in order to improve men’s track and field training, the training results are made more stable.

4.2.3. *Data Analysis of Women’s Track and Field.* The experiment is shown in the following figure. By studying and analyzing the fixed-base ratio of linear 100 m, linear 200 m, and linear 400 m in women’s track and field, and then comparing and analyzing the results of 100 m, 200 m, and 400 m with the fixed-base ratio, the behavior analysis of the performance stability and changing trend is carried out. Through relevant research, calculation, and analysis, it is known that the absolute values of linear 100-meter, linear 200-meter, and linear 400-meter fixed-base ratio scores are

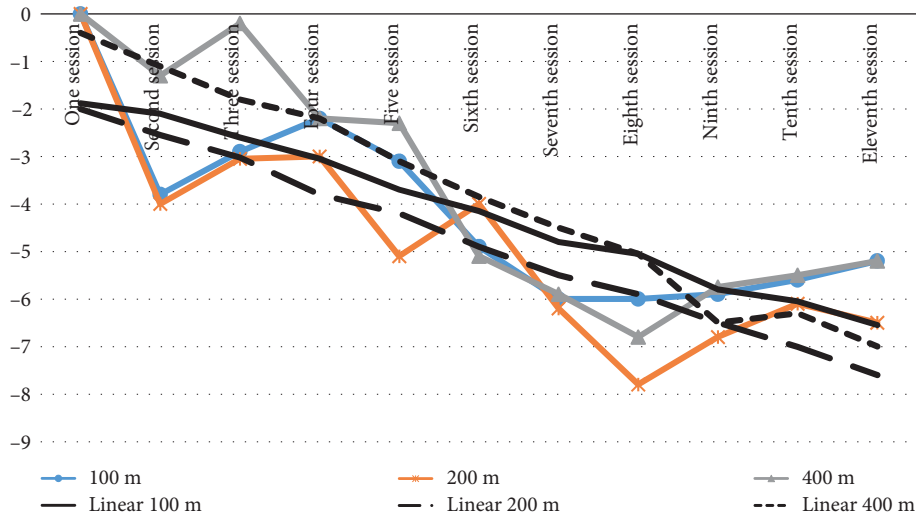


FIGURE 6: Analysis of men's track and field.

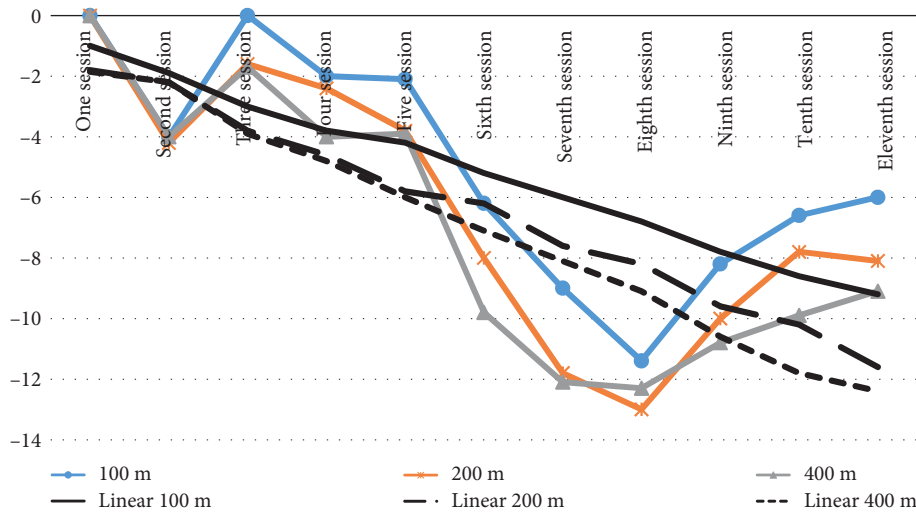


FIGURE 7: Analysis of women's track and field.

1.9, 2.2, 2.2, and  $2.2 > 1.9$  respectively, which shows that women's 400-meter and 200-meter scores are more stable than 100-meter scores. From the average progression coefficient of sprint, we can see that the absolute value of women's events is greater than the average value of men's events, which shows that women's track and field sprint performance is more stable than that of men. Through the experiment and the development trend of the image curve, it can be seen that the absolute value of the fixed-base ratio of women's track and field sprint in 100 meters, 200 meters, and 400 meters that reached the highest in the 8th competition, with the results of 10.93 s, 22.33 s, and 50.69 s, respectively. In order to make track and field performance more stable and shorten the time, the ATI model under machine learning should be used to analyze related sports behaviors through track and field big data, so as to improve the stability of track and field performance and shorten the competition time, as shown in Figure 7.

### 4.3. Comparison of Analysis Models

**4.3.1. Error of Data Behavior Analysis.** In order to analyze the error rate of the ATI model under machine learning in track and field big data behavior analysis, the model is analyzed through 1000, 2000, 3000, 4000, 5000, and 10000 data. It can be seen from the experimental data that, when the amount of data is increasing, the error rate of the ATI model, ATT model, ATT-Net model, and WAT model for behavior analysis is slightly increased, but the error rate of the ATI model proposed in this study is lower than that of the other three models. Therefore, the results obtained by the ATI model proposed in this study for behavior analysis of track and field big data are more accurate. Through the ATI model to track and field athletes' behavior analysis, from many aspects to improve the athletes' behavior, the stability of sports performance is improved and the competition time is shortened, as shown in Table 3.

TABLE 3: Behavior analysis data sheet.

| Model   | Behavioral analysis data | 1000 (%) | 2000 (%) | 3000 (%) | 4000 (%) | 5000 (%) | 10000 (%) |
|---------|--------------------------|----------|----------|----------|----------|----------|-----------|
| ATI     |                          | 2        | 2.40     | 2.70     | 3.50     | 3.60     | 3.30      |
| ATT     |                          | 2.40     | 3        | 3.70     | 4.60     | 5        | 5.40      |
| ATT-net | Error rate               | 2        | 3.10     | 3        | 4.50     | 6        | 5.50      |
| WAT     |                          | 7        | 7.30     | 8        | 8.40     | 11       | 11.30     |

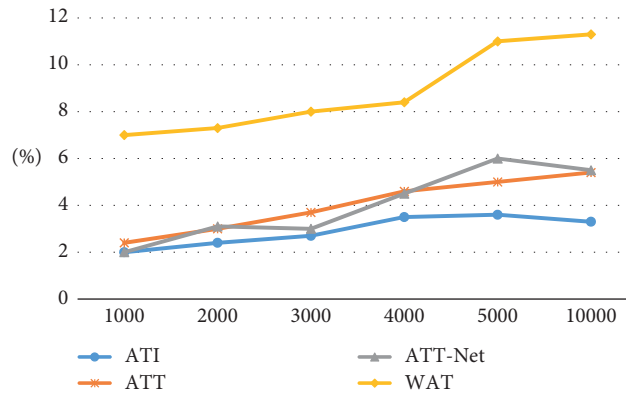


FIGURE 8: Error rate analysis.

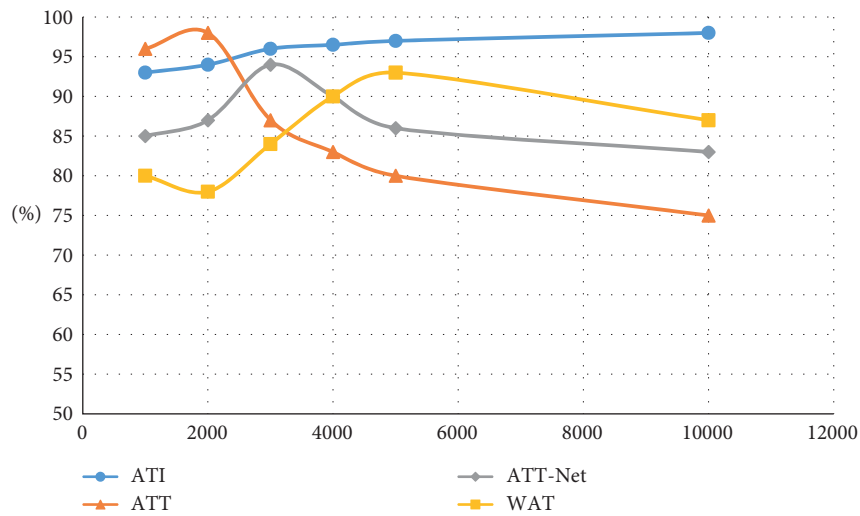


FIGURE 9: Coverage analysis.

Through the related experiments to draw experimental graphics, from the curve movement trend of the image, it can be seen that in the analysis of 1000–10000 behavior data, with the increase in data, the error rate of the comparison model slightly increases, showing an upward trend. But through the correlation image curve, we can see that the ATI model curve is always at the bottom, which shows that the error rate of the ATI model is the lowest under the condition of increasing behavior data, and it is more accurate for correlation behavior analysis, as shown in Figure 8.

4.3.2. Coverage Analysis of Big Data Behavior Analysis. Through the ATI model, ATT model, ATT-Net model, and WAT model, the coverage of big data behavior analysis is

analyzed. Through the relevant experimental analysis of the relevant information, the ATI model for behavior analysis coverage of 1000–10000 will be carried out in coverage analysis, and error rates in this range are small or neglected. For the ATT model, the analysis coverage rate is about 1000–3000, and there is a high accuracy rate in this coverage range, but when the big data behavior increases, there is a large error in the error rate. For the ATT-Net model, its coverage rate is about 2000–5000, and there is a high accuracy rate in this range. The coverage rate of the WAT model is within 4000–10000 data analysis, but the accuracy rate is relatively unstable when there are few data behavior analyses. Therefore, to sum up, the ATI model has wider coverage ability, higher accuracy, and relatively stable error rate within its coverage range, while the ATT model, ATT-

Net model, and WAT model have a coverage shortage range, and the behavior analysis outside the coverage range is unstable. Therefore, in order to obtain stable and more accurate behavior analysis of big data, the ATI model should be preferred to analyze behavior data, as shown in Figure 9.

## 5. Conclusions

In this study, the loss of the ATI model and the correlation analysis of learning rate, through the experiment and related data can be seen when the learning rate is 0.1, the loss is the lowest, when the learning rate is 0.0001, the loss is higher, and in order to reduce the unnecessary loss in the experimental process, we should give priority to the learning rate of 0.1 for the experiment. Next, the ATI model proposed in this study explores the change in NRMSE value when the hidden neurons and dropout rate change. The results show that when the number of neurons is fixed, the NRMSE value also increases with the increase in the dropout rate, and when the dropout rate is constant, the NRMSE value decreases with the increase in hidden neurons. Finally, the ATI model and other models for error rate and behavioral analysis coverage comparative analysis draw the conclusion that the ATI model compared with the rest of the model error rate is lower and has more extensive coverage. For track and field big data behavior analysis under the machine learning model, in order to improve the accuracy and stability of related behavior analysis, this study proposes the ATI model under machine learning. Through the analysis of the ATI model, the sports mode and arrangement are improved to get better results.

## Data Availability

The experimental data used to support the findings of this study are available from the corresponding author upon request.

## Conflicts of Interest

The authors declare that they have no conflicts of interest regarding this work.

## References

- [1] T. T. T. Nguyen and G. Armitage, "A survey of techniques for internet traffic classification using machine learning," *IEEE Communications Surveys & Tutorials*, vol. 10, no. 4, pp. 56–76, 2008.
- [2] G. Cauwenberghs and T. Poggio, "Incremental and decremental support vector machine learning," *Advances in Neural Information Processing Systems*, vol. 13, no. 5, pp. 409–412, 2001.
- [3] A. Doan, P. Domingos, and A. Y. Halevy, "Reconciling schemas of disparate data sources," *ACM SIGMOD Record*, vol. 30, no. 2, pp. 509–520, 2001.
- [4] T. Chen, Z. Du, N. Sun et al., "DianNao," *ACM Sigplan Notices*, vol. 49, no. 4, pp. 269–284, 2014.
- [5] I. Arel, D. C. Rose, and T. P. Karnowski, "Deep machine learning—a new frontier in artificial intelligence research," *IEEE Computational Intelligence Magazine*, vol. 5, no. 4, pp. 13–18, 2010.
- [6] S. García, A. Fernández, J. Luengo, and F. Herrera, "A study of statistical techniques and performance measures for genetics-based machine learning: accuracy and interpretability," *Soft Computing*, vol. 13, no. 10, pp. 959–977, 2009.
- [7] A. K. Mccallum, K. Nigam, J. Rennie, and K. Seymore, "Automating the construction of internet portals with machine learning[J]," *Information Retrieval*, vol. 3, no. 2, pp. 127–163, 2000.
- [8] K. Mithoefer, R. J. Williams, R. F. Warren, T. L. Wickiewicz, and R. G. Marx, "High-impact athletics after knee articular cartilage repair," *The American Journal of Sports Medicine*, vol. 34, no. 9, pp. 1413–1418, 2006.
- [9] J. M. Alonso, A. Junge, P. Renström, L. Engebretsen, M. Mountjoy, and J. Dvorak, "Sports injuries surveillance during the 2007 IAAF world athletics championships," *Clinical Journal of Sport Medicine*, vol. 19, no. 1, pp. 26–32, 2009.
- [10] J. G. Ingram, S. K. Fields, E. E. Yard, and R. D. Comstock, "Epidemiology of knee injuries among boys and girls in US high school athletics," *The American Journal of Sports Medicine*, vol. 36, no. 6, pp. 1116–1122, 2008.
- [11] T. Timпка, J.-M. Alonso, J. Jacobsson et al., "Injury and illness definitions and data collection procedures for use in epidemiological studies in Athletics (track and field): consensus statement," *British Journal of Sports Medicine*, vol. 48, no. 7, pp. 483–490, 2014.
- [12] S. D. Barber-Westin and F. R. Noyes, "Objective criteria for return to athletics after anterior cruciate ligament reconstruction and subsequent reinjury rates: a systematic review," *The Physician and Sportsmedicine*, vol. 39, no. 3, pp. 100–110, 2011.
- [13] N. Sousa, O. Almeida, and C. T. Wotjak, "A hitchhiker's guide to behavioral analysis in laboratory rodents," *Genes, Brain and Behavior*, vol. 5, no. s2, pp. 5–24, 2010.
- [14] D. R. Albrecht and C. I. Bargmann, "High-content behavioral analysis of *Caenorhabditis elegans* in precise spatiotemporal chemical environments," *Nature Methods*, vol. 8, no. 7, pp. 599–605, 2011.
- [15] D. Carneiro, J. C. Castillo, P. Novais, A. Fernández-Caballero, and J. Neves, "Multimodal behavioral analysis for non-invasive stress detection," *Expert Systems with Applications*, vol. 39, no. 18, pp. 13376–13389, 2012.
- [16] A. D. Mazzocca, F. M. Brown, D. S. Carreira, J. Hayden, and A. A. Romeo, "Arthroscopic anterior shoulder stabilization of collision and contact athletes," *The American Journal of Sports Medicine*, vol. 33, no. 1, pp. 52–60, 2005.
- [17] L. B. Mayers, D. A. Judelson, B. W. Moriarty, and K. W. Rundell, "Prevalence of body art (body piercing and tattooing) in university undergraduates and incidence of medical complications," *Mayo Clinic Proceedings*, vol. 77, no. 1, pp. 29–34, 2002.
- [18] L. T. Rameson, A. B. Satpute, and M. D. Lieberman, "The neural correlates of implicit and explicit self-relevant processing," *NeuroImage*, vol. 50, no. 2, pp. 701–708, 2010.
- [19] J.-M. Alonso, P. Edouard, G. Fischetto, B. Adams, F. Depiesse, and M. Mountjoy, "Determination of future prevention strategies in elite track and field: analysis of Daegu 2011 IAAF Championships injuries and illnesses surveillance," *British Journal of Sports Medicine*, vol. 46, no. 7, pp. 505–514, 2012.
- [20] S. E. Hobfoll, "Social and psychological resources and adaptation," *Review of General Psychology*, vol. 6, no. 4, pp. 307–324, 2002.

- [21] E. Schramm, I. Zobel, D. Schoepf et al., "Cognitive behavioral analysis system of psychotherapy versus escitalopram in chronic major depression," *Psychotherapy and Psychosomatics*, vol. 84, no. 4, pp. 227–240, 2015.
- [22] R. J. Schwartzman, "A Behavioral analysis of complete unilateral section of the pyramidal tract at the medullary level in macaca mulatta," *Annals of Neurology*, vol. 4, no. 3, pp. 234–244, 1978.
- [23] T. Baluchnejadmojarad and M. Roghani, "Effect of naringenin on intracerebroventricular streptozotocin-induced cognitive deficits in rat: a behavioral analysis," *Pharmacology*, vol. 78, no. 4, pp. 193–197, 2006.
- [24] J. Jun Luo, L. Lei Zhang, L. Li Zhang, W. Yan, and Y. Zhiping, "Behavioral analysis and optimization of CMOS CML dividers for millimeter-wave applications," *IEEE Transactions on Circuits and Systems II: Express Briefs*, vol. 62, no. 3, pp. 256–260, 2015.
- [25] L. M. Mccracken and S.-Y. Yang, "A contextual cognitive-behavioral analysis of rehabilitation workers' health and well-being: influences of acceptance, mindfulness, and values-based action," *Rehabilitation Psychology*, vol. 53, no. 4, pp. 479–485, 2008.

## Research Article

# Hybrid Genetic Algorithms for the Asymmetric Distance-Constrained Vehicle Routing Problem

Zakir Hussain Ahmed <sup>1</sup>, Asaad Shakir Hameed <sup>2,3</sup> and Modhi Lafta Mutar <sup>2,4</sup>

<sup>1</sup>Department of Mathematics and Statistics, Imam Mohammad Ibn Saud Islamic University (IMSIU), Riyadh, Saudi Arabia

<sup>2</sup>Department of Mathematics, General Directorate of Thi-Qar Education, Ministry of Education, Al-Haboubi str., Nasiriyah 64001, Iraq

<sup>3</sup>Data Mining and Optimization Group, Centre of Artificial Intelligence, Faculty of Information Science and Technology, National University of Malaysia, B. B. Bangi 43600, Selangor, Malaysia

<sup>4</sup>Department of Medical Instruments Engineering Techniques, Al-Turath University College, Mansour str., Baghdad 12013, Iraq

Correspondence should be addressed to Zakir Hussain Ahmed; [zaahmed@imamu.edu.sa](mailto:zaahmed@imamu.edu.sa)

Received 22 March 2022; Revised 15 May 2022; Accepted 19 May 2022; Published 22 June 2022

Academic Editor: Shimin Wang

Copyright © 2022 Zakir Hussain Ahmed et al. This is an open access article distributed under the Creative Commons Attribution License, which permits unrestricted use, distribution, and reproduction in any medium, provided the original work is properly cited.

We aim to suggest a simple genetic algorithm (GA) and other four hybrid GAs (HGAs) for solving the asymmetric distance-constrained vehicle routing problem (ADVVP), a variant of vehicle routing problem (VRP). The VRP is a difficult NP-hard optimization problem that has numerous real-life applications. The VRP aims to find an optimal tour that has least total distance (or cost) to provide service to  $n$  customers (or nodes or cities) utilizing  $m$  vehicles so that every vehicle starts journey from and ends journey at a depot (headquarters) and visits every customer only once. The problem has many variations, and we consider the ADVVP for this study, where distance traveled by every vehicle must not exceed a predefined maximum distance. The proposed GA uses random initial population followed by sequential constructive crossover and swap mutation. The HGAs enhance the initial solution using 2-opt search method and incorporate a local search technique along with an immigration procedure to obtain effective solution to the ADVVP. Experiments have been conducted among the suggested GAs by solving several restricted and unrestricted ADVVP instances on asymmetric TSPLIB utilizing several vehicles. Our experiments claim that the suggested HGAs using local search methods are very effective. Finally, we reported a comparative study between our best HGA and a state-of-the-art algorithm on asymmetric capacitated VRP and found that our algorithm is better than the state-of-the-art algorithm for the instances.

## 1. Introduction

The vehicle routing problem (VRP) is very complicated traditional NP-hard combinatorial optimization problem (COP) that was presented by Dantzig and Ramser [1]. The problem determines minimum distance (cost or time) route for a vehicle set to serve a customer set. It has several real-life applications such as shipments delivery, transportation networks, and street cleaning. The VRP is a widely studied problem that has several variants such as the VRP with Backhauls (VRPB), the VRP with pickup and delivery (VRPPD), the split delivery VRP (SDVRP), the VRP with time window (VRPTW), and the multi-depot VRP (MDVRP) [2].

We consider another variant of the VRP, called distance-constrained VRP (DVRP) in which total distance toured by every vehicle in the tour is constrained by a predefined maximum distance. The problem determines minimum cost route for a vehicle set so that every customer is provided service once by exactly one vehicle, every vehicle starts journey and ends journey at the same depot, and the entire distance traveled by each vehicle must not exceed the predefined maximum distance. Methods that have been used to solve the DVRP as well as COPs are categorized as exact and heuristic methods [3]. Branch and bound, branch and price, branch and cut, and lexsearch are some examples of exact methods which obtain exact solutions [4]. However, these methods take lots of computational effort. However, heuristic

and metaheuristic methods obtain near exact solutions quickly, so they are normally used in large-scale DVRP instances. Metaheuristic methods are more advanced than the heuristic methods. Genetic algorithm (GA), simulated annealing (SA), differential evolution algorithm (DEA), tabu search (TS), artificial bee colony (ABC), ant colony optimization (ACO), and particle swarm optimization (PSO) are some examples of metaheuristic methods. They can obtain suitable solutions to various kinds of optimization problems in a realistic time [5]. Among them, GA is commonly applied to find effective solution to the COPs in a reasonable time.

GA is a popular metaheuristic algorithm, which was first introduced by John Holland [6]. The major assumption of GA is that just the stronger individuals/chromosomes can live longer. Normally, a random population of chromosomes is generated first, and then using possibly three operators—selection, crossover, and mutation, (hopefully) new population is created in each generation. The process is replicated till the stopping criterion is reached. The purpose is to find solution with higher fitness value that is close to the optimal solution.

A common problem with GAs is premature convergence to obtain optimal solution which is due to the population diversity loss. If it is low, the convergence will be fast; otherwise, convergence will be time-consuming and sometimes it is a wastage of computational efforts. So, it is important to balance between exploitation and exploration of search area. In general, the effectiveness of GAs extremely depends on genetic operators. Among them, crossover operator plays a very important role and accordingly many researchers used/developed different crossovers for the VRP. Usually, crossover techniques that were used/developed for the usual traveling salesman problem (TSP) are used in other COPs also. Among crossover operators, sequential constructive crossover (SCX) was found very good for some COPs [7, 8]. Though simple GA using SCX is very good, sometimes it gets stuck in local optima. So, one can go for hybrid GA that merges simple GA with a local search (or heuristic) method.

The main contribution of this paper is to propose a simple GA and four hybrid GAs (HGAs) for the ADVRP. In our proposed HGAs, initial population is generated randomly that is further enhanced by 2-opt local search, offspring are created by SCX, random alteration of two genes by swap mutation, solutions are improved by one of three different local search methods, and stagnation/premature convergence is removed by immigration method. Experiments have been conducted among the suggested GAs by solving several restricted and unrestricted ADVRP instances on asymmetric TSPLIB utilizing several vehicles. Our experiments claim that the suggested HGAs using different local search methods are very effective. Finally, we did a comparative study between our best HGA and a state-of-the-art algorithm [9] on some asymmetric capacitated VRP (ACVRP) and found that our algorithm is better than the competing algorithm for the instances.

This paper is arranged as follows: Section 2 defines the problem, Section 3 provides a literature survey for the

problem, Section 4 develops the simple GA and hybrid GAs for the problem, Section 5 introduces results of experiments, and finally Section 6 introduces discussion and conclusion.

## 2. Problem Definition

The ADVRP determines the minimum cost route to serve a customer set. The cost is defined by total traveling distance. Customers are scattered across several locations, and each of them is to be visited only once by a single vehicle. Generally, the vehicles have the same distance constraints.

*2.1. Assumptions.* Following are the assumptions for defining the problem:

- (i) Each customer is visited exactly once by exactly one vehicle
- (ii) Each vehicle route starts and ends at the same depot
- (iii) Each vehicle's route can only pass through one depot exactly once
- (iv) A non-negative distance-constrained for all vehicle is defined, and the distance traveled by each vehicle cannot exceed the distance-constrained
- (v) The sum of route of all vehicles must be minimum

*2.2. Notation.* Following is the list of notations that will be used in this study (Table 1).

The objective of the ADVRP is to find a least cost optimal tour set that visit all cities using all vehicles, every vehicle starts journey from and ends journey at the same headquarters, each city is visited exactly once, and the distance traveled by each vehicle must not exceed  $D_{\max}$ . If  $d_{ij} = d_{ji}$ , the matrix  $D$  is symmetric, otherwise, asymmetric. The mathematical model of the ADVRP is given below [10].

The objective function:

$$f(S) = \min \sum_{i=0}^{n-1} \sum_{j=0}^{n-1} d_{ij} x_{ij}. \quad (1)$$

Subject to

$$\sum_{i=0}^{n-1} x_{ij} = 1 \quad j = 1, 2, \dots, n-1, \quad (2)$$

$$\sum_{j=0}^{n-1} x_{ij} = 1 \quad j = 1, 2, \dots, n-1, \quad (3)$$

$$\sum_{j=0}^{n-1} x_{0j} = m, \quad (4)$$

$$\sum_{i=0}^{n-1} x_{i0} = m, \quad (5)$$

TABLE 1: List of notations that will be used in this study.

| Notation                    | Description  |
|-----------------------------|--|
| $n$                         | Number of cities (or customers or nodes)   |
| $N = \{0, 1, 2, \dots, n\}$ | Set of cities, where “city 0” is the depot   |
| $M$                         | Number of vehicles   |
| $D = [d_{ij}]$              | Distance matrix  |
| $d_{ij}$                    | The traveled distance from city $i$ to city $j$  |
| $D_{\max}$                  | Maximum traveled distance-constrained  |
| $x_{ij}$                    | The decision binary variable that is equal to 1 if a vehicle travels from city $i$ to city $j$ and 0 otherwise             |
| $z_{ij}$                    | The variable that presents the shortest distance traveled from the depot to city $j$ , where $i$ is the predecessor of $j$ |

$$\sum_{j=0, j \neq i}^{n-1} z_{ij} - \sum_{j=0, j \neq i}^{n-1} z_{ji} - \sum_{j=0}^{n-1} d_{ij} x_{ij} = 0 \quad i = 1, 2, \dots, n-1, \quad (6)$$

$$z_{ij} \leq (D_{\max} - d_{j0}) x_{ij} \quad j \neq 0, \quad (7)$$

$$z_{ij} \leq (D_{\max}) x_{i0} \quad i = 1, 2, \dots, n-1, \quad (8)$$

$$z_{ij} \geq (d_{ij} + d_{0i}) x_{ij} \quad i \neq 0, \quad (9)$$

$$z_{0i} = d_{0i} x_{0i} \quad i = 1, 2, \dots, n-1, \quad (10)$$

$$x_{ij} \in \{0, 1\}. \quad (11)$$

In this formulation, the constraint (1) shows the objective function that minimizes the total routes' distance. The constraints (2) and (3) are the constraints that ensure that each node (or customer) is visited exactly once, whereas the constraints (4) and (5) ensure that only  $m$  vehicles are allowed. The constraint (6) is a flow constraint that is identified as a flow-based model which states that the distance from city  $i$  to another city  $j$  on a tour must be same as the difference between the distance from headquarters (depot) to city  $i$  and the distance from headquarters to city  $j$ . The constraint (7) claims that the distance from headquarters to city  $j$  must not exceed the difference between the predefined maximum distance ( $D_{\max}$ ) and the distance from city  $j$  to depot. The constraint (8) verifies that the distance traveled up to the depot must not exceed the predefined maximum distance. Additionally, the constraint (9) states that the total distance from depot to city  $j$  must not be less than the distance from the depot to city  $i$  plus the distance from city  $i$  to city  $j$ . The constraint (10) shows the initial value of  $z_{0i}$  that equals the distance from the depot to city  $i$ . The constraint (11) states that the decision variables  $x_{ij}$  are binary variables.

### 3. Literature Review

There is enough literature for the CVRP, but very few literature are available for the DVRP as it is not a common variant [2]. A branch and bound (B&B) method is developed in [10] for finding exact solution to the ADVRP. A multistart B&B method is developed in [11] for solving the ADVRP.

Computational results show that the algorithm can provide exact solutions for some instances. But, for some instances, it could not find a feasible solution. Additionally, when distance restriction is tight, solving the problem instance becomes very hard, and the method is terminated before it might find any feasible solution. A lexicsearch algorithm is developed in [4] for the DVRP and applied on various problem instance types. The results show that as the number of vehicles increases the computational time and optimal solution value also increase. Further, for some instances, the algorithm failed to prove the optimality of the solutions within restricted time limit. In general, exact algorithms cannot provide exact solutions for large problem instances, and hence many heuristic algorithms are developed for solving large problem instances.

Rachid et al. [12] compared some crossover operators for the VRP and found that partially mapped crossover (PMX) is better than ordered crossover (OX), and OX is better than merge #2. The PMX arbitrarily chooses two crossover points, copies the sub-chromosome between the points from any parent into one offspring, and then creates the full offspring by adding remaining cities from other parent in the mapped process. The OX arbitrarily chooses two crossover points, copies the sub-chromosome between the points from any parent into one offspring, and then creates the full offspring by adding remaining cities from other parent in the same order as they appear therein. The merge #2 operator is based on the global precedence among the genes and is independent of any of the chromosomes.

Krunoslav and Robert [13] compared eight crossover operators for the VRP and showed that alternate edge crossover (AEX) is best among them. The AEX chooses edges subsequently from the parents or arbitrarily chooses a legal edge if an illegal edge exists, for creating offspring.

Alabdulkareem and Ahmed [7] conducted a comparative study among four crossover methods—cycle crossover (CX), SCX, AEX, and PMX, for the DVRP and observed that SCX is the best. The CX takes positions and values from any parent so that the cities are reproduced from every parent in alternative cycles for creating offspring. The SCX creates an offspring using better links (edges) from the parents. Sometimes, it introduces better new edges which are not consistent in any parent. So, the chance of creating better offspring is very high [8].

Simple heuristic procedures have some drawbacks, such as stagnation and premature convergence. Hybrid techniques are used to overcome such drawbacks. Hybridization



can be done by combining the better sides of various exact methods or heuristic methods [14]. Several hybridization methods have been described in the literature for the VRP.

A hybrid swarm-based method (PSO-VNS) is proposed for the distance-constrained CVRP in [15], by combining a variable neighborhood search (VNS) within the PSO. As reported, the algorithm shows high-quality solutions compared to the existing algorithms.

The variable neighborhood SA (VNSA) algorithm is proposed for the CVRP in [16] by combining a modified VNS and SA. The algorithm is tested on 39 CVRP instances and then is compared against some existing algorithms. As reported, the algorithm could solve some large and very large instances efficiently.

A hybrid algorithm (LNS-ACO) is proposed for the capacitated VRP (CVRP) in [5] by embedding the solution by the ACO into the large neighborhood search (LNS) algorithm. The performance of the algorithm is tested on 88 CVRP instances and then is compared against other LNS algorithms. As reported, the algorithm has a suitable performance in solving the instances.

Four hybrid algorithms—improved intelligent water drops (IIWD), advanced cuckoo search (ACS), local search hybrid algorithm (LSHA), and post-optimization hybrid algorithm (POHA)—are proposed for the CVRP in [17]. Experimental results on some instances are compared to the best known solutions and found that LSHA and POHA algorithms could obtain best known solutions for most of the instances.

An enhanced perturbation-based VNS with adaptive selection mechanism method (PVNS-ASM) is developed in [18] by combining perturbation-based VNS (PVNS) with an adaptive selection mechanism (ASM). The algorithm is tested on 21 CVRP instances and then is compared against existing heuristics. The computational results show the efficiency of the algorithm.

A hybrid firefly algorithm (CVRP-FA) is proposed for the CVRP in [19] by integrating 2 h-opt and improved 2-opt algorithms for improving solution quality obtained by PMX and two mutation operators, and then tested on 82 instances. The computational results show that the algorithm has faster convergence rate and higher computational accuracy.

An improved SA (ISA) algorithm with crossover operator (ISA-CO) is developed for the CVRP in [20] where a population-based SA algorithm is applied. Further, the solutions are improved using four local search methods—swap, scramble, insertion, and reversion—and two crossover operators—PMX and OX operators. The algorithm was applied on 91 instances. The computational results show that the algorithm has a better performance compared to other algorithms.

A hybrid algorithm that combines the randomized VNS (RVNS) and TS is proposed in [9] to solve the ADVRP. In addition, the intensification and diversification stages are also incorporated to find optimal solutions. Computational results show that the algorithm is competitive in finding quality solutions.

There is some literature available for other VRP variants. A hybrid GA is proposed to solve the VRP with drones

(VRPD) [21]. Experiments were carried out on different instances and found good performance of the algorithm. A novel hybrid algorithm by combining the GA and modified VNS (MVNS) for the VRP with cross-docking (VRPCD) is proposed in [22]. To prove the usefulness of the hybrid algorithm, a comparative study is carried out on some problem instances. It is found from the computational study that the proposed algorithm is more efficient than other algorithms to find best solutions in less computational time. A hybrid multi-objective genetic local search (HGLS) algorithm is proposed for the prize-collecting VRP (PCVRP) in [23]. Experiments on some instances are performed to evaluate the performance of the algorithm that shows the superiority of the algorithm.

#### 4. The HGAs for the ADVRP

In this present section, a simple GA and four HGAs are proposed for the ADVRP. Following is the list of notations that will be used in our algorithms (Table 2).

*4.1. The Solution Encoding and Initial Population.* For applying GA to solve any problem, a way to represent (encode) a solution as chromosome (individual) must be defined first. In our GAs, a solution is encoded by an integer chromosome called path representation whose length is  $n + m - 1$ , where  $n$  is the number of cities and  $m$  is the number of vehicles. In this representation, there are  $m - 1$  extra cities that represent duplicate depot cities to show the beginning of new vehicles [24]. A chromosome consisting of all routes of the vehicles is created randomly such that distance constraint is not violated. An initial population of size  $P_s$  is created using Algorithm 1.

An example of a chromosome with  $n = 10$  cities and  $m = 3$  vehicles is given in Figure 1(a), where the integer 1 and integers bigger than 10 are the depot and the others are intermediate cities. The routes of the vehicles are shown in the VRP version in Figure 1(b), while the graphical interpretation of the routes is given in Figure 1(c). Thus, the given distance matrix is to be augmented to show the duplicate depot cities. For this,  $m - 1$  copy of the depot (city 1) row and column (i.e., 1st row and 1st column) is added to the given original matrix.

*4.2. Fitness Function and Selection Operator.* The objective function value of a chromosome (solution) is the total traveled distance of the routes by all vehicles. The distance of every route is computed by adding the distances between the cities. Since the ADVRP is minimization problem, so the fitness function is the inverted objective function. In the selection procedure, a subpopulation (some chromosomes) is chosen from the current population for forming the next population. The performance of GA is affected by choosing a better selection operator without which GA is a like random sampling that gives various results in the generations. Several selection procedures are present in the literature. We implement the fitness proportional selection (FPS) [25] for our GAs, which is very popular operator where the fitness

TABLE 2: List of notations that will be used in our algorithms.

| Notation    | Description   |
|-------------|---|
| $P_s$       | Population size   |
| $P_c$       | Crossover probability                                       |
| $P_{mut}$   | Mutation probability  |
| MaxGen      | Maximum generation allowed                                  |
| $G_i$       | Population in $i$ th generation                             |
| $f_i$       | Fitness of $i$ th chromosome                                |
| $prob_i$    | Selection probability of $i$ th chromosome in a generation  |
| $cP_i$      | Cumulative probability of $i$ th chromosome in a generation |
| $C_j$       | The $j$ th chromosome                                       |
| $B_i$       | Best solution in $i$ th generation                          |
| $D_{route}$ | Distance of the route of a vehicle                          |
| BS          | Best solution   |
| BT          | Best tour   |

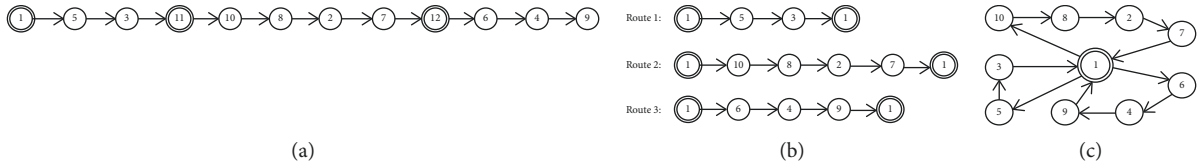


FIGURE 1: (a) An example chromosome, (b) the VRP routes, and (c) the graphical interpretation.

**Input:**  $n, D_{max}, P_s$ .

**Output:** Population of chromosomes.

**for**  $i = 1$  **to**  $P_s$  **do**

**Set** first city  $p = 1$ .

    Current chromosome contains only “city 1.”

    Prepare a list of remaining cities except dummy cities.

**for**  $j = 2$  **to**  $n$  **do**

        Select a city (suppose city  $q$ ) randomly from the list of remaining cities.

        If the distance of the route of present vehicle is less than or equal to  $D_{max}$ , then add it to the current chromosome and then remove it from the list to make sure that it is not repeated.

        If the distance of the route greater than  $D_{max}$  then add a dummy depot (city  $q$ ).

        Rename the “city  $q$ ” as “city  $p$ ” and continue.

**end for**

**end for**

Improve the population by 2-opt local search

**Return** the population

ALGORITHM 1: Initial population creation algorithm.

value of every chromosome in a population relates the area of roulette-wheel portions. Then, a chromosome is pointed by the roulette-wheel pointer after it is rotated. Depending on the fitness value of each chromosome, a probability  $prob_i$  of selection is calculated as follows:

$$prob_i = \frac{f_i}{\sum_{j=1}^{P_s} f_j}; \quad i \in \{1, 2, \dots, P_s\}, \quad (12)$$

where  $P_s$  is the population size and  $f_i$  is the fitness function value for the chromosome  $i$ . Thus, better fitness value chromosomes have higher chance of being selected as

parents. There is no variation of the segment size and selection probability during the selection process. This process is very simple to implement, and it gives unbiased distributed probabilities to the chromosomes and assigns a high probability to the best chromosome. This procedure is called roulette-wheel selection procedure [6] that is presented in Algorithm 2.

**4.3. The Crossover Operator.** The selection procedure gives a trade-off between exploration and exploitation of search area. The crossover is a major procedure in GAs that is

**Input:**  $P_s$ , Population of chromosomes.  
**Output:** New population of chromosomes.  
 Calculate the fitness  $f_i$ , probability  $prob_i$ , and then cumulative probability  $cp_i$  of each chromosome ( $1 \leq i \leq P_s$ ) of the population. Note that  $cp_0 = 0$ .  
**for**  $i = 1$  **to**  $P_s$  **do**  
     Generate a random number  $r \in [0, 1]$ .  
     **if** ( $cp_{j-1} < r \leq cp_j$ ) (for any  $j, 1 \leq j \leq P_s$ ) **then**  
         Copy the chromosome  $j$  to the population.  
     **end if**  
**end for**  
**Return** the new population

ALGORITHM 2: Roulette-wheel selection algorithm.

TABLE 3: The given distance matrix.

| City | 1     | 2     | 3     | 4     | 5     | 6     | 7     |
|------|-------|-------|-------|-------|-------|-------|-------|
| 1    | 99999 | 2     | 11    | 10    | 8     | 7     | 6     |
| 2    | 6     | 99999 | 1     | 8     | 8     | 4     | 6     |
| 3    | 5     | 12    | 99999 | 11    | 8     | 12    | 3     |
| 4    | 11    | 9     | 10    | 99999 | 1     | 9     | 8     |
| 5    | 11    | 11    | 9     | 4     | 99999 | 2     | 10    |
| 6    | 12    | 8     | 5     | 2     | 11    | 99999 | 11    |
| 7    | 10    | 11    | 12    | 10    | 9     | 12    | 99999 |

employed on a chromosome pair to generate offspring(s) within a subspace restricted by the parents. Combinedly, selection and crossover operators are very strong operators that accelerate the convergence of GAs. The basic one-point or multi-point crossover operators do not work with respect to our encoding. The crossover operators which are valid for the TSP can be applied to the VRP and its variants. Several crossover operators are present in the literature for the TSP, and we are using the SCX; as it is observed to be one of the best crossovers for the DVRP [7], we apply this SCX with some modifications. The SCX algorithm is presented in Algorithm 3.

We demonstrate the SCX applying on a 7-city ( $n = 7$ ) and 2-vehicle ( $m = 2$ ) instance together with distance matrix given in Table 3. Further, suppose that maximum allowed distance is 60.

We modify the given distance matrix by combining one copy of the depot (city 1) row and column (i.e., 1st row and 1st column) to the matrix [14] that is provided in Table 4.

Let  $P_1: (1, 2, 4, 8, 3, 6, 5, 7)$  and  $P_2: (1, 3, 8, 5, 2, 7, 4, 6)$  be parent chromosomes. The objective function value of a chromosome is determined by summing the tour distances of all vehicles. The objective function value (total distance) of the 1st parent chromosome is 75 with the 1st and 2nd vehicle distances 54 and 21, respectively. The objective function value of the 2nd parent chromosome is 72 with the 1st and 2nd vehicle distances 56 and 16, respectively.

The calculation is begun from the city 1 (depot). After city 1, cities 2 in  $P_1$  and 3 in  $P_2$  are un-visited cities with distances  $d_{12} = 2$  and  $d_{13} = 11$ . Since  $d_{12} < d_{13}$ , city 2 is combined that generates the offspring as (1, 2). Since  $2 = D_{route} < D_{max} = 60$ , continue to build offspring. After city 2, cities 4 in  $P_1$  and 7 in  $P_2$  are legitimate cities with distances

$d_{24} = 8$  and  $d_{27} = 6$ . Since  $d_{27} < d_{24}$ , city 7 is combined that generates the offspring as (1, 2, 7). Since  $8 = D_{route} < D_{max} = 60$ , continue to build offspring. After city 7, city 4 is in  $P_2$  with distances  $d_{74} = 10$ , but no city in  $P_1$ . So, for  $P_1$ , search from the starting and find legitimate city 4 with  $d_{74} = 10$ . Since both are same cities, city 4 is combined that generates the offspring as (1, 2, 7, 4). Since  $18 = D_{route} < D_{max} = 60$ , continue to build offspring. After city 4, cities 8 in  $P_1$  and 6 in  $P_2$  are legitimate cities with distances  $d_{48} = 11$  and  $d_{46} = 9$ . Since  $d_{46} < d_{48}$ , city 6 is combined that generates the offspring as (1, 2, 7, 4, 6). Since  $27 = D_{route} < D_{max} = 60$ , continue to build offspring. After city 6, cities 5 are in  $P_1$  with distances  $d_{65} = 11$ , but there is no city in  $P_2$ . So, for  $P_2$ , search from the starting and city 3 with  $d_{63} = 5$  is found. Since  $d_{63} < d_{65}$ , city 3 is combined that generates the offspring as (1, 2, 7, 4, 6, 3). Since  $32 = D_{route} < D_{max} = 60$ , continue to build offspring. After city 3, cities 5 in  $P_1$  and 8 in  $P_2$  are legitimate cities with distances  $d_{35} = 8$  and  $d_{38} = 5$ . Since  $d_{38} < d_{35}$ , city 8 is combined that generates the offspring as (1, 2, 7, 4, 6, 3, 8). This completes route for the first vehicle whose distance is 37. Continue to build route for the next vehicle as well as the offspring. After city 8, the un-visited city 5 is in both parents, with distance  $d_{85} = 8$ . So, city 5 is added that produces the offspring as (1, 2, 7, 4, 6, 3, 8, 5). Since  $8 = D_{route} < D_{max} = 60$ , continue to build offspring. However, this is the complete offspring chromosome, and so, we stop. The distance of the route of the 2nd vehicle is 19, and total distance of the offspring is  $37 + 19 = 56$  which is less than the distance of the parents. For this example, the SCX obtains an offspring that has value better than the values of both parent chromosomes. Figure 2(a) shows parent chromosomes ( $P_1$  and  $P_2$ ), Figure 2(b) shows the offspring chromosome (O),

```

Input:  $D, P_c, D_{\max}$ , Pair of parent chromosomes.
Output: Offspring chromosome.
Generate a random number  $r \in [0, 1]$ .
if ( $r \leq P_c$ ) then do
  Set  $p = 1$ .
  The offspring chromosome contains only "city 1."
  for  $i = 2$  to  $n$  do
    In each chromosome consider the first "legitimate" (un-visited) city existed after "city  $p$ ."
    if no legitimate city is existed in a parent, then
      Examine from starting of the parent and choose the first legitimate city existed after "city  $p$ ."
    end if
    Assume that "city  $\alpha$ " and "city  $\beta$ " are selected from 1st and 2nd parents, respectively.
    if ( $d_{p\alpha} < d_{p\beta}$ ) then do
      Add "city  $\alpha$ " to the offspring chromosome.
    else
      Add "city  $\beta$ " to the offspring chromosome.
    end if
    If after combining the current city,  $D_{\text{route}} > D_{\max}$ 
    then
      Drop the current city and add a dummy depot in the route as the end city of the route.
    end if
    Rename the present city as "city  $p$ " and continue.
  end for
end if
Return the offspring chromosome

```

ALGORITHM 3: Sequential constructive crossover algorithm.

TABLE 4: The modified distance matrix.

| City | 1    | 2    | 3    | 4    | 5    | 6    | 7    | 8    |
|------|------|------|------|------|------|------|------|------|
| 1    | 9999 | 2    | 11   | 10   | 8    | 7    | 6    | 9999 |
| 2    | 6    | 9999 | 1    | 8    | 8    | 4    | 6    | 6    |
| 3    | 5    | 12   | 9999 | 11   | 8    | 12   | 3    | 5    |
| 4    | 11   | 9    | 10   | 9999 | 1    | 9    | 8    | 11   |
| 5    | 11   | 11   | 9    | 4    | 9999 | 2    | 10   | 11   |
| 6    | 12   | 8    | 5    | 2    | 11   | 9999 | 11   | 12   |
| 7    | 10   | 11   | 12   | 10   | 9    | 12   | 9999 | 10   |
| 8    | 9999 | 2    | 11   | 10   | 8    | 7    | 6    | 9999 |

Figure 2(c) shows ADVRP routes of the offspring, and Figure 2(d) shows the graphical interpretation of the offspring chromosome. In general, the crossover operator that maintains better attributes of parents in their offspring(s) is supposed to be better crossover, and SCX is supposed to be better in this respect. In Figure 2(b), six boldface edges are from either parent chromosome.

This SCX obtains only one offspring chromosome. The parent chromosomes are chosen based on the predefined crossover probability. If the offspring has better fitness value than the parent, the first parent is substituted by the offspring in the new population.

**4.4. Mutation Operator.** To diversify the population, mutation operator is applied with a prespecified probability. Generally, mutation probability is set very low compared to crossover probability. The exchange mutation that chooses randomly two places in a chromosome and exchanges their

values, if neither of them is dummy depot, is applied here. The exchange mutation is presented in Algorithm 4.

For example, let the chromosome: (1, 2, 7, 4, **6**, 3, 8, 5) with distance 56 be allowed for the mutation, and the 5th and 8th positions with their values are swapped. Then, the muted chromosome will be muted: (1, 2, 7, 4, 5, 3, 8, **6**) with distance of 1st and 2nd vehicles 33 and 19, respectively, and with total distance equal to  $33 + 19 = 52$  which is less than the distance of the original chromosome. Figure 3 shows this mutation process. However, we do not see whether the value of muted chromosome is better than the original chromosome, we only see whether the distance constraint is valid, and if it is not valid, then the mutated chromosome is not accepted.

**4.5. Local Search Approach.** Local search approaches are used to hybridize the simple GA that improve the solution quality and convergence level of the simple GA. In this study, the local

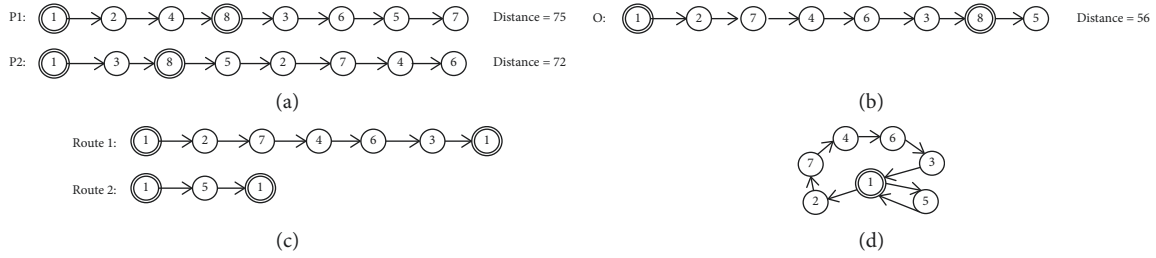


FIGURE 2: (a) Parent chromosomes, (b) the offspring, (c) the ADVRP routes of the offspring, and (d) the graphical interpretation of the offspring.

**Input :** A chromosome,  $P_{mut}$ .  
**Output:** Muted chromosome.  
 Generate a random number  $r \in [0, 1]$ .  
**if** ( $r \leq P_{mut}$ ) **then do**  
     Select randomly two different cities except dummy depots, suppose “city  $\alpha$ ” and “city  $\beta$ ” in the chromosome.  
     “city  $\alpha$ ”  $\leftrightarrow$  “city  $\beta$ ,” provided that they do not violate the distance constraint.  
**end if**  
 Return the mutated chromosome

ALGORITHM 4: Exchange mutation algorithm.

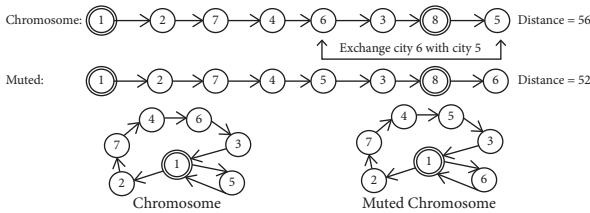


FIGURE 3: Exchange mutation process.

search approaches based on swap, insertion, and inversion mutations are used. Swap search chooses two cities (genes) randomly and swaps them. Insertion search inserts a randomly chosen city into a position in a chromosome randomly. Inversion search inverts the sub-chromosome between two randomly chosen places in a chromosome. Let  $(\alpha_1, \alpha_2, \alpha_3, \dots, \alpha_n)$  be a chromosome, then we define these three mutations as local search techniques in our HGAs as follows.

**4.5.1. Insertion Search.** The insertion search is presented in Algorithm 5. Figure 4 shows the implementation of the insertion search approach.

**4.5.2. Inversion Search.** The inversion search is presented in Algorithm 6. Figure 5 shows the implementation of the inversion search approach.

**4.5.3. Swap Search.** The swap search is presented in Algorithm 7. Figure 6 shows the implementation of the swap search approach.

In the proposed local search technique, one of these three local searches is chosen for the first three HGAs. For the

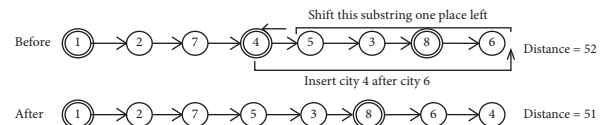


FIGURE 4: Implementation of the insertion search.

fourth HGA, we choose any of the above local search approaches randomly with a probability of 1/3.

**4.6. Immigration Method.** Although GAs are robust approaches, however, occasionally they get trapped in local optima. It might be caused by similar population, and so, the population should be diversified to escape from the local optima. The immigrant procedure increases population diversity by substituting some chromosomes of the current population with newly generated chromosomes every generation. We use the following immigration procedure. If there is no improvement of solution within last 10% generations of maximum predefined generations, then 10% of population is replaced by random chromosomes which is further improved by 2-opt local search approach.

**4.7. The Algorithms.** We propose one simple GA and four HGAs for the ADVRP. The GA begins with randomly generated initial population and goes repeatedly through roulette-wheel selection, sequential constructive crossover, and exchange mutation procedures to enhance the population gradually, until a predefined maximum number of generations is reached, hoping that a near-optimal solution is obtained. In addition to the operators in GA, one of the

```

Input: A chromosome.
Output: New chromosome.
for  $i = 2$  to  $n - 1$  do
  for  $j = i + 1$  to  $n$  d
    If inserting city  $ai$  after city  $aj$  reduces the distance of the chromosome and does not violate distance constraint, then insert the city  $ai$  after the city  $aj$ .
  end for
end for
Return the new chromosome

```

ALGORITHM 5: Insertion search algorithm.

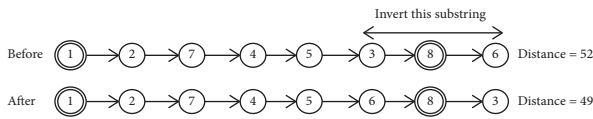


FIGURE 5: Implementation of the inversion search.

following local search approaches and above defined immigration approach are incorporated in the HGAs.

GA-INS: GA + insertion search + immigration approach.

GA-INV: GA + inversion search + immigration approach.

GA-SWP: GA + swap search + immigration approach.

GA-ADP: GA + adaptive search that randomly selects one of three local searches—insertion, inversion, and swap search + immigration approach.

The algorithm of the proposed HGAs is presented in Algorithm 8.

## 5. Experimental Results

The proposed GA and HGAs are encoded in Visual C++ and run on a Laptop with i7-1065G7 CPU@1.30 GHz and 8 GB RAM under MS Windows 10. The proposed GAs are executed for different parameter settings on some TSPLIB instances [26]. For setting parameters, ftv70 with 2 vehicles and infinite maximum distance constraint are used for the pilot runs. As the higher crossover probability can produce (hopefully) better solutions, we kept crossover probability fixed at 1.00 and run all algorithms for all combinations of  $P_s = 20, 30, 40, 50, 60, 70, 80, 90,$  and 100 and  $P_{mut} = 0.05, 0.06, 0.07, 0.08, 0.09, 0.10, 0.11, 0.12, 0.13, 0.14,$  and 0.15. We observed that for  $P_s = 50$  and  $P_{mut} = 0.10$ , almost all algorithms could obtain better solutions; hence, these values are considered for the study. However, looking at the computational time and solution improvement in the successive generations, for termination condition, we considered 2000 generations for GA and 200 generations for HGAs. The parameter values are reported in Table 5.

We compare the performance of GA and four HGAs on asymmetric TSPLIB instances of various sizes with various numbers of vehicles.

In Figure 7, each GA is represented by a curve that indicates improvement of the solution in successive generations. The curve for simple GA shows that it starts the search process with the worst solutions compared to the HGAs at the initial stage. It shows variation in solutions within first 25 generations, and after that it shows no variation. So, it gets stuck in local minimum quickly and is found to be the worst one. Among HGAs, the curve for GA-INV shows that it starts the search process with the worst solutions at the initial stage, and shows variation in solutions within only first 10 generations. So, it gets stuck in local minimum very quickly and is found to be the worst one among HGAs. However, compared to simple GA, it is far better. The curve for GA-INS shows that it starts the search process with the best solutions compared to other HGAs at the initial stage and shows variation in solutions within first 30 generations. However, after 30 generations, it shows no variation. So, it gets stuck in local minimum quickly and is not the best one. The curves for GA-SWP and GA-ADP show that they start the search process with better solutions and are competing within first few generations. However, GA-SWP shows no variation in solutions after first 20 generations. The variation of solutions by GA-ADP continues up to 35 out of 50 generations, and it obtains best solution. So, GA-ADP is positioned in 1st position and GA-SWP is positioned in 2nd position.

We report relative studies among GA and HGAs on fifteen asymmetric TSPLIB instances of various sizes with 2 and 3 vehicles. Note that we suppose br17 with 2 vehicles is one instance and br17 with 3 vehicles is another instance. So, the total number of tested instances is thirty. The descriptions of the different column titles are as follows (Table 6).

Table 7 reports the results for 30 unrestricted ADVRP instances where  $D_{max} = \text{Inf}$  (infinity). The formula for AI is as follows:

$$AI = \frac{100(AS_1 - AS_2)}{AS_2}, \quad (13)$$

where  $AS_1$  and  $AS_2$  are average solutions found by the GA and a HGA, respectively.

The results are evaluated based on average solution, and SD and average improvement (%) of the HGAs over simple GA. From Table 7, it is noticed that all algorithms could find best average solutions for the instance br17 with both 2 and 3 vehicles. The algorithms GA-INS, GA-INV, GA-SWP, and GA-ADP could obtain best average solutions for 6, 5, 10, and

**Input:** A chromosome.

**Output:** New chromosome.

**for**  $i = 2$  **to**  $n - 1$  **do**

**for**  $j = i + 1$  **to**  $n$  **do**

    If inverting substring between the cities  $\alpha_i$  and  $\alpha_j$  reduces the distance of the chromosome and does not violate distance constraint, then invert the substring

**end for**

**end for**

**Return** the new chromosome

ALGORITHM 6: Inversion search algorithm.

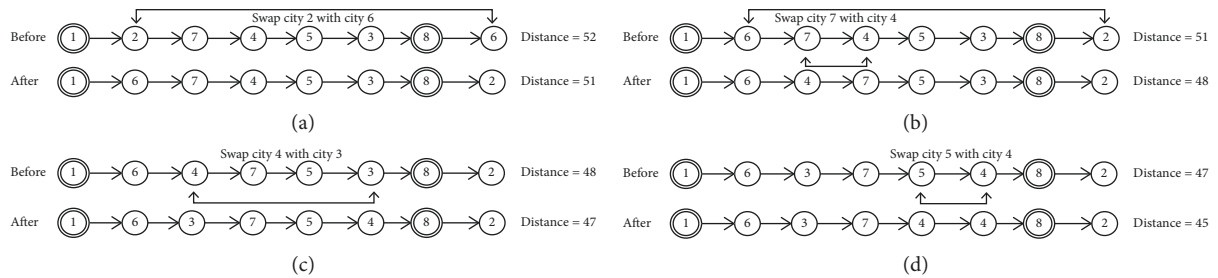


FIGURE 6: Implementation of the swap search.

**Input:** A chromosome.

**Output:** New chromosome.

**for**  $i = 2$  **to**  $n - 1$  **do**

**for**  $j = i + 1$  **to**  $n$  **do**

    If swapping cities  $\alpha_i$  and  $\alpha_j$  reduces the distance of the chromosome and does not violate distance constraint, then swap them

**end for**

**end for**

**Return** the new chromosome

ALGORITHM 7: Swap search algorithm.

18 instances, respectively. On average, GA-ADP, GA-SWP, GA-INS, and GA-INV have average improvement (%) as 7.75, 7.51, 7.13, and 5.08, respectively. It shows that the average improvement of GA-ADP is the largest, GA-SWP is the second largest, GA-INS is the third largest, and GA-INV shows the smallest average improvement. From these results, we can tell that GA-ADP is the best one, GA-SWP is the second best, GA-INS is the third best, and GA-INV is positioned in fourth position. Further, by looking at SD, we can say that results by GA-ADP are stable because its obtained solutions have lowest SD. Figure 8 shows the average improvements (%) that also signifies the appropriateness of the HGAs, especially GA-ADP and GA-SWP. Note that b17.2 means the instance br17 with 2 vehicles. So, for these asymmetric unrestricted instances GA-ADP is the best method and GA-SWP is the second best method. Regarding the computational time, almost all HGAs are taking same time. However, simple GA takes less time. We further can see in this table that a number of vehicles have significant

effect on the solution; i.e., as the number of vehicles increases, solution also increases.

From the above outcomes on the asymmetric unrestricted instances, we can see that HGAs have showed very good enhancements in the solutions over GA, and GA-ADP and GA are the best and worst algorithms, respectively. To confirm whether average solutions obtained by GA-ADP are statistically and significantly distinct from the average solutions found by other HGAs, we conducted Student's  $t$ -test applying the (14) below [27]. The  $t$ -test is utilized to measure not only improvement of an algorithm over another, but significant performance by the better algorithm.

$$t = \frac{\bar{X}_1 - \bar{X}_2}{\sqrt{(SD_1^2/n_1 - 1) + (SD_2^2/n_2 - 1)}}, \quad (14)$$

where  $\bar{X}_1$  is average of first sample,  $SD_1$  is standard deviation of first sample,  $\bar{X}_2$  is average of second sample,  $SD_2$  is

```

Input:  $n$ , MaxGen.
Output: BS and BT
 $G_0$  = Generate initial population using Algorithm 1
Evaluate ( $G_0$ )
BS = Find the best solution in this population
 $i = 0$ 
while ( $i \leq$  MaxGen) do
     $i = i + 1$ 
     $G_i$  = Population after selection using Algorithm 2
    for  $j = 1$  to  $P_s$  do
         $C_j$  = offspring chromosome using crossover Algorithm 3
         $C_j$  = mutated chromosome using mutation Algorithm 4
         $C_j$  = improved chromosome using a local search Algorithm 5, 6, or 7
    end for
     $G_i$  = New population
    Evaluate ( $G_i$ )
     $B_i$  = Find the best solution in this generation
    if ( $B_i <$  BS) then
        BS =  $B_i$ 
        BT = Best tour;
    else if (number of generation till last update  $>$   $0.10 * \text{MaxGen}$ ) then
        Apply immigration
    end if
end while
Print BS and BT
    
```

ALGORITHM 8: Hybrid genetic algorithm.

TABLE 5: Parameter settings for the GAs.

| Parameters                    | Values  |
|-------------------------------|---|
| $P_s$                         | 50  |
| $P_c$                         | 100%  |
| $P_{mut}$                     | 10%   |
| Termination condition         | For GA, 2000 generations<br>For HGAs, 200 generations |
| No. of runs for each instance | 20 times  |

TABLE 6: Description of different notations used in the tables that contain results.

| Notation | Description   |
|----------|---|
| INST     | Name of a TSPLIB instance   |
| Opt      | Optimal solution  |
| AS       | Average solution in 20 runs   |
| SD       | Standard deviation of obtained solutions  |
| AT       | Average computational time in seconds in 20 runs  |
| AI       | Average percentage of improvement of average solution obtained by a HGA over average solution obtained by simple GA |
| $Max_i$  | The maximum distance traveled by a vehicle among $m$ vehicles in a route  |

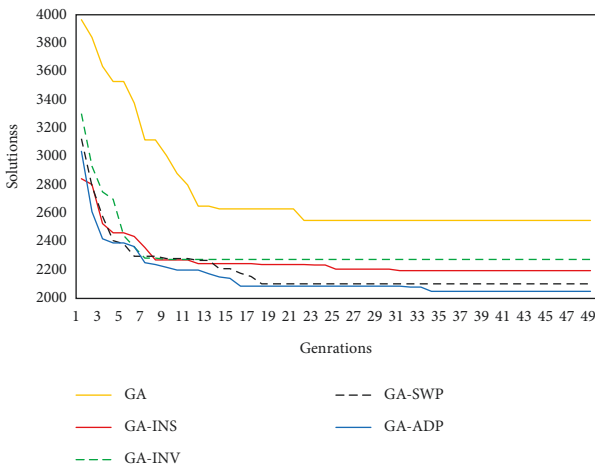


FIGURE 7: Solutions for ftv70 with 2 vehicles and infinite maximum distance constraint within only first 50 generations by GA and HGAs.

standard deviation of second sample,  $n_1$  is first sample size, and  $n_2$  is second sample size.

Here,  $\bar{X}_2$  and  $SD_2$  are found by GA-ADP, and  $\bar{X}_1$  and  $SD_1$  are found by remaining HGAs. Table 8 reports t-statistic values, which can be positive or negative. As the problem is a minimization problem, positive value implies that GA-ADP found better solution than its rival HGA found, and negative value implies that the rival HGA found better solution than GA-ADP found. We applied 95% confidence level ( $t_{0.05} = 1.73$ ), so if t-value is higher than 1.73, they have significant difference. So, if t-value is positive, then GA-ADP is significantly better; otherwise, its competitive HGA is better. If t-value is smaller than 1.73, then they have no statistical and significant differences. We further report the name of better algorithm.



TABLE 7: Results of unrestricted ADVRP on TSPLIB asymmetric instances.

| INST    | n | M   | D <sub>max</sub> | Max1     | GA     |         |          | GA-INS |       |         | GA-INV   |        |       | GA-SWP  |          |        | GA-ADP |         |          |        |       |
|---------|---|-----|------------------|----------|--------|---------|----------|--------|-------|---------|----------|--------|-------|---------|----------|--------|--------|---------|----------|--------|-------|
|         |   |     |                  |          | AS     | SD      | AT       | AS     | SD    | AT      | AS       | SD     | AT    | AS      | SD       | AT     | AS     | SD      | AT       | AS     | SD    |
| br17    | 2 | Inf | 39               | 39.00    | 0.00   | 0.02    | 39.00    | 0.00   | 0.00  | 0.00    | 0.00     | 0.00   | 39.00 | 0.00    | 0.00     | 39.00  | 0.00   | 0.00    | 39.00    | 0.00   | 0.00  |
|         | 3 | Inf | 31               | 42.00    | 0.00   | 0.00    | 42.00    | 0.00   | 0.00  | 0.00    | 0.00     | 0.00   | 42.00 | 0.00    | 0.00     | 42.00  | 0.00   | 0.00    | 42.00    | 0.00   | 0.00  |
| ftv33   | 2 | Inf | 1216             | 1381.78  | 13.07  | 0.17    | 1352.07  | 26.52  | 0.22  | 2.20    | 1356.70  | 23.92  | 0.25  | 1.85    | 1353.37  | 23.13  | 0.18   | 2.10    | 1346.72  | 24.07  | 0.11  |
|         | 3 | Inf | 1195             | 1400.20  | 15.48  | 0.18    | 1371.03  | 16.70  | 0.16  | 2.13    | 1365.07  | 20.14  | 0.22  | 2.57    | 1365.10  | 24.61  | 0.18   | 2.57    | 1356.47  | 21.52  | 0.12  |
| ftv35   | 2 | Inf | 1463             | 1563.25  | 23.68  | 0.26    | 1491.50  | 9.59   | 0.34  | 4.81    | 1499.03  | 16.53  | 0.34  | 4.28    | 1494.30  | 17.92  | 0.22   | 4.61    | 1492.60  | 6.25   | 0.16  |
|         | 3 | Inf | 1393             | 1558.00  | 14.31  | 0.23    | 1517.83  | 13.84  | 0.31  | 2.65    | 1524.93  | 12.88  | 0.31  | 2.17    | 1519.27  | 13.93  | 0.23   | 2.55    | 1517.10  | 11.21  | 0.18  |
| ftv38   | 2 | Inf | 1533             | 1637.23  | 27.51  | 0.66    | 1546.33  | 11.33  | 0.79  | 5.88    | 1574.97  | 19.42  | 0.42  | 3.95    | 1560.90  | 19.07  | 0.33   | 4.89    | 1547.32  | 4.71   | 0.21  |
|         | 3 | Inf | 886              | 1619.12  | 24.45  | 0.63    | 1576.57  | 8.64   | 0.61  | 2.70    | 1596.03  | 19.65  | 0.55  | 1.45    | 1592.10  | 20.60  | 0.39   | 1.70    | 1576.57  | 8.02   | 0.22  |
| p43     | 2 | Inf | 5617             | 5645.56  | 2.28   | 1.07    | 5634.83  | 3.04   | 1.21  | 0.19    | 5633.00  | 0.00   | 0.82  | 0.22    | 5633.07  | 2.61   | 0.56   | 0.22    | 5633.00  | 0.00   | 0.21  |
|         | 3 | Inf | 5613             | 5720.42  | 3.76   | 1.08    | 5688.63  | 4.23   | 1.19  | 0.56    | 5685.00  | 0.00   | 0.91  | 0.62    | 5685.17  | 3.55   | 0.61   | 0.62    | 5685.00  | 0.00   | 0.18  |
| ftv44   | 2 | Inf | 1609             | 1765.41  | 28.14  | 1.13    | 1650.67  | 20.87  | 1.13  | 6.95    | 1670.07  | 40.69  | 0.95  | 5.71    | 1646.10  | 32.45  | 0.85   | 7.25    | 1654.60  | 28.23  | 0.53  |
|         | 3 | Inf | 1547             | 1786.88  | 16.69  | 1.02    | 1680.88  | 21.09  | 1.19  | 6.31    | 1704.77  | 47.25  | 1.06  | 4.82    | 1685.40  | 31.95  | 0.91   | 6.02    | 1678.17  | 20.15  | 0.56  |
| ftv47   | 2 | Inf | 1311             | 2062.06  | 104.55 | 1.13    | 1876.53  | 22.21  | 1.49  | 9.89    | 1890.23  | 47.82  | 1.18  | 9.09    | 1872.00  | 34.85  | 1.05   | 10.15   | 1858.17  | 31.16  | 0.74  |
|         | 3 | Inf | 1672             | 2169.50  | 68.78  | 1.12    | 1942.43  | 27.10  | 1.26  | 11.69   | 1967.57  | 56.26  | 1.22  | 10.26   | 1943.37  | 26.29  | 1.15   | 11.64   | 1933.23  | 27.42  | 0.84  |
| ry48p   | 2 | Inf | 14255            | 16263.01 | 188.67 | 1.36    | 14923.97 | 125.70 | 1.96  | 8.97    | 14828.96 | 66.17  | 1.28  | 9.67    | 14972.56 | 136.60 | 1.31   | 8.62    | 14835.00 | 51.33  | 1.41  |
|         | 3 | Inf | 14119            | 16326.01 | 202.59 | 1.27    | 15181.33 | 99.35  | 2.03  | 7.54    | 15087.63 | 56.77  | 2.01  | 8.21    | 15226.03 | 118.73 | 1.42   | 7.22    | 15083.16 | 47.57  | 1.74  |
| ft53    | 2 | Inf | 4461             | 8380.06  | 242.42 | 2.07    | 7198.50  | 141.50 | 2.80  | 16.41   | 7374.43  | 192.59 | 2.03  | 13.64   | 7203.68  | 122.46 | 1.93   | 16.33   | 7128.80  | 160.23 | 1.77  |
|         | 3 | Inf | 3452             | 8307.16  | 180.16 | 2.13    | 7333.50  | 103.49 | 2.98  | 13.28   | 7661.60  | 217.87 | 2.12  | 8.43    | 7390.27  | 98.26  | 2.06   | 12.41   | 7305.03  | 135.92 | 1.82  |
| ftv55   | 2 | Inf | 1053             | 1861.16  | 43.79  | 2.28    | 1719.70  | 23.68  | 2.36  | 8.23    | 1748.90  | 31.06  | 2.23  | 6.42    | 1716.57  | 29.70  | 2.09   | 8.42    | 1697.23  | 22.66  | 1.86  |
|         | 3 | Inf | 947              | 1919.06  | 40.38  | 2.33    | 1789.63  | 30.09  | 2.71  | 7.23    | 1827.70  | 28.15  | 2.17  | 5.00    | 1781.30  | 33.32  | 2.16   | 7.73    | 1774.03  | 21.02  | 1.98  |
| ftv64   | 2 | Inf | 1786             | 2131.36  | 32.85  | 3.47    | 1903.07  | 28.84  | 3.92  | 12.00   | 1957.00  | 48.76  | 3.01  | 8.91    | 1883.33  | 41.35  | 2.73   | 13.17   | 1884.13  | 29.65  | 2.72  |
|         | 3 | Inf | 1679             | 2090.06  | 44.66  | 3.33    | 1917.40  | 26.45  | 3.85  | 9.00    | 1971.60  | 53.26  | 3.14  | 6.01    | 1916.17  | 20.67  | 2.94   | 9.07    | 1909.27  | 29.17  | 2.91  |
| ft70    | 2 | Inf | 38585            | 41879.88 | 241.22 | 4.03    | 39942.93 | 187.13 | 4.17  | 4.85    | 40898.37 | 229.28 | 3.96  | 2.40    | 39751.03 | 305.59 | 3.01   | 5.36    | 39762.73 | 250.41 | 3.01  |
|         | 3 | Inf | 22295            | 42709.01 | 270.83 | 4.16    | 40758.00 | 264.21 | 4.11  | 4.79    | 41774.53 | 189.39 | 3.80  | 2.24    | 40696.80 | 294.00 | 3.35   | 4.94    | 40701.40 | 235.31 | 3.02  |
| ftv70   | 2 | Inf | 1938             | 2187.36  | 39.83  | 4.53    | 2002.83  | 38.13  | 4.59  | 9.21    | 2131.10  | 45.18  | 4.03  | 2.64    | 2007.77  | 43.45  | 3.75   | 8.94    | 2022.33  | 24.79  | 3.04  |
|         | 3 | Inf | 1888             | 2240.89  | 38.73  | 4.78    | 2073.70  | 37.76  | 4.96  | 8.06    | 2165.27  | 34.41  | 4.16  | 3.49    | 2039.90  | 43.05  | 3.90   | 9.85    | 2047.93  | 25.10  | 3.13  |
| kro124p | 2 | Inf | 27336            | 43753.76 | 746.76 | 5.43    | 39387.77 | 603.29 | 7.27  | 11.08   | 40520.10 | 470.44 | 6.58  | 7.98    | 38541.40 | 321.72 | 5.28   | 13.52   | 38427.57 | 310.33 | 5.02  |
|         | 3 | Inf | 22203            | 44607.76 | 528.36 | 5.44    | 39329.70 | 442.91 | 8.16  | 13.42   | 41207.70 | 359.10 | 6.84  | 8.25    | 39038.83 | 508.58 | 6.53   | 14.27   | 39073.87 | 425.54 | 5.21  |
| ftv170  | 2 | Inf | 2900             | 3611.78  | 66.87  | 14.81   | 3211.37  | 90.66  | 32.88 | 12.47   | 3379.13  | 82.69  | 31.15 | 6.88    | 3103.03  | 57.46  | 25.12  | 16.40   | 3157.23  | 76.97  | 29.66 |
|         | 3 | Inf | 1877             | 3569.32  | 44.16  | 14.37   | 3206.30  | 66.34  | 39.37 | 11.32   | 3391.97  | 88.52  | 39.08 | 5.23    | 3115.27  | 77.41  | 31.05  | 14.57   | 3140.53  | 80.42  | 31.63 |
| Average |   |     | 9007.60          | 109.83   | 3.30   | 8309.67 | 83.16    | 9.26   | 7.13  | 8515.81 | 83.27    | 8.46   | 5.08  | 8260.50 | 83.44    | 9.14   | 7.51   | 8243.67 | 70.31    | 8.78   |       |

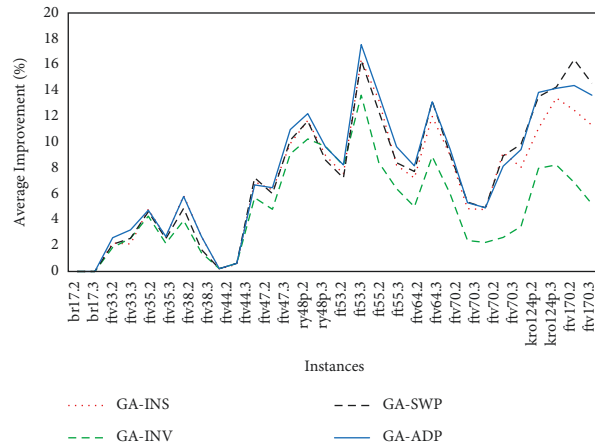


FIGURE 8: Average improvement (%) of solution by HGAs over solution by GA for TSPLIB asymmetric instances.

TABLE 8: The  $t$ -values against GA-ADP and the result about HGAs that found significantly better solutions for the unrestricted ADVRP.

| INST    | GA-INS | GA-INV | GA-SWP | Instance       | GA-INS | GA-INV | GA-SWP |
|---------|--------|--------|--------|----------------|--------|--------|--------|
| br17.2  | —      | —      | —      | ry48p.3 better | 6.24   | 0.42   | 7.82   |
| Better  | —      | —      | —      |                | GA-ADP | —      | —      |
| br17.3  | —      | —      | —      | ft53.2         | 2.28   | 6.86   | 2.60   |
| Better  | —      | —      | —      | Better         | GA-ADP | GA-ADP | GA-ADP |
| ftv33.2 | 1.05   | 2.06   | 1.39   | ft53.3         | 1.17   | 9.72   | 3.56   |
| Better  | —      | GA-ADP | —      | Better         | —      | GA-ADP | GA-ADP |
| ftv33.3 | 3.74   | 2.04   | 1.85   | ftv55.2        | 4.80   | 9.41   | 3.62   |
| Better  | GA-ADP | GA-ADP | GA-ADP | Better         | GA-ADP | GA-ADP | GA-ADP |
| ftv35.2 | -0.67  | 2.55   | 0.63   | ftv55.3        | 2.98   | 10.69  | 1.29   |
| Better  | —      | GA-ADP | —      | Better         | GA-ADP | GA-ADP | —      |
| ftv35.3 | 0.29   | 3.21   | 0.85   | ftv64.2        | 3.21   | 8.94   | -0.11  |
| Better  | —      | GA-ADP | —      | Better         | GA-ADP | GA-ADP | —      |
| ftv38.2 | -0.56  | 9.69   | 4.84   | ftv64.3        | 1.45   | 7.19   | 1.35   |
| Better  | —      | GA-ADP | GA-ADP | Better         | —      | GA-ADP | —      |
| ftv38.3 | 0.00   | 6.42   | 4.92   | ft70.2         | 4.04   | 23.41  | -0.21  |
| Better  | —      | GA-ADP | GA-ADP | Better         | GA-ADP | GA-ADP | —      |
| p43.2   | 4.21   | —      | 0.19   | ft70.3         | 1.12   | 24.87  | -0.09  |
| Better  | GA-ADP | —      | —      | Better         | —      | GA-ADP | —      |
| p43.3   | 6.01   | —      | 0.34   | ftv70.2        | -3.00  | 14.77  | -2.04  |
| Better  | GA-ADP | —      | —      | Better         | GA-INS | GA-ADP | GA-SWP |
| ftv44.2 | -0.78  | 2.19   | -1.38  | ftv70.3        | 3.98   | 19.28  | -1.13  |
| Better  | —      | GA-ADP | —      | Better         | GA-ADP | GA-ADP | —      |
| ftv44.3 | 0.65   | 3.62   | 1.34   | kro124p.2      | 9.91   | 25.99  | 1.78   |
| Better  | —      | GA-ADP | —      | Better         | GA-ADP | GA-ADP | GA-ADP |
| ftv47.2 | 3.36   | 3.93   | 2.07   | kro124p.3      | 2.92   | 26.83  | -0.37  |
| Better  | GA-ADP | GA-ADP | GA-ADP | Better         | GA-ADP | GA-ADP | —      |
| ftv47.3 | 1.67   | 3.84   | 1.87   | ftv170.2       | 3.19   | 13.75  | -3.95  |
| Better  | —      | GA-ADP | GA-ADP | Better         | GA-ADP | GA-ADP | GA-SWP |
| ry48p.2 | 4.59   | -0.50  | 6.60   | ftv170.3       | 4.42   | 14.72  | -1.58  |
| Better  | GA-ADP | —      | GA-ADP | Better         | GA-ADP | GA-ADP | —      |

The algorithms GA-ADP and GA-INS have no statistical and significant differences on thirteen instances. On the sixteen instances, GA-ADP is better than GA-INS, and only on ftv70.2, GA-INS is better than GA-ADP. On six instances, GA-ADP and GA-INV have no statistical and significant differences. On the remaining twenty-four instances, GA-ADP is better than GA-INV. On eighteen instances, GA-ADP and GA-SWP have no statistical and significant

differences. On two instances—ftv70.2 and ftv170.2, GA-SWP is better than GA-ADP, and on the other ten instances, GA-ADP is better than GA-SWP. From these experimental results, we can tell that GA-ADP is statistically significant and is the best among the HGAs for unrestricted ADVRP instances.

Further, we conducted  $t$ -test to check whether average solutions obtained by GA-SWP are statistically and

TABLE 9: Results of restricted ADVRP where  $D_{max} = 0.9 * Max_1$  is used.

| INST    | n | m   | $D_{max}$ | Max1     | GA     |         |          | GA-INS |       |         | GA-INV   |        |       | GA-SWP  |          |        | GA-ADP |         |          |        |       |       |
|---------|---|-----|-----------|----------|--------|---------|----------|--------|-------|---------|----------|--------|-------|---------|----------|--------|--------|---------|----------|--------|-------|-------|
|         |   |     |           |          | AS     | SD      | AT       | AS     | SD    | AT      | AI       | AS     | SD    | AT      | AI       | AS     | SD     | AT      | AI       | AS     | SD    | AT    |
| br17    | 2 | Inf | 39        | 39.00    | 0.00   | 0.02    | 39.00    | 0.00   | 0.00  | 0.00    | 0.00     | 0.00   | 0.00  | 39.00   | 0.00     | 0.00   | 0.00   | 39.00   | 0.00     | 0.00   | 0.00  | 0.00  |
|         | 3 | Inf | 31        | 42.00    | 0.00   | 0.00    | 42.00    | 0.00   | 0.00  | 0.00    | 0.00     | 0.00   | 0.00  | 42.00   | 0.00     | 0.00   | 0.00   | 42.00   | 0.00     | 0.00   | 0.00  | 0.00  |
| ftw33   | 2 | Inf | 1216      | 1381.78  | 13.07  | 0.17    | 1352.07  | 26.52  | 0.22  | 2.20    | 1356.70  | 23.92  | 0.25  | 1.85    | 1353.37  | 23.13  | 0.18   | 2.10    | 1346.72  | 24.07  | 0.11  | 2.60  |
|         | 3 | Inf | 1195      | 1400.20  | 15.48  | 0.18    | 1371.03  | 16.70  | 0.16  | 2.13    | 1365.07  | 20.14  | 0.22  | 2.57    | 1365.10  | 24.61  | 0.18   | 2.57    | 1356.47  | 21.52  | 0.12  | 3.22  |
| ftw35   | 2 | Inf | 1463      | 1563.25  | 23.68  | 0.26    | 1491.50  | 9.59   | 0.34  | 4.81    | 1499.03  | 16.53  | 0.34  | 4.28    | 1494.30  | 17.92  | 0.22   | 4.61    | 1492.60  | 6.25   | 0.16  | 4.73  |
|         | 3 | Inf | 1393      | 1558.00  | 14.31  | 0.23    | 1517.83  | 13.84  | 0.31  | 2.65    | 1524.93  | 12.88  | 0.31  | 2.17    | 1519.27  | 13.93  | 0.23   | 2.55    | 1517.10  | 11.21  | 0.18  | 2.70  |
| ftw38   | 2 | Inf | 1533      | 1637.23  | 27.51  | 0.66    | 1546.33  | 11.33  | 0.79  | 5.88    | 1574.97  | 19.42  | 0.42  | 3.95    | 1560.90  | 19.07  | 0.33   | 4.89    | 1547.32  | 4.71   | 0.21  | 5.81  |
|         | 3 | Inf | 886       | 1619.12  | 24.45  | 0.63    | 1576.57  | 8.64   | 0.61  | 2.70    | 1596.03  | 19.65  | 0.55  | 1.45    | 1592.10  | 20.60  | 0.39   | 1.70    | 1576.57  | 8.02   | 0.22  | 2.70  |
| p43     | 2 | Inf | 5617      | 5645.56  | 2.28   | 1.07    | 5634.83  | 3.04   | 1.21  | 0.19    | 5633.00  | 0.00   | 0.82  | 0.22    | 5633.07  | 2.61   | 0.56   | 0.22    | 5633.00  | 0.00   | 0.21  | 0.22  |
|         | 3 | Inf | 5613      | 5720.42  | 3.76   | 1.08    | 5688.63  | 4.23   | 1.19  | 0.56    | 5685.00  | 0.00   | 0.91  | 0.62    | 5685.17  | 3.55   | 0.61   | 0.62    | 5685.00  | 0.00   | 0.18  | 0.62  |
| ftw44   | 2 | Inf | 1609      | 1765.41  | 28.14  | 1.13    | 1650.67  | 20.87  | 1.13  | 6.95    | 1670.07  | 40.69  | 0.95  | 5.71    | 1646.10  | 32.45  | 0.85   | 7.25    | 1654.60  | 28.23  | 0.53  | 6.70  |
|         | 3 | Inf | 1547      | 1786.88  | 16.69  | 1.02    | 1680.88  | 21.09  | 1.19  | 6.31    | 1704.77  | 47.25  | 1.06  | 4.82    | 1685.40  | 31.95  | 0.91   | 6.02    | 1678.17  | 20.15  | 0.56  | 6.48  |
| ftw47   | 2 | Inf | 1311      | 2062.06  | 104.55 | 1.13    | 1876.53  | 22.21  | 1.49  | 9.89    | 1890.23  | 47.82  | 1.18  | 9.09    | 1872.00  | 34.85  | 1.05   | 10.15   | 1858.17  | 31.16  | 0.74  | 10.97 |
|         | 3 | Inf | 1672      | 2169.50  | 68.78  | 1.12    | 1942.43  | 27.10  | 1.26  | 11.69   | 1967.57  | 56.26  | 1.22  | 10.26   | 1943.37  | 26.29  | 1.15   | 11.64   | 1933.23  | 27.42  | 0.84  | 12.22 |
| ry48p   | 2 | Inf | 14255     | 16263.01 | 188.67 | 1.36    | 14923.97 | 125.70 | 1.96  | 8.97    | 14828.96 | 66.17  | 1.28  | 9.67    | 14972.56 | 136.60 | 1.31   | 8.62    | 14835.00 | 51.33  | 1.41  | 9.63  |
|         | 3 | Inf | 14119     | 16326.01 | 202.59 | 1.27    | 15181.33 | 99.35  | 2.03  | 7.54    | 15087.63 | 56.77  | 2.01  | 8.21    | 15226.03 | 118.73 | 1.42   | 7.22    | 15083.16 | 47.57  | 1.74  | 8.24  |
| ft53    | 2 | Inf | 4461      | 8380.06  | 242.42 | 2.07    | 7198.50  | 141.50 | 2.80  | 16.41   | 7374.43  | 192.59 | 2.03  | 13.64   | 7203.68  | 122.46 | 1.93   | 16.33   | 7128.80  | 160.23 | 1.77  | 17.55 |
|         | 3 | Inf | 3452      | 8307.16  | 180.16 | 2.13    | 7333.50  | 103.49 | 2.98  | 13.28   | 7661.60  | 217.87 | 2.12  | 8.43    | 7390.27  | 98.26  | 2.06   | 12.41   | 7305.03  | 135.92 | 1.82  | 13.72 |
| ftw55   | 2 | Inf | 1053      | 1861.16  | 43.79  | 2.28    | 1719.70  | 23.68  | 2.36  | 8.23    | 1748.90  | 31.06  | 2.23  | 6.42    | 1716.57  | 29.70  | 2.09   | 8.42    | 1697.23  | 22.66  | 1.86  | 9.66  |
|         | 3 | Inf | 947       | 1919.06  | 40.38  | 2.33    | 1789.63  | 30.09  | 2.71  | 7.23    | 1827.70  | 28.15  | 2.17  | 5.00    | 1781.30  | 33.32  | 2.16   | 7.73    | 1774.03  | 21.02  | 1.98  | 8.18  |
| ftw64   | 2 | Inf | 1786      | 2131.36  | 32.85  | 3.47    | 1903.07  | 28.84  | 3.92  | 12.00   | 1957.00  | 48.76  | 3.01  | 8.91    | 1883.33  | 41.35  | 2.73   | 13.17   | 1884.13  | 29.65  | 2.72  | 13.12 |
|         | 3 | Inf | 1679      | 2090.06  | 44.66  | 3.33    | 1917.40  | 26.45  | 3.85  | 9.00    | 1971.60  | 53.26  | 3.14  | 6.01    | 1916.17  | 20.67  | 2.94   | 9.07    | 1909.27  | 29.17  | 2.91  | 9.47  |
| ft70    | 2 | Inf | 38585     | 41879.88 | 241.22 | 4.03    | 39942.93 | 187.13 | 4.17  | 4.85    | 40898.37 | 229.28 | 3.96  | 2.40    | 39751.03 | 305.59 | 3.01   | 5.36    | 39762.73 | 250.41 | 3.01  | 5.32  |
|         | 3 | Inf | 22295     | 42709.01 | 270.83 | 4.16    | 40758.00 | 264.21 | 4.11  | 4.79    | 41774.53 | 189.39 | 3.80  | 2.24    | 40696.80 | 294.00 | 3.35   | 4.94    | 40701.40 | 235.31 | 3.02  | 4.93  |
| ftw70   | 2 | Inf | 1938      | 2187.36  | 39.83  | 4.53    | 2002.83  | 38.13  | 4.59  | 9.21    | 2131.10  | 45.18  | 4.03  | 2.64    | 2007.77  | 43.45  | 3.75   | 8.94    | 2022.33  | 24.79  | 3.04  | 8.16  |
|         | 3 | Inf | 1888      | 2240.89  | 38.73  | 4.78    | 2073.70  | 37.76  | 4.96  | 8.06    | 2165.27  | 34.41  | 4.16  | 3.49    | 2039.90  | 43.05  | 3.90   | 9.85    | 2047.93  | 25.10  | 3.13  | 9.42  |
| kro124p | 2 | Inf | 27336     | 43753.76 | 746.76 | 5.43    | 39387.77 | 603.29 | 7.27  | 11.08   | 40520.10 | 470.44 | 6.58  | 7.98    | 38541.40 | 321.72 | 5.28   | 13.52   | 38427.57 | 310.33 | 5.02  | 13.86 |
|         | 3 | Inf | 22203     | 44607.76 | 528.36 | 5.44    | 39329.70 | 442.91 | 8.16  | 13.42   | 41207.70 | 359.10 | 6.84  | 8.25    | 39038.83 | 508.58 | 6.53   | 14.27   | 39073.87 | 425.54 | 5.21  | 14.16 |
| ftw170  | 2 | Inf | 2900      | 3611.78  | 66.87  | 14.81   | 3211.37  | 90.66  | 32.88 | 12.47   | 3379.13  | 82.69  | 31.15 | 6.88    | 3103.03  | 57.46  | 25.12  | 16.40   | 3157.23  | 76.97  | 29.66 | 14.40 |
|         | 3 | Inf | 1877      | 3569.32  | 44.16  | 14.37   | 3206.30  | 66.34  | 39.37 | 11.32   | 3391.97  | 88.52  | 39.08 | 5.23    | 3115.27  | 77.41  | 31.05  | 14.57   | 3140.53  | 80.42  | 31.63 | 13.65 |
| Average |   |     | 9007.60   | 109.83   | 3.30   | 8309.67 | 83.16    | 9.26   | 7.13  | 8515.81 | 83.27    | 8.46   | 5.08  | 8260.50 | 83.44    | 9.14   | 7.51   | 8243.67 | 70.31    | 8.78   | 7.75  |       |

significantly distinct from the average solutions found by GA-INS. We saw (not reported here) that for 25 instances there is no statistical difference between them, and for 5 instances, GA-SWP is better than GA-INS. So, GA-SWP is the second best.

Table 9 reports the results for restricted ADVRP instances where  $D_{\max} = 0.9 * \text{Max}_1$  is used to find  $\text{Max}_2$ . From this table, it is seen that the GA could find best average solutions for the instance br17 with both 2 and 3 vehicles. The algorithms GA-INS, GA-INV, GA-SWP, and GA-ADP could find best average solutions for 4, 2, 6, and 22 instances, respectively. On average, GA-ADP, GA-SWP, GA-INS, and GA-INV have average improvement (%) as 10.97, 9.97, 9.72, and 6.59, respectively. It shows that the average improvement of GA-ADP is the largest, GA-SWP is the second largest, GA-INS is the third largest, and GA-INV shows the smallest average improvement. From these results, we can tell that GA-ADP is the best one, GA-SWP is the second best, GA-INS is the third best, and GA-INV is positioned in fourth position. Further, by looking at SD, we can say that results by GA-ADP are stable because its obtained solutions have lower SD. It is to be noted that no algorithm could solve the instance p43 with both 2 and 3 vehicles, so their results are not stated in Table 9. Figure 9 shows the average improvements (%) that also signifies the appropriateness of the HGAs, especially GA-ADP and GA-SWP. So, for these restricted ADVRP instances GA-ADP is the best algorithm and GA-SWP is the second best algorithm. Regarding the computational time, almost all HGAs are taking same time. However, simple GA takes less time. We further can see in this table that a number of vehicles have significant effect on the solution; i.e., almost for all instances, as the number of vehicles increases, solution also increases.

We see from the experiment that HGAs have fantastic improvements in the solution over GA for the restricted ADVRP instances. Among the algorithms, GA-ADP is the best and GA is the worst. To confirm whether average solutions obtained by GA-ADP are statistically and significantly distinct from the average solutions found by other HGAs, Student's *t*-test is performed, and the results are shown in Table 10. There is no statistical and significant difference between GA-INS and GA-ADP on twelve instances. On the remaining sixteen instances, GA-ADP is better than GA-INS. There is no statistical and significant difference between GA-INV and GA-ADP on five instances. On the remaining twenty-three instances, GA-ADP is better than GA-INV. There is no statistical and significant difference between GA-SWP and GA-ADP on ten instances. On the seventeen instances, GA-ADP is better than GA-SWP. On only the instance ftv38 with 3 vehicles, GA-SWP is better than GA-ADP. From this experiment, we can say that GA-ADP is statistically significant and is the best among the HGAs for the restricted ADVRP instances also.

Further, we conducted *t*-test to check whether average solutions obtained by GA-SWP are statistically and significantly distinct from the average solutions found by GA-INS. We saw (not reported here) that for 20 instances there is no statistical difference between them, for 3 instances GA-INS is better than GA-SWP, and for 5 instances GA-SWP is

better than GA-INS. So, GA-SWP is the second best and GA-INS is the third best one.

We further report the results in Table 11 for restricted ADVRP instances where  $D_{\max} = 0.9 * \text{Max}_2$  is used to find  $\text{Max}_3$ . It is seen that no algorithm could solve the instances p43, ftv53, and ftv170 with both 2 and 3 vehicles; ftv35, ftv38, ftv44, ftv47, ftv55, ftv70, and kro124p with 2 vehicles; and br17 with 3 vehicles. It seems that these problem instances are more complex. So, we did not report them, and we reported the results on 17 instances only.

Among the reported instances, GA could not solve kro124p with 2 vehicles; GA-INV could not solve ftv38 with 3 vehicles, and ftv64 and kro124p with 2 vehicles; however, the algorithms GA-INS, GA-SWP, and GA-ADP could solve these instances. It is noticed that the GA could find best average solutions for the instance br17 with 2 vehicles only. The algorithms GA-INS, GA-INV, GA-SWP, and GA-ADP could find best average solutions for 2, 1, 5, and 12 instances, respectively.

On average, GA-ADP, GA-INS, GA-SWP, and GA-INV have average improvement (%) as 10.77, 9.90, 8.98, and 6.17, respectively. It shows that the average improvement of GA-ADP is the largest, GA-INS is the second largest, GA-SWP is the third largest, and GA-INV shows the smallest average improvement. From these results, we can tell that for these restricted ADVRP instances GA-ADP is the best one, GA-INS is the second best, GA-SWP is the third best, and GA-INV is positioned in fourth position. Further, by looking at SD, we can say that results by GA-ADP are stable because its obtained solutions have lowest SD.

We further can see in this table that a number of vehicles have significant effect on the solution; i.e., almost for all instances, as the number of vehicles increases, solution also increases. It is also observed that as the distance-constrained becomes tight finding feasible solution becomes difficult. Regarding the computational time, almost all HGAs are taking same time. However, simple GA takes less time.

To prove whether average solutions found by GA-ADP are statistically and significantly different from the average solutions found by remaining HGAs, we conducted Student's *t*-test and reported the results in Table 12. There is no statistical and significant difference between GA-INS and GA-ADP on five instances. On one instance, GA-INS is better, and on the other ten instances GA-ADP is better. There is no statistical and significant difference between GA-INV and GA-ADP on four instances. On the remaining twelve instances, GA-ADP is better. There is no statistical and significant difference between GA-SWP and GA-ADP on three instances, on one instance GA-SWP is better, and on the other twelve instances GA-ADP is better. From this experiment, we can say that GA-ADP is the best for the restricted ADVRP instances also. However, GA-INS and GA-SWP are still competing for 2nd rank. We further perform Student's *t*-test between GA-SWP and GA-INS but found them equivalent. From all above experiments, we can assume that GA-ADP is the best, GA-SWP and GA-INS are the second best, and GA is the worst.

We further report a performance comparison of GA-ADP against HVT algorithm [9] on some asymmetric CVRP

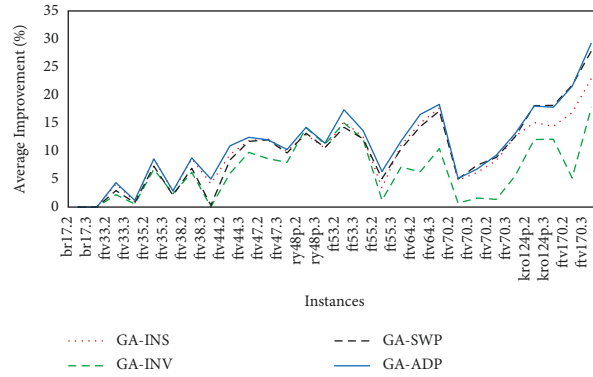


FIGURE 9: Average improvement (%) of solution by HGAs over solution by GA for TSPLIB asymmetric instances.

TABLE 10: The  $t$ -values against GA-ADP and the result about HGAs that found significantly better solutions for the restricted ADVRP.

| INST    | GA-INS | GA-INV | GA-SWP | Instance       | GA-INS      | GA-INV      | GA-SWP      |
|---------|--------|--------|--------|----------------|-------------|-------------|-------------|
| br17.2  | —      | —      | —      | ftv53.2 better | 2.86 GA-ADP | 2.99 GA-ADP | 4.01 GA-ADP |
| Better  | —      | —      | —      |                |             |             |             |
| br17.3  | —      | —      | —      | ftv53.3 better | 1.58        | 2.07 GA-ADP | 2.06 GA-ADP |
| Better  | —      | —      | —      |                |             |             |             |
| ftv33.2 | 1.13   | 7.64   | 4.80   | ftv55.2        | 10.56       | 12.43       | 3.33        |
| Better  | —      | GA-ADP | GA-ADP | Better         | GA-ADP      | GA-ADP      | GA-ADP      |
| ftv33.3 | 1.20   | 5.58   | 5.49   | ftv55.3        | 1.68        | 12.97       | 6.16        |
| Better  | —      | GA-ADP | GA-ADP | Better         | —           | GA-ADP      | GA-ADP      |
| ftv35.2 | -0.26  | 5.88   | 2.80   | ftv64.2        | 4.82        | 13.55       | 5.44        |
| Better  | —      | GA-ADP | GA-ADP | Better         | GA-ADP      | GA-ADP      | GA-ADP      |
| ftv35.3 | 0.98   | 1.65   | 1.85   | ftv64.3        | 3.48        | 21.04       | 5.44        |
| Better  | —      | —      | GA-ADP | Better         | GA-ADP      | GA-ADP      | GA-ADP      |
| ftv38.2 | 0.84   | 11.39  | 7.68   | ftv70.2        | 1.75        | 27.89       | 0.58        |
| Better  | —      | GA-ADP | GA-ADP | Better         | GA-ADP      | GA-ADP      | —           |
| ftv38.3 | 2.00   | 5.01   | 11.78  | ftv70.3        | 5.06        | 29.94       | -2.30       |
| Better  | GA-ADP | GA-ADP | GA-ADP | Better         | GA-ADP      | GA-ADP      | GA-SWP      |
| ftv44.2 | 4.50   | 7.19   | 4.95   | ftv70.2        | 1.93        | 18.94       | 0.75        |
| Better  | GA-ADP | GA-ADP | GA-ADP | Better         | GA-ADP      | GA-ADP      | —           |
| ftv44.3 | 2.90   | 5.38   | 4.40   | ftv70.3        | 1.07        | 19.95       | 1.53        |
| Better  | GA-ADP | GA-ADP | GA-ADP | Better         | —           | GA-ADP      | —           |
| ftv47.2 | -0.81  | 3.75   | -0.11  | kro124p.2      | 6.02        | 15.31       | -0.05       |
| Better  | —      | GA-ADP | —      | Better         | GA-ADP      | GA-ADP      | —           |
| ftv47.3 | 1.65   | 6.00   | 1.58   | kro124p.3      | 7.01        | 17.21       | -0.98       |
| Better  | —      | GA-ADP | —      | Better         | GA-ADP      | GA-ADP      | —           |
| ry48p.2 | 6.13   | 0.99   | 5.72   | ftv170.2       | 9.88        | 16.42       | -0.31       |
| Better  | GA-ADP | —      | GA-ADP | Better         | GA-ADP      | GA-ADP      | —           |
| ry48p.3 | 4.11   | 1.34   | 5.19   | ftv170.3       | 5.90        | 9.02        | 1.75        |
| Better  | GA-ADP | —      | GA-ADP | Better         | GA-ADP      | GA-ADP      | GA-ADP      |

(ACVRP) instances [28] of sizes from 34 to 71. As in [9], we run each instance 10 times. Further, we increase in the maximum generations to 250 generations for each run. The results are reported in Table 13. The percentage of gap (Gap) is calculated by

$$\text{Gap} = \frac{100(\text{BS} - \text{Opt})}{\text{Opt}}. \quad (15)$$

Looking at the best solutions, HVT could not find optimal solution for the A065-03f, whereas our proposed GA-ADP could find optimal solutions of all instances at least once in ten runs. So, in terms of best solution, our proposed

algorithm GA-ADP is better than HVT. Looking at the average solutions, for the first four instances, both algorithms could obtain same average solutions, for the remaining three instances—A048-03f, A065-03f, and A071-03f, our GA-ADP is better than HVT, whereas only for the instance A056-03f, HVT is better than GA-ADP. Overall, our proposed algorithm GA-ADP is better than HVT. Regarding the computational time, HVT was executed on Intel Pentium core i7 duo 2.10 GHz CPU with 8 GB RAM, whereas our algorithm is executed on Intel Pentium core i7 1.30 GHz CPU with 8 GB RAM. It shows that their machine is faster than our machine. Looking at the computer specifications of both machines and computational times,

TABLE 11: Results of restricted ADVRP where  $D_{\max} = 0.9 * \text{Max}_2$  is used.

| INST    | n   | M     | $D_{\max}$ | Max3    | GA       |        |          | GA-INS   |        |      | GA-INV  |          |        | GA-SWP |          |          | GA-ADP  |          |        |       |
|---------|-----|-------|------------|---------|----------|--------|----------|----------|--------|------|---------|----------|--------|--------|----------|----------|---------|----------|--------|-------|
|         |     |       |            |         | AS       | SD     | AT       | AS       | SD     | AT   | AS      | SD       | AT     | AS     | SD       | AT       | AS      | SD       | AT     | AS    |
| br17    | 17  | 2     | 28         | 28      | 46.00    | 0.00   | 0.00     | 0.00     | 0.00   | 0.00 | 0.00    | 46.00    | 0.00   | 0.00   | 46.00    | 0.00     | 0.00    | 46.00    | 0.00   | 0.00  |
| ftv33   | 34  | 2     | 790        | 786     | 1478.23  | 23.02  | 0.24     | 1408.43  | 19.41  | 0.12 | 4.96    | 1426.78  | 17.18  | 0.37   | 3.61     | 1436.07  | 22.15   | 1405.73  | 19.21  | 0.06  |
| ftv35   | 36  | 3     | 790        | 748     | 1484.30  | 26.33  | 0.34     | 1393.30  | 14.25  | 0.15 | 6.53    | 1409.30  | 43.93  | 0.26   | 5.32     | 1403.23  | 22.79   | 1388.00  | 0.00   | 0.10  |
| ftv38   | 39  | 3     | 798        | 780     | 1769.78  | 61.73  | 0.24     | 1625.03  | 29.24  | 0.35 | 8.91    | 1703.43  | 149.72 | 0.32   | 3.90     | 1681.20  | 76.93   | 1617.07  | 70.57  | 0.21  |
| ftv44   | 45  | 3     | 716        | 671     | 1853.23  | 73.12  | 0.35     | 1693.50  | 26.58  | 0.26 | 9.43    | —        | —      | —      | 1778.37  | 42.81    | 1687.27 | 77.94    | 0.34   |       |
| ftv47   | 48  | 3     | 823        | 657     | 2049.86  | 78.32  | 1.03     | 1828.80  | 72.03  | 0.34 | 12.09   | 1987.73  | 95.21  | 0.34   | 3.13     | 1890.27  | 65.21   | 1860.50  | 59.94  | 0.65  |
| ry48p   | 48  | 2     | 11226      | 10872   | 17090.50 | 288.57 | 1.03     | 15048.43 | 115.14 | 1.39 | 13.57   | 14946.30 | 119.80 | 1.27   | 14.35    | 15124.60 | 193.42  | 14945.57 | 112.57 | 1.54  |
| ftv55   | 56  | 3     | 766        | 736     | 2011.18  | 81.42  | 1.39     | 1820.17  | 20.66  | 1.80 | 10.49   | 1880.20  | 43.50  | 1.81   | 6.97     | 1822.70  | 44.53   | 1798.93  | 32.57  | 2.13  |
| ftv64   | 65  | 3     | 955        | 705     | 2318.26  | 92.56  | 2.05     | 2073.07  | 45.03  | 1.62 | 11.83   | 2157.27  | 75.26  | 2.31   | 7.46     | 2010.07  | 64.82   | 1939.73  | 36.53  | 2.53  |
| ftv70   | 70  | 3     | 18059      | 16232   | 44730.41 | 304.83 | 3.63     | 41931.23 | 162.88 | 2.56 | 6.68    | 43881.17 | 410.78 | 4.54   | 1.94     | 42129.47 | 405.29  | 41776.10 | 421.49 | 5.17  |
| ftv70   | 71  | 3     | 1467       | 1067    | 2320.18  | 25.16  | 3.57     | 2166.03  | 62.12  | 2.98 | 7.12    | 2297.43  | 44.00  | 4.44   | 0.99     | 2076.40  | 39.24   | 2082.90  | 31.18  | 4.33  |
| kro124p | 100 | 2     | 20751      | 19719   | —        | —      | —        | 40602.53 | 894.25 | 5.82 | —       | —        | —      | —      | 40109.33 | 684.12   | 5.96    | 40351.37 | 423.12 | 8.02  |
| Average | 3   | 17638 | 14999      | 9351.08 | 115.96   | 1.57   | 10286.84 | 173.26   | 1.52   | 9.90 | 9586.54 | 117.85   | 1.95   | 6.17   | 10209.22 | 153.36   | 8.98    | 139.08   | 2.53   | 10.77 |

TABLE 12: The  $t$ -values against GA-ADP and the result about HGAs that found significantly better solutions for the restricted ADVRP.

| INST    | GA-INS        | GA-INV        | GA-SWP        | Instance  | GA-INS        | GA-INV        | GA-SWP        |
|---------|---------------|---------------|---------------|-----------|---------------|---------------|---------------|
| ftv33.2 | 0.69          | 5.72          | 7.24          | ftv55.3   | 3.85          | 10.47         | 3.02          |
| Better  | —             | <b>GA-ADP</b> | <b>GA-ADP</b> | Better    | <b>GA-ADP</b> | <b>GA-ADP</b> | <b>GA-ADP</b> |
| ftv33.3 | 2.60          | 3.39          | 4.68          | ftv64.2   | 3.70          | —             | 6.62          |
| Better  | <b>GA-ADP</b> | <b>GA-ADP</b> | <b>GA-ADP</b> | Better    | <b>GA-ADP</b> | —             | <b>GA-ADP</b> |
| ftv35.3 | 0.73          | 3.65          | 4.30          | ftv64.3   | 1.19          | 6.59          | 5.27          |
| Better  | —             | <b>GA-ADP</b> | <b>GA-ADP</b> | Better    | —             | <b>GA-ADP</b> | <b>GA-ADP</b> |
| ftv38.3 | 0.53          | —             | 7.17          | ft70.3    | 2.40          | 25.04         | 4.23          |
| Better  | —             | —             | <b>GA-ADP</b> | Better    | <b>GA-ADP</b> | <b>GA-ADP</b> | <b>GA-ADP</b> |
| ftv44.3 | -2.37         | 7.92          | 2.35          | ftv70.2   | 8.37          | 27.85         | -0.91         |
| Better  | <b>GA-INS</b> | <b>GA-ADP</b> | <b>GA-ADP</b> | Better    | <b>GA-ADP</b> | <b>GA-ADP</b> | —             |
| ftv47.3 | 2.04          | 7.88          | 4.49          | ftv70.3   | 1.00          | 20.99         | -0.32         |
| Better  | <b>GA-ADP</b> | <b>GA-ADP</b> | <b>GA-ADP</b> | Better    | —             | <b>GA-ADP</b> | —             |
| ry48p.2 | 4.47          | 0.03          | 5.60          | kro124p.2 | 4.16          | —             | -4.00         |
| Better  | <b>GA-ADP</b> | —             | <b>GA-ADP</b> | Better    | <b>GA-ADP</b> | —             | <b>GA-ADP</b> |
| ry48p.3 | 4.41          | 2.73          | 6.86          | kro124p.3 | 5.80          | 16.36         | -0.70         |
| Better  | <b>GA-ADP</b> | <b>GA-ADP</b> | <b>GA-ADP</b> | Better    | <b>GA-ADP</b> | <b>GA-ADP</b> | —             |

TABLE 13: A comparative study between HVT [9] and GA-ADP on the ACVRP.

| INST     | $n$ | $m$ | Opt  | HVT  |         |      |      | GA-ADP |         |      |      |
|----------|-----|-----|------|------|---------|------|------|--------|---------|------|------|
|          |     |     |      | BS   | AS      | Gap  | Time | BS     | AS      | Gap  | Time |
| A034-02f | 34  | 2   | 1406 | 1406 | 1406.00 | 0.00 | 0.27 | 1406   | 1406.00 | 0.00 | 0.16 |
| A036-03f | 36  | 3   | 1644 | 1644 | 1644.00 | 0.00 | 0.31 | 1644   | 1644.00 | 0.00 | 0.18 |
| A039-03f | 39  | 3   | 1654 | 1654 | 1654.00 | 0.00 | 0.44 | 1654   | 1654.00 | 0.00 | 0.26 |
| A045-03f | 45  | 3   | 1740 | 1740 | 1740.00 | 0.00 | 0.52 | 1740   | 1740.00 | 0.00 | 0.53 |
| A048-03f | 48  | 3   | 1891 | 1891 | 1891.51 | 0.00 | 0.59 | 1891   | 1891.23 | 0.00 | 0.74 |
| A056-03f | 56  | 3   | 1739 | 1739 | 1739.00 | 0.00 | 0.63 | 1739   | 1739.01 | 0.00 | 1.96 |
| A065-03f | 65  | 3   | 1974 | 1976 | 1976.21 | 0.10 | 2.61 | 1974   | 1975.06 | 0.00 | 2.63 |
| A071-03f | 71  | 3   | 2054 | 2054 | 2054.51 | 0.00 | 2.80 | 2054   | 2054.35 | 0.00 | 2.95 |

one can say that our computational time is comparable with that of HVT. Overall, looking at the solution quality and computational time, our suggested GA-ADP is found to be better than HVT.

A real-life application of the ADVRP may be the sales representative who visits customers without pick up or delivery constraints but with distance constraints. This study uses three local search methods to develop three separate HGAs and adaptive search that randomly selects one of three local search methods to develop fourth HGA to solve the ADVRP. The fourth HGA, i.e., GA-ADP, provides cost-effective optimal solution to the problem. The proposed GA-ADP provides a cost-effective optimal routing plan to the sales representative. It is observed that as the number of vehicles increases solution value also increases, so removal of a vehicle from the fleet can reduce the workers. Hence, this gives managerial interpretation for the optimal fleet sizing and route designing.

## 6. Conclusion and Future Works

This paper developed a simple GA and four hybrid HGAs for solving the asymmetric distance-constrained vehicle routing problem (ADV RP). The proposed GA used random initial

population followed by sequential constructive crossover and swap mutation. The HGAs improved the initial solution using 2-opt search method and incorporated local search techniques along with an immigration procedure to find better solution to this problem. Experimental study has been carried out among the proposed GA and HGAs, by solving some TSPLIB asymmetric instances of various sizes.

Three sets of experiments were performed on asymmetric TSPLIB instances. The first experiment was unrestricted ADVRP that used a very big predefined maximum distance for every vehicle, in the 2nd experiment, the predefined maximum distance was restricted by multiplying 0.9 to the maximum distance obtained in the 1st experiment, and the third experiment used the maximum distance as 0.9 multiple of maximum distance obtained in 2nd experiment. Our computational experience reveals that the suggested HGAs are very good. From the experiments, we found that HGA using adaptive search is the best, and HGA using swap search is the second best for the restricted and unrestricted ADVRP instances. We further performed Student's  $t$ -test and confirmed our claim. However, since no research reported the exact solutions for the instances, hence, we could not claim how good our obtained solutions are. So, one can verify the optimality of our best solutions, which is also

under our next investigation. However, it is observed that as the distance-constrained becomes tight finding feasible solution becomes difficult. Finally, we reported a comparative study between our GA-ADP and a state-of-the-art algorithm on asymmetric capacitated VRP and found that our algorithm is better than the state-of-the-art algorithm for the instances.

Though the proposed HGAs found very effective solutions with small differences among average solutions, we acknowledge that still there is possibility to enhance the solutions by merging better local search approaches and/or heuristic procedures and perturbation technique to the algorithms which will be our investigation. Also, proposing a new metaheuristic procedure for solving many other instances effectively could be very interesting for the researchers.

### Data Availability

The data set used to support the findings of this study is available from the corresponding author upon request.

### Conflicts of Interest

The authors declare that they have no potential conflicts of interest.

### Acknowledgments

The authors extend their appreciation to the Deanship of Scientific Research at Imam Mohammad Ibn Saud Islamic University for funding this work through research group no. RG-21-09-17.

### References

- [1] G. B. Dantzig and J. H. Ramser, "The truck dispatching problem," *Management Science*, vol. 6, no. 1, pp. 80–91, 1959.
- [2] F. Daneshzand, "The vehicle-routing problem," *Logistics Operations and Management*, vol. 8, pp. 127–153, 2011.
- [3] P. Toth and D. Vigo, Eds., *Vehicle Routing: Problems, Methods, and Applications*, Society for Industrial and Applied Mathematics, 3600 University City Science Center Philadelphia, PA, USA, 2014.
- [4] Z. H. Ahmed, "A lexisearch algorithm for the distance-constrained vehicle routing problem," *International Journal of Mathematical and Computational Methods*, vol. 1, pp. 165–174, 2016.
- [5] S. Akpinar, "Hybrid large neighbourhood search algorithm for capacitated vehicle routing problem," *Expert Systems with Applications*, vol. 61, pp. 28–38, 2016.
- [6] D. E. Goldberg, *Genetic Algorithms in Search, Optimization, and Machine Learning*, Addison-Wesley, New York, USA, 1989.
- [7] K. Alabdulkareem and Z. H. Ahmed, "Comparison of four genetic crossover operators for solving distance-constrained vehicle routing problem," *IJCSNS International Journal of Computer Science and Network Security*, vol. 20, no. 7, pp. 114–123, 2020.
- [8] Z. H. Ahmed, "Genetic algorithm for the traveling salesman problem using sequential constructive crossover operator," *International Journal of Biometric and Bioinformatics*, vol. 3, no. 6, pp. 96–105, 2010.
- [9] H.-B. Ban and P. K. Nguyen, "A hybrid metaheuristic for solving asymmetric distance-constrained vehicle routing problem," *Computational Social Networks*, vol. 8, no. 1, p. 3, 2021.
- [10] G. Laporte, Y. Nobert, and S. Taillefer, "A branch-and-bound algorithm for the asymmetrical distance-constrained vehicle routing problem," *Journal of Mathematical Modelling*, vol. 9, no. 12, pp. 857–868, 1987.
- [11] S. Almoustafa, S. Hanafi, and N. Mladenović, "New exact method for large asymmetric distance-constrained vehicle routing problem," *European Journal of Operational Research*, vol. 226, no. 3, pp. 386–394, 2013.
- [12] M. H. Rachid, W. R. Cherif-Khettaf, P. Chatonnay, and C. Bloch, "A study of performance on crossover and mutation operators for vehicle routing problem," in *Proceedings of the 3rd International Conference on Information Systems, Logistics and Supply Chain - ILS'2010*, Casablanca, Morocco, April 2010.
- [13] P. Krunoslav and M. Robert, "Comparison of eight evolutionary crossover operators for the vehicle routing problem," *Mathematical Communications*, vol. 18, pp. 359–375, 2013.
- [14] Z. H. Ahmed, "A hybrid algorithm combining lexisearch and genetic algorithms for the quadratic assignment problem," *Cogent Engineering*, vol. 5, no. 1, Article ID 1423743, 2018.
- [15] T. Tlili, S. Faiz, and S. Krichen, "A hybrid metaheuristic for the distance-constrained capacitated vehicle routing problem," *Procedia - Social and Behavioral Sciences*, vol. 109, pp. 779–783, 2014.
- [16] Y. Xiao, Q. Zhao, I. Kaku, and N. Mladenovic, "Variable neighbourhood simulated annealing algorithm for capacitated vehicle routing problems," *Engineering Optimization*, vol. 46, no. 4, pp. 562–579, 2014.
- [17] E. Teymourian, V. Kayvanfar, G. M. Komaki, and M. Zandieh, "Enhanced intelligent water drops and cuckoo search algorithms for solving the capacitated vehicle routing problem," *Information Sciences*, vol. 334–335, pp. 354–378, 2016.
- [18] A. Faiz, S. Subiyanto, and U. M. Arief, "An efficient metaheuristic algorithm for solving capacitated vehicle routing problem," *International Journal of Advances in Intelligent Informatics*, vol. 4, no. 3, pp. 212–225, 2018.
- [19] A. M. Altabeeb, A. M. Mohsen, and A. Ghallab, "An improved hybrid firefly algorithm for capacitated vehicle routing problem," *Applied Soft Computing*, vol. 84, Article ID 105728, 2019.
- [20] İ. İlhan, "An improved simulated annealing algorithm with crossover operator for capacitated vehicle routing problem," *Swarm and Evolutionary Computation*, vol. 64, Article ID 100911, 2021.
- [21] J. Euchí and A. Sadok, "Hybrid genetic-sweep algorithm to solve the vehicle routing problem with drones," *Physical Communication*, vol. 44, Article ID 101236, 2021.
- [22] A. Baniamerian, M. Bashiri, and F. Zabihi, "A modified variable neighborhood search hybridized with genetic algorithm for vehicle routing problems with cross-docking," *Electronic Notes in Discrete Mathematics*, vol. 66, pp. 143–150, 2018.
- [23] J. Long, Z. Sun, P. M. Pardalos, Y. Hong, S. Zhang, and C. Li, "A hybrid multi-objective genetic local search algorithm for the prize-collecting vehicle routing problem," *Information Sciences*, vol. 478, pp. 40–61, 2019.



- [24] J. K. Lenstra and A. H. G. R. Kan, "Some simple applications of the travelling salesman problem," *Operational Research Quarterly (1970-1977)*, vol. 26, no. 4, pp. 717–733, 1975.
- [25] Z. H. Ahmed, A. S. Hameed, M. L. Mutar, M. F. Alrifaie, and M. M. Taresh, "Experimental study of hybrid genetic algorithms for the maximum scatter travelling salesman problem," *International Journal of Advanced Computer Science and Applications*, vol. 12, no. 8, pp. 471–482, 2021.
- [26] G. Reinelt, "TSPLIB," <http://comopt.ifi.uni-heidelberg.de/software/TSPLIB95/>.
- [27] Z. H. Ahmed, "Adaptive sequential constructive crossover operator in a genetic algorithm for solving the traveling salesman problem," *International Journal of Advanced Computer Science and Applications*, vol. 11, no. 2, pp. 593–605, 2020.
- [28] M. Fischetti, P. Toth, and D. Vigo, "A branch-and-bound algorithm for the capacitated vehicle routing problem on directed graphs," *Operations Research*, vol. 42, no. 5, pp. 846–859, 1994, <http://www.vrp-rep.org/datasets/item/2017-0002.html>.

## Research Article

# Lithium Battery Allocation Decision-Making Scheme Based on *K*-Means Algorithm

Dandan Ma <sup>1</sup> and Xiangge Qin <sup>2</sup>

<sup>1</sup>Information Science & Electronic Technology, Jiamusi University, Jiamusi 154007, Heilongjiang, China

<sup>2</sup>Materials Science & Engineering, Jiamusi University, Jiamusi 154007, Heilongjiang, China

Correspondence should be addressed to Xiangge Qin; [qinxiangge@jmsu.edu.cn](mailto:qinxiangge@jmsu.edu.cn)

Received 24 March 2022; Revised 27 May 2022; Accepted 31 May 2022; Published 20 June 2022

Academic Editor: Hangjun Che

Copyright © 2022 Dandan Ma and Xiangge Qin. This is an open access article distributed under the Creative Commons Attribution License, which permits unrestricted use, distribution, and reproduction in any medium, provided the original work is properly cited.

Lithium-ion batteries, the core components of electric vehicles, have received unprecedented attention and undergone development in the era of huge energy demand. The traditional clustering algorithm cannot meet the requirement of the consistency of lithium battery distribution. In this study, we provide an improved *K*-means algorithm to meet the battery distribution needs of enterprises and combine it with reality. This model includes an early data processing model and a battery comparison method based on the new *K*-means algorithm. In the battery data processing model, the preprocessing process approach and actual production standards preclude problematic batteries. In the battery comparison algorithm, the number of batteries in each cluster becomes equal after the battery comparison. The algorithm can ensure the internal characteristics of lithium-ion power batteries, and, at the same time, after the matching is completed, the number of lithium batteries in each cluster is equal.

## 1. Introduction

At present, energy and environmental issues have received global attention. Governments have taken a series of measures to slow down energy consumption and solve environmental pollution. Electric vehicles are supported by the government because they do not directly consume oil resources and can effectively reduce environmental pollution. It has gradually become an important development direction in the automotive field [1]. In order to support the operation of electric vehicles, lithium-ion batteries are used as the power source of electric vehicles due to their high density, long life, high safety, and high discharge platform.

As an indispensable part of new energy vehicles, the performance of power battery will affect the life, safety, and overall usage of the vehicle [2]. The capacity and voltage of a battery are relatively small. The voltage of a battery is usually about 3.6 B, but the voltage required for a powered vehicle is usually 300–400 B, which cannot meet the needs for high voltage and large energy accumulation. The daily electric battery is a battery consisting of several independent units, in

series and in parallel, to meet the high voltage and high energy requirements of the car. However, in the actual production process, due to the complexity of the physical and chemical changes in the production process, the parameters of each battery cannot be exactly the same. The battery pack formed by these single cells with different characteristics will cause differences in charge and discharge characteristics due to the differences between the single cells. Cells with different characteristics form a battery pack, during the charging process, because in a battery pack, the single battery with small capacity is fully charged first. But the large capacity is not full yet. If you continue to charge, then the small capacity single battery will be overcharged. If you do not continue to charge, then there will be a battery that has been undercharged. During the discharge process, in a battery pack, the single battery with small capacity is the first to complete the discharge, but the battery with a large capacity does not fully release energy. If it continues to discharge, the single battery with lesser capacity will be over-discharged, and there will be a series of problems such as potential safety hazards. If the performance of individual

cells in the battery pack varies greatly, it will not only cause energy waste but also affects the total and lifetime of the battery [3]. Unagreed battery characteristics can make it difficult to track the battery state [4] and charge state [5].

Therefore, more and more manufacturers conduct simple parameter performance consistency sorting. However, this approach is not suitable because it cannot use production process data or internal characteristics of individual cells. Therefore, the battery coordination method that considers the internal characteristics of the battery and the consistency of the production process can effectively improve the consistency of the battery. In order to solve the inconsistent characteristics in production, lithium battery factories are also constantly improving the material quality and manufacturing process. However, improving the quality of battery materials requires a lot of time and resources. Therefore, a more efficient and economical approach is to compare elements with different characteristics with different cells to make the charging and discharging characteristics of the same cell more consistent.

Improving the stability of lithium-ion batteries requires a more complex process for producing them. Consistency and automation can greatly reduce human and mechanical errors in the manufacturing process and improve the reliability of lithium-ion batteries. Whether it is to improve the production line or update the automatic production equipment, the production cost has risen significantly, which will not be realized in the short term. In the current case, the performance of the battery can be used to produce more accurate battery cells and maximize the internal discharge characteristics of the battery, thus greatly improving the stability of the battery.

In response to the problem of battery inconsistency, researchers have proposed many battery balancing methods, which are mainly divided into passive balancing and active balancing [5, 6]. Passive balancing is an energy-consuming balancing method. Its hardware structure is simple and easy to implement. Higher voltage battery capacity is mainly consumed by external resistors to solve internal battery consistency problems and improve the total available capacity of the battery. Active balancing consumes almost no battery capacity. It transfers high-voltage battery energy to low-voltage batteries through components such as transformers or capacitors to achieve complementary energy balance between batteries. Although this equalization method reduces the energy loss, the circuit design is complex and the hardware implementation cost is high. In some studies, a new type of equalization circuit is designed by combining the advantages of active equalization and passive equalization, which improves the equalization efficiency to a certain extent and simplifies the circuit design [7–10]. In addition to improving balance efficiency and reducing balance time, different balancing strategies are proposed, which are mainly defined according to the battery cell voltage or the remaining capacity of the single battery. Due to the randomness of the operating conditions of the vehicle, the voltage of the single cells inside the battery pack will

fluctuate with the operating conditions. This leads to failure of the voltage equalization strategy. The equilibrium strategy cannot be balanced or the equilibrium effect is not obvious in the dynamic environment of vehicle operation. The balance strategy based on the remaining capacity of the battery usually takes the average value of the remaining capacity of each cell as the balance target. Although this balancing method ensures the stability of the balancing, taking the average residual capacity of the monomer as the balancing target cannot guarantee the balancing efficiency.

The equalization strategy is the method basis for the equalization circuit to start working. The quality of the balancing method directly affects the quality of the balancing effect. A lithium power battery factory has a production capacity of 210,000 cells per day. Human and mechanical errors cause the consistency of lithium-ion batteries to fail to meet production requirements. Therefore, it is necessary to improve the production process to achieve more accurate battery packs. According to the existing equalization circuits, this paper proposes an optimal efficiency equalization strategy based on the *K*-means algorithm. The algorithm selects the optimal energy balance point, which can achieve the balance effect efficiently and quickly.

## 2. Lithium Battery Matching Technology

*2.1. The Working Principle of the Lithium Battery.* The basic structure of a lithium-ion battery mainly includes positive and negative electrodes, lithium salt electrolyte, diaphragm, positive temperature coefficient (PTC), and a safety valve. The positive and negative electrode materials mainly determine the basic performance of the battery. The separator between the positive and negative electrodes is used to isolate the conduction of electrons, allowing only ions to pass through. The electrolyte is usually a lithium salt electrolyte doped with an organic solvent, which is responsible for transporting ions. The settings of the PTC element and the safety valve are to prevent abnormality inside the battery [11]. The working principle of a lithium-ion battery is illustrated in Figure 1.

As can be observed from Figure 1, both the positive and negative electrodes of the lithium-ion battery are immersed in the lithium salt electrolyte. The charge and discharge process is achieved by extracting and introducing lithium ions between the positive and negative poles. When the battery is charged, lithium ions are extracted from lithium compounds in the positive electrode. They move to the negative electrode through the electrolyte and are embedded in the micropores of the negative electrode graphite material. The charging capacity of a lithium battery depends on the number of lithium ions embedded. When the battery is discharged and in use, lithium ions embedded in the carbon layer of the negative electrode are extracted and returned to the positive electrode through an electrolyte solution. When the lithium ions return to the positive electrode, they release more capacitance [12].

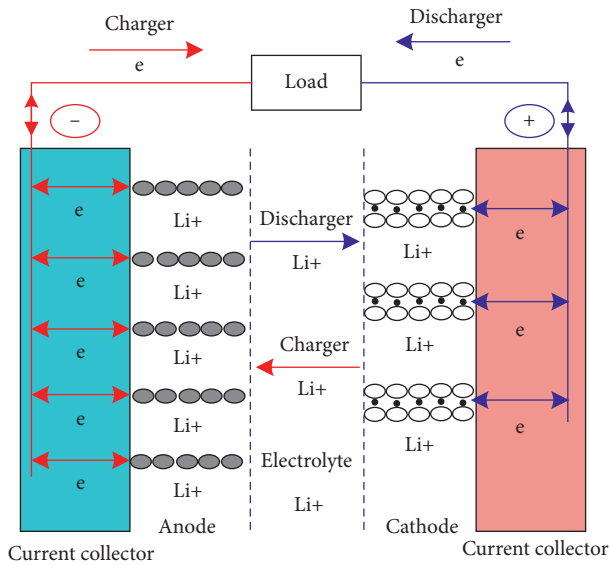


FIGURE 1: The working principle of the lithium battery.

**2.2. Characteristics of Lithium Batteries.** Lithium-ion batteries will inevitably show decline in battery life during use and storage. The degradation effect of batteries is usually manifested as changes in the electrical properties of the battery, especially the capacity and power of the battery will decrease with the aging of the battery. Battery life includes cycle life and calendar life. The cycle life takes into account the deterioration caused by the charge-discharge cycle of the power battery in the electric vehicle, and the calendar life refers to the battery deterioration caused by the storage of the battery without going through the charge-discharge cycle. In practical applications, the power battery will be in a state of charge, discharge, and static, so the cycle aging and calendar aging of the battery need to be considered [13, 14].

As shown in Figure 2, according to the manufacturing process manual, after the lithium battery is injected, the nonactivated battery first undergoes constant current charging. Among them, the current is 0.05 C, the time is 2 h, and the voltage limit is 3.45 V. After constant current charging, the current is 0.2 C, the time is 2 h, and the voltage limit is 3.9 SV. Finally, through constant voltage charging, the current reaches 0.5 C, the time is 2.5 h, the voltage is limited to 4.2 V, and the current is limited to 4 mA. The power supply phase of the lithium battery is completed. After completing the above process, the lithium battery is activated. After the lithium battery is fully charged, it is first discharged with a constant current. Among them, the current is 200 m, the time is 80 minutes and the voltage limit is 2.75 V. After constant voltage charging, the current is 200 m, the time is 25 h, the voltage limit is 380 V, and the current limit is 44 mA. After the above process is completed, the recorded process is as shown in Figure 3. According to the battery voltage curve and capacity, registered as automatic production equipment, after the discharge process has been completed and after standing for a short time, the battery is recharged at a constant voltage. Static termination voltage was recorded after standing for 15 minutes and after

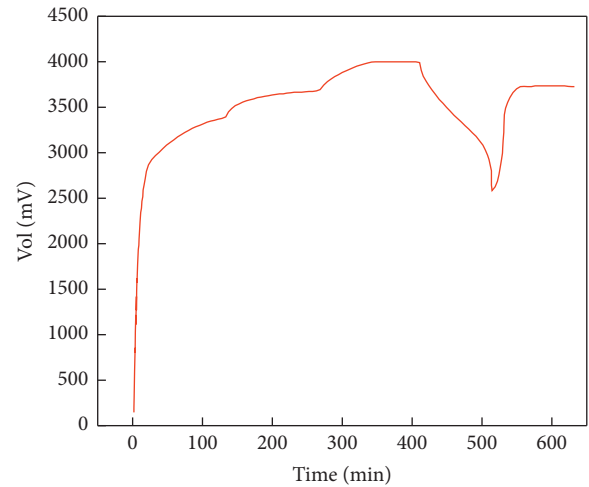


FIGURE 2: Activation process of the lithium battery.

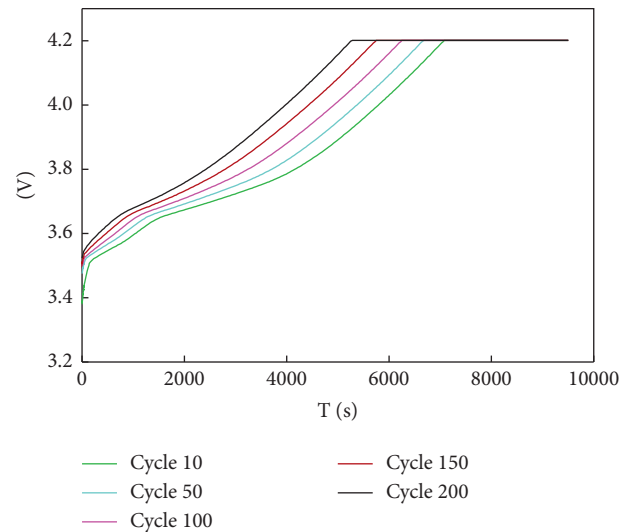


FIGURE 3: Lithium battery charging voltage curve under different cycle times.

charging was completed. After the above process is expected to be completed, the lithium battery is assembled.

As a battery ages, some noticeable changes occur in its charge-discharge process. In order to intuitively analyze the characteristic changes during the charging and discharging process of the battery, Figure 3 depicts the changing law of the charging voltage of the lithium battery under different cycles. In the constant current charging stage, as the aging of the battery intensifies, the time it takes for the battery voltage to reach the charging cutoff voltage is gradually shortened, that is, the duration of the constant current charging is gradually reduced. The duration of the constant current charging phase determines how much power the battery can charge. This to some extent represents the polarization characteristics of the battery. As the battery ages, the polarization characteristics of the battery gradually intensify, resulting in a decrease in the duration of the constant current

charging phase. Conversely, when the duration of the constant current charging phase gradually decreases, the constant current charging time of the battery gradually increases. The constant current charging mode of the battery is used to eliminate the polarization caused by the constant current charging, so that the battery can be fully charged. The longer the charging duration is, the more difficult it is to intercalate lithium ions in the negative electrode and the more serious the battery aging is.

The variation curve of voltage with the number of cycles during battery discharge is shown in Figure 4. It can be seen from the figure that the slope of the discharge voltage curve will change significantly as the number of cycles increases. That is, the voltage drop rates corresponding to different cycle times are different. If the battery is discharged at a constant current or under constant working conditions, the length of the discharge time directly represents how much capacity the battery can release, and the state of health of the battery can be directly calculated from the maximum discharge capacity. Therefore, the change of the discharge process of the battery can be used as a health factor to characterize the aging of the battery. Considering that in the actual application process, the battery rarely discharges at 100% state of charge and discharges to 0% state of charge, so the discharge time corresponding to part of the voltage range can be used as a health factor.

Figure 3 shows that when charge/discharge process curves are used as a basis for battery configuration, the battery curves are relatively close to each other. Therefore, they must be connected to a battery unit. When the clustering algorithm is complete, each cell must be recombined into the same cell block.

**2.3. Inconsistency of Lithium Battery Performance.** The inconsistency of battery performance is mainly caused by two aspects. The first is that the battery is produced during the manufacturing process. The second is generated during use. During battery production, due to manufacturing process issues and differences in materials, the internal structure of the battery will vary to some extent. Therefore, even batteries produced from the same batch will have inconsistent performance [15]. When batteries are used in electric vehicles, environmental and operational factors can increase the variability between batteries.

The inconsistency of the battery will bring certain harm during use. For example, the small-capacity battery in the cell gets overloaded during charging and charging. This reduces the length of the battery cycle, reduces the performance of the battery, and creates a number of safety issues [16], such as spontaneous combustion. After the batteries are grouped, the energy density and capacity of the batteries will decrease due to the differences between the batteries, thereby shortening the cycle time of the batteries [17]. Improving the consistency of the battery can start from the following two aspects. First, control the consistency of raw materials in the production process of batteries, inspect raw materials according to strict standards, and ensure that each process is within the specified error range [18]. Second,

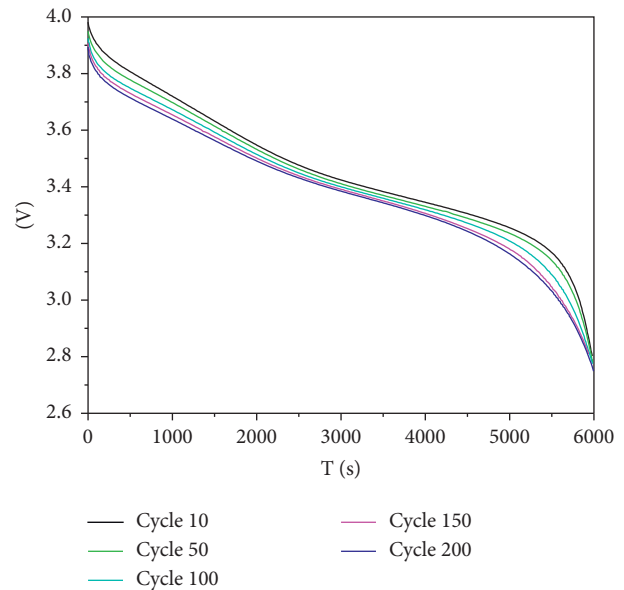


FIGURE 4: Discharge process of lithium battery.

the battery is prescreened by the voltage and internal resistance of the battery before use. Batteries with excellent correlation are selected for use as a group [19].

**2.4. Lithium Battery Matching Method.** Battery matching technology that has been proposed can be divided into single-parameter, multiparameter, and dynamic characteristics matching [20].

Single-parameter matching is to sort according to a certain characteristic of the battery. It is based primarily on one of the terminal voltage, capacity, or internal resistance of the battery for sorting. The voltage matching method is to hold the battery for about 12 hours after being fully charged, measure the terminal voltage of the battery, and then sort the battery based on the size of the terminal voltage. The capacity matching method is generally to discharge the battery at the same rate after the battery is fully charged, calculate the discharge capacity of the battery, and group the batteries with a small difference in discharge capacity into a group. The internal resistance matching method is to measure the internal resistance of the battery and group the batteries with similar internal resistance into a group. The voltage matching method is commonly used in the single-parameter matching method. The battery voltage can indirectly reflect the performance of other batteries. For example, voltage indirectly reflects electrolyte concentration in a battery. The pressure release velocity of the battery in static state reflects the self-exploding velocity of the battery [21]. Therefore, the persistence of battery voltage is an important factor to ensure battery stability.

The multiparameter matching method is mainly based on the comparison and classification of multiple battery performance parameters. Compared with single-parameter matching, multiparameter matching is relatively comprehensive. However, like the single-parameter matching

group, some changes in the performance of the battery during the working process are not considered. Even if the single cells in the battery pack are consistent at the beginning, their performance will change during use and the variability of the cells will continue to increase [22]. Therefore, multiparameter matching still has great defects in practical applications.

The dynamic characteristics are classified according to the battery voltage change curve during charging and discharging. It classifies batteries with similar charge/discharge curves as in [23]. Therefore, balancing battery voltage plays an important role in improving battery stability. However, the combination of static characteristics cannot reflect the changes in the performance of the battery during the working process [24]. Researchers believe that the battery is a relatively complex electrochemical system. There are certain physical differences between single cells, and this difference will gradually enlarge during use [25]. The method of adjusting dynamic characteristics according to the voltage change curve of battery operation fully considers some characteristics of the battery in the working process and indirectly reflects some static characteristics of the battery. For example, if a battery is exhausted at a certain current, the discharge time indirectly reflects the battery capacity. Battery voltage can also indirectly reflect the resistance and concentration of electrolytes in the battery [26]. The dynamic characteristic matching scheme overcomes the shortcomings of the above two matching methods. Therefore, this paper adopts a battery arrangement scheme based on dynamic characteristics.

The process of sorting the charge-discharge curve of the battery can also be regarded as a clustering process of the time series. In this paper, by discharging the battery and collecting its voltage in real time, the time series of its discharge voltage is obtained. Then, each time series is clustered to achieve the purpose of battery matching. The time cluster algorithm based on raw data considers the time series as a whole without considering the characteristics of time series. Then, we cannot understand some of the internal structure of the time series. Moreover, when the dimension of the time series becomes longer, the efficiency of its calculation will decrease and the effect of clustering will become worse [27]. Therefore, relatively speaking, feature-based clustering algorithms have advantages.

This paper discharges the battery and collects a voltage value at the same interval. The composite sequence of battery discharge voltage has uneven length and large size. Computational complexity is relatively high when raw data is used. Moreover, in arrays, similarities can only be found if they do not affect the array's internal mechanisms. Therefore, this paper uses a function-based time series cluster. First, the features of the battery sequence collected in the first batch are retrieved, which are used to represent the battery, and the similarity between the two batteries is measured according to the retrieved features. Finally, the clustering algorithm is used.

### 3. K-Means Algorithm

*3.1. The Principle of K-Means Algorithm.* The K-means clustering algorithm has a long tradition. Its concept was

proposed by Macqueen in 1967, and its research purpose is mainly derived from the fact that the mean or centroid of the points in the cluster can be regarded as the center point of the cluster [28]. This algorithm is typical of the iterative descent of grouped datasets. The K-means algorithm is one of the easiest ways to teach without a teacher. It automatically identifies clusters and central points without the need for tags [29]. The K-means algorithm is widely used in science, industry, business, and other fields.

The K-means algorithm is a classical partition-based clustering method. The algorithm can be widely used in  $n$ -dimensional data space. The K-means algorithm divides data objects into different classes through continuous iteration, so that each class is as compact as possible and unique from other classes. The basic principle of K-means algorithm is to first determine the value of K parameter and that the dataset must be divided into K classes as the initial cluster center. The distance equation then calculates the distance from all remaining data objects to the center of the cluster, and the calculated data objects are decomposed into the nearest data center. Therefore, you can have the cluster distribution with the data object K as the initial center point. For the divided initial cluster distribution, the center point of each class is recalculated according to a certain rule (usually a distance formula) and a new class is formed with the calculated point as the center. If the calculated class center point is different from the previous calculated class center point, the rules are used again to redistribute and adjust the dataset. This cycle repeats until the new class center point is the same as the previous class center point. All data objects are not repartitioned, marking the end of the algorithm [30]. The K-means algorithm continuously changes the position of the center point through iteration, so that the sum of the distances from all data objects to the center point of its class becomes the smallest, so that the objective function can be minimized [31].

*3.2. Steps of K-Means Algorithm.* The K-means algorithm is the process of calculating the cluster center points by continuously iterating on the data objects. The algorithm is simple, is efficient, and has fast convergence speed. The specific steps are as follows:

- (1) Randomly select data objects from the dataset, and use these data objects as the initial center of the cluster. We have  $C_1$ ,  $C_2$ , and  $C_k$  as the initial center of the cluster. This determines how many classes the dataset needs to be divided into.
- (2) Calculate the distance from each remaining data object in the dataset to the  $k$  initial center points, and divide each data object into the nearest class to form a class centered on the  $k$  initial center points. For example,  $Xp$  objects are decomposed into  $C_i$  classes if they are closest to  $C_i$ .
- (3) Recalculate the center point of each cluster according to formula  $C_i = (1/n_i) \sum_{x \in u_i} X$ ; then, we get  $C_1^*, C_2^*, \dots, C_k^*$ .

- (4) Repeat steps (2) and (3) until the center point of the statistical cluster matches the center point of the precomputed cluster. If there is no change, it means that the clustering results have reached convergence.
- (5) This produces clustered results. According to the basic procedure of K-means algorithm, Figure 5 shows a simplified flowchart of the algorithm.

#### 4. Improved K-Means Algorithm and Experiment

**4.1. Introduction.** The K-means algorithm is an iterative optimization algorithm. In the iterative process, it is often easy to converge to the local optimum, so that the expected effect cannot be obtained. And in the process of algorithm initialization, if the center of the K-means algorithm is not properly initialized, this can greatly increase the cost of the calculation process and ultimately lead to incorrect results. Therefore, it is sensitive to iterative initialization, and a good initialization strategy will effectively improve the K-means algorithm model. When the original dataset is large, an effective initialization strategy will effectively improve the number of iterations of the K-means algorithm and accelerate the convergence speed. When many K-means algorithms initialize cluster center selection, many data centers are often initialized directly. The data density or mean value is directly used as the data center, but this method of selecting the center, in turn, is often ignored, resulting in a large difference between the final calculated data center and the final iteration convergence point. Today, many improved K-means algorithms for related applications have been proposed. However, there is always the problem of selecting the initialization center in the algorithm process. Due to the simple implementation of the algorithm, many center initialization methods have been proposed in corresponding applications at this stage. However, the problem of hard clustering of data in the iterative process still exists. And after the algorithm is clustered, the amount of data in each cluster is not the same, which cannot meet the application requirements of having the exact same amount of data in each cluster. In order to solve the problem that the amount of data in each cluster is not equal to the K-means algorithm, the K-means algorithm is improved to meet the existing requirements and actual situations of applications.

**4.2. Improved K-Means Algorithm.** As a classic clustering algorithm, the K-means algorithm is widely used in big data algorithm processing due to its fast calculation speed, simple principle, excellent clustering effect, high scalability, and high efficiency. The traditional K-means algorithm includes hard clustering in the algorithm process, and the amount of data in each cluster is usually not equal to after the cluster is completed. However, when producing lithium batteries, the technical specifications of lithium batteries are the same and the number of lithium batteries per battery pack is the same. Therefore, the traditional method of this algorithm cannot meet the existing requirements of lithium batteries.

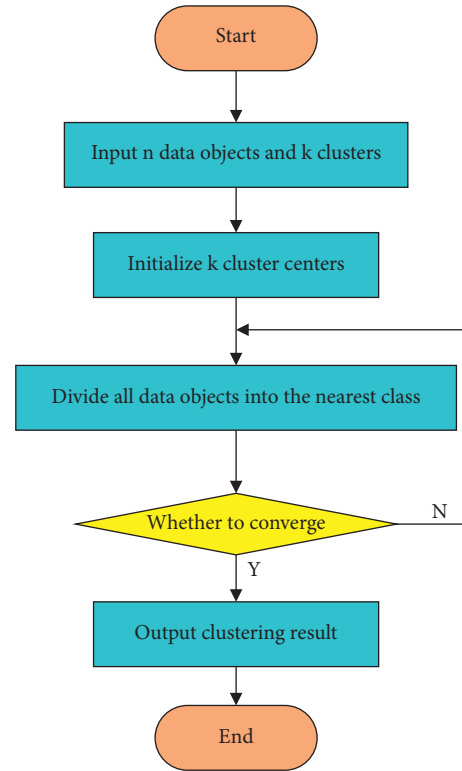


FIGURE 5: Flowchart of the K-means algorithm.

**4.2.1. Data Preprocessing.** The process data of lithium battery production cannot be directly applied to the current algorithm model, and it needs to undergo certain data preprocessing to adapt to the new improved algorithm. The data is processed according to the production process data. According to equation (1), the lithium battery discharge sequence is processed and the fault data is eliminated.

$$d_i^j = \sqrt{\sum_l (\rho_l |V_l^i - V_l^j|^2 + \mu |C^i - C^j|^2)}, \quad (1)$$

where  $\rho_l$  and  $\mu$  are balance coefficients,  $V_l^i$  represents the voltage value of lithium battery  $i$  at a certain time, and  $C^i$  represents the capacity obtained by the  $i$ -th battery after the lithium battery is discharged. The calculation formula is shown in

$$C^i = \int_0^t Idt. \quad (2)$$

The average voltage distribution curve of the first cell is defined as

$$S_i = \frac{d_i^1 + d_i^2 + \dots + d_i^n}{n}, \quad (3)$$

where  $d_i^1, d_i^2, \dots, d_i^n$  represents the distance between the  $i$ -th battery and other batteries calculated according to formula (1).

**4.2.2. Improved K-Means Algorithm Model.** The general clustering algorithm divides the data of similar

characteristics into the same cluster. The data characteristics in the same cluster maintain a certain similarity according to the division principle. In the application of lithium battery distribution, the clustering algorithm used in lithium battery distribution is different from the general clustering algorithm. It cannot be directly applied to lithium battery matching applications and needs to be optimized and modified according to the actual need to meet the corresponding need. In the application of lithium battery matching, it is necessary to ensure that the number of clusters in each cluster is equal. This is because, in the process of producing lithium batteries, the number of lithium batteries in each battery is the same. It is urgent to improve the K-means algorithm according to this special requirement.

K-means algorithm is a widely used uncontrolled clustering algorithm. In K medium-sized centers,  $N$  clusters were randomly selected and the data was divided into  $N$  clusters based on distance, similarity, and user criteria. The distance function shown in the following equation is often used as a standard function of the K-means algorithm:

$$E = \sum_{n=1}^N \sum_{x \in c_n} \|x - u_n\|^2. \quad (4)$$

The traditional K-means algorithm randomly initializes K data points as the original cluster centers. However, the K-means algorithm is very sensitive to cluster centers and has strong randomness and chance. Different random initialization methods will get different cluster centers. Industrial production processes require a certain degree of stability. However, in the K-means algorithm, using different random initialization methods will have a certain probability to obtain different clustering results, which violates the principle of stability in the process. Therefore, it is very interesting to study the initialization of the K-means algorithm. Kd tree is a very efficient initialization algorithm. The initialization effect of K-means algorithm is greater than that of random initialization.

The clustering rules of the K-means algorithm are modified in this paper to solve the problem of placing lithium batteries in actual production. The ultimate goal of the algorithm is to divide battery data into  $N$  clusters.

## 5. Results and Discussion

The accuracy of the improved K-means algorithm is tested in the method of comparing batteries. The batteries that have been assembled should be connected and tested. However, its analysis is too complicated, the experimental conditions are limited, and parallel or series batteries cannot be obtained, so the corresponding results cannot be obtained.

In actual production, the static tuning voltage is between 3860 MB and 3880 MB. Batteries with capacities over 2160 MHz are suitable batteries. The accuracy of battery cells depends on the degree of aggregation of charge/discharge curves of each cell. The capacity is increased to 20 MHz at a time according to the certified battery, which will be the first layer of battery matching. The matching parameter of  $M$  is

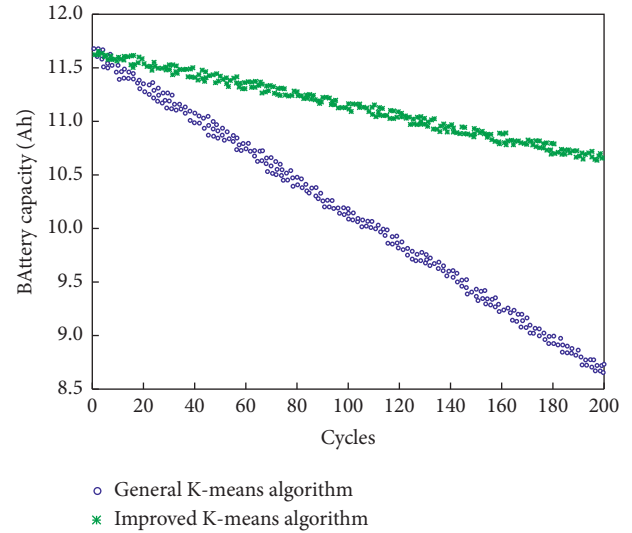


FIGURE 6: Comparison of two matching methods.

set to 5. That is, every 5 batteries are a battery pack after the batteries are assembled.

In this paper, 5 batteries based on the general K-means algorithm and 5 batteries based on the improved K-means algorithm model are selected to test the energy storage performance for comparing the energy storage capacity of the batteries of the two matching methods. At the same time, two groups of batteries were selected for charge-discharge cycles, and the capacity changes during multiple charge-discharge processes were measured.

In this experiment, two groups of battery packs were, respectively, subjected to cyclic charge-discharge experiments and their capacity changes were recorded. First, the battery pack is charged at 0.5 C. When the voltage reaches 42 V, we must switch to constant voltage charging and stop charging when the current is about 0.05 C. Then, the battery was put aside for a period of time for constant current discharge with a discharge current of 0.5 C. The capacity of the battery pack is recorded. The above process is repeated continuously. The change in capacity of the battery after 200 charge-discharge cycles is observed and compared, as shown in Figure 6.

As shown in Figure 5, the battery capacity of the battery pack based on the general K-means algorithm decreases faster than the battery pack based on the improved K-means algorithm model as the number of cycles increases. It can be seen from this experiment that the performance of the battery pack based on the improved K-means algorithm model is better than that of the battery pack under the general K-means algorithm.

## 6. Conclusion

Lithium battery coordination technology is a widely used technology, which can effectively improve battery life and stability. In this paper, we provide an improved K-means algorithm model for configuring lithium-ion batteries. You can integrate your model according to traditional



comparison methods, ensuring that each cluster has the same number of cells and conforms to the actual production process. The method has remarkable effectiveness compared with the actual method. At the same time, the improved K-means algorithm can also be used in other applications with the same requirements. Once clustering is complete, you can ensure that the amount of data in each cluster is the same. The results of clustering show that after completing a particular group, the distance within the group is smaller than that of the typical K-means algorithm.

In this study, under the existing production conditions, combined with the production process of lithium batteries, a lithium battery matching algorithm model was designed. Compared with the traditional lithium battery assembly method, the performance of the battery assembly under this method is significantly improved.

### Data Availability

The dataset can be accessed upon request to the corresponding author.

### Conflicts of Interest

The authors declare that they have no conflicts of interest.

### References

- [1] O. I. Al-Sanjary, M. A. B. Roslan, R. A. A. Helmi, and A. A. Ahmed, "Comparison and detection analysis of network traffic datasets using K-means clustering algorithm," *Journal of Information and Knowledge Management*, vol. 19, no. 3, 2020.
- [2] Y. Cheng, D. Song, Z. Wang, C. Lu, and N. Zerhouni, "An ensemble prognostic method for lithium-ion battery capacity estimation based on time-varying weight allocation," *Applied Energy*, vol. 266, 2020.
- [3] Y. Ding and I. W. Selesnick, "Artifact-Free wavelet denoising: non-convex sparse regularization, convex optimization," *IEEE Signal Processing Letters*, vol. 22, no. 9, pp. 1364–1368, 2015.
- [4] F. Flamarly-Mespoulie, A. Boulineau, H. Martinez et al., "Lithium-rich layered titanium sulfides: c," *Energy Storage Materials*, vol. 26, pp. 213–222, 2020.
- [5] D. Gaissmaier, D. Fantauzzi, and T. Jacob, "First principles studies of self-diffusion processes on metallic lithium surfaces," *The Journal of Chemical Physics*, vol. 150, no. 4, 2019.
- [6] S. R. Gampa, K. Jasthi, P. Goli, D. Das, and R. C. Bansal, "Grasshopper optimization algorithm based two stage fuzzy multiobjective approach for optimum sizing and placement of distributed generations, shunt capacitors and electric vehicle charging stations," *Journal of Energy Storage*, vol. 27, 2020.
- [7] M. S. Garapati and R. Sundara, "Synergy between interconnected porous carbon-sulfur cathode and metallic MgB<sub>2</sub> interlayer as a lithium polysulfide immobilizer for high-performance lithium-sulfur batteries," *ACS Omega*, vol. 5, no. 35, Article ID 22379, 2020.
- [8] S. Ghassa, A. Farzanegan, M. Gharabaghi, and H. Abdollahi, "The reductive leaching of waste lithium ion batteries in presence of iron ions: process optimization and kinetics modelling," *Journal of Cleaner Production*, vol. 262, 2020.
- [9] R. Gogoana, M. B. Pinson, M. Z. Bazant, and S. E. Sarma, "Internal resistance matching for parallel-connected lithium-ion cells and impacts on battery pack cycle life," *Journal of Power Sources*, vol. 252, pp. 8–13, 2014.
- [10] T. A. Gunawan, I. Williamson, D. Raine, and R. F. D. Monaghan, "Decarbonising city bus networks in Ireland with renewable hydrogen," *International Journal of Hydrogen Energy*, vol. 46, no. 57, Article ID 28870, 2021.
- [11] X. Guo, J. Zhang, and Q. Tian, "Modeling the potential impact of future lithium recycling on lithium demand in China: a dynamic SFA approach," *Renewable and Sustainable Energy Reviews*, vol. 137, 2021.
- [12] D. Gupta and G. M. Koenig, "Analysis of chemical and electrochemical lithiation/delithiation of a lithium-ion cathode material," *Journal of the Electrochemical Society*, vol. 167, no. 2, Article ID 020537, 2020.
- [13] K. Hamid, "Improving performance of classification on severity of ill effects (SEV) index on fish using K-Means clustering algorithm with various distance metrics," *Water Practice and Technology*, vol. 14, no. 1, pp. 101–117, 2019.
- [14] M. Hilbert, "Big data for development: a review of promises and challenges," *Development Policy Review*, vol. 34, no. 1, pp. 135–174, 2016.
- [15] M. S. Hossain Lipu, M. A. Hannan, A. Hussain et al., "Data-driven state of charge estimation of lithium-ion batteries: algorithms, implementation factors, limitations and future trends," *Journal of Cleaner Production*, vol. 227, no. 12, 2020.
- [16] A. Islam, S. Roy, M. A. Khan et al., "Improving valuable metal ions capturing from spent Li-ion batteries with novel materials and approaches," *Journal of Molecular Liquids*, vol. 338, 2021.
- [17] J. Arias, I. A. Gamez, and J. M. Puerta, "Learning distributed discrete bayesian network classifiers under MapReduce with Apache spark," *Knowledge-Based Systems*, vol. 117, 2017.
- [18] R. Jothi, S. K. Mohanty, and A. Ojha, "DK-means: a deterministic K-means clustering algorithm for gene expression analysis," *Pattern Analysis & Applications*, vol. 22, no. 2, pp. 649–667, 2019.
- [19] T. R. Jow, S. A. Delp, J. L. Allen, J.-P. Jones, and M. C. Smart, "Factors limiting Li+Charge transfer kinetics in Li-ion batteries," *Journal of the Electrochemical Society*, vol. 165, no. 2, pp. A361–A367, 2018.
- [20] A. Karrech, M. R. Azadi, M. Elchalakani, M. A. Shahin, and A. C. Seibi, "A review on methods for liberating lithium from pegmatities," *Minerals Engineering*, vol. 145, no. 1, 2020.
- [21] B. Ludwig, Z. Zheng, W. Shou, Y. Wang, and H. Pan, "Solvent-free manufacturing of electrodes for lithium-ion batteries," *Scientific Reports*, vol. 6, 2016.
- [22] V. Marangon, L. Minnetti, M. Adami, A. Barlini, and J. Hassoun, "Lithium-Metal batteries using sustainable electrolyte media and various cathode chemistries," *Energy & Fuels*, vol. 35, no. 12, Article ID 10284, 2021.
- [23] M. J. Rothenberger, J. Safi, J. Liu, J. Anstrom, S. Brennan, and H. K. Fathy, "Improving lithium-ion battery pack diagnostics by optimizing the internal allocation of demand current for parameter identifiability[J]," *Journal of Dynamic Systems, Measurement and Control, Transactions of the ASME*, vol. 139, no. 8, 2017.
- [24] K. P. Sinaga and M.-S. Yang, "Unsupervised K-means clustering algorithm," *IEEE Access*, vol. 8, no. 8, Article ID 80716, 2020.
- [25] Y. Wang, Z. Sun, X. Li, X. Yang, and Z. Chen, "A comparative study of power allocation strategies used in fuel cell and ultracapacitor hybrid systems," *Energy*, vol. 189, 2019.

- [26] J. Wessel, A. Turetskyy, O. Wojahn, C. Herrmann, and S. Thiede, "Tracking and tracing for data mining application in the lithium-ion battery production," *Procedia CIRP*, vol. 93, pp. 162–167, 2020.
- [27] N. Wilson, E. Meiklejohn, B. Overton et al., "A physical allocation method for comparative life cycle assessment: a case study of repurposing Australian electric vehicle batteries," *Resources, Conservation and Recycling*, vol. 174, 2021.
- [28] Z. Wu and Z. Wu, "An enhanced regularized k-means type clustering algorithm with adaptive weights," *IEEE Access*, vol. 8, no. 8, Article ID 31171, 2020.
- [29] Y. Yang, M. Gao, Z. He, and C. Wang, "A robust battery grouping method based on a characteristic distribution model," *Energies*, vol. 10, no. 7, p. 1035, 2017.
- [30] J. Yang, F. Gu, and J. Guo, "Environmental feasibility of secondary use of electric vehicle lithium-ion batteries in communication base stations," *Resources, Conservation and Recycling*, vol. 156, 2020.
- [31] Z. Yuan, W. Wang, H. Wang, and A. Yildizbasi, "A new methodology for optimal location and sizing of battery energy storage system in distribution networks for loss reduction," *Journal of Energy Storage*, vol. 29, 2020.

## *Retraction*

# **Retracted: Study on Intelligently Designed Business Innovation Service Models Driven by Big Data**

### **Mathematical Problems in Engineering**

Received 18 July 2023; Accepted 18 July 2023; Published 19 July 2023

Copyright © 2023 Mathematical Problems in Engineering. This is an open access article distributed under the Creative Commons Attribution License, which permits unrestricted use, distribution, and reproduction in any medium, provided the original work is properly cited.

This article has been retracted by Hindawi following an investigation undertaken by the publisher [1]. This investigation has uncovered evidence of one or more of the following indicators of systematic manipulation of the publication process:

- (1) Discrepancies in scope
- (2) Discrepancies in the description of the research reported
- (3) Discrepancies between the availability of data and the research described
- (4) Inappropriate citations
- (5) Incoherent, meaningless and/or irrelevant content included in the article
- (6) Peer-review manipulation

The presence of these indicators undermines our confidence in the integrity of the article's content and we cannot, therefore, vouch for its reliability. Please note that this notice is intended solely to alert readers that the content of this article is unreliable. We have not investigated whether authors were aware of or involved in the systematic manipulation of the publication process.

Wiley and Hindawi regrets that the usual quality checks did not identify these issues before publication and have since put additional measures in place to safeguard research integrity.

We wish to credit our own Research Integrity and Research Publishing teams and anonymous and named external researchers and research integrity experts for contributing to this investigation.

The corresponding author, as the representative of all authors, has been given the opportunity to register their agreement or disagreement to this retraction. We have kept a record of any response received.

### **References**

- [1] H. Liu, J. Shang, and G. Wan, "Study on Intelligently Designed Business Innovation Service Models Driven by Big Data," *Mathematical Problems in Engineering*, vol. 2022, Article ID 4468240, 15 pages, 2022.

## Research Article

# Study on Intelligently Designed Business Innovation Service Models Driven by Big Data

Huiying Liu <sup>1,2</sup>, Jianfeng Shang <sup>2,3</sup> and Gang Wan<sup>4</sup>

<sup>1</sup>Graduate School, Jose Rizal University, Manila 1552, Philippines

<sup>2</sup>Shenzhen Perth Industrial Design Co., Ltd., Shenzhen 518038, China

<sup>3</sup>College of Computer Science and Electronic Engineering, Hunan University, Changsha 410082, China

<sup>4</sup>Talkweb Yunchuang Technology Co., Ltd., Changsha 410000, China

Correspondence should be addressed to Jianfeng Shang; [jf\\_shang@hnu.edu.cn](mailto:jf_shang@hnu.edu.cn)

Received 16 March 2022; Revised 11 April 2022; Accepted 15 April 2022; Published 20 June 2022

Academic Editor: Hangjun Che

Copyright © 2022 Huiying Liu et al. This is an open access article distributed under the Creative Commons Attribution License, which permits unrestricted use, distribution, and reproduction in any medium, provided the original work is properly cited.

Although conventional business models have been increasingly affected in front of the big data technology application, it has also brought new opportunities and challenges for enterprise development. In order to create a higher value, enterprises should keep pace with the times and actively develop business innovation service models. The greatest value brought by data is to help enterprises find potential business value. It can provide a broader user market and channels, avoid homogeneous competition, and realize the integration of upstream and downstream value chains. In addition, it abandons the extensive development under the traditional model and allows enterprises to return to real value services, which is also an irresistible trend of business model transformation. This paper studies and analyzes business innovation service models. First, the business model as required is presented, and the management system and risk evaluation method are introduced. Then, the construction of the business service model is discussed, and the typical big data technologies are reviewed. Next, according to the evaluation theory of business model, the index system of business innovation service model is explored, which can examine the development of business model objectively and comprehensively. Last, the operations of the business model under the big data are analyzed. The research on the business model in this paper can be provided with universality and has a certain practical value for the development of business innovation service.

## 1. Introduction

Business model innovation takes customers as the starting point and source, adopts initiative market orientation, and is open to the bilateral market. It makes systematic innovation in many key links of a business model such as value model, operation model, marketing model, and profit model, enables customer value grows by leaps, creates new markets or restructures the existing industries, changes the competition rules and nature, and helps firms get excess profit and rapid growth [1, 2]. In order to better target user groups in the Internet Age, enterprises center on users, take product strategy as the fundamental principle, continuously optimize the products and services, restructure their own business models based on the user data analysis, and take into account

how to provide more innovative products or services with new features given the existing market products and services in order to better satisfy users' demands [3]. The business model design of a company determines what products or services it provides to its users. But users' experience on products or services changes all the time, which is a process of motion capture. It has already been very difficult to effectively meet the personalized requirements of users with only the resources of an enterprise [4]. Meanwhile, the design of organizational structure of the enterprise shall also pay attention to how to maneuver the idle resources in a more efficient manner and quickly respond to users' demand. With the constantly expanding Internet application scope, the data volume required to be processed increases exponentially, which directly promotes the development of

big data processing technique [5]. Such technology can process plenty of multitype data in a real-time manner, ensure the authenticity and safety of data, and accomplish the data mining, which cannot be done by conventional architecture. In the rapidly changing global information market, decision-makers of enterprises are challenged to quickly understand and analyze data. Lack of data in traditional business system results in weak supporting ability; worse still, the characteristics of a single visualized icon and complex information understanding make it unable to meet the demands of enterprises' data analysis [6]. Big data-driven intelligent business service models can provide the technology and methods for corporates to quickly analyze data, including data collection, management, and analysis, so that the companies can convert it into use information to support the decision-making. Based on the enterprise data warehouse, it builds data cube, achieves the multidimensional query of data, and obtains the hidden business information by means of data mining and information mining tools so as to help users acquire data from multiple perspectives, assist in, and support the business decision-making in the entire process [7, 8]. Nowadays, the pop-up contents from on-shopping APPs and short videos are realized by big data technique. For decision-makers, they can from the intelligent business platforms under big data technology track users' focus of attention and analyze the user traffic so as to promote the decision-making from a certain extent [9].

This paper conducts research of the intelligent and business innovation service models driven by big data, and the key research content includes the following: first, the business model as required is presented, and the management system and risk evaluation method are introduced; then, the construction of the business service model is discussed, and the typical big data technologies are reviewed; next, according to the evaluation theory of business model, the index system of business innovation service model is explored, which can examine the development of business model objectively and comprehensively; and last, the operations of the business model under the big data are analyzed.

The remainder of this paper is organized as follows: Section 2 discusses related work, followed by design of business innovation service model driven by big data in Section 3. Section 4 shows construction of evaluation index of business innovation service model. Research on business model operation based on big data is presented in Section 5, and Section 6 concludes the paper with a summary and future research directions.

## 2. Related Work

The concept of "business model" first appeared in the 1950s, but it has not attracted extensive attention gradually until the continuous development of Internet and big data technology in recent years. The rapid rise of numerous Internet enterprises has given a more intuitive understanding of the importance of business model to all walks of life, and it is even considered as the key element of the enterprise competition and development now [10]. Business model

innovation is further development of the study on business models. Through the innovation of business model, enterprises can gain more resources and competitive advantages and finally reach the purpose of enhancing strength and acquiring profits [11]. Scholars have conducted related research on business model innovation. The innovation of business model was to upset the plans of competitors, create new value for customers, and create new wealth for stakeholders to restructure the existing business models of the industries [12]. It helps enterprises share the value created in the industry more efficiently. Business model innovation by overturning the existing rules and changing the competition nature restructures the exiting business models and market and achieves high-speed growth of enterprises while greatly increasing customer value [13]. Business model innovation subverts the existing business rules by redefining customer segmentation criteria, customer demand, product manufacturing, and delivery method or new products development and introduces new ones [14]. An increasing number of people have faith in that business model innovation can bring stronger competitiveness and profit value to enterprises than innovation of conventional products, services, and techniques. One of the key factors that drive the innovation of business model is the emergence of new technology [15]. With the popularization and swift growth of Internet, the data generated by various application systems are exploding. Big data is another technical revolution in the information industry after cloud computing, business intelligence, and Internet, and it has a profound impact on the decision-making, organization, and business process of a company [16]. Big data has four major features: a large amount of data, a great variety of data, a fast data processing speed, and high data authenticity. Consequently, big data can process plenty of multitype data in a real-time manner, ensure the authenticity and safety of data, and effectively analyze the information, which is valuable to enterprises. However, many traditional and medium-sized enterprises do not have much internal data or technology advantage. They only have a blurry concept of data value, which they hope to improve but do not know how to integrate with their own strengths [17]. Those enterprises are still at a low level of informatization. On the contrary, they still make use of the conventional business intelligence model, which results in slow, inaccurate, and untimely statistical analysis of the data in product sales, purchase, and other processes in the market. The shortcomings mainly include insufficient evaluation on business intelligence construction, lack of specialized personnel in data processing, and incomplete analytical results [18, 19]. Therefore, only the combination of big data technology and business innovation service model can resolve the complicated and diversified data analysis problems in various business models. With the help of data, the production and operation vigor of enterprises are stimulated.

Chen [20] analyzed the transition direction of traditional manufacturing enterprises from the business model perspective in the big data background. It focused on three prominent aspects of business model—customer value proposition, business system, and profit mode—combined

with applications of big data, and finally put forward transformation direction for reference. Sun et al. [21] examined incorporation of business analytics into enterprise information system through proposing a model for business analytics service-based enterprise information system. The proposed method contributed to the research of business service and business innovation. Fernandez-Manzano and Gonzalez-Vasco [22] commented on the implications of data management in social networks. They discussed the privacy and security risks associated with this novel scenario and briefly commented on tools that aid in securing the privacy of business intelligence within this context. Loebbecke and Picot [3] studied the potential mechanism of how digital and big data analysis can promote enterprise and social transformation and outlined the potential impact of digital and big data analysis on employment, especially in the context of cognitive tasks. The analysis and discussion of Yablonsky [23] led to a multidimensional framework of innovations, with a particular emphasis on a technology stack, business models, products, services, and platform innovations. Wang [24] thought management must transform enterprise-centric into customer-centric with the big changing of the business service, and a business innovation model was presented. Li [25] analyzed in detail the organization and innovative ideas of the business model of online travel service companies by taking Ctrip as the object for the case study. Adopting the business model canvas to analyze its business model, the paper finally concluded four perspectives, namely concentration on differentiated development, establishment of a perfect service system, improvement on technological competence, multi-dimensional channels both online and offline, and reinforce the establishment of key resources. Duan et al. [26] studied the relationship between business analytics and innovation by theoretically and empirically investigating. At present, the data accumulation of the whole industry is still in its infancy, and the development of big data technology is also a big bottleneck. The value of big data has not yet been revealed through mature operation mode. We need to treat this problem rationally, any new technology will experience a bubble stage at the early stage of development, and this is the inevitable result of the massive influx of resources [27–30]. When people's lives are completely recorded by data, data driven will become an indispensable element of existence. The evolution of innovation model will gradually form a perfect business system, and big data will play an increasingly important role in this business ecosystem. The greatest value of data is that it can help enterprises find potential business value, provide a broader user market and channels, avoid homogeneous competition, and realize the integration of upstream and downstream value chains. It abandons the rough development under the traditional model and allows enterprises to return to real value services, which is also the inevitable trend of business model transformation. This paper takes big data, artificial intelligence, and business model innovation of service-type enterprises as a whole. By integrating the definition of business model innovation, enterprises change a certain link or many links in their previous value proposition, creation, and realization so as to better discover, lead, and meet customer needs and create greater value.

### 3. Design of Business Innovation Service Model Driven by Big Data

**3.1. Business Innovation Service Model Management System.** We should determine all kinds of resources needed for business model innovation and determine the key resources and key innovation factors from the process of enterprise value creation. We should also correctly locate the target. Generally speaking, the purpose of business model innovation is to create more value, which can be expressed as value maximization or profit maximization. However, according to the development status of each enterprise, the specific objectives and manifestations of business model innovation may be different. Business model innovation is an active role of enterprise managers in the objective environment. In this process, based on some basic principles, we must make the innovation mechanism simple and efficient. The management system of business innovation service model is shown in Figure 1.

Enterprises should determine the innovation strategy. Choosing an appropriate innovation strategy requires entrepreneurs to fully grasp innovation resources and have the ability to adapt and take charge of the overall situation. Generally, there are three innovation strategies that can be selected by enterprises: cumulative innovation, explosive innovation, and progressive innovation, as shown in Figure 2:

**3.2. Design Ideas and Methods.** A business model is not a set of static methods, and it will change with the external environment. Therefore, the design of enterprise business model should first identify its environment and its own characteristics; it is also necessary to analyze the macro environment and industrial environment of the enterprise market, as well as the business strategy of the company after SWOT analysis under such environmental background. However, in order to design the strategic means into a systematic business model and make it competitive enough, we must dig out the essence of user needs. After grasping the needs of users, the business model improvement design can be carried out: the first step is to compare the advantages and disadvantages of the company after SWOT analysis with the needs of users to confirm that preliminary improvement points can be formed; and the second step is to decompose the business model to the business model of the company and form the improvement solution according to the business model.

**3.3. Functional Requirements Analysis of Business Model Innovation.** The business intelligence system based on big data hopes to realize real-time monitoring and management of enterprise business systems, including production, sales, and inventory. The requirements of each function focus on the design and implementation of data warehouse based on Hadoop. On this basis, ETL data processing, online analysis, data mining, and data visualization are realized to help enterprises realize the intellectualization of management. The system can regularly and incrementally obtain the data

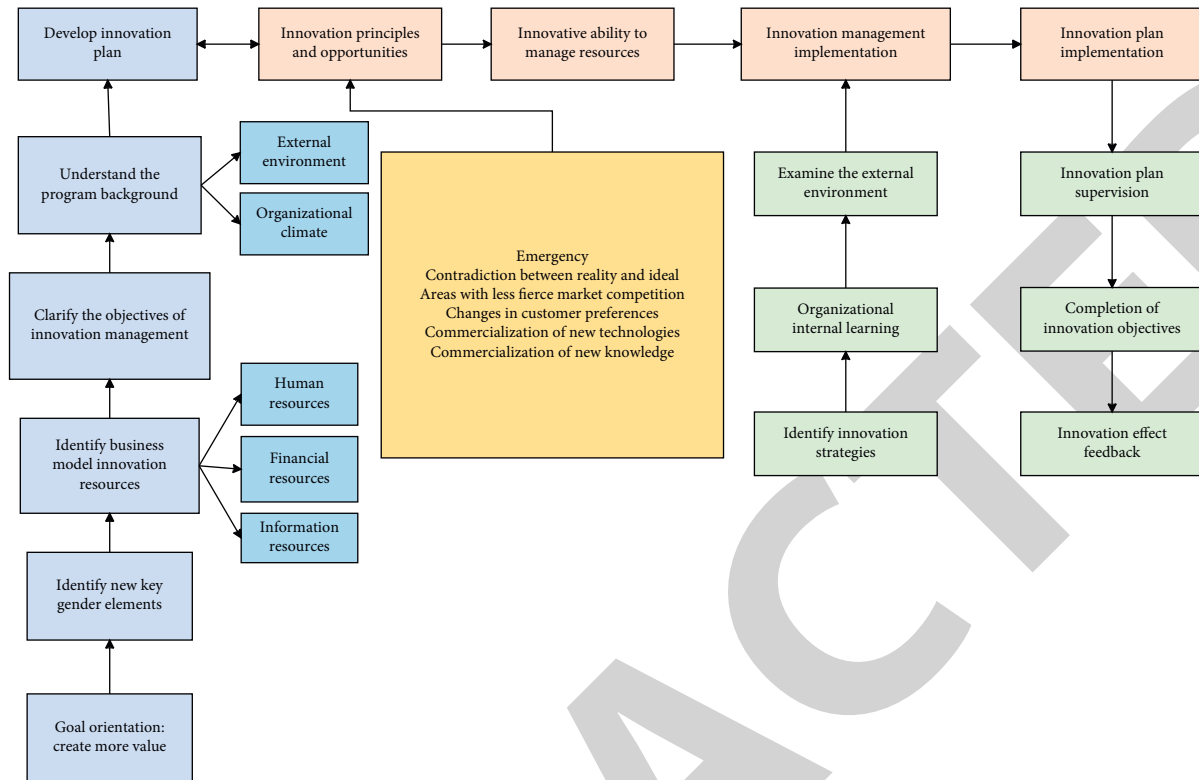


FIGURE 1: Business innovation service model management system.

|                     |                            |                        |
|---------------------|----------------------------|------------------------|
|                     | Innovation matrix          |                        |
| New technique       | Progressive innovation     | Explosive innovation   |
| Original technology | Cumulative innovation      | Progressive innovation |
|                     | Similar to existing models | New business model     |

FIGURE 2: Selection structure of business model innovation mode.

of each business system, realize regular data analysis according to the demand, and provide visual reports for relevant users for decision support. The functional requirements are shown in Figure 3.

3.4. *Big Data Infrastructure Analysis.* At present, many industries are building big data systems, but few can continue to have vitality and form business models. Massive data needs a scientific, standardized, and unified architecture. The big data infrastructure is composed of resource center, user center, application center, and big data center. The four centers coordinate and depend on each other, so as to complete the collection, cleaning, and processing of big data for decision analysis and finally show it to management and decision-makers in the form of graphical reports and provide analysis and decision-making purposes. In terms of function, it is mainly divided into four parts: data warehouse

model design, data collection and summary, data warehouse processing, and upper layer interactive management. Among them, the big data center will provide the underlying technical support for the realization of the above-mentioned whole big data collection, processing, and analysis. The function diagram of big data center is shown in Figure 4.

The whole process of building a big data service center can be divided into the steps shown in Figure 5.

#### 4. Construction of Evaluation Index of Business Innovation Service Model

Nowadays, various business models emerge one after another, and enterprises are facing an unprecedented turbulent market environment. In the new market environment, enterprises have to innovate business models. How to objectively and comprehensively evaluate the development of

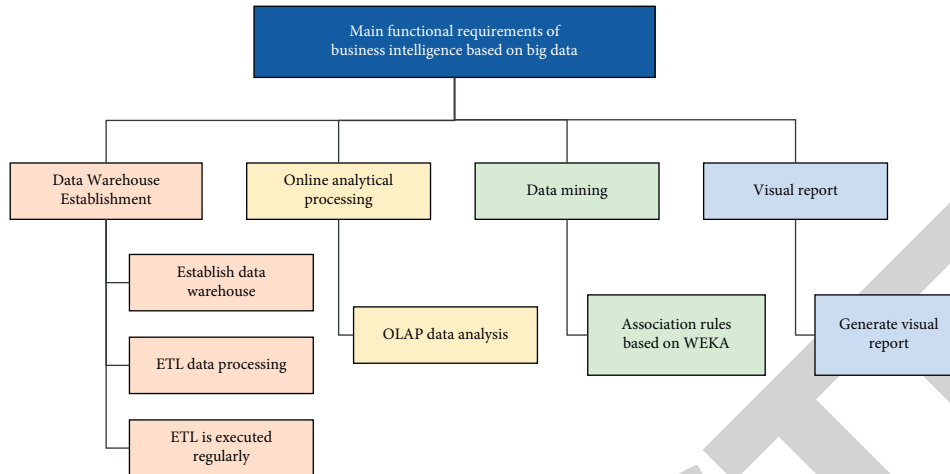


FIGURE 3: Diagram of functional requirements.

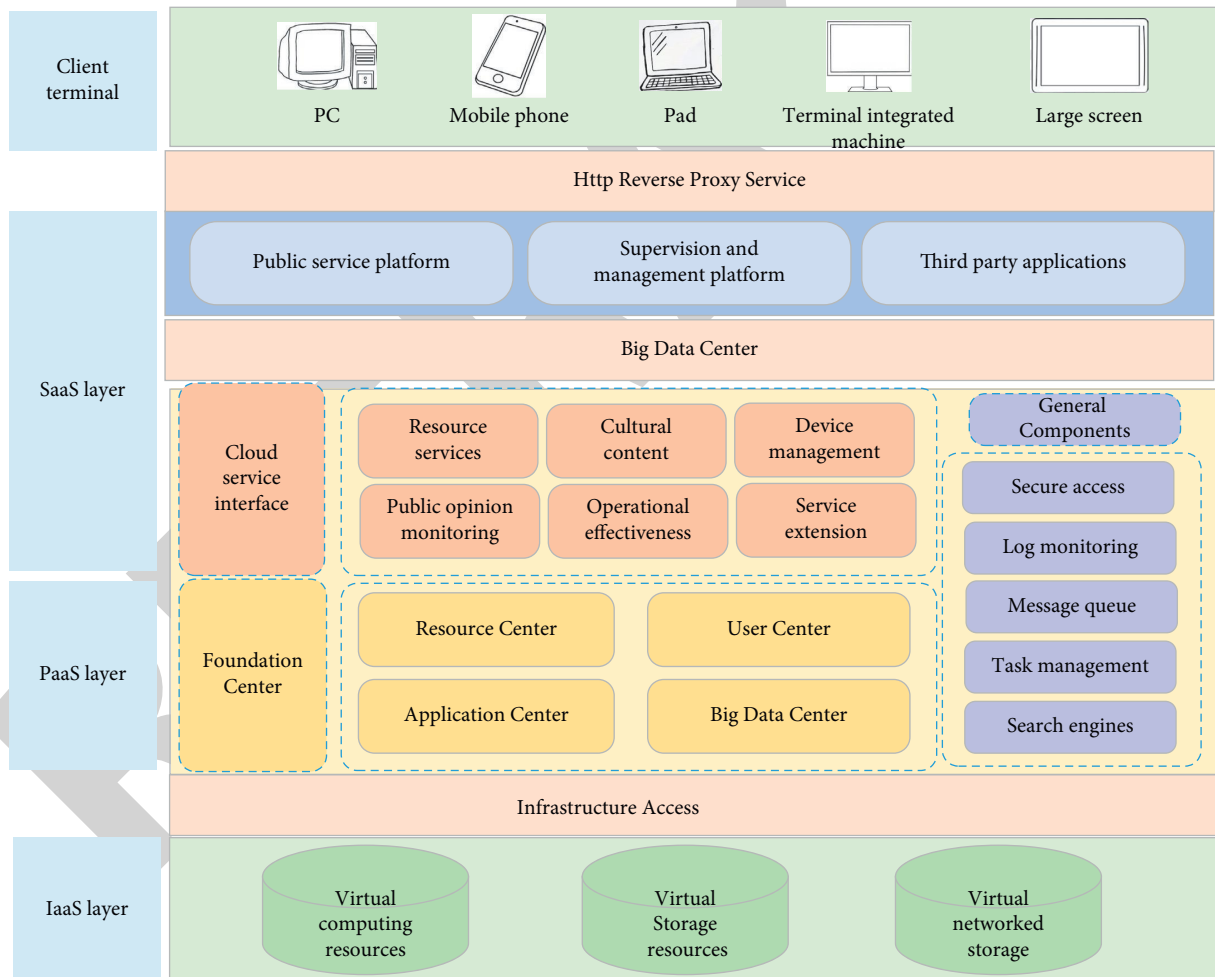


FIGURE 4: Big data infrastructure.

innovative business service models is an urgent problem to be solved. Based on the study of business model evaluation theory, this paper constructs the evaluation index system of business model innovation.

4.1. Selection Principle and Process of Evaluation Indicators for Business Innovation Service Model. The selection of evaluation indicators for the innovation effect of business service model will affect the accuracy of evaluation results and



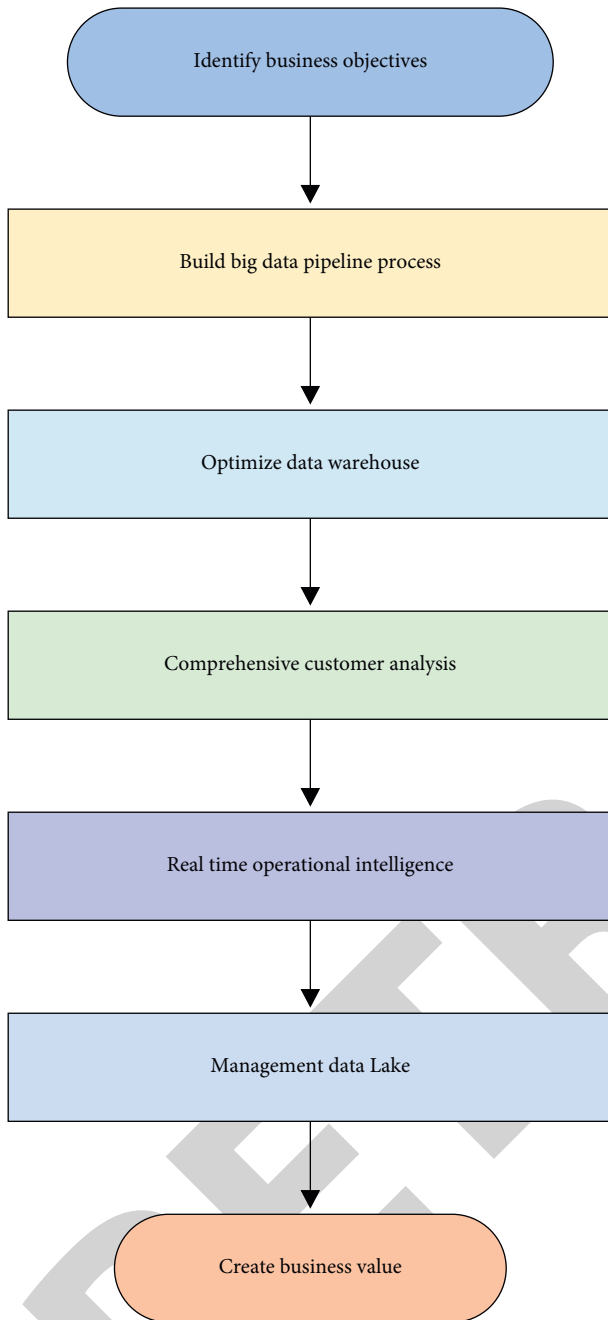


FIGURE 5: Construction process of big data service center.

indirectly affect the scientificity and accuracy of research conclusions. The establishment of business model innovation evaluation index system is the core step of business model evaluation. Scientific and effective methods must be applied for strict screening and screening. The principle relationship of indicator selection is shown in Figure 6.

There are many methods of index screening, such as time difference correlation analysis, cluster analysis, and comprehensive induction. Comprehensive induction developed relatively early. It combines objective statistical analysis data with subjective scientific description data to ensure the scientificity and effectiveness of index selection to a certain extent. Therefore, comprehensive induction can be used to

screen the index system. The specific process of establishing the index system is shown in Figure 7.

*4.2. Construction of Evaluation Index of Business Innovation Service Model.* The basic viewpoint of stakeholder theory is that the purpose of enterprise business model innovation is to create more value for stakeholders. Based on this basic view, we should carry out the innovation and reform of enterprise business model around the goal of maximizing the interests of enterprises and their stakeholders. The first step is to analyze the internal and external resources of the enterprise, make full use of the existing enterprise resources, actively find the external resources that may be used, and even actively explore some resources that are not owned by the enterprise and necessary for enterprise innovation. The second step, a very important part of business model innovation, is to redesign the organizational system. There may be some personnel changes, but major changes should be reduced as far as possible, so as not to cause employees' panic about job instability, so as to reduce the internal resistance of enterprise business model innovation. Business model innovation is not only a model change but also a process of organizational management innovation. The third step is to adjust the profit model of the enterprise. For stakeholders to realize their rights and interests, it may be necessary to broaden enterprise marketing channels, change marketing means, apply new technologies to reduce commodity circulation costs, etc. Through the above steps to maximize the interests of enterprises and meet the needs of maximizing individual value, that is, to pursue the promotion of personal value in the development of the enterprise, the personal value of employees is based on the enterprise value. Without the enterprise, the embodiment of personal value becomes empty talk. At the same time, the realization of personal value by employees is also the fundamental driving force to promote the development of the enterprise, and the two are interdependent and pull each other.

Based on the stakeholder theory, this paper reclassifies the enterprise stakeholders and puts forward the primary indicators to evaluate the business innovation service model, such as economic value, capital value, market value, product value, and production value. This paper proposes the initial index system model of business innovation service model, as shown in Figure 8.

The function of business model innovation is to realize the highly unified collective choice equilibrium between individual rationality and collective rationality of many transaction subjects within the enterprise boundary, so as to realize this team production mode, reduce transaction costs through this mechanism design, and realize Pareto optimal balance. The realization condition of this equilibrium state is not only to establish a perfect value creation mechanism through business model innovation but also to have a value sharing mechanism of benefit distribution, which is the essence of enterprise business model innovation. The flowchart of business model innovation is shown in Figure 9.

*4.3. Selection and Improvement of Evaluation Index System of Business Innovation Service Model.* This paper studies

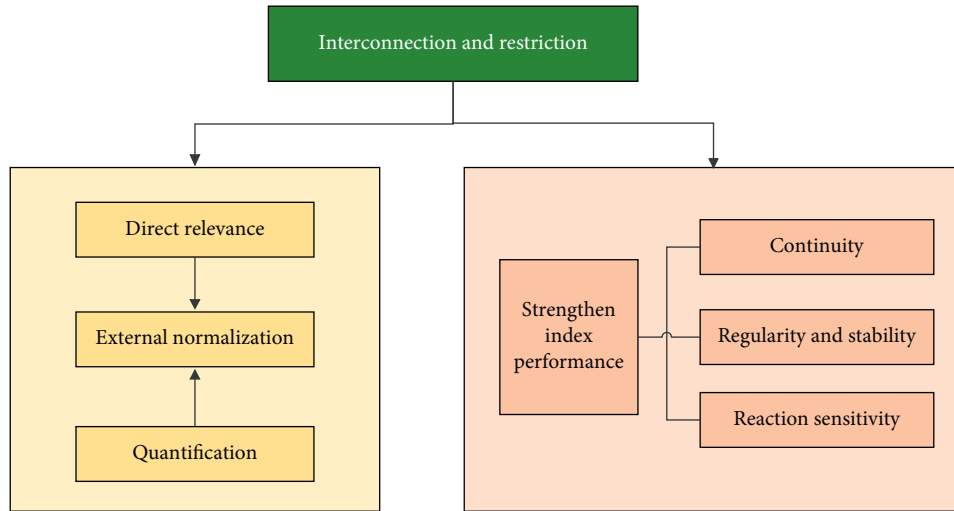


FIGURE 6: Relationship diagram of indicator selection principles.

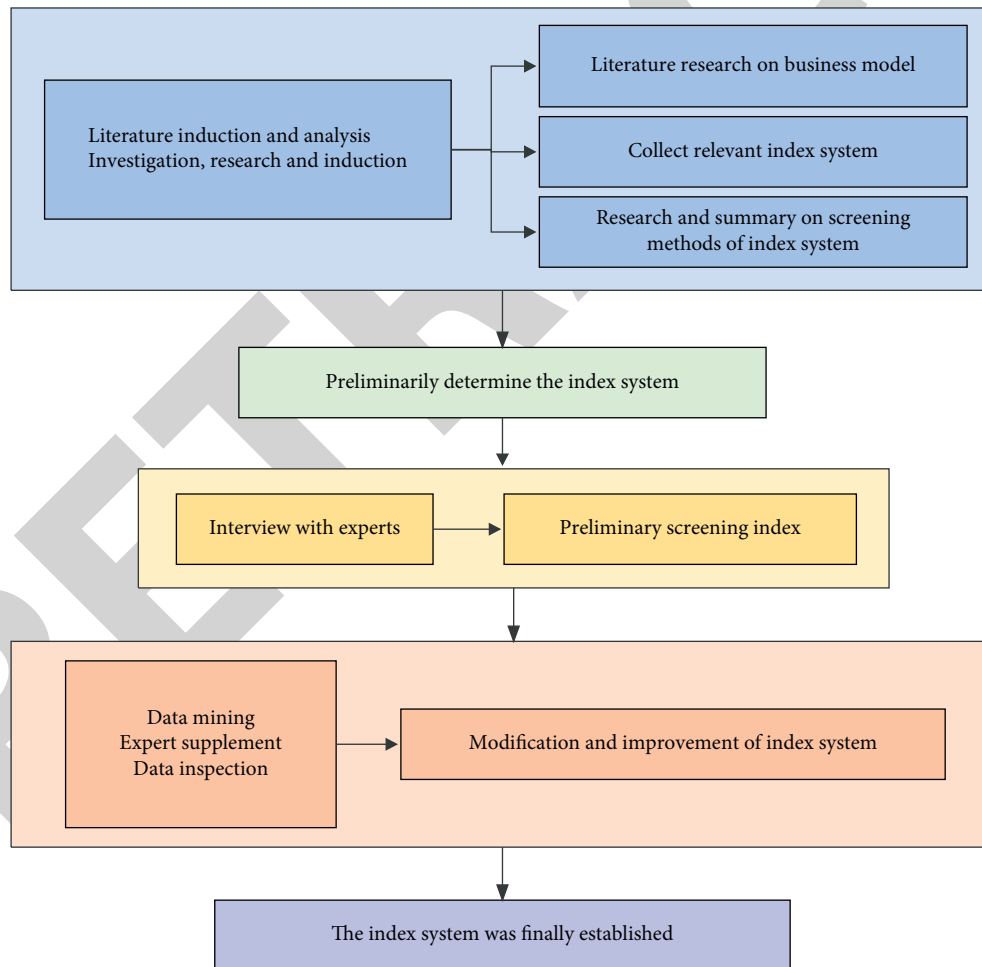


FIGURE 7: Specific process of determining the index system.

stakeholder theory and analyzes the expectations and risks of internal staff. After referring to relevant research data and conducting exploration and analysis of operation models of many enterprises, it has preliminarily built the

evaluation index system of business innovation service model. For the evaluation indexes with part of similar contents, just take one of them. Therefore, the new index set includes 18 indexes: bonus, rent, enterprise scale, corporate

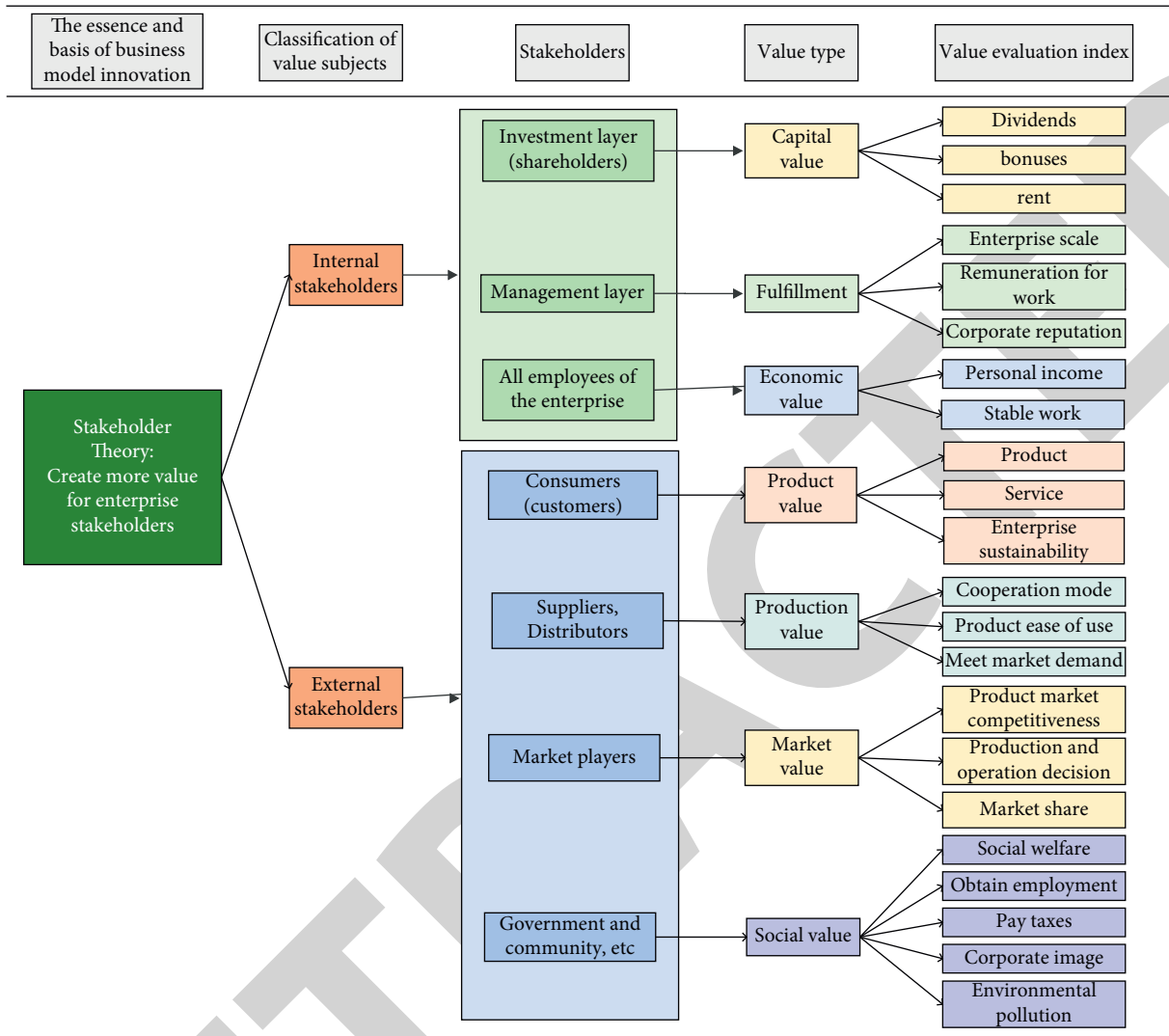


FIGURE 8: Initial model of business innovation service model evaluation index system.

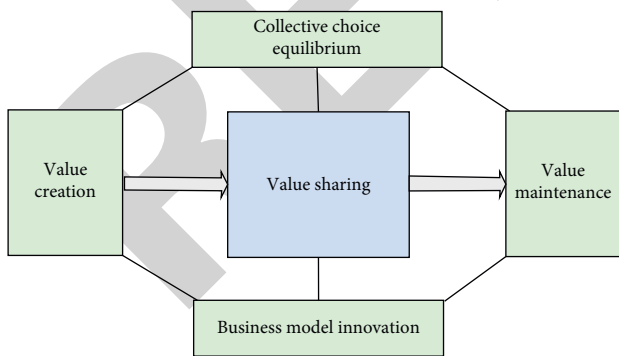


FIGURE 9: Business model innovation flowchart.

reputation, personal income, employees work stably, product, service, cooperation model, product ease of use, meeting market demand, market competitiveness of products, production and operation decision-making, market share, social welfare, obtain employment, taxation, and environmental pollution.

Besides, as it is difficult to acquire the data of many evaluation indexes and most indexes are difficult to quantize, this paper have replaced some indexes with quantitative ones with the same concept and add some necessary indexes. The finally determined evaluation index set includes enterprise profitability, enterprise scale, corporate reputation, employee income, employees work stably, product quality, product price, user satisfaction, enterprise information interaction, distribution strategy, new product innovation ability, master core technology, proportion of enterprise R&D investment, market share, enterprise capital turnover, and taking advantage of the original network and obtain employment.

In order to build the index system that can objectively assess the business innovation service model, it is necessary to conduct deeper-level analysis on the preliminarily built index set and make technical screening on the index set so as to build the business model innovation evaluation model with the evaluation layer. Comprehensive optimization chemotaxis algorithm is a science-based computing method, and it takes the dialectical decision-making of experts and typical data computing as the basis and combines qualitative and quantitative analysis in the

entire screening process. It first filters the indexes with 6 methods in a sequential order and revises and improves the built index system. One or more methods can be used repeatedly until the requirement is met. The index system confirmed by this method has higher scientificity and rationality, as shown in Figure 10.

According to the above principle of index system screening, determine the initial index set and set up a valuable index system  $Z = \{z_1, z_2, \dots, z_k, \dots, z_n\}$ .

#### 4.3.1. Filtering of Index Set

##### Step 1. Set filtering method

By means of set, filter unnecessary indexes and keep the remaining indexes. Assume the initial index system  $Z = \{z_1, z_2, \dots, z_k, \dots, z_n\}$ . Assume invite  $K$  experts and screen  $n$  indexes so as to preserve the important and indispensable indexes. Assume that the 1<sup>st</sup> expert selects  $t_1$  indexes:  $Z_1 = \{z_{11}, z_{12}, z_{13}, \dots, z_{1t_1}\}$ , the 2<sup>nd</sup> expert  $t_2$ :  $Z_2 = \{z_{21}, z_{22}, z_{23}, \dots, z_{2t_2}\}$ , and the  $K$ th expert  $t_k$ :  $Z_k = \{z_{k1}, z_{k2}, z_{k3}, \dots, z_{kt_k}\}$ . Then,  $U_i^k = z_i$  is the index system recognized by these experts and  $U_i^k = z_k$  is the complete index system all experts can accept.  $-U_i^k = z_k$  is the filtered index set, which might be an empty set.  $Z^0 = U_i^k = z_k = \{Z_1^0, Z_2^0, Z_3^0, \dots, Z_k^0\}$  is the index system selected.

##### Step 2. Weighted filtering method

In this process, indexes with small weight are filtered. Assume the index system is  $Z = \{z_1, z_2, \dots, z_k, \dots, z_n\}$ , and the corresponding weight coefficient is  $a_i = \{a_1, a_2, \dots, a_n\}$ . For the given  $a \in [0, 1]$ ,

$$Z^* = Z_a = \{Z_i | a_i \geq a, i = 1, 2, \dots, n\} = \{X_1^*, X_2^*, \dots, X_n^*\}, \quad (1)$$

where  $Z^*$  is the filtering index system to  $a$ , which is a very small positive number and the value of which shall be determined by experts according to specific principles and actual circumstance.

##### Step 3. Validity purification of index set

With this step, it can further improve the rationality of the index system. Validity is a measurement on the accuracy and effectiveness of the index results. Mark it as  $\beta$ , and the computing result is as follows:

Assume the index system is  $Z = \{z_1, z_2, \dots, z_k, \dots, z_n\}$  and that there are  $S$  evaluation object persons. Their score set on index  $Z_i$  is  $\{F_1^{(i)}, F_2^{(i)}, F_3^{(i)}, \dots, F_S^{(i)}\}$ . They divide them into 3 groups (high, medium, and low scores) according to the scores  $F_1^{(i)}, F_2^{(i)}, F_3^{(i)}, \dots, F_S^{(i)}$ , and the number of people in high- and low-score groups shall take up around 1/4 of the total people  $S$ .

Assume that  $\bar{F}_{1i}$  is the average score of the high-score group of  $Z_i$ ,  $\bar{F}_{2i}$  is the average score of the low-score group of  $Z_i$ , and  $F_i$  is the full score of  $Z_i$ . Then, the validity of  $Z_i$  is  $\beta_i = \bar{F}_{1i}/F_i - \bar{F}_{2i}/F_i, i = 1, 2, \dots, n$ , and the average validity of index system  $Z$  is  $\bar{\beta}_i = 1/n \sum_{i=1}^n \beta_i$ . Generally speaking, when

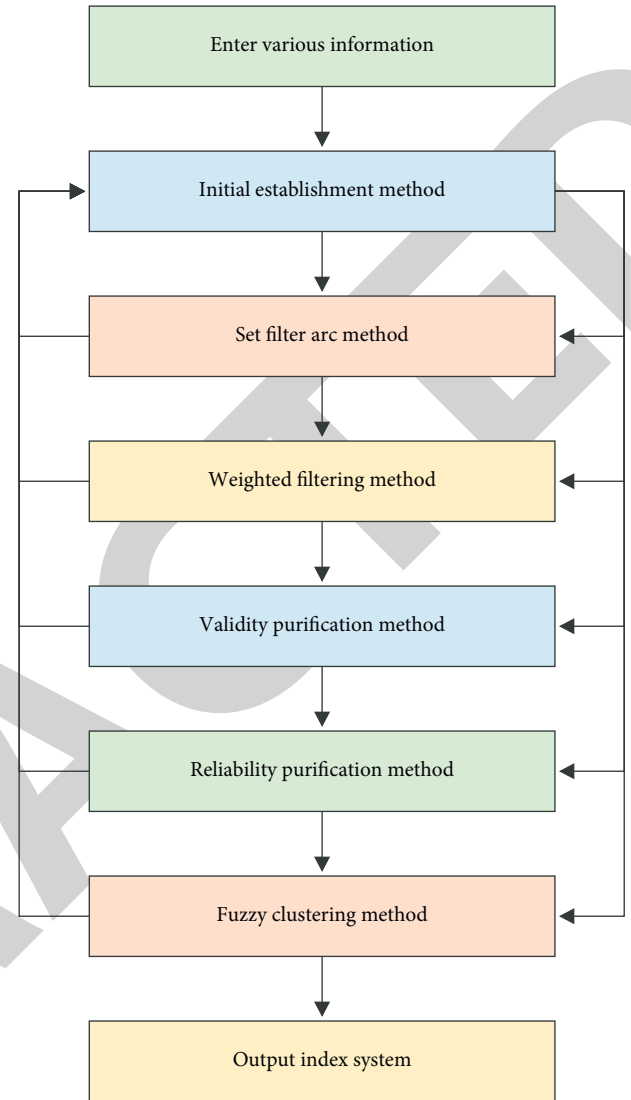


FIGURE 10: Specific procedures of comprehensive optimization chemotaxis algorithm creation of initial indexes.

the evaluation result of  $\beta_i$  or  $\bar{\beta}$  to  $z_i$  is good, it shall be kept; when  $\beta_i$  is within the scope of 0.2 – 0.4, the evaluation result is so-so and  $z_i$  shall be corrected; and when  $\beta_i$  is smaller than 0.2, the evaluation result is bad and  $z_i$  shall be modified or eliminated.

##### Step 4. Reliability purification of index set

This method is a kind of purification for the stability and reliability of index set. The so-called reliability refers to the correlation coefficient of 2 evaluation results on the same index. Assume that  $\bar{Y}$  is the average value of the 1<sup>st</sup> evaluation on  $z_1$  and  $\bar{X}$  the average value of the 2<sup>nd</sup> evaluation on  $z_1$ .

$$\bar{X} = \frac{1}{n} \sum_{i=1}^n X_i, \quad (2)$$

$$m\bar{Y} = \frac{1}{n} \sum_{i=1}^n Y_i.$$

Then, the reliability of the index system  $Z = \{z_1, z_2, \dots, z_k, \dots, z_n\}$  is

$$\rho = \frac{\sum_{i=1}^n (Y_i - \bar{Y}) - (X_i - \bar{X})}{\sqrt{\sum_{i=1}^n (Y_i - \bar{Y})^2 \cdot \sum_{i=1}^n (X_i - \bar{X})^2}} \quad (3)$$

Assume that the objects are evaluated in the stationary normality and they have no significant changes in the 2 evaluations, then:

When  $\rho$  is within the range of 0.90 ~ 0.95, this index system has excellent stability and reliability; when  $\rho$  is within 0.80 ~ 0.90, it has good stability and reliability; when  $\rho$  is within 0.65 ~ 0.80, it has so-so stability and reliability; and when  $\rho$  is within 0.65, it has bad stability and reliability, indicating that certain indexes in the system have significant differences in these 2 evaluations. The following methods can be adopted in order to find these indexes:

Assume that  $R_i^{(1)} = \{Y_{i1}^{(1)}, Y_{i2}^{(1)}, Y_{i3}^{(1)} \dots Y_{im}^{(1)}\}$  and  $R_i^{(2)} = \{Y_{i1}^{(2)}, Y_{i2}^{(2)}, Y_{i3}^{(2)} \dots Y_{im}^{(2)}\}$  are the evaluation vectors made by the evaluation objects on  $Z_i, i = 1, 2, \dots, n$ . Cluster  $\{R_1^{(1)}, R_2^{(1)} \dots R_n^{(1)}, R_1^{(2)}, R_2^{(2)} \dots R_n^{(2)}\}$ . If the predesigned input values  $R_i^{(1)}$  and  $R_i^{(2)}$  are in different classes, take out  $Z_i$  and then make qualitative analysis. If the differences of the 2 evaluation results are caused by  $Z_i$ , then modify or eliminate  $Z_i$ .

**Step 5. Fuzzy clustering method**

This method is a kind of purification on the between-index compatibility. With this method, it can merge the indexes with bigger compatibility into one term or modify it or reduce the compatibility between indexes in order to make the index system more independent, scientific, and simple. Assume that all data involved are acquired under the stable state and the fuzzy relation matrix of index system  $Z = \{z_1, z_2, \dots, z_k, \dots, z_n\}$  is

$$Q = \begin{pmatrix} q_{11} & K & q_{1n} \\ M & O & M \\ q_{m1} & K & q_{mn} \end{pmatrix}, \quad (4)$$

where  $Q_{ii}$  represents the similarity coefficient between  $Z_i$  and  $Z_i$  and can be calculated with the following formula:

$$q_{ij} = \frac{\sum_{k=1}^m (r_{ik} - \bar{r}_i) - (r_{jk} - \bar{r}_j)}{\sqrt{\sum_{k=1}^m (r_{ik} - \bar{r}_i)^2 \cdot \sum_{k=1}^m (r_{jk} - \bar{r}_j)^2}}, \quad (5)$$

where  $r_{ik}$  is the evaluation vector of the evaluation object  $P_t$  (representative typical evaluation object) to  $Z$ ,

$$\bar{r}_i = \frac{1}{m} \sum_{k=1}^m r_{ik}, \quad (6)$$

$$\bar{r}_j = \frac{1}{m} \sum_{k=1}^m r_{jk}.$$

According to the relevant fuzzy theories, assume that (a)  $q_{ii} = 1, \forall i \in [0, 1]$ ; (b)  $q_{ij} = q_{jk}, \forall i, j, q_{ij} \in [0, 1]$ ; and (c)  $q_{ij} \leq q_{jk} \leq q_{ik}, \forall i, j, k = 1, 2, 3, \dots, k, \dots, n$ .

Calculate  $a < b = \min\{a, b\}$ . At this time, matrix  $Q = (q_{ij})_{m \times n}$  is called as the fuzzy equivalent matrix  $Q = (q_{ij}^\lambda)_{m \times n}$ , where

$$q_{ij}^\lambda = \begin{cases} 1, & q_{ij} \geq \lambda, \\ 0, & q_{ij} < \lambda. \end{cases} \quad (7)$$

Apparently, different  $Z$  has different  $Q_\lambda$  and  $\lambda$ . For the given  $\lambda$ , it is a matrix formed by 0 and 1. If the elements in the  $i$ th column are completely equal to those in the  $j$ th column, then  $z_i$  and  $z_j$  are of the same class. In this way, for different  $\lambda$ , it has different classes. Such  $\lambda$  shall be selected. It leads to small differences in the index within the same class, but the differences between classes are significant. Such  $\lambda$  is the optimal, and the cluster corresponding to the optimal  $\lambda$  is called as the optimal cluster and is marked as

$$Z_{Pt} = \left\{ \left\{ Z_1^{(1)}, Z_2^{(1)}, Z_3^{(1)} \dots Z_{n1}^{(1)} \right\}, \left\{ Z_1^{(2)}, Z_2^{(2)}, Z_3^{(2)} \dots Z_{n2}^{(2)} \right\} \dots \right\} \\ \left\{ Z_1^{(c)}, Z_2^{(c)}, Z_3^{(c)} \dots Z_{nc}^{(c)} \right\} \dots \left\{ Z_{pt}^{(1)} K Z_{pt}^{(c)} \right\} \quad (8)$$

where  $Z_{pt}^i = \{Z_1^i, Z_2^i, Z_3^i K Z_{ni}^i\}$  is called as the subclass of  $Z_{pt}$ .

Assume that there are  $S$  evaluation object persons.  $\{Z_{pt} | t = 1, 2, 3, \dots, k, \dots, s\}$ .  $Z_{pt}$  is the optimal cluster to the evaluation objects; obviously  $Z_i$  belongs to a certain subclass of  $Z_{pt}$ . If  $Z_{i1}, Z_{i2}, Z_{i3} \dots Z_{ib}$  all belong to the same subclass, then  $Z_{i1}, Z_{i2}, Z_{i3} \dots Z_{ib}$  are called as the same class.

Assume that  $Z_{i1}, Z_{i2}, Z_{i3} \dots Z_{ib}$  are of the same kind as  $k$  elements in  $\{Z_{pt} | t = 1, 2, 3, \dots, k, \dots, s\}$ . Then  $\varphi = k/s$  and  $1 \leq k \leq s$  is the clustering degree between  $Z_{i1}$  and  $Z_{i1}, Z_{i2}, Z_{i3} \dots Z_{ib}$ . Obviously,  $0 \leq \varphi \leq 1$ . If  $\varphi \geq 0.8$ , merge  $Z_{i1}, Z_{i2}, Z_{i3} \dots Z_{ib}$  into a term; if  $\varphi < 0.8$ , do not merge but keep them. Adjustments shall be made to the indexes, which can be merged into 2 or more terms in order to merge them into just one term.

The above clustering is taken into account from a quantity perspective, and whether to merge terms requires analysis from a qualitative angle. For the indexes to be merged, efforts shall be made to reduce the compatible parts. Due to fuzziness, the boundary between indexes is not clear; therefore, the reduction of compatible components is relative. At the end, get the evaluation index system model of business innovation service model, as shown in Figure 11.

Finally, give weight to the evaluation index of business model, including expert sorting method or comprehensive weighting method. Analyze the data collected with the optimal weight combination so as to provide more targeted opinions and suggestions for the healthy development of enterprises.

**5. Research on Business Model Operation Based on Big Data**

Generally speaking, operation is a series of human intervention activities aimed at product promotion. How to use big data to realize the operation of intelligent business service mode is a relatively new research topic. The operation scope of business intelligence services under big data

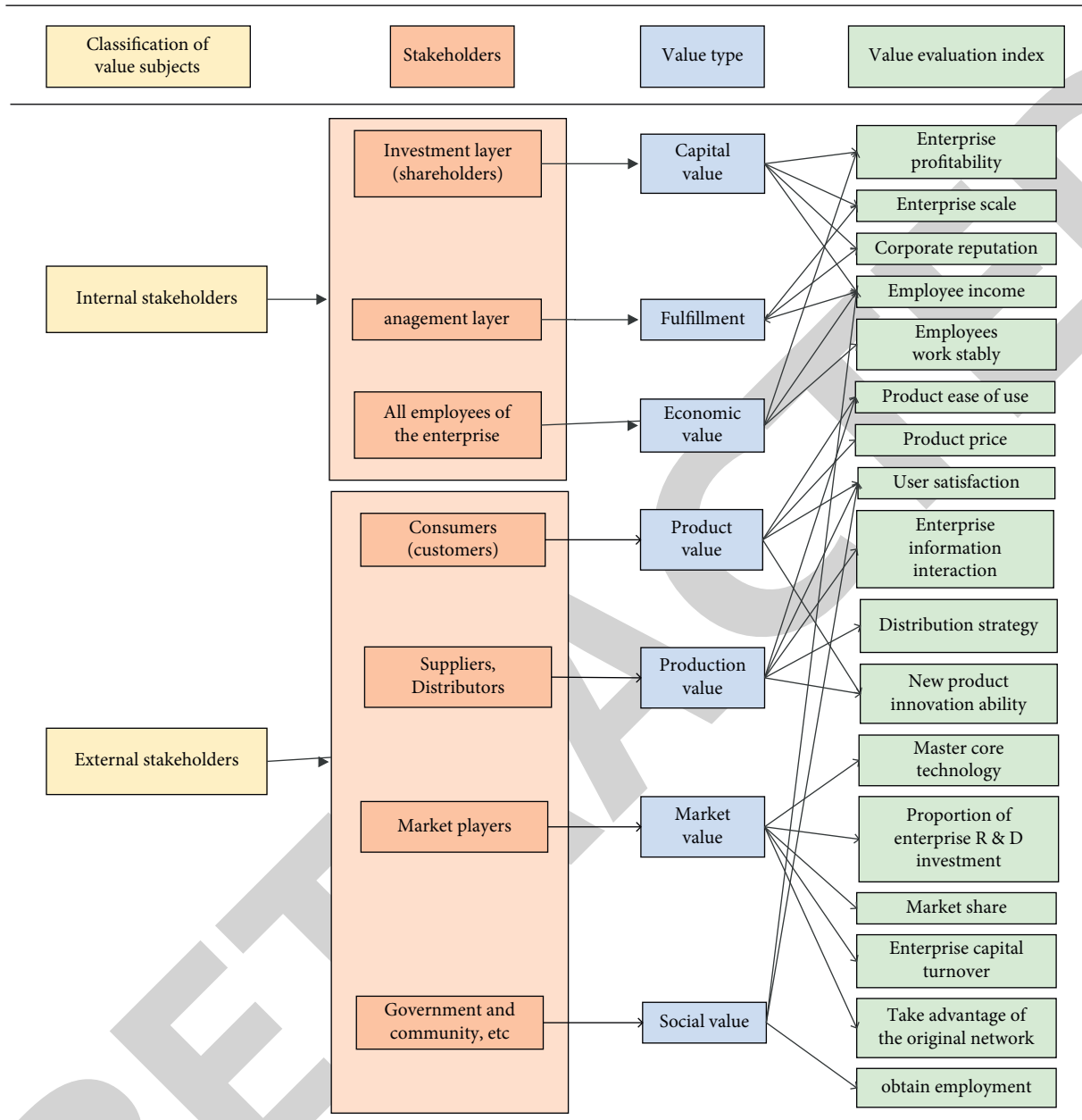


FIGURE 11: Evaluation cross index model of business innovation service model.

proposed in this paper includes construction industry big data standards, daily data operation, data-driven operation, content operation, user operation, publicity and promotion operation, and other services, as shown in Figure 12.

5.1. Construction of Industry Big Data Standard. Standardization construction is the basic pillar of the big data center. Only through the construction and use of standards can we ensure the interconnection of various kinds of service information and reduce risks. The construction of industrial big data standards mainly provides support for the organization, preservation, classification, resource exchange, and other related work of big data warehouse, takes into account the digital resource technical

standards of different institutions, enhances the capacity of co-construction and sharing of digital resource content, and ensures the long-term benign and sustainable development of public cultural big data service system. At the same time, the industry standards shall comply with the definition principles of digital resource type, user type, terminal type, and network environment and formulate standards and specifications based on national standards, industry standards, and technical standards of co-construction units, so as to achieve inheritance, compatibility, practicability, and expansibility.

5.2. Daily Data Operation. The daily operation of data mainly ensures the safe and stable operation of big data and

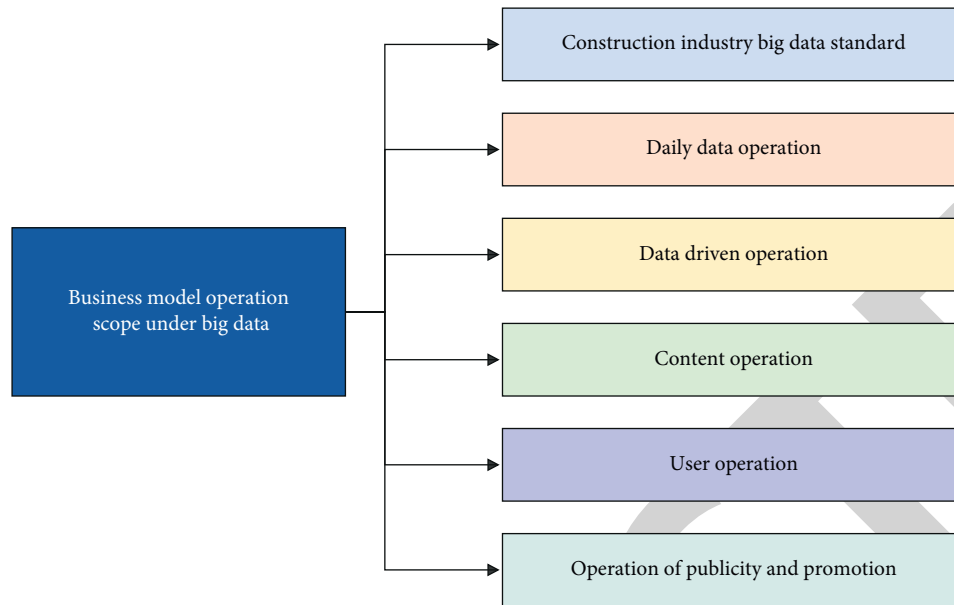


FIGURE 12: Operation scope of business intelligence model based on big data.

ensures the maintenance of big data system and infrastructure. The operation center shall regularly test the effectiveness of big data warehouse, data lake, and microservice to ensure the normal operation of source code and data integrity. In case of system problems, it shall feedback and deal with them in time.

Big data security protection is also an important part of daily data operation. Enterprise big data often contains a large number of personal private contents, including personal avatar, mobile phone, address, family members, and other sensitive information. The operation center needs to consider the personal information security of the data and shall not provide it to a third party without the consent of the person to whom the information belongs. Even if the data is not personal information, the damage caused by information loss is huge. Therefore, it is necessary to establish the big data service information security management system and various operation and maintenance security management systems, conduct regular security inspection and evaluation, and establish continuous tracking and improvement schemes for potential security risks and related problems. During operation, the operation center shall actively take necessary technical measures for security control, regularly repair loopholes, and prevent malicious tampering of external services and important data facilities and make disaster recovery backups in different places regularly to ensure rapid recovery after being attacked and tampered with. In enterprises, big data services cover a wide range and the number of users is huge. Therefore, it is necessary to establish and improve the fault emergency response mechanism.

**5.3. Data-Driven Operation.** Data-driven operation refers to the process of using the results of big data service analysis to drive the improvement of operation quality. Big data enables

the operation center to collect, store, organize, analyze, and visualize any real-time data and generate operable intelligence. This intelligence provides impetus for the sustainable development of the industry and is the information infrastructure available to each organization. Data-driven operation needs to focus on three aspects: data planning, data acquisition, and data analysis. Its dimensions include all aspects, which can be improved from the following four parts:

- (1) According to the analysis of operation data, help relevant departments to establish an assessment and evaluation system and present it through the platform
- (2) Use big data to collect, analyze, and solve problems and provide services more in line with users' needs
- (3) Guide and help users more accurately, and efficiently enjoy the sense of gain brought by intelligent business services according to big data
- (4) According to the user's use data and evaluation feedback, form iterative suggestions for system improvement, and submit them to the operation center for service optimization and upgrading

Data-driven operation is also the self-optimization and improvement of the big data algorithm. Through data accumulation and learning, big data can upgrade and improve the original algorithm through self-learning of data, so as to predict the future trend of the market and make scientific decisions for enterprises.

**5.4. Content Operation.** Through big data services to achieve efficient content operation, business intelligence services will have repeatable processes to create effective content. Content operation mainly includes content audit,

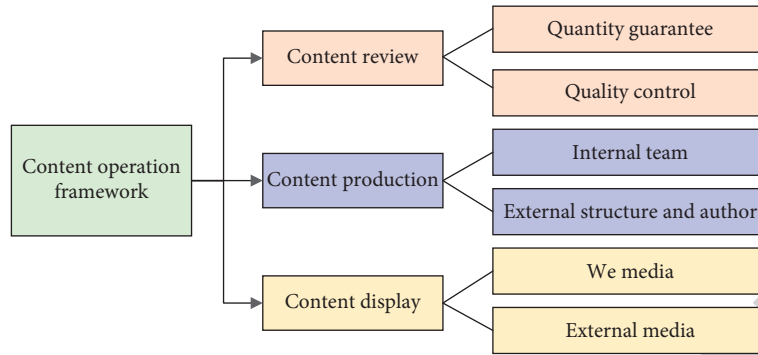


FIGURE 13: Content operation framework.

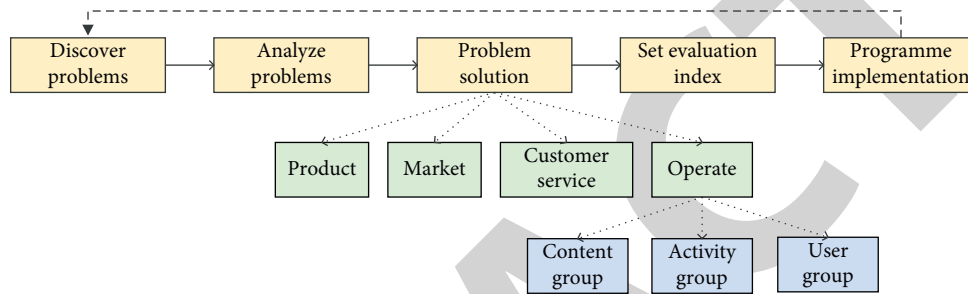


FIGURE 14: User operation workflow.

content production, and content display. Content audit is mainly responsible for quality and quantity to ensure that business intelligence services have sufficient and high-quality content. Content production consists of internal team, external structure, and author. Content display refers to the specific presentation form of content. It can be displayed through self-media such as channels and columns or through external media to realize the internal and external dissemination of information. The three parts jointly realize the content operation of intelligent business service mode, so as to provide various information services for enterprises. The specific framework is shown in Figure 13:

**5.5. User Operation.** Users are the foundation of an enterprise or product, and all business departments focus on user services. User operation plays the role of a thread in the enterprise and coordinates the resources between various departments. Its most important job is to control the needs of users. After discovering the problems and analyzing the causes of the problems, user operations should distribute requirements to relevant business departments. If multiple parties need to work together, user operations need to coordinate resources and the relationship between various departments. Monitoring the implementation process and results of the scheme is also an extremely important work and puts forward reasonable improvement suggestions for the scheme in real time. The evaluation index link is set in the process, that is, whether the time, money, and other labor costs paid for doing a thing meet the psychological expectations. Through this process, the user operation realizes the

rapid transformation of value. The specific workflow is shown in Figure 14.

**5.6. Publicity, Promotion, and Operation.** Publicity and promotion operation mainly refers to the integration of various online and offline business services within the enterprise and targeted publicity and promotion. This is a big data model promotion process, and the purpose is to achieve full coverage of services. Publicity, promotion, and operation include the basic work of processing, integration, review, uploading, and initial promotion of resources of various departments in the enterprise. On the basis of continuous operation and promotion, it is needed to focus on the construction of enterprise characteristic service system to expand the effect; then focus on promoting users to become the application, creator, and provider of the system; and finally promote the system to become a new operation mode benefiting the whole enterprise.

## 6. Conclusions

This paper has mainly studied the business intelligence service model based on big data technology. It has firstly summarized the defects of conventional business models and the characteristics of big data. Then, it has combined big data technology with business innovation service model, designed the big data-driven business innovation service model, including management system, risk assessment, and functional and nonfunctional demands, and analyzed the big data architecture. After that, it has studied the construction of big data-driven business innovation service model,



analyzed the construction process, and established the evaluation index system of the completed business models so as to evaluate its development status in a comprehensive and objective manner. Finally, it has studied and analyzed the operations of business model under big data so as to provide certain ideas for business model innovation. The methods and evaluation index system in this paper on data mining and analysis and business model design have certain universality and significance in helping enterprises to realize the big data business innovation service model.

## Data Availability

The simulation experiment data used to support the findings of this study are available from the corresponding author upon request.

## Conflicts of Interest

The authors declare that there are no conflicts of interest regarding the publication of this paper.

## Acknowledgments

This work was supported in part by the National Key R&D Program of China (2018YFB1402600).

## References

- [1] J. H. Yang and D. N. Liu, "The big data business model of smart power based on information value theory," in *Proceedings of the 2015 International Symposium on Energy Science and Chemical Engineering (ISESCE 2015)*, vol. 45, pp. 14–17, Guangzhou, China, December 2015.
- [2] V. L. F. Minatogawa, M. M. V. Franco, I. S. Rampasso et al., "Operationalizing business model innovation through big data analytics for sustainable organizations," *Sustainability*, vol. 12, no. 1, 2020.
- [3] C. Loebbecke and A. Picot, "Reflections on societal and business model transformation arising from digitization and big data analytics: a research agenda," *The Journal of Strategic Information Systems*, vol. 24, no. 3, pp. 149–157, 2015.
- [4] R. Schuritz and G. Satzger, "Patterns of data-infused business model innovation," in *Proceedings of the 2016 IEEE 18th International Conference on Business Informatics (CBI)*, vol. 1, pp. 133–142, Paris, France, September 2016.
- [5] M. Paiola and H. Gebauer, "Internet of things technologies, digital servitization and business model innovation in btob manufacturing firms," *Industrial Marketing Management*, vol. 89, pp. 245–264, 2020.
- [6] F.-J. Molina-Castillo, A.-L. Meroño-Cerdan, and C. López-Nicolás, "Impact of business model objectives on marketing innovation activities," *European Journal of Innovation Management*, vol. 23, no. 1, pp. 177–195, 2019.
- [7] M. Geissdoerfer, D. Vladimirova, K. V. Fossen, and S. Evans, "Product, service, and business model innovation: a discussion," *Procedia Manufacturing*, vol. 21, pp. 165–172, 2018.
- [8] A. Calabrese, G. Forte, and N. L. Ghiron, "Fostering sustainability-oriented service innovation (SOSI) through business model renewal: the SOSI tool," *Journal of Cleaner Production*, vol. 201, pp. 783–791, 2018.
- [9] C.-Y. Song and E.-S. Cho, "A business service identification techniques based on XL-BPMN model," *KIPS Transactions on Software and Data Engineering*, vol. 5, no. 3, pp. 125–138, 2016.
- [10] J. Yang, W. Zhang, J. Liu, J. Wu, and J. Yang, "Generating de-identification facial images based on the attention models and adversarial examples," *Alexandria Engineering Journal*, vol. 61, no. 11, pp. 8417–8429, 2022.
- [11] X. Yang, T. Yu, and H. Xu, "A novel framework of using petri net to timed service business process modeling," *International Journal of Software Engineering and Knowledge Engineering*, vol. 26, no. 4, pp. 633–652, 2016.
- [12] J. Kim and B. Yang, "A smart city service business model: focusing on transportation services," *Sustainability*, vol. 13, no. 19, Article ID 10832, 2021.
- [13] P. Ateetanan, S. Usanavasin, K. Shirahada, and T. Supnithi, "From service design to enterprise architecture: the alignment of service blueprint and business architecture with business process model and notation," *Serviceology for Services*, vol. 10371, pp. 202–214, 2017.
- [14] P. P. Pieroni, T. C. McAlloone, and D. C. A. Pigosso, "Configuring new business models for circular economy through product-service systems," *Sustainability*, vol. 11, no. 13, pp. 1–8, 2019.
- [15] W. Wei, B. Zhou, D. Połap, and M. Woźniak, "A regional adaptive variational PDE model for computed tomography image reconstruction," *Pattern Recognition*, vol. 92, pp. 64–81, 2019.
- [16] Y. Liu, D. Jiang, B. Tao et al., "Grasping posture of humanoid manipulator based on target shape analysis and force closure," *Alexandria Engineering Journal*, vol. 61, no. 5, pp. 3959–3969, 2022.
- [17] J.-S. Kyung and W. Cho, "The study of business model development of support service Program for small and medium enterprise using process modeling," *The e-Business Studies*, vol. 14, no. 4, pp. 99–118, 2013.
- [18] G. Li, J. Li, Z. Ju, Y. Sun, and J. Kong, "A novel feature extraction method for machine learning based on surface electromyography from healthy brain," *Neural Computing & Applications*, vol. 31, no. 12, pp. 9013–9022, 2019.
- [19] O. Turetken, P. Grefen, R. Gilsing, and O. E. Adali, "Service-dominant business model design for digital innovation in smart mobility," *Business & Information Systems Engineering*, vol. 61, no. 1, pp. 9–29, 2019.
- [20] J. Chen, "The influence of big data on transformation of traditional manufacturing enterprises from business model perspective," in *Proceedings of the Fourth International Symposium - Management, Innovation & Development, Bk One & Two*, pp. 460–465, Berlin, Germany, December 2018.
- [21] Z. H. Sun, K. Strang, and S. Firmin, "Business analytics-based enterprise information systems," *Journal of Computer Information Systems*, vol. 57, no. 2, pp. 169–178, 2017.
- [22] E. P. Fernandez-Manzano and M. I. Gonzalez-Vasco, "Analytic surveillance: big data business models in the time of privacy awareness," *El Profesional de la Información*, vol. 27, no. 2, p. 402, 2018.
- [23] S. Yablonsky, "Smart wearable multi-sided fashion product platforms," *Business Models and Ict Technologies for the Fashion Supply Chain*, vol. 413, pp. 135–150, 2017.
- [24] S. Wang, "Research on the paths of business model innovation," *Proceedings of The Second International Conference on Economic and Business Management (FEBM 2017)*, vol. 33, pp. 732–738, 2017.
- [25] Y. Li, "Research on the business model innovation in online tourism services: a case study of Ctrip," in *Proceedings of the 2018 2nd International Conference on Management*

## Research Article

# Evaluation and Analysis of High-Quality Development of New Urbanization Based on Intelligent Computing

**Haoran Cheng** 

*School of Business, Yuxi Normal University, Yuxi 653100, China*

Correspondence should be addressed to Haoran Cheng; [chenghaoran1984@yxnu.edu.cn](mailto:chenghaoran1984@yxnu.edu.cn)

Received 11 April 2022; Revised 16 May 2022; Accepted 26 May 2022; Published 17 June 2022

Academic Editor: Man Fai Leung

Copyright © 2022 Haoran Cheng. This is an open access article distributed under the Creative Commons Attribution License, which permits unrestricted use, distribution, and reproduction in any medium, provided the original work is properly cited.

Urbanization construction is an important part of China's economic development. New urbanization is a new development direction proposed by China in order to adapt to social development. China's urbanization construction must be changed. The construction of new urbanization is not only committed to expanding the scale of cities and towns but also promotes the industrial upgrading of cities and towns and improves the efficiency of urban production to meet the needs of economic growth. Under China's high-quality economic development model, various problems of ecological environment pollution and low productivity have emerged. New urbanization has become an effective strategy to promote high-quality economic development. The research results of this paper show that (1) the level of coordinated development among urbanization systems is low, and the population agglomeration and industrial economic development, urban land resource utilization, urban public welfare development, and urban ecological environment development are not coordinated during the process of population urbanization, it is necessary to strengthen the development capacity of the economy, space, society, and green urbanization, and only the coordinated development of various systems can promote the high-quality development of urbanization. (2) From 2006 to 2017, the urbanization development coefficient of the five northwestern provinces and regions has increased year by year, and the high-quality development level of urbanization has gradually increased. Except for the urbanization system development coefficient of urbanization from 2016 to 2017, which was higher than 0.3 and was in a relatively imbalanced stage, the coefficients of the other provinces were all lower than 0.2 in each year, which was in a highly imbalanced stage. (3) The loss value of the intelligent computing development evaluation model proposed in the article is the lowest among the detection models. When the number of iterations is 20, the final loss value of the article is 0.1. With the increase in the number of iterations, the accuracy rate is basically in a stable growth state, when the number of iterations is 20, and the accuracy rate reaches a peak value of 99%, which is close to 100%. The experimental results can also show that the performance of the intelligent computing development evaluation model structure is better than the evaluation of high-quality urbanization development.

## 1. Introduction

As a strong driving force for high-quality development, urbanization is not only an important driving force for population agglomeration within urban space but also an important support for industrial agglomeration and technological innovation. In the process of urbanization construction, policy dividends have opened up prerequisites for industrial agglomeration. At this stage, my country's urbanization construction is still in a critical period of improving quality. The article shows that the

problem of low quality of urbanization in my country is becoming increasingly prominent and proposes that the high-quality development of urbanization should be promoted by improving total factor productivity, strengthening urban quality construction, building characteristic small towns, and cultivating new types of farmers [1]. The article puts forward the current development status of my country's urbanization and gives relevant suggestions [2]. Based on the panel data of 30 provinces in China from 2004 to 2018, this paper constructs an evaluation system for the rapid development of townships [3]. Using the GIS

technology and the coordination degree model, the spatial pattern of urbanization quality and resource utilization coordination in 288 cities above the prefecture level in China is analyzed, and the potential reasons are being discussed [4]. Based on the new perspective of “urbanization quality improvement,” this paper summarizes the connotation of urbanization quality in developed areas by analyzing the experience and practice of village renovation in the Southwest Village of Zengcheng County [5]. This paper describes the great significance of the government’s strong support for township construction [6]. Based on the analysis of relevant literature at home and abroad, the article gives a brand-new goal for the development direction of my country’s towns and villages [7]. According to the relationship between urbanization development and industrialization development since my country’s reform and opening up, this paper makes a quantitative analysis of I/U and N/U [8]. This paper calculates the development index of new urbanization and industrial structure in Shandong Province and establishes a coupling coordination degree model of new urbanization and industrial structure [9]. The article analyzes the overall trend of agglomeration in the economic pattern of Northeast China and shows that the development characteristics of Northeast China are different, and the role of urban agglomerations needs to be strengthened [10]. This paper analyzes the economic development status of cities and towns in the five northwestern provinces over the past five years and makes a simple forecast for the future economic development [11]. The article explains the necessity and importance of township construction for national economic development [12]. The article illustrates that promoting high-quality development is an inherent requirement of new urbanization and an objective requirement of rural revitalization [13]. Based on the Guangxi research, this paper believes that private enterprises should adhere to the new development concept, firmly grasp, and make good use of five opportunities, namely, high-end industry, population urbanization, green development, social informatization, economic globalization, and exploring the new era of enterprise high A new path for quality development [14]. By analyzing the development path of urbanization, this paper considers the agglomeration efficiency and the fairness of urban and rural spaces in a thoughtful manner [15].

## 2. Construction of Development Evaluation Model

*2.1. Research Purpose and Significance.* With the continuous deepening of the urbanization process, the shortcomings of the traditional urbanization model have become prominent, the ecological environment has been seriously damaged, the development of cities and rural areas is not coordinated, and the construction of urban infrastructure is not perfect. This kind of large-scale urbanization construction is not in line with the current development concept of our country, and it also leads to the problem of spatial disequilibrium in the quality of urbanization in different regions. These problems

need to find new solutions. Throughout the construction process of my country’s urbanization, urbanization is based on large-scale population space migration. Today, my country is seeking to transform from “seeking wealth” to “strengthening the country”, and the concept of guiding urbanization construction is no longer the best way. Development” and “rapid development” are “how to better seek new development”. The current is in the new period of the “14th Five-Year Plan”, and it is also the historical meeting period of the first two-hundred-year “great goals of struggle”, and at this critical period, perfecting the new-type urbanization development strategy has great practical significance for my country to realize socialist modernization and cope with the complex international situation. Rural areas have also achieved balanced development.

*2.2. Construction of the Indicator System.* Combined with the characteristics of the current era of increasing double circulation, the article constructs a development evaluation system, as shown in Table 1 [16].

## 3. Evaluation and Analysis of High-Quality Urban Development

*3.1. Calculation and Evaluation of Urbanization Efficiency.* In order to test the effect of new urbanization on high-quality industrial development, the following model is constructed [17].

$$IDQ_{it} = \beta_0 + \beta_1 urb_{it} + \beta_2 Z_{it} + u_i + v_i + \varepsilon_{it}, \quad (1)$$

where  $i$  is the individual or each province,  $t$  is the year,  $IDQ_{it}$  is the comprehensive level of high-quality industrial development,  $urb_{it}$  is the comprehensive level of new urbanization,  $Z_{it}$  is the control variable, and  $u_i$  is the individual fixed effect, which is used to control changes over time. The individual heterogeneity of  $v_i$  is the time dummy variable, and  $\varepsilon_{it}$  is the random disturbance term.

Test the effect of new urbanization on high-quality industrial development:

$$IDQ_{it} = \alpha_0 + \alpha_1 urb_{it} + \alpha_2 zit + u_i + v_i + \varepsilon_{it}. \quad (2)$$

The regression results of the new urbanization on the intermediary variable [18] are as follows:

$$Mit = \beta_0 + \beta_1 urb_{it} + \beta_2 Z_{it} + u_i + v_i + \varepsilon_{it}, \quad (3)$$

$$IDQ_{it} = \gamma_0 + \gamma_1 urb_{it} + \gamma_2 Mit + \gamma_3 zit + u_i + v_i + \varepsilon_{it}.$$

Considering the multiple correlations of resource element structure transformation in the process of urbanization, the mainstream spatial panel model can be set as SAR and SEM types.

$$Urban_{it} = \alpha + \rho \sum_{j=1}^n W_{ij} Urban_{jt} + \gamma Rstru_{it} + \delta X_{it} + \varepsilon_{it}, \quad (4)$$

$$Urban_{it} = \alpha + \gamma Rstru_{it} + \delta X_{it} + \varepsilon_{it}.$$

Build a dynamic space panel model:

TABLE 1: Indicators of high-quality urban development.

| First-level indicator                        | Secondary indicators   | Three-level indicator   |
|--|--|---|
| High-quality urbanization development system | Population of town   | The resident population ratio of the town (%)   |
|  |  | Urban population density (person/Km <sup>2</sup> )  |
|  |  | Proportion of employment in the secondary industry (%)                                      |
|  |  | Proportion of employment in the tertiary industry (%)                                       |
|  |  | Provincial per capita GDP/national per capita GDP   |
|  |  | Value of nonagricultural industries/number of business people in nonagricultural industries |
|  | Economic urbanization  | Nonfixed output value/fixed output value  |
|  |  | Population urbanization rate as a percentage of nonagricultural industry structure          |
|  |  | The ratio of population urbanization rate to GDP growth rate                                |
|  |  | The ratio of total import and export to GDP (%)   |
|  |  | FDI to GDP ratio (%)  |
|  |  | OFDI to GDP ratio (%)   |
| Spatial urbanization                         | Spatial urbanization   | Fiscal deficit ratio (%)  |
|  |  | Inflation rate (%)  |
|  |  | Ratio of construction area to total area (%)  |
|  |  | Per capita built-up area (m <sup>2</sup> /person)   |
|  |  | Ratio of urban construction land to total area (%)  |
|  |  | Per capita road area (m <sup>2</sup> /person)   |
|  | Social urbanization  | Completed building area (10000m <sup>2</sup> )  |
|  |  | Per capita social consumption   |
|  |  | Urban registered unemployment rate  |
|  |  | Income ratio of urban and rural residents   |
|  |  | Human capital   |
|  |  | Ratio of urban and rural Engel coefficients   |
| Green urbanization                           | Ratio of personnel in urban and rural health institutions      |   |
|  | Number of patents granted                                      |   |
|  | R&D input intensity  |   |
|  | Science and technology fiscal expenditure                      |   |
|  | Social security investment level                               |   |
|  | Green coverage   |   |
| Green urbanization                           | Daily treatment capacity of urban sewage (10,000 cubic meters) |   |
|  | Domestic garbage removal volume (10,000 tons)                  |   |
|  | Forestry investment/GDP  |   |
|  | Industrial pollution investment/secondary GDP                  |   |
|  | Per capita park green space (square meters)                    |   |
|  | CO <sub>2</sub> emissions per capita                           |   |

$$\begin{aligned}
 \text{Urban}_{it} &= \beta \text{Urban}_{it-1} + \rho \sum_{j=1}^n W_{ij} \text{Urban}_{it} + \gamma \text{Rstru}_{it} \\
 &+ \delta X_{it} + \varepsilon_{it}, \\
 \varepsilon_{it} &= \lambda \sum_{j=1}^n W_{ij} \varepsilon_{it} + \mu_{it}.
 \end{aligned} \tag{5}$$

Ratio of service sector to industrial output is as follows:

$$\text{Rstru}_{B_{ij}} = \sum_{j=1}^n \frac{v_{ijt}}{v_{it}} \ln \left( \frac{lp_{ijt}}{lp_{jt}} \right). \tag{6}$$

3.2. Variables and Data Description. Based on the two dimensions of time and cross section, the panel data containing  $m$  evaluation indicators in  $n$  regions in  $T$  years are split, so that there is one cross-sectional data every year [19].

$$X^T = (x_{ij})_{n \times m}. \tag{7}$$

The  $T$ -year cross-sectional data are sorted by time and region to form a  $nT \times m$  global evaluation matrix [20].

$$X = (X^1, X^2, \dots, X^T)_{nT \times m} = (x_{ij})_{nT \times m}. \tag{8}$$

For positive indicators,

$$x_{ij} = \frac{x_{ij} - \min x_{ij}/i}{\max x_{ij}/i - \min x_{ij}/i} \times 99 + 1, 1 \leq i \leq nT, 1 \leq j \leq m. \tag{9}$$

For negative indicators,

$$x_{ij} = \frac{\max x_{ij}/i - x_{ij}}{\max x_{ij}/i - \min x_{ij}/i} \times 99 + 1, 1 \leq i \leq nT, 1 \leq j \leq m. \tag{10}$$

Calculate the information entropy of the  $j$ -th index [21]:

$$e_j = \frac{1}{\ln(nT)} \times \sum_{i=1}^{nT} (f_{ij} \times \ln f_{ij}), 1 \leq i \leq nT, 1 \leq j \leq m. \quad (11)$$

Calculate the information entropy redundancy of the  $j$ -th indicator [22]:

$$g_j = 1 - e_j. \quad (12)$$

Indicator weight calculation [23]:

$$\omega_j = \frac{g_j}{\sum_{j=1}^m g_j}. \quad (13)$$

Calculate the high-quality development level of the economy [24]:

$$F_i = \sum_{j=1}^m \omega_j \times x_{ij}. \quad (14)$$

Urban high-quality development index[25]:

$$hstruc = \sum_{j=1}^5 (W_j \theta_j). \quad (15)$$

## 4. Simulation Experiments

**4.1. Spatial and Temporal Analysis of Development.** In order to understand the changing trend of the coordinated development of the urbanization system, the experiment selected five different towns in five different provinces in the northwest region and recorded the changes in their development coefficients in recent years. The experimental results show that from 2006 to 2017, the urbanization development coefficient of the five northwestern provinces and regions has increased year by year, and the high-quality development level of urbanization has gradually increased. In terms of provinces and regions, the development coefficient of urban one ranks first among the five provinces and regions in the northwest. The development coefficient of town one was 0.240 in 2006 and has been on an upward trend since then, reaching 0.320 in 2017. Urban 2 was 0.191 in 2006, showing an upward trend in fluctuations. In 2017, it was 0.240, ranking fourth. Urban 3 was 0.163 in 2006 and has been on an upward trend, reaching 0.210 in 2017, ranking last among the five northwestern provinces. In 2006, the urban area 4 was 0.240, showing a fluctuating upward trend, and it reached 0.260 in 2017, ranking second. The development coefficient of town five in 2006 was 0.220, showing an upward trend, and it reached 0.250 in 2017, ranking third. The statistics of the urbanization development coefficient are shown in Figure 1.

As shown in Figure 1, although the urban development coefficient of the five northwestern provinces is on the rise, the level of development schedule is low. Except for the urban development coordination degree in 2016–2017, which was higher than 0.3, which was in a relatively imbalanced stage, the urbanization development coordination degree of other provinces in each year was lower than 0.2, which was in a highly imbalanced stage. The Northwest is in

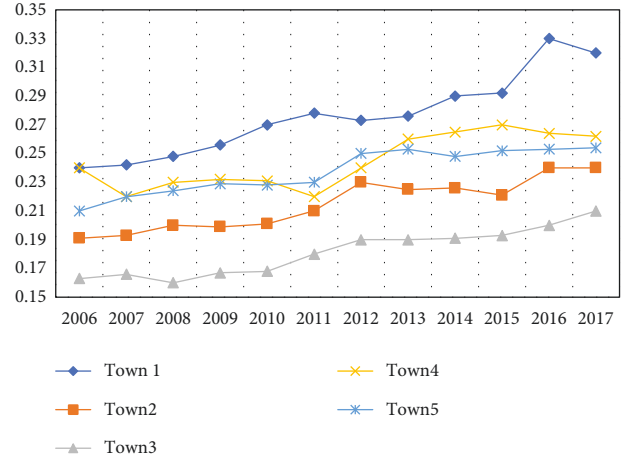


FIGURE 1: Regional urbanization development coefficient of the five northwestern provinces.

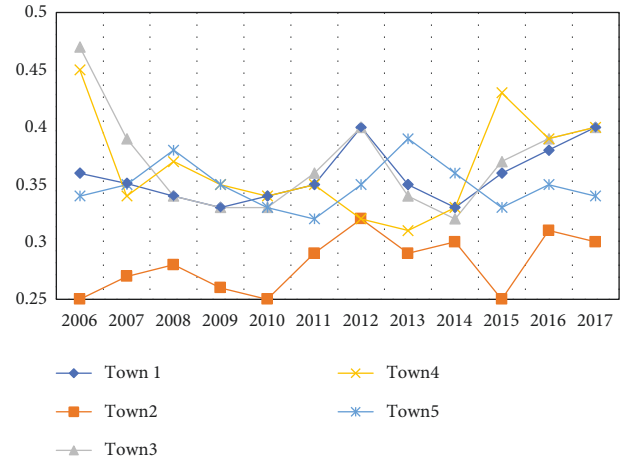


FIGURE 2: Urban economic development coefficient.

a stage of serious imbalance as a whole, indicating that the quality of urbanization in the Northwest is low. The level of coordinated development among urbanization systems is low, and there is an inconsistency between population agglomeration and industrial economic development, urban land resource utilization, urban public welfare development, and urban ecological environment development. In the process of population urbanization, people constantly emphasize economy, space, society, and green. The development capacity of urbanization is very important for the rapid development of cities and towns. Only by achieving stable and coordinated development among various regions, we can correctly achieve the goal of high-quality development of urban construction.

As shown in Figure 2, from the perspective of the urban economic development coefficient, the overall value is between 0.2 and 0.4, which is in a relatively high imbalance stage. The coefficients of Urban 1, Urban 2, and Urban 5 and 3 provinces are relatively stable and are also in a relatively high imbalance stage. The coefficients of Urban 3 and Urban 4 fluctuate and decrease and tend to be stable.

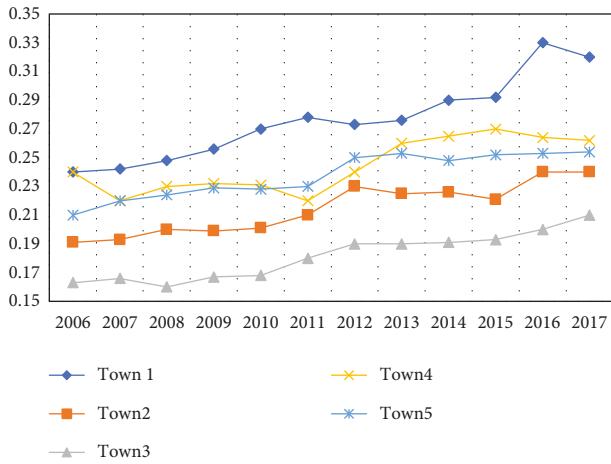


FIGURE 3: Urban spatialization development coefficient.

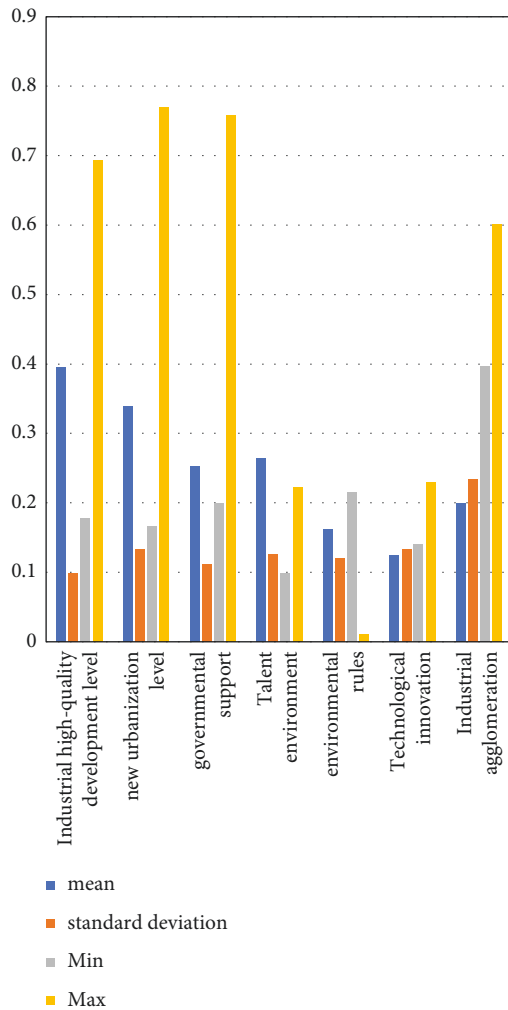


FIGURE 4: Descriptive statistics result from graph.

This is related to the weak economic foundation of the five northwestern provinces and regions. The key to the quality of urbanization development lies in economic development. As the basic guarantee for urban development, the

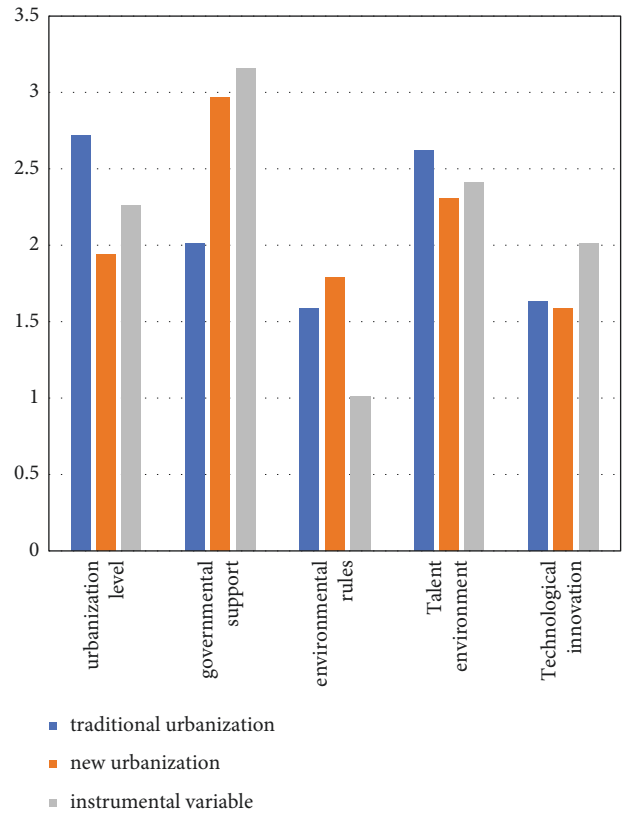


FIGURE 5: Statistics of regression results.

economy is a necessary factor to determine whether the high-quality urban development is successful. From the industrial development of the northwest provinces, we can see that except for the urban four and two industries in the northwest provinces, the growth rate of the four and two industries is positive and has a downward trend. This reflects the unstable foundation of high-quality development of urbanization and inhibits the high-quality development of urbanization.

As shown in Figure 3, from the perspective of the urban spatialization development coefficient, the development coefficient of the northwest provinces shows a gradual upward trend, evolving from a high imbalance to a moderate coordination. The coefficients of Town 1 and Town 4 are in a moderate coordination stage in each year. The coefficients of Town 2 and Town 5 have evolved from high imbalance to moderate coordination. Although the coefficient of Town 3 is on the rise, it has been in a relatively high imbalance stage. Judging from the gradual increase in the development coefficient of population and spatial urbanization in Northwest China, the level of urban spatial development has gradually met the needs of population urbanization, but the degree of coordinated development still needs to be improved. Because the northwest is located in an ecologically fragile area, especially in the second, third, and fifth cities, the urban spatial development is greatly affected by natural factors, and it is more necessary to make scientific planning in terms of land resource utilization to improve the level of spatial urbanization.

TABLE 2: Descriptive statistics.

| Variable                                  | Sample size | Mean   | Standard deviation | Min    | Max    |
|---|-------------|--------|--------------------|--------|--------|
| Industrial high-quality development level | 360         | 0.3955 | 0.0988             | 0.1780 | 0.6941 |
| New urbanization level                    | 360         | 0.3387 | 0.1326             | 0.1655 | 0.7702 |
| Governmental support                      | 360         | 0.2523 | 0.1112             | 0.1998 | 0.7582 |
| Talent environment                        | 360         | 0.2642 | 0.1257             | 0.0989 | 0.2221 |
| Environmental rules                       | 360         | 0.1614 | 0.1203             | 0.2160 | 0.0110 |
| Technological innovation                  | 360         | 0.1249 | 0.1327             | 0.1402 | 0.2287 |
| Industrial agglomeration                  | 360         | 0.1987 | 0.2348             | 0.3964 | 1.6003 |

TABLE 3: Benchmark regression results and instrumental variable regression.

| Variable                 | Traditional urbanization | New urbanization | Instrumental variable |
|--------------------------|--------------------------|------------------|-----------------------|
| Urbanization level       | 2.72                     | 1.94             | 2.26                  |
| Governmental support     | 2.01                     | 2.97             | 3.16                  |
| Environmental rules      | 1.59                     | 1.79             | 1.01                  |
| Talent environment       | 2.62                     | 2.31             | 2.41                  |
| Technological innovation | 1.63                     | 1.59             | 2.01                  |

*4.2. Analysis of Empirical Results.* In order to explore the impact of new urbanization on high-quality industrial development, the experiment uses a fixed-effect model for regression analysis. By comparing the impact of traditional urbanization and new urbanization on the quality of industrial development, we can find out the important factors that affect the high-quality development of cities and towns. The experimental results are shown in Figures 4 and 5.

According to the data in Tables 2 and 3, in the stage of traditional urbanization, the results show that the coefficient of influence of traditional urbanization on high-quality industrial development is 0.315, and it can significantly promote development at the level of 1%. Traditional urbanization focuses on the expansion of population and space. To a certain extent, population aggregation and spatial expansion are conducive to the expansion of industrial scale and the improvement of efficiency and to improve the overall development quality of cities and towns. In the new-type urbanization stage, the influence coefficient of new-type urbanization on the high-quality industrial development is much higher than that of traditional urbanization, and at the level of 1%, its promotion effect is much greater than that of traditional urbanization. As far as control variables are concerned, the influence coefficient of government support on high-quality industrial development is not at a significant level in the traditional urbanization stage, indicating that government support has little impact on high-quality industrial development at this stage, while the influence coefficient in the new-type urbanization stage is small and more significant. Under the environmental rules, the difference between the coefficients of traditional towns and new-type urbanization is relatively small, indicating that environmental rules have little influence on the construction of new-type urbanization, and the influence of the talent environment and technological innovation on traditional and new-type towns is within the control range.

*4.3. Model Validation.* In order to verify the performance of the model, the experiment was compared with the other two models, and the evaluation results of urban development were analyzed. The loss value and exact value are set under the model. Among them, the experimental set is a set of samples set aside during the model training process, which can be used to adjust the hyperparameters of the model and to initially evaluate the ability of the model, and the test set is used to evaluate the generalization ability of the final model, but it cannot be used as the basis for algorithm-related selections such as parameter tuning and feature selection. In order to make the model run better, each model is set for 20 iterations. The model test loss value is shown in Figure 6.

According to the experimental results in Figure 6, it can be known that the loss value of the intelligent computing development evaluation model proposed in the article is the smallest value in the test model. When the number of iterations is 20, the final loss value of the article is 0.1. The final loss value of the development evaluation model is 0.3, the final loss value of the grey relational development evaluation model is 0.48, the loss value of the intelligent computing development evaluation model decreases slowly with the increase of the number of iterations, showing a relatively stable state, and the other two models have a more tortuous decline. Therefore, in terms of loss value, the model proposed in this paper has a lower loss value and higher robustness. The correct rate curves of the three different models are shown in Figure 7.

According to the data in the figure, we can know that the correct rate of the intelligent computing development evaluation model proposed in the article is the one with the largest value in the test model. With the increase in the number of iterations, the correct rate is basically in a steady growth state. When the number of iterations is 20, the accuracy rate peaks at 99%, which is close to 100%. The accuracy rate of the grey relational development evaluation model is the lowest among the three models. When the number of iterations is 20, the accuracy rate reaches 78%. The accuracy rate of the AHP development evaluation model is 92%, which is between the two models. Due to the limited

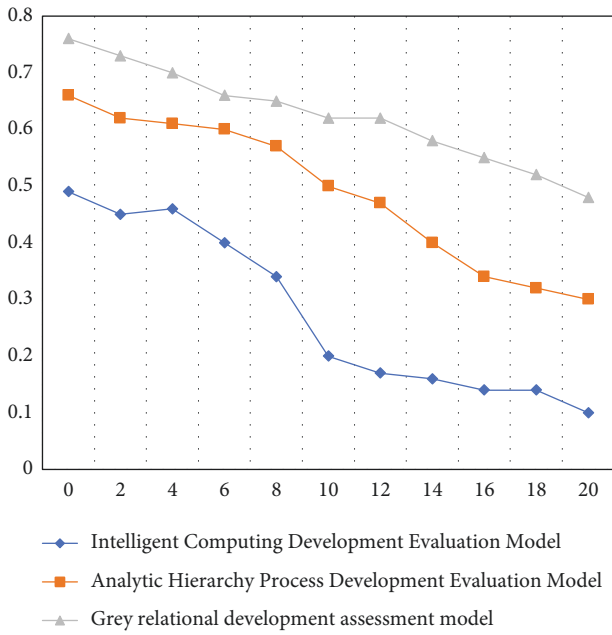


FIGURE 6: Model loss value test.

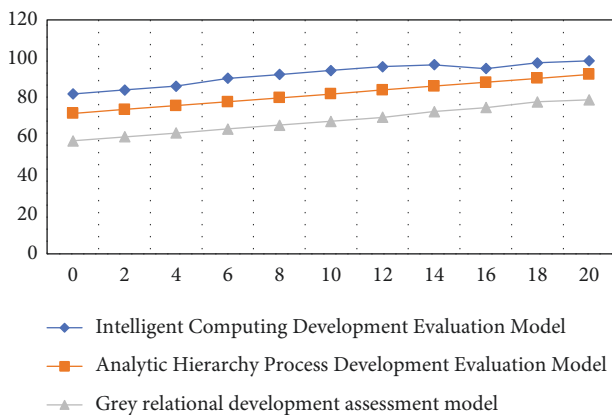


FIGURE 7: Model accuracy test.

TABLE 4: Model test comparison results.

| Model category  | Correct rate (%) | F1     | Loss value |
|---|------------------|--------|------------|
| Intelligent computing development evaluation model      | 96.23            | 0.8843 | 0.0647     |
| Analytic hierarchy process development evaluation model | 90.25            | 0.7406 | 0.1945     |
| Grey relational development assessment model            | 86.23            | 0.6452 | 0.2453     |

data set and the number of experiments, the two indicators cannot accurately compare the performance of the model. Therefore, the article also introduces the  $F1$  indicator, which can better reflect the specific performance of the model on different test sets. Based on the above model verification results, the performance of the three models is compared and analyzed, and the results are shown in Table 4.

As shown in the data in Table 4, we can know that the performance of the intelligent computing development evaluation model structure is better than the other two models in terms of accuracy,  $F1$ , and loss value. Therefore, it can be shown that the intelligent computing development evaluation model structure is very important for urbanization. The quality development assessment performed better than the other two models.

### 5. Conclusion

The current international environment is complex, and economic globalization has entered a period of adjustment. Under the background of the new development pattern, my country should give the correct development concept to solve the problem of high-quality development of the domestic economy. The key lies in the coordinated development of urban and rural areas. On the one hand, it is necessary to strengthen the implementation of the rural revitalization strategy, further improve the total factor productivity of agriculture, improve the level of rural revitalization, release more rural labor force, and promote the transformation efficiency of migrant workers into citizens. On the other hand, based on the construction of new urbanization, accelerate the high-quality development of urbanization and strengthen the coordinated development of urban and rural areas. Based on the panel data of five provinces and regions in Northwest China in recent years, this paper constructs an indicator system for high-quality urbanization development and concludes that my country's new-type urbanization and industrial high-quality development levels are gradually improving, but there are regional differences between the two. This result shows that my country's industrial development is gradually transforming into a high-quality direction, but the current level of development needs to be further improved. In the future research work, we should focus on the following aspects:

- (1) Accelerating the construction of new urbanization provides an important support platform for the high-quality development of the industry. First, under the guidance of the government, accelerate the reform of the household registration system to realize the real citizenization of migrant workers and promote more rural laborers to gather in cities and towns. Second, speed up the urban infrastructure construction and expand the space for industrial agglomeration to realize the free flow of factors, so as to realize the balanced development of cities and towns and solve the problem of unbalanced labor distribution.
- (2) In the process of promoting new-type urbanization, reasonably introduce industries and build industrial parks according to the factor endowments of each region. Through continuous adjustment and optimization of industrial layout and structure, resource elements can be reasonably circulated, thereby reducing industrial production costs, improving production efficiency, and promoting high-quality industrial development.



- (3) In the critical period of improving the quality of new-type urbanization, through the construction of new-type urbanization, continuously lead the technological innovation of industrial enterprises, and provide strong support for promoting the high-quality development of the industry. In the information age, more emphasis is placed on the diffusion of information technology, so as to optimize resource efficiency and promote high-quality industrial development.

## Data Availability

The experimental data used to support the findings of this study are available from the corresponding author upon request.

## Conflicts of Interest

The authors declare that they have no conflicts of interest regarding this work.

## References

- [1] Z. Yang, "Research on strategies for promoting the high-quality development of urbanization[J]," *Academic Journal of Zhongzhou*, vol. 03, no. 11, pp. 21–26, 2018.
- [2] L. Chen, Q. Wei, and Q. Fu, "Spatiotemporal evolution analysis of habitat quality under high-speed urbanization: a case study of urban core area of China lin-gang free trade zone," *The Journal*, vol. 05, no. 3, pp. 56–79, 2021.
- [3] M. Atiquzzaman, N. Yen, and Z. Xu, "Big data analytics for cyber-physical system in smart city," *BDCPS: International conference on Big Data Analytics for Cyber-Physical-Systems(BDCPS 2020)*, Shanghai, China, vol. 1303, 2020.
- [4] L. Wei, "Coordination of urbanization quality and resource utilization in inclusive perspective: taking 288 cities in China as an example [J]," *Ying yong sheng tai xue bao = The journal of applied ecology*, vol. 29, no. 12, pp. 4119–4127, 2018.
- [5] J. Zhang, Y. Sun, and K. Shan, "Research of reconstruction of village in the urban fringe based on urbanization quality improving - a case study of xi'nan village[J]," *EDP Sciences*, vol. 03, no. 11, pp. 110–121, 2014.
- [6] C. S. Santos Ferreira, R. Walsh, and M. D. L. Costa, "Dynamics of surface water quality driven by distinct urbanization patterns and storms in a Portuguese peri-urban catchment[J]," *Journal of Soils and Sediments*, vol. 16, no. 11, pp. 1–16, 2016.
- [7] B. Liang and M. Chen, "Improving the quality of China's urbanization through new-type urbanization," *Chinese Journal of Urban and Environmental Studies*, vol. 02, no. 2, Article ID 1450011, 2014.
- [8] X. W. Hou, "Research on the balanced development of China's urbanization and industrialization in eastern, central, western and northeastern regions[J]," *Asian Agricultural Research*, vol. 3, pp. 5–11, 2011.
- [9] W. Zhao and W. Hui, *The Research of the Coordinated Development of New Urbanization and Industrial Structure in Shandong Province*, vol. 12, no. 3, pp. 56–59, 2008.
- [10] L. I. Yao and A. N. Shu-Wei, "Research on the high-quality development of Northeast China's economy[J]," *Urban and Environmental Studies*, vol. 06, no. 11, pp. 89–99, 2019.
- [11] C. Fang, "Basic rules and key paths for high-quality development of the new urbanization in China[J]," *Geographical Research*, vol. 06, no. 4, pp. 45–56, 2019.
- [12] X. Yuan, L. I. Caijuan, and L. I. Zhaopeng, "Present situation, perplexity and prospect of high-quality development of Chinese economy[J]," *Journal of Xi'an Jiaotong University*, vol. 06, no. 14, pp. 56–69, 2019.
- [13] Y. Wang, Z. He, and Q. An, "Constraints and breakthroughs in the high-quality development of county urbanization[J]," *Academic Journal of Zhongzhou*, vol. 03, no. 11, pp. 23–36, 2018.
- [14] W. J. Zheng and W. University, "Five paths and opportunities for the high-quality development of private enterprises in the new era[J]," *Journal of Guangxi University for Nationalities*, vol. 03, no. 8, pp. 89–96, 2019.
- [15] L. Hua, "Binary urbanization:high quality urban development path considering the balance of agglomeration[J]," *Journal of Macro-Quality Research*, vol. 07, no. 3, pp. 45–56, 2014.
- [16] C. Fang, "The regularity and key direction of high-quality development of new urbanization in China [J]," *Geographical Research*, vol. 38, no. 1, pp. 13–22, 2019.
- [17] Z. Yang, "Research on strategies to promote high-quality development of urbanization," *J Zhongzhou Journal*, vol. 8, pp. 44–46, 2018.
- [18] J. Ding, "A comparative study on the high-quality development of urbanization in China and Japan, based on the empirical analysis of the two countries from 1985 to 2014 [J]," *Jiangxi Social Sciences*, vol. 38, no. 5, pp. 44–53+254, 2018.
- [19] W. Zhang, J. Xu, R. Ma, and G. Liu, "The connotation, status quo and development orientation of high-quality urban development in China: based on the perspective of resident survey [J]," *Urban Planning*, vol. 43, no. 11, pp. 13–19, 2019.
- [20] Li Jing, L. Zhuang, and S. Shu, "Calculation of the coordinated development degree of urbanization quality and industrial structure [J]," *Statistics and Decision-Making*, vol. 19, pp. 145–147, 2014.
- [21] W. Xu, Z. Xu, and J. Zheng, "Research on the spatial characteristics of urbanization quality and its threshold effect [J]," *Urban Issues*, vol. 2, pp. 22–30, 2020.
- [22] Li Wang and J. Li, "Quality evaluation and dynamic mechanism of urbanization in northwest provincial capitals under the background of new urbanization," *Journal of Economic Geography*, vol. 34, no. 12, pp. 55–61, 2014.
- [23] W. Lili, "Measurement and evaluation of urbanization quality in Northwest minority areas—taking linxia prefecture in gansu province as an example [J]," *Lanzhou Journal*, vol. 12, pp. 185–190, 2014.
- [24] Q. Zhou and D. Liu, "Research on the coordinated development of urban resilience and urbanization level in the Yangtze River Delta urban agglomeration [J]," *Research of Soil and Water Conservation*, vol. 27, no. 4, pp. 286–292, 2020.
- [25] B. Ye and B. Dai, "Coordinated development of agricultural modernization and new urbanization: mechanism of action and spatial and temporal evolution—taking the main grain producing areas in my country as an example [J]," *Theory Monthly*, vol. 6, pp. 97–105, 2020.

## Research Article

# Sports-Assisted Education Based on a Support Vector Machine and Genetic Algorithm

**ChengZhao Li** 

*Physical Education College, Pingdingshan University, Pingdingshan 467000, China*

Correspondence should be addressed to ChengZhao Li; 3049@pdsu.edu.cn

Received 4 March 2022; Revised 14 April 2022; Accepted 12 May 2022; Published 16 June 2022

Academic Editor: Man Fai Leung

Copyright © 2022 ChengZhao Li. This is an open access article distributed under the Creative Commons Attribution License, which permits unrestricted use, distribution, and reproduction in any medium, provided the original work is properly cited.

A sports-assisted education method based on a support vector machine (SVM) is proposed to address the problem of complex and variable sports actions leading to easy ghosting of target detection and high dimensionality of feature extraction, which reduces the low accuracy of sports action recognition. The ViBe target detection algorithm is improved by using Wronskian function and the “4-linked algorithm” seed filling algorithm, which effectively solves the ghosting problem and obtains clearer human sports targets. By using the genetic algorithm to fuse the eight-star model with sports action features extracted by the Zernike moment, redundant features are reduced and differentiability between different classes is ensured. Sports action classification was achieved by using a one-to-one construction of an SVM classifier. The results show that the proposed method can effectively recognize sports movements with an average recognition accuracy of more than 96%, which can assist physical education and has a certain practical application value.

## 1. Related Work

With the popularity of artificial intelligence technology in various industries, machine vision is playing an increasingly important role in people’s lives. As a hot research direction in machine vision, sports action recognition is widely used in sports analysis and sports-assisted education, which is based on target detection. Sports action features are extracted to analyze them, and an automatic classifier is used for recognition. At present, commonly used target detection algorithms mainly include hybrid Gaussian background modeling, visual background extraction (ViBe), and average background model. [1]. For example, Farag Wael detected autonomous vehicles by hybrid Gaussian background modeling to achieve fast real-time target detection. Zhao Xiaolei et al. applied the ViBe algorithm to achieve multi-scale target detection in high-resolution remote sensing images [2]. Zhao Weidong et al. achieved the target detection of steel defects by the average background model [3]. Compared with hybrid Gaussian background modeling and the average background model, the ViBe algorithm has good fault tolerance, high computing speed, and detection

accuracy [4]. Therefore, the ViBe algorithm is used as the target detection algorithm in this paper for sports action recognition. In terms of feature extraction, the main feature extraction methods include the eight-star model, Zernike moments, and other approaches. Liu Jing et al. extracted hyperspectral remote sensing image features. An eight-star model is used to improve the recognition effect of images [5]. Wang et al. used Zernike moments to extract MRI image features and used SVM classification to identify them for rectal cancer T-stage prediction [6]. Sports actions are complex, and multifeature fusion is beneficial to improve the accuracy of subsequent action recognition. Therefore, in this paper, a genetic algorithm is used to fuse the eight-star model with features extracted from Zernike moments. For image classification recognition, it mainly includes a dynamic time regularization algorithm and probability-based statistical recognition methods. Based on the former, it is usually not used for complex sports action classification recognition due to its susceptibility to noise [7]. The classification methods based on probability statistics include hidden Markov models and SVM models. The SVM model is highly useable and generalizable in dealing with high-

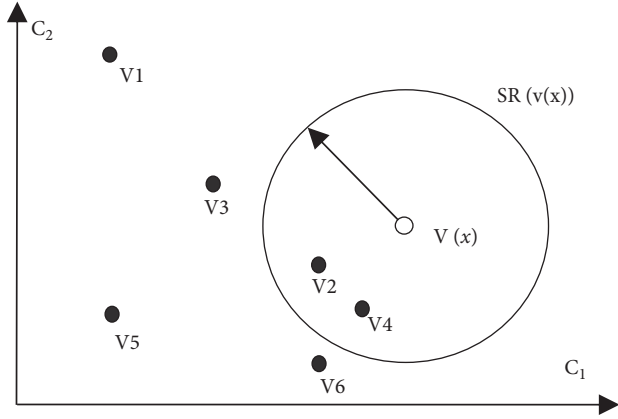


FIGURE 1: Pixel classification diagram in Euclidean space.

dimensional pattern recognition and nonlinear problems, and it is applicable to this paper for sports action classification [8]. Thus, SVM is selected as a classifier to classify sports actions through target detection and multifeature fusion, so as to achieve sports-assisted education.

## 2. Basic Algorithms

### 2.1. Target Detection Algorithm

**2.1.1. An Introduction to ViBe Algorithm.** A ViBe algorithm is a pixel-level detection algorithm with the characteristics of occupying a small hardware memory and a high recognition rate, and its specific steps are as follows:

- (1) Background modeling: let  $M(x)$  be the set of background pixel values  $v(x)$  of the pixel point  $x$ . Then, the background model can be obtained as

$$M(x) = \{v_1, v_2, \dots, v_N\}. \quad (1)$$

- (2) Foreground detection: the new pixel value  $v(x)$  with  $M(x)$  is compared. If  $v(x)$  is close to the sampled value in  $M(x)$ ,  $v(x)$  belongs to the background point. Suppose  $S_R(v(x)) \cap \{v_1, v_2, \dots, v_N\}$  is a sphere space with  $v(x)$  as the center and  $R$  as the radius and  $S_R(v(x)) \cap \{v_1, v_2, \dots, v_N\}$  denotes finding the cross section in the space. In Figure 1,  $C_1$  and  $C_2$  are the components of  $(C_1, C_2)$  in the two-dimensional Euclidean space,  $\#$  is the number of intersecting elements of the set, and  $\min$  is the decision threshold, then the decision process is expressed as

$$v(x) \in \begin{cases} \text{foreground} & \text{if } \# \{S_R v(x) \cap M(x)\} < \text{Min} \\ \text{background} & \text{otherwise} \end{cases}. \quad (2)$$

If the number of  $M(x)$  in the space  $< \min$ ,  $x$  is a foreground pixel point.

- (3) Background model updating:  $P_G$  is the pixel point in the random point  $x$  eight neighborhood in the background model, as in Figure 2(a), input  $P_t$ , as in Figure 2(b), and  $P_G$  needs to be updated when  $P_t(x)$

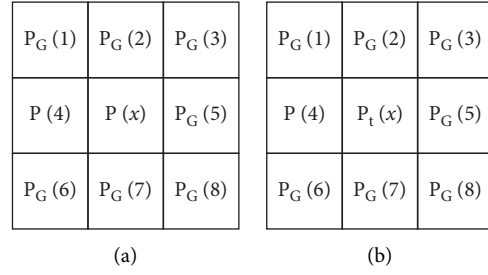
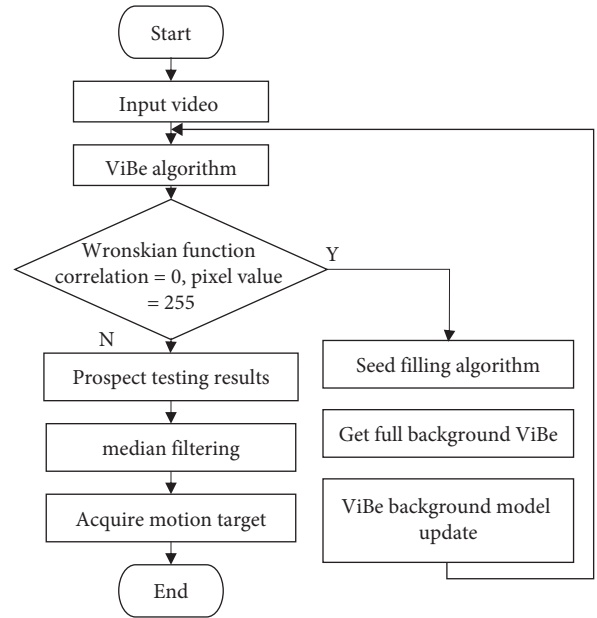
FIGURE 2: background model update strategy. (a) The background model randomly selects  $P_G$ . (b) New frames in the video sequence.

FIGURE 3: ViBe algorithm improvement process.

is judged to be the background. Spatial randomness is the random replacement of pixels  $P_G(r)$  in the  $P_G(x)$  eight neighborhoods by  $P_t(x)$ .

**2.1.2. ViBe Algorithm Improvement.** The ViBe algorithm has the advantage of constructing a background model from the first frame of the video sequence, but at the same time, it also has the problem of ghosting regions. To solve this problem, this paper improves it by the means of Wronskian function [9] and the “4-linked algorithm” seed filling algorithm [10], as shown in Figure 3. In addition, the steps of improvement are as follows:

- (1). After preprocessing the collected data, the ViBe algorithm is used to detect the motion target
- (2). The pixel values are judged according to equation (3) to obtain the ghosting area:

$$|W| = \left( \left( \frac{F'_t(x, y)}{F'_{t-1}(x, y)} \right)^2 - \frac{F'_t(x, y)}{F'_{t-1}(x, y)} \right) = 0, \quad (3)$$

where  $F_t(x, y)$ ,  $F_{t-1}(x, y)$  are the gray values of the pixel point  $(x, y)$  at moments  $t$  and  $t-1$

- (3) The ghost region is filled with the “4-linked algorithm” and acquire the moving target by median filtering

## 2.2. Feature Extraction Algorithm

**2.2.1. Eight-Star Model.** The process of extracting sports action features from the eight-star model is as follows: we assume that the silhouette pixel points are  $N$ , and we calculate the sports pose silhouette centroid coordinates  $(x_c, y_c)$ .

$$\begin{aligned} x_c &= \frac{1}{N} \sum_{i=1}^N x_i, \\ y_c &= \frac{1}{N} \sum_{i=1}^N y_i. \end{aligned} \quad (4)$$

According to  $(x_c, y_c)$ , the motion target is divided into four parts: top, bottom, left, and right, and the Euclidean distance from the extreme value point of the silhouette contour of each part to the center of mass is calculated as

$$d_i = \sqrt{(x_i - x_c)^2 + (y_i - y_c)^2}, i = 1, 2, \dots, 8. \quad (5)$$

We connect the center of mass of each part with the contour extreme point, and we calculate the angle between each line and the horizontal line as shown in

$$\theta_i = \arccos\left(\left|\frac{x_i - x_c}{d_i}\right|\right) \times \frac{180}{\pi}. \quad (6)$$

By internalizing the sports action gesture silhouette in a semicircle, the eccentricity is used to determine the amplitude of sports movements as shown in

$$e = \sqrt{1 - \frac{a^2}{b^2}}, \quad (7)$$

where  $b$  is the short semiaxis of the ellipse, i.e., silhouette height, and  $a$  is the long semi-axis of the ellipse, i.e., silhouette width. Based on the above information, the sports action feature vector extracted by the eight-star model can be obtained as

$$F = (d_1, d_2, d_3, d_4, d_5, d_6, d_7, d_8, \theta_1, \theta_2, \theta_3, \theta_4, \theta_5, \theta_6, \theta_7, \theta_8, e). \quad (8)$$

**2.2.2. Zernike Moments.** Zernike moments are calculated by computing the orthogonal set of the projection of the image  $f(x, y)$  on the set of complex-valued functions  $\{V_{pq}(x, y)\}$  on the unit circle  $x^2 + y^2 = 1$  in the following form:

$$V_{pq}(x, y) = V_{pq}(\rho)e^{jq\theta},$$

$$R_{pq}(\rho) = \sum_{s=0}^{(p-|q|)/2} (-1)^s \frac{(p-s)!}{s!(p+|q|/2-s)!(p-|q|/2-s)!} \rho^{p-2s}, \quad (9)$$

where  $\rho$  and  $\theta$  are the length of the pixel point  $(x, y)$  in the unit circle from the origin and the angle information with the  $x$ -axis and  $R_{pq}(\rho)$  is the radial polynomial of  $(x, y)$ .

From Zernike moment polynomial properties, it is known that there exists a unique expression of  $f(x, y)$ .

$$f(x, y) = \sum_{p=1}^{\infty} \sum_{q=0}^{\infty} Z_{pq} V_{pq}(\rho, \theta), \quad (10)$$

where  $Z_{pq}$  is the Zernike moment, which is defined in

$$Z_{pq} = \frac{p+1}{\pi} \iint_{x^2+y^2 \leq 1} f(x, y) V_{pq}^*(\rho, \theta) dx dy. \quad (11)$$

The eigenvectors corresponding to Zernike moments are  $\log|Z_{11}|$ ,  $\log|Z_{20}|$ ,  $\log|Z_{31}|$ ,  $\log|Z_{33}|$ ,  $\log|Z_{40}|$ ,  $\log|Z_{42}|$ , and  $\log|Z_{44}|$ .

**2.3. Classification Recognition Algorithm.** SVM is a classification algorithm that performs nonlinear classification by a kernel method. The core idea of the SVM algorithm is to use mathematical methods to construct the optimal classification surface in the original space or the projected high-dimensional space, so that the given binary categories can be distinguished [11]. The specific procedure is as follows:

Suppose the input data is  $x$  and  $x$  is mapped to a high-dimensional space by a nonlinear mapping function  $\phi(x): R^d \rightarrow F$  as shown in Figure 4. The estimation function is then used to linearly estimate:

$$R(w) = \frac{1}{2} \|w\|^2 + C \sum_{i=1}^n f^\varepsilon(y_i, d_i), \quad (12)$$

where  $C$  is the penalty coefficient, and the larger its value, the stronger the penalty;  $\varepsilon$  is the insensitive loss function; and  $d_i$  is the true output of SVM. For finding the minimum value of  $R(w)$ , i.e., by introducing the dot product function  $K(x_i, y_i)$  with the use of Wolfe pairwise solution [12], the dual solution of equation (15) is

$$\min \left( \frac{1}{2} \|w\|^2 + C \sum_{i=1}^n \xi_i + \xi_i^* \right). \quad (13)$$

The constraint of equation (16) is [13]

$$y_i - (w - x_i) - b \leq \zeta + \zeta_i, i = 1, 2, 3 \dots n, \quad (14)$$

$$(w - x_i) + b - y_i \leq \zeta + \zeta_i^*, i = 1, 2, 3 \dots n, \quad (15)$$

$$\zeta \geq 0, \zeta_i^* \geq 0, \quad (16)$$

where  $\xi, \xi^*$  are relaxation variables.

Introducing the Lagrange multiplier method, the estimated function  $f(x)$  can be transformed as [13]

$$f(x) = \sum_{i=1}^n (a_i - a_i^*) K(x_i, x) + b. \quad (17)$$

The constraint is  $0 < a_i < C, 0 < a_i^* < C$ , where  $K(x_i, x)$  is the kernel function of SVM.

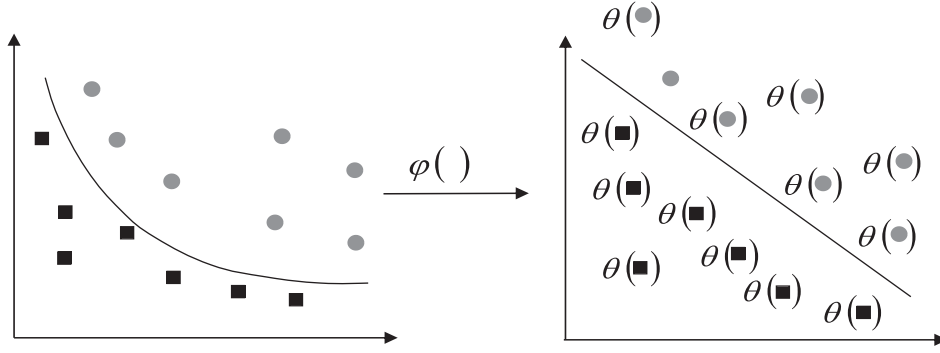


FIGURE 4: SVM classification principle.

The estimation function is then used to linearly estimate in

$$R(w) = \frac{1}{2}\|w\|^2 + C \sum_{i=1}^n J^\varepsilon(y_i, d_i), \quad (18)$$

where  $C$  is the penalty coefficient, and the larger its value, the stronger the penalty;  $\varepsilon$  is the insensitive loss function; and  $d_i$  is the true output of SVM. For finding the minimum value of  $R(w)$ , i.e., by introducing the dot product function  $K(x_i, y_i)$  with the use of the Wolfe pairwise solution [12], the dual solution of (19) is

$$\min \left( \frac{1}{2}\|w\|^2 + C \sum_{i=1}^n \xi_i + \xi_i^* \right). \quad (19)$$

The constraint of (20) is [13]

$$y_i - (w - x_i) - b \leq \zeta + \zeta_i, i = 1, 2, 3 \dots n, \quad (20)$$

$$(w - x_i) + b - y_i \leq \zeta + \zeta_i^*, i = 1, 2, 3 \dots n, \quad (21)$$

$$\zeta \geq 0, \zeta_i^* \geq 0, \quad (22)$$

where  $\xi, \xi^*$  are relaxation variables.

Introducing the Lagrange multiplier method, the estimated function  $f(x)$  can be transformed in [13]

$$f(x) = \sum_{i=1}^n (a_i - a_i^*) K(x_i, x) + b. \quad (23)$$

The constraint is  $0 < a_i < C, 0 < a_i^* < C$ , where  $K(x_i, x)$  is the kernel function of SVM.

Although SVM has a strong ability to be used and generalized, it still has some limitations when facing complex and changing sports. Therefore, this paper selects SVM as a classifier to build a classification model to identify sports actions and then assist in sports education.

### 3. Multifeature Fusion-Based SVM Sports Action Recognition Classification Method

**3.1. Feature Fusion.** Feature extraction is central to the implementation of sports action recognition [14]. In this paper, we combine the characteristics of sports action,

consider the comprehensiveness of feature extraction and the description of local features, and use the eight-star model and Zernike moments commonly used in sports posture multifeature extraction to extract sports action multifeatures. In order to reduce the redundancy of features and the dimensionality of the feature vector, this paper uses a genetic algorithm-based approach to fuse the above extracted features [15]:

- (1) We use the binary method with “0” and “1” code to indicate the unchecked and selected features
- (2) initialize the generated population and calculate the fitness function of all features, randomly select individuals for inheritance, and eliminate unselected individuals according to a predetermined strategy, such as the random traversal sampling method
- (3) We use crossover probability of 0.7 [16] and a variance probability of 0.5 [17] to generate new individuals
- (4) continue iterating until the algorithm satisfies termination condition

**3.2. Recognition Model Construction.** Using a one-to-one approach, a multiclassifier with radial kernel function SVM is constructed, and the specific implementation process is shown in Figure 5, which indicates that six SVMs are required for the input of four classes of samples. Set class a as positive samples and class b as negative samples and train to get the classifier SVMab. When classifying votes, the test samples are input to the classifier to get the cumulative values of votes corresponding to the four categories, and the maximum cumulative value corresponding to labels is used as the classification result. Taking SVMab as an example, if the output is determined to be class a, the voting score of a is  $\text{sum}(i) = \text{sum}(i) + 1$ , and the maximum value corresponding to the label is found from it.

The above classifier is applied to human sports action recognition to construct a feature fusion multiclass classifier as shown in Figure 6. The training samples are input to the model for training, the best model is saved and input to the test samples, and the category corresponding to the maximum cumulative value is selected as the classification result output, which is the model recognition result.

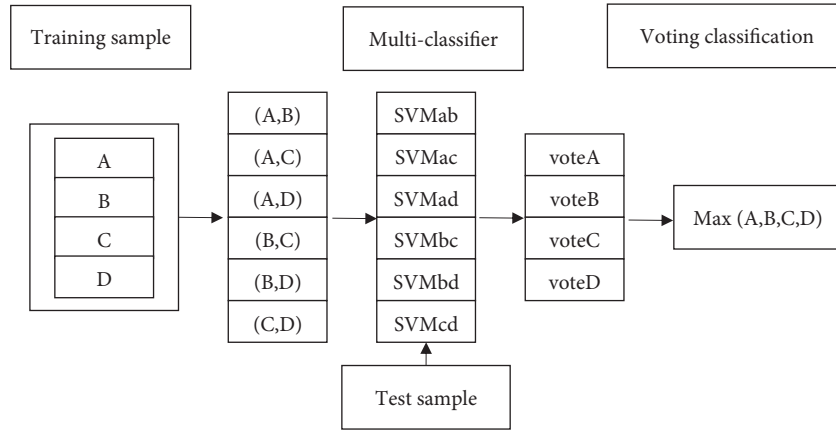


FIGURE 5: Schematic diagram of multiclassifier.

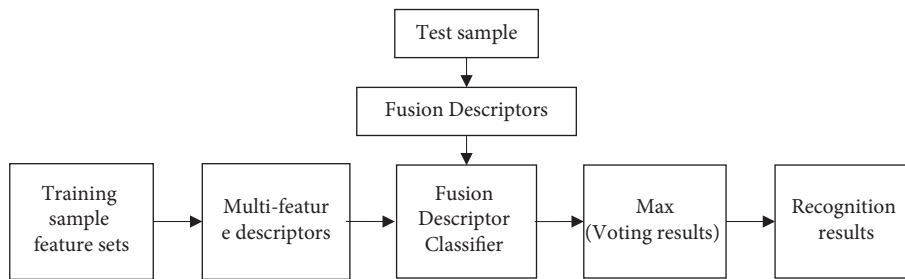


FIGURE 6: SVM classification recognition model based on multifeature fusion.

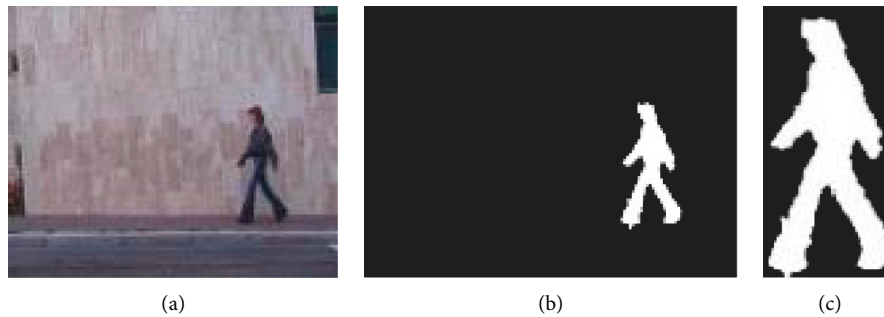


FIGURE 7: Video frame normalization results. (a) Original frame rate. (b) Motion target detection result map. (c) Normalized silhouette map.

## 4. Simulation Experiments

**4.1. Experimental Environment Construction.** The experiment runs on 64-bit Windows 7 operating system with Inter(R) Core(TM) i5-2450M CPU@2.5 GHz CPU, 8 GB RAM, Microsoft Visual Studio 2010+Opencv2.4.1 software development environment, and Visual C++ as the development language.

**4.2. Data Source and Preprocessing.** The test and competition datasets are selected as the experimental datasets for evaluating the target detection effectiveness of the proposed method [18]. Among them, the test dataset contains 111 video frames with a resolution of 320 \* 240 and a frame rate of 25

fps, and the competition dataset contains 396 video frames with a resolution of 720 \* 480 and a frame rate of 29 fps.

KTH, Weizmann, and UCF-Sport datasets, which are commonly used for human motion pose recognition, are selected as experimental data [19, 20]. KTH contains 160 \* 120 resolution, 25 fps frame rate, 599 videos, and 6 kinds of actions; Weizmann contains 180 \* 144 resolution, 25 fps frame rate, 90 videos, and 10 kinds of actions; UCF-Sport contains 720\*480 resolution, 10fps frame rate, 150 videos, and 10 kinds of actions.

Since videos in the above dataset usually contain clips without human behavioral activities and video frames without motion targets, which increase the model computation and recognition time, invalid video frames are

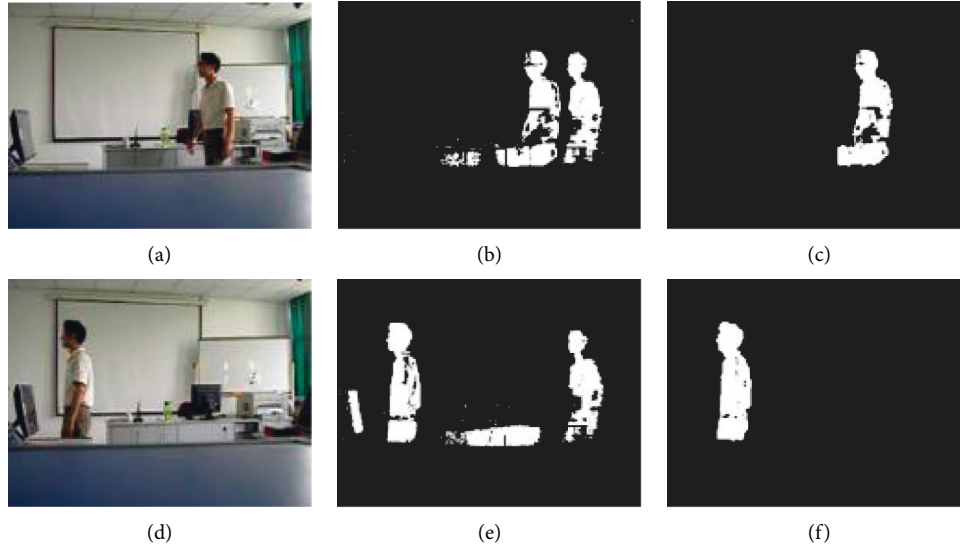


FIGURE 8: Comparison of test dataset target detection results. (a) Frame 15 original image. (b) Frame 15 ViBe algorithm result. (c) Frame 15 result of the proposed algorithm. (d) Frame 64 original image. (e) Frame 64 ViBe algorithm result. (f) Frame 64 result of the proposed algorithm.

removed in this experiment. Taking the KTH dataset as an example, we first calculate the area of the motion target silhouette area in each frame of a video, set 1/2 of the maximum area value as the threshold value, and then classify the video frames smaller than the threshold value as invalid video for deletion processing.

In addition, considering that the human motion changes with the motion distance from camera position, there is a difference in the size of the target detection motion area. To eliminate this discrepancy, experiments are performed using a bilinear interpolation method [21], as shown in (24), with scale normalization for each video frame.

$$\text{newR} * \text{newC} = M * \frac{n}{m} \times M, \quad (24)$$

where  $m * n$  is the motion target region,  $M$  is the height, and  $\text{newR} * \text{newC}$  is the preprocessing result. The normalized result of the original video frame is shown in Figure 7.

**4.3. Evaluation Indexes.** In this experiment, precision, recall, false positive rate (FPR), and  $F$ -measure are selected as evaluation metrics of the proposed method, which are calculated as follows [22, 23]:

$$\begin{aligned} \text{precision} &= \frac{\text{TP}}{\text{TP} + \text{FP}}, \\ \text{recall} &= \frac{\text{TP}}{\text{TP} + \text{FN}}, \\ \text{FPR} &= \frac{\text{FP}}{\text{FP} + \text{TN}}, \\ F - \text{measure} &= \frac{2 \times \text{precision} \times \text{recall}}{\text{precision} + \text{recall}}, \end{aligned} \quad (25)$$

where TP, TN, FP, and FN correspond to true positive, true negative, false positive, and false negative, respectively.

#### 4.4. Experimental Results

**4.4.1. Target Detection Algorithm Verification.** To verify the results of the proposed method on target detection and the suppression effect of ghosting, experiments are tested on test and competition datasets, and the results are shown in Figures 8 and 9. From figures, it can be seen that the conventional ViBe algorithm detects the ghost shadow in the background of the target, and there is an occluding reflective shadow. The ViBe algorithm improved by the Wronskian can eliminate the ghost shadow and reflective shadow well, which has no effect on multimotion targets. This shows that the proposed algorithm has a good detection effect in the target detection process.

In order to quantitatively analyze the effectiveness of the proposed method in target detection, the performance of the algorithm before and after the improvement is experimentally analyzed, and the results are shown in Table 1. As can be seen from the table, compared with the traditional ViBe algorithm and the Wronskian algorithm, the proposed algorithm performs better in terms of precision, recall, false positive rate, and  $F$ -measure indexes, which indicates that the improvement of the algorithm in this paper is effective.

**4.4.2. Multifeature Fusion Results.** To verify the effect of the proposed method on the multifeature fusion, the 39 feature quantities of walking, running, and jumping movements extracted from the eight-star model and Zernike moments are experimentally fused with normalized and normalized features, and the results are shown in Figure 10. As can be seen from the figure, there is a certain interval between the feature data of walking, running, and jumping after the

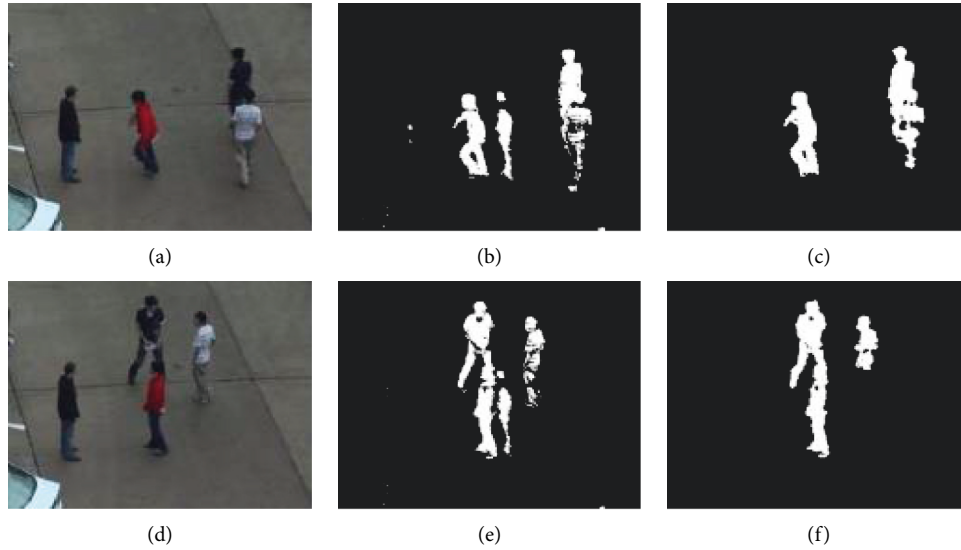


FIGURE 9: Comparison of target detection results for the competition dataset. (a) Frame 179 original image. (b) Frame 179 ViBe algorithm result. (c) Frame 179 result of the proposed algorithm. (d) Frame 253 original image. (e) Frame 253 ViBe algorithm result. (f) Frame 253 result of the proposed algorithm.

TABLE 1: Comparison of performance metrics of different algorithms.

| Algorithm ViBe                  | Precision | Recall | False positive rate | Comprehensive evaluation |
|---------------------------------|-----------|--------|---------------------|--------------------------|
| ViBe algorithm                  | 0.721     | 0.812  | 0.020               | 0.764                    |
| Wronskian model                 | 0.675     | 0.837  | 0.017               | 0.748                    |
| The proposed improved algorithm | 0.796     | 0.898  | 0.011               | 0.844                    |

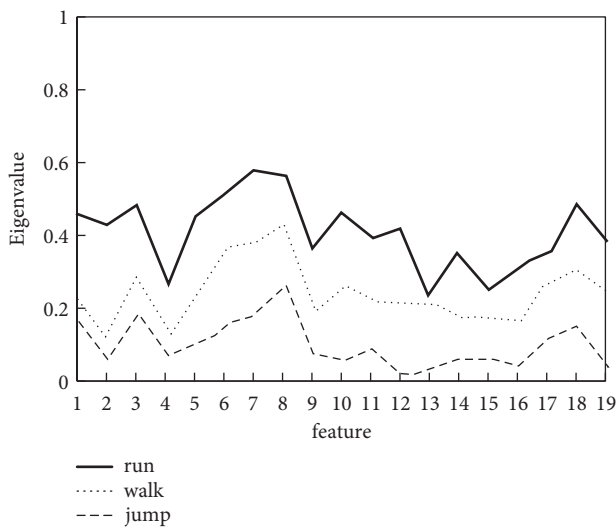


FIGURE 10: Multifeature fusion results.

multifeature fusion, which indicates that the differences between different categories of sports actions after the multifeature fusion are obvious and easy to classify.

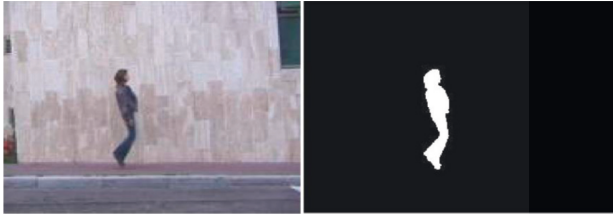
4.4.3. *Identification Results.* To verify the effectiveness of the proposed method, experiments are tested on the pre-processed Weizmann and UCF-Sport data. Among them, three common movement postures of walking, running, and

jumping are selected for testing on the Weizmann dataset, with walking and running movements recorded by 10 volunteers individually and jumping by 9 volunteers; three common movement postures of golf, diving, and gymnastics are selected for testing on the UCF-Sport dataset. Figure 11 shows the test results of the proposed method on the Weizmann dataset. From the figure, it can be seen that the proposed method can effectively identify sports targets and accurately classify the sports movements of walking and jumping, but there is a classification error of misidentifying running as walking. The reason for this is that some of the key frames of running and walking are similar in posture profile, so the separability of extracted features needs to be improved, which in turn leads to classification errors.

Figure 12 shows the test results of the proposed method on the UCF-Sport dataset. As can be seen from the figure, the proposed method has good recognition results for videos with a single background and can well recognize the sports action of playing golf, but there are false recognition cases for sports actions such as diving and gymnastics with complex backgrounds, the cause of which is that sports such as diving and gymnastics have more action transformations that are not conducive to feature extraction, which in turn leads to wrong recognition of individual video frames.

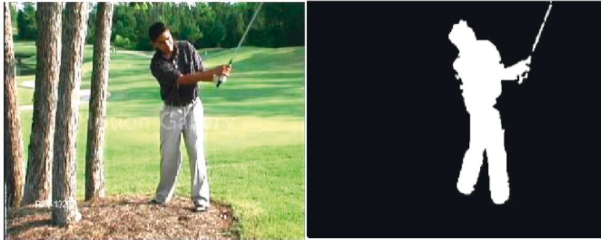
To further verify the effectiveness of the proposed method, experiments compare the recognition results of the proposed model with those of the commonly used sports recognition methods on the experimental dataset. Table 2 shows the recognition results of different recognition





test7,flag=3 Posture: jump

FIGURE 11: Test results on the Weizmann dataset.



test10,flag=6 Posture: Golf

FIGURE 12: Test results on UCF-Sport dataset.

TABLE 2: Comparison of identification results of different methods on the KTH dataset.

| Posture | SIFT | SIFT feature | Multifeature | This article algorithm |
|---------|------|--------------|--------------|------------------------|
| Walk    |      | 45.36        | 93.08        | 95.33                  |
| Run     |      | 60.28        | 90.73        | 95.01                  |

TABLE 3: Comparison of identification results of different methods on the Weizmann dataset.

| Posture | SIFT | SIFT feature | Multifeature | This article algorithm |
|---------|------|--------------|--------------|------------------------|
| Walk    |      | 40.2         | 95.28        | 100                    |
| Run     |      | 48.21        | 89.43        | 95.04                  |
| Jump    |      | 63.52        | 97.92        | 100                    |

TABLE 4: Comparison of identification results of different methods on UCF-Sport dataset.

| Video library | SIFT feature | Multifeature | This article algorithm | This article algorithm |
|---------------|--------------|--------------|------------------------|------------------------|
| UCF-sport     | 68.59        | 81.37        | 88.92                  | 91.02                  |

methods on the KTH dataset for walking and running, Table 3 shows the recognition results of different recognition methods on the Weizmann dataset for walking, running, and jumping, and Table 4 shows the recognition results of different recognition methods on the UCF-Sport dataset. As can be seen from the tables, compared with SIFT features and multifeatures recognition methods on different experimental datasets, the recognition accuracy of the proposed method has been improved to different degrees, and the average recognition accuracy reaches more than 95%, which has good recognition results.

TABLE 5: Accuracy rate of sports posture recognition.

| Moving posture | Accuracy rate |
|----------------|---------------|
| Walk           | 97.36         |
| Run            | 93.01         |
| Jump           | 99.67         |

**4.4.4. Example Validation.** To verify the generalization ability of the proposed method, experiments are tested on the above standard experimental dataset in addition to the self-built video dataset. A 48-megapixel camera is used to capture three sports postures of walking, running, and striping in both indoor and outdoor scenes, and the proposed method is used to test them. The average recognition rate of the proposed method is shown in Table 5. As can be seen from figures, the proposed method can detect the complete motion target, and there is no shadow interference and trailing shadow adhesion between the target and the surrounding environment, which is conducive to the extraction of physical signs, and the overall recognition effect is good with an average recognition accuracy of more than 96%. However, due to the small difference between walking and running movement transformation and posture, there is still the problem of recognition error, but it has no effect on the overall recognition effect and can better realize movement recognition and then assist physical education.

## 5. Conclusion

In summary, the proposed deep learning-based sports-assisted education method improves the ViBe algorithm by using Wronskian function and the “4-linked algorithm” seed filling algorithm, which effectively solves the ghosting problem and can obtain clearer targets of human sports. By using the genetic algorithm to fuse the eight-star model with sports action features extracted by Zernike moments, redundant features are reduced, and differentiability between different classes is ensured. By using one-to-one construction of the SVM classifier, sports action classification recognition is achieved with a comprehensive recognition accuracy of more than 96%, which can be used for actual sports action classification recognition. The innovation of this research lies in the systematic processing of moving images from all links and the improvement of classification algorithm, so as to comprehensively improve the classification accuracy of moving images.

However, due to these conditions, there are some problems in this paper to be further deepened and improved. When SVM is selected for classification, its kernel parameters and penalty factors have a large impact on classification results and affect the generalizability of the model, while the influence of kernel function is ignored in this paper. Therefore, in the subsequent research, the SVM model should also be further improved from the above aspects in order to enhance the generalization ability and the classification effect of the model.

## Data Availability

The experimental data used to support the findings of this study are available from the corresponding author upon request.

## Conflicts of Interest

The authors declared that they have no conflicts of interest regarding this work.

## References

- [1] F. Wael, "Kalman-filter-based sensor fusion applied to road-objects detection and tracking for autonomous vehicles," *Proceedings of the Institution of Mechanical Engineers - Part I: Journal of Systems & Control Engineering*, vol. 235, no. 7, pp. 1125–1138, 2021.
- [2] X. Zhao, J. Zhang, J. Tian, L. Zhuo, and J. Zhang, "Multiscale object detection in high-resolution remote sensing images via rotation invariant deep features driven by channel attention," *International Journal of Remote Sensing*, vol. 42, no. 15, pp. 5764–5783, 2021.
- [3] W. Zhao, F. Chen, H. Huang, D. Li, and W. Cheng, "A new steel defect detection algorithm based on deep learning," *Computational Intelligence and Neuroscience*, vol. 2021, Article ID 5592878, 13 pages, 2021.
- [4] J. Liu, Y. Zhang, J. Xie, Y. Wei, Z. Wang, and M. Niu, "Head detection based on DR feature extraction network and mixed dilated convolution module," *Electronics*, vol. 10, no. 13, pp. 1565–1567, 2021.
- [5] J. Liu, Z. Yang, Y. Liu, and C. Mu, "Hyperspectral remote sensing images deep feature extraction based on mixed feature and convolutional neural networks," *Remote Sensing*, vol. 13, no. 13, p. 2599, 2021.
- [6] Y. Wang, "A feature extraction based support vector machine model for rectal cancer T-stage prediction using MRI images," *Multimedia Tools and Applications*, vol. 80, no. 20, pp. 1–11, 2021.
- [7] D. Bastian Nathaniel, "A dual U-Net algorithm for automating feature extraction from satellite imagery," *The Journal of Defense Modeling and Simulation: Applications, Methodology, Technology*, vol. 18, no. 3, pp. 193–205, 2021.
- [8] W. Hu, "LE-MSFE-DDNet: a defect detection network based on low-light enhancement and multi-scale feature extraction," *The Visual Computer*, pp. 1–15, 2021.
- [9] S. K. Ho, H. C. Nedunuri, W. Balachandran, J. Kanfoud, and T.-H. Gan, "Monitoring of industrial machine using a novel blind feature extraction approach," *Applied Sciences*, vol. 11, no. 13, pp. 5792–5798, 2021.
- [10] S. Zhang, D. Jiang, and Yu Cheng, "A mixed depthwise separation residual network for image feature extraction," *Wireless Networks*, pp. 1–12, 2021.
- [11] X. Zhong, X. Gao, Q. Mei, T. Huang, and X. Zhao, "Fault feature extraction method of gear based on optimized minimum entropy deconvolution and accugram," *Journal of Intelligent and Fuzzy Systems*, vol. 40, no. 6, Article ID 12265, 2021.
- [12] L. V. Stanislawski, E. J. Shavers, S. Wang et al., "Extensibility of U-net neural network model for hydrographic feature extraction and implications for hydrologic modeling," *Remote Sensing*, vol. 13, no. 12, p. 2368, 2021.
- [13] H. Xu, "A novel automatic method on pseudo-invariant features extraction for enhancing the relative radiometric normalization of high-resolution images," *International Journal of Remote Sensing*, vol. 42, no. 16, pp. 6155–6186, 2021.
- [14] A. B. Wicaksono Putra, W. Putra, Mulyanto, B. Suprpty, and A. F. Onnilita Gaffar, "A performance of combined methods of VCG and 16BCD for feature extraction on HSV," *International Journal of Image, Graphics and Signal Processing*, vol. 13, no. 3, pp. 13–32, 2021.
- [15] A. Mendes, T. Palmer, A. Berens et al., "Mapathons versus automated feature extraction: a comparative analysis for strengthening immunization microplanning," *International Journal of Health Geographics*, vol. 20, no. 1, pp. 27–29, 2021.
- [16] Z. Mu, T. Yu, X. Liu, H. Zheng, L. Wei, and J. Liu, "FEGS: a novel feature extraction model for protein sequences and its applications," *BMC Bioinformatics*, vol. 22, no. 1, pp. 297–299, 2021.
- [17] K. Vandana and P. Shukla, "A 3 Tier CNN model with deep discriminative feature extraction for discovering malignant growth in multi-scale histopathology images," *Informatics in Medicine Unlocked*, vol. 43, Article ID 100616, 2021.
- [18] X.-a. Bi, Y. Xie, H. Wu, and L. Xu, "Identification of differential brain regions in MCI progression via clustering-evolutionary weighted SVM ensemble algorithm," *Frontiers of Computer Science*, vol. 15, no. 6, Article ID 156903, 2021.
- [19] J. Fan, G. Huang, M. Chi et al., "Prediction of chemical reproductive toxicity to aquatic species using a machine learning model: an application in an ecological risk assessment of the Yangtze River, China," *The Science of the Total Environment*, vol. 796, Article ID 148901, 2021.
- [20] X. Li, J. Yang, Y. Fan, M. Xie, X. Qian, and H. Li, "Rapid monitoring of heavy metal pollution in lake water using nitrogen and phosphorus nutrients and physicochemical indicators by support vector machine," *Chemosphere*, vol. 280, Article ID 130599, 2021.
- [21] N. Hemanth, I. Keita, and T. Yamamoto, "Non-invasive diagnosis of colorectal cancer by Raman spectroscopy: recent developments in liquid biopsy and endoscopy approaches," *Spectrochimica Acta Part A: Molecular and Biomolecular Spectroscopy*, vol. 258, Article ID 119818, 2021.
- [22] J. B. Mohapatra, P. Jha, M. K. Jha, and S. Biswal, "Efficacy of machine learning techniques in predicting groundwater fluctuations in agro-ecological zones of India," *The Science of the Total Environment*, vol. 785, Article ID 147319, 2021.
- [23] S. İlkin, T. H. Gençtürk, F. Kaya Gülağız, H. Özcan, M. A. Altuncu, and S. Şahin, "hybSVM: bacterial colony optimization algorithm based SVM for malignant melanoma detection," *Engineering Science and Technology, an International Journal*, vol. 24, no. 5, pp. 1059–1071, 2021.

## Research Article

# Tumor Detection on Microarray Data Using Grey Wolf Optimization with Gain Information

**K. Dhana Sree Devi,<sup>1</sup> P. Karthikeyan,<sup>2</sup> Usha Moorthy ,<sup>3</sup> K. Deeba,<sup>4</sup> V. Maheshwari,<sup>2</sup> and Shaikh Muhammad Allayear<sup>5</sup>**

<sup>1</sup>Department of Computer Science and Engineering, CVR College of Engineering, Hyderabad, Telangana, India

<sup>2</sup>School of Information Technology and Engineering, Vellore Institute of Technology, Vellore, Tamil Nadu, India

<sup>3</sup>School of Computer Science and Engineering, REVA University, Bangalore, India

<sup>4</sup>Department of Computer Applications, Auxilium College (Autonomous)-Vellore, India

<sup>5</sup>Department of Multimedia and Creative Technology, Daffodil International University, Daffodil Smart, Khagan, Ashulia, Dhaka, Bangladesh

Correspondence should be addressed to Usha Moorthy; [ushmitha@gmail.com](mailto:ushmitha@gmail.com)

Received 17 March 2022; Revised 9 May 2022; Accepted 13 May 2022; Published 15 June 2022

Academic Editor: Shimin Wang

Copyright © 2022 K. Dhana Sree Devi et al. This is an open access article distributed under the Creative Commons Attribution License, which permits unrestricted use, distribution, and reproduction in any medium, provided the original work is properly cited.

Microarray data are becoming a more essential source of gene expression data for interpretation and analysis. To improve the detection accuracy of tumors, the researchers try to use the lowest feasible collection of the most gene expression studies, and relevant gene expression patterns are found. The purpose of this article is to use a data mining strategy and an optimized feature selection method focused on a limited dense tree forest classifier to evaluate and forecast colon cancer data. More specifically, merging the “gain information” and “Grey wolf optimization” was incorporated as a feature selection approach into the random forest classifier, to improve the prediction model’s accuracy. Our suggested technique can decrease the load of high-dimensional data, and it allows quicker computations. In this research, we provided a comparison of the analysis model with feature selection accuracy over model analysis without feature selection accuracy. The extensive experimental findings have shown that the suggested method with selecting features is beneficial, outperforming the good classification performances.

## 1. Introduction

Most colon cancers have become a considerable public health issue, and most of these cancers have expanded speedily worldwide. GLOBOCAN Database 2018 examined new 1,849,518 colorectal cancer (CRC) instances and 880,792 CRC-related deaths. The CRC is 0.33% the main cause of most cancer-associated deaths in the USA, 2019. The latest study by Wong Martin [1] suggests that about 25 percent of CRC instances contain a genetic propensity. At initial stage, generic cancers classification technique is build totally on DNA microarray gene expression monitor [2]. They additionally recommended similar microarray data would possibly give a classification technique for most cancers. The microarray technology, which largely

constructs the expression of genes, has widely utilized in prognosis additionally assessment of colon-related malignancies. Timely identification of cancer is crucial in accurate detection and therapy. Microarray-based data contain hundreds of gene information, and subsample sizes are often smaller. They had a difficult time identifying the most significant genes using microarray data because not every gene had adequate check-out facts and many of them are redundant. The two current strategies, feature transformation and selection of acquiring feature genes for most cancer classification, were built totally on gene expression data [3].

Feature transformation is a technique for creating a unique set of modern datasets from existing ones to achieve feature reductions, even if the author requires strong

discriminating power, typically to not retain the biological data in the initial sequence. The loss of data is reflected in data transformation interpretability, and it is not possible to spot a list of cancer-related target genes unlike methods for feature transformation and selection that do not generate a new set of features. Ghazavi and Liao take off nonredundant and relevant functions and keep their exceptional classification performance accuracy [4]. Feature selection now no longer contains replacing original features hence lowering the dimensionality information trouble to create a trust model of the dataset used. Even though, the techniques with a characteristic selection have received a similar interest aspect. The selection techniques may be separated into 3 major categories: filters, wrappers, and embedded techniques [5]. The filter method is a way of selecting features that is dependent on any future machine learning techniques and is based on a few statistical feature performances. They were technically quick and completely dependent on dataset characteristics. One of the most significant dangers is the overlook function connections. Wrapping-based methods were primarily focused on finding algorithms, which iteratively evaluate data against a set of machine learning rules to get the best subset of features. For datasets with numerous properties, algorithms are not only slower than filters but also computationally costly. Because they interact with the classifiers for the selection of features, embedded methods are minimally computationally expensive and faster than the other types of feature selection algorithms. Different forms of random forests, decision trees, and artificial neural networks are popular embedded methods. Gain information (GI) and Grey Wolf optimization were presented as strategies for choosing variables (GWO). An classifier is then developed for analyzing colon cancer. GWO is the most efficient swarm intelligence-based metaheuristic method. GWO is used in several optimization methods such as clustering applications, design and tuning controllers, power dispatch problems, robotics and path planning, scheduling problems, wireless sensor networks, and medical and biomedical applications [6]. While researching the usage of GWO in various engineering problems, we found that GWO has an ability to handle huge variable numbers and to escape local solutions while solving a large-scale problem. Since GWO has the ability to handle a large amount of variable with better solution, we intend to apply GWO for microarray data as it is a more essential source of gene expression data for interpretation and analysis.

For different environments, scholars have proposed abundant selection algorithms. There are several optimization algorithms inspired from nature or purely mathematical-driven methods. Some of them include monarch butterfly optimization (MBO), which optimizes the search strategy by decreasing the local optima, which in turn decreases the premature convergence and reduces the number the local maxima. This behavior is inspired from the monarch butterflies [7]. The slime mould algorithm is another kind of optimization algorithm inspired from the slime mould mode in nature. This algorithm mimics its behavior from the morphological changes of slime mould physisarum

polycephalum in completing its lifecycle. The entire lifecycle is modeled into a mathematical one, and the authors found it can be useful for optimization problems [8]. There is an algorithm inspired from the orientation of moths called moth swarm algorithm (MSA) [9]. MSA is modeled by capturing the movements of moths in moonlight. This can be used to create a learning based on association yielding an immediate memory, which utilizes levy-based mutation ethics to increase the cross-population environment and movement in spiral. Hunger Games Search (HGS) [10] optimization is based on inheriting the characteristics from hunger behavior of animals. The hunger-driven behavior of wild animals is inherited and modeled to a mathematical model and applied to solve a range of optimization problems. The RUNge Kutta optimizer [11] is different from bio-inspired algorithms and is meant to solve a variety of optimization problems in future. RUN utilizes the slope variation logic that is computed by the Runge–Kutta method as a searching mechanism. The drawback in this method is that this optimization works on large datasets only. The colony predation algorithm (CPA) is an efficient optimization method that focuses on utilizing a mathematical method inspired from the hunting group of animals such as prey encircling, prey dispersing, targeting hunters, animal strategy, and adjusting strategy [12]. Weighted mean of vectors is the most commonly used optimization algorithm in the literature prior to the discovery of bio-inspired algorithms. It works on the simple logic of assigning weights to the elements present in the vectors using a normalized function and computing the solution for the question set [13]. However, scheduling problem with no-wait constraints widely exists in the real-life process of steel production, computer systems, food processing, chemical industry, pharmaceutical industry, concrete products, etc. Many experts and scholars have studied optimization problems with zero constraints. For instance, to overcome no-wait scheduling idea with m-machine, a hybrid algorithm is taken based on the genetic algorithm and simulated annealing. To minimize the makespan of Flow Shop scheduling idea, several variants of descending search and Tabu search algorithm were proposed, and a strategy based on a dynamic Tabu list was also proposed, which enhanced the algorithm's ability to jump out of local optimum to a certain extent. A hybrid optimization algorithm based on variable neighborhood descent and PSO was used to solve Flow Shop scheduling with two optimization goals. To minimize the weighted sum of maximum completion time and total completion time, the literature proposed a TOB (trade-off balancing) algorithm based on machine idle times. For Job Shop scheduling optimization in which each job has its optimization strategy, the literature proposed a hybrid genetic algorithm, in which the genetic operation is treated as a subproblem and transformed into asymmetric travelling salesman problem. In the abovementioned commonly used production scheduling algorithms, no consideration is given to the great product structure differences, processing parameter differences, and the need for further deep processing after assembly of jobs in the real-life manufacturing process of nonstandard products.

In fact, to quickly respond to the ever-changing market and alleviate the pressure of nonstandard products in research and trial production, some enterprises have established dedicated production workshops to improve production efficiency of less-than-truckload, personalized products and nonstandard products. However, some order-oriented SMEs organize production according to orders. During the production process, there are a large number of nonstandard products that demand scribbling, hand lapping, scraping, and precision templates. Big differences exist in product structure and component parameters and jobs demand further deep processing after assembly, so parts cannot be predicted and prepared in advance, and production must be advanced according to BOM (bill of material) [14]. The problem of requiring further deep processing after jobs assembly is often referred to as integrated scheduling problem (ISP). For ISP, literatures discussed a hybrid optimization method of bottleneck shifting and genetic algorithm. The literature pointed out that common no-wait scheduling algorithms can only deal with the case where the number of no-wait child nodes is 1. However, in ISP, there are abundant cases in which further deep processing is required after jobs assembly; that is, the number of no-wait child nodes can be greater than 1 in ISP. Therefore, ISP with no-wait constraints is more complicated [15]. Some of the recent heuristic algorithms include monarch butterfly optimization (MBO), slime mould algorithm (SMA), moth search algorithm (MSA), hunger games search (HGS), Runge-Kutta method (RUN), and Harris hawks optimization (HHO). There are several optimization algorithms in the literature using various nature-inspired techniques for optimization but still GWO is not utilized in the field of microarray detection and so we proposed in this work. While researching the above published works, it is clear that optimization is still a major issue.

Our Contributions include the following:

- (1) A data mining strategy and a feature selection method based on a threshold optimized forest classifier are proposed to optimize the feature selection
- (2) Ensemble of “gain information” and “Grey wolf optimization” was incorporated as a feature selection approach into the random forest classifier, to improve the prediction model’s accuracy
- (3) Provided a comparison of model analysis with feature selection over model analysis without feature selection

## 2. Literature Survey

A detailed review on gene selection proves that feature selection is a significant thing for data mining procedure. Xian et al. proposed a particle deletion using a strategy with a computed fitness value through clustering, and the corresponding particles are generated using the importance of feature and this ensemble of the two algorithms is used to compute the crossover of both qualities of particles. Salem et al. published a study that used gene

expression profiles to classify human cancers [16]. In this feature selection technique, from the initial microarray, the information gain (IG) was used to identify genes. In addition, the genetic algorithm (GA) was used for reducing the features utilizing the IG. For cancer categorization using genetic programming (GP) (or diagnosis), data mining algorithms are used. Seven cancer gene expression datasets were utilized to verify the technique. The author established accuracy of 85.48 percent for colon cancer and 88.87 percent for breast cancer (central nervous system *cancer*), 96.05 percent (leukaemia72), 72.3 percent (lung *cancer* in Ontario), and 100 percent for all cancers (lung cancer, Michigan), 93.7 percent (DLBCL, Harvard), and 100 percent (lung cancer, Michigan) (prostate).

Bennett et al. provided an ensemble feature technique that combines the support vector machine feature selection reduction (SVM-RFE) technique with Bayes error filter (BBF) for accuracy improvement as a hybrid genetic algorithm strategy [17]. The attributes were sorted using SVM-RFE, and the superfluous sorted attributes were removed using BBF. After that, the dataset was classified using the SVM method. The best classification accuracy for the Leukaemia73 dataset was 96.1 percent.

On 10 datasets, the authors of Gunavathi et al. investigated the effects of GA combined with k-nearest-neighbors (KNN) and are analyzed using SVM classifiers [18]. Three filters were used to decrease the number of characteristics identified by the GA. The SVM ensembles with KNN algorithms are utilized to predict the data at the end. Accuracy of the SVM is nearly identical to that of the KNN classifier on most datasets; the only exception was the Leukaemia72 dataset, for which the authors used fivefold cross-validation.

Canedo et al. developed a new method of bifurcation of classifiers. The researchers utilized a voting mechanism to classify the samples [19]. They used tenfold cross-validation to apply their methods to ten microarray datasets, and classification accuracy rates are well improved for several datasets, and moreover, the authors tried to focus on the level of possible parameter optimization in gene selection using the GA. This is considered the best performing area in optimization methodology.

Using a gene expression dataset, in a combination of four classifiers for cancer classification, a GA-based optimization was utilized for gene selection. As classifiers, naive Bayes feature selector, SVM hyperplane optimization, CUBIST, and decision tree forests classifiers were employed [20]. Lymphoma, Lung, CNS, Colon, Leukaemia38, and Leukaemia73 were the six datasets studied, with top prediction rates of 97.1 percent, 99.03 percent, 81.3 percent, 87.8%, 100 percent, and 97.06 percent, respectively.

Salem and Hanaa highlighted the results of a study that used gene expression to classify early breast cancer [21]. Their method uses an IG approach to identify important genes from both the initial microarray data and then gives it as an input to a GA-based arithmetic material to enable the optimization at a better speed. The specificity of classification was 100 percent.

Bouazza and Sara Haddou presented findings from a study that used SVM and KNN classifiers to classify cancer [22]. This study analyzed the data using various feature selection techniques (such as Fisher, Relief, SNR, and T-Statistics) on multiple gene regulation account sets of data (Prostate, Colon, and Leukaemia) for both KNN and SVM classifiers on 3 datasets of profiled gene expression. Merging the SNR feature selection with SVM yielded the best results. The best classification accuracy rates were 95 percent for the colon and breast data and 100 percent for leukaemia-based data utilizing SNR feature selection with the KNN classifier.

Wang et al. [23] proposed an ensemble feature selection method based on the sampling method. The feature vector is sampled using the threshold value set by a sample selector, and the sampled features are ranked using the bootstrapping method. Based on the ranking, the top-ranked features are aggregated using a data aggregation function. High-dimensional microarray data are utilized to test the proposed ensemble model, and the results show the efficiency of the proposed algorithm is better compared to benchmark optimization algorithms. A detailed review of feature selection methods for microarray data for cancer disease classification is detailed by Esra'a Alhenawi [24].

There are several classification mechanisms proposed by various researchers using different approaches. One such novel approach is carried out by Konstantina et al. [25]. The authors utilized the transcriptomics dataset for modeling the gene expression data. Deep learning-based time series modeling is used for time series analysis to provide inference on network regulatory. The authors achieved an accuracy of 98%. Several experiments were carried out to show the efficiency of the proposed algorithm in gene expression time series data.

A concept of altruism is proposed by Rohit Kundu et al. [26]. Altruism concept is embedded in the WOA to manipulate the candidate solutions to reach the local optima over the fitness value of the iterations. This method of alteration increased the fitness value of the WOA. The efficiency of altruistic WOA is tested on the microarray dataset for optimized feature selection. The authors used eight microarray datasets from cancer data repository to show the supremacy of the proposed algorithm in these datasets.

There are three phases to the proposed technique. After the data are provided in the feature learning process, the IG filter identifies one of the essential features. The GWO algorithm then minimizes the volume of features that have been selected. The system's final stage involves using the SVM classifier to generate cancer classification. The following is a summary of the technique shown in Figure 1.

### 3. Proposed System

The ensemble model of gain information and grey wolf optimization is the proposed system, and we utilized in this research. Since the ensemble model provides better performance than benchmark optimization algorithms, we used this ensemble technique for performance improvement. The

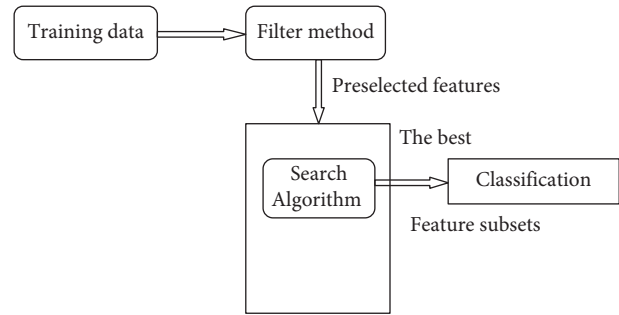


FIGURE 1: Information gain process.

methodology of this analysis is depicted in Figure 2. Firstly, the data collection plays a very crucial in the process. The data from the first stage were then moved to the second stage, where they were classified. We employed two techniques in the third stage to choose MDI and MDG features for data training and testing. A comparative architecture analysis was carried out.

**3.1. Data Samples.** During the collection process of the concerned data, data on colon cancer gene expression were collected from Alon et al. [27]. There are 63 samples (testing) and approximately 2000 genes (attributes) among colon cancer patients in the databases. There are 42 cancer cell samples among them, as well as 22 normal biopsies. The data from colon tumor samples are shown in Table 1.

**3.2. Classification Performance Evaluation in the Absence of Feature Selection.** With all of the attributes in this technique, an RF classification with tenfold cross-connection was utilized to evaluate the model's results.

**3.3. Evaluation of Feature Selection with Classification.** MDG and MDA were utilized as a feature selection approach to predict the more relevant to the meaningful feature. We then used selected features to build a robust model and followed the same process as defined in the previous phase.

**3.4. Performance Measures.** We compare the effectiveness of the system without feature selection with the model with feature selection in this procedure. To evaluate the classification's consistency, we used recalls, accuracy, correctness, and F1-score measures. The neural network, which is used to analyze the quality of classifiers, produces predictable results.

Tables 1 and 2 show the confusion matrix's interpretation and the algorithm for calculating performance indicators, evenly. Recalls, also known as sensitivity, are the proportion to properly predict positive instances of every discovery in the label class. The precision metric reveals which of the positive results are correct. This shows that the ratio of accurately predicted classes to total classes is the accuracy of a classifier. The F1-score is calculated using a weighted average of accuracy and recall. When there is an unbalanced class percentage, the F1-

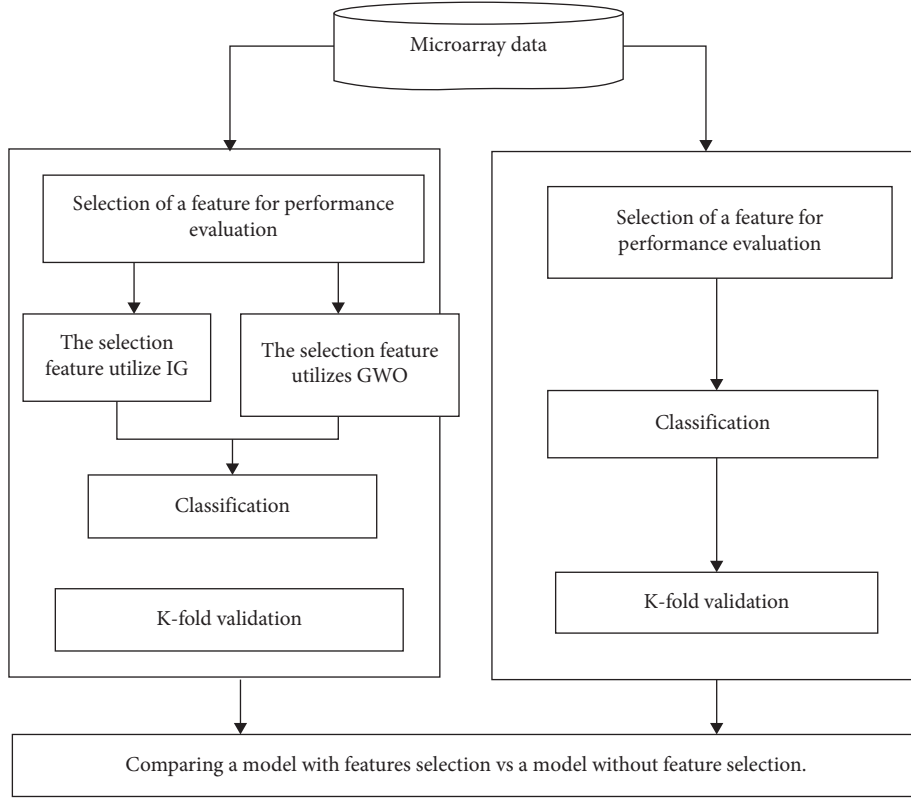


FIGURE 2: Framework of the proposed model.

TABLE 1: Confusion matrix.

| Predicted          | Actual               |                       |
|--------------------|----------------------|-----------------------|
|                    | Positive             | Negative              |
| Predicted positive | True positives (TPs) | False negatives (FNs) |
| Predicted negative | False positive (FPs) | True negatives (TNs)  |

TABLE 2: Performance measure representation.

| Performance metrics | Formula                                       |
|---------------------|---|
| Recall              | $TP/TP + FN$                                  |
| Precision           | $TP/TP + FP$                                  |
| F1-score            | $2 * Recall * Precision / Recall + Precision$ |
| Accuracy (%)        | $TP + TN / TP + FP + FN + TN$                 |

score is frequently the most important than the precision since it accounts for either false positives or false negatives:

$$VI(x_j) = \frac{1}{n_{tree}} \sum_{t=1}^{n_{tree}} \frac{|\sum_{i \in OOB} I(y_i = f(X_i)) - \sum_{i \in OOB} I(y_i = f(X_i^j))|}{|OOB|} \quad (1)$$

where  $VI(x_j)$  denotes the value significance of  $x_j$ . If ignoring (or permuting) a variable decreases the random forest's accuracy, it is regarded as more significant. As a

result, variables that have a considerable mean drop in precision are the most important for accuracy.

## 4. Feature Selection Algorithm Description

**4.1. Gene Selection Using Entropy and Information Gain (Ig).** Entropy is considered a fundamental term in the information theory that is used to calculate the homogeneity of features. For instance, homogeneous samples have an entropy of zero, while evenly split samples have one value for entropy. A high feature dimensionality data and a minimum size make data categorization exceedingly challenging. A minimal percentage of millions of gene characteristics analyzed are more relevant for given disease data. As a result, only the most important features should be kept. A thorough analysis of the gene profiles would aid in the selection of the gene, which is the most significant for problem identification.

$E(Z) = -D^+ \log_2(D^+) - D^- \log_2(D^-)$  for a sample with negative and positive attributes.

The entropy model can be summarized as the following equation [28]:

$$\text{Entropy}(Z) = \sum_{i=1}^v -(D_i \log_2 D_i) \quad (2)$$

where  $D_i$  is the probability of categorical variables a priori, and  $Z$  and  $k$  are indexes in the classification systems that indicate a certain category.

Consider the case of 2 classification issues in particular ( $V$  is known for classes). We consider gene with  $n$  potential values ( $j_1, j_2, \dots, j_n$ ). The following is the entropy:

$$\text{Entropy}\left(\frac{k}{j}\right) = \sum_{j=1}^n p(j) \sum_{k=1}^v p\left(\frac{k}{j}\right) \log_2\left(p\left(\frac{k}{j}\right)\right), \quad (3)$$

where  $p(k|j)$  is called probability distribution in variation  $K$  assuming variable  $J$  remains static and is computed across full variables with subclasses. In calculating  $IG$ , entropy is their most important factor [29]. The entropy across all variables in the sample of data is determined by the distribution of the features in the data sample. The information is then divided into feature sections. The entropy of each group to be measured independently, and the overall entropy can be computed by combining the entropy data of all groups. The entropy of particular groupings of sample data is then subtracted from their total entropy of the dataset distribution [30]:

$$IG(J) = \text{Entropy}(S) - \text{Entropy}\left(\frac{k}{j}\right). \quad (4)$$

When gene  $J$  and category  $K$  are unrelated,  $IG(J) = \text{Entropy}(S) - \text{Entropy}(k|j) = \text{zero}$ , while when they are related,  $\text{Entropy}(S) > \text{Entropy}(k|j)$ , resulting in  $IG(J) > 0$ . A greater association between  $J$  and  $K$  is directly proportional to a larger discrepancy between  $K$  and  $J$ . For classification, a feature selection within a higher  $IG$  value is more relevant. As an outcome, genes with higher  $IG$  values are chosen first from the original set of high-dimension genes to serve as the sample for feature gene selection [31].

Those steps of the  $IG$  algorithm have illustrated the form of the  $IG$  flowchart in Figure 2. The suitable output is a subgroup  $Y$  of the real variable  $W$ , with a group of attributes  $W$  in the input data set. The attributes that will be used for classifiers are first analyzed. Second, for each class, the entropy of all subsamples is calculated using (1). The probability of every value of one attribute is then computed, but the conditional entropy for each attribute is calculated using (2). For all attributes, the  $IG$  is calculated using (3). The resulting  $IG$  values are sorted ascendingly, with all values over a particular threshold value being selected.

**4.2. The Mathematical Model of GWO.** Mirjalili and Lewis established the GWO method to discover proper, restricted, and uncontrolled objective functions [32]. Grey wolves' social hierarchy serves as inspiration for the GWO algorithm. Artificial wolves in a virtual environment imitate tracking, encircling, and attacking actions, among others. The GWO social hierarchy divides wolves into four groups: alpha ( $\alpha$ ), beta ( $\beta$ ), delta ( $\delta$ ), and omega ( $\omega$ ). The best option is to think of wolves. The second- and third-placed options are known as  $\beta$  wolves and  $\delta$  wolves, respectively. Wolves guide  $\alpha$ ,  $\beta$ ,  $\delta$  wolves' hunting activity, which reflects optimization procedures. The remaining population is regarded as  $\omega$ , and their movements are conditioned by those three dominant wolves. Figure 3 depicts the power hierarchy of a wolf pack. The wolf commands all of the subordinates,

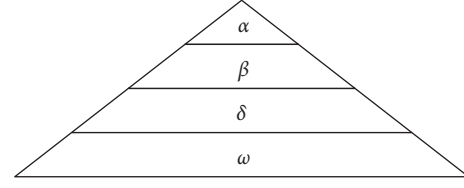


FIGURE 3: Hierarchical orders of grey wolves in nature.

according to the dominance hierarchy. Similarly,  $\beta$  and  $\delta$  wolves have an influence on the wolves in their social roles.

Grey wolves begin their hunting behavior by enveloping their target. The following equations are used to represent the encircling behavior in mathematics:

$$\begin{aligned} \vec{D} &= \left| \vec{C} \cdot \vec{X}_p(t) - \vec{X}(t) \right|, \\ \vec{X}(t+1) &= \vec{X}_p(t) - \vec{A} \cdot \vec{D}. \end{aligned} \quad (5)$$

where  $t$  represents iterations,  $\vec{A}$  and  $\vec{C}$  are coefficient vectors,  $\vec{X}_p$  in  $\vec{X}$  is the location vectors of a grey wolf, and  $Y$  is the position vector of the prey. The coefficients vector is donated in the following way:

$$\begin{aligned} \vec{A} &= 2 \vec{a} \cdot \vec{r} - \vec{a}, \\ \vec{C} &= 2 \cdot \vec{r}_2. \end{aligned} \quad (6)$$

The variable of the constant vectors  $\vec{X}$  decreases linear from 2 to 0 as a  $(t) = 2 - (t-1) / (2/\text{maxIter})$ , where  $\text{maxIter}$  is the maximum number of iterations.

Hunting behavior follows their circling in the prey. The movements of grey wolves are regulated by donates wolves ( $\alpha$ ,  $\beta$ ,  $\delta$ ):

$$\vec{D}_\alpha = \vec{C}_1 \vec{X}_\alpha - \vec{X}, \quad (7)$$

$$\vec{D}_\beta = \vec{C}_2 \vec{X}_\beta - \vec{X}, \quad (8)$$

$$\vec{D}_\delta = \vec{C}_3 \vec{X}_\delta - \vec{X}, \quad (9)$$

$$\vec{X}_1 = \vec{X}_\alpha - \vec{A}_1 \cdot \vec{D}_\alpha, \quad (10)$$

$$\vec{X}_2 = \vec{X}_\beta - \vec{A}_2 \cdot \vec{D}_\beta, \quad (11)$$

$$\vec{X}_3 = \vec{X}_\delta - \vec{A}_3 \cdot \vec{D}_\delta, \quad (12)$$

$$\vec{X}(t+1) = \frac{\vec{X}_1 + \vec{X}_2 + \vec{X}_3}{3}, \quad (13)$$

where  $\beta$ ,  $\xi$  represents the number of iterations,  $D$  and  $C$  are coefficients vectors,  $X$  is the space vectors of a grey wolf, and  $Y$  is the position vector of the prey.  $\vec{X}(t+1)$  is the resultant vector. The coefficient vector is donated in the following way.

The above equations were utilized to arithmetically model the wolf pack's hunting behavior in this regard. In the simulated environment, (7)–(13). Table 3 concludes with the



TABLE 3: The GWO's pseudocode.

---

- (1). initialize GWO population of solution vectors
- (2). define coefficient vectors  $\vec{A}$ ,  $\vec{C}$  and  $\vec{a}$
- (3). evaluate fitness value  $f(x_i)$ ,  $i = 1, \dots, nWolf$
- (4). determine  $\vec{X}_\alpha$ ,  $\vec{X}_\beta$ , and  $\vec{X}_\delta$
- (5). **while** iter < maxIter
- (6).   **for**  $i = 1:nWolf$
- (7).     movement of grey wolves, according to Equation 18
- (8).   **end for**
- (9).   update coefficients  $\vec{A}$ ,  $\vec{C}$  and  $\vec{a}$
- (10).   calculate fitness values  $f(x_i)$ ,  $i = 1, \dots, n$
- (11).   update  $\vec{X}_\alpha$ ,  $\vec{X}_\beta$ , and  $\vec{X}_\delta$
- (12).   iter  $\leftarrow$  iter + 1
- (13). **end while**
- (14). return  $\vec{X}_\alpha$ ,  $f(\vec{X}_\alpha)$

---

GWO's pseudocode. The fitness value is calculated by dividing the survival rate by the highest survival rate.

**4.3. Classification Algorithm Description.** In this study, the prediction of colon cancer was tested using random forest, a well-known classification method for prediction models. CART is a mixed classifier made up of unpruned decision trees, whereas RF is a collection of unpruned data sets (classification and regression trees). The CART method is described in great depth in this book [33]. When conducting classification research, the RF forecast is the intermediate majority of each tree category votes [34]. The architecture of an RF model for predicting colon class is shown in Figure 2.

## 5. Algorithm Description for Random Forest

Here, initial datasets are  $D(X, Y)$  and RF creates a simple decision tree: where  $n$  is training observations,  $K$  is classes, and  $(x_i, y_i)$  collection of cases whose class membership is determined  $(X, Y)$ .  $(x_i, y_i)$  can be used to represent the combined classifier  $(X, Y)$ . Find the best classifier that minimizes error in comparison with the original dataset [35].

## 6. Description of K-Fold Cross-Validation

Cross-validation is a recreation sample technique in the test machine learning methods on a bounded set of data samples. The unique argument in the technique is  $k$ , which denotes the number of sample groups that should be conquered into a set of datasets. As a result, that approach is called as  $k$ -fold cross-validation. This technique is known as tenfold cross-validation when the values of  $k$  are set to 10 [36].

The steps for training  $K$ -fold cross-validation are as follows:

- (i) Divided full dataset into  $k$  equivalent sections, each one of which is referred to as a fold. The names of the folds should be  $f_1, f_2 \dots f_k$ .
- (ii) For  $i = 1$  to  $k$ , preserve the  $f_i$  bend in the validated model and the subsequent  $k-1$ -fold in the classification model.

TABLE 4: Confusion matrix without feature selection.

---

| Actual   | Predicted class |        |
|----------|-----------------|--------|
|          | Abnormal        | Normal |
| Abnormal | 35              | 5      |
| Normal   | 5               | 12     |

---

TABLE 5: Performance analysis of the model without feature selection.

---

| Classes              | Recall   | Precision | F1-score | Accuracy (%) |
|----------------------|----------|-----------|----------|--------------|
| Abnormal             | 00.85724 | 00.89     | 00.90    | 84.870       |
| Normal               | 00.81    | 00.7277   | 00.7618  |              |
| Weighted measure (%) | 82.58    | 82.85     | 82.67    |              |

---

TABLE 6: Confusion matrix with feature selection.

---

| Actual   | Predict classes |        |
|----------|-----------------|--------|
|          | Abnormal        | Normal |
| Abnormal | 38              | 2      |
| Normal   | 3               | 22     |

---

TABLE 7: Performance of feature selection with the analysis of the models.

---

|                      | Recall   | Precisions | F1-scores | Accuracy (%) |
|----------------------|----------|------------|-----------|--------------|
| Abnormal             | 00.95123 | 00.976     | 00.9628   | 96.166       |
| Normal               | 00.95240 | 00.90908   | 00.9702   |              |
| Weighted measure (%) | 96.15    | 96.15      | 96.13     |              |

---

- (iii) Create a model given a dataset, and test its accuracy using the validation data.
- (iv) The model's value is defined by the accuracy average of all  $k$ -fold cross-validation occurrences.

### 6.1. System Requirements. Anaconda Enterprise 4.

CPU:  $2 \times 64$  bit 2.8 GHz 8.00 GT/s CPUs.

RAM: 32 GB (or 16 GB of 1600 MHz DDR3 RAM).

Storage: 300 GB.

These experimental data from the three phases are summarized in this section: classification assessment without feature selection, classifiers evaluations with feature selection, and comparison analyzed evaluations. The complete dataset is divided into two groups for experimental testing: normal and abnormal, using each of the 3000 genes. Table 4 shows the correlation coefficient, as well as the performance evaluation between the two groups in terms of recalls, clarity, F1-score, and accurate scores. Our random forest classification model can correctly classify 53 of 63 objects, as shown in Tables 5, yielding weighted recalls, accurate, and F1-scores of 82.78 percent, 82.77 percent, and 82.775 percent, respectively.

TABLE 8: Comparison of analysis of the models.

| Model                            | Evaluation metric |            |              |              |
|----------------------------------|-------------------|------------|--------------|--------------|
|                                  | Precision (%)     | Recall (%) | F1-score (%) | Accuracy (%) |
| Models without feature selection | 84.87             | 84.68      | 84.68        | 84.871       |
| Models with feature selection    | 96.15             | 96.15      | 96.13        | 96.166       |

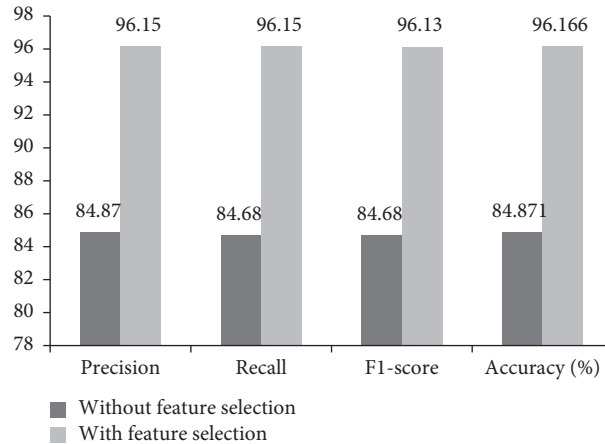


FIGURE 4: Comparison of analysis of the models.

TABLE 9: Comparison of the performance with different methods.

| Publications            | Methods         | Number of attributes | Accuracy (%) | Time complexity | Time (ms)   |
|-------------------------|-----------------|----------------------|--------------|-----------------|-------------|
| Simone A et al. [13]    | FDT             | 22                   | 79.13        | $O(n \log n)$   | 0.54        |
| Nguyen et al. [14]      | MAPH + PNN      | 5                    | 85.19        | $O(n * n)$      | 0.21        |
| Lingyun Gao et al. [15] | FCBFS + SVM     | 14                   | 90.45        | $O(n \log n)$   | 0.43        |
| Salem H et al. [16]     | GP + IG + GA    | 60                   | 84.68        | $O(n + k)$      | 0.34        |
| Our proposed method     | <b>IG + GWO</b> | <b>33</b>            | <b>95.16</b> | $O(\log n)$     | <b>0.12</b> |

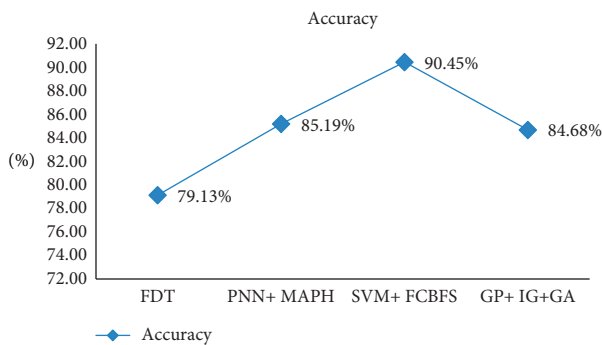


FIGURE 5: Graphical comparison of the model for various evaluation metric.

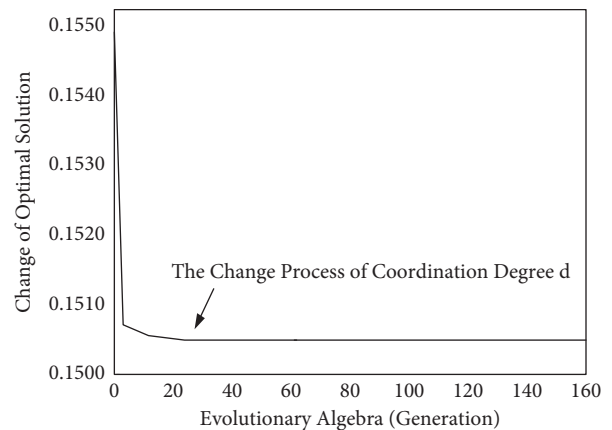


FIGURE 6: Process execution evolutionary timeline for the proposed system.

Using all genes, this model is 84.870 percent accurate. To eliminate the more relevant and redundant genes from every dataset, we used mean decreased with accuracy and means decreased Gini as feature selection methods. In Tables 6 and 7, the finally confusion matrix and efficiency measures depend upon the top 33 genes, respectively.

The models depending upon the top 35 identified genes could accurately recognize 57 samples out of 61 samples with a 95.161 percent accuracy. In addition, the models received

94.10 percent for weighted recalls, accuracy, and F1-scores, and 94.10 percent for weighted recalls, accuracy, and F1-scores. Table 7 shows a comparison of the model with and without feature selection [37–47].

When the models with feature selection were utilized, all of the measured parameters outperform their equivalents

when the model without feature selection was employed, as shown in Table 8. Figure 4 depicts the model's overall findings based on performance metrics in a graphical representation. Table 9 shows that the time complexity of our proposed system is the best.

Figure 5 shows a comparison of our suggested models and previous techniques. Table 9 illustrates that our technique outperforms all other procedures with less information about the expression of genes. Figure 6 describes the process execution evolutionary timeline for the proposed system.

## 7. Conclusion

A “gain information”- and “Grey wolf optimization”-based ensemble model was incorporated as an optimal feature selection approach into the random forest classifier to improve the prediction model's accuracy. Our suggested technique can decrease the load of high-dimensional data, and it allows quicker computations. Additionally, we provided the comparison of classification model analytics for feature selection over prediction analysis without feature selection. The extensive experimental findings have shown that the suggested method with selecting features is beneficial, outperforming the good classification performances. In fact, feature selection is an accurate method, and its time complexity increases exponentially with the problem scale. In order to alleviate the running time of large-scale instance, multilevel window technology can be adopted. That is, the preprocessing scheme could be subdivided for multiple levels of windows to reduce the number of jobs in a window. By making full use of the time period in which the tasks of the previous window are being processed, the tasks of the next window are solved by using constraint programming solver. Therefore, this work can serve as the research basis for feature selection problem. [47].

## Data Availability

The data used to support the findings of this study are included within the article.

## Conflicts of Interest

The authors declare that there are no conflicts of interest regarding the publication of this article.

## References

- [1] M. C. Wong, H. Ding, J. Wang, P. S. Chan, and J. Huang, “Prevalence and risk factors of colorectal cancer in Asia,” *Intestinal research*, vol. 17, no. 3, pp. 317–329, 2019.
- [2] T. R. Golub, D. K. Slonim, P. Tamayo et al., “Molecular classification of cancer: class discovery and class prediction by gene expression monitoring,” *Science*, vol. 286, no. 5439, pp. 531–537, 1999.
- [3] M. Xi, J. Sun, L. Liu, F. Fan, and X. Wu, “Cancer feature selection and classification using a binary quantum-behaved particle swarm optimization and support vector machine,” *Computational and Mathematical Methods in Medicine*, vol. 20169 pages, Article ID 3572705, 2016.
- [4] S. N. Ghazavi and T. W. Liao, “Medical data mining by fuzzy modeling with selected features,” *Artificial Intelligence in Medicine*, vol. 43, no. 3, pp. 195–206, 2008.
- [5] A. L. Blum and P. Langley, “Selection of relevant features and examples in machine learning,” *Artificial Intelligence*, vol. 97, no. 1-2, pp. 245–271, 1997.
- [6] M. S. Kumar and J. Prabhu, “A hybrid model collaborative movie recommendation system using K-means clustering with ant colony optimisation,” *International Journal of Internet Technology and Secured Transactions*, vol. 10, no. 3, p. 337, 2020.
- [7] M. S. Kumar and J. Prabhu, “Comparison of multi-criteria recommendation system for improving accurate prediction,” *Journal of Advanced Research in Dynamical & Control Systems*, vol. 10, no. 8, 2018.
- [8] G. G. Wang, S. Deb, and Z. Cui, “Monarch butterfly optimization,” *Neural Computing & Applications*, vol. 31, no. 7, pp. 1995–2014, 2019.
- [9] M. S. Kumar and J. Prabhu, “Hybrid model for movie recommendation system using fireflies and fuzzy c-means,” *International Journal of Web Portals*, vol. 11, no. 2, pp. 1–13, 2019.
- [10] D. Oliva, S. Esquivel-Torres, S. Hinojosa et al., “Opposition-based moth swarm algorithm,” *Expert Systems with Applications*, vol. 184, Article ID 115481, 2021.
- [11] M. Sandeep Kumar and J. Prabhu, “A case study on recommendation systems based on big data,” in *Smart Intelligent Computing and Applications*, pp. 407–417, Springer, Singapore, 2019.
- [12] I. Ahmadianfar, A. A. Heidari, A. H. Gandomi, X. Chu, and H. Chen, “RUN beyond the metaphor: an efficient optimization algorithm based on Runge Kutta method,” *Expert Systems with Applications*, vol. 181, Article ID 115079, 2021.
- [13] J. Tu, H. Chen, M. Wang, and A. H. Gandomi, “The colony predation algorithm,” *Journal of Bionics Engineering*, vol. 18, no. 3, pp. 674–710, 2021.
- [14] I. Ahmadianfar, A. A. Heidari, S. Noshadian, H. Chen, and A. H. Gandomi, “INFO: an efficient optimization algorithm based on weighted mean of vectors,” *Expert Systems with Applications*, vol. 195, Article ID 116516, 2022.
- [15] H. N. Nguyen, T. N. Vu, S. Y. Ohn, Y. M. Park, M. Y. Han, and C. W. Kim, “Feature elimination approach based on random forest for cancer diagnosis,” in *Proceedings of the Mexican International Conference on Artificial Intelligence*, pp. 532–542, Springer, Berlin, Germany, November 2006.
- [16] X. F. Song, Y. Zhang, Y. N. Guo, X. Y. Sun, and Y. L. Wang, “Variable-size cooperative coevolutionary particle swarm optimization for feature selection on high-dimensional data,” *IEEE Transactions on Evolutionary Computation*, vol. 24, no. 5, pp. 882–895, 2020.
- [17] H. Salem, G. Attiya, and N. El-Fishawy, “Classification of human cancer diseases by gene expression profiles,” *Applied Soft Computing*, vol. 50, pp. 124–134, 2017.
- [18] J. Bennet, C. Ganaprakasam, and N. Kumar, “A hybrid approach for gene selection and classification using support vector machine,” *The International Arab Journal of Information Technology*, vol. 12, pp. 695–700, 2015.
- [19] C. Gunavathi and K. Premalatha, “Performance analysis of genetic algorithm with kNN and SVM for feature selection in tumor classification,” *International Journal of Comput Electronic Automation Control and Information Engineering*, vol. 8, no. 8, pp. 1490–1497, 2014.

- [20] V. B. Canedo, N. S. Maroño, and A. A. Betanzos, "An ensemble of filters and classifiers for microarray data classification," *Pattern Recognition*, vol. 45, no. 1, pp. 531–539, 2012.
- [21] J. Y. Yeh, "Applying data mining techniques for cancer classification on gene expression data," *Cybernetics & Systems*, vol. 39, no. 6, pp. 583–602, 2008.
- [22] H. Salem, G. Attiya, and N. El-Fishawy, "Early diagnosis of breast cancer by gene expression profiles," *Pattern Analysis & Applications*, vol. 20, no. 2, pp. 567–578, 2017.
- [23] A. Wang, S. Ve, W. A. Hatamleh, K. D. Haouam, B. Venkatesh, and D. Sweidan, "Advanced lightweight feature interaction in deep neural networks for improving the prediction in click through rate," *Annals of Operations Research*, pp. 1–15, 2021.
- [24] A. Wang, H. Liu, J. Yang, and G. Chen, "Ensemble feature selection for stable biomarker identification and cancer classification from microarray expression data," *Computers in Biology and Medicine*, vol. 142, Article ID 105208, 2022.
- [25] E. A. Alhenawi, R. Al-Sayyed, A. Hudaib, and S. Mirjalili, "Feature selection methods on gene expression microarray data for cancer classification: a systematic review," *Computers in Biology and Medicine*, vol. 140, Article ID 105051, 2022.
- [26] K. Kourou, G. Rigas, C. Papaloukas, M. Mitsis, and D. I. Fotiadis, "Cancer classification from time series microarray data through regulatory dynamic bayesian networks," *Computers in Biology and Medicine*, vol. 116, Article ID 103577, 2020.
- [27] R. Kundu, S. Chattopadhyay, E. Cuevas, and R. Sarkar, "AltWOA: altruistic whale optimization algorithm for feature selection on microarray datasets," *Computers in Biology and Medicine*, vol. 144, Article ID 105349, 2022.
- [28] Z. M. Hira and D. F. Gillies, "A review of feature selection and feature extraction methods applied on microarray data," *Advances in bioinformatics*, vol. 201513 pages, Article ID 198363, 2015.
- [29] U. Alon, N. Barkai, D. A. Notterman et al., "Broad patterns of gene expression revealed by clustering analysis of tumor and normal colon tissues probed by oligonucleotide arrays," *Proceedings of the National Academy of Sciences*, vol. 96, no. 12, pp. 6745–6750, 1999.
- [30] J. C. Baez, T. Fritz, and T. Leinster, "A characterization of entropy in terms of information loss," *Entropy*, vol. 13, no. 11, pp. 1945–1957, 2011.
- [31] M. Walowe Mwadulo, "A review on feature selection methods for classification tasks," *International Journal of Computer Applications Technology and Research*, vol. 5, no. 6, pp. 395–402, 2016.
- [32] S. Ve, C. Shin, and Y. Cho, "Efficient energy consumption prediction model for a data analytic-enabled industry building in a smart city," *Building Research & Information*, vol. 49, no. 1, pp. 127–143, 2021.
- [33] S. Mirjalili, S. M. Mirjalili, and A. Lewis, "Grey wolf optimizer," *Advances in Engineering Software*, vol. 69, pp. 46–61, 2014.
- [34] D. J. Hand, "Principles of data mining," *Drug Safety*, vol. 30, no. 7, pp. 621–622, 2007.
- [35] R. Harb, X. Yan, E. Radwan, and X. Su, "Exploring precrash maneuvers using classification trees and random forests," *Accident Analysis & Prevention*, vol. 41, no. 1, pp. 98–107, 2009.
- [36] L. Y. Chang and H. W. Wang, "Analysis of traffic injury severity: an application of non-parametric classification tree techniques," *Accident Analysis & Prevention*, vol. 38, no. 5, pp. 1019–1027, 2006.
- [37] S. Sucharita, B. Sahu, and T. Swarnkar, "A comprehensive study on the application of grey wolf optimization for microarray data," *Data Analytics in Bioinformatics: A Machine Learning Perspective*, pp. 211–248, 2021.
- [38] S. Ve and Y. Cho, "A rule-based model for Seoul Bike sharing demand prediction using weather data," *European Journal of Remote Sensing*, vol. 53, no. 1, pp. 166–183, 2020.
- [39] V. E. Sathishkumar, J. Park, and Y. Cho, "Using data mining techniques for bike sharing demand prediction in metropolitan city," *Computer Communications*, vol. 153, pp. 353–366, 2020.
- [40] R. M. Aziz, "Nature-inspired metaheuristics model for gene selection and classification of biomedical microarray data," *Medical & Biological Engineering & Computing*, vol. 60, pp. 1–20, 2022.
- [41] O. A. Alomari, S. N. Makhadmeh, M. A. Al-Betar et al., "Gene selection for microarray data classification based on Gray Wolf Optimizer enhanced with TRIZ-inspired operators," *Knowledge-Based Systems*, vol. 223, Article ID 107034, 2021.
- [42] R. M. Aziz, *Application of Nature Inspired Soft Computing Techniques for Gene Selection: A Novel Frame Work for Classification of Cancer*, Springer, Berlin, Germany, 2022.
- [43] A. Hajieskandar, J. Mohammadzadeh, M. Khalilian, and A. Najafi, "Molecular cancer classification method on microarrays gene expression data using hybrid deep neural network and grey wolf algorithm," *Journal of Ambient Intelligence and Humanized Computing*, pp. 1–11, 2020.
- [44] R. Aziz, C. K. Verma, M. Jha, and N. Srivastava, "Artificial neural network classification of microarray data using new hybrid gene selection method," *International Journal of Data Mining and Bioinformatics*, vol. 17, no. 1, p. 42, 2017.
- [45] A. Dabba, A. Tari, S. Meftali, and R. Mokhtari, "Gene selection and classification of microarray data method based on mutual information and moth flame algorithm," *Expert Systems with Applications*, vol. 166, Article ID 114012, 2021.
- [46] N. Yuvaraj, K. Srihari, G. Dhiman et al., "Nature-inspired-based approach for automated cyberbullying classification on multimedia social networking," *Mathematical Problems in Engineering*, vol. 202112 pages, Article ID 6644652, 2021.
- [47] R. A. Musheer, C. K. Verma, and N. Srivastava, "Novel machine learning approach for classification of high-dimensional microarray data," *Soft Computing*, vol. 23, no. 24, pp. 13409–13421, 2019.

## *Retraction*

# **Retracted: Strategy of Maintainable Renewal of Assembled Residential Buildings Based on PSO-ELM**

### **Mathematical Problems in Engineering**

Received 19 September 2023; Accepted 19 September 2023; Published 20 September 2023

Copyright © 2023 Mathematical Problems in Engineering. This is an open access article distributed under the Creative Commons Attribution License, which permits unrestricted use, distribution, and reproduction in any medium, provided the original work is properly cited.

This article has been retracted by Hindawi following an investigation undertaken by the publisher [1]. This investigation has uncovered evidence of one or more of the following indicators of systematic manipulation of the publication process:

- (1) Discrepancies in scope
- (2) Discrepancies in the description of the research reported
- (3) Discrepancies between the availability of data and the research described
- (4) Inappropriate citations
- (5) Incoherent, meaningless and/or irrelevant content included in the article
- (6) Peer-review manipulation

The presence of these indicators undermines our confidence in the integrity of the article's content and we cannot, therefore, vouch for its reliability. Please note that this notice is intended solely to alert readers that the content of this article is unreliable. We have not investigated whether authors were aware of or involved in the systematic manipulation of the publication process.

Wiley and Hindawi regrets that the usual quality checks did not identify these issues before publication and have since put additional measures in place to safeguard research integrity.

We wish to credit our own Research Integrity and Research Publishing teams and anonymous and named external researchers and research integrity experts for contributing to this investigation.


The corresponding author, as the representative of all authors, has been given the opportunity to register their agreement or disagreement to this retraction. We have kept a record of any response received.

### **References**

- [1] Y. Zhang, Y. Wu, J. Sui, and M. Lee, "Strategy of Maintainable Renewal of Assembled Residential Buildings Based on PSO-ELM," *Mathematical Problems in Engineering*, vol. 2022, Article ID 5813577, 7 pages, 2022.

## Research Article

# Strategy of Maintainable Renewal of Assembled Residential Buildings Based on PSO-ELM

Yitong Zhang,<sup>1</sup> Yuhang Wu,<sup>1</sup> Jing Sui<sup>2,3</sup> ,<sup>2,3</sup> and Min Lee<sup>1</sup> 

<sup>1</sup>Graduate School of Technical Design Staff, Kookmin University, Seoul 02707, Republic of Korea

<sup>2</sup>Kookmin University, Graduate School of Techno Design (TED), Seoul 02707, Republic of Korea

<sup>3</sup>LuXun Academy of Fine Arts, Shenyang 110003, China

Correspondence should be addressed to Min Lee; [liwen@kookmin.ac.kr](mailto:liwen@kookmin.ac.kr)

Received 15 February 2022; Revised 3 March 2022; Accepted 25 May 2022; Published 9 June 2022

Academic Editor: Man Fai Leung

Copyright © 2022 Yitong Zhang et al. This is an open access article distributed under the Creative Commons Attribution License, which permits unrestricted use, distribution, and reproduction in any medium, provided the original work is properly cited.

Based on the PSO-ELM model, we analyze the key elements of safety input to respond to accidents and construct and evaluate its resource input optimization scheme. Based on the PSO-ELM cost prediction model, we analyze the key safety inputs for accident response and construct and evaluate the optimal allocation of resources. The results show that improving the technical level of component lifting is the key point of safety management in the construction of assembled buildings; increasing the strength of safety inspection before delivery of components, enhancing the technical performance of component safety status identification, and reasonably planning the frequency of using special transportation vehicles for components are effective ways to achieve the balance of safety, schedule, and cost of the project.

## 1. Introduction

With the leap-forward development of the economy, the construction industry, represented by residential construction, has become one of the pillars of the national economy [1]. With the continuous improvement of people's quality of life, the problems exposed by the traditional construction industry have become more and more prominent. In the past, residential construction mainly used on-site pouring operation mode, and on the one hand, the ecological environment was seriously polluted, the use of resources was inefficient, and the noise generated during the construction process affected the life of the surrounding residents [2, 3]. On the other hand, construction safety accidents occurred from time to time, and the quality of construction was difficult to be guaranteed. In order to cope with such problems, the government proposes to accelerate the process of residential industrialization, improve the quality of housing, and promote the transformation and upgrading of the construction industry [4].

With the expansion of the construction scale of assembled buildings, the construction activities of assembled

buildings are distributed in parallel to their component production, logistics and transportation, on-site assembly, and other operation spaces, which are very prone to construction safety accidents at this stage with insufficient reserves of safety technology and management measures [5]. Facing the increasingly severe construction safety management situation, how to find effective technologies and strategies to deal with safety accidents in the construction of assembled buildings with limited investment in safety resources is a key issue that needs to be solved [6].

As an important carrier of residential industrialization, the development of assembled housing is an important way to achieve green and efficient construction. In September 2016, Premier Li Keqiang emphasized at the State Council executive meeting hosted by the State Council that "assembled construction can accelerate the process of building a new type of urbanization, and assembled construction should be vigorously developed." Assembled construction has huge advantages over the traditional cast-in-place model, and according to the statistics of an assembled house, the construction schedule can be advanced by about 20%, water resources can be saved by about 41%, labor can be

reduced by about 9.5%, and construction waste can be reduced by about 56% [7–9].

Compared with traditional housing, assembled housing has obvious advantages in terms of comprehensive quality and social benefits, and because of its industrialized production method, it is highly reproducible, greatly shortens the construction cycle of residential projects, and is energy efficient and environmentally friendly [10]. However, the high cost of assembled housing is an inescapable problem, and how to control the cost and be able to effectively reduce it is the key to promote assembled housing. This paper studies the cost of assembled houses, analyzes the factors affecting the cost of assembled houses, and establishes a cost prediction model by combining the characteristics of assembled houses, based on which it is important to forecast the cost [11].

The cost prediction model established in this paper can quickly estimate the cost of assembled housing projects; however, in the process of predicting the cost of pending assembled housing projects, sufficient sample data are needed to ensure the smooth prediction [12, 13]. Therefore, the construction of the cost prediction model is conducive to the improvement of the enterprise's own engineering information database and the promotion of the enterprise's development in the direction of informationization and digitalization to ensure the enterprise's advantage in the future intelligent era.

## 2. Related Studies

In recent years, domestic and foreign scholars have made representative research results in the configuration of safety inputs in traditional building construction [14], but it is difficult to apply them directly due to the differences in assembly building projects. Most of the current assembly building construction safety management results stay in the qualitative research stage, and some scholars try to introduce quantitative analysis means such as gray clustering [15], attribute mathematics [16], and finite element [17] to study assembly building construction safety accidents so as to propose management countermeasures [18, 19], and the method can be used to analyze and identify key safety input elements, but its drawback is that it cannot determine the optimal ratios of elemental inputs, while the multiobjective programming (MOP) method can be used to analyze and identify key safety input elements [20–22].

The authors of [23] systematically reviewed the evolution of assembled housing in the UK and analyzed it through a literature review, while suggesting that further research is needed to enrich the field. The authors of [5] used artificial neural network algorithms to establish a dynamic decision system to analyze the factors affecting the development of industrialized housing and found that high cost is the most important influencing factor limiting its development. The authors of [6] compared the costs of four different structural systems of industrialized housing in the UK and concluded that efficiency learning, technological innovation, the establishment of an efficient on-site construction organization mode, and strengthening the production management of

prefabricated components can effectively reduce the costs [7]. The authors of [8] established a database of 179 prefabricated assembled houses, and through a detailed case study of five residential communities, the results showed that standardized design can improve the design efficiency and the production scale of prefabricated components. Meanwhile, the authors of [9] found that projects using assembly construction methods are concentrated in the public sector, while the private sector still tends to build using traditional construction methods requiring extensive scaffolding, formwork, wet work on-site, and cast-in-place concrete, despite the advantages of assembly construction over the traditional construction. The authors of [10] introduced an Internet of Things (IoT)-based multidimensional BIM platform (MITBIMP) for real-time visibility and traceability of prefabricated components and validated it with an actual construction project in Hong Kong as a pilot project, showing its good practicality to facilitate decision making and real-time cost control by project builders. The authors of [11] designed and developed a virtual simulation system to support the simulation of the whole process from architectural design to prefabricated component production and construction and installation in order to optimize the construction process of assembled buildings for cost-saving purposes. The authors of [12] proposed an ice formwork system based on high-performance concrete (HPCfr) with a frost-proof design in order to solve the problem of high costs required for the production of precast components, thus reducing the number of labor as well as material wastage during the production of precast components. The authors of [18] took a residential project as an example, and by comparing the construction cost difference between prefabricated assembly type and traditional cast-in-place type, it was found that the prefabricated components and their installation cost were the main factors of the high construction cost of assembly type.

In summary, although scholars have achieved promising results in the study of the cost of assembled housing, there are still gaps compared with developed countries, and further research is needed. Scholars' research on the cost of assembled houses mainly focuses on the analysis of influencing factors, economic analysis, and the method of comparing the cost of assembled buildings with that of cast-in-place structures, which is a single method. The use of intelligent algorithms for cost prediction of assembled houses is relatively rare, so it is necessary to study this aspect to help understand the impact of assembled houses' own characteristics on their costs and to take targeted measures for cost control.

## 3. Overview of Assembled Housing

The assembled house is mainly built in an industrial way, where the required prefabricated components are processed in a component factory, transported to the construction site, and assembled into a complete residential building through professional joining operations [9]. During the construction of the assembled concrete house, some parts of the building and the prefabricated component connections still need to

be poured because they are not installed in the strict sense of “building blocks.” The structural system of assembled houses can be divided into concrete, wood, and steel systems depending on the material of the components [3]. When residences are built with the wood structure system, a large amount of forest resources are required, which affects the ecological environment; although residences with the steel structure system can meet the requirements of residential industrialization to the maximum extent, the excessive use of steel causes very high engineering costs, which hinders their large-scale development. Compared with the above two structures, the concrete structure system is more in line with China’s national conditions and the concept of ecological protection, so the assembled concrete houses are more frequently used in the field of assembled houses in China. This paper takes assembled concrete houses as the research object, and for the sake of simplicity, the assembled houses appearing in this paper refer to assembled concrete houses exclusively.

#### 4. PSO-ELM Based Cost Prediction Model for Assembled Houses

**4.1. Network Structure Design of PSO-ELM.** The extreme learning machine is improved from the feedforward neural network, and the design of the network structure is a very important task when using the extreme learning machine for assembled housing cost prediction. The design of the network structure is a very important task when using the extreme learning machine for assembled house cost prediction. The so-called design of the network structure is first to solve the problem of the number of input nodes, hidden layer nodes, and output nodes in the network structure [6]. Up to now, there is not a perfect and exact theory to guide how to determine the number of hidden layer nodes in the network structure. Whether the design of the network model is reasonable is directly related to the convergence state of the network model, and choosing a suitable network model structure can significantly enhance the training ability of the samples and improve the accuracy of the cost prediction of assembled houses.

**4.2. ELM Parameter Optimization Based on PSO Algorithm.** Through the preliminary study of the limit learning machine and the particle swarm algorithm above, two aspects need to be considered in the optimization process of the limit learning machine using the particle swarm algorithm.

**4.2.1. Input Weights and Hidden Layer Bias Values.** The input weights and hidden layer bias values of the ELM are optimized by the PSO algorithm, and the input weights and hidden layer bias values are used as the particles in the PSO algorithm, and the length  $D$  of the particles is denoted as

$$D = K(n + 1),$$

$$\theta^m = [\omega_{11}^m, \omega_{11}^m, \dots, \omega_{11}^m, \omega_{21}^m, \omega_{21}^m, \dots, \omega_{2k}^m, \dots, \omega_{n1}^m, \omega_{n2}^m, \omega_{nk}^m, \dots, b_1^m, b_2^m, \dots, b_k^m], \quad (1)$$

where  $K$  is the number of nodes in the hidden layer,  $n$  is the number of samples in the input layer,  $\omega_{ij}^m, b_j^m$  is the random number in  $[-1, 1]$ .

**4.2.2. Adaptation Function.** The fitness is a measure to evaluate the position of the particle and also indirectly portrays the generalization performance of the limit learning machine. The input weight matrix and bias value of the limit learning machine can be used to derive the output weight matrix, that is, to derive the prediction value, and to judge whether the prediction value meets the accuracy requirement, which is often expressed in the following mean square error equation:

$$f = \frac{1}{n} \sum_{i=1}^n (y_j - \hat{y}_j)^2, \quad (2)$$

where  $y_j$  denotes the actual output value of the  $j$ th sample and  $\hat{y}_j$  denotes the predicted value obtained by the limit learning machine.

**4.3. PSO-ELM Based Cost Forecasting Steps for Assembled Housing.** In the process of limit learning machine prediction, the input weights and bias values are searched in a certain range with the help of the particle swarm algorithm, and the mean square error equation is used as the fitness function of the particle swarm algorithm while minimizing  $f$  in equation (2), at which time particle  $\theta^m$  is the optimal input vector and bias value of the limit learning machine. The steps for optimizing the cost prediction of assembled houses using the particle swarm algorithm for the limit learning machine are as follows.

Step 1: collect sample data of assembled housing costs, divide them into training samples and validation samples, and form a sample matrix

Step 2: establish the limit learning machine network structure model and determine the parameters of the network model

Step 3: random training to obtain the weights and hidden layer node bias values, using the input weights and bias value range as the particle velocity and position seeking a range

Step 4: initialize various parameters in the particle swarm algorithm, such as the maximum number of iterations, population size, acceleration constant, inertia weight, and particle dimension

Step 5: combine the training samples to obtain the fitness of the particle and compare it with its own optimal fitness and the global optimal fitness to obtain the individual optimal position  $P_{\text{best}}$  and the global optimal position  $G_{\text{best}}$

Step 6: iterate and keep updating the velocity and position of the particles until the stopping condition (maximum number of iterations or minimum fitness value) is met, exit, and decode them as the input



weights and hidden layer node bias values of the limit learning machine

Step 7: assign the output optimal parameters to the extreme learning machine prediction model, train the training samples with this model, and after training, input the validation sample data for prediction

The prediction flowchart based on PSO optimized ELM is shown in Figure 1.

## 5. Cost Forecast for Assembled Housing

**5.1. Model Training and Simulation.** After the data normalization process is completed, the data samples to be used for cost prediction are divided into two parts: training data and test data. The first 30 groups of the sample data are taken as training samples, and the remaining 5 groups are taken as test samples. In the training sample, the training sample is divided into two parts:  $p\_train$  and  $t\_train$ .  $p\_train$  record 11 cost prediction indexes of floor area, structure type, number of floors, and height of floors in the first 30 groups of samples, and  $t\_train$  records one-sided cost data. In the test sample,  $t\_text$  records 11 cost predictors such as floor area, structure type, number of floors, and number of stories in the test sample. In order to be able to better verify the superiority of the extreme learning machine optimized by particle swarm algorithm, three machine learning algorithms, BP neural network, ELM, and PSO-ELM, are used in the MATLAB platform to model and simulate the cost of assembled houses respectively.

**5.1.1. ELM Model.** To establish the standard ELM model, first of all, we need to program in MATLAB2018a platform to get the ELM algorithm program [24]. The best performance of the Sigmoid was found through simulation analysis of the excitation function in the same number of hidden layers and regularization [8]. Therefore, in this paper, the Sigmoid function is chosen as the excitation function for the simulation prediction. After the two parameters are determined, the prediction results are plotted using the plot plotting function, and the obtained prediction results are shown in Figure 2.

**5.1.2. PSO-ELM Model.** Before optimizing the input weights  $w_i$  and bias values  $b_i$  in the ELM model using the PSO algorithm, the parameters of the particle swarm algorithm need to be set in conjunction with the study of the parameters of the particle swarm algorithm in Chapter 4, with the population size  $sizpop = 20$ , the maximum number of iterations  $maxgen = 200$ , the inertia weight  $\omega = 1$ , the acceleration constant  $c_1 = c_2 = 1.5$ , and the mean square error of the training sample as the fitness value of the particles. After the parameters of the particle swarm algorithm are set, the PSO-ELM model is established, and the unilateral cost of the test sample is obtained as shown in Figure 3.

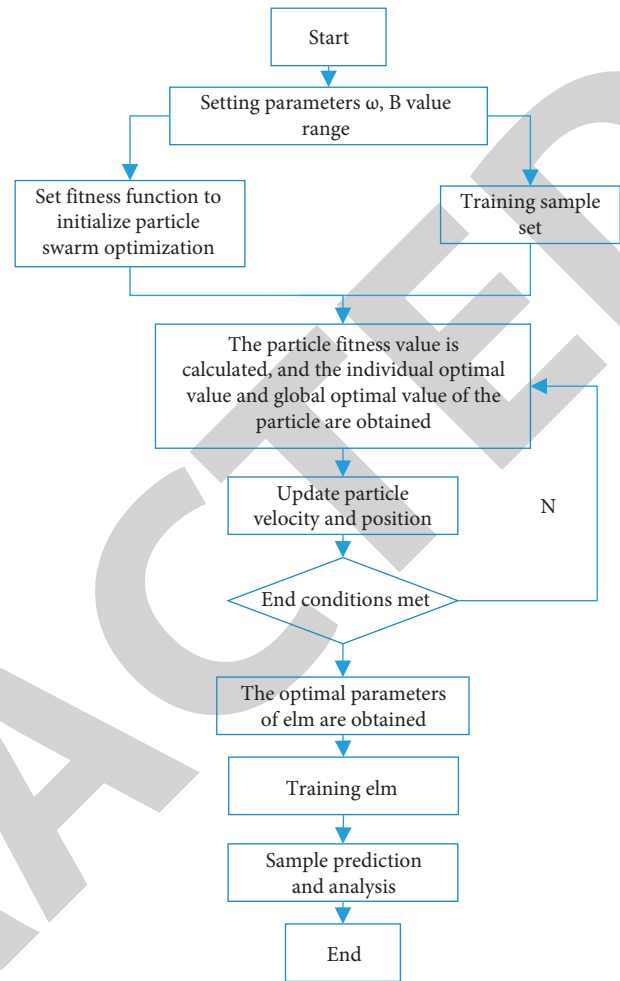


FIGURE 1: Flowchart of PSO-based optimized ELM prediction.

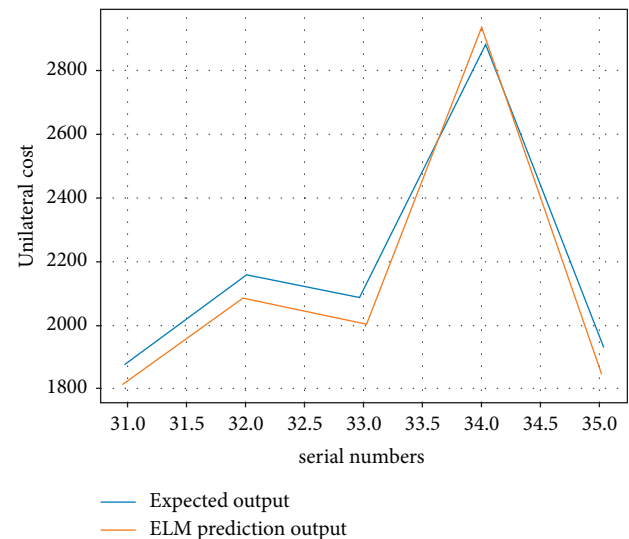


FIGURE 2: Comparison of prediction curves of ELM model.

**5.1.3. BP Neural Network Model.** When using the BP neural network model for cost prediction, it is necessary to first create a neural network using the function `newff()`, and the

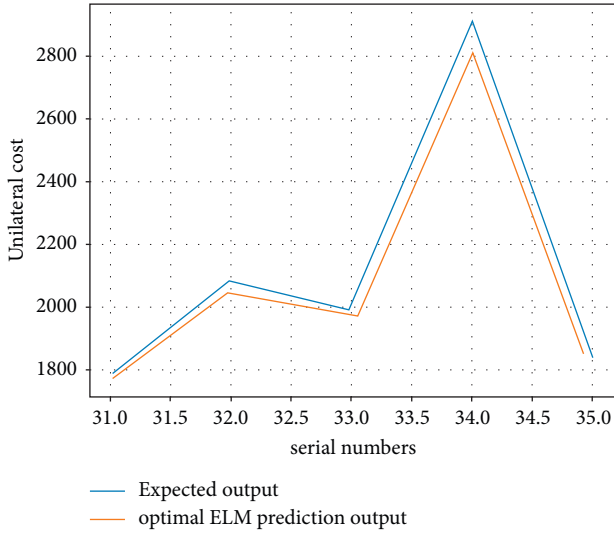


FIGURE 3: Comparison of prediction curves of PSO-ELM model.

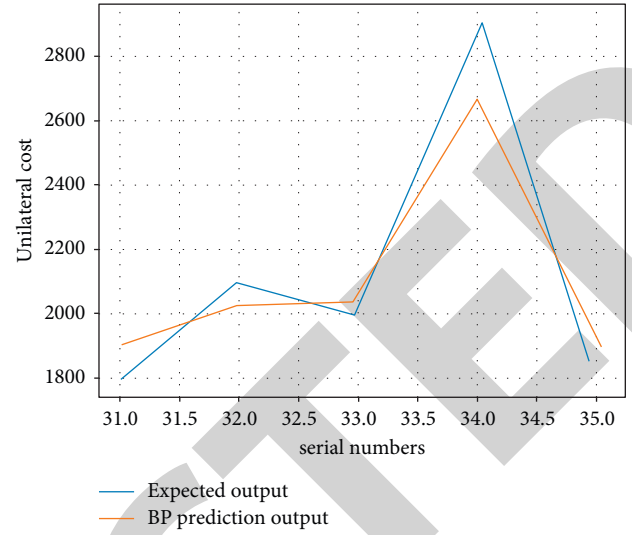


FIGURE 4: Comparison of prediction curves of BP neural network models.

excitation function on the neurons is chosen logsig () function. The number of nodes in the hidden layer can be initially determined by using the formula  $m = 2n + 1$ , based on which the number of nodes can be increased or decreased according to the training error. The number of hidden layers is determined as 25, the maximum number of iterations is set as 1000, the learning rate is 0.1, and the momentum factor is 0.01. Finally, the trained neural network is used to predict the test sample, the plot() function is called to draw the prediction image, and the prediction image of the test sample is shown in Figure 4.

**5.2. Analysis of Prediction Results.** The prediction effect of the three prediction models, ELM, PSO-ELM, and BP neural network, is put under the same coordinates, and their prediction curves are compared as shown in Figure 5. Although the prediction curve comparison graph can reflect the prediction trend of each method, it cannot reflect the prediction effect of the three prediction methods on the cost of assembled houses quantitatively well, so this paper selects the relative error  $\partial$ , the average absolute relative error MAPE, and the running time to reflect the effect of cost prediction, and the specific results are shown in Table 1. Among them,

$$\partial = \frac{y_i - \hat{y}_i}{y_i}, \tag{3}$$

$$\text{MAPE} = \frac{1}{n} \sum_{i=1}^n |\partial| \times 100\%,$$

where  $y_i$  represents the actual cost of the  $i$ -th sample,  $\hat{y}_i$  represents the predicted cost of the  $i$ -th sample,  $n$  represents the number of samples tested,  $\partial$ , and the magnitude of MAPE reflects the predictive power of the prediction model, with smaller values indicating stronger predictive power of the model and vice versa.

From Table 1, we can see that the average absolute relative error of all three prediction models is less than 10%

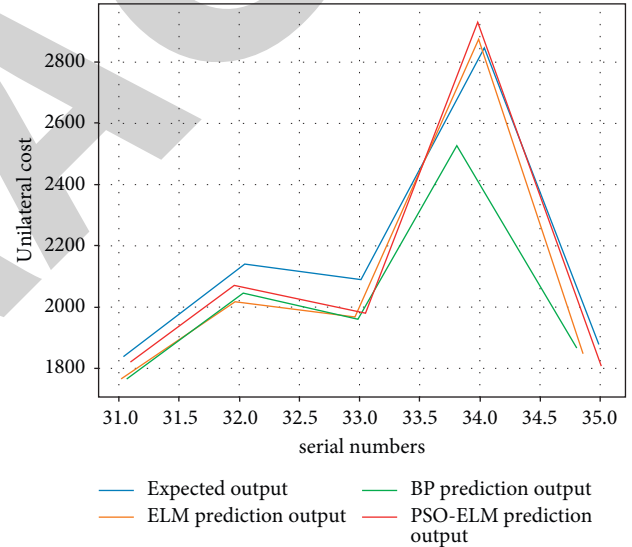


FIGURE 5: Comparison of prediction curves of ELM, PSO-ELM, and BP neural network models.

(the error range of investment estimation is  $\pm 10\%$ ), which indicates that the cost prediction using these three methods is successful and can be applied to the cost prediction of assembled houses. The main reason is that the BP neural network model requires a large number of samples for cost prediction to achieve high prediction accuracy, which makes it more difficult to collect data for the developing assembled housing projects. The optimized ELM prediction accuracy was significantly improved, indicating that it is practical to optimize the extreme learning machine using the particle swarm algorithm. The running time of the BP neural network-based prediction model is 9.83 s, that of the ELM-based prediction model is 1.83 s, and that of the PSO-ELM-based model is 3.56 s. The running times of all three are very fast.

TABLE 1: Comparison of prediction effects of different models.

| Number           | Actual value (yuan/m <sup>2</sup> ) | Estimate (yuan/m <sup>2</sup> ) |         |          | Relative error (%) |         |       |
|------------------|-------------------------------------|---------------------------------|---------|----------|--------------------|---------|-------|
|                  |                                     | ELM                             | PSO-ELM | BP       | ELM                | PSO-ELM | BP    |
| 31               | 1811.59                             | 1898.35                         | 1824.58 | 1923.25  | 4.85               | 0.56    | 6.65  |
| 32               | 2135.09                             | 2189.48                         | 2100.01 | 20064.84 | 2.58               | -1.65   | -3.35 |
| 33               | 2035.75                             | 2125.09                         | 2043.78 | 2072.82  | 4.50               | 0.48    | 1.93  |
| 34               | 3028.89                             | 2978.12                         | 2918.89 | 27.58.05 | -1.65              | -3.63   | -8.95 |
| 35               | 1868.54                             | 1942.92                         | 1879.53 | 1951.78  | 3.94               | 0.55    | 4.42  |
| MAPE (%)         | —                                   | —                               | —       | —        | 3.48               | 1.37    | 5.04  |
| Running time (s) | —                                   | —                               | —       | —        | 1.39               | 3.67    | 9.81  |

The prediction time of the PSO-ELM model is slower than that of the ELM model, but the prediction accuracy of the former is higher. The standard limit learning machine does not require iteration in the prediction process, and the input weights and bias values are given randomly, and its operation speed becomes very fast, but the PSO-ELM model uses the particle swarm algorithm to optimize the randomly given input weights and bias values by iterating continuously until the best parameters are obtained, which reduces the instability of the standard limit learning prediction. Through the analysis of the performance of the three prediction models, this paper selects the PSO-ELM model as a better guide for the cost prediction of assembled houses with better results.

## 6. Conclusions

This paper considers that the response to safety accidents in assembly building construction is no longer limited to the traditional safety and civilization construction measures specified in the scope, but also from the production of components, logistics and transportation, on-site assembly multispace, to achieve the optimal allocation of safety inputs under the conditions of resource constraints. Strong conditions are provided for the maintenance and renewal of assembled residential buildings. The method of this paper on the safety performance of components is the focus of more attention to respond to safety accidents in assembly building construction, should enhance the frequency of safety inspection before the delivery of components and the use of the whole process of safety state identification technology accounted for, to ensure the stable articulation of the safety performance of each space components to lay a solid foundation for the later maintenance.

## Data Availability

The experimental data used to support the findings of this study are available from the corresponding author upon request.

## Conflicts of Interest

The authors declare that they have no conflicts of interest regarding this work.

## References

[1] D. C. W. Ho, Y. Yau, S. W. Poon, and E. Liusman, "Achieving sustainable urban renewal in Hong Kong: Strategy for

dilapidation assessment of high rises," *Journal of Urban Planning and Development*, vol. 138, no. 2, pp. 153–165, 2012.

[2] N. de Silva, M. F. Dulaimi, F. Y. Ling, and G. Ofori, "Improving the maintainability of buildings in Singapore," *Building and Environment*, vol. 39, no. 10, pp. 1243–1251, 2004.

[3] H. Che and J. Wang, "A nonnegative matrix factorization algorithm based on a discrete-time projection neural network," *Neural Networks*, vol. 103, pp. 63–71, 2018.

[4] A. S. Asmone, S. Conejos, and M. Y. Chew, "Green maintainability performance indicators for highly sustainable and maintainable buildings," *Building and Environment*, vol. 163, Article ID 106315, 2019.

[5] H. Che and J. Wang, "A collaborative neurodynamic approach to global and combinatorial optimization," *Neural Networks*, vol. 114, pp. 15–27, 2019.

[6] J. Li, Q. Wang, and H. Zhou, "Establishment of key performance indicators for green building operations Monitoring—an application to China case study," *Energies*, vol. 13, no. 4, p. 976, 2020.

[7] R. Matos, F. Rodrigues, H. Rodrigues, and A. Costa, "Building condition assessment supported by building information Modelling," *Journal of Building Engineering*, vol. 38, Article ID 102186, 2021.

[8] H. Che, C. Li, X. He, and T. Huang, "A recurrent neural network for adaptive beamforming and array correction," *Neural Networks*, vol. 80, pp. 110–117, 2016.

[9] F. M. Abd Al Galil, S. P. Zambare, F. A. Al-Mekhlafi, and L. Al-Keridis, "Effect of dimethoate on the developmental rate of forensic importance Calliphoridae flies," *Saudi Journal of Biological Sciences*, vol. 28, no. 2, pp. 1267–1271, 2021.

[10] D. J. Weeks and F. Leite, "Minimizing facility corrective maintenance: Benchmarking Preventative-to-corrective maintenance ratios using maintenance data and building age in Dormitories," *Journal of Management in Engineering*, vol. 38, no. 1, Article ID 04021086, 2022.

[11] M. Marzouk and M. Hanafy, "Modelling maintainability of healthcare facilities services systems using BIM and business intelligence," *Journal of Building Engineering*, vol. 46, Article ID 103820, 2022.

[12] S. Qi, X. Ning, G. Yang et al., "Review of multi-view 3D object Recognition methods based on Deep learning," *Displays*, vol. 69, no. 1, Article ID 102053, 2021.

[13] L. Zhang, W. Li, L. Yu, L. Sun, X. Dong, and X. Ning, "GmFace: an explicit function for face image representation," *Displays*, vol. 69, no. 1, 2021.

[14] P. An, Z. Wang, and C. Zhang, "Ensemble unsupervised autoencoders and Gaussian mixture model for cyberattack detection," *Information Processing & Management*, vol. 59, no. 2, Article ID 102844, 2022.

## *Retraction*

# **Retracted: Research on the Efficiency Evaluation of Cross-Organizational Knowledge Synergy in Industry University Cooperation Based on BP Neural Network Algorithm**

### **Mathematical Problems in Engineering**

Received 18 July 2023; Accepted 18 July 2023; Published 19 July 2023

Copyright © 2023 Mathematical Problems in Engineering. This is an open access article distributed under the Creative Commons Attribution License, which permits unrestricted use, distribution, and reproduction in any medium, provided the original work is properly cited.

This article has been retracted by Hindawi following an investigation undertaken by the publisher [1]. This investigation has uncovered evidence of one or more of the following indicators of systematic manipulation of the publication process:

- (1) Discrepancies in scope
- (2) Discrepancies in the description of the research reported
- (3) Discrepancies between the availability of data and the research described
- (4) Inappropriate citations
- (5) Incoherent, meaningless and/or irrelevant content included in the article
- (6) Peer-review manipulation

The presence of these indicators undermines our confidence in the integrity of the article's content and we cannot, therefore, vouch for its reliability. Please note that this notice is intended solely to alert readers that the content of this article is unreliable. We have not investigated whether authors were aware of or involved in the systematic manipulation of the publication process.

Wiley and Hindawi regrets that the usual quality checks did not identify these issues before publication and have since put additional measures in place to safeguard research integrity.

We wish to credit our own Research Integrity and Research Publishing teams and anonymous and named external researchers and research integrity experts for contributing to this investigation.

The corresponding author, as the representative of all authors, has been given the opportunity to register their

agreement or disagreement to this retraction. We have kept a record of any response received.

### **References**

- [1] L. Jing, "Research on the Efficiency Evaluation of Cross-Organizational Knowledge Synergy in Industry University Cooperation Based on BP Neural Network Algorithm," *Mathematical Problems in Engineering*, vol. 2022, Article ID 1873862, 8 pages, 2022.

## Research Article

# Research on the Efficiency Evaluation of Cross-Organizational Knowledge Synergy in Industry University Cooperation Based on BP Neural Network Algorithm

Li Jing 

*School of Management and Economics, Jingdezhen Ceramic University, Jingdezhen 333403, China*

Correspondence should be addressed to Li Jing; 022515@jci.edu.cn

Received 26 April 2022; Revised 21 May 2022; Accepted 27 May 2022; Published 8 June 2022

Academic Editor: Man Fai Leung

Copyright © 2022 Li Jing. This is an open access article distributed under the Creative Commons Attribution License, which permits unrestricted use, distribution, and reproduction in any medium, provided the original work is properly cited.

The difference of decision-making knowledge among members is conducive to the successful realization of group cooperative production. In the actual production, if the different knowledge environments between organizations can cooperate and penetrate each other, the common knowledge of groups can be formed, which is a key step to successfully solve the social and economic problems of public resources. The final efficiency of cross-organizational knowledge collaboration is the key to measure the success or failure of collaboration. Because the cross-organizational knowledge synergy efficiency of industry university cooperation is the result of the cross-influence of many factors, the general linear regression model is difficult to describe the relationship between these influencing factors and knowledge synergy efficiency. Based on the analysis of the importance of cross-organizational knowledge sharing efficiency evaluation of industry university cooperation, this study constructs the efficiency evaluation index system from different angles. At the same time, based on the field investigation of the index system, BP network model is established to effectively evaluate the collaborative efficiency.

## 1. Introduction

For a single member, how to make a decision or what kind of decision to make mainly depends on the decision-making knowledge of a single member, and even the decision-making environment will affect the result of the decision. In real life, it is not difficult to find that some people are good at calculating and free riding. Events like this can be seen everywhere, but more often, some people or organizations cannot calculate clearly, so some people will introduce to others the benefits of new collective action and how to take collective action. The main reason is that some people do not really understand the interests, so there must be “understanding people” to tell the interests. In fact, as far as public resources are concerned, the decision-making state of individual members can be summarized as whether there are new collective action reserves and whether there are payment expectations of prisoners’ dilemma, which are the decision-making knowledge state of individual members [1]. Obviously, there must be knowledge differences among

members, which is mainly reflected in the distribution of new knowledge and collective action cooperation strategy, because this is a necessary condition for realizing knowledge cooperation, which is embodied in the following two aspects: first, if there is no such new knowledge, it means that there is no knowledge gap between members, so it is difficult for a single member to spontaneously invest. The noncooperative equilibrium of individual decision-making has nothing to do with the degree of knowledge. Second, if there is this new knowledge gap and this new knowledge is widely distributed, it will be conducive to the development of individual spontaneous investment, so as to realize cooperative production and supply [2].

It can be seen from the above that before the formation of new common knowledge, some “ignorant” are not free riders in the real sense [3]. If they are punished too early, they will bring more serious consequences, which cannot be ignored. Therefore, in the process of transforming the obtained information into new common knowledge, some members must determine the accuracy and timeliness of the

information, because it will directly affect the formation of new common knowledge and is also an important link that cannot be ignored. In the next process of the formation of new common knowledge, the heterogeneity of other dimensions will play a leading role, which cannot be replaced in the formation of collective cooperation strategies and benefited new knowledge. Taking the preference difference between members as an example, for members, the greater the difference, the smaller the difference between the output levels of public resources cooperated by members, and the supply of public resources will be borne by the members with larger preference [4]. If the output level is larger, the members providing supply will tend to be consistent. Although there is a monotonous relationship between one-dimensional differences and cooperative production, it is also possible to play the same role under the joint action of multi-dimensional differences [5].

With the advent of the era of knowledge economy, a single enterprise is also unable to learn and create knowledge. The specialized division of labor of knowledge learning and innovation based on the enterprise is becoming more and more obvious. Only through specific business experience and coordination of low-cost industry university cooperation can enterprises continuously acquire and accumulate proprietary knowledge. Therefore, as mentioned above, how to choose partners, efficient knowledge collaboration in the alliance, and the ability to continuously accumulate and create new knowledge are of great concern to many enterprises in the process of participating in the inter-organizational knowledge collaboration of the alliance, and it is also the core of collaboration efficiency [6].

## 2. Influencing Factors of Efficiency

*2.1. Organizational Difference Elements.* In general, the realization of cross-organizational knowledge collaboration of industry university cooperation often occurs between organizations with equal knowledge stock and knowledge collaboration ability. However, due to the problems of information asymmetry and entry barriers of industry university cooperation itself, there will be obvious deficiencies in distinguishing the knowledge synergy ability of its member organizations. For example, a series of problems such as organizational knowledge management system, knowledge stock, knowledge coding degree, knowledge staff quality, and corporate culture are difficult to make accurate judgments in a reasonable time [7]. If the knowledge collaboration capabilities of member organizations differ greatly, it will increase the transaction cost, lead to disharmony in the collaboration process, reduce the value of synergy, and then reduce the efficiency of knowledge collaboration. On the other hand, due to the different survival and development environment of different member organizations, their knowledge stock is different, and the paths of knowledge learning and knowledge accumulation are also different. Therefore, there are differences in the knowledge required by different projects in industry university cooperation [8]. This gap often leads to the inconsistency and knowledge conflict of partners, improves the transaction

cost, and affects the synergy efficiency. For example, in the collaborative innovation process of the atmospheric pollution control alliance initiated and established by environmental protection, there are relatively complete agreed terms before technology research and development to avoid subsequent income disputes [9].

In the initial stage of industry university cooperation, member organizations are often unfamiliar with each other, and there are differences in the overall cognition of knowledge synergy, especially in the expectation of synergy benefits. This is because each partner will recognize, assume, design, and specify the key issues of the whole knowledge sharing according to their past experience, which may eventually lead to cognitive differences among partners on many issues. It is manifested in the differences in the expectation of cooperation objectives, the expectation of benefit acquisition, the confidence of cooperation, and the understanding of knowledge itself. Therefore, in order to improve the efficiency of collaboration, the selection of partners in cross-organizational knowledge collaboration of industry university cooperation is more critical, and the matching and collaboration among member organizations are the main factors to be considered [10].

Due to the implicit characteristics of knowledge, the private knowledge owned by knowledge employees participating in cross-organizational knowledge collaboration is often difficult to measure, which will bring unpredictable results to the efficiency of knowledge collaboration. On the one hand, employees with richer knowledge have better overall knowledge structure and stronger ability to modulate and absorb knowledge. In the process of participating in knowledge collaboration, they have stronger learning ability and faster speed of acquiring knowledge, and are in an advantageous position and higher benefit in collaboration, which is the expected goal of all alliance organizations [11]. However, due to the complex environment of knowledge collaboration, some knowledge workers are prone to leakage of private knowledge, resulting in collaboration failure or infringement of organizational intellectual property rights. Therefore, the cognitive structure and psychological structure of employees will be analyzed to make a reasonable impact on their cognitive and collaborative response to knowledge structure.

*2.2. Risk Elements.* At present, under the condition of market economy, the possibility of opportunistic behavior increases in order to maximize interests and minimize costs. This opportunistic behavior is embodied in the following aspects: first, in terms of technology and intellectual property rights, there is a potential competition between members in the same alliance. Sometimes, some members will steal the core technology of other members, thus weakening the competitive advantage of competitors; in terms of cooperation, some members of the alliance hold a negative attitude toward the operation of the enterprise, which cannot guarantee the quality of the project, so it brings irreparable losses to the alliance; in terms of credit, due to the imperfection of the overall law of the alliance, the

members unilaterally broke the contract, falsely reported information, leaked secrets, and other acts, resulting in the leakage and misappropriation of knowledge, leading to the disintegration of the alliance; in terms of incentive, when the benefits obtained by alliance members are not commensurate with the risks they bear, they will take measures to damage other members of the alliance, so as to maximize their own interests. The existence of the above behavior directly affects the interests and ultimate goal of the alliance, and even poses a threat to the cooperation among the members of the alliance, thus affecting the stability of the alliance and causing the risk of disintegration of the alliance.

As shown in Figure 1, the cause of alliance opportunistic behavior and alliance relationship risk is the specificity of enterprise technology assets. For the development of the enterprise alliance, a special investment must be set up for the technology research and development of the alliance. For example, in order to ensure the smooth progress of the project, the alliance must provide some professional technical talents and management personnel. If the human resources of the enterprise cannot meet the demand, it will directly affect the progress of the project. Therefore, the human resources department should strengthen the training of talents in this field; therefore, funds must be injected into the decision. In practice, the technology alliance does not agree that enterprises have business exchanges with enterprises different from itself, because the enterprise technical standards, enterprise culture, internal information exchange mode, and R&D operation form must be suitable for the corresponding adjustment of partners. At the same time, in order to meet the R&D requirements of enterprise projects, enterprises must provide professional equipment. All these require investment. These investments only have high value within the alliance and small value to the outside world, which is the so-called specific transaction investment [12].

Therefore, enterprises' choice of alliance operation mode mainly takes into account the stability of the alliance, which is the choice that alliance member enterprises have to face. The utilization and protection of resources by enterprises can reflect that enterprises have to face the integration and protection of resources in the alliance, which is the trade-off made by enterprises in a dilemma, and the existence of opportunistic behavior is a major obstacle to this. Therefore, the choice of alliance operation mode is the response of alliance enterprises to opportunism and alliance risk relationship [13].

**2.3. Environmental Elements.** Environment is the element of any activity. Obviously, the efficiency of inter-organizational knowledge synergy of industry university cooperation is also affected by the environment, that is, the interactive environment among alliance members. In essence, industry university cooperation is an economic community, which is composed of multiple enterprises or institutions within a certain space. Industry university cooperation contains rich knowledge, which includes various types of knowledge activities. These activities mainly include knowledge acquisition, learning, and creation. This is a complex activity, in

which knowledge innovation is the foundation, knowledge transfer is the key, and the application of knowledge is the key. Such a structural form determines the enrichment of the content of knowledge activities, and knowledge innovation is the core of knowledge activities. From the perspective of system engineering, the knowledge, knowledge activities, and its management process contained in industry university cooperation are a complex system, but it is a knowledge collaboration system [14].

Industry university cooperation is an organizational form with "local embeddedness," "spatial agglomeration," and "industrial relevance." It is not only a social system, but also an economic system. From the perspective of social technology system, industry university cooperation is also a technical system, so it is a technical, economic, and social system. The technical activities and economic activities of industry university cooperation are affected by various factors, which makes the relationship between them more complex. The reason is that they are affected by cultural and social factors. Therefore, to a more accurate extent, industry university cooperation is not only a technical system, but also a social and cultural system. These two systems have their corresponding networks in technology alliance, namely, value network and social network [15].

With the continuous development of economy, no knowledge system of industry university cooperation can maintain its own operation, which means that the technology alliance itself cannot carry out knowledge activities in a "closed door" way. It must widely absorb foreign knowledge and supplement its own shortcomings, so as to form an inseparable and close relationship with foreign knowledge. In this way, industry university cooperation can timely absorb the latest scientific and technological knowledge and production and management information, so as to overcome the problems faced by industry university cooperation in operation and promote itself to take the road of sustainable development. To sum up, a complete knowledge collaboration system of industry university cooperation must be open.

**2.4. Behavioral Elements.** There are both interdependence and competition among members of cross-organizational knowledge collaboration. The reason why industry university cooperation can exist is that in order to maximize the interests, members can reach a collaborative relationship in the form of collaboration, so as to better seek interests. Therefore, members of technology alliance need to apply this way of collaborative cooperation to complete difficult tasks in this complex environment. This mutually beneficial relationship between members has formed a trend. This relationship is mainly maintained by the equal coordination relationship between organizations, not based on the price mechanism, which has laid a solid foundation for the stability of industry university cooperation.

Behavior mechanism is the mechanism to deal with the relationship between organizations. Because many knowledge resources in the organization are often secret, if you want to obtain the secret knowledge resources of other

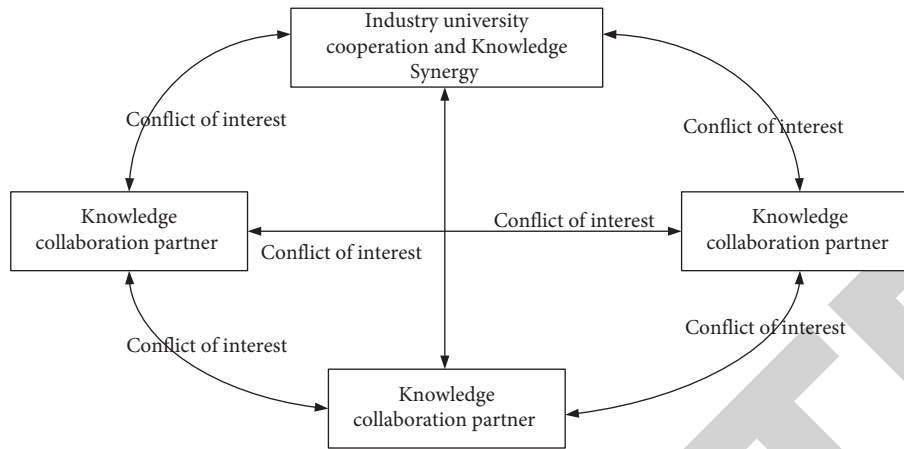


FIGURE 1: Conflict risk of knowledge collaboration.

organizations, you must consult with them to reach an agreement, and the behavior mechanism plays a vital role in this process. The behavior mechanism can not only make the members of industry university cooperation better use of their own learning resources, but also promote the harmonious relationship with other organizations. Especially in this social network, the exchange and flow of knowledge resources must rely on a certain mechanism for protection, so as to efficiently transfer knowledge resources and form a good speed of cooperation.

The transfer of knowledge resources cannot be directly applied to the recipient, it needs to be sorted and reconstructed, so the coordination and cooperation between the two sides can promote the improvement of knowledge synergy efficiency. At the same time, it can also improve the speed of knowledge collaboration, so as to promote the establishment of knowledge resource sharing among industry university cooperation members and make the collaboration of knowledge resources more convenient. Through the corresponding cooperation adjustment, it can promote the cooperation and exchange between the members of the technology alliance and increase their understanding of each other. At the same time, it can also promote the members to be familiar with the industry terminology, professional vocabulary, communication language, and common transaction rules, so as to ensure the smooth cooperation between the members of the industry university cooperation. The adjustment of industry university cooperation norms and systems can promote the ability, knowledge, and preference of industry university cooperation members to lock in a certain range, so as to ensure the consistency of rules and regulations, beliefs, and language symbols in the process of cooperation, because language and symbols are the main tools of social group communication. Only by determining the language and symbols between industry university cooperation members can we ensure the realization of knowledge synergy. Under the common language and symbol, the members of industry university cooperation can promote the knowledge collaboration of technology alliance to achieve the expected results, ensure the smooth operation of industry university

cooperation, and promote the sustainable development of industry university cooperation.

### 3. Efficiency Evaluation Index System

**3.1. Importance of Efficiency Evaluation.** The maximum expected goal of industry university cooperation members refers to the best result obtained in a relatively ideal state of knowledge collaboration, in which there are no negative influence and interference factors and knowledge collaboration obstacles. However, in practice, there will be various interfering factors in the process of knowledge collaboration, resulting in the reduction of its knowledge collaboration efficiency. There are relative difference and distance between the actual knowledge collaboration effect and the maximum expected target effect. Knowledge collaboration efficiency is difficult to achieve in practical operation. The maximum expected goal set belongs to the ultimate goal pursued by cross-organizational knowledge collaboration of industry university cooperation. It is unscientific to directly measure the efficiency of cross-organizational knowledge collaboration from the theoretical concept, because the maximum expected goal of knowledge collaboration under the theoretical condition cannot be possessed or nonexistent under the realistic condition. However, taking the maximum expected goal as an important standard to measure efficiency, if the actual result of knowledge collaboration is close to the maximum expected goal, it can indicate that the actual efficiency of knowledge collaboration is high; otherwise, it indicates that the efficiency of knowledge collaboration is low. In order to achieve the purpose of fair evaluation, a large number of experts must participate in the evaluation process. The evaluation subject is required to be an expert or scholar who is proficient in the law and evaluation law of cross-organizational knowledge synergy efficiency of industry university cooperation, defines and understands the goal of knowledge synergy efficiency in industry university cooperation and innovation, and forms an evaluation team. The group members shall include industry scholars, entrepreneurs, alliance managers, government departments, middle-level cadres of enterprises, core knowledge workers,



skilled workers, etc. Only in this way can the evaluation activities of cross-organizational knowledge synergy efficiency of industry university cooperation make appropriate evaluation according to the law and goal of knowledge synergy development.

In inter-organizational knowledge management mechanism of industry university cooperation, the evaluation of knowledge synergy efficiency is an important content of management. The goal of cross-organizational knowledge management behavior of industry university cooperation is to improve the innovation ability and adaptability of a single member organization by using the collective knowledge of members based on the external sharing way of tacit knowledge or explicit knowledge. Building an effective cross-organizational knowledge coordination mechanism can realize the repeated investment of a single organization in knowledge innovation, avoid problems, save certain knowledge resources, and carry out knowledge innovation from a relatively high starting point, so as to improve the practical efficiency of knowledge innovation, and then enhance the knowledge competitiveness of member organizations. However, in the process of the operation of the knowledge collaboration mechanism of industry university cooperation, how to judge and measure the operation effect of the mechanism has become an important problem in the application of the mechanism. If there are problems in the operation mechanism itself, it is necessary to consider whether an effective feedback monitoring mechanism can be set, and the mechanism can be corrected through the capture and feedback of existing problems. In order to ensure the operation quality of the knowledge collaboration mechanism, the knowledge sharing evaluation mechanism is introduced, and the evaluation mechanism is used as a feedback mechanism to reflect whether there is coordination and consistency in the strategies, objectives, and changes in the cross-organizational operation of the industry university cooperation. The member behavior coordination is carried out through the feedback mechanism to ensure the smooth realization of the organizational knowledge management objectives.

The practical functions of the evaluation mechanism of knowledge synergy efficiency are as follows: first, through the evaluation mechanism, it can promote all organization members to recognize the differences between cooperation goals, behaviors, confidence, and various expected results, and promote members to more rationally recognize and evaluate the cognitive gap existing in knowledge synergy; second, the evaluation mechanism urges the organization members to think about the degree of trust, fairness of benefit distribution, and cultural compatibility, so as to provide support for creating a better knowledge coordination atmosphere and environment; third, give play to the incentive role of the evaluation mechanism, coordinate and optimize the behavior of managers and organization members under the feedback results of the evaluation mechanism, encourage them to carry out knowledge collaboration in a better state, and effectively improve the efficiency of knowledge collaboration. It can be seen that the evaluation mechanism plays an important role in the cross-

organizational knowledge management of industry university cooperation.

Based on certain standards and purposes, the evaluation mechanism of knowledge collaboration efficiency adopts scientific and reasonable methods to evaluate and judge the value of the evaluation object. The operation goal of the mechanism is to optimize and improve the cross-organizational knowledge collaboration activities of industry university cooperation, so as to improve the efficiency of knowledge collaboration to the greatest extent and ensure the smooth completion of the goal of knowledge sharing.

*3.2. Basic Idea of Efficiency Evaluation.* In the cooperative innovation of industry university cooperation, the process of knowledge collaboration is very obvious, and it itself is a complex process. Therefore, the purpose of paying attention to the evaluation of knowledge collaboration process is mainly to analyze and adjust the process in time, so we can achieve the goal of improving the efficiency of knowledge collaboration. In the cooperative innovation of industry university cooperation, the evaluation subject of knowledge collaboration efficiency must clarify the main objective system of the whole process of knowledge collaboration, evaluate the situation or behavior of each stage of knowledge collaboration on this basis, and revise the objectives and guidance plans of each stage according to the evaluation results.

Because the process of inter-organizational knowledge collaboration of industry university cooperation is cyclic, this study can divide the knowledge collaboration process in industry university cooperation innovation into four stages according to time: preparation period, behavior start period, operation integration period, and coordination application period. Firstly, in the preparation period, the potential difference between alliance organizations must have a far-reaching impact on the process and efficiency of knowledge collaboration. Therefore, the evaluation in this period should reflect the compatibility of knowledge collaboration strategy matching between organizations, that is, the driving problem, find out the key indicators that affect the understanding difference of knowledge collaboration itself, and achieve the goal of driving organizations to carry out knowledge collaboration behavior. Through evaluation, we can find out the differences and differences between organizations in the value chain of knowledge collaboration, and find out the root causes affecting the efficiency of knowledge collaboration. Secondly, at the beginning of behavior, different organizations in the alliance form knowledge collaboration teams. These organizations must face the complex environment and the basis of knowledge collaboration efficiency, such as partner selection and income distribution. Through the evaluation of the corresponding indicators, we can find the existing problems. Third is the operation integration period. Through the understanding of the above evaluation process, knowledge collaboration does not necessarily produce high efficiency in the innovation of industry university cooperation and needs to be adjusted and integrated in the process of knowledge collaboration. Therefore, the key to

improve the efficiency of knowledge collaboration lies in the adjustment of the operation process, mainly including the construction of organizational model, organizational stability, and ability training. These are the efficiency evaluation of integration for the problems in operation, which is in the core position in the efficiency evaluation of knowledge collaboration. Fourth is collaborative application period. During this period, knowledge collaboration has been more mature, which directly shows the efficiency of knowledge collaboration. Due to the lag of collaborative efficiency, it is necessary to evaluate the indicators in the coordination application stage. These indicators reflect the continuity and sustainable development of the later knowledge collaboration process. Although knowledge synergy efficiency is directly related to the contribution of member organizations, the cross-organizational knowledge synergy efficiency of industry university cooperation is more affected by the factors that are difficult to quantify, and its knowledge synergy effect cannot be expressed immediately. Its efficiency performance has the characteristics of lag and delay. When evaluating the efficiency of knowledge collaboration, we need to comprehensively consider the impact of the interaction and relationship between member organizations, which are difficult to quantify.

#### 4. Efficiency Evaluation Based on BP Neural Network

The basic BP algorithm formula mainly includes the forward propagation of signal and the back propagation of error.

**4.1. Forward Propagation Process of Signal.** Let the input mode of the network be  $x = (x_1, x_2, \dots, x_n)^T$ , the hidden layer has  $h$  units, the output of the hidden layer is  $y = (y_1, y_2, \dots, y_h)^T$ , the output layer has  $m$  units, and the target output is  $z = (z_1, z_2, \dots, z_m)^T$ . Let the transfer function from the hidden layer to the output layer be  $f$  and the transfer function of the output layer be  $g$ .

Thus,  $y_j = f(\sum_{i=1}^n w_{ij}x_i - \theta) = f(\sum_{i=0}^n w_{ij}x_i)$ .

Among them,  $w_{0j} = -\theta, x_0 = 1$ .

$z_k = g(\sum_{j=0}^h w_{jk}y_j)$ : output of the  $k$ th neuron in the output layer.

At this time, the error between the network output and the target output is  $\varepsilon = 1/2 \sum_{k=1}^m (t_k - z_k)^2$ . Obviously, it is a function of  $w_{ij}, w_{jk}$ .

The next step is to find a way to adjust the weight to reduce the  $\varepsilon$ .

From the knowledge of advanced mathematics, we know that the direction of negative gradient is the direction in which the value of function decreases fastest.

Therefore, you can set a step size and adjust units along the negative gradient direction each time, that is,  $\eta$ , and the weight can be adjusted as follows:

$\Delta w_{pq} = -\eta \partial \varepsilon / \partial w_{pq}$ ,  $\eta$  in neural networks, and it is called learning rate.

It can be proved that the error will be gradually reduced by adjusting this method.

The adjustment order of BP neural network (back propagation) is  $v_k = \sum_{j=0}^h w_{jk}y_j$ .

Partial derivative formula of composite function is as follows.

If  $g(x) = f(x) = 1/1 + e^{-x}$ , then  $g'(u_k) = e^{-v_k}/(1 + e^{-v_k})^2 = 1/1 + e^{-v_k}(1 - 1/1 + e^{-v_k}) = z_k(1 - z_k)$ .

Therefore, the weight adjustment iterative formula from hidden layer to output layer is as follows.

The iterative formula for weight adjustment from input layer to hidden layer is as follows.

Note: the  $j$ th neuron in the hidden layer is connected with each neuron in the output layer; that is, it involves all weights, so

$$\frac{\partial \varepsilon}{\partial y_j} = \sum_{k=0}^m \frac{\partial (t_k - z_k)^2}{\partial z_k} \frac{\partial z_k}{\partial u_k} \frac{\partial u_k}{\partial y_j} = - \sum_{k=0}^m (t_k - z_k) f'(u_k) w_{jk}. \quad (1)$$

As shown in Figure 2, first, set the number of layers of the network by adding neurons in the middle layer to reduce the error and improve the accuracy. Secondly, the number of neurons in the middle layer was calculated. You can determine the increased number by training and comparing different numbers of situations. In addition, the setting of initial weight is key, and its size has a great impact on learning efficiency.

**4.2. The Learning Process and Steps of BP Network.** Weight each connection  $w_{ij}, v_{jt}, \theta_j, \gamma_t$  ending interval  $(-1, 1)$ .

Select a set of input and target samples at random:  $P_k = (a_1^k, a_2^k, \dots, a_n^k), T_k = (y_1^k, y_2^k, \dots, y_q^k)$ .

Set input samples:

$$s_j = \sum_{i=1}^n w_{ij}a_i^k - \theta_j, \quad j = 1, 2, \dots, p, \quad (2)$$

$$b_j = f(s_j), \quad j = 1, 2, \dots, p.$$

Output of middle layer  $L_t = \sum_{j=1}^p v_{jt}b_j - \gamma_t, t = 1, 2, \dots, q, C_t = f(L_t), t = 1, 2, \dots, q$ .

Using network target vector:  $T_k = (y_1^k, y_2^k, \dots, y_q^k)$ , calculate the generalization error of each element in the output layer:  $d_t^k$ .

$$d_t^k = (y_t^k - C_t) \cdot C_t \cdot (1 - C_t), \quad t = 1, 2, \dots, q. \quad (3)$$

Calculate the generalization error of each element in the middle layer:  $e_j^k$ .

$$e_j^k = \left[ \sum_{t=1}^q d_t^k \cdot v_{jt} \right] b_j (1 - b_j). \quad (4)$$

Modified connection right:  $v_{jt}, \gamma_t$ .

$$v_{jt}(N+1) = v_{jt}(N) + \alpha \cdot d_t^k \cdot b_j$$

$$\gamma_t(N+1) = \gamma_t(N) + \alpha \cdot d_t^k \quad (5)$$

$$t = 1, 2, \dots, q, j = 1, 2, \dots, p, 0 < \alpha < 1.$$

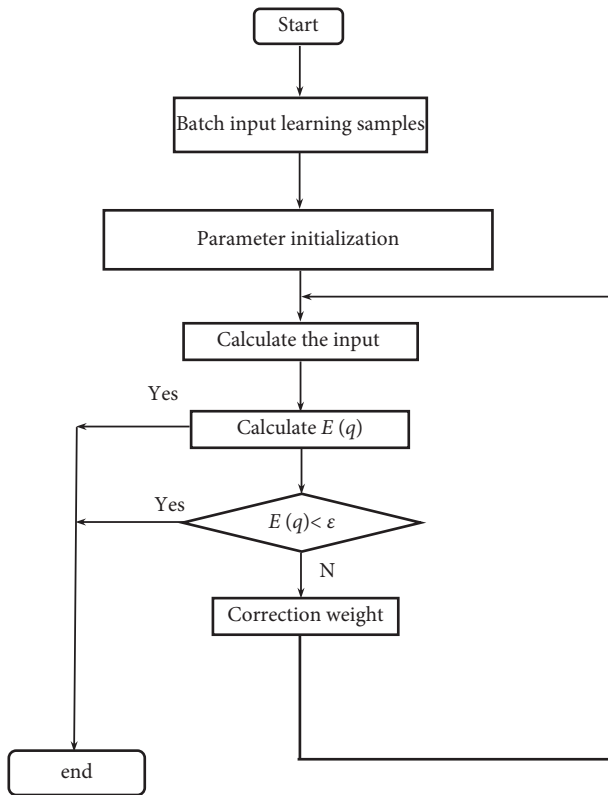


FIGURE 2: BP algorithm program flowchart.

Using the generalization error of each unit in the middle layer:  $e_j^k$ , modified connection right:  $w_{ij}, \theta_j \dots$

$$\begin{aligned}
 w_{ij}(N+1) &= w_{ij}(N) + \beta \cdot e_j^k \cdot a_i^k \\
 \theta_j(N+1) &= \theta_j(N) + \beta \cdot e_j^k \quad (6) \\
 i &= 1, 2, \dots, n, j = 1, 2, \dots, p, 0 < \beta < 1.
 \end{aligned}$$

Finally, the next learning sample vector is randomly selected and provided to the network until the training sample is trained.

## 5. Conclusion

The research shows that the efficiency evaluation of cross-organizational knowledge collaboration of industry university cooperation, as a complete system, is complex. In the industry university cooperation, multi-selection neural network model is used as the basic model for the evaluation of knowledge collaboration efficiency. Neural network model can also be applied to management practice, economy, and other fields. It has the advantages of fast and reliable calculation. Through this model, the relationship between knowledge collaboration efficiency index and knowledge collaboration efficiency can be described relatively objectively. In order to realize the objective description of the essence and law of knowledge collaboration, it is necessary to build a perfect index system. However, the operation of the index system composed of many indicators is difficult to achieve. A single index can describe one or

more attribute characteristics of the knowledge synergy efficiency evaluation system. Therefore, in the process of constructing the index system, select more representative main indexes for analysis and processing to ensure the rationality and scientificity of the construction of the evaluation index system, which is the basis of scientific evaluation and judgment of the actual efficiency of knowledge synergy. At the same time, based on the evaluation of knowledge collaboration efficiency and related factors, this study selects three main elements in the analysis of knowledge collaboration efficiency, namely, organizational differences, knowledge collaboration real environment, and behavior elements, and realizes knowledge collaboration efficiency through the integration and operation of the three elements. The result of knowledge collaboration efficiency is the result of its comprehensive effect. According to the final evaluation results, this study can calculate the cross-organizational knowledge synergy efficiency of production learning cooperation within a certain confidence interval.

## Data Availability

The simulation experiment data used to support the findings of this study are available from the corresponding author upon request.

## Conflicts of Interest

The authors declare that there are no conflicts of interest regarding the publication of this paper.

## Acknowledgments

This work was supported in part by the National Social Science Foundation of China (Grant no. 15BJY073).

## References

- [1] Y. Song and Y. Yan, "Analysis of the impact of knowledge differences on member cooperation," *Industrial technology and economy*, vol. 30, no. 3, pp. 52–57, 2011.
- [2] P. S. Ring and H. Andrew, "Structure cooperative relationships between organizations," *Strategic Management Journal*, vol. 13, no. 7, pp. 483–498, 1992.
- [3] M. Bell and M. Albu, "Knowledge systems and technological dynamism in industrial clusters in developing countries," *World Development*, vol. 27, no. 9, pp. 1715–1734, 1999.
- [4] B. Cai and M. Nie, "The impact of social network on technological innovation of industrial clusters," *Science of science and management of science and technology*, vol. 7, no. 7, pp. 57–60, 2003.
- [5] Y. Zhu, "On the innovation advantages of industrial clusters," *China soft science*, vol. 7, no. 7, pp. 107–112, 2003.
- [6] H. Bathelt, A. Malmberg, and P. Maskell, "Clusters and knowledge: local buzz global pipelines and the process of knowledge creation," *Progress in Human Geography*, vol. 28, no. 1, pp. 31–56, 2004.
- [7] J. Candace, W. S. Hesterly, and S. P. Borgatti, "A general theory of network governance: exchange conditions and social mechanisms," *Academy of Management Review*, vol. 22, no. 4, pp. 911–945, 1997.

## Research Article

# Comparative Study on the Plastic Zone of Circular Hole Surrounding Rock in Anisotropic In Situ Stress Conditions

Pei Zhou <sup>1,2</sup> and Peng Wu <sup>3,4</sup>

<sup>1</sup>China University of Geosciences, Wuhan 430074, China

<sup>2</sup>Engineering Research Center of Rock-Soil Drilling and Excavation and Protection, Ministry of Education, Wuhan 430074, China

<sup>3</sup>School of Electronics and Information, Yangtze University, Jingzhou 434023, China

<sup>4</sup>National Engineering Research Center for GIS, China University of Geosciences, Wuhan 430074, China

Correspondence should be addressed to Peng Wu; [wupeng@yangtzeu.edu.cn](mailto:wupeng@yangtzeu.edu.cn)

Received 1 April 2022; Revised 25 April 2022; Accepted 5 May 2022; Published 6 June 2022

Academic Editor: Hangjun Che

Copyright © 2022 Pei Zhou and Peng Wu. This is an open access article distributed under the Creative Commons Attribution License, which permits unrestricted use, distribution, and reproduction in any medium, provided the original work is properly cited.

Anisotropic in situ ground stress is an objective stress state of rock mass that should be taken into account when calculating the plastic zone of the circular hole surrounding rock. The point stress method and approximate plastic condition method for calculating plastic zone are derived, and the finite element numerical calculation is carried out. Different analytical and finite element approaches are employed for calculation based on the representative parameters. The outcomes of the calculations are thoroughly examined. There are four shapes of plastic zone, among which the butterfly plastic zone can be obtained only by approximate plastic condition method and finite element method. The distribution of plastic zone calculated by using the point stress method and the Ruppneyt formula is identical, with only small deviations. The modified Fenner formula should not be used to calculate the plastic zone under in situ stress anisotropy since it would result in an underestimation of the maximum plastic radius. The detailed calculation and results comparison of this paper can provide a reference for more comprehensive and reasonable evaluation of the surrounding rock plastic zone.

## 1. Introduction

The in situ stress state of surrounding rock changes as a result of the excavation of circular hole (e.g., roadway and tunnel). When the redistributed stress meets the yield condition, the surrounding rock enters the plastic state [1, 2]. The distribution shape and size of the plastic zone serve as the foundation for evaluating the stability of the surrounding rock, as well as an essential basis for supporting design [3, 4].

The in situ stress field was simplified to uniform distribution in early elastic-plastic analyses of surrounding rock, and the theory represented by the modified Fenner formula was proposed. Many scholars later optimized and improved this method in combination with the physical and mechanical properties of geotechnical materials, resulting in the development of a series of analytical calculation methods [5–8]. It is able to obtain a detailed analytical calculation

theory of stress, strain, displacement, and plastic zone distribution. The plastic zone of circular hole surrounding rock is axisymmetric under isotropic stress conditions.

The true in situ stress field, on the other hand, is generally anisotropic. Due to the stress redistribution effect, it is difficult to solve the exact mechanical field under the condition of anisotropic in situ stress after the surrounding rock enters the plastic state. Obviously, the distribution of the plastic zone is axi-asymmetric, and researchers have proposed some approximate solutions [9–13]. The shape and size of the plastic zone obtained by different methods differ due to different assumptions and mathematical solutions.

In practice, the choice of calculation methods is currently subjective, and there is a lack of comparative analysis of different methods. Considering anisotropic in situ stress state, the point stress method and approximate plastic condition method for plastic zone calculation are derived.

Based on the representative parameters, calculation is performed using four analytical methods: modified Fenner formula, Ruppneyt solution, point stress method, and approximate plastic condition method. Moreover, the nonlinear finite element software ABAQUS is used for comprehensive calculations in this paper.

## 2. Analytical Solution

The analytical solution is based on the reasonable mechanical model which is an idealized analysis model based on practical engineering problems that grasps the mechanical essence and major principles while making appropriate assumptions and simplifications. The basic assumptions for elastic-plastic analysis of circular hole surrounding rock are as follows: the cross section of hole is circular, the length of hole is much larger than its diameter, and the mechanical model is simplified to plane strain

problem; geotechnical materials are homogeneous and isotropic; they are infinite boundary media; the gravity stress gradient is not considered, and in situ stress is regarded as the initial pressure acting on the boundary. The Mohr–Coulomb strength criterion is adopted as the condition for judging plastic yield. The basic mechanical model is shown in Figure 1.

Kirsch was the first to investigate the elastic stress distribution of a tensile-stressed infinite plate, while other scholars updated and revised it, which later became well-known as the Kirsch equation [14–16]. Airy function trial methodology or the complex variable approach can be used to obtain Kirsch equation; detailed solution process is given in references [17, 18].

The stress distribution of the hole surrounding rock in the elastic state is as follows based on Kirsch equation:

$$\begin{aligned}\sigma_r &= \frac{1}{2}\sigma_v\left((1+K_0)\left(1-\left(\frac{R}{r}\right)^2\right)-(1-K_0)\left(1-4\left(\frac{R}{r}\right)^2+3\left(\frac{R}{r}\right)^4\right)\cos(2\theta)\right)+P_i\left(\frac{R}{r}\right)^2, \\ \sigma_\theta &= \frac{1}{2}\sigma_v\left((1+K_0)\left(1+\left(\frac{R}{r}\right)^2\right)+(1-K_0)\left(1+3\left(\frac{R}{r}\right)^4\right)\cos(2\theta)\right)-P_i\left(\frac{R}{r}\right), \\ \tau_{r\theta} &= \frac{1}{2}\sigma_v\left((1-K_0)\left(1+2\left(\frac{R}{r}\right)^2-3\left(\frac{R}{r}\right)^4\right)\sin(2\theta)\right).\end{aligned}\quad (1)$$

**2.1. Modified Fenner Formula.** It is the elastic solution of isotropic stress condition when the lateral pressure coefficient in Kirsch equation is equal to 1. If the actual support force is less than the critical support force, the surrounding rock becomes plastic, and the radius of the plastic zone is [16]

$$R_p = R \left[ \frac{(\sigma_v + c \cot \varphi)(1 - \sin \varphi)}{(P_i + c \cot \varphi)} \right]^{(1 - \sin \varphi)/(2 \sin \varphi)}. \quad (2)$$

The modified Fenner formula, also known as the Kastner formula, is shown above. This approach is widely used and

has a straightforward calculation. This assumption of in situ stress isotropy, on the other hand, is clearly incompatible with actual situations.

**2.2. Ruppneyt Solution.** Due to the stress redistribution effect, it is difficult to compute the exact mechanical field when in situ stress anisotropy exists. There are some approximate answers available at present, among which the Ruppneyt solution is a representative calculating approach [19]:

$$R_p = R \left\{ \frac{[(\sigma_v(1+K_0) + 2c \cot \varphi)](1 - \sin \varphi)}{2P_i + 2c \cot \varphi} \right\}^{(1 - \sin \varphi)/(2 \sin \varphi)} \times \left\{ 1 + \frac{\sigma_v(1 - K_0)(1 - \sin \varphi)\cos 2\theta 3}{[\sigma_v(1 + K_0) + 2c \cot \varphi]\sin \varphi} \right\}. \quad (3)$$

Ruppneyt equation considering anisotropic in situ stress conditions has an explicit expression and has been widely applied in engineering [20].

**2.3. Point Stress Method.** A plastic radius equation was proposed by Cai and Cai [21], and the results of the original literature are modified in this study.

Assume that the circular hole surrounding rock is an axisymmetric plane strain solution after entering the plastic state, and the circumferential stress equation is as follows:

$$\sigma_{\theta p} = A(P_i + c \cot \varphi)\left(\frac{r}{R}\right)^{A-1} - c \cot \varphi. \quad (4)$$

The Kirsch equation is satisfied by the stress solution in the elastic region. The radial stress at the elastic-plastic

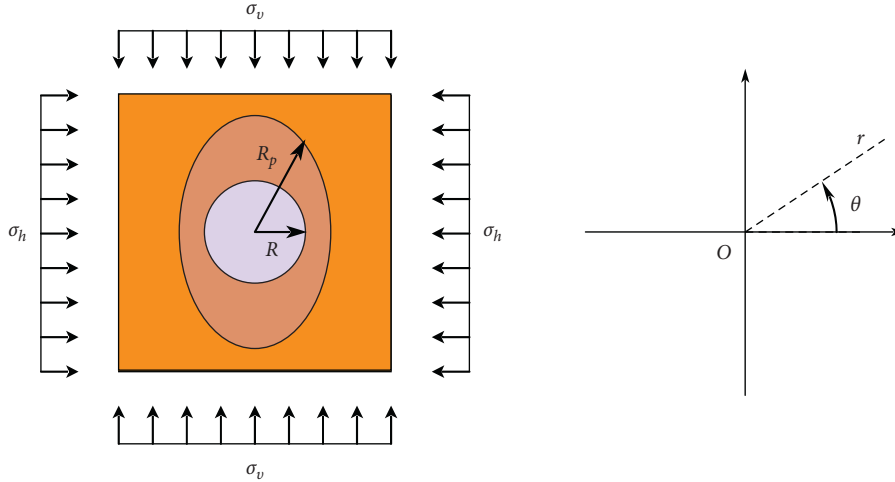


FIGURE 1: Basic mechanical model.

interface is utilized to replace the support force, and the boundary radius of the plastic zone is used to replace the hole radius. The following equation can be obtained:

$$\sigma_{\theta} = \frac{1}{2}\sigma_v \left( (1 + K_0) \left( 1 + \left( \frac{R_p}{r} \right)^2 \right) + (1 - K_0) \left( 1 + 3 \left( \frac{R_p}{r} \right)^4 \right) \cos(2\theta) \right) - (\sigma_v(1 - \sin \varphi) - c \cos \varphi) \left( \frac{R_p}{r} \right)^2. \quad (5)$$

The radius of the plastic zone is calculated using simultaneous (4) and (5):

$$R_p = R \left( \frac{(1 - \sin \varphi) (2\sigma_v \cos 2\theta (1 - K_0) + \sigma_v (K_0 + \sin \varphi) + c (\cos \varphi + \cot \varphi))}{(1 + \sin \varphi) (P_i + c \cot \varphi)} \right)^{(1 - \sin \varphi) / (2 \sin \varphi)}. \quad (6)$$

This approach is called point stress method since it is based on the equal circumferential stress of individual points.

**2.4. Approximate Plasticity Condition Method.** Kastner proposed to ignore the stress redistribution caused by elastic-plastic deformation, i.e., the stress field of the hole surrounding rock is still the same as Kirsch equation during plastic deformation, and the boundary line equation of approximate plastic zone is obtained based on the geometric relationship of stress Mohr circle [22]. This method has

recently been used in the stability analysis of roadway surrounding rock [23–28]. Taking the supporting force into account, the boundary line equation is rederived in this study.

The following equation can be obtained after a series of operations such as the combination of similar terms and the transformation of trigonometric functions (the specific calculation and simplification process are omitted):

$$M_8 \left( \frac{R}{r} \right)^8 + M_6 \left( \frac{R}{r} \right)^6 + M_4 \left( \frac{R}{r} \right)^4 + M_2 \left( \frac{R}{r} \right)^2 + M_0 = 0, \quad (7)$$

in which

$$\begin{aligned}
M_8 &= 9(K_0 - 1)^2, \\
M_6 &= -6\left(2(K_0 - 1)^2 + \cos(2\theta)(K_0^2 - 1)\right) + 12\frac{P_i}{\sigma_v}\cos(2\theta)(K_0 - 1), \\
M_4 &= \left((K_0 - 1)^2\left(\cos(4\theta)\left(6 - 2\frac{(A - 1)^2}{(A + 1)^2}\right) + 4 - 2\frac{(A - 1)^2}{(A + 1)^2}\right) + 4\cos(2\theta)(K_0^2 - 1) + (K_0 + 1)^2\right) \\
&\quad - 4\frac{P_i}{\sigma_v}(K_0 + 1 + 2\cos(2\theta)(K_0 - 1)) + 4\left(\frac{P_i}{\sigma_v}\right)^2, \\
M_2 &= \left(-4\cos(4\theta)(K_0 - 1)^2 - 2\cos(2\theta)(K_0^2 - 1)\left(1 - \frac{2(A - 1)^2}{(A + 1)^2}\right)\right) \\
&\quad + 4\cos(2\theta)(K_0 - 1)\left(\frac{P_i}{\sigma_v} + \frac{2B(A - 1)}{(A + 1)^2}\frac{1}{\sigma_v}\right), \\
M_0 &= \left((K_0 - 1)^2 - \frac{(K_0 + 1)^2(A - 1)^2}{(A + 1)^2}\right) - \frac{4B(K_0 + 1)(A - 1)}{(A + 1)^2}\frac{1}{\sigma_v} - \frac{4B^2}{(A + 1)^2}\left(\frac{1}{\sigma_v}\right)^2, \\
A &= \frac{1 + \sin\varphi}{1 - \sin\varphi}, \\
B &= \frac{2c\cos\varphi}{1 - \sin\varphi}.
\end{aligned} \tag{8}$$

The issue with this method is that the stress distribution in the plastic stage is identical to that in the elastic stage, making it a rough estimating method. Therefore, it is called approximate plastic condition method.

**2.5. Calculation Results of Analytical Methods.** Typical calculation parameters are adopted [29]:  $R = 2$  m,  $\gamma = 25$  kN/m<sup>3</sup>,  $H = 600$  m,  $\varphi = 30^\circ$ , and  $c = 1$  MPa. The plastic zone boundary lines are depicted in Figures 2–4 using the Ruppneyt solution, point stress technique, and approximated plastic condition method, respectively.

### 3. Finite Element Method

Finite element software ABAQUS is used for numerical calculation in order to evaluate the accuracy of the analytical solution derived by various ideas and methodologies. There are two stages of the numerical simulation: in situ stress balance and hole excavation [30].

The calculation parameters are identical to those used in the previous analytical calculations. The model's width and height are both 40 m, and the hole is located in the center. The horizontal displacement at the left and right sides of the model is zero, and the vertical displacement at the bottom is also zero. The gravity of the rock mass is taken into account in the numerical simulation. As a result, a pressure of 14.5 MPa is applied on the top boundary, and the pressure on the left and right sides is determined according to lateral pressure coefficient. The element type of surrounding rock in the model is CPE4 solid element. To achieve excellent

precision, the model has a total of 201,550 elements. Eight groups of numerical simulation are carried out in this research, with the calculated plastic zone distribution illustrated in Figure 5.

### 4. Comparison and Analysis

The numerical results clearly show that the plastic zone has four shapes: butterfly, curved rectangle with concave horizontal direction and convex vertical direction, approximate ellipse, and circle. Specifically, the plastic zone is butterfly when  $K_0 = 0.3 \sim 0.5$ ; when  $K_0 = 0.6$ , it is a curved rectangle with concave horizontal direction and convex vertical direction; when  $K_0 = 0.7 \sim 0.9$ , the plastic zone is approximate ellipse; and when  $K_0 = 1$ , it is round.

Among various analytic approaches, only the approximate plastic condition method can calculate the butterfly-shaped plastic zone. At  $K_0 = 0.3 \sim 0.4$ , there is an obvious butterfly plastic zone which is not noticeable at  $K_0 = 0.5$ . Ruppneyt solution and point stress method, although considering the anisotropy of in situ stress, cannot reflect the distribution characteristics of butterfly plastic zone.

When  $K_0 = 0.7 \sim 0.9$ , the plastic zone obtained from the two analytical methods (Ruppneyt solution and point stress method) and numerical simulation are approximate elliptical. Specifically, when  $K_0 = 0.7$ , the plastic radius calculated by Ruppneyt solution is 3.45~4.72 m and the result of the point stress method is 2.99~4.77 m; the numerical simulation solution is 3.24~4.73 m. When  $K_0 = 0.8$ , the plastic radii calculated by these three methods (Ruppneyt solution, point

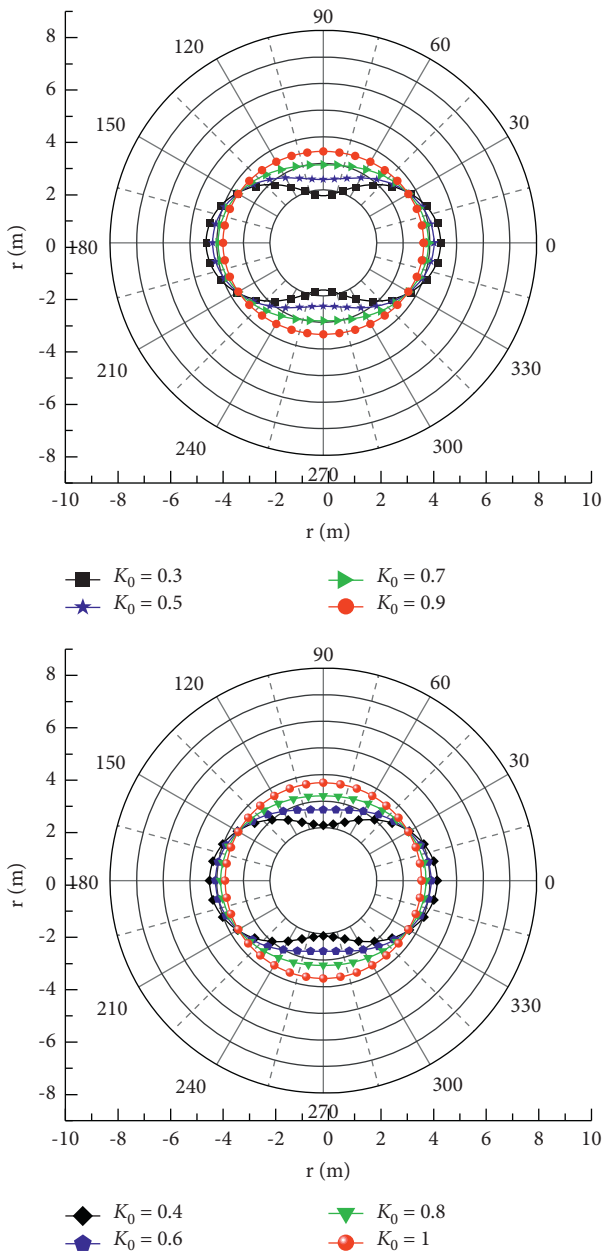


FIGURE 2: Boundary lines of plastic zone based on Ruppneyt solution.

stress method, and finite element method) are 3.78~4.61 m, 3.52 ~ 4.65 m, and 3.67~4.66 m, respectively. These three methods are 4.09~4.50 m, 3.98~4.52 m, and 4.03~4.59 m, respectively, at  $K_0=0.9$ . Obviously, the results of these three methods are very close.

Although the approximate plastic condition method can also obtain the elliptical plastic zone when  $K_0=0.8 \sim 0.9$ , the plastic radius is significantly smaller than the results of the previous three calculation methods. When  $K_0=0.8$ , the plastic radius is 2.59 ~2.73 m and it is 2.64~2.70 m when  $K_0=0.9$ .

The distribution of the plastic zone calculated using the point stress method and the Ruppneyt solution is nearly identical, with only minor differences. Specifically, when  $K_0=0.3$ , the vertical direction of the inner boundary of

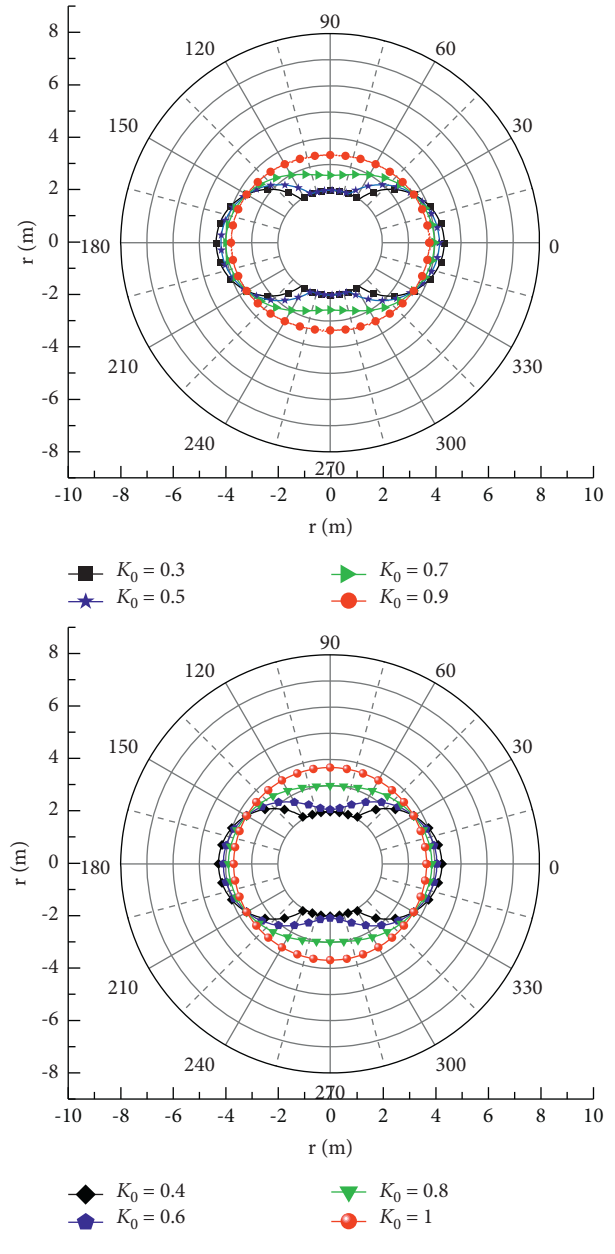


FIGURE 3: Boundary lines of plastic zone based on the point stress method.

circular hole has an elastic range ( $85^\circ \sim 95^\circ$  and  $25^\circ \sim 275^\circ$ ) according to Ruppneyt solution.

When  $K_0=0.3 \sim 0.5$ , there are elastic zones in this position calculated by the point stress method, and the range is larger than results of Ruppneyt solution. When  $K_0=0.3$ , the range is  $59^\circ \sim 121^\circ$  and  $239^\circ \sim 301^\circ$ . The range is  $64^\circ \sim 116^\circ$  and  $244^\circ \sim 296^\circ$  when  $K_0=0.4$ ; the range is  $73^\circ \sim 107^\circ$  and  $253^\circ \sim 287^\circ$  when  $K_0=0.5$ .

When the lateral pressure coefficient is equal to 1, the boundary line of the plastic zone is circular. The plastic radii calculated using the modified Fenner formula, Ruppneyt solution, point stress method, and finite element method are 4.39 m, 4.40 m, 2.68 m, and 4.32~4.51 m, respectively. The plastic radius computed by other methods is quite close, with the exception of the approximate plastic condition method.



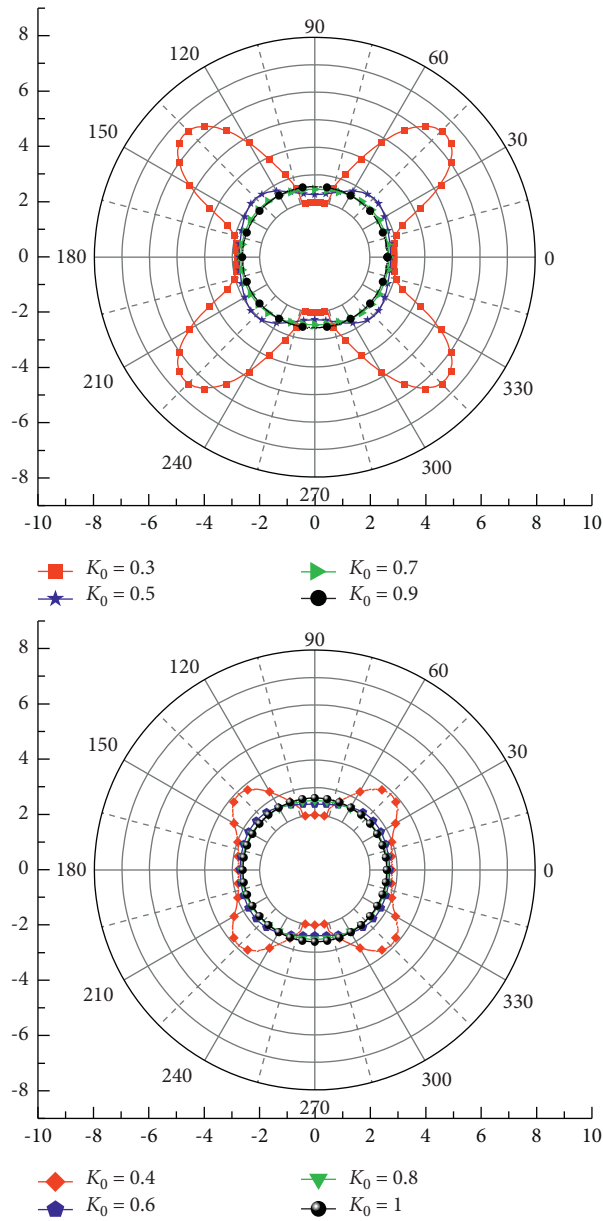


FIGURE 4: Boundary lines of plastic zone based on the approximate plastic condition method.

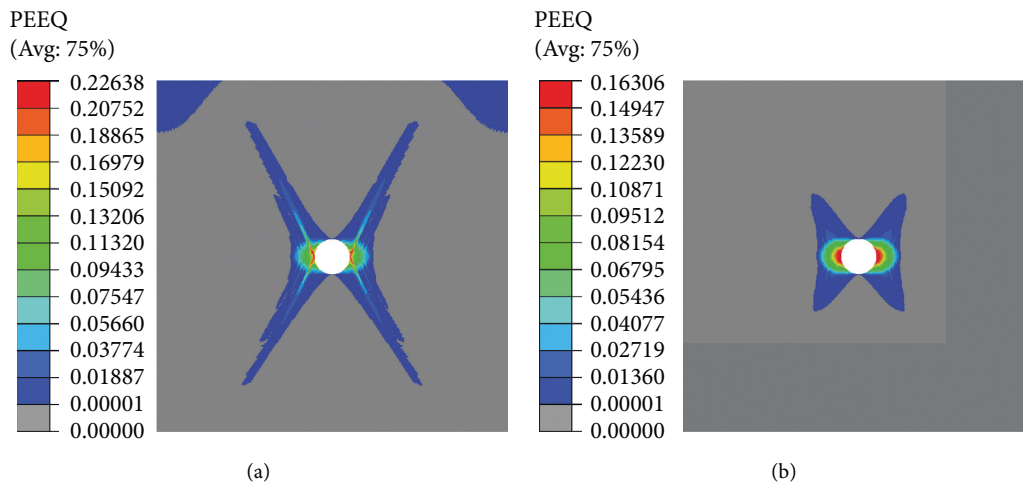


FIGURE 5: Continued.

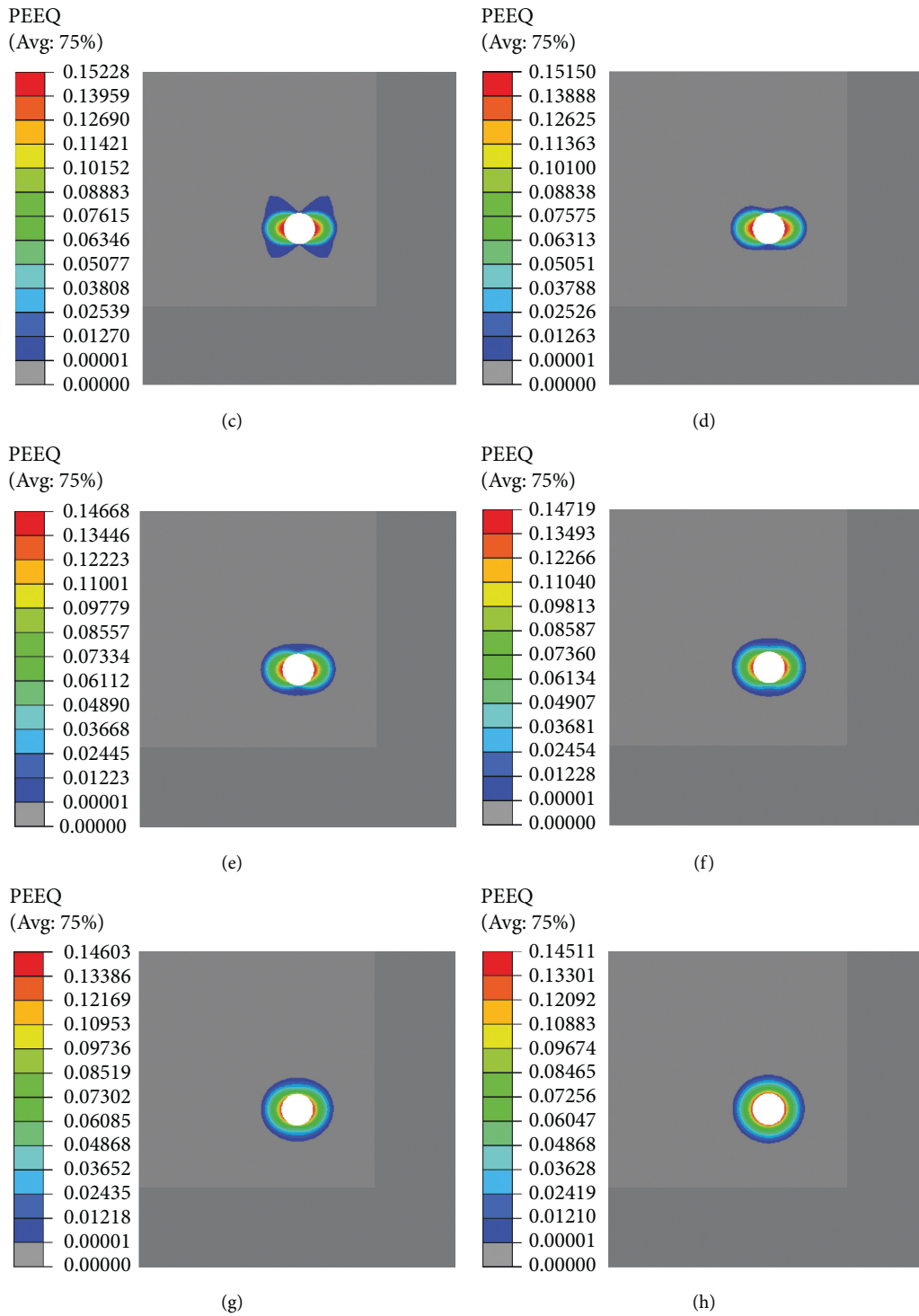


FIGURE 5: Distribution of plastic zone based on the finite element method: (a)  $K_0 = 0.3$ ; (b)  $K_0 = 0.4$ ; (c)  $K_0 = 0.5$ ; (d)  $K_0 = 0.6$ ; (e)  $K_0 = 0.7$ ; (f)  $K_0 = 0.8$ ; (g)  $K_0 = 0.9$ ; (h)  $K_0 = 1.0$ .

When the anisotropy of in situ stress is strong, the maximum plastic radius calculated by numerical simulation is much larger than the result of modified Fenner formula which is based on the assumption of in situ stress isotropic.

## 5. Conclusions

In this research, the plastic zone of circular hole surrounding rock is calculated and compared using four analytical approaches (modified Fenner formula, Ruppneyt solution, point stress method, and approximate plasticity condition method) and finite element method. Some key conclusions are reached through in-depth comparison and analysis with various methods.

- (1) Four shapes of plastic zone (butterfly, curved rectangle with concave horizontal direction and convex vertical direction, approximate ellipse, and circle) can be obtained by using the finite element method and approximate plastic condition method. Other analytic approaches cannot get butterfly shape. Therefore, the approximate plastic condition method has advantages in describing the shape of plastic zone.
- (2) In the distribution and evolution of the plastic zone, the degree of in situ stress anisotropy is critical. The butterfly distribution appears when the horizontal stress differs significantly from the vertical stress (when  $K_0 < 0.5$  or  $K_0 > 2$ ), which is the key shape of the plastic radius with a significant abrupt change. The modified Fenner formula will severely underestimate the plastic zone range at this time.
- (3) When lateral pressure coefficient is close to 1, Ruppneyt solution, point stress method, and finite element method calculation results are similar. The shape of the plastic zone calculated by the approximate plastic condition method is similar to that calculated by other methods, but the plastic radius is significantly underestimated.
- (4) In the supporting design, the anisotropic in situ stress conditions need to be carefully considered. While using an anchor, the length of anchor should be greater than the maximum plastic radius. When in situ stress anisotropy is considerable, the appropriate plastic zone calculation method and support scheme must be carefully chosen.

## Notation

$R$ : Radius of circular hole  
 $R_p$ : Radius of plastic zone of surrounding rock  
 $r$ : The distance between any point in the surrounding rock and the circular roadway's center  
 $P_i$ : Support force  
 $\sigma_v$ : Vertical in situ stress  
 $\sigma_h$ : Horizontal in situ stress  
 $\theta$ : Angle, starting horizontally to the right and increasing counterclockwise  
 $K_0$ : Lateral pressure coefficient

$\sigma_r$ : Radial stress  
 $\sigma_\theta$ : Circumferential stress  
 $\tau_{r\theta}$ : Shear stress  
 $\sigma_{\theta p}$ : Circumferential stress of plastic zone  
 $\varphi$ : Friction angle of rock mass  
 $c$ : Cohesion of rock mass  
 $\gamma$ : Unit weight of rock mass  
 $H$ : Depth of underground hole.

## Data Availability

The data used to support the findings of this study are available from the corresponding author upon request.

## Conflicts of Interest

The authors declare that they have no conflicts of interest regarding the publication of this paper.

## References

- [1] E. Komurlu, A. Kesimal, and R. Hasanpour, "In situ horizontal stress effect on plastic zone around circular underground openings excavated in elastic zones," *Geomechanics and Engineering*, vol. 8, no. 6, pp. 783–799, 2015.
- [2] Y. H. Hao and R. Azzam, "The plastic zones and displacements around underground openings in rock masses containing a fault," *Tunnelling and Underground Space Technology*, vol. 20, no. 1, pp. 49–61, 2005.
- [3] T. Ogawa and K. Y. Lo, "Effects of dilatancy and yield criteria on displacements around tunnels," *Canadian Geotechnical Journal*, vol. 24, no. 1, pp. 100–113, 1987.
- [4] S. H. Du, D. Y. Li, and J. Sun, "Stability control and support optimization for a soft-rock roadway in dipping layered strata," *Geotechnical and Geological Engineering*, vol. 37, no. 3, pp. 2189–2205, 2019.
- [5] H. S. Yu, *Cavity Expansion Methods in Geomechanics*, Kluwer Academic Publishers, Dordrecht, Netherlands, 2000.
- [6] S. K. Sharan, "Analytical solutions for stresses and displacements around a circular opening in a generalized Hoek–Brown rock," *International Journal of Rock Mechanics and Mining Sciences*, vol. 45, no. 1, pp. 78–85, 2008.
- [7] C. G. Zhang, J. H. Zhao, Q. H. Zhang, and X. D. Hu, "A new closed-form solution for circular openings modeled by the Unified Strength Theory and radius-dependent Young's modulus," *Computers and Geotechnics*, vol. 42, pp. 118–128, 2012.
- [8] Q. Zhang, B. S. Jiang, S. L. Wang, X. R. Ge, and H. Q. Zhang, "Elasto-plastic analysis of a circular opening in strain-softening rock mass," *International Journal of Rock Mechanics and Mining Sciences*, vol. 50, no. 1, pp. 38–46, 2012.
- [9] Y. Ma, A. Z. Lu, H. Cai, and X. T. Zeng, "Analytical solution for determining the plastic zones around two unequal circular tunnels," *Tunnelling and Underground Space Technology*, vol. 120, no. 1, Article ID 104267, 2022.
- [10] Y. C. Ma, A. Z. Lu, X. T. Zeng, and H. Cai, "Analytical solution for determining the plastic zones around twin circular tunnels excavated at great depth," *International Journal of Rock Mechanics and Mining Sciences*, vol. 136, Article ID 104475, 2020.
- [11] C. Li, J. H. Xu, J. Z. Pan, and C. Ma, "Plastic zone distribution laws and its types of surrounding rock in large-span roadway,"

- International Journal of Mining Science and Technology*, vol. 22, no. 1, pp. 23–28, 2012.
- [12] M. J. Leitman and P. Villaggio, “Plastic zone around circular holes,” *Journal of Engineering Mechanics*, vol. 135, no. 12, pp. 1467–1471, 2009.
- [13] G. Y. Gao, Q. S. Chen, Q. S. Zhang, and G. Q. Chen, “Analytical elasto-plastic solution for stress and plastic zone of surrounding rock in cold region tunnels,” *Cold Regions Science and Technology*, vol. 72, pp. 50–57, 2012.
- [14] C. Kirsch, “Die theorie der elastizitat und die bedurfnisse der festigkeitslehre,” *Zeitschrift des Vereines Deutscher Ingenieure*, vol. 42, pp. 797–807, 1898.
- [15] Y. Hiramatsu and Y. Oka, “Determination of the stress in rock unaffected by boreholes or drifts, from measured strains or deformations,” *International Journal of Rock Mechanics and Mining Sciences & Geomechanics Abstracts*, vol. 5, no. 4, pp. 337–353, 1968.
- [16] S. P. Wu, L. P. Li, and X. P. Zhang, *Rock Mechanics*, Higher education press, Beijing, China, 2021.
- [17] J. C. Jaeger, N. G. Cook, and R. Zimmerman, *Fundamentals of Rock Mechanics*, John Wiley & Sons, Hoboken, NJ, U.S.A, 4th edition, 2009.
- [18] Y. Y. Xiang, *Introduction to Tunnel Mechanics*, Science Press, Beijing, China, 2014.
- [19] K. B. Ruppneyt, *Several Problems in Mining Rock Mechanics*, China Coal Industry Publishing House, Beijing, China, 1960.
- [20] Z. S. Zou, J. Yang, Z. M. Wang, and H. Y. Liu, “The plastic zone of tunnel surrounding rock under unequal stress in two directions based on the unified strength theory,” *Mathematical Problems in Engineering*, vol. 2021, Article ID 8842153, 11 pages, 2021.
- [21] X. H. Cai and Y. P. Cai, *Stress Calculation of Hydraulic Pressure Tunnel Structure*, China Water Resources and Hydropower Press, Beijing, China, 2004.
- [22] H. Kastner, *Statik des Tunnel-und Stollenbaues*, Springer, Berlin, Germany, 1971.
- [23] X. F. Guo, Z. Q. Zhao, X. Gao, X. Y. Wu, and N. J. Ma, “Analytical solutions for characteristic radii of circular roadway surrounding rock plastic zone and their application,” *International Journal of Mining Science and Technology*, vol. 29, no. 2, pp. 263–272, 2019.
- [24] N. J. Ma, J. Li, and Z. Q. Zhao, “Distribution of the deviatoric stress field and plastic zone in circular roadway surrounding rock,” *Journal of China University of Mining & Technology*, vol. 44, no. 2, pp. 206–213, 2015.
- [25] H. S. Jia, N. J. Ma, and Q. K. Zhu, “Mechanism and control method of roof fall resulting from butterfly plastic zone penetration,” *Journal of China Coal Society*, vol. 41, no. 6, pp. 1384–1392, 2016.
- [26] N. J. Ma, X. F. Guo, Z. Q. Zhao, X. D. Zhao, and H. T. Liu, “Occurrence mechanisms and judging criterion on circular tunnel butterfly rock burst in homogeneous medium,” *Journal of China Coal Society*, vol. 41, no. 11, pp. 2679–2688, 2016.
- [27] J. Li, X. B. Qiang, N. J. Ma, R. G. Zhang, and B. Li, “Formation mechanism and engineering application of the directionality of butterfly leaf in the butterfly plastic zone of roadway rock surrounded,” *Journal of China Coal Society*, vol. 46, no. 9, pp. 2838–2852, 2021.
- [28] Z. Q. Zhao, N. J. Ma, H. T. Liu, and X. F. Guo, “A butterfly failure theory of rock mass around roadway and its application prospect,” *Journal of China University of Mining & Technology*, vol. 47, no. 5, pp. 969–978, 2018.
- [29] A. Z. Lu, X. L. Zhang, and S. J. Wang, “Analytic method for elasto-plastic analysis of circular tunnels under non-axisymmetric stresses,” *Chinese Journal of Rock Mechanics and Engineering*, vol. 37, no. 1, pp. 14–22, 2018.
- [30] S. Helwany, *Applied Soil Mechanics with ABAQUS Applications*, John Wiley & Sons, Hoboken, NJ, U.S.A, 2007.

## *Retraction*

# **Retracted: DARSegNet: A Real-Time Semantic Segmentation Method Based on Dual Attention Fusion Module and Encoder-Decoder Network**

### **Mathematical Problems in Engineering**

Received 19 September 2023; Accepted 19 September 2023; Published 20 September 2023

Copyright © 2023 Mathematical Problems in Engineering. This is an open access article distributed under the Creative Commons Attribution License, which permits unrestricted use, distribution, and reproduction in any medium, provided the original work is properly cited.

This article has been retracted by Hindawi following an investigation undertaken by the publisher [1]. This investigation has uncovered evidence of one or more of the following indicators of systematic manipulation of the publication process:

- (1) Discrepancies in scope
- (2) Discrepancies in the description of the research reported
- (3) Discrepancies between the availability of data and the research described
- (4) Inappropriate citations
- (5) Incoherent, meaningless and/or irrelevant content included in the article
- (6) Peer-review manipulation

The presence of these indicators undermines our confidence in the integrity of the article's content and we cannot, therefore, vouch for its reliability. Please note that this notice is intended solely to alert readers that the content of this article is unreliable. We have not investigated whether authors were aware of or involved in the systematic manipulation of the publication process.

Wiley and Hindawi regrets that the usual quality checks did not identify these issues before publication and have since put additional measures in place to safeguard research integrity.

We wish to credit our own Research Integrity and Research Publishing teams and anonymous and named external researchers and research integrity experts for contributing to this investigation.

The corresponding author, as the representative of all authors, has been given the opportunity to register their agreement or disagreement to this retraction. We have kept a record of any response received.

### **References**

- [1] Y. Xing, L. Zhong, and X. Zhong, "DARSegNet: A Real-Time Semantic Segmentation Method Based on Dual Attention Fusion Module and Encoder-Decoder Network," *Mathematical Problems in Engineering*, vol. 2022, Article ID 6195148, 10 pages, 2022.

## Research Article

# DARSegNet: A Real-Time Semantic Segmentation Method Based on Dual Attention Fusion Module and Encoder-Decoder Network

Yongfeng Xing <sup>1,2</sup>, Luo Zhong <sup>1</sup>, and Xian Zhong <sup>1</sup>

<sup>1</sup>School of Computer Science and Artificial Intelligence, Wuhan University of Technology, Wuhan 430070, China

<sup>2</sup>School of Software, Nanyang Institute of Technology, Nanyang 473000, China

Correspondence should be addressed to Yongfeng Xing; xingyongfeng@whut.edu.cn

Received 27 April 2022; Revised 17 May 2022; Accepted 21 May 2022; Published 6 June 2022

Academic Editor: Hangjun Che

Copyright © 2022 Yongfeng Xing et al. This is an open access article distributed under the Creative Commons Attribution License, which permits unrestricted use, distribution, and reproduction in any medium, provided the original work is properly cited.

The convolutional neural network achieves excellent semantic segmentation results in artificially annotated datasets with complex scenes. However, semantic segmentation methods still suffer from several problems such as low use rate of the features, high computational complexity, and being far from practical real-time application, which bring about challenges for the image semantic segmentation. Two factors are very critical to semantic segmentation task: global context and multilevel semantics. However, generating these two factors will always lead to high complexity. In order to solve this, we propose a novel structure, dual attention fusion module (DAFM), by eliminating structural redundancy. Unlike most of the existing algorithms, we combine the attention mechanism with the depth pyramid pool module (DPPM) to extract accurate dense features for pixel labeling rather than complex expansion convolution. Specifically, we introduce a DPPM to execute the spatial pyramid structure in output and combine the global pool method. The DAFM is introduced in each decoder layer. Finally, the low-level features and high-level features are fused to obtain semantic segmentation result. The experiments and visualization results on Cityscapes and CamVid datasets show that, in real-time semantic segmentation, we have achieved a satisfactory balance between accuracy and speed, which proves the effectiveness of the proposed algorithm. In particular, on a single 1080ti GPU computer, ResNet-18 produces 75.53% MIoU at 70 FPS on Cityscapes and 73.96% MIoU at 109 FPS on CamVid.

## 1. Introduction

These years, convolutional neural network is making great progress for semantic image segmentation. Semantic segmentation is a basic topic in the field of computer vision. It is a pixel-level classification and plays an important role in the fields of automatic driving, video surveillance, geographic information system, medical image analysis, and so on [1], [2]. Traditional segmentation methods are limited by feature extraction methods, and the image segmentation effect is poor in complex scenes. The convolutional neural network achieves good segmentation results in artificially annotated datasets with complex scenes [3]. However, recent semantic segmentation methods still suffer from several problems such as low use rate of the features, high computational

complexity, and being far from practical application, which bring about challenges for the image semantic segmentation field. Current research mainly focuses on two aspects: applying different network structures to improve the segmentation accuracy and reducing network parameters and computational overheads to meet the real-time requirements with a relatively real-time segmentation accuracy [4].

Real-time segmentation algorithm has attracted more and more attention. Recently, some new real-time semantic segmentation algorithms have been proposed. There are two methods. One is to use GPU efficient backbone, especially ResNet-18, MobileNet, and so forth. Other algorithms have developed complex lightweight coders trained from scratch, and one algorithm BiSeNet [5] has reached a new peak in real-time performance. In short, the current mainstream

semantic segmentation framework has some defects, which cannot meet the good balance of high speed and high precision simultaneously. In this paper, we propose a dual attention network with deep high-resolution representation.

Figure 1 shows a comparison of speed and MIoU on the Cityscapes [6] test set. Red color refers to our methods, while green color refers to other methods. We achieve a good speed-accuracy trade-off.

In practical applications such as automatic driving, robotics, and security monitoring, real-time segmentation may be more valuable than accurate segmentation. The lightweight network model aims to reduce the complexity of parameters of the neural network model, while maintaining the accuracy of the model. Lightweight networks not only include in-depth research on network structure but also include the application of model compression technologies such as knowledge extraction and pruning. Together, they promote the application of convolutional neural network technology in mobile terminals and embedded terminals and make due contributions to the development of all walks of life [7–9].

However, the current mainstream semantic segmentation framework has some defects in real-time semantic segmentation field, which cannot meet the good balance between high speed and high precision simultaneously. At present, deep learning has excellent results in various image processing tasks, but a large number of redundant parameter calculations seriously hinder its use in practical projects. It is difficult to comply with real-time requirements in both mobile terminals and embedded devices [2]. For example, the parameters of ResNet-101 are more than 170 MB of storage resources. For instance, images with a  $224 \times 224$  resolution require more than 7.6 billion floating-point operations, and the parameter memory consumption is 170 MB. This will seriously affect the user's personal experience. Therefore, it is particularly urgent to design a lightweight and efficient neural network.

Compared with the network based on pyramid structure, multibranch network will not increase the output resolution of high-level feature map by changing the reference network. Its operation speed will be faster, but there is a defect that makes it difficult to be applied to real-time semantic segmentation; that is, the contradiction between its spatial branch depth and speed is difficult to coordinate.

At present, the real-time algorithms based on multi-branch networks use relatively simple high-resolution branches. Although they run fast, their segmentation accuracy is low. Some branch information will be extracted in different network contexts. The deep branches of the network use separable convolution and other lightweight operations to obtain semantic context information, and the shallow branches use convolution to retain effective spatial details. The network model with this structure is lighter and promotes the real-time application of semantic segmentation, but it is difficult to extract effective semantic context information. In addition, there is a large gap between the two pieces of feature information, so the fusion cannot produce good results.

Although real-time semantic segmentation has made good progress, there are still three main problems [4]. Firstly, the image may contain similar objects with different scales, such as cars and houses. How to capture and integrate different proportions of image features is very important for semantic segmentation. In the mainstream semantic segmentation framework, image classification network is usually used to extract features, while pyramid feature fusion is used to extract multiscale feature information, such as spatial pyramid pooling module. In this case, a lot of computing resources are generally required. Secondly, the multiscale context extraction module of this pyramid method is not flexible enough and needs to manually set the kernel size, so it can only extract a limited feature scale range, which is not conducive to the learning of network semantic features. Finally, the deep convolution neural network has a hierarchical structure, and the characteristics of different levels are different. The high level has rich semantics but lacks accurate location information, while the low one contains spatial detail information but lacks discriminative semantic features. Because semantic segmentation involves object positioning, there are different levels of feature fusion. If the information flow in the model is not well controlled, some redundant features, including background noise in low level and rough boundary in high level, will be introduced into subsequent features and may lead to network performance degradation.

## 2. Related Work

The segmentation accuracy largely depends on the choice of backbone network. Generally speaking, the more accurate the segmentation model is, the better the relative effect of semantic segmentation is. There are three very important indicators: accuracy, speed, and memory. The performance of these indicators depends on the CNN you choose and any modifications you make to it. Networks have different trade-offs on these indicators. In addition, these network structures can be modified, such as by reducing some layers and adding some layers. Usually, adding more layers will improve accuracy, while sacrificing some speed and memory. However, researchers have realized that this trade-off is subject to marginal effects; that is, the more layers are added, the less accuracy improvement will be brought by adding each layer.

The segmentation accuracy and speed of some classification network models are shown in Table 1.

Generally speaking, using a larger convolution kernel will always lead to the highest accuracy, but it will lose both speed and memory. However, this is not always the case, because it has been found many times that using a large convolution kernel will make the network difficult to diverge. Using smaller cores, such as  $3 \times 3$  convolution, the effect will be better. ResNet [10] and VGGNet [11] both fully explain this fact, as shown in the papers related to these two models.

In this paper, ResNet-18, the lightweight form of ResNet, is taken as the backbone network of semantic segmentation. Compared with ResNet-50, ResNet-101, and ResNet-152,

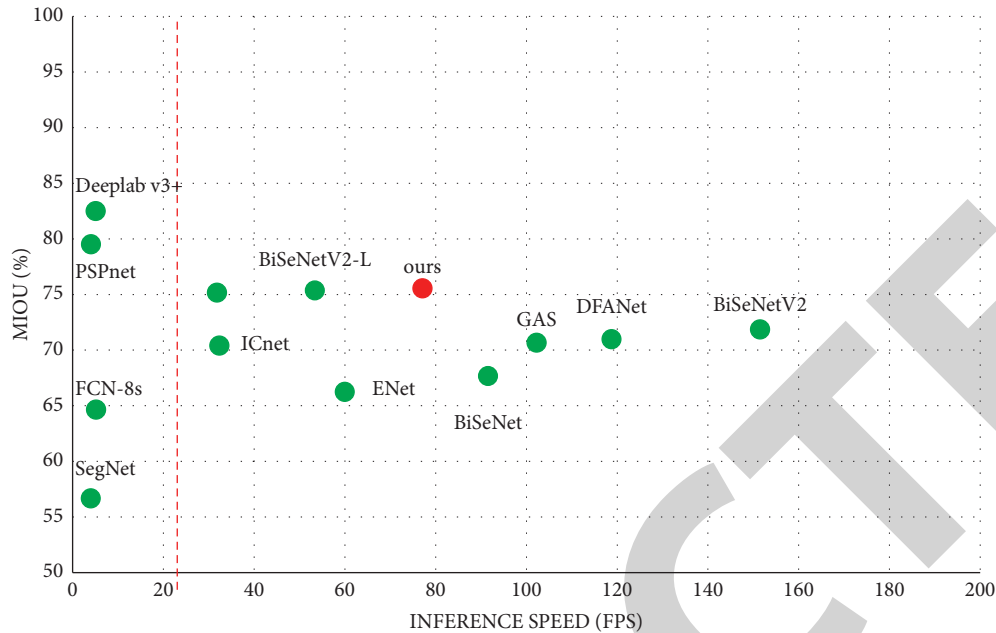


FIGURE 1: Comparison of speed and MIOU on the Cityscapes dataset.

ResNet-18 has fewer network layers and output channels. Although the information classification accuracy of the network is sacrificed, it can significantly improve the running speed of it. ResNet-18 is also composed of convolution layer, pool layer, and four blocks, but each block of ResNet-18 is not composed of bottleneck units but of more lightweight residual units. It can be seen that each block of ResNet-18 contains two residual units, a number which is far less than the number of units of each block in the backbone network ResNet-101, making it run faster. According to the data provided by ResNet [10], its detection speed is 31.54 ms and 156.44 ms, respectively.

Now the mainstream image semantic segmentation methods mainly focus on the improvement of network performance. Although the segmentation method based on deep convolution neural network has significantly improved the performance of image segmentation, it still faces a lot of computational overhead. However, for the real-time semantic segmentation method, the biggest concern is how to construct a real-time system with low delay. In order to solve this problem, many researchers have studied the lightweight image semantic segmentation model and summarized some experience, which is also reflected in our paper. For example, there are some achievements in the lightweight convolution structure, such as  $1 \times 1$  convolution, decomposition convolution, grouping convolution, and depth separation convolution.

### 3. Real-Time Semantic Segmentation Network Architecture

**3.1. Dual Channel Attention Mechanism Network.** Therefore, reducing the communication between high-level and low-level feature maps is the most effective way to improve their fusion efficiency. Inspired by the GAU

TABLE 1: Classification performance of common network models.

| Network    | Layers | Top-1 error | Top-5 error | Speed (ms) |
|------------|--------|-------------|-------------|------------|
| VGG-16     | 16     | 27.00       | 8.80        | 128.62     |
| ResNet-18  | 18     | 30.43       | 10.76       | 31.54      |
| ResNet-101 | 101    | 22.44       | 6.21        | 156.44     |

attention module in PANet, we strengthen its performance and use it as part of the attention mechanism we proposed. The attention part of the upper channel is shown in Figure 2. GDAM is a structure that can be used to enhance acquisition ability of lower feature map. For high-level feature map, GDAM first uses average pooling and max pooling to reduce its resolution to  $1 \times 1$ . There is one more maximum pooling operation than the original GAU module. In paper [12], the authors proved that global average pooling is not the optimal choice for channel attention, and global maximum pooling will also extract some unique features of objects, which can infer more meaningful feature information. Then, combining BN and sigmoid function uses  $1 \times 1$  convolution to generate channel attention mask. For the low-level feature map, GDAM uses  $3 \times 3$  combining BN and ReLU convolution layer to optimize it; here  $3 \times 3$  convolution is combined with  $1 \times 3$  and  $3 \times 1$  convolution.

**3.2. DARSegNet Semantic Segmentation Model.** With the asymmetric encoder-decoder and the dual attention mechanism, the DARSegNet (deep asymmetric real-time semantic segmentation network model) is illustrated in Figure 3.

In this section, we first describe in detail our proposed segmented network DARSegNet. In addition, we also explain the effectiveness of these two paths accordingly. Finally, we show how to combine the features of these two



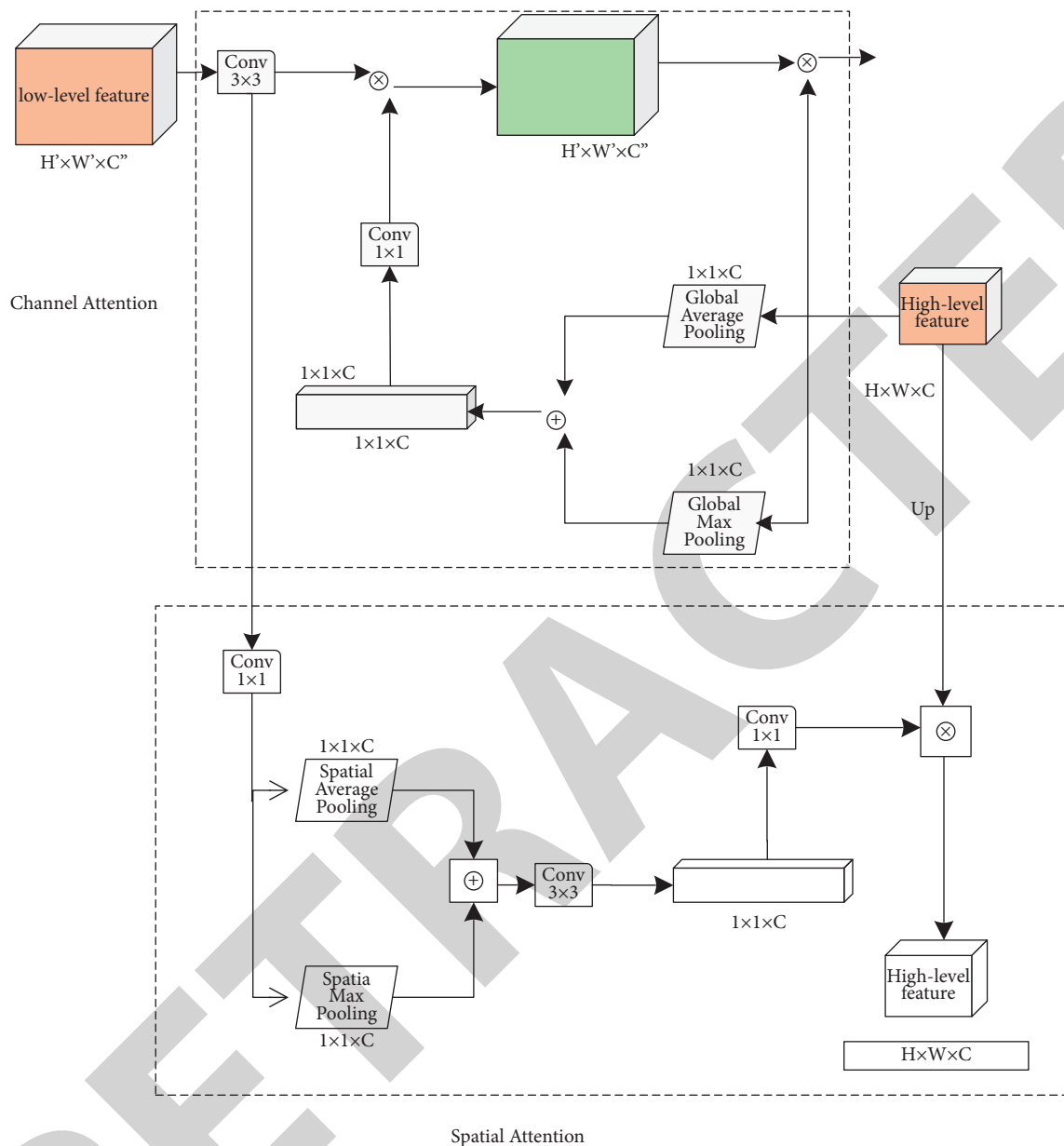


FIGURE 2: Dual channel attention mechanism network.

paths with the feature fusion module and the overall architecture of our DARSegNet.

DARSegNet combines the sequential and parallel structure of the general network model and can provide multiscale visualization. Because DARSegNet can provide multiscale processing of image features, it can effectively improve the accuracy of image segmentation. Compared with other segmentation methods, the hierarchical convolution module used in DARSegNet model can effectively reduce the depth of the network model and improve the coupling of the model under the condition of providing receptive fields of the same size. The global pooling layer in the model can effectively reduce the computational complexity and prevent overfitting in the training process. The module uses the attention mechanism, combined with the high-level and low-level features of the network and the

introduced supervision strategy to correct the wrong details in the features, which can obtain more accurate results in the image segmentation task.

The image segmentation model DARSegNet combines the sequential and parallel structure of the general network model and can provide multiscale visualization. Because DARSegNet segmentation model can provide multiscale processing of image features, it can effectively improve the accuracy of image segmentation. Compared with other segmentation methods, the hierarchical convolution module used in DARSegNet model can effectively reduce the depth of the network model and improve the coupling of the model under the condition of providing receptive fields of the same size. The global pooling layer in the model can effectively reduce the computational complexity and prevent overfitting in the training process. The module uses the attention

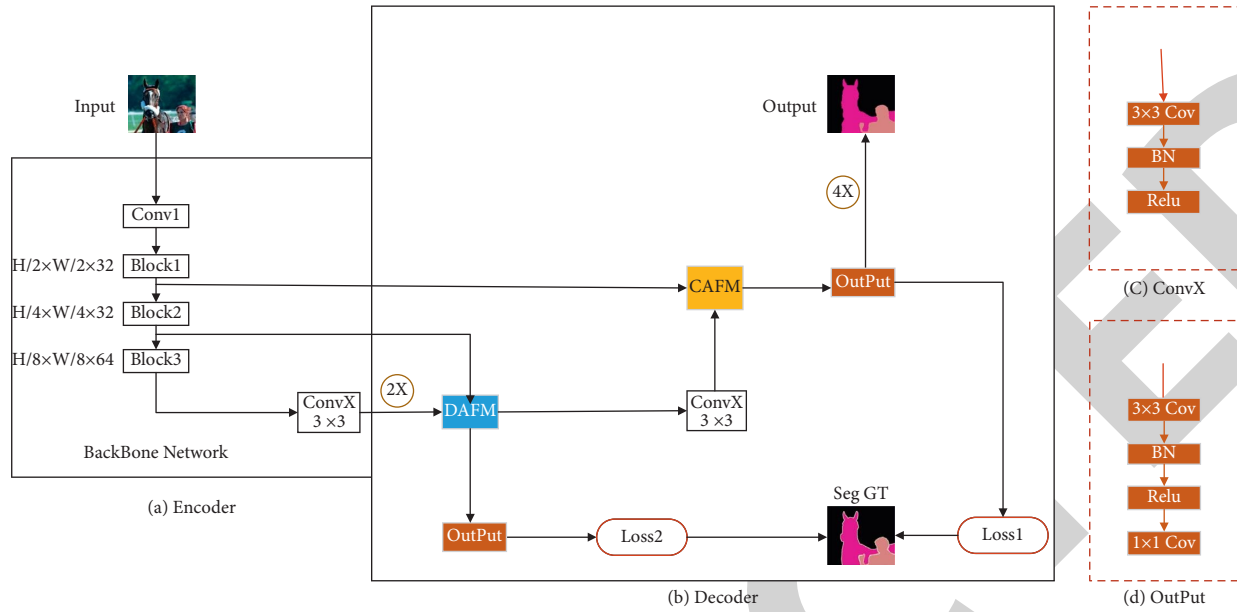


FIGURE 3: The architecture of the asymmetric encoder-decoder and attention mechanism of the semantic segmentation model.

mechanism, combined with the high-level and low-level features of the network and the introduced supervision strategy to correct the wrong details in the features, which can obtain more accurate results in the image segmentation task.

The encoder-decoder model is improved, the basic network structure of the encoder module is redesigned, and the feature extraction ability of the encoder is improved. On the one hand, an asymmetric convolution block (ACB) is connected behind each convolution of the backbone network. On the other hand, combining several atrous convolutions [13] with different expansion rates, according to the idea of dense connection, a dense atrous spatial pyramid pooling (DASPP) module is proposed; that is, ACB and DASPP together constitute the encoder for feature extraction. In order to improve the efficiency of the decoder to fuse high-level feature maps, a dual channel attention decoder (DCAM) is proposed, which can significantly reduce the information gap between high-level and low-level feature maps by using the attention mechanism and provide guarantee for the accurate fusion of high-level and low-level feature maps. Experimental results show that the proposed network and module can significantly improve the segmentation accuracy of the network [14].

After summarizing the above, combined with our proposed feature processing module, this paper proposes a new asymmetric encoder network model DARSegNet. The model in this chapter combines the general sequential and parallel structure and can provide multiple scales of visual domain. Therefore, the method in this chapter provides a feature of multiscale processing, which effectively improves the accuracy of the algorithm. In addition, compared with other methods, the hierarchical convolution module of the segmentation model in this chapter effectively reduces the depth of the network model when providing the same size of receptive field. The global pooling layer included in the model effectively reduces the computational overhead and

prevents the training from overfitting. The module uses the hop connection strategy, combined with the characteristics of the lower layer of the network and the strategy of intermediate supervision to correct the wrong details in the features, so as to get more precise and accurate results in image segmentation.

The encoder-decoder model is improved, the basic network structure of the encoder module is redesigned, and the feature extraction ability of the encoder is improved. On the one hand, asymmetric convolution blocks (ACBs) are connected behind each convolution in the backbone. On the other hand, combining several ATOS convolutions with different expansion rates, according to the idea of dense connection, a dense atrous (dilated) spatial pyramid pool (DASPP) module is proposed; that is, ACB SegNet and DASPP together constitute an encoder for feature extraction. In order to improve the efficiency of the decoder in fusing high-level feature maps, a dual channel attention decoder (DCAM) is proposed. The decoder uses the attention mechanism to significantly narrow the information gap between high-level and low-level feature maps, which provides a guarantee for the accurate fusion of high-level and low-level feature maps. The experimental results show that the proposed network and module can significantly improve the segmentation accuracy of the network.

**3.3. Loss Function.** We also use the auxiliary loss function to supervise the training of DARSegNet. In order to make the semantic segmentation model converge effectively, similar to PSPNet [15], the model proposed adding supervision information in the backbone network; that is, additional auxiliary loss function is introduced to supervise and learn the initial segmentation results generated by the model. The auxiliary loss function and the main loss function of the final segmentation result use loss function, as shown in formula

(4). Softmax function is shown in formula (1), pred is the prediction segmentation diagram,  $Y_t$  is the truth segmentation diagram, Cost (\*) represents the multivariate cross entropy loss function, and its definition is shown in formula (3), where  $n$  is the number of samples.

Loss function is an important part of convolution network. It is used to calculate the difference between the network prediction result and the true value, so as to update the network parameters through the back-propagation algorithm. The most widely used loss function in deep learning semantic segmentation is softmax cross entropy.

$$\text{soft max}(Z_i) = \frac{e^{z_i}}{\sum e^{z_j}}, \quad (1)$$

$$\text{Loss}(\text{pred}, Y_t) = \text{Cost}(\text{soft max}(\text{pred}), Y_t), \quad (2)$$

$$\text{Cost} = -\frac{1}{N} \sum_i ((1 - Y_t) \times \log(1 - \text{soft max}(\text{pred})) + Y_t \times \log(\text{soft max}(\text{pred}))). \quad (3)$$

In general, additional supervision in the model training stage can optimize the deep convolution neural network.

$$\text{Loss}_f = \alpha_1 \text{Loss}_1 + \alpha_2 \text{Loss}_2. \quad (4)$$

Here,  $\text{Loss}_f$ ,  $\text{Loss}_1$ , and  $\text{Loss}_2$ , respectively, represent the final loss, main loss, and auxiliary loss;  $\alpha_1$  and  $\alpha_2$  represent the balance parameters of main loss and auxiliary loss. According to a large number of experiments [5], when  $\alpha_1 = 1$  and  $\alpha_2 = 0.4$ ,  $\text{Loss}_f$  is the joint loss function.

## 4. Experiments

This section is the experimental part. We will introduce the effect of semantic segmentation, configuration environment, network structure, and experimental results.

**4.1. Experiment Environment.** Facebook developed the PyTorch framework based on Python and used the Python version of the torch library in image processing. The advantage is that it provides dynamic calculation diagrams, which means that images are generated at runtime and are easier to run on GPU. However, due to the short development time and lack of reference materials, it is still to be developed.

This paper selects the advanced PyTorch platform. The specific configuration is shown in Table 2.

This section makes relevant experiments on the Cityscapes [6] and CamVid [16] datasets and compares the performance with those of other advanced models. The software and hardware configuration of the experimental platform is shown in Table 2.

### 4.2. Datasets

**Cityscapes.** It contains 2975 images for training, 500 images for verification, and 1525 images for testing. It has 19 dense pixel annotations. Cityscapes is a new large-scale dataset

TABLE 2: Real-time image semantic segmentation model environment.

| Item                 | Configuration         |
|----------------------|-----------------------|
| OS                   | Ubuntu 16.04          |
| CPU                  | Intel Core i7 4790K   |
| GPU                  | GeForce 1080TI 11 GB  |
| RAM                  | 32 G                  |
| Framework            | PyTorch 1.6           |
| Programming language | Python 3.6            |
| GPU acceleration     | CUDA 10.2/cuDNN 7.6.5 |

containing street scenes from 50 different cities. In addition to 20000 weak annotation frames, it also contains 5000 high-quality pixel level annotation frames [6].

**CamVid.** CamVid (the Cambridge driving labeled video database) dataset was released by the Engineering Department of Cambridge University in 2008. It is the first video set with target category semantic tags. It is the first video dataset containing semantic labels of object classes. It is selected from driving videos taken during the day and dusk. It contains 701 color images and notes of 11 semantic classes. The dataset consists of four video clips, each of which contains an average of 5000 frames with a resolution of  $720 \times 960$  pixels, about 40 K frames [16].

### 4.3. Parameter Setting

**Cityscapes Setting.** Following [5], the SGD optimizer with initial learning rate of 0.01, momentum of 0.9, and weight attenuation of 0.0001 is used in this paper. The learning strategy with power of 0.9 is adopted to reduce the learning rate, and data enhancement methods including random clipping image, random scaling from 0.5 to 2.0, and random horizontal flip are used. The image is randomly cropped to  $1024 \times 1024$  for training following [5]. We use the linear warmup strategy, from  $0.1 \times \text{lr}$  (learning rate) to  $1 \times \text{lr}$  which only works in the previous 5000 iterations.

**CamVid Setting.** The initial learning rate is 0.001, and models are trained in 968 stages. The image is randomly cropped to  $960 \times 720$  pixels for subsequent training stages. Other settings followed Cityscapes.

**4.4. Analysis of Network Training Process.** This section mainly analyzes the network training process of DARSegNet model and introduces and analyzes the loss rate, MIoU, and PA in the network training process of DARSegNet in the Cityscapes dataset.

**4.4.1. Loss Rate Analysis of the Network Model.** During the training on the Cityscapes dataset, the change of loss rate of DARSegNet model can be seen in Figure 4, in which the blue one indicates the change of loss rate.

The network convergence process is stable. In the first 10,000 iterations, the loss rate of the DARSegNet network model decreases rapidly and steadily, and the network model

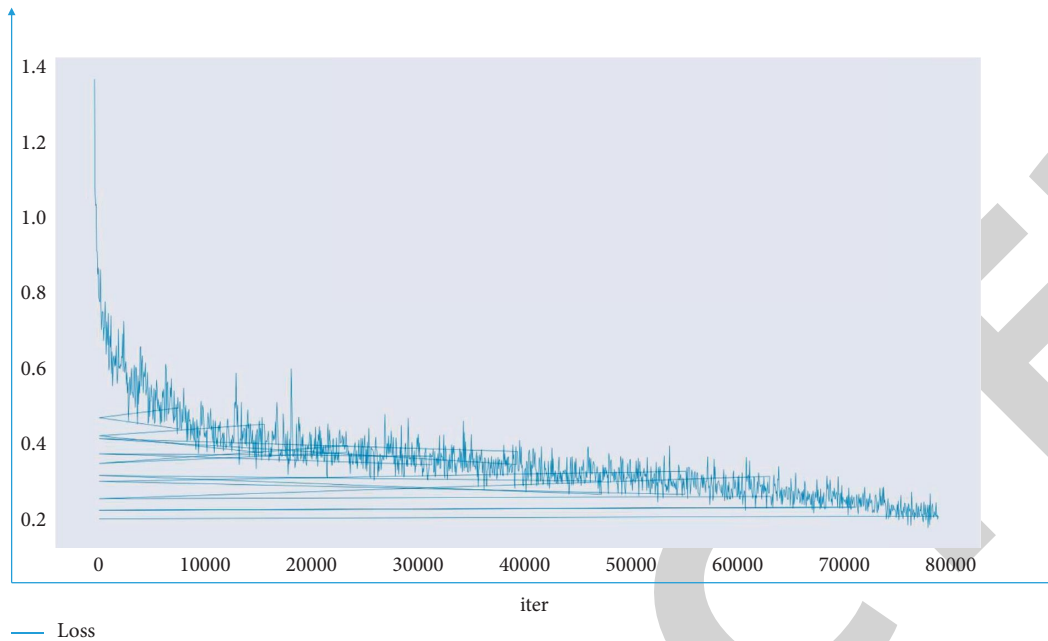


FIGURE 4: Decline curve of loss rate during network training.

converges quickly. During 10,000 to 18,000 iterations, the loss rate drop of the network model slows down rapidly. In the process of 18,000 to 20,000 iterations, the loss rate of the model fluctuates greatly. After 20,000 iterations of the model, the loss rate slowly decreased in the oscillation. At 70,000 epochs, the loss rate of the training model was about 0.20, and then the loss rate dropped to about 0.10. After 80,000 iterations, the loss value stabilized, and the loss rate hardly decreased.

**4.4.2. Network Model MIoU Analysis.** The network model has carried out 100,000 iterations in total. Around 25,000 iterations, MIoU fluctuates slightly, which is consistent with the time of loss value oscillation of loss rate in Figure 5. After that, MIoU increased rapidly and the effect was good. From 59,000 iterations to 60,000 iterations, MIoU rose very slowly in the shock, and, after the shock, MIoU began to stabilize. Near 80,000 iterations, MIoU increases to about 72%. In the process of 90,000 to 100,000 iterations, MIoU has only very small changes and tends to be stable as a whole. After 100,000 iterations, the MIoU value tends to be stable and hardly decreases, and the MIoU value is about 75%. It can be seen from the trend of the curve in Figure 5 that the MIoU of the network model rises rapidly in the early stage, the convergence speed of the model is good and tends to be stable in the later stage, there is no obvious large fluctuation, and finally it stabilizes at about 75%.

**4.4.3. Pixel Accuracy Analysis of the Network Model.** On the Cityscapes dataset, the changes of the pixel accuracy in the training are shown in Figure 6.

The network model has carried out 100,000 iterations in total. Around 25,000 iterations, MIoU fluctuates slightly, which is consistent with the time of loss value oscillation of

loss rate in Figure 6. After that, MIoU increased rapidly and the effect was good. From 59,000 iterations to 60,000 iterations, MIoU rose very slowly in the shock, and, after the shock, MIoU began to stabilize. Near 80,000 iterations, MIoU increases to about 72%. In the process of 90,000 to 100,000 iterations, MIoU has only very small changes and tends to be stable as a whole. After 100,000 iterations, the MIoU value tends to be stable and hardly decreases, and the MIoU value is about 75%. It can be seen from the trend of the curve in Figure 6 that the MIoU of the network rises rapidly in the early stage, the convergence speed of the model is good and tends to be stable in the later stage, there is no obvious large fluctuation, and it finally stabilizes at about 75%.

The pixel accuracy of the network model increases rapidly. Although there is a small fluctuation in the middle, the pixel accuracy is stable around 0.948 in the end.

On the Cityscapes dataset, the comparisons of accuracy, speed, and parameters of some lightweight segmentation model are shown in Table 3.

Using a single GTX 1080Ti GPU card, with 32 G memory, DARSegNet achieves 75.53% MIoU and carries out image segmentation test at the speed of 70 FPS. In the Cityscapes test set, its performance is better than that of the current SOTA BiSeNet V2, with an increase of 0.8%, respectively, while the number of parameters is reduced by about 23%, and FPS is nearly twice that. The visualization of image segmentation results is shown in Figure 7.

**4.4.4. Comparative Analysis of Experiments on the CamVid Dataset.** It can be seen that the method proposed in this paper also achieves competitive accuracy and speed on CamVid dataset and realizes a good balance between accuracy and speed. As shown in Table 4, DARSegNet achieves 73.96% MIoU and 109 FPS test speed.

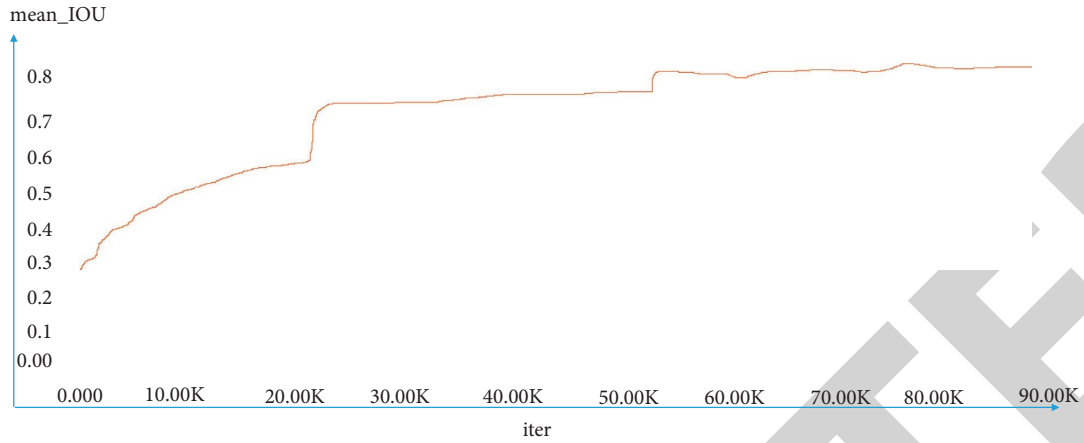


FIGURE 5: Changes of MIoU during training.

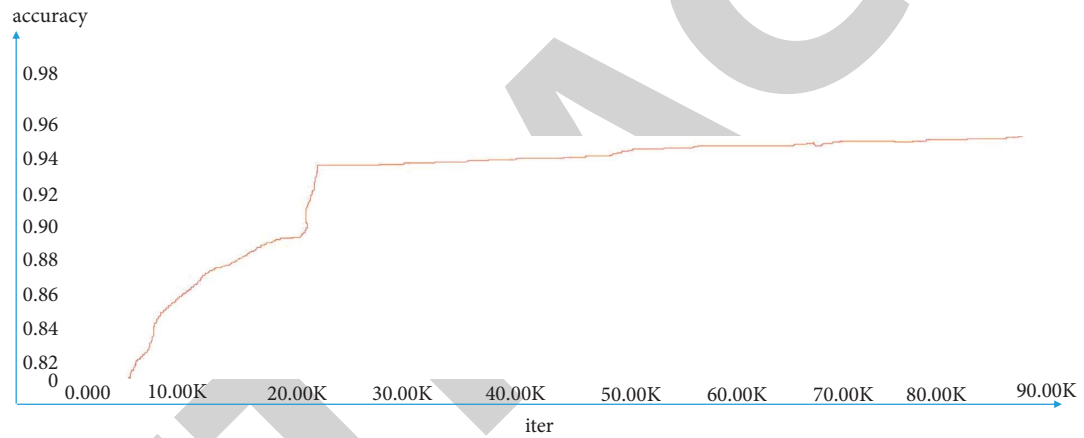


FIGURE 6: Changes in pixel accuracy during training.

TABLE 3: Comparison on cityscapes test set.

| Method           | Pretraining | GPU      | MIoU        | Speed (FPS) | Params |
|------------------|-------------|----------|-------------|-------------|--------|
| SegNet           | ImageNet    | TitanX   | 56.1        | 15          | 29.5 M |
| ENet             | No          | TitanX   | 58.3        | 31          | 0.36 M |
| ESPNet           | No          | TitanX   | 60.3        | 113         | 0.36 M |
| CGNet            | No          | 1080Ti   | 64.8        | 17          | 0.50 M |
| ContextNet       | ImageNet    | 1080Ti   | 66.1        | 18          | 0.85 M |
| EDANet           | No          | 1080Ti   | 67.3        | 81          | 0.68 M |
| ERFNet           | No          | 1080Ti   | 68.0        | 42          | 2.10 M |
| BiseNet          | ImageNet    | 1080Ti   | 68.4        | 106         | 5.80 M |
| ICNet            | ImageNet    | TitanX M | 69.5        | 30          | 7.80 M |
| DABNet           | No          | 1080Ti   | 70.1        | 28          | 0.80 M |
| BiSeNet V2       | No          | 1080Ti   | 73.4        | 156         | 49M    |
| BiSeNet V2-L     | No          | 1080Ti   | <b>75.8</b> | 47.3        | NULL   |
| DARSegNet (ours) | No          | 1080Ti   | 75.49       | 69.3        | 4.15 M |
| DARSegNet (ours) | ImageNet    | 1080Ti   | 75.53       | 69.5        | 4.15 M |

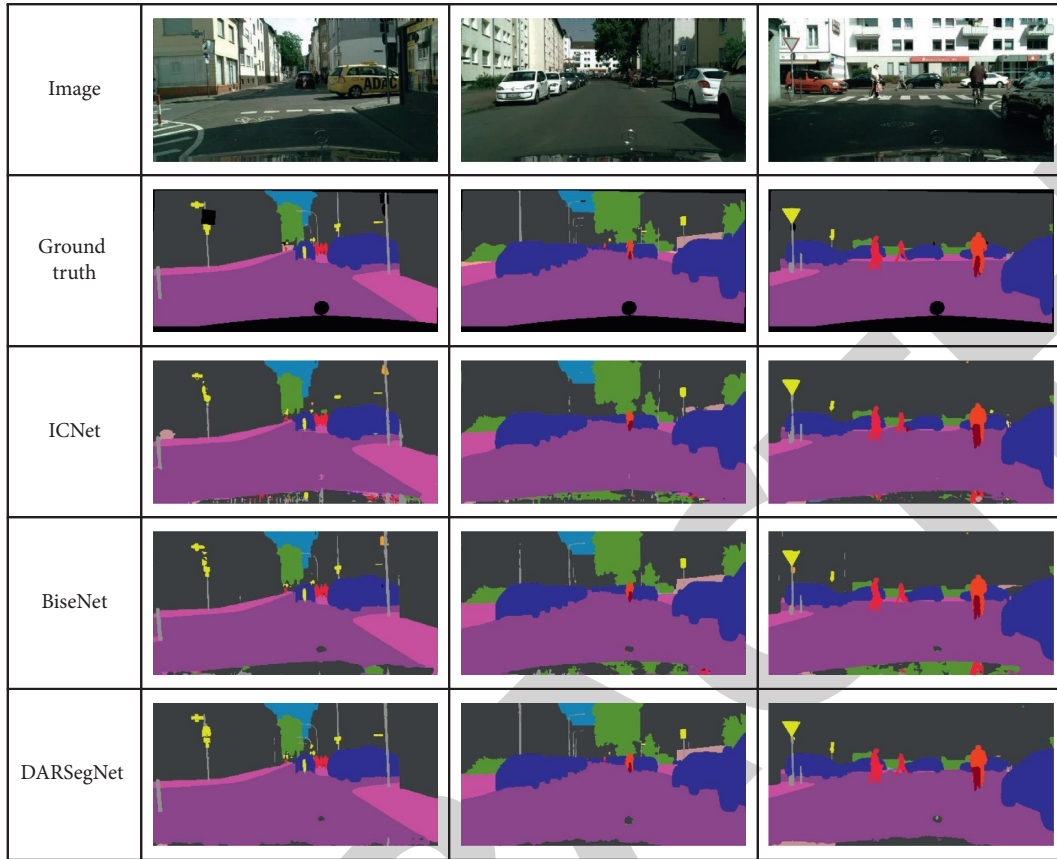


FIGURE 7: Visualization results on the Cityscapes test set.

TABLE 4: Comparison of accuracy, speed, and parameters of the lightweight segmentation model on the CamVid test set.

| Method           | Pretraining | GPU      | MIOU (%) | Speed (FPS) |
|------------------|-------------|----------|----------|-------------|
| SegNet           | ImageNet    | TitanX   | 55.6     | 15          |
| ENet             | No          | TitanX   | 51.3     | 61.2        |
| BiSeNet          | ImageNet    | 1080Ti   | 65.6     | 175         |
| ICNet            | ImageNet    | TitanX   | 67.1     | 34.5        |
| SFNet (DF2)      | No          | 1080Ti   | 70.4     | 134         |
| CAS              | No          | Titan Xp | 71.2     | 169         |
| BiSeNet V2       | No          | 1080Ti   | 68.7     | 116         |
| BiSeNet V2       | No          | 1080Ti   | 73.2     | 32.7        |
| SwiftNet         | No          | 1080Ti   | 72.6     | 75.9        |
| DARSegNet (ours) | No          | 1080Ti   | 73.27    | 109         |
| DARSegNet (ours) | ImageNet    | 1080Ti   | 73.96    | 109         |

The best results in each class are shown in bold.

According to the setting of [5], the split network model is trained with a combined dataset consisting of training set and validation set. The MIOU is measured using the test set. To test the running speed of the network, an image with a size of  $720 \times 960 \times 3$  resolution was input to each network, and the FPS of each network was measured.

## 5. Conclusions

In this paper, we propose an effective real-time semantic segmentation network model for asymmetric encoder and decoder. This segmentation result is efficient and in

real time and has been recognized. We improve the performance by using asymmetric encoder structure and dual attention module, increasing the receptive field of backbone network. We introduce a novel attention mechanism to increase the accuracy of semantic segmentation without losing local details and balance the speed. The real-time segmentation performance is verified by several experiments in the Cityscapes and CamVid datasets. We also propose a lightweight decoder module, which has better performance than the ordinary decoder. The next research will focus on improving the generalization performance.

## Research Article

# Research on Prediction of Physical Fitness Test Results in Colleges and Universities Based on Deep Learning

Jiwen Wang,<sup>1</sup> Binghui Wu,<sup>1</sup> Yun Jiang,<sup>2</sup> and Yidan Yuan<sup>3</sup> 

<sup>1</sup>Shijiazhuang Information Engineering Vocational College, Shijiazhuang 050000, Hebei, China

<sup>2</sup>Shanghai Open University Minhang Branch, Shanghai 201100, China

<sup>3</sup>The Department of Basic Education, Shanghai Urban Construction Vocational College, Shanghai 201415, China

Correspondence should be addressed to Yidan Yuan; [yuanyidan@succ.edu.cn](mailto:yuanyidan@succ.edu.cn)

Received 31 March 2022; Revised 5 May 2022; Accepted 17 May 2022; Published 6 June 2022

Academic Editor: Man Fai Leung

Copyright © 2022 Jiwen Wang et al. This is an open access article distributed under the Creative Commons Attribution License, which permits unrestricted use, distribution, and reproduction in any medium, provided the original work is properly cited.

All-round development strategy of quality education makes primary and secondary school students not only pursue the improvement of achievement but also carry out physical exercise. Physical training is the material basis for students to study other disciplines, and the core is to improve students' own physical quality and increase their physique. Having a strong body helps students have certain physical strength to study in other courses. In recent years, in the background of the scientific era, college students in China obviously have some problems, such as insufficient awareness of physical exercise and serious decline in physical fitness. Nowadays, teenagers are addicted to games and go out to become members of the low-headed people. Nowadays, it is very unhealthy for teenagers to go out with their mobile phones as "low-headed people." In order to avoid college students getting rid of this living condition, colleges and universities carry out physical fitness tests every year to promote contemporary college students to strengthen exercise. College students, as the main force in the future construction of the motherland, should not only master professional knowledge but also improve their physical fitness. Good health is the greatest capital in one's life. Every year, some students fail to pass the physical fitness test in universities. It stands to reason that college students are in the age of high youth, and physical fitness test should be a piece of cake for them. In the face of the inconsistency between the predicted results and the actual results, this paper analyzes this. Based on the above situation, With the aim of improving students' training efficiency and physical performance, the physical performance prediction model of deep learning is designed and analyzed to predict the performance, analyze the influencing factors of the model and how to reduce the influencing components of the factors, and analyze and compare the performance of various prediction models to find out the best model, so as to make the predicted value closer to the true value.

## 1. Introduction

Contemporary college students in China are the main force in revitalizing the Chinese nation and improving comprehensive national strength, and their physical quality is closely related to the prosperity and development of the country. Digital storytelling, student engagement, and deep learning are applied to geography [1]. This study aims to provide insight into the usefulness of integrating digital stories in teaching and learning activities in Geography in higher education [1]. Using convolution neural network, ion current is decoded in high-dimensional feature space, which can visually reflect the hidden signal of rapid

translocation movement of objects in nanoscale catheter [2]. Deep learning classifies galaxy morphology into 3-way and 4-way CNNs [3]. In Deep Merge-II, robust deep learning algorithms are constructed for cross-domain merger galaxy identification [4]. The paper aims to address the tracking algorithm based on deep learning and four deep learning tracking models developed [5]. This paper presents a literature survey and discusses how SOA can be enabled by as well as can facilitate the use of deep learning approaches in different types of environments for different levels of users [6]. Deep learning reduces blindness due to retinopathy of prematurity [7]. In publisher correction, a convolutional neural network is used to convert tabular

data into images for deep learning [8]. We believe that deep learning technology-based systems will be on the front line of monitoring and investigation of microorganisms [9]. Deep learning is the automatic segmentation of middle skull base structures in augmented navigation [10]. Deep learning is an artificial intelligence (AI) function that imitates the workings of the human brain in processing data and creating patterns for use in decision making. Deep learning is a subset of machine learning in artificial intelligence that has networks capable of learning unsupervised from data that are unstructured or unlabeled, and it also known as deep neural learning or deep neural network [11]. We present a comprehensive exploration of the use of GPU-based hardware acceleration for deep learning inference within the data reconstruction workflow of high energy physics [12]. Application of deep learning is detection of obsolete scaphoid fractures with artificial neural networks [13]. Deep learning now accurately predicts physicochemical properties of peptides from their sequence, including tandem mass spectra and retention time [14]. This reiterates the idea that even if ML/DL algorithms are trained to make some hydrologic predictions accurately, they must be designed and trained to provide each user-required output if their results are to be used to improve our understanding of hydrologic systems [15]. Deep learning methods are applied to genotype data to predict eye color and type-2 diabetes phenotypes [16]. Deep learning and machine learning are applied to sketch image retrieval [17]. Time series and deep learning algorithms are applied to predict the gold price in India [18]. The article considers the possibilities of using the deep learning convolutional neural network ResNet in computer vision and image classification problems [19]. The differences and common points are abstract from the classification, and it is found that there are sensitive points in the counter disturbance, and the fluctuation of the sensitive points affects the classification of the deep learning model [20]. A systematic literature search was undertaken of the Web of Science, PubMed, Cochrane Library, and Embase, with an emphasis on the deep learning-based diagnosis of precancerous lesions in the upper GI tract. The status of deep learning algorithms in upper GI precancerous lesions has been systematically summarized [21]. This paper also discusses the challenges and expected future trends in the application of deep learning to heart sounds classification with the objective of providing an essential reference for further study [22]. Supervised multitask deep learning with convolutional neural networks (CNNs) on frontal chest radiographs was able to predict many underlying patient comorbidities represented by hierarchical condition categories (HCCs) from the International Classification of Diseases, Tenth Revision, including those corresponding to diabetes with chronic complications, morbid obesity, congestive heart failure, cardiac arrhythmias, and chronic obstructive pulmonary disease [23]. This article reviews deep learning applications in biomedical optics with a particular emphasis on image formation [24].

## 2. The Importance of Physical Quality Education

*2.1. Physical Training.* Physical fitness is the material basis of energy output based on the three functional systems of human body, and physical fitness is improved through repeated movements of skeletal muscles. Physical training is an important part of sports training, which is divided into general physical training and special physical training. General physical training is the basis of special physical training. Physical training refers to improving the basic quality, extension ability, and sports level of the body to make it a skill of the trainees. The core task is to strengthen one's own physique, improve the technical level of physical training projects, and obtain high scores. The fundamental purpose is to promote college students to take physical exercise, improve their life types, and make them develop good exercise habits. Its core significance lies in participating in training to improve their physical fitness and improve the performance level of physical fitness test, so as to achieve the three views of shaping their own posture, cultivating good temperament, and establishing positive and healthy in this process. This paper takes college students as the main body, including archery, yoga, running, rope skipping, and other sports training.

*2.2. Sports Attitude.* In fact, the formation of sports attitude is that people get their own sports concepts and corresponding lifestyles under the environment of social development by observing the imitation of people's actions around them. Among them, sports attitude is mainly to learn from other people's life experience as a third party to gain their own insights. Sports attitude is parents' expectation for their children's physical training. First, parents' actual support attitude towards children's physical training, parents' and children's motivation to participate in sports together, the attitude of parents to support their children's sports equipment, the guidance and support of parents to their children's sports events, and the process support attitude of parents to their children's physical training during the epidemic. Second, the different attitudes include the attitude support of parents accompanying together, the different attitude support of unilateral parents accompanying, and the potential attitude support of children participating alone. It also explores the direct attitude relationship between children's performance and parents accompanying in physical training outside school. Third, the linkage attitude includes the attitude synergy between parents and their children's education, There are four aspects of sports attitude support: attitude adjustment of children's mutual assistance and growth in peer relationship, attitude guidance of teacher-student relationship to children's physical education assistance, attitude integration of family relationship in parent-child relationship, and attitude coordination of family and society synergy in parent-coach relationship.



### 3. Prediction Algorithm and Model

**3.1. Logistic Regression Model.** Logistic regression is based on linear regression model with sigmoid function, and the output value is the same as the input value.

Sigmoid function is as follows:

$$f(z) = \frac{1}{1 + e^{-z}}. \quad (1)$$

The conditional probability calculation formula is as follows:

$$p(Y = 1|x) = \frac{\exp(w \cdot x + b)}{1 + \exp(w \cdot x + b)}, \quad (2)$$

$$p(Y = 0|x) = \frac{1}{1 + \exp(w \cdot x + b)}.$$

The input training set is as follows:

$$D = \{(x_1, y_1), (x_2, y_2), \dots, (x_n, y_n)\}, \quad (3)$$

where the likelihood function of  $x_i \in R$ ,  $x_i \in \{0, 1\}$  is as follows:

$$\prod_{i=1}^n [\psi(x_i)]^{y_i} [1 - \psi(x_i)]^{1-y_i}. \quad (4)$$

Logarithmic expression of the above function is as follows:

$$L(w) = \log \left\{ \prod_{i=1}^n [\psi(x_i)]^{y_i} [1 - \psi(x_i)]^{1-y_i} \right\}, \quad (5)$$

$$= \sum_{i=1}^n [y_i \log \pi(x_i) + (1 - y_i) \log (1 - \pi(x_i))].$$

The final model result is as follows:

$$p(Y = 1|x) = \frac{\exp(\hat{w} \cdot x + b)}{1 + \exp(\hat{w} \cdot x + b)}, \quad (6)$$

$$p(Y = 0|x) = \frac{1}{1 + \exp(\hat{w} \cdot x + b)}.$$

**3.2. KNN Classification Algorithm.** KNN judges whether the new target prediction point belongs to this category by calculating the existing sites closest to it and the category to which the most sites belong.

The characteristics in the sample set are as follows:

$$x = (x^1, x^2, \dots, x^m). \quad (7)$$

The Euclidean distance between samples is as follows:

$$d(x^1, x^2) = \sqrt{\sum_{i=1}^m (x_1^i - x_2^i)^2}. \quad (8)$$

The shortest distance sample of 1 is as follows:

$$X\{X_1, X_2, X_{k1}\} = \min_{k1} (d(x_i, y)). \quad (9)$$

Quantity in each category is as follows:

$$W_y = \{n_1, n_2, L, n_w\}. \quad (10)$$

Its maximum value is as follows:

$$\max W_y = n_{\max}. \quad (11)$$

**3.3. Support Vector Regression Model.** Assume that the training data set is  $D = \{(x_1, y_1), (x_2, y_2), \dots, (x_n, y_n)\}$ .

Expression of planning problem is as follows:

$$\min \frac{1}{2} w^2 + C \sum_{i=1}^n \delta_i. \quad (12)$$

Constraints are as follows:

$$\text{s.t. } y_i (w \cdot x_i + b) \geq 1 - \delta_i, \quad \delta_i \geq 0, 1, \dots, n. \quad (13)$$

Introducing Lagrange multipliers and transforming them into dual problems,

$$\min L(w, b, a) = \frac{1}{2} \sum_{i=1}^n \sum_{j=1}^n a_i a_j y_i y_j (x_i \cdot x_j) - \sum_{i=1}^n a_i. \quad (14)$$

Constraints are as follows:

$$\text{s.t. } \sum_{i=1}^n a_i y_i = 0, \quad 0 \leq a_i \leq C, \quad i = 1, 2, \dots, n. \quad (15)$$

The optimal solution problem is transformed into the optimal solution:

$$w = \sum_{i=1}^n a_i y_i x_i, \quad (16)$$

$$b = y_j - \sum_{i=1}^n y_i a_i (x_i \cdot x_j).$$

The optimal hyperplane obtained is

$$f(x) = \text{sign} \left( \sum_{i=1}^n a y_i (x_i \cdot x_j) + b \right). \quad (17)$$

Output real value as

$$y_j = \sum_{i=1}^n a y_i (x_i \cdot x_j) + b. \quad (18)$$

**3.4. Deep Neural Network.** The structure of the deep neural network is shown in Figure 1.

The input of each moving track is enhanced after summation, and the correlation function is as follows.

The Sigmoid activation function takes the form of

$$f(z) = \frac{1}{1 + \exp(-z)}. \quad (19)$$

The corresponding derivative function is

$$f'(z) = f(z)(1 - f(z)). \quad (20)$$

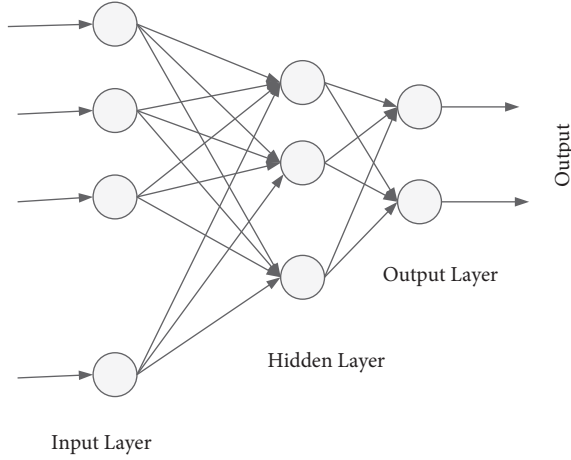


FIGURE 1: Structure diagram of deep neural network.

The Tanh activation function takes the form of

$$f(z) = \tanh(z) = \frac{e^z - e^{-z}}{e^z + e^{-z}}. \quad (21)$$

The corresponding derivative function is

$$f'(z) = 1 - (f(z))^2. \quad (22)$$

The ReLU activation function takes the form of

$$f(z) = \max(0, z). \quad (23)$$

The corresponding derivative function is

$$f'(z) = \begin{cases} 1, & z > 0, \\ 0, & z \leq 0. \end{cases} \quad (24)$$

## 4. Experiment

### 4.1. Influence of Various Factors on Model Performance

**4.1.1. Effect of Quantity Set on Model Performance.** In this experiment, the ADMF model is trained on the above three data sets. Data set 1 represents the experimental results of 5 skipping groups, data set 2 represents the experimental results of 5 archery groups, and data set 3 represents the experimental results of 10 running groups. The analysis of the above results shows that on the three data sets, the more data, the better the prediction effect of the ADMF model. The experimental results of the ADMF model on three data sets are shown in Figure 2.

In the data set, the physical performance of 5 groups of students participating in different projects is randomly selected to predict the prediction accuracy of the model, as shown in Table 1.

**4.1.2. Influence of Physical Fitness on Model Performance.** Self-physical quality is an important feature that affects physical performance. Therefore, in this experiment, different students' physical quality and the potential characteristics of different courses have different weights and

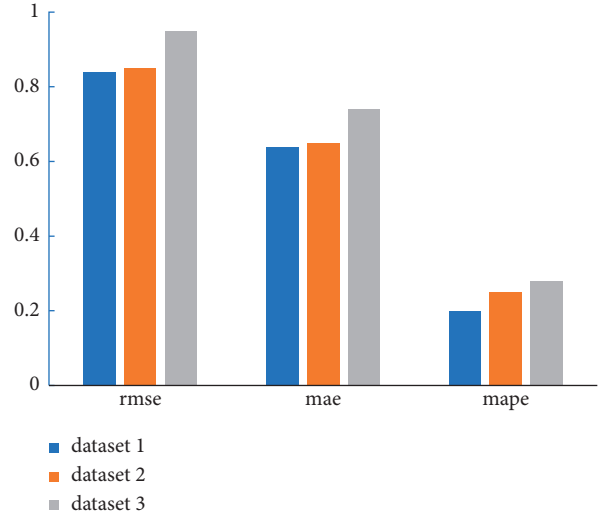


FIGURE 2: Prediction effect of different data sets.

TABLE 1: Comparison of predicted and true values.

| Group | Sports             | Predicted value (%) | Actual value (%) |
|-------|--------------------|---------------------|------------------|
| 1     | 3 km long-distance | 90.12               | 88.3             |
| 2     | Running            | 92.2                | 89.1             |
| 3     | 100-meter sprint   | 93.1                | 90.2             |
| 4     | Skipping rope      | 95.21               | 91.1             |
| 5     | Archery yoga       | 94.23               | 89.7             |

TABLE 2: Comparison of experimental results.

| Method | Rmse  | Mae   | Mape  |
|--------|-------|-------|-------|
| Dmf    | 1.503 | 1.106 | 0.564 |
| Admf   | 1.266 | 0.872 | 0.255 |

different influences on students' performance. The experimental results are compared with those in Table 2.

The data in the above table are counted into a two-dimensional bar chart, as shown in Figure 3.

**4.1.3. Effect of Liking for Sports Events on Model Performance.** Different students have different affection for sports events, which also has certain influence on the performance of the model. We study and analyze the performance of the model with three different affection degrees: special affection, general affection, and disaffection. The experimental results are as shown in Table 3.

The data in the above table are counted into a two-dimensional bar chart, as shown in Figure 4.

### 4.2. Model Comparison

**4.2.1. Effect of Activation Function on Model.** Because this paper is a combined and single-structure model and because ReLU and Tanh are better applied in the deep learning

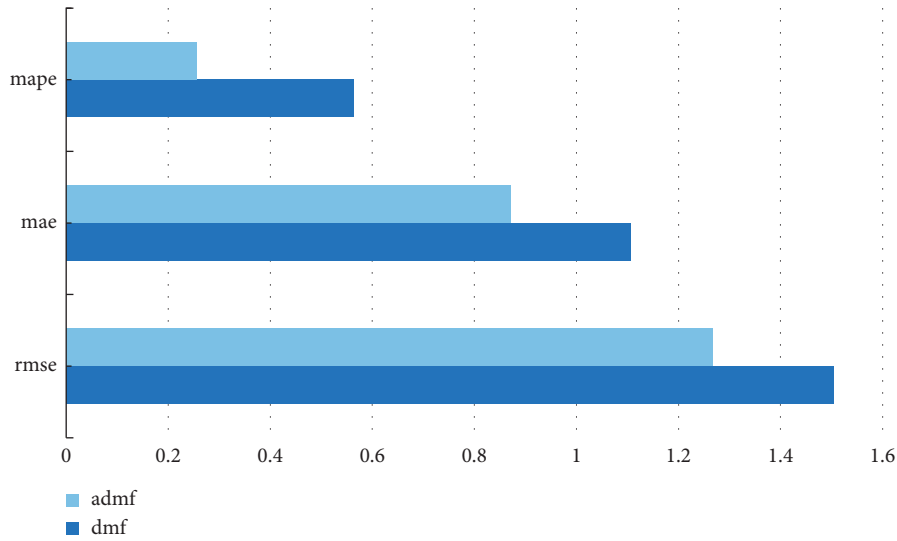


FIGURE 3: Comparison of experimental results.

TABLE 3: Comparison of experimental results.

| Degree of liking  | Rmse  | Mae   | Mape  |
|-------------------|-------|-------|-------|
| Especially liking | 1.208 | 0.886 | 0.332 |
| Generally like    | 1.084 | 0.621 | 0.219 |
| Dislike           | 0.651 | 0.449 | 0.105 |

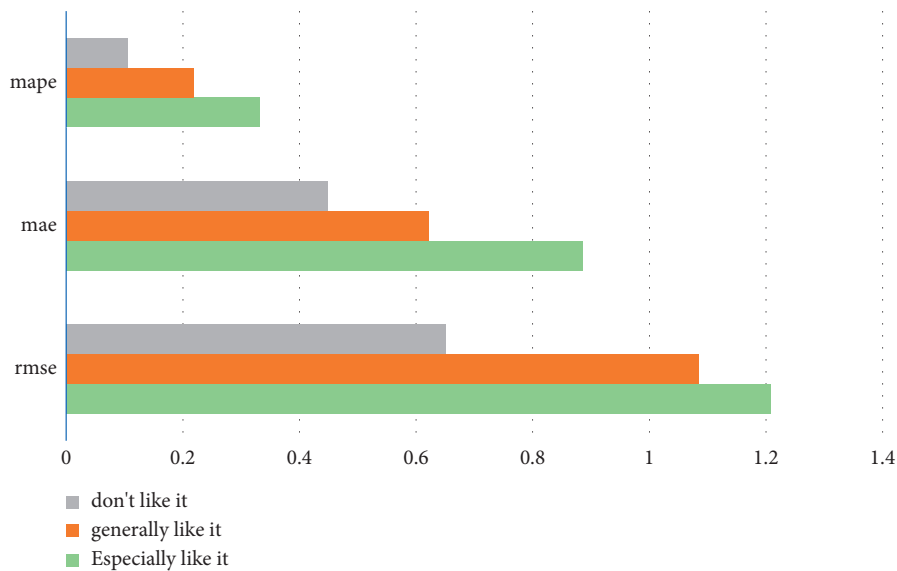


FIGURE 4: Comparison of experimental results.

TABLE 4: Comparison of the prediction of skipping rope by the number of activated culverts.

| Activation function | Accuracy | Precision | Recall | F1    | AUC   |
|---------------------|----------|-----------|--------|-------|-------|
| Tanh                | 0.912    | 0.886     | 0.923  | 0.752 | 0.802 |
| ReLU                | 0.890    | 0.885     | 0.943  | 0.771 | 0.819 |

TABLE 5: Comparison of prediction of archery events by activation function.

| Activation function | Accuracy | Precision | Recall | F1    | AUC   |
|---------------------|----------|-----------|--------|-------|-------|
| Tanh                | 0.932    | 0.876     | 0.915  | 0.789 | 0.823 |
| ReLU                | 0.880    | 0.885     | 0.945  | 0.799 | 0.854 |

TABLE 6: Comparison of prediction of running events by activation function.

| Activation function | Accuracy | Precision | Recall | F1    | AUC   |
|---------------------|----------|-----------|--------|-------|-------|
| Tanh                | 0.905    | 0.891     | 0.941  | 0.738 | 0.844 |
| ReLU                | 0.911    | 0.902     | 0.952  | 0.747 | 0.865 |

TABLE 7: Comparison of yoga project prediction by activation function.

| Activation function | Accuracy | Precision | Recall | F1    | AUC   |
|---------------------|----------|-----------|--------|-------|-------|
| Tanh                | 0.918    | 0.876     | 0.954  | 0.763 | 0.802 |
| ReLU                | 0.895    | 0.892     | 0.949  | 0.799 | 0.819 |

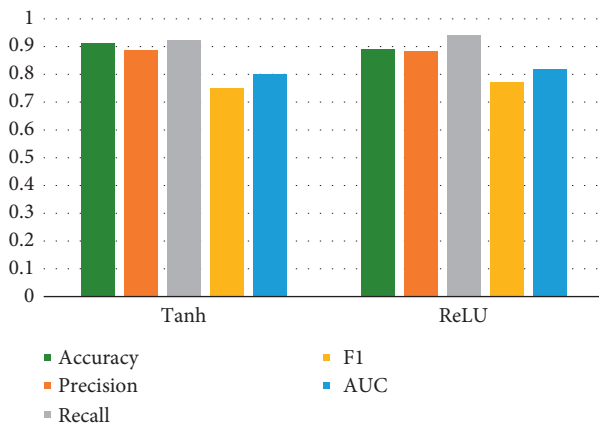


FIGURE 5: Comparison diagram of activation function.

TABLE 8: Comparison results of hidden layer number on skipping project prediction.

| Number of layers | Accuracy | Precision | Recall | F1   | AUC  |
|------------------|----------|-----------|--------|------|------|
| 1                | 0.75     | 0.86      | 0.95   | 0.91 | 0.81 |
| 2                | 0.76     | 0.85      | 0.94   | 0.88 | 0.82 |
| 3                | 0.61     | 0.65      | 0.73   | 0.72 | 0.69 |

model, this experiment only compares the hidden layer neuron activation function with ReLU activation function and Tanh activation function. The experimental results of the prediction model for skipping rope, archery, running, and yoga by activation function are shown in Tables 4–7.

The data comparison table of the overall impact of the two activation functions on the four projects is counted as a bar chart, as shown in Figure 5.

TABLE 9: Comparison results of hidden layer number on archery project prediction.

| Number of layers | Accuracy | Precision | Recall | F1   | AUC  |
|------------------|----------|-----------|--------|------|------|
| 1                | 0.74     | 0.86      | 0.92   | 0.88 | 0.81 |
| 2                | 0.76     | 0.85      | 0.84   | 0.85 | 0.82 |
| 3                | 0.68     | 0.65      | 0.85   | 0.78 | 0.69 |

TABLE 10: Contrast results of prediction of running events by hidden layer number.

| Number of layers | Accuracy | Precision | Recall | F1   | AUC  |
|------------------|----------|-----------|--------|------|------|
| 1                | 0.77     | 0.86      | 0.95   | 0.98 | 0.86 |
| 2                | 0.73     | 0.88      | 0.86   | 0.88 | 0.84 |
| 3                | 0.75     | 0.75      | 0.73   | 0.87 | 0.76 |

TABLE 11: Comparative results of hidden layer number on yoga project prediction.

| Number of layers | Accuracy | Precision | Recall | F1   | AUC  |
|------------------|----------|-----------|--------|------|------|
| 1                | 0.78     | 0.68      | 0.85   | 0.95 | 0.83 |
| 2                | 0.79     | 0.73      | 0.87   | 0.90 | 0.82 |
| 3                | 0.68     | 0.75      | 0.88   | 0.72 | 0.79 |

4.2.2. Influence of the Number of Hidden Layers on the Model. For DNN and PNN single-segment neural networks, we set the number of hidden layers and the number of neurons in each layer to be the same and change the number of hidden layers. The experimental results of the prediction model of hidden layer number for skipping rope, archery, running and yoga are shown in Tables 8–11:

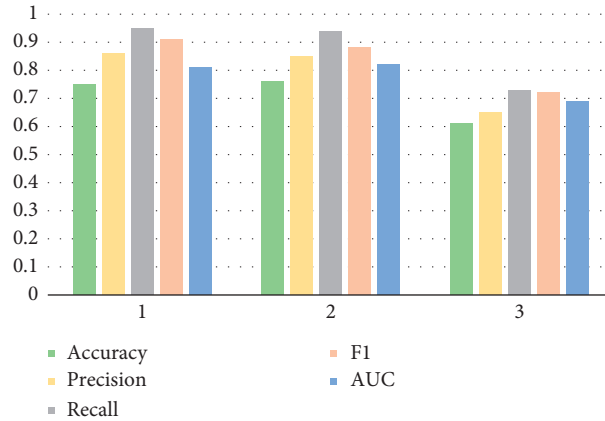


FIGURE 6: Contrast diagram of hidden layer number.

TABLE 12: Structural comparison.

| Structure | Accuracy | Precision | Recall | F1    | AUC   |
|-----------|----------|-----------|--------|-------|-------|
| FM        | 0.813    | 0.861     | 0.891  | 0.791 | 0.815 |
| DNN       | 0.824    | 0.854     | 0.882  | 0.832 | 0.824 |
| DeepFM    | 0.841    | 0.860     | 0.883  | 0.814 | 0.803 |
| PNN       | 0.852    | 0.866     | 0.873  | 0.853 | 0.815 |
| DNN + PNN | 0.887    | 0.871     | 0.838  | 0.856 | 0.887 |
| FM + PNN  | 0.876    | 0.875     | 0.841  | 0.814 | 0.882 |
| FDPN      | 0.868    | 0.882     | 0.859  | 0.816 | 0.792 |

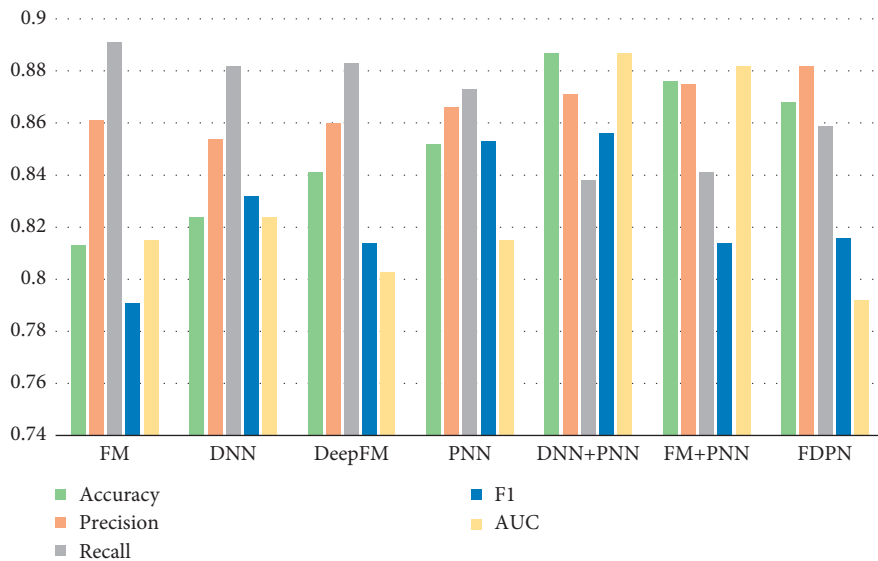


FIGURE 7: Structural comparison diagram.

Compare the overall model performance indicators of the above projects with different hidden layers, such as Figure 6.

4.2.3. *Influence of Model Structure on Model.* In this paper, seven mixed structures are used to predict the results of physical fitness test. In this experiment, we compare different feature combinations and observe the influence of

structure on model performance. The experimental results are shown in Table 12.

According to the influence of different structures on the model, it is compared and counted into a bar chart, as shown in Figure 7.

4.3. *Contrast Experiment.* The model presented in this chapter is compared with the traditional methods used in predicting students' physical performance including KNN,

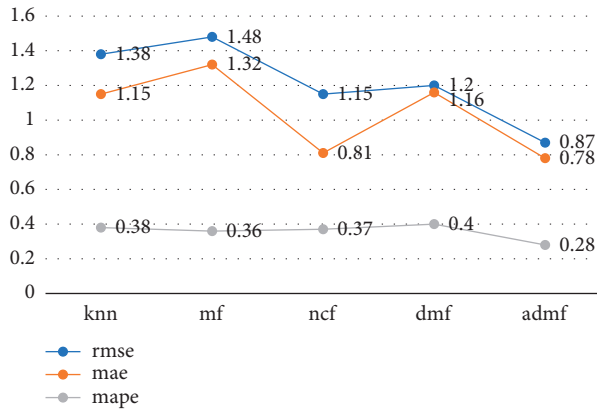


FIGURE 8: Comparison diagram of prediction algorithms.

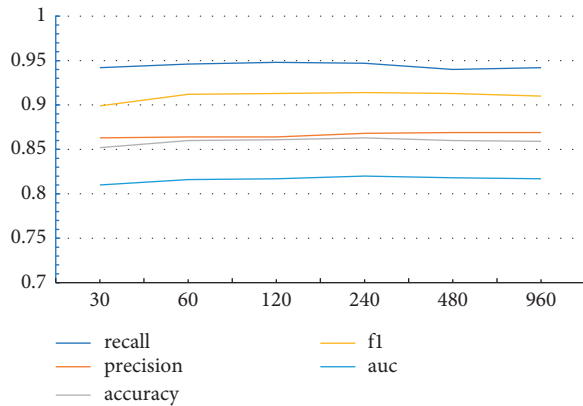


FIGURE 9: Influence of different parameters on FDPN.

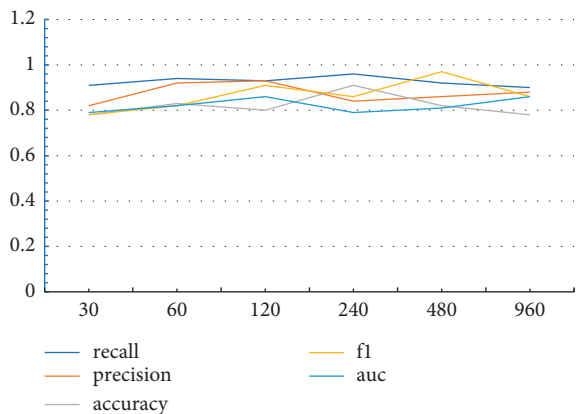


FIGURE 10: Influence of different parameters on DNN + PNN.

MF, NCF, and DMF. The test was carried out on the sample set, and the final experimental results are shown in Figure 8.

Different parameters affect the performance of FDPN, DNN + PNN, and FM + PNN models. Through a large number of experiments with different neuron numbers, the learning comparison of students' physical fitness

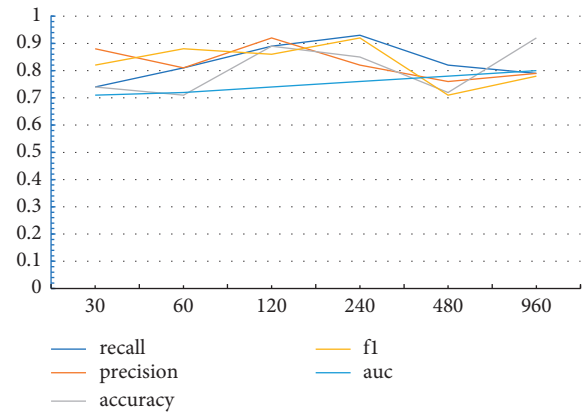


FIGURE 11: Influence of different parameters on FM + PNN.

performance prediction models is obtained, as shown in Figures 9–11.

## 5. Conclusion

With the development of social intelligence, our research on the prediction of students' physical performance has made great significance in the aspects of accurate management and scientific decision making. This paper discusses a variety of prediction models to study and analyze the prediction of physical fitness test scores in colleges and universities. The results are as follows:

- (1) In the experiment of the influence of data set on the model, the amount of training data in data set 2 and data set 3 is obviously lower than that in data set 1. The analysis of the above results shows that on the three data sets, the more data, the better the prediction effect of the ADMF model.
- (2) Taking students' physical quality and students' love for sports as independent variables, students with good physical quality and love for sports will naturally have better physical test scores.
- (3) In the comparative experiment, we select different numbers of neurons to carry out the experiment. It can be seen that when it comes to deep neural network training, the number of neurons needs to be continuously compared by model training and learning, and the optimal number of neurons should be selected.
- (4) In the experiment of exploring the influence of model structure on the model, the results show that the effect of single structure is slightly worse, and the combined feature learning of two structures is slightly better than that of single structure. The FDPN model has a good prediction effect and can improve the performance of performance prediction.

## Data Availability

The experimental data used to support the findings of this study are available from the corresponding author upon request.

## Conflicts of Interest

The authors declare that they have no conflicts of interest regarding this work.

## References

- [1] A. Wally and A. Jørund, "Digital storytelling, student engagement and deep learning in Geography," *Journal of Geography in Higher Education*, vol. 45, no. 3, pp. 380–396, 2021.
- [2] T. Makusu, "Back cover: deep learning-enhanced nanopore sensing of single-nanoparticle translocation dynamics (small methods 7/2021)," *Small Methods*, vol. 5, no. 7, 2021.
- [3] M. K. Cavanagh, K. Bekki, and B. A. Groves, "Morphological classification of galaxies with deep learning: comparing 3-way and 4-way CNNs," *Monthly Notices of the Royal Astronomical Society*, vol. 506, no. 1, pp. 659–676, 2021.
- [4] A. Ćiprijanović and D. K. Kafkes, "DeepMerge-II. Building robust deep learning algorithms for merging galaxy identification across domains," *Monthly Notices of the Royal Astronomical Society*, vol. 506, no. 1, pp. 677–691, 2021.
- [5] E. Kiyak and G. Unal, "Small aircraft detection using deep learning," *Aircraft Engineering & Aerospace Technology*, vol. 93, no. 4, pp. 671–681, 2021.
- [6] C. K. W. Dickson, "A review on the integration of deep learning and service-oriented architecture," *Journal of Database Management*, vol. 32, no. 3, pp. 95–119, 2021.
- [7] D. M. Moshfeghi and M. T. Trese, "Reducing blindness resulting from Retinopathy of prematurity using deep learning," *Ophthalmology*, vol. 128, no. 7, pp. 1077–1078, 2021.
- [8] Y. Zhu and T. F. Brettin, "Publisher Correction: Converting tabular data into images for deep learning with convolutional neural networks," *Scientific Reports*, vol. 11, no. 1, Article ID 14036, 2021.
- [9] Y. Zhang and H. T. M. Jiang, "Deep learning for imaging and detection of microorganisms," *Trends in Microbiology*, vol. 29, no. 7, pp. 569–572, 2021.
- [10] C. A. Neves and E. D. Tran, "Deep learning automated segmentation of middle skull-base structures for enhanced navigation," *International Forum of Allergy & Rhinology*, vol. 11, no. 12, pp. 1694–1697, 2021.
- [11] I. Mohammad, "Introduction to deep learning," *International Journal of Swarm Intelligence and Evolutionary Computation*, vol. 10, no. 6, 1 page, 2021.
- [12] J. Krupa, "GPU coprocessors as a service for deep learning inference in high energy physics," *Machine Learning: Science and Technology*, vol. 2, no. 3, 2021.
- [13] A. P. Yoon and K. C. Chung, "Application of deep learning: detection of obsolete scaphoid fractures with artificial neural networks," *Journal of Hand Surgery*, vol. 46, no. 8, pp. 914–916, 2021.
- [14] J. G. Meyer, "Deep learning neural network tools for proteomics," *Cell Reports Methods*, vol. 1, no. 2, Article ID 100003, 2021.
- [15] M. A. Moghaddam and P. A. Ferre, "Can deep learning extract useful information about energy dissipation and effective hydraulic conductivity from gridded conductivity fields?" *Water*, vol. 13, no. 12, 1668 pages, 2021.
- [16] M. Muhammad and H. Andreas, "Correction to: Eye-color and Type-2 diabetes phenotype prediction from genotype data using deep learning methods," *BMC Bioinformatics*, vol. 22, no. 1, 319 pages, 2021.
- [17] D. Sivasankaran, "Sketch based image retrieval using deep learning based machine learning," *Regular issue*, vol. 10, no. 5, pp. 79–86, 2021.
- [18] P. S. Shankar and M. K. Reddy, "Forecasting gold Prices in India using time series and deep learning algorithms," *Regular issue*, vol. 10, no. 5, pp. 21–27, 2021.
- [19] K. E. Tokarev, "Convolutional neural network of deep learning in computer vision and image classification problems," *IOP Conference Series: Earth and Environmental Science*, vol. 786, no. 1, 2021.
- [20] Z. Chang, "Research and implementation of deep learning counter attack defense strategy," *Journal of Physics: Conference Series*, vol. 1952, no. 3, 2021.
- [21] T. Yan, P. K. Wong, and Y. Y. Qin, "Deep learning for diagnosis of precancerous lesions in upper gastrointestinal endoscopy: a review," *World Journal of Gastroenterology*, vol. 27, no. 20, pp. 2531–2544, 2021.
- [22] W. Chen and Q. X. Sun, "Deep learning methods for heart sounds classification: a systematic review," *Entropy*, vol. 23, no. 6, 667 pages, 2021.
- [23] A. Pyrros, A. E. Flanders, and J. M. Rodríguez-Fernández, "Predicting prolonged hospitalization and supplemental oxygenation in patients with COVID-19 infection from ambulatory chest radiographs using deep learning," *Academic Radiology*, vol. 28, no. 8, pp. 1151–1158, 2021.
- [24] L. Tian and B. M. Hunt, "Deep learning in biomedical optics," *Lasers in Surgery and Medicine*, vol. 53, no. 6, pp. 748–775, 2021.

## Research Article

# Deep Learning for Chinese Language Sentiment Extraction and Analysis

Zhu Zhu 

*School of Education, Yunnan Open University, Kunming 650500, China*

Correspondence should be addressed to Zhu Zhu; zhuzhu@ynou.edu.cn

Received 30 March 2022; Revised 20 April 2022; Accepted 26 April 2022; Published 2 June 2022

Academic Editor: Man Fai Leung

Copyright © 2022 Zhu Zhu. This is an open access article distributed under the Creative Commons Attribution License, which permits unrestricted use, distribution, and reproduction in any medium, provided the original work is properly cited.

In recent years, vocabulary emotion processing has become immensely popular and the requirements for language emotion analysis mining and processing have become significantly abundant. The sentiment extraction and analysis work has always been very challenging; especially, the Chinese word segmentation operation is difficult to deal with effectively, the multiple combinations of implicit and explicit words make the task of sentiment analysis mining more difficult, and, in particular, the efficiency of machine analysis of language sentiment is feeble. We use some expressions and sentiment vocabulary dictionaries combined with hybrid structures and use information synergy methods to get in touch with sentiment analysis methods. We use the relevant sentiment to evaluate the explicit or implicit emotional association of the emotional connection of the vocabulary and add the unique emotional word matrix to analyze the related clustering results of the emotional words to continuously optimize and upgrade the performance, so that our sentiment analysis results are systematic in terms of efficiency and significantly improved.

## 1. Introduction

In recent years, the processing of language vocabulary sentiment has gradually increased and sentiment analysis mining processing is an important source of reviewing the author's opinion and attitude. We focus on the study of the time span and causal connection of emotion. Combining the dual connection of time and causality, a corresponding data model can be established and emotional data analysis can be performed on it to predict related events. Using deep learning series algorithms to analyze data units such as image networks, statistical results are obtained. The algorithm operation of the convolutional network has become the preferred method in the application of analytical images. Metrics tuning of deep learning performance has huge benefits, enabling the perfect combination of flexibility and uniformity. We use POS (part of speech) tagging and maximum entropy (ME) modeling to develop text-based sentiment detection models to explore mutual sentimental connections between words and objective transactions and perform multiple analyses of word sentiment data.

## 2. Introduction to the CLSTM Model

The application of the LSTM model has the following advantages: (1) It is convenient for sequential modeling work. (2) The memory function of the model is relatively powerful, and it can carry out long-term memory. (3) The model implementation scheme is relatively simple. (4) It solves some problems of long sequences, such as gradient disappearing and exploding. The CLSTM model is a neural network prediction model based on deep learning. On the model's attention mechanism, it can quickly distinguish between regular words and analysis words with emotional tendencies and compare with the traditional LSTM model. Its advantages are used in time. It is more obvious, and the classification and analysis efficiency of vocabulary is greatly improved. The CLSTM model is constructed to realize the language emotion analysis of deep learning, improve the accuracy of emotion extraction and analysis, optimize the processing and analysis results, and then realize the function of language emotion analysis [1]. The CLSTM model is shown in Figure 1.



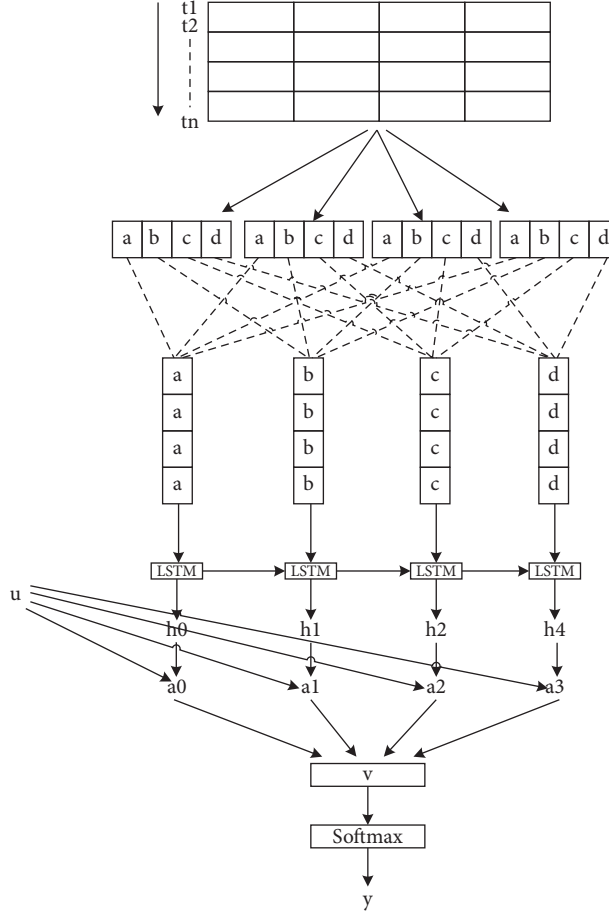


FIGURE 1: CLSTM model with attention mechanism.

**2.1. Calculation of the Model.** To realize the specific classification mechanism of the CLSTM algorithm, the specific implementation formula of the related algorithm is as follows:

$$T = (t_1, t_2, \dots, t_n), \quad (1)$$

$$i_t = \sigma(w_i \cdot [h_{t-1}, x_t] + b_i), \quad (2)$$

$$f_t = \sigma(w_f \cdot [h_{t-1}, x_t] + b_f), \quad (3)$$

$$O_t = \sigma(W_0 \cdot [h_{t-1}, X_t] + b_0), \quad (4)$$

$$\tilde{c}_t = \tan h(w_c \cdot [h_{t-1}, x_t] + b_c), \quad (5)$$

$$C_t = f_t \cdot C_{t-1} + i_t \cdot \tilde{C}_t, \quad (6)$$

$$h_t = o_t \cdot \tan h(c_t), \quad (7)$$

$$u_t = \tan h(w_s h_t + b_s), \quad (8)$$

$$a_t = \text{soft max}(u_t^T, u_s), \quad (9)$$

$$v = \sum_t a_t h_t, \quad (10)$$

$$y = \text{soft max}(v). \quad (11)$$

**2.2. Final Output of the Model.** The CLSTM model combines the advantages of CNN and LSTM. CNN effectively extracts the n-gram features of the text, and LSTM has the ability to effectively capture contextual information. The CLSTM model combines these two advantages and derives its own unique advantages and uses the unique neural network data elements to effectively distinguish text data [2].

Among them, in the convolution layer, feature maps have different color information; if feature maps have the same color, it means that the convolution kernel has selected a unified operation value, and the same color will be automatically spliced to form a new vector. At this time, we can get the matrix formula as

$$w = [C_1; C_2; \dots; C_n]. \quad (12)$$

“Semicolon” represents vector splicing, that is, a value obtained by the convolution behavior of different convolution kernels in the feature map, and the dotted line part represents the generation of a new vector. A filter  $f \in R^{m \times k}$  with a step size of 1 can completely get  $w \in R^{(n-m+1) \times n}$ ; then, we should apply the new vector and gradually input it into

the LSTM, and finally, the softmax layer can output the classification probability.

In the training set, the preprocessing operation is performed, the text is vectorized, and feature extraction is performed. Finally, through the system display of the model training, a suitable model is obtained for sentiment analysis of related language texts [3]. The left-path process is the preprocessing training work. We conduct research on the training model just because we need to test the optimal results of the algorithm, so we use the optimal algorithm model to output the formula. After the left-path training model is gradually formed, we can get the right-hand training set of the standard model. Therefore, the left-hand training model must be used to determine the best model, and then the right-hand process must be carried out. The operation process is shown in Figure 2.

As mentioned earlier, CNN can be combined with LSTM to form a new CLSTM model. Here, we also call it a CLSTM model that introduces residual connections. In the past, we may have encountered a series of problems, such as loss of network parameter update data or disappearance of vocabulary gradients, not to mention that better analytical work can be achieved after concatenating the residuals. The residual connection of the CLSTM model is shown in Figure 3.

$W_1$  is the text representation word vector, and the output-related features of the language can be expressed as  $C^i = \{C_1^i, C_2^i, \dots, C_n^i\}$ ; after the residual connection makes  $-w_{i-1}$  and  $c_i$  as the module input, the output is  $h^i = \{h_1^i, h_2^i, \dots, h_n^i\}$ , and the calculation formula is as follows:

$$h_j^i = C_j^i + w_j^{i-1}, \quad (j = 1, 2, 3, \dots, n). \quad (13)$$

### 3. Improvement of the CLSTM Model

The specific implementation of the superimposed application of this model is shown in Figure 4.

The superposition of the algorithm is used not to randomly perform mixed operations, but to find the comprehensive performance advantages of the superposition algorithm through specific applications. In Figure 4, what we need to add is the specific operation of the hybrid operation of the CLSTM algorithm and PML and experimental steps need to be added to reflect the effectiveness and superiority of its superposition algorithm.

**3.1. The PMI Model Algorithm Design.** Here, we add a reference to the degree of language lexical association and use the SO-PMI algorithm to calculate the emotional trend weighted value of language vocabularies, record the language emotion comparison differences of related vocabularies, and calculate whether the emotional correlation and the degree of connection are close [4]. The formula for calculating the similarity of language vocabulary is as follows:

$$\text{PMI}(w_1, w_2) = \log_2 \left( \frac{P(w_1 \& w_2)}{P(w_1)P(w_2)} \right). \quad (14)$$

Here,  $P(w_1 \& w_2)$  represents the probability of  $w_1$  and  $w_2$  appearing at the same time and  $P(w_1)P(w_2)$  represents the probability of  $w_1$  and  $w_2$  appearing alone. In fact,  $\text{PMI}(w_1, w_2) = \log_2(M \cdot df(w_1 \& w_2) / df(w_1)df(w_2))$  in the article is composed of the basic formula  $\text{PMI}(w_1, w_2) = \log_2(p(w_1 \& w_2) / p(w_1)p(w_2))$ , combined with  $p(\text{word}) = df(\text{word}) / M$ . In this formula,  $p(w_1 \& w_2)$  represents the probability of word 1 and word 2 appearing together and  $p(w_1)$  and  $p(w_2)$  represent the probability of each word appearing alone. The basic idea is to use statistical methods to calculate the common probability of two words appearing in a text, and the size of the probability reflects the degree of association between the two words.

After performing the SO-PMI algorithm, we can get the emotional tendency of the language emotion of words, which can be roughly divided into neutral words, positive words, and negative words. We then add and subtract weights to determine neutral words as 0, positive words as 1, and negative words as  $-1$  [5]. In general, if the final calculation result of the weight value is positive, the sentence can be judged to be a positive sentence; if the final calculation result of the weight value is negative, it can be judged that the sentence is a negative sentence. The algorithm can make sentiment analysis results more accurate than before in the application of word linking [6]. The implementation process is roughly as shown in Figure 5.

#### 3.2. Introduction of the Auxiliary Algorithm Formula

**3.2.1. Gradient Descent Algorithm.** In this paper, the gradient descent algorithm is used simply to solve the problem of the optimal solution of the vocabulary in the current gradient, and the algorithm will explore the optimal solution of the vocabulary along the negative direction of this gradient. With the deepening of the training of the deep learning model, the difficulty level and complexity of the vocabulary will gradually deepen. Therefore, we use the negative direction to explore, so that the loss function decreases the fastest. The Taylor calculation formula of the relevant  $f(x)$  is as follows:

$$f(x + a \vec{d}) = f(x_k) + a \vec{g}_k^T \vec{d} + o(a), \quad a > 0. \quad (15)$$

Here, the unit vector is  $\vec{d}$  and  $\theta$  is the angle between  $\vec{d}$  and  $-\vec{g}_k$ ; then,

$$\vec{g}_k^T \vec{d} = -\vec{g}_k \cos \theta. \quad (16)$$

When  $\theta = 0$ ,  $\vec{g}_k^T \vec{d}$  will reach the minimum value and the speed of  $f(x)$  will reach the maximum value.

The descent algorithm is shown in Figure 6.

**3.2.2. Sentiment Word Feature Formula Application.** A piece of text is composed of many words, so we say that words are the basis of text composition [7]. In particular, the emotional vocabulary that appears in the text will greatly affect the language emotional tendency of the entire sentence. The amount of emotional vocabulary has a great effect on the appeal of the language. We supplement the emotional

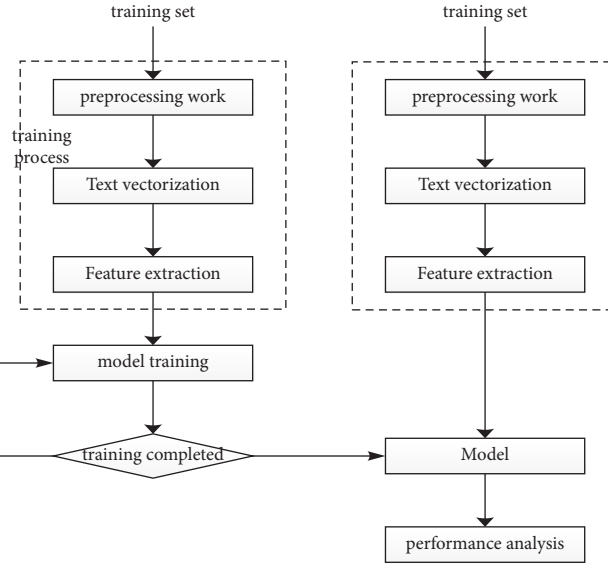


FIGURE 2: Text recognition sentiment analysis model process.

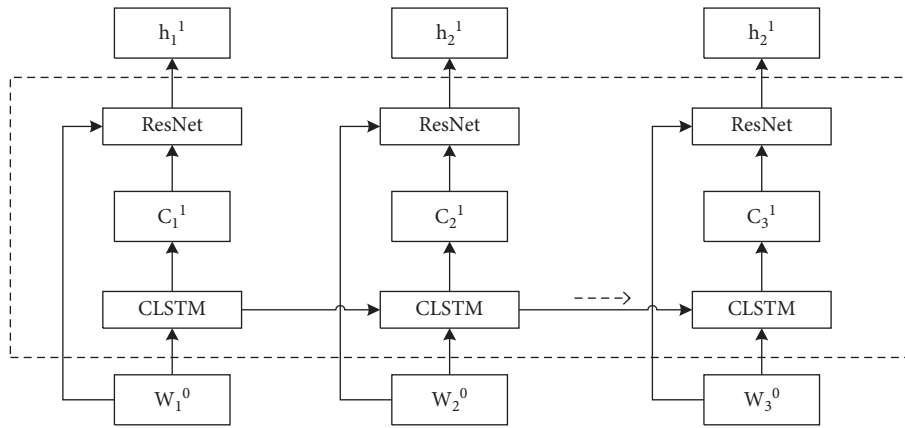


FIGURE 3: CLSTM model with residual connections.

dictionary here, which can make the emotional attribute  $f_{\text{sentiment}}(s_i)$  look like the following formula:

$$f_{\text{sentiment}}(s_i) = \frac{\sum_{k=1}^m \text{estimate}(\text{word}_{i,k})}{m}. \quad (17)$$

Here, word represents vocabulary,  $\text{word}_{i,k}$  is the  $k$ th word in the  $s_i$  sentence, and  $m$  represents the number of words. When  $\text{estimate}(\text{word}_{i,k}) = 0$ , the word is not an emotional word, and when  $\text{estimate}(\text{word}_{i,k}) = 1$ , the word is an emotional word. When using the relevant sentiment calculation formula, we can still add some auxiliary formulas, so on the basis of it, we have added the scoring formula calculation associated with it.

$$f_{\text{keyword}}(s_i) = \sum_{j=1}^n \text{keyword}(w_{ij}), \quad (18)$$

$$\text{keyword}(w_{ij}) = \begin{cases} 1; & w_{ij} \text{ a keyword,} \\ 0; & w_{ij} \text{ not a keyword.} \end{cases}$$

Here,  $w_{ij}$  represents the  $j$ th word in the sentence  $s_i$ ; we traverse it, and if it is a keyword, the feature score can be +1.

Of course, the analysis of all languages is inseparable from the huge language storage database. Under the relevant operations of deep learning, we use relevant equipment to remove language redundancy and extract relevant information [8]. After a series of word segmentation operations, the language is carried out. Sentiment classification, combined with the weighted value operation of the previous technology, can make a better judgment, so as to realize the extraction of the text language [9].

$w_c$  is the central reference vocabulary of the model application, which can effectively discriminate the context content  $w_o$  and make probabilistic analysis. The relevant formulas applied by the model are as follows:

$$P(w_o|w_c) = \frac{\exp(u_o^T v_c)}{\sum_{i \in V} \exp(u_i^T v_c)}. \quad (19)$$

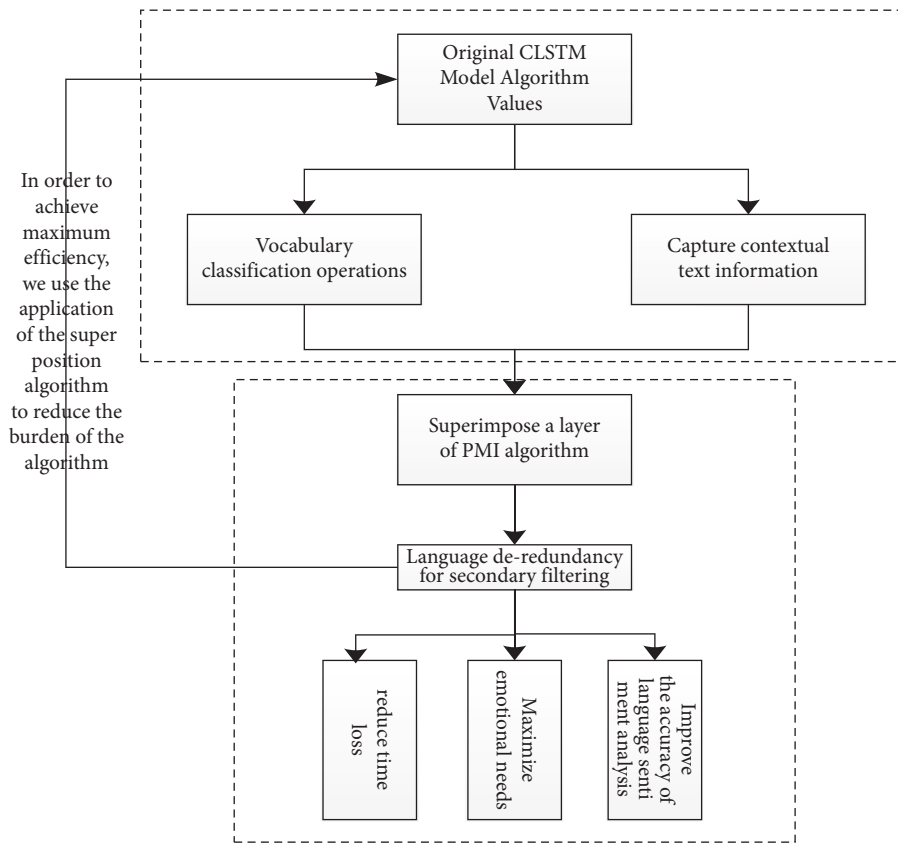


FIGURE 4: Superposition application of the CLSTM model algorithm.

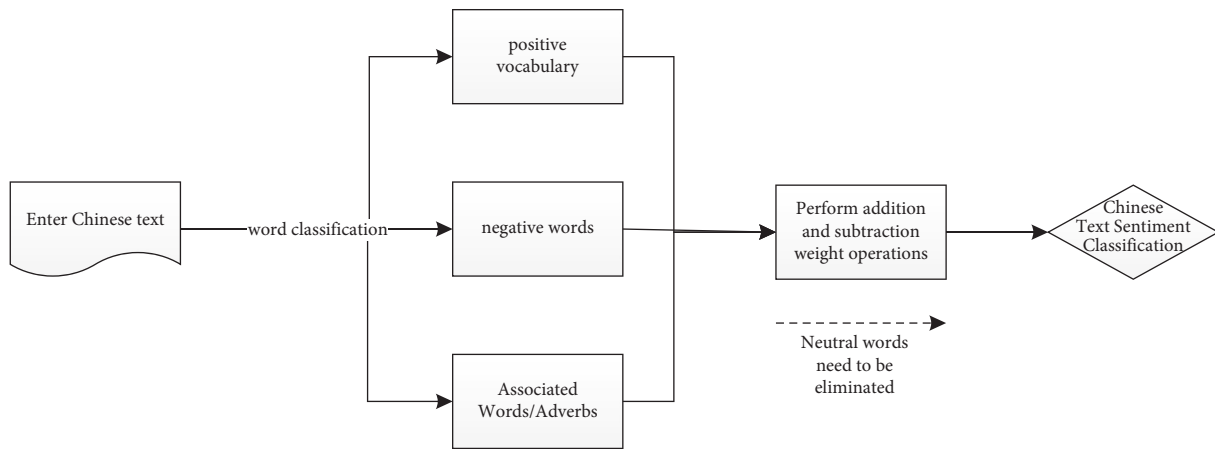


FIGURE 5: Flowchart of Chinese language emotion classification.

$v_c$  is the center word vector, and  $u_i$  is the background word vector. We can make the corresponding flow chart, as shown in Figure 7.

Extracting and analyzing common vocabulary and selecting this formula can restore the emotional data of the original text to the greatest extent.

$$p(x_i) = \left( \sqrt{\frac{Z(x_i)}{t}} + 1 \right) \times \frac{t}{Z(x_i)} = \sqrt{\frac{t}{Z(x_i)}} + \frac{t}{Z(x_i)}. \quad (20)$$

$x_i$  represents the original vocabulary,  $Z(x_i)$  represents the probability that the sampled vocabulary is extracted

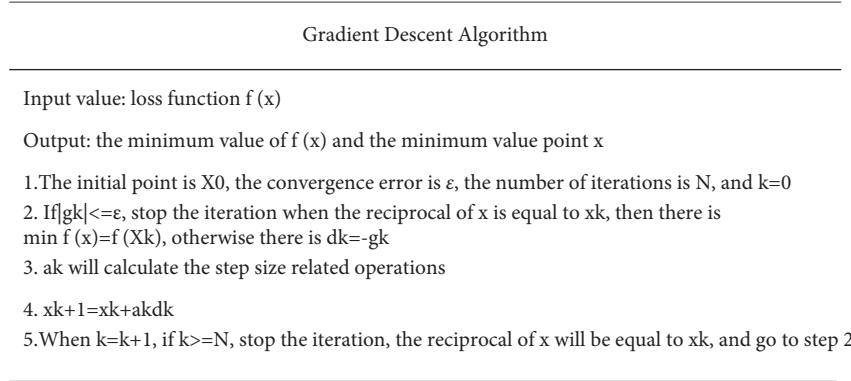


FIGURE 6: The detailed process of the gradient descent algorithm.

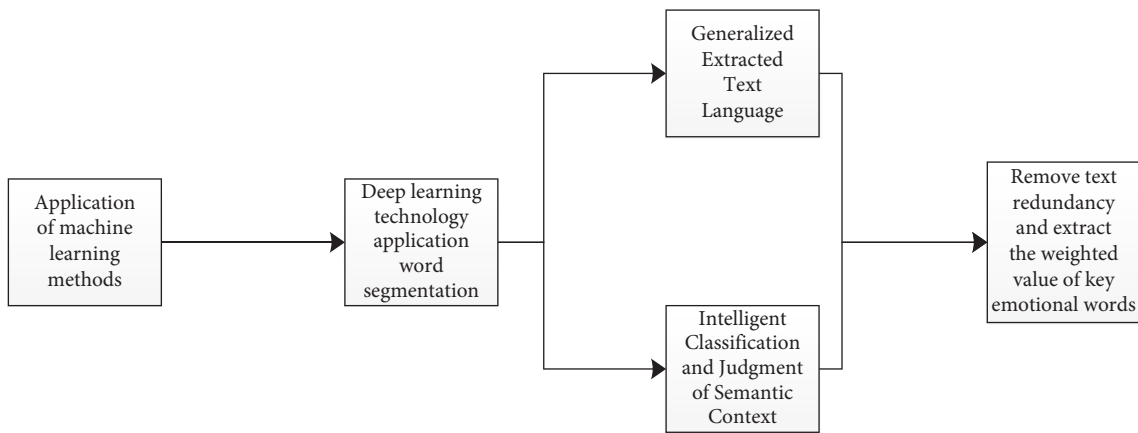


FIGURE 7: De-redundancy exclusion operation of machine learning.

from the entire data set, and  $t$  is the threshold of the sampled vocabulary, which is 0.001 by default. The larger the value unit, the greater the difference in the sampling probability. For the same vocabulary, the larger the  $t$  value, the greater the probability of the sampled value being deleted [10].

**3.3. Actual SO-PMI Algorithm Operation.** We can introduce relevant calculation algorithms of the probability theory. Assuming that the total number of text data is  $M$ , what we need to count is the specific number of text words, that is to say, the frequency problem in the text data set [11]. We can set it as  $df(\text{word})$ , which has the corresponding probability calculation formula of

$$p(\text{word}) = \frac{df(\text{word})}{M}. \quad (21)$$

Then, we can convert the SO-PMI algorithm to the formula, and the new word similarity calculation formula can be obtained as

$$\text{PMI}(w_1, w_2) = \log_2 \left( \frac{M \cdot df(w_1 \& w_2)}{df(w_1)df(w_2)} \right). \quad (22)$$

In this calculation, we use the base 2 logarithmic formula, so that the statistical result is always between 0 and 1,

so the similarity of words can be easily expressed. If the PMI value is greater than 0, it can indicate that the words have a correlation; if the PMI value is equal to 0, the words are independent of each other; if the PMI value is less than 0, the words have no correlation [12].

We now continue the introduction of the formula, and we get the calculation formula of emotional tendency. At the beginning, we need to select words with clear emotions as reference objects and calculate the PMI difference, so as to judge the difference of language emotional tendency [13]. The relevant calculation formula is as follows:

$$\text{SO-PMI}(w) = \sum_{i=1}^k \text{PMI}(\text{key} - p_i, w) - \sum_{i=1}^k \text{PMI}(\text{key} - n_i, w). \quad (23)$$

Here,  $\text{key} - p_i$  represents the  $i$ th positive word in the vocabulary statistics and  $\text{key} - n_i$  represents the  $i$ th derogatory word in the vocabulary statistics.

The following three judgment results for judging the Chinese language vocabulary are given as follows:

If the value obtained by SO-PMI is greater than 0, the sentiment tendency of the word  $w$  is positive.

If the value obtained by SO-PMI is equal to 0, the emotional tendency of the word  $w$  is neutral.

If the value obtained by SO-PMI is less than 0, the sentiment tendency of the word  $w$  is negative.

At the beginning of this algorithm, the first thing to do is the preprocessing of the text.

At this time, we need to extract candidate words according to the emotional language vocabulary database and judge whether the words in the text are emotional words [14]. If it has become an emotional vocabulary, the operation process can be directly skipped. If the text contains words that are not emotional words, the formula is used for calculation and evaluation.

The SO-PMI value between the word and the benchmark word is calculated. If the result is greater than zero, it can be judged as a positive value and then added to the analysis operation; if the result is less than zero, it is judged as a derogatory word and added to the analysis. After all the judgment operation steps are finished, the algorithm can be judged to be finished. Due to the diversity and complexity of the Chinese language vocabulary, we can synonymously divide the selected positive and derogatory words in consideration of the benchmark value.

Please note the following: when the target algorithm starts to execute, the corpus must be preprocessed and analyzed, then the part-of-speech judgment criteria are added after the word division and classification work, and finally, the regions are allocated [15]. This is based on the difficulty of the Chinese language. The Chinese phrase system is too large, and it is inevitable that there will be some omissions in the emotional thesaurus. Moreover, in today's society in the Internet age, the number of emotional vocabulary updates is far greater than the number of thesauri stored. Therefore, we need to design an algorithm to judge the emotion of words. The SO-PMI algorithm in the figure is one of them. The specific implementation of the SO-PMI algorithm is shown in Figure 8.

## 4. Simulation Experiments

*4.1. Data Budget Processing.* In order to realize the superiority of related operation analysis of superimposed applications, we perform superimposition processing on the SO-PML algorithm, taking 5000+ Chinese language emotion data as an example, using the following methods to deeply analyze language emotion [16]. The specific experimental methods are as follows:

Option 1: we model and cite the CLSTM model separately to analyze Chinese lexical sentiment

Option 2: the CLSTM model uses the auxiliary gradient descent algorithm to calculate the optimal solution for the Chinese vocabulary

Option 3: combined application of the CLSTM model in the auxiliary gradient descent algorithm and the emotional vocabulary formula is performed

Option 4: The comprehensive application of the CLSTM model superimposed on the SO-PMI algorithm, the auxiliary gradient algorithm, and the emotional vocabulary formula calculation is done at the same time

*4.2. Comparison Results of Experimental Algorithms.* In the above scheme, we carried out data comparison operations, respectively, and obtained the comparison results of the Chinese language sentiment analysis, as shown in Tables 1–4. Comparing the data in the table, we can clearly see that the data in scheme 1 is significantly lower than that of the other three schemes. We analyzed about 3000 words, but the algorithm's sentiment extraction and analysis efficiency is only 50.7%, which is far lower than other algorithms [17]. Scheme 2 adds an auxiliary gradient descent algorithm to the CLSTM model to process the optimal solution of the vocabulary, and the rate and accuracy of analyzing vocabulary sentiment are slightly improved, but the overall change is not large and there are still major problems. Scheme 3 then analyzes the changes brought by the emotion formula to the CLSTM model. It can be seen that there are obvious changes compared to Scheme 1, but the analysis of the emotional state after too many words is still unsatisfactory. After all the tests, we finally designed the fourth scheme and it was successfully selected. It has its uniqueness in addition to the advantages of other algorithms, which greatly improves the efficiency of sentiment analysis. Therefore, this scheme has obvious advantages compared with other schemes, and its computing speed and the accuracy of the language sentiment analysis make its comprehensive level the best [18].

We compared the line graphs of the analysis times for scenarios 1–4. The number of words from left to right in the figure is 100, 500, 1500, and 3000, respectively. We can clearly see the overall superiority of this scheme. When the number of vocabulary is larger, the more obvious the advantage is [19]. In this line chart, the larger the change of the line, the more obvious the distinction between the pros and cons of the model. We can clearly see from Figure 9 that when 100 text data is used as the standard, the line is basically a horizontal line with little change. When 3000 text data is used as the standard, the variation of schemes 1–4 is huge, which better verifies the superior performance of our selected algorithm.

The comparison effect is shown in Figure 10.

Here, we take the 3000 language vocabulary benchmarks as an example and list the line chart to compare the data of schemes 1–4 in detail. It can be clearly seen that the comprehensive performance of scheme 4 is significantly better than the other schemes [20]. The effect is shown in Figure 9.

*4.3. Analysis of the SO-PMI Algorithm Model for Superposition Application.* In the above case analysis, using this algorithm, when the number of the Chinese language vocabulary is about 2000, it can make the language sentiment analysis efficiency and language sentiment analysis accuracy achieve the best comprehensive performance.

Based on the comprehensive application of the CLSTM model superimposed on the SO-PMI algorithm proposed by the verification, that is, in the case of scheme 4, the number of 2000 Chinese language vocabulary is cited as the benchmark and the deep learning analyzes the emotional distribution of the vocabulary, conducts a comprehensive

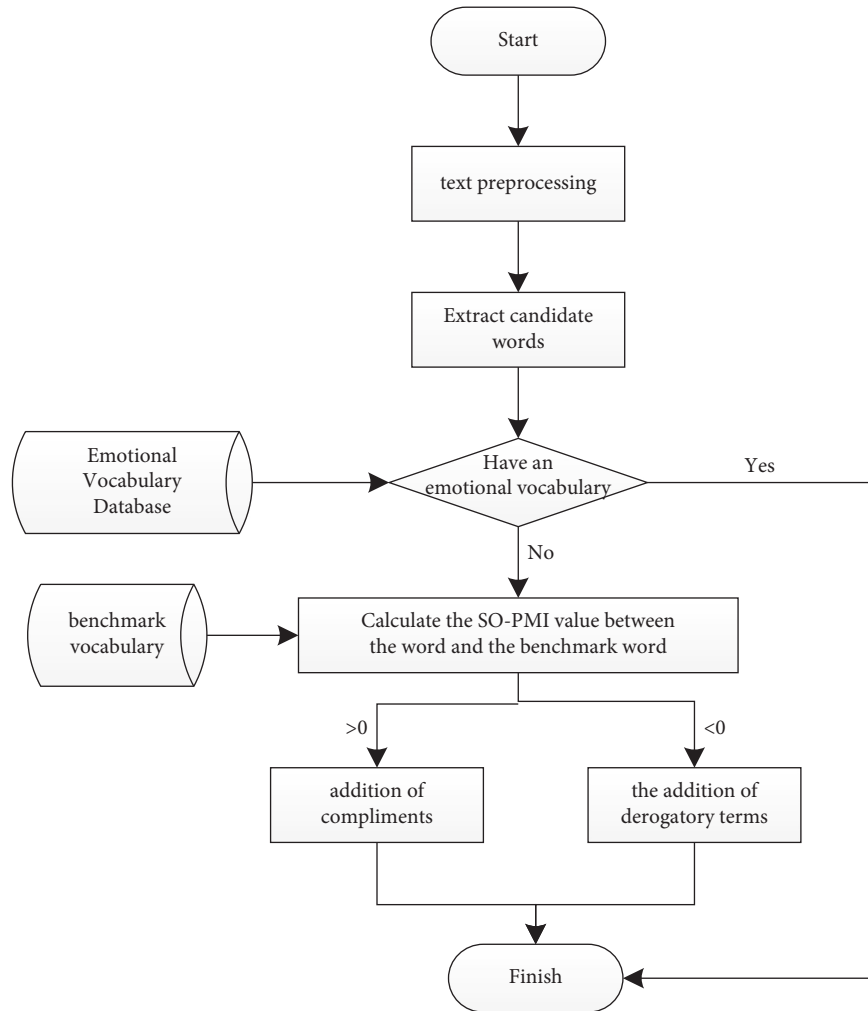


FIGURE 8: SO-PMI algorithm implementation.

TABLE 1: Chinese language sentiment extraction and analysis in scheme 1.

| The number of emotion words extracted | Sentiment analysis rate (min) | Language sentiment analysis accuracy (%) |
|---------------------------------------|-------------------------------|--|
| 100                                   | 0.5                           | 70.8                                     |
| 500                                   | 3.0                           | 65.4                                     |
| 1500                                  | 10.1                          | 59.6                                     |
| 3000                                  | 21.7                          | 50.7                                     |

performance analysis on it, and shows the superior performance of the algorithm [21].

When the number of Chinese language vocabulary is 2000, its comprehensive performance index is shown in Figure 11.

When the number of words reaches 2000, it can meet the role of general article language sentiment analysis. The speed of language sentiment analysis is significantly improved compared with the previous algorithm. Based on 2000 words, the application waits about 4.5 minutes to meet people's general needs, which is the time to wait [22].

Text length is an important indicator of language sentiment analysis. If the text length is too short, it is difficult to

reflect the superior performance of each algorithm. If the text is too long, it will increase the burden of the algorithm model.

Therefore, we counted the distribution of language text length in general life, and Figure 12 is a graphic representation of its distribution. We control most of the text within a reasonable range (this article uses 3000 as the range), so the algorithm can effectively perform related sentiment analysis work [23]. The distribution of language texts in daily life is shown in Figure 12.

Similarly, we analyze the actual emotional needs in this field. The language emotion function can be applied to emotion retrieval, emotion summary, emotion question answering, and many places such as movie reviews, product

TABLE 2: Chinese language sentiment extraction and analysis in scheme 2.

| The number of emotion words extracted | Sentiment analysis rate (min) | Language sentiment analysis accuracy (%) |
|---------------------------------------|-------------------------------|--|
| 100                                   | 0.4                           | 78.9                                     |
| 500                                   | 2.8                           | 70.5                                     |
| 1500                                  | 8.5                           | 64.9                                     |
| 3000                                  | 16.4                          | 60.5                                     |

TABLE 3: Chinese language sentiment extraction and analysis in scheme 3.

| The number of emotion words extracted | Sentiment analysis rate (min) | Language sentiment analysis accuracy (%) |
|---------------------------------------|-------------------------------|--|
| 100                                   | 0.25                          | 81.2                                     |
| 500                                   | 1.5                           | 74.3                                     |
| 1500                                  | 6.0                           | 65.9                                     |
| 3000                                  | 14.8                          | 61.7                                     |

TABLE 4: Chinese language sentiment extraction and analysis in scheme 4.

| The number of emotion words extracted | Sentiment analysis rate (min) | Language sentiment analysis accuracy (%) |
|---------------------------------------|-------------------------------|--|
| 100                                   | 0.11                          | 98.8                                     |
| 500                                   | 0.6                           | 89.3                                     |
| 1500                                  | 3.5                           | 82.7                                     |
| 3000                                  | 8.1                           | 77.6                                     |

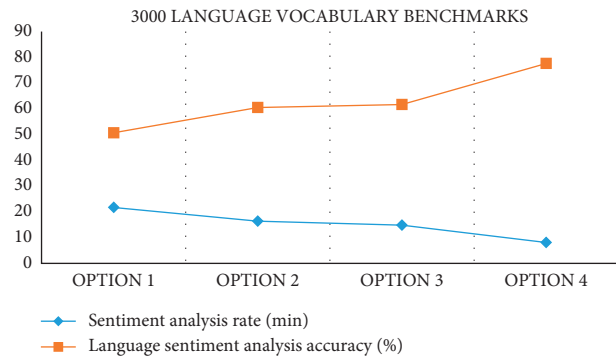


FIGURE 9: Comprehensive comparison of 4 algorithms on 3000 language vocabulary benchmarks.

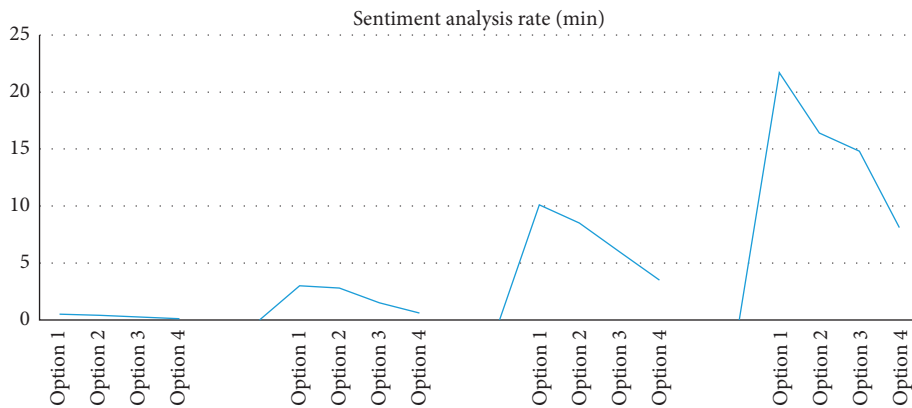


FIGURE 10: Overall comparison of sentiment analysis time for schemes 1–4.



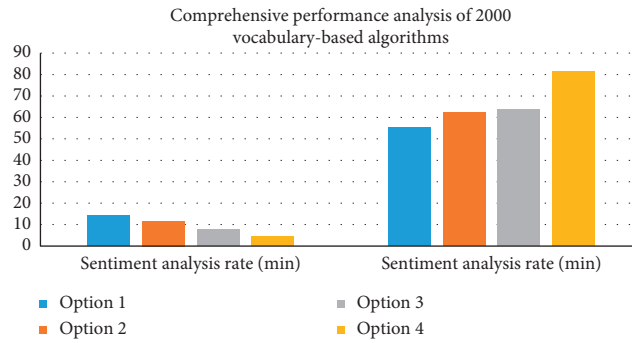


FIGURE 11: Comprehensive performance analysis of the 2000-word-based algorithm.

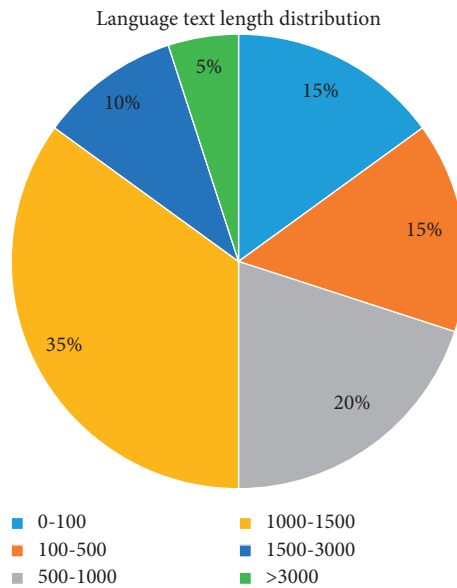


FIGURE 12: Statistical distribution display of language text length.

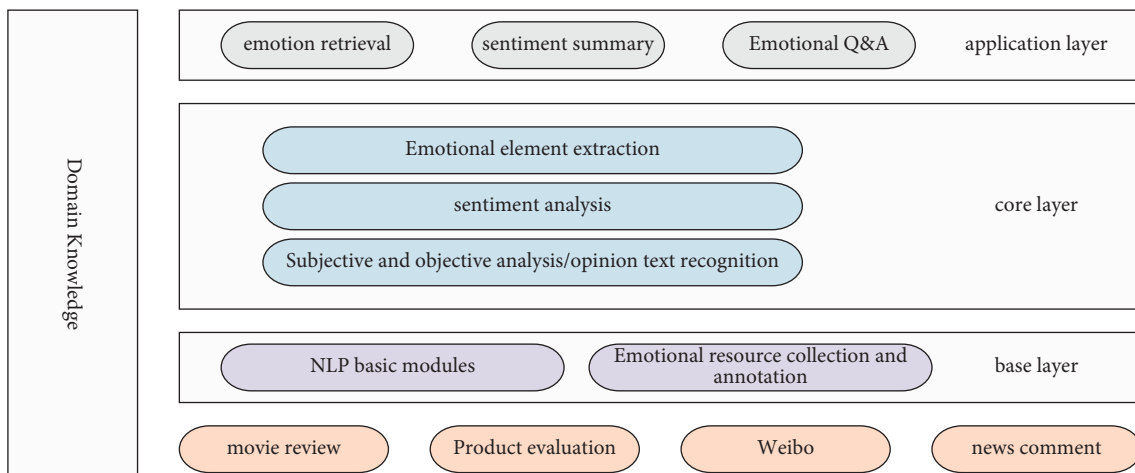


FIGURE 13: The main adaptation map of language emotion.

evaluations, microblogs, and news. It can be seen that its application field is broad, and the information given above shows that the comprehensive performance of the algorithm

is superior and it is easy to meet the needs of language sentiment analysis in people's daily life [24]. The overall block diagram of the language statistics is shown in Figure 13.

We need to transform traditional algorithmic sentiment analysis methods, improve the extraction and analysis of key words, and expand the coverage of key sentences to improve their representativeness. At the same time, emoji is also a major direction of its sentiment analysis. We also need to increase the related construction tasks of the symbol dictionary and combine it with text language analysis, expand the sentiment dictionary on the SO-PMI algorithm, and formulate a corresponding set of sentiment rules calculation.

## 5. Conclusion

As mentioned above, the deep learning of this research is used for Chinese language sentiment extraction and analysis, through the reference of the original CLSTM model, plus the calculation of the auxiliary gradient algorithm and the emotional vocabulary formula  $f\_sentiment(s_i)$  and the synthesis of the SO-PMI algorithm model. The application can substantially improve the efficiency and accuracy of language emotion extraction and analysis. The algorithm we propose performs de-redundancy operations on some unnecessary neutral words and can extract and analyze language sentiment after a series of word segmentation operations. Compared with other single algorithms, the comprehensive performance of this algorithm is the best, which significantly improves the efficiency and accuracy of sentiment analysis. Under the premise of 2000-word vocabulary, the algorithm fully meets the needs of daily life. In the traditional language sentiment analysis work, we add the new text extraction opinion vocabulary to explore the mutual emotional connection between vocabulary and objective affairs [25]. Combined with the extraction of opinion relations in the application of tree kernels, a new kernel reference is developed, multiple analyses is performed on the emotional vocabulary data model, and finally, the overall performance improvement of the efficiency of language sentiment analysis is achieved. The algorithm also has imperfections. Our emotional vocabulary is imperfect, and the Chinese text language is extremely difficult to analyze. In addition, there are some special sentence structure analyses, such as antonyms. We still need to increase the extraction of key sentence patterns and explore more advantageous algorithms to make the extraction of text information more representative.

## Data Availability

The experimental datasets used to support the findings of this study are available from the author upon request.

## Conflicts of Interest

The author declares no conflicts of interest regarding this work.

## References

- [1] V. Gulshan, L. Peng, M. Coram et al., "Development and validation of a deep learning algorithm for detection of diabetic retinopathy in retinal fundus photographs," *Journal of the American Medical Association*, vol. 316, no. 22, p. 2402, 2016.
- [2] G. Litjens, T. Kooi, B. E. Bejnordi, A. Setio, and C. I. Sánchez, "A survey on deep learning in medical image analysis," *Medical Image Analysis*, vol. 42, no. 9, pp. 60–88, 2017.
- [3] B. C. Ng, C. Cui, and F. Cavallaro, "The annotated lexicon of Chinese emotion words," *Word*, vol. 65, no. 2, pp. 73–92, 2019.
- [4] Z.-T. Liu, M. Wu, W.-H. Cao, Y. Mei, and J.-W. Mao, "Speech emotion recognition based on an improved brain emotion learning model," *Neurocomputing*, vol. 309, pp. 145–156, 2018.
- [5] Y. Chen, Z. Lin, Z. Xing, G. Wang, and Y. Gu, "Deep learning-based classification of hyperspectral data," *IEEE Journal of Selected Topics in Applied Earth Observations and Remote Sensing*, vol. 7, no. 6, pp. 2094–2107, 2017.
- [6] S. Ding and R. A. Saunders, "Talking up China: an analysis of China's rising cultural power and global promotion of the Chinese language," *East Asia*, vol. 23, no. 2, pp. 3–33, 2006.
- [7] A. Sengupta, S. Roy, and G. Ranjan, "LJST: a semi-supervised joint sentiment-topic model for short texts," *SN Computer Science*, vol. 2, no. 4, p. 256, 2021.
- [8] Y. H. Lee and K. S. Ang, "Brand name suggestiveness: a Chinese language perspective," *International Journal of Research in Marketing*, vol. 20, no. 4, pp. 323–335, 2003.
- [9] R. V. Kübler and A. Colicev, "Social media's impact on the consumer mindset: when to use which sentiment extraction tool?" *Journal of Interactive Marketing*, vol. 50, no. 1, pp. 136–155, 2020.
- [10] Y. Wu, W. Gang, and H. Li, "A Chinese word segmentation algorithm based on N-gram model and machine learning," *Journal of Electronics and Information*, vol. 11, pp. 1148–1153, 2001.
- [11] S. Wan, J. Tang, and X. Yang, "Research on big data of customer product reviews based on text sentiment extraction and statistical analysis," *Academic Journal of Humanities & Social Sciences*, vol. 3, no. 3, 2020.
- [12] V. Radhakrishnan, C. Joseph, and K. Chandrasekaran, "Sentiment extraction from naturalistic video," *Procedia Computer Science*, vol. 143, pp. 626–634, 2018.
- [13] M. Tubishat, N. Idris, M. A. M. Abushariah, and M. Abushariah, "Implicit aspect extraction in sentiment analysis: review, taxonomy, oppportunities, and open challenges," *Information Processing & Management*, vol. 54, no. 4, pp. 545–563, 2018.
- [14] P. G. Preethi, V. Uma, and A. Kumar, "Temporal sentiment analysis and causal rules extraction from tweets for event prediction," *Procedia Computer Science*, vol. 48, pp. 84–89, 2015.
- [15] R. Shettar and S. Taorem, "Sentiment extraction and analysis of product reviews at sentence level," *Current Trends in Information Technology*, vol. 1, 2011.
- [16] S. Wang, A. Yang, and D. Li, "Research on sentence sentiment tendency classification based on Chinese sentiment vocabulary," *Computer Engineering and Applications*, vol. 45, no. 24, pp. 153–155+161, 2009.
- [17] Y. Zhang and H. Wang, "Chinese text sentiment analysis based on att-BiGRU-CRF model," *Journal of Tianjin University of Technology*, vol. 37, no. 6, pp. 31–35, 2021.
- [18] Z. Chen, Y. Qian, and W. Zhao, "Research on sentiment classification model of bullet screen text—based on Chinese pre-training model and bidirectional long short-term memory network," *Journal of Hubei University of Technology*, vol. 36, no. 6, pp. 56–61, 2021.

- [19] Z. Pan, L. Zhao, L. Yuan, and H. Wang, "FastText Chinese sentiment polarity analysis based on Borderline-Smote algorithm improvement," *Computer Applications and Software*, vol. 38, no. 11, pp. 295–299+349, 2021.
- [20] B. Zhang, H. Zhang, T. Li, and J. Shang, "A sentiment analysis method for Chinese reviews based on multi-input model and syntactic structure," *Big Data*, vol. 7, no. 6, pp. 41–52, 2021.
- [21] T. Diao, J. Zhang, C. Yao, and W. Li, "Application of Chinese text sentiment classification based on recurrent neural network," *Wireless Internet Technology*, vol. 18, no. 19, pp. 96–97, 2021.
- [22] Y. Yuan, "Research on sentiment classification of online review texts based on Naive Bayes," *Inner Mongolia Science and Technology and Economy*, vol. 18, pp. 91–94, 2021.
- [23] H. Zhang, H. Huang, and W. Li, "Speech emotion database for emotion change detection," *Computer Simulation*, vol. 38, no. 9, pp. 448–455, 2021.
- [24] Y. Wang, "On the emotional penetration and integration in the process of Chinese teaching in higher vocational colleges," *University*, vol. 35, pp. 128–130, 2021.
- [25] Z. Huang, X. Wu, Y. Wu, and J. Ling, "Chinese text sentiment classification combined with BERT and BiSRU-AT," *Computer Engineering and Science*, vol. 43, no. 9, pp. 1668–1675, 2021.

## *Retraction*

# **Retracted: Study on the Integration of Computer-Assisted Teaching Methods for Teaching Volleyball in College Physical Education**

### **Mathematical Problems in Engineering**

Received 26 September 2023; Accepted 26 September 2023; Published 27 September 2023

Copyright © 2023 Mathematical Problems in Engineering. This is an open access article distributed under the Creative Commons Attribution License, which permits unrestricted use, distribution, and reproduction in any medium, provided the original work is properly cited.

This article has been retracted by Hindawi following an investigation undertaken by the publisher [1]. This investigation has uncovered evidence of one or more of the following indicators of systematic manipulation of the publication process:

- (1) Discrepancies in scope
- (2) Discrepancies in the description of the research reported
- (3) Discrepancies between the availability of data and the research described
- (4) Inappropriate citations
- (5) Incoherent, meaningless and/or irrelevant content included in the article
- (6) Peer-review manipulation

The presence of these indicators undermines our confidence in the integrity of the article's content and we cannot, therefore, vouch for its reliability. Please note that this notice is intended solely to alert readers that the content of this article is unreliable. We have not investigated whether authors were aware of or involved in the systematic manipulation of the publication process.

Wiley and Hindawi regrets that the usual quality checks did not identify these issues before publication and have since put additional measures in place to safeguard research integrity.

We wish to credit our own Research Integrity and Research Publishing teams and anonymous and named external researchers and research integrity experts for contributing to this investigation.

The corresponding author, as the representative of all authors, has been given the opportunity to register their agreement or disagreement to this retraction. We have kept a record of any response received.

### **References**

- [1] J. Zhang, "Study on the Integration of Computer-Assisted Teaching Methods for Teaching Volleyball in College Physical Education," *Mathematical Problems in Engineering*, vol. 2022, Article ID 5028705, 8 pages, 2022.

## Research Article

# Study on the Integration of Computer-Assisted Teaching Methods for Teaching Volleyball in College Physical Education

Jinfeng Zhang 

*Sport College of Zhoukou Vocational and Technical College, Zhoukou 466000, China*

Correspondence should be addressed to Jinfeng Zhang; 2005090009@zkvtc.edu.cn

Received 12 April 2022; Accepted 25 April 2022; Published 29 May 2022

Academic Editor: Man Fai Leung

Copyright © 2022 Jinfeng Zhang. This is an open access article distributed under the Creative Commons Attribution License, which permits unrestricted use, distribution, and reproduction in any medium, provided the original work is properly cited.

Computer-aided network (CAI) teaching method is to establish a volleyball teaching forum on campus network, upload graphic materials related to volleyball teaching, combine inside and outside classes, and combine teaching with self-study. This article studies the volleyball teaching of physical education in colleges and universities by comprehensively using the computer-aided teaching method, and discusses its role in improving the teaching quality, interest, and self-study ability, to improve the teaching effect. The results show that the computer network teaching method is an effective supplement to the teaching mode of students' autonomous learning and cooperative learning. It is an effective way to fully mobilize students' subjective initiative and improve the effect of volleyball teaching. At the same time, it is considered that the key to popularize and develop this teaching method is to improve the computer operation standards of physical education teachers.

## 1. Introduction

With the continuous promotion and application of computer network technology in various fields, the reform of physical education classroom teaching with computer-aided instruction (CAI) as the main feature is imperative [1]. Demonstration effect is one of the important characteristics in the process of physical education teaching. Students can constantly correct and improve their actions through teachers' demonstration, to achieve a better physical education teaching effect [2]. Teachers' energy is limited, as well as the limitations of space, class time, and class size, which may be the factors limiting the effectiveness of physical education teaching. How can students see enough presentations and have enough time to learn and imitate [3]? How to stimulate students' enthusiasm and interest in learning and make sports a habit in their daily life have become an urgent problem to be solved in college students' physical education at this stage [4].

With the increasing maturity of computer network technology and its popularization in various fields, physical education teaching methods based on classroom teaching and supplemented by computer teaching have emerged [5].

At present, the main way of physical education teaching is that teachers personally demonstrate in class and students imitate teachers' actions [6]. Teachers need to remind and correct students' actions and practice repeatedly to achieve better results [7, 8], [9–11]. Therefore, at this stage, several problems need to be solved in physical education teaching: how to give students enough time to learn and imitate correct actions; how to improve students' enthusiasm and interest in sports; and how to make sports become a part of students' daily life. Students' enthusiasm for learning and interest in sports will become an indispensable part of their daily life [12].

The purpose of computer network (CAI) teaching is to mobilize students' passion and love for physical education learning, improve students' volleyball technical ability, make students good at finding problems in the learning process, cultivate students to think independently, analyze problems, solve problems, find the fun of volleyball in the course of lessons, understand volleyball more deeply, discover the laws of volleyball, and develop the awareness of their exercise [13]. The main way of online teaching as described in this article is to upload image materials, text materials, and video materials in the volleyball section of the campus network for

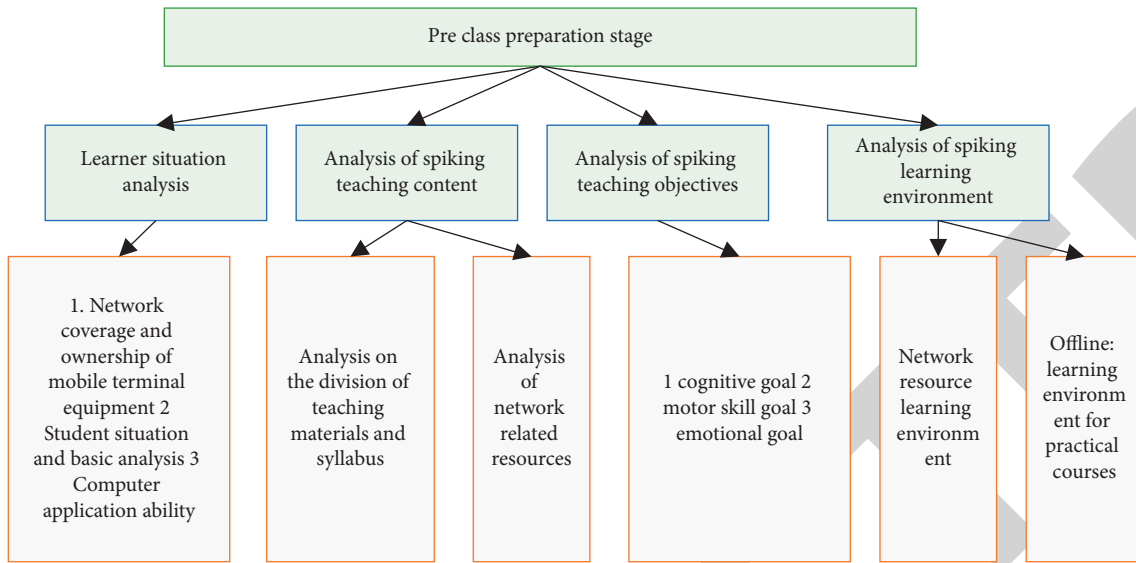


FIGURE 1: List of preparation contents in the pre-course preparation stage.

students to learn [14, 15]. The machine network teaching method supplements the insufficient part of in-class learning, enhances students' independent learning ability, fully mobilizes students' subjective initiative, and then achieves volleyball teaching effect [16, 17]. Therefore, in this article, we choose students who took volleyball as a physical education elective to conduct a study to explore how the computer network (CAI) teaching method can improve teaching quality, cultivate students' interest in volleyball and their ability to learn volleyball by themselves, achieve teaching purposes, and provide teaching opinions [18, 19]. In view of this, this study takes volleyball elective students as the experimental subjects to explore the promotion effect of the computer network (CAI)-assisted teaching method on improving the teaching effect of students' volleyball techniques, and to provide a reference for the reform and development of physical education courses in higher education institutions [20].

## 2. Detailed Construction and Analysis of the Teaching Model of Volleyball Bucketing Technique

**2.1. Pre-Course Preparation Stage.** The pre-course preparation stage is the first step of constructing the teaching mode of the Internet + volleyball bucketing technique, and it is also the front-end preparation. The design diagram of the pre-course preparation stage is shown in Figure 1.

It is important to improve the complete learning experience in the pre-course preparation phase as an indispensable part of the constructed Internet + volleyball bucketing technique teaching model. The analysis of learners' situation is mainly about the school network coverage and students' ownership of mobile devices, the availability of the basics of snapping learning, and the ability to use computers. Whether the student learning environment has network coverage and the student's ability to

simply use the computer are important factors affecting the quality of learning, and the learning of the Internet + bucketball technology learning resources integrated into the teacher is based on the network and the equipment to provide support. Internet mobile terminal devices are the receivers at the end of the students, such as computers, smartphones, and tablets. These devices provide online technical support and are the key factor in achieving "Internet+."

In the new context of building a new teaching mode of buckling technique, the analysis of teaching content is divided into the analysis of traditional teaching materials and teaching progress, and the analysis of Internet learning resources of buckling technique. The dunking technique can be divided into five parts such as preparation posture, running, jumping, aerial strike, and landing. Through watching experts' video resources, interviewing experts, and reading textbooks, it is found that it is more difficult to learn the consistency of swinging arm, control of human ball distance, and the striking part when learning arm whipping action; to master the height of the step and pace rhythm when learning running and jumping, and to learn the timing of jumping, aerial strike, and the control of the human ball distance when learning complete dunking.

**2.2. Pre-Class Self-Learning Stage Based on Learning Task List.** The pre-class self-learning stage based on the bucketing task list (Figure 2) is the most critical part of building the Internet + volleyball bucketing technique teaching model, and this stage is an important stage for students' knowledge self-construction and ability development.

There are four main steps in the production of the online learning platform of bucketing technique: the first step is the collection of Internet video resources of bucketing technique (including Gif motion pictures), videos recorded by famous teachers, text, patterns, and picture resources of bucketing technique learning. The second step is to process and classify

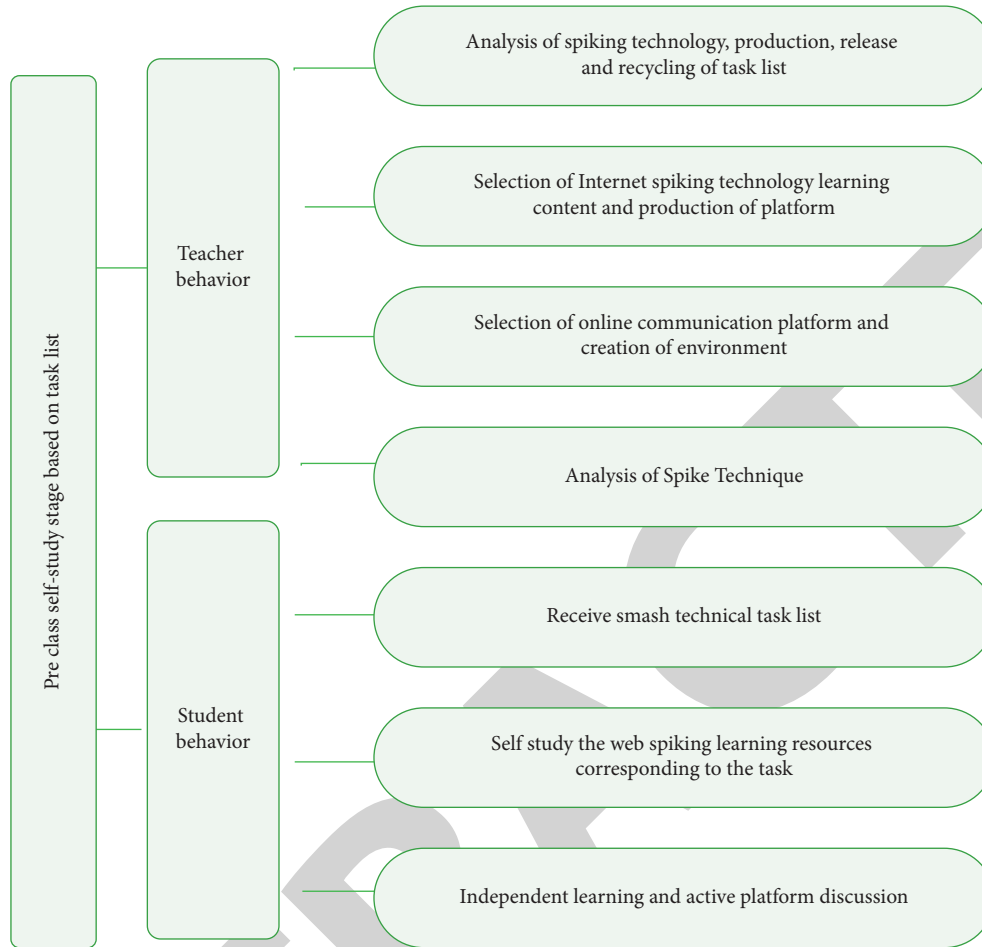


FIGURE 2: List of teacher and student behaviors in the pre-class self-study stage.

the resources by using information technology (such as editing software and image processor) and auxiliary tools according to the teaching progress of bucketing technique and students' situation. In the third step is to analyze the teaching content, carry out the teaching expected results vision, and integrate the resources, such as the layout of video text and pictures of the swinging arm whipping action. The fourth step is to create a web page using Dreamweaver to compile the classified snapping technique required to visualize intuitively and classify with clear knowledge points (Figure 3).

The video resources should not be too long and can come from the videos on Youku, Akiyip, Tencent, or other platforms about teaching content, the videos recorded by famous teachers on the teaching of bucketing technique, and the bucketing teaching videos quoted by other online learning platforms. The viewing time of the integrated video resources is limited to 10 minutes in learning, and cultivate their feelings about sports.

Online learning resources must be selected and self-built according to the requirements of the syllabus and teaching objectives, and coincide with the teaching content of offline face-to-face teaching, and the online learning resources constructed should fully reflect the richness, sharing, and openness of the Internet resources.

The editing of board settings and content is the key point of the effectiveness of web page production. The whole layout of the web page should be simple and clear, not too cumbersome, and students can form a clear cognition through learning. The author's web page for learning the snapping technique is shown in Figure 4.

### 3. Analysis of the Effects of Teaching Volleyball Bucketing

*3.1. Research Object and Method.* The research object is to study the application of the computer network (CAI) teaching method to assist volleyball teaching in colleges and universities. For the determination of the experimental group and control group, four teaching classes of volleyball elective courses in our school were randomly selected, two classes as the experimental group and the other two classes as the control group (Table 1).

Before the experiment, a diagnostic survey was conducted in all four classes to understand the initial level of students' volleyball. The results showed that the students' volleyball skills in the four classes were basically in synchronization, and more than 80% of the students did not know how to play volleyball; three experts were asked to evaluate the basic volleyball skills of the two groups of

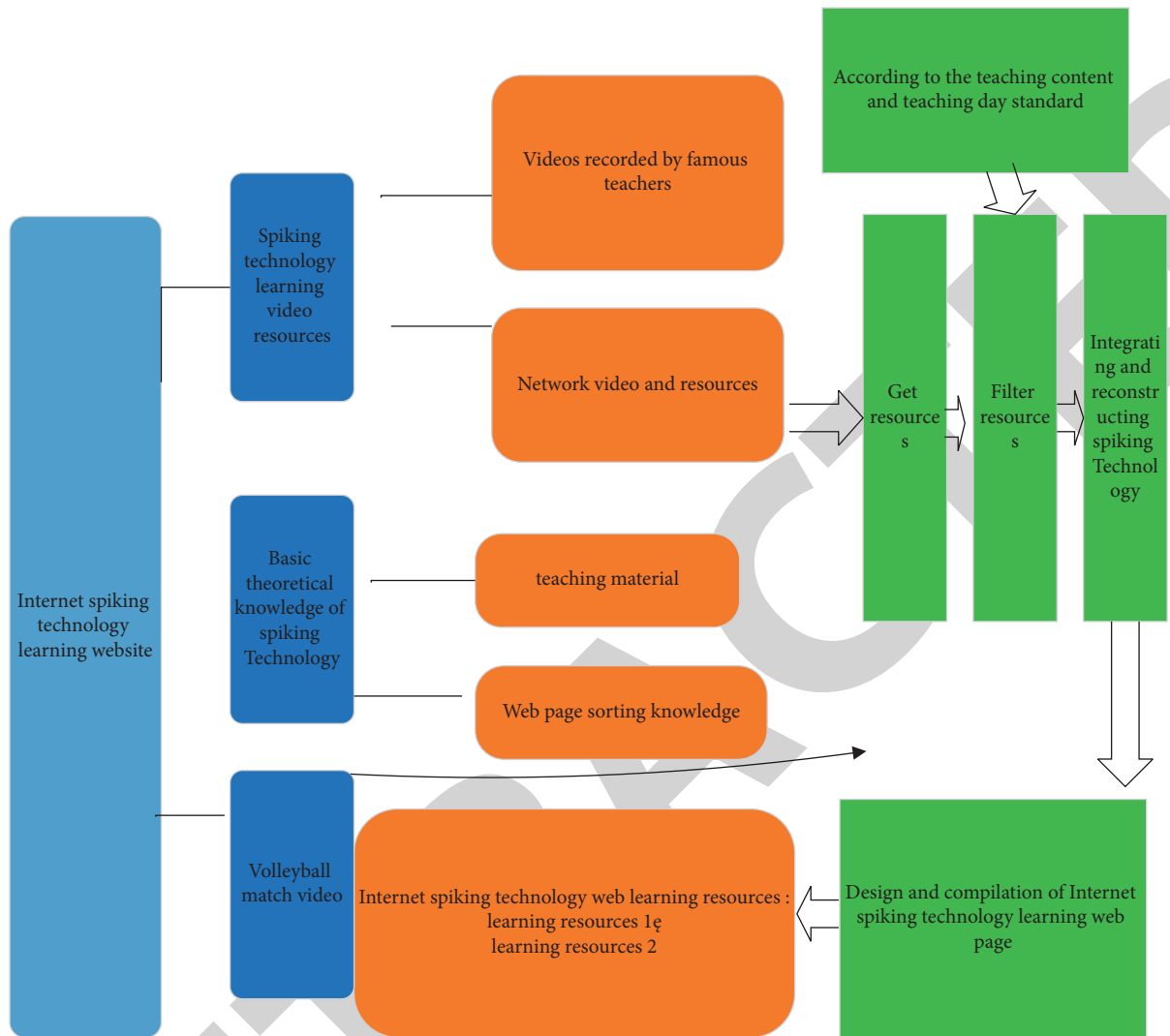


FIGURE 3: Diagram of the process of creating a web page for learning Internet bucketing techniques.

students before the experiment, and the experts thought that there was no significant difference between the skills of the two groups of students; and both groups of students qualified to complete the study and assessment of the compulsory freshman physical education course, which were 50 m running, front throwing solid ball, 12 minutes running (men 2400 m, women 2000 m). The results were analyzed and the students in both groups completed their freshman physical education courses, including 50 m run, solid ball throw, standing long jump, and 12 minutes run (2400 m for men and 2000 m for women). The analysis of the results showed that there was no significant difference in the special physical quality between the two groups of students. From the above raw volleyball technical level, technical evaluation, and special physical quality of students, the test conditions were the same, and the experimental and control groups were determined reasonably and effectively [21–23].

The teaching experiment was conducted on the campus network of Jiaotong University with multimedia audio, video, text, and picture resources, mainly including volleyball teaching videos by Professor Ge Chunlin of Beijing

Sport University, volleyball training videos by Wang Jiawei, former head coach of the national men's volleyball team, and teachers' teaching videos. Both the control group and the experimental group were taught by the author of this article, and both the control group and the experimental group were taught 32 hours (90 minutes/2 hours/week, 16 weeks in total). The on-site survey revealed that 100% of the students in the experimental group had easy access to the campus network, which provided the necessary material basis for the smooth implementation of the teaching experiment.

The experimental group adopted the "computer network (CAI) teaching method" to assist in teaching. The teacher first taught according to the traditional physical education process, except that on the basis of students' basic mastery of passing and matting techniques, students were allowed to try to serve and dunk the ball according to the online materials, log on to the homepage of "Zhixing BBS Forum" on the campus network and enter the "Volleyball World" section. "Through the comparison with the correct movements, they can find out their shortcomings and give feedback to the forum in time, so that teachers can understand the students'



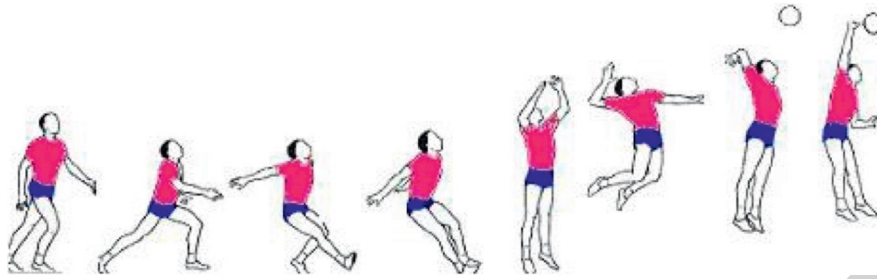


FIGURE 4: Screenshot of the dunking technique learning page.

TABLE 1: Sex and age distribution of experimental subjects.

|                     | Boys/<br>person | Girls/<br>person | Total/<br>person | Age/year     |
|---------------------|-----------------|------------------|------------------|--------------|
| Experience<br>group | 28              | 36               | 64               | 20.00 ± 0.62 |
| Control group       | 33              | 31               | 64               | 20.00 ± 0.45 |

situation in real-time and formulate corresponding teaching contents and methods, and focus on practicing in the next class. Repeat this process many times until the examination [24].

The control group used the traditional physical education teaching method, i.e., the combination of explanation and demonstration and practice to correct errors, to teach the four techniques of volleyball matting, passing, serving, and dunking, and finally, the test was conducted uniformly with the experimental group.

Therefore, it is important to measure and assess the students' learning effectiveness. The assessment of the scores of the experimental and control classes' sinking techniques was evaluated by qualitative and quantitative methods. The assessment of the qualitative scores was mainly evaluated by the scores of the two volleyball experts invited, while the quantitative assessment was to specify the number of sinking balls and count the number of valid balls. The paired samples *t*-test with a 95% confidence interval was used to evaluate the scores of the experimental and control classes' snapping technique, and the results of the analysis are shown.

According to the analysis results of Table 2, the results of the deduction of the experimental class show significant differences in the quantitative evaluation after the experiment, while the clocking performance of the control class also shows significant differences. But the number of spike in the experimental class is lower than that of the control class before the experiment. The number of the deduction of the experimental class is higher than that of the control class after the experiment, and the increase is larger, which indicates that the Internet plus volleyball spiking technique teaching mode is applied in the teaching of smash skills. It can improve the effect of students' learning spiking. From the analysis of the technical evaluation results, there is a significant difference between the test results of Expert 1 and Expert 2. From the analysis of the test results, we can see that the technical assessment scores of the experimental class before the experiment were lower than those of the control

class, but the technical assessment test results of both the experimental class and the control class after the experiment were better than those of the control class, and the difference between the mean values of the experimental class and the control class before and after the experiment were 2.58 and 2.11, showing a difference, which can indicate that the growth of the level of the bucketing technique of the experimental class was greater than that of the control class [25, 26].

**3.2. Results and Analysis.** The assessment of the experimental and control classes was conducted separately so that they could not interfere with each other. The four techniques of pad, pass, serve, and dunk were scored independently and the scores obtained were averaged.

In the comparison of the scores of the four techniques of padding, passing, serving, and dunking of the players in the experimental and control classes, the players' mastery of these four techniques could be seen (Table 3). The experimental group and the control group showed significant differences ( $P < 0.05$ ) in the scores of three techniques, namely, matting, passing, and serving, which indicated that the computer network (CAI)-assisted teaching method was beneficial to the players in learning and mastering these three volleyball techniques, while the statistical difference between the scores of the two groups in the spiking technique was not significant and not statistically significant. The reason for this is that the dunking technique is more likely to be affected by the players' perceptual ability, which makes it more difficult to master, and the CAI-assisted teaching method cannot fully play its supporting role in the teaching class.

Table 4 shows that the comparison between the experimental group and the control group is also obvious, according to the standard of student's performance set by the school's Academic Affairs Office, the students are classified as: 90–100 as excellent; 80–90 as good; 70–80 as moderate; and 60–70 as poor. The specific assessment data were 15 students in the experimental group and 6 in the control group with the excellent grade; 30 students in the experimental group and 22 in the control group with the good grade; 11 students in the experimental group and 24 in the control group with the medium grade; and 2 students in the experimental group and 6 in the control group with the poor grade. It can be seen that the computer network (CAI)-assisted teaching method has helped students in the

TABLE 2: Comparison of the results of the before-and-after bucketing technique test between the experimental class and the control class at a glance.

| Content                    |                    | Before experiment ( $n = 18$ ) | After experiment ( $n = 18$ ) | After $x =$ before $x$ | $t$ value | $P$   |
|----------------------------|--------------------|--------------------------------|-------------------------------|------------------------|-----------|-------|
| Spiking skill evaluation 1 | Experimental class | $2.13 \pm 0.29$                | $4.75 \pm 0.10$               | 2.68                   | -16.520   | 0.000 |
| Spiking skill evaluation 1 | Contrast class     | $2.16 \pm 0.38$                | $4.29 \pm 0.36$               | 2.12                   | -17.655   | 0.000 |
| Spiking skill evaluation 2 | Experimental class | $1.51 \pm 0.56$                | $4.18 \pm 0.31$               | 2.78                   | -16.498   | 0.000 |
| Spiking skill evaluation 2 | Contrast class     | $1.68 \pm 0.58$                | $3.35 \pm 0.46$               | 2.71                   | -7.446    | 0.000 |
| Up to standard             | Experimental class | $1.52 \pm 1.03$                | $4.19 \pm 0.88$               | 2.69                   | -7.665    | 0.000 |
| Up to standard             | Contrast class     | $1.68 \pm 1.45$                | $3.36 \pm 1.01$               | 2.29                   | -3.178    | 0.000 |

TABLE 3: Difference test of the four technical scores ( $x \pm S$ ) between the experimental and control groups.

| Group            | Number of people | Cushion          | Pass the ball  | Serve            | Spiking          |
|------------------|------------------|------------------|----------------|------------------|------------------|
| Experience group | 64               | $82.68 \pm 5.88$ | $88.5 \pm 3.6$ | $83.55 \pm 8.98$ | $66.23 \pm 8.29$ |
| Control group    | 64               | $78.8 \pm 5.69$  | $80.9 \pm 6.9$ | $76.59 \pm 6.89$ | $66.66 \pm 5.58$ |
| $t$              |                  | -2.686           | -2.088         | -3.088           | -0.107           |
| sig.             |                  | 0.019            | 0.032          | 0.003            | 0.896            |

Note. \*indicates a significant difference in technical scores between experimental and control groups ( $P < 0.05$ ).

experimental group to improve their performance, and the number of students who got excellent and good grades in the final examination was significantly higher than that of the control group, which can be said to have achieved the expected vision of the teaching experiment.

Students use the BBS system to access the volleyball forum for computer network-assisted teaching. Students can access the campus network in various ways: laptops, tablets, and even cell phones, and learn volleyball techniques and knowledge freely anywhere and anytime. The frequency of students' access to the BBS system (Table 5).

Therefore, the establishment of a volleyball BBS on the campus network is an effective way of computer network (CAI)-assisted teaching method. The main function of the forum is to allow students to discuss and communicate freely, in this section of the volleyball BBS, about volleyball techniques that cannot be adequately conducted in class. Of course, this free discussion and speaking are only possible within the teacher's control. Teachers can use their class time to upload more videos, pictures, texts, and other materials related to the classroom content to the volleyball BBS in the form of postings. At the same time, students can also spontaneously search for more volleyball information of interest on the Internet and upload it under the intervention and guidance of teachers for other students who log on to this forum to share, thus changing the scope of traditional volleyball classroom teaching and making volleyball techniques, tactics, physical training, theoretical knowledge, and many other aspects fully shared on the Internet, becoming an indispensable supplement to physical education classroom teaching in the new situation This has become an indispensable supplement to physical education classroom teaching in the new situation (Table 6).

Through the Internet (for example, the establishment of a small website for everyone), volleyball teaching can make full use of its convenient and widespread characteristics, with classroom teaching as the main focus and volleyball forums as a supplement, guiding students to pay attention to volleyball forums and develop the habit of browsing volleyball forums to

TABLE 4: Comparison of the total scores of the final examination of the experimental and control groups.

| Fraction           | Experience group |                | Control group    |                |
|--------------------|------------------|----------------|------------------|----------------|
|                    | Number of people | Percentage (%) | Number of people | Percentage (%) |
| 90~100 (excellent) | 24               | 26.9           | 8                | 11.5           |
| 80~90 (good)       | 32               | 52.8           | 25               | 38.6           |
| 70~80 (average)    | 15               | 19.8           | 29               | 44.5           |
| 60~70 (poor)       | 3                | 3.6            | 8                | 10.9           |

achieve better teaching results. At the beginning of the forum, teachers should fully mobilize students' enthusiasm and assign browsing the volleyball forum as a class assignment. At the same time, teachers should pay attention to the quality of posts, which should be relevant, practical, and interesting, so that students can get more knowledge and increase their interest in volleyball by browsing the forum. The teaching mode of the forum is a good solution to the problem of continuity of teaching based on in-class teaching, which makes teachers and students fully interact and form a virtuous cycle, gradually making the forum not only a platform for spreading knowledge, but also a communication platform for students to actively participate in the construction of the forum and join the ranks of spreading volleyball knowledge, and participation in the forum is not limited to students who take the course, but any other students interested in volleyball knowledge can participate in it. Any other students who are interested in volleyball knowledge can participate in it, which also makes the forum teaching mode have a wider meaning. Through the summarization of the questionnaire results and the statistics of the data, it is found that the volleyball forum is a good solution to the problem of the limitation of classroom teaching, and it is a teaching method for students to receive volleyball knowledge delightfully.

TABLE 5: How and how often students use the BBS system to log into the volleyball section.

| Investigation content                     | Option content               | Effective number (62 persons) | Percentage (%) |
|---|------------------------------|-------------------------------|----------------|
| Mobile terminal login                     | Used                         | 25                            | 42.8           |
|   | Not used                     | 37                            | 59.8           |
| Fixed computer login                      | Used                         | 62                            | 100            |
|   | Not used                     | 0                             | 0              |
| Login frequency of BBS volleyball section | Less than once a week        | 0                             | 0              |
|   | Once a week                  | 22                            | 38.5           |
|   | Twice a week                 | 28                            | 49.8           |
|   | More than three times a week | 12                            | 17.6           |

TABLE 6: Reasons for students to visit BBS volleyball section.

| Reason for visit   | Effective number (62) | Percentage (%) |
|--|-----------------------|----------------|
| Acquire relevant knowledge of Volleyball                   | 62                    | 100            |
| Keep in touch with teachers and classmates                 | 38                    | 61.1           |
| Participate in the discussion of relevant volleyball games | 31                    | 50             |
| Have problems that need teachers' help to solve,           | 29                    | 49.2           |
| Others   | 6                     | 11.2           |

#### 4. Conclusions

Computer network-assisted instruction is an effective supplement to the traditional physical education teaching mode, and the teaching experiment effect is remarkable. The application of computer network-assisted volleyball teaching is a further improvement of traditional teaching methods. It is a teaching method to optimize the teaching effect by using modern teaching means. Computer network (CAI)-assisted teaching method can fully mobilize students' subjective initiative, improve students' ability to learn volleyball technology, cultivate independent thinking ability, enable students to find problems in observation, analyze problems in thinking, and solve problems in practice, which is helpful for students to further understand volleyball, find rules and cultivate the consciousness of lifelong physical exercise.

Teachers should pay attention to the improvement of their quality, establish the awareness of modern sports information, combine professional knowledge with modern educational technology, create a network teaching sports resources, and let more students learn sports knowledge better through the network. If possible, teachers should receive systematic computer network course production training to improve their network course production level. Schools should allocate more sports network resources, such as campus network services, establish sports network media courses, and realize the modernization of college sports teaching.

#### Data Availability

The experimental data used to support the findings of this study are available from the corresponding author upon request.

#### Conflicts of Interest

The authors declared that they have no conflicts of interest regarding this work.

#### References

- [1] D. A. El-Moneim, "The effects of multimedia computer-assisted instruction on learning basic ballet skills with physical education students," *Physical Culture and Sport, Studies and Research*, vol. 63, no. 1, pp. 36–41, 2014.
- [2] D. Metwaly, "The effects of multimedia computer assisted instruction on learning the swimming basic skills for physical education students," *Science, Movement and Health*, vol. 16, no. 1, pp. 49–53, 2016.
- [3] Z. Liping, "research on the new college physical education pattern based on information technology," in *Proceedings of the 2017 International Conference on Smart Grid and Electrical Automation (ICSGEA)*, pp. 679–682, IEEE, Changsha, China, May 2016.
- [4] B. Wang, "A study on application of CAI dynamic image-guided method in college physical education technical course," *Research Journal of Applied Sciences, Engineering and Technology*, vol. 5, no. 3, pp. 982–985, 2013.
- [5] G. Gunawan, D. Firmansyah, and W. Widiastuti, "Effect of interactive multimedia learning to learn skills of students sports volleyball," *Journal of Education, Health and Sport*, vol. 9, no. 9, pp. 263–270, 2019.
- [6] S. Kubiyeva, A. Akhmetova, K. Islamova, N. Mambetov, A. Aralbayev, and G. Sholpankulova, "Electronic physical education textbook: effective or not? Experimental study," *International Journal of Emerging Technologies in Learning*, vol. 15, no. 15, pp. 64–78, 2020.
- [7] C.-C. Kao and Y.-J. Luo, "Effects of multimedia-assisted learning on learning behaviors and student knowledge in physical education lessons: using basketball game recording as an example," *International Journal of Emerging Technologies in Learning*, vol. 15, pp. 119–139, 2020.
- [8] H. Deng and J. Wang, "Optimization of computer-aided teaching network management system for college physical education courses," *Computer-Aided Design and Applications*, vol. 18, no. S4, pp. 158–167, 2020.
- [9] H. Che and J. Wang, "A two-timescale duplex neurodynamic approach to mixed-integer optimization," *IEEE Transactions on Neural Networks and Learning Systems*, vol. 32, no. 1, pp. 36–48, 2021.
- [10] H. Che and J. Wang, "A two-timescale duplex neurodynamic approach to biconvex optimization," *IEEE Transactions on Neural Networks and Learning Systems*, vol. 30, no. 8, pp. 2503–2514, 2019.
- [11] Z. Chen, "preliminary design and realization of the computer aided teaching software of volleyball tactics," in *Proceedings of the 2021 4th International Conference on Information Systems and Computer Aided Education*, pp. 1209–1213, Dalian, China, September 2021.
- [12] V. Shute, S. Rahimi, G. Smith et al., "Maximizing learning without sacrificing the fun: stealth assessment, adaptivity and

## Research Article

# Performance Prediction and Action Performance Analysis of Sports Competitive Events Based on Deep Learning

Xiaoying Zhang<sup>1</sup> and Jianqiang Lou <sup>2</sup>

<sup>1</sup>Department of Physical Education University, Communication University of Zhejiang, Hangzhou 310018, China

<sup>2</sup>College of Physical Education and Health, Wenzhou University, Wenzhou 325035, China

Correspondence should be addressed to Jianqiang Lou; 00041058@wzu.edu.cn

Received 22 February 2022; Revised 18 April 2022; Accepted 29 April 2022; Published 27 May 2022

Academic Editor: Man Fai Leung

Copyright © 2022 Xiaoying Zhang and Jianqiang Lou. This is an open access article distributed under the Creative Commons Attribution License, which permits unrestricted use, distribution, and reproduction in any medium, provided the original work is properly cited.

Physical education performance in primary and secondary school classroom education seems mediocre, and many students treat it as a minor subject. With parents and schools paying attention to physical education, physical education performance is very important now, whether in primary and secondary schools or universities. Nowadays, college students have less and less physical exercise, and sports achievements are one of the index achievements for evaluating scholarships. Many teachers also arrange appropriate physical training reasonably in order to improve students' sports achievements. Forecasting sports achievements is the key to making scientific sports training plans. According to the study of college students' group sports achievements, we can predict students' follow-up learning achievements, collect, sort out, and study students' sports achievements information regularly, so as to better guarantee the quality of college sports teaching. This paper compares and analyzes the sports achievements of various schools from the aspects of strength, endurance, and sensitivity. At the same time, it compares and analyzes the sports achievements of major universities. Finally, from the perspective of physical education, this paper analyzes and studies the situation of individual schools and then finds out the pedagogical factors that make them achieve excellent physical education results and puts forward the teaching strategies to improve physical education results, as well as the positive influence of physical education teachers on teaching, school physical education results, and students' physical quality. When teaching courses, use big data mining technology to find qualified students to study the actual teaching needs, recommend an efficient learning curriculum system to students with reference to research conclusions, and give rich material resources. Teachers can teach students in accordance with their aptitude with reference to their usual learning situation, instead of "one size fits all."

## 1. Introduction

In today's new era, physical education is particularly important. Under the expectation of the country, schools, and parents, students' physical education achievements in schools always affect students' general subject achievements. For the prediction of students' sports achievements, teachers arrange a series of different sports trainings to teach students in accordance with their aptitude. Literature [1] expounds the influence of extracurricular sports on academic achievements. References [2, 3], respectively, use particle swarm optimization and PSO-SVM learning methods to predict sports performance. Literature [4] proposes a sports performance prediction algorithm combining gray

prediction features with CNNs and optimizes the sports competition performance prediction model of extreme learning machine based on the Drosophila algorithm in literature [5], so that the performance prediction can achieve higher prediction accuracy and computational efficiency. Reference [6] uses factor analysis to study and analyze the performance of the prediction model. Literature [7] puts forward a prediction model with higher accuracy, which provides a new research idea for the prediction of sports achievements. Using the information technology in reference [8], this paper predicts and analyzes the sports training plan and quantitative load arrangement. Based on the machine learning in literature [9] and literature [10], this paper predicts and analyzes the college sports achievements.

For the calculation of students' endurance scores, the management system of students' exercise prescription based on BP neural network in literature [11] is used. Through the hybrid genetic neural network in literature [12], the special performance of athletes is predicted. Literature [13] expounds the neural network prediction model to predict the performance of speed skating. Literature [14] expounds the application and prospect analysis of artificial neural network in competitive sports. Literature [15] studies the analysis of influencing factors of sports performance and the ways to improve sports performance mentioned in literature [16]. Literatures [17, 18] analyze various factors affecting sports performance. This paper analyzes the influence of school factors on students' sports achievements [19]. Literature [20] uses intelligent technology to improve the reference value of academic performance and models based on the LSTM model in literature [21] and puts forward the main factors affecting academic performance and judgment methods. The trend of performance change is proposed to analyze the factors affecting performance in the literature [22]. Literature [23] expounds the application of multiple linear regression in college achievement prediction. Literature [24] predicts and empirically analyzes CET-4 scores, while literature [25] judges the difficulty of learning and studies and analyzes the accuracy of scores.

## 2. Influencing Factors and Improvement Methods of Sports Achievements

*2.1. Influence of Physical Training on Sports Performance.* Physical fitness plays a significant role in promoting human health, developing physical fitness, and improving immunity. The diversity of training also determines the enthusiasm of students to carry out physical training in physical education. Due to the relative lag of physical training, there are few studies on the influence of physical training methods on sports achievements. Under the background of the new curriculum standard of physical education and health, students cannot do without physical training if they want to have sports skills and get strong physique. Offering physical education courses in schools can effectively improve students' strength, speed, sensitivity, and other sports skills and promote students' healthy development. Training in this area has a positive role in promoting. It should be pointed out that in the teaching process, teachers should, according to the characteristics of sports events, focus on developing students' physical fitness. According to different training purposes, physical training to improve students' fitness ability can usually be subdivided into general physical training and special physical training. Among them, general physical training is the basis of special physical training. The main purpose is to improve the individual's physical function level and promote the all-round development of physical quality, while special physical training is highly related to special physical training, which mainly develops the specific sports quality needed to complete specific skills and tactics in special projects, and is the basis for improving and enhancing special sports ability. Reasonable training of physical fitness can certainly promote the best sports

performance. The framework diagram of the physical fitness system is shown in Figure 1.

*2.2. Effective Means to Improve Sports Performance.* In recent years, with the implementation and promotion of physical education entrance examination in all parts of the country, the scores of physical education entrance examination have been improved in some areas, which make the importance of preparing for physical education entrance examination increasingly prominent. This paper analyzes the present situation of endurance quality of junior high school students. It is found that the third grade students' knowledge and understanding of endurance events are not complete, their scores in endurance events are relatively poor in physical examination, and their enthusiasm for physical training is not high at ordinary times. A large number of students feel that endurance events have great room for improvement. Junior three students are not interested in endurance quality training, and their grades improve slowly. The reasons can be summarized as three aspects: monotonous practice methods, insufficient venues and facilities, and insufficient attention from schools and parents. For endurance training, change the traditional training methods, increase the interest of training content, and stimulate students' training interest and participation enthusiasm. Increase the publicity of endurance quality, improve students' understanding of endurance quality, and strengthen the communication and contact between schools and parents through the combination of home and school. Increase capital investment, improve equipment and site construction, improve teachers' teaching ability and professional quality, and create good conditions for students' endurance quality training. The framework diagram of endurance training is shown in Figure 2.

*2.3. The Influence of Physical Condition on Performance.* Students' training performance is determined by their comprehensive physical condition. In the research, it is difficult to judge that a certain physical health index has a direct impact on sports performance. This time we studied the influence of a single index on 1000 m long-distance running. The morning pulse is analyzed, as shown in Figure 3.

In Figure 3, we can see that the morning pulse is unstable because the physical strength and physical condition are exhausted during training, so the performance drops obviously in the subsequent training.

## 3. Deep Learning Sports Performance Prediction

Deep learning framework diagram is shown in Figure 4.

*3.1. Neural Network.* BP neural network is the fastest and most flexible algorithm among all neural networks, which can accurately describe the curve change characteristics of the system. Let the input of the system be  $x(i)$ ,  $i = 1, 2, \dots, n$ ,

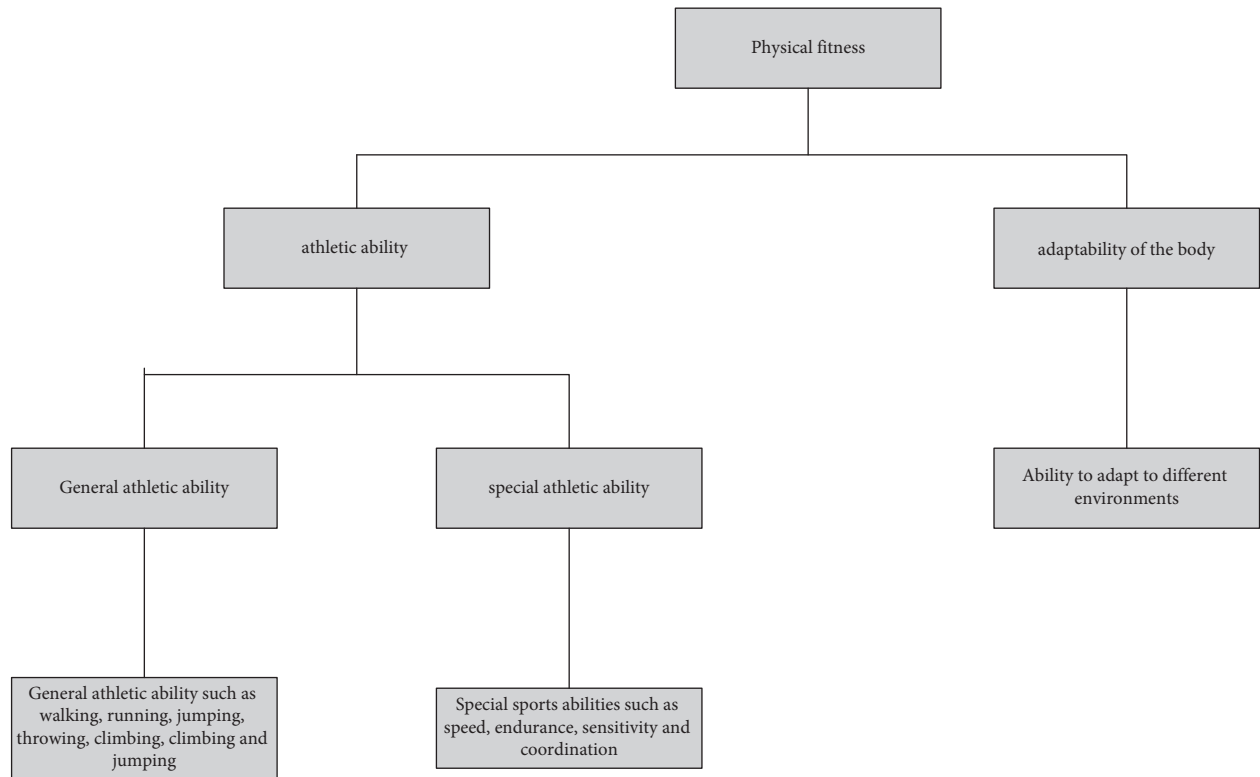


FIGURE 1: Macroscopic system diagram of physical fitness.

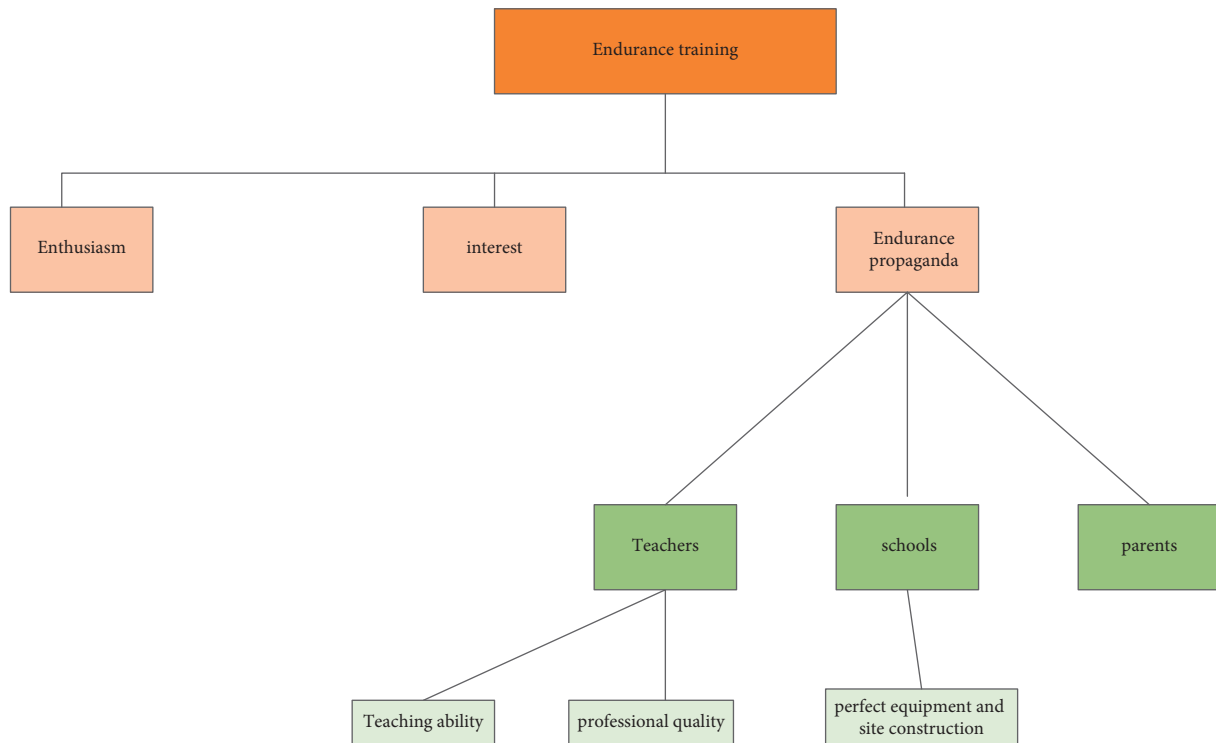


FIGURE 2: Endurance training frame diagram.

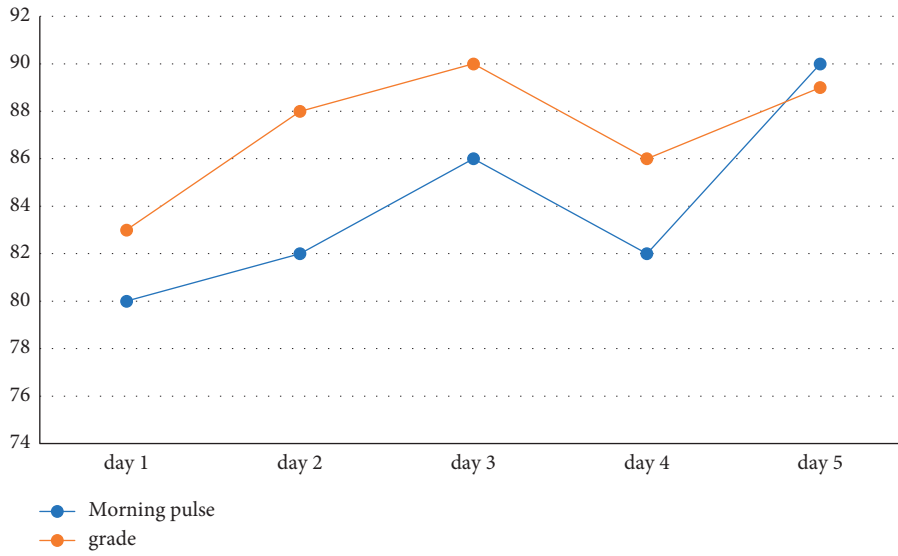


FIGURE 3: Relationship between morning pulse and performance.

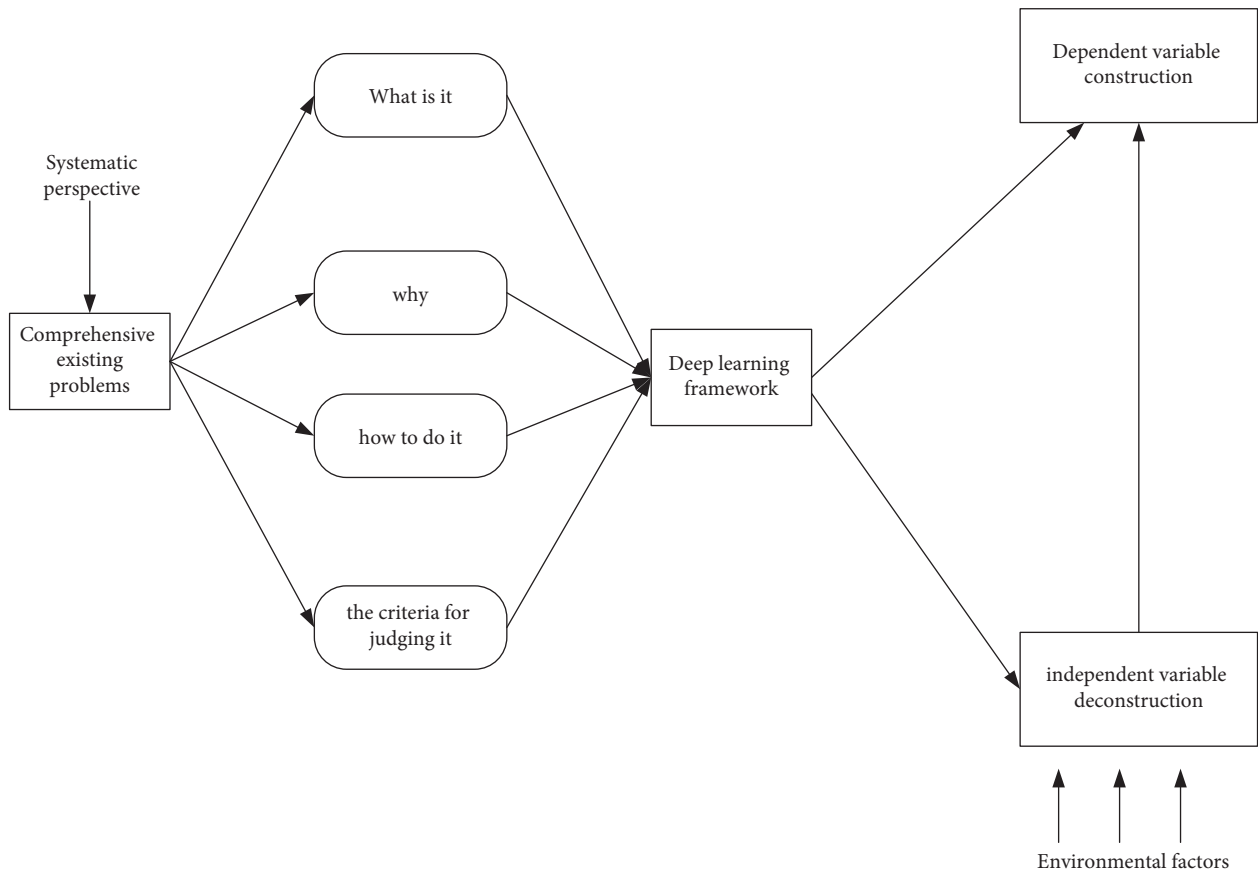


FIGURE 4: Deep learning framework.

and the expressions of the input vector and output vector of the hidden layer of the neural network are as follows:

$$S_i = \sum_{i=1}^m w_{ij}x(i) - \theta_j, \quad (1)$$

$$b_j = \exp\left(\sum_{i=1}^n w_{ij}x_i - \theta_j\right). \quad (2)$$

The input vectors and output vectors of the output layer are as follows:

$$L = \sum_{j=1}^p w_{jk}b_j - \theta_k, \quad (3)$$

$$x_{i+1} = \exp\left(\sum_{j=1}^n v_jb_j - \gamma\right). \quad (4)$$

**3.2. Optimize Neural Network Algorithm.** According to the luminous form of fireflies to attract other fireflies [26], different positions of fireflies represent different solutions of the problem and the luminous brightness corresponds to the fitness function. The greater the fitness value, the stronger the luminous brightness. The firefly with weak brightness is getting closer and closer to the firefly with strong brightness and keeps approaching the firefly with the strongest brightness. Because the position of the firefly with the strongest brightness indicates the optimal solution of the problem, the following assumptions are made first:

Brightness is determined by the fitness function of the problem: on the basis of satisfying the above assumptions, the brightness  $M_0$  and attractiveness of fireflies are defined to represent the brightness of a firefly itself, so the received brightness of fireflies is as follows:

$$M = M_0e^{-\gamma r}, \quad (5)$$

where  $\gamma$  is the light intensity absorption factor and  $r$  is the distance.

The attractivity calculation formula is as follows:

$$\beta = \beta_0e^{-\gamma r}. \quad (6)$$

If  $r=0$ , the attractivity is  $\beta_0$ .

If the two fireflies are  $i$  and  $j$ , respectively, and the condition  $M_0(i) > M_0(j)$  is satisfied, then  $i$  is attracted by  $j$  and changes its position; that is, there are

$$x_i t + 1 = x_i t + \beta_0 e^{-\gamma r} (x_j t - x_i t) + \partial \epsilon_i, \quad (7)$$

where  $\partial$ ,  $\epsilon_i$  is a random number.

The attractivity coefficient is improved, and the change rule is as follows:

$$\beta_0 = \begin{cases} \beta_{\text{begin} \times \sigma_\beta, \beta_0 > \mu} \\ \mu, \beta_0 < \mu \end{cases}, \quad (8)$$

$$\gamma = \gamma_{\text{begin} \times \sigma_\gamma}. \quad (9)$$

At the initial stage, the value of  $\beta_0$  is relatively large and the search range is large, as the number of moves increases. With the increase in iteration times, the attractiveness becomes smaller, and the optimal position can be found quickly.

**3.3. Sports Performance Prediction Model.** The data value of sports achievements can be regarded as a group of irregular time series, and the fitting state model of sports achievements described by a multivariate statistical characteristic equation is as follows:

$$\begin{pmatrix} X \\ P(X) \end{pmatrix} = \begin{cases} a_1, a_2, a_3, \dots, a_n \\ p(a_1), p(a_2), p(a_3), \dots, p(a_n) \end{cases}. \quad (10)$$

Through discrete analytic processing of data, the information entropy of distribution characteristics of sports achievements is as follows:

$$H(X) = E(I(a_i)) = \sum_{i=1}^m p(a_i) \log_2 p(a_i). \quad (11)$$

The auxiliary spatial test cumulant of time series  $X$  for sports achievements is as follows:

$$C = \frac{(x_n - \bar{x})(x_{n-d} - \bar{x})(x_{n-D} - \bar{x})}{(x_n - \bar{x})^3}. \quad (12)$$

Take the average value

$$\langle x(n) \rangle = \frac{1}{N} \sum_{n=1}^N x(n). \quad (13)$$

For the statistical sequence  $x(n)$  of sports achievements with multivariate variables, the statistical characteristic quantities of sports achievements expressed by scores and generalized integro-differential equations are as follows:

$$\begin{aligned} c_{1x}T &= E\{xn\} = 0, \\ c_{2x}T &= E\{xnxn + T\} = r(T), \\ c_{kx}T_1, T_2, T_3, \dots, T_{k-1} &= 0, k \geq 3. \end{aligned} \quad (14)$$

Constraints are as follows:

$$\delta_x(\omega) = \ln \varphi_x(\omega) = -\frac{1}{2}\omega^2 \sigma^2. \quad (15)$$



The constraint variables of environmental factors are

$$\begin{aligned} c_k &= \frac{1}{j^k} \left[ \frac{d_k}{w_k} \ln \varnothing_x \omega \right]_{w=0} \\ &= -j^k \left[ \frac{d_k}{w_k} \ln \varnothing_x \omega \right]_{w=0} \\ &= -j^k \varnothing_x^k 0. \end{aligned} \quad (16)$$

In order to maintain the initial data characteristics of sports achievements, the statistical model is reconstructed:

The information characteristic state equation of statistical sports achievements obtained by the mathematical method of least square estimation is as follows:

$$E((u(t)), u_t t) = \int_{IR} \frac{1}{2} (|\nabla u t|^2 + |u t|^2) + \frac{1}{6} |u t|^6 dx. \quad (17)$$

The control objective function of sports performance prediction is as follows:

$$\begin{aligned} &\max_{x_{a,b,d,p}} \sum_{a \in A} \sum_{b \in B} \sum_{d \in D} \sum_{p \in P} x_{a,b,d,p} V_p^3 \\ &\sum_{a \in A} \sum_{b \in B} \sum_{d \in D} \sum_{p \in P} x_{a,b,d,p} R_p^{bw} \leq K_b^{bw} S, b \in B. \end{aligned} \quad (18)$$

$R_p$  denotes prediction factor and  $K_b$  denotes prediction plus carrier.

The probability density functional coefficient of sports performance prediction is as follows:

$$K = (4\beta\tau P\sigma^{-a})^{1/2} \cdot (2^{-a/2} P\sigma^{-a} - \beta N_0)^{-1/a} + 1 + \sqrt{2}. \quad (19)$$

The confidence degree of the accuracy of sports performance prediction is as follows:

$$\begin{aligned} &c_1 e^{\lambda_1 t} + c_2 e^{\lambda_2 t} (\lambda_1 \neq \lambda_2), \\ &f(x_1, x_2, i) - g(y_1, y_2, i) \\ &+ \int (h(x_1, x_2, i) - g(y_1, y_2, i)) dx < x(|x - y|^2 + x|x - y|^2). \end{aligned} \quad (20)$$

The eigendecomposition values of the self-similar regression model meet the following requirements:

$$Y(P, Q, ) = Y[re d(P, Q, \beta), Q, \beta]. \quad (21)$$

## 4. Experiments

**4.1. Contents of the Experiment.** A 1000 m long-distance running of 30 college students in a university is selected as an experimental object. The neural network adopted has three input nodes and one output node. The population of the particle swarm optimization method is  $m = 20$ , and the initial value of inertia weight is 1. With the gradual decrease in iteration times, the inertia weight is reduced to 0.5. When the iteration times reach the maximum, the iteration stops. Comparing the prediction data of this method with other common neural network optimization methods, the results are shown in Table 1.

In the data of Table 1, the prediction error and convergence time of the BP neural network algorithm are obviously better than those of the other two sports performance prediction methods. Judging from the prediction error of college students' sports achievements, the prediction error of this method is always lower than that of the other two methods, which shows that BP neural network method has the best prediction effect.

Ten college students were randomly selected to predict the performance of 100-meter sprint, which were compared by the BP neural network method, GDX method, and LM method under deep learning. Channel theory formula is a method of buying and selling stocks by technical means and empirical judgment. This formula smoothes and corrects the trend line, which reflects the running law of stock price more accurately. When the stock price rises to the pressure line, investors sell the stock, and when the stock price falls to the support line, investors make up accordingly. The difference between the predicted results and the actual demerits is tested as shown in Figures 5–7.

It can be seen from Figures 5–7 that the difference between the actual value and the predicted value of sports achievements predicted by the BP neural network algorithm is not big, and the other two algorithms have large errors, which shows that the prediction efficiency and accuracy of sports achievements predicted by the BP neural algorithm are higher.

**4.2. Simulation Experiment.** The samples are selected from the sports achievements of college students, including 3 km long-distance running, 100 m sprint, skipping rope, archery, and yoga. Various sports can also test the universality of the prediction model under deep learning. All the data are analyzed according to three methods, and the waveform description diagram of sports performance prediction is obtained as shown in Figure 8.

The prediction effect of sports performance is universal in various events, as shown in Table 2.

The results of five sports events were compared with the prediction model such as genetic algorithm [27] and particle swarm optimization algorithm [28] as shown in Table 3.

The fitting accuracy is the deviation between the predicted value and the actual value in the past five years after we make a time series model and determine the model parameters.

Taking the sports performance statistics collected above as the test sample set, the simulation analysis of the sports performance prediction model is carried out, and the comparison results of prediction errors under different algorithms are obtained as shown in Figure 9.

Test the performance of the model to evaluate whether the model for predicting sports performance has practical applicability. The test results are as shown in Table 4.

**4.3. Model Comparison.** The prediction accuracy of the model is compared, as shown in Figure 10.

TABLE 1: Prediction results of different neural network methods.

| Method | BP               |                      | GDX              |                      | LM               |                      |
|--------|------------------|----------------------|------------------|----------------------|------------------|----------------------|
|        | Prediction error | Convergence time (s) | Prediction error | Convergence time (s) | Prediction error | Convergence time (s) |
| 100    | 0.021            | 4.1                  | 0.028            | 8.3                  | 0.031            | 15.1                 |
| 200    | 0.032            | 5.2                  | 0.041            | 15.3                 | 0.042            | 16.2                 |
| 300    | 0.043            | 5.6                  | 0.047            | 15.9                 | 0.053            | 16.9                 |
| 400    | 0.048            | 6.3                  | 0.052            | 16.6                 | 0.068            | 17.3                 |
| 500    | 0.052            | 7.1                  | 0.055            | 17.5                 | 0.072            | 18.1                 |
| 600    | 0.059            | 7.9                  | 0.062            | 18.3                 | 0.079            | 18.9                 |
| 700    | 0.064            | 8.6                  | 0.066            | 18.8                 | 0.084            | 19.6                 |
| 800    | 0.071            | 9.2                  | 0.074            | 19.4                 | 0.091            | 20.4                 |
| 900    | 0.079            | 9.6                  | 0.082            | 20.1                 | 0.099            | 22.1                 |
| 1000   | 0.083            | 10.1                 | 0.089            | 20.9                 | 0.103            | 25.6                 |

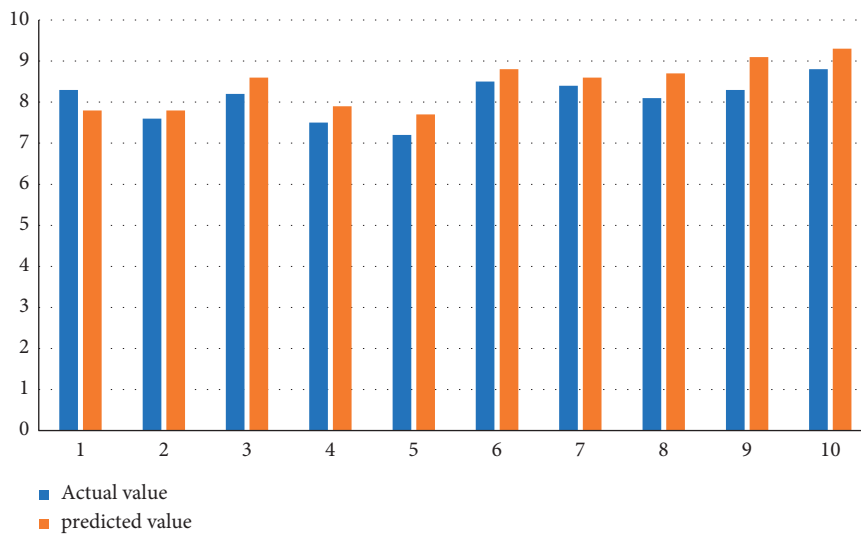


FIGURE 5: GDX prediction method.

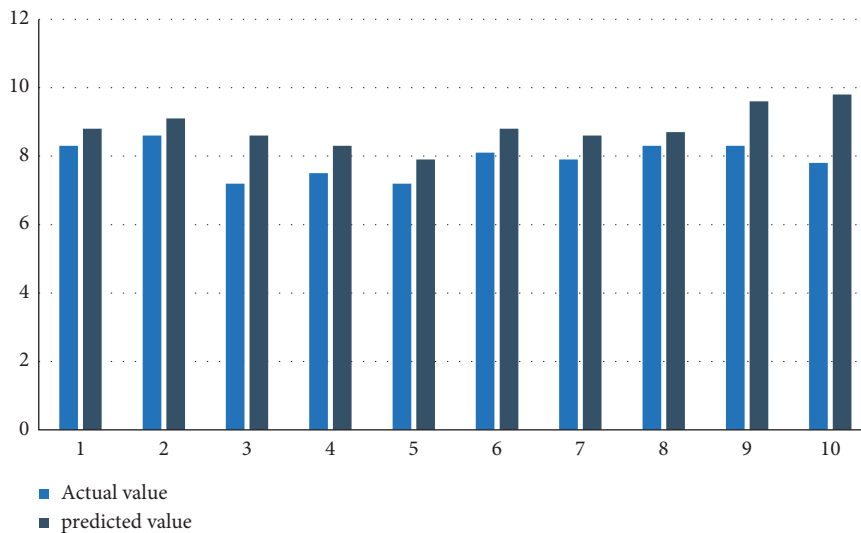


FIGURE 6: LM prediction method.

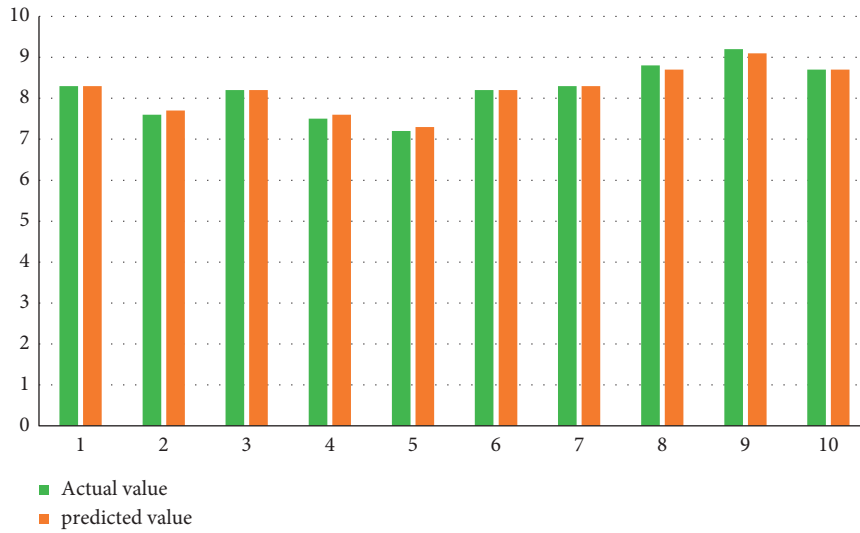


FIGURE 7: BP neural network prediction method.

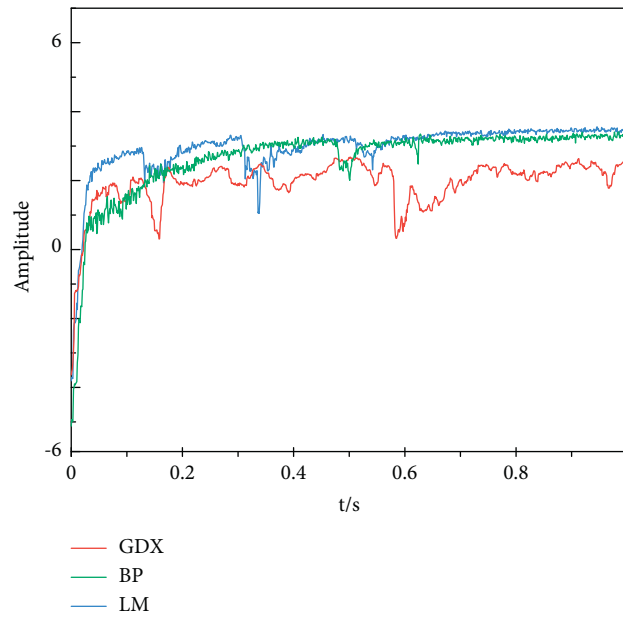


FIGURE 8: Time domain waveform diagram of sports achievements.

TABLE 2: Versatility testing.

| Numbering | Sports events              | Fitting accuracy (%) | Prediction accuracy (%) |
|-----------|----------------------------|----------------------|-------------------------|
| 1         | 3 km long-distance running | 90.12                | 88.3                    |
| 2         | 100 m sprinting            | 92.2                 | 89.1                    |
| 3         | Skipping rope              | 93.1                 | 90.2                    |
| 4         | Archery                    | 95.21                | 91.1                    |
| 5         | Yoga                       | 94.23                | 89.7                    |

TABLE 3: Test results of the universal model.

| Numbering | Model   | Fitting accuracy (%) | Prediction accuracy (%) |
|-----------|---|----------------------|-------------------------|
| 1         | Multiple regression model                     | 84.65                | 82.4                    |
| 2         | Genetic algorithm                             | 82.3                 | 81.3                    |
| 3         | Particle swarm optimization algorithm         | 85.6                 | 84.8                    |
| 4         | Firefly optimizes BP neural network algorithm | 96.5                 | 97.4                    |

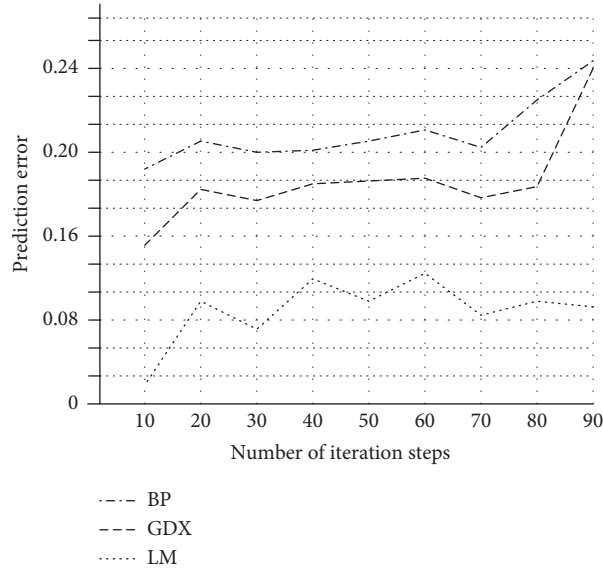


FIGURE 9: Error analysis of sports performance prediction.

TABLE 4: Performance comparison of three methods.

| Performance          | BP     | LM     | GDX    |
|----------------------|--------|--------|--------|
| Convergence speed    | Fast   | Medium | Slow   |
| Model structure      | Simple | Medium | Medium |
| Anti-noise strength  | Strong | Medium | Medium |
| Data requirements    | Medium | High   | High   |
| Prediction accuracy  | High   | Low    | Low    |
| Application range    | Wide   | Medium | Medium |
| Development prospect | Big    | Medium | Medium |

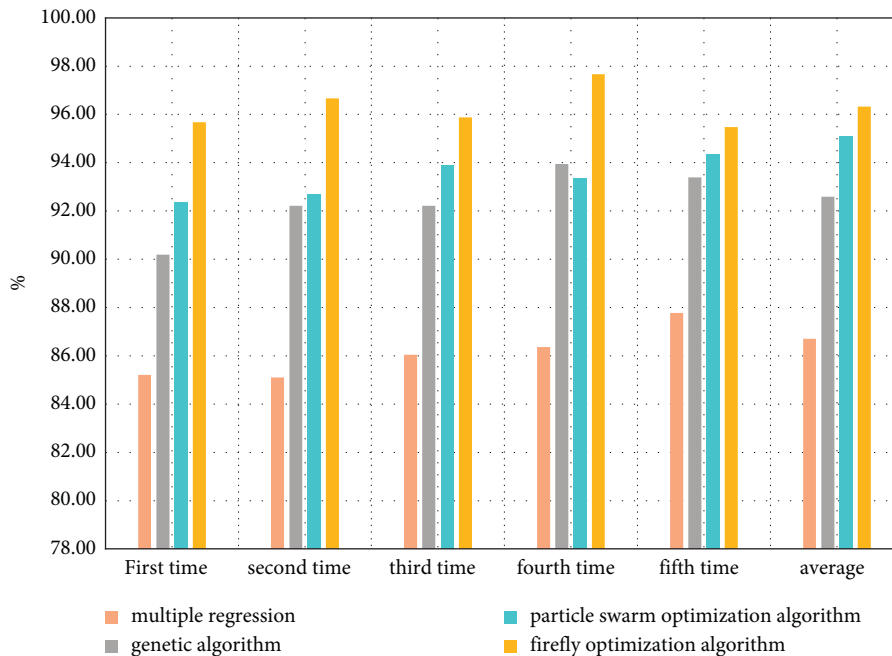


FIGURE 10: Comparison of prediction accuracy of different models.

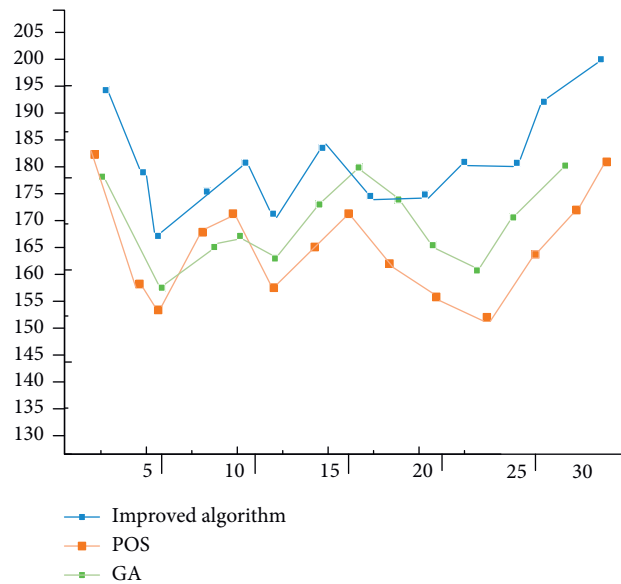


FIGURE 11: Algorithm comparison experiment.

4.4. *Comparison of Optimization Algorithms.* Comparison diagram combined with the firefly algorithm and neural network BP algorithm for optimization and improvement is as shown in Figure 11.

## 5. Conclusion

Reasonable physical training in schools can improve students' physical quality on the one hand and get higher physical performance on the other hand. In order to improve students' overall academic performance, teachers make different physical training plans according to different physical indicators of each student, so as to make students' predicted physical performance reach the best. Combined with the deep learning method, this paper constructs an optimization model that can make the predicted value of sports achievements achieve high precision and low error, as follows:

- (1) The BP algorithm, LM algorithm, and GDX algorithm are compared with the difference of prediction error and convergence time. It is obvious that the error value of the BP neural network algorithm is obviously lower than that of the other two algorithms, and the convergence time is also higher than the other two algorithms.
- (2) According to the three algorithms, the difference between the actual value and the predicted value of sports achievements is compared, and it is obvious that the actual value and the predicted value of sports achievements predicted by the other two algorithms are quite different.
- (3) According to the simulation experiment, different sports items are selected to test the universality of the model. The fitting accuracy and prediction accuracy of the firefly optimized BP algorithm are obviously more than 5% higher than those of the three models.

- (4) By comparing the performance of three algorithms under deep learning, it can be concluded that the BP neural network model is more practical.
- (5) Select five different samples, mathematical model, neural network algorithm, optimization algorithm, and other four different models to test and compare the prediction accuracy. The error under the mathematical model is the largest, and the firefly algorithm based on the neural network algorithm is the best.

## Data Availability

The experimental data used to support the findings of this study are available from the corresponding author upon request.

## Conflicts of Interest

The authors declare that they have no conflicts of interest.

## References

- [1] Y. Dong and C. Zhu, "Research on the influence of teenagers' extracurricular sports on academic performance-also on the mediating effect of non-cognitive ability," *Physical Education Research*, vol. 34, no. 6, pp. 52–62, 2020.
- [2] S. Wang, "Prediction of college students' sports performance based on particle swarm optimization neural network," *Microcomputer Applications*, vol. 36, no. 9, pp. 143–145 +159, 2020.
- [3] H. Guo and H. Yang, "Sports performance prediction model based on PSO-SVM," *Electronic Measurement Technology*, vol. 43, no. 17, pp. 87–91, 2020.
- [4] X. Zhang, C. Guo, Z. Guo, and Z. Xin, "Combining gray prediction characteristics with CNNs' information service sports performance prediction," *Journal of Shenyang University of Technology*, vol. 42, no. 4, pp. 432–436, 2020.

- [5] W. Zhang, M. Yan, Z. Gao, and Z. Liu, "Research on sports competition performance prediction based on Drosophila algorithm to optimize extreme learning machine," *Micro-computer Applications*, vol. 34, no. 3, pp. 58–61, 2018.
- [6] J. Yao, L. Yan, X. Chen, and J. Su, "Research on the promotion effect of peer dialogue feedback based on real-time interaction on college students' classroom deep learning," *Audio-visual Education Research*, vol. 43, no. 1, pp. 113–121, 2022.
- [7] H. Liu and S. S. Y. Au-Yeung, "Reliability of transcranial magnetic stimulation induced corticomotor excitability measurements for a hand muscle in healthy and chronic stroke subjects," *Journal of Neurological Sciences*, vol. 341, no. 1-2, pp. 105–109, 2014.
- [8] D. Wang, "Research on applying information technology to determine load prescription and performance prediction in sports training," *Contemporary Sports Science and Technology*, vol. 3, no. 2, pp. 21–22, 2013.
- [9] J. Wong, "Prediction and analysis of college sports achievements based on machine learning," *Modern Electronic Technology*, vol. 40, no. 17, pp. 116–119, 2017.
- [10] X. Shen, B. Zhang, and F. Rui, "Research on deep learning activities in blended learning environment: trio of design, implementation and evaluation," *Audio-visual Education Research*, vol. 43, no. 1, pp. 106–112+121, 2022.
- [11] X. Liu, L. Zhou, and Y. Yan, "Student exercise prescription management system based on BP neural network," *Zhejiang Sports Science*, vol. 37, no. 5, pp. 79–84, 2015.
- [12] De Ma, S. Li, and J. Zhang, "Design of athletes' special performance prediction system based on hybrid genetic neural network," *Modern Electronic Technology*, vol. 41, no. 8, pp. 183–186, 2018.
- [13] Y. Li and Y. Sheng, "Neural network model for predicting speed skating performance," *Ice and Snow Sports*, vol. 32, no. 3, pp. 60–63, 2010.
- [14] Nankai, "Application and prospect analysis of artificial neural network in competitive sports," *Journal of Jilin Institute of Physical Education*, vol. 25, no. 3, pp. 39–40, 2009.
- [15] D. Fang, "Research on the influencing factors of sports performance created by sports teams in colleges and universities-Taking Guilin Institute of Aerospace Technology as an example," *Contemporary Sports Science and Technology*, vol. 11, no. 29, pp. 93–95, 2021.
- [16] J. Chen and J. Lin, "Study on the influencing factors and ways to improve the sports scores of the senior high school entrance examination-taking Fuzhou Pingtung Middle School as an example," *Contemporary Sports Science and Technology*, vol. 11, no. 11, pp. 216–219, 2021.
- [17] Y. E. Zhang, "The influence of subjective and objective factors on students' grades in the physical examination for junior high school graduation," *Neijiang Science and Technology*, vol. 34, no. 2, pp. 197–198, 2013.
- [18] Y. Tang, "Multivariate analysis of influencing the test results of physical examination in rural middle schools in Hengyang City," *Contemporary Sports Science and Technology*, vol. 5, no. 7, pp. 124–125, 2015.
- [19] Jeff, "Analysis of the influence of school factors on the academic performance of students majoring in physical education," *Contemporary Sports Science and Technology*, vol. 4, no. 18, p. 53 +55, 2014.
- [20] G. Li and Y. Qi, "Research on the competency model of university teachers under the background of curriculum ideological and political education," *2021 3rd International Conference on Applied Machine Learning (ICAML)*, vol. 33, no. 1, pp. 36–41, 2021.
- [21] H. Cao and X. Jin, "Research on LSTM-based academic performance prediction and its influencing factors," *Journal of Beijing University of Posts and Telecommunications*, vol. 22, no. 6, pp. 90–100, 2020.
- [22] S. Li, Y. Su, C. Huang, P. Wang, and T. Ren, "Multi-task performance prediction model based on performance change trend," *Journal of Changchun University of Science and Technology (Natural Science Edition)*, vol. 42, no. 5, pp. 122–127, 2019.
- [23] H. Wang, "Application of multiple linear regression in college achievement prediction," *Journal of Baoshan University*, vol. 39, no. 5, pp. 84–88, 2020.
- [24] G. Zhao, S. Wang, and H. Sun, "Construction and empirical analysis of CET-4 score prediction model," *Western China Science and Technology*, vol. 14, no. 4, pp. 94–95 +98, 2015.
- [25] H. Wu and D. Zhang, "An experimental study on the influence of task cues on the judgment and accuracy of learning difficulty," *Psychological Science*, vol. 36, no. 3, pp. 566–570, 2013.
- [26] J. Senthilnath, S. N. Omkar, and V. Mani, "Clustering using firefly algorithm: performance study," *Swarm and Evolutionary Computation*, vol. 1, no. 3, pp. 164–171, 2011.
- [27] O. E. Canyurt and H. K. Öztürk, "Three different applications of genetic algorithm (GA) search techniques on oil demand estimation," *Energy Conversion and Management*, vol. 47, no. 18–19, pp. 3138–3148, 2006.
- [28] N. Zeng, H. Zhang, Y. Chen, B. Chen, and Y. Liu, "Path planning for intelligent robot based on switching local evolutionary PSO algorithm," *Assembly Automation*, vol. 36, no. 2, pp. 120–126, 2016.

## Research Article

# Residential Energy-Saving Lighting Based on Bioinspired Algorithms

Yuhang Wu,<sup>1</sup> Yitong Zhang,<sup>1</sup> Nah Ilmin ,<sup>1</sup> and Jing Sui <sup>2,3</sup>

<sup>1</sup>Graduate School of Technical Design Staff, Kookmin University, Seoul 02707, Korea

<sup>2</sup>Kookmin University, Graduate School of Techno Design (TED), Seoul 02707, Korea

<sup>3</sup>LuXun Academy of Fine Arts, Shenyang 110003, China

Correspondence should be addressed to Nah Ilmin; [ilminnah@kookmin.ac.kr](mailto:ilminnah@kookmin.ac.kr) and Jing Sui; [suijing@lumei.edu.cn](mailto:suijing@lumei.edu.cn)

Received 4 March 2022; Revised 12 April 2022; Accepted 30 April 2022; Published 27 May 2022

Academic Editor: Man Fai Leung

Copyright © 2022 Yuhang Wu et al. This is an open access article distributed under the Creative Commons Attribution License, which permits unrestricted use, distribution, and reproduction in any medium, provided the original work is properly cited.

Traditional residential lighting systems have the problem of high energy consumption. Based on artificial neural network (ANN), combined with particle swarm optimization algorithm, and genetic algorithm to optimize the initial weights and thresholds, an improved ANN prediction model for residential energy-saving lighting is proposed, and an actual residential lighting project is taken as an example to verify it. The results show that the proposed method can quickly predict the number of residential lighting lamps under the premise of meeting the standard illumination of residential lighting. The prediction accuracy can reach 98.45%, which has the characteristics of high prediction accuracy and small error. Compared with the ANN model and ANFIS model, the average relative error of the proposed prediction model is reduced by 2.29% and 0.87%, respectively, which has certain effectiveness and superiority. It provides a new idea for residential energy-saving lighting.

## 1. Introduction

In line with the concept of scientific and sustainable development, people's awareness of energy conservation and environmental protection has gradually been raised, which is manifested in water conservation, energy conservation, and emission reduction. Moreover, residential buildings are the essential material form of human beings, and their energy conservation and environment protection can save social resources to a large extent, which has important significance for the environment protection and pollution abatement. Energy-saving and environmental protection of residential buildings can be realized in various ways. For example, N. Thejo Kalyani et al studied different organic materials synthesized by organic light-emitting diodes. A new organic light-emitting diode (OLED) is prepared, and energy-saving lighting is realized [1]. Sadeghian Omid et al analyzed the potential of different energy-saving schemes and their environmental impact, discussed the use of renewable energy and energy-saving lamps and other direct energy-saving schemes, and realized the energy-saving and emission

reduction by using alternating energy storage system control strategies and technologies [2]. Under different climate conditions, Maučec Damjan et al. carried out sensitivity analysis on different input parameters where global sensitivity analysis technology based on elementary effect is adopted. The main design parameters affecting energy saving are determined, and the energy saving of timber structure building is realized by adjusting these parameters [3]. Grobe Oliver Lars innovated the windowing irregular reflection and transmission, and thus, the solar radiation is redirected, selectively admitted, or blocked. Also, the modeling technology of optical complex fenestration is proposed. Finally, the design of energy-saving green buildings is realized [4]. In the environment of the oil crisis and global warming caused by emissions of greenhouse gases, Vasiliu A et al. took Romania residence as the research object and adopted a cross-dialectical analysis method to analyze passive energy-saving buildings, such as low energy consumption, green house, and net zero-energy buildings. Thus, they thought that residential building designed according to Nzeb standard can meet the low energy

consumption residential minimum requirements [5]. Rijal Hom B et al collected 19,081 pieces of thermal comfort data from 94 households in 69 apartments in Japan, connected indoor comfort temperature with outdoor temperature, quantified changes in the thermal environmental comfort temperature of Japanese residential buildings with seasons, and established a domestic adaptability model of Japanese high-insulation residential buildings. Adaptive thermal comfort energy-saving building is designed [6]. Based on data mining techniques, Himmetoğlu Salih et al. proposed a multifactor PSACONN analysis framework to study the influence of climate and building enclosure structure on building heat (heat and cold) energy consumption at the design stage. It is found that the estimation accuracy of this framework reaches 99% and 98%, respectively, which can effectively find the envelope combination that provides the minimum energy consumption for different climate regions and realize the residential energy saving [7]. Wu Weidong et al. reconstructed the reference building envelope and renewable energy system with zero-energy consumption, constructed the control function, and optimized the solution to obtain the optimal reconstruction scheme, which provides guidance for the reconstruction of zero-energy residential buildings [8]. Among them, under the premise of ensuring the standard lighting intensity, using limited resources to create a good lighting environment and realize energy saving is the most common way at present. However, as the characteristics of three-dimensional spatial distribution and dynamic time change of residential lighting, there are many nonlinear relationship problems in residential lighting, which is a great challenge to the design of residential energy-saving lighting.

## 2. Basic Methods

**2.1. ANN Networks.** ANN network is a complex network system that simulates human brain behavior and consists of a large number of neurons. It has intelligent processing functions such as learning and computing. There are many ANN network models, including the Hopfield model and BP model. For the convenience of explanation, the BP network model is used to illustrate where the input and output of BP network model can be expressed by activation function or transfer function, and neurons at each layer have a certain threshold and internal state [9]. In the BP model, there are three layers: input layer, hidden layer, and output layer. Furthermore, each layer of neurons only receives the neurons' output of the previous layer, and output information is generated through the weight of each layer and changes of each neuron, which are shown in Figure 1.

As can be seen from the figure, input  $X_j$  and output  $O_j$  of the neuron at layer  $j$  can be expressed as

$$\begin{aligned} X_j &= \sum_i W_{ji} \bullet O_i, \\ O_j &= F(X_j), \end{aligned} \quad (1)$$

where  $W_{ji}$  is the weight of layer  $j$  and layer  $i$ ;  $f$  is the activation function, usually an S-type function.

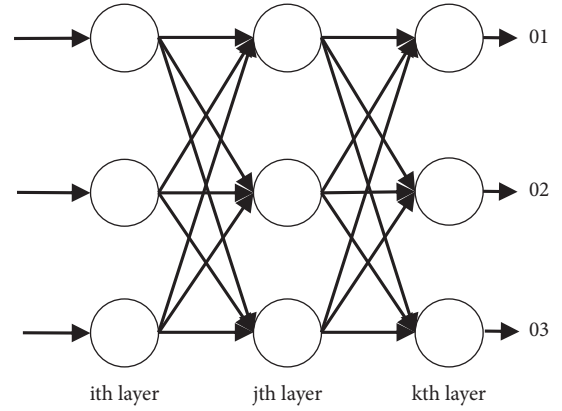


FIGURE 1: Schematic diagram of BP network model.

$$f(x) = \frac{1}{1 + \exp[-\beta(x - \theta)]}, \quad (2)$$

where  $\beta$  is the slope of the activation function;  $\theta$  is the neuron threshold.

For  $k$  samples, BP network training output error is

$$\varepsilon_k = t_k - O_k, \quad (3)$$

where  $t_k$  and  $O_k$  are the target output and real output of  $k$ .

The total error function is

$$E = \frac{1}{2} \sum_k (t_k - O_k)^2. \quad (4)$$

In the whole BP network training, the adjustment rule of weight is as follows [10]:

$$\Delta W_{kj} = -\eta \bullet \frac{\partial E}{\partial W_{kj}}, \quad (5)$$

where  $\eta$  is the learning rate. By substituting the above formula into (4), the adjustment rules of weight can be obtained.

$$\Delta W_{kj}(n+1) = \eta \bullet \delta_k \bullet O_j, \quad (6)$$

$$\Delta W_{ji}(n+1) = \eta \bullet \delta_j \bullet O_i. \quad (7)$$

Node  $\delta_j$  of hidden layer and node  $\delta_k$  of output layer can be expressed as

$$\delta_j = O_j(1 - O_j) \bullet \sum_k W_{kj} \bullet \delta_k, \quad (8)$$

$$\delta_k = (t_k - O_k) \bullet (1 - O_k).$$

In practical application, the momentum factor is usually introduced to adjust weight, so (6) and (7) can be rewritten as

$$\Delta W_{kj}(n+1) = \eta \bullet \delta_k \bullet O_j + \alpha \bullet W_{kj}(n), \quad (9)$$

$$\Delta W_{ji}(n+1) = \eta \bullet \delta_j \bullet O_i + \alpha \bullet W_{ji}(n),$$

where  $\alpha$  is the momentum factor, and its value range is (0,1).



The threshold values of the hidden layer and output layer can be used as the expansion of neuron input of this layer, and its adjustment rules can be expressed as

$$\begin{aligned}\Delta\theta_j(n+1) &= -\eta\bullet\delta_j + \alpha\bullet\Delta\theta_j(n), \\ \Delta\theta_i(n) &= -\eta\bullet\delta_i + \alpha\bullet\Delta\theta_i(n).\end{aligned}\quad (10)$$

BP network has powerful computing capacity and can process more data quickly, but it also has certain limitations. For initial weight and threshold assignment, the different assignment has a certain influence on the performance of the network. In order to avoid this problem, this paper combines the highly complementary searching ability to conduct search optimization on the optimal assignment of initial weights and thresholds, so as to improve the prediction accuracy of the ANN network [11].

**2.2. Improvement of ANN Algorithm.** The specific operation process of adopting PSO and GA to optimize the initial weights and thresholds of the ANN network is as follows:

- (1) Combine initial weights and thresholds of the ANN network according to the binary real-number coding method. The parameters to be optimized in each coding group represent genes, and each coding group is an individual. In reverse solution, binary numbers can be converted into decimal numbers through (11) [12].

$$F(a_{i1}, a_{i2}, n, a_{il}) = R_i + \frac{T_i - R_i}{2^l - 1} \sum_{j=1}^l a_{ij} 2^{j-1}, \quad (11)$$

where  $a_{i1}, a_{i2}, n, a_{il}$  is the  $i$  section with  $l$  length, and  $a_{i1} = 0$  or  $a_{i1} = 1$ .  $T_i$  and  $R_i$  are the endpoints of the definition domain  $i$ .

The population containing  $S$  individuals is denoted as  $M$ , and the genome of individual  $u$  is  $M_u$ , which are denoted as

$$\begin{aligned}M &= (M_1, M_2, \dots, M_s), \\ M_u &= (M_{u1}, M_{u2}, \dots, M_{u\sigma}),\end{aligned}\quad (12)$$

where  $\sigma$  is the total number of weights and thresholds.

- (2) The purpose of ANN network training is to make the predicted value  $y$  approximate the real value  $b$ , so the fitness function can be determined as [13]

$$F = \sum_0 |y_0 - b_0|. \quad (13)$$

- (3) Calculate individual fitness values and population fitness values of PSO and GA initial populations, respectively, and select the optimal value as the optimal value group to form the initial parent population.

Where the update formulas for the position and speed of PSO are

$$\begin{aligned}v_{i,j}(t+1) &= \rho v_{i,j}(t) + c_1 r_1 [pbest_i - x_{i,j}(t)] \\ &\quad + c_2 r_2 [gbest - x_{i,j}(t)], \\ x_i(t+1) &= x_i(t) + v_i(t+1),\end{aligned}\quad (14)$$

where  $\rho$  represents inertia weight;  $c_1$  and  $c_2$  are particle accelerations;  $r_1$  and  $r_2$  are random vectors;  $p_{best_i}$  represents the local optimal value of the current particle;  $g_{best}$  represents the global optimal value.

- (4) For the initial parent population, the PSO algorithm and GA algorithm are adopted to update the population, respectively, which means that the PSO algorithm updates the population by updating individual speed and position space [14]. GA algorithm realizes population renewal through selection, mutation, and crossover operation [15].
- (5) When the PSO algorithm and GA algorithm meet the termination conditions, the best individual is selected and input it into the ANN network for training;
- (6) Calculate the network error, and stop the iteration when the termination condition is met.

The process can be illustrated in Figure 2.

**2.3. Prediction Model Construction of Residential Energy-Saving Lighting Based on Improved ANN.** According to the residential energy-saving lighting requirements, the specific design of the PSO algorithm and GA algorithm optimizing and improving the ANN network model is as follows.

**2.3.1. Network Layers.** The theory proves that a three-layer neural network structure can achieve any nonlinear mapping [16]. Therefore, this paper sets the residential energy-saving lighting prediction ANN network as a three-layer network model that includes an input layer, hidden layer, and output layer.

**2.3.2. Neurons of Input Layer.** The function of the input layer is to receive the input model data and transmit it to the hidden layer. According to the residential energy-saving lighting requirements, it can be seen that the efficiency of lamps, luminous flux of light source, average reflectance ratio of wall surfaces, the installation height of lamps, working area, maintenance coefficient of lamps, effective floor reflectance, and effective ceiling reflectance have a significant impact on residential energy-saving lighting [17–21]. Therefore, the above 8 types of data are selected as input data, and the number of neurons in the input layer is 8.

**2.3.3. Neurons of Output Layer.** The prediction of residential energy-saving lighting is mainly to determine the number of lamps and illumination value, so the number of neurons in the output layer can be determined as 2.

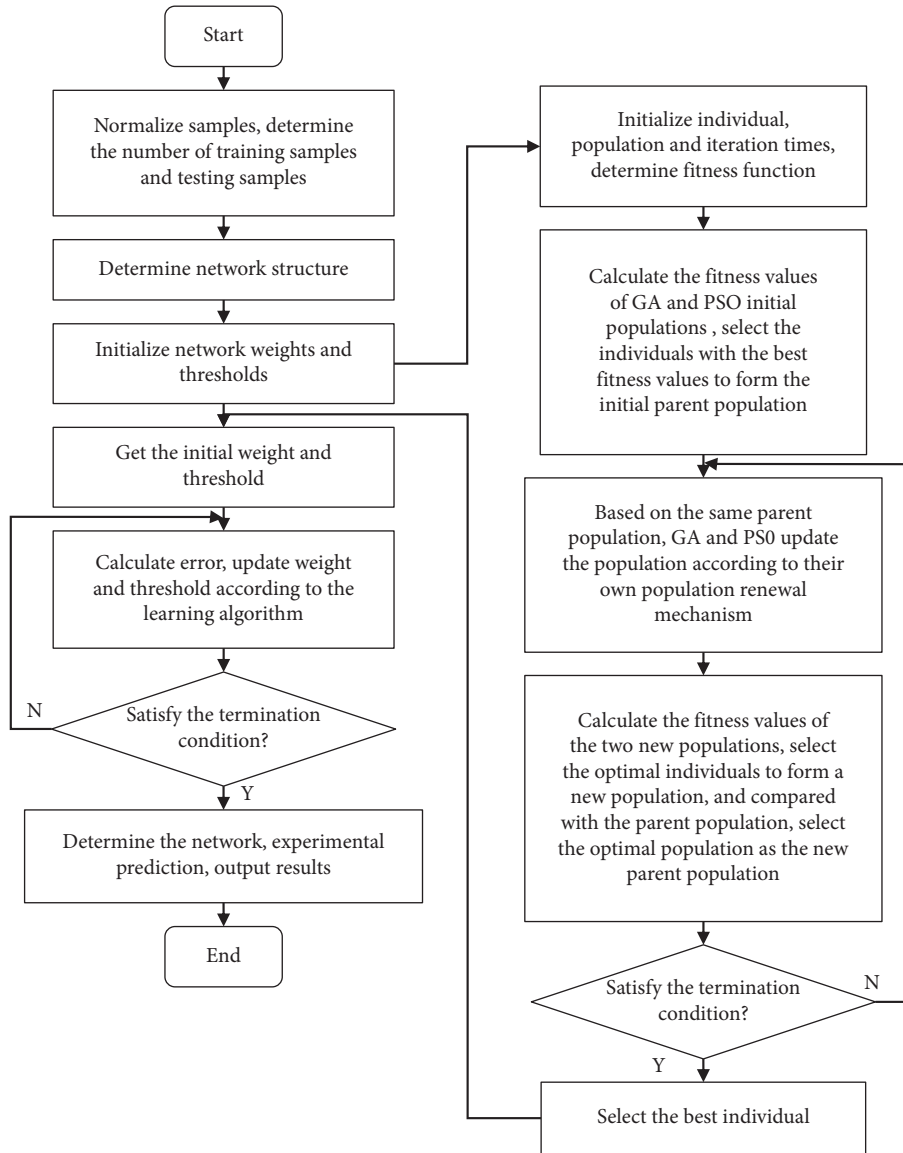


FIGURE 2: Optimization flowchart.

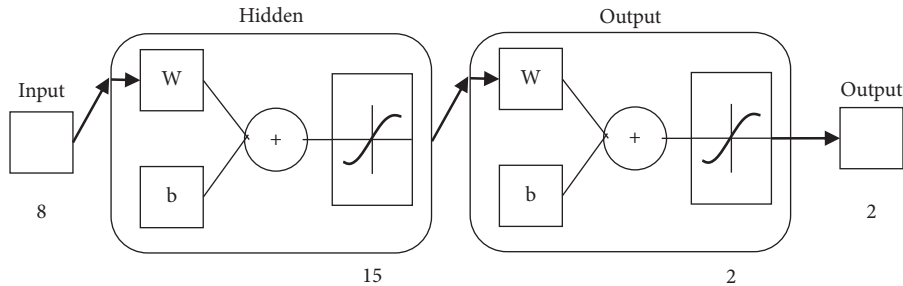


FIGURE 3: Structure diagram of the optimized ANN network.

2.3.4. *Neurons of Hidden Layer.* For a three-layer ANN network, the number of neurons  $X$  in the hidden layer is generally determined by the following equation [21]:

$$x = \sqrt{m + n} + a, \tag{15}$$

where  $m$  and  $n$  are the number of nodes in the input layer and output layer, respectively;  $a$  is a constant between 0 and 10. Combined with PSO and GA algorithm to optimize ANN parameters, the number of neurons in the hidden layer is 15.

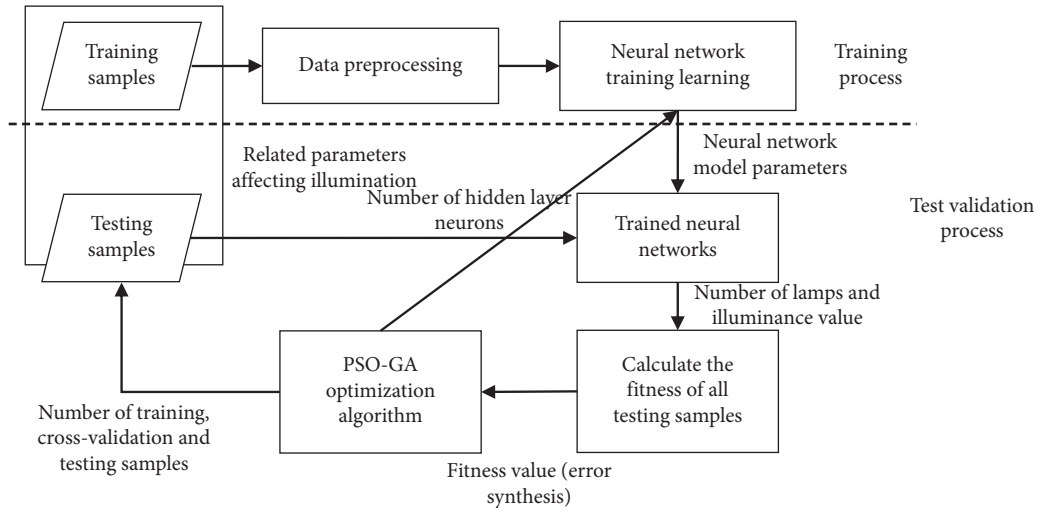


FIGURE 4: Prediction process of residential energy-saving lighting based on improved ANN.

Based on the above analysis, the structure of the improved ANN network is shown in Figure 3.

Therefore, according to the actual situation of residential lighting, the realization process of residential energy-saving lighting prediction is shown in Figure 4. Firstly, the model sample data are determined, and the samples after preprocessing are divided into the training set, testing set, and cross-validation set according to a certain proportion. Moreover, the initial weights and thresholds of the network are optimized. Thus, the network structure and related model parameters are determined, and the optimal ANN network model is obtained. Finally, the number of lamps and illuminance of residential energy-saving lighting are predicted through the optimal ANN network model.

### 3. Simulation Experiment

**3.1. Experimental Environment.** In this experiment, the improved PSO prediction model is constructed on MATLAB2014 software. The operating system is Windows7, and the CPU is Intel(R) Core(TM) i7-7770hq 2.8 GHz. Moreover, the memory is 8G.

**3.2. Data Sources and Preprocessing.** Data in this experiment are the lighting-related data of dozens of residential buildings of different sizes from May to December 2020 in Xi'an, Shaanxi, including 100 sets of data, such as indoor area, isometric efficiency, and the number of lamps [22, 23].

Considering that the dimensions of sample data are different and the span of data is large, it is easy to cause difficulties in subsequent model analysis. To solve this problem, deviation standardization is adopted to normalize sample data in the experiment, as shown in the following equation [24]:

$$A = \frac{(A_0 - A_{\min})}{(A_{\max} - A_{\min})}, \quad (16)$$

where  $A$  is the data whose value range is  $[0,1]$ ;  $A_0$  is the original data value;  $A_{\max}$  and  $A_{\min}$  are the maximum and minimum values of  $A_0$ .

There are 70 groups of samples randomly selected from the experimental samples as the training set, 15 groups of samples as the testing set, and 15 groups of sample data as the cross-validation set.

**3.3. Evaluation Indicators.** In the experiment, average relative error (MAPE) is selected as the indicator to evaluate model performance, and its calculation method is as follows [25]:

$$MAPE = \frac{1}{n} \sum_{i=1}^n \left| \frac{\text{actual}(t) - \text{forecast}(t)}{\text{actual}(t)} \right| * 100\%. \quad (17)$$

### 3.4. Experimental Results

**3.4.1. Model Verification.** To verify the effectiveness of the proposed model, the predicted results of the model on the number of lights and illuminance are tested experimentally and compared with the actual values, which are shown in Figure 5 where the predicted value curve of the proposed model for the number of lights and illumination has a good fitting effect with the actual value curve, which almost coincides with each other, indicating that the proposed model has a good prediction accuracy.

Figure 6 shows the error convergence curves on the training set, testing set, and cross-validation sample set before and after the ANN model is improved. It can be seen that when it is iterated for 9 times before improvement, the mean square error of the ANN model is 44.45. When it is iterated for 14 times after improvement, the mean square error is 5.89. Therefore, PSO and GA algorithms can improve the convergence speed of the ANN model.

Figure 7 shows the linear regression diagram of the proposed model before and after improvement. As can be seen that the fitting accuracy of training samples and cross-validation samples before model improvement is  $R = 0.9768$ , the fitting accuracy of validation samples is  $R = 0.9538$ , and the overall fitting accuracy is  $R = 0.9845$ . After model

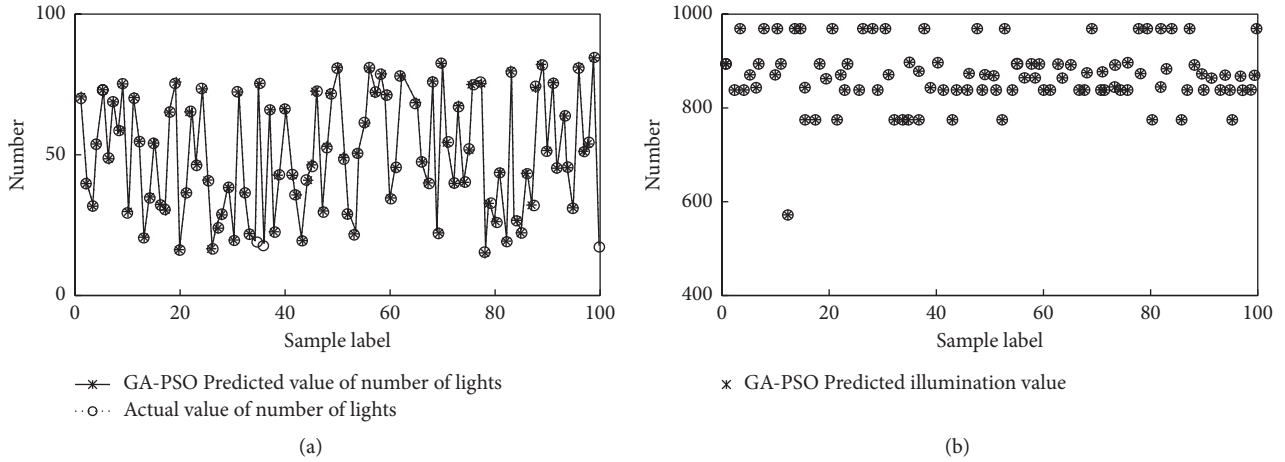


FIGURE 5: Prediction results of improved PSO.

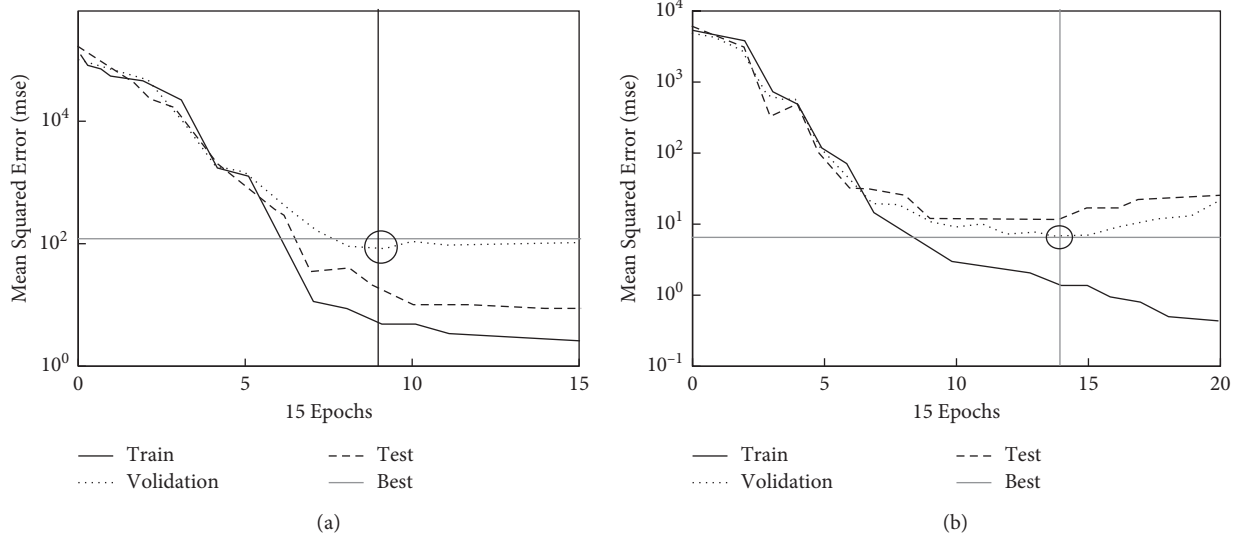


FIGURE 6: Error convergence curve of models. (a) ANN network. (b) Improved ANN network.

improvement, the fitting accuracy of training samples, cross-validation samples, validation samples, and overall fitting samples is  $R = 0.99999$ . Therefore, after optimizing the ANN network by PSO and GA algorithms, the prediction accuracy of the model can be improved, and the proposed model has a high prediction accuracy of residential energy-saving lighting.

In conclusion, the improved ANN model has a high prediction accuracy for residential energy-saving lighting, which reaches 98.45%. In addition, the convergence speed of the model is fast. It can predict and calculate the number of lamps and illuminance degree of residences under the design requirements of the residential energy-saving lighting prediction model.

**3.4.2. Model Comparison.** To further verify the validity of the proposed model, the experiment compares the prediction effect of the proposed model with the common prediction model ANN and fuzzy neural network model (ANFIS) on the experimental data set, and the results are

shown in Table 1 where the ANFIS network structure and initial parameters are determined by the fuzzy C-means clustering algorithm. After debugging, the initial number of clusters is set to 2; the target error is set to 0.1; the classification matrix index is set to 10; and the maximum number of iterations is set to 100. At this time, ANFIS has good prediction accuracy. Compared with ANN and ANFIS models, the prediction error of the proposed model is 1.28%, and the average relative error decreases to varying degrees, which means that the proposed model has better performance and is more suitable for solving the residential energy-saving lighting problem.

**3.4.3. Example Verification.** To verify the prediction effect of the proposed model in the actual residential energy-saving lighting, a senior residence is taken as the research object for verification. Compared with the prediction results of the ANN network and fuzzy neural network before improvement, the results are shown in Table 2. Here, the predicted

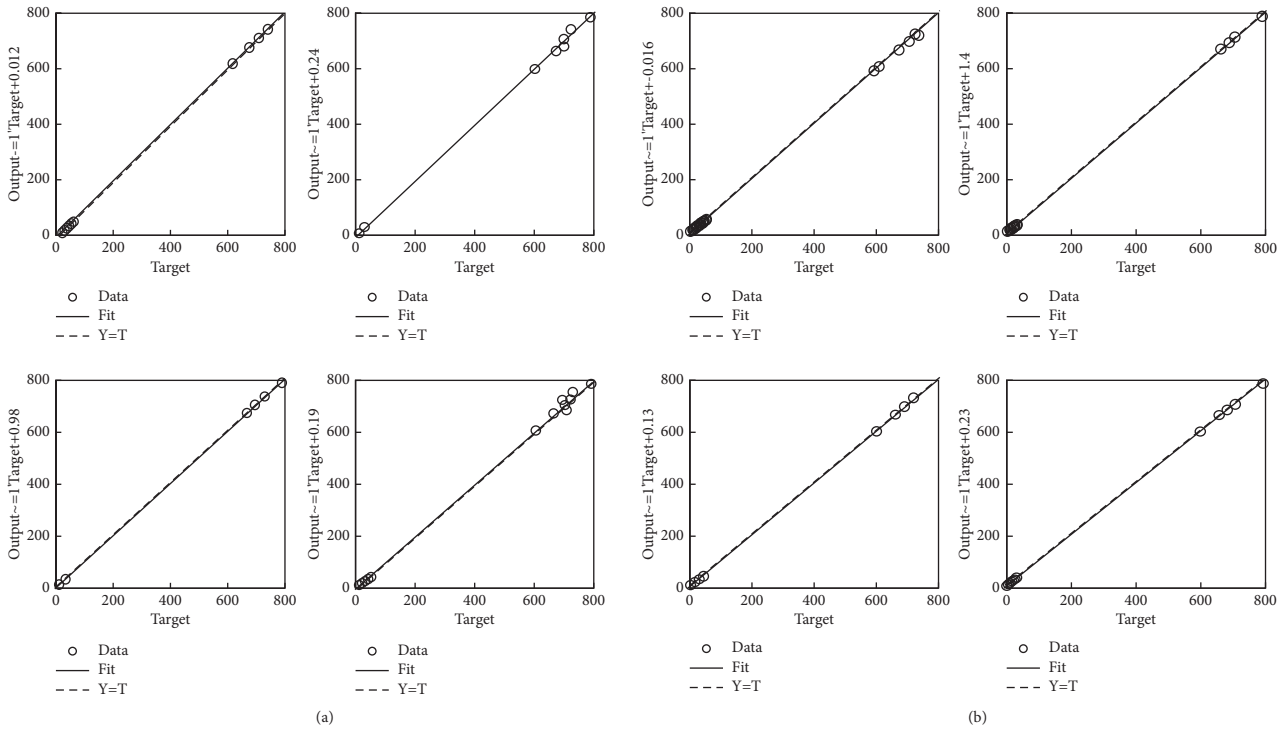


FIGURE 7: Linear regression diagram of models. (a) PSO network. (b) Improved PSO network.

TABLE 1: Comparison of average relative errors of models.

| Indicator | Improved ANN (%) | ANN (%) | ANFIS (%) |
|-----------|------------------|---------|-----------|
| MAPE      | 1.28             | 3.57    | 2.15      |

TABLE 2: Comparison of prediction results of different models.

| Model   | Number of lamps/lamp | Illumination/lm | Standard illumination/lm |
|---|----------------------|-----------------|--------------------------|
| Neural network calculation method                 | 76                   | 912             | 750                      |
| Fuzzy neural network calculation method           | 71                   | 795             | 750                      |
| BP network calculation method optimized by PSO-GA | 69                   | 765             | 750                      |

TABLE 3: Comparison of illumination index values of different models.

| Category    | Average illumination (lx) | Minimum illumination (lx) | Maximum illumination (lx) | Minimum illumination/average illumination | Minimum illumination/maximum illumination |
|-------------|---------------------------|---------------------------|---------------------------|---|---|
| ANN         | 912                       | 729                       | 1101                      | 0.81                                      | 0.66                                      |
| ANFIS       | 795                       | 680                       | 930                       | 0.86                                      | 0.73                                      |
| Improve ANN | 765                       | 704                       | 832                       | 0.92                                      | 0.85                                      |

TABLE 4: Comparison of GR values of different models.

| Category    | GR observation point 1 | GR observation point 2 | GR observation point 3 | GR observation point 4 | GR observation point 5 |
|-------------|------------------------|------------------------|------------------------|------------------------|------------------------|
| ANN         | 34                     | 32                     | 34                     | 35                     | 35                     |
| ANFIS       | 31                     | 32                     | 30                     | 32                     | 30                     |
| Improve ANN | 30                     | 28                     | 30                     | 29                     | 30                     |

results of the proposed model, ANN network model, and fuzzy neural network model all meet the standard value of illumination requirements of relevant national specifications. On this basis, the use of lamps in the proposed model is the least (69 lamps), and the value of illumination is closer to the standard value. Therefore, compared with the ANN model and fuzzy neural network model, the proposed model meets the requirements of residential energy-saving lighting and has certain effectiveness and superiority.

**3.4.4. Simulation Results of DIALux Modeling.** To verify the generalization ability of the proposed model, DIALux lighting software is used for modeling and simulation. DIALux lighting software can provide a variety of parameters for calculation according to the actual residential building requirements and can be compared and analyzed according to the input set value. DIALux lighting software is used to simulate the residential illumination values, and the results are shown in Table 3. Compared with the ANN model and ANFIS model, the average illuminance value of the proposed model is the smallest and closest to the standard illuminance (750lx), which is 765lx. Furthermore, the illuminance uniformity is the largest, which is 0.85. So it indicates that the proposed model can provide a better lighting environment with more uniform illumination and energy saving under the premise of ensuring lighting requirements.

Table 4 shows the comparison of GR values of glare index of different models at 5 observation points. As can be seen from the table, the GR values of the five observation points of the ANN model are all over 30, and there are three observation points that GR values of the ANFIS model are all over 30. The GR values of the five observation points of the proposed model are all within 30 (including 30), which meets the maximum glare index (30) stipulated by the state. Therefore, the proposed model meets the requirements of the national specification.

## 4. Conclusion

To sum up, the PSO and GA algorithms can optimize the initial weights and thresholds of the ANN network, and then, the proposed residential energy-saving lighting prediction model based on machine vision can improve the model convergence speed and prediction accuracy. The prediction accuracy can reach 99.999%. Compared with the ANN model and ANFIS model, the prediction average relative error of the proposed model is reduced by 2.29% and 0.87%, respectively. Under the premise of meeting the standard illumination of residential energy-saving lighting, the proposed model can use fewer lamps, and it can get closer to the standard illumination value, which has certain effectiveness and superiority. The innovation of this research is to apply artificial intelligence algorithm to energy-saving lighting, which provides a new way and way for scientific optimization of lighting. However, due to the influence of external factors, there are still certain limitations, which are mainly the number of data samples. To meet the requirements, the next step is to expand the collection range of

sample data to improve the accuracy of model training and the generalization ability of the model.

## Data Availability

The experimental data used to support the findings of this study are available from the corresponding author upon request.

## Conflicts of Interest

The authors declare that they have no conflicts of interest regarding this work.

## References

- [1] N. T. Kalyani and S. J. Dhoble, "Organic light emitting diodes: energy saving lighting technology-A review," *Renewable and Sustainable Energy Reviews*, vol. 16, no. 5, pp. 2696–2723, 2012.
- [2] S. Omid, A. Moradzadeh, M. Ivatlo, and M. Abapour, "A Comprehensive Review on Energy Saving Options and Saving Potential in Low Voltage Electricity Distribution Networks: Building and Public lighting," *Sustainable Cities and Society*, vol. 72, 2021.
- [3] M. Damjan, P. Miroslav, and L. Žegarac, "Use of sensitivity analysis for a determination of dominant design parameters affecting energy efficiency of timber buildings in different climates," *Energy for Sustainable Development*, vol. 63, pp. 86–102, 2021.
- [4] G. Lars, "Irregular light scattering properties of fenestration for comfortable and energy-efficient buildings," *International Journal of Digital Innovation in the Built Environment (IJDIIBE)*, vol. 10, no. 2, pp. 1–16, 2021.
- [5] O. Nedelcu, O. Salisteanu, and I. C. Sălișteanu, "Modern concepts of energy-efficient civil and residential buildings. Case study: analysis of a residential building according to Nzeb c," *Scientific Bulletin of Electrical Engineering Faculty*, vol. 21, no. 1, pp. 39–45, 2021.
- [6] B. H. Rijal, K. Yoshida, A. Humphreys, and F. Nico, "Development of an adaptive thermal comfort model for energy-saving building design in Japan," *Architectural Science Review*, vol. 64, no. 1-2, pp. 109–122, 2021.
- [7] H. Salih, D. Yilmaz, and E. Kızılkaya, "PSACONN mining algorithm for multi-factor thermal energy-efficient public building design," *Journal of Building Engineering*, vol. 34, Article ID 102025, 2021.
- [8] W. Wu, Q. Meng, Y. Lv et al., "An optimization and evaluation method construction of zero-energy residential building renovation," *IOP Conference Series: Earth and Environmental Science*, vol. 675, no. 1, Article ID 012089, 2021.
- [9] L. Chen, Y. Li, and X. Lu, "Research on energy-saving design of thermal insulation structure of residential buildings in severe cold areas," *IOP Conference Series: Earth and Environmental Science*, vol. 638, no. 1, Article ID 012128, 2021.
- [10] X. Zhang, "Energy-saving design of civil engineering buildings based on FPGA and embedded system," *Microprocessors and Microsystems*, vol. 83, Article ID 103976, 2021.
- [11] J. Seo, B. Yun, J. Park, J. Park, M. Shin, and S. Park, "Prediction of instantaneous real-world emissions from diesel light-duty vehicles based on an integrated artificial neural network and vehicle dynamics model," *The Science of the Total Environment*, vol. 786, Article ID 147369, 2021.

- [12] D. Thiruselvi, S. Aathika, Y. Mani, and D. Jagadiswary, "Application of Artificial Neural Network as a nonhazardous alternative on kinetic analysis and modeling for green synthesis of cobalt nanocatalyst from *Ocimum tenuiflorum*," *Journal of Hazardous Materials*, vol. 416, Article ID 125725, 2021.
- [13] S. Sudhakar, S. Pasupuleti, S. Singha, and R. Singh, "Prediction of groundwater quality using efficient machine learning technique," *Chemosphere*, vol. 276, Article ID 130275, 2021.
- [14] Y. Liu, H. Fan, D. Dong et al., "Computed tomography-based radiomic model at node level for the prediction of normal-sized lymph node metastasis in cervical cancer," *Translational Oncology*, vol. 14, no. 8, Article ID 101123, 2021.
- [15] B. S. Kumar, K. Pyrgaki, S. Salih, and T. Tiyasha, "Prediction of copper ions adsorption by attapulgite adsorbent using tuned-artificial intelligence model," *Chemosphere*, vol. 276, Article ID 130168, 2021.
- [16] X. Li and J. Lu, "Energy-saving feature extraction method for urban buildings with near-zero energy-consuming based on SVR," *International Journal of Global Energy Issues*, vol. 42, no. 5/6, pp. 375–392, 2020.
- [17] K. Oleksandra, K. Dikarev, D. Rodinov, and O. Martysh, "Geothermal energy use for the additional heat supply of a residential building," *Slovak Journal of Civil Engineering*, vol. 28, no. 4, pp. 15–22, 2020.
- [18] L. K. Udaya, K. Ramya, G. Radhakrishnan, V. Gomathy, and S. R. Sheeba, "IoT based energy efficient architecture for integrated Smart Grid," *IOP Conference Series: Materials Science and Engineering*, vol. 993, no. 1, Article ID 012096, 2020.
- [19] M. Hatem and R. Ayman, "Urban geometry optimization to mitigate climate change: towards energy-efficient buildings," *Sustainability*, vol. 13, no. 1, pp. 27–29, 2020.
- [20] X. Han, "Economic analysis and evaluation of energy-efficient renovation of existing buildings based on the whole life cycle," in *Proceedings of the E3S Web of Conferences*, Article ID 02098, Banda Aceh (Virtually), Indonesia, October 2021.
- [21] R. Qin and X. Li, "A preliminary study on green building 3D modelling energy-saving design combined with traditional ecological concepts," in *Proceedings of the E3S Web of Conferences*, Article ID 03028, Banda Aceh (Virtually), Indonesia, October 2021.
- [22] S. Stetsky and N. Galaeva, "Contemporary types of energy-efficient buildings: an architectural and structural review," in *Proceedings of the E3S Web of Conferences*, Article ID 05022, Banda Aceh (Virtually), Indonesia, October 2021.
- [23] N. Ding and H. Guo, "Energy-saving design of office buildings considering light environment and thermal environment," *Applied Mathematics and Nonlinear Sciences*, vol. 6, no. 1, pp. 269–282, 2021.
- [24] M. Zhang, Y. Liu, and Z. Shen, "Effects of energy saving and emission reduction in the heating system part of the energy-saving renovation of existing buildings—based on China's first residential area with a 75% energy saving standard," *IOP Conference Series: Earth and Environmental Science*, vol. 647, no. 1, Article ID 012148, 2021.
- [25] W. Yu, S. Tang, and K. Wang, "Research on energy-saving performance of low-energy consumption green buildings," in *Proceedings of the E3S Web of Conferences*, Article ID 011109, Banda Aceh (Virtually), Indonesia, October 2021.

## *Retraction*

# **Retracted: Fractal Visual Art Graphic Design Based on Computer-Aided Algorithms**

### **Mathematical Problems in Engineering**

Received 18 July 2023; Accepted 18 July 2023; Published 19 July 2023

Copyright © 2023 Mathematical Problems in Engineering. This is an open access article distributed under the Creative Commons Attribution License, which permits unrestricted use, distribution, and reproduction in any medium, provided the original work is properly cited.

This article has been retracted by Hindawi following an investigation undertaken by the publisher [1]. This investigation has uncovered evidence of one or more of the following indicators of systematic manipulation of the publication process:

- (1) Discrepancies in scope
- (2) Discrepancies in the description of the research reported
- (3) Discrepancies between the availability of data and the research described
- (4) Inappropriate citations
- (5) Incoherent, meaningless and/or irrelevant content included in the article
- (6) Peer-review manipulation

The presence of these indicators undermines our confidence in the integrity of the article's content and we cannot, therefore, vouch for its reliability. Please note that this notice is intended solely to alert readers that the content of this article is unreliable. We have not investigated whether authors were aware of or involved in the systematic manipulation of the publication process.

Wiley and Hindawi regrets that the usual quality checks did not identify these issues before publication and have since put additional measures in place to safeguard research integrity.

We wish to credit our own Research Integrity and Research Publishing teams and anonymous and named external researchers and research integrity experts for contributing to this investigation.

The corresponding author, as the representative of all authors, has been given the opportunity to register their agreement or disagreement to this retraction. We have kept a record of any response received.

### **References**

- [1] Q. Zhou, T. Liu, G. Wu, and X. Chen, "Fractal Visual Art Graphic Design Based on Computer-Aided Algorithms," *Mathematical Problems in Engineering*, vol. 2022, Article ID 3345037, 7 pages, 2022.



## Research Article

# Fractal Visual Art Graphic Design Based on Computer-Aided Algorithms

Qihao Zhou,<sup>1</sup> Teng Liu,<sup>1</sup> Guorong Wu ,<sup>2</sup> and Xuhui Chen<sup>2</sup>

<sup>1</sup>College of Fine Arts, Wonkwang University, Iksan 54538, Republic of Korea

<sup>2</sup>College of Art and Design, Nanchang University, NanChang 330031, China

Correspondence should be addressed to Guorong Wu; wuguorong@ncu.edu.cn

Received 24 March 2022; Revised 8 May 2022; Accepted 10 May 2022; Published 27 May 2022

Academic Editor: Man Fai Leung

Copyright © 2022 Qihao Zhou et al. This is an open access article distributed under the Creative Commons Attribution License, which permits unrestricted use, distribution, and reproduction in any medium, provided the original work is properly cited.

Embedded machine vision algorithm development platform is of great significance. Based on the elaboration of visual communication design, this paper further details the design of fractal visual art graphics based on computer-aided algorithms to design edge detection schemes, where edges represent sudden changes in the signal and are able to characterize the rich information of an image. In response to the problems of poor robustness and difficult parameter selection of the currently widely used edge detection algorithms, the platform encapsulates joint edge detection graphic components in a higher-order processing library to achieve the requirements of high-precision detection and to realise enhanced edge detection effects. Finally, the experimental analysis shows that the proposed algorithm has a more accurate detection effect and can meet the user's high-precision detection requirements.

## 1. Introduction

As the times have developed, Internet information technology has also developed rapidly and has become popular in many areas of society, especially in the application of mathematical and web design [1]. With the rapid development of society, people's needs are constantly growing, and in the specific visual communication design, the individual needs of web users need to be taken into account, as well as the rationality of web design and other requirements [2]. For this reason, visual communication design in the Internet era often requires consideration of a wider range of requirements. The so-called visual communication design mainly refers to the implementation of information-based communication design based on the combination of art and communication, while the use of visual symbols for auxiliary expression is also very important and has a strong application type [3]. At the beginning of visual communication design, a variety of forms of expression exist, which, in summary, include four main forms: painting, sculpture, architecture and design [4]. As the development of visual communication design is inevitably linked to many media, it has been influenced to a certain extent by the rapid

development of the Internet, which has also given rise to a variety of new forms [5]. For this reason, in the specific visual communication design, the visual intention needs to be fully considered, including its own intention as well as the client's intention [6]. Only in this way can designers be comprehensive in their visual communication design and thus help to ensure that the visual communication design meets the individual needs of web users.

There are two main types of machine vision systems available, one relying on general purpose computers for processing and computing, and the other based on embedded architectures [7]. Commonly used machine vision systems generally carry out data processing via general-purpose computers, but with the increase in the number of inspection objects and the demand for real-time inspection, machine vision systems based on embedded architectures help to reduce the burden on data transmission and computer resources, enabling real-time monitoring, multipoint detection, distributed computing, and highly modular multitasking [8], and are increasingly being used in manufacturing industries.

Existing algorithm development platforms are often incompatible with system versatility and ease of use [9].

Some platforms use sequential function diagrams and ladder diagrams in order to meet generality, which still require a certain level of programming literacy on the part of the developer, and the design process is more complex and the interaction is more cumbersome, not intuitive or easy to use. The algorithm development platforms that can meet the ease of use are often industry-specific platforms, which cannot be downloaded across platforms and have to be redesigned by software developers for functional iterations, and generally suffer from poor generality and low reuse rate [10]. As users' needs are polymorphic and algorithms are designed for thousands of people, the value of personalised services and customised solutions is increasingly evident in the manufacturing industry, with more and more customised solutions being used to replace standardised products in the field of machine vision. Existing platforms can no longer meet the requirements of a wide range of applications for embedded systems [11]. The ideal vision algorithm development platform should reduce the difficulty and complexity of machine vision system development for developers, enable easy iteration and updating of system functions, and meet the diverse functional requirements of different situations [12].

Therefore, the research of an algorithm development platform for embedded machine vision is of great significance. Users can perform interactive programming in a graphical development environment, complete the rapid development of vision systems, and download them to the embedded devices with a single click, with low error rate, high versatility, and high reliability, which has become the future development trend of embedded machine vision systems [13]. In this study, a machine learning-like algorithm was used to develop a high-precision tool recognition system to meet the requirements of high-precision detection and achieve enhanced edge detection. Aiming at the problems of poor robustness and difficult parameter selection of the currently widely used edge detection algorithms, this research designs an edge detection scheme, combined with edge detection graphics components and encapsulated in a high-level processing library to meet the requirements of high-precision detection.

## 2. Joint Edge Detection Graphic Element

The joint edge detection graphical element not only solves the problem of poor algorithm robustness by using a composite wrapper model and an adaptive algorithm, but also solves the problem of difficult selection of edge detection threshold parameters by using an automatic parameter finding algorithm, making it very adaptable to images that change due to irresistible factors [14].

The graphical component combines the common Roberts, Sobel, and Prewitt edge detection operators in a composite package, and uses the Canny algorithm to perform non-maximum suppression and double thresholding on the gradient images obtained under the different operators to output more accurate single-edge results [15]. First, the target image is segmented by  $N$  equal parts (default is four equal parts) based on the adaptive algorithm, and the segmented subimages are processed separately. Then, the

gradient image is obtained for each subimage under different operators, and the upper and lower threshold combinations corresponding to the Canny algorithm are automatically found based on the gradient image, respectively [16]. Finally, more accurate single-edge information is obtained based on the Canny algorithm, and the optimal edge of each subimage is selected by an objective evaluation method and combined to obtain the complete output edge as shown in figure 1 [17].

**2.1. Automatic Parameter Optimization.** The aim of the automatic parameter finding algorithm is to solve the problem of difficult parameter selection during the actual development of the algorithm and to improve the dynamic adaptability of the algorithm. Although not all graphical elements are suitable for automatic parameter selection, and human debugging of some image algorithms is still irreplaceable, the parameter auto-optimisation algorithm encapsulated by the joint edge detection graphical element is a good solution to the problem of difficult threshold selection in Canny edge detection.

The parameter optimization algorithm of the joint edge detection graphic element introduces the image entropy [18], which can characterize the aggregation property of the image grey-scale distribution, and proposes the method of maximum entropy ratio of class groups to achieve the automatic threshold optimization of the Canny algorithm. According to the maximum entropy theory, it is known that the greater the variation of the grayscale value of a class group, the greater the entropy, so the optimal segmentation threshold is found by calculating the maximum value of the entropy ratio between intraclass and interclass.

Let the number of image pixels be  $N$ , the range of gray levels be  $[0, L - 1]$ , and the number of pixels corresponding to gray level  $i$  be  $n_i$ , with probability.

$$p_i = \frac{n_i}{N}, \quad (i = 0, 1, 2, \dots, L - 1). \quad (1)$$

In the gray level range,  $k$  is set as the most segmentation threshold, and the threshold  $k$  is used to classify the nonedge  $C_0$  and the edge  $C_1$  into two categories,  $C_0$  in the range  $[0, k]$  and  $C_1$  in the range  $[k, L - 1]$ . Then, the image entropy of nonedge  $C_0$  and edge  $C_1$  is expressed as

$$H_0 = - \sum_{i=0}^k P \frac{\log P_i}{\rho_0}; \quad (2)$$

$$H_1 = - \sum_{i=k+1}^{L-1} P \frac{\log P_i}{\rho_1},$$

where the probabilities  $\rho_0$  and  $\rho_1$  of nonedge  $C_0$  and edge  $C_1$  are

$$\rho_0 = \sum_{i=0}^k P_i, \quad (3)$$

$$\rho_1 = \sum_{i=k+1}^{L-1} P_i.$$

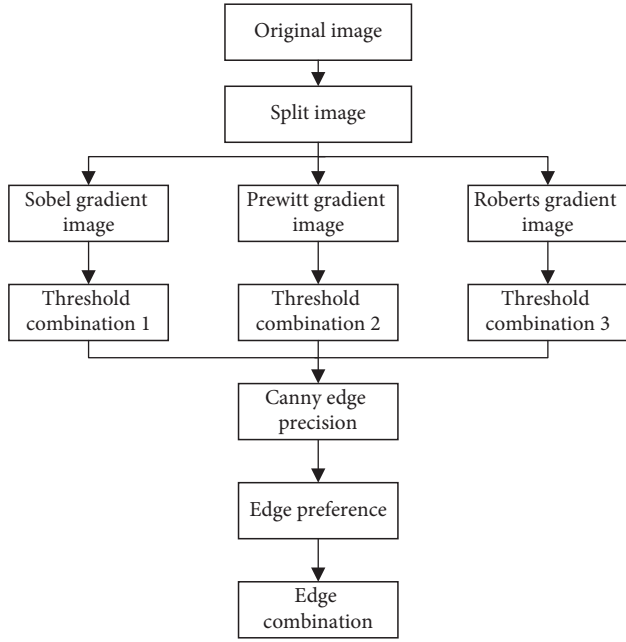


FIGURE 1: Flowchart of edge detection algorithm.

The total mean image entropy  $H$  is

$$H = - \sum_{i=0}^{L-1} P_i \log P_i. \quad (4)$$

The expression for the entropy ratio  $\Delta\eta$  of the nonedge class to the edge class is

$$\Delta\eta = \frac{\eta_2^2(k)}{\eta_1^2(k)}, \quad (5)$$

where the interclass entropy variance  $\eta_2^2(k)$  is defined as

$$\eta_2^2(k) = \rho_0 (H_0 - H)^2 + \rho_1 (H_1 - H)^2. \quad (6)$$

The intraclass entropy variance  $\eta_1^2(k)$  is defined as

$$\eta_1^2(k) = \rho_0 \sum_{i=0}^k (i - H_0)^2 + \rho_1 \sum_{i=k+1}^{L-1} (i - H_1)^2. \quad (7)$$

When  $k$  is the optimal partitioning threshold such that the interclass entropy is maximized while the intraclass entropy is minimized, the derivative of  $k$  in (7) is therefore

$$\frac{\partial \Delta \eta(k)}{\partial k} = 0. \quad (8)$$

The  $k$  value solved according to (8) is used as the upper threshold TH1 in Canny's algorithm, while the lower threshold is chosen based on the empirical coefficient of proportionality, i.e., TH2 =  $\alpha$ TH1, and the final  $\alpha$  value was chosen as 0.4 after several experiments.

**2.2. Edge Evaluation Model.** The selection of the best edge in the joint edge detection graphical component relies on a reference-free evaluation method, i.e., there is no baseline reference edge information, and an evaluation model is built

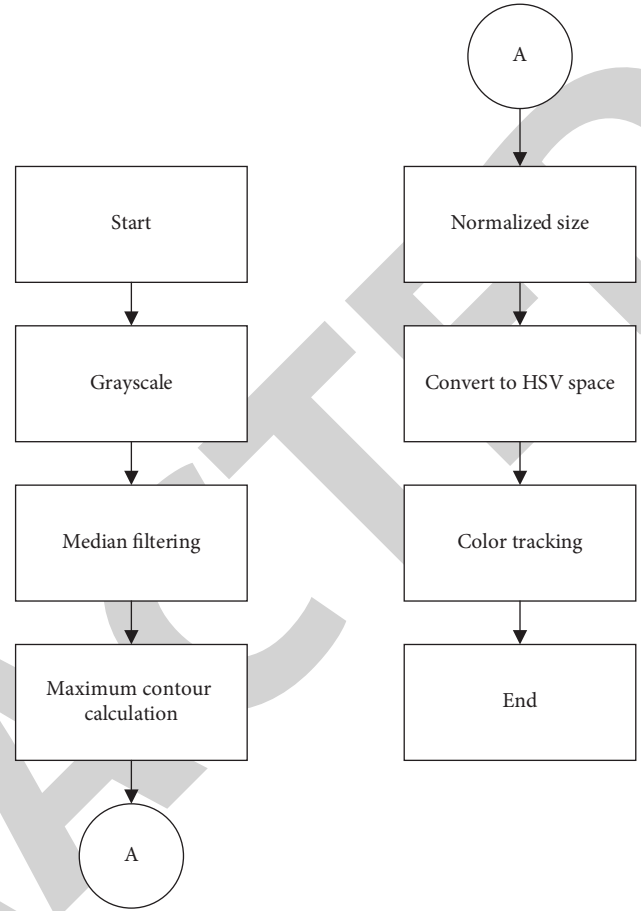


FIGURE 2: Image preprocessing and feature extraction.

to objectively score the edge result image and select the highest score as the final output. The edge detection evaluation model is based on the connected component analysis method [19], where the ratio of the 4- to 8-connected component scores reflects the degree of edge line connectivity, and the influence of the degree of edge line connectivity on edge detection is reflected in the error and miss detection.

In order to score the edge result image specifically, the quantitative model fitting of the principle of connected components is used as an evaluation model to complete the selection of the edge algorithm in this paper. An edge map is a binary image with pixel values consisting of only 0 and 1. For the total number of edges  $A$ , 4-connected components  $B$ , and 8-connected components  $C$  in the edge map, mathematical induction shows that the magnitude of the values of  $C/A$  and  $C/B$  is linearly and positively correlated with the effect of the extracted edges.

Let the edge score be  $G$ , the edge evaluation index be  $M = B/C$ ,  $N = A/C$ , and the weight coefficients be  $\alpha$  and  $\beta$ , respectively; then, the linear model of the edge score  $G$  with  $M$  and  $N$  can be expressed as

$$G = \alpha \times M + \beta \times N. \quad (9)$$

For each set of edge results, the ratio of 4- to 8-connectedness score  $M$  and the ratio of total number of edges to

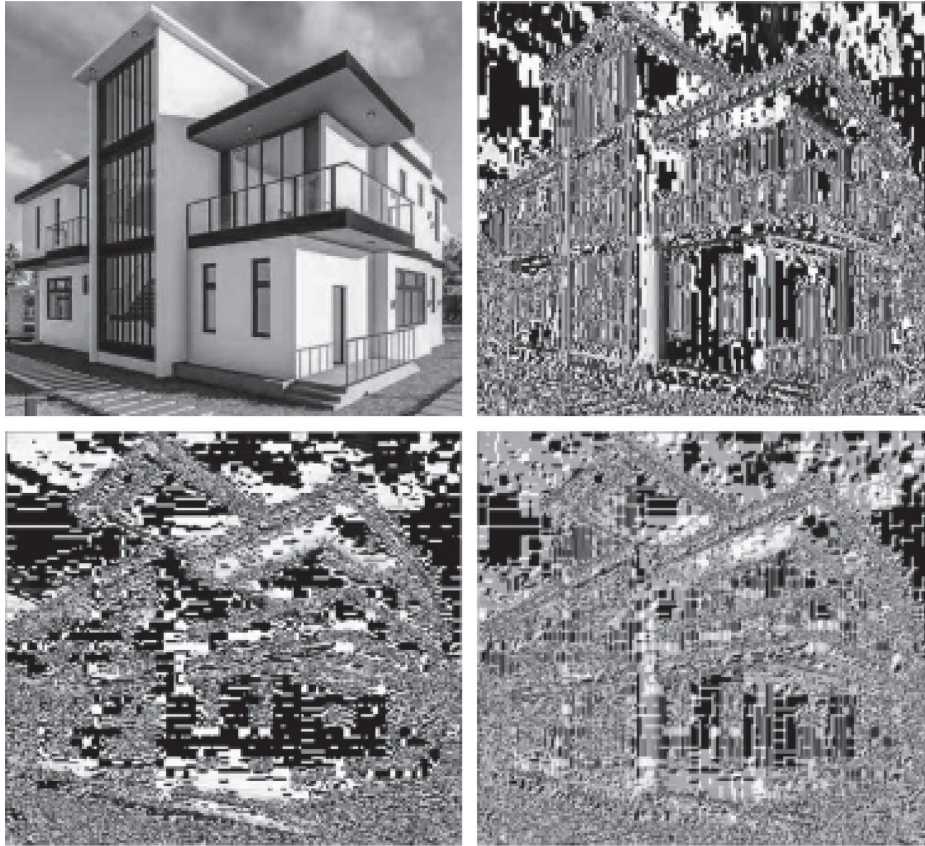


FIGURE 3: Comparison of edge detection results of Experiment 1.

8-connectedness score  $N$  were calculated, and a subjective score was assigned to each of the 100 edge results and fitted to the model. The final ratio of  $\alpha$  to  $\beta$  is approximately  $(4.8e^2)e^2:1$ . The evaluation model formula in equation (10) shows that the ratio of 4- to 8-linked scores  $M$  is the main variable for the edge score  $G$ , with a correlation coefficient  $r$  of 0.98.

$$G = 4.8M + e^{-2}N. \quad (10)$$

### 3. Enhanced Effect Validation

After obtaining a dataset with a sufficient number of samples, the image needs to be preprocessed first; the purpose of which is to improve the image quality and exclude the redundant images other than the tool, to segment the tool from the complex background; the program flowchart is shown in Figure 2.

In order to remove the redundant parts other than the backpack part, the backpack region is first segmented from the background using binarization. Then, the backpack location is further determined based on the maximum contour extraction method, and the image is cropped according to the location coordinates to achieve the backpack region extraction. In the next step, the image is scaled to a uniform size of  $128 \times 128$  by dragging and dropping the image crop graphic component, taking into account the

uniform size of the training samples of the machine learning model. Finally, the tool is separated from the backpack using a colour tracking method. The image is first converted to the HSV colour space, which is more suitable for tracking a given colour as HSV is an intuitive colour model that describes the image by hue  $H$ , saturation  $S$ , and luminance  $V$ . In the X-ray image, the tool colours are distributed in the range (70, 43, 46) to (130, 255, 255), and the tool segmentation is achieved using the threshold settings in the colour tracking graphic element.

To verify whether the above joint edge detection graphic element provides enhanced edge detection, two experiments were selected for analysis and testing. The house image shown in Figure 3 was selected for the edge detection experiment. Figure 3 shows the results of the Robert's operator, Prewitt operator and Sobel operator edge detection combined with the Otsu threshold selection method compared to the edge detection algorithm encapsulated by the graphical element, respectively. It can be seen visually that the composite edge detection elements of the platform can effectively suppress spurious edges and obtain better continuity of edge results.

Experiment 2 selected Figure 3 for contrast edge detection, and the experimental comparison results are shown in Figure 4. Since the pixel values of an edge image consist of only 0 and 1, the edge detection algorithm to be evaluated can be considered as a binary classifier, and the result of its classification is also the result of edge detection. In order to

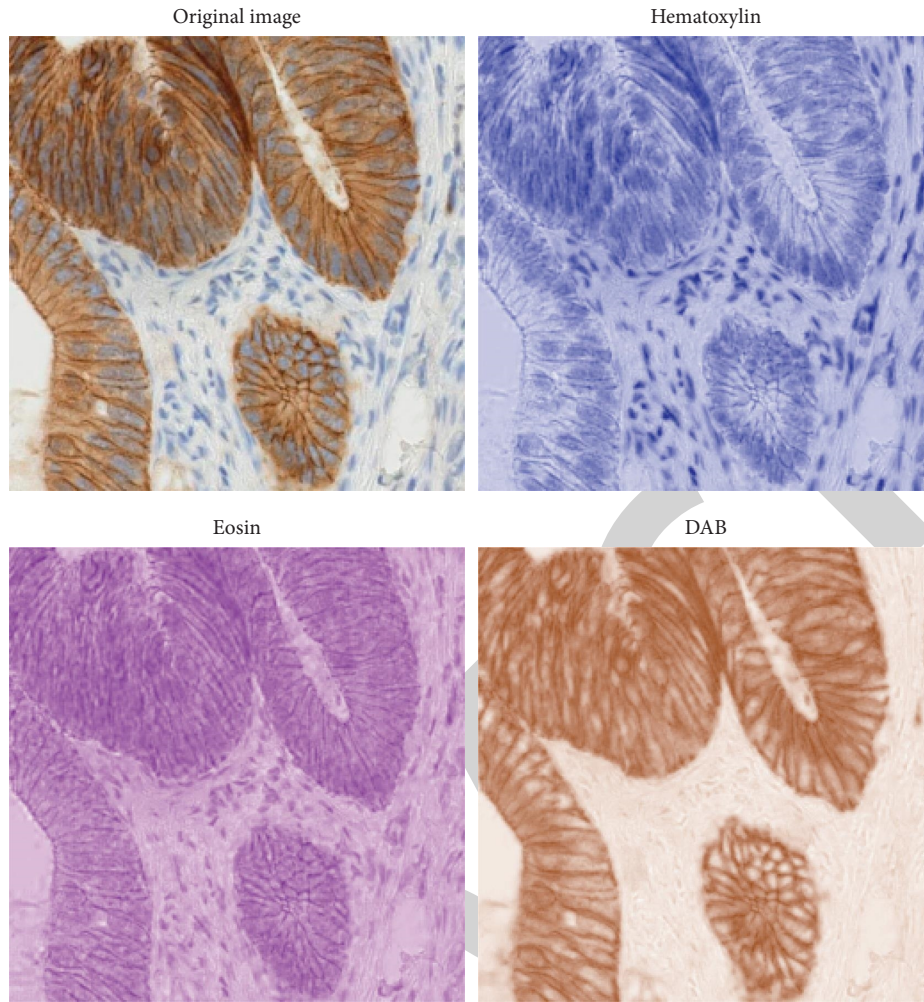


FIGURE 4: Comparison of the edge detection results of Experiment 2.

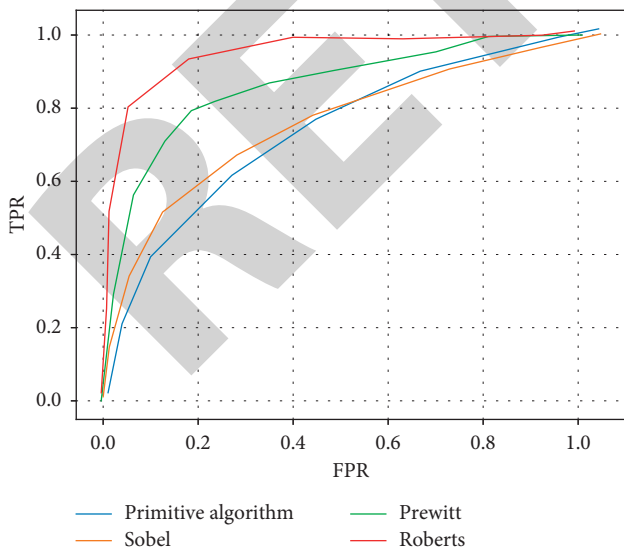


FIGURE 5: ROC plot of edge detection algorithm.

better characterize the edge detection performance of the detection algorithm, a receiver operating characteristic (ROC) curve was introduced for algorithm performance

TABLE 1: Algorithm performance comparison table.

| Evaluating indicator | Roberts | Prewitt | Sobel | Primitive algorithm |
|----------------------|---------|---------|-------|---------------------|
| AUC                  | 0.707   | 0.712   | 0.762 | 0.854               |
| Running time/s       | 0.995   | 0.874   | 1.23  | 1.854               |

evaluation, which was used to illustrate the relationship between the correct and incorrect edge detection rates [20–22].

The measure of correct edge detection results is the edge information reference map, which represents an ‘ideal’ edge detection effect and often requires constant debugging and subjective judgement by the human visual system. The reference map for Experiment 2 is shown in Figure 5 and the total number of benchmark edges is calculated to be 2066 [23–25].

A comparison of the performance of the four algorithms based on the ROC curve is shown in Table 1, where the area enclosed by the axes under the ROC curve is defined as the metric AUC for the mathematical morphological gradient method, and the closer the value is to 1, the more realistic the detection algorithm is. As can be seen, although the edge

detection algorithm in this paper sacrifices runtime to a certain extent, the detected edges are more accurate than the single operator Canny edge detection combined with the Otsu threshold selection method.

#### 4. Conclusions

In summary, in the network era, visual communication design is not only very rich in content but also has very significant features, specifically navigation design content, page and graphic design, features specifically freedom, and interactivity and timeliness. Traditional recognition methods generally achieve the classification problem through image feature description and detection, but due to the high complexity of images in practical applications, traditional methods are difficult to perform the detection work. This paper therefore builds on traditional vision algorithms to develop a high-precision tool recognition system using machine learning-like algorithms in an algorithm development platform. In this way, in the rapidly developing information technology network era, to better visual communication design, designers need to continuously conduct in-depth research in order to improve the level of visual communication design.

#### Data Availability

The raw data supporting the conclusions of this article will be made available by the authors, without undue reservation.

#### Conflicts of Interest

The authors declared that they have no conflicts of interest regarding this work.

#### References

- [1] A. Radwan, K. M. S. Huq, S. Mumtaz, K. F. Tsang, and J. Rodriguez, "Low-cost on-demand C-RAN based mobile small-cells," *IEEE Access*, vol. 4, pp. 2331–2339, 2016.
- [2] C. Shi, "Design of fractal art design image based on one-dimensional MFDMA algorithm," in *Proceedings of the International Conference on Big Data Analytics for Cyber-Physical-Systems*, pp. 247–251, Springer, Singapore, December 2020.
- [3] D. Wu, Y. Lei, M. He, C. Zhang, and L. Ji, "Deep Reinforcement Learning-Based Path Control and Optimization for Unmanned Ships," *Wireless Communications and Mobile Computing*, vol. 2022, Article ID 7135043, 8 pages, 2022.
- [4] Y. Zheng, C. Chen, and M. Sarem, "A computer aided inbetweening algorithm for color fractal graphics," in *Proceedings of the International Conference on Natural Computation*, pp. 651–659, Springer, Berlin, Germany, September 2006.
- [5] W. L. Lee, Y. C. Chen, Y. C. Chen, and K. S. Hsieh, "Un-supervised segmentation of ultrasonic liver images by multi-resolution fractal feature vector," *Information Sciences*, vol. 175, no. 3, pp. 177–199, 2005.
- [6] M. Gletsos, S. G. Mougiakakou, G. K. Matsopoulos, K. S. Nikita, A. S. Nikita, and D. Kelekis, "A computer-aided diagnostic system to characterize CT focal liver lesions: design and optimization of a neural network classifier," *IEEE Transactions on Information Technology in Biomedicine A Publication of the IEEE Engineering in Medicine and Biology Society*, vol. 7, no. 3, pp. 153–162, 2003.
- [7] W. Pang and K. C. Hui, "Interactive evolutionary 3D fractal modeling with modified IFS," *Computer-Aided Design and Applications*, vol. 6, no. 1, pp. 55–67, 2009.
- [8] Ali, Rahman, Muhammad Hameed Siddiqi, and Sungyoung Lee, "Rough set-based approaches for discretization: a compact review," *Artificial Intelligence Review*, vol. 44, no. 2, pp. 235–263, 2015.
- [9] Z. Zhang, C. Zhang, H. Li, and X. Tao, "Multipath transmission selection algorithm based on immune connectivity model," *Journal of Computer Applications*, vol. 40, no. 12, p. 3571, 2020.
- [10] Z. W. Zhang, D. Wu, and C. J. Zhang, "Study of cellular traffic prediction based on multi-channel sparse LSTM," *Computer Science*, vol. 48, no. 6, pp. 296–300, 2021.
- [11] F. M. Abd Algalil and S. P. Zambare, "Effects of temperature on the development of Calliphorid fly of forensic importance *Chrysomya megacephala* (Fabricius, 1794)," *Indian Journal of Applied Research*, vol. 5, no. 2, pp. 767–769, 2015.
- [12] M. H. Yap, E. A. Edirisinghe, and H. E. Bez, "A novel algorithm for initial lesion detection in ultrasound breast images," *Journal of Applied Clinical Medical Physics*, vol. 9, no. 4, pp. 2741–3199, 2008.
- [13] F. A. Al-Mekhlafi, R. A. Alajmi, Z. Almusawi et al., "A study of insect succession of forensic importance: Dipteran flies (diptera) in two different habitats of small rodents in Riyadh City, Saudi Arabia," *Journal of King Saud University-Science*, vol. 32, no. 7, pp. 3111–3118, 2020.
- [14] S. G. R. Mougiakakou, S. Golemati, I. Gousias, A. N. Nicolaides, and K. S. Nikita, "Computer-aided diagnosis of carotid atherosclerosis based on ultrasound image statistics, laws' texture and neural networks," *Ultrasound in Medicine and Biology*, vol. 33, no. 1, pp. 26–36, 2007.
- [15] U. Raghavendra, U. Rajendra Acharya, A. Gudigar et al., "Fusion of spatial gray level dependency and fractal texture features for the characterization of thyroid lesions," *Ultrasonics*, vol. 77, pp. 110–120, 2017.
- [16] S. Guo and B. Wang, "Application of computer aided modeling design in the expression techniques of sculpture art space," *Computer-Aided Design and Applications*, vol. 19, no. S3, pp. 1–12, 2021.
- [17] J. Tang, R. M. Rangayyan, J. Xu, I. El Naqa, and Y. Yang, "Computer-aided detection and diagnosis of breast cancer with mammography: recent advances," *IEEE Transactions on Information Technology in Biomedicine A Publication of the IEEE Engineering in Medicine and Biology Society*, vol. 13, no. 2, pp. 236–251, 2009.
- [18] R. Abdulaziz, Abdulaziz, A. Badry et al., "Intraspecific molecular variation among *Androctonus crassicauda* (Olivier, 1807) populations collected from different regions in Saudi Arabia," *Journal of King Saud University-Science*, vol. 34, no. 4, p. 101998, 2022.
- [19] Z. He, X. You, L. Zhou, Y. Cheung, and J. Du, "Writer identification using fractal dimension of wavelet subbands in gabor domain," *Integrated Computer-Aided Engineering*, vol. 17, no. 2, pp. 157–165, 2010.
- [20] H. Che and J. Wang, "Browse Journals & Magazines," *IEEE Transactions on Neural Networks and Learning Systems*, vol. 30, no. 8, pp. 2503–2514, 2019.
- [21] H. Che and J. Wang, "A nonnegative matrix factorization algorithm based on a discrete-time projection neural

## Research Article

# Research on Optimization and Allocation of English Teaching Resources

Chongya Liu  and Jue Xia

*School of Foreign Languages, NanYang Institute of Technology, NanYang 473000, China*

Correspondence should be addressed to Chongya Liu; [sophia\\_liu@nyist.edu.cn](mailto:sophia_liu@nyist.edu.cn)

Received 15 March 2022; Revised 12 April 2022; Accepted 12 May 2022; Published 27 May 2022

Academic Editor: Man Fai Leung

Copyright © 2022 Chongya Liu and Jue Xia. This is an open access article distributed under the Creative Commons Attribution License, which permits unrestricted use, distribution, and reproduction in any medium, provided the original work is properly cited.

To rationally allocate teaching resources in English teaching, a teaching resource optimization and allocation management method is proposed based on a convolutional neural network (CNN) and Arduino device. By constructing a 9-layer CNN classification and recognition model and the English education resource library of the Arduino device and applying them to the recognition program design of the Arduino device, the rational optimization and allocation of teaching resources are realized. Simulation results show that the recognition accuracy of the proposed method is over 90% for Arduino devices, and the recognition accuracy is over 80% for real English teaching scenarios, which means that the proposed method has a certain practical application value. Moreover, the interaction mode between English learners and English teaching resources is innovated, which contributes to the optimization and allocation of English teaching resources. Thus a new idea is generated to integrate the English teaching resources.

## 1. Related Work

With the globalization of economics, the communication and connection between countries have been closer and closer. As an international language, English is widely used in the world and it has become one of the main languages for communication between countries. In order to promote the communication between countries, China has launched a nationwide English education campaign. However, due to regional differences, English education resources in China are unevenly allocated. In recent years, online education has solved the problem of uneven allocation of English teaching resources to a certain extent. Ronkowitz Kenneth et al. believed that online education is conducive to integrate the online courses into higher education and balance the allocation of educational resources, which plays a positive role in promoting the education system [1]. SerranoSolano Beatriz et al. took Galaxy as an e-learning platform and realized accessible online education by providing a training material library of high-quality community library [2]. On this basis, data, tools, and other teaching resources are easy to obtain,

and learners' teaching resources can be shared. Çoban Atakan applied the Algodoo program to the teaching and evaluation process of physics courses, thus application that can arouse students' attention to the course is designed, which improves learners' learning motivation and facilitates the sharing of educational resources [3]. Zhang Rongbo and Afrouz Rojan et al. constructed the construction paradigm of the online education evaluation model by analyzing the application of the current scientific paradigm. The proposal of a new education concept has promoted the development of a new paradigm, and the paradigm constructs a series of educational evaluation models from macro, Miso, and micro levels, which play a positive role in the research of various aspects of related fields [4, 5]. Ren T and Kim Jihyun et al. improved the ease of use of online networks and further optimized teaching resources with the aid of artificial intelligence (AI) technology [6, 7]. Arnab Kundu reviewed the role of self-efficacy in online education, and thus, an overall framework for strengthening participants' self-efficacy is put forward. At this time, online education becomes effective and impressive. In addition, participants' self-efficacy is easy

to be improved, and the rational allocation of teaching resources is realized. The results show that online education plays a positive role in the optimization and allocation management of teaching resources [8]. However, the above studies only focus on the preliminary allocation and management of educational resources and do not conduct an in-depth discussion. To solve this problem, a teaching resource optimization and allocation management method for English teaching is proposed based on the CNN and Arduino device, so as to deeply study the optimization and allocation of teaching resources.

## 2. Introduction to CNN

CNN is a classification and recognition algorithm proposed based on biological vision, which is often used for the classification and recognition of images, texts, audio signals, and other fields. The basic results are shown in Figure 1 [9].

The input layer is used to preprocess input data. The convolution layer is responsible for learning and extracting sample features of input data, and when invalid data sample features are filtered, the mathematical description is shown in formula (1). The pooling layer includes average pooling and maximum pooling operations, as shown in formulas (2) and (3), respectively, which are responsible for reducing the amount of data to avoid overfitting problems of the model. The full connection layer is the output layer of the CNN, which acts as a classifier and is used to output the final classification calculation results. Its mathematical description is shown in (4).

$$y = f\left(\sum w_{ij}x + b\right), \quad (1)$$

$$S_j = \frac{1}{t} \sum_{i \in R_j, r_i \leq t} a_i, \quad (2)$$

$$y = f(\beta \text{ down}(x) + b), \quad (3)$$

$$y = f(wx + b). \quad (4)$$

In formula (1),  $x$  and  $y$  are the input and output image features;  $W_{ij}$  stands for two-dimensional convolution kernel;  $b$  represents the offset term; and  $f(\bullet)$  is the activation function.

In formula (2),  $t$  represents the sequential threshold of activation value. In addition, pooling domain  $R_j$  belongs to the  $j$ th feature graph, and the index value  $i$  of activation value is in  $R_j$ .  $R_i$  and  $a_i$  represent the sequence and activation value of  $i$ , respectively. In formula (3),  $x$  and  $y$  represent pooled input feature and output feature of the convolution layer, respectively;  $\beta$  and  $b$  represent multiplicative and additive bias terms, respectively; and  $\text{down}(\bullet)$  stands for pooled function. In formula (4),  $y$  represents the fully connected output;  $f(\bullet)$  represents activation function;  $x$  represents the input of full connection layer;  $W$  stands for weight; and  $b$  means offset term.

CNN usually adopts the cross entropy function as the loss function, and its calculation formula is shown in the following formula [10, 11]:

$$H(p, q) = - \sum_x p(x) \log q(x), \quad (5)$$

where  $p$  and  $q$  are actual value and predicted value, respectively. The higher the value, the better the model performance.

CNN is characterized by parameter sharing and translation invariance and is mainly delinearized by activation function [12, 13]. The activation functions mainly have the following centralized forms [14, 15]:

$$\text{sigmoid function : } f(x) = \text{sigmoid}(x),$$

$$\text{tanh function : } f(x) = \text{tanh}(x), \quad (6)$$

$$\text{ReLU function : } f(x) = \max(0, x).$$

Among them, the sigmoid function and tanh function usually have the problem of "gradient dispersion" and are more suitable for shallow networks. However, the ReLU function almost completely transmits the gradient to each layer of the network losslessly, so that the weight of each layer of the network can be trained [16]. Therefore, the ReLU function is adopted as the activation function of the CNN model. For image recognition tasks, the parameter sharing and translational invariance of the CNN can effectively reduce nonessential parameters of the network and retain important parameters, so as to make the network achieve a better learning effect.

## 3. Optimization and Allocation of English Teaching Resources

**3.1. Overall Design.** Based on the above analysis, the method of optimizing and allocating English teaching resource is divided into two parts: the first is to use the CNN design recognition program; the second is to collect and organize existing English education resources to build an Arduino device resource library. Figure 2 shows the processes.

### 3.2. Design of Arduino Recognition Program Based on CNN

**3.2.1. Design of Recognition Program.** The basic idea of the design of the Arduino recognition program based on the CNN is to collect the data set composed by images of Arduino devices to train the CNN, so as to obtain an optimal CNN recognition model whose output value is closest to the actual value. Then, the model is used to classify and recognize the samples to be tested, and categories can be output. The specific idea is shown in Figure 3.

According to the characteristics of Arduino devices, there are two convolution layers and three full connection layers set for the preliminary CNN model. Among them, the last full connection layer adopts the Softmax function, as shown in the following formula:

$$S_i = \frac{e^{Z_i}}{\sum_c e^{Z_c}}, \quad (7)$$

where  $Z_i$  represents the output value of node  $i$ , and  $c$  represents the number of output nodes. When the value



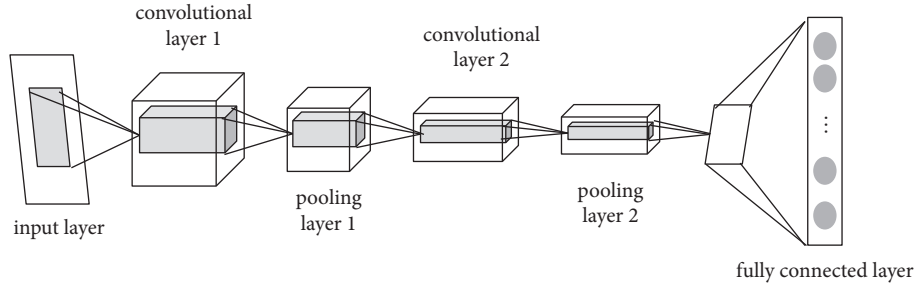


FIGURE 1: Structure of CNN.

overflows, the Softmax function can be optimized by subtracting the maximum value  $D$  from the output value.

$$\text{soft max}(z_i) = \frac{e^{z_i - D}}{\sum_c e^{z_c - D}}, \quad (8)$$

$$D = \max(z).$$

3.2.2. *Optimization of Recognition Program.* To explore a more reasonable CNN structure and improve the classification and recognition performance of the model, the CNN model is adopted to optimize the network structure of the mode. There are one convolution layer and pooling layer added, and one full connection layer reduced. The steps of optimizing CNN construction are as follows:

- (1) Convert input images to meet the requirements of CNN input images. Assume that the initial threshold of image gray value is  $T_0$ , the part greater than  $T_0$  is  $A_1$ , and the part less than  $T_0$  is  $A_2$ . Calculate the normalized gray histogram  $h(t)$  and normalized cumulative histogram  $H(t')$  of  $A_1$  and  $A_2$ , respectively, as shown in the following formulas:

$$h(t) = \frac{n(t)}{M * N}, \quad (9)$$

$$H(t') = \sum_{t=0}^{t'} h(t), \quad (10)$$

where  $t$  and  $t'$  are pixel gray level;  $n(t)$  is pixel point with gray level  $t$ ;  $M$  and  $N$  are the numbers of pixel rows and columns, respectively. Then, gray mean  $X_1$  and  $X_2$  of  $A_1$  and  $A_2$  can be expressed as follows:

$$X_1 = \frac{\sum_{t=0}^{T_0} t \cdot h(t)}{H(T_0)}, \quad (11)$$

$$X_2 = \frac{\sum_{t=T_0}^1 t \cdot h(t)}{(1 - H(T_0))}.$$

Calculate and update the threshold as follows:

$$T_1 = \frac{1}{X_1 + X_2}. \quad (12)$$

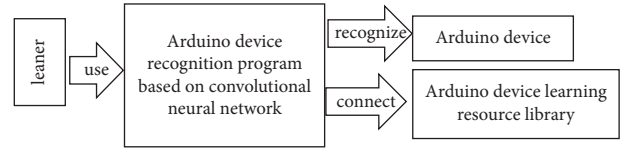


FIGURE 2: Optimization and allocation of English teaching resource based on CNN.

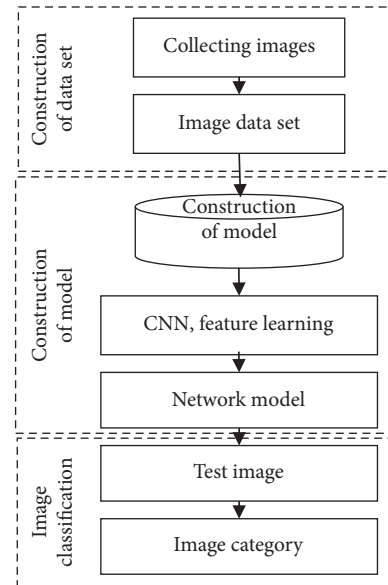


FIGURE 3: Classification and recognition process of Arduino devices based on CNN.

- (2) Set the depth of the convolution kernel of the three-layer convolution layer to 64, 128, and 256. In addition, both height and width are set to 7, and the move step is 1.
- (3) Adopt maximum pooling and obtain the final classification results by the Softmax regression model.

As can be seen, the optimized CNN model is constructed. Inputting the data set into the constructed CNN model for iterative training, the optimal classification recognition CNN model can be obtained.

During model training, the loss function is used to describe the performance of the model. When the value of the loss function is large, there is an obvious gap between the

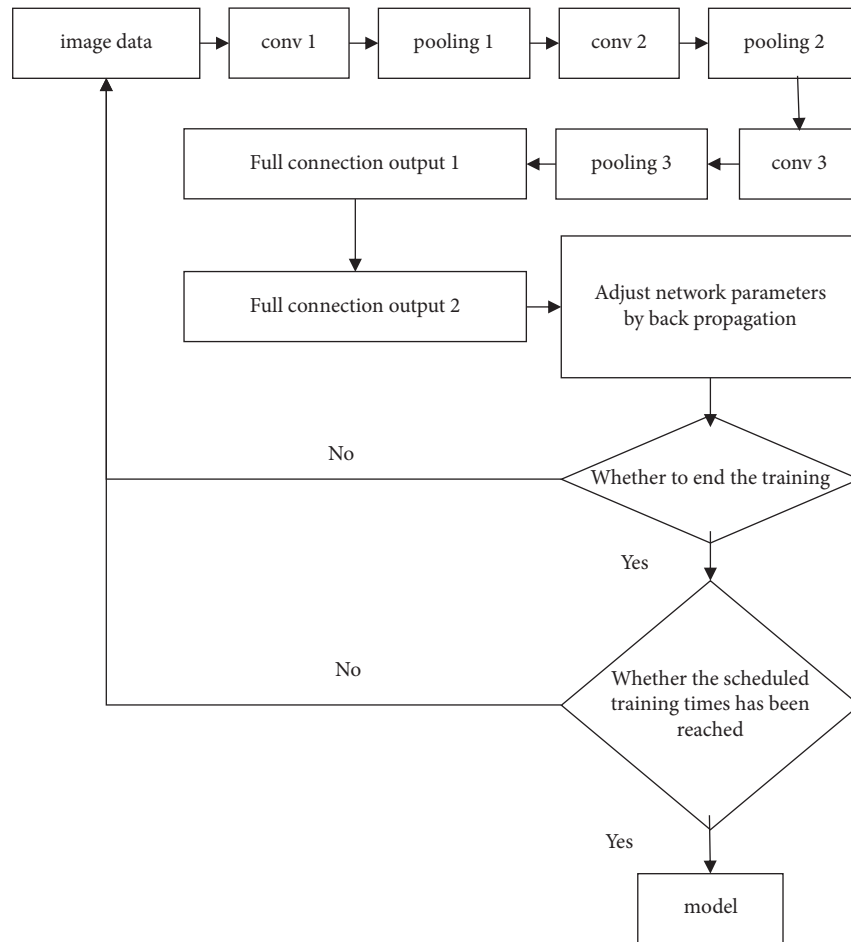


FIGURE 4: Training process of CNN model.

output value of the model and the actual value. At this time, the back propagation algorithm should be used to adjust the model parameters and continue training the model. When the loss function value is small and the iteration termination condition is met, it indicates that the model has reached the best state. At this point, the model is the best classification recognition model, and the model is saved and output. Figure 4 shows the training process of the optimized CNN model.

**3.2.3. Construction of English Education Resource Library for Arduino Devices.** Arduino is easy to learn and can adapt products to the environment by connecting different sensors in different environments, so as to immerse learners in the world of learning [17]. At present, Arduino learning resources are abundant. To achieve targeted learning and training for learners, English education video resources are collected and sorted out from the Internet. Thus an English education resource library for Arduino devices is built. When CNN successfully identifies Arduino devices, the Arduino recognition program automatically pushes links of relevant English education resources in the resource library to learners. Learners can click the links to open and view corresponding English learning resources in the browser.

## 4. Simulation Experiment

**4.1. Construction of Experimental Environment.** This experiment is carried out on the Windows7 operating system. Tensorflow deep learning framework is used to construct the CNN classification recognition model, and Python language is used to design the model.

**4.2. Data Sources and Preprocessing.** In this experiment, 10 English education resource libraries of Arduino device images collected on-site are selected as experimental data, including Arduino UNO board, L298 N drive board, Hall sensor, active buzzer, rocker, serial wireless transparent transmission module, PIR human body sensor, potential device, and ultrasonic module and LCD [18, 19]. Each device collects 500 images, and a total of 5000 images are collected.

CNN is adopted to learn and extract data features, but the number of images collected in this experiment is still small. In order to expand sample data and improve the applicability of the model, the experimental data set is expanded. Firstly, more sample images are obtained by searching similar images on the Internet, and then the sample images are further expanded by converting image angles and rotating images. Through the above-

TABLE 1: Accuracy of model with different network layers.

| Number of network layers | 5     | 6     | 7     | 8     | 9    | 10          |
|--------------------------|-------|-------|-------|-------|------|-------------|
| Accuracy (%)             | 45.37 | 48.64 | 40.62 | 56.22 | 91.3 | Overfitting |

TABLE 2: Accuracy of model with different iterations.

| Number of iterations | 2000  | 3000  | 4000  | 5000  | 6000  | 7000  | 8000  | 9000  | 10000 |
|----------------------|-------|-------|-------|-------|-------|-------|-------|-------|-------|
| Accuracy (%)         | 56.12 | 69.32 | 64.56 | 70.12 | 86.32 | 65.74 | 50.36 | 60.35 | 72.13 |

TABLE 3: Accuracy of model with different batch sizes.

| Batch size   | 10    | 30    | 50    | 70    | 100   | 150   |
|--------------|-------|-------|-------|-------|-------|-------|
| Accuracy (%) | 55.23 | 76.08 | 85.11 | 84.36 | 90.12 | 90.46 |

mentioned processing, there are 8200 sample images obtained.

**4.3. Evaluation Indicators.** Generally, there are accuracy, precision, recall, and F1 values selected as evaluation indicators, which are used to evaluate the performance of classification models. In this experiment, only accuracy is selected as an indicator to evaluate the classification performance of the model. The calculation methods are as follows [20]:

$$\text{Accuracy} = \frac{(TP + TN)}{(P + N)}. \quad (13)$$

Here,  $TP$  and  $TN$  represent true positive and true negative;  $P$  and  $N$  represent all positive and negative; and  $FP$  and  $FN$  represent false positive and false negative.

**4.4. Parameter Settings.** CNN parameters include the number of the network layer, iterations, batch size, and learning rate, whose setting has a great influence on the recognition accuracy of the CNN model [21, 22]. In order to ensure the recognition accuracy of the model as far as possible, the experiment determines the values of the above parameters through debugging.

**4.4.1. Number of Network Layers.** The more network layers of CNN, the more complex the model structure and the more extracted feature information. However, too many network layers will greatly increase the model training time, resulting in overfitting problems [23]. The fewer network layers, the simpler the model structure and the shorter the model training time. However, too few network layers will make the number of extracted features limited, and the error function is prone to non-convergence and falls into local optimization, resulting in low accuracy of final model recognition [24, 25]. To determine the number of network layers of the model, there are 5,6,7,8, 9, and 10 layers set up for model training, and the results are shown in Table 1. When the CNN has 9 layers, the recognition accuracy is the highest. When the number of network layers is less than or greater than 9, the model cannot achieve the ideal effect.

TABLE 4: Accuracy of model with different learning rates.

| Learning rate | 0.1            | 0.01  | 0.001 |
|---------------|----------------|-------|-------|
| Accuracy (%)  | Nonconvergence | 72.36 | 48.67 |

Therefore, the network layer of the CNN model in this experiment is set as 9 layers.

**4.4.2. Number of Iterations.** Table 2 shows the accuracy of the model with different iterations. When the number of iterations is 6000, the accuracy of the model is the highest, reaching 86.32%. The accuracy of the model greater than or less than 6000 times decreases. Thus when the number of iterations increases, the recognition accuracy of the model firstly increases to a critical value and then decreases, and the critical value in this experiment is 6000. Therefore, the iterations of the CNN model in this experiment is set to 6000.

**4.4.3. Batch Size.** Table 3 shows the recognition accuracy of the model with different batch sizes. With the increase of batch size, the recognition accuracy of the model increases gradually, and the increased range of model accuracy increases first and then decreases. When batch size reaches 100, the accuracy of the model does not increase significantly and tends to be stable. Therefore, the batch size of the CNN model is set to 100 in this experiment.

**4.4.4. Learning Rate.** If the learning rate is too high, the model will not be converged. However, if the learning rate is too low, the optimization speed will be reduced. The accuracy of the observation model with different learning rates is set, and the results are shown in Table 4. Here, when the learning rate is 0.01, the accuracy of the CNN model is the highest, which is 72.36%. When the learning rate is less than or greater than 0.01, the accuracy reduces greatly. Therefore, the learning rate of the CNN model is set as 0.01 in this experiment.

Through the above experiments, the parameters of the optimized CNN model are finally set as follows: 9-layer network structure, 6000 iterations, batch size of 100, and learning rate of 0.01.

TABLE 5: Recognition results of the model before CNN structure optimization.

|  | Total number of devices | Number of successful recognition | Number of failure recognition | Success rate of recognition (%) |
|--|-------------------------|----------------------------------|-------------------------------|---------------------------------|
| Arduino UNO board                                      | 128                     | 116                              | 12                            | 90.6                            |
| Potential device                                       | 108                     | 97                               | 11                            | 89.8                            |
| LCD  | 114                     | 103                              | 11                            | 90.4                            |
| Serial wireless transparent transmission module APC220 | 119                     | 107                              | 12                            | 89.9                            |
| Active buzzer  | 109                     | 89                               | 20                            | 81.7                            |
| Ultrasonic module                                      | 154                     | 135                              | 19                            | 87.7                            |
| L298 N drive board                                     | 122                     | 110                              | 12                            | 89.8                            |
| Hall sensor  | 130                     | 110                              | 20                            | 84.6                            |
| Rocker   | 141                     | 124                              | 17                            | 87.9                            |
| PIR human body sensor                                  | 152                     | 136                              | 16                            | 89.5                            |

TABLE 6: Recognition results of the model after CNN structure optimization.

|  | Total number of devices | Number of successful recognitions | Number of failure recognitions | Success rate of recognition (%) |
|--|-------------------------|-----------------------------------|--------------------------------|---------------------------------|
| Arduino UNO board                                      | 200                     | 192                               | 8                              | 96                              |
| Potential device                                       | 200                     | 186                               | 14                             | 93                              |
| LCD  | 200                     | 196                               | 4                              | 98                              |
| Serial wireless transparent transmission module APC220 | 200                     | 187                               | 13                             | 93.5                            |
| Active buzzer  | 200                     | 179                               | 21                             | 90.0                            |
| Ultrasonic module                                      | 200                     | 181                               | 19                             | 90.5                            |
| L298 N drive board                                     | 200                     | 190                               | 10                             | 95                              |
| Hall sensor  | 200                     | 182                               | 18                             | 91                              |
| Rocker   | 200                     | 185                               | 15                             | 92.5                            |
| PIR human body sensor                                  | 200                     | 194                               | 6                              | 97                              |

TABLE 7: Recognition results under real English teaching scenarios.

|                   | Number of successful recognitions | Number of failure recognitions | Success rate of recognition (%) |
|-------------------|-----------------------------------|--------------------------------|---------------------------------|
| Arduino UNO board | 27                                | 3                              | 90                              |
| Active buzzer     | 24                                | 6                              | 80                              |
| Ultrasonic module | 25                                | 3                              | 83.3                            |

#### 4.5. Experimental Results

**4.5.1. Model Verification.** To verify the optimization effect of the proposed method on CNN structure, the recognition accuracy of the model before and after optimization for the English education resource library of the Arduino device is compared. Table 5 shows the recognition results of the model before CNN structure optimization, and Table 6 shows the recognition results of the model after CNN structure optimization. As can be seen from Table 5, the recognition accuracy of CNN structure before optimization on different device images is high and the recognition accuracy of larger devices reaches more than 90%, such as the Arduino UNO board and the L298 N driver board. The recognition accuracy of smaller devices is also more than 80%, such as the active buzzer. Therefore, the recognition method of Arduino devices based on CNN has certain effectiveness and can accurately identify Arduino device images in different scenarios, which is conducive to reasonable optimization and manage English education resources. As can be seen from Table 6, the overall recognition

accuracy of the model after CNN structure optimization for Arduino device images is 90% or more, and the recognition accuracy of the Arduino UNO board, LCD, and PIR human induction sensor is more than 95%. Compared with the model before optimization, the optimized CNN model has a better recognition effect. Therefore, the optimization of the CNN model is effective, and the recognition accuracy of the model can be improved.

**4.5.2. Method Verification.** To verify the application effect of the proposed method in the actual English teaching environment, a bow alarm based on the proposed method is constructed for English teaching activities. The alarm will sound when learners' head is down or close to the desk. At the beginning of the experiment, there are 30 students scanning Arduino devices through a mobile phone mini program and the mini program recommends English learning resources to students according to the scanning results for them to learn by themselves. Table 7 shows the usage of the recognition program. As can be seen, the

recognition program of the proposed method also has a high recognition accuracy in the real English teaching scenarios, which is more than 80%. Compared with the laboratory test environment, the success rate of recognition is lower, but it can still meet the design requirements and has certain practicability.

## 5. Conclusion

In conclusion, the number of network layers of the CNN classification model is 9. Among them, there is only 1 input layer. In addition, the number of convolution layers and pooling layers both are 3, and the number of full connection layers is 2. On this basis, the proposed optimization and allocation method of English teaching resources can realize the recognition of Arduino devices and recommendation of English teaching resources. Moreover, the interaction way between English learners and English teaching resources is innovated, which promotes the optimization and management of English teaching resources. As can be seen that the recognition accuracy of the proposed method is more than 90% for Arduino devices, and the recognition accuracy is more than 80% for real English teaching scenarios, which has certain practical application value and is helpful for the optimization and allocation management of English teaching resources. Thus a new idea has emerged to integrate English teaching resources. This paper takes deep learning as the main line and the optimal allocation of teaching resources as the carrier and applies it to the field of teaching, so as to provide a new reference way for the informatization of teaching points.

## Data Availability

The experimental data used to support the findings of this study are available from the corresponding author upon request.

## Conflicts of Interest

The authors declare that they have no conflicts of interest regarding this work.

## References

- [1] R. Kenneth and R. L. Condro, "Choosing transformation over tradition: the changing perception of online education," *The American Journal of Economics and Sociology*, vol. 80, no. 1, pp. 205–229, 2021.
- [2] S. Beatriz, M. C. Foll, C. G. Alba, A. Erxleben, and H. Rasche, "Fostering accessible online education using Galaxy as an e-learning platform," *PLoS Computational Biology*, vol. 17, no. 5, Article ID e1008923, 2021.
- [3] Ç. Atakan, "Algodoo for online education: impulse and momentum activities," *Physics Education*, vol. 56, no. 2, Article ID 025017, 2021.
- [4] R. Zhang, W. Zhao, and Y. Wang, "Big data analytics for intelligent online education," *Journal of Intelligent and Fuzzy Systems*, vol. 40, no. 2, pp. 2815–2825, 2021.
- [5] A. Rojan and R. Crisp Beth, "Online education in social work, effectiveness, benefits, and challenges: a scoping review," *Australian Social Work*, vol. 74, no. 1, pp. 55–67, 2021.
- [6] T. Ren, Y. Q. Wu, Y. T. Han, and Q. Y. Meng, "[Analysis of online education for public health and preventive medicine]," *Zhonghua yu fang yi xue za zhi [Chinese journal of preventive medicine]*, vol. 54, no. 12, pp. 1484–1486, 2020.
- [7] J. Kim, K. Merrill, and K. Xu, "My teacher is a machine: understanding Students' Perceptions of AI teaching assistants in online education," *International Journal of Human-Computer Interaction*, vol. 36, no. 20, pp. 1902–1911, 2020.
- [8] A. Kundu, "Toward a framework for strengthening participants' self-efficacy in online education[J]," *Asian Association of Open Universities Journal*, vol. 15, no. 3, pp. 351–370, 2020.
- [9] A. Shahzad, M. Raza, and J. H. Shah, "Categorizing white blood cells by utilizing deep features of proposed 4B-AdditionNet-based CNN network with ant colony optimization," *Complex & Intelligent Systems*, vol. 33, pp. 1–17, 2021.
- [10] K. Ioannis, S. Ilham, and M. Sanjay, "A modified CNN network for automatic pain recognition using facial expressions," *Journal of Software Engineering and Applications*, vol. 14, no. 8, pp. 400–417, 2021.
- [11] Y. Guo, L. Bi, Z. Zhu, and D. D. Feng, "Automatic left ventricular cavity segmentation via deep spatial sequential network in 4D computed tomography," *Computerized Medical Imaging and Graphics*, vol. 91, Article ID 101952, 2021.
- [12] Y. Lei, Y. Tingxiao, K. Hiroki, and Y. Yuichiro, "An automatic detection approach of traumatic bleeding based on 3D CNN networks:special section on image media quality," *IEICE - Transactions on Fundamentals of Electronics, Communications and Computer Sciences*, vol. E104.A, no. 6, pp. 887–896, 2021.
- [13] C. Wang, L. Liang, Y. Chenggang, and W. Zhan, "Cross-modal semantic correlation learning by Bi-CNN network," *IET Image Processing*, vol. 15, no. 14, pp. 3674–3684, 2021.
- [14] Y. Su, "A parallel computing and mathematical method optimization of CNN network convolution," *Microprocessors and Microsystems*, vol. 80, Article ID 103571, 2021.
- [15] K. Jalaldeen, M. Malathi, and B. Sinthia, "An automatic recognition of lung tumor by using CNN network and fuzzy-clustering algorithm," *Materials Today Proceedings*, vol. 45, no. P2, pp. 2921–2924, 2021.
- [16] S. Tanzila, A. Rehman, N. S. M. Jamail, and S. L. M. Sainte, "Categorizing the students' activities for automated exam proctoring using proposed deep L2-GraftNet CNN network and ASO based feature selection approach," *IEEE Access*, vol. 9, Article ID 47639, 2021.
- [17] B. He, Q. Lu, J. Lang, and H. Yu, "A new method for CTC images recognition based on machine learning," *Frontiers in Bioengineering and Biotechnology*, vol. 8, pp. 897–899, 2020.
- [18] X. Guan, "An algorithm based on simple CNN and BI\_LSTM network for Chinese word segmentation," *Journal of Physics: Conference Series*, vol. 1621, no. 1, Article ID 012001, 2020.
- [19] X. Pan, S. Zhang, and W. P. Guo, "Video-based facial expression recognition using deep temporal-spatial networks," *IETE Technical Review*, vol. 37, no. 4, pp. 402–409, 2020.
- [20] B. Jiang, H. Jinrong, and Y. Shuqin, "Fusion of machine vision technology and AlexNet-CNNs deep learning network for the

- detection of postharvest apple pesticide residues,” *Artificial Intelligence in Agriculture*, vol. 1, no. C, pp. 1–8, 2019.
- [21] G. Wang, W. Li, X. Chen, and X. Yin, “Blurring-effect-free CNN network of structural edge for focus stacking,” *IEEE Access*, vol. 7, Article ID 167672, 2019.
- [22] M. Moshfeghi Darius and T. Trese Michael, “Reducing blindness resulting from retinopathy of prematurity using deep learning,” *Ophthalmology*, vol. 128, no. 7, pp. 1077–1078, 2021.
- [23] M. Zheng, T. Li, R. Zhu et al., “Traffic accident’s severity prediction: a deep-learning approach-based CNN network,” *IEEE Access*, vol. 7, Article ID 39897, 2019.
- [24] G. Jack, “An overview of artificial intelligence/deep learning,” *Pathology*, vol. 53, no. S1, pp. S6–S9, 2021.
- [25] T. Y. Han, D. H. Kim, S. Lee, and B. C. Song, “Infrared image super-resolution using auxiliary convolutional neural network and visible image under low-light conditions,” *Journal of Visual Communication and Image Representation*, vol. 51, pp. 191–200, 2018.

## Research Article

# Research on Intelligent Retrieval Method of Teaching Resources on Large-Scale Network Platform

Xiaofeng Su<sup>1</sup> and Tianjing Zhang <sup>2</sup>

<sup>1</sup>*Xi'an Siyuan University, Xi'an, Shaanxi 330022, China*

<sup>2</sup>*Hebei Academy of Fine Arts, Shijiazhuang, Hebei 050000, China*

Correspondence should be addressed to Tianjing Zhang; [tianjing@hbafa.edu.cn](mailto:tianjing@hbafa.edu.cn)

Received 12 April 2022; Revised 7 May 2022; Accepted 11 May 2022; Published 27 May 2022

Academic Editor: Man Fai Leung

Copyright © 2022 Xiaofeng Su and Tianjing Zhang. This is an open access article distributed under the Creative Commons Attribution License, which permits unrestricted use, distribution, and reproduction in any medium, provided the original work is properly cited.

With the increase in information on various cloud computing platforms, there are more and more teaching documents and videos, which provide sufficient resources for people to learn. Facing the large-scale digital teaching resources, how to quickly and accurately retrieve the required content has become an important research direction in the information field. Especially in the face of heterogeneous, dynamic, and large-scale teaching resources stored in the cloud computing platform, the traditional cloud computing resource retrieval has poor performance and low work efficiency. To solve this problem, a cloud computing platform retrieval method based on genetic algorithm is proposed, which is suitable for intelligent retrieval of teaching resources. Firstly, the teaching resource storage system based on cloud computing platform is analyzed, and the overall architecture of the system and the network topology of cloud storage data are given. Then, a resource retrieval method suitable for cloud computing platform is designed by genetic algorithm, and the convergence performance of genetic algorithm is improved by ant colony algorithm. Finally, the selection algorithm in genetic algorithm is optimized by using random numbers and increasing the number of cycles. The experimental results show that the proposed intelligent retrieval method has greatly improved the Recall and Precision compared with the traditional retrieval methods.

## 1. Introduction

With the increase in information on various cloud computing platforms, there are more and more teaching documents and videos. Different from local storage, users using cloud data can greatly improve work efficiency and reduce hardware investment costs [1–4]. Many products and services based on cloud computing are constantly being introduced, and the scale and fields involved in the computer industry are constantly expanding. “Cloud Computing-Aided Instruction” (CCAI) has become a new means for colleges and universities to set up modern teaching [5–7], which has effectively improved the teaching quality technically. The features of CCAI mode are very beneficial to the information management of teaching, reduce the capital investment and maintenance costs, improve the network

security, and help to build a personalized teaching environment.

However, with the continuous growth of digital teaching resources on the cloud computing platform, how to quickly and accurately retrieve the required content has become an important research direction in the information field [8, 9]. In most cases, these network resources are unorganized, or each has a different organizational structure, which brings a lot of pressure for users to inquire about resources. Although the emergence of search engines has eased the pressure of resource inquiry, most search engines are not satisfactory in recall and precision. Most of the time, users cannot find the resources they need from a large number of inquiry results. In this case, the user experience is poor, and the user still has not got rid of the trouble of too much information. Web information retrieval belongs to the category of information

retrieval and is an important development stage in the field of information retrieval.

Genetic algorithm [10, 11] is a globally optimized intelligent probability search algorithm developed by referring to the natural selection and genetic evolution mechanism of organisms. The genetic algorithm is an effective method for finding the optimal solution in a large solution space. Searching for an optimal query in large-scale information retrieval system can also be regarded as a problem of searching for the optimal solution in a large solution space. Therefore, how to apply the retrieval method based on the genetic algorithm to the cloud computing teaching platform to improve the retrieval effect is the key research content of this paper. The results show that the genetic algorithm is effective in query optimization, and it can overcome the shortcomings of low Recall and Precision of the retrieval system, so that users can accurately and efficiently obtain the required network teaching resources.

## 2. Related Works

At present, the resource retrieval methods of cloud computing teaching platform are mostly based on manual classification or keyword matching technology [12, 13]. These two retrieval methods have not optimized the user's query requirements, which lead to the unsatisfactory retrieval results of these teaching platforms.

There are many disadvantages in the retrieval method of manual classified catalog. The first is inefficient. Administrators of resource management systems need to upload resources based on manually categorized directories. However, once there is any objection to the manual classification catalog, the administrator shall be contacted to modify relevant catalog. The second is poor compatibility. Resources in one system are hard to reuse in another. To use these resources, the administrator needs to enter them one by one in another system. If we want to overcome these shortcomings, we need to provide a unified resource storage method, and the resource storage method based on cloud computing platform is a good solution.

The retrieval method based on keyword matching has great limitations in the semantic disclosure of information, and it is difficult to guarantee the accuracy and precision of information. The retrieval system simply matches the keywords entered by the user. Many resources that should be retrieved are not retrieved, while resources that should not be retrieved are retrieved. This requires query optimization. Global analysis is an early query optimization method with practical application value. Roul [14] proposed a global analysis method based on Latent Semantic Indexing, which realized effective semantic clustering and topic sorting of web documents. However, when the document set is very large, it is often infeasible in time and space to establish a global dictionary of word relations, and the update cost after the document set changes is huge.

At present, the popular local analysis methods mainly include Relevance Feedback and Pseudo Feedback. Pseudo Feedback is developed on the basis of Relevance Feedback.

Relevance Feedback is a very important mechanism for query optimization in information retrieval. Because of the remarkable effect of relevant feedback, it has been widely applied and studied in information retrieval. Zhang et al. [15] proposed a method to improve the query effect by using relevant feedback. This method expands and shrinks the query at the same time, thus obtaining a high recall rate. Pseudo-relevance feedback does not need to interact with users. It directly regards the first N documents retrieved by the first query as relevant documents and optimizes the query based on this. Wang et al. [16] proposed a pseudo-relevance feedback framework for information retrieval, which combines relevance matching and semantic matching. However, the selection of keywords in Pseudo Feedback is more important. Generally speaking, keywords with higher weights are selected for query expansion. This selection method ensures the importance of keyword selection, but it does not guarantee that keywords are related to the topic.

Although information retrieval technology has made some progress, the performance of retrieval engines in large-scale network platforms still cannot meet users' expectations. Because of the huge retrieval data set and the diversity and complexity of the factors that affect retrieval efficiency, the above optimization techniques are not ideal in practical application. The introduction of the genetic algorithm provides a new way to solve information retrieval problems. Therefore, a cloud computing platform retrieval method based on the genetic algorithm is proposed. The main innovations and contributions are as follows: (1) try to apply the genetic algorithm, which is suitable for finding the best solution in large space, to retrieval optimization, and design a resource retrieval method suitable for Spark platform, so as to overcome the low Recall and Precision of the retrieval system; (2) the ant colony algorithm is used to improve the convergence performance of the genetic algorithm, and the selection algorithm in the genetic algorithm is optimized by using random numbers and increasing the number of cycles.

## 3. Teaching Resource Storage System Based on Cloud Computing Platform

### 3.1. Cloud Computing Theory and Related Technologies.

Cloud computing is a research hotspot in computer science and technology at present, which has attracted the attention of many enterprises and related Internet experts, and is an important trend of computer network technology development in the future. The concept of cloud computing was first put forward by Ehrlich Schmidt, CEO of Google Inc., at the Internet Conference in 2006. A typical cloud computing platform needs to have (1) a gridded data storage matrix network; (2) firewall equipment; and (3) computing resource equipment, allowing users to remotely use an expandable cloud storage space by leasing, to realize cloud application services [17], as shown in Figure 1.

A complete cloud computing architecture should include access layer, core layer, resource convergence layer,



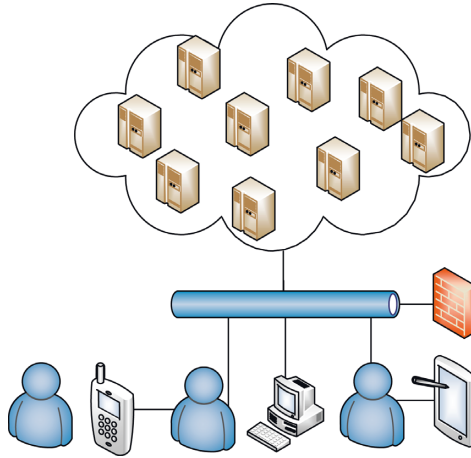


FIGURE 1: Principle of cloud computing services.

API interface layer, and application layer [18], as shown in Figure 2.

3.2. *Cloud Storage System Network Topology.* The teaching resource system under CCAI mode needs to meet the requirements of all-weather, all-geographical, and all-connection. In this paper, C/S mode [19] is adopted to construct the service system architecture of network teaching resources, and all data are stored in the data server, as shown in Figure 3. In the teacher’s office, upload or access the online teaching server through the campus network. Students on campus can access learning resources through campus network in dormitory or library. On the other hand, off-campus personnel can also remotely access the training and learning resources through the Internet, thus realizing the efficient sharing of limited teaching resources, breaking the geographical space limitation, and reducing the input cost of manpower and material resources.

At present, there are many excellent learning resource banks, some of which are all open, and the construction of these network resource banks has laid the foundation for the improvement of network education. However, these learning resources have a disadvantage; that is, they are difficult to be compatible with each other, that is, different systems have different learning resources, and the construction standards of these resources are different, so they cannot share resources. If you want to use the resources of another system in one system, you need to rebuild the resources according to the resource construction scheme of this system. In this situation, the learning resource pool has not been shared in the real sense.

#### 4. Intelligent Retrieval of Teaching Resources Based on Genetic Algorithm

4.1. *Design of Resource Retrieval Method Based on Genetic Algorithm.* As mentioned above, faced with the heterogeneous and large-scale teaching resources stored in the cloud computing platform, the traditional cloud computing

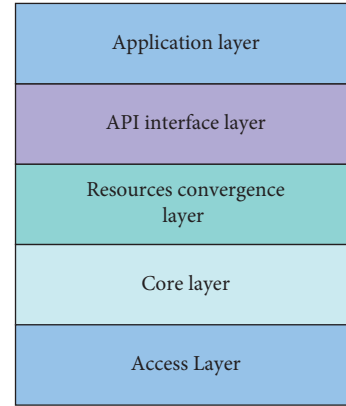


FIGURE 2: Cloud computing architecture.

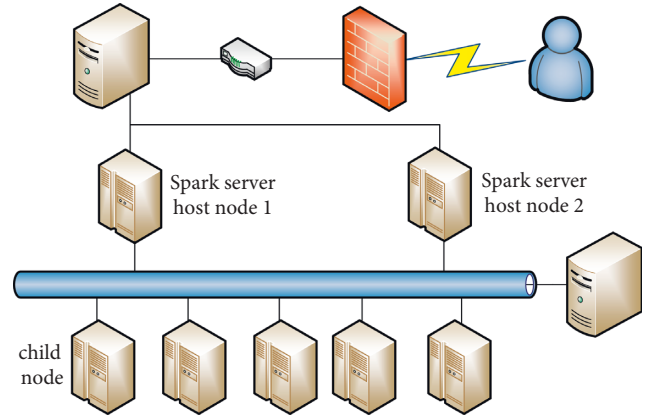


FIGURE 3: Network topology of the cloud storage system.

resource retrieval has poor performance and low work efficiency. Therefore, this paper uses the genetic algorithm to realize the retrieval of cloud computing resources. First, suppose that there are  $m$  hosts  $H$  in the resource retrieval task, and  $n$  virtual machines  $V$  are installed on these hosts, and each genetic individual is coded  $\{k_0, k_1, \dots, k_{n-1}\}$  by coding mapping [20–22]. For example, as shown in Figure 4, in the mapping relationship between virtual machines and hosts, if the sequence length is 5, then the number of 0–5 of  $V$  is  $\{1, 0, 2, 0, 2\}$ . The number in the sequence is the number of host  $H$ , and then the population is initialized.

Let the total number of constituent objects of a retrieval task be  $N$  and the fitness of each of the  $N$  constituent objects be  $f_i$ . Then, the probability of the  $i$ -th object being selected for evolution is as follows:

$$P = \frac{f_i}{\sum_{i=1}^N f_i} \quad (1)$$

Let the position change of the retrieval task in a certain period of time be  $\delta(H)$ . While the probabilities of selection crossover and change of the genetic algorithm are  $P_c$  and  $P_m$ , respectively, the expected value of the next generation belonging to the dynamic process of retrieval task is as follows:

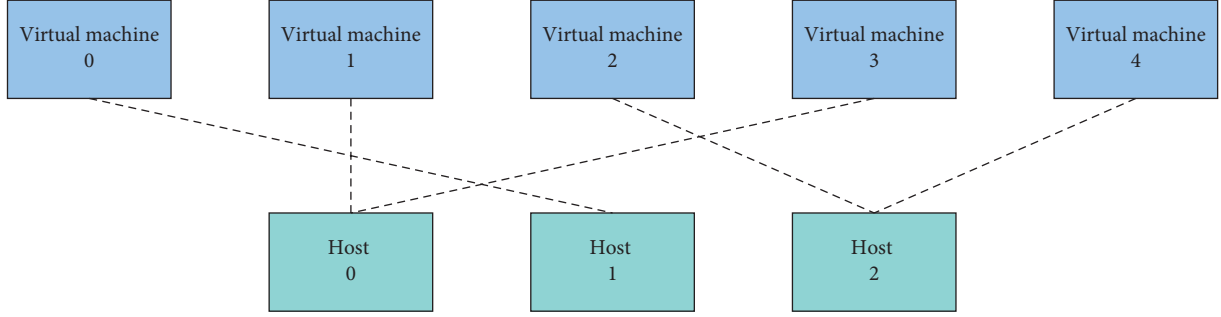


FIGURE 4: Schematic diagram of virtual machine and host mapping.

$$E[m(H, t + 1)] \geq m(H, t) \cdot \frac{f(H, t)}{\bar{f}(t)} \left[ 1 - P_c \frac{\delta(H)}{L-1} - O(H)P_m \right], \quad (2)$$

where  $O(H)$  is the dynamic order of task [23]. The longest distance of transmission is  $L$ , and  $m(H, t)$  is the number of objects in the next generation that need to be transmitted by the retrieval task.  $f(H, t)$  and  $\bar{f}(t)$  are the fitness and average fitness of the next generation of objects that need to be retrieved.

In the process of retrieval task, in order to ensure the integrity of the object and prevent the local data loss due to the change of retrieval task, the probability of selecting crossover operation must satisfy the following formula:

$$P_s \geq 1 - P_c \frac{\delta(H)}{L-1} \quad (3)$$

Then, according to formulas (2) and (3), we can get the following:

$$E[m(H, t + 1)] \geq m(H, t) \cdot \frac{f(H, t)}{\bar{f}(t)} - P_c \frac{\delta(H)}{L-1},$$

$$E[m(H, t + 1)] \geq m(H, t) \cdot \frac{f(H, t)}{\bar{f}(t)} \cdot \left[ 1 - P_c \frac{\delta(H)}{L-1} \right] (1 - P_m)^{O(H)}. \quad (4)$$

In formula (4), generally, the value of  $P_m$  is very small and then formula (4) can be further optimized to obtain as follows:

$$(1 - P_m)^{O(H)} \approx 1 - O(H) \cdot P_m$$

$$\left( 1 - P_c \frac{\delta(H)}{L-1} \right) (1 - O(H) \cdot P_m) \geq 1 - P_c \frac{\delta(H)}{L-1} - O(H) \cdot P_m \quad (5)$$

If  $f(H, t)/\bar{f}(t) > C$  ( $C$  is constant), it means that the operation has not reached the optimal solution calculated by the algorithm. Let  $K$  be given as follows:

$$K = C \cdot \left[ 1 - P_c \frac{\delta(H)}{L-1} - O(H) \cdot P_m \right]. \quad (6)$$

If  $K > 1$ , there are:

$$E[m(H, t + 1)] \geq m(H, t) \cdot K. \quad (7)$$

From this, we can recursively get the following:

$$E[m(H, t + 1)] \geq m(H, 0) \cdot K. \quad (8)$$

After the object of the retrieval task is iteratively calculated by the genetic algorithm, the position change of the resource object required by the retrieval task in a certain period of time can be obtained. During the training of position change, the ant colony algorithm is used to improve the convergence performance of the genetic algorithm.

**4.2. Genetic Algorithm after Ant Colony Optimization.** Let the number of ants in the nest be  $R$  and the set of elements to be optimized be  $D$ , where  $D_{\phi_i}$  represents its  $i$ -th element. In order to solve the initial population problem, the number of all parameters to be optimized in this paper is  $n$ . Assuming that there are  $K$  possible values of these elements  $\phi_i$ , then  $\zeta_j(D_{\phi_i})(0)$  is the pheromone of the  $j$ th element under the initial condition.

According to formula (9), the  $t$ -th ant calculated its parameters to distinguish the probability of each possible value [24–26].

$$k(\zeta_j^t(D_{\phi_i})) = \frac{\zeta_j(D_{\phi_i})}{\sum_{i=1}^n \zeta_j(D_{\phi_i})}. \quad (9)$$

Then, elements are selected from the set  $D_{\phi_i}$  with high probability and adjusted according to the following formula:

$$\zeta_j(D_{\phi_i})(t + \Delta) = \zeta_j(D_{\phi_i})(t) + \Delta\zeta_j(D_{\phi_i}), \quad (10)$$

where  $\Delta\zeta_j(D_{\phi_i})$  is the information increment on element  $\phi_i$ , representing the sum of pheromones left by all ants passing through this element. Its calculation method is as follows:

$$\Delta\zeta_j(D_{\phi_i}) = \sum_k^R \Delta\zeta_j^k(D_{\phi_i}). \quad (11)$$

The above process was repeatedly performed until the maximum allowed number of iterations was reached, or all the ants could obtain the unique element, thus obtaining the optimized initial population-related parameters.

After the initial population is generated by the ant colony algorithm, it is necessary to continue the genetic operation. The main contents of genetic operation are selection operator, crossover operator, and mutation operator. The operation of the traditional genetic process will lead to

premature convergence, so this paper improves the selection operator in the genetic operation in order to improve the convergence speed of the addition algorithm and obtain a better solution. This paper improves the selection algorithm based on traditional roulette. In the improved roulette method, the selection operator will also cycle  $m$  times, but the condition of the cycle is modified: whether  $m$  chromosomes have been selected. If yes, these selected chromosome markers will be used as the next generation, otherwise keep turning. Therefore, the required individuals will be generated only after  $M$  random numbers are generated in each cycle, thus ensuring the diversity of the next generation population and improving the chance of selecting the best chromosome.

**4.3. Design of Fitness Function.** In order to achieve the performance balance (reduce the energy consumption) on the premise of improving the work efficiency, this paper combines the service quality constraint and the energy consumption constraint to construct the fitness function. Among them, the total QoS violation  $Q_{total}$  of virtual machines is calculated as follows:

$$Q_{total} = 1 - \frac{MIPS_{total\_L} - MIPS_{total\_M}}{MIPS_{total\_L}}, \quad (12)$$

where  $MIPS_{total\_L}$  and  $MIPS_{total\_M}$  are all allocated millions of instructions per second and those that are not allocated on time, respectively.

Total system energy consumption  $E$  is calculated as follows:

$$E = \sum_{i=0}^{m-1} Host_i, \quad (13)$$

where  $Host_i$  is the energy consumption of the  $i$ -th host in cloud computing retrieval. A double index constraint composed of quality and cost is adopted as the fitness function. The fitness function is defined as follows:

$$fitness = 1 - a \times Q_{total} - b \times E, \quad (14)$$

where  $a$  and  $b$  are the weights corresponding to service quality violations and total energy consumption, respectively.

## 5. Experimental Results and Analysis

**5.1. Experimental Setup.** In order to test the performance of the proposed retrieval method based on the genetic algorithm, it is compared with Pseudo Feedback and extended retrieval method based on local context analysis (LCA). Experimental data were from the CISI test set. The CISI test set is a test set on information science, which consists of 1460 documents and 112 searches. The test set source url is [http://www.dcs.gla.ac.uk/idom/ir/resources/test\\_collections/](http://www.dcs.gla.ac.uk/idom/ir/resources/test_collections/). The test set contains the full text of the document, the retrieved initial text, and a list of document relationships. In the list of retrieved and document relationships, each retrieved related document has been given.

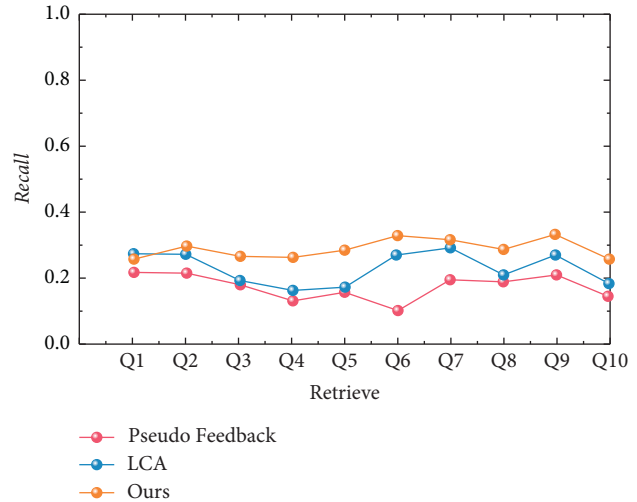


FIGURE 5: The Recall of three different algorithms (the first 10 documents).

Each document and the initial retrieval are preprocessed (stop words eliminated). A word stem extraction algorithm is adopted to extract the word stem and establish a keyword dictionary. Extract keywords from the dictionary and calculate their weights. At the same time, the retrieval of each document is vectorized. The cosine similarity calculation method is adopted to calculate the similarity between the initial retrieval and the documents, and the documents are sorted in descending order according to the size of the similarity. The more advanced the document is, the closer it is to retrieval. In genetic algorithms, generally speaking, selecting a larger initial population can handle more solutions at the same time, so it is easy to find the global optimal solution. The disadvantage is that it increases the time of each generation selection [27, 28], so the population size is generally 20–100. In the optimization process, the crossover probability always controls the crossover operator which plays a dominant role in genetic operations. The crossover probability controls how often crossover operations are used. The higher the frequency is, the greater the probability for each generation to produce new individuals is, and the better the diversity of the population is, and the faster it can converge to the optimal solution region. However, too high a frequency may also lead to premature convergence, generally taking the value of 0.4–0.9. When the maximum evolutionary algebra is used as the termination condition of the genetic algorithm, it is generally between 100 and 500 generations. In the experiment of this paper, the setting parameters of the genetic algorithm were as follows: initial population was 30, crossover probability was 0.4, mutation probability was 0.3, and maximum evolution algebra was 100.

**5.2. Evaluation Indicators.** Recall and Precision are widely used evaluation criteria of Web information retrieval effect [29]. Recall is the ratio of the number of relevant documents retrieved to all relevant documents in the document collection, and Precision is the ratio of the number of relevant

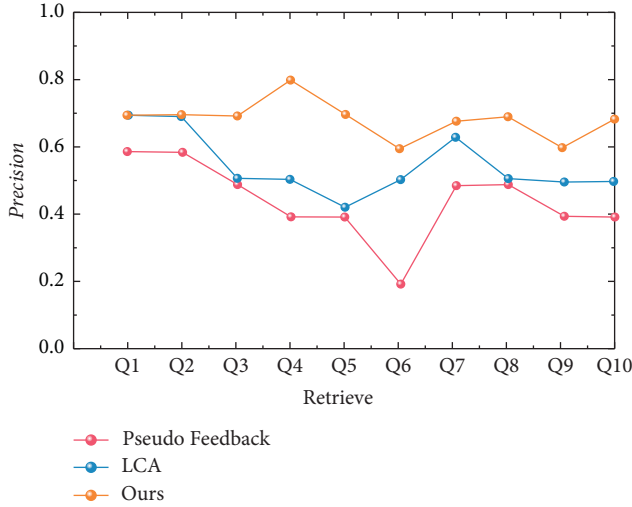


FIGURE 6: The Precision of three different algorithms (the first 10 documents).

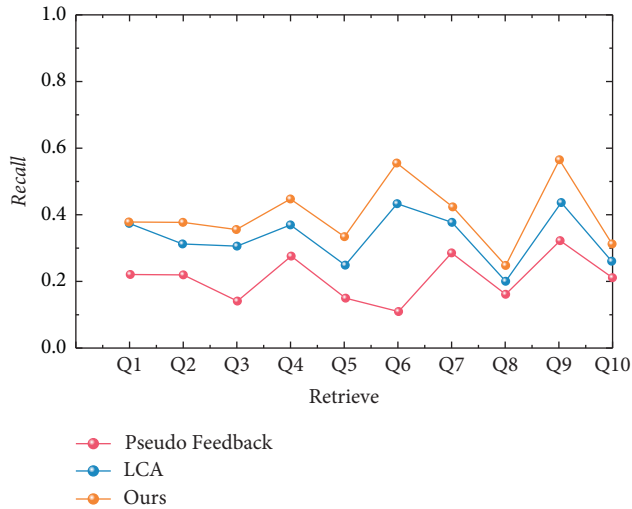


FIGURE 7: The Recall of three different algorithms (the first 20 documents).

documents retrieved to the total number of documents retrieved. Recall and Precision are defined as follows:

$$\text{Recall} = \frac{\text{number of related documents retrieved}}{\text{all related documents in the document set}} \times 100\%, \quad (15)$$

$$\text{Precision} = \frac{\text{number of related documents retrieved}}{\text{total number of documents retrieved}} \times 100\%.$$

In search engines, the first 10 or 20 documents usually reflect the results of the first page and the first two pages. Therefore, this paper uses the Recall and Precision of the first 10 or 20 retrieved documents as the evaluation indicators.

**5.3. Result Analysis.** Figures 5 and 6 show the Recall and Precision (the first 10 documents) of 10 different searches using three different algorithms, respectively. Note that, as mentioned in the previous section, only the first 10 documents retrieved are counted here.

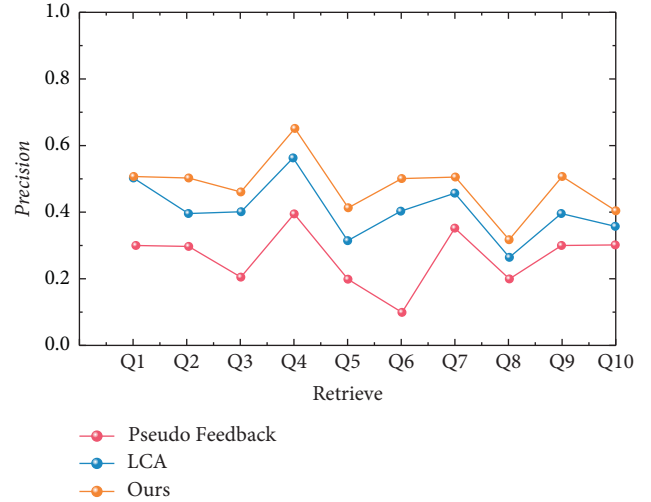


FIGURE 8: The Precision of three different algorithms (the first 20 documents).

TABLE 1: Retrieval performance comparison results.

| Algorithm       | First 10 documents |                   | First 20 documents |                   |
|-----------------|--------------------|-------------------|--------------------|-------------------|
|                 | Average recall     | Average precision | Average recall     | Average precision |
| Pseudo feedback | 0.18               | 0.45              | 0.22               | 0.27              |
| LCA             | 0.23               | 0.55              | 0.34               | 0.4               |
| Ours            | 0.29               | 0.69              | 0.4                | 0.47              |

Figures 7 and 8 show the Recall and Precision (the first 20 documents) of 10 different searches using three different algorithms, respectively. Table 1 shows the comparison results of retrieval performance of the three algorithms.

As can be seen from Table 1, compared with Pseudo Feedback and local context analysis-based retrieval extension method (LCA), the retrieval method based on the optimized genetic algorithm has higher Recall and Precision, that is, better retrieval performance. The number of false feedback detected is very large, and the proportion of the relevant literature is relatively low; that is, its Precision is relatively low. This retrieval mode has poor user experience, and users need to find the information they need by themselves from a large number of check-out results. However, the algorithm proposed in this paper does a good job in this respect, and most of the checked-out documents are related to the retrieval topic; that is, most of the checked-out results are the information that users need. It does not take users too much time to pick and choose the materials they need from the results.

## 6. Conclusions

Aiming at the poor performance of traditional cloud computing resource retrieval, this paper proposes a cloud computing platform retrieval method based on the genetic algorithm. The genetic algorithm is used to design a resource retrieval method suitable for cloud computing platform, so as to overcome the problems of low Recall and Precision. In

addition, the ant colony algorithm is used to improve the convergence performance of the genetic algorithm, and the selection algorithm in the genetic algorithm is optimized by using random numbers and increasing the number of cycles. The proposed method has achieved good retrieval performance in Recall and Precision, which verifies its feasibility. However, because there are not enough teaching resources in this system, the performance of the system has not improved much. If more types of teaching resources such as video resources and audio resources can be provided, the Recall and Precision of the proposed retrieval method will be obviously improved.

## Data Availability

The experimental data used to support the findings of this study are available from the corresponding author upon request.

## Conflicts of Interest

The authors declare that they have no conflicts of interest to report regarding the present study.

## References

- [1] S. Namasudra, "An improved attribute-based encryption technique towards the data security in cloud computing," *Concurrency and Computation: Practice and Experience*, vol. 31, no. 3, p. 4364, 2019.
- [2] L. Mingtong, "Research on the mechanism and influence factors of urban style building based on cloud computing logistics information," *Cluster Computing*, vol. 22, no. s6, pp. 13873–13880, 2019.
- [3] P. Zheng, Z. Wu, J. Sun et al., "A pu-based content retrieval system for distributed h imagery repository on cloud computing platforms," *Remote Sensing*, vol. 13, no. 2, pp. 176–186, 2021.
- [4] N. Ashammakhi, B. D. Unluturk, O. Kaarela, and I. F. Akyildiz, "The cells and the implant interact with the biological system via the Internet and cloud computing as the new mediator," *Journal of Craniofacial Surgery*, vol. 32, no. 5, pp. 1655–1657, 2021.
- [5] K. Sreenu and M. Sreelatha, "W-Scheduler: Whale optimization for task scheduling in cloud computing," *Cluster Computing*, vol. 22, no. S1, pp. 1087–1098, 2019.
- [6] P. W. Leclercq, A. Kääb, and B. Altena, "Brief communication: D," *The Cryosphere*, vol. 15, no. 10, pp. 4901–4907, 2021.
- [7] F. J. Abdullayeva, "Cloud computing virtual machine workload prediction method based on variational autoencoder," *International Journal of Systems and Software Security and Protection*, vol. 12, no. 2, pp. 33–45, 2021.
- [8] M. J. Mahdi, A. F. Aljuboori, and M. Hussein Ali, "Smart stadium using cloud computing and Internet of things (IoT): Existing and new models," *International Journal of Computer Applications Technology and Research*, vol. 10, no. 05, pp. 111–118, 2021.
- [9] L. Zhao, B. Liu, and J. Ma, "Virtual machine allocation method for cloud computing based on multi-objective evolutionary algorithm," *International Journal of Information and Communication Technology*, vol. 18, no. 2, pp. 207–216, 2021.
- [10] D. W. Gong, J. Sun, and Z. Miao, "A set-based genetic algorithm for interval many-objective optimization problems," *IEEE Transactions on Evolutionary Computation*, vol. 22, no. 1, pp. 47–60, 2018.
- [11] M. Gulić, B. Vrdoljak, and M. Ptiček, "Automatically specifying a parallel composition of matchers in ontology matching process by using genetic algorithm," *Information*, vol. 9, no. 6, pp. 138–145, 2018.
- [12] H. Yin, W. Wang, X. U. Zhang, Y. Lyu, G. Min, and D. Guo, "UMCR: User interaction-driven mobile content retrieval," *ACM Transactions on Intelligent Systems and Technology*, vol. 9, no. 1, pp. 1–19, 2018.
- [13] X. Liu, F. Zhu, Y. Fu, and Q. Liu, "A resource retrieval method of multimedia recommendation system based on deep learning," *International Journal of Autonomous and Adaptive Communications Systems*, vol. 13, no. 4, pp. 400–408, 2020.
- [14] R. K. Roul, "An effective approach for semantic-based clustering and topic-based ranking of web documents," *International Journal of Data Science and Analytics*, vol. 5, no. 4, pp. 269–284, 2018.
- [15] H. Zhang, G. V. Cormack, M. R. Grossman, and M. D. Smucker, "Evaluating sentence-level relevance feedback for high-recall information retrieval," *Information Retrieval*, vol. 23, no. 3, pp. 36–47, 2018.
- [16] J. Wang, M. Pan, T. He, X. Huang, and X. Tu, "A Pseudo-relevance feedback framework combining relevance matching and semantic matching for information retrieval," *Information Processing & Management*, vol. 57, no. 6, pp. 112–119, Article ID 102342, 2020.
- [17] H. Dawid and M. Kopel, "On economic applications of the genetic algorithm: A model of the cobweb type," *Journal of Evolutionary Economics*, vol. 8, no. 3, pp. 297–315, 1998.
- [18] J. Bhagwan and S. Kumar, "Independent task scheduling in cloud computing using meta-heuristic HC-CSO algorithm," *International Journal of Advanced Computer Science and Applications*, vol. 12, no. 7, pp. 281–291, 2021.
- [19] A. Khaliq, A. Umair, R. Khan, S. Iqbal, and A. Abbass, "Leadership and dm: Management accounting information and the moderating role of cloud computing," *Business Ethics and Leadership*, vol. 5, no. 2, pp. 78–95, 2021.
- [20] E. Bradford, A. M. Schweidtmann, and A. Lapkin, "Efficient multiobjective optimization employing Gaussian processes, spectral sampling and a genetic algorithm," *Journal of Global Optimization*, vol. 71, no. 2, pp. 407–438, 2018.
- [21] L. Michaeli and A. Bahabad, "Genetic algorithm driven spectral shaping of supercontinuum radiation in a photonic crystal fiber," *Journal of Optics*, vol. 20, no. 5, pp. 76–85, Article ID 055501, 2018.
- [22] A. Mustafa, A. Heppenstall, H. Omrani, I. Saadi, M. Cools, and J. Teller, "Modelling built-up expansion and densification with multinomial logistic regression, cellular automata and genetic algorithm," *Computers, Environment and Urban Systems*, vol. 67, no. 4, pp. 147–156, 2018.
- [23] M. Giassi and M. Goteman, "Layout design of wave energy parks by a genetic algorithm," *Ocean Engineering*, vol. 154, no. 4, pp. 252–261, 2018.
- [24] A. Kumar, P. B. Kumar, and D. R. Parhi, "Intelligent navigation of humanoids in cluttered environments using regression analysis and genetic algorithm," *Arabian Journal for Science and Engineering*, vol. 43, no. 12, pp. 7655–7678, 2018.
- [25] S. Mozaffari, "Parallel image encryption with bitplane decomposition and genetic algorithm," *Multimedia Tools and Applications*, vol. 77, no. 10, pp. 1–21, 2018.

- [26] S. Kalsi, H. Kaur, and V. Chang, "DNA cryptography and deep learning using genetic algorithm with NW algorithm for key generation," *Journal of Medical Systems*, vol. 42, no. 1, pp. 17–28, 2018.
- [27] J. S. Lee, I. Y. Choi, I. K. Kim, and S. H. Hwang, "Tamping and renewal optimization of ballasted track using track measurement data and genetic algorithm," *Journal of Transportation Engineering Part A Systems*, vol. 144, no. 3, Article ID 04017081, 2018.
- [28] L. Z. Zhai and S. H. Feng, "A novel evacuation path planning method based on improved genetic algorithm," *Journal of Intelligent and Fuzzy Systems*, vol. 42, no. 3, pp. 1813–1823, 2022.
- [29] C. C. Lin, H. H. Chin, and W. B. Chen, "Balancing latency and cost in software-defined vehicular networks using genetic algorithm," *Journal of Network and Computer Applications*, vol. 116, no. 8, pp. 35–41, 2018.

## *Retraction*

# **Retracted: Practice and Research of Blended Learning Model Guided by Deep Learning Model**

### **Mathematical Problems in Engineering**

Received 18 July 2023; Accepted 18 July 2023; Published 19 July 2023

Copyright © 2023 Mathematical Problems in Engineering. This is an open access article distributed under the Creative Commons Attribution License, which permits unrestricted use, distribution, and reproduction in any medium, provided the original work is properly cited.

This article has been retracted by Hindawi following an investigation undertaken by the publisher [1]. This investigation has uncovered evidence of one or more of the following indicators of systematic manipulation of the publication process:

- (1) Discrepancies in scope
- (2) Discrepancies in the description of the research reported
- (3) Discrepancies between the availability of data and the research described
- (4) Inappropriate citations
- (5) Incoherent, meaningless and/or irrelevant content included in the article
- (6) Peer-review manipulation

The presence of these indicators undermines our confidence in the integrity of the article's content and we cannot, therefore, vouch for its reliability. Please note that this notice is intended solely to alert readers that the content of this article is unreliable. We have not investigated whether authors were aware of or involved in the systematic manipulation of the publication process.

Wiley and Hindawi regrets that the usual quality checks did not identify these issues before publication and have since put additional measures in place to safeguard research integrity.

We wish to credit our own Research Integrity and Research Publishing teams and anonymous and named external researchers and research integrity experts for contributing to this investigation.

The corresponding author, as the representative of all authors, has been given the opportunity to register their agreement or disagreement to this retraction. We have kept a record of any response received.

### **References**

- [1] F. Yang and Y. Rao, "Practice and Research of Blended Learning Model Guided by Deep Learning Model," *Mathematical Problems in Engineering*, vol. 2022, Article ID 8915162, 6 pages, 2022.

## Research Article

# Practice and Research of Blended Learning Model Guided by Deep Learning Model

Fan Yang <sup>1</sup> and Yutai Rao <sup>2</sup>

<sup>1</sup>Software Engineering Institute, Hubei Open University, Wuhan 430074, Hubei, China

<sup>2</sup>Teaching Quality Management and Evaluation Center, Hubei Open University, Wuhan 430074, Hubei, China

Correspondence should be addressed to Yutai Rao; 2079406@qq.com

Received 10 March 2022; Revised 1 May 2022; Accepted 6 May 2022; Published 26 May 2022

Academic Editor: Hangjun Che

Copyright © 2022 Fan Yang and Yutai Rao. This is an open access article distributed under the Creative Commons Attribution License, which permits unrestricted use, distribution, and reproduction in any medium, provided the original work is properly cited.

An innovative approach to education and teaching, with a deeper integration of teaching and learning through a deeper mix of learning and study was proposed. The new organisational format combines independent learning in the form of microlessons and flipped classrooms with communication and cooperation in forums. In the context of the rapid development of Internet + education, big data information technology, and the accelerated promotion of education informatization by the Ministry of Education, this paper studies how to use the blended learning model to achieve the deep integration of information technology and classroom teaching through the innovative form of “microlesson and flipped classroom,” so as to improve students’ independent learning ability. Taking the university course of dynamic web design as an example, this course aims to achieve the teaching objectives of this course by using a deep learning model to guide the deep integration of information technology and classroom in a blended learning mode.

## 1. Introduction

The rapid development of information technology has brought new development opportunities for teaching informatization [1]. The Chinese government’s work report proposes to “formulate an “Internet +” action plan and promote the rapid development of the mobile Internet, cloud computing, big data, and the Internet of Things .....,” and the main points of the work of the Ministry of Education’s also mention “speeding up the informatization of education” [2–4]. This has led to a deeper integration of information technology and classroom teaching. However, there is a one-sided or even wrong understanding among teachers, who think that as long as they apply multimedia or courseware in the classroom, they are integrating information technology with classroom teaching, so the integration of information technology with classroom teaching stays at the primary level [5–8].

University education is the key to higher education teaching and is an important reflection of the quality and

level of talent cultivation in universities as well as the core of talent cultivation [9]. However, the inquisitive scientific literacy of our university students is relatively lacking, and this literacy is precisely the important source for the formation of university students’ ability to analyse problems, solve them, and think critically [10–12]. This literacy is indispensable for the future entrepreneurship and innovation of university students, and these also prompt us to carry out teaching reforms [13].

Information technology is beginning to be used in all areas of education, providing convenient and effective teaching aid to better achieve subject teaching objectives [5]. It provides a convenient and effective teaching aid to better achieve the teaching objectives of the subject. The majority of teaching activities are now based on information technology, and the scope of its use in the scope of application of information technology in teaching is expanding [6]. At present, research on the integration of information technology and the teaching of Civic studies in colleges and universities has been conducted at home and abroad, and



certain progress has been made, which can serve as a reference for further research. However, the current research on the integration of the two has not been analyzed in-depth from the nature of the curriculum of the college Civics course, and there is no real in-depth integration between the teaching of the college Civics course and information technology in the content.

In recent years, more and more online education and large-scale open network courses have emerged in China, and the combination of various teaching methods such as flipped classroom, catechism, and microlesson has been widely popularized, which makes information technology gain a broader application space and development opportunities in the field of education [14]. However, there is a one-sided or even wrong understanding among teachers, who think that as long as they apply multimedia or courseware in the classroom, they are integrating IT with the curriculum, which makes the integration of IT with the curriculum stay at the most elementary level [15].

Professor He Keban points out that the implementation of the deep integration of information technology and classroom teaching requires a deep understanding of the specific content of the structural changes in classroom teaching, the implementation of teaching models that can effectively change the structure of classroom teaching, on the basis of fundamental changes in the structure of classroom teaching to achieve a significant improvement in the quality of subject teaching and the overall quality of students [16–19]. In this paper, we adopt a deep blended learning model of “learning,” and use the innovative form of “microlesson and flipped classroom” to realise the deep integration of information technology and classroom teaching. In this paper, we will adopt a deep blended learning model of “learning” and “learning,” through the innovative form of “microlesson and flipped classroom,” to realise the deep integration of information technology and classroom teaching, and improve students’ independent learning ability and their scientific literacy in the spirit of exploration [20].

## 2. Blended Learning Model

A blended learning model is simply a combination of traditional learning styles and *E* learning, with the teacher playing a leading role in guiding, inspiring, and managing classroom teaching and learning, and with the student as the main subject [21–24]. Blended learning is a very effective mode of teaching and learning, but another phenomenon is that we rarely see examples of successful blended learning. Either the form of blended learning is relatively simple and does not achieve good results, or the blended approach tends to be more complex, making it difficult to carry out the teaching process [25]. The reasons for these phenomena are mainly due to the fact that many teachers do not have a deeper understanding of the blended education model and do not grasp the key points of the blended learning model, which is generally limited to the blending of online learning with traditional learning, and is understood at a lower level, so it is difficult to bring out the advantages of the blended learning model [26].

Blended learning consists of several levels of application, the third of which is the blending of learning and learning. “A deeper blend of learning and learning is what blended learning is really all about [27]. Generally speaking, we only compare “learning” to studying, but in practice we always ignore “learning,” and most teaching processes or e-learning are limited to “learning.” Most teaching and learning processes or e-learning are limited to the level of ‘learning,’ but do not reach a deeper level of learning and learning in a mixed mode [28].

## 3. Innovative Forms of Teaching

In the context of the teaching concept of deep integration of information technology and university teaching, a deep “learning” and “learning” hybrid learning model combining microlesson and flipped classroom is proposed, which helps to promote further reform of the teaching model and enhance students’ independent learning ability and exploration spirit.

*3.1. Teaching Methods.* The “teaching carrier” has changed. In traditional classroom teaching, the process of transferring professional skills and knowledge is mainly achieved through the teacher’s lectures in the classroom, and the understanding and digestion of professional knowledge are mainly achieved by students through after-class assignments and exercises. In the combination of microlesson and flipped classroom, this form of teaching is greatly changed. The transfer of knowledge and skills is mainly achieved before class through new media such as network technology and mobile terminals, while the understanding and digestion of knowledge is completed in class through the teacher’s Q&A (question and answer) and cooperation among students. In the implementation of the microlesson, students are allowed to learn the important and difficult points of teaching through the microlesson first, and then master and internalise the knowledge in the classroom through the teacher’s guidance and students’ collaboration, realising the classroom flip of learning before teaching.

*3.2. Innovative Teaching Formats.* An innovative approach to education and teaching, with a deeper integration of teaching and learning through a deeper mix of learning and study, is proposed. The new organisational format combines independent learning in the form of microlessons and flipped classrooms with communication and cooperation in forums, which will not be limited to the traditional classroom lecture format but will enable deeper development of teacher-student discussions, student discussions, and student independent learning, thus achieving a deeper level of “learning” and “learning.”

*3.3. Innovations in Appraisal and Evaluation Methods.* The rapid development of information technology has led to significant changes in examinations and assessment. The traditional assessment and evaluation method of a final exam has resulted in incomplete and somewhat delayed

assessment of students' learning knowledge. With mobile learning, a staged form of assessment can be used. A combination of staged and task-based assessment can also be used. Three or five students are divided into a learning team, and the project is required to be realised within a specified time frame and to achieve the expected results. The knowledge learnt can be used in an integrated way, with team members designing and implementing the project, and the team completing the project, with assessment marks given through the project and the implementation process. It is also possible to incorporate a combination of mutual assessment among students and teacher evaluation to achieve a multifaceted and comprehensive assessment of students' learning outcomes.

#### 4. Key Perspectives on Blended Learning

The current understanding of blended learning has resulted in different definitions depending on the way in which "blended" is used (online and offline learning; synchronous and asynchronous learning); integration of learning resources (traditional and networked or digital media resources); integration of learning participants (learners, teachers, experts, and networked computers); etc. The aim of this integration is to 'draw on the strengths of all' and to complement each other to achieve effective learning for learners. However, over-generalised definitions tend to lose the inherent character of 'blending' and its practical implications. In summarising the new stage of development of China's education informatisation, Mr. Nan Guonong, a renowned expert in education technology, took the theory of blended learning as the leading theory in the further development stage of China's education informatisation, with the basic idea that "the best learning effect can be achieved by combining the advantages of traditional learning methods with those of digital learning so that the advantages of both can complement each other." Moskal et al. [6] define blended learning as "a combination of face-to-face instruction with online learning."

In this study, the blended learning model is used as a guiding theory for constructing a learning system framework, and the deeper learning cycle (DELIC) proposed by Eric Jensen and LeAnn Nickelsen (shown in Figure 1) is used as a practical guide for the implementation of blended learning, aiming to combine traditional teaching and online teaching in a rational way so as to promote effective learning and achieve the purpose of deep learning.

#### 5. Take the Course "Dynamic Web Design" as an Example

I have taught the dynamic web design course at university for many years and have accumulated a wealth of teaching experience. I have explored the teaching format of "micro-learning and flipped classroom" in the Dynamic Web Design course. The teacher records and edits the course video in advance and puts it on the learning resources. Students are encouraged to study in advance through the Internet and other new media after class and can also communicate with the teacher and discuss and communicate with each other through the Internet. In the classroom, the teacher mainly

answers students' questions to achieve a student-centred approach and to highlight the characteristics of personalised tutorials.

The course will also set the task of implementing a website, allowing students to find a team (3–6 people) in the class freely and communicate with the team members through the online platform as well as communicating with the teacher online about the task, which greatly enhances students' enthusiasm to participate in the task and is also a good way for students to grasp the knowledge in an integrated way.

By comparing the results of the summative tests of this course in the Computer Network Technology major in years 14 and 15 of the school, the blended learning mode is effective in practical teaching. The course, Dynamic Web Design, is very hands-on, and the blended learning is effective in developing operational skills and overall competencies.

*5.1. System Testing and Analysis of Results.* The system can easily be built and deployed in minutes with a complete online evaluation system by distributing Docker Mirror and Docker Compose deployment profiles. By further extending this, a highly available solution can be implemented for the entire system, with a cluster structure in a highly available state, as shown in Figure 2. On the other hand, with the introduction of Continuous Integration (CI), any changes to the system source code are fed back into the image in real time, and when the version is tested and stable with few bugs, a new version can be released directly, truly automating the deployment and making it easy for users to test or update the system [29].

*5.2. Stress Test Results.* The stress test for this evaluation system is for data from 5 000 people online at the same time. The system was deployed on the same server. As shown in Figure 3, when deployed on a single machine, the system was able to support more than 5,000 people online at the same time and completed 250,000 requests in 2 minutes, and due to the increasing number of people, it is known that the system carried more user requests in the final phase than in the pretest period [30].

The topic described has been presented comprehensively. The different figures, diagrams, tables, and schemes have facilitated the reader's understanding of the document. Regarding the results, to assess these statistical data, it is necessary to know details related to the trial and the sample size.

Compared to the traditionally used online assessment system, this system separates test maintenance and assessment from the overall system, making it a new, almost completely independent system. The independent maintenance of test questions brings a higher level of security. It is well known that the least expensive solution to achieving a fully secure computer system is to take computers containing confidential information offline. By making test maintenance and evaluation independent, the system allows users to use a separate instance of Problem CI when creating questions, and then access the public "Thousand Practices"

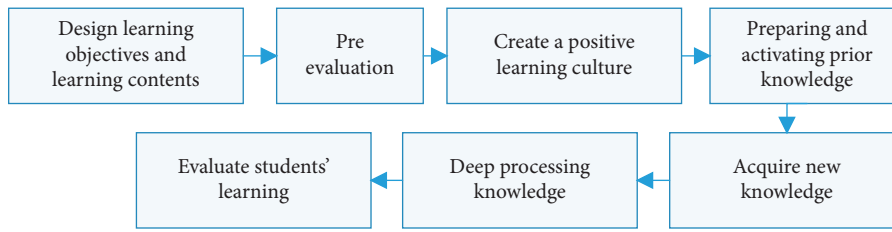


FIGURE 1: DELC deep learning route.

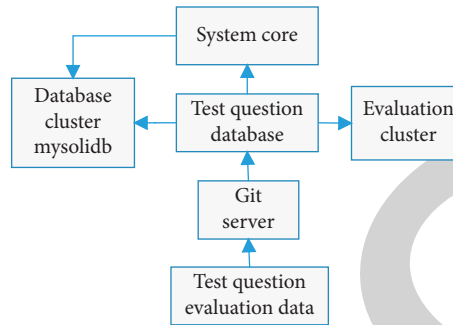


FIGURE 2: High availability implementation plan.

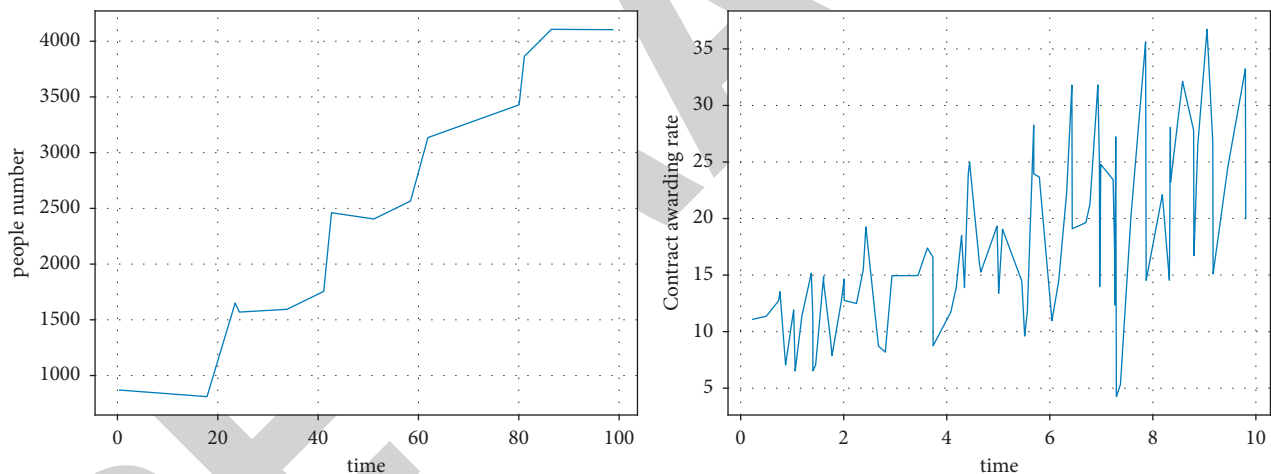


FIGURE 3: “Thousand Practices 2.0” system performance test.

system when it comes to the actual competition, with no degradation to the end user experience of the platform [31].

In terms of their understanding of blended learning, blended learning is a combination of traditional face-to-face teaching and digital learning, but this combination is not a mechanical superimposition of learning styles, but a rational product of the process of informatization in education, a new way of learning that emerges from reflecting on the application of learning theories and technologies when attempts to reform or replace traditional classroom teaching with E-learning are not as effective as they could be. It is a new way of learning that emerges when people try to reform or replace traditional classroom teaching with E-learning, reflecting on the way in which learning theories and technologies are applied, and bringing back traditional classroom teaching to complement the strengths of E-learning. It

emphasises the integration of teaching-centred and student-centred teaching modes, and focuses on effective communication between teachers and students in the classroom and the self-construction of the content learned in online learning. It no longer places one-sided emphasis on the role of the online learning environment at the expense of classroom teaching, on student-centredness at the expense of the teacher’s leading role, on constructivism at the expense of the guiding role of other learning theories, or on the application of online resources at the expense of the role of traditional media.

As shown in Figure 4, different students learn effectively under blended learning. Many existing open source online assessment systems lack an easy-to-use question generation aid, and in order to generate questions, teachers often need complex command line operations, which are not very user-

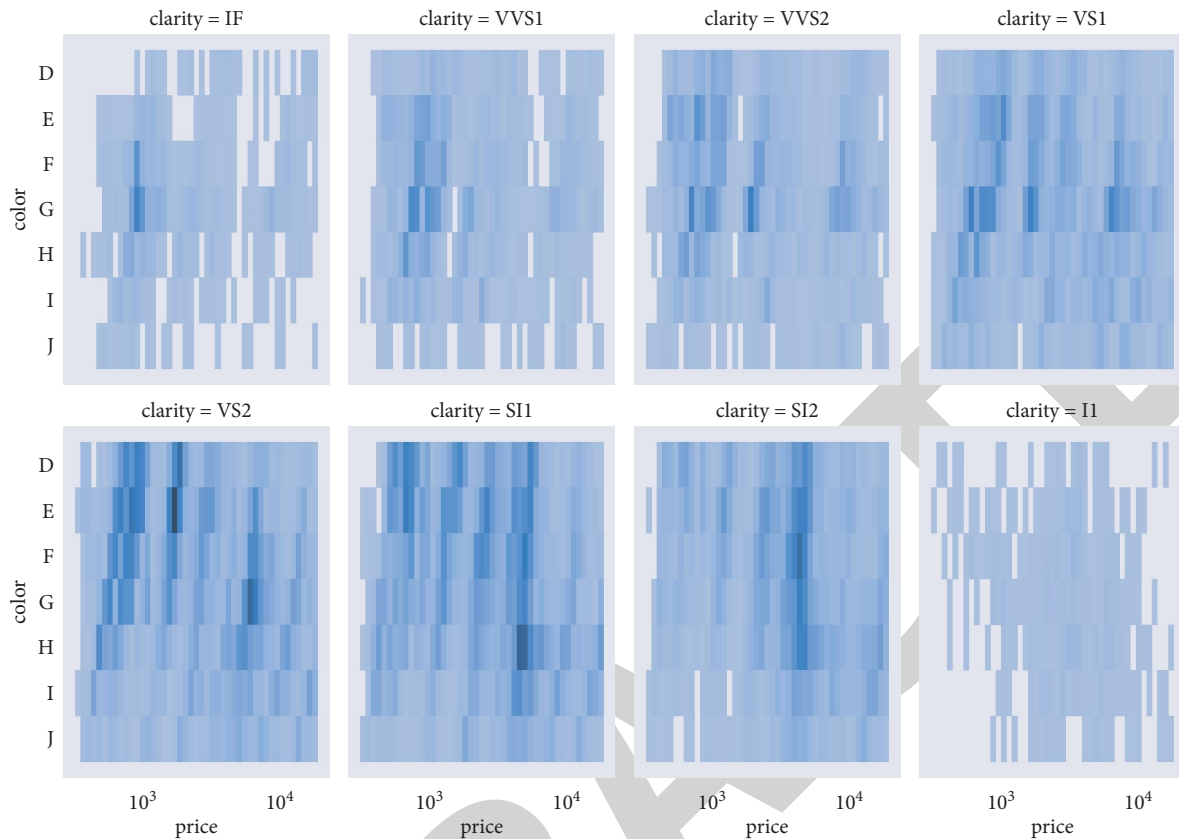


FIGURE 4: Student learning intensity for different blended learning.

friendly for nonexpert operators and pose problems of misuse. While other systems often require users to understand the details of the system's assessment specifications, Problem CI's question editor offers the ability to perform complex operations, but for most questions, the user does not need to have any knowledge of the assessment principles and only needs to upload data, select a comparator, set a time limit, write a question, and other necessary operations to construct a legitimate question. The easy management of test questions facilitates the use of teachers and also allows students to use them for daily self-training and testing. The two main functions of the teaching aid system, "teaching" and "learning," are truly realised.

## 6. Conclusions

Blended learning mode, in fact, does not have a standard definition, whether it is the use of MOOC, or big data analysis technology or even just the teacher with students in online case discussions, as long as the teaching methods can make full use of the Internet and play with imagination are all blended.

In this paper, good results have been achieved by applying it in the Dynamic Web Design course to enhance student learning. It shows that the deep integration of information technology and classroom teaching based on a deep blended learning model has implementable feasibility, using a combination of microlessons and flipped classrooms,

using the concept of blended teaching, to achieve the purpose of optimising teaching content, teaching format, and teaching mode. In the future, this model will be further applied in a number of courses to further explore this topic.

## Data Availability

The raw data supporting the conclusions of this article will be made available by the authors, without undue reservation.

## Conflicts of Interest

The authors declare that they have no conflicts of interest regarding this work.

## Acknowledgments

This work is supported by General topics of Educational Science Planning of Hubei Province in 2021: Research on online and offline integrated teaching mode based on Artificial Intelligence, 2021GB193; Key topics of Educational Science Planning of Hubei Province in 2021: Research and Practice on the Integration and Development of Open Education and Vocational Education, 2021GA113; Open project of Hubei Vocational Education Development Research Institute: A comparative study on inter provincial policies for the construction of "double high plan," 2021Z01.

## Research Article

# The Database Construction of Intangible Cultural Heritage Based on Artificial Intelligence

**Haixing Zhao** <sup>1,2,3,4</sup>

<sup>1</sup>The Development Research Center of the Three Gorges Culture and Economic Society, China Three Gorges University, Yichang 443002, Hubei, China

<sup>2</sup>Bachu Art Culture Research Center, China Three Gorges University, Yichang 443002, Hubei, China

<sup>3</sup>Research Center of Film and Television Culture and Industry, China Three Gorges University, Yichang 443002, Hubei, China

<sup>4</sup>Research Center for Regional Social Management Innovation and Development, China Three Gorges University, Yichang 443002, Hubei, China

Correspondence should be addressed to Haixing Zhao; zhaohaixing@ctgu.edu.cn

Received 18 March 2022; Accepted 22 April 2022; Published 25 May 2022

Academic Editor: Man Fai Leung

Copyright © 2022 Haixing Zhao. This is an open access article distributed under the Creative Commons Attribution License, which permits unrestricted use, distribution, and reproduction in any medium, provided the original work is properly cited.

At present, the protection of material cultural heritage is spread all over the world, but the protection of intangible cultural heritage is relatively backward. With the development of information technology, database technology provides a new retrieval method. Therefore, based on database technology, this paper constructs the database system of intangible cultural heritage, where MySQL is used as the system database, Struts 2 framework is selected in MVC to realize the separation of business logic and data display, and retrieval and query are realized through Lucene. In addition, the system takes Mongolian stringed instruments as the carrier, constructs the metadata framework, and forms the database structure. Moreover, the system is divided into six functional modules and the front and back functions of the system are managed. Finally, the system function test and performance test are carried out. The test results show that the system has good functionality, which is helpful to realize the effective protection of intangible cultural heritage.

## 1. Introduction

Excellent national culture is the most profound soft power. Since China carried out the reform and open policy, especially since the 16th National Congress, the party and the state have paid more and more attention to inheriting and carrying forward the national cultural tradition and protecting the national cultural heritage [1, 2]. According to the convention for the protection of intangible cultural heritage of UNESCO (United Nations Educational, Scientific and Cultural Organization), the definition of intangible cultural heritage is given from the international perspective, which must be reconsidered in combination with the historical and cultural background of China. Yuan Li, the author of “Intangible Cultural Heritage,” believes that human beings were created in history and inherited in a living form, which has important value in traditional cultural matters such as

literature and art, technology, and rituals. The database of intangible cultural heritage refers to the resource database which has the functions of standardized description, structured storage, diversified retrieval and query, Web-based access, and sharing. It is directly used for the preservation and management of intangible cultural heritage and directly assists the inheritance and protection of projects about intangible cultural heritage.

At the same time, the management of cultural resources in China is not perfect and there is still a lack of in-depth research on information standards, digital protection of copyright, integration, and sharing of resource [3–5]. With the development of information society, although a large number of national cultural researchers have devoted themselves to the digital research of intangible culture, there is not a complete and standardized platform for collecting, storing, protecting, managing, and sharing traditional

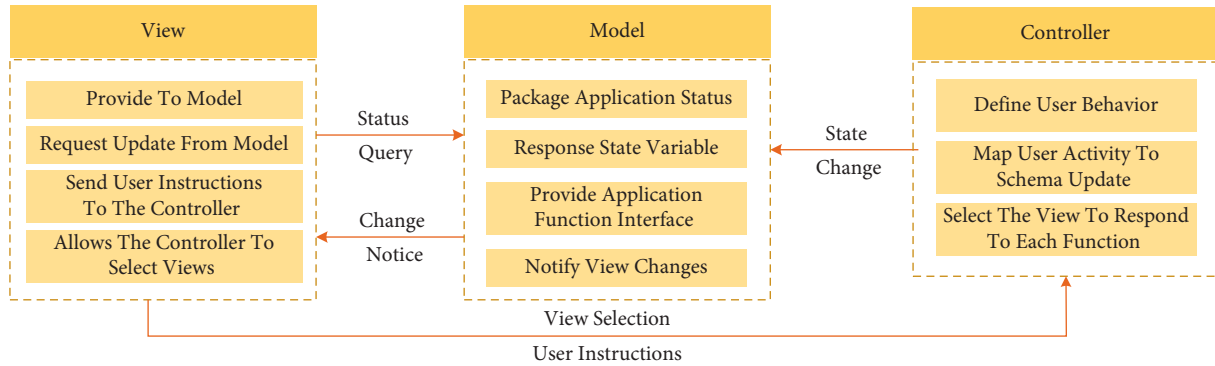


FIGURE 1: MVC framework structure.

intangible cultural resources in China. More importantly, the existing database systems about cultural communication at home and abroad have poor scalability and low reusability, so it is impossible to establish a universal and customizable database for cultural resources [6]. We need to establish a database system of intangible cultural heritage with high expansibility in combination with the corresponding standards, so as to provide a solid foundation for the rescue, inheritance, and standardized management of cultural resources. Therefore, this paper has taken the spread of Mongolian string instruments as the carrier, where the database system of China's intangible cultural heritage protection is constructed by using database technology.

## 2. Analysis of Key Technologies of Database System

The development of thematic database system is to reorganize special data to form a new database. First of all, complex information needs to be screened to ensure the gold content of literature information. The process of selecting, sorting, and organizing documents is a process of knowledge management, which is related to the quality of the whole database. It needs to be completed by professionals. The screened data are divided into different subdatabases according to their knowledge system and finally form a thematic database [7, 8].

*2.1. Selection of MVC Framework.* MVC is a program development and design mode, which realizes the separation of business logic and data display [9], improves the maintainability, portability, extensibility, and reusability of the program, and reduces the difficulty of program development. The MVC framework includes three cores: model, view, and controller, and its structure is shown in Figure 1.

Model is the main part of MVC application, which mainly includes business logic module (Action class in Web project) and data module (POJO class). The model has high reusability and can provide data for different views, so it can greatly reduce the code repetition rate [10]. View is the interface for users to interact with it, which is generally composed of JSP and HTML, while the controller itself does not make any processing, which only receives the user's

input request, and calls the model and view to complete their requirements.

The commonly used MVC frameworks are Struts and Webwork, and their comparison is shown in Figure 2.

Struts 2 framework combines the advantages of the above two frameworks, so this system adopts Struts 2 framework as the technical scheme to realize the separation of business logic and data display. The structure of Struts 2 controller is shown in Figure 3, which consists of three parts: scheduler, interceptor, and business controller. The configuration file manages and maintains the relationship between them, and the Struts 2 controller works as follows:

- (1) After the scheduler obtains the page http request, it selects the corresponding interceptor group to pre-process it and then calls the corresponding service controller
- (2) The service controller calls the service logic layer interface to process the request
- (3) Return the result to the interceptor group, and then return it to the page for rendering after processing it

Struts 2, as the controller component of the system, reduces the coupling between front-end page presentation, front-end data interaction, and page jumping and greatly improves the scalability and maintainability of the system.

*2.2. Database Selection.* For the protection of intangible cultural heritage, this system must use databases to manage cultural heritage data. At present, the mainstream databases commonly used are MySQL and Oracle [11], and the comparison between them is shown in Figure 4.

As string instruments are an important part of intangible cultural heritage, intangible culture with distinct personality determines the regionality of data resources. At the same time, the shape, color, structure, production technology, traceability, and legend of each kind of Mongolian stringed instruments are different, and the resulting data also contain rich contents. In addition, the data resources of Mongolian string instruments are diverse, including physical resources, historical resources, heritage and protection resources, laws and regulations resources, and inheritors' archives resources, which determines the variety of their data.

|                        | Struts Framework                | Webwork Framework             |
|------------------------|---------------------------------|-------------------------------|
| Class Structure Design | Design For Abstract Classes     | For Interface Design          |
| Test Method            | Difficult To Complete Unit Test | Unit Tests Can Be Completed   |
| Dependence             | Dependent Servlet               | Servlet Independent           |
| Thread Safety          | Thread Safety Required          | Thread Safety Is Not Required |

FIGURE 2: Comparison of different MVC frameworks.

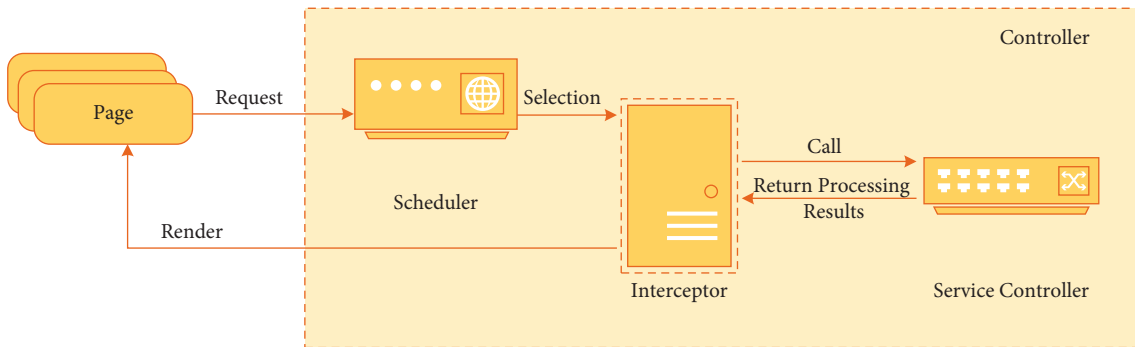


FIGURE 3: The structure of Struts 2 controller.

|                           | Oracle Database                         | MySQL Database                        |
|---------------------------|---|---------------------------------------|
| Database Management       | Complex And High Technical Requirements | Simple And Low Technical Requirements |
| Data Recovery Costs       | High Cost                               | Low Cost                              |
| Database Connection       | Slow Speed                              | Faster Speed                          |
| Requirements For Hardware | High Requirements                       | Low Requirements                      |
| Security                  | Higher                                  | Lower                                 |

FIGURE 4: Comparison of different database technologies.

Therefore, through the above comparative analysis, MySQL database is simpler and more convenient in management and data recovery, whose database connection speed is faster. In addition, it takes up less resources and requires less hardware [12]. Therefore, according to the requirements of database management in this system, this paper uses MySQL as the system database.

2.3. *Lucene System.* Lucene is a full-text search engine toolkit, which provides the functions of data index and full-

text search. It consists of three parts: infrastructure package module, external interface module, and index core module. The index core module directly operates index files, which is the focus of the whole system. Lucene index contains a number of files, which are stored in groups according to their respective segment. The same group index files have the same file name, but different extensions [13]. There is a correspondence between index files and information files, which means that the information files are arranged according to the order of index files.

The entire search process of Lucene is as follows:

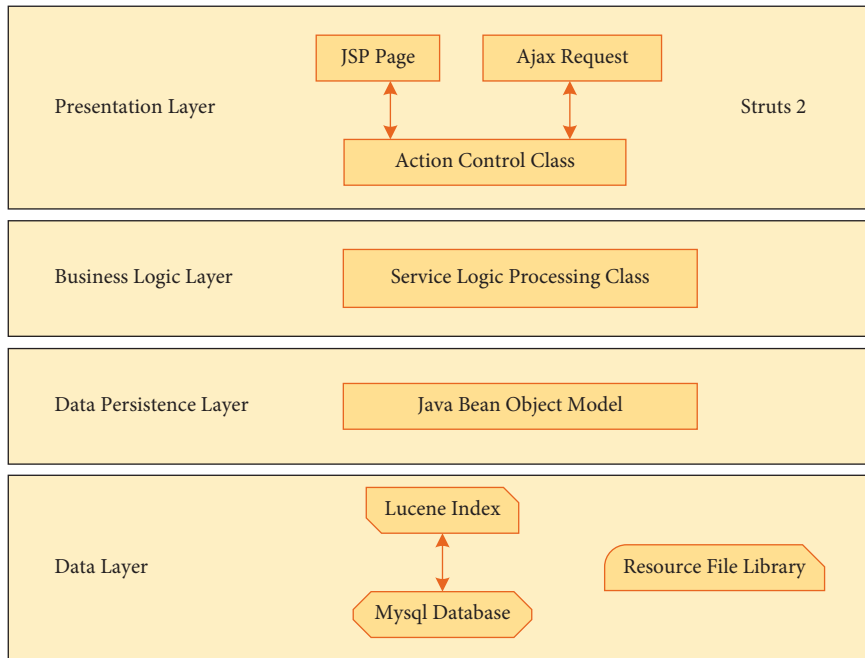


FIGURE 5: Overall structure of intangible cultural heritage database.

- (1) Build a text database, save all the information that users may retrieve, and then determine the index text model.
- (2) Establish the index according to the database text. In this process, it is necessary to correctly select the index mode according to the scale of the retrieval system.
- (3) Make the search that the user first submits a search request; the system analyzes the request and then carries out corresponding processing through text operation.
- (4) Filter and sort the search results according to certain rules, and finally return them to users.

### 3. Design of Intangible Cultural Heritage Resources Database

*3.1. Design of Overall Framework.* In order to make the system have good expansibility and maintainability, this system adopts hierarchical design idea and divides the system implementation into the following four levels: presentation level, business logic level, data persistence level, and data level. This system uses Java language and Tomcat as the server, and the hierarchical framework of the system is shown in Figure 5.

**Presentation layer:** it is responsible for receiving the user's request data and submitting it to the business logic layer for processing. At the same time, the response data processed by the business logic layer are displayed to the interface to present dynamic Web content for users. In addition, it provides a controller to call business logic and a model for display. On the one hand, using the rich tag library of Struts 2 framework can make it more convenient for the

presentation layer to accept page requests. On the other hand, the powerful page jump control function of Struts 2 framework is used to manage all page jump control in the configuration file, which makes the code more concise and the management more convenient.

**Business logic layer:** in the middle of the presentation layer and the data persistence layer, it is responsible for receiving the request data submitted by the presentation layer in the system and calling the corresponding business logic for processing. After obtaining the data through the data persistence layer for processing, the results are returned to the presentation layer.

**Data persistence layer:** it is located in the middle of business logic layer and data layer, which is responsible for processing operations such as reading and writing data that business logic layer needs to access, and separates business logic layer from other operations. In the data persistence layer, JavaBeans are used to encapsulate the data, which makes the operation data as simple as the operation object, enhances the reusability of the code, and makes the code easy to write, maintain, and use.

**Data layer:** the data layer is located at the bottom of the hierarchical framework of the system, which is responsible for the data processing in the system, including database operation and the establishment of Lucene index. Through Lucene technology, the index of relevant data in the database is established, so that the business logic layer can directly obtain the required data from Lucene index, which greatly improves the efficiency of database query. At the same time, the response speed of the system is improved.

*3.2. Database Metadata Framework.* Metadata refers to the data of data. It is a structured description of resource



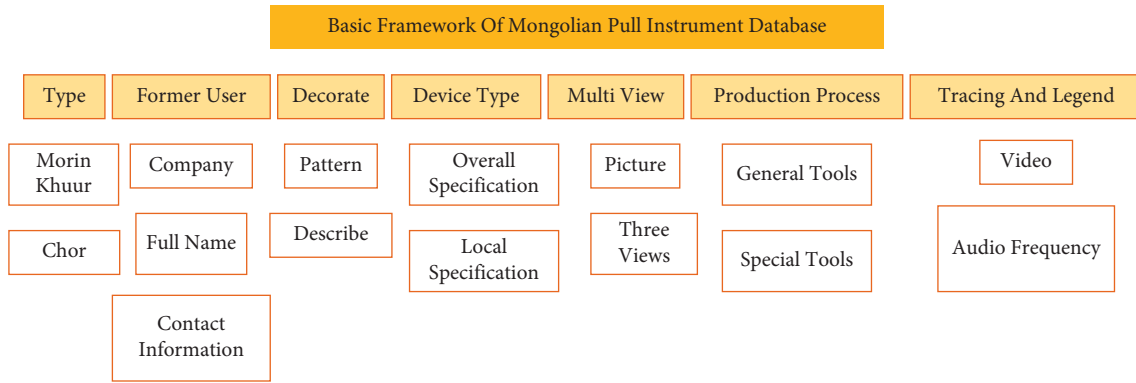


FIGURE 6: Division of data structure.

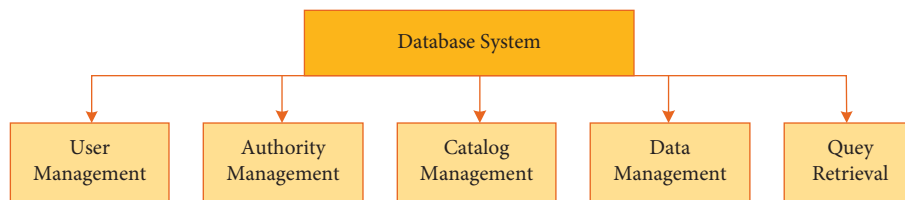


FIGURE 7: Function of resource database system.

information, which provides standard description and retrieval tools for various forms of data-based information units and resource integration. It is the basis of constructing database, digital museum, and multimedia library. Metadata has specific definitions and applications in various fields.

The metadata of Mongolian stringed instruments means the data that describe the attributes of Mongolian stringed instruments. By describing the resource data and resource attributes, the organization and discovery of information resources can be promoted, while the text, image, voice, and other information can be sorted out at the same time. The various attributes of metadata resources of Mongolian stringed instruments are described, and it is necessary to manage the classification, naming, and value range of its attributes by depending on its classification system, category, and essence, that is, what kind of category it belongs to, what naming requirements it has, and what range of range it is, etc.

Establishing a database is to create a warehouse for organizing, storing, and managing data. The attribute description of the metadata of the database about stringed musical instruments is to informationize the relevant data of the Mongolian stringed instruments and manage the tasks of data collection, coding, transmission, storage, retrieval, display, statistical analysis, etc., which provides a theoretical basis for the subsequent database construction service.

The metadata elements of Mongolian stringed instruments are described, and then they are combined into different categories to establish the basic framework of database structure. The metadata framework of Mongolian stringed instruments is composed of 16 different element categories, and each element contains subelements, which can be further split and nested, as shown in Figure 6.

3.3. *Function Module Design.* The database system of stringed instruments is mainly composed of the following functions that are shown in Figure 7.

3.3.1. *User Management Function.* After all types of users enter the system, they can view, modify, and add personal information in the user management module. Through this module, users can set system permissions. Each user can add and modify personal information and personal login password, query personal work log, browse, download, and upload historical information. Senior administrators can view the work content of research directors and researchers, query user information, leave messages, and limit users' rights. They can also manage the personnel of the database to avoid data confusion and improve the accuracy.

3.3.2. *Authority Management Function.* It mainly refers to the function of setting permissions for users who enter the database system of stringed instruments. Users who enter the repository system must have certain permissions that have different operation functions according to different levels. In order to ensure the security and order of the system, it is necessary to divide the permissions for the users who enter the system. As shown in Figure 8, the system user rights are divided into senior administrator, research director, researcher, and visitor.

Senior administrators: they are the owner with the highest authority and can be assigned to other users, to improve the system settings, management directory and resource integration, and other functions.

Research director: their authority is assigned by the senior administrator to enable users to view data and browse

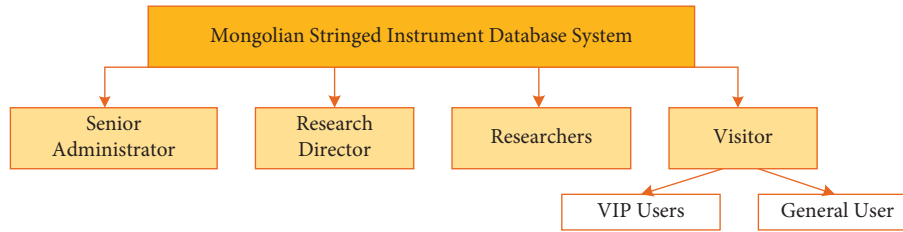


FIGURE 8: Authority management function.

the status of data input, statistical analysis, and log management.

**Researcher:** the authority is assigned by the senior administrator, who can complete the input, upload, download, and modification of resource data, as well as query the historical input data. In addition, they can view the status of its entry and approval.

**Visitor:** visitors are external users that are not allowed to enter the background system, but can view the results of the system at any time, and they are divided into VIP users and ordinary users. They can view the published pictures, text, video, 2D resources, and 3D resources at any time, while VIP users can download some resources through payment points and ordinary users have no right to download.

Senior administrators can modify, delete, and assign permissions to users of various roles in the system. The superadministrator's actions are automatically combined with the log module, and all operations are automatically entered into the log database.

The string instrument database system needs to store and manage all the input information. These resources need to be classified and stored in an organized way. The specific classification can be set by the superadministrator. The directory management module is a module subsystem that provides directory planning and directory creation and maintenance for superadministrators.

**3.3.3. Catalog Management Function.** The directory structure adopts the tree directory to realize the management of the tree directory. There is no restriction on the directory hierarchy that is allowed to create the top-level directory and the lower directory at any level. The module is provided for the superadministrator of the system to create top-level directory and subdirectory, modify directory name and directory merge, and delete empty directory, as well as set directory view permission, where tree display of all directories supports expansion and collapse.

At the same time, the system provides the authority assignment for all top-level directories, that is, it can be assigned to some users in the role of scientific research director, so that only the research director who owns the top-level directory and his subordinate researchers can carry out various operations in this directory. The directory in the system is to better store the included data resources, and each directory sets the serial number, creation date, storage type, and other fields. Finally, the system can generate the data report based on the directory according to the date in the directory.

**3.3.4. Data Management Function.** Data management function mainly refers to the storage of the original data in the system. The original data in the database of stringed instrument include text, picture, audio, video, two-dimensional image, original scanning information of three-dimensional model, registration information, number information, and feature information.

All kinds of information in the database are formed into original pictures, videos, two-dimensional graphics, and three-dimensional models through graphic processing software, video editing software, and data modeling software, which are stored in the database system through the original data module. After inputting various additional information of the data, the system can automatically number each original data according to the predefined numbering rule. The number is unique and cannot be changed which is used to index and locate the original data in the database. All the information is input into the corresponding directory system (systematic directory generated by the directory management module) according to the method of symbol classification, which allows researchers to view or modify the symbol information. However, if necessary, the deletion of information must be approved by the research director.

The data management function stores all original text, pictures, videos, audio, and 2D data and 3D data information. The system provides the view and full-text search of them and supports a variety of formats to download. In the dynamic thumbnail window, users can view the video, audio, and 3D data.

**3.3.5. Query and Retrieval Function.** Query and retrieval function are the most important function of the system which can perform a variety of query and retrieval on all the data stored in the numbered warehouse. The methods include the following: first, users can select retrieval by module of isomorphic tree directory management and obtain the query results that meet the user's needs through one or more conditions. Meanwhile, they can also enter the query page by entering keywords that can be one or more words. The result of the query is multiple data containing keywords, and each condition is associated with a space.

The relevant information of the query is arranged in the form of update date and displayed as the name of the information. The small window that appears after clicking the selected information can support online preview and download of all types of files.

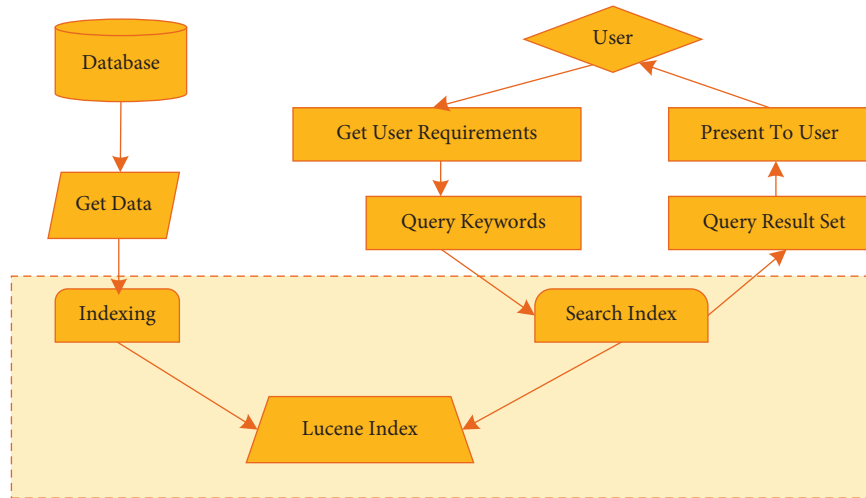


FIGURE 9: Process of data retrieval.

#### 4. Realization of Database System

User is the core of module design. The premise is to provide an interface for users to operate, rather than to provide an interface for operating users. Module is the basic medium of interaction between system and user. It not only provides users with excellent visual experience but also provides a simple and standard interaction process, which can also guide users to gradually form good operating habits, thus greatly improve efficiency.

**4.1. Foreground Systematic Management Module.** The foreground system of string instrument database is a network platform for users to visit, which can browse the contents published publicly, such as Mongolian string instrument information, inheritors, and intangible cultural heritage. The auxiliary functions of the system, such as the homepage interface, the data browsing interface, and the information searching interface, are designed according to the characteristics of Mongolian stringed instruments, where the positioning of the whole front desk system is clear, and the function is comprehensive, so that users can better experience the charm of Mongolian string instrument.

**4.1.1. Home Page of System.** In order to meet the different needs of users, according to the different visual areas of different devices, the front-end web pages adapted to various situations are quickly developed, and the goal of displaying different interface layouts for different devices is achieved, which creates a better learning and communication platform for users.

**4.1.2. Data Browsing.** The data browsing interface satisfies the user's classification browsing of data. The user selects any classification item to enter the relevant classification interface, and the data information displayed in the interface, such as inheritor information and data resources, is displayed in the form of a table, which is convenient for the user to click and view. For example, when browsing the data

window of Mongolian stringed instruments, users can click the switch button and realize the browsing of all Mongolian stringed instrument information in the database.

**4.1.3. Data Retrieval.** The global search module includes two core functions: establishing function of Lucene index and global search. Among them, the establishment of Lucene index is the core foundation of global search. When users search resource data globally, they are actually searching for the established Lucene index, which makes global search not only realize the powerful fuzzy search function but also greatly improve the indexing speed. Global search is the core function of this system, which enables users to get all similar matching results conveniently and quickly. As shown in Figure 9, the global search process is divided into the following two parts.

When users know the key words or some important information of the queried data, they can retrieve the required related data through accurate query. Users only need to directly input keywords to search, and the system will automatically find the data information that meets the search conditions. If users want to inquire about the information of the inheritors of Morin Khuur in Hohhot, select "Hohhot" in the drop-down list of "Location" in the window, then select "art inheritor," and click "Query." Then, the search results are all art inheritors in Hohhot.

**4.2. Background Systematic Management Module.** Background system is the foundation of information management, which provides guarantee for the release, update, and deletion of daily files and facilitates statistics and management. It is a rapid operation and management system for databases and files, which can update and adjust front-end content more conveniently and quickly, whose interface design mainly includes user login interface and data management interface.

**4.2.1. User Login.** In the database system of Mongolian stringed instruments, managers are the publishers and

TABLE 1: Results of systematic functional test.

| Test item              | Test method             | Result | Description  |
|------------------------|-------------------------|--------|--|
| Interface test         | Style judgment          | Good   | The style and color tone of interface are unified<br>The compatibility effect of IE6/IE7 browser is not as good                              |
|                        | Compatibility           | Common | as IE8 and above, the layout effect of input box in the page is not good enough, and the layout is disordered in the case of incompatibility |
| Link test<br>Form test | User experience         | Good   | The layout is reasonable, the page results are divided according to functions, and the positions of operation buttons are uniform            |
|                        | Run test cases manually | Pass   | Bugs are managed through Redmine, and all found bugs have been fixed and the test cases have passed  |

TABLE 2: Parameters of performance test.

|                                    |  |                                 |
|------------------------------------|--|---------------------------------|
| Concurrent parameter configuration | Number of threads                        | 100                             |
|                                    | Thread startup completion time           | 0                               |
|                                    | Number of request sending cycles (times) | 5                               |
| Request parameter configuration    | Server                                   | Localhost                       |
|                                    | Port number                              | 8080                            |
|                                    | Path                                     | /Fund/admin/project!list.action |
|                                    | Request mode                             | GET                             |

updaters of data resources and the guardians of the stability, security, integrity, and high performance of the database management system. After the manager logs in to the database background system, they can enter the user name and password in the user login interface and then can enter the management interface to modify, delete, update, and publish the metadata of Mongolian stringed instruments in the database.

**4.2.2. Data Management.** Data management is the core content of database background system, which directly affects the presentation of Mongolian stringed instrument data. The metadata entry interface is a general framework based on the data collection table of Mongolian stringed instruments, where some of them are designed as a selective drop-down menu, which can be added, deleted, or sorted by administrators, while some conceptual and descriptive data need to be entered manually.

## 5. Systematic Test

### 5.1. Test Environment and Tools

- (1) Test tool: LoadRunner 11.0.
- (2) Hardware test environment:
  - Server model: IBM System X3850.
  - Client model: Lenovo ThinkPad X1 Carbon.
- (3) Software testing environment:
  - Operating system: Windows Server 2008; Client: Windows 7 Professional.
  - Database: MySQL 5.5.
  - Browser: Internet Explorer 6.0 and above.
  - Environmental temperature and humidity: the temperature is 20°C and the relative humidity is 65%.

**5.2. Functional Test of System.** The functional test refers to testing various functions of the system and testing item by item to check whether the system meets the requirements of users. The functional test of this system mainly includes the following two parts:

- (1) Interface test: Test whether the system interface is reasonable, beautiful, and coordinated and whether it is consistent with the design and easy to use, which mainly includes navigation test, form test, and overall interface test
- (2) Link test: Test whether all links or function buttons of each page jump to the target page according to the design and whether the linked page exists to ensure that all links are valid and correct
- (3) Form test: Test the input contents of the search input box for string, value, required items, and keywords to check whether the submitted form parameters are correct and whether the response to critical values is accurate

The front and back modules of the system are tested in the above way, and the results are shown in Table 1.

**5.3. Performance Test.** The purpose of performance testing is to count the performance parameters of the system, which mainly includes response speed, throughput, and other parameters. The system performance is judged according to the performance parameters to ensure an excellent experience. Because the portal subsystem is a system that directly contacts users, the number of users is large and the database is frequently operated in the retrieval process, so the biggest load in this system is the retrieval page. The specific parameters of performance test are configured as shown in Table 2, where JMeter is used to multithread concurrent access single-category page, test the average response time of the page, and simulate the heavy load environment to test the performance of the system in this environment.

TABLE 3: Test results of systematic performance.

|   |       |
|---|-------|
| Total samples   | 500   |
| Average request response time (m/s)                             | 182   |
| The response time of 90% requests is less than this value (m/s) | 580   |
| The minimum response time (m/s)                                 | 43    |
| The maximum response time (m/s)                                 | 375   |
| Request error percentage  | 0%    |
| Throughput (per second)   | 276.9 |

The test results are shown in Table 3.

As can be seen from Table 3, the system can still guarantee a short corresponding time and a high throughput under heavy load, which will not cause a large network delay. Therefore, this system has high performance, can meet the concurrent access of large amounts of data, and has a good user experience.

The test results also show that various functions and the interaction between systems are designed and developed, where the flexible combination of functions in the whole database system is realized, and the data management in the field of Mongolian stringed instruments crosses from traditional manual management to modern management. At the same time, it accelerates the accumulation of Mongolian stringed instrument resources in industrial clusters, which improves the quality of cultural exchanges and cooperation.

Through the testing of the functional modules and performance of the intangible cultural heritage database system, its function can meet the functional requirements of stable running performance and strong running environment security. The intangible cultural heritage database designed in this paper has the following capabilities: first, it can effectively realize the classified management, data query, collection, and download of data resources in the database; meanwhile, users of the background system can also add, modify, and delete data; and finally, the background management of the system runs normally.

## 6. Conclusion

Through the establishment of intangible cultural heritage database, the preservation, display, and education of intangible cultural heritage resources can be better realized. In this paper, Mongolian stringed instruments are taken as the carrier and the intangible cultural heritage protection system is designed, where MySQL is used as the system database and Struts 2 framework in MVC architecture is selected to realize the separation of business logic and data display. The test results show that the system can meet the requirements of stable operation, and its database has the following capabilities: first, it can effectively realize the classified management, data query, collection, and download of data resources in the database; at the same time, users of the background system can also add, modify, and delete data; and finally, the background management of the system runs normally.

## Data Availability

The dataset can be accessed upon request.

## Conflicts of Interest

The authors declare that they have no conflicts of interest.

## Acknowledgments

This work was supported by TheDevelopment Research Centerof the Three Gorges Culture and Economic Society, Key Research Base of Humanities and Social Science in Hubei Province (project no. SXKF202105); Bachu Art Culture Research Center, Key Research Base of Humanities and Social Science in Hubei Province (project no. 2018KF07); Research Center of Film and Television Culture and Industry, Key Research Base of Humanities and Social Science in Hubei Province (project no. 2021yskf09); and Research Center for Regional Social Management Innovation and Development, Key Research Base of Humanities and Social Science in Hubei Province (project no. 2021SDSG07).

## References

- [1] I. Lee and F. Zhou, "Overview of digital protection technology of national cultural heritage," *Computer Knowledge and Technology*, vol. 9, no. 15, pp. 3643–3645, 2013.
- [2] C. Fu and C. Geng, "The Protection and Development Model of Contemporary Chinese Heritage," *Journal of Hubei University (Philosophy and Social Sciences)*, vol. 37, no. 4, pp. 93–98, 2010.
- [3] B. Liu, *Research and Implementation of Heterogeneous Data Visualization Sharing Mechanism of Intangible Cultural Heritage Based on G/S Model [D]* Chengdu University of Technology, 2011.
- [4] Z. Zhao, "Visual analysis of the evolution path and hot Frontier of digital research on cultural heritage [J]," *Library Forum*, vol. 33, no. 02, pp. 33–40, 2013.
- [5] G. Lei, "Five levels of intangible cultural heritage database construction needs [J]," *Three Gorges Forum*, vol. 33, no. 1, pp. 84–89, 2009.
- [6] Erbihe, *The Role of Modern Digital Technology in the Establishment of Intangible Cultural Heritage Database [J]*no. Z1, , pp. 25–28, Erdos Culture, 2014.
- [7] Q. Chen, "Research on digital protection of intangible cultural heritage [J]," *Science and Technology of Energetic Materials*, vol. 28, no. 23, pp. 67–69, 2015.

- [8] Y. Guo and Ye Yao, "Design and implementation of experimental platform for database management [J]," *Digital Technology and Application*, vol. 28, no. 11, pp. 162–164, 2017.
- [9] M. Guo and H. Jiang, "Application of Struts in realizing MVC framework," *Computer and Modernization*, vol. 34, no. 1, pp. 37–40, 2004.
- [10] Yi Tang and C. Yang, "Research on MVC framework principle based on pattern design," *Educational Technology Guide*, vol. 48, no. 6, pp. 40-41, 2008.
- [11] S. M. Stephens, J. Y. Chen, and M. G. Davidson, "Oracle Database 10g: a platform for BLAST search and Regular Expression pattern matching in life sciences," *Nucleic Acids Research*, vol. 23, no. 1, pp. 675–679, 2004.
- [12] M. Di Giacomo and M. MySQL, "MySQL: lessons learned on a digital library," *IEEE Software*, vol. 22, no. 3, pp. 10–13, 2005.
- [13] X. Wu, H. Xia, and G. Zhao, "Application and improvement of full-text search engine based on Lucene," *Journal of Wuhan University of Technology*, vol. 30, no. 7, pp. 145–148, 2008.

## *Retraction*

# **Retracted: Question and Answer Techniques for Financial Audits in Universities Based on Deep Learning**

### **Mathematical Problems in Engineering**

Received 18 July 2023; Accepted 18 July 2023; Published 19 July 2023

Copyright © 2023 Mathematical Problems in Engineering. This is an open access article distributed under the Creative Commons Attribution License, which permits unrestricted use, distribution, and reproduction in any medium, provided the original work is properly cited.

This article has been retracted by Hindawi following an investigation undertaken by the publisher [1]. This investigation has uncovered evidence of one or more of the following indicators of systematic manipulation of the publication process:

- (1) Discrepancies in scope
- (2) Discrepancies in the description of the research reported
- (3) Discrepancies between the availability of data and the research described
- (4) Inappropriate citations
- (5) Incoherent, meaningless and/or irrelevant content included in the article
- (6) Peer-review manipulation

The presence of these indicators undermines our confidence in the integrity of the article's content and we cannot, therefore, vouch for its reliability. Please note that this notice is intended solely to alert readers that the content of this article is unreliable. We have not investigated whether authors were aware of or involved in the systematic manipulation of the publication process.

Wiley and Hindawi regrets that the usual quality checks did not identify these issues before publication and have since put additional measures in place to safeguard research integrity.

We wish to credit our own Research Integrity and Research Publishing teams and anonymous and named external researchers and research integrity experts for contributing to this investigation.

The corresponding author, as the representative of all authors, has been given the opportunity to register their agreement or disagreement to this retraction. We have kept a record of any response received.

### **References**

- [1] Q. Li, "Question and Answer Techniques for Financial Audits in Universities Based on Deep Learning," *Mathematical Problems in Engineering*, vol. 2022, Article ID 4875859, 8 pages, 2022.

## Research Article

# Question and Answer Techniques for Financial Audits in Universities Based on Deep Learning

**Qiang Li** 

*Jiangsu College of Engineering and Technology, Nantong 226007, Jiangsu, China*

Correspondence should be addressed to Qiang Li; [liqiang991631@jcet.edu.cn](mailto:liqiang991631@jcet.edu.cn)

Received 22 March 2022; Revised 24 April 2022; Accepted 10 May 2022; Published 25 May 2022

Academic Editor: Hangjun Che

Copyright © 2022 Qiang Li. This is an open access article distributed under the Creative Commons Attribution License, which permits unrestricted use, distribution, and reproduction in any medium, provided the original work is properly cited.

Financial auditing in universities is highly specialized, with a huge knowledge system and rapid updates. Auditors will encounter various problems and situations in their work and need to acquire domain knowledge efficiently and accurately to solve the difficulties they encounter. The existing audit information software, however, is mostly aimed at the management of audit affairs and lacks the relevant functions to acquire and retrieve knowledge of specific audit domains. In this study, we use deep learning theory as support to conduct an in-depth study on the key technologies of question and answer systems in the field of financial auditing in universities. In the question-answer retrieval stage, the local information and the global information of the sentence are first modelled using a two-way coding model based on the attentional mechanism, and then, an interactive text matching model is used to interact directly at the input layer, and a multilayer convolutional neural network model cable news network (CNN) is used to extract the fine-grained matching features from the interaction matrix; this study adopts two matching methods. We have conducted comparative experiments to verify the effectiveness and application value of the entity recognition algorithm based on this study's algorithm and the question-answer retrieval model based on multi-granularity text matching in the university financial audit domain.

## 1. Introduction

In recent years, China's financial auditing of colleges and universities has been developed in an unprecedented way by combining national conditions, absorbing international advanced ideas, and groping on the road of practice, constantly improving and refining. With the flourishing development of computer science and technology, audit informatization has become a wave that promotes the development and progress in the field of financial auditing in universities, improving audit efficiency, and saving audit costs [1].

Financial auditing in colleges and universities is a scout to punish and prevent corruption. Financial audit of colleges and universities refers to the auditing and supervision of the assets, funds, profit and loss, and liabilities of state-owned colleges and universities and their holding colleges and universities independently, objectively, and impartially according to laws and regulations, to judge whether they are

true and lawful and to give evaluation and audit opinions in the form of audit reports [2]. The purpose of financial audit of universities is to verify and reveal the true operation status of state-owned universities and their holding universities; to investigate and deal with illegal and irregular behaviors in financial income and expenditure; and to prevent the loss of state-owned assets and to facilitate the macro-control of the government [3].

In this process, the majority of university financial auditors are eager to quickly and fully understand the knowledge and new policies of all aspects of university financial auditing, so that they can have justifications and evidence to obtain the corresponding domain knowledge efficiently and accurately in the face of university financial auditing affairs [4]. As a result, university financial auditors have a huge and urgent need for domain knowledge in their work and are eager to learn domain knowledge quickly to solve the problems they encounter [5]. Therefore, it is necessary to provide them with a Q&A service that can



answer questions and solve problems in a professional and intelligent manner [6].

Financial auditors in higher education can satisfy their need for domain knowledge acquisition using search engines (e.g., Baidu and Google) to retrieve information on the Internet [7]. However, traditional search engines return to the user a large number of links to keyword-related Web pages based on the keywords entered by the user, and there are many unsatisfactory aspects, mainly in the following areas [8].

Because traditional search engines cannot meet people's needs for accurate and efficient access to information, many large companies, research institutes, and scholars at home and abroad have turned their attention to more intelligent, professional, and personalized automatic question and answer systems and are constantly researching and exploring them. Question answering system (QA) can answer questions in natural language (a sentence or a paragraph of text, or even a named entity such as a person's name or a place's name) based on the user's input, which is more efficient, accurate, and concise than traditional search engines that are accurate, concise, and clear [9].

In view of the high degree of specialization in university financial auditing, the huge knowledge system, and the large workload of auditors who are eager to obtain domain knowledge efficiently and accurately, it is necessary for us to use advanced theoretical knowledge in natural language processing and machine learning to build a question and answer system for auditors in the field of university financial auditing, which can answer auditors' questions intelligently, efficiently, professionally, and concisely and help auditors obtain domain knowledge accurately, thus assisting auditors to improve work efficiency and audit quality [10].

## 2. Related Work

In the 21st century, computer technology has developed rapidly and widely spread to all aspects of production and life [11]. At the same time, domestic universities have absorbed the advanced ideas of international universities and kept in line with them, so China's auditing work has also entered the era of information technology and is on par with international standards [12]. The financial audit of contemporary universities has significant characteristics, the scope and field of audit are expanding, the content of audit becomes more and more complex, the audit subject is also developing along the trend of diversification, and the corresponding audit technology is also more scientific [13].

Reference [14] proposed a semantic Web-based question and answer system built on the powerful and easy-to-use structured data of freebase. A typical representative of a semantic Web-based Q&A system is jacana-freebase [15], where natural language interrogatives entered by the user are transformed by the Q&A system into graph query statements against the semantic Web knowledge base.

Reference [16] used a recurrent neural network to represent the interrogative sentences as word vectors, considering the dependent syntax of the interrogative sentences. In addition,  $t$  implemented a question and answer system for

single-relationship problems using convolutional neural networks, the main idea of which is to train matching relations between entities and entities, which are represented by semantic vectors. Reference [17] proposed the concept of word vectors, which is a distributed representation of meaningful words using neural networks. Reference [18] proposed a neural network language model, i.e., modelling the  $n$ -gram, which solves the problem of word vector dimensional catastrophe. Reference [19] proposed the widely known Centralne Biuro Obrotu Wierzytelnościami (CBOW) word vector model and Skip-gram word vector model using more contextual information to share parameters through recurrent neural networks, and its open-source project word2vec was more widely used by researchers, and the distributed representation technique of words matured. In [16], based on word vectors and word-level neural networks, the transfer probability matrix is added to the named entity recognition task to improve performance; Collobert constructed a multilayer convolutional neural network model for four annotation tasks, with input raw sentences for vector representation without artificial features. Kim proposed a multichannel CNN model for the sentence classification task [20].

## 3. Preprocessing of the Corpus

Corpus preprocessing is to remove useless and invalid phrases from the large amount of unstructured text crawled, so that the efficiency of domain entity recognition can be improved and the recognition effect can be better. The corpus preprocessing mainly includes three stages: sentence division, word division, and screening of deactivated words.

- (1) Split-sentence processing.
- (2) Word processing.
- (3) Deactivation word screening.
- (4) Dependency syntax analysis. Research has shown that every word in a sentence is dependent in some way on another word. Dependency syntax analysis allows the identification of semantic dependencies between words and the understanding of their relational categories. In entity recognition tasks, dependency syntax analysis can be used to capture functional information about entities and improve the quality of sequence annotation.

Typically, the dependency syntax analysis algorithm starts at the root node and expands downwards from the top to generate a dependency syntax analysis tree. For ease of understanding, this study uses the Dependency Viewer tool to build the dependency syntax analysis tree.

Taking the question "What are the steps in a fixed asset audit?" as an example, the dependency syntax analysis gives an example of the dependency syntax analysis tree in Figure 1.

After dividing the corpus into sentences and words in the field of university financial auditing, 8304 words were collected, and after filtering them for deactivated words, a total of 5873 valid words were obtained.

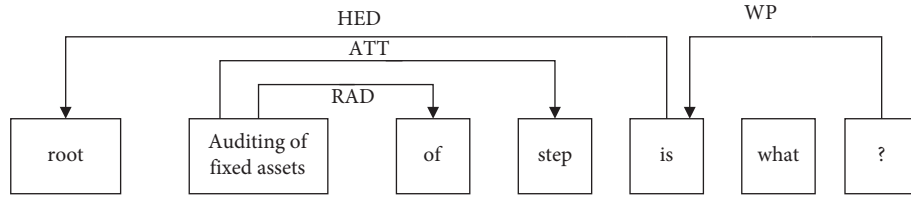


FIGURE 1: Example of a dependency syntax analysis tree.

TABLE 1: Training data format.

| User questions  | Knowledge point title                    | Knowledge point answer | Label |
|---|--|------------------------|-------|
| What is accounting statement audit?                     | Definition of accounting statement audit | Corresponding answer a | 1     |
| What is the significance of accounting statement audit? | Definition of accounting statement audit | Corresponding answer a | 0     |
| What are the steps of accounting statement audit?       | Audit steps of accounting statements     | Corresponding answer b | 1     |
| How to audit accounting statements?                     | Audit steps of accounting statements     | Corresponding answer b | 1     |
| What are the key points of accounting statement audit?  | Audit steps of accounting statements     | Corresponding answer b | 0     |

#### 4. Question and Answer Search Model

We divide the Q&A system into two modules: entity recognition, as a pre-step of Q&A retrieval, plays an important role for Q&A retrieval, and it can be used as an important feature for Q&A matching. From our experimental analysis later, we can see that the entity information identified in the entity recognition stage can improve the accuracy of the Q&A retrieval model.

In the question-answer retrieval phase, the goal of question-answer matching is to find the most similar answer from the candidate knowledge base to return to the user, which can be abstracted into two academic tasks, one is question-question matching (paraphrase identification), which aims to calculate the semantic similarity of two interrogative sentences and determine one is question-answer selection, which aims to determine whether the answer can answer the corresponding question and is a question-answer relationship. Both can be defined as text matching tasks, and this section presents them in a unified way, with the following abstract definition:

$$\text{score} = F(x_1, x_2), \quad (1)$$

where  $x_1, x_2$  denotes the word sequence of the two input texts,  $F$  denotes the implicit relationship function learned by our model, for the question-question matching task,  $F$  denotes the degree of similarity, and for the question-answer matching task,  $F$  denotes the degree of correlation between the question and the answer.

**4.1. Data Preprocessing.** We crawled a huge knowledge base of questions and answers in the field of university financial auditing from Internet resources, processed it by some rules (special character processing, spam identification, etc.), generated question-answer knowledge in the form of questions and answers and possible descriptions of all user questions, and retrieved the knowledge base question—answer is retrieved from the candidate set of all user questions based on retrieval, and 10 items of each knowledge are recalled and manually reviewed and marked as our

training data. The format of the training data is shown in Table 1.

“User question” indicates the question asked by the user, “knowledge point title” indicates the knowledge base question we crawled, “knowledge point answer” indicates the answer to the knowledge point, and “label” indicates whether the knowledge point answer can be used as the answer to the user question. The “label” indicates whether the knowledge answer can be used as an answer to the user question, with “1” meaning that it can be used as an answer and “0” meaning that it cannot be used as an answer. The general question and answer matching only considers the relevance of the user question and the knowledge answer, but there may be some noise in the knowledge base we crawl, so the effect of matching the user question with the answer is not particularly satisfactory.

After constructing the training data, data preprocessing is required as input to the model. Traditional methods require extensive data preprocessing including word separation, dependent syntactic analysis, and feature construction, while the proposed question-answer matching model is based on the deep learning end-to-end model, which does not require excessive data preprocessing and manual feature definition and extraction and only requires word separation for the training data.

#### 4.2. Multi-Granularity Question and Answer Matching Model.

We fuse information at different levels of granularity, and the overall model structure is shown in Figure 2. The model consists of three modules: an input layer, a representation layer, and a matching layer. Based on the input matrix mapped in the input layer, the representation layer maps the two input texts into the same semantic space through two-way coded text relationship modelling, interactive text relationship modelling, entity information fusion, and attentional mechanism. Finally, the matching layer uses cosine similarity for the question-question matching (paraphrase identification) task based on the semantic vectors modelled in the representation layer, and the question-answer matching (answer selection) task is computed using an implicit semantic relation function.

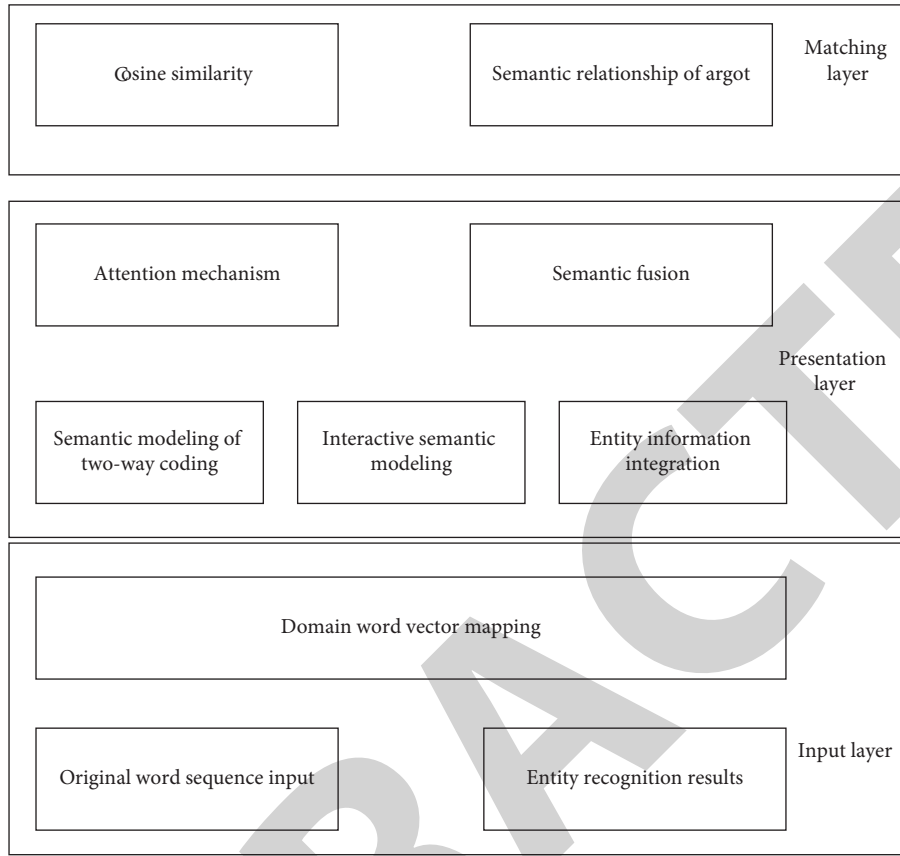


FIGURE 2: Structure of this matching model.

**4.3. Input Layer.** The input layer is the input to the whole model, including the raw word sequence input, and the input from the entity recognition results in Section 3. Assume that the two sentences input are  $S_1 = \{w_1, w_2, \dots, w_n\}$  and  $S_2 = \{w'_1, w'_2, \dots, w'_n\}$ . Using the entity recognition results from the square in Section 3 as  $E_1 = \{e_1, e_2\}$  and  $E_2 = \{e'_1\}$ , where  $w^{\text{word}} \in R^{d^{\text{word}} \times |V^{\text{word}}|}$  and  $d^{\text{word}}$  denote an entity that can consist of multiple words, the word sequence input is mapped to a word vector representation via a word vector matrix, where  $e_i$  denotes the word vector dimension,  $V^{\text{word}}$  denotes the lexicon size, and  $w^{\text{word}}$  is word learned through the model, as shown as follows:

$$r^k = w^{\text{word}} \cdot v^w. \quad (2)$$

Similarly, the entity inputs are mapped by means of an entity vector matrix  $w^{\text{entity}} \in R^{d^{\text{entity}} \times p^{\text{entity}}}$ ,  $d^{\text{entity}}$  denotes the entity vector dimension, which is small in order to be adequately trained, typically 10,  $v^{\text{entity}}$  denotes the number of entity types, and  $w^{\text{entity}}$  is also automatically learned by the model to obtain an entity vector representation; see the following equation:

$$r^e = w^{\text{entity}} \cdot v^e. \quad (3)$$

**4.4. Representation Layer.** The role of the representation layer is mainly to encode the input and map it to the same semantic space, as, for the input features of the matching layer, mainly including the two-way encoding semantic modelling based on attentional mechanism, interactive semantic modelling, entity information integration, and other major parts.

In terms of recurrent neural network (CRNN) modelling, the RNN model can retain the contextual information of each word, and it is difficult to train the traditional model because it is difficult to solve the problem of long-distance dependency; therefore, we use the bidirectional long- and short-term memory recurrent neural network model (BiLSTM) for training, and the BiLSTM model can solve the problem of long-distance dependency, and the bidirectional LSTM model, which not only models the above information of words but also preserves the below information of words, enables a richer representation of word levels. For example, in the questions “What is the objective of the financial audit of the university?” and “what are the parts of the audit?” the input of the hidden unit corresponding to “objective” can not only retain “audit” but also include in the question “What is the objective of the audit?”. The BiLSTM model maps the two-word sequences to vectors in the same semantic space, as follows:

$$\begin{aligned}
h_i^{\text{forward}} &= \text{LSTM}^{\text{forward}}(s_i\{r_1^w, r_2^w, \dots, r_n^w\}), \\
h_i^{\text{backward}} &= \text{LSTM}^{\text{backward}}(s_i\{r_1^w, r_2^w, \dots, r_n^w\}), \\
h_i &= h_i^{\text{forward}} \cdot h_i^{\text{backward}},
\end{aligned} \quad (4)$$

where  $s_i$  denotes the input word vector matrix, LSTM denotes the long- and short-term memory recurrent neural network model operation, as described in detail in Section 2, and  $h_i$  denotes the forward and backward computation, respectively, and  $h_i$  denotes the concatenation of the forward and backward computed LSTM representation vectors as the semantic representation of the word.

We introduce attentional mechanisms. Combined with our model and the characteristics of the domain, we introduce two attentional mechanisms, one based on entity information and one based on answers. The two attentional mechanisms are only different in representation, and the principles are the same, so they are introduced in unison. The core idea of the attentional mechanism is to assign different weights to different words in a sentence, with the different weights representing the importance of the words, which is calculated as follows:

$$\begin{aligned}
\alpha_i &= \sigma(r_q^T M_q h_i), \\
h'_i &= \alpha_i \times h_i,
\end{aligned} \quad (5)$$

where  $M$  denotes the parameter matrix of the attentional mechanism, which is learned automatically by the model;  $r_q^T$  denotes the context vector involved in the weight calculation, which can be either the entity vector or the hidden layer vector of the BiLSTM hidden layer output by max-pooling or average pooling;  $\sigma$  denotes the nonlinear transformation function;  $\alpha_i$  denotes the different weights of each word based on the attentional mechanism;  $h_i$  denotes the hidden layer output of the BiLSTM; and  $h'_i$  denotes the hidden layer output after weighting based on the different weights. The attentional mechanism allows each word to be given a different weight based on different contextual information (different entities, different answers, etc.).

In terms of convolutional neural network (CNN) modelling, local features are generally extracted based on the original word vector through the convolution and pooling operations of the CNN model [21], while we use the output of each hidden layer (forward and backward outputs are concatenated) in the BiLSTM as the CNN model is calculated as follows:

$$r'_i = f\left(\text{conv}\left(h_i^{\text{Bi-LSTM}}\right)\right) + \text{bias}, \quad (6)$$

where conv represents the convolutional and pooling formulas in the convolutional neural network, which are described in detail in Section 2;  $h_i^{\text{Bi-LSTM}}$  represents the output of the bidirectional long- and short-term memory recurrent neural network model,  $f$  represents the nonlinear function, bias represents the bias, and  $r'_i$  represents the text semantic vector represented by the two-way coded text relationship modelling. In summary, the two-way encoding model based on the attention-based mechanism is shown in Figure 3.

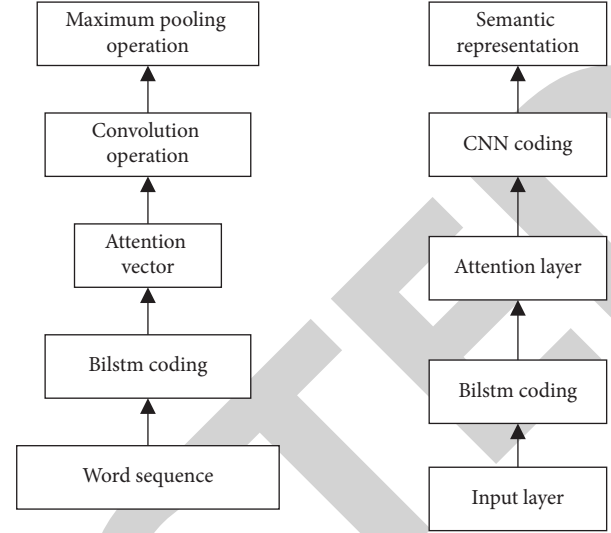


FIGURE 3: Two-way coding model with attentional mechanism.

**4.5. Matching Layer.** The matching layer is mainly based on the semantic representation of the representation layer for matching score calculation. In our knowledge base, a knowledge point has both questions and answers, and these data are mined from the Internet without manual review, and if we simply match from the question dimension or the answer dimension, it may bring large deviations; for example, the questions are similar, but the answers are not good enough to solve the user's problem. Based on this difference, different matching methods are used for the two matching models.

**4.6. Model Training and Parameter Tuning.** Again, we developed the model based on the TensorFlow deep learning development environment developed by Google. The parameters of the model are word vector, entity type vector, LSTM parameters, CNN parameters, implicit relation parameters, and fully connected layer parameters [24, 25], where the implicit relation parameters represent the implicit relation matrix  $M$  in the question-answer matching process, and for all hyperparameters, we iterate through a gradient search to find the best combination of parameters. The final model parameters are shown in Table 2.

## 5. Financial Audit Entity Identification Experiments

To verify the advantages and disadvantages of the model proposed in this study and the effectiveness of the features introduced in this study, we have done two sets of experiments, one set of experiments is to compare the effect of the entity recognition model proposed in this study with the traditional method [26] and the other set of experiments is to compare the different features introduced in this study, and the detailed analysis is as follows.

**5.1. Experiments Comparing the Model in This Study with Traditional Methods.** As the area of study for this study is

TABLE 2: Table of model parameters.

| Parameter name | Word vector dimension | Entity vector dimension | LSTM hidden layer dimension | LSTM layers                  | Convolution kernel size |
|----------------|-----------------------|-------------------------|-----------------------------|------------------------------|-------------------------|
| Value          | 128                   | 128                     | 128                         | 1                            | [128,3]                 |
| Parameter name | Matrix size           | Dropout                 | Wight                       | Number of hidden layer nodes | Number of hidden layers |
| Value          | [128, 64]             | 0.8                     | 0.8                         | 128                          | 2                       |

TABLE 3: Experimental results of entity recognition models.

| Model                 | Accuracy (%) | Recall rate (%) | F1 value (%) |
|-----------------------|--------------|-----------------|--------------|
| CRF-based             | 78.52        | 77.48           | 78.94        |
| BiLSTM-based          | 80.01        | 79.87           | 80.12        |
| BiLSTM + CRF + model  | 81.45        | 80.03           | 80.07        |
| BiLSTM + CRF + Deixis | 81.47        | 81.29           | 80.97        |
| Paper model           | 80.14        | 83.47           | 82.59        |

the specialist field of financial auditing in universities, there is no publicly available experimental dataset on the Internet. To compare the experimental results and to validate the results of this study, the dataset used in this study was manually annotated by the author's team.

To compare this model with other models, we have selected three models that work well in other domains for implementation and tested them on our dataset, of which the CRF-based, BiLSTM-based, and LSTM-CRF-based models use manual feature design and feature extraction as input to the model, and BiLSTM-based and BiLSTM-CRF models use raw word input and learn automatically through deep learning models without introducing domain knowledge features similar to those proposed in this study. The model in this study is the BiLSTM and CRF model-based entity recognition method that fuses domain knowledge proposed in this study. The experimental results are shown in Table 3.

From the experimental results, it can be seen that the proposed multi-granular entity recognition model incorporating domain knowledge outperforms the traditional model in terms of accuracy, recall, and F1 value in the test set, fully validating the effectiveness of introducing domain knowledge features on top of the popular BiLSTM + CRF model. To illustrate the effectiveness of the different features, we have also conducted corresponding comparison experiments for different feature combinations.

**5.2. Validation Experiments for Domain Knowledge.** We added different features such as lexicality, entity lexicon, and indicator word information to the standard BiLSTM + CRF model for experimental validation to illustrate the role of different features separately, as shown in Table 4.

From the experimental results, it can be seen that a variety of features introduced in this study can be useful for entity recognition. The lexical features can be seen as an additional supplement to the word vector information; for example, nouns are generally considered to be more likely to be entities, and this information can be learned automatically by the model, but as the word vector information is already rich in semantics, the introduction of lexical features

is not very useful. In contrast, the introduction of entity features improves the  $n$  value by 1.24% relative to the BiLSTM + CRF model, while the recall rate improves by 1.47%, indicating that the candidate domain entity lexicon can play an important role for some sparse entities. This is reflected in the significant increase in the recall rate; the introduction of the indicator information improves the F1 value by 0.87% relative to the BiLSTM + CRF model, while the accuracy rate improves by 0.92%, indicating that the indicator information can correct those entities that are easily misidentified and improve the accuracy rate. Finally, it can be seen that the combination of the three features can further improve the recognition effect compared with the introduction of entity words or indicator words alone, indicating that these features are complementary to each other and the combination can improve the final entity recognition effect.

**5.3. Question and Answer Search Experiment.** In the experiments, two types of evaluation criteria were chosen for evaluating the model, one is the AUC, which is not related to the selection threshold of the classification criteria, and the AUC is usually used to evaluate the goodness of the dichotomous classification model; the other is the metrics such as MAP and MRR, which are related to the ranking of the information retrieval, MAP denotes the mean accuracy rate.

Attentional mechanism plays an important role in the model of this study, we introduced answer attention and entity attentional mechanism, the difference between the two is that the answer attentional mechanism calculates the weight of each word in the question based on the coding vector of the answer, while the entity attentional mechanism calculates the weight of each word in the question based on the coding vector of the entity. The detailed results are shown in Table 5.

From the experimental results, we can see that the introduction of the attentional mechanism can improve the model's effectiveness to a certain extent, in which the entity attentional mechanism improves the effect better than the answer attentional mechanism, indicating that the entity attentional mechanism can make the model pay more

TABLE 4: Results of domain knowledge validity experiments.

| Model                         | Accuracy (%) | Recall rate (%) | F1 value (%) |
|-------------------------------|--------------|-----------------|--------------|
| BiLSTM + CRF model            | 81.21        | 80.12           | 84.12        |
| BiLSTM + CRF + part of speech | 81.02        | 82.03           | 82.04        |
| BiLSTM + CRF + entity         | 82.24        | 82.39           | 82.79        |
| BiLSTM + CRF + Deixis         | 82.47        | 83.12           | 82.90        |
| Paper model                   | 82.74        | 84.57           | 86.35        |

TABLE 5: Experimental results of the attentional entry mechanism.

| Model   | Auc (%) | MAP (%) | MRR (%) |
|---|---------|---------|---------|
| This model does not introduce attentional mechanism | 79.01   | 67.47   | 65.98   |
| This study models entity attentional mechanism      | 78.92   | 68.74   | 66.87   |
| This study models the answer attentional mechanism  | 80.54   | 67.98   | 67.89   |
| Paper model   | 81.23   | 70.01   | 69.53   |

TABLE 6: Experimental results for entry entity characteristics.

| Model   | Auc (%) | MAP (%) | MRR (%) |
|---|---------|---------|---------|
| This model does not introduce entity features         | 81.11   | 70.01   | 69.21   |
| In this study, model + entity features are introduced | 82.37   | 69.47   | 68.71   |

attention to the entity information and reflect the core semantics of the user when performing the question representation.

To illustrate the importance of the entity feature information identified in the question-answer matching process, we compared the models without the introduction of entity features and the models with the introduction of entity features, respectively, and the detailed results are shown in Table 6.

From the experimental results, it can be seen that the introduction of entity features has an important role in the improvement of the question and answer matching model, with 0.74%, 0.85%, and 0.81% improvement in the Auc, MAP, and MRR indexes, respectively, and the introduction of entity features can incorporate the a priori knowledge of entity features into the model, which can automatically learn the role of entity features for the final matching relationship through a large amount of training data.

## 6. Conclusions

In this study, we propose a question and answer retrieval model based on multi-granularity text matching, incorporating matching features of different granularities. Firstly, a two-way code model, i.e., a long- and short-term memory recurrent neural network (BiLSTM) and a CNN model, is used to model the contextual and local information of the sentence, while an attentional mechanism is introduced to assign different weights to different words, allowing the model to focus more on the expression of specific words; then, an interactive text matching model is used in the input layer directly; finally, by fusing the entity recognition information, entity features are introduced to enhance the effectiveness of question and answer matching.

## Data Availability

The dataset used in this study is available from the corresponding author upon request.

## Conflicts of Interest

The authors declare that they have no conflicts of interest regarding this work.

## Acknowledgments

This work was sponsored by the Research on the Cost of Higher Education under the Government Accounting System—A Case Study of Jiangsu College of Engineering and Technology (2020SJB1281).

## References

- [1] A. O. A. Semasaba, W. Zheng, X. Wu, and S. A. Agyemang, "Literature survey of deep learning-based vulnerability analysis on source code," *IET Software*, vol. 14, no. 6, pp. 654–664, 2020.
- [2] C. Zhang, "Intelligent process automation in audit," *Journal of Emerging Technologies in Accounting*, vol. 16, no. 2, pp. 69–88, 2019.
- [3] M. Schreyer, T. Sattarov, B. Reimer, and D. Borth, "Adversarial learning of deepfakes in accounting," 2019, <https://arxiv.org/abs/1910.03810>.
- [4] L. Li, F. Zhu, H. Sun, Y. Hu, Y. Yang, and D. Jin, "Multi-source information fusion and deep-learning-based characteristics measurement for exploring the effects of peer engagement on stock price synchronicity," *Information Fusion*, vol. 69, pp. 1–21, 2021.
- [5] A. Radwan, K. M. S. Huq, S. Mumtaz, K. F. Tsang, and J. Rodriguez, "Low-cost on-demand C-RAN based mobile small-cells," *IEEE Access*, vol. 4, pp. 2331–2339, 2016.

## Research Article

# Research and Analysis on the Integration of Artificial Intelligence in College English Teaching

Dashan Jiang,<sup>1</sup> Yubing Pei ,<sup>2</sup> Gongping Yang,<sup>3</sup> and Xue Wang<sup>4</sup>

<sup>1</sup>International Education College, Kaifeng University, Kaifeng 475000, China

<sup>2</sup>School of Foreign Languages and Business, Shenzhen Polytechnic, Shenzhen 518055, China

<sup>3</sup>Human Resource Department, Shanghai Xingjian College, Shanghai 200072, China

<sup>4</sup>Foreign Language Department College, Shanghai Xingjian College, Shanghai 200072, China

Correspondence should be addressed to Yubing Pei; [probinpei@szpt.edu.cn](mailto:probinpei@szpt.edu.cn)

Received 3 March 2022; Revised 11 April 2022; Accepted 15 April 2022; Published 21 May 2022

Academic Editor: Man Fai Leung

Copyright © 2022 Dashan Jiang et al. This is an open access article distributed under the Creative Commons Attribution License, which permits unrestricted use, distribution, and reproduction in any medium, provided the original work is properly cited.

With the rapid development of modern information technology, students' education and computer technology begin to blend, and the modern teaching mode is quite different from the traditional education mode known in the past. In view of the current college English teaching in the information age, this study puts forward the way of integrating computer information technology with college English teaching, improves MLP algorithm, puts forward a new artificial intelligence algorithm, improves its calculation efficiency, and uses the optimized GA-MLP-NN (Genetic Neural Network Algorithm for the Multilayer Perceptron) algorithm in college students' oral correction program. Firstly, GA-MLP-NN algorithm is used to optimize college English teaching so that more complex structures can be learned and dealt with. Incremental hidden layer unit neural network is added, which makes the operation more accurate based on S-type recursive function. Then, the oral English system is established, using the GA-MLP-NN neural network model. Finally, we evaluate the parameters of the model, design a comparative experiment and a questionnaire survey to verify the rationality and feasibility of the guess, which proves that this method can deal with more complex programs, and make students learn English more handy and close to students' needs by using computer technology.

## 1. Introduction

Due to the development of computer information technology, many traditional industry models have undergone tremendous changes. Traditional English teaching methods are gradually declining in the era of rapid development of big data industry. Traditional English teaching is facing great challenges, which are both a crisis and a challenge for the traditional teaching mode. In recent decades, computer deep learning can imitate the learning process of the human brain and obtain the inherent characteristics and natural rules of data such as sound, video, and image, which can be applied to all walks of life. Ding et al. [1] have designed a deep learning method which can be used to assist and improve college English online teaching by combining the multilayer neural network model with K-means clustering algorithm. If we want to improve the level of college English teaching, we cannot avoid creating a good oral environment. Therefore,

the spoken English dialogue system based on computer big data analysis and artificial neural network is very important. Liu [2] proposed an evaluation model connecting specific time-delay neural network (TDNN) layers by previous feedback. By using different feature representations of each word, abundant information can be obtained and the number of model parameters can be reduced. In oral English teaching, it is inevitable to detect oral grammar. In college English grammar detection, oral grammar is the content with the highest error rate. Du [3] proposed in the research of intelligent error correction of college oral English grammar based on GA-MLP-NN algorithm that compared with the traditional multilayer perceptron prediction, the optimized algorithm significantly improves the running efficiency of the model and shortens the prediction time. During the university period, in the large-scale classroom teaching, teachers often cannot interact effectively with every student, which leads to a significant reduction in teaching

effect. Therefore, relevant research and investigation have been done. Wang et al. [4] found that PDA classroom teaching can achieve a central balance between teachers and classmates, improve the interaction between teachers and classmates, and increase students' absorption of knowledge. Yang et al. [5] found that there are still many problems in English teaching mode based on multisource information fusion algorithm through the investigation of college language teaching. Tian [6] found that the intervention of multimedia makes educational resources richer, pays more attention to students' status, and improves educational management. Hu [7] pointed out that, after the integration of computer information technology and foreign teachers' courses, traditional teaching elements (textbooks and contents) were replaced by new teaching technologies (multimedia and network programs). Nael et al. [8] put forward AraScore. Through empirical research and investigation using the baseline model, RNN, LSTM, and other language models, it is found that using the ELECTRA language model to realize the task at hand in language teaching is the best system, which highlights the powerful performance of computer deep learning in language teaching. Giosue et al. [9] introduced an ATE system based on RNN, which was tested in Italian and English, and concluded that it can solve the complexity evaluation problem of different languages. In the overall framework of English learning, considering the integrity and overall situation of learning, Wu et al. [10] refer to the combination of Einstein's cognition, emotion, behavior, and attitude with modern classroom teaching to form an overall goal classification framework suitable for university teaching mode. Alshara et al. [11] apply the interdisciplinary learning model in SEE portal to computer network and education, which is used to overcome the teaching and island model, so that software engineers can communicate with relevant knowledge in the field of education. Based on deep learning, Yan and Dong [12] analyzed iSmart platform and offline classroom and constructed a teaching mode combining the two. Brauer et al. [13], in the HCI study, elucidate Web-based software application interactions between Web analysts and users. Waiganjo [14] has studied the views and attitudes of integrating information technology into teaching in rural areas. The government should strengthen ICT construction and strengthen the popularization of information and communication technology in schools. Ruby and David [15] provide a way to make English learning learn and practice in an unknowable environment, using NLN to provide standards. Li [16] explores the hybrid model of college English based on modern educational technology and computer technology. Yuan [17] analyzes the connotation of artificial intelligence technology and the technical problems in ETIP and gathers contemporary information to prove that the construction of college English education needs to follow the traditional educational concept and add artificial intelligence technology to the educational mode. Haet al. [18] studied the attitudes and thoughts of students and teachers on oral corrective feedback and discussed the influence of language education, teachers, and project designers on teaching. Mohammad and Junji [19] developed the application of Wordhyve according

to image memory, which can regard learning experience as a trigger to enhance the vocabulary of a second foreign language and help users learn a language better by analyzing logs. Zhang [20] proposes an innovative teaching model of college English reverse classroom through intermediary intelligent adjustment algorithm [21], in which virtual multimedia teaching [22] needs to be used to replace outdated technology and specify specific teaching schemes related to it. Yanhong YUE [23] established a quality-oriented hierarchical process model of educational evaluation analysis for college English teaching reform [24]. Pemba et al. designed software, which can provide learning interaction, arrange small learning tasks that are more suitable for users' English, and reflect the evaluation to the background analysis of learning. Song [25] proposed that the English multimedia teaching mode will become an inevitable trend of English teaching reform and development. It is necessary to stimulate students' learning winter and learn more independently; the principle of taking teachers as the leading factor and students as the main body avoids repetition and improves classroom teaching efficiency. In the related literature description, the corresponding intelligent methods are generally used to realize the application and analysis of spoken English, and the corresponding neural network is also used to realize the detection and application of English grammar in order to improve the recognition rate. There is also an analysis of the corresponding English application scenarios, and relevant applications are carried out through the curriculum characteristics.

## 2. Experimental Model

*2.1. Computer Intelligent Computing and Neuroscience.* Neural network can be applied to computer image analysis and the regression method can be used to make machines imitate and learn human computation process. MLP algorithm is one of many algorithms about artificial intelligence. In machine learning, MLP algorithm can improve the model's data error and achieve comprehensive optimization performance. However, there are also obvious drawbacks. The MLP calculation is too inefficient, resulting in a particularly slow machine learning and training process. In the traditional multilayer perceptron model, the operation on single data cannot achieve the desired effect, as shown in Figure 1.

In order to solve the problem of low computational efficiency of MLP algorithm, we propose another artificial intelligence algorithm. On the basis of MLP algorithm, the number of nodes of network nerves is improved when working cooperatively at different levels. The optimized GA-MLP-NN algorithm can complete the function of multidirectional computation at the same time, which greatly improves the efficiency of the model in machine learning training and greatly saves time and cost.

*2.2. GA-MLP-NN Arithmetic.* GA-MLP-NN algorithm [26, 27] is a research technique for oral grammar correction. It is one of the artificial intelligence algorithms that can deal



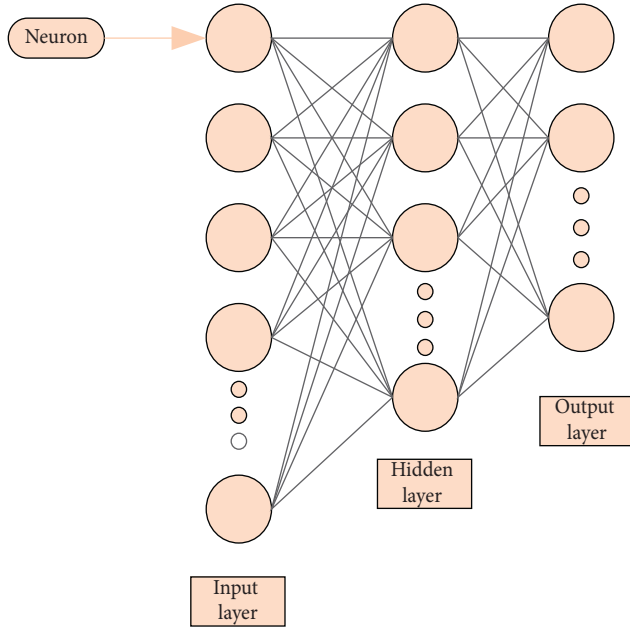


FIGURE 1: Network structure block diagram of multilayer perceptron system.

with a large amount of data and information, realize multinode output, and solve practical problems:

$$A = f(W_1^T * X), \quad (1)$$

$$Y = f(W_2^T * A). \quad (2)$$

The purpose of training is to reduce the fault tolerance of data and achieve the ultimate goal of optimization. In the training process, only the weights need to be adjusted out of the appropriate range to achieve the goal.

Then, the minimum distance solution under the hidden layer can be obtained:

$$W_2^T * R - S_2 = \min. \quad (3)$$

Using the transfer function in the model, we can determine the range of parameter values for matrix R:

$$W_2^T * \Delta R - (S - W_2^T * A)_2 = \min. \quad (4)$$

The linear regression model used in the experimental analysis is as follows:

$$W_T = [W_1 W], \quad (5)$$

$$X_r = [XR], \quad (6)$$

$$Y = a + bX + \varepsilon. \quad (7)$$

The formula includes constant term, linear regression coefficient, and error value. To sum up, it is the function variables that have a great influence on the whole expected experimental data. For the significance test of integrity, the required calculation formula is as follows:

$$ESS = \sum (\hat{Y}_i - \bar{Y})^2, \quad (8)$$

$$RSS = \sum (Y_i - \hat{Y})^2. \quad (9)$$

The entire multilayer perceptron of the model needs to insert the known variables into the activation function, and the expected result factor after the change is obtained through the control of the model function. The formula for the activation function can be expressed as follows:

$$t = \frac{R}{\sqrt{(1 - R^2)(n - 2)}}. \quad (10)$$

The result can be expressed as

$$\phi(v) = \tanh(v), \quad (11)$$

$$\hat{y} = \tanh\left(d \sum_{d=1, n=1}^n w_d x_n\right). \quad (12)$$

The above model is studied by adjusting the range of weight parameters in the function, and the final result is approximate to the actual data:

$$w_j^{k+1} = w_j^k + \beta(y_i - y_i^k)x_{ij}. \quad (13)$$

If the experimental results are close to or consistent with the expected results, the current values can continue to be used; otherwise, the weights and thresholds need to be updated for adjustment. In this model, we set two variables, which are the total number of data syntax and the syntax error correction rate:

$$h_t = f(h_{t-1}, x_t), \quad (14)$$

$$C = q(h_1, h_2, h_3, \dots, h_t). \quad (15)$$

Through the decoding function of the model, the data variables can be decoded, and the next syntax can be corrected by using the obtained results.

In this process, the required calculation formula is as follows:

$$y_t = \arg \max P(y_t), \quad (16)$$

$$y_t = \prod_{t=1}^T P(y_t | \{y_1, y_2, \dots, y_{t-1}\}, C). \quad (17)$$

In the whole model, because the data length is too long, it may lead to information loss and other problems, which is not conducive to computer model calculation. Therefore, we introduce an intelligent learning system transformation mechanism to solve such problems. The model formula is as follows:

$$h_t' = f(h_{t-1}', y_{t-1}, C). \quad (18)$$

**2.3. TDNN Model.** For college oral English teaching, we also propose another spoken English recognition model, which is an evaluation estimation model connected with

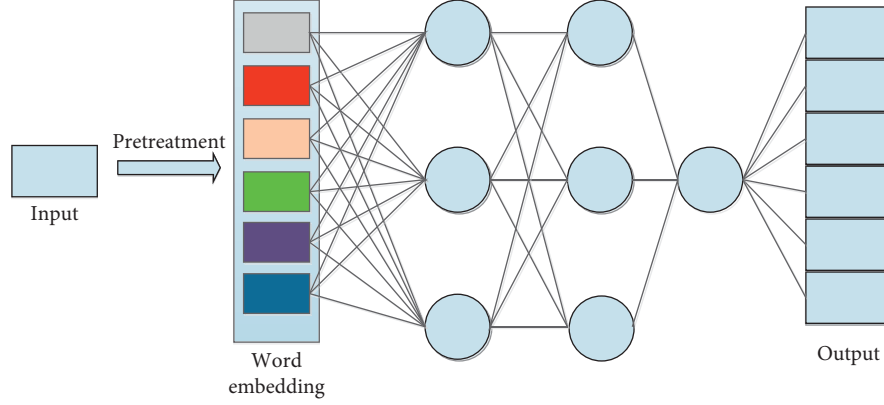


FIGURE 2: Structure diagram of the word embedding model system of neural network.

specific TDNN levels by previous feedback. The main way is to obtain more abundant context information according to the different performance characteristics of different target words in the TDNN layer, so as to reduce the number of model parameters, as shown in Figure 2 and Figure 3.

In Figure 3,  $T$  represents time and  $X$  represents the data state when the system enters the hidden layer at time  $H$ . The matrices  $W$ ,  $V$ , and  $N$  represent the weight matrix, and its calculation formula is as follows:

$$h_t = \text{fuc}(Uh_{t-1} + Wx_t + b), \quad (19)$$

$$O_t = Vh_t, \quad (20)$$

$$C_t^* = \tanh(W_c x_t + U_c h_{t-1} + b_c), \quad (21)$$

$$c_t = f_t \circ c_{t-1} + i_t \circ c_t^*, \quad (22)$$

$$h_t = O_t \circ \tanh(C_t). \quad (23)$$

Among them,  $f_t$ ,  $i_t$ , and  $O_t$  are three valve controllers, and the valve control mechanism is a systematic method of information selection and differentiation. Its value range is between 0 and 1, so there is a certain information flow rate.  $D$  denotes the dot product operation of the matrix, and  $C$  is the time before the state of the memory cell.

In the literature on speech recognition, a time-delay neural network is proposed, which is a multilayer neural feedback system, and each layer has strong information extraction ability. In the process of machine learning, there is no need to mark and locate the learned ones. The training method of the neural network is backpropagation algorithm.

In the TDNN model, the model structure is similar to the traditional model, so the time complexity of a single convolution layer can be expressed as

$$\text{Time} \sim O(M^2 \times K^2 \times C_{in} \times C_{out}), \quad (24)$$

where  $M$  is the secondary side length of the feature graph output of each convolution kernel of the model and  $K$  is the main side length. As shown in the formula, enter  $C_{in}$ , output  $C_{out}$ , and convolution kernel  $K^2$  are three influencing factors that affect the feature properties of the feature map:

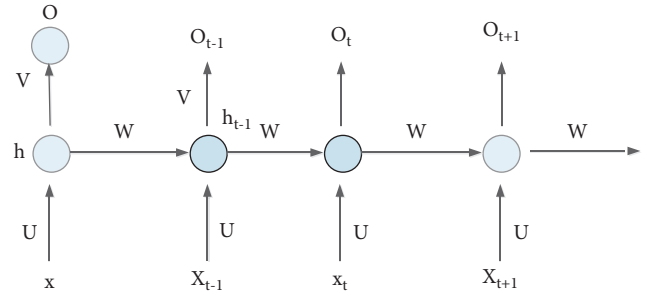


FIGURE 3: Single-layer RNN network structure diagram.

$$M = \frac{(X - K + 2 * \text{Padding})}{\text{Stride} + 1}, \quad (25)$$

$$\text{Time} \sim O\left(\sum_{\rho=1}^D M_{\rho}^2 \times K_{\rho}^2 \times C_{\rho-1} \times C_{\rho}\right), \quad (26)$$

$$\text{Space} \sim O\left(\sum_{\rho}^D K_{\rho}^2 \times C_{\rho-1} \times C_{\rho}\right). \quad (27)$$

In many NLP-related tasks, the current high-usage approach is to construct a data dictionary in the dataset, known as a dataset. Each id of the data dictionary corresponds to a word. Input different ids will be converted into word vector sets corresponding to their ids, and then, all vector sets will be spliced.  $W$  is the size of the spliced word window. Therefore, in sequence  $t$ , we should enter the following format:

$$E_t = [e_{t-w}, \dots, e_{t-1}, e_t, e_{t+1}, \dots, e_{t+w}]. \quad (28)$$

Finally, a more accurate linearized probability distribution is obtained by using the activation function of the last layer of the neural network layer. In this experiment, we used the following objective functions:

$$L = -\frac{1}{N} \sum_{t=1}^N \sum_{c=1}^C y_t, c \log \hat{y}_{t,c}. \quad (29)$$

Thus, although the traditional RNN network model can process sequence data, it also has the problem of insufficient

TABLE 1: Student performance evaluation table.

| Type      | Group              | Max score | Min score | Average score |
|-----------|--------------------|-----------|-----------|---------------|
| Listening | Experimental group | 98        | 82        | 88.3          |
|           | Control group      | 86        | 66        | 70.2          |
| Speaking  | Experimental group | 93        | 81        | 87.5          |
|           | Control group      | 83        | 64        | 70.35         |
| Reading   | Experimental group | 97        | 80        | 88.9          |
|           | Control group      | 80        | 63        | 76.2          |
| Writing   | Experimental group | 94        | 78        | 86.3          |
|           | Control group      | 73        | 46        | 66.19         |

TABLE 2: Questionnaire survey results.

| Type               | Contents of the survey  | Satisfaction (%) |
|--------------------|---|------------------|
| Experimental group | Is there a new understanding of the world in connection with the international community          | 73               |
| Control group      |   | 56               |
| Experimental group | Satisfaction with one's own progress after learning oral English, listening, reading, and writing | 85               |
| Control group      |   | 76               |
| Experimental group | Are you satisfied with your understanding of learning tasks                                       | 88               |
| Control group      |   | 69               |
| Experimental group | Satisfied with the diversity of English   | 82               |
| Control group      |   | 62               |

long-term memory. Therefore, the TDNN model proposed by us can realize the input sequence in time, which greatly solves the problem of insufficient memory. TDNN model is a model based on BACK SPREAD algorithm, which is a fast algorithm and makes every layer of TDNN model have abstraction ability.

### 3. Experimental Simulation

3.1. Investigation and Analysis of College English Online Teaching Mode Based on Deep Learning. In a Chinese university, two classes were selected. Before entering the school, their overall English level was the same, and they were instructed by the same teacher. The control class was mainly taught by the teacher face-to-face, and the other experimental class was mainly learned online.

We used the experimental control method to verify the reliability of this method according to the final score and questionnaire survey.

It can be seen from Table 1 and 2 that the application of computer information technology in college English learning can help students to improve their enthusiasm for English, help them to have a further understanding of English, improve the basic English literacy of common

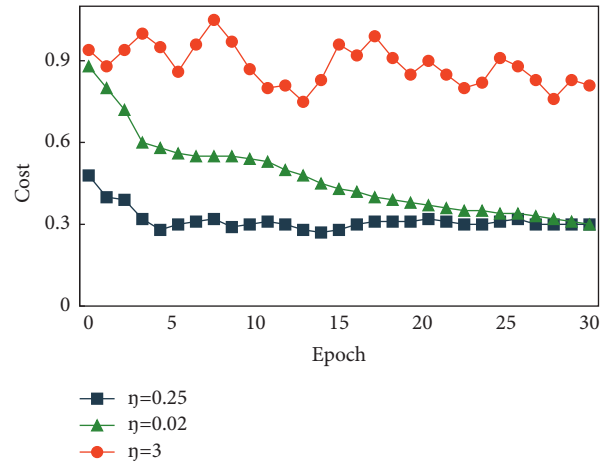


FIGURE 4: Test diagram of the first experiment.

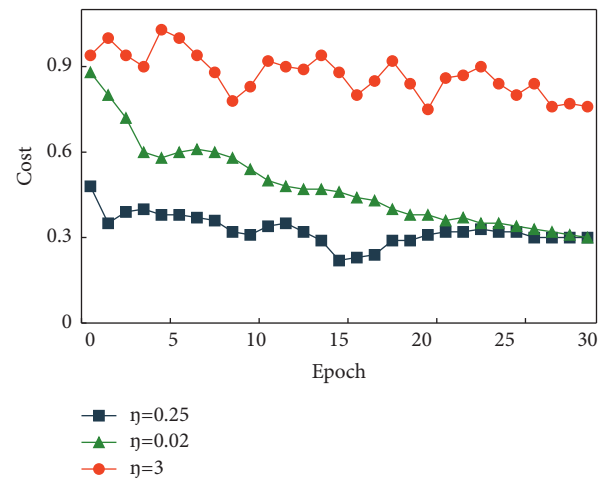


FIGURE 5: Test diagram of the second experiment.

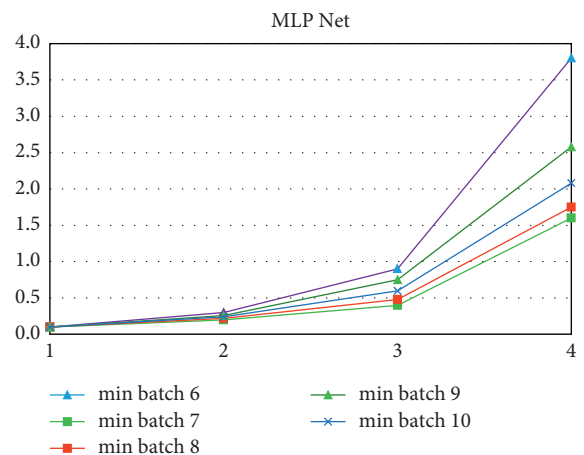


FIGURE 6: Gradient change diagram during MLP network training.

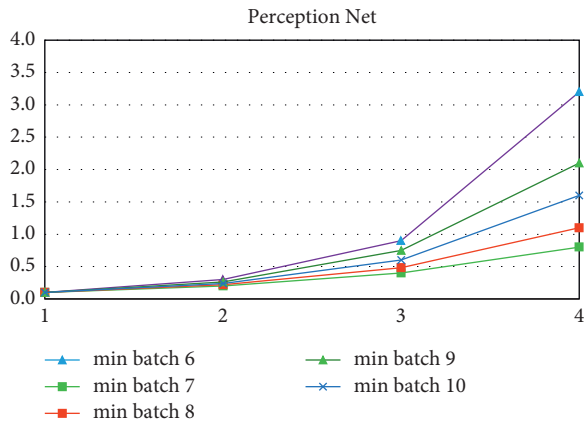


FIGURE 7: Gradient change diagram in the training process of perceptron network.

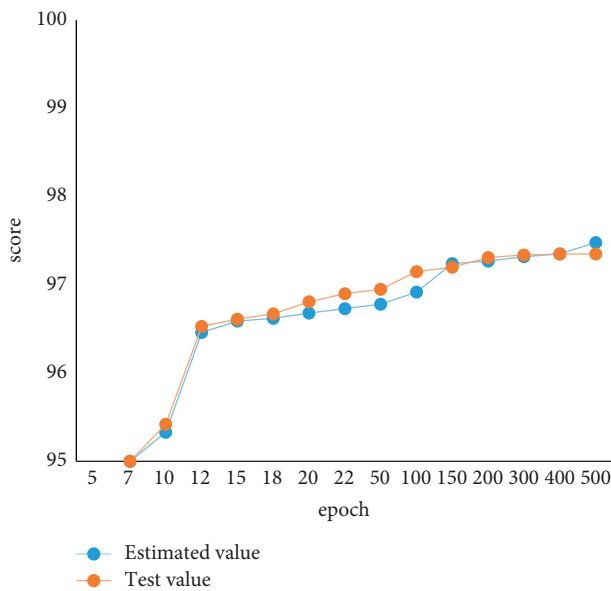


FIGURE 8: CNN gradient change diagram.

students, clarify the bad habits and tasks, and make students more targeted and clear when learning English.

3.2. *Experimental Comparison Diagram.* In order to reduce the error, we compare the learning parameters in MLP network and reduce the related neurons appropriately.

- (1) Influence curve (different learning rates on network convergence): SGD algorithm is used to train parameters. In the dataset, the gradient changes of perceptron training and MLP training are compared.
- (2) The gradient change diagram during the training process of perceptron network: CNN and MLP models are used to compare the experimental results in the verification set and dataset.
- (3) Gradient change diagram of MLP network during training.

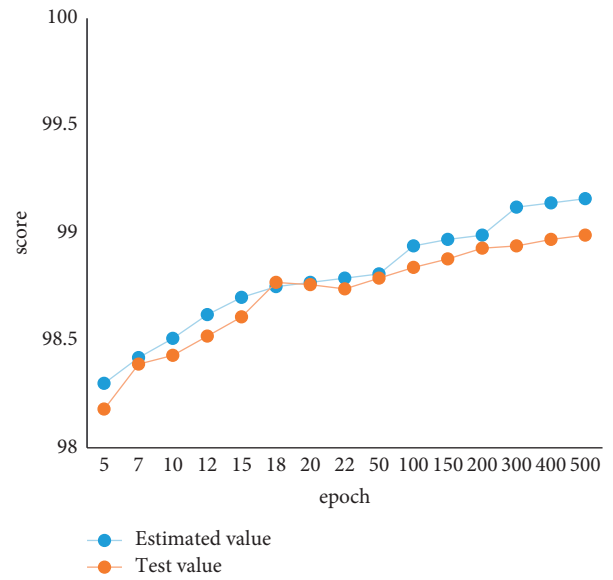


FIGURE 9: MLP gradient change diagram.

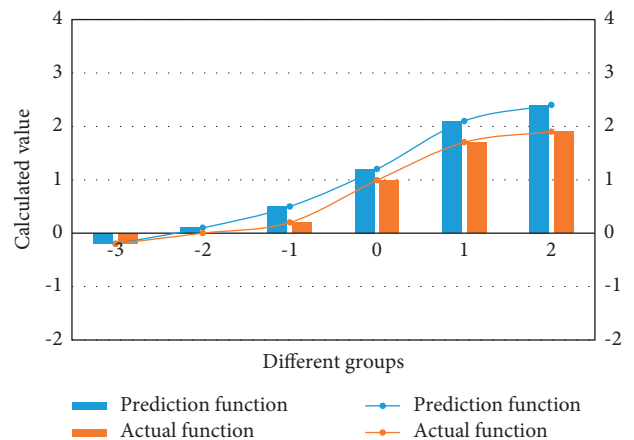


FIGURE 10: Column chart of S-type function prediction change.

Next, the recognition results of CNN and MLP on training set and test set are discussed and analyzed.

The data in Figure 4–9 show that it is useful to apply functions to deep learning and optimize the college students' English learning model. In the learning process, functions play a role and are effective for the blending of computer information technology and college English teaching.

3.3. *Optimization Effect.* By using progressive hidden layer element neural network, s-type recursive function is used to perform precise continuous operation. Using the weight matrix in each layer, the change of function value is predicted based on s-type function.

It can be seen from Figure 10 that the trend of this function is gradually rising, indicating that, under the traditional forward neural network, the operation of gradient function based on S-type will be more accurate. In order to improve the operation efficiency, the traditional S-type hidden layer unit neural network is increased, and the

number of layers and nodes in it is gradually increased, so the algorithm of GA-MLP-NN is optimized.

#### 4. Conclusion

This study integrates computer information technology into college English teaching and proposes an optimized artificial intelligence algorithm. Ga-mlp-nn algorithm in spoken English correction program is optimized, and multilevel precise continuous operation is carried out by using progressive hidden layer unit neural network and S-type recursive function. The neural network model is constructed and evaluated. In order to establish a more complete learning system, experimental verification is designed to make it more convenient for students to learn English in college.

#### Data Availability

The experimental data used to support the findings of this study are available from the corresponding author upon request.

#### Conflicts of Interest

The authors declare that they have no conflicts of interest regarding this work.

#### References

- [1] H. Ding, Y. Chen, and L. Wang, "College English online teaching model based on deep learning," *Hindawi Security and Communication Networks*, vol. 2021, Article ID 8919320, 11 pages, 2021.
- [2] H. Liu, "College oral English teaching reform driven by big data and deep neural network technology," *Wireless Communications and Mobile Computing*, vol. 2021, Article ID 8389469, 8 pages, 2021.
- [3] Y. Du, "Intelligent error correction of college English spoken grammar based on the GMLP-NN algorithm," *Hindawi-Computational Intelligence and Neuroscience*, vol. 2021, Article ID 7371416, 9 pages, 2021.
- [4] H. Wang, H. Fu, and D. Wang, "Research on teaching practice of college English PAD class with multi-modality plus mutual evaluation," *Creative Education*, vol. 12, no. 05, pp. 966–973, 2021.
- [5] B. Yang, L. Mou, and H. Tang, "Research on higher English internationalization education model and evaluation index system based on multi-source information fusion," *Computational Intelligence and Neuroscience*, vol. 2021, Article ID 1599007, 8 pages, 2021.
- [6] Z. Tian, "Research on optimization of college English classroom teaching based on computer network environment," *Journal of Physics: Conference Series*, vol. 1648, no. 4, Article ID 042030, 2020.
- [7] L. Hu, *Revista Ibérica de Sistemas e Tecnologias de Informação*, pp. 243–253, Lousada Iss. 17A, Lousada, Portugal, 2016.
- [8] O. Nael, Y. ELmanyalawy, and N. Sharaf, "AraScore: a deep learning-based system for Arabic short answer scoring," *Array*, vol. 13, Article ID 100109, 2022.
- [9] L. B. Giosue, P. Giovanni, and S. Daniele, "DeepEva: a deep neural network architecture for assessing sentence complexity in Italian and English languages," *Array*, vol. 12, Article ID 100097, 2021.
- [10] H. Wu, Y. Li, and S. Dong, "A feasibility data study on the necessity of ideological and political education in college English courses based on computer technology," *Journal of Physics: Conference Series*, vol. 1578, no. 1, Article ID 012049, 2020.
- [11] O. K. Alshara and M. Ibrahim, "Business Integration Using the Interdisciplinary Project Based Learning Model (IPBL)," in *Human Interface and the Management of Information*, M. J. Smith and G. Salvendy, Eds., Springer-Verlag, Berlin, Germany, 2007pp. 823–833, Lecture Notes in Computer Science.
- [12] J.-Y. Yan and H. Dong, "A study on the "iSmart + offline classroom" teaching method based on deep learning in college English," *Journal of Changji University*, vol. 92-94, no. 1, 2019.
- [13] C. Brauer, D. Reischer, and F. Mödritscher, "What Web Analysts Can Do for Human-Computer Interaction?," in *HCI in Business*, F. F.-H. Nah, Ed., Springer International Publishing, New York City, NY, USA, 2014pp. 471–481, Lecture Notes in Computer Science.
- [14] I. N. Waiganjo, "Teachers' perceptions and use of information and communication technology in teaching and learning: kajimi circuit, kavango west, Namibia," *OALib*, vol. 08, no. 3, pp. 1–21, 2021.
- [15] I. Ruby and S. David, "Natural-Language Neutrality in Programming Languages: Bridging the Knowledge Divide in Software Engineering," in *Learning and Collaboration Technologies*, P. Zaphiris and A. Ioannou, Eds., Springer International Publishing, New York City, NY, USA, 2016pp. 628–638, Lecture Notes in Computer Science.
- [16] Y. Li, "Research on the construction of college English mixed teaching model based on modern educational technology and computer technology," *Journal of Physics: Conference Series*, vol. 1915, no. 2, Article ID 022091, 2021.
- [17] X. Yuan, "Design of college English teaching information platform based on artificial intelligence technology," *Journal of Physics: Conference Series*, vol. 1852, no. 2, Article ID 022031, 2021.
- [18] X. V. Ha, L. T. Nguyen, and B. P. Hung, "Oral corrective feedback in English as a foreign language classrooms: a teaching and learning perspective," *Heliyon*, vol. 7, no. 7, Article ID e07550, 2021.
- [19] N. H. Mohammad, W. Junji, Wordhyve: "a context-aware language learning app for vocabulary enhancement through images and learning contexts," *Procedia Computer Science*, vol. 192, pp. 3432–3439, 2021.
- [20] Y. Zhang, "Innovative development of college English education based on the media information," *Journal of Physics: Conference Series*, vol. 1992, no. 3, Article ID 032116, 1992.
- [21] Z. Xiu-miao and Y. Jun, "Reflection and exploration of interactive teaching in college English intensive reading classroom of newly built universities under network environment in minority areas," in *Proceedings of the 2011 international conference on future computer science and education*, pp. 513–517, Xi'an, China, August 2011.
- [22] C. Macdonald and M. Pinheiro, "Working in the zone of proximal development (zpd) in the English classroom: a case study on the teaching of literature," *Journal for Language Teaching*, vol. 49, no. 1, pp. 141–1342, 2015.
- [23] Y. Yue, "The AHP model of evaluation on quality-oriented education in college English teaching," *International Journal of Education and Management Engineering*, vol. 2, no. 5, pp. 37–42, 2012.

- [24] D. Pemba, V. Mann, T. Sarkar, and K. Azartash, "Learning English in China: a tablet-based app using the voices of native speakers," *Open Journal of Social Sciences*, vol. 04, no. 07, pp. 85–91, 2016.
- [25] C. Song, "College English teaching based on information technology -- exploration of English multimedia teaching mode based on computer and network," *Journal of Changchun University of Science and Technology (Social Science Edition)*, vol. 23, no. 1, 2010.
- [26] R. Akkaya, A. A. Kulaksız, and Ö. Aydoğdu, "DSP implementation of a PV system with GA-MLP-NN based MPPT controller supplying BLDC motor drive," *Energy Conversion and Management*, vol. 48, no. 1, pp. 210–218, 2007.
- [27] D. K. Choubey, S. Paul, and S. Paul, "GA\_MLP NN: a hybrid intelligent system for diabetes disease diagnosis," *International Journal of Intelligent Systems and Applications*, vol. 8, no. 1, pp. 49–59, 2016.

## Research Article

# Research on National Costume Design Based on Virtual Reality Technology

Chunnan Cao  and Yiping Gao 

*Qiongtai Normal University College of Fine Arts, Haikou, Hainan 571100, China*

Correspondence should be addressed to Chunnan Cao; 125411058@qq.com

Received 14 March 2022; Revised 8 April 2022; Accepted 13 April 2022; Published 20 May 2022

Academic Editor: Hangjun Che

Copyright © 2022 Chunnan Cao and Yiping Gao. This is an open access article distributed under the Creative Commons Attribution License, which permits unrestricted use, distribution, and reproduction in any medium, provided the original work is properly cited.

Cheongsam has the unique costume culture characteristics of the Chinese nation and is a classic style of traditional Chinese costumes. At the same time, with the rapid development of science and technology, 3D virtual technology plays an increasingly important role in the garment intelligent manufacturing industry. Therefore, how to combine 3D virtual technology with the development of women's cheongsam clothing products is of great significance, which can overcome the limitations of time and space and effectively improve the efficiency of clothing pattern design. To solve this problem, a design method for national costume based on virtual reality technology is proposed. First of all, the modeling and structural characteristics of cheongsam are analyzed. Secondly, different curve fitting methods are applied to human body feature recognition, and cubic polynomial fitting is selected to complete the feature recognition of the human body model in a virtual environment. Then, in order to prevent the penetration between clothing and the human body, the collision detection function based on the AABB bounding box is added, and a method based on linear sensitivity is used to map 2D to 3D. Finally, the model of a cheongsam costume is created by using the clothing simulation Marvelous Designer software, and the effectiveness of the proposed virtual cheongsam costume simulation design method is verified by subjective evaluation indexes.

## 1. Introduction

The traditional cheongsam in the Republic of China plays an important role in the history of Chinese national costume. It reflects the evolution from tradition to modernity in the modeling structure of Chinese traditional national costume and is a typical representative of Chinese women's traditional costume. With the progress of the times, people pay more attention to the cultural heritage of costumes, and national costumes gradually show vigorous vitality. In recent years, the booming development of the Hanfu industry and high-end customization industry in China is the best example. However, with the popularity of COVID-19 in the world, fashion designers cannot communicate face-to-face with customers in the real world. In this situation, people have an unprecedented demand for virtual fitting and virtual dynamic display of clothing [1–6].

For fashion designers, reliable and real 3D clothing simulation can accurately convey the details and wearing

styles of clothing and make consumers more intuitive to understanding the shape of clothing. Clothing manufacturing mode based on a 3D model is also helpful for enterprises to realize flexible production and reduce inventory pressure and capital chain tension. For consumers, a more intuitive clothing display can help them accurately judge whether the clothing is suitable for their own conditions, which greatly promotes clothing consumption [7–10]. For schools, 3D clothing simulation can serve teaching well. For the museum, 3D costume simulation can help the inheritance and development of traditional national costume culture.

In the aspect of 3D modeling, Poser, Marvelous Designer (MD), CLO3D, Style 3D, and other software which are more suitable for human body modeling and virtual clothing design simulation in the clothing industry have been born since the traditional Maya and 3Dmax [11–14]. In the field of anthropometry, the popularization and application of phase grating technology, 3d scanner, and reverse engineering

technology have laid a good foundation for accurate anthropometry [15–17]. In two-dimensional plate making, pattern design, and fabric design, various advanced systems also provide support for small-scale, flexible customized production of clothing. Each link of virtual clothing design can be completed more accurately and quickly by new technology step by step. Virtual garment last section system can greatly reduce the cycle and cost of garment design. The key problems of virtual clothing design can be classified into three aspects: feature recognition of the human body model, real-time interaction, and fabric model. This paper mainly studies the first two problems.

First of all, the recognition of human body features is a key link in the process of virtual clothing design. The accuracy of feature point recognition is directly related to the progress of digital clothing research and development and the quality of products. How to obtain the position of human feature points accurately and quickly at the same time with low cost is the research content of many scholars and scientific research institutions. Li et al. [18] used the improved Canny algorithm to identify feature points and combined it with subjective artificial marking points to accurately identify human feature points. Zhang et al. [19] proposed to recognize 3D human feature points by a random forest algorithm. Zou et al. [20] proposed to obtain human body parameters by fitting the distance between feature points. At present, the types of functions that can be used for curve fitting include polynomial, exponential function, parametric spline curve, B spline curve, Gaussian function, Fourier function, and interpolation function. In this paper, different curve fitting methods are applied to human feature recognition. Through the comparison of different effects, the advantages, disadvantages, and adaptation surfaces of different ways are discussed, and finally, cubic polynomial fitting is selected for human feature recognition.

Secondly, the real-time interaction between the human body and clothing is another difficult problem that clothing design needs to face in the virtual environment. In order to avoid the situation where the cloth penetrates the human body when the cloth collides with the human body, it is necessary to add real-time interaction of collision detection and response. Park et al. [21] combined multilevel modeling methods to improve the accuracy of collision detection and solved the problem of low collision detection efficiency caused by the complexity of multilevel modeling. Nakai et al. [22] used a two-stage filtering algorithm to realize the continuous collision detection of objects, aiming at detecting the continuous collision state and collision feedback so as to improve the detection efficiency of continuous collision of objects.

Therefore, aiming at these two problems, this paper designs a cheongsam clothing simulation method based on virtual reality technology. Due to the powerful technology of MD clothing simulation, it is gradually being favored by fashion designers. As a new 3D clothing software, MD has plenty of room for innovation and development in the clothing field. Therefore, this research will use the Marvelous Designer 9 platform and Unity engine to realize virtual clothing design. The main work includes the following: (1)

Aiming at the problem of human model recognition, different curve fitting methods are applied to human feature recognition, and different effects are compared; (2) Aiming at the real-time interaction problem, the collision detection method based on AABB bounding box is adopted to prevent the penetration phenomenon between clothing and the human body, and a method based on linear sensitivity is adopted to map 2D to 3D, which can more truly simulate the influence of mouse drag on 3D clothing state.

The rest of the paper is organized as follows: In Section 2, the structural analysis of traditional cheongsam clothing is studied in detail, while Section 3 provides the human feature point recognition in virtual environments. Section 4 provides the collision detection techniques in virtual interaction. Section 5 provides the virtual clothing design presentation and evaluation. Finally, the paper is concluded in Section 5.

## 2. Structural Analysis of Traditional Cheongsam Clothing

The modeling structure features of cheongsam are analyzed, including cheongsam standup, cheongsam sleeve, cheongsam body piece, and cheongsam slit. First of all, whether it is a traditional cheongsam or a modern cheongsam, standup up is its representative feature and an important modeling language of cheongsam. Standup is a subtle detail that plays a finishing role in the whole cheongsam. By measuring the standing up of 25 cheongsams in the Republic of China, it is found that the circumference of the standing up is about 34 cm, and the maximum value is no more than 37 mm. The greater the rise of the standup, the tighter the standup will be to the top of the neck, creating a small amount of space, which is not conducive to human movement. Therefore, there is a certain limit to the amount of rise, generally between 1 cm and 2.5 cm. In short, the internal structural features of the cheongsam standup, although varying slightly, are directly related to the modeling features of the collar, reflecting people's dress code and aesthetic requirements.

Secondly, the sleeves of the cheongsam are roughly divided from a structural perspective into loose sleeves, modest sleeves, and semiwestern sleeves. As the sleeves and body pieces of the traditional cheongsam are flat, this shape requires that the sleeves and the body piece of the garment must become a single unit.

The fabric of the cheongsam in the Republican period was mainly silk fabric, which was soft and delicate and not easy to fix when cutting. In order to ensure the accuracy of the values when cutting, a two-dimensional flat structure was adopted. The front and back body is symmetrical in the horizontal direction with the shoulder and sleeve line, and the left and right body are symmetrical in the vertical direction with the front and back centerline.

Finally, in terms of construction, the slash is mainly to facilitate the body's movement. The height of the slash depends on the length of the cheongsam and the distance that the legs can travel when the body is in motion. The slash does not need to be too high to allow for movement.



Depending on the height of the hemline, the cheongsam can be divided into long and short cheongsams, as shown in Figure 1.

### 3. Human Feature Point Recognition in Virtual Environments

*3.1. Experimental Analysis of Human Bust Line Curve Fitting.* In the process of garment design and manufacturing, the bust line is a key part of human body shape analysis, and the curve structure is complex and difficult to fit, so the right section of the 160/84A bust line is selected as the experimental object for curve fitting in this paper. By comparing the fitting effects of different fitting methods, the fitting equations suitable for calculating the curvature and circumference of the human body at a later stage are sought [23–25].

In terms of the selection of the fitted functions, the spline curve, although a good fit, has a large number of equations and high complexity, so the spline curve was not part of the examination for this experiment. The types of functions finally chosen for the experiment were polynomial, Gaussian, sine, and Fourier functions. Due to the relatively even distribution of the point cloud data, the bust line was divided roughly equally into 10 segments, the effect of which is shown in Figure 2.

In this experiment, 12 fitting methods (4 functions, multiple orders) were applied to the 10-segment bust sample data for a total of 140 fitting trials, and the accuracy of each order of the different fitting functions is shown in Table 1.

The polynomial of the 3rd order was not only fitted with an accuracy mostly above 0.99 but also with a relatively simple equation and a small number of parameters, making it easy to carry out the subsequent derivative integration operation. In combination with the analysis of human characteristics in the subsequent operation, the amount of data selected was moderate and evenly distributed, so the final choice was to fit a 3rd order polynomial for the calculation of curvature, tangent point, slope, arc length, etc.

*3.2. Human Feature Point Localisation in Virtual Environments.* There is a certain variability between people because of regional differences caused by different growing environments, height differences caused by different age stages, and the influence of genetic material on human body shape. The object of this research is the individualized female body shape in the production of clothing design. For the identification of the main feature points, firstly, according to the proportional relationship between human feature points and height (assuming a height of 1.00), the human torso is divided into regions consisting of the neck, shoulders, underarms, chest, waist, and hips. For computational convenience, the three-dimensional human body is projected onto the YZ and XZ planes in this paper.

*3.2.1. Breast Point (BP).* The BP is the highest point of the breast and is the reference point for measuring bust circumference and one of the most important reference points

in garment construction. The absolute value of the coordinate  $x$  is obtained from the data of the gallery in the area where the breast point is located on the side view of the body. The point with the largest absolute value is then used as the BP, so the detection area  $\Omega_{BP}$  for the BP can be expressed as follows:

$$\Omega_{BP} = \{P \in G_{ZX} | 0.67H < z_p < 0.77H\}, \quad (1)$$

where  $G_{ZX}$  denotes the set of all points on the chest in the side view and  $H$  denotes height.

*3.2.2. Scapular Point (SP).* The SP is the most convex point of the human scapula and is the key point of the posterior garment piece. In the real human body, it has a more ambiguous amount of projection compared to the BP point and is more difficult to locate. It is analyzed by means of the coordinates of the 3D human body point cloud data. As the measurement unit is millimeters, even small bumps can cause significant changes in the coordinates. The detection area  $\Omega_{SP}$  of the SP can be expressed as follows:

$$\Omega_{SP} = \{P \in G_{ZX} | 0.70H < z_p < 0.80H\}. \quad (2)$$

First extract the gurney data for the region, i.e., extract the data with the smallest  $x$ -value for each layer on the region in the side view. As with BP, for the obtained human back corridor data, the absolute value of each coordinate  $x$  is found, and the maximum value is selected as the SP.

*3.2.3. Posterior Neck Point (BNP).* The BNP is the seventh cervical protrusion point and is the reference point for measuring dorsal length. This point is highlighted when the neck is bent forward. This effect is particularly evident in the 3D body point cloud data map. The detection area  $\Omega_{BNP}$  of the BNP can be represented as follows:

$$\Omega_{BNP} = \{P \in G_{ZX} | 0.81H < z_p < 0.91H\}. \quad (3)$$

*3.2.4. Side Waist Node (SWP).* The SWP is located in the middle of the side waist area of the body. It is the division between the front waist and the back waist and is also the reference point for measuring the size of the side seam of the garment. It is in the waist area of the front view of the body and has a distinctive concave feature. The detection area  $\Omega_{SWP}$  of the SWP can be expressed as follows:

$$\Omega_{SWP} = \{P \in G_{zy} | 0.58H < z_p < 0.68H\}. \quad (4)$$

*3.2.5. Side Neck Point (SNP).* The SNP is at the intersection of the anterior aspect of the trapezius muscle of the neck with the shoulder. The curvature of the data of the rotunda on the front view of the body in the area where the SNP is located is found and the point of maximum curvature is found as the SNP. The detection area  $\Omega_{SNP}$  of the SNP can be expressed as follows:



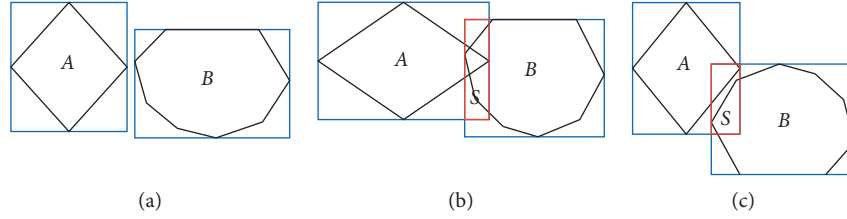


FIGURE 3: AABB enclosure collision detection method. (a) No crossing and no collision, (b) crossing and collision, and (c) crossing and no collision.

$$\Omega_{\text{SNP}} = \{P \in G_{zy} | 0.80H < z_p < 0.90H\}. \quad (5)$$

The Cftool tool in the Matlab toolbox was used to perform the 3-polynomial fit. To facilitate the fit, the  $z$ -coordinate values were used as the horizontal coordinates and the  $y$ -coordinate values were used as the vertical coordinates in the SNP fit.

#### 4. Collision Detection Techniques in Virtual Interaction

**4.1. Enclosure Intersection for Collision Detection.** In order to avoid the situation where the fabric penetrates the body when it is colliding with it, collision detection is incorporated into the virtual simulation process. Collision detection in virtual reality generally uses the method of enclosure [26]. Figure 3 shows the AABB fenestration collision detection method.

Figure 3 has 2 objects A and B. The objects are projected onto the 2D plane as a rhombus and an octagon, respectively. The blue color indicates the enclosure of the 2 objects and the red S part indicates the intersection of the 2 enclosures. In Figure 3(a), there is no intersection between the enclosures of A and B. It is straightforward to decide that A and B will not collide. When object A in Figure 3(a) is rotated  $90^\circ$  clockwise to the state in Figure 3(b), there is an enclosure crossover S between A and B. In Figure 3(b), objects A and B collide, but the enclosure crossover does not necessarily mean that the 2 objects will collide. In Figure 3(c), A and B appear to be enclosed by the crossover S, but they do not collide. In summary, it is not possible to determine whether an object has collided based on the enclosure intersection alone, and further identification is required by other methods. In this paper, we take the enclosing intersection part as the starting point and perform mesh feature extraction on the enclosing intersection part.

#### 4.2. Mathematical Description of Object Collision Detection.

Let objects A and B in the enclosing intersection space.  $a_i$  and  $b_j$  denote the features of objects A and B, respectively.  $i$  takes the value  $[1, M]$  and  $j$  takes the value  $[1, N]$ .  $i$  and  $j$  denote the feature number of object A and the feature number of object B, respectively.  $M$  and  $N$  are the total number of features, respectively.  $F(p)$  is the set of distances of similar features of objects A and B. If  $F(p) \leq \delta$ , then it means that A and B will collide, where  $\delta$  is the collision threshold [27].

Assume that the velocity and position of an object have 2 components.

$$\begin{aligned} X &= \{X_a, X_b\} = \{(x_a, y_a, z_a), (x_b, y_b, z_b)\}, \\ V &= \{V_a, V_b\} = \{(v_{ax}, v_{ay}, v_{az}), (v_{bx}, v_{by}, v_{bz})\}. \end{aligned} \quad (6)$$

The fitness function can be expressed as follows:

$$F(X_a, X_b) = (x_a - x_b)^2 + (y_a - y_b)^2 + (z_a - z_b)^2. \quad (7)$$

After each update, the spatial distribution of the object's state is determined by both its velocity  $V$  and its position  $X$ .

#### 4.3. Collision Detection Based on AABB Bounding Boxes.

The bounding box technique is a common method for collision detection in virtual reality environments, with simple algorithms and fast detection speeds. Commonly used bounding boxes are bounding sphere, AABB and OBB.

The bounding sphere is used to enclose the object and is suitable for objects with rounded edges.

$$R = \{(x, y, z) | (x - O_x)^2 + (y - O_y)^2 + (z - O_z)^2 < r^2\}, \quad (8)$$

where the three-dimensional coordinates of the centre of the sphere are  $O_x = (x_{\max} + x_{\min})/2$ ,  $O_y = (y_{\max} + y_{\min})/2$ ,  $O_z = (z_{\max} + z_{\min})/2$  and the radius of the sphere is as follows:

$$r = \frac{1}{2} \sqrt{(x_{\max} - x_{\min})^2 + (y_{\max} - y_{\min})^2 + (z_{\max} - z_{\min})^2}, \quad (9)$$

where  $(x_{\min}, x_{\max})$ ,  $(y_{\min}, y_{\max})$  and  $(z_{\min}, z_{\max})$  represent the minimum and maximum values of the projection of all edge points of the object onto the  $x$ ,  $y$ , and  $z$  axes, respectively.

The AABB bounding box uses a rectangle parallel to the coordinate axes to enclose the object. The equation relating the center point of the rectangle to the radius is as follows:

$$R = \{(x, y, z) | x_c - x^2 \leq r_x, |y_c - y|^2 \leq r_y, |z_c - z|^2 \leq r_z\}, \quad (10)$$

where  $(x_c, y_c, z_c)$  is the 3D coordinate center of the bounding box.  $(r_x, r_y, r_z)$  is the 3D radius.

The OBB bounding box uses a hexahedral form for object bounding. Compared to spheres and AABB boxes, the OBB is able to surround objects more closely to their edges, with a mathematical representation of the region as follows:

TABLE 2: System development environment.

| System composition   | Specification parameter  |
|----------------------|--|
| Development platform | Windows 10   |
| Development tools    | Marvelous designer 9, Photoshop CC2017, Unity 2017.2.0f3, Visual studio 2017, MATLAB 2019b |
| Development language | C#, MATLAB   |
| Hardware environment | CPU: AMD ryzen 7 4800H with radeon graphics, GPU:NVIDIA GeForce RTX 2060, 2.90 GHz, 16.0GB |

$$R = \{O + ar_1v_1 + ar_2v_2 + ar_3v_3 | a, b, c \in (-1, 1)\}, \quad (11)$$

where  $O$  is the centre of the OBB.  $r_1$ ,  $r_2$  and  $r_3$  are the radii on the directional axes, respectively.  $v_1$ ,  $v_2$  and  $v_3$  are vectors orthogonal to each other and to the regular coordinate axes. Compared to the sphere and AABB, the OBB is slightly more complex to create and calculate than the sphere and AABB, although it can wrap around the edges of the object more closely. This paper uses the AABB to implement the bounding box for collision detection between the fabric and the human body.

**4.4. Interactive Mapping Based on Linear Sensitivity.** Most current virtual clothing systems use physical models for fabric simulation, requiring a large number of calculations to obtain the convergence process of the garment. Such calculations are more than computationally intensive, so the real-time simulation cannot be achieved when using physical modeling. In this paper, therefore, a linear sensitivity-based approach is used for 2D to 3D mapping.

In the determination of the garment model, it is assumed that the 2D garment piece is  $x$  and the 3D garment piece is  $X$ . Both can be represented using a mesh of  $n$  vertices. Setting  $F$  as the combined external force and  $Q$  as the combined internal force, the equations for the equilibrium forces on the virtual garment system are shown as follows:

$$R(x, X) = F(x, X) - Q(x, X) = 0. \quad (12)$$

The determination solution for this dynamic simulation method is very computationally intensive and time consuming. Sensitivity analysis is a frequently used analysis method in the engineering field and can be used to mathematically establish a sensitivity mapping function. The position of the mouse,  $\Delta x_{\text{mouse}}$ , is set as the independent variable and  $\Delta X$  represents the value of the function in the static draped state of the fabric. If the static function is set to be an approximately linear function, the derivative of the amount of change in mouse position can be used to derive the rate of change of the 3D fabric as the mouse moves.

$$\Delta X \approx \frac{\partial X}{\partial x_{\text{mouse}}} \Delta x_{\text{mouse}}. \quad (13)$$

The relationship between a change in the 3D fabric state and a change in the 2D garment mesh can be represented by

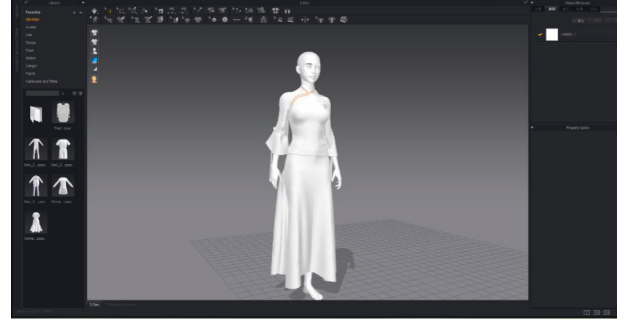


FIGURE 4: Interface of the virtual cheongsam costume design.

a sensitivity response. Setting  $S$  to denote linear sensitivity, the change from 2D to 3D can then be represented by an approximate linear mapping as follows:

$$\Delta X = S\Delta x = \left( \frac{\partial R}{\partial x} \Delta x \right) + \left( \frac{\partial R}{\partial X} \Delta X \right). \quad (14)$$

As can be seen, this method allows a more realistic simulation of the effect of mouse dragging on the state of a 3D costume, which is close to the real results.

## 5. Virtual Clothing Design Presentation and Evaluation

**5.1. Development Environment and Running Hardware Requirements.** The development environment of the virtual cheongsam costume design system and the hardware conditions for system operation are shown in Table 2. The hardware environment for system development is highly configured, which helps to meet the operation rate requirements for system development.

In the traditional garment industry model, when the customer proposes changes to the design, the designer needs to make repeated design changes and produce sample garments. This not only increases the turnaround time but is also a less than ideal user experience for the customer. The virtual cheongsam costume design system is able to recreate the design file according to the customer's needs and present it in real time. Virtual cheongsam costume design is the technology used to virtually try on cheongsams on the computer. The interface of the virtual cheongsam design is shown in Figure 4.

**5.2. Collision Detection Performance Analysis.** The collision detection of garments was performed on a set of 1000 human samples, with the number of sampled feature pairs being  $100 \times 100$ ,  $300 \times 300$ ,  $500 \times 500$ , and  $700 \times 700$ . The virtual cheongsam garment samples were simulated using the bounding sphere, OBB, and AABB algorithms, respectively. The detection accuracy RMSE and detection time of the three algorithms were compared, as shown in Table 3.

As can be seen from Table 3, the collision detection accuracy RMSE of all three algorithms decreases as the amount of sampled features increases. This is mainly because the more the amount of features sampled, the better the

TABLE 3: Collision detection time and RMSE under different sampling scales.

| Algorithm       | Characteristic quantity | RMSE       | Testing time (ms) |
|-----------------|-------------------------|------------|-------------------|
| Bounding sphere | 100*100                 | 8.163E-02  | 131.211           |
|                 | 300*300                 | 7.643 E-02 | 198.712           |
|                 | 500*500                 | 6.229 E-02 | 313.739           |
|                 | 700*700                 | 5.728 E-02 | 481.661           |
| OBB             | 100*100                 | 7.671 E-02 | 152.374           |
|                 | 300*300                 | 5.294 E-02 | 246.244           |
|                 | 500*500                 | 4.426 E-02 | 388.860           |
|                 | 700*700                 | 3.211 E-02 | 633.525           |
| AABB            | 100*100                 | 6.502 E-02 | 161.588           |
|                 | 300*300                 | 4.128 E-02 | 262.643           |
|                 | 500*500                 | 3.081 E-02 | 410.183           |
|                 | 700*700                 | 2.764 E-02 | 722.241           |



FIGURE 5: The final display effect of virtual cheongsam.

TABLE 4: Evaluation scores of each index for the cheongsam simulation effect.

| Index                | Rating score (%) |      |      |      |      |      |      | Average score |
|----------------------|------------------|------|------|------|------|------|------|---------------|
|                      | 4                | 5    | 6    | 7    | 8    | 9    | 10   |               |
| Overall profile      | 0                | 0    | 6.7  | 3.3  | 23.3 | 46.7 | 20   | 8.7           |
| Standup structure    | 0                | 3.3  | 6.7  | 6.7  | 36.7 | 33.3 | 13.3 | 8.3           |
| Closure structure    | 0                | 0    | 10   | 40   | 40   | 10   | 0    | 7.5           |
| Sleeve structure     | 0                | 0    | 3.3  | 13.3 | 40   | 36.7 | 6.7  | 8.3           |
| Body piece structure | 0                | 3.3  | 3.3  | 20   | 16.7 | 46.7 | 10   | 8.3           |
| Fabric texture       | 0                | 6.7  | 13.3 | 30   | 30   | 20   | 0    | 7.433         |
| Slash                | 0                | 0    | 16.7 | 26.7 | 36.7 | 20   | 0    | 7.6           |
| Fabric drapability   | 3.3              | 0    | 13.3 | 23.3 | 33.3 | 23.3 | 3.3  | 7.667         |
| Hue                  | 0                | 3.3  | 10   | 36.7 | 40   | 10   | 0    | 7.433         |
| Color saturation     | 0                | 0    | 16.7 | 36.7 | 40   | 6.7  | 0    | 7.367         |
| Color value          | 0                | 0    | 20   | 46.7 | 26.7 | 6.7  | 0    | 7.2           |
| Attachment           | 10               | 26.7 | 30   | 13.3 | 20   | 0    | 0    | 6.067         |
| Facing               | 3.3              | 6.7  | 6.7  | 43.3 | 30   | 6.7  | 3.3  | 7.233         |

collision detection of object edges. The comparison of the 3 algorithms reveals that the AABB algorithm has the best RMSE performance, with an RMSE of only 2.764 E-02 when the feature pair is 700\*700.

In terms of detection time, the bounding sphere technique takes the least time to detect the same sampled feature pairs, followed by OBB and AABB. This is mainly due to the fact that the secondary detection of AABB takes more time and that improving the step size increases the calculation

time of the rate of change. The number of features has the greatest impact on the detection time of the three algorithms, as the increase in the number of features sampled causes the amount of computation involved in collision detection to increase. When selecting the feature pairs to be involved in training, the collision detection accuracy requirements and the detection time requirements should be fully considered, and the feature sampling frequency should be set according to the actual situation.

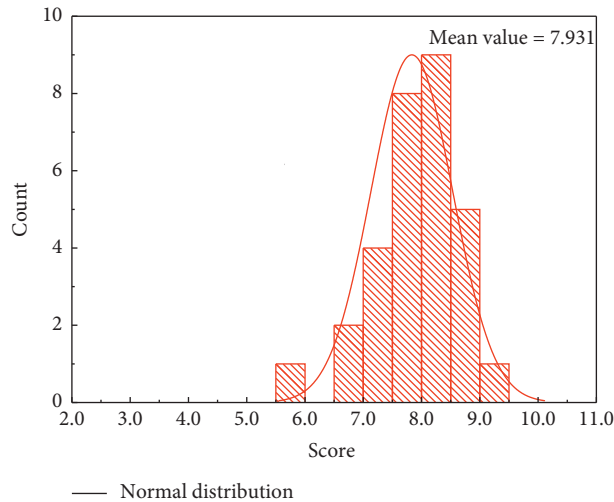


FIGURE 6: Score distribution histogram of cheongsam evaluation.

**5.3. Costume Model Simulation Effect Evaluation.** To ensure the validity of the experimental data, the evaluation was completed by 30 students majoring in clothing. The respondents had all used the apparel virtual design system and had a professional foundation in the concept of virtual clothing, thus being able to improve the accuracy of the evaluation results. The evaluation questionnaire was based on a 10-point Likert scale, where 1 means that the virtual costume is very unlike the real costume and 10 means that the virtual costume is very similar to the real costume. The observer scores the simulation effect of each element of the virtual costume based on the pictures. The final display of the virtual cheongsam is shown in Figure 5.

The percentage and statistical mean results of each evaluation score in the simulation evaluation index are shown in Table 4.

Looking at the mean values of each evaluation indicator, the number of those with mean values above 6 is high, indicating that the overall level of each evaluation is above the middle level. The evaluation of each indicator shows that the overall profile is rated high. The evaluation scores of each section were multiplied and aggregated with the corresponding weights to obtain the overall evaluation scores. The histogram of the distribution of evaluation scores is shown in Figure 6.

The mean value of the total score is 7.931 with a standard deviation of 0.732. The results show that the total score of all the evaluators is mainly distributed on the right side of the 7-point scale. The total score was compared to a medium score level of “5” using a one-sample  $t$ -test. The results showed a value of 21.95,  $p < 0.001$ , which means that the mean score for the virtual cheongsam design was significantly higher than 5, indicating that the virtual simulation was generally better.

## 6. Conclusions

This paper presents a virtual reality-based approach to the design of national costumes. Different curve fitting methods

are applied to the recognition of human features, and an AABB box-based collision detection method is used to prevent penetration between the garment and the body. The virtual costume design is implemented using the Marvelous Designer 9 platform and the Unity engine. The results of the subjective simulation effect evaluation show that the mean score of the virtual cheongsam design is 7.931 with a standard deviation of 0.732, which verifies the effectiveness of the virtual simulation effect. This paper uses hierarchical analysis to achieve the subjective evaluation of the virtual costume simulation effect, which may have the problem of imprecise weight distribution. Subsequently, we will try to use principal component analysis or factor analysis to find out the weights and establish more accurate and effective evaluation indexes for the virtual costume simulation effect.

## Data Availability

The experimental data used to support the findings of this study are available from the corresponding author upon request.

## Conflicts of Interest

The authors declare that they have no conflicts of interest to report regarding the present study.

## Acknowledgments

This study was supported by the research results of the 2020 Planning project of philosophy and Social Sciences in Hainan Province “Research on digital design of Li traditional schema”, Item No: HNSK(YB)21-60, and in 2019, the research results of the key research topic of science and education innovation of the Institute of Educational Sciences, Chinese Academy of Management Sciences “Research on the inheritance and protection of Li traditional handicrafts from the perspective of intangible cultural heritage”, Item No: KJJCX17598.

## References

- [1] S. C. Hidayati, C.-W. You, W.-H. Cheng, and K.-L. Hua, "Learning and recognition of clothing genres from full-body images," *IEEE Transactions on Cybernetics*, vol. 48, no. 5, pp. 1647–1659, 2018.
- [2] M. M. Ahmad, J. Batish, and K. Maira, "Consumer perceptions of counterfeit clothing and apparel products attributes," *Marketing Intelligence & Planning*, vol. 12, no. 4, pp. 254–268, 2018.
- [3] O. Gefeller, "The Garment Protection Factor: further advances in labelling sun-protective clothing," *British Journal of Dermatology*, vol. 178, no. 4, pp. 835–836, 2018.
- [4] J. N. Down and L. S. Harrison, "A comprehensive approach to evaluating and classifying sun-protective clothing," *British Journal of Dermatology*, vol. 36, no. 2, pp. 309–317, 2018.
- [5] A. M. Magee, M. Breathnach, S. Doak, and F. C. L. G. Thornton, "Wearer and non-wearer DNA on the collars and cuffs of upper garments of worn clothing," *Forensic Science International: Genetics*, vol. 34, no. 8, pp. 152–161, 2018.
- [6] R. Osmud and Y. Hong, "A study of Canadian female baby boomers: physiological and psychological needs, clothing choice and shopping motives," *Journal of Fashion Marketing and Management*, vol. 22, no. 3, pp. 509–526, 2018.
- [7] D. A. Assaad, S. Yang, and D. Licina, "Particle release and transport from human skin and clothing: a CFD modeling methodology," *Indoor Air*, vol. 11, no. 8, pp. 89–103, 2021.
- [8] M. Deng, M. Tian, and Y. Wang, "Quantitatively evaluating the effects of flash fire exposure on the mechanical performance of thermal protective clothing," *International Journal of Clothing Science & Technology*, vol. 12, no. 4, pp. 19–28, 2020.
- [9] Y. Song and J. Wirta, "Anthropometric clothing measurements from 3D body scans," *Machine Vision and Applications*, vol. 31, no. 1, pp. 59–71, 2020.
- [10] R. F. H. Nunes, N. Dittrich, R. Duffield, and M. C. T. M. D. F. L. G. A. Serpa, "Effects of finfrared emitting ceramic material clothing on recovery after maximal eccentric exercise," *Journal of Human Kinetics*, vol. 70, no. 1, pp. 135–144, 2019.
- [11] Y. Chen, R. Chen, M. Liu, and A. D. S. Xiao, "Indoor visual positioning aided by CNN-based image retrieval: training-free, 3D modeling-f," *Sensors*, vol. 18, no. 8, pp. 2692–2638, 2018.
- [12] G. D. Fleishman, G. M. Nita, N. Kuroda, and S. Jia, "Revealing evolution of nonthermal electrons in solar flares using 3D modeling," *The Astrophysical Journal*, vol. 859, no. 1, pp. 112–129, 2018.
- [13] R. Winzenrieth, M. S. Ominsky, Y. Wang, and L. Humbert, "Differential effects of abaloparatide and teriparatide on hip cortical volumetric BMD by DXA-based 3D modeling," *Osteoporosis International*, vol. 32, no. 6, pp. 33–45, 2021.
- [14] F. Radicioni, A. Stoppini, G. Tosi, and L. Marconi, "Necropolis of Palazzone in Perugia: geomatic data integration for 3D modeling and geomorphology of underground sites," *Transactions in GIS*, vol. 25, no. 5, pp. 2553–2570, 2021.
- [15] Y. Perez-Perez, M. Golparvar-Fard, and K. El-Rayes, "Segmentation of point clouds via joint semantic and geometric features for 3D modeling of the built environment," *Automation in Construction*, vol. 125, no. 7, Article ID 103584, 2021.
- [16] L. Ding, W. Jiang, Y. Zhou, and C. S. Zhou, "BIM-based task-level planning for robotic brick assembly through image-based 3D modeling," *Advanced Engineering Informatics*, vol. 43, no. 13, Article ID 100993, 2020.
- [17] H. Huang, C. Lin, and D. Cai, "Enhancing the learning effect of virtual reality 3D modeling: a new model of learner's design collaboration and a comparison of its field system usability," *Universal Access in the Information Society*, vol. 20, no. 3, pp. 429–440, 2020.
- [18] K. Li, T. Wu, and Q. Q. Liu, "Human contour extraction based on depth map and improved Canny algorithm," *Computer Technology and Development*, vol. 31, no. 5, pp. 6–12, 2021.
- [19] W. Zhang, D. Kong, S. Wang, and Z. Wang, "3D human pose estimation from range images with depth difference and geodesic distance," *Journal of Visual Communication and Image Representation*, vol. 59, no. 2, pp. 272–282, 2019.
- [20] K. Zou, Li Ma, Li Rong, and C. Xu, "Image-based non-contact measurement method of human body parameters," *Computer Engineering and Design*, vol. 38, no. 2, pp. 6–11, 2017.
- [21] C. Park, J. S. Park, and D. Manocha, "Fast and bounded probabilistic collision detection for high-DOF trajectory planning in dynamic environments," *IEEE Transactions on Automation Science and Engineering*, vol. 15, no. 3, pp. 980–991, 2018.
- [22] Y. Nakai, T. Miwa, and H. Shigemune, "Four-dimensional collision detection and behaviour based on the physics-based calculation," *Expert Systems*, vol. 144, no. 2, pp. 645–663, 2021.
- [23] J.-H. Park and B. Lee, "Holographic techniques for augmented reality and virtual reality near-eye displays," *Light: Advanced Manufacturing*, vol. 3, no. 1, pp. 1–14, 2022.
- [24] K. T. Martono, D. Eridani, D. I. S. Isabella, and H. Alfian, "The design of recognition system of children basic activities based on virtual reality," *IOP Conference Series: Earth and Environmental Science*, vol. 704, no. 1, Article ID 012019, 2021.
- [25] F. Tian, "Immersive 5G virtual reality visualization display system based on big-data digital city technology," *Mathematical Problems in Engineering*, vol. 2021, no. 3, Article ID 6627631, 9 pages, 2021.
- [26] V. Brua, J. Byka, J. Mian, and B. Kozlíková, "VRdeo: creating engaging educational material for asynchronous student-teacher exchange using virtual reality," *Computers & Graphics*, vol. 11, no. 2, pp. 65–71, 2021.
- [27] A. Rahouti, R. Lovreglio, and S. Datoussad, "Prototyping and validating a non-immersive virtual reality serious game for healthcare fire safety training," *Fire Technology*, vol. 7, no. 13, pp. 1–38, 2021.

## Research Article

# A Research on Library Space Layout and Intelligent Optimization Oriented to Readers' Needs

**Binli Gu** <sup>1</sup> and **Kenichi Tanoue**<sup>2</sup>

<sup>1</sup>Graduate School of Design, Kyushu University, Fukuoka 815-8540, Japan

<sup>2</sup>Faculty of Design, Kyushu University, Fukuoka 815-8540, Japan

Correspondence should be addressed to Binli Gu; [gu.binli.438@s.kyushu-u.ac.jp](mailto:gu.binli.438@s.kyushu-u.ac.jp)

Received 10 February 2022; Revised 2 March 2022; Accepted 19 March 2022; Published 19 May 2022

Academic Editor: Man Fai Leung

Copyright © 2022 Binli Gu and Kenichi Tanoue. This is an open access article distributed under the Creative Commons Attribution License, which permits unrestricted use, distribution, and reproduction in any medium, provided the original work is properly cited.

With the rapid development of the Internet age, all walks of life have been affected to a certain extent. The layout of a traditional library is an extremely important part of the library. A good layout can make full use of the space in the library to maximize the use of space and give readers a better sense of experience. It is better to study or work in the library. At the same time, with the rapid development of the Internet, all walks of life have been affected to a certain extent. For the library, the intelligent library based on GA-RFID technology can improve both the readers and the staff in the library. Reading books can improve the efficiency of study or work. In this article, some comparisons are made between the intelligent library based on GA-RFID technology and various types of libraries, and the technology is compared from many aspects, thus reflecting that this technology is beneficial to readers.

## 1. Introduction

The library is an institution that specializes in the collection, sorting, preservation, and dissemination of documents and the use of science, culture, education, and science. It is the material basis for the library to carry out all work. In terms of design concepts, the traditional library space is a “book” space, while for the intelligent library [1], it is a “human” space in my opinion. For these two spaces, the layout of the library is extremely important. The layout of the library that makes readers feel comfortable will directly increase the reader’s sense of experience and interest in coming to the library. The layout generally refers to the overall layout of the building [2] and overall design [3]. With the rapid development of the Internet, the library is no longer a rigid building. It is an intelligent library with vitality. For readers, the more important thing about the spatial layout in the library is whether it allows them to find the books they want more easily and quickly. At this time, we can introduce more intelligent content to achieve high efficiency [4] to meet the readers’ desires. This kind of intelligent library based on RFID technology [5] can better improve the efficiency of readers in finding, borrowing, and returning books. If the RFID

capture effect [6] probability value [7] is higher, the capture speed will be faster; at the same time, RFID-based book carts can be set up, which can better help readers complete the functions they want to achieve and can help working people with similar tasks such as putting new books on the shelves. Finally, the comparison of the average time spent by readers in traditional libraries and RFID-based intelligent libraries [8] and the comparison of related indicators [9] are carried out. From the comparison, it can be concluded that the RFID-based intelligent libraries are used by readers, the operation efficiency will be higher, and the reader’s sense of experience will be better [10].

So far, nearly 100 institutions in Singapore, Australia, India, and other countries have adopted RFID technology in their library automatic management systems [11]. The National Library of Singapore is the first library to implement an RFID system. Every book in the library has an RFID tag [12]. In this library, borrowing and returning books are self-service [13]. At the same time, the staff can quickly understand the type and location of books through the scanning device [14]. In China, on February 20, 2006, the Chengyi College Library of Xiamen Jimei University was officially opened to the public. The supporting “RFID Smart



Collection Management System” was also announced to be completed and put into trial operation, becoming the first domestic library with complete functional modules [15] and entering the practical stage.

## 2. Library Layout Requirements

The library is composed of reading rooms, book stacks, computer equipment rooms, etc., but when arranging the entire library, these should not only be considered but also the aisles, stairs, lighting, ventilation, and other aspects should be affected by each other. The layout of the rooms should be combined, the specific role of each section should be considered, and the overall planning should be carried out to achieve the optimal layout result.

*2.1. Requirements for the Layout of Reading Rooms and Library.* For readers, the reading room is the most important part of the entire library. It should have basic requirements such as quietness, good light, and fresh air. The second is to consider the size of the tables and chairs in the reading room and calculate the optimal arrangement distance and the number of tables and chairs in the reading room. For these data, it is necessary to have a certain understanding of the reading room area and the number of people that may be accommodated. The most important thing in the reading room is the bookshelf, so the layout of the bookshelf is a problem we must consider. After establishing the length, width, and height of the bookshelf, we can know how many books can be accommodated in the current library and can be able to know the usage area of the library. Generally speaking, if there are many people in the reading room and the number of tables and chairs in the reading room, the area invested must be large. At the same time, the requirements for lighting and ventilation are relatively high, and the height of the floor must be increased. At the same time, if there are relatively few people using the library, the position of the bookshelves remains unchanged, and the floor height of the room is reduced accordingly. For general reference, the following standards are used: the floor height of the reading room is 3.6 m~4.8 m; the floor height of the bookshelves is 2.4 m~3.6 m. For readers, setting the height of the bookshelf to a height that makes them comfortable will allow readers to get a better experience when choosing books in the library.

*2.2. Requirements for the Layout of Computer Equipment Rooms.* With the rapid development of electronic information technology, libraries should also follow the footsteps of and incorporate computer equipment into the library, so as to provide users with a better sense of use. Just like the layout of the library, it is necessary to set up computer rooms, databases, multimedia reading rooms, and so on. For these rooms, it needs to have the basic requirements of quietness, good light, and fresh air and also strictly manage the use of these devices, such as timely updating the system and software, to provide readers with a better sense of use.

*2.3. Requirements for Aisles and Stairs.* For the library, whether it is to buy or borrow books or read books in the library, there will always be an endless stream of people. Therefore, the layout of the corridors and stairs of the library is also very important because of its traffic. The connection layout is very frequent, so the width of the stairs and aisles can be slightly wider; generally, the approved width is 1.4 m~2.2 m. This width is also a suitable length for the reader, and it is not too spacious and appears to be open. For the setting of the safety exit, it is necessary to be clear, so that readers can know where it is for the first time.

*2.4. Lighting and Ventilation Requirements.* For a library, good lighting conditions are also very important. It is necessary to ensure that every place in the library is well-lit, but at the same time, it should not be dazzling; second, there should be good ventilation conditions to ensure the entire indoor air. At the same time, some green plants can be set up in the library. Green plants will not only make the entire library more dynamic but also allow readers to relax when they are tired.

Generally speaking, the internal space of a library building consists of several use spaces and connecting spaces. The layout must be based on the functional characteristics and needs of the library, and the various parts of the space must be organized rationally.

*2.5. Basic Facilities Required by the Library.* The basic facilities required by the library and the main functions of the functional areas are shown in the following Table 1.

## 3. Layout Optimization

When conducting related research on the layout of the library, we can regard the library as a system. The various spaces of the library will cause the movement of people. The connection between the book stocks and people forms a spatial connection, and the result is to form a layout with multiple styles. Topological analysis of the library is performed to obtain the degree of travel and integration to reflect the basic variables of library accessibility.

The degree of traversal is the number of times the shortest distance traversed within any two spaces in the space system in the entire space of the library. The more the number of times, the more convenient and quicker the readers will move in the various spaces in the library, that is, the room. The specific expression is as follows:

$$NAchoic_i = \frac{\log(ACH_r + 1)}{\log(ATD_r + 3)} \quad (1)$$

In the above formula,  $NAchoic_i$  is expressed as the standard degree of travel,  $r$  is expressed as the standard topological structure,  $ACH_r$  is expressed as the selectivity under the radius  $r$ , and  $ATD_r$  is expressed as the depth value under  $r$ .

The degree of integration  $li$  indicates the degree of agglomeration or dispersion of a space unit and other space units. When the value of the integration degree is greater, the

TABLE 1: Names and functions of library functional areas and service facilities.

| Serial number | Function area and service facility name | Main functions of functional areas and service facilities  |
|---------------|---|--|
| 1             | Query machine                           | Assist in querying the specific location of books and newspapers   |
| 2             | Reading room                            | Provide a place to read all kinds of books   |
| 3             | Computer equipment room                 | Provide computer equipment to help readers reach a project   |
| 4             | Newspaper reading room                  | Provide access to various periodicals and magazines  |
| 5             | Learning commons                        | Provide one or more integrated common spaces for various informal learning behaviors, including solitary and collaborative |
| 6             | Locker                                  | Provide a location for storing personal belongings   |
| 7             | Lounge                                  | Provide a place to read and rest   |
| 8             | Fire room                               | Store firefighting equipment and emergency supplies  |
| 9             | Bathroom                                | Provide a place to solve personal physiological needs  |
| 10            | Waterhouse                              | Provide drinking water   |
| 11            | Library                                 | Where to store books   |

space, that is, the room, is in a more convenient position in the system (library).

$$I_i = RA_i = \frac{2(MD_i - 1)}{n - 2}. \quad (2)$$

where MD<sub>i</sub> is the average depth, and  $n$  is the number of spatial nodes. Based on the above, it is possible to calculate which room in the library will be more integrated, so that the room is located in a more convenient location for readers.

From the reader's point of view, this article considers the spatial layout of the library and asks to bring the best sense of experience to the readers. Therefore, the problem of optimizing the spatial layout of the library is transformed into how to achieve the results they want faster (including reading, borrowing, returning) after the readers come to the library and how to use the advantages of the layout to improve the reader's the question of experience.

For example, there are  $n$  libraries with demand points  $P_i(x_i, y_i)$  ( $i = 1, 2, \dots, n$ ), and  $b_i(i = 1, 2, \dots, n)$  is the demand for each reader. Also, suppose that there are  $m$  library candidate points  $Q_j(u_j, v_j)$  ( $j = 1, 2, \dots, m$ ).  $g$  bookshelves are selected from the  $m$  candidate points to serve the  $n$  readers' demand points in the library so that the distance between the  $n$  demand points and the place they want to reach is the shortest.  $T_{ij}$  and  $d_{ij}$  ( $i=1, 2, \dots, n; j=1, 2, \dots, m$ ) are, respectively, the books provided by the library candidate point  $Q_j(u_j, v_j)$  to the demand point  $P_i(x_i, y_i)$  and the distance between the two points. If  $w_i$  is recorded as the demand at the demand point  $P_i$ , and  $a_{ij}$  is the weight coefficient, then the target equation is

$$\min \left( \sum_{i=1}^n \sum_{j=1}^m a_{ij} w_i d_{ij} \right). \quad (3)$$

The corresponding constraints are

$$\begin{aligned} \sum_{i=1}^n a_{ij} &= 1, \quad i = 1, 2, \dots, n, \\ \sum_{j=1}^m \left( \prod_{i=1}^n a_{ij} \right) &= g, \quad g \leq m \leq n. \end{aligned} \quad (4)$$

The above two constraints are to ensure that each reader's demand point can be searched on a certain bookshelf, and there are at least  $g$  bookshelves.

**3.1. Buffer Model.** From a mathematical point of view, buffer analysis is a distance analysis based on the topological relationship between spatial objects (this article refers to libraries and readers), and its basic model is a given set of spatial objects  $O = \{O_i / i = 1, 2, \dots, n\}$ , where  $O_i$  is a target of the space, and the buffer of  $O_i$  is defined as

$$B_i = \{d(x, O_i) \leq d_i\}. \quad (5)$$

where  $d(x, O_i)$  is the distance between  $x$  and  $O_i$ ;  $d_i$  is the radius of the field, or called buffer analysis, and sometimes,  $d_i$  is a constant.

For the spatial target set  $O = \{O_i / i = 1, 2, \dots, n\}$ , the buffer is usually defined as

$$B = \bigcup_{i=1}^n B_i. \quad (6)$$

**3.2. Find the Mathematical Model of the Nearest Bookshelf.** After optimizing the spatial layout of the library, it is necessary to check the rationality of the optimized library spatial layout. The mathematical model of finding the nearest facility (referring to a certain bookshelf in this article) can enable readers at the demand point to find the nearest bookshelf. The mathematical model of the shortest path is as follows.

Let  $G = \langle V, E \rangle$  be a nonempty simple finite graph,  $V$  is the set point, and  $E$  is the edge set. For any  $e = (v_i, v_j) \in E$ ,  $w(e) = a_{ij}$  is the weight of edge  $(v_i, v_j)$ .  $P$  is a directed path between two points in  $G$  and defines the weight of  $P$ .

$$W(P) = \sum_{e \in E(P)} w(e). \quad (7)$$

Then, the directional path with the smallest weight between two points in  $G$  is called the best path of these two points, that is, the best path for readers to complete the service they want based on the library after the optimized spatial layout. The shortest path model is

$$\min \sum_{(v_j, v_i) \in E} a_{ij} x_{ij}. \quad (8)$$

The constraints of the above formula are

$$x_{ij} \geq 0, \quad (9)$$

$$\sum_{(v_j, v_i) \in E} a_{ij} x_{ij} - \sum_{(v_j, v_i) \in E} a_{ij} x_{ij} = \begin{cases} 0, & i = 1 \\ 0, & 2 \leq i \leq n-1 \\ -1, & i = n \end{cases}$$

Among them,  $x_{ij}$  is the number of occurrences of  $(v_i, v_j)$  in a limited path.

Through this model, we can randomly select multiple demand points, calculate the total distance from the demand point to the optimized bookshelf, and compare the total distance from the demand point to the bookshelf before optimization. In order to verify the rationality of the optimized spatial layout of the library, readers need to reach the required location in a relatively short time.

**3.3. Objective Function and Constraints.** There are many layout planning goals that need to be followed for the spatial layout of the library, such as making the best use of the area of each space, facilitating readers to achieve the desired purpose in the library, providing good infrastructure services, and providing good books. But in order to simplify the processing and the efficiency in data acquisition, only the following goals are considered, that is, to make the best use of the area of each space to facilitate readers to achieve the desired purpose in the library. Making the best use of the area of each space is to understand and plan the functionality of each space in the library. For example, a room is used as a reading room or an electronic equipment reading room, and how many bookshelves, tables, and chairs are more appropriate in a room. Therefore, the objective function of the problem can be expressed as

$$\begin{aligned} \text{Min} & \sum_{i=1}^N \sum_{j=1}^M \sum_{k=1}^K C_{ijk} X_{ijk}, \\ \text{Max} & \sum_{i=1}^N \sum_{j=1}^M \sum_{k=1}^K \sum_{i'=1}^N \sum_{j'=1}^M \sum_{k'=1}^K L_{ij, i' j'} H_{k, k'}. \end{aligned} \quad (10)$$

Similarly, the problem also needs to meet the following constraints.

The number of space utilization types for each unit must meet the predefined structural ratio.

$$\sum_{i=1}^N \sum_{j=1}^M X_{ijk} = X_k, \forall k. \quad (11)$$

There must be a sufficient area in each space unit.

$$\sum_{k=1}^K X_{ijk} = 1, \forall ij. \quad (12)$$

A production unit is adjacent to at least another unit.

$$S_{Li, j, i' j'} \geq 1, \forall (ij, i' j'). \quad (13)$$

The spatial adjacency constraints of the production units of the same type are relative. It is better to generate a

completed area with the same type of production units. This is the need for planning the library and to make the distribution of each type of space more complete. If  $m_{i_1 j_1 k_1, i_2 j_2 k_2}$  represent the Manhattan distance of 2 units  $(i_1 j_1)$  and  $(i_2 j_2)$  of space utilization type  $k$ , there are certain requirements.

$$m_{i_1 j_1 k_1, i_2 j_2 k_2} = 1. \quad (14)$$

**Distance constraint:** It is necessary to maintain a certain distance between different types of production units. For example, a certain distance must be maintained between the reading room and the bookshelves and tables and chairs. It is not easy to satisfy the distance constraint between space objects of arbitrary shape in vector space, but it is relatively easy to deal with the distance between two space objects of different shapes in grid space. If  $d_{i_1 j_1 k_1, i_2 j_2 k_2}$  is used to represent the Euclidean distance between a unit of space use type  $k_1$   $(i_1 j_1)$  and a unit of land use type  $k_2$   $(i_2 j_2)$ , and it is required to be greater than  $D$ , the distance constraint can be expressed as follows:

$$d_{i_1 j_1 k_1, i_2 j_2 k_2} > D. \quad (15)$$

**Convenience constraints.** For example, the emergency exit in the library should be set up at the most convenient location.  $B_{ij}$  represents the most convenient unit set for a certain spatial unit  $(i, j)$ , as shown in Equation 19:

$$i \notin B_{ij} \& j \notin B_{ij}. \quad (16)$$

In addition to this, there may be other corresponding constraints in a specific practical problem.

In the above expression, the objective function and constraint conditions are nonlinear and multidimensional, which is a combined problem, while the size of the problem increases exponentially with the increase in the number of spatial planning units, and many spatial constraints and spatial objectives are more important. The objective function and constraints increase the complexity and size of the problem. Conventional accurate algorithms are difficult or even impossible to solve, and the above method is another way to solve the problem.

## 4. Intelligent Library

So far, the traditional library business model familiar to readers has been relatively mature, but for most people, including staff, the overall impression of a traditional library is still the oldest and relatively traditional one. He believes that a library is still just a place for reading and borrowing books, a "book collection center" in the traditional sense. But in fact, the basic functions of traditional libraries have not changed. For this kind of service concept, in today's relatively advanced science and technology, it must be developed in the direction of multifunctionality and omnipotence, so as to expand the functions of today's traditional libraries.

For example, with the fierce growth of the Internet, libraries should also integrate with it to achieve more intelligent services, so as to provide more readers with a better sense of experience and more convenient use for readers.

The accelerated development of the new generation of information technology is related to my country's ability to seize the opportunities of the new cycle of technological revolution and industrial transformation. At present, with the rapid development of Internet-related information technologies such as big data, cloud computing, and the Internet of Things, the application of artificial intelligence in different industries and fields will become more and more extensive and in-depth. As a collector, inheritor of human culture, and a promoter of social civilization, libraries must also seize the opportunity to combine intelligence with the improvement of service functions, the optimization of the hardware environment, and the targeted implementation of data. New state and function design are carried out, the renovation and upgrade are completed, and an intelligent library that meets the requirements of the new era is built. For readers, by optimizing the use environment of the library, allowing readers to enjoy reading more effectively, based on this expectation, library intelligence can achieve this.

The intelligence of the library is reflected in the hardware, such as smart technology, data resources; at the same time, it can also be well reflected in the management, service, and other software parts. The conclusion is that the two-way co-construction of technology and services must be linked to the intelligent construction of the library to truly narrow the gap between readers and the library, and let artificial intelligence become an intermediary between people and the library. With the continuous innovation of intelligent wearable devices, RFID tags, chips, and other technologies, artificial intelligence-related products such as shelf sorting robots and reading service robots are applied to the work of libraries to serve readers to the greatest extent. In the improvement of service and management level, the library site is transformed into a comfortable, tidy and bright space, so that readers have a better reading environment, enjoy the reading environment better, and greatly improve their spiritual life. The main modules of library intelligence are as follows in Figure 1.

With the intelligent analysis of relevant information, intelligent information transmission, and intelligent human-computer interaction, the big data of book information resources and readers' reading behavior can be better integrated, analyzed, and applied. At the same time, relying on big data of information resources, big data of reader behavior, etc., readers' knowledge portraits and charts are constructed, and the law of interaction between book information resources and readers are analyzed and understand not only carry out customized, segmented, and accurate library resource recommendation but also can focus on single-point information. Providing diversified and comprehensive relevant information greatly improves the efficiency of readers' information capture and meets the needs of readers to the greatest extent. An intelligent security-related system can also be built. The library is a public place with intensive personnel and knowledge. To ensure safety, artificial intelligence technology can be used to build an intelligent security system, which can effectively

improve the safety factor in all aspects and protect the library's safety. Safe operation: In terms of data management, intelligent security is strengthened, library network confidentiality is improved, and network attacks, virus transmission, intrusion, and other issues are effectively prevented. In terms of circuit management, through the intelligent security system, intelligent diagnosis, analysis, and processing of faults in the library operation process are carried out, and the temperature of various electronic components is controlled around the clock to reduce the overload of electronic circuits. In terms of facility management, intelligent monitoring collects data such as the flow of people and logistics. Real-time fire safety monitoring ensures the safety of the central area.

*4.1. RFID Technology Introduction.* The emergence of RFID technology and its application in libraries have enabled libraries to take a step toward an intelligent library, but, at the same time, they have also brought challenges.

RFID technology is a radio frequency technology and a noncontact automatic identification technology. At the same time, this technology can also be called an electronic tag. To put it simply, when we are shopping in the supermarket, we scan the QR code of the product and show the payment code. The clerk uses the machine to scan it using this technology.

Applying this technology to the library can be used when readers borrow and return books. When the reader needs to scan the barcode, it will show which bookshelf the book belongs to and all related information. This kind of operation can realize the self-service borrowing and returning of readers to improve efficiency. At the same time, we can also configure RFID tags as a management method, through document recognition and portable scanning, to change the traditional library's contribution to only relying on manpower to locate bookshelves and count books. This technology can realize the real time and accuracy of book storage in various tasks such as new book storage, book location changes, and book inventory.

For the logistics classification in RFID technology, we can also use this concept to develop smart book carts, which are in line with the smart transmission equipment of smart libraries. In view of the limited static physical location of the smartbook cart, it is expected that the correspondence between the wireless dynamic document address data and the classification principle can be used to provide on-board computers and multiunit document classification for the book cart. RFID readers and computers can better and faster determine the specific location of books that the reader wants by identifying books and bookshelves. In this way, the query and delivery process of books in a certain area can be realized. This RFID-based technology enables this book cart to have functions such as document shelving and arranging at the same time as shown in Figure 2.

We can compare the high efficiency that this technology brings to libraries. The results of libraries that use this technology with the results of libraries that have not applied this technology are compared, so as to understand intelligence more intuitively.

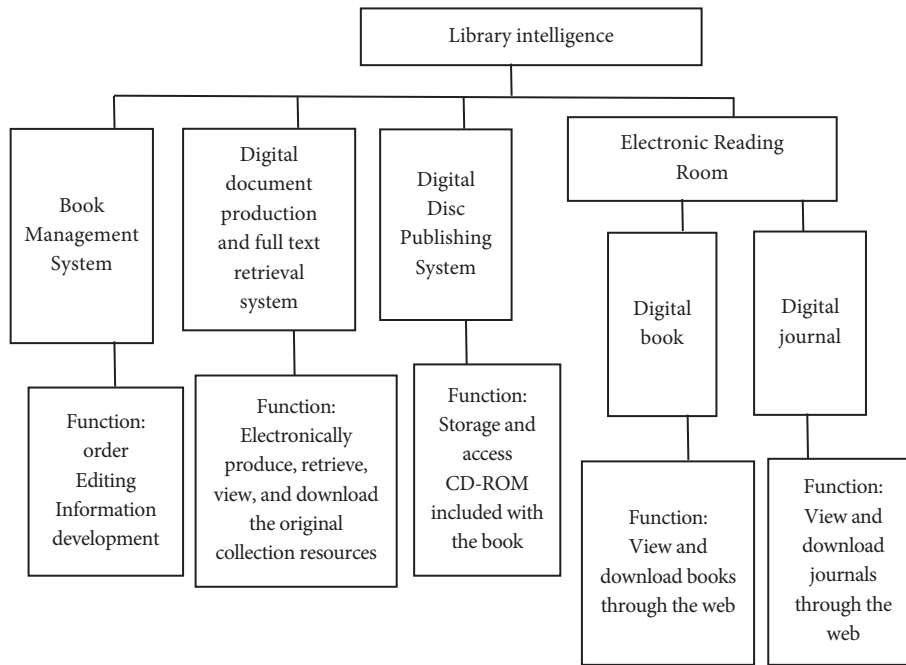


FIGURE 1: Main functional modules of library intelligence.

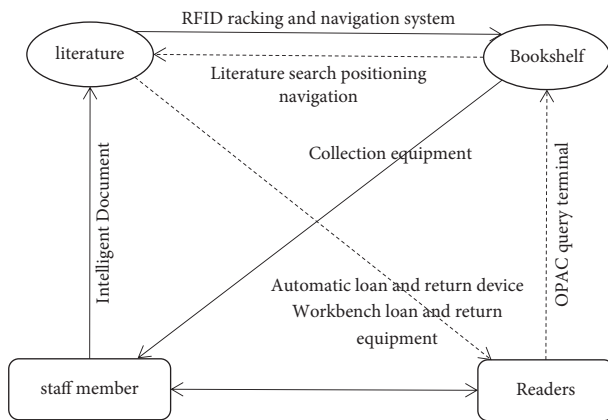


FIGURE 2: Functions that can be realized by the smartbook cart.

4.2. GA Genetic Algorithm. The genetic algorithm (GA) was first proposed by John Holland in the United States in the 1970s. The algorithm was designed and proposed according to the evolutionary laws of natural organisms. It is a computational model that simulates the biological evolution process of natural selection and the genetic mechanism of Darwin’s biological evolution theory. It is a method to find the optimal solution by simulating the natural evolution process. The algorithm uses computer simulation to transform the problem-solving process into a process similar to the hybridization and mutation of chromosomal genes in biological evolution. When solving more complex combinatorial optimization problems, it is usually faster to obtain better optimization results than some conventional optimization algorithms. Genetic algorithms have been widely used in fields such as combinatorial optimization, machine learning signal processing, adaptive control, and artificial life.

In the process of researching genetic algorithm, genetic operations such as selection, crossover, and mutation are random, but the genetic algorithm is not a blind search. It can select relatively better individuals from the previous generation group according to its own reproductive ability. Therefore, each generation of the population can continue to evolve and eventually converge to the individual with the highest fitness function level in the coding space. Since the standard genetic algorithm has a relatively fixed algorithm execution process, only a few important factors need to be defined when using the genetic algorithm. These important factors include parameter coding, initial population selection, adaptive function design, genetic manipulation design, control parameter settings.

4.2.1. Genetic Manipulation Design. Choose: The choice to adopt an adaptive ratio will be implemented in the form of a roulette wheel. The specific operation is as follows: for a given population  $X = \{x_1, x_2, x_3, \dots, x_n\}$  with population size  $n$ , calculate the fitness value of individual  $x_i$  ( $x_i \in X$ ) as  $f(x_i)$ , then the selected concept size is

$$P_i(x_i) = \frac{f(x_i)}{\sum_{j=1}^n f(x_j)}. \tag{17}$$

The above formula determines the survival probability of each individual in the offspring population. After the selection operation, the expected number of parent individuals in the next generation population is

$$N(x_i) = n \cdot p_i(x_i). \tag{18}$$

Mutations: The mutation operation is implemented according to the mutation operator used in the genetic algorithm using binary coding. For a given random individual

$S = a_1 a_2 a_3 \dots a_L$  and the new individual after mutation  $S' = a'_1 a'_2 a'_3 \dots a'_L$ , the specific operation is as follows:

$$O(P_m, S): ai' = \begin{cases} 1 - a_i & x \leq P_m \\ a_i & x > P_m \end{cases} \quad (19)$$

In the above formula, the termination condition of 2 adopts the maximum algebra method, and the maximum iteration algebra is set to 100, and then, the calculation is performed according to the genetic algorithm process, and the obtained coordinates  $(x, y, z)$  are the preliminary position estimates of the tags to be located, plus the correction factor to get the final positioning result. For this technology, we can apply it to the library to locate books when searching and, at the same time, combine RFID technology with it to achieve better results.

**4.3. GA-RFID Technology Realization.** A static RFID system consists of identification devices, namely readers, databases, and a large number of passive tags. The identification device and all tags share all wireless channels, and the identification device does not have any specific quantity and prior information about the tags before identification. The interrogation response is used for communication between the identification device and the tag. The tag can only perform simple calculations, storage, and communication capabilities, and the tags do not communicate with each other. Based on the above information, we can obtain the probability of capturing effects under the influence of different channel environments, so that the application of GA-RFID technology in the library can be easily accepted by readers.

For the communication line in the GA-RFID system in this article, including the forward channel and the reverse channel, the identification device sends query commands through the forward channel and provides a continuous carrier signal, while the tag will communicate in the reverse direction. The scattering method obtains the ability from the carrier signal of the identification device and responds with certain information to the reader. The identification device needs to comprehensively consider the forward and reverse link loss in the cascaded channel when receiving the power of the label reply signal. Let  $P_{tx}$  be the transmission power of the identification device, and the power  $P_{r,T}$  of the identification device signal received by the tag is as follows:

$$P_{r,T} = \rho LP_{tx} G_T G_R L(d_f) |h_f|^2 \quad (20)$$

Here, PL is the polarization loss factor (PLF) matching the identification device and the transition, and GR and GT are the antenna gains of the identification device and the tag, respectively. The tag obtains the information through backscattering and gives a reply, so the information power  $P_{r,R}$  of a tag that the identification device can receive is

$$P_{r,R} = \tau v_T \rho LP_{tx} |G_T|^2 G_R^f G_R^b \quad (21)$$

In the above information,  $T$  is the normalization coefficient, which represents the difference in the received power

of the identification device caused by the encoding and modulation methods;  $v_T$  is the power transmission efficiency between the tag chip and the identification device;  $f$  and  $b$ , respectively, represent the forward link and the reverse link;  $R$  and  $T$  represent identification devices and tags, respectively.

The effect of tag capture in the GA-RFID system is defined according to the power model as follows. When  $n$  tags send signals at the same time, if the signal strength of a certain tag is much greater than the sum of the information strengths of all other tags, the identification device will have a capture effect, as shown in the following:

$$P_{r,R-i} \geq Z \left\{ \sum_{i \neq j} P_{r,R-i} + N \right\} \quad (22)$$

In the above information, it is the power ratio threshold, which is the minimum interference ratio required after the identification device successfully receives the signal from the book. For a general narrowband system,  $1 < Z < 10$ . At this time, “ $_i$ ” in the formula represents the received power of tag  $i$ , and  $N$  is additive noise, which is a negligible value. Therefore, when there are  $n$  tags transmitting information in the same time period, the probability of a capture effect is

$$q_n = \text{prob} \left\{ \frac{P_{r,R-i}}{\sum_{j \neq i}^k P_{r,R-j} + N} \right\} n \quad (23)$$

Among the above information, if there are  $n$  tags sending information at the same time, the probability that the capture effect occurs is  $q_n$ . When the value of  $q_n$  is larger, that is, the information on the book, such as the two-dimensional code and the like, is more likely to be captured. For readers, they can get it on the library smart device based on GA-RFID. A better sense of experience can be completed with higher efficiency in order to meet certain needs.

## 5. Intelligent Distribution of Books

In the process of borrowing and returning books, we can understand which books are more popular at the moment, so that we can better plan them, just like placing the hottest books in the most conspicuous way. Readers can see these books intuitively. Of course, the realization of this idea is also combined with intelligence and realized by using certain formulas, which fundamentally saves time and costs and achieves the effect of enhancing the reader’s sense of experience.

We can use the book trolley mentioned in the previous article to know which bookshelf or which bookshelves have the most readers and use the kernel density estimation method to perform a calculation. We can move the book trolley to a certain bookshelf. The position is the center, and the books in a certain range of radius  $h$  are set with the bookshelf as the center. The closer the center point is, the maximum attribute value decreases as the distance increases. The formula is as follows:

$$F(x) = \frac{1}{nh} \sum_{i=1}^n k\left(\frac{x-x_i}{h}\right), \quad (24)$$

where  $F(x)$  is the kernel density function at position  $x$ ,  $h$  is the threshold radius ( $>0$ ), and  $K$  is the kernel density equation.  $x-x_i$  is the distance from the element point  $x$  to  $x_i$ .

A relevant data set is established based on the book cart data and grid the data, and the grid center is used as the demand point to reduce data errors caused by data errors. The specific steps are as follows.

In the first step, for each supply point, that is, bookshelf  $j$ ,

$$R_j = \frac{S_j}{\sum_{i \in \{d_{ij} \leq d_n\}} P_i \times g(d_{ij})}. \quad (25)$$

In the second step, for each demand point  $i$ ,

$$A_i = \sum_{j \in \{d_{ij} \leq d_n\}} R_j \times g(d_{ij}). \quad (26)$$

$g(d_{ij})$  is the Gaussian equation considering the distance attenuation, and the calculation formula is as follows:

$$g(d_{ij}) = \begin{cases} e^{-1/2 \times (d_{ij}/d_n)^2} - e^{-1/2} & , d_{ij} \leq d_n \\ 0 & , d_{ij} > d_n \end{cases} \quad (27)$$

In the above formula,  $R_j$  is the supply ratio of the library's supply to the total number of people demanded within the supply radius of the supply point bookshelf  $j$ ,  $S_j$  is the area of the supply point bookshelf  $j$ ,  $k$  is the space function of the supply point  $j$ , and the internal demand point  $D_{ij}$  is the representation of the distance between demand point  $i$  and supply point  $j$ ;  $d_n$  is the service radius of a book cart;  $P_i$  is the number of library people at demand point  $i$ ;  $A_i$  is the final process matching index of each demand point, that is, taking the demand point  $i$  as the center, sum up all  $R_j$  within the service radius of a specific bookshelf in the library.

## 6. Experiment Comparison

According to the information mentioned in the above article, we can compare the average duration of GA-RFID-based library intelligent equipment with that of traditional libraries, that is, using manual registration. Of course, under the same environment and conditions for comparison, this comparison can better highlight the advantages and disadvantages of different algorithms. At the same time, we can carry out a simulation of borrowing, returning, and finding books in the library environment and check the average market performance required for each operation, as shown in Figure 3.

For readers, there are several indicators in the reading library that can be used as evaluation indicators for the overall evaluation of the library. At the same time, we can also integrate and optimize the overall layout and various aspects of the library based on these indicators, as shown in Figure 4.

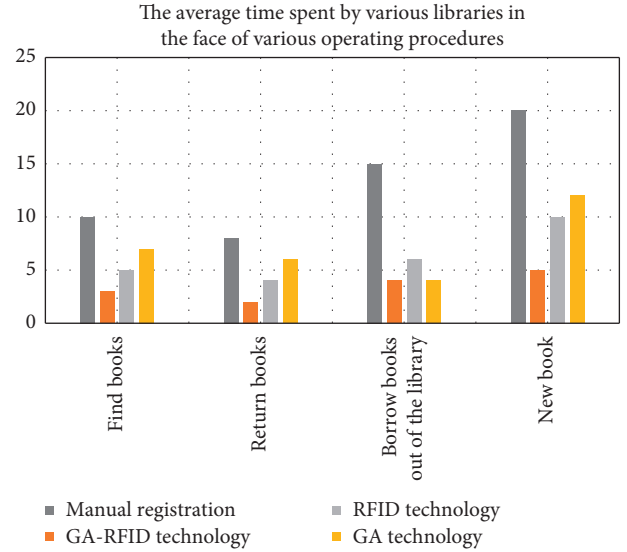


FIGURE 3: The average time spent by various libraries in the face of various operating procedures.

People who come to the library at different ages will have different acceptance of intelligent equipment. For older people, they will actually be more inclined to the traditional form of library, which is to use manual registration; for middle-aged people, if they are relatively familiar with GA-RFID technology, they will choose to use this technology, so it is necessary for us to design this technology more simply and clearly, and for young people, young people are more receptive, and they will be more inclined to intelligent equipment; for younger children, they will be novel about intelligent equipment (especially robots), and they need to work at this time. The staff gave a guide to the children, as shown in Figure 5.

The frequency of use of various functions of intelligent equipment by visitors to the library is integrated in various time periods, so as to use this as a data source for planning or upgrading the library, as shown in Figure 6.

Based on this comparison, we can understand which function readers are more inclined to in each time period, so as to specifically improve the role of related functions in a certain time period.

In order to better compare these three methods, we can extract some books in the library to observe the results expressed by readers based on these three technologies, so as to compare the required efficiency and correct rate of these three methods. The reader's satisfaction and other factors are compared, as shown in Figure 7.

In the above chart, the efficiency is the length of time it takes to find a book based on this technology, and the correct rate is whether the book found is what the current reader wants. When optimizing the layout of the library space, different spaces need to be paid differently. For example, the proportion of the reading room must be more important. From this, you can compare each space to understand each space. Therefore, detailed

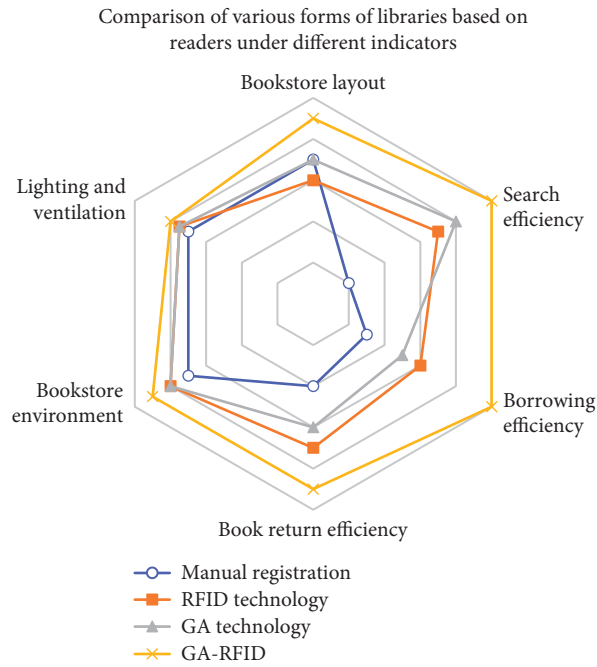


FIGURE 4: Comparison of various forms of libraries based on readers under different indicators.

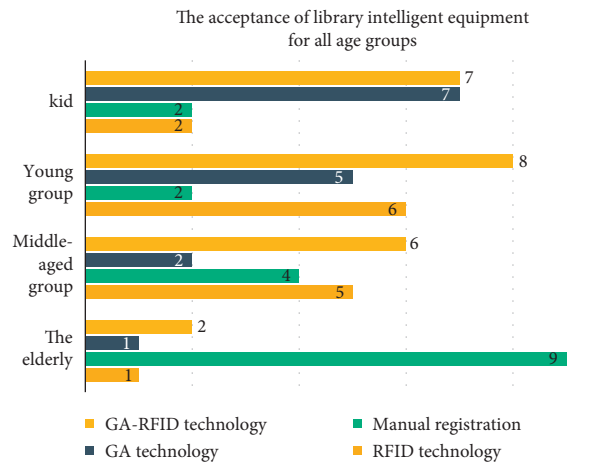


FIGURE 5: The acceptance of library intelligent equipment for all age groups.

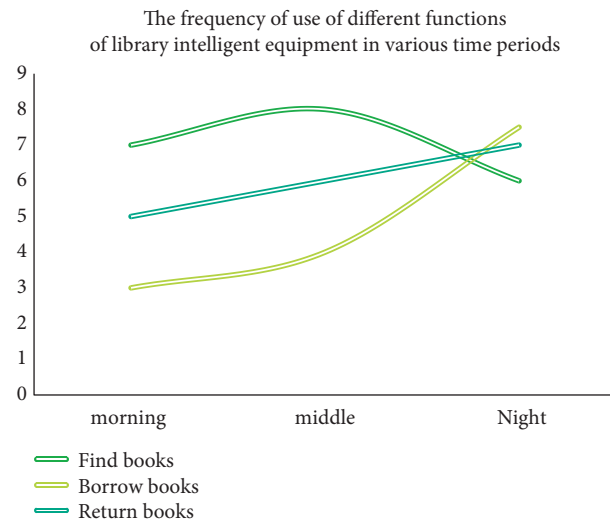


FIGURE 6: The frequency of use of different functions of library intelligent equipment in various time periods.



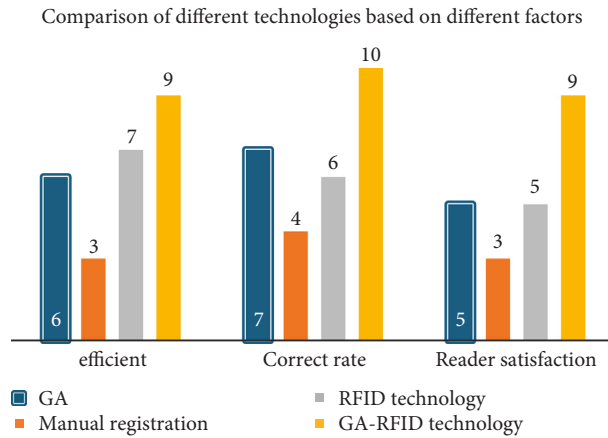


FIGURE 7: Comparison of different technologies based on different factors.

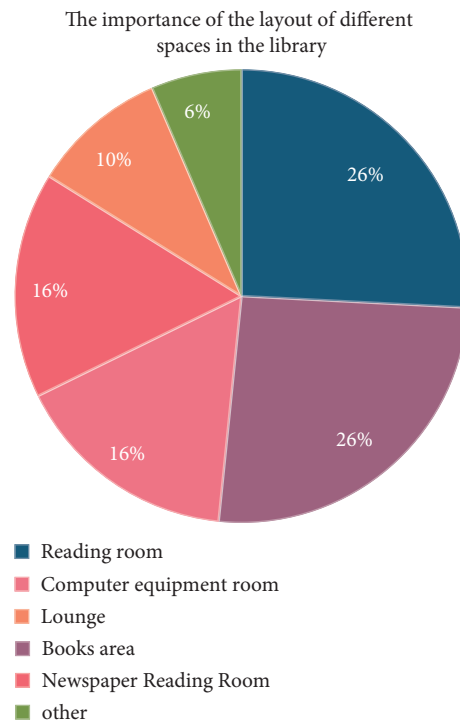


FIGURE 8: The importance of the layout of different spaces in the library.

planning of each space layout is carried out, as shown in Figure 8.

We can compare the time of these four technologies when looking for books with different numbers of books, so as to see the efficiency of searching books of different technologies, and choose a better technology for library intelligence, as shown in Figure 9.

Based on the above information, it is not difficult to see that the GA-RFID technology has considerable advantages when searching for books.

The processing time of this technology is shorter whether it is facing a large number of books or a small number of books. This high-efficiency result can bring a better sense of experience to readers, and books the staff in the museum can

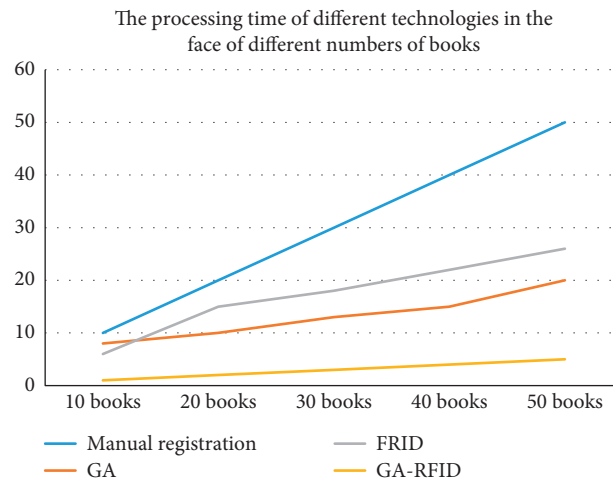


FIGURE 9: The processing time of different technologies in the face of different numbers of books.

also greatly improve the efficiency of the staff when they work again.

## 7. Conclusion

For a library, the layout of the library is a very important issue. A good layout, such as quiet, bright, transparent, is the most important indicator for readers to evaluate a library. If you want to bring readers to have a better experience, it is necessary to continuously optimize and upgrade the layout of each space in the library. With the development of the Internet, a faster and better bridge can be established between books and readers, just like the intelligent library based on GA-RFID technology in this article can help libraries save manpower and material resources to a certain extent, and at the same time, more importantly, it can give readers a better sense of experience and higher processing efficiency. This technology not only helps libraries upgrade their intelligence but can also apply this technology to other fields to achieve the purpose of improvement. The intelligent effect and operational efficiency of the library realized through GA-RFID technology will only be better. Furthermore, with the introduction of Learning Commons in library, this GA-RFID technology would be expected to be transplanted into the management of spatial units of Learning Commons, replacing the objects “books” with spatial units of Learning Commons, and it will be possible to be utilize the efficient use and visual management of Learning Commons

## Data Availability

The experimental data used to support the findings of this study are available from the corresponding author upon request.

## Conflicts of Interest

The authors declare that they have no conflicts of interest regarding this work.

## Acknowledgments

This work was supported by the JST SPRING (Grant no. JPMJSP2136).

## References

- [1] P. J. Fagan, E. Hauptman, R. Shapiro, and A. Casalnuovo, “Using intelligent/random library screening to design focused libraries for the optimization of homogeneous catalysts: Ullmann ether formation,” *Journal of the American Chemical Society*, vol. 122, no. 21, pp. 5043–5051, 2000.
- [2] H. Chen, J. Zhang, S. J. Cai, and D. Wang, “The influence from water supply system to the overall layout of the residential building in village,” *Advanced Materials Research*, vol. 798–799, pp. 1174–1177, 2013.
- [3] J. Scheffczyk, P. Schäfer, L. Fleitmann et al., “COSMO-CAMPD: A framework for integrated design of molecules and processes based on COSMO-RS,” *Molecular Systems Design & Engineering*, vol. 3, 2018.
- [4] E. Couto, M. L. Calijuri, P. Assemany, and P. R. Cecon, “Evaluation of high rate ponds operational and design strategies for algal biomass production and domestic wastewater treatment,” *The Science of the Total Environment*, vol. 791, Article ID 148362, 2021.
- [5] J. L. Gay, K. E. Carmichael, C. C. LaFlamme, and P. J. O’Connor, “Novel use of radio frequency identification (RFID) provides a valid measure of indoor stair-based physical activity,” *Applied Ergonomics*, vol. 95, Article ID 103431, 2021.
- [6] Y.-C. Lai and L.-Y. Hsiao, “General binary tree protocol for coping with the capture effect in RFID tag identification,” *IEEE Communications Letters*, vol. 14, no. 3, pp. 208–210, 2010.
- [7] X. Ning, K. Gong, W. Li, L. Zhang, X. Bai, and S. Tian, “Feature refinement and filter network for person re-identification,” *IEEE Transactions on Circuits and Systems for Video Technology*, vol. 31, no. 9, pp. 3391–3402, 2021.
- [8] G. Chen, L. Wang, and M. M. Alam, “Intelligent group prediction algorithm of GPS trajectory based on vehicle communication,” *IEEE Transactions on Intelligent Transportation Systems*, vol. 22, no. 7, pp. 3987–3996, 2020.

- [9] D. Rand and I. Cooper, "Caspase-1: an important player and possible target for repair of the blood-brain barrier underlying neurodegeneration," *Neural Regeneration Research*, vol. 16, no. 12, pp. 2390–2392, 2021.
- [10] A. Maitra, M. R. Kamdar, D. M. Zulman et al., "Using ethnographic methods to classify the human experience in medicine: A case study of the presence ontology," *Journal of the American Medical Informatics Association*, vol. 28, no. 9, pp. 1900–1909, 2021.
- [11] G. Kuang and Z. Sun, "Management information system, Internet of things, RFID technology, radio frequency identification, non-contact automatic identification, wireless sensor networks," *Astronomy & Astrophysics*, vol. 565, no. 9, pp. 89–93, 2014.
- [12] A. P. Renold and R. J. Rani, "An internet based RFID library management system," in *Proceedings of the 2013 IEEE Conference on Information & Communication Technologies*, pp. 932–936, Thuckalay, India, 11-12 April 2013.
- [13] C. Nichols, "Self-help groups as platforms for development: The role of social capital," *World Development*, vol. 146, Article ID 105575, 2021.
- [14] R. Anemone, C. Emerson, and G. Conroy, "Finding fossils in new ways: An artificial neural network approach to predicting the location of productive fossil localities," *Evolutionary Anthropology: Issues, News, and Reviews*, vol. 20, no. 5, pp. 169–180, 2011.
- [15] B. H. Lee, R. Wang, I. M. Moberg et al., "A species-specific functional module controls formation of pollen apertures," *Nature plants*, vol. 7, no. 7, pp. 966–978, 2021.

## Research Article

# 3D Reconstruction Method of Virtual and Real Fusion Based on Machine Learning

Wenyao Zhu  and Shuyue Zhou 

College of Engineering, Lishui University, Lishui 323000, Zhejiang, China

Correspondence should be addressed to Wenyao Zhu; [zwj@lsu.edu.cn](mailto:zwj@lsu.edu.cn)

Received 9 March 2022; Revised 6 April 2022; Accepted 18 April 2022; Published 19 May 2022

Academic Editor: Man Fai Leung

Copyright © 2022 Wenyao Zhu and Shuyue Zhou. This is an open access article distributed under the Creative Commons Attribution License, which permits unrestricted use, distribution, and reproduction in any medium, provided the original work is properly cited.

With the continuous development of computer vision technology, people are paying more and more attention to the method of using computers to simulate actual 3D scenes, and the requirements for 3D reconstruction technology are getting higher and higher. Virtual and real fusion refers to combining the virtual environment generated by the computer with the actual scenes around the user through photoelectric display, sensors, computer graphics, multimedia, and other technologies. This is a technology that can obtain more convenient and direct expressions, and it is also a technique for expressing content more abundantly and accurately. The key to virtual and real fusion technology is the registration of virtual objects and real scenes. It means that the system should be able to correctly estimate the position and posture of the camera in the real world, and then place the virtual object where it should be. Machine learning is a multifield interdisciplinary subject that specializes in how computers simulate or realize human learning behaviors. It is the core of artificial intelligence and the fundamental way to make computers intelligent. Its applications are in all the fields of artificial intelligence. This article introduces the virtual-real fusion 3D reconstruction method based on machine learning, compares the performance of the method with other algorithms through experiments, and draws the following conclusion: the algorithm in this study is the fastest, with an average speed of 72.9% under different times. To evaluate the image acquisition indicators of each algorithm, the algorithm in this study has the lowest error rate. The matching accuracy of each algorithm is tested, and it is found that the average matching accuracy of the algorithm in this study is about 0.87, which is the highest.

## 1. Introduction

*1.1. Background.* The twenty-first century is the information century and the Internet century. Computer technology is increasingly inseparable from people's daily life and has become a part of their lives. Whether it is military, education, etc., which are related to the country's centuries-old plan, or life, shopping, and people's other livelihoods, computer technology plays a very important role. With the vigorous development of applications such as virtual reality, 3D animation, three-dimensional measurement, virtual teaching, photomicrography, computer fluid mechanics, and military simulation, the research on the fusion of virtual

and real three-dimensional reconstruction technology under different backgrounds has become more and more important. The research of 3D reconstruction has experienced the initial modeling of small and medium-sized objects, followed by the modeling of large buildings. The three-dimensional reconstruction of indoor scenes has been developed for many years in the field of scientific research. In this process, various implementation methods have been proposed and improved. Many scholars have proposed various 3D reconstruction methods. Among them, the three-dimensional reconstruction technology based on the machine learning theory algorithm has the advantages of small error, high degree of restoration, and good stability.

*1.2. Significance.* As a new technology in the Internet era, 3D reconstruction technology is developing rapidly. Three-dimensional reconstruction is an important communication bridge between the computer and the real scene and plays an important role in the interaction between virtual reality and humans and computers. At the same time, it can effectively guide human life and is widely used in various fields. Three-dimensional reconstruction is a reverse engineering from reality to the virtual world. The combination of virtual and real means to combine the virtual world of 3D reconstruction with reality to present a good visual effect, which is of great significance to industries such as medicine, artificial intelligence, and education. Machine learning is the core of artificial intelligence, which is the basic method to make computers intelligent. Machine learning mainly studies the methods of computer simulation or implementation of human learning actions to learn new knowledge and skills. The virtual-real fusion 3D reconstruction technology based on machine learning can shorten the image matching time, reduce the error rate of image matching, and increase the accuracy of image matching. The research of virtual and real 3D reconstruction technology based on machine learning can improve the efficiency of 3D reconstruction and bring a better experience to technicians, which has important practical significance.

*1.3. Related Work.* The emergence of 3D reconstruction technology has had a significant impact on the fields of artificial intelligence, robotics, and unmanned driving. So far, many scholars have researched it. Watanabe T used a focused ion beam scanning electron microscope to examine the three-dimensional organization of GAG chains in the Achilles tendons of mature rats embedded with epoxy resin. After staining with cupra iron blue, he specifically dyed the GAG chain. He also used 250 serial backscattered electron images (at 10 nm intervals) in the longitudinal section for reconstruction. The three-dimensional image shows that the GAG chain forms a ring-shaped network structure, each ring surrounds the collagen fibrils in the d-band and merges with adjacent rings to form a planar network. The disadvantage of this study is the lack of practical data support [1]. Zhu et al. set up two sets of experiments to compare and analyze the degree of agreement between the three-dimensional reconstruction data and the actual tumor classification found after surgery, as well as the difference between the estimated liver volume of the two-dimensional and three-dimensional images. The average intraoperative blood loss, operation time, and extubation time were significantly reduced, but there was no statistical difference in the postoperative hospital stay and the total complication rate between the two groups. Among the patients in the observation group, the coincidence rate of the bismuth Colette classification by three-dimensional reconstruction and the actual results was 86.7%. There was no statistical difference between the estimated hepatectomy volume calculated by the two-dimensional and three-dimensional techniques. It is concluded that the three-dimensional reconstruction can provide accurate preoperative evaluation

for hilar cholangiocarcinoma. It has certain guiding significance for the surgical treatment of hilar cholangiocarcinoma [2]. Ficker Tomá outlines various microreconstruction techniques based on optical sectioning. He used graphical and numerical methods to compare the 3D copy of this special reconstruction frequency method with the 3D copy of the confocal method. Based on comparative studies, it was concluded that the quality of conventional replicas of surfaces with moderately high irregular textures is acceptable, and it is almost the same quality as the confocal replica, but the disadvantage of this experiment is the lack of detailed design [3]. Zhang et al. introduced the high-precision reconstruction method of sinusoidal motion and the factors that affect the reconstruction accuracy. First, he established a stereo vision reconstruction error model that considered delay time, frequency, amplitude, and parallax. He analyzed theoretically and experimentally the accuracy of sinusoidal motion reconstruction considering subpixel interpolation in the entire cycle. Peak recognition is the key to sinusoidal motion reconstruction, with the highest accuracy. But the experiment is more complicated and not practical [4]. Min et al. studied the impact of 23G minimally invasive vitrectomy assisted by optical coherence tomography three-dimensional reconstruction on patients with proliferative diabetic retinopathy. The follow-up time was about 6 months. The operation time, intraoperative complication rate, and postoperative complication rate of the observation group were significantly lower than those of the control group. The BCVA of the observation group was significantly higher than that of the control group, while the intraocular pressure and retinal thickness were significantly lower than that of the control group. In summary, with the aid of OCT three-dimensional imaging, 23G surgery for PDR can improve the efficacy and reduce complications [5]. Terao et al. have developed an accurate method for three-dimensional reconstruction of microstructures to analyze mass transfer phenomena in the microporous layer (MPL). The method he proposed involves the use of focused ion beam scanning electron microscopy tomography. He used the reconstruction results to perform numerical calculations on the structure and mass transfer characteristics of MPL and found that these results are in good agreement with the experimental results, which proves the accuracy of the new method. The disadvantage of this method is that it has higher requirements for the experimental environment [6]. In recent years, there has been a large amount of literature outlining the use of three-dimensional (3D) reconstruction and printing techniques. However, precise guidance articles describing the step-by-step method of reconstructing 3D images from computed tomography (CT) or magnetic resonance imaging (MRI) are still limited. To solve these problems, Chen D described a detailed agreement. This agreement will allow readers to easily perform 3D reconstructions in their future research. It allows investigation of appropriate surgical anatomy and allows innovative design of new screw fixation techniques or preoperative surgical planning. The experiment is innovative but the description of the agreement is not complete [7].

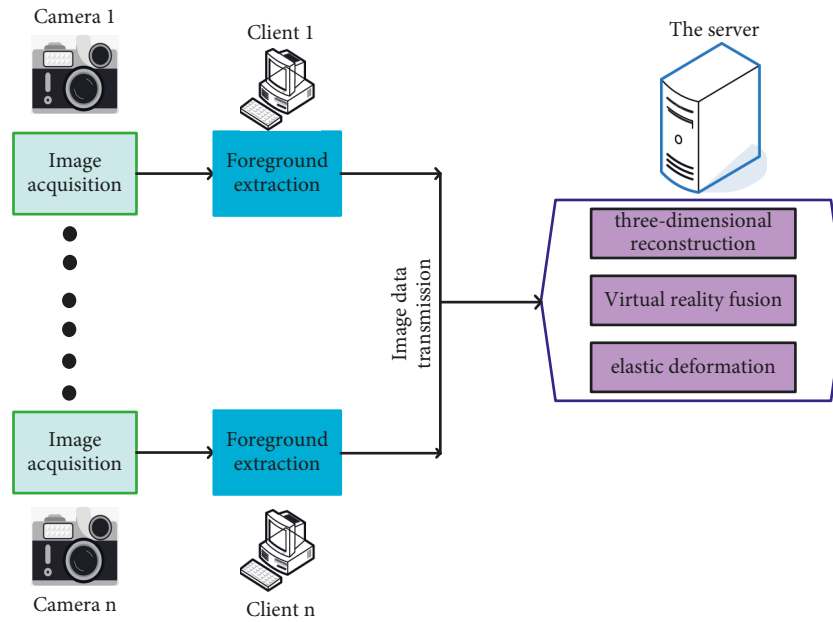


FIGURE 1: Three-dimensional reconstruction and virtual-real interaction design.

**1.4. Innovation.** The innovations of this article are: (1) This article combines machine learning with virtual and real 3D reconstruction technology. This article introduces the virtual and real 3D reconstruction algorithm based on machine learning and explains the algorithm process. (2) This article designs a comparative experiment. The virtual-real fusion 3D reconstruction algorithm based on machine learning is compared with other commonly used algorithms to verify the superiority of the performance of the virtual-real fusion 3D reconstruction algorithm based on machine learning.

## 2. 3D Reconstruction Method of Virtual and Real Fusion Based on Machine Learning

### 2.1. 3D Reconstruction and Fusion of Virtual and Real

#### 2.1.1. Overview of 3D Reconstruction and Virtual-Real Fusion

(1) *Three-dimensional reconstruction.* Generally speaking, the 3D reconstruction technology first uses the vision sensor to obtain the image information in the real world and then obtains the 3D information of the object through techniques such as information matching in the 3D reconstruction. This means that 3D reconstruction is a computer vision method that uses 2D projection to recover 3D information. There are many types of 3D reconstruction techniques, but generally speaking, they can be divided into two types: non-contact method and non-contact method. The non-contact method can be divided into active vision and passive vision. There are more subdivided types, so I will not repeat them here [8].

(2) *Fusion of virtual and real.* The fusion of virtuality and reality, as the name suggests, refers to the fusion of computer-generated virtual objects with real scenes. The most important thing in the fusion of virtual and real is the

presentation of the fusion of virtual and real. The virtual and real fusion presentation includes the rendering of the virtual model and the occlusion processing of the virtual and real targets.

For the occlusion processing part, the result of virtual and real fusion must correctly simulate the relationship between occlusion and occlusion of virtual objects in the actual scene. The correct occlusion relationship is an important condition for achieving excellent fusion effects. However, most of the existing virtual and real fusion systems only overlap the virtual object with the actual scene image, so the virtual image always obstructs the actual scene. Once there is a real object that is closer to the virtual object, the wrong occlusion relationship will be highlighted and will seriously affect the perception.

The rendering of the virtual model affects the integration of the virtual target in the real environment, including information such as color and lighting. Due to the rapid development of computer graphics technology, many types of rendering technologies have emerged, and people can choose according to the desired effect of the image [9].

**2.1.2. Three-Dimensional Reconstruction and Virtual-Real Fusion Structure Design Method.** The design of 3D reconstruction and virtual-real interaction is shown in Figure 1. The system consists of a client host, a camera, and a server. The modeling service sends instructions to the client. Multiple client programs extract images collected by multiple cameras. Then the client sends the data to the server and the server uses the relevant 3D reconstruction algorithm to reconstruct the space to realize the interaction of virtual elastic objects. In this process, a three-dimensional reconstruction method with the combination of virtual and real can be realized.



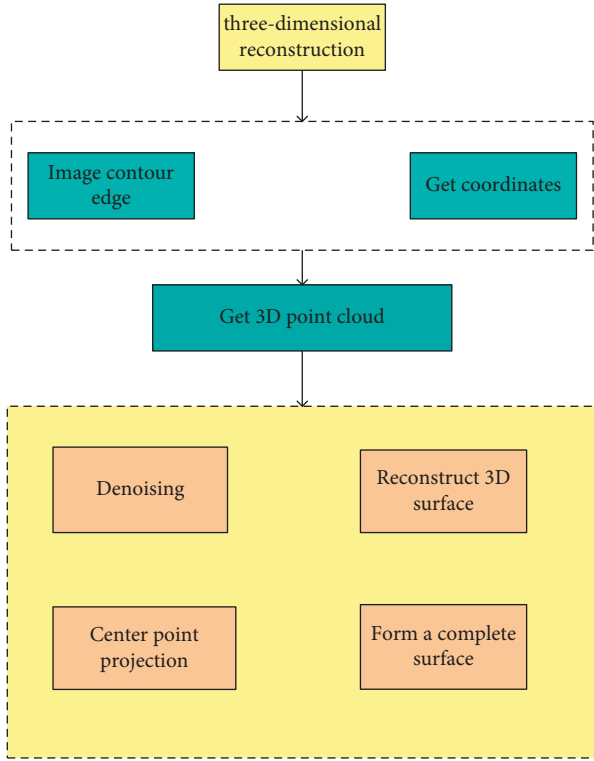


FIGURE 3: Three-dimensional reconstruction process.

fitting function of the approximate point set is  $x$ , the point set is split and the approximate fitting function is as follows:

$$\eta_x = \sum_c p(x)\partial^c \quad (8)$$

where  $\eta_x$  is the fitting function,  $\partial$  means the number of basis functions, and  $p$  means the number of point sets [15].

**2.3. Model Matching 3D Reconstruction Technology Based on Machine Learning.** This section introduces the 3D reconstruction method based on model matching. Based on the segmentation of the two-dimensional image, the image of the indoor scene elements is extracted and then the three-dimensional model is matched through the convolutional neural network based on machine learning. Finally, the extracted matching model is combined with the virtual three-dimensional model constructed by the computer [16] and the final three-dimensional reconstruction product is obtained.

**2.3.1. Foundation of Convolutional Neural Network.** A convolutional neural network is an efficient recognition method that has been developed in recent years and has attracted widespread attention. It is one of the more popular deep learning architectures in recent years, which is inspired by the visual perception of the human brain in the real world. The convolutional neural network can obtain the effective information of the original image. That is, without or after less preprocessing, some reliable rules can be distinguished from the original image [17]. Machine learning is

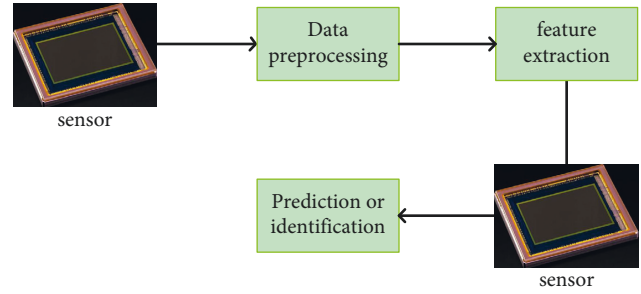


FIGURE 4: Basic problem solving process of machine learning.

a theory that learns knowledge and skills through a series of computer research and continues to improve. The idea of solving the problem is roughly shown in Figure 4. First, the sensor performs data preprocessing, then features extraction, and finally performs prediction or recognition instructions. However, most of the machine learning is a manual selection of features, which not only requires time and effort. The characteristics of manual selection are not necessarily effective, and the selection is almost random. Therefore, people put forward the concept of deep learning on this basis. Deep learning itself is a field of machine learning.

The following introduces a very important unit module convolution layer in the convolutional neural network [18], the following is the formula for convolution forward calculation:

$$x_j^l = F\left(\sum_{i=m_j} x_j^{l-1} * k_{i,j}^l + b_j^l\right). \quad (9)$$

The following is the residual calculation formula of the convolutional layer:

$$\delta_j^l = \beta_j^{l+1}(F(\mu_j^l) \cdot \text{up}(\delta_j^{l+1})). \quad (10)$$

Among them, the  $l+1$  layer is extended to an operation of the same size as the  $l$  layer. The following is the gradient calculation formula of the convolutional layer:

$$\frac{\partial E}{\partial b_j} = \sum_{u,v} (\delta_j^l)_{uv}, \quad \frac{\partial E}{\partial k_{i,j}^l} = \sum_{u,v} (\delta_j^l)_{uv} (p_i^{l-1})_{uv}. \quad (11)$$

**2.3.2. Model Matching Method Based on Convolutional Neural Network.** Model matching refers to the establishment of a corresponding relationship between image pairs based on the extracted features. That is, the imaging points of the same physical space point in two different images are mapped one by one.

The next stage of the work is to compare the 3D model that is most similar to the known image blocks in the 3D model library. It configures it in an appropriate position to reconstruct the three-dimensional scene. A model matching method based on a convolutional neural network is proposed here. Since the detailed classification categories contained in different scene elements are different, to



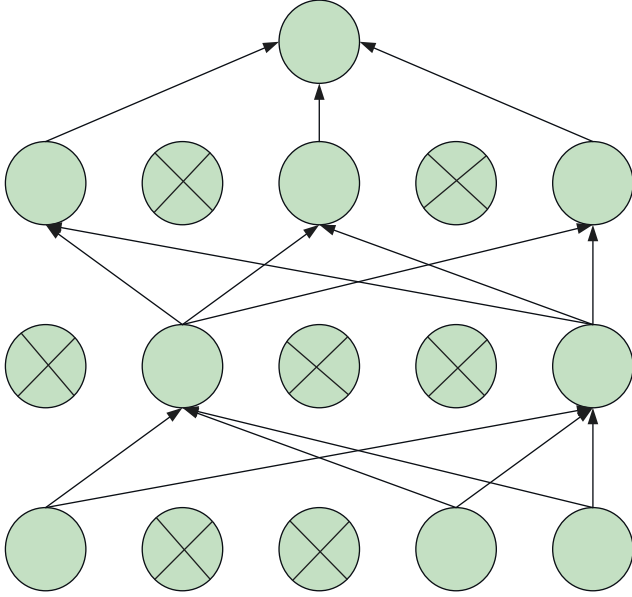


FIGURE 5: Dropout diagram.

achieve the purpose of classification and matching, the network structure of different elements themselves is designed [19]. The following is a summary of the important modules of the network structure.

(1) *Pooling*. As a result of pooling, features are reduced. The parameter reduction is to maintain a certain invariance (such as rotation, translation, etc.) in the process of image processing at each layer. Its error generation in feature extraction mainly comes from two aspects: one is the variance of the estimated value caused by the limited size of the neighborhood. The second is the deviation of the estimated value caused by the parameter error of the convolutional layer. According to the characteristics of the problem in this article, we choose max pooling as the downsampling layer here.

(2) *Dropout layer*. The dropout method is a breakthrough in the field of deep learning. Figure 5 is a schematic diagram of Dropout. It refers to temporarily suspending the state of certain neurons with a certain probability during the training process so that these neurons are temporarily separated from the information transmission process of this neural network. These neurons are temporarily ignored, but their weights must be maintained and continue to participate in the work during the next sample input [20].

(3) *Activation function*. The activation function is very important for the artificial neural network model to learn and understand very complex and non-linear functions. They introduce nonlinear characteristics into our network. Its main purpose is to convert the input signal of a node in the A-NN model into an output signal. This output signal is now used as the input for the next layer in the stack. In this chapter, an activation function is added after each convolutional layer of the network structure [21]. The RELU function is selected here, and its formula is:

$$f(x) = \max(0, x). \quad (12)$$

The advantage of this function is high efficiency and a small amount of calculation.

2.3.3. *Interactive Image Semantic Segmentation and Annotation*. To segment the RGBD image obtained by the user into labeled image blocks, we use a conditional random field (CRF) model to solve the labeling problem. The conditional random field energy function for label  $C$  is as follows:

$$E(C) = \sum_i E_1(C_i; X_i) + \lambda E_2(C_i; X_j), \quad (13)$$

where  $E_1(C_i; X_i)$  represents the possibility that pixel  $i$  belongs to the category and is the feature of pixel  $i$ .  $E_2(C_i; X_j)$  is a compatibility item, which measures the consistency of the categories between two adjacent pixels.

(1) *Principle of semantic segmentation*. Semantic segmentation is a typical computer vision problem. It involves taking some raw data (e.g., flat images) as input and converting them into a mask with highlighted regions of interest. What is evaluated is the possibility that the feature of pixel  $i$  belongs to the category label [22]. It is composed of the sum of two data items, the appearance model and the geometric model, which are obtained by the color information and the depth map information obtained by the depth camera:

$$E_1(C_i; X_i) = E_a(C_i; X_i^a) + E_g(C_i; X_i^g). \quad (14)$$

The former item represents the appearance item and the latter item represents the geometric item. For the local appearance feature, the local color information is used to compute the geometric feature. The appearance term is calculated as follows:

$$E_a(C_i; X_i^a) = -\log(1 - \alpha_p) p(C_i | X_i^a) + \alpha_p p(C_i | X_i^a). \quad (15)$$

We extract SIFT features from each pixel in the RGB image and the depth image. Then connect them into RGBD SIFT features, and use a two-layer neural network and a supervised learning method of cross-entropy loss function to calculate. We combine the classification results of all pixels as the result of image segmentation, and then use RGB data to perform K-means operation [23]. The calculation formula is as follows:

$$p(C_i | X_i^a) = \frac{1/(-d(X_i^a, C_i) + \epsilon)}{\sum_j 1/(-d(X_i^a, C_j) + \epsilon)}, \quad (16)$$

where  $d(X_i^a, C_i)$  represents the distance between the current RGB pixel and the nearest cluster center and  $\epsilon$  is a minimal parameter.

The calculation formula for geometric terms is as follows:

$$E_g(C_i; X_i^g) = -\log(1 - \alpha_g) p(C_i | X_i^g) + \alpha_g p(C_i | X_i^g). \quad (17)$$

TABLE 1: Hardware configuration.

| Equipment | To configure  |
|-----------|---|
| Kinect    | Microsoft kinect for Xbox<br>Kinect power adapter                   |
| Computer  | Operating system:Windows 7 64 bit<br>CPU:i5-4200U,1.6GHZ<br>RAM: 4G |

$p(C_i|X_i^g)$  is trained from the depth data of the scene data set and  $p(C_i|X_i^g)$  is the segmentation result of the previous layer [24].

The basic plane image is used to extract local geometric features instead of local depth data because the basic plane image has less noise than the depth data. The information extraction of the basic floor plan uses the more efficient RANSAC algorithm.

Compatibility items are used to enhance the smoothness of labels between adjacent pixels. The calculation method is as follows:

$$E_2(C_i:C_j) = d(C_i \neq C_j) \text{sim}(F_i:F_j). \quad (18)$$

Among them,  $F_i = [r, g, b, t]^T$ , where  $F_i$  is the connection vector of the RGB value and the depth value at pixel  $i$ . The similarity calculation method between two pixels is:

$$\text{sim}(F_i:F_j) = \exp\left(-\frac{F_i - F_j^2}{2d^2}\right), \quad (19)$$

where,  $d$  is the average distance between features [25].  $F_i$  and  $F_j$  respectively refer to two pixels and the similarity of these two pixels is calculated by exp.

### 3. 3D Reconstruction Technology Experiment Based on Virtual and Real Fusion Based on Machine Learning

#### 3.1. Test System Design

**3.1.1. Hardware Platform Configuration.** The experimental system of this study uses Kinect sensor as the input device to obtain depth data, and the processing part uses a computer, and the computer reconstructs the obtained image data. This system only uses one Kinect device, no additional auxiliary equipment is needed, and the hardware platform is easy to build. In this experiment, holding the Kinect device to scan the object, or fixing the Kinect sensor, and rotating the target to realize the complete collection of object information. The hardware platform and configuration are shown in Table 1. Kinect sensors are superior in terms of performance and price, and computers with higher running memory are more suitable for 3D reconstruction.

The following focuses on the Kinect depth sensor, which is an important equipment in the experiment.

(1) *Kinect*. Kinect is a fusion of many current advanced machine vision technologies, which can collect the color and depth information of the object at the same time. Compared

TABLE 2: Kinect basic parameters.

| Characteristic specification | Parameter         |
|------------------------------|-------------------|
| Maximum frame rate           | 30 fps            |
| Depth range                  | 40 cm–400 cm      |
| Depth image resolution       | 640 × 480, 11 bit |
| Color image resolution       | 640 × 480, 8 bit  |

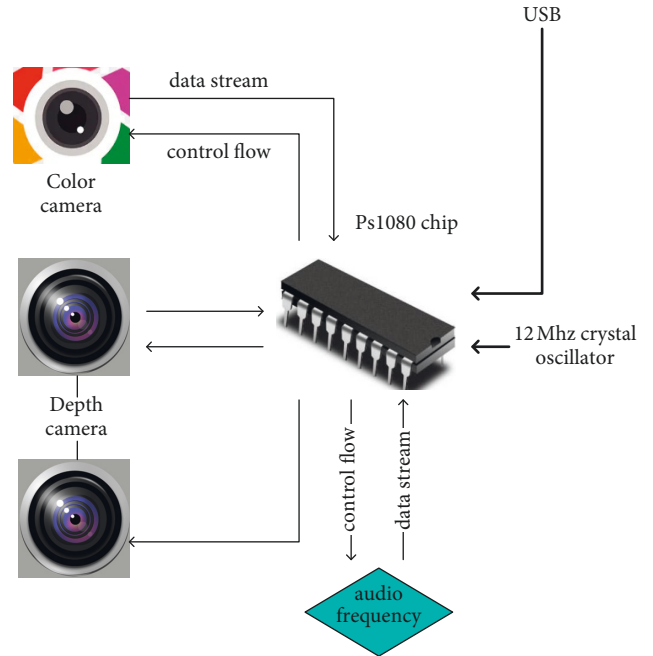


FIGURE 6: Kinect working principle diagram.

with other devices, Kinect is not only cheap but also can obtain high-resolution depth maps and color maps at the same time. The hardware structure is mainly divided into three parts. They are a system-on-chip, three cameras, and a four-element microphone array. The basic parameters of Kinect are shown in Table 2:

Kinect can obtain 640 \* 480 pixel depth information and color information at a frame rate of up to 30 fps. By combining the infrared CMOS sensor and the color camera, the three-dimensional information of the target can be projected onto the screen. Its working principle is shown in Figure 6:

The shooting frame rate of Kinect has reached 30 fps, which will not be a shortcoming of the system frame rate. The processing speed of the system is often lower than the input speed of the image, so the processing speed determines the frame rate of the final system. The main hardware factors that affect the frame rate are the video memory capacity and the number of cores of the graphics card. After testing on different devices, the results are shown in Table 3:

**3.1.2. Software Platform Configuration.** The development environment used in this article is Win7 64 bit, the development platform is Visual Studio 2010, and the interface is

TABLE 3: System frame rate.

| Memory size (GB) | Memory size (MB) | Number of CUDA cores | Frame rate (fps) |
|------------------|------------------|----------------------|------------------|
| 4                | 512              | 192                  | Cannot execute   |
| 4                | 1024             | 576                  | 12               |
| 8                | 2048             | 1344                 | 21               |

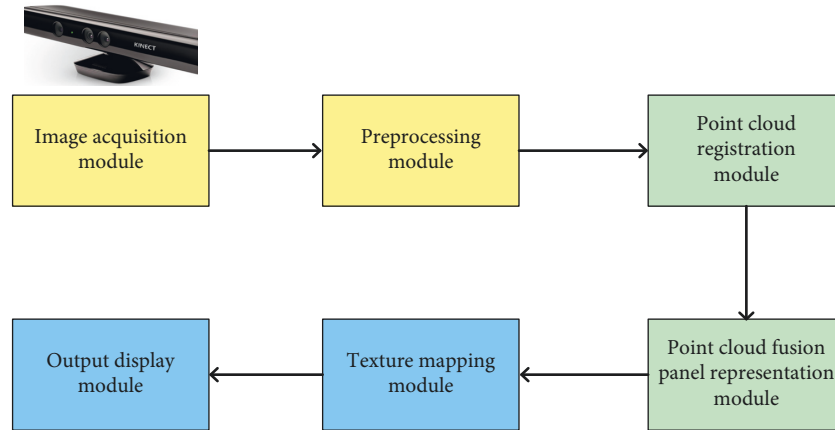


FIGURE 7: 3D reconstruction function module.

designed with Qt4.8. Although Microsoft provides a software development kit Kinect SDK and related drivers, these software development kits are mainly for somatosensory control, gesture recognition, tracking, and voice control. The latest Kinect SDK 1.7 is more powerful and also includes the realization of algorithms such as KinectFusion. The focus of this article is to achieve the three-dimensional reconstruction of the target object. The existing open-source library contains a large number of resources, which is convenient for learning and using.

**3.1.3. System Structure Design.** Although different methods use different 3D reconstruction techniques, the main process of 3D reconstruction is roughly the same. The system function module is shown in Figure 7:

The six functional modules we designed for the 3D reconstruction system are image acquisition module, registration module, surface extraction module, preprocessing module, texture mapping module, and output display module. Aiming at these six functional modules, the software architecture of the reconstruction system is designed. In this architecture, the Kinect sensor is first used to obtain depth image information and color image information. Since the image contains noise information, the data needs to be preprocessed. The depth information is coordinate-converted into 3D point cloud data and then filtering and denoising operation is performed, and then the registration and alignment operation is performed on the 3D point cloud data set under multiple viewing angles. After registration, the point cloud data is fused according to the corresponding spatial conversion relationship, and the color RGB image is used for texture mapping, so as to output a complete 3D reconstruction model of the target object.

**3.1.4. Comparative Test Design.** The experiment is based on the built hardware and software platform using Kinect sensors and computers to analyze the performance of the above-mentioned virtual-real fusion 3D reconstruction technology is based on machine learning, and the experiment selects other 3D reconstruction techniques for comparison to obtain the performance data of each algorithm, such as speed, error rate, correct rate, and other information, so as to understand whether the 3D reconstruction fusion method based on machine learning is more superior. The comparison algorithms selected in this experiment are SGM, SFM, and CMMs (coordinate measuring machines). These algorithms belong to different kinds of algorithms in 3D reconstruction and they are used frequently. The performance data of each algorithm is obtained through experiments, and the performance of the virtual and real 3D reconstruction algorithm based on machine learning is understood.

## 3.2. Test Results and Analysis

**3.2.1. Image Reconstruction Speed.** Testing the speed of image reconstruction in the figure below for each algorithm, increasing the number of experiments, calculating the average value of the speed under different number of experiments, and getting the speed data of each algorithm is shown in Figure 8:

According to the data in Figure 8, the speed of the 3D reconstruction algorithm based on machine learning in this article first slowly increases with the increase of the number of trials. After the number of times is greater than 30, the speed increases, and this algorithm is always faster than the other several algorithms. The average speed under different test times is 72.9%. Therefore, it is concluded that the 3D

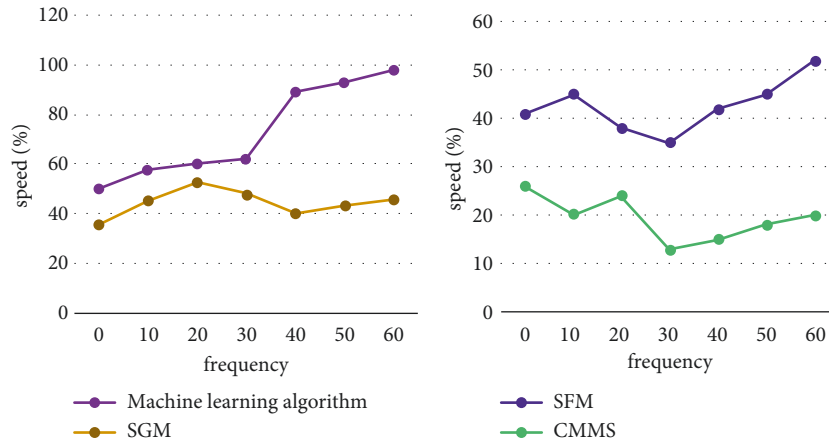


FIGURE 8: The speed of different algorithms.

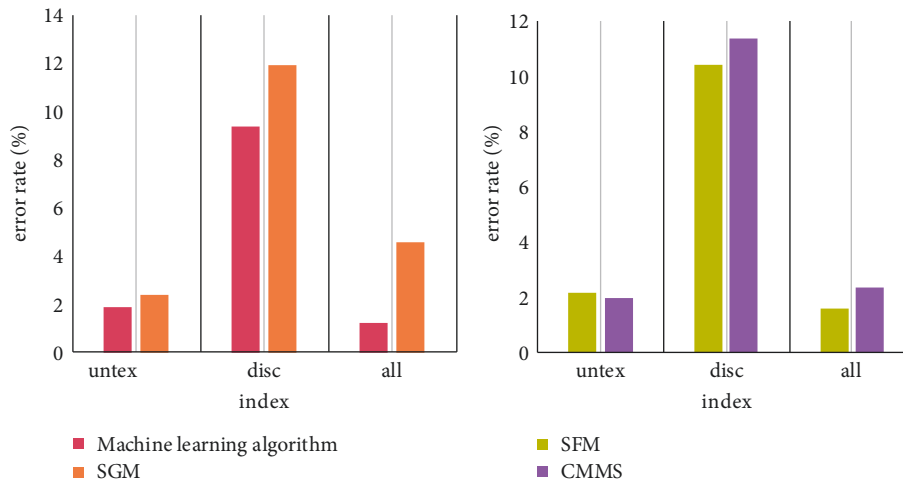


FIGURE 9: Evaluation values of various indicators in the image test set of different algorithms.

reconstruction algorithm based on machine learning can greatly reduce the image reconstruction time and increase the efficiency of 3D reconstruction processing.

**3.2.2. The Evaluation Value of Each Index in the Image Test Set.** In this part of the experiment, the experiment chose to compare 3 quantitative parameters, namely the non-texture area matching error percentage (untex), all pixel matching error percentage (all), parallax discontinuous area matching error percentage (disc) and matching, and the time used (time). The evaluation values of these indicators of the four algorithms are all measured, and the data obtained is shown in Figure 9:

It can be seen from Figure 9 whether it is the test result of the nontexture area matching error percentage, all pixel matching error percentage, or parallax discontinuous area matching error percentage. The error percentage of the 3D reconstruction algorithm based on machine learning is the lowest, among them, and 3d reconstruction algorithm based on machine learning has the lowest error rate on untex index and the highest error rate on disc. But the error rate for each indicator was less than 10%, which proves that the 3D

reconstruction algorithm based on machine learning has a low error rate and high efficiency.

**3.2.3. Accuracy Comparison.** In this part of the experiment, we put the reconstructed object indoors through the matching of indoor objects, tables, lamps, sofas, chairs, and beds to understand the matching accuracy of each algorithm and recorded the data. The results are shown in Figure 10:

It can be seen from Figure 10 that the 3D reconstruction algorithm based on machine learning has the highest matching accuracy no matter which object is in the room. Among them, the chair matching accuracy is the highest and the bed matching accuracy is the lowest. But the accuracy was better than 0.8 for any object. After calculation, for different objects, the average matching accuracy of the 3D reconstruction algorithm based on machine learning is about 0.87. The average matching accuracy of other algorithms SGM, SFM, and CMMS for different objects is about 0.84, 0.84, and 0.83, respectively. It can be seen that the accuracy of the matching rate of several algorithms is relatively close, but the accuracy of the 3D reconstruction algorithm based on machine learning is the best.

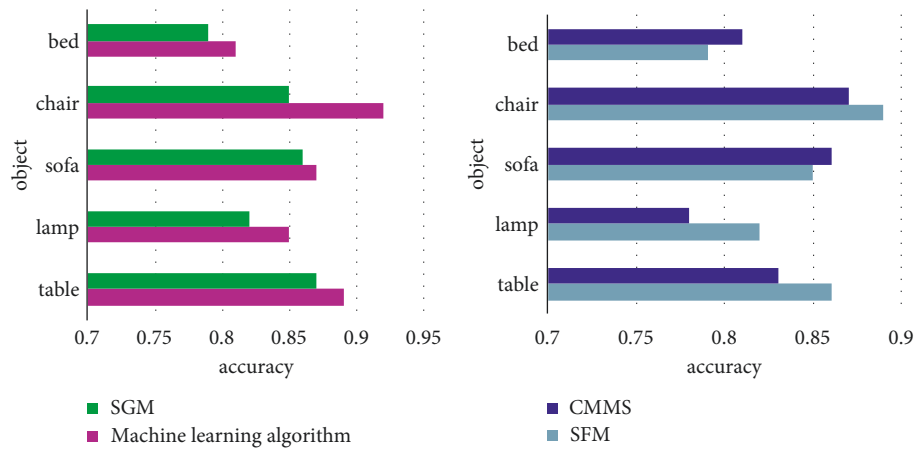


FIGURE 10: Matching accuracy of different algorithms.

#### 4. Discussion

The three-dimensional model is more superior than the two-dimensional image because the three-dimensional image has the advantage of more than one dimension, so the appearance and structure of the object can be expressed more clearly. For e-commerce, for example, businesses can construct a three-dimensional model to represent the appearance of the product, so that customers can gain a clearer and more intuitive understanding of the product. At the same time, 3D models can also be used in 3D movies, TV animations, medical imaging, and other fields. Also, the digital geometric processing of three-dimensional geometric data has become an important technology in the study of computer graphics, computer vision, and image processing. As a new form of information carrier, three-dimensional geometric models have gradually changed the way people explore and understand the world due to their unparalleled advantages such as high fidelity and intuitive visualization. The combination of 3D reconstruction technology and virtual and real fusion can combine the scene reconstructed by calculation with the real scene. This plays an important role in many fields such as augmented reality and artificial intelligence. Theories such as convolutional neural networks and deep learning in machine learning can be used in 3D reconstruction technology to improve the efficiency and accuracy of 3D reconstruction.

#### 5. Conclusion

This article introduces the background significance of virtual and real fusion and 3D reconstruction technology, as well as the combination of the two. This article introduces the theory of machine learning, combines the theory with 3D reconstruction, and introduces the 3D reconstruction algorithm based on machine learning. Finally, this article designs experiments and designs the hardware and software and basic architecture of the system. This article compares the 3D reconstruction algorithm based on machine learning with several other common algorithms and draws a conclusion as follows: (1) the 3D reconstruction algorithm based on machine learning is the fastest, with an average speed of 72.9% under different times. (2)

Evaluating the image acquisition indicators of each algorithm and finding that the error rate of the 3D reconstruction algorithm based on machine learning is low. (3) Testing the matching accuracy of each algorithm. The average matching accuracy of the 3D reconstruction algorithm based on machine learning is about 0.87, which is the highest. Experiments in this article verify the superiority of the performance of the 3D reconstruction algorithm based on machine learning, but there are a few performance indexes in the test. If more indexes are added, it will be more convincing, AND due to practical reasons, the equipment available for the experiment is limited. If given the chance, a better job can be made.

#### Data Availability

The experimental data used to support the findings of this study are available from the corresponding author upon request.

#### Conflicts of Interest

The authors declare that they have no conflicts of interest regarding this work.

#### Acknowledgments

This research was supported by Public Technology Application Research of Zhejiang Province (Project Code: LGG20F020020) and Lishui Major Research and Development Program (Project Code: 2019ZDYF03). These supports are appreciated. The authors also acknowledge the support from the government agencies during the research.

#### References

- [1] T. Watanabe, K. Kametani, Y.-i. Koyama, and D. Y. K. K. Suzuki, "Ring-mesh model of proteoglycan glycosaminoglycan chains in tendon based on three-dimensional reconstruction by focused ion beam scanning electron microscopy," *Journal of Biological Chemistry*, vol. 291, no. 45, pp. 23704–23708, 2016.
- [2] Y. Zhu, E. E. Roselli, J. J. Idrees, and S. L. Kapadia, "sCombined transapical transcatheter aortic valve

- replacement and thoracic endovascular aortic repair for severe aortic stenosis and arch aneurysm," *Aorta*, vol. 04, no. 05, pp. 175–177, 2016.
- [3] F. Tomá and M. Dalibor, "Three-dimensional reconstructions of solid surfaces using conventional microscopes," *Scanning*, vol. 38, no. 1, pp. 21–35, 2016.
  - [4] J. Zhang, P. Zhang, H. Deng, and J. Wang, "High-accuracy three-dimensional reconstruction of vibration based on stereo vision," *Optical Engineering*, vol. 55, no. 9, Article ID 091410, 2016.
  - [5] F. Min, X. Lu, and H. Hu, "Effect of three-dimensional reconstruction-assisted 23G micro-invasive vitrectomy in patients with proliferative diabetic retinopathy," *Experimental and Therapeutic Medicine*, vol. 13, no. 6, pp. 2912–2916, 2017.
  - [6] T. Terao, G. Inoue, M. Kawase, and N. M. K. T. K. Y. T. Kubo, "Development of novel three-dimensional reconstruction method for porous media for polymer electrolyte fuel cells using focused ion beam-scanning electron microscope tomography," *Journal of Power Sources*, vol. 347, no. 15, pp. 108–113, 2017.
  - [7] D. Chen, C.-H. Chen, L. Tang, and K. Y.-Z. K. A.-M. Wang, "Three-dimensional reconstructions in spine and screw trajectory simulation on 3D digital images: a step by step approach by using Mimics software," *Journal of Spine Surgery*, vol. 3, no. 4, pp. 650–656, 2017.
  - [8] M. Santagata, N. Sgaramella, I. Ferrieri, and G. G. S. Corvo, "Segmental sandwich osteotomy and tunnel technique for three-dimensional reconstruction of the jaw atrophy: a case report," *International Journal of Implant Dentistry*, vol. 3, no. 1, p. 14, 2017.
  - [9] L. Boissière, B. Moal, O. Gille, and E. M. I. V. J.-M. W. De-Roquefeuil, "Lumbar spinal muscles and spinal canal study by MRI three-dimensional reconstruction in adult lumbar spinal stenosis," *Orthopaedics and Traumatology: Surgery & Research*, vol. 103, no. 2, pp. 279–283, 2017.
  - [10] T. Guan, C. Fang, Z. Mo, and N. J. N. Xiang, "RETRACTED: long-term outcomes of hepatectomy for bilateral hepatolithiasis with three-dimensional reconstruction: a propensity score matching analysis," *Journal of Laparoendoscopic & Advanced Surgical Techniques*, vol. 26, no. 9, pp. 680–688, 2016.
  - [11] S. Usuki, K. Tamaki, and K. T. Miura, "Three-dimensional reconstruction by time-domain optical coherence tomography microscope with improved measurement range," *International Journal of Automation Technology*, vol. 11, no. 5, pp. 787–794, 2017.
  - [12] T. Simpfendorfer, Z. Li, C. Gasch, F. M. Droszol, and M. L. M. D. Müller, "Three-dimensional reconstruction of preoperative imaging improves surgical success in laparoscopy," *Journal of Laparoendoscopic & Advanced Surgical Techniques*, vol. 27, no. 2, pp. 181–185, 2017.
  - [13] D. Feng and W. Chen, "Structure filling and matching for three-dimensional reconstruction of buildings from single high-resolution SAR image," *IEEE Geoscience and Remote Sensing Letters*, vol. 13, no. 6, pp. 752–756, 2016.
  - [14] Y. Li, "Identification of solitary pulmonary nodule based on chest CT three-dimensional reconstruction," *Chest*, vol. 149, no. 4, p. A284, 2016.
  - [15] Z. Sun, Y. Qiao, and Z. Jiang, "An accurate Fourier-based method for three-dimensional reconstruction of transparent surfaces in the shape-from-polarization method," *IEEE Access*, no. 99, p. 1, 2020.
  - [16] P. Reischig and W. Ludwig, "Three-dimensional reconstruction of intragranular strain and orientation in polycrystals by near-field X-ray diffraction," *Current Opinion in Solid State & Materials Science*, vol. 24, no. 5, Article ID 100851, 2020.
  - [17] M. Yushan, Y. Alike, A. Keremu, and A. P. A. Abulaiti, "Precise rmunder assistance of three-dimensional reconstruction technology: a case report," *The Journal of Foot and Ankle Surgery*, vol. 59, no. 1, pp. 125–127, 2020.
  - [18] B. Tla, B. Vra, and D. BMC, "The impact of body-mass index on the frontal knee alignment estimation using three-dimensional reconstruction based on movement analysis," *The Knee*, vol. 27, no. 1, pp. 89–94, 2020.
  - [19] M. Jian, J. Dong, M. Gong, and H. L. Y. K.-M. Yu, "Learning the traditional art of Chinese calligraphy via three-dimensional reconstruction and assessment," *IEEE Transactions on Multimedia*, vol. 22, no. 4, pp. 970–979, 2020.
  - [20] F. D. León-Cázares, C. Kienl, and C. M. F. Rae, "Three-dimensional reconstruction of planar deformation features from single electron micrographs," *Metallurgical and Materials Transactions A*, vol. 51, no. 3, pp. 1163–1172, 2020.
  - [21] H. Wang, Y. Zhang, W. Ding et al., "Trends and influencing factors of perinatal birth defects in Huai'an from 2008 to 2020," *Journal of Zhejiang University. Medical Sciences*, vol. 50, no. 7, pp. 1–9, 2021.
  - [22] Z. Gu, J. Chen, and C. Wu, "Three-dimensional reconstruction of welding pool surface by binocular vision," *Chinese Journal of Mechanical Engineering*, vol. 34, no. 47, pp. 1–13, 2021.
  - [23] H. Almansour, W. Pepke, J. Rehm, and T. D. M. Bruckner, "Interrater reliability of three-dimensional reconstruction of the spine," *Orthopäde, Der*, vol. 49, no. 4, pp. 350–358, 2020.
  - [24] S. Li, Q. Wang, X. Wei, and Z. Q. Cao, "Three-dimensional reconstruction of integrated implosion targets from simulated small-angle pinhole images," *Optics Express*, vol. 28, no. 23, Article ID 34848, 2020.
  - [25] M. Sun and J. Zhang, "Single-pixel imaging and its application in three-dimensional reconstruction," *Infrared and Laser Engineering*, vol. 48, no. 6, Article ID 603003, 2019.

## Research Article

# A Multimixed Strategy Improved Sparrow Search Algorithm and Its Application in TSP

Weizheng Li <sup>1</sup>, Mengjian Zhang <sup>2</sup>, Jing Zhang <sup>1</sup>, Tao Qin,<sup>1</sup> Wei Wei,<sup>3</sup> and Jing Yang <sup>1,4</sup>

<sup>1</sup>Electrical Engineering College, Guizhou University, Guiyang 550025, China

<sup>2</sup>School of Computer Science and Engineering, South China University of Technology, Guangzhou 510006, China

<sup>3</sup>Power China Guizhou Electric Power Engineering Co., Ltd., Guiyang 550025, China

<sup>4</sup>Key Laboratory of Advanced Manufacturing Technology of Ministry of Education, Guizhou University, Guiyang 550025, China

Correspondence should be addressed to Jing Yang; [jyang7@gzu.edu.cn](mailto:jyang7@gzu.edu.cn)

Received 8 February 2022; Revised 25 March 2022; Accepted 6 April 2022; Published 18 May 2022

Academic Editor: Man Fai Leung

Copyright © 2022 Weizheng Li et al. This is an open access article distributed under the Creative Commons Attribution License, which permits unrestricted use, distribution, and reproduction in any medium, provided the original work is properly cited.

Aiming at the shortcomings of the sparrow search algorithm (SSA), such as falling into local optimum and slow convergence speed, an improved sparrow search algorithm based on multimixed strategy (MISSA) is proposed in this paper. In the initial stage, the iterative chaotic mapping is used to initialize the population in order to improve the diversity of population. In the foraging stage, the golden sine algorithm and nonlinear convergence factor strategy are introduced to optimize the discoverer-follower model, which make search process more comprehensive and extensive for the discoverer. The elite opposition-based learning strategy is used to update the optimal solution and the population obtained in each iteration to improve the self-learning ability of the algorithm. To verify the rationality of the multimixed strategy selection and efficiency of the proposed algorithm, MISSA is compared with three derived single-strategy improved algorithms, other improved SSAs, and five typical swarm intelligence algorithms using ten basic benchmark functions and CEC 2014 function. The optimization results, diversity analysis, and Wilcoxon rank-sum test results certify that the proposed MISSA has better optimization accuracy, convergence speed, and robustness than other compared methods. Moreover, the practicability and feasibility of MISSA are verified by solving the traveling salesman problem (TSP).

## 1. Introduction

**1.1. Research Background.** Optimization problems can be found in various fields, such as combinatorial optimization problems and engineering design problems. In general, the optimization problems and methods can be classified as shown in Figure 1. A general optimization problem can mathematically be described as follows [1]:

$$\begin{cases} \min F(x) = f_1(x), f_2(x), \dots, f_m(x), \\ g_i(x) \leq 0, i = 1, 2, \dots, p, \\ h_j(x) = 0, j = 1, 2, \dots, q, \\ x_l^i \leq x^i \leq x_u^i, i = 1, 2, \dots, N, \end{cases} \quad (1)$$

where  $x = (x_1, x_2, \dots, x_n)^T \in \Omega$  is the feasible solution with  $n$  decision variables or real parameters,  $F(x)$  is the function

with  $m$  objectives, and  $g_i(x)$  and  $h_j(x)$  are the  $i^{\text{th}}$  and  $j^{\text{th}}$  constraint functions, respectively.  $x_l^i \leq x^i \leq x_u^i$  is a bound constrained over the searching space  $x$ .

As shown in Figure 1, optimization methods are mainly based on mathematical methods or stochastic methods. Traditional mathematical methods are susceptible to type constraints and fall into the dimension disaster when solving high-dimensional problems, as well solve the multicriteria, nonlinear, and nondifferentiable problems [2, 3] with slight effectiveness. Metaheuristic algorithm benefits from the randomness of the optimization principle and can escape the local optimal solution when dealing with high-dimensional optimization problems. Metaheuristic algorithms also have the advantages of simple structure, high efficiency, and strong robustness. Therefore, many metaheuristic algorithms were proposed for solving the high-dimensional optimization problems.

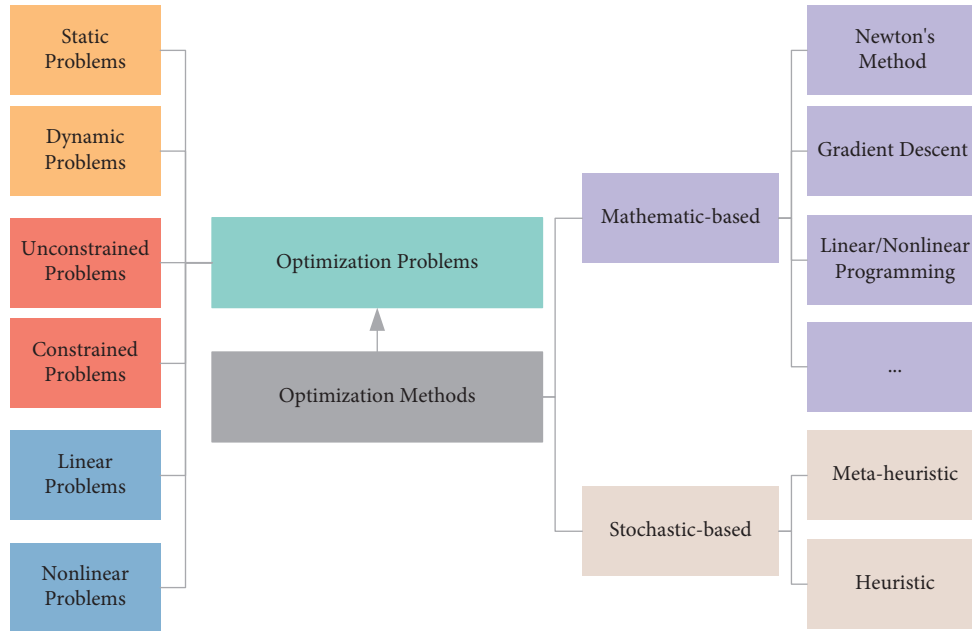


FIGURE 1: Classification of optimization problems and methods.

In general, metaheuristic algorithms are usually classified into four categories: (1) biological evolution-based algorithms, such as genetic algorithm (GA) [4] and differential evolution (DE) [5]; (2) physics-based algorithms, such as simulated annealing (SA) [6], black hole algorithm (BHA) [7], and Runge–Kutta optimizer (RUN) [8]; (3) human social behavior-based algorithms, such as teaching-learning-based optimization (TLBO) [9], imperialist competitive algorithm (ICA) [10], and Hunger Games Search (HGS) [11]; (4) swarm-based algorithms, such as particle swarm optimization (PSO) [12], ant colony optimization (ACO) [13], whale optimization algorithm (WOA) [14], grey wolf algorithm (GWO) [15], coot optimization algorithm (COOT) [16], naked mole-rat algorithm (NMR) [17], Harris Hawk Optimization (HHO) [18], slime mould algorithm (SMA) [19], and colony predation algorithm (CPA) [20].

The swarm-based algorithm simulates the behavior characteristics of a certain type of biological population in nature and performs random retrieval in the solution space to obtain the optimal solution. In addition, it is the focus of the metaheuristic algorithm due to its remarkable optimization performance and has been widely used in engineering optimization, image processing, machine learning, and other high-dimensional optimization fields.

The traveling salesman problem is a typical NP-hard combinatorial optimization problem, which was first proposed by Menger in 1959. TSP has attracted the attention of the operations research, logistics science, applied mathematics, computer science, graph theory, and other disciplines. TSP has an important practical significance and is widely used in logistics and distribution [21], aircraft route arrangement [22], integrated circuit wiring [23], and other fields, which can be solved by transforming them into TSP problems. Due to the high versatility and controllable complexity of TSP, it is used as a benchmark case to test the

ability of methods to deal with complex combinatorial optimization problems.

*1.2. Related Work.* The sparrow search algorithm is a new swarm-based algorithm proposed by Xue and Shen [24] in 2020, which was inspired by foraging and antipredation behavior of sparrow population. SSA has the advantages of few control parameters and high optimization precision. It has been used in the diagnosis on wheelset bearings [25], configuration of distributed generation [26], and gear fault detection [27]. But, the algorithm is prone to premature convergence in the later iterations and converges slowly when dealing with complex optimization problems.

In order to enhance the optimization ability of the sparrow algorithm, Liu et al. [28] proposed an enhanced sparrow algorithm based on the merit function mechanism for improving the accuracy of the tumor diagnosis identified by the convolutional neural network. Zhang and Ding [29] proposed a chaotic sparrow search algorithm to optimize the parameters for the stochastic configuration network, which has enhanced the regression performance. Mao and Zhang [30] introduced sine-cosine algorithm and Lévy flight strategy to balance the local and global exploitation ability of SSA. Lv et al. [31] enhanced the global search ability of SSA through Tent chaotic map, generated Tent chaotic sequence based on the stagnant solution, and finally applied the algorithm to image segmentation. Tang et al. [32] introduced the logarithmic spiral strategy, adopted an adaptive stepping strategy to balance the searching abilities, and then applied the algorithm to traditional engineering problems. Ouyang et al. [33] designed an adaptive sparrow search algorithm based on the lens reverse learning strategy and sine-cosine guidance mechanism, which has better optimization ability in robot path planning. Yuan et al. [34] proposed an



improved sparrow search algorithm which can track the maximum power point more accurately in the photovoltaic microgrid system.

Compared with the original SSA, the above improved sparrow algorithms have many improvements in the optimization ability. However, some shortcomings are summarized as follows:

- (1) Many researchers use the chaos theory to improve the diversity of the initial population but ignore the diversity of the population in subsequent iterations and the diversity analysis
- (2) The existing improvement strategies have not fundamentally changed the searching mechanism of SSA. The shortcoming of insufficient self-learning ability in SSA has not been improved
- (3) Some improved SSAs are only optimized for basic benchmark functions, which is not enough to explain the superiority and practicability of the improved algorithm

**1.3. Contribution.** To solve the above shortcomings, a novel multimixed strategy improved sparrow search algorithm is proposed in this paper, including four strategies: iterative chaotic mapping, golden sine algorithm, nonlinear convergence factor strategy, and elite opposition-based learning approach. The iterative chaotic map strategy is used to initialize the population in order to enhance the diversity of the population. The golden sine algorithm and nonlinear convergence factor strategies are used to improve the ability of discoverer-follower model for searching the solution space, which enhance the convergence speed and global exploration ability of the algorithm. The elite opposition-based learning strategy is used to update optimal solution and population to improve the diversity, self-learning ability, and local exploitation ability of the algorithm. In addition, we use MISSA to solve the traveling salesman problem. The innovations and main contributions of this paper are described as follows:

- (i) A novel MISSA is proposed in this paper, and four improved strategies of iterative chaotic map strategy, golden sine strategy, nonlinear convergence factor strategy, and elite opposition-based learning strategy are used to enhance the performance of the proposed algorithm for solving the complex optimization problems.
- (ii) Ablation experiments are designed to verify the specific impact of different strategies on population diversity and optimization performance of SSA.
- (iii) Comprehensive experiments are designed and accomplished to fully verify the efficiency of the MISSA by basic benchmark functions and CEC 2014 function. Eight algorithms are compared, including SSA, other improved SSAs, WOA, GWO, COOT, and PSO.
- (iv) MISSA is used to settle TSP, and the results verified the practicality of MISSA in solving the combinatorial optimization problem.

## 2. The Original Sparrow Search Algorithm

The original SSA algorithm was mainly inspired by foraging and antipredation behavior of sparrow population. The population of SSA can be divided into discoverers, followers, and scouts [24]. The discoverers with high fitness value are responsible for searching for food and guiding the migration direction of the population, which accounts for 10%–20% of the entire sparrow population, and others are followers. The followers search for food in the direction pointed by the discoverers, and in order to increase the predation rate, they will constantly monitor the discoverers and compete for food with high-intake individuals. The scouts belong to the discoverers and followers, usually about 10%–20% individuals randomly within the population to detect danger and alarm the population. When predators invade, they will chirp alarming signals to make the sparrow population migrate to the safe area.

The location of discoverers is updated as follows:

$$X_{i,j}^{t+1} = \begin{cases} X_{i,j}^t \cdot \exp\left(\frac{-i}{\alpha \cdot \text{iter}_{\max}}\right), & \text{if } R_2 < ST, \\ X_{i,j}^t + Q \cdot L, & \text{if } R_2 \geq ST, \end{cases} \quad (2)$$

where  $X_{i,j}^t$  denotes the position of the  $i^{\text{th}}$  sparrow in the  $j^{\text{th}}$  dimension under the current  $t^{\text{th}}$  iteration,  $\text{iter}_{\max}$  is the maximum number of iterations,  $\alpha \in (0, 1)$  is a random number, and  $R_2 \in [0, 1]$  and  $ST \in [0.5, 1]$  represent the alarm value and the safety threshold, respectively.  $Q$  is the migration control coefficient, which is a random number that obeys the standard normal distribution.  $L$  is a matrix of  $1 \times d$  for which each element inside is 1. If  $R_2$  is less than  $ST$ , it indicates the foraging environment is safe and the discoverers perform global search mode. If  $R_2$  is greater than or equal to  $ST$ , it indicates some individuals have detected predators and the discoverers will lead the population to migrate to the safe area quickly.

The location of followers is updated as follows:

$$X_{i,j}^{t+1} = \begin{cases} Q \cdot \exp\left(\frac{X_{\text{worst}}^t - X_{i,j}^t}{t^2}\right), & i > \frac{N}{2}, \\ X_p^{t+1} + |X_{i,j}^t - X_p^{t+1}| \cdot A^+ \cdot L, & \text{other}, \end{cases} \quad (3)$$

where  $X_{\text{worst}}^t$  represents the current global worst position and  $X_p^{t+1}$  denotes the optimal position of the discoverers in the  $(t+1)^{\text{th}}$  iteration.  $A$  is a matrix of  $1 \times d$  in which each element inside is 1 or  $-1$ , and  $A^+ = A^T (AA^T)^{-1}$ . When  $i$  is greater than  $N/2$ , it indicates that the  $i^{\text{th}}$  follower with a lower fitness value is most likely to be hungry, which needs to go to other areas for foraging.

The location of scouts is updated as follows:

$$X_{i,j}^{t+1} = \begin{cases} X_{\text{best}}^t + \beta \cdot |X_{i,j}^t - X_{\text{best}}^t|, & \text{if } f_i > f_g, \\ X_{i,j}^t + k \cdot \left(\frac{|X_{i,j}^t - X_{\text{worst}}^t|}{(f_i - f_w) + \varepsilon}\right), & \text{if } f_i = f_g, \end{cases} \quad (4)$$

where  $X_{\text{best}}^t$  represents the current global optimal position.  $\beta$  is the step size control coefficient, which is a normal distributed random number with a mean value of 0 and variance value of 1.  $k \in [-1, 1]$  is a random number which represents the direction of the sparrow movement.  $\varepsilon$  is the smallest constant for avoiding from zero-division error.  $f_i$  represents the fitness value of the current individual.  $f_g$  and  $f_w$  represent the current global optimal value and worst fitness value, respectively. When  $f_i$  is greater than  $f_g$ , it indicates the individual is on the fringe of the population and vulnerable to predators. If  $f_i$  is equal to  $f_g$ , it means the individuals in the center of the population are aware of the danger of being attacked by predators and need to fly closer to the safe area.

### 3. A Multimixed Strategy Improved Sparrow Search Algorithm

Through the research on the algorithm searching mechanism, the shortcomings of SSA are mainly caused by three aspects: the method of population initialization relies on a simple random number, which cannot provide good diversity for the population; the algorithm relies on the discoverer-follower model to search the solution space, which is slow and not comprehensive enough; the algorithm lacks the learning and upgrading mechanism of the optimal individual and does not make effective use of the optimal solution during the iteration process. Based on these aspects, this paper proposes four strategies to optimize the mechanism of the algorithm. The iterative chaotic map strategy is used to initialize the population, the golden sine algorithm and nonlinear convergence factor strategies are used to improve the discoverer-follower model, and the elite opposition-based learning strategy is used to update optimal solution and population.

**3.1. Iterative Chaotic Map Strategy.** The original SSA uses a random method to generate the initial position of the sparrow population, which is likely to cause uneven distribution of individuals, resulting in poor population diversity. Chaotic motion is characterized by pseudo-randomness, ergodicity, and high sensitivity to initial conditions and parameters [35, 36].

Chaotic mapping can be used to initialize the population to obtain good diversity. The iterative map has better chaotic ergodicity, hyperchaotic behavior, and high complexity. The Lyapunov exponent of the iterative map is better than one-dimensional maps such as Singer chaotic map, Tent chaotic map, and sinusoidal chaotic map [37]. The simulation results of four chaotic maps under 500 iterations are shown in Figure 2.

The chaotic variables generated by the Singer chaotic map have small periods and an uneven distribution phenomenon between 0.6 and 0.9. The Tent chaotic map has small periods and an unstable periodic phenomenon between 0 and 0.2, as well as the problem of easily falling into fixed points. The chaotic variables generated by the sinusoidal chaotic map have certain bimodal distribution characteristics, which are more evenly distributed in the middle of the chaotic attraction domain and densely

distributed at both ends. In contrast, the distribution of iterative mapping from 0 to 1 is the most uniform. Therefore, this paper uses the iterative chaotic map strategy to initialize the population, and the equation is as follows:

$$x_{i+1} = \sin\left(\frac{bx_i}{x_i}\right), \quad (5)$$

where  $b \in (0, 1)$  is the control parameter, which is usually set to 0.7.

**3.2. Golden Sine Algorithm Strategy.** The current environment is safe when the alarm value ( $R_2$ ) is under the safety threshold (ST), and the discoverers will lead the population to forage in this area. The algorithm performs deeper local exploitation of the current solution space. Local exploitation and global exploitation are two important stages of optimization algorithms. Excessive local exploitation will inhibit the tendency of algorithm to search for global optimal solution, and too much global exploitation will reduce the optimization accuracy.

The golden sine algorithm (Gold-SA) is a mathematical heuristic algorithm presented by Tanyildizi and Demir in 2017, which is inspired by the sine function and golden section coefficient [38]. The mathematical relationship between the unit circle and the sine function is shown in Figure 3. The coordinates on the sine function correspond to the  $y$ -axis coordinates of the point on the unit circle centered on the origin with a radius of 1. Gold-SA improves the global exploitation ability by traversing the points on the sine function which in turn traverses the points on the unit circle.

The golden section coefficient is widely used in the field of art because of its strict proportionality, artistry, and harmony. Gold-SA introduces the golden section coefficient to separate the solution space in each iteration. The coefficient with fixed shrink step does not require gradient information. Therefore, combining the sine function with the golden section coefficient can help Gold-SA comprehensively search the solution space where the optimal solution can be generated, thereby improving the local exploitation ability of algorithm. The key of Gold-SA is the golden section coefficient, which is represented by  $\theta_1$  and  $\theta_2$ . The mathematical expression is as follows:

$$\begin{aligned} \theta_1 &= a(1-h) + bh, \\ \theta_2 &= ah + b(1-h), \end{aligned} \quad (6)$$

where  $a$  and  $b$  are the initial values of the golden section; according to the relationship between the period of the standard sine function and the unit circle, we set  $a$  to  $\pi$  and  $b$  to  $-\pi$ .  $h$  is the golden section coefficient. The golden section coefficient will separate the solution space every time it goes through an iteration. The position update formula is as follows:

$$X_{i,j}^{t+1} = X_{i,j}^t \left| \sin(r_1) \right| - r_2 \sin(r_1) \left| \theta_1 \cdot X_p^t - \theta_2 \cdot X_{i,j}^t \right|, \quad (7)$$

where  $X_{i,j}^t$  represents the position of the  $i^{\text{th}}$  sparrow in the  $j^{\text{th}}$  dimension under the current  $t^{\text{th}}$  iteration.  $r_1$  and  $r_2$  are random numbers, where  $r_1 \in (0, 2\pi)$  and  $r_2 \in (0, \pi)$ .

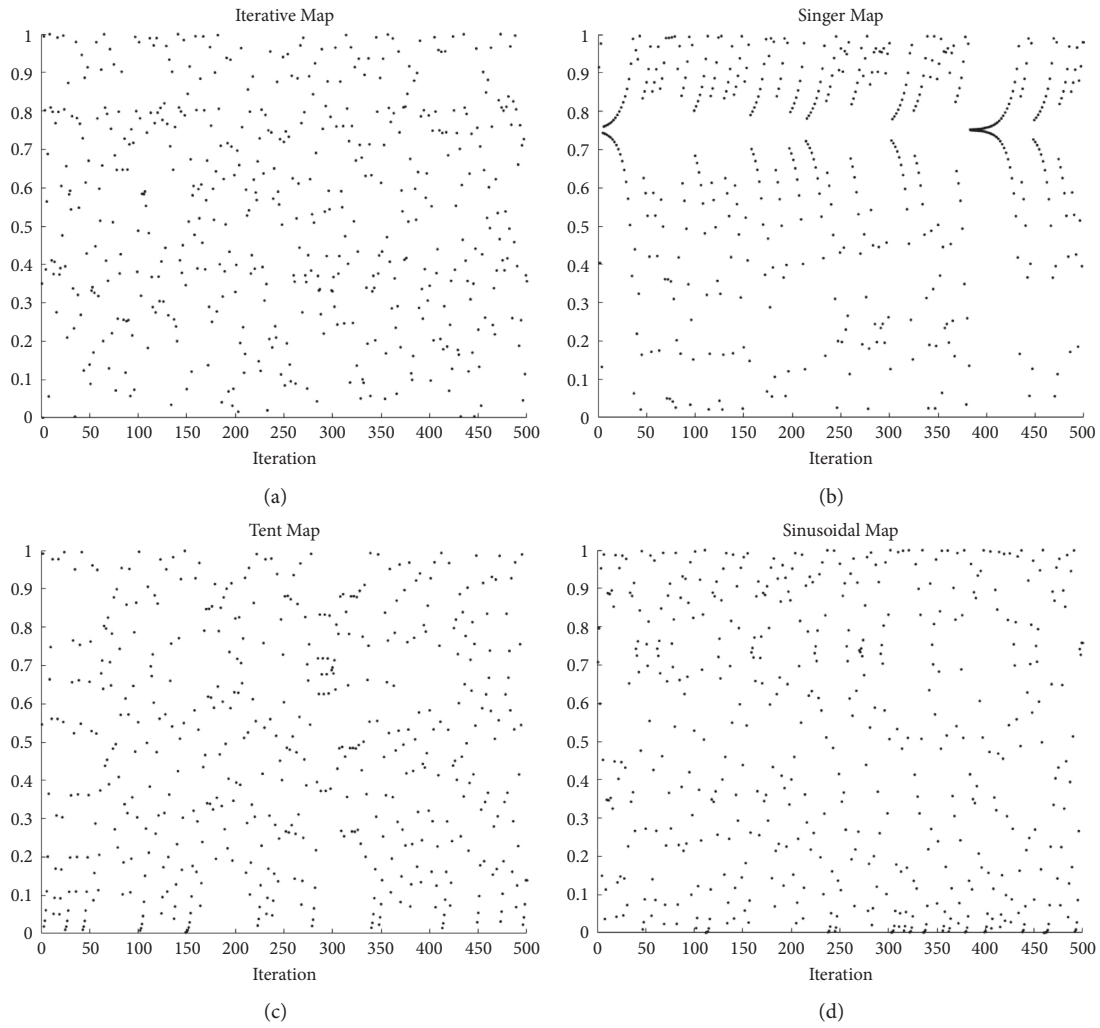


FIGURE 2: Chaotic map. (a) Iterative map. (b) Singer map. (c) Tent map. (d) Sinusoidal map.

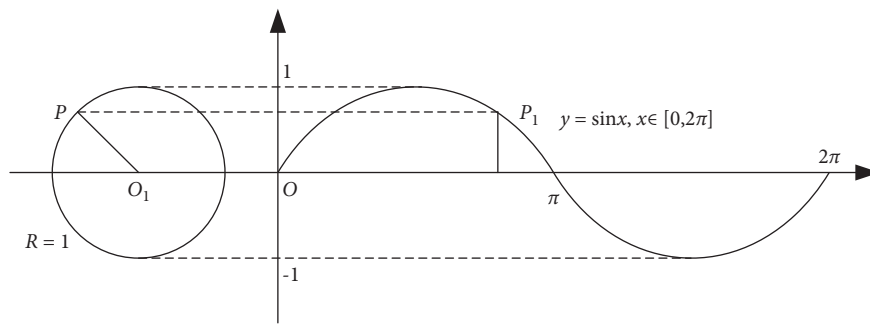


FIGURE 3: Correspondence diagram between the unit circle and the sine function.

**3.3. Nonlinear Convergence Factor Strategy.** When the alarm value ( $R_2$ ) reaches or exceeds the safety threshold (ST), the discoverers will migrate with the population to avoid the predators. The algorithm performs a broader global search. The migration distance depends on the migration control coefficient  $Q$  in equation (2). In the original SSA,  $Q$  is a random number that obeys the standard normal distribution. Although the strong randomness of the migration control coefficient has the probability to help the algorithm

jump out of the local optimum, the shortcoming of this strategy is also obvious. When  $Q$  cannot migrate or the migration distance is very short, the global exploitation ability and robustness of algorithm will be reduced.

Therefore, this paper optimizes the coefficient and uses the nonlinear convergence factor  $\omega$  as the new migration control coefficient. We refer to the study of nonlinear convergence factor adjustment [39], and the parameter control strategy can be expressed as

$$\omega(t) = 1 - \sin\left(\left(\frac{t}{\text{iter}_{\max}}\right)^2 \cdot \frac{\pi}{2}\right), \quad (8)$$

where  $\omega$  is the new migration control coefficient instead of  $Q$  in (2) and  $\text{iter}_{\max}$  is the maximum number of iterations.

As shown in Figure 4, at the beginning of the iteration, the value of  $\omega$  is large and the changing rate is slow, keeping a large migration distance, so the discoverers can lead the population to fully explore the solution space and enhance the global optimization ability. The changing rate of  $\omega$  in the middle term of the iteration is faster, which is beneficial to improving the convergence speed of the algorithm and the ability to jump out of the local optimal solution. In the later stage of the iteration, the changing rate of  $\omega$  slows down and the individuals perform a local exploitation on the current solution space to enhance the local optimization ability of the algorithm.

Considering the GA strategy and the nonlinear convergence factor strategy, the discoverer location formula is updated as follows:

$$X_{i,j}^{t+1} = \begin{cases} X_{i,j}^t |\sin(r_1)| - r_2 \sin(r_1) |\theta_1 \cdot X_p^t - \theta_2 \cdot X_{i,j}^t|, & R_2 < ST, \\ X_{i,j}^t + \omega \cdot L, & R_2 \geq ST, \end{cases} \quad (9)$$

where the meaning of each parameter is the same as in (2).

**3.4. Elite Opposition-Based Learning Strategy.** Tizhoosh [40] proposed opposition-based learning (OBL) in 2005, and it was proved that the probability of the opposite solution approaching the optimal solution was 50% higher than the current solution through experiments. The strategy can increase the population's diversity effectively. The OBL strategy calculates the opposite solution of the current solution, finally selects a better fitness solution from the current solution and the corresponding opposite solution, and updates the individual.

**Definition 1** (opposite solution). Suppose that a feasible solution of the current population in the  $D$ -dimensional solution space is expressed as  $X = (x_1, x_2, \dots, x_D)$ ,  $x_j \in [a_j, b_j]$ ; then, its corresponding opposite solution is  $\bar{X} = (\bar{x}_1, \bar{x}_2, \dots, \bar{x}_D)$ , where  $\bar{x}_j = \lambda(a_j + b_j) - x_j$ ,  $\lambda \in [0, 1]$  is a uniformly distributed random number.

Since OBL solves the problem in a certain space, it has the risk of falling into the local optimum and the problem of making the algorithm fall into premature convergence. The generated opposite solution may have difficulty to search for the optimal value than the current solution space [41, 42]. Elite opposition-based learning (EOBL) was proposed and successfully used to improve the characteristics of this algorithm. Sihwail et al. [43] introduced it in the HHO algorithm to improve population diversity and speed up the convergence process.

The EOBL takes advantage of the fact that elite individuals carry more effective information than ordinary individuals. First, the opposite population is formed through

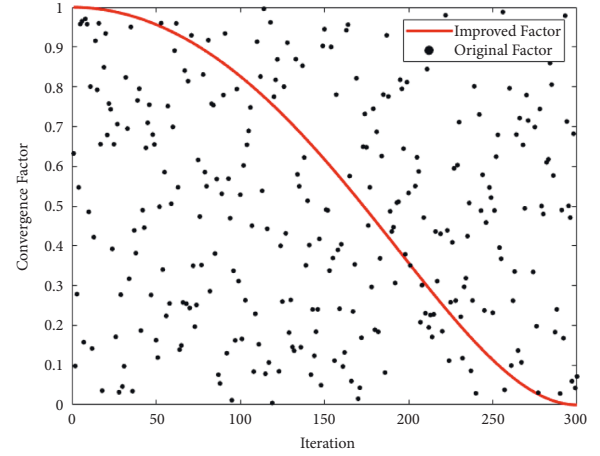


FIGURE 4: Variation curve of the migration control coefficient.

elite individuals with high adaptability in the population; then, elite individuals are selected as a new population from the opposite population and the current population. The EOBL strategy increases the diversity and quality of the population and improves the ability of the algorithm to jump out of the local optimum solution.

**Definition 2** (elite opposite solution). Suppose that the extreme point corresponding to the general individual in the current population is elite individuals, which is expressed as  $X_{i,j}^e = (X_{i,1}^e, X_{i,2}^e, \dots, X_{i,D}^e)$ ; then, its corresponding opposite solution is  $\bar{X}_{i,j}^e = (\bar{X}_{i,1}^e, \bar{X}_{i,2}^e, \dots, \bar{X}_{i,D}^e)$ . We select the individuals whose fitness value is in the top 10% of the population after each iteration as elite individuals. The equation for the elite opposite solution is as follows:

$$\bar{X}_{i,j}^e = \lambda \times (lb_j + ub_j) - X_{i,j}^e, \quad (10)$$

where  $\lambda \in [0, 1]$  is a uniformly distributed random number,  $X_{i,j}^e \in [lb_j, ub_j]$ ,  $lb_j = \min(X_{i,j})$ , and  $ub_j = \max(X_{i,j})$ .  $lb_j$  and  $ub_j$  are the lower and upper bounds of the dynamic boundary. Compared with the fixed boundary, the dynamic boundary can save the search experience and reduce the optimization time of the algorithm. When  $\bar{X}_{i,j}^e$  exceeds the boundary, it is reset by the equation as follows:

$$\bar{X}_{i,j}^e = \text{rand}(lb_j + ub_j). \quad (11)$$

**3.5. Pseudo-Code and Flow Chart of MISSA.** The pseudo-code and flow chart of MISSA is shown in Algorithm 1 and Figure 5.

### 3.6. Complexity Analysis of MISSA

**3.6.1. Time Complexity.** Assuming the population size and the solution space dimension are  $N$  and  $D$  and the maximum iteration is  $T$ , the time complexity of the original SSA includes the following: the population initialization complexity is  $O(1)$ , the fitness value of calculation complexity is

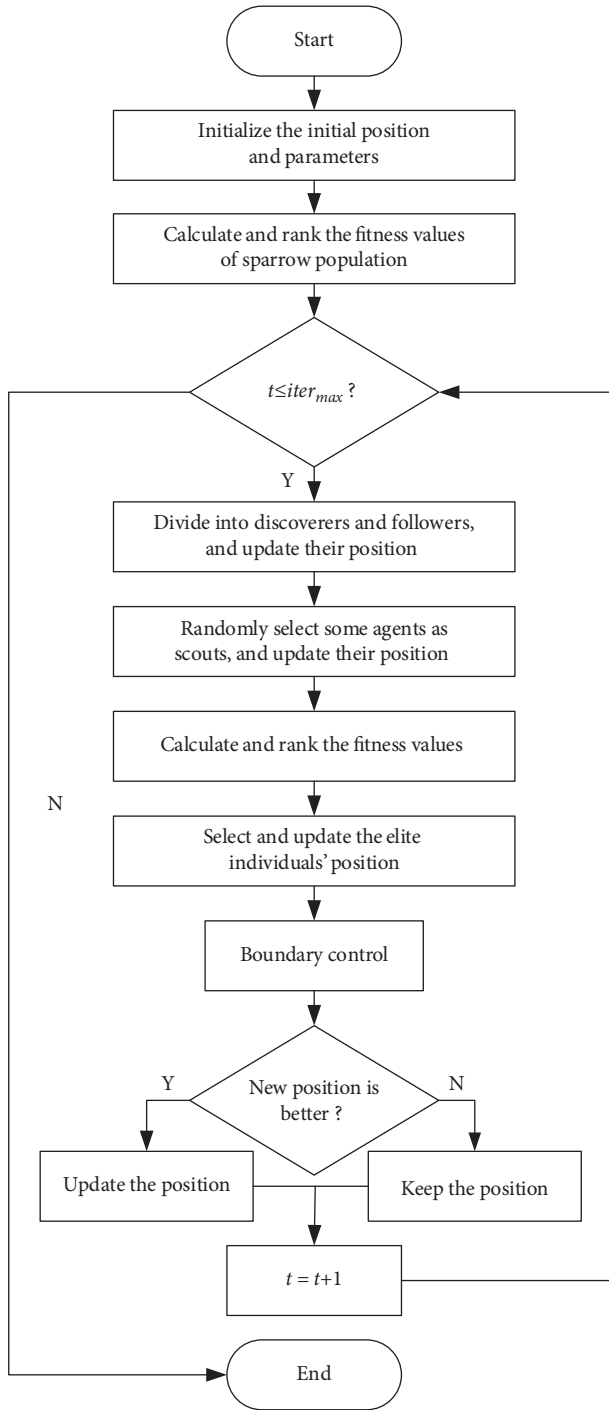


FIGURE 5: Flow chart of MISSA.

$O(N)$ , the complexity of exploration and exploitation phases is  $O(T * N * D)$ , and the total time complexity of SSA is  $O(1) + O(N) + O(T * N * D) = O(T * N * D)$ .

MISSA does not change the structure of SSA. The chaotic mapping strategy does not increase the complexity of population initialization, and the time complexity of initializing the population is still  $O(1)$ . The Gold-SA strategy and the nonlinear convergence factor strategy only improve

the position update method of the discoverers without additional operations, so the time complexity of this stage is still  $O(N * D)$ , and the time complexity of the EOBL strategy is  $O(N * D)$ . In regard to this, the total time complexity of MISSA is  $O(T * N * D)$ , which is the same as that of SSA, indicating that the multimixed strategy used in MISSA does not affect the efficiency of the algorithm.

**3.6.2. Space Complexity.** The storage space consumed by an algorithm can be defined as the space complexity. Assume that the ratio of elite individuals is  $R$ . Compared with SSA, only the EOBL strategy increases a certain amount of computational complexity of  $O(T * R * N * D)$ . The addition of multimixed strategies does not improve the order of magnitude of SSA. Thus, the space efficiency of the proposed strategy is effective and stable.

#### 4. Experimental Simulation and Result Analysis

**4.1. Experimental Design and Parameter Settings.** To verify the rationality of the multimixed strategy selection and efficiency of the proposed algorithm, two sets of comparative experiments are designed in this paper:

- (1) In order to verify the rationality of the multimixed strategy, three derivative algorithms with a single mechanism were proposed: ITSSA (using the iterative chaotic map strategy), GS-NSSA (using the Gold-SA and nonlinear convergence factor strategies for discoverers), and OBLSSA (using the EOBL strategy).
- (2) In order to verify the proposed algorithm's efficiency, MISSA has been compared to eight optimization algorithms. The comparison algorithms are SSA [24], the improved sparrow search algorithm (ISSA) [30], the chaotic sparrow search algorithm (CSSA) [31], a chaos sparrow search algorithm based on logarithmic spiral search strategy and adaptive step size strategy (CLSSA) [32], COOT [16], WOA [14], GWO [15], and PSO [12].

All the experimental tests are carried out with a Windows 10 system using Intel (R) Core (TM) i5-7300HU @2.50 GHz CPU with 16 G RAM and MATLAB 2018b in this paper. The population size and maximum iteration number of each algorithm are 30 and 300, respectively. In addition, other parameters are shown in Table 1. In this paper, a comparison test of 30-dimensional, 50-dimensional, and 100-dimensional function optimization is carried out on ten benchmark functions with different characteristics. The specific information of the test functions is shown in Table 2.  $f_1-f_5$  are unimodal functions used to examine the local exploitation ability of the algorithm, and  $f_6-f_{10}$  are multimodal functions used to examine the global exploration ability of the algorithm. To understand the difficulty of searching process intuitively, the two-dimensional graphs of each benchmark functions are illustrated in Figure 6.

```

/*Initialization*/
(1) Input:
(2) POP: the number of sparrows;
(3) itermax: the maximum number of iterations;
(4) PD: the proportion of discoverers in the population;
(5) SD: the proportion of scouts in the population;
(6) R2: the alarm value;
(7) ST: the safety threshold;
(8) Initialize the position of POP sparrows using equation (5);
(9) Rank the fitness values and divide the population into discoverers and scouts;
/*Iterative search*/
(10) while ( $t \leq \text{iter}_{\max}$ )
(11)    $R_2 = \text{rand}(1)$ ;
(12)   for  $i = 1 : \text{POP} * \text{PD}$ 
(13)     Update the discoverer's position using equation (7);
(14)   end for
(15)   for  $i = (\text{POP} * \text{PD}) + 1 : \text{POP}$ 
(16)     Update the follower's position using equation (3);
(17)   end for
(18)   for  $i = 1 : \text{POP} * \text{SD}$ 
(19)     Update the scout's position using equation (4);
(20)   end for
(21)   Calculate and rank the fitness values;
(22)   for  $i = 1 : \text{POP} * 10\%$ 
(23)     Update the elite individuals' position using equation (10);
(24)     If the position exceeds the boundary, using equation (11) to reset;
(25)     If the new position is better than before, update it;
(26)   end for
(27)   Rank the fitness values and find the current best position;
(28)    $t = t + 1$ ;
(29) end while
(30) Output  $X_{\text{best}}$  and  $f_g$ 

```

ALGORITHM 1: Pseudo-code of MISSA.

TABLE 1: Algorithm parameter settings.

| Algorithm                      | Parameter settings  |
|--------------------------------|---|
| SSA/CSSA/CLSSA /GS-NSSA/OBLSSA | $ST = 0.6, PD = 0.7, SD = 0.2$                                    |
| ISSA                           | $ST = 0.6, PD = 0.7, SD = 0.2, \theta = 0.05$                     |
| MISSA/ITSSA                    | $ST = 0.6, PD = 0.7, SD = 0.2, b = 0.7$                           |
| COOT                           | $p = 0.5$   |
| WOA                            | $b = 1, p = 0.5$  |
| GWO                            | $a_{\text{first}} = 2, a_{\text{final}} = 0, r_1, r_2 \in (0, 1)$ |
| PSO                            | $V_{\max} = 0.9, V_{\min} = -0.9, C_1 = C_2 = 2, \omega = 0.7$    |

## 4.2. Ablation Experiment of the Multimixed Strategy

**4.2.1. Optimization Results for Different Strategies.** In order to analyze the rationality of the multimixed strategy and the specific impact of each strategy on the performance of proposed algorithm, MISSA, ITSSA, GS-NSSA, and OBLSSA are compared to optimize several basic benchmark functions as in Table 2. The parameters of each algorithm are shown in Table 1. To avoid the bias caused by the contingency of the algorithm, and considering the difference of the algorithms in dealing with different dimensions, three algorithms are independently run 50 times on the four test functions for dimensions 30, 50, and 100, respectively. We

select the best value (Best), worst value (Worst), mean value (Mean), and standard deviation (Std) as the evaluation criterion. The Best and Worst reflect the quality of the solution, the Mean reflects the optimization accuracy of the algorithm, and Std reflects the robustness and stability of the algorithm. Table 3 shows the optimization results of the unimodal functions  $f_1$  and  $f_2$  and the multimodal functions  $f_6$  and  $f_{10}$  in three different dimensions.

From a macroperspective, MISSA basically occupies all the optimal values except the function  $f_{10}$  obtained by GS-NSSA in 100 dimensions. Combined with the experiment results of the three derivative algorithms, the performance of MISSA has been comprehensively improved.

TABLE 2: Benchmark functions.

| Name                 | Type | Test function   | Range         | Optimum       |
|----------------------|------|---|---------------|---------------|
| Sphere               | UN   | $f_1 = \sum_{i=1}^n x_i^2$  | [-100, 100]   | 0             |
| Schwefel 2.22        | UN   | $f_2 = \sum_{i=1}^n  x_i  + \prod_{i=1}^n  x_i $  | [-10, 10]     | 0             |
| Schwefel 1.2         | UN   | $f_3 = \sum_{i=1}^n (\sum_{j=1}^i x_j)^2$   | [-100, 100]   | 0             |
| Schwefel 2.21        | UN   | $f_4 = \max\{ x_i , 1 \leq i \leq n\}$  | [-100, 100]   | 0             |
| Step                 | UN   | $f_5 = \sum_{i=1}^n (x_i + 0.5)^2$  | [-100, 100]   | 0             |
| Generalized Schwefel | MU   | $f_6 = \sum_{i=1}^n -x_i \sin(\sqrt{ x_i })$  | [-500, 500]   | -418.9829 × n |
| Rastrigin            | MU   | $f_7 = \sum_{i=1}^n (x_i^2 - 10 \cos(2\pi x_i) + 10)$   | [-5.12, 5.12] | 0             |
| Ackley               | MU   | $f_8 = -20 \exp\left(-0.2 \sqrt{\frac{1}{\text{Dim}} \sum_{i=1}^n x_i^2}\right)$  | [-32, 32]     | 0             |
| Griewank             | MU   | $-\exp\left(\frac{1}{n} \sum_{i=1}^n \cos(2\pi x_i)\right) + 20 + e$<br>$f_9 = \frac{1}{4000} \sum_{i=1}^n x_i^2 - \prod_{i=1}^n \cos\left(\frac{x_i}{\sqrt{i}}\right) + 1$ | [-600, 600]   | 0             |
| Penalized            | MU   | $f_{10} = 0.1 \left\{ \sin^2(3\pi x_i) + \sum_{i=1}^n (x_i - 1)^2 [1 + \sin^2(3\pi x_i + 1)] + (x_i)^2 (1 + \sin^2 2\pi x_i) \right\} + \sum_{i=1}^n u(x_i, 5, 100, 4)$     | [-50, 50]     | 0             |

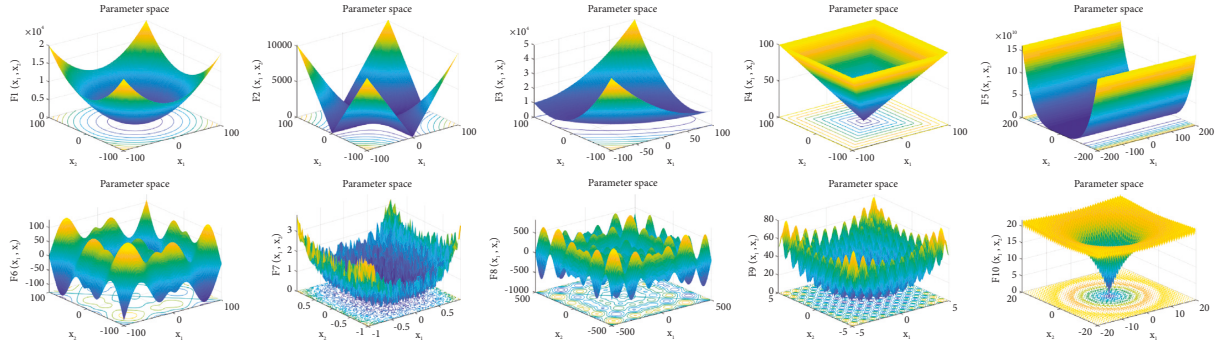


FIGURE 6: 2-D diagrams of the benchmark functions.

From a microperspective, ITSSA based on the iterative chaotic map does not fundamentally change the individual searching mechanism of sparrows and it can easily fall into the local optimal solution as SSA when dealing with complex problems. OBLSSA based on the EOBLS strategy has obvious effect on the optimization of unimodal functions, indicating that the opposite solutions of the elite individuals play a dominant role in improving the local exploitation ability. The optimization effect of GS-NSSA based on the Gold-SA and the nonlinear convergence factor on multimodal functions is obvious, which shows the improved location update formula of discovers enhances the global exploration and anti-premature abilities.

Overall, MISSA integrates the advantages of different single strategies, synergizes the optimization ability of each strategy, and proves the rationality of multimixed strategy selection.

**4.2.2. Diversity Analysis for Different Strategies.** To distinguish the effect of different strategies on population diversity, this paper takes the Schwefel 2.22 function and performs diversity analysis on derived algorithms to visualize the diversity of agents in the process of global exploration and local exploitation. Besides, to verify the superiority of the iterative chaotic map, a comparative analysis of four chaotic mapping methods introduced in Section 3.1 is carried out.

The diversity [44, 45] is defined as follows:

$$\text{Div}(t) = \sum_{j=1}^D \frac{1}{N} \text{Div}_j = \frac{1}{N} \sum_{j=1}^D \text{Div}_j, \quad (12)$$

$$\text{Div}_j = \frac{1}{N} \sum_{i=1}^N \sqrt{\sum_{j=1}^D (X_{i,j} - \bar{X}_j)^2} \bar{X}_j = \frac{1}{N} \sum_{i=1}^N X_{i,j},$$

where  $\text{Div}(t)$  represents the population diversity in the  $t^{\text{th}}$  iteration,  $N$  represents the population size, and  $D$  is the dimension of the problem.  $\bar{X}_j$  represents the mean value of current position in the  $j^{\text{th}}$  dimension, and  $\text{Div}_j$  represents mean population diversity in the  $j^{\text{th}}$  dimension. Thus, the exploration and exploitation percentage of the search process can be defined as follows:

$$\text{exploration}(\%) = \frac{\text{Div}_t}{\text{Div}_{\max}} \times 100\%, \quad (13)$$

$$\text{exploitation}(\%) = \frac{|\text{Div}_t - \text{Div}_{\max}|}{\text{Div}_{\max}} \times 100\%,$$

where  $\text{Div}_{\max}$  represents the maximum diversity of the whole group's population diversity.

Figure 7 shows the exploration and exploitation percentage curves of population diversity in the search space while solving the Schwefel 2.22 function. Diversity of the algorithm increases with the addition of chaotic initialization methods. Due to the small periods and unstable periodic phenomenon in Singer and Tent maps and the bipolar distribution phenomenon in sinusoidal map, the diversity curves of algorithms fluctuate greatly, which means the improved SSA is not stable. The diversity analysis is the same as the Lyapunov exponent analysis of chaotic maps in [37]. Thus, the iterative chaotic map has the best effect on improving population diversity.

The curve of GS-NSSA indicates that the Gold-SA and the nonlinear convergence strategies sacrifice part of the stability but rapidly separate the solution space in order to improve the convergence speed. However, the EOBLS strategy reconstructs the population through the opposite solution, which greatly improves the stability of population diversity. Ultimately MISSA guarantees stable and abundant population diversity. Notably, combined with optimization results in Table 3, MISSA can balance the capabilities between exploration and exploitation phases to push sparrow agents to the global optimal solution.

### 4.3. Benchmark Function Test

**4.3.1. Optimization Results for Different Dimensions.** The experimental parameter settings are consistent with the rationality experiment in Section 4.2. The nine swarm intelligence algorithms performed 50 independent runs on the ten benchmark functions for low dimension (30), medium dimension (50), and high dimension (100). The specific experimental results are reported in Table 4.

As shown in Table 4, the optimization accuracy of MISSA for ten benchmark functions is significantly better than of the other nine swarm intelligence algorithms under the same conditions.



TABLE 3: Optimization results of different improvement strategies.

| F        | Dim   | Algorithm | D = 30    |           |           |           |           | D = 50    |           |           |           |           | D = 100   |           |  |  |  |
|----------|-------|-----------|-----------|-----------|-----------|-----------|-----------|-----------|-----------|-----------|-----------|-----------|-----------|-----------|--|--|--|
|          |       |           | Best      | Worst     | Mean      | Std       | Best      | Worst     | Mean      | Std       | Best      | Worst     | Mean      | Std       |  |  |  |
| $f_1$    | ITSSA | 0.00E+00  | 1.35E-68  | 2.70E-70  | 1.91E-69  | 0.00E+00  | 7.30E-48  | 1.46E-49  | 1.03E-48  | 0.00E+00  | 1.26E-49  | 2.63E-51  | 1.82E-50  |           |  |  |  |
|          |       |           | 9.28E-149 | 1.43E-43  | 1.01E-42  | 1.80E-158 | 8.11E-49  | 1.71E-35  | 1.21E-34  | 1.74E-159 | 5.51E-43  | 1.10E-44  | 7.79E-44  |           |  |  |  |
|          |       |           | 0.00E+00  | 2.35E-57  | 5.00E-59  | 3.43E-58  | 0.00E+00  | 2.04E-77  | 1.76E-90  | 1.24E-89  | 0.00E+00  | 9.22E-61  | 1.84E-62  | 1.30E-61  |  |  |  |
|          |       |           | 0.00E+00  | 8.18E-98  | 2.20E-99  | 1.22E-98  | 0.00E+00  | 5.24E-129 | 1.05E-130 | 7.40E-130 | 0.00E+00  | 5.00E-118 | 2.00E-119 | 9.90E-119 |  |  |  |
| $f_2$    | ITSSA | 0.00E+00  | 2.78E-22  | 5.56E-24  | 3.93E-23  | 0.00E+00  | 3.69E-23  | 5.56E-24  | 5.22E-24  | 0.00E+00  | 4.28E-22  | 8.56E-24  | 6.06E-23  |           |  |  |  |
|          |       |           | 8.92E-78  | 2.05E-21  | 5.14E-23  | 2.98E-22  | 3.28E-89  | 1.04E-21  | 2.08E-23  | 1.47E-22  | 3.22E-86  | 1.04E-19  | 2.09E-21  | 1.48E-20  |  |  |  |
|          |       |           | 0.00E+00  | 1.80E-35  | 3.92E-37  | 2.55E-36  | 0.00E+00  | 1.58E-30  | 3.17E-32  | 2.24E-31  | 0.00E+00  | 2.10E-36  | 4.19E-38  | 2.97E-37  |  |  |  |
|          |       |           | 0.00E+00  | 1.37E-55  | 2.76E-57  | 1.93E-56  | 0.00E+00  | 2.61E-45  | 5.21E-47  | 3.69E-46  | 1.01E-179 | 4.57E-64  | 1.00E-65  | 6.47E-65  |  |  |  |
| $f_6$    | ITSSA | -1.26E+04 | -6.39E+03 | -9.80E+03 | 1.90E+03  | -2.09E+04 | -9.92E+03 | -1.58E+04 | 3.63E+03  | -3.97E+04 | -1.94E+04 | -3.32E+04 | 6.90E+03  |           |  |  |  |
|          |       |           | -1.26E+04 | -6.60E+03 | -1.14E+04 | -2.09E+04 | -1.09E+04 | -1.91E+04 | 2.24E+03  | -4.19E+04 | -4.19E+04 | -1.89E+04 | -3.82E+04 | 5.35E+03  |  |  |  |
|          |       |           | -1.16E+04 | -4.54E+03 | -7.69E+03 | -2.07E+03 | -7.88E+03 | -1.38E+04 | 3.97E+03  | -4.13E+04 | -4.13E+04 | -1.31E+04 | -2.98E+04 | 7.12E+03  |  |  |  |
|          |       |           | -1.26E+04 | -1.04E+04 | -1.22E+04 | 4.02E+02  | -2.09E+04 | -1.36E+04 | -1.94E+04 | -4.19E+04 | -4.19E+04 | -4.02E+04 | -4.14E+04 | 3.95E+02  |  |  |  |
| $f_{10}$ | ITSSA | 1.14E-04  | 2.10E-02  | 4.02E-03  | 6.85E-03  | 2.04E-04  | 2.86E-02  | 5.31E-03  | 8.80E-03  | 1.33E-04  | 3.36E-02  | 3.36E-03  | 6.80E-03  |           |  |  |  |
|          |       |           | 3.92E-08  | 3.26E-05  | 3.45E-06  | 1.13E-09  | 6.06E-05  | 4.32E-06  | 1.14E-05  | 1.26E-10  | 3.80E-05  | 5.99E-06  | 9.85E-06  |           |  |  |  |
|          |       |           | 6.70E-05  | 2.19E-02  | 4.74E-03  | 1.13E-04  | 2.90E-02  | 4.63E-03  | 8.80E-03  | 1.65E-03  | 3.37E-02  | 2.92E-03  | 5.82E-03  |           |  |  |  |
|          |       |           | 1.40E-10  | 2.78E-05  | 2.92E-06  | 1.40E-10  | 6.78E-05  | 4.96E-06  | 1.15E-05  | 1.16E-09  | 1.43E-04  | 1.09E-05  | 2.74E-05  |           |  |  |  |

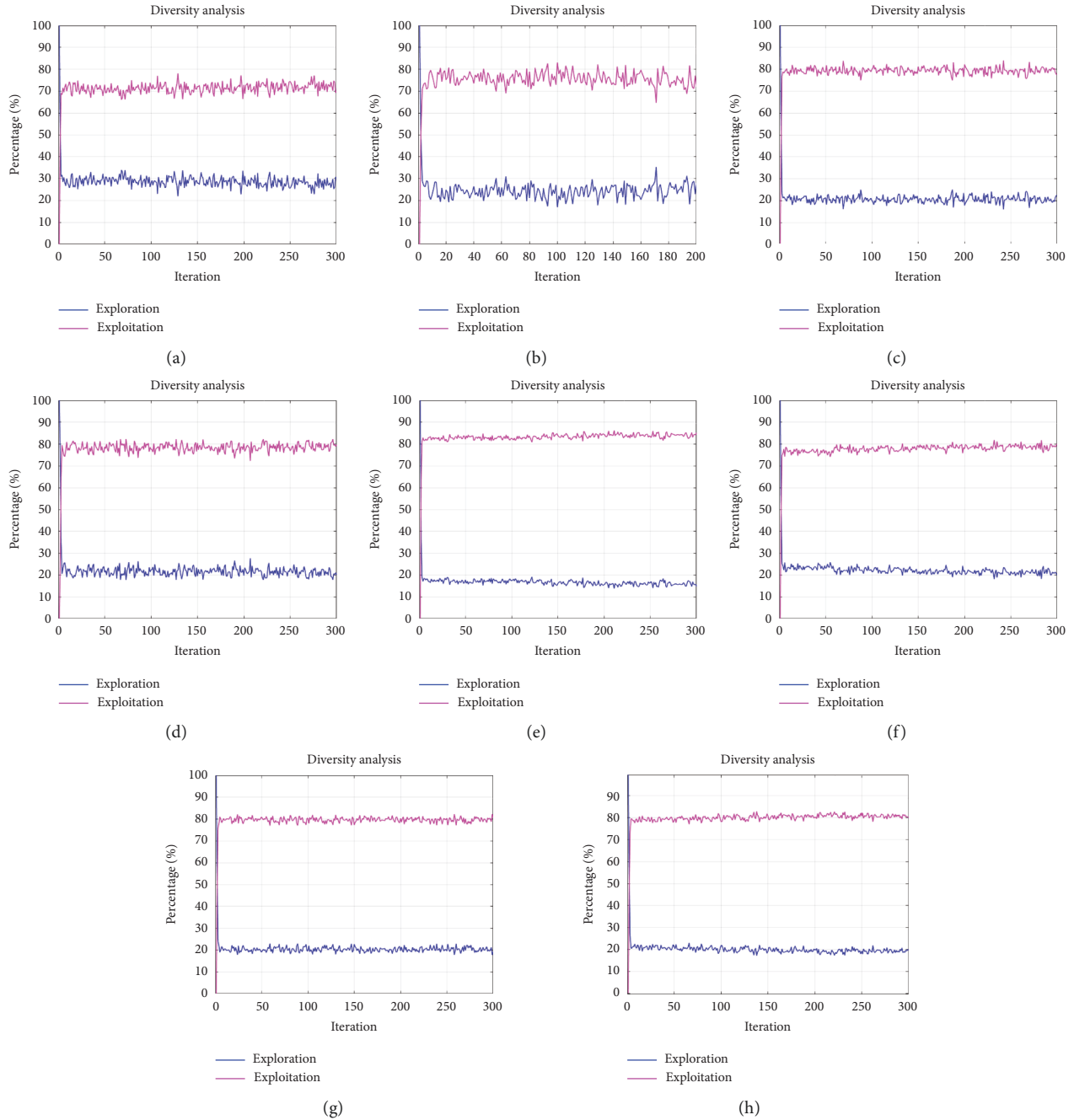


FIGURE 7: Average diversity analysis of different strategies with 20 times. (a) SSA. (b) SSA with Tent map. (c) SSA with Singer map. (d) SSA with sinusoidal map. (e) ITSSA (SSA with iterative algorithm). (f) GS-NSSA. (g) OBLSSA. (h) MISSA.

In the experiments on unimodal functions, MISSA can quickly find the optimal values with high optimization accuracy. For  $f_1$ – $f_4$ , MISSA, CSSA, CLSSA, and SSA can all converge to the theoretical optimal value, indicating that MISSA does not reduce the search accuracy of the original SSA algorithm. Although ISSA has not converged to the theoretical value, its accuracy is more than a dozen orders of magnitude better than of other algorithms, which shows the superiority of the original SSA itself. In addition, MISSA is better than the original SSA and other improved SSAs in the evaluation of the Mean and Std, which is better than dozens

of orders of magnitude in  $f_1$ – $f_4$ . Besides, the trend of superiority is further improved with the increase in dimensions, showing that MISSA has better stability. For  $f_5$ , although MISSA fails to find the theoretical optimal solution, the Mean, Std, and quality of its optimal solution in each dimension have been significantly better than other algorithms.

In the experiments on multimodal function, MISSA demonstrates excellent global optimization ability to deal with complex problems. For  $f_6$ , only MISSA and CSSA converge to the theoretical optimal solution, but the

TABLE 4: Results for ten basic benchmark functions.

| F     | Dim       | Algorithm | D = 30    |           |             |             |           | D = 50    |           |           |           |           | D = 100   |          |          |          |  |
|-------|-----------|-----------|-----------|-----------|-------------|-------------|-----------|-----------|-----------|-----------|-----------|-----------|-----------|----------|----------|----------|--|
|       |           |           | Best      | Worst     | Mean        | Std         |           | Best      | Worst     | Mean      | Std       |           | Best      | Worst    | Mean     | Std      |  |
| $f_1$ | SSA       | SSA       | 0.00E+00  | 1.57E-48  | 3.21E-50    | 2.25E-49    | 0.00E+00  | 1.99E-29  | 1.79E-66  | 1.25E-65  | 0.00E+00  | 2.96E-24  | 5.92E-26  | 4.19E-25 |          |          |  |
|       |           | ISSA      | 4.39E-102 | 6.97E-28  | 1.40E-29    | 9.86E-29    | 8.18E-86  | 6.83E-47  | 1.33E-27  | 9.39E-27  | 3.97E-57  | 7.95E-59  | 5.62E-58  |          |          |          |  |
|       |           | CSSA      | 0.00E+00  | 1.73E-26  | 3.45E-28    | 2.44E-27    | 0.00E+00  | 5.14E-27  | 1.04E-28  | 7.27E-28  | 6.60E-32  | 1.48E-33  | 9.54E-33  |          |          |          |  |
|       |           | CLSSA     | 0.00E+00  | 2.00E-52  | -1.38E-47   | 9.74E-47    | 0.00E+00  | 6.77E-53  | 1.36E-54  | 9.58E-54  | 8.26E-57  | 2.79E-99  | 1.39E-49  |          |          |          |  |
|       |           | MISSA     | 0.00E+00  | 1.57E-48  | 7.91E-106   | 5.34E-105   | 0.00E+00  | 6.09E-128 | 1.24E-129 | 8.71E-129 | 4.39E-123 | 9.55E-125 | 6.48E-124 |          |          |          |  |
|       |           | COOT      | 1.69E-31  | 2.56E-11  | 9.54E-13    | 4.70E-12    | 1.85E-32  | 1.46E-05  | 2.92E-07  | 2.06E-06  | 3.15E-13  | 9.72E-15  | 4.72E-14  |          |          |          |  |
|       |           | WOA       | 4.97E-51  | 1.13E-40  | 5.56E-42    | 3.04E-41    | 7.01E-53  | 4.57E-37  | 9.14E-39  | 6.46E-38  | 2.65E-38  | 5.35E-40  | 3.74E-39  |          |          |          |  |
|       |           | GWO       | 1.16E-16  | 3.00E-14  | 4.86E-15    | 6.77E-15    | 3.46E-11  | 7.37E-10  | 2.21E-10  | 1.89E-10  | 2.69E-05  | 7.99E-06  | 4.19E-06  |          |          |          |  |
|       |           | PSO       | 0.00E+00  | 3.62E-104 | 7.91E-106   | 5.34E-105   | 1.44E+00  | 6.09E+02  | 8.19E+01  | 2.27E+02  | 4.15E+01  | 7.72E+02  | 5.77E+02  |          |          |          |  |
|       |           | $f_2$     | SSA       | SSA       | 0.00E+00    | 8.21E-22    | 1.73E-23  | 1.17E-22  | 0.00E+00  | 2.22E-20  | 4.44E-22  | 3.14E-21  | 0.00E+00  | 1.60E-25 | 3.24E-27 | 2.27E-26 |  |
| ISSA  | 2.57E-50  |           |           | 5.05E-17  | 3.27E-18    | 1.03E-17    | 7.68E-51  | 4.52E-16  | 2.11E-17  | 8.48E-17  | 4.71E-53  | 1.31E-16  | 2.68E-18  | 1.85E-17 |          |          |  |
| CSSA  | 0.00E+00  |           |           | 8.24E-12  | 1.65E-13    | 1.17E-12    | 0.00E+00  | 2.51E-16  | 5.06E-18  | 3.55E-17  | 0.00E+00  | 6.52E-13  | 1.62E-14  | 9.44E-14 |          |          |  |
| CLSSA | 0.00E+00  |           |           | 8.15E-50  | 2.86E-51    | 1.45E-50    | 0.00E+00  | 1.44E-44  | 2.88E-46  | 2.04E-45  | 0.00E+00  | 3.23E-41  | 6.46E-43  | 4.57E-42 |          |          |  |
| MISSA | 0.00E+00  |           |           | 1.39E-54  | 2.80E-56    | 1.97E-55    | 0.00E+00  | 2.03E-48  | 4.07E-50  | 2.87E-49  | 0.00E+00  | 2.06E-61  | 4.12E-63  | 2.92E-62 |          |          |  |
| COOT  | 2.12E-16  |           |           | 9.51E-06  | 3.51E-07    | 1.63E-06    | 3.97E-15  | 3.06E-03  | 6.12E-05  | 4.32E-04  | 4.66E-16  | 1.18E-04  | 3.68E-06  | 1.89E-05 |          |          |  |
| WOA   | 4.05E-35  |           |           | 5.61E-28  | 2.38E-29    | 9.67E-29    | 1.02E-34  | 2.56E-28  | 2.27E-29  | 5.22E-29  | 2.36E-28  | 2.10E-29  | 4.92E-29  |          |          |          |  |
| GWO   | 5.00E-10  |           |           | 7.45E-09  | 1.70E-09    | 1.19E-09    | 3.13E-07  | 1.56E-06  | 7.55E-07  | 2.63E-07  | 2.53E-04  | 6.47E-04  | 9.74E-05  |          |          |          |  |
| PSO   | 1.01E-167 |           |           | 1.39E-54  | 2.80E-56    | 1.97E-55    | 1.32E+00  | 3.18E+00  | 2.01E+00  | 4.30E-01  | 1.13E+01  | 2.17E+01  | 1.54E+01  | 1.99E+00 |          |          |  |
| $f_3$ | SSA       |           |           | SSA       | 0.00E+00    | 9.96E-35    | 2.03E-36  | 1.42E-35  | 0.00E+00  | 2.43E-71  | 4.98E-73  | 3.44E-72  | 0.00E+00  | 5.96E-59 | 1.22E-60 | 8.52E-60 |  |
|       |           | ISSA      | 1.84E-83  | 2.62E-20  | 5.25E-22    | 3.71E-21    | 1.68E-109 | 1.81E-24  | 3.75E-26  | 2.56E-25  | 3.17E-88  | 1.22E-28  | 2.46E-30  | 1.73E-29 |          |          |  |
|       |           | CSSA      | 0.00E+00  | 1.55E-22  | 3.44E-24    | 2.23E-23    | 0.00E+00  | 9.06E-23  | 1.81E-24  | 1.28E-23  | 0.00E+00  | 4.67E-27  | 9.55E-29  | 6.68E-28 |          |          |  |
|       |           | CLSSA     | 0.00E+00  | 4.56E-28  | 9.12E-30    | 6.46E-29    | 0.00E+00  | 1.24E-31  | 4.99E-33  | 2.44E-32  | 0.00E+00  | 1.13E-24  | 2.31E-26  | 1.59E-25 |          |          |  |
|       |           | MISSA     | 0.00E+00  | 3.72E-67  | 7.43E-69    | 5.26E-68    | 0.00E+00  | 9.81E-91  | 1.96E-92  | 1.39E-91  | 0.00E+00  | 5.10E-76  | 1.16E-77  | 7.68E-77 |          |          |  |
|       |           | COOT      | 3.01E-32  | 6.79E-10  | 1.36E-11    | 9.61E-11    | 1.44E-30  | 2.66E-09  | 5.31E-11  | 3.75E-10  | 4.16E-34  | 8.65E-11  | 3.37E-12  | 1.63E-11 |          |          |  |
|       |           | WOA       | 4.79E+04  | 1.35E+05  | 6.04E+04    | 1.82E+04    | 1.46E+05  | 3.54E+05  | 2.37E+05  | 4.24E+04  | 5.74E+05  | 1.82E+06  | 1.14E+06  | 3.41E+05 |          |          |  |
|       |           | GWO       | 1.86E-04  | 3.77E-01  | 7.86E-02    | 1.01E-01    | 4.24E+00  | 3.31E+02  | 3.99E+01  | 5.78E+01  | 2.77E+02  | 1.57E+04  | 4.23E+03  | 3.04E+03 |          |          |  |
|       |           | PSO       | 2.92E-296 | 3.72E-67  | 7.43E-69    | 5.26E-68    | 1.18E+03  | 3.44E+04  | 6.39E+03  | 6.57E+03  | 8.91E+03  | 7.49E+04  | 2.92E+04  | 1.53E+04 |          |          |  |
|       |           | $f_4$     | SSA       | SSA       | 0.00E+00    | 2.06E-31    | 3.69E-04  | 9.54E-04  | 0.00E+00  | 2.67E-28  | 5.33E-30  | 3.77E-29  | 0.00E+00  | 1.09E-41 | 2.22E-43 | 1.55E-42 |  |
| ISSA  | 4.83E-58  |           |           | 2.93E-23  | 7.61E-29    | 9.41E-29    | 1.95E-55  | 9.17E-31  | 7.39E-17  | 2.78E-16  | 9.81E-46  | 7.57E-16  | 1.87E-17  | 1.07E-16 |          |          |  |
| CSSA  | 0.00E+00  |           |           | 4.44E-14  | 9.25E-16    | 6.41E-15    | 0.00E+00  | 7.97E-13  | 1.60E-14  | 1.13E-13  | 0.00E+00  | 2.80E-16  | 7.72E-18  | 4.21E-17 |          |          |  |
| CLSSA | 0.00E+00  |           |           | 9.99E-57  | -4.62E-49   | 3.24E-48    | 0.00E+00  | 4.67E-48  | 9.35E-50  | 6.61E-49  | 0.00E+00  | 2.51E-48  | 4.61E-48  | 3.54E-49 |          |          |  |
| MISSA | 0.00E+00  |           |           | 1.12E-123 | 3.2682E-125 | 1.7339E-124 | 0.00E+00  | 5.09E-58  | 1.11E-59  | 7.21E-59  | 0.00E+00  | 1.42E-64  | 2.95E-66  | 2.01E-65 |          |          |  |
| COOT  | 1.06E-48  |           |           | 2.23E-15  | 5.74E+00    | 7.66E+00    | 2.29E-17  | 3.98E-07  | 1.27E-08  | 5.83E-08  | 5.96E-16  | 1.64E-06  | 4.64E-08  | 2.44E-07 |          |          |  |
| WOA   | 3.80E-03  |           |           | 9.15E+01  | 1.63E-36    | 4.47E-36    | 1.32E+01  | 9.54E+01  | 6.75E+01  | 2.47E+01  | 2.60E+01  | 9.54E+01  | 7.70E+01  | 1.96E+01 |          |          |  |
| GWO   | 3.95E-16  |           |           | 1.35E-13  | 4.24E-22    | 1.17E-21    | 3.57E-02  | 1.26E-01  | 4.92E-02  | 2.62E-02  | 8.04E-01  | 1.52E+01  | 4.91E+00  | 2.62E+00 |          |          |  |
| PSO   | 1.27E-01  |           |           | 2.76E-01  | 6.00E-69    | 1.65E-68    | 8.08E+00  | 9.05E+00  | 6.01E+00  | 1.17E+00  | 7.54E+00  | 1.26E+01  | 9.98E+00  | 1.18E+00 |          |          |  |

TABLE 4: Continued.

| F              | Dim            | Algorithm | D = 30    |           |           |           |           | D = 50    |           |           |           |           | D = 100   |          |      |     |  |
|----------------|----------------|-----------|-----------|-----------|-----------|-----------|-----------|-----------|-----------|-----------|-----------|-----------|-----------|----------|------|-----|--|
|                |                |           | Best      | Worst     | Mean      | Std       |           | Best      | Worst     | Mean      | Std       |           | Best      | Worst    | Mean | Std |  |
| f <sub>5</sub> | f <sub>5</sub> | SSA       | 5.23E-05  | 2.06E-03  | 4.07E-04  | 4.09E-04  | 3.97E-05  | 4.53E-04  | 1.61E-03  | 1.92E-03  | 1.38E-03  | 1.85E+00  | 3.23E-01  | 3.45E-01 |      |     |  |
|                |                | ISSA      | 1.27E-10  | 1.24E-04  | 7.24E-06  | 1.87E-05  | 2.24E-10  | 1.18E-04  | 1.08E-05  | 2.31E-05  | 1.48E-07  | 2.42E-02  | 3.16E-03  | 6.02E-03 |      |     |  |
|                |                | CSSA      | 4.87E-11  | 4.65E-05  | 1.47E-06  | 6.59E-06  | 1.64E-08  | 6.53E-05  | 4.72E-06  | 1.05E-05  | 2.57E-11  | 4.47E-05  | 4.05E-05  | 9.02E-05 |      |     |  |
|                |                | CLSSA     | 4.60E-10  | 2.96E-05  | 1.64E-06  | 4.47E-06  | 1.06E-08  | 2.57E-05  | 2.18E-06  | 4.42E-06  | 3.55E-09  | 2.94E-04  | 1.33E-05  | 4.22E-05 |      |     |  |
|                |                | MISSA     | 3.15E-14  | 4.15E-05  | 5.03E-06  | 8.74E-06  | 1.42E-09  | 9.85E-06  | 3.50E-06  | 4.01E-06  | 5.42E-12  | 7.18E-05  | 2.74E-05  | 6.44E-05 |      |     |  |
|                |                | COOT      | 2.49E-01  | 6.76E+00  | 1.29E+00  | 1.30E+00  | 2.16E+00  | 3.45E+01  | 6.29E+00  | 6.40E+00  | 9.86E+01  | 9.77E+03  | 6.50E+02  | 1.56E+03 |      |     |  |
|                |                | WOA       | 2.74E-01  | 1.60E+00  | 9.22E-01  | 3.36E-01  | 7.38E-01  | 4.06E+00  | 2.19E+00  | 6.63E-01  | 9.77E+01  | 9.86E+01  | 9.83E+01  | 1.34E-01 |      |     |  |
|                |                | GWO       | 1.98E-04  | 2.51E+00  | 9.99E-01  | 4.50E-01  | 2.00E+00  | 5.24E+00  | 3.47E+00  | 6.68E-01  | 9.62E+01  | 9.82E+01  | 9.82E+01  | 5.16E-01 |      |     |  |
|                |                | PSO       | 1.05E-01  | 3.05E+01  | 1.28E+00  | 4.41E+00  | 1.80E+00  | 4.70E+02  | 3.64E+01  | 8.28E+01  | 1.06E+03  | 2.56E+03  | 1.59E+03  | 3.67E+02 |      |     |  |
|                |                | SSA       | -1.18E+04 | -4.90E+03 | -8.25E+03 | 2.23E+03  | -2.06E+04 | -7.41E+03 | -1.49E+04 | 4.02E+03  | -4.15E+04 | -1.20E+04 | -3.15E+04 | 7.89E+03 |      |     |  |
| ISSA           | -1.22E+04      | -3.92E+03 | -9.72E+03 | 2.43E+03  | -2.08E+04 | -6.77E+03 | -1.72E+04 | 3.80E+03  | -4.19E+04 | -2.14E+04 | -3.64E+04 | 5.51E+03  |           |          |      |     |  |
| CSSA           | -1.26E+04      | -5.01E+03 | -8.80E+03 | 3.11E+01  | -2.08E+04 | -8.01E+03 | -1.72E+04 | 3.72E+03  | -4.18E+04 | -1.10E+04 | -3.30E+04 | 7.80E+03  |           |          |      |     |  |
| CLSSA          | -8.00E+03      | -5.22E+03 | -9.60E+03 | 8.60E+02  | -2.09E+04 | -8.73E+03 | -1.62E+04 | 4.41E+03  | -4.16E+04 | -1.46E+04 | -3.39E+04 | 6.80E+03  |           |          |      |     |  |
| MISSA          | -1.26E+04      | -1.04E+04 | -1.22E+04 | 4.01E+02  | -2.09E+04 | -1.33E+04 | -1.88E+04 | 1.70E+03  | -4.19E+04 | -3.99E+04 | -4.12E+04 | 5.45E+02  |           |          |      |     |  |
| COOT           | -8.17E+03      | -4.81E+03 | -6.84E+03 | 7.60E+02  | -1.42E+04 | -7.36E+03 | -1.04E+04 | 1.49E+03  | -2.11E+04 | -1.11E+04 | -1.69E+04 | 2.82E+03  |           |          |      |     |  |
| WOA            | -1.26E+04      | -7.43E+03 | -9.66E+03 | 1.34E+03  | -2.09E+04 | -1.32E+04 | -1.68E+04 | 2.89E+03  | -4.19E+04 | -2.12E+04 | -3.25E+04 | 5.86E+03  |           |          |      |     |  |
| GWO            | -7.17E+03      | -2.78E+03 | -5.66E+03 | 1.02E+03  | -1.07E+04 | -4.06E+03 | -8.80E+03 | 1.59E+03  | -2.00E+04 | -5.69E+03 | -1.44E+04 | 3.95E+03  |           |          |      |     |  |
| PSO            | -3.86E+03      | -1.64E+03 | -2.66E+03 | 4.15E+02  | -4.57E+03 | -2.54E+03 | -3.31E+03 | 5.03E+02  | -6.03E+03 | -3.70E+03 | -4.84E+03 | 6.17E+02  |           |          |      |     |  |
| SSA            | 0.00E+00       | 0.00E+00  | 0.00E+00  | 0.00E+00  | 0.00E+00  | 0.00E+00  | 0.00E+00  | 0.00E+00  | 0.00E+00  | 0.00E+00  | 0.00E+00  | 0.00E+00  |           |          |      |     |  |
| ISSA           | 0.00E+00       | 0.00E+00  | 0.00E+00  | 0.00E+00  | 0.00E+00  | 0.00E+00  | 0.00E+00  | 0.00E+00  | 0.00E+00  | 0.00E+00  | 0.00E+00  | 0.00E+00  |           |          |      |     |  |
| CSSA           | 0.00E+00       | 0.00E+00  | 0.00E+00  | 0.00E+00  | 0.00E+00  | 0.00E+00  | 0.00E+00  | 0.00E+00  | 0.00E+00  | 0.00E+00  | 0.00E+00  | 0.00E+00  |           |          |      |     |  |
| CLSSA          | 0.00E+00       | 0.00E+00  | 0.00E+00  | 0.00E+00  | 0.00E+00  | 0.00E+00  | 0.00E+00  | 0.00E+00  | 0.00E+00  | 8.69E-09  | 9.00E-10  | 1.60E-09  |           |          |      |     |  |
| MISSA          | 0.00E+00       | 0.00E+00  | 0.00E+00  | 0.00E+00  | 0.00E+00  | 0.00E+00  | 0.00E+00  | 0.00E+00  | 0.00E+00  | 0.00E+00  | 0.00E+00  | 0.00E+00  |           |          |      |     |  |
| COOT           | 0.00E+00       | 3.14E-07  | 6.29E-09  | 4.44E-08  | 0.00E+00  | 4.68E-09  | 1.13E-10  | 6.63E-10  | 0.00E+00  | 6.44E-09  | 1.54E-10  | 9.13E-10  |           |          |      |     |  |
| WOA            | 0.00E+00       | 5.68E-14  | 1.14E-15  | 8.04E-15  | 0.00E+00  | 1.14E-13  | 4.55E-15  | 2.25E-14  | 0.00E+00  | 0.00E+00  | 0.00E+00  | 0.00E+00  |           |          |      |     |  |
| GWO            | 9.44E-12       | 2.59E+01  | 7.60E+00  | 5.88E+00  | 1.35E-05  | 2.81E+01  | 1.17E+01  | 6.97E+00  | 3.56E+00  | 8.64E+01  | 3.45E+01  | 1.67E+01  |           |          |      |     |  |
| PSO            | 2.16E+01       | 8.34E+01  | 4.40E+01  | 1.44E+01  | 7.29E+01  | 1.67E+02  | 9.99E+01  | 1.85E+01  | 2.56E+02  | 4.74E+02  | 3.53E+02  | 4.95E+01  |           |          |      |     |  |
| SSA            | 8.88E-16       | 8.88E-16  | 8.88E-16  | 0.00E+00  | 8.88E-16  | 8.88E-16  | 8.88E-16  | 0.00E+00  | 8.88E-16  | 8.88E-16  | 8.88E-16  | 0.00E+00  |           |          |      |     |  |
| ISSA           | 8.88E-16       | 4.44E-15  | 1.23E-15  | 1.07E-15  | 8.88E-16  | 1.96E-13  | 8.28E-15  | 3.05E-14  | 8.88E-16  | 8.88E-16  | 8.88E-16  | 0.00E+00  |           |          |      |     |  |
| CSSA           | 8.88E-16       | 8.88E-16  | 8.88E-16  | 0.00E+00  | 8.88E-16  | 8.88E-16  | 8.88E-16  | 0.00E+00  | 8.88E-16  | 8.88E-16  | 8.88E-16  | 0.00E+00  |           |          |      |     |  |
| CLSSA          | 8.88E-16       | 8.88E-16  | 8.88E-16  | 0.00E+00  | 8.88E-16  | 8.88E-16  | 8.88E-16  | 0.00E+00  | 8.88E-16  | 8.88E-16  | 8.88E-16  | 0.00E+00  |           |          |      |     |  |
| MISSA          | 8.88E-16       | 8.88E-16  | 8.88E-16  | 0.00E+00  | 8.88E-16  | 8.88E-16  | 8.88E-16  | 0.00E+00  | 8.88E-16  | 8.88E-16  | 8.88E-16  | 0.00E+00  |           |          |      |     |  |
| COOT           | 4.44E-15       | 1.54E-05  | 6.83E-07  | 3.01E-06  | 8.88E-16  | 7.45E-05  | 1.49E-06  | 1.05E-05  | 4.44E-15  | 8.52E-06  | 1.77E-07  | 1.20E-06  |           |          |      |     |  |
| WOA            | 8.88E-16       | 1.51E-14  | 7.13E-15  | 3.95E-15  | 8.88E-16  | 2.22E-14  | 5.93E-15  | 3.45E-15  | 4.44E-15  | 1.51E-14  | 6.93E-15  | 2.41E-15  |           |          |      |     |  |
| GWO            | 2.50E-09       | 4.00E-08  | 1.18E-08  | 7.32E-09  | 8.94E-07  | 7.22E-06  | 2.35E-06  | 1.08E-06  | 1.83E-04  | 5.24E-04  | 3.18E-04  | 8.37E-05  |           |          |      |     |  |
| PSO            | 5.78E-02       | 4.08E+00  | 5.00E-01  | 8.25E-01  | 4.65E-01  | 2.94E+00  | 1.21E+00  | 5.50E-01  | 2.32E+00  | 4.35E+00  | 2.93E+00  | 3.93E-01  |           |          |      |     |  |

TABLE 4: Continued.

| F     | Dim      | Algorithm | D = 30   |          |          |          | D = 50   |          |          |          | D = 100  |          |          |          |          |
|-------|----------|-----------|----------|----------|----------|----------|----------|----------|----------|----------|----------|----------|----------|----------|----------|
|       |          |           | Best     | Worst    | Mean     | Std      | Best     | Worst    | Mean     | Std      | Best     | Worst    | Mean     | Std      |          |
| $f_9$ |          | SSA       | 0.00E+00 | 0.00E+00 | 0.00E+00 | 0.00E+00 | 0.00E+00 | 0.00E+00 | 0.00E+00 | 0.00E+00 | 0.00E+00 | 0.00E+00 | 0.00E+00 | 0.00E+00 |          |
|       |          | ISSA      | 0.00E+00 | 0.00E+00 | 0.00E+00 | 0.00E+00 | 0.00E+00 | 0.00E+00 | 0.00E+00 | 0.00E+00 | 0.00E+00 | 0.00E+00 | 0.00E+00 | 0.00E+00 |          |
|       |          | CSSA      | 0.00E+00 | 0.00E+00 | 0.00E+00 | 0.00E+00 | 0.00E+00 | 0.00E+00 | 0.00E+00 | 0.00E+00 | 0.00E+00 | 0.00E+00 | 0.00E+00 | 0.00E+00 |          |
|       |          | CLSSA     | 0.00E+00 | 0.00E+00 | 0.00E+00 | 0.00E+00 | 0.00E+00 | 0.00E+00 | 0.00E+00 | 0.00E+00 | 0.00E+00 | 0.00E+00 | 0.00E+00 | 0.00E+00 |          |
|       |          | MISSA     | 0.00E+00 | 0.00E+00 | 0.00E+00 | 0.00E+00 | 0.00E+00 | 0.00E+00 | 0.00E+00 | 0.00E+00 | 0.00E+00 | 0.00E+00 | 0.00E+00 | 0.00E+00 |          |
|       |          | COOT      | 0.00E+00 | 7.89E-14 | 3.42E-15 | 1.30E-14 | 0.00E+00 | 8.32E-12 | 1.73E-13 | 1.18E-12 | 0.00E+00 | 0.00E+00 | 7.73E-10 | 1.55E-11 | 1.09E-10 |
|       |          | WOA       | 0.00E+00 | 3.74E-01 | 2.95E-02 | 9.14E-02 | 0.00E+00 | 3.20E-01 | 6.39E-03 | 4.52E-02 | 0.00E+00 | 1.11E-16 | 2.22E-18 | 1.57E-17 |          |
|       |          | GWO       | 3.11E-15 | 3.11E-02 | 6.10E-03 | 9.41E-03 | 1.29E-02 | 3.99E-02 | 5.31E-03 | 1.12E-02 | 5.57E-02 | 7.00E-02 | 8.65E-03 | 2.02E-02 |          |
|       |          | PSO       | 1.60E+02 | 2.18E+02 | 1.87E+02 | 1.59E+01 | 3.10E+02 | 3.73E+02 | 3.40E+02 | 1.64E+01 | 6.69E+02 | 7.92E+02 | 7.25E+02 | 3.00E+01 |          |
|       |          | $f_{10}$  |          | SSA      | 8.48E-06 | 1.96E-02 | 2.81E-03 | 5.68E-03 | 3.38E-06 | 3.58E-02 | 4.73E-03 | 8.95E-03 | 2.35E-05 | 4.16E-02 | 5.26E-03 |
| ISSA  | 1.66E-10 |           |          | 6.50E-05 | 4.86E-06 | 1.24E-05 | 1.03E-08 | 7.67E-05 | 8.08E-06 | 1.67E-05 | 1.61E-08 | 1.76E-04 | 1.56E-05 | 3.31E-05 |          |
| CSSA  | 1.66E-10 |           |          | 2.26E-05 | 1.73E-06 | 1.34E-05 | 1.52E-09 | 8.80E-06 | 2.47E-06 | 3.30E-06 | 1.89E-08 | 1.03E-05 | 3.69E-06 | 5.26E-06 |          |
| CLSSA | 3.60E-09 |           |          | 1.17E-05 | 1.87E-06 | 2.73E-06 | 2.33E-09 | 3.86E-05 | 3.37E-06 | 7.89E-06 | 1.73E-08 | 1.79E-05 | 5.26E-06 | 4.00E-06 |          |
| MISSA | 4.15E-10 |           |          | 7.66E-05 | 5.51E-06 | 3.63E-06 | 3.89E-10 | 1.60E-05 | 3.95E-06 | 5.35E-06 | 7.97E-09 | 2.78E-05 | 2.64E-07 | 4.55E-07 |          |
| COOT  | 6.01E-01 |           |          | 2.60E+00 | 8.21E-01 | 4.61E-01 | 1.77E+00 | 1.18E+01 | 4.08E+00 | 2.09E+00 | 8.03E+00 | 2.29E+01 | 1.17E+01 | 2.68E+00 |          |
| WOA   | 1.50E-01 |           |          | 1.67E+00 | 8.00E-01 | 3.89E-01 | 4.91E-01 | 3.17E+00 | 1.60E+00 | 6.08E-01 | 1.41E+00 | 6.39E+00 | 3.86E+00 | 1.20E+00 |          |
| GWO   | 4.26E-01 |           |          | 1.50E+00 | 9.30E-01 | 2.76E-01 | 1.40E+00 | 3.55E+00 | 2.48E+00 | 4.51E-01 | 5.91E+00 | 8.74E+00 | 7.58E+00 | 5.93E-01 |          |
| PSO   | 1.75E-03 |           |          | 3.62E+00 | 1.60E-01 | 7.11E-01 | 6.09E-02 | 5.22E+01 | 4.77E+00 | 1.22E+01 | 2.63E+00 | 1.24E+02 | 5.85E+01 | 4.20E+01 |          |

accuracy of the evaluation criterion for MISSA increases up to one or two orders of magnitudes than of other algorithms including CSSA. For  $f_7$  and  $f_9$ , the original SSA and other improved SSAs can search for the theoretical optimal solution in all dimensions and the Mean and Std are both 0, indicating the rationality and superiority of the algorithm itself. For  $f_8$ , neither MISSA nor other test algorithms have found the theoretical optimal solution, but the Std of MISSA is 0, which indicates that MISSA has been optimized to the theoretical maximum accuracy. For  $f_{10}$ , all the evaluation criteria of MISSA are optimal and the superiority becomes more significant when the dimension increases. The mathematical principle of other swarm intelligence algorithms is inferior to that of the sparrow algorithm, and it is easy to fall into local optimum when solving complex problems.

Overall, the experiments verify the significant difference between the results obtained by MISSA and other compared algorithms in almost all cases. With the increase in the dimension, other swarm intelligence algorithms such as COOT, WOA, and GWO are not effective enough in solving complex optimization problems. However, the original SSA benefits from the superiority of mathematical principles, which still has the opportunity to jump out of the local optimal solution in high-dimensional optimization, but the stability of the algorithm is obviously reduced. MISSA has prominent stability and robustness, which can balance the global exploitation and local exploitation abilities to fully explore the solution space.

**4.3.2. Convergence Curve Analysis.** Notably, to completely analyze the convergence speed and optimization accuracy of the compared algorithms, the convergence curves of the ten benchmark functions ( $D=30$ ) are shown in Figure 8. We select the semilogarithmic coordinate axis to draw the convergence curve. The  $y$ -axis and  $x$ -axis represent the fitness value and iteration, respectively.

As shown in Figure 8, the convergence curves clearly illustrate the advantages of MISSA in integrating the global exploration and local exploitation abilities into the search process. Under the premise of ensuring the optimization accuracy, the convergence speed of MISSA is better than that of other test algorithms.

The smooth convergence curves of MISSA on benchmark functions  $f_1$ ,  $f_3$ ,  $f_4$ ,  $f_6$ ,  $f_7$ , and  $f_9$  indicate that the improved optimization mechanism is more capable to search the solution space and the algorithm does not tend to fall into local optimum when dealing with these types of benchmark functions. Especially for  $f_7$ – $f_9$ , although both MISSA and other SSAs can converge to the theoretical optimal solution, MISSA has the fastest convergence speed.

The steplike fluctuant convergence curves of MISSA on the benchmark functions  $f_2$ ,  $f_5$ ,  $f_8$ , and  $f_{10}$  indicate that MISSA can jump out of the local optimum and can be effectively implemented to avoid premature convergence. After the algorithm is temporarily trapped in a local optimum, the EOBL strategy for elite individuals helps the algorithm escape the local optimum.

Combined with the optimization results in Table 4, MISSA not only improves the stability and robustness but also ensures the optimization accuracy and convergence speed of the algorithm.

**4.3.3. Wilcoxon Rank-Sum Test.** To further verify the difference from the perspective of statistics between MISSA and the comparison algorithms, the Wilcoxon rank-sum test is carried out at the  $P=5\%$  significance level in this paper [46]. Table 5 shows the corresponding results of the Wilcoxon rank-sum test on the benchmark functions ( $D=30$ ), in which the value of significance level is set to 0.05. There is a significant advantage between MISSA and the comparison algorithm if the  $P$  value is less than 0.05. On the contrary, the optimization performance of MISSA is equal to or worse than the comparison algorithm. NaN means the results of the comparison algorithms are close, and the significance judgment cannot be made. The sign “+/-” means that the MISSA is “better than/equivalent or inferior to” other algorithms in performance.

For the  $P$  value in Table 5, MISSA has a significant difference with other eight algorithms. For  $f_7$ – $f_9$ , due to the superiority of the SSA, SSAs can converge to the theoretical optimal value, so the difference is not obvious and the optimization ability is equivalent.

**4.4. CEC 2014 Function Test.** Compared to the basic benchmark functions, the CEC 2014 [47] is more complicated and can evaluate the effectiveness and robustness of the proposed algorithm better. The CEC 2014 consists of unimodal functions ( $F1$ – $F3$ ), simple multimodal functions ( $F4$ – $F16$ ), hybrid functions ( $F17$ – $F22$ ), and composition functions ( $F23$ – $F30$ ). According to the evaluation criteria of CEC 2014, the number of iterations is  $10,000 \times \text{dim}$ , the dimension is 30, the search range is  $[100, 100]$ , and other parameter settings are the same as in Section 4.1.

Table 6 illustrates that MISSA has a better optimization effect on CEC 2014. From the Wilcoxon rank-sum test, it is seen that MISSA is significantly different from other algorithms, showing better advantages, and some composition functions are similar to SSAs because of the superiority of the sparrow search algorithm itself which is analyzed in benchmark functions  $f_7$ – $f_9$ . Generally, MISSA has high effectiveness and robustness and is more suitable for some complex optimization problems than other algorithms.

## 5. Inductive Analysis of Strategies

MISSA improves the original SSA from three aspects: initialization method, discoverer-follower model, and optimal solution. After the experiments and analysis in Section 4, we generalize the impact influence of four strategies, as shown in Table 7; the sign “ $\uparrow/\downarrow/-$ ” means “enhance/reduce/no significant change.”

From Table 7, the abundance of population diversity has been improved after the addition of different strategies. The chaotic map enhances the diversity of the population and slightly improves the algorithm’s ability to deal with

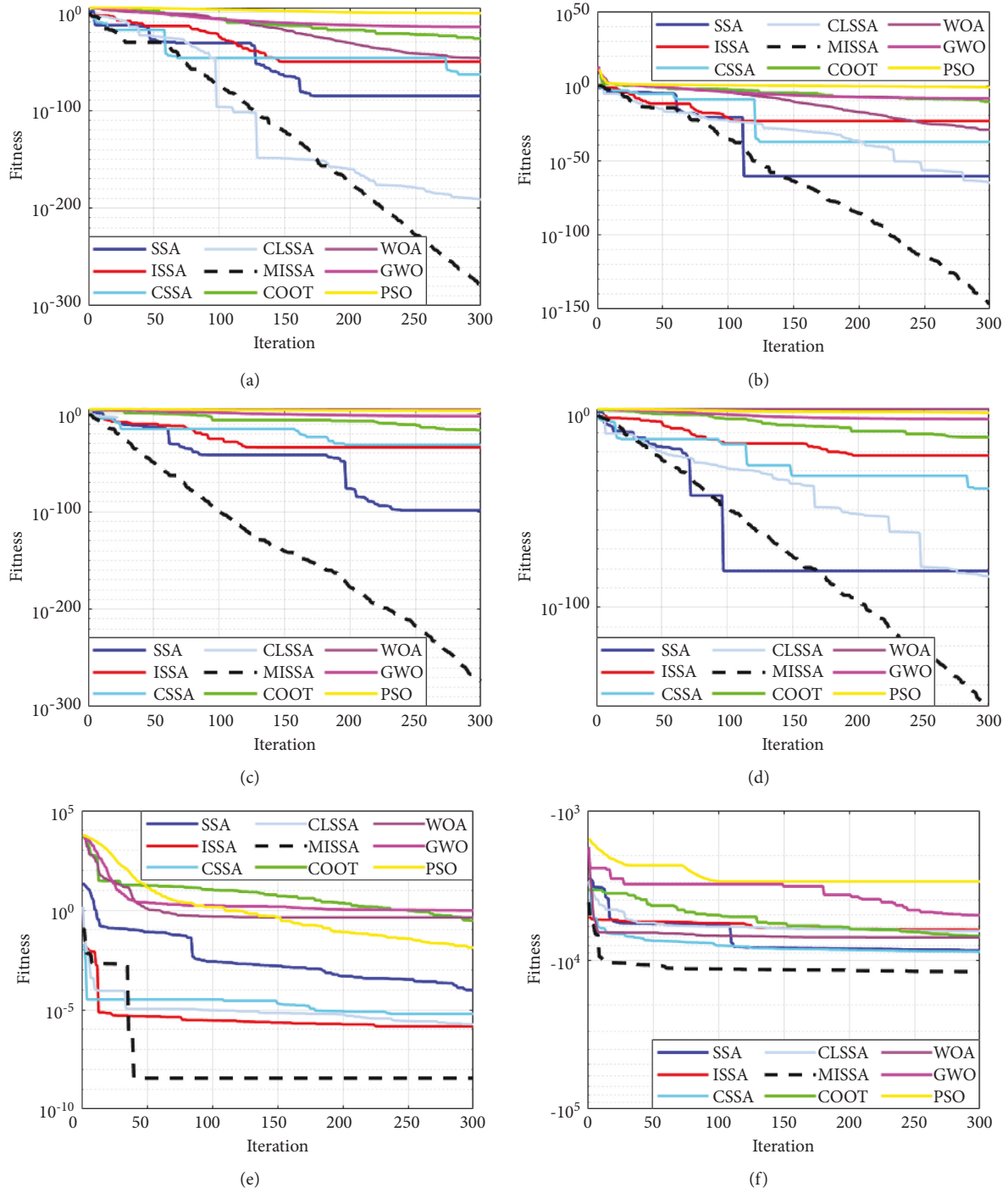


FIGURE 8: Continued.

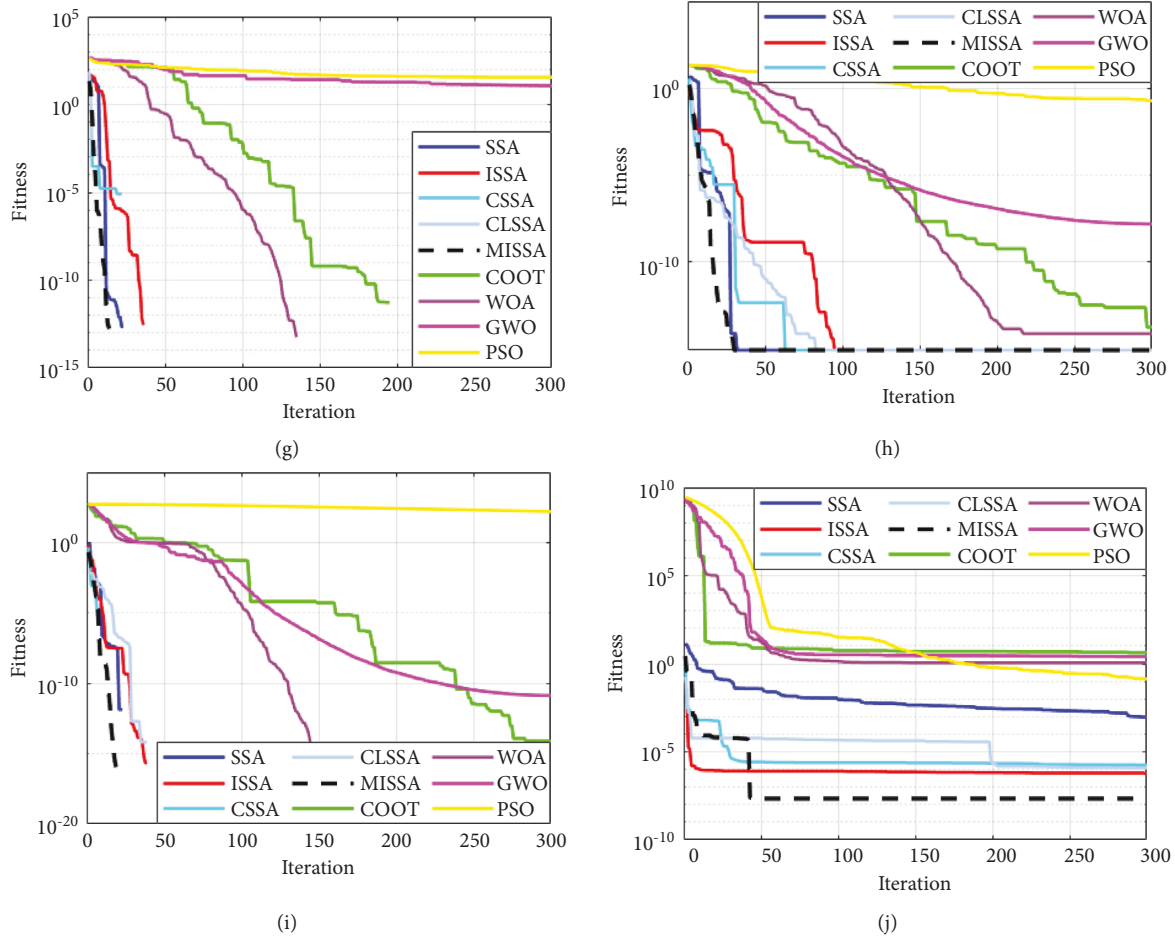


FIGURE 8: Convergence curves of ten benchmark functions. (a)  $f_1$ . (b)  $f_2$ . (c)  $f_3$ . (d)  $f_4$ . (e)  $f_5$ . (f)  $f_6$ . (g)  $f_7$ . (h)  $f_8$ . (i)  $f_9$ . (j)  $f_{10}$ .

TABLE 5: Results of the Wilcoxon rank-sum test.

| Function | SSA        | ISSA       | CSSA       | CLSSA      | COOT       | WOA        | GWO        | PSO        |
|----------|------------|------------|------------|------------|------------|------------|------------|------------|
| $f_1$    | $6.43E-11$ | $1.12E-18$ | $8.49E-02$ | $4.81E-01$ | $1.12E-18$ | $1.12E-18$ | $1.12E-18$ | $1.12E-18$ |
| $f_2$    | $8.16E-06$ | $1.52E-17$ | $1.66E-02$ | $4.00E-03$ | $1.52E-17$ | $3.31E-15$ | $1.52E-17$ | $1.52E-17$ |
| $f_3$    | $3.36E-06$ | $1.34E-18$ | $1.98E-02$ | $7.11E-02$ | $1.34E-18$ | $1.34E-18$ | $1.34E-18$ | $1.34E-18$ |
| $f_4$    | $1.33E-05$ | $3.41E-17$ | $1.17E-01$ | $3.21E-02$ | $3.41E-17$ | $3.41E-17$ | $3.41E-17$ | $3.41E-17$ |
| $f_5$    | $7.07E-18$ | NaN        | $4.04E-05$ | $6.96E-03$ | $7.07E-18$ | $7.07E-18$ | $7.07E-18$ | $7.07E-18$ |
| $f_6$    | $2.54E-16$ | $1.93E-11$ | $1.77E-10$ | $6.98E-18$ | $7.07E-18$ | $7.68E-15$ | $7.07E-18$ | $7.07E-18$ |
| $f_7$    | NaN        | NaN        | NaN        | NaN        | $1.73E-07$ | $3.27E-01$ | $3.31E-20$ | $3.31E-20$ |
| $f_8$    | NaN        | $4.28E-02$ | NaN        | NaN        | $8.24E-17$ | $2.32E-15$ | $8.24E-17$ | $8.24E-17$ |
| $f_9$    | NaN        | N/A        | NaN        | NaN        | $6.50E-05$ | $2.31E-02$ | $3.31E-20$ | $3.31E-20$ |
| $f_{10}$ | $1.54E-17$ | $2.50E-03$ | $4.63E-02$ | $4.46E-02$ | $7.07E-18$ | $7.07E-18$ | $7.07E-18$ | $7.07E-18$ |
| NaN/+/-  | 3/7/0      | 3/7/0      | 3/6/1      | 3/6/1      | 0/10/0     | 0/9/1      | 0/10/0     | 0/10/0     |

unimodal functions. The Gold-SA with nonlinear convergence factor strategies can quickly search the solution space and improve the convergence speed of the algorithm and the ability to deal with multimodal functions, but it reduces the stability of population diversity. The EOBL has a strong ability to handle unimodal functions by opposite solution and population reconstruction of elite individuals. However, when EOBL is used alone, the algorithm does not improve the ability to handle multimodal functions,

because the reverse learning of the current optimal solution amplifies the probability of the algorithm falling into a local optimum.

Notably, the EOBL improves the stability of population diversity, which was reduced by Gold-SA with the nonlinear convergence factor, and Gold-SA with nonlinear convergence factor can help EOBL to escape local optimum, which shows that there is a complementary relationship between them when strategies are mixed.



TABLE 6: Results of each algorithm in CEC 2014.

| <i>F</i>   | Criteria | SSA       | ISSA      | CSSA      | CLSSA     | COOT      | WOA       | GWO       | PSO       | MISSA     |
|------------|----------|-----------|-----------|-----------|-----------|-----------|-----------|-----------|-----------|-----------|
| <i>F1</i>  | Best     | 1.592E+08 | 2.567E+06 | 8.560E+06 | 3.745E+06 | 2.400E+05 | 5.548E+06 | 8.723E+06 | 2.585E+07 | 9.413E+04 |
|            | Worst    | 5.321E+08 | 1.321E+07 | 2.380E+07 | 2.012E+07 | 8.529E+05 | 2.382E+07 | 1.308E+08 | 6.025E+09 | 6.025E+05 |
|            | Mean     | 1.601E+08 | 7.609E+06 | 1.399E+07 | 1.255E+07 | 5.334E+05 | 1.217E+07 | 4.544E+07 | 8.539E+08 | 3.239E+05 |
|            | Std      | 1.760E+08 | 3.806E+06 | 5.323E+06 | 5.995E+06 | 2.033E+05 | 5.486E+06 | 3.635E+07 | 1.961E+09 | 1.776E+05 |
|            | <i>P</i> | 2.827E−03 | 1.402E−02 | 1.827E−04 | 1.827E−04 | 2.202E−03 | 1.827E−04 | 1.827E−04 | 1.827E−04 | 1.827E−04 |
| <i>F2</i>  | Best     | 4.636E+02 | 4.473E+02 | 2.172E+04 | 3.446E+04 | 2.807E+03 | 3.581E+04 | 4.116E+07 | 1.330E+10 | 2.025E+02 |
|            | Worst    | 2.450E+04 | 2.220E+04 | 2.221E+10 | 1.092E+05 | 3.197E+04 | 1.102E+05 | 3.098E+09 | 2.225E+10 | 8.635E+03 |
|            | Mean     | 1.107E+04 | 6.900E+03 | 1.784E+10 | 8.130E+04 | 1.286E+04 | 6.618E+04 | 1.240E+09 | 1.681E+10 | 1.771E+03 |
|            | Std      | 8.510E+03 | 7.633E+03 | 6.515E+09 | 2.312E+04 | 1.035E+04 | 3.005E+04 | 9.874E+08 | 3.162E+09 | 2.787E+03 |
|            | <i>P</i> | 2.827E−03 | 1.402E−02 | 1.827E−04 | 1.827E−04 | 2.202E−03 | 1.827E−04 | 1.827E−04 | 1.827E−04 | 1.827E−04 |
| <i>F3</i>  | Best     | 7.248E+04 | 1.796E+05 | 6.625E+04 | 6.504E+04 | 6.012E+04 | 4.606E+04 | 1.845E+04 | 3.142E+02 | 3.195E+03 |
|            | Worst    | 9.039E+04 | 2.869E+05 | 8.757E+04 | 8.525E+04 | 8.190E+04 | 1.264E+05 | 6.590E+04 | 9.248E+03 | 9.734E+03 |
|            | Mean     | 8.405E+04 | 2.408E+05 | 8.303E+04 | 7.839E+04 | 7.289E+04 | 7.405E+04 | 3.928E+04 | 5.238E+03 | 5.071E+03 |
|            | Std      | 5.338E+03 | 3.171E+04 | 7.377E+03 | 6.719E+03 | 7.671E+03 | 3.116E+04 | 1.268E+04 | 3.596E+03 | 1.952E+03 |
|            | <i>P</i> | 1.827E−04 | 1.827E−04 | 1.827E−04 | 1.827E−04 | 1.827E−04 | 1.827E−04 | 1.827E−04 | 1.827E−04 | 6.776E−01 |
| <i>F4</i>  | Best     | 1.246E+03 | 8.594E+02 | 1.064E+03 | 4.056E+03 | 5.858E+02 | 5.583E+02 | 5.651E+02 | 4.694E+02 | 4.222E+02 |
|            | Worst    | 3.336E+03 | 2.445E+03 | 8.607E+03 | 1.021E+04 | 1.062E+03 | 7.400E+02 | 7.834E+02 | 4.774E+02 | 5.259E+02 |
|            | Mean     | 1.838E+03 | 1.770E+03 | 6.405E+03 | 6.818E+03 | 7.996E+02 | 6.711E+02 | 6.650E+02 | 4.717E+02 | 4.774E+02 |
|            | Std      | 6.265E+02 | 5.105E+02 | 2.253E+03 | 1.927E+03 | 1.578E+02 | 5.354E+01 | 7.403E+01 | 8.878E+00 | 2.131E+01 |
|            | <i>P</i> | 1.817E−04 | 1.817E−04 | 1.817E−04 | 1.817E−04 | 1.817E−04 | 1.817E−04 | 1.817E−04 | 1.817E−04 | 8.747E−03 |
| <i>F5</i>  | Best     | 5.200E+02 | 5.200E+02 | 5.200E+02 | 5.200E+02 | 5.200E+02 | 5.203E+02 | 5.209E+02 | 5.200E+02 | 5.200E+02 |
|            | Worst    | 5.204E+02 | 5.205E+02 | 5.202E+02 | 5.202E+02 | 5.208E+02 | 5.207E+02 | 5.211E+02 | 5.209E+02 | 5.200E+02 |
|            | Mean     | 5.200E+02 | 5.201E+02 | 5.201E+02 | 5.200E+02 | 5.203E+02 | 5.205E+02 | 5.210E+02 | 5.205E+02 | 5.200E+02 |
|            | Std      | 1.153E−01 | 1.587E−01 | 5.872E−02 | 5.831E−02 | 2.534E−01 | 1.138E−01 | 4.143E−02 | 3.427E−01 | 1.618E−03 |
|            | <i>P</i> | 4.309E−04 | 1.315E−03 | 1.620E−01 | 3.281E−04 | 2.461E−04 | 1.827E−04 | 1.827E−04 | 2.461E−04 | 1.827E−04 |
| <i>F6</i>  | Best     | 6.360E+02 | 6.384E+02 | 6.398E+02 | 6.384E+02 | 6.367E+02 | 6.328E+02 | 6.102E+02 | 6.295E+02 | 6.173E+02 |
|            | Worst    | 6.454E+02 | 6.466E+02 | 6.486E+02 | 6.456E+02 | 6.438E+02 | 6.420E+02 | 6.182E+02 | 6.421E+02 | 6.264E+02 |
|            | Mean     | 6.425E+02 | 6.419E+02 | 6.421E+02 | 6.432E+02 | 6.390E+02 | 6.370E+02 | 6.145E+02 | 6.352E+02 | 6.214E+02 |
|            | Std      | 2.816E+00 | 2.521E+00 | 2.621E+00 | 2.168E+00 | 2.203E+00 | 3.012E+00 | 2.642E+00 | 4.779E+00 | 3.423E+00 |
|            | <i>P</i> | 1.827E−04 | 1.827E−04 | 1.827E−04 | 1.827E−04 | 1.827E−04 | 1.827E−04 | 1.827E−04 | 7.685E−04 | 1.827E−04 |
| <i>F7</i>  | Best     | 7.305E+02 | 7.476E+02 | 7.241E+02 | 8.942E+02 | 7.000E+02 | 7.013E+02 | 7.040E+02 | 7.016E+02 | 7.000E+02 |
|            | Worst    | 8.443E+02 | 8.490E+02 | 1.110E+03 | 1.050E+03 | 7.000E+02 | 7.061E+02 | 7.643E+02 | 7.021E+02 | 7.021E+02 |
|            | Mean     | 7.919E+02 | 7.898E+02 | 9.265E+02 | 9.743E+02 | 7.000E+02 | 7.022E+02 | 7.239E+02 | 7.019E+02 | 7.017E+02 |
|            | Std      | 3.405E+01 | 3.439E+01 | 1.467E+02 | 5.949E+01 | 8.745E−03 | 1.401E+00 | 1.837E+01 | 2.292E−01 | 6.519E−01 |
|            | <i>P</i> | 1.827E−04 | 1.827E−04 | 1.827E−04 | 1.827E−04 | 2.827E−03 | 8.796E−01 | 1.827E−04 | 3.195E−01 | 1.827E−04 |
| <i>F8</i>  | Best     | 9.640E+02 | 9.291E+02 | 9.277E+02 | 9.383E+02 | 9.572E+02 | 9.170E+02 | 8.681E+02 | 9.015E+02 | 8.627E+02 |
|            | Worst    | 1.025E+03 | 9.887E+02 | 1.016E+03 | 1.007E+03 | 1.024E+03 | 1.094E+03 | 9.615E+02 | 9.731E+02 | 9.473E+02 |
|            | Mean     | 9.860E+02 | 9.675E+02 | 9.743E+02 | 9.710E+02 | 9.750E+02 | 9.908E+02 | 8.951E+02 | 9.389E+02 | 9.046E+02 |
|            | Std      | 1.838E+01 | 1.669E+01 | 2.236E+01 | 2.075E+01 | 2.076E+01 | 5.343E+01 | 2.629E+01 | 2.009E+01 | 2.765E+01 |
|            | <i>P</i> | 1.827E−04 | 3.298E−04 | 3.298E−04 | 2.461E−04 | 1.827E−04 | 1.008E−03 | 3.847E−01 | 1.726E−02 | 1.827E−04 |
| <i>F9</i>  | Best     | 1.100E+03 | 1.093E+03 | 1.124E+03 | 1.117E+03 | 9.995E+02 | 1.065E+03 | 1.001E+03 | 1.021E+03 | 9.914E+02 |
|            | Worst    | 1.130E+03 | 1.161E+03 | 1.188E+03 | 1.183E+03 | 1.039E+03 | 1.228E+03 | 1.139E+03 | 1.097E+03 | 1.131E+03 |
|            | Mean     | 1.117E+03 | 1.132E+03 | 1.160E+03 | 1.144E+03 | 1.015E+03 | 1.133E+03 | 1.031E+03 | 1.063E+03 | 1.095E+03 |
|            | Std      | 1.069E+01 | 2.137E+01 | 2.410E+01 | 2.383E+01 | 1.339E+01 | 5.343E+01 | 5.097E+01 | 2.220E+01 | 3.958E+01 |
|            | <i>P</i> | 1.041E−01 | 1.133E−02 | 4.396E−04 | 1.706E−03 | 2.827E−03 | 1.859E−01 | 4.362E−02 | 1.133E−02 | 1.827E−04 |
| <i>F10</i> | Best     | 4.708E+03 | 3.946E+03 | 5.095E+03 | 4.458E+03 | 3.416E+03 | 4.487E+03 | 3.473E+03 | 3.617E+03 | 2.752E+03 |
|            | Worst    | 5.737E+03 | 7.185E+03 | 7.089E+03 | 6.473E+03 | 4.740E+03 | 6.788E+03 | 6.226E+03 | 5.298E+03 | 4.153E+03 |
|            | Mean     | 5.153E+03 | 5.484E+03 | 5.926E+03 | 5.397E+03 | 4.164E+03 | 5.735E+03 | 5.049E+03 | 4.569E+03 | 3.598E+03 |
|            | Std      | 3.121E+02 | 8.421E+02 | 6.559E+02 | 6.528E+02 | 4.148E+02 | 6.061E+02 | 8.830E+02 | 5.878E+02 | 4.754E+02 |
|            | <i>P</i> | 1.827E−04 | 4.396E−04 | 1.827E−04 | 1.827E−04 | 1.402E−02 | 1.827E−04 | 1.315E−03 | 4.586E−03 | 1.827E−04 |
| <i>F11</i> | Best     | 4.599E+03 | 5.689E+03 | 4.942E+03 | 5.895E+03 | 4.321E+03 | 5.239E+03 | 4.910E+03 | 4.251E+03 | 2.714E+03 |
|            | Worst    | 7.325E+03 | 7.937E+03 | 8.411E+03 | 7.682E+03 | 5.879E+03 | 7.681E+03 | 7.039E+03 | 9.197E+03 | 4.860E+03 |
|            | Mean     | 6.390E+03 | 6.570E+03 | 6.584E+03 | 6.748E+03 | 4.954E+03 | 6.531E+03 | 5.671E+03 | 5.882E+03 | 3.875E+03 |
|            | Std      | 8.529E+02 | 7.063E+02 | 1.036E+03 | 6.091E+02 | 5.479E+02 | 8.841E+02 | 7.064E+02 | 1.360E+03 | 6.634E+02 |
|            | <i>P</i> | 3.298E−04 | 1.827E−04 | 1.827E−04 | 1.827E−04 | 4.586E−03 | 1.827E−04 | 1.827E−04 | 7.685E−04 | 1.827E−04 |

TABLE 6: Continued.

| <i>F</i> | Criteria | SSA       | ISSA      | CSSA      | CLSSA     | COOT      | WOA       | GWO       | PSO       | MISSA     |
|----------|----------|-----------|-----------|-----------|-----------|-----------|-----------|-----------|-----------|-----------|
| F12      | Best     | 1.201E+03 | 1.201E+03 | 1.201E+03 | 1.201E+03 | 1.201E+03 | 1.201E+03 | 1.200E+03 | 1.201E+03 | 1.201E+03 |
|          | Worst    | 1.203E+03 | 1.203E+03 | 1.203E+03 | 1.202E+03 | 1.202E+03 | 1.203E+03 | 1.203E+03 | 1.202E+03 | 1.202E+03 |
|          | Mean     | 1.202E+03 | 1.202E+03 | 1.202E+03 | 1.202E+03 | 1.202E+03 | 1.202E+03 | 1.203E+03 | 1.202E+03 | 1.201E+03 |
|          | Std      | 7.197E-01 | 5.079E-01 | 6.170E-01 | 3.856E-01 | 4.297E-01 | 6.000E-01 | 8.211E-01 | 4.977E-01 | 3.077E-01 |
|          | <i>P</i> | 1.399E-01 | 1.388E-02 | 1.207E-01 | 7.910E-01 | 1.613E-01 | 4.362E-02 | 2.786E-03 | 3.840E-01 |           |
| F13      | Best     | 1.303E+03 | 1.303E+03 | 1.306E+03 | 1.306E+03 | 1.300E+03 | 1.300E+03 | 1.300E+03 | 1.300E+03 | 1.300E+03 |
|          | Worst    | 1.305E+03 | 1.305E+03 | 1.308E+03 | 1.308E+03 | 1.301E+03 | 1.301E+03 | 1.303E+03 | 1.301E+03 | 1.303E+03 |
|          | Mean     | 1.304E+03 | 1.304E+03 | 1.307E+03 | 1.307E+03 | 1.300E+03 | 1.301E+03 | 1.301E+03 | 1.301E+03 | 1.301E+03 |
|          | Std      | 5.492E-01 | 8.018E-01 | 7.393E-01 | 6.089E-01 | 1.261E-01 | 1.122E-01 | 8.971E-01 | 1.260E-01 | 7.857E-01 |
|          | <i>P</i> | 1.827E-04 | 1.827E-04 | 1.827E-04 | 1.827E-04 | 5.795E-03 | 3.447E-01 | 2.413E-01 | 4.390E-02 |           |
| F14      | Best     | 1.467E+03 | 1.475E+03 | 1.422E+03 | 1.420E+03 | 1.400E+03 | 1.400E+03 | 1.400E+03 | 1.400E+03 | 1.400E+03 |
|          | Worst    | 1.507E+03 | 1.515E+03 | 1.491E+03 | 1.510E+03 | 1.401E+03 | 1.400E+03 | 1.416E+03 | 1.401E+03 | 1.438E+03 |
|          | Mean     | 1.491E+03 | 1.493E+03 | 1.457E+03 | 1.464E+03 | 1.400E+03 | 1.400E+03 | 1.404E+03 | 1.400E+03 | 1.418E+03 |
|          | Std      | 1.373E+01 | 1.367E+01 | 2.338E+01 | 2.428E+01 | 1.708E-01 | 3.211E-02 | 5.397E+00 | 3.465E-01 | 1.235E+01 |
|          | <i>P</i> | 1.827E-04 | 1.827E-04 | 5.828E-04 | 5.828E-04 | 1.133E-02 | 5.795E-03 | 3.121E-02 | 1.133E-02 |           |
| F15      | Best     | 4.278E+03 | 4.537E+03 | 2.272E+03 | 2.263E+03 | 1.571E+03 | 1.555E+03 | 1.508E+03 | 1.540E+03 | 1.518E+03 |
|          | Worst    | 1.537E+04 | 2.229E+04 | 6.568E+03 | 1.394E+04 | 2.222E+03 | 1.691E+03 | 1.885E+03 | 1.570E+03 | 1.533E+03 |
|          | Mean     | 7.556E+03 | 8.870E+03 | 4.873E+03 | 4.617E+03 | 1.746E+03 | 1.624E+03 | 1.610E+03 | 1.552E+03 | 1.523E+03 |
|          | Std      | 3.669E+03 | 5.508E+03 | 1.524E+03 | 3.448E+03 | 2.256E+02 | 4.273E+01 | 1.200E+02 | 1.035E+01 | 4.466E+00 |
|          | <i>P</i> | 1.817E-04 | 1.827E-04 | 1.827E-04 | 1.827E-04 | 1.827E-04 | 1.827E-04 | 1.827E-04 | 1.827E-03 | 1.827E-04 |
| F16      | Best     | 1.613E+03 | 1.613E+03 | 1.613E+03 | 1.613E+03 | 1.612E+03 | 1.612E+03 | 1.614E+03 | 1.612E+03 | 1.612E+03 |
|          | Worst    | 1.614E+03 | 1.614E+03 | 1.614E+03 | 1.614E+03 | 1.613E+03 | 1.613E+03 | 1.613E+03 | 1.613E+03 | 1.613E+03 |
|          | Mean     | 1.613E+03 | 1.613E+03 | 1.613E+03 | 1.613E+03 | 1.612E+03 | 1.613E+03 | 1.613E+03 | 1.613E+03 | 1.613E+03 |
|          | Std      | 3.827E-01 | 2.789E-01 | 2.316E-01 | 3.621E-01 | 3.050E-01 | 3.664E-01 | 6.362E-01 | 5.379E-01 | 4.230E-01 |
|          | <i>P</i> | 2.409E-04 | 1.786E-04 | 1.688E-04 | 2.786E-03 | 1.726E-02 | 3.447E-01 | 3.298E-04 | 3.440E-01 |           |
| F17      | Best     | 8.051E+05 | 6.594E+05 | 4.092E+05 | 3.200E+05 | 3.505E+04 | 6.989E+05 | 2.133E+05 | 1.236E+05 | 7.154E+03 |
|          | Worst    | 9.578E+06 | 3.698E+06 | 7.083E+06 | 4.444E+06 | 2.988E+05 | 7.565E+06 | 1.656E+06 | 9.602E+05 | 5.006E+04 |
|          | Mean     | 3.533E+06 | 2.071E+06 | 2.808E+06 | 1.874E+06 | 1.515E+05 | 3.003E+06 | 7.017E+05 | 4.927E+05 | 2.645E+04 |
|          | Std      | 2.477E+06 | 1.136E+06 | 2.262E+06 | 1.442E+06 | 9.963E+04 | 2.469E+06 | 5.702E+05 | 3.004E+05 | 1.383E+04 |
|          | <i>P</i> | 1.827E-04 | 1.827E-04 | 1.827E-04 | 1.827E-04 | 5.828E-04 | 1.827E-04 | 1.827E-04 | 1.827E-04 | 1.827E-04 |
| F18      | Best     | 3.365E+03 | 8.957E+03 | 7.399E+04 | 6.574E+08 | 2.092E+04 | 2.067E+04 | 4.002E+03 | 2.193E+03 | 1.885E+03 |
|          | Worst    | 1.290E+08 | 2.893E+07 | 3.872E+09 | 4.259E+09 | 1.574E+05 | 6.860E+05 | 7.632E+07 | 5.631E+07 | 7.298E+03 |
|          | Mean     | 2.185E+07 | 6.500E+06 | 1.435E+09 | 2.713E+09 | 4.205E+04 | 1.514E+05 | 1.738E+07 | 1.035E+07 | 3.291E+03 |
|          | Std      | 4.097E+07 | 9.788E+06 | 1.311E+09 | 1.395E+09 | 4.222E+03 | 2.037E+05 | 2.603E+07 | 1.943E+07 | 1.761E+03 |
|          | <i>P</i> | 4.586E-03 | 1.827E-04 | 1.827E-04 | 1.827E-04 | 4.708E-03 | 1.827E-04 | 4.396E-04 | 1.133E-02 |           |
| F19      | Best     | 2.066E+03 | 2.052E+03 | 2.060E+03 | 2.065E+03 | 1.912E+03 | 1.928E+03 | 1.912E+03 | 1.959E+03 | 1.918E+03 |
|          | Worst    | 2.331E+03 | 2.199E+03 | 2.332E+03 | 2.364E+03 | 1.971E+03 | 2.094E+03 | 2.002E+03 | 2.038E+03 | 1.946E+03 |
|          | Mean     | 2.160E+03 | 2.141E+03 | 2.146E+03 | 2.216E+03 | 1.920E+03 | 1.994E+03 | 1.946E+03 | 2.005E+03 | 1.927E+03 |
|          | Std      | 8.977E+01 | 4.816E+01 | 1.006E+02 | 1.008E+02 | 1.819E+01 | 5.239E+01 | 3.136E+01 | 2.448E+01 | 8.322E+00 |
|          | <i>P</i> | 1.827E-04 | 1.827E-04 | 1.827E-04 | 1.827E-04 | 2.827E-03 | 5.828E-04 | 2.123E-01 | 1.827E-04 |           |
| F20      | Best     | 9.172E+04 | 1.226E+05 | 3.271E+04 | 6.443E+04 | 5.353E+03 | 2.061E+04 | 1.262E+04 | 2.486E+04 | 3.490E+03 |
|          | Worst    | 3.861E+05 | 2.749E+06 | 5.141E+05 | 4.471E+05 | 2.929E+04 | 1.165E+05 | 3.594E+04 | 3.048E+05 | 1.041E+04 |
|          | Mean     | 2.281E+05 | 7.579E+05 | 1.972E+05 | 1.969E+05 | 1.854E+04 | 6.012E+04 | 2.709E+04 | 1.308E+05 | 6.484E+03 |
|          | Std      | 1.031E+05 | 9.890E+05 | 1.451E+05 | 1.151E+05 | 8.090E+03 | 2.632E+04 | 7.251E+03 | 8.808E+04 | 2.063E+03 |
|          | <i>P</i> | 1.827E-04 | 1.827E-04 | 1.827E-04 | 1.827E-04 | 1.315E-03 | 1.827E-04 | 1.827E-04 | 1.827E-04 |           |
| F21      | Best     | 1.357E+06 | 1.514E+06 | 2.552E+05 | 2.722E+05 | 4.970E+04 | 1.156E+06 | 6.811E+04 | 1.346E+06 | 2.009E+04 |
|          | Worst    | 5.335E+07 | 3.639E+07 | 2.150E+07 | 4.371E+07 | 4.151E+05 | 1.029E+07 | 1.846E+06 | 1.521E+07 | 1.177E+05 |
|          | Mean     | 1.192E+07 | 1.237E+07 | 9.264E+06 | 1.412E+07 | 2.425E+05 | 6.436E+06 | 5.982E+05 | 6.043E+06 | 7.626E+04 |
|          | Std      | 1.498E+07 | 1.137E+07 | 8.219E+06 | 1.505E+07 | 1.483E+05 | 3.172E+06 | 5.877E+05 | 4.241E+06 | 3.785E+04 |
|          | <i>P</i> | 1.817E-04 | 1.817E-04 | 1.817E-04 | 1.817E-04 | 1.398E-02 | 1.817E-04 | 5.777E-03 | 1.817E-04 |           |
| F22      | Best     | 3.098E+03 | 3.245E+03 | 3.235E+03 | 3.248E+03 | 2.376E+03 | 3.003E+03 | 2.389E+03 | 2.873E+03 | 2.821E+03 |
|          | Worst    | 4.849E+03 | 5.707E+03 | 4.393E+03 | 5.464E+03 | 3.132E+03 | 3.499E+03 | 2.869E+03 | 3.998E+03 | 3.658E+03 |
|          | Mean     | 3.824E+03 | 4.160E+03 | 3.877E+03 | 3.745E+03 | 2.768E+03 | 3.264E+03 | 2.602E+03 | 3.380E+03 | 3.260E+03 |
|          | Std      | 5.866E+02 | 7.812E+02 | 3.807E+02 | 6.163E+02 | 1.998E+02 | 1.645E+02 | 1.427E+02 | 3.380E+02 | 2.635E+02 |
|          | <i>P</i> | 1.726E-02 | 4.586E-03 | 2.202E-03 | 1.402E-02 | 7.685E-04 | 9.698E-01 | 2.461E-04 | 3.447E-02 |           |

TABLE 6: Continued.

| <i>F</i>   | Criteria | SSA       | ISSA      | CSSA      | CLSSA     | COOT      | WOA       | GWO       | PSO       | MISSA     |
|------------|----------|-----------|-----------|-----------|-----------|-----------|-----------|-----------|-----------|-----------|
| <i>F23</i> | Best     | 2.500E+03 | 2.500E+03 | 2.500E+03 | 2.500E+03 | 2.615E+03 | 2.640E+03 | 2.626E+03 | 2.614E+03 | 2.500E+03 |
|            | Worst    | 2.500E+03 | 2.500E+03 | 2.500E+03 | 2.500E+03 | 2.616E+03 | 2.678E+03 | 2.662E+03 | 2.614E+03 | 2.500E+03 |
|            | Mean     | 2.500E+03 | 2.500E+03 | 2.500E+03 | 2.500E+03 | 2.615E+03 | 2.657E+03 | 2.641E+03 | 2.614E+03 | 2.500E+03 |
|            | Std      | 0.000E+00 | 0.000E+00 | 0.000E+00 | 0.000E+00 | 1.123E-01 | 1.380E+01 | 1.208E+01 | 1.228E-03 | 0.000E+00 |
|            | <i>P</i> | NaN       | NaN       | NaN       | NaN       | 6.386E-05 | 6.386E-05 | 6.386E-05 | 6.386E-05 | 6.386E-05 |
| <i>F24</i> | Best     | 2.600E+03 | 2.600E+03 | 2.600E+03 | 2.600E+03 | 2.625E+03 | 2.605E+03 | 2.600E+03 | 2.621E+03 | 2.600E+03 |
|            | Worst    | 2.600E+03 | 2.600E+03 | 2.600E+03 | 2.600E+03 | 2.631E+03 | 2.617E+03 | 2.600E+03 | 2.651E+03 | 2.600E+03 |
|            | Mean     | 2.600E+03 | 2.600E+03 | 2.600E+03 | 2.600E+03 | 2.628E+03 | 2.611E+03 | 2.600E+03 | 2.633E+03 | 2.600E+03 |
|            | Std      | 0.000E+00 | 0.000E+00 | 0.000E+00 | 0.000E+00 | 1.989E+00 | 5.162E+00 | 5.381E-03 | 1.063E+01 | 0.000E+00 |
|            | <i>P</i> | NaN       | NaN       | NaN       | NaN       | 6.386E-05 | 6.386E-05 | 6.386E-05 | 6.386E-05 | 6.386E-05 |
| <i>F25</i> | Best     | 2.700E+03 | 2.700E+03 | 2.700E+03 | 2.700E+03 | 2.700E+03 | 2.716E+03 | 2.706E+03 | 2.711E+03 | 2.700E+03 |
|            | Worst    | 2.700E+03 | 2.700E+03 | 2.700E+03 | 2.700E+03 | 2.718E+03 | 2.759E+03 | 2.719E+03 | 2.731E+03 | 2.700E+03 |
|            | Mean     | 2.700E+03 | 2.700E+03 | 2.700E+03 | 2.700E+03 | 2.713E+03 | 2.727E+03 | 2.711E+03 | 2.719E+03 | 2.700E+03 |
|            | Std      | 0.000E+00 | 0.000E+00 | 0.000E+00 | 0.000E+00 | 4.821E+00 | 1.472E+01 | 4.320E+00 | 5.773E+00 | 0.000E+00 |
|            | <i>P</i> | NaN       | NaN       | NaN       | NaN       | 1.576E-04 | 5.511E-05 | 6.340E-05 | 6.386E-05 | 6.386E-05 |
| <i>F26</i> | Best     | 2.702E+03 | 2.703E+03 | 2.701E+03 | 2.707E+03 | 2.718E+03 | 2.800E+03 | 2.800E+03 | 2.800E+03 | 2.700E+03 |
|            | Worst    | 2.800E+03 | 2.800E+03 | 2.800E+03 | 2.800E+03 | 2.800E+03 | 2.800E+03 | 2.800E+03 | 2.800E+03 | 2.701E+03 |
|            | Mean     | 2.790E+03 | 2.771E+03 | 2.773E+03 | 2.783E+03 | 2.792E+03 | 2.800E+03 | 2.761E+03 | 2.800E+03 | 2.700E+03 |
|            | Std      | 3.089E+01 | 4.648E+01 | 4.427E+01 | 3.524E+01 | 2.598E+01 | 0.000E+00 | 5.082E+01 | 1.902E-02 | 1.288E-01 |
|            | <i>P</i> | 8.745E-05 | 1.317E-04 | 2.438E-04 | 1.107E-04 | 8.745E-05 | 6.386E-05 | 5.828E-04 | 1.727E-04 | 6.386E-05 |
| <i>F27</i> | Best     | 2.900E+03 | 2.900E+03 | 2.900E+03 | 2.900E+03 | 3.111E+03 | 3.177E+03 | 3.192E+03 | 3.106E+03 | 2.900E+03 |
|            | Worst    | 2.900E+03 | 2.900E+03 | 2.900E+03 | 2.900E+03 | 3.835E+03 | 4.170E+03 | 3.699E+03 | 4.477E+03 | 2.900E+03 |
|            | Mean     | 2.900E+03 | 2.900E+03 | 2.900E+03 | 2.900E+03 | 3.592E+03 | 3.785E+03 | 3.417E+03 | 3.787E+03 | 2.900E+03 |
|            | Std      | 0.000E+00 | 0.000E+00 | 0.000E+00 | 0.000E+00 | 1.978E+02 | 3.861E+02 | 1.412E+02 | 5.854E+02 | 0.000E+00 |
|            | <i>P</i> | NaN       | NaN       | NaN       | NaN       | 6.386E-05 | 6.386E-05 | 6.386E-05 | 6.386E-05 | 6.386E-05 |
| <i>F28</i> | Best     | 3.000E+03 | 3.000E+03 | 3.000E+03 | 3.000E+03 | 3.796E+03 | 4.711E+03 | 3.689E+03 | 6.271E+03 | 3.000E+03 |
|            | Worst    | 3.000E+03 | 3.000E+03 | 3.000E+03 | 3.000E+03 | 5.108E+03 | 5.966E+03 | 4.747E+03 | 8.157E+03 | 3.000E+03 |
|            | Mean     | 3.000E+03 | 3.000E+03 | 3.000E+03 | 3.000E+03 | 4.432E+03 | 5.351E+03 | 4.009E+03 | 7.026E+03 | 3.000E+03 |
|            | Std      | 0.000E+00 | 0.000E+00 | 0.000E+00 | 0.000E+00 | 4.163E+02 | 3.647E+02 | 3.494E+02 | 6.857E+02 | 0.000E+00 |
|            | <i>P</i> | NaN       | NaN       | NaN       | NaN       | 6.386E-05 | 6.386E-05 | 6.386E-05 | 6.386E-05 | 6.386E-05 |
| <i>F29</i> | Best     | 3.100E+03 | 3.100E+03 | 3.100E+03 | 3.100E+03 | 5.558E+03 | 2.146E+06 | 9.872E+03 | 4.580E+03 | 3.100E+03 |
|            | Worst    | 3.100E+03 | 3.100E+03 | 3.100E+03 | 3.100E+03 | 1.644E+07 | 2.111E+07 | 1.683E+06 | 4.343E+05 | 3.100E+03 |
|            | Mean     | 3.100E+03 | 3.100E+03 | 3.100E+03 | 3.100E+03 | 6.121E+06 | 1.269E+07 | 2.989E+05 | 1.071E+05 | 3.100E+03 |
|            | Std      | 0.000E+00 | 0.000E+00 | 0.000E+00 | 0.000E+00 | 6.805E+06 | 5.525E+06 | 5.341E+05 | 1.387E+05 | 0.000E+00 |
|            | <i>P</i> | NaN       | NaN       | NaN       | NaN       | 6.386E-05 | 6.386E-05 | 6.386E-05 | 6.386E-05 | 6.386E-05 |
| <i>F30</i> | Best     | 3.200E+03 | 3.200E+03 | 3.200E+03 | 3.200E+03 | 1.068E+04 | 1.172E+05 | 1.817E+04 | 5.782E+03 | 3.200E+03 |
|            | Worst    | 3.200E+03 | 3.200E+03 | 3.200E+03 | 3.200E+03 | 2.423E+04 | 1.124E+06 | 1.441E+05 | 5.947E+04 | 3.200E+03 |
|            | Mean     | 3.200E+03 | 3.200E+03 | 3.200E+03 | 3.200E+03 | 1.539E+04 | 4.686E+05 | 5.813E+04 | 1.648E+04 | 3.200E+03 |
|            | Std      | 0.000E+00 | 0.000E+00 | 0.000E+00 | 0.000E+00 | 4.192E+03 | 2.990E+05 | 3.914E+04 | 1.642E+04 | 0.000E+00 |
|            | <i>P</i> | NaN       | NaN       | NaN       | NaN       | 6.386E-05 | 6.386E-05 | 6.386E-05 | 6.386E-05 | 6.386E-05 |
| NaN/+/-    |          | 7/21/2    | 7/23/0    | 7/21/2    | 7/21/2    | 0/29/1    | 0/25/5    | 0/27/3    | 0/26/4    |           |

TABLE 7: Impact influence of the strategy.

| Aspect                    | Strategy                                  | Diversity |           | Searching ability |              |
|---------------------------|---|-----------|-----------|-------------------|--------------|
|                           |   | Abundance | Stability | Exploration       | Exploitation |
| Population initialization | Iterative chaotic map                     | ↑         | ↑         | —                 | —            |
| Discoverer-follower model | Gold-SA with nonlinear convergence factor | ↑         | ↓         | ↑                 | —            |
| Optimal solution          | EOBL                                      | ↑         | ↑         | —                 | ↑            |

### 6. Experimental Simulation and Result Analysis

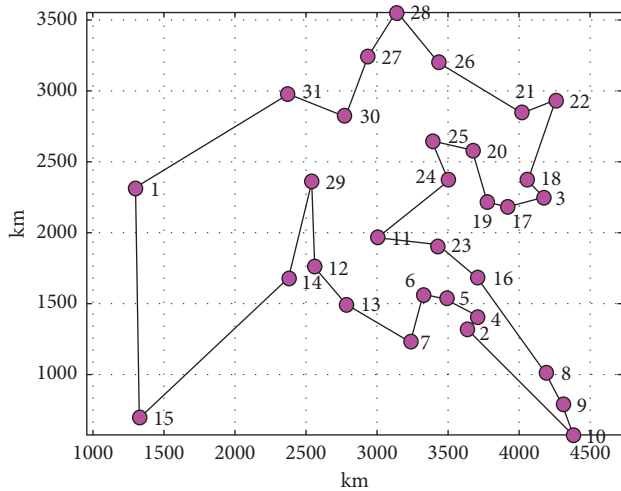
In order to verify the efficiency of the proposed MISSA in dealing with combinatorial optimization problems, Section 6 applies the proposed MISSA to the traveling salesman problem, the tourism route planning problems of 31 provincial capital cities in China, the standard TSPLIB instance

is selected for testing, and the results are compared with SSA [24], ISSA [30], GWO [15], and PSO [12].

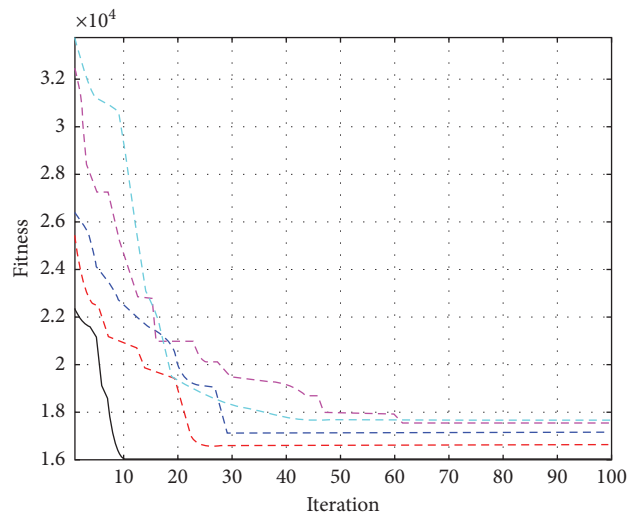
6.1. The Traveling Salesman Problem. The traveling salesman problem is a well-known problem in combinatorial optimization filed, which can be described as follows: the traveling

TABLE 8: City coordinates.

| Order | Coordinate   |
|-------|--------------|
| 1     | (1304, 2312) |
| 2     | (3639, 1315) |
| 3     | (4177, 2244) |
| 4     | (3712, 1399) |
| 5     | (3488, 1535) |
| 6     | (3326, 1556) |
| 7     | (3238, 1229) |
| 8     | (4196, 1004) |
| 9     | (4312, 790)  |
| 10    | (4386, 570)  |
| 11    | (3007, 1970) |
| 12    | (2562, 1756) |
| 13    | (2788, 1491) |
| 14    | (2381, 1676) |
| 15    | (1332, 695)  |
| 16    | (3715, 1678) |
| 17    | (3918, 2179) |
| 18    | (4061, 2370) |
| 19    | (3780, 2212) |
| 20    | (3676, 2578) |
| 21    | (4029, 2838) |
| 22    | (4263, 2931) |
| 23    | (3429, 1908) |
| 24    | (3507, 2367) |
| 25    | (3394, 2643) |
| 26    | (3439, 3201) |
| 27    | (2935, 3240) |
| 28    | (3140, 3550) |
| 29    | (2545, 2357) |
| 30    | (2778, 2826) |
| 31    | (2370, 2975) |



(a)



(b)

FIGURE 9: Provincial capitals tourism route planning. (a) Optimal route of MISSA. (b) Convergence curves.

TABLE 9: TSPLIB instances.

| TSPLIB | Instance | burma14  | bayg29   | dantzig42 | eil51    | eil76    |
|--------|----------|----------|----------|-----------|----------|----------|
|        | D        | 14       | 29       | 42        | 51       | 76       |
|        | TO       | 3.09E+01 | 9.07E+03 | 6.99E+02  | 4.26E+02 | 5.38E+02 |
| MISSA  | Best     | 3.09E+01 | 9.07E+03 | 6.88E+02  | 4.26E+02 | 5.38E+02 |
|        | RE       | 0.00%    | 0.00%    | 0.14%     | 0.40%    | 0.89%    |
|        | Mean     | 3.09E+01 | 9.07E+03 | 7.00E+02  | 4.28E+02 | 5.43E+02 |
| ISSA   | Best     | 3.09E+01 | 9.13E+03 | 6.99E+02  | 4.35E+02 | 5.52E+02 |
|        | RE       | 0.91%    | 1.21%    | 1.57%     | 5.15%    | 6.32%    |
|        | Mean     | 3.12E+01 | 9.18E+03 | 7.10E+02  | 4.48E+02 | 5.72E+02 |
| SSA    | Best     | 3.09E+01 | 9.23E+03 | 7.01E+02  | 4.38E+02 | 5.62E+02 |
|        | RE       | 1.17%    | 2.21%    | 2.72%     | 6.09%    | 8.00%    |
|        | Mean     | 3.12E+01 | 9.27E+03 | 7.18E+02  | 4.52E+02 | 5.81E+02 |
| GWO    | Best     | 3.09E+01 | 9.24E+03 | 7.21E+02  | 4.83E+02 | 6.35E+02 |
|        | RE       | 1.69%    | 2.09%    | 4.43%     | 12.96%   | 17.89%   |
|        | Mean     | 3.14E+01 | 9.26E+03 | 7.31E+02  | 5.06E+02 | 6.74E+02 |
| PSO    | Best     | 3.09E+01 | 9.23E+03 | 7.26E+02  | 6.38E+02 | 5.82E+02 |
|        | RE       | 2.01%    | 3.09%    | 5.01%     | 16.57%   | 21.61%   |
|        | Mean     | 3.15E+01 | 9.35E+03 | 7.34E+02  | 4.97E+02 | 6.54E+02 |

salesman intends to sell goods in  $n$  cities, selecting one of the cities as the starting point and visiting all the remaining cities without repetition, and finally returns to the starting point to select the shortest path among all routes [48].

In the graph theory, TSP can be described as finding a Hamilton cycle with the lowest weight in a complete weighted graph. Let  $G=(V, E)$  be a complete weighted graph, where  $V = \{1, 2, \dots, n\}$  represents the vertex set and  $E$  represents the edge set. Each edge has a nonnegative weight  $m(e)$  on  $e=(I n, j) \in E$  and finds the Hamiltonian cycle  $C$  of  $G$ , in which the total weight of  $C$  satisfies  $M(C) = \min_{\sum_{E(C)} m(e)}$ . The matrix  $W$  of distance between cities is as follows:

$$W = \begin{bmatrix} d_{(1,1)} & \cdots & d_{(1,n)} \\ \vdots & \ddots & \vdots \\ d_{(n,1)} & \cdots & d_{(n,n)} \end{bmatrix}, \quad (14)$$

where  $d_{(i,j)}$  represents the distance from the  $i^{\text{th}}$  city to the  $j^{\text{th}}$  city,  $d_{(i,j)} \geq 0, i, j \in v$ . The mathematical model of the objective function and constraint function of TSP are established as follows:

$$f = \min\left(\sum \sum d_{(i,j)} x_{(i,j)}\right),$$

$$\text{s.t.} \begin{cases} \sum_{j \neq 1} x_{(i,j)} = 1, & i \in V, \\ \sum_{i \neq j} x_{(i,j)} = 1, & j \in V, \\ \sum_{i,j \in S} x_{(i,j)} = |S| - 1, & S \subseteq V, \\ x_{(i,j)} \in \{0, 1\}, & i, j \in V, \end{cases} \quad (15)$$

$$x_{(i,j)} = \begin{cases} 1, & (i, j) \in \text{optimal path}, \\ 0, & \text{other}, \end{cases}$$

where  $|S|$  represents the number of vertices in the set  $S$ . The constraint functions show that there is only one outgoing edge and one incoming edge for each vertex and no subloops will be generated.

6.2. Practical Problem Test. Suppose a tourist wants to travel around China passing through 31 provincial capital cities, an appropriate travel route to reduce economic costs is an important issue. The tourism scheme can be abstracted into a typical TSP problem, and the proposed MISSA, ISSA, SSA, GWO, and PSO are used for solving and comparative analysis. The city coordinates are shown in Table 8. To ensure the consistency of the comparative experiments, the population size and maximum iteration number of each algorithm are 30 and 300, respectively. In addition, other parameters are as shown in Table 1.

Figure 9(a) shows the optimal travel route searched by MISSA, which does not show a crossed route and is consistent with the theoretical optimal solution. Figure 9(b) shows the convergence curves of the four algorithms. MISSA converges to the theoretical optimal solution in the 10<sup>th</sup> iteration, and the optimization accuracy and convergence speed are better than of compared algorithms.

To further verify the practicality and feasibility of the proposed MISSA, the algorithm is applied to five standard TSPLIB instances [49] in Table 9. We select the Euclidean distance as the calculation standard, and four algorithms are run 20 times on the five TSPLIB instances independently. The theoretical optimal (TO) value is the current optimal solution given by TSPLIB. The relative error (RE) is defined as follows:

$$RE = \frac{\text{Mean} - \text{TO}}{\text{TO}}. \quad (16)$$

Table 9 illustrates that the solution precision and dimension of MISSA have been greatly improved in TSPLIB instances. For the instances tested, MISSA can converge to the theoretical optimal value with a lower relative error. For dantzig42, the Best of MISSA is better than the theoretical optimal value. Notably, as the dimensionality and dense distribution of cities increase, the requirements for algorithms to handle complex problems increase explosively. The relative error of the compared algorithms increases rapidly in eil51 and eil76, especially for GWO and PSO, which indicates the algorithms are falling into the

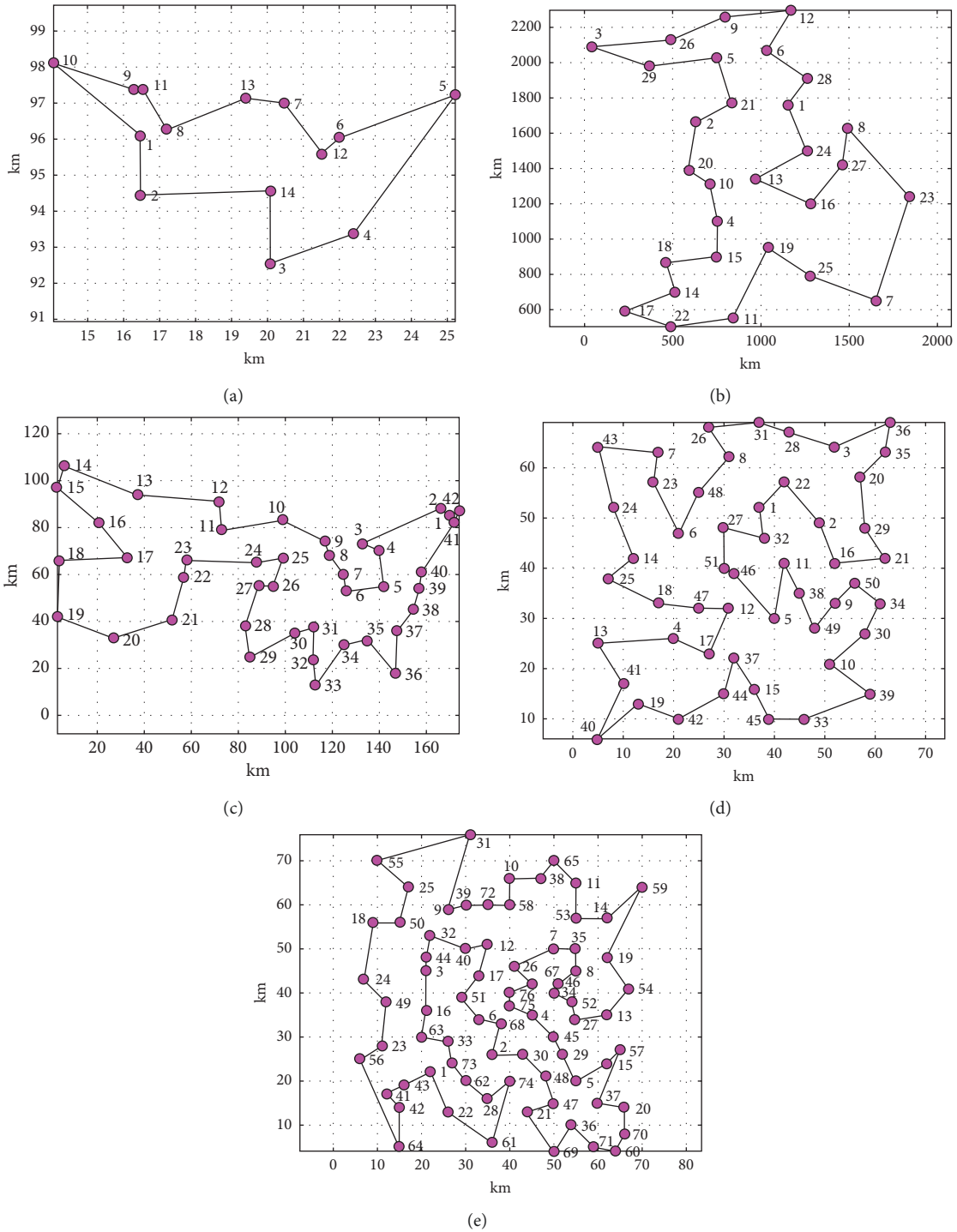


FIGURE 10: Optimal routes of MISSA. (a) burma14. (b) bayg29. (c) dantzig42. (d) eil51. (e) eil76.

local optimum. However, MISSA still maintains excellent optimization ability, indicating that the multimixed strategy is useful. The chaotic map provides good population diversity, the improved discoverer-follower model rapidly separates the solution space, and the EOBL mechanism upgrades the optimal solution and reconstructs the population. The multimixed strategy helps MISSA solve complex optimization problems with high dimensions. Figure 10 shows the optimal routes

obtained by MISSA for burma14, bayg29, dantzig42, eil51, and eil76. None of the optimal routes obtained by MISSA have a crossed route.

### 7. Conclusion

A multimixed strategy improved sparrow search algorithm is proposed in this paper, overcoming the shortcomings of

the original SSA, and we apply it to TSP. The original SSA is improved from three aspects: population initialization method, individuals' location update principle, and optimal solution mutation strategy. The iterative chaotic mapping is used to improve the diversity of the initial population, making the population to be distributed more uniformly. The Gold-SA and nonlinear convergence factor strategies are introduced to enhance the discoverer-follower model, which make the discoverer's searching process more comprehensive and extensive. Besides, the optimal solution and population are updated by the EOBL strategy, which enable the algorithm to increase self-learning ability.

Compared with three derived algorithms through four basic benchmark functions and diversity analysis, the rationality of the multimixed strategy selection is proved. Through the optimization and Wilcoxon rank-sum test of ten basic benchmark functions and CEC 2014 function, MISSA is certified to have better optimization accuracy, convergence speed, and robustness than SSA, ISSA, CSSA, CLSSA, WOA, GWO, COOT, and PSO. Finally, the practicability of MISSA is verified by TSP. Experimental results demonstrate the feasibility of MISSA to solve complex combinatorial optimization problems.

In the future, the application of MISSA in TSP will be further studied in generalized fields. Further research will be done on the multimixed strategy to stabilize population diversity while improving global exploration ability. The convergence of MISSA will be researched theoretically, and it will be used to solve large-scale combinatorial optimization problems.

## Data Availability

The data used to support the findings of this study are included within the article.

## Conflicts of Interest

The authors declare that they have no conflicts of interest.

## Acknowledgments

The authors are grateful for the support provided by the Guizhou Provincial Key Laboratory of Internet+Intelligent Manufacturing, Guiyang 550025, China. This work was supported by the National Natural Science Foundation of China (No. 61640014), Innovation Group of Guizhou Education Department (No. Qianjiaohe KY[2021]012), Industrial Project of Guizhou Province (No. Qiankehe Zhicheng [2022]017, [2019]2152), Science and Technology Fund of Guizhou Province (No. Qiankehe [2020]1Y266), Platform of IOT Personnel from Guiyang High Technology Industry Development Zone (No. 2015), and Postgraduate Case Library (No. KCALK201708).

## References

- [1] W. K. Mashwani, R. Haider, and S. Brahim Belhaouari, "A multiswarm intelligence algorithm for expensive bound constrained optimization problems," *Complexity*, vol. 2021, pp. 1–18, Article ID 5521951, 2021.
- [2] G. Wu, W. Pedrycz, P. N. Suganthan, and R. Mallipeddi, "A variable reduction strategy for evolutionary algorithms handling equality constraints," *Applied Soft Computing*, vol. 37, pp. 774–786, 2015.
- [3] W. K. Mashwani, A. Hamdi, M. Asif Jan, and A. F. Göktaş, "Large-scale global optimization based on hybrid swarm intelligence algorithm," *Journal of Intelligent and Fuzzy Systems*, vol. 39, no. 1, pp. 1257–1275, 2020.
- [4] J. H. Holland, "Genetic algorithms," *Scientific American*, vol. 267, no. 1, pp. 66–72, 1992.
- [5] R. A. Sarker, S. M. Elsayed, and T. Ray, "Differential evolution with dynamic parameters selection for optimization problems," *IEEE Transactions on Evolutionary Computation*, vol. 18, no. 5, pp. 689–707, 2014.
- [6] I. Dupanloup, S. Schneider, and L. Excoffier, "A simulated annealing approach to define the genetic structure of populations," *Molecular Ecology*, vol. 11, no. 12, pp. 2571–2581, 2002.
- [7] A. Hatamlou, "Black hole: a new heuristic optimization approach for data clustering," *Information Sciences*, vol. 222, pp. 175–184, 2013.
- [8] I. Ahmadianfar, A. A. Heidari, A. H. Gandomi, and X. H. Chu, "RUN beyond the metaphor: an efficient optimization algorithm based on Runge Kutta method," *Expert Systems with Applications*, vol. 181, p. 115079, 2021.
- [9] R. V. Rao, V. J. Savsani, and D. P. Vakharia, "Teaching-learning-based optimization: a novel method for constrained mechanical design optimization problems," *Computer-Aided Design*, vol. 43, no. 3, pp. 303–315, 2011.
- [10] E. Atashpaz-Gargari and C. Lucas, "Imperialist Competitive Algorithm: An Algorithm for Optimization Inspired by Imperialistic Competition," in *Proceedings of the 2007 IEEE congress on evolutionary computation*, pp. 4661–4667, Singapore, September 2007.
- [11] Y. Yang, H. Chen, A. A. Heidari, and A. H. Gandomi, "Hunger games search: visions, conception, implementation, deep analysis, perspectives, and towards performance shifts," *Expert Systems with Applications*, vol. 177, Article ID 114864, 2021.
- [12] J. Kennedy and R. Eberhart, "Particle swarm optimization," *Proceedings of ICNN'95 - International Conference on Neural Networks*, vol. 4, pp. 1942–1948, 1995.
- [13] M. Dorigo and G. D. Caro, "Ant colony optimization: a new meta-heuristic," *Proceedings of the 1999 congress on evolutionary computation-CEC99*, vol. 2, pp. 1470–1477, 1999.
- [14] S. Mirjalili and A. Lewis, "The whale optimization algorithm," *Advances in Engineering Software*, vol. 95, pp. 51–67, 2016.
- [15] S. Mirjalili, S. M. Mirjalili, and A. Lewis, "Grey wolf optimizer," *Advances in Engineering Software*, vol. 69, pp. 46–61, 2014.
- [16] I. Naruei and F. Keynia, "A new optimization method based on COOT bird natural life model," *Expert Systems with Applications*, vol. 183, Article ID 115352, 2021.
- [17] R. Salgotra and U. Singh, "The naked mole-rat algorithm," *Neural Computing & Applications*, vol. 31, no. 12, pp. 8837–8857, 2019.
- [18] A. A. Heidari, S. Mirjalili, H. Faris, and I. M. H. Aljarah, "Harris hawks optimization: algorithm and applications," *Future Generation Computer Systems*, vol. 97, pp. 849–872, 2019.

- [19] S. Li, H. Chen, M. Wang, and A. A. S. Heidari, "Slime mould algorithm: a new method for stochastic optimization," *Future Generation Computer Systems*, vol. 111, pp. 300–323, 2020.
- [20] J. Tu, H. Chen, M. Wang, and A. H. Gandomi, "The colony predation algorithm," *Journal of Bionics Engineering*, vol. 18, no. 3, pp. 674–710, 2021.
- [21] X. Hua, X. Hu, and W. Yuan, "Research optimization on logistics distribution center location based on adaptive particle swarm algorithm," *Optik*, vol. 127, no. 20, pp. 8443–8450, 2016.
- [22] E. K. Burke, P. De Causmaecker, G. De Maere, and J. M. G. Mulder, "A multi-objective approach for robust airline scheduling," *Computers & Operations Research*, vol. 37, no. 5, pp. 822–832, 2010.
- [23] T.-H. Hou, C.-H. Su, and H.-Z. Chang, "An integrated multi-objective immune algorithm for optimizing the wire bonding process of integrated circuits," *Journal of Intelligent Manufacturing*, vol. 19, no. 3, pp. 361–374, 2008.
- [24] J. Xue and B. Shen, "A novel swarm intelligence optimization approach: sparrow search algorithm," *Systems Science & Control Engineering*, vol. 8, no. 1, pp. 22–34, 2020.
- [25] Z. Xing, C. Yi, J. Lin, and Q. Zhou, "Multi-component fault diagnosis of wheelset-bearing using shift-invariant impulsive dictionary matching pursuit and sparrow search algorithm," *Measurement*, vol. 178, Article ID 109375, 2021.
- [26] H. Wang and J. Xianyu, "Optimal configuration of distributed generation based on sparrow search algorithm," *IOP Conference Series: Earth and Environmental Science*, vol. 647, no. 1, Article ID 012053, 2021.
- [27] J. Gai, K. Zhong, X. Du, and K. J. Yan, "Detection of gear fault severity based on parameter-optimized deep belief network using sparrow search algorithm," *Measurement*, vol. 185, Article ID 110079, 2021.
- [28] T. Liu, Z. Yuan, L. Wu, and B. Badami, "An optimal brain tumor detection by convolutional neural network and Enhanced Sparrow Search Algorithm," *Proceedings of the Institution of Mechanical Engineers - Part H: Journal of Engineering in Medicine*, vol. 235, no. 4, pp. 459–469, 2021.
- [29] C. Zhang and S. Ding, "A stochastic configuration network based on chaotic sparrow search algorithm," *Knowledge-Based Systems*, vol. 220, Article ID 106924, 2021.
- [30] Q. H. Mao and Q. Zhang, "Improved sparrow algorithm combining Cauchy mutation and Opposition-based learning," *Journal of Frontiers of Computer Science and Technology*, vol. 15, pp. 1155–1164, 2021.
- [31] X. Lu, X. D. Mu, J. Zhang, and Z. Wang, "Chaos sparrow search optimization algorithm," *Journal of Beijing University of Aeronautics and Astronautics*, vol. 47, pp. 1712–1720, 2021.
- [32] A. Tang, H. Zhou, T. Han, and L. Xie, "A chaos sparrow search algorithm with logarithmic spiral and adaptive step for engineering problems," *Computer Modeling in Engineering and Sciences*, vol. 130, no. 1, pp. 331–364, 2022.
- [33] C. Ouyang, D. Zhu, and F. Wang, "A learning sparrow search algorithm," *Computational Intelligence and Neuroscience*, vol. 2021, pp. 1–23, Article ID 3946958, 2021.
- [34] J. Yuan, Z. Zhao, Y. Liu, and B. L. B. He, "DMPPT control of photovoltaic microgrid based on improved sparrow search algorithm," *IEEE Access*, vol. 9, Article ID 16623, 2021.
- [35] S. Pervaiz, W. Haider Bangyal, A. Ashraf et al., "Comparative research directions of population initialization techniques using PSO algorithm," *Intelligent Automation & Soft Computing*, vol. 32, no. 3, pp. 1427–1444, 2022.
- [36] M. Abdel-Basset, M. Mohamed, Y. Zhou, and I. Hezam, "Multi-criteria group decision making based on neutrosophic analytic hierarchy process," *Journal of Intelligent and Fuzzy Systems*, vol. 33, no. 6, pp. 4055–4066, 2017.
- [37] J. Feng, J. Zhang, X. Zhu, and W. Lian, "A novel chaos optimization algorithm," *Multimedia Tools and Applications*, vol. 76, no. 16, pp. 17405–17436, 2017.
- [38] E. Tanyildizi and G. Demir, "Golden sine algorithm: a novel math-inspired algorithm," *Advances in Electrical and Computer Engineering*, vol. 17, no. 2, pp. 71–78, 2017.
- [39] M. J. Zhang and D. Y. Long, "Improved gray wolf optimization algorithm based on nonlinear control parameter combination strategy," *Computer Applications and Software*, vol. 38, pp. 250–255+322, 2021.
- [40] H. R. Tizhoosh, "Opposition-based learning: a new scheme for machine intelligence," in *Proceedings of the International Conference on Computational Intelligence for Modelling, Control and Automation and International Conference on Intelligent Agents, Web Technologies and Internet Commerce (CIMCA-IAWTIC'06)*, pp. 695–701, Vienna, Austria, November 2005.
- [41] S. Gupta and K. Deep, "A hybrid self-adaptive sine cosine algorithm with opposition based learning," *Expert Systems with Applications*, vol. 119, pp. 210–230, 2019.
- [42] X. Qian and W. Fang, "Opposition-based learning competitive particle swarm optimizer with local search," *Control, Decision*, vol. 36, pp. 779–789, 2021.
- [43] R. Sihwail, K. Omar, K. A. Z. Ariffin, and M. Tubishat, "Improved Harris hawks optimization using elite opposition-based learning and novel search mechanism for feature selection," *IEEE Access*, vol. 8, Article ID 121127, 2020.
- [44] K. Hussain, M. N. M. Salleh, S. Cheng, and Y. Shi, "On the exploration and exploitation in popular swarm-based meta-heuristic algorithms," *Neural Computing & Applications*, vol. 31, no. 11, pp. 7665–7683, 2019.
- [45] S. Cheng, Y. Shi, Q. Qin et al., "Population diversity maintenance in brain storm optimization algorithm," *Journal of Artificial Intelligence and Soft Computing Research*, vol. 4, no. 2, pp. 83–97, 2014.
- [46] R. Salgotra, U. Singh, and S. Saha, "New cuckoo search algorithms with enhanced exploration and exploitation properties," *Expert Systems with Applications*, vol. 95, pp. 384–420, 2018.
- [47] J. J. Liang, B. Y. Qu, and P. N. Suganthan, "Problem definitions and evaluation criteria for the CEC 2014 special session and competition on single objective real-parameter numerical optimization," vol. 635, p. 490, 2013.
- [48] O. Cheikhrouhou and I. Khoufi, "A comprehensive survey on the multiple traveling salesman problem: applications, approaches and taxonomy," *Computer Science Review*, vol. 40, Article ID 100369, 2021.
- [49] G. Reinelt, "TSPLIB-A traveling salesman problem library," *ORSA Journal on Computing*, vol. 3, no. 4, pp. 376–384, 1991.



## Research Article

# Study on Strength Theory Effect of Plastic Zone Distribution of Roadway Surrounding Rock

Pei Zhou <sup>1,2</sup> and Peng Wu <sup>3,4</sup>

<sup>1</sup>Faculty of Engineering, China University of Geosciences, Wuhan 430074, China

<sup>2</sup>Engineering Research Center of Rock-Soil Drilling & Excavation and Protection, Ministry of Education, Wuhan 430074, China

<sup>3</sup>School of Electronics and Information, Yangtze University, Jingzhou 434023, China

<sup>4</sup>National Engineering Research Center for GIS, China University of Geosciences, Wuhan 430074, China

Correspondence should be addressed to Peng Wu; [wupeng@yangtzeu.edu.cn](mailto:wupeng@yangtzeu.edu.cn)

Received 16 March 2022; Revised 2 April 2022; Accepted 7 April 2022; Published 18 May 2022

Academic Editor: Hangjun Che

Copyright © 2022 Pei Zhou and Peng Wu. This is an open access article distributed under the Creative Commons Attribution License, which permits unrestricted use, distribution, and reproduction in any medium, provided the original work is properly cited.

The plastic zone of surrounding rock is an important basis for evaluating the stability of roadway, and the distribution of plastic zone is closely related to the strength theory. The equation of boundary line of plastic zone is derived by using the approximate plastic condition method. According to specific parameters, the plastic zone is calculated. When the lateral pressure coefficient increases from 0.3 to 1, almost all the plastic zones calculated by different strength criteria have four shapes: butterfly, curved rectangle with concave horizontal direction and convex vertical direction, approximate ellipse, and circle, but the butterfly shape based on DP1 is not obvious. There are differences in the maximum plastic radius calculated by different strength criteria with the same lateral pressure coefficient from large to small: DP3 criterion, DP2 criterion, Mohr–Coulomb criterion/UST ( $b=0$ )/DP5 criterion, UST ( $b=0.25$ ), DP4 criterion, UST ( $b=0.5$ ), UST ( $b=0.75$ ), Matsuoka–Nakai criterion, UST ( $b=1$ ), Mogi–Coulomb criterion, Lade–Duncan criterion, and DP1 criterion. With the increase in lateral pressure coefficient, the difference between the results calculated by different strength criteria is smaller. When  $K_0=0.3$ , the maximum plastic radius is distributed at  $43^\circ\sim 47^\circ$ . The results of this paper show that the strength theory effect of plastic zone distribution cannot be ignored, which enriches the theory of approximate plastic condition method and can provide an important reference for roadway stability evaluation and support design.

## 1. Introduction

The shallow resources of the earth are gradually decreasing due to high intensity mining all the year round, and the rational development and utilization of deep resources are of great significance to the development of the future society. However, a series of challenges and technical problems such as high ground stress, strong mining, and large deformation faced by deep mining need to be solved urgently [1, 2]. It is inseparable from the theoretical guidance of rock mechanics and effective engineering technical measures to mine safely and efficiently. The distribution range and size of plastic failure zone of surrounding rock are important indexes to

analyze and evaluate the stability of roadway and have guiding function for effective support design.

In the early elastoplastic analysis of roadway surrounding rock, the theory represented by the Fenner equation is put forward based on the assumption of uniform distribution of initial ground stress. On this basis, scholars have developed a series of analytical calculation theories combined with the physical and mechanical characteristics of geomaterials [3–6]. Detailed stress, strain, displacement field, and plastic zone distribution can be obtained. However, under the condition that there is a great difference between horizontal in situ stress and vertical in situ stress, whether the assumption of uniform distribution of initial in situ stress field is reasonable is a question worthy of study.

Recent studies have shown that butterfly shape of the plastic zone of roadway surrounding rock may appear under the condition of nonuniform and high ground stress. The butterfly plastic failure theory obtains the distribution of plastic zone by solving the boundary equation, and the distribution and expansion law of butterfly plastic zone has been verified by numerical simulation. Moreover, the effects of physical and mechanical parameters (including rock mass gravity, friction angle, cohesion, lateral pressure coefficient, roadway radius, buried depth, and support force), roadway section shape, and deflection of principal stress direction are quantitatively calculated and discussed. The research fruits have been verified and applied in engineering fields such as rockburst, roadway roof fall, layered stratum penetration, and earthquake [7–11]. It highlights the theoretical value and practical significance of the approximate plastic condition method.

It is particularly noteworthy that the boundary line equation of plastic zone is calculated based on stress field and strength criterion. The mathematical expressions of each strength criterion are different, so the boundary lines of plastic zone are also different. Obviously, the distribution of plastic zone strongly depends on the strength theory adopted.

Because of the multiphase complexity of geotechnical materials, its strength theory involves tension-compression anisotropy (SD), hydrostatic pressure effect, stress Lode angle effect, intermediate principal stress effect, intermediate principal stress interval effect, nonlinear characteristics, and so on [12, 13]. It is difficult to have a single strength criterion to fully reflect all the influencing factors, and the strength theory of rock mass mechanics is called the unsolved centennial problems [14]. Among hundreds of strength theories, there are two common problems: first, the strength theories put forward by different scholars have different definitions and symbols for some physical quantities, which lead to inconveniences and errors in the application; second, the selection of strength theory is arbitrary in the concrete research. There are many literature reports on the study of strength theory effect in the aspects of tunnel surrounding rock stability analysis, slope stability, earth pressure, foundation bearing capacity, and so on [15–17]. Studies have shown that the influence of different strength criteria on the results cannot be ignored.

At present, for the important subject of boundary line equation of plastic zone of surrounding rock of roadway, most kinds of literatures are based on the Mohr–Coulomb criterion, and a few works of literatures are based on the Drucker–Prager criterion, lacking the comparative calculation and analysis on strength theory effect. Therefore, this paper studies the influence of strength theory on the distribution of plastic zone, including the morphological characteristics of plastic zone, the maximum plastic radius, and its location.

## 2. Summary of Strength Criterion

The research history of strength theory is very long, and hundreds of strength criteria have been obtained, forming a

rich strength theory system. In the existing literature, some of the strength theory equations are positive for tensile stress, some are positive for compressive stress, some are expressed by principal stress, and some are expressed by stress invariants. Due to the differences in algebraic sign convention and physical quantities and coefficients adopted, it is inconvenient for calculation and comparative analysis.

This article unifies the physical quantity expression of each equation based on compressive stress which is positive by selecting six classical strength criteria that are commonly utilized in engineering. For the brevity of writing expression, the unified form of stress invariants is used to sort out and summarize the six classical strength criteria. Hereinafter,  $I_1$ ,  $I_2$ , and  $I_3$  are the first, second, and third invariant of the stress tensor, respectively,  $J_2$  is the second invariant of the deviatoric stress tensor,  $\theta$  is the Lode angle of stress,  $\varphi$  is the friction angle, and  $c$  is the cohesion.

The stress invariants expressed by principal stresses  $\sigma_1$ ,  $\sigma_2$ , and  $\sigma_3$  are as follows:

$$\begin{aligned} I_1 &= \sigma_1 + \sigma_2 + \sigma_3, \\ I_2 &= \sigma_1\sigma_2 + \sigma_2\sigma_3 + \sigma_3\sigma_1, \\ I_3 &= \sigma_1\sigma_2\sigma_3, \\ J_2 &= \frac{1}{6} [(\sigma_1 - \sigma_2)^2 + (\sigma_2 - \sigma_3)^2 + (\sigma_3 - \sigma_1)^2]. \end{aligned} \quad (1)$$

Haigh–Westergaard principal stress space and projection in the  $\pi$  plane are shown in Figure 1.

**2.1. Mohr–Coulomb Criterion.** The Mohr–Coulomb criterion assumes that when the shear stress reaches a certain extreme value, the material fails. This extreme value is not a constant but is related to normal stress on the failure plane. The function expression is as follows:

$$\begin{aligned} &\sqrt{J_2} \left( \sin\left(\theta + \frac{\pi}{3}\right) - \frac{1}{\sqrt{3}} \cos\left(\theta + \frac{\pi}{3}\right) \sin\varphi \right) \\ &\quad - \frac{1}{3} I_1 \sin\varphi - c \cos\varphi = 0. \end{aligned} \quad (2)$$

This criterion is the most widely used and controversial strength theory for geomaterials, and the biggest problem of the Mohr–Coulomb criterion is that the influence of intermediate principal stress on yield and failure is not considered [18].

**2.2. Lade–Duncan Criterion.** The Lade–Duncan criterion is put forward according to the true triaxial test results of sand, and then it is further extended to cohesive soil and rock [19–21], which is expressed as follows:

$$\frac{I_1^3}{I_3} - \frac{(3 - \sin\varphi)^3}{1 - \sin\varphi - \sin^2\varphi + \sin^3\varphi} = 0. \quad (3)$$

When the criterion is extended to rock and soil with cohesive strength (i.e.,  $c \neq 0$ ), stress translation

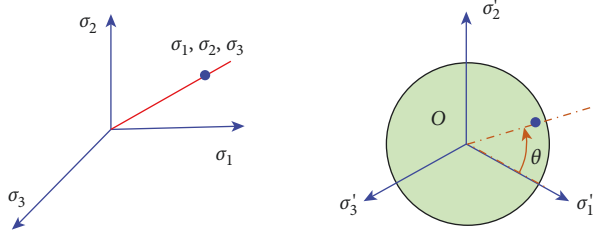


FIGURE 1: Haigh–Westergaard principal stress space and projection in  $\pi$  plane.

transformation is made:  $\sigma'_{ii} = \sigma_{ii} + c \cot \varphi$ .  $\sigma_{ii}$  represents the principal stress of sand, and the principal stress of cohesive geotechnical materials is represented by  $\sigma'_{ii}$ .

$$\left[ 3\sqrt{3} - 2\sqrt{3} \left( \cos\left(\theta + \frac{2\pi}{3}\right) + \cos \theta \right) \sin \varphi \right] \sqrt{J_2} - 2 \sin \varphi I_1 - 6c \cos \varphi = 0. \quad (4)$$

**2.4. A Series of Drucker–Prager Criteria.** The Drucker–Prager criterion proposed by Drucker and Prager in 1972 is the approximation of the Mohr–Coulomb criterion, which has no corner and considers the influence of hydrostatic pressure on strength [26]. It is equivalent to adding hydrostatic pressure term to the Huber–Mises criterion, so this criterion is also called the generalized Mises criterion. Later, scholars put forward some amendments on this basis and formed a series of Drucker–Prager criteria [27]. A series of Drucker–Prager criteria can be written as follows:

$$-\alpha I_1 + \sqrt{J_2} - k = 0. \quad (5)$$

The analytical expressions of parameters and of yield criteria (DP1~5) are given in Table 1.

**2.5. Matsuoka–Nakai Criterion.** Matsuoka and Nakai considered that the three Mohr circles in the three-dimensional principal stress state have influence on the strength, and the geomaterials failure occurs when the ratio of shear stress to normal stress reaches a certain value, and the failure surface

$$\left. \begin{aligned} \frac{I_1}{3} (1 - \alpha) + (2 + \alpha) \frac{\sqrt{J_2}}{\sqrt{3}} \cos \theta + \frac{\alpha(1 - b)}{1 + b} \sqrt{J_2} \sin \theta - \sigma_t = 0 \quad 0^\circ \leq \theta \leq \theta_b \\ \frac{I_1}{3} (1 - \alpha) + \left( \frac{2 - b}{1 + b} + \alpha \right) \frac{\sqrt{J_2}}{\sqrt{3}} \cos \theta + \left( \alpha + \frac{b}{1 + b} \right) \sqrt{J_2} \sin \theta - \sigma_t = 0 \quad \theta_b \leq \theta \leq 60^\circ \end{aligned} \right\}, \quad (7)$$

in which  $\alpha = (1 - \sin \varphi)/(1 + \sin \varphi)$ ,  $\sigma_t = (2c \cos \varphi)/(1 + \sin \varphi)$ ,  $\theta_b = \arctan(\sqrt{3}(2 + \sin \varphi)/(6 - \sin \varphi))$ , and  $b$  is the influence coefficient of medium principal stress. When  $b = 0$ , it can be reduced to the Mohr–Coulomb criterion, and when  $b = 1$ , it is a double shear yield criterion.

**2.3. Mogi–Coulomb Criterion.** Mogi carried out true triaxial test of rock earlier and studied the influence of intermediate principal stress on strength [22, 23]. Al-Ajmi and Zimmerman established the Mogi–Coulomb criterion, which can reflect the effect of rock intermediate principal stress and its interval influence, based on a large number of test data and the Mogi empirical criterion combined with the Coulomb criterion [24, 25]. The mathematical expression is as follows:

in this three-dimensional stress state is called spatially moved plane (SMP) [28, 29]. The equation of the criterion is as follows:

$$\frac{I_1 I_2}{I_3} - 8 \tan^2 \varphi - 9 = 0. \quad (6)$$

Similarly, when the Matsuoka–Nakai criterion is applied to geomaterials with cohesive strength, stress translation transformation is also needed as the Lade–Duncan criterion.

**2.6. Unified Strength Theory (UST).** Yu carried out systematic study on strength theory and put forward the unified strength theory based on the double shear stress yield criterion, double shear stress strength theory, and generalized double shear stress yield criterion [17].

When the two major principal shear stresses on the double shear element and the influence function of the corresponding normal stress on the plane reach a certain limit value, the material begins to yield or fail.

Through derivation, calculation, and simplification, the above strength criteria under the condition of plane strain can be uniformly expressed as follows:

$$\sigma_1 = A\sigma_3 + B. \quad (8)$$

TABLE 1: Parameters' expressions of yield criteria (DP1~5).

| Yield criteria | Amendments                        | A  | k  |
|----------------|-----------------------------------|--|--|
| DP1            | M-C exterior angle circumcircle   | $2 \sin\varphi / (\sqrt{3} (3 - \sin\varphi))$                     | $2\sqrt{3}c \cos\varphi / (3 - \sin\varphi)$                         |
| DP2            | M-C interior angle circumcircle   | $2 \sin\varphi / (\sqrt{3} (3 + \sin\varphi))$                     | $2\sqrt{3}c \cos\varphi / (3 + \sin\varphi)$                         |
| DP3            | M-C inscribed circle              | $\sin\varphi / (\sqrt{3} \sqrt{3 + \sin^2\varphi})$                | $\sqrt{3}c \cos\varphi / \sqrt{3 + \sin^2\varphi}$                   |
| DP4            | M-C equivalent area circle        | $\sqrt{2} \sqrt[3]{3} \sin\varphi / \sqrt{\pi(9 - \sin^2\varphi)}$ | $3\sqrt{2} \sqrt[3]{3}c \cos\varphi / \sqrt{\pi(9 - \sin^2\varphi)}$ |
| DP5            | M-C nonassociated matching circle | $\sin\varphi/3$  | $c \cos\varphi$  |

Coefficients A and B in the equation are given in Table 2.

In Table 2,  $s = (3 - \sin\varphi) / \sqrt[3]{1 - \sin\varphi - \sin^2\varphi + \sin^3\varphi} - 1$ ,  $t = \sqrt{8\tan^2\varphi + 9} - 1$ ,  $\sin\varphi_{UST} = 2(b+1)\sin\varphi_{UST} / (2+b(1+\sin\varphi_{UST}))$ , and  $c_{UST} = 2(b+1)c \cos\varphi_{UST} / ((2+b(1+\sin\varphi_{UST})) / \cos\varphi_{UST})$ .

### 3. Derivation of Unified Boundary Line Equation

Mechanical model is an idealized analytical model based on practical engineering problems, grasping its mechanical

essence and main laws and making necessary assumptions and simplifying some conditions. The section of roadway is round, and its length is much larger than the diameter of roadway, so it can be simplified as plane strain problem. It is assumed that the surrounding rock is a homogeneous and isotropic material. The basic mechanical model is shown in Figure 2.

In the elastic state, the stress field distribution of surrounding rock called Kirsch equation is as follows [30]:

$$\left. \begin{aligned} \sigma_r &= \frac{1}{2}\sigma_v \left( (1+K_0) \left( 1 - \left( \frac{R_0}{r} \right)^2 \right) - (1-K_0) \left( 1 - 4 \left( \frac{R_0}{r} \right)^2 + 3 \left( \frac{R_0}{r} \right)^4 \right) \cos(2\theta) \right) \\ \sigma_\theta &= \frac{1}{2}\sigma_v \left( (1+K_0) \left( 1 + \left( \frac{R_0}{r} \right)^2 \right) + (1-K_0) \left( 1 + 3 \left( \frac{R_0}{r} \right)^4 \right) \cos(2\theta) \right) \\ \tau_{r\theta} &= \frac{1}{2}\sigma_v \left( (1-K_0) \left( 1 + 2 \left( \frac{R_0}{r} \right)^2 - 3 \left( \frac{R_0}{r} \right)^4 \right) \sin(2\theta) \right) \end{aligned} \right\}, \quad (9)$$

in which  $\sigma_r$  is the radial stress,  $\sigma_\theta$  is the circumferential stress,  $\tau_{r\theta}$  is the shear stress,  $R_0$  is the radius of roadway,  $\sigma_v$  is the vertical in situ stress,  $\sigma_h$  is the horizontal in situ stress,  $K_0$  is the lateral pressure coefficient,  $\theta$  is the angle starting horizontally to the right and increasing counterclockwise, and  $r$  represents the distance between any point in the surrounding rock and the circular roadway's center.

Rewrite the stress component in polar coordinates  $\sigma_{ij}^{r\theta}$  to the stress component in rectangular coordinates  $\sigma_{ij}^{xy}$ :

$$[\sigma_{ij}^{xy}] = \mathbf{L}^T [\sigma_{ij}^{r\theta}] \mathbf{L}, \quad (10)$$

in which  $\mathbf{L} = \begin{bmatrix} \cos\theta & \sin\theta \\ -\sin\theta & \cos\theta \end{bmatrix}$ .

Solve the principal stress equation from the stress equation expressed by rectangular coordinates:

$$\begin{aligned} \sigma_1 &= \frac{\sigma_x + \sigma_y}{2} + \frac{1}{2} \sqrt{(\sigma_x - \sigma_y)^2 + 4\tau_{xy}^2}, \\ \sigma_3 &= \frac{\sigma_x + \sigma_y}{2} - \frac{1}{2} \sqrt{(\sigma_x - \sigma_y)^2 + 4\tau_{xy}^2}. \end{aligned} \quad (11)$$

Substitute the principal stress equation simplified in the above steps into the unified form of yield equation (8). After a series of operations and simplification such as merging similar terms and trigonometric function conversion, the following results are obtained:

TABLE 2: Coefficient A and B of unified form of strength theory.

| Strength criterion                  | A   | B  |
|-------------------------------------|---|--|
| Mohr–Coulomb criterion              | $(1 + \sin\varphi)/(1 - \sin\varphi)$                   | $2c \cos\varphi/(1 - \sin\varphi)$                     |
| Lade–Duncan criterion               | $1/4(s + \sqrt{s^2 - 4})^2$                             | $(1/4(s + \sqrt{s^2 - 4})^2 - 1)c \cot\varphi$         |
| Mogi–Coulomb criterion              | $(\sqrt{3} + 2 \sin\varphi)/(\sqrt{3} - 2 \sin\varphi)$ | $(4c \cos\varphi)/(\sqrt{3} - 2 \sin\varphi)$          |
| A series of Drucker–Prager criteria | $(1 + 3\alpha)/(1 - 3\alpha)$                           | $2k/(1 - 3\alpha)$                                     |
| Matsuoka–Nakai criterion            | $1/4(t + \sqrt{t^2 - 4})^2$                             | $(1/4(t + \sqrt{t^2 - 4})^2 - 1)c \cot\varphi$         |
| Unified strength theory (UST)       | $(1 + \sin\varphi_{UST})/(1 - \sin\varphi_{UST})$       | $(2c_{UST} \cos\varphi_{UST})/(1 - \sin\varphi_{UST})$ |

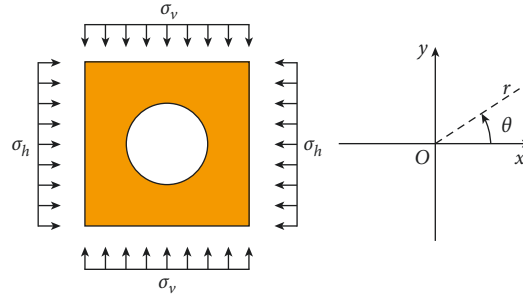


FIGURE 2: Basic mechanical model.

$$M_8 \left(\frac{R_0}{r}\right)^8 + M_6 \left(\frac{R_0}{r}\right)^6 + M_4 \left(\frac{R_0}{r}\right)^4 + M_2 \left(\frac{R_0}{r}\right)^2 + M_0 = 0, \quad (12) \quad \text{in which}$$

$$M_8 = 9(K_0 - 1)^2 \sigma_v^2,$$

$$M_6 = -6(2(K_0 - 1)^2 + \cos(2\theta)(K_0^2 - 1)) \sigma_v^2,$$

$$M_4 = \left( (K_0 - 1)^2 \left( \cos(4\theta) \left( 6 - 2 \frac{(A-1)^2}{(A+1)^2} \right) + 4 - 2 \frac{(A-1)^2}{(A+1)^2} \right) + 4 \cos(2\theta)(K_0^2 - 1) + (K_0 + 1)^2 \right) \sigma_v^2,$$

$$M_2 = \left( -4 \cos(4\theta)(K_0 - 1)^2 - 2 \cos(2\theta)(K_0^2 - 1) \left( 1 - \frac{2(A-1)^2}{(A+1)^2} \right) \right) \sigma_v^2 \quad (13)$$

$$+ 4 \cos(2\theta)(K_0 - 1) \frac{2B(A-1)}{(A+1)^2} \sigma_v,$$

$$M_0 = \left( (K_0 - 1)^2 - \frac{(K_0 + 1)^2 (A-1)^2}{(A+1)^2} \right) \sigma_v^2 - \frac{4B(K_0 + 1)(A-1)}{(A+1)^2} \sigma_v - \frac{4B^2}{(A+1)^2}.$$

#### 4. Calculation and Analysis

In order to analyze the distribution characteristics of plastic zone of deep roadway surrounding rock, typical parameters are selected: roadway radius of 2 m, weight of 25 kN/m<sup>3</sup>, buried depth of 800 m, internal friction angle of 30°, and cohesion of 2 MPa [31]. Considering the symmetry of the model, it is equivalent to rotating the plastic zone of 1/K<sub>0</sub> by

90 degrees when K<sub>0</sub> > 1. Thus, this paper only calculates and analyzes the distribution and morphological characteristics of the plastic zone with K<sub>0</sub> < 1.

##### 4.1. Morphological Distribution Characteristics of Plastic Zone.

Figure 3 shows the distribution of plastic zone calculated by the Mohr–Coulomb criterion (UST, b = 0) and double shear

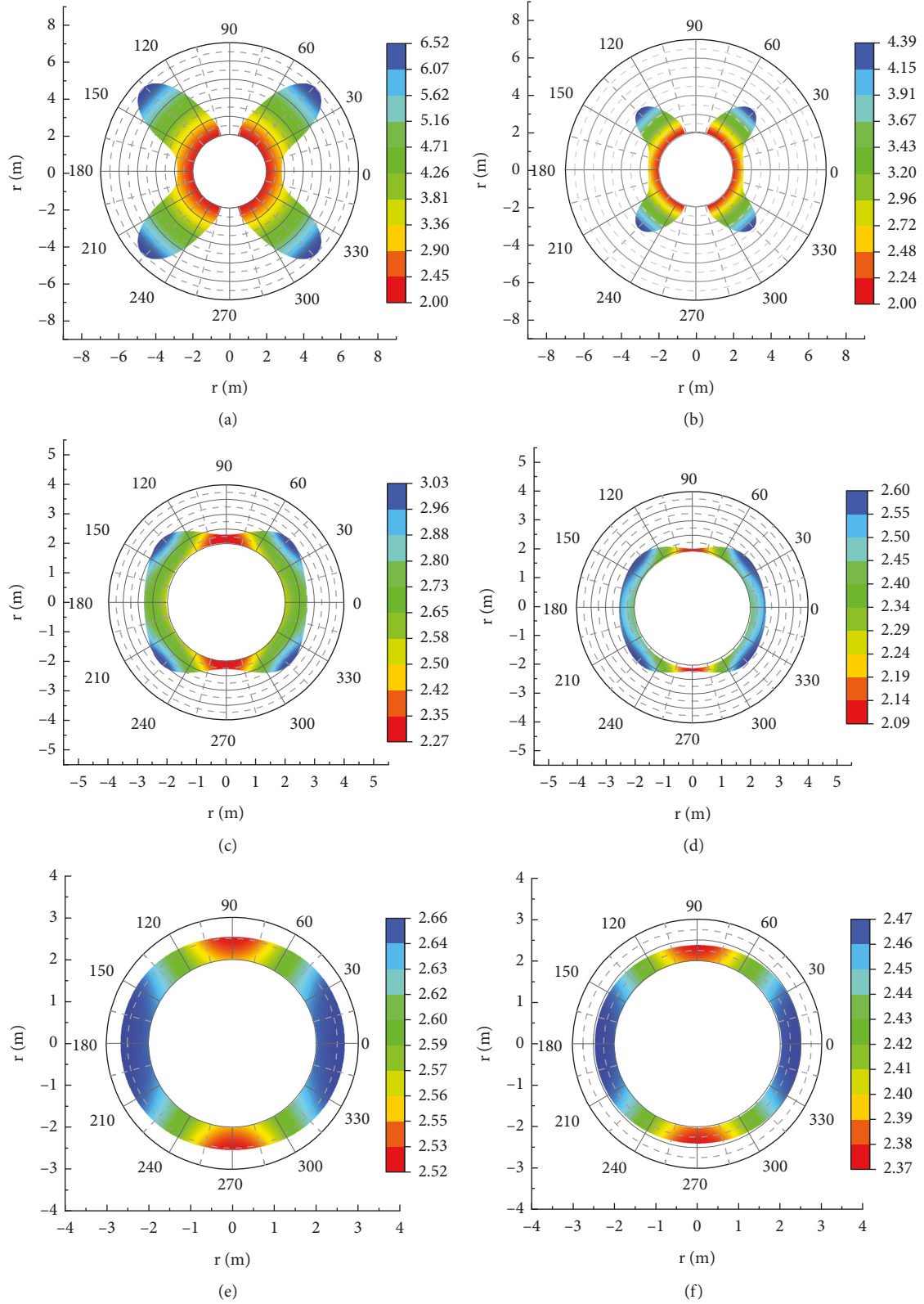


FIGURE 3: Distribution of plastic zone based on UST: (a)  $b = 0$  and  $K_0 = 0.3$ ; (b)  $b = 1$  and  $K_0 = 0.3$ ; (c)  $b = 0$  and  $K_0 = 0.5$ ; (d)  $b = 1$  and  $K_0 = 0.5$ ; (e)  $b = 0$  and  $K_0 = 0.8$ ; (f)  $b = 1$  and  $K_0 = 0.8$ .

TABLE 3: Maximum plastic radius and position calculated by different strength criteria.

| Strength theory                           | Lateral pressure coefficient |                    |                    |                    |                    |               |               |       |
|---|------------------------------|--------------------|--------------------|--------------------|--------------------|---------------|---------------|-------|
|   | 0.3                          | 0.4                | 0.5                | 0.6                | 0.7                | 0.8           | 0.9           | 1     |
| Mohr–Coulomb criterion                    | 6.51*                        | 3.90               | 3.03               | 2.78               | 2.69               | 2.66          | 2.63          | 2.61  |
| /UST ( $b = 0$ )/DP5 criterion            | 43/137/223/<br>317**         | 44/136/224/<br>316 | 43/137/223/<br>317 | 37/143/217/<br>323 | 26/154/206/<br>334 | 0/180/<br>360 | 0/180/<br>360 | 0~360 |
| UST ( $b = 0.25$ )                        | 5.49                         | 3.52               | 2.85               | 2.67               | 2.61               | 2.58          | 2.56          | 2.55  |
|   | 44/136/224/<br>316           | 45/135/225/<br>315 | 43/137/223/<br>317 | 44/136/224/<br>316 | 23/157/203/<br>337 | 0/180/<br>360 | 0/180/<br>360 | 0~360 |
| UST ( $b = 0.5$ )                         | 4.95                         | 3.28               | 2.73               | 2.60               | 2.55               | 2.53          | 2.52          | 2.50  |
|   | 45/135/225/<br>315           | 46/134/226/<br>314 | 43/137/223/<br>317 | 34/146/214/<br>326 | 19/161/199/<br>341 | 0/180/<br>360 | 0/180/<br>360 | 0~360 |
| UST ( $b = 0.75$ )                        | 4.61                         | 3.12               | 2.65               | 2.55               | 2.51               | 2.50          | 2.48          | 2.47  |
|   | 46/134/226/<br>314           | 47/133/227/<br>313 | 42/138/222/<br>318 | 33/147/213/<br>327 | 15/165/195/<br>345 | 0/180/<br>360 | 0/180/<br>360 | 0~360 |
| Double shear criterion/<br>UST( $b = 1$ ) | 4.38                         | 3.00               | 2.60               | 2.51               | 2.48               | 2.47          | 2.46          | 2.44  |
|   | 46/134/226/<br>314           | 47/133/227/<br>313 | 42/138/222/<br>318 | 31/149/211/<br>329 | 9/171/189/<br>351  | 0/180/<br>360 | 0/180/<br>360 | 0~360 |
| Lade–Duncan criterion                     | 4.13                         | 2.86               | 2.54               | 2.47               | 2.45               | 2.44          | 2.43          | 2.41  |
|   | 47/133/227/<br>313           | 48/132/228/<br>312 | 41/139/221/<br>319 | 28/152/208/<br>332 | 0/180/360          | 0/180/<br>360 | 0/180/<br>360 | 0~360 |
| Matsuoka–Nakai criterion                  | 4.60                         | 3.11               | 2.65               | 2.54               | 2.51               | 2.49          | 2.48          | 2.47  |
|   | 46/134/226/<br>314           | 47/133/227/<br>313 | 42/138/222/<br>318 | 32/148/212/<br>328 | 15/165/195/<br>345 | 0/180/<br>360 | 0/180/<br>360 | 0~360 |
| Mogi–Coulomb criterion                    | 4.27                         | 2.94               | 2.57               | 2.49               | 2.47               | 2.46          | 2.44          | 2.43  |
|   | 46/134/226/<br>314           | 48/132/228/<br>312 | 41/139/221/<br>319 | 30/150/210/<br>330 | 3/177/183/<br>357  | 0/180/<br>360 | 0/180/<br>360 | 0~360 |
| DP1 criterion                             | 2.27                         | 2.26               | 2.25               | 2.25               | 2.24               | 2.23          | 2.23          | 2.22  |
|   | 33/147/213/<br>327           | 0/180/360          | 0/180/360          | 0/180/360          | 0/180/360          | 0/180/<br>360 | 0/180/<br>360 | 0~360 |
| DP2 criterion                             | 6.77                         | 3.98               | 3.07               | 2.80               | 2.71               | 2.67          | 2.65          | 2.62  |
|   | 43/137/223/<br>317           | 44/136/224/<br>316 | 43/137/223/<br>317 | 37/143/217/<br>323 | 26/154/206/<br>334 | 0/180/<br>360 | 0/180/<br>360 | 0~360 |
| DP3 criterion                             | 7.69                         | 4.24               | 3.19               | 2.87               | 2.76               | 2.72          | 2.69          | 2.66  |
|   | 43/137/223/<br>317           | 43/137/223/<br>317 | 42/138/222/<br>318 | 37/143/217/<br>323 | 27/153/207/<br>333 | 0/180/<br>360 | 0/180/<br>360 | 0~360 |
| DP4 criterion                             | 5.30                         | 3.44               | 2.81               | 2.64               | 2.59               | 2.57          | 2.55          | 2.53  |
|   | 45/135/225/<br>315           | 46/134/226/<br>314 | 43/137/223/<br>317 | 35/145/215/<br>325 | 22/158/202/<br>338 | 0/180/<br>360 | 0/180/<br>360 | 0~360 |

Note. \* Maximum plastic radius (unit: m); \*\* Location where the maximum plastic radius appears (unit: degree).

criterion (UST,  $b = 1$ ). It can be clearly seen that the shape of the plastic zone is basically similar regardless of the Mohr–Coulomb criterion (UST,  $b = 0$ ) or double shear criterion (UST,  $b = 1$ ).

When  $K_0 = 0.3$ , the shape of the plastic zone is butterfly, and obviously the maximum plastic radius is between the  $x$  and  $y$  axes. When  $K_0 = 0.5$ , the range of plastic zone decreases rapidly and the butterfly almost disappears, and the plastic zone becomes an approximate rectangle with curved edges, showing concave in the upper and lower horizontal directions and convex in the left and right vertical directions. At this time, the maximum plastic radius is still between the  $x$  and  $y$  axes. The outer angle of the plastic zone disappears, and the shape is approximately elliptical with the maximum plastic radius on the  $x$  axis when  $K_0 = 0.8$ .

Further calculation and analysis show that all the criteria have obvious butterfly failure zones except DP1 when  $K_0 = 0.3$ .

4.2. Maximum Plastic Radius and Position Analysis. In practical engineering application, the maximum plastic radius and its position are important characteristic parameters of plastic zone distribution. It can be seen from Table 3 that the maximum plastic radius value and position calculated by different strength criteria are different. When  $K_0$  takes the same value, the maximum plastic radius calculated by strength criteria from large to small is DP3 criterion, DP2 criterion, Mohr–Coulomb criterion/UST ( $b = 0$ )/DP5 criterion, UST ( $b = 0.25$ ), DP4 criterion, UST ( $b = 0.5$ ), UST ( $b = 0.75$ ), Matsuoka–Nakai criterion, UST ( $b = 1$ )/Double shear criterion, Mogi–Coulomb criterion, Lade–Duncan criterion, and DP1 criterion. The smaller the value of  $K_0$ , the larger the difference of the maximum plastic radius calculated by different strength criteria. The calculation results of each strength criterion are getting closer with the increase in  $K_0$ . All the shapes of plastic zone

calculated by each criterion are circle, and value of the plastic radius is about 2.22 m to 2.66 m.

Butterfly shape with bigger plastic radius has a great influence on the stability of roadway, which can also explain the practical engineering phenomena such as roadway damage, large deformation, and difficult support in the tectonic stress zone. Further calculation and analysis show that all the criteria have obvious butterfly failure zones except DP1 when  $K_0 = 0.3$ , and the maximum plastic radius is distributed near the angle bisector (43–48 degree) of major and minor principal stress direction. With the increase in  $K_0$ , the maximum plastic radius gradually shifts to the direction of small principal stress. The value of the maximum plastic radius calculated by DP1 is 2.27 m, which is significantly less than the results obtained by other criteria (4.13–7.69 m) when  $K_0 = 0.3$ .

## 5. Conclusion

In this paper, different strength theories are used to calculate and compare the distribution of plastic zone of surrounding rock in detail. A series of meaningful conclusions are drawn as follows:

- (1) The shape of the plastic zone of roadway surrounding rock may be butterfly, horizontally concave, and vertically convex curved rectangle, ellipse, and circle. The results calculated by different strength criteria all reflect the morphological distribution characteristics of the plastic zone mentioned above, but DP1 is not applicable.
- (2) When  $K_0$  takes the same value, the maximum plastic radius calculated by strength criteria from large to small is DP3 criterion, DP2 criterion, Mohr–Coulomb criterion/UST ( $b = 0$ )/DP5 criterion, UST ( $b = 0.25$ ), DP4 criterion, UST ( $b = 0.5$ ), UST ( $b = 0.75$ ), Matsuoka–Nakai criterion, UST ( $b = 1$ )/Double shear criterion, Mogi–Coulomb criterion, Lade–Duncan criterion, and DP1 criterion, and using the DP1 criterion is not safe in practical engineering.
- (3) Strength theory has influence on the shape and size of plastic zone distribution, which cannot be ignored when carrying out support design.

## Data Availability

The data used to support the findings of this study are available from the corresponding author upon request.

## Conflicts of Interest

The authors declare that they have no conflicts of interest regarding the publication of this paper.

## References

- [1] H. P. Xie, “Research review of the state key research development program of China: deep rock mechanics and mining theory,” *Journal of China Coal Society*, vol. 44, no. 5, pp. 1283–1305, 2019.
- [2] J. Bai and C. J. Hou, “Control principle of surrounding rocks in deep roadway and its application,” *Journal of China University of Mining & Technology*, vol. 35, no. 2, pp. 145–148, 2006.
- [3] C. Carranza-Torres and C. Fairhurst, “Application of the convergence-confinement method of tunnel design to rock masses that satisfy the Hoek-Brown failure criterion,” *Tunnelling and Underground Space Technology*, vol. 15, no. 2, pp. 187–213, 2000.
- [4] S. K. Sharan, “Analytical solutions for stresses and displacements around a circular opening in a generalized Hoek-Brown rock,” *International Journal of Rock Mechanics and Mining Sciences*, vol. 45, no. 1, pp. 78–85, 2008.
- [5] C. G. Zhang, J. H. Zhao, Q. H. Zhang, and X. D. Hu, “A new closed-form solution for circular openings modeled by the Unified Strength Theory and radius-dependent Young’s modulus,” *Computers and Geotechnics*, vol. 42, no. 1, pp. 118–128, 2012.
- [6] Q. Zhang, B. S. Jiang, S. L. Wang, X. R. Ge, and H. Q. Zhang, “Elasto-plastic analysis of a circular opening in strain-softening rock mass,” *International Journal of Rock Mechanics and Mining Sciences*, vol. 50, no. 1, pp. 38–46, 2012.
- [7] N. J. Ma, X. F. Guo, Z. Q. Zhao, X. D. Zhao, and H. T. Liu, “Occurrence mechanisms and judging criterion on circular tunnel butterfly rock burst in homogeneous medium,” *Journal of China Coal Society*, vol. 41, no. 11, pp. 2679–2688, 2016.
- [8] H. S. Jia, N. J. Ma, and Q. K. Zhu, “Mechanism and control method of roof fall resulting from butterfly plastic zone penetration,” *Journal of China Coal Society*, vol. 41, no. 6, pp. 1384–1392, 2016.
- [9] Z. Q. Zhao, N. J. Ma, H. T. Liu, and X. F. Guo, “A butterfly failure theory of rock mass around roadway and its application prospect,” *Journal of China University of Mining & Technology*, vol. 47, no. 5, pp. 969–978, 2018.
- [10] X. Guo, Z. Zhao, X. Gao, X. Wu, and N. Ma, “Analytical solutions for characteristic radii of circular roadway surrounding rock plastic zone and their application,” *International Journal of Mining Science and Technology*, vol. 29, no. 2, pp. 263–272, 2019.
- [11] J. Li, X. B. Qiang, N. J. Ma, R. G. Zhang, and B. Li, “Formation mechanism and engineering application of the directionality of butterfly leaf in the butterfly plastic zone of roadway rock surrounded,” *Journal of China Coal Society*, vol. 46, no. 9, pp. 2838–2852, 2021.
- [12] M. H. Yu, G. Y. Xia, and V. A. Kolupaev, “Basic characteristics and development of yield criteria for geomaterials,” *Journal of Rock Mechanics and Geotechnical Engineering*, vol. 1, no. 1, pp. 71–88, 2009.
- [13] Y. R. Zheng and L. Kong, *Geotechnical Plastic Mechanics*, China Building Industry Press, Beijing, 2nd edition, 2019.
- [14] Y. S. Zhao, “Retrospection on the development of rock mass mechanics and the summary of some unsolved centennial problems,” *Chinese Journal of Rock Mechanics and Engineering*, vol. 40, no. 7, pp. 1297–1336, 2021.



- [15] T. Ogawa and K. Y. Lo, "Effects of dilatancy and yield criteria on displacements around tunnels," *Canadian Geotechnical Journal*, vol. 24, no. 1, pp. 100–113, 1987.
- [16] Y. Mitsutoshi, X. R. Hu, M. H. Yu, and W. Fan, "Influences of the strength theory on geotechnical structure analysis," *Chinese Journal of Rock Mechanics and Engineering*, vol. 21, no. 2, pp. 2314–2317, 2002.
- [17] M. H. Yu, *Unified Strength Theory and its Applications*, Springer-Verlag, Berlin, Germany, 2nd edition, 2017.
- [18] M. H. Yu, "Advances in strength theories for materials under complex stress state in the 20th century," *Applied Mechanics Reviews*, vol. 55, no. 3, pp. 169–218, 2002.
- [19] P. V. Lade and J. M. Duncan, "Elastoplastic stress-strain theory for cohesionless soil," *Journal of the Geotechnical Engineering Division*, vol. 101, no. 10, pp. 1037–1053, 1975.
- [20] P. V. Lade, "Elasto-plastic stress-strain theory for cohesionless soil with curved yield surfaces," *International Journal of Solids and Structures*, vol. 13, no. 11, pp. 1019–1035, 1977.
- [21] R. T. Ewy, "Wellbore-stability predictions by use of a modified Lade criterion," *SPE Drilling and Completion*, vol. 14, no. 2, pp. 85–91, 1999.
- [22] K. Mogi, "Effect of the intermediate principal stress on rock failure," *Journal of Geophysical Research*, vol. 72, no. 20, pp. 5117–5131, 1967.
- [23] K. Mogi, "Effect of the triaxial stress system on the failure of dolomite and limestone," *Tectonophysics*, vol. 11, no. 2, pp. 111–127, 1971.
- [24] A. M. Al-Ajmi and R. W. Zimmerman, "Relation between the Mogi and the Coulomb failure criteria," *International Journal of Rock Mechanics and Mining Sciences*, vol. 42, no. 3, pp. 431–439, 2005.
- [25] A. M. Al-Ajmi and R. W. Zimmerman, "Stability analysis of vertical boreholes using the Mogi-Coulomb failure criterion," *International Journal of Rock Mechanics and Mining Sciences*, vol. 43, no. 8, pp. 1200–1211, 2006.
- [26] D. C. Drucker and W. Prager, "Soil mechanics and plastic analysis or limit design," *Quarterly of Applied Mathematics*, vol. 10, no. 2, pp. 157–165, 1952.
- [27] C. J. Deng, G. J. He, and Y. R. Zheng, "Studies on Drucker-Prager yield criterions based on MC yield criterion and application in geotechnical engineering," *Chinese Journal of Geotechnical Engineering*, vol. 28, no. 6, pp. 735–739, 2006.
- [28] H. Matsuoka and T. Nakai, "Stress-deformation and strength characteristics of soil under three different principal stresses," *Proceedings of the Japan Society for Comparative Endocrinology*, vol. 1974, no. 232, pp. 59–70, 1974.
- [29] T. Luo, Y. P. Yao, and H. Matsuoka, "Soil strength equation in plane strain based on SMP," *Rock and Soil Mechanics*, vol. 21, no. 4, pp. 390–393, 2000.
- [30] H. S. Yu, *Cavity Expansion Methods in Geomechanics*, Kluwer Academic Publishers, Dordrecht, 2000.
- [31] A. Z. Lu, X. L. Zhang, and S. J. Wang, "Analytic method for elasto-plastic analysis of circular tunnels under non-axisymmetric stresses," *Chinese Journal of Rock Mechanics and Engineering*, vol. 37, no. 1, pp. 14–22, 2018.

## Research Article

# An Improved JADE Hybridizing with Tuna Swarm Optimization for Numerical Optimization Problems

MuLai Tan , YinTong Li , DaLi Ding , Rui Zhou, and ChangQiang Huang

Aviation Engineering School, Air Force Engineering University, Xi'an 710038, China

Correspondence should be addressed to DaLi Ding; kgdddl@sina.com

Received 13 February 2022; Revised 20 March 2022; Accepted 7 April 2022; Published 16 May 2022

Academic Editor: Shimin Wang

Copyright © 2022 MuLai Tan et al. This is an open access article distributed under the Creative Commons Attribution License, which permits unrestricted use, distribution, and reproduction in any medium, provided the original work is properly cited.

In this paper, we propose IJADE-TSO, a novel hybrid algorithm in which an improved adaptive differential evolution with optional external archive (IJADE) has been combined with the tuna swarm optimization (TSO). The proposed algorithm incorporates the spiral foraging search and parabolic foraging search of TSO into the mutation strategy in IJADE to improve the exploration ability and population diversity. Additionally, to enhance the convergence efficiency, crossover factor ( $CR$ ) ranking,  $CR$  repairing, top  $\alpha r_1$  selection, and population linear reduction strategies have been included in the algorithm. To evaluate the superiority of the proposed algorithm, IJADE-TSO has been benchmarked with its state-of-the-art counterparts using the CEC 2014 test set. Finally, to check the validity of IJADE-TSO, we apply it to photovoltaic (PV) parameter identification and compare its performance with those of other recently developed well-known algorithms. The statistical results reveal that IJADE-TSO outperforms the other compared algorithms.

## 1. Introduction

There are an increasing number of optimization problems regarding engineering design and industrial production calling for more effective optimization methods in the real world [1, 2]. One efficient approach is the stochastic heuristic algorithm, which can be divided into three categories [3]: evolution-based algorithms [4, 5], physical-phenomena-based algorithms [6, 7] and swarm-based algorithms [8, 9]. Differential evolution (DE) [10], one of the most excellent heuristic algorithms, has been widely used to solve complex optimization problems such as mechanical engineering [11], optimal power flow [12], parameter optimization [13], neural network training [14, 15], and complex control system [16]. The simplicity and efficiency of the DE algorithm has been attracting extensive exploration of it since its proposition by Storn and Price in 1995.

The performance of DE algorithm is sensitive to the mutation strategy and parameters and prone to fall into a local optimum. To fix these defects, a series of DE variants were proposed over the past two decades. These DE variants can be easily traced through the result of the competition organized

by IEEE Congress on Evolutionary Computation (CEC), where DE-based variant algorithms have ranked the top 3 in successive years except for 2013. According to the ways of improvement, current improvement methods can be classified into three main categories: optimizing mutation scheme, adaptive setting of control parameters, and hybridization.

*1.1. Optimizing Mutation Scheme.* Zhang and Sanderson [17] proposed JADE which implements the current-to-best mutation strategy for the first time with adaptively set  $CR$  and mutant factors ( $F$ ) achieved through evolving the mutation factors and crossover probabilities based on their historical record of success. Based on current-to- $p$ best strategy, V. Stanovov et al. [17] developed current-to- $p$ best/ $r$ , a new mutation strategy in LSHADE-RSP, which performs better in comparison with the alternative algorithms.

*1.2. Adaptive Setting of Control Parameters.* As an improvement upon the robustness of JADE, SHADE [18] enhances the adaptive performance of control parameters by adopting a diverse set of parameters to guide control parameter

adaptation based on the historical memory of successful parameter settings of JADE. As an extension of the SHADE algorithm, LSHADE [19] incorporates the linear population size reduction strategy to balance the exploration and exploitation. iL-SHADE, an improved version of LSHADE, was proposed by J. Brest et al. [20], in which the memory update mechanism is modified from LSHADE and the initial value of CR is set to 0.8 to enhance population diversity.

**1.3. Hybridization.** Hybridization is another important strategy to modify DE as plentiful hybridized algorithms concerning DE have been developed. C. Zhang et al. [21] proposed DE-PSO algorithm, where DE is hybridized with PSO for enhancing the exploration ability with most new individuals generated by the modified DE operator. However, the algorithm was only tested on the basic benchmark functions. S. Y. Du and Z. G. Liu [22] proposed PSOJADE by introducing a multicrossover operation and JADE to enhance the global exploration and the local exploitation in PSO. W. Gong et al. [23] proposed DE/BBO, a hybrid DE with BBO, which combines the exploration of DE with the exploitation of BBO effectively, enabling it to generate the promising candidate solutions. A. W. Mohamed et al. [24] proposed a hybridization framework in which CMA-ES is hybridized with LSHADE through adaptive approach, and semiparameter adaptation is adopted to effectively adapt the values of  $F$ .

Nevertheless, conventional current-to- $p$ best mutation strategy in the above hybrid algorithms can only capture the interindividual differential information to form the trial vector, which is single and prone to stagnation. Therefore, it is judicious to integrate it with other algorithms with strong global exploitation capabilities to improve its performance. However, roughly hybridizing swarm-based algorithms with DE rarely performs well. Hence, it is crucial to find an effective way to hybridize the DE algorithm with other algorithms.

Tuna swarm optimization [25] is one of the excellent swarm-based algorithms proposed by L. Xie et al. It shows a strong global search ability due to spiral foraging and parabolic foraging search behavior. This paper introduces TSO into the mutation strategy instead of simply hybridizing TSO with IJADE. In the iteration of each generation, individuals in the population except the optimal individual are selected with a certain probability to generate offspring individuals by IJADE or TSO, respectively. Similarly, the mutation vectors generated by TSO are subject to crossover operations. In addition, a series of improvements are made to improve the convergence efficiency.

The main contributions of this paper are as follows: (1) A novel hybrid mutation strategy is proposed. In the mutation operator, spiral foraging and parabolic foraging are incorporated into classical "current-to- $p$ best" mutation strategy. (2) To enhance the convergence efficiency of JADE, CR sorting mechanism and CR repairing are introduced. (3) A top  $\alpha$   $r_1$  selection strategy is proposed to accelerate convergence efficiency. (4) The linear population size reduction strategy is introduced to approximate the optimal individual in the final phase of the search.

## 2. Brief Review of DE and JADE

Optimization problems are common in the real world. The common form is shown as follows [10]:

$$\begin{aligned} \text{Objective function: } & f(\mathbf{x}), \quad \mathbf{x} = (x_1, x_2, \dots, x_D), \\ \text{Constraint: } & L_j \leq x_j \leq U_j. \end{aligned} \quad (1)$$

We have that  $\mathbf{x} = (x_1, x_2, \dots, x_D)$  is the optimization vector,  $D$  is the dimension of the optimization problem, and  $L_j$  and  $U_j$  are the boundaries.

**2.1. Differential Evolution.** At the beginning of the optimization problem, DE stochastically generates populations in the search space. The individuals in the population create the next generation in an evolutionary manner. When the individual explores a new location with a better fitness value, the individual moves to that location. There are four main operators in DE, that is, initialization, mutation, crossover, and selection operations. These operations will be discussed in detail as follows.

**2.1.1. Initialization.** Like other swarm intelligence optimization algorithms, the population is initialized first.

$$\{\mathbf{x}_i | L_j \leq x_{i,j} \leq U_j, \quad i = 1, 2, \dots, NP; j = 1, 2, \dots, D\}, \quad (2)$$

where  $\mathbf{x}_i$  is the  $i$ th individual,  $j$  represents the  $j$ th dimension, and  $NP$  is the initial population number.

$$x_{i,j} = L_j + \text{rand}(0, 1)(U_j - L_j). \quad (3)$$

**2.1.2. Mutation.** For each individual  $\mathbf{x}_i$  in the population, the mutant vector of DE is generated in the following way:

$$\frac{\text{DE/rand}}{1}: \mathbf{v}_{i,g+1} = \mathbf{x}_{r1,g} + F(\mathbf{x}_{r2,g} - \mathbf{x}_{r3,g}). \quad (4)$$

In the above formula,  $r1$ ,  $r2$ , and  $r3$  are randomly selected in the population and  $r1 \neq r2 \neq r3$ . Parameter  $F$  is used to control the amplification of the difference vector and  $0 \leq F \leq 2$ .

In addition, the mutant vector can be generated in other ways [26].

$$\frac{\text{DE/best}}{1}: \mathbf{v}_{i,g+1} = \mathbf{x}_{\text{best},g} + F(\mathbf{x}_{r1,g} - \mathbf{x}_{r2,g}),$$

$$\begin{aligned} \frac{\text{DE/current-to-best}}{1}: \mathbf{v}_{i,g+1} &= \mathbf{x}_{i,g} + \lambda(\mathbf{x}_{\text{best},g} - \mathbf{x}_{i,g}) \\ &+ F(\mathbf{x}_{r1,g} - \mathbf{x}_{r2,g}), \end{aligned}$$

$$\frac{\text{DE/best}}{2}: \mathbf{v}_{i,g+1} = \mathbf{x}_{\text{best},g} + F(\mathbf{x}_{r1,g} - \mathbf{x}_{r2,g} + \mathbf{x}_{r3,g} - \mathbf{x}_{r4,g}),$$

$$\frac{\text{DE/rand}}{2}: \mathbf{v}_{i,g+1} = \mathbf{x}_{r5,g} + F(\mathbf{x}_{r1,g} - \mathbf{x}_{r2,g} + \mathbf{x}_{r3,g} - \mathbf{x}_{r4,g}). \quad (5)$$

**2.1.3. Crossover.** The trial vector  $\mathbf{u}_{i,g}$  is obtained through replacing some components of target vector  $\mathbf{x}_{i,g}$  with corresponding mutant vector  $\mathbf{v}_{i,g}$ .

$$\mathbf{u}_{i,j,g} = \begin{cases} \mathbf{v}_{i,j,g} & \text{if } \text{rand} < \text{CR or } \text{randi}(1, D) = j, \\ \mathbf{x}_{i,j,g} & \text{else.} \end{cases} \quad (6)$$

$\text{randi}(1, D)$  generate a random integer between 0 and  $D$ .  $\text{CR} \in (0, 1)$  is the crossover factor which decides the proportion of replaced components in  $\mathbf{x}_{i,g}$ .

**2.1.4. Selection.** In the selection operation, according to the greedy strategy, the individual of next generation is selected by comparing the trail vector  $\mathbf{u}_{i,g}$  and the target vector  $\mathbf{x}_{i,g}$  in DE. The selection method is as follows:

$$\mathbf{x}_{i,g+1} = \begin{cases} \mathbf{u}_{i,g}, & \text{if } f(\mathbf{u}_i) < f(\mathbf{x}_i), \\ \mathbf{x}_{i,g}, & \text{else.} \end{cases} \quad (7)$$

**2.2. JADE.** The JADE algorithm is a variant of DE that was proposed by Zhang J. et al. [27] in 2009. In recent years, many excellent algorithms have been established based on JADE, and their advantages are as follows.

**2.2.1. DE/Current-to-pbest Strategy.** The most important improvement is that the new mutation strategy DE/current-to-pbest is implemented with the optional external archive, which uses historical information to provide evolution direction information.

Mutation strategy without external archive is

$$\mathbf{v}_{i,g} = \mathbf{x}_{i,g} + F_i \left( \mathbf{x}_{\text{best},g}^p - \mathbf{x}_{i,g} \right) + F_i \left( \mathbf{x}_{r1,g} - \mathbf{x}_{r2,g} \right). \quad (8)$$

Mutation strategy with external archive is

$$\mathbf{v}_{i,g} = \mathbf{x}_{i,g} + F_i \left( \mathbf{x}_{\text{best},g}^p - \mathbf{x}_{i,g} \right) + F_i \left( \mathbf{x}_{r1,g} - \tilde{\mathbf{x}}_{r2,g} \right). \quad (9)$$

The difference between the above two mutation strategies is the element  $\tilde{\mathbf{x}}_{r2,g}$ . In the strategy with external archive, there is a certain possibility for  $\tilde{\mathbf{x}}_{r2,g}$  to be selected from either the current group or the external archive, which enhances the diversity of the population.

**2.2.2. Adaptive Control Parameters of  $F$  and  $CR$ .** The control parameters  $F$  and  $CR$  are updated adaptively to improve the optimization performance.

$CR$  is generated according to the normal distribution with mean  $\mu_{CR}$  and standard deviation equal to 0.1, and  $F$  is generated according to the Cauchy distribution with mean  $\mu_F$  and standard deviation equal to 0.1.  $\mu_{CR}$  and  $\mu_F$  are initially set to 0.5.

$S_{CR}$  is a collection for storing the  $CR$  value of each generation of successful individuals. Similarly,  $S_F$  is a collection for storing the  $F$  value of each generation of successful individuals.

After each iteration, the values of  $\mu_{CR}$  and  $\mu_F$  are updated as follows:

$$\begin{aligned} \mu_{CR} &= (1 - c) \cdot \mu_{CR} + c \cdot \text{mean}_A(S_{CR}), \\ \mu_F &= (1 - c) \cdot \mu_F + c \cdot \text{mean}_L(S_F). \end{aligned} \quad (10)$$

We have that  $c$  is the learning rate, which is set to 0.1,  $\text{mean}_A(\cdot)$  refers to the arithmetic mean, and  $\text{mean}_L(\cdot)$  represents the Lehmer mean, which is defined as follows:

$$\text{mean}_L(S_F) = \frac{\sum_{F \in S_F} F^2}{\sum_{F \in S_F} F}. \quad (11)$$

In general, the control parameters of the DE algorithm are not adaptive [28] and the convergence performance is undesired. Although the convergence speed of JADE is high [29], the single mutation strategy results in poor population diversity and liability of falling into local optimum.

### 3. IJADE-TSO

**3.1. Tuna Swarm Optimization.** The JADE algorithm uses a single mutation strategy, giving rise to a greater possibility of the algorithm falling into a local optimum. To compensate for this, two foraging search strategies in tuna swarm optimization (TSO) [25] have been introduced into the mutation operation of IJADE. The two mutation strategies account for a respective percentage of the population to improve population diversity and avoid local optimum.

Tuna swarm optimization is a novel swarm-based metaheuristic algorithm for global optimization. The inspiration for TSO comes from the cooperative foraging behavior of tuna swarm. It mainly consists of two foraging behaviors of tuna swarm: spiral foraging and parabolic foraging. Its global exploration capacity excels its exploitation capacity.

**3.1.1. Spiral Foraging.** When foraging, the tuna group will form a spiral formation to round up the target in the face of the rapid position change of the target fish group. If a small part of tuna group moves firmly towards a certain direction, the surrounding tuna group will gradually adjust their directions and follow to round up. Each tuna will follow the previous tuna while chasing the target, forming a chain of information transmission. The position of the most important lead tuna is updated by the mutation strategy of IJADE, which augments the foraging efficiency. The mathematical model of the spiral foraging strategy is as follows:

$$\begin{aligned}
\mathbf{v}_{i,g} &= \alpha_1 \cdot \left( \mathbf{x}_{\text{best},g} + \beta \cdot \left| \mathbf{x}_{\text{best},g} - \mathbf{x}_{i,g} \right| \right) \\
&\quad + \alpha_2 \cdot \mathbf{x}_{i-1,g}, \quad i = 2, 3, \dots, NP, \\
\alpha_1 &= a + (1 - a) \cdot \frac{g}{g_{\max}}, \\
\alpha_2 &= (1 - a) - (1 - a) \cdot \frac{g}{g_{\max}}, \\
\beta &= e^{bl} \cdot \cos(2\pi b), \\
l &= e^{3 \cos(((g_{\max}+1/g)-1)\pi)}.
\end{aligned} \tag{12}$$

We have that  $\mathbf{x}_{i,g}$  is the  $i$ th individual of the  $g+1$  generation,  $\mathbf{x}_{\text{best},g}$  is the current optimal individual (lead tuna),  $\alpha_1$  and  $\alpha_2$  are weight coefficients that control the tendency of individuals to move towards either the optimal individual or the previous individual,  $a$  is a constant used to determine the extent to which the tuna follows the optimal individual or the previous individual in the initial phase,  $g$  denotes the number of current iterations,  $g_{\max}$  is the maximum number

of iterations, and  $b$  is a random number uniformly distributed between 0 and 1.

In the initial stage of foraging, the prey tracked by the lead fish is not necessarily the fish group that provides the most abundant food. Therefore, the whole tuna group needs to scatter to find the location of the fish group with the most abundant food. It is more efficient to stochastically select a point in the space and spirally search around it. The specific mathematical model is described as follows:

$$\begin{aligned}
\mathbf{v}_{i,g} &= \alpha_1 \cdot \left( \mathbf{x}_{\text{ran } d,g} + \beta \cdot \left| \mathbf{x}_{\text{ran } d,g} - \mathbf{x}_{i,g} \right| \right) \\
&\quad + \alpha_2 \cdot \mathbf{x}_{i-1,g}, \quad i = 2, 3, \dots, NP.
\end{aligned} \tag{13}$$

We have that  $\mathbf{x}_{\text{ran } d,g}$  is a randomly generated reference point in the search space.

Metaheuristic algorithms usually perform extensive global exploration in the early stage and then gradually transition to precise local exploitation. Therefore, TSO changes the reference points of spiral foraging from random individuals to optimal individuals with the increase in iteration. In summary, the final mathematical model of the spiral foraging strategy is as follows:

$$\mathbf{v}_{i,g} = \begin{cases} \alpha_1 \cdot \left( \mathbf{x}_{\text{best},g} + \beta \cdot \left| \mathbf{x}_{\text{best},g} - \mathbf{x}_{i,g} \right| \right) + \alpha_2 \cdot \mathbf{x}_{i-1,g}, & i = 2, 3, \dots, NP, \quad \text{if } \text{rand} < \frac{t}{t_{\max}}, \\ \alpha_1 \cdot \left( \mathbf{x}_{\text{ran } d,g} + \beta \cdot \left| \mathbf{x}_{\text{ran } d,g} - \mathbf{x}_{i,g} \right| \right) + \alpha_2 \cdot \mathbf{x}_{i-1,g}, & i = 2, 3, \dots, NP, \quad \text{if } \text{rand} \geq \frac{t}{t_{\max}}. \end{cases} \tag{14}$$

**3.1.2. Parabolic Foraging.** To prevent preys from escaping, in addition to spiral foraging, tunas also adopt parabolic foraging. Tuna forms a parabolic formation with prey as a reference point. Meanwhile, tuna forage preys by searching areas around themselves. The two approaches are performed simultaneously, with the assumption that the selection probabilities are 50% for both. The specific mathematical model is described as follows:

$$\mathbf{v}_{i,g} = \begin{cases} \mathbf{x}_{\text{best},g} + \text{rand} \cdot \left( \mathbf{x}_{\text{best},g} - \mathbf{x}_{i,g} \right) \\ \quad + TF \cdot p^2 \cdot \left( \mathbf{x}_{\text{best},g} - \mathbf{x}_{i,g} \right), & \text{if } \text{rand} < 0.5, \\ TF \cdot p^2 \cdot \mathbf{x}_{i,g}, & \text{if } \text{rand} \geq 0.5. \end{cases} \tag{15}$$

$$p = \left( 1 - \frac{t}{t_{\max}} \right)^{(t/t_{\max})}, \tag{16}$$

where  $TF$  is a random number with a value of 1 or  $-1$ .

Tuna work cooperatively with the two foraging strategies to hunt for the prey. In each iteration, each individual randomly executes one of the two foraging strategies.

**3.2. Crossover Rate Sorting Mechanism and CR Repairing.** In order to establish the relationship between  $CR$  and the individual fitness values, the  $CR$  sorting mechanism [30] is

introduced. Firstly, the  $CR$  values are generated by Gaussian distribution and then are sorted in an ascending order. This is shown as follows:

$$\begin{aligned}
CR' &= \text{sort}(CR, 'ascen d'), \\
\text{index} &= \text{sort}(f(X), 'ascen d'), \\
CR(\text{index}) &= CR'.
\end{aligned} \tag{17}$$

A variant of JADE is introduced in [31], which modifies the crossover factor according to the real crossover rate of each generation. In this way, the adaption of the crossover factor is improved. Its crossover operation becomes

$$b_{i,j} = \begin{cases} 1, & \text{if } \text{rand} < CR \text{ or } \text{randi}(1, D) = j, \\ 0, & \text{else,} \end{cases} \tag{18}$$

$$CR_i = \frac{\sum_{j=1}^D b_{i,j}}{D}.$$

By sorting the  $CR$  values, the individuals with better fitness are given smaller  $CR$ , so their next generation can retain more characteristics of the parent individuals. Meanwhile the poor individuals will be given larger  $CR$  and a larger proportion of components will be replaced by the

mutated individuals. This helps to improve the exploration efficiency.

With the  $CR$  sorting mechanism, the issue of neglecting the relationship between  $CR$  values and the individual fitness values in JADE can be effectively addressed. Through  $CR$  correction, the actual crossover rate is introduced into the calculation of the crossover factor in the next generation.

**3.3. Top  $\alpha$   $r_1$  Selection.** In LSHADE-RSP [17], a ranking-based approach was proposed for the selection of  $r_1$  and  $r_2$ . In the JADE algorithm, the selection of the  $r_1$  individual is random. To improve the convergence efficiency of the algorithm, we use the top  $\alpha$   $r_1$  selection strategy. The selection of  $r_1$  is shown as follows:

$$r_1 = \text{floor}(1 + \alpha \cdot NP \cdot \text{rand } d). \quad (19)$$

We have that  $\alpha \cdot NP$  is the number of candidates for the selection of  $r_1$ , and  $\text{rand } d$  is a random value selected in  $[0, 1]$ . The individuals with better fitness values will be more likely to be selected. In this way, it is easier to form a difference vector that evolves towards the current optimal individual and expedite convergence.

**3.4. Linear Population Size Reduction.** The linear population size reduction strategy is introduced to accomplish depth exploration around the optimal individual and facilitate algorithm convergence in the final stage of the search. The mathematical formula is as follows:

$$NP = \text{round}\left[\left(\frac{NP_{\min} - NP_{\text{init}}}{FES_{\max}}\right) \times FES + NP_{\text{init}}\right]. \quad (20)$$

$NP_{\min}$  and  $NP_{\text{init}}$  represent the minimum population and the number of initial populations, respectively. However, the increasing number of populations will result in a decrease in population diversity, making it liable to be trapped in local optimum. Therefore, rather than setting  $NP_{\min}$  to 4 in [19],  $NP_{\min}$  is set to 50 in this paper.

The algorithm pseudocode is shown as Table 1 and the corresponding flowchart of IJADE-TSO algorithm is shown in Figure 1.

## 4. Numerical Experiment and Discussion

**4.1. CEC 2014.** In this section, we use the 2014 IEEE CEC test suite to verify the performance of the IJADE-TSO by comparing it with state-of-the-art algorithms, including LSHADE [19], iLSHADE [20], SPS-LSHADE-EIG [32], CPI-JADE [33], GEDGWO [34], and DOLTLBO [35]. Among them, LSHADE won a prize at the 2014 IEEE CEC. The first four are all improved algorithms based on JADE. GEDGWO is a variant of GWO [8] applying the Gauss probability model to estimate the distribution. DOLTLBO is an enhanced teaching-learning-based optimization algorithm proposed in 2019. The parameters are the same as the recommended settings in the original works, as reported in Table 2.

TABLE 1: Pseudocode of IJADE-TSO algorithm.

| Algorithm: IJADE-TSO  |
|---|
| Initialise population   |
| $\mu_{CR} = 0.5, \mu_F = 0.8, A = \emptyset, p = 0.11, Ar = 2.6, NP_{\min} = 50, \alpha = 0.6$  |
| for $g = 1$ to $g_{\max}$ do  |
| for $i = 1:NP$  |
| $CR_i = \text{rand } dn_i(\mu_{CR}, 0.1), F_i = \text{rand } dc_i(\mu_F, 0.1)$  |
| End   |
| $CR = \text{sort}(CR)$  |
| for $i = 1:NP$  |
| if $\text{rand} < 0.9$ or $i = 1$   |
| Generate $r_1, r_2, \mathbf{x}_{\text{best}}^p$   |
| $\mathbf{v}_{i,g} = \mathbf{x}_{i,g} + F_i(\mathbf{x}_{\text{best},g}^p - \mathbf{x}_{i,g}) + F_i(\mathbf{x}_{r_1,g} - \bar{\mathbf{x}}_{r_2,g})$ |
| Else  |
| if $\text{rand} < 0.5$  |
| generate $\mathbf{v}_{i,g}$ According to equation (19)  |
| else  |
| generate $\mathbf{v}_{i,g}$ According to equation (20)  |
| end   |
| end   |
| if $\text{rand } d < CR$ or $\text{rand } di(1, D) = j$   |
| $u_{i,j,g+1} = v_{i,j,g}, b_{i,j} = 1$  |
| else  |
| $u_{i,j,g+1} = x_{i,j,g}, b_{i,j} = 0$  |
| end   |
| $CR_i' = \sum_{j=1}^D b_{i,j}/D, CR = CR'$  |
| if $f(u_i) \leq f(x_i)$   |
| $x_{i,G+1} = u_{i,G}, x_{i,G} \rightarrow A, CR_i \rightarrow S_{CR}, F_i \rightarrow S_F$  |
| else  |
| $x_{i,G+1} = x_{i,G}$   |
| end   |
| end   |
| Update $\mu_{CR}, \mu_F$ and $NP$   |
| Update archive size by removing worst solutions   |
| Update population size by removing worst solutions  |
| end   |

The definitions and optimal values of CEC 2014 test suite are provided in [36]. The number of maximum function evaluations ( $MaxFES$ ) is set to  $D \times 10000$ , and  $D$  is set to 30 in this paper. Each function is evaluated 51 times independently for statistics. The error value between the best obtained solution and the optimal solution is recorded as the result.

All experiments are performed on a computer with AMD R7 4800U (1.80 GHz) processor and 16 GB of RAM. The programs are implemented by MATLAB 2016B platform.

From Table 3, It is apparent that, for unimodal functions, IJADE-TSO outperforms all other comparison algorithms, and the optimal value can be stably obtained, which confirms the excellent performance of IJADE-TSO in solving unimodal functions. As for the multimodal and hybrid functions, IJADE-TSO ranked in the top four except F5 and F12. IJADE-TSO ranks in the top two except F26 in solving composition functions. It is worth noting that the latter two groups of test functions are more complex, so the superiority of IJADE-TSO in solving complex optimization problems is better demonstrated. SPS-LSHADE-EIG performs well in multimodal functions except for F14, unimodal and

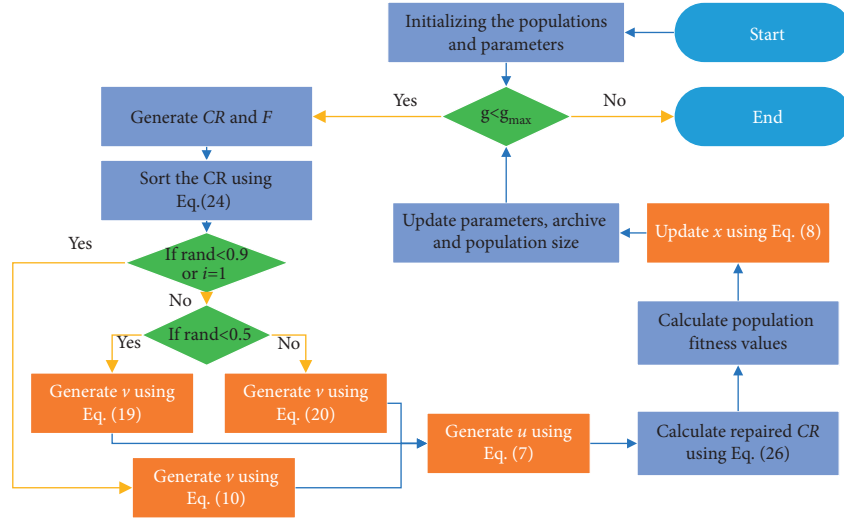


FIGURE 1: The flowchart of the IJADE-TSO algorithm.

TABLE 2: Parameter settings for the seven algorithms in the CEC 2014 test.

| Algorithms     | Parameter settings  |
|----------------|---|
| IJADE-TSO      | $NP_{\min} = 50, \mu_{CR} = 0.5, \mu_F = 0.8, p = 0.11, r^{arc} = 2.6, \alpha = 0.6$                              |
| SPS-LSHADE-EIG | $NP_{\min} = 4, ER_{init} = 1, p = 0.11, H = 6, M_F = 0.5, M_{CR} = 0.5, Q = 64$                                  |
| LSHADE         | $NP_{init} = 18 \cdot D, NP_{\min} = 4, r^{arc} = 2.6, p = 0.11, H = 6, M_F = 0.5, M_{CR} = 0.5$                  |
| CPI-JADE       | $NP_{init} = 500, \mu_{CR} = 0.5, \mu_F = 0.5, c = 0.1, p = 0.05$   |
| iLSHADE        | $NP_{init} = 12 \cdot D, NP_{\min} = 4, Ar = 2.6, p_{init} = 0.2, p_{\min} = 0.1, H = 6, M_F = 0.5, M_{CR} = 0.8$ |
| GEDGWO         | $NP_{init} = 500, r_3 \in (0, 1), r_4 \in (0, 1), r_5 \in (0, 1)$   |
| DOLTLBO        | $NP_{init} = 500, jr = 0.3, w = 10$   |

multimodal functions, and hybrid functions but performs poorly in composition functions except F26. LSHADE and iLSHADE are similar to SPS-LSHADE-EIG, but LSHADE shows poor performance in F19 and iLSHADE performs poorer than SPS-LSHADE-EIG for composition functions. The performances of CPI-JADE and GEDGWO are poor. DOLTLBO performs well in F23, F25, F26, and F28 of composition functions but poor in other functions.

Figure 2 shows the ranking of the algorithm in each test function. The closer to the center of the circle, the higher the ranking, and vice versa. The area enclosed by the curves shows the overall ranking of the algorithms.

**4.1.1. Friedman Test.** The Friedman test is used [37] to analyze the performance difference of algorithms on the 30 test functions. Table 4 shows the average ranking results of each algorithm.

The ranking value of IJDAE-TSO is 2.92, ranking the top among all algorithms. The rankings of the other six algorithms are as follows: SPS-LSHADE-EIG, iLSHADE, LSHADE, GEDGWO, CPI-JADE, and DOLTLBO. Note that, compared with the improved variant of JADE, CPI-JADE, which ranks sixth, IJDAE-TSO ranks the first, proving the effectiveness of the improvement strategies. The  $p$  value calculated by Iman-Davenport test is  $4.43e-11$ , showing that there is a significant difference between algorithms.

**4.1.2. Wilcoxon Signed-Rank Test.** Reference [38] shows that it is insufficient to analyze and compare the algorithms only according to the average value. Because, in some tests, the results produced by the algorithms are slightly different, and the occurrence of these differences may be accidental, to verify whether the statistical difference between IJADE-TSO and the comparison algorithms is accidental or not, the Wilcoxon signed-rank test is used to analyze the performances of the IJADE-TSO and the other six algorithms. Table 5 lists the Wilcoxon signed-rank test [39] results of each competitor and IJADE-TSO with the significance level set to 0.05. In Table 5, “+” indicates that the optimization result of IJADE-TSO is better than the competitor, “-” denotes the opposite, and “=” represents that the optimization results are similar. “R+” denotes the magnitude with which IJADE-TSO surpasses the comparison algorithm, and “R-” indicates the opposite result. The statistical results of the test are also given in the last row of the table. According to the statistical results in Table 5, among the 30 test functions of CEC 2014 test set, IJADE-TSO shows a performance that is similar to those of SPS-LSHADE-EIG, LSHADE, and iLSHADE and precedes CPI-JADE in all test functions except F5, F7, F12, and F14.

**4.1.3. Convergence Curve of Algorithms.** To further illustrate the convergence performance of IJADE-TSO, the average error convergence curves in solving the test function are given in Figure 3.

TABLE 3: Comparison of statistical results derived from seven algorithms for CEC 2014 test suite.

| No. | Types                       | IJADE-TSO |          | SPS-LSHADE-EIG |          | LSHADE   |          | CPI-JADE |          | GEDGWO   |          | iLSHADE  |          | DOLTLBO  |          |
|-----|-----------------------------|-----------|----------|----------------|----------|----------|----------|----------|----------|----------|----------|----------|----------|----------|----------|
|     |                             | Mean      | SD       | Mean           | SD       | Mean     | SD       | Mean     | SD       | Mean     | SD       | Mean     | SD       | Mean     | SD       |
| F01 | Unimodal functions          | 1.42E-14  | 8.04E-15 | 1.50E-14       | 8.72E-15 | 1.73E-14 | 7.69E-15 | 1.10E-04 | 5.66E-05 | 9.88E-03 | 1.15E-02 | 2.01E-14 | 1.34E-14 | 8.82E+05 | 7.11E+05 |
| F02 |                             | 0.00E+00  | 0.00E+00 | 0.00E+00       | 0.00E+00 | 1.11E-15 | 5.57E-15 | 1.57E-09 | 1.23E-09 | 3.18E-04 | 1.12E-03 | 1.11E-15 | 5.57E-15 | 4.96E+02 | 7.91E+02 |
| F03 |                             | 0.00E+00  | 0.00E+00 | 0.00E+00       | 0.00E+00 | 3.34E-15 | 1.35E-14 | 5.74E-11 | 4.39E-11 | 1.27E-05 | 9.49E-06 | 3.34E-15 | 1.35E-14 | 3.50E+00 | 3.32E+00 |
| F04 | Simple multimodal functions | 4.90E-14  | 3.41E-14 | 1.05E-13       | 9.33E-14 | 8.92E-14 | 4.44E-14 | 6.21E-01 | 6.24E-01 | 5.62E-04 | 3.95E-03 | 5.24E-14 | 2.50E-14 | 5.78E+01 | 3.75E+01 |
| F05 |                             | 2.06E+01  | 2.40E-01 | 2.01E+01       | 6.58E-02 | 2.01E+01 | 3.05E-02 | 2.06E+01 | 4.91E-02 | 2.09E+01 | 5.55E-02 | 2.01E+01 | 1.27E-01 | 2.09E+01 | 5.95E-02 |
| F06 |                             | 0.00E+00  | 0.00E+00 | 1.93E-02       | 1.38E-01 | 0.00E+00 | 0.00E+00 | 1.24E-01 | 2.64E+00 | 1.09E-01 | 3.08E-01 | 1.93E-02 | 1.38E-01 | 1.73E+01 | 3.26E+00 |
| F07 | 0.00E+00                    | 0.00E+00  | 0.00E+00 | 0.00E+00       | 0.00E+00 | 0.00E+00 | 0.00E+00 | 0.00E+00 | 0.00E+00 | 1.60E-09 | 3.72E-09 | 0.00E+00 | 0.00E+00 | 1.62E-02 | 1.97E-02 |
| F08 | 2.49E-01                    | 1.78E+00  | 1.56E-13 | 6.81E-14       | 1.92E-13 | 7.71E-14 | 2.83E-01 | 2.10E+00 | 4.11E+01 | 1.06E+01 | 1.14E-13 | 0.00E+00 | 7.35E+01 | 1.71E+01 |          |
| F09 | 7.97E+00                    | 1.67E+00  | 7.96E+00 | 3.49E+00       | 6.47E+00 | 1.68E+00 | 7.93E+01 | 5.43E+00 | 4.71E+01 | 1.35E+01 | 7.59E+00 | 1.69E+00 | 8.49E+01 | 2.36E+01 |          |
| F10 | 6.16E+00                    | 3.41E+00  | 4.90E-03 | 1.15E-02       | 3.27E-03 | 7.65E-03 | 1.17E+03 | 1.18E+02 | 1.75E+03 | 5.03E+02 | 7.35E-03 | 1.37E-02 | 2.93E+03 | 6.12E+02 |          |
| F11 | 1.94E+03                    | 3.05E+02  | 1.09E+03 | 4.35E+02       | 1.24E+03 | 2.02E+02 | 4.14E+03 | 2.46E+02 | 2.90E+03 | 5.77E+02 | 1.08E+03 | 2.58E+02 | 3.48E+03 | 7.63E+02 |          |
| F12 | 1.78E+00                    | 5.81E-01  | 1.02E-01 | 3.49E-02       | 1.63E-01 | 2.25E-02 | 9.10E-01 | 1.06E-01 | 1.42E+00 | 5.52E-01 | 1.87E-01 | 1.51E-01 | 1.82E+00 | 2.33E-01 |          |
| F13 | 1.27E-01                    | 1.85E-02  | 4.79E-02 | 9.91E-03       | 1.19E-01 | 1.64E-02 | 2.51E-01 | 3.41E-02 | 2.49E-01 | 5.35E-02 | 9.90E-02 | 2.08E-02 | 3.65E-01 | 7.23E-02 |          |
| F14 | 2.28E-01                    | 3.98E-02  | 2.80E-01 | 3.75E-02       | 2.34E-01 | 2.92E-02 | 2.39E-01 | 2.56E-02 | 2.52E-01 | 4.05E-02 | 1.66E-01 | 3.39E-02 | 2.35E-01 | 3.75E-02 |          |
| F15 | 2.85E+00                    | 3.27E-01  | 2.91E+00 | 7.26E-01       | 2.15E+00 | 2.33E-01 | 8.72E+00 | 7.85E-01 | 3.82E+00 | 1.14E+00 | 1.89E+00 | 3.20E-01 | 7.97E+00 | 2.77E+00 |          |
| F16 | 9.96E+00                    | 5.94E-01  | 7.21E+00 | 9.30E-01       | 8.57E+00 | 4.37E-01 | 1.13E+01 | 1.13E+01 | 2.64E-01 | 7.26E-01 | 7.85E+00 | 7.79E-01 | 1.16E+01 | 2.99E-01 |          |
| F17 | 2.31E+02                    | 1.21E+02  | 1.65E+02 | 9.74E+01       | 1.71E+02 | 9.15E+01 | 7.58E+02 | 1.76E+02 | 2.56E+02 | 2.58E+02 | 2.01E+02 | 1.20E+02 | 5.10E+03 | 4.38E+03 |          |
| F18 | 5.84E+00                    | 2.88E+00  | 5.78E+00 | 2.65E+00       | 6.21E+00 | 2.48E+00 | 4.25E+01 | 5.98E+00 | 3.95E+01 | 2.37E+01 | 4.84E+00 | 2.03E+00 | 2.44E+02 | 5.01E+01 |          |
| F19 | 3.46E+00                    | 7.68E-01  | 2.86E+00 | 7.08E-01       | 3.77E+00 | 5.85E-01 | 4.48E+00 | 4.63E-01 | 4.48E+00 | 7.52E-01 | 2.84E+00 | 8.20E-01 | 1.07E+01 | 8.34E+00 |          |
| F20 | 3.48E+00                    | 2.58E+00  | 2.86E+00 | 1.26E+00       | 2.97E+00 | 1.25E+00 | 1.67E+01 | 1.91E+00 | 1.80E+01 | 1.49E+01 | 2.59E+00 | 1.05E+00 | 1.78E+02 | 5.44E+01 |          |
| F21 | 1.52E+02                    | 1.12E+02  | 7.23E+01 | 7.11E+01       | 8.00E+01 | 7.29E+01 | 4.21E+02 | 1.40E+02 | 2.51E+02 | 2.33E+02 | 1.06E+02 | 8.55E+01 | 2.78E+03 | 1.82E+03 |          |
| F22 | 3.58E+01                    | 1.91E+01  | 2.78E+01 | 2.87E+01       | 2.91E+01 | 2.34E+01 | 1.07E+02 | 4.66E+01 | 1.99E+02 | 1.03E+02 | 3.77E+01 | 4.28E+01 | 2.13E+02 | 9.12E+01 |          |
| F23 | 2.00E+02                    | 1.89E-01  | 3.15E+02 | 4.16E-13       | 3.15E+02 | 4.02E-13 | 3.15E+02 | 4.02E-13 | 2.00E+02 | 1.28E+00 | 3.15E+02 | 4.02E-13 | 2.00E+02 | 0.00E+00 |          |
| F24 | 2.00E+02                    | 0.00E+00  | 2.24E+02 | 1.32E+00       | 2.24E+02 | 1.00E+00 | 2.22E+02 | 6.45E-01 | 2.00E+02 | 2.85E-03 | 2.14E+02 | 1.07E+01 | 2.00E+02 | 5.03E-11 |          |
| F25 | 2.00E+02                    | 4.10E-03  | 2.03E+02 | 5.26E-02       | 2.03E+02 | 4.40E-02 | 2.03E+02 | 2.80E-02 | 2.02E+02 | 9.64E-01 | 2.03E+02 | 1.34E-01 | 2.00E+02 | 0.00E+00 |          |
| F26 | 2.00E+02                    | 1.88E-02  | 1.00E+02 | 1.40E-02       | 1.00E+02 | 1.62E-02 | 1.00E+02 | 2.95E-02 | 1.00E+02 | 5.30E-02 | 1.00E+02 | 2.77E-02 | 1.00E+02 | 6.91E-02 |          |
| F27 | 1.00E+02                    | 1.10E-02  | 3.00E+02 | 1.11E-13       | 3.00E+02 | 2.56E-13 | 3.59E+01 | 4.98E+01 | 3.65E+01 | 4.80E+01 | 3.04E+02 | 1.47E+01 | 2.08E+02 | 1.88E+01 |          |
| F28 | 2.02E+02                    | 1.23E+01  | 8.40E+02 | 1.35E+01       | 8.45E+02 | 1.55E+01 | 8.44E+02 | 1.57E+01 | 5.51E+02 | 3.03E+02 | 8.46E+02 | 1.96E+01 | 2.00E+02 | 2.51E-01 |          |
| F29 | 6.48E+02                    | 1.00E+02  | 7.16E+02 | 3.16E+00       | 7.16E+02 | 3.44E+00 | 7.16E+02 | 1.71E+00 | 1.41E+02 | 8.70E+01 | 7.16E+02 | 3.67E+00 | 2.64E+04 | 1.77E+05 |          |
| F30 | 8.38E+02                    | 8.18E+02  | 1.27E+03 | 5.75E+02       | 1.23E+03 | 5.65E+02 | 9.30E+02 | 1.52E+02 | 4.34E+02 | 6.02E+01 | 2.22E+03 | 1.01E+03 | 1.95E+03 | 5.92E+02 |          |



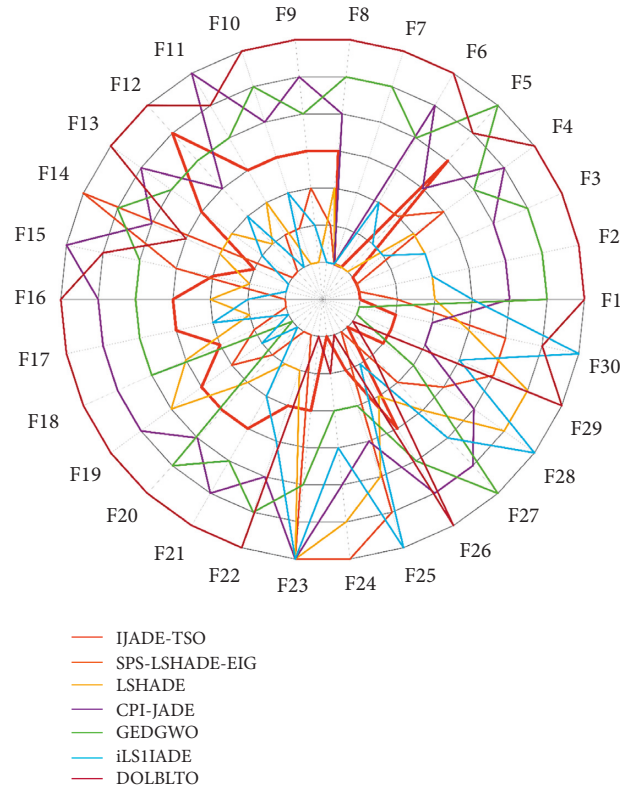


FIGURE 2: Radar figure of algorithm rankings.

TABLE 4: Friedman test.

| Algorithm | IJADE-TSO | SPS-LSHADE-EIG | LSHADE | CPI-JADE | GEDGWO | iLSHADE | DOLTLBO |
|-----------|-----------|----------------|--------|----------|--------|---------|---------|
| Rank      | 2.92      | 2.93           | 3.23   | 5.22     | 4.77   | 3.10    | 5.83    |

Friedman test:  $p$  value is  $4.43e-11$ ; Chi-square is 60.03.

For most unimodal functions, simple multimodal functions, and hybrid functions, IJADE-TSO shows better convergence accuracy and higher convergence speed compared to GEDGWO, CPI-JADE, and DLOTLBO and slower convergence speed compared to LSHADE, iLSHADE, and SPS-LSHADE-EIG. For the composite function, the convergence curve of IJADE-TSO drops slightly at the initial stage of iteration and then falls into local optimization, but it breaks through local optimization at the later stage of iteration and shows a significant decline. For composition functions, LSHADE, SPS-LSHADE-EIG, and iLSHADE converge quickly, but their accuracy is significantly worse than that of IJADE-TSO, and they are apt to fall into the local optimum. As mentioned above, IJADE-TSO possesses both strong convergence ability and the capacity to break through local optimization.

**4.1.4. Box Graph of the Results.** The following box graphs are drawn to analyze the distribution characteristics of the results for CEC 2014 test functions.

As shown in Figure 4, the center mark of each box represents the median value of the results of 51 runs, and the bottom and upper edges of each box represent the third and

fourth quartiles, respectively. Outliers are drawn separately with “+.” IJADE-TSO has no outliers in 13 test functions (F2-F3, F5-F7, F9, F13-F14, F17, F19, F24, F26, and F29). The distribution of the IJADE-TSO solutions is more centralized, with rarely produced outliers, except for F30. Thus, it is safe to conclude that IJADE-TSO is more robust than the competing algorithms.

#### 4.2. Parameters Identification of Photovoltaic Models.

Global warming has become an increasingly serious issue threatening the survival of mankind nowadays. In response to the environmental impact of global warming, solar energy has become widely exploited as a clean energy source [40]. Solar energy has many advantages, such as being nonpolluting, renewable, cheap, and easy to obtain. Photovoltaic systems are commonly used in daily life as an important device for collecting solar energy. PV models are crucial for PV systems, as they are used to imitate the response of real PV cells, fitting measured current-voltage (I-V) data under all operating conditions. The most widely used PV systems are single-diode model (SDM), double-diode model (DDM), and PV module model [41]. It is necessary to identify the parameters in the established photovoltaic models to make

TABLE 5: Wilcoxon signed-rank test.

| No.   | SPS-LSHADE-EIG |        |      |     | LSHADE   |       |      |     | CPI-JADE |      |      |     | GEDGWO   |      |      |     | iLSHADE  |        |      |     | DOLTLBO  |        |      |     |
|-------|----------------|--------|------|-----|----------|-------|------|-----|----------|------|------|-----|----------|------|------|-----|----------|--------|------|-----|----------|--------|------|-----|
|       | p value        | R+     | R-   | Win | p value  | R+    | R-   | Win | p value  | R+   | R-   | Win | p value  | R+   | R-   | Win | p value  | R+     | R-   | Win | p value  | R+     | R-   | Win |
| F1    | 6.27E-01       | 193    | 158  | =   | 3.56E-02 | 170.5 | 60.5 | +   | 5.15E-10 | 1326 | 0    | +   | 5.15E-10 | 1326 | 0    | +   | 1.53E-02 | 140    | 31   | +   | 5.15E-10 | 1326   | 0    | +   |
| F2    | 1.00E+00       | 0      | 0    | =   | 5.00E-01 | 3     | 0    | =   | 5.15E-10 | 1326 | 0    | +   | 5.15E-10 | 1326 | 0    | +   | 5.00E-01 | 3      | 0    | =   | 5.15E-10 | 1326   | 0    | +   |
| F3    | 1.00E+00       | 0      | 0    | =   | 2.50E-01 | 6     | 0    | =   | 5.15E-10 | 1326 | 0    | +   | 5.15E-10 | 1326 | 0    | +   | 2.50E-01 | 6      | 0    | =   | 5.15E-10 | 1326   | 0    | +   |
| F4    | 4.62E-05       | 529.5  | 65.5 | +   | 5.82E-05 | 421.5 | 43.5 | +   | 5.15E-10 | 1326 | 0    | +   | 5.15E-10 | 1326 | 0    | +   | 6.82E-01 | 115    | 95   | =   | 5.15E-10 | 1326   | 0    | +   |
| F5    | 5.15E-10       | 0      | 1326 | -   | 5.15E-10 | 0     | 1326 | -   | 4.04E-01 | 574  | 752  | +   | 2.80E-09 | 1297 | 29   | +   | 1.67E-09 | 20     | 1306 | -   | 2.65E-09 | 1298   | 28   | +   |
| F6    | 1.00E+00       | 0      | 0    | =   | 1.00E+00 | 0     | 0    | =   | 5.15E-10 | 1326 | 0    | +   | 5.15E-10 | 1326 | 0    | +   | 1.00E+00 | 0      | 0    | =   | 5.15E-10 | 1326   | 0    | +   |
| F7    | 1.00E+00       | 0      | 0    | =   | 1.00E+00 | 0     | 0    | =   | 1.00E+00 | 0    | 0    | =   | 5.15E-10 | 1326 | 0    | +   | 1.00E+00 | 0      | 0    | =   | 5.15E-10 | 1326   | 0    | =   |
| F8    | 1.69E-09       | 7      | 1218 | -   | 2.51E-09 | 7     | 1169 | -   | 5.15E-10 | 1326 | 0    | +   | 5.15E-10 | 1326 | 0    | +   | 1.62E-09 | 0      | 1176 | -   | 5.15E-10 | 1326   | 0    | +   |
| F9    | 8.37E-01       | 641    | 685  | =   | 1.08E-04 | 250   | 1076 | -   | 5.15E-10 | 1326 | 0    | +   | 5.15E-10 | 1326 | 0    | +   | 3.99E-01 | 573    | 753  | =   | 5.15E-10 | 1326   | 0    | +   |
| F10   | 5.15E-10       | 0      | 1326 | -   | 5.15E-10 | 0     | 1326 | -   | 5.15E-10 | 1326 | 0    | +   | 5.15E-10 | 1326 | 0    | +   | 5.15E-10 | 0      | 1326 | -   | 5.15E-10 | 1326   | 0    | +   |
| F11   | 9.66E-09       | 51     | 1275 | -   | 5.46E-10 | 1     | 1325 | -   | 5.15E-10 | 1326 | 0    | +   | 9.87E-10 | 1315 | 11   | +   | 5.46E-10 | 1      | 1325 | -   | 6.15E-10 | 1323   | 3    | +   |
| F12   | 5.15E-10       | 0      | 1326 | -   | 5.15E-10 | 0     | 1326 | -   | 4.42E-09 | 37   | 1289 | -   | 1.64E-03 | 327  | 999  | -   | 5.46E-10 | 1      | 1325 | -   | 9.55E-01 | 657    | 669  | =   |
| F13   | 5.15E-10       | 0      | 1326 | -   | 1.27E-02 | 397   | 929  | -   | 5.15E-10 | 1326 | 0    | +   | 5.46E-10 | 1325 | 1    | +   | 3.77E-07 | 121    | 1205 | -   | 5.15E-10 | 1326   | 0    | +   |
| F14   | 1.87E-07       | 1219   | 107  | +   | 3.30E-01 | 767   | 559  | =   | 1.13E-01 | 832  | 494  | =   | 3.45E-03 | 975  | 351  | +   | 1.97E-08 | 64     | 1262 | -   | 1.96E-01 | 801    | 525  | =   |
| F15   | 5.93E-01       | 720    | 606  | =   | 1.32E-09 | 16    | 1310 | -   | 5.15E-10 | 1326 | 0    | +   | 2.21E-06 | 1168 | 158  | +   | 5.46E-10 | 1      | 1325 | -   | 5.15E-10 | 1326   | 0    | +   |
| F16   | 5.15E-10       | 0      | 1326 | -   | 7.35E-10 | 6     | 1320 | -   | 5.46E-10 | 1325 | 1    | +   | 1.11E-01 | 833  | 493  | =   | 5.46E-10 | 1      | 1325 | -   | 5.15E-10 | 1326   | 0    | +   |
| F17   | 1.86E-03       | 331    | 995  | -   | 2.01E-02 | 415   | 911  | -   | 5.15E-10 | 1326 | 0    | +   | 9.18E-01 | 652  | 674  | =   | 1.71E-01 | 517    | 809  | =   | 5.15E-10 | 1326   | 0    | +   |
| F18   | 8.37E-01       | 641    | 685  | =   | 2.85E-01 | 777   | 549  | =   | 5.15E-10 | 1326 | 0    | +   | 1.11E-09 | 1313 | 13   | +   | 8.98E-02 | 482    | 844  | =   | 5.15E-10 | 1326   | 0    | +   |
| F19   | 6.91E-04       | 301    | 1025 | =   | 2.63E-02 | 900   | 426  | +   | 3.03E-08 | 1254 | 72   | +   | 2.79E-05 | 216  | 1110 | -   | 5.06E-04 | 292    | 1034 | =   | 5.15E-10 | 1326   | 0    | +   |
| F20   | 4.88E-01       | 589    | 737  | =   | 5.42E-01 | 598   | 728  | +   | 5.15E-10 | 1326 | 0    | +   | 1.18E-09 | 1312 | 14   | +   | 1.77E-01 | 519    | 807  | =   | 5.15E-10 | 1326   | 0    | +   |
| F21   | 1.00E-04       | 248    | 1078 | -   | 3.19E-04 | 279   | 1047 | =   | 1.05E-09 | 1314 | 12   | +   | 4.69E-02 | 875  | 451  | +   | 2.63E-02 | 426    | 900  | -   | 5.15E-10 | 1326   | 0    | +   |
| F22   | 5.85E-07       | 130    | 1196 | -   | 2.29E-07 | 111   | 1215 | -   | 2.10E-09 | 1302 | 24   | +   | 7.35E-10 | 1320 | 6    | +   | 2.04E-03 | 334    | 992  | -   | 5.15E-10 | 1326   | 0    | +   |
| F23   | 5.13E-10       | 1326   | 0    | +   | 5.13E-10 | 1326  | 0    | +   | 5.13E-10 | 1326 | 0    | +   | 1.10E-05 | 1132 | 194  | +   | 5.13E-10 | 1326   | 0    | +   | 2.40E-09 | 0      | 1128 | -   |
| F24   | 5.14E-10       | 1326   | 0    | +   | 5.15E-10 | 1326  | 0    | +   | 5.15E-10 | 1326 | 0    | +   | 5.15E-10 | 1326 | 0    | +   | 5.15E-10 | 1326   | 0    | +   | 5.14E-10 | 1326   | 0    | +   |
| F25   | 5.15E-10       | 1326   | 0    | +   | 5.15E-10 | 1326  | 0    | +   | 5.15E-10 | 1326 | 0    | +   | 5.15E-10 | 1326 | 0    | +   | 5.15E-10 | 1326   | 0    | +   | 1.63E-09 | 0      | 1176 | -   |
| F26   | 5.15E-10       | 0      | 1326 | -   | 2.51E-02 | 424   | 902  | =   | 5.15E-10 | 1326 | 0    | +   | 5.15E-10 | 1326 | 0    | +   | 4.74E-05 | 229    | 1097 | -   | 5.15E-10 | 1326   | 0    | +   |
| F27   | 5.12E-10       | 1326   | 0    | +   | 5.12E-10 | 1326  | 0    | +   | 5.15E-10 | 1326 | 0    | +   | 5.15E-10 | 1326 | 0    | +   | 5.14E-10 | 1326   | 0    | +   | 5.46E-10 | 1325   | 1    | +   |
| F28   | 5.15E-10       | 1326   | 0    | +   | 5.15E-10 | 1326  | 0    | +   | 5.15E-10 | 1326 | 0    | +   | 6.93E-10 | 1321 | 5    | +   | 5.15E-10 | 1326   | 0    | +   | 1.49E-06 | 139    | 1136 | -   |
| F29   | 2.68E-05       | 1111   | 215  | +   | 6.02E-05 | 1091  | 235  | +   | 3.87E-05 | 1102 | 224  | +   | 5.46E-10 | 1    | 1325 | -   | 4.55E-04 | 1037   | 289  | +   | 7.80E-10 | 1319   | 7    | +   |
| F30   | 3.89E-03       | 971    | 355  | +   | 2.96E-03 | 980   | 346  | +   | 2.06E-02 | 910  | 416  | +   | 6.56E-03 | 373  | 953  | -   | 6.36E-08 | 1240   | 86   | +   | 2.18E-07 | 1216   | 110  | +   |
| +/-/= |                | 9/12/9 |      |     | 10/11/9  |       |      |     | 26/1/3   |      |      |     | 24/4/2   |      |      |     |          | 8/13/9 |      |     |          | 24/3/3 |      |     |

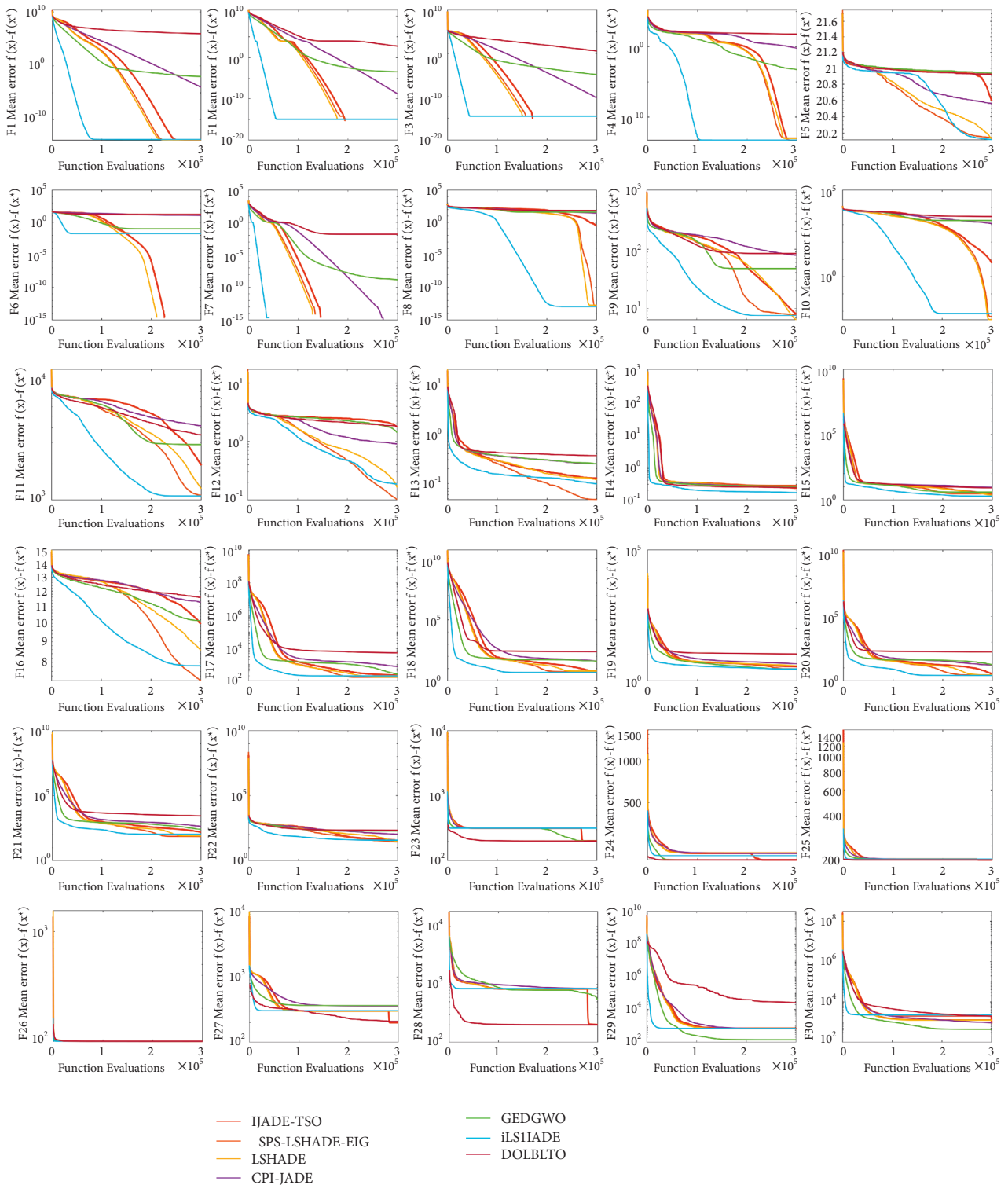


FIGURE 3: Convergence curve of algorithms.

the model more consistent with the measured data. In this section, the proposed IJADE-TSO algorithm is used to identify parameters of photovoltaic models.

**4.2.1. Problem Statement.** In [42], there are three PV models, single-diode model, double-diode model, and PV

module model, which are not repeated in this paper. The PV parameter identification models referenced from [41, 42] are as follows.

In general, parameters extraction problem is usually transformed into a class of optimization problem to leverage the optimization algorithms. Similar to [42], the root mean

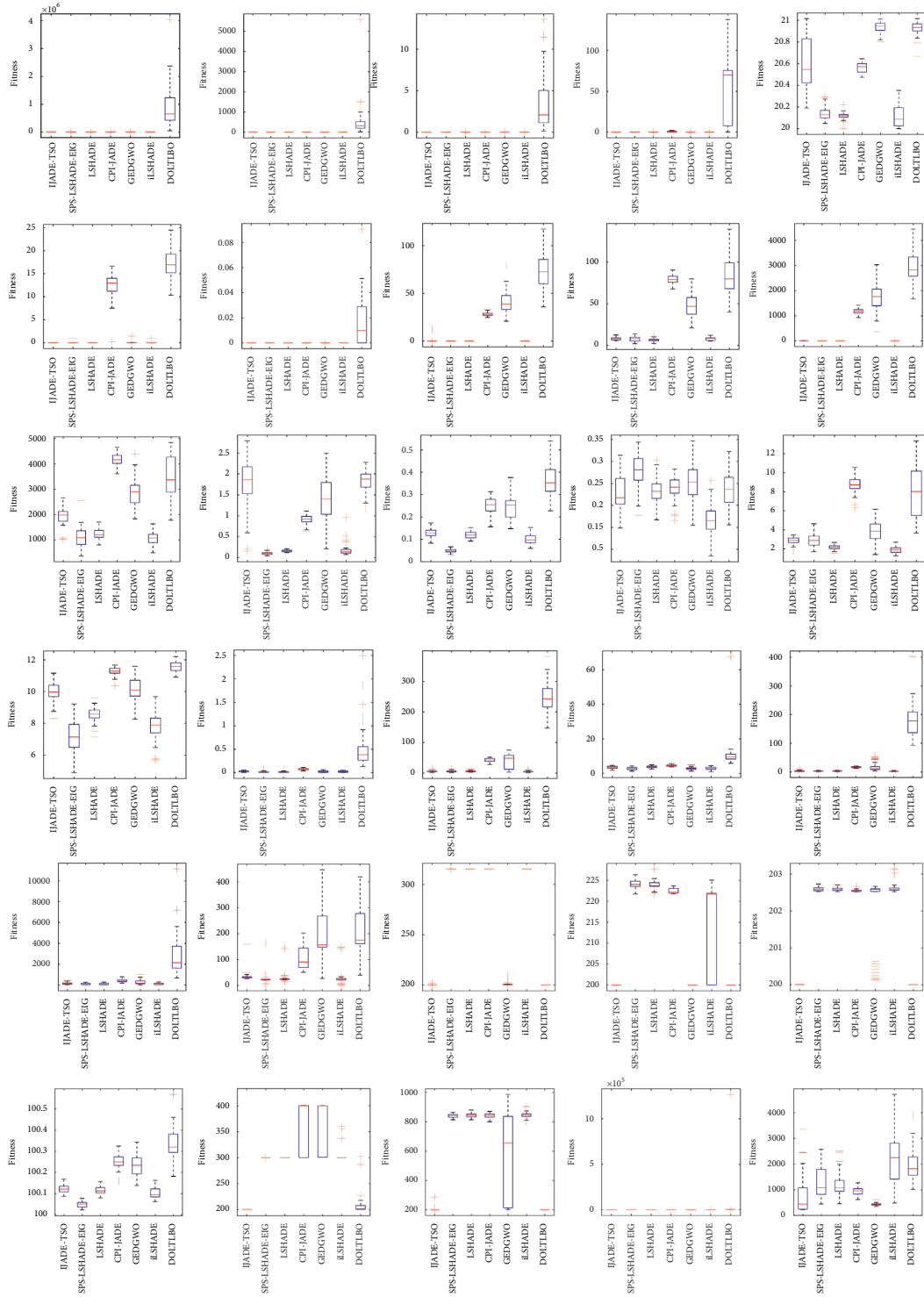


FIGURE 4: Box plots of algorithms on CEC 2014 test functions. (a) F1, (b) F2, (c) F3, (d) F4, (e) F5, (f) F6, (g) F7, (h) F8, (i) F9, (j) F10, (k) F11, (l) F12, (m) F13, (n) F14, (o) F15, (p) F16, (q) F17, (r) F18, (s) F19, (t) F20, (u) F21, (v) F22, (w) F23, (x) F24, (y) F25, (z) F26, (aa) F27, (ab) F28, (ac) F29, and (ad) F30.

square error (RMSE) is also used as the objective function in this study, which is defined as follows:

$$RMSE(x) = \sqrt{\frac{1}{N} \sum_{k=1}^N f(V_k, I_k, \mathbf{x})^2}, \quad (21)$$

where  $N$  is the number of measured  $I$ - $V$  data samples and  $\mathbf{x}$  is a vector that concludes the unknown parameters to be extracted. For different PV models, their objective functions are represented as follows.

For single-diode model,

TABLE 6: IAE of IJADE-TSO for each measurement on single-diode model.

| Item | $V_m$ (V) | $I_m$ (A) | $I_c$ (A) | IAE        |
|------|-----------|-----------|-----------|------------|
| 1    | -0.2057   | 0.764     | 0.7641    | 8.7704E-05 |
| 2    | -0.1291   | 0.762     | 0.7627    | 6.6309E-04 |
| 3    | -0.0588   | 0.7605    | 0.7614    | 8.5531E-04 |
| 4    | 0.0057    | 0.7605    | 0.7602    | 3.4601E-04 |
| 5    | 0.0646    | 0.76      | 0.7591    | 9.4479E-04 |
| 6    | 0.1185    | 0.759     | 0.7580    | 9.5765E-04 |
| 7    | 0.1678    | 0.757     | 0.7571    | 9.1654E-05 |
| 8    | 0.2132    | 0.757     | 0.7561    | 8.5864E-04 |
| 9    | 0.2545    | 0.7555    | 0.7551    | 4.1313E-04 |
| 10   | 0.2924    | 0.754     | 0.7537    | 3.3612E-04 |
| 11   | 0.3269    | 0.7505    | 0.7514    | 8.9097E-04 |
| 12   | 0.3585    | 0.7465    | 0.7474    | 8.5385E-04 |
| 13   | 0.3873    | 0.7385    | 0.7401    | 1.6172E-03 |
| 14   | 0.4137    | 0.728     | 0.7274    | 6.1777E-04 |
| 15   | 0.4373    | 0.7065    | 0.7070    | 4.7265E-04 |
| 16   | 0.459     | 0.6755    | 0.6753    | 2.1985E-04 |
| 17   | 0.4784    | 0.632     | 0.6308    | 1.2417E-03 |
| 18   | 0.496     | 0.573     | 0.5719    | 1.0716E-03 |
| 19   | 0.5119    | 0.499     | 0.4996    | 6.0702E-04 |
| 20   | 0.5265    | 0.413     | 0.4136    | 6.4879E-04 |
| 21   | 0.5398    | 0.3165    | 0.3175    | 1.0101E-03 |
| 22   | 0.5521    | 0.212     | 0.2122    | 1.5494E-04 |
| 23   | 0.5633    | 0.1035    | 0.1023    | 1.2487E-03 |
| 24   | 0.5736    | -0.01     | -0.0087   | 1.2825E-03 |
| 25   | 0.5833    | -0.123    | -0.1255   | 2.5074E-03 |
| 26   | 0.59      | -0.21     | -0.2085   | 1.5277E-03 |

$$f(V, I, \mathbf{x}) = I_{ph} - I_o \left[ \exp\left(\frac{V + IR_s}{aV_t}\right) - 1 \right] - \frac{V + IR_s}{R_{sh}} - I,$$

$$\mathbf{x} = [I_{ph}, I_o, R_s, R_{sh}, a].$$
(22)

For double-diode model,

$$f(V, I, \mathbf{x}) = I_{ph} - I_{o1} \left[ \exp\left(\frac{V + IR_s}{a_1 V_t}\right) - 1 \right]$$

$$- I_{o2} \left[ \exp\left(\frac{V + IR_s}{a_2 V_t}\right) - 1 \right] - \frac{V + IR_s}{R_{sh}} - I$$
(23)

$$\mathbf{x} = [I_{ph}, I_{o1}, I_{o2}, R_s, R_{sh}, a_1, a_2].$$

For PV module based on the SDM,

$$f(V, I, \mathbf{x}) = I_{ph} - I_o \left[ \exp\left(\frac{V + IR_s}{aV_t}\right) - 1 \right] - \frac{V + IR_s}{R_{sh}} - I,$$

$$\mathbf{x} = [I_{ph}, I_o, R_s, R_{sh}, a].$$
(24)

data of SDM and DDM are obtained from [43], which are measured on a 57 mm diameter commercial (R.T.C France) silicon solar cell under 1000 W/m<sup>2</sup> at 33°C.

(1) *Results for the Three Models.* In order to further show the quality of the results, we have introduced individual absolute error (IAE).

$$IAE = |I_m - I_c|. \quad (25)$$

$I_m$  is the measured current and  $I_c$  is the simulated current. IAE represents the absolute error between them.

The  $I$ - $V$  characteristics obtained by IJADE-TSO and the individual absolute error (IAE) between the experimental data and simulated data are shown in Tables 6–8 and the  $I$ - $V$  characteristics are plotted in Figure 5. In addition, Tables 6–8 present the individual absolute error (IAE) between the measured data and calculated data. From Table 6, all the IAE values of single-diode model are smaller than 2.5434E-03. From Table 7, all the IAE values of double-diode model are smaller than 1.6284E-03. From Table 8, all the IAE values of double-diode model are smaller than 4.8328E-03. The results show that the calculated data obtained by IJADE-TSO are remarkably in accordance with the measured data over the whole voltage range, which indicates that IJADE-TSO identifies highly accurate parameters.

4.2.2. *Experimental Results and Analysis.* To evaluate the performance of IJADE-TSO, we employ it to extract parameters of SDM, DDM, and PV module model. The  $I$ - $V$

(2) *Statistical Results and Convergence Speed.* To validate the superior performance of IJADE-TSO, the comparisons are carried out with other algorithms including MLHADE [44],

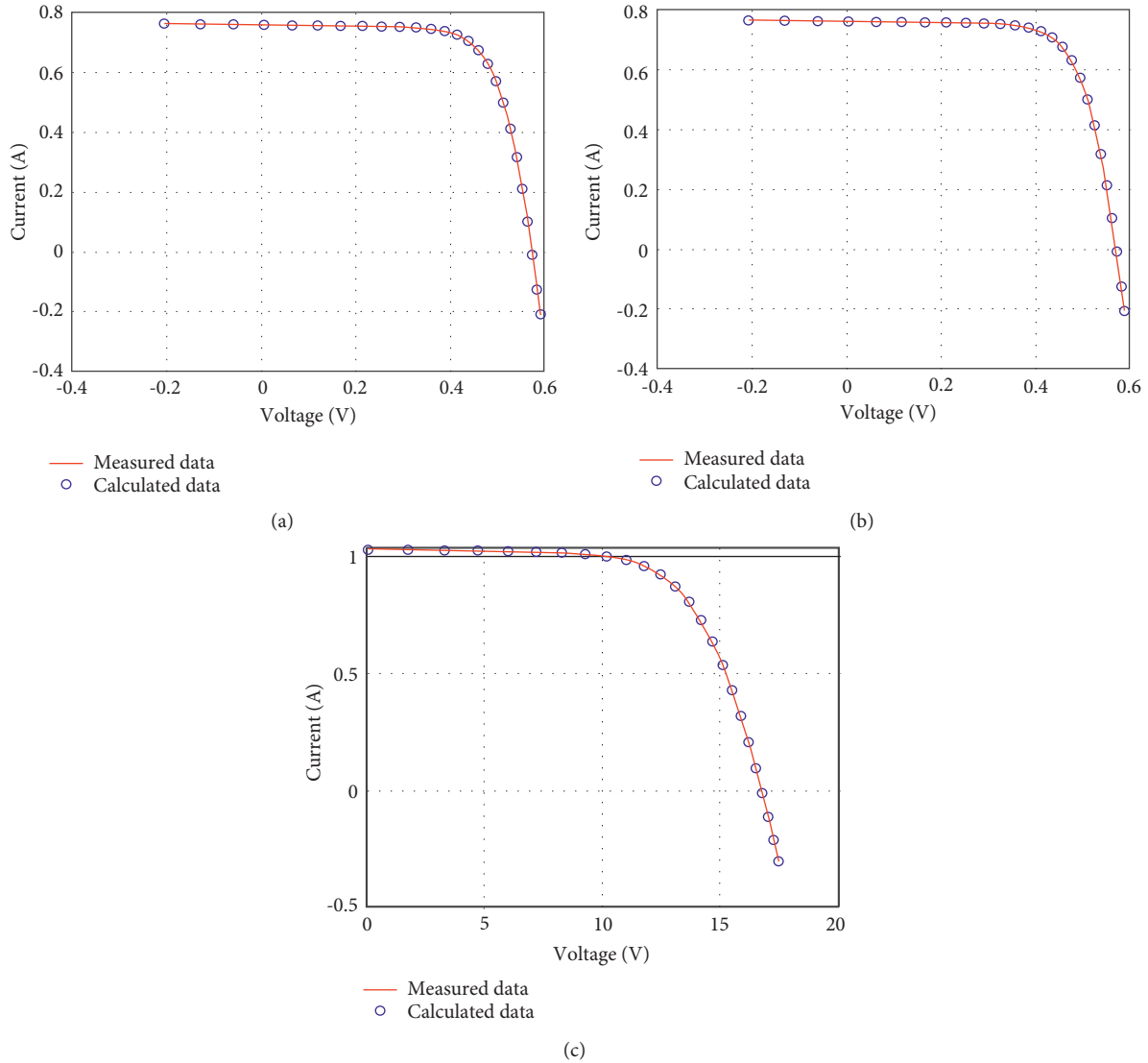


FIGURE 5: Comparisons between measured data and calculated data for three models.

improved JAYA [45], JADE [27], crow search algorithm (CSA) [46], and multiple learning backtracking search algorithm (MLBSA) [47]. Among the above algorithms, MLSHAPE, MLBSA, IJAYA, and CSA are excellent algorithms that have been applied in the field of photovoltaic parameter identification in recent years. JADE is the prototype of the improved algorithm in this paper. For fair comparison, the value of function evaluations of all algorithms is set to 50000 for all problems. Meanwhile, each algorithm is tested 30 times independently. The population sizes of all compared algorithms are set to 50. Other algorithm parameter settings are the same as the references.

The statistical results are reported in Table 9. For single-diode model, IJADE-TSO has the same accuracy as MLSHADE and MLBSA. The Min RMSE searched by all algorithms have no difference except IJAYA. As for standard deviation, IJADE-TSO is better than its competitors. For double-diode model, only IJADE-TSO and MLSHADE algorithms obtain the same Min RMSE, but the Mean and SD

RMSE of IJADE-TSO ranks the first. For PV module model, the minimum RMSE of PV model obtained by all algorithms are no different. Only MLBSA, IJADE-TSO, and JADE ranked the first in the Mean RMSE. The SD value obtained by IJADE-TSO ranks the first. Overall, IJADE-TSO has better search ability and robustness than the comparison algorithms and can steadily obtain the minimum RMSE value in all three PV parameter identification models.

The convergence curves among all competitors for three PV models are shown in Figure 6. Obviously, for the single-diode model, the descent curve of the IJADE-TSO algorithm is significantly higher compared to the other algorithms in the initial parts, and then it declines fastest and obtains the best results after 10,000 function evaluations. Although MLSHADE and MLBSA also obtain the best results, they are significantly slower than IJADE-TSO. For the double-diode model, IJADE-TSO achieves the best results with the least number of function evaluations. For the PV model, IJADE-TSO, MLBSA, and JADE all achieve the best results, but IJADE-TSO uses the least

TABLE 7: IAE of IJADE-TSO for each measurement on double diode model.

| Item | $V_m$ (V) | $I_m$ (A) | $I_c$ (A) | IAE        |
|------|-----------|-----------|-----------|------------|
| 1    | -0.2057   | 0.764     | 0.7640    | 1.6588E-05 |
| 2    | -0.1291   | 0.762     | 0.7626    | 6.0410E-04 |
| 3    | -0.0588   | 0.7605    | 0.7613    | 8.3770E-04 |
| 4    | 0.0057    | 0.7605    | 0.7602    | 3.2621E-04 |
| 5    | 0.0646    | 0.76      | 0.7591    | 8.9232E-04 |
| 6    | 0.1185    | 0.759     | 0.7581    | 8.7858E-04 |
| 7    | 0.1678    | 0.757     | 0.7572    | 1.8861E-04 |
| 8    | 0.2132    | 0.757     | 0.7562    | 7.5639E-04 |
| 9    | 0.2545    | 0.7555    | 0.7552    | 3.2270E-04 |
| 10   | 0.2924    | 0.754     | 0.7537    | 2.7765E-04 |
| 11   | 0.3269    | 0.7505    | 0.7514    | 8.9913E-04 |
| 12   | 0.3585    | 0.7465    | 0.7473    | 8.0144E-04 |
| 13   | 0.3873    | 0.7385    | 0.7400    | 1.5107E-03 |
| 14   | 0.4137    | 0.728     | 0.7272    | 7.5305E-04 |
| 15   | 0.4373    | 0.7065    | 0.7069    | 3.5030E-04 |
| 16   | 0.459     | 0.6755    | 0.6752    | 2.8946E-04 |
| 17   | 0.4784    | 0.632     | 0.6308    | 1.2392E-03 |
| 18   | 0.496     | 0.573     | 0.5720    | 1.0053E-03 |
| 19   | 0.5119    | 0.499     | 0.4997    | 7.0614E-04 |
| 20   | 0.5265    | 0.413     | 0.4137    | 7.3367E-04 |
| 21   | 0.5398    | 0.3165    | 0.3175    | 1.0462E-03 |
| 22   | 0.5521    | 0.212     | 0.2121    | 1.2300E-04 |
| 23   | 0.5633    | 0.1035    | 0.1022    | 1.3367E-03 |
| 24   | 0.5736    | -0.01     | -0.0088   | 1.2082E-03 |
| 25   | 0.5833    | -0.123    | -0.1255   | 2.5434E-03 |
| 26   | 0.59      | -0.21     | -0.2084   | 1.6284E-03 |

TABLE 8: IAE of IJADE-TSO for each measurement on PV module model.

| Item | $V_m$ (V) | $I_m$ (A) | $I_c$ (A) | IAE        |
|------|-----------|-----------|-----------|------------|
| 1    | 0.1248    | 1.0315    | 1.0291    | 2.3808E-03 |
| 2    | 1.8093    | 1.03      | 1.0274    | 2.6189E-03 |
| 3    | 3.3511    | 1.026     | 1.0257    | 2.5820E-04 |
| 4    | 4.7622    | 1.022     | 1.0241    | 2.1072E-03 |
| 5    | 6.0538    | 1.018     | 1.0223    | 4.2918E-03 |
| 6    | 7.2364    | 1.0155    | 1.0199    | 4.4307E-03 |
| 7    | 8.3189    | 1.014     | 1.0164    | 2.3631E-03 |
| 8    | 9.3097    | 1.01      | 1.0105    | 4.9615E-04 |
| 9    | 10.2163   | 1.0035    | 1.0006    | 2.8710E-03 |
| 10   | 11.0449   | 0.988     | 0.9845    | 3.4516E-03 |
| 11   | 11.8018   | 0.963     | 0.9595    | 3.4783E-03 |
| 12   | 12.4929   | 0.9255    | 0.9228    | 2.6612E-03 |
| 13   | 13.1231   | 0.8725    | 0.8726    | 9.9663E-05 |
| 14   | 13.6983   | 0.8075    | 0.8073    | 2.2574E-04 |
| 15   | 14.2221   | 0.7265    | 0.7283    | 1.8365E-03 |
| 16   | 14.6995   | 0.6345    | 0.6371    | 2.6380E-03 |
| 17   | 15.1346   | 0.5345    | 0.5362    | 1.7131E-03 |
| 18   | 15.5311   | 0.4275    | 0.4295    | 2.0113E-03 |
| 19   | 15.8929   | 0.3185    | 0.3188    | 2.7448E-04 |
| 20   | 16.2229   | 0.2085    | 0.2074    | 1.1105E-03 |
| 21   | 16.5241   | 0.101     | 0.0962    | 4.8328E-03 |
| 22   | 16.7987   | -0.008    | -0.0083   | 3.2539E-04 |
| 23   | 17.0499   | -0.111    | -0.1109   | 6.3517E-05 |
| 24   | 17.2793   | -0.209    | -0.2092   | 2.4727E-04 |
| 25   | 17.4885   | -0.303    | -0.3009   | 2.1364E-03 |

TABLE 9: Statistical results of RMSE of different algorithms for three models.

| Model              | Algorithm | IJADE-TSO         | MLSHADE           | MLBSA             | IJAYA             | JADE              | CSA               |
|--------------------|-----------|-------------------|-------------------|-------------------|-------------------|-------------------|-------------------|
| Single-diode model | Min       | <b>9.8602E-04</b> | <b>9.8602E-04</b> | <b>9.8602E-04</b> | 9.8613E-04        | <b>9.8602E-04</b> | <b>9.8602E-04</b> |
|                    | Mean      | <b>9.8602E-04</b> | <b>9.8602E-04</b> | <b>9.8602E-04</b> | 1.0030E-03        | 9.8624E-04        | 1.0362E-03        |
|                    | SD        | <b>1.9126E-17</b> | 3.6556E-17        | 7.0565E-11        | 6.1010E-05        | 1.1128E-06        | 1.0178E-04        |
| Double-diode model | Min       | <b>9.8248E-04</b> | <b>9.8248E-04</b> | 9.8249E-04        | 9.8354E-04        | 9.8863E-04        | 9.8467E-04        |
|                    | Mean      | <b>9.8296E-04</b> | 9.8336E-04        | 9.8647E-04        | 1.0128E-03        | 1.1220E-03        | 1.3258E-03        |
|                    | SD        | <b>1.2228E-06</b> | 1.4528E-06        | 5.1996E-06        | 6.7236E-05        | 1.6138E-04        | 5.1016E-04        |
| PV module model    | Min       | <b>2.4251E-03</b> | <b>2.4251E-03</b> | <b>2.4251E-03</b> | <b>2.4251E-03</b> | <b>2.4251E-03</b> | <b>2.4251E-03</b> |
|                    | Mean      | <b>2.4251E-03</b> | 2.4373E-03        | <b>2.4251E-03</b> | 2.4377E-03        | <b>2.4251E-03</b> | 2.6458E-03        |
|                    | SD        | <b>1.9641E-17</b> | 4.6443E-05        | 1.6392E-08        | 2.9308E-05        | 1.9823E-17        | 6.2071E-04        |

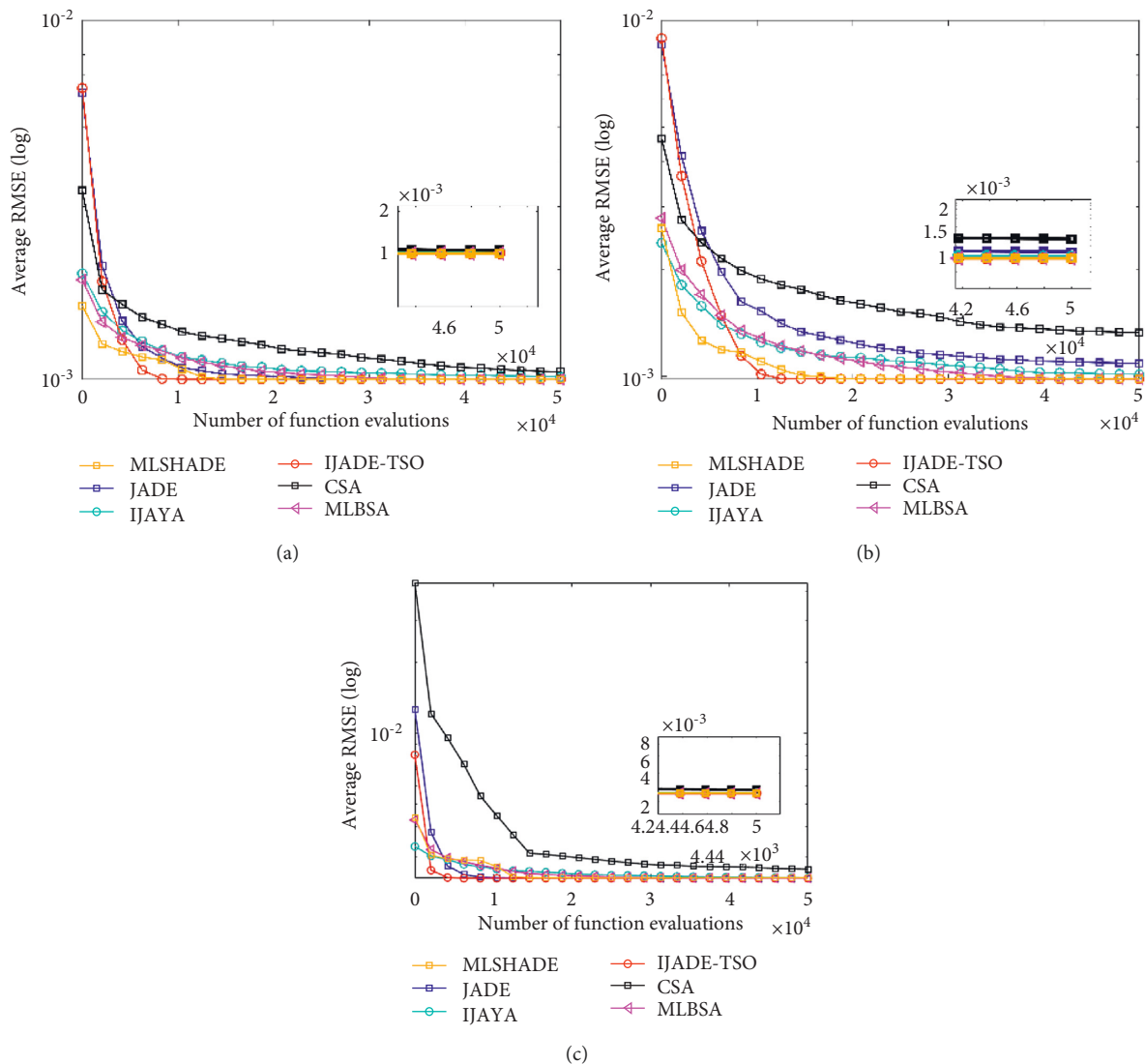


FIGURE 6: Convergence curves for three models.

number of function evaluations and its iteration curve declines the fastest. Among the three PV models, the descent curve of the IJADE-TSO declines the fastest compared with other algorithms and achieves the best results.

In order to comprehensively compare the performances of all algorithms in the three PV models, we conducted a Friedman test with a significance of 0.05, and the results are shown in Table 10.



TABLE 10: Friedman test results.

| Algorithms              | IJADE-TSO | MLSHADE | MLBSA | IJAYA | JADE | CSA  |
|-------------------------|-----------|---------|-------|-------|------|------|
| Min ranks <sup>a</sup>  | 1         | 2       | 3.67  | 5     | 4    | 5.33 |
| Mean ranks <sup>b</sup> | 1         | 2.67    | 3     | 4.67  | 3.67 | 6    |
| SD ranks <sup>c</sup>   | 1         | 3       | 3     | 4.33  | 3.67 | 6    |

<sup>a</sup>Friedman test:  $p$  value is 0.0305; Chi-square is 12.33. <sup>b</sup>Friedman test:  $p$  value is 0.0262; Chi-square is 12.71. <sup>c</sup>Friedman test:  $p$  value is 0.0382; Chi-square is 11.76.

In terms of Min, Mean, and SD of RMSE, IJADE-TSO excels all other algorithms, ranking the first, which shows that IJADE-TSO has an excellent performance in terms of accuracy, robustness, and computational efficiency.

## 5. Conclusions

This paper proposed a novel hybrid algorithm, named IJADE-TSO. The spiral foraging search and parabolic foraging search of TSO are introduced into the mutation strategy in IJADE to improve the exploration ability and population diversity. Meanwhile, this paper integrates JADE with three strategies: CR sorting mechanism and CR repairing, top  $\alpha r_1$  selection, and population linear reduction.

The proposed IJADE-TSO is evaluated using CEC 2014 benchmarks with dimensionality of 30 and photovoltaic parameter identification problem. Although the statistical results of the CEC 2014 benchmarks demonstrate that IJADE-TSO is slightly superior to SPS-LSHADE-EIG and iLSHADE, IJADE-TSO is significantly better than other comparison algorithms such as MLHADE in solving photovoltaic parameter identification problem. This shows that the two mutant strategies combined contributed significantly to expanding the search scope and avoiding local optimization, and three other strategies are conducive to improve the convergence efficiency. IJADE-TSO achieves a good balance in exploration and exploitation and demonstrates great value in solving practical engineering problems.

The current spiral foraging and parabolic foraging strategies are selected with a stationary probability, which means the selected strategy may not be optimal and an adaptive selection strategy needs to be developed in the future.

## Data Availability

The codes used to support the findings of this study can be downloaded at <https://github.com/lailaidaren/Matlab-code-of-IJADE-TSO.git>.

## Conflicts of Interest

The authors declare that they have no conflicts of interest.

## Acknowledgments

The authors acknowledge funding received from the following science foundations: the National Natural Science Foundation of China (no. 62101590), the Science Foundation of the Shanxi Province, China (2021JM-223, 2022JQ-584, and 2021JM-224), and Military Scientific Research Project (KJ2020C009002).

## References

- [1] S. S. Rao, *Engineering Optimization: Theory and Practice*, Wiley, Hoboken, 2019.
- [2] Y. Li, X. Zhu, and J. Liu, "An improved moth-flame optimization algorithm for engineering problems," *Symmetry*, vol. 12, no. 8, p. 1234, 2020.
- [3] W. Hare, J. Nutini, and S. Tesfamariam, "A survey of non-gradient optimization methods in structural engineering," *Advances in Engineering Software*, vol. 59, pp. 19–28, 2013.
- [4] J. Liang, K. Qiao, C. Yue et al., "A clustering-based differential evolution algorithm for solving multimodal multi-objective optimization problems," *Swarm and Evolutionary Computation*, vol. 60, Article ID 100788, 2021.
- [5] S. Katoch, S. S. Chauhan, and V. Kumar, "A review on genetic algorithm: past, present, and future," *Multimedia Tools and Applications*, vol. 80, no. 5, pp. 8091–8126, 2021.
- [6] Z. Shang, J. Gu, and J. Wang, "Improved simulated annealing algorithm for capacitated vehicle routing problem," *Jisuanji Jicheng Zhizao Xitong/Computer Integr. Manuf. Syst. CIMS*, vol. 27, pp. 2260–2269, 2021.
- [7] B. Gao, Z. Bai, and Y. Song, "Optimal placement of sensors in bridge monitoring based on an adaptive gravity search algorithm," *Zhendong yu Chongji/Journal Vib. Shock*, vol. 40, 2021.
- [8] S. Mirjalili and S. M. Mirjalili, "Lewis, A. Grey wolf optimizer," *Advances in Engineering Software*, vol. 69, pp. 46–61, 2014.
- [9] G.-G. Wang, S. Deb, and Z. Cui, "Monarch butterfly optimization," *Neural Computing & Applications*, vol. 31, no. 7, pp. 1995–2014, 2019.
- [10] R. Storn and K. Price, "Differential evolution - a simple and efficient heuristic for global optimization over continuous spaces," *Journal of Global Optimization*, vol. 11, no. 4, pp. 341–359, 1997.
- [11] H. Abderazek, A. R. Yildiz, and S. M. Sait, "Mechanical engineering design optimisation using novel adaptive differential evolution algorithm," *International Journal of Vehicle Design*, vol. 80, no. 2/3/4, pp. 285–329, 2019.
- [12] S. Li, W. Gong, L. Wang, X. Yan, and C. Hu, "Optimal power flow by means of improved adaptive differential evolution," *Energy*, vol. 198, Article ID 117314, 2020.
- [13] Y. Cai, D. Wu, S. Fu, and S. Zeng, "Self-regulated differential evolution for real parameter optimization," *Applied Intelligence*, vol. 51, no. 8, pp. 5873–5897, 2021.
- [14] O. Yilmaz, E. Bas, and E. Egrioglu, "The training of pi-sigma artificial neural networks with differential evolution algorithm for forecasting," *Computational Economics*, vol. 59, pp. 1699–1711, 2022.
- [15] F. Arce, E. Zamora, H. Sossa, and R. Barrón, "Differential evolution training algorithm for dendrite morphological neural networks," *Applied Soft Computing*, vol. 68, pp. 303–313, 2018.
- [16] H. Ma, D. Dong, C.-C. Shu, Z. Zhu, and C. Chen, "Quantum learning control using differential evolution with equally-

- mixed strategies,” *Control Theory and Technology*, vol. 15, no. 3, pp. 226–241, 2017.
- [17] V. Stanovov, S. Akhmedova, and E. Semenkin, “LSHADE algorithm with rank-based selective pressure strategy for solving CEC 2017 benchmark problems,” in *Proceedings of the 2018 IEEE Congress on Evolutionary Computation, CEC 2018*, Rio de Janeiro, Brazil, July 2018.
- [18] R. Tanabe and A. Fukunaga, “Success-history based parameter adaptation for differential evolution,” in *Proceedings of the 2013 IEEE Congress on Evolutionary Computation, CEC 2013*, pp. 71–78, Cancun, Mexico, June 2013.
- [19] R. Tanabe and A. S. Fukunaga, “Improving the search performance of SHADE using linear population size reduction,” in *Proceedings of the 2014 IEEE Congress on Evolutionary Computation, CEC 2014*, pp. 1658–1665, Beijing, China, July 2014.
- [20] J. Brest, M. S. Maučec, and B. Bošković, “IL-SHADE: improved L-SHADE algorithm for single objective real-parameter optimization,” in *Proceedings of the 2016 IEEE Congress on Evolutionary Computation, CEC 2016*, pp. 1188–1195, Vancouver, BC, Canada, July 2016.
- [21] C. Zhang, J. Ning, S. Lu, D. Ouyang, and T. Ding, “A novel hybrid differential evolution and particle swarm optimization algorithm for unconstrained optimization,” *Operations Research Letters*, vol. 37, no. 2, pp. 117–122, 2009.
- [22] S.-Y. Du and Z.-G. Liu, “Hybridizing particle swarm optimization with JADE for continuous optimization,” *Multi-media Tools and Applications*, vol. 79, no. 7-8, pp. 4619–4636, 2020.
- [23] W. Gong, Z. Cai, and C. X. Ling, “DE/BBO: a hybrid differential evolution with biogeography-based optimization for global numerical optimization,” *Soft Computing*, vol. 15, no. 4, pp. 645–665, 2010.
- [24] A. W. Mohamed, A. A. Hadi, A. M. Fattouh, and K. M. Jambi, “LSHADE with semi-parameter adaptation hybrid with CMA-ES for solving CEC 2017 benchmark problems,” in *Proceedings of the 2017 IEEE Congress on Evolutionary Computation, CEC 2017*, pp. 145–152, Donostia, Spain, June 2017.
- [25] L. Xie, T. Han, H. Zhou, Z. R. Zhang, B. Han, and A. Tang, “Tuna swarm optimization: a novel swarm-based meta-heuristic algorithm for global optimization,” *Computational Intelligence and Neuroscience*, vol. 2021, Article ID 9210050, 22 pages, 2021.
- [26] A. K. Qin, V. L. Huang, and P. N. Suganthan, “Differential evolution algorithm with strategy adaptation for global numerical optimization,” *IEEE Transactions on Evolutionary Computation*, vol. 13, no. 2, pp. 398–417, 2009.
- [27] J. Jingqiao Zhang and A. C. Sanderson, “JADE: adaptive differential evolution with optional external archive,” *IEEE Transactions on Evolutionary Computation*, vol. 13, no. 5, pp. 945–958, 2009.
- [28] T. Eltaieb and A. Mahmood, “Differential evolution: a survey and analysis,” *Applied Sciences*, vol. 8, no. 10, p. 1945, 2018.
- [29] M. Yang, Z. Cai, C. Li, and J. Guan, “An improved JADE algorithm for global optimization,” in *Proceedings of the 2014 IEEE Congress on Evolutionary Computation, CEC 2014*, Beijing, China, July 2014.
- [30] Y.-Z. Zhou, W.-C. Yi, L. Gao, and X.-Y. Li, “Adaptive differential evolution with sorting crossover rate for continuous optimization problems,” *IEEE Transactions on Cybernetics*, vol. 47, no. 9, pp. 2742–2753, 2017.
- [31] W. Gong, Z. Cai, and Y. Wang, “Repairing the crossover rate in adaptive differential evolution,” *Applied Soft Computing J.* vol. 15, pp. 149–168, 2014.
- [32] S. M. Guo, J. S. H. Tsai, C. C. Yang, and P. H. Hsu, “A self-optimization approach for L-SHADE incorporated with eigenvector-based crossover and successful-parent-selecting framework on CEC 2015 benchmark set,” in *Proceedings of the 2015 IEEE Congress on Evolutionary Computation, CEC 2015*, pp. 1003–1010, Sendai, Japan, May 2015.
- [33] Y. Wang, Z.-Z. Liu, J. Li, H.-X. Li, and G. G. Yen, “Utilizing cumulative population distribution information in differential evolution,” *Applied Soft Computing*, vol. 48, pp. 329–346, 2016.
- [34] X. Wang, H. Zhao, T. Han, H. Zhou, and C. Li, “A grey wolf optimizer using Gaussian estimation of distribution and its application in the multi-UAV multi-target urban tracking problem,” *Applied Soft Computing*, vol. 78, pp. 240–260, 2019.
- [35] Y. Xu, Z. Yang, X. Li, H. Kang, and X. Yang, “Dynamic opposite learning enhanced teaching-learning-based optimization,” *Knowledge-Based Systems*, p. 188, 2020.
- [36] J. J. Liang, B. Y. Qu, and P. N. Suganthan, “Problem definitions and evaluation criteria for the CEC 2014 special session and competition on single objective real-parameter numerical optimization,” *IEEE Congr. Evol. Comput.*, pp. 1–32, 2014.
- [37] B. B. Frey, “Friedman test,” in *The SAGE Encyclopedia of Educational Research, Measurement, and Evaluation* Sage, Thousand Oaks, 2018.
- [38] D. W. Zimmerman and B. D. Zumbo, “Relative power of the Wilcoxon test, the friedman test, and repeated-measures ANOVA on ranks,” *The Journal of Experimental Education*, vol. 62, no. 1, pp. 75–86, 1993.
- [39] D. Rey and M. Neuhäuser, *Wilcoxon-signed-rank test, International Encyclopedia of Statistical Science*, pp. 1658–1659, Springer, Berlin, Germany, 2011.
- [40] L.-q. Liu, Z.-x. Wang, H.-q. Zhang, and Y.-c. Xue, “Solar energy development in China-A review,” *Renewable and Sustainable Energy Reviews*, vol. 14, no. 1, pp. 301–311, 2010.
- [41] D. F. Alam, D. A. Yousri, and M. B. Eteiba, “Flower pollination algorithm based solar PV parameter estimation,” *Energy Conversion and Management*, vol. 101, pp. 410–422, 2015.
- [42] L. L. Jiang, D. L. Maskell, and J. C. Patra, “Parameter estimation of solar cells and modules using an improved adaptive differential evolution algorithm,” *Applied Energy*, vol. 112, pp. 185–193, 2013.
- [43] T. Easwarakhanthan, J. Bottin, I. Bouhouch, and C. Boutrit, “Nonlinear minimization algorithm for determining the solar cell parameters with microcomputers,” *International Journal of Solar Energy*, vol. 4, no. 1, pp. 1–12, 1986.
- [44] Q. Hao, Z. Zhou, Z. Wei, and G. Chen, “Parameters identification of photovoltaic models using a multi-strategy success-history-based adaptive differential evolution,” *IEEE Access*, vol. 8, pp. 35979–35994, 2020.
- [45] K. Yu, J. J. Liang, B. Y. Qu, X. Chen, and H. Wang, “Parameters identification of photovoltaic models using an improved JAYA optimization algorithm,” *Energy Conversion and Management*, vol. 150, pp. 742–753, 2017.
- [46] A. Omar, H. M. Hasanien, M. A. Elgendy, and M. A. L. Badr, “Identification of the photovoltaic model parameters using the crow search algorithm,” *Journal of Engineering*, vol. 2017, no. 13, pp. 1570–1575, 2017.
- [47] K. Yu, J. J. Liang, B. Y. Qu, Z. Cheng, and H. Wang, “Multiple learning backtracking search algorithm for estimating parameters of photovoltaic models,” *Applied Energy*, vol. 226, pp. 408–422, 2018.

## Research Article

# Green City Landscape Design and Planning Based on GIS and Analytic Hierarchy Process Model

Daochun Liu,<sup>1</sup> Mingming Tang,<sup>2</sup> and Nan Dong <sup>1</sup>

<sup>1</sup>School of Forestry Science, Xinyang Agriculture and Forestry University, XinYang 464000, China

<sup>2</sup>School of Agronomy, Xinyang Agriculture and Forestry University, XinYang 464000, China

Correspondence should be addressed to Nan Dong; 2017290003@xyafu.edu.cn

Received 10 February 2022; Revised 13 April 2022; Accepted 18 April 2022; Published 16 May 2022

Academic Editor: Man Fai Leung

Copyright © 2022 Daochun Liu et al. This is an open access article distributed under the Creative Commons Attribution License, which permits unrestricted use, distribution, and reproduction in any medium, provided the original work is properly cited.

The spiritual connotation of contemporary cities has gradually become rich and colorful, and the concept of a green city has also been accepted by the public. People living in cities have higher and higher requirements for landscape, but traditional landscape design cannot achieve efficient and accurate planning. Therefore, the old design method, which cannot meet the complex and changeable urban needs and cannot keep up with the development and changes of the times, is doomed to be eliminated and replaced. This study introduces a GIS system and uses an AHP method to assist landscape design. Through rational resource utilization of topography, vegetation growth, population density, and other conditions, the city can be green and environmentally friendly, reduce energy consumption, and meet people's concept of healthy life. The experimental results show that: (1) through the GIS system, a multidecision model is constructed to choose a reasonable location for the garden. Based on the opinions and scores of all parties, the B place with a score as high as 8.97 was selected. (2) Using comprehensive landscape sensitivity to divide four levels of landscape land-use value and looking for the best landscape vision, it is divided into five scenic functional areas and 12 scenic spots. SPEI and NDVI were used to select cultivated plants and landscapes. (3) Route multifactor comprehensive model is designed to plan garden route. The coincidence degree between the model and the actual road condition is about 87.62%. Citizen satisfaction is between 7 and 9 points, and the comprehensive evaluation is high. (4) The evaluation system of landscape architecture, in which both B-level index and C-level index are higher than 7 points is constructed, which is in line with the expectations of the public and experts and convenient for feedback correction. The method based on this study is feasible and can be further optimized.

## 1. Introduction

In recent years, the propaganda of green urbanism can better help people know, understand, and build the cities they have lived in for generations. On the basis of a deep understanding of the green city and the integration of the essential characteristics of landscape architecture design, the ultimate goal is to make people and nature achieve a harmonious and unified realm. At present, there are a lot of documents about the application of urban planning and design, which can provide us with more methods for reference. Compact urban areas can be identified by using GIS and AHP, and the function and spatial structure can be fully developed [1]. The spatial distribution data were extracted by GIS and ENVI

software to evaluate the natural suitability of the environment [2]. The GIS system is introduced to make the spatial accuracy error less than 4%, and the urban landscape planning and design under light pollution are completed [3]. Further, introducing high-resolution image recognition technology can obtain data more effectively and simulate the green city landscape platform [4]. In addition, GIS remote sensing information collection can effectively monitor the ecological environment quality [5]. The evaluation thinking framework based on the entropy method and GIS can comprehensively evaluate the general situation of green cities [6]. Modeling cities was based on GIS to reduce energy consumption and greenhouse gas emissions [7]. To meet the special needs of landscape management, the landscape GIS

system should improve the manageability of each area [8]. Mediterranean Green City uses GuidosToolBox software, GIS modeling technology, and MSPA to evaluate the connectivity of the natural framework [9]. Taking the design of Libo World Natural Heritage Theme Park in Karst of South China as an example, this study analyzes the application advantages of the GIS system [10]. The route selection of scenic roads in mountainous areas of southern Anhui by GIS-AHP method conforms to the development of transportation planning and tourism and recreation [11]. The ecological sensitivity of Qingcheng Mountain-Dujiangyan scenic spot under the construction pressure was evaluated by GIS [12]. Based on RS and GIS, combined with DEM and remote sensing image data, the ecological risk of Emei Mountain Scenic Area was analyzed and evaluated [13]. This study briefly summarizes the application of GIS in landscape architecture in the past 30 years [14]. Appropriate ideological and political education elements were incorporated and the course of GIS technology application in landscape architecture was reformed [15].

Since science and technology have never been valued by traditional art design, they are often despised or even ignored. Therefore, the landscape design relying on computers was not optimistic at first. The above literature boldly breaks through the limitations and abandons the single messy and blind pursuit of the inspiration construction method. Using various angles and technical methods to design landscape, we try to scientifically discuss the construction of a green city and related decision-making and scheduling. Combining landscape design with modern science and technology through powerful computer technology, the actual scene is better conceived and designed, and the traditional design is revolutionized so that it retains the original landscape design characteristics, and at the same time, it is more diversified, inclusive, and a true complex. Due to its strong logic, easy to use, powerful data processing function, and many other advantages, the GIS system has been gradually introduced into landscape design and has brought new value and scientific achievements. This study presents a GIS system, which uses the AHP method to assist landscape design. Through the rational utilization of resources in topography, vegetation growth, population density, and other conditions, the city can be green and environmentally friendly, reduce energy consumption, and meet the concept of people's healthy life. Through the GIS system, a multivariate decision-making model is built, and a comprehensive landscape sensitivity to divide four levels of landscape land use value is used to find the best landscape vision. SPEI and NDVI are used to select cultivated plants and landscapes. The evaluation system of landscape architecture is constructed, and the B-level index and C-level index are both higher than 7 points, which meets the expectations of the public and experts and is convenient for feedback correction. The method based on this study is feasible and can be further optimized.

## 2. Related Works

**2.1. Green City.** For Green City [16], in the theory of urban sustainable development, energy is used. For a prosperous

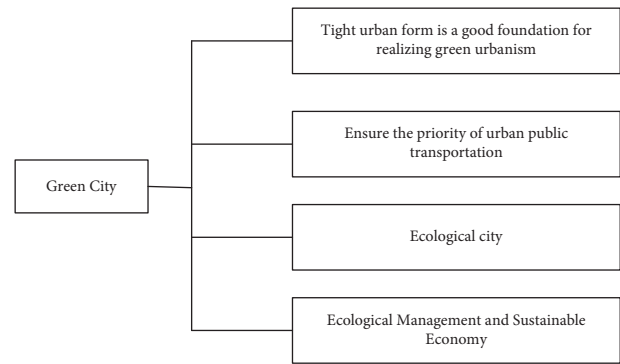


FIGURE 1: Characteristics of green cities.

and developing city, the uncontrolled and high-speed development of the city will inevitably cause a series of injuries to the natural living environment. It is a theory put forward in the “Green Movement,” aiming at protecting the environment. In the theory of urban sustainable development, the use of energy can further promote the stable development of the economy. Designing a garden landscape in the city is just in line with the spiritual connotation of the green city. Great importance is attached to the neglected natural resources in cities and rational transformation and utilization are made so as to drive more sustainable economic development through the landscape. This is in line with the requirements of ecological balance advocated in green cities.

Problems such as environmental pollution, insufficient resources, and serious losses are becoming more and more serious, which cause irreversible harm and threat to human survival and development. Therefore, the traditional development concept in the past needs to be changed. A more reasonable ecological environment is constructed, and resources are used better. Man and nature are harmonious and unified, and the goal lies in the common development of economy and environment. While protecting nature, it drives the economy and emphasizes the overall balance of ecology. To try to point out the future and direction of people's healthy life and civilized development, scholar Timshi Bitley summed up several characteristics of green cities, as shown in Figure 1:

**2.2. Urban Landscape Architecture.** The normal operation of the city will inevitably transform the original natural landscape. At this time, how to coordinate people, urban architecture, and natural landscape has become a problem that people should think about. Landscape architecture was born. By using this kind of planning, people can better coordinate the relationship between the living environment and natural science. Designers strive to create an efficient, comfortable, safe, and healthy living environment for people living in this land. For cities, it is of great significance.

The core of traditional urban garden design lies in artistic literariness. Designers are easily limited by individuals in the process of design and planning and they pay great attention to the generation of inspiration. The creation of artistic conception and the interest in poetry and painting are the

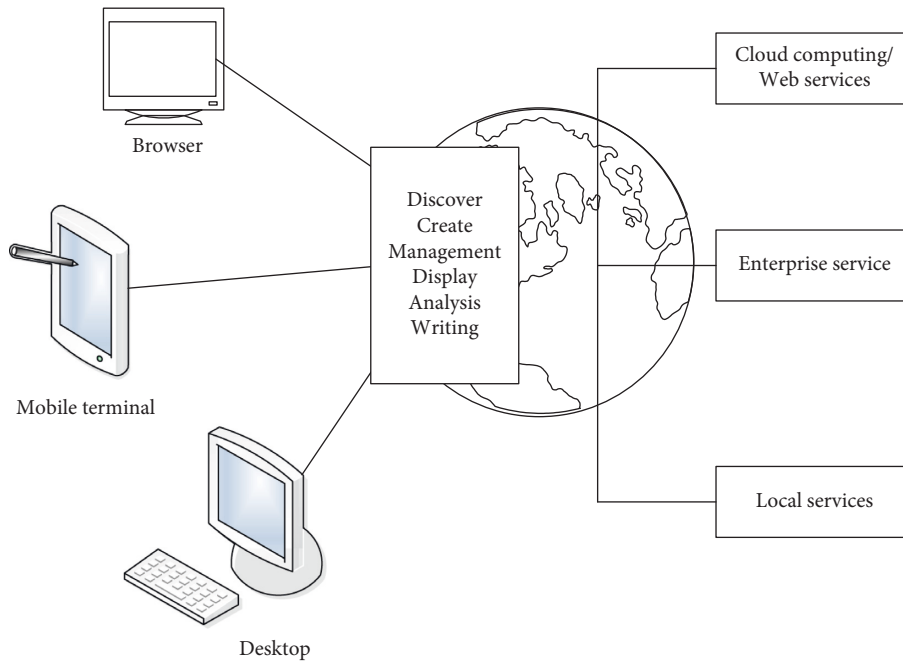


FIGURE 2: ArcGIS infrastructure.

soul of garden creation. Therefore, people will have a prejudice in the design of gardens. That is, this kind of planning and design is not logical and scientific, and cannot be measured concretely by parameters. This leads to the late integration design of modern science and technology with this discipline, which lags behind and has a broad prospect. However, to adapt to the complex and changeable social needs, the traditional landscape design system can not meet the requirements and can not reasonably explain the logic and internal relations of landscape design, breakthrough the traditional cognitive concept and create digital aesthetics. Let all landscape elements interweave harmoniously to create a scientific and dynamic garden system.

**2.3. GIS Technology.** GIS [17], the Chinese name is Geographic Information System. This is a computer system based on geographic information and spatial database that was gradually developed in the 20th century. It can collect and sort out the scattered spatial data (map data, remote sensing data, statistical data, etc.) and analyze and build a geographical model. This reduces a lot of tedious and unnecessary field exploration work and capital loss and greatly improves the work efficiency of the designers. As an instrumental subject, it has a wide range of uses, such as transportation, environmental protection, agriculture, and these industries, through the use of the GIS system for spatial analysis, can be associated with spatial location and attribute relationship, showing a three-dimensional spatial relationship. ArcGIS is the mainstream GIS platform software in the market so far, and it is a mature and complete product, as shown in Figure 2:

In ArcGIS operation, several kinds of data are involved, as shown in Table 1:

**2.4. Analytic Hierarchy Process.** AHP [22], whose Chinese name is “analytic hierarchy process,” combines qualitative and quantitative analysis when dealing with complex decision-making problems. This method is simple and clear, and the basic idea of solving problems is similar to people’s way of thinking, especially the process of judgment is roughly the same. The basic steps of AHP are as follows:

**2.4.1. Establish Hierarchical Structure Model.** It is expressed by a structural model with clear levels. All the factors that need to be considered into the model are put, which can be divided into: the highest level, the middle level, and the lowest level.

**2.4.2. Constructing Paired Comparison Matrices.**

$$A = (a_{ij})_{n \times n}. \tag{1}$$

Among them, let  $n$  elements participate in the comparison, and the relative weight  $a_{ij}$  is used to describe the comparison of the importance of a certain factor between the  $i$ -th element and the  $j$ -th element.

We can get the characteristics of paired comparison matrices:

$$a_{ij} > 0, a_{ij} = 1, a_{ij} = \frac{1}{a_{ji}}, \tag{2}$$

$$a_{ij} = 1 \quad (i = j).$$

**2.4.3. Consistency Test.** Theoretically, if it is an identical paired comparison matrix, then

TABLE 1: Categories of different data.

| Data name               | Specific introduction   |
|-------------------------|---|
| Vector data             | The data precision is high, the storage capacity is small, and the operation is fast. The way to express the position of spatial objects is to write down the coordinates and spatial relations of spatial objects. Vector map data is composed of geometric data of geographical elements and attribute data.                        |
| Raster data [18]        | The accuracy of data expression is low and the amount of data is large. Its graphics operation is simple and inefficient. However, its digital simulation is easy, cheap and easy to achieve data sharing, and the remote sensing image format is close to the same. The data structure is mainly represented by regular pixel array. |
| Irregular triangulation | Abbreviated as "TIN" [19]. It is a special data structure, which is between vector data and raster data. It represents the terrain surface by connecting a bunch of non-overlapping and non-intersecting triangular surfaces.   |
| Attribute data [20]     | Descriptive data that describes the characteristics of geospatial elements. For vector data and raster data, attribute data are different.  |
| Metadata [21]           | Data quality has great influence on GIS application. Metadata can describe objects such as information resources or data.   |

$$a_{ij}a_{jk} = a_{ik} \quad 1 \leq i, j, k \leq n. \quad (3)$$

In case of inconsistency, the following indicators are calculated:

$$CI = \frac{\lambda_{\max}(A) - n}{n - 1}, \quad (4)$$

$$CR = \frac{CI}{RI}.$$

Among them,  $RI$  is only related to the matrix order  $n$ , which can be obtained by specific query.

Judgment method: when there is only  $CR < 0.1$ , the inconsistency degree of paired comparison matrix is satisfactory and can be accepted; otherwise, we will continue to adjust the pair comparison matrix until we are satisfied.

The method of calculating the maximum eigenvalue of paired comparison matrices:

$$U_k = \frac{\sum_{j=1}^n a_{kj}}{\sum_{i=1}^n \sum_{j=1}^n a_{ij}},$$

$$U = (u_1, u_2, \dots, u_n)^z \quad (5)$$

$$\lambda = \frac{1}{n} \sum_{i=1}^n \frac{(AU)_i}{u_i} = \frac{1}{n} \sum_{i=1}^n \frac{\sum_{j=1}^n a_{ij} u_j / u_i}{\sum_{j=1}^n a_{ij} u_j / u_i}.$$

**2.4.4. Hierarchical Total Sorting [23].** For example, after a series of calculations in the previous three steps,  $y_1, y_2, y_3$  are sorted to give a decision.

$$y_3 > y_1 > y_2, \text{ choose } y_3. \quad (6)$$

**2.5. NDVI and SPEI.** NDVI [24], the Chinese name is normalized vegetation index. Using this index in this study, we can reflect the coverage degree of surface vegetation and the growth of vegetation; at the same time, it is also one of the important indicators reflecting the growth and nutrition information of crops. In the calculation process, the spectral reflection characteristics of different bands are mainly used. If  $NIR$  is the reflection value in the near infrared band and  $R$

is the reflection value in the red band, the definition formula of normalized vegetation index can be obtained as follows:

$$NDVI = \frac{NIR - R}{NIR + R}. \quad (7)$$

The range of NDVI values is  $[-1, 1]$ . A positive value represents plant coverage, and the greater the calculated NDVI value, the greater the vegetation density; the smaller the NDVI value, the smaller the vegetation density. Therefore, in this study, we can reasonably choose suitable plants for cultivation in gardens according to the monitored vegetation coverage, which is of great significance. Of course, it is not completely appropriate for practical application to calculate only by definition. Therefore, there are several NDVI estimation models as follows:

#### 2.5.1. Modis Algorithm [25]

$$NDVI = \frac{\text{Band}_2 - \text{Band}_1}{\text{Band}_2 + \text{Band}_1}. \quad (8)$$

#### 2.5.2. TM/ETM Algorithm

$$NDVI = \frac{\text{Band}_4 - \text{Band}_3}{\text{Band}_4 + \text{Band}_3}, \quad (9)$$

$$NDVI = \frac{CH_2 - CH_1}{CH_2 + CH_1}.$$

**2.5.3. AVHRR Algorithm.** We can use the standardized precipitation evapotranspiration index (SPEI) to assess the temporal and spatial effects of drought on soil wetness. The larger the SPEI value, the wetter the area is. The smaller the value, the drier the area. It can provide great reference significance when selecting plants.

$$SPEI = w - \frac{C_0 + C_1 w + C_2 w^2}{1 + d_1 w + d_2 w^2 + d_3 w^3}. \quad (10)$$

### 3. Landscape Design Based on GIS

According to the goal of green city, the overall design is carried out, and the urban landscape elements are analyzed

TABLE 2: Model comparison.

| Model name                | Disadvantages  |
|---------------------------|--|
| Scale model               | The layout of the model is simple and easy to understand. The final effect is intuitive, but it is easy to be constrained by boundaries; No spatial change can be seen, and the transportation distance and cost cannot be calculated; Layout optimization is incompetent and difficult. |
| Distance model            | The calculation of this model is simple, and it is difficult to accord with the actual situation only by measuring the rationality of distance in planning. Unable to find the best location.  |
| Location allocation model | This model is suitable for simple problems, and the optimal conclusion is obtained by comparing them one by one. If the amount of data is large, the amount of computation increases and the problem is complex, there may not be an optimal solution.                                   |

by using ArcGIS software in GIS system. It is necessary to consider the site selection and specific functions of scenery, the flow of vehicles and people, and the convenience of transportation are also necessary to consider the integration and coordination between the landscape architecture and the surrounding environment, and the selection of plants in the landscape. After considering all the above factors, it is necessary to use the AHP method to evaluate the whole landscape concretely, and the designer will make corresponding adjustments and designs for landscape planning according to the feedback obtained.

3.1. *Location Model.* Landscape planning needs to choose a suitable geographical location in the city. Due to the complexity of the spatial layout, we usually simplify and eliminate unnecessary related objects, establish a clear model, and carry out specific analysis process in this model.

3.1.1. *Scale Model*

$$p = \frac{D_n}{S_n}, \tag{11}$$

where  $S_n$  is the total number of existing facilities in the study area and  $D_n$  is the total number of required facilities.

3.1.2. *Distance Model*

$$D_{ij} < \rho, \tag{12}$$

where  $D_{ij}$  is the distance from the facility supply position to the service demand position. Satisfaction means reasonable spatial layout.

3.1.3. *Location Allocation Model*

$$\min Z = \sum_i \sum_j a_i d_{ij} x_{ij}, \tag{13}$$

where  $a_i$  is the weight of the  $i$ -th demand point;  $d_{ij}$  is the distance;  $x_{ij}$  is the decision variable. The ultimate goal is to find the minimum value of the objective function, that is, the minimum weighted distance.

Three spatial models are compared, as shown in Table 2:

In view of the shortcomings of the three models the problems we need to solve were , cleared and finally we choose to build a multicriteria decision-making location

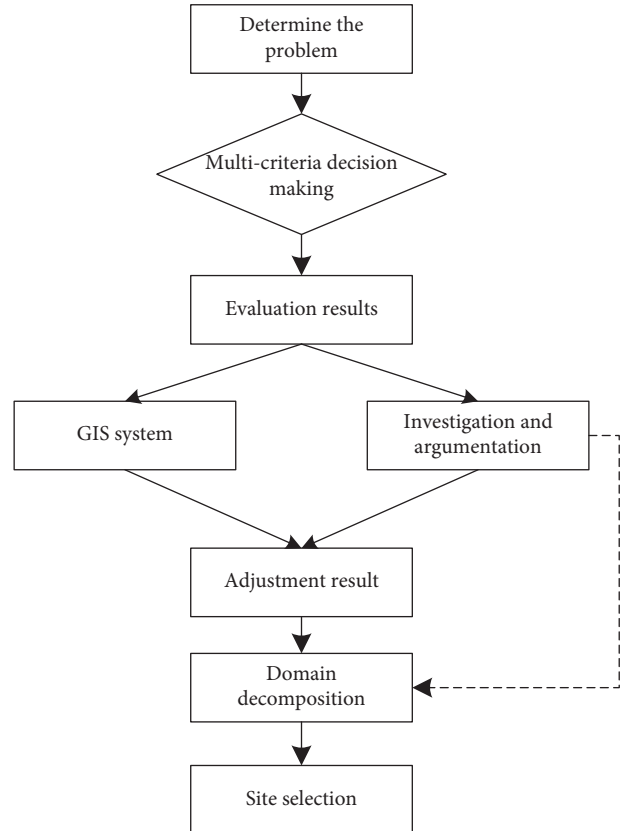


FIGURE 3: Optimal location model in this paper.

model based on the GIS system. Based on the GIS system and the method of investigation and demonstration, Dijkstra algorithm is used to solve the shortest path, and a single optimal address is obtained through a series of solutions, as shown in Figure 3:

Shortest path:

$$d(v_i, x) = \min\{d(v_i, v_p) + b(v_p, x), d(v_i, v_q) + b(v_q, x)\}. \tag{14}$$

Build a mathematical model:

$$\begin{aligned} \min & \sum_{i=1}^n h_i d(v_i, x), \\ \text{s.t.} & \max_{1 \leq i \leq n} d(v_i, x) \leq \lambda \quad x \in G, \end{aligned} \tag{15}$$

where  $G$  is a tree and the solution is simple:

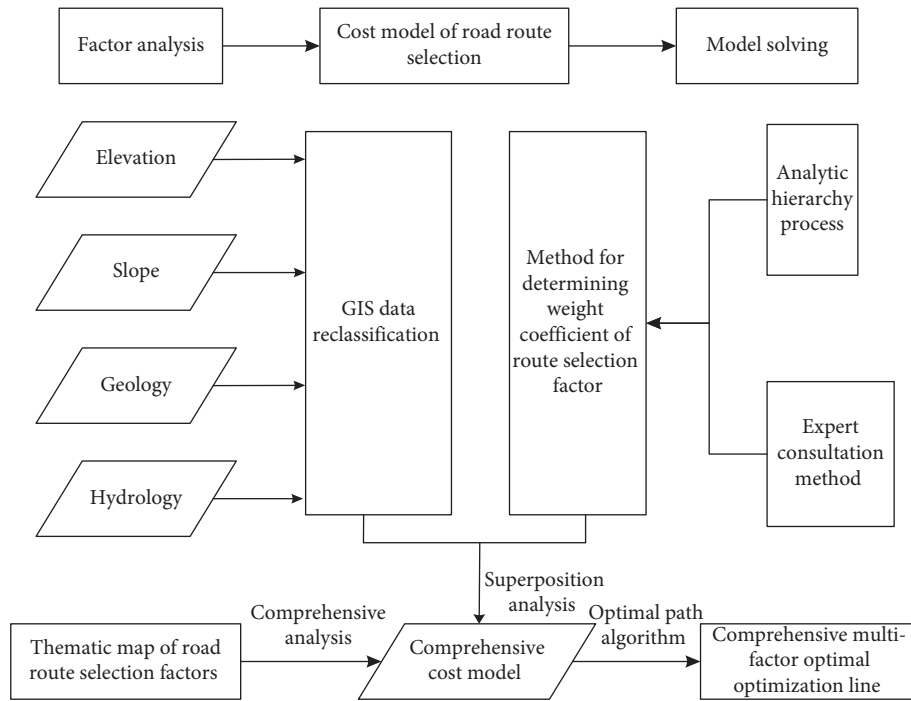


FIGURE 4: Multifactor comprehensive model of the garden route.

$$d(v_i, x): G \longrightarrow R \text{ Is a convex function.} \quad (16)$$

$G$  is a general network, which is complicated to solve:

$$d(v_i, x): G \longrightarrow R \text{ Is not a convex function.} \quad (17)$$

**3.2. Garden Route Design.** Determining the road route is the most important basic work to connect the whole landscape. Therefore, we need to give full consideration to the road route arrangement of urban landscape. To fully consider a variety of factors that can affect the road, it must be reasonable in the economy and also ensure green environmental protection. The whole garden keeps coordination in the environment and finally achieves the goal of people-orientation. Using the powerful function of the computer to choose the most suitable garden route, reduce the

investment of capital cost and the waste of manpower and material resources. As shown in Figure 4:

Four single factors related to road route determination are considered comprehensively. The weight of each factor is determined by the analytic hierarchy process and expert consultation. On this basis, using GIS system, the map of each topic is analyzed by weight superposition, and the comprehensive cost model is established. Finally, through this model, the optimal route design is selected. Using the Raster Calculator function of ArcGIS software and Spatial Analyst module. Calculation model:

$$S = \sum_{i=1}^n F_i W_i (i = 1, 2, \dots, n). \quad (18)$$

Based on the raster data, the optimal road path is analyzed. Mathematical model:

$$W(P) = \sum_{e \in E(P)} \omega(e), \left\{ \begin{array}{l} \min \sum_{(v_i, v_j) \in E} a_{ij} x_{ij}, x_{ij} \geq 0, \\ \sum_{(v_i, v_j) \in E} x_{ij} - \sum_{(v_i, v_j) \in E} x_{ji} = \begin{cases} 0, & i = 1 \\ 0, & 2 \leq i \leq n-1 \\ -1, & i = n \end{cases} \end{array} \right. \quad (19)$$

**3.3. Landscape and Architectural Analysis.** When the landscape architecture is built, the original ecological environment in the city will be destroyed. To conform to the spirit of green urbanism, the designers in this study can measure the conspicuous degree of landscape and the clarity of attention with the help of a landscape sensitivity method. The most valuable ecological features to the

greatest extent are preserved, people are shown the best landscape vision, and people are let enjoy the beautiful scenery of the garden. In addition, to coordinate construction and protection, we also need to pay attention to the height of buildings and landscape buildings around the city and architectural planning with the help of the GIS system.



(1) Slope landscape sensitivity

$$Sa = \sin \cdot \alpha \quad (0^\circ \leq \alpha \leq 90^\circ). \quad (20)$$

(2) Distance landscape sensitivity

$$Sd = \begin{cases} 1, d \leq D, \\ \frac{D}{d}, d > D. \end{cases} \quad (21)$$

(3) Visual probability landscape sensitivity

$$St = \frac{t}{T}, \quad (22)$$

$$St = \frac{l}{L}.$$

(4) Comprehensive analysis of landscape sensitivity

$$S = k_1 Sa + k_2 Sd + k_3 St. \quad (23)$$

“Plants” are the most important part of landscape composition. The landscape in the garden is not single, and the actual terrain is complex. The choice of plants should adapt to local conditions and follow the general law of plant growth. With the help of the GIS system, factors such as light, temperature, moisture, and soil are fully considered, and indicators such as NDVI and SPEI are used to provide scientific suggestions for the scientific cultivation of plants so that plants can grow and form beautiful landscapes. As shown in Table 3:

3.4. *Construction of the Evaluation System.* It is very important to construct the evaluation system of landscape architecture for the evaluation and optimization of landscape architecture ability. Function expression:

$$A = \sum_{k=1}^m B_k E_k = \sum_{k=1}^m \left( \sum_{j=1}^n c_j D_j \right) E_k. \quad (24)$$

We set the following landscape evaluation indicators. As shown in Table 4:

## 4. Experimental Analysis

The experimental project of this study is to create a natural landscape that meets the requirements of a green city in a city. It is necessary not only to meet the needs of citizens for daily play and recuperation but also to show the city’s characteristic culture, pay attention to the ecological harmony between man and nature, and give the city a green leisure comprehensive scenic spot.

4.1. *Reasonable Degree of Site Selection.* A suitable place is chosen in the city for garden transformation. According to geography, space, length, topography, convenient transportation, and other factors, the experiment uses the multidecision site selection model based on the GIS system and

TABLE 3: Influencing factors of plant selection.

| Influencing factors of garden plant design |                              |
|--|------------------------------|
| Climate                                    | Illumination                 |
|  | Precipitation                |
|  | Temperature and humidity     |
| Region                                     | Soil type                    |
|  | Topography and geomorphology |
|  | Nutrient content             |
| Microenvironment                           | Plant disturbance            |
|  | Microbial interference       |
|  | Abiotic action               |

gives three garden site selection sites: A, B, and C. The location of these three locations in the city environment is a relatively good place, and then through expert interviews and public questionnaires, we carried out the evaluation of the reasonable degree of site selection, as shown in Figure 5:

We use the 10-point scoring standard to comprehensively evaluate the scores of models, experts, and citizens, and find that the comprehensive scores of A, B, and C are about 8.81, 8.97 and 8.53. Among them, location B scored the highest; among the scores given by models, experts, and citizens. Location B is also the most popular and the best choice location.

### 4.2. Master Plan of Landscape Architecture

4.2.1. *Landscape Sensitivity Synthesis.* According to the GIS system and relevant design experts, the weights of slope landscape sensitivity ( $Sa$ ), distance landscape sensitivity ( $Sd$ ), and visual probability landscape sensitivity ( $St$ ) can be determined As shown in Figure 6:

$$S = 0.3Sa + 0.3Sd + 0.4St. \quad (25)$$

According to the comprehensive landscape sensitivity ( $S$ ) stratification in each class, we can divide the landscape sensitivity areas in the landscape, as shown in Table 5:

All the land in the garden planning area is divided according to the classification table. We can clearly see the different sensitivity levels in different regions, as shown in Figure 7:

The higher the sensitivity of landscape, the more scenery tourists see and the more it is suitable for sightseeing. Class I landscape sensitive areas account for 35.10% of the total planned garden area, and basically the best viewing areas are all over the two sides of the road. Among them, the sensitive land area of scenic appreciation area is as high as 14.80%. Class II and Class III landscape sensitive areas are mainly scenic sightseeing and cultural entertainment areas, accounting for 33.70% and 26.60% of the total planned garden area respectively. Level IV area is only 5% of the land area, scattered in various areas, with the lowest viewing value, which is difficult to be developed and visited.

4.2.2. *Landscape Functional Zoning.* According to the needs of gardens, based on the original mountain vegetation and water flow area, most of the mountains and ecological

TABLE 4: Landscape evaluation index.

| Criterion layer (B)        | Weight | Factor layer (C)                               | Weight |
|----------------------------|--------|--|--------|
| Ecological benefits (B1)   | 0.365  | Plant species richness (C1)                    | 0.052  |
|                            |        | Green coverage area (C2)                       | 0.086  |
|                            |        | Species diversity (C3)                         | 0.030  |
|                            |        | Water body area (C4)                           | 0.084  |
|                            |        | Completeness of ecological elements (C5)       | 0.032  |
|                            |        | Landscape Ecological Sustainability (C6)       | 0.081  |
| Aesthetic Experience (B2)  | 0.163  | Plant landscape level and color change (C7)    | 0.062  |
|                            |        | Harmony between plants and hard landscape (C8) | 0.053  |
|                            |        | Diversity of ornamental characteristics (C9)   | 0.048  |
| Behavioral perception (B3) | 0.242  | Accessibility of scenic spots (C10)            | 0.065  |
|                            |        | Landscape Scale Comfort (C11)                  | 0.072  |
|                            |        | Interaction between people and landscape (C12) | 0.056  |
|                            |        | Road density (C13)                             | 0.049  |
| Social function (B4)       | 0.230  | Infrastructure integrity (C14)                 | 0.083  |
|                            |        | Recreational and sports facilities (C15)       | 0.037  |
|                            |        | Service leisure facilities (C16)               | 0.067  |
|                            |        | Disaster prevention and refuge (C17)           | 0.043  |

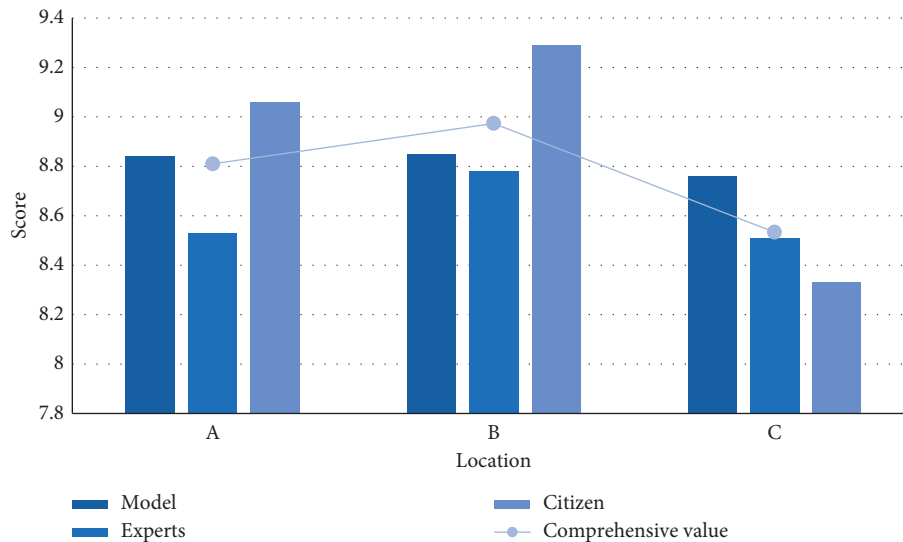


FIGURE 5: Comparison of site selection rationality.

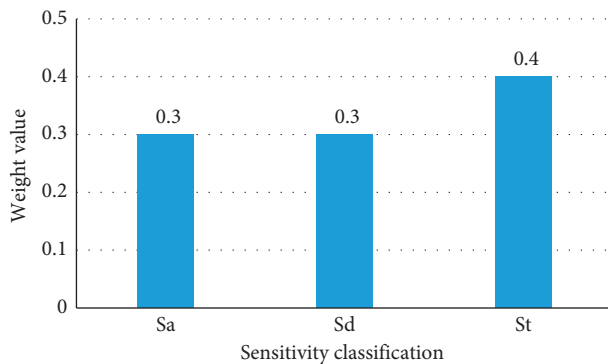


FIGURE 6: Sensitivity weights.

landscapes are preserved, such as digging and starting work are reduced and the damage to the soil and vegetation is minimized. It is divided into the following five regions (12

landscape spots in total): (1) building area: the areas with a poor environment are developed into building areas, artificial greening, and cultivation are used to restore the environment, and the landscape effect and atmosphere are set off by combining human landscape. (2) Cultural and entertainment areas: at the same time, exhibition education with cultural characteristics will be carried out, and activity areas for citizens to play and recuperate will be developed. (3) Economic and industrial zone: the land with great economic utilization value will be developed into an economic and industrial zone to drive the economic development of the city. (4) Ecological restoration area: natural protection and ecological restoration are carried out for some landscapes that have no development value but have been ecologically damaged. (5) Landscape appreciation area: transform the remaining landscape for viewing and sight-seeing, as shown in Figure 8:

TABLE 5: Landscape sensitivity grading.

| S Classification | Distribution and characteristics   |
|------------------|--|
| I                | In the visible area of close-range zone ( $0m \leq d < 100m$ ) or steep slope ( $30^\circ \leq \alpha < 90^\circ$ )                              |
| II               | Except grade I, in the visible area of close-range zone or middle-range zone ( $100m \leq d < 200m$ ) or ( $14.5^\circ \leq \alpha < 30^\circ$ ) |
| III              | Except grade ii, in the near, middle and long-term zones ( $200m < d$ ) or ( $\alpha < 14.5^\circ$ )   |
| IV               | Invisible area   |

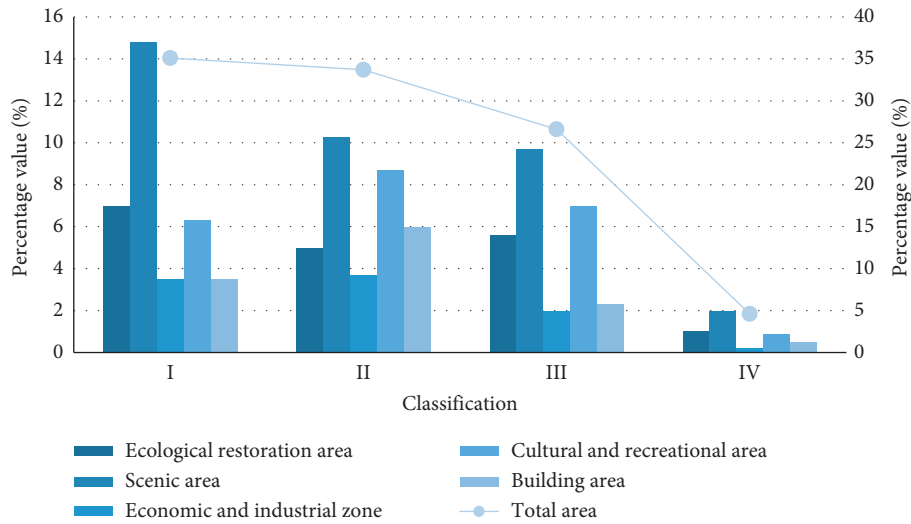


FIGURE 7: Sensitive area of planned land use.

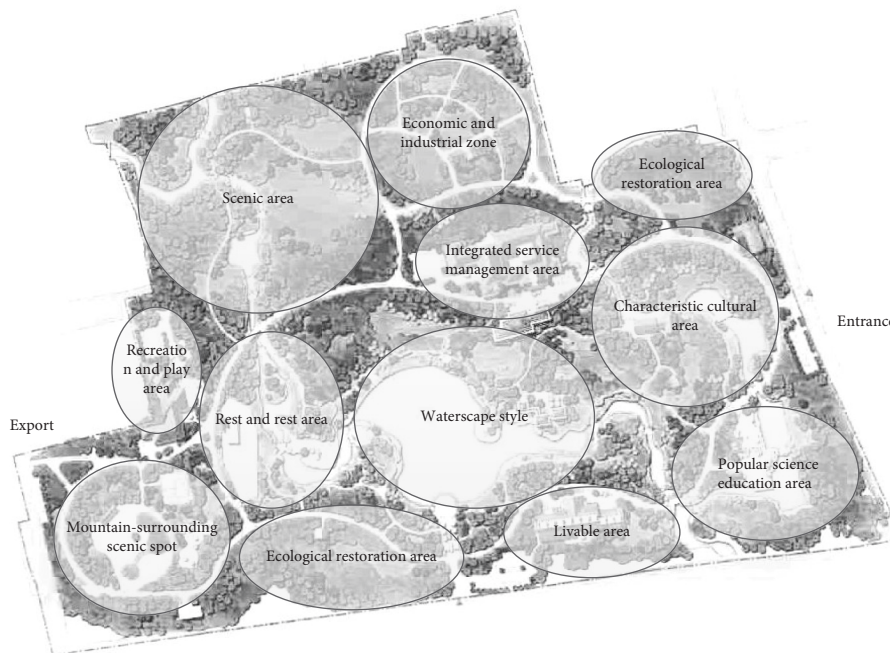


FIGURE 8: Functional structure of landscape in a city.

4.3. Facilitation Analysis of Route Design. Based on ArcGIS software and route multifactor comprehensive model, we got the total design of the garden route in this experiment. As shown in Figure 9:

To explore the rationality and convenience of route setting in more detail, we measure the coincidence between

the specific actual road condition construction and the route given by the model and the route selected by experts. Twelve landscape spots were set for wiring, and the feelings of citizens in five groups (200 people in each group, 1000 people in total) were comprehensively considered, as shown in Figure 10:

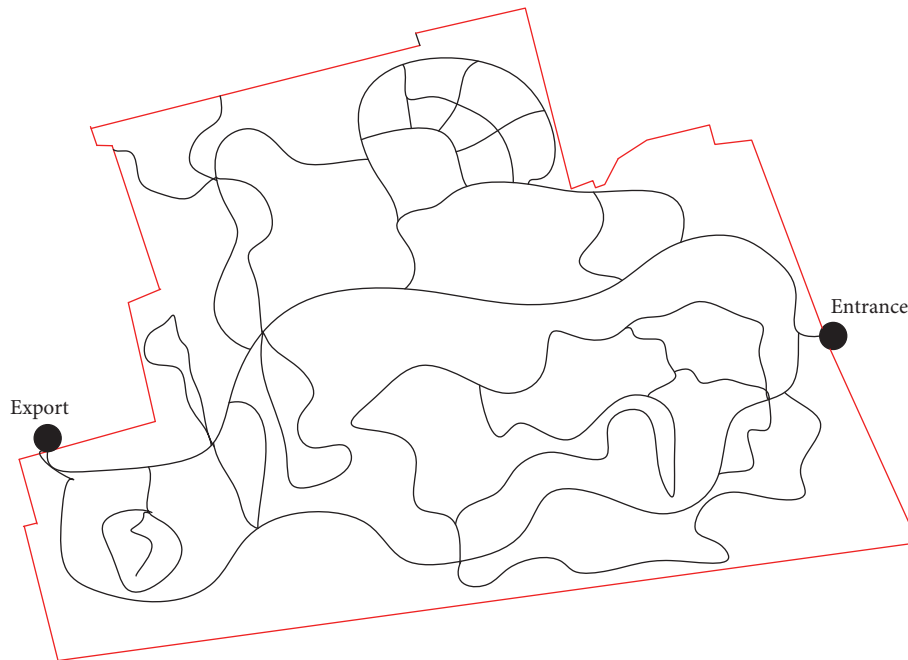


FIGURE 9: Schematic diagram of garden route plan.

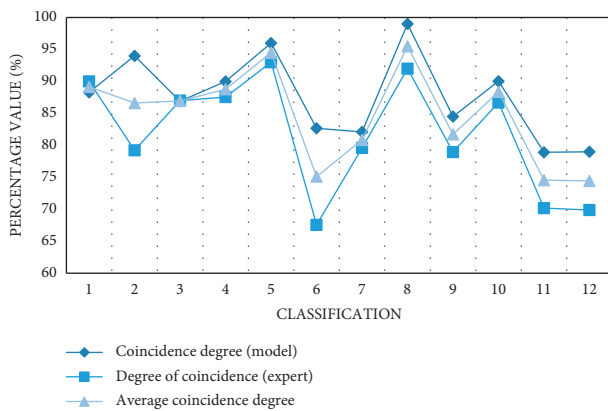


FIGURE 10: Determination of route coincidence.

We can find from Figure 10 that the garden route given by the model is the most consistent with the actual road conditions, with a coincidence degree of about 87.62%, while the coincidence degree of the route given by experts is about 81.81%. Their average coincidence was 84.71%. This shows that the optimal path given by the model through multi-factor consideration is effective and feasible, and has a high practical value.

With the 10-point scoring system, each citizen has different situations, so his subjective evaluation is different. The comprehensive score for each landscape spot is between 7 and 9 points. This shows that the route setting basically meets the travel needs of citizens, as shown in Figure 11:

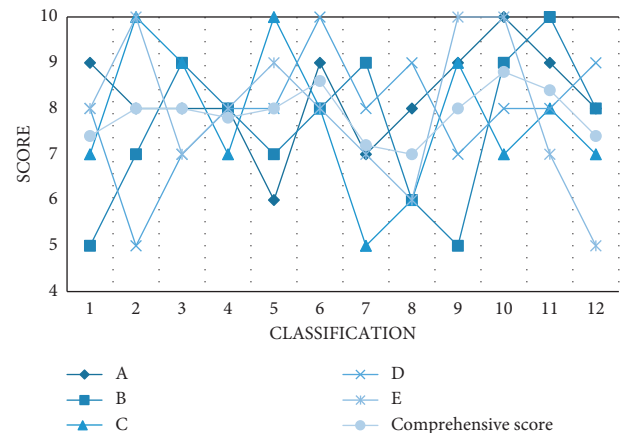


FIGURE 11: Route satisfaction measurement.

NDVI in recent 10 years from 2011 to 2020. The plant cover in the scenic area and the economic and industrial area increased with the increase in the number of years, indicating that precipitation and vegetation grew well. However, the plant coverage in ecological restoration areas and building areas decreases sharply, and the environment is harsh, as shown in Figure 12.

Therefore, in terms of plant selection, we mainly choose drought-resistant, wind-resistant, and sun-loving plants in ecological restoration areas and building areas to stabilize water and soil and restore the original ecological environment. For other areas, we choose to keep the original tree species and plants without making too many ecological changes. More water-resistant plants can be planted in water flow areas, while flower lawns and sparse forest landscapes can be created in flat areas.

4.4. *Vegetation Analysis.* We count the SPEI trend and NDVI of the landscape planning area in the past 10 years, as shown in Table 6:

TABLE 6: SPEI change trend statistics/%.

| Project               | Variation trend of SPEI in years and seasons |        |        |        |        |
|-----------------------|--|--------|--------|--------|--------|
|                       | Year   | Spring | Summer | Autumn | Winter |
| Increasing trend      | 8  | 22     | 36     | 33     | 38     |
| Significant increase  | 6  | 3      | 3      | 4      | 6      |
| Reducing trend        | 4  | 31     | 64     | 62     | 52     |
| Significant reduction | 2  | 53     | 12     | 19     | 7      |

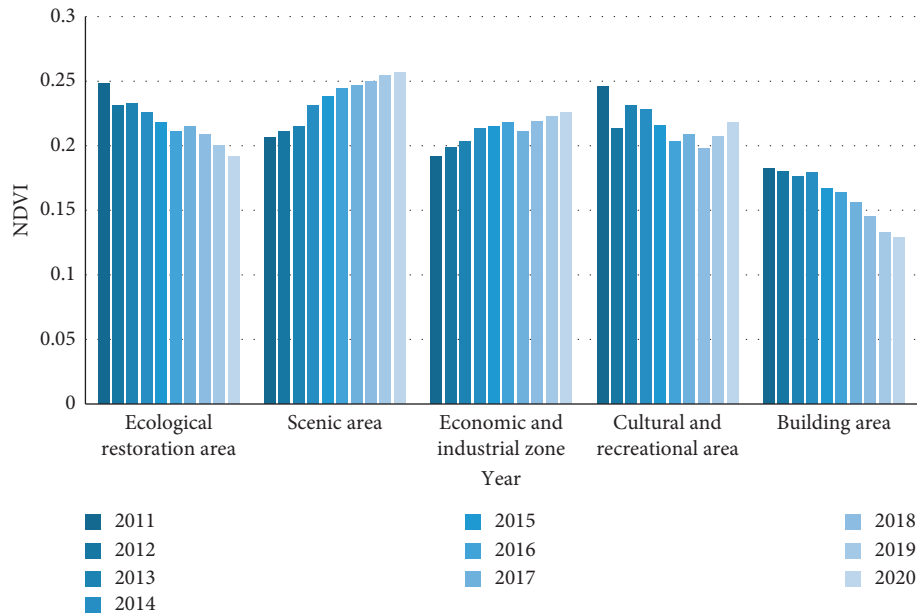


FIGURE 12: NDVI situation.

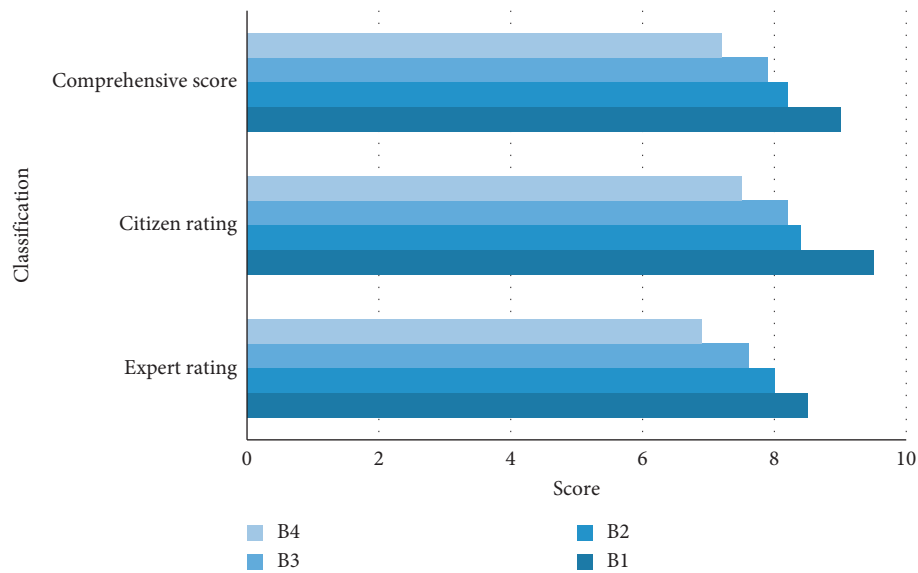


FIGURE 13: Landscape scoring statistics (B index).

4.5. Evaluation and Analysis. The indexes in the evaluation system of landscape architecture are scored. Citizen scores are generally higher than expert scores. In the

comprehensive score, the score of the ecological benefit index is the highest, up to 9 points, which shows that gardens give people real comfort for landscape design and ecological

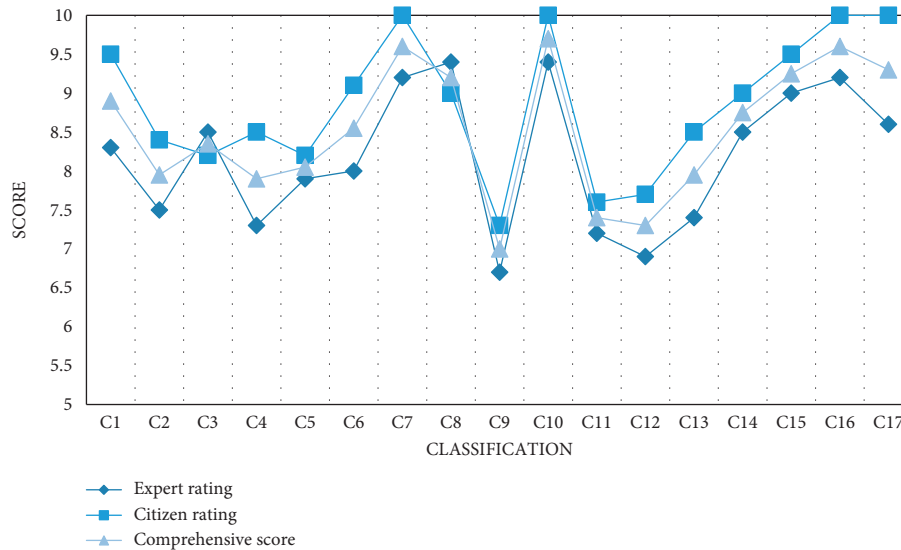


FIGURE 14: Landscape scoring statistics (C index).

protection. The aesthetic experience index is as high as 8.2, and aesthetics has been recognized by experts and the public. The score of behavior feeling is 7.9, which is slightly lower and should be given more attention and changes. The effect of social function is the worst, with a score of 7.2, and related facilities and equipment should be further improved in the follow-up. The C-grade index scores are all greater than 7 points, which shows that it basically meets the requirements of landscape design, and has been generally recognized by experts and the public in rationality, as shown in Figures 13 and 14:

## 5. Conclusion

In this study, the concept of green city is integrated into landscape design and the GIS system is used to improve the original traditional design method, which has a strong innovative concept. The research results of this study show the following:

- (1) To choose a reasonable landscape location for a city, it is necessary to build a multidecision site selection model through the GIS system. Taking full account of the opinions and scores of experts, models, and citizens, the B site with a score as high as 8.97 is selected as the site selection for landscape design from three sites: A, B, and C.
- (2) Using comprehensive landscape sensitivity to divide the land use value. The garden area is divided into four levels, and the functions of the different sensitive levels are different, so as to find the best landscape vision. Following the general law of ecological environment, five scenic functional areas and 12 landscape spots are divided. According to SPEI and NDVI, the cultivated plants and landscapes were selected.
- (3) design a multifactor comprehensive model of the garden route and give the master plan of the garden route. According to the actual road conditions, the rationality and convenience of the route is explored.

The coincidence degree of the model is about 87.62%, and the effect is very good. Citizens' satisfaction with the route is between 7 and 9 points, and the comprehensive evaluation is high.

- (4) construct a landscape evaluation system with 4 B-level indexes and 17 C-level indexes. Both B-level index and C-level index are higher than 7 points, which is in line with the expectations of the public and experts. Subsequent optimization can be optimized and fed back according to index details.

The final experimental results prove the feasibility and superiority of this method. Although GIS technology has been widely used, relying solely on the use of the GIS system for landscape design will cause aesthetic defects. This requires the designer to measure subjectively. In addition, due to the problem of network security, the GIS system should also strengthen the security work to avoid the risk of data leakage caused by some interference factors.

## Data Availability

The experimental data used to support the findings of this study are available from the corresponding author upon request.

## Conflicts of Interest

The authors declare that they have no conflicts of interest regarding this work.

## References

- [1] K. Ogrodnik and Ł. Kolendo, "Application of gis technology and AHP to determine the areas with fully developed, compact functional and spatial structure: a case study of Bialystok, Poland," *Land Use Policy*, vol. 109, no. 11, Article ID 105616, 2021.
- [2] T. Liu, "Natural suitability evaluation of habitat environment in transition zone based on GIS spatial analysis technology-taking beichun county as an example [J]," *Journal of Earth*

- Science and Environmental Protection (English)*, vol. 9, no. 8, p. 12, 2021.
- [3] M. Yu, "Research on urban landscape planning method based on GIS," *International Journal of Environmental Technology and Management*, vol. 24, no. 3/4, pp. 248–263, 2021.
  - [4] H. Zhou and Z. Dai, "Green urban garden landscape simulation platform based on high-resolution image recognition technology and GIS," *Microprocessors and Microsystems*, vol. 82, Article ID 103893, 2021.
  - [5] D. Yao, "Application of GIS remote sensing information integration in eco-environmental quality monitoring," *International Journal of Environmental Technology and Management*, vol. 24, no. 5/6, pp. 375–389, 2021.
  - [6] X. Sun, "Green city and regional environmental economic evaluation based on entropy method and GIS," *Environmental Technology & Innovation*, vol. 23, no. 9, p. 7, Article ID 10166, 2021.
  - [7] G. Mutani and V. Todeschi, "GIS-based urban energy modelling and energy efficiency scenarios using the energy performance certificate database," *Energy Efficiency*, vol. 14, no. 5, pp. 1–28, 2021.
  - [8] L. Yu, X. Xie, and L. Wei, "Green urban garden landscape design and soil microbial environmental protection based on Virtual Visualization System," *Arabian Journal of Geosciences*, vol. 14, no. 12, pp. 1–16, 2021.
  - [9] E. E. Mironova, "GIS modeling of green infrastructure of mediterranean cities for the management of urbanized ecosystems," *Arid Ecosystems*, vol. 11, no. 2, pp. 149–155, 2021.
  - [10] X. Han and J. Qi, "Application of GIS technology in landscape architecture design--Taking the design of Libo World Natural Heritage theme park in karst of South China as an example," *Engineering Construction and Design*, vol. 2, no. 18, pp. 26–27, 2020.
  - [11] X. Tang, X. Liu, and L. Zheng, "Study on route selection of scenic roads in mountainous areas of southern Anhui based on GIS-AHP," *Journal of Inner Mongolia Agricultural University (Natural Science Edition): Natural Science Edition*, vol. 41, no. 5, p. 7, 2020.
  - [12] S. Wang, Y. Gao, S. Liang et al., "Ecological sensitivity evaluation of Qingcheng Mountain-Dujiangyan scenic spot based on GIS," *Metallurgical Series*, vol. 005, no. 002, pp. 243–244, 2020.
  - [13] S. Huang, Q. Hu, and H. Li, "Ecological risk assessment of Mount Emei scenic spot based on RS and GIS," *Environmental Science Research*, vol. 33, no. 12, pp. 2745–2751, 2020.
  - [14] C. Xue, "Preliminary study on the application of GIS in landscape architecture in the era of science and technology," *Science and Technology Economic Guide*, vol. 28, pp. 26–27, 2020.
  - [15] Q. Zhu, "Discussion on teaching reform of landscape architecture GIS technology application course based on curriculum ideological and political education," *Asia-Pacific Education*, vol. 2, no. 17, pp. 84–85, 2021.
  - [16] G. Chen, L. Wang, and M. M. Alam, "Intelligent group prediction algorithm of GPS trajectory based on vehicle communication," *IEEE Transactions on Intelligent Transportation Systems*, vol. 22, no. 7, pp. 3987–3996, 2020.
  - [17] Z. Shi and K. Lv, "Green highway evaluation based on Big Data GIS and BIM technology," *Arabian Journal of Geosciences*, vol. 14, no. 11, pp. 1–15, 2021.
  - [18] C. Liu and R. Zhao, "Study on land ecological assessment of villages and towns based on GIS and remote sensing information technology," *Arabian Journal of Geosciences*, vol. 14, no. 6, pp. 1–10, 2021.
  - [19] W. Huang, J. Ren, T. Yang, and Y. Huang, "Research on urban modern architectural art based on artificial intelligence and GIS image recognition system," *Arabian Journal of Geosciences*, vol. 14, no. 10, pp. 1–13, 2021.
  - [20] J. Shao and H. Yan, "Retracted ARTICLE: evaluation of urban land green utilization efficiency with a view of GIS images," *Arabian Journal of Geosciences*, vol. 14, no. 7, p. 629, 2021.
  - [21] A. K. Abd El Aal, M. Kamel, and S. H. Alyami, "Environmental analysis of land use and land change of najran city: GIS and remote sensing," *Arabian Journal for Science and Engineering*, vol. 45, no. 10, pp. 8803–8816, 2020.
  - [22] X. Xu, Z. Zhang, T. Long, S. Sun, and J. Gao, "Mega-city region sustainability assessment and obstacles identification with GIS-entropy-TOPSIS model: a case in Yangtze River Delta urban agglomeration, China," *Journal of Cleaner Production*, vol. 294, Article ID 126147, 2021.
  - [23] X. Bai, "Virtual garden landscape planning based on FPGA and GIS platform," *Microprocessors and Microsystems*, vol. 79, Article ID 103314, 2020.
  - [24] X. Jiang, S. Fan, L. Huang et al., "Study on landscape ecological evaluation of bamboo forest park based on GIS--A case study of Yixing Zhuhai Scenic Spot," *Acta Bamboo Sinica*, vol. 39, no. 4, p. 10, 2020.
  - [25] X. Ning, K. Gong, W. Li, L. Zhang, X. Bai, and S. Tian, "Feature refinement and filter network for person re-identification," *IEEE Transactions on Circuits and Systems for Video Technology*, vol. 31, no. 9, pp. 3391–3402, 2021.

## Research Article

# Basketball Motion Posture Recognition Based on Recurrent Deep Learning Model

FeiPeng Liu<sup>1</sup> and Wei Zhang <sup>2</sup>

<sup>1</sup>Changsha Medical University, Changsha 410219, Hunan, China

<sup>2</sup>Zhengzhou University, Zhengzhou 450000, Henan, China

Correspondence should be addressed to Wei Zhang; zhangwei0909@zzu.edu.cn

Received 28 March 2022; Revised 19 April 2022; Accepted 25 April 2022; Published 16 May 2022

Academic Editor: Man Fai Leung

Copyright © 2022 FeiPeng Liu and Wei Zhang. This is an open access article distributed under the Creative Commons Attribution License, which permits unrestricted use, distribution, and reproduction in any medium, provided the original work is properly cited.

In order to improve the training effect of athletes and effectively identify the movement posture of basketball players, we propose a basketball motion posture recognition method based on recurrent deep learning. A one-dimensional convolution layer is added to the neural network structure of the deep recurrent Q network (DRQN) to extract the athlete pose feature data before the long short-term memory (LSTM) layer. The acceleration and angular velocity data of athletes are collected by inertial sensors, and the multi-dimensional motion posture features are extracted from the time domain and frequency domain, respectively, and the posture recognition of basketball is realized by DRQN. Finally, the new reinforcement learning algorithm is trained and tested in a time-series-related environment. The experimental results show that the method can effectively recognize the basketball motion posture, and the average accuracy of posture recognition reaches 99.3%.

## 1. Introduction

In the process of basketball training and competition, coaches need to formulate corresponding training plans according to the individual conditions of different players to improve the players' basketball skills. The traditional training method is that coaches formulate training plans based on their own training theory and training experience, combined with the skill level of basketball players [1]. This training mode is highly subjective, and coaches need to spend a lot of time analyzing the posture of athletes, and it is difficult to objectively evaluate the training effect of athletes [2]. The core of modern physical training is precision and efficiency. If the coach can accurately control the movement posture of the athlete, the training effect can be greatly improved. Therefore, collecting and analyzing the posture data of basketball players and accurately identifying the movement posture has significant significance for improving the scientificity of the coaches' training plan and improving the training effect of the athletes, which is a new research direction [3].

With the rapid development of computer computing power, it has become possible to introduce deep learning into reinforcement learning to solve continuous state space problems. In 2015, the deep Q-network (DQN) proposed by Mnih and colleagues solved the instability problem by employing experience replay and target network techniques, reaching the level of human players on more than 2,600 Atari games, bringing depth. Since then, various improvements to DQN have emerged. Reference [4] proposes priority experience replay, which allows important experience to be used more frequently, thereby improving the efficiency of reinforcement learning. The deep double-Q network proposed by [5] in 2016 solves the problem of overestimation. In the same year, literature [6] added a competitive structure to DQN, which improved the learning efficiency of DQN. This DQN with a competitive structure is called a competitive deep Q-network [7].

DQN and its derived reinforcement learning algorithms have already been regarded as powerful algorithms, and in many areas, such as simple 2D games, the performance is



beyond the level of ordinary people. However, this excellent performance often only stays in the environment of artificially specified rules, such as most chess and games and other fields. DQN still has problems that are difficult to implement in real-world problems. This is own to in the past research on reinforcement learning algorithms, we usually default to the state of the environment that we can fully obtain. But in the real world, we obviously don't have the God's perspective like in chess and games, and our acquisition of the state of the environment is obtained through observation. However, there will inevitably be information errors or even loss in observation, which makes it impossible to obtain a complete state through observation. At this time, the performance of the DQN based on the Markov decision process will naturally be greatly affected.

In order to solve the above problems, reference [8] proposed a deep recurrent Q network (DRQN), and on the basis of DQN, the first fully connected layer was changed to a long short-term memory (LSTM) layer of the same size, which solved the problem of reality environmental part observation problem. To solve the contradiction between reinforcement learning and feedback neural network parameter update, Matthew Hausknecht et al. proposed two matching parameter update methods: sequential bootstrap update and random bootstrap update. In the partially observed Markov environment, DRQN has a significant improvement over DQN.

Basketball motion posture recognition is a kind of human gesture recognition. At present, the methods of human posture recognition mainly include two categories: posture recognition based on inertial sensors and posture recognition based on image acquisition. Posture recognition based on image acquisition can be divided into monocular video recognition and multi-eye video recognition according to the number of image acquisition devices. The general idea of image capture gesture recognition is to first use the camera to capture the image or video of the athlete, and then extract the motion features hidden in the image and video. Finally, a classifier is designed to recognize the sports posture of athletes [9–13]. The image acquisition posture recognition technology has a relatively high maturity, and the accuracy of posture recognition is also very high. However, the defects of this type of method are that there are dead spots in video surveillance, a large amount of equipment, and a heavy data processing burden, which is not conducive to popularization and application [14]. The basic idea of inertial sensor recognition is that the athlete wears a simple and lightweight data acquisition sensor, sends the collected data to the processing terminal in real time, and recognizes the athlete's posture according to various posture data [15]. This kind of method can make up for the shortcomings of image acquisition and recognition, has low requirements on the use environment and high recognition efficiency, and has become a hot method in basketball posture recognition research.

Based on these studies, we propose a basketball motion posture recognition method based on inertial sensors and DRQN. First, a data acquisition module of basketball motion posture based on inertial sensor is designed, and the features for basketball motion posture recognition are extracted from

time domain and frequency domain, respectively. Then, we build a posture recognition model for basketball players based on one-dimensional convolutional layers and DRQN. Finally, we conduct experiments and evaluations on the model, and the experimental results verify the effectiveness and accuracy of the method.

## 2. Background

*2.1. Deep Recurrent Q Network.* In a real environment, it is often difficult for an agent to obtain a complete state. In other words, real-world environments usually do not strictly conform to Markov properties [8]. Partially Observable Markov Decision Processes (POMDPs) mathematically model the connection between observations and the true state. Therefore, it can better describe the dynamics of the real environment [16]. POMDP introduces observation space  $\Omega$  and conditional observation probability function  $O$  on the basis of Markov decision process (MDP), and defines the agent's primary perception of the environment as observation  $o \in \Omega$ . There is a certain connection between the observation and the real state, and this connection is described by probability, that is,  $o \sim O(s)$ . In this way, the POMDP can be described by six parameters ( $S, A, P, R, \Omega, O$ ), which represent the state space, action space, state transition probability function, reward function, and the newly added observation space  $\Omega$  relative to MDP, and the conditional observation probability function  $O$ . Obviously, when the observation  $o$  corresponds to the state  $s$  one-to-one, the POMDP becomes the MDP. The DRQN proposed by Matthew Hausknecht and Peter Stone in 2017 modified the network structure of DQN by changing its first fully connected layer to an LSTM layer of the same size. Because of the introduction of memory capabilities, neural networks are better able to combat incomplete information due to observations. The neural network structure of DRQN is shown in Figure 1.

*2.2. Input and Output Structure.* The hardware structure of data acquisition is shown in Figure 2. The functions of the hardware part include data acquisition and data transmission, including four data acquisition nodes and one data transmission base station. The data acquisition node consists of a three-axis gyroscope MPU3050 three-axis accelerometer and a magnetometer LSM303DLH, which, respectively, collect the angular velocity and acceleration data of the human body. The core component of the data sending base station is the wireless transceiver nRF24L01, which receives the data collected by the node and sends the data to the data terminal through the wireless network. The core processing function of the data acquisition module is completed by the 32-bit ARM microcontroller STM32F103. The energy supply of the data acquisition module is responsible for a 3.7 V lithium-ion battery.

The signal transmission of the entire data acquisition module includes two parts: First, the sensor node sends the collected human body posture data to the data transmission base station. The second is that the data transmission base

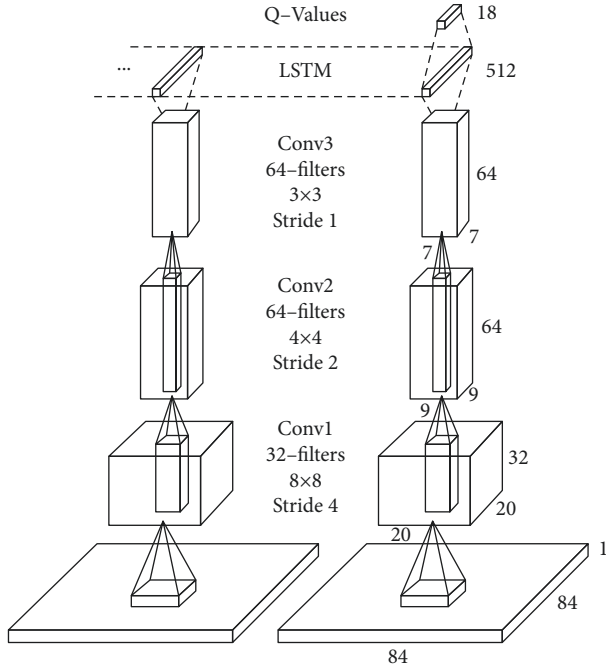


FIGURE 1: The neural network structure framework of DRQN.

station sends data to the signal transmission between the processing terminal sensor node and the data transmission base station, which is realized based on the wireless sensor network. The problem that needs to be overcome is to minimize the data collision rate, reduce data loss, and improve the accuracy of data collection. The signal transmission between the data transmission base station and the processing terminal is realized based on the star topology network, and the time division multiplexing protocol is adopted. The problem that needs attention is to calibrate the clock deviation between different nodes and keep the time uniform.

In data collection, multiple sensor nodes are generally used to collect relevant information. In addition to the structure of the node itself, the effective and complete transmission of data is another major problem. At present, according to different data transmission media, data transmission forms are mainly wired and wireless. The wired transmission mode is more stable and reliable, but it has not been widely used because of its complex installation and wiring and many restrictions on motion detection. There are many advantages in the field of human body posture recognition; often using wireless communication technology has Bluetooth, Zig Bee, wireless radio frequency identification, wireless transmission mode can reduce the influence of the sensors on the normal activity, so most systems adopt the form of data transmission. In the design of wireless transfer protocol, it forms the network architecture. Among the common network topology, star topology and mesh topology are widely used in practical applications. In the application of body area network, star topology requires multiple nodes to be directly connected to the receiving node, so it is often used because of its simple communication structure and convenient implementation.

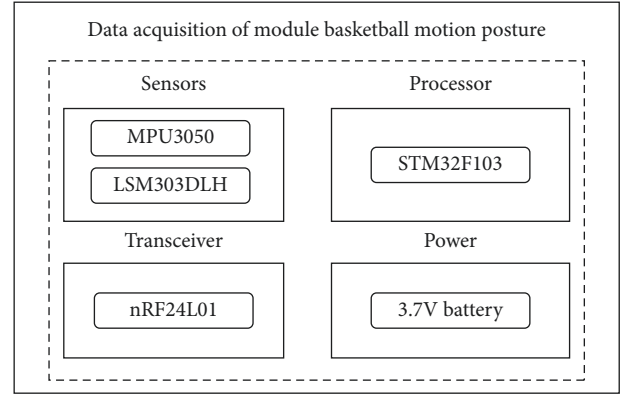


FIGURE 2: The hardware structure of data acquisition.

Compared with star topology structure, network topology structure is more complex, but it can be used in a multiple way to reduce the path loss caused by diffraction, and the data transmission is only between adjacent nodes, can envoys point to keep the smaller energy transmission network protocol setting need according to their own research needs in setting reasonable network structure.

### 3. The Proposed Model

**3.1. Feature Extraction of Basketball Motion Posture.** The basketball player posture acquisition data that mainly includes acceleration information and angular velocity information, respectively, uses  $a_n^x$ ,  $a_n^y$ ,  $a_n^z$  to represent the acceleration of the  $x$ ,  $y$ ,  $z$  axes of the  $n$ -th sampling point.  $g_n^x$ ,  $g_n^y$ ,  $g_n^z$  represent the angular velocity of the  $x$ ,  $y$ , and  $z$  axes of the  $n$ -th sampling point. The vector sum of the acceleration at the  $n$ -th point is

$$a_n = \sqrt{(a_n^x)^2 + (a_n^y)^2 + (a_n^z)^2}. \quad (1)$$

Similarly, the vector sum of the angular velocity at the  $n$ -th point is

$$g_n = \sqrt{(g_n^x)^2 + (g_n^y)^2 + (g_n^z)^2}. \quad (2)$$

Combine the three acceleration vectors, three angular velocity vectors input by the data acquisition module, and the vector sum of the acceleration and angular velocity calculated by equations (1) and (2) into an eight-dimensional feature matrix. If a total of  $N$  samples are collected point, each sample is an  $N \times 8$  feature matrix. The time-domain features of basketball player posture recognition are mean and variance, and the mean of each point is

$$\mu_a = \frac{1}{N} \sum_{n=1}^N a_n. \quad (3)$$

The variance of each sampling point is

$$\sigma^2 = \frac{1}{N} \sum_{n=1}^N (a_n - \mu_a)^2. \quad (4)$$

The extracted time-domain features include four dimensions of the acceleration sensor  $x$ ,  $y$ , and  $z$  axis and the

mean value of the acceleration vector sum; four dimensions of the angular velocity sensor  $x$ ,  $y$ , and  $z$  axis and the mean value of the angular velocity vector sum; four dimensions of the acceleration sensor  $x$ ,  $y$ , and  $z$  axis and the variance of the acceleration vector sum and the angular velocity sensor. The variance of the  $x$ ,  $y$ , and  $z$  axis and the angular velocity vector sum has a total of four dimensions, and a total of 16-dimensions of time-domain attitude parameters.

Next, based on the Fourier transform principle, the time-domain acquisition data is transformed into the frequency domain, and the formula is

$$S(n) = \sum_{n=1}^{N-1} a_i e^{-i(2\pi/N^n)}, \quad (5)$$

where  $S(n)$  represents the  $n$ th adoption point value in the frequency domain. The frequency-domain feature for basketball player posture recognition is the peak value of the Fourier transform, that is,

$$f = \frac{Kf_s}{N}, \quad (6)$$

where  $K$  is the number of sampling points in the frequency domain and  $f$  is the frequency used by the data acquisition sensor.

The extracted frequency-domain features include the frequency-domain peak value of the acceleration sensor  $x$ ,  $y$ , and  $z$  axis and the six-dimensional frequency value corresponding to the peak value, the acceleration vector and the two-dimensional frequency value corresponding to the frequency-domain peak value and peak value, and the angular velocity sensor. The frequency-domain peak value of the  $x$ ,  $y$ , and  $z$  axis and the corresponding frequency value of the peak value are six dimensional. The angular velocity vector and the frequency-domain peak value and peak value corresponding to the frequency value are two dimensional, with a total of 16-dimensional features.

**3.2. Model Establishment.** Feature selection is a variable selection method, also known as attribute selection or variable subset selection, which is a process of selecting a subset of relevant attributes in order to build a classification model. The primary reason for feature selection is that in the feature set obtained by feature extraction, not all attributes are relevant and useful, and the selection of some attributes may be redundant. The introduction of those irrelevant attributes not only has no effect on the construction of the model, but also makes the constructed model more complex due to the redundancy and irrelevance of the data. Therefore, it is extremely necessary to conduct reasonable feature screening. There is a big difference between feature selection and feature extraction. The purpose of feature extraction is to extract feature vectors from the original data, while feature selection is to select a suitable subset of feature vectors from these feature vectors. There are three main purposes of feature selection: (1) simplify the model and reduce the computational complexity; (2) shorten the training time; and (3) strengthen the promotion to avoid the

problem of overfitting. Commonly used feature selection algorithms are generally obtained by combining evaluation functions with algorithms such as sequential forward/backward search, decision tree, best-first search, and genetic algorithm. Among them, the evaluation algorithm is a function that can reflect the pros and cons of the selected feature subset, and can be used to solve the correlation between features and classification, classifier error rate, etc. In addition, the commonly used methods for feature selection to reduce the feature dimension and reduce the amount of system computation are: linear discriminant analysis (LDA), principal component analysis (PCA), and other algorithms [17].

The recognition of basketball motion posture is to construct a classifier that can recognize the athlete's posture according to the features of the data collected by the sensor. The extracted pose features are input into the classification, and the classifier outputs a specific basketball action. After feature extraction, a 16-dimensional feature parameter set for identifying the posture of basketball players is obtained. However, some of these feature parameters are features that are not related to the basketball player's posture, or have low correlation. There are also some features that represent redundant information. If these features are input into the classifier at the same time, it will not only reduce the recognition performance of the classifier, but also seriously affect the recognition efficiency of the classifier. Therefore, it is necessary to select features before performing basketball pose recognition. The purpose of feature selection is to reduce dimensionality in the data. At the same time, the feature parameters that are highly relevant to the posture recognition of basketball players are screened out. After experimental testing, the PCA method was selected to realize the selection of characteristic parameters.

In the 16-dimensional feature, the optimal feature is selected based on the PCA method. Next, the classifier is constructed to recognize the posture of the basketball player. Both DQN and DRQN neural networks contain two-dimensional convolutional layers. Typically, if the input is not an image, but just a feature vector, the neural network used by DQN and DRQN will not contain convolutional layers. However, the feature extraction capability of convolutional layers can be applied not only to extract image features, but also to extract features in the temporal dimension [18]. Therefore, this model utilizes the temporal dimension feature extraction capability of a 1-dimensional convolutional layer to extract temporal features of athlete poses.

The network structure of the proposed model is shown in Figure 3. On the basis of the neural network used in DRQN, a one-dimensional convolutional layer is added, which is called a one-dimensional convolutional recurrent neural network. The one-dimensional convolutional layer will convolve the input data in the time dimension and extract its features in the time dimension. Experiments show that this can improve the feature extraction ability and fitting ability of the neural network, thereby improving the decision-making level of the agent, and making the agent perform better in the environment related to time series.

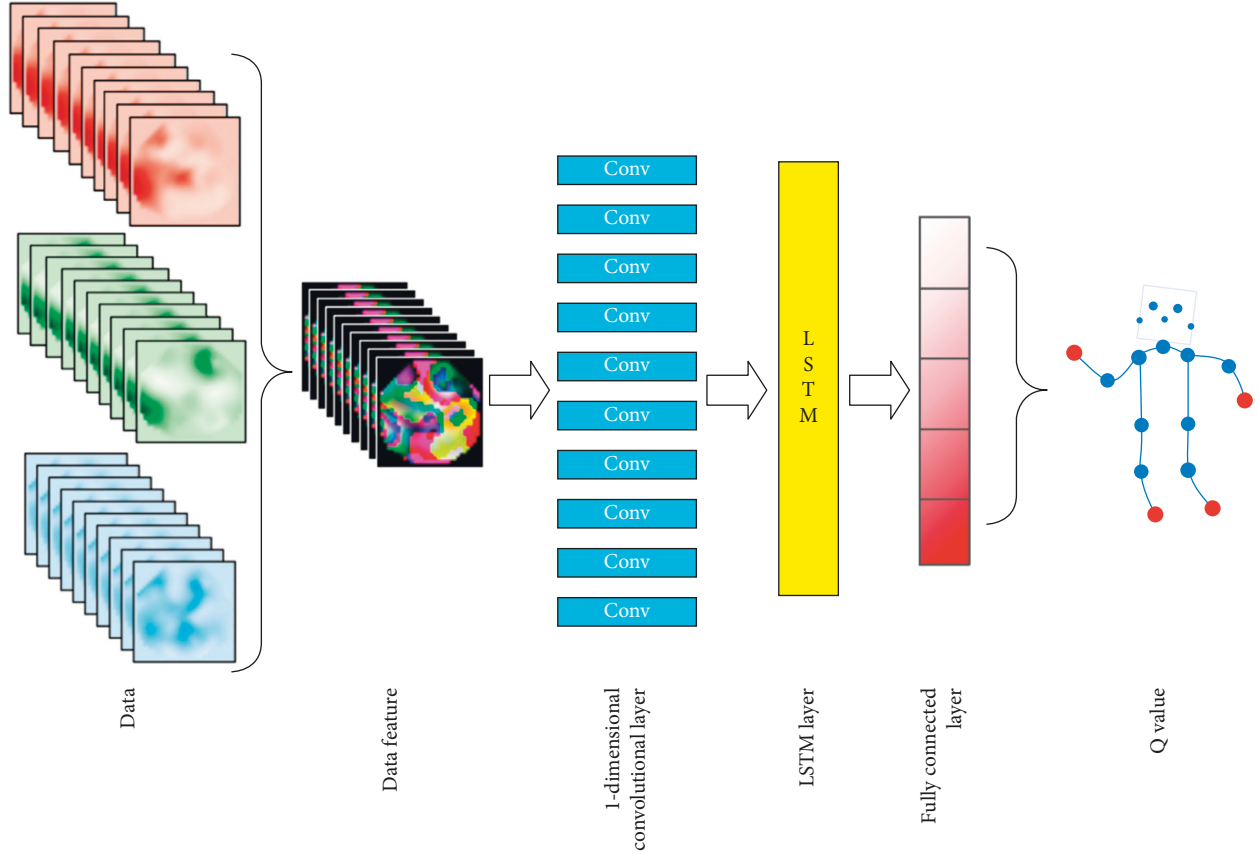


FIGURE 3: The neural network structure framework of our scheme.

**3.3. The Recognition of Basketball Motion Postures.** To solve the convergence problem of deep reinforcement learning in the environment with large state-space dimension, this study uses a one-dimensional convolutional layer to extract the features of the state in the time dimension. Let the input be  $X \in R^{N \times C_{in} \times L_{in}}$  and the output be  $Y \in R^{N \times C_{out} \times L_{out}}$ , then the mathematical expression of the one-dimensional convolutional layer is

$$Y[i, j, :] = \beta[j] + \sum_{k=0}^{c_{in}-1} \alpha[j, k, :] \otimes Y[i, k, :]. \quad (7)$$

In (7), the symbol  $\otimes$  is the cross-correlation operation.  $N$  is the size of a batch of training data.  $C_{in}$  and  $C_{out}$  are the number of channels of input and output data, respectively.  $L_{in}$  and  $L_{out}$  are the lengths of input and output data, respectively. A `kernel_size` represents the one-dimensional convolution kernel size.  $\alpha \in R^{C_{out} \times C_{in} \times \text{kernel\_size}}$  is the one-dimensional convolution kernel of this layer.  $\beta \in R^{C_{out}}$  is the bias term of this layer.

The LSTM layer is a recurrent neural network that brings memory capabilities to the neural network. Generally, the input of the LSTM layer is a time series  $x$  of a certain feature vector  $x \in R^{N \times L_{in} \times H_{in}}$ . For simplicity, assume that a batch contains only one piece of data and the feature vector contains only one feature, that is,  $x \in R^{L_{in}}$ . It can be seen that  $x = [x_1, x_2, \dots, x_t, \dots, x_{L_{in}}]^T$ , then for the element  $x_t$  at any time in  $x$ , the mathematical expression of the LSTM layer is

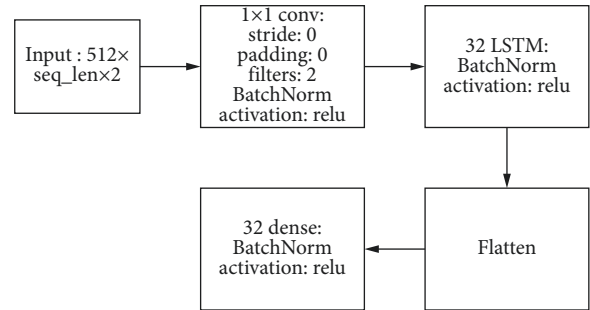


FIGURE 4: The detail neural network structure framework of our scheme.

$$\begin{cases} i_t = \sigma(W_{ii}x_t + b_{ii} + W_{hi}h_{t-1} + b_{hi}), \\ f_t = \sigma(W_{if}x_t + b_{if} + W_{hf}h_{t-1} + b_{hf}), \\ g_t = \tanh(W_{ig}x_t + b_{ig} + W_{hg}h_{t-1} + b_{hg}), \\ o_t = \sigma(W_{io}x_t + b_{io} + W_{ho}h_{t-1} + b_{ho}), \\ c_t = f_t \odot c_{t-1} + i_t \odot g_t, \\ h_t = o_t \odot c_t. \end{cases} \quad (8)$$

In (8), the symbol  $\odot$  represents the Hadamard product.  $N$  is the size of a batch of training data.  $L_{in}$  is the length of the time series in the time dimension.  $H_{in}$  is the feature number included by the time series.  $i_t$ ,  $f_t$ ,  $g_t$ , and  $o_t$  are called input

TABLE 1: The comparison of experimental results.

| Postures  | Random forest/% | Support vector machine/% | SOM neural network/% | Bayesian network/% | Our model/% |
|-----------|-----------------|--------------------------|----------------------|--------------------|-------------|
| Shooting  | 87.9            | 96.9                     | 93.2                 | 93.9               | 98.9        |
| Passing   | 86.3            | 98.3                     | 94.1                 | 89.1               | 99.6        |
| Dribbling | 90.2            | 97.1                     | 95.8                 | 90.7               | 99.2        |
| Catching  | 93.2            | 96.2                     | 94.2                 | 92.2               | 99.5        |
| Average   | 89.4            | 97.1                     | 94.3                 | 91.4               | 99.3        |

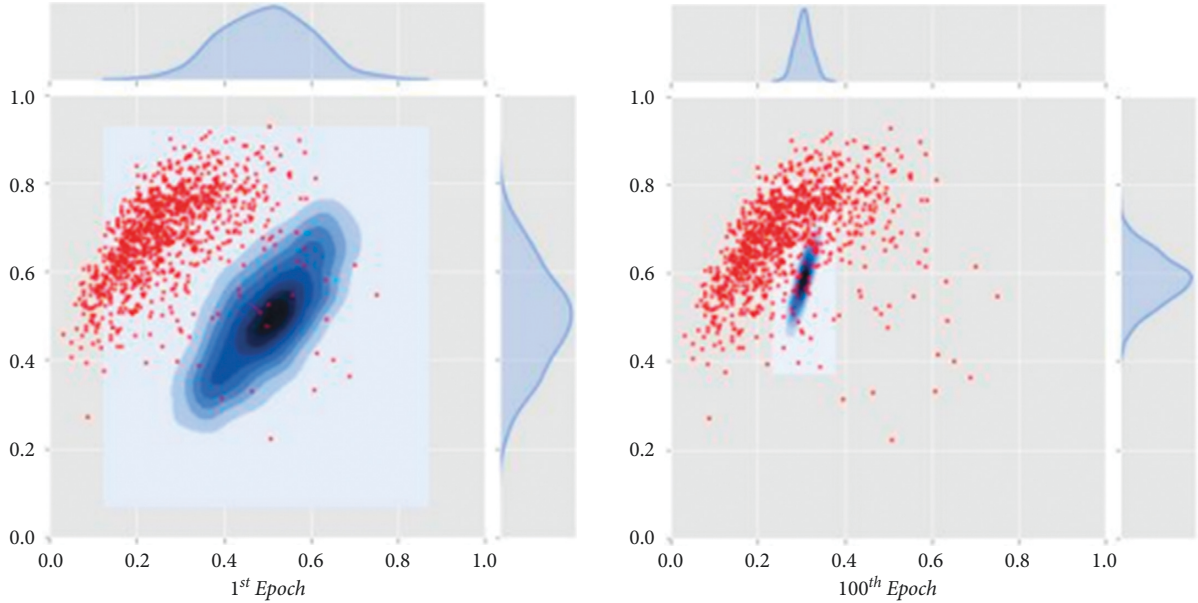


FIGURE 5: The training results of our model.

gates, forget gates, cell gates, and output gates at time  $t$ , respectively.  $c_t$  and  $h_t$  are called time  $t$ , which denote cell states and hidden states, respectively.

The fully connected layer is the most classic component of the neural network. According to the classical form, let the input of the fully connected layer be the feature vector  $X \in \mathbb{R}^{N \times H_{in}}$  and the output be  $Y \in \mathbb{R}^{N \times H_{out}}$ , then the mathematical expression of the fully connected layer is

$$Y[i, :] = \sigma(X[i, :]A + b), \quad (9)$$

where  $\sigma$  is a nonlinear activation function, commonly used are sigmoid function and ReLU function.  $N$  is the size of a batch of training data.  $H_{in}$  and  $H_{out}$  are the number of features of the input and output data, respectively.  $A$  is the weight of the layer, and  $b$  is the bias term of the layer. As seen in Figure 4, the detail neural network structure framework of our scheme is given.

#### 4. Experimental Results and Evaluation

In the experimental process, a total of 100 basketball players were collected in four postures: shooting, passing, dribbling, and catching. About 100 sets of data were collected for each posture, and 40,000 sample data were obtained. These data were iterated 100 times in the above model. In the process of collecting basketball motion

posture data, the testers completed the prescribed basketball movements according to the preset posture and according to their usual exercise habits. According to the characteristics of the body movements of the athletes, a classifier is constructed to identify the posture of the basketball players. Four classical classifier, that is, random forest, support vector machine, SOM neural network, and Bayesian network, as a comparison with our model, is verified with the validation set of basketball motion pose. The comparison of experimental results is shown in Table 1.

The experimental results show that for the recognition of basketball poses, our model has the highest average recognition accuracy, reaching 99.3%. Among other models, the SVM algorithm has the highest recognition accuracy, with an average recognition accuracy of 97.1%. The average recognition accuracies of SOM neural network, Bayesian network, and random forest are 91.5%, 90.8%, and 89.4%, respectively. This result verifies the accuracy of the proposed basketball motion recognition method based on multi-feature fusion and DRQN. This is because compared with these traditional machine learning algorithms, DRQN has a deeper network structure and extract more in-depth features of basketball poses, thereby improving the accuracy of recognition.

Figure 5 shows the distribution of the output results of the model after the first epoch and the 100-th epoch. The red dots are the characteristic distribution of the samples, and

the blue dots are the characteristic distribution of the model results. It can be seen that after the 100-th epoch, the training results are more in line with the feature distribution of the original data than the first epoch.

## 5. Conclusion

In recent years, with the development of wireless sensor networks, and microelectronics equipment technology, the human body gesture recognition has attracted extensive attention in various fields, such as health sports game movie. Based on posture recognition based on the human body, posture recognition of the movement of athletes in the field of basketball was studied and analysis.

In this study, the problem of basketball pose recognition is studied, and a new basketball posture recognition method based on DRQN is proposed. Inertial sensors are used to collect athletes' posture data. After the features are extracted, PCA is used to reduce the dimensionality of the features. The introduction of the LSTM layer enables our model to have a certain memory capacity. The addition of a one-dimensional convolutional layer gives our model a stronger feature extraction ability on the basis of its memory ability, and then it can process information in the time dimension more efficiently. At the same time, the one-dimensional convolutional layer also increases the fitting ability and stability of the neural network, making the training process of deep reinforcement learning more stable. After 100-th epoch, the accuracy of recognizing basketball poses is significantly improved. Compared with other methods for recognizing basketball motion posture, our model has better performance.

## Data Availability

The raw data supporting the conclusions of this article will be made available by the authors, without undue reservation.

## Conflicts of Interest

The authors declare that they have no conflicts of interest regarding this work.

## Acknowledgments

The work was not supported by any funding.

## References

- [1] W.-F. Wang, C.-Y. Yang, and D.-Y. Wang, "Analysis of movement effectiveness in badminton strokes with accelerometers," *Genetic and Evolutionary Computing*, pp. 95–104, Springer, Berlin, Germany, 2016.
- [2] F. Dadashi, A. Arami, F. Crettenand et al., "A hidden Markov model of the breaststroke swimming temporal phases using wearable inertial measurement units," in *Proceedings of the Body Sensor Networks (BSN)*, pp. 1–6, Cambridge, MA, USA, May 2013.
- [3] L. A. Schwarz, A. Bigdelou, and N. Navab, "Learning Gestures for Customizable Human-Computer Interaction in the Operating Room," *Med Image Comput Comput Assist Interv*, vol. 14, 2011.
- [4] T. Schaul, J. Quan, I. Antonoglou, and D. Silver, "Prioritized Experience Replay," in *Proceedings of the ICLR*, San Juan, Puerto Rico, May 2016.
- [5] H. V. Hasselt, A. Guez, and D. Silver, "Deep Reinforcement Learning with Double Q-learning," in *Proceedings of the Thirtieth AAAI Conference on Artificial Intelligence*, Phoenix, Arizona, February 2015.
- [6] Z. Wangz, M. Hessel, T. Schaul, and L. Marc, "Dueling Network Architectures for Deep Reinforcement Learning," in *Proceedings of the International Conference on Machine Learning*, PMLR, pp. 1995–2003, London, UK, June 2016.
- [7] V. Mnih, K. Kavukcuoglu, D. Silver, A. A. Rusu, and D. Hassabis, "Human-level control through deep reinforcement learning," *Nature*, vol. 518, no. 7540, pp. 529–533, 2015.
- [8] M. Hausknecht and P. Stone, "Deep Recurrent Q-Learning for Partially Observable MDPs," 2015, <https://arxiv.org/abs/1507.06527>.
- [9] Y. L. Hsu, J. S. Wang, Y. C. Lin et al., "A Wearable Inertial-Sensing-Based Body Sensor Network for Shoulder Range of Motion assessment," in *Proceedings of the 2013 International Conference on Orange Technologies (ICOT)*, March 2013.
- [10] S. Asai, K. Watanabe, and Y. Kurihara, "Measurement and Analysis of Running Form Using 3-D Acceleration and Gyroscopic sensor," in *Proceedings of the SICE Annual Conference (SICE)*, IEEE, Akita, Japan, August 2012.
- [11] B. Longstaff, S. Reddy, and D. Estrin, "Improving Activity Classification for Health Applications on mobile Devices Using Active and Semi-supervised learning," in *Proceedings of the Pervasive Computing Technologies for Healthcare International Conference*, Munich, Germany, March 2006.
- [12] L. Oudre, M. Doron, and C. Simon, "Segmentation and classification of dynamic activities from accelerometer signals," *Journal of Innovation Impact*, vol. 6, 2013.
- [13] Y. Wang, "Real-time collection method of athletes' abnormal training data based on machine learning," *Mobile Information Systems*, vol. 2021, Article ID 9938605, 11 pages, 2021.
- [14] G. M. Paul, B. P. David, and L. M. Clare, "The physical and physiological demands of basketball training and competition," *International Journal of Sports Physiology and Performance*, vol. 5, no. 1, pp. 75–86, 2010.
- [15] A. D. Ignatov and V. V. Strijov, "Human activity recognition using quasiperiodic time series collected from a single tri-axial accelerometer," *Multimedia Tools and Applications*, vol. 75, no. 12, pp. 7257–7270, 2016.
- [16] M. Spaan, "Fuzzy Reinforcement Learning Control for Decentralized Partially Observable Markov Decision processes," in *Proceedings of the IEEE International Conference on Fuzzy Systems*, June 2011.
- [17] N. Y. Ke and R. Sukthankar, "PCA-SIFT: A More Distinctive Representation for Local Image descriptors," in *Proceedings of the IEEE Computer Society Conference on Computer Vision & Pattern Recognition*, June 2004.
- [18] S. Albawi, T. A. Mohammed, and S. Alzawi, "Understanding of a Convolutional Neural Network," in *Proceedings of the International Conference on Engineering and Technology*, Antalya, Turkey, August 2017.

## *Retraction*

# **Retracted: Effect of Evaluation of Popular Song Creation and Literature Based on RITNN Model**

### **Mathematical Problems in Engineering**

Received 18 July 2023; Accepted 18 July 2023; Published 19 July 2023

Copyright © 2023 Mathematical Problems in Engineering. This is an open access article distributed under the Creative Commons Attribution License, which permits unrestricted use, distribution, and reproduction in any medium, provided the original work is properly cited.

This article has been retracted by Hindawi following an investigation undertaken by the publisher [1]. This investigation has uncovered evidence of one or more of the following indicators of systematic manipulation of the publication process:

- (1) Discrepancies in scope
- (2) Discrepancies in the description of the research reported
- (3) Discrepancies between the availability of data and the research described
- (4) Inappropriate citations
- (5) Incoherent, meaningless and/or irrelevant content included in the article
- (6) Peer-review manipulation

The presence of these indicators undermines our confidence in the integrity of the article's content and we cannot, therefore, vouch for its reliability. Please note that this notice is intended solely to alert readers that the content of this article is unreliable. We have not investigated whether authors were aware of or involved in the systematic manipulation of the publication process.

Wiley and Hindawi regrets that the usual quality checks did not identify these issues before publication and have since put additional measures in place to safeguard research integrity.

We wish to credit our own Research Integrity and Research Publishing teams and anonymous and named external researchers and research integrity experts for contributing to this investigation.

The corresponding author, as the representative of all authors, has been given the opportunity to register their agreement or disagreement to this retraction. We have kept a record of any response received.

### **References**

- [1] R. Song, "Effect of Evaluation of Popular Song Creation and Literature Based on RITNN Model," *Mathematical Problems in Engineering*, vol. 2022, Article ID 4643674, 9 pages, 2022.

## Research Article

# Effect of Evaluation of Popular Song Creation and Literature Based on RITNN Model

Rui Song 

College of Sport and Art Shandong Sport University, Jinan 250001, Shandong, China

Correspondence should be addressed to Rui Song; [songrui@sdpei.edu.cn](mailto:songrui@sdpei.edu.cn)

Received 16 March 2022; Revised 12 April 2022; Accepted 16 April 2022; Published 14 May 2022

Academic Editor: Man Fai Leung

Copyright © 2022 Rui Song. This is an open access article distributed under the Creative Commons Attribution License, which permits unrestricted use, distribution, and reproduction in any medium, provided the original work is properly cited.

The era of modernity and information technology has entered people's lives, which has brought new challenges to innovative culture and art to a great extent, especially changing the relationship between traditional culture and pop music creation. In order to better automate music creation, this paper proposes a mixed model of cultural term evaluation of Chinese pop songs based on RITNN, which sets up RNN structure composition models of different channels. Through this method, a data reconstruction model of important cultural elements of simultaneous interpretation is established. The experiment fully proves that the pop music creation in traditional cultural materials not only integrates the essence of traditional cultural elements but also makes new creation. This scheme can evaluate the integration effect of traditional cultural elements in pop music creation.

## 1. Introduction

The age of modernity and information technology has entered our lives. New materials and new technologies are emerging all the time, and we are overwhelmed by them to a large extent; this has brought new challenges to innovative culture and art [1–3]. The text therefore analyses the successful cases of pop music creation in China and abroad, analyses the fusion and innovation of traditional musical elements in pop music creation, and explores the essence of traditional culture to experience the fusion and creation of new musical concepts.

In the course of the long development of society, people have created a brilliant culture and art. The art of singing is one of the oldest; from the ancient rock paintings of Dunhuang to the opera “Silk Road” [4, 5]; from the old records of the industrial revolution to the electronic music of high technology; from the early whispers of pop songs to the current star-studded pop scene. People have come a long way from ancient time. The creative arts have also progressed and developed; and these have never left the traditional culture in the journey of history [6]. Traditional culture has made to the present day. The achievements of today are the traditional culture of the future. Excellent traditional culture has always

been the source of water on which humanity depends. So, while people are enjoying modern culture, they should cherish traditional culture, but the youth of today has a shallow understanding of traditional culture. After the reform and opening up, songs such as “I Only Care About You” by Teresa Teng and “The Fragrance of the Night” by Xu Xiaofeng were introduced to the mainland, but many people did not know that these songs were old pop songs from Shanghai [7–9].

In fact, in the 1930s and 1940s, Chinese pop music spread both at home and abroad, with present-day Malaysian singers such as Wu Qixian and Hua Yi Bao, Pan Xiuqiong, and Sun Yanzhi, all of whom sang songs from this period. To this day, we can also hear the classic songs of this period in many film and television productions. It is easy to see that the creation of the so-called pop songs is based on traditional culture. For example, as Lai Jinhui, the founder of pop music [10–12], said: “I took as my material the poetry of famous writers from the past and present, Western poetry, folk ditties, songs in the native style, as well as Western ditties and love songs from the South Pacific area.” So the main characteristic of early Chinese pop songs is that “Chinese pop songs are the Chinese version of world pop music, and they are directly or indirectly connected with the



international community, not only maintaining the traditional nature of their own national music culture, but also cleverly combining with foreign culture.”

In the mid-nineteenth century, the song “Shanghai by Night,” with lyrics by Fan Yanqiao and music by Chen Gexin, became an iconic piece of music in Shanghai. The lyrics of “Shanghai by Night” reflect the complex, helpless, miserable, uncertain, and awakening inner activities of the protagonist in the midst of the glamour of the nightclubs and the monologue of his heart. The lyrics of “Shanghai by Night” are also based on the stanza structure of song lyrics and Yuan songs, and fully express the helplessness and awakening of the old Shanghai dancers. This is why in the late 1990s, Hong Kong’s Great Wall Pictures brought “Shanghai by Night” to the big screen [13]. This is a classic song that can be found here. This is why in the last eighty years of Chinese pop music and its songwriting, there has been a strong sense of nationalism and an openness to embrace elements of global culture. In many major international song competitions, very little traditional music has won awards. On the contrary, those who create music that incorporates traditional culture and ethnicity are more likely to attract the attention of the judges. So, there is no such thing as a single traditional culture, only a fusion of innovative culture and modernity can be truly innovative.

## 2. Integration and Innovation of Traditional Cultural Elements and Popular Songwriting

The fusion of traditional culture and pop music is mainly based on the word “new.” This innovation lies in the fact that the compositions are drawn from tradition, but are not simply repetitions, copies, or displaced variations, but rather extracts some of the cultural essence from traditional cultural elements, expresses it with a modern sense of innovation, and recreates it [14–16]. As a result, new works are created that not only leave behind the traditional artistic flavour but are also very contemporary and have a new popular artistic image. In 1986, the first concert of the singers was a great success. The song “Let the world be full of love” became a national hit. From then on, pop music composers were emerging and the pop stars were gathering, and pop music began to diversify and explore. The song has been around for more than a decade, but “Sea grows the sky” still has the spirit of the band beyond. This is what beyond had to endure in their songwriting. But that is what made beyond the avant-garde band that they are, and their appeal has remained intact for decades. As the lyrics go, “The sea is wide, you and I, but how many times have we faced the scorn and ridicule? We’ve never given up on our ideals.” It is for this reason that beyond has created music based on traditional cultural elements that are contemporary and encourage dreamers to follow their dreams. They are at the forefront of music creation, both spiritually and mentally, and it is their innovation that gives us the spiritual strength to pursue and innovate, and they have created a work that will be remembered and remembered as the most valuable for us to learn from.

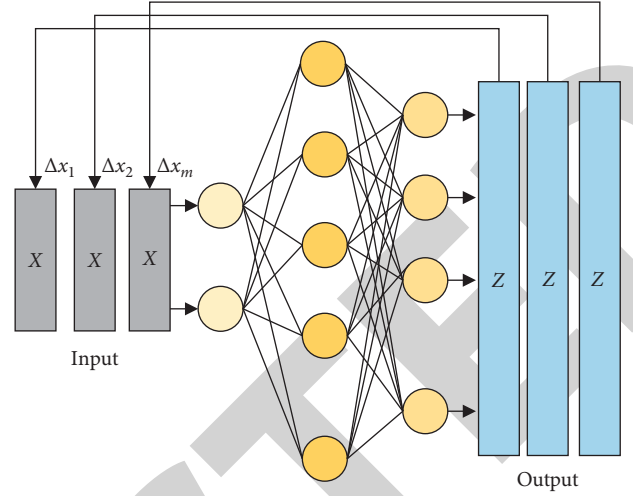


FIGURE 1: Illustration of the RITNN network structure.

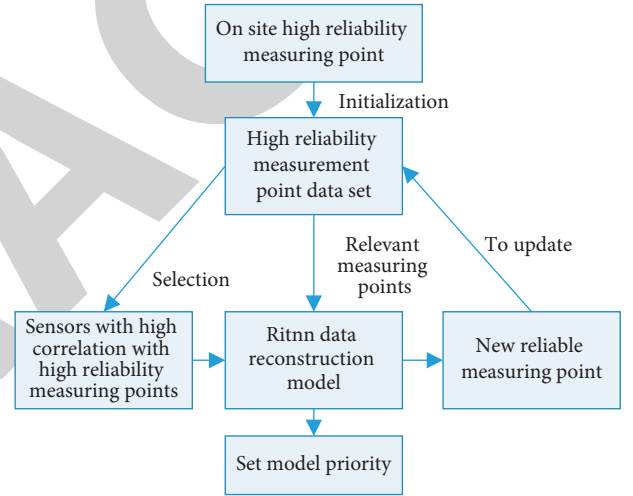


FIGURE 2: Modelling process.

**2.1. Robust Input Training Neural Network.** The RITNN consists of 3 parts: the input layer, the hidden layer, and the output layer, as shown in Figure 1 [17].

The RITNN network is trained using the error back-propagation gradient descent method to adjust the internal weights of the network as well as the input values, and  $m$  sets of training samples containing  $n$  variables are normalized to obtain  $t_{pk}$ , and the network training objective function is

$$E = \frac{1}{2} \sum_{p=1}^m \sum_{k=1}^n (z_{pk} - t_{pk})^2, \quad (1)$$

where  $z_{pk}$  is the network output value.

The activation function of the hidden layer of the network uses a single-level Sigmoidal function  $\sigma(x) = 1/1 + e^{-x}$ , while the input and output layers use a linear activation function  $f(x) = x$  so that  $z_{pk}$  can be expressed as

$$z_{pk} = \sum_j w_{2,jk} \sigma \left( b_j + \sum_j w_{1,ij} x_{pi} \right), \quad (2)$$

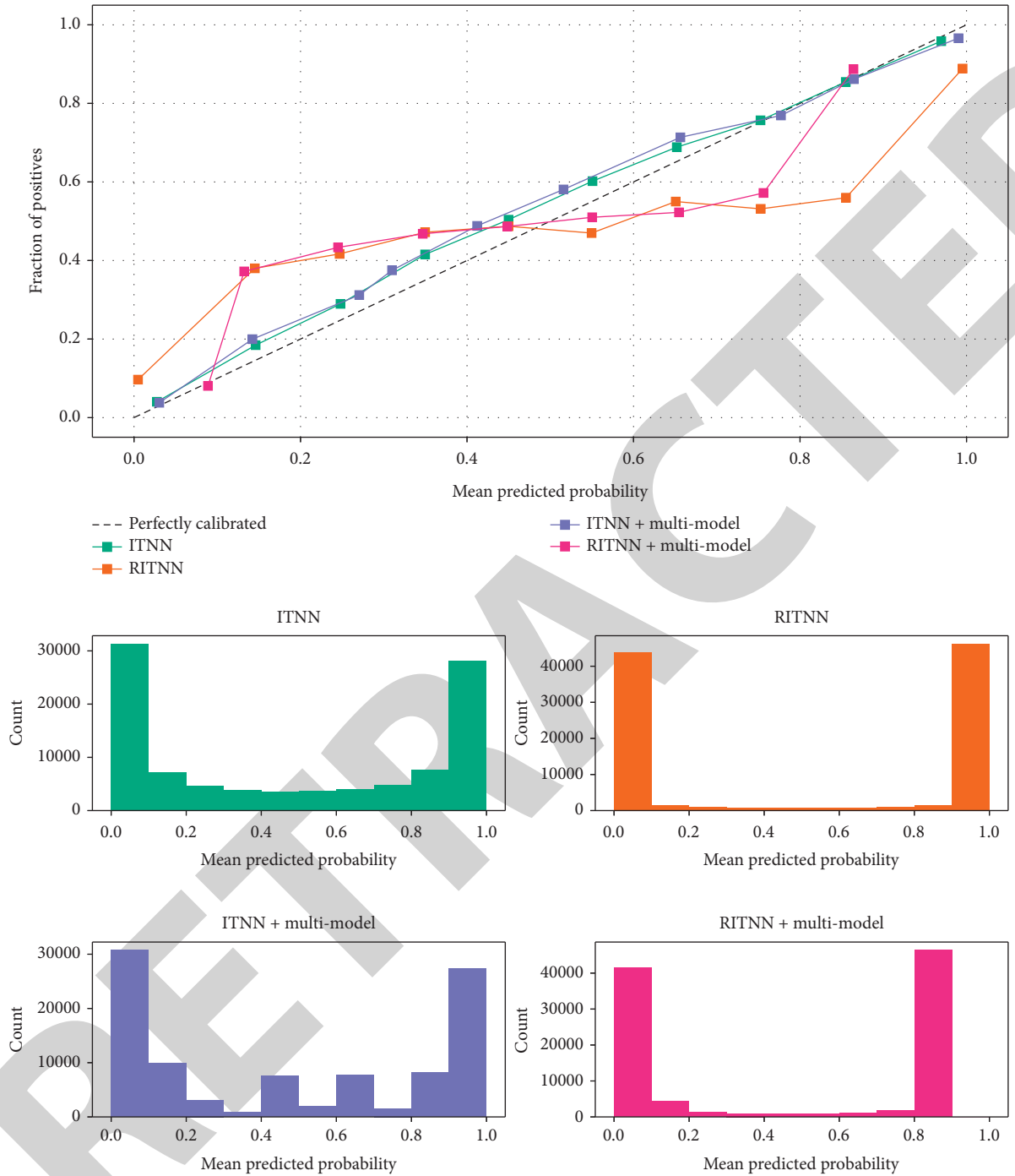


FIGURE 3: 5 comparisons of cultural elements and concurrent cultural elements.

where  $w_{1ij}$  and  $w_{2jk}$  are the network weights between the input layer and the hidden layer, respectively;  $b_j$  is the  $j$ th hidden layer node threshold, and the network parameters are adjusted as follows:

$$\Delta x_{pi} = \sum_j w_{1ij} \sigma' \left( b_j + \sum_i w_{1ij} x_{pi} \right) \sum_k w_{2jk} (t_{pk} - z_{pk}), \quad (3)$$

where  $\sigma'$  is the derivative of  $\sigma$ .

$$\begin{aligned} \Delta w_{1ij} &= \sum_p x_{pi} \sigma' \left( b_j + \sum_i x_{pi} w_{1ij} \right) \sum_k w_{2jk} (t_{pk} - z_{pk}), \\ \Delta w_{2jk} &= \sum_p \sigma \left( b_j + \sum_i x_{pi} w_{1ij} \right) (t_{pk} - z_{pk}). \end{aligned} \quad (4)$$

In general, when the reliability of a cultural element is high and the probability of occurrence of a cultural element is small, it corresponds to a larger reliability coefficient; conversely, a cultural element parameter that is prone to occurrence of a

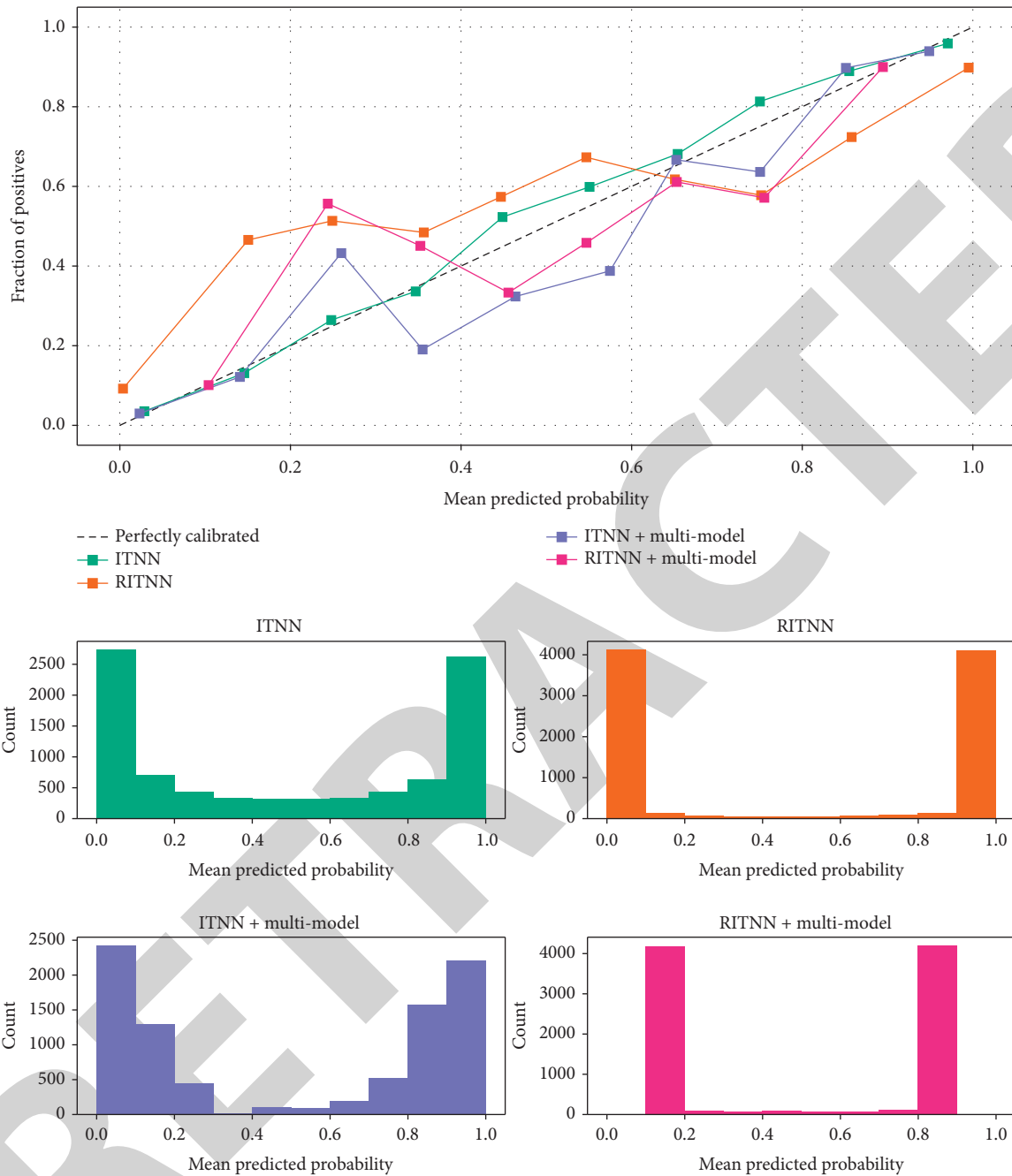


FIGURE 4: 10 comparisons of cultural elements and concurrent cultural elements.

cultural element corresponds to a smaller reliability coefficient [18–20]. When a cultural element occurs, RITNN reduces the weight of the cultural element parameter error in the objective function through the reliability coefficient, reducing the residual contamination of other parameters and providing a reliable guarantee for the next influential factor function.

### 3. Collaborative Songwriting Based on Multiple RITNN Models

3.1. Multiple RITNN Model Data Reconstruction. Although RITNN has a certain suppression effect on the residual effects of cultural element data when dealing with

multiple cultural elements, the number of cultural elements and pop song composition cultural elements is large, and if numerous measurement parameters are built into only 1 RITNN model, it will lead to a decrease in modelling accuracy; in addition, the number of high reliability measurement points in the field is very limited. In order to ensure the accuracy of reconstructed data in the case of multiple cultural elements occurring at the same time, this paper adopts the collaborative data reconstruction method of multiple RITNN models, grouping cultural elements of popular song composition through the analysis of the mechanistic relationship between parameters and the correlation of historical data, establishing multiple RITNN

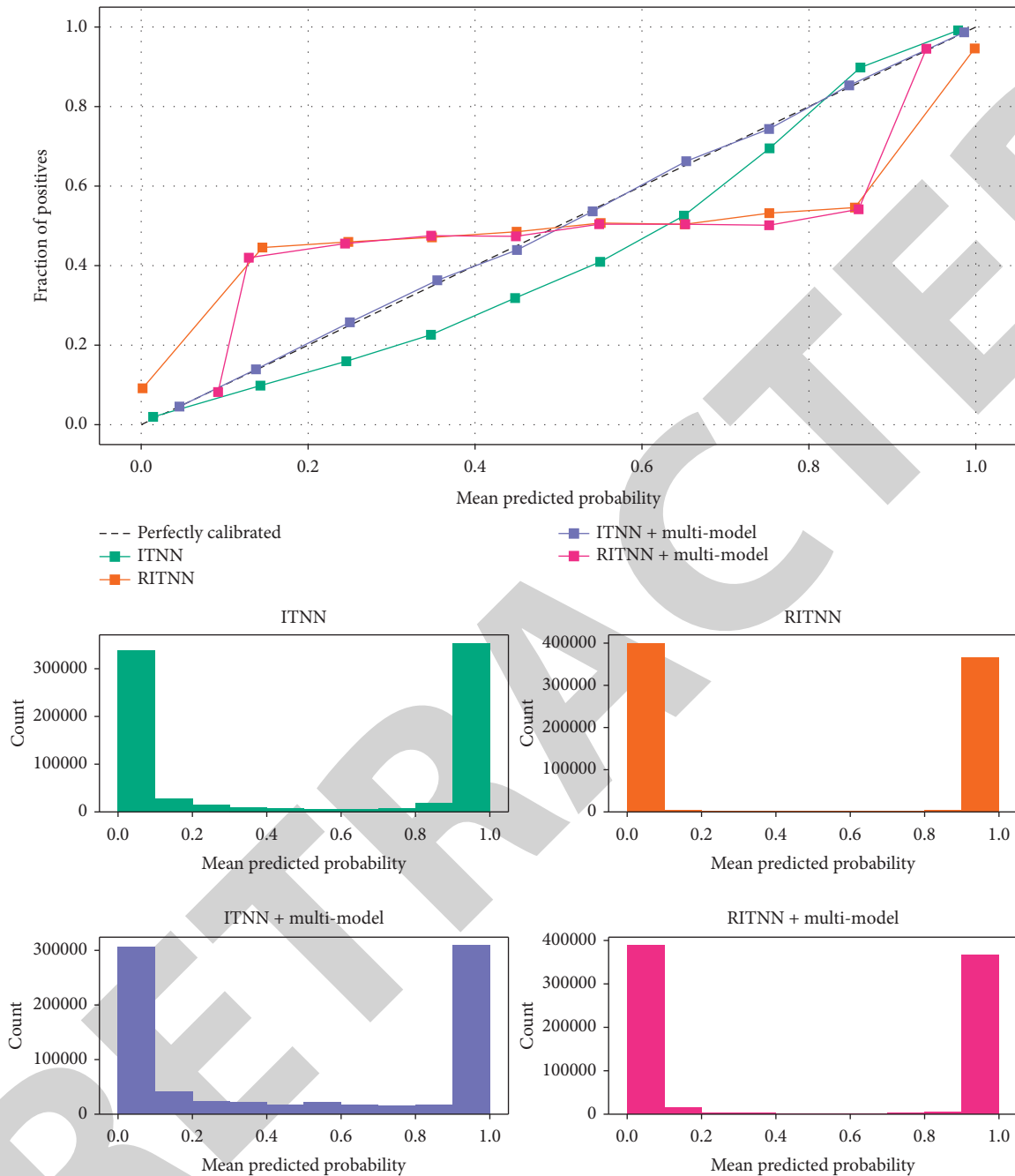


FIGURE 5: Comparison of 20 cultural elements and concurrent cultural elements.

models [21–23], and dividing the model priorities according to the order of data reconstruction, in series and parallel manner to form a complete data reconstruction module.

The modelling process of the multi-RITNN model collaborative data reconstruction method is shown in Figure 2, where the first step is to establish a high reliability measurement point dataset, which only contains high reliability measurement point data in the initial state. The parameters of the selected and completed cultural elements will become new reliable measurement points, which will be updated to the high reliability measurement point dataset. The process is

repeated until a data reconstruction model is built for all cultural elements. As each round of modelling is completed, the priority of the reconstructed model is set, with the earlier the model is built, the higher the priority will be.

Cultural elements and pop songwriting operate in a hostile environment for long periods of time and are prone to degradation and other cultural elements that can lead to inconsistent relationships. Therefore, it is necessary to update the model parameters to eliminate the effects of changes in degraded cultural elements on the fusion of popular songwriting.

TABLE 1: Results of the 3 methods of popular songwriting.

|                           |          | Average detection number | Average number of missed inspections | Average number of false detections | Average detection rate% | Average false detection rate |
|---------------------------|----------|--------------------------|--------------------------------------|------------------------------------|-------------------------|------------------------------|
| Single-ITNN model         | 5 fault  | 6.07                     | 0.029                                | 1.10                               | 99.4                    | 2.2                          |
|                           | 10 fault | 17.45                    | 0.026                                | 7.47                               | 99.7                    | 16.6                         |
|                           | 20 fault | 29.67                    | 0.052                                | 9.72                               | 99.7                    | 27.8                         |
| Single-RITNN model        | 5 fault  | 5.8                      | 0.031                                | 0.83                               | 99.4                    | 1.7                          |
|                           | 10 fault | 11.62                    | 0.062                                | 1.68                               | 99.4                    | 3.7                          |
|                           | 20 fault | 23.11                    | 0.026                                | 3.14                               | 99.9                    | 9.0                          |
| Collaborative multi model | 5 fault  | 5.64                     | 0.000                                | 0.67                               | 100.0                   | 1.3                          |
|                           | 10 fault | 10.90                    | 0.013                                | 0.91                               | 99.9                    | 2.0                          |
|                           | 20 fault | 21.16                    | 0.021                                | 1.24                               | 99.9                    | 3.5                          |

#### 4. Example Analysis and Validation

**4.1. Fusion Composition of Popular Songs.** The most recent historical data were selected as the test data, with a sampling interval of 10 s. A total of 3,000 sets of data were collected, and a random error of 10% to 50% was superimposed on the 1,300 to 2,200 sets of data as the culture element test sample [24, 25]. The cultural element types included accuracy degradation, drift, constant deviation, and complete failure.

RMSE (F) and RMSE (H) were calculated separately for the cultural element data segment of the test sample to measure the reconstruction accuracy of the cultural element variables and the extent to which the health variables were contaminated by residuals, as shown in equations (5) and (6). The smaller the RMSE (F), the higher the reconstruction accuracy of the cultural element variables; the smaller the RMSE (H), the less the health variables are contaminated by the residuals of the cultural element parameters, and the lower the error detection rate of the corresponding healthy cultural elements [26–28].

$$RMSE(F) = \sqrt{\frac{1}{m} \frac{1}{n_F} \sum_{p=1}^m \sum_{k=1}^{n_F} (z_{pk} - t_{pk})^2}, \quad (5)$$

$$RMSE(H) = \sqrt{\frac{1}{m} \frac{1}{n_H} \sum_{p=1}^m \sum_{k=1}^{n_H} (z_{pk} - t_{pk})^2}, \quad (6)$$

where  $n_F$  is the number of failed sensors in one test sample;  $n_H$  is the number of healthy cultural elements in the same test sample;  $m$  is the number of cultural element test samples;  $t_{pk}$  is the raw data normalisation result for the cultural element samples;  $z_{pk}$  is the network output value.

5 cultural elements and concurrent cultural elements. The RMSE (F) distribution, RMSE (H) distribution, and

natural logarithm of error detection rate  $\ln(T)$  for each group of 10 randomly selected parameter combinations of 5 cultural elements for the multiple RITNN model synergy approach, single RITNN model approach, and single ITNN model approach are shown in Figure 3.

10 sensor concurrent failure. The RMSE (F) distribution, RMSE (H) distribution, and natural logarithm of the error detection rate  $\ln(T)$  for each of the 10 groups of 10 cultural elements selected randomly for the multi-RITNN model synergy approach, the single RITNN model approach, and the single ITNN model approach are shown in Figure 4.

20 sensors with concurrent failure. The distribution of RMSE (F) [29], RMSE (H), and the natural logarithm of the error detection rate  $\ln(T)$  for each of the 10 sets of 20 randomly selected cultural element parameter combinations for the multiple RITNN model synergy approach, the single RITNN model approach, and the single ITNN model approach are shown in Figure 5.

A status determination was made for the ITNN failed data segments [29–32] of the song parametric test samples, and the results of the 3 methods of diagnosis are shown in Table 1. Figure 6 shows the data reconstruction of the four cultural element variables for one of the 20 culture element concurrent cultural element groups, with the culture element types of reduced precision, complete failure, drift, and constant deviation.

As can be seen from Figures 4–6 and Table 1, the accuracy of the single RITNN model method and the single ITNN model method for reconstructing data decreases in the case of simultaneous failure of multiple cultural elements, and although a certain detection rate of cultural elements can still be guaranteed, the residual contamination of cultural element data has a greater impact, resulting in a higher false detection rate of health data. The detection rate of cultural elements in this paper was found to be high. The paper's series-parallel multiple RITNN models can effectively overcome the reconstruction difficulties caused by

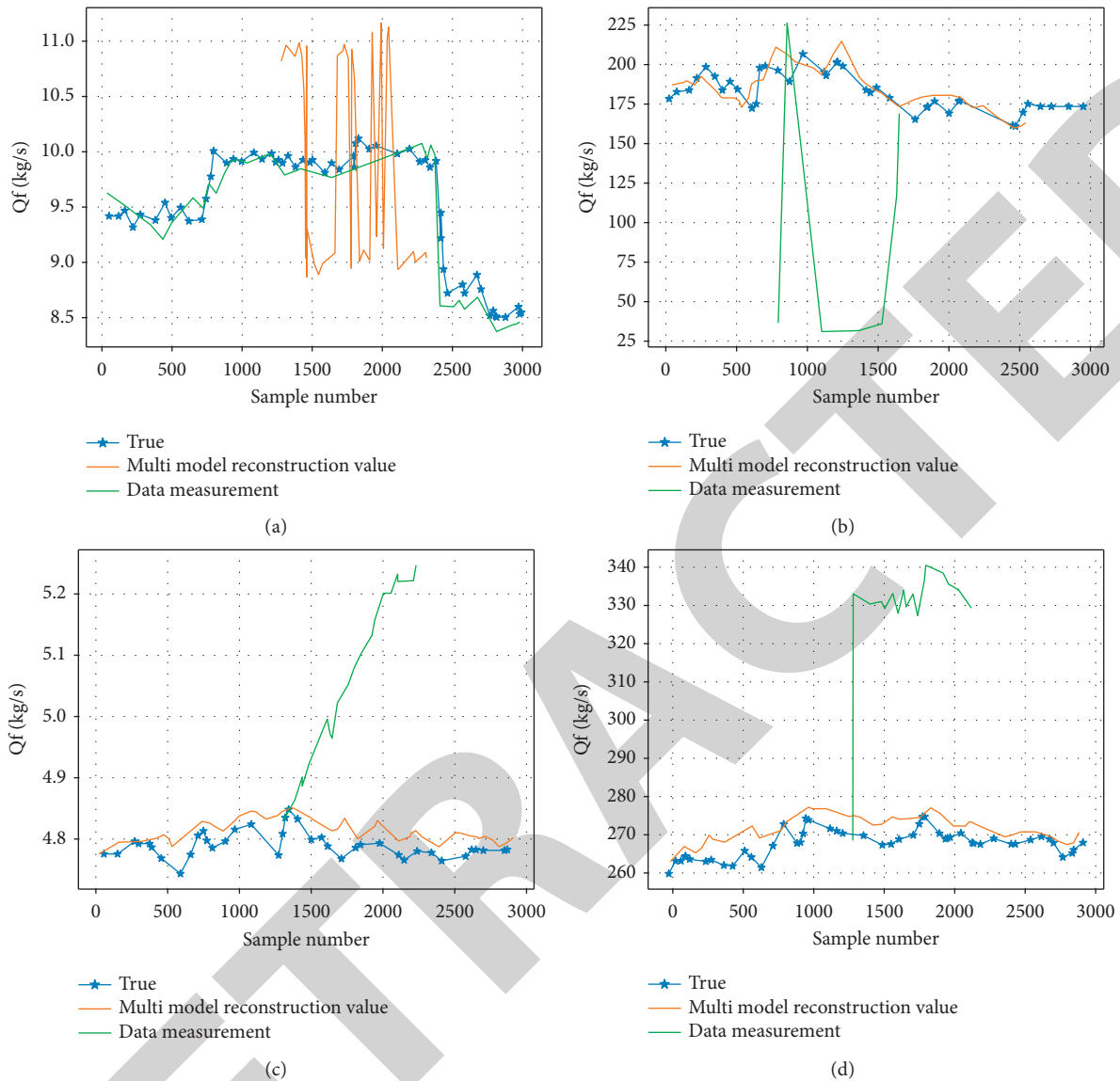


FIGURE 6: Reconstruction results for 3,000 sets of test data for 4 cultural element variables. (a)  $Q_f$ , (b)  $T_{7L}$ , (c)  $P_{ht}$ , and (d)  $Th$ .

multiple target cultural elements, and the reconstruction accuracy of cultural element parameters is maintained at a high level, and the detection rate of cultural elements is nearly 100%, and the influence of significant errors in cultural element data is well suppressed, which greatly reduces the residual pollution and keeps the false detection rate of health data in a low range, and significantly improves the accuracy of the accuracy of popular songwriting.

## 5. Conclusions

The above analysis of the songs shows that modern pop music carries all the ideas of today's life. It is the most typical, direct, and quickest way of creating music that maps out the reality of people's lives, using Koranic media technology to awaken and inspire self-confidence and pride. The creation of today's pop music is a sign of cultural progress. People are

putting a lot of information into music. The visualisation of notes and words is with simple, individual words. There is a strong call to create a new atmosphere of a spirit. The main trend in today's society is the exchange, fusion, and innovation of Chinese and foreign cultures. In our pluralistic and integrated society, it is important to have not only the characteristics of the local traditional culture but also the pioneering ideas of modern music creation. It is only in this way that the creators of popular music can continue to innovate and develop, as there is a collision of new elements. Only then can they stand on the platform at the time, thus enriching their cultural heritage and drawing on various genes. This is how traditional guitars and pop music can be fused and innovated. Inheriting traditional cultural elements and developing advanced pop music culture, this will lead to innovative forms of music art and promote the development of Chinese music art.

## Data Availability

The raw data supporting the conclusions of this article will be made available by the authors, without undue reservation.

## Conflicts of Interest

The authors declared that they have no conflicts of interest regarding this work.

## Acknowledgments

This work supported by 2021 Undergraduate Teaching Reform Research Project of Shandong Education Department “Research on The Theory and Practice of Collaborative Education of Dance Performance Majors in Sports Colleges under the Background of New Liberal Arts Construction” M2021321.

## References

- [1] S.-H. Han, “A review of research on restaurant brand personality: a focus on the hospitality and tourism journals listed at Korea Research Foundation,” *Journal of Tourism Sciences*, vol. 35, no. 2, pp. 337–353, 2011.
- [2] K. J. Bae, J. W. Jeong, M. Y. Jung, and S. J. Kim, “Reviewing research on the treatment and study of fracture in Korean journals objective - focus on domestic thesis,” *Journal of Korean Medicine Rehabilitation*, vol. 25, no. 3, pp. 27–36, 2015.
- [3] A. Legendijk, “The accident of the region: a strategic relational perspective on the construction of the region’s significance,” *Regional Studies*, vol. 41, no. 9, pp. 1193–1208, 2007.
- [4] A. E. Öztürk and S. Sözeri, “Diyanet as a Turkish foreign policy tool: evidence from The Netherlands and Bulgaria,” *Politics and Religion*, vol. 11, no. 3, pp. 624–648, 2018.
- [5] F. Guo, “Research on Hegel’s view of Practice,” *World Journal of Educational Research*, vol. 6, no. 3, p. p435, 2019.
- [6] A. Soo-Chan, “A meta analysis of Korean journalism studies: focus on the research papers in 12 journals (1990~2014),” *Korean Journal of Journalism & Communication Studies*, vol. 59, no. 6, pp. 246–280, 2015.
- [7] R. H. Mcguire and L. A. Wurst, “Struggling with the past,” *International Journal of Historical Archaeology*, vol. 6, no. 2, pp. 85–94, 2002.
- [8] J. Favret-Saada, “Benjamin and us,” *Hau Journal of Ethnographic Theory*, vol. 4, no. 3, pp. 317–328, 2014.
- [9] E. H. . Louai, “Retracing the concept of the subaltern from Gramsci to Spivak: historical developments and new applications,” *African Journal of History and Culture*, vol. 4, no. 1, 2012.
- [10] C. S. Dempwolf and L. W. Lyles, “The uses of social network analysis in planning: a review of the literature,” *Journal of Planning Literature*, vol. 27, no. 1, pp. 3–21, 2012.
- [11] A. Ayman, K. Mohammed Saidul Huq, S. Mumtaz, K.-F. Tsang, and J. Rodriguez, “Low-cost on-demand C-RAN based mobile small-cells,” *IEEE Access*, vol. 4, pp. 2331–2339, 2016.
- [12] R. G. Rajan and L. Zingales, “The firm as a dedicated hierarchy: a theory of the origins and growth of firms,” *Quarterly Journal of Economics*, vol. 116, no. 3, pp. 805–851, 2001.
- [13] M. Bould, “The dreadful credibility of absurd things: a tendency in fantasy theory,” *Historical Materialism*, vol. 10, no. 4, pp. 51–88, 2002.
- [14] C. H. Cao, Y. N. Tang, and D. Y. Huang, “IIBE: An Improved Identity-Based Encryption Algorithm for WSN Security,” *Security and Communication Networks*, vol. 2021, Article ID 8527068, 2021.
- [15] D. Wu, C. Zhang, L. Ji, R. Ran, H. Wu, and Y. Xu, “Forest fire recognition based on feature extraction from multi-view images,” *Traitement du Signal*, vol. 38, no. 3, pp. 775–783, 2021.
- [16] L. Wang, C. Zhang, and Q. Chen, “A Communication Strategy of Proactive Nodes Based on Loop Theorem in Wireless Sensor Networks,” in *Proceedings of the 2018 Ninth International Conference on Intelligent Control and Information Processing (ICICIP)*, pp. 160–167, Wanzhou, China, November 2018.
- [17] H. Li, D. Zeng, and L. Chen, “Immune Multipath Reliable Transmission with Fault Tolerance in Wireless Sensor Networks,” in *Proceedings of the International Conference on Bio-Inspired Computing: Theories and Applications*, pp. 513–517, Springer, Singapore, January 2016.
- [18] M. J. Fortner, “The “silent majority” in black and white,” *Journal of Urban History*, vol. 40, no. 2, pp. 252–282, 2013.
- [19] C. Hay, “The obligation to resist oppression,” *Journal of Social Philosophy*, vol. 42, no. 1, pp. 21–45, 2011.
- [20] S. S. Fainstein, “My career as a planner,” *Journal of the American Planning Association*, vol. 80, no. 3, pp. 268–275, 2014.
- [21] S. A. . McClennen, “Exilic perspectives on “alien nations,”” *CLCWeb: Comparative Literature and Culture*, vol. 7, no. 1, pp. 45–55, 2005.
- [22] E. Sine, M. K. Schmidt, D. Bocquet et al., *Planning Perspectives*, vol. 26, no. 4, pp. 663–682, 2011.
- [23] A. Antliff, “Anarchist modernism: art, politics, and the first American avant-garde,” *Journal of American History*, vol. 10, no. 1, pp. 670–671, 2004.
- [24] T. Dai, “The applicative research on DOI in the digital publication of Chinese sci-tech journals,” *Management & Engineering*, no. 18, pp. 47–50, 2015.
- [25] Y. Mei, Z. Shihui, and Z. Wanlan, “The analysis of knowledge base, theme evolution and research hotspot of ideological and political theory course in Colleges and universities based on CiteSpace,” in *Proceedings of the 2021 2nd international conference on artificial intelligence and education (ICAIE)*, pp. 460–467, 2021.
- [26] Y. Liu, S. Chen, and B. Guan, “Layout optimization of oil-gas gathering and transportation system in constrained three-dimensional space,” *Chinese Science Bulletin*, vol. 65, no. 9, pp. 834–846, 2020.
- [27] Y. Liu, S. Chen, B. Guan, and P. Xu, “Layout optimization of large-scale oil-gas gathering system based on combined optimization strategy,” *Neurocomputing*, vol. 332, no. 7, pp. 159–183, 2019.
- [28] B. Guan, S. Chen, Y. Liu, X. Wang, and J. Zhao, “Wave patterns of (2+1)-dimensional nonlinear Heisenberg ferromagnetic spin chains in the semiclassical limit,” *Results in Physics*, vol. 16, Article ID 102834, 2020.
- [29] Y. Song, K. Du, and Z. Xu, “Knowledge mapping analysis to research of symbiosis based on big data method,” in *Proceedings of the 2021 2nd international conference on big data*

## Research Article

# Research on the Change in Public Art Landscape Pattern Based on Deep Learning

Lei Zhao  and Congcong Tang 

*School of Architecture and Art Design, Hebei Academy of Fine Arts, Shijiazhuang 050700, China*

Correspondence should be addressed to Lei Zhao; zhaolei2021@hbafa.edu.cn

Received 7 February 2022; Revised 16 March 2022; Accepted 21 March 2022; Published 11 May 2022

Academic Editor: Man Fai Leung

Copyright © 2022 Lei Zhao and Congcong Tang. This is an open access article distributed under the Creative Commons Attribution License, which permits unrestricted use, distribution, and reproduction in any medium, provided the original work is properly cited.

With the limited design level of urban external space and place environment, however, the city image design and public art design play an important role in urban development, which leads to the lack of rational understanding that vague urban style is the effective implementation. In this article, a deep learning model is proposed to study the changes in public art landscape pattern in urban space, and it is constantly found that the changes in urban spatial layout have an impact on urban development. Firstly, the landscape index was analyzed effectively, and the Markov model was used to predict land use change, which provided a theoretical basis for the analysis of urban landscape change. Then the GeoSOS-FLUS model based on deep learning is used to make up for the lack of diversity of land use types by using the suitability probability calculation module of ANN and the adaptive inertia and competition mechanism, and the competition between different land use types is introduced. The experimental results show that the GeoSOS-FLUS framework based on deep learning model has good prediction effect and application ability.

## 1. Introduction

With the prevalence of art planning forms that use public art to render urban vitality and promote urban culture in major cities, public art works gradually assume the important role of “city business cards.” The research on the dynamic change in artistic landscape in public places shows that landscape structure, landscape function, and landscape spatial pattern are the core issues of landscape ecology. Landscape pattern refers to the arrangement of landscape patches with different sizes, shapes, and attributes in landscape space. Literature [1] elaborates that people’s environmental needs for public streets far exceed simple material enjoyment but pay more attention to people’s real feelings about landscape structure. Literature [2] describes the Humanistic design of public places around the characteristics of art design and city image. Literature [3] analyzes the three intervention ways of cities’ art design in public territory, and then analyzes how to apply public art design in public territory from four aspects, namely scientific and technological innovation, experience service, interaction and cooperation, and citizen aesthetics,

so as to build a good city image and promote the new round of construction and development of urban culture. In literature [4], the combination of public art landscape pattern design and regional culture is studied. Literature [5] focuses on the two characteristics of public space and public art in urban centers and studies the relationship among public art, people, and natural environment. The paper expounds how to combine the characteristics of the city to carry out artistic transformation [6]. Literature [7] describes the concept of public art design, literature [8] thinks around the concept of public art design, and literature [9] expounds that the change in landscape pattern is due to the process of landscape change. Understanding the driving mechanism of landscape pattern evolution is the premise and foundation of landscape pattern analysis combined with patch scale. Literature [10] describes the quantitative research method of landscape pattern. Literature [11] shows the changes in landscape pattern indicators to different landscape patterns, and the main data source of literature [12] is remote sensing images, which systematically studies the evolution of landscape pattern from three aspects: situation, relationship, and



mechanism. Literature [13] vividly expounds the characteristics of urban ecosystem landscape pattern and the development direction of landscape pattern optimization in literature [14], and literature [15] makes an in-depth study on public art design under the influence of history and culture. Literature [16] puts forward a method based on deep learning and uses landscape model to make two deforestation hotspots, which shows that the reliability of monthly forest harvesting mapping using Sentinel-1 data is high; the average IoU is superior to the traditional object-based method. Samples collected at a specific time in a place are trained, and sparse local samples from the new area are used for fine tuning to achieve the best performance. Therefore, when applied to a new research site, the workload of training data collection can be greatly reduced. Literature [17] is applied to urban landscape design and proposed the processing and application of urban landscape images to analyze landscape changes.

## 2. Publicity of Public Art

Public space is the material space carrier of people's public activities, communication and life, and the place of public life, which embodies the functional attributes of society. Because public space is changeable, that is to say, the ownership of space will change with time, urban space is the possibility of mutual transformation from private space to public space. Urban public space should be a region that concentrates all elements and functions in the city. This region can be a space shared by individuals and collectives, and they enjoy the services and convenience brought by this space. Urban public space is a traditional sense of public space, such as streets, riverside squares, parks, green spaces, etc. Today, it includes museums, shopping centers, transportation hubs, etc. The meaning of public space is becoming more broader. Words such as "popular," "common," "public pragmatic," and "shared" are used to describe "public." This shows from the side of a word that the characteristics of what we call public space lie in that it is different from the space form, which generally belongs to private field, nonpublic nature, and nonpublic welfare nature. Habermas thinks that publicity embodies fairness and democratization in all fields of society. His exposition is of great significance for explaining art about public areas. Herzberg thinks that "public" and "private" can be regarded as homosexual words related to "collective" and "individual," and the meaning of "public space" lies in the area that anyone can enter at any time. Publicity firstly means openness, no matter in principle or form, anyone can enter freely, and everyone has the right to express their opinions and be respected. Secondly, publicity means universal application, which specifically refers to the needs of all the contents in the public space that are applicable to all the subjects in the space. Finally, publicity also means public interests. Compared with emphasizing the interests of individuals, classes, and groups, publicity is the interests of all existing subjects, and the public sphere seeks public welfare rather than private interests. As a popular art, the essence of public art is to realize its social value through "publicity," regardless of its

appearance or design concept. Publicity must be a common feature of shared space and public art, and the publicity of shared space promotes the communication and sharing between people. As the art of shared space, shared art is to better serve the public and meet people's psychological and spiritual needs, and it is an effective way to realize the publicity of shared space (Figure 1).

*2.1. Development and Evolution of Rural Public Buildings.* The organizational form of rural public buildings has changed from autonomous form to organized form in the early stage of the founding of the People's Republic of China. In the period of new rural construction, it presents a government-led organizational form. In terms of spatial characteristics, it has changed from the original closed and single to diversified and modern characteristics. The role of space is becoming more and more colorful. From the original traditional architectural forms such as stage, school, ancestral hall, and cooperative, the villagers' activity center with weaving and planning has gradually begun to form (Table 1).

*2.2. Digital Reform of Public Art.* The fundamental purpose of digital public art is to serve the public and meet the needs of the public. Communication thinking is the basic demand of the public for digital public art, and interactive thinking is the main guiding ideology. It is a form of interactive thinking in creation that creates communicative thinking. Communication thinking is a two-way interactive behavior, a unique expression of digital public art, and also the purpose of digital public art creation (Figure 2).

## 3. Study on Landscape Pattern

*3.1. Landscape Index Analysis Method.* Landscape index analysis is an extensive method for the quantitative evaluation of landscape bureau at present. Referring to previous research methods and combining with the characteristics of the study area, this article selects the indicators that can best reflect the landscape index from two types, patch type level and landscape level, to quantitatively describe the landscape pattern change process, and further expounds the relationship between the future trend and process of landscape in timescale in connection with ecological process. Four landscape classification vector maps in 2012, 2014, 2016, and 2018 were transformed into  $t_{ij}$  grid images with a granularity of 30 m by using ArcGIS.4.1 vector-to-grid theory, and then imported into Fragstats.4.2 software to calculate each landscape index.

This article analyzes the dynamic changes in landscape pattern from two levels: patch type level and landscape level. At the level of patch type, patch area (CA), landscape percentage (PLAND), patch number (NP), patch density (PD), landscape shape index (LSI), maximum patch area index (LPI), average patch area (AREA-MN), aggregation degree (AI), and cohesion index (COHESION) were selected. At the landscape level, patch number (NP), patch density (PD), landscape shape index (LSI), edge density (ED), perimeter area fractal dimension (PAFRAC),

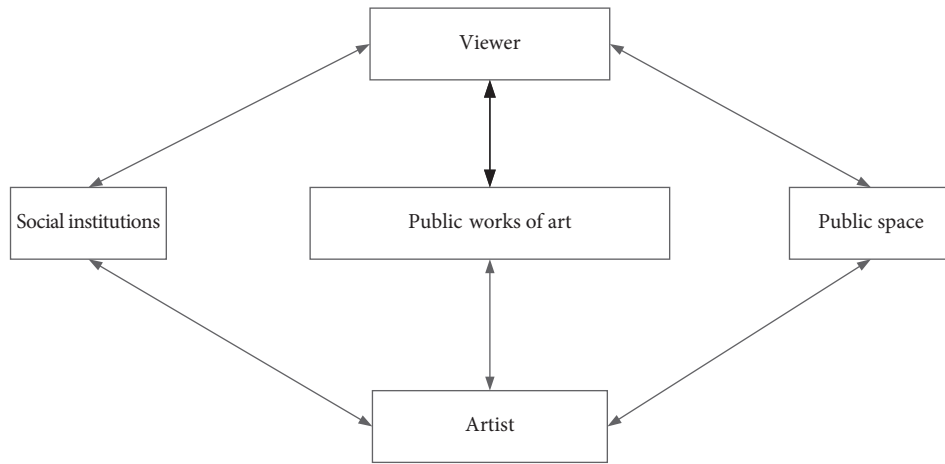


FIGURE 1: The relationship between shared works of art, shared space, viewers, social institutions, and artists.

TABLE 1: Changes in organizational forms and other characteristics of rural public buildings.

| Time  | Organizational form       | Spatial characteristics                    | Function of public space shelf                           | The nature of public space                          |
|---|---------------------------|--|--|---|
| Before the founding of the People's Republic of China | Self-organizing form      | Closed, single                             | Get outside information, living and entertainment places | Have a strong breath of life                        |
| Economic planning period                              | Organized form            | Open and unitary                           | The main place of political propaganda                   | Strong political color                              |
| After the reform                                      | Take "family" as the unit | Public space is diversified and modernized | Social place   | Diversification of public space forms               |
| New rural construction period                         | Passive organization      | Bottom-up construction mode                | Become the center of government activities               | There are no traditional customs in the countryside |

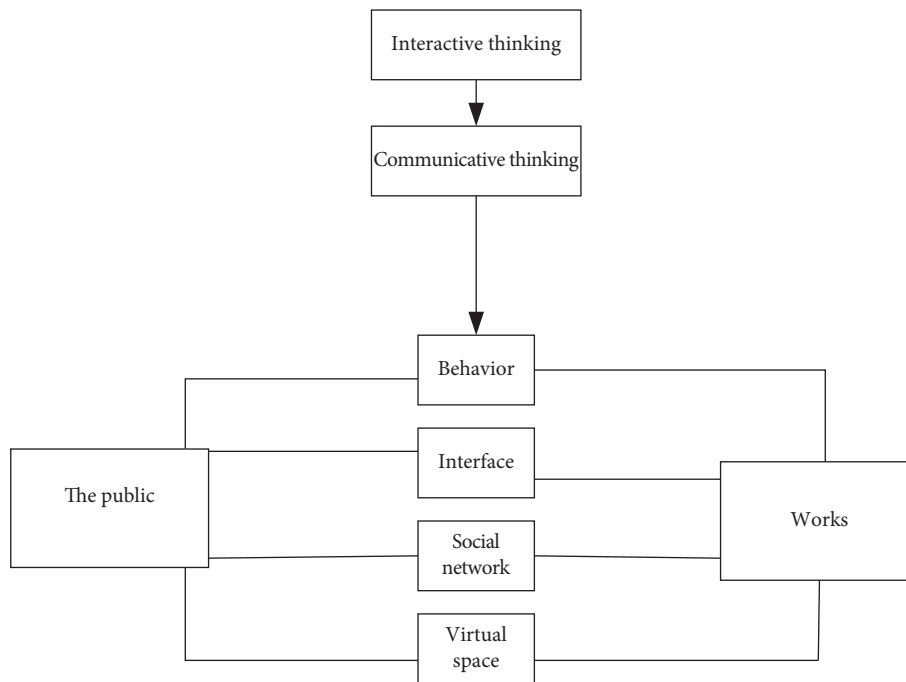


FIGURE 2: Digital public art.

maximum patch area index (LPI), aggregation degree (AI), cohesion index (COHESION), contagion degree (CONTAG), separation degree (DIVISION), Shannon diversity index (SHDI), and Shannon evenness index (SHEI) were selected. The ecological meaning of each index is listed in the Table 2:

(1) Plaque area  $CA$

$$CA = \sum_{j=1}^n a_{ij} \frac{1}{10000}, \quad (1)$$

where  $a_{ij}$  indicates the area of type  $i$  patch and  $n$  is the total number of type plaques.

(2) PLAND

$$PLAND = \frac{\sum_{j=1}^n a_{ij}}{A} (100), \quad (2)$$

where  $a_{ij}$  represents the covered area of patch  $j$  of type  $i$  and  $A$  is the overall landscape area, with a value of 0–100.

(3) Plaque number  $NP$

$$NP = N_i, \quad (3)$$

where  $N_i$  is the number of patches of type  $i$  or the total number in all landscapes.

(4) Plaque density  $PD$

$$PD = \frac{N_i}{A} (10000) (100), \quad (4)$$

where  $N_i$  is the total area of Class  $I$  landscape elements or the total area within all landscapes.

(5) Landscape shape index LSI

$$LSI = \frac{0.25E}{\sqrt{A}}, \quad (5)$$

where  $E$  is the total boundary length of patch type or landscape,  $LSI \geq 1$ , and there is no upper limit.

(6) Maximum patch area index LPI

$$LPI = \frac{\text{MAX}_{j=1}^n (a_{ij})}{A} \times 100. \quad (6)$$

Max is the maximum number of patches or landscape pixels that may be adjacent, and the value is 0–100.

(7) Average patch area  $AREA-MN$

$$\begin{aligned} AREA - MN &= LPI \\ &= \frac{\text{MAX}_{j=1}^n (a_{ij})}{N_i} \times \left( \frac{1}{10000} \right). \end{aligned} \quad (7)$$

(8) Degree of polymerization  $AI$

$$AI = \left[ \sum_{i=1}^n \left( \frac{g_{ii}}{\max g_{ii}} \right) p_i \right] (100). \quad (8)$$

$g_{ii}$  represents the number of adjacent pixels of type  $i$  or landscape patches, and  $p_i$  contains the landscape percentage of type  $i$  patches or landscapes, with a value of 0–100.

(9) Cohesion index COHESION

$$COHESION = \left[ 1 - \frac{\sum_{i=j}^m \sum_{j=1}^n d_{ij}}{\sum_{i=j}^m \sum_{j=1}^n d_{ij} \cdot \sqrt{a_{ij}}} \right] \frac{1}{[1 - \sqrt{A}]}. \quad (9)$$

$n$  is the total number of types of plaques and  $m$  is the number of all types. For example,  $d_{ij}$  is the perimeter of plaque  $ij$ , and the value is 0–10.

(10) Edge density  $ED$

$$ED = \frac{\sum_{j=1}^n e_{ij}}{A} (10000), \quad (10)$$

where  $e_{ij}$  is the total edge length of patches in the landscape.

(11) Perimeter area fractal dimension PAFRAC

$$PAFRAC = \frac{2(n_i \sum_{j=1}^n \ln a_{ij})}{\left[ n_i \sum_{i=1}^n (\ln a_{ij} - \ln d_{ij}) \right] - \left[ \left( \sum_{j=1}^n a_{ij} \right) \left( \sum_{j=1}^n d_{ij} \right) \right]}. \quad (11)$$

(12) Spreading degree CONTAG

$$CONTAG = \left[ 1 + \frac{\sum_{i=1}^m \sum_{k=1}^m [p_i (g_{ik} / \sum_{k=1}^m g_{ik})] [\ln p_i (g_{ik} / \sum_{k=1}^m g_{ik})]}{2 \ln(m)} \right], \quad (12)$$

where  $g_{ik}$  is the number of adjacent plaques of type  $i$  and type  $k$ , and the value is 0–100.

(13) Separation degree DIVISION

$$DIVISION = \left[ 1 - \sum_{i=j}^m \sum_{j=1}^n \left( \frac{a_{ij}}{A} \right)^2 \right], \quad (13)$$

(14) Diversity Index SHDI

$$SHDI = - \sum_{i=1}^m (p_i \ln p_i). \quad (14)$$

(15) Evenness index SHEI

TABLE 2: Landscape pattern analysis indicators.

| Serial number | Index name                          | English abbreviation | Meaning   | Horizontal level |
|---------------|-------------------------------------|----------------------|---|------------------|
| 1             | Patch area                          | CA                   | The total patch area of a certain patch type reflects the difference of information flow such as species, energy, and nutrients during the period.                        | Plaque type      |
| 2             | Percentage of landscape             | PLAND                | The ratio of a patch type to the total landscape area measures the dominant landscape elements of landscape components.   | Plaque type      |
| 3             | Number of patches                   | NP                   | The patch type indicates the total number of patches in a certain category.   | Plaque type      |
| 4             | Patch density                       | PD                   | Ratio of landscape area.  | Plaque type      |
| 5             | Landscape shape index               | LSI                  | Refers to the total edge length of patch type or landscape divided by the minimum possible value of the total edge length.  | Plaque type      |
| 6             | Maximum patch area index            | LPI                  | Refers to the proportion of the maximum patch area to the patch type area or landscape area.  | Plaque type      |
| 7             | Average patch area                  | AREA-MN              | The total area of a patch divided by the total number of patches.   | Plaque type      |
| 8             | Degree of polymerization            | AI                   | Refers to the number of nodes of patch type or landscape divided by the maximum number of nodes when the type or landscape first comes together.                          | Plaque type      |
| 9             | Cohesion index                      | COHESION             | Reflects the degree of aggregation of a certain type of patch or landscape.   | Plaque type      |
| 10            | Edge density                        | ED                   | The degree of edge segmentation is a direct response to the degree of landscape fragmentation.  | Plaque type      |
| 11            | Fractal dimension of perimeter area | PAFRAC               | Refers to the relationship between the shape and area size of landscape patches. When the value is 1–2, the closer the value is to 1, the more regular the patch shape is | Landscape type   |
| 12            | Spreading degree                    | CONTAG               | Describes the degree or extension trend of different patches in the landscape.  | Landscape type   |
| 13            | Separation degree                   | DIVISION             | Refers to the degree of separation of individual distribution of different patches in a landscape.  | Landscape type   |
| 14            | Shannon diversity index             | SHDI                 | Refers to the diversity of landscape elements or ecosystem structure and function changing with time.   | Landscape type   |
| 15            | Shannon evenness index              | SHEI                 | It reflects the uniformity of each patch in the area of landscape.  | Landscape type   |

$$SHEI = \frac{-\sum_{i=1}^m (pi, \ln pi)}{\ln(m)}, \quad (15)$$

$pi$  is the percentage of landscapes that contain type  $i$  patches or landscapes,  $\ln pi$  is the logarithm of the landscape percentage.

### 3.2. Analysis Method of Spatial Development Pattern

3.2.1. *Markov Prediction Model.* Markov model was put forward by Soviet mathematician Markov, which is often used to predict land use transformation, and it is also called discrete-time stochastic process model Markov chain. This model emphasizes the stochastic process with discrete states and is a probabilistic prediction method based on stochastic processes. Therefore, the model has time homogeneity, that is, during the transition from time  $T_{n-1}$  to time  $T_n$ , it is found that the state of the system at time  $T$  is only related to the state of the system at time  $T_{n-1}$  in a certain period of time. The process of land use type conversion has typical Markov model characteristics. In a specific area, land use types can be converted to each other, However, the transformation between land use types is predicted and expressed by mathematical functions, which is the most distressing. Markov model can obtain the conversion probability matrix

of land use according to the state of land use at the beginning and end of the period, so as to predict the future land use. Its calculation process is as follows:

$$C_{Tn} = C_{Tn-1} \times P, \quad (16)$$

$$P = P_{ab}$$

$$= \begin{bmatrix} P_{11} & \cdots & P_{1n} \\ \vdots & \ddots & \vdots \\ P_{n1} & \cdots & P_{nn} \end{bmatrix}$$

In the formula,  $P$  denotes the probability of conversion between various types of land in the region,  $P_{ab}$  denotes the probability of conversion of land use type  $a$  to  $b$ ,  $n$  denotes land use type  $n$  in formula (17) and the total number of land use types in formula (17), so the matrix should satisfy the following two conditions:

$$0 \leq P_{ab} \leq 1, \quad (17)$$

$$\sum_{b=1}^n P_{ab} = 1 \quad (a, b = 1, 2, 3, \dots, n)$$

Therefore, when  $n = 0$ , that is, at the initial time, the matrix of land use type state is as follows:

$$C^{(0)} = [C_1^{(0)} \ C_2^{(0)} \ C_3^{(0)} \ \dots \ C_n^{(0)}]. \quad (18)$$

The land use status after  $n$  times of land use type conversion can be expressed as follows:

$$C^{(n)} = C^{(0)} \times P^{(n)}, \quad (19)$$

where  $P^{(n)}$  is the probability matrix of the land use type at the initial moment after  $n$  transformations, so:

$$\begin{aligned} C^{(n)} &= C^{(n-1)} \times P = C^{(n-2)} \times P^2 \\ &= C^{(n-3)} \times P^3 = \dots \dots C^{(0)} \times P^n, \end{aligned} \quad (20)$$

$$\text{Get: } P^{(n)} = P^n.$$

In  $C^{(n)} = C^{(n-1)} * P^1 = C^{(n-2)} * P^2 = C^{(0)} * P^n$  formula, the sum of the exponents of the variables on the left and right sides of the equal sign is always equal to  $n$ .

Therefore, according to the land use state and probability matrix at the initial time, the land use state at any time in the future can be calculated. The conversion between land use types depends on the land use status. By studying the state transition of land use types at the initial and final moments in a certain time, the probability matrix describes the change value of each point in the process of land use transition probability. According to the land use state at the initial moment, the land use, evolution law, and development trend at any time in the future can be predicted.

**3.2.2. GeoSOS-FLUS Model.** The change in urban spatial development pattern is manifested in the change in land use and has large spatial autocorrelation. Traditional analysis models of urban spatial development pattern include CA and its improved model. This kind of model is widely used in the delineation of urban growth boundary and the spatio-temporal dynamic simulation of urban land use. However, because the cellular automata model only pays attention to the conversion between urban construction land and non-construction land, ignoring the diversity of land use types, it cannot meet the reality of analyzing the conversion between various types of land. The GeoSOS-FLUS model contains module 1: ANN-based suitability probability calculation module (ANN-based suitability probability estimation); and module 2: self-adaptive inertia and competition mechanism CA based on autonomous adaptive inertial mechanism. CA model makes up for the lack of diversity of land use types, and the model introduces the competition between different land types, reflects the relationship between various land use types, and proposes the nonconstruction area as the ecological constraints of FLUS model, more realistic simulation ability. Cellular automaton model is the most commonly used network dynamics model. Network dynamics models include cellular automata, Boolean networks, neural networks, and L-systems. Cellular automata are dynamic models with discrete time and space.

Module 1: The suitability probability calculation based on neural network is used to analyze the suitability probability of mutual conversion among various land use types. The probability is related to the current situation of urban

land use and the driving factors affecting urban spatial expansion. Generally, natural influence factors and human influence factors are included, and root mean square error (RMSE) is provided in the calculation results to test the accuracy of the simulated plot. The sum of suitability probabilities for all land use types of a grid in the simulated plot is 1, and the formula is as follows:

$$sp(p, i, t) = \sum_j w_{i,j \times 1/1+e^{-net(p,t)}} \sum_j sp(p, i, t) = 1. \quad (21)$$

where  $sp(p, i, t)$  is the calculated suitability probability,  $i$  is the land use type,  $p$  represents the grid,  $j$  is the set hidden layer,  $w_{ij}$  is the weight, and  $net(p, t)$  is the received signal.

Module 2: The suitability probability data obtained by the above modules are imported into module 2 for analysis, and the land use data of previous years are input. The parameters such as the ability, rules, iteration times, and limiting conversion conditions between land use types are set, and the future land use results are obtained by simulation. FLUS model adopts selection method to realize the competitive relationship between each different land. In the simulation process, the total probability of convertible land use type on grid  $p$  is calculated, and then the land use type  $i$  is given to grid  $p$ , and the formula is as follows:

$$\begin{aligned} TP_{p,i}^t &= sp(p, i, t) \times Inertia_i^t \\ &\cdot \left( 1 - sc_{c \rightarrow i} \times \frac{\sum_{N \times N} \text{con}(c_p^{t-1} = i)}{N \times (N-1)} \right) \times W_i, \end{aligned} \quad (22)$$

where  $TP_{p,i}^t$  is an index of the total probability of land use type  $i$  on grid  $p$  at  $t$  time node,  $sc_{c \rightarrow i}$  is an index of the cost of land use type conversion,  $\sum_{N \times N} \text{con}(c_p^{t-1} = i)$  is the quantitative index of land use type  $i$  in the calculation results, and  $W_i$  represents the domain weight of various land use types.

## 4. Experimental Part

**4.1. Model Testing.** In this article, GeoSOS-FLU model is used to study and analyze the future land use from the perspective of deep learning, and the model needs to be tested before using this model.

**4.1.1. Model Comparison.** We compare Markov prediction model with GeoSOS-FLU model, evaluate and analyze the future land use, and compare their accuracy (Figure 3).

By comparing the two prediction models, GeoSOS-FLU model is more suitable for the calculation of land use transformation than Markov model, and the accuracy is above 60%, which shows that this model is more suitable for future land use analysis.

**4.1.2. Performance Comparison.** In this experiment, the neural network-based suitability calculation method of GeoSOS-FLU model proposed in this article is compared

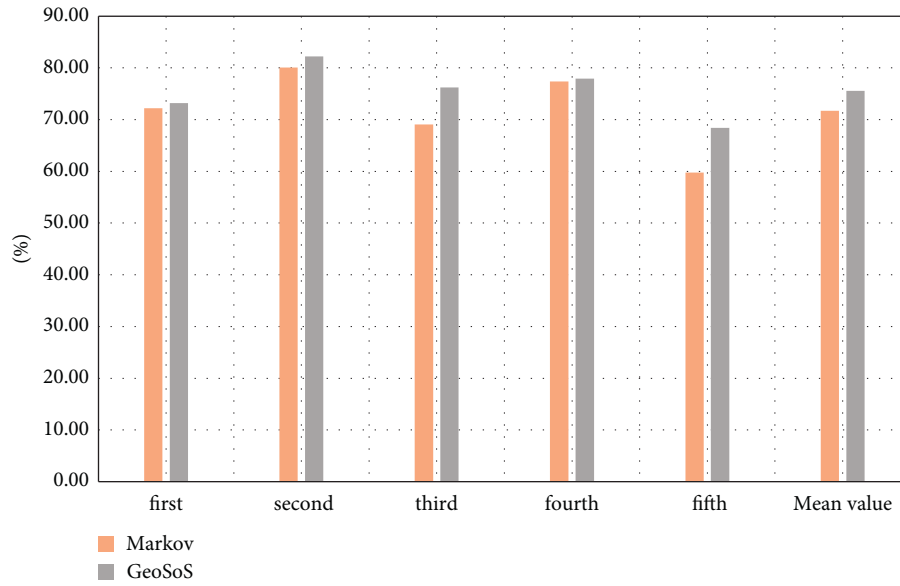


FIGURE 3: Model comparison of Markov and GeoSoS.

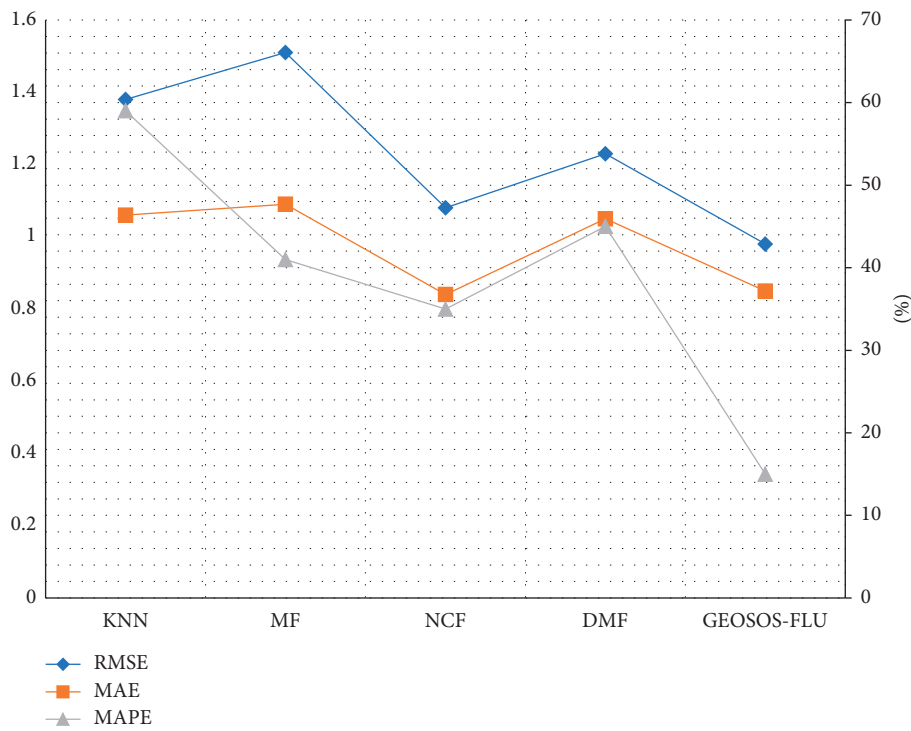


FIGURE 4: Performance comparison of different models.

TABLE 3: Comparative experiment of deep learning model.

| Type       | Accuracy | Precision | Recall | F1     | AUC    |
|------------|----------|-----------|--------|--------|--------|
| LR         | 0.7990   | 0.8401    | 0.8728 | 0.8561 | 0.7557 |
| SVM        | 0.8324   | 0.8464    | 0.9229 | 0.8830 | 0.7793 |
| FM         | 0.8431   | 0.8552    | 0.9281 | 0.8902 | 0.7933 |
| DNN        | 0.8440   | 0.8554    | 0.9294 | 0.8908 | 0.7939 |
| DeepFM     | 0.8485   | 0.8603    | 0.9297 | 0.8937 | 0.8008 |
| PNN        | 0.8576   | 0.8646    | 0.9392 | 0.9004 | 0.8098 |
| GeoSOS-FLU | 0.8768   | 0.8780    | 0.9599 | 0.9171 | 0.8279 |

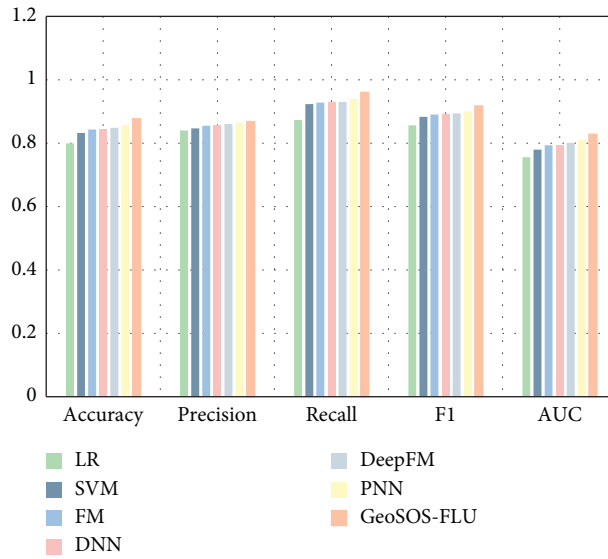


FIGURE 5: Comparative test.

TABLE 4: Index survey result.

| Land type          | Patch area | Number of patches | Landscape shape index | Dispersion index | Degree of polymerization |
|--------------------|------------|-------------------|-----------------------|------------------|--------------------------|
| Farming            | 568.11     | 650               | 23.24                 | 100.34           | 93.21                    |
| Grassland          | 233.21     | 346               | 43.45                 | 93.5             | 96.34                    |
| Woodland           | 500.57     | 345               | 32.67                 | 38.71            | 83.21                    |
| Place of residence | 343.37     | 678               | 78.32                 | 76.34            | 93.41                    |
| Mining site        | 277.66     | 56                | 38.21                 | 84.00            | 90.32                    |
| Water area         | 8.92       | 124               | 67.02                 | 37.00            | 92.21                    |

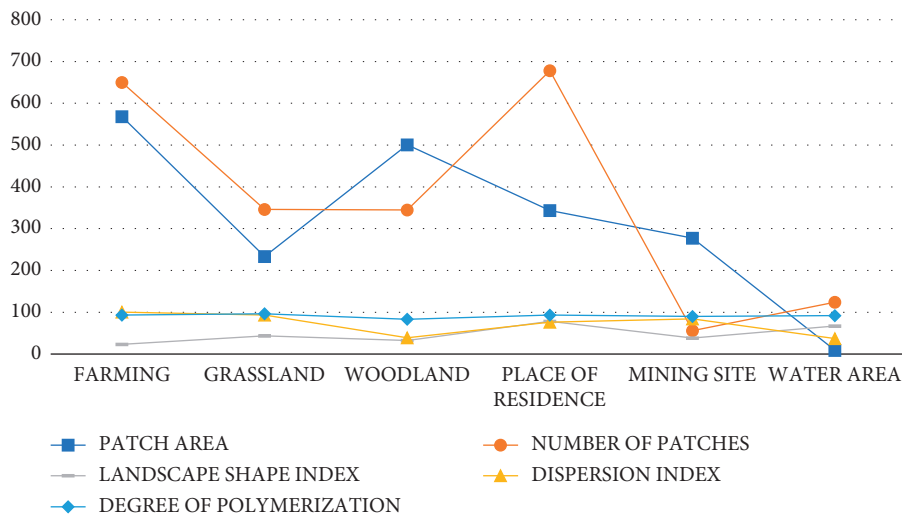


FIGURE 6: Index analysis diagram of six landscape patterns.

with (KNN, MF, NCF, and DMF). The final experimental results are shown in Figure 4:

It can be seen from the experimental results that the deep learning GeoSOS-FLU model has achieved better evaluation results than KNN, MF, NCF, and DMF methods. GeoSOS-

FLU model has the smallest difference between RMSE and MAE and has obvious advantages in model execution results. In the MAPE evaluation, the MAPE of GeoSOS-FLU model has the minimum value, and the evaluation of the model has a good performance.

TABLE 5: Land use type area and change range from 2012 to 2018.

| Land type       | Area ( $km^2$ ) |           |           | Amplitude of change (%) |                |           |
|-----------------|-----------------|-----------|-----------|-------------------------|----------------|-----------|
|                 | 2014 Year       | 2016 Year | 2018 Year | 2012-2014 Year          | 2014-2016 Year | 2016-2018 |
| Cultivated land | 7330.23         | 9340.44   | 13034.67  | 9.2%                    | -0.3%          | 12.3%     |
| Woodland        | 8999.32         | 10034.21  | 15880.11  | -2.1%                   | -3.1%          | 5.3%      |
| Grassland       | 10002.1         | 8977.3    | 6668.1    | -10.2%                  | -1.2%          | 11.3%     |
| Water area      | 12005.2         | 10344.3   | 9998.2    | 3.19%                   | 1.05%          | 7.4%      |

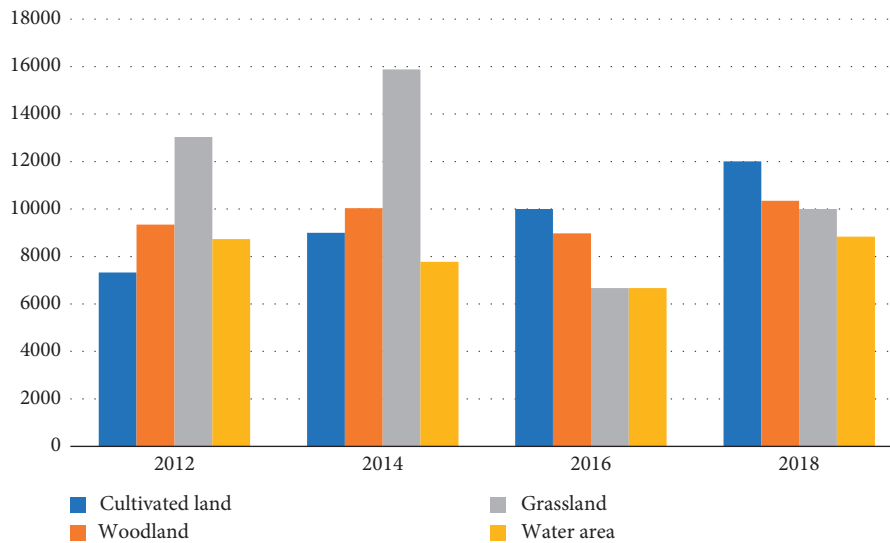


FIGURE 7: Landscape pattern in different years.

GeoSOS-FLU model is the best learning method for future land use analysis and research. GeoSOS-FLU model has stronger prediction ability, flexibility, and accuracy.

4.1.3. *Contrast Experiment.* In this article, LR, SVM, FM, DNN, DeepFM, and PNN deep learning models are compared with GeoSOS-FLU deep learning models. The results are shown in Table 3:

According to the data in the table, a chart is drawn as shown in Figure 5.

From the experimental results in Figure 5, it can be seen that the accuracy and AUC of GeoSOS-FLU model are improved by 2.3% compared with the best traditional method, and the three indexes of precision, recall, and F1 are also significantly improved. By comparing the models proposed in this article, good evaluation results have been achieved.

4.2. *Application Effect of Landscape Pattern Change Model.* Using the model of landscape pattern change in this article, the landscape pattern change of a certain area is analyzed and studied based on the landscape index of that region.

4.2.1. *Survey Results of Five Landscape Indexes.* Six different land types were selected, according to the patch area, patch number, landscape shape index, dispersion index, and aggregation of five landscape indexes on the future changes in

landscape pattern of the impact of specific analysis (Table 4 and Figure 6).

Based on GeoSOS-FLU model, some land types, landscape indexes of different regions, and analysis factors matching with specific regions are selected, and a perfect index system is constructed to expand the practicality of the study.

4.2.2. *Index Survey Results in Different Years.* In different periods, four different types of land were selected, according to the patch area, patch number, landscape shape index, dispersion index, and aggregation degree of these five landscape indexes to analyze the landscape pattern change range (Table 5 and Figure 7).

## 5. Conclusion

With the rapid development of economy, the natural environment in which we live has gradually lost its original balance system, and how the landscape pattern will change dynamically in the future has become a problem that we need to predict now. Mastering the future utilization rate of land has also become an answer that people are eager to get. The landscape pattern change model under deep learning proposed in this article can analyze the future change trend in landscape pattern more accurately. The research results show that:



- (1) By comparing GeoSOS-FLU model with Markov prediction model, the accuracy of GeoSOS-FLU model is over 60% in five comparisons and it is higher than Markov prediction model.
- (2) In the model comparison stage, GeoSOS-FLU deep learning method is compared with several traditional methods (KNN, MF, NCF, and DMF), and the RMSE, MAE, and MAPE of GeoSOS-FLU method are higher than the other four traditional methods.
- (3) Compared with the best traditional method, the accuracy and AUC of GeoSOS-FLU model are improved by 2.3%, and the accuracy, recall, and F1 of GeoSOS-FLU model are also improved significantly.
- (4) Through the analysis of five landscape indexes of six different land types, such as patch area, patch number, landscape shape index, dispersion index, and aggregation degree, it is concluded that the dynamic analysis of landscape pattern mainly depends on two levels, namely patch type level and landscape level.
- (5) In order to analyze the changing trend in landscape pattern, the cultivated land area increases year by year, the grassland and water area decrease year by year, and the woodland area tends to be balanced [18–25].

## Data Availability

The experimental data used to support the findings of this study are available from the corresponding author upon request.

## Conflicts of Interest


The authors declared that they have no conflicts of interest regarding this work.

## References

- [1] W. Feng, J. Hu, and M. Funk, "Practice and experience evaluation of interactive digital public art design," *Zhuangshi Chinese Journal of Design*, vol. 9, pp. 96–97, 2015.
- [2] J. Sharp, V. Pollock, and R. Paddison, "Just art for a just city: public art and social inclusion in urban regeneration," *Urban Studies*, vol. 42, no. 5/6, pp. 1001–1023, 2005.
- [3] Y. Lei and w. Yang, "Exploring the intervention and application of public art design in urban public space," *Western Leather*, vol. 43, no. 8, p. 2, 2021.
- [4] F. Xia, "Research on regional cultural integration in public art landscape design," *Think Tank Era*, vol. 3, no. 18, p. 2, 2019.
- [5] J. M. Zhou, "Environment and space-public art design in city," *Journal of Hubei University of Technology*, vol. 16, no. 3, pp. 11–12, 2001.
- [6] E. Heffernan, T. Heffernan, and W. Pan, "The relationship between the quality of active frontages and public perceptions of public spaces," *Urban Design International*, vol. 19, no. 1, pp. 92–102, 2014.
- [7] G. Liu, "The casting of soul-thinking on the concept of public art design," *The Literary Review*, vol. 6, p. 3, 2006.
- [8] J. Cai and T. Xu, "Infiltration of ecological concept in the design of small and medium-sized rivers treatment project," *Jiangxi Building Materials*, vol. 7, pp. 110–112, 2019.
- [9] Q. Zhang, B. Fu, and L. Chen, "Several problems on the study of landscape pattern evolution," *Journal of Geography Science*, vol. 11, no. 3, pp. 264–270, 2003.
- [10] J.-t Zhang, Y. Qiu, and F.-y Zheng, "Quantitative research method of landscape pattern," *Acta Montana Sinica*, vol. 18, no. 4, p. 7, 2000.
- [11] L. I. Xiuzhen, B. U. Rencang, C. Yu et al., "The response of landscape metrics against pattern scenarios response to different landscape patterns," *Acta Ecologica Sinica*, vol. 24, no. 1, pp. 123–134, 2004.
- [12] W. Yue, *Study on Urban Landscape Pattern and its thermal Environment Effect Based on Remote Sensing Images*, Science Press, Beijing, China, 2008.
- [13] W. Li, Z. Ouyang, R. Wang, and X. Wang, "Landscape pattern characteristics and formation mechanism of urban ecosystem," *Journal of Ecology*, vol. 24, no. 4, p. 5, 2005.
- [14] W. Han, Y. Chang, Y. Hu, X. Li, and R. Bu, "Research advance in landscape pattern optimization," *Chinese Journal of Ecology*, vol. 24, no. 12, pp. 1487–1492, 2005.
- [15] X. Zhang and W. University, "Research on design strategy of public art from the perspective of urban culture," *Journal of Yancheng Institute of Technology*, vol. 32, no. 2, pp. 87–90, 2019.
- [16] F. Zhao, R. Sun, L. Zhong et al., "Monthly mapping of forest harvesting using dense time series Sentinel-1 SAR imagery and deep learning," *Remote Sensing of Environment*, vol. 269, Article ID 112822, 2022.
- [17] S. Shumack, P. Hesse, and W. Farebrother, "Deep learning for dune pattern mapping with the AW3D30 global surface model," *Earth Surface Processes and Landforms*, p. 45, 2020.

## Research Article

# Design and Research of Dynamic Evolution System in Football Tactics Under Computational Intelligence

Jianming Wang<sup>1</sup> and Jing Chen<sup>2</sup> 

<sup>1</sup>Department of Physical Education, Tongling University, Tongling 244061, Anhui, China

<sup>2</sup>Department of Physical Education, Jiangsu University, Zhenjiang 212013, Jiangsu, China

Correspondence should be addressed to Jing Chen; jean0430@ujs.edu.cn

Received 7 March 2022; Revised 11 April 2022; Accepted 19 April 2022; Published 11 May 2022

Academic Editor: Man Fai Leung

Copyright © 2022 Jianming Wang and Jing Chen. This is an open access article distributed under the Creative Commons Attribution License, which permits unrestricted use, distribution, and reproduction in any medium, provided the original work is properly cited.

With the rapid development of computer vision, it has been widely used in football. Aiming at the problems of incomplete collection of information, poor operability of system, and bad practical application in the field of football match, an analysis system of football tactics is designed in this paper. Combining the requirements of functions and performance, the analysis system is divided into management of basic information, collection of tactical information, detection of passing pattern, inquiry of tactical information, and visual display, which puts forward the method of the detection of passing pattern based on model. Through the intelligent design, the visual display of the information of athlete, team, competition, tactics, and passing pattern is realized under computational intelligence, which has certain practical value in application.

## 1. Introduction

Football is the most popular competitive sport in the world, which attracts hundreds of millions of spectators and has high commercial value. It is not only colorful in technology but also unpredictable in tactics that its flexibility and variability attract countless audiences to be fascinated, and it also stimulates the enthusiasm of research by scholars. Strategies are a significant component that influences the presentation of football players, and whether it is applied properly is the decisive factor that affects the result of football matches [1]. Consequently, to work on the strategic level in football, it is important to set up a logical strategic examination framework to help mentors to settle on logical choices by concentrating on the strategic principles in football.

With the rapid development of computer vision, computer vision technology has been widely used in football. Examples include video assistant referee (VAR) and goal line technology. In recent years, computer intelligent algorithm has been widely used in the tactical decision-making research of competitive football. Machine learning algorithms

are used to make judgements about events and situations during matches and perform qualitative or quantitative analysis of the attributes of the event, such as rating the quality of threatening shots or passes. In addition, Artificial Neural Networks (ANN) are often used in the research of football tactics, which can analyze tactics according to position data. By running a simulation to see how Artificial Intelligence (AI) teams behave in certain situations, AI teams are created by “ghosting” the features of ordinary and top teams. Deep imitation learning is used here by AI teams to compare the actions of their players to the league average or the top teams in the league.

Thanks to these devices and technologies, people can easily collect a large number of fine-grained data in football matches, such as the behavior and spatial position of players at every moment, so as to master the tactical skills and rules of football players. In addition, with the help of computer technology, collecting and processing complex data of football matches to complete football tactical analysis has become the current focus, which has high academic value and broad prospects of application. At present, some scholars have studied the analysis system of football tactics,

put forward the information collection scheme consistent with the football match, and established the model of corresponding data [2]. The video information is integrated into the tactical information, and at the same time, simple data is input by mouse and keyboard to analyze more complicated information intelligently, which breaks away from the traditional manual statistical mode to the maximum extent [3]. However, the systems are only limited to the collection of football tactical information, which is lack of detection on football tactical tracking. Based on this, the design of analysis system of football tactics in this paper can extract useful information from football matches more conveniently and make the collected data more complete, which is of practical significance to the development of China's football industry.

## 2. Requirements Analysis of Football Tactical Analysis System

*2.1. Analysis Functional Requirements.* Football tactical analysis system is a subsystem of the research project of the State Sports General Administration. Its purpose is to realize the collection and tracking of football tactics information of players, so as to master the tactics skills and rules of football players and guide the daily training of players and the on-the-spot decisions of coaches.

The football tactical analysis system is an interactive system, which includes the detection module of backend passing pattern and the frontend visual analysis module, which concretely realizes the following basic functions.

*2.1.1. Management of Basic Information.* Management of basic information is the basic function of football tactics analysis system, which mainly manages information of players, teams, and competitions by adding, modifying, deleting, and inquiring.

*2.1.2. Collection of Tactical Information.* Collection of tactical information mainly includes the collection of the information of athlete's position and event. Among them, location information is collected by sensors, and event data is marked manually.

*2.1.3. Detection of Passing Pattern.* Passing pattern detection is the core function of football tactical analysis system, which provides the basis for tactical analysis. According to the players' passing strategies, their tendency is analyzed by focusing on the grasp of the scale of football passing and the judgement of their patterns and strategies.

*2.1.4. Inquiry of Tactical Information.* By inputting related keywords such as specific competitions, specific teams, and specific athletes, the tactical information of athletes can be searched and queried, and the categories of tactics and relevant information can also be inquired.

*2.1.5. Visual Display.* The visual display of football tactical analysis system mainly displays basic information management, collection of tactical information, detection of passing pattern, and inquiry of tactical information.

*2.2. Analysis of Performance Requirement.* In addition to meeting the functional requirements above, the system also needs to meet the performance requirements.

*2.2.1. Applicability.* Combined with the characteristics of the football field, the football tactical analysis system adopts the interface in mainstream design style, so that the operation of the interface is professional, simple, and smooth, which conforms to the operation habits of football practitioners [4]. In this paper, Action Script3.0 is adopted, and the interface of football tactics analysis system is designed by using programmable and visual operation mode. The function controls and football and player controls in the system can be redesigned and can be redeveloped by dragging and setting attribute, which will improve the applicability and expansibility of the system.

*2.2.2. Maintainability and High Scalability.* As the antagonistic sport of football is constantly developing, and the tactics and rules of football are constantly progressing [5], it is necessary that the football tactics analysis system designed in this paper has strong maintainability and high expansibility to ensure that football practitioners can continue to use the system through the expansion and maintenance of it when the demand for the system is expanded.

*2.2.3. Stability.* Football tactical analysis is not only used in normal teaching and training, but also used in on-the-spot matches. It is necessary to ensure the stability of the function when designing the function of football tactics analysis system [6]. If tactical analysis and rehearsal fail due to unstable functions, the consequences will be unimaginable.

*2.2.4. Sensitivity.* For the football tactics analysis system designed in this paper is mainly used for the analysis and rehearsal of football tactics, football practitioners need to explain and speak tactics [7] by controlling the football and players' controls, which requires the football tactics analysis system to be highly sensitive in the processing of control movement, and quickly respond to the user's actions, to make the tactics be explained smoothly.

## 3. Design of Football Tactics Analysis System

Combining the analysis of functional requirements and performance requirements of the football tactical analysis system, the overall framework and core functions of the system are designed.

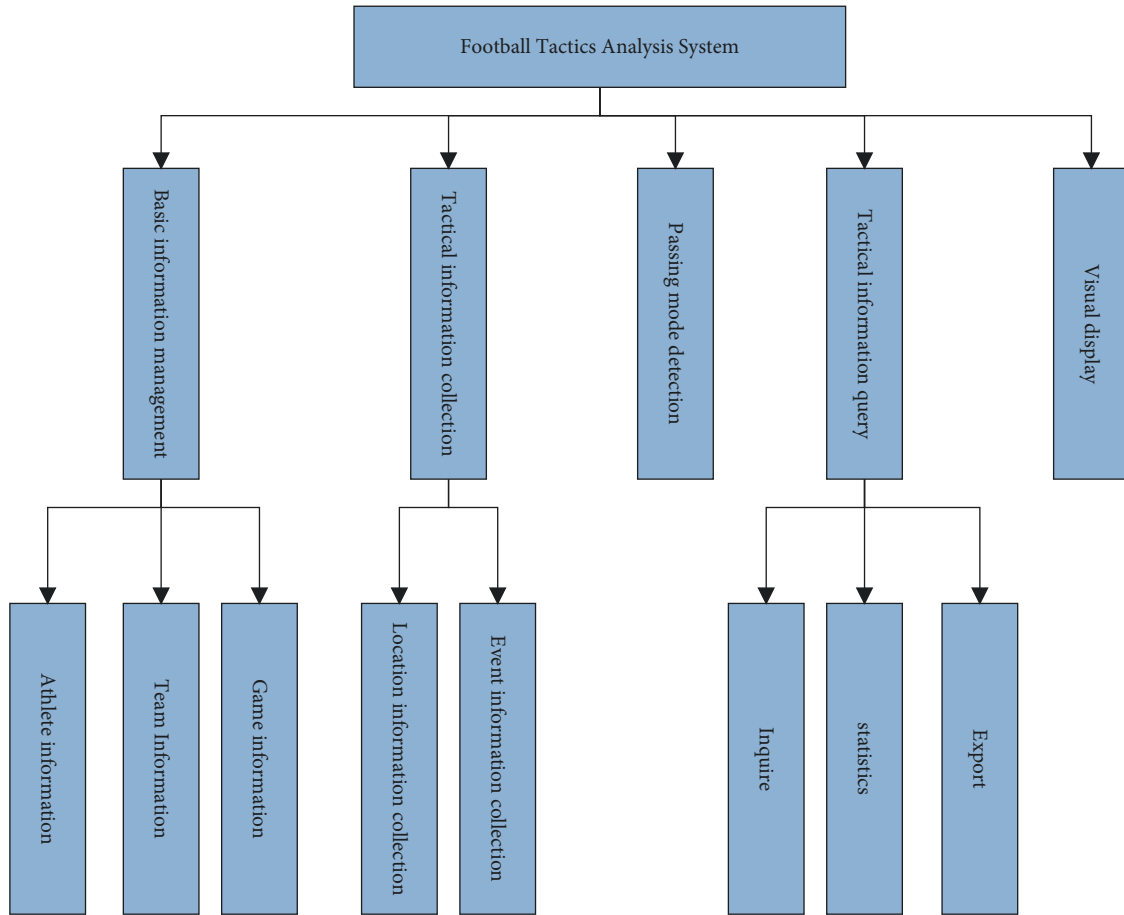


FIGURE 1: Functional structure diagram of football tactics analysis system.

3.1. *Requirements of System Architecture.* The architecture requirements of the football tactics analysis system designed in this paper are as follows:

- (1) The football tactics analysis system is designed with three-tier architecture, and the programming language is Action Script 3.0 [8].
- (2) The system runs in C/S mode.
- (3) Data storage of football tactics analysis system uses XML to process and interact with data [9].
- (4) The system adopts modular design [10], which enhances the expansibility of the system, reduces the coupling degree between the functional modules of the system, and provides convenience for the upgrade of the system.
- (5) The system is built with knowledge base [11], SQL SERVER 2005 is used to build the database for the data needed for retrieval, and XML documents are built for the information described by tactics and rules.

3.2. *Design of Core Function.* Through the demand analysis of football tactical analysis system, its core functions can be divided into management of basic information, collection of tactical information, detection of passing pattern, inquiry of

tactical information, visual display, and others. The functional structure of the system is shown in Figure 1.

The basic information module is the preparation part of data, including athlete information, competition information, etc. Passing pattern detection is the core function of football tactical analysis system. Tactical information collection, tactical information query, and visual display are the key modules of football tactical analysis system, which realize the collection logic and analysis and statistics logic, respectively.

3.2.1. *Basic Information Management.* The executives of essential data is comprised of three sections, specifically competitor data, group data, and contest data. Each sort of data is recorded by a different information base table in the data set. Athlete information, team information, and competition information are stored relatively independently, and the association among them is established in the database with the AthleteIn-Match table [12]. In the system, every kind of basic information can be added and modified.

Basic information is the important related information of tactical acquisition and the subject of information analysis, so it is very important to record basic information correctly. In the football tactics analysis system, the correctness of basic information will be checked, such as whether necessary information is added and whether the

team information and player information corresponding to the game are correct which will be further checked before data collection. For example, in a football match, each team is required to have 11 players. Before data collection, the system will automatically detect the number of players of the two teams in the match. When the basic information is incorrect, a prompt will be given correctly, and the data acquisition module will not be open.

**3.2.2. Collection of Tactical Information.** Module of collection of tactical information is the main logic module of football tactical analysis system. The module of game integrates the function of video playback, which can be played back in a single frame, fast forward, fast rewind, and select the playback speed [13]. It can be collected after opening the corresponding game video.

Collection tactical information mainly includes the data of position and event of players.

At present, scholars mainly use image gray information to segment images in video sequences [14]. However, the information of the image's original color is ignored when recognizing the football trajectory, so the results often have problems with large error and slow recognition speed. Compared with traditional tracking of pedestrian, athletes often move quickly with unpredictable directions, such as sudden stop, deceptive feint, and collision with players, which increases the difficulty of tracking. Therefore, the selection of acceleration sensor is adopted to collect data of players' position. Kalman filter model [15] is introduced to filter the data collected by sensors; the model [16] can be expressed by formula (1):

$$x_m = \phi_m x_m + \delta_m, \quad (1)$$

where  $x_m$  matrix represents system state,  $\phi_m$  represents a matrix of system state transition, and  $\delta_m$  indicates system noise. The data of motion trajectory is input into the Kalman filter model, and the new state data collected are sequentially input into the update equation to obtain the dynamic data of football motion trajectory with the elimination of noise. Then, the estimated value is updated, the noise variance and forward prediction are calculated according to the measured value, while the estimated value is returned to the Kalman filter model again, and the cycle is also repeated. Finally, the filtering is stopped until the motion of the soccer curve ball stops and all the values of updated input are 0.

Event data refers to a series of events that happen on the court [17], such as passing, shooting, and scoring. Event data is marked manually. Users browse the game video on an interactive interface and mark events by clicking and recording. A user needs about 90 minutes to complete the event collection of a game.

In the football tactical analysis system, a storage object and related processing method of technical information and tactical information in attack sequence are provided to realize the encapsulation of storage and management of tactical information [18], in which the storage objects of technical information and tactical information are sat Recs and tactics Rec, respectively. In the process of collecting,

every technical action is abstracted as the process of catching and delivering the football. The process corresponds to a technical record, which records the team in ball control, players in ball control, positions of starting and ending site, technical action types, video clips, and other information. The algorithm only needs to operate in the memory to realize the function of recovery, without frequently reading and writing, which improves the system effectively. The logic flow of acquisition is shown in Figure 2.

**3.2.3. Detection of Passing Pattern.** In the football tactical analysis system, detection of passing pattern is the core function where scholars mainly adopt the network-based method [19] and the sequence-based method [20]. The organization based technique totals players' passing records to get a coordinated graph [21], in which the hubs address players and the lines address recurrence of passing between players. Arrangement based strategy respects a progression of successive passes in a group assault as a grouping, while in view of the examination of example mining in arrangement information, the discovery of passing examples is like the model of text. The cooccurrence of players observed in the passing sequence is the result of implementing the passing strategy (which cannot be directly observed in the data) [22]. This is very similar to the idea of topic modeling; that is, the cooccurrence of word observed in natural text sequences is determined by the potential subjects [23].

On the basis of previous results, the detection of passing patterns based on topic model is proposed [24].

According to the passing strategy, players have a tendency to pass the ball. For example, when adopting the long pass strategy, the defender tends to pass the ball directly to the striker and attack. In this attack mode, the striker and defender will appear in the passing sequence at the same time with high frequency, while that is relatively rare in the midfield. Therefore, different strategies will lead to different cooccurrence modes of players, where patterns can make a more in-depth analysis of passing strategies. Therefore, subject modeling is used to detect the passing pattern, as shown in Figure 3.

First, establish a dictionary of players. For each stage, the continuous passing is transformed into a player sequence (A). Then, the model of word bag is used to transform the sequence of players into the one-hot vector pattern (B), where a number of football stages constitute the text library in the model. The text library is defined where  $n$  represents the total number of football stages and  $m$  represents the total number of players (C). Nonnegative matrix factorization (NMF) is used to extract subject model [25]. Compared with other algorithms, NMF has the advantage that it can easily support acceleration of parallelization.

Nonnegative Matrix Factorization (NMF) was proposed by Lee et al. [26], which first proposed block processing of data, providing a new idea for large-scale data processing. The principle of the algorithm is to express the original nonnegative matrix as the product of two small nonnegative matrices, improving the efficiency of data processing. Nonnegative matrix decomposition algorithm is introduced

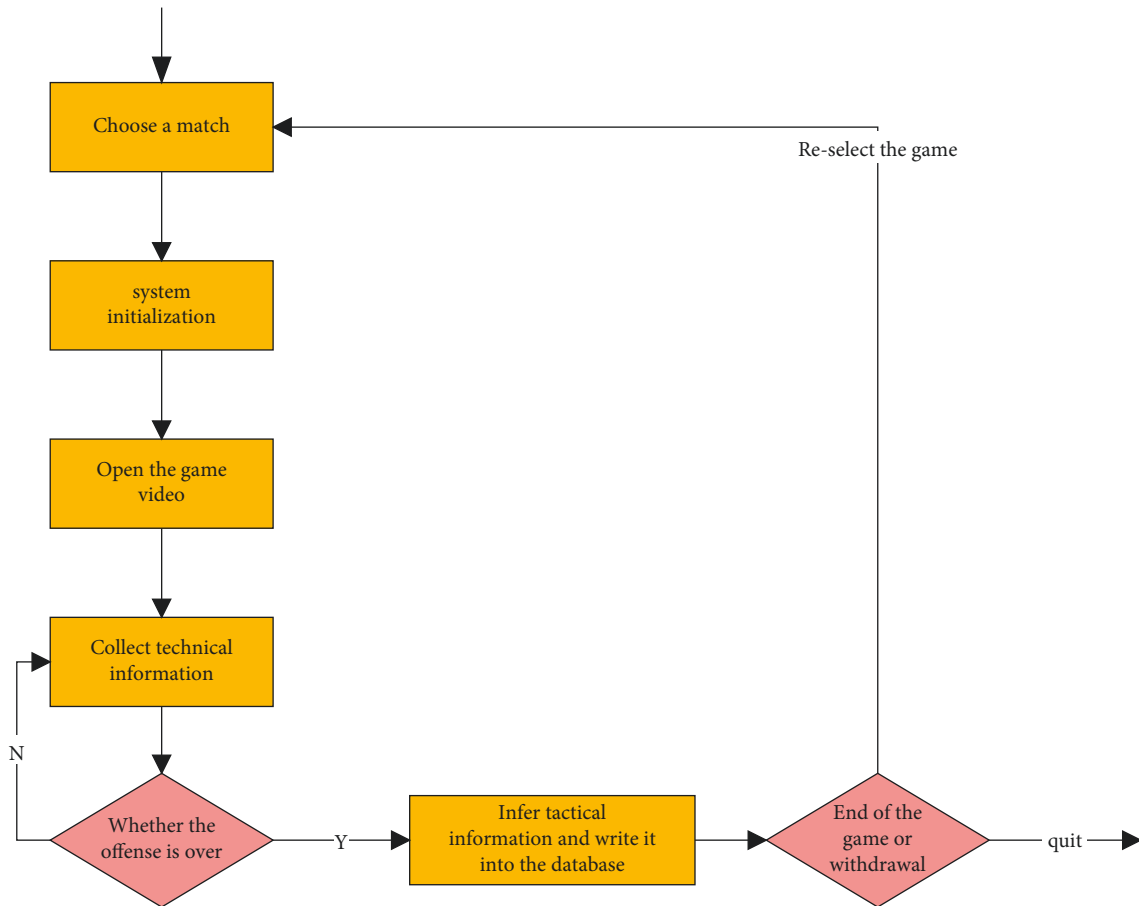


FIGURE 2: Flowchart of collection of tactical information.

into data processing according to the principle that physiological human perception as a whole is composed of local perception (pure additive) and constitutes global data by accumulating all parts of data [27]. Different from other feature extractions, NMF algorithm ensures that all data are nonnegative during processing. It has the advantages of interpretability, physical meaning, simple calculation, and small storage space, so it is widely used in pattern recognition, computer vision, biomedical, and other fields. Now, it has been applied to face recognition, image restoration, blind source separation, gene detection, and other directions [28]. NMF directly uses the relationship between data for matrix factorization, resulting in incomplete data mining. For data without labels, the essential high-dimensional features and sparse performance of the data are ignored, resulting in information waste and complex calculation. The NMF algorithm is used directly for the built-in label information, causing the label information to be ignored.

In order to describe the process of detection conveniently, this section will first describe the traditional NMF algorithm, which can be expressed as formula (2):

$$\min_{W,H} \|X - W \cdot H\|, \quad \text{s.t. } W > 0, H > 0, \quad (2)$$

where  $W \in \mathbb{R}^{m \times k}$ ,  $H \in \mathbb{R}^{k \times n}$ ,  $\|\cdot\|$  represents the distance of L2, and  $k$  represents the number of subjects. The subjects are

represented by columns in the  $W$  matrix. Each subject is about the distribution of players ( $D$ ), and then the distribution of players is transformed into a passing pattern by extracting keywords, that is, a group of players who frequently pass each other. Next, judge which passing mode the passing in each stage belongs to, which can be accomplished by  $H$  matrix. Each column in the  $H$  matrix, namely,  $c_i$ , represents the weight of each football stage in each passing mode. According to the common allocation of subjects, the passing mode with the highest weight is allocated to the football stage [29]. Through this method, a group of passing patterns and the labels of each football stage can be successfully detected.

The implementation scheme of NMF algorithm is as follows:

- (1) All football stages in the match are divided into two categories, namely, the stage of defensive counter-attack and the stage of positional attack. Counter-attack defense represents a direct way of playing in which a team plays an attack with a small number of passes. Positional play means that the team makes a series of passes to control the ball and complete the attack. The two forms of attack are so different that experts often discuss them separately when conducting tactical analyses.

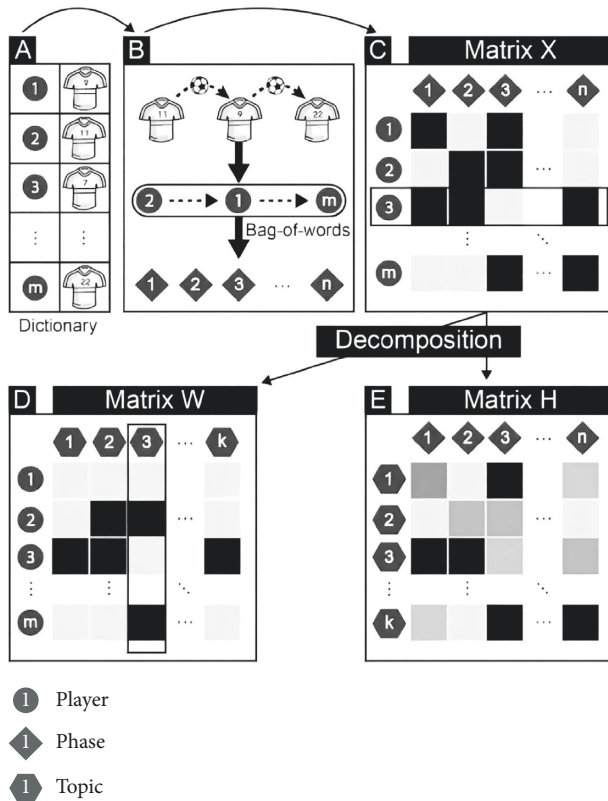


FIGURE 3: Detection of passing pattern based on subject model.

- (2) In this detection method, words can be likened to different football attributes. For example, users can apply the method to study the spatial information of passes. The user can divide the pitch into a number of spatial areas and convert each phase of the pass into a sequence of spatial areas. By comparing each area of space to a word, the user can use the topic model to detect patterns in the area of space during passing. A player's movement on the pitch is largely influenced by his role (striker, midfielder, etc.) and this role information can be revealed by the player's identity.
- (3) The substitution of players is a common situation in matches, and the dictionary of players should be expanded to deal with this situation. Specifically, the resulting theme will contain the weight of substitute players, which can be used to explain the passing pattern including substitute players.

**3.2.4. Tactical Information Inquiry.** The football tactical analysis system provides the query function of flexible combination of multiple conditions. In the query module, users can query the technical and tactical information of specific competitions, specific teams, and specific athletes, respectively, and also query the categories of tactics, so that the system has the ability to analyze information from multiple angles.

The query can be modified. When the technical information is modified, the system will automatically update the corresponding tactical information to keep it correct and

consistent. The module integrates functions of video preview, cutting, and merging and then selects one or more records from the queried tactical information to preview their corresponding video clips. These clips can also be cut and merged into a video file, which is conducive to the preservation and extraction of effective information.

In addition, the system also has an important function of analysis; that is, the data can be counted by Excel and then be exported. According to the data commonly used in football, the system designs several templates of Excel data. Users only need to select the templates, and the system will statistically analyze the data in the background and then return the tables filled with corresponding data to the users, which makes the statistical data more comprehensive and correct.

**3.2.5. Visual Display.** Visualization has been widely used in analysis of football matches. Analysis of football tactics involves many kinds of data and models such as background, players, tactics, passing, and so on; in order to visually display football tactics, the system supports visual display, which mainly realizes visual display of basic information, tactical information, and passing patterns, which provides an effective tool for analysis of football tactics.

## 4. Visualization of Football Tactics Analysis System

Combined with the design of football tactical analysis system, the core functions of the system are displayed visually.

**4.1. Visualization of Basic Information Management.** Basic management is the basic function of football tactics analysis system, which mainly realizes the basic settings of the information of players, team, and competition. After determining the competition plan, it can be given priority to rapid formation. There are two teams in a football match; each team consists of 11 players. The players of each team can be divided into four roles: Goalkeeper, defender, midfielder, and striker, which indicates the relative positions of players on the court. Players' roles can be subdivided according to their responsibilities, tactical needs, or players' characteristics, such as left midfielder, attacking midfielder, and shadow striker. The formation of football tactical analysis system describes the position of players on the field, as shown in Figure 4.

**4.2. Visualization of Collection of Tactical Information.** Collection of tactical information is mainly realized by moving the controls of football and players, and at the same time, it records the trajectory of football and players in real time by drawing lines. Interface of tactical acquisition is shown in Figure 5. Firstly, the system determines whether the color selected by the user is red or blue. In the process of implementation, a status sign is set to TRUE when the user selects red; then the line follows the player's movement and draws a red line.

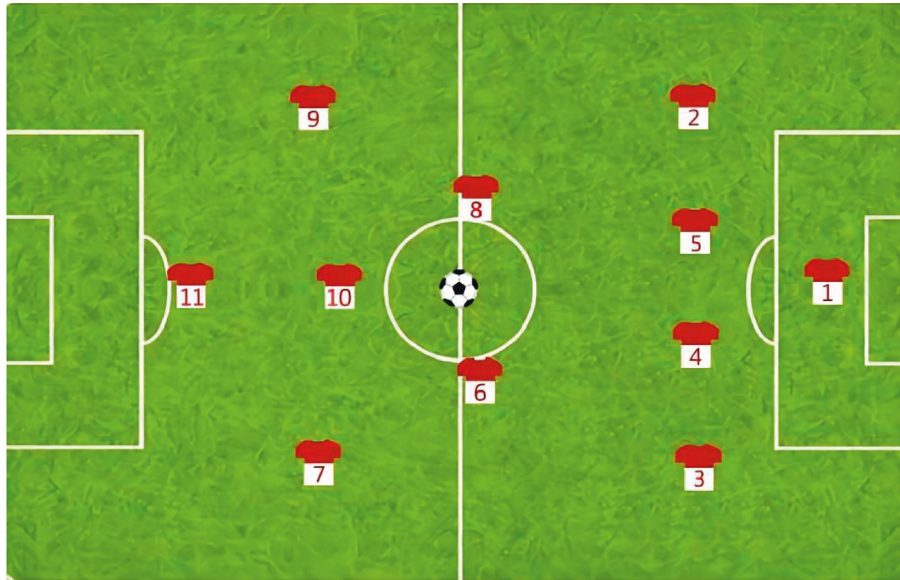


FIGURE 4: Interface of fast arrangement.

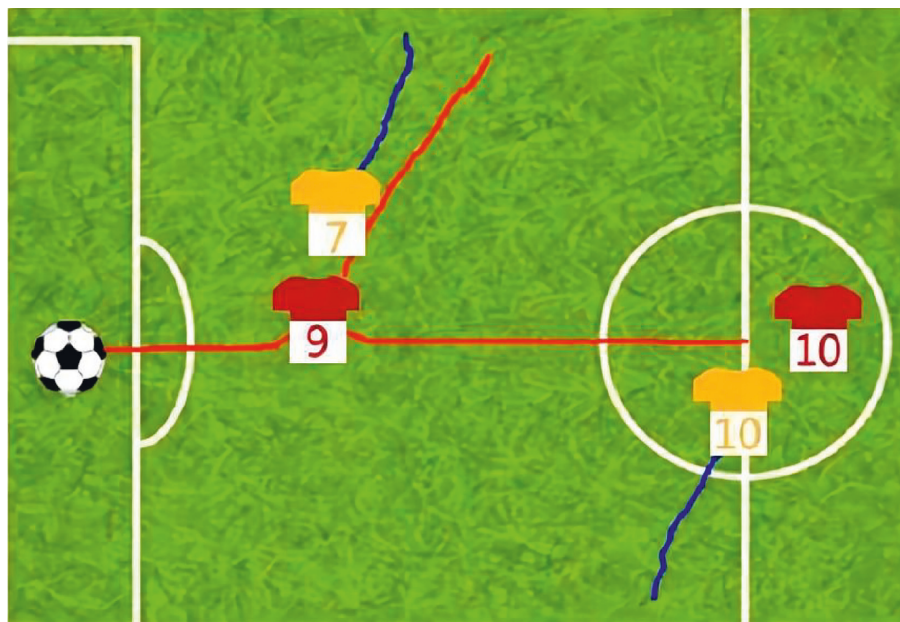


FIGURE 5: Collection of tactical information.

4.3. *Visualization of Detection of Passing Pattern.* There are two types of information features in passing pattern detection, namely, the player’s identity and the player’s spatial position, as shown in Figure 6.

Figure 6 shows the passing pattern and its characteristics. Each node in (b) represents 11 players, and each small court on the right represents a passing pattern. The passing mode at the bottom represents the stage of defensive counterattack, while other passing modes represent the stage of positional attack. The heat map (B2) on the small court is used to indicate the position of players when passing the ball. By extracting the starting position and ending position of each passing trajectory, and expressing this spatial information through heat map, the diagram shows the statistical

information of passing patterns. C2 shows the defensive effect of the defender, which is expressed by the coverage area of the defender that the higher the height, the worse the defensive effect.

The visual display of passing pattern is shown in Figure 7.

In this visualization, each column consists of a series of icons, which represents the multidimensional information of passing in a stage. There are different technologies for visualizing multidimensional information, among which parallel coordinates and reduced-dimension projection are typical examples. According to the reference, the information of the first passer and the last catcher is considered as the most representative in a series of passing in the stage. Therefore, the information of both of them is used to



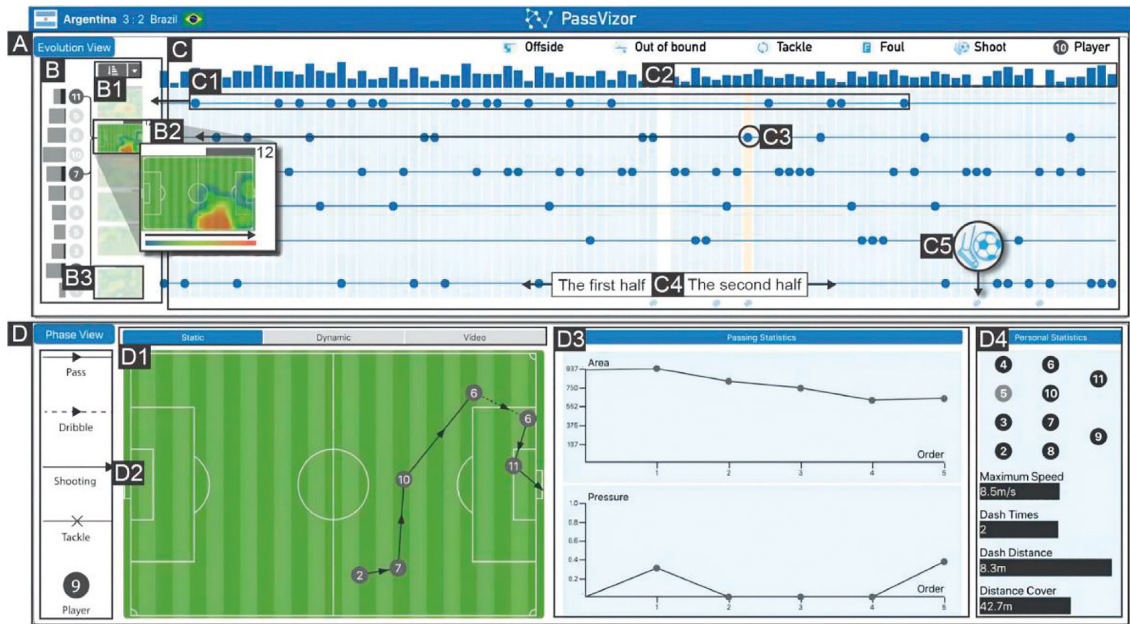


FIGURE 6: Identity and spatial position of players.

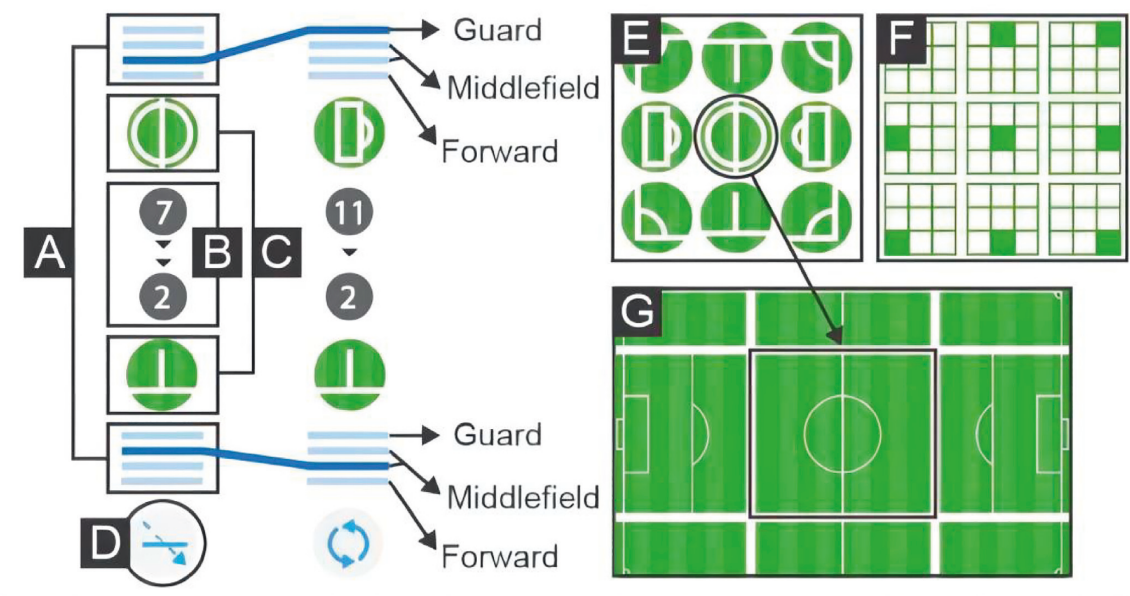


FIGURE 7: Visual display of passing pattern.

characterize the passing in a stage. For each stage, icons are used to show three types of information, namely, formation (A), player identity (B), and spatial position (C). The end event of the stage is placed at the bottom of the column (D). The density of the triangle in the middle of the column represents the number of passing in the stage.

The football tactical analysis system helps users to identify the similarities and differences of passing in different stages more quickly by displaying visualization of icon of multiple stages side by side. At the same time, cause-and-effect simulations can be done using

dimensional and tabular views. Take Causality Explorer as an example to realize the simulation of football game, as shown in Figure 8. In the dimensional view, each histogram represents the data distribution of a variable in the data. The height of the column codes the proportion of each value to complete the interactive process of simulation deduction.

In particular, Flash software development tools are used to describe and demonstrate the interactive patterns and movement paths required in the football tactical rehearsal system. By using multitouch technology, the design and



FIGURE 8: Game simulation and deduction.

rehearsal of football tactics with fingers are realized, and the process of tactical rehearsal is recorded and played back.

4.4. *Visualization of Query of Tactical Information.* Tactical information can be queried by the input of keywords. Take an athlete as an example; the visual display of his position is shown in Figure 9.

In order to save or print it permanently, it is necessary to export this tactical map from the system and store it in jpg format. Firstly, use Bitmap Data class to create an object containing the picture data obtained from the component, encode it into JPEG or PNG format by using the method provided by mx.graphics.codec package, and then save it locally by using the File and File Stream provided by AIRAPI.

## 5. Analysis of Systematic Effectiveness

5.1. *Evaluation Methods.* The data used in the system evaluation was a football tournament organized by CONMEBOL, which was the final match between Argentina and Brazil. In order to verify the effectiveness of the system, in the case study, the senior coach (E) with the Asian Football Confederation coaching certificate was invited to analyze the match between Argentina and Brazil, who already know the outcome of the game (i.e., the score, winner, and type of goal) before analyzing it. But this is the first time they have analyzed the game from a passing point of view. Before the case study, we demonstrated the use of the system to the experts. After the case study, we interviewed experts to gather their feedback and suggestions.

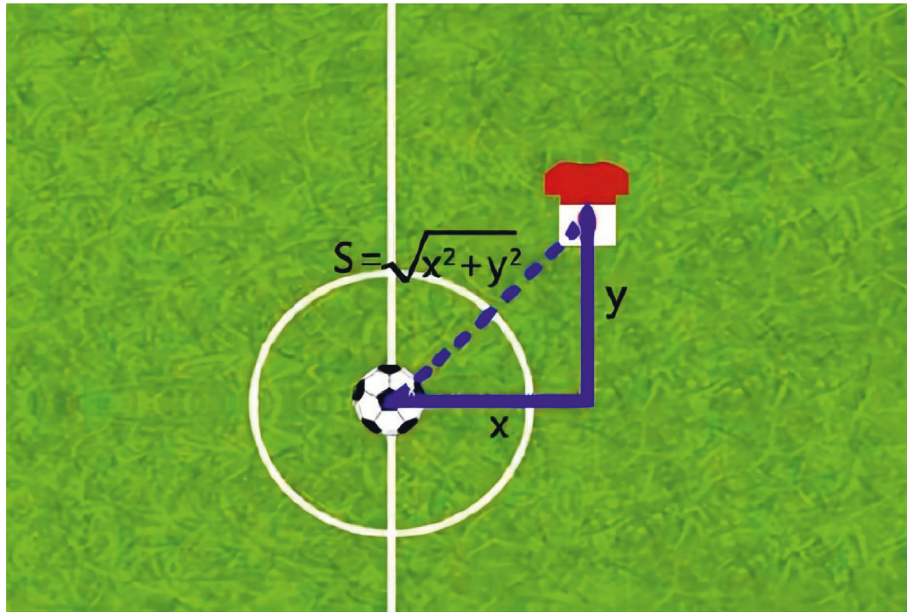


FIGURE 9: Visual display of location query.

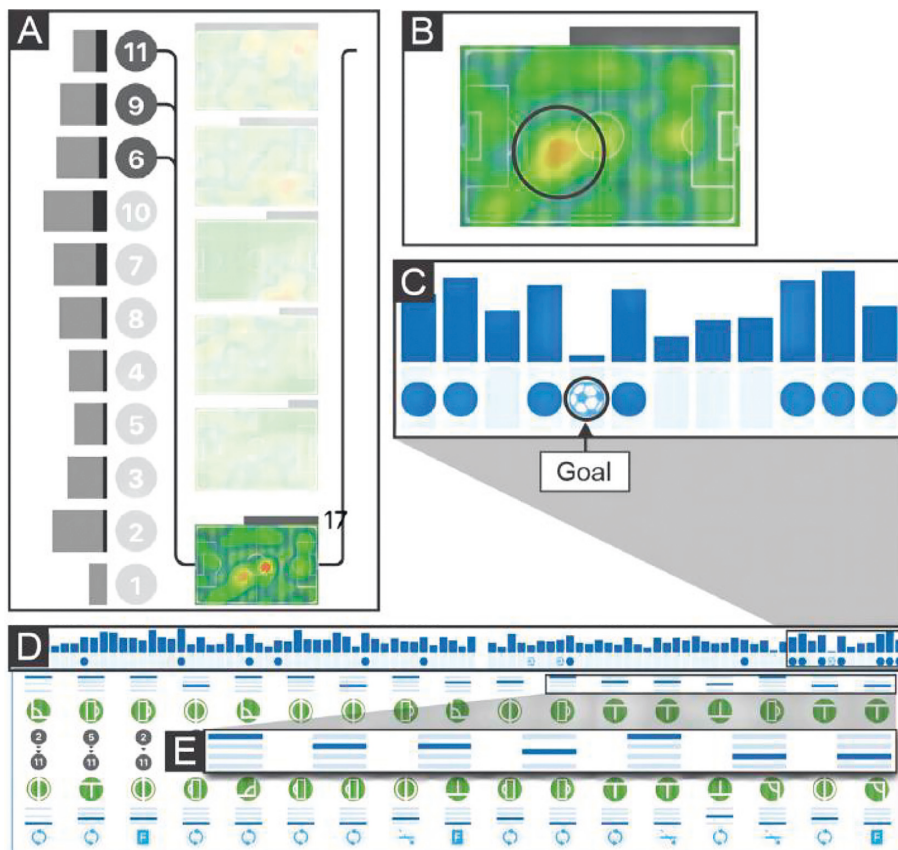


FIGURE 10: Analysis of counterattack strategy.

5.2. *Evaluation Results.* As there are many football tactics, this paper only tests the system with the counterattack strategy. The result is shown in Figure 10.

In this case, *E* was invited to analyze the match between Argentina and Brazil. *E* is very interested in passing on

counterattack. At the beginning of the analysis, *E* hovered over the pass pattern representing the defensive counter to see which players were deeply involved in the defensive counter. According to the bar chart of the players, *E* found three important players in the counterattack defense,

namely, the two forward 9 and 11 players and a midfield 6 player (Figure A). According to the identities of the players, *E* judged that most of the defensive counterattacks were initiated and completed by these three players. *E* then look at the thermal map of the defensive counterattack to learn the specific spatial position information. *E* stands for counter-attack, usually when the team recovers the ball by closing down and moves the ball forward quickly to launch an attack. In the thermal map, *E* found a highlighted area in the middle half of the circle (Figure B). *E* says this means most of the counterattacks are likely to come from the back.

*E* then turns to the mode stream to see when the team has used the counterattack and the result. The bar chart of defensive effectiveness, shown in Figure D, shows that Argentina most of the time attacked when the opposition was defending poorly. *E* says it is a reasonable counterattack strategy. Through the time distribution of the stages, it is further found that the occasions of Argentina's defensive counterattack are random. But towards the end of the second half (Figure C), Argentina's attacking pattern changed and they began to play consistently on the counterattack. According to the end of the period, *E* found that the switch allowed Argentina to take a one-goal lead (Figure C) and to continue to counter defensively at the end of the game after gaining the advantage. *E* said Argentina reduced possession to avoid mistakes in the final stages to maintain their lead. *E* then turns to the mode flow at the detail level to see the details of the counterattack defense.

Based on the observations, *E* focuses on Argentina's counterattack in the final period. According to the formation icon, *E* finds that the position of the first passer in the formation gradually moves forward in the three reciprocal phases (Figure E). This meant that Argentina had more players involved in defensive pressing, leading to a shift in tackling positions. The defensive counterattack for the scoring opportunity was initiated by the number four on the right and ended by the number six being robbed out of bounds. In order to have a deeper understanding of how the counterattack creates goal chances, *E* then jumps to the phase view to see the detailed process of the counterattack. *E* found the counterattack created a corner for Argentina. Argentina then took advantage of the corner to score. Therefore, *E* believes that the counterattack played an important role in Argentina's victory. In this case, the expert found and studied the phenomenon of Argentina changing its passing strategy and using defensive counterattack through the model graph, which was consistent with the prediction results.

## 6. Conclusion

Football is a complex event of team sports. The traditional collection of skills and tactics is generally received by coaches, and then the participation of teams or players in the game are counted manually. Manual collection of information not only is cumbersome and inefficient, but also causes incomplete data and high rate of error, which will adversely affect the analysis of follow-up game. Through the investigation of football tactics, the design of football tactics

analysis system is put forward in order to extract useful information from football matches more conveniently. In the design of the system, the emphasis is on the analysis of data collection and passing mode, while the method of collecting position data and event data of players is also put forward. The model of subject is used to detect the passing pattern. Through the design, the visualization of management of basic information, collection of tactical information, detection of passing pattern, query of tactical information, and other functions is realized, which has important practical significance and value.

## Data Availability

The dataset can be accessed upon request.

## Conflicts of Interest

The authors declare that there are no conflicts of interest.

## References

- [1] K. Chen, S. Zhao, N. Lv, and E. Cestino, "Network monitoring information collection in the SDN-enabled airborne tactical network," *International Journal of Aerospace Engineering*, vol. 2018, pp. 1–20, Article ID 1940842, 2018.
- [2] D. Gu, "Analysis of tactical information collection in sports competition based on the intelligent prompt automatic completion algorithm," *Journal of Intelligent and Fuzzy Systems*, vol. 35, no. 3, pp. 2927–2936, 2018.
- [3] Z. Liu, "Research on design of collection and intellectual analysis system of technical and tactical information in basketball matches," *Advanced Materials Research*, vol. 3181, no. 926-930, p. 234, 2014.
- [4] M. C. Ernesto, O. M. D. Marcel, and M. N. Vladimi, "System for the analysis of significant tactical actions of hand- ball teams," *Revista Cubana de Ciencias Informáticas*, vol. 12, no. 1, pp. 49–51, 2018.
- [5] S. L. Rubén, E. Ibon, and C. Julen, "Validation of a football competence observation system (FOCOS), linked to procedural tactical knowledge," *Sustainability*, vol. 13, no. 12, pp. 214–216, 2021.
- [6] G. Ramchandani, R. Millar, and D. Wilson, "The relationship between team ability and home advantage in the English football league system," *German Journal of Exercise and Sport Research*, vol. 121, pp. 147–149, 2021.
- [7] D. R. Anamisa, Y. Kustiyaningsih, M. Yusuf et al., "A selection system for the position ideal of football players based on the AHP and TOPSIS methods," *IOP Conference Series: Materials Science and Engineering*, vol. 1125, no. 1, pp. 178–180, 2021.
- [8] V. F. Della, P. S. Di, D. Santagati et al., "A 2D video-analysis scoring system of 90° change of direction technique identifies football players with high knee abduction moment," *Knee Surgery, Sports Traumatology, Arthroscopy*, vol. 178, pp. 45–48, 2021.
- [9] M. Zhou and D. Li, "Research on arm embedded system for football robot," *Microprocessors and Microsystems*, vol. 81, pp. 221–223, 2021.
- [10] C. Xiao and L. Sun, "Campus football application based on FPGA system and GPS wearable electronic equipment," *Microprocessors and Microsystems*, vol. 81, p. 456, 2021.

- [11] L. M. Christian and R. Fabio, "Analysis system for emotional behavior in football (ASEB-F): matches of FC red bull salzburg without supporters during the COVID-19 pandemic," *Humanities and Social Sciences Communications*, vol. 8, no. 1, pp. 221–223, 2021.
- [12] S. Wojciech, S. Andrii, P. Dragan et al., "A fuzzy inference system for players evaluation in multi-player sports: the football study case," *Symmetry*, vol. 12, no. 12, pp. 68–70, 2020.
- [13] V. Rago, "Training load monitoring in football: application of field systems in professional male players (PhD Academy Award)," *British Journal of Sports Medicine*, vol. 55, no. 12, pp. 131–135, 2020.
- [14] C. Daniel, S. C. Micael, J. Brito, F. Pedro, R. J. Lopes, and A. Duarte, "Using optical tracking system data to measure team synergic behavior: synchronization of player-ball-goal angles in a football match," *Sensors*, vol. 20, no. 17, p. 222, 2020.
- [15] W. A. Young and G. R. Weckman, "A team-compatibility decision support system for the national football league," *International Journal of Computer Science in Sport*, vol. 19, no. 1, pp. 345–346, 2020.
- [16] E. Berber, B. McLean, and S. Read, "Defining the attributes for specific playing positions in football match-play: a complex systems approach," *Journal of Sports Sciences*, vol. 38, no. 11–12, pp. 161–168, 2020.
- [17] M. Xia, Z. Li, S. Wang et al., "A video information driven football recommendation system," *Computers & Electrical Engineering*, vol. 85, no. 85, pp. 245–249, 2020.
- [18] T. Pereira, J. Ribeiro, F. Grilo, and D. Barreira, "The Golden Index: a classification system for player performance in football attacking plays," *Proceedings of the Institution of Mechanical Engineers - Part P: Journal of Sports Engineering and Technology*, vol. 233, no. 4, pp. 467–477, 2019.
- [19] B. Gong, B. Gong, Y. Cui, Y. Gai, Q. Yi, and M. Á. Gómez, "The validity and reliability of live football match statistics from champdas master match analysis system," *Frontiers in Psychology*, vol. 10, no. 10, pp. 38–39, 2019.
- [20] F. Yandun and A. Fernando, "Auat Cheein, Daniela Lorca, Omar Acevedo, Cecilia Auat Cheein. Design and evaluation of sound-based electronic football soccer training system for visually impaired athletes," *BioMedical Engineering Online*, vol. 18, no. 1, pp. 121–124, 2019.
- [21] G. E. Bayliff, B. H. Jacobson, M. Moghaddam, and C. Estrada, "Global positioning system monitoring of selected physical demands of NCAA division I football players during games," *The Journal of Strength & Conditioning Research*, vol. 33, no. 5, pp. 1185–1191, 2019.
- [22] B. Wang, W. Shen, F. S. Chen, and D. Zeng, "Football match intelligent editing system based on deep learning," *KSII Transactions on Internet and Information Systems (TIIS)*, vol. 13, no. 10, p. 1111, 2019.
- [23] J. Castellano, D. Casamichana, M. A. Campos-Vázquez, and A. Langarika-Rocafort, "Interchangeability of two tracking systems to register physical demands in football: multiple camera video versus GPS technology," *Archivos de Medicina del Deporte*, vol. 36, no. 3, pp. 268–269, 2019.
- [24] M. Z. Z. Abidin, M. K. B. M. Nawawi, and M. M. Kasim, "Identifying players' selection criteria for the development of decision support system for football and hockey," *Advanced Science Letters*, vol. 24, no. 11, pp. 96–99, 2018.
- [25] Schutt Sports, "Schutt sports reclaims #1 spot in Virginia tech STAR football helmet rating system," *Journal of Engineering*, vol. 38, no. 78, p. 1112, 2018.
- [26] D. D. Lee and H. S. Seung, "Learning the parts of objects by non-negative matrix factorization," *Nature*, vol. 401, no. 6755, pp. 788–791, 1999.
- [27] L. Li and Y. Zhang, "Review of nonnegative matrix factorization algorithms," *Acta Electronica Sinica*, vol. 36, no. 4, pp. 737–743, 2008.
- [28] W. Yuan, *Research on multi-view personalized recommendation method for sparse data*, Shandong Normal University, China, 2018.
- [29] L. Tao and C. Liu, "Research on the theoretical system of athletes' physical fitness training based on the characteristics of competition system," in *Proceedings of the 2019 Asia-Pacific Conference on Emerging Technologies and Engineering (ACETE 2019)*, pp. 349–352, Francis Academic Press, London, U K, July 2019.

## Research Article

# Prediction of Phishing Susceptibility Based on a Combination of Static and Dynamic Features

Rundong Yang <sup>1</sup>, Kangfeng Zheng <sup>1</sup>, Bin Wu,<sup>1</sup> Chunhua Wu <sup>1</sup> and Xiujuan Wang <sup>2</sup>

<sup>1</sup>School of Cyberspace Security, Beijing University of Posts and Telecommunications, Beijing 100876, China

<sup>2</sup>School of Computer Science, Beijing University of Technology, Beijing 100124, China

Correspondence should be addressed to Kangfeng Zheng; [kfzheng@bupt.edu.cn](mailto:kfzheng@bupt.edu.cn)

Received 13 March 2022; Accepted 13 April 2022; Published 10 May 2022

Academic Editor: Man Fai Leung

Copyright © 2022 Rundong Yang et al. This is an open access article distributed under the Creative Commons Attribution License, which permits unrestricted use, distribution, and reproduction in any medium, provided the original work is properly cited.

Phishing is a very serious security problem that poses a huge threat to the average user. Research on phishing prevention is attracting increasing attention. The root cause of the threat of phishing is that phishing can still succeed even when anti-phishing tools are utilized, which is due to the inability of users to correctly identify phishing attacks. Current research on phishing focuses on examining the static characteristics of the phishing behavior phenomenon, which cannot truly predict a user's susceptibility to phishing. In this paper, a user phishing susceptibility prediction model (DSM) that is based on a combination of dynamic and static features is proposed. The model investigates how the user's static feature factors (experience, demographics, and knowledge) and dynamic feature factors (design changes and eye tracking) affect susceptibility. A hybrid Long Short-Term Memory (LSTM) and LightGBM prediction model is designed to predict user susceptibility. Finally, we evaluate the prediction performance of the DSM by conducting a questionnaire survey of 1150 volunteers and an eye-tracking experiment on 50 volunteers. According to the experimental results, the correct prediction rate of the DSM is higher than that for individual feature prediction, which reached 92.34%. These research experiments demonstrate the effectiveness of the DSM in predicting users' susceptibility to phishing using a combination of static and dynamic features.

## 1. Introduction

With the continuous development of the Internet and the increasing popularity of electronic payments, the problem of online fraud has gradually become a focus of attention. Phishing refers to a category of fraudulent behaviors in which attackers use social engineering techniques to guide users to visit fake websites that appear to be real through SMSs, emails, fake advertisements, and live chat tools, among other ways, to fraudulently obtain users' private information, such as private account passwords, payment passwords, and credit card information.

Phishing is currently one of the biggest threats in cybersecurity and is widely used. Many expert researchers and government authorities give great attention to the phishing problem and expect the phishing threat to become more serious in the future [1, 2]. The reason for this phishing threat is simple: many phishing incidents succeed because

users are unable to recognize phishing [3]. Historically, many disruptive security attacks have occurred, and one of the more threatening security attacks was a phishing security attack called the Locky ransomware attack [4]. When a user with enough access to an organization's server opens a phishing e-mail from an attacker, the attacker extorts the organization by obtaining a large amount of encrypted data. Researchers in fields that are related to cybersecurity [5, 6] and in governments [1, 7] have warned businesses and individual users about the growing phishing threat.

If anti-phishing tools and phishing detection techniques alone cannot effectively prevent phishing, the user is the ultimate defense against phishing [8]. According to an APWG report, 1,520,832 phishing websites and 1,031,347 phishing emails were detected in 2020, and the number of phishing websites peaked in October 2020, with 369,254 phishing attacks occurring in January alone; phishing activity is still at an all-time high [9].

Several recent studies have found that Internet users are unable to effectively distinguish legitimate sites from phishing sites and are unable to avoid transactions on phishing sites [10–12]; summarizing previous work, studies have found that 40–80% of users are unable to correctly identify phishing sites [10, 13, 14] and more than 70% of transactions are made on phishing sites [10, 11]. Many studies have used anti-phishing tools to prevent users from visiting phishing websites, which mainly include web browser security toolbars and plug-ins [15–17]. Although these tools are highly accurate in detecting phishing websites, phishing still has a high success rate, and these software tools fail to attract users' attention or warnings are ignored [18]. Internet users always ignore the warnings of anti-phishing tools because users believe that the warnings are not directed to them [19].

Internet users are unable to recognize the threat of phishing, and they click on links because they lack security awareness, which depends mainly on their static awareness. Static awareness is formed by a user before performing a security action, so it does not correctly reflect the real situation of the user at the time of performing the action [12, 20, 21].

The central issue for phishing prevention and detection is security awareness. Is the user thinking through the process of performing actions when he or she is subjected to a phishing attack? To solve this problem, we mainly consider the influence of personal characteristics (e.g., demographic characteristics, personality traits, experience, and knowledge) and e-mail characteristics (e.g., sender address and outgoing connections) on the person [22].

Static awareness cannot be addressed in the case where the user is performing the action and the static role is separated. Since human behavior when subjected to phishing attacks is determined by the interactions with human perceptions of phishing attacks, awareness in this interactive scenario is called dynamic awareness. Dynamic awareness, which is derived from situational awareness, is represented by a cyclical model (PCM) [15], which considers both knowledge states and processes.

In contrast to previous studies that treat static aspects of consciousness as separate from the actual situation, we adopt an approach that is based on the assumption that safety-related behaviors are generated by the interaction between the person and the perception of the situation. Thus, our basic premise is that security-related behaviors are based on the context of the environment in which they occur and require an assessment of the encountered situation. To conceptualize the actual awareness of individuals in security-related situations, we introduce the construct of situational information security awareness. It is derived from the perceptual cycle model (PCM) of situational awareness [15], which considers both products (knowledge states) and processes (how knowledge is created through intelligent interactions).

The approach that is used in this study differs from previous approaches in that, instead of predicting a single phishing attack, we predict the user's phishing

susceptibility. In this paper, we define the user's susceptibility as the degree of interaction between the user and the phishing attack. Our approach can truly reflect the user's susceptibility level, analyze the factors of susceptibility, and provide personalized warning messages to the user.

We propose a hybrid phishing susceptibility prediction model that is based on static and dynamic features. The model integrates the key features of static and dynamic features. These static features mainly include individual-level features such as experience, personal attributes, and other features. To obtain the static features, we use questionnaires to collect the personal static features of 1150 volunteers. In addition, to more realistically reflect the real situation of users facing phishing, it is necessary to obtain the dynamic features of users in the scenario. We conduct eye-tracking experiments and questionnaires on 50 volunteers. We use a hybrid model for static features, we mainly use an LSTM model for feature extraction, and we apply the LightGBM model for dynamic feature prediction, in which the LightGBM algorithm is utilized to predict the user's susceptibility. Finally, after the prediction stage, the prediction results of the two models are combined. The combined model integrates the respective characteristics of the two models, which can not only explore the intrinsic connections between the time-series data but also avoid the influence of discontinuous features on the prediction results. The test results show that the combined model can realize lower error than a single model in special scenarios and has more stable prediction results.

Although phishing has been studied for many years, predicting users' susceptibility to phishing is a new challenge in proactive defense against phishing attacks. Many experts and scholars have emphasized that anti-phishing tools are not effective in preventing users from being phished [23–25]. Therefore, according to the scientific guidelines [26], our work can be regarded as an improvement to previous work, and the main contributions of this paper are as follows:

- (1) Previous studies have not analyzed the prediction of users' susceptibility to phishing emails but have focused on developing or testing behavioral models, and the present model demonstrates the feasibility of susceptibility prediction.
- (2) Previous phishing studies have analyzed user susceptibility with a static set of personal characteristics in the model. The present model combines static personal characteristics while taking into account interactivity and incorporates eye movement by using eye movement data as a dynamic response to threat perception for dynamic feature extraction. This model yields more accurate prediction results.

The remainder of the paper is organized as follows: Section 2 reviews the series of phishing susceptibility studies that have been conducted, Section 3 discusses the proposed work, Section 4 presents the detailed results of the data analysis and discusses the limitations of the model, and Section 5 discusses and summarizes the full paper.

## 2. Related Work

Traditional anti-phishing efforts have focused on designing and developing anti-phishing tools [26] and designing better algorithms to improve the accuracy of detection [27]. Despite researching anti-phishing techniques, phishing is still able to attack successfully, and phishing attacks have become one of the most threatening digging attacks for network security. To solve the problem of phishing attacks, more and more researchers have started to shift the focus of their research to user susceptibility analysis.

In recent years, a survey of Dutch cybercrime victims [28] has been conducted to determine which user behaviors increase the risk of being phished, using a multivariate risk analysis approach. The results of the analysis were used to determine several behaviors that increase the user's risk.

Leukfeldt [28] used risk perception theory, theory of planned behavior, and decision theory to construct a model to analyze the factors influencing spear phishing attacks on users. The experiments were conducted mainly in Middle Eastern countries, and the final results analyzed the behavioral factors that increase cyber network susceptibility and help to evaluate and select the use of phishing tools.

According to the research findings [20], some users are more susceptible to phishing attacks due to attack scenarios and personality factors, and experiments were conducted through individuals and companies to analyze how personality traits affect human behavior.

Lin et al. [29] investigated the factors affecting users' susceptibility by conducting a study on phishing emails and analyzing the impact of psychological, demographic, and cultural characteristics on susceptibility to phishing, and the experimental results showed that age had the greatest impact on phishing.

Luo et al. [30] designed a heuristic system model to investigate the impact of users' psychology and behavior on phishing susceptibility through a qualitative study. The model can explain the factors of user number victimization.

Lillo et al. [31] showed that the factors influencing susceptibility to phishing include demographics, knowledge, experience, and self-efficacy, which affect the user's access to the browser and transactional behavior on the phishing site.

Sheng et al. [32] proposed a phishing susceptibility assessment model (DRKM) that analyzes multiple demographic variables including age, education, and gender as well as knowledge and experience aspects mainly considering awareness of phishing, technical skills, etc. Based on the analysis of the model, the final implementation results showed that the susceptibility of users to phishing can be effectively predicted by gender, age, and risk propensity.

Abbasi et al. [33] proposed a phishing funnel model (PFM) for phishing susceptibility analysis, which divides the user's susceptibility into multiple stages and predicts the user's susceptibility by performing susceptibility analysis for each stage separately.

Yang et al. [34] proposed a model for phishing susceptibility analysis, which mainly extracts features of pairs of

dimensions, including demographics, personality, knowledge experience, and computer knowledge, and uses these features to predict the susceptibility of users.

## 3. Proposed Method

In this section, we propose a user phishing susceptibility prediction model that is based on static and dynamic features. Based on the combined LSTM and LightGBM model, the prediction of phishing susceptibility using static features and dynamic features is realized. A flowchart of the model is presented in Figure 1.

The model has three main components. The first component obtains data for preprocessing. A lot of these static data are obtained using a normalization method. The original static features and dynamic features are obtained for preprocessing. The converted data, which contain a variety of factors that affect susceptibility, are conducive to the prediction of user susceptibility. Then, we design an LSTM model, set the LSTM parameters, use the LSTM model to predict susceptibility for static features, and use the LightGBM model to predict susceptibility for dynamic features. Finally, the prediction of user phishing susceptibility is realized by combining the prediction results of the static susceptibility prediction model and the dynamic susceptibility prediction model.

*3.1. Data Preprocessing.* When the LSTM and LightGBM hybrid model is applied for network phishing susceptibility prediction, the input feature vectors of the component models consist of questionnaires and eye-tracking experiment data, and feature values with different magnitudes and large differences in values are obtained. According to the characteristics of the network model, the data are directly input into the model because the weighted accumulator data will become abnormally large, thereby resulting in the network failing to converge; therefore, the input data vector needs to be normalized before the data are input. The commonly used method is the min-max normalization method because it is easy to use and fast, so it is applied in this paper, and the formula is presented below.

$$x^* = \frac{x - x_{\min}}{x_{\max} - x_{\min}}. \quad (1)$$

In the above equation,  $x_{\max}$  is the maximum value of the sample data, and  $x_{\min}$  is the minimum value of the sample data.

In this paper, the data obtained by questionnaires and eye tracking, in which the input and output values vary widely, are normalized using the min-max normalization method, which can reduce the error of the model and map the data into the interval [0, 1]. The data are obtained from static features such as personal attributes (e.g., gender, age, income, experience, and knowledge) and dynamic feature data (e.g., the time of eye gaze and the number of gazes during user interaction) through questionnaires and eye tracking. Table 1 presents the acquired data.



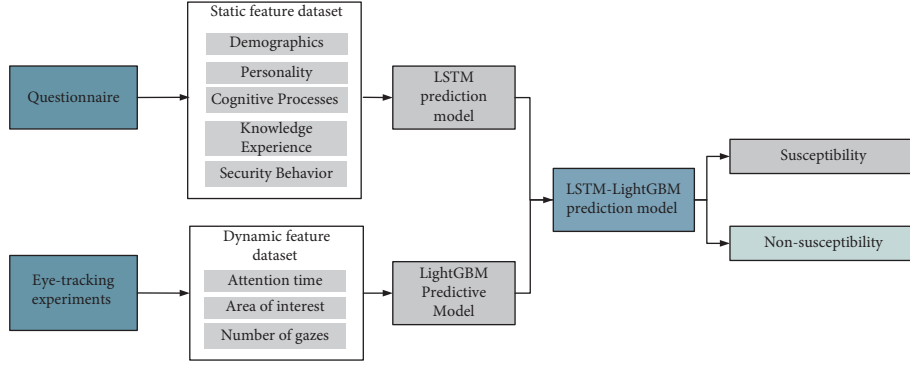


FIGURE 1: DSM flow.

Normalization is performed using the extreme values via (1) for the above data, and the normalized data are presented in Table 2.

3.2. *LSTM*. An LSTM is a special RNN network. RNNs have the problems of gradient disappearance and gradient explosion. An LSTM, through a cell gate switch to achieve temporal memory function and prevent gradient disappearance, can learn the long-term dependence on information, preserve the information, and overcome the disadvantages of RNNs [22]. Its algorithm structure is illustrated in Figure 2. The current loss  $x^t$  of an LSTM and the last state that is passed down  $h^{t-1}$  are used to obtain four states by splicing training, and the state formula is as follows:

$$z = \tanh(w_h^{(z/2)t-1}), \quad (2)$$

$$z^i = \sigma(w_h^{it}), \quad (3)$$

$$z^f = \sigma(wx^t h^{t-1}), \quad (4)$$

$$z^o = \sigma(w_h^{oxt}), \quad (5)$$

$z^i$ ,  $z^f$ , and  $z^o$  in (2) and (3) are converted to values between 0 and 1 by a sigmoid activation function after multiplying the splicing vector by the weight matrix as a gating state. In (2),  $z$  is the result converted to a value between  $-1$  and  $1$  by the tanh activation function.  $\odot$  denotes multiplication of the corresponding elements in the operation matrix, which requires that the two multiplied matrices be of the same type [12].  $+$  denotes matrix addition.  $c^t$ ,  $h^t$ , and  $y^t$  are calculated as follows:

$$c^t = z^f \odot c^{t-1} + z^i \odot z, \quad (6)$$

$$h^t = z^o \odot \tanh(c^t), \quad (7)$$

$$y^t = \sigma(W^f h^t). \quad (8)$$

The computational process of the LSTM model is divided into three main phases: the forgetting phase, the input phase, and output phase. In the forgetting phase, the previously

TABLE 1: Collected data.

| ID | Age (years) | Annual income (yuan) | Duration of gaze (s) |
|----|-------------|----------------------|----------------------|
| 1  | 23          | 100,000              | 0.3                  |
| 2  | 24          | 50,000               | 0.0087               |
| 3  | 54          | 80,000               | 0.2                  |
| 4  | 12          | 300,000              | 0.0374               |
| 5  | 38          | 200,000              | 0.3551               |
| 6  | 21          | 400,000              | 0.008                |

TABLE 2: Data normalization.

| ID | Age (years) | Annual income (yuan) | Duration of gaze (s) |
|----|-------------|----------------------|----------------------|
| 1  | 0.26        | 0.11                 | 0.33                 |
| 2  | 0.28        | 0.04                 | 0.00                 |
| 3  | 0.85        | 0.08                 | 0.22                 |
| 4  | 0.06        | 0.36                 | 0.03                 |
| 5  | 0.55        | 0.24                 | 0.39                 |
| 6  | 0.23        | 0.49                 | 0.00                 |

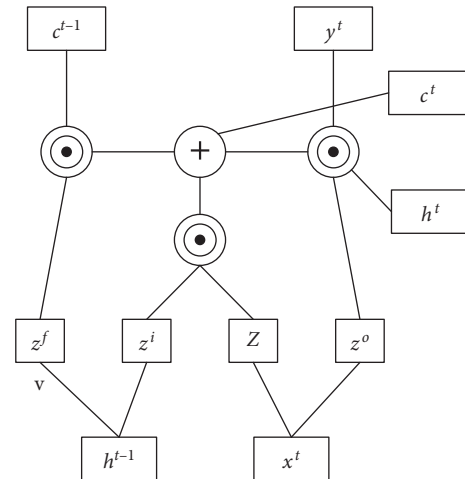


FIGURE 2: LSTM structure.

unused information is forgotten. The forgetting gate decides which information will be forgotten based on the input  $x^t$  of the current node, the state  $c^{t-1}$  of the previous node, and the output  $h^{t-1}$  of the previous node. The input phase determines which information will be left behind for the current

input data. The main memory selection is made for the input  $x^t$ . The current input content is expressed by (2).

$z$  is derived, and the selection gating signal is controlled by  $z^i$ . From (2) to (4), the  $c^t$  value that is transmitted to the next state is obtained by (5). The output stage determines the output value. After obtaining the latest node state  $c^t$ , the LSTM combines the output  $h^{t-1}$  of the previous node and the input  $x^t$  of the current node to determine the output  $y^t$  of the current node, which is obtained by changing  $h^t$  in (6) and (7).  $z^o$  in (6) is used to perform control and scaling of the state  $c^t$  (which is transformed by the tanh activation function) [12].

3.3. *LightGBM*. LightGBM is a distributed gradient boosting GBDT framework that is based on a decision tree algorithm, and the GBDT algorithm faces substantial challenges in terms of performance and accuracy in a data environment with large training samples and high-dimensional features. To overcome these problems, LightGBM was developed. LightGBM has the features of fast training speed, low memory occupation, high accuracy, and support for parallelized learning, and it can handle large-scale data [11].

LightGBM mainly uses some optimization algorithms in the gradient algorithm.

- (1) Gradient-based one-sided sampling algorithm (GOSS): LightGBM uses the GOSS algorithm to optimize the training sample sampling. The basic strategy of the GOSS algorithm is to first sort the training set data according to the gradient, apply a preset proportion, and keep the data samples with gradients that are higher than the proportion among all samples; the data samples with gradients that are lower than the proportion are not discarded directly but are sampled according to a sampling proportion. To compensate for the impact on the sample distribution, the GOSS algorithm calculates the information gained by multiplying the data with smaller gradients by a factor to amplify them. The algorithm can give more attention to the “under-trained” sample data when calculating the information gain.
- (2) EFB (exclusive feature bundling) algorithm: The LightGBM algorithm not only optimizes the sampling of training samples by the GOSS algorithm but also performs feature extraction to further optimize the training speed of the model. In the algorithm, a table of nonzero-valued features can be created for each feature. By scanning the data in the table, the time complexity of creating the histogram can be effectively reduced.
- (3) Histogram algorithm: LightGBM uses a histogram-based algorithm that discretizes continuous feature values into  $K$  integers, constructs a histogram of width  $K$ , traverses the training data, and counts the cumulative statistics of each discrete value in the histogram. In selecting the splitting points of the features, only the discrete values of the sorted

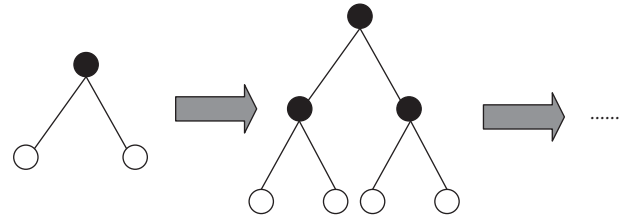


FIGURE 3: Level-wise strategy map.

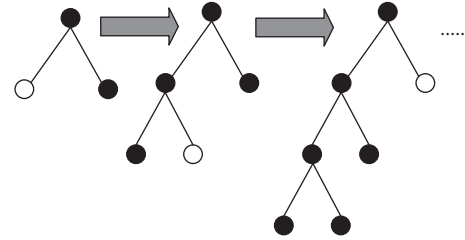


FIGURE 4: Leaf-wise strategy map.

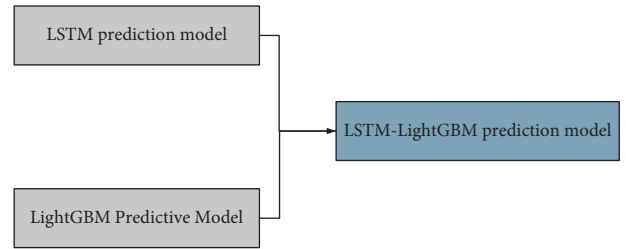


FIGURE 5: LSTM-LightGBM prediction model.

histogram need to be traversed. The histogram algorithm reduces the computational cost and memory consumption.

- (4) Grow-by-leaf (leaf-wise) algorithm: Most decision tree learning algorithms for tree generation use the grow-by-level (level-wise) strategy loss, as illustrated in Figure 3.

LightGBM uses a more efficient leaf-wise strategy algorithm, as illustrated in Figure 4. This strategy finds the leaf node with the largest splitting gain among all the leaf nodes of the current decision tree to split in each round. This mechanism reduces the splitting computation for the leaf nodes with lower gain. Compared with the level-wise strategy, the leaf-wise strategy can reduce the error and yield higher accuracy with the same number of splits. The disadvantage of the leaf-wise algorithm is that it may generate a deeper decision tree. Therefore, LightGBM adds a parameter to limit the maximum depth on the leaf-wise decision tree to prevent overfitting while ensuring the efficiency of the algorithm.

3.4. *LSTM-LightGBM Model*. Because the two models have different advantages for data processing, we linearly combine the two prediction results by applying a weighting factor  $\alpha$  as follows:

**Survey Questionnaire**

Hello! I'll appreciate it if you can help me complete the survey questionnaire. Thank you for your time and cooperation.

---

\*1. Name: \_\_\_\_\_  
 Age: \_\_\_\_\_  
 tel: \_\_\_\_\_

\*2. What kind of work do you do?  
 A. Heads of state organs, party organizations, enterprises and institutions  
 B. Clerical and related personnel  
 C. Professional and technical personnel  
 D. Commercial and service personnel  
 E. Agriculture, forestry, animal husbandry, fisheries, water conservancy production personnel  
 F. Production, transport equipment operators and related personnel  
 G. Military personnel  
 H. Other employees inconvenient to classify

\*3. Your annual income? (Single choice)  
 A. Less than 30,000  
 B. 30-100,000  
 C. 100,000-200,000

FIGURE 6: Questionnaire experiment.



FIGURE 7: Experimental diagrams of eye tracking. (a) Trajectory diagram. (b) Heat diagram.

$$o = \alpha o_1 + (1 - \alpha) o_2, \tag{9}$$

where  $o_1$  is the prediction probability of the LSTM model,  $o_2$  is the prediction model of the LightGBM model,  $o$  is the final prediction result, and the value of  $\alpha$  is determined by the final evaluation metric; namely, the best  $\alpha$  value on the validation set is chosen. The structure of the combined model is illustrated in Figure 5.

### 4. Results and Discussion

To evaluate the effectiveness of the proposed model for predicting users' susceptibility to phishing based on a combination of static and dynamic features, the static feature dataset using LSTM and the dynamic feature dataset using LightGBM are analyzed and studied, and all experiments in this paper are conducted on a laptop with an Intel 8-core 2.8 GHz processor, 32 GB RAM, and a 1 TB hard disk using Python 3.6.

**4.1. Experiment Setup and Dataset.** In this study, to evaluate the effectiveness of the method that is proposed in this paper, the experimental dataset is mainly obtained by using questionnaires and eye-tracking methods. Two datasets are generated: a dynamic dataset and a static dataset. Static

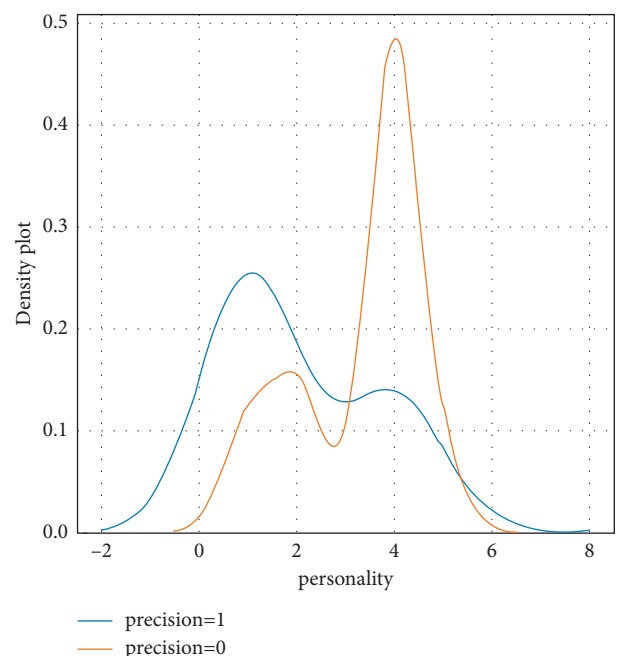


FIGURE 8: Distribution of susceptibility characteristics.

features are collected by using questionnaires; they consist mainly of users' characteristics, including name, gender, age, income, experience, and knowledge. Data are collected from 1150 volunteers. The susceptibility of users is judged by the phishing detection of users. One of the survey questionnaires is shown in Figure 6.

Fifty volunteers are selected from 1150 volunteers to conduct eye-tracking experiments to build a dynamic feature dataset, which is the user's interaction behavior when receiving phishing requests. The dynamic features are interaction behavior features, including gaze time, number of gazes, and area of interest. One of the eye-tracking experiments is shown in Figure 7. Because the testers are mostly Chinese, the phishing emails in the questionnaire and eye-tracking experiments are in Chinese, considering that volunteers will experience ambiguity when they are recognizing English.

In this experiment, two datasets are generated. For the static dataset, 19 characteristics, such as name, age, income, and knowledge, of 1150 volunteers are collected through 144 questions. Eighty percent of these are randomly selected as the training dataset, and the rest are selected as the test dataset. A dynamic feature dataset is obtained through an eye-tracking experiment on 50 people who are randomly selected from 1150 people for the experiment, and the dynamic features include six dimensions. Before the experiment, the data need to be preprocessed.

**4.2. Feature Analysis.** For static features, in this paper, 19-dimensional features, including gender, age, and knowledge, are constructed mainly from the data that are obtained from the questionnaire. To better make predictions, all the features are analyzed, and by analyzing the distributions of the categories and quantities of data, one can better understand the data and improve the model's correctness rate.

**4.3. Analysis of Static Data.** Personality is a very important characteristic that impacts the susceptibility of users; the distribution of personality characteristics in both categories is shown below. According to Figure 8, the neurotic personality is the most common in susceptible users, and the pleasant personality is the most common in nonsusceptible users.

Previous studies have shown that education level is an important factor that influences users' susceptibility, but according to the experimental results of this paper, education level has little effect on phishing susceptibility; the results are shown in Figure 9.

The cybersecurity knowledge scores of susceptible and nonsusceptible users are shown in Figure 10. The cybersecurity knowledge scores of users who are susceptible are distributed relatively evenly, but the scores of nonsusceptible users are mainly concentrated at the average level.

The distributions of other characteristic data, such as age, annual income, and gender, are shown in Table 3. The distribution of gender is relatively even. The number of users with annual incomes of less than 30,000 RMB is the highest, followed by the number of users with incomes of

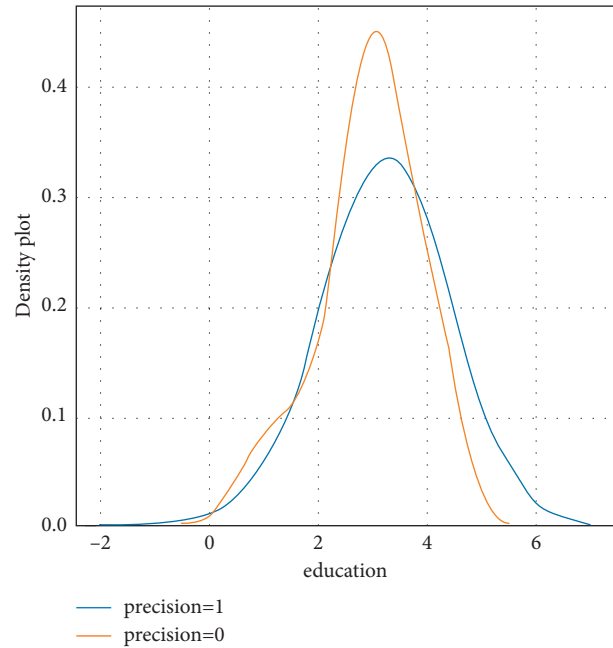


FIGURE 9: Distribution of educational level characteristics.

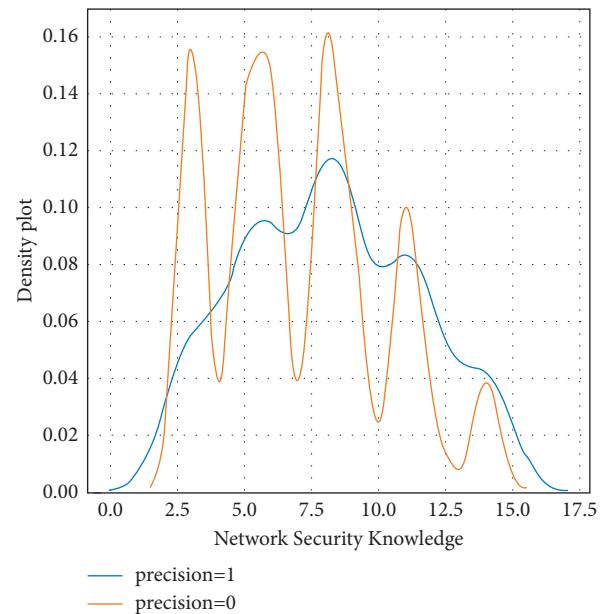


FIGURE 10: Network security knowledge feature distribution.

30–100,000, and the number of users with incomes of more than 200,000 is the smallest. The ages are mainly distributed in the range of 20–30 years old, because the volunteers are mostly college students.

**Experiment 1.** Prediction of phishing susceptibility based on static features.

In this experiment, the LSMT model is mainly used to predict the susceptibility of users to network phishing using static features as input. It is also compared with several other machine learning models for analysis.

TABLE 3: Distributions of other characteristics.

| Attribute         | Feature         | Category                           | Frequency |
|-------------------|-----------------|------------------------------------|-----------|
| Demographics      | Age             | <20                                | 67        |
|                   |                 | 20–30                              | 720       |
|                   |                 | 30–40                              | 107       |
|                   |                 | 40–50                              | 128       |
|                   |                 | >50                                | 83        |
|                   | Education level | Below high school                  | 61        |
|                   |                 | Vocational high school/high school | 109       |
|                   |                 | Undergraduate                      | 610       |
|                   | Gender          | Graduate or above                  | 325       |
|                   |                 | Male                               | 555       |
|                   | Annual income   | Female                             | 550       |
|                   |                 | <¥30,000                           | 477       |
|                   |                 | ¥30,000–¥100,000                   | 369       |
| ¥100,000–¥200,000 |                 | 178                                |           |
| >¥200,000         |                 | 81                                 |           |

First, the input data are organized into a three-dimensional structure, as required for LSTM, which is denoted as (TrainX, SeqLen, Dim\_in). The first dimension, TrainX, represents the corresponding sample; the second dimension, SeqLen, represents the sequence data (specified sequence length) that are collected for that sample; and the third dimension, Dim\_in, represents the corresponding feature dimension of the static feature variables in the dataset of this paper. The dataset is divided into a training set and a test set according to this three-dimensional structure [20].

Second, the LSTM model is constructed. The model structure is represented as (Units, Input\_Shape, Activation, Recurrent\_dropout). Units is the number of neurons in the hidden layer, Input\_Shape is the structural form of the input dataset, Activation is the activation function, and Recurrent\_dropout is the learning rate. The sample size and characteristics of the dataset are analyzed to obtain the best model values. In this paper, Units is 45; Activation is the activation function, which is “ReLU”; and Recurrent\_dropout is 0.01.

Third, the LSTM model is trained. The training model structure is (X\_Train, Y\_Train, Epochs, Batch\_Size, Validation\_Split). X\_Train and Y\_Train are the model training data; Epochs is the number of iterations; Batch\_Size is the number of batch samples; and Validation\_Split is the training validation set splitting ratio. The values of the training model parameters are based on a priori knowledge and many experiments. In this paper, Epochs is set to 100, Batch\_Size to 16, and Validation\_Split to 0.8.

To compare and analyze the static feature prediction models, a variety of machine learning models are selected, such as RF [35], SVM [36], and KNN [37], and their experimental results are presented in Table 4.

In this experiment, the main dataset used is a static feature dataset for the analysis of users’ phishing susceptibility keys. The LSTM static feature prediction model was designed for comparison with other machine learning models. According to the experimental results, LSTM obtains the highest correctness rate of 89.71%, which is better than the rates of other models.

TABLE 4: Evaluation of LSTM on special static datasets with various classifiers.

| Classifier | Accuracy (%) | Precision (%) | Sensitivity (%) | F-measure (%) |
|------------|--------------|---------------|-----------------|---------------|
| RF         | 87.00        | 89.00         | 88.00           | 87.98         |
| SVM        | 88.04        | 88.42         | 88.23           | 88.25         |
| KNN        | 88.59        | 83.31         | 85.88           | 84.26         |
| LSTM       | 89.71        | 89.49         | 88.90           | 90.15         |

*Experiment 2.* Dynamic feature network-based phishing susceptibility prediction.

In this experiment, the main objective is to predict the user network phishing susceptibility using dynamic features as input to the LightGBM model. This model is also compared with several other machine learning models for analysis.

The dynamic feature dataset is divided into training and validation sets, and the scaling factor between the training and validation sets is set to 0.8. The parameters of the model are set based on a priori knowledge and many experiments, and the core parameters of the LightGBM training model are set as follows for the experimental data.

objective: task type. The task type options are regression, binary, and multiclass, among others. In this paper, the task is to make predictions, and the type is set to regression.

num\_leaves: the number of leaf nodes. This parameter determines the complexity of the tree model. The larger it is, the more accurate the model is; however, larger values may lead to overfitting. This parameter is set to 120.

max\_depth: controlling the maximum depth of the tree. This parameter can explicitly limit the depth of the tree. It is generally set to a value no greater than  $\log_2(\text{num\_leaves})$  and is set to 7 in this paper.

min\_data\_in\_leaf: the minimum number of samples per leaf node. It is an important parameter for dealing with overfitting of the leaf-wise tree. By setting it to a larger value, generation of an overly deep tree can be avoided, but a larger value may also lead to underfitting. In this paper, it is set to 16.

TABLE 5: Evaluation of LightGBM on the dynamic feature dataset with various classifiers.

| Classifier | Accuracy (%) | Precision (%) | Sensitivity (%) | F-measure (%) |
|------------|--------------|---------------|-----------------|---------------|
| DT         | 82.66        | 84.66         | 83.66           | 83.64         |
| LR         | 83.70        | 84.08         | 83.89           | 83.91         |
| XGBoost    | 84.25        | 78.97         | 81.54           | 79.92         |
| LightGBM   | 85.37        | 85.15         | 84.56           | 85.81         |

TABLE 6: Evaluation of LSTM-LightGBM on the feature dataset with various classifiers.

| Classifier    | Accuracy (%) | Precision (%) | Sensitivity (%) | F-measure (%) |
|---------------|--------------|---------------|-----------------|---------------|
| LSTM          | 89.71        | 89.49         | 88.90           | 90.15         |
| LightGBM      | 85.37        | 85.15         | 84.56           | 85.81         |
| LSTM-LightGBM | 92.34        | 91.26         | 92.29           | 92.26         |

learning\_rate: the learning rate of the training model. A larger learning rate will accelerate the convergence but reduce the accuracy, and the default value is 0.1. The learning rate can be adjusted according to the size of the dataset and is set to 0.05 in this paper.

Experiments are conducted on dynamic datasets to predict susceptibility using the LightGBM model, and a performance comparison is conducted with several other machine learning models, such as DT [38], LR [39], and XGBoost [40]. The experimental results are presented in Table 5.

In this experiment, the dataset is a dynamic feature dataset, which is used to analyze the users' susceptibility to phishing. The designed dynamic feature prediction model, namely, LightGBM, is compared with other machine learning models. According to the experimental results, LightGBM obtains the highest correctness rate of 85.37% among the compared models.

*Experiment 3.* Susceptibility prediction of phishing based on hybrid features.

In the experiments in this section, users' susceptibility to phishing is predicted using a combined LSTM-LightGBM model, in which the static feature variables personal attributes, personality, knowledge, and experience data are input into the LSTM training model, and each static feature variable can be calculated to predict users' susceptibility to phishing. The dynamic feature multidimensional prediction values are fed into the LightGBM model as input variables, from which the user's phishing susceptibility prediction values can be derived.

In this paper, a static feature dataset and dynamic feature dataset are selected as test samples, and the test results of the LSTM model alone, LightGBM model alone, and combined model are presented in Table 6. According to Table 6, the combined model has the highest correctness value and the best result compared with the stand-alone models; not only is it sensitive to timing, but it can also handle large batch data to effectively predict the phishing susceptibility.

## 5. Conclusions

In this paper, based on static and dynamic data of users, a prediction algorithm was used to predict the susceptibility analysis of users to phishing. First, susceptibility prediction was performed using an LSTM model for 19-dimensional features, such as the annual income, occupation, age, knowledge, and experience of users. Then, we used the LightGBM model to predict the susceptibility using dynamic features. Finally, we used a hybrid LSTM-LightGBM model to predict the susceptibility of users to phishing. By comparing the susceptibility prediction results that were obtained using the LSTM model alone and the combined LSTM-LightGBM model, we concluded that the prediction accuracy of the combined LSTM-LightGBM model was higher, namely, 92.34%, and that its prediction results were closer to the real situation. In this paper, we combined dynamic features and static prediction of phishing susceptibility, and by predicting user susceptibility, we identified users who were susceptible to phishing, for whom a more secure phishing defense could be implemented.

Although the proposed model can predict the susceptibility of users, there are still several areas for improvement in future work. For example, the testers in this paper were mainly college students, and the sample data were not evenly distributed. More data on occupation and age groups can be collected in the future to improve the model's robustness and accuracy rate.

## Data Availability

The processed data required to reproduce these findings cannot be shared at this time as the data also form part of an ongoing study.

## Conflicts of Interest

The authors declare that there are no conflicts of interest.

## Acknowledgments

This research was funded by the National Key R&D Program of China (2017YFB0802800) and Beijing Natural Science Foundation (4202002).

## References

- [1] K. Erb, *IRS Warns on Surge of New Email Phishing Scams*, 2018.
- [2] M. Landewe, "Four phishing attack trends to look out for in 2019," 2019, <https://www.forbes.com/sites/forbestechcouncil/2019/01/10/four-phishing-attack-trends-to-look-out-for-in-2019/#6b7a63d4ec20>.
- [3] J. Hong, "The state of phishing attacks," *Communications of the ACM*, vol. 55, no. 1, pp. 74–81, 2012.
- [4] L. Mathews, "Massive ransomware attack unleashes 23 Million emails in 24 hours," 2017, <https://www.forbes.com/sites/leemathews/2017/08/31/massive-ransomware-attack-unleashes-23-million-emails-in-24-hours/>.
- [5] M. Vergelis, T. Shcherbakova, T. Sidorina, and T. Kulikova, "Spam and phishing in 2018," *Secure List*, 2019, <https://securelist.com/spam-and-phishing-in-2018/89701>.

- [6] R. Brewer, "Ransomware attacks: detection, prevention and cure," *Network Security*, vol. 2016, no. 9, pp. 5–9, 2016.
- [7] A. Chanthadavong, "US, Canada issue alert on ransomware," 2017, <http://www.zdnet.com/article/us-canada-issue-alert-on-ransomware/>.
- [8] J. Wang, Y. Li, and H. R. Rao, "Coping responses in phishing detection: an investigation of antecedents and consequences," *Information Systems Research*, vol. 28, no. 2, pp. 378–396, 2017.
- [9] S. Grazioli and S. L. Jarvenpaa, "Perils of Internet fraud: an empirical investigation of deception and trust with experienced Internet consumers," *IEEE Transactions on Systems, Man, and Cybernetics-Part A: Systems and Humans*, vol. 30, no. 4, pp. 395–410, 2000.
- [10] T. N. Jagatic, N. A. Johnson, M. Jakobsson, and F. Menczer, "Social phishing," *Communications of the ACM*, vol. 50, no. 10, pp. 94–100, 2007.
- [11] L. Li, E. Berki, M. Helenius, and S. Ovaska, "Towards a contingency approach with whitelist- and blacklist-based anti-phishing applications: what do usability tests indicate?" *Behaviour & Information Technology*, vol. 33, no. 11, pp. 1136–1147, 2014.
- [12] R. Dhamija, J. D. Tygar, and M. Hearst, "Why phishing works," in *Proceedings of the SIGCHI Conference on Human Factors in Computing Systems*, pp. 581–590, Montréal, Canada, 2006.
- [13] A. Herzberg and A. Jbara, "Security and identification indicators for browsers against spoofing and phishing attacks," *ACM Transactions on Internet Technology*, vol. 8, no. 4, pp. 1–36, 2008.
- [14] L. Li and M. Helenius, "Usability evaluation of anti-phishing toolbars," *Journal in Computer Virology*, vol. 3, no. 2, pp. 163–184, 2007.
- [15] A. Abbasi, F. Zahedi, and Y. Chen, "Impact of anti-phishing tool performance on attack success rates," in *Proceedings of the 2012 IEEE International Conference on Intelligence and Security Informatics*, pp. 12–17, IEEE, Washington, DC, USA, June 2012.
- [16] D. Zhang, Z. Yan, H. Jiang, and T. Kim, "A domain-feature enhanced classification model for the detection of Chinese phishing e-Business websites," *Information & Management*, vol. 51, no. 7, pp. 845–853, 2014.
- [17] D. Akhawe and A. P. Felt, "Alice in warningland: a {Large-Scale} field study of browser security warning effectiveness," in *Proceedings of the 22nd USENIX Security Symposium (USENIX Security 13)*, pp. 257–272, Washington, DC, USA, August 2013.
- [18] H. Chen, R. H. L. Chiang, and V. C. Storey, "Business intelligence and analytics: from big data to big impact," *MIS Quarterly*, vol. 36, no. 4, pp. 1165–1188, 2012.
- [19] M. Alsharnouby, F. Alaca, and S. Chiasson, "Why phishing still works: user strategies for combating phishing attacks," *International Journal of Human-Computer Studies*, vol. 82, pp. 69–82, 2015.
- [20] G. D. Moody, D. F. Galletta, and B. K. Dunn, "Which phish get caught? an exploratory study of individuals' susceptibility to phishing," *European Journal of Information Systems*, vol. 26, no. 6, pp. 564–584, 2017.
- [21] A. R. Dennis and R. K. Minas, "Security on autopilot: why current security theories hijack our thinking and lead us astray," *ACM SIGMIS-Data Base: The DATABASE for Advances in Information Systems*, vol. 49, no. SI, pp. 15–38, 2018.
- [22] K. Smith, P. A. Hancock, and A. Peter, "Situation awareness is adaptive, externally directed consciousness," *Human Factors: The Journal of the Human Factors and Ergonomics Society*, vol. 37, no. 1, pp. 137–148, 1995.
- [23] L. Musthaler, *Security Analytics Will Be the Next Big Thing in IT Security*. Network World (May 31), 2013.
- [24] B. Taylor, *How Big Data Are Changing the Security Analytics Landscape*. TechRepublic (January 2), 2014.
- [25] S. Gregor, A. R. Hevner, and A. R. Hevner, "Positioning and presenting design science research for maximum impact," *MIS Quarterly*, vol. 37, no. 2, pp. 337–355, 2013.
- [26] Y. Zhang, S. Egelman, L. Cranor, and J. Hong, "Phishing phish: Evaluating anti-phishing tools," in *Proceedings of the 14th Annual Network and Distributed System Security Sympos*, pp. 1–16, San Diego, CA, USA, 2007.
- [27] S. Li and R. Schmitz, "A novel anti-phishing framework based on honeypots," in *Proceedings of the 2009 eCrime Researchers Summit*, Tacoma, WA, USA, September 2009.
- [28] E. R. Leukfeldt, "Phishing for suitable targets in The Netherlands: routine activity theory and phishing victimization," *Cyberpsychology, Behavior, and Social Networking*, vol. 17, no. 8, pp. 551–555, 2014.
- [29] T. Lin, D. E. Capecci, D. M. Ellis et al., "Susceptibility to spear-phishing emails: effects of internet user demographics and email content," *ACM Transactions on Computer-Human Interaction*, vol. 26, no. 5, pp. 1–28, 2019.
- [30] X. Luo, W. Zhang, S. Burd, and A. Seazzu, "Investigating phishing victimization with the Heuristic-Systematic Model: a theoretical framework and an exploration," *Computers & Security*, vol. 38, pp. 28–38, 2013.
- [31] C. Bravo-Lillo, L. F. Cranor, J. Downs, and S. Komanduri, "Bridging the gap in computer security warnings: a mental model approach," *IEEE Security & Privacy Magazine*, vol. 9, no. 2, pp. 18–26, 2011.
- [32] S. Sheng, M. Holbrook, P. Kumaraguru, L. F. Cranor, and J. Downs, "Who falls for phish?: a demographic analysis of phishing susceptibility and effectiveness of interventions," in *Proceedings of the SIGCHI Conference on Human Factors in Computing Systems*, pp. 373–382, ACM, New York, NY, USA, 2010.
- [33] A. Abbasi, D. Dobolyi, A. Vance, and F. M. Zahedi, "The phishing funnel model: a design artifact to predict user susceptibility to phishing websites," *Information Systems Research*, vol. 32, no. 2, pp. 410–436, 2021.
- [34] R. Yang, K. Zheng, B. Wu, D. Li, Z. Wang, and X. Wang, "Predicting user susceptibility to phishing based on multi-dimensional features," *Computational Intelligence and Neuroscience*, vol. 2022, Article ID 7058972, 11 pages, 2022.
- [35] J. G. Bartlett, R. F. Breiman, L. A. Mandell, and T. M. File, "Community-acquired pneumonia in adults: guidelines for management," *Clinical Infectious Diseases*, vol. 26, no. 4, pp. 811–838, 1998.
- [36] C. Schuldt, I. Laptev, and B. Caputo, "Recognizing human actions: a local SVM approach," in *Proceedings of the 17th International Conference on Pattern Recognition, 2004*, pp. 32–36, IEEE, Cambridge, UK, August 2004.
- [37] G. Guo, H. Wang, D. Bell, Y. Bi, and K. Greer, "KNN model-based approach in classification," in *Proceedings of the OTM Confederated International Conferences On the Move to Meaningful Internet Systems*, pp. 986–996, Berlin, Heidelberg, Germany, 2003.
- [38] S. R. Safavian and D. Landgrebe, "A survey of decision tree classifier methodology," *IEEE Transactions on Systems, Man, and Cybernetics*, vol. 21, no. 3, pp. 660–674, 1991.
- [39] A. DeMaris, "A tutorial in logistic regression," *Journal of Marriage and Family*, vol. 57, no. 4, pp. 956–968, 1995.
- [40] T. Chen and C. Guestrin, "Xgboost: a scalable tree boosting system," in *Proceedings of the 22nd acm SIGKDD International Conference on Knowledge Discovery and Data Mining*, pp. 785–794, San Francisco, CA, USA, August 2016.

## Research Article

# Market Risk Early Warning Based on Deep Learning and Fruit Fly Optimization

Liang Chen<sup>1</sup> and Rui Ma<sup>2</sup> 

<sup>1</sup>School of Economics and Management, Southwest Petroleum University, Chengdu 610500, China

<sup>2</sup>Health and Rehabilitation College, Chengdu University of Traditional Chinese Medicine, Chengdu 610032, China

Correspondence should be addressed to Rui Ma; marui19840213@cdutcm.edu.cn

Received 4 March 2022; Revised 14 April 2022; Accepted 18 April 2022; Published 9 May 2022

Academic Editor: Man Fai Leung

Copyright © 2022 Liang Chen and Rui Ma. This is an open access article distributed under the Creative Commons Attribution License, which permits unrestricted use, distribution, and reproduction in any medium, provided the original work is properly cited.

To improve the ability of market to avoid and prevent credit risk and strengthen the awareness of market risk early warning, SMOTE is used to process the unbalanced sample, and fruit fly optimization algorithm (FOA) is utilized to optimize the parameters of support vector machine (SVM), and thus an improved SVM market risk early warning model is proposed. The simulation results show that the proposed model has excellent stability and generalization ability, and it can predict market credit risk accurately. Compared with the prediction model based on FOA-SMOTE-BP and FOA-SMOTE-Logit, the proposed model performs better on the indicators of G value, F value, and AUC value, which provides a reference for market credit risk prediction.

## 1. Introduction

Market risk early warning is an important measure to prevent market risk and unknown loss and improve market normalization. In recent years, with the development of intelligent technology, deep learning has been widely used in various fields, including market risk warning. So far, the relevant researchers achieved market risk early warning through the use of deep learning. On the basis of in-depth study of rough set theory (RST), Guan et al. proposed a financial operation risk early warning model based on BP neural network, which effectively realizes the prediction of financial operation risk and profit risk of family farm [1]. In the cross-border environment, scholars put forward the marginal expected gap, delta conditional value at risk, and conditional capital gap to measure the system risk. The feature pair method based on bilateral balance sheet data is different from the paradoxical risk measurement method based on market price. Thus, a systemic risk early warning method based on the network spectral feature pair method analyzing the core global banking system is proposed. The method provides risk early warning for the unstable financial markets based on turning points similar to  $R$  numbers in

popular models [2]. Figini et al. improved the sample performance of parametric models and nonparametric models in credit risk estimation, so as to propose a multi-variable outlier detection technology based on local outliers, which can support financial institutions to make decisions and avoid falling into corporate credit risks [3]. In view of the credit risk assessment of the Internet finance industry, Yang and Yuan applied RBF network to analyze the statistical data of online peer-to-peer lending platform and evaluated the credit risk of the platform, and thus a new early warning method of RBF neural network model is proposed, which can reasonably predict the credit risk status of the industry development [4]. Based on the fuzzy theory and related theories of financial risk early warning management, Ding proposed the fuzzy comprehensive evaluation method, which realizes more accurate early warning and assessment of potential and obvious risks of financial enterprises. In addition, the safety of financial enterprise management is greatly improved, and the losses caused by various risks are reduced [5]. Based on BP neural network, Li constructed a risk assessment model of knowledge transfer in transforming enterprises to realize knowledge management risk warning [6]. Dong adopted the improved K-means



algorithm of quantum evolution to divide the risk warning interval by combining the given initial value and the value at risk measured by well-known Chinese online financial companies [7, 8]. Zhang and Chen used the autoregressive conditional Fréchet (ACF) model to predict the tail risk of the capital market, so as to identify major crisis sources [9]. Ouyang et al. applied the deep learning algorithm to the early warning of market risk. The results show that the algorithm has high accuracy compared with the traditional BP and others [10].

Among them, SVM algorithm is widely used in the field of classification because of its nonlinear and small sample advantages, but the parameter optimization of SVM is a research hotspot. For example, Jerlin Rubini and Perumal proposed to optimize the SVM algorithm by using the Drosophila algorithm and applied the optimized algorithm to the classification of chronic kidney disease, showing a good classification effect, indicating that the Drosophila algorithm has great advantages in optimizing SVM [11]. Tian and others used the fruit fly algorithm to optimize the echo state network, which greatly improved the accuracy of prediction [12]. Lu et al. applied the fruit fly algorithm and SVM to the prediction of urban gas load, which greatly improved the accuracy of short-term prediction. It can be seen from the above that the combination of Drosophila algorithm and SVM for classification or prediction has become the focus of current research [13]. The above early warning models based on deep learning realize the early warning of market risks to a certain extent. However, the prediction accuracy needs to be improved. To solve this problem, this paper applies the SVM model with excellent predictive performance and constructs a market risk early warning model by optimizing its parameters and unbalanced samples.

## 2. Basic Methods

**2.1. SVM Model.** SVM is a generalized linear classifier, which is proposed based on statistical learning theory and the principle of minimizing structural risk. Its basic principle is to construct an optimal hyperplane to maximize the distance between samples of two different categories, which is shown in Figure 1 [14]. Here, circles and squares represent two different types, respectively, and the optimal hyperplane is to maximize the range between the two dotted lines.

Suppose, dataset =  $(x_i, y_i), i = 1, 2, \dots, n, x \in R, y \in \{-1, 1\}$ ,  $y$  is the category number. When  $y = 1$ , it means that  $x$  belongs to the first category. Also, when  $y = -1$ , it means that  $x$  belongs to the second category. Its linear discriminant function is usually expressed as [15]

$$g(x) = w' \cdot x + b, \quad (1)$$

where  $w'$  is the inertia weight and  $b$  is a constant.

The classification gap is  $2/\|w'\|^2$ . When  $\|w'\|^2$  is minimum, the classification spacing is maximum. The form of standard SVM is [16]

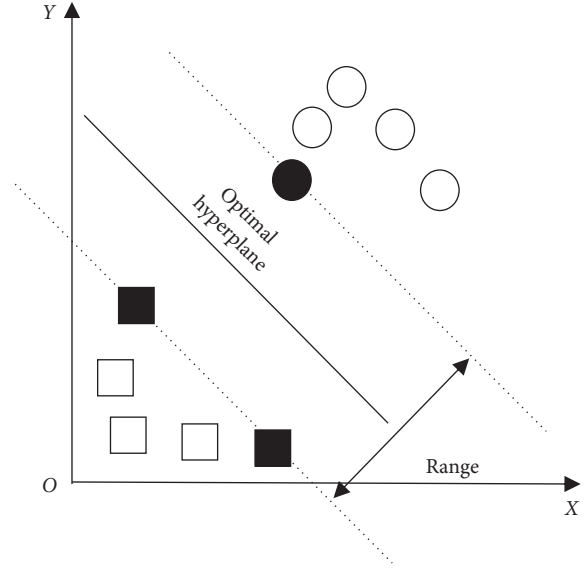


FIGURE 1: SVM for classification data example.

$$\min g(w') = \left( \frac{1}{2} \|w'\|^2 + c \sum_{i=1}^n \varepsilon_i^2 \right), \text{ s.t. } y_i (w'^T x_i + b^T x_i + b) \geq 1 - \varepsilon_i, \quad (2)$$

$$\varepsilon_i \geq 0, i = 1, 2, \dots, n,$$

where  $c$  is the penalty function and  $\varepsilon$  is the slack variable.

SVM is used to perform nonlinear transformation for undivided linear sample data, namely,  $\varphi: R^d \rightarrow H$ . Thus, the data sample space can be mapped in high-dimensional space. When solving, it should meet the requirement of [17]

$$Q(a) = \sum_{i=1}^n a_i - \frac{1}{2} \sum_{i,j=1}^n a_i a_j y_i y_j K(x_i, x_j), \quad (3)$$

where  $a_i$  is the Lagrange multiplier and  $\sum_{i=1}^n y_i a_i = 0$ . Since the above equation is constrained by the inequality, there is a unique optimal solution corresponding to the Lagrange multiplier  $a_i^*$ . The optimal classification discriminant function is [18]

$$f(x) = \text{sgn} \left\{ \sum_{i=1}^n a^* y_i K(x_i, y_i) + b^* \right\}, \quad (4)$$

where  $b^*$  is the  $b$  value obtained from formula (2) and  $K(x_i, x_i)$  is the kernel function. Take the radial basis function (RBF) as an example, which can be expressed as [19]

$$K(x, y) = \exp(-\sigma \|x - y\|^2), \quad (5)$$

where  $\sigma$  is the RBF kernel parameter. According to formulas (4) and (5), the optimal classification discriminant function is

$$f(x) = \text{sgn} \left\{ \sum_{i=1}^n a^* y_i \exp(-\sigma \|x_i - y_i\|^2) + b^* \right\}. \quad (6)$$

As can be seen from the above analysis, the classification effect of the SVM model mainly depends on two aspects: one is whether the number of classification samples is balanced, and the other is whether the kernel parameters and penalty factors of the model are optimal, while the standard SVM model does not consider the situation [20]. Therefore, in order to improve the classification effect of the SVM model, this paper improves the model from the above two aspects.

## 2.2. SVM Model Improvements

**2.2.1. Unbalanced Sample Processing.** For the unbalanced classification samples, the Synthetic Minority Oversampling Technique (SMOTE) is used to deal with them from the data level [21]:

- (1) Determine a few sample categories  $X$ , calculate the Euclidean distance  $d$  between samples in  $X$ , and select  $K$  samples with the smallest distance  $d$ .
- (2) Sample  $X$  with the multiplier of  $N = \text{minority sample} / \text{majority sample}$ , and select  $X_i (i = 1, 2, \dots, N)$  from  $K$  samples.
- (3) According to formula (7),  $X_i$  and  $X$  are synthesized into a new sample:

$$X_{\text{new}} = X + \text{rand}(0, 1) \times (X_i - X). \quad (7)$$

- (4) Combine  $X_{\text{new}}$  and  $X$  as a new training set to learn on the SVM model.

**2.2.2. Optimization of Model Parameters.** To optimize kernel parameters and penalty factors of the SVM model, this paper adopts fruit fly optimization algorithm (FOA) with high searching accuracy to process. Figure 2 shows simulated behavior of fruit fly foraging process [22]. The basic operation is as follows.

- (1) Initialize model maximum iteration, population size, fruit fly population location range (LR), and other parameters. In 2D coordinates  $(X, Y)$ , the initial position of each individual fruit fly is

$$\begin{aligned} X_{\text{axis}} &= \text{rand}(LR), \\ Y_{\text{axis}} &= \text{rand}(LR). \end{aligned} \quad (8)$$

- (2) Assign flight direction and distance to all fruit flies and olfactory search is utilized to update [23]

$$\begin{aligned} X_i &= X_{\text{axis}} + \text{rand}(FR), \\ Y_i &= Y_{\text{axis}} + \text{rand}(FR), \end{aligned} \quad (9)$$

where  $FR$  represents the single flight range of fruit fly.

- (3) According to formula (12), the distance between the individual position of fruit fly and the origin is calculated [24].

$$\text{DIST}_i = \sqrt{X_i^2 + Y_i^2}. \quad (10)$$

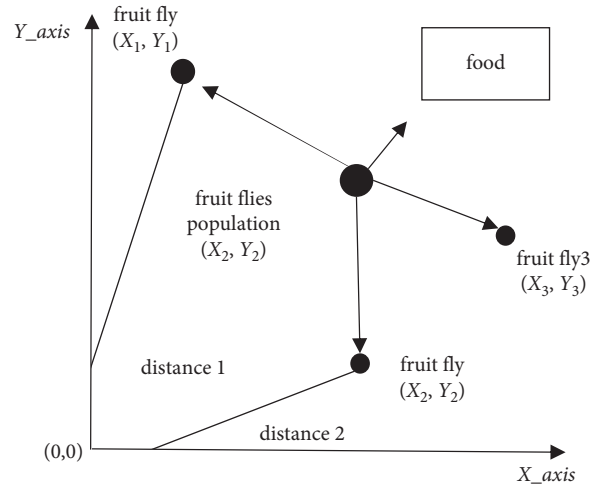


FIGURE 2: Simulation of fruit fly foraging behavior.

- (4)  $\text{Smell}_i$  and  $S_i$  are calculated according to fitness:

$$\text{Smell}_i = \text{fitness}(S_i),$$

$$S_i = \frac{1}{\text{DIST}_i}, \quad (11)$$

where fitness is the discriminant function,  $\text{smell}_i$  is the flavor concentration value, and  $S_i$  is the judgment value of smell.

- (5) Update bestSmell and bestIndex:

$$[\text{bestSmell}, \text{bestIndex}] = \min(\text{Smell}). \quad (12)$$

- (6) Use visual search to make other fruit flies fly to the best position [25]:

$$\begin{aligned} \text{SmellBest} &= \text{BestSmell}, \\ X_{\text{axis}} &= X(\text{bestIndex}), \\ Y_{\text{axis}} &= Y(\text{bestIndex}). \end{aligned} \quad (13)$$

- (7) Repeat steps (2)–(6) until the algorithm iterates to the set number.

FOA guides the search by the current optimal solution and makes the result close to the optimal solution, so as to realize the parameter optimization.

## 3. Market Credit Risk Early Warning Model Based on Improved SVM

$S_{\text{min}}$  and  $S_{\text{maj}}$  are used to represent the samples of market credit risk and noncredit risk, and  $S$  is the set of all samples. Based on the above improvements, the construction process of the market credit risk early warning model is designed as follows:

- (1) Calculate  $k$  nearest neighbor points of each sample point  $(x_{\text{smi}}, y_{\text{smi}})$  in  $S_{\text{min}}$ , randomly select a neighbor point  $|S_{\text{maj}} - S_{\text{min}}|/2$  to subtract  $(x_{\text{smi}}, y_{\text{smi}})$  and multiply it by the random number  $\delta$  in the

interval  $[0, 1]$ , and then add  $(x_{smin}, y_{smin})$  to obtain a new credit risk sample  $x_{new}$ , and thus there is

$$x_{new} = x_{smin} + (\overline{x_{min}} - x_{smin}) \times \delta. \quad (14)$$

- (2) Repeat the above steps until the number of  $x_{new}$  reaches  $|S_{maj}-S_{min}|/2$ .
- (3) Initialize relevant parameters of SVM and FOA. In this paper, referring to reference [26], the maximum iteration number of FOA is set to 100, and the population size is set to 20.
- (4) Use FOA to optimize the parameters of the SVM model, and the judgment value of flavor concentration is calculated according to  $DIST_i = \sqrt{X_i^2 + Y_i^2}$  and  $S_i = 1/DIST_i$ .
- (5) Continue to iterate until the optimal bestsmell is less than the set value, and then the value is the optimal parameter.
- (6) Plug optimal parameters and  $x_{new}$  to construct the improved SVM model and perform prediction.

The above process is illustrated in Figure 3.

## 4. Simulation Experiment

**4.1. Experimental Environment Construction.** This experiment is run on 64-bit Windows 7 professional edition system. The CPU is Intel(R)Xeon(R) e5-2620v3 2.40ghz, and the GPU is Tesla K80. In addition, the memory is 16G. The model was built with MATLAB2018a.

### 4.2. Data Sources and Preprocessing

**4.2.1. Data Sources.** The financial data of 260 listed manufacturing enterprises in Shenzhen and Shanghai from 2018 to 2020 are selected as the experiment data. Through references [21, 27, 28], there are a total of 20 financial indicators selected as credit risk warning indicators of listed companies, including 6 first-level indicators such as enterprise operation capacity, growth capacity, profitability, and so on, and 20 second-level indicators such as total asset turnover rate, net asset growth rate, return on net asset, and so on. The indicators are listed in detail in Table 1.

### 4.2.2. Data Preprocessing

(1) *Descriptive Statistics.* Since there are significant differences between the mean of the above indicator variables and standard deviation and maximum and minimum values, descriptive statistics of indicator variables are carried out, and the results are shown in Table 2.

(2) *Normalization.* Considering the dimensional level of index variables, z-score is adopted for normalization, which is shown in the following formula:

$$x_j^* = \frac{x_j - \mu(x_j)}{\sigma(x_j)}, \quad (15)$$

where  $\mu(x_j)$  and  $\sigma(x_j)$  represent the sample mean and standard deviation corresponding to index  $j$ , respectively.

After normalization, descriptive statistics of each indicator variable are shown in Table 3.

(3) *Significance Testing.* For the selection of indicators that can distinguish credit risks and nonuse risks of listed companies, this paper adopts independent sample  $T$ -test to test them, and the results are shown in Table 4. The  $P$  value of 7 indicators, such as net asset-liability ratio and operating profit growth rate, is more than 10%, which indicates that it is unable to distinguish the credit risk and noncredit risk, so it is deleted in this paper.

**4.3. Evaluation Indicators.** Set average accuracy (G), F value, and AUC are used to evaluate the prediction performance of model. Confusion matrix is used to represent the dichotomous dataset of credit risk, which is shown in Table 5.

The model sensitivity (SE), specificity (SP), and precision (P) can be calculated as follows:

$$\begin{aligned} SE &= \frac{|TSmin|}{(|TSmin| + |TSmin|)}, \\ SP &= \frac{|TSmin|}{(|TSmin| + |TSmin|)}, \\ P &= \frac{|TSmin|}{(|TSmin| + FSmin)}. \end{aligned} \quad (16)$$

Through the above three indicators, the following can be calculated:

$$G = 0.1044, \quad (17)$$

$$F\_measure = 2 * SE * \frac{SP}{(SE + P)}$$

The larger the selected index value is, the better the model performance is.

### 4.4. Experimental Results

**4.4.1. Model Verification.** The samples are divided into training sets and testing sets according to different proportions, and experiments are carried out under different kernel functions and different optimal parameter values. The results are shown in Table 6. Under the division condition of different sample proportion, models corresponding to different kernel functions and optimal parameter values perform well in G value, F value, and AUC value, and the differences are small, which indicates that the proposed model has good prediction performance and strong generalization ability [29].

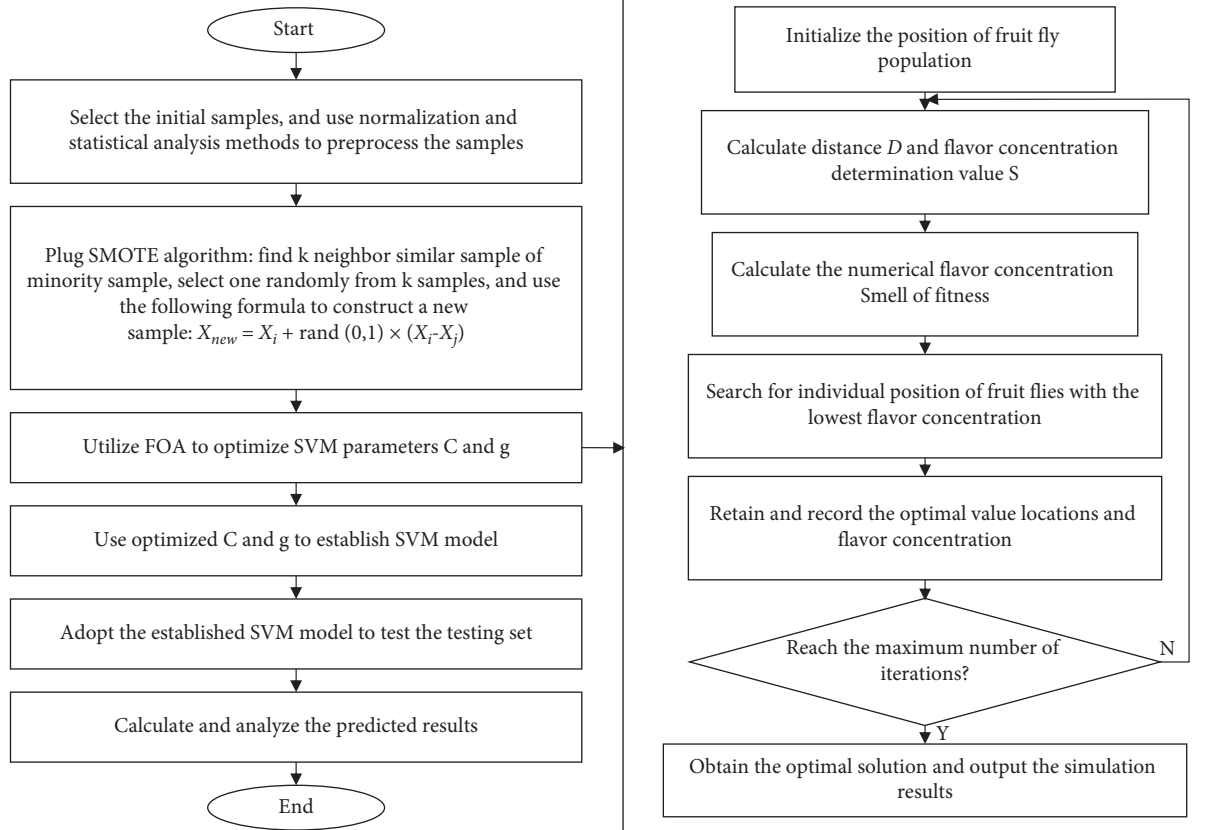


FIGURE 3: Prediction process of market credit risk early warning model based on improved SVM.

TABLE 1: Index selection.

| Index type          | Index name   |
|---------------------|--|
| Debt paying ability | Current ratio (X <sub>1</sub> )                            |
|                     | Quick ratio (X <sub>2</sub> )                              |
|                     | Net asset-liability ratio (X <sub>3</sub> )                |
| Operation ability   | Fixed asset turnover ratio(X <sub>4</sub> )                |
|                     | Total asset turnover ratio (X <sub>5</sub> )               |
|                     | Receivable turnover ratio (X <sub>6</sub> )                |
| Profit ability      | Return on net assets (X <sub>7</sub> )                     |
|                     | Return on total assets (X <sub>8</sub> )                   |
|                     | Net interest rate in sale (X <sub>9</sub> )                |
| Growth ability      | Growth rate of basic earnings per share (X <sub>10</sub> ) |
|                     | Growth rate of total operating revenue (X <sub>11</sub> )  |
|                     | Operating profit growth rate (X <sub>12</sub> )            |
|                     | Growth rate of net assets (X <sub>13</sub> )               |
| Index per share     | Earning per share (X <sub>14</sub> )                       |
|                     | Net assets per share (X <sub>15</sub> )                    |
|                     | Retained earnings per share (X <sub>16</sub> )             |
|                     | Operating revenue per share (X <sub>17</sub> )             |
| Asset structure     | Asset-liability ratio (X <sub>18</sub> )                   |
|                     | Rights multiple (X <sub>19</sub> )                         |
|                     | Capital fixed ratio (X <sub>20</sub> )                     |

In order to more intuitively reflect the prediction performance of different kernel functions and optimal parameter values under different training sample proportions, the prediction results in the above table are plotted in

Figures 4–6. Figure 4 shows that under different ratios of training set and testing set, the fluctuation range of G values of different kernel functions is small. Compared with the sigmoid and polynomial models, linear and RBF models have higher G values, which indicates that linear and RBF models have slightly better performance. On the other hand, Figure 5 shows that under different proportions of training sets and testing sets, F values of different kernels fluctuate greatly, but the overall F value is high. There is no trend indicating that the model F value of certain kernels type has the highest value, and thus the proposed model has good generalization ability. As can be seen from Figure 6, the AUC value of the proposed model fluctuates greatly, but the proposed model also achieves good results on this index. To sum up, the model proposed in this paper has good generalization ability and good prediction performance.

Considering that evaluating the model performance only through evaluation indexes lacks a certain scientific character, paired sample *T* test is adopted to test the prediction performance of different kernel function models, and the results are shown in Table 7. On the G value, the statistics of RBF and polynomial model, linear, and sigmoid model are all less than 10%, which rejects the null hypothesis, indicating that the performance of RBF and polynomial model is significantly different from that of linear and sigmoid model. On the *F* value, the statistics of all kernel function models are less than 10%, and all accept the null hypothesis, indicating that the performance of different kernel function models is less

TABLE 2: Descriptive statistical results of indicators.

| Financial indicators | Mean      | Standard deviation | Minimum value | Maximum value |
|----------------------|-----------|--------------------|---------------|---------------|
| X <sub>1</sub>       | 2.5217    | 2.9850             | 0.15          | 33.17         |
| X <sub>2</sub>       | 2.0907    | 2.7981             | 0.13          | 33.17         |
| X <sub>3</sub>       | 1.4701    | 1 1.5760           | -151.94       | 231.66        |
| X <sub>4</sub>       | 3.5915    | 4.4036             | 0.17          | 47.23         |
| X <sub>5</sub>       | 0.7471    | 0.3703             | 0.03          | 2.64          |
| X <sub>6</sub>       | 9.1016    | 9.0790             | 0.00          | 108.47        |
| X <sub>7</sub>       | 2.7914    | 134.5795           | -3106.24      | 871.51        |
| X <sub>8</sub>       | 7.89869   | 7.8307             | -60.11        | 48.03         |
| X <sub>9</sub>       | 7.8415    | 15.9206            | -222.31       | 153.66        |
| X <sub>10</sub>      | -35.1845  | 549.6023           | -6200.00      | 4550.49       |
| X <sub>11</sub>      | 14.9435   | 37.1203            | -90.05        | 467.03        |
| X <sub>12</sub>      | 1857.6662 | 52257.2278         | -41692.61     | 1398352.86    |
| X <sub>13</sub>      | 25.4540   | 76.0995            | -1281.86      | 691.26        |
| X <sub>14</sub>      | 0.4146    | 0.6626             | -5.75         | 4.37          |
| X <sub>15</sub>      | 4.7500    | 3.7401             | -3.04         | 70.53         |
| X <sub>16</sub>      | 1.6847    | 2.6542             | -5.95         | 51.75         |
| X <sub>17</sub>      | 6.1740    | 5.9962             | 0.06          | 72.55         |
| X <sub>18</sub>      | 38.5987   | 23.5712            | 3.03          | 326.20        |
| X <sub>19</sub>      | 2.6128    | 9.8620             | 0.00          | 232.68        |
| X <sub>20</sub>      | 136 0941  | 769.6847           | -12085.50     | 13048.27      |

TABLE 3: Descriptive statistics of index variables after normalization.

| Financial indicators | Mean | Standard deviation | Minimum value | Maximum value |
|----------------------|------|--------------------|---------------|---------------|
| X <sub>1</sub>       | 0    | 1                  | -0.7976       | 10.2645       |
| X <sub>2</sub>       | 0    | 1                  | -0.7032       | 11.1042       |
| X <sub>3</sub>       | 0    | 1                  | -13.25121     | 19.8845       |
| X <sub>4</sub>       | 0    | 1                  | -0.7785       | 9.9074        |
| X <sub>5</sub>       | 0    | 1                  | -1.9700       | 5.0861        |
| X <sub>6</sub>       | 0    | 1                  | -1.0026       | 10.9445       |
| X <sub>7</sub>       | 0    | 1                  | -23.1019      | 6.4551        |
| X <sub>8</sub>       | 0    | 1                  | -8.6845       | 5.1242        |
| X <sub>9</sub>       | 0    | 1                  | -14.4564      | 9.1595        |
| X <sub>10</sub>      | 0    | 1                  | -11.2170      | 8.3437        |
| X <sub>11</sub>      | 0    | 1                  | -2.8287       | 12.1791       |
| X <sub>12</sub>      | 0    | 1                  | -0.8335       | 26.7232       |
| X <sub>13</sub>      | 0    | 1                  | -17.1797      | 8.7492        |
| X <sub>14</sub>      | 0    | 1                  | -9.2881       | 5.9572        |
| X <sub>15</sub>      | 0    | 1                  | -2.0798       | 17.5859       |
| X <sub>16</sub>      | 0    | 1                  | -2.8729       | 18 8525       |
| X <sub>17</sub>      | 0    | 1                  | -1.0214       | 11.0679       |
| X <sub>18</sub>      | 0    | 1                  | -1.5097       | 12.2011       |
| X <sub>19</sub>      | 0    | 1                  | -0.2650       | 23.3276       |
| X <sub>20</sub>      | 0    | 1                  | -15.8788      | 16.7760       |

TABLE 4: Independent sample T-test results of index variables.

| Financial indicators | T value | P value | Financial indicators | T value | P value |
|----------------------|---------|---------|----------------------|---------|---------|
| X <sub>1</sub>       | 9.015   | 0.000   | X <sub>11</sub>      | 2.163   | 0.032   |
| X <sub>2</sub>       | 9.958   | 0.000   | X <sub>12</sub>      | 0.174   | 0.864   |
| X <sub>3</sub>       | 0.223   | 0.827   | X <sub>13</sub>      | 2.772   | 0.014   |
| X <sub>4</sub>       | 2.118   | 0.035   | X <sub>14</sub>      | 3.862   | 0.002   |
| X <sub>5</sub>       | 2.533   | 0.012   | X <sub>15</sub>      | 3.601   | 0.000   |
| X <sub>6</sub>       | 2.085   | 0.038   | X <sub>16</sub>      | 4.695   | 0.000   |
| X <sub>7</sub>       | 1.711   | 0.105   | X <sub>17</sub>      | 1.246   | 0.215   |
| X <sub>8</sub>       | 7.660   | 0.000   | X <sub>18</sub>      | -4.182  | 0.002   |
| X <sub>9</sub>       | 6.117   | 0.000   | X <sub>19</sub>      | -1.504  | 0.153   |
| X <sub>10</sub>      | 1.588   | 0.132   | X <sub>20</sub>      | 0.176   | 0.863   |

TABLE 5: Confusion matrix of credit risk dataset.

|                                  | Judged as noncredit risk sample | Judged as credit risk sample |
|----------------------------------|---------------------------------|------------------------------|
| Actually a noncredit risk sample | $ TS_{maj} $                    | $ FS_{min} $                 |
| Actually a sample of credit risk | $ FS_{maj} $                    | $ TS_{min} $                 |

TABLE 6: Prediction results.

| Kernel function | Proportion of training samples (%) | Proportion of testing samples (%) | Optimal parameter value                          | G      | F      | AUC    |
|-----------------|------------------------------------|-----------------------------------|--|--------|--------|--------|
| RBF             | 90                                 | 10                                | $c = 0.6509, g = 0.6666$                         | 0.6954 | 0.2023 | 0.6071 |
|                 | 80                                 | 20                                | $c = 0.0836, g = 0.0806$                         | 0.7659 | 0.2224 | 0.7946 |
|                 | 70                                 | 30                                | $c = 0.0908, g = 0.0798$                         | 0.7083 | 0.4576 | 0.7338 |
|                 | 60                                 | 40                                | $c = -0.7157, g = -0.6259$                       | 0.7578 | 0.2888 | 0.7821 |
|                 | 50                                 | 50                                | $c = 0.1384, g = 0.1355$                         | 0.7151 | 0.2143 | 0.7490 |
| Polynomial      | 90                                 | 10                                | $c = 2.1547, g = 0.7367, d = 6.8425, r = 0.9121$ | 0.7071 | 0.2667 | 0.6843 |
|                 | 80                                 | 20                                | $c = 3.0080, g = 0.8021, d = 2.0911, r = 1.1900$ | 0.6157 | 0.2222 | 0.5429 |
|                 | 70                                 | 30                                | $c = 4.5994, g = 0.4957, d = 0.9812, r = 1.8810$ | 0.6279 | 0.4000 | 0.5514 |
|                 | 60                                 | 40                                | $c = 2.6578, g = 0.7339, d = 1.8111, r = 2.7077$ | 0.6684 | 0.0909 | 0.5786 |
|                 | 50                                 | 50                                | $c = 0.2456, g = 0.0897, d = 0.0835, r = 0.0810$ | 0.6673 | 0.2353 | 0.5677 |
| Linear          | 90                                 | 10                                | $c = 1.6133$                                     | 0.7098 | 0.2349 | 0.7465 |
|                 | 80                                 | 20                                | $c = 0.1$  | 0.7641 | 0.2311 | 0.7935 |
|                 | 70                                 | 30                                | $c = 0.0887$                                     | 0.7761 | 0.4295 | 0.8024 |
|                 | 60                                 | 40                                | $c = 15.6392$                                    | 0.6488 | 0.2127 | 0.6530 |
|                 | 50                                 | 50                                | $c = 0.1044$                                     | 0.6954 | 0.2110 | 0.7108 |
| Sigmoid         | 90                                 | 10                                | $c = 5.7636, g = 0.7344, r = 0.7683$             | 0.7011 | 0.2879 | 0.7243 |
|                 | 80                                 | 20                                | $c = 1.9080, g = 0.6945, r = 0.8052$             | 0.6970 | 0.1319 | 0.7154 |
|                 | 70                                 | 30                                | $c = 3.3143, g = 0.5031, r = 0.8505$             | 0.7061 | 0.3002 | 0.7212 |
|                 | 60                                 | 40                                | $c = 2.4913, g = 0.7543, r = 1.1081$             | 0.6267 | 0.2199 | 0.5436 |
|                 | 50                                 | 50                                | $c = 0.2223, g = 0.0758, r = 0.0757$             | 0.6443 | 0.1900 | 0.5981 |

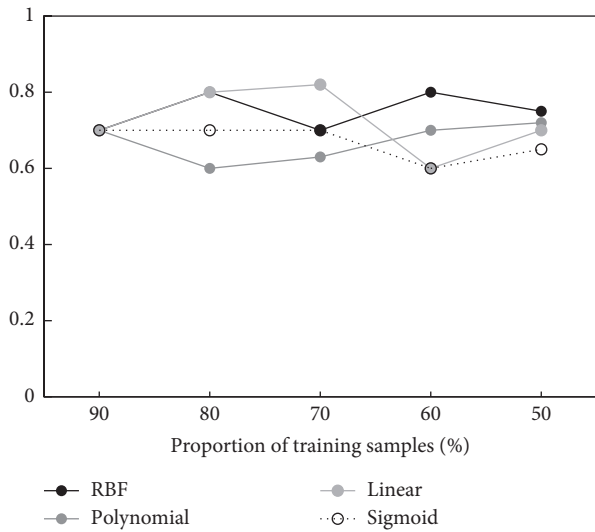


FIGURE 4: G values of the model under different kernel functions.

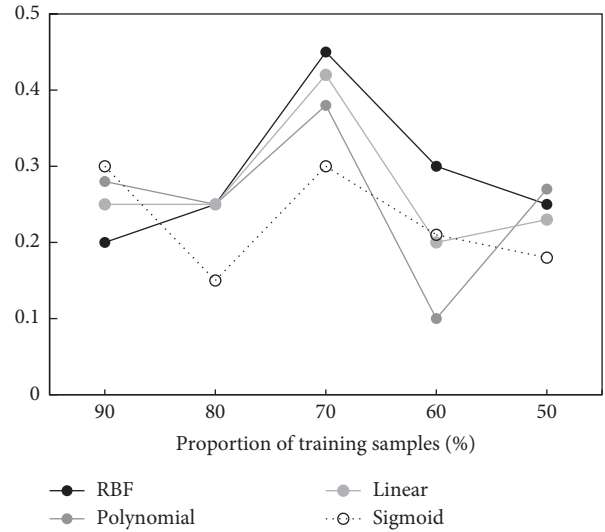


FIGURE 5: F values of the model under different kernel functions.

different. On the AUC value, the statistics of all models are less than 10%, which rejects the null hypothesis, indicating that the performance of linear and polynomial, sigmoid and polynomial, and RBF models is significantly different.

In conclusion, the change of kernel function has little influence on the prediction performance of the proposed model, which means that the prediction performance of the proposed model is relatively stable.

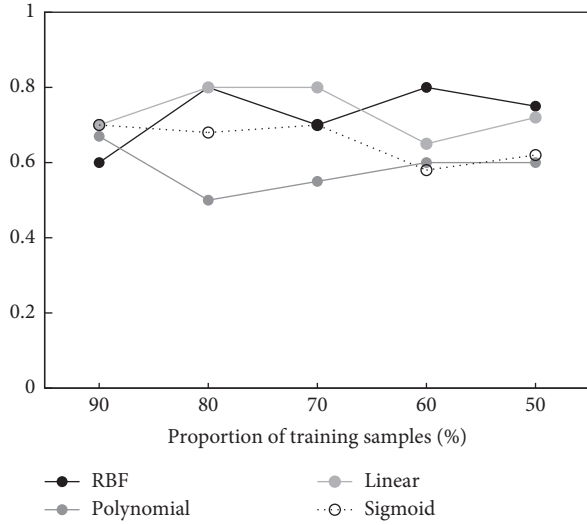


FIGURE 6: AUC values of the model under different kernel functions.

TABLE 7: Paired *T*-test results of model prediction performance under different kernel functions.

| Evaluation indicators | Kernel function | Polynomial | RBF   | Sigmoid |
|-----------------------|-----------------|------------|-------|---------|
| G                     | Linear          | 0.164      | 0.754 | 0.023   |
|                       | Polynomial      |            | 0.055 | 0.531   |
|                       | RBF             |            |       | 0.101   |
| F                     | Linear          | 0.492      | 0.514 | 0.324   |
|                       | Polynomial      |            | 0.495 | 0.708   |
|                       | RBF             |            |       | 0.274   |
| AUC                   | Linear          | 0.019      | 0.871 | 0.008   |
|                       | Polynomial      |            | 0.062 | 0.140   |
|                       | RBF             |            |       | 0.296   |

TABLE 8: Comparison of prediction performance of different models.

| Model           | G      | F      | AUC    |
|-----------------|--------|--------|--------|
| FOA-SMOTE-SVM   | 0.7083 | 0.4576 | 0.7338 |
| FOA-SMOTE-BP    | 0.6377 | 0.1760 | 0.6855 |
| FOA-SMOTE-Logit | 0.7026 | 0.2563 | 0.7219 |

**4.4.2. Model Comparison.** To further verify the validity of the proposed model, the prediction performance of the proposed model is compared with that of other models. The results are shown in Table 8. Compared with FOA-SMOTE-BP and FOA-SMOTE-Logit, the proposed model has the best performance on the indicators of G value, F value, and AUC value, indicating that the model proposed in this paper has the best prediction performance.

In order to observe the prediction performance of different models intuitively, the results of the above table are drawn as shown in Figure 7. It can be seen from the figure that the G value, F value, and AUC value curves of the proposed model are significantly higher than those of the

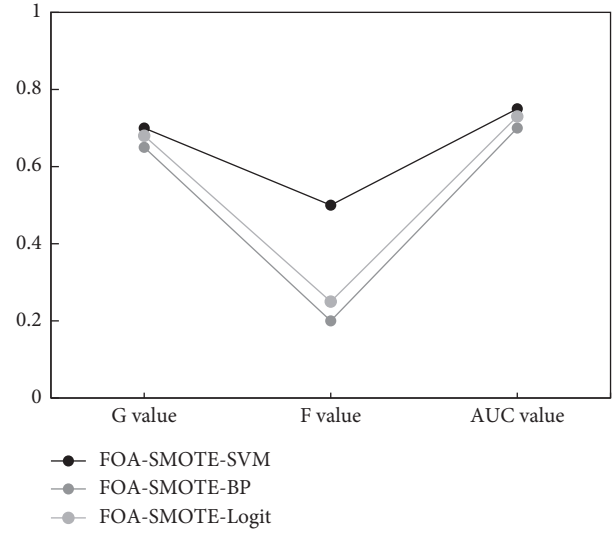


FIGURE 7: Comparison of every indicator of different models.

comparison model, indicating that the proposed model has better prediction performance.

## 5. Conclusion

In summary, the proposed market risk early warning method based on deep learning takes SVM as basic model and uses SMOTE to deal with unbalanced sample. In addition, minority samples are subjected to oversampling, and FOA is utilized to tune model parameters. Thus, the classification effect of the model is improved. The empirical results show that the proposed model has excellent stability and generalization ability and can accurately predict market credit risk. Compared with FOA-SMOTE-BP and FOA-SMOTE-Logit models, the proposed model performs better on G value, F value, and AUC value indicators and has better prediction performance, which provides a reference for market credit risk prediction research. The contribution of this study is to use a new improved SVM to predict the market risk. It provides a new reference for information management and prevention of the market. However, as the limitation of conditions, there are still some deficiencies to be improved. In the selection of market credit risk indicators, they are selected just through references, without considering the actual situation of China's manufacturing industry, which may affect the final market risk prediction results. To avoid the influence of index selection on prediction accuracy, the next research will try to independently determine the relevant index variables affecting market credit risk.

## Data Availability

The experimental data used to support the findings of this study are available from the corresponding author upon request.

## Conflicts of Interest

The authors declare that they have no conflicts of interest.


## References

- [1] Z. Guan, Y. Zhao, and G. Geng, "The risk early-warning model of financial operation in family farms based on back propagation neural network methods," *Computational Economics*, vol. 73, pp. 1–24, 2021.
- [2] S. Markose, S. Giansante, N. A. Eterovic, and M. Gatkowski, "Early warning of systemic risk in global banking: eigen-pair R number for financial contagion and market price-based methods[J]," *Annals of Operations Research*, vol. 163, pp. 1–39, 2021.
- [3] S. Figini, F. Bonelli, and E. Giovannini, "Solvency prediction for small and medium enterprises in banking," *Decision Support Systems*, vol. 102, pp. 91–97, 2017.
- [4] Y. Yang and Y. Yuan, "Research on credit risk early warning based on RBF neural network—taking Internet financial trading platform as an example[J]," *Modeling and Simulation*, vol. 10, no. 02, pp. 257–267, 2021.
- [5] Q. Ding, "Risk early warning management and intelligent real-time system of financial enterprises based on fuzzy theory," *Journal of Intelligent and Fuzzy Systems*, vol. 40, no. 4, pp. 6017–6027, 2021.
- [6] W. Li, "Research on project knowledge management risk early warning based on b neural network," *Journal of Physics: Conference Series*, vol. 1744, no. 3, pp. 032250–032255, 2021.
- [7] M. S. Dong, "Intelligent early warning of Internet financial risks based on mobile computing," *International Journal of Mobile Computing and Multimedia Communications*, vol. 11, no. 2, pp. 61–78, 2020.
- [8] K. Noureddine, "Using multivariate stochastic dominance to enhance portfolio selection and warn of financial crises[J]," *The Quarterly Review of Economics and Finance*, vol. 80, pp. 480–493, 2021.
- [9] Z. Zhang and Y. Chen, "Tail risk early warning system for capital markets based on machine learning algorithms," *Computational Economics*, pp. 21–23, 2021.
- [10] Z. S. Ouyang, X. T. Yang, and Y. Lai, "Systemic Financial Risk Early Warning of Financial Market in China Using Attention-LSTM model," *North American Journal of Economics and Finance*, vol. 56, Article ID 101383, 2021.
- [11] L. Jerlin Rubini and E. Perumal, "Efficient classification of chronic kidney disease by using multi-kernel support vector machine and fruit fly optimization algorithm," *International Journal of Imaging Systems and Technology*, vol. 30, no. 3, pp. 660–673, 2020.
- [12] Z. Tian, "Echo state network based on improved fruit fly optimization algorithm for chaotic time series prediction[J]," *Journal of Ambient Intelligence and Humanized Computing*, pp. 1–20, 2020.
- [13] H. Lu, M. Azimi, and T. Iseley, "Short-term load forecasting of urban gas using a hybrid model based on improved fruit fly optimization algorithm and support vector machine," *Energy Reports*, vol. 5, no. C, pp. 666–677, 2019.
- [14] F. Meng, "Safety warning model of coal face based on fcm fuzzy clustering and GA-BP neural network," *Symmetry*, vol. 13, no. 6, pp. 1082–1087, 2021.
- [15] V. Coudert and J. Idier, "Reducing model risk in early warning systems for banking crises in the euro area," *International Economics*, vol. 156, pp. 98–116, 2018.
- [16] J. Beutel, S. List, and V., "Does machine learning help us predict banking crises?" *Journal of Financial Stability*, vol. 45, no. C, pp. 100693–100698, 2019.
- [17] E. Markus and F. Presbitero Andrea, "Commodity prices and banking crises[J]," *Journal of International Economics*, vol. 131, pp. 103474–103479, 2021.
- [18] T. Jiang, M. Zhou, W. Xuan, S. Wen, T. Shao, and J. Lu, "Dynamics in bank crisis model," *Mathematical Problems in Engineering*, vol. 2015, no. Pt.2, pp. 1–5, 2015.
- [19] I. Ilić, S. Pizarov, and P. S. Schmidt, "Preaching water but drinking wine? Relative performance evaluation in international banking[J]," *Swiss Journal of Economics and Statistics*, vol. 155, no. 1, pp. 1–25, 2019.
- [20] X.-A Bi and Y. Xie, H. Wu and L. Xu, Identification of differential brain regions in MCI progression via clustering-evolutionary weighted SVM ensemble algorithm," *Frontiers of Computer Science*, vol. 15, no. 6, pp. 156903–156909, 2021.
- [21] J. Fan and G. Huang, M. Chi, Y. Shi, J. Jiang, C. Feng, and Z. Xu, Prediction of chemical reproductive toxicity to aquatic species using a machine learning model: an application in an ecological risk assessment of the Yangtze River, China," *The Science of the Total Environment*, vol. 796, pp. 148901–148908, 2021.
- [22] X. Li, J. Yang, Y. Fan, M. Xie, X. Qian, and H. Li, "Rapid monitoring of heavy metal pollution in lake water using nitrogen and phosphorus nutrients and physicochemical indicators by support vector machine," *Chemosphere*, vol. 280, pp. 130599–130605, 2021.
- [23] S. İlkin, T. H. Gençtürk, and F. Kaya Gülağız, H. Özcan, M. A. Altuncu, and S. Şahin, HybSVM: bacterial colony optimization algorithm based SVM for malignant melanoma detection," *Engineering Science and Technology, an International Journal*, vol. 24, no. 5, pp. 1059–1071, 2021.
- [24] H. Hu and J. Li, "Research on reference crop evapotranspiration forecast based on FOA-GRNN[J]," *International Core Journal of Engineering*, vol. 7, no. 5, pp. 108–116, 2021.
- [25] C. Lan, S. Li, H. Chen, W. Zhang, and H. Li, "Research on running state recognition method of hydro-turbine based on FOA-PNN," *Measurement*, vol. 169, pp. 108498–110852, 2021, (prepublish).
- [26] L. Li, H. Yang, L. Jiang, J. Gu, and Y. Zhang, "Optimal measurement area determination algorithm of articulated arm measuring machine based on improved FOA," *Measurement and Control*, vol. 53, no. 9-10, pp. 2146–2158, 2020.
- [27] V. Jaiswal, A. Negi, and T. Pal, "A review on current advances in machine learning based diabetes prediction," *Primary Care Diabetes*, vol. 15, no. 3, pp. 435–443, 2021.
- [28] Y. Tian, C. Chen, X. Chen, X. Chen, and R. Sun, "Research on real-time analysis technology of urban land use based on support vector machine," *Pattern Recognition Letters*, vol. 133, no. prepublsh, pp. 320–326, 2020.
- [29] D. Sun, B. Wang, X. Hu, and W. Wang, "A fault diagnosis method based on improved pattern spectrum and FOA-SVM," *International Journal of Acoustics and Vibration*, vol. 24, no. 2, pp. 312–319, 2019.



## Research Article

# Research on the Evaluation of Industrial Poverty Alleviation under the Background of the Internet

Ying Tao,<sup>1</sup> Jiazhi Xie,<sup>1</sup> and Jinqiao Yang <sup>2</sup>

<sup>1</sup>School of Economics and Management of Southwest University, Chongqing 400715, China

<sup>2</sup>China Post Insurance Heilongjiang Branch, Harbin Bank, Harbin 15000, China

Correspondence should be addressed to Jinqiao Yang; [zhuhangying@hrbb.com.cn](mailto:zhuhangying@hrbb.com.cn)

Received 15 March 2022; Revised 7 April 2022; Accepted 12 April 2022; Published 5 May 2022

Academic Editor: Man Fai Leung

Copyright © 2022 Ying Tao et al. This is an open access article distributed under the Creative Commons Attribution License, which permits unrestricted use, distribution, and reproduction in any medium, provided the original work is properly cited.

With the advent of the information age in the 21st century, Internet technology has developed rapidly. With the development of agriculture, industry, and service industry, Internet technology has also achieved further innovation and cross-border integration. The rapid development of Internet technology has provided new ideas for poverty alleviation in poor areas of China and accelerated the speed of poverty alleviation in poor areas. Based on the assumption of China's industrial poverty alleviation and the analysis of the implementation center, this paper puts forward an evaluation method of industrial poverty alleviation effect based on the fuzzy comprehensive evaluation method, which is evaluated from three aspects: income structure, expenditure structure, and labor resources. Taking Wuxi County as an example, this paper discusses the combination of human capital theory and multidimensional poverty theory. The evaluation of poverty alleviation effectiveness includes four indicators (comprehensive analysis, evaluation system, policy implementation, poverty alleviation funds) and 21 secondary indicators. Fuzzy comprehensive evaluation is an objective, fair, and comprehensive evaluation of the overall level of poverty alleviation and development in Wuxi. The expert scoring method is used to calculate the weight of each index and determine the level of members and the industrial situation of China's industrial poverty alleviation. According to the scores of each evaluation index, the poor households in Wuxi County are very satisfied with the person in charge of help, the villager group, the way of helping, and the effect of helping.

## 1. Introduction

In 2006, the State Council issued the Guiding Opinions on Promoting the Action Plan of "Internet plus." It is pointed out that it is necessary to conform to the development trend of "Internet plus" in the world and create new advantages and new impetus for social and economic development. Under the background of the Internet in the Internet plus, poverty needs to seize the opportunity of the Internet. Through the "high-speed train" of information technology, we can realize the high connection between resources in poverty-stricken areas and external markets [1, 2]. In the era of Internet plus, we should gradually explore new poverty alleviation strategies for economic and social development in poverty-stricken areas and innovate poverty alleviation concepts, policies, and methods [3].

At present, the research direction of poverty alleviation effect evaluation system in China is mostly in the field of poverty degree evaluation and poverty identification, which is too inclined to economic development and ignores the sustainable development of human society and ecological environment. Government departments pay too much attention to the investment of poverty alleviation funds and the formulation of poverty alleviation policies and have less evaluation on the effect of industrial poverty alleviation [4]. How to evaluate the effect of industrial poverty alleviation in poverty-stricken areas and sum up experiences and lessons can not only provide reference and guidance for the current evaluation of poverty alleviation effect but also put forward suggestions for the further development of poverty alleviation in the future [5]. This is the practical significance of this study.

On the basis of defining relevant concepts, this paper analyzes the present situation and characteristics of industrial poverty alleviation in Wuxi County and evaluates the effect of industrial poverty alleviation in Wuxi County by using fuzzy comprehensive evaluation method [6, 7]. At present, fuzzy comprehensive analysis method is mainly used to explore and analyze the risks of several projects. The theoretical significance of this paper lies in applying the creative fuzzy comprehensive evaluation method to the evaluation of industrial poverty alleviation effect, which opens up a new perspective for the theoretical system of poverty alleviation effect evaluation [8].

In this paper, the fuzzy evaluation model is used to evaluate and apply the industrial structure, which provides a theoretical basis for the design of the evaluation system of industrial poverty alleviation. Through fuzzy evaluation method, the evaluation system of industrial poverty alleviation effect is designed. By designing scientific and reasonable evaluation indexes, the evaluation index system of industrial poverty alleviation effect is established, including a comprehensive evaluation system of 4 first-class indexes and 21 second-class indexes so as to make an objective and fair evaluation of the industrial poverty alleviation effect in poverty-stricken areas.

## 2. Definition and Theoretical Basis of Related Concepts of Industrial Poverty Alleviation

### 2.1. Definition of Related Concepts

**2.1.1. Industrial Poverty Alleviation.** Industrial poverty alleviation refers to the process of poverty alleviation and development with market as the guide, economic benefits as the center, and industrial development as the lever. It is an effective way to promote the development of poor areas and increase the income of poor farmers [9]. It is the strategic focus and main task of poverty alleviation and development. Industrial poverty alleviation is an endogenous development mechanism, which aims to promote the coordinated development of poor individuals and poor areas, take root in development genes, activate development momentum, and cut off poverty momentum.

**2.1.2. Fuzzy Comprehensive Evaluation.** Fuzzy comprehensive evaluation method is a comprehensive analysis and evaluation method based on reasoning, quantitative and qualitative, correct, and fuzzy combination. A system analysis method is suitable for “fuzzy” evaluation of things. Membership theory in fuzzy mathematics is its basic principle. When analyzing some complex system problems, the fuzzy comprehensive evaluation method has incomparable advantages over other correct analysis methods. Therefore, in recent years, it has become the preferred tool to deal with complex problems and has been widely used in many research fields [10]. The fuzzy decision model generally requires the following steps: (1) establish the factor set of comprehensive evaluation, (2) establish the evaluation set of comprehensive evaluation, (3) carry out single-factor

fuzzy evaluation to obtain an evaluation matrix, (4) determine a factor weight vector, (5) establish a comprehensive evaluation model, and (6) determine the total system score.

### 2.2. Theoretical Basis

**2.2.1. Human Capital Theory.** Different from other material capital, human capital is immaterial intangible capital, which refers to the skills, experience, knowledge, and other qualities attached to workers. Education investment such as continuing education, training, and social practice is its main investment form [11]. For the invested individuals, human investment can achieve the synchronization of personal development and income growth. The same amount of labor can bring additional benefits and accelerate economic development.

**2.2.2. Multidimensional Poverty Theory.** The multidimensional poverty theory was put forward by Indian economist and Nobel Prize winner Amartya Fair in 1984. The main point is that human poverty includes not only income poverty but also subjective perception of welfare through objective indicators such as drinking water and roads [12].

## 3. Evaluation Method of Industrial Poverty Alleviation Effectiveness Based on Fuzzy Evaluation

### 3.1. Fuzzy Evaluation Steps

**Step 1.** The judgment matrix determines the weight of each index.

Analytic hierarchy process (AHP) mainly determines the weights of indicators at all levels including target level, standard level, and scene level. Its main idea is to establish a judgment matrix to determine the importance of each element. According to the judgment of the expert group, the two factors are compared and evaluated according to the importance of each factor [13, 14]. The index  $C$  is chosen as the evaluation criterion, and the importance degree of elements  $U_1, U_2, U_3, \dots, U_n$  relative to element  $C$  is the next index controlled by it, that is, the weight. The scale of 1 ~ 9 is used to quantify the importance of elements  $U_i$  and  $U_j$  to criterion  $C$  as shown in Table 1.

**Step 2.** Consistency test.

When calculating the weight, consistency test must also be carried out. The inspection method and process are given in Table 2.

Step A: calculate the consistency index (CI):

$$CI = \frac{\lambda_{\max} - n}{n - 1}. \quad (1)$$

Because the CI value changes with the change of the deterministic matrix, it is necessary to introduce RI as the matrix matching index to verify the matching of different next deterministic matrices.

TABLE 1: Importance scale of evaluation factors.

| Important scale $a_{ij}$           | Meaning  |
|------------------------------------|--|
| 1                                  | $i$ and $j$ are equally important  |
| 3                                  | $i$ is slightly more important than $j$  |
| 5                                  | $i$ is obviously more important than $j$   |
| 7                                  | $i$ is more important than $j$   |
| 9                                  | $i$ is more important than $j$   |
| 1, 2, 6, 8                         | Corresponding intermediate scale   |
| The reciprocal of the above values | If the importance ratio of element $i$ to $j$ is $a_{ij}$ , then the importance ratio of element $j$ to element $i$ is $a_{ji} = 1/a_{ij}$ |

TABLE 2: Random index RI.

| Matrix order | 1 | 2 | 3    | 4    | 5    | 6    | 7    | 8    | 9    |
|--------------|---|---|------|------|------|------|------|------|------|
| RI           | 0 | 0 | 0.58 | 0.90 | 1.12 | 1.24 | 1.32 | 1.41 | 1.45 |

Step B: find the corresponding average random index (RI)

Step C: calculate the consistency ratio (CR)

$$CR = \frac{CI}{RI} \quad (2)$$

Only when the CR value of the matrix is less than 0.1 can the matrix pass the consistency check and have consistency. Otherwise, the judgment matrix needs to be corrected twice.

When checking the consistency of the judgment matrix, it is necessary to calculate the maximum characteristic of the matrix, and the formula can be used:

$$\lambda_{\max} = \sum_{i=1}^n \frac{(AW)_i}{nw_i} = \frac{1}{n} \sum_{i=1}^n \frac{\sum_{j=1}^n a_{ij}w_j}{w_i} \quad (3)$$

Step 3. Establish the evaluation set of fuzzy comprehensive evaluation.

The evaluation index in AHP is based on hierarchical structure, and comprehensive evaluation is carried out on this basis, so the evaluation index in AHP can be used directly. In the fuzzy comprehensive evaluation method, the grades of comments are called fuzzy grades, such as good, good, fair, and bad, which constitute the comment set  $V = \{V_1, V_2, \dots, V_3\}$ .

Step 4. Establish membership matrix  $R$ .

According to the expert evaluation, the membership degree of each element of the index set to each comment is obtained, and the membership matrix is constructed.

Step 5. Calculate the fuzzy comprehensive evaluation vector.

The fuzzy evaluation vector  $B_i$  of each evaluation index can be calculated by using the calculation model  $B_i = W_i * R_i$  of fuzzy comprehensive evaluation.

Step 6. Synthesize the result vector of fuzzy comprehensive evaluation.

### 3.2. Construction of the Evaluation Index System for Industrial Poverty Alleviation

3.2.1. Principles of Indicator Selection. The establishment of industrial poverty alleviation effect evaluation index is an important part of industrial poverty alleviation effect evaluation in Wuxi County [10, 15]. Therefore, when constructing the effect evaluation system, we must follow the following index selection principles: good faith principle, scientific principle, focusing principle, and usability principle.

3.2.2. Construction of the Evaluation Index System. Index system of industrial poverty alleviation effectiveness evaluation is shown in Table 3.

### 3.3. Determination of Weight of the Index System

#### 3.3.1. Determination of the Weight of the First-Class Index

(1) Principle of Good Faith. Wuxi County's poverty alleviation through business development refers to the support for all the poor people in the county, not limited to one household in 13 townships within the jurisdiction, but the whole county. Therefore, when choosing the evaluation index that can reflect the effect of poverty alleviation in the whole county, we should pay attention to the integrity.

(2) Scientific Principles. The indicators of the poverty alleviation effect evaluation system in Wuxi County should objectively and fairly reflect the actual results and substantive characteristics of the county's poverty alleviation through business development. The evaluation index should have certain scientific significance and should not overlap with other indicators.

(3) Focus Principle. The content of industrial poverty alleviation activities is very extensive. In the several areas covered, it is not possible to select indicators that reflect all aspects, so we can only select representative key indicators to reflect these indicators.

(4) Availability Principle. Although there are many indicators that can reflect the same performance, the data of some indicators are easy to obtain, and the data of some indicators are not easy to obtain, so we must choose the common evaluation indicators that are easy to start and easy for statistical analysis.

The  $A-B_n$  judgment matrix is shown in Tables 4–6.

3.3.2. Determination of the Weight of Secondary Indicators. The weight calculation and consistency test of B1 index of living standard improvement are shown in Table 7.

TABLE 3: Index system of industrial poverty alleviation effectiveness evaluation.

| Target layer   | Criterion layer                              | Scenario layer  |
|--|--|---|
| Effectiveness evaluation of industrial poverty alleviation A | Living standard B1                           | Source of income C1                                   |
|  |  | Expenditure structure C2                              |
|  |  | Food and clothing guarantee rate C3                   |
|  |  | Housing security rate C4                              |
|  | Policy implementation B2                     | Ex situ poverty alleviation and relocation C5         |
|  |  | Industrial poverty alleviation C6                     |
|  |  | Renovation of dilapidated buildings C7                |
|  |  | Ecological poverty alleviation C8                     |
|  |  | Poverty alleviation through education C9              |
|  |  | Medical assistance C10                                |
|  | Improvement of poor villages B3              | Workforce skills training C11                         |
|  |  | Rural drinking water safety rate C12                  |
|  |  | Hardening rate of rural roads C13                     |
|  |  | Village collective economy C14                        |
|  |  | Health and medical facilities C15                     |
|  |  | Cultural and sports facilities C16                    |
|  |  | Kindergarten and primary school C17                   |
|  |  | Satisfaction with helping those responsible C18       |
|  | Accurate poverty alleviation satisfaction B4 | Satisfaction with helping methods C19                 |
|  |  | Satisfaction with the resident team C20               |
|  |  | Satisfaction with the effectiveness of assistance C21 |

TABLE 4: A-Bn (n = 1, 2, 3, 4) judgment matrix table.

| A  | B1  | B2  | B3  | B4 |
|----|-----|-----|-----|----|
| B1 | 1   | 1/5 | 1/3 | 2  |
| B2 | 5   | 1   | 4   | 5  |
| B3 | 3   | 1/4 | 1   | 3  |
| B4 | 1/2 | 1/5 | 1/3 | 1  |

TABLE 5: Weight calculation table.

| Column normalization of judgment matrix | Sum by row | Weight |
|---|------------|--------|
| 0.1053                                  | 0.1212     | 0.0588 |
| 0.5263                                  | 0.6061     | 0.7059 |
| 0.3158                                  | 0.1515     | 0.1765 |
| 0.0526                                  | 0.1212     | 0.0588 |
|   |            | 0.1818 |
|   |            | 0.4545 |
|   |            | 0.2727 |
|   |            | 0.3236 |
|   |            | 0.4671 |
|   |            | 0.1168 |
|   |            | 0.5732 |
|   |            | 0.2291 |
|   |            | 0.0809 |

TABLE 6: Consistency inspection table.

| AW     | AW/W   | $\lambda_{max}$              | RI           |
|--------|--------|------------------------------|--------------|
| 0.4696 | 4.0211 | 4.1603                       | 0.90         |
| 2.4781 | 4.3232 | $CI = (\lambda - n)/(n - 1)$ | $CR = CI/RI$ |
| 0.9654 | 4.2136 |                              |              |
| 0.3303 | 4.0831 | 0.0534                       | 0.0594       |

If  $CR = 0.0594 < 0.1$ , it will pass the consistency test.

The weight calculation and consistency test of B2 index of policy implementation are shown in Table 8.

The weight calculation and consistency test of B3 index for the promotion of poor villages are shown in Table 9.

The weight calculation and consistency test of B4 index of industrial poverty alleviation satisfaction are shown in Table 10.

Through calculation, the matching check of all decision matrices is less than 0.1, that is,  $CR < 0.1$ , which shows that

TABLE 7: B1-Cn (n = 1, 2, 3, 4) judgment matrix table.

| B1 | C1  | C2 | C3  | C4  | Weight | RI          |
|----|-----|----|-----|-----|--------|-------------|
| 1  | 1   | 3  | 1/3 | 1/3 | 0.1611 | 0.9         |
| C2 | 1/3 | 1  | 1/4 | 1/4 | 0.0806 | CI          |
| C3 | 3   | 4  | 1   | 1   | 0.3792 | 0.0282      |
| C4 | 3   | 4  | 1   | 1   | 0.3792 | CR = 0.0313 |

$CR = 0.0313 < 0.1$  passed the consistency test.

TABLE 8: B2-Cn (n = 5, 6, 7, 8, 9, 10, 11) judgment matrix table.

| B2  | C5  | C6 | C7  | C8 | C9 | C10 | C11 | Weight | RI     |
|-----|-----|----|-----|----|----|-----|-----|--------|--------|
| C5  | 1   | 3  | 2   | 3  | 3  | 1/3 | 2   | 0.1883 | 1.32   |
| C6  | 1/3 | 1  | 1/3 | 1  | 1  | 1/5 | 1/2 | 0.0598 | CI     |
| C7  | 1/2 | 3  | 1   | 3  | 3  | 1/3 | 1/2 | 0.1362 | 0.0448 |
| C8  | 1/3 | 1  | 1/3 | 1  | 1  | 1/5 | 1/2 | 0.0598 |        |
| C9  | 1/3 | 1  | 1/3 | 1  | 1  | 1/5 | 1/2 | 0.0598 |        |
| C10 | 3   | 5  | 3   | 5  | 5  | 1   | 4   | 0.3406 |        |
| C11 | 1/2 | 2  | 2   | 2  | 2  | 1/4 | 1   | 0.1555 |        |

$CR = 0.0339 < 0.1$  passed the consistency test.

TABLE 9: B3-Cn (n = 12, 13, 14, 15, 16, 17) judgment matrix table.

| B3  | C12 | C13 | C14 | C15 | C16 | C17 | Weight | RI     |
|-----|-----|-----|-----|-----|-----|-----|--------|--------|
| B12 | 1   | 3   | 3   | 4   | 1   | 2   | 0.3425 | 1.32   |
| B13 | 1/3 | 1   | 3   | 3   | 4   | 1/3 | 0.1365 | CI     |
| B14 | 1/3 | 1   | 1   | 3   | 4   | 1/3 | 0.1365 | 0.0448 |
| B15 | 1/4 | 1/3 | 1/3 | 1   | 3   | 1/4 | 0.0726 |        |
| B16 | 1/5 | 1/4 | 1/4 | 1/3 | 1   | 1/5 | 0.0417 |        |
| B17 | 1/2 | 3   | 3   | 4   | 5   | 1   | 0.2702 |        |

If  $CR = 0.0486 < 0.1$ , it passes the consistency test.

the selected weight value is expected and effective, and the satisfaction degree of the matrices constructed in this paper is consistent.

TABLE 10: B4-Cn (n = 18, 19, 20, 21) judgment matrix table.

| B4  | C18 | C19 | C20 | C21 | Weight | RI          |
|-----|-----|-----|-----|-----|--------|-------------|
| C18 |     | 1/3 | 1/2 | 1/5 | 0.0858 | 0.9         |
| C19 | 3   | 1   | 3   | 1/2 | 0.2887 | CI          |
| C20 | 2   | 1/3 | 1   | 1/4 | 0.1296 | 0.019       |
| C21 | 5   | 2   | 4   | 1   | 0.4959 | CR = 0.0211 |

If  $CR = 0.0211 < 0.1$ , it passes the consistency test.

TABLE 11: Weight comprehensive ranking table.

| A  | B criterion layer index                      | Index weight | C Scheme layer indicators                                  | Index weight | Composite weight | Sort |
|--|--|--------------|--|--------------|------------------|------|
| Index system for evaluating the effectiveness of industrial poverty alleviation work | B1 improvement of living standards           | 0.1168       | C1 source of income  | 0.1611       | 0.0188           | 16   |
|  |  |              | C2 expenditure structure                                   | 0.0806       | 0.0094           | 20   |
|  |  |              | C3 food and clothing guarantee rate                        | 0.3792       | 0.0443           | 7    |
|  |  |              | C4 housing security rate                                   | 0.3792       | 0.0443           | 7    |
|  |  |              | C5 ex situ poverty alleviation and relocation              | 0.1883       | 0.1079           | 2    |
|  |  |              | C6 industry helps the poor                                 | 0.0598       | 0.0343           | 10   |
|  |  |              | C7 renovation of dilapidated buildings                     | 0.1362       | 0.0781           | 5    |
|  | B2 policy implementation                     | 0.5732       | C8 ecological poverty alleviation                          | 0.0598       | 0.0343           | 10   |
|  |  |              | C9 education for poverty alleviation                       | 0.0598       | 0.0343           | 10   |
|  |  |              | C10 medical assistance                                     | 0.3406       | 0.1952           | 1    |
|  |  |              | C11 workforce skills training                              | 0.1555       | 0.0891           | 3    |
|  |  |              | C12 rural drinking water safety rate                       | 0.3425       | 0.0785           | 4    |
|  | B3 improvement of poor villages              | 0.2291       | C13 hardening rate of rural roads                          | 0.1365       | 0.0313           | 13   |
|  |  |              | C14 village collective economy                             | 0.1365       | 0.0313           | 13   |
|  |  |              | C15 health and medical facilities                          | 0.0726       | 0.0166           | 17   |
|  |  |              | C16 cultural and sports facilities                         | 0.0417       | 0.0096           | 19   |
|  |  |              | C17 kindergarten and primary school                        | 0.2702       | 0.0619           | 6    |
|  |  |              | C18 satisfaction with helping those responsible            | 0.0858       | 0.0069           | 21   |
|  |  |              | C19 satisfaction with help methods                         | 0.2887       | 0.0234           | 15   |
|  | B4 accurate poverty alleviation satisfaction | 0.0809       | C20 satisfaction with the resident team                    | 0.1296       | 0.0105           | 18   |
|  |  |              | C21 satisfaction with the effectiveness of assistance work | 0.4959       | 0.0401           | 9    |

3.3.3. *Determination of Comprehensive Weight and Ranking Statistics of Each Index.* Weight comprehensive ranking is shown in Table 11.

3.3.4. *Indicator Weight Description.* It can be seen from the data in the table that the weight of improving living standards is 0.11168, the weight of policy implementation is 0.5732, the weight of poor villages is 0.291, and the weight of industrial poverty alleviation satisfaction is 0.0809. The evaluation results show that among the evaluation indicators affecting the effect of industrial poverty alleviation, policy implementation

has the highest proportion and is also the most important indicator. Therefore, the implementation of poverty alleviation policy is an important factor to promote poverty alleviation in rural poor areas and poor people. The implementation of this policy is directly related to the improvement of production and life of poor families, and experts have paid more attention to it. Second, the improvement of poor villages is mainly because the infrastructure conditions of poor villages are still an important bottleneck affecting poverty alleviation in poor areas. By vigorously building infrastructure, the development environment and conditions in poverty-stricken areas can be greatly improved, which is an

important indicator to measure the effect of poverty alleviation. Third, improve living standards. Only by implementing poverty alleviation policies and improving the infrastructure of poor villages can people's living standards be improved. Therefore, compared with the first two indicators, the given weight is lower. Finally, the poverty alleviation through business development satisfaction is evaluated. After the implementation of poverty alleviation policy, the living conditions of poor villages and poor households have improved. If income increases, many poor families are very satisfied, so experts give the lowest weight.

Through the analysis of standard level indicators, among the indicators for improving living standards, the weight of income source is 0.1611, the weight of expenditure structure is 0.0806, the weight of food and clothing security rate is 0.3792, and the weight of housing security rate is 0.3792, which is consistent with clothing weight and food safety rate and higher than the other two indicators. This is because the safety of food, clothing, and housing is the foundation of human survival. It is the material basis to ensure the sustainable development of mankind. In the process of policy implementation, the proportion of poverty alleviation transfer subsidy is 0.188, and the proportion of industrial poverty alleviation, ecological poverty alleviation, and education poverty alleviation is 0.0598. The importance of various poverty alleviation policies is the same. The two complement each other. The weight of reconstruction of dilapidated buildings is 0.162, the weight of medical assistance is 0.3406, and the weight of labor skills training is 0.1555, among which medical assistance has the highest weight, indicating that a healthy body is the capital and foundation of all human activities. In the process of promoting poor villages, the weight of rural drinking water safety rate is 0.3425, the weight of rural road hardening rate is 0.165, the weight of rural collective economy is 0.165, the weight of health and medical facilities is 0.0726, the weight of sports facilities is 0.0417, and the ratio of kindergarten to primary school is 0.272. The weight of satisfaction with village groups is 0.11296, and the weight of satisfaction with aid effectiveness is 0.4959. Among them, satisfaction accounts for the highest proportion in the effect of poverty alleviation activities. The effect of poverty alleviation activities is the final index to test poverty alleviation activities, so we should focus on poverty alleviation.

After determining the comprehensive weight of each index, the first six indexes have the greatest influence on medical assistance, and the other five indexes are sorted according to the comprehensive weight: poverty alleviation transfer in different places, labor skills training, rural drinking water safety rate, reconstruction of old houses, and kindergartens and primary schools. The other 15 index factors are arranged according to comprehensive weight: residents' safety rate, food safety rate, clothing safety rate, satisfaction with assistance effect, industrial poverty alleviation, ecological poverty alleviation, education poverty alleviation, rural road hardening rate, village collective economy, rescue mode, income source, health and medical facilities, village team, sports facilities, and expenditure structure. To a certain extent, the comprehensive weight

ranking of these indicators reflects experts' concern about the effect of industrial poverty alleviation.

#### 4. Comprehensive Evaluation of Industrial Poverty Alleviation in Wuxi County, Chongqing

*4.1. Introduction of Wuxi County.* Wuxi County is one of the key poverty alleviation counties in Chongqing, located in the northeast of Chongqing, at the southern foot of the eastern bus section. This is a typical mountainous agricultural county. Wuxi County is located at the junction of Chongqing, Shaanxi, and Hubei provinces, bordering Shennongjia Forest Region and Zhuxi County in Hubei Province in the east, Fengjie County and Wushan County in the south, Kaizhou District and Yunyang County in the west, and Chengkou County and Zhenping County in Shaanxi Province in the north. As of 2017, the total area of Wuxi County has reached 4,030 square kilometers. According to the data of the seventh census, as of November 1, 2020, the resident population of Wuxi County was 388,600 with 810,000 mu of cultivated land. In addition, due to the uneven distribution of rainfall in time and space, the rainstorm is concentrated and the convergence speed is fast, which forms a very serious water shortage problem in this project. In particular, predatory reclamation has seriously damaged the ecological environment of the whole county. The area of soil erosion is 2537 square kilometers, accounting for 63% of the total area of the county, and the living environment is further deteriorated. Once upon a time, the poverty rate here reached 18%, ranking first in Chongqing. By the end of 2020, all 150 poverty-stricken villages in Wuxi County have been lifted out of poverty, with a decrease of 105,000 people and a decrease of 0.65% in the incidence of poverty, and they have successfully withdrawn from the national key poverty alleviation and development counties. The result is shown in Figure 1.

*4.2. Expert Score to Determine the Membership Matrix of Evaluation Index.* Firstly, the comment set is established as  $V = \{V_1, V_2, \dots, V_n\}$ , where  $V_j (j = 1, 2, \dots, n)$ . The comments of industrial poverty alleviation indicators in Wuxi County are set as "very good," "good," "medium," "poor," and "difference." Then, the comments represented in the order of  $n = 5$  and  $V_1 - V_5$  are "very good," "good," "medium," "poor," and "difference." In this manual, the annotation set can be regarded as vector  $C$  and assigned values. The added value of the annotation set is shown in Figure 2.

Next, it needs to decide the membership degree, and the membership degree value of each annotation is the proportion of the number of experts who selected the annotation. Table 12 shows the membership degree determined by expert score.

According to the expert evaluation, the membership degree of each element of the index set to each comment is obtained, and the membership matrix is constructed. The results are as follows:

$$\begin{aligned}
 R1 &= \begin{pmatrix} 0.2 & 0.4 & 0.3 & 0.1 & 0 \\ 0.1 & 0.2 & 0.4 & 0.2 & 0.1 \\ 0.7 & 0.3 & 0 & 0 & 0 \\ 0.6 & 0.3 & 0.1 & 0 & 0 \end{pmatrix}, \\
 R2 &= \begin{pmatrix} 0.1 & 0.5 & 0.4 & 0 & 0 \\ 0.2 & 0.3 & 0.4 & 0.1 & 0 \\ 0.3 & 0.4 & 0.3 & 0 & 0 \\ 0.2 & 0.3 & 0.3 & 0.2 & 0 \\ 0.3 & 0.5 & 0.2 & 0 & 0 \\ 0.3 & 0.4 & 0.3 & 0 & 0 \\ 0.1 & 0.2 & 0.4 & 0.2 & 0 \end{pmatrix}, \\
 R3 &= \begin{pmatrix} 0.1 & 0.4 & 0.4 & 0.1 & 0 \\ 0.2 & 0.3 & 0.4 & 0.1 & 0 \\ 0.1 & 0.2 & 0.5 & 0.1 & 0.1 \\ 0.3 & 0.5 & 0.2 & 0 & 0 \\ 0.2 & 0.3 & 0.3 & 0.2 & 0 \\ 0 & 0.2 & 0.3 & 0.3 & 0.2 \end{pmatrix}, \\
 R4 &= \begin{pmatrix} 0.3 & 0.3 & 0.3 & 0.1 & 0 \\ 0.4 & 0.3 & 0.2 & 0.1 & 0 \\ 0.2 & 0.4 & 0.4 & 0 & 0 \\ 0.3 & 0.3 & 0.4 & 0 & 0 \end{pmatrix}.
 \end{aligned}
 \tag{4}$$

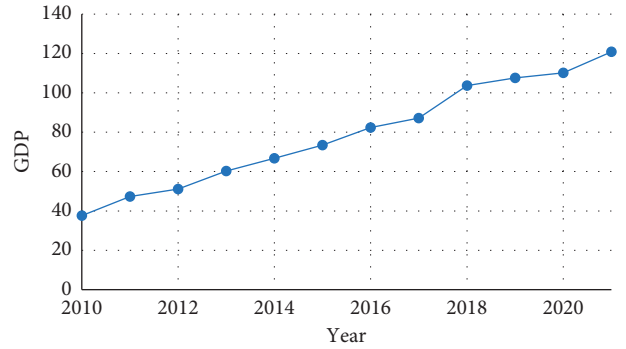


FIGURE 1: Trend chart of conceptual GDP in Wuxi County.

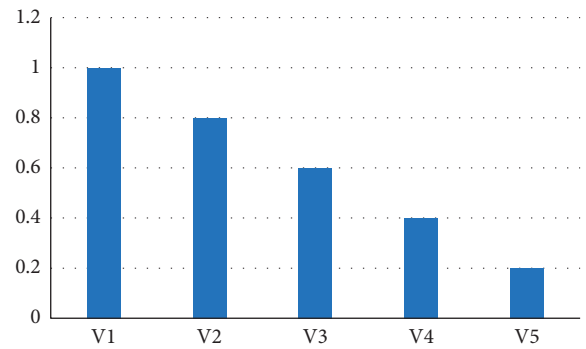


FIGURE 2: Added value of the annotation set.

4.3. Determining the Fuzzy Evaluation Vector. The fuzzy evaluation vector  $B_i$  of each evaluation index can be

calculated by using the calculation model  $B_i = W_i * R_i$  of fuzzy comprehensive evaluation method.

$$\begin{aligned}
 B_i &= W_i * R_i, \\
 W &= (0.1168, 0.5732, 0.2291, 0.0809), \\
 W1 &= (0.0188, 0.0094, 0.0443, 0.0443), \\
 W2 &= (0.1079, 0.0343, 0.0781, 0.0343, 0.0343, 0.1952, 0.0891), \\
 W3 &= (0.0785, 0.0313, 0.0313, 0.0166, 0.0096, 0.0619), \\
 W4 &= (0.0069, 0.0234, 0.0105, 0.0401),
 \end{aligned}
 \tag{5}$$

$$B1 = (0.0188, 0.0094, 0.0443, 0.0443) * \begin{pmatrix} 0.2 & 0.4 & 0.3 & 0.1 & 0 \\ 0.1 & 0.2 & 0.4 & 0.2 & 0.1 \\ 0.7 & 0.3 & 0 & 0 & 0 \\ 0.6 & 0.3 & 0.1 & 0 & 0 \end{pmatrix}.$$

Get

$$B1 = (0.06229, 0.03598, 0.01383, 0.00376, 0.00094). \tag{6}$$

Calculate  $B2$ ,  $B3$ , and  $B4$  in the same way.

Comprehensive synthesis of fuzzy evaluation vectors:  $B = W * R$ ,  $R = (B1, B2, B3, B4)$ ,  $R$  is the data in Table 13, resulting in

$$B = (0.08692, 0.14786, 0.13298, 0.02472, 0.00877). \tag{7}$$

TABLE 12: Expert scoring table.

| Indicators   | Very good | Better | Medium | Poor | Difference |
|--|-----------|--------|--------|------|------------|
| Source of income                                       | 0.2       | 0.4    | 0.3    | 0.1  | 0          |
| Expenditure structure                                  | 0.1       | 0.2    | 0.4    | 0.2  | 0.1        |
| Food and clothing guarantee rate                       | 0.7       | 0.3    | 0      | 0    | 0          |
| Housing security rate                                  | 0.6       | 0.3    | 0.1    | 0    | 0          |
| Ex situ poverty alleviation and relocation             | 0.1       | 0.5    | 0.4    | 0    | 0          |
| Industrial poverty alleviation                         | 0.2       | 0.3    | 0.4    | 0.1  | 0          |
| Renovation of dilapidated buildings                    | 0.3       | 0.4    | 0.3    | 0    | 0          |
| Ecological poverty alleviation                         | 0.2       | 0.3    | 0.3    | 0.2  | 0          |
| Poverty alleviation through education                  | 0.3       | 0.5    | 0.2    | 0.0  | 0          |
| Medical assistance                                     | 0.3       | 0.4    | 0.3    | 0    | 0          |
| Labor skill training                                   | 0.1       | 0.2    | 0.4    | 0.2  | 0.1        |
| Rural drinking water safety rate                       | 0.1       | 0.4    | 0.4    | 0.1  | 0          |
| Hardening rate of rural roads                          | 0.2       | 0.3    | 0.4    | 0.1  | 0          |
| Village economy  | 0.1       | 0.2    | 0.5    | 0.1  | 0.1        |
| Health and medical facilities                          | 0.3       | 0.5    | 0.2    | 0    | 0          |
| Cultural and sports facilities                         | 0.2       | 0.3    | 0.3    | 0.2  | 0          |
| Kindergarten and primary school                        | 0         | 0.2    | 0.3    | 0.3  | 0.2        |
| Satisfaction with helping those responsible            | 0.3       | 0.3    | 0.3    | 0.1  | 0          |
| Satisfaction with the way of helping                   | 0.4       | 0.3    | 0.2    | 0.1  | 0          |
| Satisfaction with the resident team                    | 0.2       | 0.4    | 0.4    | 0    | 0          |
| Satisfaction with the effectiveness of assistance work | 0.3       | 0.3    | 0.4    | 0    | 0          |

TABLE 13: Calculation table of the fuzzy evaluation vector.

|    |         |         |         |         |         |
|----|---------|---------|---------|---------|---------|
| B1 | 0.06229 | 0.03598 | 0.01383 | 0.00373 | 0.00094 |
| B2 | 0.1257  | 0.21882 | 0.19166 | 0.02811 | 0.00891 |
| B3 | 0.02414 | 0.07061 | 0.08434 | 0.0346  | 0.01551 |
| B4 | 0.02556 | 0.02532 | 0.02699 | 0.00303 | 0       |

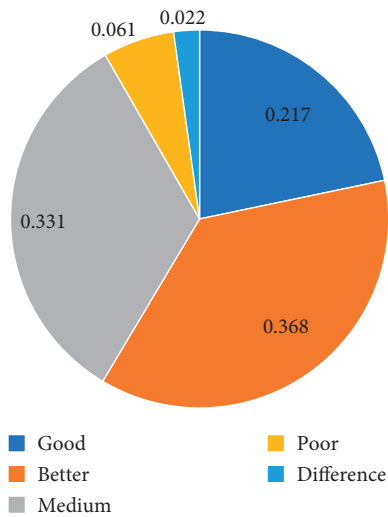


FIGURE 3: Proportion of experts' evaluation of industrial poverty alleviation in Wuxi County.

Normalizing  $B$  results in

$$B = (0.21663, 0.36849, 0.33141, 0.06160, 0.02186). \quad (8)$$

According to the results of fuzzy evaluation vector, the membership degree belonging to the "better" level is the largest, which is 0.36849; that is, nearly 36.8% of experts think that the industrial poverty alleviation effect in Wuxi County is at a good level. According to the principle of maximum subordination, the effect of industrial poverty

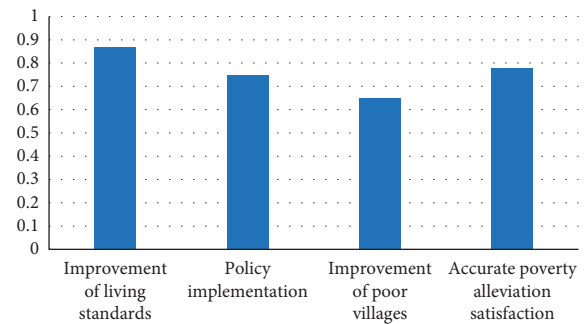


FIGURE 4: Scores of various indicators of industrial poverty alleviation in Wuxi County.

alleviation is at a "good" level. In addition, 21.7% of the experts answered "good," 33.1% thought it was "medium," and 6.1% answered "poor." Only 2.2% of experts thought it was "bad," as shown in Figure 3.

4.4. Comprehensive Score of Industrial Poverty Alleviation Effectiveness. The above research results only qualitatively evaluate the effect of industrial poverty alleviation in Wuxi County, and the evaluation results are generally vague. Therefore, the quantification score is used to quantify the evaluation result. Five levels of performance evaluation (very good, good, medium, poor, and difference). Multiply the evaluation ratio by the index dependence matrix to obtain the single factor score:

$$\begin{aligned}
 C1 &= (0.2, 0.4, 0.3, 0.1, 0) * (1, 0.8, 0.6, 0.4, 0.2)^T = 0.74, \\
 C2 &= 0.1, 0.2, 0.4, 0.2, 0.1 * (1, 0.8, 0.6, 0.4, 0.2)^T = 0.6, \\
 C3 &= (0.7, 0.3, 0, 0, 0) * (1, 0.8, 0.6, 0.4, 0.2)^T = 0.94, \\
 C4 &= (0.6, 0.3, 0.1, 0, 0) * (1, 0.8, 0.6, 0.4, 0.2)^T = 0.9.
 \end{aligned} \quad (9)$$



TABLE 14: Evaluation scores of indicators at all levels.

| Criterion layer                           | Scenario layer                                    | Score | Target level score |
|---|---|-------|--------------------|
| Improvement of living standards           | Source of income                                  | 0.74  |                    |
|   | Expenditure structure                             | 0.6   |                    |
|   | Food and clothing guarantee rate                  | 0.94  |                    |
|   | Housing security rate                             | 0.90  |                    |
|   | Ex situ poverty alleviation and relocation        | 0.74  |                    |
| Policy implementation                     | Industrial poverty alleviation                    | 0.72  |                    |
|   | Renovation of dilapidated buildings               | 0.8   |                    |
|   | Ecological poverty alleviation                    | 0.7   |                    |
|   | Poverty alleviation through education             | 0.82  |                    |
|   | Medical assistance                                | 0.8   |                    |
|   | Labor skill training                              | 0.6   | 0.74               |
|   | Rural drinking water safety rate                  | 0.7   |                    |
| Improvement of poor villages              | Hardening rate of rural roads                     | 0.72  |                    |
|   | Village collective economy                        | 0.62  |                    |
|   | Health and medical facilities                     | 0.82  |                    |
|   | Cultural and sports facilities                    | 0.7   |                    |
|   | Kindergarten and primary school                   | 0.5   |                    |
| Accurate poverty alleviation satisfaction | Satisfaction with helping those responsible       | 0.76  |                    |
|   | Satisfaction with the way of helping              | 0.8   |                    |
|   | Satisfaction with the resident team               | 0.76  |                    |
|   | Satisfaction with the effectiveness of assistance | 0.78  |                    |

The score of criterion level index can be calculated by multiplying the weight of scheme level index by the score of each index (taking the improvement of living standard as an example).

$$B1 = (0.1611, 0.0806, 0.3792, 0.3792)^* (0.74, 0.60, 0.94, 0.9)^T = 0.87. \tag{10}$$

The score of the target layer is the weight of the index of the criterion layer multiplied by the score of each index, as shown in Figure 4.

**4.5. Evaluation Results and Problem Analysis.** It can be seen from Table 14 that the final comprehensive score of industrial poverty alleviation effect in Wuxi County is 0.74, and the industrial poverty alleviation effect in Wuxi County is at a “good” level, in which the living standard is improved by 0.87, the policy implementation is 0.75, 0.65 is used to improve poor villages, and 0.78 is used to meet industrial poverty assistance.

In terms of improving living standards, the score of income source is 0.74; the score of expenditure structure is 0.60; the score of food, clothing, housing, and transportation security rate is 0.94; and the score of housing security rate is 0.90. According to the scores of various evaluation indicators, the living standards of poor households have improved significantly since Wuxi County launched industrial poverty alleviation activities. The income sources are not only crop planting but also characteristic aquaculture, five-in-one financial poverty alleviation, coordinated dividends, and solar power generation industry, which greatly increased the income of poor families. The main reason for the low score of expenditure structure is the large expenditure on medical and health care. More than 50% of poor families in Wuxi County are poor due to illness. Medical expenses account for half of the total income, daily expenses account for 33%, and

operating expenses account for 8%. The expenditure structure is unreasonable. Food and clothing security rate and housing security rate reached a good level. Poor households in Wuxi County basically have no worries about food and clothing, and their housing is basically guaranteed.

Under the policy implementation, the scores of relocation, poverty alleviation, and transfer are 0.74, 0.72, 0.80, 0.70, 0.82, 0.80, and 0.60 respectively. Judging from the scores of various evaluation indicators, Wuxi County has done a good job in relocation and poverty alleviation so that farmers’ income will continue to increase. In the renovation of dilapidated buildings, the renovation has been completed by means of new construction, replacement, and repair, but there are some poor families giving up the renovation. The government should pay special attention to finding out the reasons. In terms of ecological poverty alleviation, since 2008, the coal industry has continuously integrated resources and closed small and medium-sized coal mining enterprises with high-ash, high-sulfur, high-gas, low-heat, and great potential safety hazards. The government vigorously protects the environment and strengthens the management of atmospheric environment. At the same time, by 2025, the forest coverage rate will reach over 25%, the urban sewage treatment rate will reach 100%, the degree of soil and water conservation management will reach 63.07%, and the energy consumption per 10,000 yuan of GDP will be reduced by 17%. Urban and rural areas will become more livable. Poor family members with labor force are employed as forest rangers. Wuxi County is better in poverty alleviation education. The enrollment rate of school-age children reached 100%. Subsidies to students in the nine-year compulsory education stage are given, subsidies of 5,000 yuan to students in more than two courses are given, and subsidies of 2,000 yuan to technical school students every year are given. The farmers are very satisfied. In terms of medical assistance, medical conditions are insufficient. Poor people are further

impoverished by illness and disability. The number of poor people due to illness in Wuxi County accounts for half of the card-building households. By providing medical assistance, the government has greatly improved the medical environment in poor areas, and medical assistance must continue to improve.

In the improvement of poor villages, the rural drinking water safety rate is 0.70, the rural road hardening rate is 0.72, the village collective economy score is 0.62, the health and medical facilities score is 0.82, the sports facilities score is 0.70, and the kindergartens and primary schools score is 0.50. Judging from the scores of each evaluation index, in terms of infrastructure construction, since poverty alleviation activities were carried out, the appearance of villages has been greatly improved, and waterways have been basically improved. However, due to the imperfect infrastructure, hardened roads, and damaged village committees and roads in some remote villages, the government must continue to improve. The collective economy of the village began to move towards zero in just two years, but it is still immature and the funds are not in place in time. In some rural areas with poor natural conditions, there is no collective economic dividend income at present, and the score of basic education is the lowest. At present, the number of kindergartens and primary schools in Wuxi County is small, so we should increase investment in basic education. Judging from the scores of each evaluation index, poor households in Wuxi County are very satisfied with the person in charge of helping, villagers' groups, helping methods, and helping effects.

## 5. Conclusion

In order to study the concrete effect of industrial poverty alleviation, this paper puts forward an evaluation method of industrial poverty alleviation based on fuzzy evaluation method. First of all, collect relevant literature at home and abroad, collate relevant data, summarize the previous research results of scholars at home and abroad, briefly introduce the concept of industrial poverty alleviation, and summarize the previous experience of industrial poverty alleviation, which provides a certain theoretical basis for the design of industrial poverty alleviation evaluation system in this study. Secondly, based on the present situation of industrial poverty alleviation in Wuxi County, this paper analyzes the natural and economic conditions of Wuxi County and obtains the present situation of extensive poverty and serious poverty in Wuxi County. By analyzing the causes of poverty in Wuxi County, we can see that natural factors, government financial supply capacity, infrastructure construction, and poverty level are the main causes of poverty in Wuxi County. At the same time, through the analysis of the effect of industrial poverty alleviation in Wuxi County, we can understand the development process and achievements of industrial poverty alleviation in Wuxi County and introduce the industrial poverty alleviation model and experience in Wuxi County in detail.

Based on fuzzy evaluation method, the evaluation system of industrial poverty alleviation effect in Wuxi County is

designed. By designing scientific and reasonable evaluation indexes, the evaluation index system of industrial poverty alleviation effect in Wuxi County is established, including a comprehensive evaluation system of 4 first-class indexes and 21 second-class indexes. Through fuzzy evaluation method, this paper analyzes the weight of each index in detail, obtains the specific status of industrial poverty alleviation effect in Wuxi County, and makes an objective and fair evaluation of industrial poverty alleviation effect in poverty-stricken areas of Wuxi County.

## Data Availability

The experimental data used to support the findings of this study are available from the corresponding author upon request.

## Conflicts of Interest

The authors declare that they have no conflicts of interest regarding this work.

## Acknowledgments

The work was supported by the project "Research on the Innovation System of Chinese Decentralization for Financial Return to Its Origin" (19XJL005).

## References

- [1] L. Wang and H. E. Puming, "Analysis on the strategy of precise poverty alleviation under the background of rural revitalization strategy," *Asian Agricultural Research*, vol. 10, no. 9, pp. 42–44, 2018.
- [2] J. Wang and L. Long, "A preliminary study on the rational utilization of land resources in the poverty-stricken mountainous areas in the upper reaches of the yangtze river: a case study of xueshan township," *Asian Agricultural Research*, vol. 9, 2020.
- [3] Q. Huang, "Realization path for inclusive finance to support rural revitalization in poverty-stricken areas," *Asian Agricultural Research*, vol. 13, no. 6, p. 5, 2021.
- [4] L. Xu, X. Deng, Q. O. Jiang, and F. Ma, "Identification and alleviation pathways of multidimensional poverty and relative poverty in counties of China," *Journal of Geographical Sciences*, vol. 31, no. 12, pp. 1715–1736, 2021.
- [5] Y. Hu and S. D. professor, "Empirical research on the educational production function of rural primary schools in western China," *Educational Research*, vol. 190, no. 1, pp. 23–31, 2009.
- [6] Z. Chen, T. Li, X. Xue, Y. Zhou, and S. Jing, "Fatigue reliability analysis and optimization of vibrator baseplate based on fuzzy comprehensive evaluation method," *Engineering Failure Analysis*, vol. 127, Article ID 105357, 2021.
- [7] S. He, D. Song, H. Mitri et al., "Integrated rockburst early warning model based on fuzzy comprehensive evaluation method," *International Journal of Rock Mechanics and Mining Sciences*, vol. 142, no. 4, Article ID 104767, 2021.
- [8] A. H. Hadna, D. Kartika, and K. W. Tong, "Evaluation of poverty alleviation policy: can conditional cash transfers improve the academic performance of poor students in Indonesia," *Cogent Social Sciences*, vol. 3, no. 1, 2017.

- [9] A. H. Jiang, "An empirical analysis on the effectiveness of China's governmental poverty alleviation fund," *Journal of Central University of Finance & Economics*, vol. 42, no. 5, pp. 2999–3008, 2008.
- [10] X. Li and L. Li, "Evaluation of China's targeted poverty alleviation policies: a decomposition analysis based on the poverty reduction effects," *Sustainability*, vol. 13, 2021.
- [11] Y. Yang, "From anti-poverty to revitalization: exploring the path of sustainable development in poverty-stricken areas," *Eco-economy: English version*, vol. 9, no. 1, 2019.
- [12] X. Cheng, J. Chen, S. Jiang et al., "The impact of rural land consolidation on household poverty alleviation: the moderating effects of human capital endowment," *Land Use Policy*, vol. 109, Article ID 105692, 2021.
- [13] Y. Du, Y. Zheng, G. Wu, and Y. Tang, "Decision-making method of heavy-duty machine tool remanufacturing based on AHP-entropy weight and extension theory," *Journal of Cleaner Production*, vol. 252, Article ID 119607, 2020.
- [14] J. Hu, B. Xu, Z. Chen, H. Zhang, J. Cao, and Q. Wang, "Hazard and risk assessment for hydraulic fracturing induced seismicity based on the Entropy-Fuzzy-AHP method in Southern Sichuan Basin, China," *Journal of Natural Gas Science and Engineering*, vol. 90, no. B1, Article ID 103908, 2021.
- [15] H. Fu and N. Wang, "Analysis on the policy of poverty alleviation in deep poverty areas of henan province," *International Core Journal of Engineering*, vol. 6, no. 5, pp. 344–349, 2020.

## *Retraction*

# **Retracted: A Deep Learning-Based Framework for Social Data Sensing and Fusion for Enterprise Management**

### **Mathematical Problems in Engineering**

Received 18 July 2023; Accepted 18 July 2023; Published 19 July 2023

Copyright © 2023 Mathematical Problems in Engineering. This is an open access article distributed under the Creative Commons Attribution License, which permits unrestricted use, distribution, and reproduction in any medium, provided the original work is properly cited.

This article has been retracted by Hindawi following an investigation undertaken by the publisher [1]. This investigation has uncovered evidence of one or more of the following indicators of systematic manipulation of the publication process:

- (1) Discrepancies in scope
- (2) Discrepancies in the description of the research reported
- (3) Discrepancies between the availability of data and the research described
- (4) Inappropriate citations
- (5) Incoherent, meaningless and/or irrelevant content included in the article
- (6) Peer-review manipulation

The presence of these indicators undermines our confidence in the integrity of the article's content and we cannot, therefore, vouch for its reliability. Please note that this notice is intended solely to alert readers that the content of this article is unreliable. We have not investigated whether authors were aware of or involved in the systematic manipulation of the publication process.

Wiley and Hindawi regrets that the usual quality checks did not identify these issues before publication and have since put additional measures in place to safeguard research integrity.

We wish to credit our own Research Integrity and Research Publishing teams and anonymous and named external researchers and research integrity experts for contributing to this investigation.

The corresponding author, as the representative of all authors, has been given the opportunity to register their agreement or disagreement to this retraction. We have kept a record of any response received.

### **References**

- [1] Y. Wang, "A Deep Learning-Based Framework for Social Data Sensing and Fusion for Enterprise Management," *Mathematical Problems in Engineering*, vol. 2022, Article ID 3606469, 8 pages, 2022.

## Research Article

# A Deep Learning-Based Framework for Social Data Sensing and Fusion for Enterprise Management

Yu Wang 

*School of Business, Tianfu College of SWUFE, Mianyang 621000, China*

Correspondence should be addressed to Yu Wang; wangyu1@tfsfwufe.edu.cn

Received 24 February 2022; Revised 5 April 2022; Accepted 11 April 2022; Published 30 April 2022

Academic Editor: Man Fai Leung

Copyright © 2022 Yu Wang. This is an open access article distributed under the Creative Commons Attribution License, which permits unrestricted use, distribution, and reproduction in any medium, provided the original work is properly cited.

How to effectively realize the perception and fusion of data in the enterprise management society is the core problem that must be solved by enterprise management. On the basis of defining the resource system of enterprise management society, a semantic-oriented metadata model is proposed, combined with the classification of user needs, to build a data fusion framework for enterprise management society based on multisource data. The study designs a multilayer convolutional neural network model to process the data and proposes a recommendation path for the implementation of user data services for the enterprise management society based on the data operation center of the enterprise management society. Finally, it proposes suggestions for the development of the data fusion of the enterprise management society by improving the data fusion standard of the enterprise management society from multiple sources, actively formulating the data opening policy, and exploring the personal data collection and storage protection scheme. Experiments show that the scheme designed in this study is 5% more accurate than the state-of-the-art scheme.

## 1. Introduction

Enterprise management societies are developed on the basis of enterprises and are the advanced form of enterprises [1]. The guidance on promoting the Healthy Development of Enterprise Management Societies, jointly issued by eight Chinese ministries and commissions, states that, “by 2020, a number of distinctive enterprise management societies will be built” [2]. The Thirteenth Five-Year Plan for National Economic and Social Development clearly states that the construction of modern information infrastructure should be strengthened and an enterprise management society should be built [3]. The Report on the Development of New Enterprise Management Societies 2017 shows that the construction of new enterprise management societies in China is developing in clusters, and at the National Conference on Network Security and Informatization in April 2018, General Secretary Xi Jinping proposed to promote the deep development of digitalisation, big data, and artificial intelligence, and the application of big data provides a

strong technical guarantee for the development of enterprise management societies [4].

Many researchers also study the use of enterprise data through the deep learning model [5]. The essence of a deep learning application is to extract and classify data features. Its research directions are mainly divided into two categories: one is to optimize the way of extracting features from data, and the quality of feature extraction directly affects the final classification results; the other is to build a good classifier based on the existing feature extraction methods [6].

The difficulty of many data processing tasks depends on the representation of information. This principle has a far-reaching impact on computer science and machine learning. For example, for tasks such as 210 divided by 6, giving the form of the problem will change the ease of calculation; if the numbers are expressed in Roman characters, the process of obtaining the results becomes less intuitive. When most modern people deal with the problem of CCX divided by VII, they first convert the numbers into Arabic numerals and then calculate them. In addition, once the

TABLE 1: Comparison of various models on CIFAR 10.

| Model name          | Training accuracy | Verification accuracy | Training time |
|---------------------|-------------------|-----------------------|---------------|
| Original network    | 0.8056            | 0.8104                | —             |
| SVM hybrid model    | 0.85711           | 0.8137                | —             |
| Enhanced network N1 | 0.79725           | 0.8195                | 1080.479      |
| Enhanced network N2 | 0.79658           | 0.8127                | 998.404       |

data representation is determined, the time spent processing the data can be quantified, for example, inserting numbers into a sequential (Table 1). If the list is implemented by a chain, the time complexity is  $O(n)$ . If the chain is implemented by a red-black tree, the time complexity can be said to be the same as good data representation, making the next machine learning task simple. For different data processing tasks, the representation of data will change [7].

There is still no uniform definition of the concept of EMS in the industry. Sun et al. [8] argue that the connotations of the enterprise management society include the fundamental role of information and communication technology, economic development and encouragement of innovation, and the promotion of resource sharing and collaborative operations among various sectors. Although researchers have interpreted the definition of the enterprise management society from different perspectives, their core concepts are basically the same, namely, the use of a new generation of information technology tools to integrate core data on enterprise operations and provide intelligent services to the public [9, 10].

Liu et al. [11] reviewed the current status of enterprise management society research through literature and concluded that enterprise management society research is more concerned with technological progress, data integration and fusion. In 2021, the National Enterprise Management Society Standardization General Group released the standard document “Enterprise Management Society Data Fusion,” which specifies the conceptual model and data coding specification for data collection, organization, interconnection, and service [12]. Based on clarifying the enterprise management social resource system, this study proposes a semantic-oriented metadata model, combines the classification of user needs, builds a framework for enterprise management social data fusion based on multisource data, enhances public participation in enterprise management, provides decision support for the government and enterprises, and innovates the enterprise management social information service model [13].

## 2. Related Work

In terms of the basic elements of enterprise construction, scholars have mostly focused on the basic elements of enterprise construction and have not discussed the technical issues. Zhou et al. [14] propose a preliminary framework for an enterprise-managed society from a system integration perspective, integrating government, residential communities, the economy, infrastructure, and the natural environment. Makkar and Kumar [15] argue that the fundamental elements of a business-managed society include people,

technology, and organization. Blake and Michalikova [16] argue that the subjects of information resource management are government, business, and society. Rowland and Porter [17] believe that the main body of enterprise operation and management is the government department, and the service targets are the government, enterprises, and individuals.

As for the application of enterprise management in society, scholars have constructed a technical framework of enterprise management in society with data mining and analysis technology as the core, in order to provide diversified application services on this basis. For example, Muhammad and Hossain [18] proposed an enterprise management social technology framework based on trajectory data analysis and mining, which is divided into three levels: trajectory sensing, knowledge discovery, and specific application; Li et al. [19] proposed an enterprise management social technology framework with a “four-level feedback” structure, including enterprise sensing and data acquisition, enterprise management social management, enterprise management social analysis, application, and service.

In the area of enterprise management social integration, scholars have built a framework for enterprise management social data integration from different perspectives. Wu et al. [20] studied emergency information fusion and proposed an information fusion framework based on emergency information and aimed at serving emergency decision-making. Ning et al. [12] proposed a theoretical architecture for multimodal data fusion in enterprises, including service information description model, metadata model, and data interconnection model, and proposed a framework for sharing and fusion of enterprise management social data. From the technical implementation level, there are enterprise management social integration framework based on Web API information integration, enterprise management social integration framework based on metadata, and enterprise management social integration framework based on semantic aggregation: the enterprise management social integration framework based on Web API is more widely used, but the disadvantage is that the open interface is inconsistent, and specific APIs only allow access to specific data or services and cannot achieve data; metadata-based enterprise management social inclusion frameworks use a unified metadata standard to aggregate enterprise operational data, but there may be cases where the same entities from different datasets are represented, ignoring the semantic relationships between entities and the corresponding matching relationships. The framework makes use of domain-specific ontologies [13] (e.g., Km4City) to collect data from enterprise operators and aggregate data that are intrinsically semantically linked so that they are integrated in a

unified, semantically interoperable multidomain ontology-based model.

### 3. Corporate Management Social Resource System

The enterprise management social resource system is a complex system formed by integrating geospatial data as a unified carrier and based on the intrinsic relationship of data in various fields within the enterprise's spatial and temporal scope. The government, enterprises, and public are the subjects of the enterprise management society. From the perspective of the system, the geospatial data are used as the root to build the enterprise management society data resource system based on the enterprise subjects, as shown in Figure 1:

The enterprise data in Figure 1 refer to the data related to the operation of the enterprise, including data formed in various aspects such as product development and design, manufacturing, marketing, and capital flow. The management enterprise system under big data thinking is based on massive data for information processing, so the traditional manual data statistics method is no longer applicable, and a big data system support system based on automatic docking must be built. Modern Internet enterprises have more complete management information systems. For example, the trading system of e-commerce platforms integrates customer management, order management, transaction management, and settlement management, and the management system of communication operators includes network management system, business management system, customer management system, marketing management system, and settlement management system [14–16]. These business systems can provide a large amount of management enterprise information, which is very useful for enterprise internal management and business decisions, but this information is scattered in various systems, in a fragmented state, and must be collected, collated, and modeled to turn into useful information, and this process must rely on the automatic docking of business systems to achieve the processing and handling of big data management enterprise information.

### 4. Semantic-Oriented Social Metadata Model for Business Management

**4.1. Metadata.** Metadata are structured data describing the attributes of a certain type of resource. A standardised enterprise management social metadata model is the basis for achieving interoperability between enterprise applications, resolving heterogeneous data conversion, achieving resource aggregation on the same topic, and providing data services for enterprise decision makers. The metadata service providers, mainly data producers and owners, publish metadata services to the enterprise's UDDI registry [13]. This study defines the metadata model as a six-tuple  $MD = \{S, E, A, I, R, C\}$ .

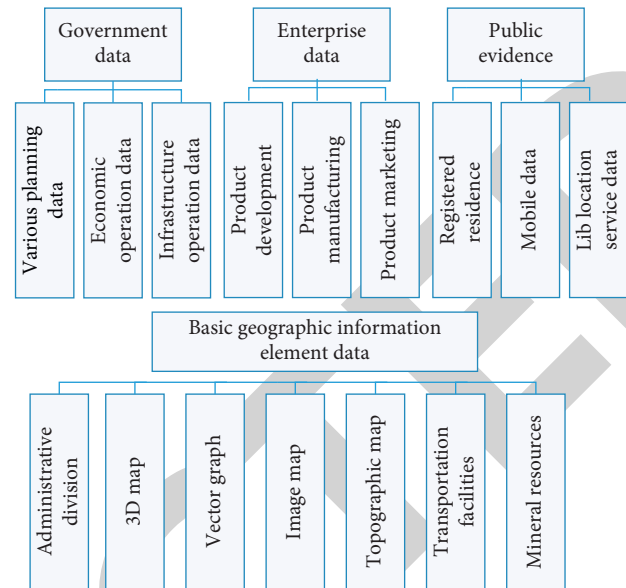


FIGURE 1: Corporate governance and social resource system.

- (1) Data source  $S$  (Source): the data sources are data from the Education Bureau, Transport Bureau, Health Bureau, Taxation Bureau, Housing and Construction Bureau, Public Security Bureau, Civil Affairs Bureau, Meteorological Bureau, Water Bureau, and so on. The set of data sources is denoted as  $= \{S_1, S_2, \dots, S_n\}$ , where  $S_i$  ( $1 < i < n$ ) denotes the  $i$ th data source [18–20].
- (2) Entity-type collection  $E$ : a generic term for the set of entities that share the same attributes. Entity types include people, objects, and spatiotemporal entities. People (agent) is a generic term for governments, businesses, and public and refers to data holders who are capable of autonomous activities. Objects include natural geographical entities (e.g., mountains, rivers, and lakes) and man-made geographical entities (e.g., buildings, roads, bridges, and streets). Temporal spatial entity refers to objects with multidimensional characteristics in space and time. The temporal spatial entity (temporal spatial entity) is an object with spatial and temporal multidimensional characteristics, as shown in Figure 2.
- (3) Entity attribute  $A$ : the set of entity attributes  $A = \{a_{11}, a_{12}, \dots, a_{mk}\}$ , where  $a_{ij}$  ( $1 < i < m, 1 < j < k$ ) represents the  $j$ th attribute of the  $i$ th entity. For example, a sensing device is a physical device that can sense changes in external information in real time and transmit the acquired information to other devices, such as sensors, GPS positioning devices, video surveillance devices, and RFID devices.
- (4) The set of instances  $I$  is the set of entity class objects. An entity is a real-world, identifiable object, and set of instance classes is denoted  $I = \{I_1, I_2, \dots, I_m\}$ , where  $I_i$  ( $1 < i < m$ ) denotes the  $i$ th entity [21].

**4.2. Deep Learning Feature Classification.** The advantage of deep learning lies in the ability of deep neural networks to fit

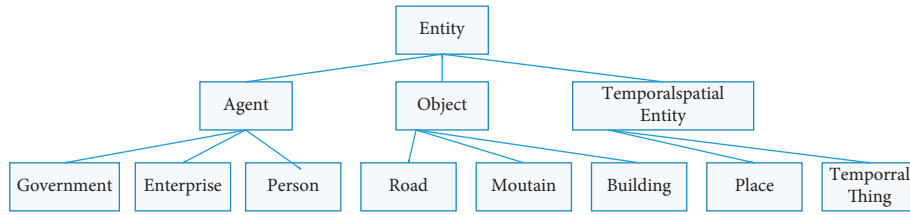


FIGURE 2: Example of a classification system for entities.

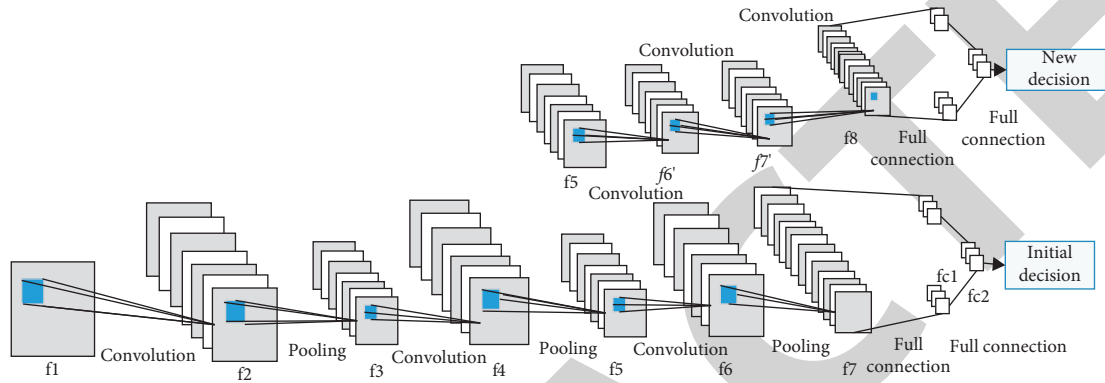


FIGURE 3: CNN augmentation model.

data, which not only brings high accuracy to deep learning but also has the disadvantage that deep neural networks require large amounts of data for training. The collection of labeled samples is labor intensive.

The specific mixture of CNN and SVM is divided into two parts. Firstly, a CNN is obtained by training on the original dataset or by pretraining on a large dataset. The second part of the hybrid model is an SVM, which follows the last layer of the CNN. During training and testing, the data is first extracted by the CNN, and the extracted features are then used as input to the SVM, thus enabling the training and testing of the SVM [22].

The hybrid model of CNN and SVM only uses the features of the last layer of the CNN and feeds them into the SVM, which does not make full use of the features of the lower layers.

The network framework is divided into two parts: the first part is the original network and the second part is the augmented network. The original network is a normal CNN, which can be trained in two ways: either on the target dataset or directly on the large-scale dataset using the same CNN structure. The second part of the network is an augmentation of the original network, which is modified from the second half of the original network and incorporates the last layer of feature mapping of the image with the original features. In Figure 3, the augmented network replicates the feature map of the original CNN from the feature map coincidentally and uses the same structure as the original network to regain the feature maps [23–25].

In general, the augmented network has two main functions: when the training set of the original network is the training set of the target task, the classification accuracy is improved without changing the original network; when the

training set of the original network is not the target training set, the original network can only be used as a feature extractor of the data; the task of the augmented network is the main body of the task implementation.

## 5. Enterprise Management Social Data Integration Framework

### 5.1. Enterprise Management Social User Needs' Classification.

The government is the operational manager of the enterprise management society, and the public is the object of the enterprise management and society management and services. Enterprise development is driven by user needs [14], user needs and feedback cannot be ignored, and meeting user needs is the key to building an enterprise management society.

The user needs are dynamic, multifaceted, and uncertain, and the enterprise management society covers specific applications in many fields, making it difficult to precisely describe their specific needs. Using the Kano model and taking into account the five stages of an individual user's lifecycle, including infancy, childhood, adolescence, adulthood, and old age, we have gradually refined the demand groups with different functional attributes (see Figure 4) and developed specific products covering different industry sectors, including smart education-related products, smart healthcare-related products, smart transport-related products, and smart community-related products [26].

5.2. Data Service Recommendation Path. Based on a multisource data fusion framework, the enterprise management social data operation center is established, responsible for



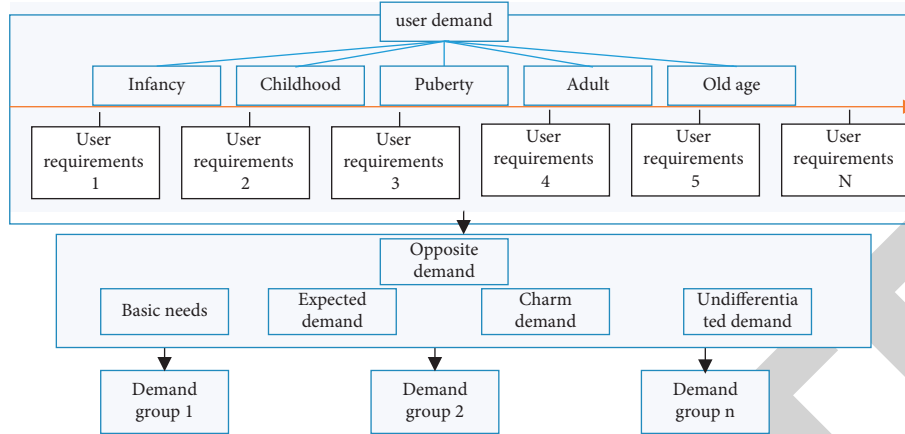


FIGURE 4: Classification of user requirements based on Kano.

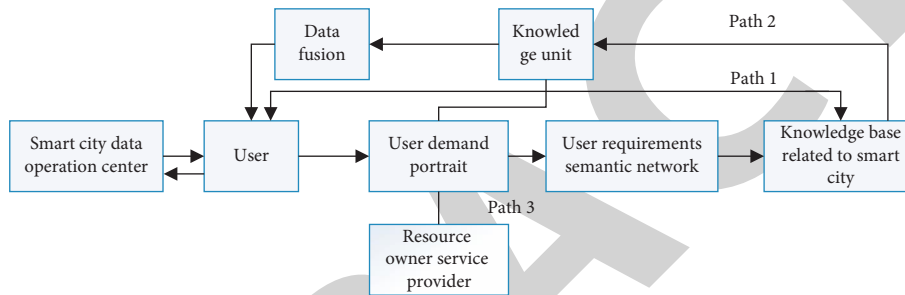


FIGURE 5: Implementation path for data service recommendations.

the collection, management, and sharing of big data in enterprise life, and establishing an enterprise-wide paradigm of multidepartmental cooperation, which can improve the current situation of inadequate horizontal collaboration among government departments. Based on the categorisation of the needs of EMS users, the data are combined with demographic attributes, usage preferences, and other data to build a profile of EMS users' needs and provide specific data recommendation services. Figure 5 illustrates the three paths of user data recommendation services: (i) path 1 is to match user demand information with the knowledge base related to the enterprise management society at a coarse-grained level and provide users with services related to the enterprise management society [27], (ii) path 2 is to match user demand semantic information with knowledge units extracted from the knowledge base of the enterprise management society at a fine-grained level, fuse the knowledge units with multidimensional data, and provide users with, and (iii) path 3 is to study how to open up data interfaces to resource owners and service providers and provide corresponding data services to them based on user demand profiles.

## 6. Simulation Experiments and Analysis of Results

6.1. *Enterprise Data Effectiveness.* The building of an enterprise management society requires the synergistic development of enterprise, data, and standardisation. In the

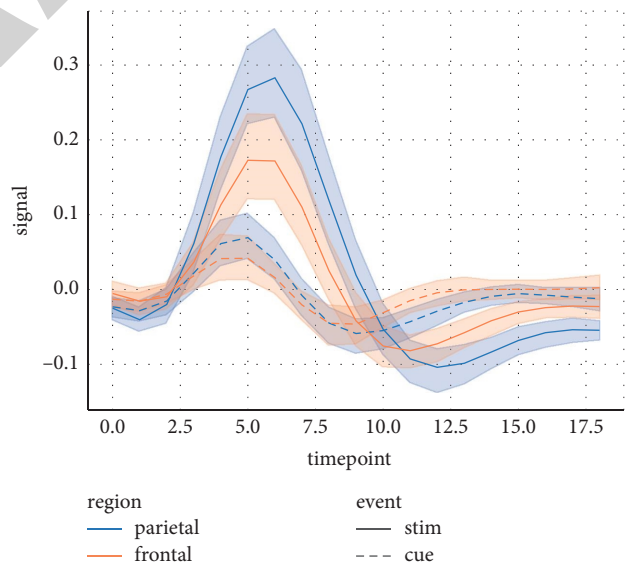


FIGURE 6: Comparison of enterprise data and standardisation effectiveness.

big data environment, the Internet of Things, cloud computing, and sensing technologies transform the information flowing within the enterprise into data, giving the attributes of data and thus presenting the development of an enterprise management society [28]. On the basis of the data coding specification, data collection specification, and municipal infrastructure data element specification, further

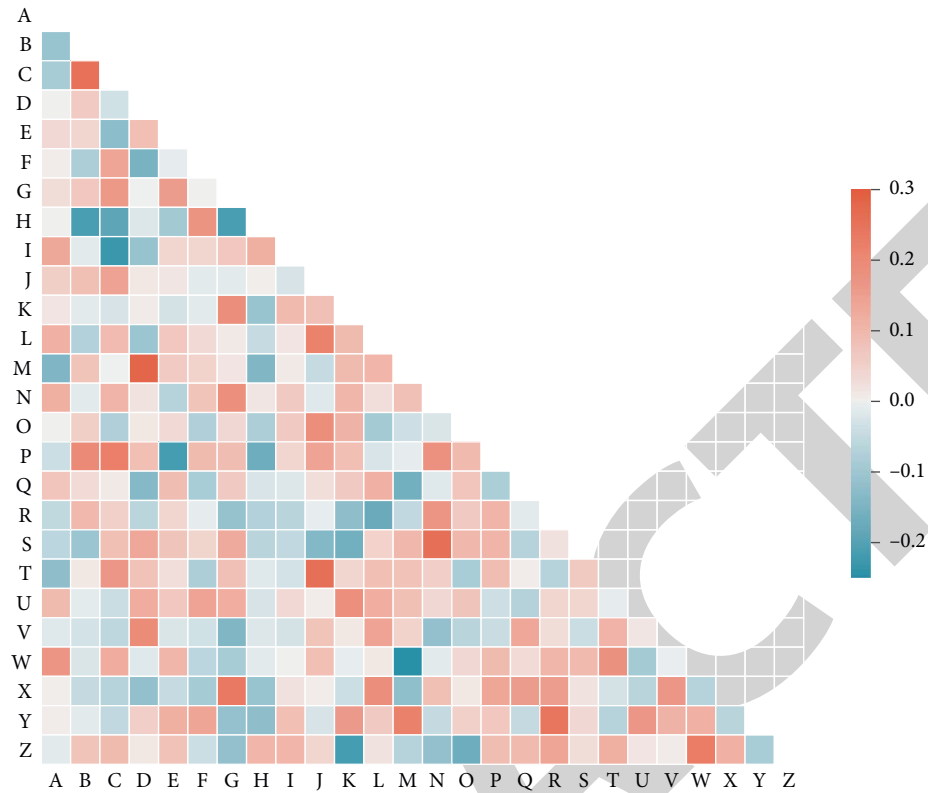


FIGURE 7: Level of data privacy.

improvement should be made to the enterprise management social multisource data fusion standard, including entity data standardisation, entity attribute standardisation, and application context standardisation, and data conversion standard and storage specification should be established to achieve cross-domain, cross-sector, and cross-level data fusion. See Figure 6.

The government provides decision optimization support, universities provide intellectual service support, and enterprises provide technology and product support and establish a data-sharing mechanism for stakeholder partnership. Data are a true reflection of the enterprise, and the construction of an enterprise management society should protect data extensively. The data privacy of the scheme in this study is shown in Figure 7. The government formulates a data opening policy to clarify the scope of data that can be opened. As a data provider, it should try to provide original data-sharing services and ensure the integrity of data fields under the premise of conforming to policy regulations; as a data recipient, it still has the responsibility to ensure information security under the premise of the reasonable use of data.

**6.2. In-Depth Performance.** The original CNN network consists of three convolutional layers, three pooling layers, and two fully connected layers. The ReLU activation function is used by default, and each convolutional operation uses a  $5 \times 5$  convolutional kernel with a step size of 1, filling a blank area of 2 pixels. The pooling layer is first a maximum pooling layer of size  $3 \times 3$  with a step size of 2, followed by an

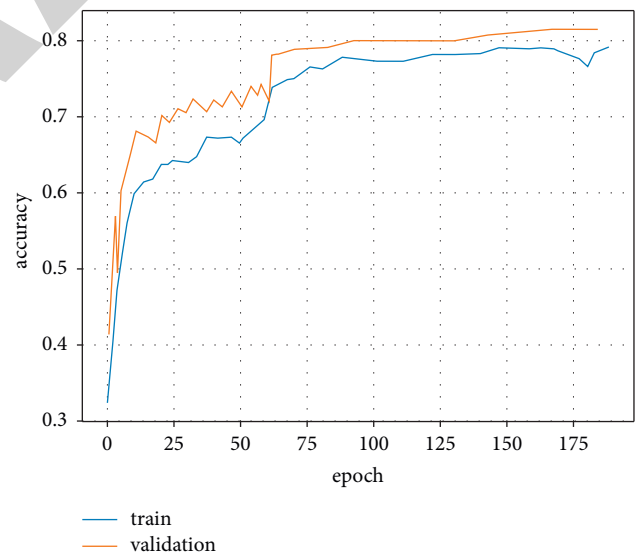


FIGURE 8: Original network training curve.

average pooling layer of size  $3 \times 3$  with a step size of 2. The number of fully connected neural units in the penultimate layer is 512, i.e., the number of output features is 512. The training curve is shown in Figure 8.

The final training accuracy of the network at the 200th epoch was 0.8059, and the validation accuracy was 0.8107. The features extracted from the original network at the 200th epoch were used in the experiment.

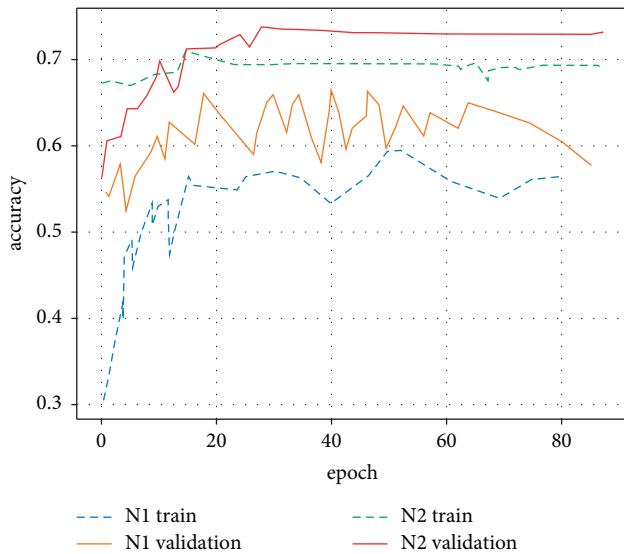


FIGURE 9: Plot of N1 and N2 training curves.

The enhanced network was trained using the feature map of the conv2 layer of the original network, and N1 was merged with pool3 of the original network at the pool3 layer. N2 was spliced with fcl of the original network at the f1 layer. The training curves of N1 and N2 are shown in Figure 9. In the training of the augmented network, both N1 and N2 were trained on the 200th epoch of the original network, with an initial training step of 0001 for 100 epochs and a step size of 01 times the original at the 16th, 32<sup>nd</sup>, and 64th epochs. In Figure 9, N2 converges on the validation set at approximately epoch 16 and N1 converges at epoch 32. The training and validation accuracies of the network at the 100th epoch are shown in Table 1.

As can be seen from Table 1, the results of either training method have improved the classification results of the original network. The augmented network N1 has the best classification result because it replicates the feature maps of the convolutional layers in the original network, which is equivalent to increasing the number of convolutional layers, and N1 makes full use of the features in the intermediate layers compared to N2. The effect of the augmented network N2 is weaker than that of the SVM hybrid model because the augmented network N2 only replicates the features in the original fully connected layer, which does not make full use of the features in the intermediate layers and increases redundancy. In the augmented network model, we can see that the training accuracy is lower than that of the SVM hybrid model, but the final performance on the test set is better, which indicates that the augmented network has good generalization.

## 7. Conclusions

This study proposes a semantic-oriented metadata model, combined with the classification of user needs, and constructs an enterprise management social data fusion framework based on multisource data. Based on the enterprise management social data operation center, this study

designs a multilayer convolution neural network model to process the data. It can be seen from the experiment that the CNN enhancement model proposed in this study is better than the hybrid model of CNN and SVM and is slightly weaker than the model that directly adds corresponding neural units to the original network, but it does not need to retrain the whole network. The CNN enhancement model proposed in this section is essentially a shallow CNN model. Compared with the original network, the enhanced network is easier to train and has faster convergence speed.

## Data Availability

The experimental data used to support the findings of this study are available from the corresponding author upon request.

## Conflicts of Interest

The author declared no conflicts of interest regarding this work.

## References

- [1] S. Pouyanfar, Y. Tao, H. Tian, S.-C. Chen, and M.-L. Shyu, "Multimodal deep learning based on multiple correspondence analysis for disaster management," *World Wide Web*, vol. 22, no. 5, pp. 1893–1911, 2019.
- [2] T. H. Do, E. Tsiligianni, X. Qin et al., "Graph-deep-learning-based inference of fine-grained air quality from mobile IoT sensors," *IEEE Internet of Things Journal*, vol. 7, no. 9, pp. 8943–8955, 2020.
- [3] J. Sun, Z. Tian, Y. Fu, J. Geng, and C. Liu, "Digital twins in human understanding: a deep learning-based method to recognize personality traits," *International Journal of Computer Integrated Manufacturing*, vol. 34, no. 7-8, pp. 860–873, 2021.
- [4] N. S. Khan and M. S. Ghani, "A survey of deep learning based models for human activity recognition," *Wireless Personal Communications*, vol. 120, no. 2, pp. 1593–1635, 2021.
- [5] P. Sundaravadivel, K. Kesavan, L. Kesavan, S. P. Mohanty, and E. Kougiianos, "Smart-log: a deep-learning based automated nutrition monitoring system in the iot," *IEEE Transactions on Consumer Electronics*, vol. 64, no. 3, pp. 390–398, 2018.
- [6] J. Jonnalagadda and M. Hashemi, "A deep learning-based traffic event detection from social media," in *Proceedings of the 2021 IEEE 22nd International Conference on Information Reuse and Integration for Data Science (IRI)*, pp. 1–8, IEEE, Las Vegas, NV, USA, 2021, August.
- [7] W. Niu, X. Zhang, X. Du, L. Zhao, R. Cao, and M. Guizani, "A deep learning based static taint analysis approach for IoT software vulnerability location," *Measurement*, vol. 152, Article ID 107139, 2020.
- [8] L. Sun, Q. Yu, D. Peng, S. Subramani, and X. Wang, "Fogmed: a fog-based framework for disease prognosis based medical sensor data streams," *Computers, Materials & Continua*, vol. 66, no. 1, pp. 603–619, 2021.
- [9] Z. Qu, H. Sun, and M. Zheng, "An efficient quantum image steganography protocol based on improved EMD algorithm," *Quantum Information Processing*, vol. 20, no. 53, pp. 1–29, 2021.
- [10] J. Wei, J. He, K. Chen, Y. Zhou, and Z. Tang, "Collaborative filtering and deep learning based recommendation system for

## Research Article

# Research on the Evaluation Model of Dance Movement Recognition and Automatic Generation Based on Long Short-Term Memory

Xiuming Yuan<sup>1</sup> and Peipei Pan <sup>2</sup>

<sup>1</sup>College of Music, St. Paul University Manila, Manila 1004, Philippines

<sup>2</sup>Academy of Music and Dance, Liaocheng University, Liaocheng 252000, China

Correspondence should be addressed to Peipei Pan; panpeipei@lcu.edu.cn

Received 9 February 2022; Revised 28 March 2022; Accepted 3 April 2022; Published 28 April 2022

Academic Editor: Man Fai Leung

Copyright © 2022 Xiuming Yuan and Peipei Pan. This is an open access article distributed under the Creative Commons Attribution License, which permits unrestricted use, distribution, and reproduction in any medium, provided the original work is properly cited.

With the development of random image processing technology and in-depth learning, it is possible to recognize human movements, but it is difficult to recognize and evaluate dance movements automatically in artistic expression and emotional classification. Aiming at the problems of low efficiency, low accuracy, and unsatisfactory evaluation in dance motion recognition, this paper proposes a long short-term memory (LSTM) model based on deep learning to recognize dance motion and automatically generate corresponding features. This paper first introduces the related deep learning model recognition methods and describes the related research background. Secondly, the method of identifying dance movements is identified concretely, and the process of identifying concretely is given. Finally, through the comparison of different dance movements through experiments, it shows that there are obvious advantages in the accuracy of action recognition, error rate, similarity, and model evaluation method.

## 1. Introduction

As time enters the twenty-first century, the technology in the computer field has made a qualitative leap, and various scientific and technological achievements have been widely used in people's daily life, constantly promoting the world to be trendy day by day. Human thought, art, and creativity are by far the most unique and difficult to replicate, and dance is one of the carriers of artistic inheritance. It is not only a grand goal but also a significant research project to make the "dance" created by machines without "emotion" recognized by human beings. It can be applied to education, entertainment, animation, games, and other fields, liberating human work and creating new artistic life. Up to now, computer-generated dance movements are stiff and out of rhythm, and the specific generation process still stays at the stage of extracting matches from the existing dance movement database, so it is impossible to automatically create new dances. In this paper, a data set of music and dance movements containing about 270,000 frames is constructed, dance posture features are extracted by human

posture detection technology, a specific music feature encoder is designed, and a system for automatic generation of dance movements is proposed based on the deep learning method. Literature [1] proposed a deep learning framework DanceNet3D. Dance is generated with parameterized motion converter. MIDI Music Emotional Annotation System integrates music and dance movements to complete automatic choreography [2]. Literature [3] made autonomous humanoid robot generate dance through real-time music input. Literature [4] designed an automatic facial animation generation system for dance characters considering emotions in dance and music. Literature [5] selected motion to generate dance according to connection similarity. Literature [6] proposed a new system of Music2Dance to solve automatic music and choreography. Literature [7] introduced a system and method for automatically generating dance symbols. Literature [8] generated a human skeleton sequence map from music to generate the final video. Literature [9] took violin or piano playing audio as input and output skeleton predicted video for animated avatars. A method is capable of generating realistic video independent

of subject directly from original audio [10]. Literature [11] proposed an effective method for real-time detection of image 2D posture by using part association fields. Literature [12] reviewed the latest trend of video-based human capture and analysis to realize automatic visual analysis of motion. Literature [13] automatically generated Labanotation from human motion capture data stored in BVH file. Literature [14] summarized the research of target detection based on convolution neural network. Literature [15] designed the LSTM recurrent neural network speech recognition system based on i-vector feature.

## 2. Theoretical Basis

Due to space limitations, only simple explanations are made such as deep learning [16], LSTM [17], dance generation algorithm [18], self-encoder [19], and so on.

**2.1. Deep Learning Model.** We divide deep learning into three categories. The first type is the commonly used convolution neural network (CNN). The second is self-coding neural network based on multilayer neurons, which includes self-coding and sparse coding; the third type is deep confidence network (DBN), which mainly uses multilayer self-coding neural network for pretraining.

There are two characteristics of deep learning. The first point is that deep learning can emphasize the depth of model structure; the second point is to clarify the importance of feature learning. It makes classification and prediction operations easier.

The high bias or high variance state of the deep network is shown in Figure 1.

In the application of deep learning, a lot of mathematical knowledge will be used. We show some formulas as follows:

(1) Upper and lower bounds are as follows:

$$\begin{aligned} \forall a \in A \Rightarrow a \leq \sup A, \\ \forall b > 0, \quad \exists a_0 \in A \Rightarrow a_0 > \sup A - b, \\ \forall a \in A \Rightarrow a \geq \inf A, \\ \forall b > 0, \quad \exists a_0 \in A \Rightarrow a_0 < \inf A + b. \end{aligned} \quad (1)$$

(2) Concave and convexity of functions are as follows [20]:

$$\begin{aligned} f(\lambda x_1 + (1 - \lambda)x_2) \leq \lambda f(x_1) + (1 - \lambda)f(x_2), \\ f(\lambda x_1 + (1 - \lambda)x_2) \geq \lambda f(x_1) + (1 - \lambda)f(x_2). \end{aligned} \quad (2)$$

(3) Sigmoid function is as follows:

$$S(x) = \frac{1}{1 + e^{-x}}. \quad (3)$$

(4) Directional derivative is as follows:

$$\frac{\partial f}{\partial l} = \frac{\partial f}{\partial x} \cos \phi + \frac{\partial f}{\partial y} \sin \phi. \quad (4)$$

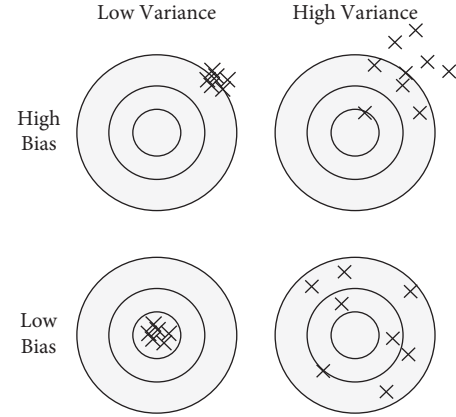


FIGURE 1: Deviation/variance diagram.

**2.2. Dance Generation Algorithm.** As shown in Table 1, we summarized some dance generation algorithms.

**2.3. LSTM.** Cyclic neural network is referred as “RNN.” It can effectively deal with the problem of time series format data.

$$\begin{aligned} O_t &= g(V \cdot S_t), \\ S_t &= f(U \cdot X_t + W \cdot S_{t-1}). \end{aligned} \quad (5)$$

The infrastructure of the cyclic neural network is shown in Figure 2. Cyclic neural network has a closed loop, which can continuously input time series information into the network layer at different times. This cyclic structure shows the close relationship between RNN and time series data.

In Figure 2,  $h_t$  is called state or hidden state and A is hidden layer, which is cyclic layer.

**Long and Short-Term Memory (LSTM) network.** It belongs to a special type of RNN. Although RNN has made amazing achievements in recent years, ordinary cyclic neural networks are mainly trained by the back propagation algorithm, and it is very difficult to learn long-term dependence. This is due to gradient disappearance and gradient explosion. LSTM can solve the problem of long-term dependence, and it works well on time series.

The state of cells in each network layer and the horizontal line passing through cells are the key to LSTM. The structure of cells is like a conveyor belt structure. Data run directly on the chain with only a small amount of linear interaction.

$$\begin{aligned} f_t &= \sigma(W_f \cdot [h_{t-1}, x_t] + b_f), \\ i_t &= \sigma(W_i \cdot [h_{t-1}, x_t] + b_i), \\ \tilde{C}_t &= \tanh(W_C \cdot [h_{t-1}, x_t] + b_C), \\ C_t &= f_t * C_{t-1} + i_t * \tilde{C}_t, \\ o_t &= \sigma(W_o \cdot [h_{t-1}, x_t] + b_o), \\ h_t &= o_t \cdot \tanh(C_t). \end{aligned} \quad (6)$$

TABLE 1: Dance generation algorithm based on deep learning.

| Algorithm  | Content  |
|--|--|
| Yi wang and other researchers proposed NPHHMM in 2005.   | This hierarchical hidden Markov model can capture action data. NPHHMM is trained to include a wide variety of ballet and disco movements.  |
| In 2006, Bai niao takagi created an action synthesis method based on motion capture system [21], which can input music synchronously.                  | When the system inputs music, this method can calculate the similarity between motion and music features. The system can use correlation tracking motion graph to generate new motion.   |
| In 2012, a new many-to-many statistical mapping framework emerged. The framework proposed by ofli et al. can learn musical features and dance figures. | The framework is also a discrete hidden Markov model. In addition, it introduces an improved Viterbi algorithm to synthesize dance sequences. It can use MFCC features to classify music and generate corresponding dance postures.  |
| Chor-RNN's system was proposed in 2016.  | RNN of LSTM type was used for modern dance training. This is the first time that deep recurrent neural network is used to automatically generate dances and generate new dance sequences.  |
| Omid alemi et al. designed an application called GrooveNet in 2017.  | This application can learn and generate dance patterns on a very small training set. It uses FCRBM and RNN to generate dance movements.  |
| A deep recurrent neural network with good performance is proposed.   | Its encoder adopts one-dimensional convolution layer and multilayer LSTM, which can process the audio power spectrum. The decoder part uses LSTM layer to generate dance movements. Sound and motion features are used to extract mapping. In order to get better performance, time index and masking methods are also used. |
| Vondrick et al. designed a deep learning model [22].   |  |

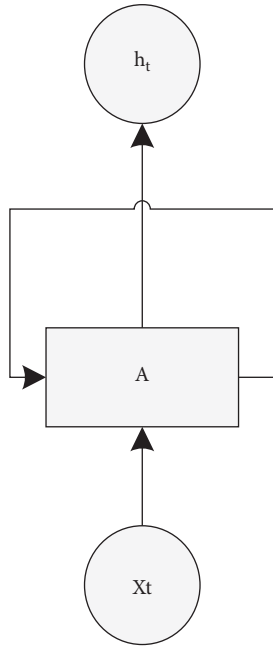


FIGURE 2: Simple cyclic neural network.

2.4. Self-Encoder. The self-encoder includes a decoder and an encoder as shown in Figure 3.

$$\begin{aligned}
 f: \chi &\longrightarrow F, \\
 g: F &\longrightarrow \chi, \\
 f, g &= \arg \min_{f, g} \|X - g[f(X)]\|^2.
 \end{aligned}
 \tag{7}$$

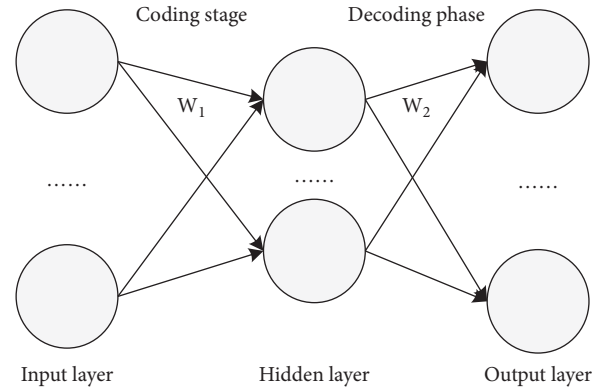


FIGURE 3: Process description of self-coding machine.

Detailed process description is as follows:

$$\begin{aligned}
 y &= \sigma_e(Wx + b), \\
 z &= \sigma_e(W'y + b'), \\
 W' &= W^T, \\
 L(xz) &= \|x - z\|^2, \\
 L_H(x, z) &= -\sum_{k=1}^n [x_k \log z_k + (1 - x_k) \log(1 - z_k)],
 \end{aligned}
 \tag{8}$$

wherein  $W$  and  $B$  are the weights and offsets of the codes and  $W'$  and  $b'$  are the weights and offsets of the decoding. The whole training process uses the traditional gradient-based training method.

The characteristics of the self-encoder are shown in Table 2.

TABLE 2: Three characteristics of self-encoder.

| Characteristic          | Content  |
|-------------------------|--|
| Data correlation        | Refers that the self-encoder can only compress data similar to its previous training data.   |
| Data lossiness [23]     | Compared with the original input, the output of self-encoder will lose information when decompressing, so self-encoder is a data lossy compression algorithm.                        |
| Automatic learning [24] | Automatic encoders learn automatically from data samples, which mean that it is easy to train a specific encoder for the input of a specified class without completing any new work. |

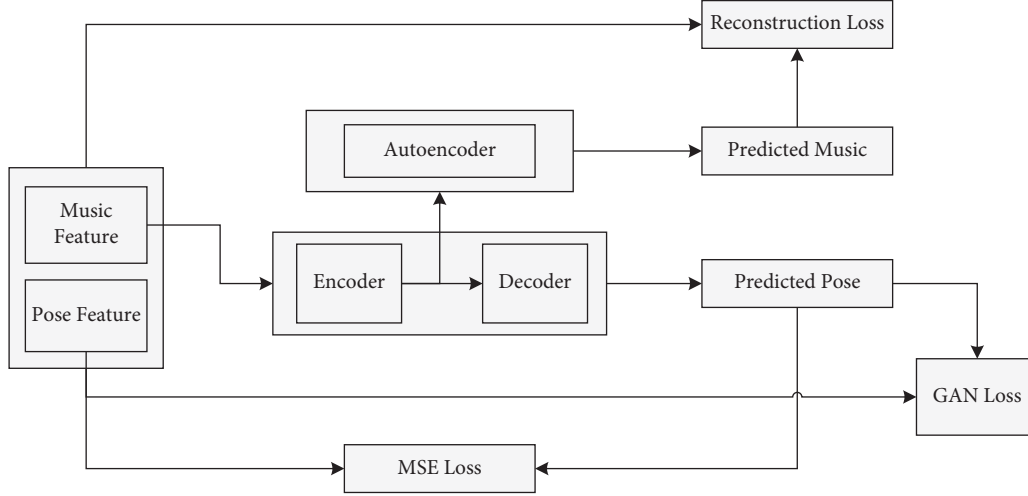


FIGURE 4: Network structure diagram of the dance generation system.

### 2.5. Attention Mechanism.

$$c_j = \sum_{i=1}^T \alpha_{ij} h_i. \quad (9)$$

The core idea of the attention model is to introduce attention weight  $\alpha$  into the input sequence and to learn by adding an extra feedforward neural network into the Sequence-to-Sequence architecture. The two states of  $h_i, S_j$  are used as the input of neural network, and then the value of  $\alpha^{ij}$  is learned.

Attention mechanism has three advantages. First, the interpretability of neural networks is improved; Second, it is linked with input length and input sequence, which affects network performance. Third, in order to improve the performance of deep learning, the model is allowed to dynamically focus on the input part.

## 3. System Design and Implementation

**3.1. General System Design.** In this chapter, the overall design of the dance automatic generation system is discussed. The timing characteristics of the generated dance data and the music data are focused. Music and dance coexist, and they cannot be well integrated, which proves that the design of this system fails as shown in Figure 4.

The system first extracts features related to audio and action. Then, the system inputs the audio features into the dance generator and then passes the audio features through the autoencoder module. In this way, we can get the predicted dance form and make MSE loss, and we can also get

TABLE 3: Prosodic characteristics.

| Audio feature  | Feature dimension     |
|----------------|-----------------------|
| MFCC           | $M_1 \dots M_{24}$    |
| Tempogram [25] | $M_{24} \dots M_{32}$ |

the audio reconstructed loss. Finally, the system puts the predicted dance form and the real MSE loss into the discriminator to discriminate the training model.

**3.2. Music Feature Extraction.** Music feature extraction is divided into rhythm and prosody. For prosody, we mainly choose the 24-dimensional Meyer frequency cepstrum feature and the 8-dimensional Tempogram feature which are closest to the field of human sound processing. Let them represent vectors so as to represent the melody of audio and make the sound have more satisfactory feature representation as shown in Table 3.

Quoting rhythm characteristics, both music and dance have fixed beats and rhythms. If this feature is not introduced, music and dance will be arranged in a messy and inconsistent way. In addition, because sound features will slowly disappear in the deep network, it is necessary to introduce rhythm features as shown in Table 4.

**3.3. Open Pose Attitude Detection.** Considering the funds and specific usage of this research, we choose from several of the most popular human posture estimation algorithms. Open Pose open-source library is selected. and human

TABLE 4: Rhythm characteristics table.

| Rhythm characteristics                        | Feature dimension |
|---|-------------------|
| Position of the whole music audio frame       | $B_1$             |
| Position of audio frame within beat           | $B_2$             |
| Relative values of audio frames within a beat | $B_3$             |

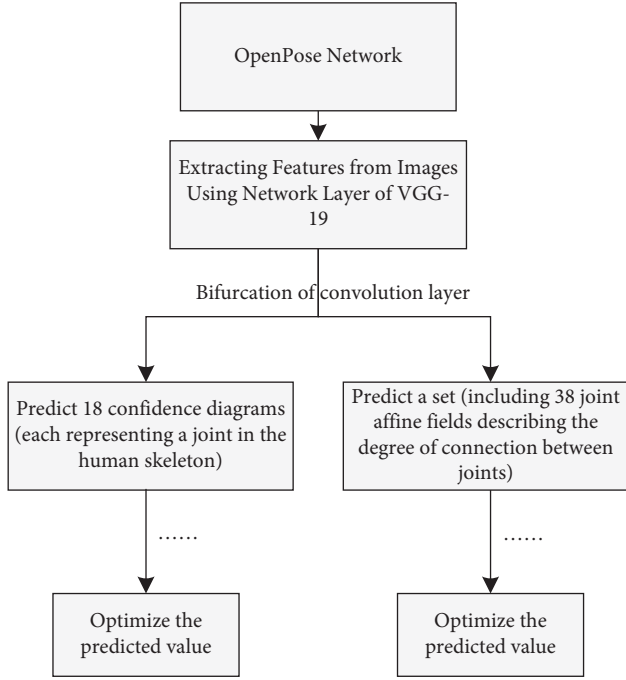


FIGURE 5: Open pose actual detection flow chart.

posture is described with connected coordinates. We can effectively detect the 2D movements of single or multiple people in dance videos.

$$\begin{aligned}
 L^t &= \phi(F, L^{t-1}), \\
 S^{T_p} &= \rho^t(F, L^{T_p}), \\
 S^t &= \rho^t(F, L^{T_p}, S^{t-1}).
 \end{aligned} \tag{10}$$

Pose detection is shown in Figures 5 and 6.

18 key points are selected. In this way, the feature representation can be well divided to represent the dance posture as shown in Table 5.

Training data is shown in Table 6.

Finally, the optimization goal of the model is shown in formula as follows:

$$\begin{aligned}
 \min_G \max_D L_{GAN}(G, D) + \lambda_1 L_{MSE}(G) \\
 + \lambda_2 L_{Recon}(Encoder, Decoder).
 \end{aligned} \tag{11}$$

**3.4. Automatic Generation Design of Dance.** In this module, we need the generator to transform the feature vector to a certain extent, and then we get the dance posture we need. Simply generating each posture of dance is not complete. We specially introduced the improved Pix2Pix algorithm to

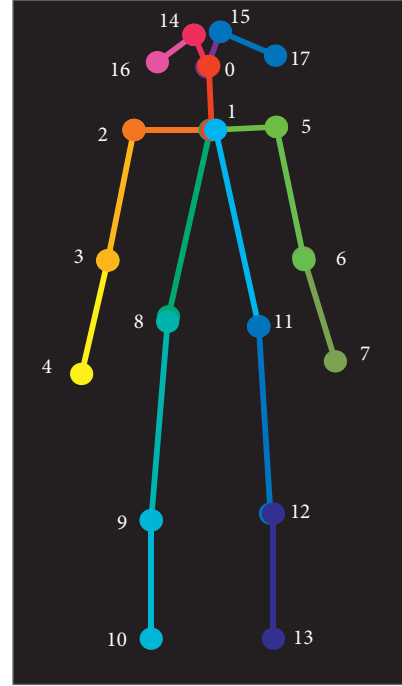


FIGURE 6: Key point model diagram of human skeleton.

TABLE 5: Characteristic representation of key points of human posture.

| Serial number of key points | Key point feature | Feature representation |
|-----------------------------|-------------------|------------------------|
| 0                           | Nose              | $P_1, P_2$             |
| 1                           | Neck              | $P_3, P_4$             |
| 2                           | Right shoulder    | $P_5, P_6$             |
| 3                           | Right elbow       | $P_7, P_8$             |
| 4                           | Right hand        | $P_9, P_{10}$          |
| 5                           | Left shoulder     | $P_{11}, P_{12}$       |
| 6                           | Left elbow        | $P_{13}, P_{14}$       |
| 7                           | Left hand         | $P_{15}, P_{16}$       |
| 8                           | Right leg         | $P_{17}, P_{18}$       |
| 9                           | Right knee        | $P_{19}, P_{20}$       |
| 10                          | Right foot        | $P_{21}, P_{22}$       |
| 11                          | Left leg          | $P_{23}, P_{24}$       |
| 12                          | Left knee         | $P_{25}, P_{26}$       |
| 13                          | Left foot         | $P_{27}, P_{28}$       |
| 14                          | Right eye         | $P_{29}, P_{30}$       |
| 15                          | Left eye          | $P_{31}, P_{32}$       |
| 16                          | Right ear         | $P_{33}, P_{34}$       |
| 17                          | Left ear          | $P_{35}, P_{36}$       |

transform the dance into a real person's posture, so as to make it smoother and more realistic.

$$\begin{aligned}
 L_{GAN}(G, D) &= E_{(x,y)}[\log D(x, y)] + E_x[\log(1 - D(x, G(x)))], \\
 L_{smooth}(G, D) &= E_{(x,y)}[\log D(x_{t-1}, x_t, y_{t-1}, y_t)] \\
 &+ E_x[\log((1 - D(x_{t-1}, x_t, G(x_{t-1}), G(x_t))))].
 \end{aligned} \tag{12}$$

Feature dimension vectors are mapped by human posture as shown in Figure 7.



TABLE 6: Representation of training data.

| Characteristic     | Feature representation                                |
|--------------------|---|
| Audio feature      | $M_i = \langle m_i^1, m_i^2, \dots, m_i^{32} \rangle$ |
| Metrical feature   | $B_i = \langle b_i^1, b_i^2, b_i^3 \rangle$           |
| Attitude feature   | $P_i = \langle p_i^1, p_i^2, \dots, p_i^{36} \rangle$ |
| Audio data         | $M = \{M_1, M_2 \dots M_n\}$                          |
| Dance posture data | $P = \{P_1, P_2 \dots P_n\}$                          |

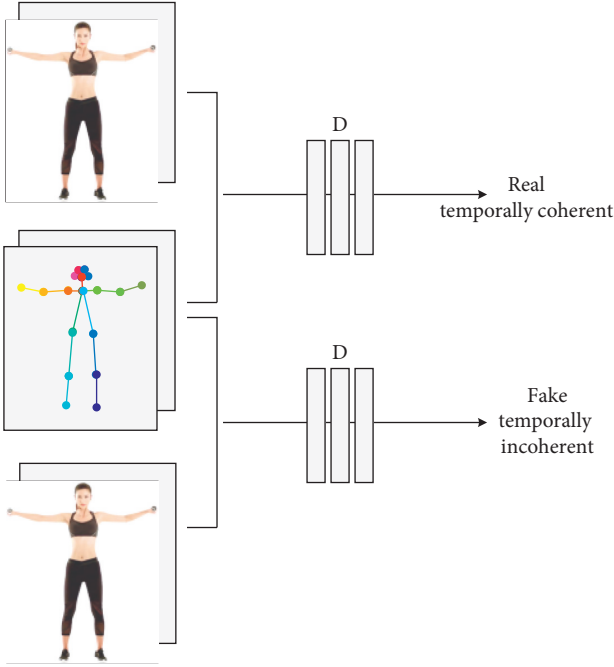


FIGURE 7: Improved training process of Pix2Pix network.

## 4. Experimental Analysis

**4.1. Experimental Environment Setting.** The specific experimental environment settings are shown in Table 7.

**4.2. Performance Comparison of LSTM.** In this part, we test the performance of LSTM when the features are different and select the best expression features. The test data of left and right legs are intercepted, and the method is unified as LSTM, and only the characteristics are different as shown in Figure 8.

We can find that LSTM based on Join + Line features has the best performance, which is 2.5% higher than the method with single features. Therefore, in the feature part of dance generation research, the best choice is Join + Line feature fusion method.

In order to better highlight the advantages of this method, we compare the performance of the LSTM method adopted in this paper with other common methods. The test data of left and right legs are intercepted. The accuracy of the two data sets is compared. We can find that the LSTM method in this paper has the highest accuracy, with an average accuracy of 94.33%, as shown in Figure 9.

TABLE 7: Experimental environment settings.

| All the experiments were completed on a NVIDIA 1080tigpu                   |  |
|--|--|
| Generator training stage   | Set the training model to train 10000 rounds. The model input dimension is 35, the encoder convolution layers are 3, the maximum length of each convolution kernel is 5, the decoder RNN dimension is 1024, the prenet dimension is 256, the learning rate is set to 0.001, the gradient clipping threshold is set to 1, the weight attenuation is set to 1e-6, the batchsize is set to 40, the seqLen is set to 125, and the optimizer uses Adam. |
| Discriminator training stage   | The discriminator is trained once every three training rounds, the learning rate of the discriminator is 0.001, the weight attenuation is 1e-6, and the optimizer uses Adam.   |
| The training set used 80% dance data, and the test set used 20% dance data |  |

**4.3. Loss Function Analysis.** The experiment in this section is mainly aimed at the stage of music feature extraction. We will analyze different data set processing methods and compare their final influence on the loss function. Filtering erroneous data are very important for the final result. If we eliminate the wrong key coordinate points of human body extracted in the extraction stage, our final result will be significantly enhanced as shown in Figure 10.

After filtering the wrong data, we can find that the generator based on the generator model has the lowest loss, with an average of 11.93; the average loss of the Generator + Discriminator model is 14.61. With autoencoder, the average loss is as high as 17.36 which has the greatest influence and the worst fitting ability as shown in Figure 11.

**4.4. Analysis of Dance Sequence Results.** The dance effect is measured by similarity. From the figure, we can find that LSTM-PCA has the highest similarity, up to 0.205; Generator + Discriminator + Autoencoder model has the best effect, and the similarity is as low as 0.063, which is superior to other methods. The details are shown in Figure 12.

**4.5. System Usage Analysis.** The basic performance of the system is tested professionally.

**4.5.1. Evaluation of Dance Authenticity.** Because our system is arranged and designed by computer machines, we need to invite the audience to score and evaluate the authenticity of this dance, and we can also use scores to test the integrity, smoothness, and rationality of the dance.

We first invited 20 ordinary spectators who volunteered to participate. Five experts related to dance music were also invited. They score the authenticity of the dances generated by our system. The dances watched are divided into 5 types, with a total of 15 dance fragments. The highest score for realistic evaluation is 10 points, and the lowest score is 0

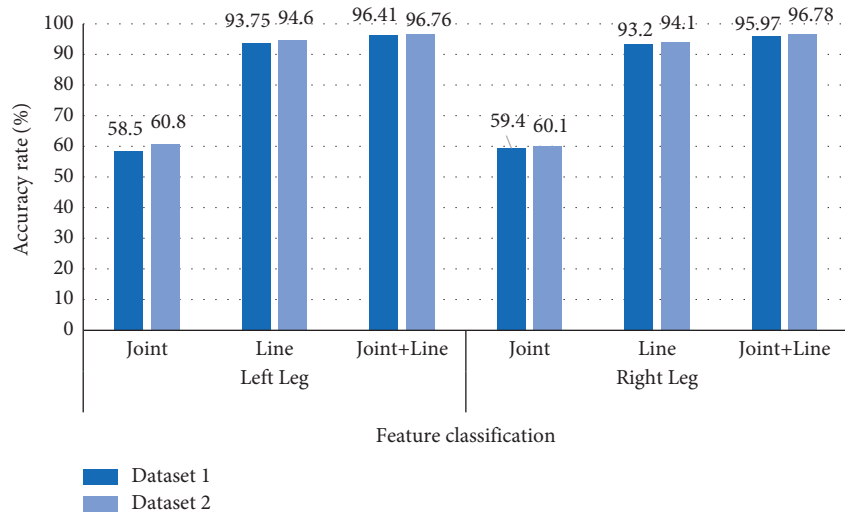


FIGURE 8: Performance comparison of different features.

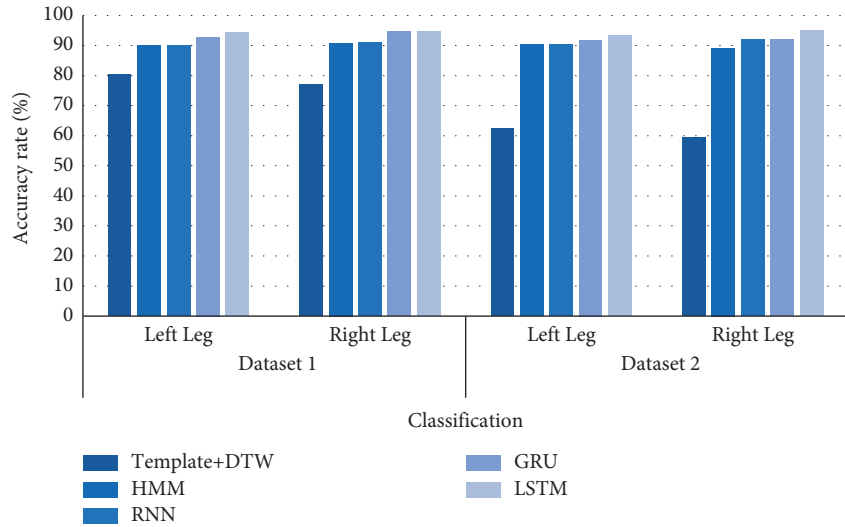


FIGURE 9: Experimental comparison with other methods.

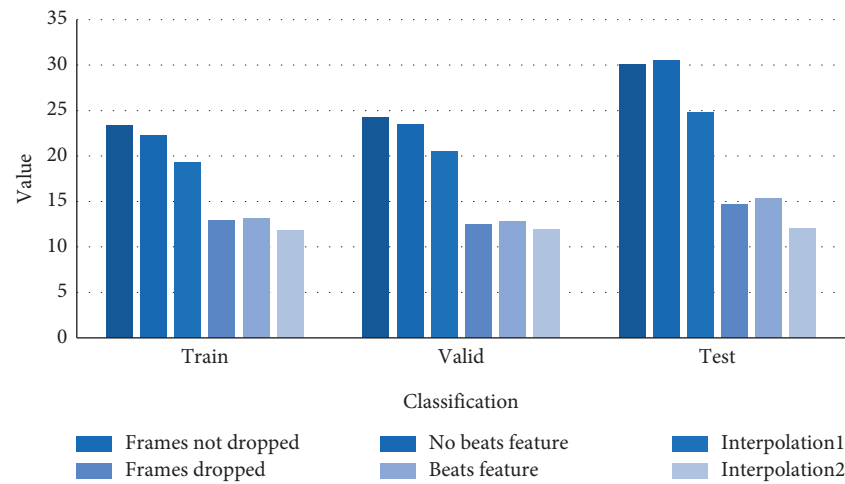


FIGURE 10: Dance dataset (1).

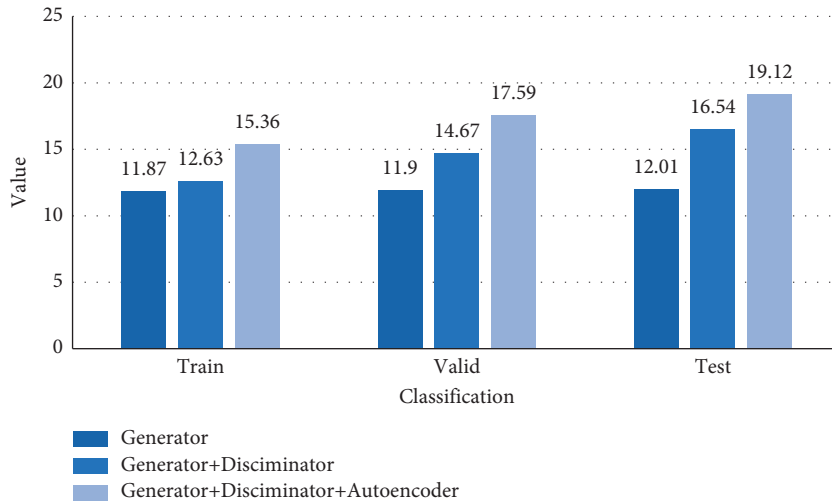


FIGURE 11: Dance dataset (2).

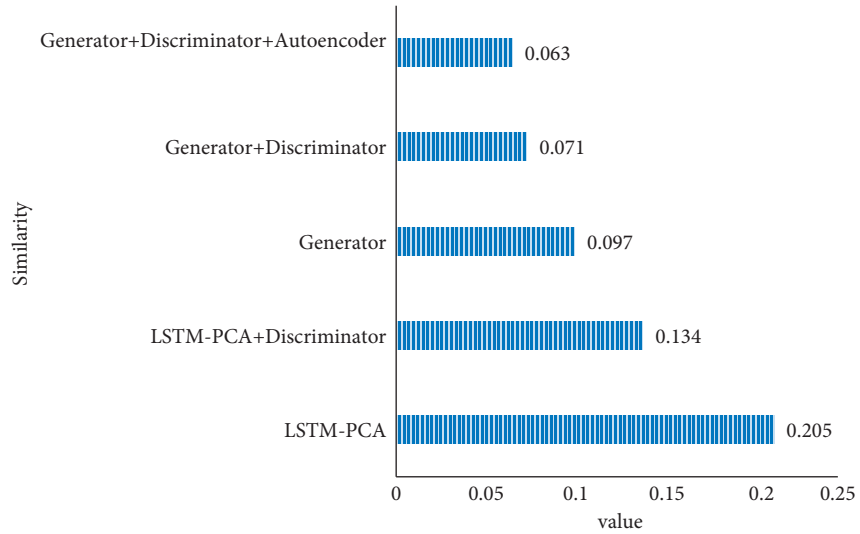


FIGURE 12: Similarity between generated dance and real dance.

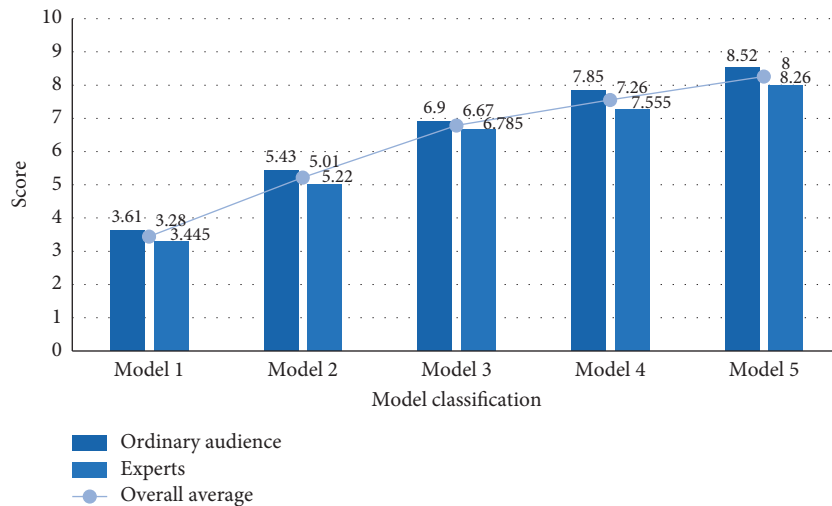


FIGURE 13: Scoring chart of dance truth.

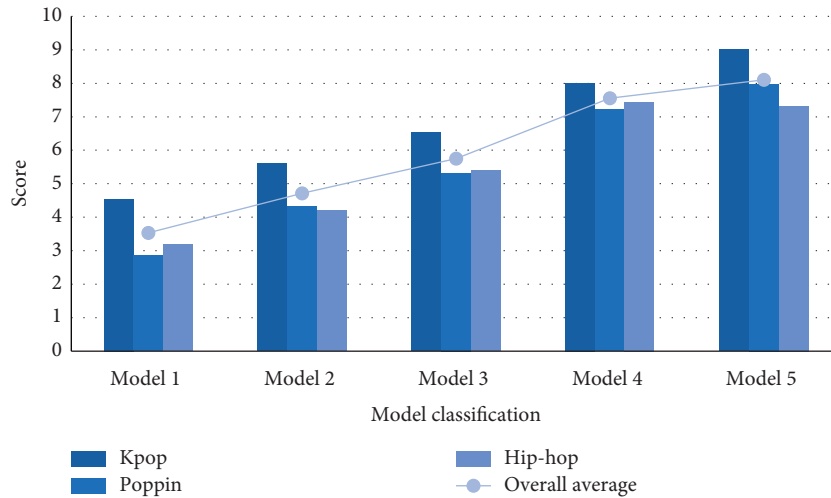


FIGURE 14: Music consistency scoring evaluation.

TABLE 8: Image quality evaluation score.

| Method                                  | BRISQUE |
|---|---------|
| Generator                               | 39.23   |
| Generator + Discriminator               | 41.40   |
| Generator + Discriminator + Autoencoder | 40.37   |

points. We can find that Model 5 has the best effect with an average truth of 8 points as shown in Figure 13.

**4.5.2. Music Consistency Evaluation.** What this system emphasizes most is the consistency of music and dance. We selected three music data sets Kpop, Poppin, and Hip-hop for testing and asked the audience to score their models, respectively. We can find that the scores of Kpop data set in five models are the highest, which are 4.54 points, 5.61 points, 6.54 points, 8.01 points, and 9.01 points, respectively. This shows that Kpop music type is most suitable for this system, and the consistency of dance generation music is high as shown in Figure 14.

**4.6. Image Quality Evaluation.** The quality of the generated image is evaluated. Generator + Investigator + Autoencoder is rated as high as 40.37 with the best image quality, more details, and obvious dance posture as shown in Table 8.

## 5. Conclusion

The results show that

- (1) From the experimental results, we can see that the LSTM method in this paper is more efficient and has the highest accuracy than other existing methods, with an average accuracy of 94.33%. The Join + Line feature performs best.
- (2) Erroneous data have the greatest influence. After filtering error data, the generator based on the Generator model has the lowest loss, averaging 11.93, and the best fitting ability.

- (3) By calculating the similarity between the generated dance and the real dance, the Generator + Discriminator + Autoencoder model has the best effect, and the similarity is as low as 0.063, which is superior to other methods.

- (4) Model 5 is the best in evaluating the degree of dance truth, and the average degree of dance truth is as high as 8 points. Kpop music type is most suitable for dance generation in this system, and its music consistency is high.

The system designed in this paper basically meets the requirements. However, the content of this system is not rich enough, simple, and simplified, and the structure constructed by deep learning is too complex. In fact, people will have different movement postures, and the automatic dance generation system is still missing and insufficient. In the future, it is necessary to add more dance data sets for data training and find better models.

## Data Availability

The experimental data used to support the findings of this study are available from the corresponding author upon request.

## Conflicts of Interest

The authors declare that they have no conflicts of interest regarding this work.

## References

- [1] B. Li, Y. Zhao, and L. Sheng, "DanceNet3D: music based dance generation with parametric motion transformer," vol. 12, no. 3, pp. 1873–1876, 2021.
- [2] P. Lv, "Automatic dance generation system based on emotion annotation," *Electronic Technology*, vol. 37, no. 5, pp. 18–32, 2008.
- [3] J. H. Seo, J. Y. Yang, J. W. Kim, and D. S. Kwon, "Autonomous humanoid robot dance generation system based on real-time

- music input,” in *Proceedings of the RO-MAN, 2013 IEEE*, no. 2, August 2013.
- [4] W. Asahina, N. Okada, N. Iwamoto, T. Masuda, T. Fukusato, and S. Morishima, “Automatic facial animation generation system of dancing characters considering emotion in dance and music,” in *Proceedings of the Siggraph Asia. ACM*, pp. 928–1021, Kobe Japan, November 2015.
  - [5] S. Baek and M. Kim, “Dance motion generation with pose constraints,” in *Proceedings of the 2013 International Conference on Sport Science and Computer Science CCCS 2013*, San Francisco, USA, October 2013.
  - [6] W. Zhuang, C. Wang, S. Xia, J. Chai, and Y. Wang, “Music2Dance: music-driven dance generation using WaveNet,” pp. 1202–1089, 2020.
  - [7] X. Zhang, Z. Miao, X. Yang, and Q. Zhang, “An efficient method for automatic generation of labanotation based on Bi-directional LSTM,” in *Proceedings of the 2019 3rd International Conference on Machine Vision and Information Technology (CMVIT 2019)*, pp. 268–273, Guangdong, China, February 2019.
  - [8] X. Ren, H. Li, Z. Huang, and Q. Chen, “Music-oriented dance video synthesis with pose perceptual loss,” 2019, <https://arxiv.org/abs/1912.06606>.
  - [9] E. Shlizerman, L. Dery, H. Schoen, and I. Kemelmacher-Shlizerman, “Audio to body dynamics,” in *Proceedings of the IEEE Conference on Computer Vision and Pattern Recognition*, pp. 7574–7583, Salt Lake City, UT, USA, June 2018.
  - [10] G. Chen and S. Li, “Network on chip for enterprise information management and integration in intelligent physical systems,” *Enterprise Information Systems*, vol. 15, no. 7, pp. 935–950, 2021.
  - [11] Z. Cao, T. Simon, S. E. Wei, and Y. Sheikh, “Realtime multi-person 2d pose estimation using part affinity fields,” in *Proceedings of the IEEE Conference on Computer Vision and Pattern Recognition*, pp. 7291–7299, Honolulu, HI, USA, July 2017.
  - [12] T. Moeslund, A. Hilton, and V. Kruger, “A survey of advances in vision-based human motion capture and analysis,” *Computer Vision and Image Understanding*, vol. 104, no. 2-3, pp. 90–126, 2006.
  - [13] H. Guo, Z. Miao, F. Zhu, G. Zhang, and S. Li, “Automatic Labanotation generation based on human motion capture data,” in *Proceedings of the Chinese Conference on Pattern Recognition*, pp. 426–435, Springer, Changsha, China, November 2014.
  - [14] X. Li, Y. Mao, and L. Tao, “A review of target detection based on convolution neural network,” *Computer application research*, vol. 34, no. 10, pp. 7–12 +17, 2017.
  - [15] G. Huang, Y. Tian, J. Kang, J. Liu, and S. H. Xia, “LSTM recurrent neural network speech recognition system based on i-vector features under low resource conditions,” *Computer Application Research*, vol. 34, no. 2, pp. 392–396, 2017.
  - [16] X. Ning, W. Li, B. Tang, and H. He, “BULDP: biomimetic uncorrelated locality discriminant projection for feature extraction in face recognition,” *IEEE Transactions on Image Processing*, vol. 27, no. 5, pp. 2575–2586.
  - [17] L. Chen, R. K. Maddox, Z. Duan, and C. Xu, “Hierarchical cross-modal talking face generation with dynamic pixel-wise loss,” in *Proceedings of the IEEE Conference on Computer Vision and Pattern Recognition*, pp. 7832–7841, Long Beach, CA, USA, June 2019.
  - [18] A. Duarte, F. Roldan, M. Tubau et al., “Wav2Pix: speech-conditioned face generation using generative adversarial networks,” in *Proceedings of the ICASSP 2019-2019 IEEE International Conference on Acoustics*, May 2019.
  - [19] a Graves and J. Schmidhuber, “Framewise phoneme classification with bidirectional LSTM and other neural network architectures,” *Neural Networks: The Official Journal of the International Neural Network Society*, vol. 18, no. 5-6, pp. 602–610, 2005.
  - [20] Y. Wang, Z. Q. Liu, and L. Z. Zhou, “Learning hierarchical non-parametric hidden Markov model of human motion,” in *Proceedings of the 2005 International Conference on Machine Learning and Cybernetics*, August 2005.
  - [21] G. Sun and C.-C. Chen, “Influence maximization algorithm based on reverse reachable set,” *Mathematical Problems in Engineering*, vol. 202112 pages, 2021.
  - [22] C. Vondrick, H. Pirsiavash, and A. Torralba, “Generating videos with scene dynamics,” in *Proceedings of the Advances in neural information processing systems*, pp. 613–621, Barcelona, Spain, 2016.
  - [23] I. Goodfellow, J. Pouget-Abadie, M. Mirza et al., “Generative adversarial nets,” in *Proceedings of the Advances in neural information processing systems*, pp. 2672–2680, Montreal, Canada, December 2014.
  - [24] F. Ofli, E. Erzin, Y. Yemez, and A. M. Tekalp, “Learn2dance: learning statistical music-to-dance mappings for choreography synthesis,” *IEEE Transactions on Multimedia*, vol. 14, no. 3, pp. 747–759, 2011.
  - [25] C. Chan, S. Ginosar, T. Zhou, and A. A. Efros, “Everybody dance now,” in *Proceedings of the IEEE International Conference on Computer Vision*, pp. 5933–5942, Seoul, Korea (South), November 2019.

## Retraction

# Retracted: Deep Learning-Based Assessment of Sports-Assisted Teaching and Learning

### Mathematical Problems in Engineering

Received 18 July 2023; Accepted 18 July 2023; Published 19 July 2023

Copyright © 2023 Mathematical Problems in Engineering. This is an open access article distributed under the Creative Commons Attribution License, which permits unrestricted use, distribution, and reproduction in any medium, provided the original work is properly cited.

This article has been retracted by Hindawi following an investigation undertaken by the publisher [1]. This investigation has uncovered evidence of one or more of the following indicators of systematic manipulation of the publication process:

- (1) Discrepancies in scope
- (2) Discrepancies in the description of the research reported
- (3) Discrepancies between the availability of data and the research described
- (4) Inappropriate citations
- (5) Incoherent, meaningless and/or irrelevant content included in the article
- (6) Peer-review manipulation

The presence of these indicators undermines our confidence in the integrity of the article's content and we cannot, therefore, vouch for its reliability. Please note that this notice is intended solely to alert readers that the content of this article is unreliable. We have not investigated whether authors were aware of or involved in the systematic manipulation of the publication process.

Wiley and Hindawi regrets that the usual quality checks did not identify these issues before publication and have since put additional measures in place to safeguard research integrity.

We wish to credit our own Research Integrity and Research Publishing teams and anonymous and named external researchers and research integrity experts for contributing to this investigation.

The corresponding author, as the representative of all authors, has been given the opportunity to register their agreement or disagreement to this retraction. We have kept a record of any response received.

### References

- [1] W. Su and J. Feng, "Deep Learning-Based Assessment of Sports-Assisted Teaching and Learning," *Mathematical Problems in Engineering*, vol. 2022, Article ID 7833292, 8 pages, 2022.

## Research Article

# Deep Learning-Based Assessment of Sports-Assisted Teaching and Learning

Wei Su<sup>1</sup> and Jian Feng <sup>2</sup>

<sup>1</sup>Basic Education Department, ShangHai Communications Polytechnic, Shang Hai 200431, China

<sup>2</sup>Department of Physical Education of Tongji University, Shang Hai 200092, China

Correspondence should be addressed to Jian Feng; 91786@tongji.edu.cn

Received 22 February 2022; Accepted 15 March 2022; Published 27 April 2022

Academic Editor: Hangjun Che

Copyright © 2022 Wei Su and Jian Feng. This is an open access article distributed under the Creative Commons Attribution License, which permits unrestricted use, distribution, and reproduction in any medium, provided the original work is properly cited.

The current Internet development situation regarding the analysis of sports teaching information is very necessary and can be a way to improve the effectiveness of sports teaching in the information environment. Aiming at the defects of strong subjectivity and low discrimination accuracy of the current sports video classification results, this paper proposes an effective sports video classification method based on deep learning, which can effectively evaluate the sports assisted teaching. Specifically, the key frame features are obtained by using the similarity coefficient key frame extraction algorithm, and the sports video image classification is established through the deep learning coding model. Thus, the ability of the school to rely on the scheme proposed in this paper to improve the teaching facilities, physical education curriculum teaching materials, assessment teaching materials, management, and so on. The results show that for different types of sports videos, the overall effect of the classification of the method in the paper is significantly better than that of other current sports-assisted teaching evaluation methods, which has significantly improved the effect of sports-assisted teaching evaluation.

## 1. Introduction

In recent years, with the development of cloud computing and big data technology, new forms of education and teaching such as digital learning, flipped classroom, catechism, and microlesson have emerged, signifying that the field of education is undergoing a revolutionary change [1]. Research on teaching informatization will help us gain a deeper understanding and a comprehensive grasp of the factors that affect teaching effectiveness, grasp the laws of informatized teaching, better apply modern information technology to teaching practice, and promote the development of education informatization. In the field of education, information technology has greatly changed the ecological structure of teaching and learning, and it is rebuilding the education, teaching, and learning process from all aspects that affect the whole education field. It is not only changing the entire educational process but also affecting the

relationship between teaching and learning in the teaching process and the value system that determines this relationship [2].

The physically active nature of PE teaching and the openness of the teaching space make it more difficult for PE teachers than teachers of other subjects to use IT in PE teaching to improve the effectiveness of their teaching [3]. In PE teaching, the level of information technology is very low, both in terms of the way PE teachers obtain various teaching information and in terms of information exchange between teachers and students and among students. In particular, in order for students to establish correct technical concepts, teachers still need to complete a large number of demonstrations of technical movements [4]. The teacher's age, gender, and physical characteristics, as well as the teacher's own level of comprehension and mastery of technical movements, psychological factors, and other conditions, may affect the effectiveness of the teacher's demonstrations.

On the other hand, as PE teaching is mainly a class-based collective teaching, there are bound to be some students who have difficulty in clearly observing the teacher's demonstration, no matter how much they adjust their formation during the demonstration of sports techniques. Therefore, the use of modern highly developed information technology to optimise the way of information exchange and transmission in the process of physical education and to improve the effectiveness of physical education is a subject that needs to be urgently studied in the informatization of physical education [5].

One of the key features of intelligent computer-assisted teaching is its suitability for individualised teaching, with Lang being able to select appropriate content and adopt appropriate teaching strategies based on the actual needs of the learners. The system needs to receive timely and accurate feedback from learners during the teaching process and to identify specific teaching strategies based on the feedback model, i.e., the preestablished learning model within the system [6]. Feedback is collected by providing a large number of content-related test questions for learners to answer during the teaching process and then analysing the results to extract useful information. The assessment system consists of three main components: firstly, the creation and maintenance of an open-ended test bank; secondly, the automatic assembly of papers for interactive testing based on the attributes of the test questions selected by the student; and finally, the comprehensive assessment of the learner's mastery of the content based on the test results and the recommendation of the student's next steps in learning based on the assessment results [2]. This is the kind of interactive testing and assessment that assessment systems provide. There are many issues that need to be studied and many mathematical algorithms that need to be analysed in order to design and develop an assessment system. In this paper, we analyse the following aspects of the algorithms.

Sports video is an important video resource with the characteristics of a wide range of users. Due to the rapid development of information technology, sports-assisted teaching evaluation research has gradually become a hot issue of concern to relevant personnel [7]. Without an efficient sports video retrieval system, the large amount of sports video information in the network will be cluttered and disorganised. Therefore, how to organise sports video resources with high efficiency and accuracy and to achieve the classification and organisation of sports videos is beneficial in assisting users to efficiently access the sports video content they need [8].

In order to overcome the shortcomings of current sports-assisted teaching evaluation methods, a sports-assisted teaching evaluation method based on deep learning is proposed and its performance is analysed through simulation experiments, in anticipation of providing reference values for sports videos and even classification problems in the image field [9].

## 2. Strategies for Improving the Effectiveness of Physical Education

### 2.1. Optimising Physical Education Curriculum Resources

*2.1.1. Teaching and Learning Materials for Physical Education Courses.* Physical education teaching materials include the teaching content used by teachers and students to complete the teaching tasks and achieve the teaching objectives, including the main teaching and learning objectives, electronic textbooks and teaching reference materials, and multimedia teaching materials (sound, pictures, videos, and teaching software platforms). With the increasingly widespread use of information technology in education, the full use of modern Internet technology and computer technology can effectively integrate all physical education curriculum resources, so as to build a physical education curriculum of teaching materials with the idea of "building blocks" as the core and use modern network technology to achieve interaction and sharing of physical education curriculum building blocks resource base. In the process of PE teaching, PE teachers can conveniently and flexibly call up and produce PE teaching materials suitable for different PE teaching contexts according to the actual needs of PE teaching, the actual situation of different teaching targets, and the corresponding teaching strategies [10].

*2.1.2. Physical Education Course Assessment Materials.* Assessment materials for PE courses are materials that assess and evaluate students' knowledge, skills, and abilities and include both objective examination questions corresponding to the knowledge of the PE subject and assessment forms for students' behavioural performance in terms of skills and abilities. The assessments are divided into pretests and posttests, which can be used by teachers as part of the teaching or learning materials as required, so that students can complete different assessments of the effectiveness of PE teaching in specific teaching sessions, as required by the teacher's teaching design.

*2.1.3. Information on the Management of Physical Education Programmes.* The PE curriculum management information is an essential part of the PE curriculum teaching package, providing PE teachers with an overview of the teaching materials and demonstrating how they can be effectively integrated with the different stages of the student's learning process. It also includes some PE teaching assessment and evaluation materials and important information about the implementation of the curriculum [11]. In addition to providing student guidance templates, the web-based teaching and learning management platform also provides teachers with technical support for course management, including the import of student lists, tracking of student progress, monitoring of learning items, online examinations, grade



management, and mechanisms for information exchange between teachers and students or among students.

*2.2. Optimising the Time Structure of Physical Education.* The process of physical education is a dynamic and changing process, and effective physical education in the information technology environment is specifically manifested in the deep integration of information technology and physical education in the process of physical education design [12].

Teaching in the information environment is a modern form of teaching performance as opposed to traditional teaching. It attaches importance to the role of modern information technologies, such as modern Internet technology, computer technology, multimedia technology, and telecommunication technology, in teaching, makes full use of modern educational technology means and modern teaching methods, mobilises a variety of teaching media and information resources, and builds a good teaching and learning environment, under the organisation and guidance of teachers. Under the guidance of teachers, the initiative, enthusiasm, and creativity of students are developed completely, so that students can really become active constructors of knowledge and information, thus achieving good teaching results [13]. The main concepts that PE teachers need to change in the information environment are the change of the teaching subject, the change of the teacher's role, and the correct understanding of information technology. The key to the integration of information technology and physical education is not how to use information technology, but to choose teaching media and teaching methods that are more suitable for developing students' abilities according to the needs of physical education at different stages [14].

### 3. Difficulty Algorithm for Sports Test Questions

At present, there are generally three methods for selecting topics in the test question bank. One is to allow users to input the required test question types and chapters and directly use random functions to randomly select test questions to form test papers. Second, use random function to select questions within the range proposed by users, so that the selected questions can indeed meet the requirements of users, but it is too cumbersome and workload for users. Third, the user will display or print all the questions in the question bank, and then manually (expert) select the questions to form the test paper, or after the user is familiar with the contents and parameters of the question bank, understand the distribution of the questions. This way of selecting questions can make the questions of the test paper more accurate. This method of question selection can be more accurate while selecting papers that meet the requirements, but this method is also too cumbersome and demanding for the user, making it difficult to reflect the advantages of a test bank. To address these problems, a mathematical model of question selection was established

using the binomial distribution function  $B(n, p)$  of a discrete random variable to determine the distribution of question type and difficulty and then a random function was used to select questions, with good results.

Since the concept of a randomly drawn test question does not depend on the results of other drawn questions, there are only two possibilities for each test question, i.e., to be drawn or not to be drawn, and it is random in nature. The randomly drawn question event can therefore be considered to conform to the binomial distribution function of a discrete random variable  $B(n, p)$ , i.e.,

$$P_n(k) = \binom{n}{k} p^k q^{n-k} = \binom{n}{k} p^k (1-p)^{n-k}, \quad (1)$$

where  $k = 1, 2, \dots, n$ ,  $n$  is a positive integer,  $1 > p > 0$ ,  $q > 0$ , and  $p + q = 1$ ; the mean of the binomial distribution is

$$Q = np. \quad (2)$$

In the model,  $k$  denotes the difficulty level,  $P_n(k)$  denotes the probability that the difficulty level is  $k$  (i.e., the proportion of questions with difficulty level  $k$  in the total number of questions), and  $Q$  denotes the average difficulty of the test paper. Because for  $n, P$  fixed binomial distribution  $B(n, p)$ , when  $k$  increases, the probability  $P\{x=k\}$  first monotonically increases to the maximum and then monotonically decreases and the probability of both ends is very small that it can be ignored, so in the actual calculation, take  $n = 6$  a total of 7 levels of difficulty, from formula (2) to find  $p, P, n, k$  into formula (1), you can find out each difficulty. The proportion of  $P_n(k)$  in the total number of questions for each difficulty level can be found by substituting  $p, n$ , and  $k$  into (1) and then multiplying  $P_n(k)$  by the total number of questions to obtain the number of questions that should be taken for each difficulty level.

The binomial function  $B(n, p)$  of discrete random variables is used to establish the mathematical model of random question selection, which can well solve the problem of difficulty distribution in the process of test bank preparation. On this basis, the random function is then used to randomly select questions within this difficulty distribution, with good randomness, and if the question type, chapter range, and other conditions are added, satisfactory questions can be automatically selected.

## 4. Evaluating Physical Education Assistance

### 4.1. Similarity Coefficient Key Frame Extraction Algorithm Based on Lens Boundaries

*4.1.1. Sports Video Feature Extraction.* Features represent a target and certain attributes that can be quantified. In the case of sports videos, these include mainly generic features and domain-specific features. Considering the efficiency of key frame extraction for sports videos, the sports video image features are set into colour histograms and colour division descriptors [15]. In general, the description of sports video image colour belongs to the colour space problem and the key frame extraction algorithm based on the similarity

coefficients of the lens boundaries used in this paper; after the image is in the HSV colour space derived from the colour histogram, the histogram index is first initialised and the similarity of the two frames  $g_a$  and  $g_b$  of the sports video histogram  $\text{Hist}_a(h, s, v)$  can be seen as follows:

$$\text{sim}(g_a, g_b) = \sum_{h=0}^{15} \sum_{s=0}^3 \sum_{v=0}^3 \min\{\text{Hist}_a(h, s, v), \text{Hist}_b(h, s, v)\}, \quad (3)$$

where 0 describes a very large difference between the colour histograms of the two images and 1 describes the same

$$\text{Dist} = \sqrt{\sum_{h=1}^{64} \omega Y h [AY_{jh} - AY_{jh}]^2} + \sqrt{\sum_{h=1}^{64} \omega C b h [ACb_{jh} - ACb_{jh}]^2} + \sqrt{\sum_{h=1}^{64} \omega C r h [ACr_{jh} - ACr_{jh}]^2}, \quad (4)$$

where  $AY_{jh}$  describes the  $h$ th term of the discrete cosine coefficient of the  $Y$  component of frame  $g_a$  and  $\omega$  describes the weight.

**4.1.2. Sports Video Boundary Detection.** The shot boundary coefficients are set according to the properties of the sports video domain transformation [6]. Assuming that the width of the domain window is  $2M + 1$ , the neighbourhood window frame difference for frame  $a$  is as follows:

$$A_{sw}(a) = \sum_{b=1}^M \frac{M-b+1}{H} A(a-b, a+b), \quad (5)$$

where  $H = H(M+1)/2$ .

The variation in shots is higher than the variation between shots; if the distance between two random frames in a shot is  $As$  and the distance between shots is  $Ab$ , then  $As < Ab$ . If at this point  $M=3$  and there is a shot mutation between frame  $H$  and frame  $H+1$ , then the sequence of constants  $U_{sw}(b)$  that can be obtained is (1, 3, 6, 6, 3, 1). The similarity coefficient of the shot boundary at frame  $a$  can be set as follows:

$$B_{sbs}(a) = \frac{\sum_{b=-M+1}^M [A_{sw}(a+b)U_{sw}(M+L)]}{\sqrt{\sum_{b=-M+1}^M [A_{sw}(a+b)]^2} \sqrt{\sum_{b=-M+1}^M [U_{sw}(M+b)]^2}} \quad (6)$$

Here, if the similarity coefficient of the shot boundaries is close to 1 when transforming between adjacent frames, there are very small values between 0 and 1 in the remaining conditions.

**4.1.3. Key Frame Sequence Clustering.** In order to reduce the iterative nature of the final key frame sequence, the key frame sequences were clustered by K-means clustering, with the final K-value set according to the cluster validity method [17], because the same footage in the same sports video can

difference between the colour histograms of the two images. For the colour segment descriptor, which is used to represent the spatial part of the colour in the sports video image, the feature extraction process is as follows: the sports video image is chunked; the dominant colour is selected; the  $Y$ ,  $Cb$ , and  $Cr$  components of the 64 pixels are discrete cosine-transformed to obtain three sets of coefficients; finally, the obtained discrete cosine coefficients are Zigzag scanned, and a small number of low-frequency coefficients are selected to create a new segment descriptor [16]. The distance between frames  $g_a$  and  $g_b$  is then set to  $Ay$ ,  $ACd$ , and  $ACR$ .

occur repeatedly, resulting in repeated key frame sequences being obtained.

The clustering performance metrics are

$$G = xScat(a) + dis(a), \quad (7)$$

where  $G$  describes the clustering result of sports video key frame sequences;  $Scat(a)$  and  $dis(a)$  both describe the key frame sequence classes; and  $x$  and  $y$  describe the interclass distances in turn.

Since these two values vary widely, a weighting factor  $dis(d_{\max})$  is set,  $d_{\max}$  indicating the maximum predetermined number of clusters. The  $d$  obtained when this value is at the minimum is the optimal number of clusters [16].

#### 4.2. Sports Video Image Classification Based on Deep Learning Coding Models.

A multilayer restricted Boltzmann machine is used to encode and learn  $G$  into a visual lexicon with representational properties. Based on the spatial information of  $G$ , the neighbouring  $G$  features are set as the input to the RBM and the RBM is trained using the CD fast algorithm to obtain the hidden layer features; afterwards, the neighbouring hidden layer features are set as the input to the lower RBM to obtain the output dictionary [18, 19]. When  $\omega_1$  and  $\omega_2$  are the connection weights of the RBM, there is one explicit layer and one hidden layer of the RBM and the neurons at the same level in the RBM are not connected based on the connection relationship [18]. When the network is trained, the connection between the hidden and explicit layers of the RBM is achieved according to a conditional chance distribution, where the conditional chance between the explicit and hidden layers is

$$q(s_i|y) = \text{sigmoid}\left(c_i + \sum_{j=1}^i \omega_{ji}y_j\right), \quad (8)$$

$$q(y_j|s) = \text{sigmoid}\left(b_i + \sum_{j=1}^i \omega_{ji}s_j\right),$$

where  $y_j$  and  $s_i$  describe the feature and coding layers of the sports video, i.e., the explicit and implicit layers in the RBM, respectively.

By setting the weight matrix  $\omega$  and the hidden layer bias vector  $c$ , the input layer features  $y$  can be encoded into a visual dictionary  $s$ . Correspondingly, by setting  $\omega$  and the explicit layer bias matrix  $b$ , the sports video features can be reconstructed from the visual dictionaries. For a set of input and encoding layers in the RBM, its energy function is

$$D(y, s) = -\lg q(y, s) = -\sum_{j=1}^i \sum_{i=1}^i y_j \omega_{ji} s_i - \sum_{i=1}^i b_j y_j - \sum_{i=1}^i c_i s_i. \quad (9)$$

We calculate the energy function to be able to obtain the joint chance distribution function of  $(y, s)$ .

$$q(y, s) = \frac{e^{-D(y, s)}}{\sum_{y, s} e^{-D(y, s)}}, \quad (10)$$

where  $e$  describes the derivation factor.

To obtain the edge distribution of the joint sports video distribution, the chance distribution of the feature input nodes is

$$q(y) = \frac{\sum_{y, s} e^{-D(y, s)}}{\sum_{y, s} e^{-D(y, s)}}. \quad (11)$$

The RBM network is trained primarily to maximize  $q(y)$ , and its gradient is

$$\frac{\partial \lg q(y)}{\partial \omega_{ji}} = \langle y_j s_i \rangle_{\text{data}} - \langle y_j s_i \rangle_{\text{model}}, \quad (12)$$

where  $\langle y_j s_i \rangle_{\text{data}}$  describes the expected value of the prior chance distribution in the sports video training dataset and  $\langle y_j s_i \rangle_{\text{model}}$  describes the expected value of the chance distribution in this model.

In general, it is possible to obtain sample models using a Monte Carlo Markov chain approach.

$$y_j = g_{\text{dec}}(s, \omega_j) = \mu \sum_{i=0}^i \omega_{ji} s_i, \quad (13)$$

where  $g_{\text{dec}}$  describes the sports video key frame feature vector.

The CD algorithm is used to implement fast learning into the RBM to improve the convergence efficiency of the parameters, and the amount of updates to obtain the weights is  $\omega_{ji}$ .

$$\Delta \omega_{ji} = \varphi(\langle y_j s_i \rangle_{\text{data}} - \langle y_j s_i \rangle_{\text{model}}), \quad (14)$$

where  $\varphi$  describes the speed of learning.

The CD algorithm is able to acquire the latest parameters of the sports video features until the parameters converge and the initial visual dictionary is acquired.

TABLE 1: Key frame missing rate of sports video images for the method in the paper.

| Extraction times | Figure skating | Badminton | Yoga |
|------------------|----------------|-----------|------|
| 1                | 0.02           | 0.02      | 0.01 |
| 2                | 0.02           | 0.02      | 0.01 |
| 3                | 0.01           | 0.02      | 0.01 |
| 4                | 0.01           | 0.02      | 0.01 |
| 5                | 0.01           | 0.03      | 0.02 |
| 6                | 0.02           | 0.03      | 0.02 |
| 7                | 0.01           | 0.02      | 0.03 |
| Mean value       | 0.01           | 0.02      | 0.02 |

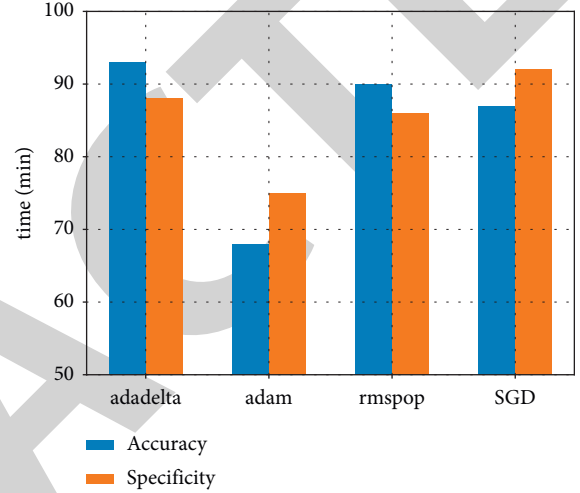


FIGURE 1: Interference of differential visual measurement point size on the method of this paper.

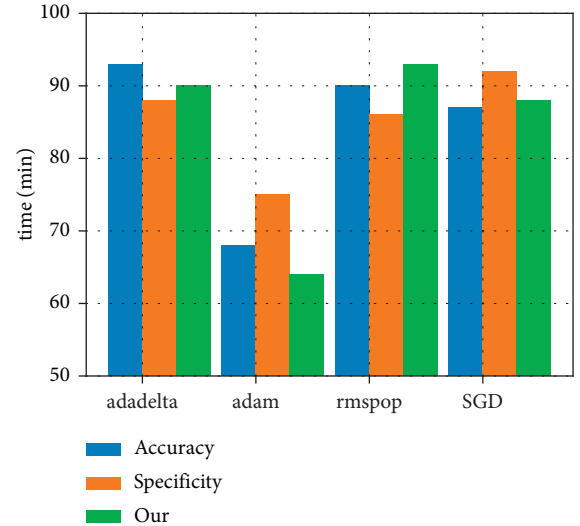


FIGURE 2: The role of fine-tuning on the effect of method classification in the text.

## 5. Simulation Experiments

**5.1. Experimental Subjects.** In order to analyse the effectiveness of the classification method in this paper, three categories of sports videos were set: figure skating, badminton, and yoga.

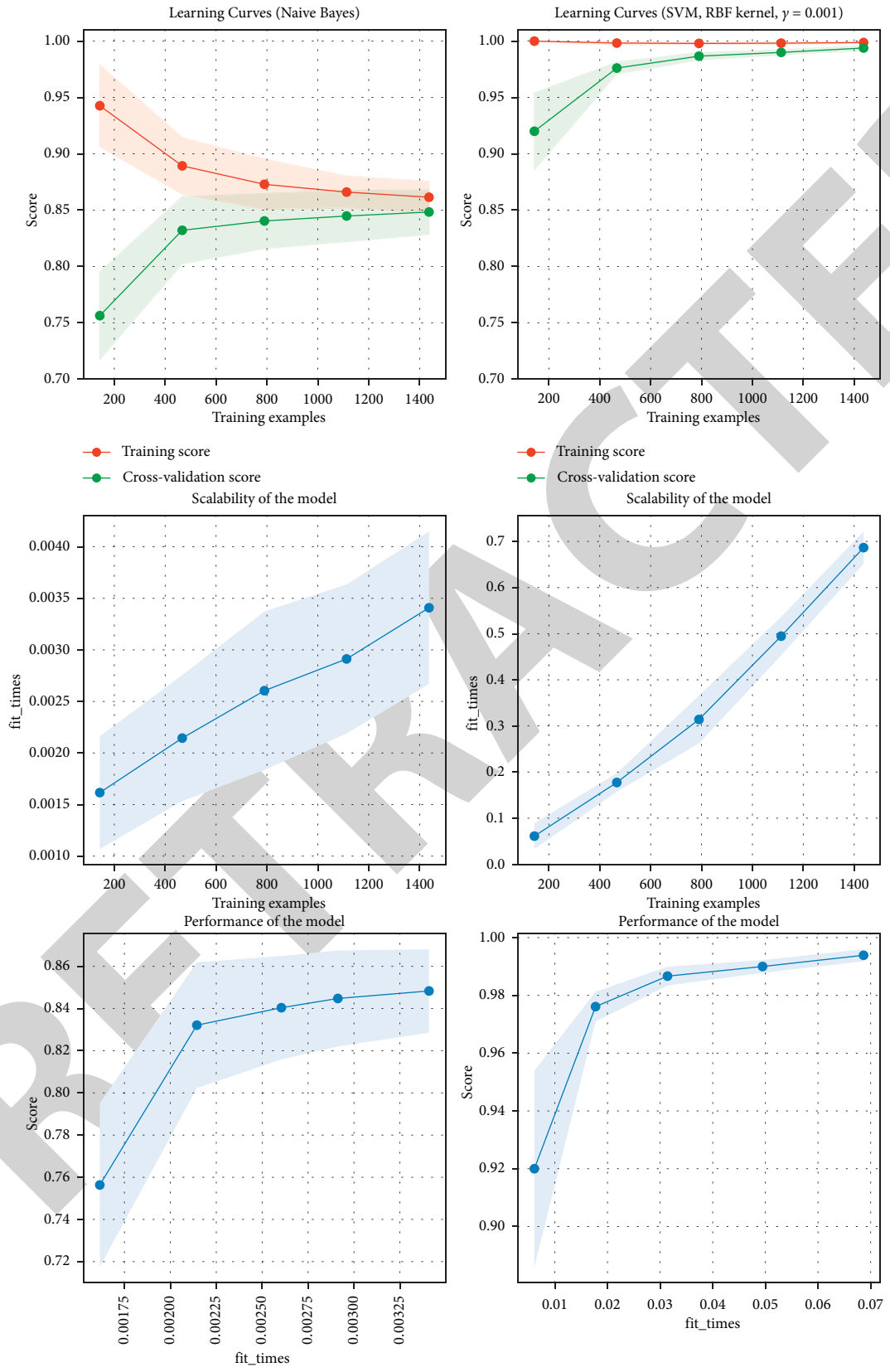


FIGURE 3: Effectiveness of different physical education systems.

**5.2. Experimental Results and Analysis.** The results are shown in Table 1, which tests the comprehensiveness of the extracted key frames of the three sports video categories: figure skating, badminton, and yoga. Table 1 shows that the average missing rate of key frame extraction is less than 0.02 for figure skating, badminton, and yoga, which indicates that the method can fully extract key frame features in sports video images.

The results are shown in Figure 1, which shows that the classification accuracy of the method increases with the size of the visual dictionary of sports videos and stabilizes at 0.98 when the size of the visual dictionary of sports videos reaches 2000 MB.

In order to test the effect of supervised fine-tuning on the classification of the in-text method, the effect of the in-text method PET assessment with and without fine-tuning is shown in Figure 2. As can be seen from Figure 2, there is a significant difference between the effect of supervised fine-tuning on in-text method classification and unsupervised fine-tuning, with supervised fine-tuning improving in-text method classification accuracy. This is due to the fact that supervised fine-tuning can adjust the parameters of each layer of the deep learning network in the form of error backpropagation to optimise the classification effect.

**5.3. Teaching Aid Effectiveness.** The information-based teaching environment should create the conditions for the creation of a modern physical education learning process or a new physical education teaching model.

We create conditions for the management and evaluation of modern physical education learning resources and information. We apply modern scientific theories and technological achievements to establish school teaching information management systems to realise the efficient collection, processing, and presentation of a wide variety of teaching information in the process of physical education teaching and make full use of modern media technology to strengthen teaching activities, such as establishing physical education teaching television monitoring, computer teaching management, school or faculty teaching management, learning resource retrieval and management, physical education teaching information feedback, and physical education teaching effect. The modern physical education teaching information resource management system with functions of assessment and evaluation is shown in Figure 3.

The informative teaching content can be transmitted and shared over long distances through the network, and learners can access the information resources they need by networking through computers and mobile terminals. The linear organisation of hypermedia is as follows: under the informatization environment, the teaching content is constructed using hypermedia technology, supporting multimedia information such as text, audio, video, image, and animation and using the hypertext way of organising and managing information nonlinearly in a mesh structure to effectively organise teaching information, which is suitable for the human brain's cognitive way of thinking and is also

conducive to effectively organising teaching information and promoting the transfer of knowledge and skills.

## 6. Conclusions

With the continuous development of information technology and the emergence of new technologies and media, information technology has become an important direction for the development and reform of physical education. In this environment, physical education teachers should firstly establish a modern concept of physical education and consciously use the theories and methods of modern information technology to improve the effectiveness of physical education. Secondly, they should think about the objectives of physical education teaching, teaching situations, teaching strategies, and teaching evaluation in the informationized environment from different levels and actively use modern information technology to create an informationized physical education teaching environment. The experimental results show that for three types of sports videos, namely, figure skating, badminton, and yoga, the classification accuracy, recall, and the maximum value of F1 of the method in the paper are better than those of the comparison method and a better evaluation result of sports-assisted teaching is obtained.

## Data Availability

The experimental data used to support the findings of this study are available from the corresponding author upon request.

## Conflicts of Interest

The authors declare that they have no conflicts of interest regarding this work.

## References

- [1] W. B. Abur, "Benefits of participation in sport for people from refugee backgrounds: a study of the South Sudanese community in Melbourne, Australia," *Issues in Scientific Research*, vol. 1, no. 2, pp. 10–26, 2016.
- [2] J. J. Crawford, A. M. Gayman, and J. Tracey, "An examination of post-traumatic growth in Canadian and American Para-Sport athletes with acquired spinal cord injury," *Psychology of Sport and Exercise*, vol. 15, no. 4, pp. 399–406, 2014.
- [3] A. Rahman, J. Hussain, M. Hameed Siddiqi, M. Hussain, and S. Lee, "H2RM: a hybrid rough set reasoning model for prediction and management of diabetes mellitus," *Sensors*, vol. 15, no. 7, pp. 15921–15951, 2015.
- [4] J. Hill, "Introduction: sport and politics," *Journal of Contemporary History*, vol. 38, no. 3, pp. 355–361, 2003.
- [5] J. N. Brownfoot, "Healthy bodies, healthy minds': sport and society in colonial malaya," *The International Journal of the History of Sport*, vol. 19, no. 2-3, pp. 129–156, 2002.
- [6] P. An, Z. Wang, and C. Zhang, "Ensemble unsupervised autoencoders and Gaussian mixture model for cyberattack detection," *Information Processing & Management*, vol. 59, no. 2, Article ID 102844, 2022.
- [7] D. E. Alvermann, A. Huddleston, and M. C. Hagood, "What could professional wrestling and school literacy practices

## Research Article

# Research on Dynamic Simulation Technology of Urban 3D Art Landscape Based on VR-Platform

Yulu Cao <sup>1</sup> and Zonghan Li<sup>2</sup>

<sup>1</sup>*School of Environmental Arts, Suzhou Art & Design Technology Institute, Suzhou 215104, Jiangsu, China*

<sup>2</sup>*School of Plastic and Integrated Arts, Hoseo University, Asan 31499, Republic of Korea*

Correspondence should be addressed to Yulu Cao; [caoyulu@sgmart.edu.cn](mailto:caoyulu@sgmart.edu.cn)

Received 16 March 2022; Accepted 4 April 2022; Published 27 April 2022

Academic Editor: Hangjun Che

Copyright © 2022 Yulu Cao and Zonghan Li. This is an open access article distributed under the Creative Commons Attribution License, which permits unrestricted use, distribution, and reproduction in any medium, provided the original work is properly cited.

With the rise of some concepts such as “Digital Earth” and “digital city,” how to realize the three-dimensional reconstruction and visualization of the urban art landscape is becoming a current research hotspot. This study takes the VR-Platform as the development platform and combines it with 3dsMax technology to study the dynamic simulation technology of urban 3D art landscapes. Additionally, this study combines the dynamic simulation technology of urban three-dimensional artistic landscape, designs the urban three-dimensional artistic landscape dynamic simulation system from the aspects of landscape modeling, texture mapping, drive integration, and so on, and finally realizes the basic functions such as roaming interaction, map navigation, information measurement, and visual display of the urban three-dimensional artistic landscape dynamic simulation system, which has a certain practical application value.

## 1. Introduction

Virtual reality technology (VR) is a multidisciplinary, interdisciplinary subject and an important direction of the development of simulation technology, which can build a virtual system with real-world shadow and physical effects [1]. With the popularization of virtual reality technology and the concept of the digital city, the application of virtual reality technology in the field of urban planning has been paid more and more attention. Urban 3D art landscape planning is that designers use three-dimensional modeling software to model according to their own landscape planning effects and generate virtual scenes through a virtual simulation platform to show the effect of urban three-dimensional art landscape planning. Applying virtual simulation technology to urban three-dimensional virtual landscape planning can not only realize the real reproduction of an urban landscape but also deeply analyze various types of spatial information by using urban VR, which can provide strong decision support for urban spatial distribution, architectural structure design, landscape

garden planning, space-time positioning, lighting analysis, road design, and other aspects. It is conducive to the realization of more scientific and reasonable urban management, thereby promoting the sustainable development of the city. In addition, virtual simulation technology is applied to the field of urban landscape planning. The current or future cities can be simulated realistically through 3D modeling and presented on a virtual platform so that multiple planning and design schemes can be seen through a virtual platform. This will help users more clearly determine the reasonable planning scheme, make users feel immersive, facilitate the communication between planning decision makers and landscape planning designers, reduce the huge losses caused by unreasonable planning, and make the planning more scientific and reasonable. The main virtual reality software used at home and abroad includes Virtools, Quest 3D, Converse 3D, and VR-Platform [2]. By comparing various 3D modeling technologies and virtual simulation technologies, this study finally chooses the VR-platform for modeling and scene planning of urban 3D art landscapes, aiming at realizing dynamic simulation and display of urban

3D art landscapes and providing reference and guidance for the application of virtual reality technology in urban landscape planning.

## 2. Dynamic Simulation Technology of Urban 3D Art Landscape

*2.1. VR-Platform Virtual Simulation Platform.* The VR-platform is the most widely used virtual reality software in China, which is extensively used in urban planning, interior design, industrial simulation, historic site restoration, bridge and road design, military simulation, and other domains [3]. Compared with other 3D virtual reality software, VR-platform can effectively solve complicated programming problems. It adopts a modular approach in the construction process, which allows visual editing of the interface and enables complex interaction functions with simple sentences [4].

The advantages of the VR-platform virtual simulation platform are prominent, mainly as follows: (1) VR-platform can obtain beautiful, realistic static light and shadow effects through lighting mapping generated by various renderers in 3dsMax and has the real-time material editing function that seamlessly transforms with 3dsMax. (2) VR-platform virtual simulation platform is embedded with script language and has a powerful secondary development interface. More required functions can be developed through the customization function [5]. (3) The display effect of the virtual simulation platform is interactive, and customized browsing is realized by setting up a walking camera, a flight camera, a role control camera, a tracking camera, and so on. (4) The VR-platform virtual simulation platform has a material library, which can be used to simulate materials in real time through simple operations. You can also set material types and adjust material properties, such as dynamic lighting, transparency, and color [6]. (5) A collision detection algorithm is introduced in VR-platform to realize efficient collision detection. (6) The association between the virtual simulation model and the database in VR-platform is also associated with multiple databases. (7) Seamless conversion is achieved with 3ds Max [7].

*2.2. Technical Process of Dynamic Simulation of Urban 3D Art Landscape.* The core content of using VR-platform software to construct a dynamic simulation system of urban 3D artistic landscape is to construct 3D virtual scenes, and 3D modeling is the foundation [8]. The establishment of urban virtual landscape environments must first be modeled and then form a virtual world according to real-time drawing and stereoscopic display of the virtual environment. The technical process of the dynamic simulation of urban 3D art landscape based on a VR-platform is shown in Figure 1.

First of all, the 3D modeling of the virtual scene of the urban 3D art landscape is carried out to obtain the relevant basic data, and the 3D modeling technology is used to establish the scene 3D model. The production of a virtual 3D landscape model mainly involves the production of terrain,

landscape trees, flowers, plants, and other models, as well as the realization of 3D terrain and landscape model fitting.

Then, the 3D model needs to be further processed. A realistic and smooth 3D virtual scene should have not only a realistic model but also a smooth operation effect, which has strict requirements on the 3D scene model. The model should be optimized as far as possible without affecting the overall effect [9]. Specifically, 3dsmax is used to establish 3D terrain and construct a 3D landscape model to realize the fit between the terrain and the model. Then, texture mapping and painting are carried out to create a realistic 3D scene.

Finally, through the real-time rendering and the three-dimensional display of the three-dimensional interactive simulation platform in the virtual simulation platform, the functions of a dynamic query, interactive roaming, and user-defined browsing of urban art landscapes are realized by designing environmental effects, adding connection database, buttoning trigger events, adding sky boxes, and setting special effects.

## 3. Design of Dynamic Simulation System for Urban 3D Art Landscape

Combined with the technical process of urban 3D art landscape dynamic simulation, VR-platform virtual simulation platform was used to design the simulation system, including the establishment of the 3D art landscape model, texture mapping, and baking of the landscape model, and integrate and drive of virtual scene simulation, and the basic functions of the urban 3D art landscape dynamic simulation system were realized.

*3.1. Establishment of the 3D Art Landscape Model.* Urban 3D art landscape model involves topography, architectural complexes, landscape trees, flowers and plants, architectural sketches, roads and rivers, and other related scenes. Therefore, 3dsMax modeling software was used to establish the scene model of the urban art landscape.

On the basis of DEM data and CAD data of the land use planning map, the topographic model was established, and in particular, DEM data and building elevation information were obtained through field measurement [10]. According to the actual situation, texture data were obtained by digital camera shooting on-site, and then, it was imported into 3DsMax to form a 3D terrain model in line with planning CAD data, as shown in Figure 2.

In urban 3D art landscape planning, exhibition halls, toilets, restaurants, and other large buildings are usually represented by body. Body shape ground objects play a crucial role in 3D modeling. The diversity of body shape, ground objects, and visual appearances add a beautiful scenery line for the city 3D art landscape. Rules are established based on the virtual reality model of 3dsMax to capture vertices or edges to sketch the general outline of the building [11]. In addition, the model is simplified by removing redundant faces and nonvisible and redundant vertices. Figure 3 shows the architectural scene model.

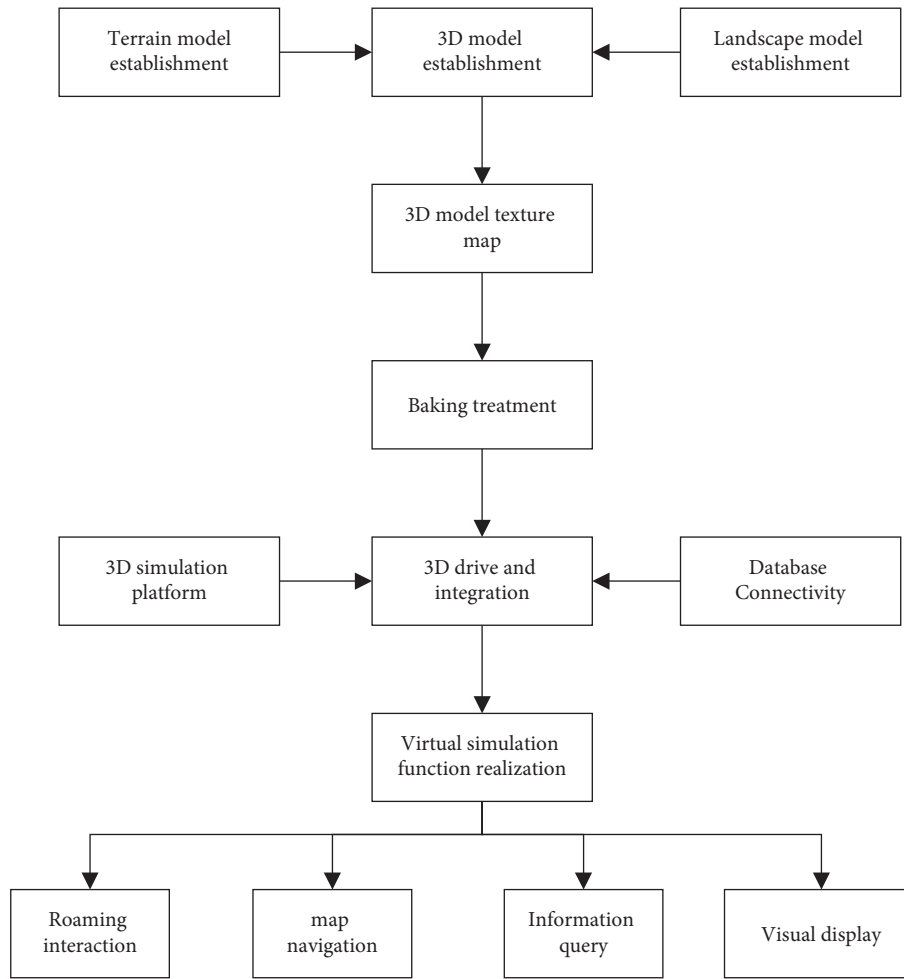


FIGURE 1: Dynamic simulation technology flowchart of the urban 3D art landscape.

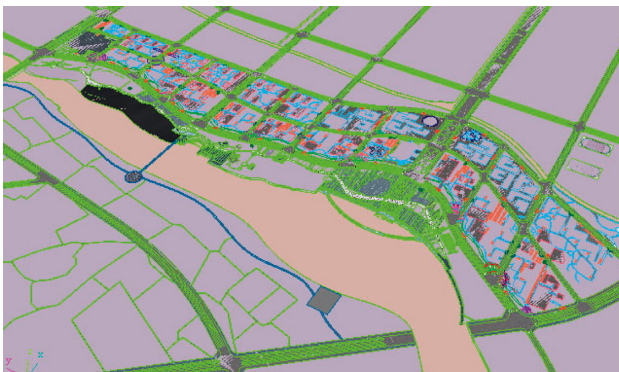


FIGURE 2: Terrain scenario model.

When making outdoor virtual reality scenes, not only buildings should be considered but also a large number of auxiliary models such as roads and green belts should be considered. Therefore, environmental scenes need to be added. For example, trees and flowers are all represented by models, which lead to a large number of model faces in VR scenes, bringing a lot of difficulties to editing and scene operation. Therefore, the green model is expressed with ten literal objects or hollow stickers. For the landscape of flowers

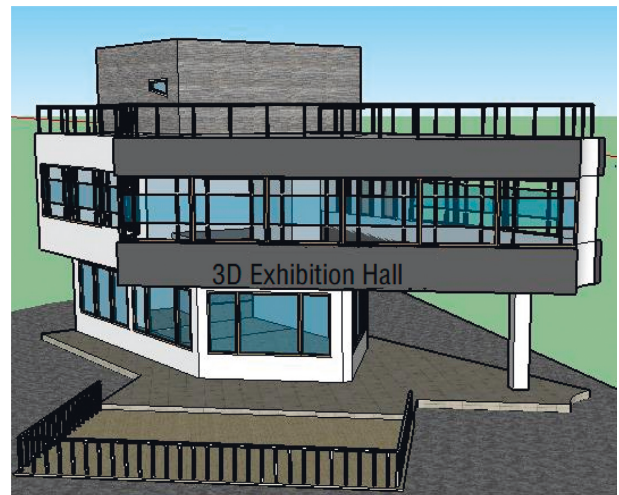


FIGURE 3: Exhibition hall scene model.

and trees, the “cross-plane” modeling method combining image and model is adopted to establish the corresponding entity model [12]. That is to say, attaching one side of the tree to two intersecting planes and then copy the same tree model by instance copy. At the same time, street lamps, rivers, and



other models of similar size in the scene are copied by instance, which improves efficiency and saves system resources. The plant scene model is shown in Figure 4.

In 3D scene, the fitting of 3D model and terrain is an important part of urban 3D art landscape planning and design. Therefore, the surface leveling tool [13] is used to place the three-dimensional model on the terrain so that the urban architectural elements are truly integrated into the irregular terrain. The fitting effect of the 3D model and the terrain is shown in Figure 5.

**3.2. Landscape Model Texture Mapping and Baking.** In order to make the 3D scene closer to the real environment of the urban art landscape, it is necessary to enhance the texture of the 3D model and improve the modeling of the 3D model through mapping. Specifically, the method of bitmap pasting can be applied to 3D urban art landscape model mapping. Firstly, select the required texture model and select a picture in the Material Editor. Then, select the bitmap in the diffuse channel and select the drawing to specify the material to a sphere model [14]. Finally, click to assign the material to the selected object and display the standard map in the viewport. When using a bitmap, 3ds Max will automatically pop up the parameter setting panel of the bitmap after the bitmap is loaded, and the relevant values of the bitmap can be set, such as offset value and angle value. Taking steps as an example, the texture mapping effect is shown in Figure 6.

At the same time, select the baking model in 3dsMax for rendering processing and rendering, and select the baked object to fill and assign the corresponding value [15]. Select Lighting Map from the output options and add relevant elements to create a new baking object. Click “Render” to complete the baking operation of the model.

**3.3. Virtual Scene Simulation Drivers and Special Effects.** The VR-platform 3D interactive simulation platform is used as the driving engine for the dynamic simulation system of the urban 3D art landscape. Firstly, the modeling is converted to 3dsMax for texture mapping and rendering, and the VR-platform export plug-in is installed to export the scenario model to VR-Platform format [16]. Click the VR-platform editor to import, edit, set, and browse on the VR-platform. Additionally, skyboxes, particle effects, water effects, smoke, collision settings, and cameras can also be added to achieve virtual scene simulation integration and drive, as shown in Figure 7.

- (1) Create a skybox. When planning a city 3D art landscape, adding a skybox to the virtual scene can make the virtual scene and skybox fusion, forming a more realistic effect. There are two ways to the add skyboxes. One is to directly add skyboxes in VR-platform [17]. The second is use 3dsMax to make skyboxes and then add skyboxes directly to the VR-platform [18]. Therefore, add the skybox to the VR-platform editor, set the sky color and display type, and add it to the 3D scene environment. The skybox



FIGURE 4: Plant scene model.



FIGURE 5: Effect of a 3D model and terrain fitting.

can also be modified by right-clicking “Modify,” as shown in Figure 8.

- (2) Set the water surface material. Only static models are not enough for the real-time virtual reality scenes. In order to create light and shadow effects, dynamic mapping technology is adopted in this study [19] to create a light and shadow effect. Specifically, adjust it into Fresnel water surface material, edit the water surface refraction group and reflection group model, and adjust water wave parameters.
- (3) Enable collision detection. Due to the change of model position and posture, it may collide with static

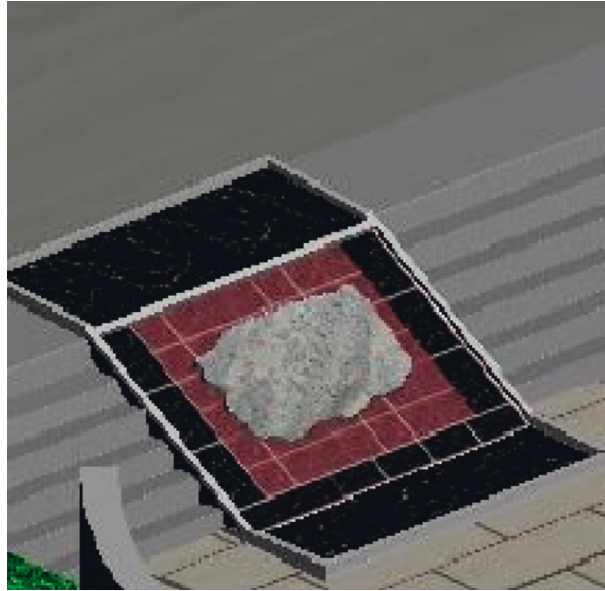


FIGURE 6: Map effect for the step scene.

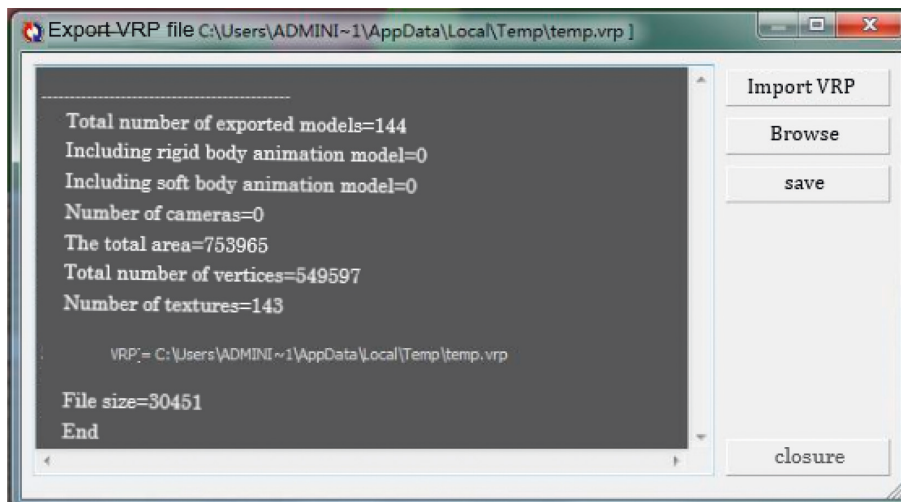


FIGURE 7: Integration and driver of virtual scene simulation.

- or dynamic models in the scene [20] during the urban 3D art landscape roaming. Collision detection is added to main models such as the ground and main structure, which can effectively improve the authenticity of roaming in virtual scenes. VR-platform has designed an efficient and accurate collision algorithm. Open the “Physical Collision” panel in the VR-Platform editor, select the model to which collision detection effects need to be added, and add collision attributes [21], and then, hide the model so that visitors cannot cross when they use the angle of view of the collision detection camera to roam. Finally, browsing is prohibited in some places in the scene, as shown in Figure 9.
- (4) Simulate different weather effects. In order to simulate the different weather conditions of the city so that visitors can browse the virtual art landscape of

the city under different weather conditions, a variety of weather effects for the current virtual scene can be added, such as fog and cloudy [22].

- (5) Add background music. In order to make the urban virtual art landscape not only visually realistic but also auditory appealing, a music background can be added to the virtual scene. Select the music file you want to add and set it as background music; the music can also be repeated [23].
- (6) Set up the camera. In order to let visitors know where they are browsing in the virtual art landscape of the city, a timely navigation map can be used to help visitors locate. Custom browsing is also possible by setting up walking, rotating, and flying cameras [24]. On the VR-platform editor interface, interactive production is used to realize the interactive functions of virtual scenes.

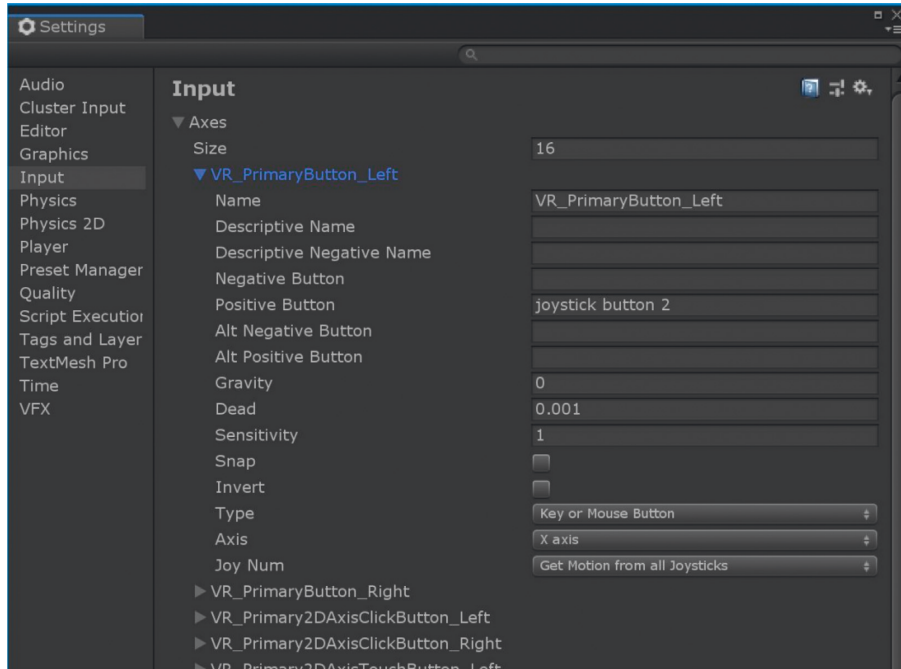


FIGURE 8: Create a skybox.



FIGURE 9: 3D renderings of urban virtual art landscape.

Based on the above design scheme, the 3D renderings of the urban virtual art landscape were obtained, as shown in Figure 9.

**3.4. Function Realization of Urban Landscape Dynamic Simulation System.** VR-platform virtual simulation platform has a powerful interface design module, a database module, a script interaction module, and a secondary development function module [25]. These functional modules are applied to the functional development of the dynamic simulation system of urban 3D art landscapes, and the following basic functions can be achieved.

- (1) Roaming interactive function: the dynamic simulation system of urban 3D art landscape realizes three

kinds of roaming functions: fixed-point roaming, path roaming, and avatar roaming [26]. The preset state is fixed-point roaming, which can directly switch to the starting point of each fixed-point camera [27]. The camera's movement can be controlled by WSDA four-letter keys or up, down, left, and right arrow keys to reach the user's desired location. Path roaming is to let the camera walk along the preset path to automatically view the scene [28]. When the user clicks "Path Roam," the window switches to a series of default path windows. Users can choose from four paths, and they can choose their favorite viewing path. The avatar tour is to create avatar characters in the scene, which allows

you to roam the scene as an avatar, roaming and browsing the scene from the avatar's perspective [29].

- (2) Map navigation function: dynamic navigation is a basic function of the dynamic simulation system of urban 3D art landscapes [30]. Roaming through virtual scenes, users mostly focus on the details of the scene, and it is difficult to fully understand the overall situation of the scene. After roaming, users often do not know which road they have taken in the scene. Therefore, it is necessary to add position and navigation functions in the system. Users can see the location of roaming on the navigation map and quickly roam to the desired place using the navigation map. Figure 10 shows the map navigation function.
- (3) Information query function: the information query function can be used to query information about buildings and planned plots in a scenario, including building name, height, area, and design concept [31]. Click the information query button on the interface, and the dynamic simulation system of the urban 3D art landscape will switch to the information query function. At this time, as long as users click on the building or plot that they want to query, the system will query relevant data from the database, and the relevant information window will pop up.
- (4) Visual display: the visual presentation function can output what is currently displayed in the scene in JPG format [32]. This feature can be used when the user needs an output screen in the current scene. By changing the parameters, the user can modify the output effect picture.

#### 4. Application Prospect of Urban 3D Art Landscape Dynamic Simulation System

With the continuous development of landscape planning, virtual simulation technology, and 3D modeling technology, the combination of these three technologies has broad application prospects [33]. With the help of virtual simulation technology and 3D modeling technology, the dynamic simulation of urban 3D art landscapes is also an objective requirement of landscape planning and development. The development and application of the dynamic simulation system of urban 3D art landscape can simulate a full three-dimensional, life-like urban landscape environment, which provides a three-dimensional and intuitive three-dimensional spatial information system for urban landscape planning, construction, and operation management and improves the level of urban landscape planning and management. Urban 3D art landscape dynamic simulation system can be widely used in all aspects of planning and bring considerable benefits. The details are as follows:

One is to show a life-like urban landscape planning scheme. Current urban landscape planning is mainly based on static or animation effects, most of which are two-

dimensional planes, lacking three-dimensional, dynamic, and immersion. It is not conducive to the overall evaluation of planning schemes. The landscape planning is designed as a 3D model, and custom browsing can be realized through virtual simulation technology so that any position in the scene can be observed, giving people an immersive feeling. In industrial augmented reality and other aspects, VR glasses, gloves, and other applications in this industry can enable the audience to experience planning and design from all aspects of vision, hearing, touch, and so on. The dynamic simulation system of urban 3D art landscape can bring realistic visual effects to users and give them an immersive experience by displaying the results of planning schemes in three dimensions. It can also obtain the data of planning projects through the database to facilitate the organization and management of projects.

The second is to avoid design risks and make the planning scheme reasonable and scientific. At present, urban art landscape planning and design are mainly based on the professional knowledge and materials mastered by planners and designers [34]. Using AD and other software to make planar graph and 3D animation effect drawing cannot reflect the rationality of planning and layout, and it is not easy to modify.

Using virtual simulation technology to generate virtual landscape planning scenes is helpful for planning designers or users to browse all angles of planning layout, find deficiencies, and modify timely. For example, you only need to set the corresponding parameters to change the height of the building, building color, green density, and so on. To some extent, it speeds up the speed and quality of planning scheme design, improves work efficiency, and saves a lot of manpower and material resources. In view of the advantages of virtual simulation technology, if it is introduced into urban landscape planning and design, it can find out whether the planning layout is reasonable without actual planning implementation. The virtual environment established by the dynamic simulation system of urban 3D art landscape is based on real and scientific data and digital models, and the landscape planning and design can be reproduced truly according to the specifications and requirements of the planning project design. Through roaming and interactive experience, users can easily find some design defects that are not easy to detect, which can reduce the loss caused by incomplete plans and greatly improve the quality of urban landscape planning.

The third is to facilitate the promotion of the urban landscape. With the development of the Internet, virtual tourism has gradually become a hot topic. After the completion of the urban art landscape planning results, the use of network technology to upload the design of a three-dimensional landscape scheme to the Internet can not only provide tourists with a realistic scene of the city's tourism scene but also provide consumers with detailed information. Let the tourists who are thousands of miles away can wander freely and customize their browsing experience, so as to facilitate the tourists to understand the overall situation of the urban landscape and find places to attract their own. At the same time, it is also convenient for tourists to increase



FIGURE 10: Map navigation function.

the publicity of popular science knowledge of urban art landscape protection.

## 5. Conclusions

At present, the application of 3D modeling and virtual simulation technology is becoming more and more extensive, and its application in urban landscape planning can make urban landscape planning scientific, reasonable, and refined. Through the research on the dynamic simulation technology of urban 3D art landscape based on VR-platform, the 3D scene modeling of urban art landscape is completed. The terrain modeling and building modeling are completed by using the 3dsMax geometric modeling method, and the environmental modeling of trees, flowers, roads, and so on is completed by means of example replication. Through virtual scene simulation integration and drive, the basic functions of the dynamic simulation system of urban 3D art landscape are finally realized, including roaming interaction, map navigation, information query, visual display, and so on. The development of a dynamic simulation system of urban 3D art landscapes has broad application prospects. It not only demonstrates the realistic urban landscape planning scheme, avoids design risk, and makes the planning scheme reasonable and scientific but also facilitates the publicity and promotion of urban landscape, which is conducive to the realization of the digital city.

## Data Availability

The dataset can be obtained from the corresponding author upon request.

## Conflicts of Interest

The authors declare that there are no conflicts of interest.

## References

- [1] Y. Wu and W. Jiang, "Analysis of key frames of square greening landscape pattern data under VR technology," *Computer Simulation*, vol. 38, no. 3, pp. 336–340, 2021.
- [2] M. S. Michel, T. Knoll, K. Ku, and P. Alken, "The URO Mentor: development and evaluation of a new computer-based interactive training system for virtual life-like simulation of diagnostic and therapeutic endourological procedures," *Bju International*, vol. 89, no. 3, pp. 174–177, 2015.
- [3] B. Ma, "Design of VR technology based 3D integration simulation system for architectural landscape features," *Modern Electronic Technique*, vol. 20, pp. 153–156, 2020.
- [4] W. Wu and Y. Wu, "Design of urban planning three-dimensional simulation design system based on VR technology," *Modern Electronic Technique*, vol. 21, pp. 145–149, 2019.
- [5] H. Zhang, "Design of landscape planning system based on 3D VR technology," *Modern Electronic Technique*, vol. 12, pp. 132–135, 2019.
- [6] X. Yang, B. Chen, W. Zhang, H. Cao, X. Li, and Q. Zhao, "Design of Virtual Campus Roaming System Based on 3d Laser Scanning Technology and VR-Platform," *Laboratory Research and Exploration*, vol. 10, pp. 110–114, 2017.
- [7] L. D. Clark, A. B. Bhagat, and S. L. Riggs, "Extending Fitts' law in three-dimensional virtual environments with current low-cost virtual reality technology," *International Journal of Human-Computer Studies*, vol. 139, Article ID 102413, 2020.
- [8] A. Fuster-Guilló, J. Azorín-López, M. Saval-Calvo, J. M. Castillo-Zaragoza, N. Garcia-D'Urso, and R. B. Fisher, "RGB-D-Based Framework to Acquire, Visualize and Measure the Human Body for Dietetic Treatments," *Sensors*, vol. 20, no. 13, 2020.
- [9] G. Burström, R. Nachabe, O. Persson, E. Edström, and A. Elmi Terander, "Augmented and Virtual Reality Instrument Tracking for Minimally Invasive Spine Surgery: A Feasibility and Accuracy Study," *Spine*, vol. 44, 2019.
- [10] W. Piedra-Cascón, V. R. Krishnamurthy, W. Att, and M. Revilla-León, "3D Printing Parameters, Supporting Structures, Slicing, and post-processing Procedures of Vat-Polymerization Additive Manufacturing Technologies:A

- Narrative review,” *Journal of Dentistry*, vol. 109, Article ID 103630, 2021.
- [11] K. Tsuchida, K. Ueno, and S. Shimada, “Motor area activity for action-related and nonaction-related sounds in a three-dimensional sound field reproduction system,” *NeuroReport*, vol. 26, no. 5, pp. 291–295, 2015.
  - [12] T. Qin, M. Cook, and M. Courtney, “Exploring chemistry with wireless, PC-less portable virtual reality laboratories,” *Journal of Chemical Education*, vol. 98, no. 2, pp. 521–529, 2021.
  - [13] F. Parisi, M. Rousian, N. A. Huijgen et al., “Periconceptional Maternal “high Fish and Olive Oil, Low Meat” Dietary Pattern Is Associated with Increased Embryonic growth,” *Ultrasound in Obstetrics & Gynecology*, vol. 6, 2017.
  - [14] C. Chang, K. Bang, G. Wetzstein, B. Lee, and L. Gao, “Toward the next-generation VR/AR optics: a review of holographic near-eye displays from a human-centric perspective,” *Optica*, vol. 7, no. 11, p. 1563, 2020.
  - [15] D. Avola, L. Cinque, G. L. Foresti, and M. R. Marini, “An interactive and low-cost full body rehabilitation framework based on 3D immersive serious games,” *Journal of Biomedical Informatics*, vol. 89, pp. 81–100, 2018.
  - [16] P. M. Maloca, B. Faludi, M. Zelechowski et al., “Validation of virtual reality orbitometry bridges digital and physical worlds,” *Scientific Reports*, vol. 10, no. 1, Article ID 11815, 2020.
  - [17] R. Johanna, T. Ralf, and T. Stefano, “The same video game in 2D, 3D or virtual reality – how does technology impact game evaluation and brand placements?” *Plos One*, vol. 13, no. 7, Article ID 200724, 2018.
  - [18] B. J. Dixon, H. Chan, M. J. Daly et al., “Three-dimensional virtual navigation versus conventional image guidance: a randomized controlled trial,” *The Laryngoscope*, vol. 126, no. 7, pp. 1510–1515, 2016.
  - [19] M. Johansson, “VR for Your Ears: Dynamic 3D audio is key to the immersive experience by mathias johansson · illustration by eddie guy,” *IEEE Spectrum*, vol. 56, no. 02, pp. 24–29, 2019.
  - [20] N. E. Werner, A. F. Jolliff, G. Casper, T. Martell, and K. Ponto, “Home is where the head is: a distributed cognition account of personal health information management in the home among those with chronic illness,” *Ergonomics*, vol. 61, no. 8, pp. 1065–1078, 2018.
  - [21] J. Egger, M. Gall, J. Wallner et al., “HTC Vive MeVisLab integration via OpenVR for medical applications,” *Plos One*, vol. 12, no. 3, Article ID 173972, 2017.
  - [22] G. A. Reina, D. W. Moran, and A. B. Schwartz, “On the relationship between joint angular velocity and motor cortical discharge during reaching,” *Journal of neurophysiology*, vol. 85, no. 6, pp. 2576–2589, 2018.
  - [23] M. Schr, C. Rsl, and A. Huber, “Preliminary experience and feasibility test using a novel 3D virtual-reality microscope for otologic surgical procedures,” *Acta Oto-Laryngologica*, vol. 141, no. 6, 2020.
  - [24] L. Bellia, A. Pedace, and F. Fragliasso, “The impact of the software’s choice on dynamic daylight simulations’ results: a comparison between Daysim and 3ds Max Design,” *Solar Energy*, vol. 122, pp. 249–263, 2015.
  - [25] A. S. Avinash, G. Klaus, C. Hsiang-Ting, and L. Chin-Teng, “The impact of hand movement velocity on cognitive conflict processing in a 3D object selection task in virtual reality - ScienceDirect,” *NeuroImage*, vol. 45, no. 01, pp. 226–228, 2020.
  - [26] J. Hamzelou, “Virtual reality puts jury in crime scene,” *New Scientist*, vol. 225, no. 3003, pp. 12–13, 2015.
  - [27] Z. Lei, H. Taghaddos, S. Han, A. Bouferguène, M. Al-Hussein, and U. Hermann, “From AutoCAD to 3ds Max: an automated approach for animating heavy lifting studies,” *Canadian Journal of Civil Engineering*, vol. 42, no. 3, pp. 190–198, 2015.
  - [28] Z. Lei, H. Taghaddos, S. Han, A. Bouferguène, M. Al-Hussein, and U. Hermann, “From AutoCAD to 3ds Max: an automated approach for animating heavy lifting studies,” *Canadian Journal of Civil Engineering*, vol. 43, no. 1, p. 84, 2016.
  - [29] G. Coelho, E. G. Figueiredo, N. N. Rabelo et al., “Development and evaluation of pediatric mixed-reality model for neuroendoscopic surgical training - ScienceDirect,” *World Neurosurgery*, vol. 64, no. 1, pp. 139–140, 2020.
  - [30] L. Baken, I. M. A. van Gruting, E. A. P. Steegers, P. J. van der Spek, N. Exalto, and A. H. J. Koning, “Design and validation of a 3D virtual reality desktop system for sonographic length and volume measurements in early pregnancy evaluation,” *Journal of Clinical Ultrasound*, vol. 43, no. 3, pp. 164–170, 2015.
  - [31] C. Jin and J. Li, “Application of VR technology in jewelry display,” *Mathematical Problems in Engineering*, vol. 2021, no. 12, pp. 1–9, 2021.
  - [32] M. Wang, A. Dhoot, A. Kimoto et al., “Responsive web-based molecule viewer for 3D communication, collaboration, and virtual reality,” *Biophysical Journal*, vol. 112, no. 3, pp. 462–463, 2017.
  - [33] N. Kato, T. Tanaka, S. Sugihara, and K. Shimizu, “Development and evaluation of a new telerehabilitation system based on VR technology using multisensory feedback for patients with stroke,” *Journal of Physical Therapy Science*, vol. 27, no. 10, pp. 3185–3190, 2015.
  - [34] C. Tang and T. Jin, “Research on product display based on virtual reality technology VR-platform,” *Modern Electronic Technique*, vol. 36, no. 2, pp. 51–55, 2021.

## Research Article

# Research on Neural Network Machine Translation Model Based on Entity Tagging Improvement

**Xijun Xu** 

Wuhan University of Technology, Wuhan 430070, China

Correspondence should be addressed to Xijun Xu; [cissyxxj@whut.edu.cn](mailto:cissyxxj@whut.edu.cn)

Received 12 March 2022; Revised 30 March 2022; Accepted 6 April 2022; Published 26 April 2022

Academic Editor: Man Fai Leung

Copyright © 2022 Xijun Xu. This is an open access article distributed under the Creative Commons Attribution License, which permits unrestricted use, distribution, and reproduction in any medium, provided the original work is properly cited.

Machine translation, as an efficient tool, can achieve equivalent conversion between different languages while preserving the original semantics. At present, machine translation models based on deep neural networks have become a hot research topic in the fields of natural language processing and image processing. However, the randomness of neural networks leads to the existing neural network machine translation models unable to effectively reflect the linguistic dependencies and having unsatisfactory results when dealing with long sentence sequences. To solve these two problems, a new neural network machine translation model with entity tagging improvement is proposed. First, for the low-frequency word translation problem, UNK entity tags replacement is used to compensate for the weakness of the randomness of neural networks and the encoding/decoding strategy of entity tagging is improved. Then, on the basis of the LSTM translation model, an attention mechanism is introduced to dynamically adjust the degree of influence of the context at the source language end on the target language sequence to improve the feature learning ability of the translation model in processing long sentences. The analysis of the experimental results shows that the translation evaluation index BLEU of the proposed translation model is significantly improved compared with various translation models, which verifies its effectiveness.

## 1. Introduction

Machine translation (MT) is an important research direction combining natural language processing and artificial intelligence [1–4]. With the development of the Internet technology, international communication has become more and more frequent. Traditional manual translation does not achieve high efficiency while consuming a lot of human and financial resources, while computers can obtain translation results quickly and efficiently.

Traditional machine translation was implemented mainly using statistical methods. In the statistical-based approach to machine translation, the translation task is abstracted as a probabilistic problem. It is necessary to establish a probability model [4–7] between any two sentences in the bilingual corpus, and the translation task is to find the corresponding target with the highest probability for the source-side utterance using a suitable method. Statistical machine translation solves the bottleneck problem of

knowledge acquisition by learning from a bilingual corpus to obtain transformation rules and no longer requires human initiative to provide language rules. The field of statistical machine translation has produced many results, mainly including language models, hidden Markov models, and models based on the idea of maximum entropy [8–10]. However, to obtain perfect translation results, statistical-based machine translation methods still have many problems [11, 12]. Data preprocessing links such as word alignment, word segmentation, and rule extraction have a great influence, so experienced experts are needed for manual processing. Choi et al. [13] used semantic role tagging information to reorder the list of candidate translations and improved the accuracy of translation preprocessing by this method. Sevens et al. [14] used dynamic, static, and topic caching techniques to improve the selection of phrase translations based on the nature of articulation, hoping that the same phrases remain consistent throughout the document. Church [15] found that unknown words are

an important factor in translation errors during cross-domain translation and proposed the use of dictionary mining techniques to solve the translation problem of unlogged words in new domains. Although statistical machine translation greatly reduces the labor cost and development cycle, the translation focuses on the conversion between source and target languages, ignoring the connection between contexts, resulting in a lack of semantic coherence in translation results.

With the development of deep learning techniques, deep neural networks have achieved remarkable results in the fields of image processing and speech recognition. Deep learning techniques provide new solutions to the challenges related to machine translation. Sennrich et al. [16] proposed an “encoding-decoding” model of neural machine translation and explained the encoding rules. Liang and Du [17] used a convolutional neural network to construct the encoder and a recurrent neural network for the decoder to obtain historical information and process variable-length strings. The current mainstream neural network machine translation approach is an end-to-end codec translation system built using recurrent neural network (RNN) models. Although the implementation of machine translation based on neural network modelling achieves significantly better results compared with traditional methods, there are still some obvious problems that constrain the performance of neural network machine translation models after the analysis of the model structure and translation results. These two problems are as follows: (1) the problem of unregistered words and low-frequency words: as the neural network approach requires modelling of word vectors for all source and target words, unregistered words and low-frequency words cannot be trained in a normal model, and the importance of this problem is particularly apparent when the language is rich in word morphology or has a large vocabulary. (2) The long-distance dependency problem: neural network-based machine translation models tend to have better translation results for inputs that are closer to the decoder, while words that are farther away lead to inaccurate translation of long sentence sequences due to the loss of information transfer.

Therefore, in order to solve the above 2 problems, a neural network machine translation model based on entity tagging improvement is proposed in this paper. The main work includes the following: (1) improvement for the low-frequency word problem. UNK entity tag replacement is used to compensate for the weakness of randomness of neural networks. Using the improved entity tagging coding/decoding strategy, all target words are mapped to a controlled size lexicon to achieve adaptation to the neural network model; (2) improvements for the model structure. The long short-term Memory (LSTM) decoder incorporates an attention mechanism, which solves the problem of gradient disappearance in the traditional RNN and solves the problem of long-distance dependence in the training of translation models through the control of three types of “gates.”

The rest of the paper is organized as follows: in Section 2, the low-frequency word processing based on improved entity tagging is studied in detail, while Section 3 provides a

neural network translation model incorporating attentional mechanisms. Section 4 provides the results and discussion. Finally, the paper is concluded in Section 5.

## 2. Low-Frequency Word Processing Based on Entity Tagging Improvement

In the traditional neural machine translation model, all unregistered words or low-frequency words are marked as <UNK> symbols. For <UNK> symbols, the current mainstream approach searches for the corresponding aligned words by sequence backtracking at the source end and performs a fill-and-replace operation. This approach provides a feasible solution for regions that cannot be covered by the dictionary, but its effectiveness is hardly guaranteed.

*2.1. Named Entity Location Tasks.* For neural network machine translation models, the coding and decoding methods with the addition of entity tags reduce the uncertainty of variables in the neural network while imposing higher requirements on some performance at the machine translation level. For example, for the decoding stage, as entity tags need to be decoded at specific locations, their semantics and context may not be quite the same as other common words, leading to error cases such as mistranslation and omission. Therefore, we make specific enhancements to the named entity localization in the decoding stage.

The main goal of the named entity localization task is to determine, during the decoding operation, whether it outputs a named entity and the class of the output named entity. This task has certain commonalities with the conventional named entity identification task, while there are differences [18–21]: (1) both are tasked with identifying named entities, but the latter operates on a determined input text and is a direct identification task. The localization task, on the other hand, determines the output type at decoding based on the encoding result of the sequence at the source and does not need to determine the specific result of decoding; (2) named entity recognition is annotated at the word level, and the goal is to annotate a single entity word or a group of entity words in multiple consecutive combinations. However, the localization task has already completed the recognition and combination of named entities during preprocessing. Therefore, only the semantics of that output is discriminated, and the need for contextual information is relatively small.

Therefore, simple named entity localization can be implemented entirely based on the neural network machine translation model, and only the dimension of the last output layer is changed. Since the codec method proposed in this paper labels tags as 4 classes, the output dimension of the output layer is  $4 + 1 = 5$ , corresponding to 4 classes of tags and other common words, respectively.

*2.2. Encoding Strategy for Entity Tagging.* For named entity words, more advanced extraction methods currently exist. Therefore, we can extend the encoding method of low-frequency words based on the features of named entity tagging. Based on the common named entity classification,



we divide low-frequency words into four categories, as shown in Table 1.

The rules and constraints for the tagging of words are as follows:

- (1) For the named entities obtained through recognition, only the individuals with lower word frequency are marked. For words like "China", "Smith," and others with high frequency, it is better to include them into the dictionary as normal words for translation.
- (2) For numeric-related entity words, the current tool does not recognize numeric entities well because of the complex format of numbers and the existence of words, abbreviations, numbers, and other forms. In addition, numbers often require different translation methods depending on the scenario, even affecting the overall semantics, and are not suitable for excision and labeling. Therefore, for the operation of entities, we choose to discard numeric entities.

According to the above rules and constraints, a dictionary of specified size is built based on the word frequency and then the entity words or phrases outside the dictionary are tagged according to the corresponding labels. Using the tagging method for low-frequency words does not mean abandoning the subword logic-based word separation method. For words other than tagged entities, there is still an option to preprocess them using double-byte encoding, thus extending the coverage of the lexicon as much as possible.

After incorporating the subword construction strategy with double-byte encoding, the new corpus preprocessing method is as follows: (1) performing the normal word-sorting operation: for different languages, the cut-off method in word sense is identified; (2) the operation of named entity identification is performed on the training corpus. Each entity word is identified with its category; (3) statistical word frequency: for entity words with word frequencies below a specific read value, tagging operation is performed according to the corresponding category and the mapping of entity tags to entity words in each sentence is saved; (4) for untagged words, the operation of cutting subwords is performed according to the double-byte encoding. The final lexicon based on subword logic and the preprocessed corpus are obtained.

For example, given a sentence "I visited Peking University in China in 2018.," it is processed to get "I visit\$ ed <LOC> in China in 20\$ 18.," and we can see that "Peking University" as an institutional entity word with low word frequency is replaced using the corresponding tag. The high-frequency word "China" is not. Among the other words, the past tense and the year numeral are cut into two words by the subword cutting method due to the dictionary size limitation, but the statistical-based features still keep them linguistically meaningful.

**2.3. Decoding Strategy for Entity Tagging.** For the problem of low-frequency words, we design an improved decoding rule for entity tags: (1) For the decoding step where the decoding output is an entity word tag, the source input sequence is

sorted according to its attention score. The search is done according to the principle of "same entity tag > other words," and the found words are translated by looking up the bilingual dictionary. (2) For other decoding steps with UNK tags, the search is carried out according to the principle of "UNK tags > other words," and the others are similar.

For example, when translating "Annie visited Peking University in China in 2018.," the output sequence is mapped by dictionary to "<PER> visited <LOC> in China in 2018." According to the above decoding rules, for the <PER> tag, it was found that the source-end sequence did not have a <PER> tag, so the output of this step was mapped to the source-end word "Annie" with the highest ATTENTION score. It is translated as "Annie" by regularization methods such as dictionary search. For the <LOC> tag, although the word with the highest attention score is "in," the source sequence contains the same <LOC> tag at this time, so we locate the position and get the correct translation result of "Peking University" by word translation, as shown in Figure 1.

### 3. A Neural Network Translation Model Incorporating Attention Mechanisms

**3.1. Neural Machine Translation Module.** To date, various neural machine translation frameworks have been proposed. Among them, self-attentive-based frameworks achieve the most advanced translation performance. The self-attentive-based framework follows an encoder-decoder architecture, where the encoder converts a source sentence  $X$  into a set of context vectors  $C$ . The decoder generates a target sentence  $Y$  from the context vectors  $C$ . Given a parallel dataset of sentence pairs  $D = \{(X, Y)\}$ , where  $X$  is the source sentence and  $Y$  is the target sentence, the loss function can be defined as follows:

$$L(D; \theta) = \sum_{(X, Y) \in D} \log p(Y|X; \theta), \quad (1)$$

where  $p$  represents the probability function and  $\theta$  represents the weight to be updated.

**3.2. LSTM Module.** Recurrent neural network (RNN) is a class of neural networks designed for the processing of serialised information. Traditional perceptrons and convolutional neural networks generally accept information as a whole and have difficulty modelling serialised information such as time and history, in which cases recurrent neural networks can be better adapted. Based on the basic ideas of recurrent neural networks, a number of quite effective improvements have been produced to address their common problems and limitations. An example is the Long Short-Term Memory Module [22, 23], also known as LSTM.

Unlike the RNN network architecture, the LSTM has three additional "gates": a forgetting gate, an input gate, and an output gate. The forgetting gate is a probability vector based on the current input, so that the information from the previous step is passed on with a certain weight. The input gate is responsible for the selective transfer of long-distance

TABLE 1: Tagging of low-frequency words.

| Category            | Tags  | Description  |
|---------------------|-------|--|
| Person name         | <PER> | Person names with low word frequency                           |
| Geographical name   | <LOC> | Geographical names with low word frequency                     |
| Organization name   | <ORG> | Organization name with a low word frequency, possibly a phrase |
| Low-frequency words | <UNK> | Other low-frequency words                                      |

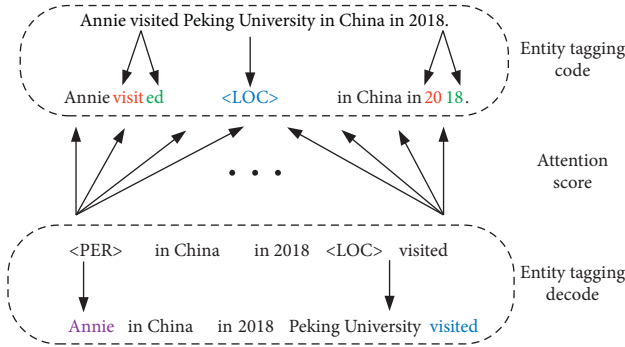


FIGURE 1: Example of coding and decoding process for entity tagging.

dependent information, so that only part of the input information of the current step is involved in the state update. For the output values, the input information is used to generate output gates that filter the updated state information. The multiple gating settings strictly control the flow of information in the sequential network and improve the performance of the RNN in long sequences, as shown in Figure 2.

The output of the next moment in the LSTM is calculated together with the output of the last moment whenever there is a new word vector input to the network. The hidden layer loops and keeps the latest state. LSTM connects the hidden layer with a traditional feedforward network as the output layer. Each node  $y_i$  in the output layer corresponds to the unnormalised log probability at the next moment, and the output  $y$  is then normalised by the softmax function. The equation for this is as follows:

$$\hat{y}_t = \text{soft max}(W^{(s)}h_t), \quad (2)$$

where  $\hat{y}_t$  is the probability distribution of the hidden layer calculated based on all vocabulary in each iteration. That is, the weights of all the predefined words in the document and the observed word vector  $x(t)$  will be determined when the model predicts the following words.

The LSTM also needs to decide which information is forgotten by the neurons. For a dataset  $X_t \in R^{m \times x}$  with sample size  $n$  and feature vector dimension  $x$  at moment  $t$ , the state of the hidden layer at the previous moment is denoted as  $H_{t-1} \in R^{n \times h}$ , at which point the forgetting gate is represented as follows:

$$f_t = \sigma(X_t \cdot W_{xf} + H_{t-1} \cdot W_{hf} + b_f). \quad (3)$$

Here,  $W_{hf}$  and  $W_{xf}$  are the learnable weight parameters and  $b_f$  is the bias vector parameter.

**3.3. Translation Models Using Attention Mechanisms.** Attentional mechanisms can model the attentional model of the human brain. When a person sees a picture, the eye focuses on certain parts of the picture rather than the whole picture. The human brain pays attention to different parts of the picture differently, and this is at the heart of the attention mechanism.

In this paper, we propose to incorporate an attention mechanism in the decoder part to solve the long-distance dependence problem of translation models dealing with long sequences. The proposed model is mainly based on an attention-based LSTM. Using the forgetting, input, and output gates of the LSTM reduces the number of features required for text encoding and allows for efficient encoding of long-range word dependencies. An LSTM incorporating an attention mechanism is able to access both previous and subsequent contextual information, treating the information obtained as two distinct text features. This feature is then fed into the attention layer, which selects the feature that is highly relevant to the entity marker, as shown in Figure 3.

Using such processing, the attention mechanism can significantly improve the accuracy of the translation and reduce the number of learnable weights required to run and efficiently learn the contextual embedded meaning of variable-length sentences around the target word.

The attention mechanism in this model uses the Bahdanau attention model, which calculates the contextual word vector for the  $i$ -th target word based on the hidden vector  $h_j$  of the source word vector and the weights  $\alpha_{ij}$ .

$$c_i = \sum_{j=1}^T \alpha_{ij} h_j. \quad (4)$$

The formula for calculating the weights is as follows:

$$\alpha_{ij} = \frac{\exp(e_{ij})}{\sum_{k=1}^T \exp(e_{ik})}. \quad (5)$$

Here,  $e_{ij}$  denotes an alignment model that refers to the fraction of the input at position  $j$  that matches the output at position  $i$ .

**3.4. Loss Functions.** In this paper, the model is trained to learn a linear Softmax classifier model by minimizing the cross-entropy loss function [24].

$$\text{Loss}(W) = - \sum_{i \in J_t} \sum_k y_{i,k} \ln(p(y_{i,k} | v_i; W)). \quad (6)$$

For the proposed Chinese-English translation model,  $W$  denotes the network model weight,  $k$  denotes the number of entity tokens,  $v_i$  denotes the entity token of the  $i$ -th text,  $n$

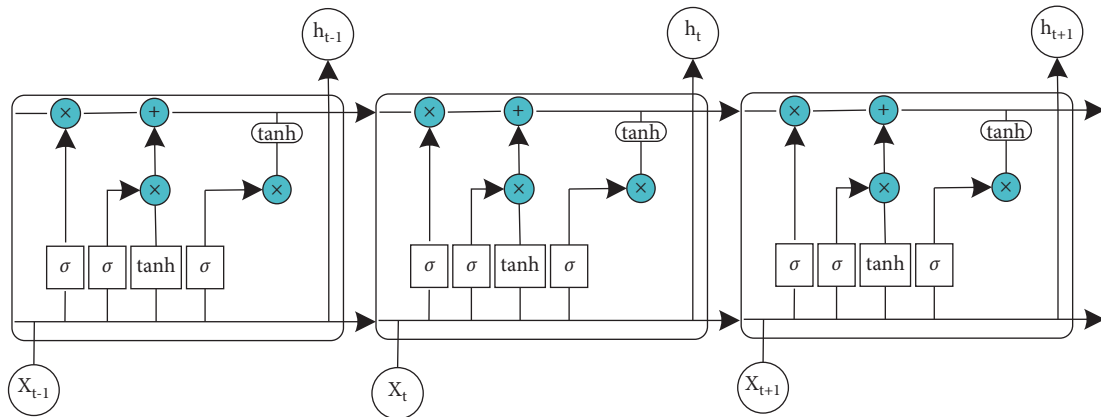


FIGURE 2: Architecture of long short-term memory.

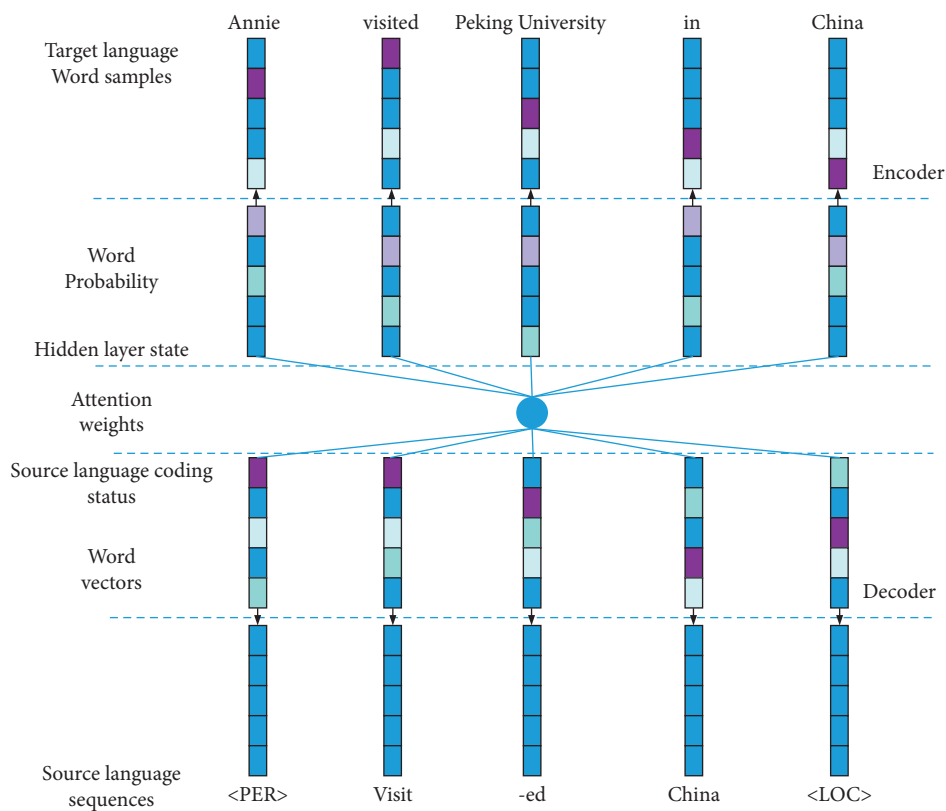


FIGURE 3: Translation model using the attention mechanism.

denotes the maximum number of texts,  $J_t$  denotes the set of training samples after text annotation, and  $y_{i,k}$  denotes the entity token corresponding to the binary representation.

#### 4. Experiment and Result Analysis

**4.1. Experimental Environment and Dataset.** In order to control the cost and ensure the effectiveness of the experiment, the CAsia2015 bilingual alignment corpus with good data quality was selected as the training dataset, containing a total of 105,000 aligned sentence pairs. The test set was selected from the newstest2017 bilingual alignment corpus, containing a total of 2002 sentence pairs. newstest2017 was

equally divided into three subsets, newstest2017-1, newstest2017-2, and newstest2017-3. The neural translation system was built on the deep learning framework TensorFlow machine translation system. For the LSTM-based translation model, the encoder is a recurrent neural network with a forward-backward depth of 2 layers each and the decoder is a unidirectional recurrent neural network with a depth of 4 layers. Based on the convergence experience, the number of running steps is set to 8 epochs.

The experiments were conducted using the deep learning framework TensorFlow to build a neural machine translation system, and the development language was Python 2.7. The hardware configuration was Intel Xeon E5-2678 CPU,

2.50 GHz main frequency, 64 GB RAM, NVIDIA GTX 1080ti GPU, and the operating system was CentOS 7. The relevant parameters are set as shown in Table 2.

**4.2. Evaluation Standards.** Translation quality is the most general measure of a good or bad translation model. The most commonly used quality evaluation metric for machine translation tasks is called BLEU (bilingual evaluation understudy) [25], which is an algorithm designed based on the co-occurrence frequency of words and phrases, and the formula for calculating BLEU is shown as follows:

$$\text{BLEU} = BP \cdot \exp\left(\sum_{n=1}^N \omega_n \log p_n\right), \quad (7)$$

where  $BP$  denotes the length penalty factor,  $\omega_n$  denotes the weight of the  $n$ -word (usually taken as a constant value of  $1/n$ ), and  $p_n$  is the matching accuracy of the  $n$ -word.

$$BP = \begin{cases} 1, & l_c > l_s, \\ \exp\left(1 - \frac{l_s}{l_c}\right), & l_c \leq l_s, \end{cases} \quad (8)$$

where  $l_c$  is the length of the candidate sentence and  $l_s$  is the length of the reference sentence.

$$P_n = \frac{\sum_i \sum_k \min(h_k(c_i), \max_{j \in m} h_k(s_{ij}))}{\sum_k \min(h_k(c_i))}, \quad (9)$$

where  $c_i$  denotes the whole sentence to be translated and  $s_i$  denotes the standard answer.  $h_k(c_i)$  denotes the number of occurrences of  $W_k$  in  $c_i$ ,  $h_k(s_{ij})$  denotes the number of occurrences of  $W_k$  in  $s_{ij}$ , and  $\max_{j \in m} h_k(s_{ij})$  denotes the number of words that occur most frequently in multiple standard answers.

**4.3. Convergence of the Named Entity Location.** When using the encoding preprocessing operation of named entity tagging, we simultaneously trained the named entity localization task for the target language. The convergence of the named entity localization task was presented as a change in the prediction accuracy of the named entity labels during training. After multiple training sessions on a dataset, cross-drops of entity labels and targets were calculated on the validation set and the resulting statistics are shown in Figure 4, with the number of training cycles as the horizontal coordinate and the cross-entropy values as the vertical coordinate.

It can be seen that the overall value of cross entropy shows a decreasing trend as training proceeds and the decreasing curve eventually converges unchanged, indicating that the proposed entity labeling improvement method effectively compensates for the weakness of the randomness of the neural network. The proposed method completes the normal training of low-frequency words, thus better adapting to the neural network machine translation model.

TABLE 2: Experimental parameter setting.

| Parameter type                     | Value    |
|------------------------------------|----------|
| Batch size                         | 64       |
| Maximum acceptable sequence length | 100      |
| Hidden variable size               | 1000     |
| Word vector size                   | 500      |
| Dropout_probability                | 0.3      |
| Attention_method                   | Bahdanau |

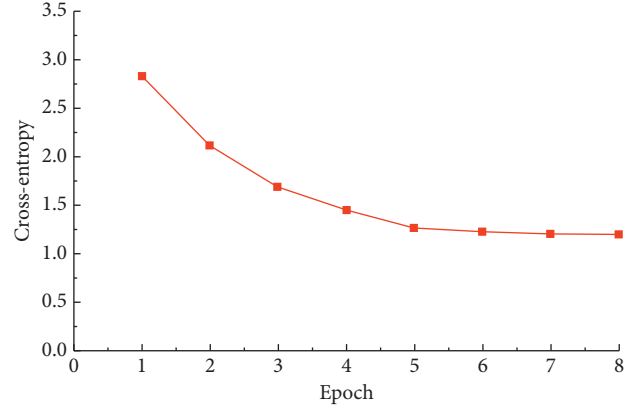


FIGURE 4: Cross-entropy change curve for named entity localization.

**4.4. Performance Comparison of Translation Models.** Different neural networks were trained separately in the translation models. The performance comparison results of the translation models with different network structures on the Chinese-English machine translation task are shown in Table 3.

As can be seen from Table 3, the performance of the LSTM-based translation models is better (larger BLEU values) compared to models with BPNN, CNN, and RNN structures without the use of the attention mechanism. The translation models incorporating the attention mechanism on the original structure each achieved improved performance. At this point, the LSTM model incorporating the attention mechanism achieves optimal performance. This is because the long-distance dependency problem is solved by enhancing the representation of contextual information at the source language end, thus improving the translation accuracy of long sentence sequences.

Next, the LSTM + Attention model with entity tagging improvement and the LSTM + Attention model without entity tagging improvement were compared for the low-frequency word problem, and the results are shown in Figure 5.

It can be seen that although the addition of the attention mechanism leads to an improvement in translation quality, the increase in scores due to tag replacement after the entity tagging improvement leads to a further improvement in overall performance, with a mean BLEU value of 24.7%. This indicates that the use of entity labeling improvement can solve the problem of randomness in neural networks, enhance the training of low-frequency words, and thus better adapt the neural network model to improve the overall performance of machine translation.

TABLE 3: Performance comparison of translation models in BLEU.

| Translation model | casia2015 | newstest2017-1 | newstest2017-2 | newstest2017-3 |
|-------------------|-----------|----------------|----------------|----------------|
| BPNN              | 12.39     | 11.87          | 11.63          | 11.79          |
| CNN               | 14.47     | 14.15          | 13.83          | 13.99          |
| RNN               | 14.49     | 14.16          | 13.85          | 14.01          |
| LSTM              | 16.21     | 15.82          | 15.49          | 15.58          |
| BPNN + Attention  | 21.34     | 16.75          | 16.41          | 16.62          |
| CNN + Attention   | 23.27     | 22.74          | 22.47          | 22.53          |
| RNN + Attention   | 23.31     | 22.77          | 22.49          | 22.55          |
| LSTM + Attention  | 24.28     | 23.86          | 23.37          | 23.41          |

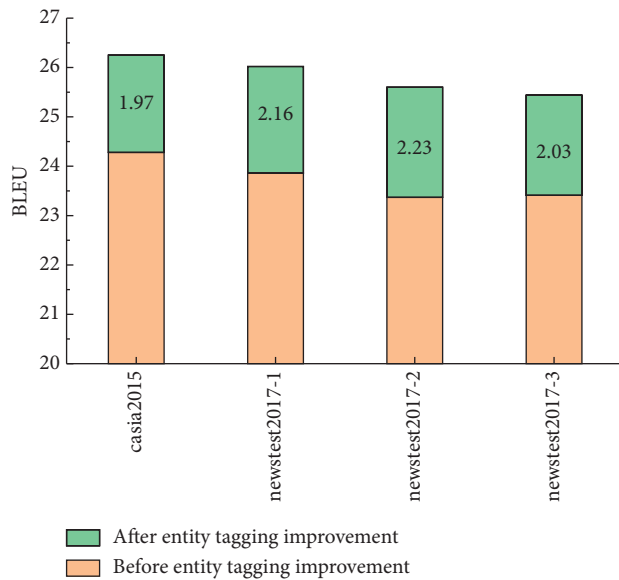


FIGURE 5: Analysis of the effect of entity tagging improvement.

## 5. Conclusions

This paper presents a neural network machine translation model based on entity tagging improvement. An improved entity tag coding/decoding strategy is used to map all target words to a controlled size lexicon to achieve an adaptation to the neural network model. In addition, the LSTM decoder enhances the representation of contextual information at the source language end by incorporating an attention mechanism, thus improving the translation accuracy of long sentence sequences. The comparison results between multiple neural network machine translation models show that the proposed model has the highest performance with a mean BLEU value of 24.7%, effectively solving the low-frequency word problem and the long-distance dependency problem. Due to the limitation of hardware conditions, a very large amount of data cannot be used in the selection of training data and similarly the parameters such as the number of training sessions and data dimension cannot be set too large. Larger scale experimental tests will be conducted on more types of datasets later.

## Data Availability

The experimental data used to support the findings of this study are available from the author upon request.

## Conflicts of Interest

The author declares that there are no conflicts of interest regarding the present study.

## Acknowledgments

This work supported by School of Foreign Languages, Wuhan University of Technology: Action Research on University English Teaching Mode from the Perspective of "Effective Failure" (Project No. 202107), and Exploration of Educational Teaching Theory and Practice of Educational Innovation, Chinese Academy of Management Sciences (No. CXS1200086201900169).

## References

- [1] S. Wu, D. Zhang, and Z. Zhang, "Dependency-to-Dependency neural machine translation," *IEEE/ACM Transactions on Audio, Speech, and Language Processing*, vol. 11, no. 26, pp. 2132–2141, 2018.
- [2] S. Tripathi and V. Kansal, "Machine translation evaluation: unveiling the role of dense sentence vector embedding for morphologically rich language," *International Journal of Pattern Recognition and Artificial Intelligence*, vol. 34, no. 1, pp. 1–18, 2020.
- [3] A. Tezcan, V. Hoste, and L. Macken, "Estimating word-level quality of statistical machine translation output using monolingual information alone," *Natural Language Engineering*, vol. 26, no. 1, pp. 73–94, 2020.
- [4] S. Bayatli, "Unsupervised weighting of transfer rules in rule-based machine translation using maximum-entropy approach," *Journal of Information Science and Engineering*, vol. 36, no. 2, pp. 309–322, 2020.
- [5] P. Dubey, "The Hindi to Dogri machine translation system: grammatical perspective," *International Journal of Information Technology*, vol. 11, no. 1, pp. 171–182, 2019.
- [6] F. Stahlberg, "Neural machine translation: a review," *Journal of Artificial Intelligence Research*, vol. 69, no. 2, pp. 343–418, 2020.
- [7] A. S. Dhanjal and W. Singh, "An automatic machine translation system for multi-lingual speech to Indian sign language," *Multimedia Tools and Applications*, vol. 81, no. 3, pp. 4283–4321, 2021.
- [8] J. G. Makin, D. A. Moses, and E. F. Chang, "Machine translation of cortical activity to text with an encoder–decoder framework," *Nature Neuroscience*, vol. 12, no. 4, pp. 19–28, 2020.
- [9] N. Herbig, S. Pal, and M. Vela, "Multi-modal indicators for estimating perceived cognitive load in post-editing of machine translation," *Machine Translation*, vol. 33, no. 2, pp. 91–115, 2019.

- [10] J. Su, X. Zhang, and Q. Lin, "Exploiting reverse target-side contexts for neural machine translation via asynchronous bidirectional decoding," *Artificial Intelligence*, vol. 27, no. 3, pp. 45–57, 2019.
- [11] N. Chatterjee and S. Gupta, "Efficient Phrase Table pruning for Hindi to English machine translation through syntactic and marker-based filtering and hybrid similarity measurement," *Natural Language Engineering*, vol. 25, no. 1, pp. 171–210, 2019.
- [12] L. Bai, J. Guo, T. Xu, and M. Yang, "Emotional monitoring of learners based on EEG signal recognition," *Procedia Computer Science*, vol. 174, no. 1, pp. 364–368, 2020.
- [13] H. Choi, K. Cho, and Y. Bengio, "Context-dependent word representation for neural machine translation," *Computer Speech & Language*, vol. 45, no. 9, pp. 149–160, 2017.
- [14] L. Sevens, V. Vandeghinste, I. Schuurman, and F. Van Eynde, "Less is more: a rule-based syntactic simplification module for improved text-to-pictograph translation," *Data & Knowledge Engineering*, vol. 117, no. 9, pp. 264–289, 2018.
- [15] K. W. Church, "Emerging trends: APIs for speech and machine translation and more," *Natural Language Engineering*, vol. 24, no. 6, pp. 951–960, 2018.
- [16] R. Sennrich, B. Haddow, and A. Birch, "Neural machine translation of rare words with subword units," *Computer Science*, vol. 12, no. 3, pp. 119–131, 2015.
- [17] J. Liang and M. H. Du, "Two-way neural network chinese-english machine translation model fused with attention mechanism," *Scientific Programming*, vol. 2022, Article ID 1270700, 11 pages, 2022.
- [18] J. Lee, K. Cho, and T. Hofmann, "Fully character-level neural machine translation without explicit segmentation," *Transactions of the Association for Computational Linguistics*, vol. 5, no. 3, pp. 365–378, 2017.
- [19] J. Zhang and C. Zong, "Deep neural networks in machine translation: an overview," *IEEE Intelligent Systems*, vol. 30, no. 5, pp. 16–25, 2015.
- [20] F. Landi and L. Baraldi, "Working memory connections for LSTM," *Neural Networks*, vol. 144, no. 2, pp. 245–252, 2021.
- [21] S. Ketu and P. K. Mishra, "India perspective: CNN-LSTM hybrid deep learning model-based COVID-19 prediction and current status of medical resource availability," *Soft Computing*, vol. 26, no. 2, pp. 645–664, 2022.
- [22] A. Sagheer and M. Kotb, "Time series forecasting of petroleum production using deep LSTM recurrent networks," *Neurocomputing*, vol. 323, no. 6, pp. 203–213, 2019.
- [23] M. S. Akhtar, P. Sawant, S. Sen, A. Ekbal, and P. Bhattacharyya, "Improving word embedding coverage in less-resourced languages through multi-linguality and cross-linguality," *ACM Transactions on Asian and Low-Resource Language Information Processing*, vol. 18, no. 2, pp. 1–22, 2019.
- [24] C. Zong, J. Y. Nie, D. Zhao, and Y. Feng, "natural language processing and Chinese computing," *Communications in Computer & Information Science*, vol. 333, no. 3, pp. 262–273, 2012.
- [25] W. Sun, P. Li, Z. Liu et al., "LSTM based link quality confidence interval boundary prediction for wireless communication in smart grid," *Computing*, vol. 103, no. 2, pp. 251–269, 2021.

## Research Article

# Application Analysis of Emotional Learning Model Based on Improved Text in Campus Review and Student Public Opinion Management

Zhaofeng Weng 

Fuzhou University Zhicheng College, Fuzhou, Fujian 350002, China

Correspondence should be addressed to Zhaofeng Weng; 02107078@fdzcxu.edu.cn

Received 1 March 2022; Revised 18 March 2022; Accepted 26 March 2022; Published 23 April 2022

Academic Editor: Man Fai Leung

Copyright © 2022 Zhaofeng Weng. This is an open access article distributed under the Creative Commons Attribution License, which permits unrestricted use, distribution, and reproduction in any medium, provided the original work is properly cited.

In an era of rapid mobile Internet development, students are increasingly expressing their views on specific events through campus comments. In the Web 2.0 era, the concept of public media participation is widely used by students, and it is important to effectively analyze online campus public opinion comments and present the findings in a rationalized form for the management of campus public opinion. In the new era of education governance modernization, the level of public opinion management in universities has become a key indicator to improve the standard of education management in higher education institutions; therefore, this paper focuses on proposing an innovative deep learning-based research method for topic management of university public opinion. Firstly, through the improved LDA module with sentiment discrimination learning capability, the sentiment of the main arguments in the campus commentary is extracted, and then the statistical sentiment intensity of the in-depth learning module is used to analyze the sentiment intensity of the thematic arguments of different events in time series, so as to achieve the long-term tracking of the trend of the sentiment intensity of the whole event.

## 1. Introduction

Public opinion, as a sociological term, refers to the subjective perception of public events in a certain context. Public opinion on campus networks refers to the attitudes and possibly related behaviors of the “subjects of public opinion,” with university students being the specific group of people, toward the events they care about on the Internet [1]. As “subjects of public opinion,” university students are significantly different from other groups in expressing their views on specific events due to their age, psychology, and cognition [2]. According to the 48th Statistical Report on the Development of China’s Internet released by China Internet Network Information Center (CNNIC) in Beijing on August 27, 2021, the number of Internet users in China reached 1.011 billion in June 2021, an increase of 21.75 million compared with December 2020, and the Internet penetration rate was as high as 71.6% [3]. This huge scale includes the most active group of students in colleges and universities. In the context of promoting the modernization of

educational governance, the management of online public opinion in colleges and universities has become an important part of improving educational management in colleges and universities [4]. College administrators must pay attention to the influence of information technology on students’ thoughts and education and strengthen public opinion management through scientific and innovative methods, and it is on this basis that this paper proposes an innovative and feasible method.

Currently, for opinion analysis and management, from an algorithmic perspective, the most focus is on LDA probabilistic topic models and deep learning models. The literature [5] used LDA models with word2vec models to construct sentiment dictionaries for the temporal analysis of sentiment intensity of hot events of students’ concern. In the literature [6], for public opinion comments in complex contexts, the sentiment value measurement algorithm was constructed and incorporated into the improved LDA-ARMA model for dynamic presentation and fine-grained classification of the sentiment of event opinion. In the topic

detection task in the opinion analysis subtask, literature [7] proposed to extend the topic distribution obtained from the LDA model with word vectors trained by Skip-gram of word2vec as the text representation and used it as the features of the SKM algorithm for cluster analysis, while optimizing the cluster number selection of SKM with the first-order difference of distance cost function values to obtain multiple text clusters as the online opinion topics. Literature [8] used a more efficient sentiment classification model based on this, which was constructed by LSTM neural network model, and the accuracy rate was improved by about 10%. Literature [9] used dimensional sentiment analysis based on Valence-Arousal, and the sentiment classification effect was significantly improved. Literature [10, 11] used a hybrid algorithm based on LSTM. LSTM + Bi further reduced the influence of irrelevant words in long texts on the classification results, while LSTM + Bert + Bi had higher accuracy and effectively solved the sentiment classification problem in public opinion. In the literature [12, 13], a logistic curve model was used to classify the stages of public opinion, and graph attention networks were used to predict the evolution of public opinion after sentiment classification. The literature [14, 15] used softsign activation function instead of tanh activation function in the LSTM model, while using regularized LSTM input weights to effectively combine the advantages of their respective models to classify the tendency of public opinion into positive and negative sentiments for early warning purposes, and the experiments proved that the performance of the enhanced model improved significantly and effectively.

The aforementioned literature applies deep learning algorithm models to various stages of opinion management from different perspectives, but from a general perspective, the following shortcomings still exist: (1) LDA models, as unsupervised machine learning techniques, adopt the bag-of-words approach to transform textual information into digital information that can be easily modeled, but the bag-of-words approach does not consider the order between words and there are difficulties in evaluating the effect; (2) word2vec, as a static approach, has strong generality but cannot be dynamically optimized for a specific task, and the problem of multiple meaning words cannot be effectively solved because the generating vector and the words are in a one-to-one relationship. Based on the above considerations, this paper improves the existing LDA model and deep learning algorithm based on the existing LDA probabilistic topic model and deep learning model from the perspectives of analysis strategy, dynamic monitoring, and effect evaluation; then combines various hybrid algorithms; and applies them to the opinion management of campus reviews. Finally, the effectiveness of the algorithmic model for campus opinion management is demonstrated with experimental validation analysis.

## 2. Related Work

As the essence of the research method proposed and applied in this paper is to use LDA models with deep learning models (word2vec, Bert), combined with sentiment dictionaries, to

perform a temporal analysis of the intensity of sentiment in campus reviews, this section will focus on three parts: probabilistic topic models, neural network language models, and sentiment analysis based on sentiment dictionaries.

*2.1. Probabilistic Topic Modeling.* In probabilistic topic modeling, as one of the most common models in topic modeling methods, the core is to extract topic information from a large amount of textual information through statistical methods and theories, and it has a wide range of applications in the field of information retrieval [16]. The most initial text representation models, the TF-IDF model [16] and the spatial vector model [17], are simpler and cannot distinguish between polysemantic words. Latent Semantic Analysis (LSA) models are therefore proposed to achieve a high-dimensional to low-dimensional spatial mapping of document words [18]. Latent Dirichlet Allocation (LDA) is a more effective probabilistic topic model for identifying latent topic information in campus reviews, using a three-layer Bayesian framework, compared to the previous models [19]. However, as the traditional LDA model uses a bag-of-words approach that lacks consideration of interword order and text-to-topic links, the improved LDA model is used to extract and analyze thematic information from the text in order to optimize the results and improve the accuracy of sentiment analysis in campus reviews.

*2.2. Neural Network Language Models.* Statistical language models aim to learn the joint probability functions of words, and their main challenge is dimensional catastrophe. The emergence of neural network language models (NNLMs) has effectively addressed this problem. The first neural network language model (NNLM) [20] was systematized by Bengio. By optimizing the training model, it is possible to eliminate dimensional disasters and to understand a number of sentences with similar meanings. Two core components make up the neural network language model: distributed representation and word embedding [21]. Neural network models have evolved considerably over the last decade or so, and various models have been proposed using the NNLM as a template, including the CBOW model and the Skip-gram model [22, 23], which are simpler than the NNLM. In addition, hierarchical Softmax algorithms and negative sample algorithms have been developed to train models faster and more efficiently [24]. Google's deep learning tool, word2vec, released in 2013, is a combination of these models and algorithms and provides a fast and effective way to obtain semantic associations between words. Based on the effectiveness of word2vec and its ability to accurately capture potential semantic similarities between words, the aim of this paper is to use an improved word2vec and Bert model to calculate the sentiment intensity of topic ideas extracted from campus reviews.

*2.3. Emotional Analysis.* Sentiment analysis is mainly implemented based on corpus, lexicon, and graph approaches. The corpus-based evaluation word extraction and



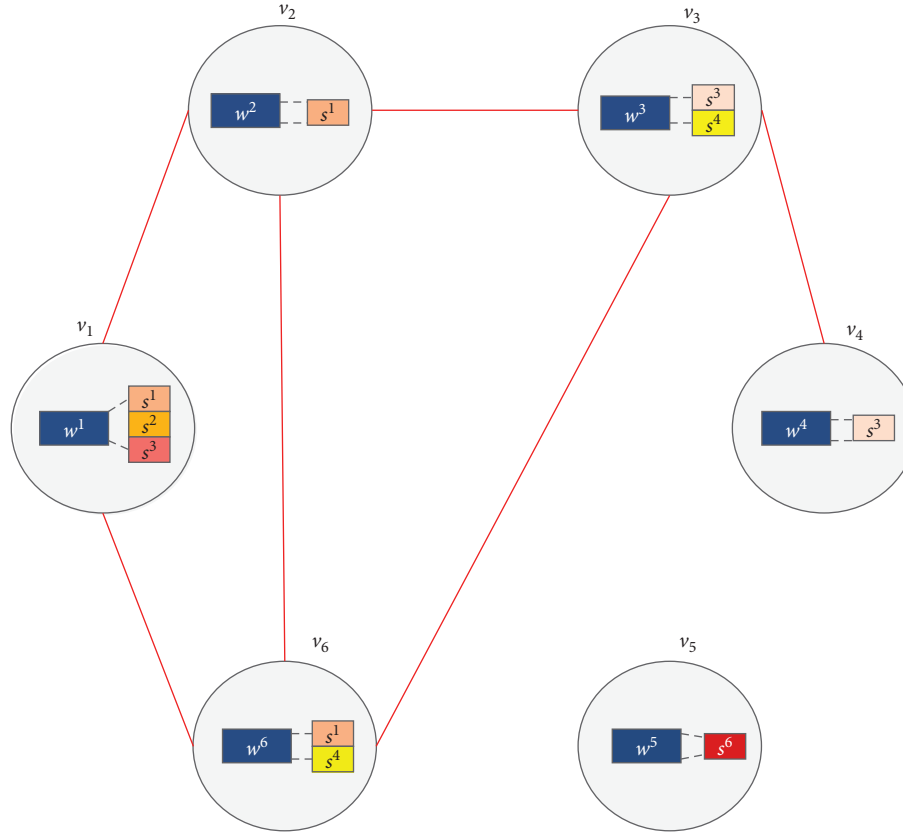


FIGURE 1: Emotional interaction diagram.

discrimination utilize the statistical properties of the corpus to mine and judge the polarity of corpus words, but the accuracy is more difficult to assess due to the limitations of the corpus. The lexicon-based evaluation word extraction and discrimination are mainly achieved through lexical links between words in the lexicon, and the HowNet sentiment lexicon is usually used for semantic similarity and semantic tendency of words based on semantic correlation fields. The calculation method, word-by-word matching for each comment text, finds all positive sentiment words and negative sentiment words in the text for sentiment calculation, and the sentiment scoring rule for each sentiment word is shown in the following equation specifically.

$$S = (-1)^n V_e W. \quad (1)$$

The sentiment score of the sentiment word in the time period is obtained by adding the sentiment scores of the same sentiment word appearing in different comment texts in the same time period, where  $S$  is the sentiment score of the sentiment word;  $n$  is the number of negative words;  $V_e$  represents the sentiment lexicality, with a value of 1 indicating a positive sentiment word and  $-1$  indicating a negative sentiment word; and  $W$  is the degree weight value.

Graph-based sentiment analysis is implemented by introducing an attention mechanism, which can solve the problem of information loss and accuracy degradation caused by the increase of coding intermediate vectors as the input text length increases when methods such as LSTM and

word2vec are used for text classification. In this paper, a self-attentive mechanism is used to reduce the dependence on external information and improve the ability to capture data features, which in turn improves the accuracy of text de-emphasis analysis. The method is implemented by acquiring sentiment words for a certain time period of comment text and associating the comment text with the sentiment words to construct a graph structure, as shown in Figure 1.

The vertices in Figure 1 are the sentiment words that appear in that time step, and if there is a sentiment word  $w$  in the comment text, the comment  $s$  is attributed to the corresponding vertex  $v$ . A vertex can contain multiple comments, and a comment can be assigned to multiple vertices. The mapping relationship also implies that the more the public comment texts associated with two sentiment words, the closer the sentiment expressed. In this paper, we propose a method for constructing edges between vertices based on the union of text structure and text content. The TF-IDF text similarity of the comment text associated with vertex  $v_i$  and vertex  $v_j$  is  $T_{ij}$ . If there are public comments on the associated comment text and the number of public comments is  $N$ , then an edge  $e_{ij}$  is added between these two vertices with the weight  $w_{ij}$ :

$$w_{ij} = \frac{a + N}{b + N}, \quad (2)$$

where  $a$  and  $b$  are the numerator and denominator, respectively, after conversion to the simplest fraction. The

threshold value of text similarity  $a$  is set to 0.3. If there is no common comment between two vertices but their text similarity  $T_{ij}$  is greater than or equal to  $a$ , an edge  $e_{ij}$  is similarly added between  $v_i$  and  $v_j$  with the weight

$$w_{ij} = T_{ij}. \quad (3)$$

**2.4. Gated Circulation Units.** GRU is the same improvement to recurrent neural networks as LSTM. The GRU model contains two gate structures, update gates and reset gates. The reset gate determines how new input information is combined with previous memory, and the update gate defines the amount of previous memory saved to the current time step. By having a more streamlined structure, the GRU model has a speedup in training compared to the LSTM model and is able to better characterize and model the text. Let the input be  $x_t$  and the output of the GRU hidden layer be  $h_t$  at moment  $t$ . The computation is shown as follows.

$$z_t = \alpha(W_z[h_{t-1}, x_t]), \quad (4)$$

$$r_t = \alpha(W_r[h_{t-1}, s_t]), \quad (5)$$

$$\bar{h}_t = \tanh(W[r_t * h_{t-1}, s_t]), \quad (6)$$

$$h_t = 1 - z_t * h_{t-1} + z_t * \bar{h}_t, \quad (7)$$

where  $w$  is the weight matrix connecting the two layers, subscripts  $r$  and  $z$  denote the reset and update gates, and  $\tanh$  and  $\sigma$  denote the activation functions.

The model in this paper uses a two-way gate to control the cyclic unit for data extraction, which fully considers the sequence information of the text and improves the accuracy of sentiment judgment.

### 3. Research Methodology and Framework

To effectively study the changing trends of sentiment intensity of topical events in campus comments, this study combines Latent Dirichlet Allocation (LDA) and deep learning. Considering the need for high timeliness in managing public opinion in campus comments, we design a sentiment intensity analysis framework based on probabilistic topic modeling and deep learning. The framework uses LDA models to discover information related to a specific topic event from campus comments; annotates the information by topic; mines students' views and opinions on the event; implements sentiment analysis through word2vec word embedding and LSTM networks, so as to obtain the sentiment intensity of the information and apply it to the topic distribution; and finally builds up the sentiment intensity through changing it under each topic by attention networks and gated recurrent units combined to form a predictive model based on graph neural networks.

**3.1. Potential Dirichlet Allocation Model.** Probabilistic topic models (PTMs) have been used for good effect in text

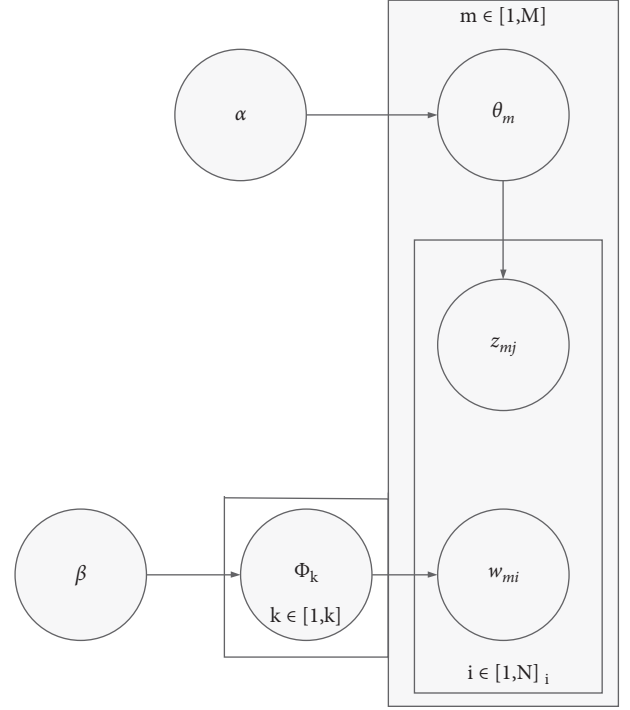


FIGURE 2: Graphical model of IDA.

classification, information retrieval, and other related fields. The basic principle of a probabilistic topic model is that a document is a mixture of probability distributions of several topics, each of which is a mixture of probability distributions of words, and can be regarded as a generative model of a document. Among the various approaches to probabilistic topics, the Latent Dirichlet Allocation (LDA) model is one of the most effective [16].

The traditional LDA-based topic modeling relies on a word cooccurrence model, which is necessarily less effective for short texts such as reviews. Therefore, this paper will improve the IDA to enable adaptive and short textual adaptation of the topic model.

**3.1.1. Model Generation Process.** The LDA is a generative probabilistic model of a 3-layer Bayesian network with the graphical model shown in Figure 2.

Each campus review is assumed to be a mixture of topics; each topic is a probability distribution over a set of words, and each word in the document is generated from a fixed topic.

The generation process is as follows:

- (1) Sample a word distribution  $\Phi_z \sim \text{Dir}(\beta)$  for any topic  $z$ .
- (2) For each comment  $d_m$ , sample a topic distribution  $\theta_d \sim \text{Dir}(\alpha)$ .
- (3) For the word  $w_{mi}$  in comment  $d_m$ , traverse  $a, b$ .
  - (a) Select a subject  $z_{mj}$ ,  $z_{mj} \sim \text{Multi}(\theta_d)$ .
  - (b) Choose a word  $w_{mi}$ ,  $w_{mi} \sim \text{Multi}(\Phi_k)$ .

$M$  denotes the number of documents  $d$  in the corpus;  $z$  denotes the topic in the corpus;  $w$  denotes the words in the corpus;  $\theta_k$  denotes the word distribution of topic  $z_k$ ;  $\theta_d$  denotes the topic distribution of document  $d$ ;  $w_m, i$  denotes the  $i$ -th word of document  $d_m$ ;  $z_m, j$  denotes the  $j$ -th topic associated with document  $d_m$ ;  $N_d$  denotes the number of words in document  $d$ ;  $z_d$  denotes the topic of document  $d$ ; and  $\alpha$  and  $\beta$  are hyperparameters, empirical values:  $\alpha = 50/k$ ,  $\beta = 0.01$ .

In the topic model,  $w_{mm}(d)$  is the known variable,  $\alpha$  and  $\beta$  are the two prior parameters of the given Dirichlet distribution, and  $z_{mm}$  is the potential topic, which is also the generating variable, so it is the document-topic distribution  $\theta_{mk}$  and the topic-word distribution  $\phi_{kt}$  that need to be estimated. Parameter estimation methods currently include the EM (expectation maximization) algorithm, GS (Gibbs sampling), variational Bayesian estimation, message passing algorithm, mean-field variational expectation maximization, and expectation propagation algorithm.

This paper focuses on the collapsed Gibbs sampling algorithm for LDA. "Collapsing" in Gibbs sampling refers to the use of statistical relationships in the form of integrals to achieve estimates of the document-topic and topic-word distributions, avoiding direct computation of the implied parameters.

Based on the model in Figure 2 and the generation process in Section 3.1.1, the joint probability distribution of the model can be calculated.

$$p(w, z|\alpha, \beta) = p(w|z, \beta)p(z|\alpha),$$

$$p(w|\alpha, \beta) = \int p(w|z, \Phi)p(\Phi|\beta)d\Phi = \prod_{m=1}^M \frac{\Delta(n_{m+\beta})}{\Delta(\alpha)},$$

$$p(z|\alpha) = \int p(z|\Theta)p(\Theta|\alpha)d\Theta = \prod_{m=1}^M \frac{\Delta(n_{m+\beta})}{\Delta(\alpha)}, \quad (8)$$

$$n_z = \{n_z^{(t)}\}_{t=1}^V,$$

$$n_m = \{n_m^{(k)}\}_{k=1}^K,$$

$$\Delta(\alpha) = \frac{\prod_{i=1}^K T(\alpha_i)}{T(\sum_{i=1}^K \alpha_i)}.$$

$n_z^{(t)}$  is the number of times a word  $t$  appears in topic  $z_k$ ;  $n_m^{(k)}$  is the number of times a word in document  $d_m$  appears in topic  $z_k$ ;  $\Theta, \theta$  are a parameter space consisting of  $\alpha, \beta$ .

$$\alpha = (\alpha_1, \dots, \alpha_k),$$

$$\alpha_1 = \alpha_2 = \dots = \alpha_k, \beta = \beta = (\beta_1, \dots, \beta_k), \beta_1 = \beta_2 = \dots = \beta_k. \quad (9)$$

Calculate the conditional posterior probability using the joint probability distribution calculated in (1).

$$p(z_i = k|z_{-i}) = \frac{p(w, z)}{p(w, z_{-i})}, \quad (10)$$

$$\begin{aligned} & \frac{p(w, z)}{p(w_{-i}|z_{-i})p(w_i|z_{-i})p(z_{-i})} \\ &= \frac{p(w, z)}{p(w_{-i}, z_{-i})} \cdot \frac{1}{p(w_i, z_{-i})} \propto \frac{\Delta(n_z + \beta)}{\Delta(n_{z_{-i}} + \beta)} \cdot \frac{\Delta(n_m + \alpha)}{\Delta(n_{m_{-i}} + \alpha)} \quad (11) \\ & \propto \frac{n_{k,-i}^{(t)} + \beta_t}{\sum_{t=1}^V n_{k,-i}^{(t)} + \beta_t} \cdot \frac{n_{m,-i}^{(t)} + \alpha_k}{\left[\sum_{k=1}^K n_m^{(k)} + \alpha_k\right] - 1}. \end{aligned}$$

Using the corollary of the prior distribution of the polynomial distribution, the Dirichlet distribution, and (10), the probability distribution of the target parameter can be obtained, and finally the estimation of the parameter is achieved.

$$p(\theta_m|w, z, \alpha) = \frac{\prod_{n=1}^{N_m} p(z_{m,n}|\theta_m)p(\theta_m|\alpha)}{\int_{\Theta} \prod_{n=1}^{N_m} p(z_{m,n}|\theta_m)p(\theta_m|\alpha)d\theta_m},$$

$$\frac{\prod_{\{i:z_i=k\}} p(w_i|\Phi_k)p(\Phi_k|\beta)}{\int_{\Theta} \prod_{\{i:z_i=k\}} p(w_i|\Phi_k)p(\Phi_k|\beta)d\Phi_k} = \text{Dir}(\Phi_k|n_k + \beta),$$

$$\Phi_{k,t} = \frac{n_k^{(t)} + \beta_t}{\sum_{t=1}^V n_k^{(k)} + \beta_t},$$

$$\theta_{m,k} = \frac{n_m^{(k)} + \alpha_k}{\sum_{k=1}^K n_m^{(k)} + \alpha_k},$$

$$\frac{\prod_{n=1}^{N_m} p(z_{m,n}|\theta_m)p(\theta_m|\alpha)}{\int_{\Theta} \prod_{n=1}^{N_m} p(z_{m,n}|\theta_m)p(\theta_m|\alpha)d\theta_m} = \text{Dir}(\theta_m|n_m + \alpha). \quad (12)$$

**3.2. Word2vec.** As a deep learning-based tool, word2vec provides a more efficient way of representing the semantic distance between words by calculating the cosine distance between the word vectors and obtaining the vector expressions of each word in the corpus, based on the corpus and optimization of the training model. Word2vec includes two word vector training models, CBOW and Skip-gram, both of which include an input layer, a projection layer, and an output layer, but the CBOW model predicts the current word from its context, whereas the Skip-gram model predicts the current word from its context. Similarly, word2vec includes two word vector optimization models, the Hierarchical Softmax model and the Negative Sampling model. The Hierarchical Softmax optimization method constructs a binary tree using the frequency of words in the corpus as weights and maps the leaf nodes to all words, while the Negative Sampling optimization method uses relatively simple resampling to improve the speed of word vector training. By combining the two training models with the two optimization methods, a total of four frameworks for training word vectors can be obtained. As a tool for training word vectors, it can quickly and efficiently represent words in a corpus as vectors and capture the semantic features and

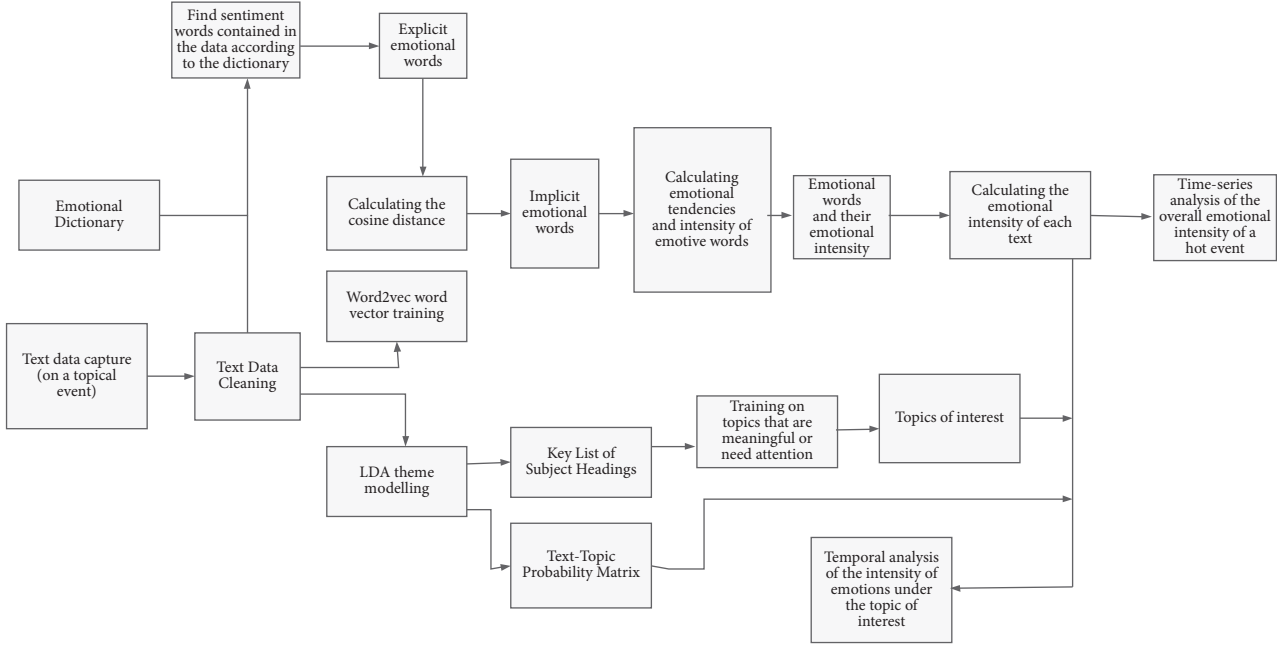


FIGURE 3: Specific process for sentiment analysis.

similarities between words for use in other related application studies. The sentiment intensity of the text data is obtained and used in the correlation analysis of the change of sentiment intensity over time for each topic.

**3.3. Specific Study Process.** In this paper, we investigate a method for sentiment intensity analysis (shown in Figure 3), using probabilistic topic modeling and deep learning to crawl text data from campus forums based on selected hot events and clean the data. Then, we train the model to analyze selected topics that are meaningful or need attention. Based on explicit sentiment words, we use word2vec to obtain implicit sentiment words in the text data and calculate the sentiment intensity of each text. Finally, we perform sentiment intensity time-series analysis under the selected topics.

- (1) Data crawling and preprocessing. The two main tasks are text data capturing and text data preprocessing. The crawler collects and crawls time-series data related to hot events. After crawling the data, the crawled data is preprocessed by word separation, spam filtering, and deactivation of words.
- (2) Topic modeling and filtering. After acquiring the data and preprocessing it, probabilistic topic modeling is carried out using the LDA model.
- (3) Sentiment intensity calculation. The calculation of sentiment intensity is carried out in parallel with the LDA theme modeling. Sentiment intensity was calculated by importing the data into word2vec for word vector cosine distance calculation and then by SO-SD.

**3.3.1. Deep Learning Sentiment Analysis Methods Incorporating Self-Attention Mechanisms.** This paper further incorporates deep learning sentiment analysis with a self-attentive

mechanism based on traditional methods, which can effectively improve the accuracy of temporal analysis.

The model in this paper is divided into six main layers: the word embedding layer, the BGRU layer, the self-attentive layer, the multi-granularity convolutional layer, the attention-based pooling layer, and the fully connected and classified layer, as shown in Figure 4.

The comment text is transformed into word sequences using a word separation library; i.e., the text data is pre-trained to achieve word vector mapping.

Implementing a word vector to a bidirectional gated cyclic unit to learn serialization features, the operation can be combined via a forward GRU and a reverse GRU, followed by the output, as shown in the following equations:

$$h_t^+ = f_{GRU}(h_{t-1}, v_t), \quad (13)$$

$$h_t^- = f_{GRU}(h_{t-1}, v_t), \quad (14)$$

$$h_t = [h_t^+, h_t^-]. \quad (15)$$

The self-attentive mechanism is used to perform an initial screening of features after sequence analysis and extract features with high task relevance. The specific form is as follows: global information is considered, word weight values  $\alpha$  are calculated, and the weights are weighted and summed with the features at each moment to obtain the highlighted new focus feature  $H_t$ . This formula is shown as follows:

$$H_t = \sum \alpha_t h_t, \quad (16)$$

where  $\alpha_t$  is the feature weight and the condition  $\sum \alpha_t = 1$  is satisfied.

This layer receives the output features from the attention layer and selects convolutional kernels of different sizes for further feature extraction using the ReLU function, which

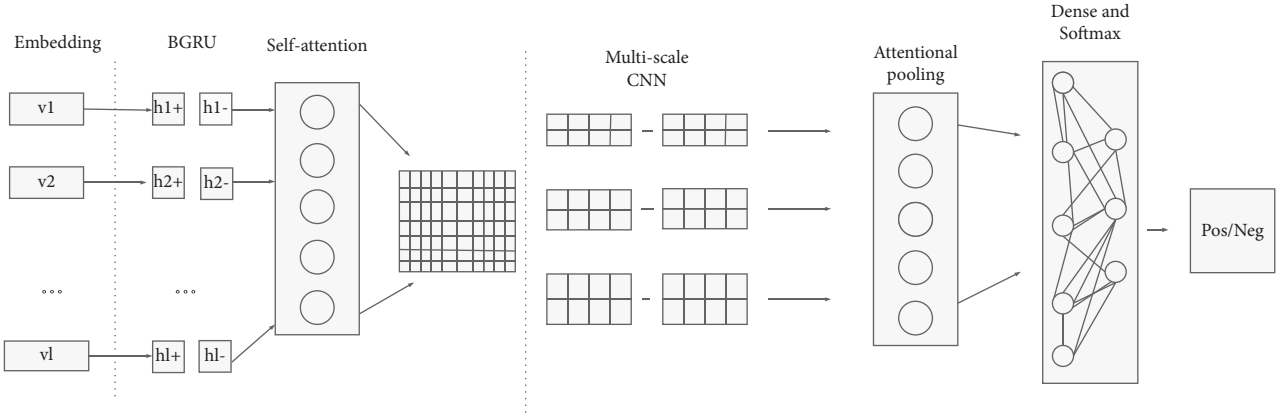


FIGURE 4: Deep learning sentiment analysis methods incorporating self-attentive mechanisms.

speeds up the training convergence and effectively avoids problems such as gradient explosion and disappearance. The feature extraction process is shown as follows:

$$c_i = f_{\text{Relu}}(w \cdot x_{i:i+h-1} + b), \quad (17)$$

where  $w$  is the convolutional kernel weight,  $h * m$  denotes the convolutional kernel window granularity, and  $f_{\text{Relu}}$  is the activation function.

After the model has obtained the feature map, pooling is used to reduce the amount of training data and model parameters to further find out the factors that have the greatest impact on the final sentiment polarity classification results, and this paper uses the attention mechanism instead of the traditional pooling layer to improve the feature extraction capability, as shown in the following equation:

$$P_t = \sum a'_i c_i, \quad (18)$$

where  $a'_i$  is the feature weight and satisfies  $\sum a'_i = 1$ .

The feature map of the data obtained in the convolution layer is extracted by self-attentive dimensionality reduction to obtain a local feature sequence. This layer feeds the feature sequence into the fully connected layer for feature fusion and is classified by the classification layer for emotional polarity. The specific operation process is as follows: the sequence is processed through the fully connected layer to obtain the feature sequence  $D^{\text{final}}$ ; the classification layer performs feature fusion analysis through Softmax and transforms  $D^{\text{final}}$  to derive the probability distribution of the two emotional polarities. The calculation formula is shown in the following equation:

$$p_i = \text{Softmax}(W \cdot D^{\text{final}} + b), \quad (19)$$

where  $p_i$  is the probability distribution of sentiment polarity,  $W$  is the weight matrix of Softmax, and  $b$  is the offset.

The sentiment intensity calculation is performed simultaneously with the LDA modeling, which is more complex compared to the topic modeling.

The processed data were transformed into word vectors, the sentiment lexicon was combined with word2vec and LSTM networks to label sentiment word lexicality, and finally SO-SD was applied to calculate sentiment intensity. The specific calculation formula is shown as follows:

$$\begin{aligned} SO - SD(\text{word}) = & \sum_{\text{poword} \in \text{Pwords}} SD(\text{word}, \text{poword}) \\ & - \sum_{\text{noword} \in \text{Nwords}} SD(\text{word}, \text{noword}), \quad (20) \end{aligned}$$

where  $\text{poword}$  denotes a positive dominant sentiment word that is highly correlated with word;  $\text{Pwords}$  denotes a positive dominant sentiment word that is most correlated with word;  $\text{noword}$  denotes a negative dominant sentiment word that is highly correlated with word; and  $\text{Nwords}$  denotes a negative dominant sentiment word that is most correlated with word. The specific formula is shown as follows:

$$SD(\text{word1}, \text{word2}) = \frac{\sum_{k=1}^n x_{1k} x_{2k}}{\sqrt{\sum_k x_{1k}^2} \sqrt{\sum_k x_{2k}^2}}, \quad (21)$$

where  $n$  is the word vector dimension,  $x_{1k}$  is the  $k$ -dimension value of the first word vector, and  $x_{2k}$  is the  $k$ -dimension value in the second word vector.

Once the SO-SD values are obtained,  $p$  and  $q$  are used as thresholds to make judgments as follows:

$$SO - SD(\text{word}) \begin{cases} > p \text{ The Word is a positive implicit emotion word,} \\ \in [p, q] \text{ The word is neutral,} \\ < q \text{ The word is a negative implicit emotion word.} \end{cases} \quad (22)$$

All positive and negative sentiment words are represented as +1 and -1, respectively. Finally, according to the emotional words and their corresponding emotional intensity, the evaluation is carried out in the campus comment text.

**3.3.2. Building Predictive Models.** Existing prediction models are mainly based on graph neural networks, using them as feature extractors, embedding nodes in vectors, and implementing sequence learning with recurrent neural networks. These methods require information about the nodes over the entire time span and have limited applicability to scenarios where the nodes change frequently. Therefore, recurrent neural networks are usually used for dynamic injection into graph convolutional network parameters to form evolving sequences to solve this problem.

This paper introduces an attention mechanism into graph neural networks on this basis, enabling adaptation to different neighbor weights shared across all edges in the graph, without relying on pre-access to the global graph structure and node features. The prediction model is based on a graph attention network and gated recurrent units, where the graph attention network is the basis and the gated recurrent network implements network parameter updates. The node features are convolved with the graph attention network to obtain a temporal node embedding matrix, and the weight matrix evolves over time through the gated cyclic unit, with the dynamic evolution of the  $l$ -th level of the weight parameter matrix being shown as follows:

$$W_t^{(l)} = \text{GRU}(H_t^{(l)}, W_{t-1}^{(l)}), \quad (23)$$

where  $W_t^{(l)}$  and  $W_{t-1}^{(l)}$  are the weight parameter matrices for time period  $t$  and time period  $t-1$ , respectively;  $H_t^{(l)}$  is the time period  $t$ ,  $l$ -layer node embedding matrix, updated in the manner shown in the following equation:

$$H_t^{(l+1)} = \text{GAT}(A_t, H_t^{(l)}, W_t^{(l)}), \quad (24)$$

where  $A_t$  is the corresponding adjacency matrix for time period  $t$ , which is used to store the inter-vertex relationship, and the node embedding matrix for time period  $t$  and layer  $l+1$  is obtained by calculation. The model can predict the possible sentiment words and the corresponding scores in the next time period by the graph structure in the time period, through the multilayer perceptron MLP, with  $x$  graph structure information, and finally all scores are summed up as the sentiment words derived from the time period prediction.

## 4. Experiments and Analysis

### 4.1. Experimental Setup

**4.1.1. Experimental Environment.** The model was trained using Ubuntu 18.04 operating system, Python 3.8 TensorFlow 1.14 deep learning framework was used for stability considerations, and the hardware configuration is shown in Table 1.

TABLE 1: Experimental environment configuration.

| Hardware    | Configuration                                 |
|-------------|---|
| CPU         | Intel Core i7-10700K; main frequency: 3.8 GHz |
| Memory (GB) | 16  |
| GPU         | NVIDIA RTX 2080 Ti; video memory: 11 GB       |

TABLE 2: Statistics for the online\_shopping\_10\_cats dataset.

| Emotional tendency | Amount | Average length | Mark |
|--------------------|--------|----------------|------|
| Positive           | 31,727 | 68.78          | 1    |
| Negative           | 21,056 | 54.97          | 0    |

TABLE 3: Statistics on the campus review dataset.

| Emotional tendency | Amount | Average length | Mark |
|--------------------|--------|----------------|------|
| Positive           | 7,000  | 112.11         | 1    |
| Negative           | 3,000  | 169.06         | 0    |

TABLE 4: Model parameter configuration.

| Hyperparameter             | Configuration |
|----------------------------|---------------|
| Word vector dimension      | 300           |
| Size of convolution kernel | (2, 3, 4, 5)  |
| Layer of BGRU              | 128           |
| Batch size                 | 50            |
| Learning rate              | 0.0012        |
| Dropout rate               | 0.5           |
| Optimizer                  | Adam          |

**4.1.2. Experimental Dataset.** To test the ability of this model to classify sentiment polarity in the Chinese corpus, two datasets, the online\_shopping\_10\_cats provided by Chinese NLP corpus and the collected campus review dataset, were used for this experiment.

The dataset contains 2 sentiment tendency labels, 0 for negative tendency sentiment and 1 for positive tendency sentiment. The experiments used 52,783 training data items and 10,000 test data items, which were balanced so that each has 5,000 positive and 5,000 negative data items. Specific examples are shown in Table 2.

The campus review dataset contains 7,000 and 3,000 positive and negative disposition sentiment data items, respectively, with 9,000 training data items and 1,000 test data items being set in this experiment; the specific parameters are shown in Table 3.

**4.1.3. Parameter Settings.** The use of moderate dimensional word embeddings preserves the deeper meaning of words and reduces the training overhead and computation. In this paper, a trained high-dimensional word vector model, Chinese Word Vectors, modified by word2vec, is used.

In order to fully extract the text features, four different convolutional kernels are used for contextual information extraction, and a dropout mechanism is added to avoid the phenomenon of fitting; the specific parameter configuration is shown in Table 4.

#### 4.2. Assessment Criteria and Comparison Experiments

**4.2.1. Assessment Methods.** In this paper, accuracy (ACC) and cross-entropy loss (CEL) functions are used to evaluate the parameters.

The formula for calculating ACC is as follows:

$$\text{ACC}(i) = \frac{T_i}{N}, \quad (25)$$

where  $T_i$  is the number of correctly classified data entries and  $N$  is the total number of data entries.

The GEL is calculated as follows:

$$\text{GEL} = -\frac{1}{N} \sum [y \ln a + (1 - y) \ln (1 - a)], \quad (26)$$

where  $a$  is the true output,  $y$  is the desired output, and  $N$  is the total number of texts.

**4.2.2. Comparative Experiments.** To demonstrate the validity of the model, this paper also compares it with other better-performing sentiment analysis models.

- (1) Text sequences were extracted using LSTM, and the comparison experiments were based on the results of the network proposed by Zaremba et al. with partial adaptations.
- (2) Bi-LSTM [25] combines contextual information to improve feature extraction of text sequences.
- (3) GRU improves model training speed by simpler structure.
- (4) Bidirectional GRU (BGRU) enhances the combination of contextual information.
- (5) ATT-BiLSTM uses an attention mechanism to differentiate the importance of the output of the BiLSTM network.
- (6) TextCNN uses CNN networks to extract local features from text.

#### 4.3. Results and Analysis

**4.3.1. Test Results.** The accuracy of each model is shown in Table 5.

Because the same dataset was used, some of the algorithms used results from the existing literature.

**4.3.2. Accuracy Analysis.** As shown in Table 5, the model in this paper achieves 92.75% accuracy on the hotel review dataset, which is the best result for the reformulation group. The experimental results prove that the model in this paper has better performance in the Chinese corpus. At the same time, considering the reasonableness test of the model results, this paper also conducts ablation experiments, and the experimental results prove that the multi-granularity convolutional neural network has certain advantages in improving the model classification, especially with long text data. This paper concludes that convolutional neural

TABLE 5: Summary of model accuracy.

| Model                | Online_shopping_10_cats | Campus comments |
|----------------------|-------------------------|-----------------|
| LSTM                 | 91.58                   | 84.09           |
| GRU                  | 91.79                   | 84.76           |
| Bi-LSTM              | 91.86                   | 85.76           |
| BGRU                 | 92.29                   | 86.43           |
| ATT-BiLSTM           | 92.38                   | 88.22           |
| TextCNN              | 91.11                   | 87.92           |
| Models in this paper | 92.94                   | 92.75           |

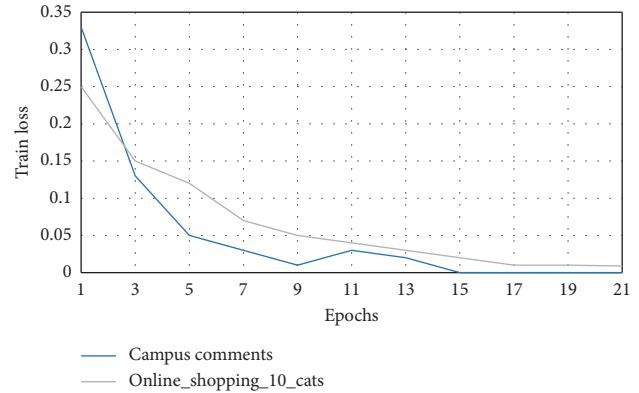


FIGURE 5: Training loss function of the model in this paper.

networks can effectively reduce the dimensionality of data and improve the local feature extraction ability of the model.

The review of the experimental data revealed that the LSTM network structure with complex results and multiple parameters is prone to overfitting in training, reducing accuracy. For recurrent neural networks, the multi-granularity approach improved the accuracy by 0.76% and 1.2% over the single convolutional kernel approach for both datasets. The results demonstrate the effectiveness of multi-scale convolutional kernel feature extraction in sentiment classification tasks, and the self-attentive mechanism further improves the model feature extraction capability and classification accuracy compared to the traditional approach.

**4.3.3. Analysis of Callback Parameters.** The analysis of each parameter of the training process of the model in this paper, as shown in Figure 5, shows that the loss function decreases rapidly with increasing number of training rounds and tends to converge.

On the online\_shopping\_10\_cats dataset, after 6 rounds of training, the loss of the training model will decrease. After 13 rounds, the loss function decreased more slowly, and finally after 18 rounds, the loss function stabilized at 0.009. In the campus comments dataset, the loss function of the model decreased faster and converged after the 8th round. After the 15th round, the loss function dropped to below 0.0001, and the best fit of the model to the dataset was achieved.

From Figure 6, it can be seen that on the online\_shopping\_10\_cats dataset, the test accuracy of the model is

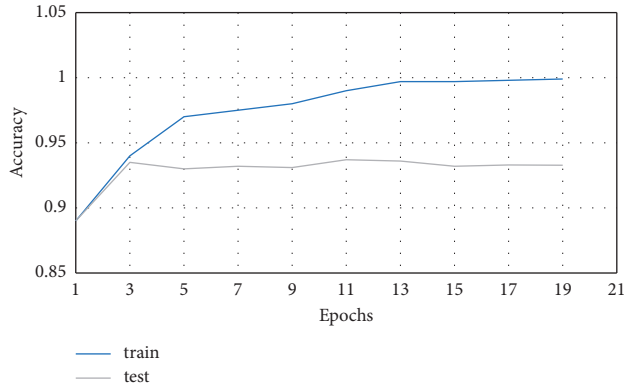


FIGURE 6: Accuracy of the model in this paper on the online\_shopping\_10\_cats dataset.

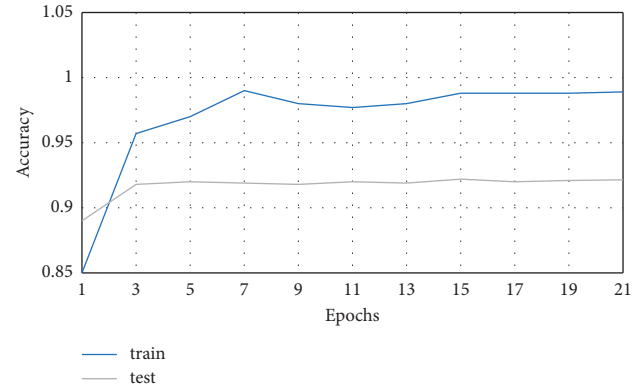


FIGURE 7: Accuracy of the model in this paper on the campus review dataset.

relatively short and the model fits the training data better as the number of experimental rounds increases, but the test accuracy does not change significantly. The test accuracy did not change significantly.

As shown in Figure 7, for the campus review data, the model's test accuracy gradually improved from the first five rounds, and in the 11th round the model performance stabilized.

As shown in Figure 8, the model uses the graph neural network and the adaptive weighting method to effectively improve the performance of evolutionary prediction and achieves good results in the evolution of emotional trends of campus comments. Leveraging the campus review text's semantic relations, structural properties, transforming the text into a graph structure, and then extracting features for predictive modeling through a graph convolutional network. The final result comparison graph proves that the improved scheme is effective.

The above experimental results show that the model can be stabilized with fewer training rounds, with fast convergence, high accuracy of sentiment prediction, and better performance.

To further validate the effectiveness and superiority of the model, this paper randomly divides the dataset into a training set and a test set in a ratio of 8:2. For each dataset, the experiment is repeated three times, and the average of accuracy, precision, recall, and AUC is taken as the final result. The main configuration parameters of the LSTM model contain the maximum number of training rounds (epoch = 10) and word embedding size (embeddingSize = 100).

Comparing this method with SVM and textCNN, as shown in Table 6, we find that textCNN is outstanding in shallow text feature extraction but is not effective in long text areas due to modeling limitations and discourse order insensitivity. LSTM, on the other hand, can capture sequence information and is more effective in sentiment analysis. In this dataset, LSTM achieves accuracy, precision, recall, and AUC of 96.1%, 84.2%, 88.9%, and 0.904 (threshold = 0.7), which are 3.2%, 0.9%, 3.3%, and 0.053 higher than textCNN and 7.2%, 4.8%, 7.7%, and 0.0821 higher than SVM, respectively. The above data demonstrate the superiority of using LSTM models for solving text sentiment analysis problems.

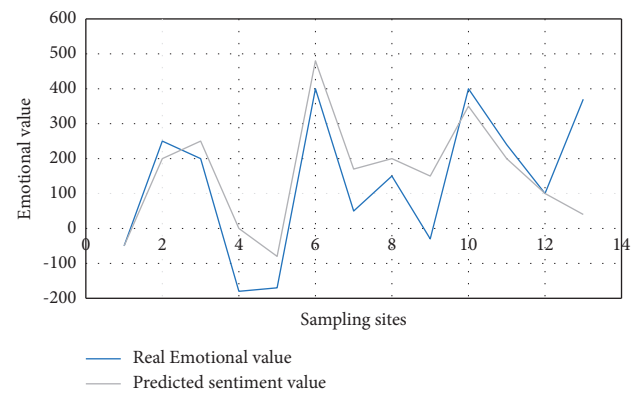


FIGURE 8: Predicted sentiment values versus true sentiment values.

TABLE 6: Comparison of LSTM with other methods.

| Methods | Accuracy (%) | Precision (%) | Recall (%) | AUC    |
|---------|--------------|---------------|------------|--------|
| SVM     | 88.9         | 79.4          | 81.2       | 0.8219 |
| TextCNN | 92.9         | 83.3          | 85.6       | 0.8510 |
| LSTM    | 96.1         | 84.2          | 88.9       | 0.9040 |

In this paper, we analyze the influence of different word vector dimensions on the performance of the model. As shown in Figure 9, word vector data with dimensions of 50, 100, 150, and 200 are processed, and the accuracy rate can reach 89.3%, 89.9%, 88.9%, and 88.6%, respectively, by comparing the LSTM model with the annotated text, and the results show that the accuracy is higher when the word vector dimension is 100. Therefore, the model is trained with a word vector dimension of 100.

In this paper, we also consider the influence of the maximum number of training rounds of the LSTM model on the results, as shown in Figure 10, the maximum number of training rounds epoch is a key parameter affecting the performance. Too many times will cause the predicted value of the fitted loss rate available estimation model to be inconsistent with the true value. The experiments were carried out with 5, 10, 15, 20, and 25 dimensions. The results showed that with the increase of dimensions, the loss rate decreased first and then increased. When the dimension was 10, the



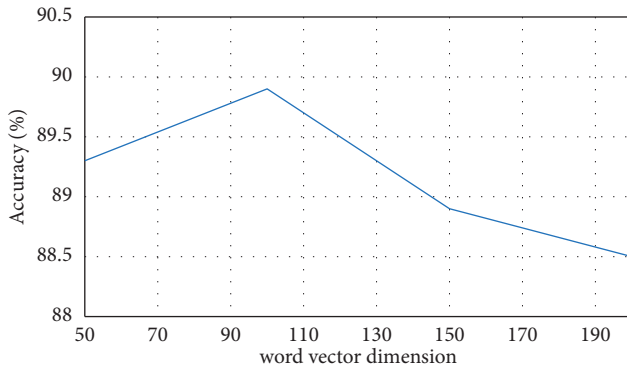


FIGURE 9: Effect of word vector dimensionality on accuracy.

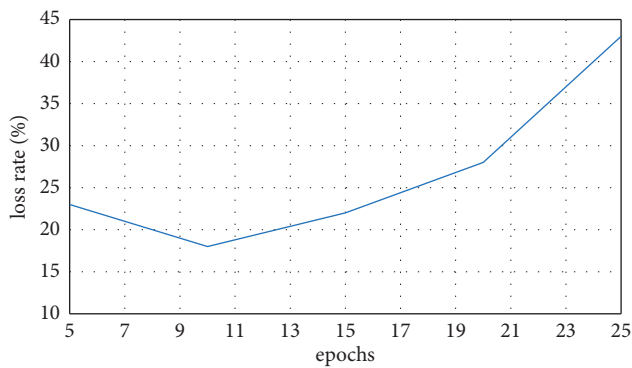


FIGURE 10: Effect of maximum number of training rounds on loss rate.

loss rate reached the best value of 16.8%. Therefore, the maximum number of training rounds in this paper was set to 10.

Overall, it can be found that the sentiment intensity analysis method based on probabilistic topic model and deep learning model proposed in this paper can obtain different views and student evaluation in public opinion based on campus comments more accurately and can reasonably and effectively analyze the change of sentiment intensity of each opinion and event over time. This method not only effectively makes up for the shortcomings of traditional opinion analysis methods in terms of not being able to obtain trends of changes in sentiment and make effective predictions for managing public opinion, but also allows for targeted sentiment analysis based on students' different views and opinions and can calculate and analyze students' public opinion and their sentiment more accurately, which is of great significance and value for monitoring and managing public opinion. The method also has a certain degree of significance in guiding students and university opinion management workers in public opinion, helping them to handle and respond to public opinion in a reasonable manner and carry out more scientific and effective opinion management.

## 5. Conclusion

For campus opinion analysis and management, which is essentially a text sentiment analysis task based on Chinese

corpus, this paper proposes a deep learning sentiment analysis method incorporating a self-attention mechanism. The model uses a recurrent neural network structure to extract the sequence features of the text; then uses the self-attentive mechanism to highlight the sentiment classification features, which are fed into a multi-granularity convolutional neural network for higher-level feature extraction; uses the self-attentive mechanism to implement the pooling function; and finally achieves the sentiment polarity determination of the text. Experiments on two typical datasets demonstrate that the model has improved the accuracy of sentiment polarity prediction compared with the current mainstream methods. In addition, this paper demonstrates the soundness of the model structure through ablation experiments. By using a combination of convolutional neural networks and recurrent neural networks, the model achieves good results on both datasets. However, in reality, there is often a lack of high-quality training data in the target domain, and how to improve the ability of deep learning models to solve cross-domain problems from existing training datasets is worthy of further research.

## Data Availability

The experimental data used to support the findings of this study are available from the author upon request.

## Conflicts of Interest

The author declares no conflicts of interest regarding this work.

## References

- [1] B. Ding, "On online public opinion," *Journalist*, vol. 28, no. 3, p. 6, 2010.
- [2] Y. Liu and Y. Li, "Analysis of the communication characteristics of online public opinion," *Journal of Beijing University of Posts and Telecommunications*, vol. 13, no. 4, pp. 1–6, 2011.
- [3] Y. He and K. Ye, "A report on the analysis of public opinion on the campus network of Beijing University of Posts and Telecommunications based on "Beiposters Forum"," *Journal of Beijing University of Posts and Telecommunications*, vol. 14, no. 2, pp. 22–31, 2012.
- [4] Y. Cui, Z. Wang, and J. Jiang, "Content analysis of policy texts on online public opinion governance in colleges and universities," *Contemporary Education and Culture*, vol. 13, no. 6, pp. 102–107, 2021.
- [5] B. Ma, N. Zhang, and T. Sun, "Big data analysis of public feedback in the context of smart cities: a probabilistic thematic modeling perspective," *E-government*, vol. 10, no. 12, pp. 9–15, 2013.
- [6] X. Tan, M. Zhuang, T. Mao, and Q. Zhang, "Analysis of large-scale online public opinion sentiment evolution based on LDA-ARMA hybrid model," *Journal of Intelligence*, vol. 39, no. 10, pp. 121–129, 2020.
- [7] X. Yang, Z. Song, K. Zhao et al., "Research on public opinion analysis of Guizhou attractions based on LDA model and sentiment analysis," *Modern Computer*, vol. 27, no. 25, pp. 36–43, 2021.

- [8] M. Q. Wu, J. M. Wu, and W. B. Xin, "Optimization of Word2Vec+LSTM multi-category sentiment classification algorithm," *Computer Systems Applications*, vol. 29, no. 1, pp. 130–136, 2020.
- [9] X. Cai and J. Yang, "Research on Twitter sentiment analysis based on word sense enhancement and attention mechanism," *Computers and Digital Engineering*, vol. 49, no. 11, pp. 2266–2270, 2021.
- [10] C.-Y. Li and J. Liu, "Sentiment analysis of car companies' public opinion based on attention and Bi-LSTM hybrid algorithm," *Information Technology and Network Security*, vol. 40, no. 1, pp. 45–49, 2021.
- [11] S. S. Tang, L. P. Lian, C. L. He et al., "A Bert and Bi-LSTM based sentiment recognition for public opinion information," *Network Security Technology and Applications*, vol. 21, no. 7, pp. 57–59, 2021.
- [12] Y. Zhu, "Logistic-based early warning model and case study of university education public opinion[J]," *Education Teaching Forum*, vol. 12, no. 34, pp. 3–6, 2020.
- [13] S. Q. Peng, A. M. Zhou, S. Liao, Y. T. Zhou, D. F. Liu, and Y. Wen, "Research on predicting the evolution of public opinion based on graph attention network," *Journal of Sichuan University (Natural Science Edition)*, vol. 59, no. 1, pp. 109–116, 2022.
- [14] R. Zhang and Q. Xiao, "Research on early warning of university online public opinion based on improved LSTM-CNN model," *Journal of Huainan Normal College*, vol. 23, no. 6, pp. 77–81, 2021.
- [15] Y. Duan, Y. Zhang, Y. Zhang, and R. Duan, "Microblog sentiment classification based on LSTM-CNNs sentiment enhancement model," *Journal of Beijing University of Information Science and Technology (Natural Science Edition)*, vol. 34, no. 6, pp. 1–7, 2019.
- [16] Y. Chen and J. Sheng, "Microblog tag generation algorithm based on LDA and Word2ve," *Computer and Modernization*, vol. 37, no. 12, pp. 37–42, 2021.
- [17] G. Salton, A. Wong, and C. S. Yang, "A vector space model for automatic indexing," *Communications of the ACM*, vol. 18, no. 11, pp. 613–620, 1975.
- [18] S. Deerwester, S. T. Dumais, G. W. Furnas, T. K. Landauer, and R. Harshman, "Indexing by latent semantic analysis," *Journal of the American Society for Information Science*, vol. 41, no. 6, pp. 391–407, 1990.
- [19] T. Hofmann, "Probabilistic latent semantic analysis," in *Proceedings of the Fifteenth conference on Uncertainty in artificial intelligence*, pp. 289–296, Morgan Kaufmann Publishers Inc, San Francisco, CA, USA, August 1999.
- [20] Y. Bengio, R. Ducharme, P. Vincent, and C. Janvin, "A neural probabilistic language model," *Journal of Machine Learning Research*, vol. 3, no. 6, pp. 1137–1155, 2003.
- [21] Y. Wang, J. Han, H. Guo, C. Liao, and L. Wang, "Bi-LSTM-based structural deformation prediction," *Computer Systems Applications*, vol. 30, no. 11, pp. 304–309, 2021.
- [22] S. S. Zhou, Z. W. Zhang, and J. Wen, "Natural language information hiding based on neural network machine translation," *Computer Science*, vol. 48, no. S2, pp. 557–564, 2021.
- [23] J. Zhao, M. Song, X. Gao, and Q. Zhu, "A study of text representation in natural language processing," *Journal of Software*, vol. 33, no. 1, pp. 102–128, 2022.
- [24] J. Lu and X. Li, "Neural network language model," *Communication World*, vol. 24, no. 9, pp. 94–95, 2017.
- [25] Z.-X. Sun, B. Ding, and X.-Y. Sun, "New cell load forecasting based on migration learning and GRU networks," *Electricity demand-side management*, vol. 24, no. 1, pp. 55–62, 2022.

## Research Article

# Analysis and Optimization of the Online Vocal Teaching System Based on Intelligent Computing

Luzhen Jiang 

*Department of Education and Modern Art, Shangqiu Institute of Technology, ShangQiu 476000, China*

Correspondence should be addressed to Luzhen Jiang; [jiangluzhen@sqgxy.edu.cn](mailto:jiangluzhen@sqgxy.edu.cn)

Received 2 March 2022; Revised 23 March 2022; Accepted 2 April 2022; Published 22 April 2022

Academic Editor: Man Fai Leung

Copyright © 2022 Luzhen Jiang. This is an open access article distributed under the Creative Commons Attribution License, which permits unrestricted use, distribution, and reproduction in any medium, provided the original work is properly cited.

With the continuous development of science and technology, network technology has become more and more advanced and network applications are widely used in all walks of life, and vocal music teaching is no exception. The Intelligent Agent plays a unique role in networked teaching by making up for the lack of intelligence, adaptiveness, autonomy, and interoperability and interactivity in all aspects of traditional teaching. This paper introduces the knowledge of Intelligent Agent and then discusses its application in the networked teaching environment. Compared with the traditional teaching environment, the intelligent network teaching environment is more conducive to the initiative and innovation of students, reflecting the characteristics of student-centred learning and achieving a variety of functions such as teaching resource sharing, information interaction, online communication, and distance learning with the support of computer network technology. It is a new field to be explored, especially opening up a new chapter of online vocal music teaching.

## 1. Introduction

In recent years, the online delivery method has been growing rapidly, with more and more students and parents recognising that online education is “time-saving and geographically unrestricted” [1]. Online web-based education can balance the educational resources of different regions, allowing children in relatively disadvantaged areas to enjoy high-quality education. In order to adapt to online education, the author has also tried to teach online vocal music courses for a long period of time, and this article briefly discusses the teaching of online vocal music courses based on his teaching experience [2].

Online courses have become a major form of learning for students at all levels, and this fast and convenient way of learning has become very common, been gradually accepted, and brought convenience to the promotion of vocal music teaching courses [3]. Cloud vocal courses and cloud concerts are already being widely disseminated in 2020. The role of digital technology in vocal music teaching is becoming increasingly important [4].

Internet technology, especially the 5G media that have been developed in recent years, is a new and modern media

based on the original digital technology, which is improved and enhanced by modern technology [5]. With the development of science, the transmission speed of 5G is more than ten times faster than 4G, greatly reducing the time to download high-definition course videos, and the course itself can carry a larger capacity of lesson transmission, thus bringing great convenience to the demonstration of vocal singing teaching and the improvement of classroom efficiency [6]. Through online teaching, students can save and play back what they have learned, digest and absorb it repeatedly, and delve into the organic integration of digital technology and vocal teaching, bringing convenience to the promotion of vocal teaching courses. The digital technology means to bring together the best talents and works from all over the country to form a collaborative singing and performance across the air [7]. How to combine digital technology with vocal teaching organically to achieve the innovative point of unifying online and offline teaching and to form a new model of vocal teaching activities is the key topic of vocal teaching research at present.

Vocal music lessons in higher education are a compulsory part of the curriculum for music majors and are traditionally taught in a “hands-on, master-apprentice”

mode [8]. This is usually a class where a vocal teacher teaches one or more students about vocal music, analyses the structure of the music, and teaches singing techniques, so it is also known as a “vocal technique class” [9]. Vocal lessons are very specialised and require the teacher to identify and solve problems in a timely manner, including musical, technical, and emotional issues. Vocal online lessons have changed the traditional mode of vocal teaching, but since it is a new thing, the cognitive study of it needs to go through a process of exploration, and in the face of many difficulties, it is a great test for vocal teachers to overcome the difficulties and make a good vocal online lesson [10].

At present, the construction of a networked teaching environment is gradually popularized, especially the construction of a networked teaching environment in higher education institutions, but the construction of an intelligent networked teaching environment is relatively lagging behind [11]. Therefore, the construction of an intelligent network teaching environment and its application to teaching have become a hot topic of discussion at present.

## 2. The Integration of Digital Technology and Vocal Skills Techniques

The 5G full media are a product of the current social development and an important part of innovative technology [12]. Vocal music teaching in the era of full media needs to create new teaching methods to test and improve the technicality and singing ability of vocal music works through digital technology. In this way, we can disseminate online courses related to vocal music teaching, follow the performances and lectures of influential figures in the vocal music industry through online platforms such as Shake, WeChat Friend Circle, and Weibo, and exchange and learn from each other, drawing on the experience and methods of the master performers and applying them to our own vocal music teaching [13]. The famous singers Dai Yuqiang’s “Dai You Sing,” Mr. Yan Weiwen’s “Master Yan Makes High Students,” Mr. Shi Yijie, Mr. Liu He Gang, Mr. Zhang Ye, etc., all conveyed their vocal learning experience to vocal learners through the Internet technology, so that the majority of vocal singers can directly gain experience and methods and quickly improve their singing ability [14].

In today’s society, vocal music teaching can only be diversified to meet the current needs of talent training and to provide more opportunities and directions for students’ future employment and further education [15], under the premise of expanding vocal teaching methods, achieving all-round and multiperspective teaching, solidly promoting students’ technical skills training in stage performance and singing, using digital technology as a carrier to achieve the integration and development of digital technology and vocal teaching, and making more people aware of the forward-looking impact of using digital 5G all-media in vocal teaching to realise the systematisation of vocal teaching. More aspirants are encouraged and supported to be placed in the development of online courses that integrate digital technology and vocal teaching, so that students can better

develop the integration of their studies and related knowledge [16].

Not only internal quality system construction is reflected in the policy and curriculum system of arts vocational education but also teachers for leading education and students as the subject of education also play an important role in education, strengthening the teacher talent training model and thus promoting the development of arts vocational schools. Voice teaching exploration and growth become an important guarantee of internal system construction in the new era of arts vocational institutions [17]. To this end, we need to use digital technology to identify, access, and respond to common and unexpected problems in the internal quality management of teaching in a timely and accurate manner; to react, reflect, and continue in-depth research in the first instance; and to promote the establishment of a highly qualified, innovative, and professional teaching staff. In the process of teaching vocal music, it is important to keep pace with the times, sing the voice of China in the new era, and use advanced technological means such as big data to establish a new model of sound internal quality system in art vocational schools [18].

## 3. Intelligent Agent Technology

*3.1. Intelligent Agent Definition.* Intelligent Agent technology is a distributed computing environment software intelligence technology and is a product of artificial intelligence and network technology, and it provides a distributed heterogeneous environment with intelligent applications to achieve intelligent coordination of a new computing model. An Intelligent Agent is a software package that has intelligent reasoning and decision-making capabilities and can take certain countermeasures in the face of changing environments. An Intelligent Agent is an intelligent computer program that can be subdivided into many small functional modules, making the program modular and flexible.

### 3.2. Smart Agent Features

- (1) **Autonomy:** the ability to adapt to changes in the environment according to the needs of the user, to take the initiative to provide services for the user, and to make appropriate responses to the impact and information from the environment
- (2) **Intelligence:** the ability to perceive the surrounding environment, reason and calculate intelligently, analyse the needs of the user, and accumulate experience to improve its ability to deal with problems
- (3) **Agent (agent):** can represent the user to complete some work or agent user software and other software to communicate and contact
- (4) **Mobility (mobility):** as a living body, able to roam across platforms on the internet to help users gather information, their state, and behavior with continuity
- (5) **Security:** to avoid damage to the computer environment caused by malicious agents

Because the Intelligent Agent has the characteristics of professionalism, the Intelligent Agent in the network teaching system must also be MAS (multiagent system). At the same time, in order to complete a complex task, it is also possible to create multiple collaborative and cooperative agent groups to improve the system's ability to solve problems.

#### 4. Intelligent Agent-Based Networked Teaching Environment

*4.1. The Concept of Intelligent Agent Networked Teaching.* Networked teaching and learning includes the teaching of teachers and the learning of students in a networked environment [19]. The agent used in the networked teaching environment is called the network teaching agent, and the network teaching agent is an agent that assists students in their learning and can interact with them; in the networked teaching environment, it must be able to coordinate with other agent systems and make judgments and decisions on the methods and steps used by the system in different environments. The environment in which the network teaching agent system is located is the student's learning environment, and the teaching agent system can give the necessary tutorials and tips to students at all stages of learning, which make them interact with the network teaching agent system, so that students feel that they are communicating with a living individual, thus improving the efficiency of learning and the quality of network teaching. At the same time, intelligent agents must provide teachers with an intelligent teaching environment [20].

*4.2. Intelligent Agent Networked Teaching Environment System Model.* The system adopts the B/A/S model, i.e., Browser/Agent/Central Server, which helps to speed up access, and the client uses the Internet/Intranet network which can provide a unified environment for complex distributed applications. The model consists of four parts: client, browser system, Intelligent Agent system, and server resource system (see Figure 1).

*4.2.1. Smart Agent Web-Based Teaching Solutions.* Based on the networked teaching environment of Intelligent Agent, the networked teaching solution was proposed and applied to the teaching of some courses in Shandong Trade Union Management Cadre College. The structure of the Intelligent Agent network teaching solution is shown in Figure 2.

A flowchart of the Intelligent Agent's web-based teaching process has been designed based on the structure diagram in Figure 3.

*4.2.2. Intelligent Agent Web-Based Teaching Solution Module Features.* The Intelligent Agent-based web-based teaching and learning solution includes three types of users: students, teachers, and administrators. There are 8 agents involved:

- (1) Student agent: It is an agent automatically generated by the system after students enter the online teaching

environment; it provides an interface for students to interact with the system, selects the teaching content dynamically according to the actual situation of students, and guides students to learn independently. They can apply for tutorials from the teacher, submit assignments or request tests, interact and discuss with other student agents, and prepare for the next step of learning based on the user's learning record.

- (2) Teacher agent: it is an agent automatically generated by the system after the teacher has logged into the online teaching environment, which can simulate the teacher's behaviour, select the appropriate knowledge to be taught to the students according to their actual situation, monitor and evaluate the students' behaviour, and provide help and select correction methods at the request of the students, whose terminal is located in each department office [21].
- (3) Administrator agent: it is an agent automatically created by the administrator after logging into the network teaching environment; the administrator agent is the organiser of the whole system, and its terminal is in each teaching management department such as the Academic Affairs Office. The administrator agent can coordinate a series of management procedures in the teaching process, such as course management, student registration management, and grade management.
- (4) Management agent: the management agent is responsible for the interaction between students, teachers, administrators, and the teaching and management subsystem and records the interaction process. The management agent is responsible for registering the current learning status of individual students and triggering the teaching agent to provide personalised teaching. It also monitors and evaluates students' learning through interactive information, giving tips, conclusions, and reference information [22].
- (5) Review training agent: teaching activity itself is an interactive process, and teachers need to understand the students' knowledge mastery and adjust their teaching methods and contents in time; students need to cooperate with teachers to master various types of knowledge and basic skills. Therefore, the review training agent provides the auxiliary learning functions of review training and automatic question and answer.
- (6) Evaluation agent: teaching evaluation is a very important part of the teaching process, and the introduction of an evaluation agent in the network teaching environment can provide dynamic teaching evaluation of the whole teaching process.
- (7) Exam and test agent: the exam and test agent is an agent responsible for testing students' questions and is used to support students' self-assessment of their current learning situation, mainly through interaction with the test bank to determine students' knowledge level and errors. The test agent gives



FIGURE 1: Networked teaching model for Intelligent Agent systems.

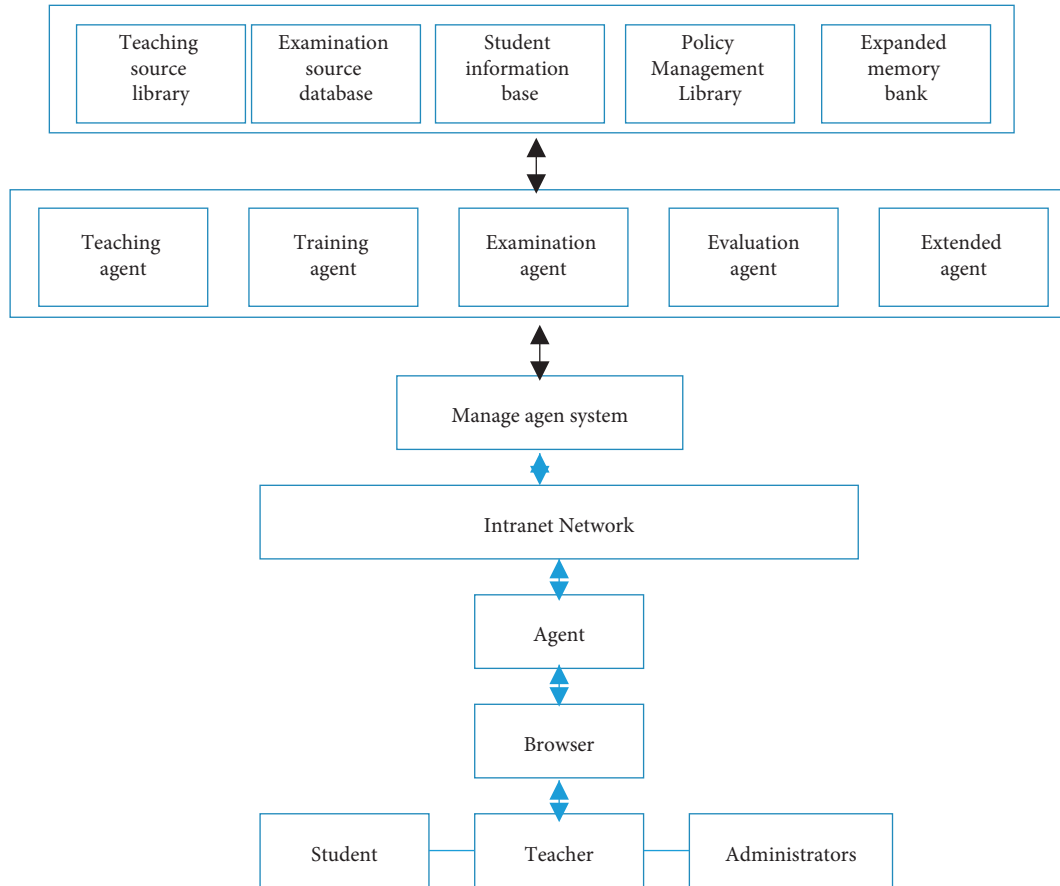


FIGURE 2: Structure of the Intelligent Agent web-based teaching solution.

correct answers and scores after the test is completed and completes the evaluation of the test results.

- (8) Extension agent: the extension agent combines the openness of the system and provides ports for the whole system to match with other systems at any time.

**4.2.3. Implementation of the System.** The development of Intelligent Agent applications can use a variety of distributed object building block technologies such as CORBA, DCOM, and Java RMI. The interface definition language IDL in CORBA also provides mapping to Java, C++, Smalltalk, and other languages, allowing easy interaction between objects from different platforms on the web. Therefore, the best solution for implementing an agent-based web-based teaching system is to use a combination of CORBA and Java technology. The B/A/S model is used, i.e., Browser/Agent/Central Server. Windows XP is used, and NT is used for the server [23, 24].

## 5. Intelligent Agent Technology in a Networked Teaching Environment

In 2020, we used traditional computer-based teaching methods, and in 2021, we piloted the implementation of networked teaching for vocal courses using Intelligent Agent technology and are now conducting a comparison experiment between the two years of the vocal course (see Table 1).

The results of the comparison and interviews with some students show that students' motivation to learn is significantly improved, their hands-on skills are significantly enhanced, and the difficulty of the course is intelligently adjusted according to the level of the students, so that the potential of each individual can be maximised and students can be effectively guided to learn better. It provides an effective platform for teachers to innovate in the curriculum, reduces duplication of effort, accurately grasps students' mastery of knowledge, provides targeted instruction, improves teaching efficiency, and is welcomed by teachers [25, 26].

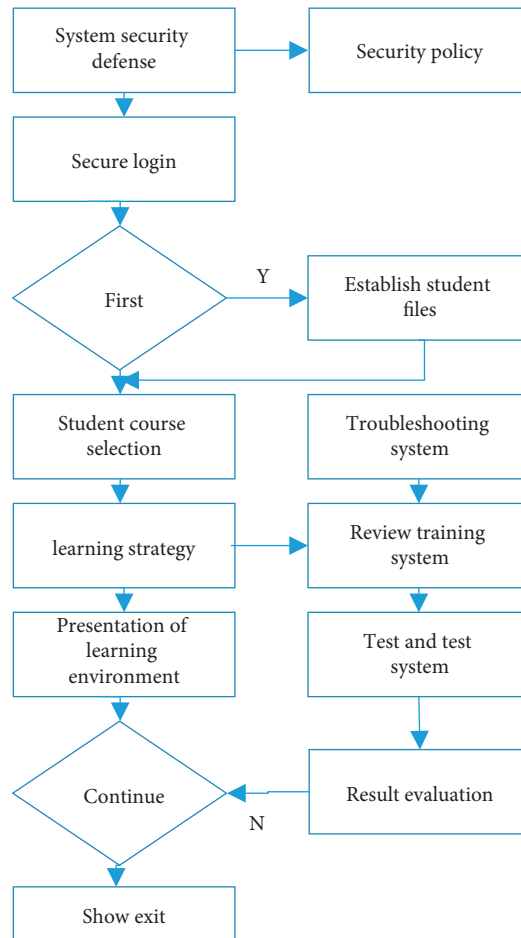


FIGURE 3: Flowchart of agent web-based teaching.

TABLE 1: Comparison of 2007 computer class results.

|                      | Fundamentals of computer (average) | Software engineering (average) | Assembly language (average) | Java language (average) | Visual basic language (average) | Network technology (average) |
|----------------------|------------------------------------|--------------------------------|-----------------------------|-------------------------|---------------------------------|------------------------------|
| Network technique    | 82.3                               | 71.2                           | 77.4                        | 77.5                    | 75.2                            | 78.2                         |
| Software technology  | 79.1                               | 73.9                           | 79.4                        | 78.1                    | 76.2                            | 79.4                         |
| Computer application | 79.2                               | 72.4                           | 79.9                        | 78.4                    | 75.2                            | 78.4                         |
| Animation technology | 79.572.8                           | 77.4                           | 77.5                        | 74.3                    | 75.2                            | 77.1                         |

As shown in Figure 4, digital full media technology brings certain facilities for vocal teaching and provides modern resources for the improvement of vocal teaching techniques. There are two sides to everything, and the same is true of modern media technology. If used accurately, it can quickly improve singing skills and enhance the knowledge and techniques we learn. The Gaussian distribution of vocal learning results across students shows that the use of full media technology in vocal performance teaching methods, which includes the promotion and dissemination of vocal performance teaching methods through digital technology,

makes it easier to improve teaching efficiency and enable students to acquire the latest knowledge [27].

As shown in Figure 5 for the vocal effect assessment, our students are recorded by video and audio at the beginning of their enrolment to create a record of their initial learning status. Through the intervention of digital teaching methods, students are able to realise their shortcomings and identify ways and means to solve their problems. At special instances when parents cannot be present to watch their students' examinations, the digital network technology allows parents to see their students' learning status at school without having

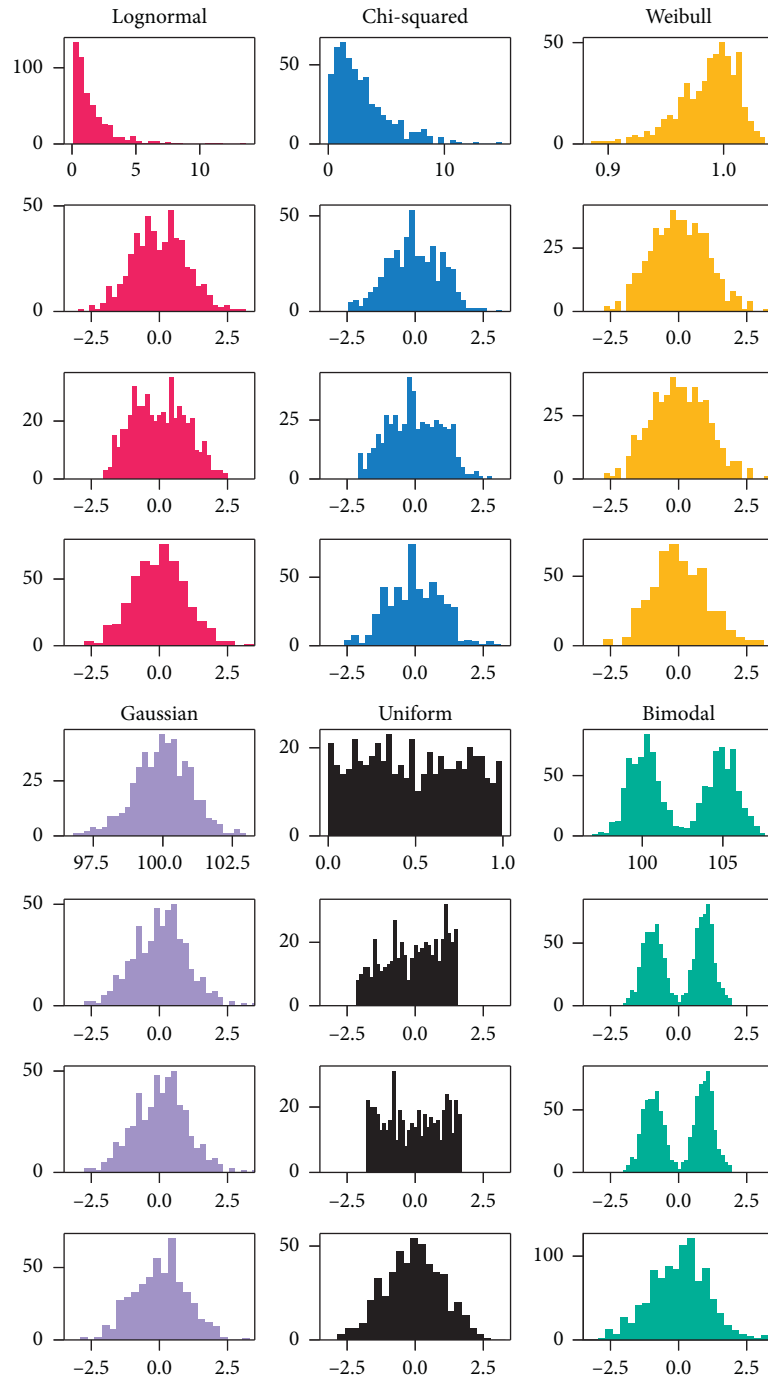


FIGURE 4: Distribution of online learning outcomes of vocal students by year.

to leave home, greatly facilitating communication between the school and parents.

In the process of learning vocal lessons in colleges and universities, vocal practice and singing songs remain an unavoidable process in vocal lessons and vocal skills are basically addressed in vocal practice pieces and songs. Due to the instability of the signal transmission or the sensitivity of receiving equipment, the transmission of

information in online courses is more or less delayed. As shown in Figure 6 for the correlation of vocal characteristics in this paper, the network reception delay can be as much as five or six seconds in some cases if the student is in a different area. Vocal lessons require student singing and teacher accompaniment at the same time, in order to reduce the delay caused by teacher accompaniment of student singing.



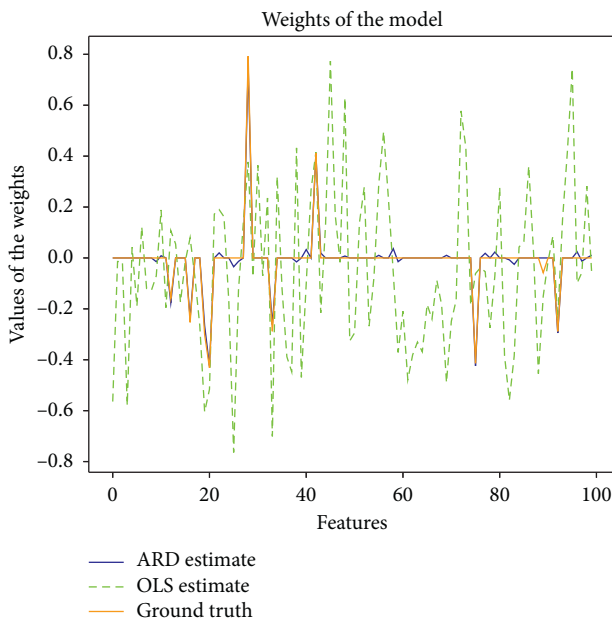


FIGURE 5: Assessment of vocal effects.

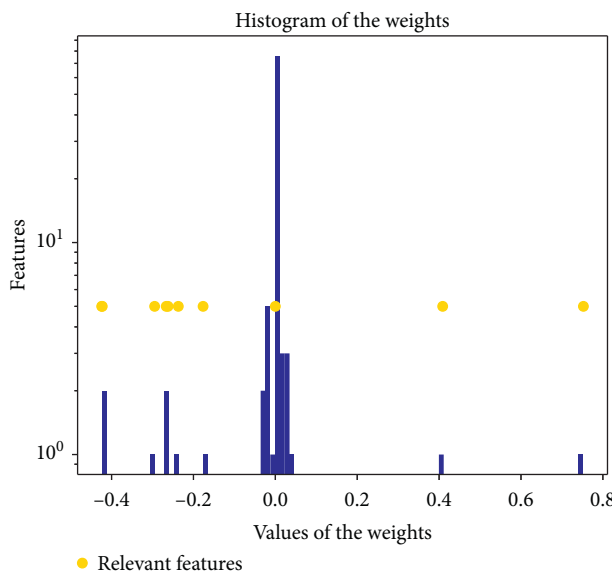


FIGURE 6: Correlation of vocal characteristics.

## 6. Conclusions

The application of Intelligent Agents in the online teaching environment of vocal music makes the teaching effect, teaching mode, and system performance much better than the traditional teaching mode, promotes the intelligence of the networked teaching environment, improves teaching efficiency, saves teaching costs, and plays a positive role in promoting the overall teaching reform and the implementation of quality education. As an auxiliary means of network teaching, the Intelligent Agent teaching system cannot completely replace the role of the teacher and the two must be combined in practical applications.

## Data Availability

The experimental data used to support the findings of this study are available from the author upon request.

## Conflicts of Interest

The author declares that there are no conflicts of interest regarding this work.

## Acknowledgments

This work was sponsored in part by Mixed Teaching Model Reform and Practice of Music Theory and Trial Singing Course Based on Smart Tree Platform (2021JGXM58).

## References

- [1] H. Swapnarekha, H. S. Behera, J. Nayak, and B. Naik, "Role of intelligent computing in COVID-19 prognosis: a state-of-the-art review," *Chaos, Solitons & Fractals*, vol. 138, Article ID 109947, 2020.
- [2] G. Malik, D. K. Tayal, and S. Vij, "An analysis of the role of artificial intelligence in education and teaching," in *Recent Findings in Intelligent Computing Techniques*, pp. 407–417, Springer, Singapore, 2019.
- [3] S. Smys, R. Bestak, and J. I.-Z. Chen, "Special issue on evolutionary computing and intelligent sustainable systems," *Soft Computing*, vol. 23, no. 18, p. 8333, 2019.
- [4] B. Ç Uslu, E. Okay, and E. Dursun, "Analysis of factors affecting IoT-based smart hospital design," *Journal of Cloud Computing (Heidelberg, Germany)*, vol. 9, no. 1, pp. 67–23, 2020.
- [5] A. Javeed, S. Zhou, L. Yongjian, I. Qasim, A. Noor, and R. Nour, "An intelligent learning system based on random search algorithm and optimized random forest model for improved heart disease detection," *IEEE Access*, vol. 7, pp. 180235–180243, 2019.
- [6] Y. Xiong and Y. Lu, "Deep feature extraction from the vocal vectors using sparse autoencoders for Parkinson's classification," *IEEE Access*, vol. 8, pp. 27821–27830, 2020.
- [7] D. Minoli, K. Sohraby, and B. Occhiogrosso, "IoT considerations, requirements, and architectures for smart buildings-Energy optimization and next-generation building management systems," *IEEE Internet of Things Journal*, vol. 4, no. 1, pp. 269–283, 2017.
- [8] O. Deperlioglu, U. Kose, D. Gupta, A. Khanna, and A. K. Sangaiah, "Diagnosis of heart diseases by a secure internet of health things system based on autoencoder deep neural network," *Computer Communications*, vol. 162, pp. 31–50, 2020.
- [9] M. S. Hossain, G. Muhammad, and N. Guizani, "Explainable AI and mass surveillance system-based healthcare framework to combat COVID-19 like pandemics," *IEEE Network*, vol. 34, no. 4, pp. 126–132, 2020.
- [10] Y. Sermet and I. Demir, "Virtual and augmented reality applications for environmental science education and training," *New Perspectives on Virtual and Augmented Reality: Finding New Ways to Teach in a Transformed Learning Environment*, Taylor & Francis Group, Abingdon, Oxfordshire, pp. 261–275, 2020.
- [11] Z. H. A. N. G. Zhengwan, Z. H. A. N. G. Chunjiang, L. I. Hongbing, and X. I. E. Tao, "Multipath transmission

- selection algorithm based on immune connectivity model,” *Journal of Computer Applications*, vol. 40, no. 12, p. 3571, 2020.
- [12] K. H. Abdulkareem, M. A. Mohammed, A. Salim et al., “Realizing an effective COVID-19 diagnosis system based on machine learning and IOT in smart hospital environment,” *IEEE Internet of Things Journal*, vol. 8, no. 21, pp. 15919–15928, 2021.
- [13] Y. Ma, Y. Wang, J. Yang, Y. Miao, and W. Li, “Big health application system based on health internet of things and big data,” *IEEE Access*, vol. 5, pp. 7885–7897, 2016.
- [14] R. K. Barik, H. Dubey, C. Misra et al., “Fog assisted cloud computing in era of big data and internet-of-things: systems, architectures, and applications,” in *Cloud Computing for Optimization: Foundations, Applications, and Challenges*, pp. 367–394, Springer, Cham, 2018.
- [15] S. B. ud din Tahir, A. Jalal, and M. Batool, “Wearable sensors for activity analysis using SMO-based random forest over smart home and sports datasets,” in *Proceedings of the 2020 3rd International Conference on Advancements in Computational Sciences (ICACS)*, pp. 1–6, Lahore, Pakistan, February, 2020.
- [16] H. Che, C. Li, X. He, and T. Huang, “A recurrent neural network for adaptive beamforming and array correction,” *Neural Networks*, vol. 80, pp. 110–117, 2016.
- [17] J. Wang, J. Wang, and H. Che, “Task assignment for multi-vehicle systems based on collaborative neurodynamic optimization,” *IEEE Transactions on Neural Networks and Learning Systems*, vol. 31, no. 4, pp. 1145–1154, 2019.
- [18] Le Sun, Q. Yu, D. Peng, S. Subramani, and X. Wang, “Fogmed: a fog-based framework for disease prognosis based medical sensor data streams,” *Computers, Materials & Continua*, vol. 66, no. 1, pp. 603–619, 2021.
- [19] Z. Qu, H. Sun, and M. Zheng, “An efficient quantum image steganography protocol based on improved EMD algorithm,” *Quantum Information Processing*, vol. 20, no. 53, pp. 1–29, 2021.
- [20] L. C. S. Afonso, G. H. Rosa, C. R. Pereira et al., “A recurrence plot-based approach for Parkinson’s disease identification,” *Future Generation Computer Systems*, vol. 94, pp. 282–292, 2019.
- [21] W. Gao, F. Tang, L. Wang et al., “AIBench: an industry standard internet service AI benchmark suite,” 2019, <https://arxiv.org/abs/1908.08998>.
- [22] N. Panda and S. K. Majhi, “How effective is the salp swarm algorithm in data classification,” in *Computational Intelligence in Pattern Recognition*, pp. 579–588, Springer, Singapore, 2020.
- [23] J. Qiu, Q. Wu, G. Ding, Y. Xu, and S. Feng, “A survey of machine learning for big data processing,” *EURASIP Journal on Applied Signal Processing*, vol. 2016, no. 1, 16 pages, 2016.
- [24] Y. Zhou, L. Liu, L. Wang et al., “Service-aware 6G: an intelligent and open network based on the convergence of communication, computing and caching,” *Digital Communications and Networks*, vol. 6, no. 3, pp. 253–260, 2020.
- [25] X. Ning, W. Li, B. Tang, and H. He, “BULDP: biomimetic uncorrelated locality discriminant projection for feature extraction in face recognition,” *IEEE Transactions on Image Processing*, vol. 27, no. 5, pp. 2575–2586, 2018.
- [26] X. Ning, F. Nan, S. Xu, L. Yu, and L. Zhang, “Multi-view frontal face image generation: a survey,” *Concurrency and Computation: Practice and Experience*, vol. 3, Article ID e6147, 2020.
- [27] R. S. Bath, A. Nayyar, and A. Nagpal, “Internet of robotic things: driving intelligent robotics of future-concept, architecture, applications and technologies,” in *Proceedings of the 2018 4th International Conference on Computing Sciences (ICCS)*, pp. 151–160, Jalandhar, India, August, 2018.

## Research Article

# Research on Fault Feature Extraction and Pattern Recognition of Rolling Bearing

**Xiaobin Miao** 

*School of Mechanical Engineering and Automation, Chongqing Industry Polytechnic College, Chongqing 401120, China*

Correspondence should be addressed to Xiaobin Miao; [miaoxb@cqipc.edu.cn](mailto:miaoxb@cqipc.edu.cn)

Received 15 February 2022; Revised 28 March 2022; Accepted 2 April 2022; Published 21 April 2022

Academic Editor: Man Fai Leung

Copyright © 2022 Xiaobin Miao. This is an open access article distributed under the Creative Commons Attribution License, which permits unrestricted use, distribution, and reproduction in any medium, provided the original work is properly cited.

Rolling bearings play a very important role. If the state of the rolling bearing is wrong, the whole equipment will fail, so we need to check the state of the running bearing. *Fault Feature Extraction of Rolling Bearings*. CEEMDAN (Complete Ensemble Empirical Mode Decomposition with Adaptive Noise) analyzes the collected oscillation signals to obtain various natural state functions. Kurtosis and Correlation Factor Evaluation Index are used to screen IMF components with a large number of error data, and independent component analysis is carried out on the selected components. The corresponding processing and reconstruction are carried out to extract the feature frequency. The built-in signal processing method can deal with the problem of bearing fault signal and identify the specific fault frequency. *Fault Pattern Recognition of Rolling Bearings*. The decomposition acceleration sensor is used to analyze the data of bearing in different states, and then, several components are obtained. The components related to the error signal are found, and the corresponding feature vectors are calculated. Then, the dimension vector is reduced, and a particle flow optimization algorithm is used to identify specific error conditions after dimension reduction. Experiments show that this method has higher detection rate in identifying specific fault states.

## 1. Introduction

The SVD (Singular Value Decomposition) method proposed in this paper can efficiently extract the fault features of bearings [1]. The cyclic spectral density method cannot identify the specific faults of bearings. Therefore, CSDK (Chi-square distribution-kernel method) is proposed in this paper, and experimental research shows that CSDK is a more effective method to solve the problem of fault feature extraction [2]. Compared with other methods, the distributed parameter extraction method is more sensitive and accurate in solving the fault problem of rolling bearings [3]. Aiming at the problem of fault feature extraction in bearings, it is concluded that the capacity distribution of the bearing frequency band can judge the state of the bearing [4]. Aiming at the problem of compound faults, this paper proposes a wavelet analysis method. The research shows that this method has great advantages in solving the problem of compound fault analysis [5]. Vibration analysis is very effective for fault feature extraction of rolling bearings. In this paper, the cyclic Wiener filter is used to further diagnose the extracted faults, and the

experiment shows that this method is very effective [6]. Rolling bearing failure will produce some major disasters; if the fault features can be effectively extracted, it will reduce the possibility of disasters. This paper verifies the effectiveness of the minimum entropy deconvolution method in solving the rolling bearing problem [7]. The fault characteristic parameters are normalized, and the neural network is used to diagnose the fault so that the ability of troubleshooting is effectively improved [8]. For fault diagnosis, the singular value decomposition method is proposed in this paper. It is concluded that the singular value decomposition method is higher in efficiency and accuracy [9]. It is very important for bearing fault identification to extract useful problem features from many problems. WPT has great advantages in extracting discriminant features [10]. Intelligent fault diagnosis is an important way to reduce maintenance costs. In this paper, a manifold learning algorithm is proposed for the intelligent diagnosis of rolling bearings, which can effectively and accurately identify different states of bearings [11]. Traditional analysis methods are not suitable for unstable bearing faults. In this paper, a neural network is proposed to identify fault

modes, and the research shows that this method has higher accuracy [12]. Feature extraction and feature classification are the core of bearing diagnosis. In this paper, a support vector machine is proposed to identify the fault of rolling bearings, and the research shows that this method is more accurate [13]. A vibration signal is developed by the pattern recognition method. The vibration signal can effectively diagnose the bearing state in the rolling bearing problem [14]. Recognition and pattern classification are the core of fault diagnosis. In this paper, a statistical pattern recognition method is proposed to solve the problem of fault classification [15]. Literature [16] uses PSO and SVM to identify rolling bearing faults, which has an obvious recognition effect in related feature extraction, kernel function, and parameter optimization. In [17], a fault diagnosis model based on the combination of CEEMD, PNN, and PSO is proposed, aiming at the high existence of non-stationarity and nonlinearity in bearing vibration signals. The feature extraction efficiency of the vibration signal is high, thus improving the recognition rate.

## 2. Bearing Fault Diagnosis Method

**2.1. Temperature Monitoring Method.** Under different working conditions, the internal temperature of rolling bearings will show different distribution characteristics due to different heating mechanisms. Holkup et al. obtained the thermal characteristics of bearings under different working conditions through experiments, so the health monitoring of bearings can be realized through the change of internal temperature of bearings. Through practice tests, temperature monitoring is really sensitive to the lubrication effect, load degree, and internal impact of bearings. However, when the bearing has early faults such as normal wear, pitting corrosion, and skin peeling, its internal temperature will hardly change, and it is impossible to accurately detect the early faults of bearings. Moreover, the temperature is easily affected by the weather and has great limitations.

**2.2. Oil Sample Collection and Analysis Method.** The oil sample collection and analysis method is mainly used to diagnose the faults by analyzing the components contained in the lubricating oil when rolling bearings are running. During the running process of the bearing, all parts contact each other and produce friction, so that the lubricating oil of the bearing will contain tiny particles produced by friction. When the wear position is different or the wear degree is different, the size, shape, and number of wear particles in lubricating oil are different. By analyzing the size, shape, and number and chemical composition of wear particles in lubricating oil, the fault severity and fault type of bearings can be monitored. However, the oil sample analysis method is not widely used because of its high cost, poor timeliness, and ease to be affected by the particles that fall off from other parts, and it can not accurately locate the fault location.

**2.3. Acoustic Emission Monitoring Method.** The acoustic emission monitoring method is also called the stress wave emission monitoring method. However, the signal-to-noise

ratio of the acoustic emission monitoring method is not high, and its wide spectrum range makes the workload of measurement and analysis heavy, the equipment is expensive, and it is easily interfered with by external noise, which requires a high test environment and noise processing, so its application and popularization in production are limited.

**2.4. Vibration Analysis Method.** When the bearing fails, the vibration signal will be abnormal. The advantage of this method is that it is suitable for diagnosing bearing faults under various types and working conditions, the vibration sensor is cheap, simple, and convenient to operate, and the diagnosis results are reliable, so it is widely used in practical engineering.

## 3. Fault Pattern Recognition of Rolling Bearings

### 3.1. Basic Theory

**3.1.1. Sample Entropy.** The sample entropy calculation method is as follows:

(1) A vector of dimension  $m$ ,  $X_m(1), \dots, X_m(N - m + 1)$ , numbered, as shown in the formula

$$X_m(i) = \{x(i), x(i + 1), \dots, x(i + m - 1)\}, 1 \leq i \leq N - m + 1. \quad (1)$$

(2) Define the distance  $d[X_m(i), X_m(j)]$  between  $X_m(i)$  and  $X_m(j)$  as the absolute value when the difference between them is the largest, as shown in the formula

$$d[X_m(i), X_m(j)] = \max(|x(i + k) - x(j + k)|). \quad (2)$$

For a given vector  $X_m(i)$ , count the distance between  $X_m(i)$  and  $X_m(j)$ ; if it is less than and equal to  $J$  number of  $R$ , where  $1 \leq j \leq N - m$ ,  $j \neq i$ , is denoted as  $B_i$ , then it is shown in the formula

$$B_i^m(r) = \frac{1}{N - m - 1} B_i. \quad (3)$$

Define  $B^{(m)}(r)$  as shown in the formula

$$B^{(m)}(r) = \frac{1}{N - m} \sum_{i=1}^{N-m} B_i^m(r). \quad (4)$$

Increase its dimension until  $m + 1$ , and then calculate the number of distances between  $X_{m+1}(i)$  and  $X_{m+1}(j)$  that are less than or equal to  $R$ , and write it as  $A_i$ ; then,  $A_i^m(r)$  is shown in the formula

$$A_i^m(r) = \frac{1}{N - m - 1} A_i. \quad (5)$$

Define  $A^m(r)$  as shown in the formula

$$A^m(r) = \frac{1}{N - m} \sum_{i=1}^{N-m} A_i^m(r). \quad (6)$$

The sample entropy is defined as shown in the formula

$$\text{sampEn}(m,r) = \lim_{N \rightarrow \infty} \left\{ -\ln \left[ \frac{A^m(r)}{B^m(r)} \right] \right\}. \quad (7)$$

If  $N$  is a finite value, it can be estimated by the formula

$$\text{sampEn}(m,r,N) = -\ln \left[ \frac{A^m(r)}{B^m(r)} \right]. \quad (8)$$

### 3.1.2. Pattern Recognition Classification Method

(1) *Support Vector Machine*. The SVM method is usually used for data classification. When classifying data, different classification situations will have different effects, but there will be an SVM best result.

Assuming that the training sample set is  $\{(x, y) | i = 1, 2, \dots, k\}$ , the optimization problem is constructed as shown in formula (10):

$$\min_{w,b} \frac{\|w\|^2}{2} + C \sum_{i=1}^k \xi_i, \quad (9)$$

$$\text{s.t. } y_i [(wx_i) + b] \geq 1 - \xi_i, i = 1, 2, \dots, k, \quad (10)$$

where  $W$  is the weight;  $C$  is the penalty parameter of error term  $\xi_i$ ,  $C > 0$ ;  $\xi_i \geq 0$ ;  $b$  is the intercept.

Solve the corresponding value and get the formula

$$f(x) = \text{sgn} \left( \sum_{i=1}^k a_i y_i K(x_i, x) + b^* \right), \quad (11)$$

where  $a_i$  is the Lagrange multiplier;  $K(x_i, x)$  is the kernel function of Mercer condition;  $b^*$  is the intercept.

In this paper, the RBF kernel function is used to analyze the results of SVM classification. As shown in the formula,

$$K(x, y) = \exp \left( -\frac{\|x - y\|^2}{2g^2} \right), \quad (12)$$

where  $g$  represents the regularity of vibration signals.

(2) *PNN Neural Network*. Classification according to probability density is the essence of a probabilistic neural network. It can output probability in a short time and maximize the probability. As shown in the formula,

$$f(X, \omega_i) = \exp \left[ -(X - \omega_i)^T \frac{(X - W_i)}{2\delta} \right], \quad (13)$$

where  $\omega_i$  is the weight;  $\delta$  is the smoothing factor.

3.1.3. *Support Vector Machine Optimized by Particle Swarm Optimization*. A particle swarm optimization algorithm is the most suitable method to find the solution. The SVM parameter  $C$  and  $G$  selection problem is actually an optimization problem that satisfies certain criteria or objectives. The classification recognition rate is directly used as the fitness to evaluate the advantages and disadvantages of the solution.

Assume that the individual extreme value is  $P_{\text{best}}$ . The global optimal solution is  $G_{\text{best}}$ . The search space contains  $m$  different particles. The position  $x_i$  and velocity  $v_i$  are brought into the functional equation for calculation. As shown in formulas (14) and (15),

$$v_i(t+1) = \alpha [\omega v_i(t) + c_1 r_1 (P_{\text{best}}(t) - x_i(t)) + c_2 r_2 (G_{\text{best}}(t) - x_i(t))], \quad (14)$$

$$x_i(t+1) = x_i(t) + v_i(t+1), \quad (15)$$

where  $c_1$  and  $c_2$  are acceleration factors;  $r_1$  and  $r_2$  obey  $[0, 1]$  distribution;  $v_i \in [-v_{\text{min}}, v_{\text{max}}]$  and  $v_{\text{max}}$  are nonnegative;  $\alpha$  is the compressibility factor,  $\alpha = 2/|2 - C - \sqrt{C^2 - 4C}|$ ;  $C = c_1 + c_2$ ;  $\omega$  is the weight. Search performance is improved through it. Use linear decreasing weights, as shown in the formula

$$\omega = \omega_{\text{max}} - \frac{(\omega_{\text{max}} - \omega_{\text{min}}) * (t - 1)}{M - 1}, \quad (16)$$

where  $t$  represents the current number of iterations and  $M$  is the maximum number of iterations.

In order to find the most suitable target value, the particle swarm optimization (PSO) algorithm is usually used to build a support vector machine (SVM) for parameter optimization of SVM. Update the speed and position of each particle. If the conditions for the completion of verification are not met, the calculation can be carried out according to equation (12), and the results can be output after ensuring that this condition is met.

3.1.4. *Comparison of Classification Effects of Different Feature Vectors*. The length of data plays a decisive role in the calculation of approximate entropy. Sample entropy does not depend on the length of data, and the calculation time is short. Therefore, this paper chooses sample entropy as a feature vector for bearing pattern recognition.

The approximate entropy of sample points  $\{x(i) | i = 1, 2, \dots, N\}$  of bearing fault signal is as shown in the formula

$$X(i) = (x(i), x(i+1), \dots, x(i+m-1)), \quad (17)$$

$$i = 1, 2, \dots, N - m + 1.$$

If the threshold value  $\varepsilon$  of similarity tolerance is set, the distance  $d(X(i), X(j))$  between  $X(i)$  and  $X(j)$  is less than the number  $B\{d(X(i), X(j)) < \varepsilon\}$  of  $\varepsilon$ ; then,  $D_{mi}(\varepsilon)$  is defined as shown in the formula

$$D_{mi}(\varepsilon) = \frac{B\{d(X(i), X(j)) < \varepsilon\}}{N - m + 1}. \quad (18)$$

The autocorrelation degree of vector  $X(i)$  is shown in the formula

$$\varphi_m(\varepsilon) = \frac{1}{N - m + 1} \sum_{i=1}^{N-m+1} \ln D_{mi}(\varepsilon). \quad (19)$$

Its approximate entropy is shown in the formula

TABLE 1: Approximate entropy of different IMF components.

| Component    | IMF1   | IMF2   | IMF3   | IMF4   | IMF5   | IMF6   | IMF7   | IMF8   |
|--------------|--------|--------|--------|--------|--------|--------|--------|--------|
| Normal       | 1.0631 | 1.121  | 0.7146 | 0.6315 | 0.6292 | 0.4228 | 0.2721 | 0.1157 |
| Status       | 0.9941 | 0.7881 | 0.6981 | 0.6674 | 0.6144 | 0.3856 | 0.2342 | 0.0977 |
| Inner ring   | 1.1442 | 0.6092 | 0.8782 | 0.6386 | 0.6261 | 0.4947 | 0.312  | 0.1189 |
| Malfunction  | 1.12   | 0.5867 | 0.8381 | 0.64   | 0.6148 | 0.4704 | 0.2916 | 0.1383 |
| Rolling body | 0.9928 | 1.1418 | 0.9041 | 0.6335 | 0.6211 | 0.4272 | 0.2966 | 0.1171 |
| Malfunction  | 0.9904 | 1.1466 | 0.9121 | 0.6265 | 0.6175 | 0.4078 | 0.2933 | 0.1026 |
| Outer ring   | 0.5872 | 0.6566 | 1.002  | 0.6412 | 0.6194 | 0.4629 | 0.2544 | 0.1227 |
| Malfunction  | 0.6068 | 0.6827 | 0.942  | 0.6483 | 0.5979 | 0.4711 | 0.3291 | 0.1195 |

TABLE 2: Classification effect of approximate entropy as a feature vector.

| Number of runs | Running time (s) | $C$    | $g$   | Fitness value | Recognition rate (%) |
|----------------|------------------|--------|-------|---------------|----------------------|
| 1              | 112.59           | 97.7   | 0.01  | 97.67         | 95                   |
| 2              | 117.86           | 4.634  | 3.656 | 97.67         | 95                   |
| 3              | 109.93           | 100    | 0.01  | 97.67         | 95                   |
| 4              | 109.15           | 96.324 | 0.01  | 97.67         | 95                   |
| 5              | 109.01           | 98.384 | 0.01  | 97.67         | 95                   |

TABLE 3: Sample entropy is the classification effect of the feature vector.

| Number of runs | Running time (s) | $C$     | $g$    | Fitness value | Recognition rate (%) |
|----------------|------------------|---------|--------|---------------|----------------------|
| 1              | 115.661          | 15.7986 | 2.2624 | 97.33         | 95                   |
| 2              | 110.928          | 100     | 1.0574 | 97.67         | 95.5                 |
| 3              | 109.904          | 91.9482 | 1.0315 | 97.67         | 95.5                 |
| 4              | 115.351          | 90.1702 | 1.176  | 97.67         | 95.5                 |
| 5              | 100.922          | 51.5063 | 0.8525 | 97.33         | 95.5                 |

$$ApEn(m, \varepsilon, N) = \varphi_m(\varepsilon) - \varphi_{m+1}(\varepsilon). \quad (20)$$

The approximate entropy of bearings in different states is shown in Table 1.

It can be seen from Table 1 that the results of approximate entropy of IMF component of vibration signal in different states of bearings are different, and it can be seen that the information contained in the signal is different.

Using the PSO-SVM classification model, the feature vectors extracted from IMF components after CEEMDAN decomposition are used for pattern recognition, and the program is run five times. The results are shown in Tables 2 and 3.

Observing Tables 2 and 3, we can get that the average classification recognition rate is 95% when approximate entropy is feature information, and the classification recognition rate is 95.5% when sample entropy is feature information.

#### 4. Application of Fault Feature Extraction Method for Rolling Bearing

*4.1. Fault Feature Extraction Method Based on Design.* In this section, the advantages of the LMD method, permutation entropy theory, multivariate feature fusion method, and LLE dimensionality reduction clustering theory are comprehensively used to propose a new method for fault feature extraction of rolling bearings. This method has the following advantages for fault feature extraction in different states.

First, aiming at the nonstationary problem of the initially collected test time series in a single scale, the initial signal is decomposed to different scales for analysis by using the adaptive decomposition ability of LMD, and the stationary component form of the signal can be obtained. The improved LMD method also preliminarily eliminates the interference information. Second, aiming at the influence of equipment structure and function coupling and uncertain signal path route, because of the complex components of vibration signals and weak fault changes, permutation entropy can better describe the complexity of signals and good sensitivity to abrupt signals and quantitatively express the fault information contained in different component signals, thus completing the initial extraction of fault features. Thirdly, in view of the "dimension disaster" and information redundancy in the process of initial signal acquisition of rotating machinery vibration signals, because of the low efficiency of fault feature recognition, the redundant information in feature vectors is removed by using the better dimension reduction ability of LLE and the clustering results are visualized, thus completing the secondary extraction of fault features and improving the accuracy of fault recognition.

There are five steps in the implementation of the fault feature extraction method, which are collecting signals, carrying out multiscale analysis on initial signals, and summarizing and sorting out all the obtained single components. The improved LMD algorithm is used to screen the PF components obtained in step 1 to obtain all effective PF

TABLE 4: Relevant specifications and parameters of test equipment.

| Category                      | Model                | Number of rolling elements | Position    | Action              |
|-------------------------------|----------------------|----------------------------|-------------|---------------------|
| Deep groove spherical bearing | 6203-2RS JEM SKF/NTN | 8                          | Fan end     | Support motor shaft |
|                               | 6205-2RS JEM SKF/NTN | 9                          | Driving end |                     |

TABLE 5: Relevant specifications and parameters of rolling bearings.

| Bearing type | Inner ring (mm) | Diameter size outer ring (mm) | Rolling body (mm) | Nodal ring (mm) | Thickness (mm) |
|--------------|-----------------|-------------------------------|-------------------|-----------------|----------------|
| 6203-2RS     | 17              | 40                            | 6.7462            | 28.4988         | 12             |
| 6205-2RS     | 25              | 52                            | 7.94              | 39.04           | 15             |

TABLE 6: Rolling bearing failure mode settings.

| Failure mode                | Loss dimension (diameter/mm) | Position setting | Source of bearing |
|-----------------------------|------------------------------|------------------|-------------------|
| Single point loss fault EDM | 0.1778                       | Inner ring       | SKFCompany        |
|                             |                              | Rolling body     |                   |
|                             |                              | 3 o'clock        |                   |
|                             |                              | Outer ring       |                   |
|                             | 0.3556                       | 6 o'clock        |                   |
|                             |                              | 12 o'clock       |                   |
|                             |                              | Inner ring       |                   |
|                             |                              | Rolling body     |                   |
|                             | 0.5334                       | 3 o'clock        | NTNCompany        |
|                             |                              | Outer ring       |                   |
|                             |                              | 6 o'clock        |                   |
|                             |                              | 12 o'clock       |                   |
| 0.7112                      | Inner ring                   |                  |                   |
|                             | Rolling body                 |                  |                   |
|                             | 3 o'clock                    |                  |                   |
|                             | Outer ring                   |                  |                   |
|                             |                              | 6 o'clock        |                   |
|                             |                              | 12 o'clock       |                   |

component sets, and the arrangement entropy of all effective PF components is calculated to complete the initial extraction of fault features. According to the selection criteria of error characteristic sensitive parameters, shielding can effectively restore the time domain and frequency domain characteristic parameters of the essential characteristics of the output signal and shield the time-frequency domain characteristics of the start-up signal. Combining the time domain characteristic index of the initial signal with the PF-PE characteristic vector obtained in step 2, a high-dimensional characteristic data set is constructed, and the high-dimensional characteristic data is reduced by LLE to obtain the low-dimensional characteristic data with good clustering, thus completing the secondary extraction of rotating machinery fault characteristics.

4.2. *Data Enhancement Technology.* Data enhancement technology can provide a spatial solution for limited problems. On the basis of the original, it can improve the size and quality of data by performing necessary transformations, such as performing various operations on the original picture in the field of computer vision. For example, when the offset is set to 100 and the sample length is 2400, the first

signal sample is intercepted from the 1st to 2400th data points of the initial signal, the second signal sample is intercepted from the 101st to 2500 data points, and so on, and an enhanced data set is obtained.

4.3. *Application of LMD and LLE*

4.3.1. *CWRU Rolling Bearing Data Description.* The structure of the rolling bearing vibration signal testing device includes a motor, power meter, sensor, decoder, and other components.

Two types of test bearings were selected for the test, and the structural description is shown in Table 4.

In Table 4, SKF and NTN represent bearing sources. The two test bearing specifications are shown in Table 5.

The default failure modes of the test are shown in Table 6.

Four working conditions were designed in the test, as shown in Table 7, and faults and no faults were set in different degrees and positions under each working condition.

4.3.2. *Experimental Analysis of Feature Extraction.* According to the data enhancement algorithm, the offset is 100, and the vibration signals of 36 different fault types

TABLE 7: Working condition setting of rolling bearings.

| Working condition number | 1    | 2    | 3    | 4    |
|--------------------------|------|------|------|------|
| Motor speed (r/min)      | 1797 | 1772 | 1750 | 1730 |
| Motor load (horsepower)  | 0    | 1    | 2    | 3    |

under four working conditions and different fault positions and diameters are selected from the CWRU data set to carry out fault diagnosis tests.

The rolling bearing failure test data set selected in this paper is shown in Table 8. Each fault contains 250 sets of data, and the sampling points of each group of samples are set to 2400 points. 4/5 samples are randomly selected as the training set of the model, and the remaining 1/5 samples are used as the test set of the model.

In order to verify the effectiveness and superiority of the proposed method, some test results of labels 11, 13, 16, and 19 are selected as examples to analyze and explain. The sample parameters of vibration signals in different states are shown in Table 9.

The main fault information calculated by the correlation coefficient method is included in the first five components.

It can be seen in Table 10 that the solution values of faults are very close, and it is difficult to distinguish them if permutation entropy is directly used as the selected feature.

Figure 1 is the distribution diagram of the arrangement entropy of different types of faults.

It can be seen that there are some differences between PE values under various working conditions, and the PE values in PF components of each level in the same signal correspond to the confusion degree at its scale.

As shown in Figures 2 and 3, it can be seen that compared with LMD permutation entropy, the features extracted by the other two methods have a serious aliasing phenomenon, which increases the difficulty of distinguishing the fault state of rolling bearings. This proves the advantage of LMD permutation entropy in feature extraction.

Figure 4 shows the distribution of LMD permutation entropy in different states.

We can also see the change law of arrangement entropy of four states. The permutation entropy is the smallest in the normal state. The permutation entropy of different faults increases in different degrees, and the permutation entropy becomes smaller and smaller with the decomposition. This is because the LMD decomposition makes the vibration signal tend to be stable continuously, and the permutation entropy is different in different states, while the entropy of different PF components in the same signal reflects the uncertainty at this scale.

In this paper, the permutation entropy and sample entropy in four states are calculated at the same time, as shown in Figures 5 and 6.

It can be seen from the figure that compared with EMD permutation entropy and LMD sample entropy, LMD permutation entropy has fewer cross-aliasing areas, and the distinction between different states is more obvious. The advantages of LMD permutation entropy in feature

extraction are proved. Some high-dimensional eigenvector values are shown in Table 11.

The eigenvectors of four kinds of fault states, which are labeled as 1U3, 16, and 19, respectively, are calculated, and then the corresponding training set and test set are obtained. Table 12 shows SVM recognition results under different eigenvalues.

It can be seen from Table 12 that the recognition rate is the lowest when only using the permutation entropy feature of the original signal, while the classification accuracy is obviously improved by using the PF-PE method, which shows that it is necessary to carry out multiscale analysis on the initial signal of rolling bearings. Compared with the PF-PE method, the recognition result of the PF-PE time-frequency domain method is improved to some extent, which shows that the method of multifeature fusion retains the essential characteristics of the initial signal well. The results of PF-PE-Time-Frequency Domain-LLE and PF-PE-Time-Frequency Domain show that LLE can eliminate redundant information and improve the clustering degree of low-dimensional features and further prove the suitability of the LLE method combined with LMD permutation entropy and multifeature fusion in feature extraction of rolling bearings.

To illustrate the universality of the extraction method designed in this paper, an additional class of rolling bearing data sets is introduced. The XJTU-SY rolling bearing test data set of Xi'an Jiaotong University is used to apply the proposed algorithm. Because the bearing data belongs to the whole cycle life test data, in order to be used in the verification of this method, to ensure that the fault information type represented by the obtained signals is clear, the samples are taken at the beginning (normal position) and the last failure position (clear fault position), and then, the test set is expanded by data enhancement.

The rolling bearing fault test data set is shown in Table 13.

According to the data enhancement algorithm, the offset is 1000, four position failure modes (early normal state, inner ring, outer ring, and cage) are selected from XJTU-SY rolling bearing accelerated life test data set, fault diagnosis test is carried out for vibration signals with different rotational speeds and single fault damage conditions, with a total of 10 different fault modes = each fault contains 250 groups of data, and the sampling points of each group of data are set to 2400 points, of which 4/5 samples are arbitrarily extracted as the training set of the model, and the remaining 1/5 samples are used as the detection set of the model. Table 14 shows the eigenvalue results of partial initial feature extraction.

Calculate the time domain and frequency domain features of the corresponding initial signal and combine the fault features extracted for the first time to obtain a high-dimensional feature vector group, and use the improved LLE algorithm to reduce its dimension. Table 15 is the eigenvalue results of partial secondary feature extraction.

SVM is used to classify and identify different eigenvalues. Table 16 shows the recognition results of SVM under different eigenvalues.

Fault feature extraction is an important part of fault diagnosis technology, and it is the basis of ensuring the



TABLE 8: Fault test data set of rolling bearing.

| Motor speed (r/min) | Fault location | Fault diameter (mm) | Training sample | Test sample | Sample label |
|---------------------|----------------|---------------------|-----------------|-------------|--------------|
| 1797                | Failure-free   | 0                   | 200             | 50          | 1            |
|                     |                | 0.1778              | 200             | 50          | 2            |
|                     |                | 0.3556              | 200             | 50          | 3            |
|                     | Inner ring     | 0.5334              | 200             | 50          | 4            |
|                     |                | 0.1778              | 200             | 50          | 5            |
|                     |                | 0.3556              | 200             | 50          | 6            |
|                     | Outer ring     | 0.5334              | 200             | 50          | 7            |
|                     |                | 0.1778              | 200             | 50          | 8            |
|                     |                | 0.3556              | 200             | 50          | 9            |
|                     | Rolling body   | 0.5334              | 200             | 50          | 10           |
| Failure-free        |                | 0                   | 200             | 50          | 11           |
|                     |                | 0.1778              | 200             | 50          | 12           |
|                     | 0.3556         | 200                 | 50              | 13          |              |
| 1772                | Inner ring     | 0.5334              | 200             | 50          | 14           |
|                     |                | 0.1778              | 200             | 50          | 15           |
|                     |                | 0.3556              | 200             | 50          | 16           |
|                     | Outer ring     | 0.5334              | 200             | 50          | 17           |
|                     |                | 0.1778              | 200             | 50          | 18           |
|                     |                | 0.3556              | 200             | 50          | 19           |
| Rolling body        | 0.5334         | 200                 | 50              | 20          |              |
|                     | Failure-free   | 0                   | 200             | 50          | 21           |
|                     |                | 0.1778              | 200             | 50          | 22           |
| 0.3556              |                | 200                 | 50              | 23          |              |
| 1750                | Inner ring     | 0.5334              | 200             | 50          | 24           |
|                     |                | 0.1778              | 200             | 50          | 25           |
|                     |                | 0.3556              | 200             | 50          | 26           |
|                     | Outer ring     | 0.5334              | 200             | 50          | 27           |
|                     |                | 0.1778              | 200             | 50          | 28           |
|                     |                | 0.3556              | 200             | 50          | 29           |
| Rolling body        | 0.5334         | 200                 | 50              | 30          |              |
|                     | Failure-free   | 0                   | 200             | 50          | 31           |
|                     |                | 0.1778              | 200             | 50          | 32           |
| 0.3556              |                | 200                 | 50              | 33          |              |
| 1730                | Inner ring     | 0.5334              | 200             | 50          | 34           |
|                     |                | 0.1778              | 200             | 50          | 35           |
|                     |                | 0.3556              | 200             | 50          | 36           |
|                     | Outer ring     | 0.5334              | 200             | 50          | 37           |
|                     |                | 0.1778              | 200             | 50          | 38           |
|                     |                | 0.3556              | 200             | 50          | 39           |
| Rolling body        | 0.5334         | 200                 | 50              | 40          |              |

TABLE 9: Sample parameters under normal and typical fault conditions.

| Working condition setting |                  | Fault setting                           | Mapping label |
|---------------------------|------------------|---|---------------|
| Model selection           | 6205-2RS JEM SKF | Failure-free                            | 11            |
| Sampling frequency        | 12999 Hz         | Inner ring fault (diameter = 0.3556 mm) | 13            |
| Rotational speed          | 1772 r/min       | Outer ring fault (diameter = 0.3556 mm) | 16            |
|                           |                  | Roller failure (diameter = 0.3556 mm)   | 19            |

effectiveness, feasibility, and accuracy of mechanical equipment fault monitoring and diagnosis. Aiming at the difficulty of the current fault feature extraction method of

vibration test signal based on acquisition in processing and aiming at the fault extraction of rolling bearings, this paper concludes that the fault feature extraction method of rolling

TABLE 10: Average value of permutation entropy of PF1.

| Malfunction | Normal state | Inner ring position | Outer ring position | Roller position |
|-------------|--------------|---------------------|---------------------|-----------------|
| Average     | 4.4516       | 5.4286              | 5.5251              | 5.0207          |

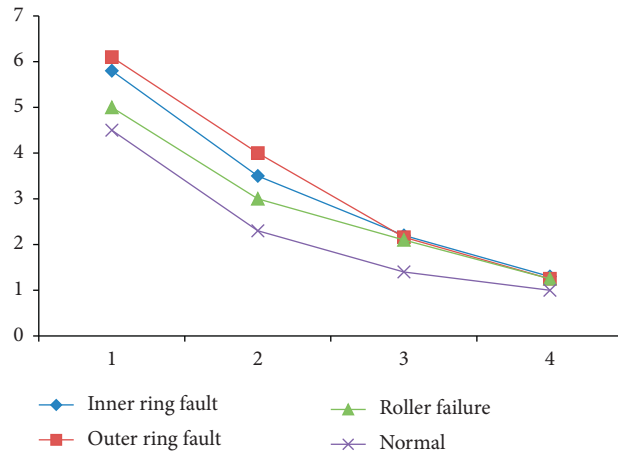


FIGURE 1: LMD permutation entropy.

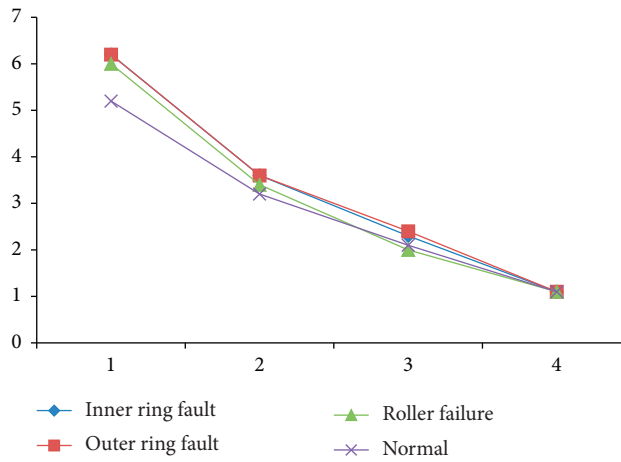


FIGURE 2: EMD permutation entropy.

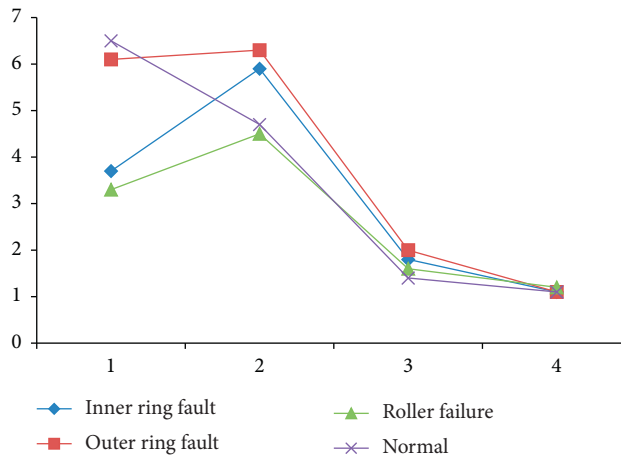


FIGURE 3: LMD sample entropy.

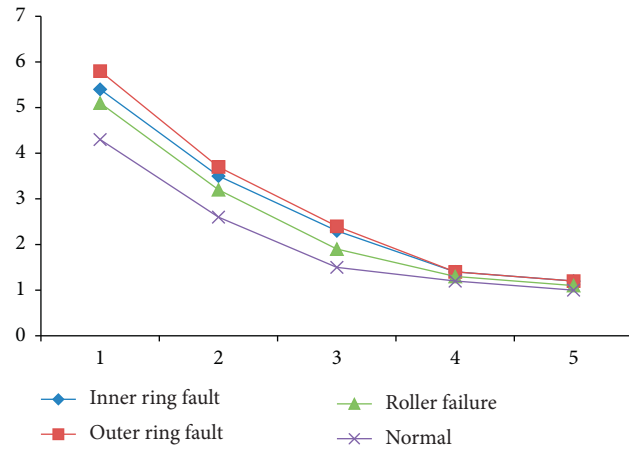


FIGURE 4: LMD permutation entropy of vibration signals in four states.

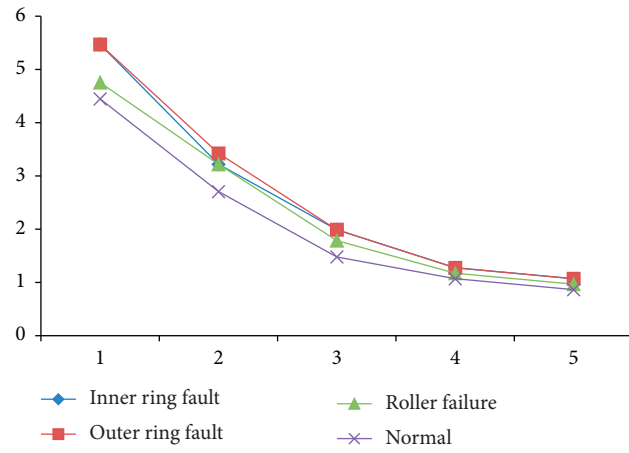


FIGURE 5: EMD permutation entropy of vibration signals in four states.

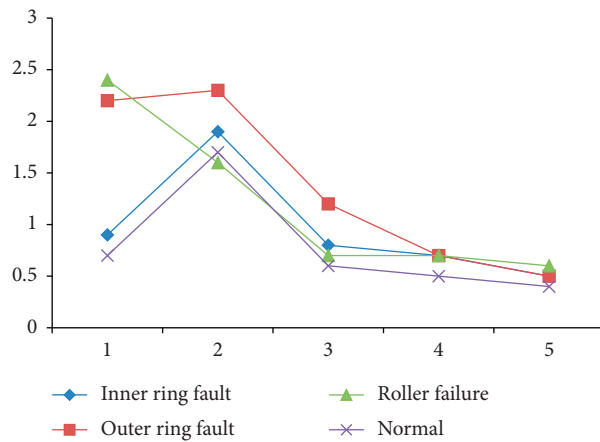


FIGURE 6: LMD sample entropy of vibration signals in four states.

TABLE 11: Partially constructed high-dimensional feature vectors.

| Eigenvector | 11     | 11     | 13      | 13      | 16     | 16     | 19     | 19      | ... |
|-------------|--------|--------|---------|---------|--------|--------|--------|---------|-----|
| 1           | 0.4032 | 0.4022 | 2.8331  | 4.0316  | 0.6487 | 0.5962 | 1.6842 | 2.2994  | ... |
| 2           | 0.0655 | 0.0648 | 0.1679  | 0.1675  | 0.0929 | 0.0921 | 0.1649 | 0.1632  | ... |
| 3           | 2.7783 | 2.769  | 19.5567 | 34.5963 | 2.9704 | 2.8728 | 5.7624 | 8.6372  | ... |
| 4           | 4.5781 | 4.6118 | 19.6046 | 27.5137 | 5.2636 | 4.6146 | 9.8718 | 12.8731 | ... |
| 5           | 4.4687 | 4.5155 | 5.4531  | 5.4495  | 5.5489 | 5.5489 | 4.9651 | 4.9272  | ... |
| 6           | 2.6808 | 2.7751 | 3.3737  | 3.448   | 3.5529 | 3.5217 | 3.118  | 3.1707  | ... |
| 7           | 1.5133 | 1.5506 | 1.9819  | 1.9906  | 2.0186 | 2.0745 | 1.7637 | 1.7449  | ... |
| 8           | 1.0364 | 1.026  | 1.3565  | 1.2851  | 1.3067 | 1.301  | 1.2552 | 1.237   | ... |
| 9           | 0.8674 | 0.8294 | 0.9622  | 0.9521  | 0.9682 | 0.9386 | 0.914  | 0.9263  | ... |

TABLE 12: Recognition results of different features.

| Feature classification          | Normal (%) | Inner ring position (%) | Outer ring position (%) | Roller position (%) | Average (%) |
|---------------------------------|------------|-------------------------|-------------------------|---------------------|-------------|
| Initial signal                  | 84.17      | 77.83                   | 75                      | 78.08               | 78.69       |
| PF-PE                           | 99.83      | 84.35                   | 88                      | 85                  | 92.25       |
| PF-PE-time-frequency domain     | 100        | 90.91                   | 90.09                   | 91.82               | 93.04       |
| PF-PE-time-frequency domain-LLE | 100        | 100                     | 100                     | 100                 | 100         |

TABLE 13: Fault test data set.

| Fault type             | Motor speed (r/min) | Training sample | Test sample | Label |
|------------------------|---------------------|-----------------|-------------|-------|
| Normal                 | 2100                | 200             | 50          | 1     |
| Normal                 | 2250                | 200             | 50          | 2     |
| Normal                 | 2400                | 200             | 50          | 3     |
| Inner ring fault       | 2250                | 200             | 50          | 4     |
| Inner ring fault       | 2400                | 200             | 50          | 5     |
| Outer ring fault       | 2100                | 200             | 50          | 6     |
| Outer ring fault       | 2250                | 200             | 50          | 7     |
| Outer ring fault       | 2400                | 200             | 50          | 8     |
| Keep and reduce faults | 2100                | 200             | 50          | 9     |
| Keep and reduce faults | 2250                | 200             | 50          | 10    |

TABLE 14: Characteristic parameters of arrangement entropy of effective components of LMD.

| Serial number        | Normal |        | Inner ring |        | Outer ring |        | Keep decreasing |        |
|----------------------|--------|--------|------------|--------|------------|--------|-----------------|--------|
| Effective component1 | 6.1312 | 6.1132 | 5.9753     | 5.9603 | 6.3119     | 6.3034 | 6.1099          | 6.1042 |
| Effective component2 | 3.1976 | 3.2602 | 3.3621     | 3.3854 | 3.0968     | 3.1051 | 3.1603          | 3.1652 |
| Effective component3 | 1.8998 | 1.8929 | 1.9508     | 1.9794 | 1.7517     | 1.7457 | 1.8545          | 1.8506 |
| Effective component4 | 1.2189 | 1.2184 | 1.2287     | 1.246  | 1.1929     | 1.1967 | 1.2056          | 1.1758 |

TABLE 15: Modified LLE dimension reduction characteristic parameters.

| Coordinates | Normal  |         | Inner ring |         | Outer ring |         | Keep decreasing |         |
|-------------|---------|---------|------------|---------|------------|---------|-----------------|---------|
| X           | 1.1681  | 1.1683  | -0.9597    | -0.9612 | -0.3832    | -0.4644 | -1.1733         | -1.173  |
| Y           | -0.3477 | -0.4483 | -1.7338    | -1.2773 | 1.9823     | 1.9901  | 0.11306         | 0.1004  |
| Z           | 0.1585  | 0.3671  | 1.0638     | 0.9573  | -0.4371    | -0.6875 | -0.4631         | -0.3956 |

TABLE 16: Recognition results of different features.

| Feature classification          | Normal (%) | Inner ring (%) | Outer ring (%) | Rolling body (%) | Average (%) |
|---------------------------------|------------|----------------|----------------|------------------|-------------|
| Initial signal                  | 86.00      | 75.00          | 73.53          | 49.01            | 70.79       |
| PF-PE                           | 91.00      | 86.00          | 89.00          | 83.50            | 86.60       |
| PF-PE-time-frequency domain     | 100.00     | 93.46          | 94.29          | 98.95            | 97.01       |
| PF-PE-time-frequency domain-LLE | 100.00     | 95.00          | 100.00         | 100.00           | 99.38       |

bearings based on LMD replacement entropy and LLE is very effective. Simulation data and experimental data of two types of rolling bearings show that the proposed method is suitable for fault feature extraction of rolling bearings.

## 5. Conclusion

The state of the bearing will affect the overall operation. Therefore, the research on the state of bearings is a very important issue. Bearing is also one of the most important mechanical fault sources. In fault diagnosis, vibration signals are usually taken as the main research object in this field, and signals containing a large amount of fault information are extracted. EMD is often used in nonstationary signal processing. It can distinguish the error characteristics of signals and compensate for the mode aliasing effect. *Identification of Rolling Bearings*. CEEMDAN can extract the features of fault signals. Two indexes are added to reconstruct the screened signals to solve the problem of fault feature extraction. Finally, the signal processing method based on CEEMDAN-ICA is verified by the measured signal. The results show that the method can separate the fault characteristic frequency of the fault bearing and then realize the fault diagnosis of the bearing. In this paper, CEEMDAN is combined with the sample entropy, Fisher point, and PSO-SVM to realize the pattern recognition of various failure states of rolling bearings.

## Data Availability

The experimental data used to support the findings of this study are available from the corresponding author upon request.

## Conflicts of Interest

The authors declare that they have no conflicts of interest regarding this work.

## Acknowledgments

This work was sponsored in part by the Digital Design and Manufacturing Chongqing Colleges and Universities Engineering Center Construction Project (Yujiao Kefa (2018) NO. 17).

## References

- [1] L. I. Zhao-Fei, Y. Chai, and L. I. Hua-Feng, "Fault feature extraction method of rolling bearing based on singular value decomposition and morphological filtering," *Application Research of Computers*, vol. 5, no. 14, pp. 128–201, 2012.
- [2] L. I. Min, J. Yang, and X. Wang, "Fault feature extraction of rolling bearing based on an improved cyclical spectrum density method," *Chinese Journal of Mechanical Engineering: English version*, vol. 28, no. 6, pp. 8–35, 2015.
- [3] P. Tao, H. Jiang, and X. Yong, "Weibull distribution parameters for fault feature extraction of rolling bearing," in *Proceedings of the Chinese Control and Decision Conference*, pp. 232–301, Mianyang, China, 23–25 May 2011.
- [4] Q. Y. Ren and L. I. Hao-Lin, "The application of wavelet packets analysis in fault feature extraction of rolling bearing," *Telecom Power Technology*, vol. 95, no. 62, pp. 158–204, 2015.
- [5] Z. Yang and L. Gao, "Wavelet analysis and fault feature extraction of rolling bearing," *Springer London*, vol. 6, no. 27, pp. 472–507, 2014.
- [6] M. Yang, C. Jin, and G. Dong, "Weak fault feature extraction of rolling bearing based on cyclic Wiener filter and envelope spectrum," *Mechanical Systems and Signal Processing*, vol. 25, no. 5, pp. 1773–1785, 2011.
- [7] H. Wang, J. Chen, and G. Dong, "Weak fault feature extraction of rolling bearing based on minimum entropy deconvolution and sparse decomposition," *Journal of Vibration and Control*, vol. 56, no. 64, pp. 323–461, 2014.
- [8] C. G. Liu, J. W. Tan, and C. Zhang, "Rolling bearing fault feature extraction technique and method," *Coal Mine Machinery*, vol. 2, no. 10, pp. 65–68, 2010.
- [9] S. . Lu, "Fault pattern recognition of rolling bearing based on singularity value decomposition and support vector machine," *Transactions of the Chinese Society of Agricultural Engineering*, vol. 9, no. 4, pp. 374–439, 2007.
- [10] C. Wang, M. Gan, and C. Zhu, "Fault feature extraction of rolling element bearings based on wavelet packet transform and sparse representation theory," *Journal of Intelligent Manufacturing*, vol. 4, no. 2, pp. 1–15, 2015.
- [11] Z. Wang, L. Yao, Y. Cai, and J. Zhang, "Mahalanobis semi-supervised mapping and beetle antennae search based support vector machine for wind turbine rolling bearings fault diagnosis," *Renewable Energy*, vol. 155, no. 155, pp. 1312–1327, 2020.
- [12] M. Li, S. Lu, D. Chen, and W. Ma, "Application of wavelet-neural network in rolling bearings fault diagnosis," in *Proceedings of the Conference Proceedings of the Seventh International Conference on Electronic Measurement & Instruments(ICEMI'2005) vol.4. College of Mechanical Science and Engineering*, pp. 35–103, Jilin University, Changchun 130025 China, 2005.
- [13] G. Chen, X. Xie, and S. Li, "Research on complex classification algorithm of breast cancer chip based on SVM-RFE gene feature screening," *Complexity*, vol. 2020, pp. 1–12, 2020.
- [14] Y. Imaizumi, T. Furue, M. Maeda, M. Azemoto, and T. Imanaka, "A study on evaluation of rolling element bearing condition using pattern recognition method," *Symposium on Evaluation & Diagnosis. The Japan Society of Mechanical Engineers*, vol. 5, no. 8, pp. 123–197, 2004.
- [15] X. Ning, K. Gong, W. Li, L. Zhang, X. Bai, and S. Tian, "Feature refinement and filter network for person re-identification," *IEEE Transactions on Circuits and Systems for Video Technology*, vol. 31, no. 9, pp. 3391–3402, 2021.
- [16] J. Ma, J. D. Wu, Y. G. Fan, X. D. Wang, and Z. K. Shao, "Fault diagnosis of rolling bearing based on the PSO-SVM of the mixed-feature," *Applied Mechanics and Materials*, vol. 380–384, pp. 895–901, 2013.
- [17] F. Liu, J. Gao, and H. Liu, "The feature extraction and diagnosis of rolling bearing based on CEEMD and LDWPSO-PNN," *IEEE Access*, vol. 8, pp. 19810–19819, 2020.

## Research Article

# Interior Space Design and Automatic Layout Method Based on CNN

WeiPing Wu<sup>1</sup> and Yanshun Feng <sup>2</sup>

<sup>1</sup>Henan Vocational College of Water Conservancy and Environment, Zhengzhou 450000, China

<sup>2</sup>Hebei Yingyi Information Technology Co., Ltd., Shijiazhuang 050000, Hebei, China

Correspondence should be addressed to Yanshun Feng; [fyscn@163.com](mailto:fyscn@163.com)

Received 24 February 2022; Revised 15 March 2022; Accepted 19 March 2022; Published 19 April 2022

Academic Editor: Man Fai Leung

Copyright © 2022 WeiPing Wu and Yanshun Feng. This is an open access article distributed under the Creative Commons Attribution License, which permits unrestricted use, distribution, and reproduction in any medium, provided the original work is properly cited.

With the rapid rise in the number of people buying houses, the demand for interior space design has also increased accordingly. The diversification of existing room types and the diversity of the public's perception of fashion make interior designers in short supply. The future of computer science and technology in the field of automatic design of indoor areas will be immeasurable. This paper proposes an automatic layout method for spatial area design based on convolutional neural networks (CNN). CNN methods are a fast and efficient method. By mimicking the designer's design process, it proposes a two-stage algorithm that defines the room first and the wall later, and the algorithm also provides a large-scale dataset called RPLAN that contains more than 80,000 interior layout plans from real residential buildings. Starting from the prediction living room, the automatic layout of the indoor areas is completed by iteration. A large number of empirical results show that the interior area design effect of this method is comparable to the interior design floor plan of professional designers.

## 1. Introduction

In the long history of 5,000 years, China has formed a unique set of architectural styles and concepts of its own, and China's architectural style and interior design have been influencing neighboring countries since the feudal society. Today's Chinese society continues to grow and develop; with the improvement of China's international status, China's traditional architecture is more valued and imitated by famous designers across the country. Chinese interior design style symbolizes traditional Chinese culture, and many contemporary designs make it possible to integrate popular elements into modern Chinese interior design while inheriting traditional Chinese architectural Wenhua, forming a new style, and promoting the development of modern interior design [1]. The automatic layout of the indoor automatic area design should consider the location of the indoor area wall and, more importantly, consider the needs of the occupants. For example, when designing a psychiatric hospital, there is a positive impact on the health

of patients [2]. In the automatic layout of interior design, the public's emphasis on natural elements has become an indispensable part of the interior landscape. To this end, the automatic layout design should add the way natural elements are reflected in the indoor landscape and the principle of using natural elements in the indoor landscape [3]. When building children's boarding schools in rural areas, it is necessary to carry out scientific automatic layout of the indoor space environment of teaching buildings, dormitories, school canteens, toilets, and activity rooms of "residual children's homes" based on psychological and behavioral psychology and architectural space theory [4] according to the purpose of promoting children's physical and mental development. In this paper, in the case of the actual floor area of the house, this paper expounds on the calculation basis and system operation process of automatic generation of interior design, puts forward the overall system design and database structure design, and summarizes the characteristics of the automatic generation system of interior decoration area [5]. Although virtual reality technology is

widely used in the automatic layout of interior design today, interior design is still a difficult field to master, without a strong, mature model to compete with the expertise of the industry. Moving away from the virtual reality trend, this paper proposes an end-to-end concept, based on a learning scoring function, to implement applications and their learning techniques to actually assess the quality of professional and realistic room furniture layouts, including different interior design guidelines, ergonomics, and common sense signs [6]. We further presented a proof of concept based on simulated annealing techniques for random optimization, aiming to generate new, reasonable, and pleasing furniture layouts that meet the strict regulations of interior design. This software tool will eventually prove that professional-quality furniture layouts in the real world can be obtained in a way that is at least semiautomatic. Using the energy function, the interdependencies of various furniture functions and styles, common practices of relative furniture positioning in the room, and other ergonomic factors that contribute to the acquisition of pleasant, livable rooms are analytically represented as cost items. Using machine learning, the ranking function parameters adapted to various types of rooms and complex furniture objects allow the method to be extended in complex interior design knowledge modeling [7]. First of all, the feature-based graphic recognition technology is modeled, the replanning of the internal space is realized by adding an automatic layout algorithm, and finally, the HTML5 Canvas 2D API is used for online graphic drawing, which realizes the allocation and management of indoor space and establishes the empty order of the internal space in partition management and timing [8]. In the era of the rise of computers, a new technology—virtual reality—has become a common and important application in people’s lives. The technology mainly imitates a real scene, reflecting the changing form of the entity so that people have a more intuitive feeling. The complex and diversified characteristics of interior design are to apply virtual reality technology as a major technology; through this technology, the design enables them to show the scene image of their own design, which makes the interior design continue to develop and progress [9]. The placement of parameter servers is an important part of distributed deep learning global model training. For the placement strategy of PSs, the training time of distributed deep learning under the minimum conditions is proposed. The whole phase is divided into two parts, the first part uses the approximation algorithm and the rounding algorithm to solve the problem, and the second part proposes to adjust algorithm 1, which reduces the amount of time spent training the global model by continuously improving the decision of the placement strategy of the PSs. Experiments have shown that both the approximation algorithm and the rounding algorithm are superior to existing algorithms [10] in terms of training time for global models. When selecting various application areas for information processing, general deep learning methods mainly consider the following three indicators: professional knowledge or knowledge of the author; the application area has successfully used deep learning techniques, such as speech recognition; and the

application area is likely to receive a significant impact on progressive learning [11]. Deep learning requires first examining the encoder-decoder concept of conformity and then classifying with spatially dominant information. Finally, the two features are merged using the new deep learning framework. From this, we can see the highest classification accuracy. The framework is a hybrid of principal component analysis (PCA), deep learning architecture, and logistic regression. Specifically, as a deep learning architecture, stacked autoencoders are designed to gain useful advanced features [12]. The latest deep learning frameworks typically use deep convolutional neural networks (CNNs) to extract image features, which are then converted into hundreds of code markers through the recurrent neural network- (RNN-) based code generators, making them through encoders. The decoder framework makes it possible to automatically convert the graphical user interface (GUI) into code. But the implementation of the framework must overcome two challenges: one is how to take full advantage of the GUI and the information contained in the Domain Specified Language (DSL) code, for which this paper addresses a model called HGui2Code, which integrates GUI features that support visual attention (extracted by CNN). It supports semantic features of DSL attention (LSTM extraction); another is how to make the build DSL code conform to syntax rules, and in response to this problem, this paper proposes the SGui2Code model, which uses the ON-LSTM network to generate syntactic correctness DSL code. Although the model does not have a big improvement on IOS and Android datasets, it is generated by the model. The DSL code is very close to the component layout [13] in the corresponding GUI. This paper mainly discusses the topology layout of wireless sensor networks and the visualization of node data, and the overall complexity of the visualization algorithm is  $2O(n)$ . The hardware design and execution part of this paper are based on the algorithm to automatically provide the main load optimization of the visual automatic layout algorithm, network control and design, module network-based research, and analysis of module serial port UART and WSN network joint monitoring platform [14]. Data representation determines the success of machine learning, and domain knowledge and learning can be used to aid design, and more, the public’s quest for artificial intelligence is inspiring the design of more powerful representation learning algorithms. Recent work in the field of unsupervised feature learning and deep learning includes probabilistic models, manifold learning, and deep learning. These works raise long-unanswered questions about the appropriate goal of learning good representations, computational representations (i.e., reasoning), and representing the geometric connections between learning, density estimation, and manifold learning [2].

## 2. Deep Learning Analysis

*2.1. Convolutional Neural Networks (CNN).* Convolutional neural network is a representative neural network in the field of deep learning technology. Compared with traditional image processing algorithms, the advantage of convolutional

neural network is that it avoids the complex image pre-processing process, and convolutional neural network can directly input the original image for work [1].

Convolutional neural networks contain convolutional operations and depth structures.

### 2.1.1. Convolution Operations Are at the Heart of Convolutional Neural Networks.

$$W = \begin{bmatrix} w_{11} & w_{12} & \cdots & w_{1n} \\ w_{21} & w_{22} & \cdots & w_{2n} \\ \cdots & \cdots & \cdots & \cdots \\ w_{m1} & w_{m2} & \cdots & w_{mn} \end{bmatrix}_{(m \times n)}. \quad (1)$$

The process of convoluting image  $X$  is to multiply each  $w$  in the convolutional kernel  $W$  with the corresponding pixel  $x$  in the original image  $X$  to be covered and then summed.

$$z = w_1 x_1 + w_2 x_2 + \cdots + w_{mn} x_{mn} = \sum_{k=1}^{mn} w_k x_k = W^T X. \quad (2)$$

In Figure 1, for example, a convolutional kernel overlays 9 pixels of the original image each time and slides four times, resulting in  $2 \times 2$  two-dimensional data. Obviously, for a raw image with a convolution kernel of  $n$ , after  $f$ -convolution operations, the output image is sized  $n-f+1$ .

2.1.2. *Step.* The convolutional step size is the spacing of the slide, and after combining the step size operation, the output image size is

$$p = \lfloor \frac{n-f}{s} \rfloor + 1, s = \text{step} \cdot \text{length}, \quad (3)$$

where  $stride = 1$  indicates that the convolutional kernel of the standard convolutional mode slides over the distance of each adjacent pixel is 1,  $stride = 2$  indicates that the movement step is 2, the adjacent pixels are skipped, and the output image is the original 1/2. By analogy, when  $stride = 3$ , the image is reduced to 1/3 of the original.

2.1.3. *Padding.* For the problem that the image loses a lot of information at the edges each time it is zoomed out, the edges of the image can be filled with "fake" pixels [15]. Assuming the fill pixel is  $p$ ,  $n$  becomes  $n+2p$ , and the dimensions of its output image are

$$p = \left\lfloor \frac{n+2p-f}{s} \right\rfloor + 1. \quad (4)$$

Fill pixels generally have two options: valid convolution and same convolution. The valid image will be reduced after calculation, and the output size is

$$p = \left\lfloor \frac{n+2p-f}{s} \right\rfloor + 1. \quad (5)$$

The same convolutional image output size remains the same; according to the above formula, the same convolutional image output size is

$$\left\lfloor \frac{n+2p-f}{s} \right\rfloor + 1 = n, \quad (6)$$

where  $P$  can be described by the following formula:

$$p = \frac{(n-1)s - n + f}{2}. \quad (7)$$

When  $s = 1$ ,

$$p = \frac{f-1}{2}. \quad (8)$$

2.2. *Deep Learning Model Framework and Design.* This paper uses graph neural networks (GNNs) to learn plan diagrams and uses both supervised and unsupervised learning strategies [16]. The system flow is shown in Figure 2.

- (1) Sample floor plans are encoded into graphs, which are data structures such as procedure 1. The nodes in the diagram represent rooms, and the edges represent the types of adjacency between rooms.
- (2) Supervised learning: use the graph neural network to embed the nodes and subgraphs in the graph to obtain the corresponding vector representation and the overall vector representation of each graph. After the training, you can extract subgraphs that have a large impact on the score as a good design, such as procedures 2 and 3.
- (3) Unsupervised learning: use GNN to map all sample plots to high-dimensional spaces and visualize them, as in procedure 4.
- (4) Structure combination: by adding new variables to combine some nodes and further using additional nodes to add new designs, manual judgment of the effectiveness of the design is required.
- (5) Generate the final conceptual design: a new drawing (graph) that conforms to the design is obtained and converted to a floor plan.

Figure 3 illustrates the graph neural network architecture used to discover the build subgraph.

Figure 4 is end-to-end learning that does not require input features and, more importantly, considers the relatively large fragments in the graph, that is, extracting the  $r$ -radius subgraph [14].  $M$  in the graph is the number of subgraphs of all  $r$  radii in a graph; of course, we need to update the subgraph vectors

$$x_i^{(t+1)} = x_i^{(t)} + \sum_{j \in N(i)} x_{ij}^{(t)}. \quad (9)$$

2.3. *Algorithm Optimization.* This paper uses the Adam algorithm to improve the algorithm model; as the name suggests, Adam integrates the first-order momentum of SGD and the second-order momentum of RMSProp.

$$m_w^{t+1} = \beta_1 m_w^t + (1 - \beta_1) \nabla L^t, \quad (10)$$

where  $m$  is a first-order moment estimate,



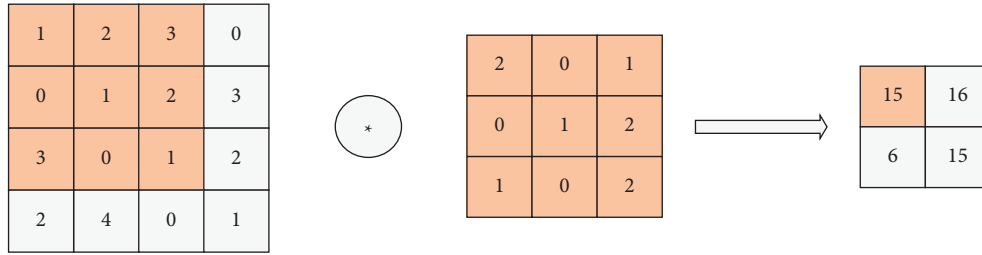


FIGURE 1: Schematic diagram of the standard 2D convolution operation process.

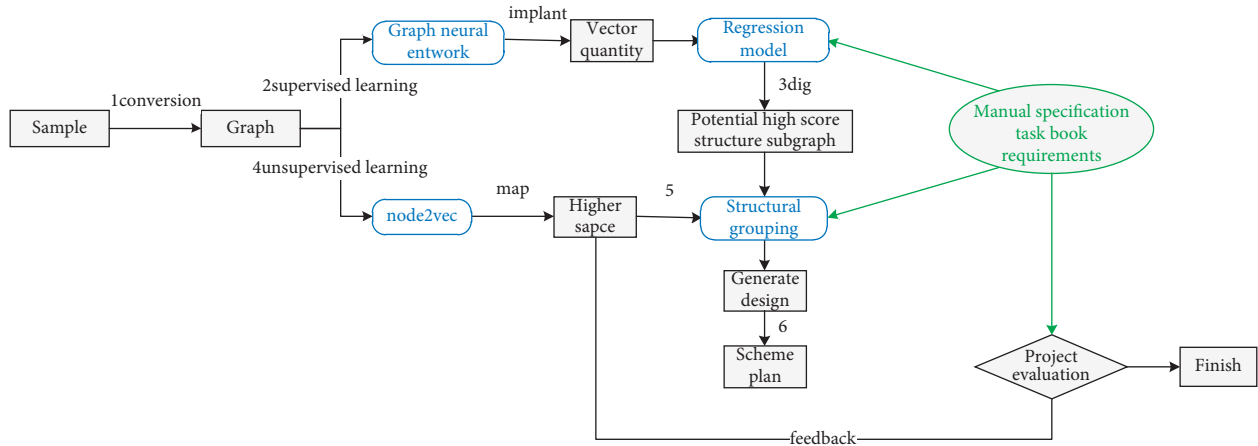


FIGURE 2: The overall process framework of the model.

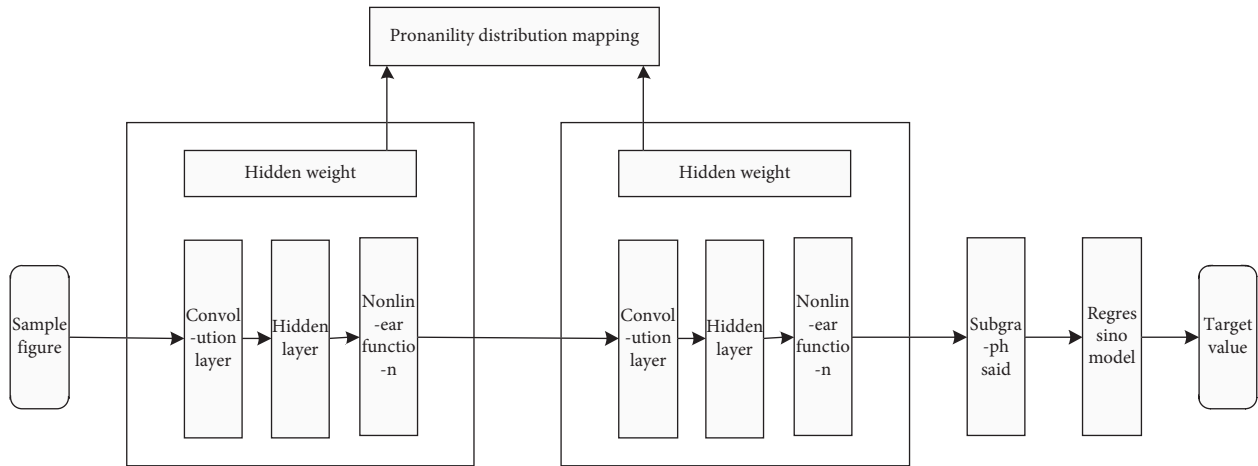


FIGURE 3: Neural network structure.

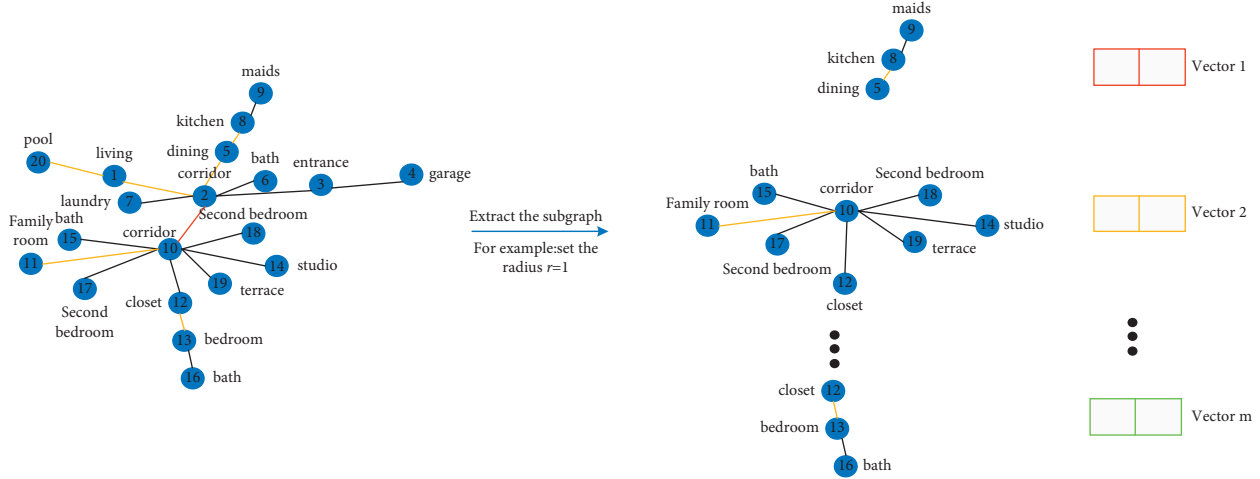


FIGURE 4: Extracting all of its subgraphs for each room and initializing each subgraph with a random vector.

$$v_w^{t+1} = \beta_2 m_w^t (1 - \beta_2) (\nabla L^t)^2; \quad (11)$$

where  $v$  is a second-order moment estimation,

$$\hat{m}_w = \frac{m_w^{t+1}}{1 - \beta_1^{t+1}}. \quad (12)$$

Estimation correction to achieve unbiased estimation is as follows:

$$\hat{v}_w = \frac{v_w^{t+1}}{1 - \beta_2^{t+1}} \quad (13)$$

The gradient method is used to optimize the parameters of the model, which can speed up the training.

The conjugate gradient method optimizes the prediction model to obtain the optimal parameter matrix of the network model, the essence of which is that the mean square error reaches the minimum value, and the definition of the mean square error is as follows:

$$\text{MSE} = E(e^T e) = E((o_d - o)^T (o_d - o)), \quad (14)$$

where  $o_d$  is the model predicts the output and  $o$  is the actual output, which is the error  $o_d - o$  between the model prediction output and the actual output [17]. The weights of the model are adjusted according to the following equation until the parameters are optimal.

$$w_{k+1} = w_k + a_k d_k, \quad (15)$$

where the search direction is  $k$  times  $d_k$  during the training of the model and the step  $a_k$  size.

When optimizing the weight matrix and paranoid matrix of the model using the conjugate gradient method, the initial value of the search direction is calculated

$$d_0 = -\nabla \text{MSE}(w_0) = -g_0. \quad (16)$$

As the number of iterations increases, the search direction for  $k+1$  is as follows:

$$d_{k+1} = -g_k + \beta_k d_k, \quad (17)$$

where  $\beta_k$  is the conjugate gradient algorithm that updates the parameters when optimizing the model, and the calculation formula is as follows:

$$\beta_k = \frac{\|g_{k+1}\|^2}{\|g_k\|^2}. \quad (18)$$

### 3. Space Layout Design

We extract design constraints from real houses, generate complex layout forms, and then use the hierarchical algorithm of complex layout structures to complete the layout design.

**3.1. Constraint Modeling.** Constraints are crucial to the layout design of indoor spaces, and there are mainly the following constraints.

**3.1.1. Dimension Constraints.** The size of the room has the range of room sizes and the specific target size of the room. Dimension range constraints  $C_{\text{size}}$  are defined as

$$\{ \underline{w}_i \leq w_i \leq \overline{w}_i, \underline{d}_i \leq d_i \leq \overline{d}_i, \quad (19)$$

where  $(\underline{w}_i, \underline{d}_i)$  and  $(\overline{w}_i, \overline{d}_i)$  are the maximum and minimum values of the  $\underline{d}_i$  room size, respectively.

**3.1.2. Scale Constraints.** Use the scale constraint of the room  $C_{\text{overlap}}$  to avoid generating a room length and width incongruity. We set a secondary binary variable for each room to represent the orientation of the room rectangle, horizontal  $w_i (>) d_i$ , or vertical ( $<$ ).  $w_i d_i$  scale constraints are defined as

$$\left\{ \begin{array}{l} \underline{r}_i \cdot d_i \leq w_i + M \cdot \sigma_i, \overline{r}_i \cdot d_i \geq w_i - M \cdot \sigma_i, \underline{r}_i \cdot w_i \leq d_i + M \cdot (1 - \sigma_i), \overline{r}_i \cdot w_i \geq d_i - M \cdot (1 - \sigma_i), \end{array} \right. \quad (20)$$

where  $(\underline{r}_i)$  is  $\overline{r}_i$  the maximum and minimum ratio between room  $w_i$   $i$   $d_i$  and  $\underline{r}_i \geq 1$ .  $\sigma_i = 0$  indicates that room  $i$  is horizontal, the range of scales is  $[\underline{r}_i, \overline{r}_i]$ , and  $\sigma_i = 1$  indicates that the room is vertical.

**3.1.3. Position Constraints.** Interior space design usually requires specifying the approximate location of the room, and we represent the guided location of the room as some points  $(x^*, y^*)$  (one or more). The position constraint of each point requires that the  $C_{\text{pos}}$  room area covers the point.

$$\left\{ \begin{array}{l} x_i \leq x^* \leq x_i + w_i, \\ y_i \leq y^* \leq y_i + d_i, \end{array} \right. \quad (21)$$

**3.1.4. Boundary Constraints.** Lighting conditions are important to boundary constraints, and to achieve this constraint, we added boundary  $C_{\text{boundary}}$  constraints.

$$\left\{ \begin{array}{l} y_i \leq y + M \cdot (1 - \rho_k), \\ x_i \leq x_2 - w_i + M \cdot (1 - \rho_k), \\ x_i \geq x_1 - M \cdot (1 - \rho_k), \\ \sum_{k=1} \rho_k \geq 1, \end{array} \right. \quad (22)$$

where  $\rho_k$  is the auxiliary binary variable,  $n$  is the number of edges of the specified boundary, and  $\rho_k = 1$  indicates that the constrained room is adjacent to the edge  $k$ .

**3.1.5. Adjacency Constraints.** Suppose that  $x_i$  rooms  $i$   $y_i$  ( $w_i$ ,  $d_i$ ) and room  $x_j$   $j$   $y_j$  ( $w_j$ ,  $d_j$ ) are adjacent, the overlap of the two rooms is implemented first, and then the nonoverlapping constraint is combined.  $C_{\text{overlap}}$  is also necessary to constrain the minimum overlapping length  $c$  of the common edge between two adjacent rooms, called the contact length. Adjacency constraints  $C_{\text{adj}}$  can be written as

$$\left\{ \begin{array}{l} x_i \leq x_j + w_j - c \cdot \theta_{i,j}, \\ x_i + w_j \geq x_j + c \cdot \theta_{i,j}, \\ y_i \leq y_j + d_j - c \cdot (1 - \theta_{i,j}), \\ y_i + d_j \geq y_j + c \cdot (1 - \theta_{i,j}), \end{array} \right. \quad (23)$$

where  $\theta_{i,j}$  is an auxiliary binary variable that determines the adjacent direction.  $\theta_{i,j} = 1$  indicates vertical neighbor; otherwise, it indicates horizontal neighbor.

**3.1.6. Extend the Target Function.** The final optimization problem is defined as

$$\min_{L, \sigma, \theta, \rho} \lambda_{\text{cover}} E_{\text{cover}}(L) + \lambda_{\text{size}} E_{\text{size}}(L). \quad (24)$$

$L = \{(x_i, y_i, w_i, d_i)\}$  is a rectangular tuple of rooms.  $\sigma$ ,  $\theta$ , and  $\rho$  are binary variables.  $\lambda_{\text{cover}}$  is the weight that  $\lambda_{\text{size}}$  balances between the area  $E_{\text{cover}}$  term and the size error term. In this document,  $E_{\text{size}}$  is set  $\lambda_{\text{cover}} = 1$ .

**3.2. Multilevel Algorithms.** Our multilevel algorithm is equivalent to further improving the details of the resulting interior space layout by extending the basic algorithm, with the advantage of being fast and efficient [18].

**3.2.1. Polygon Layout Area Representation.** A set of rectangles is used to describe the layout area of a polygon, the rectangular area marked as an obstacle cannot overlap any room, and the rectangular area marked as an obstacle remains unchanged.

**3.2.2. Subregion Selection.** If there is an indoor area that is not filled, then we will select this subarea to continue optimization.

**3.2.3. Initialize.** For a rectangular room of subarea, we randomly divide it into two subelements of the same size as shown in Figure 5, and the subelement inherits the parent rectangle label.

**3.2.4. Constraint Updates.** For the newly given layout area, we make the following constraint update. Start by updating the internal constraints and nonoverlapping constraints with the new layout area and the initial  $C_{\text{inside}} C_{\text{overlap}}$  layout. Second, for a room with a location constraint  $C_{\text{pos}}$ , you need to set a new location constraint for its subfolders and update the boundary constraint in the same way. Then, we add an adjacency constraint  $C_{\text{boundary}}$  to each sublevel, making sure that there are no neighbors to the sublevel. Finally, add a subdivision constraint for each pair of child rectangles  $C_{\text{refine}}$  to replace the dimension constraints of the parent rectangle. The main goal  $C_{\text{size}}$  is to avoid major changes in the layout of the interior space that is eventually generated. Assuming a vertically oriented decomposition, as shown in the image above, the segmentation constraint is  $C_{\text{refine}}$  defined as

$$\left\{ \begin{array}{l} x_{i1} \geq x_i - \delta \\ x_{i1} \leq x_i \\ y_{i1} \geq y_i - \delta \\ y_{i1} \leq y_i \\ y_{i1} + d_{i1} \geq y_i + d_i \\ y_{i1} + d_{i1} \leq y_i + d_i + \delta \\ x_{i2} + w_{i2} \geq x_i + w_i \\ x_{i2} + w_{i2} \leq x_i + w_i + \delta, \\ y_{i2} \geq y_i - \delta \\ y_{i2} \leq y_i \\ y_{i2} + d_{i2} \geq y_i + d_i \\ y_{i2} + d_{i2} \leq y_i + d_i + \delta \end{array} \right. \quad (25)$$

For horizontal decomposition, the subdivision constraint for dimensions is defined

$$\left\{ \begin{array}{l} x_{i1} \geq x_i - \delta \\ x_{i1} \leq x_i \\ x_{i1} + w_{i1} \geq x_i + w_i \\ x_{i1} + w_{i1} \leq x_i + w_i + \delta \\ y_{i1} + d_{i1} \geq y_i + d_i \\ y_{i1} + d_{i1} \leq y_i + d_i + \delta \\ x_{i2} \geq x_i - \delta \\ x_{i2} \leq x_i \\ y_{i2} \geq y_i - \delta \\ y_{i2} \leq y_i \\ x_{i2} + w_{i2} \geq x_i + w_i \\ x_{i2} + w_{i2} \leq x_i + w_i + \delta \end{array} \right. , \quad (26)$$

where  $(x_{i1}, y_{i1}, w_{i1})$  is the shape parameter of  $d_{i1}$  the subfold i1  $(x_{i2}, y_{i2})$  is the shape parameter of the  $w_{i2}$  subpolar  $d_{i2}$  i2, and  $\delta$  is the range of variation of the size breakdown.

**3.2.5. Optimize.** We represent the objective function as equation (24), which also requires that the update constraint on the subarea be satisfied [19]. Once all subregions have been subdivided and optimized, proceed to the next iteration process. The rational hierarchy algorithm framework performs indoor space layout generation. When each room size is less than the threshold, stop iteration. Merge rectangular rooms with the same labels to get the final layout result.

## 4. Algorithm Examples and Result Analysis

**4.1. Experimental Procedure.** The 12 types of room types that appear in a typical indoor space are summarized in Table 1.

**Room positioning:** the living room is an essential part, often as a core area, connected to other rooms. So first predict the living room location, as shown in Figure 6. The room connectivity of the indoor space is obtained by

detecting the adjacent relationship between the living room and other rooms. Through comparison, it is found that the living room prediction model alone helps to improve the prediction accuracy and the overall rationality of the indoor space layout.

**Wall positioning:** the next step is to use the method of constraint satisfaction to locate the wall, using the position of the room as a design constraint to allocate a reasonable space for each room. Since too many design constraints can lead to unworkable optimization problems, we need to use a prediction-based positioning strategy at a time, as shown in Figure 7 [20]. Specifically, the encoder-decoder network is used to predict the pixel-level wall based on the input ring and room position, and then the predicted wall is converted into a vector representation through some postprocessing.

**User research:** for floor plans with the same screenplay as a group, we mandate users to compare and choose a better floor plan. The actual number of participants was 100, and people of different ages and different jobs voted for the designer works and the deep learning network automatic layout works, recording the votes of the two teams. It is shown in Table 2.

**4.2. Evaluation Indicators.** In this paper, two evaluation indicators are introduced, mean squared error (MSE) and mean relative error (MAE), to measure the performance of the deep confidence network model in spatial design layout prediction so as to illustrate the prediction ability of the model [21].

$$\begin{aligned} \text{MSE}(y, \hat{y}) &= \frac{\sum_{i=1}^n (y_i - \hat{y}_i)^2}{n} \\ \text{MAE}(y, \hat{y}) &= \sum_{i=1}^n |y_i - \hat{y}_i|. \end{aligned} \quad (27)$$

**4.3. Analysis of Experimental Results.** According to the above experimental and evaluation indicators, we can know the difference between the overall effect before and after optimization. It shown in Figures 8–18.

It can be seen that, after using the conjugate gradient method, the correct rate of the model converges quickly during training, and the accuracy rate is the best.

The complexity of traditional machine algorithms is high compared with traditional machine learning methods; the popularity of deep learning image processing is much higher than that of traditional algorithms because the current operation speed of traditional machine algorithms is much lower than the speed of deep learning, which makes deep learning have better development prospects, and the following figure shows why deep learning gradually replaces traditional machine learning.

Through the survey, we can get the results as shown in the figure. Ordinary users of the design of the space area prefer the deep learning network design of the interior space,

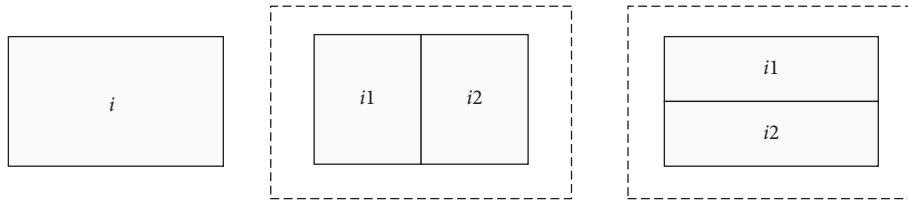


FIGURE 5: Room decomposition in a multilevel algorithm.

TABLE 1: Room types.

| Serial number | Room name      | Remark   |
|---------------|----------------|--|
| 0             | Living room    | Living room  |
| 1             | Master bedroom | One of the bedrooms of each type of apartment must be the size of a master bedroom, generally with a separate bathroom, which is the largest bedroom |
| 2             | Second bedroom | Bedrooms other than the master bedroom generally do not have a bathroom  |
| 3             | Restaurant     | Generally connected to the kitchen   |
| 4             | Toilet         | When there is only one bathroom in the home, you must choose a larger bathroom   |
| 5             | Laundry room   |  |
| 6             | Storage room   |  |
| 7             | Wardrobe       | Generally designed in the master bedroom   |
| 8             | Studio         | Den  |
| 9             | Corridor       | Extra rectangular space connecting the room  |
| 10            | Terrace        | A platform that extends out of the outdoors  |
| 11            | Maid's room    |  |

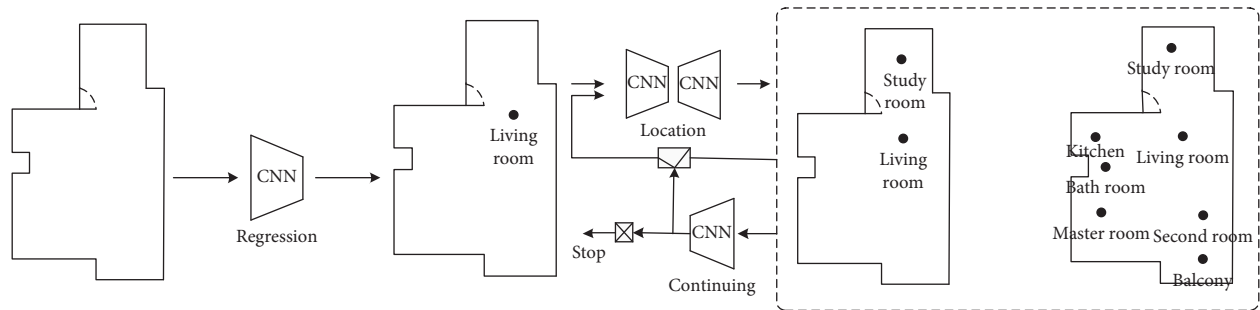


FIGURE 6: An iterative model of room types and locations.

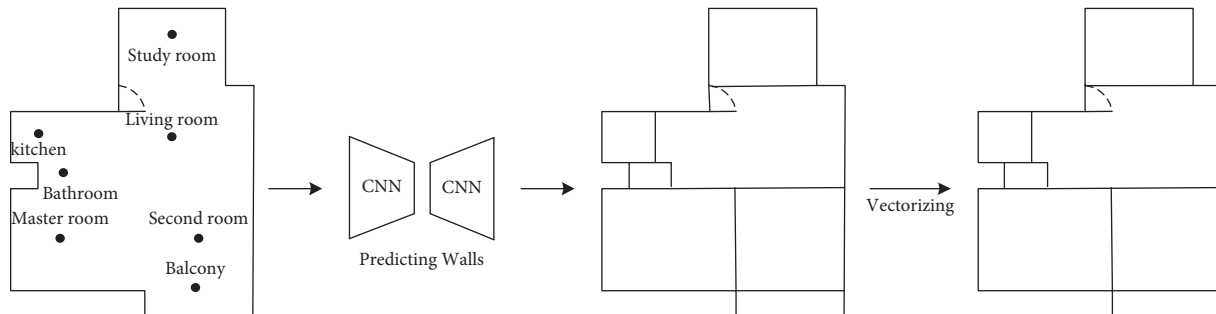


FIGURE 7: Convert a prediction wall to a vector.

mainly because the design professionals will spend more cost, slower time, and less space utilization.

The layout models of different types of bedrooms are evaluated experimentally according to MSE and MAE.

- (1) Mouth-shaped bedroom.
- (2) L-type bedroom.
- (3) Vertical hall-type living room.

TABLE 2: User votes.

|              | Designer votes | Deep learning votes | Cumulative votes |
|--------------|----------------|---------------------|------------------|
| Voting users | 42             | 58                  | 100              |

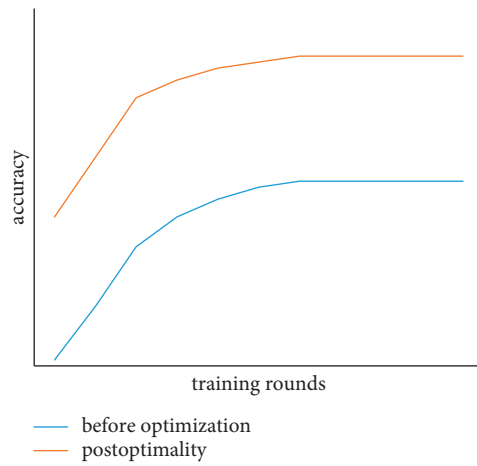


FIGURE 8: The correct rate of the strategy model before and after optimization.

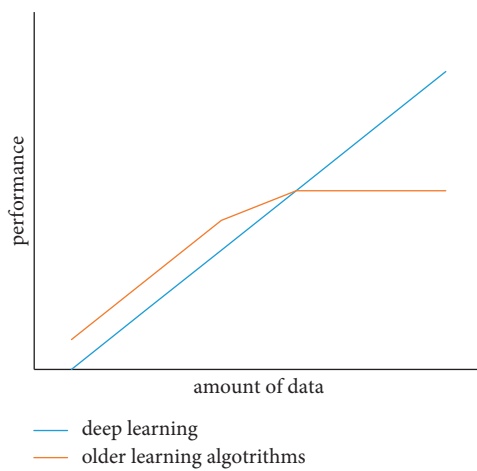


FIGURE 9: Algorithm advantages and disadvantages.

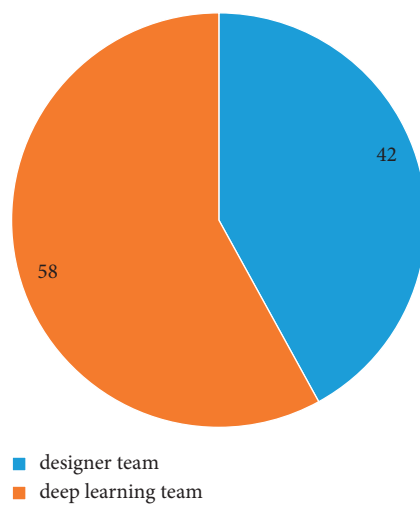


FIGURE 10: Comparison of user satisfaction.

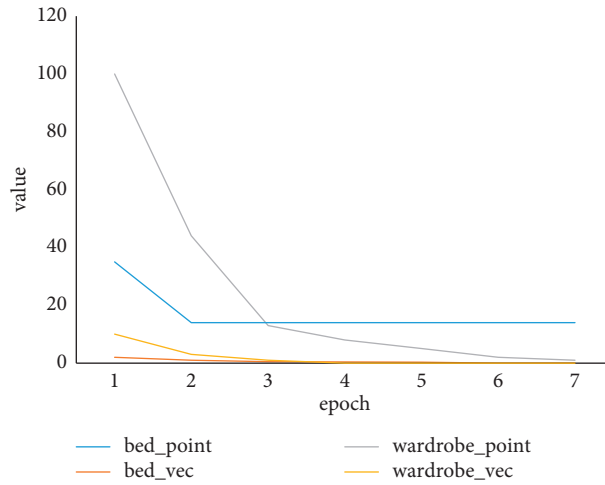


FIGURE 11: Oral-type bedroom MAE.

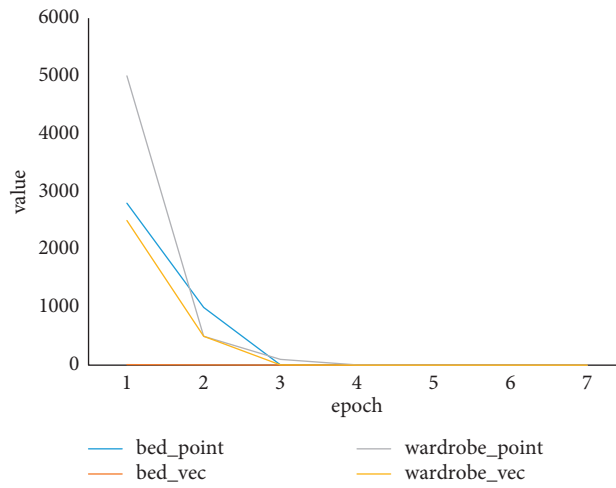


FIGURE 12: Type bedroom MSE indicator.

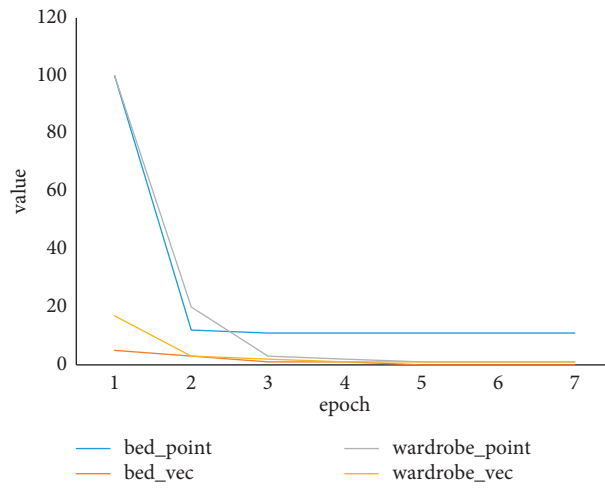


FIGURE 13: MAE index of type L bedroom.

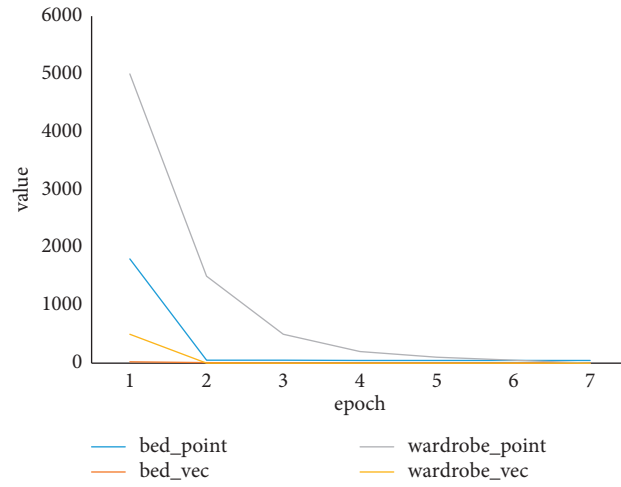


FIGURE 14: MSE indicator of type L bedroom.

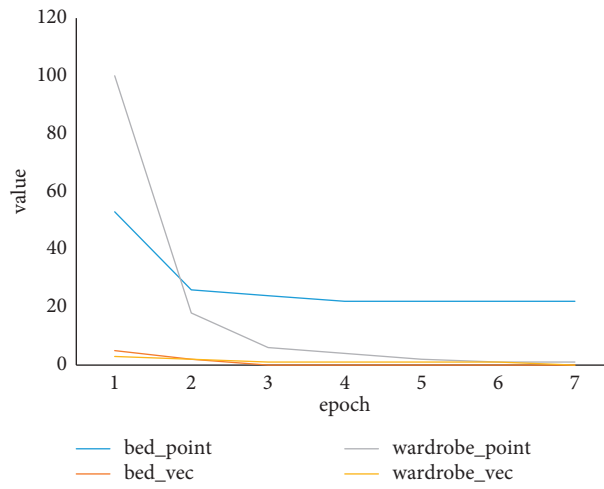


FIGURE 15: MAE index of vertical hall-type living room.

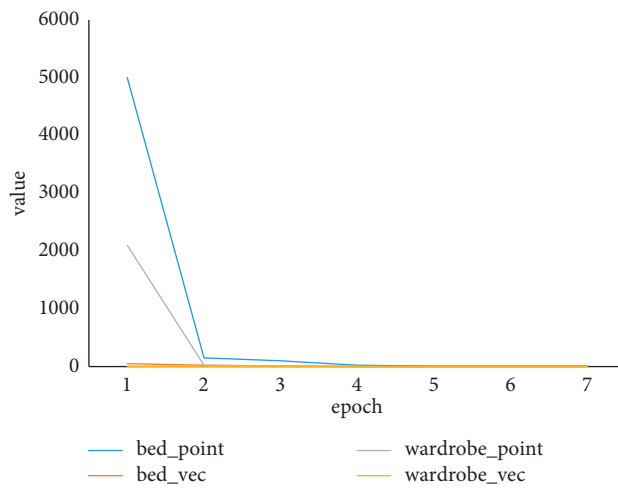


FIGURE 16: MSE index of vertical hall-type living room.



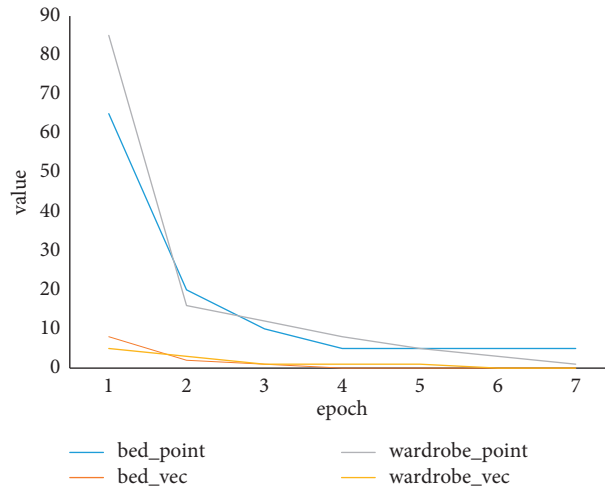


FIGURE 17: The MAE index of the horizontal hall-type living room.

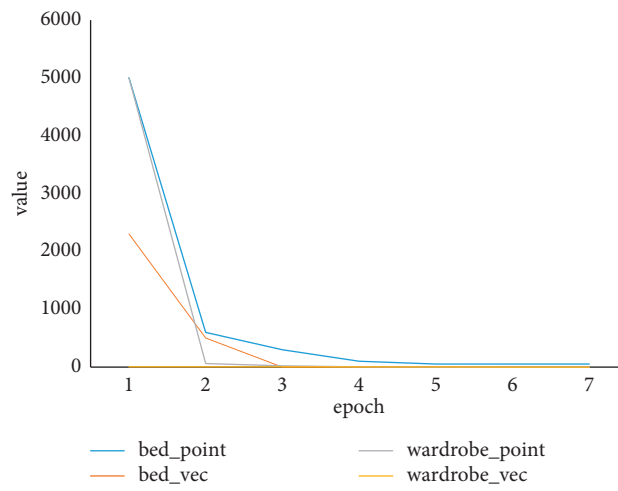


FIGURE 18: MSE index of the horizontal hall-type living room.

TABLE 3: Oral-type bedroom evaluation index table.

| Parameter      | MAE | MSE  |
|----------------|-----|------|
| Bed_point      | 7.1 | 68.7 |
| Bed_vec        | 0.6 | 0.04 |
| Wardrobe_point | 1.8 | 0.5  |
| Wardrobe_vec   | 0.5 | 0.03 |

TABLE 4: L-type bedroom evaluation indicators table.

| Parameter      | MAE | MSE  |
|----------------|-----|------|
| Bed_point      | 7.5 | 77.9 |
| Bed_vec        | 0.9 | 0.09 |
| Wardrobe_point | 1.1 | 1.8  |
| Wardrobe_vec   | 0.4 | 0.01 |

TABLE 5: Evaluation index table of vertical hall-type living room.

| Parameter      | MAE  | MSE   |
|----------------|------|-------|
| Bed_point      | 6.9  | 67.7  |
| Bed_vec        | 0.43 | 0.42  |
| Wardrobe_point | 0.36 | 0.2   |
| Wardrobe_vec   | 0.15 | 0.039 |

TABLE 6: Evaluation indicators of horizontal hall living room.

| Parameter      | MAE  | MSE  |
|----------------|------|------|
| Bed_point      | 7.9  | 87.8 |
| Bed_vec        | 0.18 | 0.01 |
| Wardrobe_point | 0.41 | 1.4  |
| Wardrobe_vec   | 0.17 | 0.04 |

#### (4) Cross-hall-type living room.

From the experimental comparison, Tables 3–6, it can be seen that the number of network iterations converges significantly after 5 to 10 times, the MAE and MSE evaluation indicators gradually decrease, and the error of the model is very small and tends to be stable [22].

## 5. Conclusion

Under the current wave of rapid development of computer networks, the industrial structure of home improvement design will also usher in an upgrade point. Based on today's scientific and technological trends and the needs of people's home decoration design, this paper has studied the automatic layout of indoor space design, Li Yong machine deep learning, imitating designers to create and carry out more scientific typography design, so that the public can get the best creative combination of interior design. First of all, this paper introduces the basic theory of deep learning, then establishes an interior design model based on deep confidence network, conducts research experiments on the model, analyzes the results, and explores the application of deep learning in interior design.

Although the deep learning in this paper has achieved some results in the field of interior area design, there are still some shortcomings in this research:

- (1) Further optimization of the deep confidence network structure is needed.
- (2) Data characteristics and processing need to be improved.
- (3) Although the deep confidence network in this paper has achieved good theoretical results, there are still many mainstream methods to be tried.

## Data Availability

The experimental data used to support the findings of this study are available from the corresponding author upon request.

## Conflicts of Interest

The authors declare that they have no conflicts of interest regarding this work.

## References

- [1] G. Purushothaman, B. B. Scott, and D. C. Bradley, "An acute method for multielectrode recording from the interior of sulci and other deep brain areas," *Journal of Neuroscience Methods*, vol. 153, no. 1, pp. 86–94, 2006.
- [2] A. E. Vaaler, G. Morken, and O. M. Linaker, "Effects of different interior decorations in the seclusion area of a psychiatric acute ward," *Nordic Journal of Psychiatry*, vol. 59, no. 1, pp. 19–24, 2005.
- [3] J. Ling, "The application of natural elements in interior landscape design and its principal analysis," *Research on architectural development*, vol. 5, no. 5, p. 4, 2021.
- [4] A. Nicolli, I. Bortoletti, S. Maso, and A. Trevisan, "Course of metal ions after a revision of malfunctioning metal-on-metal total hip prostheses," *Medicina*, vol. 57, no. 2, p. 115, 2021.
- [5] W. Baomin, "Experience in structural design of industrial buildings," *Shanxi Architecture*, vol. 37, no. 14, pp. 33–34, 2011.
- [6] Ji-S. Lee, "Real survey on interior surface area and applied finishes in recently-planned apartment houses," *The International Journal of the Korea Institute of Ecological Architecture and Environment*, vol. 10, no. 6, pp. 115–121, 2010.
- [7] J. Selga, A. Rodriguez, M. Gil, J. Carbonell, V. E. Boria, and F. Martin, "Towards the automatic layout synthesis in resonant-type metamaterial transmission lines," *IET Microwaves, Antennas & Propagation*, vol. 4, no. 8, pp. 1007–1015, 2010.
- [8] G. Shao, "Research on the construction of communication machine room and equipment layout," *Telecom construction*, vol. 6, pp. 54–56, 2002.
- [9] X. Han, "Application of virtual reality in the teaching of interior design," *Journal of Contemporary Educational Research*, vol. 5, no. 9, pp. 1–4, 2021.
- [10] L. Deng and D. Yu, "Deep learning: methods and applications," *Foundations & Trends in Signal Processing*, vol. 7, no. 3, pp. 197–387, 2014.
- [11] Y. Chen, Z. Lin, and Z. Xing, "Deep learning-based classification of hyperspectral data," *Ieee Journal of Selected Topics in Applied Earth Observations and Remote Sensing*, vol. 7, no. 6, pp. 2094–2107, 2017.
- [12] X. Pang, Y. Zhou, P. Li, W. Lin, W. Wu, and J. Z. Wang, "A novel syntax-aware automatic graphics code generation with attention-based deep neural network," *Journal of Network and Computer Applications*, vol. 161, Article ID 102636, 2020.
- [13] J. Sun, J. Zhang, and X. Zhang, "A deep learning-based method for heat source layout inverse design," *IEEE Access*, vol. 8, p. 1, 2020.
- [14] P. Seokyoung, "A study on the technological connections between BIM (building information modeling) and interior architecture design -focusing on the applications of spatial object and its properties-," *Journal of Korea Design Knowledge*, no. 34, pp. 35–44, 2015.
- [15] G. Chen, Q. Pei, and M. M. Kamruzzaman, "Remote sensing image quality evaluation based on deep support value learning networks," *Signal Processing: Image Communication*, vol. 83, Article ID 115783, 2020.
- [16] J.-K. Lee, "A case study on the remodeling design through BIM (building information modeling)," *Journal of the Korean*

- Digital Architecture Interior Association*, vol. 12, no. 4, pp. 125–132, 2012.
- [17] Y.-C. Han, “A study on the PBL based teaching-learning model using BIM tools for interior architecture design studio,” *Journal of the Korean Digital Architecture Interior Association*, vol. 12, no. 3, pp. 67–79, 2012.
- [18] G. Sun, C.-C. Chen, and S. Bin, “Study of cascading failure in multisubnet composite complex networks,” *Symmetry*, vol. 13, no. 3, p. 523, 2021.
- [19] S. Levine, P. Pastor, and A. Krizhevsky, “Learning hand-eye coordination for robotic grasping with deep learning and large-scale data collection,” *The International Journal of Robotics Research*, vol. 37, pp. 421–436, 2016.
- [20] Y. Lv, Y. Duan, and W. Kang, “Traffic flow prediction with big data: a deep learning approach,” *IEEE Transactions on Intelligent Transportation Systems*, vol. 16, no. 2, pp. 865–873, 2015.
- [21] M. Paul, E. Schkufza, and V. Koltun, “Computer-generated residential building layouts,” *ACM Transactions on Graphics*, vol. 29, no. 6, pp. 1–12, 2010.
- [22] J.-Y. Zhu, T. Park, and P. Isola, “Unpaired image-to-image translation using cycle-consistent adversarial networks,” in *Proceedings of the 2017 IEEE International Conference on Computer Vision (ICCV)*, pp. 2242–2251, Venice, Italy, October, 2017.

## Research Article

# Improved Cam Shift Algorithm for Detecting Athletes' Action Targets in Sports Videos

Yi Yuan 

Hunan University of Science and Technology, Xiangtan 411201, China

Correspondence should be addressed to Yi Yuan; 1170061@hnust.edu.cn

Received 25 February 2022; Accepted 25 March 2022; Published 18 April 2022

Academic Editor: Man Fai Leung

Copyright © 2022 Yi Yuan. This is an open access article distributed under the Creative Commons Attribution License, which permits unrestricted use, distribution, and reproduction in any medium, provided the original work is properly cited.

The detection and tracking of athletes in sports videos is of great importance, as it helps to automate the analysis of sports videos, thus providing advanced tools and instruments for sports training. The Cam Shift algorithm uses the colour information of objects to achieve tracking of moving targets, so it is very important to choose a suitable colour space when obtaining the colour information of objects. To this end, this paper improves the Cam Shift algorithm by converting the visual system mechanism to perceive the colour characteristics of the image processing, i.e., converting the video image from the RGB colour space to the HSV colour space, using the H (hue) component to model the target object. Experiments show that the improved athlete detection and tracking algorithm is more robust in practical applications. The improved tracking algorithm also has better real-time performance, with a processing speed of 20 fps during the experiments.

## 1. Introduction

In sports videos, the movement of athletes is irregular and their posture changes in various ways as they move [1]. The colours of the athletes and the scenes may be similar, and there is often mutual occlusion between the athletes. The unique nature of sports videos poses many challenges to the process of athlete detection and tracking. Therefore, the main objective of this paper is to analyse and investigate the main current methods for motion target detection and tracking, to propose an effective algorithm for athlete detection and tracking in sports videos, and to develop a prototype system to verify the correctness of the algorithm [2].

The detection and tracking of motion targets involves many disciplines such as image processing, computer vision, signal processing, and pattern recognition. In these fields, much of the processing of images and videos relies on target detection and tracking techniques, so research into motion target detection and tracking methods, and the improvement and refinement of related algorithms, is important for the advancement of these fields [3].

Motion target detection and tracking can be applied to many fields such as human-computer interaction, video

surveillance, video analysis, and sports training. In the field of human-computer interaction, the combination of human detection and tracking technology with other technologies such as audio can be used to develop multichannel user interfaces, which can both broaden the bandwidth of human-computer interaction and make the human-computer interaction more efficient and natural [4]. In the field of video analysis, motion target detection and tracking can be used to extract meaningful video objects from the video and analyse their behaviour, thus helping to implement content-based video retrieval techniques. Motion target detection and tracking technology can also be applied to sports video analysis; through the detection and tracking of athletes, you can obtain a variety of athletes' motion parameters and human posture parameters, which is conducive to the analysis of athletes' motion trajectory, and determine the normality of their movements, but also conducive to the application of these parameters for three-dimensional reconstruction, in a three-dimensional way to realistic simulation, design, and analysis of technical movements. It is important to improve the training effect of athletes [5].

In addition, traditional machine learning algorithms are limited in their ability to process raw kinematic data, cannot

effectively train on discontinuous, noisy, and high-dimensional data with missing values [6], and always require preprocessing of the raw data, including Kalman filter, fast Fourier transform (FFT), and vector coding techniques [7].

It is worth noting that the balance between robustness, accuracy, and effectiveness of a competition-based computer vision motion analysis system relies on improved algorithms and hardware optimisation compared to 3D motion capture analysis in a laboratory environment [8, 9].

## 2. Related Work

In markerless action recognition based on generative algorithms, the pose shape of the human body is determined by matching the human model with information extracted from the image. For example, for a given set of model parameters (body shape, bone length, joint angles, etc.), the corresponding model prediction parameters can first be generated and subsequently compared with the image-extracted features to calculate a single “error value” which can represent the degree of difference between the hypothesis and the observed values [10]. One study [11] projected the predicted 3D mesh onto a 2D image, adjusted to maximise the degree of overlap between the mesh and the capture target contours, and the iterative closest point (ICP) algorithm allowed for a comparison of the match between the visual shell of the image and each vertex of the capture target. The key to generative algorithms is the accurate definition of the algorithm function so that specific assumptions can be compared to image information; if the algorithm function is out of calibration, matching of optimal model parameters cannot be achieved, resulting in reduced motion constraints and increased probability of outliers [12]. Constructing highly robust algorithm functions for higher image noise and lower model configurations is more difficult, on the one hand, because generative algorithms require reasonably reliable initial speculation on model parameters and, on the other hand, the captured target needs to be initially calibrated in a specific pose at the beginning of the phase [13]. Without human intervention, the algorithmic function is not self-correcting and reversible due to degradation inaccuracy caused by occlusion, image noise, or other factors. Previous studies [14] attempted to improve the relevant algorithm functions or to address this difficulty by combining generative and discriminative algorithms.

## 3. Applying the Cam Shift Algorithm to Track Athletes

*3.1. Colour Characteristics of Statistical Targets.* Colour information is insensitive to translation, rotation, and deformation of the target and is therefore often used as a feature for target tracking. Among the many statistical methods used to characterise the colour distribution of an object, the histogram is one of the most commonly used. It is

a parameter-free density estimator obtained by counting the number of pixels with the same pixel value in a region of interest. In order to calculate the colour histogram of a target object, the colour of the target is quantified into different classes so that pixels with similar colours can be clustered into the same histogram class while at the same time reducing the time and space complexity of the calculation process. The traditional histogram is calculated as follows: for a histogram with  $m$  rank values  $\{q_u\}_{u=1\dots m}$ ,

$$q_u = \sum_{x \in R} \sum_{y \in R} \delta[c(x, y) - u]. \quad (1)$$

This is the target area for which the histogram is to be calculated, and function  $\mathfrak{R}^2 \rightarrow \{1, \dots, m\}$  is used to convert the pixel values with coordinates  $(x, y)$  to the corresponding histogram level values.  $\delta$  is the Kronecker symbol.

$$\delta[i - j] = \begin{cases} 1, & \text{if } i = j, \\ 0, & \text{otherwise.} \end{cases} \quad (2)$$

In order to obtain a probability distribution within the range  $[0, 255]$ , the histogram needs to be scaled. The following formula scales each level of the histogram from  $[0, q_{\max}]$  to  $[0, 255]$ :

$$p_u = \min\left(\frac{255}{q_{\max}}q_u, 255\right), \quad (3)$$

where  $u = 1, \dots, m$  and  $q_{\max} = \{\max(q_u)\}_{u=1, \dots, m}$ .

*3.2. Calculating Probability Distribution Charts.* The Cam Shift algorithm tracks a moving target by iteratively finding peak points in a probability distribution. A probability distribution is a special type of image in which each pixel value represents the probability that the pixel belongs to the target object. Any method that relates the value of a pixel to the probability that the pixel belongs to the target object can produce a probability distribution map, with the most commonly used method being the histogram back-projection [15].

The histogram back-projection is calculated by first obtaining the colour information of the target object, representing it as a colour histogram, and then processing the input image as follows: for each pixel in the image, the pixel value is used as an index to find the histogram and replacing the pixel value with this statistic to obtain the probability distribution. It is usually necessary to scale the pixel values of the probability distribution so that the values are in the range  $[0, 255]$ . The steps to calculate the probability distribution are as follows:

- (1) Convert the video image to HSV colour space and extract the values of the H component.
- (2) Calculate the colour histogram of the target object.
- (3) Calculate the probability distribution map. Let the value of the pixel located at  $(xy)$  in the video image be

$f(x, y)$  and  $P$  be the probability distribution map corresponding to this image. Then,

$$P(x, y) = p_{f[I(x, y)]}, \quad (4)$$

where  $\{p_u\}_{u=1\dots m}$  is the colour histogram and function  $f[I(x, y)]$  finds the corresponding grade value in the histogram based on the value of  $I(x, y)$ .

### 3.3. Applying the Cam Shift Algorithm to Track Targets.

The Mean Shift algorithm can only be used for static probability distributions as the search window remains constant during the iterative process, whereas the Cam Shift algorithm can dynamically update the size and position of the search window during the iterative process of using the Mean Shift algorithm, thus being able to handle dynamic probability distributions [16]. The Cam Shift algorithm first selects a suitable colour space and then calculates the colour information of the target in that colour space. As the colour information of the target changes due to deformation, partial occlusion, and shadow interference during the target's motion, the Cam Shift algorithm needs to recalculate the colour information of the target in each frame and generate the corresponding probability distribution map when tracking the target [17]. In order to dynamically adapt to changes in the probability distribution caused by target motion, the Cam Shift algorithm applies spatial moments to adjust the size and position of the search window during the iterative process, which is the main difference from the traditional Mean Shift algorithm. The main steps of the Cam Shift algorithm are as follows [18]:

- (1) Select the initial position of the search window.
- (2) Apply the Mean Shift algorithm and save the results of the calculation (the centre of mass position and the zero-order moment of the window).
- (3) Reset the position and size of the search window according to the saved zero-order moments.
- (4) Repeat steps 2 and 3 until the algorithm converges. The Cam Shift algorithm can dynamically set the position and size of the search window during operation. The initial centre of the search window for the next frame is the same as the centre of the current search window, and the size and orientation can be calculated as follows: let,  $I(x, y)$  be the value of the pixel located at  $x$  and  $y$  in the probability distribution, and  $x$  and  $y$  take values throughout the search window.

Calculating the second-order moments of the search window,

$$\begin{aligned} M_{20} &= \sum_x \sum_y x^2 I(x, y), \\ M_{02} &= \sum_x \sum_y y^2 I(x, y), \\ M_{11} &= \sum_x \sum_y xy I(x, y). \end{aligned} \quad (5)$$

Assumptions:

$$\begin{aligned} a &= \frac{M_{20}}{M_{00}} - x_c^2, \\ b &= 2 \left( \frac{M_{11}}{M_{00}} - x_c y_c \right), \\ c &= \frac{M_{02}}{M_{00}} - y_c^2, \end{aligned} \quad (6)$$

where  $x_c y_c$  is the window centre of mass; the length and width of the search window for the next frame are as follows:

$$\begin{aligned} l &= 2 * \sqrt{\frac{(a+c) + \sqrt{b^2 + (a-c)^2}}{2}}, \\ w &= 2 * \sqrt{\frac{(a+c) - \sqrt{b^2 + (a-c)^2}}{2}}. \end{aligned} \quad (7)$$

The direction of movement of the search window can be calculated using the following formula:

$$\theta = \frac{1}{2} \tan^{-1} \left( \frac{b}{a-c} \right). \quad (8)$$

When using the above steps to track the target, the Cam Shift algorithm calculates the centroid and area of the window within the range of the search window and resets the position and size of the next search window according to the calculation results [19]. Therefore, in the subsequent tracking process, it is not necessary to recalculate the probability distribution map of the whole image, but we only need to calculate the centroid of the current search window as the central position; a probability distribution map of the area slightly larger than the search window can be used, which can greatly reduce the amount of calculation [20]. Therefore, when the Cam Shift algorithm is used to track athletes in sports videos, its steps can be improved to the following form [21]:

- (1) In the first image, set the calculation area of the probability distribution to the whole image.

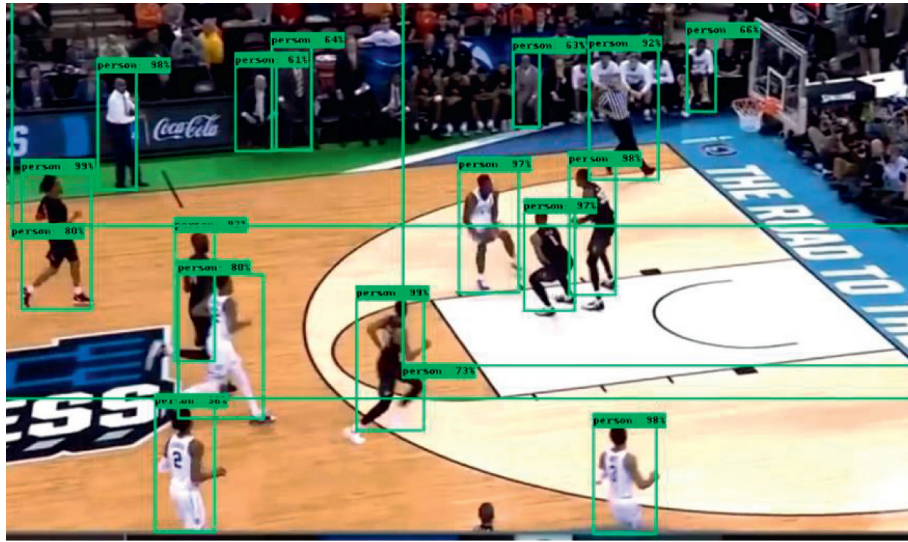


FIGURE 1: Effectiveness of system athlete detection.

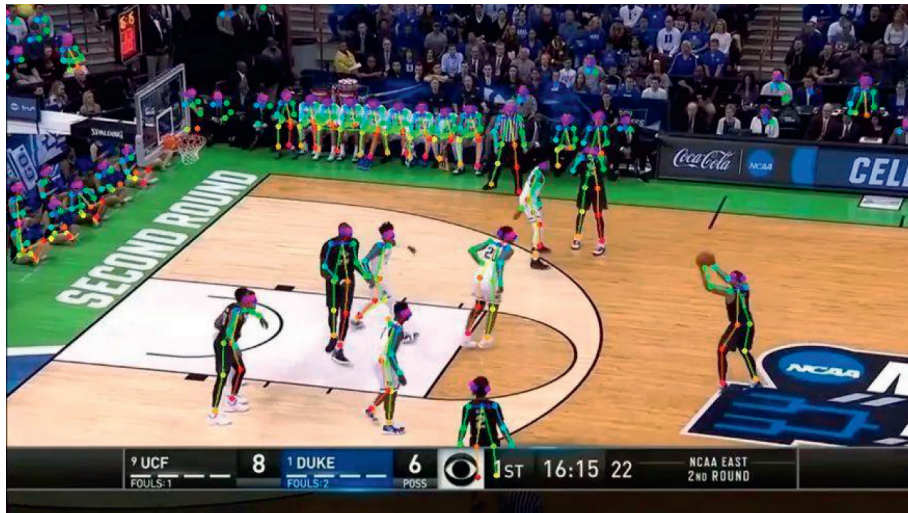


FIGURE 2: Systematic athlete tracking effect.

TABLE 1: Experimental data statistics.

| Experimental video | Count frames | Athlete detection accuracy (%) | Precision of traditional Cam Shift algorithm (%) | Precision of improved Cam Shift algorithm (%) |
|--------------------|--------------|--------------------------------|--|---|
| Group A            | 80 frames    | 98.6                           | 92   | 94  |
| Group B            | 80 frames    | 97.5                           | 62   | 86  |

- (2) Select the initial position and size of the Mean Shift search window. This window generally corresponds to the target object.
- (3) Calculate the probability distribution for the current search area. The centre of this area is the same as the centre of the search window, and the area is slightly larger than the search window.
- (4) Iterate through the probability distribution using the Mean Shift algorithm and calculate the mass-preserving zero-order moments of the probability distribution (the area of the distribution).
- (5) After calculating the centre of mass and zero-order moments in step 4, reset the position and size of the search window. Move the centre of the search window

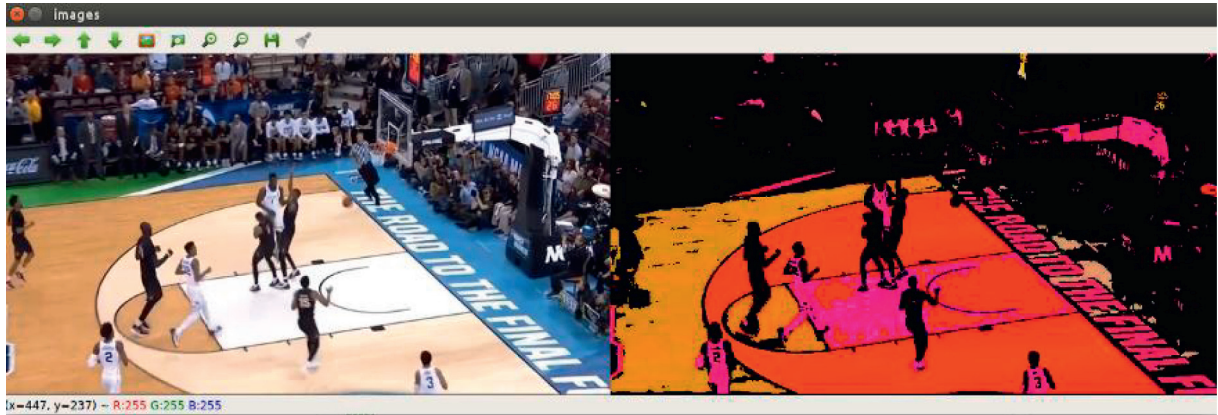


FIGURE 3: Different tracking effects.

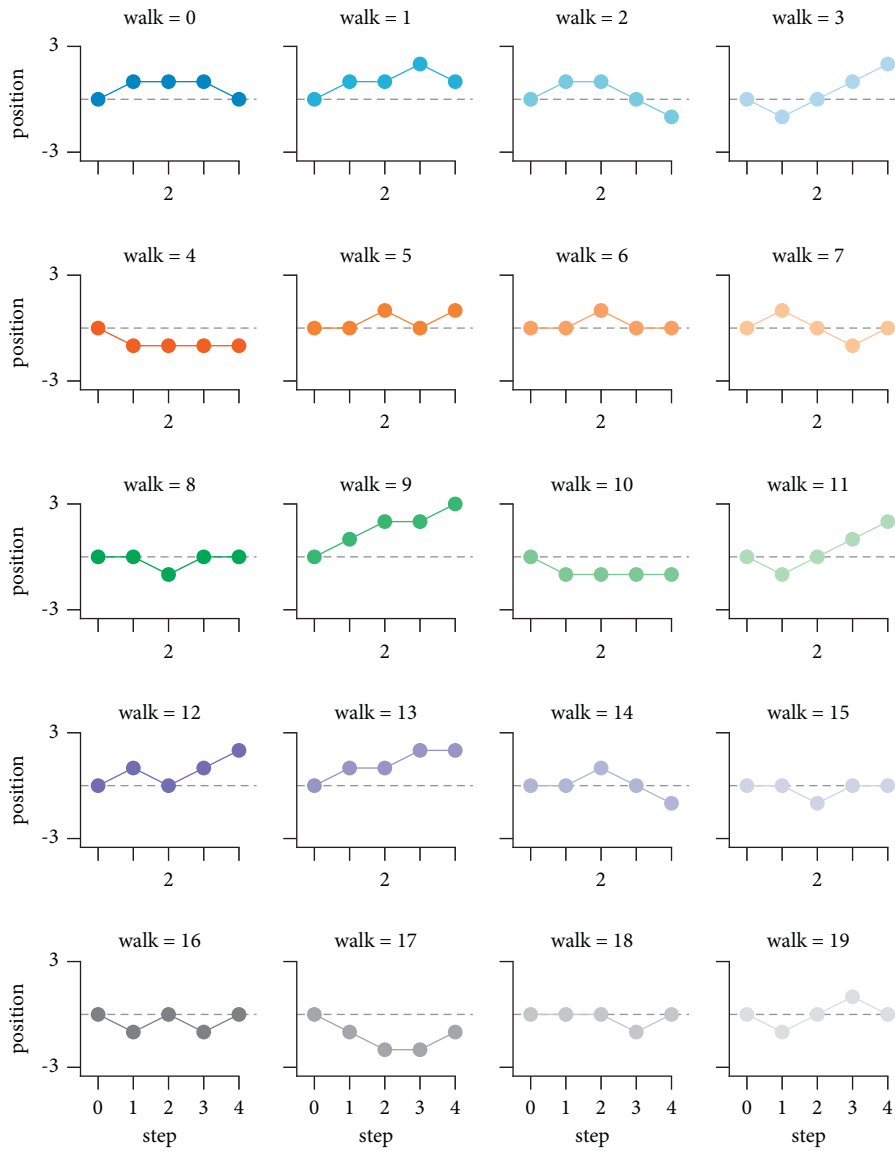


FIGURE 4: Different tracking errors.



to the centre of mass of the conservation and the area as a function of the zero-order moments. Go to step 3.

The above way of calculating the probability distribution reduces the amount of computation and improves real-time tracking [22, 23].

#### 4. Experimental Results

The experimental data for the analysis of this system were obtained from an NBA game video with a size of  $20 \times 240$ . The video was divided into two groups: group A and group B. The colour distribution of the players in group A was not similar to the background, while the colour distribution of the players in group B was more similar to the background [24, 25]. Both videos were captured with a still camera. The athlete detection effect of the system is shown in Figure 1; the upper half of the figure is the detection effect of group A video, and the lower half is the detection effect of group B video. The athlete tracking effect is shown in Figure 2; the upper half of the figure is the video tracking effect of group A, and the lower half is the video tracking effect of group B.

In order to better analyse the algorithm proposed in this paper, the formula proposed in [26] is used to measure the efficiency of the algorithm.

$$\text{Precision rate} = \frac{\text{correct athlete area detected (tracked)}}{\text{all athlete areas detected (tracked)}}. \quad (9)$$

Based on the experimental results, the data in Table 1 were obtained.

The experimental results show that the improved athlete detection and tracking algorithm in this paper has higher robustness in practical applications. The improved tracking algorithm also has better real-time performance, with a processing speed of 20 frames/second during the experiments.

Compared to the Microsoft Kinect camera based on red, green, and blue (Red-Green-Blue, RGB) depth images, deep learning algorithms have fewer constraints on the distance between the camera and the target to be measured and the sampling frequency of the video recording. Current methods based on deep learning have been implemented to automatically estimate the centre of a human joint from a 2D RGB image and output the 2D coordinates in the image. Different tracking effects are shown in Figure 3. Also, by using multiple cameras in conjunction, synchronising the 2D joint positions of the human body in multiview camera images and combining them with deep learning algorithms enables the localisation of human joint centroids and key bony marker points in 3D spaces. Deep learning computer vision research based on 3D human pose recognition is attempting to use an algorithm for pose position estimation and tracking, and studies have explored different tracking errors for 3D human pose recognition based on monocular cameras as shown in Figure 4.

Based on the above research status, this paper reveals the potential applications of markerless motion capture in the field of motion detection and feature motion recognition, such as the interference-free recognition and fast feedback of

athletes' movements in daily training competitions, which can provide reference for coaches' training decisions.

#### 5. Conclusions

In this paper, the Cam Shift algorithm is improved to perceive the colour characteristics of the image processing based on the view system mechanism, i.e., converting the video image from RGB colour space to HSV colour space, using the H (hue) component to model the target object. Experiments in this paper show that the improved athlete detection and tracking algorithm has higher robustness in practical applications. The improved tracking algorithm also has better real-time performance, with a processing speed of 20 frames/second during the experiments.

#### Data Availability

The experimental data used to support the findings of this study are available from the author upon request.

#### Conflicts of Interest

The author declares that there are no conflicts of interest regarding this work.

#### Acknowledgments

The author would like to thank reference [27] for providing the improvement and innovation ideas of this paper. The author would like to thank CSIA: The International Conference on Cyber Security Intelligence and Analytics (<https://link.springer.com/book/10.1007/978-3-030-15235-2>) for providing the source data and paper. This work was supported by the Key Project of Teaching Reform in Universities of Hunan Province (HNJG-2021-0106).

#### References

- [1] N. Liu and P. Liu, "Goaling recognition based on intelligent analysis of real-time basketball image of Internet of Things," *The Journal of Supercomputing*, vol. 78, no. 1, pp. 123–143, 2022.
- [2] M. H. Zhu, "Detection and tracking system for long jumping skilled videos," in *Applied Mechanics and Materials* vol. 543-547, , pp. 4673–4676, Trans Tech Publications Ltd, 2014.
- [3] Z. Feng, "High speed moving target tracking algorithm based on mean shift for video human motion," in *Journal of Physics: Conference Series* vol. 1744, no. 4, IOP Publishing, Article ID 42180, 2021.
- [4] D. Dahmani, M. Cheref, and S. Larabi, "Zero-sum game theory model for segmenting skin regions," *Image and Vision Computing*, vol. 99, Article ID 103925, 2020.
- [5] C. Cuiping, "Badminton video analysis based on player tracking and pose trajectory estimation," in *Proceedings of the 2021 Thirteenth International Conference on Measuring Technology and Mechatronics Automation (ICMTMA)*, pp. 471–474, IEEE, Beihai, China, January 2021.
- [6] W. Wei, "Three-dimensional human motion simulation and video analysis system for physical training," in *Proceedings of the The International Conference on Cyber Security Intelligence*

- and Analytics*, pp. 807–813, Springer, Haikou, China, February 2020.
- [7] C. Xu and Y. Li, “Sports video moving object detection and tracking technology based on hybrid algorithm,” *Lecture Notes in Electrical Engineering. In Innovative Computing*, Springer, Singapore, pp. 1799–1803, 2022.
- [8] X. Ju, C. Li, X. He, and G. Feng, “A proximal neurodynamic model for solving inverse mixed variational inequalities,” *Neural Networks*, vol. 138, pp. 1–9, 2021.
- [9] H. Che, C. Li, X. He, and T. Huang, “An intelligent method of swarm neural networks for equalities-constrained nonconvex optimization,” *Neurocomputing*, vol. 167, pp. 569–577, 2015.
- [10] Y. Song, “Development and application of sports video analysis platform in sports training in the big data era,” in *Proceedings of the The International Conference on Cyber Security Intelligence and Analytics*, pp. 541–548, Springer, Shenyang, China, March 2021.
- [11] Z. Zhengwan, Z. Chunjiang, L. Hongbing, and X. Tao, “Multipath transmission selection algorithm based on immune connectivity model,” *Journal of Computer Applications*, vol. 40, no. 12, p. 3571, 2020.
- [12] R. Yan, “Researches on hybrid algorithm for moving target detection and tracking in sports video,” *Cluster Computing*, vol. 22, no. 2, pp. 3543–3552, 2019.
- [13] M. C. Hu, M. H. Chang, J. L. Wu, and L. Chi, “Robust camera calibration and player tracking in broadcast basketball video,” *IEEE Transactions on Multimedia*, vol. 13, no. 2, pp. 266–279, 2010.
- [14] W. L. Lu, K. Okuma, and J. J. Little, “Tracking and recognizing actions of multiple hockey players using the boosted particle filter,” *Image and Vision Computing*, vol. 27, no. 1-2, pp. 189–205, 2009.
- [15] R. Gade and T. B. Moeslund, “Constrained multi-target tracking for team sports activities,” *IPSJ Transactions on Computer Vision and Applications*, vol. 10, no. 1, pp. 1–11, 2018.
- [16] M. Xu, J. Orwell, L. Lowey, and D. Thirde, “Architecture and algorithms for tracking football players with multiple cameras,” *IEE Proceedings - Vision, Image and Signal Processing*, vol. 152, no. 2, pp. 232–241, 2005.
- [17] C. W. Lu, C. Y. Lin, C. Y. Hsu, M. F. Weng, L. W. Kang, and H. Y. M. Liao, “Identification and tracking of players in sport videos,” in *Proceedings of the Fifth International Conference on Internet Multimedia Computing and Service*, pp. 113–116, Huangshan, China, August 2013.
- [18] B. Bacic, Q. Meng, and K. Y. Chan, “Privacy preservation for eSports: a case study towards augmented video golf coaching system,” in *Proceedings of the 2017 Tenth International Conference on Developments in eSystems Engineering (DeSE)*, pp. 169–174, IEEE, Paris, France, June 2017.
- [19] G. Li and C. Zhang, “Automatic detection technology of sports athletes based on image recognition technology,” *EURASIP Journal on Image and Video Processing*, vol. 2019, no. 1, pp. 1–9, 2019.
- [20] Y. Wang, Le Sun, and S. Subramani, “CAB: classifying arrhythmias based on imbalanced sensor data,” *KSII Transactions on Internet & Information Systems*, vol. 15, no. 7, pp. 2304–2320, 2021.
- [21] M. Manafifard, H. Ebadi, and H. Abrishami Moghaddam, “A survey on player tracking in soccer videos,” *Computer Vision and Image Understanding*, vol. 159, pp. 19–46, 2017.
- [22] A. Nelikanti, G. Venkata Rami Reddy, and G. Karuna, “An optimization based deep LSTM predictive analysis for decision making in cricket,” in *Innovative Data Communication Technologies and Application*, pp. 721–737, Springer, Singapore, 2021.
- [23] X. Ning, K. Gong, W. Li, and L. Zhang, “JWSAA: joint weak saliency and attention aware for person re-identification,” *Neurocomputing*, vol. 453, pp. 801–811, 2021.
- [24] X. Ning, P. Duan, W. Li, and S. Zhang, “Real-time 3D face alignment using an encoder-decoder network with an efficient deconvolution layer,” *IEEE Signal Processing Letters*, vol. 27, pp. 1944–1948, 2020.
- [25] Y. Liao, X. Lu, C. Zhang, Y. Wang, and Z. Tang, “Mutual enhancement for detection of multiple logos in sports videos,” in *Proceedings of the IEEE International Conference on Computer Vision*, pp. 4846–4855, Venice, Italy, October 2017.
- [26] L. Y. Ling-Yu Duan, M. Min Xu, Q. Qi Tian, C. S. Chang-Sheng Xu, and J. S. Jin, “A unified framework for semantic shot classification in sports video,” *IEEE Transactions on Multimedia*, vol. 7, no. 6, pp. 1066–1083, 2005.
- [27] J. Li and H. Du, “Research on the sports biomechanics modeling of the human motion technical movements,” in *Proceedings of the The International Conference on Cyber Security Intelligence and Analytics*, pp. 243–248, Springer, Shenyang, China, February 2019.

## Research Article

# Effect of Deep Learning on College Students' Career Planning

**Xianhui Gu** 

*Henan Mechanical and Electrical Vocational College, Zhengzhou 451191, China*

Correspondence should be addressed to Xianhui Gu; [hnjdgxh@hnjd.edu.cn](mailto:hnjdgxh@hnjd.edu.cn)

Received 10 February 2022; Revised 15 March 2022; Accepted 22 March 2022; Published 16 April 2022

Academic Editor: Hangjun Che

Copyright © 2022 Xianhui Gu. This is an open access article distributed under the Creative Commons Attribution License, which permits unrestricted use, distribution, and reproduction in any medium, provided the original work is properly cited.

It is difficult for college students to find jobs after graduation, which is the most important problem to be solved now. This paper chooses the statistical analysis method to analyze the career planning of college students under different circumstances. Four aspects are analyzed, which are decision-making action, current situation evaluation, career exploration, and self-understanding level. The main conclusions of this paper are as follows. In this study, the gender differences of college students have a certain impact on their career. Generally speaking, the career planning level of boys is higher than that of girls. The job-hunting needs of college graduates are students who enter social work. Family factors affect the level of college students' career planning. It is found that students' school experience is the most important factor affecting the level of career planning, and school experience is also reflected in whether students have class committee experience.

## 1. Introduction

Deep learning is an advanced abstraction of modeling data, which is a branch of machine learning [1]. Deep learning uses a backpropagation algorithm to command machines to change their internal entries, thus discovering complex structures in large data sets [2]. This paper shows how to solve the research problems by training the deep network of learning features and how to share the representation learning patterns and evaluate them on a specific task [3]. In this paper, through a series of experimental studies, it is proved that deep learning can solve the problem of face recognition well. Face recognition task increases the difference between people by extracting verification features from different identities, while face verification task reduces the difference between people by combining verification features extracted from the same identity, which are necessary for face recognition [4]. Through a large number of systematic experiments, this paper shows why traditional methods cannot explain the generalization ability of large neural networks [5]. This paper briefly describes the application research of deep learning in each field. The most advanced technology at present is summarized, and the future research direction is given [6]. Although deep learning technology is widely used in various fields, it cannot

capture the uncertainty of the model. Although the Bayesian model can reason the uncertainty of the model, its calculation cost is very high [7]. The specificity of DNA binding to protein can be determined by deep learning technology. Experiments show that this algorithm is more excellent than other algorithms [8]. In this paper, an algorithm is created by deep learning, which can be applied to the field of medical imaging [9]. This paper analyzes the trend and key points of college students' career development and provides guiding principles for college students' career planning [10]. Career planning is a compulsory course for contemporary college students, which can avoid blind employment. Therefore, the school helps college students to plan their internship career through system and reform [11]. Nowadays, there are many problems in college students' career planning. If we can make correct guidance for students' career planning, it will help students and the development of society. In this paper, PDCA theory is used to improve and upgrade it, so that college students' career planning is optimized [12]. Nowadays, the employment difficulties of college students are becoming more and more obvious. In order to improve the education of college students' career planning, a series of measures should be taken [13]. Nowadays, more and more attention has been paid to the employment of college students. In view of this problem, this paper analyzes the

existing problems in college students' career planning and puts forward some suggestions and countermeasures [14]. Learning to plan one's career after graduation is a compulsory course for college students. It can help students better understand their own situation and then make their own employment plan [15].

## 2. An Empirical Study on Career Planning

*2.1. Gender and Career Planning of College Students.* There are many differences caused by gender, which are also reflected in graduates' career planning. Most scholars believe that there are significant differences between different genders in many aspects, including career awakening, career awareness, career experience, and career development. However, Chinese scholar Chen Lijuan found through research that girls are more mature than boys in physiological development, but in career planning, boys' career maturity is higher than girls' in college and beyond. However, there are many influencing factors, and only gender has differences in the two dimensions of goal planning and interpersonal relationship.

*2.2. Major and Career Planning of College Students.* The difference between occupation and social life is significant, and the difference between occupation experience and occupation attitude is extremely significant. Some scholars have done relevant research and found through empirical research that when students learn different subjects, their factors are not significant in terms of their understanding, status, and need for career planning.

*2.3. Grade.* There are some differences among college students in different grades, and their understanding of occupation will increase with the increase of grades. Domestic scholars take the college students trained by exam-oriented education under China's national conditions as the research object. Wang Shengnan found that the differences in professional grades are significant in different grades, while grades 1 and 4 are significantly higher than grades 2 and 3, especially grades 1 and 4.

*2.4. Career Counseling Experience and College Students' Career Planning.* Not only experts or scholars but also general education practitioners or most ordinary people believe that career counseling is of positive significance to college students in all aspects. Therefore, through practical experiments, it can be concluded that if a group of students who have received relevant vocational counseling are compared with the same number of students who have not received counseling help, the former will be found to be better. Therefore, schools should increase counseling centers and train professional tutors.

*2.5. Career Planning of College Students Experienced by Student Cadres.* It is a manifestation of students' ability and an opportunity to exercise. Therefore, the work unit recognizes student cadres. However, some scholars have found that this is not the case. For example, Zhang's survey results

show that there is no significant difference between the size of all career planning and that of nonstudent cadres, but the report shows that, in the future life, students who have been student cadres will pay more attention to exploring their careers, have stronger self-awareness, and have better planning and better interpersonal coordination ability.

## 3. Deep Reinforcement Learning

A complete Markov decision process consists of a quintuple  $[S, A, P, R, \gamma]$ :  $S$  represents the set of environmental states;  $A$  represents the set of actions;  $P$  represents the state transition matrix  $P_{ss'}^a = P[S_{t+1} = s' | S_t = s, A_t = a]$ ;  $R$  represents the reward function,  $R(s, a) = E[R_{t+1} | S_t = s, A_t = a]$ ;  $\gamma$  denotes the attenuation factor;  $\gamma \in (0, 1)$ .

Reinforcement learning agents need to use strategy  $\pi$  to determine the behavior mechanism. Different reinforcement learning can adopt fixed strategies or unfixed strategies. Getting a perfect strategy to describe agent behavior is the ultimate goal of reinforcement learning. Formula (1) can be obtained by using strategy  $\pi$  for functions:

$$v_\pi(s) = E[G_t | S_t = s]. \quad (1)$$

Further decomposing it into the current reward and the subsequent status can result in formula (2):

$$v_\pi(s) = E_\pi[R_{t+1} + \gamma v_\pi(S_{t+1}) | S_t = s]. \quad (2)$$

Then, using strategy  $\pi$ , formula (3) can be obtained:

$$q_\pi(s, a) = E_\pi[G_t | S_t = s, A_t = a]. \quad (3)$$

Decompose the function into subsequent states and current rewards to obtain formula (4):

$$q_\pi(s, a) = E_\pi[R_{t+1} + \gamma q_\pi(S_{t+1}, A_{t+1}) | S_t = s, A_t = a]. \quad (4)$$

They can be transformed into each other, as shown in formula (5):

$$v_\pi(s) = \sum_{a \in A} \pi(a|s) q_\pi(s, a) \quad q_\pi(s, a) = R(s, a) + \gamma \sum_{s' \in S} P_{ss'}^a v_\pi(s'). \quad (5)$$

The median optimal value function of all strategies is found by reinforcement learning as shown in formulas (6) and (7):

$$v_*(s) = \max_\pi v_\pi(s), \quad (6)$$

$$q_*(s, a) = \max_\pi q_\pi(s, a). \quad (7)$$

In order to find the optimal value function, the recursive relationship between the optimal  $Q$  function and the optimal  $V$  function is used, as shown in formulas (8) and (9):

$$v_*(s) = v_{\pi_*}(s) = \sum_{a \in A} \pi_*(a|s) q_{\pi_*}(s, a) = \max_a q_{\pi_*}(s, a) = \max_a q_*(s, a), \quad (8)$$

$$q_*(s, a) = R(s, a) + \gamma \sum_{s' \in S} P_{ss'}^a v_*(s'). \quad (9)$$

Through continuous iteration, the optimal function can be obtained.

**3.1. Q-Learning.** In Q-Learning,  $Q$  means that  $Q(s, a)$  is the expectation that ( $s \in S$ ) and ( $a \in A$ ) actions can get benefits at a certain moment  $s$ . The environment gives feedback rewards to agents according to the actions taken by agents, then constructs Q-Table through states and actions to store the learned Q values, and selects the actions that can get the maximum benefits according to the Q values, as shown in Table 1.

By defining the problem as an MDP process, it can be expressed as formula (10):

$$\text{Goal : } \max_{\pi} E \left[ \sum_{t=0}^H \gamma^t R(S_t, A_t, S_{t+1}) | \pi \right], \quad (10)$$

where the state value function of  $q_{\pi}(s, a)$  can be defined as in formulas (11) and (12):

$$q_{\pi}(s, a) = E_{\pi} \left[ r_{t+1} + \gamma r_{t+2} + \gamma^2 r_{t+3} + \dots | A_t = a, S_t = s \right], \quad (11)$$

$$q_{\pi}(s, a) = E_{\pi} [G_t | A_t = a, S_t = s], \quad (12)$$

where  $G_t$  is the total discount reward starting at time  $t$ , and  $\gamma \in (0, 1)$ , when it is closer to 1, means that it pays more attention to the value of subsequent states, and when it is closer to 0, it means that it pays more attention to the current income. The optimal value function  $Q$  can be expressed as formula (13):

$$Q^*(s, a) = \max_{\pi} Q^*(s, a). \quad (13)$$

Expand the desired formula as shown in formulas (14)–(16):

$$Q^*(s, a) = \sum_{s'} P(s' | s, a) (R(s, a, s') + \gamma \max_{a'} Q^*(s', a')), \quad (14)$$

$$Q_{k+1}^*(s, a) \leftarrow \sum P(s' | s, a) (R(s, a, s') + \gamma \max_{a'} Q_k^*(s', a')), \quad (15)$$

$$Q(s, a) \leftarrow Q(s, a) + \alpha \left[ r + \gamma \max_{a'} Q(s', a') - Q(s, a) \right]. \quad (16)$$

Then, the Q-Table is updated in a time difference manner as shown in equation (17):

$$Q(s, a) \leftarrow Q(s, a) + \alpha \left[ r + \gamma \max_{a'} Q(s', a') - Q(s, a) \right], \quad (17)$$

where  $\gamma$  is the decay factor,  $\alpha$  is the learning rate, and the next state  $s$  is selected and updated according to the corresponding position in Q-Table. Q-Learning is shown in Algorithm 1.

**3.2. Strategy Gradient.** Q-Learning cannot deal with reinforcement learning. Therefore, reinforcement learning

TABLE 1: Q-Table example.

| Q-Table | a1        | a2        |
|---------|-----------|-----------|
| s1      | q (s1,a1) | q (s1,a2) |
| s2      | q (s2,a1) | q (s2,a2) |
| s3      | q (s3,a1) | q (s3,a2) |

- (1) Random initialization  $Q(s, a)$
- (2) Initializations
- (3) repeat
- (4) For every step in every paragraph
- (5) Select the best action in the current  $s$  through Q-Table  $a$
- (6) Take action  $a$ , get reward  $r$  and new status  $s'$
- (7)  $Q(s, a) \leftarrow Q(s, a) + \alpha [r + \gamma \max_{a'} Q(s', a') - Q(s, a)]$
- (8)  $s \leftarrow s'$
- (9) until Until  $s$  reaches the termination state

ALGORITHM 1: Q-Learning.

method is produced, which is to find the optimal strategy by learning the gradient information of strategy parameters. The specific strategy can be described as a function with parameter  $\theta$ , as shown in formula (18):

$$\pi_{\theta}(s, a) = P(a | s, \theta) \approx \pi(a | s). \quad (18)$$

The original strategy is transformed into a continuous function to find the optimal strategy. Specifically, the optimization target is set to the expectation in the initial state, as shown by formula (19):

$$J_1(\theta) = V_{\pi_{\theta}}(s_1) = E_{\pi_{\theta}}(G_1). \quad (19)$$

The strategy gradient can be expressed by multiplying the strategy by the reciprocal of a likelihood function, which becomes the score function, where the Softmax-based score function is expressed as formula (20):

$$\begin{aligned} & \nabla_{\theta} \log \pi_{\theta}(s, a), \\ &= \nabla_{\theta} \log \frac{e^{\phi(s, a)^T \theta}}{\sum e^{\phi(s, a)^T \theta}}, \\ &= \nabla_{\theta} \log e^{\phi(s, a)^T \theta} - \nabla_{\theta} \log \left( \sum e^{\phi(s, a)^T \theta} \right), \\ &= \phi(s, a) - \frac{1}{\sum e^{\phi(s, a)^T \theta}} \left[ \sum e^{\phi(s, a)^T \theta} \cdot \phi(s, a) \right], \\ &= \phi(s, a) - \left[ \sum \left( \frac{e^{\phi(s, a)^T \theta}}{\sum e^{\phi(s, a)^T \theta}} \right) \cdot \phi(s, a) \right], \\ &= \phi(s, a) - \left[ \sum \pi(s, a) \cdot \phi(s, a) \right], \\ &= \phi(s, a) - E_{\pi_{\theta}}[\phi(s, \cdot)]. \end{aligned} \quad (20)$$

The score function of the Gaussian distribution can be expressed as formula (21):

$$\nabla_{\theta} \log \pi_{\theta}(s, a) = \frac{(a - \mu(s))\phi(s)}{\sigma^2}. \quad (21)$$

The gradient is then obtained by derivation, as shown by formulas (22) and (23):

$$\begin{aligned} J(\theta) &= E_{\pi_{\theta}}[r] \\ &= \sum_{s \in S} d(s) \sum_{a \in A} \pi_{\theta}(s, a) R_{s,a}, \end{aligned} \quad (22)$$

$$\begin{aligned} \nabla_{\theta} J(\theta) &= \sum_{s \in S} d(s) \sum_{a \in A} \pi_{\theta}(s, a) \nabla_{\theta} \log \pi_{\theta}(s, a) R_{s,a} \\ &= E_{\pi_{\theta}}[\nabla_{\theta} \log \pi_{\theta}(s, a) r]. \end{aligned} \quad (23)$$

Selecting an action to maximize the reward and selecting the optimal action depending on the current state and action, the expectation of the reward multiplies the score function to obtain the derivative of the reward function, resulting in formula (24):

$$\nabla_{\theta} J(\theta) = E_{\pi_{\theta}}[\nabla_{\theta} \log \pi_{\theta}(s, a) r]. \quad (24)$$

Expectations in the reward function are replaced by samples, and after the end of a segment, the parameters are updated with each step in the segment. The policy gradient is shown in Algorithm 2.

## 4. Experimental Analysis

**4.1. Performance Comparison.** Deep learning, analytic hierarchy process, and fuzzy recognition are frequently used in daily experiments. In order to make the experiment more accurate and concise, we counted the performance capabilities of deep learning, analytic hierarchy process, and fuzzy recognition in information acquisition, model recognition, and model recognition accuracy for 10 times, and the results are shown in Figures 1–3.

By analyzing Figures 1–3, we come to the conclusion that deep learning is the best in information acquisition ability, followed by analytic hierarchy process, the worst is fuzzy recognition, the best in model recognition ability, the worst is analytic hierarchy process, the best in model recognition accuracy, the second is fuzzy recognition, and the worst is analytic hierarchy process. It is concluded that deep learning is superior to other AHP and fuzzy recognition in all aspects, so we choose deep learning for the next research.

The accuracy of Mean, PMF, AutoRec, NADE, DLTSR, REda, and DMF in five data sets was tested, and the lowest RMSE, MSE, and MAE were compared in Figures 4–8. On the whole, compared with general methods, AutoRec, NADE, DLTSR, REda, and DMF have significant improvement in accuracy compared with other methods, and DMF has achieved certain advantages in the process of comparing with other comparison methods, and DMF has a fast convergence speed in the training process. AutoRec, NADE, DLTSR, and REda all take the user's scoring history behavior as input information, but they all use an adjacency matrix to encode, which leads to extremely high-dimensional and sparse input

- (1) Random initialization  $Q(s, a)$
- (2) Initializations
- (3) repeat
- (4) In every paragraph  $s_1, a_1, r_2, \dots, s_{T-1}, s_{T-1}, r_T \in \pi_{\theta}$
- (5)  $\theta \leftarrow \theta + \alpha \nabla_{\theta} \log \pi_{\theta}(s_t, a_t) v_t$
- (6)  $s \leftarrow s'$
- (7) until Until  $s$  reaches the termination state
- (8) Return  $\theta$

ALGORITHM 2: Strategy gradient.

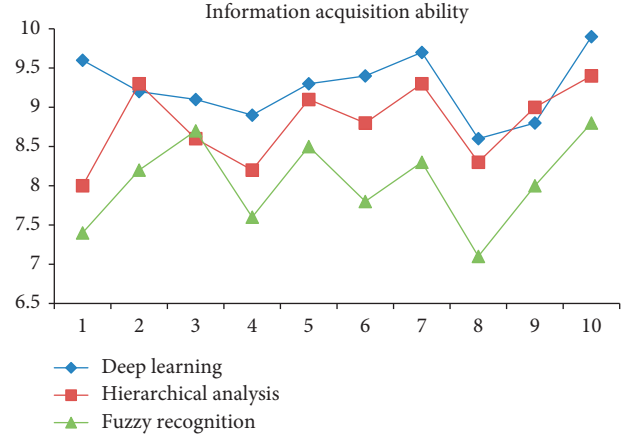


FIGURE 1: Information acquisition capability.

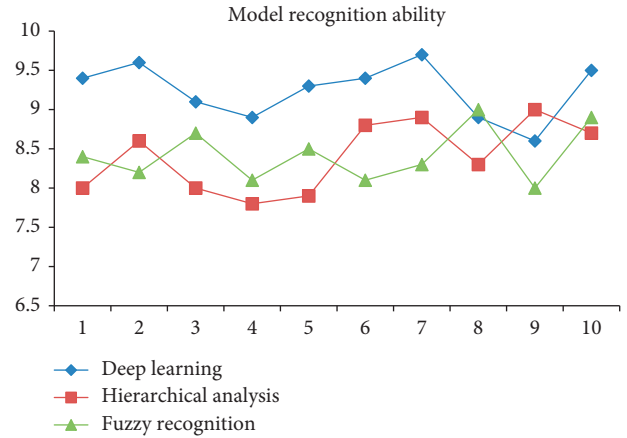


FIGURE 2: Model recognition ability.

information of the model, which makes the number of parameters of the model extremely large. Different from these models, DMF uses the IFE model to encode historical behavior, which reduces the number of parameters of the model and improves the training efficiency of the model. It can be observed that DMF has great advantages in training efficiency compared with AutoRec, NADE, DLTSR, and REda.

### 4.2. Analysis of the Present Situation of College Students' Career Planning

**4.2.1. Overall Status Analysis.** It can be seen from Table 2 that the average score of students' self-status evaluation level

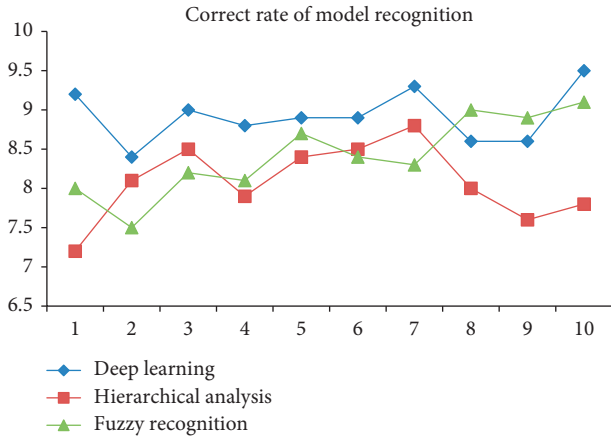


FIGURE 3: Correct rate of model recognition.

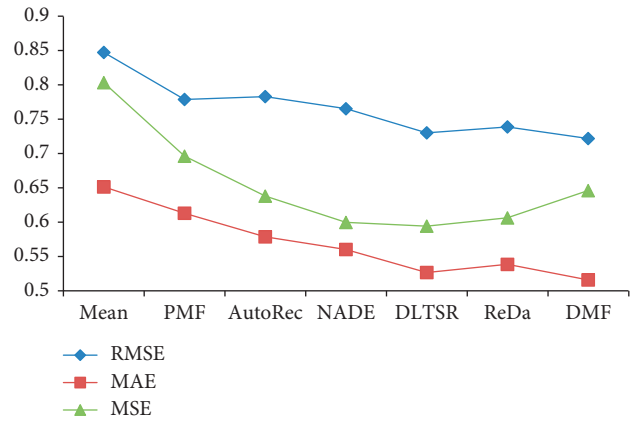


FIGURE 6: Comparison of RMSE, MSE, and MAE on the third data set.

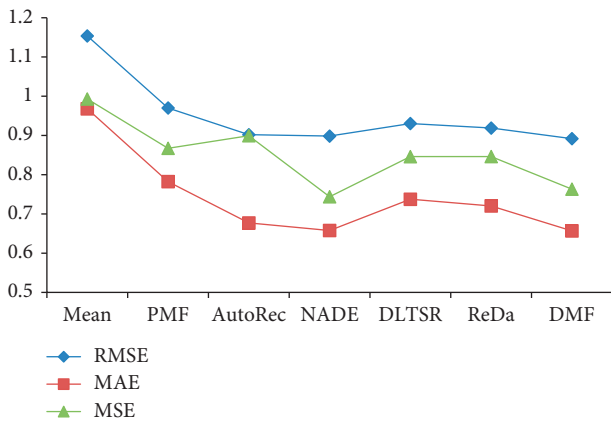


FIGURE 4: Comparison of RMSE, MSE, and MAE on the first data set.

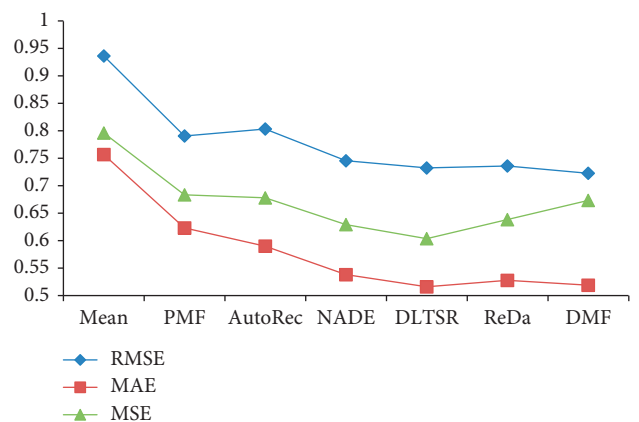


FIGURE 7: Comparison of RMSE, MSE, and MAE on the fourth data set.

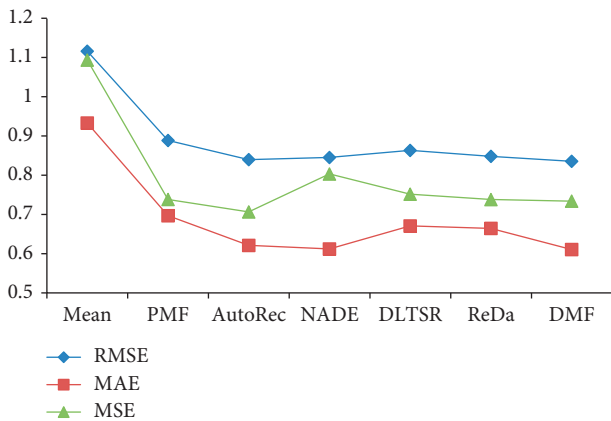


FIGURE 5: Comparison of RMSE, MSE, and MAE on the second data set.

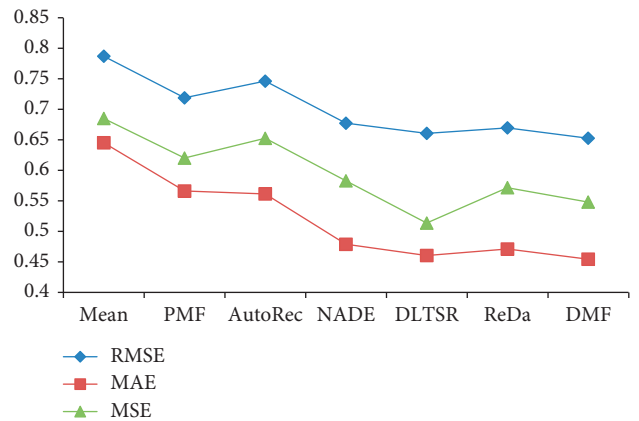


FIGURE 8: Comparison of RMSE, MSE, and MAE on the fifth data set.

after calculation is 31.72 points, which is higher than the average score of 30 points corresponding to “conformity,” indicating that students have a good understanding of career planning. The average score of students’ self-understanding (including interests, personalities, values, and skills) is 27.18. Although it is already in the second place, it is far below the average score of 33, which is the middle level of achieving

“conformity.” It shows that although students have a better sense of career planning, there is some confusion in planning behavior, which comes from their own understanding and does not know what they really want and for. Finally, we can see that the average score of career exploration and decision-making in Table 1 is no more than 30, which is lower than the average score, indicating that students “talk but do not do,” lack action, only realize its importance, but lack decisive

TABLE 2: General situation.

|                 | Sample    |         | Average value | Standard deviation value | Skewness        |                | Kurtosis        |                |
|-----------------|-----------|---------|---------------|--------------------------|-----------------|----------------|-----------------|----------------|
|                 | Effective | Invalid |               |                          | Numerical value | Standard error | Numerical value | Standard error |
| Limit           | 3215      | 0       | 31.72         | 5.467                    | 0.492           | 0.104          | 0.319           | 0.206          |
| Understand      | 3215      | 0       | 16.93         | 3.2                      | 0.761           | 0.103          | 1.043           | 0.206          |
| Explore         | 3213      | 2       | 27.18         | 5.651                    | 0.443           | 0.104          | 0.894           | 0.207          |
| Decision-making | 3213      | 2       | 16.15         | 3.542                    | 0.398           | 0.104          | 0.119           | 0.206          |

career line and clear career goals, so they have no concrete actions.

In addition, it can be seen from Table 2 that the distribution at each level is right-sided.

(1) *Current Situation Evaluation and Analysis.* Table 3 gives descriptive statistics on the evaluation of college students' professional status. It can be seen from the table that students have the highest score of environmental awareness, which is 11.47 points, indicating that students still have a good understanding of the employment environment, and it may also be that schools and society instill more in this respect for college students. After excluding environmental cognition, the scores of the other two parts are not high, which shows that students are a little deficient in these two aspects and need to improve their clear understanding of their hobbies, personalities, and interests.

(2) *Analysis of Self-Understanding Level.* Table 4 shows the descriptive statistics of students' self-understanding. Here, it is divided into two categories: "self-adaptation" and "expected goal." The value of self-adaptation and expected goal is generally low, which indicates that students cannot determine which jobs are suitable for themselves in the process of career planning, and there is a gap between the jobs they want to engage in and their personal abilities.

(3) *Career Exploration Analysis.* It can be seen from Table 5 that the scores of these three parts are not much different, and they are all about 9 to 10 points, which are not high. But generally speaking, the scores of interpersonal relationship are higher than those of the other two, which shows that students think that good interpersonal relationship is very important for employment and their career planning process, such as having good teacher-student relationship and good relationship with classmates and roommates.

(4) *Analysis of Decision-Making Action Level.* Table 6 makes a statistical analysis of the decision-making action level of college students' career planning. From the table, we can see that the scores of these two parts are very low, which is lower than those of the three tables analyzed above, which shows that students lack mobility and action awareness in career planning. In particular, the average score of the evaluated career goals is only 7.37, which indicates that students basically will not set the revision and action of goals, let alone make evaluation and feedback, which is consistent with the research results of career goals.

(5) *Analyze by Item.* Table 7 gives an analysis of some of the most representative items. According to the average value and standard deviation analysis in the table, the students' scores are not very optimistic. In the table, there are 11 questions with an average score of more than 3 points, accounting for one-third, while the remaining 20 questions have low average scores. This result shows that the overall situation of college students' career planning should prove the theory mentioned in the second section of this study.

It can be seen that the average score of the third question in the question is the highest, so it can be concluded that college students are still very aware of the importance and necessity of career planning, so they are still happy to participate in relevant training in the school. Another high score item is Question 27: It is believed that college students should "strive to learn professional knowledge well and improve professional quality." This title is 3.57 points, which is higher than the above topic. It shows that students think that the most important thing in their career planning is to learn professional knowledge to enhance their competitiveness. Only in this way is an effective way to achieve high-quality employment; after analyzing the high-scoring items, let us look at the low-scoring situation. We can see that the average score of the 20th question in the table, "Often consult relevant experts about work knowledge," is the lowest, as low as less than 2 points, which shows that there is a lack of professional exploration spirit, which is manifested in the lack of professional consultation and help from teachers in the school employment guidance center. This phenomenon deserves the double attention of universities and society.

To sum up, the high-scoring items all lie in the self-understanding and current situation cognition of career planning, and the average scores of these two levels are optimistic, while the scores of other items are not so optimistic. Especially in the decision-making action level, the average scores of basically every item are very low, which shows that college students generally feel confused when facing employment.

#### 4.2.2. Difference Analysis

(1) *Personal Characteristic Variable.* As mentioned above, gender is usually regarded as a prominent variable in many human nature studies because there are obvious differences between men and women in many aspects. In this study, it can



TABLE 3: Distribution characteristics of current situation evaluation scores.

|                         | Sample    |         | Average value | Standard deviation value | Skewness        |                | Kurtosis        |                |
|-------------------------|-----------|---------|---------------|--------------------------|-----------------|----------------|-----------------|----------------|
|                         | Effective | Invalid |               |                          | Numerical value | Standard error | Numerical value | Standard error |
| Career awakening        | 3215      | 0       | 10.59         | 2.571                    | 0.67            | 0.103          | -0.439          | 0.206          |
| Self-cognition          | 3215      | 0       | 9.67          | 2.417                    | 0.461           | 0.103          | -2.49           | 0.206          |
| Environmental cognition | 3215      | 0       | 11.47         | 2.719                    | 0.643           | 0.104          | 0.35            | 0.207          |

TABLE 4: Distribution characteristics of self-understanding scores.

|                 | Sample    |         | Average value | Standard deviation value | Skewness        |                | Kurtosis        |                |
|-----------------|-----------|---------|---------------|--------------------------|-----------------|----------------|-----------------|----------------|
|                 | Effective | Invalid |               |                          | Numerical value | Standard error | Numerical value | Standard error |
| Self-regulation | 3215      | 0       | 8.25          | 2.228                    | 0.767           | 0.103          | 0.573           | 0.206          |
| Expected goal   | 3215      | 0       | 8.69          | 1.78                     | 0.384           | 0.103          | 8.03            | 0.206          |

TABLE 5: Distribution characteristics of career exploration level.

|                            | Sample    |         | Average value | Standard deviation value | Skewness        |                | Kurtosis        |                |
|----------------------------|-----------|---------|---------------|--------------------------|-----------------|----------------|-----------------|----------------|
|                            | Effective | Invalid |               |                          | Numerical value | Standard error | Numerical value | Standard error |
| Career exploration         | 3215      | 0       | 9.99          | 2.471                    | 0.512           | 0.104          | 1.005           | 0.207          |
| Interpersonal relationship | 3215      | 0       | 10.31         | 2.817                    | 0.461           | 0.103          | 0.43            | 0.206          |
| Self-improvement           | 3215      | 0       | 9.48          | 2.019                    | 0.443           | 0.104          | 0.194           | 0.206          |

TABLE 6: Decision-making actions.

|                 | Sample    |         | Average value | Standard deviation value | Skewness        |                | Kurtosis        |                |
|-----------------|-----------|---------|---------------|--------------------------|-----------------|----------------|-----------------|----------------|
|                 | Effective | Invalid |               |                          | Numerical value | Standard error | Numerical value | Standard error |
| Goal evaluation | 3124      | 1       | 7.37          | 2.2                      | 0.491           | 0.103          | 0.787           | 0.206          |
| Revised plan    | 3124      | 1       | 8.78          | 2.198                    | 0.443           | 0.103          | 0.34            | 0.26           |

be found from Table 8 that the  $P$  value of the  $t$ -test in total table is 0.005, which is a significant difference. From a numerical point of view, the average score of male students' career planning level is higher than that of female students that is, there are significant differences between male and female college students in all aspects of career planning. Among these four levels, only the self-understanding level has little difference in scores between men and women. Except for it, there are significant differences between male students and female students in status assessment, career exploration, and decision-making actions, and this difference is that male students are generally higher than female students.

Because the topic of this study is college students' career planning, majors are naturally worth discussing for college students. In order to study the influence of majors on them, it is concluded in Table 9 that the  $P$  value of the  $t$ -test in the total table is 0.692, which is not significant, indicating that professional differences (only divided into arts and sciences to discuss here) do not lead to various differences in college students' career planning level.

When students are discussed by grades, it can be known from Table 9 that the  $P$  value of the  $t$ -test of total scale is significant; that is to say, there are significant differences in grades. In addition, from the numerical point of view, the  $F$  test  $P$  values of status assessment and self-understanding level are 0.015 and 0.002, respectively, which is very significant, indicating that there are significant differences in students' cognitive level of themselves in different grades. According to psychological research, this is because students' cognitive level is gradually rising with age.

Through Table 10 and Table 11, multiple comparison tables of different grades, it is found that the evaluation level of sophomores at all levels is significantly lower than that of graduating class. For example, in the single level of self-understanding, the level of graduating class students is significantly higher than that of freshmen, sophomores, and juniors. On the overall level, sophomores and juniors are still obviously lower than graduating class students. Generally speaking, senior students in graduating class have higher career planning level than other grades, but sophomores and

TABLE 7: Distribution characteristics of scores of each item.

|                        | Title expression  | Average | Standard deviation |
|------------------------|---|---------|--------------------|
| Self-understanding     | It is considered that career planning plays a great role in personal development                  | 3.45    | 0.949              |
|                        | Think you need to plan your career at present   | 3.44    | 0.974              |
|                        | It is necessary to carry out career planning in college   | 3.7     | 0.943              |
|                        | Understand one's own personality characteristics and hobbies                                      | 3.44    | 0.877              |
|                        | Be clear about what you like and dislike  | 3.19    | 0.992              |
|                        | Know what kind of work your major is suitable for   | 3.04    | 0.95               |
|                        | Know which professionals are in short supply nowadays   | 2.47    | 0.835              |
|                        | Know the specific requirements of the career you want to pursue in the future                     | 2.81    | 0.901              |
|                        | Understand the content and characteristics of ideal work  | 2.9     | 0.908              |
|                        | Have clear personal career development goals  | 2.74    | 0.962              |
| Status assessment      | Believe in the results of various career tests  | 2.64    | 0.727              |
|                        | Different stages have different personal development goals  | 2.85    | 0.839              |
|                        | I plan to participate in more social practice activities to accumulate "social experience"        | 3.44    | 0.898              |
|                        | I thought about asking the school's employment guidance center for help                           | 2.61    | 0.858              |
|                        | Have the habit of setting short-term and long-term goals  | 2.66    | 0.857              |
|                        | I will always keep abreast of the latest news in my ideal industry                                | 2.64    | 0.944              |
|                        | Ask relevant people for their experience in finding a job   | 2.75    | 0.88               |
|                        | Understand yourself by testing your personality and professional ability                          | 2.62    | 0.872              |
|                        | Consult with relevant experts frequently  | 1.99    | 0.73               |
|                        | Take the initiative to contact seniors and teachers who are beneficial to their future job search | 2.52    | 0.915              |
| Career exploration     | Actively participate in various school and off-campus activities and make more friends            | 2.75    | 0.885              |
|                        | Usually, I prefer to associate with classmates who are helpful to my career development           | 2.46    | 0.879              |
|                        | Take the initiative to exercise one's interpersonal skills  | 3.03    | 0.846              |
|                        | Take the initiative to find further education plans to improve their competitiveness              | 2.88    | 0.899              |
|                        | Ask some relatives and friends with good work experience for advice                               | 2.58    | 0.894              |
|                        | Work hard to learn professional knowledge and improve professional quality                        | 3.57    | 0.864              |
|                        | Will regularly check the achievement of the scheduled career goals                                | 2.41    | 0.839              |
|                        | Have your own career development plan and will implement it                                       | 2.36    | 0.737              |
|                        | Regularly assess the achievement of your career goals   | 2.61    | 0.871              |
|                        | My understanding of myself will often change  | 2.99    | 0.911              |
| Decision-making action | There has been a change in views on the current employment situation                              | 3.02    | 0.929              |
|                        | In the last year, I adjusted my interpersonal communication scope                                 | 2.77    | 0.913              |

TABLE 8: Analysis of gender differences.

|                        | Gender | Sample    |         | Average value | Standard deviation value | <i>t</i> -test value | Significance value |
|------------------------|--------|-----------|---------|---------------|--------------------------|----------------------|--------------------|
|                        |        | Effective | Invalid |               |                          |                      |                    |
| Status assessment      | Male   | 1060      | 0       | 32.7          | 5.684                    | 2.328                | 0.020*             |
|                        | Woman  | 2155      | 0       | 31.77         | 5.425                    |                      |                    |
| Self-understanding     | Male   | 1060      | 0       | 17.92         | 3.143                    | 2.356                | 0.019*             |
|                        | Woman  | 2155      | 0       | 16.96         | 3.007                    |                      |                    |
| Career exploration     | Male   | 1060      | 0       | 27.14         | 5.88                     | 1.895                | 0.59               |
|                        | Woman  | 2153      | 2       | 25.26         | 5.313                    |                      |                    |
| Decision-making action | Male   | 1059      | 1       | 16.1          | 5.587                    | 2.383                | 0.017*             |
|                        | Woman  | 2154      | 1       | 15.25         | 3.483                    |                      |                    |
| Total amount table     | Male   | 1059      | 1       | 97.02         | 15.119                   | 2.819                | 0.005**            |
|                        | Woman  | 2152      | 3       | 93.31         | 14.398                   |                      |                    |

juniors in middle grades have the lowest career planning level. In addition, there are significant differences in four aspects of career planning, namely, current situation evaluation, self-understanding, career exploration, and decision-making action. The *P* values of *t*-test are  $0.007 < 0.01$ ,  $0.002 < 0.01$ ,  $0.0005 < 0.001$ , and  $0.0009 < 0.001$ , respectively.

(2) *Family Variable*. Family has a great influence on children, especially on adolescent children. In order to verify this point, in Table 12, the *P* value of the *t*-test of the total size of college students from different families is 0.009, which is significant, indicating that there are significant differences in the level of career planning between college students from

TABLE 9: Difference analysis of specialties.

|                        | Specialties | Sample    |         | Average value | Standard deviation value | <i>t</i> -test value | Significance value |
|------------------------|-------------|-----------|---------|---------------|--------------------------|----------------------|--------------------|
|                        |             | Effective | Invalid |               |                          |                      |                    |
| Status assessment      | Wen         | 1929      | 0       | 31.7          | 5.509                    | -0.142               | 0.887              |
|                        | Tube        | 1286      | 0       | 31.77         | 5.425                    |                      |                    |
| Self-understanding     | Wen         | 1929      | 0       | 16.92         | 3.143                    | -0.131               | 0.896              |
|                        | Tube        | 1286      | 0       | 16.96         | 3.297                    |                      |                    |
| Career exploration     | Wen         | 1928      | 1       | 27.14         | 5.88                     | -0.234               | 0.815              |
|                        | Tube        | 1285      | 1       | 27.26         | 5.313                    |                      |                    |
| Decision-making action | Wen         | 1929      | 0       | 16.1          | 5.587                    | -0.485               | 0.628              |
|                        | Tube        | 1284      | 2       | 16.25         | 3.483                    |                      |                    |
| Total amount table     | Wen         | 1928      | 1       | 94.36         | 15.081                   | -0.396               | 0.692              |
|                        | Tube        | 1283      | 3       | 94.86         | 14.245                   |                      |                    |

TABLE 10: Difference analysis of different grades.

|                        | Grade                          | Sample    |         | Average value | Standard deviation value | F test value | Significance value |
|------------------------|--------------------------------|-----------|---------|---------------|--------------------------|--------------|--------------------|
|                        |                                | Effective | Invalid |               |                          |              |                    |
| Status assessment      | Freshman year                  | 2572      | 0       | 31.93         | 5.669                    | 4.26         | 0.015*             |
|                        | Sophomore year and junior year | 189       | 0       | 30.83         | 4.892                    |              |                    |
|                        | Graduating class               | 643       | 0       | 32.43         | 5.716                    |              |                    |
| Self-understanding     | Freshman year                  | 2572      | 0       | 16.91         | 3.169                    | 0.903        | 0.406              |
|                        | Sophomore year and junior year | 189       | 0       | 16.72         | 3.113                    |              |                    |
|                        | Graduating class               | 643       | 0       | 17.17         | 3.319                    |              |                    |
| Career exploration     | Freshman year                  | 2571      | 1       | 26.58         | 5.296                    | 6.313        | 0.002**            |
|                        | Sophomore year and junior year | 189       | 0       | 26.6          | 5.281                    |              |                    |
|                        | Graduating class               | 642       | 1       | 28.39         | 6.183                    |              |                    |
| Decision-making action | Freshman year                  | 2572      | 0       | 16.11         | 3.311                    | 1.576        | 0.208              |
|                        | Sophomore year and junior year | 189       | 0       | 15.86         | 3.655                    |              |                    |
|                        | Graduating class               | 641       | 2       | 16.51         | 3.638                    |              |                    |
| Total amount table     | Freshman year                  | 2571      | 1       | 94.12         | 13.989                   | 4.577        | 0.011*             |
|                        | Sophomore year and junior year | 189       | 0       | 92.53         | 13.687                   |              |                    |
|                        | Graduating class               | 640       | 3       | 97.08         | 16.17                    |              |                    |

TABLE 11: Multiple comparisons of different grades.

| <i>I</i>       | <i>J</i>         | Status assessment | Self-understanding | Career exploration | Decision-making action | Total amount table |
|----------------|------------------|-------------------|--------------------|--------------------|------------------------|--------------------|
| Freshman year  | Sophomore year   | 1.1               | 0.18               | -0.02              | 0.26                   | 1.6                |
|                | Graduating class | -0.5              | -0.26              | -1.8               | -0.39                  | -2.95              |
| Sophomore year | Graduating class | -1.6              | -0.44              | -1.78              | -0.65                  | -4.55              |

cities and rural areas; that is to say, the level of career planning of college students from cities is higher than that of students from rural areas. It is possible that this is because students who grew up in cities have more knowledge and opportunities, which will naturally have a positive impact on their career planning. In addition, there are significant differences between urban and rural students in terms of current situation assessment and career exploration; specifically, urban students are generally higher than rural students.

(3) *School Experience Variable.* The student cadres mentioned above are a manifestation of students' ability in school, which can be obtained from Table 13. The *t*-test *P* value of the total table is 0.002, which is significant, indicating that there is a very significant difference. It shows that the level of students who have experienced student cadres is higher than that of students who have not been student cadres. This conclusion supports the previous hypothesis H2.5; that is to say, there are significant differences in all levels of career planning among those who have work

TABLE 12: Difference analysis of different family locations.

|                        | Location | Sample    |         | Average value | Standard deviation value | F test value | Significance value |
|------------------------|----------|-----------|---------|---------------|--------------------------|--------------|--------------------|
|                        |          | Effective | Invalid |               |                          |              |                    |
| Status assessment      | Town     | 1929      | 0       | 32.18         | 5.472                    | 2.415        | 0.016              |
|                        | Village  | 1286      | 0       | 31.04         | 5.4                      |              |                    |
| Self-understanding     | Town     | 1929      | 0       | 17.1          | 3.151                    | 1.533        | 0.126              |
|                        | Village  | 1286      | 0       | 16.68         | 3.262                    |              |                    |
| Career exploration     | Town     | 1928      | 1       | 27.62         | 5.695                    | 2.24         | 0.026              |
|                        | Village  | 1285      | 1       | 26.53         | 5.534                    |              |                    |
| Decision-making action | Town     | 1929      | 0       | 16.39         | 3.531                    | 1.917        | 0.056              |
|                        | Village  | 1284      | 2       | 15.8          | 3.537                    |              |                    |
| Total amount table     | Town     | 1928      | 1       | 95.87         | 14.387                   | 2.617        | 0.009              |
|                        | Village  | 1283      | 3       | 92.54         | 15.055                   |              |                    |

TABLE 13: Difference analysis of student cadres' experiences.

|                        | Student cadres | Sample    |         | Average value | Standard deviation value | F test value | Significance value |
|------------------------|----------------|-----------|---------|---------------|--------------------------|--------------|--------------------|
|                        |                | Effective | Invalid |               |                          |              |                    |
| Status assessment      | Have           | 868       | 0       | 32.04         | 5.462                    | 1.982        | 0.048              |
|                        | None           | 2347      | 0       | 30.44         | 5.426                    |              |                    |
| Self-understanding     | Have           | 868       | 0       | 17.8          | 3.139                    | 1.553        | 0.121              |
|                        | None           | 2347      | 0       | 16.74         | 3.347                    |              |                    |
| Career exploration     | Have           | 866       | 2       | 27.43         | 5.669                    | 4.306        | 0.005              |
|                        | None           | 2687      | 0       | 26.67         | 5.267                    |              |                    |
| Decision-making action | Have           | 867       | 1       | 16.27         | 3.429                    | 0.998        | 0.319              |
|                        | None           | 2346      | 1       | 15.9          | 3.837                    |              |                    |
| Total amount table     | Have           | 865       | 3       | 95.3          | 14.804                   | 3.129        | 0.002              |
|                        | None           | 2346      | 1       | 91.25         | 14.097                   |              |                    |

TABLE 14: Difference analysis.

|                        | Part-time experience | Sample    |         | Average value | Standard deviation value | F test value | Significance value |
|------------------------|----------------------|-----------|---------|---------------|--------------------------|--------------|--------------------|
|                        |                      | Effective | Invalid |               |                          |              |                    |
| Status assessment      | Have                 | 2829      | 0       | 31.95         | 5.462                    | 2.623        | 0.009              |
|                        | None                 | 386       | 0       | 31.44         | 5.426                    |              |                    |
| Self-understanding     | Have                 | 2829      | 0       | 17.8          | 3.139                    | 3.01         | 0.003              |
|                        | None                 | 386       | 1       | 15.74         | 3.347                    |              |                    |
| Career exploration     | Have                 | 2829      | 0       | 27.43         | 5.669                    | 2.565        | 0.013              |
|                        | None                 | 385       | 1       | 16.67         | 5.267                    |              |                    |
| Decision-making action | Have                 | 2829      | 0       | 16.27         | 3.429                    | 0.123        | 0.902              |
|                        | None                 | 382       | 3       | 16.9          | 3.837                    |              |                    |
| Total amount table     | Have                 | 2829      | 0       | 95.3          | 14.798                   | 2.618        | 0.009              |
|                        | None                 | 381       | 5       | 90.25         | 14.164                   |              |                    |

experience as student cadres. Outstanding in the current situation assessment and career exploration level, there are obvious differences in the work experience of student cadres, and the  $P$  values of the  $t$ -test are  $0.048 < 0.05$  and  $0.000 < 0.001$ , respectively.

Part-time job or internship is a way for students to contact the society, and it is also necessary. On the premise of ensuring safety, it should be advocated in large quantities. I believe that there should be differences in career planning level with or without part-time internship experience, which is also confirmed by Table 14. The  $t$ -test  $P$  value of the total table is 0.009, which is significantly different. In addition, the  $P$  values of the  $t$ -test are  $0.009 < 0.01$ ,  $0.003 < 0.01$ , and  $0.013 < 0.05$ , respectively, which shows that students will take part-time jobs and internships, which is very helpful to

students' personal employment and career planning. Therefore, students with internship and part-time jobs must be stronger than students without these experiences in many aspects.

Very few students spontaneously have a higher level of career planning, so students must have external forces such as career counseling to promote. From Table 15, the  $t$ -test  $P$  value of the total scale is 0.000, which shows that there is a very significant difference; that is, the level of students who consult employment information and have relevant career counseling experience is significantly higher than that of students who have not experienced these that is, there are significant differences among students with different career counseling experiences at all levels. Similarly, students with career counseling experience are higher than those without.

TABLE 15: Difference analysis.

|                        | Career coaching | Sample    |         | Average value | Standard deviation value | F test value | Significance value |
|------------------------|-----------------|-----------|---------|---------------|--------------------------|--------------|--------------------|
|                        |                 | Effective | Invalid |               |                          |              |                    |
| Status assessment      | Have            | 547       | 0       | 33.04         | 5.895                    | 2.702        | 0.007              |
|                        | None            | 2688      | 0       | 31.44         | 5.313                    |              |                    |
| Self-understanding     | Have            | 547       | 0       | 17.8          | 3.245                    | 3.069        | 0.002              |
|                        | None            | 2687      | 1       | 16.74         | 3.126                    |              |                    |
| Career exploration     | Have            | 547       | 0       | 29.43         | 6.206                    | 4.565        | 0.673              |
|                        | None            | 2687      | 1       | 26.67         | 5.395                    |              |                    |
| Decision-making action | Have            | 547       | 0       | 17.27         | 3.509                    | 3.594        | 0.044              |
|                        | None            | 2685      | 3       | 15.9          | 3.507                    |              |                    |
| Total amount table     | Have            | 547       | 0       | 100.3         | 15.798                   | 4.472        | 0.003              |
|                        | None            | 2683      | 5       | 93.25         | 14.164                   |              |                    |

First, it is very important for students to understand the social employment environment in which they are currently located. They should always understand that there are still many aspects that need self-improvement and maintain a positive and progressive attitude. Second, as a university, it is necessary to understand the particularity and difference of career planning guidance, and functional departments should change their working methods and try their best to ensure that employment services and guidance can follow up with every student.

## 5. Conclusion

Generally speaking, there are many successful places in China's university education, and the enrollment data can be enough to show that China's university education has made great achievements; at least the public enjoys the right to receive higher education. However, China's total population ranks among the best in the world, with a large population and surplus labor force, so people's employment pressure can be imagined. Graduates from good universities are better at finding jobs, while students from ordinary universities are relatively difficult to find jobs. For the development of our society, we must pay attention to the disadvantages of college students' lack of career planning. From the above analysis, it can be concluded that decision-making action is very lacking in college students nowadays, and it is the last step of personal career planning, which is very important. In the process of visiting and investigating some students offline, it is found that most students do not know what decision-making actions are, are too lazy to act, or are confused and indecisive when acting. Therefore, under the current situation of no action, the overall level of college students' career planning is naturally not high, which deserves great attention.

## Data Availability

The experimental data used to support the findings of this study are available from the corresponding author upon request.

## Conflicts of Interest

The author declares that there are no conflicts of interest regarding this work.

## References

- [1] X. Hao, G. Zhang, and S. Ma, "Deep learning," *International Journal of Semantic Computing*, vol. 10, no. 03, pp. 417–439, 2016.
- [2] Y. Lecun, Y. Bengio, and G. Hinton, "Deep learning," *Nature*, vol. 521, no. 7553, pp. 436–444, 2015.
- [3] J. Ngiam, A. Khosla, and M. Kim, "Multimodal deep learning," *DBLP in Proceedings of the International Conference on Machine Learning*, vol. 37, no. 4, pp. 256–289, Washington, BC, USA, 2009.
- [4] S. Yi, X. Wang, and X. Tang, "Deep learning face representation by joint identification-verification," *Advances in Neural Information Processing Systems*, vol. 27, no. 7, pp. 58–97, 2014.
- [5] C. Zhang, S. Be Ngio, and M. Hardt, "Understanding deep learning requires rethinking generalization," in *Proceedings of the 5th International Conference on Learning Representations (ICLR 2017)*, Toulon, France, April 2017.
- [6] Geert and T. Litjens, "A survey on deep learning in medical image analysis," *Medical Image Analysis*, vol. 17, no. 9, pp. 45–89, 2017.
- [7] Y. Gal and Z. Ghahramani, "Dropout as a bayesian approximation: representing model uncertainty in deep learning," *JMLR.org*, vol. 8, no. 3, pp. 29–53, 2015.
- [8] G. Chen, L. Wang, and M. M. Alam, "Intelligent group prediction algorithm of GPS trajectory based on vehicle communication," *IEEE Transactions on Intelligent Transportation Systems*, vol. 22, no. 7, pp. 3987–3996, 2020.
- [9] V. Gulshan, L. Peng, and M. Coram, "Development and validation of a deep learning algorithm for detection of diabetic retinopathy in retinal fundus photographs," *JAMA*, vol. 2, no. 7, pp. 19–35, 2016.
- [10] Y. Y. Yan, "Career planning of college students," *Technological Development of Enterprise*, vol. 3, no. 7, pp. 43–91, 2010.
- [11] R. T. Jiang, "On career planning of university students and the mechanism reform of talent train of higher education," *Journal of Xiangtan University (Philosophy and Social Sciences Edition)*, vol. 31, no. 3, pp. 421–496, 2004.

- [12] Y. Wang, L. I. Yongneng, and Liu, "Discussion on the path of ascension of occupational career planning of college students based on PDCA theory," *Journal of Yunnan Agricultural University*, vol. 20, no. 1, pp. 1–8, 2015.
- [13] W. U. Wen-Qun and R. Zeng, "The necessary study of the career planning of university students in our country," *Journal of Huaihua University*, vol. 8, no. 13, pp. 329–341, 2007.
- [14] Z. Zhao and W. U. Nan, "Reflections on career planning of university students," *Hebei Academic Journal*, vol. 2, no. 1, pp. 19–35, 2013.
- [15] Y. Ji-Jun, "The problems and strategies on career planning of college students," *Education and Teaching Research*, vol. 6, no. 4, pp. 278–341, 2009.

## Research Article

# Lute Acoustic Quality Evaluation and Note Recognition Based on the Softmax Regression BP Neural Network

Lili Liu 

Taiyuan University of Technology Taiyuan City, Taiyuan 030024, China

Correspondence should be addressed to Lili Liu; liulili01@tyut.edu.cn

Received 22 February 2022; Revised 14 March 2022; Accepted 21 March 2022; Published 12 April 2022

Academic Editor: Man Fai Leung

Copyright © 2022 Lili Liu. This is an open access article distributed under the Creative Commons Attribution License, which permits unrestricted use, distribution, and reproduction in any medium, provided the original work is properly cited.

Note recognition technology has very important applications in instrument tuning, automatic computer music recognition, music database retrieval, and electronic music synthesis. This paper addresses the above issues by conducting a study on acoustic quality evaluation and its note recognition based on artificial neural networks, taking the lute as an example. For the acoustic quality evaluation of musical instruments, this paper uses the subjective evaluation criteria of musical instruments as the basis for obtaining the results of the subjective evaluation of the acoustic quality of the lute, similar to the acoustic quality evaluation, extracts the CQT and MFCC note signal features, and uses the single and combined features as the input to the Softmax regression BP neural network multiclassification recogniser; the classification coding of standard tones is used as the target for supervised network learning. The algorithm can identify 25 notes from bass to treble with high accuracy, with an average recognition rate of 95.6%; compared to other recognition algorithms, the algorithm has the advantage of fewer constraints, a wider range of notes, and a higher recognition rate.

## 1. Introduction

Traditional Chinese music is an important component of music that makes up the world, containing a rich resource of historical, cultural, and folk traditions, representing the accumulation of national history and ideology, a living tradition. In the world of musical instruments, western instruments dominate the field, and our national instruments are not yet comparable to them. Our national musical instruments need to move out of the country to promote our excellent traditional culture, as well as vigorously promote national musical instruments [1]. At present, the musical instrument manufacturing industry of China lags behind that of the west by 20 years and there is a need to change the current situation. The study of the acoustic quality of musical instruments will help the inheritance, development, and promotion of folk musical instruments, play a vital role in improving the quality of musical instruments, promote the development of musical instrument manufacturing and related cultural industries, and provide guidance to the buyers of musical instruments [2]. In today's context, the

development of science and technology and the prosperity of culture and art have brought about the integration of technology and culture, resulting in a prosperous scene of cultural development. The new discipline of music technology is a product of the combination of music and technology. The recent emergence of music information retrieval (MIR) technology is an important part of the music technology field. Note recognition is an important branch of music information retrieval (MIR) [3]. Note recognition is an important area of research in the field of music signal analysis and processing, and note recognition technology has important applications in the tuning of musical instruments, automatic computerised score recognition, music database retrieval, and electronic music synthesis. Note recognition is of great importance in promoting the development of music technology and new electronic industries [2].

With the development of science and technology, new tools and technologies are changing day by day and artificial intelligence (AI) has become synonymous with the new era [4]. In this paper, we focus on the subjective evaluation of the

acoustic quality of musical instruments, which does not objectively and comprehensively reflect the acoustic quality of musical instruments due to the difference in individual's musicianship and preferences, as well as the following problems in the study of note recognition: the estimated pitch is difficult to correspond to the standard pitch, the range of recognisable pitches is narrow, the recognition process is not robust, and the recognition rate is low. Using machine learning in the field of artificial intelligence (AI), a new idea is proposed: an artificial neural network-based assessment of the acoustic quality of the pipa and its note recognition, which eliminates the human subjective factor and the uncertainty that arises in the subjective evaluation process. The pipa is the most ethnically distinctive of China's traditional musical instruments, and it is known as the "king of musical instruments" due to its complexity, versatility, and representativeness [4]. Therefore, the pipa was chosen as the object of this study to facilitate the subsequent study of other instruments.

## 2. Related Work

From the relevant domestic and international literature reviewed so far on the research methods for evaluating the acoustic quality of musical instruments, they can be broadly divided into three categories: first, subjective evaluation; second, objective evaluation; third, a combination of subjective and objective evaluation, with subjective evaluation being the main focus and objective evaluation being supplementary. However, most of the literature focuses on the human subjective sense of listening and finally gives the instrument a corresponding evaluation through subjective feelings. In the absence of a unified objective evaluation standard, it is not yet possible to use an advanced and independent objective evaluation for the assessment of the acoustic quality of musical instruments and scholars at home and abroad are currently exploring a scientific method that can replace subjective evaluation. Alternatively, it may be possible to combine the evaluation of some measurable physical parameters (frequency, amplitude, time, etc.) and the physical characteristics of the instrument (material, mechanics, size and resonance characteristics, etc.) with subjective perception. The study in [5, 6] systematically discusses terminology, technical preparation, and methods related to evaluation, giving specific evaluation methods; for the first time, it proposes the use of seven subjective parameters for scoring and evaluation. The study in [7] presents a comprehensive overview of the issues to be taken into account in the behind-the-scenes appraisal (subjective evaluation) of the acoustic quality of musical instruments; the study in [8] proposes a system for evaluating the acoustic quality of musical instruments according to the different purposes, positions, and perspectives of people [9]. A two-channel FFT analyser, a 0.62 cm condenser microphone, and a preamplifier were used to analyse the sound waves generated by the instrument and thus to evaluate its performance. The study in [10] objectively evaluated the acoustic quality of musical instruments from a mechanical perspective by means of simulation analysis. The study in [11]

used a new objective acoustic quality evaluation metric, the difference in fractal dimensionality in the time-frequency domain (DFDTF), which is no longer an objective evaluation metric in the traditional simple sense of frequency, amplitude, and time. The study in [12] established a link between subjective evaluation and objective quantitative analysis and described the importance of establishing subjective and objective evaluation methods. Different evaluations of the violin by the study in [13] ultimately make an assessment of the instrument and the musician from the subjective perception, while the physicist from the vibrational properties of the violin. A system of subjective and objective sound quality evaluation methods for the improvement of bass string instruments was investigated by the study in [14], where the objective evaluation was done by analysing the frequency spectrum of the sound signal, the acoustic sound pressure level, and the dynamic range of the sound intensity [15].

In summary, subjective evaluation is still the most important method for evaluating the acoustic quality of musical instruments, and there is no scientific evaluation method that can replace it; the study of objective evaluation is also challenging, and it is not easy to achieve the effect of subjective evaluation [16]. The ultimate goal of research into methods for evaluating the acoustic quality of musical instruments is to replace human subjective perceptions, to replace subjective evaluation as far as possible, and to achieve artificial intelligence. It is hoped that the results of this paper will make a small contribution to this goal.

## 3. Pipa Music Signal Library

The music signal is acquired using the audio signal acquisition system set up for the subjective evaluation of the music used in the evaluation, and both the subjective evaluation process and the pipa music signal acquisition process are carried out simultaneously. Each music file is acquired in 30 s, and each lute is subjectively evaluated and acquired three times. The principle process of building a pipa music signal library is shown in Figure 1.

*3.1. Note Signal Library.* The audio signal acquisition system is used for the acquisition of the pipa note signals. The acquisition process is carried out after the pipa music signal has been acquired and a library of the various types of pipa note audio to be identified is created. Prior to note acquisition, the timing of each single note audio needs to be determined to facilitate subsequent experimental studies. In terms of string vibration, the longer the vibrating string length, the longer the duration of the audio, because more overtones are produced; conversely, the shorter the vibrating string length, the shorter the duration of the audio and the fewer the overtones produced [17]. To ensure that the four phases of each single note (silent section, transition section, musical section, and ending section) are all within the determined time, the captured notes should be complete. The duration of each single note was determined to be 3 s. To facilitate the control of each note within 3 s and reduce



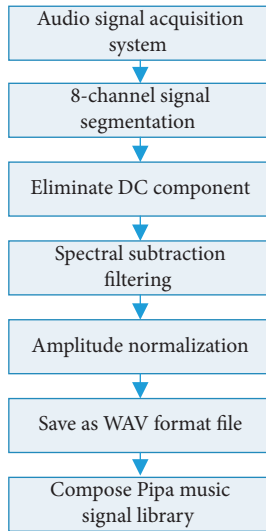


FIGURE 1: The specific principle process of building a pipa music signal library.

repetitive recording operations and improve efficiency, each type of note was played three times at intervals of about 2 s. The acquisition time was set to 20 s to ensure the integrity of each type of note signal [18]. The specific principle process of building a pipa note signal library is shown in Figure 2.

#### 4. Evaluation of the Acoustic Quality of the Lute and Its Note Recognition Model

The determination and establishment of a model for the evaluation of the acoustic quality of the lute and its note recognition is the core of this research and a key part of the solution to the research problem. The model will directly affect the results of the research; therefore, the selection and construction of a suitable model is the focus of this chapter.

**4.1. Modelling Ideas for the Evaluation of the Acoustic Quality of the Lute.** The ultimate goal of the research on the lute acoustic quality evaluation method is to replace the subjective feelings of human beings, to replace subjective evaluation as far as possible, and to achieve artificial intelligence. Using artificial neural networks with the function of mimicking the behavioural characteristics of the human brain, a modelling analysis is carried out using BP neural networks and a model based on BP neural networks is constructed for the evaluation of the acoustic quality of the pipa, the basic idea of which is shown in Figure 3. A library of subjectively evaluated pipa music signals is established, which contains samples to be trained, test samples, and validation samples. The parameters (CC, CQT, and MFCC) that are more representative and closer to human ear perception are extracted from the time, frequency, and cepstrum domains of the lute signal and fed into the evaluation model for learning and training, resulting in the best predicted evaluation results.

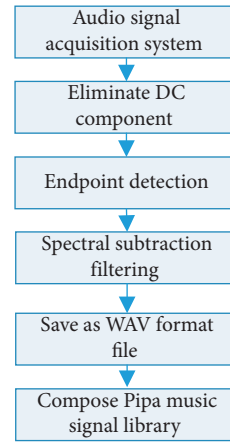


FIGURE 2: Building a pipa note signal library.

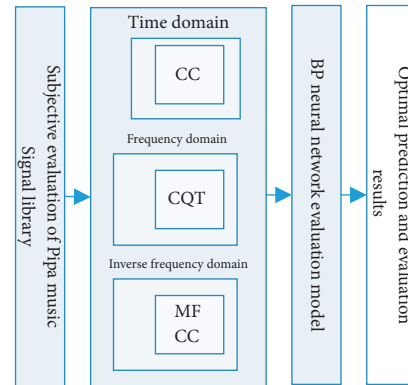


FIGURE 3: Block diagram of the basic idea of modelling the acoustic quality evaluation of the lute.

**4.2. Pipa Note Recognition Modelling Ideas.** The idea of multiclassification recognition is used to recognise the notes of the lute. As it is considered that BP neural network has a good recognition effect for binary classification problems, for multiclassification problems, the recognition effect is not good and it cannot meet the requirements of this paper for note recognition. The Softmax regression model has a great advantage in the multiclassification problem, and combined with the good nonlinear mapping ability, self-learning ability, and fault tolerance ability of BP neural networks, therefore this paper proposes a method combining Softmax regression with BP neural network that has the ability of multiclassification recognition and constructs a multiclassification note recognition model of BP neural network based on Softmax regression. The basic idea of the modelling is shown in Figure 4. A pipa note signal library is established, which contains samples to be trained and test samples. The frequency domain features (CQT) and inverse frequency domain features (MFCC) of the lute note signal are extracted and input as feature parameters into the multiclassification recognition model for learning and training, and the optimal recognition and classification results are obtained.

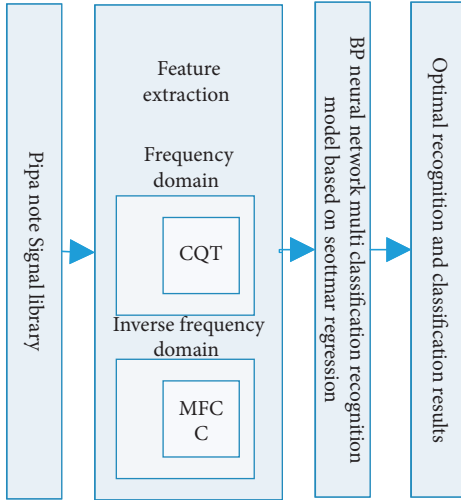


FIGURE 4: Block diagram of the basic idea of pipa note recognition modelling.

**4.3. BP Neural Network Based on Softmax Regression.** Based on the above analysis of the modelling idea of lute note recognition, the advantages of Softmax regression model in multiclassification problems are utilised and combined with the good nonlinear mapping ability, self-learning ability, and fault tolerance of BP neural networks. With reference to the structure of multilayer BP neural networks, a Softmax regression-based BP neural network multiclassification recogniser is constructed and the structure is shown in Figure 5. Based on the experimental sample size, the single implicit layer is unable to meet the experimental requirements and there are problems of large computational effort, long training time, and low recognition rate. Therefore, the number of neurons in the input layer is determined by the dimensionality of the input features, two layers are used in the hidden layer (which has been verified to be the optimal number of layers), and the Softmax regression model is used in the output layer.

The multiclassification problem solved in this paper is a one-vs-all classification problem, where the output  $y$  is expected to be a vector:

$$y \in \left\{ \begin{bmatrix} 1 \\ 0 \\ 0 \\ \vdots \\ 0 \end{bmatrix}, \begin{bmatrix} 0 \\ 1 \\ 0 \\ \vdots \\ 0 \end{bmatrix}, \begin{bmatrix} 0 \\ 0 \\ 1 \\ \vdots \\ 0 \end{bmatrix}, \dots, \begin{bmatrix} 0 \\ 0 \\ 0 \\ \vdots \\ 1 \end{bmatrix} \right\}_{25 \times 25}. \quad (1)$$

The immediate reason for using one-hot coding is that the output layer of Softmax classification outputs a probability distribution and therefore requires that the input target labels also appear as probability distributions, which makes it easier to calculate the cross entropy for loss-supervised network learning. One-hot coded labels give the sample the true probability distribution, where only one occurs with probability 1 and the others occur with probability 0.

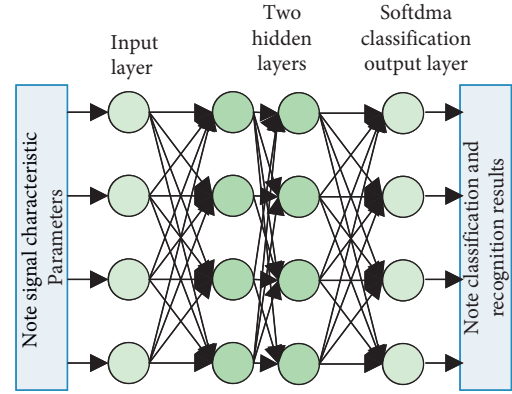


FIGURE 5: Structure of BP neural network multiclassifier recogniser with Softmax regression.

## 5. Experimental Results and Performance Analysis

**5.1. Model Evaluation Indicators.** The purpose of the model evaluation indicators is to analyse and evaluate the performance of the lute acoustic quality evaluation model and the lute note recognition model constructed in this paper and whether they are suitable for the object of study in this paper.

Average accuracy is used as the evaluation index of the pipa acoustic quality evaluation model, which is defined as follows:

$$\text{average accuracy} = \left( 1 - \frac{\sum_{i=1}^N |Y_i^p - Y_i^e| / Y_i^e}{N} \right) \times 100\%. \quad (2)$$

Five evaluation metrics were used to evaluate the classification performance of this classifier: the ConfusionMatrix P 84], Accuracy, i.e., recognition rate, Recall, Precision, and the composite metric  $F$ -Score.

The recognition rate (accuracy) is defined by the following equation:

$$A = \frac{O_{cd}}{O_{cd} + O_{fn} + O_{fp}}. \quad (3)$$

Precision is defined by

$$P = \frac{O_{cd}}{O_{cd} + O_{fp}}. \quad (4)$$

Recall is defined by the following equation:

$$R = \frac{O_{cd}}{O_{cd} + O_{fn}}. \quad (5)$$

The composite indicator  $F$ -Score is defined by the following formula:

$$F = \frac{2PR}{P + R}. \quad (6)$$

In equations (3)-(6),  $O_{cd}$  is the number of correct classifications,  $O_{fn}$  is the number of unrecognised classifications, and  $O_{fp}$  is the number of incorrect classifications. Precision ( $P$ ) and recall ( $R$ ) are two mutually constraining metrics, and the  $F$ -value is a combination of  $R$  and  $P$  [19].

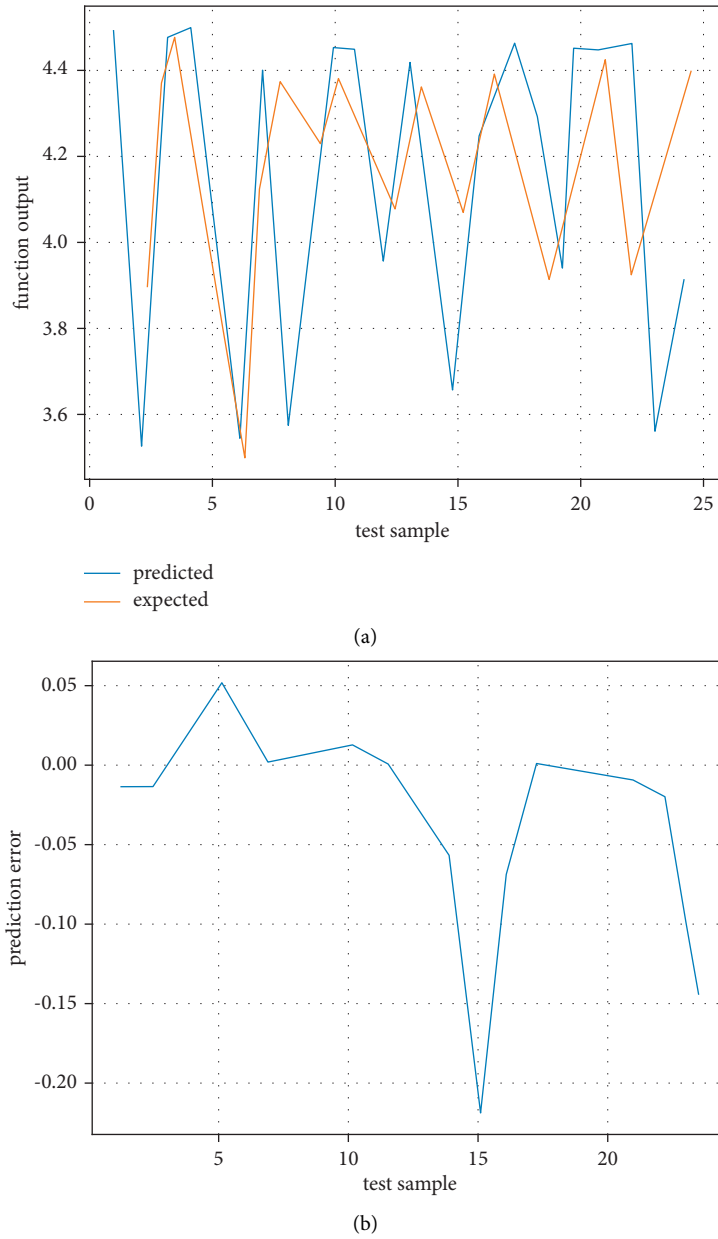


FIGURE 6: Predicted output and error analysis curves of the lute acoustic quality evaluation network.

TABLE 1: Average accuracy of varying the number of training samples for different feature inputs.

| Input           | 10 sets of samples | 30 sets of samples | 50 sets of samples | 70 sets of samples | 90 sets of samples | 110 sets of samples |
|-----------------|--------------------|--------------------|--------------------|--------------------|--------------------|---------------------|
| MFCC            | 91.63              | 95.09              | 95.48              | 95.64              | 94.92              | 95.70               |
| CQT             | 92.57              | 97.33              | 96.81              | 97.81              | 98.41              | 98.50               |
| MFCC + CQT      | 96.16              | 96.1               | 97.24              | 97.21              | 98.68              | 99.14               |
| MFCC + CC       | 94.79              | 95.7               | 95.09              | 96.11              | 96.15              | 96.72               |
| CQT + CC        | 92.16              | 97.25              | 97.77              | 98.06              | 98.55              | 98.82               |
| MFCC + CQT + CC | 94.61              | 94.78              | 97.89              | 98.7               | 99.36              | 99.68               |

5.2. Experiment to Evaluate the Acoustic Quality of the Lute. The fused features (MFCC + CQT + CC) were used as feature parameters input into the lute acoustic quality evaluation network model for learning and training in the

MATLABR2016a environment. In the experiments, the subjective evaluation results were used as expectation values to supervise the learning and training of this network model; of 144 sets of samples, 110 sets were used as training samples,

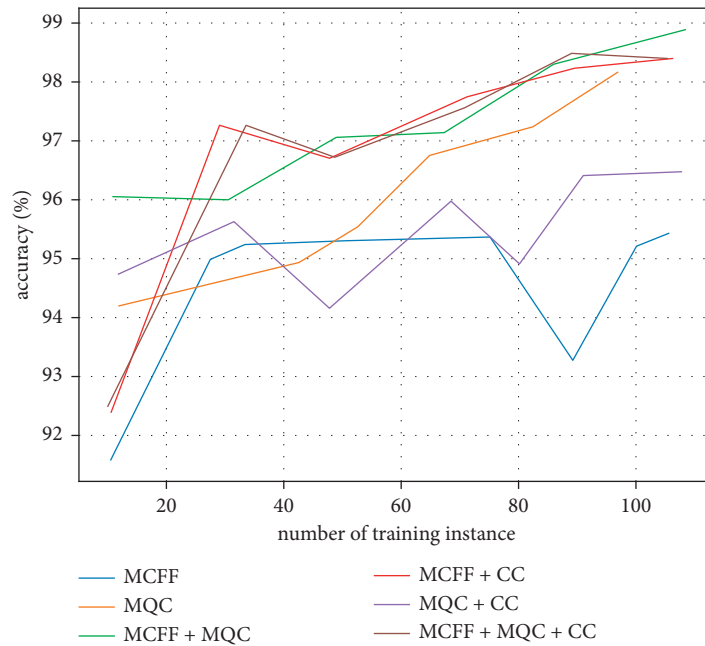


FIGURE 7: Average accuracy curve of varying the number of training samples with different feature inputs.

24 sets as testing samples, and 10 sets as validation samples. According to the characteristics of the experimental samples and the structure of the network model, logsig (Sigmoid function) was used for the activation function of the implicit layer and linear purelin was used for the activation function of the output layer; the training function of the model network was trainlm, and the training algorithm was Levenberg–Marquardt algorithm. The optimal network parameter configuration was obtained by adjusting the network parameters through several experimental comparisons. With the optimal prediction evaluation results obtained, the number of layers of the hidden layers and the number of neurons in each layer were {10, 20, 150, 50, 10, and 10} [20, 21].

For further validation, the use of fused features (MFCC + CQT + CC) as feature parameters input to the BP neural network-based lute acoustic quality evaluation model was the best way to fuse the features. Additional comparison experiments were conducted, using single features and different combinations of features as well as exploratory experiments varying only in the number of training samples.

The results obtained in the preliminary experiments are shown in Figure 6. As can be seen in Figure 6, the predicted output values are very similar to the desired output values, with some individual samples not being predicted very well, but overall, the predictions are very good. The average accuracy of the test samples was 99.68%, and the average accuracy of the validation samples was also 99.49%.

The results of further exploratory experiments are shown in Table 1 and Figure 7, and the results obtained are all under the optimal network parameter configuration. From Table 1 and Figure 7, it can be seen that the average accuracy shows an overall increasing trend with the increase in the number of training samples and the prediction effect of the fused features (MFCC + CQT + CC) is stronger than several other feature

fusions after the number of samples reaches 50 groups; on the whole, the single feature MFCC and its combined features (MFCC + CC) are not as effective in prediction.

The experimental results show that the best predictive evaluation is obtained by fusing the features (MFCC + CQT + CC), which maximizes the characterization of the pipa sound quality; the BP neural network-based pipa acoustic quality evaluation model constructed in this paper is reliable and has good predictive evaluation performance; the pipa acoustic quality evaluation method proposed in this paper is very novel and feasible.

## 6. Conclusions

Based on the subjective evaluation criteria of musical instruments, this paper proposes Softmax regression BP neural network multiclassification recogniser input based on obtaining the results of subjective evaluation of lute acoustic quality, similar to acoustic quality evaluation; the classification code of standard tones is used as the target label for supervised network learning, resulting in an optimised model for lute note recognition. The experimental results show that this scheme can achieve high precision recognition of 25 notes from bass to treble, with an average recognition accuracy of 95.6%.

## Data Availability

The experimental data used to support the findings of this study are available from the author upon request.

## Conflicts of Interest

The author declares that there are no conflicts of interest regarding this work.

## References

- [1] V. Eyharabide, I. E. I. Bekkouch, and N. D. Constantin, "Knowledge graph embedding-based domain adaptation for musical instrument recognition," *Computers*, vol. 10, no. 8, p. 94, 2021.
- [2] P. Peso Parada, D. Sharma, J. Lainez, D. Barreda, T. V. Waterschoot, and P. A. Naylor, "A single-channel non-intrusive C50 estimator correlated with speech recognition performance," *IEEE/ACM Transactions on Audio, Speech, and Language Processing*, vol. 24, no. 4, pp. 719–732, 2016.
- [3] M. Walczyński and J. Fica, "Comparison of selected acoustic signal parameterization methods in the problem of machine recognition of classical music styles," in *Progress in Image Processing, Pattern Recognition and Communication Systems*, pp. 181–190, Springer, Cham, 2021.
- [4] B. Jia, J. Lv, and D. Liu, "Deep learning-based automatic downbeat tracking: a brief review," *Multimedia Systems*, vol. 25, no. 6, pp. 617–638, 2019.
- [5] D. Kiela and S. Clark, "Learning neural audio embeddings for grounding semantics in auditory perception," *Journal of Artificial Intelligence Research*, vol. 60, pp. 1003–1030, 2017.
- [6] D. Herremans, C. H. Chuan, and E. Chew, "A functional taxonomy of music generation systems," *ACM Computing Surveys*, vol. 50, no. 5, pp. 1–30, 2017.
- [7] L. Verde, G. De Pietro, M. Alrashoud, A. Ghoneim, K. N. Al-Mutib, and G. Sannino, "Dysphonia detection index (DDI): a new multi-parametric marker to evaluate voice quality," *IEEE Access*, vol. 7, pp. 55689–55697, 2019.
- [8] Z. H. A. N. G. Zhengwan, Z. H. A. N. G. Chunjong, L. I. Hongbing, and X. I. E. Tao, "Multipath transmission selection algorithm based on immune connectivity model," *Journal of Computer Applications*, vol. 40, no. 12, p. 3571, 2020.
- [9] L. Su, C.-C. M. Yeh, J.-Y. Liu, J.-C. Wang, and Y.-H. Yang, "A systematic evaluation of the bag-of-frames representation for music information retrieval," *IEEE Transactions on Multimedia*, vol. 16, no. 5, pp. 1188–1200, 2014.
- [10] X. L. Zhang and J. Wu, "Deep belief networks based voice activity detection," *IEEE Transactions on Audio Speech and Language Processing*, vol. 21, no. 4, pp. 697–710, 2012.
- [11] D. G. Bhalke, C. B. R. Rao, and D. S. Bormane, "Automatic musical instrument classification using fractional fourier transform based- MFCC features and counter propagation neural network," *Journal of Intelligent Information Systems*, vol. 46, no. 3, pp. 425–446, 2016.
- [12] V. Lostanlen, J. Andén, and M. Lagrange, "Extended playing techniques: the next milestone in musical instrument recognition," in *Proceedings of the 5th International Conference on Digital Libraries for Musicology*, pp. 1–10, Paris, France, 2018, September.
- [13] R. Martinek, M. Kelnar, J. Vanus, P. Bilik, and J. Zidek, "A robust approach for acoustic noise suppression in speech using ANFIS," *Journal of Electrical Engineering*, vol. 66, no. 6, pp. 301–310, 2015.
- [14] C. Halkiopoulos and B. Boutsinas, "Automatic interactive music improvisation based ON data mining," *The International Journal on Artificial Intelligence Tools*, vol. 21, no. 04, Article ID 1250016, 2012.
- [15] P. Jain, S. C. P. Coogan, S. G. Subramanian, M. Crowley, S. Taylor, and M. D. Flannigan, "A review of machine learning applications in wildfire science and management," *Environmental Reviews*, vol. 28, no. 4, pp. 478–505, 2020.
- [16] I. E. I. Bekkouch, N. D. Constantin, V. Eyharabide, and F. Billiet, "Adversarial domain adaptation for medieval instrument recognition, Lecture Notes in Networks and Systems," in *Proceedings of the SAI Intelligent Systems Conference*, pp. 674–687, Amsterdam, 2021 September.
- [17] D. G. Bhalke, C. B. R. Rao, and D. S. Bormane, "Fractional fourier transform based features for musical instrument recognition using machine learning techniques," in *Proceedings of the International Conference on Frontiers of Intelligent Computing: Theory and Applications (FICTA) 2013*, pp. 155–163, Bhubaneswar, Odisha, India, 2014.
- [18] C. Dai, H. Che, and M.-F. Leung, "A neurodynamic optimization approach for L1 minimization with application to compressed image reconstruction," *The International Journal on Artificial Intelligence Tools*, vol. 30, no. 1, Article ID 2140007, 2021.
- [19] Y. Wang, J. Wang, and H. Che, "Two-timescale neurodynamic approaches to supervised feature selection based on alternative problem formulations," *Neural Networks*, vol. 142, pp. 180–191, 2021.
- [20] J. H. Calvo-Zaragoza and A. Pacha, "Understanding optical music recognition," *ACM Computing Surveys*, vol. 53, no. 4, pp. 1–35, 2020.
- [21] T. Dissanayake, T. Fernando, S. Denman, S. Sridharan, H. Ghaemmaghami, and C. Fookes, "A robust interpretable deep learning classifier for heart anomaly detection without segmentation," *IEEE Journal of Biomedical and Health Informatics*, vol. 25, no. 6, pp. 2162–2171, 2020.

## Research Article

# Convolutional Neural Networks for Structural Damage Identification in Assembled Buildings

Chunhua You , Wenxiang Liu, and Lei Hou

*School of Civil and Constructional Engineering, Hunan Institute of Technology, Hengyang 421002, China*

Correspondence should be addressed to Chunhua You; 2005001486@hnit.edu.cn

Received 21 February 2022; Accepted 4 March 2022; Published 11 April 2022

Academic Editor: Hangjun Che

Copyright © 2022 Chunhua You et al. This is an open access article distributed under the Creative Commons Attribution License, which permits unrestricted use, distribution, and reproduction in any medium, provided the original work is properly cited.

This paper investigates the migration learning AlexNet-based algorithm for the recognition of assembly building structures and the recognition based on an improved algorithm, and gives an analysis of the results. The structure of AlexNet convolutional neural network is introduced and the basic principles of migration learning are analysed. The optimal model for the ceiling damage recognition task was obtained through parameter adjustment, with a test accuracy of 96.6%. The maximum improvement in test accuracy is about 4%, with 82.6% and 79.7% for beam and column damage recognition and infill wall damage recognition respectively.

## 1. Introduction

In the aftermath of a disaster, rapid assessment of the extent of damage has become an important basis for the allocation of emergency search and rescue resources following an earthquake [1]. The traditional method of assessment mainly involves a group of trained professional engineers and academic researchers visiting the site to survey the extent of the damage. While this approach is accurate, the safety of the assessment team personnel is not guaranteed given the occurrence of aftershocks, and the unsafe elements within the building, and the whole process lasts longer and is less efficient. But with another development in artificial intelligence, computer vision is starting to come into the picture. Intelligent classification and labelling of image data using deep learning methods has become the new craze [2, 3].

The rapid assessment system for postearthquake building damage proposed in this paper has no restrictions on the professionalism of the photographers and can even use drones to enter the interior to take pictures, which greatly accelerates the efficiency of postearthquake assessment and provides suggestions for further investigation [4].

In order to enable people in the earthquake zone to work safely and urgently after the earthquake, a rapid assessment of postearthquake building damage is needed, and relatively

safe houses can be used to prevent people from having nowhere to live and sleeping on the streets. This will provide the basic basis for the government to make scientific and effective regulation [5]. The assessment is divided into structural and nonstructural elements, with structural elements including beams and columns, and nonstructural elements including infill walls and ceilings [6]. The damage to structural elements is directly related to the safety of the overall building. From the photographic data recorded in the Wenchuan and Lushan earthquakes, the damage to beams and columns in houses that did not collapse was mainly as follows: slight cracks in the beams and columns, crushed external concrete, crushed concrete with yielding steel reinforcement, example pictures are shown in Figure 1.

Since the reform and opening up, with the development of the economic level, the quality of China's urban and rural buildings has improved significantly, and in the medium earthquake, there is rarely any damage to the load-bearing elements of houses. Through a large number of post-earthquake disaster picture data the analysis revealed that the infill walls, as the first line of seismic protection for reinforced concrete frame structures, were very seriously damaged, as shown in Figure 2.

Convolutional neural networks are trained on a large amount of data. Theoretically, the richer the data, the better



FIGURE 1: Damage to structural elements in the Wenchuan earthquake.



FIGURE 2: Damage to infill wall in the Lushan earthquake.

the learning ability of the trained convolutional neural network and the better the classification results. CNN have been known for their excellent performance in image classification since their inception. In recent years, the development of CNN has become more and more rapid and has gradually surpassed the human's own ability to classify images, which lays the foundation for using CNN in this paper to perform damage recognition of buildings after earthquakes [7]. In deep learning, training a deep neural network usually requires a large amount of labelled data as the training set, however, in many practical situations, obtaining sufficient data samples is very difficult. Training a model with an inadequate training set runs the risk of overfitting the model, resulting in poor generalisation of the trained model and failure to achieve the expected accuracy on the test data set [8]. The idea of migration learning, which has emerged in recent years, better solves the problem of inadequately large datasets in deep learning. In this paper, we collected a large amount of image data from the Institute of Engineering Mechanics of the China Earthquake Administration in the Wenchuan and Lushan earthquakes, which laid a solid foundation for the establishment of the dataset.

Compared with traditional recognition methods, we do not need to personally extract the damaged areas of the components for feature input, and can avoid the disadvantages of manual feature extraction, for example: (a) it is generally difficult to express complex high-level semantics of images based on some lifting layer feature information of the graph (e.g. colour, texture, etc.), so the generalisation ability is generally weak. (b) These methods are generally designed for specific applications in specific domains, and their generalisation and migration capabilities are mostly weak.

The convolutional neural network-based recognition method only requires us to build a convolutional neural network with completed training and upload the image in the visual operation interface to recognize the result, ensuring the intelligence, simplicity and practicality of the system. In the future, there is still a broad prospect for the development of postearthquake building damage recognition algorithms based on convolutional neural networks.

## 2. Related Work

Nowadays, more people have become aware of the importance of deep learning, especially in the field of machine learning, which has become more effective. The reason for this is that deep learning has advanced and developed very significantly in several areas, such as sound and text, and most crucially, the use of Internet technology, which has led to an artificial intelligence revolution. Reference [9] proposes a method capable of recovering the properties of cracks. In this method, crack points are first located by means of state-of-the-art crack detection techniques. Then, the skeletal structure of each point is identified using image refinement methods. These structures are integrated into the distance field of the crack point by means of a distance transformation. In this way, crack width, length and direction can be automatically recovered. Reference [10] proposes a new method for detecting spalling regions on the surface of reinforced concrete columns. The properties of the spalling regions are obtained from the image data, according to which the spalling regions are first separated using a threshold-holding algorithm based on local entropy [11]. Based on this, a new global adaptive thresholding algorithm was combined to measure the longitudinal reinforcement

(spalling depth in the column) and the spalling length in the column. A new detection method for postdisaster image classification is proposed in [12], which has four steps: firstly raw data screening, secondly scene classification, then target detection and finally damage assessment. The method was validated in the classification of specific examples. Distinguishing themselves from previous work, [13] et al. propose a new method for structural damage detection using deep CNNs that automatically obtains information from low-level waveform signals rather than relying on manual labelling. The method implements structural damage detection based on data alone without relying on human expert knowledge, and numerical simulations are performed to obtain the response data of the structure, followed by data preprocessing, data augmentation, and finally training of the augmented dataset by a deep CNN to estimate its classification performance for damage localization, and demonstrates superiority compared to another damage extraction method [14].

### 3. Data Set Creation and Expansion

**3.1. Data Set Creation.** Most of the data set in this paper comes from the picture data of the Wenchuan and Lushan earthquakes provided by the Institute of Engineering Mechanics of the China Earthquake Administration, and a small part of the data comes from the Internet, as shown in Figure 3.

In this paper, according to the damage characteristics of the building, the frame building is divided into two parts: structural elements, beams and columns, and nonstructural elements, infill walls and nonstructural ceiling elements. The specific classification levels and condition descriptions are shown in Table 1:

**3.2. Data Preprocessing.** (a) Samples from the seismic images were selected to meet the experimental requirements and the target region of interest in the images was made central by manual processing.

The histogram of a grey-scale image in the grey-scale range  $[0, L-1]$  is defined as shown in (1):

$$h(r_k) = n_k. \quad (1)$$

Here  $r_k$  — kth level of grey in the image;  $n_k$  — Number of pixels in the image with a grey level of  $r_k$ .

$$p(r_k) = h(r_k) = \frac{n_k}{MN}, \quad (2)$$

where  $M$  — Number of rows of grayscale charts;  $N$  — Number of columns in the grey-scale chart;  $MN$  — Total number of pixels in the image.

$1/MN$  is the histogram defined in the normalisation (2), which after normalisation  $p(r_k)$  can be interpreted as an estimate of the probability that grey level  $r_k$  will occur in the image. The histogram is the basis for a variety of other image processing techniques, and the spatial domain processing of images can be expressed as equation (3)

$$g(x, y) = T[f(x, y)], \quad (3)$$

where  $f(x, y)$  is the input image.  $g(x, y)$  is the transformed image.  $T$  is a transform function defined on the neighbourhood of the point  $(x, y)$ .

The smallest domain of this equation is  $1 \times 1$ , in which case  $g$  depends only on the value of  $f$  at point  $(x, y)$ , while  $T$  in equation (3) becomes a grey-scale transform function shaped as in equation (4):

$$s = T(r). \quad (4)$$

The immediate effect of equation (4) is to convert the input grey-scale values to other values for the purposes of contrast stretching, binarisation, etc. Histogram equalisation is a special conversion method in the form of equation (4). There exists a very important transformation function in the image domain of the following form:

$$s = T(r) = (L - 1) \int_0^r p_r(w)dw, \quad (5)$$

where  $w$  — Integral dummy variables;  $p_r(w)$  — The probability density function of a random variable  $r$ .

The integral part of the right-hand side of the formula is the cumulative distribution function of the random variable  $r$ . Because the probability density function of the random variable  $r$  is always positive, the cumulative distribution function is increasing and has a maximum value of 1. Therefore, the transformation  $T(r)$  is an increasing function and has a value range of  $[0, L-1]$ . When the random variable is a continuous random variable, the random variable  $s$  obtained by the above transformation will be a uniform probability density variable. The pixel values in an image can be treated as if the interval were  $[0, L-1]$  a discrete variable, and according to equation (5) the histogram equalisation is obtained, which changes in the following form:

$$\begin{aligned} s_k = T(r_k) &= (L - 1) \sum_{j=0}^k p_r(r_j) \\ &= \frac{(L - 1)}{MN} \sum_{j=0}^k n_j, k = 0, 1, \dots, L - 1. \end{aligned} \quad (6)$$

In equation (6),  $r_k$ ,  $MN$ ,  $n_k$ , and  $p_r(r_k)$  all correspond to the converted values as described previously, and  $L$  is the number of grey levels in the image. The histogram equalisation conversion formula ensures two important conditions: the conversion function  $T(r)$  is a monotonically increasing function on the interval  $0 \leq r \leq L-1$ ; on the interval  $0 \leq r \leq L-1$ , there is  $0 \leq T(r) \leq L-1$ .

**3.3. Data Enhancement.** In the case of insufficient data samples, data augmentation is often used to expand the sample. A common means of data augmentation is geometric transformation, and in this paper the sample is expanded by means of rotation and mirroring. In the field of image recognition, the rotation, translation and mirroring of an image do not actually change the essential information of





FIGURE 3: Damage to structural elements—beams and columns. (a) in good condition or slightly damaged. (b) Moderate damage. (c) Severe damage.

TABLE 1: Criteria for classifying the damage state of beams and columns.

| Failure state                         | State description   |
|---------------------------------------|---|
| Basically intact and slightly damaged | Basically, there is no crack or slight crack, which does not affect the structural safety                               |
| Moderate damage                       | Large cracks appear on the concrete surface, a small part of the concrete is crushed, and the reinforcement is not bent |
| Severe damage                         | Large areas of concrete are crushed, steel bars are bent, and even tilt or collapse                                     |

the image. Moreover, by rotating, panning and mirroring the image, the sample can be obtained from multiple angles and directions with different sizes [15]. This transformation can improve the recognition accuracy of the convolutional

neural network, because it can effectively avoid the possibility that the convolutional neural network is not well trained due to the different shooting equipment or shooting angles, thus causing errors in recognition. In this paper, the



(a)



(b)



(c)



(d)



(e)



(f)

FIGURE 4: Continued.

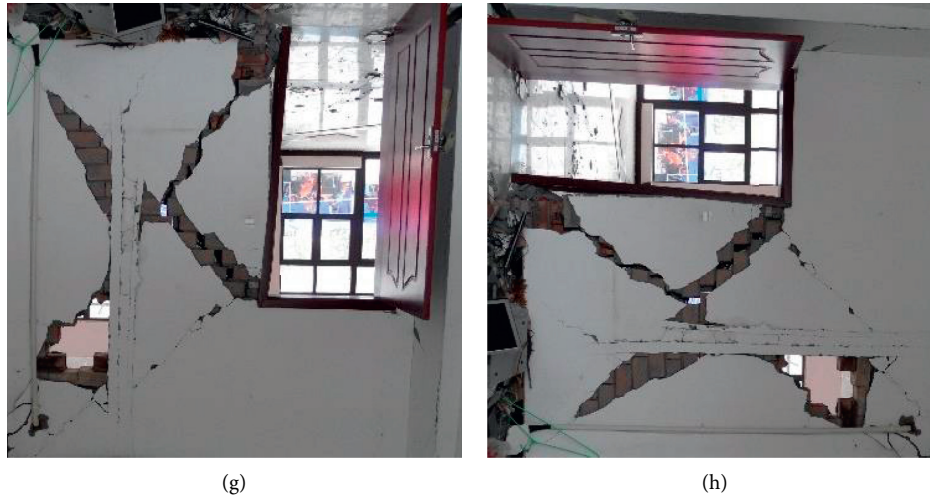


FIGURE 4: Geometric transformation diagram. (a) Original. (b) Original rotated by  $90^\circ$ . (c) Original rotated by  $180^\circ$ . (d) Original rotated by  $270^\circ$ . (e) Mirror image. (f) Mirror rotation  $90^\circ$ . (g) Mirror rotation  $180^\circ$ . (h) Mirror rotation  $270^\circ$ .

original image is rotated and mirrored to increase the number of images to 8 times the original size, as shown in Figure 4.

#### 4. Based on the Improved AlexNet

In this paper, AlexNet has a low accuracy for the task of identifying the extent of damage to beams and columns and the extent of damage to infill walls, and cannot be significantly improved by simply adjusting the hyper-parameters, so improvements to the original AlexNet are considered. In recent years, many scholars have modified and enhanced AlexNet to improve neural network recognition accuracy. In [16], the WN (Weight Normalization) was proposed to replace the LRN layer with the LRN (Local Response Normalization), and the WN was placed after all pooling layers to improve the accuracy of AlexNet model training. In [17], a fusion segmentation algorithm of ReLU6 and Swish was proposed to address the problem of partial failure to update the weights and gradient explosion of the ReLU activation function in AlexNet, which improved the convergence speed and accuracy of AlexNet model training and also alleviated the occurrence of overfitting [18].

*4.1. An Improved AlexNet Network Structure.* However, as the number of layers increases the disadvantages of a small data set become apparent, as not only does the test error become higher when the network is deeper, but its training error is surprisingly higher as well. Deeper networks are associated with gradient disappearance and explosion problems, which hinder the convergence of the network, and this phenomenon of deeper networks with reduced performance is generally referred to as the degradation problem.

However, in order to prevent the model from being trained poorly due to the increase in parameters after the

addition of the convolutional layer, we choose to combine the residual structure of ResNet with AlexNet to achieve the goal of increasing the convolutional layer without a surge in parameters, so as to improve the problem of low accuracy and loss of convergence in multitask recognition [19, 20].

Assuming that the input to a particular segment of the neural network is  $x$  and the desired output is  $H(x)$ , i.e.,  $H(x)$  is the desired complex potential mapping, it would be more difficult to train such a model if it were to be learnt; recalling the previous assumption, if a more saturated accuracy has been learnt (or when the error in the lower layers is found to become larger), then the next learning goal shifts to the learning of a constant mapping, i.e. making the input  $x$  approximate the output  $H(x)$  to keep from causing a drop in accuracy in the later layers.

In Figure 5, the residual network structure is shown by means of "shortcut connections", where the input  $x$  is passed directly to the output as the initial result, and the output is  $H(x) = F(x) + x$ . If  $F(x) = 0$ , then  $H(x) = x$ , which is the above mentioned constant mapping. Thus, ResNet is equivalent to changing the learning goal from learning a complete output to the difference between the target value  $H(x)$  and  $x$ , also known as the residual  $F(x) = H(x) - x$ . Thus, the training goal later is to approximate the residual result to 0, so that the accuracy does not decrease as the network deepens.

The two structures in Figure 6 are for ResNet34 and ResNet50/101/152 respectively, and their purpose is mainly to reduce the number of parameters. The left figure shows two  $3 \times 3 \times 256$  convolutions with the number of parameters:  $3 \times 3 \times 256 \times 256 = 1179648$ , while the right figure first reduces the 256-dimensional channels to 64 dimensions by  $1 \times 1$  convolution and finally recovers them by  $1 \times 1$  convolution, using the overall number of parameters:  $1 \times 1 \times 256 \times 64 + 3 \times 3 \times 64 \times 64 + 1 \times 1 \times 64 \times 256 = 69632$ . The number of parameters is reduced by a factor of 16.94 compared to the left graph, so the main purpose of the right graph is to reduce the number of parameters and hence the computational effort [21].

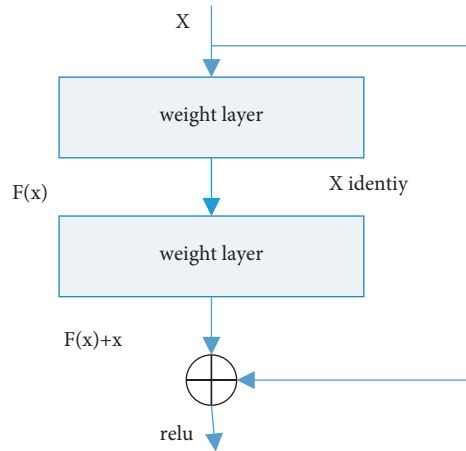


FIGURE 5: Structure of the residuals.

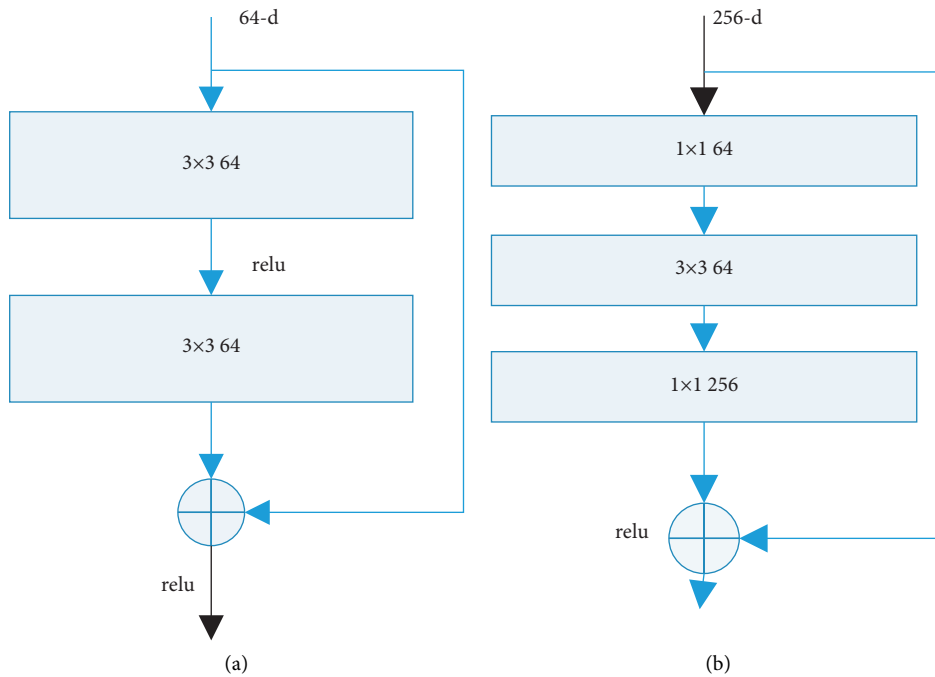


FIGURE 6: Two forms of residual structure. (a) Basic block. (b) Bottleneck.

For a regular ResNet (Figure 6(a)), basic block can be used for networks with 34 layers or less. (Figure 6(b)) Bottleneck is used for deeper networks (e.g. 101 layers) with the aim of reducing the number of computations and parameters. This paper therefore considers adding the Basic block module after the convolutional layer of AlexNet, replacing the three fully-connected layers with one. The AlexNet convolutional layer is used to extract the feature information of the images in the dataset, and a comparison experiment is set up to add one Basic block block, two Basic block blocks and three Basic block blocks to the classification layer, and then the accuracy of the network is tested after the training is completed. The network improvement scheme is shown in Figure 7.

## 5. Damage Recognition Experiments

*5.1. Vibration Recognition.* The time-frequency response of the sensor was tested at different frequencies and accelerations. The time and frequency response of the sensor is shown in Figure 8 for external excitation frequencies of 90 Hz and 350 Hz and accelerations of 1.0 g and 3.0 g respectively. The output waveform of the FBG vibration sensor is a sinusoidal waveform, as can be seen from the time domain signal; Figure 8(b) and (d) show the frequency spectrum obtained from the Fast Fourier Transform (FFT) of the time domain signal. The results are consistent with the experimentally set frequency parameters.

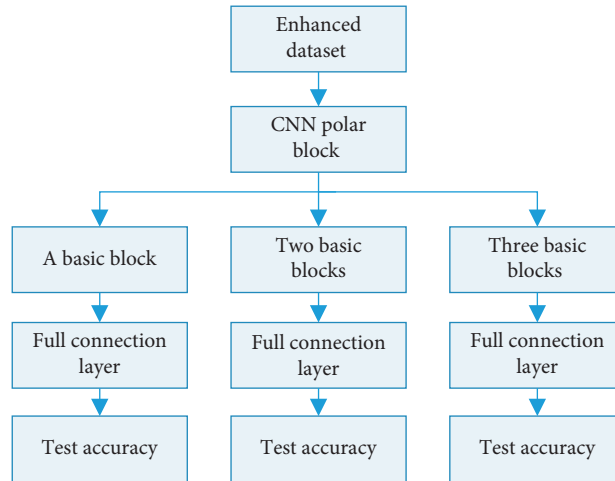


FIGURE 7: Design options for network improvements.

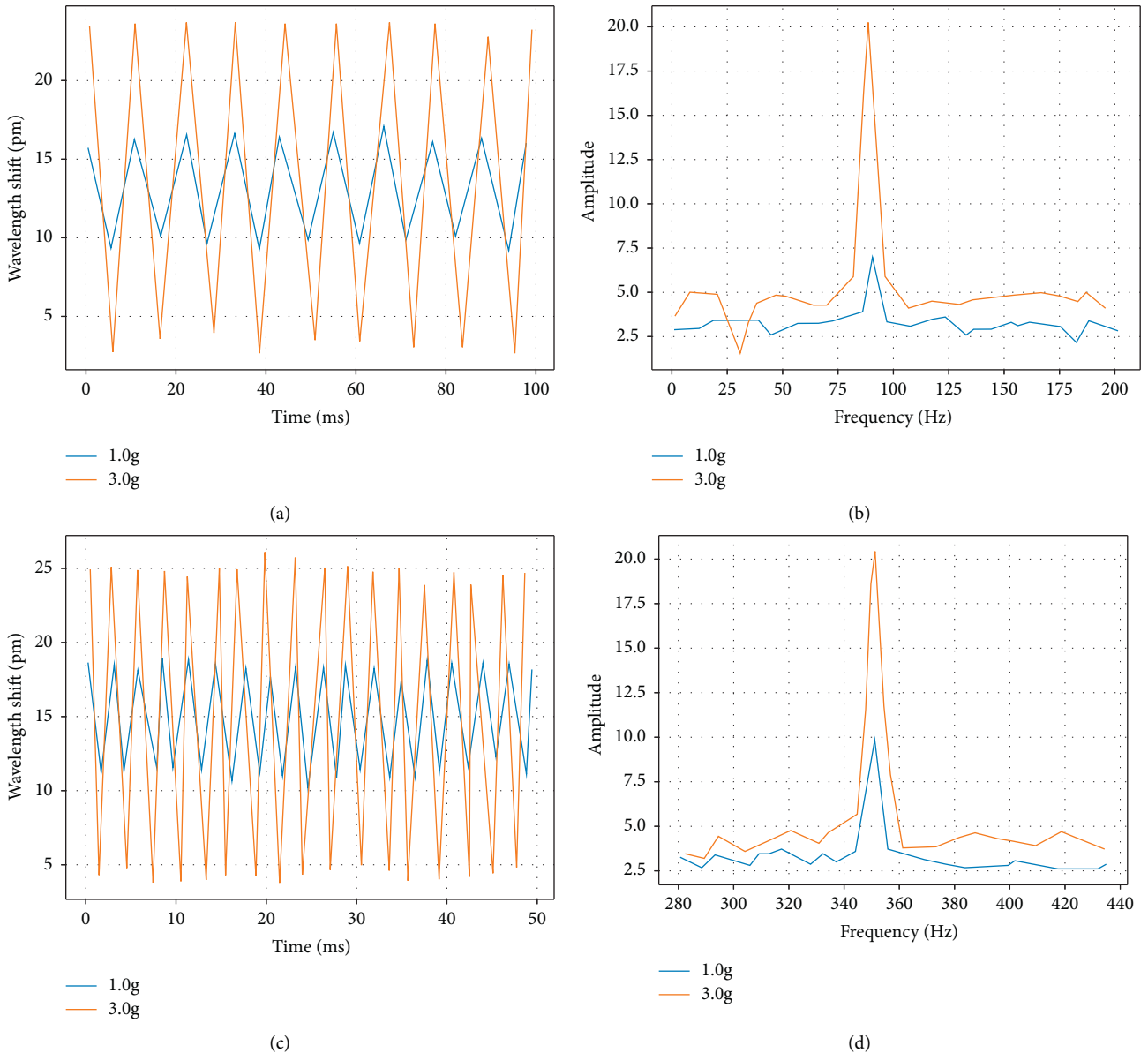


FIGURE 8: Response curves of the time-frequency characteristics of the sensor. (a) 90 Hz time domain; (b) 90 Hz frequency domain; (c) 350 Hz time domain; (d) 350 Hz frequency domain.

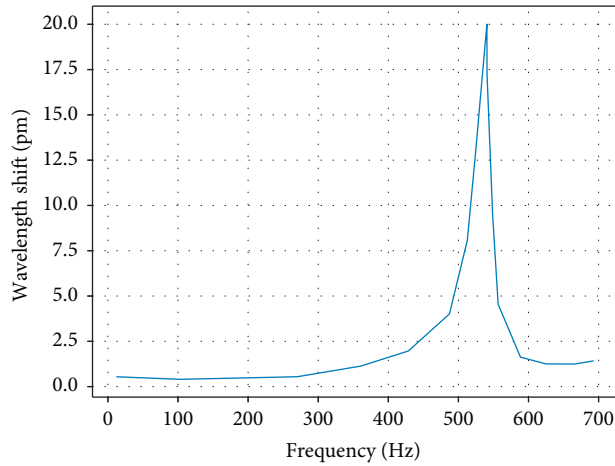


FIGURE 9: Amplitude frequency response curve of sensor.

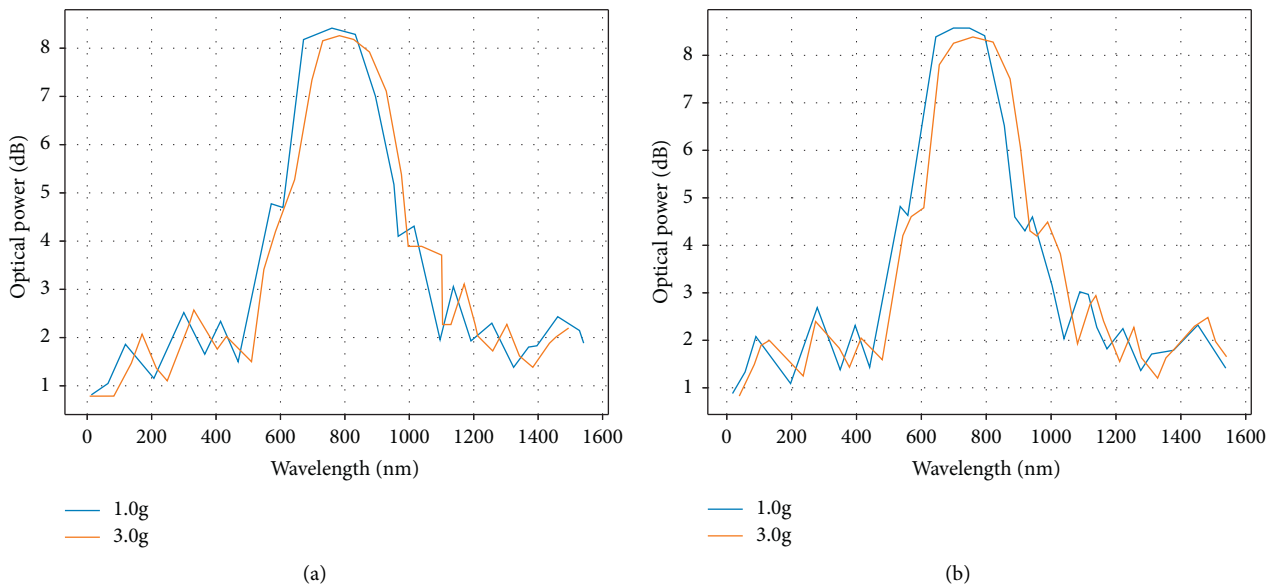


FIGURE 10: Spectra of short grating at different frequencies.(a) 90 Hz; (b) 350 Hz.

To verify the amplitude-frequency characteristics of the sensor, the maximum drift of the central wavelength of the sensor was investigated under certain conditions of acceleration, corresponding to different frequencies. The maximum value of the centre wavelength of the sensor was recorded and the curve is shown in Figure 9. It can be seen that the inherent frequency of the sensor at this acceleration is approximately 543.9 Hz, which is in good agreement with the simulated result of 568.6 Hz. The slight deviation in frequency is due to the sensor assembly error and other reasons.

The spectrograms of the sensor were measured at different frequencies and acceleration excitations. The spectra of the sensor are shown in Figure 10 for external excitation frequencies of 90 Hz and 350 Hz and accelerations of 1.0 g and 3.0 g respectively. It can be seen that the FBG spectrum did not broaden with increasing acceleration, indicating that the chirp phenomenon was effectively avoided.

The acceleration response of the sensor was tested at a certain frequency. The acceleration response of the sensor was tested at a frequency of 300 Hz with an external excitation of 0.2 g. The results showed that the acceleration and wavelength shift of the sensor were quasi-linear, with a linear fit of 99% or more and good linearity; the sensitivity of the sensor was 6.7 pm/g; the repeatability error of the sensor was about 1.7%, with good repeatability

5.2. Comparison of Whether Damage Is Identified or Not. In Scheme 1 for determining whether damage is present, as shown in Figure 11, the accuracy of both CNN1 and CNN2 is below 70% and the accuracy of LSTM is over 95%, so only LSTM can meet the requirements in this step of damage identification. The accuracy of CNN2 is improved by only 2.23% over CNN1, while LSTM is improved by 35.42% over CNN1, which indicates that in

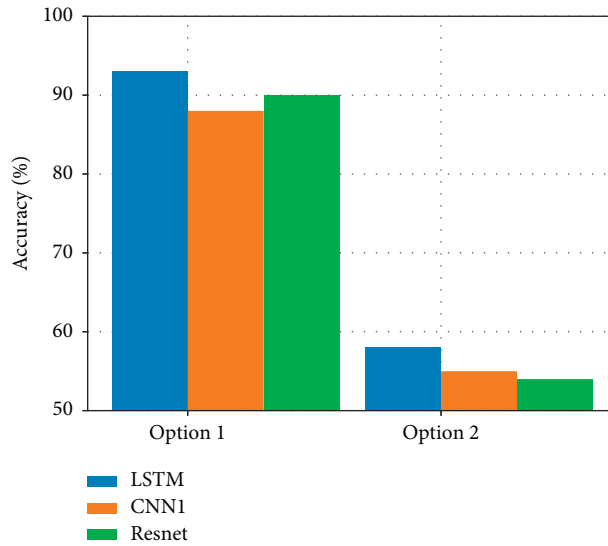


FIGURE 11: Accuracy of whether or not an injury was sustained.

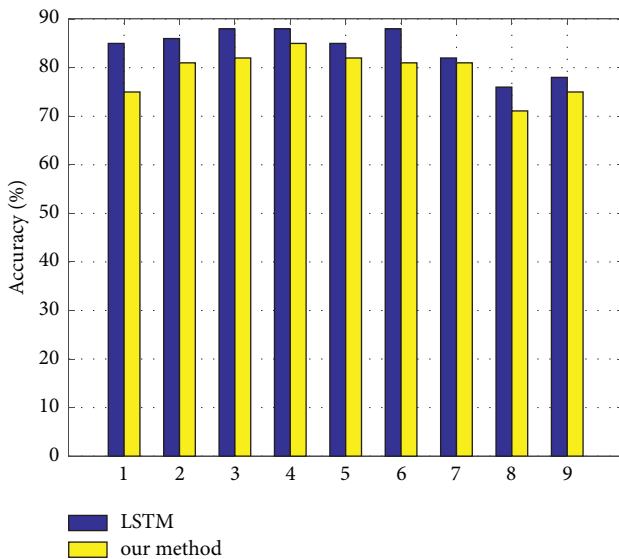


FIGURE 12: Accuracy of damage localization by location.

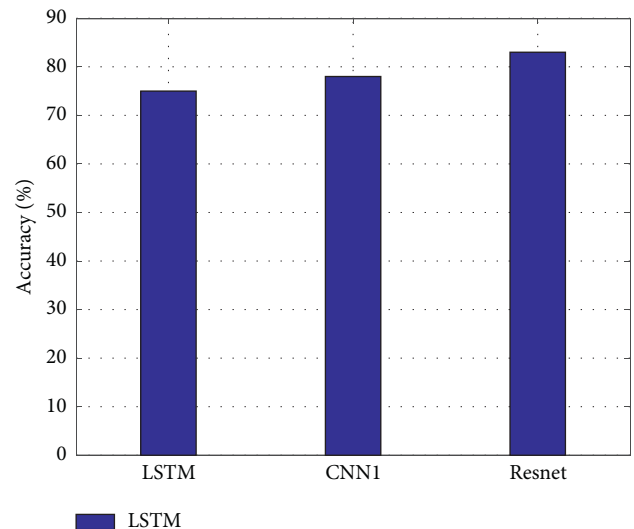


FIGURE 13: Overall average accuracy of injury localization.

Scheme 1, the The increase in sample data is not critical but the method of recognition, and therefore the LSTM method is more appropriate than the CNN method in Scenario 1.

In Scheme 2, as shown in Figure 11, the accuracy of all three methods is relatively high, so all three methods are possible. However, the recognition in Scheme 2 is more tedious and has to be divided into 10 to identify each one.

Combining the accuracy of the three methods of Option 1 and Option 2, it is more appropriate to adopt Option 1 and use the LSTM method when determining whether the damage is.

In the recognition of damage localization, as shown in Figures 12 and 13, the accuracy of damage localization at each location and the overall average accuracy are LSTM > CNN2 > CNN1, where the accuracy of both CNN1

and CNN2 is about 75, while the accuracy of LSTM can reach 91.76%, among which only LSTM meets the requirements.

## 6. Conclusions

Through the comparative experiments in this paper, it can be seen that these two methods effectively alleviate the AlexNet network’s overfitting problem. At this point, the improved convolutional neural network algorithm has effectively solved the problem of framed building vandalism. The evaluation of the entire postearthquake frame building will be carried out quickly. Experimentation with the number of parameters involved in training shows that with the feature extractor training approach, the model only needs to retrain the function of the last fully-connected layer.

## Data Availability

The experimental data used to support the findings of this study are available from the corresponding author upon request.

## Conflicts of Interest

The authors declared that they have no conflicts of interest regarding this work.

## References

- [1] O. Abdeljaber, O. Avci, S. Kiranyaz, M. Gabbouj, and D. J. Inman, "Real-time vibration-based structural damage detection using one-dimensional convolutional neural networks," *Journal of Sound and Vibration*, vol. 388, pp. 154–170, 2017.
- [2] S. Kiranyaz, O. Avci, O. Abdeljaber, T. Ince, M. Gabbouj, and D. J. Inman, "1D convolutional neural networks and applications: a survey," *Mechanical Systems and Signal Processing*, vol. 151, Article ID 107398, 2021.
- [3] Y.-J. Cha, W. Choi, and O. Büyüköztürk, "Deep learning-based crack damage detection using convolutional neural networks," *Computer-Aided Civil and Infrastructure Engineering*, vol. 32, no. 5, pp. 361–378, 2017.
- [4] C. Li and M. Wand, "Combining Markov random fields and convolutional neural networks for image synthesis," in *Proceedings of the IEEE Conference on Computer Vision and Pattern Recognition*, pp. 2479–2486, San Juan, PR, USA, June, 2016.
- [5] X. Tao, D. Zhang, W. Ma, X. Liu, and D. Xu, "Automatic metallic surface defect detection and recognition with convolutional neural networks," *Applied Sciences*, vol. 8, no. 9, p. 1575, 2018.
- [6] O. Abdeljaber, O. Avci, M. S. Kiranyaz, B. Boashash, H. Sodano, and D. J. Inman, "1-D CNNs for structural damage detection: verification on a structural health monitoring benchmark data," *Neurocomputing*, vol. 275, pp. 1308–1317, 2018.
- [7] K. Wang, X. Wang, L. Lin, M. Wang, and W. Zuo, "3D human activity recognition with reconfigurable convolutional neural networks," in *Proceedings of the 22nd ACM International Conference on Multimedia*, pp. 97–106, New York, NY, USA, 2014, November.
- [8] D. Wu, C. Zhang, L. Ji, R. Ran, H. Wu, and Y. Xu, "Forest fire recognition based on feature extraction from multi-view images," *Traitement du Signal*, vol. 38, no. 3, pp. 775–783, 2021.
- [9] O. Avci, O. Abdeljaber, S. Kiranyaz, M. Hussein, M. Gabbouj, and D. J. Inman, "A review of vibration-based damage detection in civil structures: from traditional methods to Machine Learning and Deep Learning applications," *Mechanical Systems and Signal Processing*, vol. 147, Article ID 107077, 2021.
- [10] Z. Waszczyszyn and L. Ziemiański, "Neural networks in mechanics of structures and materials—new results and prospects of applications," *Computers & Structures*, vol. 79, no. 22–25, pp. 2261–2276, 2001.
- [11] M. Mahdianpari, B. Salehi, M. Rezaee, F. Mohammadimanesh, and Y. Zhang, "Very deep convolutional neural networks for complex land cover mapping using multispectral remote sensing imagery," *Remote Sensing*, vol. 10, no. 7, p. 1119, 2018.
- [12] D. Cho, Y.-W. Tai, and I. Kweon, "Natural image matting using deep convolutional neural networks," in *European Conference on Computer Vision*, pp. 626–643, Springer, New York, NY, USA, 2016.
- [13] L. Jing, T. Wang, M. Zhao, and P. Wang, "An adaptive multi-sensor data fusion method based on deep convolutional neural networks for fault diagnosis of planetary gearbox," *Sensors*, vol. 17, no. 2, p. 414, 2017.
- [14] C. V. Dung and L. D. Anh, "Autonomous concrete crack detection using deep fully convolutional neural network," *Automation in Construction*, vol. 99, pp. 52–58, 2019.
- [15] A. Payan and G. Montana, "Predicting Alzheimer's disease: a neuroimaging study with 3D convolutional neural networks," 2015, <https://arxiv.org/abs/1502.02506>.
- [16] R. Oullette, M. Browne, and K. Hirasawa, "Genetic algorithm optimization of a convolutional neural network for autonomous crack detection," vol. 1, pp. 516–521, in *Proceedings of the 2004 congress on evolutionary computation (IEEE Cat. No. 04TH8753)*, vol. 1, pp. 516–521, IEEE, Portland, OR, USA, 2004, June.
- [17] Y. Xue and Y. Li, "A Fast detection method via region-based fully convolutional neural networks for shield tunnel lining defects," *Computer-Aided Civil and Infrastructure Engineering*, vol. 33, no. 8, pp. 638–654, 2018.
- [18] J. Kawahara, C. J. Brown, S. P. Miller et al., "BrainNetCNN: convolutional neural networks for brain networks; towards predicting neurodevelopment," *NeuroImage*, vol. 146, pp. 1038–1049, 2017.
- [19] M. Sahin and R. A. Sheno, "Quantification and localisation of damage in beam-like structures by using artificial neural networks with experimental validation," *Engineering Structures*, vol. 25, no. 14, pp. 1785–1802, 2003.
- [20] X. Yang, H. Sun, X. Sun, M. Yan, Z. Guo, and K. Fu, "Position detection and direction prediction for arbitrary-oriented ships via multitask rotation region convolutional neural network," *IEEE Access*, vol. 6, Article ID 50839, 2018.
- [21] S. H. Lee, C. S. Chan, P. Wilkin, and P. Remagnino, "Deep-plant: plant identification with convolutional neural networks," in *Proceedings of the 2015 IEEE International Conference on Image Processing (ICIP)*, pp. 452–456, IEEE, Quebec City, QC, Canada, 2015, September.



## Research Article

# Studying the Coupling and Coordination of Regional Economic and University Development Levels Based on a Deep Learning Model

Yongfeng Bai <sup>1,2</sup>, Zaixun Song,<sup>2</sup> and Weimiao Cui<sup>3</sup>

<sup>1</sup>Office of Academic Research, Handan University, Hebei, Handan, 056005, China

<sup>2</sup>Department of Business Administration, Woosuk University, Jeonju, 565701, Republic of Korea

<sup>3</sup>Administration Office, Handan University, Handan 056005, Hebei, China

Correspondence should be addressed to Yongfeng Bai; [baiyongfeng@hdc.edu.cn](mailto:baiyongfeng@hdc.edu.cn)

Received 24 February 2022; Revised 25 March 2022; Accepted 28 March 2022; Published 11 April 2022

Academic Editor: Hangjun Che

Copyright © 2022 Yongfeng Bai et al. This is an open access article distributed under the Creative Commons Attribution License, which permits unrestricted use, distribution, and reproduction in any medium, provided the original work is properly cited.

Universities are not only an important foundation of China's education but also have an important role in promoting the development of the local economy. The interaction between local universities and regional economic development is very significant, and the two promote each other and develop symbiotically. This paper designs a coupled coordination model based on autoencoder (AE) for the development level of regional economy and higher education institutions, and this paper analyses the mutual needs between local universities and regional economy in terms of talent demand, technology research, and material base puts forward the potential advantages of symbiosis, points out the weaknesses and shortcomings in the current symbiotic development, provides a basis for the symbiotic development of the two, and provokes thoughts to promote the symbiosis and win-win situation between the two.

## 1. Introduction

Local universities and higher education institutions directly under the Ministry of Education are both educational institutions that train talents for the society and also have the responsibilities of conducting scientific research, providing social services and realising cultural heritage and innovation, which are essentially providing services for the society [1]. In addition to providing social services to the local community, local universities also contribute to the development of the regional economy. The development of the regional economy also provides a broader development space for the further expansion of local universities [2]. At present, there are still problems of missing mechanism in the process of good interaction development between many local colleges and universities and regional economic development. In this current situation, it is significant to discuss how local universities can seek the key point for the symbiotic development of the two based on the actual local conditions [3].

Local universities refer to general higher education institutions that are affiliated to provinces, autonomous regions, municipalities directly under the central government, and special zones in Hong Kong and Macao and are mainly supported by local finances and allocated funds by local administrative departments [4, 5]. In this management system, the main body of local universities' operation and investment is mainly the local government departments. The meaning of regional economy is actually a geographical concept, which refers to the comprehensive economic development of the region [6]. Symbiosis theory mainly refers to the existence of different kinds of things that live together due to the existence of some kind of real-life connection. Symbiosis theory began as a biological theory, but when viewed from the perspective of the social sciences, the concept of symbiosis theory becomes a social form in which different types of material objects cooperate amicably with each other and thus achieve a mutually beneficial development [7]. Local universities and regional economy form

an interdependent and cogrowing relationship due to their natural geographical location [8].

Talent is always the most dynamic and valuable element in economic development. For the regional economy to achieve further development, it must have a stable source of supply of comprehensive and high-quality talents [9]. Although there are many sources of talent, they are mainly local universities. In addition to the advantages of geographical location, local universities have the advantage of talent training that is targeted to meet the actual needs of local talent [10]. At the same time, in order to achieve economic transformation and promote the upgrading and adjustment of industrial structure, the demand for comprehensive talents with excellent vocational skills is constantly increasing [11].

One of the key points of the role of local universities in promoting regional economic construction is that they can provide technical support for local industrial restructuring and enterprise project development [12]. Enterprises provide a platform to support the transformation of knowledge achievements of universities, and universities provide a technical basis for the development of enterprises. This is also a key node for local universities to establish ties with local enterprises [13]. Universities differ according to their actual situation, with undergraduate institutions focusing on technical support and higher education institutions focusing on service support. Cases abound where universities at home and abroad have established close cooperation with local enterprises to effectively promote progress in research, achieve technological innovation, and contribute to regional economic development, such as the Industrial Liaison Office at Cambridge University [14]. On the one hand, these institutions find markets for the research achievements of university teachers and researchers; on the other hand, they introduce the topics and business dynamics of enterprises to university teachers and researchers, playing the role of "matchmaking." At present, many higher vocational institutions in China, such as Changzhou Information Vocational Technology College, have built a key laboratory for intelligent technology of high-end manufacturing equipment on campus [15].

## 2. Analysis of Universities for Regional Economic Development

Local universities are not only a source of talent as well as a technical basis for regional economic construction but they are also able to provide industrial creation for local economic construction. By combining new technologies with practical social practice capabilities with practical conditions, universities can serve as technical support for new high-tech enterprises and promote the development of local high-tech industries, thus promoting industrial restructuring and driving regional economic growth. By establishing cooperation with local enterprises, local universities realise the organic combination of production, learning, and research, while the government provides support and a platform for independent innovation and employment for

students [16]. By establishing science and technology parks, the government has involved local universities and local enterprises in the research and development of various new technologies and the transformation of their achievements, forming a complete chain of cooperation among industry, university, and research, promoting the development of high-tech industries and facilitating the process of industrial upgrading and restructuring.

For local universities to gain further development, they need not only sufficient financial support but also the support of various social resources. Among them, the support from the local government is very important. The key to local government investment is whether it can play a role in promoting local economic development [17].

A solid material foundation is the key to the sustainable development of universities, while another basis for the development of local universities is to meet the changing needs of regional economic development. Both of these are external manifestations of local economic development. It is important to constantly bring into play the advantages of policies to meet the financial support needed for the development of universities and to improve their research strength [18].

Due to the vast territory, the level of economic development and the industrial structure of different regions of the country vary greatly, and the focus of economic development varies greatly at different times in the same region, which makes the level of demand for talents as well as the type and quantity of talents different [19]. At the same time, the country is currently in a critical period of industrial restructuring, and local universities are therefore adjusting their development strategies to serve society. With the upgrading and optimisation of the regional industrial structure, the direction of talent training in local universities will also be adjusted, and the main body will match the regional talent structure adjustment. For example, during the current rapid development of e-commerce, especially during the epidemic, community e-commerce, live-streaming with goods and other e-commerce models provide business opportunities for local economic development, and the demand for related e-commerce talents has suddenly increased [20].

## 3. A Model of Regional Economic Growth and University Coupling

*3.1. Coupled Coordination Models.* With the help of physical capacity coupling based on the orderly combination degree of the two subsystems, so as to obtain the coupling model as  $C_n = (u_1, u_2, \dots, u_m) \prod (u_i + u_j) 1/n$ , where the coupling degree value  $C \in [0, 1]$ . Thirdly, according to the specific coupling situation, we can judge that when  $C=0$ , the coupling degree between regional economy and university factors is extremely small, and economic growth and universities are in a state of mutual incoherence. When  $C \in (0, 0.3]$ , the regional economy is in a state of low uneven coupling with universities. When  $C \in (0.3, 0.5]$ , the coupling is in the collapsing phase.

**3.2. Coupled Simulation Index Analysis.** The analysis of the cubic function model and coupling indices of university indicators and economic indicators in each province of China can determine that the three current indicators of industrial emissions of waste water, industrial solid waste, and industrial emissions of exhaust gases in China are generally on a decreasing trend. Firstly, the coupling index of typical university indicators is relatively good, in which the overall decrease of industrial waste water emissions can be explained by the increasing emphasis on environmental protection in the growth of GDP per capita in China, and it is also related to the increasingly strict requirements of environmental protection laws in China. Secondly, emissions are still a serious problem in China, with vehicle emissions and industrial production emissions remaining high in recent years, and the coupling between this indicator and universities is extremely low. Thirdly, the problem of seasonal universities is still very prominent, and the problem of pollution in our winter climate universities is serious, which also has a very general relationship with economic development.

#### 4. Denoising Automatic Coder

**4.1. AE.** AE is a three-layer unsupervised neural network [12], which is divided into two parts: the encoding network and the decoding network, as shown in Figure 1.

Given an unlabeled sample set  $\{\mathbf{x}^m\}_{m=1}^M$  of mechanical health conditions, the coding network transforms each training sample  $\mathbf{x}^m$  into a coding vector  $\mathbf{h}^m$  by means of a coding function  $f_\theta$ .

$$\mathbf{h}^m = f_\theta(\mathbf{x}^m) = s_f(W\mathbf{x}^m + b). \quad (1)$$

Then, the encoding vector  $\mathbf{h}^m$  is inversely transformed into a reconstructed representation  $\hat{\mathbf{x}}^m$  of  $\mathbf{x}^m$  by the decoding function  $g_{\theta'}$ , such as (2) and (3).

$$\begin{aligned} \hat{\mathbf{x}}^m &= g_{\theta'}(\mathbf{h}^m) \\ &= s_g(W\mathbf{h}^m + d), \end{aligned} \quad (2)$$

$$L(x, \hat{x}) = \frac{1}{M} \|x - \hat{x}\|^2. \quad (3)$$

The variation in working conditions due to complex tasks lead to fluctuations in the properties of the samples under the same health conditions, so the autoencoder needs to be given certain constraints so that it learns a robust feature representation. The DAE solves this problem by reconstructing sample data containing noise to solve this problem [13].

Firstly, random noise is added to the sample  $\mathbf{x}^m$  according to  $q_D$  the distribution [14] to make it a noisy sample  $x^{m'}$ , such as

$$x^m \sim q_D(x^{m'} | x^m), \quad (4)$$

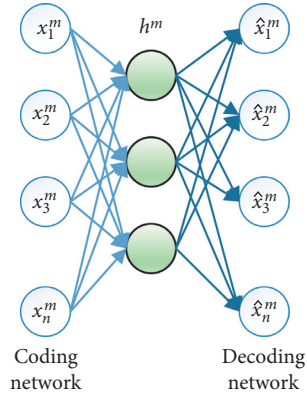


FIGURE 1: Model structure of AE.

where  $q_D$  is the binomial random hidden noise.

The DAE is then trained by optimising the following objective function such as

$$\arg \min_{\theta, \theta'} L(\mathbf{x}^m, g_{\theta'}(f_\theta(\mathbf{x}^{m'}))). \quad (5)$$

#### 4.2. Pretraining and Fine-Tuning of Deep Neural Networks.

The core of the deep neural networks, hereinafter referred to as (DNN) pretraining algorithm is the unsupervised stacking of multiple DAE layers to form a DNN hidden layer structure, as shown in Figure 2 [14–16]. Firstly, sample  $\mathbf{x}^m$  is used to train DAE<sub>1</sub> and  $\mathbf{x}^m$  is encoded as (6) and (7).

$$h_1^m = f_{\theta_1}(\mathbf{x}^m), \quad (6)$$

$$h_N^m = f_{\theta_N}(h_{N-1}^m). \quad (7)$$

Pretraining connects multiple DAEs to each other to form a DNN hidden layer structure to achieve layer-by-layer extraction of fault information [17]. After pretraining, the output layer with classification function is added in order to monitor the economic health of the diagnosed area, and the DNN parameters are fine-tuned using the BP algorithm. The output of the DNN is represented as

$$\mathbf{y}^m = f_{\theta_{N+1}}(\mathbf{h}_N^m), \quad (8)$$

where  $\theta_{N+1}$  is the parameter of the output layer. The health condition type of  $\mathbf{x}^m$  is set to  $\mathbf{d}^m$  and the DNN fine-tunes by minimising  $\phi_{\text{DNN}}(\Theta)$  such as

$$\phi_{\text{DNN}}(\Theta) = \frac{1}{M} \sum_m L(\mathbf{y}^m, \mathbf{d}^m), \quad (9)$$

where  $\Theta$  is the set of parameters of the DNN and  $\Theta = \{\theta_1, \theta_2, L, \theta_{N+1}\}$ .

The fine-tuned DNN optimises the representation of regional economic health information and provides the ability to monitor and diagnose regional economic health conditions.

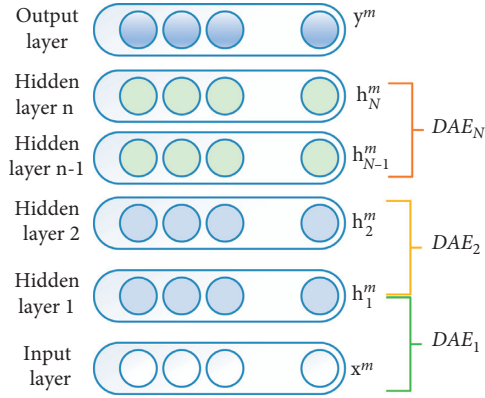


FIGURE 2: Pretraining process of DNN.

**4.3. Regional Economic and University Coupling Analysis.** Universities are harsh and volatile, so the vast amount of data collected by their monitoring systems contain a wealth of variable fault information about the various components of the regional economy. Traditional intelligent diagnostic methods rely on signal processing and diagnostic experience to extract features from the regional economy signals and use machine learning models for intelligent diagnosis. However, signal processing-based feature extraction methods tend to extract features with a deep understanding of the signal characteristics and are “inadequate” to extract typical features reflecting the health of the regional economy in the face of the massive signals of the regional economy with alternating working conditions, heavily coupled fault information, and unknown and variable patterns. In addition, traditional methods use shallow models to identify regional economic health conditions, resulting in poor monitoring and diagnostic capabilities and generalisation performance [18–20].

This paper combines the characteristics of regional economic big data with the advantages of deep learning and proposes a deep learning-based method for monitoring the health of regional economies. The method achieves the organic combination of unsupervised learning and supervised learning and can simultaneously complete the adaptive extraction of big data fault features and the identification of regional economic health, overcoming the shortcomings of traditional methods in feature extraction and fault identification. The method flow is shown in Figure 3, and the steps can be summarized as follows.

Firstly, the frequency domain signal of the regional economy, i.e., the spectrum, is obtained and the spectrum is used as the training sample; secondly, the number of hidden layers of the DNN,  $N$ , is determined and  $N$  DAEs are trained layer by layer in an unsupervised manner, i.e., the output of each DAE is used as the input of the next DAE until the training of  $N$  DAEs is completed; then, the output layer is added and the DNN parameters are fine-tuned according to the type of health condition of the sample to complete the training of the DNN; finally, the DNN is used to monitor and diagnose the health condition of the regional economy [21–23].

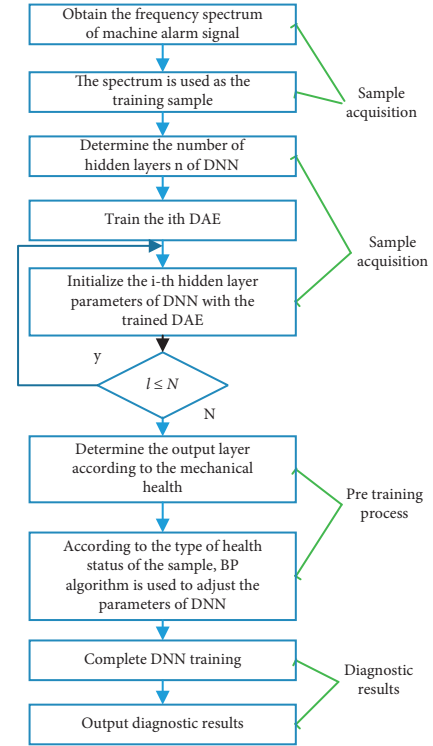


FIGURE 3: Flow chart analysis of the proposed method.

## 5. Empirical Analysis

**5.1. Coupling.** The coupling degree of coordinated development of regional economy and universities is in the fly down stage in all provinces, except Jiangsu, Guangdong, Shandong, and Zhejiang, which are in the grinding stage, and the level of coupling is relatively low, which fully indicates that there is still much room for improvement in terms of improving universities in each province. As shown in Figure 4, the coupling degree of each region shows obvious regional differences. Provinces with low coupling degree account for about 55% of the total number of coupling types in the country. Coupling coordination is also uneven in spatial distribution, usually the regional economy in the more economically developed areas in the south has a higher coupling degree with colleges and universities, while the coupling degree between the economy and colleges and universities in relatively economically backward areas is lower [24–26]. Thirdly, provinces with faster economic growth are more sensitive to the influence of colleges and universities, and some provinces, though with faster economic development, also have more serious problems for colleges and universities, even beyond the carrying capacity of natural colleges and universities, and ecological colleges and universities are not yet able to complete full absorption of the problems brought about by the influence of colleges and universities due to economic growth.

**5.2. Spatial Pattern Characterisation.** There is also a significant correlation between the regional economic development and the coupling degree of universities in the spatial pattern; as shown in Figure 5, each year the regional

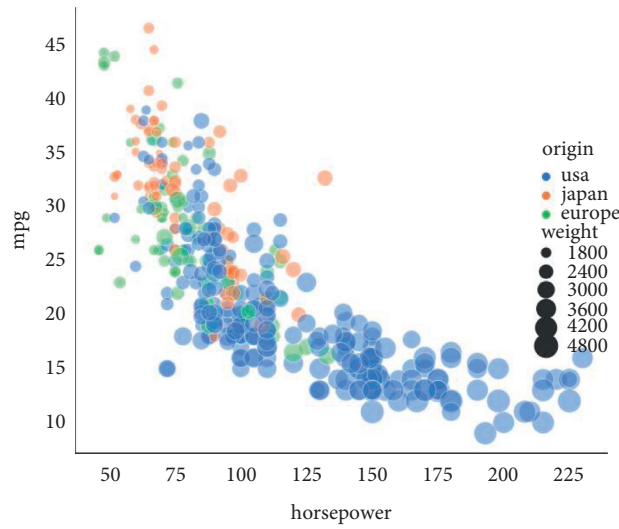


FIGURE 4: Coupling.

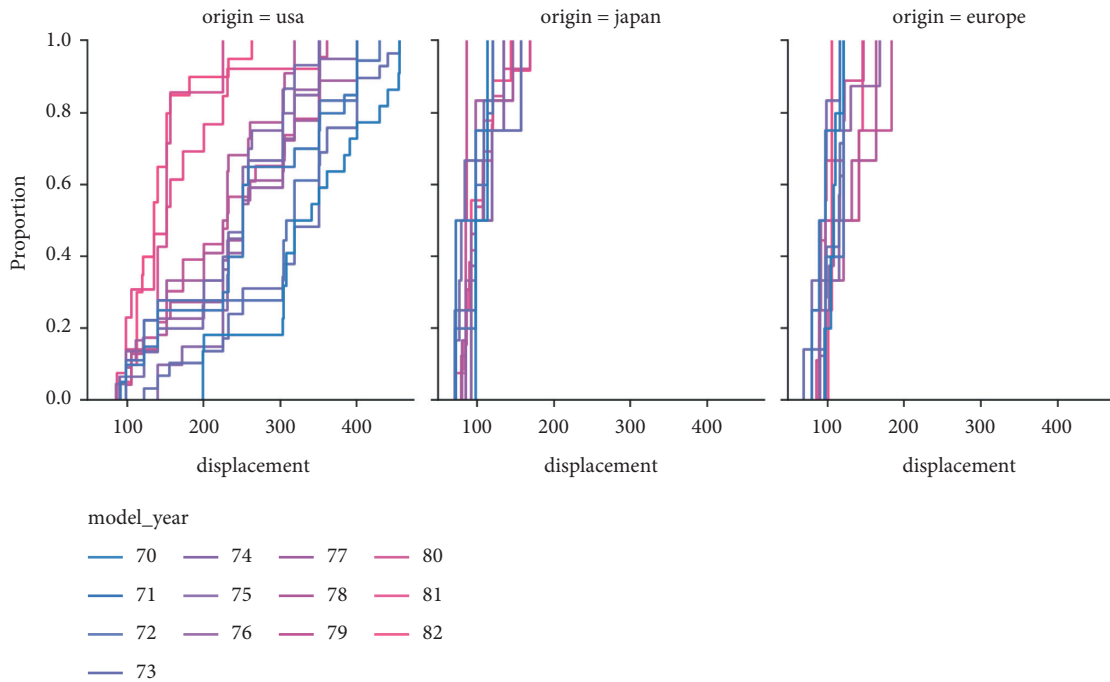


FIGURE 5: Spatial pattern characterization for each year.

coordination is higher compared to the national inland cities, but there is no significant advantageous gathering area, especially the coordination of economy and universities in the central and western regions is the main direction of future research [7]. The state has taken systematic supportive measures to break the unbalanced pattern in the central and western regions, thus the relationship between regional economic indicators and universities is showing a steady increase year by year. In response to the above problems, a coordinated development protection strategy of economy and universities should be adopted to continuously enhance the friction between universities and economy so

that the two can develop in a coordinated and sustainable direction and achieve the goal of friendly development of economy and universities.

## 6. Conclusions

For local universities, only by fully establishing a symbiotic relationship with the regional economy and insisting on mutual benefit and win-win situation can we achieve further development of both. As a talent training base, local universities should strengthen exchanges and cooperation with local enterprises and institutions, deepen the basis of

cooperation, and realise resource sharing. At the same time, the local government should also strengthen the financial and policy support of resources to enhance the awareness of local universities in serving the regional economy, so as to truly achieve sustainable symbiotic development. In the process of development, universities attach too much importance to the circle of land, people, and professions and do not know enough about their social service function and the importance of win-win cooperation with regional economic development. In the process of running the university, the traditional teaching mode is still the main one, and the large and comprehensive construction of disciplines is pursued excessively. The scientific research of many disciplines is detached from the reality, and awards are the focus, ignoring the social foundation, and all scientific research work premised on various fame and profit demands or materialistic demands is lacking in connotation, and discipline construction should be carried out on the premise of serving society, and scientific research innovation should be promoted on the basis of serving local construction.

### Data Availability

The experimental data used to support the findings of this study are available from the corresponding author upon request.

### Conflicts of Interest

The authors declare that they have no conflicts of interest regarding this work.

### Acknowledgments

This work was supported by the Handan Science and Technology Research and Development Plan (No. 21422304154).

### References

- [1] M. Batty, K. W. Axhausen, F. Giannotti et al., "Smart cities of the future," *The European Physical Journal - Special Topics*, vol. 214, no. 1, pp. 481–518, 2012.
- [2] H. W. Kang and H. B. Kang, "Prediction of crime occurrence from multi-modal data using deep learning," *PLoS One*, vol. 12, no. 4, Article ID e0176244, 2017.
- [3] W. Li, H. Fu, L. Yu, and A. Cracknell, "Deep learning based oil palm tree detection and counting for high-resolution remote sensing images," *Remote Sensing*, vol. 9, no. 1, p. 22, 2017.
- [4] T. Knudsen and K. Srikanth, "Coordinated e," *Administrative Science Quarterly*, vol. 59, no. 3, pp. 409–441, 2014.
- [5] H. Che and J. Wang, "A collaborative neurodynamic approach to global and combinatorial optimization," *Neural Networks*, vol. 114, pp. 15–27, 2019.
- [6] H. Che, C. Li, X. He, and T. Huang, "A recurrent neural network for adaptive beamforming and array correction," *Neural Networks*, vol. 80, pp. 110–117, 2016.
- [7] M. Jamshidi, A. Lalbakhsh, J. Talla et al., "Artificial intelligence and COVID-19: deep learning approaches for diagnosis and treatment," *IEEE Access*, vol. 8, Article ID 109595, 2020.
- [8] B. Asheim, "Differentiated knowledge bases and varieties of regional innovation systems," *Innovation: The European Journal of Social Science Research*, vol. 20, no. 3, pp. 223–241, 2007.
- [9] B. T. Asheim and L. Coenen, "Contextualising regional innovation systems in a globalising learning economy: on knowledge bases and institutional frameworks," *The Journal of Technology Transfer*, vol. 31, no. 1, pp. 163–173, 2006.
- [10] W. Lamine, S. Mian, A. Fayolle, M. Wright, M. Klofsten, and H. Etzkowitz, "Technology business incubation mechanisms and sustainable regional development," *The Journal of Technology Transfer*, vol. 43, no. 5, pp. 1121–1141, 2018.
- [11] J. Liu, Y. Pan, M. Li et al., "Applications of deep learning to MRI images: a survey," *Big Data Mining and Analytics*, vol. 1, no. 1, pp. 1–18, 2018.
- [12] S. J. Fong, G. Li, N. Dey, R. G. Crespo, and E. Herrera-Viedma, "Composite Monte Carlo decision making under high uncertainty of novel coronavirus epidemic using hybridized deep learning and fuzzy rule induction," *Applied Soft Computing*, vol. 93, Article ID 106282, 2020.
- [13] D. G. Brown, R. Riolo, D. T. Robinson, M. North, and W. Rand, "Spatial process and data models: toward integration of agent-based models and GIS," *Journal of Geographical Systems*, vol. 7, no. 1, pp. 25–47, 2005.
- [14] L. An, "Modeling human decisions in coupled human and natural systems: review of agent-based models," *Ecological Modelling*, vol. 229, pp. 25–36, 2012.
- [15] C. Ansell, "The networked polity: regional development in Western Europe," *Governance*, vol. 13, no. 2, pp. 279–291, 2000.
- [16] Y. Wang, L. Sun, and S. Subramani, "Classifying arrhythmias based on imbalanced sensor data," *KSII Transactions on Internet & Information Systems*, Jul.vol. 15, no. 7, pp. p2304–2320, 2021.
- [17] L. Sun, Q. Yu, D. Peng, S. Subramani, and X. Wang, "Fogmed: a fogbased framework for disease prognosis based medical sensor data streams," *Computers, Materials & Continua*, vol. 66, no. 1, pp. 603–619, 2021.
- [18] Z. Zhengwan, Z. Chunjong, L. I. Hongbing, and X. Tao, "Multipath transmission selection algorithm based on immune connectivity model," *Journal of Computer Applications*, vol. 40, no. 12, p. 3571, 2020.
- [19] A. Zlotnik, L. Roald, S. Backhaus, M. Chertkov, and G. Andersson, "Coordinated scheduling for interdependent electric power and natural gas infrastructures," *IEEE Transactions on Power Systems*, vol. 32, no. 1, pp. 600–610, 2016.
- [20] J. Zhang and J. Peck, "Variegated capitalism, Chinese style: regional models, multi-scalar constructions," *Regional Studies*, vol. 50, no. 1, pp. 52–78, 2016.
- [21] B. S. Silvestre, "Capability accumulation, innovation, and technology diffusion: lessons from a Base of the Pyramid cluster," *Technovation*, vol. 34, no. 5-6, pp. 270–283, 2014.
- [22] J. L. Campbell and O. K. Pedersen, "The varieties of capitalism and hybrid success," *Comparative Political Studies*, vol. 40, no. 3, pp. 307–332, 2007.
- [23] Y. Huang, X. Chen, T. Yu, Z. Huang, and F. Gu, "Agricultural remote sensing big data: management and applications,"

*Journal of Integrative Agriculture*, vol. 17, no. 9, pp. 1915–1931, 2018.

- [24] J. Q. James, “Citywide traffic speed prediction: a geometric deep learning approach,” *Knowledge-Based Systems*, vol. 212, Article ID 106592, 2021.
- [25] C. Wang, J. Zhou, B. Xiao et al., “Uncertainty estimation for stereo matching based on evidential deep learning,” *Pattern Recognition*, vol. 124, Article ID 108498, 2021.
- [26] S. Collinson and G. Gregson, “Knowledge networks for new technology-based firms: an international comparison of local entrepreneurship promotion,” *R & D Management*, vol. 33, no. 2, pp. 189–208, 2003.

## Research Article

# Regional Tourism Economic Forecasting Model Based on GM Grey Forecasting Method

Bin Li<sup>1</sup> and Jing Gao <sup>2</sup>

<sup>1</sup>Culinary and Food College, Zhengzhou Tourism College, Zhengzhou 451464, China

<sup>2</sup>Business Administration School, Guangxi University, Nanning 530004, China

Correspondence should be addressed to Jing Gao; 2102402004@st.gxu.edu.cn

Received 23 February 2022; Accepted 15 March 2022; Published 7 April 2022

Academic Editor: Hangjun Che

Copyright © 2022 Bin Li and Jing Gao. This is an open access article distributed under the Creative Commons Attribution License, which permits unrestricted use, distribution, and reproduction in any medium, provided the original work is properly cited.

On the basis of regional tourism economic development, this paper uses the entropy method and the coupling coordination model to analyse the comprehensive development level and the degree of coupling coordination between tourism and regional development and uses the GM (1, 1) grey prediction model to forecast the degree of coupling coordination between tourism and regional development in China in the next five years, based on the data related to tourism and regional development in China from 1996 to 2015. The results show that the degree of coupling and coordination between tourism and regional development is steadily increasing, with the coupling level moving from low level coupling to antagonistic stage and the coupling coordination level reaching from low level disorder to good level coordination.

## 1. Introduction

Since China's 18th National Congress, the Chinese government has clearly put forward that "tourism is an important engine for stable growth, an important grasp of people's livelihood, an important support for the construction of ecological civilisation and an important carrier of prosperous culture," and the important strategic position of tourism in the national economy and social development has become more prominent [1]. Territorial tourism is the overall strategy of China's tourism development in the new era and is a new regional development concept and model that uses tourism as a regional advantageous industry in the era of mass tourism to drive and promote coordinated economic and social development [2]. Therefore, the academic research on the relationship between tourism industry and regional development in the context of all-area tourism has certain theoretical guidance significance for the implementation of all-area tourism strategy [3].

Before the 1990s, scholars mainly used traditional quantitative methods to forecast tourism demand and tourist flows, where quantitative studies used causal analysis [4] in addition to econometric methods such as moving

average models and ARMA models [5]. Such methods were mainly achieved by analysing the influencing factors of tourism flows, with the disadvantage that the influencing factors are difficult to determine and too costly. After the 1990s, with the emergence and development of artificial intelligence methods and their excellent performance in the field of forecasting, scholars also began to try to introduce such methods into the forecasting of tourism traffic and tourism revenue, the most used of which are mainly BP neural networks, grey system GM (1, 1) models, and multifactor dynamic coarse forecasting models in rough set theory, genetic algorithms, etc. [6]. There is no shortage of comparisons between the results obtained using traditional research methods and artificial intelligence methods, but the final conclusions show the significant advantages of artificial intelligence methods in the field of forecasting. Because of the unique advantages of AI methods in forecasting, when the support vector machine method was introduced and performed well in the forecasting field, scholars were quick to apply it to the study of tourism demand and tourism traffic forecasting as well [7].

In support vector machine methods, the core part is the parameter selection problem, which is essentially an



optimisation search process. Before the birth of evolutionary algorithms, scholars did not find an optimal way to deal with parameter selection. With the emergence and rise of intelligent population algorithms, more and more scholars have discovered its outstanding performance in dealing with optimisation problems. Therefore, some scholars have also tried to use population intelligence algorithms, such as particle swarm algorithms and genetic algorithms, to deal with the parameter selection problem in support vector machines when doing prediction work using support vector machine methods [8].

In this paper, the GM algorithm is applied to the parameter optimisation of support vector regression and applied to regional tourism forecasting. Accurate forecasting of regional tourism traffic is beneficial not only to the management department in providing reasonable guidance on the operation and management of scenic spots, but also to the regional government in formulating relevant supportive policies and driving the overall development of the national economy with the development of tourism as the leading industry; and accurate forecasting of regional tourism revenue can also provide complete data support to the local government in formulating and improving tourism economic policies [9].

## 2. Related Work

The interaction between tourism and regional development has always been a hot content of academic research. Foreign research has started earlier and the relevant studies are more mature, mainly focusing on the interaction between tourism and economy and environment. Reference [10] has analysed the influence mechanism between tourism activities and ecological environment. The empirical analysis of tourism and economic growth concluded that there is an uneven relationship between tourism and economic growth in Korea [11]. Reference [12] used a comparative analysis to analyse the impact of energy and environment on regional development in China and the United States from the perspective of sustainable development.

A comprehensive analysis of the environmental conditions of tourism destinations was conducted, and it was concluded that tourism development has both positive and negative effects on the ecological environment [13]. Reference [14] proposes a method to quantitatively measure the contribution of tourism to regional economic development, using theories such as tourism economics and input-output analysis. In [15] using a panel analysis of 254 prefecture-level cities, it was verified that the development of tourism plays an important role in driving the development of the tertiary industry and narrowing the regional development gap. An in-depth study of the degree of coordination between tourism and the ecological environment in China was carried out based on principal component analysis [16]. Reference [17] analysed the degree of coordination between tourism and regional economy and its influencing factors in 17 cities of Shandong Province using the coupling coordination model and grey correlation analysis. Reference [18] analysed the mechanism of the interaction between tourism,

economy and ecological environment, and conducted an empirical study on the coastal areas of Jiangsu provinces and cities along the Yangtze River Economic Belt and Turpan using the coupled coordination model.

In general, domestic and foreign research on the relationship between tourism and regional development has mostly focused on three aspects: tourism and economy, tourism and ecological environment, and tourism-economy-ecological environment, without considering the region as a whole in a systematic way, and the content of the research has not taken into account the impact of tourism activities on social progress, which is lacking in the context of the new era. The research content does not take into account the impact of tourism activities on social progress and lacks in-depth consideration of the relationship between tourism and regional development in the context of the new era. In this paper, on the basis of exploring the mechanism of interaction between regional tourism and regional development, we construct a tourism development system and a regional development system from a regional perspective, analyse the comprehensive development level and the degree of coupling and coordination between tourism and regional development using the entropy value method and the coupling and coordination model, and forecast the degree of coupling and coordination between tourism and regional development in China in the next five years using the GM (1, 1) grey prediction model, with a view to providing a basis for it. The GM (1, 1) grey prediction model is used to forecast the degree of coordination between tourism and regional development in China in the next five years, in order to provide reference for the transformation and upgrading of China's tourism industry and the implementation of the regional tourism strategy.

## 3. Mechanisms of the Role of Regional Tourism Development

In essence, regional development and tourism are intrinsically linked, with the two being mutually coupled, mutually conditional, and mutually reinforcing (see Figure 1). Tourism in the region is seen as an industry with regional advantages. By optimising and enhancing industrial, environmental, and social resources, tourism is organically integrated with the region and its resources and industries and shared by tourists and residents, thus promoting coordinated regional development [19].

As a new engine for regional development, regional tourism has become an important driving force for coordinated regional development. In recent years, the country's economic development has entered a new normal, with economic growth rates continuing to decline, ecological and environmental issues coming to the fore, manufacturing, investment, and export pulling, and growth drivers gradually shifting from investment-driven and factor-driven to innovation-driven and consumption-driven. The tourism industry, on the other hand, has continued to grow at a high rate under the new normal, with record numbers of visitors and total tourism revenue, becoming an important means of driving domestic demand. The implementation of an all-area

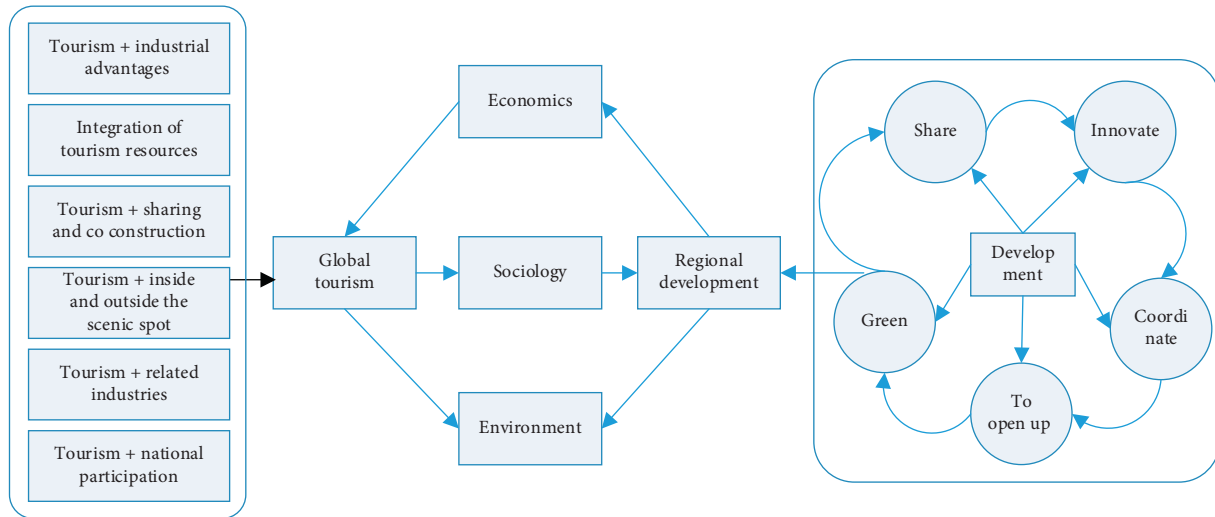


FIGURE 1: Mechanism of interaction and coupling between regional tourism and regional development.

tourism strategy will give full play to the tourism industry’s comprehensive and driving characteristics and promote coordinated regional development.

Regional development is a multilevel complex system, covering economic, social, and environmental aspects, and coordinated regional development can provide strong support and guarantee for the implementation of the all-area tourism strategy. First of all, regional economic development can provide financial guarantee for the development of all-area tourism. Tourism itself has the characteristics of large investment, long cycle, slow benefits, etc., and the whole area of tourism development will expand the scope of tourism from attractions to the entire region, construction areas, construction content, and construction goals to achieve all need sufficient sources of funding. In addition, the region is both a tourist destination and a tourist source. The rapid economic development of the region promotes the income level of local residents, which increases the likelihood that residents will change from potential tourists to real tourists, expanding the market of tourism sources. Secondly, the improvement of the regional social environment creates a good human environment for all-area tourism. The participation of the whole population in all-area tourism can make tourists and local residents more friendly and harmonious, the residents benefit from it, the tourists improve their tourism experience, and the tourist places increase their popularity, achieving a multiwin situation. Finally, the ecological environment is an important guarantee for the development of tourism. A beautiful ecological environment provides rich natural tourism resources for tourism development and becomes a major driving force for tourism development.

#### 4. Research Methodology and Data Sources

4.1. *Indicator System Construction.* The tourism development system and the regional development system are complex. Considering the aforementioned coupling mechanism between regional tourism and regional development

and previous research results, according to the principles of comprehensiveness, scientificity, and operability in the construction of the index system, fully considering the characteristics of regional tourism development, attaching importance to the selection of basic and dominant indicators, and constructing a coupled and coordinated evaluation index system of tourism development and regional development in China.

4.2. *Research Methodology.* This paper borrows the capacity coupling coefficient and coupling coordination degree from physics and constructs the coupling coordination degree model of tourism development and regional development by referring to the ideas of scholars at home and abroad on the establishment of the coupling coordination degree model between systems. The specific calculation formula is

$$C = \frac{\sqrt{(u_1 \times u_2)}}{(u_1 + u_2)},$$

$$D = \sqrt{C \times T},$$

$$T = \alpha u_1 + \beta u_2,$$
(1)

where  $C$  is the coupling degree value,  $D$  is the coupling coordination degree value,  $T$  is the comprehensive coordination index of tourism development and regional development,  $u_1$ 、 $u_2$  represents the combined level value of tourism development and regional development, respectively, and  $\alpha$  and  $\beta$  are weights to be determined. As tourism development is only one factor contributing to regional development, regional development is the result of a combination of factors, so the values of  $\alpha$  and  $\beta$  are set to 0.4 and 0.6, respectively.  $c \in [0, 1]$ ,  $d \in [0, 1]$ , the closer the value of  $c$  is to 1, the better the coupling between tourism development and regional development system is, the closer the value of  $d$  is to 1, the more the two systems tend to orderly coordination.

Referring to the study of [20] on the classification of coupled coordination levels, the coupled coordination status of tourism development and regional development was classified into two categories and twelve levels (see Table 1). Further, according to the comparison between tourism development and regional development levels, if  $u_1 > u_2$ , the level of regional development is relatively lagging; if  $u_1 = u_2$ , tourism development is synchronised with regional development; if  $u_1 < u_2$ , the level of tourism development is relatively lagging [21].

The tourism development system and the regional development system are complex giant systems, and the coupling process of the two has the characteristics of stage, uncertainty, dynamics, etc. [22]. It is difficult for the general linear or nonlinear model to accurately predict its development trend. Grey system theory is a kind of system theory for specific description, prediction, decision making, and control of systems with incomplete information. Grey prediction includes topological prediction, disaster prediction, series prediction, etc. In this paper, we adopt series prediction method to quantitatively predict the development change of tourism development and regional development coupling degree and coupling coordination degree. The modelling method and specific steps are as follows:

(i) Set the original time series:

$X_0 = \{x_0(1), x_0(2), \dots, x_0(n)\}$  generating a new sequence by  $x_1(k) = \sum_{i=1}^k x_0(i)$ ,  $k = 1, 2, 3, \dots, n$  accumulation:

$$X_1 = \{x_1(1), x_1(2), \dots, x_1(n)\}. \quad (2)$$

(ii) Defining the immediately adjacent mean series:

$$Z_1 = (z_1(2), z_1(3), \dots, z_1(n)), \quad (3)$$

where

$$z_1(k) = 0.5x_1(k) + 0.5x_1(k-1), \quad k = 2, 3, \dots, n.$$

(iii) The column of least squares estimated parameters for GM (1, 1) model  $x_0k + az_1k = b$  satisfies

$$\begin{aligned} \alpha &= (a, b)^T \\ &= (B^T B)^{-1} B^T Y_n, \end{aligned} \quad (4)$$

where

$$B = \begin{bmatrix} -z_{(1)}(2) & 1 \\ -z_{(1)}(3) & 1 \\ \dots & \dots \\ -z_{(1)}(n) & 1 \end{bmatrix}, \quad (5)$$

$$Y_n = \begin{bmatrix} x_{(0)}(2) \\ x_{(0)}(3) \\ \dots \\ x_{(0)}(n) \end{bmatrix}.$$

Constructing whitening equations for grey differential equations:

$$\frac{dx_1(k)}{dk} + ax_1(k) = b. \quad (6)$$

A direct solution gives the GM (1, 1) differential equation:

$$\hat{\alpha}_{(0)}(k+1) = [1 - e^{-a}] \left( x^{(0)}(1) - \frac{b}{a} \right) e^{-ak}. \quad (7)$$

(iv) The error test of the grey prediction model was carried out in Table 2 to determine the accuracy of the prediction results based on the magnitude of the P and C values.

**4.3. Research Data.** The data required for this paper mainly come from the China Statistical Yearbook, the China Tourism Statistical Yearbook, the China State of the Environment Bulletin, and the China Environment Statistical Bulletin from 1996 to 2016, supplemented in part by the China Regional Economic Statistical Yearbook and the tourism statistical yearbooks of some provinces from 2000 to 2016 [23]. The concept of all-area tourism has been proposed for a short period of time, and a longitudinal comparison of the coupled and coordinated relationship between the tourism industry and regional development in different years from the perspective of all-area tourism can highlight the differences in the coupled and coordinated relationship between the tourism industry and regional development before and after the introduction of all-area tourism.

## 5. Analysis of Results

Figures 2 and 3 show the raw series of regional tourism overnight receipts and tourism revenue from 2010 to 2015, respectively, and the seasonally adjusted series of each component. From the raw series of data in Figures 2 and 3, it can be seen that both the regional tourism overnight receipts and tourism revenue have a clear seasonal effect: the two sets of data start to increase slowly around October each year, reaching a peak around the Lunar New Year in January-February, and then the data start to fall gradually, reaching a minimum around April each year [24, 25]. This seasonal trend in tourism numbers and revenue can be seen more clearly in the seasonally adjusted seasonal trend graphs. As can be seen from the trend element curves in Figures 2 and 3, both the number of overnight stays and tourism receipts show a clear trend of growth. This indicates that as the economy develops, people's disposable income gradually increases, the number of overnight stays and the amount of tourism spending on Hainan Island are increasing year by year. The irregular element curves in Figures 2 and 3 show that there are large fluctuations around the Chinese New Year each year. This may be due to the fact that since the construction of the regional international tourism island started in 2010, the regional government has intensified the comprehensive management of the regional tourism environment, regulated the price order of the regional tourism market, enriched the supply of tourism products, and improved the level of tourism services, and the successful

TABLE 1: Coupling coordination levels.

| Coupling value C | Coupling                    | Coordination value D | Coordination level    |
|------------------|-----------------------------|----------------------|-----------------------|
| $C = 0.1$        | Lowest level coupling       | $L = 0$              | Uncoordinated         |
| $0 < C < 0.5$    | Low level coupling          | $0 < L < 0.3$        | Low coordination      |
| $0.1 < C < 0.2$  | Antagonism                  | $0.3 < L < 0.5$      | Moderate coordination |
| $0.4 < C < 0.7$  | Running-in                  | $0.6 < L < 0.7$      | Goodness coordination |
| $0.5 < C < 1$    | High level coupling         | $0.5 < L < 0.9$      | Highly coordinated    |
| $C = 0.9$        | Highest horizontal coupling | $L = 0.9$            | Extreme coordination  |

TABLE 2: Evaluation of tourism revenue projections.

|                               | Training set |        |        | Test set |        |        |
|-------------------------------|--------------|--------|--------|----------|--------|--------|
|                               | RMSE         | MAE    | MPE    | RMSE     | MAE    | MPE    |
| ARMA (no seasonal adjustment) | 7.082        | 5.4366 | 0.1588 | 10.464   | 8.7537 | 0.1475 |
| ARMA (seasonal adjustment)    | 0.2757       | 0.240  | 0.0066 | 12.8034  | 10.417 | 0.1751 |
| GA-SVR (seasonally adjusted)  | 0.5469       | 0.3856 | 0.0115 | 8.5108   | 6.4582 | 0.1059 |
| PSO-SVR (seasonal adjustment) | 0.5767       | 0.3897 | 0.0112 | 3.3001   | 2.7273 | 0.0473 |
| FWA-SVR (seasonally adjusted) | 0.5591       | 0.4003 | 0.0115 | 2.7070   | 2.2637 | 0.0411 |

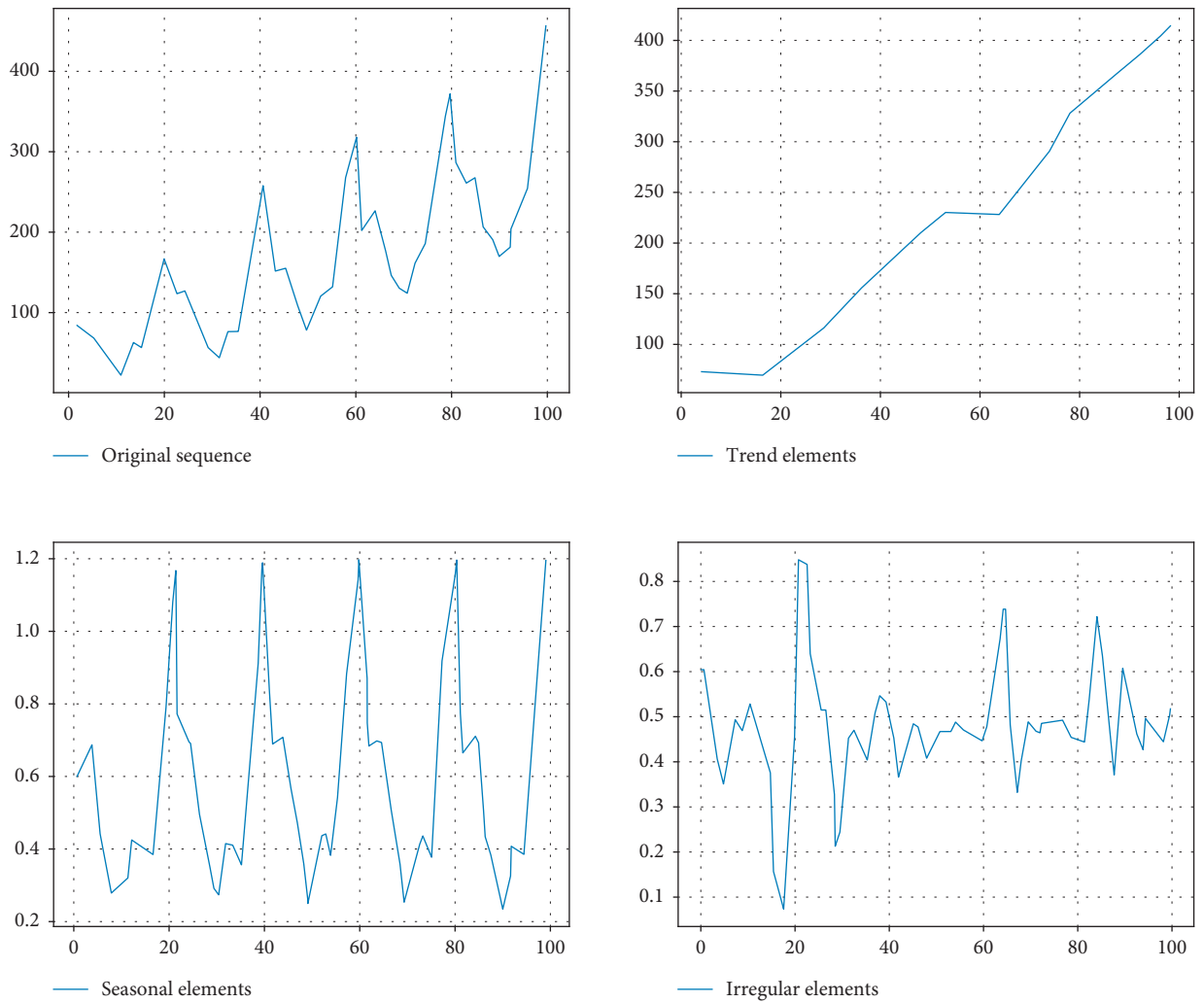


FIGURE 2: Seasonal adjustment of overnight tourist arrivals.

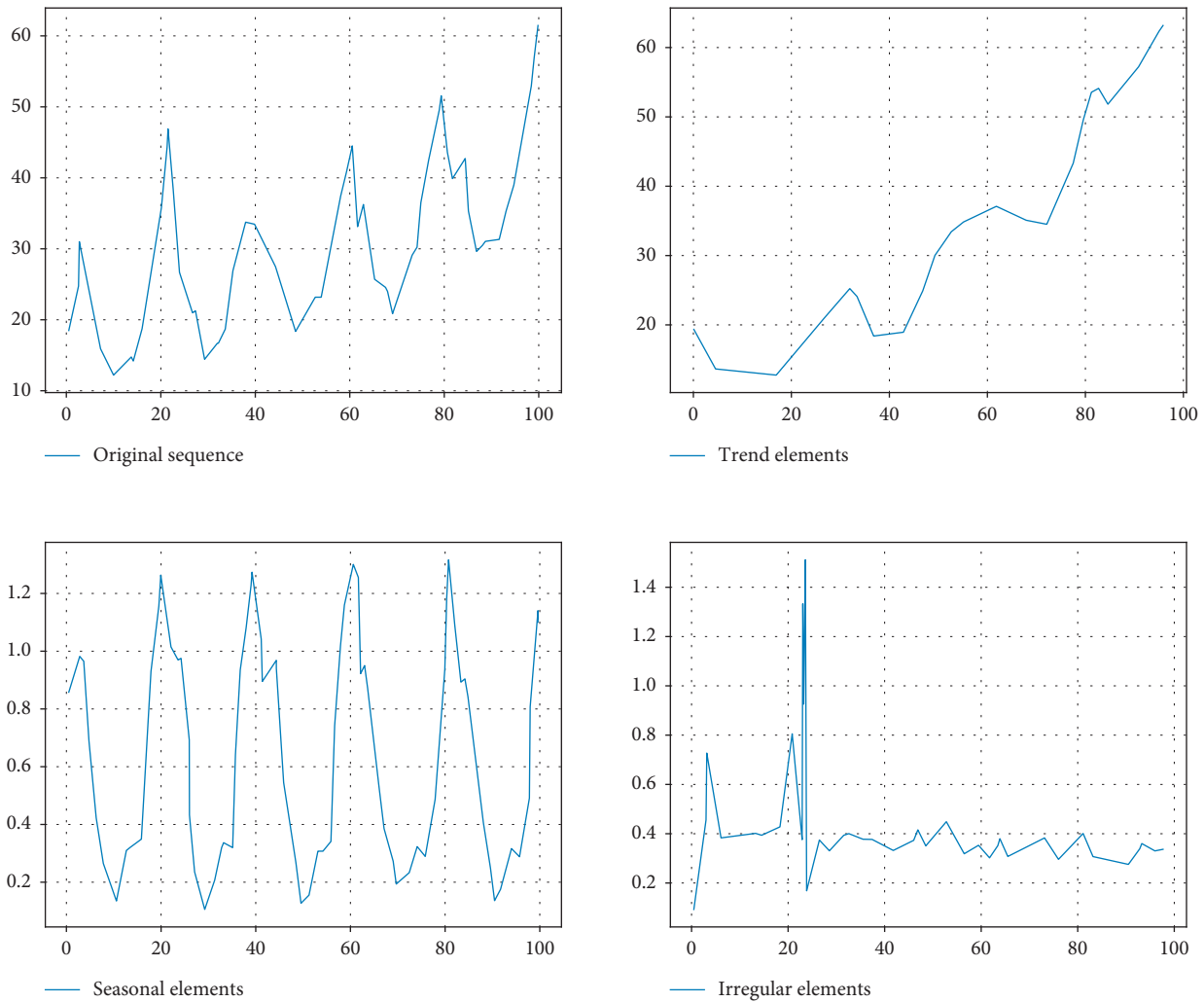


FIGURE 3: Seasonal adjustment of tourism receipts.

implementation of these measures has attracted more domestic and foreign tourists to come to the region to celebrate the Spring Festival holiday.

The fluctuations in the data in Figures 2 and 3 are consistent with the current state of tourism on Hainan International Tourism Island: on the one hand, as people's disposable income increases, so does their demand for tourism consumption and their ability to actually spend. In terms of trends, since 2010, when Hainan International Tourism Island became a major national strategic deployment, the region has attracted many tourists from home and abroad with its first-class tourism resources, and the number of tourist arrivals has continued to grow rapidly, and tourism revenue has also been rising. On the other hand, in terms of the seasonal element sequence, as a typical tropical maritime monsoon climate, Hainan's tourism data has typical seasonal characteristics, with the peak season generally occurring from early winter to early spring when it is warm and suitable, and the low season occurring from early spring to early winter when it is hot [26, 27].

Figures 4 and 5 show the results of the regional tourism overnight receipts and tourism revenue data after using the

seasonally adjusted FWA-SVR model for forecasting, respectively. In Figures 4 and 5, in addition to the FWA-SVR model proposed in this paper, the prediction results of two other types of models are used for comparison: the ARMA model without seasonal adjustment and the ARMA model with seasonal adjustment, as well as the SVR model based on the genetic algorithm and the particle swarm algorithm, respectively. The prediction evaluation results of each model are shown in Tables 2 and 3.

The trends of the curves in Figures 4 and 5 show that, in general, the seasonally adjusted forecasting model is significantly better than the nonseasonally adjusted ARMA forecasting model, which indicates that seasonal adjustment is necessary for forecasting seasonal series. The results of the forecasting evaluation in Tables 2 and 3 also show that, without seasonal adjustment, the ARMA model is not very effective in forecasting either tourism overnight receipts or tourism revenue, and the mean squared error (RMSE) is very large. After seasonal adjustment, the predictive power of the ARMA model is significantly improved. This indicates that the seasonally adjusted data is more conducive to forecasting.

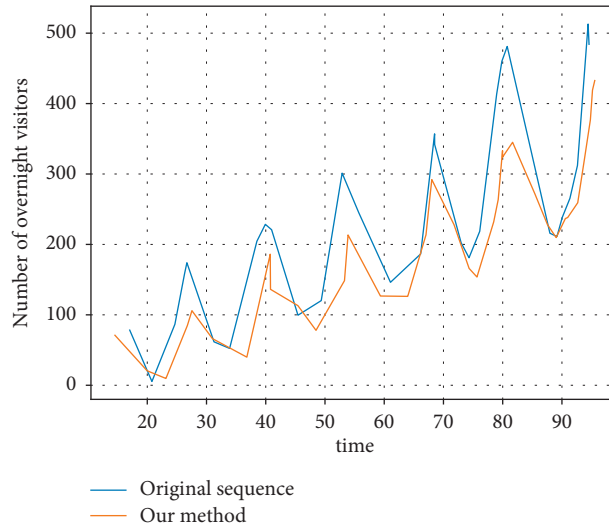


FIGURE 4: Forecast of tourism overnight stays.

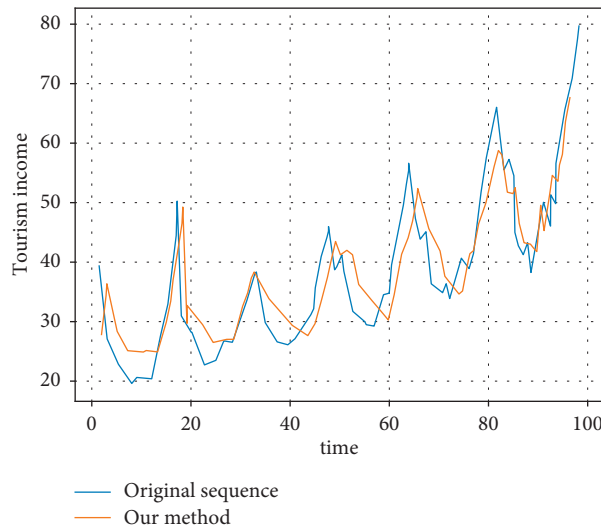


FIGURE 5: Tourism revenue projections.

TABLE 3: Evaluation of tourism overnight stay projections.

|                               | Training set |         |        | Test set |         |        |
|-------------------------------|--------------|---------|--------|----------|---------|--------|
|                               | RMSE         | MAE     | MPE    | RMSE     | MAE     | MPE    |
| ARMA (no seasonal adjustment) | 41.1866      | 34.4256 | 0.1095 | 56.0652  | 47.8624 | 0.1121 |
| ARMA (seasonal adjustment)    | 0.7355       | 0.6211  | 0.0021 | 90.0152  | 7.3781  | 0.0175 |
| GA-SVR (seasonally adjusted)  | 1.2346       | 1.0279  | 0.0035 | 8.8530   | 7.4832  | 0.0182 |
| PSO-SVR (seasonal adjustment) | 1.3845       | 1.109   | 0.0037 | 8.9617   | 7.7097  | 0.0198 |
| FWA-SVR (seasonally adjusted) | 1.2378       | 1.024   | 0.0035 | 8.8457   | 7.5264  | 0.0185 |

As can be seen in Figure 6, the comprehensive development indexes  $u_1$  and  $u_2$  of China's tourism development and regional development from 1996 to 2015 show a gradual upward trend. From 1996 to 2002, in order to stimulate the domestic consumption market and boost domestic consumption demand, the state put forward the reform idea of "double holiday" and "long holiday" system, gradually making tourism a strategic pillar industry

of the country. In order to stimulate the domestic consumer market and boost domestic consumer demand, the state introduced the idea of reforming the 'double holiday' and 'long holiday' system, gradually establishing tourism as a national strategic pillar industry and a regional advantage. During this period, China's tourism industry continued to develop rapidly in the context of the country's new normal.

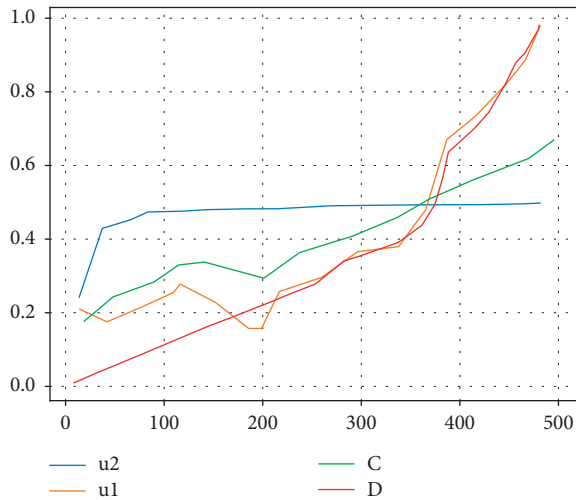


FIGURE 6: Changes in China's tourism development and regional development index and coupling coordination, 1996 to 2015.

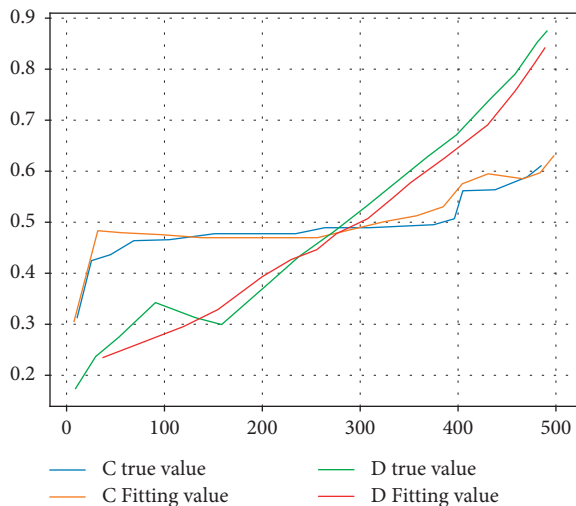


FIGURE 7: Forecast of coupling and coordination between tourism development and regional development in China (2016 ~ 2020).

As can be seen from Figure 7, the value of the coupling between tourism development and regional development in China from 2016 to 2020 ranges from 0.5131 to 0.5225, with an overall slow upward trend. The coupling level crosses from the lower level coupling antagonism stage to the benign coupling friction stage, and the growth rate of coupling value in this stage is significantly faster than that of antagonism stage. China's tourism development and regional development coupling coordination degree value increased from 0.7011 in 2016 to 0.8715 in 2020, with an average annual growth rate of 4.45%, still maintaining a relatively fast growth rate. The coupling coordination level has achieved a leap from the good coordination to the high coordination stage and is rapidly evolving to a higher level of coupling coordination stage. The predicted results show that the coupling and coordination between China's tourism development and regional development will generally improve significantly in the next few years, and both the coupling

level and coordination level have achieved a stage breakthrough, but the coupling level and coordination level have not improved and evolved at the same speed, and the coupling level during the teething period makes the two systems promote each other and coordinate development still needs a longer time.

## 6. Conclusions

This paper introduces a new intelligent optimisation algorithm to optimise the parameter selection process in the support vector regression model and considers the seasonal factors in tourism economic behaviour to construct a seasonally adjusted GM algorithm support vector regression model. The coupling and coordination between tourism and regional development will be significantly improved, and the coupling level and coordination level will enter into the grinding stage and high coordination stage, respectively, but the speed of improvement and development trajectory of the two are not consistent, and it will still take time for tourism and regional development to reach a high level of coordination.

## Data Availability

The experimental data used to support the findings of this study are available from the corresponding author upon request.

## Conflicts of Interest

The authors declare that they have no conflicts of interest regarding this work.

## References

- [1] S. Tuo, T. Chen, H. He et al., "A regional industrial economic forecasting model based on a deep convolutional neural network and big data," *Sustainability*, vol. 13, no. 22, p. 12789, 2021.
- [2] H. Duan and Y. Liu, "Research on a grey prediction model based on energy prices and its applications," *Computers & Industrial Engineering*, vol. 162, Article ID 107729, 2021.
- [3] S. Wei and X. Yanfeng, "Research on China's energy supply and demand using an improved Grey-Markov chain model based on wavelet transform," *Energy*, vol. 118, pp. 969–984, 2017.
- [4] C. Liu, R. Zhang, M. Wang, and J. Xu, "Measurement and prediction of regional tourism sustainability: an analysis of the Yangtze River Economic Zone, China," *Sustainability*, vol. 10, no. 5, p. 1321, 2018.
- [5] L. Xiao, W. Shao, M. Yu, J. Ma, and C. Jin, "Research and application of a combined model based on multi-objective optimization for electrical load forecasting," *Energy*, vol. 119, pp. 1057–1074, 2017.
- [6] H. Lan, C. Xu, and Z. Meng, "GM(1,1) model based leshan's industries shift-share analysis and prediction," in *Proceedings of the International Conference on Management Science and Engineering Management*, pp. 129–139, Springer, Kanazawa, Japan, June 2017.
- [7] L. Xiao, W. Shao, T. Liang, and C. Wang, "A combined model based on multiple seasonal patterns and modified firefly

- algorithm for electrical load forecasting,” *Applied Energy*, vol. 167, pp. 135–153, 2016.
- [8] J. Wang, P. Du, H. Lu, W. Yang, and T. Niu, “An improved grey model optimized by multi-objective ant lion optimization algorithm for annual electricity consumption forecasting,” *Applied Soft Computing*, vol. 72, pp. 321–337, 2018.
- [9] X. Ma, Z. Liu, and Y. Wang, “Application of a novel nonlinear multivariate grey Bernoulli model to predict the tourist income of China,” *Journal of Computational and Applied Mathematics*, vol. 347, pp. 84–94, 2019.
- [10] K. Li and T. Zhang, “A novel grey forecasting model and its application in forecasting the energy consumption in Shanghai,” *Energy Systems*, vol. 12, no. 2, pp. 357–372, 2021.
- [11] A. D. La Foucade, S. Gabriel, E. Scott, K. Theodore, and C. Metivier, “A survey of selected grey forecasting models with application to medical tourism forecasting,” *Theoretical Economics Letters*, vol. 09, no. 04, pp. 1079–1092, 2019.
- [12] Z. Zhengwan, Z. Chunjiong, L. I. Hongbing, and X. Tao, “Multipath transmission selection algorithm based on immune connectivity model,” *Journal of Computer Applications*, vol. 40, no. 12, p. 3571, 2020.
- [13] X. Liu and N. Xie, “A nonlinear grey forecasting model with double shape parameters and its application,” *Applied Mathematics and Computation*, vol. 360, pp. 203–212, 2019.
- [14] Y. Dong, X. Ma, C. Ma, and J. Wang, “Research and application of a hybrid forecasting model based on data decomposition for electrical load forecasting,” *Energies*, vol. 9, no. 12, p. 1050, 2016.
- [15] H. Che and J. Wang, “A two-timescale duplex neurodynamic approach to mixed-integer optimization,” *IEEE Transactions on Neural Networks and Learning Systems*, vol. 32, no. 1, pp. 36–48, 2021.
- [16] X. Liu, B. Moreno, and A. S. García, “A grey neural network and input-output combined forecasting model. Primary energy consumption forecasts in Spanish economic sectors,” *Energy*, vol. 115, pp. 1042–1054, 2016.
- [17] L. Sun, Y. Wang, Z. Qu, and N. X. Xiong, “Beatclass: a sustainable ecg classification system in iot-based ehealth,” *IEEE Internet of Things Journal*, vol. 1, 2021.
- [18] Y. Wang, L. Sun, and S. Subramani, “CAB: classifying arrhythmias based on imbalanced sensor data,” *KSII Transactions on Internet & Information Systems*, Jul.vol. 15, no. 7, pp. p2304–p2320, 2021, (Computer Science Q3, 0.858).
- [19] H.-S. Dang, T.-M.-T. Nguyen, C.-N. Wang, J.-D. Day, and T. M. H. Dang, “Grey system theory in the study of medical tourism industry and its economic impact,” *International Journal of Environmental Research and Public Health*, vol. 17, no. 3, p. 961, 2020.
- [20] Y.-C. Hu, “Electricity consumption prediction using a neural-network-based grey forecasting approach,” *Journal of the Operational Research Society*, vol. 68, no. 10, pp. 1259–1264, 2017.
- [21] K. Ni, J. Wang, G. Tang, and D. Wei, “Research and application of a novel hybrid model based on a deep neural network for electricity load forecasting: a case study in Australia,” *Energies*, vol. 12, no. 13, p. 2467, 2019.
- [22] Y.-C. Hu, P. Jiang, and P.-C. Lee, “Forecasting tourism demand by incorporating neural networks into Grey-Markov models,” *Journal of the Operational Research Society*, vol. 70, no. 1, pp. 12–20, 2019.
- [23] X. Ning, K. Gong, W. Li, and L. Zhang, “JWSAA: joint weak saliency and attention aware for person re-identification,” *Neurocomputing*, vol. 453, pp. 801–811, 2021.
- [24] X. Ning, P. Duan, W. Li, and S. Zhang, “Real-time 3D face alignment using an encoder-decoder network with an efficient deconvolution layer,” *IEEE Signal Processing Letters*, vol. 27, pp. 1944–1948, 2020.
- [25] X. Ning, W. Li, B. Tang, and H. He, “BULDP: biomimetic uncorrelated locality discriminant projection for feature extraction in face recognition,” *IEEE Transactions on Image Processing*, vol. 27, no. 5, pp. 2575–2586, 2018.
- [26] J. Zhang, Y. Qin, X. Zhang, G. Che, X. Sun, and H. Duo, “Application of non-equidistant GM (1, 1) model based on the fractional-order accumulation in building settlement monitoring,” *Journal of Intelligent and Fuzzy Systems*, vol. 42, no. 3, pp. 1559–1573, 2022.
- [27] C. Zheng, W.-Z. Wu, W. Xie, Q. Li, and T. Zhang, “Forecasting the hydroelectricity consumption of China by using a novel unbiased nonlinear grey Bernoulli model,” *Journal of Cleaner Production*, vol. 278, Article ID 123903, 2021.



## *Retraction*

# **Retracted: Construction and Knowledge Mining of Traditional Chinese Medicine Ancient Books Bibliographic Abstracts Database Based on Genetic Algorithm and BP Neural Network**

### **Mathematical Problems in Engineering**

Received 18 July 2023; Accepted 18 July 2023; Published 19 July 2023

Copyright © 2023 Mathematical Problems in Engineering. This is an open access article distributed under the Creative Commons Attribution License, which permits unrestricted use, distribution, and reproduction in any medium, provided the original work is properly cited.

This article has been retracted by Hindawi following an investigation undertaken by the publisher [1]. This investigation has uncovered evidence of one or more of the following indicators of systematic manipulation of the publication process:

- (1) Discrepancies in scope
- (2) Discrepancies in the description of the research reported
- (3) Discrepancies between the availability of data and the research described
- (4) Inappropriate citations
- (5) Incoherent, meaningless and/or irrelevant content included in the article
- (6) Peer-review manipulation

The presence of these indicators undermines our confidence in the integrity of the article's content and we cannot, therefore, vouch for its reliability. Please note that this notice is intended solely to alert readers that the content of this article is unreliable. We have not investigated whether authors were aware of or involved in the systematic manipulation of the publication process.

Wiley and Hindawi regrets that the usual quality checks did not identify these issues before publication and have since put additional measures in place to safeguard research integrity.

We wish to credit our own Research Integrity and Research Publishing teams and anonymous and named external researchers and research integrity experts for contributing to this investigation.

The corresponding author, as the representative of all authors, has been given the opportunity to register their

agreement or disagreement to this retraction. We have kept a record of any response received.

### **References**

- [1] Y. Wang, S. Ren, L. Song, and J. Zhang, "Construction and Knowledge Mining of Traditional Chinese Medicine Ancient Books Bibliographic Abstracts Database Based on Genetic Algorithm and BP Neural Network," *Mathematical Problems in Engineering*, vol. 2022, Article ID 6838714, 15 pages, 2022.

## Research Article

# Construction and Knowledge Mining of Traditional Chinese Medicine Ancient Books Bibliographic Abstracts Database Based on Genetic Algorithm and BP Neural Network

Yongmei Wang <sup>1</sup>, Shujun Ren,<sup>2</sup> Li Song,<sup>1</sup> and Jiang Zhang<sup>1</sup>

<sup>1</sup>School of Computer Science and Technology, Hefei Normal University, Hefei 230031, China

<sup>2</sup>Library of Anhui University of Traditional Chinese Medicine, Hefei 230038, China

Correspondence should be addressed to Yongmei Wang; wangymfddy@hfnu.edu.cn

Received 8 March 2022; Revised 20 March 2022; Accepted 23 March 2022; Published 6 April 2022

Academic Editor: Man Fai Leung

Copyright © 2022 Yongmei Wang et al. This is an open access article distributed under the Creative Commons Attribution License, which permits unrestricted use, distribution, and reproduction in any medium, provided the original work is properly cited.

With the rapid development of modern science technology and Internet technology, the establishment of a unified and standardized bibliographic summary database to realize the exchange and resource sharing of ancient Chinese medicine bibliography, is the inevitable trend of ancient Chinese medicine bibliography digital service. Firstly, this paper formulates the bibliographic metadata specification of traditional Chinese medicine ancient books (TCMAB), extracts each cataloging file into an XML document in line with the bibliographic metadata specification of TCMAB. Secondly, this paper realizes the unified description of ancient book resources in the database system of TCMAB, uses the native XML database eXist to store and manage the XML documents of all traditional Chinese medicine ancient book resources, and integrates the multimedia data with XML data. Finally, genetic algorithm and BP neural network are used for knowledge mining and discovery, the overall model design of TCMAB bibliographic abstracts database system is proposed based on the construction process of knowledge map. The system platform adopts B/S mode, eXist database management system, PowerSSP streaming media and video server for audio video processing.

## 1. Introduction

Traditional Chinese medicine ancient books are precious resources to carry forward traditional culture. We should make full use of the resources of TCMAB to serve the development of traditional Chinese medicine culture, which will help to promote the inheritance and develop traditional Chinese medicine culture [1]. The construction of digital database is conducive to enriching online resources and promoting the transformation of ancient books potential resources into real productivity. The digital database system can provide more comprehensive information in one aspect online for the needs of readers, improve the service quality, and is conducive to the innovative development of traditional Chinese medicine [2]. The establishment of database can improve the efficiency of resource sharing. The resources of the database should be operated according to certain

standards and norms in the process of construction, which is conducive to promoting the co-construction and sharing of resources. In addition, the database plays an irreplaceable role in the process of optimizing and developing the existing literature [3]. It can systematically sort out the scattered resources and carry out data processing and preservation of traditional Chinese medicine resources according to the relevant requirements, which will help to strengthen the integration and sharing of traditional Chinese medicine resources. The needs of users are the basis for the system to carry out services, only by closely combining the needs of users can we provide efficient services for users [4]. The needs of users can generally be described from two levels, one is general and basic needs, such as users' daily access to data, on the other hand, it is to meet the characteristic needs of scientific research, such as finding relevant materials, which helps to meet the needs of multi-level social users. At

present, the traditional Chinese medicine ancient books are scattered all over the country, and there has not been a database dedicated to the bibliographic summary information of traditional Chinese medicine ancient books [5]. This paper aims to extract the bibliography and abstract information of TCMAB from the paper books by using metadata description on the basis of analyzing the paper bibliography and abstract books, and use the existing technology to transform the bibliography and abstract information of TCMAB into digital resources, and then on this basis, build a special bibliography and abstract database of ancient doctors. On the premise of network application, carry out the collection, integration and processing of online Chinese medicine literature summary information resources, provide special information retrieval services, realize the networking of Chinese medicine ancient book summary information organization and services, develop value-added products of information resources, and produce various types of special databases according to the market demand [6].

The specific contributions of this paper include the following:

- (1) Digital description and information extraction of traditional Chinese medicine ancient books bibliographic abstracts, formulating metadata specifications of traditional Chinese medicine ancient books.
- (2) In this paper, genetic algorithm and BP neural network are used for knowledge mining in TCMAB, The scientific storage and management of bibliographic data of TCMAB can effectively manage the digital content of traditional Chinese medicine ancient books in semi-structured form.
- (3) Realizing remote access to the digital resource database of TCMAB bibliographic abstracts, and form a local bibliographic abstracts system of TCMAB with local characteristics, which has practicality, network environment support and all-round retrieval function.
- (4) The research results of this paper can help establish digital standards of TCMAB, enrich the existing digital theory, make TCMAB bibliographic abstracts database more practical.

The rest of this paper is organized as follows. Section 2 discusses related work, followed by the analysis of ancient books digitization process in Section 3. The metadata specification of TCMAB bibliography is discussed in Section 4. Section 5 proposes the design of database system for TCMAB bibliographic abstracts, and Section 6 concludes the paper with a summary and future research directions.

## 2. Related Work

Traditional Chinese medicine ancient books are an important part of Chinese ancient book resources, and their quantity ranks first among ancient books of various disciplines. The digitization of traditional Chinese medicine ancient books has made some achievements both in theory

and in database construction. The bibliographic database of ancient books is the initial stage of ancient books digital resources construction [7]. It is a database formed by inputting the information such as the title, author, version, volume number, abstract and source of ancient books into the computer, and provides users with a large catalog database for the retrieval of relevant ancient book data resources in the form of computer network system [8]. Readers can retrieve the relevant information of an ancient book through the title and author of the book. The ancient books bibliographic database can meet the needs of modern works, and it is the basis for the further digitization of ancient books. At present, the bibliographic database of TCMAB is mainly concentrated in colleges and universities of traditional Chinese medicine, scientific research institutes and their libraries, mainly to reveal the collection, serve teaching and scientific research. At present, many traditional Chinese medicine libraries and scientific research institutions have bibliographic databases in their collections of ancient books, but due to the inconsistency of standards, the depth and breadth of documents revealed by the database are also different [9–14]. For example, the Chinese medical code has collected more than 1000 major works of traditional Chinese medicine in the past dynasties. Using the library classification method, the collected ancient books are divided into 12 categories: medical classics, diagnostic methods, materia medica, prescription books, acupuncture and massage, typhoid golden chamber, febrile disease, comprehensive medical books, clinical and syndrome disciplines, external treatment of health and diet therapy, medical theory and medical records, and others, involving all disciplines of traditional Chinese medicine [15–19].

Current research progress in studies on linked data, the challenge with linked data is that databases are constantly evolving and cached content quickly becomes outdated. To overcome this challenge, Qian et al. [20] proposed a change metric that quantifies the evolution of a linked dataset and determines when to update cached content. Zhao et al. [21] proposed a query language framework for probabilistic RDF data (an important uncertain link data), in which each triplet has a probability, called pSRARQL, which is based on SPARQL. Liu et al. [22] presented a new method of web form integration based on linked data and VDIS (View based Data Integration System) architecture. They proposed WebQuinLD, an alternative new method based on linked data principle, which can combine a single WQI into a single IWQI of a given domain.

## 3. Analysis of Ancient Books Digitization Process

The digitization of ancient books uses computer technology to convert the words or images in ancient books into digital forms that can be recognized by computer, make ancient books bibliographic database, ancient books full-text database and ancient books knowledge base, save and disseminate through CD-ROM, network and other forms. So as to reveal the rich information and knowledge resources contained in ancient books and documents, protecting, utilizing

and mining ancient books and documents. The digitization of ancient books is developing rapidly, but at the same time, we should also see all kinds of problems in the process of ancient books digitization.

**3.1. Inconsistent Standards.** In today's digitization of ancient books, the problem of inconsistent standards is very serious and widely exists in the world. The non-uniform standards mainly focus on: version standard of digital ancient books, bibliographic classification standard, character set standard, storage format standard, digital image standard, retrieval system standard, metadata description standard, etc. These problems are perplexing the benign development of ancient books digitization.

The problem of non-uniform bibliographic classification standards, that is, what kind of bibliographic classification standards should be followed in the digitization of TCMAB, has become a problem that must be solved before digitization. Combined with the actual situation of TCMAB, the simple use of four part classification method or Chinese library classification method is not appropriate. In the digitization of TCMAB, we can refer to the classification methods of "The General Summary of Traditional Chinese Medicine Ancient Books" and "Xin'an Medical Books", which are divided into "Medical Classics" (including the basic theory of traditional Chinese medicine), "Typhoid Fever" (including febrile diseases), "Diagnostic Methods", "Materia Medica", "Acupuncture and Moxibustion", "Treatise on Prescription" (1-5), "Medical Records", "Health Preservation", "Series" (including reference books of medical history) "Textual Research on Medical Records" and "Appendix", a total of 15 parts. In this way, different classification standards can be avoided, which provides a prerequisite for the production of bibliographic summary database, and is also the basis for the construction of retrieval database in the future.

**3.2. Technical Difficulties.** The digital processing of ancient books mainly includes two aspects: the simple digital conversion and reproduction of the external form or content form of ancient books; after completing the text to digital conversion, related processing work, such as retrieval, content relation and so on. The main technical problem at this stage is the conversion of text from image data to text data. If such conversion cannot be realized, the related work of later text and content relation cannot be completed. OCR optical character recognition technology need to convert ancient book images into characters. OCR technology can convert the characters in the image into characters that can be seen in the computer through recognition.

There are many kinds of ancient books, but the current OCR software design only aims at an extremely limited part of them, which makes the reliability of this kind of software very limited in the text process. It is also necessary to have a deeper understanding of different ancient books and provide targeted technical processing methods for more different types of ancient books, in this way, OCR technology can better deal with a variety of ancient books in different

situations. In order to achieve a more comprehensive identification, we need more development in technology, so as to further promote the development of ancient books digitization.

Knowledge base is the combination of artificial intelligence and database. It stores knowledge in a unified form. The knowledge of knowledge base is highly structured symbolic data. Users can carry out deep knowledge mining to realize the relation retrieval of multiple knowledge points from bibliography to full text, or one author can retrieve other relevant authors. Therefore, we can find the causes and solutions of these problems in the continuous development of ancient Chinese medicine. The overall model design of TCMAB bibliographic abstracts database system is based on the construction process of knowledge map. The system platform adopts B/S mode, eXist database management system, and PowerSP streaming media and video server for audio video processing.

## 4. Metadata Specification of TCMAB Bibliography

Metadata's purpose is to provide an intermediate level description according to people can determine information package, which they want to browse or retrieve without retrieving a large number of irrelevant full-text. The metadata of ancient books can be simply defined as information object. Ancient book metadata is divided into three types: descriptive metadata, management metadata and application metadata.

**4.1. Metadata Specification of Ancient Books.** In the field of ancient books and documents, common standards related to metadata include the metadata specification of ancient books, the metadata specification of special digital object description, and the international Dublin Core metadata set (DC). The cultural industry standard of the people's Republic of China WH/T 66-2014 metadata specification for ancient books issued and implemented by the Ministry of Culture in 2014 is the metadata specification for ancient book resources. It is formulated to unify and standardize the description of the ancient books content characteristics and better manage ancient book resources. It is proposed by China's Digital Library and standard specification construction project. This specification is used to describe the content and appearance characteristics of paper books and digital ancient books. The resource objects described in the standard are ancient books, which are similar to the resource object types described in this paper. At the same time, the standard reuses some elements in DC as the core elements, and individual elements in ancient document types as the core elements of resource types. At the same time, several modifiers are added to the core elements according to the characteristics of Chinese ancient books, it provides an important reference for this paper to formulate the bibliographic metadata specification of TCMAB.

## 4.2. Formulating the Metadata Specification of TCMAB Bibliography

**4.2.1. Standard Design Principles of TCMAB Bibliographic Metadata.** The design of TCMAB bibliographic metadata specification follows the design principles of China's special metadata specification, that is, simplicity and accuracy, specificity and universality, interoperability and easy conversion, scalability and meeting the needs of users. Simplicity mainly means that the metadata standard of bibliography of TCMAB should be easy to master in the practice of description. The accuracy of TCMAB bibliographic metadata specification can improve the accuracy of cataloging of TCMAB. Specificity refers to determining the corresponding metadata specification according to the specific resource entity requirements, while universality requires that the metadata specification be universal within a certain range. The metadata specification designed in this paper is designed with reference to the cataloguing documents of ancient Chinese medicine books such as "General Outline of Ancient Chinese Medicine Books" and "Xin'an Medical Books", so as to achieve universality in the field of ancient Chinese medicine books. The interoperability of metadata refers to the feature that data can be shared among different systems. This feature ensures that metadata can be operated by application systems established by other organizations or institutions while providing services for itself. This requires that the metadata specification designed in this paper needs to meet the sharing requirements of TCMAB resource database. When designing the metadata specification of TCMAB, we need to carefully consider the definition of elements and modifiers in the metadata specification. Therefore, when designing the metadata specification of TCMAB, we refer to the "Metadata Specification of Special Digital Object Description", "Metadata Specification of Ancient Books" and the Dublin core element set widely supported abroad. The extensibility of metadata specification means that user-defined elements or modifiers can be expanded according to the specific application needs of users. Based on this feature, when formulating the metadata specification of TCMAB, corresponding elements and modifiers will be added according to the characteristics of TCMAB cataloging files collected in this paper. Considering that the purpose of formulating metadata specification is to more fully display information resources to users, user requirements are taken as an important standard to weigh the quality of metadata specification. Therefore, when designing the bibliographic metadata specification of ancient Chinese medicine books, reference is made to the bibliographic cataloguing books of ancient Chinese medicine books such as "Chinese Medical Books" and "Xin'an Medical Books", in order that the designed bibliographic metadata specification of ancient Chinese medicine books can meet the needs of users in all aspects.

**4.2.2. Establishment of Metadata Standard for Bibliography of TCMAB.** The metadata specification of TCMAB takes traditional Chinese medicine ancient books as the root node.

In this paper, we study the sub-node of paper TCMAB. The structure of elements and their modifiers in the bibliographic metadata specification of ancient Chinese medicine books designed in this paper is shown in Figure 1.

Dublin Core terms are reused in the node (<http://purl.org/dc/terms>), at the same time, metadata object description scheme is reused (<http://www.loc.gov/mods>), the location element definition in. The contents can be summarized into book title (including alias), dynasty, author, source of the book, volume number, preservation and loss, content summary, edition collection, notes, etc.

**4.2.3. Data Modeling of Bibliography of TCMAB.** The data model mainly displays the entities and attributes involved in TCMAB and the relationship between them in a more intuitive way. This paper makes a link research on the information of the responsible person, version, publishing place and so on. In the data model of TCMAB in Figure 2, it is marked with URI. The version part is the link inside the Drupal site, which is marked with node. Figure 3 shows the specific process of HTTP content negotiation mechanism for related data.

**4.3. Abstract Information Extraction of Ancient Books Based on Metadata Specification of TCMAB Bibliography.** This paper formulates the metadata specification of TCMAB bibliography. How to use this specification to extract the information of TCMAB bibliography and realize the digitization of the bibliographic abstracts of ancient books is the focus of this section. Abstract is a brief introduction and evaluation of the content, thought, author and version source of the literature, so as to effectively help readers use the literature correctly and play the role of reading guide. The "General Summary of Traditional Chinese Medicine Ancient Books" (referred to as "General Summary") contains well-documented medical literature before 1949, including existing literature and lost literature. "Xin'an Medical Books" collects ancient Chinese medical books from Shennong era to the middle of Qing Dynasty, including famous authors, ages and volumes, to provide help for the study of traditional Chinese medicine bibliography. "Xin'an" is the name of a region in Chinese history. It was first seen in the first year of Taikang in the Western Jin Dynasty (280 years). There are numerous medical books written by famous experts in this area in Chinese dynasties, of which the Ming and Qing Dynasties account for a large proportion, which naturally forms an important position of "Xin'an Medical Books" in the field of Chinese medical literature.

"General Summary", "Xin'an Medical Books" and the cataloging documents of ancient Chinese medicine books all have the characteristics of ancient books cataloging. Because the ancient books bibliographic information belongs to semi-structured data, the composition is relatively simple and has obvious regularity. The digitization process of traditional Chinese medicine ancient books is mainly to scan the "General Summary" of paper books into pictures and store them as PDF files. Then, through OCR (optical character recognition), the text file and picture file are obtained, in which the text file contains the title of Chinese characters and the bibliographic content of ancient books.

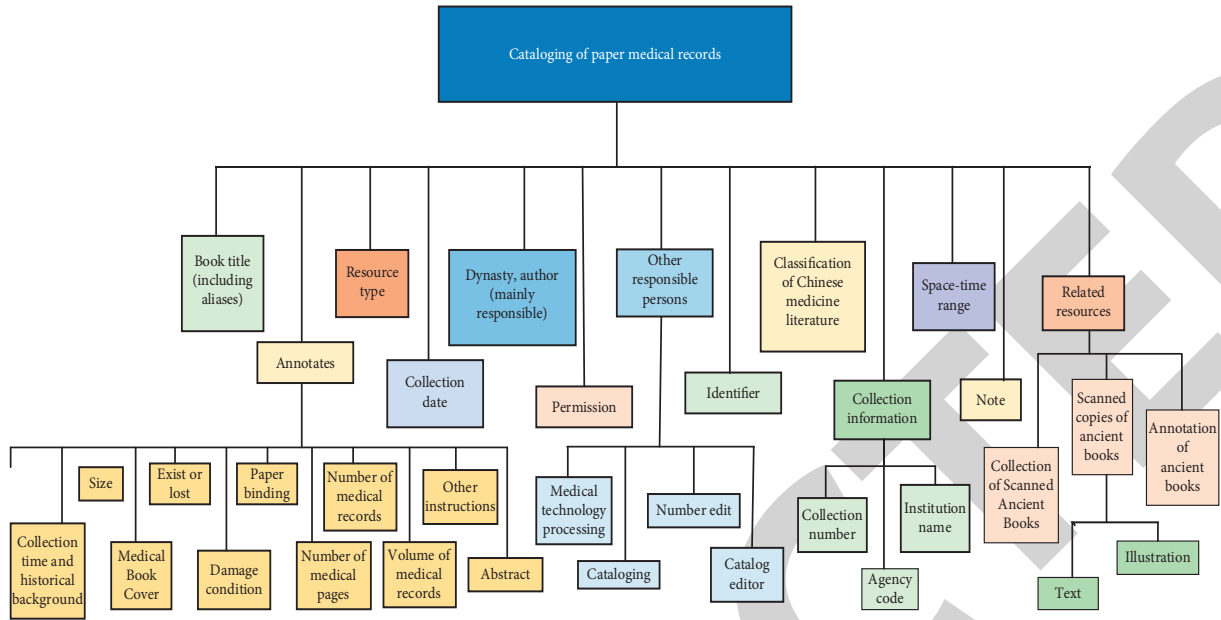


FIGURE 1: Elements and their modifiers under the nodes of TCMAB.

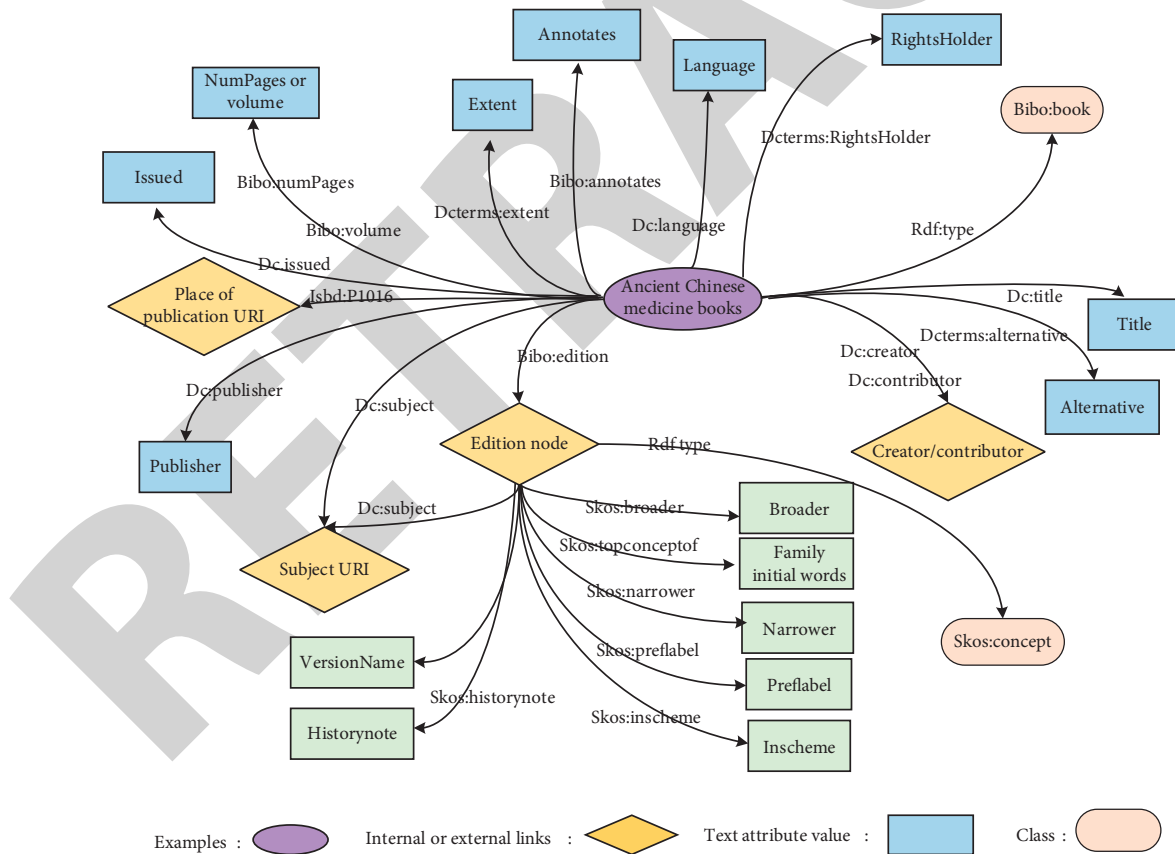


FIGURE 2: Data model of TCMAB.

Proofread the semi-structured document, and then extract the text according to the template. Name the recognized picture with the title of Chinese characters. The specific process of digitization of paper books is shown in Figure 4 [23].

The eXist is an open source native XML database management system, which has developed rapidly in recent years. Its characteristics can ensure that eXist can efficiently store and retrieve XML documents, which is also the reason why this paper chooses eXist to store and manage TCMAB.

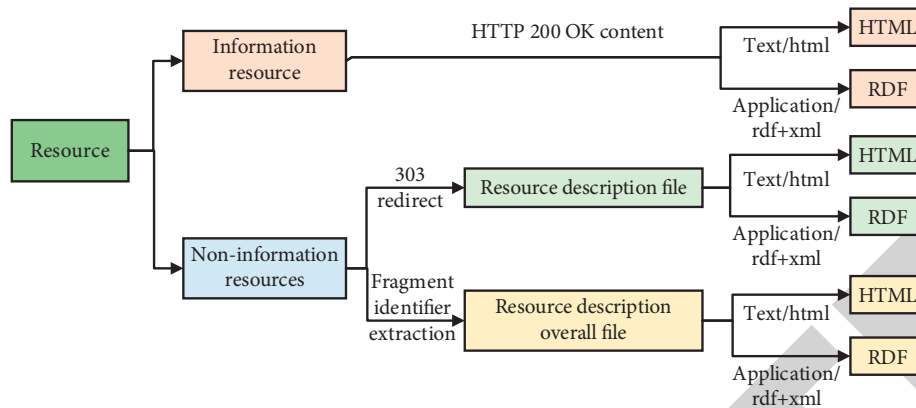


FIGURE 3: URI naming and content negotiation acquisition mechanism.

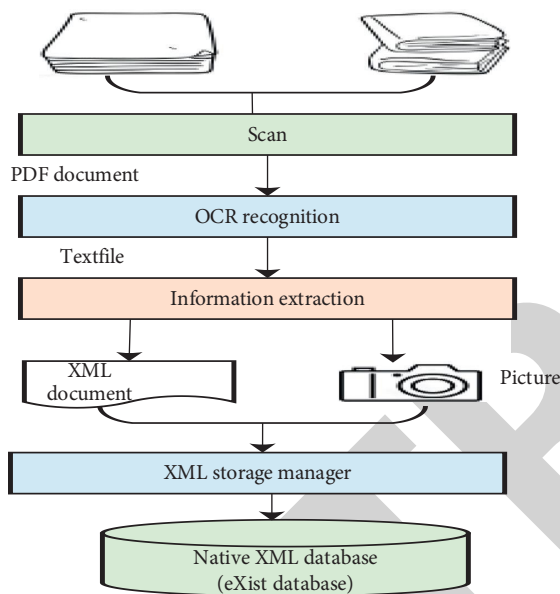


FIGURE 4: Digital process of paper books.

The goal of information extraction of TCMAB is to extract the contents of paper books and text files to form semi-structured data with standardized metadata of traditional Chinese medicine.

Before extracting information from TCMAB, we should first analyze the text characteristics of ancient books cataloging bibliography according to the different contents of metadata. The information extraction method used in this paper is the template extraction method based on regular expression. Taking “Materia Medica Preparation” in the catalogue of TCMAB in Anhui as an example, the contents can be summarized into book name (including alias), dynasty, author, source of the book, volume number, preservation and loss, content summary, edition collection, notes, etc. A large number of medical books written by doctors before the end of the Qing Dynasty have been verified, corrected, supplemented and studied from the aspects of book name, author, volume number, preservation and loss, version collection, content and notes.

Secondly, according to the writing rules of regular expression, the extraction template of ancient books in the “General Summary” is designed. According to the extraction template of books in the “General Summary”, the information of the target ancient book catalogue is extracted, and after the extraction result is compared with the content of ancient books before information extraction, the XML document after information extraction is finally obtained.

Finally, in order to test the performance of the information extraction method proposed in this paper, analyze the performance of the extraction method by using the recall rate and accuracy rate, select some ancient books in the “General Summary” as the test set for information extraction, calculate and analyze the recall rate and accuracy rate. If the results are correct, it shows that the template based information extraction method proposed in this paper can correctly extract the contents of ancient books according to the characteristics of TCMAB bibliography in the “General Summary”. Through this method, the information of the books that need to be digitized in this paper is extracted, which provides a data basis for the follow-up research work of this paper.

## 5. Application of Knowledge Discovery in the TCMAB Based on Genetic Algorithm and BP Neural Network

There may be a lot of noise in the data in the database, and knowledge mining tools can efficiently mine the laws and values hidden in the data, and find the qualitative relationship between data attributes, such as dependency. The trained neural network can give the quantitative and qualitative description of data attributes. In this paper, BP neural network and genetic algorithm are used for knowledge discovery and trend analysis in the database. Database technology can quantitatively analyze the management information system with technology as the core needed by knowledge discovery. In the transaction processing, data is the most processed in the database. Knowledge among database attributes is an important problem, knowledge discovery is an accurate reflection of functional relations.

**5.1. BP Neural Network.** BP neural network is a feedforward network where neurons are distributed in layers: input layer, output layer and hidden layer(s). The output of neurons in each layer is transmitted to the next layer. This transmission can have enhancing, weakening or inhibiting effects on the outputs through connection weight. Apart from the neurons in the input layer, the weighted sum of the output of neurons in the previous layer when the net input of neurons in the hidden layer and output layer. Each neuron is activated by its input, activation function and threshold. Its working process consists of two periods, one for learning and the other for working. The former covers two processes: forward propagation of input information and back propagation of error. In the first process, the input data are processed layer by layer, the input, hidden and output layers sequentially. The state of neurons in each layer merely affects that of the neurons in the next layer. If the output of the output layer is inconsistent with the expected output of the given sample, the output error is calculated, transferred to the error back propagation process, and the error is returned along the original connection path. By modifying the weights between neurons in each layer, the error is minimized. Through training with large quantities of learning samples, the connection right between neurons in each layer is fixed and transferred to the working period. There is only forward propagation of input information during the working period. The forward propagation is calculated according to the working process of the previous neuron model. Thus, the key to the calculation of BP neural network lies with the error back propagation process in the learning period, which is completed by minimizing an objective function. Usually, the objective function is defined as the sum of the error squares between the actual output and the expected output or the error function, and the calculation formula can be derived by using the gradient descent method.

The specific process of BP algorithm is described as follows:

The initial value of learning times is  $t = 0$ , and the network weights  $W_{ij}(t) \in [-1, 1]$ ,  $W_{jk}(t) \in [-1, 1]$  and threshold  $\theta_j(t) \in [-1, 1]$  and  $\theta_k(t) \in [-1, 1]$  are initialized with random numbers.

- (1) Enter a learning sample  $(X_p, T_p)$ , where  $p \in (1, 2, \dots, N)$  and  $N$  is the number of samples,  $(X_p \in R^n, T_p \in R^m)$ .
- (2) Calculate the output value of each node in the hidden layer.

$$Y_j^2 = f\left(\sum_{i=1}^{n_1} W_{ij} Y_i^1 - \theta_j\right) = f\left(\sum_{i=1}^{n_1} W_{ij} X_{ip} - \theta_j\right). \quad (1)$$

it's action function is log\_sigmoid type function.

$$f(x) = \frac{1}{1 + e^{-\lambda}}, j \in \{1, 2, \dots, n_2\}. \quad (2)$$

- (3) Calculate the output value of each node of the output layer.

$$Y_k^3 = f\left(\sum_{j=1}^{n_2} W_{jk} Y_j^2 - \theta_k\right). \quad (3)$$

its action function is linear Purelin function.

$$f = ax, k \in \{1, 2, \dots, m\}. \quad (4)$$

- (4) Calculate the correction value of the connection weight between the output layer node and the hidden layer node.

$$\sigma_k = (T_k - Y_k^3) Y_k^3 (1 - Y_k^3), k \in \{1, 2, \dots, m\}. \quad (5)$$

- (5) Calculate the correction of the connection weight between the hidden layer node and the input layer node.

$$\sigma_j = Y_j^2 (1 - Y_j^2) \sum_{k=1}^m \sigma_k W_{jk}, j \in \{1, 2, \dots, n_2\}. \quad (6)$$

- (6) Correct the connection weight  $W_{jk}$  of the output layer node  $K$  and the hidden layer node  $J$ , and correct the threshold of the output layer node  $K$ . The following is the error correction amount calculated in step (5).

$$W_{jk}(t+1) = W_{jk}(t) + \alpha \sigma_k Y_j^2 \quad (7)$$

$$\theta_k(t+1) = \theta_k(t) + \beta \sigma_k.$$

- (7) Modify the connection weight  $W_{ij}$  of hidden layer node  $J$  and input layer node  $I$ , and modify the threshold of hidden layer node  $j$ . The following is the error correction amount calculated in step (6).

$$W_{ij}(t+1) = W_{ij}(t) + \alpha \sigma_j Y_i^1 \quad (8)$$

$$\theta_j(t+1) = \theta_j(t) + \alpha \sigma_j.$$

- (8) If the complete learning sample is not taken, go to step (2).
- (9) Calculate the error function  $E$  and judge whether it is less than the specified upper limit of error. If it is less than the upper limit of error or the limit of learning times, the algorithm ends. Otherwise, update the learning times ( $t = t + 1$ ) and return to step (2).

The following Figure 5 is the flow chart of BP neural network.

**5.2. Genetic Algorithm.** In genetic algorithms of each generation, individuals are chosen in accordance with the fitness of individuals in the problem domain and combined crossover and mutation are performed aided by genetic operators so as to generate a population which represents the new solution set. The process will cause the population's offspring to be more adaptive to the environment than their previous generation, just like what happens in natural



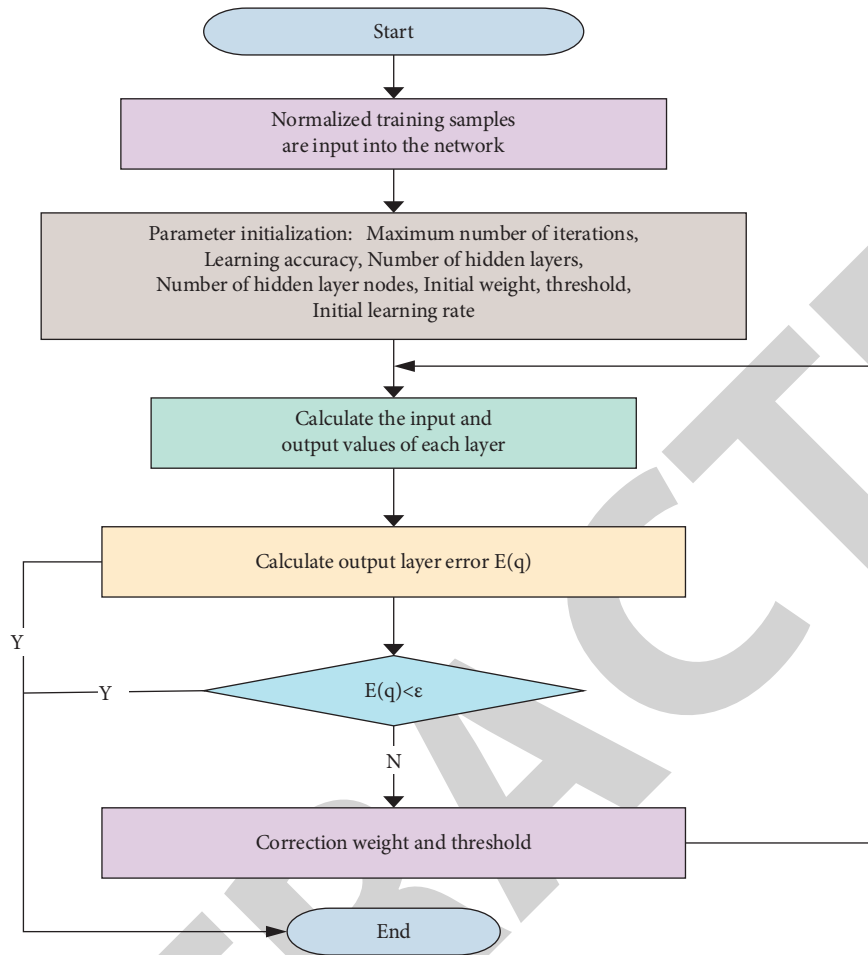


FIGURE 5: BP neural network flow chart.

evolution. When the decoding is completed, the optimal individual in the last generation of population can be regarded as the approximate optimal solution of the problem. Genetic algorithm undergoes the following basic steps:

- The coding strategy is selected to transform the parameter set (feasible solution set) into chromosome structure space;
- Define fitness function to calculate fitness value;
- Determining genetic strategies, including selecting population size, selection, crossover and mutation methods, and determining genetic parameters such as crossover probability and mutation probability;
- Randomly generate initialization population;
- Calculate the fitness value of individuals or chromosomes in the population after decoding;
- According to the genetic strategy, the selection, crossover and mutation operators are used to act on the population to form the next generation population;
- Judge whether the population performance meets a certain index or has completed the predetermined

number of iterations. If not, return to step 5, or modify the genetic strategy and return to step 6.

The flow chart of genetic algorithm is shown in Figure 6.

### 5.3. BP Neural Network Optimized by Genetic Algorithm.

Because the initial weight and threshold in BP neural network are randomly generated, the model obtained through learning may not be optimal and may fall into local optimal solution. At the same time, BP neural network is able to perform self-learning and negative back propagation of training error in the internal structure of the network. Therefore, genetic algorithm can be used to optimize and analyze the weight and threshold of BP neural network, the sum of the output absolute error of the optimized BP neural network is deemed as the fitness function of the genetic algorithm. The lower the fitness value of the response value, the better the approximation effect of the neural network, and the smaller the sum of the corresponding absolute error, thus optimizing the BP network and iteratively obtaining the optimal BP network weight and threshold. Finally, the global optimal solution is obtained by fine tuning with BP algorithm. The flow chart of BP neural network optimized by GA is shown in Figure 7.

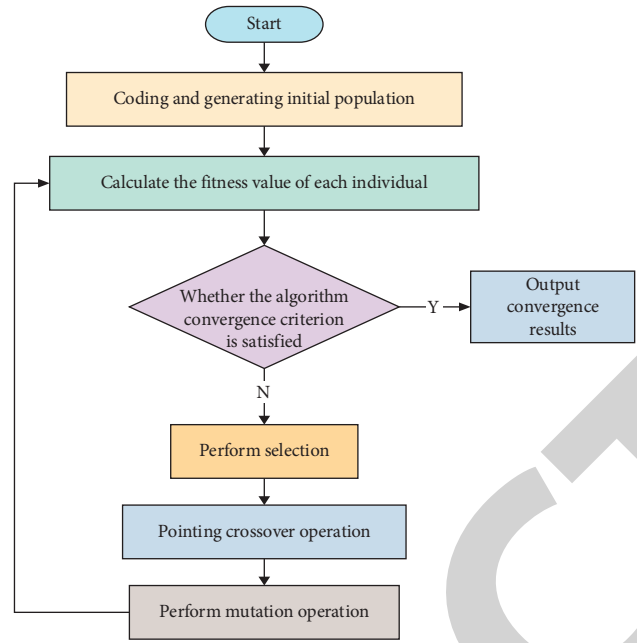


FIGURE 6: Flow chart of genetic algorithm.

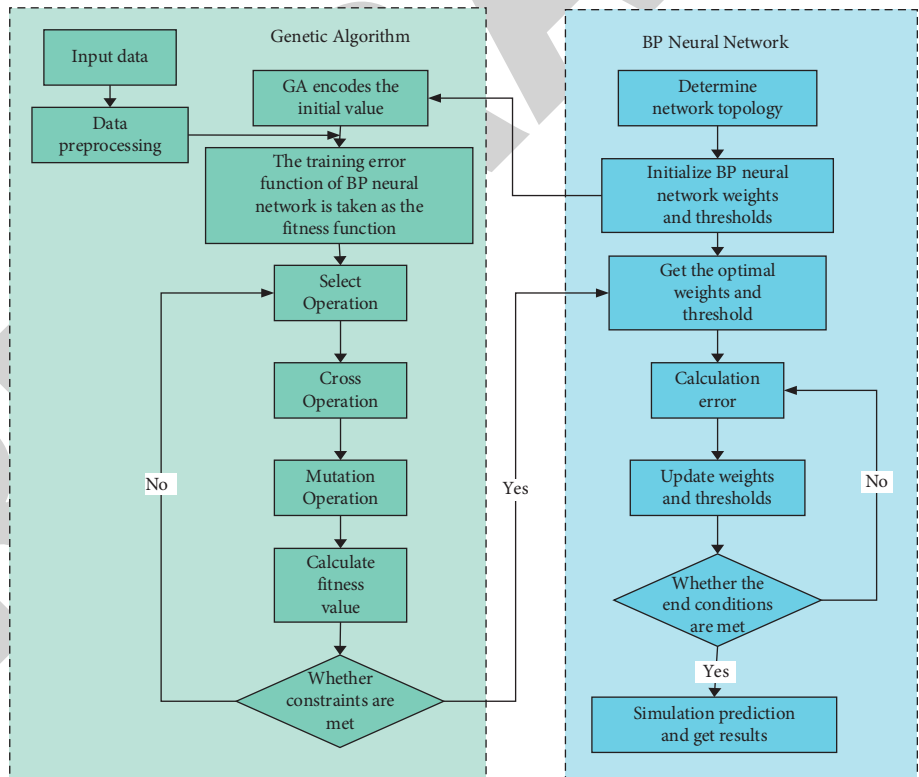


FIGURE 7: Flow chart of BP neural network optimized by GA.

In this paper, genetic algorithm and BP neural network are used for knowledge discovery and trend analysis in TCMAB. It has a fast response to the analysis between linear and nonlinear uncertain attributes. It can effectively manage

the digital content of semi-structured ancient books of traditional Chinese medicine, realize the remote access of TCMAB, and form a practical, leading and omni-directional retrieval function of TCMAB.

## 6. Design of Database System for TCMAB Bibliographic Abstracts

The overall model design of the database system of TCMAB bibliographic abstracts is based on the construction process of knowledge map. The system platform adopts B/S mode, eXist database management system, PowerSSP streaming media and video server for audio video processing. This section first analyzes the design objectives and functional requirements, then expounds the structural design based on XML database and the construction scheme of TCMAB bibliographic database system.

*6.1. Design Goal.* The database system of TCMAB bibliographic abstracts is the premise and foundation of TCMAB resource sharing. How to effectively manage the resources of TCMAB is the key to construct the resource management system of TCMAB. The design principle of TCMAB bibliographic abstracts database system should be able to provide efficient storage and management for all kinds of ancient Chinese medicine books cataloging documents, and provide users with convenient fast storage and retrieval functions at the same time. The design shall meet the following requirements.

- (1) According to the “Metadata Specification for Ancient Books”, “Metadata Specification for Special Digital Object Description” and international DC metadata, formulate the metadata specification for the bibliography of TCMAB, extract each cataloging file into an XML document conforming to the metadata specification for the bibliography of TCMAB, and realize the unified description of ancient book resources in the bibliographic summary database system of TCMAB, for the cross platform sharing of ancient book resources.
- (2) The native XML database exist is used to store and manage the XML documents of all TCMAB resources to ensure that the structural information in the XML document can be completely saved.
- (3) In the process of collecting TCMAB, there are relevant multimedia resources such as ancient book interpretation recording and introduction animation or video of medicinal materials, prescriptions and characters. Using the metadata specification of TCMAB, the multimedia data and XML data are integrated to display TCMAB to users in an all-round way.
- (4) The TCMAB are classified according to their different sources, and different access rights are set for different users.
- (5) According to the metadata specification of TCMAB, it can support multi-condition retrieval and keyword retrieval. At the same time, due to the particularity of XML database, users can directly use XQuery statements to retrieve, so that users can retrieve the required content accurately and flexibly.

*6.2. System Functional Requirements.* System users are divided into ordinary users and administrators. The following Figure 8 is use case diagram and Figure 9 is UML class diagram. Ordinary users do not need login authentication to directly enter the main page of the bibliographic summary database system of TCMAB. Ordinary users only have the retrieval function and can query the resources in the system vaguely or accurately, after the search conditions are submitted, the system will return the search result list. Ordinary users have the permission to view the details and can view the details of the ancient book bibliography, the database system of TCMAB bibliographic abstracts provides the function of resource download for ordinary users.

Compared with ordinary users, the administrator needs user login verification. After successful login, enter the home page of the administrator’s bibliographic summary database system of ancient Chinese medicine. In addition to all the permissions of ordinary users, the administrator can manage the ancient book resource data uploaded by the system, including adding, deleting and modifying. You can not only add bibliographic records of ancient books one by one, but also upload a catalogue file of ancient books.

*6.3. Design of Database Model Based on Knowledge Map.* By collecting the bibliographic data of TCMAB and studying the related technology of knowledge map, the knowledge map model of ancient books designed in this paper is shown in Figure 10. The model includes resource acquisition layer, knowledge unit processing layer, relation representation layer and application layer.

In Figure 10, the resource acquisition layer is at the bottom of the model, its main function is to obtain resource information through existing literature, paper and electronic data. The resource acquisition layer is the main source of database information. The knowledge unit processing layer is mainly responsible for the correlation analysis of the data obtained by the resource acquisition layer, to form an independent knowledge unit and establish an index for it. The main function of the relation presentation layer is to reveal the relationship between knowledge nodes links and knowledge relations. By establishing the correlation between each knowledge node, the knowledge units with different structures are connected in series to form an intertwined knowledge network, so as to provide basic data for cross database retrieval and correlation analysis of traditional Chinese medicine book knowledge in the application layer. The application layer is mainly responsible for providing friendly human-computer interaction interface, and different users provide different services. For ordinary Internet users, the system mainly provides users with basic traditional Chinese medicine knowledge browsing and query. For traditional Chinese medicine experts and administrators, the system mainly provides deeper knowledge maintenance, knowledge index and knowledge relation services.

As can be seen from Figure 10, this paper constructs the model from two perspectives. The first perspective is from the system administrator. The model improves the knowledge service of traditional Chinese medicine books layer by

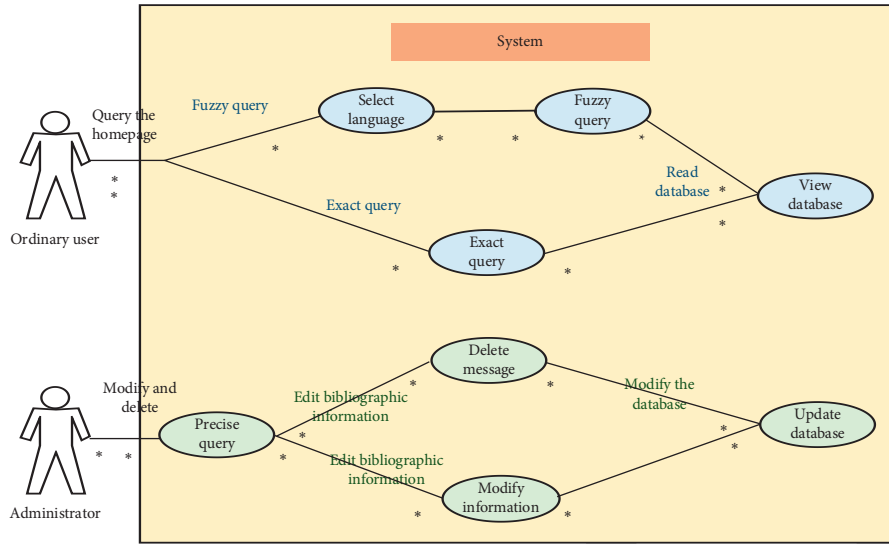


FIGURE 8: System user use case diagram.

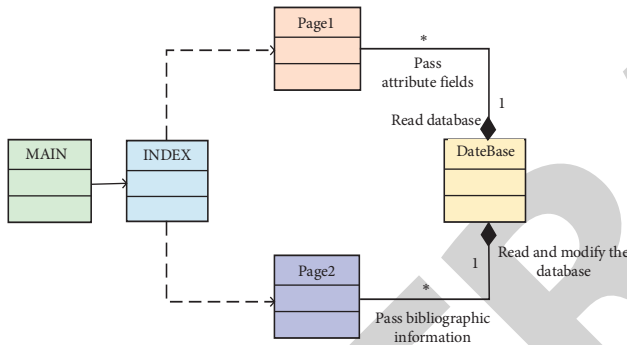


FIGURE 9: UML class diagram.

layer from resources to services, and from bottom to top by continuously deepening the humanistic knowledge service. From the perspective of user-friendly query, we can provide users with the information from the perspective of user-friendly query. The second problem is to provide users with a convenient query interface.

6.4. Retrieval Method.

- (1) Forward consistent retrieval. When the user enters any phrase in the specified search input port, the system will display all records starting with the phrase in the corresponding fields of the database. For example, if you enter "Jilin Province" in the "title" input box, the system will display all records whose "title" begins with "Jilin Province".
- (2) Arbitrary word retrieval. When the user enters any phrase in the specified search input port, the system will display all records containing the phrase in the corresponding fields of the database. Any content can be entered in the search box for search, including book name, author, keyword and other information. Advanced search can be used between multiple search items. The search result page can realize

cluster search, and can see the definition, word network and item information contained in the keyword. For example, enter "Jiutai" in the "title" input box, and the system will display all records containing "Jiutai" in the "title".

- (3) Completely consistent retrieval. When the user enters any phrase in the specified search input port, the system will display all records containing only the phrase in the corresponding fields of the database. For example, if "Xin'an Medical Books" is entered in the "title" input box, the system will display all records whose "title" is "Xin'an Medical Books".
- (4) Full text search. The system can retrieve any phrase or phrase combination in a field of the database and display their records. For example, enter "Changchun City" + "Jiutai" in the "content introduction" search entry, and the system will display the records containing "Changchun City" and "Jiutai" in the content introduction, in which "Changchun City" and "Jiutai" are highlighted in other colors.
- (5) Classified retrieval. It contains clinical knowledge base, classic prescriptions, materia medica, health preservation library and famous doctor library. It contains medical figures from ancient legends to the late Qing Dynasty, which can be classified and searched.
- (6) Knowledge map analysis and presentation. Use knowledge map technology to realize visualization, support the analysis, presentation of word network, knowledge discovery and book academic development trend map.
- (7) Retrieval approach. The system can search a record through multiple search points, such as title, author, collection place, content introduction, or combine multiple search points through the logical relationship of "and", "or". Support the multi-channel

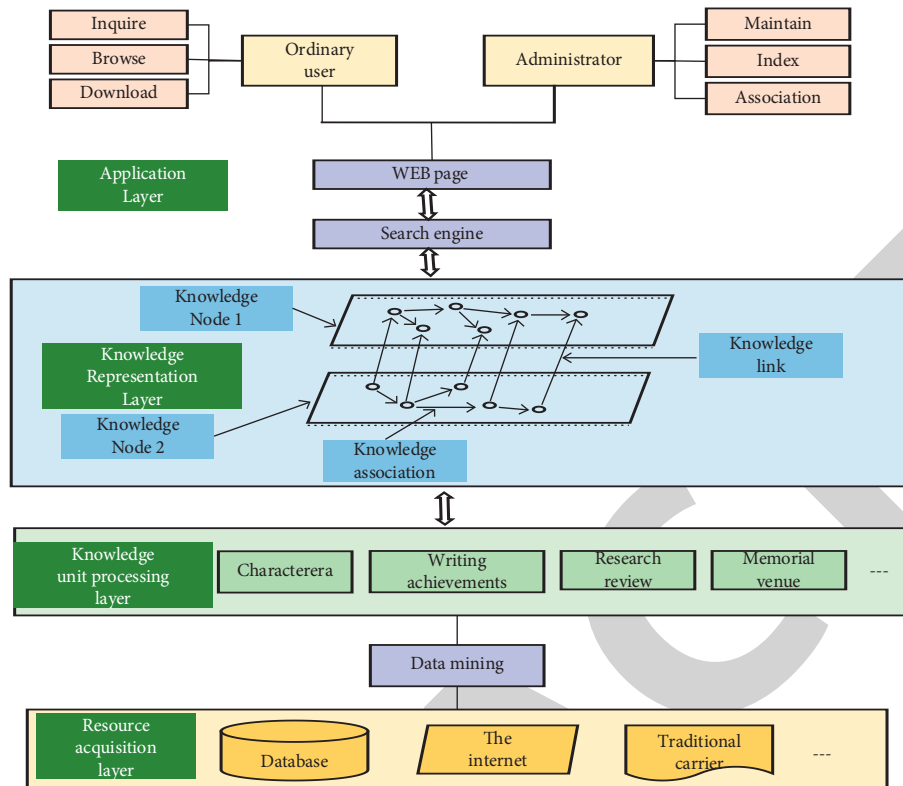


FIGURE 10: Database construction model based on knowledge map.

knowledge classification acquisition of medical books, can enter the conditions of any search item for combined search, and quickly find the required books or materials.

**6.5. Streaming Media Technology.** In the process of collecting TCMAB, there are relevant multimedia resources such as interpretation recording of ancient books, introduction videos of medicinal materials, prescriptions and characters. Streaming media technology integrates multimedia data with XML data to display TCMAB to users in an all-round way.

Streaming media video server is the center of media data storage and publishing. The storage capacity, number of concurrent users, stability and image quality of VOD are directly determined by the performance of streaming video server. PowerSSP streaming media video service system is based on a distributed architecture, which unifies PC streaming media, ipTV and mobile streaming media on one platform, adopts the platform structure of centralized governance and distributed services, realizes CDN content distribution, supports hierarchical program distribution and storage, adopts more optimized active and intelligent global content management and system load dynamic balance.

PowerSSP streaming media video service platform includes three layers: streaming media service layer (PowerMedia), CDN content distribution layer (PowerCDN) and customer layer. The architecture of PowerSSP streaming media video service platform is shown in Figure 11.

PowerSSP adopts loose coupling structure to realize interconnection among streaming media service layer, CDN content distribution layer and customer service layer through application program interface. CDN Content distribution layer can not only provide CDN content distribution, but also realize CDN content distribution to third-party streaming media system through API.

**6.6. Function Design of Background Data Processing System.** The background data processing system platform of TCMAB bibliography database is divided into four functional modules: document database maintenance, picture database maintenance, character database maintenance and audio and video database maintenance. The functions of adding, deleting and modifying document information, picture information, character information and audio video information are realized respectively. The data entry personnel log in to different function modules according to different permissions. When adding data, the system first checks the duplicate, that is, judge whether there is duplication according to the entered book name, and then judge whether to enter the next entry operation according to the query results. The specific data processing flow is shown in Figure 12.

The background data sorting of the application system can automatically realize the background data sorting without manual intervention. After setting the specific content and time interval of background data sorting, the system will process it automatically and regularly without

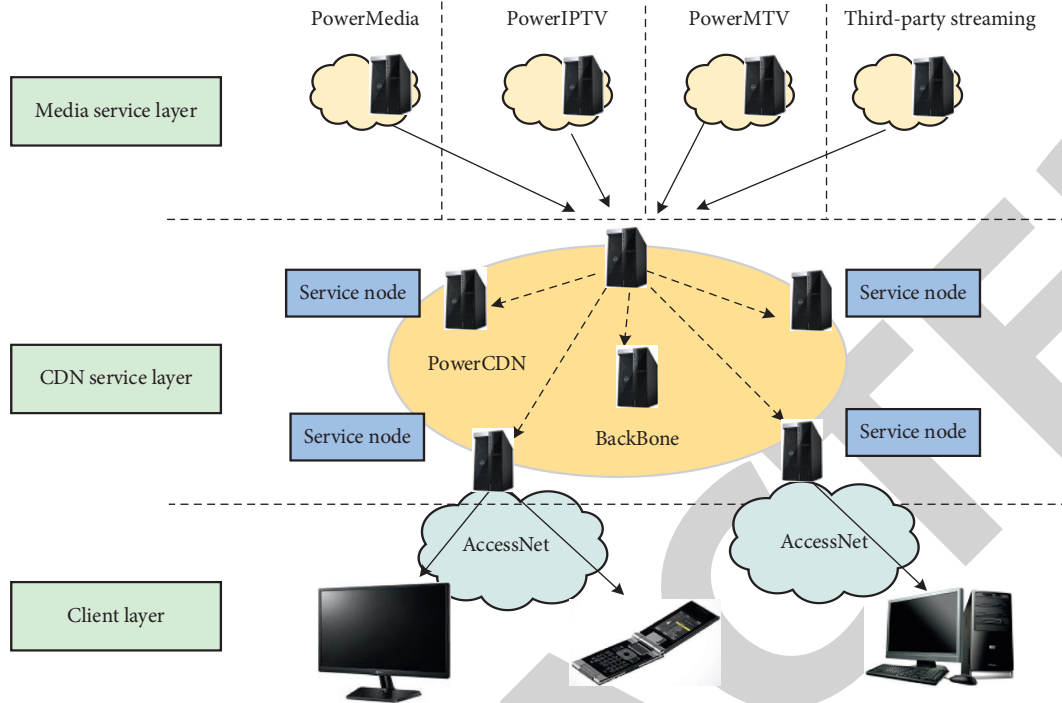


FIGURE 11: Streaming media video service platform architecture.

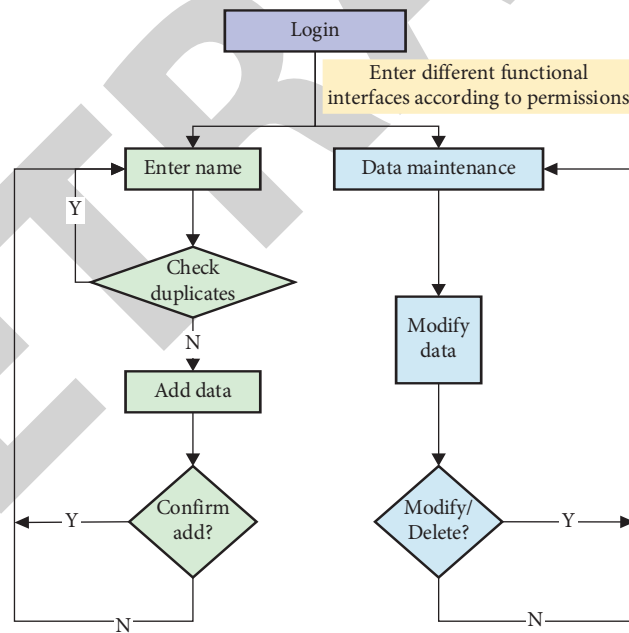


FIGURE 12: Background data processing flow of database.

affecting the foreground application and manual confirmation, it is convenient for users to manage. The content of data processing can change with the change of users' needs. The time of background data storage can be easily controlled from the foreground interface, which is convenient for users to manage. It can also effectively sort out the data. The outdated garbage data can be removed in time, which can adapt to the cleaning of various data quantities. No matter

how the content of data sorting changes, it can ensure the effectiveness of data sorting, automatic dump and storage of historical data. In order to ensure the query and calculation speed of the application system, data storage is divided into two parts: daily database and historical database. Background data sorting should automatically realize the dump of daily data from daily database to historical database, and ensure the integrity and consistency of data logical

relationship. The background data sorting of the database job mechanism realizes the automatic scheduling and execution of the job. The user modifies the data saving time in the client foreground interface, which is actually the content of the database job. Each time the user modifies the data saving time, the system automatically resubmits the database job, and the content of the data sorting can be changed according to the new needs of the user, so as to realize the purpose of controlling data sorting from the client.

## 7. Conclusion and Future Work

The construction of TCMAB knowledge base has become one of the future development directions of ancient books digitization. The means of sorting TCMAB by using modern information technology is gradually improving, the knowledge organization and processing of TCMAB have become more detailed, and the computer expression of TCMAB knowledge has also made a creative breakthrough. The establishment of a unified and standardized bibliographic database to realize the exchange and resource sharing of TCMAB bibliography is also the inevitable trend of TCMAB bibliography digital service. Relying on knowledge mining and other technologies, this paper establishes a bibliographic summary database of TCMAB with unified standards, rules and formats, and realizes the exchange of TCMAB through online resource sharing. The bibliographic database of TCMAB is constantly adjusted, modified and improved in the process of building the database. The field description information suitable for non-professional cataloguers is set, which can be input at one time and searched in multiple directions. This is a centralized sorting and bibliographic information mining of the existing TCMAB, which facilitates network retrieval, improves the utilization rate of bibliographic resources of TCMAB. The research results of this paper is practical and valuable for comprehensively understanding, obtaining version information, discovering and mining knowledge of traditional Chinese medicine.

## Data Availability

The simulation experiment data used to support the findings of this study are available from the corresponding author upon request.

## Conflicts of Interest

The authors declare that there are no conflicts of interest regarding the publication of this paper.

## Acknowledgments

This work was supported by the Scientific Research Project of the Education Department of Anhui Province (Grant no. KJ2021A0903), And The authors wish to thank the anonymous reviewers who helped to improve the quality of the paper.

## References

- [1] F. Xiong and G. Song, "Investigation and research on the construction of digital resources of ancient Chinese medicine books in colleges and universities," *Inner Mongolia Science Technology & Economy*, vol. 7, no. 1 5, pp. 97–107, 2020.
- [2] X. Cao and L. Pei, "Practice analysis and countermeasures of digitization construction of ancient books of traditional Chinese medicine," *Library Science Research*, vol. 16, no. 13, pp. 42–44, 2016.
- [3] W. Shu, K. Cai, and N. N. Xiong, "Research on strong agile response task scheduling optimization enhancement with optimal resource usage in green cloud computing," *Future Generation Computer Systems*, vol. 124, pp. 12–20, 2021.
- [4] J. Yang, J. Liu, R. Han, and J. Wu, "Transferable face image privacy protection based on federated learning and ensemble models," *Complex & Intelligent Systems*, vol. 7, no. 5, pp. 2299–2315, 2021.
- [5] W. W. X. Xia, M. Wozniak, X. Fan, R. Damaševičius, and Y. Li, "Multi-sink distributed power control algorithm for Cyber-physical-systems in coal mine tunnels," *Computer Networks*, vol. 161, pp. 210–219, 2019.
- [6] Z. J. Liu, "Problems and countermeasures of digitization of ancient books," *Library Work and Study*, vol. 10, pp. 50–52, 2019.
- [7] Y. Sun, C. Xu, G. Li et al., "Intelligent human computer interaction based on non redundant EMG signal," *Alexandria Engineering Journal*, vol. 59, no. 3, pp. 1149–1157, 2020.
- [8] W. Shu and Y. Li, "A novel demand-responsive customized bus based on improved ant colony optimization and clustering algorithms," *IEEE Transactions on Intelligent Transportation Systems*, vol. 2022, 2022.
- [9] L. Wang, X. Qi, and S. Yu, "Digital research of traditional Chinese medicine literature," *Journal of Traditional Chinese Medicine Information*, vol. 22, no. 10, 2015.
- [10] U. Akhtar, A. Sant'Anna, and S. Lee, "A dynamic, cost-aware, optimized maintenance policy for interactive exploration of linked data," *Applied Sciences-Basel*, vol. 9, no. 22, 2019.
- [11] S. Chun, J. Jung, and K.-H. Lee, "Proactive policy for efficiently updating join views on continuous queries over data streams and linked data," *IEEE Access*, vol. 7, pp. 86226–86241, 2019.
- [12] J. Hernandez, H. M. Marin-Castro, and M. Morales-Sandoval, "WebQuln-LD: a method of integrating web query interfaces based on linked data," *IEEE Access*, vol. 9, pp. 115664–115675, 2021.
- [13] S. Jeter, C. Rock, B. Benyo et al., "Semantic links across distributed heterogeneous data," in *Proceedings of the Distributed Computing and Artificial Intelligence, 16th International Conference*, vol. 1003, pp. 107–115, Ávila, Spain, June 2020.
- [14] P. Chhaya, C.-H. Choi, K.-H. Lee, W.-S. Cho, and Y.-S. Lee, "KMLoD: linked open data service for Korean medical database," *The Journal of Supercomputing*, vol. 76, no. 10, pp. 7758–7776, 2020.
- [15] J. L. Sánchez-Cervantes, L. O. Colombo-Mendoza, and G. Alor-Hernández, "LINDASearch: a faceted search system for linked open datasets," *Wireless Networks*, vol. 26, no. 8, pp. 5645–5663, 2020.
- [16] A. D. Goncalves and M. D. D. Jacyntho, "A method for linked data semantic publishing of conventional databases and a real case study of academic papers," *Transinformacao*, vol. 32, 2020.

## *Retraction*

# **Retracted: Construction of an Optimal Scheduling Method for Campus Energy Systems Based on Deep Learning Models**

### **Mathematical Problems in Engineering**

Received 18 July 2023; Accepted 18 July 2023; Published 19 July 2023

Copyright © 2023 Mathematical Problems in Engineering. This is an open access article distributed under the Creative Commons Attribution License, which permits unrestricted use, distribution, and reproduction in any medium, provided the original work is properly cited.

This article has been retracted by Hindawi following an investigation undertaken by the publisher [1]. This investigation has uncovered evidence of one or more of the following indicators of systematic manipulation of the publication process:

- (1) Discrepancies in scope
- (2) Discrepancies in the description of the research reported
- (3) Discrepancies between the availability of data and the research described
- (4) Inappropriate citations
- (5) Incoherent, meaningless and/or irrelevant content included in the article
- (6) Peer-review manipulation

The presence of these indicators undermines our confidence in the integrity of the article's content and we cannot, therefore, vouch for its reliability. Please note that this notice is intended solely to alert readers that the content of this article is unreliable. We have not investigated whether authors were aware of or involved in the systematic manipulation of the publication process.

Wiley and Hindawi regrets that the usual quality checks did not identify these issues before publication and have since put additional measures in place to safeguard research integrity.

We wish to credit our own Research Integrity and Research Publishing teams and anonymous and named external researchers and research integrity experts for contributing to this investigation.

The corresponding author, as the representative of all authors, has been given the opportunity to register their agreement or disagreement to this retraction. We have kept a record of any response received.


### **References**

- [1] J. Li and H. Zhao, "Construction of an Optimal Scheduling Method for Campus Energy Systems Based on Deep Learning Models," *Mathematical Problems in Engineering*, vol. 2022, Article ID 5350786, 10 pages, 2022.



## Research Article

# Construction of an Optimal Scheduling Method for Campus Energy Systems Based on Deep Learning Models

Jingyun Li <sup>1,2</sup> and Hong Zhao<sup>1,3</sup>

<sup>1</sup>School of Economics and Management, University of Chinese Academy of Sciences, Beijing 100190, China

<sup>2</sup>Xinjiang Tianfu Jinyang New Energy Co., Ltd, Shihezi 832000, China

<sup>3</sup>Sino-Danish College, University of Chinese Academy of Sciences, Beijing 100190, China

Correspondence should be addressed to Jingyun Li; [lijingyun18@mails.ucas.edu.cn](mailto:lijingyun18@mails.ucas.edu.cn)

Received 10 February 2022; Accepted 7 March 2022; Published 31 March 2022

Academic Editor: Man Fai Leung

Copyright © 2022 Jingyun Li and Hong Zhao. This is an open access article distributed under the Creative Commons Attribution License, which permits unrestricted use, distribution, and reproduction in any medium, provided the original work is properly cited.

Aiming at the problem of high cost and low efficiency of planning and scheduling caused by load uncertainty of campus energy system, a 3-layer planning and scheduling model based on multivariate load prediction is proposed, mainly including prediction layer, planning layer, and scheduling layer; a long-term and short-term prediction model of multivariate load is constructed based on random forest regression network and long and short-term memory network. With the objective of minimizing the comprehensive planning and scheduling cost and the scheduling operation cost, the optimal comprehensive system cost and configuration scheme are obtained by using improved particle swarm algorithm and CPLEX solver; the equipment status and system cost are analyzed by planning and scheduling under different scenarios. By comparing the planning and scheduling results of the constructed 3-layer model with the conventional two-layer model, the economy and reliability of the 3-layer planning and scheduling model are demonstrated.

## 1. Introduction

Overdependence on fossil energy has always been one of the serious problems limiting energy development. According to the current demand of energy for social development of each country, the storage of oil, fossil, and other nonrenewable energy sources will no longer be able to supply the sustainable development of human society in the long term. Facing the serious energy problem, China tries to find the solution to the problem from the perspective of “integrated energy” which is complemented by renewable energy and traditional energy [1]. Therefore, under the background of national strong support for the construction of renewable energy power plants, the new energy generation led by wind power and photovoltaic has been developed rapidly.

When wind power and photovoltaic power generation units are connected to the power grid, the random fluctuation of their output will have an impact on the safe and reliable operation environment of the power grid. Although

experts and scholars at home and abroad are carrying out research on improving the accuracy of wind power and photovoltaic output prediction, it is difficult for the prediction results to achieve satisfactory accuracy and there are prediction errors. In recent years, with the continuous expansion of renewable energy entering the power market, the operation of power grid is to ensure safety and reliability, and reduce the proportion of power generation from other energy sources. These phenomena are consistent with the national energy development trend [2]. Integrated energy system is a small energy system that organically combines wind power, PV, and other distributed renewable power sources, user multienergy demand, energy coupling equipment, and multienergy storage devices, with self-management and control functions, providing an effective solution for new energy access and consumption [3].

In the integrated energy system, multiple forms of energy flow in the system, effectively promoting the complementary and coordinated use of energy sources, while

helping to improve energy utilization efficiency, increase the penetration rate of renewable energy in the grid, reduce  $CO_2$  emissions, reduce the pollution caused by fossil energy to the environment, and achieve the purpose of reducing operating costs [4]. The park-level integrated energy system is an important carrier to achieve energy synergy and complementarity, and the coupling of multiple energy sources and the coordination of power output between devices in the park can be used to achieve efficient utilization of energy, while reducing operating costs and increasing the consumption of renewable energy. In summary, it is important to conduct in-depth research on the integrated energy system at the campus level [5].

In summary, this paper takes multienergy complementarity, cost saving, efficient energy use, and green environment protection as the starting point, addresses the problems of complex energy coupling in the system, difficulty in optimal scheduling, and uncertainties on the supply side and user side, takes the actual industrial park as an example, and establishes the park based on the analysis of the mathematical model of the park equipment and prediction uncertainties; combined with conditional risk value assessment CVaR theory and model prediction control the project is based on the analysis of the mathematical model of the park equipment and the prediction determinism. The project inherits and carries forward the advantages of integrated energy system optimal scheduling from existing research and has practical significance [6].

## 2. Related Work

At present, domestic and foreign scholars' research on integrated energy systems mainly focuses on four aspects: modeling and energy flow analysis, market multiactor game, coordinated planning, and optimal scheduling. In terms of energy flow analysis research, [7] introduces the concept of probabilistic energy flow in integrated energy systems, and [8] analyzes the energy flow of electricity-gas hybrid networks based on the maximum entropy principle. Paper [9] analyzed in detail the coupling and conversion of energy sources in the system based on the energy hub model for optimal scheduling of regional integrated energy systems. For the uncertainties of wind power and PV access and electric and thermal loads, [10] establishes interval energy flow models and probabilistic optimal models, respectively, to reduce the impact of uncertainties on the system. In terms of the market multisubject game, [11] constructed a stochastic optimization model of the park considering cooperative alliances and a multisubject benefit distribution model. According to different game subjects, the study of multisubject game in integrated energy system covers dynamic game among power generation companies, grid companies, and natural gas companies [12], master-slave game among energy sellers and combined cooling, heating, and power operators and load aggregators [13], and demand response evolution game among users based on nodal energy prices [14], etc. In terms of integrated energy system coordination planning, [15] established a regional system planning model considering interconnection interactions

and analyzed the model in terms of energy station planning, energy network planning, and joint station-network planning in different scenarios to provide an outlook. In [16], a source-side capacity planning model that takes into account economy and safety is established to realize the siting and capacity determination of power generation devices and energy storage devices. In [16], a phased planning model and a multistage planning model for integrated energy systems were developed and solved with the objective of minimizing investment cost and operation cost, respectively.

As for the optimal scheduling of integrated energy systems, experts and scholars at home and abroad mostly study the output scheduling plan of each unit when the system operating cost is minimal from the perspective of system economy and have achieved certain research results. Paper [17] considered the energy storage characteristics of water storage tanks and their influence on the operating cost of the park from the actual industrial park and established a day-ahead economic dispatching model. Paper [18] used the distribution robust optimization method to deal with the uncertainty of wind power output and established a day-ahead economic dispatch opportunity constraint model. Paper [19] conducted a two-stage day-ahead economic dispatch based on load forecast uncertainty and introduced customer-side demand response. Paper [14] also established a multilayer economic dispatch model with the objective of minimizing operating cost. Among them, the upper layer of the model is a mixed integer linear programming MILP model and the lower layer is transformed into a Karush-Kuhn-Tucker optimality condition, and the model is solved more efficiently. In [15], a regional integrated energy system is studied and PV plants and energy storage devices are added to the model to give the corresponding dispatching strategies. In [16], the optimization model of electric and thermal integration is established from the perspective of heat network complexity. The objective function of the model is to minimize the operating cost and the amount of abandoned wind, and the results of the example verify the promotion of wind power consumption by the energy synergy and complementarity of electricity-thermal system.

Based on the mathematical model of the park system, [16] points out two key points in the future research of the integrated energy system model of the park from the perspective of practical requirements: first, to consider the imbalance of the scheduling results caused by the prediction errors on both sides of the source-load and to construct an optimized scheduling model with good robustness. Secondly, the system should combine day-ahead scheduling with intraday real-time scheduling to build a refined scheduling model when operating optimally. To verify the advantages of the integrated energy system of the multi-energy complementary park over the traditional single energy system in terms of economy, a two-stage optimal scheduling model of the park system was established in [17]. The results show that the integrated energy system of the park has more advantages and benefits in terms of economy, energy consumption, and pollution compared with the traditional single energy system. To verify the advantages of the integrated energy system in enhancing energy

utilization, [18] established evaluation indexes and evaluation models for the system regarding energy efficiency to reflect the utilization characteristics of multiple energy sources. The final results show that the proposed evaluation indexes can be effectively applied to the preevaluation of the energy efficiency of the integrated energy system in the park. It has implications for the optimal scheduling of the park system.

### 3. Modeling and Analysis of Integrated Energy Systems in Parks

**3.1. Integrated Energy System Structure of the Campus.** An industrial park is used as an example for optimal scheduling research. The structure diagram of the integrated energy system of the park is shown in Figure 1. The main energy equipment in the park includes gas turbines and supporting waste heat boiler equipment, gas boilers, steam drive equipment, air conditioning and refrigeration systems, ice storage and cooling units, absorption refrigeration units, photovoltaic units, battery energy storage devices, etc. The system supplies the electrical load through a centralized busbar. Thermal energy is used in a stepwise manner to supply the steam load, hot water load, and cooling load of the system.

According to the energy flow direction in Figure 1, it can be seen that the total electrical load in the park contains the AC load and DC load for production in the park, the input electrical power for air conditioning and cooling, and the input electrical power for the ice storage and cooling device, and the electrical energy is supplied by the superior power grid, gas turbine, photovoltaic unit, and electric energy storage device together. The steam load of the park is fully supplied by the steam-driven equipment. The thermal load contains the hot water load and the thermal power consumed by the absorption chiller for cooling, which is supplied jointly by the waste heat boiler and the thermal energy recovered by the steam-driven equipment. The cooling load of the park is supplied by a combination of air conditioning and ice storage cooling units.

The heat energy of the park exhibits a graded utilization characteristic. Stepped utilization of thermal energy refers to the classification of thermal energy in the system into high-grade heat, medium-grade heat, and low-grade heat according to temperature requirements. Grade refers to the proportion of available energy per unit of energy, and the higher the temperature, the higher the grade of thermal energy. The park improves energy utilization efficiency and reduces energy consumption through graded utilization of thermal energy. The high-grade heat in the heat energy gradient is used in high-temperature thermal cycle equipment such as gas turbine, which is manifested by the combustion of natural gas in the combustion chamber to produce high-temperature flue gas of 1000°C into the gas turbine to expand and do work for power generation. The discharged 500°C high-temperature flue gas is recovered by the waste heat boiler and processed into medium-grade heat, which is used to supply steam load or as heat source for other energy conversion equipment. Low-grade heat from the

waste heat boiler flue gas recovery temperature is lower, usually about 100°C, demand is small, and the utilization rate is often not high, usually only used to supply hot water load or as a heat source for absorption chillers.

**3.2. Equipment Mathematical Model.** To optimize the scheduling of the integrated energy system in the industrial park for optimal analysis of investment decisions, the mathematical modeling of the equipment in Figure 1 is performed first. The mathematical model of each equipment is as follows.

From the perspective of power system, gas turbine is also a kind of distributed power supply, which has the characteristics of high controllability, rapid start-stop, small size, low operating environment requirement, and high energy utilization rate. It converts natural gas into electricity, and the heat released in the conversion process is recovered by the supporting waste heat boiler, and the recovered heat energy is distinguished into medium-grade heat energy and low-grade heat energy according to the temperature. The correlation equations are shown in equations (1) to (3).

$$P_{GT,i}^t = \eta_{GT}^e \lambda_{gas} G_{GT,i}^t, \quad (1)$$

$$H_{WH,mid,i}^t = \eta_{WH,mid}^h (1 - \eta_{GT}^e) \lambda_{gas} G_{GT,i}^t, \quad (2)$$

$$H_{WH,low,i}^t = \eta_{WH,low}^h (1 - \eta_{GT}^e) \lambda_{gas} G_{GT,i}^t, \quad (3)$$

where  $P_{GT,i}^t$ ,  $G_{GT,i}^t$  are the electric power output and natural gas power input of the  $i$ -th gas turbine at time  $t$ .  $\eta_{GT}^e$  is the gas turbine conversion efficiency.  $\lambda_{gas}$  is the natural gas calorific value.  $H_{WH,low,i}^t$ ,  $H_{WH,mid,i}^t$  are the waste heat boiler medium-grade heat and low-grade heat recovery power.  $\eta_{WH,low}^h$ ,  $\eta_{WH,mid}^h$  are the waste heat boiler medium-grade heat and low-grade heat recovery efficiency.

As a common heat producing equipment in integrated energy systems, gas boilers consume natural gas to produce medium-grade hot steam to meet the system's steam load and hot water load in a campus. The input natural gas power and output medium-grade hot steam power of a gas boiler have the following relationship:

$$H_{GB,i}^t = \eta_{GB}^h \lambda_{gas} G_{GB,i}^t, \quad (4)$$

where  $H_{GB,i}^t$  and  $G_{GB,i}^t$  are the medium-grade thermal power and the input natural gas power of the  $i$ -th gas boiler at time  $t$ .  $\eta_{GB}^h$  is the heating efficiency of gas boiler.

Absorption chillers are important cold and heat coupling equipment in industrial production processes. Absorption chillers utilize medium-grade heat and low-grade heat for refrigeration operations, and the refrigeration power is

$$F_{Br,i}^t = I_{Br}^c H_{Br,in,i}^t, \quad (5)$$

where  $F_{Br,i}^t$ ,  $H_{Br,in,i}^t$  are the output cooling power and input thermal power of the  $i$ -th absorption chiller at time  $t$ .  $I_{Br}^c$  is the refrigeration energy efficiency ratio.

The air conditioning and refrigeration system provides the necessary temperature environment for industrial

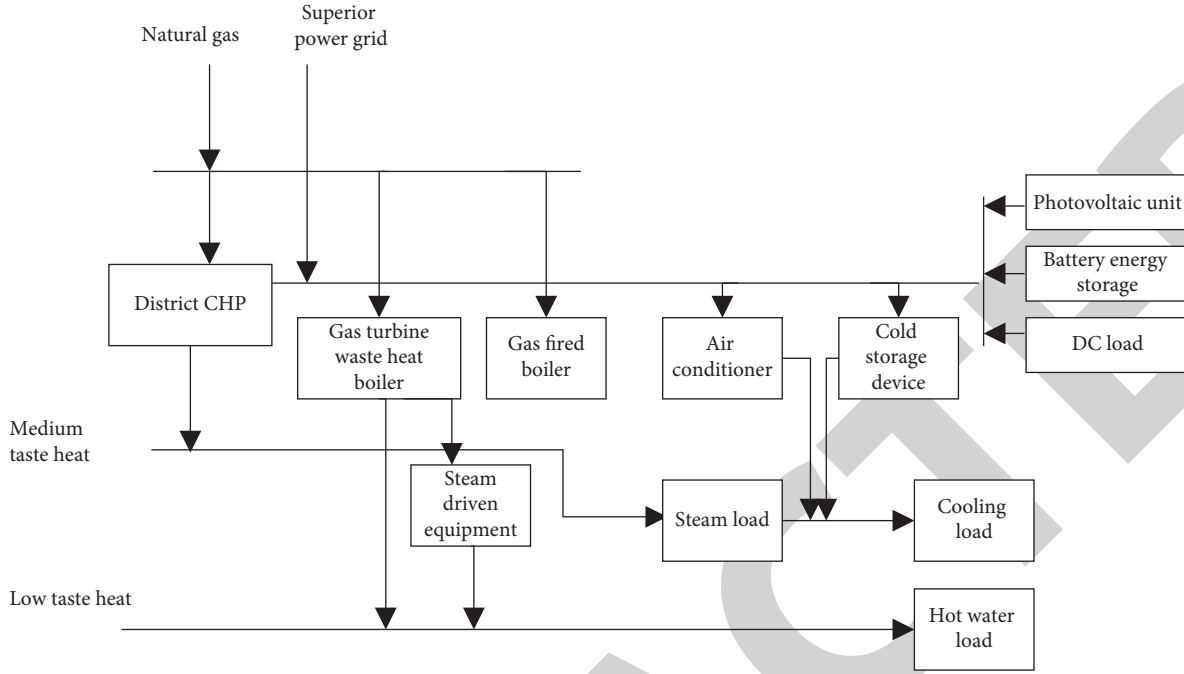


FIGURE 1: Structure diagram of the integrated energy system of the industrial park.

production and is an important electric refrigeration equipment with a refrigeration power of

$$F_{\text{air},i}^t = I_{\text{air}}^c P_{\text{air},i}^t, \quad (6)$$

where  $F_{\text{air},i}^t$ ,  $P_{\text{air},i}^t$  are the cooling power output and the electrical power input of the  $i$ -th air conditioning unit in time period  $t$ .  $I_{\text{air}}^c$  is the cooling energy efficiency ratio of the air conditioner.

#### 4. Predictive Layer Model

**4.1. Long-Term Load Forecasting Model.** The integrated energy planning stage requires long-term planning and coordination of the system by equipment life cycle as well as annual repair and maintenance costs, while the cooling, heating, and electrical loads require long-term forecast data to meet the long-term reliability requirements in the planning stage. The random forest regression (RFR) algorithm [10] has the advantages of low parameter setting and fast convergence  $G(k, \nu)$  and can still show strong generalization ability when dealing with large amounts of data and can effectively avoid overfitting problems, which is suitable for long-term load forecasting scenarios with large amounts of data. The algorithm integrates several classification and regression trees (CART), and the best cut points and cut features can be selected by traversing the features and feature values during model training, and then the weighted sum of the impurity of the cut nodes is obtained to measure the merits of the cut points to obtain accurate prediction values. In this paper, the impurity function of squared average error is used for calculation, as shown in the following equation:

$$G(k, \nu) = \frac{1}{s} \left( \sum_{j_i \in J_{\text{left}}} (j_i - \bar{j}_{\text{left}})^2 + \sum_{j_i \in J_{\text{right}}} (j_i - \bar{j}_{\text{right}})^2 \right), \quad (7)$$

where  $k, \nu$  are the value of the tangent variable and the tangent component, respectively;  $s$  is the number of all training samples of the current node;  $J_{\text{left}}, J_{\text{right}}$  are the set of training samples of the left and right subnodes, respectively; and  $\bar{j}_{\text{left}}, \bar{j}_{\text{right}}$  are the average of the training samples of the left and right subnodes, respectively. RFR obtains the prediction output by averaging all CART predictions integrated internally. The multivariate load long-term prediction model is shown in Figure 2.

**4.2. Short-Term Load Forecasting Model.** The integrated energy system needs to be optimally adjusted according to the short-term load in order to obtain a better solution and a more economical system operation cost during the actual operation, so the load forecasting needs to be performed for the scheduling phase with short-term forecasting. The long short-term memory (LSTM) [12] prediction algorithm has better robustness and memory capability in the process of load prediction, and it can overcome the problem of lack of long-term memory capability and gradient anomaly in recurrent neural networks and has more accurate prediction results than other algorithms. LSTM prediction can be generally divided into 3 stages.

Stage 1: Selecting the forgetting stage. The forgetting gate determines the discarded information, which is processed by the sigmoid unit, and the weight is set to a value between 0 and 1. When the weight is 0, all the information is discarded, and when the weight is 1, all

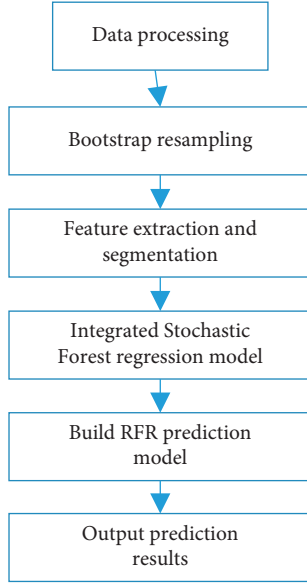


FIGURE 2: Long-term multivariate load forecasting process based on RFR.

the information is kept, and after processing, we get  $f_t$ ,  $m_t$ .

Stage 2: Selective update stage. First, the input gate is selectively updated by  $y_{t-1}$  and  $x_t$ , and then the updated state information is obtained through the tanh layer  $\tilde{u}_t$ , and the newly formed  $\tilde{u}_t$  is added to the selection information to obtain the new information  $u_t$ .

Stage 3: Output stage. The new  $u_t$  is processed with the input  $y_{t-1}$  and  $y_t$  by the sigmoid unit to obtain  $o_t$ , and the information  $u_t$  is multiplied with the new information by the tanh layer to obtain the output  $y_t$ . The specific equation is as follows:

$$\begin{cases} f_t = \sigma(\mathbf{W}_f[y_{t-1}, x_t] + b_f), \\ m_t = \sigma(\mathbf{W}_m[y_{t-1}, x_t] + b_m), \\ \tilde{u}_t = \tanh(\mathbf{W}_u[y_{t-1}, x_t] + b_u), \\ u_t = f_t u_{t-1} + m_t \tilde{u}_t, \\ o_t = \sigma(\mathbf{W}_o[y_{t-1}, x_t] + b_o), \\ y_t = o_t \tanh(u_t), \end{cases} \quad (8)$$

where  $W$  is the weight matrix in the corresponding state;  $b$  is the bias vector in the corresponding state;  $x_t$  is the current moment input;  $y_t$ ,  $y_{t-1}$  are the current moment and the previous moment output, respectively;  $o_t$  is the current moment information;  $u_t$ ,  $u_{t-1}$ ,  $\tilde{u}_t$  are the current moment and the previous moment output state and the update phase state, respectively.

Construct a short-term prediction model based on LSTM, set the number of implicit network layers to 1, set the regularization parameter to 0.2, choose the sigmoid function as the activation function, input load data and feature data to train the model and adjust the network parameters

according to Adam's algorithm, and take the mean square error (MSE) function as the loss function.

$$E_{\text{MSE}} = \frac{1}{s} \sum_{i=1}^s (z_i - \hat{z}_i)^2, \quad (9)$$

where  $z_i$ ,  $\hat{z}_i$  are the true value and predicted value, respectively;  $E_{\text{MSE}}$  is the mean square error value.

4.3. *Planning Layer Model.* The planning layer takes the number of equipment types and start-stop status of the integrated energy system as the optimization variables and the overall planning and scheduling cost  $C$  of the system as the objective function, including the initial investment cost of the equipment  $C_B$  and the scheduling and operation cost of the system  $C_{\text{OP}}$ , which is calculated as follows:

$$\begin{aligned} \min C &= C_B + C_{\text{OP}}, \\ C_B &= \sum_{n=1}^N \frac{\tau(\tau+1)^l}{(\tau+1)^l - 1} Q_n \theta_n, \end{aligned} \quad (10)$$

where  $n$  is the equipment index;  $N$  is the total number of  $n$  types of equipment;  $\tau$  is the discount rate for the planning period of the equipment (taken as 6%);  $l$  is the planning life cycle of the equipment;  $Q$  is the rated capacity of the equipment;  $\theta$  is the unit capacity cost of the equipment; the technical and economic parameters of the equipment are given in [13].

$$C_{\text{OP}} = C_{\text{MC}} + C_{\text{EC}} + C_{\text{GC}} + C_{\text{ENV}}, \quad (11)$$

where  $C_{\text{MC}}$  is the operation and maintenance cost;  $C_{\text{EC}}$  is the cost of electricity purchased from the external network;  $C_{\text{GC}}$  is the cost of gas purchased from the external network;  $C_{\text{ENV}}$  is the cost of pollutant treatment, and the equation is as follows:

$$\begin{aligned} C_{\text{MC}} &= v_d \sum_{t=1}^T \sum_n \psi_n P_{\text{out}}^{n,t} \Delta t, \\ C_{\text{EC}} &= v_d \sum_{t=1}^T \lambda_e^t P_e^t \Delta t, \\ C_{\text{GC}} &= v_d \sum_{t=1}^T \lambda_g^t P_g^t \Delta t, \\ C_{\text{ENV}} &= v_d \sum_{t=1}^T (\lambda_e^t P_e^t + \lambda_g^t P_g^t) \Delta t, \end{aligned} \quad (12)$$

where  $v_d$  is the length of the planning period;  $T$  is the length of the optimization period ( $T$  is 24 h);  $\Delta t$  is the dispatch step ( $\Delta t = 1$ );  $\psi$  is the maintenance cost per unit capacity of the equipment;  $P_{\text{out}}^{n,t}$  is the power output of equipment  $n$  at the time;  $\lambda_e^t$  and  $\lambda_g^t$  are the unit prices of electricity and gas energy from the external network at the time;  $P_e^t$  and  $P_g^t$  are the input power of electricity and gas energy at the time  $t$ ;  $\lambda_e$ ,  $\lambda_g$  are the equivalent pollutant emission treatment cost of the system at the time for electricity and gas energy, respectively.

**4.4. Model Solving.** In this paper, we construct a 3-layer model of integrated energy system and apply RFR and LSTM forecasting algorithms to predict long-term and short-term loads, respectively, in the forecasting layer; apply CPLEX solver to plan based on the load forecasting data in the planning layer to obtain the seasonal equipment allocation scheme and the planning initial investment cost; the scheduling layer, based on the allocation scheme in the planning layer and the short-term load forecasting data in the forecasting layer, performs the scheduling operation optimization of the system based on the improved particle swarm algorithm [9] to optimize the scheduling operation of the system and obtain the optimal output state of the equipment and return the obtained scheduling operation cost to the planning layer to calculate the overall planning and scheduling cost of the system to realize the optimal planning and scheduling of the system. The specific model solution is shown in Figure 3.

## 5. Analysis of Algorithm Results

This section is divided into two parts: description of the data of the day-ahead-intraday coordinated optimization model based on the model predictive control MPC and the conditional value-at-risk CVaR and analysis of the scheduling results of the model. In the analysis of the results, we focus on the analysis of the model predictive control MPC and conditional value-at-risk CVaR based on the scheduling results to improve the model economy and the ability to cope with uncertainty risk and to verify the effectiveness of the proposed model.

**5.1. Algorithm Base Data.** The integrated energy system optimal scheduling model established in this paper, day-ahead optimal scheduling, aims to calculate the capacity plan of energy storage devices based on the short-term forecast data of PV output and load demand and through the coupling and complementation between multiple energy devices, with the aim of reducing system operating costs. The results of the scheduling plans of other devices are then input to the intraday rolling optimal scheduling model as a reference. The intraday optimal scheduling further adjusts the power purchase contract and equipment output in real time according to the ultra-short-term forecast of load at each moment, so that the system can maximize the reduction of operating cost without extreme load loss [20]. The intraday rolling optimization scheduling period is 4 hours, and the solution calculation time interval is 15 min, and the scheduling plan is rolled over every 1 hour for a total of 24 times. The data of equipment parameter table, equipment start-up and shut-down maintenance unit cost, and time-of-day tariff of the model based on the model prediction control strategy are the same as those of the model in Section 3. In consideration of minimizing the risk of load loss under extreme scenarios during park operation, the risk preference coefficient in the model built in this paper is taken as  $\lambda = 0.353$ .

Based on the ultra-short-term forecasts of intraday rooftop PV and load demand, the scenario uncertainty is

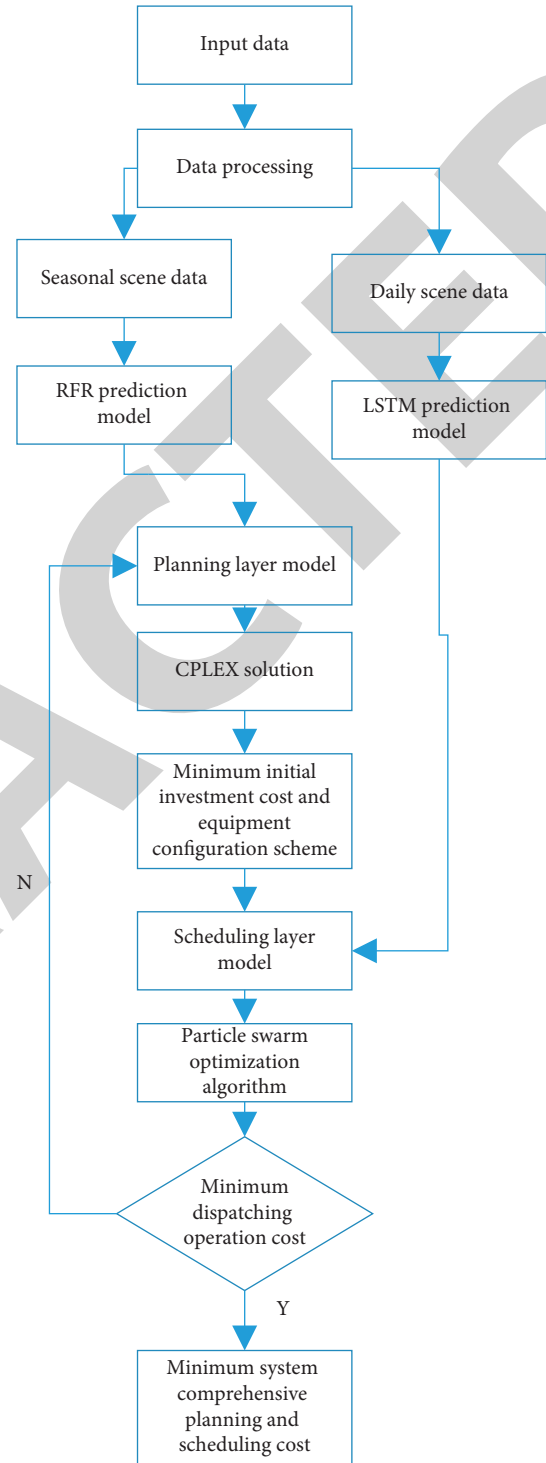


FIGURE 3: Integrated energy system 3-layer model solving process.

processed and the scenario generation and reduction methods are applied to generate five typical scenarios of PV output and load demand as shown in Figures 4 and 5.

**5.2. Analysis of Operating Cost Results.** The intraday rolling optimization corrects the power purchase contract plan of the higher-level grid obtained from the previous day's

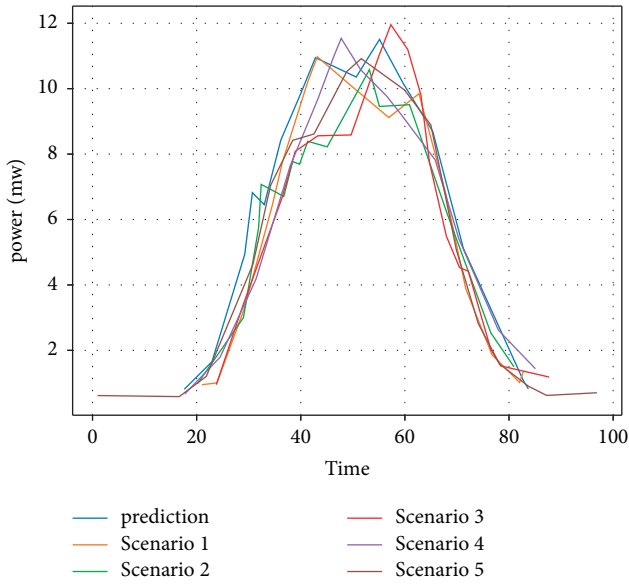


FIGURE 4: A set of typical scenarios for ultra-short-term forecasting of photovoltaic output.

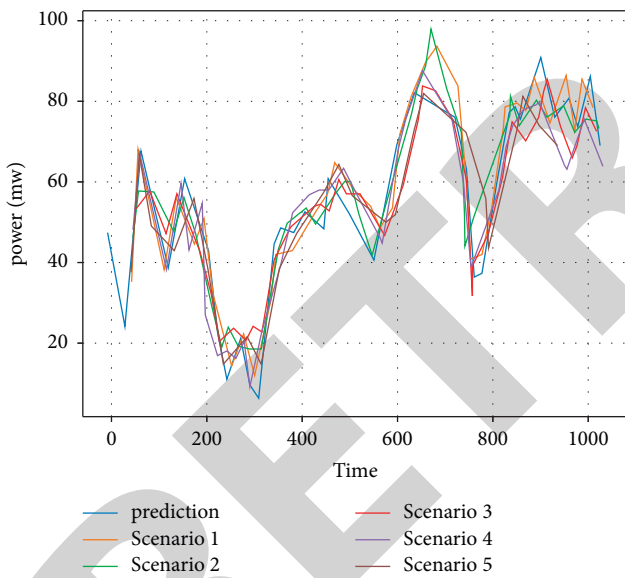


FIGURE 5: A set of typical scenarios for ultra-short-term forecasting of load demand.

dispatch, and the curves before and after the power purchase contract correction are shown in Figure 6.

In the day-ahead-internal coordinated optimal scheduling established in this paper, the intraday rolling optimization corrects the purchased power at each moment of the park in order to reduce the operating cost and uncertainty load loss risk by more accurate scheduling based on

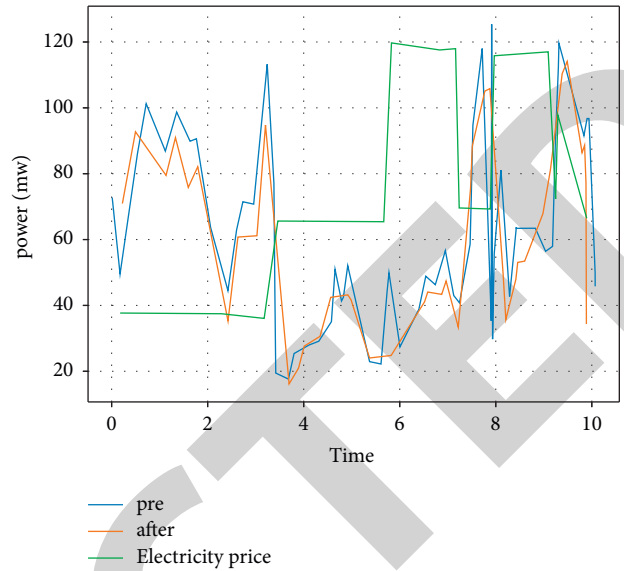


FIGURE 6: The electricity purchase contract in the day-to-day.

the intraday ultra-short-term forecast data. From Figure 6, it can be concluded that the purchased power varies more during off-peak hours of electricity prices, and during peak hours of electricity prices, the purchased power varies less, and the corrected purchased power appears to decrease instead of increase in some moments.

The total cost of electricity, heat, and gas purchased by the park in a day is \$1649,168, \$287,059, and \$519,944. Figure 7 records the variation of electricity, heat, and gas purchase cost of the park in one day for each time period.

*5.3. Analysis of the Effect of Considering CVaR Loss of Load Risk Assessment Under Model Predictive Control Strategy.* In this paper, we add the CVaR evaluation index describing the risk of lost load to the intraday rolling optimal dispatch based on the model predictive control MPC to minimize the risk of lost load under multiple scenarios of system uncertainty and minimize the total cost of the park including the operating cost and risk cost. The operating costs of the MPC and CVaR-based campus scheduling model established in this paper and the traditional MPC scheduling model under five scenarios are shown in Figures 8 and 9, respectively.

Five uncertain typical scenarios of dispatching costs based on model predictive control MPC with conditional risk assessment CVaR and traditional MPC optimal dispatching model show that after considering the uncertainty of PV output and load demand, establishing a typical set of prediction scenarios, and applying conditional risk value CVaR to assess the risk of power loss load in the park, most of the time the park's energy purchase cost, light

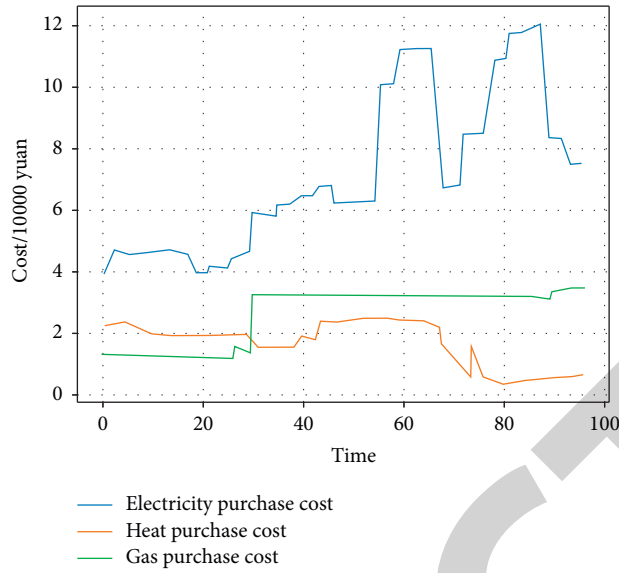


FIGURE 7: Day-to-day coordination and optimization of energy purchase costs.

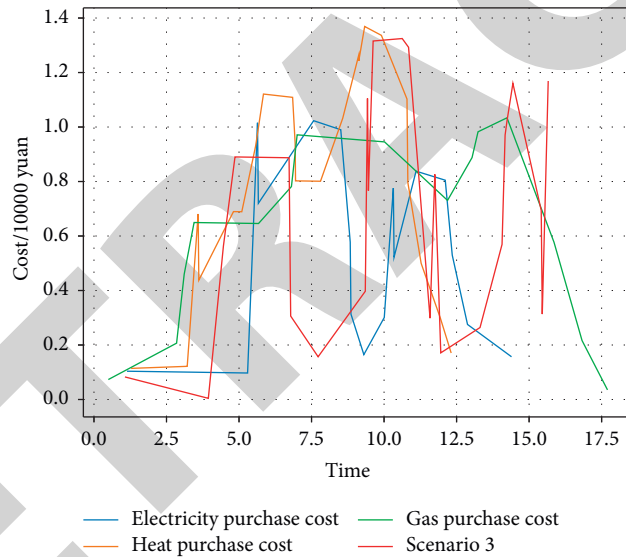


FIGURE 8: Comparison of results under scenario 1 between the scheduling model based on CVaR and MPC and the traditional MPC model.

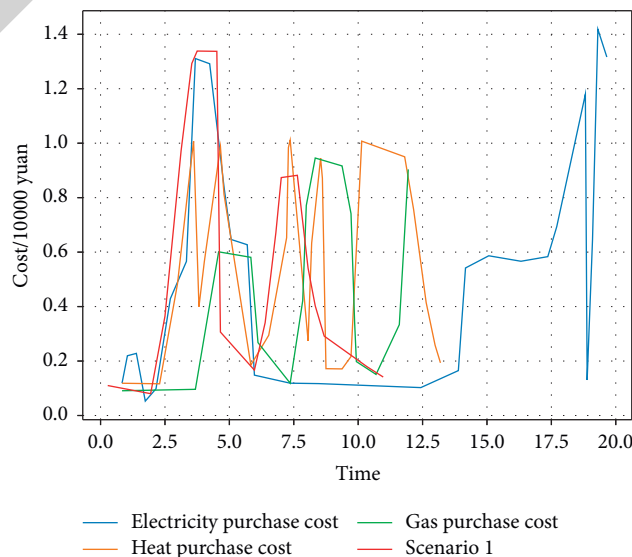


FIGURE 9: Comparison of CVaR and MPC based scheduling model with traditional MPC model under scenario 2.



abandonment penalty cost, and grid power purchase default costs increase, but the cost of compensating for lost load decreases significantly, which is because the model increases the supply of electricity at a certain moment in order to reduce the risk of lost load, and accordingly, the increase of abandonment occurs in some scenarios.

## 6. Conclusions

Compared with the traditional rolling optimization model based on model predictive control, the dispatching model considering the risk assessment of lost load under the model predictive control strategy established in this paper, the abandonment penalty cost, and power purchase contract default cost of the model under five scenarios increase to different degrees, but the cost of compensating lost load decreases, and the total cost of each scenario decreases to some extent. Considering that forecast fluctuations may cause system operation to lose load or abandon light, an optimization model based on CVaR theory is developed based on the day-ahead dispatch to address this uncertainty, aiming at minimizing system operation costs while minimizing system load loss under probabilistic scenarios. The scheduling results reduce the total cost of scheduling from 2.7591369 million yuan to 2.61311588 million yuan compared with the day-ahead economic scheduling, while the model enhances the park's ability to cope with forecast uncertainty and makes the scheduling plan more secure and reliable. In summary, the effectiveness of the day-ahead-intraday coordinated optimal scheduling model established in this paper is verified in terms of scheduling economy and handling uncertainty.

## Data Availability

The experimental data used to support the findings of this study are available from the corresponding author upon request.

## Conflicts of Interest

The authors declare that they have no conflicts of interest regarding this work.

## Acknowledgments

This study was supported by Major Science and Technology Project of the Eighth Division in Xinjiang (2021ZD002): Study on Key Technologies of Integrated Energy Collaboration Planning and Integrated Operation of PV& Storage Demonstration under the Condition of Independent Power Grid.

## References

- [1] Y. Li, R. Wang, and Z. Yang, "Optimal scheduling of isolated microgrids using automated reinforcement learning-based multi-period forecasting," *IEEE Transactions on Sustainable Energy*, vol. 13, no. 1, pp. 159–169, 2021.
- [2] D. Zhang, X. Han, and X. Han, "Review on the research and practice of deep learning and reinforcement learning in smart grids," *CSEE Journal of Power and Energy Systems*, vol. 4, no. 3, pp. 362–370, 2018.
- [3] M. Mohammadi, Y. Noorollahi, B. Mohammadi-ivatloo, H. Yousefi, and S. Jalilinasrabad, "Optimal scheduling of energy hubs in the presence of uncertainty—a review," *Journal of energy management and technology*, vol. 1, no. 1, pp. 1–17, 2017.
- [4] L. Luo, S. S. Abdulkareem, A. Rezvani et al., "Optimal scheduling of a renewable based microgrid considering photovoltaic system and battery energy storage under uncertainty," *Journal of Energy Storage*, vol. 28, Article ID 101306, 2020.
- [5] Y. Chen, Y. Shi, and B. Zhang, "Modeling and optimization of complex building energy systems with deep neural networks," in *Proceedings of the 51st Asilomar Conference on Signals, Systems, and Computers*, pp. 1368–1373, Pacific Grove, CA, USA, 2017, October.
- [6] E. Mocanu, D. C. Mocanu, P. H. Nguyen et al., "On-line building energy optimization using deep reinforcement learning," *IEEE Transactions on Smart Grid*, vol. 10, no. 4, pp. 3698–3708, 2018.
- [7] L. Suganthi, S. Iniyan, and A. A. Samuel, "Applications of fuzzy logic in renewable energy systems—a review," *Renewable and Sustainable Energy Reviews*, vol. 48, pp. 585–607, 2015.
- [8] J. Zhou, "Real-time task scheduling and network device security for complex embedded systems based on deep learning networks," *Microprocessors and Microsystems*, vol. 79, Article ID 103282, 2020.
- [9] L. Zhang and Y. Li, "A game-theoretic approach to optimal scheduling of parking-lot electric vehicle charging," *IEEE Transactions on Vehicular Technology*, vol. 65, no. 6, pp. 4068–4078, 2015.
- [10] A. T. Eseye, M. Lehtonen, T. Tukia, S. Uimonen, and R. J. Millar, "Machine learning based integrated feature selection approach for improved electricity demand forecasting in decentralized energy systems," *IEEE Access*, vol. 7, Article ID 91463, 2019.
- [11] S. Chen, T. Liu, F. Gao et al., "Butler, not servant: a human-centric smart home energy management system," *IEEE Communications Magazine*, vol. 55, no. 2, pp. 27–33, 2017.
- [12] P. An, Z. Wang, and C. Zhang, "Ensemble unsupervised autoencoders and Gaussian mixture model for cyberattack detection," *Information Processing & Management*, vol. 59, no. 2, Article ID 102844, 2022.
- [13] J. J. Zhang, D. W. Gao, Y. Zhang et al., "Social energy: mining energy from the society," *IEEE/CAA Journal of Automatica Sinica*, vol. 4, no. 3, pp. 466–482, 2017.
- [14] G. Hafeez, K. S. Alimgeer, and I. Khan, "Electric load forecasting based on deep learning and optimized by heuristic algorithm in smart grid," *Applied Energy*, vol. 269, Article ID 114915, 2020.
- [15] H. Li, Z. Wan, and H. He, "Real-time residential demand response," *IEEE Transactions on Smart Grid*, vol. 11, no. 5, pp. 4144–4154, 2020.
- [16] A. Mosavi, M. Salimi, S. Faizollahzadeh Ardabili, T. Rabczuk, S. Shamshirband, and A. R. Varkonyi-Koczy, "State of the art of machine learning models in energy systems, a systematic review," *Energies*, vol. 12, no. 7, Article ID 1301, 2019.
- [17] J. Wan, B. Chen, S. Wang, M. Xia, D. Li, and C. Liu, "Fog computing for energy-aware load balancing and scheduling in smart factory," *IEEE Transactions on Industrial Informatics*, vol. 14, no. 10, pp. 4548–4556, 2018.

## *Retraction*

# **Retracted: Application and Analysis of Taekwondo Techniques, Tactics, and Movement Trajectories Based on Multi-Intelligent Decision Making**

### **Mathematical Problems in Engineering**

Received 18 July 2023; Accepted 18 July 2023; Published 19 July 2023

Copyright © 2023 Mathematical Problems in Engineering. This is an open access article distributed under the Creative Commons Attribution License, which permits unrestricted use, distribution, and reproduction in any medium, provided the original work is properly cited.

This article has been retracted by Hindawi following an investigation undertaken by the publisher [1]. This investigation has uncovered evidence of one or more of the following indicators of systematic manipulation of the publication process:

- (1) Discrepancies in scope
- (2) Discrepancies in the description of the research reported
- (3) Discrepancies between the availability of data and the research described
- (4) Inappropriate citations
- (5) Incoherent, meaningless and/or irrelevant content included in the article
- (6) Peer-review manipulation

The presence of these indicators undermines our confidence in the integrity of the article's content and we cannot, therefore, vouch for its reliability. Please note that this notice is intended solely to alert readers that the content of this article is unreliable. We have not investigated whether authors were aware of or involved in the systematic manipulation of the publication process.

Wiley and Hindawi regrets that the usual quality checks did not identify these issues before publication and have since put additional measures in place to safeguard research integrity.

We wish to credit our own Research Integrity and Research Publishing teams and anonymous and named external researchers and research integrity experts for contributing to this investigation.

The corresponding author, as the representative of all authors, has been given the opportunity to register their

agreement or disagreement to this retraction. We have kept a record of any response received.

### **References**

- [1] W. Lu and X. Lin, "Application and Analysis of Taekwondo Techniques, Tactics, and Movement Trajectories Based on Multi-Intelligent Decision Making," *Mathematical Problems in Engineering*, vol. 2022, Article ID 8411550, 8 pages, 2022.

## Research Article

# Application and Analysis of Taekwondo Techniques, Tactics, and Movement Trajectories Based on Multi-Intelligent Decision Making

Weian Lu<sup>1</sup> and Xiaotao Lin<sup>2</sup> 

<sup>1</sup>Guizhou University of Finance and Economics Sports Department, Guiyang 550025, China

<sup>2</sup>College of National Culture and Cognitive Science, Guizhou Minzu University, Guiyang 550025, China

Correspondence should be addressed to Xiaotao Lin; 04403001@gzmu.edu.cn

Received 11 February 2022; Accepted 4 March 2022; Published 31 March 2022

Academic Editor: Man Fai Leung

Copyright © 2022 Weian Lu and Xiaotao Lin. This is an open access article distributed under the Creative Commons Attribution License, which permits unrestricted use, distribution, and reproduction in any medium, provided the original work is properly cited.

The aim of this study is to compare the trajectory of cross-kick technical movements of excellent taekwondo players in different weight classes and to investigate the relationship between weight class differences and the characteristics of cross-kick technical movements and the extent to which they affect the speed of movements. To this end, an artificial intelligence system is proposed for taekwondo field decision making, combining computer and applied mathematics knowledge. The angles, angular velocities, and moments of the joints of the lower limbs, as well as the movement time, displacement, and speed of the lower limbs, of the athletes in the three weight classes were significantly different ( $P < 0.05$ ).

## 1. Introduction

Artificial intelligence (AI) is a branch of computer science, which is a new technical science that studies and develops theories, methods, techniques and application systems for simulating, extending, and extending human intelligence [1]. One of its main goals is to enable machines to perform complex tasks that would normally require human intelligence. It has developed rapidly in recent years and is widely used in many fields such as military, economy, and management. The main objective of this idea is to build an artificial intelligence-assisted system for taekwondo field decision making based on a database and through an expert system platform (data mining, online analysis, artificial intelligence, and virtual reality) [2].

Taekwondo, as one of the more typical skill-driven same-field confrontation events in the East [3], was first listed as an official event of the Sydney Olympic Games in 2000. Due to the relatively few weight classes established, competition is relatively fierce. In competition, the horizontal kick technique has the advantages of speed, power, difficulty, short

range of motion, and less cushioning, and has become the most frequently used technical movement by athletes [4]. In the cross-kick technique, the body accelerates and brakes according to the major and minor links in sequence so that the momentum moment is transferred to the end links, which is a typical whipping action [5]. Because of the great speed and power that can be generated at the end of the kinetic chain, the horizontal kick technique has become an important scoring tool in Taekwondo and a key technique in determining the winner of a match. In order to improve the effectiveness of this technique, some scholars have studied the scoring effect [6], training methods [7], structural characteristics [8], biomechanical characteristics [9], as well as the body composition [10], sports injury, and prevention [11] of the athletes [12], the results of which have laid the foundation for improving the effectiveness of the use of the cross-kick technique. In recent years, due to new rules and the use of electronic protective gear [13], the speed of the cross-kick technique plays a decisive role in improving the effectiveness of striking [14] and has once again become a new hot spot of common concern among researchers.

However, a review of domestic and foreign research literature on the movement speed of the horizontal kick technique reveals that the research mainly focuses on individual weight classes [15], gender differences [16], regional differences [17], training methods [18], the effect of old and new rules on movement speed, and its comparison with the speed of other technical movements [19]. As there is a distinction between weight classes in taekwondo competitions, there are individual differences in the height and mass of athletes. Therefore, the key to improving the speed of horizontal kicks and the effectiveness of the strikes is to find out the intrinsic connection between the weight class differences and the speed of the athletes' movements. Based on this, the biomechanical characteristics of cross-kick movements of athletes in different weight classes were analysed and compared with the weight class set in the men's taekwondo competition at the Summer Olympic Games, using a 3D motion capture system and analysis software.

The aim is to provide theoretical reference for the improvement of cross-kick movements, increase the speed of movements, and enhance the hitting effect of taekwondo players of different weight classes.

The contributions of this paper are as follows:

We propose to establish an artificial intelligence assistant system for taekwondo on-site decision making. Using a vicon nexus three-dimensional motion capture system, we can collect the motion trajectories of athletes of different weight levels when hitting the target position.

Based on D-H modelling, we can describe the posture angle of Taekwondo trainer ontology with the Euler angle.

In this experiment, according to the weight level set in the men's Taekwondo competition of the summer Olympic Games, all subjects did not carry out high-intensity training within 24 hours. Under the knowledge of this system, the training effect was improved.

## 2. Feasibility Analysis

The basis of the artificial intelligence assisted system for taekwondo field decision making is data. It is the large amount of data and information accumulated during daily training and competition that provides a solid foundation for the system, and the rich knowledge and experience of the coaches in field command that provides a reliable support for adjusting and optimising the system. The data mining, online analysis, and virtual technology involved in this system are all relatively mature technologies and have been widely used in many fields such as military, economy, and management, and have been successful. The application of artificial intelligence in various industries is also becoming more and more widespread, and the robot football simulation game has become quite mature. Artificial intelligence is of course based on data and models, which can be built on the basis of data mining analysis of various relationships and laws, or combined with basketball expertise and the experience of coaches and experts. The model can be used to obtain valuable information from a large amount of data and to display this information in an intuitive form so that the

data can be used to benefit, and the model can be dynamically added to or subtracted from and improved through practical application. In addition, tactical rehearsals, virtual arenas, and virtual pavilions are becoming more sophisticated.

A literature search shows that as early as the 1990s, about 20 NBA teams in the US used the advanced scout system, a data mining application developed by IBM, to provide relevant game data information to optimise their tactical combinations and predict game formats. Some of the technical and tactical research in China has also started to move towards informationization and digitalization, such as the use of the "transfer matrix" for table tennis simulation and diagnosis; the video analysis and rapid feedback system for diving technical training and diving training data management and analysis system of Tsinghua University; the multimedia database for basketball techniques and tactics developed by Chen Jian of Shanghai Sports Institute, etc. research and development, etc.

By providing a wealth of data and a large number of analysis tools, the artificial intelligence assisted system can assist coaches in making on-site analysis and decisions, and can also propose targeted training objectives for daily training.

## 3. Based on D-H Modelling

Based on the principles of conservation of momentum and conservation of angular momentum, the conceptual model of the SR system with  $n$  degrees of freedom is studied based on the kinematic and model transformation, where the posture angles of the taekwondo trainer's body are described by  $z-x-y$  Euler angles  $\alpha$ ,  $\beta$ , and  $\gamma$ , and the relevant notation is agreed as follows:

$\sum A$ : inertial coordinate system;  $\sum 0$ : coordinate system fixed to the center of mass  $C_0$  of the taekwondo trainer's body;  $n$ : number of degrees of freedom of the system

$\sum i$ : the coordinate system defined on the link  $i$  whose  $z$ -axis coincides with the axis of the joint  $i$ ;  $m_i$ : the mass of the link  $i$

${}^A\mathbf{R}_i \in \mathbf{R}^{3 \times 3}$ : coordinate transformation matrix from  $\sum i$  to  $\sum A$ ;  $k_i$ : unit vector along the  $z$ -axis of  $\sum i$

${}^A\mathbf{R}_0 \in \mathbf{R}^{3 \times 3}$ : the posture matrix of the taekwondo trainer's body relative to  $\sum A$ ;  $C$ : the whole system center-of-mass position vector (PV)

$C_i^*$ : center of mass of the composite subsystem formed by the  $i$ -th link to the end effector link  $n$

And the vector product matrix of vector  $r = [r_x \ r_y \ r_z]^T$  is defined as

$$\hat{r} = \begin{bmatrix} 0 & -r_z & r_y \\ r_z & 0 & -r_x \\ -r_y & r_x & 0 \end{bmatrix}. \quad (1)$$

The superscript to the left of the symbol (e.g.,  $A$  in symbol  ${}^A\mathbf{R}_i$ ) indicates the coordinate system in which the

vector is described.  $\sum A$  this superscript is omitted when the vector is represented in the coordinate system Gua.

**3.1. Single-Degree-of-Freedom Models.** We consider first the SR system with a single DOF at  $n = 1$ , which consists of the body of the taekwondo trainer (link 0) and a link (link 1) connected by a rotating joint.

First, the total system momentum  $P$  and the total angular momentum  $L$  with respect to the  $\sum A$  origin can be expressed as

$$\begin{aligned} \text{gathered } \mathbf{P} &= \sum_{i=0}^1 m_i \dot{\mathbf{r}}_i = m_C \dot{\mathbf{r}}_C, \\ \mathbf{L} &= \sum_{i=0}^1 (\mathbf{I}_i \boldsymbol{\omega}_i + m_i \mathbf{r}_i \times \dot{\mathbf{r}}_i) = \mathbf{I}_C \boldsymbol{\omega}_C + m_C \mathbf{r}_C \times \dot{\mathbf{r}}_C. \end{aligned} \quad (2)$$

According to the D I H method, the velocity relationship between chain rod 0 and chain rod 1 is

$$\begin{aligned} \dot{\mathbf{r}}_1 &= \dot{\mathbf{r}}_0 + \boldsymbol{\omega}_0 \times (\mathbf{p}_1 - \mathbf{p}_0) + \dot{\theta}_1 \mathbf{k}_1 \times \mathbf{a}_1, \\ \boldsymbol{\omega}_1 &= \boldsymbol{\omega}_0 + \dot{\theta}_1 \mathbf{k}_1. \end{aligned} \quad (3)$$

Based on the above relationship, the equation  $\mathbf{v}_0$  can be derived for the proprioceptive speed of a taekwondo trainer:

$$\mathbf{v}_0 = \mathbf{J}_0 \dot{\theta}_1 + \mathbf{H}_0 \mathbf{v}_C, \quad (4)$$

where

$$\mathbf{J}_0 = \begin{bmatrix} \mathbf{k}_1 \times \left( \frac{m_1}{m_C} \mathbf{a}_1 \right) + p_0 \mathbf{I}_C^{-1} \bar{\mathbf{I}}_1 \mathbf{k}_1 \\ -\mathbf{I}_C^{-1} \bar{\mathbf{I}}_1 \mathbf{k}_1 \end{bmatrix}, \quad (5)$$

$$\begin{aligned} \bar{\mathbf{I}}_1 &= \mathbf{I}_1 - m_1 p_1 \mathbf{a}_1, \\ \mathbf{H}_0 &= \begin{bmatrix} \mathbf{E}_3 & -p_0 \\ 0 & \mathbf{E}_3 \end{bmatrix}. \end{aligned} \quad (6)$$

In turn, wood-end effector speeds can be obtained as  $\mathbf{v}_E$ .

$$\dot{\mathbf{r}}_E = \dot{\mathbf{r}}_0 + \boldsymbol{\omega}_0 \times (\mathbf{p}_E - \mathbf{p}_0) + (\dot{\theta}_1 \mathbf{k}_1) \times \mathbf{l}_{E,1}, \quad (7)$$

$$\boldsymbol{\omega}_E = \boldsymbol{\omega}_0 + \dot{\theta}_1 \mathbf{k}_1,$$

thus obtaining the end effector speed:

$$\mathbf{v}_E = \mathbf{J}_E \dot{\theta}_1 + \mathbf{H}_E \mathbf{v}_C, \quad (8)$$

$$\mathbf{J}_E = \begin{bmatrix} \mathbf{k}_1 \times \left( \mathbf{l}_{E,1} - \frac{m_1}{m_C} \mathbf{a}_1 \right) + P_E \mathbf{I}_C^{-1} \bar{\mathbf{I}}_1 \mathbf{k}_1 \\ \mathbf{k}_1 - \mathbf{I}_C^{-1} \bar{\mathbf{I}}_1 \mathbf{k}_1 \end{bmatrix}, \quad (9)$$

$$\mathbf{H}_E = \begin{bmatrix} \mathbf{E}_3 & -P_E \\ 0 & \mathbf{E}_3 \end{bmatrix}. \quad (10)$$

Equations (5) and (10) are the equations of motion for a single white yawl SR; matrices  $\mathbf{J}_E$  and  $\mathbf{J}_0$  in equations (6) and

(11) are the generalized Jacobi moments (GJMs) of the  $6 \times 1$  underdetermined instanton and end effector.

**3.2. Multidegree-of-Freedom Models.** The kinematic equations of the multidegree SR can be derived recursively from the conservation equations for linear and angular momentum and from the DH method. In general, the equations for the SR of  $n$  degrees of freedom can be described by the plant-meaning Jacobi matrix (GJM)  $^{[1]} \mathbf{J}_E^* \in R^{6 \times n}$ , which represents the relationship between the end-effector velocity  $\mathbf{v}_E$  and the joint velocity  $\dot{\theta}_M$  of the manipulator:

$$\mathbf{v}_E = \mathbf{J}_E^* \dot{\theta}_M + \mathbf{h}_E, \quad (11)$$

where

$$\begin{aligned} \mathbf{h}_E &= \mathbf{H}_E \cdot \mathbf{v}_C, \\ \mathbf{H}_E &= \begin{bmatrix} \mathbf{E}_3 & -P_E \\ 0 & \mathbf{E}_3 \end{bmatrix}, \end{aligned} \quad (12)$$

where  $\mathbf{H}_E$  represents the end effector velocity when  $\dot{\theta}_M = 0$ , which only occurs when the system has nonzero momentum. Clearly, the key to kinematic modelling is the calculation of the Jacobi matrix. Based on the formulation proposed by Orin and Schrader for the fixed-base Jacobi, the  $i$ -th column of the generalized Jacobi matrix  $\mathbf{J}_E^*$  in equation (13) can be interpreted as the end-effector velocity  $\mathbf{v}_E$  when  $H_E = 0$ , and only the  $i$ -th element of  $\dot{\theta}_M$  has value  $\dot{\theta}_i$  of 1. Therefore, in order to derive the  $i$ -th column element of the GM, the system can be viewed as consisting of only two composite link sub-systems connected by the  $i$ -th joint, and its  $i$ -th column element can be calculated using the results of the previous section, thus allowing a multidegree-of-freedom SR model to be built.

Let  $\mathbf{J}_E^* = [\mathbf{J}_{1E} \dots \mathbf{J}_{nE}]$ , where the column element  $\mathbf{J}_{iE} \in R^{6 \times 1}$  represents the contribution of the joint velocity  $\dot{\theta}_i$  to the end effector velocity, and using the section to obtain the result, corresponding to equation (13), yields  $\mathbf{J}_{iE}$ :

$$\mathbf{J}_{iE} = \begin{bmatrix} \mathbf{k}_i \times \left( \mathbf{l}_{E,i} - \frac{m_i}{m_C} \mathbf{a}_i^* \right) + P_E \mathbf{I}_C^{-1} \bar{\mathbf{I}}_i \mathbf{k}_i \\ \mathbf{k}_i - \mathbf{I}_C^{-1} \bar{\mathbf{I}}_i \mathbf{k}_i \end{bmatrix}, \quad (13)$$

where

$$\bar{\mathbf{I}}_i = \mathbf{I}_i^* - m_i^* P_i^* A_i^*. \quad (14)$$

The kinematic equations of SR with the reference point on the end effector can be derived in the same way as the kinematic equations of other forms with the reference point not on the end effector but on the body of the taekwondo trainer. This kinematic equation can be expressed as

$$\begin{aligned}
\mathbf{v}_0 &= \mathbf{J}_0^* \dot{\theta}_M + \mathbf{h}_0, \\
\mathbf{h}_0 &= \mathbf{H}_0 \cdot \mathbf{v}_C, \\
\mathbf{H}_0 &= \begin{bmatrix} \mathbf{E}_3 & -P_0^* \\ 0 & \mathbf{E}_3 \end{bmatrix}, \\
\mathbf{J}_0^* &= [\mathbf{J}_{10} \ \cdots \ \mathbf{J}_{n0}] \in \mathbf{R}^{6 \times n}, \\
\mathbf{J}_{i0} &= \begin{bmatrix} \mathbf{k}_i \times \left( -\frac{m_i^*}{m_C} \mathbf{a}_i^* \right) + \hat{\mathbf{s}}_0^* \mathbf{I}_C^{-1} \bar{\mathbf{I}}_i \mathbf{k}_i \\ -\mathbf{I}_C^{-1} \bar{\mathbf{I}}_i \mathbf{k}_i \end{bmatrix}, \\
\mathbf{v}_0 &= \mathbf{J}_0^* \dot{\theta}_M + \mathbf{h}_0.
\end{aligned} \tag{15}$$

#### 4. Continuous Motion Trajectory Control (Continual Motion Trajectory Control)

This section investigates the continuous motion trajectory control algorithm for SR. When the linear and angular momentum are conserved and the initial momentum is zero, the end-effector velocity can be expressed as

$$\mathbf{v}_E = \mathbf{J}_E^* \cdot \dot{\theta}_M. \tag{16}$$

With the aid of the GJM, the relationship between the velocity of the SR end effector and the angular velocity of the joint is formally the same as that described for the ground robot. If  $\mathbf{J}_E^*$  is invertible, then

$$\dot{\theta}_M = (\mathbf{J}_E^*)^+ \cdot \mathbf{v}_E. \tag{17}$$

The solution of the inverse kinematics at the velocity level of SR is obtained by (17), according to which the motion paths of the joints of the manipulator can be planned according to the given spatial task to realize the spatial continuous motion trajectory control of SR. In this paper, a continuous motion trajectory control algorithm based on the visual feedback and RMRC method is proposed. Let the desired position of the spatial target be  $\mathbf{T}_e = \begin{bmatrix} \mathbf{n}_e \mathbf{o}_e \mathbf{a}_e & \mathbf{r}_e \\ 0 & 1 \end{bmatrix}$  and the position of the end effector of the manipulator measured by the vision system installed on the body of the SR be  $\mathbf{T}_d = \begin{bmatrix} \mathbf{n}_d \mathbf{o}_d \mathbf{a}_d & \mathbf{r}_d \\ 0 & 1 \end{bmatrix}$ , and the position error of the end effector is  $e_p$ , and the attitude error is  $e_R$ .

$$\begin{aligned}
\mathbf{e}_p &= \mathbf{r}_d - \mathbf{r}_e, \\
\mathbf{e}_R &= \frac{(\mathbf{n}_e \times \mathbf{n}_d + \mathbf{o}_e \times \mathbf{o}_d + \mathbf{a}_e \times \mathbf{a}_d)}{2}, \\
\dot{\theta}_M &= (\mathbf{J}^*)^+ \mathbf{v}_E, \\
\mathbf{v}_E &= \frac{\mathbf{e}_p}{\Delta t},
\end{aligned} \tag{18}$$

where  $\Delta t$  is the sampling period.

The feedback control input joint torque is

$$\tau = K_p J_v^T + K_R J_\omega^T e_R + K_\theta \dot{\theta}_M, \tag{19}$$

where  $K_p$  is the translational gain factor,  $K_R$  is the attitude gain factor, and  $K_\theta$  is the angular acceleration gain factor.

#### 5. Subjects and Methods

**5.1. Test Subjects.** Thirty Korean taekwondo athletes in three weight classes, 58 kg, 68 kg, and 80 kg, were selected for testing according to the weight class set for the men's taekwondo competition at the Summer Olympic Games. Of these, 12 were from the Taeryeong Village (4 players/class) and 18 from the Yongin University team (6 players/class), all of whom were athletes at the rank of athlete and above. All subjects were athletes of fitness level or above. All subjects had not undergone heavy training within 24 h before the test and had not intentionally increased or decreased their body mass or suffered any sports injuries to their lower limb joints within 3 months, and their physical condition and athletic ability were normal. The basic information of the subjects is shown in Table 1.

**5.2. Research Process.** The signals collected by the 3D motion capture system are set according to the movement characteristics of the cross-kick technique, observing the moment when the supporting foot and the attacking leg touch the ground reaction on the force measuring table, the movement of the reflective marker ball attached to the target, the minimum flexion and maximum extension of the knee joint angle of the attacking leg, etc. The time interval from one moment to the next is the time periodas shown in Figure 1.

Ready moment (E1): the moment the supporting foot touches the floor of the dynamometer

Moment of flexion (E2): the moment of minimum knee flexion when the attacking leg is flexed

Moment of strike (E3): the moment of maximum extension of the knee joint during the strike of the attacking leg

Moment of recovery (E4): the moment the attacking leg is recovered and touches the floor of the dynamometer

P1: from the end of the preparation period to the beginning of the knee flexion period (E1 → E2)

Striking time (P2): from the end of the knee flexion to the beginning of the striking time (E2 → E3)

Recovery (P3): from the end of the strike to the beginning of the recovery (E3 → E4)

The results of the one-way RMANOVA are shown in Figure 2. The amplitude and direction of motion of the hip joint vary to varying degrees. At the moment of preparation (E1), the amplitude of flexion on the X-axis for the 58 kg and 68 kg, 68 kg and 80 kg weight classes, and the amplitude of abduction on the Y-axis for the three weight classes; at the moment of flexion (E2), the amplitude of flexion on the

TABLE 1: Summary of subjects' basic information.

| Group (kg) | <i>N</i> | Age        | Height (cm) | Body weight (kg) | Training years |
|------------|----------|------------|-------------|------------------|----------------|
| 58         | 10       | 20.2 ± 0.6 | 172.5 ± 2.3 | 56.7 ± 2.6       | 9.4 ± 1.3      |
| 68         | 10       | 20.2 ± 0.5 | 178.4 ± 2.5 | 66.6 ± 3.2       | 9.3 ± 1.3      |
| 80         | 10       | 19.9 ± 0.7 | 185.4 ± 2.7 | 77.3 ± 3.1       | 8.7 ± 1.3      |

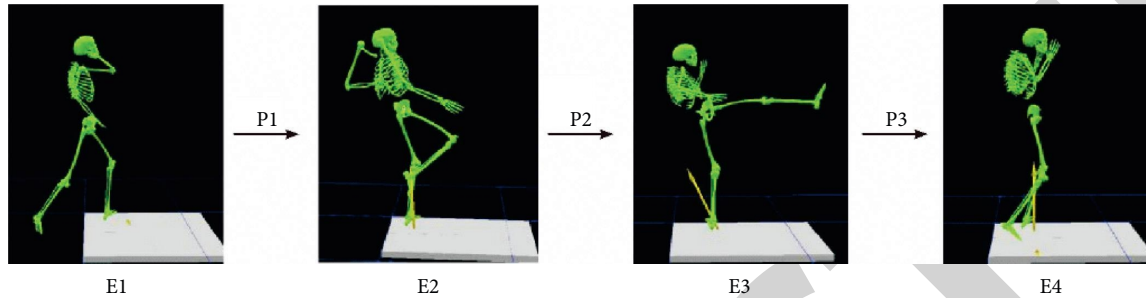


FIGURE 1: Time and period.

X-axis for the 58 kg and 68 kg weight classes, and the amplitude of rotation on the Z-axis for the 68 kg and 80 kg weight classes; at the moment of strike (E3), the amplitude of flexion on the X-axis for the 58 kg and 68 kg weight classes, and the amplitude of rotation on the Z-axis for the 58 kg and 80 kg weight classes. At the moment of strike (E3) the flexion amplitude of the 58 kg and 68 kg weight classes on the X-axis, the abduction amplitude of the 58 kg and 68 kg, 68 kg and 80 kg weight classes on the Y-axis and the rotation amplitude of the three weight classes on the Z-axis; at the moment of recovery (E4), the flexion amplitude of the 68 kg and 80 kg weight classes on the X-axis and the inversion amplitude of the 58 kg and 68 kg weight classes on the Y-axis were different ( $P > 0.05$ ), but not statistically significant. The differences were not statistically significant.

The results of the one-way RM ANOVA are shown in Figure 3, where the amplitude of knee flexion and extension movements differed between the four moments. The differences between the 58 kg and 68 kg weight classes in extension at the moment of preparation, between the 68 kg and 80 kg weight classes in flexion at the moment of knee flexion, and between the 58 kg and 68 kg weight classes in flexion at the moment of strike ( $P > 0.05$ ) were not statistically significant.

The angular velocities and moments of the knee joints of the athletes in the three periods were 58 kg > 68 kg > 80 kg, and the maximum moments of the 58 kg and 68 kg weight classes differed in the striking period (P2) ( $P > 0.05$ ) but were not statistically significant.

The results of the one-way RM ANOVA are shown in Figure 4, which shows the differences in movement time, displacement, and speed between the three weight classes. The movement time and movement displacement were 58 kg < 68 kg < 80 kg, and the movement speed was 58 kg > 68 kg > 80 kg. There were differences ( $P > 0.05$ ), but they were not statistically significant.

In order to verify the effectiveness of the kinematic modelling method proposed in this paper and its GJM and continuous motion trajectory control algorithms, a

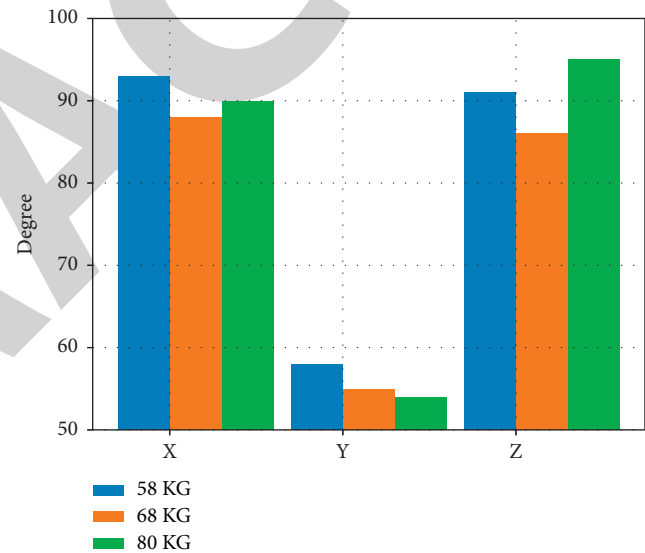


FIGURE 2: Schematic diagram of the angular characteristics of the hip joint of the supporting leg.

computer simulation study of the trajectory control of a failed taekwondo trainer was carried out using a 6DOF PUMA type SR model as an example. Figures 5 and 6 show the time course of the SR taekwondo trainer's body posture angle and the change of the robot's joint angle.

## 6. Discussion

The aim of the study is to investigate the similarities and differences in the movement trajectories of cross-kick technical movements of athletes of different weight classes, the angles, angular velocities, and moments of the joints of the lower limbs, as well as the displacement and speed of the technical movements at the four set moments and three time periods, and the degree of their influence on the speed of the movements. The study explores the biomechanical characteristics of the cross-kick technical movements of athletes of

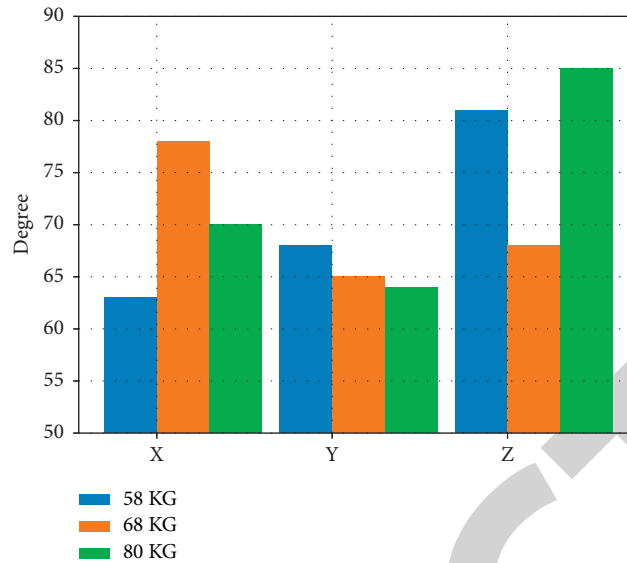


FIGURE 3: Schematic diagram of the hip joint angle characteristics of the attacking leg.

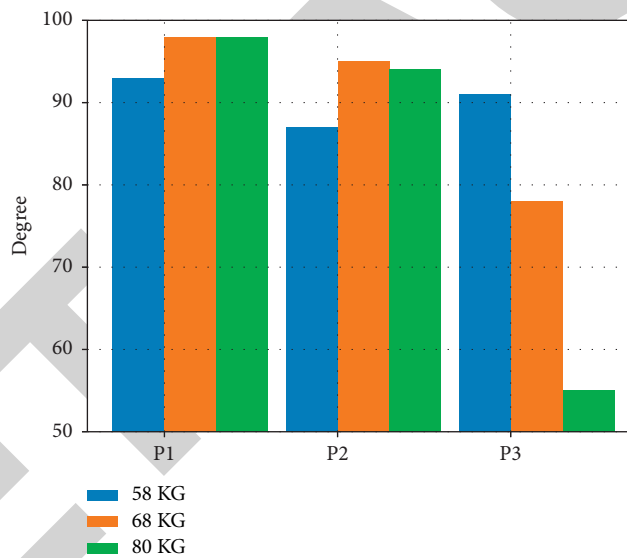


FIGURE 4: Schematic diagram of knee joint angle, angular velocity, and moment characteristics.

different weight classes and identifies the links between the differences in weight classes and movement speed, using theoretical knowledge of kinesiology and physiology and the author's training practice [20]. The results of the test revealed that there were significant differences in the biomechanical characteristics of the cross-kick movements of athletes in different weight classes. At the start of the horizontal kick, the trunk and supporting leg first rotate around the longitudinal axis, with the magnitude of rotation being  $58\text{ kg} > 68\text{ kg} > 80\text{ kg}$ . The smaller the weight class, the

greater the magnitude of rotation around the axis. It has been suggested that the rotation of the trunk and lower limb joints around the axis is consistent with the anatomy of the human body and that the supporting leg should be abducted first in order to facilitate the attacking leg movement [21]. The movement trajectory of the attacking leg is similar to that of the supporting leg in terms of flexion and extension, adduction and abduction, and internal and external rotation, starting from the preparation moment of the technical movement, with the overall performance of



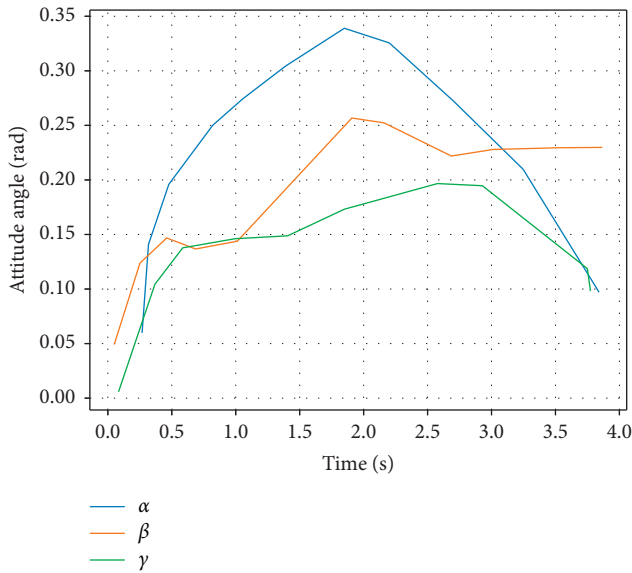


FIGURE 5: Time course of change in the proprioceptive stance angle of taekwondo trainers.

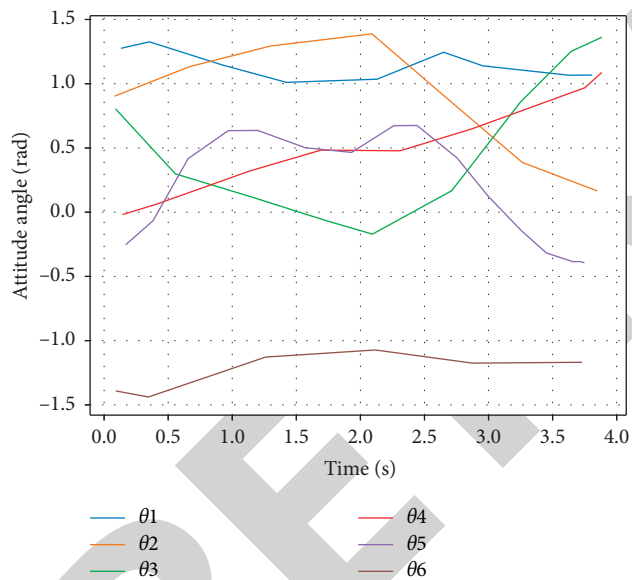


FIGURE 6: Time course of SR joint angle change.

58 kg > 68 kg > 80 kg. This shows that the difference in weight class has a direct effect on the rotation of the trunk and support leg as well as the attacking leg, especially on the knee flexion of the attacking leg.

## 7. Conclusions

The weight difference between the weight classes of the best taekwondo athletes has a significant effect on the speed of the cross kick technique; the lower the weight class of the athlete, the better the agility of the body, the faster the speed of the movement, the more reasonable the movement characteristics of the cross kick technique, and the relatively small effect on the speed of the movement; the higher the weight

class of the athlete, the less agility of the body, although the distance of the strike is relatively long, but the effect on the speed of the movement is relatively obvious. The greater the weight class the less agile the athlete is, and although the distance is longer, the effect on speed is more pronounced. When formulating training plans or carrying out special training, coaches should improve body agility and standardise cross-kick technical movements according to the differences in the characteristics of cross-kick technical movements of athletes of different weight classes and the degree of influence on movement speed, combining the characteristics of cross-kick technical movements and the principle of whipping movements, and according to the individual differences in athletes' agility, in accordance with the training principle of low weight and fast speed.

## Data Availability

The experimental data used to support the findings of this study are available from the corresponding author upon request.

## Conflicts of Interest

The authors declare that they have no conflicts of interest regarding this work.

## References

- [1] D. Bloznelis, "Salmon price volatility: a weight-class-specific multivariate approach," *Aquaculture Economics and Management*, vol. 20, no. 1, pp. 24–53, 2016.
- [2] I. N. Junejo, E. Dexter, I. Laptev, and P. Pérez, "Cross-view action recognition from temporal self-similarities," in *European Conference on Computer Vision*, pp. 293–306, Springer, Berlin, Heidelberg, 2008.
- [3] X. Yang and Y. L. Tian, "Eigenjoints-based action recognition using naive-bayes-nearest-neighbor," in *Proceedings of the 2012 IEEE Computer Society Conference on Computer Vision and Pattern Recognition Workshops*, pp. 14–19, IEEE, Providence, RI, USA, 2012, June.
- [4] B. Follmer, R. A. Dellagrana, and E. P. Zehr, "Head trauma exposure in mixed martial arts varies according to sex and weight class," *Sport Health*, vol. 11, no. 3, pp. 280–285, 2019.
- [5] J. Guo, Y. Lou, X. Zhang, and Y. Song, "Effect of aerobic exercise training on cardiometabolic risk factors among professional athletes in the heaviest-weight class," *Diabetology & Metabolic Syndrome*, vol. 7, no. 1, pp. 78–79, 2015.
- [6] A. A. Chaaoui, J. R. Padilla-López, P. Climent-Pérez, and F. Flórez-Revuelta, "Evolutionary joint selection to improve human action recognition with RGB-D devices," *Expert Systems with Applications*, vol. 41, no. 3, pp. 786–794, 2014.
- [7] I. B. Mandell, T. Maclaurin, and S. Bittenhan, "Effects of carcass weight class and postmortem aging on carcass characteristics and sensory attributes in grain-fed veal," *Journal of Food Science*, vol. 66, no. 5, pp. 762–769, 2001.
- [8] J. Nilsson, P. Tveit, and O. Eikrehagen, "Cross-country skiing," *Sports Biomechanics*, vol. 3, no. 1, pp. 85–108, 2004.
- [9] G. G. Artioli, F. Scagliusi, D. Kashiwagura, E. Franchini, B. Gualano, and A. L. Junior, "Development, validity and reliability of a questionnaire designed to evaluate rapid weight loss patterns in judo players," *Scandinavian Journal of*

## *Retraction*

# **Retracted: Deep Neural Network-Based Business Data Classification in Intelligent Business Management**

### **Mathematical Problems in Engineering**

Received 18 July 2023; Accepted 18 July 2023; Published 19 July 2023

Copyright © 2023 Mathematical Problems in Engineering. This is an open access article distributed under the Creative Commons Attribution License, which permits unrestricted use, distribution, and reproduction in any medium, provided the original work is properly cited.

This article has been retracted by Hindawi following an investigation undertaken by the publisher [1]. This investigation has uncovered evidence of one or more of the following indicators of systematic manipulation of the publication process:

- (1) Discrepancies in scope
- (2) Discrepancies in the description of the research reported
- (3) Discrepancies between the availability of data and the research described
- (4) Inappropriate citations
- (5) Incoherent, meaningless and/or irrelevant content included in the article
- (6) Peer-review manipulation

The presence of these indicators undermines our confidence in the integrity of the article's content and we cannot, therefore, vouch for its reliability. Please note that this notice is intended solely to alert readers that the content of this article is unreliable. We have not investigated whether authors were aware of or involved in the systematic manipulation of the publication process.

Wiley and Hindawi regrets that the usual quality checks did not identify these issues before publication and have since put additional measures in place to safeguard research integrity.

We wish to credit our own Research Integrity and Research Publishing teams and anonymous and named external researchers and research integrity experts for contributing to this investigation.

The corresponding author, as the representative of all authors, has been given the opportunity to register their agreement or disagreement to this retraction. We have kept a record of any response received.

### **References**

- [1] B. Wang, "Deep Neural Network-Based Business Data Classification in Intelligent Business Management," *Mathematical Problems in Engineering*, vol. 2022, Article ID 7104750, 8 pages, 2022.

## Research Article

# Deep Neural Network-Based Business Data Classification in Intelligent Business Management

**Bihong Wang** 

*School of International Trade, Zhejiang Institute of Economics and Trade, Hangzhou 310018, China*

Correspondence should be addressed to Bihong Wang; [wbh@zjiet.edu.cn](mailto:wbh@zjiet.edu.cn)

Received 10 February 2022; Revised 2 March 2022; Accepted 7 March 2022; Published 31 March 2022

Academic Editor: Man Fai Leung

Copyright © 2022 Bihong Wang. This is an open access article distributed under the Creative Commons Attribution License, which permits unrestricted use, distribution, and reproduction in any medium, provided the original work is properly cited.

The purpose of this paper is to explore how intelligent data mining technology can be used to improve the customer service capability of commercial companies. Based on extensive research on commercial business, this paper uses data mining and machine learning techniques to build an overall framework for applying intelligent technologies to business improvement, and uses multilayer perceptrons and integrated learning algorithms to build classifiers for customer segmentation; uses association rule mining to assist commercial companies in business decisions; uses clustering algorithms and visualization techniques to further analyze claims cases and assist in commercial fraud detection. The multilayer perceptron classification makes the classification of commercial customers more detailed and reasonable, and the company's business staff can sell products in a more targeted manner; association rule mining greatly improves the quality and efficiency of the company's management's decision making.

## 1. Introduction

With the rapid development of China's market economy, the competition among industries is becoming more and more intense. In order to gain a competitive advantage and win the initiative in the fierce market competition, enterprises need to use information technology tools, and business intelligence can effectively guide the business of enterprises and play a supporting role in specific business decisions [1]. In order to promote the further development of enterprises and seize the first opportunity in the market, it is necessary to adapt to the current market development requirements and make full use of advanced information technology for guidance, which is the application of data mining technology of business intelligence in enterprises. In the 1980s, the concept of data mining began to be put forward by the academic community, and in the subsequent practice, its theoretical value and real economic value began to be discovered, so it became popular in the market, and many enterprises began to apply this technology, at this time, the market for data mining has initially formed. In the following 10 years [2, 3], it was continuously practiced and further

researched by various enterprises, and data mining technology in this period has formed a unique branch of research, which is formed on the basis of continuously absorbing excellent and new research results from other frontier disciplines. Although the data mining system has been developed for a long time and continuously optimized, it is not perfect and free of any problems, among which, there are still some problems that need to be studied and explored more deeply [4].

With the continuous development of IT technology, more and more business enterprises are realizing the importance of IT technology. When the construction of IT infrastructure system is maturing, the establishment and implementation of BI system will provide a unified view for the enterprise, which means that the application of BI can centralize and present the data from various systems, provide the management with various useful data needed, and improve the quality and efficiency of the management's decision making [5, 6].

In this paper, the database design and establishment for commercial business, using data mining and machine learning technology to explore the auxiliary analysis of

commercial business, to a certain extent, has a wide range of implications [7]. The data warehouse establishes an exclusive information database for business customer groups, which can not only meet customer needs in a timely manner and ensure customer information security, but also improve customer service capability and creditworthiness, and help accumulate customer resources and business expansion.

## 2. Related Work

The first is to understand the retention patterns of customers by classifying policyholders into two categories: renewals and terminations [8]. The second is to better understand customer claims patterns and thus identify higher risk policyholder types, both of which can simultaneously affect decisions on pricing strategies for policyholders and thus directly impact the company's profitability. Using a database of medical business companies, [9] investigates the characteristics of knowledge discovery and data mining algorithms to demonstrate how they can be used to predict health outcomes and inform the management of hypertension. Reference [10] applied data mining techniques to detect anomalous data in U.S. agricultural crop commerce to uncover commercial fraud, concluding that data mining methods to investigate individual instances are more effective than current random selection techniques. The focus of [11] is on the application of data mining techniques in commerce with data warehousing in the hope of addressing the problem of high mobility of commercial agents in Hong Kong. Reference [12] tries to construct a customer evaluation index system for commercial companies by analyzing the characteristics of commercial business and treating customers as evaluation variables in commercial business. Taking the customer data of a domestic commercial company as an example, a customer evaluation model is established using data mining theory. Through testing, it is shown that the BP neural network model can realize the correct evaluation and classification of commercial company's customers, thus helping commercial companies to avoid reasonable operational risks. Reference [13] proposed a three-stage data mining method that detects and screens out customers who are more likely to buy a specific commercial at the expiration of a commercial contract and is able to identify a loyal customer base and plan appropriate commercial sales plans for them accordingly, which has considerable accuracy and has been practically applied to a commercial company in Iran. Reference [14] analyzed the risk of commercial business based on data mining techniques, and the database of commercial companies was the basis of their analysis, which contains information about policies and claims, based on which they discovered the different characteristics of the insured who had made claims, and in the process found the areas of greater risk and obtained the appropriate control methods. In [15], it is argued that "business intelligence" is important for companies to find effective data quickly and make optimal business decisions, and by analyzing the value chain of commercial companies and taking customer relationship management of

commercial companies as an example, the application of business intelligence, data mining and other technologies in commercial business management is explained, and it is concluded that business intelligence can find best strategies and apply them in business, mainly in three areas: claims management, customer relationship management, and sales channel optimization, and the return on investment obtained in this way is relatively large and enables the company to develop a competitive advantage in the market. Reference [16] argued that with the development of the economy, competition among commercial enterprises is no longer purely price competition, and the concept of customer-centeredness is being promoted by more and more companies. Reference [17] studied the architecture of data mining and customer relationship management framework, and designed a data mining-based customer relationship mining algorithm with a commercial company's customer relationship management system as an example.

## 3. Mining Algorithms and Corresponding Models

**3.1. Association Rule Algorithm.** In data mining, association rules are knowledge patterns that describe the rules of simultaneous occurrence between all possible events in an experiment. That is, association rules reveal implicit new relationships that are achieved by quantifying experiments. If we let  $T = \{t_1, t_2, \dots, t_m\}$  be a set of items and  $W$  be a set of transactions. Each transaction  $R$  in the set of  $W$  is a set of items,  $R \in T$ . Here if there exists a set  $A$  of items and a set  $R$  of transactions, if  $A \in R$ , then we say that the  $R$  transactions support the set of  $T$  items. The association rule is thus formalized as follows: if  $a \Rightarrow b$ , here  $a$  and  $b$  are a set of items,  $a \in T$ ,  $b \in T$ , and  $a \cap b = \emptyset$ . To describe the properties of the association rule, four parameters are often used: credibility ( $C$ ); support ( $S$ ); expected credibility ( $E$ ); usefulness ( $L$ ) [18].

Among the four attributes of association rules, the attributes that provide a more intuitive picture of the nature of association rules are support and credibility. In real life, people are only concerned about these two attributes, so the two values obtained Both values must be within a certain threshold, i.e., the minimum value of each, and the association rule is specified, these two minimum values must be satisfied. In the case that these two conditions are satisfied, we call It is called a strong rule.

**3.2. Clustering Algorithm.** The concept of cluster analysis is that a dataset is partitioned into various classes (Classes) that are relatively similar to each other and individually distinct, subject to a specific criterion, which is often expressed as a certain distance. Intuitively, each of the final clusters formed is a dense region in space.

The operation of the classical K-Means clustering algorithm can be described by the following image in Figure 1.

In the Figure 1(a), there are 5 samples of ABCDE. At the beginning, the 2 initial centroids on the right are selected,  $K=2$ , and all of them have different colors, and there is no concept of class or distinction [19].

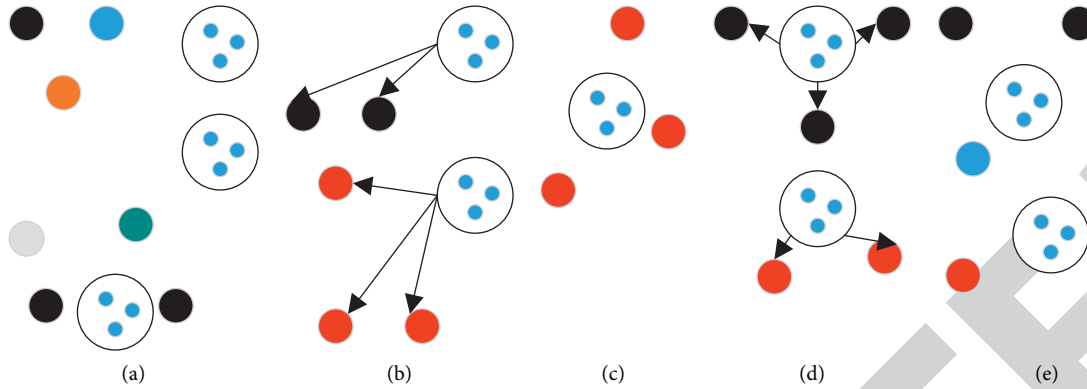


FIGURE 1: K-Means clustering algorithm process.

In Figure 1(b), the 5 samples calculate the distance to the 2 initial centroids, and choose the one with the closest distance, then the 5 samples are divided into 2 groups of red and black.

In Figure 1(c), after the calculation in Figure 2, the 2 initial centroids disappear, and 2 new centroids reappear at the center of each of the 2 classes, and the sum of the distances of these 2 new centroids from the samples in the class must be the smallest.

In Figure 1(d), the new centers and categories appear, and the categories are divided differently.

(Figure 1(d) in the above Figure 1(f)) The centers of the original two clusters disappear and the new centers (with the smallest sum of examples of each sample in the category) appear, at which point it is found that the divided categories do not change and converge.

**3.3. Classification Algorithm.** Decision tree algorithm is an algorithm to determine the category to which the data belongs in data mining, it is a relatively basic class of classification algorithm in data mining.

Figure 2 is one of the most basic decision tree models, as a tree-like decision structure, where circles represent internal nodes, identifying a feature or attribute, and squares represent leaf nodes, indicating a classification. A complete decision path is represented as an extension of the root node to each leaf node, where each branch node has a role in that they detect a specific feature in the sample and assign the sample to one of the child nodes, corresponding to their respective different special fetch values. Assuming that a predicted sample now exists, the complete process from the root of the tree to the corresponding subtree and then to the leaf nodes, each with different responsibilities, first detects the features of the sample and transmits them according to the fetched values, and then repeats the same operation in the second process, gradually extending down to the final node where the fetched values, or class markers, are formed as the final predicted result [20].

In the above description, it is clear that the merit of feature selection will directly determine the efficiency of the whole algorithm. That means with what criteria are the features selected? This explains that splitting attributes is a crucial step in decision trees. The concept of splitting attributes is to construct

different branches to nodes based on different divisions of feature attributes, with the goal that each subset of the splits will be “pure”. The “pure” criterion is to create a collection of subsets that are classified in the same category as much as possible. The key to decision tree learning is the selection of the optimal division attributes, with the goal of increasing the “purity” of the branch nodes. The different measures of “purity” have led to two common algorithms, the ID3 algorithm and the C4.5 algorithm. So how to measure this “purity”? Three concepts are introduced here: information entropy, conditional entropy, and information gain.

Information entropy is the most common measure of uncertainty (purity) of a sample set. It is defined as follows:

$$H(x) = - \sum_{k=1}^N p_k \ln(p_k). \quad (1)$$

Where:  $n$  represents the type of all samples and the proportion of class  $k$  samples. It is agreed that when  $p_k = 0$ ,  $H(x) = 0$ . Information entropy can be understood as uncertainty. The higher the information entropy of a system, the greater the uncertainty of the system. Corresponding to the space composed of all samples, the larger the information entropy, the more average the classification of samples, and the smaller the information entropy, the more inclined the samples are to a certain class.

The conditional entropy represents the complexity (uncertainty) of a random variable under a given condition [21].

The information gain is the information entropy minus the conditional entropy, which defines the information gain of partitioning the sample set  $D$  using the attribute  $a$ :

$$G(D, a) = H(x) - \sum_{v=1}^V \frac{|D^v|}{|D|} H(D^v). \quad (2)$$

$V$  is all possible values of attribute  $a$ .  $|D^v|/|D|$  represents the ratio of the number of samples to the overall number of samples when attribute  $a$  is taken as  $v$ . Here, it represents the weight of information entropy. This weight measures the importance of these samples in the calculation. A higher information gain means that the samples are more discriminated when they are divided by  $a$ .

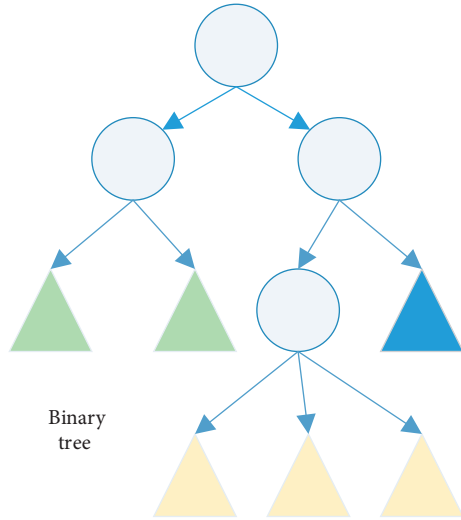


FIGURE 2: Decision tree model.

In the ID3 algorithm, the quantity used for the measure of purity is the information gain, for which the selection is made so that its features are most evident by performing the splitting. The information gain is a measure of the effectiveness of the selected division feature. To make the information gain greater, it is necessary to make  $\sum_{v=1}^V (|D^v|/|D|)H(D^v)$  smaller. Ignoring the previous weights first when considering, it can be seen that the smaller is needed. According to the definition of information entropy, the samples are more unbalanced, and at the extreme, all of them are in the same category (positive or negative samples), so that the purpose of classification is achieved.

In C4.5 algorithm, instead of using information gain, information gain rate is used. C4.5 algorithm can be seen as an improvement of ID3 algorithm. If a feature has so many categories in the total sample that it is unique to each sample (e.g., a person's ID number), ID3 will give priority to such a feature because each sample is divided into a separate node with maximum information gain, but this will have a negative impact on our decision tree [22, 23]. Because we want the decision tree to focus more on the attributes that the samples have in common, so that the new samples can be classified by our trained decision tree (with generalization ability). To balance the information gain and the number of attributes, the information gain rate is introduced:

$$G_r = \frac{G(D, a)}{IV(a)}, \quad (3)$$

where  $IV(a) = (|D^v|/|D|)\log_2(|D^v|/|D|)$ .

The formula for the information gain rate suggests that features with a small number of samples are preferred when the information gain is the same. However, another problem arises at this point, the C4.5 algorithm will have a preference for features with a small number of attributes. In order to balance the relationship between information gain and the number of attributes again, we can give priority to a few attributes with high information gain when considering features, and then consider the features with the highest information gain rate [24].

**3.4. Models Induced by Algorithms.** The cross-selling model based on the association rule algorithm is mainly analyzed from the perspective of products. Through the analysis, potential patterns in customers' purchasing behavior and those product combinations that are purchased at high frequencies are discovered, and commercial companies can conduct targeted marketing planning based on this implied information, or redevelop products with product combination characteristics to achieve the purpose of cross-selling [25].

The overall cross-selling model can be divided into four parts, as shown in Figure 3.

The first is customer classification, which differentiates customer groups according to the type of commercial products purchased and the amount of premiums; the second is to determine the input data related to the consumption set of insurance products. It mainly includes product items and parameters.

The third is association rule analysis, selecting the appropriate association rule algorithm for product set fact association mining. Finally is the analysis of mining results, a comprehensive and in-depth analysis of the algorithm output to identify cross-selling opportunities and select the optimal product set.

Here is the application of decision tree ID3 algorithm in commercial individual customer data analysis to illustrate how decision tree algorithm plays a very important role in facilitating customer relationship management [26].

A commercial company is planning to introduce a certain critical illness insurance product to the market this year. The information is basic information about gender, age, income, credit and other attributes, and whether or not to buy critical illness insurance is the category attribute of this group, i.e., customers are divided into two types, either they have already bought other critical illness insurance products of the company, or they have never bought this product.

## 4. Case Study

In business companies, the research of their customers and their segmentation according to group characteristics is not done by subjective. In the current buyer's market conditions, because each consumer has different business needs. Although commercial companies have a wide range of products, they cannot develop products that meet all the different individual needs. Therefore, it is necessary for business enterprises to segment their customers. Here, customer segmentation can be defined as a typical classification problem, and in this paper, decision trees and deep neural networks (multilayer perceptron) are used to train the classifiers respectively. The classifiers are trained separately using decision trees and deep neural networks (multilayer perceptron), and then integrated together using integrated learning to obtain better performance.

**4.1. Classification Using Decision Tree Algorithm.** An example of the use of decision trees is given below. A decision tree represents a knowledge, which is based on whether or

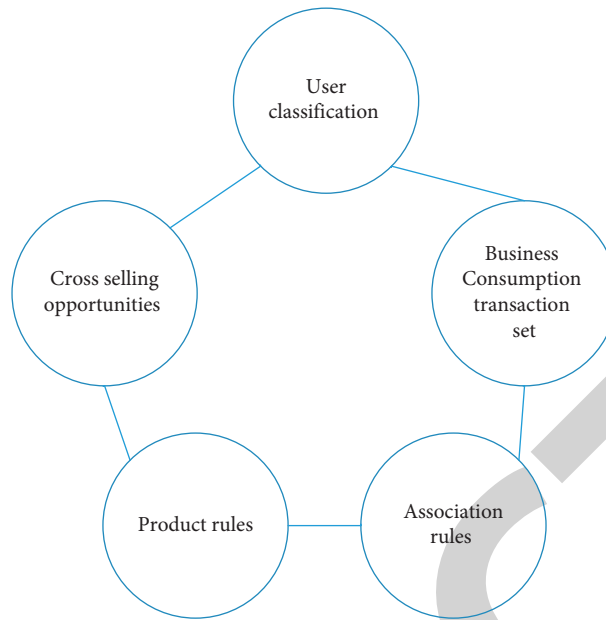


FIGURE 3: Cross-selling model based on association rules.

not a customer will take out a policy, and based on this knowledge can effectively predict the purchase intention of a particular customer. This knowledge is used to predict the purchase intention of a customer. Table 1 shows a simplified training set for a commercial company to analyze whether a customer is insured or not.

A serial number is a customer, that is, a specific example, and the other information in the table are the respective attributes of the specific customer. The objective of this analysis and prediction is set as whether the customer is insured or not, then the column of the table is the prediction attribute or the mining attribute, and the column where the insurance is located is the prediction column, and the prediction of this attribute has two results, either YES or NO. An example of the decision tree for processing the classification model of Table 1 is Figure 4.

In Figure 4, we train the first 10 steps and predict after 11 steps, so we do not show the first 10 steps in Figure 4. We usually design algorithms with a two-tier structure, which is the only way to make the class data table of nodes to be classified more open and efficient to build. The data mining middleware, a link between the data warehouse and the tree-building algorithm, is set up. The data mining client makes a request to it, which is about the class count table; secondly, the middleware extracts the relevant data from the data warehouse, then builds the class count table and sends them to the data mining client. These two queues make a connection between the middleware and the data mining client.

**4.2. Construction of Classifiers Using Integrated Learning Algorithms and Analysis of Results.** Assemble-learning accomplishes a learning task by building and combining multiple learners, also known as a multi-classifier system. It is a technical framework that allows the combination of

underlying models according to different ideas and purposes.

Using a scalable decision tree classification algorithm combined with a deep neural network classifier, the resulting customer segmentation model is a relatively accurate one, which automatically classifies customers based on their intrinsic characteristics. The model is analyzed for all situations of the business customer during the business period and thus understands the the characteristics that each customer has. This enables commercial companies to better understand the characteristics of different types of customers and to differentiate the use of marketing methods according to their situation. The customer records of a branch in 2007-2008 are shown in Table 2, where we can find the proportion and characteristics of each type of customer. This is shown in Figure 5.

From the information in the table above, it is found that business companies have to rely on the differentiation of a huge number of customer groups data mining techniques, in which there are four types of customers, which are divided according to their value, the higher the grade customers, the smaller the number, but their contribution to the business is the largest, in terms of the overall insurance. The higher the class, the smaller the number of customers, but they contribute the most to the business and account for a larger share of the overall sales of the entire insurance.

Using the input information such as gender, marital status, education level, occupation and age of the insured and the insured as the input of the above classifier, the output information predicting the type of insurance purchased by the customer can be relatively accurate, and 85% of the output entries are accurate, i.e. the accuracy rate reaches 85%. And the percentage of the retrieved accurate entries to the total entries reaches 79%, i.e., the recall rate reaches 79%. This result has considerable reference value in

TABLE 1: Training set for analyzing whether a customer buys a policy or not.

| Serial number | Gender | Age   | Education          | Income | Insure |
|---------------|--------|-------|--------------------|--------|--------|
| 1             | Male   | <35   | Research           | High   | Yes    |
| 2             | Male   | <35   | Junior college     | Low    | Yes    |
| 3             | Female | 35-45 | University         | Centre | Yes    |
| 4             | Male   | >45   | High school        | Low    | No     |
| 5             | Male   | >45   | Junior high school | High   | No     |
| 6             | Female | 35-45 | Primary school     | Centre | No     |
| 7             | Male   | <35   | High school        | Low    | Yes    |

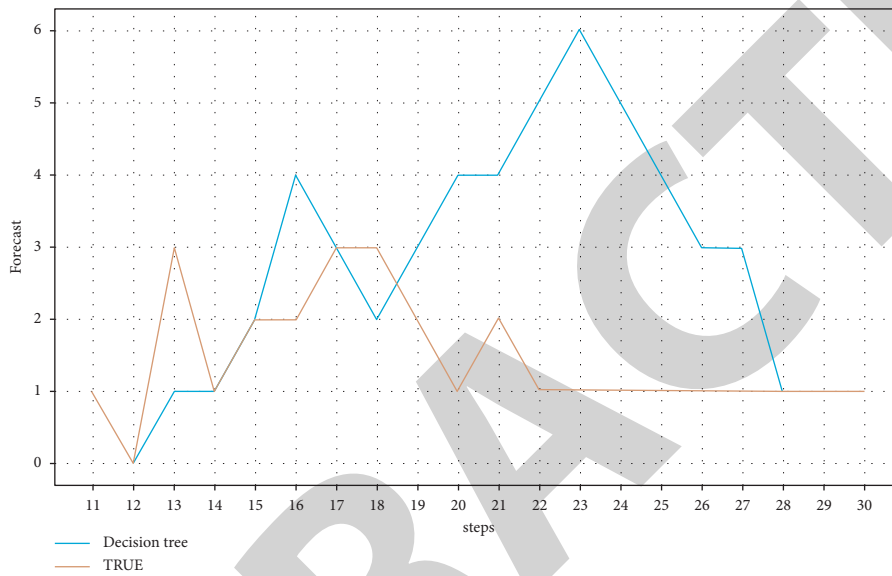


FIGURE 4: Decision tree prediction processing.

TABLE 2: Classification mining results.

| Customer type      | Proportion (%) | Characteristic information  |
|--------------------|----------------|---|
| VIP customers      | 0.99           | Occupational category = 6 and annual income $\geq 50000$ and population influence = $a$ |
| Quality customer   | 4.03           | Occupation category = 5 or 6 and $100000 \leq$ annual income $\leq 50000$               |
| Ordinary customers | 22.4           | Occupation type = 304 and age $\leq 38$ and $60000$ annual income $\leq 10000$          |
| Small customers    | 72.5           | Occupational category = 2 or other and $25000 \sim$ annual income $\leq 400$            |

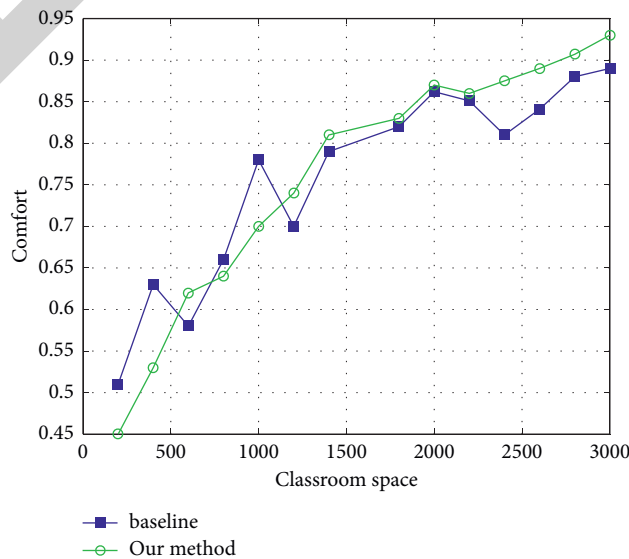


FIGURE 5: Boosting.



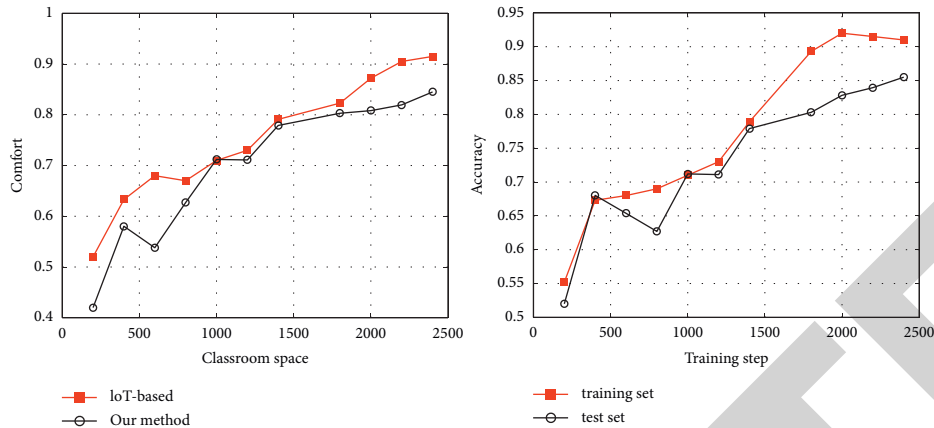


FIGURE 6: Effect of data classification of commercial companies.

practical use. In the later practical use, it enables the renewal management of the company to predict the secondary product purchase tendency of the insured customers more accurately, and provides a reference direction for the formulation of the company's product policy and business policy. The effect of commercial classification is shown in Figure 6.

## 5. Conclusions

Based on extensive research on commercial business, this paper uses data mining and machine learning techniques to build an overall framework for applying intelligent technologies to business improvement, and uses multilayer perceptrons and integrated learning algorithms to build classifiers for customer segmentation; uses association rule mining to assist commercial companies in business decisions; uses clustering algorithms and visualization techniques to further analyze claims cases and assist in commercial fraud detection. The use of clustering algorithms and visualization techniques to further analyze claims and assist in commercial fraud detection. Association rule mining has greatly improved the quality and efficiency of decision making by company managers.

## Data Availability

The experimental data used to support the findings of this study are available from the corresponding author upon request.

## Conflicts of Interest

The authors declare that they have no conflicts of interest regarding this work.

## References

- [1] S. Ryu, J. Noh, and H. Kim, "Deep neural network based demand side short term load forecasting," *Energies*, vol. 10, no. 1, p. 3, 2017.
- [2] X. Ning, K. Gong, W. Li, L. Zhang, X. Bai, and S. Tian, "Feature refinement and filter network for person re-identification," *IEEE Transactions on Circuits and Systems for Video Technology*, vol. 31, no. 9, pp. 3391–3402, 2021.
- [3] M. A. Khan, M. Y. Javed, M. Sharif, T. Saba, and A. Rehman, "Multi-model deep neural network based features extraction and optimal selection approach for skin lesion classification," in *2019 international conference on computer and information sciences (ICCIS)*, pp. 1–7, IEEE, Sakaka, Saudi Arabia, 3–4 April 2019.
- [4] X. Ning, K. Gong, W. Li, and L. Zhang, "JWSAA: Joint weak saliency and attention aware for person re-identification," *Neurocomputing*, vol. 453, pp. 801–811, 2021.
- [5] R. F. Mansour, "A robust deep neural network based breast cancer detection and classification," *International Journal of Computational Intelligence and Applications*, vol. 19, no. 01, Article ID 2050007, 2020.
- [6] K. Chen, D. Zhang, L. Yao, B. Guo, Z. Yu, and Y. Liu, "Deep learning for sensor-based human activity recognition: Overview, challenges, and opportunities," *ACM Computing Surveys (CSUR)*, vol. 54, no. 4, pp. 1–40, 2021.
- [7] H. Zhang, H. Nguyen, X.-N. Bui et al., "Developing a novel artificial intelligence model to estimate the capital cost of mining projects using deep neural network-based ant colony optimization algorithm," *Resources Policy*, vol. 66, Article ID 101604, 2020.
- [8] X. Ning, W. Li, B. Tang, and H. He, "BULDP: Biomimetic uncorrelated locality discriminant projection for feature extraction in face recognition," *IEEE Transactions on Image Processing*, vol. 27, no. 5, pp. 2575–2586, 2018.
- [9] X. Liu, Y. Zhou, and Z. Wang, "Deep neural network-based recognition of entities in Chinese online medical inquiry texts," *Future Generation Computer Systems*, vol. 114, pp. 581–604, 2021.
- [10] X. Ning, F. Nan, S. Xu, L. Yu, and L. Zhang, "Multi-view frontal face image generation: a survey," *Concurrency and Computation: Practice and Experience*, vol. 3, 2020.
- [11] P. An, Z. Wang, and C. Zhang, "Ensemble unsupervised autoencoders and Gaussian mixture model for cyberattack detection," *Information Processing & Management*, vol. 59, no. 2, Article ID 102844, 2022.
- [12] X. Ning, P. Duan, W. Li, and S. Zhang, "Real-time 3D face alignment using an encoder-decoder network with an efficient deconvolution layer," *IEEE Signal Processing Letters*, vol. 27, pp. 1944–1948, 2020.
- [13] D. Wu, C. Zhang, L. Ji, R. Ran, H. Wu, and Y. Xu, "Forest fire recognition based on feature extraction from multi-view

## Retraction

# Retracted: Clustering Merchants and Accurate Marketing of Products Using the Segmentation Tree Vector Space Model

### Mathematical Problems in Engineering

Received 18 July 2023; Accepted 18 July 2023; Published 19 July 2023

Copyright © 2023 Mathematical Problems in Engineering. This is an open access article distributed under the Creative Commons Attribution License, which permits unrestricted use, distribution, and reproduction in any medium, provided the original work is properly cited.

This article has been retracted by Hindawi following an investigation undertaken by the publisher [1]. This investigation has uncovered evidence of one or more of the following indicators of systematic manipulation of the publication process:

- (1) Discrepancies in scope
- (2) Discrepancies in the description of the research reported
- (3) Discrepancies between the availability of data and the research described
- (4) Inappropriate citations
- (5) Incoherent, meaningless and/or irrelevant content included in the article
- (6) Peer-review manipulation

The presence of these indicators undermines our confidence in the integrity of the article's content and we cannot, therefore, vouch for its reliability. Please note that this notice is intended solely to alert readers that the content of this article is unreliable. We have not investigated whether authors were aware of or involved in the systematic manipulation of the publication process.

Wiley and Hindawi regrets that the usual quality checks did not identify these issues before publication and have since put additional measures in place to safeguard research integrity.

We wish to credit our own Research Integrity and Research Publishing teams and anonymous and named external researchers and research integrity experts for contributing to this investigation.

The corresponding author, as the representative of all authors, has been given the opportunity to register their agreement or disagreement to this retraction. We have kept a record of any response received.

### References

- [1] X. Ding, Z. Wu, and M. Li, "Clustering Merchants and Accurate Marketing of Products Using the Segmentation Tree Vector Space Model," *Mathematical Problems in Engineering*, vol. 2022, Article ID 7353151, 11 pages, 2022.

## Research Article

# Clustering Merchants and Accurate Marketing of Products Using the Segmentation Tree Vector Space Model

Xuwu Ding,<sup>1,2</sup> Zhong Wu ,<sup>1</sup> and Meng Li<sup>3</sup>

<sup>1</sup>Business School, University of Shanghai for Science and Technology, Shanghai 200093, China

<sup>2</sup>School of Management, Shanghai University of Engineering and Science, Shanghai 201620, China

<sup>3</sup>Metallurgical Automation and Industrial Big Data Technology Engineering Department, Beijing Research Institute of Automation for Machinery Industry Co., Ltd., Beijing 100120, China

Correspondence should be addressed to Zhong Wu; 201670084@st.usst.edu.cn

Received 21 February 2022; Revised 2 March 2022; Accepted 7 March 2022; Published 29 March 2022

Academic Editor: Hangjun Che

Copyright © 2022 Xuwu Ding et al. This is an open access article distributed under the Creative Commons Attribution License, which permits unrestricted use, distribution, and reproduction in any medium, provided the original work is properly cited.

Using social commerce users as the data source, a reasonable and effective interest expression mechanism is used to construct an interest graph of sample users to achieve the purpose of clustering merchants and users as well as realizing accurate marketing of products. By introducing an improved vector space model, the segmentation tree vector space model, to express the interests of the target user group and, on this basis, using the complex network analysis tool Gephi to construct an interest graph, based on the user interest graph, we use Python to implement the K-means algorithm and the users of the sample set according to interest topics for community discovery. The experimental results show that the interests of the sample users are carefully divided, each user is divided into different thematic communities according to different interests, and the constructed interest graph is more satisfactory. The research design of the social commerce user interest mapping scheme is highly feasible, reasonable, and effective and provides new ideas for the research of interest graph, and the boundaries of thematic communities based on interests are clear.

## 1. Introduction

With the widespread popularity of the Internet, the e-commerce industry has made rapid development. Traditional e-commerce often ignores the user's interests and needs and simply explores the user's potential needs from the shopping basket history or browsing traces without paying attention to the influence of social relationships in social media on the user's shopping behavior. In addition, the continuous innovation of business models has led to the emergence of a large number of goods and various e-commerce platforms; the problems of how to get the goods you need from this large number of goods and how to identify the credibility of e-commerce have become the bottleneck limiting the development of e-commerce model. The emergence of social commerce has achieved a breakthrough of this bottleneck, and its media, social, and business attributes can well realize the combination of social media and e-commerce and carry out business activities based on the interests of users. Therefore, the key step to the success of social commerce is to

explore the interest graph of users in e-commerce and realize the gathering of interest-themed communities.

Using social circles, an interest graph can be utilized to attract a wide range of people. On the one hand, it may achieve accurate product marketing by grouping and clustering users' interests; on the other hand, it can build a community with the same or comparable interests as the core, allowing users and merchants to communicate more effectively. This study starts with user interest modeling, then builds the text expressing user interests using the upgraded VSM, segmentation tree VSM, and then uses the complex network analysis tool Gephi to generate the interest graph. Data mining algorithms are utilized to realize the discovery of topic communities based on this.

*1.1. Personalized Recommendation.* Traditional e-commerce sites' personalized recommendations suffer from data scarcity and a lack of complete knowledge about users'

interests; however, cross-domain recommendations based on e-commerce sites and community mining can be a useful alternative. Study [1] outlined the drawbacks of similarity recommendation based on customer ties in existing social networks and offered a cross-domain recommendation system that included social networking sites like Facebook. Study [2] considered the multidimensional nature of customer information to recommend other domains based on customer preferences for a specific domain. Study [3] improved the accuracy of product recommendation by defining the cross-domain personality trait classification problem and using the predictive text embedding method to introduce the user's personality traits into cross-domain recommendation. Study [4] integrated interests from different domains using the Latent Dirichlet Allocation ensemble probability model (LDA) to achieve cross-domain personalized recommendation. Study [5] proposed a cross-domain recommendation system framework based on Folksonomies. The premise of the cross-domain recommendation algorithm is similar to that of the collaborative filtering algorithm, which primarily addresses two issues. The first is the detection and integration of cross-domain users' knowledge. Study [6] constructed a set of cross-system unified user ontology modeling and identification theory. Study [7] focused on the user modeling problem and proposed a context-aware user modeling theory based on context-awareness as well as the FOAF (Friend of a Friend) standard and cross-social network user model Mypes. The other is the cross-domain data integration problem. Study [8] analyzed the representative Linked Data databases Open Linked Data including DBpedia, Freebase, and Linked-MDB, which have automatically or semiautomatically converted the data of traditional web pages into Linked Data, among which DBpedia is one of the world's largest multidomain knowledge ontologies and is widely used for cross-domain recommendations. However, these data are mainly focused on information retrieval and news domains and less involved in the domain of product recommendation [9].

Although the field of personalized recommendation is mature in terms of algorithm and technology, the training data set is from a single source, primarily focusing on users' browsing records and shopping basket records, and lacks the support of users' interests, according to the summary analysis of the above literature. From the perspective of developing a user interest graph, this work addresses this weakness and adds to the field of product suggestion in personalized recommendation.

*1.2. Interest Graph.* As the core element of cross-domain recommendation, the rationality of user interest graph construction will directly affect the effectiveness of the recommendation algorithm. There are various ways to classify user interests, which are generally divided into "long-term interests" and "short-term interests." Study [10] classified interests into one-time interests, long-term constant interests, periodic interests, periodic instantaneous interests, and irregular interests. The basic principle of interest recommendation is based on content, collaborative

filtering, and similar labeling methods, focusing on the problem of interest graph construction. Study [11] pointed out that "social graph" is based on your personal acquaintance social connection, so the circle is limited; while "interest graph" is based on common interests, there is no need to know each other, so it greatly extends the depth and breadth of social interaction, which has the following features: (a) one-way focus, not two-way friends; (b) organization around shared interests, not personal real social relationships; (c) default public, not default private; (d) common struggle: it does not matter what you were or what you are; what matters is what you will be. The process of building user interest graph can be divided into two steps: firstly, interest mining process, the traditional user interest mining is based on the user's historical information (such as commodity browsing path) way [12], along with the emergence of social networks Facebook, Microblog, and so on, broadened the channel of interest mining, there is user interest modeling and interest mining [13]; the other is the interest graph integration process. Accenture believes that recommendations can be made by acquiring customers' interests in different websites, such as recommending luxury off-road vehicles with LCD screens to customers when they know that they love excursions and skiing, prefer Rolex watches, and have purchased a tablet computer. The Digital Enterprise Research Institute (DERI) at the National University of Galway in Ireland proposed the concept of semantic-based customer interest mapping modeling across websites [14], where they obtained complete customer interest graphs by integrating customer information shared on private websites and made recommendations using hybrid link prediction and content-based diffusion activation methods [15], and the study [16] proposed the concept of group interest. Studies [17, 18] employed a user interest graph for user community segmentation and proposed a method for assessing user influence on social media based on distinct interest areas.

Study [19] proposed a basic approach to construct interest mapping by analyzing a large number of social media, in which interest selection, classification, data collection, and interest integration are the main steps. Study [20], on the other hand, applied the ensemble probability model to the integration of social network users' interests and realized a personalized information push service. In terms of stimulating user emotions, interest mapping can effectively stimulate the positive emotions of users [21]. Studies [22, 23] found that personalized news push has data sparsely problems, and to solve such problems, it has been used to improve the satisfaction of news push audience by constructing short- and long-term interest models of users to clarify the interaction between users, news, and potential topics. Study [24] proposed a dynamic Top-K interest subgraph discovery method with large-scale labeled graphs (commonly used in information networks, biological networks, etc.), which can effectively find users' interest graphs and cluster them in a large-scale network space.

The researchers mentioned above studied interest graph from many angles and developed ways for personalizing recommendations, stimulating users' emotions, and

increasing traffic using interest graph. They did not, however, focus on how to design an interest graph, and some of them just proposed certain imagined stages without putting them into action. As a result, in this research, we offer a user interest modeling mechanism in personalized services and utilize Gephi, a complex network analysis software, to build interest mapping of social commerce users and study the thematic communities of social commerce from this perspective.

## 2. Materials and Methods

The study takes the Chinese social commerce platform “Mogu” (Mogu is positioned as a new type of buyer community, focusing on providing a Chinese social commerce platform for discovering beauty and fashion, sharing shopping fun, making friends with like-minded people, and communicating freely. Users browse Mogu to find their favorite items and then link to Taobao (China’s largest C2C e-commerce platform) to share both the fun of shopping and their various creations on the online store) as an example, uses the web crawler technology based on HttpClient and HtmlParser [25, 26] components to obtain the research data, then uses the user interest modeling method in personalization service to express the user’s interest in the form of text, and introduces the social network relationship values into the calculation of user interests to realize the extraction and integration of user interests, so as to get the comprehensive interests of users. Based on this, we use Gephi, a visual complex network analysis tool, to construct a user’s interest graph. Figure 1 shows the program flowchart.

**2.1. USER Interest Extraction.** The social commerce site selected for the study is Mogu, an e-commerce platform similar to Pinterest [27] social photo sharing. The users of this platform are involved in shopping, food, photography, sports, and many other aspects, and they share their favorite products or experiences on social media while shopping, thus increasing the popularity of the social commerce platform. Therefore, this study selects users of Mogu as the source of data based on the following principles: (1) the user base is relatively large; (2) the platform is developing well; (3) the data collection is convenient, and the data format is relatively uniform.

By analyzing the structure of the Mogu website, user interests can be extracted from the following four areas.

**2.1.1. Personal Tags.** Personal tags are simple descriptions of users’ basic attributes, such as their profession, interests, and areas of expertise. In social commerce, personal tags can be used to quickly match users with each other and find “like-minded” friends or “opinion leaders” who can provide reference advice.

**2.1.2. Following.** According to the classic Pareto principle, 80% of the content on the web is created by 20% of the people, and the same is true in social commerce. The purpose

of users using social commerce is to get information and suggestions, so users’ following behavior becomes the most important way to get their interest.

**2.1.3. Sharing.** The sharing behavior of social commerce users focuses on the sharing of products, shopping experience, and store evaluation, and the content of sharing is mainly based on images and supplemented by text. As the topics shared by users may change frequently, it is easy to cause drift when extracting.

**2.1.4. Liking.** Like content contains a more precise amount of information compared to shared content, not only limited to products, shopping experience, store reviews, and so on but also including interesting pictures, artwork, and celebrities.

**2.2. User Interest Representation.** In order to better describe users’ interests, it is necessary to analyze them quantitatively and assign different weights to different interests to measure them more accurately. Therefore, in order to build the interest graph of social commerce users, this paper adopts the segmentation tree vector space model (a modified vector space model (VSM)) [28–33]. This model can classify and assign weights to different interests of users, that is, expressing users’ interests in the form of text, then extracting interest keywords from them for classification, and then calculating the interest distribution by weights. This representation can both visually represent user interests and initially cluster users according to thematic interest categories to facilitate subsequent community discovery [34–37]. Figure 2 presents the segmentation tree vector space model.

Thus, the user interest in social e-commerce can be expressed as

$$U^{IM} = \{(SI_1, W_1)\} (SI_2, W_2), \dots, (SI_n, W_n), \quad (1)$$

where  $SI_k$  denotes the user’s topic interest class and  $W_k$  denotes the weight of  $SI_k$ . The specific calculation method will be described in detail later.

**2.3. Calculation of User Interest.** In order to facilitate the organization and generalization of the collected data and the subsequent research, the following assumptions were made in calculating user interest for this study:

- (a) There is no distinction between long-term and short-term user interests
- (b) Users’ interests do not drift
- (c) Users’ interests are represented by the content they share and like

The basic idea of the algorithm: the user’s interest is divided into individual interest and group interest to be calculated separately and then synthesized by a parameter with a value between [0~1]. Among them, the calculation of individual interest is mainly derived from personal tags,

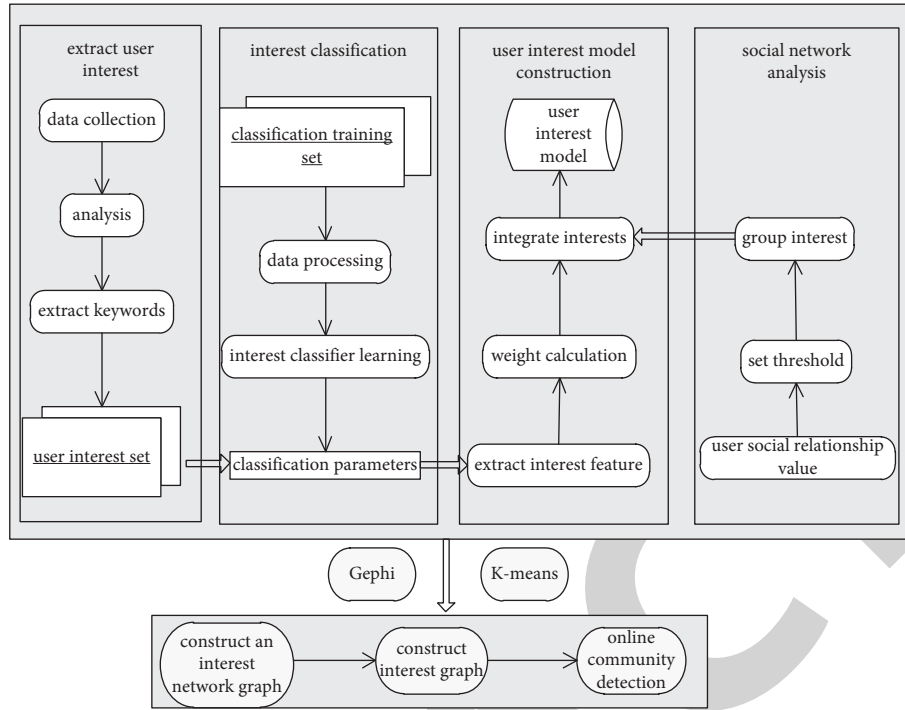


FIGURE 1: Program flowchart.

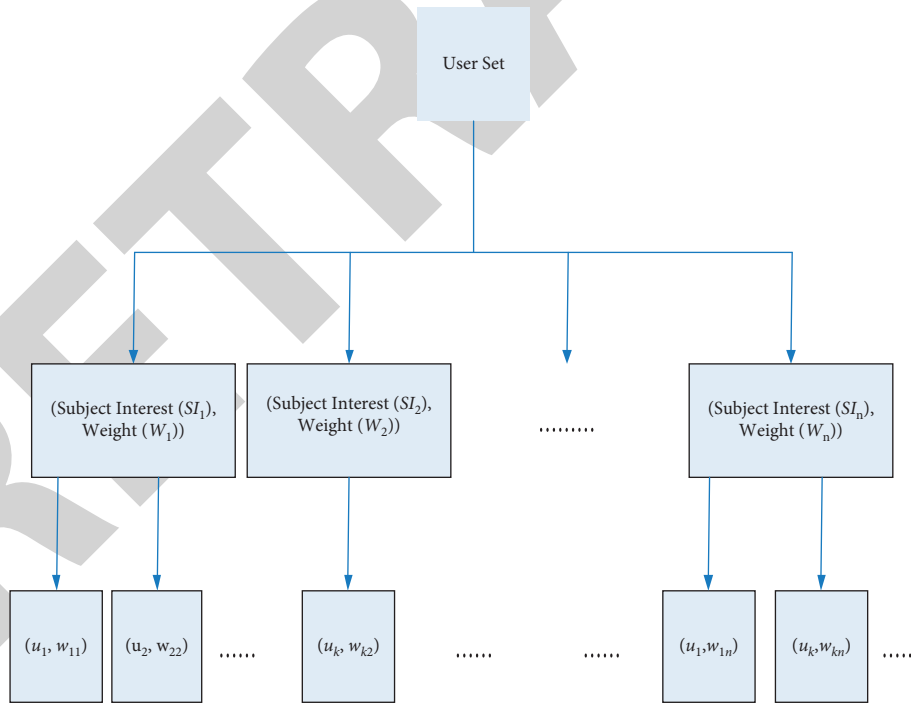


FIGURE 2: Segmentation tree vector space model.

followers, shares, and favorite content. By sorting the collected data, the key texts expressing users' interests are extracted, then the TF-IDF algorithm is used to calculate the values of each part, and then the weighted summation is performed. The group interest is calculated by introducing the social relationship value and the importance of the user

based on the completed calculation of the individual interest, and the three parts are weighted and summed.

As shown in Figure 2, user interest  $U_k^{IM}$  can be represented by the following equation:

$$U_k^{IM} = \alpha \text{Individual}(U_k^{IM}) + (1 - \alpha)\text{Groups}(U_k^{IM}), \quad (2)$$

where Individual ( $U_k^{IM}$ ) denotes individual interest and Groups ( $U_k^{IM}$ ) denotes the group interest of the user.  $\alpha$  is the adjustment coefficient, owing to the fact that the user's interest is divided into two parts: individual interest and group interest, with individual interest occupying the dominating position in previous studies, and when paired with the actual data obtained, the final determination is 0.75. And the individual interest of the user can be expressed as

$$\text{Individual}(U_k^{IM}) = \{SI_i, h(W_{\text{tag}_{ik}}, W_{\text{follow}_{ik}}, W_{\text{share}_{ik}}, W_{\text{like}_{ik}})\}, \quad (3)$$

where  $SI_i$  denotes the  $i$ -th interest component of the user and the function  $h(W_{\text{tag}_{ik}}, W_{\text{follow}_{ik}}, W_{\text{share}_{ik}}, W_{\text{like}_{ik}})$  represents the weight of  $SI_i$ , which is calculated by the formula

$$h(W_{\text{tag}_{ik}}, W_{\text{follow}_{ik}}, W_{\text{share}_{ik}}, W_{\text{like}_{ik}}) = \beta W_{\text{tag}_{ik}} + \gamma W_{\text{follow}_{ik}} + \delta W_{\text{share}_{ik}} + \varepsilon W_{\text{like}_{ik}}, \quad (4)$$

where

$$W_{\text{tag}_{ik}} = \frac{\sum n_{\text{tag}_i}}{N_{\text{tag}}}, \quad (5)$$

where  $n_{\text{tag}_i}$  denotes the number of tags in the user tags that indicate topic interest  $SI_i$  and  $N_{\text{tag}}$  represents the total number of tags for the user.

$$W_{\text{follow}_{ik}} = \frac{\sum n_{\text{follow}_i}}{N_{\text{follow}}}, \quad (6)$$

where  $n_{\text{follow}_i}$  is the number of users' followers who also have topic interest  $SI_i$  and  $N_{\text{follow}}$  denotes the number of users' followings.

$$W_{\text{share}_{ik}} = \frac{\sum n_{\text{share}_i}}{N_{\text{share}}}, \quad (7)$$

where  $n_{\text{share}_i}$  denotes the number of  $SI_i$  about the topic interest among all the content shared by the user and  $N_{\text{share}}$  is the total amount shared by the user.

$$W_{\text{like}_{ik}} = \frac{\sum n_{\text{like}_i}}{N_{\text{like}}}, \quad (8)$$

where  $n_{\text{like}_i}$  represents the number of  $SI_i$  about the topic interest in the content that the user likes and  $N_{\text{like}}$  represents its total amount.

Also in (4),  $\beta + \gamma + \delta + \varepsilon = 1$  indicates that, for different users, the weight assignments of the above four terms will vary. The four features of each user's tag set, the category of the item of interest, the material shared, and the content liked, must be restricted by the values of  $\beta$ ,  $\gamma$ ,  $\delta$ , and  $\varepsilon$ . Because the tag set is so significant in determining users' interests,  $\beta$  is given a value of 0.4, and  $\gamma$ ,  $\delta$ , and  $\varepsilon$  are given an average value of 0.2 and a threshold value of 0.1 for the range of the above three values. If user A's tag set is (astrologer, dresser, photographer) and the objects of interest and favorite content are mostly in these three sets, but the material shared is less (the amount of content shared is 20), then the values of  $\gamma$  and  $\varepsilon$  are 0.3, and the value of  $\delta$  is 0.

In (2), Groups ( $U_k^{IM}$ ) represents the interest of the user's group, and in calculating it, we need to consider the value of social relations between users SR and the importance of users UW.

$$SR(U_1, U_2) = \frac{|O(U_1) \cap O(U_2)|}{|O(U_1) \cup O(U_2)|}, \quad (9)$$

where  $O(U_1)$  denotes the objects associated with  $U_1$  (where the objects not only are users but also include interests) and  $O(U_2)$  denotes the objects associated with  $U_2$ .  $|O(U_1) \cap O(U_2)|$  denotes the number of objects jointly associated with two users, and  $|O(U_1) \cup O(U_2)|$  denotes the total number of objects jointly associated with two users.

$$UW_k = (1 - d) + d \left( \frac{UW_{p_1}}{\text{Follow}(p_1)} + \frac{UW_{p_2}}{\text{Follow}(p_2)} + \dots + \frac{UW_{p_m}}{\text{Follow}(p_{1m})} \right), \quad (10)$$

where  $p_1, p_2, \dots, p_m$  are the followers of user  $k$ ,  $\text{Follow}(p_m)$  is the number of followers of user  $p_m$ , and the damping factor,  $d$ , has a value between 0 and 1, and it indicates the likelihood that user  $k$  will continue to click into another user's space. The damping factor is used since it is impossible for a user to read all of the content provided by all of his followers. In social media, the damping factor is mainly applied in the process of calculating the PageRank value, which generally takes the value of 0.75.

So the group interest can be expressed as

$$\text{Groups}(U_k^{IM}) = \sum_{j \in H} SR(U_k, U_j) * UW_j * \text{Individual}(U_j^{IM}). \quad (11)$$

Individual ( $U_j^{IM}$ ) denotes the individual interest of user  $U_j$ ,  $H$  denotes the interest group in which  $U_k$  is located, and

$SR(U_1, U_2)$  denotes the social relationship values of users  $U_j$  and  $U_k$ .  $UW_j$  denotes the importance of user  $U_j$ .

### 3. Results and Discussion

**3.1. User Interest Model Construction and Interest Value Calculation.** The program collected the public information of Mogu users and obtained the information of 328 influencers in total, each of which has at least 5,000 fans. Considering the carrying capacity of the database and the efficiency of the analysis software, 20 of these fans were randomly selected for data collection. A total of 6840 pieces of data information were collected, and 5454 users' information was collected by eliminating the duplicated and useless data. By processing these 5454 users' sharing

contents, following magazine contents, personal tags, and favorite contents, and using ICTCLAS, a word division system of CAS, for word division and word annotation, we found that the interests of the sample users were concentrated in the following fields: apparel, street shot, constellation, fitness, tourism, cosmetology, and photography. The specific breakdown of each interest is shown in Figure 3.

Take user 136592 as an example; after using the NLTK library in Python to split words, we found that he has three personal tags, namely “astrologer,” “clothing matching,” and “photography enthusiast.” After analyzing his 1355 texts, we found 846 texts reflecting his interests, which were scattered in 5 interest sets, including 387 in constellation, 220 in apparel, 150 in photography, 50 in cosmetology, and 39 in ornament. At the same time, the analysis of their followings and followings of the magazine was carried out, the top 15 users were extracted according to the weighted values of social relationship value and user importance to form the 136592 interest groups, the maximum weighted value of these 15 users was 0.82, and the minimum was 0.39.

After obtaining the above information, the algorithm involved in the study was used to find the interest model of user 136592 as {(astrology, 0.41), (vintage, 0.18), (fashion, 0.02), (scenery, 0.23), (skincare, 0.06), (group purchase, 0.08), (glasses, 0.08)}.

**3.2. Constructing Interest Graph.** Before constructing an interest graph using Gephi, the interests of the entire sample set of users need to be processed briefly because Gephi only accepts two types of csv files, namely, edge data csv files and point data csv files. In order to better construct the interest graph of the sample users, edge data files are used in this study; that is, edges are constructed between each user and the interests they have. Through filtering, a total of 3193 nodes as well as 9739 edges were obtained (in the interest graph, the nodes are divided into two categories, one is the user’s ID number and the other is the interest topic, and the connecting line between two nodes indicates which interests the user has). The interest graph is as follows.

In Figure 4, we can see that the users in the sample are divided into different communities according to their interests. The size of the font in the figure is divided by the “modularity” index in Gephi; from the figure, we can see that fashion and folk in street photography have very high modularity value; through the analysis of the Mushroom Street website, we also found that a large part of its content is about some trend, fashion picture sharing. There are some intermediate users who play the role of bridge between different interest communities.

**3.3. Community Discovery.** Figure 5 shows that, using the modularity function in Gephi, it can be derived that the user interest profile can be roughly divided into 8 aggregation zones. Therefore, for the sample users, the initial number of cores of mass in the K-means algorithm can be set to 8. To verify its reasonableness, the study introduces the silhouette coefficient, which takes values in the range of  $[-1, 1]$ , and the larger the value, the better the clustering effect. The

implementation code of the silhouette coefficient is written using Python, and a graph of the relationship between the silhouette coefficient and the K-means core number (K-value for short) can be derived, as shown in Figure 6. From the graph, it can be seen that the silhouette coefficient has a maximum value when K-value = 8. This further validates the feasibility and effectiveness of using an interest graph to determine the K-value.

After the K-value was determined, the K-means algorithm was implemented in Python to perform community discovery on the sample, and the results were as follows.

As seen in Table 1, the square sum of the distance between clusters accounts for 81.25% of the square sum of overall distance, and these data also indicate that the clustering between different clusters achieves the maximum. Therefore, the clustering effect is good.

Table 2 shows the comparison of the mean values of each indicator in different clusters, and it can be seen from the table that the differences between different clusters are very obvious, which further verify the validity of the cluster analysis results.

Finally, the results of community discovery using K-means are shown in Figure 7, from which it can be seen that the sample set is divided into 8 communities of different sizes.

**3.4. Analysis of Results.** The results from the community discovery show that there is a high degree of coupling between the communities internally, indicating that the members within each community in Mogu have a high degree of association with each other, and the same conclusion can be drawn from the interest graph. In these interest communities, Mogu’s influencers act as community opinion leaders, which is also an important development direction of social commerce at present. Through the mining, operation, and maintenance of the influencers, these influencers are encouraged to share their shopping experience more often to attract customers. In addition, the analysis of community members reveals that a large part of them come from Weibo, Qzone, and so on, which also reflects its social characteristics. The obvious differences between communities allow users to quickly and accurately find the right community for them based on their interests and to get the information they need from the community members. This is the biggest benefit that a social commerce platform like Mogu brings to its users. Moreover, as we can see from the previous study, Mogu has carefully categorized users’ interests to satisfy different interest groups as much as possible.

Although the connection between the members of the community in Mogu is relatively close, the connection between the community is relatively small, which also reflects the lack of development of most of the social commerce platforms like Mogu in China. As a representative of domestic social commerce platforms, the development of Mogu has its own characteristics. First, the entrance of Mogu users is mainly Taobao, Baidu, Weibo, and social networking sites. Second, the core of social commerce development is a



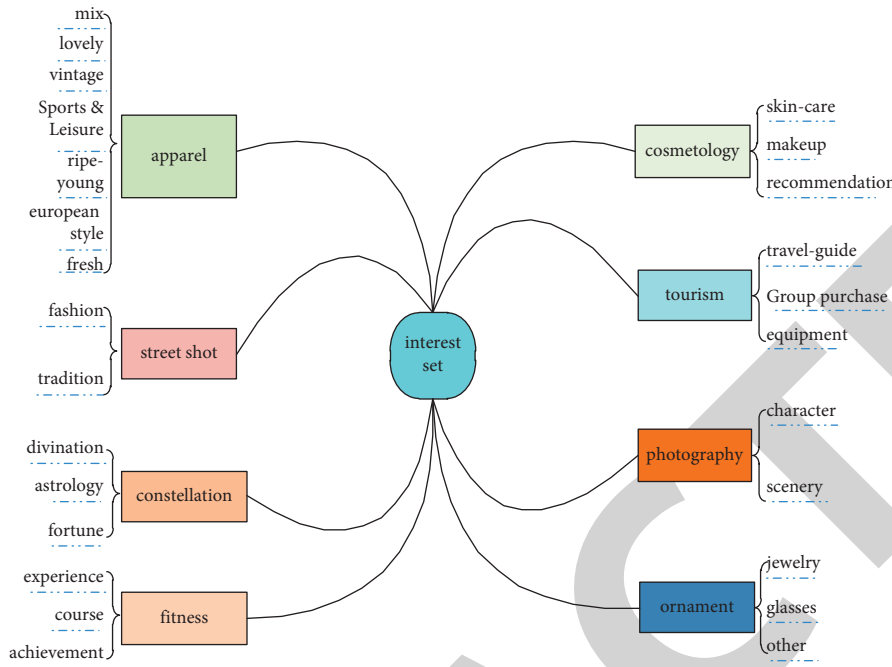


FIGURE 3: User interest segmentation tree.

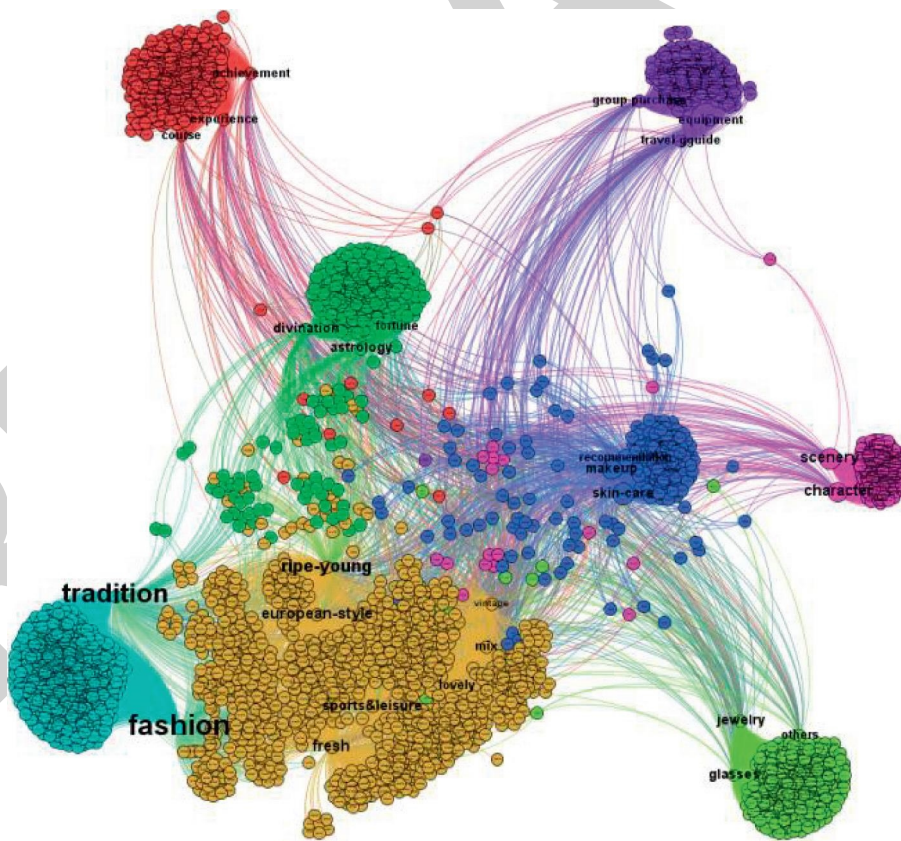


FIGURE 4: Mogu users interest graph.

common interest, and the source of development is driven by some commonality in users themselves and their temperament. Although the characteristics of each community in Mogu are more prominent, the connection between

communities is not close enough, which leads to the inability to effectively use user resources within the whole platform. Third, the source of commodity information is relatively single, most of the commodity purchase links in Mogu are

Results:  
 Modularity: 0.692  
 Number of Communities: 8



FIGURE 5: Modularization results of the interest graph.

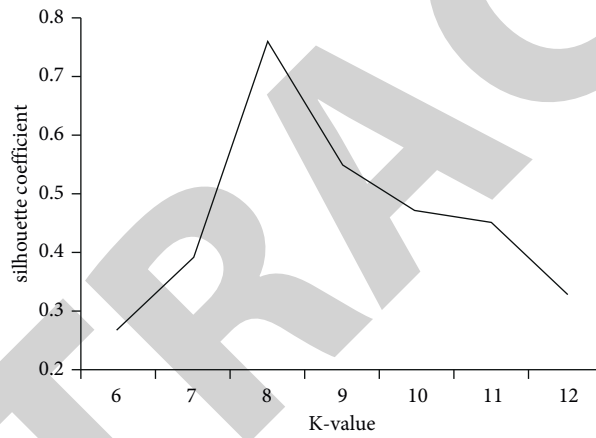


FIGURE 6: Plot of silhouette coefficient versus K-value.

TABLE 1: The square sum of internal distance in every cluster.

| Cluster   | 1      | 2      | 3      | 4      | 5      | 6      | 7      | 8      |
|---|--------|--------|--------|--------|--------|--------|--------|--------|
| Square sum of internal distance between_SS/total_SS | 1.6357 | 2.5234 | 5.3257 | 4.4712 | 1.2478 | 0.8974 | 2.2587 | 2.4244 |
|   | 81.25% |        |        |        |        |        |        |        |

TABLE 2: The table of variance analysis.

|                    | Cluster     |    | Error       |      | F        | Sig.   |
|--------------------|-------------|----|-------------|------|----------|--------|
|                    | Mean square | df | Mean square | df   |          |        |
| Mix                | 8.831       | 7  | 0.001       | 3250 | 7741.034 | ≤0.001 |
| Vintage            | 0.290       | 7  | 0.005       | 3250 | 52.814   | ≤0.001 |
| Lovely             | 5.999       | 7  | 0.002       | 3250 | 2665.849 | ≤0.001 |
| Sports and leisure | 1.725       | 7  | 0.014       | 3250 | 126.376  | ≤0.001 |
| European style     | 2.734       | 7  | 0.016       | 3250 | 174.567  | ≤0.001 |
| Fresh              | 1.843       | 7  | 0.014       | 3250 | 127.430  | ≤0.001 |
| Ripe young         | 3.689       | 7  | 0.016       | 3250 | 235.727  | ≤0.001 |
| Fashion            | 18.448      | 7  | 0.004       | 3250 | 4478.154 | ≤0.001 |
| Tradition          | 18.914      | 7  | 0.004       | 3250 | 5180.555 | ≤0.001 |
| Divination         | 0.382       | 7  | 0.011       | 3250 | 34.891   | ≤0.001 |
| Astrology          | 0.395       | 7  | 0.011       | 3250 | 37.399   | ≤0.001 |

TABLE 2: Continued.

|                | Cluster     |    | Error       |      | F        | Sig.   |
|----------------|-------------|----|-------------|------|----------|--------|
|                | Mean square | df | Mean square | df   |          |        |
| Fortune        | 0.348       | 7  | 0.009       | 3250 | 37.199   | ≤0.001 |
| Experience     | 0.469       | 7  | 0.014       | 3250 | 34.147   | ≤0.001 |
| Course         | 0.465       | 7  | 0.014       | 3250 | 33.870   | ≤0.001 |
| Achievement    | 0.467       | 7  | 0.014       | 3250 | 34.030   | ≤0.001 |
| Skincare       | 0.172       | 7  | 0.008       | 3250 | 22.637   | ≤0.001 |
| Makeup         | 0.106       | 7  | 0.005       | 3250 | 21.121   | ≤0.001 |
| Recommendation | 0.098       | 7  | 0.004       | 3250 | 21.824   | ≤0.001 |
| Travel guide   | 0.234       | 7  | 0.005       | 3250 | 44.024   | ≤0.001 |
| Group purchase | 0.388       | 7  | 0.010       | 3250 | 40.709   | ≤0.001 |
| Equipment      | 0.902       | 7  | 0.020       | 3250 | 45.759   | ≤0.001 |
| Character      | 7.766       | 7  | 0.001       | 3250 | 7754.478 | ≤0.001 |
| Scenery        | 7.744       | 7  | 0.001       | 3250 | 7117.170 | ≤0.001 |
| Jewelry        | 0.492       | 7  | 0.011       | 3250 | 45.012   | ≤0.001 |
| Glasses        | 0.484       | 7  | 0.011       | 3250 | 44.444   | ≤0.001 |
| Others         | 0.481       | 7  | 0.011       | 3250 | 44.134   | ≤0.001 |

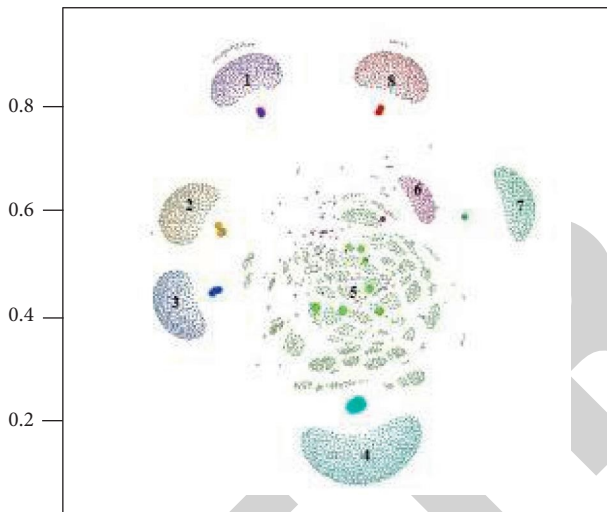


FIGURE 7: Community discovery by using K-means.

from Taobao, and there is no good connection with other shopping sites, which also leads to the homogenization of information on the platform which is more serious.

#### 4. Conclusions

For precisely detecting user interests, clustering people, and conducting word-of-mouth marketing, the creation of a user interest graph and the finding of e-commerce communities are critical. The findings of this study can be used to provide a referential idea for how to design a social commerce user interest graph on the one hand and to make suggestions for merchants, platforms, and users that are in accordance with their own development on the other hand.

*4.1. Countermeasure Suggestions for Merchants.* The construction of social commerce user interest graph and their community discovery are important tools for merchants to realize accurate marketing and improve marketing efficiency. On the one hand, the wide variety of interests

contained in the interest graph provides merchants with a source of information to promote products for different interests; on the other hand, online communities composed of the same interests have a high density of internal connections and are likely to generate several “opinion leaders,” so merchants can focus their marketing on them to improve efficiency. Merchants can do this in the following three ways: (1) seize the main interests to achieve precise marketing; (2) explore opinion leaders to realize e-commerce community; (3) play social attributes to achieve traffic multiplication.

*4.2. Countermeasure Suggestions for the Platform.* The construction of interest graphs and their community discovery are of great importance for e-commerce platforms. On the one hand, it can provide advertising placement efficiency; for both e-commerce platforms and social media platforms, bidding advertising has been the main way of their profit. A social commerce platform built on user interest mapping can not only improve the accuracy of its advertising but also increase the conversion rate from advertising effects to actual purchases. On the other hand, it can realize the sharing of user traffic between social and e-commerce platforms. In order to realize the enhancement of user wandering, the platform can be carried out in the following four aspects: (1) play the strong interactive, interactive, and interest consistency characteristics of the platform; (2) improve user experience and increase the import rate of customer traffic; (3) improve the interest tagging mechanism of the platform; (4) pay attention to the role of interest communities.

*4.3. Countermeasure Suggestions for Users.* For ordinary users, social commerce not only satisfies users’ shopping needs but also achieves the purpose of socializing with people. But to make better use of social commerce platforms to enhance their experience and avoid unnecessary product recommendations and spam, users need to (1) improve personal interest tags; (2) focus on privacy protection; (3) effectively use the platform’s user experience program.

Social commerce is currently on the rise, although the research work in this paper provides a detailed description of the development and form of social commerce and focuses on one of the most representative forms. However, there are still many shortcomings in the theoretical scope of application and the practical process of experimental results that need to be improved and perfected. The following two aspects need to be considered in future research. One is to enrich the research object, expand the sample sources of the study, and conduct the mining of social commerce users' interest graph and the discovery of online communities through comparative studies. This ensures the authenticity of the research process and the extensiveness and objectivity of the research data sources and also makes the results of the study applicable to different types of social e-commerce platforms. Secondly, the problem of user interest drift is considered. Interest graph is the basis of social commerce model development, and the interest graph constructed in this paper is based on the static formal description of users' interests. However, in the process of daily interaction, users' interests will change over time (i.e., user interest drift). If the user interest model is not updated in time when the interest changes, the performance of the constructed user interest graph will be degraded, which in turn affects the effectiveness of online community discovery. Therefore, how to establish an effective update mechanism to cope with the user interest drift becomes the difficulty and focus of the next work.

## Data Availability

The simulation experiment data used to support the findings of this study are available from the corresponding author upon request.

## Conflicts of Interest

The authors declare that there are no conflicts of interest regarding the publication of this paper.

## Acknowledgments

This work was supported by the soft science research project of the Shanghai Science and Technology Committee (Grant no. 22692104000).

## References

- [1] B. Shapira, L. Rokach, and S. Freilikhman, "Facebook single and cross domain data for recommendation systems," *User Modeling and User-Adapted Interaction*, vol. 23, no. 2, pp. 211–247, 2013.
- [2] S. Tan, J. Bu, X. Qin, C. Chen, and D. Cai, "Cross domain recommendation based on multi-type media fusion," *Neurocomputing*, vol. 127, pp. 124–134, 2014.
- [3] H. Wang, Z. Yuan, Li Hong, and J. Wu, "Cross-domain recommendation with user personality," *Knowledge-Based Systems*, vol. 213, p. 10, Article ID 106664, 2021.
- [4] Yu. Cheng, D. Agarwal, and A. Smola, "Multiple domain user personalization," in *Proceedings of the 17th ACM SIGKDD International Conference on Knowledge Discovery and Data Mining*, pp. 123–131, Association for Computing Machinery, San Diego, CA, USA, August 2011.
- [5] Y. Guo and X. Chen, "A framework for cross-domain recommendation in folksonomies," *Journal of Automation and Control Engineering*, vol. 1, no. 4, pp. 326–331, 2013.
- [6] F. Carmagnola, F. Cena, and C. Gena, "User model interoperability: a survey," *User Modeling and User-Adapted Interaction*, vol. 21, pp. 285–331, 2011.
- [7] S. Berkovsky, T. Kuflik, and F. Ricci, "Mediation of user models for enhanced personalization in recommender systems," *User Modeling and User-Adapted Interaction*, vol. 18, no. 3, pp. 245–286, 2008.
- [8] R. Mirizzi, T. D. Noia, and Ragone, "Movie recommendation with DBpedia," in *3rd Italian information retrieval workshop, CEUR Workshop Proceedings*, vol. 835, pp. 101–112, 2012.
- [9] C. Bizer, T. Heath, and T. Berners-Lee, "Linked Data - the story so far," *International Journal on Semantic Web and Information Systems*, vol. 5, no. 3, pp. 1–22, 2009.
- [10] R. Kawase and E. Herder, "Classification of user interest patterns using a virtual folksonomy," in *Proceedings of the 11th Annual International ACM/IEEE Joint Conference on Digital Libraries*, pp. 105–108, Ottawa, Canada, June 2011.
- [11] B. R. Venture, "Interest graphs will change social networks and the future of business," 2014, <http://www.199it.com/archives/24788.html>.
- [12] M. Nicoletti, S. Schiaffino, and D. Godoy, "Mining interests for user profiling in electronic conversations," *Expert Systems with Applications*, vol. 40, no. 2, pp. 638–645, 2013.
- [13] H. Bao, Q. Li, S. S. Liao, S. Song, and H. Gao, "A new temporal and social PMF-based method to predict user's interests in micro-blogging," *Decision Support Systems*, vol. 55, no. 3, pp. 698–709, 2013.
- [14] F. Orlandi, "Multi-source provenance-aware user interest profiling on the social semantic web, User Modeling, Adaptation, and Personalization," in *Proceedings of the 20th International Conference on User Modeling, Adaptation, and Personalization*, vol. 7379, pp. 378–381, Heidelberg, Germany, 2012.
- [15] B. Heitmann and M. Dabrowski, "Personalization of Social Web Services in the enterprise Using Spreading Activation for Multi-Source, Cross-Domain Recommendation," in *Proceedings of the Association for the Advancement of Artificial Intelligence*, pp. 46–51, Worldwide, January 2012.
- [16] D. Li, Q. Lv, X. Xie et al., "Interest-based real-time content recommendation in online social communities," *Knowledge-Based Systems*, vol. 28, pp. 1–12, 2012.
- [17] L. Zhai, J. Wang, C. Hu, and J. Li, "User influence in microblog based on interest graph," *International Journal of Software Engineering and Knowledge Engineering*, vol. 28, no. 2, pp. 207–217, 2018.
- [18] S. Dhelim, N. Aung, and H. Ning, "Mining user interest based on personality-aware hybrid filtering in social networks," *Knowledge-Based Systems*, vol. 206, Article ID 106227, 2020.
- [19] Lynne, "The interest graph architecture - social modeling and information fusion," *Proceedings of SPIE—signal processing, sensor fusion, and target recognition XXI*, vol. 8392, pp. 46–48, 2012.
- [20] A. Christiyana Arulselvi, S. Sendhilkumar, and G. S. Mahalakshmi, "Identifying trusted similar users using stochastic model and next-closure based knowledge model in online social networks," *Cluster Computing*, vol. 22, no. 6, pp. 14625–14635, 2019.
- [21] H. Benjamin, "An open framework for multi-source, cross-domain personalization with semantic interest graphs," in

## Retraction

# Retracted: Intelligent Analysis and Evaluation Method of Athletics Running Data Based on Big Data Statistical Model

### Mathematical Problems in Engineering

Received 18 July 2023; Accepted 18 July 2023; Published 19 July 2023

Copyright © 2023 Mathematical Problems in Engineering. This is an open access article distributed under the Creative Commons Attribution License, which permits unrestricted use, distribution, and reproduction in any medium, provided the original work is properly cited.

This article has been retracted by Hindawi following an investigation undertaken by the publisher [1]. This investigation has uncovered evidence of one or more of the following indicators of systematic manipulation of the publication process:

- (1) Discrepancies in scope
- (2) Discrepancies in the description of the research reported
- (3) Discrepancies between the availability of data and the research described
- (4) Inappropriate citations
- (5) Incoherent, meaningless and/or irrelevant content included in the article
- (6) Peer-review manipulation

The presence of these indicators undermines our confidence in the integrity of the article's content and we cannot, therefore, vouch for its reliability. Please note that this notice is intended solely to alert readers that the content of this article is unreliable. We have not investigated whether authors were aware of or involved in the systematic manipulation of the publication process.

Wiley and Hindawi regrets that the usual quality checks did not identify these issues before publication and have since put additional measures in place to safeguard research integrity.

We wish to credit our own Research Integrity and Research Publishing teams and anonymous and named external researchers and research integrity experts for contributing to this investigation.

The corresponding author, as the representative of all authors, has been given the opportunity to register their agreement or disagreement to this retraction. We have kept a record of any response received.

### References

- [1] Y. Ge, "Intelligent Analysis and Evaluation Method of Athletics Running Data Based on Big Data Statistical Model," *Mathematical Problems in Engineering*, vol. 2022, Article ID 5624482, 8 pages, 2022.

## Research Article

# Intelligent Analysis and Evaluation Method of Athletics Running Data Based on Big Data Statistical Model

Yushan Ge 

ChongQing Industry Polytechnic College, Chongqing 401120, China

Correspondence should be addressed to Yushan Ge; geys@cqipc.edu.cn

Received 18 February 2022; Accepted 17 March 2022; Published 29 March 2022

Academic Editor: Hangjun Che

Copyright © 2022 Yushan Ge. This is an open access article distributed under the Creative Commons Attribution License, which permits unrestricted use, distribution, and reproduction in any medium, provided the original work is properly cited.

To investigate the effectiveness of pedometry in athletics at different running speeds and on different walking surfaces, and to test whether it can be used for running for fitness and for pedometry on hardened concrete surfaces in daily life. The steps were measured under laboratory conditions using a running platform at 5 min at 5 speeds of 3.2 km/h, 4.8 km/h, 6.4 km/h, 8.0 km/h, and 9.6 km/h (actual steps were accurately determined by video playback), followed by 300 steps each at low, normal and fast speeds on an outdoor plastic athletics track. There were significant differences between the smart bracelet and the mobile phone sports app at low running speeds on four different surfaces: outdoor plastic track, dirt, concrete and mountainous terrain. The difference was not significant in normal pace and fast walking.

## 1. Introduction

Athletics is a regular sporting event for many schools and local sporting bodies. Long distance running lap counting in athletics is a tedious task for referees and requires a large number of experienced and professional referees. Even so, there are still some problems in the process of officiating, and in serious cases, there are also misjudgements and omissions, leading to errors in the results of the competition and requiring a lot of time to correct them, which greatly affects the smoothness of the competition. In the information collection layer, the information of athletes is collected by means of voice recognition, which greatly reduces the errors that may be generated by manual lap counting; in the data transmission, it is directly uploaded to the cloud platform by means of GPRS, which facilitates the work of referees and improves the work efficiency. The system is low cost, easy to use and has a certain value and application prospect [1].

With the development of society and technology, a sedentary lifestyle with inadequate physical activity as the main characteristic due to the motorisation of transport, real-time communication and social networking is endangering the health of the general public [2]. Walking is one of the most fundamental forms of physical activity for humans,

and its health benefits are becoming increasingly important. The easy and accurate measurement of walking is a key area of research in this field, as well as the most convenient and intuitive way for people to understand their physical activity levels on a daily basis [3]. From pedometers to triaxial accelerometers, there has been a constant quest for easier and more effective pedometry tools [4]. The advent of the smartphone has not only changed the single communication function of mobile phones, but has also changed the way people live and act, and it has become a new trend to use smartphone exercise APPs for fitness. At the same time, smart bracelets have also developed rapidly to guide healthy living by recording daily exercise data, which can be synchronised and shared with smart phones. To date, there have been reports on the development of smart bracelets and smartphone exercise applications (APPs) and gait recognition in China [5], but there is little literature on the accuracy of the pedometry function, which is assessed in two ways, namely at different walking speeds and on different walking surfaces [6].

The effectiveness of different pace counting functions based on the iPhone4siOS7 fitness app has been reported in the literature [7], but little has been reported on the effectiveness of different pace counting functions of smart bracelets and smartphone sports apps on different walking

surfaces (e.g. running on plastic athletic fields, hiking in the wild, climbing mountains and walking on city streets, etc.). This study is based on existing research in China and investigates the accuracy of the smartband and smartphone sports app for different walking speeds and running surfaces.

## 2. Related Work

With the popularity of the pedometer function, the research results of step detection algorithms have increased. At present, the step detection algorithms based on acceleration sensors at home and abroad can be divided into the following eight categories, including: normalised autocorrelation, peak detection, finite state machine, etc.

In [8], a step detection algorithm is implemented based on autocorrelation coefficient analysis. The method detects the step count results of  $y$ -axis and  $z$ -axis acceleration data separately, and then selects the largest result as the final detection result. The final example of the method in the step detection algorithm research work of [9] was to exclude the influence of nonreal walking data on the step counting results, and the authors matched the extracted nonrunning data template with the actual acceleration data for calculation based on autocorrelation coefficient analysis, thus ensuring the accuracy of the step counting. [10] used autocorrelation coefficient analysis to design a smartphone pedometer. Due to the uncertainty of the human stride period, the authors used an add-frame calculation to try to find the optimal stride period and validate the acceleration signal corresponding to the largest correlation coefficient result as a valid step. In [11], the same correlation coefficient analysis was used for step detection in the design of a Zee-based positioning navigation system, and invalid acceleration data was filtered by a threshold of signal variance.

[12] set thresholds for acceleration maximum, minimum, and variance to trigger step counting in work investigating hybrid navigation systems [13]. [14] implemented a peak detection pedometry algorithm using a plus-minus score mechanism.

A filtering method is also proposed in the pedometry algorithm study of [15], which normalises the peak features so that an acceleration point with a value of 1 after filtering represents the generation of a step. In the work on the pedometry algorithm of [16], the authors extracted features such as the number of relationships and the degree of deviation from positive and negative values of the acceleration data, and then set thresholds for each feature; only acceleration peaks that reached the threshold setting were selected as candidate peaks. In the 3D positioning system research work of [17], the authors implemented an adaptive peak counting algorithm that improves the adaptability of the peak detection pedometry algorithm under multiple movements by setting different peak thresholds for different movements. [18] designed an adaptive peak detection pedometry algorithm using different threshold ranges based on the characteristic that running and walking produce different ranges of acceleration peaks, improving the adaptiveness of the peak detection method for running and walking movements. [19] implemented a step detection

algorithm based on finite state machines, in which the authors decomposed the one-step acceleration signal into six states. [20] used a Kalman filter to preprocess the acceleration signal when designing the finite state machine based step counting algorithm, making the acceleration signal smoother and therefore allowing the process of noise processing to be removed in the finite state machine, effectively improving the step counting efficiency of the finite state machine based step counting algorithm by reducing the number of state transitions.

## 3. Human Running and Acceleration Signals

*3.1. Analysis of the Human Running Process.* In this paper, the following phases are distinguished from the other phases: supported phase, single foot lift forward phase, upright phase and heel landing phase. By analysing the changes in acceleration amplitude during these phases, the relationship between acceleration data and gait changes can be further identified. Figure 1 illustrates the continuous changes in the body as the pedestrian completes a two-step manoeuvre.

As can be seen from Figure 1, during the actual continuous walking process, one step is actually completed during the double-legged support phase. After the support phase, the body gradually leans forward while lifting one foot forward, and the entire foot of the unlifted foot gradually comes into full contact with the ground until the lower limb of the body is approximately perpendicular to the ground, at which point the zero speed phenomenon, as indicated in the zero speed correction method occurs.

*3.2. Starting Point Marking Method.* The start point is the moment in the acceleration data that may indicate the start of a step, and each start point will correspond to the sampling time of a specific acceleration sampling point. When the acceleration sensor is located in the hand, trouser pocket and chest area of the body in Figure 1, the collected acceleration signal will exhibit the acceleration signal characteristics respectively. Although noise is present in the acceleration data, the acceleration signal for normal walking maintains a certain periodicity when viewed as a whole. It is assumed that the linear synthetic acceleration collected and calculated over a given time period is  $A(n,t)$ , where  $n$  denotes the number of sampling points,  $t$  denotes the sampling time and  $a_k(t_k)$  denotes the sample point of linear synthetic acceleration with the value  $a_k$  collected and calculated at the  $t_k$  time, where  $k = 1, 2, \dots, n$ . In this paper, the following method is used to mark the starting points and record them as a set  $TP_s$ :

$$TP_s = \{t_k | a_k(t_k) \geq Th_s \cap a_{k-1}(t_{k-1}) < Th_s, k = 1, 2, \dots, n\}, \quad (1)$$

where  $Th_s$  is the starting point detection threshold. It should be noted that the linear synthetic acceleration calculated in this paper has lost the vector characteristics of the three axes and the gravity component, directly reflecting the acceleration changes generated by the sensor at a fixed part of the



FIGURE 1: Decomposition of human walking motion.

body during walking. The theoretical output value of the acceleration sensor at rest is  $g = (0, 0, 9.8)\text{m/s}^2$ , so the linear synthetic acceleration magnitude should be zero under the ideal resting action. Due to the process material and measurement accuracy of the sensor itself, this can lead to errors in the sampling value at rest. The sensor used in this paper reads around  $g = (0.2, 0.2, 10.1)\text{m/s}^2$  at rest, and is therefore set here  $Th_s = 0.5\text{m/s}^2$ . Figure 2 shows the starting point in the acceleration signal detected by the accelerometer as it swings with the arm.

The detection of the start point allows a better representation of the periodicity of the data, and the recorded  $TP_s$  and linear acceleration series  $A(n,t)$  will be used in the next stage of the pacing algorithm. The effectiveness of this method is demonstrated in the literature [10], where it is used as a threshold for starting point detection, i.e. to filter errors.

#### 4. Design of a Pedometry Algorithm Based on Autocorrelation Coefficient Analysis

Combined with the results of the start point detection in Figure 2, it can be seen that the data period in this case is different from the signal period when the accelerometer is in the trouser pocket and chest area. In addition to this, in terms of peak variation, it can be seen from Figure 2 that there is a peak in some cycles, some of which have a small amplitude, which can cause large pacing errors if the peak detection method is used for detection processing. Therefore, the design of the step counting algorithm can be considered from the perspective of calculating the similarity of the acceleration signal. In view of these factors, a step counting algorithm based on autocorrelation analysis was implemented to process the step detection of this action.

##### 4.1. Design of a Pedometry Algorithm Based on Peak Detection.

When the action detection result is a relatively stable action, this paper uses a pacing algorithm based on peak detection, which requires a threshold variable  $Th_{peak}$ , and in order to improve the adaptive nature of the peak, the threshold is set at the beginning of the algorithm execution  $Th_{peak} = 0.2g$  ( $g = 9.8\text{m/s}^2$ ), after which the  $Th_{peak}$  threshold will change in the following way:

$$Th_{peak} = \frac{1}{M} \sum_{j=1}^M peak_j, \quad (2)$$

where  $peak_j$  is the peak acceleration in the current window that has been validated and  $M$  is the number of

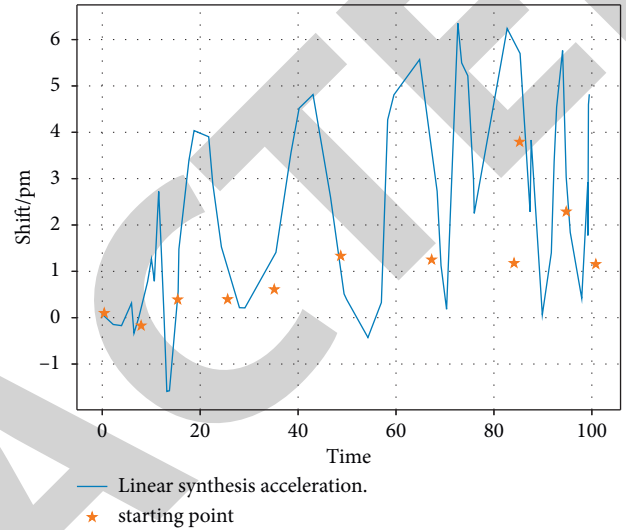


FIGURE 2: Starting points in the acceleration signal.

validated peaks in the analysis window, the meaning of the above equation is that after a period of time,  $Th_{peak}$  is set to the mean value of the validated peaks. Suppose that the algorithm is processing a starting point in  $TP_s$ , denoted  $TP_{s\_ur}$  [21].

**4.2. Step Detection Compensation Strategy.** When a pedestrian makes a transition during walking, this can cause significant noise interference in the acceleration signal. It is important to emphasise that the analysis window for action recognition in this paper is also the analysis window for the pedometry algorithm, so when just one transition action occurs within an analysis window, the system should recognise the acceleration signal within this analysis window as the acceleration signal under the transition action. For the case that the action recognition result belongs to the transition action, the acceleration data in one running cycle may produce several pseudo-peaks, and the frequency characteristics and variance characteristics of the whole acceleration signal are also less regular, for this situation, this paper tries to use a compensation method to detect the number of steps in the transition state as far as possible, the compensation method is as follows:

$$CSC = \left[ \frac{TP_{s\_new} - TP_{s\_old}}{LS_{last}} \right], \quad (3)$$

where  $TP_{s\_new}$  and  $TP_{s\_old}$  denote the most recent and latest moments in the set of starting points  $TP_s$  of the transition



movement acceleration sequence and  $LS_{\text{last}}$  denotes the period of the last valid step. The strategy adopted in the above equation is to default the period of the run under the transition action to be consistent with the period of the previous step or steps, and to update the CSC value to the TSC in time after each compensated pacing is completed. The final TSC result will consist of the autocorrelation coefficient analysis pacing algorithm, the pacing calculation for peak detection and the compensated pacing result.

## 5. Case Studies

**5.1. Research and Test Subjects.** The subjects of this study are smart bracelets and smartphone sports APPs with pedometer function, three smart bracelets from Xiaomi, Lexin and SmartHealth, and four sports APPs from Goudong, Yueyun Circle, Yidong GPS and Dynamic as test subjects.

**5.2. Pedometer Validity Tests on Different Surfaces.** The test was conducted outdoors on four different running surfaces: plastic, dirt, concrete and hills. During the test, the participant wore an arm bag with an iPhone 5s phone (on the outside of the upper arm) and began to adapt to low speed, normal speed and fast speed for 3 minutes each (low speed, normal speed and fast speed were determined by the participant's own subjective perception of speed). Afterwards, the Pro-Active App (which was determined to be more effective in the first part of the study) was activated, the phone was placed in the arm bag and the Heart of Joy bracelet was worn on the left wrist at the same time. The participant then walked 300 steps at a low, normal and fast pace (the number of steps was calculated by the participant), stopping at the end and recording the number of steps recorded by the APP at this time, 5 times for each venue. To avoid fatigue affecting the test results, there was a 5 min break between each exercise. During the test, a staff member held a video camera to follow the test and the participant counted 300 steps after the start of the walk and then finished the test.

**5.3. Study Results.** Table 1 shows the average of the recorded and actual step counts and the dispersion (standard deviation) for each of the five speed levels of 3.2 km/h, 4.8 km/h, 6.4 km/h, 8.0 km/h and 9.6 km/h for the three smart bracelets. As can be seen from the table, the most significant increase in the cumulative number of steps in 5 min occurred when the step rate was increased from 3.2 km/h to 4.8 km/h. Thereafter, the increase in the cumulative number of steps in 5 min slowed down with each 1.6 min increase. As the speed increases, the cumulative number of steps in 5 min decreases between the different rings and the difference between the actual number of steps decreases.

At the lowest speed level of 3.2 km/h, the Xiaomi bracelet had a highly significant difference ( $p < 0.01$ ) in the actual number of steps taken as a control, while the other two bracelets had a highly significant difference ( $p < 0.01$ ) in the Xiaomi bracelet as a control.

As seen in Table 2, similar to the three smart bands, the most significant increase in the cumulative number of steps in 5 min was observed when the four sports APPs were increased from 3.2 km/h to 4.8 km/h. Thereafter, the increase in the cumulative number of steps in 5 min slowed down with each 1.6 min increase. Again, as the speed increases, the cumulative number of steps in 5 min decreases between the different rings and the difference between the actual number of steps decreases. At the lowest speed level of 3.2 km/h, there was a highly significant difference between the four sports APPs in terms of actual steps ( $p < 0.01$ ).

From the scatter diagram of linear regression analysis (Figures 3, 4 and 5, where  $x$ -axis is the number of samples), it can be seen that with the increase of running speed, the actual steps of the three bracelets show a good linear correlation with the steps recorded by the three bracelets,  $R^2$  being 0.982, 0.998 and 0.998 respectively. With the improvement of running speed, the consistency between Xiaomi bracelet and the actual steps is slightly weaker than the other two bracelets. As can be seen from Figures 6 and 7 (where  $x$ -axis is the number of step), with the increase of walking speed, the actual steps of the four sports apps also show a good linear correlation with the steps recorded by the three bracelets,  $R^2$  being 0.997, 0.997, 0.994 and 0.997 respectively.

As the speed increases, the three smart bracelets with the best stability of the step-keeping function are the Le Xin bracelet, as analysed in Figures 2 to 4 and Table 3. From Figures 5 to 7, as the speed increases, the 4 sports APPs with the best stability of the step recording function are Yidong and Goudong. Therefore, the effectiveness of the pedometer on different running surfaces was tested with the Le Xin Bracelet and Yidong APPs respectively. As shown in Figure 5, with the increase of running speed, the Le Xin smart bracelet was significantly different from the actual step count on concrete and mountainous terrain at low walking speed, with  $p$ -values  $< 0.01$  and  $< 0.05$  respectively, while the Yidong APP was also significantly different from the actual step count on concrete and mountainous terrain, with  $p$ -values  $< 0.05$ .

## 6. Discussion

Based on three smartbands and four smartphone movement apps, this study investigated the effectiveness of the smartbands/phone movement apps in counting steps at different walking speeds and on different walking surfaces. Firstly, the single factor ANOVA showed that the measured step counts of the three smartbands were only significantly different from the actual step counts at the speed class of 3.2 km/h ( $p < 0.01$ ) for all five speed states, while the other four speed classes did not show significant differences. This result is consistent with previous research literature on pedometers [11]. The same results were also found for the four smartphone sports apps, where the measured number of steps in the five walking speed states was only very significantly different from the actual number of steps in the speed class of 3.2 km/h ( $p \leq 0.01$ ). The reason for this may be related to the pacing principle of the smart bracelet and

TABLE 1: Analysis of the results of the different speed tests of the 3 smart bracelets.

|              | 3.2 km/h      | 4.8 km/h     | 6.4 km/h     | 8.0 km/h     | 9.6 km/h      |
|--------------|---------------|--------------|--------------|--------------|---------------|
| Actual steps | 481 ± 10.86   | 545.6 ± 8.47 | 577.8 ± 9.62 | 720.6 ± 7.08 | 734.51 ± 6.95 |
| Millet       | 453.6 ± 49.17 | 552.6 ± 8.27 | 585.4 ± 8.49 | 724 ± 9019   | 738.8 ± 6.47  |
| Happy heart  | 482.8 ± 8.59  | 549.6 ± 9.2  | 548.8 ± 9.75 | 720.2 ± 9.65 | 738.8 ± 8.94  |
| Smarthealth  | 479.8 ± 12.21 | 544.2 ± 9.68 | 577 ± 10.29  | 729 ± 6.20   | 738.5 ± 6.54  |

TABLE 2: Analysis of the results of the 4 sports APPs in the lab running table.

|              | 3.2 km/h      | 4.8 km/h      | 6.4 km/h       | 8.0 km/h       | 9.6 km/h      |
|--------------|---------------|---------------|----------------|----------------|---------------|
| Actual steps | 464.8 ± 4.171 | 541.6 ± 7.124 | 622.4 ± 22.601 | 731.6 ± 5.727  | 750 ± 5.478   |
| Move         | 444 ± 3.123   | 540.2 ± 8.075 | 625 ± 21.79    | 732.41 ± 7.085 | 750 ± 5.241   |
| Yidong       | 444 ± 3.125   | 540.2 ± 8.337 | 625.6 ± 27.415 | 732.2 ± 7.257  | 750 ± 5.241   |
| Yue Pao      | 445.8 ± 2.247 | 540.8 ± 12.09 | 628.8 ± 27.635 | 732.6 ± 15.587 | 753.2 ± 7.147 |
| Gudong       | 444 ± 3.162   | 540.2 ± 8.075 | 625.6 ± 21.789 | 732.4 ± 7.045  | 750 ± 5.241   |

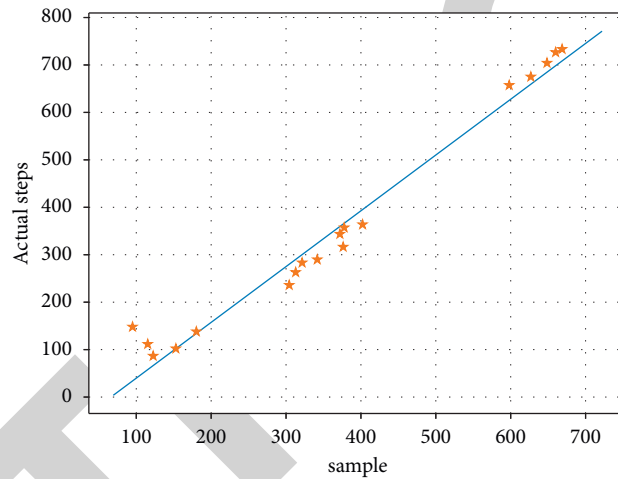


FIGURE 3: Linear regression scatter plot of the number of steps recorded and the actual number of steps taken by Xiaomi's bracelet at different speed levels.

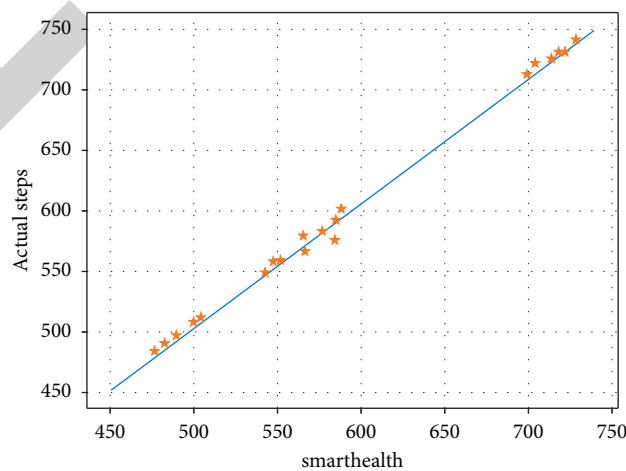


FIGURE 4: Scatter plot of the number of steps recorded by the Smarthealth bracelet versus the actual number of steps taken at different speed levels.

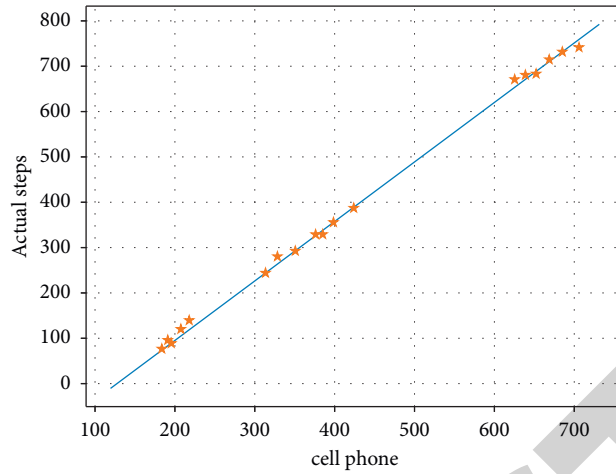


FIGURE 5: Linear regression scatter plot of recorded steps and actual steps for different speed levels.

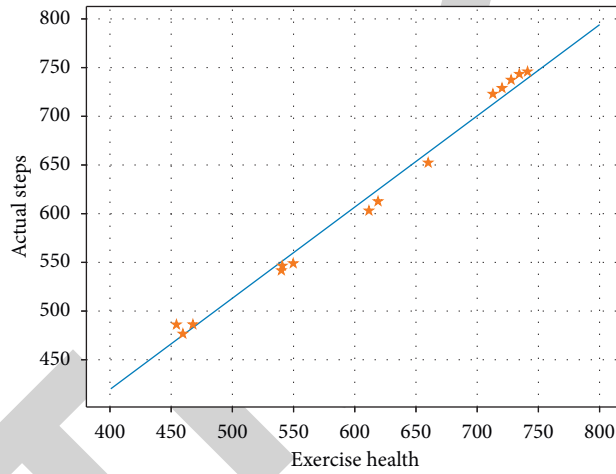


FIGURE 6: Linear regression scatter plot of the number of steps recorded by Kinetic APP and the actual number of steps at different speed levels.

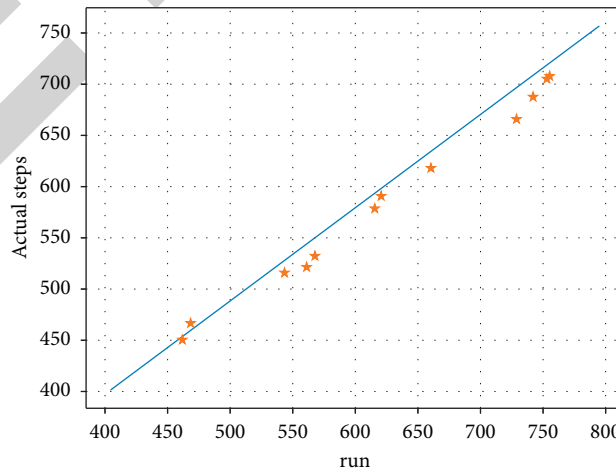


FIGURE 7: Linear regression scatter plot of the number of steps recorded at different run speed.

smart phone movement APP. The acceleration generated during walking causes the electrons in the sensor to move, resulting in a change in electrode position, and eventually

the change in capacitance difference is integrated by the chip and the voltage value is output, resulting in a count. The “threshold value” of the pedometer is not sufficient to affect

TABLE 3: Correlation analysis of the number of steps recorded by the 3 smartbands at different speed levels.

|             |                                 | Smarthealth | Happy heart | Millet |
|-------------|---------------------------------|-------------|-------------|--------|
| Smarthealth | Pearson correlation coefficient | —           | 0.998       | 0.989  |
|             | P                               | —           | 0           | 0      |
|             | N                               | —           | 25          | 25     |
| Happy heart | Pearson correlation coefficient | 0.988       | —           | 0.992  |
|             | P                               | 0           | —           | 0      |
|             | N                               | 25          | —           | 25     |
| Millet      | Pearson correlation coefficient | 0.989       | 0.992       | —      |
|             | P                               | 0           | 0           | —      |
|             | N                               | 25          | 25          | —      |

the recording [12, 13]. The disadvantages of the method are that the period of the acceleration signal is not taken into account, and that the thresholds controlling the state transitions are fixed, making the method less adaptive overall.

## 7. Conclusions

This paper first analyses the track and field running data and further analyses the start point marking method adopted in this paper. The start point marker is critical to the size of the analysis window in this paper. In the actual system implementation process, when the moment of the currently detected start point meets a time length, the system will input the sampled data within this length into the action detection module for action recognition, and then apply the corresponding step counting algorithm according to the recognition result. The specific pacing algorithms are then described in detail, including the autocorrelation coefficient based pacing algorithm, the peak detection based pacing algorithm and the compensation algorithm. The pacing algorithm based on autocorrelation coefficient analysis gives better pacing results when the action recognition result is a swinging motion M2.

## Data Availability

The experimental data used to support the findings of this study are available from the corresponding author upon request.

## Conflicts of Interest

The authors declared that they have no conflicts of interest regarding this work.

## References

- [1] R. Rein and D. Memmert, "Big data and tactical analysis in elite soccer: Future challenges and opportunities for sports science," *SpringerPlus*, vol. 5, no. 1, pp. 1410–1413, 2016.
- [2] R. Agarwal and V. Dhar, "Editorial-Big data, data science, and analytics: The opportunity and challenge for IS research," *Information Systems Research*, vol. 25, no. 3, pp. 443–448, 2014.
- [3] S. Shafqat, S. Kishwer, R. U. Rasool, J. Qadir, T. Amjad, and H. F. Ahmad, "Big data analytics enhanced healthcare systems: A review," *The Journal of Supercomputing*, vol. 76, no. 3, pp. 1754–1799, 2020.
- [4] B. Gupta, M. Goul, and B. Dinter, "Business intelligence and big data in higher education: Status of a multi-year model curriculum development effort for business school undergraduates, MS graduates, and MBAs," *Communications of the Association for Information Systems*, vol. 36, no. 1, p. 23, 2015.
- [5] G. Vossen, "Big data as the new enabler in business and other intelligence," *Vietnam Journal of Computer Science*, vol. 1, no. 1, pp. 3–14, 2014.
- [6] J. Li, L. Xu, L. Tang, S. Wang, and L. Li, "Big data in tourism research: A literature review," *Tourism Management*, vol. 68, pp. 301–323, 2018.
- [7] G. Liu, J. Yang, Y. Hao, and Y. Zhang, "Big data-informed energy efficiency assessment of China industry sectors based on K-means clustering," *Journal of Cleaner Production*, vol. 183, pp. 304–314, 2018.
- [8] C. Cao, Y. Tang, D. Huang, W. Gan, and C. Zhang, "IIBE: an improved identity-based encryption algorithm for WSN security," *Security and Communication Networks*, vol. 2021, p. 8, Article ID 8527068, 2021.
- [9] M. Cantabella, R. Martínez-España, B. Ayuso, J. A. Yáñez, and A. Muñoz, "Analysis of student behavior in learning management systems through a Big Data framework," *Future Generation Computer Systems*, vol. 90, pp. 262–272, 2019.
- [10] P. P. Maglio and C.-H. Lim, "Innovation and big data in smart service systems," *Journal of Innovation Management*, vol. 4, no. 1, pp. 11–21, 2016.
- [11] S. Batistič and P. van der Laken, "History, evolution and future of big data and analytics: A bibliometric analysis of its relationship to performance in organizations," *British Journal of Management*, vol. 30, no. 2, pp. 229–251, 2019.
- [12] V. C. Storey and I.-Y. Song, "Big data technologies and management: What conceptual modeling can do," *Data & Knowledge Engineering*, vol. 108, pp. 50–67, 2017.
- [13] S. Sharma, U. S. Tim, J. Wong, S. Gadia, and S. Sharma, "A brief review on leading big data models," *Data Science Journal*, vol. 13, pp. 138–157, 2014.
- [14] M. Haghghat, H. Rastegari, N. Nourafza, N. Branch, and I. Esfahan, "A review of data mining techniques for result prediction in sports," *Advances in Computer Science: An International Journal*, vol. 2, no. 5, pp. 7–12, 2013.
- [15] J. Wang, Y. Yang, T. Wang, R. S. Sherratt, and J. Zhang, "Big data service architecture: A survey," *Journal of Internet Technology*, vol. 21, no. 2, pp. 393–405, 2020.
- [16] E. E. Cust, A. J. Sweeting, K. Ball, and S. Robertson, "Machine and deep learning for sport-specific movement recognition: A systematic review of model development and performance," *Journal of Sports Sciences*, vol. 37, no. 5, pp. 568–600, 2019.

## *Retraction*

# **Retracted: Construction of an Assessment System for Business English Linguistics Based on RNN Multidimensional Models**

### **Mathematical Problems in Engineering**

Received 18 July 2023; Accepted 18 July 2023; Published 19 July 2023

Copyright © 2023 Mathematical Problems in Engineering. This is an open access article distributed under the Creative Commons Attribution License, which permits unrestricted use, distribution, and reproduction in any medium, provided the original work is properly cited.

This article has been retracted by Hindawi following an investigation undertaken by the publisher [1]. This investigation has uncovered evidence of one or more of the following indicators of systematic manipulation of the publication process:

- (1) Discrepancies in scope
- (2) Discrepancies in the description of the research reported
- (3) Discrepancies between the availability of data and the research described
- (4) Inappropriate citations
- (5) Incoherent, meaningless and/or irrelevant content included in the article
- (6) Peer-review manipulation

The presence of these indicators undermines our confidence in the integrity of the article's content and we cannot, therefore, vouch for its reliability. Please note that this notice is intended solely to alert readers that the content of this article is unreliable. We have not investigated whether authors were aware of or involved in the systematic manipulation of the publication process.

Wiley and Hindawi regrets that the usual quality checks did not identify these issues before publication and have since put additional measures in place to safeguard research integrity.

We wish to credit our own Research Integrity and Research Publishing teams and anonymous and named external researchers and research integrity experts for contributing to this investigation.

The corresponding author, as the representative of all authors, has been given the opportunity to register their agreement or disagreement to this retraction. We have kept a record of any response received.

### **References**

- [1] Y. Shi and H. Shi, "Construction of an Assessment System for Business English Linguistics Based on RNN Multidimensional Models," *Mathematical Problems in Engineering*, vol. 2022, Article ID 8446281, 8 pages, 2022.

## Research Article

# Construction of an Assessment System for Business English Linguistics Based on RNN Multidimensional Models

Yu Shi<sup>1</sup> and Hu Shi<sup>2</sup> 

<sup>1</sup>School of Foreign Languages, Shaoyang University, Shaoyang 422000, Hunan, China

<sup>2</sup>Software Institute, Dalian Jiaotong University, Dalian 116028, Liaoning, China

Correspondence should be addressed to Hu Shi; [shihu@djtu.edu.cn](mailto:shihu@djtu.edu.cn)

Received 23 February 2022; Accepted 4 March 2022; Published 27 March 2022

Academic Editor: Man Fai Leung

Copyright © 2022 Yu Shi and Hu Shi. This is an open access article distributed under the Creative Commons Attribution License, which permits unrestricted use, distribution, and reproduction in any medium, provided the original work is properly cited.

The current teaching evaluation system of the course “Introduction to Business English Linguistics” has many problems and should be reformed according to the requirements of the relevant professional syllabus. This paper proposes a recurrent neural network (RNN) modelling technique, which has achieved good results in modelling business English language models. The RNN modelling method is applied to Chinese language modelling according to the characteristics of Chinese language, and the advantages of the two models are combined to propose a fusion model. The experimental results demonstrate that this paper focuses on the process, diversity, and humanity of teaching evaluation and discusses the construction of the evaluation system model of the course “Introduction to Business English Linguistics” in terms of the content and criteria of teaching evaluation and the methods of teaching evaluation, so as to provide a new model for the teaching reform of the course “Introduction to Business English Linguistics”.

## 1. Introduction

The Syllabus for Business English for Business English Majors in Higher Education stipulates that linguistics, as an important course in the professional knowledge category of business English, is a compulsory course for senior undergraduate students of business English. In the current implementation of specific teaching, it has various names, such as General Linguistics, Introduction to Business English Linguistics, and Introduction to Business English Linguistics. The aim of its teaching is to make students aware of the rich achievements of human language research, to raise their awareness of the importance of language in social, humanistic, economic, technological and personal cultivation aspects, to cultivate linguistic awareness, and to develop rational thinking [1].

This syllabus sets out the requirements for students' knowledge of linguistics and their ability to analyse and apply language theory [2]. The main teaching task of Introduction to Linguistics is therefore to enable students to understand and master the basic knowledge and theories of

linguistics, to describe, explain, analyse, and solve practical linguistic problems using the knowledge and theories they have learned, and to improve their linguistic cultivation and language quality [3]. However, to date, the domestic Introduction to Business English Linguistics course does not have an examination syllabus and teaching evaluation system to match the syllabus, and the content and form of the course's teaching evaluation is very subjective and arbitrary, emphasising only the memorisation of knowledge, but not the assessment of ability [4].

The teaching of “Introduction to Business English Linguistics” focuses on the transmission of knowledge but not on the cultivation of ability, and the teaching assessment system is seriously inadequate [5]. At present, the teaching evaluation method of this course mainly adopts a single summative evaluation method, i.e., using examinations, tests, and quizzes as one-off tests to judge students' learning results and teaching quality by the level of achievement, and examinations are equivalent to evaluation [6]. The content of such summative examinations is textbook and formatted, teachers are taught what to test, students are tested on what

to learn, the difficulty of the knowledge assessed is very limited, only in the understanding of terminology and language theory and the reproduction of memory, the examination of the thinking component is small, the linguistic knowledge of the students' ability to use and expand the ability assessment is basically ignored [7]. This has a serious impact on the content and teaching style of the course and consequently on the teaching objectives of the course; i.e., it is not conducive to the development of students' ability to use their linguistic knowledge and theories to analyse linguistic phenomena and solve language learning problems [8]. To change this situation, it is necessary to reconstruct the teaching assessment system of the "Introduction to Business English Linguistics" course, i.e., to change the current single summative assessment method and increase the formative assessment, so that the two are organically combined and a new assessment system is constructed [9].

The "Introduction to Business English" course is designed to give students not only basic knowledge and skills but also the ability to explore on their own, through a variety of learning activities, such as cooperative group learning and classroom discussions [10]. In this way, students can learn and master the scientific method of exploring knowledge while gaining a deeper understanding of it. Therefore, in the process of teaching evaluation, special attention should be paid to the dynamic learning process of students, guiding them to pay more attention to, recognise, grasp, and improve the microprocesses of their own learning, and through teachers and students jointly monitoring, reflecting and regulating the whole process of teaching, prompting changes in teachers' teaching styles and students' learning methods [11].

The plurality of teaching evaluation is manifested in several aspects such as the content, evaluation subjects, and evaluation criteria. In terms of content, the "Introduction to Linguistics" course not only evaluates students' level of mastery of basic linguistic knowledge but also the development and improvement of individual students' interests, attitudes, and strategies in the learning process; in terms of the subject of evaluation, it changes from a single teacher's evaluation to a combination of teacher evaluation, student self-evaluation, and student mutual evaluation. In terms of evaluation criteria, it has both evaluation criteria for students' basic knowledge and skills and evaluation criteria for students' practical application ability, thinking ability, critical ability and innovation ability [12]. The two are combined and complement each other to evaluate students' learning status.

## 2. Related Work

It is an essential part of the teaching and learning process and is designed to check and facilitate teaching and learning. The famous American educator Bloom divides teaching evaluation into three main categories: diagnostic evaluation, formative evaluation, and summative evaluation. These three types of assessment correspond to the distinction that

is made before, during, and at the end of a sequence of educational activities [13]. Formative assessment was introduced in 1967 by M. Scriven, an American expert in evaluation, and later by Bloom, an American educationalist, into the field of teaching. Formative assessment emphasises the evaluation of students' knowledge acquisition and competence development in the educational process, including the evaluation of learning outcomes, the evaluation of various input conditions, and the evaluation of educational programmes and instructional methods. Its aim is to enable both teachers and students to receive timely feedback to improve the teaching and learning process and enhance the quality of teaching and learning. Howard Garden-er, a developmental psychologist at Harvard University, put forward the theory of multiple intelligences in 1983, and he advocated an educational evaluation that is conducted through multiple channels and in multiple forms [14]. Wiegrefe and Pinter [15] chose test questions similar to the wrong ones for practice. This is a mock exposure design that attempts to control the exposure of the overall question pool and remove highly exposed questions, but there is a gap with the real exposure design, which is still not practical enough. Reference [16] on the other hand starts from the evaluation aspect of the exercise and applies a knowledge map to manage the exercise questions.

While the theoretical results of adaptive testing are fruitful, the practical applications are also very extensive [17]. For example, the Graduate Record Examination (GRE) is used to find more suitable students and to provide students with the opportunity to choose a more suitable school and major; the US Army Vocational Aptitude Battery (ASVAB) allows people to enter a more suitable branch of the military and to perform at the highest level of operational efficiency; the National Assessment of Educational Progress (NAEP) optimises the entire US education system and allows students to learn more efficiently [18]. Domestic educational Internet companies are also beginning to consider such methods to high overall efficiency, reduce costs, and high the possibility of supplying the market with more cost-effective options for more children [19]. In addition, CAT has gained the attention of experts, scholars, and frontline engineers in various fields, and Internet education companies are devoting more attention to this area, which has good practical value and broad development prospects [20].

## 3. RNN Model in This Paper

**3.1. N-Gram Language Model.** The n-gram language model with statistical rules, introduced in 1980, is a widely used language model that uses the Markov assumption that the probability of occurrence of each predictor variable is related only to the context of length  $n - 1$ . If the historical information of word  $w_i$  is expressed as  $h_i = w_1 w_2 \dots w_{i-1}$ , then the probability of occurrence of word  $w_i$  and sentence  $s$  according to the conditional probability formula and Markov's hypothesis are as follows:

$$\begin{aligned}
p(w_i|w_1, w_2, \dots, w_{i-1}) &= p(w_i|h_i) \\
&= p(w_i|w_{i-n+1}^{i-1}), \\
p(s) &= p(w_1, w_2, \dots, w_N) \quad (1) \\
&= \prod_{i=1}^N p(w_i|h_i).
\end{aligned}$$

For n-gram language models, a large corpus is usually trained, and the more frequent words in the corpus tend to be trained better, while low frequency words are not trained as well.

In addition, the higher the order  $n$ , the more binding the model is, but as  $n$  increases, the size of the model grows exponentially, increasing the computational complexity of training and placing greater demands on storage space. The appropriate value of  $n$  is therefore a compromise between accuracy and complexity of the language model [21]. In a practical recognition system,  $n=3$  is generally chosen to construct a Tri-gram language model; i.e., the probability of each word occurring in a sentence from the training data is only related to its first two words, which can be expressed as

$$p(w_i|h_i) \approx p(w_i|w_{i-2}, w_{i-1}). \quad (2)$$

In this paper, we improve the language model in the Chinese speech recognition system and use the RNN language model to re-score the initial recognition candidates and perform postrecognition processing to complete the recognition process of the whole system, while the other modules of the baseline system remain unchanged.

**3.2. RNN Language Models.** Reference [14] states that a recurrent neural network, also known as an Elman network, has the structure shown in Figure 1 and consists of three network layers, the input layer, the implicit layer, and the output layer, with the storage layer acting as part of the input and preserving the state of the implicit layer at the previous moment [22]. After the text corpus is trained by this RNN structure, the probability of the current word  $w_i$  occurring is expressed as

$$\begin{aligned}
p(w_i|h_i) &= p_{rnn}(w_i|w_{i-1}, h_{i-1}) \\
&= p_{rnn}(w_i|h_i). \quad (3)
\end{aligned}$$

Reference [15] also states that the input word sample of the network at time  $t$  is assumed to be  $w(t)$ , i.e., the vector of current words; dimensionality is determined by the number of word samples in the corpus  $|V|$ ; the state of the implicit layer  $h(t)$  is determined by both the input current word vector  $w(t)$  and the state of the implicit layer at the previous moment, i.e., the history information  $h(t-1)$ , through the connection from the implicit layer to the input layer, and the state of the implicit layer at time  $t-1$  as part of the input at time  $t$ ; the output layer  $y(t)$  represents information about the probability distribution of the subsequent words under the current history; and the number of nodes in the output layer is the same as the number of nodes in the input layer also  $|V|$ .

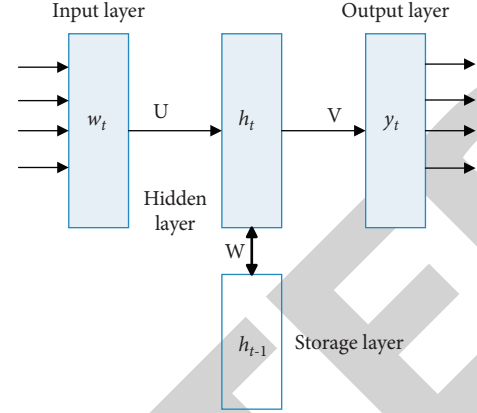


FIGURE 1: Recurrent neural network framework.

The computational relationship between the layers is represented by the following equation:

Inputs to the implicit layer :  $x(t) = w(t) + h(t-1)$ ,

$$\text{Implicit layer state : } h_j(t) = f\left(\sum_i x_i(t)u_{ji}\right). \quad (4)$$

Compared to business English speech, Chinese speech recognition is more complex. There are more than 6,000 commonly used characters in Mandarin Chinese, with about 60 phonemes, 407 untuned syllables, and 1,332 toned syllables, each of which consists of a vowel, a rhyme, and a tone, and each character represents a syllable. At the same time, there are also a large number of homophones and polysyllabic characters in Chinese, which must be constrained by high-level nonacoustic knowledge such as contextual background in order to complete recognition [23].

In terms of language, business English utterances focus on structure, while Chinese utterances focus on semantics, where the same word has different meanings in different contexts and the long-distance dependencies between words are relatively tight. When RNN is used to train the language model, more high-level semantic information is taken into account, which can better reflect the binding relationship between Chinese words. Therefore, RNN modelling techniques will be more suitable for training Chinese language models.

In addition, there are obvious spaces between words in the English corpus, so the corpus can be trained directly with a little processing. Unlike the Chinese corpus, there is no clear boundary between words in the Chinese sentences, and the training corpus needs to be divided into subword units according to the word separation model. After a series of processing to obtain a pure text corpus, the model can be trained.

The Chinese training corpus is shown in Figure 2, where the text corpus is cleaned to remove noisy information such as letters and punctuation marks from the coarse corpus and to remove redundant information; there are a large number of numbers in the corpus, and the regularisation of the numbers is completed to convert the Arabic numbers in the corpus into Chinese characters; thus, only Chinese



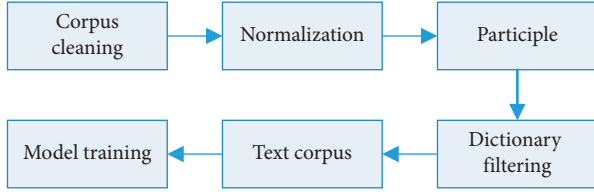


FIGURE 2: Processing flow of the Chinese corpus.

characters exist in the corpus. The lexical filtering removes English boundary characters and nonlexical sentences from the corpus. This results in a corpus that can be used for training. The model is then trained.

**3.3. RNN Model and n-Gram Model Fusion Modelling.** The higher the frequency of words in the corpus, the better the n-gram modelling technique can be trained, while the opposite is true for lower frequency words. When using RNN to train the corpus, some words in the corpus can be trained well despite their low frequency, which can effectively complement the n-gram model. In order to fully exploit the advantages of both modelling techniques and obtain better recognition results, this paper investigates a fusion modelling method based on the RNN model and the n-gram model.

As shown in Figure 3, for the same speech, the n-best list can be obtained from the word map (lattice) generated by the decoder, and the trained RNN language model is then used to re-score the n-best list. The n-gram model score information of the n-best list is then interpolated and fused with the re-score information of the RNN model to calculate a new language model score for each candidate unit.

Among the fusion algorithms for models, linear interpolation fusion is currently the more common approach, predicting the probability of the current word  $w_i$  based on the context  $h_i$ :

$$p_x(w_i|h_i) = \sum_j^L \lambda_j p_j(w_i|h_i), \quad (5)$$

$$p(w_i|h_i) = \lambda_1 p_{rm}(w_i|h_i) + \lambda_2 p_{ng}(w_i|h_i).$$

where  $L$  is the number of interpolation models and the interpolation weights  $\lambda_j$  of each model are nonnegative and sum to 1; i.e.,  $\sum_{j=1}^L \lambda_j = 1$ . The log-likelihood score is re-scaled for each n-best list sentence after model fusion:

$$\lg L(s) = \sum_{i=1}^n asc_i + \text{lms} \sum_{i=1}^n \lg p_x(w_i|h_i) + n.wp, \quad (6)$$

where  $n$  is the number of words in the sentence;  $wp$  is the penalty score of the word;  $asc_i$  is the word  $w_i$  acoustic model score;  $\text{lms}$  is the model size; and  $p_x(w_i|h_i)$  represents the fusion score of the n-gram and RNN model for each word. The overall score of each list is calculated by combining the linguistic and acoustic model scores and the penalty score, and the highest score is selected as the final recognition result of this n-best list.

## 4. Teaching Evaluation Methods and Experimental Analysis

**4.1. Model Evaluation Criteria.** The evaluation of the performance of the language model is based on information-theoretic knowledge. The performance of a language model is measured by calculating the magnitude of its perplexity on the test text. The perplexity is the inverse of the geometric mean of the probabilities of occurrence of each word in a given text set when predicted by the language model. Assuming that there are  $M$  words in the test text, the perplexity is

$$\text{perplexity} = \frac{1}{\sqrt[M]{\sum_{i=1}^M \log_2 P(w_i|w_{i-n+1}, \dots, w_{i-1})}} \quad (7)$$

In general, the smaller the value, the more binding the language model is to the language and the better the performance of the trained model. In addition to measuring language models in terms of perplexity, the most intuitive idea is to apply the model to a system and measure it by testing the system's Word Error Rate (WER). In general, a well-trained model will result in a high recognition rate. In this paper, the two evaluation criteria are combined to test the language model.

**4.2. Experimental Design.** Experiment 1 was used to verify the effectiveness of RNN language models in Chinese speech recognition. In this experiment, RNN and n-gram models were trained on the same dataset, and different RNN language models were trained by varying the number of nodes in the implicit layer of the RNN to investigate the changes in the perplexity and recognition rate of the RNN model with different parameters and to compare the performance with that of the n-gram model. Experiment 2 was used to verify the effectiveness of the proposed model fusion algorithm. The n-gram model trained in Experiment 1 was fused with the RNN model by linear interpolation, and the change in recognition rate was tested. In order to accelerate the training of RNN models, the training of RNN models was performed on a GPU (NVIDIA GTX 650) server with CUDA Toolkit 5.5, which is two to three times faster than the training on a CPU and shortens the training time of RNN models [24].

**4.3. Experimental Data.** The training data were obtained from the annotated data of the Chinese telephone speech transcription task provided by KODA XUNFE, with a total of 16 M, containing 550 thousand sentences and 4342 thousand words. The model perplexity test set is 9332 sentences containing 23 thousand words, and the speech test set is a 100-best list of 3433 sentences decoded from telephone speech, with a size of 87 kB. The number of nodes in the implicit layer for the RNN training model is set with six sets of parameters [25].

**4.4. Experiment 1.** The n-gram language model was trained using the Kneser-Ney backward smoothing algorithm with good smoothing performance, and the model order was 3,

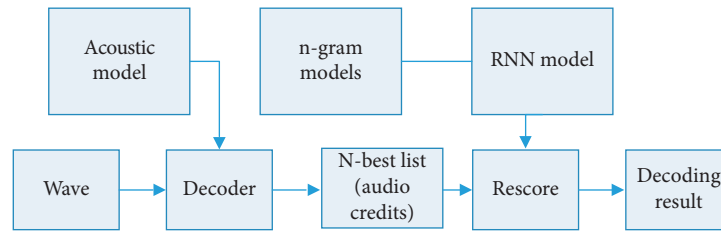


FIGURE 3: English model.

i.e., 3-gram, constructed from the SRILM toolbox. The number of n-grams in the model was  $30274 + 6568660 + 13830707 = 20429641$ , and the model size was 463599 kB. The RNN language model was then trained with the same training data, and the changes in the PPL values and the WER of the recognition system were tested. The experimental results are shown in Table 1.

As can be seen from Table 1, the RNN and 3-gram language models were trained with the same training data, and the confusion level of the RNN language model was reduced by about 7%; the error rate of speech recognition was reduced by about 5%, which proved the effectiveness of the RNN language model in Chinese speech recognition. In general, the lower the perplexity of the generated model, the higher the recognition rate of the system.

In addition, Table 1 also shows that (1) with the increase of the number of nodes in the hidden layer, the perplexity of the RNN language model and the system error rate gradually decrease, indicating that the learning ability of the network increases with the increase of the number of nodes; (2) when the number of nodes in the hidden layer increases to a certain degree, the perplexity of the generated model increases and the system recognition rate decreases, indicating that the more the number of nodes in the hidden layer. The more complex the network structure is, the smaller the error of the training samples can be reduced to a sufficient size through learning; however, excessive pursuit of learning on the training samples will produce overtraining. With a limited number of training samples, if the average training relative error of the learning sample set continues to decrease after a certain stage of learning, while the average test relative error (generalisation error) of the test sample set increases, the generalisation ability of the network will be reduced, affecting the performance of the trained model. Therefore, for different sizes of training corpus, the parameters need to be adjusted when using RNN training in order to achieve better experimental results.

The guiding principle of promoting the all-round development of all students through assessment, as shown in Figure 4, treats students as individuals with individual characteristics and different interests and needs, recognises their individual differences in their development levels, and examines all aspects of their knowledge, intelligence, and emotional factors; making horizontal comparisons fully considers students' vertical development; while assessing students teaches them to self-assess. The course is designed to help students develop a learning style that is truly effective and in line with their individual characteristics, fully

reflecting the characteristics of the student as the main subject and making them the master of learning. As a humanities subject, "Introduction to Business English Linguistics" should strive to create a relaxed and friendly atmosphere, reduce students' tension, evaluate students' achievements with a developmental and humanistic perspective, focus on students' subjectivity, and make students feel their own progress and development, so that their interest and creativity are stimulated and their self-confidence is enhanced. Self-confidence is enhanced, fully reflecting the humanistic spirit of respecting students' individuality.

**4.5. Experiment 2.** On the basis of the recognition results of Experiment 1, a linear interpolation method was used to interpolate and re-score the language model score of each word in the 100-best list by both sets of models, and then the probability of each sentence was calculated according to equation (11) combined with the acoustic model score, from which the highest score was selected as the recognition result of that speech, as shown in Table 2. The interpolation coefficient in the experiment is 0.6, i.e.,  $\lambda_1 = 0.6$  achieved a better recognition result.

As can be seen from Table 2, after linear interpolation, the recognition rate of the model decreases by about 8% compared to the 3-gram model and by about 3% compared to the RNN model, and the recognition rate after model fusion improves more significantly compared to that of the n-gram model because the RNN model is better trained for low-frequency words and can effectively solve the data sparsity problem. It can also be seen that the recognition rate of the fused models is higher than that of either model alone, indicating that the two models are complementary and demonstrating the effectiveness of the model fusion approach. In a practical recognition system, an n-gram language model with a large corpus can be trained and used as a general model and then interpolated and fused with the RNN model trained with a small corpus in the post-processing module of the speech recognition system, using this method to postprocess the decoding results to improve the recognition rate of the system. In this experiment, due to the limited training corpus, the overall recognition rate of the system is not very high, but it can still show the superiority of RNN in modelling Chinese language models and the effectiveness of the model fusion construction method.

The content of the course "Introduction to Business English Linguistics," as shown in Figure 5, is determined by its teaching objective, which is "to enable students to

TABLE 1: Performance comparison of RNN language model and 3-gram language model.

| Number of hidden layer nodes | n-gram (KN3) |         | RNN   |         | Decline rate of ppl (%) | Decrease rate of WER (%) |
|------------------------------|--------------|---------|-------|---------|-------------------------|--------------------------|
|                              | PPL          | WER (%) | PPL   | WER (%) |                         |                          |
| 100                          | 166.3        | 42.09   | 158.3 | 40.2    | 4.81                    | 4.49                     |
| 200                          | 166.3        | 42.09   | 157.6 | 40.1    | 5.23                    | 4.72                     |
| 300                          | 166.3        | 42.09   | 156.6 | 40.08   | 5.83                    | 4.77                     |
| 400                          | 166.3        | 42.09   | 155.4 | 39.96   | 6.55                    | 5.06                     |
| 55                           | 166.3        | 42.09   | 154.5 | 39.87   | 7.1                     | 5.27                     |
| 600                          | 166.3        | 42.09   | 155.2 | 39.39   | 6.67                    | 5.13                     |

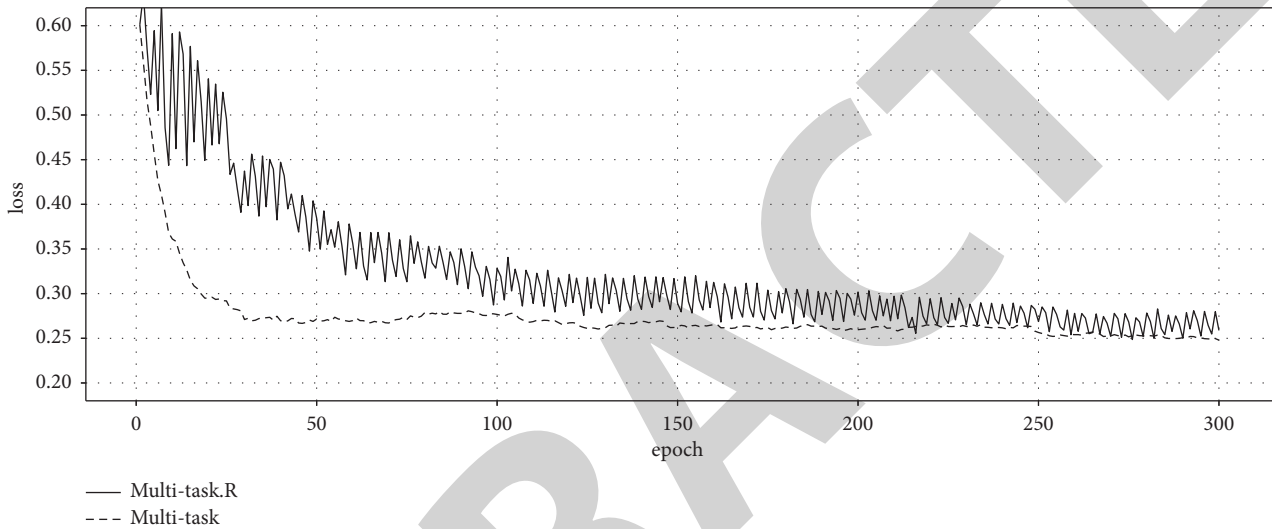


FIGURE 4: Student education learning outcomes.

TABLE 2: Comparison of recognition performance after fusion of the two models.

| Number of hidden layer nodes | RNN + n-gram | n-gram | RNN   | Decline rate compared with n-gram (%) | Decline rate compared with RNN (%) |
|------------------------------|--------------|--------|-------|---------------------------------------|------------------------------------|
|                              | WER%         | WER %  | WER % |                                       |                                    |
| 100                          | 39.23        | 42.09  | 40.2  | 6.97                                  | 2.41                               |
| 200                          | 39.14        | 42.09  | 40.1  | 7                                     | 2.39                               |
| 300                          | 38.6         | 42.09  | 40.08 | 8.29                                  | 3.69                               |
| 400                          | 38.62        | 42.09  | 39.69 | 8.24                                  | 3.28                               |
| 500                          | 38.62        | 42.09  | 39.87 | 8.38                                  | 3.28                               |
| 600                          | 38.59        | 42.09  | 39.39 | 8.31                                  | 3.35                               |

understand and master the basic knowledge and theories of linguistics, to describe, explain, analyse, and solve practical linguistic problems using the knowledge and theories they have learned, and to improve their language skills and quality.” The aim of the course is to “enable students to understand and master the basic knowledge and theories of linguistics, to use their knowledge and theories to describe, interpret, analyse and solve practical language problems, and to improve their language skills and quality.” The students

are assessed in two ways: their mastery of basic linguistic theory is assessed in terms of the syllabus and the examination syllabus, and their ability to grasp the knowledge structure as a whole is assessed in a quantitative way. The ability to apply theoretical knowledge in linguistics should be assessed in a comprehensive way (combining in-class and out-of-class) to evaluate students’ ability to apply theoretical knowledge, in a variety of forms, using a qualitative assessment approach.

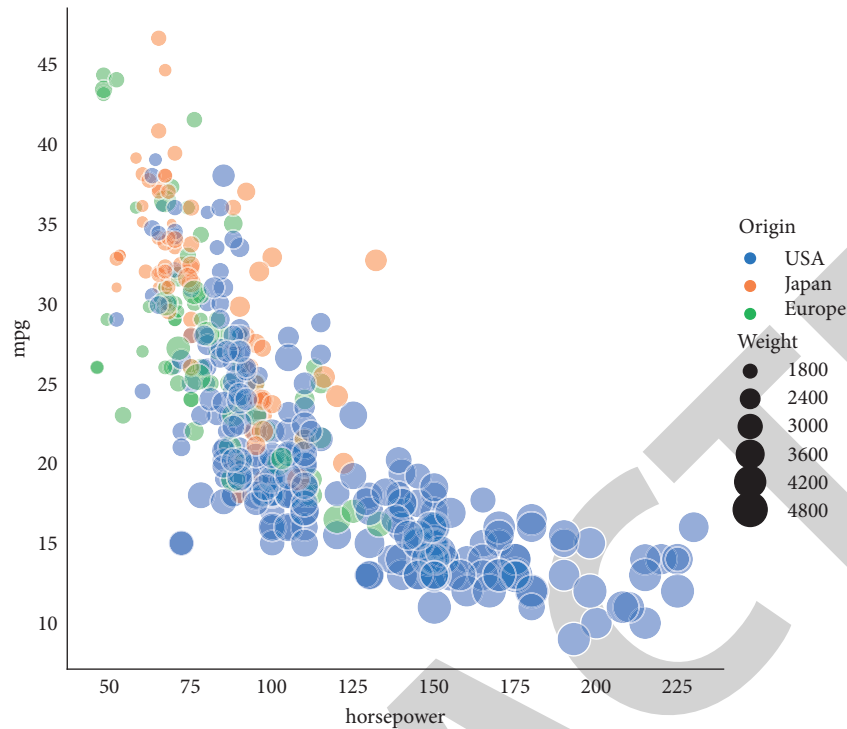


FIGURE 5: Effectiveness of teaching evaluation.

## 5. Conclusions

This paper applies RNN language model modelling to English language teaching assessment and verifies the effectiveness of the RNN modelling approach in Chinese language processing by comparing the generated model with the traditional n-gram model, which reduces the perplexity by about 7%. The reconstruction of the teaching evaluation system model of the Introduction to Business English course is a complex systemic project, which cannot be established without the related reform of teaching management, teaching content, teaching methods, teaching materials, and other aspects.

## Data Availability

The raw data supporting the conclusions of this article will be made available by the authors, without undue reservation.

## Conflicts of Interest

The authors declare that they have no conflicts of interest regarding this work.

## References

- [1] N. Basnin, L. Nahar, and M. S. Hossain, "An integrated CNN-LSTM model for Bangla lexical sign language recognition," in *Proceedings of the International Conference on Trends in Computational and Cognitive Engineering*, pp. 695–707, Malaysia, Asia, January 2021.
- [2] Z. Chen, Y. Wu, F. Yin, and C. L. Liu, "Simultaneous script identification and handwriting recognition via multi-task learning of recurrent neural networks," vol. 1, pp. 525–530, in *Proceedings of the 2017 14th IAPR international conference on document analysis and recognition (ICDAR)*, vol. 1, pp. 525–530, IEEE, Kyoto, Japan, November 2017.
- [3] S. Ghosh, M. Chollet, E. Laksana, L. P. Morency, and S. Scherer, "Affect-lm: a neural language model for customizable affective text generation," 2017, <https://aclanthology.org/P17-1059>.
- [4] I. Serban, A. Sordoni, R. Lowe et al., "A hierarchical latent variable encoder-decoder model for generating dialogues," in *Proceedings of the AAAI Conference on Artificial Intelligence*, vol. 31, no. 1, Vancouver, Canada, 2017 February.
- [5] F. Klubička, A. Toral, and V. M. Sánchez-Cartagena, "Quantitative fine-grained human evaluation of machine translation systems: a case study on English to Croatian," *Machine Translation*, vol. 32, no. 3, pp. 195–215, 2018.
- [6] M. Richardson, C. Abraham, and R. Bond, "Psychological correlates of university students' academic performance: a systematic review and meta-analysis," *Psychological Bulletin*, vol. 138, no. 2, pp. 353–387, 2012.
- [7] K. Adnan and R. Akbar, "An analytical study of information extraction from unstructured and multidimensional big data," *Journal of Big Data*, vol. 6, no. 1, pp. 1–38, 2019.
- [8] J. T. Downer, R. C. Pianta, X. Fan, B. K. Hamre, A. Mashburn, and L. Justice, "Effects of web-mediated teacher professional development on the language and literacy skills of children enrolled in prekindergarten programs," *NHSA dialog*, vol. 14, no. 4, pp. 189–212, 2011.
- [9] K. Zhu, K. L. Kraemer, and J. Dedrick, "Information technology payoff in e-business environments: an international perspective on value creation of e-business in the financial services industry," *Journal of Management Information Systems*, vol. 21, no. 1, pp. 17–54, 2004.
- [10] X. I. E. Tao, C. Zhang, and Y. Xu, "Collaborative parameter update based on average variance reduction of historical

## Research Article

# A Comparative State-of-the-Art Constrained Metaheuristics Framework for TRUSS Optimisation on Shape and Sizing

**Bahareh Etaati** <sup>1</sup>, **Amin Abdollahi Dehkordi**,<sup>2</sup> **Ali Sadollah** <sup>3</sup>, **Mohammed El-Abd** <sup>4</sup>,  
**and Mehdi Neshat** <sup>5</sup>

<sup>1</sup>Amirkabir University of Technology, Department of Computer Engineering and Information Technology, Tehran, Iran

<sup>2</sup>Computer Engineering Department, Najafabad Branch, Islamic Azad University, Najafabad, Iran

<sup>3</sup>Department of Mechanical Engineering, University of Science and Culture, Tehran, Iran

<sup>4</sup>College of Engineering and Applied Sciences, American University of Kuwait, Salmiya, Kuwait

<sup>5</sup>Center for Artificial Intelligence Research and Optimisation, Torrens University Australia, Brisbane, Australia

Correspondence should be addressed to Bahareh Etaati; [b.etaati91@aut.ac.ir](mailto:b.etaati91@aut.ac.ir)

Received 4 February 2022; Revised 27 February 2022; Accepted 28 February 2022; Published 26 March 2022

Academic Editor: Man Fai Leung

Copyright © 2022 Bahareh Etaati et al. This is an open access article distributed under the Creative Commons Attribution License, which permits unrestricted use, distribution, and reproduction in any medium, provided the original work is properly cited.

In order to develop the dynamic effectiveness of the structures such as trusses, the application of optimisation methods plays a significant role in improving the shape and size of elements. However, conjoining two heterogeneous variables, nodal coordinates and cross-sectional elements, makes a challenging optimisation problem that is nonlinear, multimodal, large-scale with dynamic constraints. To handle these challenges, evolutionary and swarm optimisation algorithms can be robust and practical tools and show great potential to solve such complex problems. This paper proposed a comparative truss optimisation framework to solve two large-scale structures, including 314-bar and 260-bar trusses. The proposed framework consists of twelve state-of-the-art bio-inspired algorithms. The experimental results show that the marine predators algorithm (MPA) performed best compared with other algorithms in terms of convergence speed and the quality of the proposed designs of the trusses.

## 1. Introduction

The dynamic performance of structures exposed to various dynamic loading is connected with their fundamental natural frequencies. For instance, prior knowledge of the natural frequencies of a structure may help prevent the vibration and noise produced under dynamic loadings, such as wind or earthquake. As a result, obtaining the optimal sizing and layout of structures with frequency constraints is exceptionally important to enhance the dynamic behaviour of structures [1].

Truss optimisation has been attracting many researchers over the past decades as one of the most significant subjects in structural engineering. Design variables include the truss sizing, shape, and topology, and the main optimisation problems include the optimisation of the design variables. In most of the case studies, the size of bars comes from a set of discrete values; therefore, the applications of the discrete

optimisation methods are considerable (for further study on the discrete optimisation methods see [2]). Most studies were conducted to obtain the optimal set of sizing variables in order to minimize the structural weight. However, the optimal structural weight depends on different design variables rather than just one. For example, the optimal truss shape is affected by its topology and size and vice versa. With this in mind, the simultaneous optimisation of design variables with frequency constraints has attracted many researchers recently.

Nevertheless, coupling shape and sizing variables may lead to mathematical difficulties, nonoptimal solutions, and occasionally divergence problems. Additionally, frequency constraints are extremely nonlinear, nonconvex, and implicit regarding design variables [3]. Therefore, global optimisation algorithms, which are able to find the global best solution in the search space, could be a good solution to truss shape and sizing optimisation with frequency constraints.

Overall, two types of optimisation methods are applied to truss optimisation problems, namely mathematical programming techniques and meta-heuristic algorithms. While mathematical programming techniques have a fast convergence speed, they are complicated and time-consuming due to the necessity of sensitivity analysis. Also, they are dependent on the starting structural design and prone to being trapped in local minima. Owing to these drawbacks of the mathematical programming techniques, meta-heuristic algorithms have been mostly used for structural optimisation as effective global optimisation methods. These stochastic search methods are bio-inspired, easy to implement, problem-independent, and flexible. Additionally, they have strong exploration and exploitation abilities, which makes them free from having prior gradient knowledge of the objective function and being sensitive to the initial point.

As already mentioned, meta-heuristic approaches inspired by biological processes are a large class of global optimisation techniques that have attracted many studies in the subject of truss optimisation [4]. Swarm intelligence-based methods, inspired by living organisms' social behaviour, are a group of population-based meta-heuristics. These algorithms proved to be great optimizers for truss problems in recent years [5–10].

In this paper, twelve modern swarm optimisation methods are deployed for the shape and sizing optimisation of a large-scale truss problem with frequency constraints. These state-of-the-art algorithms include grey wolf optimizer (GWO) [11], moth flame optimizer (MFO) [12], multi-verse optimizer (MVO) [13], dragonfly algorithm (DA) [14], equilibrium optimizer (EO) [15], arithmetic optimisation algorithm (AOA) [16], Generalized Normal Distribution optimisation (GNDO) [17], Salp Swarm Algorithm (SSA) [18], Marine Predator Algorithm (MPA) [19], Henry Gas Solubility optimisation (HGSO) [20], Neural Network Algorithm (NNA) [21], and Water Cycle Algorithm (WCA) [22]. GWO simulates grey wolves' leadership hierarchy and hunting behavior in nature, MFO is inspired by moths' navigation behavior, MVO is based on white hole, black hole, and wormhole concepts in cosmology, DA is based on searching behavior of dragonflies in static and dynamic swarms, EO is inspired by control volume mass balance models applied for dynamic and equilibrium states' estimation, AOA is based on the distribution behavior of arithmetic operators in mathematics, GNDO uses generalized normal distribution models to update the population, SSA is inspired by salps' swarming behavior during navigation and foraging in oceans, MPA is motivated by foraging strategy and optimal rate policy between prey and predator in oceans, and HGSO simulates the Henry's law behavior. All the algorithms are compared in terms of the optimal weight of truss structures concerning frequency constraints. In short, the main contributions of the paper are as follows:

- (1) Evaluating two large-scale truss problems (314-bar and 260-bar) with frequency constraints in order to optimise the shape and sizing variables
- (2) A comparison of twelve state-of-the-art bio-inspired optimisation methods

- (3) Tuning the population size of the best-performed optimisation method

The rest of the paper is organized as follows: Section 2 provides a brief review of meta-heuristic algorithms recently proposed for truss optimisation problems. Section 3 describes two truss problem case studies in more detail. Section 4 explains the optimisation methods applied to the truss problem. The given experimental results of the methods' performance on the case studies are represented in Section 5. Lastly, Section 6 concludes and provides a couple more beneficial suggestions for future work.

## 2. Related Work

This section focuses on recently proposed meta-heuristic algorithms for truss optimisation problems. Rahami et al. [23] employed a genetic algorithm (GA) coupled with a force method for truss sizing, shape, and topology optimisation. This study aimed to decrease the number of input variables, increasing the GA's convergence speed and reducing its computational cost. In another work, Wei et al. [1] proposed a Niche Hybrid Parallel Genetic Algorithm (NHPGA) to optimise truss shape and sizing. The authors combined GA, parallel computing, and simplex search with a niche approach in order to speed up the GA's search ability to find optimal solutions. An improved differential evolution (ReDE) was introduced in [24] for structural shape and size optimisation that used the roulette wheel selection technique to improve the efficiency of the basic DE.

Additionally, a novel hybrid DE and symbiotic organism search algorithm (SOS) was proposed in [25] to optimise the shape and sizing of truss structures. The algorithm utilised the global searching ability of DE and the local searching ability of SOS to achieve optimal solutions. Lamberti [26] proposed a multi-level population-based simulated annealing algorithm called CMLPSA for sizing and shape optimisation. Azad [27] hybridised an adaptive dimensional search with two versions of the big bang-big crunch algorithm for sizing optimisation of truss structures. In [28], a mine blast algorithm was proposed for truss sizing optimisation. The algorithm was inspired by the explosion of mine bombs in the real world.

The most popular swarm optimisation method applied to this kind of problem is particle swarm optimisation (PSO) [5] inspired by the birds flock or fish school's social behaviour. As an example, in [6], Kaveh et al. proposed a democratic PSO (DPSO) for truss sizing and topology optimisation with frequency constraints. This research aimed to alleviate the basic PSO premature convergence in frequency constraints. Other classical swarm methods applied for truss optimisation include ant colony optimisation (ACO) [7], artificial bee colony (ABC) algorithm [29, 30], and shuffled frog leaping (SFL) [31] to name but a few. More recently, new modern swarm optimisation algorithms have been proposed and developed for structural design optimisation. For example, in [32], a new swarm method named ray optimisation, motivated by Snell's law of light refraction, was proposed for truss optimisation. Then, in [33], the

authors proposed an improved ray optimisation method to optimise the sizing and topology of truss structures. Other new swarm-intelligence methods applied to truss problems include firefly algorithm [8, 34], dolphin echolocation [9, 35], teaching-learning based optimisation [36], grey wolf optimizer [10], political optimizer [37], and imperialist competitive algorithm [38, 39], to name but a few.

### 3. Truss Problem Formulation

Overall, in a truss sizing and shape optimisation problem with multiple frequency constraints, the primary purpose is to minimize the truss weight while meeting the constraints on natural frequencies. Nodal coordinates and cross-sectional areas are design variable, which change persistently during design process. In this problem, the truss topology is supposed to be unalterable and predetermined. Additionally, design variables may be limited to a specific interval. Hence, the optimisation problem can be stated as follows:

$$\begin{aligned}
 & \text{\text{Find}}: X = \{A, C\} \text{ \nonumber} \\
 & \text{\text{Where}}: A = \{A_{1}, A_{2}, \dots, A_{n}\} \text{ \nonumber} \\
 & \text{\text{and}} C = \{C_{1}, C_{2}, \dots, C_{m}\} \text{ \nonumber} \\
 & \text{\text{Minimize}}: f(X) = \sum_{i=1}^n \rho_i A_i L_i \\
 & \text{\text{Subjected}}: \omega_j \geq \omega_{j\text{Lb}} \text{ \nonumber} \\
 & \omega_k \leq \omega_{k\text{Ub}} \text{ \nonumber} \\
 & A \text{Lb} \leq A \leq A \text{Ub} \text{ \nonumber} \\
 & C \text{Lb} \leq C \leq C \text{Ub} \text{ \nonumber} \\
 & \text{\nonumber} \\
 & \text{\end{align}}
 \end{aligned}$$

Here,  $X$  vector includes both cross-sectional areas and the nodal coordinates of the structure.  $C_i$  is nodal coordinates of the  $i$ th node of the structure.  $f(X)$  is the structural weight, and  $\rho_i$ ,  $A_i$ , as well as  $L_i$  are the material density, cross-sectional area, and length of  $i$ th element, respectively. Also,  $n$  and  $m$  represent the number of structural cross-sectional areas and nodal coordinates confined to lower and upper bounds  $[A^{Lb}, A^{Ub}]$  and  $[C^{Lb}, C^{Ub}]$ , respectively. Additionally,  $\omega_j$  and  $\omega_k$  denote  $j$ th and  $k$ th natural frequencies restricted to the lower and upper bounds  $\omega_j^{Lb}$  and  $\omega_j^{Ub}$  [1].

In order to convert the constrained problem into an unconstrained one, we employed the function below:

$$\begin{aligned}
 & \text{\begin{equation}} \\
 & f_{\text{penalty}}(X) = f(X) + (n\text{TotalConstVio} \times \text{PF}), \\
 & \text{\quad } n\text{TotalConstVio} = \sum_{i=1}^k (C_{\text{vio}_{i}} \\
 & \text{\quad } + A_{\text{vio}_{i}}) \\
 & \text{\end{equation}}
 \end{aligned}$$

where  $f_{\text{penalty}}(X)$  is the new objective function,  $n\text{TotalConstVio}$  and  $\text{PF}$  are the total amount of constraint violations, and the penalty factor, respectively. Also,  $\text{vio}_i$  is the violation value for  $i$ th constraint, which is set to zero for

satisfied constraints. Here, the constraints include nodal displacement and element stress constraints.

Also, different values of the penalty factor  $\text{PF}$  were tested to tune this parameter. Finally,  $\text{PF}$  was set to 1000. The penalty function used is mostly similar to static penalties proposed in [40].

**3.1. Case Study.** In this paper, we aim to optimise two large-scale structural design problems proposed by the International Student Competition in Structural optimisation (ISCSO) in 2018 and 2019 [41], respectively. In the following subsection, the truss problems are explained in more detail.

**3.1.1. 314-Bar Truss.** The 314-bar problem introduced in [42] is a large-scale truss structure, and the main goal is to minimize the weight of a truss structure, including 314 bars and 84 nodes, according to the given constraints. The challenge is to obtain the optimal truss sizing and shape, while its topology is considered to be unalterable. Thus, the design variables include 314 sizing ( $A$ ) and 14 shape ( $C$ ) variables (treated as discrete decision variables). Figure 1 shows this truss structure in more detail.

The optimal solution is to minimize the structural weight, where no nodes and members violate the stress and displacement constraints. It means that the feasible solution possesses a value of zero for the amount of constraint violation, which is given by the function below:

$$\begin{aligned}
 & \text{\begin{equation}} \\
 & [W, S_{\text{Vio}}, D_{\text{Vio}}] = \text{objective\_function}(A, C). \\
 & \text{\end{equation}}
 \end{aligned}$$

Here, the function inputs include  $A$  and  $C$  denoting the cross-sectional areas and nodal coordinates, respectively. The outputs include the structural weight, the amount of stress and displacement violations, which are represented with  $W$ ,  $DV_{io}$  and  $SV_{io}$ , respectively. Moreover, the sizing and shape variables can take only integer values limited to the lower and upper bounds [1, 37] and [9000, 20000], respectively.

**3.1.2. 260-Bar Truss.** The 260-bar problem introduced in [42] is to minimize the weight of a large-scale steel truss, consisting of 260 bars and 76 nodes, while satisfying the stress and displacement constraints. Also, the number of sizing ( $A$ ) and shape ( $C$ ) variables are considered 260 and 10, respectively. Additionally, the shape variables can take only integer values in  $[-25000, 3500]$ . The rest of the problem is similar to the ISCSO 2018. Figure 2 shows this truss problem in more detail.

## 4. Methodology

Optimising both structural parameters, sizing and shape based on the mass to considerable frequency constraints is challenging because the nature of these problems is highly nonlinear, multimodal, discrete and complex. Another difficulty of the truss optimisation problems is the mixing of

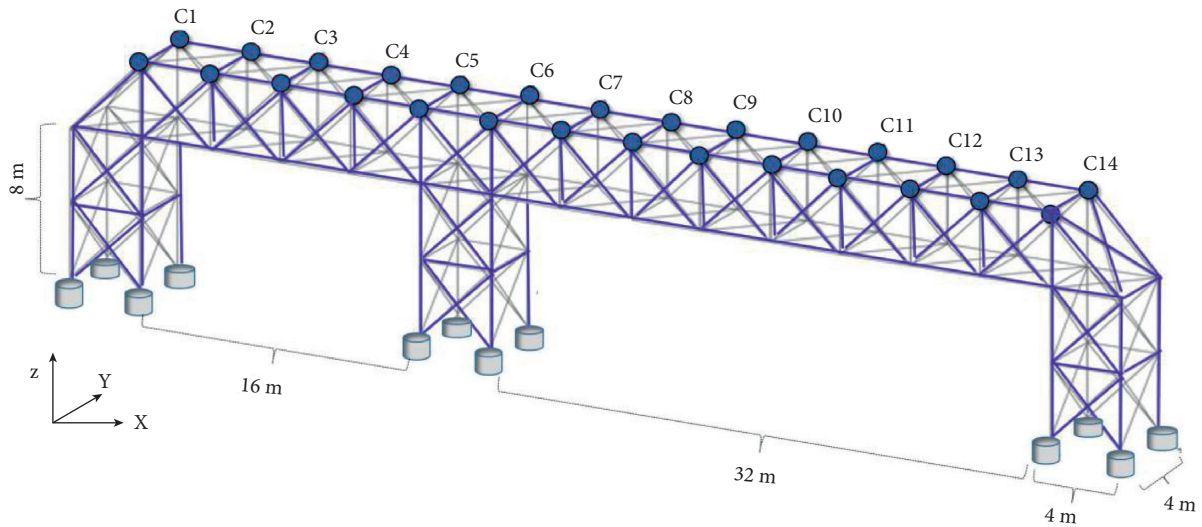


FIGURE 1: 3D steel truss structure with 314 bars and 84 nodes. The whole decision variables include 14 shape (C) and 314 sizing (A) elements. The shape variables show by  $C_i$  and total number of decision variables is 328.

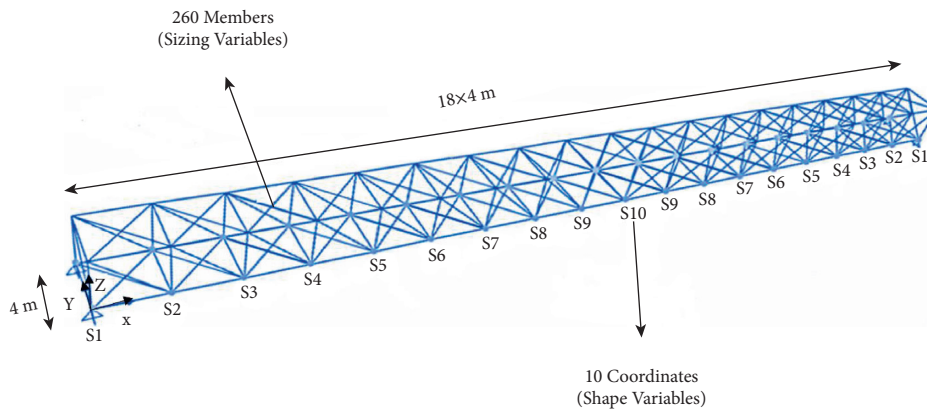


FIGURE 2: 3D steel truss structure with 260 bars and 76 nodes. The whole decision variables include 10 shape and 260 sizing elements. The shape variables show by  $C_i$  and total number of decision variables is 270.

two various parameters, cross-sectional and nodal coordinates which makes a heterogeneous search space. In order to evaluate the performance of the modern metaheuristics proposed in the last years, we developed a comparative platform of the twelve famous bio-inspired optimisation methods.

There are two most significant features of each bio-inspired search algorithm, including diversification and intensification. In the first step, in order to explore the search space and produce diverse solutions globally, an optimisation algorithm should be developed by a strong diversification technique. However, we need an alternative strategy to converge to a suitable solution that is the intensification process. In this step, the search focuses on the local areas to exploit and improve the current solutions. In this study, we applied and evaluated a wide range of optimisation methods with specific characteristics in order to propose the best-performed truss optimizer. Table 1 shows the initial control parameters of the optimisation methods applied in this study based on the recommended in the literature. As in this work

we evaluated and compared 12 optimisation methods, we just focus on the development of best performing method in this section to avoid lengthy discussions. In order to find more technical details about the algorithms applied, we refer to Ref. [11–22].

**4.1. Marine Predators Algorithm (MPA).** Faramarzi et al. [19] introduced MPA, one recently evolved nature-inspired meta-heuristic algorithms, to address optimisation problems. This algorithm's basic structure focuses on mimicking various foraging patterns by ocean predators and their optimal behaviours in attempting to deal with this biological situation. For optimal foraging, marine predators typically employ two strategies: (i) Levy flight and (ii) Brownian motions. To choose between these two strategies, predators calculate the ratio of the prey's velocity to their own.

MPA's primary goal is to provide a practical and straightforward meta-heuristic algorithm based on marine predator foraging patterns. Like other (population-based)



TABLE 1: The configuration details of optimisation methods applied the truss shape and sizing problem. Npop is the initial population size.

---

```

%-----
\begin{table}(H)
\Centering
\Caption{ The configuration details of optimisation methods applied the truss shape and sizing problem. $N_{pop}$ is the initial population size.}
\label{table:meta-details}
\scalebox{0.9}{
\begin{tabular}{|l|l|p{6cm}|}
\hline
& \textbf{Name} & \textbf{$N_{pop}$} & \textbf{Predefined Settings} \\ \hline
1 & Grey Wolf Optimizer (GWO)~\cite{mirjalili2014grey} & 50 & $\alpha$ decreases linearly from 2 to 0 \\ \hline
2 & Moth Flame Optimizer (MFO)~\cite{mirjalili2015moth} & 50 & $\alpha$ linearly decreases from -1 to -2 \\ \hline
3 & Multi Verse Optimizer (MVO)~\cite{mirjalili2016multi} & 50 & minimum and maximum of Wormhole existence probability: WEP$_{Max}$ = 1$,~ WEP$_{Min}$ = 0.2$, $\rho$ = 6$. \\ \hline
4 & Dragonfly Algorithm (DA)~\cite{mirjalili2016dragonfly} & 50 & $w = 0.9-0.2$, $s = 0.1$, $a = 0.1$, $c = 0.7$, $f = 1$, $e = 1$. \\ \hline
% 5 & Sine Cosine Algorithm (SCA)~\cite{mirjalili2016sca} & 50 & $\alpha = 2$, $r_1 = \alpha$ decreases linearly from $\alpha$ to 0 \\ \hline
5 & Henry Gas Solubility optimisation (HGSO)~\cite{hashim2019henry} & 50 & $N_g = 5$, $l_1 = 0.05$, $l_2 = 100$, $l_3 = 0.01$, $\alpha = 1$, $\beta = 1$, $c_1 = 0.1$, $c_2 = 0.2$ \\ \hline
6 & Equilibrium Optimizer (EO)~\cite{faramarzi2020equilibrium} & 50 & $\omega_1 = 1$,~ $\omega_2 = 2$, $GP = 0.5$ (=generation probability), $V = 1$. \\ \hline
7 & Arithmetic optimisation Algorithm (AOA)~\cite{abualigah2021arithmetic} & 50 & $MOP_{Max} = 1$, $MOP_{Min} = 0.2$, $C_{iter} = 1$, $\alpha = 5$, $\mu = 0.499$ \\ \hline
8 & Generalized Normal Distribution (GNDO)~\cite{zhang2020generalized} & 50 & applied the default settings. \\ \hline
9 & Salp Swarm Algorithm (SSA)~\cite{mirjalili2017salp} & 50 & $c_1$ decreased from 2 to zero. $c_2 = rand$ and $c_3 = rand$ \\ \hline
10 & Marine Predators Algorithm (MPA)~\cite{faramarzi2020marine} & 50 & $p = 0.5$, $FAD = 0.2$ \\ \hline
11 & Neural Network Algorithm (NNA)~\cite{sadollah2018dynamic} & 50 & pre-defined settings \\ \hline
12 & Water Cycle Algorithm (WCA)~\cite{eskandar2012water} & 50 & $N_{sr} = 4$, $D_{max} = 10^{-5}$ \\ \hline
\end{tabular}
}
\end{table}
%-----

```

---

algorithms, this algorithm begins by generating a random population in the problem searching space. As demonstrated by the survival of the fittest theory, efficient predators are always better off in terms of foraging in nature. The best solution is used in the MPA to construct an elite matrix. This matrix’s arrays contain prey position information for searching and finding prey [19]. The following is the definition of the elite matrix:

$$\begin{equation}
 E = \left[ \begin{array}{cccc} X_{1,1} & X_{1,2} & \dots & X_{1,d} \\ X_{2,1} & X_{2,2} & \dots & X_{2,d} \\ \vdots & \vdots & \vdots & \vdots \\ X_{n,1} & X_{n,2} & \dots & X_{n,d} \end{array} \right]
 \end{equation}$$

Here,  $\vec{X}^k$  (top predator’s vector) is replicated  $n$  times in order to build an elite matrix. Furthermore, in this equation,  $n$  represents the number of search agents, while  $d$  represents the size of the dimensions. Predators and prey are regarded as search agents in MPA. Predators and prey are regarded as search agents in MPA. In other words, when a predator looks

for his prey, the prey looks for food as well. The food chain in nature-inspired this trend. The strongest predator is at the top of the food chain, and the weakest predators are subdivided into the stronger predator group. Obviously, when a stronger predator appears in this chain, this predator is moved to the top of the chain and replaces the previous hunter. The MPA imitates this concept by updating the elite matrix.

Prey is the name of another MPA matrix. This matrix has dimensions similar to the Elite matrix, and hunters adjust their positions based on it. More specifically, the initial MPA population is recognized as prey, while the best ones are selected as predators, forming the elite matrix. The prey matrix looks like this:

$$\begin{equation}
 py = \left[ \begin{array}{cccc} X_{1,1} & X_{1,2} & \dots & X_{1,d} \\ X_{2,1} & X_{2,2} & \dots & X_{2,d} \\ \vdots & \vdots & \vdots & \vdots \\ X_{n,1} & X_{n,2} & \dots & X_{n,d} \end{array} \right]
 \end{equation}$$

Here,  $X_{(i,j)}$  depicts the  $i$ th prey with  $j$ th dimension. In general, the entire optimisation process in MPA is dependent on these two matrices.

Given the various phases and patterns of hunting for both marine predators and prey and the impact of the predator and prey speed on the modelling of this process, the MPA algorithm is divided into three significant steps. The following are the steps:

- (i) High-velocity: during this phase, the prey's speed exceeds that of the predator
- (ii) Unity-velocity: the speed of the predator and prey would be the same in this phase
- (iii) Low-velocity: the prey is slower than the predator at this phase

Although predator and prey movements in nature follow unique rules and inspire the main phases of the algorithm, the MPA assigns the specified number of iterations to these phases.

**4.1.1. Phase 1: (High-Velocity).** This phase is used in early MPA iterations where the prey outruns the predators. Predators have the least movement during this phase, so staying in their positions is the best strategy. The MPA defines this phase as follows:

```
\begin{equation}
\{\text{while}\};\;t < \frac{1}{3} * t_{\{\rm\max\}}
\{\rm\max\}}\}\longrightarrow.
\{\overrightarrow{\text{Step}}\}_i = \{\vec{R}\}_B \otimes
\text{imes}\left(\{\overrightarrow{\text{Elite}}\}_i - \{\vec{R}\}_B
\otimes \overrightarrow{\text{prey}}_{\{i\}}\right)\longrightarrow.
\overrightarrow{\text{prey}}_{\{i\}} = \overrightarrow{\text{prey}}_{\{i\}} + P * \vec{R} \otimes
\overrightarrow{\text{Step}}_{\{i\}}
\end{equation}
```

where  $R_B$  is a random number generated using the normal distribution and displaying Brownian motion, the  $\otimes$  symbol represents entry-wise multiplications. Prey movements are simulated by multiplying  $R_B$  by prey. The uniform random numbers [0, 1] are arranged in a vector, and the constant number 0.5 is assigned to  $P$ .  $t$  and  $t_{\max}$  are the current and maximum iterations, respectively. This phase takes place when the algorithm's initial iterations necessitate a high level of exploration capability.

**4.1.2. Phase 2: (Unity-Velocity).** Predators and prey move at the same speed in the second phase of the MPA algorithm. This stage in nature indicates that they are both looking for their own prey. The occurrence of this phase in the middle of the optimisation process demonstrates the algorithm's early stages of transition from exploration to exploitation. The MPA characterizes the prey for exploration and the predators for exploitation in this specific instance. Furthermore, during this phase, the prey moves according to

the Levy theorem and the predators according to Brownian motions. This phase will be modelled in the following manner:

```
%-----
\begin{equation}
\{\text{while}\};\;\frac{1}{3} * t_{\{\rm\max\}}
< t < \frac{2}{3} * t_{\{\rm\max\}}.
\end{equation}
\begin{equation} \label{eq:phase2-1}
\overrightarrow{\text{Step}}_i = \{\vec{R}\}_L \otimes
\left(\{\overrightarrow{\text{Elite}}\}_i - \{\vec{R}\}_L \otimes
\overrightarrow{\text{prey}}_{\{i\}}\right) \longrightarrow.
\overrightarrow{\text{prey}}_{\{i\}} = \overrightarrow{\text{prey}}_{\{i\}} + P * \vec{R} \otimes
\overrightarrow{\text{Step}}_{\{i\}}.
\end{equation}
\begin{equation} \label{eq:phase2-2}
\overrightarrow{\text{Step}}_i = \{\vec{R}\}_B \otimes
\text{imes}\left(\{\vec{R}\}_B \otimes \{\overrightarrow{\text{Elite}}\}_i -
\overrightarrow{\text{prey}}_{\{i\}}\right) \longrightarrow.
\overrightarrow{\text{prey}}_{\{i\}} = \overrightarrow{\text{Elite}}_{\{i\}} + P * \{\rm\{CF\}} \otimes
\overrightarrow{\text{Step}}_{\{i\}}.
\end{equation}
%-----
```

It is critical to emphasize that equation (8) is applied to the first half of the MPA population. This equation  $R_L$  generates random numbers based on the Levy distribution to simulate the Levy movement [43]. In the Levy strategy, the multiplications of  $R_L$  and prey are used to simulate the movements of prey. The MPA's exploitation phase is performed using the strategy introduced in this phase. Equation (9) is how the second part of this step is simulated for the rest of the population:

In equation (10),  $CF$  is used as an adaptive parameter to control the step size of the predator's movement. Furthermore, in the Brownian strategy, the predator's movement is simulated by multiplying  $R_B$  by Elite. The position of the prey is improved as a result of the predator's Brownian movements during this phase.

```
%-----
\begin{equation}
\label{eq:cf}
\{\rm\{CF\}} = \left(1 - \frac{t}{t_{\{\rm\max\}}}\right) \left(2 \frac{t}{t_{\{\rm\max\}}}\right).
\end{equation}
%-----
```

**4.1.3. Phase 3: (Low-Velocity).** This process was simulated in order to provide MPA with a high level of exploitation potential. This step is put in place in the algorithm when the prey's speed is slower than the predator's. Predators employ

Levy's strategy to ensure that this process is carried out correctly in the MPA. This procedure is modelled as follows:

```
%-----
\begin{equation}
\{\text{while}\};\{\text{it}\} > \frac{2}{3} * \{\text{max\_}
\{\text{iter}\}\} \ \text{longrightrightarrow.}
\{\{\text{overrightarrow}\{\text{Step}\}\}_i\} = \{\{\text{vec}\{\text{R}\}\}_L\} \text{otimes}
\left(\{\{\text{vec}\{\text{R}\}\}_L\} \text{otimes} \{\{\text{overrightarrow}\{\text{Elite}\}\}_i\} - \{\{\text{overrightarrow}\{\text{prey}\}\}_i\} \right) \ \text{longrightrightarrow.}
\{\{\text{overrightarrow}\{\text{prey}\}\}_i\} = \{\{\text{overrightarrow}\{\text{Elite}\}\}_i\} + P * \{\text{CF}\} \text{otimes} \{\{\text{overrightarrow}\{\text{Step}\}\}_i\}
\end{equation}
%-----
```

In the Levy strategy, predator movement is defined by the multiplication of  $R_L$  and Elite. Besides, Elite includes a step size to mimic predator movement in this equation and assist prey in updating their position.

**4.1.4. Eddy Formation and FAD's Effect.** Several factors could influence marine predators' foraging patterns in general. Environmental issues are one of the significant factors that can have a crucial impact on the behaviour of these predators. Eddy currents and fish aggregating devices (FAD) are two major environmental issues in these behavioural changes. Filmlalter et al. [43] discovered that sharks spend the vast majority of their hunting time (nearly 80%) near FADs in the wild. Furthermore, the remainder of the shark hunting time is spent locating areas with specific prey distributions. These FADs are regarded as local optimum points in the MPA, capable of trapping the algorithm. As a result, the effect of FADs on the MPA algorithm is as follows:

```
\begin{equation}
\{\{\text{overrightarrow}\{\text{prey}\}\}_i\} = \left[ \{\{\text{overrightarrow}\{\text{prey}\}\}_i\} + \{\text{CF}\} \left[ \left\{ \{\{\text{vec}\{\text{X}\}\}_{\min}\} + R \text{otimes} (\{\{\text{vec}\{\text{X}\}\}_{\max}\} - \{\{\text{vec}\{\text{X}\}\}_{\min}\}) \right\} \right] \text{otimes} \{\text{U}\} \ \& \ \{\text{if}\} \ r < \{\text{FADs}\} \right]
\{\{\text{overrightarrow}\{\text{prey}\}\}_i\} + \left[ \left\{ \{\text{FADs}\} \left[ (1 - r) \right] + r \right\} \left[ \{\{\text{overrightarrow}\{\text{prey}\}\}_{r_1}\} - \{\{\text{overrightarrow}\{\text{prey}\}\}_{r_2}\} \right] \right] \ \& \ \{\text{if}\} \ r > \{\text{FADs}\} \ \end{array}
\end{equation}
%-----
```

Here,  $\vec{X}_{\min}$  and  $\vec{X}_{\max}$  are the lower and upper bounds of the dimensions, respectively.  $\vec{U}$  creates a binary vector consisting of zero and one array. The FAD factor is the probability of FADs influencing the optimisation process, and its value is set to 0.2. On the other hand,  $r$  is defined as a uniform random number that generates values between [0, 1]. Subscript of  $r_1$  and  $r_2$  denotes random prey matrix indexes.

## 5. Experimental Results

In this section, we demonstrate the optimisation outcomes achieved by twelve state-of-the-art meta-heuristics in order to minimize the total weight of two truss structures. For all search algorithms, the originally recommended parameters with the same population size were applied to provide a fair comparison framework.

In Figure 3, each curve represents the development of the average truss's weight plus the penalty of 314-bar case study that yielded by the best-found design for each optimisation method over 105 evaluation iterations. From this convergence plot, we can observe that the optimisation methods can be classified into two groups. First, optimisation strategies with a high convergence rate. These methods have a heightened exploitation ability include AOA, DA, GNDO, MPA, HGSO, and SSA. In the second group, we can see four methods with slow convergence speed, such as GWO, EO, MFO and MVO. In this case study (314-bar), the fastest convergence rate is related to the MPA, which could find a relative-optimal structure; however, it struggled with a local optimum and could not escape from this situation. To have a general observation from Figure 3, except for DA, all methods in the second group were converged to a local optimum design in the same iteration approximately. The DA could improve the best-found solutions after  $4 \times 10^4$  evaluation number.

In order to provide an accurate comparison framework for these twelve optimisation methods' performance, we plotted Figure 4. In this figure, each box shows the 25% and 75% percentiles of the best-found solutions (upper and lower edges) and the median of the outcomes represented by the central tag. On each box, we can see the extended whiskers for the data points with larger variance, and finally, the outliers are depicted by the '+' symbol. From Figure 4, the most important observation is that both MPA and DA are the best-performed optimisation methods compared with other algorithms.

A comparison of the convergence rate of twelve optimizers for the 260-bar truss can be seen in Figure 5. The Figure depicts that SSA and GNDO have the most considerable convergence speed; however, the mean weight of 260-bar proposed by MPA can be significantly better. Interestingly, the whole methods applied for this large truss could not improve the quality of the solutions after 24 iterations. This premature convergence shows these meta-heuristics are not able to exit from the local optima. The highly dynamic constraints and large number of decision variables of the this truss problem can be the most significant reason for the premature convergence issue. The statistical results of the best-found solutions for twelve algorithms summarize in Figure 6. The Figure illustrates that both MPA and AOA could propose the best configuration of 260-bar compared with others methods applied. Moreover, the performance of the SSA and GNDO is considerable. In the 260-bar case study, the DA's exploration and exploitation strategies were not effective in figuring out the challenging constraints of the problem.

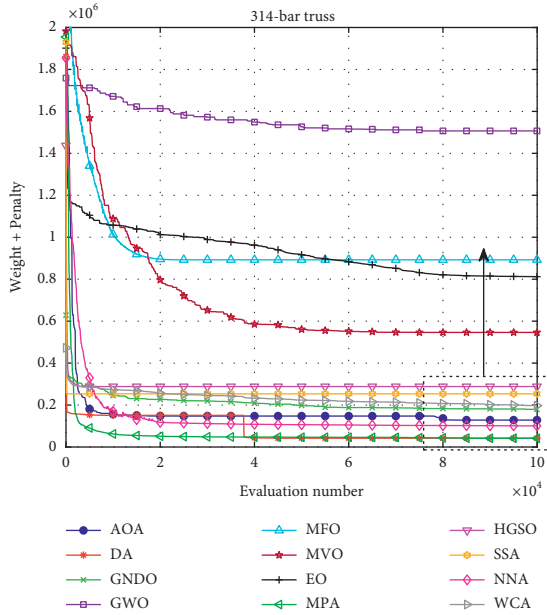


FIGURE 3: A convergence rate comparison of twelve optimisation methods applied for the large-scale 314-bar truss problem. The maximum number of evaluation is 105. Total number of decision variables is 328.

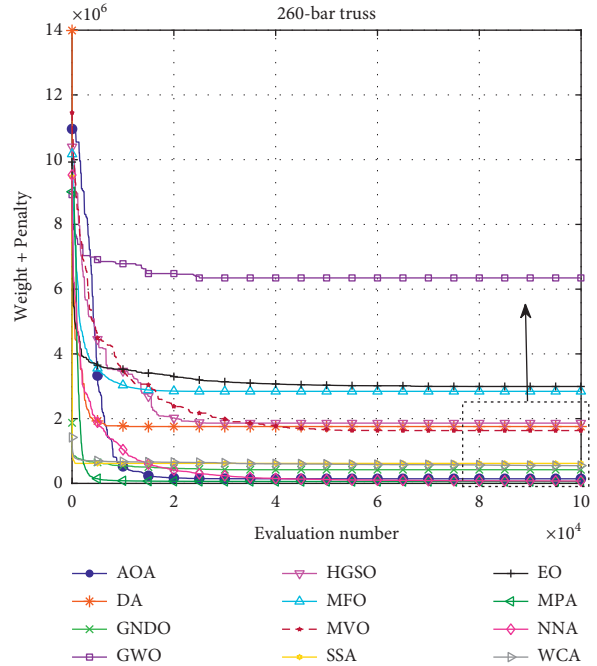


FIGURE 5: A convergence rate comparison of twelve optimisation methods applied for the large-scale 260-bar truss problem. The maximum number of evaluation is 105. Total number of decision variables is 270.

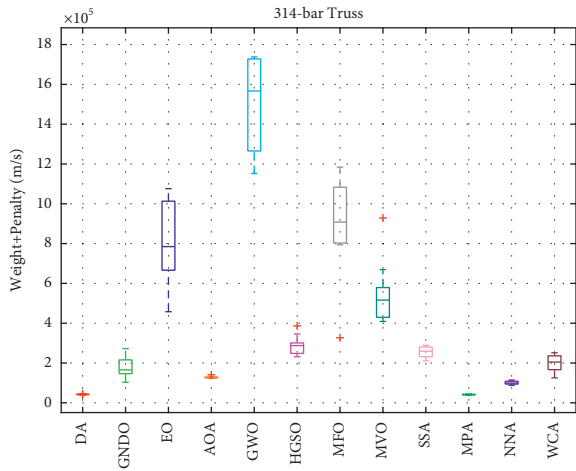


FIGURE 4: box plot of twelve various optimisation methods' performance for 314-bar truss problem.

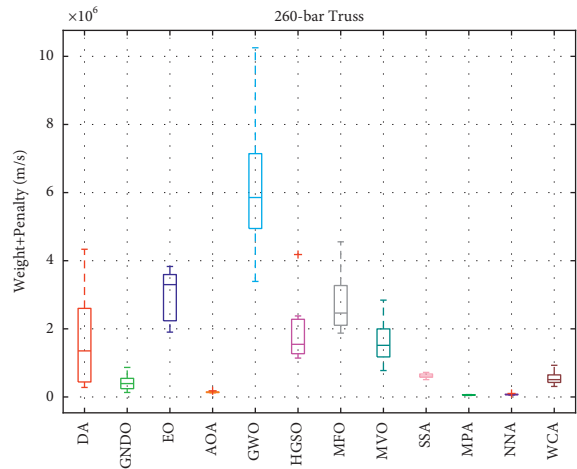


FIGURE 6: Statistical analysis of the optimisation methods' performance for 260-bar truss problem. The best-found solution per each run.

The statistical performance (best, worst, average, median and standard deviation) of these optimisation methods is quantified in Table 2 for both case studies, 314-bar and 260-bar. It can be seen that the best-found designs were proposed by the MPA in both truss problems. It is noted that the reported solutions in Table 3 are an accumulated structure weight and the penalty value. The second best method is the AOA on average in both truss problems.

In order to tune a proper population size for the MPA, we tested four population sizes consisting of 50, 100, 250,

and 500 with the same evaluation number at 105. Figure 7 shows the convergence speed of this competition among four sizes of the MPA population. It can be seen that the performance of MPA with a population size of 100 outweighs other settings in terms of designs weight. The significant observation from Figure 7 is that the population size of 50 cannot be an efficient setting for the MPA and wakened the optimisation process.

TABLE 2: The statistical results of the best-found truss structures for 12 optimisation methods.

---

```

\begin{table}[]
\centering
\caption{ The statistical results of the best-found truss structures for 12 optimisation methods.}
\label{table:best_found}
\scalebox{0.7}{
\begin{tabular}{|l|l|l|l|l|l|l|l|l|l|l|l|}
\hlineB{4}
& \multicolumn{10}{c}{260-bar truss} & \multicolumn{1}{c}{} & \multicolumn{1}{c}{} \\
& DA & GNDO & EO & AOA & GWO & HGSO & MFO & MVO & SSA & MPA & NNA & WCA \\
\hlineB{3}
Min & 2.793E+05 & 1.318E+05 & 1.904E+06 & 1.204E+05 & 3.392E+06 & 1.141E+06 & 1.874E+06 & 7.753E+05 & 5.091E+05 & \textbf{4.452E+04} & 5.537E+04 & 3.086E+05 \\
Max & 4.336E+06 & 8.669E+05 & 3.831E+06 & 1.801E+05 & 1.025E+07 & 4.181E+06 & 4.555E+06 & 2.843E+06 & 7.212E+05 & 7.031E+04 & 1.025E+05 & 9.297E+05 \\
Mean & 1.756E+06 & 4.224E+05 & 2.994E+06 & 1.423E+05 & 6.347E+06 & 1.862E+06 & 2.844E+06 & 1.632E+06 & 6.182E+05 & 5.777E+04 & 7.305E+04 & 5.485E+05 \\
Median & 1.352E+06 & 3.930E+05 & 3.298E+06 & 1.399E+05 & 5.855E+06 & 1.545E+06 & 2.464E+06 & 1.516E+06 & 6.146E+05 & 5.836E+04 & 6.973E+04 & 5.091E+05 \\
STD & 1.482E+06 & 2.372E+05 & 7.436E+05 & 1.811E+04 & 2.029E+06 & 9.217E+05 & 1.002E+06 & 6.528E+05 & 6.302E+04 & 7.729E+03 & 1.306E+04 & 1.781E+05 \\
\hlineB{4}
& \multicolumn{10}{c}{314-bar truss} & \multicolumn{1}{c}{} & \multicolumn{1}{c}{} \\
& DA & GNDO & EO & AOA & GWO & HGSO & MFO & MVO & SSA & MPA & NNA & WCA \\
\hlineB{3}
Min & 3.934E+04 & 1.031E+05 & 4.578E+05 & 1.223E+05 & 1.152E+06 & 2.315E+05 & 3.269E+05 & 4.089E+05 & 2.107E+05 & \textbf{3.888E+04} & 8.769E+04 & 1.254E+05 \\
Max & 4.598E+04 & 2.723E+05 & 1.076E+06 & 1.408E+05 & 1.738E+06 & 3.864E+05 & 1.184E+06 & 9.286E+05 & 2.885E+05 & 4.430E+04 & 1.145E+05 & 2.515E+05 \\
Mean & 4.217E+04 & 1.795E+05 & 8.122E+05 & 1.283E+05 & 1.507E+06 & 2.882E+05 & 8.925E+05 & 5.463E+05 & 2.536E+05 & 4.145E+04 & 1.006E+05 & 1.975E+05 \\
Median & 4.192E+04 & 1.653E+05 & 7.848E+05 & 1.279E+05 & 1.567E+06 & 2.875E+05 & 9.080E+05 & 5.161E+05 & 2.590E+05 & 4.121E+04 & 9.906E+04 & 2.048E+05 \\
STD & 1.647E+03 & 5.375E+04 & 2.141E+05 & 5.298E+03 & 2.303E+05 & 4.896E+04 & 2.389E+05 & 1.602E+05 & 2.784E+04 & 1.697E+03 & 8.896E+03 & 4.533E+04 \\
\hlineB{4}
\end{tabular}
}
\end{table}
%-----

```

---

TABLE 3: Shows the average sum-rank Friedman test for the 314-bar and 260-bar problems using twelve optimisation methods. It can be observed that the MPA achieved the first rank in both case studies on average, and in the following the NNA, AOA and GNDO placed the second, third, and fourth rank of the truss optimisation.

---

```

\begin{table}[]
\centering
\caption{ The average performance rank of 12 optimisation methods based on the best-found designs. significant level of the Friedman test is 0.05.}
\label{table:rank}
\scalebox{0.8}{
\begin{tabular}{|l|l|l|l|l|l|l|l|l|l|l|l|}
\hlineB{4}
& {DA} & {GNDO} & {EO} & {AOA} & {GWO} & {HGSO} & {MFO} & {MVO} & {SSA} & {MPA}&{NNA} & {WCA} \\
\hlineB{3}
314-bar & 2&5&10&4&12&8&11&9&7&1&3&6 \\
260-bar & 8&4&11&3&12&9&10&7&6&1&2&5 \\
Mean rank & 5&4.5&10.5&3.5&12&8.5&10.5&8&6.5&1&2.5&5.5 \\
\hlineB{4}
\end{tabular}
}
\end{table}

```

---

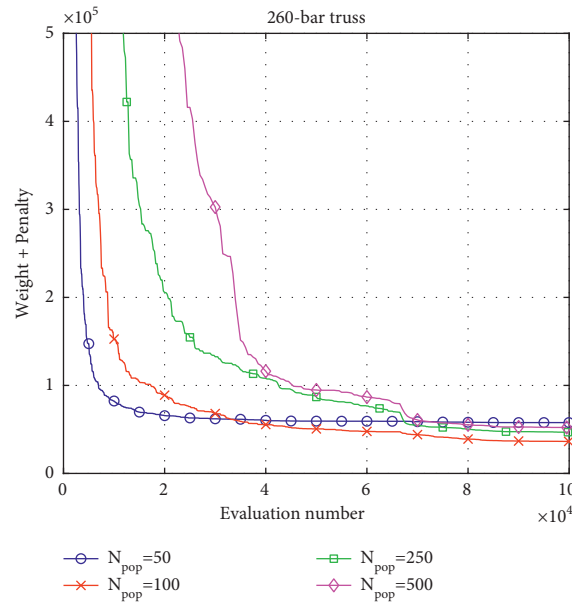


FIGURE 7: A convergence rate comparison of four different population sizes of MPA optimisation method applied for the large-scale 260-bar truss problem. The maximum number of evaluation is 105. A zoom version of the figure can be seen in top right side.

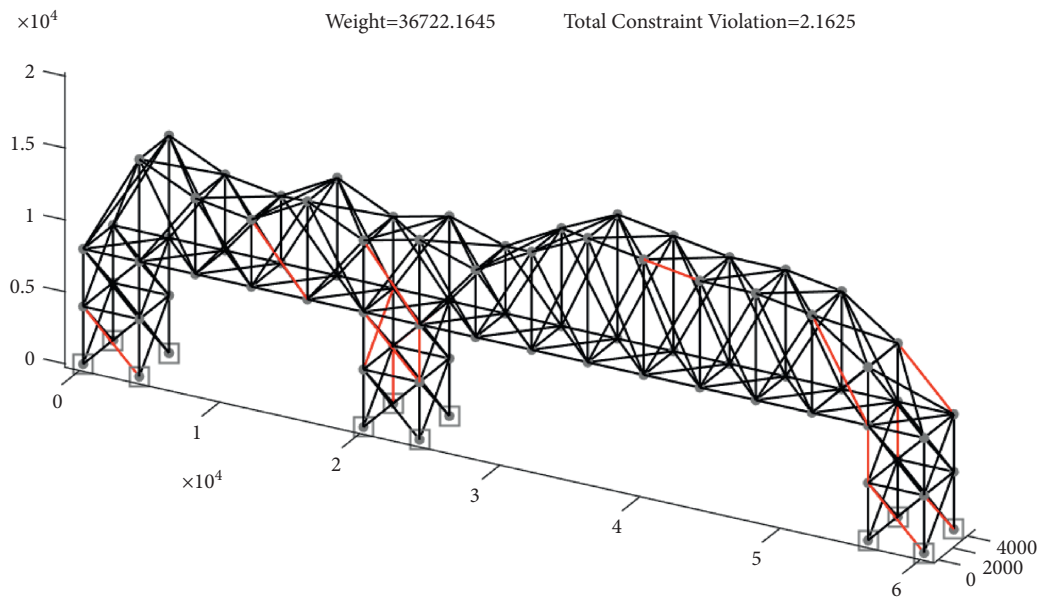


FIGURE 8: Best-found design of 314-bar structure. The violated bars are highlighted by red color.

In order to show the best-found structure of two case studies, 314, and 260-bar trusses, Figure 8 and Figure 9 are plotted. In both designs, we can see a few number of bars that are violated under stress and displacement forces (highlighted by red colour). The total sum violations are low in both cases;

however, in the real applications, these violations should be minimised as much as possible near to zero. This comparative optimisation framework obviously shows that the metaheuristics applied in this study need to be improved in terms of the constraint handling methods specifically.

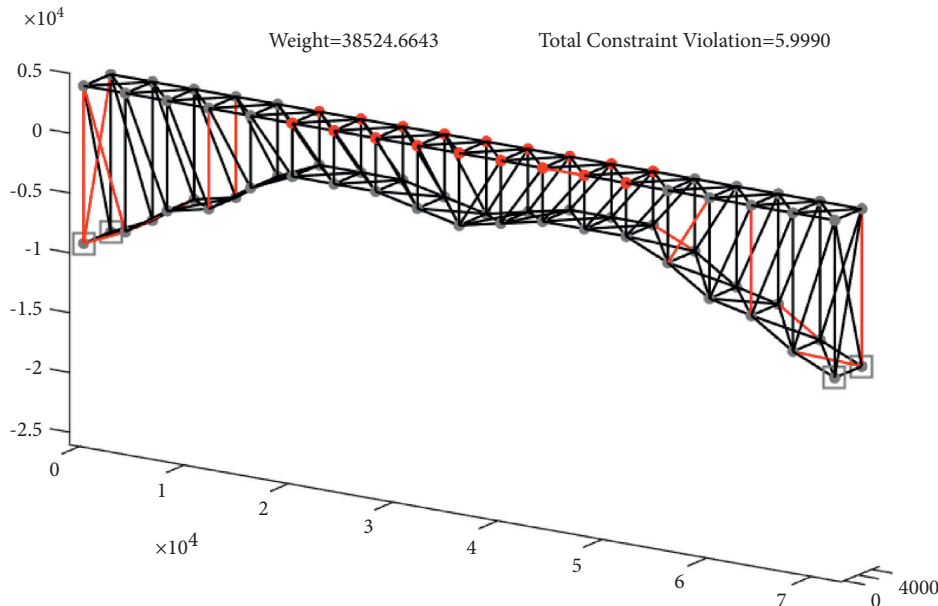


FIGURE 9: Best-found design of 260-bar structure. The violated bars are highlighted by red color.

## 6. Conclusion

This paper used 12 modern meta-heuristic algorithms to consider the truss shape and sizing optimisation problem. To handle the violation of constraints, we applied a penalty function that is a popular method in this way. Different penalty factors were evaluated to find the best value in terms of best-found designs. Two various truss problems are used in this study. Both of them have a large structure composed of 314 and 260 bars, respectively. It is assumed that the topology of the truss should be fixed and unalterable. The optimal truss shape and sizing variables should be obtained by minimizing the structural weight with respect to nodal displacement constraints, element stress constraints, and natural frequencies. These complex constraints make a challenging optimisation problem, which is large-scale, nonlinear, multimodal with dynamic constraints. As global optimisation algorithms are mostly efficient and robust, we mainly focus on the application of metaheuristics, especially modern swarm optimisation methods, to the truss optimisation problems in this study. Indeed, we applied twelve different bio-inspired optimisation methods in order to evaluate and develop a comparative framework for the large-scale truss problems. To have a fair comparison, all control parameters were set according to literature recommendations for each optimisation algorithm. This is because there is no simple way to obtain the best parameter values. From an engineering point of view, the performance of the MPA method is better than other optimisation methods used in this study because of a combination of fast and effective exploration and exploitation search strategies. Furthermore, we tuned the population size of the MPA and showed that 100 could be a better option than other dimensions.

## Data Availability

In this study, we did not apply a specific dataset.

## Conflicts of Interest

The authors declare that they have no conflicts of interest.

## References

- [1] L. Wei, T. Tang, X. Xie, and W. Shen, "Truss optimization on shape and sizing with frequency constraints based on parallel genetic algorithm," *Structural and Multidisciplinary Optimization*, vol. 43, no. 5, pp. 665–682, 2011.
- [2] B. Doerr and F. Neumann, "A survey on recent progress in the theory of evolutionary algorithms for discrete optimization," *ACM Transactions on Evolutionary Learning and Optimization*, vol. 1, no. 4, pp. 1–43, 2021.
- [3] M. Khatibinia, S. Sadegh Naseralavi, and S. Sadegh Naseralavi, "Truss optimization on shape and sizing with frequency constraints based on orthogonal multi-gravitational search algorithm," *Journal of Sound and Vibration*, vol. 333, no. 24, pp. 6349–6369, 2014.
- [4] C. Renkavieski and R. Stubs Parpinelli, "Meta-heuristic algorithms to truss optimization: literature mapping and application," *Expert Systems with Applications*, vol. 182, Article ID 115197, 2021.
- [5] J. Kennedy and E. Russell, "Particle swarm optimization," *Proceedings of ICNN'95-international conference on neural networks*, IEEE, vol. 4, pp. 1942–1948, 1995.
- [6] A. Kaveh and A. Zolghadr, "Democratic pso for truss layout and size optimization with frequency constraints," *Computers & Structures*, vol. 130, pp. 10–21, 2014.
- [7] J. A. Bland, "Optimal structural design by ant colony optimization," *Engineering Optimization*, vol. 33, no. 4, pp. 425–443, 2001.

- [8] Q. X. Lieu, D. Tt Do, and J. Lee, "An adaptive hybrid evolutionary firefly algorithm for shape and size optimization of truss structures with frequency constraints," *Computers & Structures*, vol. 195, pp. 99–112, 2018.
- [9] M. Arjmand, M. Sheikhi Azqandi, and M. Delavar, "Hybrid improved dolphin echolocation and ant colony optimization for optimal discrete sizing of truss structures," *Journal of rehabilitation in civil engineering*, vol. 6, no. 1, pp. 70–87, 2018.
- [10] A. Kaveh and P. Zakian, "Improved gwo algorithm for optimal design of truss structures," *Engineering with Computers*, vol. 34, no. 4, pp. 685–707, 2018.
- [11] S. Mirjalili, S. Mohammad Mirjalili, S. M. Mirjalili, and A. Lewis, "Grey wolf optimizer," *Advances in Engineering Software*, vol. 69, pp. 46–61, 2014.
- [12] S. Mirjalili, "Moth-flame optimization algorithm: a novel nature-inspired heuristic paradigm," *Knowledge-Based Systems*, vol. 89, pp. 228–249, 2015.
- [13] S. M. Mirjalili and A. Hatamlou, "Multi-Verse Optimizer: a nature-inspired algorithm for global optimization," *Neural Computing & Applications*, vol. 27, no. 2, pp. 495–513, 2016.
- [14] S. Mirjalili, "Dragonfly algorithm: a new meta-heuristic optimization technique for solving single-objective, discrete, and multi-objective problems," *Neural Computing & Applications*, vol. 27, no. 4, pp. 1053–1073, 2016.
- [15] A. Faramarzi, M. Heidarinejad, B. Stephens, and S. Mirjalili, "Equilibrium optimizer: a novel optimization algorithm," *Knowledge-Based Systems*, vol. 191, Article ID 105190, 2020.
- [16] L. Abualigah, A. Diabat, S. M. Mohamed, A. Elaziz, and A. H. Gandomi, "The arithmetic optimization algorithm," *Computer Methods in Applied Mechanics and Engineering*, vol. 376, Article ID 113609, 2021.
- [17] Y. Zhang, Z. Jin, and S. Mirjalili, "Generalized normal distribution optimization and its applications in parameter extraction of photovoltaic models," *Energy Conversion and Management*, vol. 224, Article ID 113301, 2020.
- [18] S. Mirjalili, A. H. Gandomi, S. Z. Mirjalili, S. Saremi, H. Faris, and S. M. Mirjalili, "Salp swarm algorithm: a bio-inspired optimizer for engineering design problems," *Advances in Engineering Software*, vol. 114, pp. 163–191, 2017.
- [19] A. Faramarzi, M. Heidarinejad, S. Mirjalili, and A. H. Gandomi, "Marine predators algorithm: a nature-inspired metaheuristic," *Expert Systems with Applications*, vol. 152, Article ID 113377, 2020.
- [20] F. A Hashim, E. H Houssein, M. S Mabrouk, W. Al-Atabany, and S. Mirjalili, "Henry gas solubility optimization: a novel physics-based algorithm," *Future Generation Computer Systems*, vol. 101, pp. 646–667, 2019.
- [21] A. Sadollah, H. Sayyaaadi, and A. Yadav, "A dynamic metaheuristic optimization model inspired by biological nervous systems: Neural network algorithm," *Applied Soft Computing*, vol. 71, pp. 747–782, 2018.
- [22] H. Eskandar, A. Sadollah, A. Bahreininejad, and M. Hamdi, "Water cycle algorithm - a novel metaheuristic optimization method for solving constrained engineering optimization problems," *Computers & Structures*, vol. 110–111, pp. 151–166, 2012.
- [23] H. Rahami, A. Kaveh, and Y. Gholipour, "Sizing, geometry and topology optimization of trusses via force method and genetic algorithm," *Engineering Structures*, vol. 30, no. 9, pp. 2360–2369, 2008.
- [24] V. Ho-Huu, T. Nguyen-Thoi, T. Khac, L. Anh, and T. Vo-Duy, "An improved differential evolution based on roulette wheel selection for shape and size optimization of truss structures with frequency constraints," *Neural Computing and Applications*, vol. 29, no. 1, pp. 167–185, 2018.
- [25] Sy. Nguyen-Van, K. T. Nguyen, V. Hai Luong, S. Lee, and Q. X. Lieu, "A novel hybrid differential evolution and symbiotic organisms search algorithm for size and shape optimization of truss structures under multiple frequency constraints," *Expert Systems with Applications*, vol. 184, Article ID 115534, 2021.
- [26] L. Lamberti, "An efficient simulated annealing algorithm for design optimization of truss structures," *Computers & Structures*, vol. 86, no. 19–20, pp. 1936–1953, 2008.
- [27] S. Kazemzadeh Azad, "Enhanced hybrid metaheuristic algorithms for optimal sizing of steel truss structures with numerous discrete variables," *Structural and Multidisciplinary Optimization*, vol. 55, no. 6, pp. 2159–2180, 2017.
- [28] S. Ali, A. Bahreininejad, H. Eskandar, and M. Hamdi, "Mine blast algorithm for optimization of truss structures with discrete variables," *Computers & Structures*, vol. 102, pp. 49–63, 2012.
- [29] F. K. J. Jawad, C. Ozturk, W. Dansheng, M. Mahmood, O. Al-Azzawi, and A. Al-Jemely, "Sizing and layout optimization of truss structures with artificial bee colony algorithm," *Structures*, Elsevier, vol. 30, pp. 546–559, 2021.
- [30] M. Sonmez, "Artificial bee colony algorithm for optimization of truss structures," *Applied Soft Computing*, vol. 11, no. 2, pp. 2406–2418, 2011.
- [31] A. Kaveh, S. Talatahari, and N. Khodadadi, "Hybrid invasive weed optimization-shuffled frog-leaping algorithm for optimal design of truss structures," *Iranian Journal of Science and Technology, Transactions of Civil Engineering*, vol. 44, 2019.
- [32] A. Kaveh and M. Khayatazad, "A new meta-heuristic method: ray optimization," *Computers & Structures*, vol. 112–113, pp. 283–294, 2012.
- [33] A. Kaveh and M. I. Ghazaan, "Layout and size optimization of trusses with natural frequency constraints using improved ray optimization algorithm," *Iranian Journal of Science and Technology Transactions of Civil Engineering*, vol. 39, no. 2, pp. 395–408, 2015.
- [34] S. Talatahari, A. H. Gandomi, and G. J. Yun, "Optimum design of tower structures using firefly algorithm," *The Structural Design of Tall and Special Buildings*, vol. 23, no. 5, pp. 350–361, 2014.
- [35] K. Ali and N. Farhoudi, "A new optimization method: dolphin echolocation," *Advances in Engineering Software*, vol. 59, pp. 53–70, 2013.
- [36] T. Dede and Y. Ayvaz, "Combined size and shape optimization of structures with a new meta-heuristic algorithm," *Applied Soft Computing*, vol. 28, pp. 250–258, 2015.
- [37] R. Awad, "Sizing optimization of truss structures using the political optimizer (po) algorithm," *Structures*, Elsevier, vol. 33, pp. 4871–4894, 2021.
- [38] A. Kaveh and S. Talatahari, "Optimum design of skeletal structures using imperialist competitive algorithm," *Computers & Structures*, vol. 88, no. 21–22, pp. 1220–1229, 2010.
- [39] M. Dehghani, M. Mashayekhi, and M. Sharifi, "An efficient imperialist competitive algorithm with likelihood assimilation for topology, shape and sizing optimization of truss structures," *Applied Mathematical Modelling*, vol. 93, no. 1–27, 2021.
- [40] C. A. C. Coello, "Theoretical and numerical constraint-handling techniques used with evolutionary algorithms: a survey of the state of the art," *Computer Methods in Applied Mechanics and Engineering*, vol. 191, no. 11–12, pp. 1245–1287, 2002.
- [41] S. Kazemzadeh Azad and O. Hasançebi, "Structural optimization problems of the iscco 2011–2015: a test set,"



*International Journal of Optimization in Civil Engineering*, vol. 6, no. 4, pp. 629–638, 2016.

- [42] B. Optimizer, “International Student Competition in Structural Optimization,” pp. 12–25, 2021, [https://www. bright-optimizer.com/](https://www.bright-optimizer.com/).
- [43] J. D. Filmalter, L. Dagorn, P. D. Cowley, and M. Taquet, “First descriptions of the behavior of silky sharks, *carcharhinus falciformis*, around drifting fish aggregating devices in the indian ocean,” *Bulletin of Marine Science*, vol. 87, no. 3, pp. 325–337, 2011.

## *Retraction*

# **Retracted: The Influence and Prediction of Industry Asset Price Fluctuation Based on the LSTM Model and Investor Sentiment**

### **Mathematical Problems in Engineering**

Received 13 September 2023; Accepted 13 September 2023; Published 14 September 2023

Copyright © 2023 Mathematical Problems in Engineering. This is an open access article distributed under the Creative Commons Attribution License, which permits unrestricted use, distribution, and reproduction in any medium, provided the original work is properly cited.

This article has been retracted by Hindawi following an investigation undertaken by the publisher [1]. This investigation has uncovered evidence of one or more of the following indicators of systematic manipulation of the publication process:

- (1) Discrepancies in scope
- (2) Discrepancies in the description of the research reported
- (3) Discrepancies between the availability of data and the research described
- (4) Inappropriate citations
- (5) Incoherent, meaningless and/or irrelevant content included in the article
- (6) Peer-review manipulation

The presence of these indicators undermines our confidence in the integrity of the article's content and we cannot, therefore, vouch for its reliability. Please note that this notice is intended solely to alert readers that the content of this article is unreliable. We have not investigated whether authors were aware of or involved in the systematic manipulation of the publication process.

Wiley and Hindawi regrets that the usual quality checks did not identify these issues before publication and have since put additional measures in place to safeguard research integrity.

We wish to credit our own Research Integrity and Research Publishing teams and anonymous and named external researchers and research integrity experts for contributing to this investigation.

The corresponding author, as the representative of all authors, has been given the opportunity to register their agreement or disagreement to this retraction. We have kept a record of any response received.

### **References**

- [1] W. Hu, H. Liu, X. Ma, and X. Bai, "The Influence and Prediction of Industry Asset Price Fluctuation Based on the LSTM Model and Investor Sentiment," *Mathematical Problems in Engineering*, vol. 2022, Article ID 1113023, 8 pages, 2022.

## Research Article

# The Influence and Prediction of Industry Asset Price Fluctuation Based on The LSTM Model and Investor Sentiment

Wenxiu Hu,<sup>1</sup> Huan Liu ,<sup>1</sup> Xiaoqiang Ma,<sup>2</sup> and Xiong Bai<sup>2</sup>

<sup>1</sup>School of Economic and Management, Xi'an University of Technology, Xi'an 710054, China

<sup>2</sup>School of Economics & Management Northwest University, Xi'an 710127, China

Correspondence should be addressed to Huan Liu; 1170511006@stu.xaut.edu.cn

Received 15 February 2022; Revised 28 February 2022; Accepted 3 March 2022; Published 21 March 2022

Academic Editor: Hangjun Che

Copyright © 2022 Wenxiu Hu et al. This is an open access article distributed under the Creative Commons Attribution License, which permits unrestricted use, distribution, and reproduction in any medium, provided the original work is properly cited.

In a real-world environment, not only can different levels of market expectations be triggered by factors such as macroeconomic policies, market operating trends, and current company developments have an impact on sector assets, but sector asset rises and falls are also influenced by a factor that cannot be ignored: market sentiment. Therefore, this paper uses LSTM to construct a forecasting model for industrial assets based on investor sentiment and public historical trading data of industry asset markets to determine future trends and obtains two conclusions: first, forecasting models incorporating investor sentiment have better forecasting effects than those without the incorporation of sentiment characteristics, indicating that the factor of investor sentiment should not be ignored when studying the problem of industry asset forecasting; secondly, investor sentiment quantified by different methods.

## 1. Introduction

As people's living standards rise, consumption is becoming a decreasing proportion of disposable income, replaced by investments, savings, and financial management [1]. Nowadays, investment and financial management are gradually coming into the public eye, and more and more people are concerned about and studying how to invest more effectively in order to allocate their disposable income rationally and maximize the return on their existing funds. The financial markets are developing at an unstoppable pace, and in the process of adapting to economic development, many investment options have emerged, most of which are based on the bond market, futures market, and the sector asset market [2]. Amongst these, the sector asset market has low investment thresholds and high liquidity, i.e., it can be quickly realized when investors need liquidity, making it the most common choice for retail investors to invest in the sector asset market to achieve a reasonable distribution of income. However, changes in the sector asset market are unpredictable and various factors, both imagined and unanticipated, may have an impact on sector assets to a greater or

lesser extent, and the market may not respond to various impacts to the same extent. The impact on asset volatility in the industry is explained in [3].

In the field of industry asset research, scholars hope to discover the overall operation and trends of industry assets through effective technical means, but after years of practice and research analysis, it is found that such ideas are difficult to realize in real life [4]. The efficient market hypothesis is considered a good theory to explain the changes in the development of the industry asset market, which believes that all effective information in the industry asset market is reflected in the historical prices of industry assets and that the future prices of industry assets are mainly affected by future information [5]. However, there are many factors that cause changes in future information that make forecasting future information very difficult, if not impossible, and therefore it is impossible to achieve forecasts of future industry assets using technical analysis under the efficient market hypothesis [6]. With the development of research and the emergence of other innovative theories, researchers have discovered that the role of investors' psychology, i.e., irrational factors, can have an impact on their financial

behavior, and this is what behavioral finance studies. With the current poor transmission mechanism in the financial markets and the time lag in information, investors have a certain speculative mentality when investing in sector assets, usually wanting to get relatively high returns for less cost, which confirms the adage “speculation is speculation.” In addition, sector assets influence investors’ decisions, which in turn influence sector assets, forming a two-way cycle, similar to the bank’s “run effect,” but investors’ decisions are often made with limited rationality mixed with some subjective judgment [7]. Family background, education, social background, etc. as the concept of behavioral finance has entered the public consciousness, some traditional theories are no longer applicable to the current financial markets. For example, while traditional asset pricing is theoretically defined based on the impact of macroeconomic policies, mesoindustry developments, and microfirm operating conditions on industry assets, there is usually a gap between asset prices in real markets and the theoretically expected prices, and behavioral finance has a unique understanding of the existence of this gap, which it sees as a result of investors’ emotional decisions. The existence of such a gap is uniquely understood by behavioral finance as a result of the “rational constraints” of investors’ emotions, which can create a systematic bias in the market as a whole and can also influence the next step in investor behavior [8].

In this paper, we consider the textual comments that reflect investors’ sentiment positively and the proxy indicators that reflect investors’ sentiment laterally, and after obtaining the textual data of investors’ sentiment, we carry out sentiment identification through sentiment analysis to obtain the negative and positive sentiment classification, based on which we obtain the textual investors’ sentiment index that represents investors’ sentiment, and together with some of the proxy indicators, we achieve the construction of a comprehensive index of investors’ sentiment through factor analysis. Finally, the index is used as the input variable of the LSTM model to build a prediction model for industry asset trends [9]. The validity of the model is tested through comparative analysis of different models and different industry backgrounds. This paper integrates the theories in the field of investor sentiment research with those in the field of industry asset forecasting research and investigates the degree of influence of investor sentiment on different styles of industries classified by CITIC style series sub-indices, which has certain theoretical significance for enriching industry asset forecasting models [10].

## 2. Related Work

The low threshold of the sector asset market and the readiness of investors to realize funds when they need them have made the equity market one of the more active markets in the financial investment sector [11]. These characteristics make the stock market a more active market in the financial investment sector. In order to invest wisely and profitably, investors focus their attention on forecasting the trend of sector assets. The common methods

used to forecast sector assets are fundamental analysis and technical analysis. Among them, the fundamental analysis method is highly subjective and mainly involves some financial researchers analyzing the future ups and downs of industry assets based on public information in the market (e.g. national policies, industry developments, company financial reports, company announcements, etc.) and combining it with their own experience, which is a test of the researcher’s professionalism and experience. For example, [12] proposed fundamental analysis methods such as the Delphi method, the principal probability method, and the cross-probability method to qualitatively forecast industry assets. Technical analysis methods are further divided into those based on statistical views and those based on data mining algorithms. Yang et al. [13] used GA-Elman neural networks to construct industry asset forecasting models, which not only achieve better forecasting results, but can also quickly calculate a large amount of data and save running time. An et al. [14] processed the mined news and financial text data and input them into a machine learning model to predict industry assets and analyzed various evaluation indicators to show that the prediction effect of the machine learning model based on text sentiment was significant.

Industry asset forecasting research has been the focus of financial researchers, and scholars have proposed many models for forecasting industry assets based on empirical and optimization studies, such as autoregressive moving average models, GRU models, and artificial neural network-type models. In order to optimize the models to achieve better forecasting results, scholars have conducted various studies: Ma et al. [15] compared BP neural networks, grey GM (1, 1) and their hybrid models, and concluded that hybrid models have better forecasting results; Thakkar and Chaudhari [16] mixed SVM models with GARCH models in order to improve the forecasting results of SVM models, and incorporated sentiment factors. In order to improve the forecasting effect of the SVM model, they mixed it with the GARCH model and incorporated the sentiment factor and investor attention into the forecasting model, and obtained a better forecasting effect. The model with the sentiment incorporated had a better effect than the model without the sentiment incorporated; Nasekin and Chen [17] chose the LSTM model to analyze the industry asset forecasting problem, and the results showed that the LSTM model could not only forecast industry assets better, but also run quickly when the data volume was large, and investors could draw on the forecasting results of the model. The results show that the LSTM model is not only good at predicting industry assets but also fast when the volume of data is large [18].

## 3. LSTM Model Based on Principal Component Analysis

*3.1. Obtaining Training Data.* The nine basic data items of the selected sector assets were obtained through the sector asset data stations of the major financial websites and the TuShare financial data interface package for Python: opening price, closing price, high price, low price, previous closing

price, up/down amount, up/down range, volume, and turnover amount. These are shown in Table 1. The KDJ and MACD indicators calculated for the underlying data are used together as training data for the model.

The KDJ indicator is a sensitive and fast technical analysis indicator that uses the real volatility of the price fluctuations of sector assets to reflect the strength of the price change trend and can signal a buy or sell before the sector assets have risen or fallen. The highest and lowest prices that have occurred in a period, the last closing price of the period, and the proportional relationship between these three are used to calculate the unripe stochastic value of RSV on the last day of the period, and then the  $K$ ,  $D$ , and  $J$  values are calculated based on the sliding average method [19].

The  $K$  value is the  $n$ -day moving average of the RSV and the  $K$  line, which is also known as the fast line, changes at a moderate rate among the 3 curves; the  $D$  value is the  $n$ -day moving average of the  $K$  value and the  $D$  line changes at the slowest rate among the 3 lines and is known as the slow line; the  $J$  value changes the fastest and is known as the ultra-fast or confirmation line as an aid to observing the buying and selling signals from the  $K$  and  $D$  lines. The three lines on the same coordinate make up the KDJ indicator, which reflects the trend of price fluctuations.

$$\begin{cases} \text{RSV} = (C_n - L_n) / (H_n - L_n) \times 100, \\ K = \frac{2}{3}K_p + \frac{1}{3}\text{RSV}, \\ D = \frac{2}{3}D_p + \frac{1}{3}K, \\ J = 3 \times K - 2 \times D, \end{cases} \quad (1)$$

where  $C_n$  is the closing price on day  $n$ ,  $L_n$  is the lowest price on day  $n$ ,  $H_n$  is the highest price on day  $n$ , and  $K_p$ , and  $D_p$  is the previous day's  $K$  and  $D$  values, both replaced by 50 if not available.

MACD is also known as the moving average of divergence. The convergence and divergence of the fast and slow averages represent changes in market trends and are a common technical indicator for sector assets. The fast and slow-moving averages, EMA, are generally chosen as the 12-day and 26-day moving averages, and their divergence, DIF, and the divergence's 9-day moving average, DEA, are calculated to give the MACD.

$$\begin{cases} \text{EMA}_{(n)} = \frac{n-1}{n+1} \times \text{PEMA}_{(n)} + \frac{2}{n+1}, \\ \text{DIF} = \text{EMA}_{(12)} - \text{EMA}_{(26)}, \\ \text{DEA} = \frac{n-1}{n+1} \times \text{PDEA}_n + \text{DIF}, \\ \text{MACD} = (\text{DIF} - \text{DEA}) \times 2, \end{cases} \quad (2)$$

where  $n$  is the number of days of moving average,  $C$  is the closing price of the day, and PEMA and PDEA are the EMA and DEA of the previous day.

**3.2. Dimensionality Reduction of Data Using Principal Component Analysis.** The principal component analysis is a method of transforming multiple interrelated raw data into a small number of linear combinations of two uncorrelated variables without changing the structure of the sample data by rotating the spatial coordinates. This reduces dimensionality and simplifies complex multidimensional problems by replacing more variables with fewer variables while maximizing the information in the original data.

To extract the principal components, the original data is first standardized, i.e., the mean of the corresponding variable is subtracted and then divided by the variance to eliminate the effect of differences in magnitudes.

$$Y_{ij}^* = \frac{x_{ij} - \bar{x}_j}{S_j}, \quad i = 1, 2, \dots, m; \quad j = 1, 2, \dots, n. \quad (3)$$

The correlation coefficient matrix  $R$  is then calculated and the eigenvalues ( $i = 1, 2, \dots, n$ ) are obtained by solving the characteristic equation  $\lambda E - R = 0$ .

The eigenvalue is the variance of each principal component. It is used to describe the amount of information contained in the direction of the corresponding eigenvector, i.e., the magnitude of the eigenvalue directly reflects the influence of each principal component. The value of an eigenvalue divided by the sum of all eigenvalues gives the variance contribution of the eigenvector.  $\lambda_i / \sum_{k=1}^n \lambda_k$  is the contribution of the  $i$ -th principal component.  $\sum_{k=1}^i \lambda_k / \sum_{k=1}^n \lambda_k$  is the cumulative contribution of the first  $i$  principal components. According to the rules for the selection of the number of principal components, the selected principal components must all have eigenvalues greater than 1 and a cumulative contribution of at least a high percentage (usually greater than 85%). It is guaranteed that the selected principal components contain most of the information of the original data.

Finally, the principal component loadings are calculated and the principal component scores are obtained as new training data.

$$T_{ij} = p(z_i, x_j) = \sqrt{\lambda_i} a_{ij}, \quad (4)$$

$$i = 1, 2, \dots, m; \quad j = 1, 2, \dots, n.$$

**3.3. Prediction Using LSTM Models.** The full form of LSTM is long term short term memory artificial neural network, a temporal recurrent neural network suitable for processing and predicting important events with relatively long intervals and delays in a time series [20]. It is a variant of the recurrent neural network, and the LSTM has an additional cellular structure in the algorithm that determines whether the information is useful or not than the recurrent neural network, as shown in Figure 1.

TABLE 1: Industry asset base data.

|      | Ts code   | Trade date | Open  | High  | Low   | Close | Pre close | Change |
|------|-----------|------------|-------|-------|-------|-------|-----------|--------|
| 0    | 000001.SZ | 20190314   | 12.33 | 12.62 | 12.55 | 12.64 | 10.20.05  | 0.184  |
| 1    | 000001.SZ | 20190313   | 12.34 | 12.55 | 12.12 | 12.37 | 0.01      | 0.0826 |
| 2    | 000001.SZ | 20190312   | 12.49 | 12.64 | 12.24 | 12.36 | 12.32     | 0.04   |
| 3999 | 000001.SZ | 20020121   | 10.19 | 9.57  | 9.6   | 10.18 | -0.59     | -5.78  |

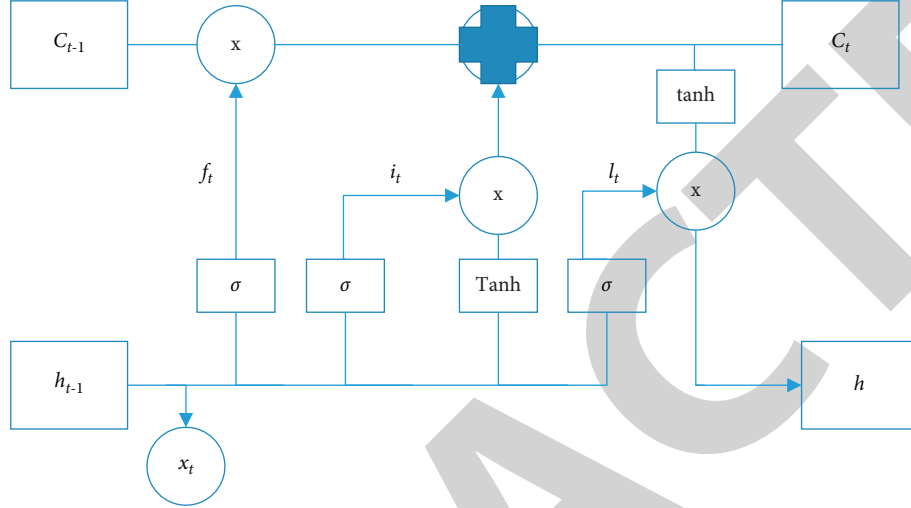


FIGURE 1: LSTM cell structure.

The LSTM has 3 gates in a cell: the forgetting gate, the input gate, and the output gate. Once a piece of data enters the LSTM's network, it is judged to be useful according to the rules, and those that match the algorithm's rules are left behind, while those that do not are forgotten through the forgetting gate. Only information that meets the algorithm's certification is left behind, while information that does not meet the rules is forgotten through the forgetting gate.

$$f_t = \sigma(W_f \cdot [h_{t-1}, x_t] + b_f). \quad (5)$$

The input gate then updates the cell state, first determining the value to be updated through the sigmoid layer, and the vector of candidate values created by the tanh layer, which are multiplied together to obtain the new candidate values.

$$\begin{cases} i_t = \sigma(W_i \cdot [h_{t-1}, x_t] + b_i), \\ C_t = \tanh(W_C \cdot [h_{t-1}, x_t] + b_C). \end{cases} \quad (6)$$

The old cell state is then multiplied by the discard information defined by the oblivion gate and the new candidate value is added to obtain the updated cell.

$$C_t = f_t \times C_{t-1} + i_t \times C_t. \quad (7)$$

Finally, based on the current cell state, the output component is determined by the sigmoid layer, which is multiplied by the tanh-processed cell state to obtain the value of the determined output

$$\begin{cases} o_t = \sigma(W_o \cdot [h_{t-1}, x_t] + b_o), \\ h_t = o_t \times \tanh(C_t). \end{cases} \quad (8)$$

In LSTM models, the model can choose what to keep and what to forget so that the model can analyze the data that is most relevant to the task. LSTM models can also learn a more abstract representation of the data so that the model learns more features of the data. These features allow LSTM models to be more effective in analyzing industry asset trends when applied to industry assets [21].

#### 4. Analysis of Results

Based on the previous analysis, we use the CITIC style index and its constituent stocks as the research object when conducting the construction of the prediction models, and this section mainly presents the results based on the financial subindices. This section constructs LSTM models based on the four forecasting scenarios mentioned above, namely, the LSTM model based on textual investor sentiment index and historical data, the LSTM model based on proxy sentiment index and historical data, the LSTM model based on composite investor sentiment index and historical data, and the LSTM model based on K-line data. Figure 2 shows the prediction results of scenario 3 on the training set compared with the real results. By tuning and optimizing the model, it can be seen that the predicted and actual values basically have the same trend, although there are certain deviations from each other, but they can capture the up and down trends well,

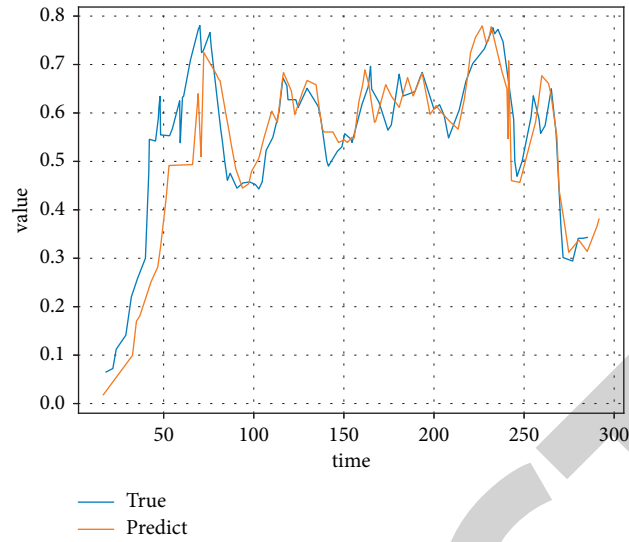


FIGURE 2: Predicted and actual values for the training set of the integrated sentiment model.

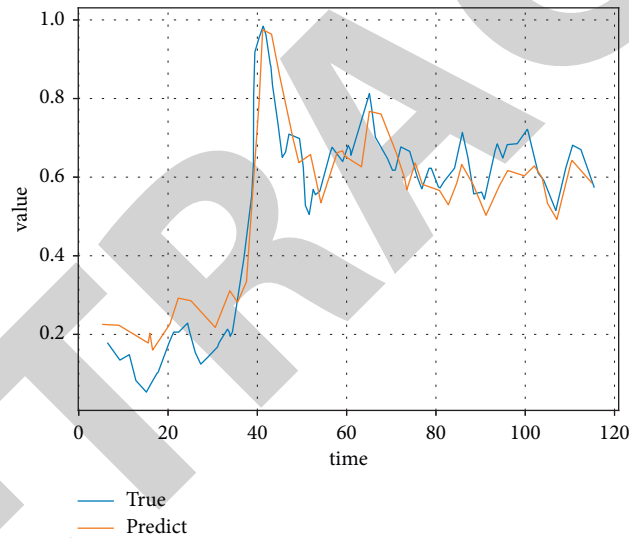


FIGURE 3: Predicted and actual values for the test set of the integrated sentiment model.

indicating that the prediction results are more satisfactory and provide a strong reference for investors' buying and selling behavior [22]. Figure 3 shows the comparison between the predicted and actual values of scenario 3 on the test set.

Figures 4–6 show the predicted versus true results for scenarios 1, 2, and 4 on the training and test sets, respectively.

Table 2 shows the performance of each evaluation indicator for each scenario based on the LSTM model. Comparing the scenarios, it can be seen that the LSTM industry asset forecasting model incorporating a composite index of investor sentiment has the best forecasting performance, the LSTM industry asset forecasting model based on a sentiment proxy index has the second-best forecasting

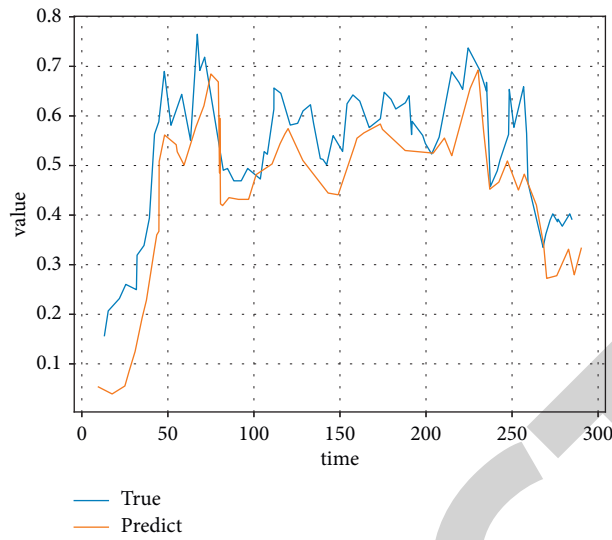


FIGURE 4: Predicted and actual values for the training set of the text sentiment prediction model.

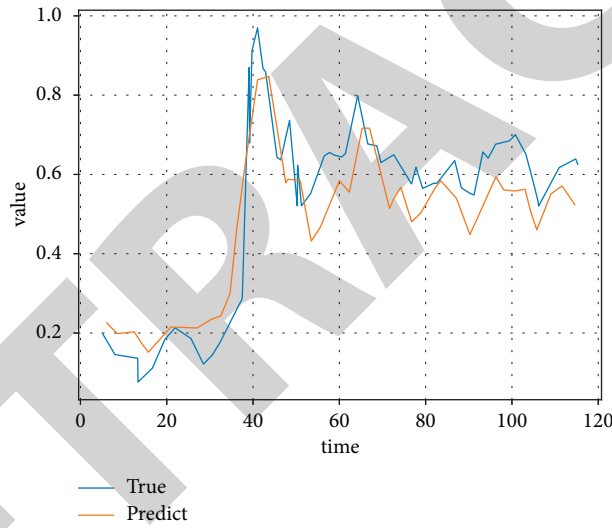


FIGURE 5: Predicted and actual values for the test set of the text sentiment prediction model.

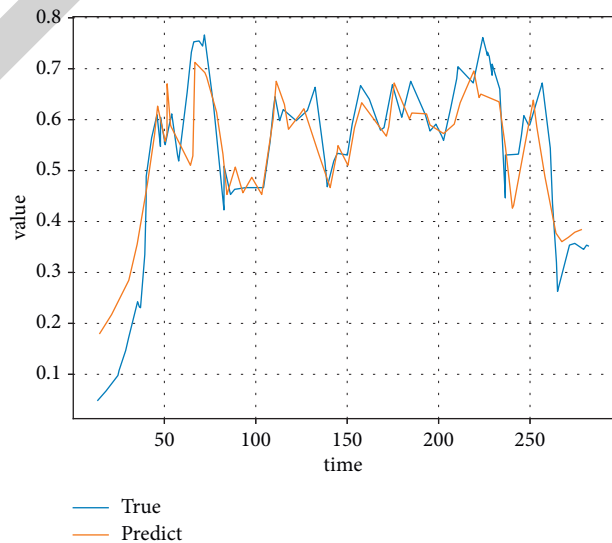


FIGURE 6: Predicted and actual values for the training set of the proxy sentiment prediction model can be seen from Figures 4–6. Scenario 3, which incorporates a composite index of investor sentiment and historical data on industry assets, has the best predictions, with the smallest difference between the true and predicted values on both the test and training sets.



TABLE 2: LSTM model evaluation metrics based on each scenario.

| Prediction scheme | Scheme I     |          | Scheme 2     |          | Scheme 3     |          | Scheme 4     |          |
|-------------------|--------------|----------|--------------|----------|--------------|----------|--------------|----------|
|                   | Training set | Test set | Training set | Test set | Training set | Test set | Training set | Test set |
| MAE               | 0.045        | 0.057    | 0.041        | 0.051    | 0.029        | 0.039    | 0.095        | 0.112    |
| MSE               | 0.0034       | 0.0041   | 0.0026       | 0.0032   | 0.00012      | 0.0001   | 0.015        | 0.0121   |
| RMSE              | 0.0591       | 0.0648   | 0.053        | 0.0558   | 0.117        | 0.0142   | 0.115        | 0.1104   |
| MAPE              | 0.52         | 0.42     | 0.41         | 0.48     | 0.26         | 0.39     | 0.4          | 0.5      |
| Accuracy          | 0.72         | 0.73     | 0.82         | 0.75     | 0.89         | 0.81     | 0.61         | 0.59     |

performance, and the K-line forecasting model based on historical industry asset data only has the worst forecasting performance.

## 5. Conclusions

In this paper, when using technical methods to build LSTM stock forecasting models, traditional methods often result in poor generalization and poor forecasting due to a large number of input data variables selected, overlapping data information, and the large impact of outliers on training. To address such problems, we propose to use principal component analysis to reduce the dimensionality of the underlying data, then combine the KDJ and MACD as input data together with stock-related technical indicators and adjust the model according to the characteristics of the stock before making predictions. The experimental results show that the PCA-S-LSTM model can reduce the average error of prediction, reduce the running time, improve the stability of prediction, and predict the closing price of Ping An Bank more accurately.

## Data Availability

The experimental data used to support the findings of this study are available from the corresponding author upon request.

## Conflicts of Interest

The authors declare that they have no conflicts of interest regarding this work.

## References

- [1] H. Wang, L. Xue, W. Du et al., "The effect of online investor sentiment on stock movements: An LSTM approach," in *Proceedings of the International Conference on Intelligence Science*, pp. 1–14, Springer, Cham, 2021, February.
- [2] Z. Huang and Z. Li, "What reflects investor sentiment? Empirical evidence from China," *Data Science in Finance and Economics*, vol. 1, no. 3, pp. 235–252, 2021.
- [3] M. Baker and J. Wurgler, "Investor sentiment in the stock market," *The Journal of Economic Perspectives*, vol. 21, no. 2, pp. 129–152, 2007.
- [4] M. Li, W. Li, F. Wang, X. Jia, and G. Rui, "Applying BERT to analyze investor sentiment in stock market," *Neural Computing & Applications*, vol. 33, no. 10, pp. 4663–4676, 2021.
- [5] G. Wang, G. Yu, and X. Shen, "The effect of online environmental news on green industry stocks: The mediating role of investor sentiment," *Physica A: Statistical Mechanics and Its Applications*, vol. 573, Article ID 125979, 2021.
- [6] Y. Li, S. Jiang, X. Li, and S. Wang, "The role of news sentiment in oil futures returns and volatility forecasting: Data-decomposition based deep learning approach," *Energy Economics*, vol. 95, Article ID 105140, 2021.
- [7] S. R. Das and M. Y. Chen, "Yahoo! for Amazon: Sentiment extraction from small talk on the web," *Management Science*, vol. 53, no. 9, pp. 1375–1388, 2007.
- [8] Y. Ren, F. Liao, and Y. Gong, "Impact of news on the trend of stock price change: An analysis based on the deep bidirectional LSTM model," *Procedia Computer Science*, vol. 174, pp. 128–140, 2020.
- [9] O. B. Sezer, M. U. Gudelek, and A. M. Ozbayoglu, "Financial time series forecasting with deep learning: A systematic literature review: 2005–2019," *Applied Soft Computing*, vol. 90, Article ID 106181, 2020.
- [10] L. Malandri, F. Z. Xing, C. Orsenigo, C. Vercellis, and E. Cambria, "Public mood-driven asset allocation: The importance of financial sentiment in portfolio management," *Cognitive Computation*, vol. 10, no. 6, pp. 1167–1176, 2018.
- [11] W. Gu, L. Zhang, H. Xi, and S. Zheng, "Stock prediction based on news text analysis," *Journal of Advanced Computational Intelligence and Intelligent Informatics*, vol. 25, no. 5, pp. 581–591, 2021.
- [12] L. Yang, T. L. J. Ng, B. Smyth, and R. Dong, "Htl: Hierarchical transformer-based multi-task learning for volatility prediction," in *Proceedings of the Web Conference 2020*, pp. 441–451, Taipei, Taiwan, 2020, April.
- [13] V. D. Ta, C. M. Liu, and D. A. Tadesse, "Portfolio optimization-based stock prediction using long-short term memory network in quantitative trading," *Applied Sciences*, vol. 10, no. 2, p. 437, 2020.
- [14] P. An, Z. Wang, and C. Zhang, "Ensemble unsupervised autoencoders and Gaussian mixture model for cyberattack detection," *Information Processing & Management*, vol. 59, no. 2, Article ID 102844, 2022.
- [15] H. Ma, J. Ma, H. Wang, P. Li, and W. Du, "A comprehensive review of investor sentiment analysis in stock price forecasting," in *Proceedings of the 2021 IEEE/ACIS 20th International Fall Conference on Computer and Information Science (ICIS Fall)*, pp. 264–268, IEEE, Xi'an, China, 2021, October.
- [16] A. Thakkar and K. Chaudhari, "Fusion in stock market prediction: A decade survey on the necessity, recent developments, and potential future directions," *Information Fusion*, vol. 65, pp. 95–107, 2021.
- [17] S. Nasekin and C. Y. H. Chen, "Deep learning-based cryptocurrency sentiment construction," *Digital Finance*, vol. 2, no. 1, pp. 39–67, 2020.
- [18] C. H. Wu, C. C. Lu, Y. F. Ma, and R. S. Lu, "A new forecasting framework for bitcoin price with LSTM," in *Proceedings of the 2018 IEEE International Conference on Data Mining*